2013

ANNUAL PROGRESS REPORT

DOE Hydrogen and Fuel Cells Program

U.S. DEPARTMENT OF ENERGY

DOE/GO-102013-4260
December 2013

U.S. Department of Energy
1000 Independence Avenue, S.W.
Washington, D.C. 20585-0121

FY 2013
PROGRESS REPORT FOR THE DOE HYDROGEN AND FUEL CELLS PROGRAM

December 2013

DOE/GO-102013-4260

Approved by Sunita Satyapal, Director, Hydrogen and Fuel Cells Program

NOTICE

This report was prepared as an account of work sponsored by an agency of the United States government. Neither the United States government nor any agency thereof, nor any of their employees, makes any warranty, express or implied, or assumes any legal liability or responsibility for the accuracy, completeness, or usefulness of any information, apparatus, product, or process disclosed, or represents that its use would not infringe privately owned rights. Reference herein to any specific commercial product, process, or service by trade name, trademark, manufacturer, or otherwise does not necessarily constitute or imply its endorsement, recommendation, or favoring by the United States government or any agency thereof. The views and opinions of authors expressed herein do not necessarily state or reflect those of the United States government or any agency thereof.

Available electronically at http://www.osti.gov/bridge

Available for a processing fee to U.S. Department of Energy
and its contractors, in paper, from:
U.S. Department of Energy
Office of Scientific and Technical Information
P.O. Box 62
Oak Ridge, TN 37831-0062
Phone: (865) 576-8401
Fax: (865) 576-5728
E-mail: mailto:reports@adonis.osti.gov

Available for sale to the public, in paper, from:
U.S. Department of Commerce
National Technical Information Service
5285 Port Royal Road
Springfield, VA 22161
Phone: (800) 553-6847
Fax: (703) 605-6900
E-mail: orders@ntis.fedworld.gov
Online ordering: http://www.ntis.gov/ordering.htm

Printed on paper containing at least 50% wastepaper, including 20% postconsumer waste

Table of Contents

I. Introduction I-1

II. Hydrogen Production II-1

II.0 Hydrogen Production Program Overview II-3

II.A Electrolysis II-11

II.A.1 Giner, Inc.: PEM Electrolyzer Incorporating an Advanced Low-Cost Membrane II-11

II.A.2 National Renewable Energy Laboratory: Renewable Electrolysis Integrated Systems Development and Testing II-15

II.A.3 Proton OnSite: High-Performance, Low-Cost Hydrogen Generation from Renewable Energy II-18

II.A.4 Proton OnSite: Low-Cost Large-Scale PEM Electrolysis for Renewable Energy Storage II-22

II.A.5 Proton OnSite: Economical Production of Hydrogen through Development of Novel, High Efficiency Electrocatalysts for Alkaline Membrane Electrolysis II-26

II.A.6 Giner, Inc.: Unitized Design for Home Refueling Appliance for Hydrogen Generation to 5,000 psi II-31

II.A.7 Proton OnSite: Hydrogen by Wire - Home Fueling System II-35

II.A.8 Proton OnSite: Low-Noble-Metal-Content Catalysts/Electrodes for Hydrogen Production by Water Electrolysis II-39

II.B Solar Thermochemical II-43

II.B.1 Argonne National Laboratory: Electrolyzer Development in the Cu-Cl Thermochemical Cycle II-43

II.B.2 Science Applications International Corporation: Solar High-Temperature Water-Splitting Cycle with Quantum Boost II-48

II.B.3 University of Colorado: Solar-Thermal Redox-Based Water Splitting Cycles II-57

II.B.4 Sandia National Laboratories: Solar Hydrogen Production with a Metal Oxide-Based Thermochemical Cycle II-62

II.B.5 Savannah River National Laboratory: Electrolyzer Development for the HyS Thermochemical Cycle II-68

II.C Photoelectrochemical II-70

II.C.1 National Renewable Energy Laboratory: Semiconductor Materials for Photoelectrolysis II-70

II.C.2 MVSystems, Incorporated: Photoelectrochemical Hydrogen Production II-75

II.C.3 Midwest Optoelectronics, LLC: Critical Research for Cost-Effective Photoelectrochemical Production of Hydrogen II-79

II.C.4 Lawrence Livermore National Laboratory: Characterization and Optimization of Photoelectrode Surfaces for Solar-to-Chemical Fuel Conversion II-84

II.C.5 University of Nevada, Reno: Metal Oxide Semiconductor Nanotubular Arrays for Photoelectrochemical Hydrogen Generation II-89

II.C.6 Los Alamos National Laboratory: Photoelectrochemical Material Synthesis at LANL II-93

II.C.7 California Institute of Technology: Next-Generation Si Microwire Array Devices for Unassisted Photoelectrosynthesis II-97

II.D Biological II-101

II.D.1 University of California, Berkeley: Maximizing Light Utilization Efficiency and Hydrogen Production in Microalgal Cultures II-101

II.D.2 National Renewable Energy Laboratory: Biological Systems for Hydrogen Photoproduction II-105

II.D.3 National Renewable Energy Laboratory: Fermentation and Electrohydrogenic Approaches to Hydrogen Production II-108

II.D.4 J. Craig Venter Institute: Hydrogen from Water in a Novel Recombinant Oxygen-Tolerant Cyanobacterial System II-113

II.D.5 National Renewable Energy Laboratory: Probing O_2-Tolerant CBS Hydrogenase for Hydrogen Production II-116

II. Hydrogen Production (Continued)

II.E Distributed Bio-Derived Liquids II-119
II.E.1 National Renewable Energy Laboratory: Distributed Bio-Oil Reforming. II-119
II.E.2 Pacific Northwest National Laboratory: Biomass-Derived Liquids Distributed Reforming II-124

III. Hydrogen Delivery III-1
III.0 Hydrogen Delivery Program Overview III-3
III.1 Argonne National Laboratory: Hydrogen Delivery Infrastructure Analysis III-11
III.2 Mohawk Innovative Technologies, Inc.: Oil-Free Centrifugal Hydrogen Compression Technology Demonstration III-16
III.3 Hexagon Lincoln: Development of High-Pressure Hydrogen Storage Tank for Storage and Gaseous Truck Delivery III-21
III.4 Savannah River National Laboratory: Fiber Reinforced Composite Pipeline III-25
III.5 Sandia National Laboratories: Hydrogen Embrittlement of Structural Steels III-29
III.6 FuelCell Energy, Inc.: Electrochemical Hydrogen Compressor III-33
III.7 Oak Ridge National Laboratory: Vessel Design and Fabrication Technology for Stationary High-Pressure Hydrogen Storage. III-37
III.8 Lawrence Livermore National Laboratory: Rapid High-Pressure Liquid Hydrogen Refueling for Maximum Range and Dormancy III-42
III.9 Sandia National Laboratories: Polymer and Composite Material Performance in Hydrogen III-46
III.10 Concepts NREC: Development of a Centrifugal Hydrogen Pipeline Gas Compressor III-48
III.11 Pacific Northwest National Laboratory: Investigation of H2 Diaphragm Compressors to Enable Low-Cost Long-Life Operation III-53

IV. Hydrogen Storage IV-1
IV.0 Hydrogen Storage Program Overview IV-3
IV.A Testing and Analysis IV-11
IV.A.1 Argonne National Laboratory: System Analysis of Physical and Materials-Based Hydrogen Storage Options IV-11
IV.A.2 Strategic Analysis, Inc.: Hydrogen Storage Cost Analysis. IV-18
IV.A.3 H2 Technology Consulting LLC: Best Practices for Characterizing Engineering Properties of Hydrogen Storage Materials. IV-24
IV.B Engineering – HSECoE . . . . . .
IV.B.1 Savannah River National Laboratory: Hydrogen Storage Engineering Center of Excellence. IV-29
IV.B.2 Pacific Northwest National Laboratory: Systems Engineering of Chemical Hydrogen Storage, Pressure Vessel, and Balance of Plant for Onboard Hydrogen Storage. IV-38
IV.B.3 United Technologies Research Center: Advancement of Systems Designs and Key Engineering Technologies for Materials-Based Hydrogen Storage. IV-46
IV.B.4 Los Alamos National Laboratory: Chemical Hydride Rate Modeling, Validation, and System Demonstration IV-53
IV.B.5 National Renewable Energy Laboratory: System Design, Analysis, Modeling, and Media Engineering Properties for Hydrogen Energy Storage IV-57
IV.B.6 General Motors Company: Thermal Management of Onboard Cryogenic Hydrogen Storage Systems IV-63
IV.B.7 Ford Motor Company: Ford/BASF-SE/UM Activities in Support of the Hydrogen Storage Engineering Center of Excellence IV-67
IV.B.8 Oregon State University: Microscale Enhancement of Heat and Mass Transfer for Hydrogen Energy Storage IV-71
IV.B.9 Hexagon Lincoln: Development of Improved Composite Pressure Vessels for Hydrogen Storage IV-76

IV. Hydrogen Storage (Continued)

IV.C Materials – Sorption IV-80
IV.C.1 National Renewable Energy Laboratory: Hydrogen Sorbent Measurement Qualification and Characterization IV-80
IV.C.2 HRL Laboratories, LLC: Room Temperature Hydrogen Storage in Nano-Confined Liquids IV-84
IV.C.3 Lawrence Berkeley National Laboratory: Hydrogen Storage in Metal-Organic Frameworks. IV-89
IV.C.4 Oak Ridge National Laboratory: The Quantum Effects of Pore Structure on Hydrogen Adsorption IV-93
IV.C.5 Northwestern University: Metallation of Metal–Organic Frameworks: En Route to Ambient Temperature Storage of Molecular Hydrogen IV-99
IV.C.6 National Renewable Energy Laboratory: Weak Chemisorption Validation. IV-103
IV.C.7 Pennsylvania State University: Hydrogen Trapping through Designer Hydrogen Spillover Molecules with Reversible Temperature and Pressure-Induced Switching IV-107

IV.D Materials – Metal Hydrides IV-112
IV.D.1 Northwestern University: Design of Novel Multi-Component Metal Hydride-Based Mixtures for Hydrogen Storage IV-112
IV.D.2 Delaware State University: Hydrogen Storage Materials for Fuel Cell-Powered Vehicles IV-121
IV.D.3 National Institute of Standards and Technology: Neutron Characterization in Support of the DOE Hydrogen Storage Sub-Program IV-126

IV.E Materials – Chemical IV-131
IV.E.1 Los Alamos National Laboratory: Fluid Phase Chemical Hydrogen Storage Materials IV-131
IV.E.2 Hawaii Hydrogen Carriers, LLC: Development of a Practical Hydrogen Storage System Based on Liquid Organic Hydrogen Carriers and a Homogeneous Catalyst. IV-135
IV.E.3 University of Oregon: Novel Carbon(C)-Boron(B)-Nitrogen(N)-Containing H2 Storage Materials IV-140
IV.E.4 Brookhaven National Laboratory: Aluminum Hydride: the Organometallic Approach IV-146
IV.E.5 Savannah River National Laboratory: Electrochemical Reversible Formation of Alane. IV-150

IV.F Advanced Tanks IV-154
IV.F.1 Oak Ridge National Laboratory: Lifecycle Verification of Polymeric Storage Tank Liners IV-154
IV.F.2 Oak Ridge National Laboratory: Melt Processable PAN Precursor for High-Strength, Low-Cost Carbon Fibers IV-160
IV.F.3 Oak Ridge National Laboratory: Development of Low-Cost, High-Strength Commercial Textile Precursor (PAN-MA) IV-165
IV.F.4 Pacific Northwest National Laboratory: Synergistically Enhanced Materials and Design Parameters for Reducing the Cost of Hydrogen Storage Tanks. IV-171

V. Fuel Cells V-1

V.0 Fuel Cells Program Overview. V-3

V.A Catalysts V-9
V.A.1 3M Company: Durable Catalysts for Fuel Cell Protection during Transient Conditions. V-9
V.A.2 National Renewable Energy Laboratory: Extended, Continuous Pt Nanostructures in Thick, Dispersed Electrodes V-14
V.A.3 Argonne National Laboratory: Nanosegregated Cathode Catalysts with Ultra-Low Platinum Loading. V-19
V.A.4 Brookhaven National Laboratory: Contiguous Platinum Monolayer Oxygen Reduction Electrocatalysts on High-Stability Low-Cost Supports. V-26
V.A.5 Los Alamos National Laboratory: The Science and Engineering of Durable Ultra-Low PGM Catalysts V-31
V.A.6 Los Alamos National Laboratory: Engineered Nano-Scale Ceramic Supports for PEM Fuel Cells V-37

V. Fuel Cells (Continued)

V.A Catalysts (Continued)

V.A.7 National Renewable Energy Laboratory: Tungsten Oxide and Heteropoly Acid-Based Systems for Ultra-High Activity and Stability of Pt Catalysts in PEM Fuel Cell Cathodes V-44

V.A.8 Illinois Institute of Technology: Synthesis and Characterization of Mixed-Conducting Corrosion Resistant Oxide Supports V-50

V.A.9 Northeastern University: Development of Novel Non-PGM Electrocatalysts for Proton Exchange Membrane Fuel Cell Applications V-54

V.A.10 General Motors Company: High-Activity Dealloyed Catalysts V-61

V.A.11 University of South Carolina: Development of Ultra-Low Platinum Alloy Cathode Catalyst for Polymer Electrolyte Membrane Fuel Cells V-68

V.A.12 Los Alamos National Laboratory: Non-Precious Metal Fuel Cell Cathodes: Catalyst Development and Electrode Structure Design V-74

V.B Membranes V-79

V.B.1 Giner, Inc.: Dimensionally Stable High Performance Membrane V-79

V.B.2 FuelCell Energy, Inc.: High-Temperature Membrane with Humidification-Independent Cluster Structure V-83

V.B.3 Ion Power Inc.: Corrugated Membrane Fuel Cell Structures V-86

V.C MEA Integration V-90

V.C.1 3M Company: High-Performance, Durable, Low-Cost Membrane Electrode Assemblies for Transportation Applications V-90

V.C.2 Argonne National Laboratory: Rationally Designed Catalyst Layers for PEMFC Performance Optimization V-95

V.D Degradation Studies V-98

V.D.1 Los Alamos National Laboratory: Durability Improvements through Degradation Mechanism Studies V-98

V.D.2 Nuvera Fuel Cells, Inc.: Durability of Low-Platinum Fuel Cells Operating at High Power Density V-104

V.D.3 Los Alamos National Laboratory: Accelerated Testing Validation V-109

V.D.4 National Renewable Energy Laboratory: Analysis of Laboratory Fuel Cell Technology Status – Voltage Degradation V-116

V.D.5 Ballard Power Systems: Development of Micro-Structural Mitigation Strategies for PEM Fuel Cells: Morphological Simulations and Experimental Approaches V-121

V.E Impurities V-129

V.E.1 National Renewable Energy Laboratory: Effect of System Contaminants on PEMFC Performance and Durability V-129

V.E.2 Hawaii Natural Energy Institute: The Effect of Airborne Contaminants on Fuel Cell Performance and Durability V-135

V.F Transport Studies V-141

V.F.1 Lawrence Berkeley National Laboratory: Fuel Cell Fundamentals at Low and Subzero Temperatures V-141

V.F.2 Giner, Inc.: Transport in PEMFCs V-147

V.F.3 General Motors Company: Investigation of Micro- and Macro-Scale Transport Processes f or Improved Fuel Cell Performance V-153

V.F.4 Nuvera Fuel Cells, Inc.: Transport Studies Enabling Efficiency Optimization of Cost-Competitive Fuel Cell Stacks V-159

V.G Balance of Plant V-162

V.G.1 Dynalene Inc.: Large-Scale Testing, Demonstration and Commercialization of the Nanoparticle-Based Fuel Cell Coolant (SBIR Phase III) V-162

V. Fuel Cells (Continued)

V.G Balance of Plant (Continued)

V.G.2 Tetramer Technologies, LLC: New High-Performance Water Vapor Membranes To Improve Fuel Cell Balance-of-Plant Efficiency and Lower Costs . . . V-166

V.G.3 Eaton Corporation: Roots Air Management System with Integrated Expander . . . V-170

V.H Analysis/Characterization. . . . V-175

V.H.1 Argonne National Laboratory: Fuel Cells Systems Analysis . . . V-175

V.H.2 Strategic Analysis, Inc.: Fuel Cell Transportation Cost Analysis. . . . V-181

V.H.3 Oak Ridge National Laboratory: Characterization of Fuel Cell Materials. . . . V-186

V.H.4 National Institute of Standards and Technology: Neutron Imaging Study of the Water Transport in Operating Fuel Cells . . . V-193

V.H.5 National Renewable Energy Laboratory: Enlarging the Potential Market for Stationary Fuel Cells Through System Design Optimization . . . V-199

V.H.6 Battelle: Stationery and Emerging Market Fuel Cell System Cost Analysis - Material Handling Equipment. . . . V-203

V.H.7 Lawrence Berkeley National Laboratory: A Total Cost of Ownership Model for Design and Manufacturing Optimization of Fuel Cells in Stationary and Emerging Market Applications . . . V-207

V.H.8 Los Alamos National Laboratory: Technical Assistance to Developers . . . V-212

V.I Portable Power . . . V-216

V.I.1 Arkema Inc.: Novel Materials for High Efficiency Direct Methanol Fuel Cells . . . V-216

V.I.2 Los Alamos National Laboratory: Advanced Materials and Concepts for Portable Power Fuel Cells . . . V-220

V.J Stationary Power . . . V-227

V.J.1 InnovaTek: Power Generation from an Integrated Biomass Reformer and Solid Oxide Fuel Cell (SBIR Phase III Xlerator Program) . . . V-227

V.K Bipolar Plates . . . V-231

V.K.1 TreadStone Technologies, Inc.: Low-Cost PEM Fuel Cell Metal Bipolar Plates . . . V-231

V.L Alkaline Fuel Cells . . . V-235

V.L.1 National Renewable Energy Laboratory: Advanced Ionomers and MEAs for Alkaline Membrane Fuel Cells . . . V-235

V.M Cross-Cutting . . . V-238

V.M.1 University of Connecticut: Improving Fuel Cell Durability and Reliability . . . V-238

V.N Basic Energy Sciences Fuel Cell Research. . . . V-243

V.N.1 University of Chicago: Computer Simulation of Proton Transport in Fuel Cell Membranes . . . V-243

V.N.2 Clemson University: Fluoropolymers, Electrolytes, Composites and Electrodes . . . V-247

V.N.3 Lehigh University: Gas Transport Across Hyperthin Membranes. . . . V-251

V.N.4 University of Texas: Theory-Guided Design of Nanoscale Multi-Metallic Catalysts For Fuel Cells . . . V-254

V.N.5 Columbia University: Structure-Property Relationship in Metal Carbides and Bimetallic Alloys . . . V-257

V.N.6 University of New Mexico: Nanostructured Catalysts for Hydrogen Production from Renewable Feedstocks . . . V-260

V.N.7 University of Texas at Austin: Fundamental Structure/Property Studies of Gas Separation Membrane Polymers. . . . V-264

V.N.8 Georgia Institute of Technology: Precisely Tunable High Performance Carbon Molecular Sieve Membranes for Energy Intensive Separations . . . V-268

V.N.9 University of Southern California, Los Angeles: Nanoporous Membranes for Hydrogen Production: Experimental Studies and Molecular Simulations . . . V-273

V. Fuel Cells (Continued)

V.N BES (Continued)

V.N.10 Argonne National Laboratory: Structure/Composition/Function Relationships in Supported Nanoscale Catalysts for Hydrogen . . . V-276

V.N.11 Brookhaven National Laboratory: Metal and Metal Oxide-Supported Platinum Monolayer Electrocatalysts for Oxygen Reduction . . . V-280

V.N.12 Brookhaven National Laboratory: Active Sites and Mechanism for the Water-Gas Shift Reaction on Metal and Metal/Oxide Catalysts. . . . V-284

V.N.13 Oak Ridge National Laboratory: Fundamentals of Catalysis and Chemical Transformations . . . V-288

V.N.14 Pacific Northwest National Laboratory: Activation of Small Molecules with Bi-Functional Ambiphilic Catalyst Complexes . . . V-292

V.N.15 Pacific Northwest National Laboratory: Bio-Inspired Molecular Catalysts for Oxidation of Hydrogen and Production of Hydrogen: Cheap Metals for Noble Tasks . . . V-295

V.N.16 University of California, Santa Barbara: Platinum-Group Metal (PGM) Substituted Complex Oxide Catalysts . . . V-298

V.N.17 University of Connecticut: Porous Transition Metal Oxides: Synthesis, Characterization, and Catalytic Activity. . . . V-301

V.N.18 University of Connecticut: Understanding the Effects of Surface Chemistry and Microstructure on the Activity and Stability of Pt Electrocatalysts on Non-Carbon Supports . . . V-305

V.N.19 Georgetown University: In Situ NMR/IR/Raman and ab initio DFT Investigations of Pt-Based Mono- and Bi-metallic Nanoscale Electrocatalysts: from Sulfur-Poisoning to Polymer Promoters to Surface Activity Indexes . . . V-309

V.N.20 Ohio State University: Investigation of the Nature of Active Sites on Heteroatom-Containing Carbon Nano-Structures for Oxygen Reduction Reaction . . . V-313

V.N.21 University of Pennsylvania: Oxide-Metal Interactions Studied on M@Oxide, Core-Shell Catalysts . . . V-318

V.N.22 University of Pennsylvania: Fundamental Studies of the Steam Reforming of Alcohols on PdZnO and Co/ZnO Catalysts . . . V-320

V.N.23 University of Pittsburgh: Theoretically Relating the Surface Composition of the Pt Alloys to Their Performance as the Electrocatalysts of Low-Temperature Fuel Cells . . . V-324

V.N.24 Rutgers University: Nanoscale Surface Chemistry and Electrochemistry of Clean and Metal-Covered Faceted Substrates: Structure, Reactivity and Electronic Properties. . . . V-328

V.N.25 University of Texas: Correlation of Theory and Function in Well-Defined Bimetallic Electrocatalysts. . . . V-331

V.N.26 Tufts University: Metal Ion Sites on Oxide Supports as Catalysts for the Water-Gas Shift and Methanol Steam Reforming Reactions . . . V-335

V.N.27 Virginia Tech: Hydrocarbon Oxidation, Dehydrogenation and Coupling over Model Metal Oxide Surfaces . . . V-340

V.N.28 Virginia Tech: Atomic Level Studies of Advanced Catalysts for Hydrodeoxygenation . . . V-343

V.N.29 University of Wisconsin: Atomic-Scale Design of Metal and Alloy Catalysts: A Combined Theoretical and Experimental Approach . . . V-347

VI. Manufacturing R&D . . . VI-1

VI.0 Manufacturing R&D Program Overview . . . VI-3

VI.1 National Renewable Energy Laboratory: Fuel Cell Membrane Electrode Assembly Manufacturing R&D . . . VI-7

VI.2 W. L. Gore & Associates, Inc.: Manufacturing of Low-Cost, Durable Membrane Electrode Assemblies Engineered for Rapid Conditioning . . . VI-11

VI.3 Rensselaer Polytechnic Institute: Adaptive Process Controls and Ultrasonics for High-Temperature PEM MEA Manufacture . . . VI-17

VI.4 National Institute of Standards and Technology: Metrology for Fuel Cell Manufacturing . . . VI-23

VI. Manufacturing R&D (Continued)

VI.5 BASF Fuel Cell, Inc.: High-Speed, Low-Cost Fabrication of Gas Diffusion Electrodes for Membrane Electrode Assemblies . . . VI-27
VI.6 Quantum Fuel Systems Technologies Worldwide, Inc.: Development of Advanced Manufacturing Technologies for Low-Cost Hydrogen Storage Vessels . . . VI-30

VII. Technology Validation . . . VII-1

VII.0 Technology Validation Program Overview . . . VII-3
VII.1 National Renewable Energy Laboratory: Technology Validation: Fuel Cell Bus Evaluations . . . VII-7
VII.2 National Renewable Energy Laboratory: Stationary Fuel Cell Evaluation . . . VII-11
VII.3 H2Pump LLC: Hydrogen Recycling System Evaluation and Data Collection . . . VII-15
VII.4 National Renewable Energy Laboratory: Hydrogen Component Validation . . . VII-18
VII.5 Proton OnSite: Validation of an Advanced High-Pressure PEM Electrolyzer and Composite Hydrogen Storage, with Data Reporting, for SunHydro Stations . . . VII-22
VII.6 National Renewable Energy Laboratory: Forklift and Backup Power Data Collection and Analysis . . . VII-26
VII.7 National Renewable Energy Laboratory: Fuel Cell Electric Vehicle Evaluation . . . VII-32
VII.8 National Renewable Energy Laboratory: Next Generation Hydrogen Infrastructure Evaluation . . . VII-36
VII.9 California Air Resources Board: Data Collection and Validation of Newport Beach Hydrogen Station Performance . . . VII-41
VII.10 California State University, Los Angeles: California State University Los Angeles Hydrogen Refueling Facility Performance Evaluation and Optimization . . . VII-43
VII.11 Gas Technology Institute: Performance Evaluation of Delivered Hydrogen Fueling Stations . . . VII-45

VIII. Safety, Codes & Standards . . . VIII-1

VIII.0 Safety, Codes & Standards Program Overview . . . VIII-3
VIII.1 National Renewable Energy Laboratory: Fuel Cell Technologies National Codes and Standards Development and Outreach . . . VIII-7
VIII.2 National Renewable Energy Laboratory: Component Standard Research and Development . . . VIII-11
VIII.3 Los Alamos National Laboratory: Hydrogen Safety, Codes and Standards: Sensors . . . VIII-14
VIII.4 Sandia National Laboratories: R&D for Safety, Codes and Standards: Materials and Components Compatibility . . . VIII-22
VIII.5 Los Alamos National Laboratory: Hydrogen Fuel Quality . . . VIII-28
VIII.6 Sandia National Laboratories: R&D for Safety Codes and Standards: Hydrogen Release Behavior . . . VIII-33
VIII.7 Sandia National Laboratories: R&D for Safety Codes and Standards: Risk Assessment . . . VIII-39
VIII.8 Pacific Northwest National Laboratory: Hydrogen Emergency Response Training for First Responders . . . VIII-43
VIII.9 Pacific Northwest National Laboratory: Hydrogen Safety Panel and Hydrogen Safety Knowledge Tools . . . VIII-46
VIII.10 Zero Carbon Energy Solutions: International Partnership for Hydrogen & Fuel Cells in the Economy - Regulations Codes and Standards Working Group . . . VIII-51
VIII.11 National Renewable Energy Laboratory: NREL Hydrogen Sensor Testing Laboratory . . . VIII-55

IX. Market Transformation . . . IX-1

IX.0 Market Transformation Program Overview . . . IX-3
IX.1 National Renewable Energy Laboratory: Direct Methanol Fuel Cell Material Handling Equipment Deployment . . . IX-7
IX.2 Pacific Northwest National Laboratory: Fuel Cell Combined Heat and Power Commercial Demonstration . . . IX-11
IX.3 Advanced Technology International: Landfill Gas-to-Hydrogen . . . IX-16

IX. Market Transformation (Continued)

IX.4 Hawaii Natural Energy Institute: Hydrogen Energy Systems as a Grid Management Tool IX-19
IX.5 Plug Power Inc.: Ground Support Equipment Demonstration IX-24
IX.6 Argonne National Laboratory: Fuel Cells as Range Extenders for Battery Electric Vehicles IX-26
IX.7 National Renewable Energy Laboratory: Hawaii Hydrogen Initiative (H2I) Financial Scenario Analysis IX-30

X. American Recovery and Reinvestment Act X-1

X.0 American Recovery and Reinvestment Act Activities. X-3
X.1 Delphi Automotive Systems, LLC: Solid Oxide Fuel Cell Diesel Auxiliary Power Unit Demonstration X-7
X.2 Plug Power Inc.: Highly Efficient, 5-kW CHP Fuel Cells Demonstrating Durability and Economic Value in Residential and Light Commercial Applications X-10
X.3 Plug Power Inc.: Accelerating Acceptance of Fuel Cell Backup Power Systems. X-13
X.4 Sprint Nextel: Use of 72-Hour Hydrogen PEM Fuel Cell Systems to Support Emergency Communications. X-16

XI. Systems Analysis XI-1

XI.0 Systems Analysis Program Overview XI-3
XI.1 Oak Ridge National Laboratory: Worldwide Status of Hydrogen Fuel Cell Vehicle Technology and Prospects for Commercialization XI-13
XI.2 University of California: Siting Strategies for Early H2 Refueling Infrastructure in California: Learning from the Gasoline Experience XI-17
XI.3 University of California: Design and Economics of an Early Hydrogen Refueling Network for California XI-21
XI.4 Oak Ridge National Laboratory: Analysis of Optimal Onboard Storage Pressure for Hydrogen Fuel Cell Vehicles XI-25
XI.5 Argonne National Laboratory: Life-Cycle Analysis of Hydrogen Onboard Storage Options XI-29
XI.6 Argonne National Laboratory: Employment Impacts of Infrastructure Development for Hydrogen and Fuel Cell Technologies XI-33
XI.7 National Renewable Energy Laboratory: Pathway Analysis: Projected Cost, Well-to-Wheels Energy Use and Emissions of Current Hydrogen Technologies XI-36
XI.8 National Renewable Energy Laboratory: Hydrogen from Biogas: Resource Assessment. XI-40
XI.9 Sandia National Laboratories: Global Hydrogen Resource Analysis XI-44
XI.10 Argonne National Laboratory: Life-Cycle Analysis of Water Use for Hydrogen Production Pathways XI-48
XI.11 National Renewable Energy Laboratory: Analysis of Fuel Cell Integration with Biofuels Production. XI-51
XI.12 National Renewable Energy Laboratory: Analysis of Community Energy XI-56

XII. Small Business Innovation Research XII-1

XII.0 Small Business Innovation Research (SBIR) Hydrogen Program New Projects Awarded in FY 2013. . . . . XII-3

Phase I Projects XII-3
XII.1 Cryogenically Flexible, Low Permeability Thoraeus Rubber H2 Dispenser Hose XII-3
XII.2 Hydrogen Leak Detector for Hydrogen Dispenser. XII-4
XII.3 Nanostructured Catalysts for Alkaline PEM Fuel Cells XII-4

Phase II Projects XII-4
XII.4 Low-Noble-Metal-Content Catalysts/Electrodes for Hydrogen Production by Water Electrolysis XII-4

XIII. Acronyms, Abbreviations and Definitions XIII-1

XIV. Primary Contacts Index XIV-1

XV. Hydrogen Program Contacts XV-1

XVI. Project Listings by State XVI-1

XVII. Project Listings by Organization XVII-1

I. INTRODUCTION

I.0 Introduction

The U.S. Department of Energy's Hydrogen and Fuel Cells Program (the Program) conducts comprehensive efforts across a range of technical and non-technical areas to enable the widespread commercialization of hydrogen and fuel cell technologies in diverse sectors of the economy. The Program is coordinated across the U.S. Department of Energy (DOE or the Department), incorporating activities in the offices of Energy Efficiency and Renewable Energy (EERE) led through the Fuel Cell Technologies Office, Science (SC), Nuclear Energy (NE), and Fossil Energy (FE). The Program's efforts are aligned with the Administration's "all-of-the-above" approach to energy and the President's Climate Action Plan and will spark the type of innovation that drives economic growth and creates American jobs, while moving our economy toward cleaner, more efficient forms of energy that will cut our reliance on foreign oil.

With emphasis on applications that will most effectively strengthen our nation's energy security and improve our efforts to cut carbon pollution, the Program engages in research, development, and demonstration (RD&D) of critical improvements in hydrogen and fuel cell technologies, as well as diverse activities to overcome economic and institutional obstacles to commercialization. The Program addresses the full range of challenges facing the development and deployment of the technologies by integrating basic and applied research, technology development and demonstration, and other supporting activities.

In Fiscal Year (FY) 2013, Congress appropriated approximately $122 million for the DOE Hydrogen and Fuel Cells Program. The Program is organized into distinct programs focused on specific areas of RD&D, as well as other activities to address non-technical challenges. More detailed discussions of Program activities and plans can be found in the *Hydrogen and Fuel Cells Program Plan*, as well as in the plans of the program offices—EERE's *Fuel Cell Technologies Office Multi-Year RD&D Plan*; FE's *Hydrogen from Coal RD&D Plan*; and SC's *Basic Research Needs for the Hydrogen Economy*. All of these documents are available at www.hydrogen.energy.gov/roadmaps_vision.html.

In the past year, the Program made substantial progress toward its goals and objectives. In addition to summarizing examples of key technical accomplishments, this report highlights major programmatic accomplishments such as the co-launching of H_2USA, a national public-private partnership to address the barriers to fuel cell electric vehicles (FCEVs) and hydrogen infrastructure.

PROGRESS AND ACCOMPLISHMENTS BY PROGRAM

This report documents more than 1,000 pages of accomplishments achieved by DOE-funded projects in the last year. The following summaries include only a few examples. More details can be found in the individual program introductions, subsequent project reports, and in the corresponding 2013 Annual Merit Review Report and Peer Evaluation Report, which can be found at http://www.hydrogen.energy.gov/annual_review13_report.html.

Fuel Cells

In 2013, the Fuel Cells program introduced several changes in the cost projection assumptions, including an increase in platinum price and an added requirement that the model system must meet the heat rejection target. These changes resulted in an increase in the projected high volume cost of transportation fuel cell systems to $55/kW in 2013. Updating previous numbers with the same assumptions and requirements shows a decrease in cost of more than 50% since 2006. This decrease stems in part from a reduction in platinum-group metal (PGM) loading and an increase in fuel cell power density, allowing the design of smaller and less expensive stacks. An interim fuel cell system cost target of $40/kW by 2020 was introduced in 2013, while the ultimate cost target was maintained at $30/kW. The $40/kW target was selected on the basis of analysis input from the U.S. DRIVE (Driving Research and Innovation for Vehicle efficiency and Energy sustainability) partnership, and responses from a Request for Information.

Successful research and development (R&D) advances continue to address critical issues with catalysts, with an emphasis on platinum levels and durability improvement. Dealloyed PtNi and PtCo catalysts were shown to have oxygen reduction reaction mass activity exceeding the 2017 target of 0.44 A/mg PGM. In addition to their high mass activity, both of these catalysts demonstrated high performance operation at high current in membrane electrode assemblies (MEAs). Researchers also developed meso-structured thin film catalysts through a new annealing process that enables specific activity eight times that of platinum. Improvements in MEAs have led to a 20% decrease since 2012 in PGM total content levels in PtNi nano-structured thin-film catalysts when operating at high temperatures of 90°C and voltages of 0.69 V. This improvement enabled achievement of a catalyst specific power level of 6.0 kW/g in

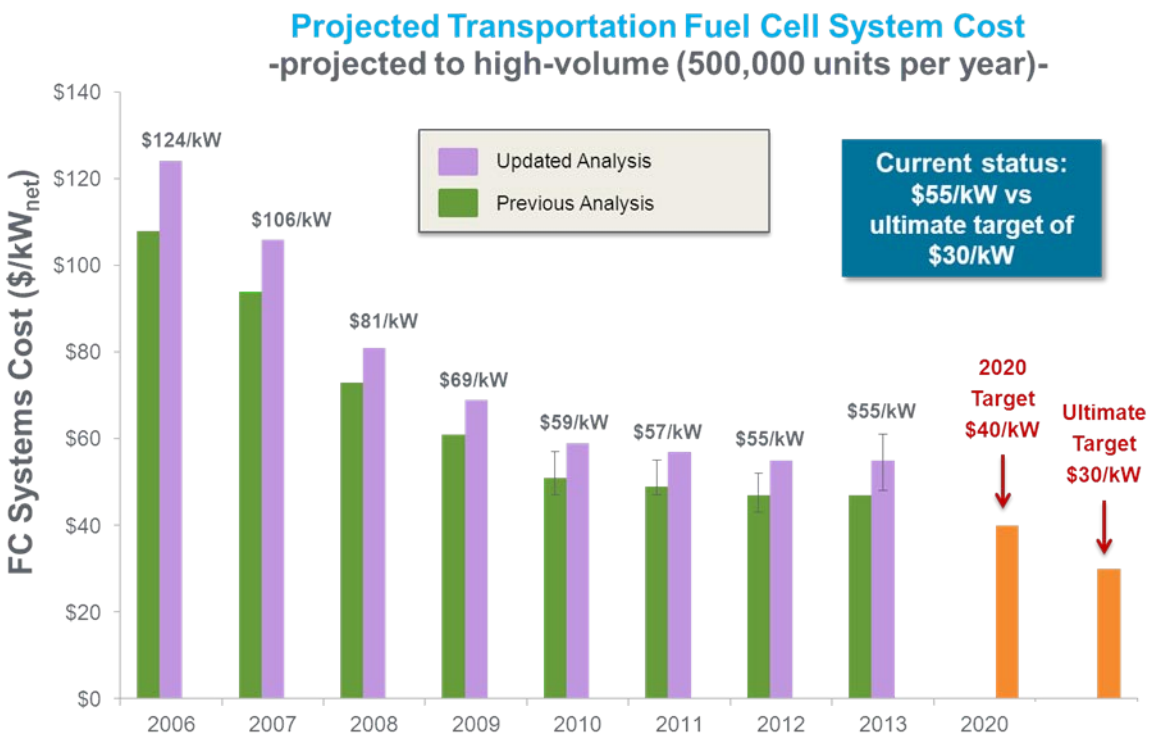

FIGURE 1. Modeled cost of an 80-kW automotive fuel cell system based on projection to high-volume manufacturing (500,000 units/year).[1]

2013, exceeding the program's milestone of 5.9 kW/g. Further R&D is required to achieve the 2020 catalyst specific power target of 8.0 kW/g, and to simultaneously meet catalyst durability targets.

Hydrogen Production

In FY 2013, the Hydrogen Production program continued to focus on developing technologies to enable the long-term viability of hydrogen as an energy carrier for a range of applications with a focus on hydrogen from low-carbon and renewable sources. Progress continued in several key areas, including biological hydrogen production, solar-thermochemical hydrogen (STCH) production, and photoelectrochemical hydrogen production.

For example, FY 2013 efforts in photobiological production led to the demonstration of an almost two times increase in hydrogen evolution rate compared to the wild-type rate for a cyanobacterial strain with a non-native hydrogenase with higher oxygen tolerance and other genetic modifications.[2] A perovskite structure was discovered that produces nine times more hydrogen than CeO_2, the current state-of-the-art metal-oxide redox material for STCH production. In addition, isothermal redox at 1,350°C for the hercynite STCH cycle was shown to be feasible with between three and twelve times the production capacity per mass of active material than hercynite and ceria, respectively, when reduced at 1,350°C and reoxidized at 1,000°C.[3] These results were recently published in *Science* magazine.

In addition, technical progress has reduced the projected costs for hydrogen production in several of the nearer-term pathways. A summary of projected high-volume cost versus targets is shown in Figure 2.

Another key accomplishment in FY 2013 was the completion of the Hydrogen Production Expert Panel (a Hydrogen and Fuel Cell Technologies Advisory Committee subcommittee) report that collected input from industry, academic, and national laboratory experts during a May 2012 workshop. The subcommittee was officially tasked by former Energy Secretary, Dr. Steven Chu, with providing recommendations to enable the widespread production of affordable, low-carbon hydrogen for both near- and long-term markets and key findings were included in the final

[1] DOE Hydrogen and Fuel Cells Program Record #13012, http://hydrogen.energy.gov/pdfs/13012_fuel_cell_system_cost.pdf.
[2] See project report *II.D.4 Hydrogen from Water in a Novel Recombinant Oxygen-Tolerant Cyanobacterial System* by Philip Weyman.
[3] See project report *II.B.3 Solar-Thermal Redox-Based Water Splitting Cycle* by Alan Weimer.

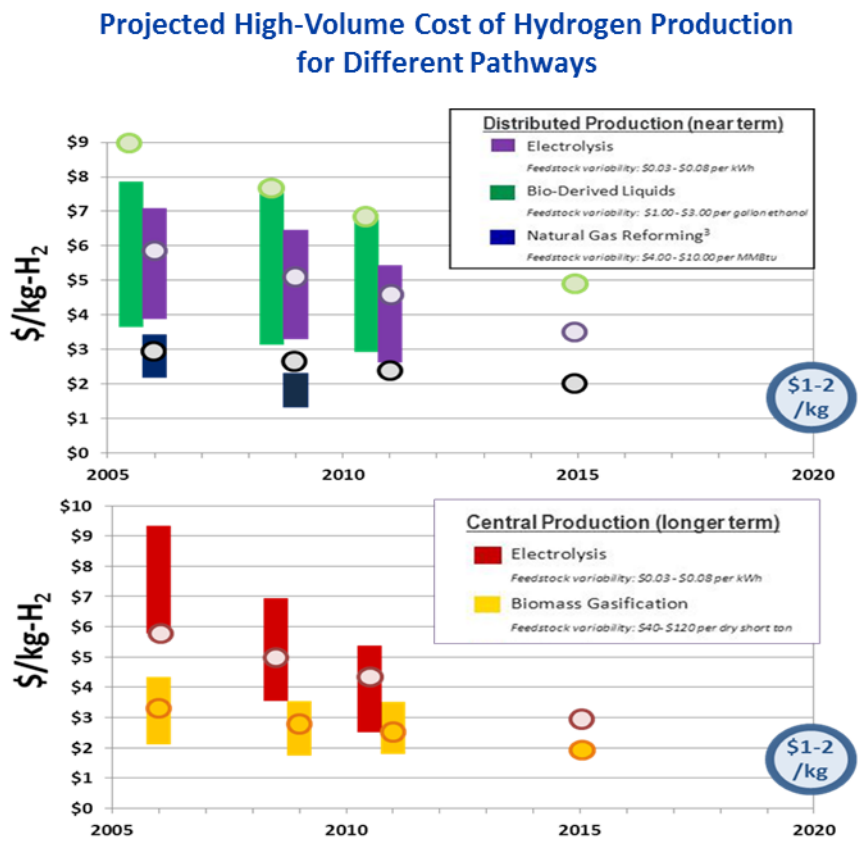

FIGURE 2. Hydrogen Production Cost Status (based on projected high-volume cost)[4]

report that is posted online.[5] The program also signed a Memorandum of Understanding with the National Science Foundation to allow for joint funding of RD&D. A major strategic outcome was a jointly funded parallel solicitation between DOE and the National Science Foundation for longer term hydrogen production R&D from renewables.

Hydrogen Delivery

In FY 2013 the Hydrogen Delivery program focused on identifying the RD&D needs for materials and components for forecourt technologies to reduce capital costs and improve system reliability. Significant cost reduction at the forecourt can be achieved through the use of high-pressure tube trailers and reliable low-cost compression. Optimization of an integrated tube trailer configuration for hydrogen delivery increased the 3,600 psi hydrogen capacity to 800 kg. This results in an increase of 30% relative to the baseline.[6]

The average hydrogen delivery cost status based on nine 700-bar delivery scenarios including pipeline, tube trailer, and liquid delivery in 2011 and 2013 and the 2015 and 2020 delivery targets are shown in Figure 3. The blue circles indicate the 2015 and 2020 cost targets and the dotted line shows the extrapolation of prior year targets against which progress can be mapped. The blue and green bars indicate the range of costs of the 350-bar and 700-bar pathways in 2011 and 2013 respectively.[7]

Developments in centrifugal compression and fiber-reinforced polymer pipelines continue to improve the economics of delivering hydrogen via pipelines. Completion of an initial validation testing of single-stage oil-free centrifugal compressor system in air and in helium at 60,000 rpm confirmed the single-stage compression ratio and thermal stability. Significant improvements in advanced forecourt technologies include a decrease of 50% in the

[4] DOE Hydrogen and Fuel Cells program Record #12002, http://hydrogen.energy.gov/pdfs/12002_h2_prod_status_cost_plots.pdf
[5] Report of the Hydrogen Production Expert Panel (May 2013), http://www.hydrogen.energy.gov/pdfs/hpep_report_2013.pdf
[6] See project report *III.3 Development of High-Pressure Hydrogen Storage Tank for Storage and Gaseous Truck Delivery* by Jon Knudsen and Don Baldwin.
[7] DOE Hydrogen and Fuel Cells Program Record #13013, http://www.hydrogen.energy.gov/pdfs/13013_h2_delivery_cost_central.pdf

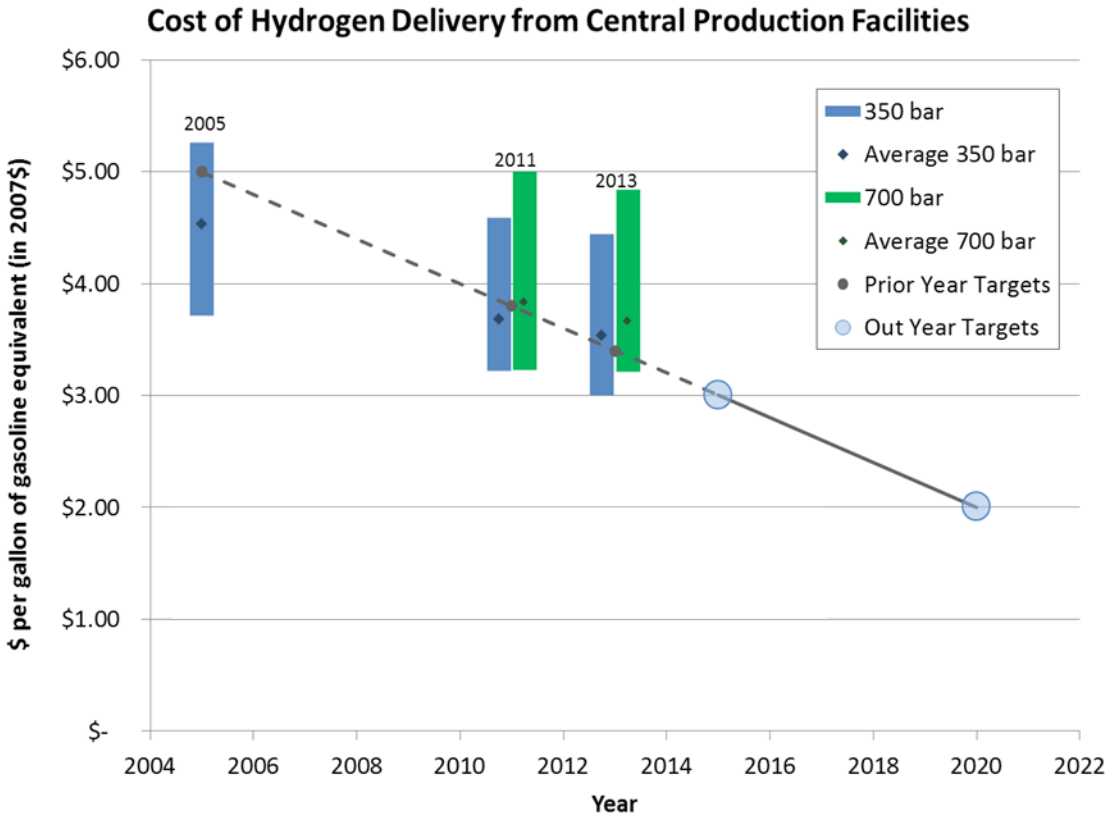

FIGURE 3. Details for the high-volume cost projection assumptions can be found in Record 13013.[8] Based on HDSAM (v2.3) analysis assuming 10% market penetration in a city with a population of 1.5M and a station size of 750 kg/day.

prototype unit cost of an electrochemical compressor since 2007 which was achieved by reducing the cell part count by half. Simultaneously a greater than three-fold increase in the stack current density and a two-fold increase in the cell active area has been achieved, which resulted in higher compressor throughput while lowering the total cells per stack.[9]

In addition to these technical accomplishments, the Hydrogen Delivery program held two workshops to discuss the current status and challenges in these areas. The first workshop, Polymer and Composite Materials Used in Hydrogen Service,[10] was held as a joint workshop with the Safety, Codes and Standards program at the DOE headquarters in October 2012 and the second workshop, Compression, Storage and Dispensing Cost Reduction,[11] was held at Argonne National Laboratory in March 2013.

Hydrogen Storage

In FY 2013, the Hydrogen Storage program focused on development of lower cost precursors and fillers for carbon fiber composites to lower the cost of high-pressure compressed hydrogen systems, system engineering for transportation applications and continued R&D efforts in materials-based storage including metal hydrides, chemical hydrogen storage materials, and hydrogen sorbents.

The Hydrogen Storage program has developed comprehensive sets of hydrogen storage targets for onboard automotive, portable power, and material handling equipment applications. In the near-term, automotive companies plan to commercialize FCEVs that use onboard compressed hydrogen systems, with system cost being one of the most important challenges to commercialization. The program, working with automotive manufacturers through the U.S.

[8] DOE Hydrogen and Fuel Cells Program Record #13013, http://www.hydrogen.energy.gov/pdfs/13013_h2_delivery_cost_central.pdf.
[9] See project report *III.6 Electrochemical Hydrogen Compressor* by Ludwig Lipp.
[10] Polymer and Composite Materials Workshop, http://www1.eere.energy.gov/hydrogenandfuelcells/mtg_poly_comp_materials.html
[11] Compression, Storage and Dispensing Cost Reduction Workshop, http://www1.eere.energy.gov/hydrogenandfuelcells/wkshp_hydrogen_csd.html

DRIVE partnership, established onboard automotive hydrogen storage system cost targets of $12/kWh of useable stored hydrogen to be reached by 2017, with $8/kWh of useable storage hydrogen as an Ultimate Full Fleet target.

As a longer-term strategy, the Hydrogen Storage program continues to pursue less mature hydrogen storage technologies that have the potential to satisfy all onboard hydrogen storage targets. Much of this activity is completed through the Hydrogen Storage Engineering Center of Excellence (HSECoE). In FY 2013, the HSECoE completed assessment of hydrogen storage systems for cryo-sorbents and liquid-phase off-board regenerable chemical hydrogen storage material systems. The HSECoE also completed an assessment of chemical hydrogen storage materials and systems that led to a decision to terminate work on these systems due to low probability of identifying materials that meet 8.5 wt% fluid gravimetric requirements and regeneration efficiencies. The HSECoE also completed an assessment of adsorbent system that led to a down selection of both the Hexcel and modular adsorbent tank insert heat exchanger designs for subscale prototype adsorbents systems.[12] Additionally, the HSECoE identified balance-of-plant components for a cryo-sorbent hydrogen storage system with a total mass of less than 9.4 kg and volume of less than 11.6 L exceeding the system targets of 17 kg and 18.5 L.

In FY 2013, the Hydrogen Storage program continued to reduce the cost of compressed hydrogen gas storage tanks by focusing efforts on low-cost, high-strength carbon fiber and advanced tank designs. The program was able

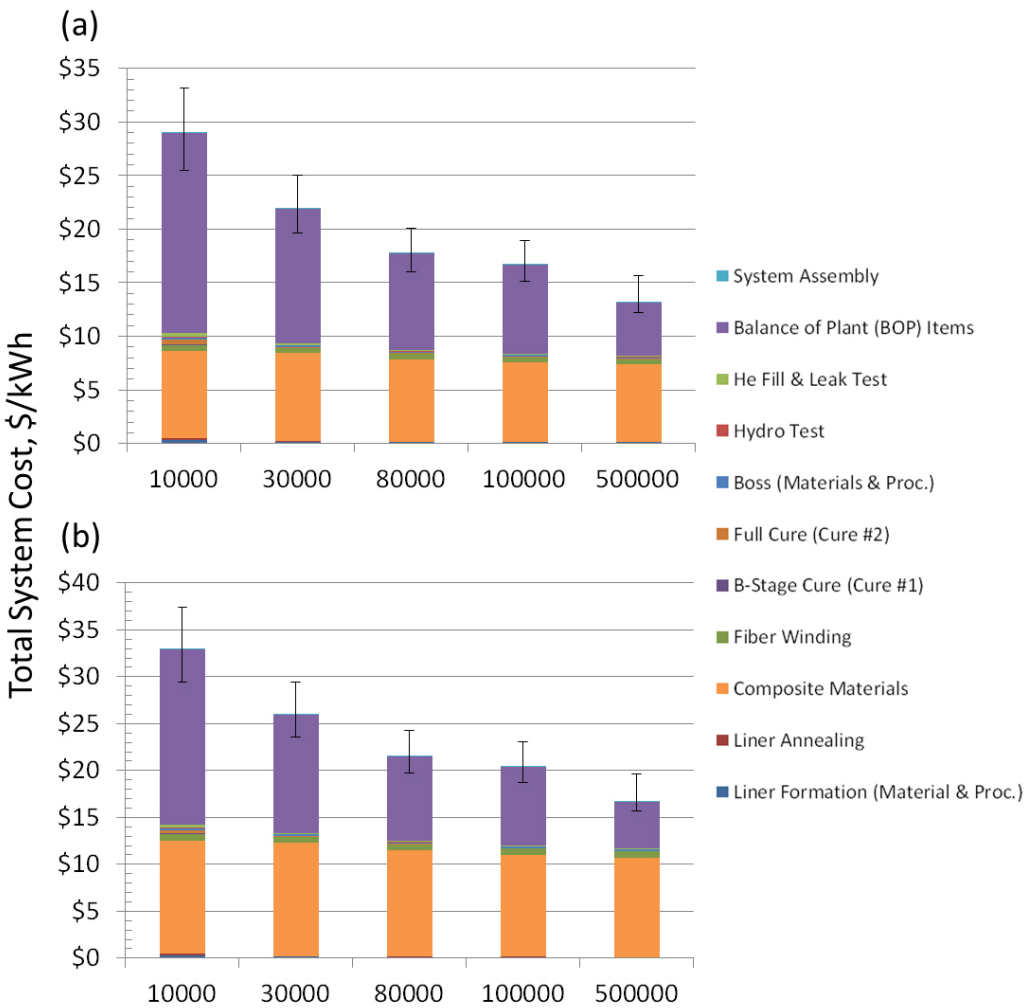

FIGURE 4. Projected costs in 2007$, at various annual manufacturing volumes, for (a) 350-bar and (b) 700-bar compressed hydrogen storage systems, sized to deliver 5.6 kg of hydrogen to the vehicle fuel cell powerplant.[13]

[12] See project report *IV.B.1 Hydrogen Storage Engineering Center of Excellence* by Donald Anton.
[13] DOE Hydrogen and Fuel Cells Program Record #13010, http://hydrogen.energy.gov/pdfs/13010_onboard_storage_performance_cost.pdf

to demonstrate strategies to reduce the cost of pressure vessels by 15% compared to the 2010 baseline of $17/kWh, through modeling and material testing including: testing properties of low-cost resins (led to a 4% cost reduction); testing properties of additives to enhance resin properties (led to a 5% cost reduction); and modeling to demonstrate alternative fiber placement and fiber types (led to a 6% cost reduction).[14]

In FY 2013, the Hydrogen Storage program continued to carry out assessments of hydrogen storage technologies and disseminate proper hydrogen storage material testing and characterization procedures to evaluate material/system performance against requirements of hydrogen fuel cell applications. Updating the Design for Manufacturing Analysis method and validating key performance parameters for pressure vessels was a critical activity and was based on discussions with industry, the U.S. DRIVE partnership, Hydrogen Storage Tech Team, the Storage System Analysis Working Group, Argonne National Laboratory, Pacific Northwest National Laboratory, HSECoE, and project collaborators.

Manufacturing R&D

In FY 2013, manufacturing projects continued in the areas of novel electrode deposition processes for MEA fabrication, reduction in the number of assembly steps for MEAs, use of scatterfield microscopy and in-line diagnostics for cell and component quality control to measure catalyst loading and detect defects in catalyst-coated membranes and gas diffusion electrodes (GDEs), and fabrication technologies for high-pressure composite storage tanks. In the area of MEAs, the Manufacturing R&D program demonstrated a "one-pass" microporous layer and catalyst coating on carbon paper, reduced labor and material costs by >30% for paper structures compared to best cloth GDEs, and demonstrated a 30% reduction in platinum loading compared to best cloth-based anodes without losing performance.[15] Using an optical reflectometry technique, the program also detected surface defects and morphology in electrode layers, in both catalyst-coated membrane and gas diffusion electrode configurations, as well as surface defects in tubular solid oxide fuel cells.

In May of 2013, the program held a fuel cell manufacturing roundtable with Assistant Secretary for Energy Efficiency and Renewable Energy Dr. David Danielson, Connecticut Governor Dannel Malloy, and members of Connecticut's fuel cell manufacturing industry. In addition to the round table, senior DOE officials were able to tour three major hydrogen and fuel cell manufacturing plants in the area.

Basic Research

The Basic Energy Sciences program in the DOE Office of Science supports fundamental scientific research addressing critical challenges related to hydrogen storage, hydrogen production, and fuel cells. These basic research efforts complement the applied R&D projects supported by other offices in the Program. Progress in any one area of basic science is likely to spill over to other areas and bring advances on more than one front.

The subjects of basic research most relevant to the Program's key technologies are:

- Hydrogen Storage: Nanostructured materials; theory, modeling, and simulation to predict behavior and design new materials; and novel analytical and characterization tools.
- Fuel Cells: Nanostructured catalysts and materials; integrated nanoscale architectures; novel fuel cell membranes; innovative synthetic techniques; theory, modeling, and simulation of catalytic pathways, membranes, and fuel cells; and novel characterization techniques.
- Hydrogen Production: Approaches such as photobiological and direct photochemical production of hydrogen.

By maintaining close coordination between basic science research and applied R&D, the Program ensures that discoveries and related conceptual breakthroughs achieved in basic research programs will provide a foundation for the innovative design of materials and processes that will lead to improvements in the performance, cost, and reliability of fuel cell technologies and technologies for hydrogen production and storage. This is accomplished in various ways—for example, through bimonthly coordination meetings between the participating offices within DOE, and at the researcher level by having joint meetings with participation from principal investigators who are funded by the participating offices.

[14] See project report *IV.F.4 Synergistically Enhanced Materials and Design Parameters for Reducing the Cost of Hydrogen Storage Tanks* by Kevin Simmons.

[15] See project report *VI.5 High-Speed, Low-Cost Fabrication of Gas Diffusion Electrodes for Membrane Electrode Assemblies* by Emory De Castro.

In May 2013, the Program included 29 presentations and posters from Basic Energy Sciences-funded researchers on fundamental science related topics in conjunction with presentations by EERE and Advanced Research Projects Agency - Energy (ARPA-E) funded researchers in the 2013 Hydrogen and Fuel Cells Annual Merit Review and Peer Evaluation (AMR).[16]

Technology Validation

In FY 2013, the Technology Validation program continued efforts toward real-world evaluation of fuel cell bus technologies at various transit authorities, and monitoring performance of fuel cells in stationary power, backup power, and material handling equipment applications. These activities led to the validation of light-duty FCEV performance and durability through analysis of dynamometer and real-world vehicle performance data. The program collected and analyzed data from fuel cell buses from three transit agencies: AC Transit (Oakland, California), CTTRANSIT (Hartford, Connecticut), and SunLine (Thousand Palms, California) and found that the new fuel cell bus designs have about 1.9 times the fuel economy of diesel buses, and approximately 2.3 times the fuel economy of compressed natural gas buses.[17]

The program was able to independently validate systems integration of commercial and advanced prototype hydrogen production, compression, dispensing, and fuel cell technologies. Specific activities included performing accelerated life testing of both diaphragm and piston hydrogen compressors. The program collected valuable data from state-of-the-art hydrogen fueling facilities, such as those operated by the California Air Resources Board (CARB), Proton OnSite, and GTI, to provide feedback on sensitive data related to hydrogen infrastructure to stakeholders. Finally, the program validated a system of reclamation and recycling of hydrogen that is wasted (flared or vented) in various industrial operations.

Safety, Codes and Standards

The Hydrogen Safety, Codes and Standards program continued to achieve significant accomplishments with respect to critical regulations, codes, and standards in FY 2013. For example, in December 2012, the Global Technical Regulation on hydrogen-fuelled vehicles was submitted to the United Nations Economic Commission for Europe Working Party 29 (UN ECE WP.29) and was accepted in June 2013. This regulation will serve as the technical underpinning for the United States Federal Motor Vehicle Safety Standard. The program also continued to support R&D to provide the technical basis for codes and standards development, with projects in a wide range of areas, including fuel specification, separation distances, materials and components compatibility, and hydrogen sensor technologies.

The program developed integrated algorithms for conducting Quantitative Risk Assessments for gaseous hydrogen facilities and vehicles that are applied to identified risk drivers and associated consequences, including further reducing separation distances and identified ignition and jet light up boundaries of jet flames for circular unintended releases with increased confidence and initiated a study on non-circular releases. The program developed a template that includes basic codes and standards requirements, including those related to the California Risk Management Plan requirements that will be used in California. The program continues to develop training material for first responders and code officials and have educated over 26,000 first responders and code officials to-date (online[18] and in-person).

The program also developed the first mobile app for the Fuel Cell Technologies Office. The app, available free of charge for iPhones and iPads, integrates H2incidents.org and H2bestpractices.org into a single, searchable application and includes safety planning guidance and checklist features.[19]

Education

The Education program facilitates hydrogen and fuel cell demonstrations and supports commercialization by providing technically accurate and objective information to key target audiences both directly and indirectly involved in the use of hydrogen and fuel cells. Funding from prior appropriations supported the program's activities.

In FY 2013 the Fuel Cell Technologies Office published more than 80 success stories through news articles, blogs, press releases, and media announcements and conducted more than 15 webinars, averaging more than 150 attendees per webinar. Activities reached at least 3,000 people at key conferences and meetings, including the Fuel Cell Expo

[16] 2013 Annual Merit Review Proceedings, http://www.hydrogen.energy.gov/annual_review13_proceedings.html

[17] Fuel Cell Buses in U.S. Transit Fleets: Current Status 2012, http://www1.eere.energy.gov/hydrogenandfuelcells/pdfs/fceb_status_2012.pdf

[18] Hydrogen Safety for First Responders, http://www.hydrogen.energy.gov/firstresponders.html and Introduction to Hydrogen Safety for Code Officials, http://www.hydrogen.energy.gov/training/code_official_training/

[19] Energy Department Launches App on Hydrogen Use, September 12, 2013, http://apps1.eere.energy.gov/news/progress_alerts.cfm/news_id=20553

in Japan, AIChE conference, and the AMR. The program is also continuing to train middle school and high school teachers based on prior years' funding through "H2 Educate!" reaching a cumulative of 10,000 teachers, in 35 states; 90% of participants stated that the training resources increased the effectiveness of their lesson plans.

Market Transformation

To ensure that the benefits of the Program's efforts are realized in the marketplace, in FY 2013 the Market Transformation program continued to facilitate the growth of early markets for fuel cells used in portable, stationary, and specialty-vehicle applications. Market Transformation activities are helping to reduce the cost of fuel cells by enabling economies of scale through early market deployments; these early deployments also help to overcome a number of barriers, including the lack of operating performance data, the need for applicable codes and standards, and the need for user acceptance.

Current key objectives of the Market Transformation program are to build on past successes in material handling equipment (MHE) (e.g., lift trucks or forklifts) and emergency backup power applications by exploring other emerging applications for market viability. FY 2013 accomplishments included launching a new project to demonstrate commercial viability of fuel cell-powered airport ground support baggage tractors, demonstrating fuel cell-powered electric medium-duty hybrid trucks for parcel delivery applications, and beginning design development of fuel cell auxiliary power systems for refrigerated trucks. These projects are highly leveraged, with an average of more than half of the projects' funds being provided by DOE's partners. The market transformation team also demonstrated the world's first landfill gas-to-hydrogen fuel system for fuel cell-powered lift trucks at the BMW plant in Greer, South Carolina, which has the world's largest fuel cell-powered lift truck fleet (more than 300) to date.

Systems Analysis and Integration

The Systems Analysis program supports decision making by providing a greater understanding of technology gaps, options and risks, and examining the interaction of individual technologies and components and their contributions to the performance of larger systems, e.g., the entire hydrogen fuel system, from production to utilization. The program also analyzes cross-cutting issues, such as the integration of hydrogen and fuel cell systems with the electrical sector and the use of renewable fuels. Particular emphasis is given to assessing stationary fuel cell applications and the implications of various approaches to establishing hydrogen infrastructure.

The Systems Analysis program activity made several significant contributions to the Program during FY 2013. The cost of hydrogen infrastructure was compared to infrastructure for other advanced fuel vehicles and opportunities of reducing the infrastructure costs were examined by utilizing using stakeholder input and exploring synergies with other fuels such as natural gas. The JOBS and economic impacts of fuel cells model continues to be enhanced by Argonne National Laboratory and RCF Economic and Financial Consulting as they add the capability to assess employment impacts of infrastructure development. Infrastructure and early market analyses were conducted to better understand early market hurdles such as cash flow and station utilization, and supply and demand issues. The Greenhouse Gases Regulated Emissions and Energy Use in Transportation (GREET) model is being enhanced to evaluate greenhouse gas emissions and petroleum use on a well-to-wheels basis for hydrogen pathways with various onboard storage options, and incorporating water consumption analysis in the model.

In addition, the Systems Analysis program conducted critical vehicle portfolio well-to-wheel analysis in collaboration with the Bioenergy Technologies and Vehicles Technologies Offices to estimate the lifecycle greenhouse gas (GHG) emissions resulting from several fuel/vehicle pathways, for a portfolio of future mid-size cars. The data and major assumptions and results are documented in a DOE records.[20] The results of the analysis show that GHG emissions could be reduced to approximately 35 g of CO_{2eq} per mile compared to the current gasoline internal combustion engine of 430 g of CO_{2eq} per mile, as shown in Figure 5.

American Recovery and Reinvestment Act of 2009 Projects

The American Recovery and Reinvestment Act of 2009 (Recovery Act or ARRA) has been a critical component of the Program's efforts to accelerate the commercialization and deployment of fuel cells in the marketplace.

As of October 2013, more than 500 fuel cell lift trucks and a total of 820 fuel cell backup power systems for cellular communications towers and stationary backup power systems had been deployed—surpassing the original deployment goal of up to 1,000 fuel cells—and over 95% of the Recovery Act project funds had been spent by the

[20] Fuel Cell Technologies Office Program Records, http://hydrogen.energy.gov/program_records.html

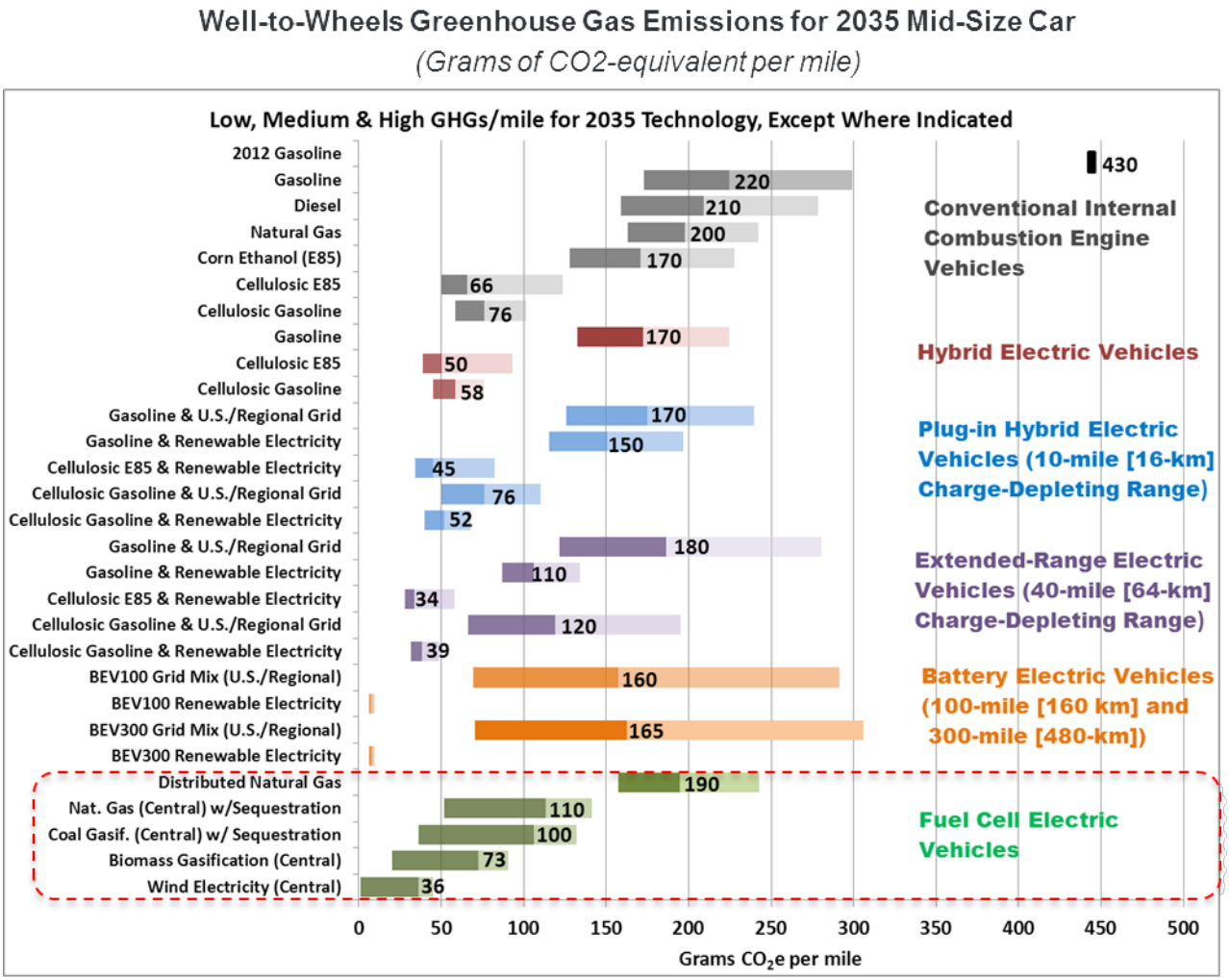

E85 – 85% ethanol 15% gasoline; BEV – battery electric vehicle; CO_2e – CO_2-equivalent

FIGURE 5. Well-to-Wheels Greenhouse Gas Emissions for 2035 Mid-Size Car.[21]

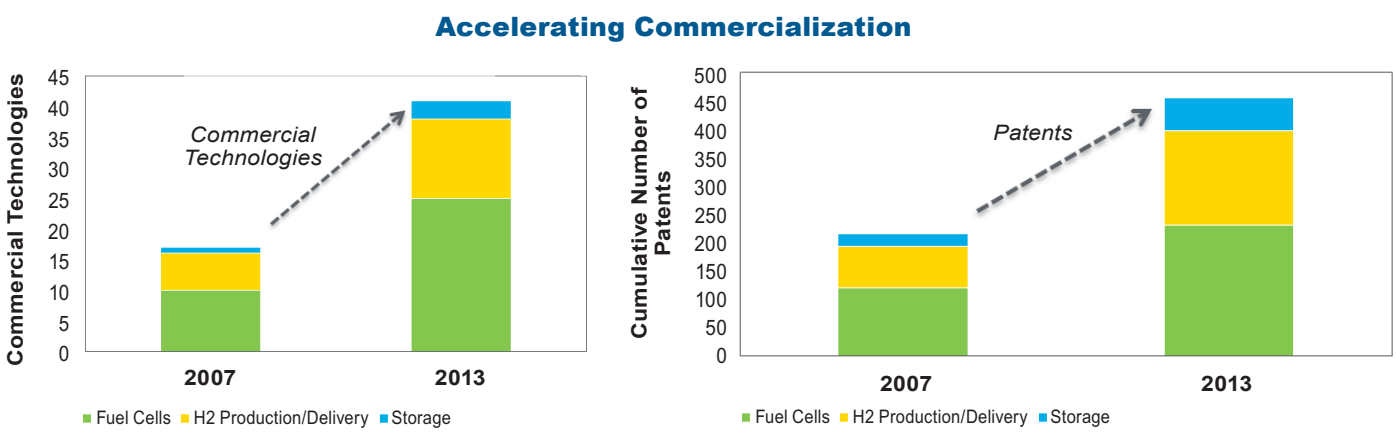

FIGURE 6. Cumulative number of commercial products on the market as a result of funding by the DOE Fuel Cell Technologies Office.[22]

[21] DOE Hydrogen and Fuel Cells Program Record #13005, http://hydrogen.energy.gov/pdfs/13005_well_to_wheels_ghg_oil_ldvs.pdf
[22] Pathways to Commercial Success: Technologies and Products Supported by The Fuel Cell Technologies Program, Pacific Northwest National Laboratory, September 2012, www.hydrogenandfuelcells.energy.gov/pdfs/pathways_2013.pdf

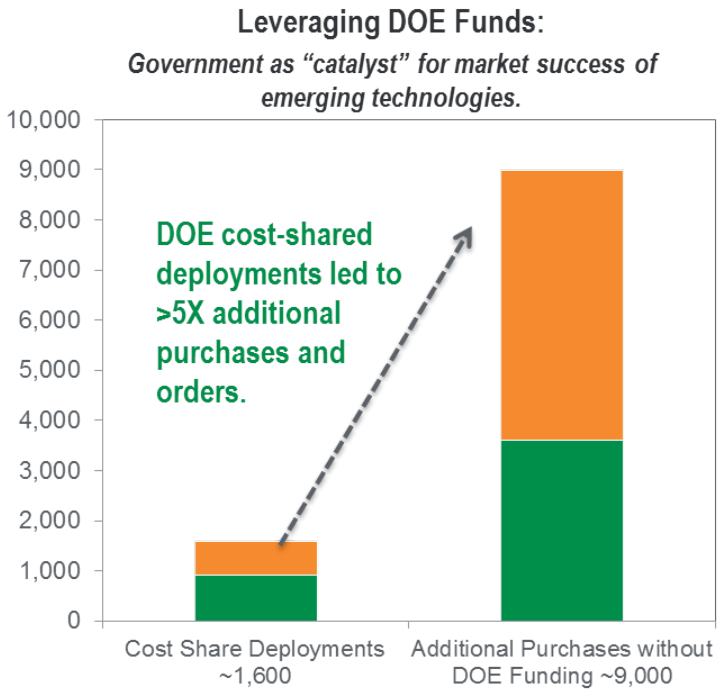

FIGURE 7. Early market deployments of approximately 1,600 fuel cells have led to approximately 9,000 additional purchases by major companies (including Coca-Cola, Sprint, Sysco, FedEx, and others) **with no additional DOE funding.**

projects. The National Renewable Energy Laboratory's (NREL's) National Fuel Cell Technology Evaluation Center (NFCTEC) has established data reporting protocols with each of the project teams. Composite Data Products (CDPs) and Detailed Data Products showing progress to date have been prepared. The CDPs are available on the NREL NFCTEC website.[23] Of the original twelve projects, nine have been successfully completed.

Successful DOE deployments of fuel cells (including deployments from ARRA funding as well as Market Transformation projects) have led to industry orders of almost 5,000 fuel cell forklifts and almost 3,500 fuel cell backup power systems, with no additional DOE funding.[24]

OTHER PROGRAM ACTIVITIES AND HIGHLIGHTS FROM FY 2013

Tracking Commercialization

One indicator of the robustness and innovative vitality of an RD&D program is the number of patents applied for and granted, and the number of technologies commercialized. The Program continued to assess the commercial benefits of funding by tracking the commercial products and technologies developed with the support of the EERE Fuel Cell Technologies Office (the Office). R&D efforts funded by the Office have resulted in more than 450 patents, 40 commercial technologies, and 65 technologies that are projected to be commercialized within three to five years.[25] In addition, EERE's investment of $50 million in specific hydrogen and fuel cell projects led to more than $300 million in revenue and investments of approximately $14 million in specific projects led to a nearly $130 million in additional private investment.

Awards & Distinctions

During the last year, a number of researchers within the Program were recognized through various awards. For example:

[23] http://www.nrel.gov/hydrogen/proj_fc_market_demo.html
[24] DOE Hydrogen and Fuel Cells Program Record #13007 and #13008, http://hydrogen.energy.gov/program_records.html
[25] 2013 Pathways to Commercial Success: Technologies and Products Supported by the Fuel Cell Technologies Office, http://www1.eere.energy.gov/hydrogenandfuelcells/pdfs/pathways_2013.pdf

- Electrocatalysis magazine dedicated its December 2012 issue to celebrate Radoslav Adzic, a Fuel Cell Technologies Office-supported research scientist at Brookhaven National Laboratory.
- Dr. Maria Ghirardi was named to NREL's Research Fellows Council, the laboratory's top advisory council comprised of internationally recognized NREL scientists and engineers.
- Dr. Felix Paulauskas, an EERE-supported fuel cell scientist, was recognized by the Oak Ridge National Laboratory (ORNL) as the 2012 Inventor of the Year for distinguished, sustained, and cumulative contributions to ORNL's patent portfolio, which are the basis for establishment of carbon fiber initiatives and significant program growth, new ORNL facilities, and future opportunities for developing and demonstrating pioneering new approaches to producing carbon fibers.
- Dr. Bryan Pivovar was recognized with the Charles W. Tobias Young Investigator Award from the Electrochemical Society for his work advancing polymer electrolyte fuels and liquid fed fuel cell systems.
- Dr. Piotr Zelenay of Los Alamos National Laboratory won the 2013 Research Award presented by the Energy Technology Division of The Electrochemical Society for his research on polymer electrolyte fuel cells, including direct-methanol fuel cells, precious-metal/non-precious metal electrocatalysis, membrane and membrane electrode assembly development, and performance optimization of fuel cell materials and components.

Key Reports/Publications

Every year, the Hydrogen and Fuel Cells Program commissions a number of key reports, providing vital information to industry and the research community. Some of these are released on an annual basis—such as the *Market Report (**2012 Fuel Cell Technologies Market Report**)*, the commercialization report (***2013 Pathways to Commercial Success: Technologies and Products Supported by the Fuel Cell Technologies Office***), and the ***State of the States: Fuel Cells in America 2013*** report—while others are published when studies are complete, projects have ended, or key milestones have been reached. Key examples include:

- The ***2012 Fuel Cell Technologies Market Report*** finds that commercial markets for fuel cells continue to expand, including in the stationary back-up power and material handling equipment markets. Approximately 30,000 fuel cell systems were shipped worldwide in 2012, up nearly 35% over 2011 and more than 320% since 2008. http://www1.eere.energy.gov/hydrogenandfuelcells/pdfs/2012_market_report.pdf
- ***2013 Pathways to Commercial Success: Technologies and Products Supported by the Fuel Cell Technologies Office,*** the Program's annual commercialization report, indicates that Fuel Cell Technologies Office efforts have successfully generated more than 450 patents, 41 commercial technologies, and 66 technologies that are projected to be commercial within the next three to five years. http://www1.eere.energy.gov/hydrogenandfuelcells/pdfs/pathways_2013.pdf
- ***State of the States: Fuel Cells in America 2013***, the fourth annual report on state activities, details fuel cell and hydrogen activities and policies in the 50 states and the District of Columbia. http://www1.eere.energy.gov/hydrogenandfuelcells/pdfs/state_of_the_states_2013.pdf
- ***Business Case for Fuel Cells 2012*** illustrates how top American companies are using fuel cells in their business operations to advance their sustainability goals, save millions of dollars in electricity costs, and reduce carbon emissions by hundreds of thousands of metric tons per year. www.hydrogenandfuelcells.energy.gov/pdfs/business_case_fuel_cells_2012.pdf
- ***REPORT ON RFI DE-FOA-000753: High-Accuracy Hydrogen Meters*** summarizes the current status of meters for hydrogen fueling with information collected from publically available documents and a Request for Information, excluding any proprietary/company sensitive information. http://www1.eere.energy.gov/hydrogenandfuelcells/pdfs/rfi_responses_hydrogen_meters.pdf
- ***Hydrogen Compression, Storage, and Dispensing Cost (CSD) Reduction Workshop Report*** includes proceedings from the Hydrogen CSD Cost Reduction Workshop that took place March 20–21, 2013. http://www1.eere.energy.gov/hydrogenandfuelcells/wkshp_hydrogen_csd.html
- ***Economic Impact of Fuel Cell Deployment in Forklifts and for Backup Power under the American Recovery and Reinvestment Act*** estimates the economic impacts associated with expenditures under the Recovery Act and includes estimates of the total employment, earnings, and economic output using the JOBS and economic impacts of Fuel Cells model, also developed by Argonne. http://www1.eere.energy.gov/hydrogenandfuelcells/fc_publications.html#fc_general

- ***Evaluation of the Total Cost of Ownership of Fuel Cell-Powered Material Handling Equipment*** assesses the total cost of ownership of fuel cell MHE and compares it to the cost of ownership of traditional battery-powered MHE. http://www1.eere.energy.gov/hydrogenandfuelcells/pdfs/fuel_cell_mhe_cost.pdf
- ***Blending Hydrogen into Natural Gas Pipeline Networks: A Review of Key Issues*** focuses on using hydrogen both as a fuel and as an energy storage tool and details the issues related to blending hydrogen into natural gas pipeline networks. http://www1.eere.energy.gov/hydrogenandfuelcells/news_detail.html?news_id=19093
- ***Vessel Cold-Ironing Using a Barge Mounted PEM Fuel Cell: Project Scoping and Feasibility*** examines the feasibility of a hydrogen-fueled polymer electrolyte membrane fuel cell barge to provide electrical power to vessels at anchorage or at berth. http://www1.eere.energy.gov/hydrogenandfuelcells/fc_publications.html#fc_aux
- ***Fuel Cell Buses in U.S. Transit Fleets: Current Status 2012*** report shows that the fuel economy of fuel cell electric buses is 1.8 to 2 times higher than conventional diesel buses (4 mpg) and compressed natural gas buses (3 mpg). http://www1.eere.energy.gov/hydrogenandfuelcells/news_detail.html?news_id=18910
- ***The Hydrogen Safety Best Practices Manual*** is an online manual that captures the wealth of knowledge and experience related to the safe handling and use of hydrogen that exists as a result of its extensive history in a wide variety of applications. http://h2bestpractices.org/

New Funding Opportunity Announcements (FOAs) and Awards

- **$1 million to advance cost-competitive hydrogen fuel.** To help meet this aggressive goal by 2020, the projects selected through this Program will help identify cost-effective materials and processes to produce hydrogen from renewable energy sources and natural gas.
- **$9 million to accelerate the development of hydrogen and fuel cell technologies for use in vehicles, backup power systems, and hydrogen refueling components.** This FOA closed on July 12, 2013.
- **$4 million to address critical challenges and barriers for low-cost, low-carbon hydrogen production.** The new funding opportunity solicits projects focused on innovative materials, processes, and systems that are needed to establish the technical and cost feasibility for renewable and low carbon hydrogen production. Concept papers were due November 26, 2013, and full applications are due January 31, 2014.
- **$4 million to address critical challenges and barriers to advanced hydrogen delivery technology development.** The new funding opportunity solicits projects focused on innovative hydrogen delivery materials, components, and systems needed to establish the technical and cost feasibility for renewable and low-carbon hydrogen delivery. Concept papers were due December 9, 2013, and full applications are due February 14, 2014.
- **$4 million to develop advanced hydrogen storage systems and novel materials to provide adequate onboard storage for a wide range of applications including FCEVs, and for emerging fuel cell applications such as material handling equipment.** Concept papers were due November 11, 2013 and full applications are due January 17, 2014.
- **$4.5 million awarded to lower the cost, improve the durability, and increase the efficiency of next-generation fuel cell systems.**
- **Small Business Innovation Research (SBIR)/Small Business Technology Transfer (STTR) Phase I Release 2 funding opportunity included a hydrogen dispenser technologies topic.** Applications were due in February 2013.
- **SBIR/STTR Phase I Release 2 Award Winners included hydrogen dispenser and hydrogen sensor projects.**
- **SBIR/STTR award winners included a hydrogen-from-water electrolysis project.**

Requests for Information (RFI)

- Automotive Fuel Cell Cost and Durability Target collected feedback from stakeholders regarding proposed cost and durability targets for fuel cells designed for automotive applications. The proposed cost target is $40/kW for automotive fuel cell systems and the proposed durability target is 5,000 hours, which corresponds to approximately 150,000 miles. This RFI closed on April 1, 2013.[26]

[26] http://www1.eere.energy.gov/hydrogenandfuelcells/news_detail.html?news_id=18989

- Hydrogen and Fuel Cell Technology Readiness collected feedback from stakeholders regarding technology validation and deployment activities aimed at ensuring commercial readiness and stimulating commercialization of fuel cell and hydrogen technologies. This RFI closed on April 10, 2013.[27]
- Home Hydrogen Refueling Systems and Potential H-Prize Topics collected feedback from stakeholders about a potential H-Prize competition involving home hydrogen refueling systems. This RFI closed on May 24, 2013.[28]
- Hydrogen Delivery Technologies collected feedback from interested stakeholders regarding hydrogen delivery research and development activities aimed at lowering the cost of hydrogen delivery technologies. This RFI closed on June 13, 2013.[29]
- Rotating Disk Electrode Diagnostics for Proton Exchange Membrane Fuel Cell Electrocatalyst Screening collected feedback from interested stakeholders regarding the use of rotating disk electrode experiments and best practices for experimental conditions for characterization of the activity and durability of proton exchange membrane fuel cell oxygen reduction reaction electrocatalysts. This RFI closed on July 12, 2013.[30]

INTERNATIONAL ACTIVITIES

International Partnership for Hydrogen and Fuel Cells in the Economy

The International Partnership for Hydrogen and Fuel Cells in the Economy (IPHE) includes 17 member countries (Australia, Austria, Brazil, Canada, China, France, Germany, Iceland, India, Italy, Japan, Norway, the Republic of Korea, the Russian Federation, South Africa, the United Kingdom, and the United States) and the European Commission. The IPHE is a forum for governments to work together to advance worldwide progress in hydrogen and fuel cell technologies. IPHE also offers a mechanism for international R&D managers, researchers, and policymakers to share program strategies. IPHE members agreed to embark upon a second term starting in November 2013. The Chair of the IPHE was recently transferred from Germany to Japan. The United States and Germany are now Vice Chairs.[31]

International Energy Agency

The United States is involved in international collaboration on hydrogen and fuel cell R&D through the International Energy Agency (IEA) implementing agreements; the United States is a member of both the Advanced Fuel Cells Implementing Agreement (AFCIA) and the Hydrogen Implementing Agreement (HIA). These agreements provide a mechanism for member countries to share the results of R&D and analysis activities. The AFCIA has several annexes: Molten Carbonate Fuel Cells, Polymer Electrolyte Fuel Cells, Solid Oxide Fuel Cells, Fuel Cells for Stationary Applications, Fuel Cells for Transportation, Fuel Cells for Portable Power, and Systems Analysis. Participating countries include Australia, Austria, Belgium, Denmark, Finland, France, Germany, Italy, Japan, Korea, Mexico, Sweden, Switzerland, and the United States. The IEA HIA is focused on RD&D and analysis of hydrogen technologies. Tasks include Hydrogen Safety, Biohydrogen, Fundamental and Applied Hydrogen Storage Materials Development, Small-Scale Reformers for On-site Hydrogen Supply, Wind Energy and Hydrogen Integration, High-Temperature Production of Hydrogen, Advanced Materials for Hydrogen from Water Photolysis, Near- Market Routes to Hydrogen by Co-Gasification with Biomass, Large Scale Hydrogen Delivery Infrastructure, Distributed and Community Hydrogen for Remote Communities, and Global Hydrogen Systems Analysis. Members of the HIA include Australia, Denmark, the European Commission, Finland, France, Germany, Greece, Iceland, Italy, Japan, Korea, Lithuania, New Zealand, Norway, Spain, Sweden, Switzerland, Turkey, Taiwan, United Nations Industrial Development Organization International Centre for Hydrogen Energy Technologies, and the United States. The United States is a strong contributor to numerous IEA tasks and activities.[32]

---

[27] http://www1.eere.energy.gov/hydrogenandfuelcells/news_detail.html?news_id=19089
[28] http://www1.eere.energy.gov/hydrogenandfuelcells/news_detail.html?news_id=19249
[29] http://www1.eere.energy.gov/hydrogenandfuelcells/news_detail.html?news_id=19306
[30] http://www1.eere.energy.gov/hydrogenandfuelcells/news_detail.html?news_id=19437
[31] International Partnership for Hydrogen and Fuel Cells in the Economy, http://www1.eere.energy.gov/hydrogenandfuelcells/international_partnership.html
[32] International Energy Agency, http://www1.eere.energy.gov/hydrogenandfuelcells/international_energy_agency.html

EXTERNAL COORDINATION, INPUT, AND ASSESSMENTS

H_2USA Partnership

In 2013, the Energy Department announced H_2USA—a new public-private partnership focused on advancing hydrogen infrastructure to support more transportation energy options for U.S. consumers, including FCEVs. The new partnership brings together automakers, government agencies, gas suppliers, and the hydrogen and fuel cell industries to coordinate research and identify cost-effective solutions to deploy infrastructure that can deliver affordable, clean hydrogen fuel in the United States. H_2USA held its launch meeting in Washington, D.C., in August. The meeting was attended by 55 representatives of the 26 current participating organizations, including U.S. Department of Energy representatives Dr. David Danielson, Assistant Secretary of Energy Efficiency and Renewable Energy and Steven Chalk, Deputy Assistant Secretary for Renewable Energy.

Hydrogen and Fuel Cells Technical Advisory Committee (HTAC)

As required by the Energy Policy Act of 2005, HTAC was created in 2006 to advise the Secretary of Energy on issues related to the development of hydrogen and fuel cell technologies and to provide recommendations regarding DOE's programs, plans, and activities, as well as on the safety, economic, and environmental issues related to hydrogen and fuel cells. HTAC members include representatives of domestic industry, academia, professional societies, government agencies, financial organizations, and environmental groups, as well as experts in the area of hydrogen safety. HTAC met three times in FY 2013—twice in person and once via webinar. In May 2013, HTAC released its fifth annual report, which summarizes hydrogen and fuel cell technology, domestic and international progress in RD&D projects, commercialization activities, and policy initiatives.[33]

Former Secretary of Energy, Dr. Steven Chu, launched an HTAC subcommittee focusing on hydrogen production in May of 2012, the Hydrogen Production Expert Panel. A major HTAC activity in FY 2012 was the publication of this committee's report. The Steering Committee of the panel offered overall recommendations after considering presentations by the expert panel as well as the findings from the working groups. The panel was charged with providing recommendations to DOE regarding both policy and investments in R&D to enable the widespread production of affordable, low-carbon hydrogen—taking into consideration relevant market and business forces, technology barriers, and policy barriers, as well as the impact of safety codes and standards. HPEP collected input from experts from industry, academia, and national laboratories during a May 2012 workshop and developed recommendations based on that input. HTAC was established under Section 807 of the Energy Policy Act of 2005 to provide technical and programmatic advice to the Energy Secretary on DOE's hydrogen research, development, and demonstration efforts. Key findings were included in the final report that is posted online.[34]

Federal Inter-Agency Coordination

The Hydrogen and Fuel Cell Interagency Task Force, mandated by the Energy Policy Act of 2005, includes senior representatives from federal agencies supporting hydrogen and fuel cell activities, with the DOE/EERE serving as chair. The Hydrogen and Fuel Cell Interagency Working Group, co-chaired by DOE and the White House Office of Science and Technology Policy, continues to meet monthly to share expertise and information about ongoing programs and results, to coordinate the activities of federal entities involved in hydrogen and fuel cell RD&D, and to ensure efficient use of taxpayer resources. A key example of interagency collaboration included a Memorandum of Understanding between DOE's Fuel Cell Technology Office and the National Science Foundation to coordinate basic and applied research, particularly on hydrogen production from renewables. In addition, the Office is working to complete an interagency federal fleet strategy plan to identify locations and vehicle classes to better pinpoint FCEV opportunities. The strategy is under development and expected to be completed in FY 2014.

The National Academies

The National Research Council (NRC) of the National Academies provides ongoing technical and programmatic reviews and input to the Hydrogen and Fuel Cells Program. The NRC has conducted independent reviews of both the Program and the R&D activities of the U.S. DRIVE partnership. Formerly known as the FreedomCAR and Fuel Partnership, the U.S. DRIVE partnership advances an extensive portfolio of advanced automotive and energy

[33] 2012 HTAC Annual Report, http://www.hydrogen.energy.gov/pdfs/2012_htac_annual_report.pdf
[34] Report of the Hydrogen Production Expert Panel (May 2013), http://www.hydrogen.energy.gov/advisory_htac.html#reports

infrastructure technologies, including batteries and electric-drive components, advanced combustion engines, lightweight materials, and hydrogen and fuel cell technologies.

Clean Energy Manufacturing Initiative

The Clean Energy Manufacturing Initiative (CEMI) is a strategic integration and commitment of manufacturing efforts across EERE's clean energy technology offices and the Advanced Manufacturing Office, focusing on American competitiveness in clean energy manufacturing. The objectives are to increase U.S. competitiveness in the production of clean energy products by strategically invest in technologies that leverage American competitive advantages and overcome competitive disadvantages, and increase U.S. manufacturing competitiveness by strategically investing in technologies and practices to enable U.S. manufacturers to increase their competitiveness through energy efficiency, combined heat and power, and taking advantage of low-cost domestic energy sources.

The Office is an active participant in CEMI and is working to increase funding for manufacturing R&D and EERE focus on energy productivity resources for manufacturers. Through an Advanced Manufacturing Office competitive funding opportunity, CEMI is supporting innovative and transformational manufacturing processes and materials across multiple technologies, including high-volume manufacturing processes for low-cost, high-quality MEAs for fuel cells.

EERE's CEMI is partnering with the Council on Competitiveness to convene the nation's private and public sector leaders in a series of successive dialogues to identify barriers to U.S. competitiveness in clean energy manufacturing, as well as solutions to overcome those barriers through public-private partnership models. The first of these regional summits was held on June 21, 2013, in Toledo, Ohio, and showcased regional clean energy manufacturing activities and encouraged a dialogue about how the Initiative can strengthen national and regional manufacturing competitiveness and foster regional stakeholder networking and partnerships. Five additional regional summits have been planned. In addition, CEMI and the Council on Competitiveness held the inaugural American Energy and Manufacturing Competitiveness Summit in December 2013, a first-of-its-kind annual gathering of preeminent leaders from industry, government, academia, labor, and the national laboratories to address critical national imperatives in manufacturing and energy. A fuel cell manufacturing session was organized by the Office in conjunction with CEMI at these summits.

National Fuel Cell Technology Evaluation Center at the Energy Systems Integration Facility

Following Energy Secretary Ernest Moniz's visit to DOE's NREL in September 2013, the Department unveiled a one-of-its-kind national secure data center dedicated to the independent analysis of advanced hydrogen and fuel cell technologies at the Department's Energy Systems Integration Facility (ESIF) located at NREL in Golden, Colorado. The National Fuel Cell Technology Evaluation Center (NFCTEC)[35] allows industry, academia, and government organizations to submit and review data gathered from projects to advance cost-effective fuel cell technology. NFCTEC will also help accelerate the commercialization of fuel cell technologies by strengthening data collection from fuel cell systems and components operating under real-world conditions, and analysis of these detailed data that can be compared to technical targets. The NFCTEC is housed within an ESIF area specifically designed for the secure management, storage, and processing of proprietary data from industry and other stakeholders. Aggregated analysis results that show the status and progress of the technology but do not identify individual companies are available to the public.

DOE Fuel Cell Tech Team

The DOE Fuel Cell Tech Team was created in November 2012 in recognition of the importance of hydrogen and fuel cells in the Department's portfolio and the benefit of greater coordination across offices. The Fuel Cell Tech Team includes members from multiple DOE offices including EERE, the Offices of Science, Fossil Energy, and the Advanced Research Projects Agency. Endorsement of the team by the Secretary and the Under Secretary of Energy along with relevant Assistant Secretaries from the Offices of Science, Fossil Energy, and ARPA-E underscore the importance of fuel cells and the need to directly address key recommendations by the Department's federal advisory committee. Examples of collaboration include best practices/protocols on diagnostics, workshop planning (e.g., natural gas for fuel cells), and biweekly meetings and presentations.

[35] National Fuel Cell Technology Evaluation Center http://www.nrel.gov/hydrogen/facilities_nfctec.html

FY 2013 Annual Merit Review and Peer Evaluation

The Program's AMR took place May 13–17 in Arlington, Virginia, and provided an opportunity for the Program to obtain expert peer reviews of the projects it supports and to report its accomplishments and progress. For the fifth time, this meeting was held in conjunction with the annual review of DOE's Vehicle Technologies Office. During the AMR, reviewers evaluate the Program's projects and make recommendations; DOE uses these evaluations, along with other review processes, to make project funding decisions for the upcoming fiscal year. The review also provides a forum for promoting collaborations, the exchange of ideas, and technology transfer. This year, more than 1,500 participants attended, and more than 200 experts peer-reviewed 145 of the Program's projects—conducting a total of more than 900 individual project reviews, with an average of more than six reviewers per project. The report summarizing the results and comments from these reviews is available at www.hydrogen.energy.gov/annual_review12_report.html. The 2014 Annual Merit Review and Peer Evaluation Meeting will be held June 16–20, in Washington, D.C.

Funds Saved through Active Project Management

The AMR is a key part of the Program's comprehensive approach toward active management of its projects. Termination of underperforming projects—identified through the AMR as well as through other Go/No-Go decisions (with criteria defined in the project scope of work)—helped the Office redirect $7.6 million in funding in FY 2013, $6.8 million in FY 2012, and over $37 million over the past five years.

DOE Cross-Cutting Activities

Grid Integration: Integration of energy efficiency and renewable energy technologies into the grid at scale is a major challenge facing deployment of all clean energy technologies. EERE is working to address some of these issues through a new cross-cutting initiative focused on integrating clean energy technologies into the energy system in a safe, reliable, and cost effective manner at a relevant scale to support the nation's goals of 80% clean electricity by 2035 and reducing oil imports by 33% by 2025. All of the participating technologies offices, including the Fuel Cell Technologies Office, are determining the high impact RD&D necessary to enable the integration of energy efficiency and renewable energy technologies into the energy system at a scale necessary to realize this vision.

Carbon Fiber: High quality carbon fiber is essential to addressing the needs of the automotive industry as well as emerging clean energy industries. Customers in these industrial markets use carbon fiber for necessary performance benefits but have not explored the full range of possibilities due to high manufacturing costs. The primary objective of EERE's cross-cutting carbon fiber initiative is to scale up the technology to market development scale (1,000-fold above the anticipated pilot scale throughput). One of the Office's goals is to produce low cost carbon fiber from novel polymer precursors in higher yield and at lower cost than the incumbent carbon fiber made from specialty-grade peroxyacetyl nitrate.

Wide Bandgap Semiconductors for Clean Energy Initiative: Wide bandgap (WBG) semiconductor materials allow power electronic components to be smaller, faster, more reliable, and more efficient than their silicon-based counterparts. These capabilities make it possible to reduce weight, volume, and life-cycle costs in a wide range of power applications. EERE's technology offices, through the Advanced Manufacturing Office, are working together to harness these capabilities to lead to dramatic energy savings in industrial processing and consumer appliances, accelerate widespread use of electric vehicles and fuel cells, and help integrate renewable energy onto the electric grid. In support of this cross-cutting initiative, the Office has successfully launched fuel cell specific efforts in the development of WBG energy conversion materials and initiated cross-office and cross-agency R&D collaborations for innovative WBG for photoelectrochemical hydrogen production. The Office has also begun to evaluate the current gaps in innovative WBG power electronics to improve efficiency and lifetime of renewable/integrated electrolysis.

CONCLUSION

The need for clean, sustainable energy, combined with the need to reduce emissions, has come together to form a global imperative—one that demands new technologies and new approaches for the way we produce and use energy. Widespread use of hydrogen and fuel cells can play a substantial role in a portfolio of clean energy technologies that will overcome key energy challenges. In addition, growing interest and investment among leading world economies, such as Germany, Japan, and South Korea, underscores the global market potential for these technologies. FY 2013

brought the renewal of the International Partnership for Hydrogen and Fuel Cells in the Economy, a global partnership on hydrogen and fuel cells, with more than 17 countries around the world.

The United States continues to be one of the world's largest and fastest growing markets for fuel cell and hydrogen technologies. In 2012, nearly 80 percent of total investment in the global fuel cell industry was made in U.S. companies.[36] Major companies—such as Coca-Cola, FedEx, Sysco, Wegmans, and Whole Foods—are deploying fuel cell forklifts in their warehouses and distribution facilities. As of October 2013, DOE's Recovery Act efforts have deployed more than 1,300 fuel cells systems, surpassing the original Recovery Act deployment goal of up to 1,000 fuel cells. In the wake of those initial purchases, private businesses have ordered more than 5,000 additional fuel cell forklifts and 3,500 fuel cell emergency backup power systems with no DOE funding.[37] These rapidly growing markets have helped create and keep jobs in the United States.

Another indicator of the robustness and innovative vitality of a thriving market is the number of patents granted, and the number of technologies commercialized. EERE-funded R&D has resulted in more than 450 patents, 40 commercial technologies, and 65 technologies that are projected to be commercialized within three to five years.[38] In addition, EERE's investment of $50 million in specific hydrogen and fuel cell projects led to more than $300 million in revenue and investments of approximately $14 million in specific projects led to a nearly $130 million in additional private investment.

FY 2013 was a productive year for the Program in terms of technical accomplishments as well. For example, the Program introduced several changes in the transportation fuel cell system cost projection assumptions, which resulted in an increase in the projected cost status to $55/kW. Updating previous numbers with the same assumptions and requirements shows a decrease in the transportation fuel cell system cost of more than 50% since 2006 and 30% since 2008.

We've made tremendous progress, but innovative R&D breakthroughs won't be enough—infrastructure remains a key challenge to the widespread adoption of FCEVs. To overcome these challenges, DOE, together with other federal agencies, automakers, state government, academic institutions, and additional stakeholders, has formed a public-private partnership called H_2USA to promote the widespread adoption of FCEVs. The partnership's first action is to form a strategy to coordinate vehicle and infrastructure rollout, conduct situational assessment and analysis, and identify synergies and opportunities to leverage other alternative fueling infrastructure—such as natural gas—to enable cost reductions and economies of scale. H_2USA is also focusing on identifying actions to incentivize early adopters and evaluating the business cases required for commercialization of FCEVs and hydrogen infrastructure technologies. While the research community is working toward finding technical solutions, this partnership is going to be working on accelerating a national infrastructure by tackling the largest barriers: location, financing, codes and standards, and equipment costs.

FY 2013 was also a landmark year for industry, with many auto manufacturers announcing FCEV commercialization plans; Toyota, Nissan, Hyundai, General Motors, Honda, Mercedes/Daimler, and Ford have all committed to putting FCEVs on the road, some as early as the 2015–2017 timeframe. In November 2013 at the Tokyo Motor Show, Toyota unveiled their concept model FCEV, stating that the cars will be on the market in 2015. Hyundai Motor Co., has said it will start leasing its Tucson FCEV in the spring of 2014 with three years of fuel and maintenance at no cost. Honda Motor Co., who has leased an FCEV for several years, unveiled its next-generation version at the Los Angeles Auto Show in November as well. Major industry partnerships were also announced: GM and Hyundai; Toyota and BMW; and Daimler, Ford, and Nissan. Major progress by independent gas providers such as Air Products, Linde, and Air Liquide was also announced.

Moving forward, the Program's emphasis on the transportation sector will be strengthened by the creation of an Office of Sustainable Transportation within EERE that will include the Vehicle Technologies Office and the Bioenergy Technology Office as well as the Fuel Cell Technologies Office. This new office will allow the opportunity for additional cross-cutting activities and a closer collaborative relationship between all advanced vehicle technology R&D. However, the Program will continue to pursue a broad portfolio of R&D activities for fuel cell applications across multiple sectors including stationary applications. Efforts will span the full spectrum of technology readiness, including near term markets like material handling equipment and backup power, mid-term markets like combined heat and power, and auxiliary power units, and longer-term markets like FCEVs.

[36] 2012 Fuel Cell Technologies Market Report, http://www1.eere.energy.gov/hydrogenandfuelcells/pdfs/2012_market_report.pdf

[37] DOE Hydrogen and Fuel Cells Program Record #13007 and 13008

[38] 2013 Pathways to Commercial Success: Technologies and Products Supported by the Fuel Cell Technologies Office, http://www1.eere.energy.gov/hydrogenandfuelcells/pdfs/pathways_2013.pdf

This is a critical time for fuel cells and hydrogen. DOE's Hydrogen and Fuel Cell Program will continue to work in close collaboration with key stakeholders, and will continue its strong commitment to effective stewardship of tax payer dollars in support of its mission to enable the energy, environmental, and economic security of the nation.

Sunita Satyapal
Director
Fuel Cell Technologies Office
U.S. Department of Energy

II. HYDROGEN PRODUCTION

II.0 Hydrogen Production Program Overview

INTRODUCTION

The Hydrogen Production program supports research and development (R&D) of technologies that will enable the long-term viability of hydrogen as an energy carrier for a diverse range of end-use applications including stationary power (e.g., backup power and combined heat and power systems), transportation (e.g., specialty vehicles, cars, trucks, and buses), and portable power. A portfolio of hydrogen production technology pathways utilizing a variety of renewable energy sources and renewable feedstocks is being developed under this program.

Multiple DOE offices are engaged in R&D relevant to hydrogen production, including:

- The Fuel Cell Technologies Office (FCTO), within the Office of Energy Efficiency and Renewable Energy (EERE), is developing technologies for distributed and centralized renewable production of hydrogen. Distributed production options under development include reforming of bio-derived renewable liquids and electrolysis of water. Centralized renewable production options include water electrolysis integrated with renewable power generation (e.g., wind, solar, hydroelectric, and geothermal power), biomass gasification, solar-driven high-temperature thermochemical water splitting, direct photoelectrochemical water splitting, and biological processes.
- The Office of Fossil Energy (FE) is advancing the technologies needed to produce hydrogen from coal-derived synthesis gas, including co-production of hydrogen and electricity. Separate from the Hydrogen and Fuel Cells Program, FE is also developing technologies for carbon capture, utilization, and storage, which will ultimately enable hydrogen production from coal to be a near-zero-emissions pathway.
- The Office of Science's Basic Energy Sciences program conducts research to expand the fundamental understanding of biological and biomimetic hydrogen production, photoelectrochemical water splitting, catalysis, and membranes for gas separation.
- The Office of Nuclear Energy (NE) has been conducting efforts in the development of high-temperature electrolysis, under the Next Generation Nuclear Plant (NGNP) project, which also includes evaluations of other end-user applications and energy transport systems. The previous activity, the Nuclear Hydrogen Initiative, was discontinued in Fiscal Year (FY) 2009 after steam electrolysis was chosen as the hydrogen production pathway most compatible with the NGNP.

GOAL

The goal of the Hydrogen Production program is to develop low-cost, highly efficient hydrogen production technologies that utilize diverse domestic sources of energy, including renewable resources (EERE), coal with sequestration (FE), and nuclear power (NE).

OBJECTIVES[1]

The objective of the Hydrogen Production program is to reduce the cost of hydrogen dispensed at the pump to a cost that is competitive on a cents-per-mile basis with competing vehicle technologies. Based on current analysis, this translates to a hydrogen threshold cost of $2–$4 per gallon gasoline equivalent (gge) (produced, delivered and dispensed, but untaxed) by 2020[2], apportioned to $1-$2/gge for production only[3]. Technologies are being developed to achieve this goal in timeframes appropriate to their current stages of development.

The objectives of FE's efforts in hydrogen production are documented in the *Hydrogen from Coal Program Research, Development and Demonstration Plan* (September 2010)[4]. They include proving the feasibility of a near-zero emissions, high-efficiency plant that will produce both hydrogen and electricity from coal and reduce the cost

[1] Note: Targets and milestones were recently revised; therefore, individual project progress reports may reference prior targets.
[2] Hydrogen Threshold Cost Calculation, Program Record (Office of Fuel Cell Technologies) 11007, US Department of Energy, 2012, http://www.hydrogen.energy.gov/pdfs/11007_h2_threshold_costs.pdf
[3] *Hydrogen Production and Delivery Cost Apportionment*, Program Record (Office of Fuel Cell Technologies) 12001), US Department of Energy, 2012
[4] *Hydrogen from Coal Program Research Development and Demonstration Plan*, Office of Fossil Energy, US Department of Energy, September 2010, http://fossil.energy.gov/programs/fuels/hydrogen/2010_Draft_H2fromCoal_RDD_final.pdf

of hydrogen from coal by 25 percent compared with current technology by 2016. The objectives of NE's efforts in hydrogen production are documented in the *Technology Roadmap for Generation IV Nuclear Energy Systems* (December 2002)[5]. They include the development of high-temperature thermochemical process for hydrogen production compatible with NGNP.

FY 2013 TECHNOLOGY STATUS AND PROGRESS

In FY 2013, significant progress was made by the Hydrogen Production program on several important fronts. For example:

- The Hydrogen Production Expert Panel (HPEP), a Hydrogen and Fuel Cell Technical Advisory Committee (HTAC) subcommittee collected input from experts from industry, academia, and national laboratories during a May 2012 workshop and developed recommendations based on that input. HPEP was tasked with providing recommendations to enable the widespread production of affordable, low-carbon hydrogen to HTAC, which was established under Section 807 of the Energy Policy Act of 2005 to provide technical and programmatic advice to the Energy Secretary on DOE's hydrogen research, development, and demonstration efforts. Key findings were included in the final report that is posted online[6] and are summarized in the next section.
- The Hydrogen Production program's chapter of the *Multi-Year Research, Development and Demonstration Plan (MYRD&DP)* was updated. Cost and performance targets for the hydrogen production pathways were identified based on new and updated Hydrogen Analysis (H2Av3) Model production pathway case studies.
- A Memorandum of Understanding with the National Science Foundation was signed allowing for joint funding of RD&D with the FCTO.
- The Hydrogen Production Roadmap was revised and updated by the U.S. DRIVE Hydrogen Production Technology Team.
- The DOE Photoelectrochemical Hydrogen Production Working Group published the Springer Brief in Energy: "Photoelectrochemical Water Splitting: Standards, Experimental Methods, and Protocols."[7]
- The Biological Hydrogen Production Workshop (September 2013) was held to identify key R&D needs.
- A funding opportunity announcement for hydrogen production pathways analysis was released and a new award was made to a team led by Strategic Analysis Inc.

Hydrogen Production Expert Panel Report

An HPEP, comprised of world leaders in hydrogen production technologies from industry, academia and the national laboratories, was established in 2012 as a subcommittee of HTAC. A workshop was held by the panel in May 2012 to formulate recommendations to HTAC about enabling pathways to the widespread production of affordable low carbon hydrogen, both for near- and long-term markets. A summary report resulting from the workshop has been completed and published by HTAC. Key recommendations from the report included: 1) providing incentives to accelerate the production of hydrogen for transportation applications with a particular focus on the steam reforming of natural gas, leveraging this abundant and low-cost domestic resource; 2) considering significant investments in hydrogen production and storage analyses and demonstrations; 3) developing a cohesive plan for all pertinent R&D programs to provide consistent and long-term guidance; and 4) establishing public-private partnerships and/or clusters to create well-defined plans for infrastructure roll-out, establishing appropriate incentives, and promoting uniform codes, standards, and safety regulations.

Production Cost Status and Targets

The status and targets for the projected cost of hydrogen production based on the pathway-specific H2Av3 case studies completed in FY 2013 are shown in Table 1. The technoeconomic assumptions used in these case studies can be found online for each pathway at http://www.hydrogen.energy.gov/h2a_production; and these cases are also fully documented in the new DOE-FCTO MYRD&DP. Targets for hydrogen production efforts in FE and NE (not included

[5] *A Technology Roadmap for Generation IV Nuclear Energy Systems*, Office of Nuclear Energy, US Department of Energy, December 2002, http://www.ne.doe.gov/genIV/documents/gen_iv_roadmap.pdf

[6] Report of the Hydrogen Production Expert Panel (a subcommittee of HTAC), May 2013, http://www.hydrogen.energy.gov/advisory_htac.html

[7] *Springer Brief in Energy*, September 2013, http://link.springer.com/book/10.1007/978-1-4614-8298-7/page/1

in Table 1), along with information on the status of the technologies, are described separately in the previously cited RD&D and roadmap documents for these programs.

TABLE 1. Cost Status and Targets for Hydrogen Production*

	$/gge (production costs only)	Current Status**	2015 Target	2020 Target	Ultimate Production Target
Distributed	Electrolysis from grid electricity	$4.20	$3.90	$2.30	$1-$2
	Bio-derived Liquids (based on ethanol reforming case)	$6.60	$5.90	$2.30	
Central	Electrolysis From renewable electricity	$4.10	$3.00	$2.00	
	Biomass Gasification	$2.20	$2.10	$2.00	
	Solar Thermochemical	NA	$14.80	$3.70	
	Photoelectrochemical	NA	$17.30	$5.70	
	Biological	NA	NA	$9.20	

*H2A v3 technoeconomic assumptions used in the projected cost status and targets for hydrogen production are consistent with the DOE-FCTO MYRD&DP; Apportionment of threshold cost: $1-$2/gge for production, $1-$2/gge for delivery is addressed in FCTO Program record #12001; new H2A v3 case studies are published at http://www.hydrogen.energy.gov/h2a_production.
** Current status as of 2011.
NA - not applicable

Reductions in the projected costs for hydrogen production in several of the nearer term pathways have been realized through continued technical progress in these technologies, as illustrated in Figure 1. Specific technical progress achieved in FY 2013 in both the nearer- and longer-term hydrogen production pathways is addressed in the following sections.

Separation Processes

Membrane separations RD&D continued through the Small Business Innovation Research (SBIR) program and FE. Technical progress included:

- Developed, through a Phase III SBIR project, a sorbent bed to operate downstream of a bulk desulfurization system as a polishing bed to provide an essentially sulfur-free biogas to a solid oxide fuel cell (SOFC). Laboratory testing of a SOFC module running on bio-gas, integration of a clean-up system and power generation module with the SOFC, and initiation of slipstream demonstrations for an integrated SOFC system was completed. The sorbent achieved 17.5 wt% sulfur capacity, with the potential for 2X higher capacity than current commercially available sorbents. (TDA Research, Inc.)
- Continued FE funding for comprehensive engineering design of advanced Pd and Pd-alloy composite membrane separations for hydrogen production from syngas derived from coal or a coal-biomass mixtures. Five membrane projects successfully designed, constructed, and tested membranes with operating gasifier and/or simulated syngas mixtures that produced 2 pounds per day (lb/day) of hydrogen. A down-select process has resulted in two project teams going forward to complete their designs and construct membrane separation modules with the capacity to produce up to 50 lbs/day of H_2. (FE)

Bio-Derived Liquid Pathways

Projects in this area addressed hydrogen production through catalytic steam reforming of pyrolysis oil and aqueous phase reforming of pyrolysis oil at moderate temperatures. Technical progress included:

- Compared hydrogen production by autothermal reforming of pyrolysis oils for three bio-oils feedstocks (oak, poplar, and pine) and demonstrated that the composition of bio-oil has a significant impact on the yield of hydrogen. The highest hydrogen yields were obtained from the poplar bio-oil (11 g H_2/100 gr bio-oil) with a process energy efficiency (70.8%) and projected high-volume cost ($4.26/gge hydrogen) exceeding the 2015 targets of 70%, and $5.90/gge, respectively. (National Renewable Energy Laboratory, NREL)
- Identified a promising pathway, using a WO_3/AL2O_3 + Ru/C catalyst system, for hydrogen production from cellulose through a two-step process: production of ethylene glycol and then short chain polyols, followed by conversion of polyols to H_2 and CO_2 via aqueous phase reforming. Demonstrated >40% ethylene glycol yield by catalytic deconstruction of cellulose in reactor tests. (Pacific Northwest National Laboratory)

Projected High-Volume Cost of Hydrogen for Near-Term Production Pathways

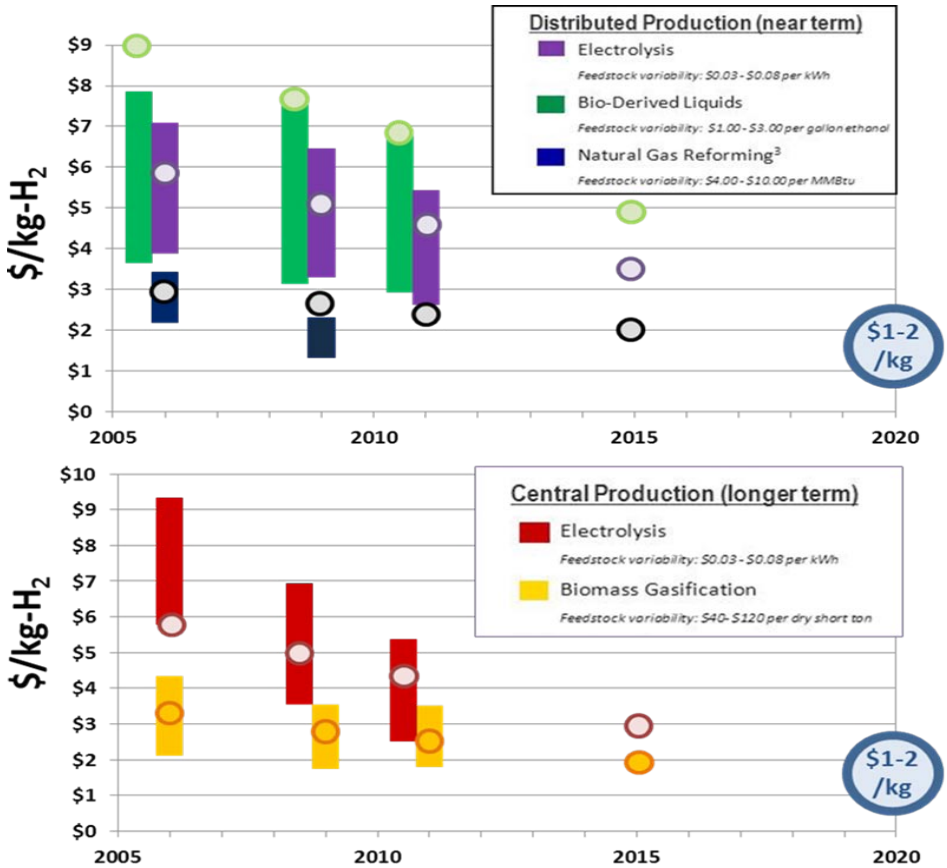

FIGURE 1. HYDROGEN PRODUCTION COST STATUS. Significant progress has been made in several hydrogen production pathways. The hydrogen threshold cost represents the cost at which hydrogen fuel cell electric vehicles are projected to become competitive on a cost-per-mile basis with competing vehicles (gasoline hybrid-electric vehicles) in 2020. Notes: (i) Costs shown do not include taxes. Costs of forecourt compression, storage, and dispensing are not included for distributed technologies, and plant-gate production costs (not including transportation, compression, storage, and dispensing) are shown for centralized technologies. Projections of distributed costs assume station capacities of 1,500 kg/day. Projections of centralized production costs assume capacities of ≥50,000 kg/day. Cost ranges for each pathway are shown in 2007 dollars, based on high-volume projections from H2A analyses, reflecting variability in major feedstock pricing and a bounded range for capital cost estimates. (ii) DOE funding of natural gas reforming projects was completed in 2009 due to achievement of the threshold cost. Incremental improvements will continue to be made by industry.

Electrolysis Hydrogen Production

The major emphases of the electrolysis projects were on cost reduction and efficiency improvement through cell and stack optimization, and validation of integration with renewable resources. Technical progress included:

- Reduced electrolyzer stack costs by 60% compared to a 2007 baseline through low-cost component development resulting in commercial electrolyzer stack products in 30, 60, and 100 cell configurations. (Giner)
- Operated proton exchange membrane (PEM) electrolyzer stacks for greater than 10,000 hours with variable wind profile. Preliminary results indicate no substantial difference in the decay rates between stacks operating under variable wind power versus operating under constant power. (NREL)
- Scaled up and validated advanced stack design with a cell active area of >500 cm^2 and demonstrated single-cell stack prototype operation. Validated a >40% stack cost reduction versus the original project baseline design. (Proton OnSite)

- Demonstrated feasibility to reach <10% catalyst loadings with nanostructured thin film electrodes on multiple membrane types without loss of performance versus baseline electrodes. (Proton OnSite)

Photoelectrochemical (PEC) Hydrogen Production

The broad focus of projects in this area was on utilizing state-of-the-art theory, synthesis, and characterization tools to develop viable PEC material systems and prototypes with improved efficiency and durability. Technical progress included:

- Durability tested multiple surface-treated tandem $GaInP_2$/GaAs electrodes under bias and demonstrated numerous samples which lasted for over a hundred hours with little sign of physical degradation or loss of performance. (NREL)
- Completed quantum molecular dynamics simulations of water electrode interfaces (GaP/InP), and formulated models of interfacial water and wetted surfaces. (Lawrence Livermore National Laboratory, LLNL)
- Applied the innovative model of PEC electrodes developed in 2012 based on the Hamiltonian approach to an unconventional photoelectrode, MoS_2, and submitted results for publication. (LLNL/Stanford)
- Experimentally validated hole-trapping corrosion mechanisms key to stability of PEC devices. (LLNL, in collaboration with the NREL Surface Validation Team)
- Achieved 500 hr durability at 4.1 mA/cm^2 (~5% solar-to-hydrogen efficiency) in a low-cost thin-film silicon-based device. (MVSystems, Inc.)
- Successfully demonstrated bandgap engineering of copper chalcopyrite thin film materials optimized for PEC applications. (MV Systems, Inc., University of Hawaii)
- Successfully demonstrated roll-to-roll production for depositing cobalt oxide films on large area amorphous silicon cells for PEC applications. (Midwest Optoelectronics, LLC)

Biological Hydrogen Production

The broad focus of the projects in the biological hydrogen production portfolio were to address key barriers such as oxygen sensitivity and feedstock utilization using molecular biology and genetic engineering techniques along with improved systems engineering. Technical progress included:

- Demonstrated 10-fold improvement in oxygen tolerance in preliminary experiments in a strain of algae carrying the bacterial Ca1 hydrogenase, which produced hydrogen photobiologically at oxygen concentrations equivalent to 80% of air, at least double the concentration that the native wild-type could tolerate, in the first *in vivo* demonstration of increased oxygen-tolerance of light-driven biological hydrogen production from intact cells. (NREL)
- Developed genetic tools to generate mutants in *Clostridium thermocellum*, and used them to knock out the pyruvate-to-formate reaction pathway that competes for substrates with the hydrogen production pathway, reducing formate production to below detectable levels. (NREL)
- Inserted new promoters for the recombinant Casa Bonita strain hydrogenase genes, which code for the hydrogen-producing machinery, increasing cells' production of the hydrogenase proteins by 16- to 44-fold. (NREL)
- Increased the hydrogen evolution rate of a recombinant, more oxygen-tolerant hydrogenase in the cyanobacteria *Synechococcus elongates* 35-fold through directed mutations of the hydrogenase protein and improvements in maturation gene expression. This new strain has nearly double the hydrogen evolution rate than that of the wild type. (J. Craig Venter Institute)
- Identified the gene mutation that increases *Chlamydomonas reinhardtii* light utilization from the wild-type baseline of 3% to 25% as coding a signal recognition protein, and characterized the role of the protein in light harvesting complex assembly in *C. reinhardtii*. (University of California, Berkeley)

Solar-Thermochemical Hydrogen (STCH) Production

Efforts in these projects were directed toward novel materials design and performance characterization for water splitting by non-volatile metal-oxide-based materials for the high-temperature cycles. For the hybrid cycles with electrolysis steps, efforts were directed toward development of membranes and catalysts for improved performance and durability during the electrolysis step. Technical progress included:

- Demonstrated unchanged current density and voltage characteristics in small 5 cm^2 CuCl electrolyzer cell after Pt loadings were reduced to less than half of the original value, i.e., down from 0.8 mg/cm^2 on both electrodes to 0.4 mg/cm^2 on the cathode and 0.1 mg/cm^2 on the anode. (Argonne National Laboratory)
- Demonstrated long-term stability of the complete electrochemical system for the Sulfur Ammonia (SA) thermochemical reaction cycle, including a greater than 500-hour durability test; and new membranes for the electrolytic cell were identified with up to 2 orders of magnitude lower sulfite flux. A phase-change thermal-storage system concept based on melting and solidification of NaCl was developed to allow for 24/7 operation of the SA cycle. (Science Applications International Corporation, SAIC)
- Discovered a perovskite structure that produces 9x more hydrogen, at a 250°C lower reduction temperature than CeO_2 (1,350°C vs. 1,500°C), the current state-of-the art metal-oxide redox material. H2Av3 analysis of a dish-based H_2 production plant (with SAIC) showed the major contributors to capital cost to be 1) the solar to hydrogen conversion ratio, 2) collector cost, 3) the solar reactor/receiver cost, and 4) electrical power generation cost. (Sandia National Laboratories)
- Isothermal redox at 1,350°C was shown to be feasible for the hercynite cyle with >3x and >12x the production capacity per mass of active material observed than for hercynite and ceria, respectively, during temperature swing water splitting (reduced at 1,350°C and reoxidized at 1,000°C). Results were recently published in *Science*[8]. (University of Colorado, Boulder)
- Modified a Pressurized Button Cell Test Facility, for operation up to 130°C and 1 MPa, for the testing of advanced membranes to reduce polarization losses and SO_2 crossover fluxes for the electrolysis step of the hybrid sulfur reaction cycle was initiated. Candidate anode electrocatalysts, including Pt,Au, PtAu, PtAg, PtPd, AuPd, AuAg, PtCr, and AuCr, that have potential to reduce anode polarization by greater than 100 mV versus state-of-art Pt catalyst, were identified. (Savannah River National Laboratory)

Analysis

The focus of the analysis efforts were on the development of standardized procedures for formulating hydrogen pathway case studies utilizing the H2Av3 tool with technical inputs from production pathway experts. Technical accomplishments included:

- Developed a comprehensive PEM Electrolysis H2Av3 Case Study based on input from four electrolyzer companies with PEM electrolysis expertise. (SAIC/NREL)

BUDGET

The FY 2013 appropriation for the Hydrogen Production and Delivery program of the FCTO was $15.7 million. Funding was distributed approximately 68% to 32% between Production and Delivery, respectively (approximately the same distribution used in FY 2012).

The request for Production and Delivery in FY 2014 is $21 million. The estimated budget breakdown for Production funding in FY 2014 is shown in Figure 2. Production has increasingly focused in past years on early development, long-term, renewable pathways such as photoelectrochemical, biological, and solar-thermochemical hydrogen production. This trend will likely continue in FY 2014 as new projects are selected from funding opportunities. However, innovative approaches to renewable or reduced carbon technologies for nearer-term distributed and/or semi-central production will also be considered for funding when appropriate.

[8] *Efficient Generation of H2 by Splitting Water with an Isothermal Redox Cycle*, Christopher L. Muhich et.al., Science 341, 540 (2013).

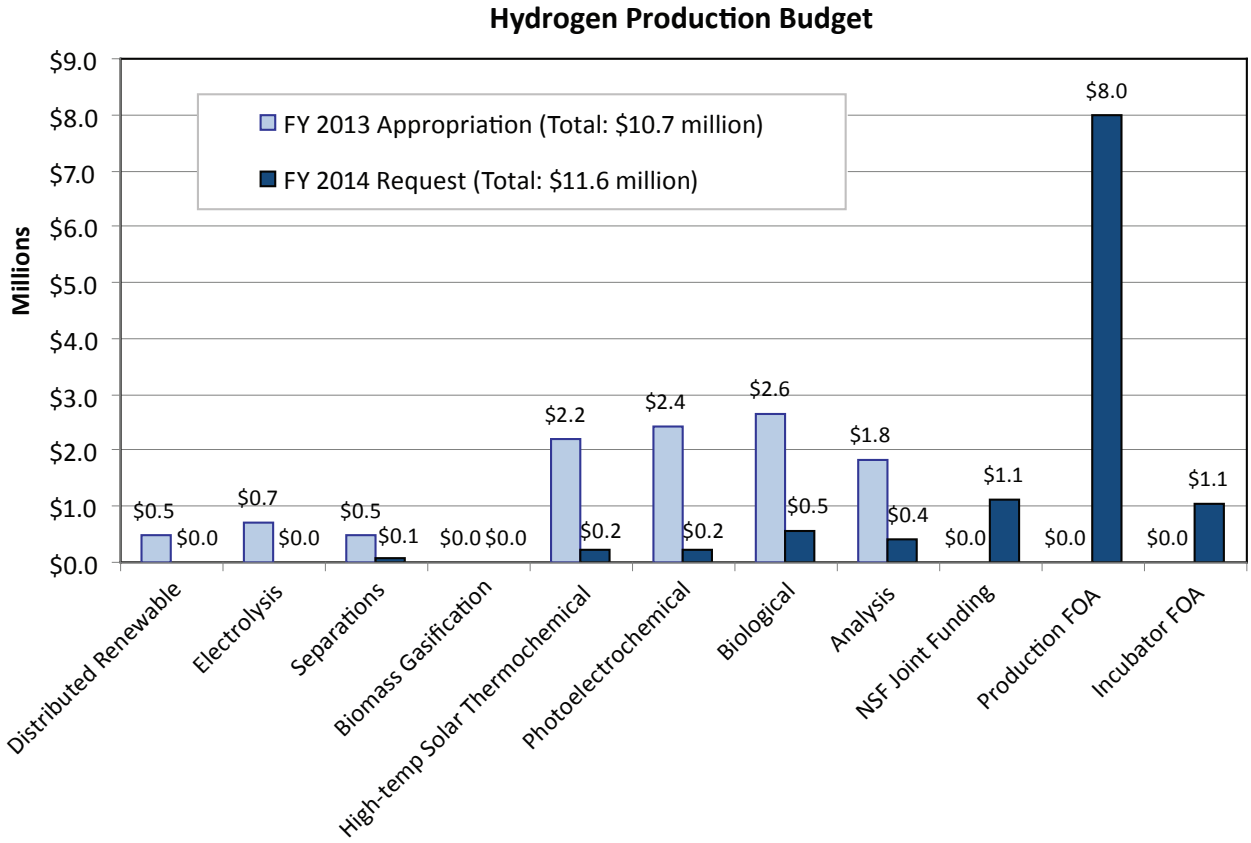

NSF – National Science Foundation; FOA – Funding Opportunity Announcement

FIGURE 2. HYDROGEN PRODUCTION BUDGET. Budget amounts for FY 2013 and projected amounts for FY 2014, contingent upon appropriations, are shown broken down by the different production pathways. Exact distribution of funds in FY 2014 will not be defined until funds have been appropriated and new projects selected.

FY 2014 PLANS

General Hydrogen Production program plans for FY 2014 include:

- Prepare and post a report on the Biological Hydrogen Production Workshop; and release a Request for Information inviting further input. Outcomes of the workshop and responses to the Request for Information will be used to inform programmatic planning.
- Continue to develop and update hydrogen production pathways analyses with the H2Av3 tool and develop a case study on fermentative hydrogen production and establishment of cost and performance baselines for new project starts.
- Continue emphasis on materials durability, production efficiency and process optimization for all pathways, and develop and refine materials characterization protocols and performance metrics for early development technologies.
- Continue coordination with the Office of Science, which funds basic research related to hydrogen and fuel cell technologies. Together with Basic Science activities, a fundamental understanding of issues related to hydrogen production (particularly in the longer-term R&D areas of photoelectrochemical and biological processes) can help address the challenges of hydrogen production. Coordination of the solar-hydrogen-related fundamental research activities in the Office of Science's Solar Fuels Innovation Hub with the EERE's hydrogen production systems-oriented R&D will be a high priority.
- Initiate RD&D projects in Production R&D through competitive funding opportunities, including a topic on renewable hydrogen for joint funding by the National Science Foundation and the FCTO.

- Validate and assess performance and design of composite separation membranes, as well as production methods to produce commercial quantities of substrates and membranes at reasonable cost. Perform economic analysis based on test results obtained to estimate costs for commercial equipment and membranes. (FE)

Important pathway-specific milestones planned for FY 2014 in the Hydrogen Production program projects include:

- Achieve continuous hydrogen photoproduction for at least 30 minutes (10x longer than wild type) with an average rate of at least 2.8 umol H_2 mg Chl-1 h^{-1}, by whole cells of a Ca1-expressing mutant strain of the alga *Chlamydomonas reinhardtii* under full solar-light intensities, in the presence of the uncoupler FCCP (mesoxalonitrile 4-trifluoromethoxyphenylhydrazone) measured continuously by the Clark electrode.
- Reduce electrolyzer cell precious metal cathode catalyst loading by 90%, compared to a baseline commercial membrane electrode assembly, to 0.12 mg/cm^2 while maintaining equivalent performance of at least 2.0 V at 1.75 A/cm^2.
- Apply nitrogen ion implantation surface passivation treatment to p-InP, a III-V semiconductor that could enable PEC water splitting efficiencies in excess of 20% solar-to-hydrogen, and evaluate the corrosion mitigation.
- Demonstrate a H_2 redox capacity of ≥300 µmole/g for one or more reaction cycles for particle-based STCH production, compared to the 2012 baseline for ceria of 150 µmole/g (at a reduction temperature of 1,550 C), indicating the potential to achieve the 2015 targets of 10% solar-to-hydrogen efficiency and 8.1E-07 kg/s m^2 production rate.

Sara Dillich
Acting Hydrogen Production & Delivery Team Lead
Fuel Cell Technologies Office
U.S. Department of Energy
1000 Independence Ave., SW
Washington, D.C. 20585-0121
Phone: (202) 586-7925
Email: Sara.Dillich@ee.doe.gov

II.A.1 PEM Electrolyzer Incorporating an Advanced Low-Cost Membrane

Monjid Hamdan (Primary Contact), Tim Norman
Giner, Inc. (Formerly Giner Electrochemical Systems, LLC.)
89 Rumford Ave.
Newton, MA 02466
Phone: (781) 529-0526
Email: mhamdan@ginerinc.com

DOE Managers
Erika Sutherland
Phone: (202) 586-3152
Email: Erika.Sutherland@ee.doe.gov
David Peterson
Phone: (720) 356-1747
Email: David.Peterson@go.doe.gov

Contract Number: DE-FG36-08GO18065

Subcontractors:
- Virginia Polytechnic Institute and University Blacksburg, VA
- Parker Hannifin Ltd domnick hunter Division, Hemel Hempstead, United Kingdom

Project Start Date: May 1, 2008
Project End Date: May 31, 2013

Overall Objective

Develop and demonstrate advanced low-cost, moderate-pressure polymer electrolyte membrane (PEM)-based water electrolyzer system to meet DOE targets for distributed electrolysis:

- Develop high-efficiency, low-cost membrane
- Develop long-life cell-separator
- Develop lower-cost prototype electrolyzer stack and system

Fiscal Year (FY) 2013 Objectives

- Deliver and demonstrate prototype electrolyzer system at the National Renewable Energy Laboratory (NREL)
- Conduct membrane evaluations under aggressive conditions:
  - High-pressure evaluation
  - High current density evaluation

Technical Barriers

This project addresses the following technical barriers from the Hydrogen Production section of the Fuel Cell Technologies Office Multi-Year Research, Development, and Demonstration (MYRDD) Plan:

(F) Capital Cost

(G) System Efficiency and Electricity Cost

Technical Targets

Table 1 presents the technical targets for this project.

TABLE 1. Giner Progress toward Meeting DOE Targets for Distributed Electrolysis Hydrogen Production

Characteristics	Units	2015/2020 Target[a]	2013 Giner Status
Hydrogen Levelized Cost[b]	$/kg H_2	3.90/<2.30	3.64[c] (5.11)[d]
System Electrolyzer Energy Efficiency	% (LHV)	72/75	65
Stack Electrolyzer Energy Efficiency	% (LHV)	76/77	74

[a] 2012 Hydrogen Production MYRDD Plan.
[b] Production Only.
[c] Utilizing H2A Ver.2 (based on electricity cost of $0.039/kW).
[d] Utilizing H2A Ver.3 (based on electricity cost of $0.057/kW).
LHV – lower heating value

FY 2013 Accomplishments

- Membrane
  - Demonstrated dimensionally stable membrane (DSM™) efficiency and performance:
    - Demonstrated high membrane efficiency of 74% LHV (>87% higher heating value, HHV)
    - Demonstrated improved membrane stability at 3x nominal operating current density of 5,000 mA/cm²
    - Demonstrated membrane operation at high differential pressure of 5,000 psig
- Cell-Separator
  - Developed cell-separator with life expectancy of >60,000 hours
- Electrolyzer Stack and System Design
  - Completed fabrication of full-scale electrolyzer stack utilizing low-cost components
  - Reduced electrolyzer stack costs by 60%
  - Commercialized electrolyzer stack in 30-, 60-, and 100-cell configurations
  - Improved stack design to accommodate up to 200 cells/stack

– Delivered and demonstrated prototype electrolyzer system at NREL:
  - Demonstrated high stack voltage efficiency: 73.6% LHV (>87% HHV) @ 1,500 mA/cm²
  - Demonstrated hydrogen dryer with efficiency of 96.6%
  - Completed DOE Joule Milestone for the project

✧ ✧ ✧ ✧ ✧

INTRODUCTION

The DOE has identified hydrogen production by electrolysis of water at forecourt stations as a critical technology for transition to the hydrogen economy, and as the hydrogen economy matures, for hydrogen production at centralized locations using renewable energy sources. However, state-of-the-art electrolyzers are not economically competitive for forecourt hydrogen production due to their high capital and operating costs. The cost of hydrogen produced by present commercially available electrolysis systems is estimated to be \$4.20/kg-H_2, considerably higher than the DOE target of <\$2.30/kg-H_2 by 2020 [1]. Analysis of electrolyzer systems performed by Giner and others using DOE's H2A model indicate that the major cost elements are the cost of electricity, the capital costs of electrolyzer stacks and systems, and the high cost of hydrogen compression, storage, and delivery.

Giner, Inc. (Giner) has developed PEM-based electrolyzer technology that operates at differential pressure for producing hydrogen at moderate to high pressure directly in the electrolyzer stack, while oxygen is evolved at near-atmospheric pressure. The goals of the project are to reduce the cost of the stack and system, improve electrolyzer efficiency, and to demonstrate electrolyzer operation at moderate pressure.

APPROACH

To reduce the cost of producing hydrogen, Giner is improving electrolyzer stack efficiency and reducing stack cost through development of an advanced low-cost, high-strength, membrane that utilizes a perforated polyimide support imbibed with perfluorosulfonic acid (PFSA) ionomer. Giner is also reducing stack capital cost and increasing stack life through development of a long-life bipolar stack cell-separator, decreasing stack costs by initiating scale up to a larger active area, and reducing the system capital cost by applying commercial production methods to PEM-based electrolyzer systems. In each of the key development areas, Giner and its team members are conducting focused development of advanced components in laboratory-scale hardware, followed by life-testing of the most promising candidate materials.

Successful development of the advanced electrolyzer stack and system will result in a high-efficiency, low-capital-cost electrolyzer that will meet the DOE cost targets for hydrogen production, assuming high-volume production. This will provide competitively priced hydrogen for delivery at forecourt stations to enable transition to the hydrogen economy.

RESULTS

A 0.5 kg-H_2/hr prototype electrolyzer system was delivered to NREL's National Wind Technology Center for validation. The high efficiency of the electrolyzer stack and system, as measured by Giner and Parker during in-house evaluations, were confirmed by NREL. During NREL's evaluation, electrolyzer stack efficiencies were measured at 74% LHV (87%, HHV) at a nominal operating current density of 1,500 mA/cm², 72% LHV (85%, HHV) at a current density of 1,900 mA/cm², and >76% LHV (90%, HHV) at current densities less than 1,000 mA/cm². A DOE Joule Milestone was also completed with the successful validation of the electrolyzer unit.

The results in each of the key development areas of this project are summarized in the following.

DSM™ Membrane Performance: To improve electrolyzer efficiency, Giner has developed an advanced supported membrane having an ionic resistance comparable to that of a 0.0020 to 0.0035-inch-thick Nafion® [2] membrane, but having significantly improved mechanical properties. This advanced membrane is referred to as a DSM™ due to the membrane support that minimizes changes in dimensions (swelling/contraction) under high-pressure operation and with changes in water content. The support structure utilized in the development of the DSM™ consists of a polyimide (Kapton®) base film with a definable open pattern. The support structure is then imbibed with 1100 equivalent-weight (EW) PFSA ionomer to a thickness of 3 mil (0.003 inch). Initially, Giner fabricated the membrane support structures using a laser-drilling procedure. In 2011, a more cost-effective technique of fabricating the support structures via chemical-etching was implemented by Giner, reducing the cost of the membrane by one order of magnitude.

Polarization scans of the DSM™ were conducted in scaled-up, 0.5 kg-H_2/hr electrolyzer stack hardware, through a current density range of 0-1,900 mA/cm², a differential pressure of 300 psid, and a temperature of 80°C. The average cell voltage was measured at 1.757 V/cell corresponding to a voltage efficiency of 74% LHV (87% HHV) at a current density of 1,500 mA/cm².

Durability of the DSM™ was also demonstrated in the scaled-up, hardware via fluoride release rate (FRR) measurements at constant-current operation. Since PFSA ionomer is used as the membrane material and in the binder for the catalyst layer, the loss of fluoride is used

as a measurement of membrane degradation. Based on electrolysis FRR results, the lifetime of the DSM™ is projected to be between 45,000 and 55,000 hours. Membrane lifetimes beyond this period were also demonstrated during high current density operation (5,000 mA/cm²) using an advanced DSM™ fabricated with a proprietary additive that mitigates membrane degradation. Finally, a significant improvement in membrane creep property and mechanical stability were demonstrated during high differential pressure operation. The high strength of the DSM™ membrane provided sealing up to an operating pressure of 5,000 psi.

Cell-Separator Development: The cell separator is a gas-impermeable conductive sheet that separates the hydrogen and oxygen compartments in the bipolar stack. The separator must be highly conductive, as well as resistant to hydrogen embrittlement and to corrosion in an oxidizing environment. Giner's legacy high-pressure naval electrolyzers use a complex multi-layer cell-separator incorporating a conductive compliant member and sheets of niobium and zirconium metal. Zirconium is used due to its high resistance to hydrogen embrittlement. Giner has previously evaluated a low-cost, dual-layer titanium cell-separator. Although performance was comparable to that of niobium/zirconium cell-separators, lifetimes were limited to 5,000 hours due to hydrogen embrittlement.

The most promising approach for long-term implementation has been achieved by coating titanium with a low-cost electrically conductive, embrittlement-resistant carbon coating. The challenge was the development of a pinhole-free, highly adherent coating with the required characteristics. Under the cell-separator development task, Giner demonstrated performance of a carbon/titanium cell separator in scaled-up 290-cm² electrolyzer stack hardware. Performance is comparable to that of the niobium-zirconium separator. In addition, life expectancy of the carbon/titanium separator, determined via hydrogen-uptake analysis over a 5,000-hour period, indicates lifetimes exceeding the 50,000-hour system requirement.

Electrolyzer Stack and System Fabrication: In addition to the use of chemically etched DSM™ and carbon/titanium cell-separators, the electrolyzer stack includes several modifications to Giner's legacy hardware: (1) an increase in cell active area from 160 to 290 cm², effectively reducing the number of cells required to produce a given amount of hydrogen, thus reducing the stack manufacturing labor; (2) an overall decrease in the parts count per cell (from 41 to 10); (3) a 75% reduction in anode and cathode catalyst loadings; (4) molded thermoplastic cell frames, resulting in a cost reduction of 95% as compared to machining this component; (5) a 33% reduction in cell frame thickness, thus reducing the anode and cathode support materials and costs by 33%; and (6) a low-cost carbon-steel end plate. As a result of the component and membrane development during this project, the overall projected capital cost of the electrolyzer stack (Figure 1) has decreased from greater than $1,000/kW in 2007 to <$350/kW in 2011.

The electrolyzer system, shown in Figure 2, required detailed planning with respect to system layout and fabrication sequence. Several factors, including specific codes and standards that are pertinent to hydrogen electrolyzer systems, were considered during the system layout. To meet these requirements, the system was designed with three separate compartments: the oxygen (O_2), the hydrogen (H_2), and the electrical (controller and power supply) compartments. The O_2 compartment contains the oxygen gas-phase separator, a circulating liquid pump, and the deionized water feed tank. The H_2 compartment encloses a novel high-efficiency (96.6%) hydrogen dryer assembly, high- and low-pressure hydrogen gas-phase separators, a heat exchanger, cooling fans, and various flow valves. The electrolyzer stack is powered via a direct-current (DC) power supply located in the electrical compartment.

The system build, undertaken at the Parker facility, was delivered and tested at NREL's National Wind Technology Center. A breakdown of the system performance is shown in Table 2. At an operating current density of 1,600 mA/cm², the electrolyzer stack exhibits an energy efficiency of 47.3 kWh/kg; the overall system (not including the H_2-dryer) is 57.5 kWh/kg, and with the H_2-dryer, 64.8 kWh/kg.

FIGURE 1. Electrolyzer Stack

FIGURE 2. Electrolyzer System

Included in the efficiency calculations are the additional power requirements for safety ventilation fans (0.7 kW) and the inefficiency of the DC power supply (4.2 kW, 80% efficient) which was below that of the manufacture's rated efficiency of 94%. Compensating for the efficiency of the DC power supply, the PEM-based electrolyzer system will operate in the range of 50.5 kWh/kg (not including the H_2-Dryer) and 54.0 kWh/kg (with the H_2-Dryer).

CONCLUSIONS AND FUTURE DIRECTIONS

Significant progress has been made in DSM™ membrane development. Giner has demonstrated membrane reproducibility and durability as well as a significant improvement in electrolyzer cell efficiency. The progress made during this program has enabled electrolyzer stack efficiencies that meet DOE's 2012 targets and that are in line with achieving DOE's 2015 efficiency goals. In addition, development efforts conducted under this project have resulted in significant cost reductions of PEM-based electrolyzer stacks and systems, an increase in the life of the cell-separators, and improved balance-of-plant components efficiency. Work on this project had been completed in May 2013, however Giner will continue to investigate methods that further reduce cost and improve the efficiency of PEM-based electrolyzer stacks and systems. Giner believes that future challenges for PEM electrolysis will include:

- Scale up of technology for large energy storage applications
- Improve pressure capabilities of stacks (6,250 and 12,688 psi) to eliminate the need for mechanical compressors

TABLE 2. Electrolyzer System Performance

Hydrogen Production & Losses	Units	1600 mA/cm²
Stack H_2-Production	kg-H_2/hr	0.468
Membrane permeation losses (-0.6%)		-0.005
Phase-Separator (-0.14%)		-0.0007
H_2-Dryer (-3.4%)		-0.015
Total H2-Production		**0.43**

Power Consumption	Units	1600 mA/cm²
Electrolyzer Stack	kW	**21.9**
DC power supply & control (~80% Efficient)		**+ 4.2**
PLC Rack		0.05
Electrolyzer Water Pump		0.30
Heat exchanger fans A & B		0.05
H_2 sensor circuit pump		0.12
Total Energy Consumption (No Dryer)		**26.6**
H_2-Dryer		0.59
Total Energy Consumption (w/Dryer)		**27.9**

Overall Efficiencies	Units	1600 mA/cm²
Electrolyzer Stack (includes permeation)	kWh/kg	**47.3**
System (No Dryer)		**57.5**
System (w/Dryer)		**64.8**

- Further improvements in membrane efficiency and costs reductions

FY 2013 PUBLICATIONS/PRESENTATIONS

1. M. Hamdan, *Evaluation and Challenges of PEM Electrolyzer for Commercial Applications. Presentation at the* NREL ESIF meeting, August 30, 2012.

2. M. Hamdan, *PEM Electrolyzer Incorporating an Advanced Low-Cost Membrane.* 2013 Hydrogen Annual Program Merit Review Meeting, Presentation #pd030, May 15, 2013.

3. M. Hamdan, *Unitized Design for Home Refueling Appliance for Hydrogen Generation to 5,000 psi.* 2012 Hydrogen Annual Program Merit Review Meeting. Presentation #PD065, May 15, 2013.

REFERENCES

1. 2012 Multi-Year Research, Development and Demonstration Plan. Hydrogen Production. DOE, Pg 3.1-14, (http://www1.eere.energy.gov/hydrogenandfuelcells/mypp/pdfs/production.pdf)

2. Nafion® and Kapton® are registered trademarks of E.I. du Pont de Nemours and Company

II.A.2 Renewable Electrolysis Integrated Systems Development and Testing

Kevin Harrison (Primary Contact), Michael Peters, Christopher Ainscough
National Renewable Energy Laboratory (NREL)
15013 Denver West Parkway
Golden, CO 80401
Phone: (303) 384-7091
Email: Kevin.Harrison@nrel.gov

DOE Manager
David Peterson
Phone: (720) 356-1747
Email: David.Peterson@go.doe.gov

Subcontractor:
Marc Mann, Spectrum Automation Controls, Arvada, CO

Project Start Date: October 1, 2003
Project End Date: Project continuation and direction determined annually by DOE

Overall Objectives

- Collaborate with industry to research, develop, and demonstrate improved integration opportunities for renewable electrolysis systems for energy storage, vehicle refueling, grid support, and industrial gas end-uses.
- Design, develop, and test advanced experimental and analytical methods to validate electrolyzer stack and system efficiency; including contributions of sub-system losses (e.g., power conversion, drying, electrochemical compression) of advanced electrolysis systems.

Fiscal Year (FY) 2013 Objectives

- Quantify stack, system efficiency, and hydrogen drying losses of the DOE-awarded electrolyzer system from Giner/Parker Hannifin.
- Demonstrate and compare 10,000 hours of variable (i.e., wind-profile) and constant power operation of proton exchange membrane (PEM) electrolyzer stacks and determine decay rates.

Technical Barriers

Electrolysis presents the opportunity for non-carbon-emitting hydrogen production when a renewable electricity source such as wind, solar, or hydropower is used. To be cost competitive, however, R&D is necessary to reduce electrolysis capital and operating costs, and the cost of electricity needs to be less than or equal to half the current average grid price of electricity.

This project addresses the following technical barriers from the Fuel Cell Technologies Office 2012 Multi-Year Research, Development, and Demonstration (MYRD&D) Plan, section 3.1.5:

(G) System Efficiency and Electricity Cost

(J) Renewable Electricity Generation Integration (for central production)

(M) Control and Safety

Technical Targets

This project is conducting applied research, development, and demonstration (RD&D) to reduce the cost of hydrogen production via renewable electrolysis for both distributed and central production pathways to help meet the following DOE hydrogen production and delivery targets found in the 2012 Multi-Year Research, Development, and Demonstration Plan:

Technical Targets: Central Water Electrolysis using Green Electricity (Table 3.1.5)

- Stack efficiency:
  - 44 kWh/kg H_2 (76% lower heating value, LHV) by 2015
  - 43 kWh/kg H_2 (78% LHV) by 2020
- System efficiency:
  - 46 kWh/kg H_2 (73% LHV) by 2015
  - 44.7 kWh/kg H_2 (75% LHV) by 2020
- By 2015 reduce the cost of central production of hydrogen from water electrolysis using renewable power to $3.00/gasoline gallon equivalent (gge) at plant gate. By 2020, reduce the cost of central production of hydrogen from water electrolysis using renewable power to ≤$2.00/gge at plant gate.

FY 2013 Accomplishments

- Installed, commissioned and completed 200 hours of operation of advanced high-efficiency electrolyzer system from Giner/Parker Hannifin.
  - First 100 hours of operation were completed by the end of June 2012, completing an FY 2012 EE-1 Joule Milestone.
  - Subsequently, the 12 kg/day electrolyzer system was moved from the National Wind Technology

Center to the Energy Systems Integration Facility in Golden, CO.

- Operated PEM electrolyzer stacks over 10,000 hours with variable wind profile to compare stack decay rate with that of a stack operating under constant power.

✧ ✧ ✧ ✧ ✧

INTRODUCTION

The capital cost of commercially available water electrolyzer systems, along with the high cost of electricity in many regions, limits widespread adoption of electrolysis technology to deliver low-cost hydrogen production. PEM electrolyzer manufacturers are working to scale up into the MW range to reduce their system energy efficiency to better compete with alkaline. Along with capital cost reductions and efficiency improvements, both technologies are developing utility-scale electrolyzers capable of advanced grid integration functionality and better integration with renewable electricity sources. Electrolytic production of hydrogen, where fossil fuels are the primary electricity source, will not lead to significant carbon emission reduction without carbon sequestration technologies.

Renewable electrolysis is inherently distributed, but large-scale wind and solar installations are being planned to take advantage of economies of scale and achieve system-level energy efficiencies less than 50 kWh/kg. Renewable electricity sources, such as wind and solar, can be closely, and in some cases directly, coupled to the hydrogen-producing stacks of electrolyzers to reduce energy conversion losses and capital costs investment of this near-zero-carbon pathway.

Large-scale hydrogen production using renewable electricity is well positioned to produce near-zero-greenhouse-gas-emission vehicle fuel in the coming years as hydrogen-powered fuel cell electric vehicles are introduced into the marketplace. An integrated system with advanced sensing and communications will enable grid operators to take advantage of the controllable nature of distributed and central water electrolysis systems to maintain grid stability.

APPROACH

Results and insights gained from this RD&D project aim to benefit the hydrogen-based industry and relevant stakeholders as the market for this equipment expands. Results from the project have demonstrated opportunities to improve efficiency and capital cost of an integrated renewably coupled electrolysis system.

The Xcel Energy/NREL Wind-to-Hydrogen collaborative RD&D project is advancing the integration of renewable electricity sources with state-of-the-art electrolyzer technology. Real-world data from 24/7 daily operations are demonstrating opportunities for improved system design and novel hardware configurations to advance the commercialization of this technology. Lessons learned and data-driven results provide feedback to industry and to the analytical components of this project. Finally, this project provides independent testing and verification of the technical readiness of advanced electrolyzer systems by operating them from the grid and renewable electricity sources.

RESULTS

Advanced Electrolyzer Testing

The DOE-awarded electrolyzer system was delivered to NREL in June 2012. The system was promptly installed, commissioned, and operated for 100 hours to achieve a DOE EE-1 Joule Milestone by the end of June.

Giner predicted that the system would produce a kilogram of hydrogen using 54 kWh of electricity. The electrolyzer control system monitors the internal pressure of the hydrogen and varies stack current to maintain 390 psig. Because of the continuous slewing of stack current, instantaneous measurements are binned and averaged, typically based on stack temperature.

Stack temperature is determined by averaging the input and output de-ionized water measurements. In addition to stack in/output temperature, NREL also instrumented the electrolyzer with the following sensors: alternating current (AC) input and voltage and stack current and voltage. Hydrogen product from the electrolyzer system was measured using an NREL designed and built volumetric mass flow device. Stack efficiency is determined based on stack voltage, temperature, and operating pressure.

The stack, designed and built by Giner, operates at 390 psig and achieved 87% (higher heating value, HHV), 73.6% (LHV) efficiency at 1,500 mA/cm^2 and 80°C (Figure 1). The balance of plant, designed and built by Parker Hannifin, achieved an overall system efficiency of 64.8 kWh/kg at

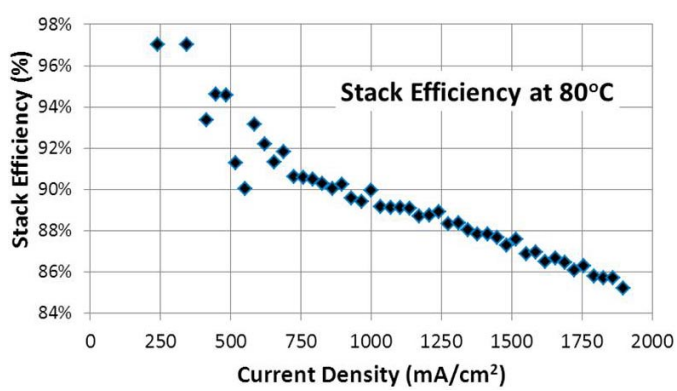

FIGURE 1. Stack Efficiency (HHV) based on Current Density

1,600 mA/cm^2. Approximately 10 kWh/kg of this specific energy requirement is attributed to lower-than-expected efficiency of the AC to direct current (DC) power supplies.

Hydrogen product from commercial electrolyzer systems is routinely dried to -20°C dew point and below. Hydrogen drying losses have been reported for these systems in the 5–10% of the rated product flow from the stacks based on full stack current. These drying losses directly reduce the system efficiency because the hydrogen used to regenerate the desiccant drying beds is vented from the system.

During the milestone testing, NREL intercepted this hydrogen drying vent from the Giner/Parker Hannifin electrolyzer system and measured the flow rate using two different methods. Both methods provided reasonably close measurements of the drying loss. First, a hydrogen mass flow sensor measured 11–12 grams per hour of hydrogen loss from the drying system. Although the hydrogen from the vent was dried using desiccant prior to the sensor, this measurement is slightly in question because it is a thermally-based technology and any entrained water vapor will disrupt the measurement.

The second method used a 5.9-liter flask and a timer. The amount of time and volume of gas was repeatedly measured to a range of 15.2–15.6 grams per hour. Giner predicted a drying loss of 18 grams per hour. The measured loss represents about 3.5% drying loss based on full stack current of 505 amps DC.

Variable vs. Constant Power Stack Operation

NREL is conducting side-by-side testing and comparison of stack voltage decay rates between constant and variable power operation. Two 34-cell stacks of an H-Series PEM electrolyzer from Proton Onsite were operated with a highly variable wind profile, achieving a total of over 10,000 hours of operation between November 2010 and March 2013. A third stack was operated over the same time with constant stack power. All three stacks were operated with the same average current.

A varying wind power profile is run on the stacks for hundreds of hours continuously and only interrupted to operate all three stacks at their full-current point for a few consecutive days to enable comparison of their steady-state voltage. Table 1 summarizes the results over 7,500 hours of operation and shows one of the variable stacks exhibiting a slightly higher decay rate than that of the constant current stack. The other variable-powered stack's decay rate is significantly higher than the others. That stack failed shortly after this 7,500 hour test was completed.

At the beginning of the 7,500 hour test, the stack's operational modes were randomly selected. Because of this, the two remaining stacks in the test were swapped and the test restarted. The reason for swapping the two stacks was to eliminate any random systematic error in stack manufacturing. Unfortunately, after the first 2,500 hours (~10,000 hours total) after swapping their operational modes another stack failed and the test was halted. Since these stack failures, Proton Onsite has provided two newer replacement stacks (manufactured in 2008) and the variable versus constant power testing is continuing.

Table 1. Average Cell Decay Rates by Operational Mode

Mode	Average Decay µV/cell-h
Variable	16.7
Variable	9.7
Constant	9.2
Hours	7,538

It is important to note that before delivery to NREL, that all three of the original electrolyzer stacks faced severe abuse with no hydration for about a year in a warehouse. Furthermore, this testing is intended only to reveal relative stack decay rates between a variable wind profile and constant current operation, if there is any difference. Normal stack decay rates of today's PEM stacks from Proton Onsite are between 2–5 µV/cell-h.

CONCLUSIONS AND FUTURE DIRECTION

NREL completed a DOE EE-1 Joule Milestone by installing, commissioning and operating an advanced electrolyzer from Giner and Parker Hannifin. The PEM electrolyzer included a high efficiency stack operating at 390 psig. Stack efficiency was determined to be 73.6% (LHV) versus the DOE's 2015 target of 76% (LHV). The system consumed 64.8 kWh/kg but 10 of those kWhs were attributed to higher-than-expected power supply conversion losses. The DOE 2015 target for system efficiency is 46 kWh/kg, noting that this would be expected of large MW-scale electrolyzers. The Giner/Parker Hannifin electrolyzer produces 12 kg/day while requiring 30-35 kW of electrical power. Hydrogen drying losses were determined to be 3.5%, based on the full rated hydrogen flow from the stack.

Three PEM electrolyzer stacks were operated in variable and constant power modes. Over 10,000 hours of operation were achieved before the test was halted due to two stack failures. All three of the original electrolyzer stacks faced severe abuse with no hydration for about a year in a warehouse. Two newer stacks (manufactured in 2008) were provided by Proton Onsite and are now under test.

In the coming year the team will complete the following:

- Complete testing of novel hydrogen drying process and show potential improvement of system efficiency.
- Achieve over 4,000 hours of variable versus constant power stack operation to determine if variable stack operation causes a different decay rate than constant power mode.

II.A.3 High-Performance, Low-Cost Hydrogen Generation from Renewable Energy

Katherine Ayers (Primary Contact), Andy Roemer
Proton Energy Systems dba Proton OnSite
10 Technology Drive
Wallingford, CT 06492
Phone: (203) 678-2190
Email: kayers@protononsite.com

DOE Managers
Erika Sutherland
Phone: (202) 586-3152
Email: Erika.Sutherland@ee.doe.gov
David Peterson
Phone: (720) 356-1747
Email: David.Peterson@go.doe.gov

Contract Number: DE-EE000276

Subcontractors:
- Entegris, Inc., Chaska, MN
- The Electrochemical Engine Center at Penn State, University Park, PA
- Oak Ridge National Laboratory, Oak Ridge, TN

Project Start Date: September 1, 2009
Project End Date: September 30, 2013

Overall Objectives

- Improve electrolyzer cell stack manufacturability through:
  - Consolidation of components
  - Incorporation of alternative materials and manufacturing methods
  - Improved electrical efficiency
- Reduce cost in electrode fabrication through:
  - Reduction in precious metal content
  - Alternative catalyst application methods
- Design scale up for economy of scale including:
  - Scale up of the design to a large active area cell stack platform
  - Development and demonstration of a robust manufacturing process for high volume plate production
- Quantification of the impact of these design changes via the H2A model.

Fiscal Year (FY) 2013 Objectives

- Verify low-cost manufacturing processes
  - Capability to meet dimensions
  - Structural testing
- Perform operational testing and stack scale up
- Develop manufacturing process (to scale) and qualify production level parts

Technical Barriers

This project addresses the following technical barriers from the Hydrogen Production section of the Fuel Cell Technologies Office Multi-Year Research, Development, and Demonstration Plan:

(F) Capital Cost

Technical Targets

The technical targets are presented in Table 1.

TABLE 1. Proton Energy Systems Progress Towards Meeting Technical Targets for Distributed Water Electrolysis Hydrogen Production

Characteristics	Units	2012 Target	2017 Target	Proton Status
Hydrogen Cost	$/gge	<3.70	<3.00	3.46
Electrolyzer Capital Cost	$/gge	0.70	0.30	0.64
Electrolyzer Energy Efficiency	% (LHV)	69	74	67

gge - gasoline gallon equivalent; LHV - lower heating value
Note: Estimates are based on H2A v2.1, for electrolysis only (compression-storage-delivery not included). Model assumes $0.05/kWh.
Electrolyzer cost based on 1,500 kg/day capacity, 500 units/year; efficiency based on system projections, technology which could be implemented within five years, and demonstrated stack efficiency of 74% LHV efficiency.

Advanced Bipolar Plate Manufacture and Cell Stack Scale Up

This project is bringing low-cost bipolar plate technology to production implementation. Two stack designs will be completed to leverage these advancements, with the following targets:

- Cost reduction of baseline stack: 40%
- Scale up to >5 times active area
- Additional 40% cost reduction based on scale

FY 2013 Accomplishments

- Implemented intermediate treatment process for 50% improved embrittlement resistance (cost share)
- Production scale stack at 0.1 ft^2 level demonstrated to >5,000 hours with advanced coatings which provide >99% reduction in hydrogen uptake
- Scale up and validation of advanced stack design to >500 cm^2 active area
  - Completed mechanical stress and flow modeling
  - Pilot run of >50 parts
- Demonstrated single cell prototype operation at large active area
- Production tooling ordered for large active area parts

✧ ✧ ✧ ✧ ✧

INTRODUCTION

This project addresses the DOE Hydrogen Program objective for distributed production of hydrogen from proton exchange membrane water electrolysis. The DOE technical targets for hydrogen cost as well as electrolyzer efficiency and capital cost will be directly addressed through the advancement of key components and design parameters. When added together, the bipolar assemblies and membrane electrode assemblies (MEAs) constitute over half of the total cell stack cost. Significant cost reductions of these components are required in order to reach the targets. This project focuses on cost reduction of the bipolar assembly through improved design and manufacturing methods, as well as scale up. Additional feasibility work was conducted on cost-reduced MEA configurations and transitioned to other projects, as described other summary reports.

The efforts of the last year culminated in the build of a >0.6 ft^2 prototype stack utilizing the selected materials, coatings and manufacturing methods for the bipolar assembly. This achievement was based on extensive modeling of mechanical stress and fluid flow in the proposed part design as well as collaboration with the supplier. Cost reductions for the new design vs. the legacy design at the same active area as well as for scale up were documented. Additional subscale stacks will be built and tested as part of the design validation effort. The scaled-up stack will form the basis for megawatt scale electrolysis systems.

APPROACH

The scope of work for this project allowed for research and development in several key areas relating to cell stack cost reduction. Topics included 1) catalyst formulation, 2) flow field design and materials, 3) computational performance modeling, and 4) flow field coating development.

Advancements in flow field design are intended to be advantageous for low-cost, high-volume manufacturing. Alternatives to the current flow field design included either 1) composite bipolar plates or 2) unitized flow fields, which consolidate parts and reduce the amount of required precious metal plating. The early investigations into the cost and manufacturability of the various design alternatives resulted in a final down-select to a unitized flow field. This approach integrated the function of several components into a single low-cost component, which also reduced the assembly labor. Computational modeling of an electrolyzer cell will allow for optimization studies to be performed around flow field material and architecture. Cell performance can be quantified in ways not typically possible with standard physical test experiments. Alternate coating strategies are also being investigated which eliminate metal plating. Validation of all of the previously mentioned design changes will be achieved through cost analysis based on the H2A model.

RESULTS

Accelerated hydrogen uptake experiments and analysis of residual stress were continued at Oak Ridge National Laboratory as a function of process steps and order of operation (Figure 1). While the long-term goal is to implement alternative coatings for cost reduction, the analysis also showed the potential for near-term improvements based on process order. Residual stress was significantly reduced depending on the current steps used to treat the plate. Based on these results, Proton leveraged non-federal funding to implement these near-term improvements. In parallel, continued validation of various nitride coatings continued. Minor loss of the coating is observed in the water channels, but the layer contacting the MEA appears

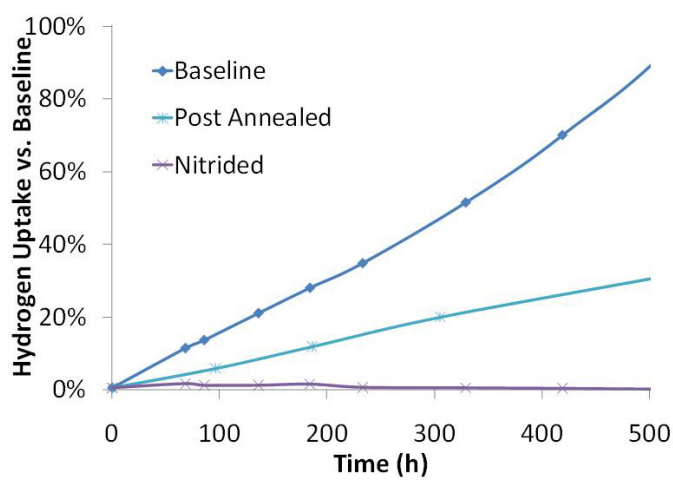

FIGURE 1. Accelerated H_2 Uptake as a Function of Surface Treatment

stable, and over 10,000 hours of performance have been demonstrated with no change in voltage. With these advanced coatings, no detectable hydrogen uptake is observed even after hundreds of hours on the accelerated uptake test. Initial plans to move forward with implementation at smaller stack sizes are underway.

For the plate design, based on the initial success and 5,000 hour validation run for the prototype stack, scale up in cell count was performed to a commercially relevant level. The first stack was disassembled to analyze the coatings discussed above. The second stack has also operated for several thousand hours and continues to operate (Figure 2). Based on these builds and quotes for parts at the 100-1000 piece level, the cost reduction of 40% vs. the baseline stack was validated, even for low production volumes. A key advantage of the manufacturing approaches chosen were the relatively low tooling costs, allowing rapid payback on the design and fewer stacks required to amortize any required design changes.

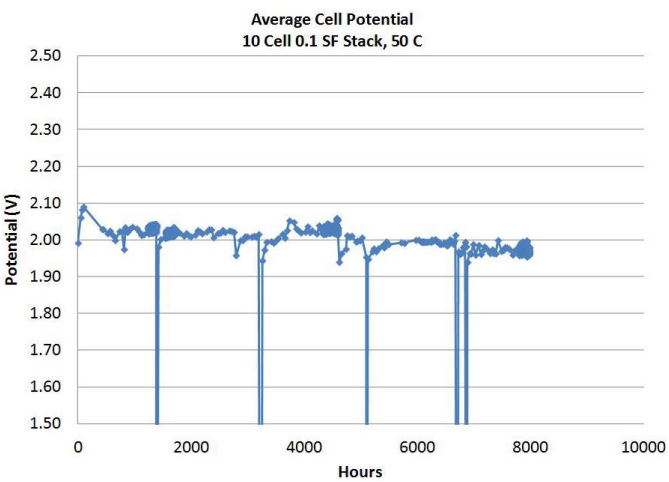

FIGURE 2. Operational Data (Average Cell Voltage), Commercial Scale Cell Stack

Detailed design work was also continued for the large active area version of the new stack design. This format required re-design of the flow features to avoid warping of the part during manufacture due to long, narrow features. A novel solution was developed to add tortuosity to the flow field while providing exceptional flow distribution. Computational fluid dynamics (CFD) modeling was performed to simulate fluid flow on the oxygen-water side of the cell to insure acceptable water distribution across the MEA. Design refinement was then performed for the large active area stack, which resulted in enabling a 15% increase in the active area vs. the original design intent, while maintaining equivalent cost reductions. Design tasks included finite element analysis of critical load-bearing components such as flow fields, frames, and endplates, as well as additional CFD analysis on sensitivity to flow rate variations at the cell level and the impact of cell count in the stack to fluid flow for each cell (Figure 3). Manufacturing considerations such as orienting features for improved registration and error-proofing during assembly were also included.

Design verification included load testing of individual parts as received to check for deformation under the design loads, and hydrostatic testing of the assembled cell configuration to verify sealing capability. Flow testing was also performed to verify the results of the CFD single-cell modeling. Once this testing was completed, final tooling was ordered and a production level run of the plates was performed. Acceptance test procedures were drafted based on similarity to existing cell stacks, including short testing, gas permeation testing, and cell resistance measurements. A single-cell stack was assembled and tested (Figure 4). The stack passed the initial acceptance test procedures and successfully operated within the expected cell voltage range. A multi-cell stack will replace this stack once an acceptable amount of run time has been achieved (1,000 hours) and the single cell stack disassembled for analysis.

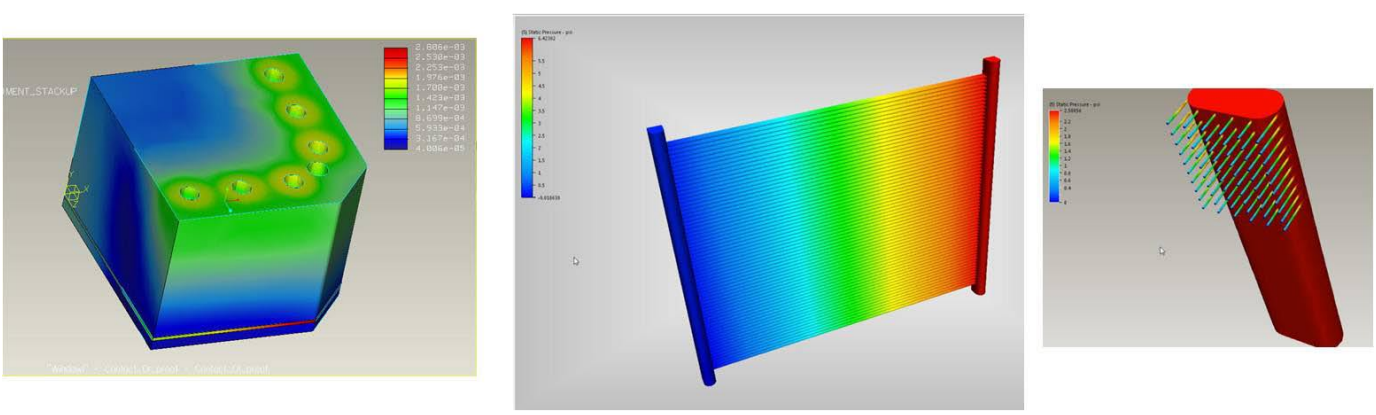

FIGURE 3. Single Cell Stack Performance, Large Active Area Stack

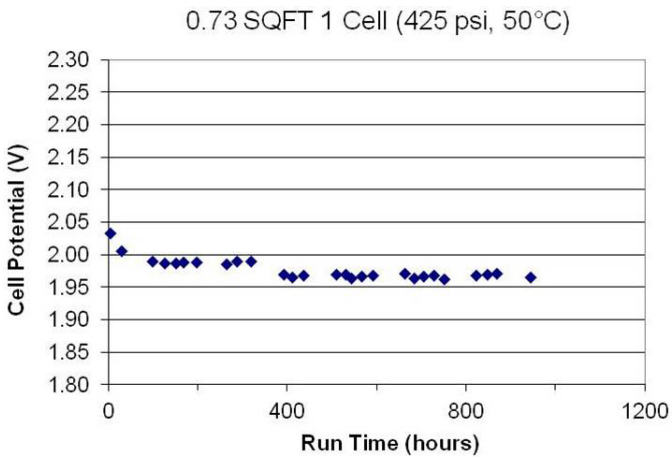

FIGURE 4. Single-Cell Stack Test

CONCLUSIONS AND FUTURE DIRECTIONS

- Initial single-cell testing has been verified at commercially relevant stack heights. Single- and multi-cell stacks have been operated for thousands of hours. Part costs for these stacks validate the 40% cost reduction target vs. the original project baseline.
- Detailed design work and modeling was completed on the large active area stack. Analysis of form factors and design limits enabled a 15% increase in active area vs. the original design intent.
- Initial testing on prototype parts for the large active area stack have matched the modeling results and electrolysis was demonstrated at 430 psi. Cost analysis for the large active area stack also validates the 40% cost reduction for this stack platform. The stack scale up contributes approximately an additional 40% in $/kg vs. the smaller active area stack.
- Alternative coatings and processes are being qualified for production vs. the baseline plate treatment. These processes have been demonstrated to reduce hydrogen uptake while providing consistent voltage performance.
- For the remainder of the project, the next step in scale up of stack count will be performed for the large active area stack. This stack will be tested in a system capable of full scale stack testing. Additional work will be performed through internal funding to release the stack to production manufacture. A final cost analysis will be provided with the final report.

FY 2013 PUBLICATIONS/PRESENTATIONS

Presentations

1. "Fueling Vehicles from Sun and Water", Fall ECS meeting, Honolulu, October 2012.

2. "Bridging the Infrastructure Gap: Cost Effective Generation of Hydrogen from Water", Department Seminar, Colorado School of Mines, November 2012.

3. "Material Advancements for Cost Effective Hydrogen Energy Storage: Megawatt Electrolysis Development", Spring ACS Meeting, Esther Takeuchi Award Symposium, New Orleans, April 2013.

4. "Development of Megawatt Scale PEM Electrolysis: A Culmination of Cell Design and System Advancements", Spring ECS Meeting, Toronto, Canada, May 2013.

II.A.4 Low-Cost Large-Scale PEM Electrolysis for Renewable Energy Storage

Katherine Ayers (Primary Contact), Chris Capuano
Proton Energy Systems dba Proton OnSite
10 Technology Drive
Wallingford, CT 06492
Phone: (203) 678-2190
Email: kayers@protononsite.com

DOE Manager
Erika Sutherland
Phone: (202) 586-3152
Email: Erika.Sutherland@ee.doe.gov

Contract Number: DE-SC0001338

Subcontractors:
- 3M, Minneapolis, MN
- University of Wyoming, Laramie, WY

Project Start Date: June 19, 2010 (Phase 1)
Project End Date: August 18, 2013 (with Phase 2 continuation)

Overall Objectives

- Demonstrate optimal membrane electrode assembly (MEA) efficiency through:
  - Refinement of catalyst composition for oxygen evolution reaction
  - Rapid screening of additional metal candidates through combinatorial methods to determine optimal anode catalyst composition
  - Fabrication of identified materials as both traditional and nano-structured thin-film (NSTF)-type electrodes
  - Integration of new catalyst materials with advanced thinner membranes
- Reduce catalyst loading through:
  - Formulation optimization of metal oxide based inks
  - Improved electrode application processes for uniform distribution
  - Application of NSTF structures
  - Demonstration in Proton's large active area format
- Demonstrate 1,000 hours system operation at >69% efficiency
- Develop a concept design to scale the system to 50,000 kg/day H_2 production including:
  - Definition of the requirements for operation and maintenance
  - Updated H2A analysis based on the actual 435 psi system cost and operation projected to 50,000 kg/day
  - Analysis of greenhouse gas and petroleum reductions that will occur with the successful implementation of the proposed technology

Fiscal Year (FY) 2013 Objectives

- Implement advanced catalyst application process for 50% reduction in catalyst loading
- Demonstrate equivalent oxygen evolution reaction (OER) activity in NSTF format to Proton baseline for 90% reduction in catalyst loading
- Manufacture NSTF or advanced catalyst process electrodes using alternate membrane and demonstrate 69% lower heating value (LHV) efficiency for 1,000 hours
- Complete environmental impact assessment based on renewable hydrogen vs. other technologies

Technical Barriers

This project addresses the following technical barriers from the Hydrogen Production section of the Fuel Cell Technologies Office Multi-Year Research, Development, and Demonstration Plan:

(F Capital Cost

(G) System Efficiency and Electricity Cost

Technical Targets

Table 1 contains the technical targets for this project.

Advanced MEA manufacture

This project is designed to take the first step in implementing substantial reductions in precious-grade metal (PGM) content in the electrodes, while demonstrating feasibility for order of magnitude reductions. Feasibility has already been demonstrated on the cathode. In addition, higher activity catalysts and more efficient membranes will be examined for application in electrolysis. While there are

TABLE 1. Proton Energy Systems Progress Towards Meeting Technical Targets for Distributed Water Electrolysis Hydrogen Production

Characteristics	Units	2012 Target	2017 Target	Proton Status
Hydrogen Cost	$/gge	<3.70	<3.00	3.46
Electrolyzer Capital Cost	$/gge	0.70	0.30	0.64
Electrolyzer Energy Efficiency	% (LHV)	69	74	67

gge - gasoline gallon equivalent
Note: Estimates are based on H2A v2.1, for electrolysis only (compression-storage-delivery not included). Model assumes $0.05/kWh.
Electrolyzer cost based on 1,500 kg/day capacity, 500 units/year; efficiency based on system projections, technology which could be implemented within five years, and demonstrated stack efficiency of 74% LHV efficiency.

no specific material metrics for electrolyzers as there are for fuel cells, the goals for this project are as follows:

- Membrane thickness <75 microns
- Total PGM loading <0.5 mg/cm^2
- Stack efficiency >72%

FY 2013 Accomplishments

- Manufactured catalyst powders based on combinatorial synthesis predictions
- Validated general performance trends in full cell testing
- Evaluated ternary catalyst compositions for 500 hours and demonstrated presence of all elements in expected ratios
- Validated 50% reduction in loading for baseline catalyst formulation with no loss in full cell performance
- Developed improved quality control methods for inspection of new electrodes
- Demonstrated high activity NSTF electrodes for OER
- Demonstrated operation of improved membrane for 10,000 hours at 80ºC
- Demonstrated >73% efficiency at stack level for advanced MEA

✧ ✧ ✧ ✧ ✧

INTRODUCTION

This project addresses the DOE Hydrogen Program objective for distributed production of hydrogen from proton exchange membrane (PEM) water electrolysis. The DOE technical targets for hydrogen cost as well as electrolyzer efficiency and capital cost will be directly addressed through the advancement of key components and design parameters. For renewable applications such as grid energy storage, a continuum of options from distributed hydrogen generation to centralized production at capacities on the order of 50,000 kg/day will be needed. The majority of the electrolysis efficiency losses arise from the oxygen evolution overpotential and the membrane ionic resistance. To reach a target system operating efficiency of 69%, new catalyst and membrane materials are needed. Especially for these large scales, it is necessary to minimize the use of precious metals. Much learning from fuel cell materials research can be applied to enable the required advancements. Design studies are also needed for PEM electrolysis at this scale to understand the capital costs, environmental impact, and operation and maintenance requirements.

APPROACH

This project addresses crucial elements of Proton's technology roadmap, with a focus on improving MEA performance. The oxygen evolution catalyst and membrane are therefore the two key areas of focus. Critical issues include long-term stability of the membrane under electrolysis conditions, particularly as it relates to long term creep with a thinner membrane, and stability of the catalyst to dissolution. Continuation of the work completed in Phase 1 includes 1) refinement of the mixed metal oxide catalyst composition for increased activity while maintaining voltage stability, 2) initial reductions in catalyst loading of 50% or greater based on implementation of improved manufacturing processes at Proton, 3) integration of optimized catalyst compositions into nanostructured thin films to demonstrate an additional order of magnitude reduction in catalyst loading and development of high-speed manufacturing capability, 4) use of reinforced membranes in order to reduce membrane thickness and ionic resistance without decreasing durability, and 5) projection of these improvements to 50,000 kg/day production levels including cost modeling, impact on reduction of greenhouse gas emissions, and conceptual system design.

Catalyst compositions were made using two techniques. Promising compositions from Phase 1 were manufactured as nanopowders through fusion of soluble metal salt precursors with sodium nitrate at high temperatures. Nanopowders were screened through fabrication of bench-scale MEAs. New candidates were made through ink jet printing and sintering,

FIGURE 1. Combinatorial Electrode Fabrication Equipment and Measurement

and were screened through a fluorescence technique to determine the relative amount of oxygen evolution at a given overpotential. The approach is shown in Figure 1. The conceptual 50,000 kg/day system design was developed through sizing calculations of the major system components and consultation with relevant industries such as chlor-alkali to determine typical redundancy factors and margins. Items such as power conversion components, water treatment facilities, pressure vessels, and storage tanks were quoted through suppliers well versed in the relevant sizes. Cell stack costs were estimated based on a module similar to Proton's largest active area platform and known design improvements validated at a prototype level.

RESULTS

Combinatorial results from FY 2012 were used to select ternary catalysts for manufacture as nanopowders. Metals examined included Ir, Pt, Al, Ru, Sn, Rh, and Pd. Synthesis was successful using Proton's standard catalyst synthesis process and powders were successfully manufactured into acceptable MEAs. After 1,500 hours of operation, the oxygen electrodes were analyzed for composition. Percentages of the three metals were very consistent with the predicted formulation (Table 2).

For the near-term catalyst application process, the formulation and process variables optimization was completed, resulting in a 50% reduction in catalyst loading vs. the baseline process. This formulation provides some design margin based on the loading studies performed. This formulation also provided efficiency benefits vs. the baseline MEA, possibly due to reduced resistance across the layer. As part of this effort, a new quality control measurement scheme was developed. One of Proton's standard acceptance testing protocols is an electrical test, which gave non-meaningful data with the new process. Investigating the full impedance data, a more appropriate test point was determined and a production rig utilized to obtain more consistent data.

For the larger reductions in catalyst loading, several iterations were performed on the NSTF electrodes from 3M.

TABLE 2. SEM Analysis, Ternary Metal Oxide Catalyst, 1,500 Hours of Operation

	Metal 1 (at%)	Metal 2 (at%)	Metal 3 (at%)
Theoretical/ Design Point	51	23	26
Operated MEA, Point 1	56.25	20.00	23.75
Operated MEA, Point 2	47.58	21.61	30.86

Initially, the anode continued to show higher voltage than the baseline, apparently due to higher activation energy, while the cathode had been successfully demonstrated to match baseline performance. Polarization curves showed very linear behavior to high current densities, implying a lack of mass transfer limitations. Alternate loadings, catalyst compositions, surface treatments and coating variables were therefore tested over the course of these experiments to improve the anode activity. Based on this series of investigations, an electrode configuration meeting the performance targets was achieved, using less than 10% of the baseline catalyst loading (Figure 2).

Thinner, high mechanical strength membranes were also utilized to manufacture MEAs with the new manufacturing process as well as the NSTF configuration. Both types of electrodes yielded very good performance, with efficiencies above 72% at normal commercial operating current densities.

Finally, an environmental assessment was performed based on the plant design developed for 50,000 kg/day hydrogen. Hydrogen equivalency was calculated to other forms of energy such as gasoline, natural gas, and coal. Scenarios were examined based on transportation, building energy, and CO_2 emissions (Table 3). The analysis showed that for the transportation market, one 50,000 kg/day plant could cut CO_2 emissions by 100,000 metric tons per year, while building emissions could be cut by four times that for the same plant size.

CONCLUSIONS AND FUTURE DIRECTIONS

- Advanced catalyst formulations have demonstrated structural stability over several hundred hours of operation, with qualitative performance trends as predicted by the combinatorial screening.
- Process optimization has validated near term catalyst reductions of 50%.
- NSTF electrodes have demonstrated feasibility to reach less than 10% catalyst loading on multiple membrane types without loss of performance vs. baseline electrodes. Stack efficiencies of 72% or greater have been demonstrated at relevant stack operating current densities.
- An environmental analysis was conducted, demonstrating potential savings of 100,000 metric tons of CO_2 annually per 50,000 kg/day plant. The 50,000 kg/day plant concept is based on a modular design which is being leveraged in Proton's megawatt-scale system development effort.
- In the remainder of the project, scaled-up samples will be tested and the system efficiency measured based on electricity to hydrogen conversion.

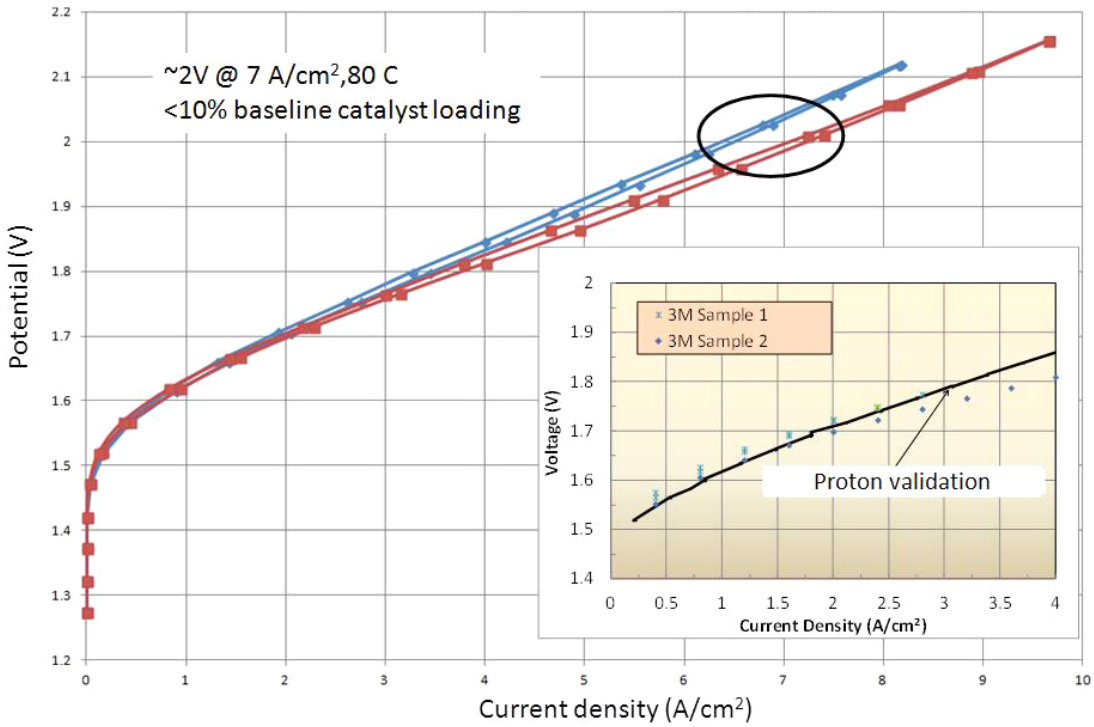

FIGURE 2. Progression of Performance for NSTF Electrodes for OER

TABLE 3. Reduction of CO_2 Emissions, 50,000 kg/day Renewable Hydrogen

	Greenhouse Gas Reductions (kg per 50,000 kg/day H_2 plant)		
	CO_2	Methane	Nitrous Oxide
Highway Vehicles	1.09E+08	3.86E+05	3.71E+06
Residential Buildings	4.06E+08		
Commercial Buildings	5.28E+08		

FY 2013 PUBLICATIONS/PRESENTATIONS

1. "Bridging the Infrastructure Gap: Cost Effective Generation of Hydrogen from Water", Department Seminar, Colorado School of Mines, November 2012.

2. "Combinatorial Search for Improved Metal Oxide Oxygen Evolution Electrocatalysts in Acidic Electrolytes", Parkinson, B.; Seley, D.; Ayers, K.; ACS Combinatorial Science, Feb. 11 2013, 15(2), pp. 82-89.

3. "Material Advancements for Cost Effective Hydrogen Energy Storage: Megawatt Electrolysis Development", Spring ACS Meeting, Esther Takeuchi Award Symposium, New Orleans, April 2013.

4. "Development of Megawatt Scale PEM Electrolysis: A Culmination of Cell Design and System Advancements", Spring ECS Meeting, Toronto, Canada, May 2013.

5. "Proton Exchange Membranes for H_2 Generation: A Tutorial on Research Needs and Challenges for PEM Electrolysis vs. Fuel Cells", Spring ECS Meeting, Toronto, Canada, May 2013.

II.A.5 Economical Production of Hydrogen through Development of Novel, High Efficiency Electrocatalysts for Alkaline Membrane Electrolysis

Katherine Ayers (Primary Contact),
Everett Anderson
Proton Energy Systems dba Proton OnSite
10 Technology Drive
Wallingford, CT 06492
Phone: (203) 678-2190
Email: kayers@protononsite.com

DOE Manager
David Peterson
Phone: (720) 356-1747
Email: David.Peterson@go.doe.gov

Contract Number: DE-SC0007574

Subcontractor:
Illinois Institute of Technology (IIT), Chicago, IL

Project Start Date: February 20, 2012
Project End Date: April 21, 2015

Overall Objectives

- Understand and optimize activity of pyrochlore catalysts for oxygen evolution based on composition and microstructure
- Determine the impact of key anion exchange membrane properties (conductivity, water uptake, gas crossover) on performance
- Derivatize polymer backbones to form new anion exchange membranes (AEMs) and characterize said AEMs for mechanical and electrochemical properties
- Select the system circulating fluid based on performance and stability
- Process promising membrane and catalyst materials into electrodes and test
- Scale up downselected materials to a relevant stack active area and height and operate in a relevant environment
- Develop a prototype system package and perform testing of up to 500 hours
- Provide product cost analysis and H2A modeling demonstrating the cost saving

Fiscal Year (FY) 2013 Objectives

- Demonstrate high activity of pyrochlore catalysts for oxygen evolution
- Optimize catalyst composition and microstructure
- Form and characterize new anion exchange membranes and demonstrate acceptable conductivity for electrolysis
- Process promising membrane and catalyst materials into MEAs
- Scale up to a relevant stack active area and height and operate in a relevant environment

Technical Barriers

This project addresses the following technical barriers from the Hydrogen Production section of the Fuel Cell Technologies Office Multi-Year Research, Development and Demonstration Plan:

(F) Capital Cost

Technical Targets

The technical targets for this project are presented in Table 1.

TABLE 1. Proton Energy Systems Progress Towards Meeting Technical Targets for Distributed Water Electrolysis Hydrogen Production

Characteristics	Units	2012 Target	2017 Target	Proton Status
Hydrogen Cost	$/gge	<3.70	<3.00	3.51
Electrolyzer Capital Cost	$/gge	0.70	0.30	0.57
Electrolyzer Energy Efficiency	% (LHV)	69	74	58

gge - gasoline gallon equivalent; LHV - lower heating value
Note: Estimates are based on H2A v2.1, for electrolysis only (compression-storage-delivery not included). Model assumes $0.05/kWh.
Electrolyzer cost based on 1,500 kg/day capacity, 500 units/year; efficiency based on system projections, and technology which could be implemented within five years.

Development of Alkaline Exchange Membrane Systems

This project is designed to significantly reduce the capital cost of hydrogen generation through elimination of the most expensive materials in the cell stack. It is likely that the AEM cells will not achieve the same efficiency as proton exchange membrane (PEM) technology for similar current densities, but not all markets will be as sensitive to electrical

cost. Proton has developed the following targets for AEM technology based on current technology status:

- Demonstrate cell voltages of 1.8 V at 500 mA/cm^2 or greater
- Increase stack durability to greater than 1,000 hours
- Reduce stack contribution to the overall system at MW scale by $100K ($100/kW)

FY 2013 Accomplishments

- Synthesized desired pyrochlores and proved structure with X-ray diffraction
- Demonstrated up to order of magnitude increase in mass activity for the oxygen evolution reaction (OER)
- Completed process trials for improved electrode adhesion and stability
- Tested cells for up to 200 hours
- Demonstrated modeling results consistent with experimental trends to give direction in Phase 2 composition refinement

✧ ✧ ✧ ✧ ✧

INTRODUCTION

There are currently two primary commercial electrolyzer options: systems based on liquid potassium hydroxide electrolyte and systems based on solid PEM electrolytes. While the PEM systems allow higher current densities and safety advantages such as lack of corrosive electrolyte and ability to run at low pressure oxygen, the materials of construction are expensive. Primary contributors to the cell cost are catalysts, membranes and flow fields. Moving to a hybrid system which uses an AEM enables the attractive operating parameters of the PEM case, while allowing use of less expensive materials. For example, flow fields can be made of stainless steel, while a larger variety of catalyst materials are stable in basic media. While AEM materials are still less stable and efficient than PEM materials, Proton has made significant progress in increasing the performance of AEMs for electrolysis. This technology has the long-term potential of reducing the stack cost by up to 75%. In the current project, work is being performed on catalyst materials to reduce the amount of noble metal needed in the baseline catalyst composition, and define the operating requirements of the system. While these catalysts still contain some PGM content, the conversion to stainless steel flow fields is still the major opportunity for AEM electrolysis in terms of cost contribution.

APPROACH

Electrolysis using anion exchange membranes introduces some new considerations to cell operating conditions. The schematic for acid-based systems vs. basic systems is shown in Figure 1. Because the water is actually consumed on the hydrogen side of the cell in the basic system, water management becomes a key consideration. Phase separation is more straightforward in an anode feed cell, because only the water transported through the separator has to be removed from the hydrogen, which becomes a smaller fraction of the total flow as the hydrogen pressure is increased. However, cathode feed would potentially enable higher current densities, by reducing any mass transfer limitations due to the rate of water transport across the membrane. Proton's past work under Advanced Research Projects Agency–Energy (ARPA-E) funding has shown that AEM electrolysis at greater than 500 mA/cm^2 is achievable with no evidence of mass transfer. Proton has therefore chosen to continue to leverage existing cell designs and balance of plant configurations established for our anode feed commercial products. A second consideration is the electrolyte. Anion exchange membranes are not at the same level of maturity as PEM materials, and tend to be less stable in strongly alkaline environments. In addition, they rapidly carbonate in air, blocking hydroxide conducting sites. While deionized water is the preferred fluid for the electrolyzer, using a buffered solution such as carbonate may provide stability enhancements without significantly impacting performance.

In the Phase 1 project, the pyrochlore class of catalysts ($A_2B_2O_{6-7}$) were investigated in AEM cells for improved activity at the oxygen electrode vs. noble metal oxide baseline catalysts. This approach leverages several advantages of the pyrochlores. First, these materials have good kinetics for oxygen evolution, as supported by density functional theory calculations performed in this project. Also, these materials are stable in basic media, such as the polymer electrolyte. Finally, it has been demonstrated that these structures can be made into nanoparticles. This characteristic is especially important, as several reports of oxygen evolution catalysts

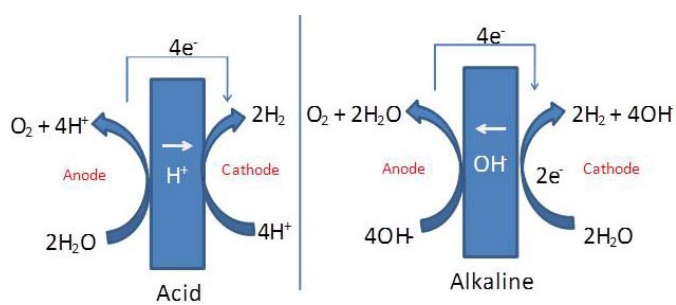

FIGURE 1. Acidic vs. Basic Membrane-Based Electrolysis Cell Schematic

exist in the literature which claim very high activity as normalized by surface area, but have not been successfully made at relevant surface areas. In the Phase 1 project, compounds using Bi or Pb for the A metal and B metals including Ru and Ir were investigated.

RESULTS

As shown in Figure 2, the desired catalyst compositions were successfully synthesized in the Phase 1 project. While some of the formulations were lower than desired in surface area, the ruthenates were acceptable, and electronic conductivities for all the samples measured were good. Even at the lower than desired surface areas for some catalysts, mass activity measurements using rotating disk electrodes (RDE) showed promise, as shown in Figure 3. While iridium oxide is not the most active known oxygen evolution catalyst in basic media, it serves as the baseline in this study. Nickel alloys and nickel-based oxides are well known for catalytic activity in the alkaline liquid systems. However, Proton's ARPA-E project has demonstrated that iridium oxide performance translates very well from RDE testing to a practical electrode configuration, while the nickel systems still require understanding around the ionomer-catalyst-membrane interface. IrO_2 is therefore still an appropriate baseline for comparison. Platinum is also included for reference, as platinum is not a very good oxygen evolution catalyst. Typical cell voltages are 300 mV higher for platinum than IrO_2.

Proton has spent considerable effort to develop AEM electrolysis electrode configurations, in collaboration with our ARPA-E project partners especially at Penn State. The AEM membranes are much less stable at high temperature vs. PEM materials and cannot withstand many of the processing conditions of traditional electrolysis MEA manufacturing. Using a gas diffusion electrode approach in which the electrodes can be directly sprayed on the gas diffusion material mitigates this stress on the membrane and results in more stable, reproducible results. Proton has also translated this technique to PEM systems and demonstrated very close to equivalent performance. In addition, the AEM materials tend to be significantly stiffer than the PEM materials, and are thinner than standard PEM electrolysis membranes. The thinner membrane is required due to the slower diffusion of hydroxide vs. protons. While the improved stiffness results in the membranes being easier to handle, these characteristics require adjustments to the cell design, particularly in the seal area, to effectively operate the stack and avoid overboard leaks while not overloading the membrane. Proton made some of these adjustments on the ARPA-E project and has continued to improve the cell on this project. Based on this background work, Proton was able to rapidly test new material candidates from IIT and compare to established performance baselines for the AEM cell.

Stack testing demonstrated good translation of the RDE results as shown in Figure 4. The lead ruthenates showed the most promise, consistent with the higher surface area of these materials. Figure 4a shows the initial performance

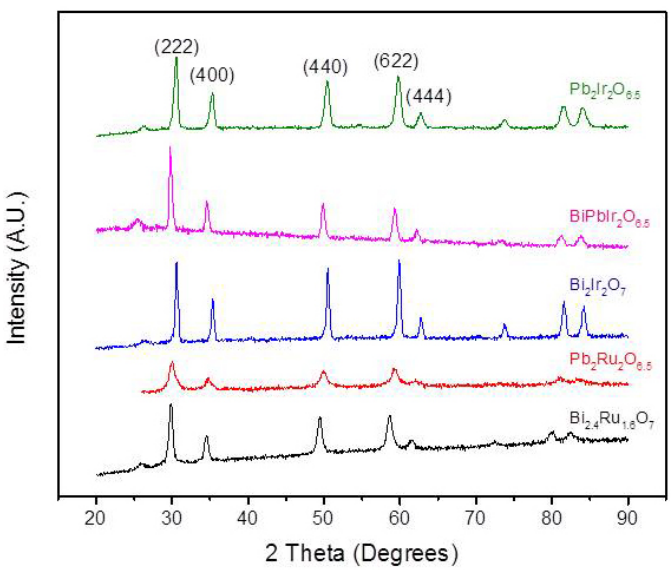

Catalyst	B.E.T. surface area (m^2/g)	Electronic conductivity S/cm
$Pb_2Ru_2O_{6.5}$	99±4	87
$Bi_{2.4}Ru_{1.6}O_7$	7.8±0.2	63
$Pb_2Ir_2O_{6.5}$	1.2±0.1	73±7
$Bi_2Ir_2O_7$	0.4±0.1	56±6
$BiPbIr_2O_{6.5}$	0.4±0.1	75±7
$Pb_2Os_2O_{6.5}$	0.8±0.3	

FIGURE 2. X-Ray Diffraction Analysis, Synthesized Pyrochlor Catalysts

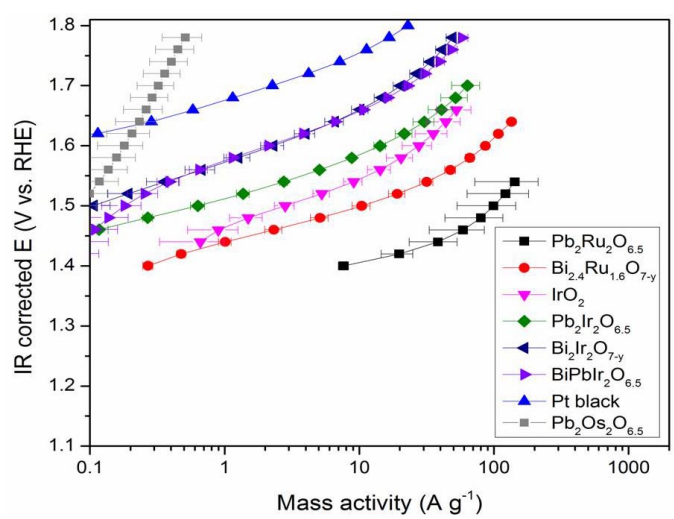

FIGURE 3. Mass Activity for OER, RDE Analysis

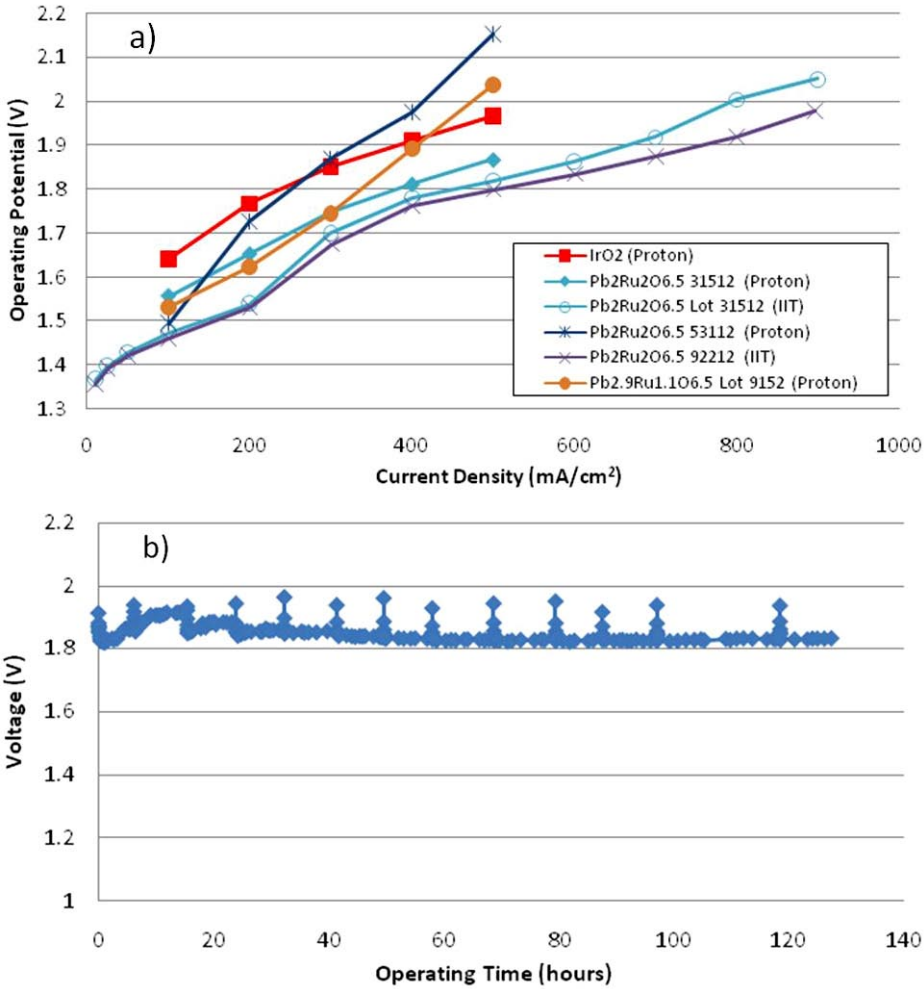

FIGURE 4. Cell Stack Performance, Lead Ruthenate Catalysts: a) Polarization Curve; b) Durability Performance at 500 mA/cm^2 in Carbonate Electrolyte

data, while Figure 4b shows stable voltage performance at good efficiencies in a carbonate electrolyte. While carbonate conductivity should be lower than hydroxide conductivity, it is believed that the performance does not significantly decline because of the increased ionic conductivity of the liquid phase and high water content of the membranes under electrolysis conditions. In addition, there was good agreement between results obtained at IIT vs. Proton in similar test hardware, demonstrating consistent electrode fabrication and test protocol. Initial performance with IIT membranes and ionomers also showed high efficiency, although durability needs to be improved.

Finally, density functional theory and d-band orbital theory were applied to the catalyst compositions tested. A four-step mechanism was proposed for the oxygen evolution reaction, with the ruthenium compounds showing higher predicted performance, as demonstrated in the cell testing. Generally good agreement was obtained between modeling and theory, particularly when corrected for surface area. Larger metal-adsorbate repulsion for the hydroxide absorption leads to lower OER activity, mainly dictated by the B cation. However, the modeling also predicts that there may be further room for improvement beyond the highest performing Phase 1 materials, if the surface area can be corrected on the bismuth materials.

CONCLUSIONS AND FUTURE DIRECTIONS

- In the Phase 1 project, improvements over past AEM electrolysis cells were demonstrated. High OER activity was achieved with lead ruthenate materials, reducing noble metal content. Future work includes determining the influence of composition on pyrochlore microstructure, physical properties, and activity.
- Initial IIT membrane performance met efficiency targets. In Phase 2, focus will be on improving durability through investigation of key AEM properties

(conductivity, ion exchange capacity, water uptake, gas crossover) and modification of membrane characteristics.

- Carbonate in the electrolyte served as a stabilizer for the AEM electrolyzer, without negatively impacting efficiency. A system trade study of electrolyte type vs. cost and stability will be performed in the next phase and a prototype lab system will be developed.

FY 2013 PUBLICATIONS/PRESENTATIONS

1. Final Report, Phase 1 Small Business Innovation Research.

2. "Bridging the Infrastructure Gap: Cost Effective Generation of Hydrogen from Water", Department Seminar, Colorado School of Mines, November 2012.

3. "Material Advancements for Cost Effective Hydrogen Energy Storage: Megawatt Electrolysis Development", Spring ACS Meeting, Esther Takeuchi Award Symposium, New Orleans, April 2013.

II.A.6 Unitized Design for Home Refueling Appliance for Hydrogen Generation to 5,000 psi

Timothy Norman (Primary Contact),
Monjid Hamdan
Giner, Inc. (Formerly Giner Electrochemical Systems, LLC)
89 Rumford Avenue
Newton, MA 02466
Phone: (781) 529-0556
Email: tnorman@ginerinc.com

DOE Manager
Eric Miller
Phone: (202) 287-5829
Email: Eric.Miller@hq.doe.gov

Contract Number: DE-SC0001486

Project Start Date: August 15, 2010
Project End Date: June 14, 2013

Overall Objectives

Design and demonstrate subsystems for a unitized proton electrolyte membrane (PEM)-based electrolyzer system for residential refueling at 5,000 psi to meet DOE targets for a home refueling appliance (HRA).

Fiscal Year (FY) 2013 Objectives

- Design, fabricate, and evaluate 5,000 psig electrolyzer stack
- Fabricate and demonstrate 5,000 psi electrolyzer system

Technical Barriers

This project addresses the following technical barriers from the Hydrogen Production section of the Fuel Cell Technologies Office Multi-Year Research, Development and Demonstration (MYRDD) Plan [1]:

(F) Capital Cost

(G) System Efficiency and Electricity Cost

Technical Targets

The technical targets for this project are listed in Table 1.

TABLE 1. Giner Progress toward Meeting DOE Targets for Hydrogen Production

Characteristics	Units	2015 Targets[a]	Giner Status
Total Hydrogen Production Cost	$/kg H_2	3.90[b]	3.98[c]/4.64[d]
Electrolyzer Capital Cost	$/kg H_2	0.50	1.05
Electrolyzer Stack Efficiency	% (LHV) (kWh/kg)	76 (44)	72[e] (47)[e]

[a] 2012 Hydrogen Production MYRDD Plan; [b] Includes delivery (compression, storage, and dispensing); [c] Based on H35 refueling; [d] Based on H70 refueling; [e] Isothermal Compression at 5,000 psig adds ~5 kWh/kg; LHV – lower heating value.

FY 2013 Accomplishments

- Membrane Development Completed
  - Developed and evaluated high-pressure, high-strength membranes compatible with 5,000 psi operation
  - Membranes exhibit high mechanical stability and improved sealing under high operating pressure
- Electrolyzer Stack Design
  - Completed fabrication of 20-cell electrolyzer stack
  - Successfully operated electrolyzer stack at a pressure of 5,000 psig
- Electrolyzer System
  - Unitize breadboard system design and fabrication complete:
  - Determined cost of hydrogen directly in stack:

✧ ✧ ✧ ✧ ✧

INTRODUCTION

U.S. automakers have invested significant resources in the research and development of hydrogen fuel cell vehicles. However, to enable the widespread use of fuel cell vehicles, an additional major investment will be required to construct an infrastructure for hydrogen production and delivery to fueling stations. In order to facilitate this transition, it has been recommended that high-pressure hydrogen, generated at 5,000 psig for home refueling of fuel cell vehicles, be implemented as an intermediary approach. An improved, low-cost process for producing high-pressure hydrogen from water by electrolysis will significantly advance the development of the hydrogen economy, providing hydrogen for fuel cell vehicles at a price competitive with

that of gasoline on a per-mile basis. The ability to produce hydrogen economically, the relatively low capital cost of the electrolyzer unit, and the low maintenance cost of the unit will allow widespread distribution of hydrogen home fueling appliances deemed necessary for the introduction of fuel cell vehicles.

The project focuses on the development of high-pressure, low-cost electrolyzer stack and balance-of-plant (BOP) components. Giner has a matured PEM-based electrolyzer technology for producing hydrogen at moderate to high pressure directly in the electrolyzer stack, while oxygen is evolved at near-atmospheric pressure. In this system, liquid water, which is a reactant as well as coolant, is introduced into the anode (O_2) side of the electrolyzer at near atmospheric pressure; high-pressure hydrogen is removed from the cathode or product side. In addition to reliability, and long maintenance intervals, safety is also a primary concern in this design due to the flammability and reactivity concerns of hydrogen and oxygen.

APPROACH

Giner recently completed a multi-year development project for DOE that reduces commercial PEM-based electrolyzer costs while simultaneously raising the efficiencies of water electrolyzer systems that operate in a moderate pressure range of 400 psi. Future extension of this technology to pressures of 5,000 psig is feasible with modifications to the electrolyzer stack, providing the ability to safely operate in a differential hydrogen/oxygen pressure mode. Based on an innovative electrolyzer stack concept and recent developments in high-strength membranes, Giner has designed a PEM-based water electrolyzer system for home refueling applications that will be able to deliver hydrogen at pressures of 5,000 psi. High-pressure hydrogen can be generated in low-cost moderate-pressure electrolyzer stacks by means of external reinforcement to the individual cell frames. Utilizing external cell reinforcement eliminates the need for bulky and costly stack parts and facilitates a method for fabricating an electrolyzer stack and system that can safely operate at 5,000 psi. In addition, a reduction of major system components and system cost is realized.

RESULTS

Membrane Evaluation: Utilizing supported dimensionally stable membrane (DSM™) membranes developed at Giner, the performance of the PEM electrolyzer stack can be optimized for a selected operating pressure and temperature. DSM™ membranes were fabricated with thickness ranging from 1 to 20 mils. Gas permeation data obtained during single-cell testing at various operating pressures and temperatures indicates that improved membrane efficiency is obtained while operating the electrolyzer stack in a differential pressure mode (hydrogen pressure over oxygen pressure) as opposed to balanced pressure in which both hydrogen and oxygen gases are generated at the same pressure. Based on membrane gas permeation (Faradaic losses), and membrane voltage efficiency, the cost of electrochemical hydrogen compression in the stack was determined to be 4 to 6 $kWh_e/kg\text{-}H_2$. At an operating pressure of 5,000 psi and 80°C, the optimal membrane thickness was determined to be between 7 and 10 mils operating in the current density range of 1,000 to 1,500 mA/cm². The supported membranes also demonstrated significant improvements in membrane creep property and mechanical stability during high differential pressure operation of 5,000 psi.

Electrolyzer Stack Fabrication: The HRA has been designed for on-demand operation. The system is designed with a 2.3-kWe, 20-cell electrolyzer stack (Figure 1), providing a vehicle tank fill of 0.5 kg of hydrogen over a 12-hour period. This will provide 30 miles of driving range based on current fuel cell vehicle fuel economy estimates of 60 miles/kg-H_2. Differential pressure operation required redesign of the electrolyzer stack hardware. Giner's initial design included the use of a pressure containment dome; the gas pressure in the pressure dome is matched to that of the electrolyzer's hydrogen and oxygen product streams to provide external stack reinforcement. In 2012, Giner developed a modified stack design that utilizes a metal containment ring externally attached to the electrolyzer-stack's cathode (H_2) cell frames. The simplified design eliminates the need for a containment dome; in addition, this technique enables high pressure operation with the use of low- and moderate-pressure PEM-based electrolyzer stacks without the need for expensive internal cell reinforcement or metal frames. The low cost of the electrolyzer stack is maintained by utilizing previously designed injection molded thermoplastic cell frames and cell components.

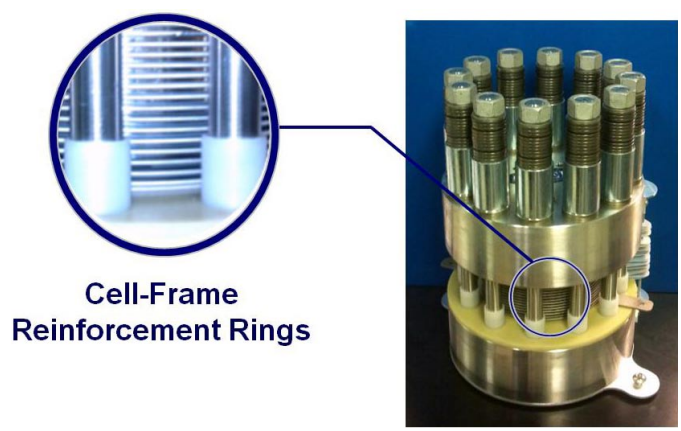

FIGURE 1. High-Pressure PEM Electrolyzer Stack with Reinforced Cell Frames (20-Cell Stack)

In addition to the use of external cell-frame reinforcement, the electrolyzer stack includes several modifications developed under a separate DOE project that further reduce stack cost. This includes: (1) an overall decrease in the parts count per cell, (2) a 75% reduction in anode and cathode catalyst loadings, (3) molded thermoplastic cell frames, resulting in a cost reduction of 95% as compared to machining this component, (4) a reduction in cell frame thickness, thus reducing the anode and cathode support materials and costs, and (5) a modified anode membrane support material that enables high pressure operation of 5,000 psi. The stack was successfully operated in 8- to 12-hour intervals at hydrogen pressures of 5,000 psi. The average cell performance is shown in Figure 2 for various operating pressures and temperatures. The power consumption of the electrolyzer stack was measured at 51.8 $kWh_e/kg\text{-}H_2$ while operating at a pressure of 5,000 psi and a current density of 1,200 mA/cm².

5,000 psi "Unitized" Electrolyzer System for Home Refueling: The HRA shown in Figure 3 features: (1) a 20-cell differential pressure electrolyzer stack that produces hydrogen at up to 5,000 psi and oxygen at ambient pressure, (2) a water tank, sized for approximately 12 hours of electrolyzer operation at rated power levels, (3) an integrated deionized water loop used to maintain water purity and temperature control of the electrolyzer stack during operation, (4) a small hydrogen dryer to maintain a hydrogen gas dew point of <-40°C, (5) sensors for monitoring the production gases to detect/prevent formation of flammable mixtures, and (6) the integration of electrolyzer subsystems to minimize the number of BOP components. An automated control system also provides safe automated operation.

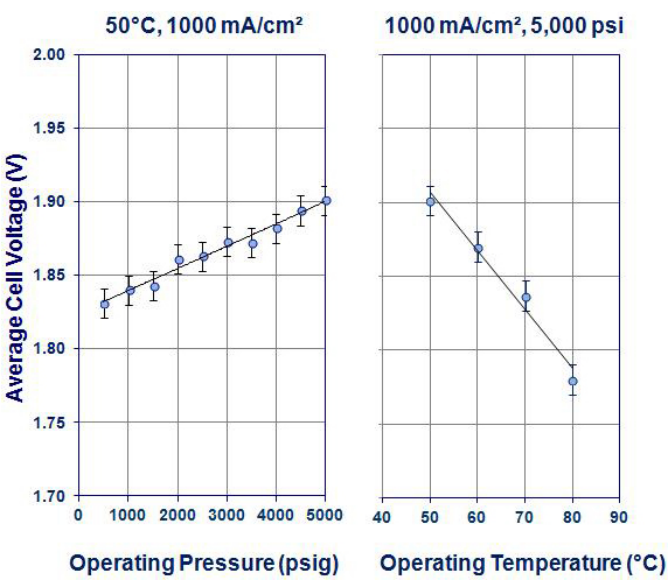

FIGURE 2. Cell Performance under Various Operating Conditions

The reactant water is supplied to the anode side of the electrolyzer stack at ambient pressure. Oxygen generated on the anode side of the electrolyzer stack is then separated from water in the oxygen gas separator which also serves as the water reservoir. Water is circulated from the oxygen gas separator to the anode of the electrolyzer stack and back to the oxygen gas separator. The circulating pump operates at low differential pressure, as it must only overcome the pressure drop in the feed loop. During electrolyzer operation water is transferred from the anode side of the electrolyzer stack to the cathode side due to electrically-osmotic transport. Water loss due to electro-osmotic drag is collected in the hydrogen gas phase separator and returned to the electrolyzer feed loop after it has been degassed. Hydrogen generated on the cathode side is then passed through a regenerative dryer consisting of dual desiccant columns.

At the end of the electrolysis cycle, which occurs when the water in the HRA system is nearing depletion, power is no longer available, or at a predetermined time or pressure, the electrolyzer system is shut down. In addition to the normal end-of-cycle operation, the control system automatically shuts down electrolyzer operation when abnormal conditions are detected. The conditions that trigger

FIGURE 3. Electrolyzer (HRA) System

electrolyzer subsystem shut down include: low water in the electrolyzer feed loop, low water flow rate, high temperatures (>80°C), over pressure (>5,000 psig), and gas detection alarms. In addition, any cell in the electrolyzer stack exhibiting a low or high cell voltage will activate a system shutdown.

CONCLUSIONS AND FUTURE DIRECTIONS

The stack and system design incorporates numerous cost-saving (and reliability enhancing) simplifications. These design features eliminate the need for bulky and costly stack and system parts, and facilitate a method for producing a low-cost electrolyzer system that can safely operate at a hydrogen pressure of 5,000 psi in a residential setting. The technology is capable of providing onsite residential hydrogen refueling at a cost that meets the DOE 2015 target of \$3.90/kg-H_2 for vehicles that have H35 (6,250 psi) refueling requirements. In addition, the hydrogen production costs for H70 (12,688 psi) refueling, have been estimated at \$4.64/kg-H_2.

Work on this project has been completed, however Giner will continue to investigate methods that further reduce cost and improve the efficiency of high-pressure PEM-based electrolyzer stacks and systems. Giner believes that future challenges for high-pressure PEM electrolysis include:

- Scale up of high-pressure stack technology to 50 cells per stack (or higher)
- Improve pressure capabilities of stacks (to 12,688 psi) for H70 refueling
- Develop membranes with reduced gas permeability (improve membrane efficiency)

FY 2013 PUBLICATIONS/PRESENTATIONS

1. M. Hamdan, *PEM Electrolyzer Incorporating an Advanced Low-Cost Membrane.* 2013 Hydrogen Annual Program Merit Review Meeting, Presentation #pd030, May 15, 2013.

2. T. Norman, and M. Hamdan, *Unitized Design for Home Refueling Appliance for Hydrogen Generation to 5,000 psi.* 2013 Hydrogen Annual Program Merit Review Meeting. Presentation #pd065, May 15, 2013.

REFERENCES

1. 2012 Multi-Year Research, Development and Demonstration Plan. Hydrogen Production. DOE, Pg 3.1-14 (http://www1.eere.energy.gov/hydrogenandfuelcells/mypp/pdfs/production.pdf)

II.A.7 Hydrogen by Wire – Home Fueling System

Luke T. Dalton
Proton Energy Systems dba Proton OnSite
10 Technology Drive
Wallingford, CT 06492
Phone: (203) 678-2128
Email: ldalton@protonenergy.com

DOE Manager
Eric Miller
Phone: (202) 287-5829
Email: Eric.Miller@ee.doe.gov

Contract Number: DE-SC0001149

Project Start Date: August 15, 2010
Project End Date: August 14, 2012

Overall Objectives

- Develop enabling technologies for 350-bar hydrogen home fueling
- Design key electrolysis cell stack and system components
- Fabricate, inspect and assemble prototype components
- Demonstrate prototype 350-bar hydrogen generation
- Demonstrate prototype 350-bar home fueling technologies

Fiscal Year (FY) 2013 Objectives

Complete demonstration of prototype 350-bar home fueling technologies including full characterization of the prototype and start/stop cycles to simulate tank fill operation

Technical Barriers

This project addresses the following technical barriers from the Hydrogen Production section of the Fuel Cell Technologies Office Multi-Year Research, Development, and Demonstration Plan:

(F) Capital Cost

(G) System Efficiency and Electricity Cost

(H) Footprint

(I) Grid Electricity Emissions (for distributed)

(K) Manufacturing

(L) Operations and Maintenance

(M) Control and Safety

Technical Targets

Table 1 presents the technical targets for this project.

TABLE 1. Progress towards Meeting Technical Targets for Hydrogen Production via Distributed Water Electrolysis

Characteristics	Units	2013 Status	2015 Target	2020 Target
Hydrogen Levelized Cost (Production Only)	$/kg	5.99[a, b]	3.90	2.30
Electrolyzer System Capital Cost	$/kg	2.62[a,b]	0.50	0.50
System Energy Efficiency	% (LHV)	57[b]	72	75
Stack Energy Efficiency	% (LHV)	66[b]	76	77
Compression, Storage, and Dispensing	$/kg	0.00	1.70	1.70
Total Hydrogen Levelized Cost (Dispensed)	$/kg	5.99	5.60	4.00

[a]Based on H2A model modified for residential (non-commercial) application
[b]Includes generation and compression to 350 bar
LHV – lower heating value

FY 2013 Accomplishments

- Demonstrated 350-bar (5,000 psig) differential pressure electrolysis
- Demonstrated several cycles from start to 350-bar generation to stop
- Demonstrated comparison of stack performance at 350 bar vs. 13 bar

✧ ✧ ✧ ✧ ✧

INTRODUCTION

Based upon the results of the Phase 1 study, the fundamental requirements for a hydrogen home fueling appliance have been defined. The conclusion of the Phase 1 study indicated that an overnight-fill proton exchange membrane (PEM) electrolysis device that fills the vehicle directly to a maximum of 350 bar with no mechanical compressor or secondary hydrogen storage can cost effectively supply the daily hydrogen for a typical commuter operating a fuel cell vehicle. The case for including the hydrogen home fueling concept in the overall mix of fueling infrastructure is strong. The home fueler can grow in production volume and geographic distribution with individual vehicles as they are placed in the market with more flexibility than centralized fueling stations. Existing utility infrastructure (water, electricity) can be utilized within

their existing capacities to cover the distribution aspect of the fueling infrastructure.

The goal of this Phase 2 project was to design and demonstrate the key hardware for 350-bar hydrogen home fueling based on PEM electrolysis. Proton Energy Systems has previously demonstrated durable PEM electrolysis equipment generating hydrogen at 165 bar. In addition, Proton has also demonstrated the ability of sub-scale prototypes to seal at the required proof pressure for 350-bar operation. Building upon this past work, designs have been developed utilizing Proton's reliable PEM electrolysis cell stack and system technologies for hydrogen generation and vehicle fueling at 350 bar.

APPROACH

The approach to the Phase 2 project was threefold. First, utilize the data and modeling results from the Phase 1 project to provide approximate sizing for the hydrogen generation rate. Second, build upon Proton's proven cell stack design and development experience to undertake the designs required for 350-bar operation. Third, utilize Proton's strong engineering processes that rely on a phased approach, with stage reviews, key written guidelines, and design output documentation to guide the successive levels of design refinement and demonstration. To that end, the project was organized into four main tasks: (1) Prototype System Design and Fabrication, (2) Prototype Stack Design, (3) Prototype Component Verification, and (4) Prototype System Testing.

Task 1 utilized engineering best practices to design and fabricate the prototype fueling system. This includes producing the plumbing and instrumentation diagram, electrical schematics, bills of materials, control schemes and component specifications for the prototype system. In addition, Task 1 included the procurement, fabrication, and acceptance testing of the prototype system. Task 2 included producing the component designs and assembly models for the cell stack in three-dimensional computer-aided design format. Moreover, it included completing design feasibility pressure testing using both sub-scale and full-scale active area components. Task 3 incorporated work on verifying the functionality of key components within the cell stack design and one or two custom components within the system design. Task 4 included assembling and checking the first electrolysis-ready version of the new prototype stack design. Furthermore, it includes integrating the prototype stack into the prototype system and operating in electrolysis to generate hydrogen at 350 bar.

RESULTS

As of last year's annual report, the project had completed all of Tasks 1, 2, and 3, and 80% of Task 4. The project is now complete and all of the goals of the project have been met.

The prototype system design is based upon Proton's commercial HOGEN® HP high-pressure hydrogen generator which delivers hydrogen at pressures of up to 2,400 psi. This high-pressure system is also derivative of Proton's highly successful HOGEN® S-series product with over 400 units now in operation. The prototype system has gone through a complete prototype design process, including schematics, drawings, and controls definition. A picture of the completed system is shown in Figure 1. System acceptance testing included leak checking, ground continuity testing, and hi-pot testing.

The final activity during Task 3 was the fabrication of an operational single-cell stack suitable for integration and testing in the prototype test bed. Leading up to the operational single-cell stack, an equivalent test article was built for cross-cell diffusion testing. The operational single-cell stack went through a complete acceptance test protocol as is typical for all of our commercial product electrolysis stacks. This acceptance test protocol included cross-cell diffusion testing up to the full operating pressure. The results of the high pressure diffusion tests for the pre-operation test article and the operational single cell are shown in Figure 2 in comparison with previously reported data.

All of the preparation, build, and acceptance testing of the complete system was described in the previous annual report. After the operational single-cell 350-bar stack was installed, the initial milestone of hydrogen production at 350-bar pressure and full differential pressure was achieved (Figure 3). Continued testing with the stack and system allowed the full tuning of system operating parameters as well as cycle testing of the stack and system through

FIGURE 1. Prototype Test System and Data Acquisition

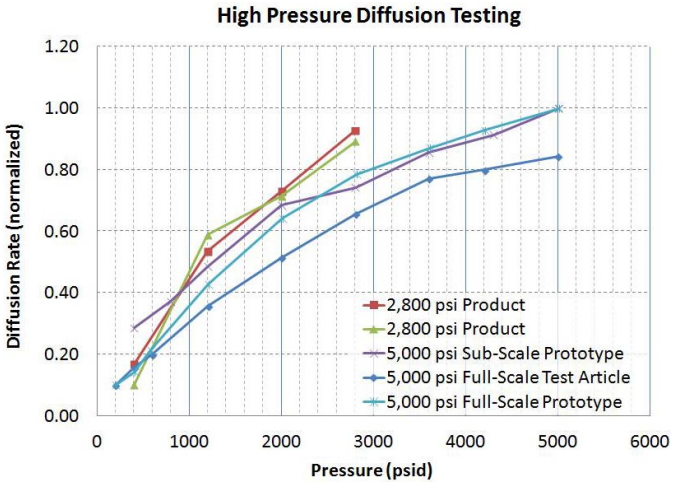

FIGURE 2. Cross-Cell Diffusion Testing at up to 350-Bar Differential Pressure

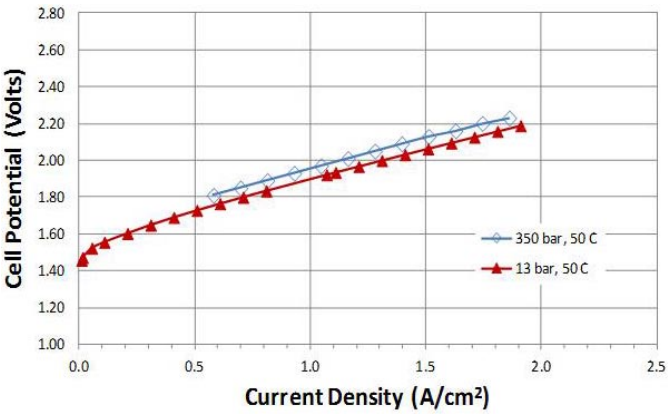

FIGURE 3. Polarization Data during 350-bar (5,000 psig) Hydrogen Generation Compared with 13-Bar Hydrogen Generation

simulated tank fills starting from zero pressure through full pressure and return to system standby (Figure 4). The key high-pressure components including the stack and high-pressure phase separator worked well throughout the test. The test was stopped due to the failure of one sensor that was newly designed for this operating pressure. The redesign of that sensor by the component supplier was beyond the scope of the project.

CONCLUSIONS AND FUTURE DIRECTIONS

All of the diligent design and development work of the project team resulted in achievement of the initial demonstration of a 350-bar capable electrolysis stack and system. This accomplishment creates a foundation from which the hydrogen output and pressure can be scaled up and also design improvements can be made to improve the efficiency and economics of this small-scale, high-pressure hydrogen generator system.

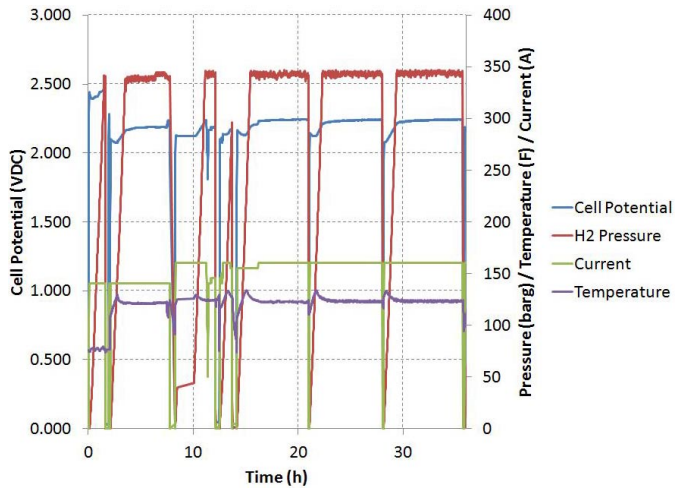

FIGURE 4. Start, Pressurization, and Return to Standby Cycle Test Data with 350-Bar (5,000 psig) Hydrogen Generation

In summary, the following tasks have been completed for the 350-bar electrolysis fueling system development effort and the parallel 350-bar electrolysis cell stack development:

- All prototype system components have been ordered and procured
- The prototype system is complete, including full system operational checkout
- The high-pressure cell stack design is finalized including overboard seal testing to proof pressures above 500 bar
- All prototype cell and stack embodiment components have been ordered and procured
- Design and verification of cell stack components is completed, including seal and active area full differential pressure testing
- The operational prototype cell stack has been assembled and acceptance tested
- The prototype system and operational stack have been integrated and operationally tested
- 350-bar hydrogen generation from water electrolysis at full differential pressure has been achieved
- Multiple cycles from start to 350 bar to stop with full system operation

FY 2013 PUBLICATIONS/PRESENTATIONS

1. Phase II Final Report.

2. "Electrochemical Compression and Purification to Enable Hydrogen Fuel Distribution, Storage, and Use", Fuel Cell Seminar, November 2012.

3. "Bridging the Infrastructure Gap: Cost Effective Generation of Hydrogen from Water", Department Seminar, Colorado School of Mines, November 2012.

4. "Proton Exchange Membranes for H_2 Generation: A Tutorial on Research Needs and Challenges for PEM Electrolysis vs. Fuel Cells", Spring ECS Meeting, Toronto, Canada, May 2013.

II.A.8 Low-Noble-Metal-Content Catalysts/Electrodes for Hydrogen Production by Water Electrolysis

Katherine Ayers (Primary Contact), Chris Capuano
Proton Energy Systems dba Proton OnSite
10 Technology Drive
Wallingford, CT 06492
Phone: (203) 678-2190
Email: kayers@protononsite.com

DOE Manager
Eric Miller
Phone: (202) 287-5829
Email: Eric.Miller@hq.doe.gov

Contract Number: DE-SC0008251

Subcontractor:
Brookhaven National Laboratory, Brookhaven, NY

Project Start Date: June 28, 2012
Project End Date: August 14, 2015

Overall Objectives

- Develop cathode catalyst materials for lower Pt concentration
- Investigate application on gas diffusion electrodes (GDEs) vs. membrane electrode assemblies (MEAs)
- Develop anode catalyst/support composition development and application methods
- Durability testing of ultra-low catalyst loaded electrodes
- Process scale up to demonstrate economic feasibility of the approach

Fiscal Year (FY) 2013 Objectives

- Optimize composition and microstructure of cathode catalysts on carbon-based substrates
- Demonstrate equivalent cathode performance to baseline with ultra-low catalyst loading
- Screen promising candidates for core-shell anode catalysts and non-carbon catalyst supports
- Demonstrate feasibility of reduced anode catalyst loadings
- Estimate the impact of noble metal reduction on the cost of hydrogen from water

Technical Barriers

This project addresses the following technical barriers from the Hydrogen Production section of the Fuel Cell Technologies Office Multi-Year Research, Development, and Demonstration Plan:

(F) Capital Cost

Technical Targets

Technical targets are presented in Table 1.

TABLE 1. Proton Energy Systems Progress Towards Meeting Technical Targets for Distributed Water Electrolysis Hydrogen Production

Characteristics	Units	2012 Target	2017 Target	Proton Status
Hydrogen Cost	$/gge	<3.70	<3.00	3.46
Electrolyzer Capital Cost	$/gge	0.70	0.30	0.64
Electrolyzer Energy Efficiency	% (LHV)	69	74	67

gge - gasoline gallon equivalent; LHV - lower heating value
Note: Estimates are based on H2A v2.1, for electrolysis only (compression-storage-delivery not included). Model assumes $0.05/kWh.
Electrolyzer cost based on 1,500 kg/day capacity, 500 units/year; efficiency based on system projections; technology which could be implemented within five years, and demonstrated stack efficiency of 74% LHV efficiency.

Ultra-Low Catalyst Loading

This project is developing methods to reduce the amount of platinum group metals (PGMs) used in the MEA, reducing the sensitivity to market fluctuations in precious metal costs. At today's precious metal prices, these advancements enable the following progress in capital cost of hydrogen:

- $0.04/kg reduction in stack capital cost
- Savings of ~$45,000 per MW
- Enables thinner membranes for lower total cost and higher efficiencies

FY 2013 Accomplishments

- Successfully synthesized and characterized catalysts for use on cathode GDEs
- Successfully fabricated catalyst coated GDEs for operational testing
- Durability target of 500 hours met and cell stack continues to operate

- Successfully synthesized and screened catalysts for oxygen evolution use.
- Surveyed anode support and gas diffusion layer (GDL) materials
- Conducted operational tests, demonstrating feasibility of the anode GDE approach

✧ ✧ ✧ ✧ ✧

INTRODUCTION

Proton OnSite has worked over the past several years to significantly reduce the cost of hydrogen production via proton exchange membrane (PEM) electrolysis. With progress made on the cost of the flow field/bipolar plate assembly, the MEA is currently the most expensive single component of the electrolysis cell. An important portion of MEA cost is related to the prices of PGMs, which are high and may rise with demand due to limited natural resources. Based on current noble metal prices, the catalyst represents half of the MEA cost. Recently, however, efforts have demonstrated that significant reductions in catalyst loading are feasible.

The high percentage of catalyst cost for electrolysis reflects the fact that MEA technology has lagged significantly behind fuel cells, for several reasons. First, the capital cost of electrolysis is already competitive in high purity industrial hydrogen applications for commercial viability, reducing the urgency of immediate change until the energy markets are more mature. Second, there has been resistance to the use of supported catalysts in electrolysis applications, because performance limitations have been noted on the cathode at fuel cell Pt loadings, and carbon supports are not stable on the anode side of the electrolysis cell. Finally, most manufacturing processes for electrolysis electrodes are still highly manual and require high loadings in order to achieve uniform catalyst distribution. This project leverages core shell catalyst structures developed for fuel cells by Brookhaven National Laboratory and application methods for improved utilization to reduce the catalyst loading by an order of magnitude or more.

APPROACH

In this project, catalyst structures developed by Brookhaven National Laboratory for fuel cells were investigated for use in electrolysis. These types of materials have achieved a large amount of attention due to their high mass activity, enabling ultra-low loading of PGMs for fuel cell MEAs. However, the conditions for electrolysis are more aggressive than in the fuel cell, and require modifications of the approach in order to translate technology from one device to the other. The Phase 1 Small Business Technology Transfer scope included advancement of initial feasibility studies on the cathode to define a durable and reproducible electrode configuration with equivalent performance to the production baseline. For the anode, the goal was to show feasibility for similar loading reductions, with more substantial development in Phase 2.

The approach to improving activity and reducing loading on the cathode (hydrogen production) side of the cell involves two steps; 1) increasing the catalyst specific surface area by synthesizing sized-controlled, core-shell nanocatalysts, and 2) achieving better utilization with a more effective GDE structure. Several GDL types and catalyst supports are being evaluated to determine the optimal interface for catalyst deposition while maintaining the required transport properties for electrolysis as well as the optimal formulation of catalyst, support, and ionomer for high utilization. Durability of the new electrode structures will be performed in commercial stack hardware. Scale up of the catalyst manufacturing process will then be performed and cost analysis documenting the savings through the new process will be provided to DOE.

RESULTS

For the cathode, improvements were made in the synthetic process for core shell catalysts, specifically on the PtRu system. Previous methods had produced a Ru-rich core and Pt-rich shell, but there were defects in the structure, causing partial alloying. In the Phase 1 project, atomic-level perfection was achieved in synthesizing core-shell electrocatalysts via green chemistry, using ethanol as the solvent and reductant without capping agents and templates. Figure 1 shows transmission electron microscopy data and schematics illustrating the improvement.

In addition, Brookhaven needed to develop a fast and sensitive technique for screening electrode configurations at the bench level, to conserve materials for larger scale testing to evaluate structures which had already shown promise at the screening level. A GDE hanging strip method was developed, in which the catalyst, support, and gas diffusion electrode material could be tested at a small but representative scale. In addition, this technique did not have the mass transport limitations of typical rotating disk electrode experiments. In general, the results translated well to full cells, except for any effects due to insufficient conductivity between the GDE and the membrane, which were not predicted in the acidic solution test.

Once the catalyst synthesis and catalyst-support systems were defined, samples were sent to Proton for screening at the 25 cm^2 level. Initial testing was performed in a non-proprietary test cell which Proton has used with several partners, in order to establish consistent and accessible benchmarks for electrolysis performance. Proton has developed techniques to test full and half MEAs and GDEs. This test cell is also simpler and faster to assemble than a

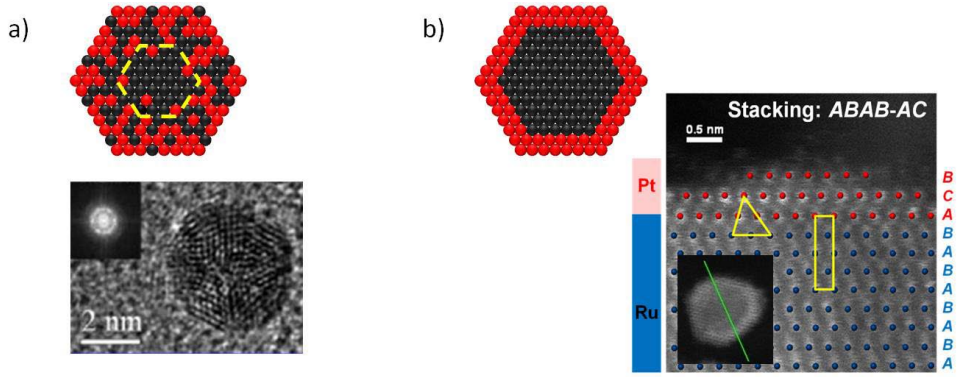

FIGURE 1. Structural Schematics and Transmission Electron Microscopy Data for Core Shell Catalysts: a) Defect-Induced Alloying; b) Atomically Perfect Core Shell

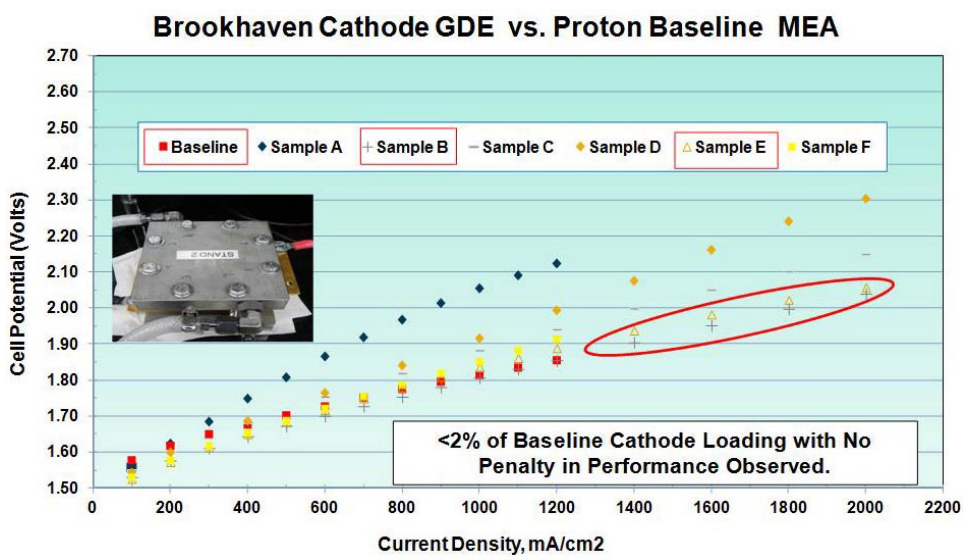

FIGURE 2. Cathode Performance Screening

full-scale commercial cell. While it cannot be operated at pressure and is not designed for long-term testing, it has been shown in other projects to yield very good predictions of performance. Several configurations were tested based on the Brookhaven cathode samples, with representative results shown in Figure 2. A Proton anode was used in all cases. The best performing samples were able to achieve equivalency to the Proton cathode, at 2% of the catalyst loading.

Based on these results, a final set of samples was created in Proton's commercial electrode format for durability testing. A three-cell stack in Proton's commercial GC format was built, using one baseline cell and two cells containing the Brookhaven-fabricated samples. All three cells operated at 2 A/cm^2 for 500 hours without measureable voltage decay, with the Brookhaven cells demonstrating performance within 0.03 V of the baseline cell.

For the anode, the GDE approach is somewhat more challenging, first because carbon-based support materials cannot be used in the formulation, and second because the porosity of the anode is designed for water flow, not gas flow. However, Proton provided GDL samples to Brookhaven for process trials, and GDE samples were successfully fabricated using unsupported core shell catalysts. While there is still room for optimization of catalyst composition and application method, the initial trials demonstrated near equivalent performance to the Proton baseline (Figure 3). These samples utilized 10-15% catalyst loading vs. Proton's internal baseline. The anode will be a focus area of the Phase 2 project.

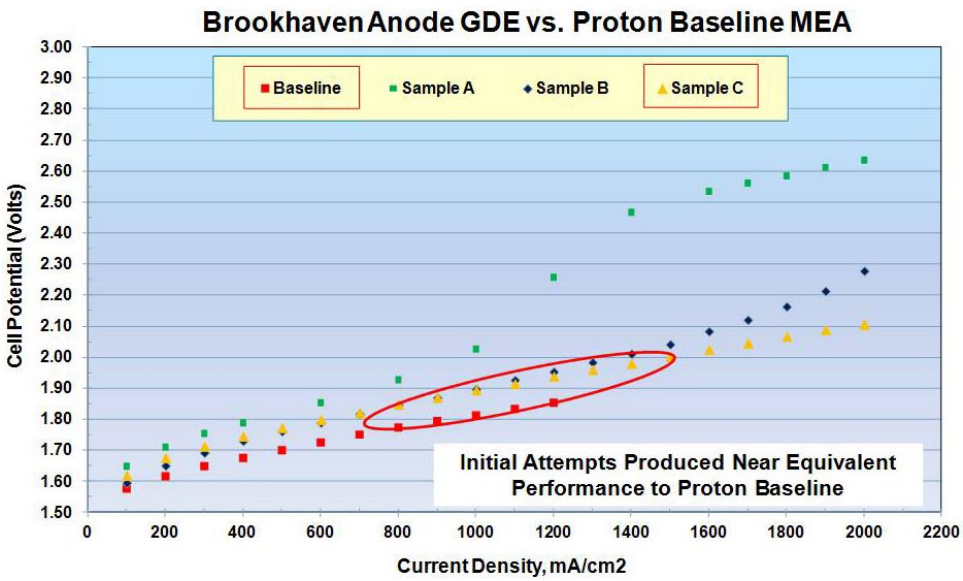

FIGURE 3. Anode Performance Screening

CONCLUSIONS AND FUTURE DIRECTIONS

- In the Phase 1 project, a screening protocol was developed to optimize the knowledge gained while maximizing efficiency and conserving materials. Results translated well from early bench tests to full cell testing.
- Catalyst syntheses were improved both in terms of removing structural defects as well as making the process more manufacturable and reducing environmental impact.
- Cathode samples demonstrated equivalent performance to baseline at 2% loading and anode samples were close to equivalence at approximately 10-15% loading. Cathode samples also passed the 500-hour durability test.
- The Phase 2 project will further develop the anode, leveraging work funded by DOE in non-carbon supports for fuel cells as well as new approaches. Catalyst composition, electrode formulation, and GDL type will be optimized.
- Technology transfer of the cathode formulations and manufacturing process development will continue for the cathode electrode.

FY 2013 PUBLICATIONS/PRESENTATIONS

1. Final Report, Phase 1 Small Business Technology Transfer.

2. "Bridging the Infrastructure Gap: Cost Effective Generation of Hydrogen from Water", Department Seminar, Colorado School of Mines, November 2012.

3. "Development of Megawatt Scale PEM Electrolysis: A Culmination of Cell Design and System Advancements", Spring ECS Meeting, Toronto, Canada, May 2013.

4. "Proton Exchange Membranes for H_2 Generation: A Tutorial on Research Needs and Challenges for PEM Electrolysis vs. Fuel Cells", Spring ECS Meeting, Toronto, Canada, May 2013.

II.B.1 Electrolyzer Development in the Cu-Cl Thermochemical Cycle

M.A. Lewis (Primary Contact), S. Ahmed
Argonne National Laboratory
9700 S. Cass Avenue
Argonne, IL 60439
Phone: (630) 881-5973
Email: lewism@cmt.anl.gov

DOE Manager
Sara Dillich
Phone: (202) 586-7925
Email: sara.dillich@ee.doe.gov

Contributors:
- S. Lvov, D. Hall, R. Schatz, and E. LaRow; Pennsylvania State University (PSU)
- C. Fan, R. Liu; Gas Technology Institute (GTI)
- D. Tatterson; Orion Enterprises, Northbrook, IL

Start Date: October 2010
Projected End Date: September 2013

Overall Objectives

- PSU: Determine effect of increased temperature on cell operation
- PSU: Reduce Pt loading
- GTI: Identify scale up issues
- ALL: Identify methods to reduce costs of H_2 production

Fiscal Year (FY) 2013 Objectives

- PSU: Complete 168-hour test in 5-cm^2 electrolyzer
- PSU: Design, build and test a 5-cm^2 electrolyzer operating at 100°C
- PSU: Reduce Pt loading by 50% in 5-cm^2 electrolyzer
- GTI: Scale up electrolyzer to 300 cm^2
- GTI: Increase number of 300-cm^2 cells from 1 to 5 and operate stack for 100 hours

Technical Barriers

This project addresses the following technical barriers from the Hydrogen Production section of the Fuel Cell Technologies Office Multi-Year Research, Development, and Demonstration Plan:

(S) High-Temperature Robust Materials

(T) Coupling Concentrated Solar Energy and Thermochemical Cycles

(W) Materials and Catalyst Development

(X) Chemical Reactor Development and Capital Costs

FY 2013 Accomplishments

- PSU: Completed a 168-hour test in a 5-cm^2 electrolyzer at the milestone value
- PSU: Reduced Pt loading by at least 50% in the 5-cm^2 electrolyzer
- GTI: Ran a 2-cell full-size stack with 65% conversion from Cu(I) to Cu(II)
- GTI: Ran a 5-cell, full-size stack at the milestone value of 0.2 A/cm^2 at 0.7 V and 60°C; a 100-hour test is ongoing

Technical Targets

The DOE cost target for H_2 production is $2.00/gallon gasoline equivalent (gge) dispensed. However, it is recognized that solar thermochemical cycles are in their early stages of development and the 2015 target is $14.80 and $3.70 for 2020 [1]. Costs for H_2 production using the CuCl cycle were calculated in 2011 using H2A v.2 with estimates of capital and operating costs based on an Aspen process design as $6.0/gge for 2015 and as $4.0-4.4/gge for 2025, depending on the number of solar fields [2].

✧ ✧ ✧ ✧ ✧

INTRODUCTION

The goal of this project is to couple the relatively low-temperature CuCl thermochemical cycle for hydrogen production with a solar power tower as a possible heat source. The power tower is near commercialization and could provide heat near the maximum process temperature of the CuCl cycle. The cycle consists of three major reactions, shown in Table 1. All have been proven in the laboratory.

TABLE 1. Major Reactions and Operating Temperatures in the CuCl Cycle

Reaction	Chemistry	Operating Temperature, °C
Hydrolysis	$CuCl_2 + H_2O \rightarrow Cu_2OCl_2 + 2HCl$	375
Decomposition	$Cu_2OCl_2 \rightarrow 0.5O_2$	450-525
Electrolysis	$CuCl + 2HCl \rightarrow CuCl_2 + H_2$	80-100(verified)-120

We have recently focused on the development of the electrolyzer. One reason was that catastrophic failure of the cell could result from copper deposition on an electrode or

membrane. It was subsequently shown that any electrolytic copper metal that may be formed dissolves immediately in the high concentrations of HCl. Another reason for emphasizing the electrolyzer was that our cost estimates for H_2 production showed that the major cost and energy usage drivers are the electrolyzer and its components. To meet the projected cost of hydrogen at $6.0/gge, both the design and operation of the electrolyzer have to meet certain specifications. The current density, which controls the number of electrolyzer units, should be 0.5 A/cm^2 or higher and the applied cell potential should be 0.7 V (in 2015) and 0.5 V (in 2025). The cost of the noble metal catalysts is high and our plan is to reduce Pt loading (by 2015) and/or substitute other lower cost catalysts (by 2025). Longer term tests are also being conducted to determine the durability of the membrane and other components. Another avenue to reduce costs is possible if Cu(I) conversion to Cu(II) in the full-scale electrolyzer is about 90%, which would allow elimination of a separation step.

APPROACH

Our approach is twofold. One path is to conduct fundamental studies with a 5-cm^2 electrolyzer that include the effects of increased temperature, lower Pt loadings, and longer duration tests. Running the electrolyzer above 80°C is demanding because of the increase in vapor pressure of HCl (above 1 bar) and the higher pressure operation needed to contain the vapors. These experiments should provide an estimate of the magnitude of the expected increase in current density with increasing temperature. Various Pt loadings and application methods are being investigated to reduce catalyst costs. Longer duration tests are being conducted to determine if degradation occurs with time. In all of the tests, the current density was measured as a function of cell potential and the H_2 production efficiency was determined. Scanning electron microscopy (SEM) was used to study the catalytic surfaces. Electrochemical impedance spectroscopy (EIS) was used to identify important cell resistances as a function of time on stream and temperature. A second path is to identify and meet challenges associated with scale up to a full-size or 300-cm^2 electrolyzer. The issues related to scale up are expected to be quite different from those used for water electrolyzers. For example, the solubility of CuCl used in the electrolyzer is very dependent on the HCl concentration and both HCl and $CuCl_2$ are very corrosive materials. Scale up involves fabricating and testing the 300-cm^2 full-size cells and then combining them to form a stack, using sufficient holding force and appropriate seals and contacts so that the mass flow distribution is even and the electrical contact is the same for all of the cells. A 100-hour test is being conducted with a 5-cell stack.

RESULTS AND DISCUSSION

S. Lvov (PI), D. Hall, R. Schatz, and E. LaRow—Pennsylvania State University

Effect of increasing temperature. Details of the chemistry, the electrolyzer system and changes made to accommodate operation at 100°C are described elsewhere [3]. The results of the tests at 40-100°C are shown in Figure 1. At 0.7 V, there was a 15% increase in current density as the temperature was increased from 80°C to 100°C. EIS measurements showed that the increase in current density was due to decreases in internal ohmic and charge transfer resistances.

Long-term tests. The results of the 168-hour test at 80°C are shown in Figure 2. The current density decreased from an initial value near 0.5 A/cm^2 to about 0.3 A/cm^2 (the milestone value) at the end of the test. The cell was operational for 168 hours while the membrane was contacted by the solution for over 400 hours. The hydrogen production efficiency was measured and found to be ≥95% of the theoretical value predicted by Faraday's Law. EIS was used to characterize the electrolyzer processes. Analysis of the EIS data is ongoing but preliminary results indicated that the internal ohmic resistance increased with time, which suggests membrane degradation.

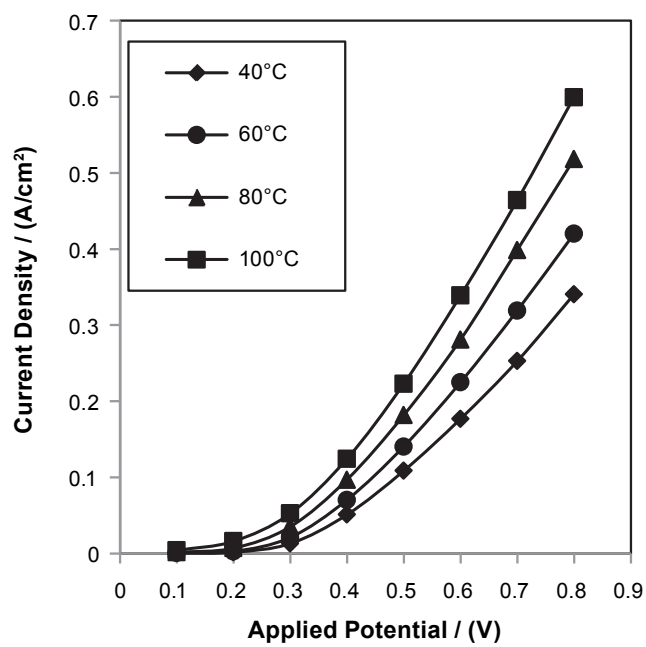

Conditions: Single Pressed Nafion® 117, Pt loading 0.8 mg/cm^2 on each electrode, 2 M CuCl in 7 M HCl, anolyte, 7 M HCl catholyte, 230 mL/min flow rate, 1-1.3 bar and 40-100°C

FIGURE 1. Polarization Curves for Four Temperatures

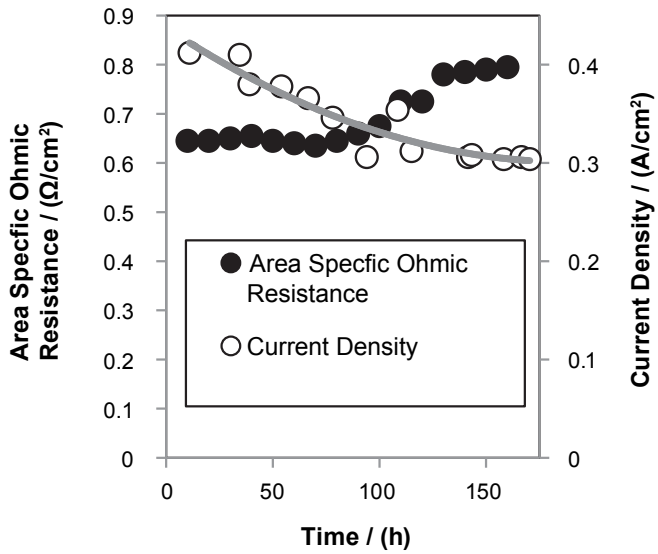

Conditions: Single pressed Nafion® 117, 20% Pt loading 0.8 mg/cm^2 on each electrode, 1-2 M CuCl in 6-7 M HCl anolyte, 7 M HCl catholyte, 230 mL/min flow rate, 80°C and 1 bar

FIGURE 2. Current Density (right) and Internal Ohmic Resistance (left) during the 168-Hour Test vs. Cell Potential

Pt loading studies. SEM images of painted electrode surfaces showed a dense catalyst deposit suggesting inactive Pt within the catalyst layer. An airbrush method was tested as a means to apply a thinner deposit. SEM images in Figure 3 show the very different surfaces. When the airbrushed Pt loadings were reduced to 0.1 and 0.4 mg/cm^2 on the anode and cathode, respectively, the current density was 0.55 A/cm^2 at 0.7 V. Past tests used 0.8 mg/cm^2 on both electrodes. GTI's tests with a 6.45-cm^2 electrolyzer showed that the current density was nearly independent of the Pt loading on the anode when the Pt loading on the cathode was 0.5 mg/cm^2. Atomic Energy of Canada Limited uses none on the anode but has not reported Pt loading on the cathode.

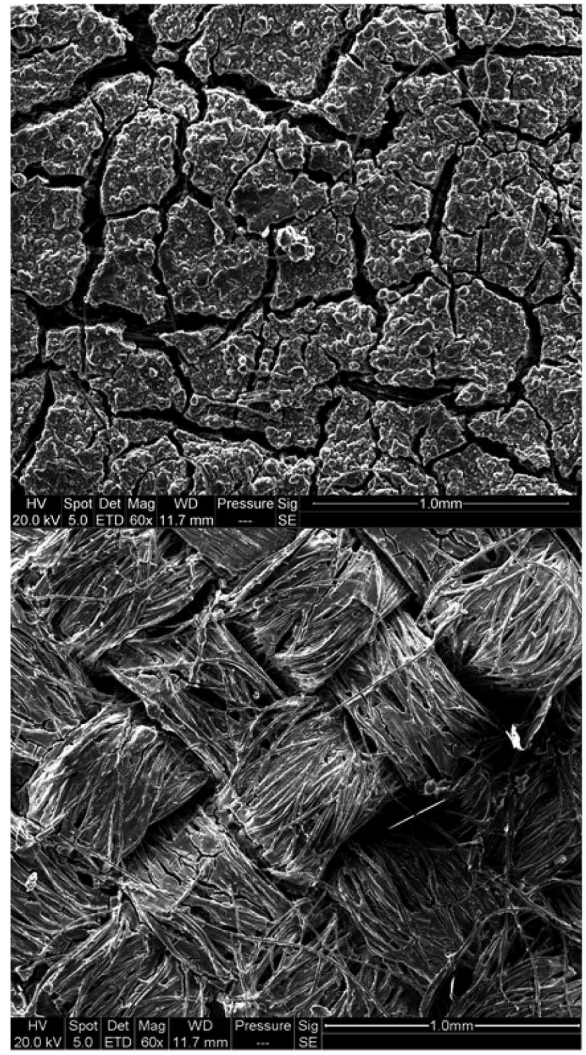

FIGURE 3. Two SEM Images Comparing Catalyst Application Differences between Painted (left) and Airbrushed (right) Electrodes (Pt loadings were 0.8 mg/cm^2 on both)

C. Fan (PI) and R. Liu—Gas Technology Institute

Scale up. Testing of the one full-size 300-cm^2 cell showed a current density of 0.55 A/cm^2 at 0.7 V and 60°C. A stack with two 300-cm^2 cells was then fabricated and tested to ensure that the mass flow distribution was even and that there were no shunt currents. At 0.7 V, the current density was 0.36 A/cm^2 and H_2 production efficiency was 98% of the theoretical value. Conversion of Cu(I) to Cu(II) was 65% when the flow rate was 210 mL/min.

Preliminary tests with the 5-cell 300-cm^2 cell stack showed a large drop off in current within 20 minutes of the start of the test, indicating much of the Cu(I) was consumed. Two major changes in the ancillary equipment were therefore necessary, i.e., a higher capacity pump to provide greater flow rates and a redesigned recycle system with a larger capacity. After these system changes, the 5-cell stack was placed in the testing facility. The current densities at several voltages were measured for each cell and the resulting polarization curves for each of the five cells overlapped each other. Figure 4 shows the results of the second set of tests with the 5-cell stack. The current density at 0.7 V varied between 0.11-0.15 A/cm^2, significantly lower than those for the one cell and the 2-cell stacks. Increases in the current densities, up to 0.19 A/cm^2 , were obtained when the recycle time for the spent anolyte was increased and when the cathodic flow rate was increased from 600 to 800 mL/min. Tests at PSU also confirmed that cathodic and anodic flow rates affected current densities. Possible reasons for the lower current densities for the 2- and 5-cell full-size 300-cm^2 stacks compared to the single 300-cm^2 cell are under investigation. Preliminary data suggest that high back pressure due to the large amount of H_2 generated is limiting hydrogen release and reducing the flow rate of the solutions.

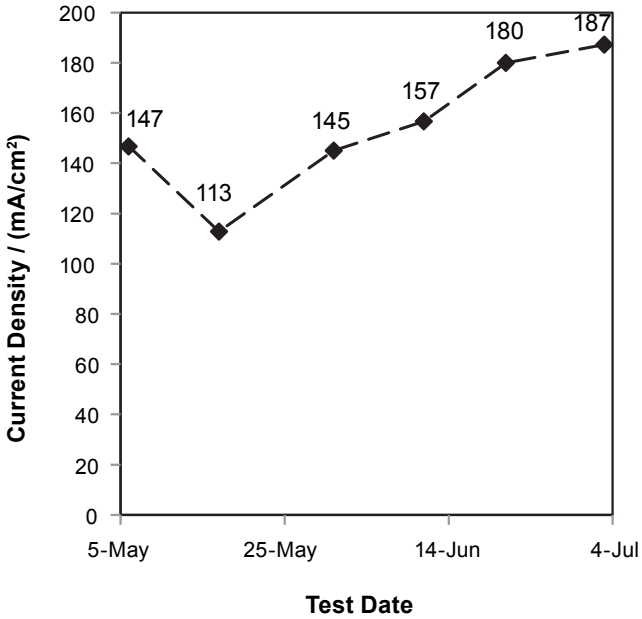

Conditions: Nafion® 112, Pt loading 0.5 mg/cm^2 on each electrode, 1 M CuCl in 7 M HCl anolyte, 7 M HCl catholyte, 600 mL/min flow rate, 60°C, 1 bar

FIGURE 4. Five-Cell Stack Performance at 0.7 V

Collaborations

Atomic Energy of Canada Limited and five Canadian universities are also working on the development of the CuCl cycle. Collaboration between the U.S. and Canada consists of an informal information exchange via biannual meetings wherein the latest results from each group are reported. For example, Atomic Energy Canada Limited has a new membrane and cell design that suppressed all copper crossover during a test of 1,600 hours at 45°C. The five Canadian universities led by the University of Ontario Institute of Technology are investigating materials of construction, hydrolysis reactor designs, new membrane materials, sensible heat recovery from the molten salt and the overall design of an integrated demonstration planned for the future. Summaries of the work in Canada are reported annually [4].

CONCLUSIONS

- PSU: Pt loadings were successfully reduced to less than half of the original value (0.8 mg/cm^2 on both electrodes to 0.4 mg/cm^2 on the cathode and 0.1 mg/cm^2 on the anode).
- PSU: Current density increased with increasing temperature.
- PSU: Degradation occurred due to an increase in internal ohmic resistance, possibly due to membrane degradation, in a 168-hour test.
- GTI: Tests with the 2- and 5-cell full-size 300-cm^2 stacks showed that mass flow was evenly distributed, shunt currents were absent and seals were durable between the cells. Further improvement is needed in the design to obtain higher current densities.
- GTI and PSU: Current density depended on cathodic and anodic flow rates.

FUTURE DIRECTIONS

- PSU: Identify degradation mechanisms observed in longer duration tests and determine methods to minimize these mechanisms.
- PSU: Design a laboratory-scale electrolyzer for operation above 100°C and pressures up to 24 bar (80°C tests are run at 1 bar, 100°C tests at 1.2-1.3 bar).
- GTI: Optimize system integration by studying flow rates, manifold hole size, pump head pressure, and possibly other variables to increase current densities in the 5-cell stack.
- All: Continue studies of methods to reduce Pt loading, study electrocatalytic properties of new catalysts, investigate other membranes that limit Cu crossover and have high durability.
- All: Continue collaboration with staff at Atomic Energy of Canada Limited and Canadian universities.

FY 2013 PUBLICATION/PRESENTATIONS

1. R. Schatz, S. Kim, S. Khurana, M.V. Fedkin, and S.N. Lvov, High Efficiency CuCl electrolyzer for Cu-Cl Thermochemical Cycle, ECS Transactions, 45(19), 2013, 153-164.

2. S. Khurana, D. Hall, R. Schatz, and S. N. Lvov, Diagnosis and Modeling of the CuCl Electrolyzer Using Electrochemical Impedance Spectroscopy, ECS Transactions, 2013 (in press).

3. D. M. Hall, R. S. Schatz, E. G. LaRow, S. N. Lvov, CuCl/HCl Electrolyzer Kinetics for Hydrogen Production via Cu-Cl Thermochemical Cycle, ECS Transactions, 2013 (submitted).

4. S. Ahmed and D. Tatterson, Electrolyzer Developments in the Cu-Cl Cycle, Ontario Research Foundation Workshop, Chalk River, Ontario, Canada, April 22, 2013 (oral presentation).

5. S.N. Lvov, R. Schatz, S. Kim, S. Khurana, A. Morse, M. Chung, and M. Fedkin, Hydrogen Production via Electrolysis in Cu-Cl Thermochemical Cycle, Pacific Rim Meeting on Electrochemical and Solid State Science, Honolulu, Hawaii, October 7–12, 2012 (an oral presentation).

REFERENCES

1. S. Dillich, Hydrogen Production and Delivery, presented at the 2013 Annual Merit Review and Peer Evaluation Meeting, Crystal City, VA, May 13, 2013.

2. M. Kromer et al., Support for Cost Analyses on Solar-Driven High Temperature Thermochemical Water-Splitting Cycles, DE-DT0000951 (Department of Energy report by TIAX LLC), 2011.

3. S.N. Lvov, R. Schatz, S. Kim, S. Khurana, A. Morse, M. Chung, and M. Fedkin, Hydrogen Production via Electrolysis in Cu-Cl Thermochemical Cycle, Pacific Rim Meeting on Electrochemical and Solid State Science, Honolulu, Hawaii, October 7–12, 2012 (an oral presentation).

4. G.F. Naterer et al., International Program on Hydrogen Production with the Copper-Chlorine Cycle, 2013, to be submitted to the International Journal of Hydrogen Energy.

II.B.2 Solar High-Temperature Water-Splitting Cycle with Quantum Boost

Robin Taylor (Primary Contact), Roger Davenport, David Genders[1], Peter Symons[1], Lloyd Brown[2], Jan Talbot[3], Richard Herz[3]
Science Applications International, Corp. (SAIC)
10260 Campus Point Drive
San Diego, CA 92121
Phone: (858) 826-9124
Email: taylorro@saic.com

DOE Managers
Sara Dillich
Phone: (202) 586-7925
Email: Sara.Dillich@ee.doe.gov
Katie Randolph
Phone: (720) 356-1759
Email: Katie.Randolph@go.doe.gov

Contract Number: DE-FG36-07GO17002

Subcontractors:
1 Electrosynthesis Co., Inc. (ESC), Lancaster, NY
2 Thermochemical Engineering Solutions (TCHEME), San Diego, CA
3 University of California, San Diego (UCSD), San Diego, CA

Project Start Date: September 1, 2007
Project End Date: January 31, 2014

Overall Objectives

- Prove the viability of a sulfur family thermochemical water-splitting cycle for large-scale hydrogen production using solar energy.
- Evaluate sulfur ammonia (SA) water-splitting cycles that employ photocatalytic (quantum boost) or electrolytic hydrogen evolution steps and perform lab testing to demonstrate feasibility of the chemistry.
- Perform economic analyses of SA cycles as they evolve.
- Develop a cycle that has high potential for meeting the DOE threshold cost goal of \$2-4/kg H_2 and solar-to-hydrogen (STH) energy conversion ultimate target of 26%.

Fiscal Year (FY) 2013 Objectives

- Improve electrolytic H_2 production by developing better anode electrocatalysts to facilitate operation at lower temperatures (80°C) while maintaining low voltage (<0.8 V) and/or identifying alternate membranes that can operate at higher temperature (up to 130°C) to take advantage of the lower thermochemical potential at higher temperature, but without an unacceptably high flux of sulfite across the membrane (<0.1 mmole/m^2/s).
- Use the Aspen Plus® modeling tool to optimize systems for input to the H2A economic model. Evaluate using heat from excess electricity production for SO_3 decomposition. Evaluate power recovery and electrical power generation alternatives.
- Perform technical and economic analyses of the SA cycle systems with and without a high-temperature storage system that would allow for 24/7 operation.

Technical Barriers

This project addresses the following technical barriers from the Hydrogen Production section (3.1.5) of the Fuel Cell Technologies Office Multi-Year Research, Development, and Demonstration Plan:

(S) High-Temperature Robust Materials

(T) Coupling Concentrated Solar Energy and Thermochemical Cycles

(U) Concentrated Solar Energy Capital Cost

(V) Heliostat Development and Cost

(Y) Diurnal Operation

(Z) Control and Safety

(AB) Chemical and Thermal Storage

(AC) Solar Receiver and Reactor Interface Development

Technical Targets

Table 1 presents the progress made, to date, in achieving the DOE technical targets as outlined in the Multi-Year Research, Development, and Demonstration Plan – Planned Program Activities for 2005-2015 (updated July 2013), Table 3.1.7/7.A: Solar-Driven High-Temperature Thermochemical Hydrogen Production.

FY 2013 Accomplishments

- Long-term stability of the complete electrochemical system was demonstrated, including a >500 hour durability run.
- New membranes for the electrolytic cell have been identified with up to 2 orders of magnitude lower sulfite fluxes.

TABLE 1. Progress towards Meeting Technical Targets for Solar-Driven High-Temperature Thermochemical Hydrogen Production

Characteristics	Units	U.S. DOE Targets[a]			Project Status
		2015	2020	Ultimate	
Solar-Driven High-Temperature Thermochemical Cycle Hydrogen Cost	$/kg H_2	14.80	3.70	2.00	10.91[b] (2015) 7.04[b] (2025)
Heliostat Capital Cost (installed cost)	$/m^2	140	75	75	97[c]
Chemical Process Energy Efficiency[d]	%	25	30	>35	20
STH Energy Conversion Ratio[e]	%	10	20	26	9.6

[a] Source: Multi-Year Research, Development, and Demonstration Plan (Updated July 2013) http://www1.eere.energy.gov/hydrogenandfuelcells/mypp/pdfs/production.pdf
[b] Electrolytic system projected costs based on latest H2A analysis.
[c] Based on SAIC glass-reinforced concrete structure with 10 sq.m. area and low production quantity.
[d] Chemical process efficiency is defined as the energy of the hydrogen produced (lower heating value, LHV) divided by the sum of the energy delivered by the solar concentrator system plus any other net energy imports (electricity or heat) required for the process.
[e] STH energy conversion ratio is the overall system efficiency defined as the LHV of the hydrogen produced divided by the sum of the solar energy incident on the solar collector field and any other net energy imports. The estimated solar field efficiency to provide 800°C energy to the storage system is 48% based on the National Renewable Energy Laboratory Solar Advisor Model calculations.

- Separation of NH_3 and SO_3 in the oxygen generation step was demonstrated using a sulfate/pyrosulfate molten salt system.
- Lower melting temperatures were achieved with a combination of sodium salts and potassium salts.
- The molten salt viscosity was measured to be low (<5.5 cP at 450°C), proving that it can be easily pumped.
- Aspen Plus® was used to model significant process improvements, including:
  - A phase-change thermal-storage system with NaCl incorporated, allowing 24/7 continuous plant operation.
  - Rankine power cycles were designed to recover excess heat and efficiently generate electricity.
  - Overall plant pressure and SO_3 decomposer temperature were varied to optimize plant efficiency and power recovery.
- The focus of the solar configuration was determined to be a 50 MW_{th} central receiver system with NaCl molten salt storage to allow 24/7 operation and produce 5,400 kg/day of H_2 per module.
- The H2A version 3 economic model was used to optimize and trade off SA cycle configurations.

✧ ✧ ✧ ✧ ✧

INTRODUCTION

Thermochemical production of hydrogen by splitting water with solar energy is a sustainable and renewable method of producing hydrogen. However, the process must be proven to be efficient and cost-effective if it is to compete with conventional energy sources.

APPROACH

To achieve the project objectives, a variation of the hybrid sulfur thermochemical water splitting cycle (*aka* the "Hybrid Sulfur," or "HyS" cycle) was developed by introducing ammonia as a working reagent (thus "sulfur-ammonia," or "SA," cycle) to allow more efficient solar interface and facile product separation steps. The thermochemical cycle SA process was originally developed by the Florida Solar Energy Center. Several versions of the SA cycle have been evaluated, both experimentally and analytically.

Two approaches were considered for the hydrogen production step of the SA cycle: photocatalytic and electrolytic oxidation of ammonium sulfite to ammonium sulfate in an aqueous solution. Also, two sub-cycles have been considered for the oxygen evolution side of the SA cycle: zinc sulfate/zinc oxide and potassium sulfate/potassium pyrosulfate sub-cycles. The laboratory testing and optimization of all the process steps for each version of the SA cycle were then carried out. Once the optimum configuration of the SA cycle has been identified and the cycle has been validated in closed loop operation in the lab, it will be ready to be scaled up and tested on-sun.

RESULTS

Cycle Evaluation and Analysis

During the past year, work focused on the electrolytic SA cycle, which is summarized in the following equations:

$$SO_{2(g)} + 2NH_{3(g)} + H_2O_{(l)} \rightarrow (NH_4)_2SO_{3(aq)}$$

$$(NH_4)_2SO_{3(aq)} + H_2O_{(l)} \rightarrow (NH_4)_2SO_{4(aq)} + H_2$$

$$(NH_4)_2SO_{4(aq)} + K_2SO_{4(l)} \rightarrow 2NH_{3(g)} + K_2S_2O_{7(l)} + H_2O_{(g)}$$

$$K_2S_2O_{7(l)} \rightarrow SO_{3(g)} + K_2SO_{4(l)}$$

$$SO_{3(g)} \rightarrow SO_{2(g)} + ½O_{2(g)}$$

The electrolytic oxidation of the ammonium sulfite solution occurs more efficiently at higher temperatures, requiring the development of a system capable of running at higher pressures. Reactions (3) and (4) form a sub-cycle by which potassium sulfate is reacted with ammonium sulfate in the low-temperature reactor, to form potassium pyrosulfate. That substance is then fed to the medium-temperature reactor, where it is decomposed to SO_3 and K_2SO_4 again, closing the sub-cycle. The potassium sulfate and pyrosulfate form a miscible liquid melt that facilitates the separations and the movement of the chemicals in reactions (3) and (4). The oxygen production step (5) occurs at high temperature over a catalyst. Separation of the oxygen from SO_2 occurs when they are mixed with water in reaction (1). The net cycle reaction represented by reactions 1-5 is the decomposition of water to form hydrogen and oxygen. All of the reaction steps described above have been demonstrated in the laboratory and shown to occur without undesirable side reactions. However, we are working to ensure that there are none in the electrolytic step and the SO_3 decomposition. Figure 1 shows a schematic of the electrolytic SA cycle.

1 - chemical absorption	110-160°C
2 - electrolytic	80-150°C
3 – adiabatic mixing	400-450°C
4 – stored thermal	790°C
5 – electric heat	850-1200°C

Electro-Oxidation of Aqueous Ammonium Sulfite Solutions

A 500-hour durability test was successfully completed using an electrochemical cell comprising a Pt/Co catalyzed anode on a carbon felt substrate and a Pt/C membrane electrode assembly cathode on a FuMaTech FX-7050 cation exchange membrane. The test was run at 100 mA/cm^2 for a total of 550 hours electrolysis time at a temperature of 100°C, which required the use of a pressurized cell reactor**.** The durability testing was done as four consecutive batch electrolyses, with each experiment being run to approximately 90% conversion of sulfite to sulfate. The coulombic efficiency for hydrogen production was 94%, and the cell voltage increased reproducibly and consistently over each batch by an amount predicted from thermodynamic calculations based on the conversion (1.09–1.17 V). Figure 2 shows excellent reproducibility for the change in concentration of sulfite for the four consecutive batches as a function of charge passed. Note that as the electrolysis proceeds, there is also a concentrating effect in the anolyte as water transfer accompanies the transport of cations across the cation exchange membrane. We measured the water transfer rate to

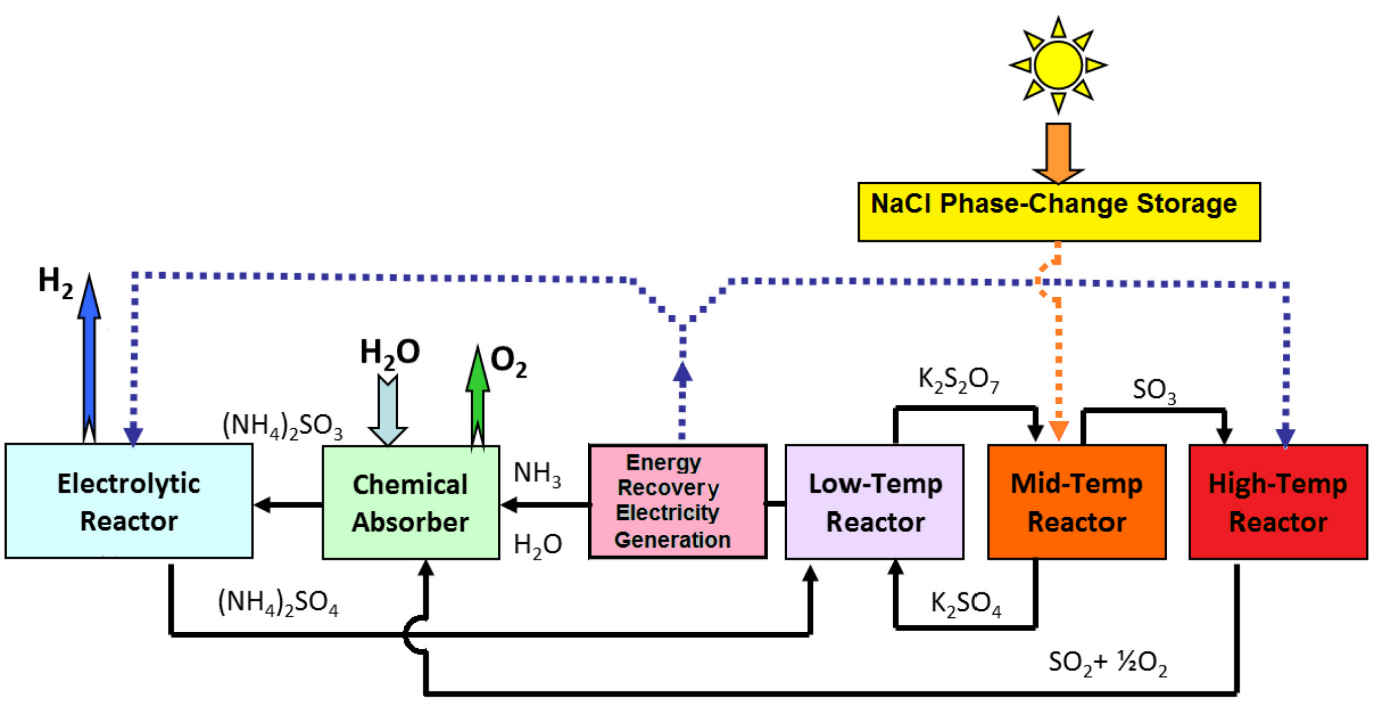

FIGURE 1. Schematic of the Electrolytic SA Cycle

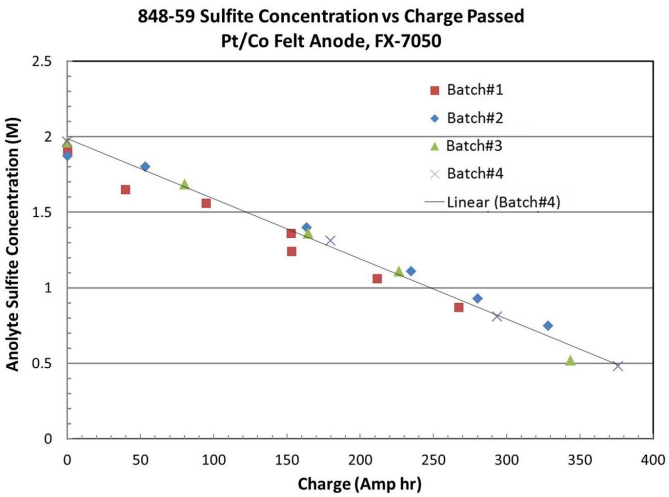

FIGURE 2. Electrochemical Oxidation of Sulfite—Plot of Sulfite Concentration vs. Charge for Four Separate Batches Totaling 550 Hours

be 3.1 moles/mole of charge passed, which is consistent with observations in other electrochemical systems.

The purpose of the durability test was to demonstrate the stability of the electrocatalysts and the membrane. This can be assessed by looking for changes in coulombic efficiency and cell voltage as a function of electrolysis time. The coulombic efficiencies were consistent over the entire run. Given the small changes in cell voltage as a function of conversion, the cell voltage needs to be compared for the same anolyte conversion for each batch. This was done towards the end of each batch and showed that the cell voltage was 1.139 V +/- 6 mV, or 0.5% variation between batches, again showing excellent stability over the 550-hour test.

Previous attempts to run durability tests at elevated temperature (100-130°C) were abandoned due to high sulfite transfer and subsequent reaction at the cathode. Using the FX-7050 membrane, the sulfite flux averaged 1.7×10^{-4} mole/m^2-s over the entire test. Since running the long-term test, we have evaluated a developmental membrane from DuPont that, in short-term testing, has shown up to two orders of magnitude reduction in sulfite flux. Initial testing in the electrolysis rig at 85°C showed this membrane gave up to 25% lower cell voltage than the cell with the FX-7050 membrane used in the long-term testing. However, attempts to use the membrane at 130°C showed a slow increase in the cell voltage, possibly due to dehydration of the membrane. Further work is required to characterize this phenomenon and understand the reasons for the apparent increase in resistance. Despite the increase in cell voltage, the coulombic efficiency for hydrogen production was very good (>95%), and the measured total flux of sulfur species was 8×10^{-5} mol/m^2-s.

UCSD synthesized cobalt ferrite and platinum cobalt nanoparticles and then used electrophoretic deposition (EPD) with two new suspension chemistries that produced thinner and more distributed layers of the catalysts. Cobalt ferrite nanoparticles were synthesized using a co-precipitation method [1]. The samples were analyzed using a scanning electron microscope (SEM), which showed particles from 4-20 nm, and an energy-dispersive X-ray spectroscope to verify composition. Pt_3Co was synthesized using a solvothermal process [2] in which nanoparticles formed in a sealed autoclave; the particle size of 20 ± 5 nm was measured using an SEM image. Nanoparticles of 30 wt% platinum cobalt on carbon were also purchased from Sigma Aldrich. SEM images showed that the Pt_3Co-loaded carbon particle size was 50 ± 15 nm.

The first EPD bath contained 2 g/L particles suspended in 90 vol% water and 10 vol% isopropanol with 0.4 g/L hexadecyltrimethlyammonium bromide (CTAB). Figure 3 compares the zeta potential of cobalt ferrite in 90 vol% water and 10 vol% isopropanol solution with and without CTAB as a function of pH as changed with the addition of nitric acid and sodium hydroxide. The zeta potential was only positive at low pH without CTAB, but remained positive with addition of CTAB over a wide range of pH values. The second bath contained 2 g/L particles suspended in 100% ethanol. The zeta potential of the cobalt ferrite nanoparticles in the CTAB bath chemistry at a pH of 6.2 was 20 ± 2 mV.

EPD of both cobalt ferrite and platinum cobalt nanoparticles was achieved from two different bath chemistries. Cobalt ferrite deposits from a 100% ethanol bath at a pH of 5 gave a 3-5 layer deposit that was evenly distributed across the substrate. This EPD method will be used to deposit particles on graphite paper to further test the electrocatalytic properties of the particles themselves. The platinum cobalt particles on carbon were large and deposited in small agglomerates from both tested baths. Sonication of the bath during EPD resulted in smaller agglomerates that were more evenly distributed in comparison with deposits conducted without sonication.

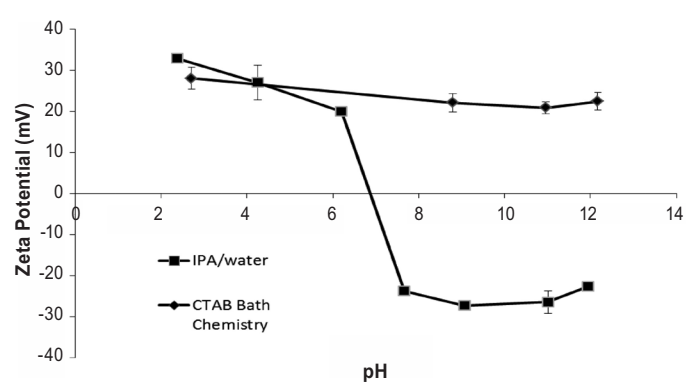

FIGURE 3. Zeta Potential vs. pH for Cobalt Ferrite Particles in a 90 vol% Water, 10 vol% Isopropanol Alcohol Solution and in a CTAB Solution

The deposits were tested for electrocatalytic properties for the oxidation of ammonium sulfite to ammonium sulfate. Linear sweep voltammetry was used to compare the electrocatalytic activity of cobalt ferrite and platinum cobalt nanoparticles deposited on graphite paper using EPD. Cobalt ferrite was deposited at 35 V for 60 s from a 100% ethanol bath. Platinum cobalt was deposited with an applied voltage of 13 V for 15 s from a CTAB bath. The deposit densities varied from 0.3 mg/cm^2 to 0.8 mg/cm^2 depending upon the EPD bath chemistry and material deposited. As shown in Figure 4, both cobalt ferrite and platinum cobalt nanoparticle deposits show enhanced electrochemical activity compared to graphite paper, that is, a higher current density for all voltages scanned. As the particle size and loading of the cobalt ferrite and platinum cobalt nanoparticles are different, it is difficult to directly compare their electrocatalytic activity, which will be done in future work. Electrosynthesis has been conducted using our electrophoretic deposition procedure to test other possible catalysts.

High-Temperature Cycle Step Evaluation

Experimental work was completed demonstrating that the all-liquid/gas high-temperature cycle steps are feasible. Specifically, the decomposition steps to evolve NH_3 and SO_3 occur at sufficiently different temperatures, the molten salts are liquid and are pumpable at the conditions required, and the melting point of the molten salts can be adjusted by addition of sodium salts to the potassium salt mixture. Specifically, experiments were conducted to show the evolution of ammonia and water vapor at ~465°C, followed by evolution of sulfur trioxide at 500°C. It was determined that it should be easy to pump these molten salts with viscosities below 5.5 cP at 450°C.

Aspen Plus® Process Analysis

The chemical process remains basically unchanged but with significant improvement in the thermal integration of the process. The major source of electrical energy used for electrolysis and electrically heated SO_3 decomposition is energy recovered from the ammonia-steam product of the low-temperature reactor. Previously, we had employed a turbine to recover this energy, but the small amount of SO_2 in the stream will result in the formation of solids in the turbine, which is unacceptable. We now use heat exchange to a separate waste heat recovery system. A trade-off analysis was undertaken to determine which working fluid would provide the highest efficiency for this system. Although water could be used, a lower boiling working fluid would give higher efficiency. Ammonia and sulfur dioxide are obvious alternatives since they are already in use in the plant and cross-contamination from heat exchanger leakage would not result in undesirable or reactive byproducts. An ammonia water mixture was also considered. Ultimately, ammonia was chosen as the working fluid as it gave a good thermal match to the source stream with minimal process complications.

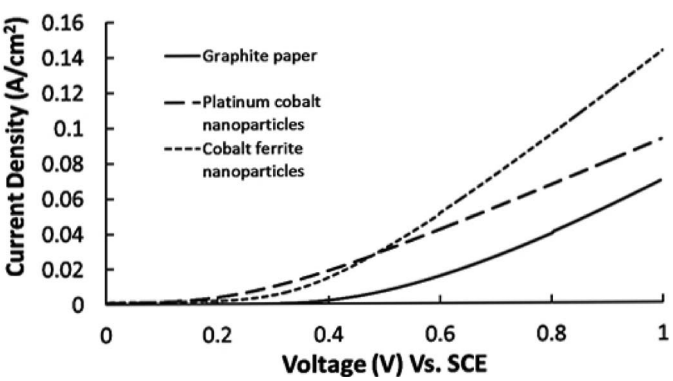

FIGURE 4. Electrocatalytic Activity of EPD Deposits Showing Current Density vs. Voltage

UCSD improved the Aspen Plus® model of the plant. A process heat integration analysis, or pinch analysis, of the plant was performed in order to place heat exchangers at optimal positions. Thermodynamic data from the literature were incorporated into the mid-temperature reactor, which decomposes molten pyrosulfates to sulfates and releases gaseous SO_3. Calculator blocks were utilized to obtain power requirements for the electrolyzer and the overall efficiency of the plant. Design specifications were placed in strategic areas of the model to aid convergence.

Figure 5 shows an overview of the latest Aspen Plus® model of the plant. Not shown is a thermal storage system that allows 24/7 operation of the plant. In the thermal storage system, the latent heat of NaCl melting and solidifying stores and releases solar thermal energy for use by the plant at night. NaCl melts at 801°C; thus, the endothermic mid-temperature reactor is operated at 790°C in order to provide heat transfer from the thermal storage system to the plant. The low-temperature reactor operates adiabatically at 400°C. The endothermic high-temperature reactor is heated electrically to 950°C by resistive heaters powered by power plants that recover heat within the main process plant and generate electricity. Two Rankine-cycle electrical power plants are coupled to the main process plant through heat exchangers. The working fluid in the Rankine-cycle power plants was selected to be ammonia in order to match the temperatures and phase changes in the process streams of the main plant. The power plant at the top of the figure recovers energy from cooling and condensation of the ammonia/water product of the low-temperature reactor. The power plant in the bottom-right of the figure recovers energy from resistive heating in the electrolyzer.

The total heat requirements of the solar reactors along with the total hydrogen product were exported to a calculator block that computes the overall efficiency of the plant. Currently, the overall process efficiency is 20%. It is anticipated that the efficiency can be increased to 28–30%

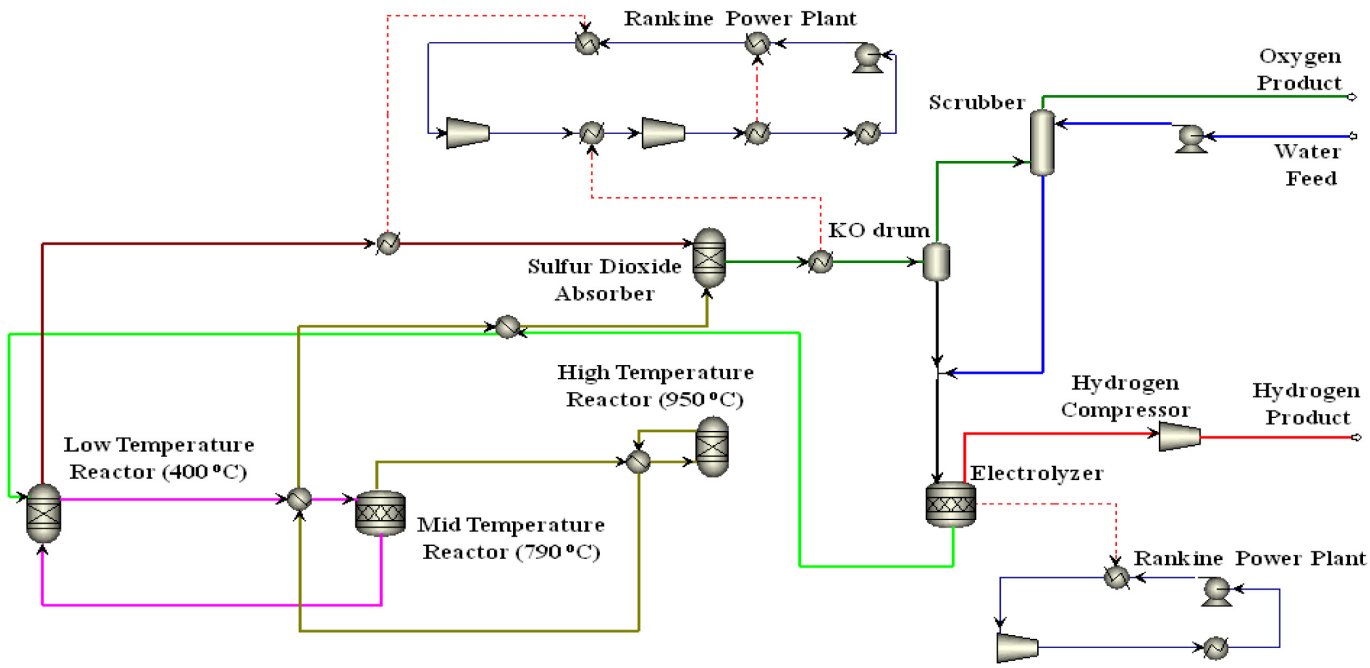

FIGURE 5. Overview of the Aspen Plus® Model

with further refinement of the heat integration and power generation portions of the system and improvement in the electrolytic process performance.

Heat Storage

To allow the chemical plant to operate 24/7, storage of solar energy is needed, and the most efficient type of storage is direct thermal storage. To provide the needs of the medium-temperature reactor, a maximum temperature of about 800°C is needed. SAIC identified a unique phase-change storage approach using molten NaCl that provides large amounts of thermal capacity (481 kJ/kg) at this temperature, as well as providing an efficient means of extracting the heat from the storage to the molten salts [3,4]. The storage consists of a tank holding a volume of NaCl, with headspace above to accommodate the expansion/contraction of the salt as it changes phase. A schematic of the conceptual system is shown in Figure 6. A thin layer of liquid sodium metal (Na) floats on top of the molten NaCl, and the headspace is filled with Na vapor at its vapor pressure, which runs from about 0.5 to 1.5 bar over the temperature range expected. Pipes carrying the molten salt materials to be heated pass through the headspace in contact with the Na vapor, and the sodium acts as a heat pipe to transfer heat from the NaCl to the pipes. Solid NaCl that forms in the Na pool sinks to the bottom (there is about a 30% reduction in volume upon solidification), so the Na remains in contact with liquid NaCl as the entire heat capacity of the storage is used. To re-melt the NaCl, pipes containing liquid sodium are placed at the bottom of the tank, and circulation from the solar receiver heats and re-melts the NaCl.

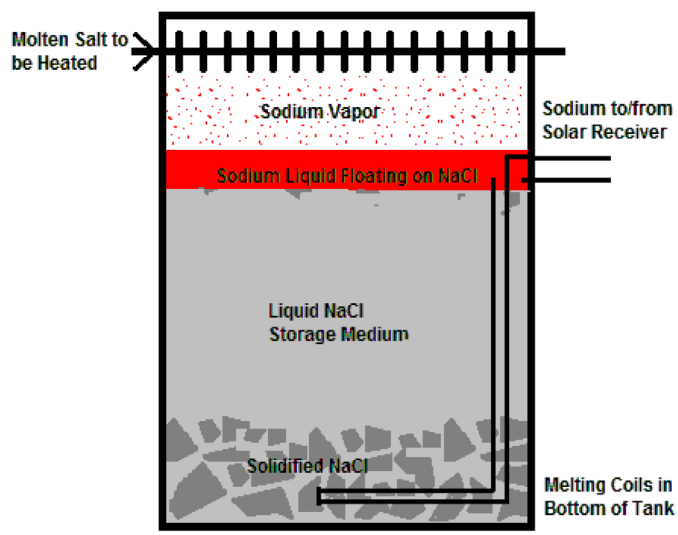

FIGURE 6. Schematic of a Conceptual NaCl Heat Storage System

SAIC summer interns from UCSD have continued to investigate the thermal storage system. Interaction with other researchers has indicated there can be problems of crust formation in the NaCl upon freezing, and ideas to mitigate this have been developed. The students are designing a demonstration testing approach that could be performed on the SAIC solar dish. Configurations with a sodium heat pipe receiver and with a sodium pumped loop have been studied (see Figure 7). Also, analogue testing with low-temperature phase-change materials is being developed to study freeze/thaw behavior and other features of the system at a bench scale.

Solar Field Optimization

A modular solar plant configured to deliver thermal power to the modular 50-MW_{th} chemical plant has been designed (see Figure 8). The central receiver solar plant includes a north-side heliostat field with 227,600 square meters of heliostats. The heliostats focus onto a 150-meter-tall tower with a cavity receiver about 12 m x 14 m in size. Energy absorbed at the receiver is delivered to the NaCl phase-change storage system at about 800°C. Performance estimates indicate a 150-MW_{th} peak absorbed power for the system, 1,196 MWh peak daily energy collection (equivalent to 50 MW_{th} continuously over 24 hours), and 32.3 MW_{th} average power over the year (65% overall capacity factor). The overall average efficiency of the solar plant, from incident solar energy to delivered thermal energy, was estimated at 48% using the National Renewable Energy Laboratory Solar Advisor Model.

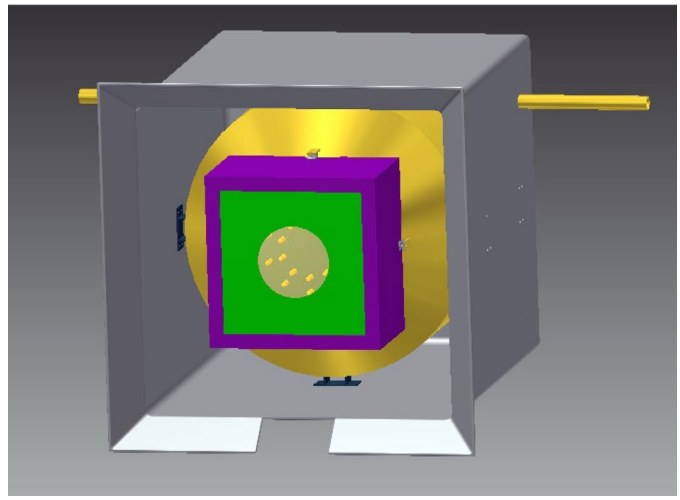

FIGURE 7. Schematic of a Heat Pipe Receiver with On-Dish NaCl Storage for Dish Demonstration

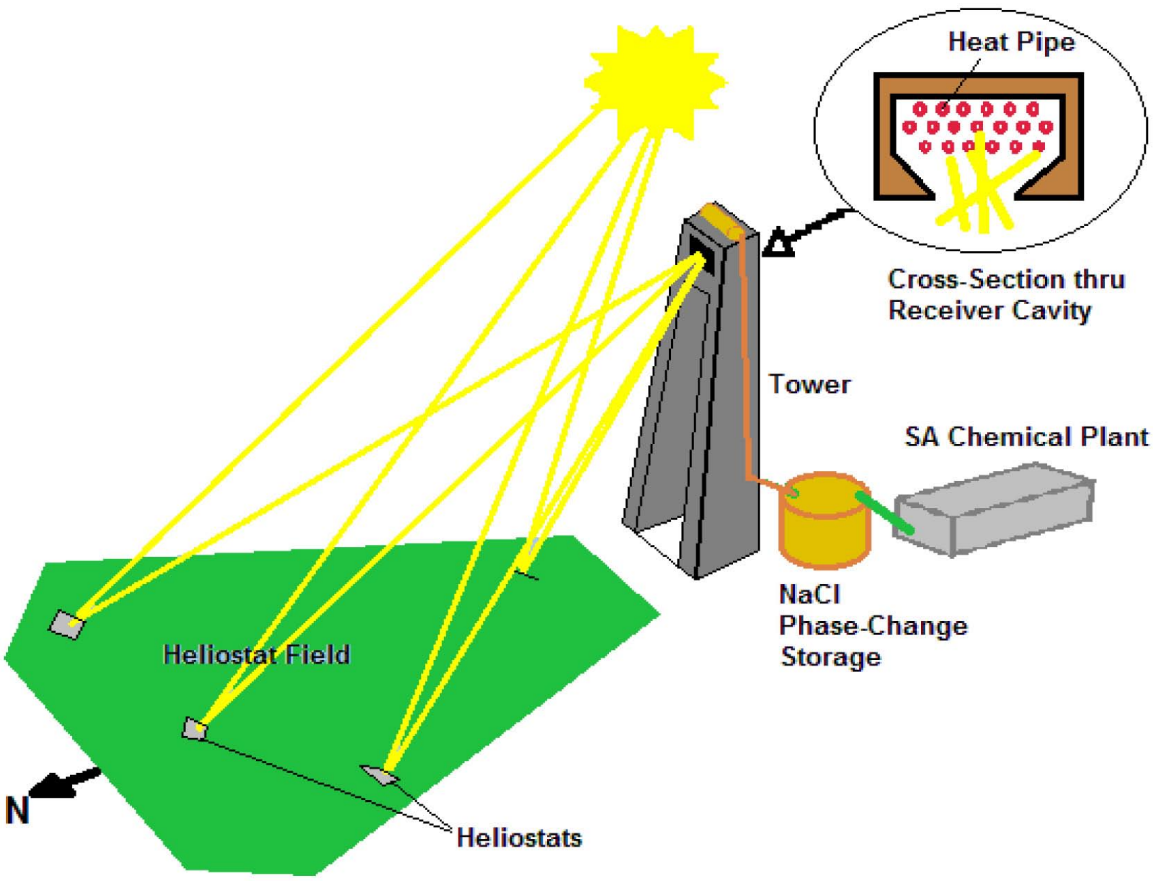

FIGURE 8. Schematic of 50-MW_{th} SA Hydrogen Production System Configuration

Economic Analysis

The H2A economic analysis was converted to version 3 of H2A, and the plant costs were updated with the most up-to-date estimates of plant and solar equipment costs, based on the 50-MW_{th} unit size. The results were a $53 million solar module cost (including NaCl storage) and a $17 million process plant cost. The 50-MW_{th} plant produces about 5,400 kg of hydrogen per day; thus, 19 plants would be needed to meet the DOE production level of 100,000 kg/day. The itemized 2015 and total 2025 production cost of hydrogen from this plant is shown in the following table:

Cost Component	Hydrogen Cost ($/kg)	Fraction of Total Cost
Capital Cost	8.96	82%
Fixed O&M	1.90	17%
Other	0.05	1%
Total 2015	10.91	
Total 2025	7.04	

O&M – operations and maintenance

The estimated hydrogen production cost for 2025 decreases to $7.04/kg based on reductions in heliostat costs and improvements in the efficiency of the chemical and electrochemical portions of the system.

CONCLUSIONS AND FUTURE DIRECTIONS

In summary:

- The SA cycle is unique in that it is an all-fluid cycle with no high-temperature solids handling. It is a relatively low-temperature plant. The solar receiver operates at 800°C when the SO_3 decomposition is achieved through electrical heating with excess electricity production of the system. All the electricity needed for the process is generated internally, and the cycle can operate 24/7 with low-cost storage.
- The long-term stability of the electrochemical system was demonstrated with a 500+ hour extended run; however, not at the optimum operating conditions. A lower temperature was used since sulfite fluxes were found to be too high at 130°C. Recently, alternate membranes were identified with up to 2 orders of magnitude lower sulfite fluxes even at higher temperatures. Durability of these membranes still needs to be evaluated.
- Experiments for the oxygen evolution sub-cycle using potassium sulfate confirmed that ammonia and sulfur trioxide can be evolved separately with a 25–50°C temperature difference, thus avoiding difficult gas separation processes. The melting points, densities, and viscosities of the $K_2SO_4/K_2S_2O_7$ molten salts were measured to prove that they have low viscosities and can be easily pumped. It was confirmed that the decomposition of SO_3 is proven technology, thus laboratory demonstration was not necessary. The entire process consists of elementary chemical engineering unit operations, all in widespread industrial use for over 100 years.
- The Aspen Plus® SA process modeling showed that a phase-change thermal-storage system with NaCl incorporated would allow 24/7 continuous plant operation. Rankine power cycles were modeled to recover excess heat and efficiently generate electricity. Overall plant pressure and SO_3 decomposer temperature were varied to optimize plant efficiency and power recovery.
- The solar configuration was focused on a 50-MW_{th} central receiver system with NaCl molten salt storage to allow 24/7 operation and produce 5,400 kg/day H_2 per module, thus requiring 19 modules to produce 100,000 kg/day H_2.
- The H2A economic analysis was converted to version 3 of H2A, and the plant costs were updated with the most up-to-date estimates of plant and solar equipment costs, based on the 50-MW_{th} module size.

Activities planned for the upcoming year include:

- Continue optimization of the electrolytic process through catalyst development and alternate membrane screening. With catalyst development, the objectives are to lower the anode over-potential at high current densities, increase effective catalyst surface area using nanoparticles, and increase the cathode hydrogen selectivity in the presence of sulfite. Achieve high-temperature operation with low sulfite flux through alternate membrane screening.
- Continue refinement of the Aspen Plus® model to maximize hydrogen production efficiency, perform trade-off studies of power recovery options, and provide input to the H2A economic model.
- Continue to evaluate NaCl phase-change storage system configuration, materials, and components to achieve 24/7 operation.
- Continue to update the H2A analysis to improve the quality of cost estimates through initial design of key process equipment.

FY 2013 PUBLICATIONS/PRESENTATIONS

1. Taylor, R., Genders, D., Brown, L., Talbot, J., Herz, R., Davenport, R., Presentation at the STCH Hydrogen Production Technology Team Review Meeting, La Jolla, California, July 10, 2012. (PowerPoint presentation).

2. Taylor, R., Genders, D., Brown, L., Talbot, J., Herz, R., Davenport, R., Presentation at the DOE Sulfur Ammonia Cycle Phase 1 Go/No-Go Meeting Teleconference, August 27, 2012. (PowerPoint presentation).

3. Tanakit, R., Luc, W., Solar Hydrogen Project, Presentation at the SAIC/UCSD Jacobs School of Engineering Intern Summit, San Diego, California, September 14, 2012. (PowerPoint presentation).

4. Tanakit, R., Luc, W., Solar Hydrogen Project, Poster presentation at the UCSD Jacobs School of Engineering Corporate Affiliates Program, La Jolla, California, September 27, 2012.

5. J. Littlefield, "Solar Thermochemical Hydrogen Production Plant Design," M.S. thesis, (2012). Thesis defense on Nov. 19, 2012.

6. Jesse Littlefield, Mimi Wang, Lloyd C. Brown, Richard K. Herz, and Jan B. Talbot, "Process Modeling and Thermochemical Experimental Analysis of a Solar Sulfur Ammonia Hydrogen Production Cycle," World Hydrogen Energy Conference 2012, *Energy Procedia* 29 (2012) 616 – 623.

7. Wesley W. Luc, Richard K. Herz, and Jan B. Talbot, "Design of a Solar Thermochemical Hydrogen Production Plant," Poster presented at the UCSD Jacobs School of Engineering Research Expo, April 18, 2013.

8. Brown, L., Symons, P., Taylor, R., Presentation at the 2013 U.S. DOE Hydrogen and Fuel Cell Program and Vehicle Technologies Program Annual Merit Review and Peer Evaluation Meeting, Washington, D.C., May 16, 2013. (PowerPoint presentation).

9. Luc, W., "A Continuous Solar Thermochemical Hydrogen Production Plant Design," M.S. thesis, University of California, San Diego, 2013.

10. Taylor, R., Davenport, R., Genders, D., Symons, P., Herz, R., Talbot, J., Brown, L., Luc, W., "Status of the Solar Sulfur Ammonia Thermochemical Hydrogen Production System for Splitting Water," Technical Paper to be presented at the SolarPACES 2013 Conference, Las Vegas, Nevada, September 17–20, 2013.

11. Ryan Tanakit, Wesley Luc, J. Talbot, "Electrophoretic Deposition of Cobalt Ferrite and Platinum Cobalt Nanoparticles as Electrocatalysts," Abstract 2306, for presentation at the 224th ECS Meeting in San Francisco, California (October 27 – November 1, 2013).

REFERENCES

1. Z. Zi, Y. Sun, X. Zhu, Z. Yang, J. Dai, and W. Song, *Journal of Magnetism and Magnetic Materials,* **321,** 1251-1255 (2009).

2. Wang, W.; Wang, G.; van der Vliet, D.; Chang, K.; Markovic, N.; Stamenkovic, V., Monodisperse Pt_3Co nanoparticles as electrocatalyst: the effects of particle size and pretreatment on electrocatalytic reduction of oxygen. *Physical Chemistry Chemical Physics*. **2010,** *12,6877-7296*.

3. Adinberg, R.; Yogev, A.; Kaftori, D., High Temperature Thermal Energy Storage an Experimental Study, J. Phys. IV France 9, 1999.

4. White, M.; Qiu, S.; Galbraith, R., Phase Change Salt Thermal Energy Storage for Dish Stirling Solar Power Systems. ASME 2013 7th International Conference on Energy Sustinability. 2013, Paper No. 18292.

II.B.3 Solar-Thermal Redox-Based Water Splitting Cycle

Alan W. Weimer (Primary Contact), Darwin Arifin, Janna Martinek, Christopher Muhich, Kayla Weston, Kimberly Zimmer, and Charles Musgrave
University of Colorado
Campus Box 596
Boulder, CO 80309-0596
Phone: (303) 492-3759
Email: alan.weimer@colorado.edu

DOE Manager
Sara Dillich
Phone: (202) 586-7925
Email: Sara.Dillich@hq.doe.gov

Contract Number: DE-FC36-05GO15044

Project Start Date: March 31, 2005
Project End Date: Project continuation and direction determined annually by DOE

Overall Objective

Develop a two-step, non-volatile metal-oxide solar-thermal water-splitting cycle to produce hydrogen.

Fiscal Year (FY) 2013 Objectives

- Demonstrate isothermal redox water-splitting in a stagnation flow reactor at a temperature of 1,350°C yielding a H_2 production per gram of total mass of active material >100 µmoles/g active material.
- Develop an understanding of temperature swing vs. isothermal redox and the relative efficiency for carrying out each.
- Demonstrate the so-called "hercynite cycle" on-sun.

Technical Barriers

This project addresses the following technical barriers from the Hydrogen Production section of the Fuel Cell Office Multi-Year Research, Development, and Demonstration Plan:

(S) High-Temperature Robust Materials

(U) Concentrated Solar Energy Capital Cost

(T) Coupling Concentrated Solar Energy and Thermochemical Cycles

Technical Targets

The technical targets for solar-driven thermochemical conversion are summarized in Table 1.

TABLE 1. Technical Targets for Solar-Driven High-Temperature Thermochemical Hydrogen Production

Characteristics	Units	2015 Target	2020 Target
Plant Gate H_2 Cost	\$/gge H_2	14.80	3.70
Installed Heliostat Capital Cost	\$/m^2	140	75
Solar-to-H_2 Energy Conversion Ratio (LHV)	%	10	20

gge – gasoline gallon equivalent; LHV – lower heating value

FY 2013 Accomplishments

- >200 µmoles/g active material was demonstrated.
- Isothermal redox was found to be more efficient than temperature-swing redox under the conditions evaluated.
- Demonstrated stable activity after the first cycle up to ~200 cycles.

✧ ✧ ✧ ✧ ✧

INTRODUCTION

Two-step solar thermochemical processes based on non-volatile metal-oxide cycles have the potential to operate at high thermal efficiencies, are chemically simple, and require less land and water to operate than competing biomass, artificial photosynthesis, and photovoltaic-driven electrolysis. Traditionally, two types of non-volatile metal-oxide redox chemistries are utilized in solar thermochemical H_2O splitting. The first is based on non-stoichiometric oxides of which ceria is a representative example. Such redox materials are thermally reduced without undergoing phase change, as the lattice is able to accommodate the strain induced by oxygen vacancy formation. These materials are thermally quite stable, although the extent of reduction, and hence cycle capacity, is small compared to other reducible oxides.

The second prototypical chemistry utilizes materials of the spinel structure that form solid solutions upon reduction. The most common are ferrites where Fe^{3+} in $M_xFe_{3-x}O_4$ is partially reduced to Fe^{2+}; here M can be any number of transition metals that form spinel type oxides with iron, though Co, Zn, and Ni are the most studied. In these redox cycles, the ferrite spinel is heated until it decomposes into a mixture of metal-oxide solid solutions that are thermodynamically stable at temperatures above which the spinel decomposes. Thus, thermal reduction yields a solid solution of oxides with mixed valence (M^{2+}, Fe^{2+}, and Fe^{3+}). While these materials theoretically exhibit greater redox potential than non-stoichiometric oxides, in practice deactivation induced by irreversible processes such

as sintering or the formation of liquid phases and metal vaporization lead to loss of active oxide.

We have developed a novel chemistry for a two-step, non-volatile metal-oxide H_2O splitting cycle that shuttles iron oxidation states ($Fe^{2+/3+}$) between $CoFe_2O_4$ and $FeAl_2O_4$ spinel compounds. This chemistry is dramatically different than current metal-oxide cycles that exploit oxygen non-stoichiometry in ceria or solid solution behavior in ferrites. The material has maintained redox productivity for over 150 thermochemical cycles. Hydrogen is produced via an isothermal two-step solar-thermal H_2O splitting cycle by removing the traditional temperature swings that are detrimental to efficiency and materials. We show that the traditional temperature swings for redox are unnecessary, and that isothermal water splitting at 1,350°C using the hercynite cycle exhibits H_2 production capacity >3 and >12 times that of the hercynite cycle and ceria, respectively, per mass of active material when reduced at 1,350°C and re-oxidized at 1,000°C. These properties provide for a technical foundation to achieve the DOE technical targets and enable the hydrogen economy.

APPROACH

The hercynite cycle reduction chemistry occurs via a reaction between decomposition products of the $CoFe_2O_4$ and Al_2O_3, forming the corresponding stable aluminates $CoAl_2O_4$ and $FeAl_2O_4$ according to the following oxygen evolution reaction:

$$CoFe_2O_4 + 3Al_2O_3 \rightarrow CoAl_2O_4 + 2FeAl_2O_4 + \tfrac{1}{2} O_2 \qquad (1)$$

During subsequent oxidation by H_2O, the cobalt ferrite spinel and alumina reform and H_2 is produced:

$$CoAl_2O_4 + 2FeAl_2O_4 + H_2O \rightarrow CoFe_2O_4 + 3Al_2O_3 + H_2 \qquad (2)$$

The oxygen evolution reaction (Equation 1) occurs to a greater extent at a temperature 150°C lower than a similarly prepared $CoFe_2O_4$-coated m-ZrO_2 (conventional ferrite) because compound formation is thermodynamically more favorable than solid solution formation. While lowering the reduction temperature is an important consideration for solar thermochemical technologies, perhaps more intriguing is the idea of binding the reduced iron in a compound that is more stable than a solid solution.

RESULTS

We used a hercynite cycle active material (47% active by mass) composed of 19.8 wt% $CoFe_2O_4$ on Al_2O_3 in a stagnation flow reactor to establish the baseline for comparison of temperature-swing water splitting (TSWS) to isothermal water splitting (ITWS). In TSWS, the active materials are reduced (Reaction 1) under inert gas flow (He) at 1,350°C and 101.3 kPa for 60 min, before being cooled to 1,000°C for water re-oxidation (Reaction 2). A gas stream of 50% by volume steam in inert He was used to oxidize the reduced materials for 25 min producing 31.4 ± 2.3 µmol of H_2 per gram of total material. The extent of reduction and water splitting capacity depends on the reduction temperature. Higher temperatures lead to a larger fraction of reduced Fe^{2+} ions. The number of available Fe^{2+} ions dictates the total H_2 generating capacity of the active material with a maximum ratio of one H_2 molecule produced to every two Fe^{2+} cations. Oxidation at 1,000°C was characterized by a slow rate of reaction (a peak H_2 generation rate of 0.06±0.04 µmol/g/s) and is likely surface-reaction limited. Because the oxidation reaction is slow, it is unlikely that most of the Fe^{2+} ions are re-oxidized to Fe^{3+} during the 25 min, which limits the total H_2 production capacity of the 1,350/1,000°C TSWS cycle.

Higher TSWS reduction and oxidation temperatures result in increased H_2 and O_2 production capacity and water splitting rates. Active material cycled between 1,500 and 1,200°C produced 93.7 ± 19.2 µmol of H_2/g with a peak rate of 0.32 µmol H_2/g·s. The higher reduction temperature resulted in more complete reduction of the active material and a larger thermodynamic driving force for H_2O splitting. The higher rates of H_2 generation at 1,500/1,200°C resulted from two factors: 1) the intrinsically higher reaction rates which arise from carrying out a kinetically limited process at a higher temperature, and 2) the larger thermodynamic driving force for oxidation which comes from the larger extent of reduction. The ability to perform water oxidation at temperatures above the onset of reduction suggests that isothermal water splitting is possible and that the current understanding of the thermodynamics of solar-thermal water-splitting is incomplete.

Hercynite cycle materials split water in a two-step isothermal redox cycle as exemplified by the 1,350°C ITWS results shown in Figure 1. H_2 generation under ITWS conditions was achieved at a temperature above the minimum reduction temperature by first flowing an inert gas through the reactor to sweep away O_2 generated during the reduction step and subsequently injecting steam during the oxidation step to produce H_2. For 1,350°C ITWS, the active particles produced 45.1 ± 7.6 µmol O_2/g during 1 hour of reduction and 102 ± 18 µmol H_2/g total (>200 µmol H_2/g active material) during a 25 min exposure to 50 vol% steam in He. During reduction, the initial O_2 plateaus arise from incomplete H_2O removal from the system. Once all steam is swept from the reactor, the O_2 peak occurs as the materials reduce followed by the normal exponential decay as the reaction goes to completion. 1,350°C ITWS produces substantially more O_2 and H_2 than 1,350/1,000°C TSWS and slightly more O_2 and H_2 than 1,500/1,200°C TSWS. The slight deviation of the 2.26:1 H_2 to O_2 ratio from the expected 2:1 ratio, though within the error, likely arises from slight differences in the sensitivities and response times of the mass spectrometer used for measuring H_2, and the O_2 analyzer. The higher gas splitting production capacity of ITWS was

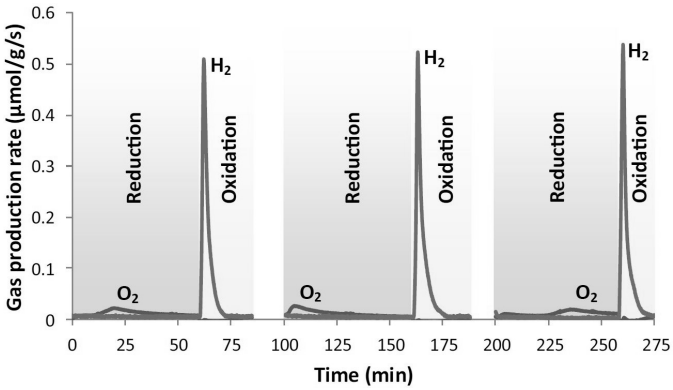

FIGURE 1. Isothermal Water Splitting at 1,350°C

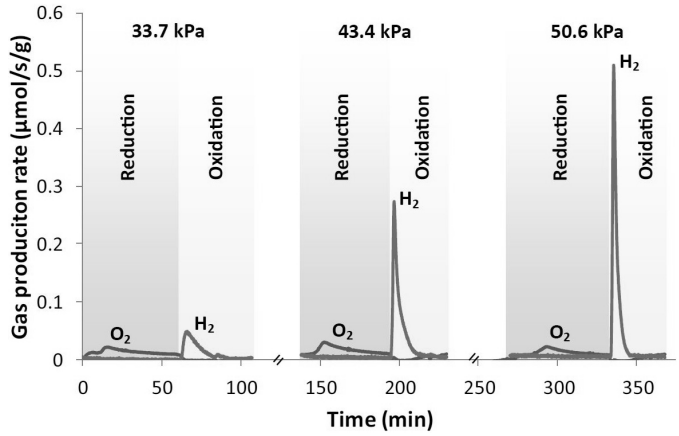

FIGURE 2. The Effect of Steam Pressure on 1,350°C ITWS

accompanied by a higher H_2 production rate of 0.55 ± 0.16 µmol H_2 per gram/s. ITWS's higher rate of H_2 generation and its lack of irreversible heat losses associated with the changes in temperature between oxidation and reduction steps (which is required for TSWS) results in ITWS having a higher theoretical efficiency than TSWS with the conditions examined in this study.

Traditional TSWS thermodynamic theory uses a closed-system model in which an oxidation temperature lower than the reduction temperature raises the chemical potential of the oxidizing gas and reduced metal oxide above that of the product gases and oxidized material in order to drive the oxidation reaction. In contrast, ITWS is an open system that uses swings in the partial pressure of the oxidizing gas to produce the chemical potential differences that drive the oxidation and reduction steps. To form a two-step water-splitting closed-cycle system, a process for the recombination of H_2 and O_2 must be included, such as a fuel cell. In the ITWS process, the partial pressure of generated gaseous reduction and oxidation products remains low by sweeping them from the reactor. The low chemical potential of O_2 during reduction and high H_2O and low H_2 chemical potentials during oxidation drive the respective reactions forward to enable ITWS. Furthermore, sweeping the product gases away from the metal-oxide prevents reverse reactions from occurring.

Not only are redox reactors open systems, but the reactions take place between gases adsorbed on the surface of the solid phase. Thus, the chemical potential and the coverage gas molecules adsorbed on the surface are the relevant quantities to consider for analyzing redox reaction thermodynamics. Because the coverage of adsorbates and, therefore, their chemical potentials are related to partial pressure, the oxidation reaction is driven by increasing the H_2O partial pressure and maintaining a low H_2 partial pressure. Therefore, ITWS relies on a chemical potential difference derived from readily adjustable gas phase partial pressures, rather than having to depend on the problematic large temperature changes of TSWS.

This analysis suggests that by increasing the partial pressure of the oxidizing gas, we can drive the water splitting reaction further toward the products. Indeed, an increased partial pressure of water resulted in higher H_2 production capacities at higher rates (see Figure 2). For 1350°C ITWS, steam concentrations in He of 33, 43 and 50% (overall pressure held at 101.3 kPa) correspond to H_2 production capacities of 40 ± 9, 72 ± 8, and 102 ± 18 µmol H_2/g and peak production rates of 0.06 ± 0.02, 0.15 ± 0.07, and 0.55 ± 0.16 µmol H_2/g·s, respectively. The increased peak production rates correspond to shorter oxidation times, as expected. The higher steam pressure results in a higher water chemical potential on the active material's surface, which provides a higher thermodynamic driving force for oxidation. Additionally, the higher steam concentrations increase the overall rate of reaction by increasing the reactant concentration. This result suggests that decreases in the time required for the oxidation step and possible increases in the ITWS temperature can be achieved by increasing the partial pressure of the oxidizing gas. Furthermore, as shown in Figure 3, the ITWS hercynite cycle produces >6 times more H_2 on a total mass basis and >12 times more H_2 on an active materials basis (47% active) compared to the 1,350/1,000°C ceria redox cycle which is considered the current state-of-the-art material for TSWS redox processing. In addition to ITWS's favorable kinetics and thermodynamics demonstrated in Figure 3, ITWS reduces both irreversible heat losses and thermal shock concerns that limit the efficiency and operations of traditional TSWS.

As can be seen from Table 2, our analysis, although simple, shows that the hercynite cycle-based ITWS is more efficient than TSWS for the conditions investigated. Because radiation losses scale as temperature to the fourth power, the solar heat required to maintain a 1,350°C reduction temperature is much less than a 1,500°C reduction temperature. This gives 1,350°C ITWS a substantial advantage over 1,500/1,000°C TSWS even though they produce similar quantities of H_2 per cycle. For all cases

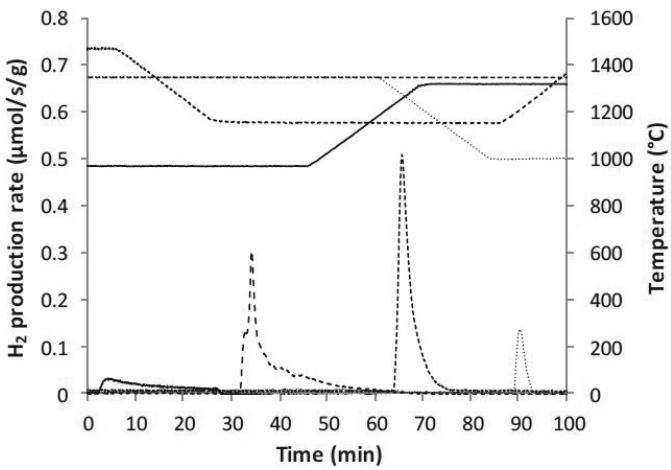

FIGURE 3. A comparison of solar-thermal water splitting. H_2 production curves are shown for hercynite cycle-based 1,350°C/1,000°C TSWS (solid line), 1,500°C/1,200°C TSWS long dashed line, 1,350°C ITWS (short dashed line), and ceria-based 1,350°C/1,000°C TSWS (dotted line).

studied, the heat input required to counteract the radiation losses during the oxidation step was small in comparison to the other losses. The difference between emission losses during reduction and oxidation for ITWS arises from the comparatively longer reduction time, despite identical reduction and oxidation temperatures. While the decrease in temperature diminishes the radiative heat losses incurred during oxidation for the TSWS cycles (and therefore the solar heat required to maintain the oxidation temperature), the much shorter time required for ITWS oxidation keeps the total solar duty of the oxidation step low, even though ITWS's oxidation step has a higher rate of heat loss.

As expected, the sensible heat necessary to heat the oxidized material back to the reduction temperature exceeds all other energy requirements considered in the simplified analysis. The solar input required ranges from 28% of the total energy required to produce a mole of H_2 in the best scenario modeled here (95% recuperation under 1,500/1,200°C TSWS conditions) to 77% in the worst scenario modeled here (90% recuperation under 1,350/1,000°C TSWS conditions). It is important to note that even the worst case scenario provides a generous coefficient of heat recuperation, which is more typical of fluid phase heat transfer than of solid systems. Additionally, it is worth pointing out that 1,350/1,000°C TSWS suffers from two negative effects: in addition to requiring a significant amount of heat to change temperatures between 1,350 and 1,000°C, the total amount of H_2 that 1,350/1,000°C TSWS can produce is small and therefore it requires multiple cycles to produce an equivalent quantity of H_2 as 1,350°C ITWS or 1,500/1,200°C TSWS can achieve in a single cycle. This necessitates more cycles, and associated temperature swings, which results in higher heat losses per mole of H_2 produced.

ITWS's higher solar efficiency and specific H_2 production capacity as compared to TSWS for the conditions examined here, suggests that ITWS has the potential to be a game changing technology in the renewable energy and, particularly, H_2 economy fields.

TABLE 2. A simplified comparison of efficiencies of hercynite cycle-based ITWS and TSWS operating conditions using the experimental results. This comparison is made up of the relative H_2 production per mass of material and solar energy inputs required for each step of the ITWS and TSWS reactions reported in kJ/mol H_2 produced in a cycle.

Reduction/Oxidation temperature (°C)		1,350/1,350°C ITWS	1,350/1,000°C TWSW	1,500/1,200°C TWSW
Oxidation Time (min)		12	24	21
Relative H_2 generation*		1.0	0.27	0.79
Solid material heat recuperation efficiency	Reaction step	Solar heat input		
ε_s = 0.95	ΔH_{red} (kJ/mol H_2)	286.4	286.4	287.8
	$Q_{rad,R}$ (kJ/mol H_2)	101.8	101.8	171.5
	$Q_{rad,O}$ (kJ/mol H_2)	20.4	15.4	28.6
	Q_{solids} (kJ/mol H_2)	0.0	665.8	191.2
	Q_{tot} (kJ/mol H_2)	408.6	1,069.5	678.9
ε_s = 0.90	ΔH_{red} (kJ/mol H_2)	286.4	286.4	287.8
	$Q_{rad,R}$ (kJ/mol H_2)	101.8	101.8	171.5
	$Q_{rad,O}$ (kJ/mol H_2)	20.4	15.4	28.6
	Q_{solids} (kJ/mol H_2)	0.0	1,331.7	382.5
	Q_{tot} (kJ/mol H_2)	408.6	1,735.3	870.2

*Relative H_2 generation is based upon the total H_2 that can be produced by the same amount of material in an eight-hour day in the same reactor.

CONCLUSIONS AND FUTURE DIRECTIONS

- The hercynite cycle active materials can be operated under isothermal conditions, reducing irreversible heat losses and thermal shock concerns that limit efficiency and operations of traditional temperature-swing water splitting cycles.
- The hercynite cycle active materials can be improved to be greater than 47% active, thus increasing H_2 production, and work is underway to develop such materials.

PATENTS ISSUED

1. "Metal Ferrite Spinel Energy Storage Devices and Methods for Making and Using Same," U.S. Patent 8,187,731 (2012)

FY 2013 PUBLICATIONS

1. Martinek, J. and A.W. Weimer, "Evaluation of Finite Volume Solutions for Radiative Heat Transfer in a Closed Cavity Solar Receiver for High Temperature Solar-thermal Processes," International Journal of Heat and Mass Transfer, 58, 585-596 (2012).

2. Lichty, P., X.H. Liang, C.L. Muhich, B. Evanko, C.Bingham and A.W. Weimer, "Atomic Layer Deposited Thin Film Metal Oxides for Fuel Production in a Solar Cavity Reactor," International Journal of Hydrogen Energy, 37, 16888-16894 (2012).

3. Arifin, D., V.J. Aston, X.H. Liang, A.H. McDaniel and A.W. Weimer, "$CoFe_2O_4$ on Porous Al_2O_3 Nanostructure for Solar Thermochemical CO_2 Splitting," Energy & Environmental Science 5, 9438-9443 (2012).

4. Scheffe, J.R., A.H. McDaniel, M.D. Allendorf and A.W. Weimer, "Kinetics and Mechanism of Solar-Thermochemical H_2 Production by Oxidation of a Cobalt Ferrite-Zirconia Composite," Energy & Environmental Science, 6, 963-973 (2013).

5. Martinek, J. and A.W. Weimer, "Design Considerations for a Multiple-Tube Solar Reactor," Solar Energy, 90, 68-83(2013).

II.B.4 Solar Hydrogen Production with a Metal Oxide-Based Thermochemical Cycle

Anthony McDaniel
Sandia National Laboratories
MS9052
PO Box 969
Livermore, CA 94550
Phone: (925) 294-1440
Email: amcdani@sandia.gov

DOE Manager
Sara Dillich
Phone: (202) 586-7925
Email: Sara.Dillich@ee.doe.gov

Subcontractors:
- Prof. Nathan Siegel, Bucknell University, Lewisburg, PA
- Dr. Jianhua Tong, Colorado School of Mines, Golden, CO
- Prof. Alan Weimer, University of Colorado, Boulder, CO

Project Start Date: October 1, 2008
Project End Date: October 1, 2013

Overall Objectives

- Verify the potential for a solar thermochemical hydrogen production cycle based on a two-step, non-volatile metal oxide to be competitive in the long term.
- Develop a high-temperature solar receiver-reactor (SRR) and redox material for hydrogen production with a projected cost of $3.00/gasoline gallon equivalent at the plant gate by 2020.

Fiscal Year (FY) 2013 Objectives

- Discover and characterize novel perovskite materials for a two-step, non-volatile metal oxide water-splitting thermochemical cycle.
- Calculate theoretical system efficiency for various SRR operating scenarios that meet or exceed a solar-to-hydrogen (STH) ratio of 26%.
- Formulate particle-based SRR designs and assess feasibility.
- Construct an engineering test stand and evaluate particle conveyance and pressure separation concepts.
- Conduct H2Av3 analysis of a dish-based particle SRR producing 100,000 kg H_2/day and identify a clear path towards meeting DOE projected cost targets for H_2.

Technical Barriers

This project addresses the following technical barriers from the Hydrogen Production section of the Fuel Cell Technologies Office Multi-Year Research, Development, and Demonstration Plan:

(S) High-Temperature Robust Materials

(T) Coupling Concentrated Solar Energy and Thermochemical Cycles

(X) Chemical Reactor Development and Capital Costs

(AC) Solar Receiver and Reactor Interface Development

Technical Targets

This project is conducting fundamental studies on materials for use in concentrated solar power applications and designing reactor concepts that, when combined, will produce H_2 from thermochemical water-splitting (WS) cycles. Insights gained from these studies will be applied toward the design and optimization of an SRR that meets the following ultimate DOE hydrogen production targets:

- Hydrogen Cost: $2/kg H_2
- Materials of Reaction Cost: $11 K/yr tonnes per day H_2
- STH Conversion Ratio: 26%
- 1-Sun Hydrogen Production Rate: 2.1×10^{-6} kg/s m^2

FY 2013 Accomplishments

- Synthesized 55 different oxides and screened them for WS activity.
- Discovered a $Sr_{1-x}La_xMn_{1-y}Al_yO_3$ perovskite that produces 9x more hydrogen (220-307 µmoles/g oxide) as compared to CeO_2 (32 µmoles/g) at a lower reduction temperature (T_{RED}). Finding more effective materials increases the likelihood of meeting the DOE targets for material cost and STH conversion ratio.
- Refined our thermodynamic model of the particle SRR and discovered an optimal ΔT (T_{RED}-T_{OXD}) that lies between the worst case (isothermal operation, ΔT = 0°C) and the highest practical reduction temperature (T_{RED} = 1,600°C). Identifying optimal operating temperatures is key to meeting the DOE STH conversion ratio target of 26%. This result was derived for ceria, however, it is anticipated that other materials will act the same.
- Constructed an engineering test stand that operates at ambient conditions, verified that a particle conveyance rate of more than 30 g/s can be achieved which exceeds

the particle flow design requirement for a 5-kW SRR. The gas permeability of surrogate particles is also lower than that required for pressure and gas separation. Achieving these two milestones is critical to demonstrating the feasibility of the particle SRR design.

- Analyzed H_2 production costs for a parabolic-dish based particle SRR for a 100,000 kg H_2/day plant. Sensitivity analysis reveals the importance of reactor efficiency to meeting DOE ultimate cost targets.
- Designed and optimized a novel full field beam-down optical system for a 5-15 MW central receiver with a flat tower reflector. This design will form the basis of an H2Av3 cost analysis for a central receiver hydrogen production plant.

✧ ✧ ✧ ✧ ✧

INTRODUCTION

This research project is focused on the development of technologies that produce hydrogen at a cost that is competitive with fossil-based fuels for transportation. A two-step, solar-driven WS thermochemical cycle is theoretically capable of achieving a STH conversion ratio that exceeds the DOE target of 26% at a scale large enough to support a hydrogen economy [1]. The challenge is to engineer an SRR that will meet the DOE cost target of \$2/kg H_2.

Conceptually, heat derived from concentrated solar energy can be used to reduce a metal oxide at high temperature producing O_2 (step 1). The reduced metal oxide is then taken off sun and re-oxidized at lower temperature by exposure to H_2O, thus producing H_2 (step 2) and completing the cycle. The ultimate commercial success of solar thermochemical H_2 production is contingent upon developing suitable redox active materials and incorporating them into an efficient SRR. There is a large pallet of material chemistries that have attributes suitable for inclusion in a thermochemical H_2 production system [2-4]. The challenge is to identify an optimally-performing material. In addition, the development of redox material and SRR are not mutually exclusive, but must be conducted in parallel [5]. This project also addresses the reactor- and system-level challenges related to the design of an efficient particle-based SRR concept [6].

APPROACH

Thermochemical WS reactors are heat engines that convert concentrated solar energy (heat) to chemical work. Our approach is to discover novel materials to accomplish the WS chemistry and pair these with a novel SRR that, when combined, can achieve an unprecedented STH conversion ratio. The material discovery work involves expanding our understanding of the underlying thermodynamics and kinetics in order to make performance improvements and/or formulate new, more redox-active compositions. Sandia's patented SRR technology is based on a moving bed of packed particles that embodies all of the design attributes essential for achieving high efficiency operation: 1) inherent sensible solid-solid heat recovery; 2) spatial separation of pressure, temperature, and reaction products; 3) continuous on sun operation; and 4) direct absorption of solar radiation by the redox-active material. Research efforts are focused on validating design concepts and deriving optimal operating conditions through detailed systems modeling.

RESULTS

Perovskite oxides are an unexplored class of materials in solar H_2 applications. Fifty-five different perovskite formulations were synthesized this FY and screened for the following attributes: 1) O_2 uptake and release, 2) onset temperature of thermal reduction, and 3) WS activity. Of those screened, three formulations of a Sr- and Mn-doped $LaAlO_3$ (SLMA) exhibited attributes that exceed the current state-of-the-art redox material, CeO_2. We found that the SLMA materials reduce to a much greater extent than CeO_2, and that the onset of thermal reduction occurs fully 300°C lower in temperature. More importantly, the SLMA family of compounds we discovered split H_2O and yield more H_2 than CeO_2. Results were reported in a high-impact journal article [4] and a patent application was filed.

Presented in Figure 1 are the H_2 production rates for SLMA perovskites and CeO_2 measured over previously reduced oxides. Nearly 9x more H_2 is produced by the SLMA compounds (220-307 µmoles/g oxide) as compared to CeO_2 (32 µmoles/g). To put this discovery in perspective, extensive efforts to improve the performance of CeO_2, focused on destabilizing the crystal structure through doping and substitution, succeeded in marginally increasing the cycle capacity [7]. Although decreasing T_{RED} while increasing cycle capacity is significant, fast oxidation kinetics are equally important because they directly influence the STH conversion ratio. Detailed numerical analysis of the H_2 production rates for SLMA1-3 found that the WS rates are comparable to CeO_2, a material noted for fast kinetics. The number of perovskite compounds that may exhibit redox and WS activity is extremely large. In fact, we discovered another material that shows WS activity comprised entirely of inexpensive earth-abundant elements ($CaTi_{1-x}Fe_xO_3$). Unfortunately this compound's redox behavior did not surpass that of CeO_2. Nonetheless, Sandia is the first to recognize the potential for these materials to achieve DOE technical targets, and we feel confident that better performing perovskites will be discovered in the near future.

In this FY, the thermodynamic model of our SRR was expanded to include a detailed accounting of the energy needed for steam production. Previously, we described the

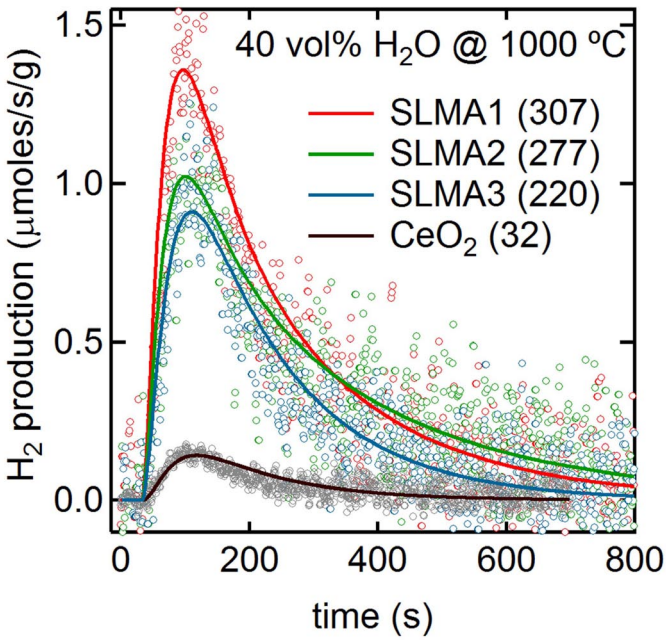

FIGURE 1. H_2 production rate as a function of time measured during oxidation in 40 vol% H_2O at 1,000°C (open symbols). SLMA1-3 and CeO_2 thermally reduced at 1,350°C in He. The total amount of H_2 produced in μmoles per g material is shown in parentheses. Solid lines are the results of detailed kinetic modeling.

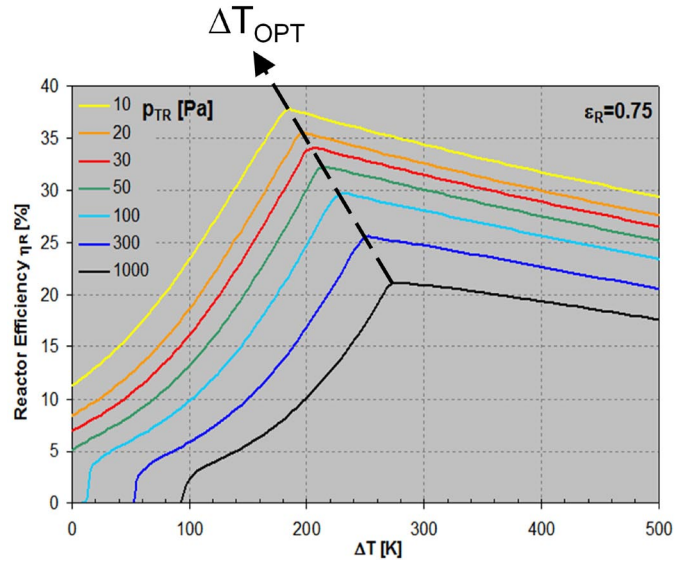

FIGURE 2. Calculated reactor efficiency (η_R) as a function of ΔT for several values of O_2 partial pressure in the reduction zone (p_{TR}) and a recuperator effectiveness (ε_R) of 0.75.

dependence of reactor efficiency on the O_2 partial pressure (p_{TR}) and recuperator effectiveness (ε_R) [6]. This analysis was conducted at a fixed value for ΔT. By extending the SRR model and relaxing the ΔT constraint, we can more thoroughly probe the thermodynamic behavior of the system. The SRR operation parameter space was explored using CeO_2 as the active oxide with special emphasis on resolving optimal values for operating points. We note that our model is easily adapted to predict the performance of other materials provided thermodynamic information on the specific redox cycle is available. To facilitate this analysis, the collection and conversion efficiencies were decoupled in the model. Thus, reactor efficiency (η_R) is reported in the subsequent figure as opposed to the STH conversion ratio. Illustrated in Figure 2 are the calculated reactor efficiencies (η_R) as a function of ΔT for several values of p_{TR} at a recuperator effectiveness of 0.75. The existence of a temperature difference value, ΔT_{OPT}, for any value of p_{TR} where η_R is greatest, is an obvious feature in the results shown in Figure 2. Additionally, it can be seen that isothermal operation (ΔT = 0) yields the lowest efficiency for any p_{TR}.

The peaks in the η_R vs. ΔT curves appear because the sensible heat of the reduced oxide is used to heat the steam to reaction temperature. Since oxide heating and steam heating are the two largest sensible heat loads, peak efficiency occurs at the point where these two terms are balanced. The reason behind poor performance at large ΔT, and even poorer performance at ΔT = 0, are easily explained. At large ΔT more sensible heat is available in the reduced oxide than is needed for heating steam, creating excess waste heat. In the isothermal operation limit, the reverse is true—no energy is needed to heat the oxide but the steam heating requirement is exceptionally large. The entirety of both these loads must be supplied by solar input, and inefficient utilization negatively impacts η_R. We also find through this expanded analysis that waste heat of sufficient quality is available to provide all of the process water via an absorption chiller; basically condense H_2O from the atmosphere. This reduces capital costs because H_2O does not have to be transported or otherwise supplied to a remote, desert location.

In this FY, Sandia constructed an engineering test stand, shown schematically in Figure 3c, in order to validate two critical design concepts, 1) particle elevation using an Olds lift, and 2) pressure separation using a packed particle bed. The data in Figure 3a shows a linear correlation between mass flow rate of particles and the rotational velocity of the chamber wall for a prototype double-helix auger designed for efficient solid-solid heat recuperation. The mass conveyance rate for this auger greatly exceeds the requirement for a 5-kW SRR, which is our design target for a high-temperature test stand. In addition, the gas permeability of a ~3-m column of surrogate steel grit particles is sufficient to stand-off an atmosphere of pressure, therefore validating our pressure separation concept at this length scale. Taken together, these results indicate no major technical barriers will prevent operation of a 5-kW, high-temperature test stand. We are currently modifying this unit to operate under vacuum at high-temperature.

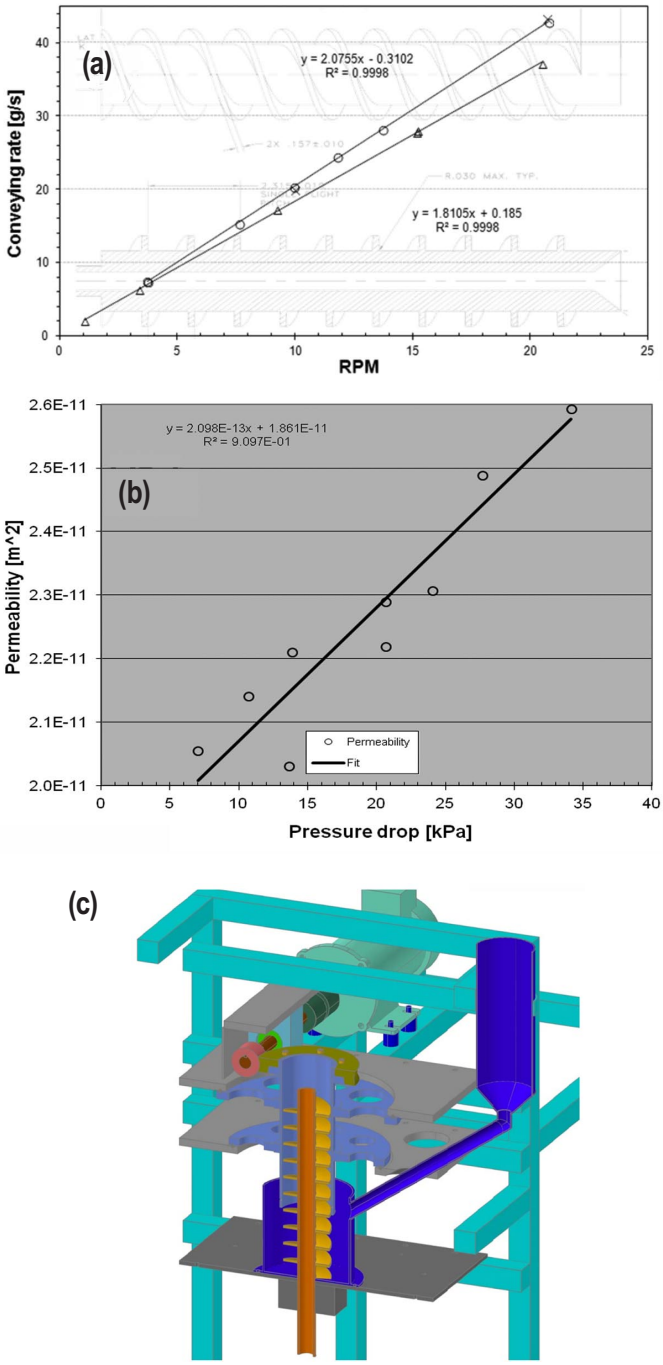

FIGURE 3. (a) The mass transport rate of particles as a function of revolutions per minute (RPM) measured in the engineering test stand at ambient conditions. (b) The gas permeability as a function of pressure drop across a packed bed of surrogate particles measured in the engineering test stand. (c) A schematic of the engineering test stand designed to operate at ambient conditions and test particle conveyance.

Significant progress was also achieved in the design and technoeconomic analysis of large-scale H_2 production plants based on Sandia SRR technology. Namely, the design and H2Av3 analysis of a dish-based H_2 production plant

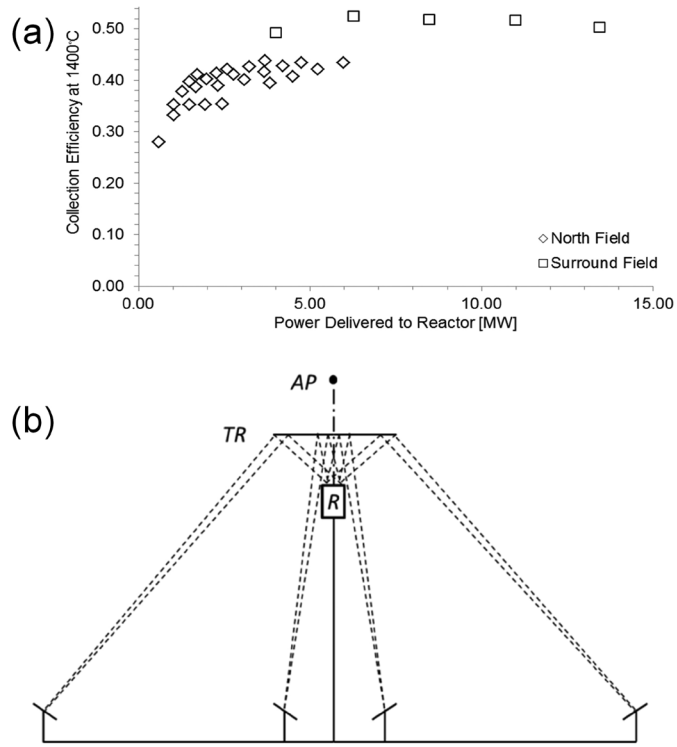

FIGURE 4. (a) The solar collection efficiency predicted for an optimal heliostat field design as a function of power delivered to the reactor aperture using a novel beam-down design. (b) A schematic of the full-field beam-down collector design. TR is the terminal reflector (flat mirror), AP is the aim point of the field, and R is the solar receiver-reactor.

capable of producing 100,000 kg H_2/day, and the design and optimization of a full-field collector array for a central receiver capable of delivering up to 15 MW to an SRR aperture. The H2Av3 work was conducted in collaboration with Strategic Analysis, Inc. (Arlington, VA). Results indicated a projected high volume cost of \$8.56/kg H_2 (produced, but not delivered or dispensed) in 2020 based on a conventional reactant material like ceria operating at an STH conversion ratio of 16.6%. The cost is projected to be near the ultimate DOE production cost target of \$2/kg H_2 for an advanced material operating in an advanced SRR at an STH conversion ratio of 34.3%. In addition, the H2Av3 analysis shows that the major contributors to capital cost are, in order, 1) STH conversion ratio, 2) collector cost, 3) SRR cost, and 4) electrical power generation cost. Research described herein addresses both the STH conversion ratio and SRR cost.

H2Av3 analysis will continue next FY using the central receiver production platform shown in Figure 4b. In this case the SRR is located on a tower as opposed to a dish, and requires a novel beam-down optical design. The collector layout was optimized using Delsol to evaluate the highest annual field efficiency for a given power level. Both north field and surround field configurations were considered.

The collection efficiencies at 1,400°C for these designs are plotted in Figure 4a. A peak collection efficiency of 53% can be achieved with a surround field design having an outer radius of 115 m providing 6.3 MW to the SRR from 9,642 heliostats. A less efficient configuration, at 50%, provides nearly 13.5 MW of power to the SRR from a total of 21,719 heliostats in a field with an outer diameter of 130 m. We will consider both cases in the pending H2Av3 study.

CONCLUSIONS AND FUTURE DIRECTIONS

- Discover additional perovskite and phase-change type oxides for improved WS activity.
- Construct a high-temperature SRR test stand sized for 5 kW.
- Conduct H2Av3 analysis of central-receiver based SRR platforms.

PATENTS ISSUED

1. A. Ambrosini, A.H. McDaniel, E. Nicholas Coker, W. Chueh, J. Tong, "A Method and System for Solar Thermochemical H_2 and CO Production", US patent, Application number: 61/808,956, filed April 05, 2013.

FY 2013 PUBLICATIONS/PRESENTATIONS

1. "$CoFe_2O_4$ on a Porous Al_2O_3 Nanostructure for Solar Thermochemical CO_2 Splitting", D. Arifin, V.J. Aston, X. Liang, A.H. McDaniel, and A.W. Weimer, *Energy & Environmental Science* 5 (2012) 9438.

2. "A New Reactor Concept for Efficient Solar-Thermochemical Fuel Production", I. Ermanoski, N.P. Siegel, and E.B. Stechel, *J. Solar Energy Engineering* 135 (2013) 031002-1.

3. "Factors Affecting the Efficiency of Solar Driven Metal Oxide Thermochemical Cycles", N.P. Siegel, J.E. Miller, I. Ermanoski, R.B. Diver, E.B. Stechel, *Industrial & Engineering Chemistry Research* 52 (2013) 3276.

4. "Kinetics and Mechanism of Solar-thermochemical H_2 Production by Oxidation of a Cobalt Ferrite–Zirconia Composite", J.R. Scheffe, A.H. McDaniel, M.D. Allendorf, and A.W. Weimer, *Energy & Environmental Science*, 6 (2013) 963.

5. "A Beam-down Central Receiver for Solar Thermochemical Hydrogen Production", N.P. Siegel, I. Ermanoski, *Proceedings of the American Solar Energy Society*, oral presentation and proceedings paper, Baltimore, MD, USA, 16–20 April, 2013.

6. "Sr- and Mn-doped $LaAlO_{3-\delta}$ for Solar Thermochemical H_2 and CO Production", A.H. McDaniel, E.C. Miller, D. Arifin, A. Ambrosini, E.N. Coker, R. O'Hayre, W. Chueh, and J. Tong, *Energy & Environmental Science*, 6 (2013) 2424.

7. "Annual Average Efficiency of a Solar Thermochemical Reactor", I. Ermanoski and N.P. Siegel, *Energy Procedia*, 19th SolarPACES poster presentation and proceedings paper, Las Vegas, NV, USA 17–20 September, 2013.

8. "Advancing Oxide Materials for Thermochemical Production of Solar Fuels", J.E. Miller, A. Ambrosini, E.N. Coker, M.D. Allendorf, and A.H. McDaniel, *Energy Procedia,* 19th SolarPACES oral presentation and proceedings paper, Las Vegas, NV, USA 17–20 September, 2013.

9. "Nonstoichiometric Perovskite Oxides for Solar Thermochemical H_2 and CO Production", A.H. McDaniel, A. Ambrosini, E.N. Coker, J.E. Miller, W.C. Chueh, R. O'Hayre, and J. Tong, *Energy Procedia*,19th SolarPACES oral presentation and proceedings paper, Las Vegas, NV, USA 17–20 September, 2013.

10. "Oxide Materials for Thermochemical CO_2 and H_2O-Splitting Using Concentrated Solar Energy", A. Ambrosini, E.N. Coker, M.D. Allendorf, A.H. McDaniel, D. Arifin, E.C. Miller, J. Tong, and J.E. Miller, ASME 7th International Conference on Energy Sustainability, Minneapolis, MN, USA, 14–19 July, 2013.

11. "Perovskite-Type Oxides for Sustainable Clean Energy", J. Tong, invited talk at the University of Tokyo, Tokyo, Japan, 14 June, 2013.

12. "Nonstoichiometric Perovskite-Type Oxides for Solar Thermochemical Fuel Production", J. Tong, invited talk at the National Institute of Materials Science, Tsukuba, Japan, 12 June 2013.

13. "Solid State Ionics Materials and Devices for Advanced Energy Conversion and Storage", J. Tong, invited talk at the National Institute of Advanced Industrial Science and Technology (AIST), Kansai Center, Osaka, Japan, 31 May, 2013.

14. "Nonstoichiometric Oxides for Solar Fuels Production: Can We Beat Ceria?", J. Tong, M. Sheng, A.H. McDaniel, W.C. Chueh, R. O'Hayre, 19th International Conference on Solid State Ionics, Kyoto, Japan, 2–7 June, 2013.

15. "Ab Initio Thermodynamics of Nonstoichiometric Oxides for Solar Thermochemical Fuel Production", A. Deml, V. Stevanović, J. Tong, R. O'Hayre, C. Musgrave, 19th International Conference on Solid State Ionics, Kyoto, Japan, 2–7 June, 2013.

16. "The Intrinsic Oxidation Kinetics of Two Step Solar Thermochemical H_2O and CO_2 Splitting with CeO_2", D. Arifin, A.H. McDaniel, and A.W. Weimer, ASME 7th International Conference on Energy Sustainability, Minneapolis, MN, USA, 14–19 July, 2013.

17. "High Temperature Splitting of Water and Carbon Dioxide Using Complex Oxides as a Route to Solar Fuels", A.H. McDaniel, J.R. Scheffe, V.J. Aston, D. Arifin, E.N. Coker, J.E. Miller, M.D. Allendorf, and A.W. Weimer, 245th ACS National Meeting & Exposition, New Orleans, LA, USA, 7–11 April, 2013.

18. "The Storage and Utilization of Solar Thermal Energy: Central Receivers for Solar Fuel Production", N.P. Siegel, NPS Defense Energy Seminar | Guest Lecturer, Monterey, CA, USA, 21 February, 2013.

REFERENCES

1. N.P. Siegel, J.E. Miller, I. Ermanoski, R.B. Diver, and E.B. Stechel, *Ind. Eng. Chem. Res.*, **52**, 3276–3286 (2013).

2. W.C. Chueh and S.M. Haile, *Philos. Trans. R. Soc. Math. Phys. Eng. Sci.*, **368**, 3269–3294 (2010).

3. R.B. Diver, J.E. Miller, M.D. Allendorf, N. P. Siegel, and R.E. Hogan, *J. Sol. Energy Eng.*, **130**, 041001(1)–041001(8) (2008).

4. A.H. McDaniel, E.C. Miller, D. Arifin, A. Ambrosini, E.N. Coker, R. O'Hayre, W.C. Chueh, and J. Tong, *Energy Environ. Sci.*, **6**, 2424–2428 (2013).

5. J.E. Miller, A.H. McDaniel, and M.D. Allendorf, *Adv. Energy Mater.*, **accepted for publication 2013**.

6. I. Ermanoski, N.P. Siegel, and E.B. Stechel, *J. Sol. Energy Eng.*, **135**, 031002 (2013).

7. A. Le Gal and S. Abanades, *J. Phys. Chem. C*, **116**, 13516–13523 (2012).

II.B.5 Electrolyzer Development for the HyS Thermochemical Cycle

William A. Summers (Primary Contact),
Hector Colon-Mercado
Savannah River National Laboratory
Savannah River Site, Building 773-41A
Aiken, SC 29808
Phone: (803) 725-7766
Email: William.Summers@srnl.doe.gov

DOE Manager
Sara Dillich
Phone: (202) 586-7925
Email: Sara.Dillich@ee.doe.gov

Project Start Date: June 1, 2013
Project End Date: Project continuation and direction determined annually by DOE

Overall Objectives

- Identify and quantify anode electrocatalysts and advanced proton-exchange membranes to improve the performance and lower the capital and operating costs for the electrolysis step of the Hybrid Sulfur (HyS) thermochemical water-splitting process
- Demonstrate electrolyzer operation at elevated temperature and pressure up to 140°C and 2 MPa
- Improve electrolyzer efficiency to achieve 600 mV cell potential at high current density

Fiscal Year (FY) 2013 Objectives

- Complete integration of major components into the Pressurized Button Cell Test Facility
- Identify and screen electrocatalysts with the potential to reduce oxidation overpotential by >20 mV versus the state-of-the-art platinum catalyst
- Characterize three or more anode catalysts in conditions of sulfur dioxide saturated solutions of 30-50 wt% H_2SO_4

Technical Barriers

This project addresses the following technical barriers from the Hydrogen Production section of the Fuel Cell Technologies Office Multi-Year Research, Development, and Demonstration (RD&D) Plan:

(T) Coupling Concentrated Solar Energy and Thermochemical Cycles

(W) Materials and Catalysts Development

(X) Chemical Reactor Development and Capital Costs

Technical Targets

This project is conducting studies to improve the performance and lower the capital and operating costs for the electrolysis step of the HyS thermochemical cycle. Insights gained from these studies will be applied toward the design and demonstration of a solar-driven HyS thermochemical cycle that meets the following DOE 2020 hydrogen production targets for high-temperature, solar-driven, thermochemical processes as given in Table 3.1.7 of the Multi-Year RD&D Plan:

- Hydrogen Cost: $3.70/kg
- Solar to Hydrogen Energy Conversion Ratio: 20%

✧ ✧ ✧ ✧ ✧

APPROACH

The DOE is supporting research to verify the potential for solar thermochemical (STCH) cycles for hydrogen production to be competitive in the long-term and by 2020 to develop this technology to produce hydrogen with a projected cost of $3.70/gasoline gallon equivalent at the plant gate. The HyS process is a promising sulfur-based STCH cycle that depends on a simple, two-step chemical process with all fluid reactants. It contains a low-energy electrolysis step, making it a thermo/electrochemical hybrid process. In this process, sulfuric acid (H_2SO_4) is thermally decomposed by solar energy at high temperature (>800°C), producing SO_2, O_2, and steam. Sulfuric acid saturated with SO_2 is then pumped into a sulfur dioxide-depolarized electrolyzer (SDE) that electrochemically oxidizes sulfur dioxide with water to form sulfuric acid at the anode and reduces protons to form hydrogen at the cathode. The reversible cell potential for this electrochemical process is -0.158 V (standard hydrogen electrode) versus -1.229 V (standard hydrogen electrode) for low-temperature water electrolysis [1]. The overall electrochemical reaction consists of the production of H_2SO_4 and H_2, while the entire cycle produces H_2 and O_2 from H_2O with no side products.

The SDE is the major developmental technology in this cycle, and the objective of the research is to identify, develop, and demonstrate new SDE components to improve the efficiency and lower the costs of this key step. The focus of the research is on the anode electrocatalyst and the proton exchange membrane. New research has shown that Pt alloys with transition metals, gold, and gold alloys can decrease the overpotential for the SO_2 oxidation reaction [2]. Another major goal of the research is to develop membranes that can operate at elevated temperature and pressure (140°C and 2 MPa) for extended periods without degradation of

performance. Higher-temperature operation is expected to reduce kinetic polarization losses at the anode and permit the use of advanced membranes (versus Nafion®). Previous low-temperature results indicate that the advanced membranes can also reduce the crossover of SO_2 through the membrane to the cathode, thereby eliminating or minimizing elemental sulfur formation that can reduce cell performance and operating lifetime.

ACCOMPLISHMENTS

This project was initiated in June 2013. Accomplishments to date include:

- Identified tantalum-coated parts as a more cost-effective alternative instead of custom-made zirconium fittings for construction of the metal parts of the Pressurized Button Cell Test Facility.
- Began modification of the original piping and instrumentation diagram from earlier large-scale testing to accommodate the changes in size and type of parts to be used in the Pressurized Button Cell Test Facility and to permit operating conditions up to 130°C and 1 MPa.
- Identified candidate anode electrocatalysts, including Pt, Au, PtAu, PtAg, PtPd, AuPd, AuAg, PtCr, and AuCr, that have potential to reduce anode polarization by greater than 100 mV versus state-of-art Pt catalyst. All chemicals and materials were purchased and received.

FUTURE DIRECTIONS

- Complete design, procurement of parts, and construction of Pressurized Button Cell Test Facility
- Integrate all major components into the Pressurized Button Cell Test Facility with the capability to increase operating conditions up to 130°C and 1 MPa
- Initiate testing of advanced, high-temperature membrane electrode assemblies
- Prepare and sputter catalysts on substrates and test activity on model solutions

REFERENCES

1. Gorensek, M.B.; Staser, J.A.; Stanford, T.G.; Weidner, J.W., A thermodynamic analysis of the SO2/H2SO4 system in SO2-depolarized electrolysis. *International Journal of Hydrogen Energy* **2009,** *34* (15), 6089-6095.

2. O'Brien, J.A.; Chemistry, U. o. N. S. o., *Solar Hydrogen: A Fundamental and Applied Electrochemical Investigation of the Hybrid Sulfur Cycle Electrolyser*. University of Newcastle: 2011.

II.C.1 Semiconductor Materials for Photoelectrolysis

Todd Deutsch (Primary Contact), John Turner, Heli Wang, Huyen Dinh
National Renewable Energy Laboratory (NREL)
15013 Denver West Parkway
Golden, CO 80401
Phone: (303) 275-3727
Email: Todd.Deutsch@nrel.gov

DOE Manager
Eric Miller
Phone: (202) 287-5829
Email: Eric.Miller@ee.doe.gov

Subcontractor:
University of Nevada Las Vegas (UNLV), Las Vegas, NV

Project Start Date: 2005
Project End Date: Project continuation and direction determined annually by DOE

Overall Objectives

Identify, synthesize, and characterize new semiconductor materials that have the capability of meeting the criteria for a viable photoelectrochemical (PEC) hydrogen-producing device, either as a single absorber or as part of a high-efficiency multi-junction device

Fiscal Year (FY) 2013 Objectives

- Optimize semiconductor surface modification for passivation against corrosion while maintaining high solar-to-hydrogen efficiency.
- Demonstrate improved durability for state-of-the-art high-efficiency III-V semiconductor electrodes.

Technical Barriers

This project addresses the following technical barriers from the Hydrogen Production section (3.1.5) of the Fuel Cell Technologies Office Multi-Year Research, Development, and Demonstration Plan:

(AE) Materials Efficiency – Bulk and Interface

(Af) Materials Durability – Bulk and Interface

(Ag) Integrated Device Configurations

(Ai) Auxiliary Materials

Technical Targets

This project is a materials discovery investigation to identify a single semiconductor material that meets the technical targets for efficiency and stability. The 2015 technical targets from the Multi-Year Research, Development, and Demonstration Plan PEC hydrogen production goals in Table 3.1.8.A are as follows:

- 15% conversion efficiency
- 900-hour replacement lifetime (1/2 year at 20% capacity factor)
- $\$300/m^2$ PEC electrode cost

This project made progress towards the stability target with material that exceeds the efficiency target. The main achievements were over 300 hours of high photocurrent operation under bias with minimal corrosion and surpassing a 100-hour lifetime at short-circuit.

FY 2013 Accomplishments

- We fabricated an acrylic photoreactor for testing PEC materials that is able to collect hydrogen and oxygen gases separately for quantitative analysis which is necessary for solar-to-hydrogen efficiency benchmarking. The photoreactor was designed for mounting on a two-axis solar tracker for outdoor testing and can be equipped with lenses for moderate optical concentration.
- Surface spectroscopic results from UNLV uncovered additional elements that played a key role in the successful nitride passivation treatment allowing us to reproduce the protective effect on additional $GaInP_2$ surfaces. In partnership with UNLV, we filed a provisional patent application on the treatment process.
- Feedback from nitrogen K-edge X-ray emission spectroscopy taken by our UNLV collaborators at the Advanced Light Source has provided quantitative results on the degree of nitride that provides the best electrode durability, giving us a target level of incorporation for ion dosing.
- We led an effort, along with Stanford and DOE, to compile and streamline PEC standardized methods documents that did not fit into our Journal of Materials Research publication [1] and submitted them to Springer for publication as a short book.
- We tested multiple treated tandem $GaInP_2$/GaAs electrodes for durability under bias and had some last for several hundred hours with little sign of physical degradation or loss of performance.

- We tested several tandem $GaInP_2$/GaAs electrodes at short-circuit that had initial starting solar-to-hydrogen efficiencies in excess of 10%. They were tested until failure and the average lifetime of fourteen electrodes was 60 hours, with three operating longer than 100 hours.

✧ ✧ ✧ ✧ ✧

INTRODUCTION

Photoelectrochemistry combines a light harvesting system and a water splitting system into a single, monolithic device. The catalyzed surface of a semiconductor is the light-harvesting component as well as one part of the water splitting system with the balance consisting of a spatially separated counter electrode. Discovering a semiconductor system that can efficiently and sustainably collect solar energy and direct it towards the water splitting reaction could provide renewable and economically competitive fuel for the hydrogen economy.

The goal of this work is to develop a semiconductor material set or device configuration that (i) splits water into hydrogen and oxygen spontaneously upon illumination without an external bias, (ii) has a solar-to-hydrogen efficiency of at least 10% with a clear pathway to 15%, and (iii) can ultimately be synthesized via high-volume manufacturing techniques with a final hydrogen production cost of $2.10/kg.

APPROACH

Our approach is to study the current material sets used in commercial solar cells as well as related materials that meet near-term solar-to-hydrogen efficiency targets and to extend their durability by surface passivation techniques. The surface passivation treatments are engineered not only to stabilize the semiconductor at the electrolyte interface but also to maintain the high native efficiencies by ensuring that charge transfer is not compromised. To help us identify the steps that initiate corrosion reactions and develop mitigation strategies, we collaborate with partners who apply state-of-the-art spectroscopic characterization skills and theory to better observe and understand our system. Another area of focus is to investigate new materials that have lower band gaps and high quantum efficiencies that could allow them to achieve the ultimate DOE solar-to-hydrogen efficiency target, which is very high.

RESULTS

Photoreactor Design and Fabrication

With the aid of intern Adolfredo Alvarez, we designed a photoreactor to facilitate on-sun testing of promising PEC water-splitting electrodes. The body was made of poly(methyl methacrylate) for optimal chemical resistance and optical transparency. The design incorporated a bracket for mounting on a two-axis solar tracker at NREL's Solar Radiation Research Laboratory. Two lower ports allow interchangeable semiconductor and counter electrode insertion and permit electrical contacts between the electrodes for circuit measurements (Figure 1). Two upper ports on the reactor allow separate hydrogen and oxygen collection and were engineered to be the high points during the full range of inclinations the cell experiences as it tracks the sun's path throughout the day. Solar-to-hydrogen efficiency can be evaluated using real-time solar spectral and intensity data collected on instruments adjacent to the tracker and compared with current measured between the water splitting electrodes. The product gas volumes can be used to determine the Faradaic efficiency. Testing of III-V tandem electrodes under on-sun conditions to benchmark efficiency and durability is ongoing.

Durability Testing on Tandem Electrodes

High efficiency III-V tandem semiconductor photoelectrochemical electrodes were tested for durability under water splitting conditions. A protective surface modification developed at NREL was applied and resulted in improved photocorrosion resistance. The best performing electrodes had lifetimes that exceeded 100 hours when tested at short-circuit and several hundred hours when a bias was applied. The durability of the modified surfaces at unprecedented photocurrent densities is a significant improvement over the severe degradation observed after only 24 hours for untreated electrode surfaces. These results demonstrate noteworthy progress towards the DOE's

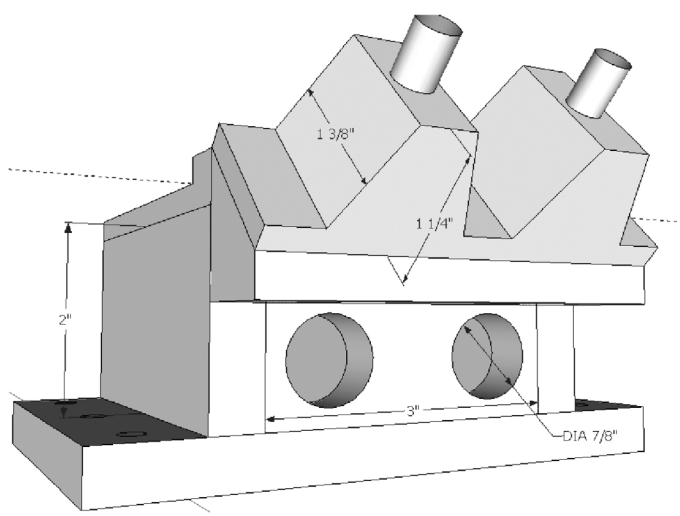

FIGURE 1. Computer-aided design rendering of the back-side of the photoreactor. The two lower ports are for the semiconductor and counter electrodes. The two upper ports connect to tubing for hydrogen and oxygen gas collection.

efficiency and durability targets required to achieve cost-competitive hydrogen production via photoelectrolysis.

After undergoing nitrogen ion implantation-based surface passivation treatments, tandem p-$GaInP_2$/GaAs photoelectrodes were potentiostatically tested for durability in 3M H_2SO_4 electrolytes with the fluorosurfactant Zonyl® FSN-100. Electrodes were illuminated by a 250-watt tungsten light source calibrated to AM1.5G with a 1.81 eV band gap $GaInP_2$ reference cell. Previously we reported 115 hours of stability on epilayer (non-tandem) p-$GaInP_2$ where a constant current of 10 mA/cm^2 was applied. The testing for tandem electrodes either had a constant circuit bias of -1.5 V or -1 V, or had no bias at all between the working and platinum black counter electrodes (short-circuit). All of the tests were accomplished in a two-terminal configuration because reference electrodes are not robust enough to withstand the harsh durability conditions.

At the conclusion of the biased durability testing, the semiconductor electrodes were disassembled and their surfaces were analyzed using an optical profilometer to determine if any physical degradation had occurred. The corrosion electrolytes were also tested for gallium and indium concentrations by inductively coupled plasma mass spectrometry (ICP-MS). The analytes were detected in ppb quantities and converted to nanomoles per Coulomb to account for variation in testing cell volumes, electrode surface areas, and overall charge passed. The ICP-MS results from the biased tests (Figure 2) demonstrate that the surface passivation treatment is effective in providing protection at very high cathodic current densities for long durations. Interference microscopy (Figure 3) revealed that nominal etching occurred for this particular electrode surface over 315 hours of passing, on average, 14.55 mA/cm^2 cathodic, hydrogen-evolution photocurrent. While untreated electrode

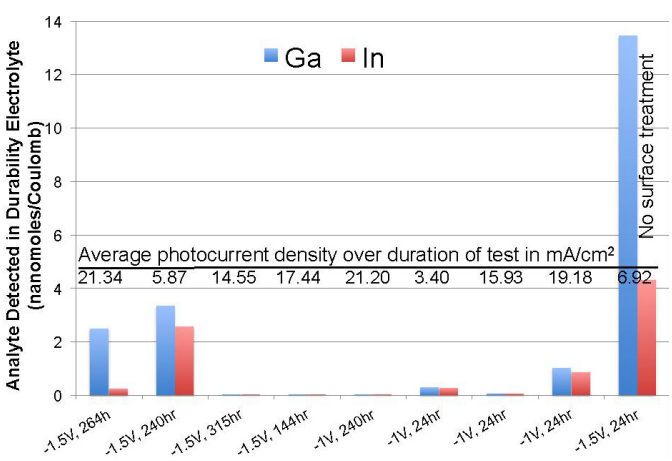

FIGURE 2. Ga and In present in 3M H_2SO_4 durability solutions of tandem electrodes detected by ICP-MS. Results are from multiple, unique electrodes that were all treated except for the one noted. Lower values for the treated electrodes suggest stability compared with the untreated sample.

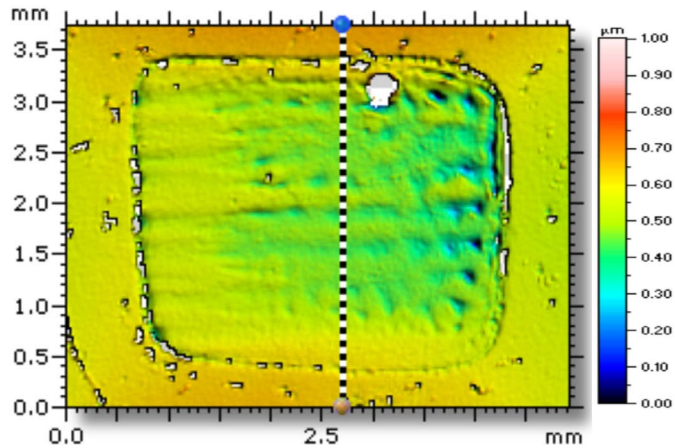

FIGURE 3. Surface profile of the deconstructed electrode subjected to 315 hours of testing at -1.5 V generated by optical interference microscopy. The perimeter of the rectangular chip was masked with epoxy leaving only the interior area exposed to electrolyte during testing. The etching of the exposed surface was minimal compared to that observed on untreated electrodes.

surfaces exhibit widespread, uniform etching about 1 µm deep after only 24 hours at 10 mA/cm^2, 315 hours at a higher current density resulted in localized surface etching that was only a few hundred nanometers deep on treated electrode surfaces.

Short-circuit testing was a measure of lifetime as all of the tests ended in catastrophic failure of the electrodes with large craters that perforated the entire epilayer and substrate. Optical profilometry and ICP-MS are not useful tools for quantitative comparisons under such failure conditions. Electrode failure under short-circuit conditions was indicated by the first appearance of anodic current, and on average the 14 treated tandem electrodes operated for 60 hours before failing. The most durable electrodes had lifetimes of 102.6, 103.2, and 110.1 hours. Even though three out of the 14 electrodes exceeded 100 hours of unbiased operation, the durability under short-circuit was not as great as when the electrodes were biased. It appears that sustaining a high cathodic photocurrent is critical to the long-term stability of the treated tandem electrode surfaces.

In addition to semiconductor degradation, another possible reason for the decline in photocurrent with time could be fouling of the counter electrode, which was observed at the conclusion of each of the durability tests. When biased testing was performed in a surfactant-free electrolyte, the counter electrode did not get fouled; however, large bubbles formed on the working electrode and severe physical degradation of the semiconductor occurred within a few hours. At the rate of gas evolution for these high efficiency water-splitting tests, surfactant is required and a fluorosurfactant was chosen because it should be resistant to oxidative decomposition. It is clear that alternative surfactants should be investigated to identify those that can

still aid bubble removal and also resist degradation. We are optimistic that the durability at short-circuit can be pushed to several hundred hours as we continue to optimize the surface treatment conditions and refine electrolyte composition.

CONCLUSIONS

- We have developed a surface passivation treatment that significantly improves the durability of p-$GaInP_2$/GaAs tandem electrode surfaces. The durability of tandem electrodes at short-circuit is greater for treated than for untreated surfaces, but still needs improvement.
- The PEC performance metrics necessary to achieve the DOE goals for cost-competitive hydrogen could be met using the high water-splitting efficiencies of these tandem devices coupled with the durability provided by an optimized surface modification.
- The durability was not as great as for electrodes tested at short-circuit as it was for those that were biased. Because a real PEC reactor will not have a bias applied, durability testing should utilize short-circuit conditions to determine how a candidate semiconductor material will perform in an actual deployed device.

FUTURE DIRECTIONS

- We will continue to optimize the surface passivation treatment by varying ion implantation parameters based upon critical feedback provided by our UNLV collaborators.
- We will evaluate the efficacy of the surface passivation treatment on other III-V PEC semiconductors to see if the protection could apply to this whole material class.
- To minimize ancillary system component contributions to circuit failure in two-electrode durability testing, we will examine alternative electrolyte/surfactant compositions and investigate other counter electrodes that are more catalytically active for water oxidation.

FY 2013 PUBLICATIONS

1. "Titanium and magnesium Co-alloyed hematite thin films for photoelectrochemical water splitting" Houwen Tang, Wan-Jian Yin, M.A. Matin, Heli Wang, Todd Deutsch, Mowafak M. Al-Jassim, John A. Turner and Yanfa Yan, *J. Appl. Phys.* **111**, 073502 (2012).

2. "Photoelectrochemical activity of as-grown, α-Fe_2O_3 nanowire array electrodes for water splitting" Boris D. Chernomordik, Harry B. Russel, Uros Cvelbar, Jacek B. Jasinski, Vivekanand Kumar, Todd Deutsch, and Mahendra K. Sunkara, *Nanotechnology*, **23**, 194009 (2012).

3. "Novel Micropixelation Strategy to Stabilize Semiconductor Photoelectrodes for Solar Water Splitting Systems" Fatima Toor, Todd G. Deutsch, Joel W. Pankow, William Nemeth, Arthur J. Nozik and Howard M. Branz, *J Phys. Chem. C*, **116**, 19262-19267, (2012).

4. "The stability of illuminated p-$GaInP_2$ semiconductor photoelectrode" Heli Wang, Todd Deutsch, Adam Welch, John A. Turner, *Int. J. Hydrogen. Energ.*, **37**, 14009-14014, (2012).

5. "$BiVO_4$/$CuWO_4$ Heterojunction Photoanodes for Efficient Solar Driven Water Oxidation" Satyananda Kishore Pilli, Todd G. Deutsch, Thomas E. Furtak, Logan D. Brown, John A. Turner and Andrew M. Herring. *Phys. Chem. Chem. Phys.*,**15**, 3273-3278, (2013).

6. "Technical and economic feasibility of centralized facilities for solar hydrogen production via photocatalysis and photoelectrochemistry" Blaise A. Pinaud, Jesse D. Benck, Linsey C. Seitz, Arnold J. Forman, Zhebo Chen, Todd G. Deutsch, Brian D. James, Kevin N. Baum, George N. Baum, Shane Ardo, Heli Wang, Eric Miller and Thomas F. Jaramillo, Energy Environ. Sci. **6**, 1983-2002, (2013).

7. "Electronic structure study of N, O related defects in GaP for photoelectrochemical applications" Muhammad N. Huda, Todd G. Deutsch, Pranab Sarker, and John A. Turner, *J. Mater. Chem A*, **1**, 8425-8431, (2013).

8. "Efficient photoelectrochemical water oxidation over cobalt-phosphate (Co-Pi) catalyst modified BiVO4/1D-WO_3 heterojunction electrodes" Satyananda Kishore Pilli, Todd G. Deutsch, Thomas E. Furtak, John Turner, Logan D. Brown, and Andrew M. Herring, Phys Chem Chem Phys, IN PRESS First published online July 9, 2013. DOI: 10.1039/C3CP52401A

FY 2013 PRESENTATIONS

1. "Photoelectrochemical water splitting", Inter-Continental Advanced Materials & Photonics (I-CAMP), 2012 Summer School on Renewable and Sustainable Energy, University of Colorado, Boulder, July 19, 2012. (Turner) *Invited*

2. "Material Properties and Economic Considerations for Photoelectrochemical Water-Splitting Systems", JX Nippon Oil & Energy Corporation", Yokohama, Japan, July 23, 2012. (Turner) *Invited*

3. "Semiconducting Materials and Structures for Photoelectrochemical Hydrogen Production", University of Tokyo, Tokyo, Japan, July 24, 2012. (Turner) *Invited*

4. "Material Properties and Economic Considerations for Photoelectrochemical Water-Splitting Systems", 1st International Workshop on Solar-Chemical Energy Storage (SolChES), Sendai, Japan, July 25, 2012. (Turner) *Invited Plenary*

5. "Protecting p-GaInP2 from Corrosion for Durable Photoelectrochemical Water Splitting", 2012 SPIE's Optics + Photonics, San Diego, CA, August 12, 2012. (Wang) *Invited*

6. "Photoelectrochemical Hydrogen Production", CRSP Fall Research Symposium, University of Colorado, Boulder, August 29, 2012. (Turner) *Invited*

7. "Material Properties and Economic Considerations for Photoelectrochemical Water-Splitting Systems", Toyota Central Research and Development Laboratory, Toyota, Japan, September 19, 2012. (Turner) *Invited*

8. "The Promise and Challenges for Photoelectrochemical Hydrogen Production", Nagoya Institute of Technology (NITech), Nagoya, Japan, September 20, 2012. (Turner) *Invited*

9. "Challenges in Photoelectrochemistry and the Impact of Coordination Chemistry", 62nd Japan Society of Coordination Chemistry Symposium, Toyoma, Japan, September 21, 2012. (Turner) *Invited Plenary* -JSCC Lectureship Award presentation.

10. "The Hydrogen Economy and Photoelectrochemical Water Splitting", NREL Fall Interns, October 3, 2012. (Turner) *Invited*

11. "Hydrogen Production from Photoelectrochemical Cells: Economic and theoretical considerations and experimental results", PRiME 2012: Joint International Meeting of the Electrochemical Society and the Electrochemical Society of Japan. Honolulu, Hawaii. October 7th, 2012. (Turner) *Invited Plenary*

12. "Photoelectrolysis on p-$GaInP_2$; Extended Durability by Nitrogen Ion Implantation", PRiME 2012: Joint International Meeting of the Electrochemical Society and the Electrochemical Society of Japan. Honolulu, Hawaii. October 9th, 2012. (Deutsch) *Contributed*

13. "Corrosion protection of p-$GaInP_2$ for durable photoelectrochemical water splitting", PRiME 2012: Joint International Meeting of the Electrochemical Society and the Electrochemical Society of Japan. Honolulu, Hawaii. October 9th, 2012. (Wang) *Contributed*

14. "Photoelectrochemical Water Splitting and the Hydrogen Economy", South Dakota School of Mines, October 18, 2012. (Turner) *Invited Sigma Xi lecture*

15. "Photoelectrochemical Water Splitting and the Hydrogen Economy", Black Hills State University, October 19, 2012. (Turner) *Invited Sigma Xi lecture*

16. "Material Properties and Economic Considerations for Photoelectrochemical Water-Splitting Systems", University of Nevada, Reno, November 30, 2012. (Turner) *Invited*

REFERENCES

1. Chen, Z., Jaramillo, T.F., Deutsch, T.G., Kleiman-shwarsctein, A., Forman, A.J., Gaillard, N., Garland, R., et al. (2010). Accelerating materials development for photoelectrochemical hydrogen production: Standards for methods, definitions, and reporting protocols. *Journal of Materials Research*, *25*(1), 3–16. doi:10.1557/jmr.2010.0020

II.C.2 Photoelectrochemical Hydrogen Production

Jian Hu
MVSystems, Incorporated (MVS)
500 Corporate Circle, Suite L
Golden, CO 80401
Phone: (303) 271-9907
Email: jhu@mvsystemsinc.com

DOE Managers
Eric Miller
Phone: (202) 287-5829
Email: Eric.Miller@hq.doe.gov
David Peterson
Phone: (720) 356-1747
Email: David.Peterson@go.doe.gov

Contract Number: DE-FC36-07GO17105, A00

Subcontractor:
University of Hawaii at Manoa (UH), Honolulu, HI

Project Start Date: September 1, 2007
Project End Date: September 30, 2013

Overall Objectives

- 5% solar-to-hydrogen (STH) conversion efficiency
- Operational life up to 500 hours
- Identify commercialization paths toward a \$22/kg-H_2 plant production cost

Fiscal Year (FY) 2013 Objectives (towards end of September)

- Work closely with the DOE Working Group on Photoelectrochemical (PEC) Hydrogen Production for optimizing PEC materials and devices, with the STH efficiency improved to 5% from current level of 4.34% (reported in May 2012), and durability at the working condition up to 500 hours.
- Develop new PEC film materials compatible with high-efficiency, low-cost hydrogen production devices.
- Demonstrate functional multi-junction device incorporating materials developed.
- Explore avenues toward manufacture-scaled devices and systems.

Technical Barriers

This project addresses the following technical barriers from the Photoelectrochemical Hydrogen Production section of the Fuel Cell Technologies Office Multi-Year Research, Development, and Demonstration Plan:

(AE) Materials Efficiency - Bulk and Interface

(AF) Materials Durability - Bulk and Interface

(AG) Integrated Device Configurations

(AI) Auxiliary Materials

(AJ) Synthesis and Manufacturing

Technical Targets

Task 2

Table 1 lists the technical targets for PEC hydrogen production using amorphous silicon carbide-compound (a-SiC), metal oxide-compound (i.e. WO_3), and I-III-VI_2 (copper chalcopyrite-based) films.

FY 2013 Accomplishments

1) Improvement in performance of the hybrid photovoltaic (PV)/a-SiC device: Increase of photocurrent density up to 4.9 mA/cm^2 (equivalent to ~6.1% STH efficiency) by combining surface modification (Ru nano-particles) and high-performance PV cells.
2) In metal oxides: theory-driven quaternary oxides engineering.
3) In copper chalcopyrites: synthesis of 'Red' (2.0 eV) copper indium gallium diselenide (CIGS).

✧ ✧ ✧ ✧ ✧

INTRODUCTION

Based on its potential to meet long-term goals, research and development (R&D) centering on multi-junction hybrid photoelectrode technology defines the scope of this collaborative project. Within this scope, particular emphasis is put in the development of low-cost photoactive materials integrated with a-Si-based solar cells as a driving force with photocurrents greater than 4 mA/cm^2, and with sufficient durability to meet lifetime requirement, i.e., ≥500 hours. In addition to the materials R&D activities, development of laboratory-scale demonstration devices and generation of preliminary energy/economic analysis for hydrogen production cost based on the developed PEC technology is included in the project scope as second-level priorities. To support the device-demonstration activities, appropriate auxiliary components are being developed for incorporation in PEC photoelectrode designs, including attention to the necessary process integration techniques.

TABLE 1. Technical Targets

Task #	Milestone	a-SiC	WO_3	I-III-VI_2
Year 1	Material photocurrent ≥3 mA/cm^2	**Achieved**	**Achieved**	**Achieved**
	Durability ≥100 hr	**Achieved**	**Achieved**	10% Achieved
Year 2	Material photocurrent ≥4 mA/cm^2	**Achieved**	90% Achieved	**Achieved**
	Durability ≥200 hr	**Achieved**	**Achieved**	**Achieved**
	Device STH efficiency ≥5%	32% Achieved	60% Achieved	62% Achieved
Passed Go/No-Go decision evaluation in November 2010				
Year 3	Device STH efficiency ≥5%	32% Achieved	60% Achieved	85% Achieved
	Durability ≥300 hr	62% Achieved	83% Achieved	66% Achieved
Year 4	Device STH efficiency ≥5%	**Achieved**	62% Achieved	87% Achieved
	Durability ≥500 hr	62% Achieved	**Achieved**	84% Achieved
	Completion of Final Energy/Economics report on scale up and commercialization toward a \$22/kg-H_2 plant production cost			

APPROACH

The general approach of this collaborative effort focuses on the DOE PEC Working Group's "feedback" philosophy integrating state-of-the-art theoretical, synthesis, and analytical techniques to identify and develop the most promising materials classes to meet the PEC challenges in efficiency, stability, and cost. Materials modeling, bulk-film optimization, film-surface enhancement, along with comprehensive material and device characterization are being employed to facilitate the R&D process. Specifically, the feedback approach are being applied to our focus material classes, including the metal oxide-, copper-chalcopyrite-, and silicon-based compounds, to enhance understanding of fundamental performance parameters and expedite development of process-compatible forms of these materials. The most promising candidate materials are being identified, with the short-term goal of demonstrating laboratory-scale water-splitting devices, and with a long-term goal of transferring the fabrication processes toward the commercial scale.

RESULTS

During this reporting period (June 2012–June 2013), extensive studies of the three materials classes under investigation have focused on understanding and improving PEC behavior, specifically by applying our theoretical, synthesis, and analytical techniques in identifying relevant aspects of structural, optoelectronic, and electrochemical properties.

1. Amorphous Silicon Carbide-Based Compound Films

The surface barrier at a-SiC/electrolyte interface impedes photocurrent to be extracted from the hybrid PV/a-SiC device. Last year, we reported improvement in surface energetics and improvement of photocurrent in the hybrid PV/a-SiC device via Ru nanoparticle surface treatment. Over this reporting period, a further improvement in the device performance has been achieved through combination of the surface treatment by Ru nanoparticles, improvement of the solar cell performance, and use of electrolyte of higher conductivity. Figure 1 shows the 2-electrode current density-voltage (JV) characteristics obtained before (blue line) and after Ru nanoparticle treatment (red line). The Ru-coated hybrid PV/a-SiC device is of the configuration SnO_2/X cell/a-SiC(p)/a-Si(i)/a-SiC(n)/Ru, where the X cell is a high-performance solar cell[1] and is series-connected with the a-SiC photoelectrode by a metal wire. Compared with the previous hybrid device, where the a-SiC photoelectrode was

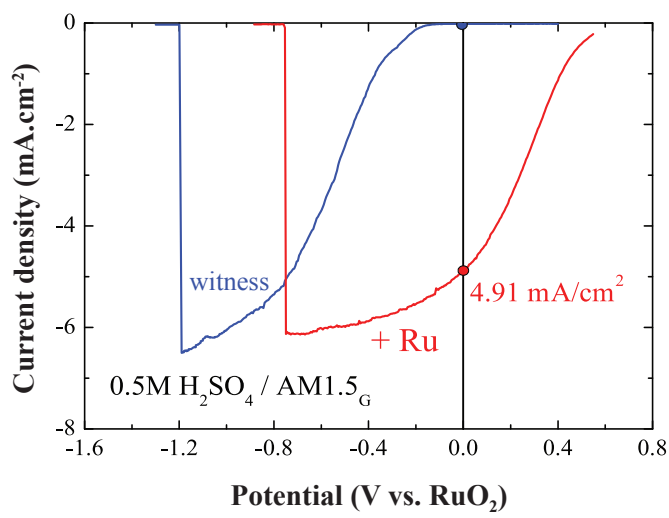

FIGURE 1. The 2-electrode current density-potential characteristics in 0.5 M H_2SO_4 solution on hybrid devices.

[1] For proprietary purpose, the details of this solar cell are not disclosed here.

of p-i configuration, the p-i-n structure here provides extra photovoltage, i.e., by 0.4-0.5 V. The Ru nanoparticle catalyst was fabricated at the University of Hawaii by sputtering technique for 15 sec. Prior to Ru deposition, SiO_2 on a-SiC photoelectrode surface was removed in 5% hydrofluorhydric acid solution for 90 sec. The current density vs. potential characteristics were measured in 0.5 M H_2SO_4 electrolyte and in 2-electrode setup using a RuO_2 counter electrode. The illumination intensity conformed with air mass 1.5_G spectrum. It was observed that the resultant photocurrent density increase up to 4.9 mA/cm^2 without external bias, or equivalent to a STH efficiency of ~6.1% (assuming 100% Faradaic efficiency). The illuminated open-circuit potential measurements confirmed an anodic shift in the flat band potential of ca. 600 mV, an ideal situation for photocathode systems.

2. Oxide Mineral-Based Compound Films

With an electronic band-gap of 2.2 eV and optimum surface energetics for water splitting, copper tungstate ($CuWO_4$) is a promising material for PEC hydrogen production. During this reporting period, our efforts were focused on improving the electronic transport properties of this system, especially evaluating the effect of the addition of foreign chemical elements on $CuWO_4$ bulk resistivity. With the help of Prof. Huda's group at the University of Texas in Arlington, we were able to identify several new tungstate-based multi-cation metal-oxides. For example, from a combined mineral data-based search and density functional theory (DFT) calculations, we were able to predict that the addition of bismuth to form quaternary copper bismuth tungstate ($CuBiW_2O_8$) should: i) lower the electron effective mass in the conduction band, and ii) suppress unfilled states present in the forbidden gap of $CuWO_4$. In other words, $CuBiW_2O_8$ should have a higher electrical conductivity when compared to $CuWO_4$. This was tested by electrical impedance analyses performed on ceramic pellets of $CuBiW_2O_8$ and $CuWO_4$ formed by solid-state reaction (powder sintering). As predicted, the bulk resistivity decreased by two orders of magnitude after addition of bismuth to a value much closer to that of our high-performance WO_3 material.

3. Copper Chalcopyrite-Based Films

Amongst all material classes currently studied for PEC H_2 production, the chalcopyrite system is the system that probably offers the best compromise between efficiency and synthesis costs. In order to integrate this class into an efficient standalone hybrid photoelectrode system, one must i) lower overpotentials originating from a valence band sitting too far from the O_2/H_2O redox level, and ii) increase its optical bandgap from 1.6 eV (the highest value for the selenide class, $CuGaSe_2$) to 2.0 eV. This year, our research was focused on selenium substitution with sulfur. Using co-evaporated 1 µm-thick $CuGaSe_2$ as the baseline system, we demonstrated that selenium could be substituted by sulfur using a simple annealing step. With this protocol, a dramatic change in optical properties was observed, with a band-gap increase from 1.6 eV ($CuGaSe_2$) to 2.4 eV ($CuGaS_2$). Then, by simply adjusting the indium content in the film during the initial growth process, the band-gap of sulfurized copper chalcopyrite was decreased from 2.4 eV to 2.2 eV and finally to 2.0 eV, as shown in Figure 2. X-ray photoelectron spectroscopy analysis performed by Prof. Heske's group at the University of Nevada in Las Vegas on the 2.0 eV copper indium gallium sulfide ($CuInGaS_2$) material indeed confirmed that all selenium at the surface of the films was replaced with sulfur. Preliminary PEC analyses reveal an anodic shift of the flatband potential with increasing band-gap. This suggests that the bandgap modification in sulfurized films primarily stems from a downward shift of the valence band, an ideal situation for p-type PEC systems.

CONCLUSIONS AND FUTURE DIRECTIONS

The photocurrent of the hybrid PV/a-SiC device has been enhanced to 4.9 mA/cm^2 at zero bias due to improved surface energetics using Ru nanoparticle surface treatment and incorporating the high-performance PV cell. Durability of such hybrid devices will be tested in a working condition, i.e., under a current bias of ~4 mA/cm^2. Progress continued on metal oxide-based compound with the evaluation of quaternary systems ($CuBiW_2O_8$), directed by advanced theoretical calculations. Copper tungstate material resistivity has been decreased by two orders of magnitude with the addition of bismuth. Several new tungstate-based multi-cation metal-oxides have also been identified. Thin film synthesis is currently underway. In copper chalcopyrite-based systems, $CuInGaS_2$ of 2 eV has been successfully fabricated by replacing Se with S and adjusting the indium

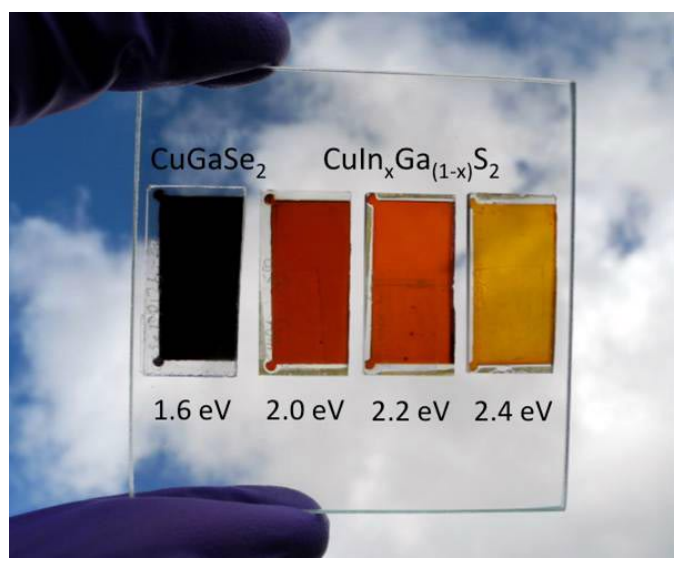

FIGURE 2. Optical image of as-deposited $CuGaSe_2$ and sulfur-annealed $CuInGaS_2$ thin films.

content in the film. A downward shift in the valence band was confirmed. Durability testing will be performed on this new type of material.

FY 2013 PUBLICATIONS/PRESENTATIONS

1. Surface Modification of a-SiC Photoelectrode Using Metal Nanoparticles, Feng Zhu, Ilvydas Matulionis, Nicolas Gaillard, Yuancheng Chang, Jian Hu, Josh Gallon, and Arun Madan, presented at MRS Spring Meeting, San Francisco, April 1–5, 2013.

2. PHOTOELECTROCHEMICAL HYDROGEN PRODUCTION, 2012 DOE H_2 Annual Merit Review meetings, Washington, DC, May 16, 2013 (presented by Nicolas Gaillard).

3. A nanocomposite photoelectrode made of 2.2 eV band gap copper tungstate (CuWO4) and multi-wall carbon nanotubes for solar-assisted water splitting, Nicolas Gaillard, Yuancheng Chang, Alexander DeAngelis, Scott Higgins, Artur Braun, International Journal of Hydrogen Energy, Volume 38, Issue 8, 19 March 2013, Pages 3166–3176.

4. Photoelectrochemical Reforming of Glucose for Hydrogen Production using a WO3–based Tandem Cell Device, D.V. Esposito, R.V. Forest, Y. Chang, N. Gaillard, S. Hou, K.H. Lee, B.E. McCandless, R.W. Birkmire, and J. Chen, Energy Environ. Sci. 5, 9091-9099 (2012).

5. Theory-driven Metal Oxide Down-selection for Photoelectrochemical Hydrogen Production: The Case of Metal Tungstates, Nicolas Gaillard, Yuancheng Chang, Dixit Prasher, S. Sarker, Muhammad N. Huda, presented at MRS Spring Meeting, San Francisco, April 1–5, 2013.

6. Development of Chalcogenide Thin Films Materials for Photoelectrochemical Hydrogen Production, Nicolas Gaillard, Stewart Mallory, Jess Kaneshiro, presented at MRS Spring Meeting, San Francisco, April 1–5, 2013.

7. Performance and Limits of 2.2eV Copper Tungstate (CuWO4) Mineral for Photoelectrochemical Hydrogen Production, N. Gaillard, Electrochemical Society PRIME meeting, symposium B10, 1741 (2012).

8. Ruthenium-Based Materials for Oxygen and Hydrogen Evolution Catalysis in Photoelectrochemical Applications, Y. Chang, J.M. Kaneshiro, N.M. Gaillard, Electrochemical Society PRIME meeting, Abstract MA2012-02 1775 (2012).

II.C.3 Critical Research for Cost-Effective Photoelectrochemical Production of Hydrogen

Liwei Xu[1] (Primary Contact), Anke E. Abken[1,2], Changyong Chen[3], Yanfa Yan[3], John Turner[4], Xunming Deng[1,3]

[1] Midwest Optoelectronics LLC (MWOE)
2801 W. Bancroft Street
Mail Stop 230
Toledo, OH 43606
Phone: (419) 215-8583
Email: xu@mwoe.com

[2] Xunlight Corporation (Xunlight), Toledo, OH

[3] University of Toledo (UT), Toledo, OH

[4] National Renewable Energy Laboratory (NREL), Golden, CO

DOE Managers

Eric Miller
Phone: (202) 287-5829
Email: Eric.Miller@ee.doe.gov

David Peterson
Phone: (720) 356-1747
Email: David.Peterson@go.doe.gov

Contract Number: DE-FG36-05GO15028

Subcontractors:
- Xunlight Corporation, Toledo, OH
- University of Toledo, Toledo, OH
- National Renewable Energy Laboratory, Golden, CO

Project Start Date: April 1, 2005
Project End Date: March 31, 2014

Overall Objectives

- To develop critical technologies required for cost-effective production of hydrogen from sunlight and water using thin film (tf)-Si based photoelectrodes.
- Two approaches are taken for the development of efficient and durable photoelectrochemical (PEC) cells:
  - An immersion-type PEC cell in which the photoelectrode is immersed in electrolyte.
  - A substrate-type PEC cell in which the photoelectrode is not in direct contact with electrolyte.

Fiscal Year (FY) 2013 Objectives

- Focus on immersion-type PEC systems, and work on improving the solar-to-hydrogen (STH) conversion efficiency and durability to achieve a cost-effective PEC system.
- Develop new designs of PEC electrodes, and explore new kinds of transparent, conducting, and corrosion-resistive coating material to improve the durability of the electrode.
- Develop new oxygen and hydrogen generation catalysts and understand how they affect the performance of the PEC system.
- Improve the PEC module case design, carry out outdoor testing of immersion-type PEC systems and study their performance under real-time conditions.

Technical Barriers

This project addresses the following technical barriers from the Hydrogen Production section 3.1.5 of the Fuel Cell Technologies Office Multi-Year Research, Development, and Demonstration Plan:

(AE) Materials Efficiency

(AF) Materials Durability

(AG) Integrated Device Configuration

(AI) Auxiliary Material

(AJ) Synthesis and Manufacturing

Technical Targets

This project focuses on the development of photoelectrode materials and triple junction tf-Si-based PEC cells to split water and generate hydrogen using sunlight. The status of this project towards the Fuel Cell Technologies Office Multi-Year Research, Development, and Demonstration Plan objective for PEC production of hydrogen is shown in Table 1.

FY 2013 Accomplishments

- Transparent, conducting, and corrosion-resistant (TCCR) coatings have been developed (Task 1). Successfully transferred results from research and development to the prototype roll-to-roll production machine for depositing cobalt oxide film on large area amorphous silicon (a-Si) triple-junction cells.
- Submitted two provisional patent applications on a novel design for immersion-type PEC cells where the illuminated side of the PEC electrode is divided into areas coated with corrosion-resistant transparent protective (CRTP) layer for light absorption and areas

TABLE 1. Progress towards Meeting Technical Targets for Immersion-Type PEC Cells and Systems

DOE Barriers	Performance Measure	Units	DOE 2013 Targets	DOE 2015 Targets	MWOE current Status
(AE) Materials Efficiency	STH Efficiency	%	8	15	5.7 (immersion-type)
(AF) Materials Durability	Hours under PEC Operation	Hours	≥1,000	≥0.5 year	480 hr (STH efficiency >1%)
	Cost	gge		$4 (2020)	TBD

gge – gasoline gallon equivalent; TBD – to be determined

coated with corrosion-resistant conducting catalytic (CRCC) layer for oxygen or hydrogen generation depending on the structure of the solar cells (Tasks 1 and 4).

- Developed complete procedures starting with standard solar cells from large-scale production, going through shunt passivation, next applying the TCCR layer and oxygen evolution reaction (OER) catalyst, and then adding hydrogen evolution reaction (HER) catalyst, and finally make a PEC electrode for photovoltaic hydrogen generation (Task 1 and 4).
- Have achieved 5.7% STH conversion efficiency for immersion type PEC cells (Task 4). This is, to our knowledge, the highest STH efficiency ever achieved for low-cost thin-film PEC electrode.
- Have achieved ~480 hours of operating life time for immersion-type PEC cells with final STH efficiency >1% (Task 4).
- Developed and evaluated a variety of hydrogen evolution catalyst materials such as plated platinum, ruthenium, electro-plated and sintered nickel (Task 4).
- Various immersion-type PEC module designs have been built to optimize the STH conversion efficiency, to extend the lifetime and reduce the cost (Task 4).

✧ ✧ ✧ ✧ ✧

INTRODUCTION

In this project, MWOE and its subcontractors are jointly developing critical technologies for cost-effective production of hydrogen from sunlight and water using tf-Si-based photoelectrodes.

Triple junction a-Si/a-SiGe/a-SiGe is an ideal material for making cost-effective PEC systems for hydrogen generation. It has the following key features:

- It has an open-circuit voltage (V_{oc}) of ~2.3 V and has an operating voltage around 1.6 V. This is ideal for water splitting. There is no need to add a bias voltage or to inter-connect more than one solar cell.
- It is made by depositing a-Si/a-SiGe/a-SiGe or a-Si/a-SiGe/μc-Si(or nc-Si) thin films on a conducting stainless steel substrate which can serve as an electrode. When we immerse a triple-junction solar cell in electrolyte and illuminate it under sunlight, the voltage is large enough to split water, generating oxygen at the Si solar cell side (for n-i-p type cells) and hydrogen at the back, which is the stainless steel side. This results in a simple and low-cost system which does not need a counter electrode or any wire connections.
- It is being produced on large rolls of 3-ft wide and up to 5,000 ft long stainless steel web in a 25-MW roll-to-roll production machine. Therefore, the corresponding PEC electrodes and systems can be made at very low cost.

However, the tf-Si solar cell is not highly stable in a strongly acidic or strongly basic electrolyte, which is typically needed for efficient and simultaneous evolution of oxygen and hydrogen. The tf-Si layers could be corroded by such electrolyte, especially under working conditions under light. In order to develop a PEC system using triple-junction tf-Si solar cells, we need to develop a coating which can be applied onto the solar cell surface, and which needs to have the following features: 1) transparent, so that the light can pass through the coating and reach the solar cells, 2) conducting, so that the voltage generated by the solar cell under sunlight can be applied to the electrolyte-electrode interface and generate oxygen and hydrogen, 3) corrosion resistant, so that it can protect the solar cell surface from being corroded in the electrolyte, and 4) capable of being deposited onto the solar cell surface at 200°C or lower, since the solar cell could be damaged if the temperature is higher than 200°C. In addition, it needs to act as an OER catalyst.

APPROACH

Five technical tasks are being performed under this grant to accomplish the project objectives:

- Task 1: Transparent, conducting and corrosion-resistant coating for triple-junction tf-Si-based photoelectrodes.
- Task 2: Hybrid multi-junction PEC electrodes having semiconductor-electrolyte junctions.
- Task 3: Understanding and characterization of photo-electrochemistry.
- Task 4: Development of device designs for low-cost, durable and efficient immersion-type PEC cells and systems.

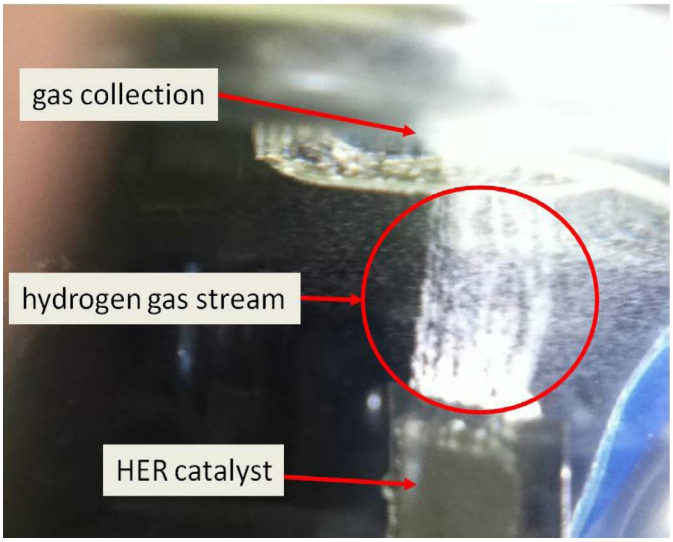

FIGURE 1. PEC electrode under operation conditions in KOH/H_3BO_3 electrolyte.

- Task 5: Development of device designs for large area, substrate-type PEC cells.

RESULTS

During last year, more work has been carried out to improve the TCCR coating (Task 1) and develop procedures to fabricate PEC electrodes from the standard solar cells by shunt passivation, applying the TCCR coating and OER catalyst and applying the HER catalyst. One of the focuses was to develop various HER catalyst materials, which have a substantial impact on the STH efficiency and durability of immersion-type PEC systems. We have studied five different types of HER catalyst. They are electroplated platinum, ruthenium, electroplated smooth Ni and porous nickel, and sintered nickel. While noble metals such as platinum and ruthenium are very good HER catalysts, Ni is considered a low-cost option for commercial-scale PEC systems for hydrogen generation. Platinum was plated from an H_2PtCl_6 solution and ruthenium was plated from a $RuCl_3$ solution. Smooth Ni was plated from a $NiCl_2/NiSO_4$ solution. To obtain porous Ni, we developed a method to co-deposit Ni and zinc from a $NiCl_2/NiSO_4/ZnCl_2$ solution and then leach out the zinc, which will leave a porous Ni coating. Sintered Ni is obtained by annealing Ni powders in a mixture of other metal powders acting as filler which then are leached out, leaving a porous Ni structure behind. The HER catalyst sheet is then attached to the backside of tf-Si-based PEC electrodes which use Co_3O_4 as the TCCR coating.

Table 2 summarizes the initial STH efficiency values obtained for PEC electrodes using these five HER materials. The highest initial STH efficiency of 5.7% has been obtained using plated ruthenium as the HER catalyst followed by plated platinum providing an STH efficiency of 5.6%. The STH for electrodes with Ni HER are somewhat lower: 4.1% for plated porous Ni, 3.0% for sintered Ni and 1.5% for plated smooth Ni catalyst materials. In comparison, the PEC electrode without any HER catalyst (last one in Table 2) has the lowest STH efficiency and worst durability, which indicates that a HER catalyst, although on the backside of photoelectrode, is essential.

TABLE 2. Comparison of Different Hydrogen Generation Catalyst

HER Catalyst	Initial STH Efficiency	Operating Hours with STH Efficiency >1%
Plated Platinum	5.6%	42 hrs
Plated Ruthenium	5.7%	37 hrs
Plated Smooth Nickel	1.5%	80 hrs
Plated Porous Nickel	4.1%	170 hrs
Sintered Nickel	3.1%	480 hrs
No HER catalyst	1.2%	8 hrs

Although the highest STH efficiency values were obtained using platinum and ruthenium as HER catalyst materials, the PEC system using Ni as the HER catalysts demonstrates much better durability (480 hours). Figure 2 shows STH efficiency versus operation time for PEC electrodes with different HER catalyst materials. More work is underway to improve both the efficiency and durability.

Examining the electrodes with decayed efficiency, corrosion is observed at the oxygen generating side, which is the solar cell/TCCR coating side of the electrode. Therefore, we concluded that even though Co_3O_4 itself is stable in electrolyte, the thickness (~70 nm) that we have been using might be too thin to protect the solar cell underneath. On the other hand, if we increase the thickness of Co_3O_4, the

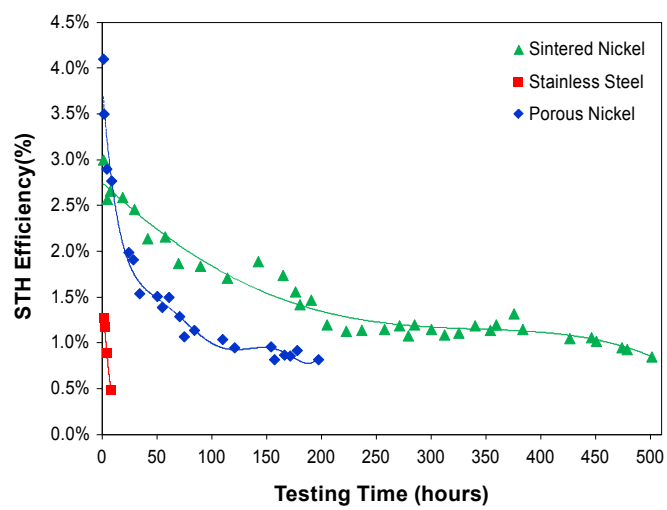

FIGURE 2. STH efficiency versus operation time for PEC electrodes with different HER catalyst materials.

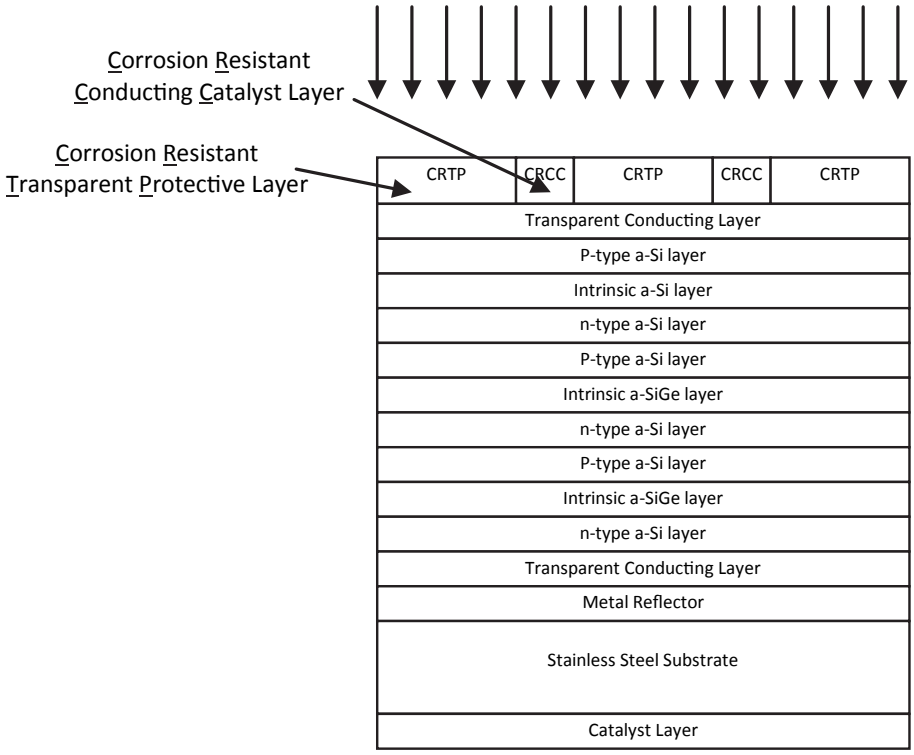

FIGURE 3. Schematic of the PEC electrode with the novel design of alternating CRCC and CRTP coating.

transparency will decrease. Recently, we have developed a novel design which would address this problem and which could lead to a PEC electrode that can generate hydrogen effectively and have a good durability.

In this novel design as shown in Figure 3 and Figure 4, we separate the solar cell surface into two types of regions, Region I and Region II. For Region I, we coat the surface with a CRTP layer, which does not need to be electrically conducting. There are many materials we can use, for example, clear coat, SiO_2 coating, etc. For region II, we coat the surface with a CRCC layer, such as Co_3O_4 material. In this design, Region II does not need to be transparent, it only needs to have good electrical conductivity and act as a good oxygen generating site. Since there is no need to be transparent, we can make much thicker Co_3O_4 coating, not being limited by the 70-nm thickness, or we can use a metal catalyst, such as platinum. Effectively, Region I will act as solar energy absorbing and electrical voltage generating sites; the indium tin oxide (ITO) layer on top of the solar cell and underneath the CRTP and CRCC coating transfers the voltage from Region I to Region II, and Region II will act as oxygen generating site with Co_3O_4 as the oxygen generating catalyst. We have filed two provisional patents based these new ideas. The experiment work is underway.

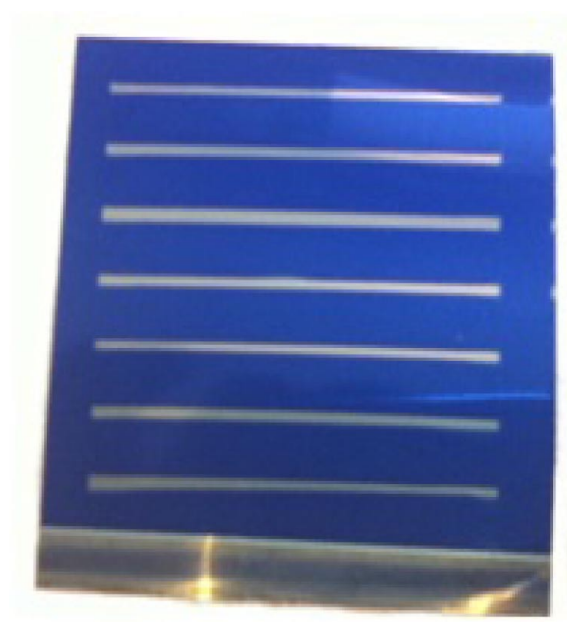

FIGURE 4. PEC electrode with CRCC/CRTP design. The silver lines are Co_3O_4-coated regions (CRCC), and the blue regions are for light absorption (CRTP). The ratio between the areas of CRCC and the CRTP regions can be adjusted to optimize the PEC performance.

CONCLUSIONS AND FUTURE DIRECTIONS

- Fabricate PEC electrodes with the novel CRTP/CRCC design which potentially could extend the durability of the PEC electrodes substantially.
- Experiment with different fabrication methods for PEC electrode preparation with respect to solar cell and ITO deposition conditions, different catalyst and fabrication process, and different conditions for applying TCCR coating both in the lab and in the large scale roll-to-roll deposition system.
- Continue to develop different module designs to optimize the STH efficiency, extend lifetime, and reduce cost.
- Develop large-area, commercial-size PEC systems and carry out tests in real-life conditions.
- Complete concept design of large-area, low-cost PEC system.
- Perform preliminary techno-economic analysis of the immersion-type PEC system based on the concept design.
- Collaborate with different research groups around the world to further PEC hydrogen generation research and development.
- This project is approaching its final phase, and one of the priorities is to document progress made and lessons learned to position for further research and commercialization in the future.

FY 2013 PUBLICATIONS/PRESENTATIONS

1. Xu, L., Deng, X., Abken, A.E., Chen, C., Turner, J., "Critical Research for Cost-effective Photoelectrochemical Production of Hydrogen", 2013 DOE Hydrogen Program and Vehicle Technologies Program Annual Merit Review and Peer Evaluation, Oral presentation, Crystal Gateway Marriott, Arlington, VA., May 16, **2013**.

II.C.4 Characterization and Optimization of Photoelectrode Surfaces for Solar-to-Chemical Fuel Conversion

Tadashi Ogitsu (Primary Contact), Woon Ih Choi, Brandon Wood
Lawrence Livermore National Laboratory (LLNL)
7000 East Ave., L-413
Livermore, CA 94550
Phone: (925) 422-8511
Email: ogitsu@llnl.gov

DOE Manager
Eric Miller
Phone: (202) 287-5829
Email: Eric.Miller@ee.doe.gov

Project Start Date: March 1, 2010
Project End Date: Project continuation and direction determined annually by DOE

Overall Objectives

- Develop theoretical tool chest for modeling photoelectrochemical (PEC) materials to be used for synergistic theory, characterization, and synthesis activities.
- Uncover underlying mechanisms of surface corrosion and hydrogen evolution at the water-photoelectrode interface.
- Elucidate relationship between stability and efficiency.
- Use derived structure-property relationships to develop device improvement strategies.

Fiscal Year (FY) 2013 Objectives

- Complete the *ab initio* simulations of water-InP and water-GaP interfaces, including data analysis and publication in peer-reviewed journals.
- Investigate corrosion mechanisms for III-V semiconductor electrodes.
- Identify chemical environments of N_2^+ bombardment-induced nitrogen impurities in $GaInP_2$, based on measured and calculated X-ray emission spectroscopy (XES) spectra.
- Publish results on simplified interfacial charge-transfer model for high-throughput assessment of PEC surface catalytic activity.
- Compile knowledge database of existing research on PEC electrode materials and interfaces, with emphasis on III-Vs and chalcogenides.

Technical Barriers

This project addresses the following technical barriers from the Hydrogen Production section (3.1) of the Fuel Cell Technologies Office Multi-Year Research, Development, and Demonstration Plan [1]:

(AE) Materials Efficiency – Bulk and Interface

(AF) Materials Durability – Bulk and Interface

Technical Targets

This project is conducting fundamental theoretical studies of mechanisms of corrosion and catalysis in semiconductor-based photoelectrode materials for PEC hydrogen production. Insights gained from these studies will be applied toward the optimization and design of semiconductor materials that meet the following DOE 2015 PEC hydrogen production targets (Table 3.1.8A in [1]):

- Solar-to-hydrogen (STH) energy conversion ratio: 15%
- Electrode replacement lifetime: 0.5 year

FY 2013 Accomplishments

- Continued with compilation, review, and sharing of available information on III-V electrode materials, catalysts, and related subjects (ongoing).
- Began gathering available information on copper indium gallium diselenide electrodes as a lower-cost alternative to high-STH III-V semiconductors.
- Completed quantum molecular dynamics of water-electrode (GaP/InP) interfaces, and submitted two papers on the properties of interfacial water and wetted surfaces [2,3].
- Applied the simple model Hamiltonian approach developed in FY 2012 to an unconventional photoelectrode, MoS_2. A paper on this topic was submitted [4].
- The National Renewable Energy Laboratory (NREL) team conducted further experiments to validate the hole-trapping corrosion mechanism. This was one of three possible corrosion mechanisms identified in FY 2011 [5], for which supporting evidence emerged during group discussions in FY 2012 [6].
- Continued collaborations with unfunded external collaborators to develop theoretical tool chest for PEC hydrogen research.

- Continued joint theoretical/experimental XES study on III-V electrode surface (continue through FY 2013 and beyond).

✧ ✧ ✧ ✧ ✧

INTRODUCTION

Certain III-V-based PEC cells, notably the $GaInP_2$/GaAs tandem cell developed at NREL, are known to demonstrate high STH conversion efficiencies that are close to the DOE FY 2015 goal [1]. However, durability of these cells has remained the key unresolved issue so far. The primary purpose of this project is to perform a detailed investigation into the microscopic properties of the water-electrode interface, and to use this information to identify correlations with device performance, as measured in terms of STH conversion efficiency and corrosion resistance. The results will provide key feedback to collaborators at NREL, helping them develop a coherent performance optimization scheme for III-V-based photoelectrodes. State-of-art X-ray spectroscopic measurements performed by the University of Las Vegas (UNLV) team will bridge remaining gaps in the knowledge obtained from our atomistic modeling, facilitating comparison with actual electrode properties. In FY 2013, we had three major accomplishments [7]. First, our findings on the interfacial properties and their implications for the hydrogen evolution reaction (HER) and corrosion reactions were summarized in two papers submitted to peer-reviewed journals [2,3]. Second, the simple model Hamiltonian-based method tested in FY 2012 [6] was applied to MoS_2, and all results were summarized and submitted to a peer-reviewed journal [4]. Third, in order to determine the chemical environment of nitrogen impurities in $GaInP_2$ introduced by N_2^+ bombardment, a rational procedure to build model atomic structures that can reproduce the measured XES was developed, and the major nitrogen states were successfully identified [8].

APPROACH

Further progress in semiconductor-based PEC photoelectrodes requires in-depth understanding of the complex relationship between surface stability and catalytic activity. This in turn relies on knowledge of the fundamental nature of the electrode-water interface, and of the chemical pathways explored during surface-active hydrogen evolution. As such, we are carrying out finite-temperature *ab initio* molecular dynamics simulations and energetics calculations based on density-functional theory to understand the chemical, structural, and electronic properties of water/electrode interfaces under equilibrium conditions, as well as to understand the competing chemical reaction pathways visited during photocatalysis. Our approach uses (001) surfaces of InP, GaP and $GaInP_2$ as model semiconductor electrodes. We are investigating on effect of the foreign chemical species on the stability and reactivity of the electrode surfaces, as suggested by our collaborators in J. Turner and T. Deutsch's group at NREL [9], as well as independent reports in the literature that surface oxygen may play a key role in motivating both the surface photocorrosion and the catalytic water splitting reaction [10,11]. Accordingly, we are evaluating the stability, structure and reactivity of the III-V(001)/water interfaces in the presence of surface oxygen, hydroxyl, and nitrogen, in order to correlate the results to experimentally observed surface compositions and morphologies. We also provide *ab initio* derived X-ray spectroscopic data to enable direct comparison with experimental results from Prof. C. Heske's group at UNLV. This information is intended to suggest a strategy for device improvement.

RESULTS

About 1,200 papers related to PEC hydrogen research have been collected, indexed, and stored. Those deemed especially relevant to III-V semiconductor-based approaches have been summarized and shared with members of the III-V Surface Validation Team (LLNL/NREL/UNLV) of the DOE Photoelectrochemical Hydrogen Production Working Group using a limited-access community web forum and traditional email communication. Particular emphasis was put on $GaInP_2$, In_2O_3, the growth interface between the two, co-catalyst, and corrosion mechanisms, since these are expected to be crucial for identifying the agent responsible for corrosion resistance and hydrogen evolution.

Detailed studies of InP and GaP (001) surfaces and their interfaces with water were summarized as two separate papers and submitted to peer reviewed journals [2,3]. As a continuation of previous studies on these surfaces and the effect of oxidation and/or hydroxylation [12], the first paper discussed how these surfaces are affected by contact with bulk water [3]. We previously showed that oxidized surfaces facilitate water dissociation, which leads to surface hydroxylation [12]. A consistent behavior was observed during *ab initio* molecular dynamics of water/III-V interfaces, where the formation of an ice-like hydrogen-bond network was observed near both InP and GaP. No major significant differences were observed in the structural and electronic properties of the two surfaces [3]. In contrast, the properties of interfacial water near GaP(001) and InP(001) were found to exhibit a peculiar difference [2]. In particular, at the GaP (001)-water interface, a clear gap in the hydrogen-bond network was found between the surface adsorbants (O, OH, or H_2O) and bulk water, while at the InP (001)-water interface, the hydrogen-bond network is continuous and dynamic. Further analysis suggested that these differences will lead to differences in surface proton transport properties at these interfaces: it is facile at the InP-water interface, while likely to be hindered at the GaP-water

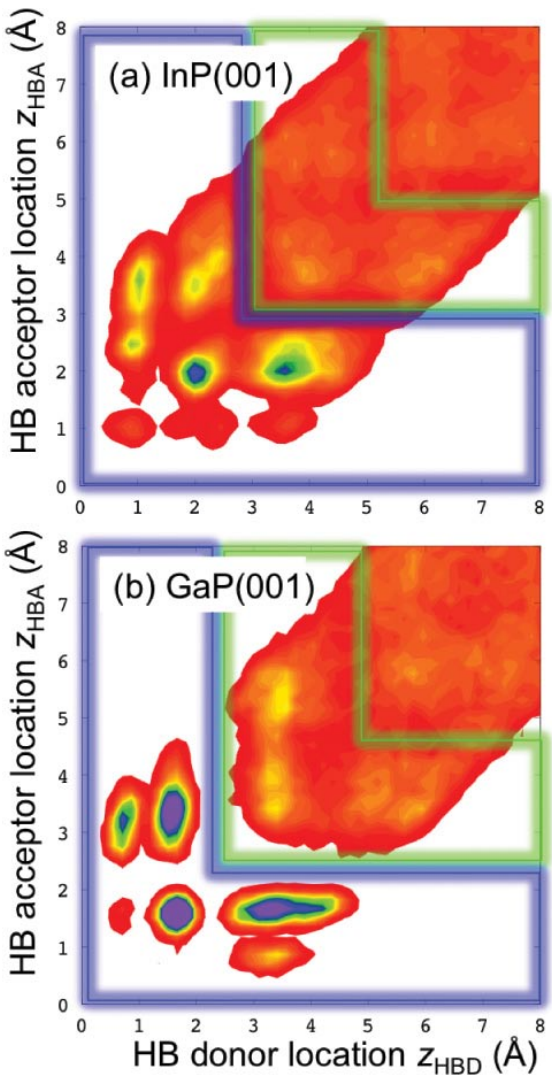

FIGURE 1. Probability density of locations (measured perpendicular to the surface) of hydrogen-bond donor-acceptor pairs in water at the interface with (a) InP(001) and (b) GaP(001). The simulations account for native surface hydroxylation [2].

interface. Possible scenarios for the relationship between the proton transport property and photoelectrode performance/corrosion resistance are discussed in detail [2]. These include differences in HER and corrosion mechanisms, as well as the influence of surface catalysts on these mechanisms.

During a Working Group teleconference held in FY 2012, we proposed a "dark" current experiment, in which electrons are provided by a power source to the cathode rather than by photoillumination. This allows one to identify whether cathodic hole transport, which is relevant only in the case of photoillumination where electrons and holes are co-generated, plays a role in the corrosion mechanism. If hole trapping is the major source of corrosion, the rate of corrosion should be greatly suppressed in a dark current experiment. In addition to the published results [13] found during the FY 2012 discussion [6], more experiments were conducted by NREL in FY 2013. It was shown that the rate of corrosion is linear to the photoillumination (i.e., hole concentration) [7]. This supports our assertion that the hole-trapping corrosion mechanism is the major contributor for III-V-based photocathode. Further investigation is desired to understand the nature of hole-traps in order to develop an effective mitigation strategy.

Motivated by the reported stability of GaN as a photoelectrode [14,15], the effect of nitrogen bombardment on the $GaInP_2$ surfaces has been being studied by NREL during FY 2012 [16] and FY 2013 [17]. The spectroscopy team at UNLV performed a series of measurements including N K-edge XES on these nitrogen-treated electrodes [18]. Our earlier XES simulations results indicated that the chemical environments of nitrogen impurities were not pure substitutional impurities. In FY 2013, we have developed a rational scheme to determine the relevant chemical environment of nitrogen based on a consideration of the following factors [7]: (1) expected shape and positions of XES peaks based on the atomic levels and their hybridization; (2) chemical shifts from the environment; and (3) spectral broadening due to vacancy-induced structural distortions. Our results indicated that a significant number of nitrogen impurities are forming various types of vacancy-interstitial complexes, suggesting that more thermodynamically driven approach might be suitable in forming a thin layer of less defective nitride compound (assuming that defects would have negative impact on STH efficiency and/or corrosion resistance). We point out that the developed procedure described above is generally applicable to an arbitrary system and currently being summarized in order to publish in a peer reviewed journal [8].

Finally, the model Hamiltonian approach developed by Santos et al. [19] tested in FY 2012 [6] was applied to the protonation process on a MoS_2 electrode. This method is based on Markus-Hush theory and the Anderson-Newns model, and is able to simultaneously address H^+ solvation, charge transfer reactions, and chemisorption very simply and with relatively low computational cost. This approach was tested with Pt in the original work [19] and with $GaInP_2$ in FY 2012 [6], where it was confirmed that the model is able to reproduce qualitatively correct behavior of protonation on these systems under a bias potential. On Pt, proton adsorption and reduction is exothermic and barrier-free, while on $GaInP_2$, it is exothermic with a large barrier. Our new results on MoS_2 showed that protonation on the Mo site has a negligibly small energy barrier with favorable binding energy for the HER. This was attributed to an appropriate strength of interaction between relevant orbitals of H and Mo (see Figure 3). The S site might have a reasonable protonation free energy profile if the surrounding atoms were able to relax fast enough compared to the time scale of protonation (quasi-adiabatic). We also found that the proton binding energy could be modulated by solvation, due to

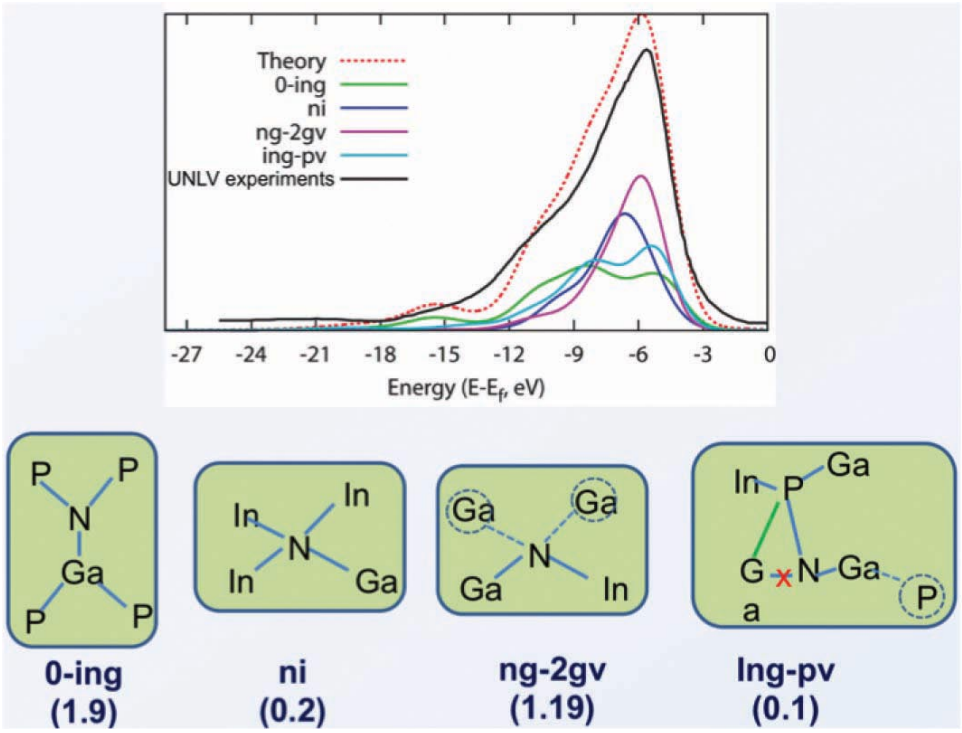

FIGURE 2. Calculated XES spectra corresponding to different possible nitrogen environments in nitridated $GaInP_2$, shown schematically below the graph. The total calculated spectrum (red dotted) is a fit to the experimental spectrum (black) based on a weighted sum of these calculated components [8].

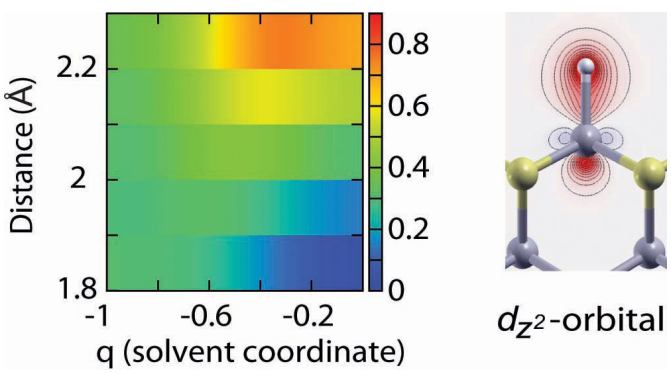

FIGURE 3. Left: calculated free energy profile for the protonation at the Mo site on MoS_2 as functions of solvent coordinate and Mo-H distance [4]. Right: the Mo-H bonding orbital that contributes to the low barrier protonation where the dz^2 character is clearly seen [4].

sizable polarization. All of these results were summarized and submitted to a peer-reviewed journal [4]. We emphasize that this approach provides a high-throughput way to gain insights on the underlying mechanisms that responsible for favorable/unfavorable free energy profile of protonation in different materials, which could be very useful for designing a novel catalytic material.

CONCLUSIONS AND FUTURE DIRECTIONS

- The studies of water/III-V interface performed during FY 2010-FY 2013 were summarized as two papers and submitted to peer-reviewed journals.
- The study of the catalytic reaction process on MoS_2 based on the *ab initio*-derived simple model Hamiltonian were summarized and submitted to a peer-reviewed journal.
- The linear relation between the hole-carrier concentration and the rate of corrosion was shown by the experiments conducted by NREL in FY 2013. Discussions for developing a research plan for understanding the precise nature of hole-traps responsible for the observed corrosion underway.
- Using theoretical and experimental N K-edge XES spectra, the procedure to construct model atomic structures of impurities in semiconductor electrode was established. Based on this, we have identified the major chemical states of nitrogen impurities that were introduced to $GaInP_2$ by N_2^+ bombardment.
- The compilation of past studies will continue in order to refine our growing understanding of the relevant issues of photoelectrochemistry, particularly with respect to III-V surfaces, their oxides, and interfaces between them.

This effort will be expanded to the other materials and catalysts in FY 2014.

- Develop deeper understanding on the role of thermodynamics and kinetics in HER and in corrosion for a given photoelectrode material in order to identify an effective corrosion mitigation strategy.

FY 2013 PUBLICATIONS/PRESENTATIONS

Publications

1. T. Ogitsu, B. Wood, W. Choi, *DOE Fuel Cell Technology Hydrogen Program Annual Merit Review* (2013).

2. B.C. Wood, E. Schwegler, W.-Ih Choi, and T. Ogitsu, "Aspects of the surface chemistry of GaP(001) and InP(001) in contact with water," submitted.

3. B.C. Wood, E. Schwegler, W.-Ih Choi, and T. Ogitsu, "Hydrogen-bond dynamics of water at the interface with InP/GaP(001) and its implications for photoelectrochemistry," submitted.

4. W.-I. Choi, B. Wood, E. Schwegler, and T. Ogitsu, "Site-dependent free energy barrier for proton reduction on MoS_2 edges," submitted.

5. W.-I. Choi, M. Weir, T. Deutsch, T. Williamson, L. Weinhardt, A. Benkert, M. Blum, F. Meyer, M. Bär, K. George, B.C. Wood, D. Prendergast, E. Schwegler, J. Turner, C. Heske, and T. Ogitsu, "Chemical environments of implanted nitrogen in $GaInP_2$ characterized with X-ray emission spectroscopy," in preparation.

Presentations

1. PRiME 2012, Honolulu, HI, Oct 2012 (invited).

2. Physics Colloquium at UT Arlington, Arlington, TX, Oct 2012 (invited seminar).

3. Invited seminar at U. South Florida, Jan 2013.

4. WIP progress report presentation at DOE PEC hydrogen WF meeting at UNLV, Jan 2013.

5. American Physical Society March Meeting in Baltimore, March 2013 (two presentations).

6. 2013 Materials Research Society Spring Meeting in San Francisco, April 2013.

7. 223rd ECS Meeting in Toronto, May 2013 (invited).

8. DOE EERE Fuel Cell Technology Annual Merit Review in Arlington, May 2013.

9. Invited seminar at Sandia National Laboratory, July 2013.

10. SPIE conference, San Diego, August 2013 (invited).

11. CPMD-Meeting 2013, Matter, life, light from ab initio molecular dynamics simulations, Leipzig, September 2013 (invited).

12. American Chemical Society Fall Meeting, Indianapolis, September 2013 (invited).

13. JSAP-MRS Joint Symposia, Kyoto, September 2013 (oral).

REFERENCES

1. DOE EERE Fuel Cell Technologies Office Multi-Year Research, Development, and Demonstration Plan, 3.1 Hydrogen Production, 2012, http://www1.eere.energy.gov/hydrogenandfuelcells/mypp.

2. B. Wood, E. Schwegler, W.-Ih Choi, and T. Ogitsu, "Hydrogen-bond dynamics of water at the interface with InP/GaP(001) and its implications for photoelectrochemistry," submitted.

3. B. Wood, E. Schwegler, W.-Ih Choi, and T. Ogitsu, "Aspects of the surface chemistry of GaP(001) and InP(001) in contact with water," submitted.

4. W.-Ih Choi, B. Wood, E. Schwegler, T. Ogitsu, "Site-dependent free energy barrier for proton reduction on MoS_2 edges," submitted.

5. T. Ogitsu, B. Wood, W. Choi, *DOE Fuel Cell Technology Hydrogen Program Annual Merit Review* (2011).

6. T. Ogitsu, B. Wood, W. Choi, *DOE Fuel Cell Technology Hydrogen Program Annual Merit Review* (2012).

7. T. Ogitsu, B. Wood, W. Choi, *DOE Fuel Cell Technology Hydrogen Program Annual Merit Review* (2013).

8. W.-I. Choi, M. Weir, T. Deutsch, T. Williamson, L. Weinhardt, A. Benkert, M. Blum, F. Meyer, M. Bär, K. George, B.C. Wood, D. Prendergast, E. Schwegler, J. Turner, C. Heske, and T. Ogitsu, "Chemical environments of implanted nitrogen in $GaInP_2$ characterized with X-ray emission spectroscopy," in preparation.

9. T.G. Deutsch, C.A. Koval, and J.A. Turner, *J. Phys. Chem. B* 110, 25297 (2006).

10. A. Heller, *Science* **223**, 1141 (1984).

11. J. Vigneron, M. Herlem, E. M. Khoumri, and A. Etcheberry, *Appl. Surf. Sci.* **201**, 51 (2002).

12. B. Wood, T. Ogitsu, and E. Schwegler, *J. Chem. Phys.* **136**, 064705 (2012).

13. T. Deutsch, C. Koval, and J. Turner, *J. Electrochem. Soc.* **145**, 3335 (1998).

14. K. Maeda et al., J. Phys. Chem. B, **109**, 20504 (2005).

15. K. Maeda et al., J. Am. Chem. Soc., **127**, 8286 (2005).

16. T. Deutsch *et al., DOE Fuel Cell Technology Hydrogen Program Annual Merit Review* (2012).

17. T. Deutsch *et al., DOE Fuel Cell Technology Hydrogen Program Annual Merit Review* (2013).

18. C. Heske *et al.*, *DOE Fuel Cell Technology Hydrogen Program Annual Merit Review* (2012).

19. E. Santos *et al.*, *Phys. Rev. B* **79**, 235436 (2009).

II.C.5 Metal Oxide Semiconductor Nanotubular Arrays for Photoelectrochemical Hydrogen Generation

Dev Chidambaram (Primary Contact), Mano Misra, York Smith, and Ruchi Gakhar
University of Nevada Reno
Chemical and Materials Engineering
Reno, NV 89557-0388
Phone: (775) 784-7066
Email: dcc@unr.edu

DOE Managers
Eric Miller
Phone: (202) 287-5829
Email: Eric.Miller@hq.doe.gov
David Peterson
Phone: (720) 356-1747
Email: David.Peterson@go.doe.gov

Contract Number: DE-FG-36-06GO86066

Subcontractors:
- National Renewable Energy Laboratory, Golden, CO
- University of Arkansas at Little Rock, Little Rock, AR
- University of Nevada Las Vegas, Las Vegas, NV

Project Start Date: October 1, 2006
Project End Date: September 30, 2014

Overall Objectives

Develop high efficiency hybrid-semiconductor nanotubular materials for hydrogen generation by water splitting

Fiscal Year (FY) 2013 Objectives

- Enhance visible light absorption of metal oxide nanotubes
- Develop new synthesis techniques for enhanced photoelectrochemical (PEC) performance

Technical Barriers

This project addresses the following technical barriers from the Hydrogen Production section of the Fuel Cell Technologies Office Multi-Year Research, Development, and Demonstration Plan:

(AE) Materials Efficiency - Bulk and Interface

(AF) Materials Durability - Bulk and Interface

(AG) Integrated Device Configurations

(AJ) Synthesis and Manufacturing

Technical Targets

The project is aimed at conducting fundamental materials and device studies related to the development of metal oxide semiconductor nanotubular arrays for PEC hydrogen generation that have high efficiency. Insights gained from these studies will be applied toward the design and synthesis of hydrogen generation materials that meet the following DOE hydrogen production targets:

- Cost: $4/gasoline gallon equivalent (gge) at plant gate by 2020
- Cost: $5/gge at plant gate by 2017
- Efficiency: 15% efficiency by 2020

FY 2013 Accomplishments

- Developed hierarchical TiO_2 nanotubes (H-T-NT) nanolace-type TiO_2 nanotubes (T-NT) in a single anodization step.
- Developed a method to extend the visible light absorbance of tantalum oxynitride nanotubes.
- Developed new synthesis techniques for higher order one-dimensional titania nanotube architectures which demonstrate enhanced PEC water splitting.

✧ ✧ ✧ ✧ ✧

INTRODUCTION

Increasing global energy demand requires the development of new sustainable and environmentally friendly energy storage and conversion systems [1]. Solar energy has the potential to play a significant role in meeting our energy demands. Solar-assisted water splitting to generate hydrogen as an energy carrier is one of the options, and utilizes the two most abundant resources, namely, solar energy and water [2]. Successful implementation of solar-based energy systems can possibly lower the cost of hydrogen to be comparable to gasoline prices [3]. PEC water splitting was first demonstrated in 1972 using TiO_2 [4]. Other metal oxides such as ZnO, WO_3, and Fe_2O_3 have been investigated for PEC water splitting [5-7]. However, TiO_2 remains the most studied material for this reaction as it retains several desirable properties such as chemical and optical stability as well as being environmentally benign.

The use of highly ordered, one-dimensional nanostructures of TiO_2, such as nanotubes, has gained much attention over the past decade due to their inherently large surface area and unidirectional flow of charges. More specifically, T-NT formed via anodic oxidation of titanium metal have demonstrated superior performance over its nanoparticle counterpart in charge transport [8]. The use of hierarchical type T-NT has demonstrated enhanced performance over plain T-NT in photovoltaic and PEC applications. The common synthesis technique adopted for growing hierarchical-type T-NT involves a two-step anodization process. First, T-NT are grown on a Ti substrate and subsequently removed via ultrasonication for a long duration, leaving a patterned Ti substrate.

APPROACH

The project approach is to increase visible light utility of metal oxide nanotubes by examining new synthesis techniques and to study the effect of surface treatment and effect of light irradiation during synthesis. Then, characterization of the prepared materials is conducted to gain a fundamental understanding of the materials properties. The materials are then evaluated for their PEC behavior by using them as photoanodes in a PEC setup. Finally, the stability of materials in the presence and absence of irradiation is studied using electrochemical methods combined with electron microscopic analysis and spectroscopic methods.

RESULTS

Figures 1 and 2 show scanning electron microscope (SEM) images of the T-NT and hierarchical type titania nanotubes (H-T-NT). The etching treatment anisotropically removes a small layer of Ti resulting in a rippled surface of titania. As nanotube formation depends on the local electric field and solution diffusion rate [9], the etching treatment prior to anodization provides a discontinuous surface where the electric field is not uniform and becomes localized at the grains. The current during the anodization was observed to stabilize rapidly, implying an initial oxide layer had already formed (via etching). The existing oxide layer that is formed is relatively smooth as the etching treatment results in the exposure of small grains. The initial pitting mechanism for nanotube formation occurs at the wells of the surface. The smooth surface from the etching treatment results in a more uniform distribution of electric field, yielding a porous top layer to the nanotubes (inset Figure 2). Previous reports show anodization of a specially processed Ti foil smoothed via mechanical polishing resulted in a nanoporous layer [10]. However, the etching treatment of the Ti substrates creates a random surface of exposed grains, which is not an entirely uniform surface. This treatment results in a larger distribution of pore sizes within the nanoporous layer formed on top of the nanotubes. Longer etching treatments of the Ti substrates forms a thicker native oxide layer prior to anodization. It was observed that the nanoporous layers become qualitatively thicker with longer etching treatments. Figure 3 shows SEM images of H-T-NT and nano-grass type titania nanotubes (N-T-NTs). Anodization at elevated temperatures increases the reaction kinetics of not only nanotubular formation, but also the chemical dissolution of the nanotubes as well (due to solvated F^- species). Etching of the tops of the nanotubes leads to inhomogeneous nanotube formation. As the walls of the nanotubes become too thin, they collapse on themselves due to capillary forces during rapid drying. Larger examination of the N-T-NT samples shows qualitatively more nanograss with increased anodization temperature.

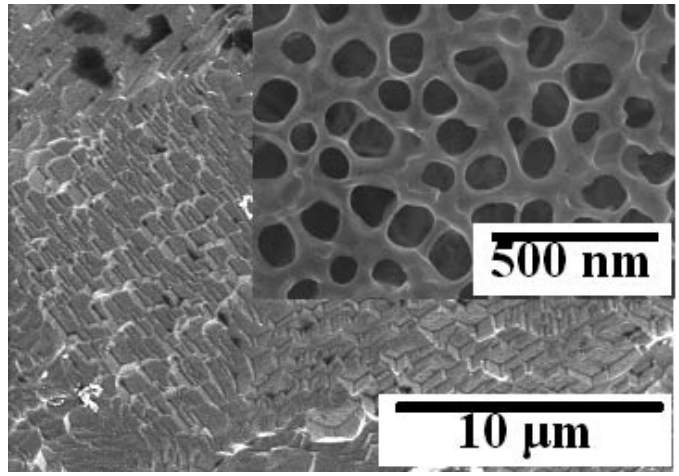

FIGURE 1. SEM Image of Plain T-NT

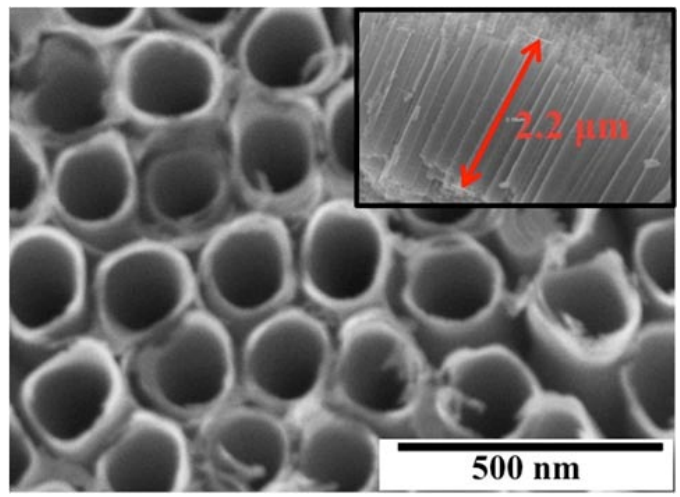

FIGURE 2. SEM image of etched Ti surface before anodization. Inset shows the formation of H-T-NT.

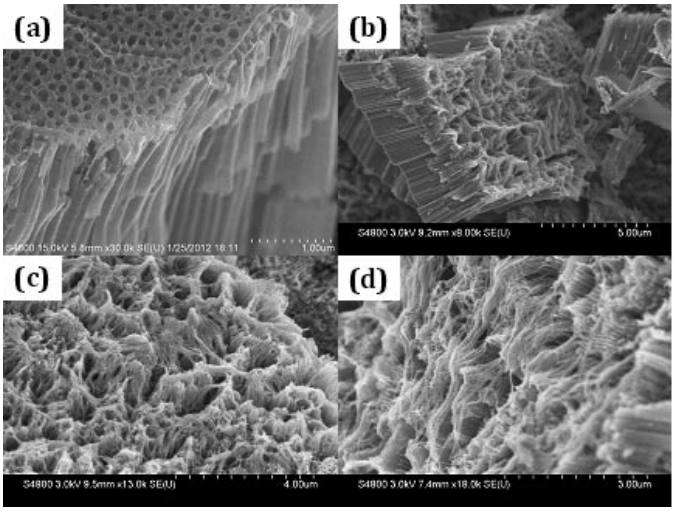

FIGURE 3. SEM Images of (a) H-T-NT, (b) N-T-NT Prepared at 40°C, (c) 50°C, and (d) 65°C

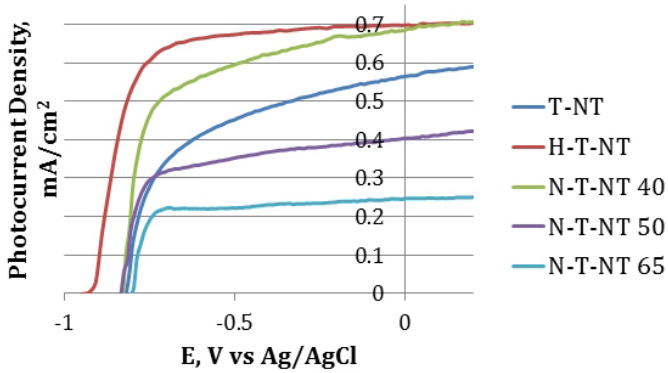

FIGURE 4. Potentiodynamic plot of various substrates under AM 1.5 irradiation in 1 M KOH electrolyte. The anodes were anodically polarized from open-circuit potential to 0.2 V (vs Ag/AgCl) at 10 mV/s.

PEC Activity

The PEC enhancement of the hierarchical nanotubes over plain nanotubes can be attributed to an increased surface area for light harvesting and electrolyte surface coverage as well as improved charge separation. Wang, et al., [11] studied the ultraviolet photoelectron spectroscopy of hierarchical and plain titania nanotubes. The study found the work function difference between the plain nanotubes and hierarchical nanotubes to be 0.05 eV, which is sufficient for improving charge separation. The nanoring/nanoporous layer on top of the tubes serves as an electron transporter for effective charge separation and rapid transport of photogenerated charges [11]. These results are further supported by the electrochemical impedance spectroscopy and Mott-Schottky studies conducted on hierarchical titania nanotubes by Zhang and Wang [12], in which they reported a reduction in charge transfer resistance between the semiconductor/electrolyte interface in conjunction with an increased charge carrier density. In a similar manner, the same argument can be said for the N-T-NT regarding improved PEC activity. However, as the layer of the nanograss becomes thicker (due to increased anodization temperature, *vide supra*) the PEC activity drastically decreases.

CONCLUSIONS AND FUTURE DIRECTIONS

The observed behavior may be attributed the entangled nanograss interfaces which act as recombination centers. The photo-induced electrons and holes have a more tortuous diffusion path within the nanograss increasing their probability or recombining within the volume of the nanograss. A similar trend was observed when the nanoporous layer on H-T-NT samples was thicker due to longer etching treatment. Future studies would include:

- Electrochemical impedance spectroscopy studies on these samples would give information on the electrolyte/photoanode interface charge resistance as well as the charge carrier density.
- Stability studies in the presence and absence of irradiation.
- Materials will be studied using spectroscopy and microscopy.

FY 2013 PUBLICATIONS/PRESENTATIONS

1. B. Sarma, A.L. Jurovitzki, Y.R. Smith, S.K. Mohanty, M. Misra, Redox-Induced Enhancement in Interfacial Capacitance of the Titania Nanotube/Bismuth Oxide Composite Electrode, ACS Applied Materials & Interfaces 5 (2013) 1688-1697.

2. B. Sarma, Y.R. Smith, A.L. Jurovitzki, R.S. Ray, S.K. Mohanty, M. Misra, Supercapacitance behavior of porous oxide layer grown on 302 type stainless steel substrate, Journal of Power Sources 236 (2013) 103-111.

3. B. Sarma, Y.R. Smith, S.K. Mohanty, M. Misra, Electrochemical deposition of CdO on anodized TiO2 nanotube arrays for enhanced photoelectrochemical properties, Materials Letters 85 (2012) 33-36.

4. Y.R. Smith, B. Sarma, S.K. Mohanty, M. Misra, Light-Assisted Anodized TiO2 Nanotube Arrays, ACS Applied Materials & Interfaces 4 (2012) 5883-5890.

REFERENCES

1. N.S. Lewis, D.G. Nocera, Powering the planet: chemical challenges in solar energy utilization, Proc Natl Acad Sci USA, 103 (2006), pp. 15729–15735.

2. T. Bak, J. Nowotny, M. Rekas, C.C. Sorrell, Photo-electrochemical hydrogen generation from water using solar energy. Materials-related aspects, Int J Hydrogen Energy, 27 (2002), pp. 991–999.

3. J.O.M. Bockris, T.N. Veziroglu, Estimates of the price of hydrogen as a medium for wind and solar sources, Int J Hydrogen Energy, 32 (2007), pp. 1605–1610.

4. A. Fujishima, K. Honda, Electrochemical photolysis of water at a semiconductor electrode, Nature, 238 (1972), pp. 37–38.

5. A. Wolcott, W.A. Smith, T.R. Kuykendall, Y. Zhao, J.Z. Zhang, Photoelectrochemical study of nanostructured ZnO thin films for hydrogen generation from water splitting, Adv Funct Mater, 19 (2009), pp. 1849–1856.

6. H. Wang, T. Lindgren, J. He, A. Hagfeldt, S.-E. Lindquist, Photolelectrochemistry of nanostructured WO_3 thin film electrodes for water oxidation: mechanism of electron transport, J Phys Chem B, 104 (2000), pp. 5686–5696.

7. S.K. Mohapatra, S.E. John, S. Banerjee, M. Misra, Water photooxidation by smooth and ultrathin alpha-Fe_2O_3 nanotube arrays, Chem Mater, 21 (2009), pp. 3048–3055.

8. Z. Liu, X. Zhang, S. Nishimoto, M. Jin, D. Tryk, T. Murakami *et al.*, Highly ordered TiO2 nanotube arrays with controllable length for photoelectrocatalytic degradation of phenol, J Phys Chem C, 112 (2008), pp. 253–259.

9. K.S. Raja, M. Misra, K. Paramguru, Electrochim Acta, Formation of self-ordered nano-tubular structure of anodic oxide layer on titanium, 51 (2005) 154-165.

10. S. Li, G. Zhang, D. Guo, L. Yu, W. Zhang, J Phys Chem C, Anodization Fabrication of Highly Ordered TiO2 Nanotubes, 113 (2009) 12759-12765.

11. F. Wang, Y. Liu, W. Dong, M. Shen, Z. Kang, Tuning TiO2 Photoelectrochemical Properties by Nanoring/Nanotube Combined Structure, J Phys Chem C 115 (2011) 14635-14640.

12. Z. Zhang, P. Wang, Optimization of photoelectrochemical water splitting performance on hierarchical TiO_2 nanotube arrays, Energy Environ Sci 5 (2012) 6506-6512.

II.C.6 Photoelectrochemical Material Synthesis at LANL

Todd L. Williamson
Los Alamos National Laboratory (LANL)
PO Box 1663, MS J565
Los Alamos, NM 87545
Phone: (505) 665-9994
Email: twilliamson@lanl.gov

DOE Manager
Eric Miller
Phone: (202) 287-5829
Email: Eric.Miller@hq.doe.gov

Project Start Date: October 1, 2010
Project End Date: Project continuation and direction determined annually by DOE

Overall Objective

The overall objective of this project is to evaluate the InGaN ternary alloy system for use as a photoelectrode for photoelectrochemical (PEC) hydrogen generation. In the past, problems with the material quality of InGaN have led to an incomplete picture for this material as a PEC photoelectrode. This project utilizes a novel molecular beam epitaxy (MBE)-type film synthesis based on a high flux beam of energetic nitrogen atoms to improve InGaN material quality.

Fiscal Year (FY) 2013 Objectives

- Improve electrical properties of n-type InGaN
- Improve electrical properties and crystallographic quality of p-type InGaN
- Determine mechanisms causing corrosion of p- and n-type InGaN and seek to find solutions to problem

Technical Barriers

This project addresses the following technical barriers from the Hydrogen Production section of the Fuel Cell Technologies Office Multi-Year Research, Development, and Demonstration Plan:

(AE) Materials Efficiency – Bulk and Interface

(AF) Materials Durability – Bulk and Interface

(AG) Integrated Device Configurations

Technical Targets

This project is conducting fundamental studies on the synthesis of InGaN films for use as PEC electrodes for hydrogen generation. Insight gained from this work will determine if wide band-gap nitride based semiconductors are suitable materials for PEC photoelectrodes. While this work is at an early stage, it has the long-term goal of addressing the ultimate, long-term DOE technical targets for hydrogen production identified in the 2012 Fuel Cell Technologies Office Multi-Year Research, Development, and Demonstration Plan, Table 3.1.8:

- PEC hydrogen cost: $2.10/kg
- Energy conversion ratio (efficiency): 25%
- 1-sun hydrogen production rate: 2.0×10^{-6} kg/s∗m^2

FY 2013 Accomplishments

- InGaN films show photocurrent at 0 V applied bias, suggesting the interfacial energetics are favorable for spontaneous photoelectrolysis.
- Have improved mobility and carrier concentration levels in n-type and p-type InGaN.
- Have improved surface morphology of n-type InGaN films, which will lead to improved stability and corrosion resistance.

✧ ✧ ✧ ✧ ✧

INTRODUCTION

The overall purpose of this work is to provide an economic solar-based technology for creating hydrogen. The bulk of hydrogen reformation currently is done using fossil fuel sources. To move away from the current fossil fuel model for hydrogen production, new technologies must be developed or made more efficient and cost effective. One proven method for hydrogen production is PEC hydrogen production, also known as photoelectrolysis.

The photoelectrolysis of water is the process whereby light, illuminating a semiconductor, is used to split water into hydrogen and oxygen. The incident light, absorbed in a semiconductor electrode, splits water directly. These water splitting systems consist of three main components, a light harvesting system (the semiconductor) and two gas evolving electrodes, one for hydrogen and one for oxygen. Combining the light harvesting electrode and the electrolyzer into a single monolithic device simplifies device design. This is accomplished by putting the semiconductor material into an aqueous solution, illuminating it with sunlight, and driving the water splitting reaction directly. With one of the gases, either hydrogen or oxygen, evolved directly off the surface of the semiconductor, the other electrode is spatially separated so that the two gasses do not mix. The result of this configuration is that sunlight is the only energy input and that

hydrogen is evolved with no external electron flow. Critical to this design is having a semiconductor material that is corrosion resistant under operating conditions.

APPROACH

Among the technical barriers limiting PEC hydrogen production, becoming widespread and economically viable are efficiency and cost. Closely related to these challenges are material quality of photoelectrodes and the stability of these materials under operating conditions.

To improve the material quality, we use a unique MBE-type growth platform called energetic neutral atom beam lithography/epitaxy (ENABLE) to grow InGaN films. ENABLE utilizes a semi-collimated beam of energetic nitrogen atoms (energies spanning 1.0 to 5.0 eV) as the reactive nitrogen source for InGaN film growth. The metals are evaporated from standard thermal sources. The advantage of ENABLE is that the reactive nitrogen atoms have sufficient energy to overcome reaction barriers involved in film growth, which reduces the need for high substrate temperatures that are required for conventional growth. High substrate temperatures are a recognized problem for high quality InGaN growth, as they lead to In phase and compositional segregation and clustering within films.

RESULTS

In previous years, we have demonstrated n-type InGaN growth on c-axis sapphire, and these films have shown non-zero current at zero bias under illumination, which may be indicative of PEC water splitting. An example of one such film can be seen in Figure 1. While this film does show non-zero current of 25 $\mu A/cm^2$, this value is well below the theoretical limit for this material under experimental conditions, ~5 mA/cm^2. Additionally, the performance of the materials degraded over time, and it appears that the material is corroding or etching under operating conditions. To address these two challenges, lower than expected efficiency and corrosion/stability of material under operating conditions, we have pursued three directions. These are improved material quality (including surface morphology), p-type doping, and growth on conductive substrates.

In previous years we demonstrated the target compositions believed to be ideal for InGaN as a PEC photoelectrode, but material quality, while state-of-the-art, was still not sufficient for use in a working PEC cell. Additionally, the electrical properties (conductivity) of the films were too low and likely limiting performance. Over this year, we have achieved a noticeable improvement in InGaN film crystallinity and surface morphology and an approximate factor of 2 increase in carrier mobility.

P-type films are desirable from a stability standpoint because they force electrons to the semiconductor/electrolyte

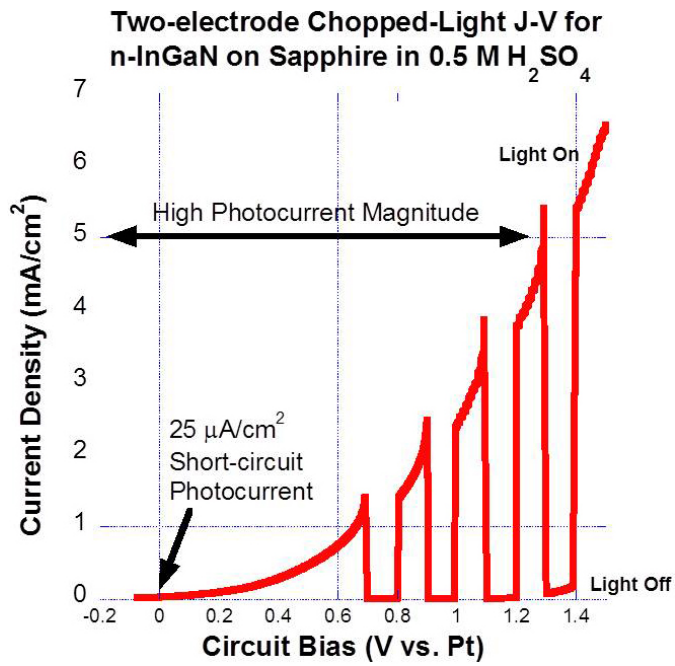

FIGURE 1. Current-voltage plot of InGaN photoelectrode showing non-zero current at zero applied volts.

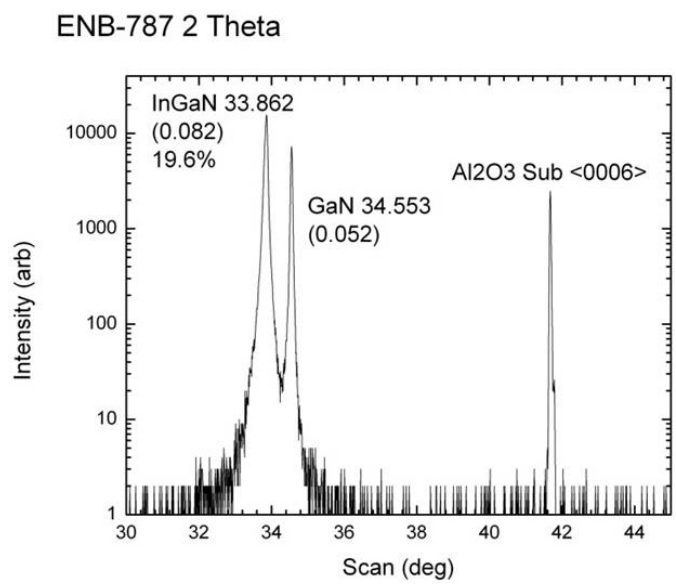

FIGURE 2. XRD pattern of InGaN film. Numbers next to peak markers are observed diffraction angles, numbers in parentheses are full width at half maximum. The InGaN film was 19.6% In

interface offering cathodic protection. This could solve the corrosion problem that is observed. Figure 2 shows an X-ray diffraction (XRD) pattern of an ~20% InGaN film that has been p-type doped. Figure 3 shows an electrochemical capacitance voltage (ECV) measurement of the same film, showing a p-type acceptor concentration of ~$6x10^{20}$ cm^{-3}. According to hall measurements, the film measures p-type

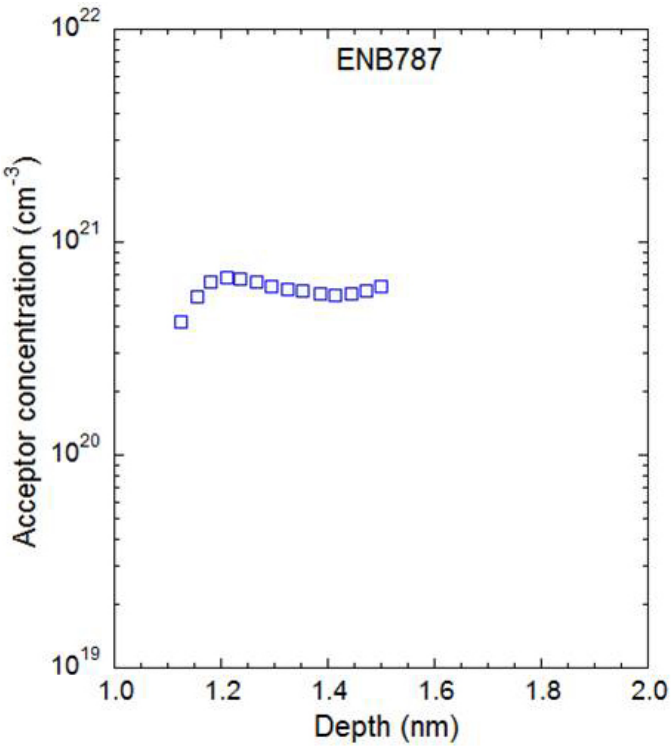

FIGURE 3. ECV plot showing acceptor concentration (p-type carriers) near the surface of the InGaN film from Figure 2.

with a carrier concentration of 2.2×10^{19} cm^{-3} with a acceptor mobility of 2.75 $cm^2/V*s$. This means ~3.5% of the acceptors are active, which is a reasonable value for a p-type III-N film. Similar p-type films have been evaluated for their PEC performance, but their efficiency and stability is not markedly different from representative n-type InGaN films (Figure 1). Likely, the reason for the stability and efficiency not improving is that the p-type films tend to be of lower crystalline and surface quality, due to the defects introduced by doping the film.

While sapphire is much simpler to use for InGaN growth, due to the Si substrate being reactive and fouling the epitaxy during initial growth phases. The non-conductive substrates (sapphire) require a non-ideal front contact configuration where majority carriers have to traverse several mm laterally for collection. This contact configuration leads to a low photon to current efficiency and prevents accurate ensemble efficiency and durability assessments. InGaN films do show excellent vertical conductivity (often more than an order of magnitude larger than lateral) due to the columnar grain structure that is intrinsic to this material system. Furthermore, a back ohmic contact enables greatly reduced collection distances and should lead to enhanced utility of photogenerated electrons. Growing on conductive substrates (Si) allows one to bypass the lateral conductivity and collection problem by having the electrical transport follow a more favorable and shorter path.

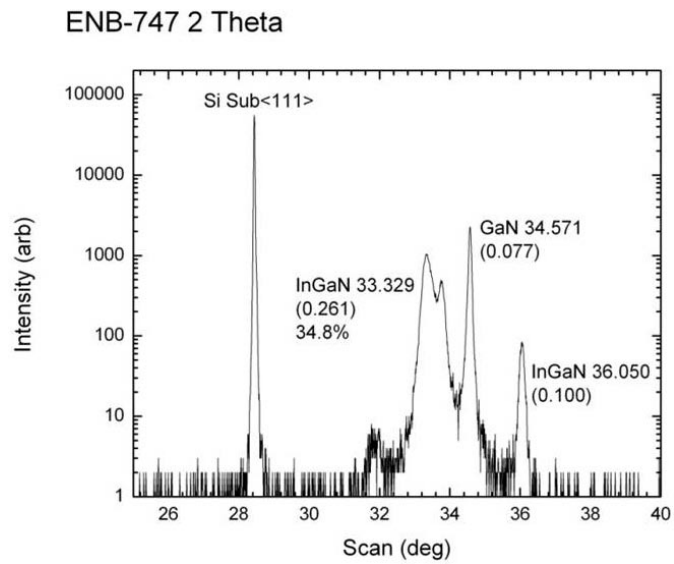

FIGURE 4. XRD pattern of InGaN film grown on Si <111>. Numbers next to peak markers are observed diffraction angles, numbers in parentheses are full width at half maximum. The InGaN film was 34.8% In.

Figure 4 shows an XRD pattern of ~35% n-type InGaN film grown on conductive <111> Si. Compared to the peak width of the InGaN in Figure 2, this peak is much wider, indicating poorer crystalline quality. Also, ECV showed that the film had a high carrier concentration of ~1×10^{21} cm^{-3}; 1×10^{18} cm^{-3} is a more typical value for films grown on sapphire. Additionally, the surface was quite rough, 30-nm root mean square as measured by atomic force microscopy, which is more than twice a typical value for a film grown on sapphire. All of these figures of merit show that the film quality on Si is far inferior to films grown on sapphire. As a result, we have not observed the enhanced performance expected by moving to a back contact and conductive substrate (Si). By improving the film quality on these substrates, a noticeable performance improvement should be observed. Most of the film quality issues are traceable to the initial buffer layer growth on the Si surface; work will focus on improving this initial phase of growth.

CONCLUSIONS AND FUTURE DIRECTIONS

While the initial results of this work are promising, more study is needed to determine if the InGaN alloy system can be made into a useful, efficient photoelectrode for PEC water splitting. Future work will focus on the following areas:

- Improved material quality. While the demonstrated InGaN films in this work are state of the art, it appears that the material quality and electrical properties remain insufficient for use as a PEC electrode. Further work optimizing crystallinity and surface morphology, both on sapphire and conductive Si substrates, will be done.

- Improve corrosion resistance/stability. It appears that some corrosion of the InGaN photoanodes is taking place. This may be because the InGaN films are N-polar, rather than metal-polar on the surface. The N-polar face is known to be less stable and will corrode in strong acids and bases. Initially, we will evaluate the corrosion resistance of N- and metal-polar GaN to validate the relationship in a PEC environment. We will then attempt to create metal polar InGaN films.
- Further improvement of p-type InGaN. P-type films are desirable from a stability standpoint because they force electrons to the semiconductor/electrolyte interface offering cathodic protection. This could solve the corrosion problem that is observed due to the use of N-polar InGaN.

FY 2013 PUBLICATIONS/PRESENTATIONS

1. 'Photoelectrochemical Material Synthesis at LANL'. Todd L. Williamson, Project # PD097. 2013 DOE HYDROGEN and FUEL CELLS PROGRAM and VEHICLE TECHNOLOGIES PROGRAM ANNUAL MERIT REVIEW, May 15, 2013.

II.C.7 Next-Generation Si Microwire Array Devices for Unassisted Photoelectrosynthesis

Shane Ardo
California Institute of Technology
1200 E. California Blvd., Mail Code 139-74
Pasadena, CA 91125
Phone: (626) 395-3964
Email: sardo@caltech.edu

DOE Manager
Eric Miller
Phone: (202) 287-5829
Email: Eric.Miller@hq.doe.gov

Contract Number: DEAC05-06OR23100

Project Start Date: November 1, 2011
Project End Date: September 15, 2013

Overall Objectives

- Demonstrate a scalable and stable Si-microwire-array-based device for sunlight to clean H_2 fuel production, through hydrohalic acid splitting.
- Optimize the fabrication protocols for n-type crystalline Si microwire arrays and tandem Si-microwire-array-based devices containing an amorphous Si top layer.
- Quantify the solar-to-hydrogen (STH) efficiency of peeled, free-standing Si microwire arrays partially embedded in Nafion® proton exchange membrane.

Fiscal Year (FY) 2013 Objectives

- Quantify the STH efficiency of free-standing Si-microwire-array devices for hydrohalic acid splitting.
- Demonstrate protection of Si from passivation and corrosion in hydrohalic acid solutions.
- Quantify the STH efficiency of tandem Si-microwire-array devices for hydrobromic acid splitting.
- Identify efficient and stable halide-oxidation catalysts.

Technical Barriers

This project addresses the following technical barriers from the Hydrogen Production section of the Fuel Cell Technologies Office Multi-Year Research, Development, and Demonstration Plan:

(AE) Materials Efficiency – Bulk and Interface

(AF) Materials Durability – Bulk and Interface

(AG) Integrated Device Configurations

Technical Targets

This project investigates efficient and economically sustainable fuel-forming photoelectrosynthetic devices consisting of arrays of Si microwires. These devices are capable of storing 0.6–0.8 V of potential as H_2 fuel, which is a priority of the Hydrogen Production sub-program. Technical targets are listed in Table 1.

TABLE 1. Progress towards Meeting Technical Targets for Photoelectrochemical Hydrogen Production (Photoelectrode System)

Characteristics	Units	2011 Status	2015	Status Herein
STH Energy Conversion Ratio	%	Not Available	15	1
Electrode Replacement Lifetime	Years	Not Available	0.5	0.05

FY 2013 Accomplishments

- Optimized radial emitter doping of n-type Si microwire arrays with boron and demonstrated >3% light-to-electrical energy conversion efficiency in aqueous hydroiodic acid solution, which is far below the 2015 DOE targets for STH energy conversion ratio.
- Demonstrated two successful tandem Si-microwire-array-based devices: one consisting of two crystalline Si microwire arrays of opposite doping configuration, partially embedded in Nafion®, and laminated back-to-back; and the other consisting of a crystalline Si microwire array with amorphous pin-doped Si deposited on top. Both generated open-circuit photovoltages in excess of 0.9 V, which is significant because a priority of the Hydrogen Production sub-program is to store 0.6–0.8 V of potential as H_2 fuel from sunlight.
- Fabricated a custom device sample holder and measurement system for the peeled, free-standing Si-microwire-array devices that was superior to previous designs.
- Discovered a method to fabricate a highly doped, axial n-type Si region at the base of microwires via in situ chemical vapor deposition. The method forms ohmic tunnel junctions with high-barrier-height contacts.
- Discovered stable catalysts for halide oxidation and materials to protect Si from corrosion and passivation: a nanoscale electrocatalyst requiring ~5 mV overpotential and that is stable for >4 hr in hydroiodic acid, at

~10 mA/cm^2; and poly(3,4-ethylenedioxythiophene): perchlorate (PEDOT:ClO_4) requiring ~20 mV overpotential and that is stable for ~20 hr in HBr, at ~10 mA/cm^2.

- Optimized the composition and synthetic protocol for an electrically and ionically conductive membrane as well as the protocol to deposit/transfer it to the backsides of p-Si microwire arrays.

✧ ✧ ✧ ✧ ✧

INTRODUCTION

A priority of the DOE Hydrogen Production sub-program is to demonstrate efficient and economically sustainable solar fuels devices that store 0.6–0.8 V of potential as hydrogen fuel. This was demonstrated in the 1980s by Texas Instruments Corporation through use of a ~9% efficient device for converting the energy in sunlight into hydrogen from hydrobromic acid solutions [1]. This efficiency is ~10 times that of photosynthesis from typical crops [2], and the reaction products can be combined in a flow battery to generate electricity when sunlight is sparse, e.g., at night. Texas Instruments Corporation used a scalable, serially connected Si–Si device; however, their device required high-purity materials and used expensive and sparse Pt–Ir alloy noble-metal electrocatalysts, which would far exceed the 2015 DOE cost target of $2.0 M/yr-tonnes H_2 per day.

The project described herein utilizes new Si-microwire-array device architectures [3], decorated with electrocatalysts and embedded in a flexible proton exchange membrane, to drive hydrogen evolution from hydrohalic acid solutions using sunlight as the only energy input. From an economic standpoint, the microwire geometry uses ~5% of the material required for conventional wafer-based solar cells, tolerates less pure Si, and the growth wafer substrate can be reused repeatedly. Such characteristics are advantageous for a technology with commercial potential and are of interest to the DOE Hydrogen Production sub-program. A >3.5% light-to-electrical efficiency for sunlight-driven oxidation of hydroiodic acid to triiodide was demonstrated, which was stable for over 200 hr of continuous operation. In addition, a serially connected Si–Si device gave >0.7 V of potential toward H_2 evolution. Lessons gleaned from these Si-microwire-array-based devices will be invaluable to future solar fuels devices.

APPROACH

Si microwire arrays were grown by chemical vapor deposition using a vapor–liquid–solid growth catalyst and doped either in situ during growth or post growth via a thermal, diffusion process. Catalysts and protective layers were deposited and Nafion® was coated into the microwire arrays via spin coating, followed by mechanical removal of the array using a razor blade. The samples were evaluated by traditional photoelectrochemical methods using a three-electrode arrangement. Peeled, free-standing devices were evaluated in a custom acrylic holder and glass cells fitted with inductive stirrers, fiber optic excitation and digital camera imaging, in situ electrochemical evaluation, and in situ and in operando product detection via mass spectrometry and optical transmission spectroscopy.

RESULTS

Three different functioning microwire arrangements were fabricated as free-standing, partially Nafion®-embedded Si microwire array devices for solar hydrogen formation from fuming hydroiodic acid: (a) radially doped pn^+-Si employing Pt electrocatalysts; (b) axially doped n^+n-Si, surface functionalized with methyl groups, and employing Pt electrocatalysts; and (c) a tandem Si–Si device consisting of a and b laminated together by an electrically and ionically conductive composite membrane. These were all milestones for the proposed project. Several apparatuses were designed and engineered to aid in the measurement of the reaction products. Each apparatus was incorporated into an ultraviolet-visual spectrophotometer and plumbed to a mass spectrometer to detect I_3^- and H_2, respectively, when formed at rates >100 µA/cm^2. The final version of the apparatus affords better forced convection of each reaction vessel through inductive stirring and in situ and in operando monitoring of hydrogen bubble formation via a digital endoscope camera.

Tandem Si–Si devices were fabricated as described above. In addition, a tandem device using amorphous Si on crystalline Si microwire arrays was demonstrated. These devices generated >1 V open-circuit photovoltage by photoelectrochemistry (Figure 1). This is extremely relevant to the DOE Hydrogen Production sub-program's desire to store 0.6–0.8 V of potential in H_2 fuel.

Original reports on hydrogen evolution from Si microwire arrays in acidic electrolytes used Pt electrocatalysts [4]. Previous reports from this DOE-funded research also utilized Pt for both hydrogen evolution and halide oxidation from hydrohalic acid solutions. FY 2013 progress included hydrogen evolution from pn^+-Si microwire arrays functionalized with electrochemically deposited amorphous MoS_x, and efficient and stable halide photo-oxidation using electropolymerized PEDOT:ClO_4 on planar n-Si–CH_3 wafers (Figure 2).

CONCLUSIONS AND FUTURE DIRECTIONS

This project demonstrated sunlight-driven, unassisted hydrogen evolution in hydroiodic acid solutions using

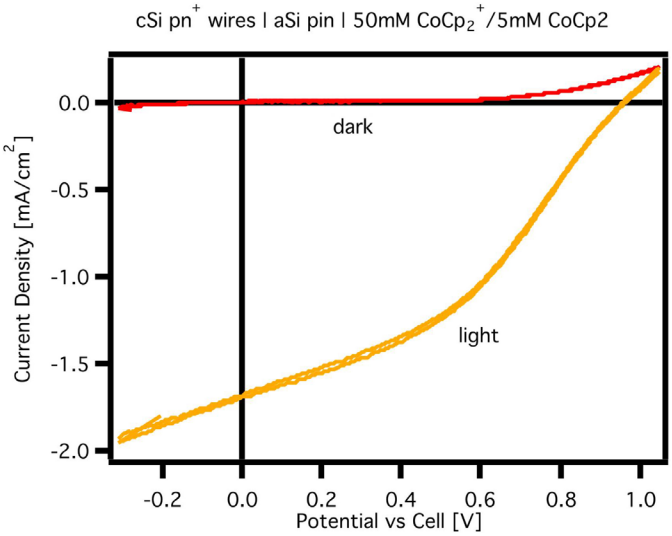

FIGURE 1. Dark and illuminated current density vs. potential relationship for a tandem Si–Si device consisting of pn$^+$-Si microwire arrays coated in a ~200-nm thick layer of amorphous pin-Si immersed in Ar-purged acetonitrile electrolyte containing cobaltocene/cobaltocenium.

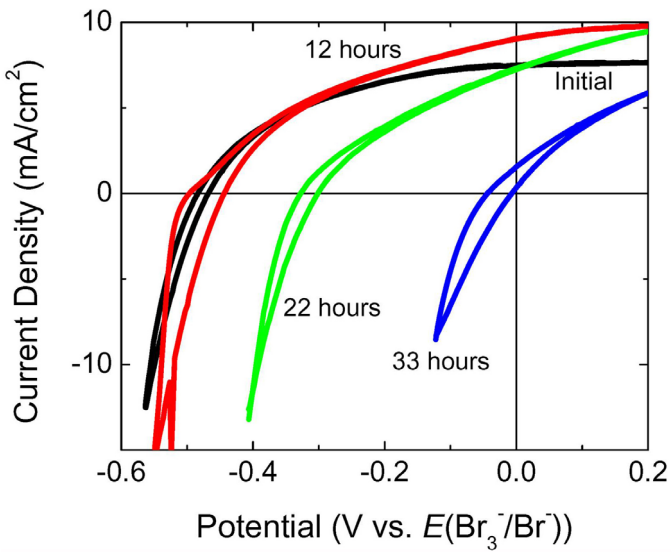

FIGURE 2. Illuminated current density vs. potential relationships at the indicated times for a planar n-Si–CH_3 wafer with electropolymerized PEDOT:ClO_4 on top immersed in Ar-purged HBr solution.

peeled, free-standing silicon microwire arrays. For FY 2013, a tandem functioning device was also demonstrated. In addition, major results this year included protection of Si from corrosion during iodide and bromide oxidation using surface chemistry and earth-abundant PEDOT:ClO_4 polymers, respectively; stable sunlight-driven hydrogen evolution using sulfide and phosphide electrocatalysts; and a transparent electrically and ionically conductive membrane.

The research challenges that remain include:

- Determining protocols for the deposition of materials on microwires to serve as protective layers from highly oxidizing electrolytes.
- Altering Si-microwire-array fabrication protocols so that dopants at the bases of the microwires are not gettered through oxidation processes, and so that emitters are conformal along the length of the microwire.
- Reinvestigating methods to cast Nafion® proton-exchange membrane and mechanically remove partially Nafion®-embedded Si microwire arrays from their growth substrate.

SPECIAL RECOGNITIONS & AWARDS/ PATENTS ISSUED

1. Postdoctoral Research Award, American Chemical Society, Physical (PHYS) Division (**2013**).

2. Ardo, S.; Lewis, N.S. *(pending)* Patent, California Institute of Technology (**2013**) (Provisional patent (**2012**) *61/697,422*). Light-Driven Hydroiodic Acid Splitting from a Free-Standing Microwire Array Partially Embedded in an Ionomer Membrane.

3. Ardo, S.; Shaner, M.; Coridan, R.; Strandwitz, N.; McKone, J.; Fountaine, Katherine; Atwater, H.A.; Lewis, N.S. *(pending)* Patent, California Institute of Technology (**2013**) *13/856,353* (Provisional patents (**2012**) *61/619,661* and (**2012**) *61/621,819*). Semiconductor Structures for Fuel Generation.

4. Ardo, S.; Lewis, N.S. *(pending)* Patent, California Institute of Technology (**2012**) *13/539,335* (Provisional patent (**2011**) *61/503,083*). A Tandem Solar Cell using a Silicon Microwire Array and Amorphous Silicon Photovoltaic Layer.

FY 2013 PUBLICATIONS/PRESENTATIONS

1. Yahyaie, I.; Ardo, S.; Oliver, D.R.; Thomson, D.J.; Freund, M.S.; Lewis, N.S. *Energy Environ. Sci.* (**2012**) *5(12)*: 9789–9794. Comparison between the electrical junction properties of H-terminated and methyl-terminated individual Si microwire/polymer assemblies for photoelectrochemical fuel production.

2. Haussener, S.; Xiang, C.; Spurgeon, J.; Ardo, S.; Lewis, N.S.; Weber, A.Z. *Energy Environ. Sci.* (**2012**) *5(12)*: 9922–9935. Modeling, simulation, and design criteria for photoelectrochemical water-splitting systems. *(Highlighted in Today at Berkeley Lab, LBNL Magazine on Jan. 16, 2013.)*

3. Pinaud, B.A.; Benck, J.D.; Seitz, L.C.; Forman, A.J.; Chen, Z.; Deutsch, T.G.; James, B.D.; Baum, K.N.; Baum, G.N.; Ardo, S.; Wang, H.; Miller, E.; Jaramillo, T.F. *Energy Environ. Sci.* (**2013**) *6(7)*: 1983–2000. Technical and economic feasibility of centralized facilities for solar hydrogen production via photocatalysis and photoelectrochemistry.

4. Shaner, M.R.; Fountaine, K.T.; Ardo, S.; Coridan, R.H.; Atwater, H.A.; Lewis, N.S. *(submitted)* Photoelectrochemistry of Core–Shell Tandem Junction n-p$^+$-Si/n-WO_3 Microwire Array Photoelectrodes.

5. Nielander, A.C.; Bierman, M.J.; Petrone, N.; Strandwitz, N.C.; Ardo, S.; Yang, F.; Hone, J.; Lewis, N.S. *(submitted)* Photoelectrochemical Behavior of n-type Si(111) Electrodes Coated by a Single Layer of Graphene.

6. McDonald, M.B.; Ardo, S.; Lewis, N.S.; Freund, M.S. *(submitted)* Use of bipolar membranes for maintaining steady-state pH gradients in membrane-supported solar-driven water splitting.

7. Ardo, S.; Warren, E.L.; Roske, C.; Brunschwig, B.S.; Atwater, H.A.; Lewis, N.S. *Materials Research Society, Spring National Meeting* (**2013**) San Francisco, CA. Demonstration of Artificial Photosynthesis with Peeled Silicon Microrod Arrays.

8. Ardo, S.; Roske, C.; Warren, E.L.; Brunschwig, B.S.; Atwater, H.A.; Lewis, N.S. *American Chemical Society, Fall National Meeting (abstract accepted)*, Indianapolis, IN.

REFERENCES

1. Johnson, E.L. *IEEE* **1981**, 2 - 6.

2. Blankenship, R.E.; Tiede, D.M.; Barber, J.; Brudvig, G.W.; Fleming, G.; Ghirardi, M.; Gunner, M.R.; Junge, W.; Kramer, D.M.; Melis, A.; Moore, T.A.; Moser, C.C.; Nocera, D.G.; Nozik, A.J.; Ort, D.R.; Parson, W.W.; Prince, R.C.; Sayre, R.T. *Science* **2011**, *332*, 805 - 809.

3. Boettcher, S.W.; Spurgeon, J.M.; Putnam, M.C.; Warren, E.L.; Turner-Evans, D.B.; Kelzenberg, M.D.; Maiolo, J.R.; Atwater, H.A.; Lewis, N.S. *Science* **2010**, *327*, 185 - 187.

4. Boettcher, S.W.; Warren, E.L.; Putnam, M.C.; Santori, E.L.; Turner-Evans, D.; Kelzenberg, M.D.; Walter, M.G.; McKone, J.R.; Brunschwig, B.S.; Atwater, H.A.; Lewis, N.S. *J. Am. Chem. Soc.* **2011**, *133*, 1216 - 1219.

II.D.1 Maximizing Light Utilization Efficiency and Hydrogen Production in Microalgal Cultures

Tasios Melis
University of California, Berkeley
Dept. of Plant & Microbial Biology
111 Koshland Hall
Berkeley, CA 94720-3102
Phone: (510) 642-8166
Email: melis@berkeley.edu

DOE Manager
Katie Randolph
Phone: (720) 356-1759
Email: Katie.Randolph@go.doe.gov

Technical Advisor
Sarah Studer
Phone: (202) 586-4031
Email: Sarah.Studer@ee.doe.gov

Contract Number: DE-FG36-05GO15041

Start Date: December 1, 2004
End Date: January 30, 2014

Overall Objectives

- Minimize, or truncate, the chlorophyll antenna size in green algae, and the phycobilisome antenna size in cyanobacteria to maximize photobiological solar energy conversion efficiency and H_2-production.
- Demonstrate that a truncated light-harvesting antenna (TLA) minimizes absorption and wasteful dissipation of bright sunlight by individual cells, resulting in better light utilization efficiency and greater photosynthetic productivity in high-density mass cultures.

Fiscal Year (FY) 2013 Objectives

- Publish the work on the *TLA3* gene and show its *modus operandi* as to how it confers a truncated Chl antenna size in *Chlamydomonas reinhardtii*.
- Provide physiological and genetic characterization of the *tla3* mutant; including mapping of the plasmid insert site and cloning of the gene affected in the *tla3* mutation.
- Apply the TLA concept in cyanobacteria.

Technical Barriers

The project addresses the following technical barriers from the Photolytic Hydrogen Production from Water (green algae or cyanobacteria) section of the Fuel Cell Technologies Office Multi-Year Research, Development, and Demonstration Plan:

(AN) Light Utilization Efficiency

Technical Targets

The Fuel Cell Technologies Office Multi-Year Research, Development, and Demonstration Plan technical target for this project was to reach a truncated Chl antenna size conferring a 20% light utilization efficiency in unicellular green algae by 2015. Progress was achieved ahead of schedule enabling us to reach this goal by 2012.

FY 2013 Accomplishments (TLA3-ΔCpSRP43 effort)

- Physiological characterization of the *tla3* mutant was completed.
- Genetic analysis and multiple crosses of the *tla3* mutant were completed.
- Mapping of the plasmid insert site in the *tla3* mutant was completed.
- The unique functional role of the CpSRP43 protein in microalgae was elucidated.
- A peer-reviewed paper was published with the following full citation: Kirst H, Garcia-Cerdan JG, Zurbriggen A, Ruehle T, Melis A (2012) Truncated photosystem chlorophyll antenna size in the green microalga *Chlamydomonas reinhardtii* upon deletion of the *TLA3-CpSRP43* gene. Plant Physiol. 160(4):2251-2260.

FY 2013 Accomplishments (TLA effort in cyanobacteria)

- Functional absorption cross section measurements for PSII in wild type and *Δcpc* mutants (10:1 WT/*Δcpc* ratio).
- Functional absorption cross section measurements for PSI in wild type and *Δcpc* mutants (unchanged 1:1 WT/*Δcpc* ratio).
- Completed comparative Light-Saturation Curves of photosynthesis in wild type and *Δcpc* mutants.
- SDS-PAGE and Western blot analysis of protein profiles in wild type and *Δcpc* mutants (verification of the absence of the phycocyanin-binding proteins).
- Growth curves of wild type and *Δcpc* mutants (*Δcpc* growth lags behind the WT at low-light intensities,

whereas growth curves of both are the same at medium-light intensities).

Table 1 summarizes project progress to date.

TABLE 1. Microalgae Milestones and Progress
Sunlight Utilization Efficiency, % of Incident Solar Energy (maximum possible = 30%)

	2000	2003	2005	2007	2008	2010	2011	2012	2015
Targets (Light Utilization efficiency)	3%	10%				15%			20%
Tla strain with the highest efficiency identified	3% (WT)	10% TLA1	15% TLA2		25% TLA3				
Gene cloning from the TLA strains				TLA1: Mov34 MPN			TLA2: FTSY	TLA3: SRP43	

✧ ✧ ✧ ✧ ✧

INTRODUCTION

The goal of the research is to generate green algal and cyanobacterial strains with enhanced photosynthetic productivity and H_2-production under mass culture conditions. To achieve this goal, it is necessary to optimize the light absorption and utilization properties of the cells [1-4]. A cost-effective way to achieve this goal is to reduce the number of Chl molecules in green microalgae, or phycobilins in cyanobacteria, that function in the apparatus of photosynthesis.

The rationale for this work is that a truncated light-harvesting antenna size in green algae or cyanobacteria will prevent individual cells at the surface of a high-density culture from over-absorbing sunlight and wastefully dissipating most of it (Figure 1). A truncated antenna size will permit sunlight to penetrate deeper into the culture, enabling many more cells to contribute to useful photosynthesis and H_2 production (Figure 2). It has been shown that a truncated Chl antenna size will enable about 3-4 times greater solar energy conversion efficiency and photosynthetic productivity than could be achieved with fully pigmented green microalgal cells [5].

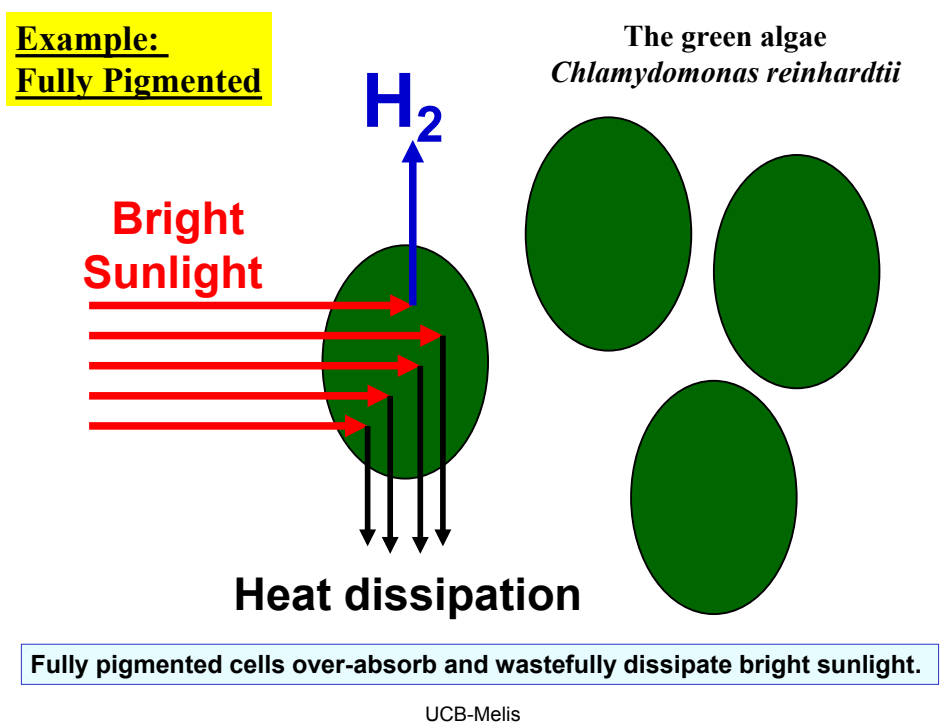

FIGURE 1. Schematic presentation of the fate of absorbed sunlight in fully pigmented (dark green) algae. Individual cells at the surface of the culture over-absorb incoming sunlight (i.e., they absorb more than can be utilized by photosynthesis), and 'heat dissipate' most of it. Note that a high probability of absorption by the first layer of cells would cause shading of cells deeper in the culture.

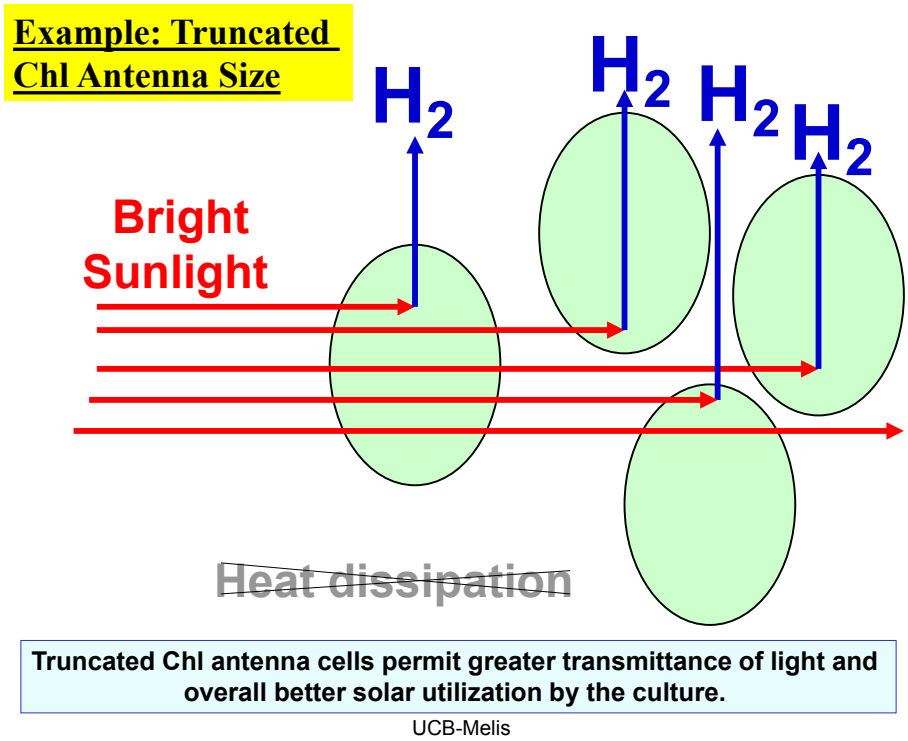

FIGURE 2. Schematic of sunlight penetration through cells with a truncated chlorophyll antenna size. Individual cells have a diminished probability of absorbing sunlight, thereby permitting penetration of irradiance and H_2 production by cells deeper in the culture.

APPROACH

The focal objective of the research is to identify genes that control the antenna size of photosynthesis and, further, to elucidate how such genes confer a truncated antenna size in the model green alga *Chlamydomonas reinhardtii* and model cyanobacterium *Synechocystis* PCC 6803. Identification of such genes will permit application of this TLA property, i.e., "truncated light-harvesting antenna size," to other microalgae and cyanobacteria of interest to the DOE Fuel Cell Technologies Office. This objective has been successfully approached through deoxyribonucleic acid (DNA) insertional mutagenesis/screening (green microalgae) or double homologous recombination and gene deletion (cyanobacteria) and biochemical/molecular/genetic analyses of the resultant TLA *Chlamydomonas reinhardtii* or *Synechocystis* PCC 6803 cells. The following specific approaches were undertaken.

- Performed *Chlamydomonas reinhardtii* genomic DNA mapping at the site of plasmid DNA insertions, followed by identification of open reading frames (ORFs = putative genes) that have been affected by the plasmid insertion.
- Performed complementation-type transformations of the *tla* mutant with each of the affected ORFs to rescue the mutation and, thus, identify the gene that confers a TLA property.
- Cloned, characterized, and manipulated gene(s) that affect the "light-harvesting antenna size" property in *Chlamydomonas reinhardtii* and *Synechocystis* PCC6803.

CONCLUSIONS

- Significant progress was achieved in terms of characterization of "truncated Chl antenna size" mutants, cloning of the respective *TLA* genes, and elucidation of the properties of the proteins encoded by these genes in both green microalgae and cyanobacteria.
- Further results and analyses on the manipulation of the *TLA1* gene [6] and deletion of the *TLA3* gene [7] for the regulation of the Chl antenna size in green microalgae were published.
- Application of the TLA concept in cyanobacteria is at a fairly advanced stage, results to be drafted in the form of a manuscript soon.

FUTURE DIRECTIONS

- Complete the work pertaining to the TLA concept in cyanobacteria. (Currently in progress.)

- Advance the exploration of the "*extended photosynthetically active radiation*" (ePAR) concept. (Proprietary design not disclosed.)

FY 2013 PUBLICATIONS/PRESENTATIONS/ PATENT

1. Kirst H, Garcia-Cerdan JG, Zurbriggen A, Ruehle T, Melis A (2012) Truncated photosystem chlorophyll antenna size in the green microalga *Chlamydomonas reinhardtii* upon deletion of the *TLA3-CpSRP43* gene. Plant Physiol. 160(4):2251-2260.

2. Mitra M, Kirst H, Dewez D, Melis A (2012) Modulation of the light-harvesting chlorophyll antenna size in *Chlamydomonas reinhardtii* by *TLA1* gene over-expression and RNA interference. Phil. Trans. R. Soc. B 367:3430-3443.

3. Melis A (2012) Using and abusing photosynthesis to produce fuels and chemicals. European Union Photosynthesis Workshop: from Science to Industry. Marie Curie Program on Training in BioSolar Research. NH Conference Centre, Leeuwenhorst, Noordwijkerhout, The Netherlands. Pp. 26-27.

4. Kirst H, Garcia-Cerdan JG, Zurbriggen A, Melis A (2013) The CrCpSRP pathway proteins CrCpSRP43 and CpFTSY are required for the assembly of the light-harvesting chlorophyll antenna in the green alga *Chlamydomonas reinhardtii*. Western Photosynthesis Conference, Asilomar Conference Grounds, Pacific Grove, CA, pages 23-24.

REFERENCES

1. Kok B (1953) Experiments on photosynthesis by *Chlorella* in flashing light. In: Burlew JS (ed), Algal culture: from laboratory to pilot plant. Carnegie Institution of Washington, Washington, D.C., pp 63-75.

2. Myers J (1957) Algal culture. In: Kirk RE, Othmer DE (eds), Encyclopedia of chemical technology. Interscience, New York, NY, pp 649-668.

3. Radmer R, Kok B (1977) Photosynthesis: Limited yields, unlimited dreams. Bioscience 29: 599-605.

4. Mitra M, Melis A (2008) Optical properties of microalgae for enhanced biofuels production. Optics Express 16: 21807-21820.

5. Melis A, Neidhardt J, Benemann JR (1999) *Dunaliella salina* (Chlorophyta) with small chlorophyll antenna sizes exhibit higher photosynthetic productivities and photon use efficiencies than normally pigmented cells. J. appl. Phycol. 10: 515-525.

6. Mitra M, Ng S, Melis A (2012) The *TLA1* protein family members contain a variant of the plain MOV34/MPN domain. Amer J Biochem Mol Biol. 2(1): 1-18.

7. Kirst H, Garcia-Cerdan JG, Zurbriggen A, Melis A (2012) Assembly of the light-harvesting chlorophyll antenna in the green alga *Chlamydomonas reinhardtii* requires expression of the *TLA2-CpFTSY* gene. Plant Physiol 158: 930–9451.

II.D.2 Biological Systems for Hydrogen Photoproduction

Maria L. Ghirardi (Primary Contact), Paul W. King, and Seth Noone
National Renewable Energy Laboratory (NREL)
15013 Denver West Parkway
Golden, CO 80401
Phone: (303) 384-6312
Email: maria.ghirardi@nrel.gov

DOE Manager
Katie Randolph
Phone: (720) 356-1759
Email: Katie.Randolph@go.doe.gov

Project Start Date: October 1, 2000
Project End Date: Project continuation and direction determined annually by DOE

Overall Objective

Develop photobiological systems for large-scale, low-cost, and efficient H_2 production from water to meet DOE's targets (see Table 1).

Fiscal Year (FY) 2013 Objectives

- Develop and characterize deoxyribonucleic acid (DNA) constructs for stable expression of the more O_2-tolerant *Clostridium acetobutylicum* [FeFe]-hydrogenase Ca1 in *Chlamydomonas reinhardtii*
- Investigate the efficiency of H_2 photoproduction in recombinant organisms

Technical Barriers

This project addresses the following technical barriers from the Hydrogen Production section of the Fuel Cell Technologies Office Multi-Year Research, Development, and Demonstration Plan.

(AO) Rate of Hydrogen Production

(AP) Oxygen Accumulation

Technical Targets

The technical targets for this project are listed in Table 1.

TABLE 1. Technical Targets for Photobiological Hydrogen Production (http://www1.eere.energy.gov/hydrogenandfuelcells/mypp/pdfs/production.pdf)

	2013 Status	2015 Target	2020 Target	Ultimate Target
Duration of continuous H_2 production under full sunlight intensity	2 min	30 min	4 h	8 h
Solar-to-Hydrogen Energy Conversion Ratio	NA	2%	5%	17%

FY 2013 Accomplishments

- Increased the stability and rates of the recombinant Ca1 hydrogenase under the regulation of the light-dependent PsaD promoter in *C. reinhardtii*.
- Demonstrated that the *in vivo* O_2-tolerance of the recombinant Ca1 is 10-20-fold higher than that of the native hydrogenases.
- Observed expression of Ca1 under the regulation of the anaerobiosis-dependent *C. reinhardtii* [FeFe]-hydrogenase (HYDA)1 promoter.
- Generated DNA expression constructs incorporating introns from other algal genes to further improve rates of H_2 photoproduction; currently testing the activity of the positive transformants.
- Achieved a 2.5-fold increase in H_2 photoproduction rates by optimizing induction of the PsaD-Ca1 gene.

✧ ✧ ✧ ✧ ✧

INTRODUCTION

The green alga *C. reinhardtii* has the biochemical machinery necessary to photoproduce H_2 from water efficiently by using hydrogenase enzymes as endogenous biological catalysts. Currently, under conditions where O_2 is a by-product of photosynthesis, sustained H_2 photoproduction cannot be maintained for more than a few minutes. This limitation is due to a number of factors, including the sensitivity of the hydrogenase enzyme to O_2 co-evolved from photosynthetic water oxidation. Other contributing factors include the down-regulation of photosynthesis by the proton gradient that is established during electron transport at high light intensity, the competition for photosynthetic reductant between H_2 photoproduction and CO_2 fixation, and the low-light saturation of the organism.

Our current project addresses the O_2 sensitivity and concomitant low rate of H_2 photoproduction by expressing

a gene encoding a more O_2-tolerant hydrogenase (from *Clostridium acetobutylicum*) in the green alga *C. reinhardtii*.

APPROACH

Previous efforts at expressing the clostridial hydrogenase in *Chlamydomonas* were hampered by the presence of two native algal hydrogenases, HYDA1 and HYDA2, which confounded the analysis of our results. Since then, we switched our host organism to an algal strain, developed by Prof. Posewitz under Ghirardi's Office of Science/ Basic Energy Sciences-funded project, that lacks native hydrogenase activity. To achieve expression of the Ca1 hydrogenase in *Chlamydomonas*, we generated DNA constructs comprised of a promoter (to turn the recombinant gene ON or OFF), a signal peptide (to direct the translated protein to the chloroplast), a codon-optimized Ca1 gene (to match the high guanine/cytosine content of the algal genome), and an algal terminator (to ensure proper conclusion of mRNA translation). Two major promoters were tested this year; the PsaD promoter is responsive to light, and the HYDA1 promoter responds to anaerobiosis. Finally, we are also incorporating intron sequences within the prokaryotic Ca1 gene, an approach that has been shown by others to promote expression of heterologous genes in *Chlamydomonas*.

The DNA constructs are introduced into a hygromycin-resistance-carrying vector that has been used extensively by the *Chlamydomonas* community. The success of each transformation is determined by the survival of cells in the presence of different levels of hygromycin. Positive transformants are screened on plates for hydrogenase activity using a novel, *in vivo* bioassay developed by Dr. Wecker under Ghirardi's Office of Science/Biological and Environmental Research Program funding. The bioassay detects H_2 as fluorescence emission by a green fluorescent protein (GFP), which is expressed from a H_2-sensing promoter in a modified bacterium *Rhodobacter capsulatus* [1]. Hydrogenase-expressing *C. reinhardtii* transformants are detected by the presence of a green, GFP halo around the colony. Each positive transformant is then assessed for H_2-photoproduction capability, stability of the phenotype, and tolerance to O_2. Modifications to the construct are then made, as needed, to achieve higher rates, stability and O_2-tolerance.

RESULTS

At the last progress report, we described the successful transformation of a double-hydrogenase knock-out strain of *Chlamydomonas* with the Ca1 gene and showed light-induced H_2 photoproduction by this transformant. Unfortunately, its H_2-photoproduction capability decreased over time. This year, we used the GFP assay to assess the homogeneity of our transformants. Figure 1A shows a plate of individual cells originated from a single transformant colony; the red dots indicate individual clones, while the green halo corresponds to H_2-producing colonies. Clearly, this sample shows a high level of heterogeneity; the best H_2-producing clone was re-plated, re-grown in liquid medium, and again assessed for H_2 production. Figure 1B indicates that the clone is now stable and homogeneous. We are investigating its H_2-production capability over time in order to determine whether this re-purification step solved the decrease in H_2-production rate observed earlier. So far, we have not observed any negative effect.

We have since generated constructs under the regulation of the HYDA promoter and tested hundreds of transformants for H_2 photoproduction. As in the case of the PsaD constructs, we successfully detected H_2 production by the GFP assay and by the Clark electrode (results not shown), although the observed rates were not as high as those obtained with the PsaD constructs.

With stable Ca1-expressing transformants in hand, we are then able to measure their tolerance to added O_2. Figure 2 shows a representative series of curves showing light-induced H_2 production by wild-type (A) and Ca1-expressing mutants (B) upon exposure to different levels of O_2. Rates of H_2 photoproduction were determined from the initial slope of each curve and fitted to a two-exponential decay equation. The results are shown in Table 2. At this point it is not clear what the origins of the slow and fast components are. However, the transformant's rate constants are significantly higher than the ones derived for the wild-type strain. These results confirm that Ca1, when expressed in *Chlamydomonas*, does display a higher tolerance to O_2. It is important to point out, though, that these measurements were done in the presence of the uncoupler carbonyl cyanide 4-(trifluoromethoxy)phenylhydrazone, which dissipates the proton gradient. As such, the observed H_2 photoproduction activity is not limited by the proton gradient during the experiment.

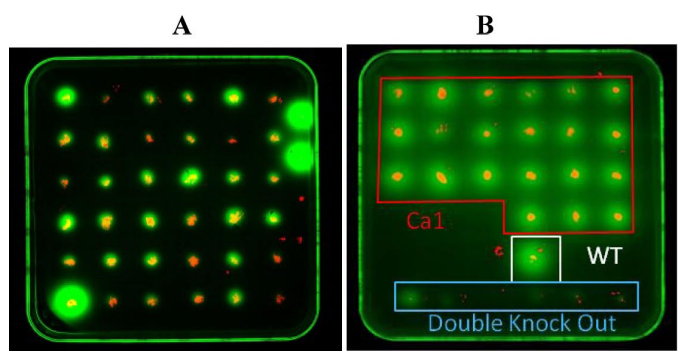

FIGURE 1. Results from the GFP screening of the PsaD-Ca1-expressing transformant (A) and from clones derived from a high H_2-producing strain from A, re-grown in liquid medium and re-plated (B). Controls: Wild-type (expressing algal hydrogenases), double knock-out (unable to express algal hydrogenases and host for Ca1 hydrogenase gene).

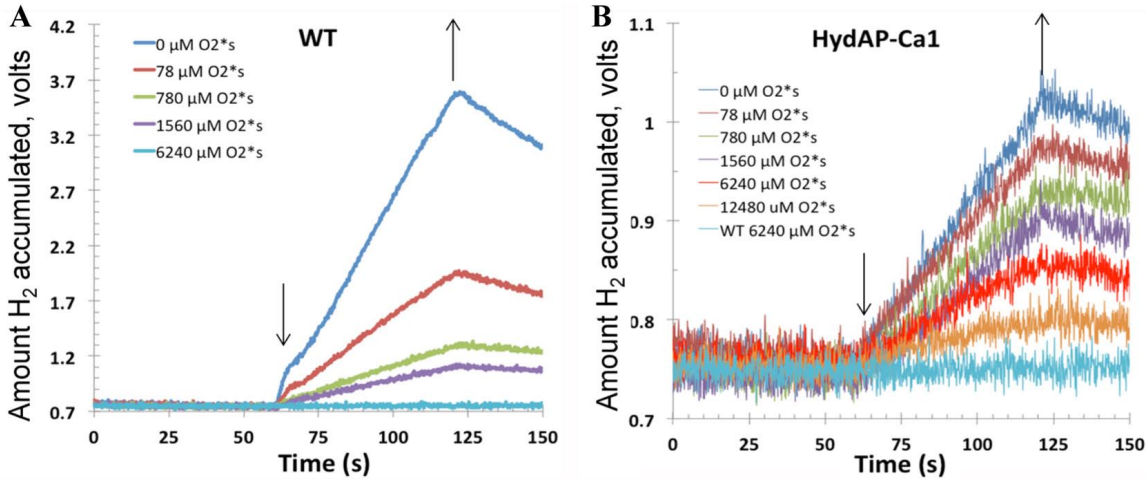

FIGURE 2. Kinetic analysis of the effect of added O_2 on the rates of H_2 photoproduction as measured by the Clark electrode by wild-type (A) and a HYDA-Ca1-expressing transformant (B). Initial rates were estimated from the slope of each curve and plotted as a function of added O_2 concentration. The results are shown in Table 2.

TABLE 2. Kinetic components derived from Figures 2A and 2B and data collected from the HYDA-Ca1 transformant. The data were better fitted to a two-exponential decay equation.

Enzyme/ Strain	O_2 Inactivation Rate Constants (τ_1 and τ_2) (µM O_2^{-1}•s^{-1})		O_2 Tolerance (Ratio to WT)	
	Fast	Slow	Fast	Slow
WT	$2.7 \times 10^{-2} \pm 2 \times 10^{-3}$	$1.7 \times 10^{-3} \pm 5.2 \times 10^{-4}$	NA	NA
PsaDP-Ca1	1.4×10^{-3}	$1 \times 10^{-4} \pm 2 \times 10^{-5}$	19	17
HydAP-Ca1	3×10^{-3}	3.5×10^{-4}	9	5

Finally, we designed alternative constructs containing introns from the Rubisco small subunit algal gene and transformed them into *Chlamydomonas*. Unfortunately, our initial selection in hygromycin suggested that the host double knock-out strain had lost some of its sensitivity to the antibiotic for unknown reasons. We are in the process of repeating the transformation with another knock-out clone.

Overall, we were able to improve the stability of the PsaD-based construct, as described above, and, by manipulating the induction conditions, have shown a 2.5-fold increase in the initial rates of H_2 photoproduction, from 5 to 12 µmoles H_2 x mg Chl^{-1} x h^{-1}.

CONCLUSION AND FUTURE DIRECTIONS

- The data have confirmed the hypothesis that the introduction into *Chlamydomonas* of a clostridial hydrogenase that is more O_2-tolerant *in vitro* than algal hydrogenases results in a recombinant organism that has increased O_2-tolerant H_2 photoproduction *in vivo*.
- A 2.5-fold increase in the rates of H_2 photoproduction was achieved by manipulating induction conditions.
- The investigation of the effect of introns in Ca1 expression will continue in FY 2014.
- A genetic effort will be initiated to combine multiple useful traits into a single algal strain, including Ca1 expression, truncated antenna, and a mutation that eliminates the formation of a proton gradient.

SPECIAL RECOGNITIONS AND AWARDS/ PATENTS ISSUED

1. Maria Ghirardi was selected as one of the two newest NREL Fellows.

FY 2013 PUBLICATIONS

1. Ghirardi, M.L. 2013. "Photobiological H_2 production: theoretical maximum light conversion efficiency and strategies to achieve it". ECS Trans. 50:47-50.

FY 2013 PRESENTATIONS

1. Ghirardi, M.L. "Photobiological H_2 production: theoretical maximum light conversion efficiency and strategies to achieve it". ECS meeting, October 2012.

2. Ghirardi, M.L. "Algal Systems for H_2 Photoproduction". EERE/ FCTO Annual Merit Program Review Meeting, May 2013.

REFERENCES

1. Wecker et al. 2011. Int. J. Hydrogen Energy 36:11229

II.D.3 Fermentation and Electrohydrogenic Approaches to Hydrogen Production

Pin-Ching Maness (Primary Contact),
Katherine Chou, and Lauren Magnusson
National Renewable Energy Laboratory (NREL)
15013 Denver West Parkway
Golden, CO 80401
Phone: (303) 384-6114
Email: pinching.maness@nrel.gov

DOE Manager
Katie Randolph
Phone: (720) 356-1759
Email: Katie.Randolph@go.doe.gov

Subcontractor:
Bruce Logan, Pennsylvania State University
College Park, PA

Start Date: October 1, 2004
Projected End Date: Project continuation and direction determined annually by DOE

Overall Objectives

- Optimize rates and yields of hydrogen production in a sequencing fed-batch bioreactor by varying hydraulic retention time and reactor volume replacement.
- Optimize genetic tools to transform *Clostridium thermocellum* and obtain mutants lacking the targeted competing pathway to improve hydrogen molar yield.
- Demonstrate hydrogen production from the NREL fermentation effluent and harness the energy in a chemical gradient to improve overall energy efficiency in hydrogen production.

Fiscal Year (FY) 2013 Objectives

- Optimize sequencing fed-batch parameters in converting cellulose to hydrogen by the cellulolytic bacterium *Clostridium thermocellum*, aimed at lowering feedstock cost.
- Develop genetic tools in *C. thermocellum*, aimed at metabolic pathway engineering to improve hydrogen molar yield via fermentation.
- Examine performance of the microbial electrolysis cell (MEC) system with boosted voltages to convert the subcomponents in the NREL fermentation effluent to hydrogen.
- Redesign a microbial reverse-electrodialysis electrolysis cell (MREC) to examine the scalability of the MREC for hydrogen production from fermentation effluent without an external energy input.

Technical Barriers

This project supports research and development on DOE Technical Task 6, (Fuel Cell Technologies Office Multi-Year Research, Development, and Demonstration Plan) subtasks "Molecular and Systems Engineering for Dark Fermentative Hydrogen Production" and "Molecular and Systems Engineering for MEC" and it addresses barriers AX, AY, and AZ.

(AX) Hydrogen Molar Yield

(AY) Feedstock Cost

(AZ) Systems Engineering

Technical Targets

TABLE 1. Progress toward Meeting DOE Technical Targets in Dark Fermentation

Characteristics	Units	Current Status	2015 Target	2020 Target
Yield of H_2 from glucose	Mole H_2/mole glucose	2–3.2	6*	9
Feedstock cost	Cents/lb glucose	13.5	10	8
Duration of continuous production (fermentation)	Time	17 days	3 months	6 months
MEC cost of electrodes	$/m^2	$2,400	$300	$50
MEC production rate	L-H_2/L-reactor-d	1	1	4

*Yield of H_2 from glucose: DOE has a 2015 target of an H_2 molar yield of 6 (4 from fermentation and 2 from MEC) from each mole of glucose as the feedstock, derived from cellulose.

Feedstock cost: The DOE Bioenergy Technologies Office is conducting research to meet its 2015 target of 10 cents/lb biomass-derived glucose. NREL's approach is to use cellulolytic microbes to ferment cellulose and hemicellulose directly, which will result in lower feedstock costs.

FY 2013 Accomplishments

- Conducted sequencing fed-batch reactor experiments and demonstrated that by using a hydraulic retention time (HRT) of 24 h and displacing 50% of the reactor liquid every 12 h, the rate of H_2 production and hydrogen molar

yield can be increased by 2.7 fold and 62%, respectively. The improved rates and yield of hydrogen production were realized via retaining those microbes that were adapted to degrade cellulose.

- Designed a proprietary plasmid suitable for deleting genes encoding the competing pathways in *C. thermocellum*. This capability will serve as the foundation for improved hydrogen molar yield in *C. thermocellum* by redirecting more electrons from cellulose toward hydrogen rather than other carbon byproducts.
- Obtained a volumetric current density of 44 A/m^3 with NREL fermentation wastewater in the MEC with 0.9 V applied voltage. The chemical oxygen demand (COD) removal was 73% and the maximum hydrogen production rate was 0.5 L-H_2 L^{-1} d^{-1}. Among the components in fermented wastewater, protein degradability (48% removal) was lower than alcohols and volatile fatty acids (>90%) and carbohydrate (89%). Increased applied voltages resulted in an increase in protein removal, but decreased H_2 yields.

✧ ✧ ✧ ✧ ✧

INTRODUCTION

Biomass-derived glucose feedstock is a major operating cost driver for economic hydrogen production via fermentation. The DOE Fuel Cell Technologies Office is taking advantage of the DOE Bioenergy Technology Office's investment in developing less expensive glucose from biomass to meet its cost target of 10 cents/lb by 2015. Meanwhile, one alternative and viable approach to addressing the glucose feedstock technical barrier (AZ) is to use certain cellulose-degrading microbes that can ferment biomass-derived cellulose directly for hydrogen production. One such model microbe is the cellulose-degrading bacterium *Clostridium thermocellum* (*C. thermocellum*), which was reported to exhibit one of the highest growth rates using crystalline cellulose [1]. Another technical barrier to fermentation is the relatively low molar yield of hydrogen from glucose (mol H_2/mol sugar; technical barrier AX), which results from the simultaneous production of waste organic acids and solvents. Biological pathways maximally yield 4 moles of hydrogen per 1 mole of glucose (the biological maximum) [2]. However, most laboratories have reported a molar yield of 2 or less [3,4]. Molecular engineering to block competing pathways is a viable option toward improving H_2 molar yield. This strategy had resulted in improved hydrogen molar yield in *Enterobacter aerogenes* [5].

A promising parallel approach to move past the biological fermentation limit has been developed by a team of scientists led by Prof. Bruce Logan at Pennsylvania State University. In the absence of O_2, and by adding a slight amount of negative potential (–250 mV) to the circuit, Logan's group has produced hydrogen from acetate (a fermentation byproduct) at a molar yield of 2.9–3.8 (versus a theoretical maximum of 4) in a modified microbial fuel cell called an MEC [6]. It demonstrates for the first time a potential route for producing eight or more moles of hydrogen per mole glucose when coupled to a dark fermentation process. Indeed, in FY 2009 the team reported a combined molar yield of 9.95 when fermentation was coupled to MEC in an integrated system [7]. Combining fermentation with MEC could therefore address technical barrier AX and improve the techno-economic feasibility of hydrogen production via fermentation.

APPROACH

NREL's approach to addressing feedstock cost is to optimize the performance of the cellulose-degrading bacterium *C. thermocellum*. To achieve this goal, we are optimizing the various parameters in a sequencing fed-batch reactor to improve longevity, yield, and rate of H_2 production. To improve hydrogen molar yield, we are selectively blocking competing metabolic pathways in this organism via genetic methods. Through a subcontract, Pennsylvania State University is testing the performance of an MEC and MREC using both a synthetic effluent and the real waste stream from lignocellulosic fermentation generated at NREL.

RESULTS

Lignocellulose Fermentation

Cellulose is a solid substrate, and with continuous feeding the system will eventually suffer from clogging of feed lines and over-exhaustion of the feed pump. A more feasible strategy for cellulose fermentation is to feed the substrate at a predetermined interval instead of using continuous feeding. This strategy can be realized via the use of a sequencing fed-batch bioreactor. This method also simultaneously retains the acclimated microbes to increase the rate of hydrogen production. We carried out the experiment in a Sartorius bioreactor with a working volume of 2 L. The medium was continuously sparged with N_2 at a flow rate of 16 ccm and agitated at 100 rpm. We tested HRT of 12, 24, and 48 h, four cycles each, with a constant carbon loading of 5.0 g/L of cellulose. At each constant HRT, we also altered the feeding strategy by displacing a varying portion of the reactor liquid at different time intervals in order to uncover the most optimal parameters. The reactor was initiated by running the fermentation using cellulose at 5 g/L for 36 h. We turned off the agitation for 1 h, during which the unfermented substrate along with the attached microbes settled, then removed 1.5 L (75%) of the clear supernatant and added back 1.5 L of fresh medium

replenished with cellulose (5.0 g/L). In the subsequent four cycles, the HRT was kept at 48 h, yet only 25% of the liquid was displaced at 12-h intervals. This was then followed by four more cycles at an HRT of 24 h with displacement of 50% of the liquid every 12 h. In the end we operated another four cycles with an HRT of 12 h and displaced 50% of the liquid volume every 6 h (Table 2).

Initial results indicate that with an HRT of 48 h, more frequent displacement of a smaller amount of reactor liquid (25% vs. 75%) led to a 38% increase in both rate and yield of hydrogen. This finding strengthens the assumption that more frequent liquid displacement retains the acclimated microbes. Collectively the data suggest that an HRT of 24 h with a 12-h interval of liquid displacement generates the highest production rate and yield of hydrogen. An HRT of 12 h is deemed impractical because it would consume a large volume of liquid.

TABLE 2. Rate and Yield of Hydrogen Production in Sequencing Fed-Batch Bioreactor with *Clostridium thermocellum* Fermenting Cellulose Substrate

HRT (h)	Liquid Displacement (%)	Interval (h)	Rate of H_2 Production (mL H_2/L/d)	H_2 Molar Yield (mol H_2/mol hexose)
48	75	36	764	0.79
48	25	12	1,057	1.09
24	50	12	2,045	1.28
12	50	6	1,179	1.21

Metabolic Engineering

The ultimate goal of this approach is to develop tools to inactivate genes encoding competing metabolic pathways, thus redirecting more cellular flux to improve hydrogen molar yield. Transformation in *C. thermocellum* has been challenging, likely due to either an inefficiency of the plasmids used or an incompatibility of the deoxyribonucleic acid (DNA) restriction system between the host and the plasmid [8]. To circumvent both challenges, we have achieved the following: (1) redesigned a commercial plasmid with a Gram-positive origin of replication suitable for *C. thermocellum*; (2) deleted the *dcm* gene in the *E. coli* host used for cloning purpose; and (3) used *C. thermocellum* strain DSM 1313 as the model cellulose-degrader. Following the protocols developed by Argyros et al. [9], we first generated a Δ*hpt* mutant of *C. thermocellum*, which was then used as the recipient strain to delete a gene of interest encoding a specific competing pathway, based on two rounds of counter-selection using two suicide substrates. The resultant double mutant (Δ*hpt*Δ*goi*) failed to produce the specific product due to the deletion of its encoding gene. The mutant produced equal amounts of total hydrogen when compared to the control, the parental strain. Yet the double mutant produced up to 60% more ethanol and exhibited a nearly 50% increase in specific rate of hydrogen production early in its growth, which warrants further investigation.

Microbial Electrolysis Cell

The prototype two-chamber MEC was designed for improved hydrogen recovery and to eliminate methane production. The reactor had a total liquid volume of 302 mL, and it was initially fed with sodium acetate (synthetic wastewater). Following that, the substrate was shifted to fermentation wastewater from NREL. The HRT was 24 h and the applied voltage was 0.9 V. Catholyte was 50 mM of phosphate buffered saline and was supplied to the cathode chamber. The volumetric current density (44 A/m^3) obtained with fermented wastewater decreased slightly compared to that obtained with the synthetic wastewater (51 A/m^3) due to the more complex substrates in the fermentation effluent (Figure 1). The use of the fermented wastewater also resulted in a slightly lower COD removal of 73%, when compared to an 87% of COD removal using synthetic waste water (acetate). The average gas volume was 159 mL with fermented wastewater, which was slightly lower than that of the synthetic wastewater (183 mL). The maximum hydrogen production rates were 0.5 L-H_2 L^{-1} d^{-1} and 0.6 L-H_2 L^{-1} d^{-1}. Among the components in fermented wastewater, protein degradability (48% removal) was lower than alcohols and volatile fatty acids (>90%) and carbohydrate (89 %).

Although more hydrogen gas was generated at increased applied voltages, H_2 yields were lower with higher applied voltage (Figure 2A). The highest H_2 yield (1.1 H_2 L/g COD) was obtained at E_{ap}= 0.9 V. Also, energy recovery (η_E=223%) was highest at E_{ap}=0.9 V, with overall energy recovery (η_{E+S}) of 64%. The increase in the applied voltages resulted in higher rates of organic matter removals; however, the amount of that organic matter going into current production (Coulombic efficiency) decreased, suggesting that this

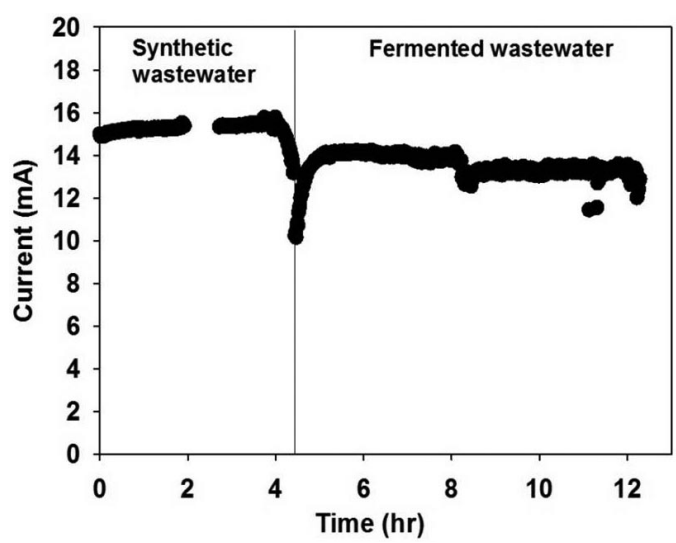

Figure 1. Current Generation from MEC using Synthetic Wastewater (Sodium Acetate) and Fermented Wastewater

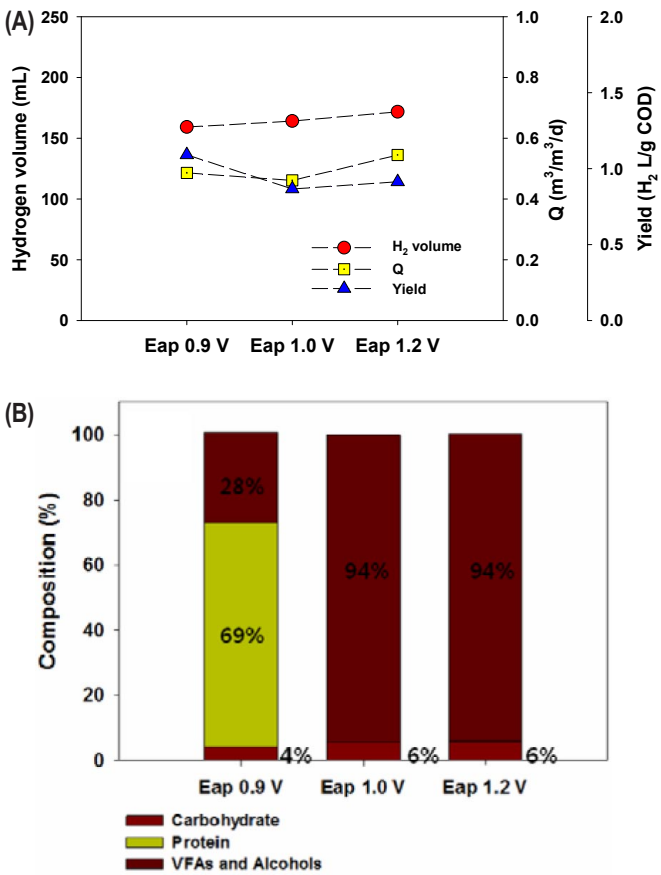

Figure 2. MEC Performance with Different Applied Voltage: (A) hydrogen generation and (B) effluent composition removal as a function of applied voltage

increase in removal did not benefit hydrogen production. Amongst the components in the MEC effluents generated at different applied voltage, protein was almost completely removed at higher applied voltage (Figure 2B). Degraded protein seemed to be used more for cell growth than electricity generation.

Microbial Reverse-Electrodialysis Electrolysis Cell

The MREC was redesigned to examine its scalability for hydrogen production from fermentation effluent without an external energy input. The MREC reactor (Figure 3) was modified to create larger anode (150 mL) and cathode (165 mL) chambers.

CONCLUSIONS AND FUTURE DIRECTION

- Using cellulose (5 g/L) as the substrate in a sequencing fed-batch reactor, we determined that using an HRT of 24 h and displacing 50% of the reactor liquid volume at 12-h intervals resulted in the highest production rate and yield of hydrogen (2.7-fold and 62% increase, respectively). Longer HRT led to retaining cultures in the inactive stationary phase of growth while shorter HRT resulted in large water consumption.
- We redesigned a commercial plasmid suited for transformation in *C. thermocellum*. We also deleted the *dcm* gene in the *E. coli* host for cloning purposes to ensure compatibility of the plasmid DNA with that in the *C. thermocellum* host. Following published protocols, we deleted the gene of interest. Yet the resultant mutant produced the same amount of total hydrogen comparing to its parental control. Nevertheless we observed a 60% increase in ethanol production as well as a 50% increase in specific rate of hydrogen production in the mutant due to the deletion of the competing pathway. The outcome should aid in future site-directed mutagenesis by deleting multiple competing pathways to improve hydrogen molar yield.
- Using an applied potential is an effective method for producing hydrogen gas. The increase in applied voltages results in higher set anode potentials, but the cathode potential does not appreciably vary. Hydrogen gas production is increased with applied potentials, as is

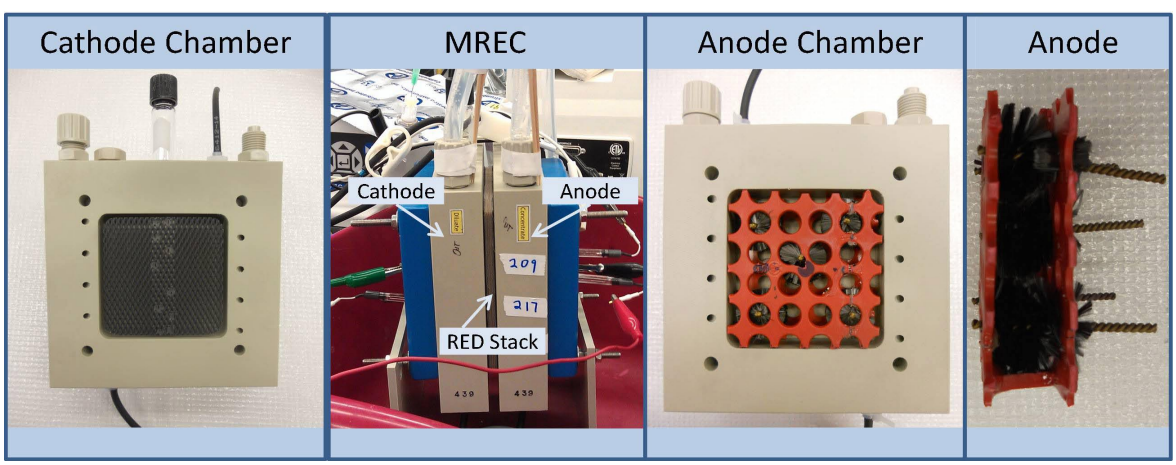

FIGURE 3. Modified MREC Reactor

COD removal. More of the protein in the fermentation effluent can be removed at the higher applied voltages.

In the future, we will operate the sequencing fed-batch bioreactor fermenting lignocellulose derived from corn stover (vs. pure cellulose) and test an HRT of 24 h with liquid volume displacement at 12-h intervals. We will test other bioreactor parameters (HRT and percent displacement) just to ensure these parameters are not substrate-dependent. We will continue to generate pathway mutants by deleting multiple competing pathways to realize an increase in hydrogen molar yield. One such candidate pathway is the ethanol pathway, since the production of one mole of ethanol consumes two moles of nicotinamide adenine dinucleotide, which could be redirected toward hydrogen production. In the future, the performance of the newly redesigned MREC will be examined and operating conditions such as HRT, salinity ratios, and concentrations of the saline solution will be optimized.

FY 2013 PUBLICATIONS/PRESENTATIONS

1. Levin, D., J. Jo, and P.C. Maness. 2012. "Biohydrogen production from cellulosic biomass." Book chapter in Integrated Forest BioRefineries, Royal Society of Chemistry, Cambridge, UK.

2. Thammannagowda, S., L. Magnusson, J.H. Jo, P.C. Maness, and M. Seibert. 2013. Renewable hydrogen from biomass. In Encyclopedia of Biol. Chem. 4: 72-75.

3. Nam, J.-Y., R.D. Cusick, Y. Kim, and B.E. Logan. 2012. Hydrogen generation in microbial reverse-electrodialysis electrolysis cells using a heat-regenerated salt solution. *Environ. Sci. Technol.* 46(9): 5240-5246.

4. Nam, J-Y., and B.E. Logan. 2012. Optimization of catholyte concentration and anolyte pHs in two chamber microbial electrolysis cells. *Int. J. Hydrogen Energy.* 37(24):18622-18628.

5. "Hydrogen production from cellulose in *Clostridium thermocellum*", poster presentation at the Clostridium XII - International Conference on the Genetics, Physiology and Biotechnology of Solvent- and Acid-forming Clostridia, Sept. 10–12, 2012, Nottingham, UK (Chou).

6. "Metabolic engineering in *Clostridium thermocellum* for hydrogen production", invited presentation at the Annual MGCB2 Review. November 5–6, 2012, Winnipeg, Canada (Maness) – paid for by Genome Canada Program.

7. "Hydrogen production via the fermentation of lignocellulosic biomass in *Clostridium thermocellum,"* poster presentation at the MGCB2 Annual Review. November 5–6, 2012, Winnipeg, Canada (Chou) – paid for by Genome Canada Program.

8. Logan, B.E. Microbial fuel cells meet salinity gradient energy. *Invited talk*, Science Writers Workshop, CASW New Horizons in Science, Raleigh, North Carolina, October 29, 2012.

9. Maness, P.C. and Logan, B. 2013. DOE Fuel Cell Technology Program Review, May 2013, Washington, DC. Presentation PD038.

REFERENCES

1. Zhang, Y.P.; Lynd, L.R. (2005). Cellulose utilization by *Clostridium thermocellum*: bioenergetics and hydrolysis product assimilation. *Proc. Natl. Acad. Sci. USA* **102**, 7321–7325.

2. Hawkes, F.R.; Dinsdale, R.; Hawkes, D.L.; Hussy, I. (2002). Sustainable fermentative hydrogen production: Challenges for process optimisation. *Intl. J. Hydrogen Energy* **27**, 1339–1347.

3. Logan, B.E.; Oh, S.E.; Kim, I.S.; Van Ginkel, S. (2002). Biological hydrogen production measured in batch anaerobic respirometers. *Environ. Sci. Technol.* **36**, 2530–2535.

4. Van Ginkel, S.; Sung, S. (2001). Biohydrogen production as a function of pH and substrate concentration. *Environ. Sci. Technol.* **35**, 4726–4730.

5. Rachman, M.A.; Furutani, Y.; Nakashimada, Y.; Kakizono, T.; Nishio, N. (1997). Enhanced hydrogen production in altered mixed acid fermentation of glucose by *Enterobacter aerogenes*. *J. Ferm. Eng.* **83**, 358–363.

6. Cheng, S.; Logan, B.E. (2007). Sustainable and efficient biohydrogen production via electrogenesis. *Proc. Natl. Acad. Sci. USA.* **104**, 18871–18873.

7. Lalaurette, E.; Thammannagowda, S.; Mohagheghi, A.; Maness, P.C.; Logan, B.E. (2009). Hydrogen production from cellulose in a two-stage process combining fermentation and electrohydrogenesis. *Intl. J. Hydrogen Energy* **34**, 6201–6210.

8. Guss, A.; Olson, D.G.; Caiazza, N.C.; Lynd, L.R. (2012). Dcm methylation is detrimental to plasmid transformation in *Clostridium thermocellum*. *Biotechnol. Biofuels* **5**, 30–41.

9. Argyros, D.; Tripathi, S.A.; Barrett, T.F.; Rogers, S.R.; Feinberg, L.F.; Olson, D.G.; Foden, J.M.; Miller, B.B.; Lynd, L.R.; Hogsett, D.A.; Caiazza, N.C. (2011). High ethanol titers from cellulose by using metabolically engineered thermophilic anaerobic microbes. *Appl. Environ. Microbiol.* **77**, 8288–8294.

II.D.4 Hydrogen from Water in a Novel Recombinant Oxygen-Tolerant Cyanobacterial System

Philip D. Weyman (Primary Contact),
Isaac A. Yonemoto, Hamilton O. Smith
J. Craig Venter Institute
10355 Science Center Dr.
San Diego, CA 92121
Phone: (858) 200-1815
Email: pweyman@jcvi.org

DOE Manager
Katie Randolph
Phone: (720) 356-1759
Email: Katie.Randolph@go.doe.gov

Technical Advisor
Sarah Studer
Phone: (202) 586-4031
Email: Sarah.Studer@ee.doe.gov

Contract Number: DE-FC36-05GO15027

National Laboratory Collaborators:
Pin-Ching Maness, Scott Noble, and Jianping Yu
National Renewable Energy Laboratory (NREL),
Golden, CO

Project Start Date: May 1, 2005
Project End Date: January 30, 2014

Overall Objective

Develop an O_2-tolerant cyanobacterial system for sustained and continuous light-driven H_2 production from water.

Fiscal Year (FY) 2013 Objective

Increase activity of environmentally derived hydrogenase by at least five-fold.

Technical Barriers

This project addresses the following technical barriers from the Hydrogen Production section (3.1.5) of the Fuel Cell Technologies Office Multi-Year Research, Development, and Demonstration Plan:

(AP) Oxygen Accumulation

Technical Targets

Barrier AP: O_2 Accumulation	2011 Status	2015 Target	2020 Target
Duration of continuous photoproduction in full sunlight	2 min	30 min	4 h

FY 2013 Accomplishments

- Increased hydrogen evolution activity for our environmentally derived hydrogenase expressed in cyanobacteria by 20-fold compared to our original strain.
- Developed an affinity-tagged purification scheme for use with the environmentally derived hydrogenase.
- Created plasmids with different combinations of cyanobacterial promoters to find optimal levels of transcription of hydrogenase accessory proteins.

✧ ✧ ✧ ✧ ✧

INTRODUCTION

Photobiological processes are attractive routes to renewable H_2 production. With the input of solar energy, photosynthetic microbes such as cyanobacteria and green algae carry out oxygenic photosynthesis, using sunlight energy to extract reducing equivalents from water. The resulting reducing equivalents can be fed to a hydrogenase system yielding H_2. However, one major difficulty is that most hydrogen-evolving hydrogenases are inhibited by O_2, which is an inherent byproduct of oxygenic photosynthesis. The rate of H_2 production is thus limited. Certain photosynthetic bacteria are reported to have an O_2-tolerant evolving hydrogenase, yet these microbes do not split water and require other more expensive feedstocks.

To overcome these difficulties, we propose to construct novel microbial hybrids by genetically transferring O_2-tolerant hydrogenases from other bacteria into cyanobacteria. These hybrids will use the photosynthetic machinery of the cyanobacterial hosts to perform the water-oxidation reaction with the input of solar energy, and couple the resulting reducing equivalents to the O_2-tolerant bacterial hydrogenase, all within the same microbe. By overcoming the sensitivity of the hydrogenase enzyme to O_2, we address one of the key technological hurdles to cost-effective photobiological H_2 production which currently limits the production of hydrogen in algal systems.

APPROACH

Our goal is to construct a novel microbial hybrid taking advantage of the most desirable properties of both cyanobacteria and other bacteria, to serve as the basis for technology to produce renewable H_2 from water. To achieve this goal, we use the following two approaches. The first approach is to transfer known O_2-tolerant hydrogenases from anoxygenic photosynthetic bacteria *Thiocapsa roseopersicina* to cyanobacteria. Since only a very limited number of O_2-tolerant hydrogenases are available, our second approach is to identify novel O_2-tolerant hydrogenases from environmental microbial communities and transfer them into cyanobacteria.

RESULTS

Previously, we reported the successful expression in cyanobacteria of active, oxygen-tolerant NiFe hydrogenases. These NiFe hydrogenases included the stable hydrogenase from *Thiocapsa roseopersicina* and a novel, environmentally derived NiFe hydrogenase, HynSL (previously named HyaAB). Although active hydrogenase was detected indicating co-expression of all required accessory proteins, the activity of this strain (RC41) was 10-fold lower than the native hydrogenase activity (strain 7942, Figure 1). To increase activity we developed two strategies. The first involved increasing the number of promoters to achieve higher transcription and higher levels of the hydrogenase activity in the cyanobacteria (strain RC41-4, Figure 1). The second strategy involved modification of the amino acid residues predicted to ligate the iron sulfur (FeS) clusters in the small subunit. Each of these strategies resulted in a four-to-five-fold increase in activity. When combined in the same plasmid, hydrogen evolution activity increased by 20-fold (strain CM12, Figure 1).

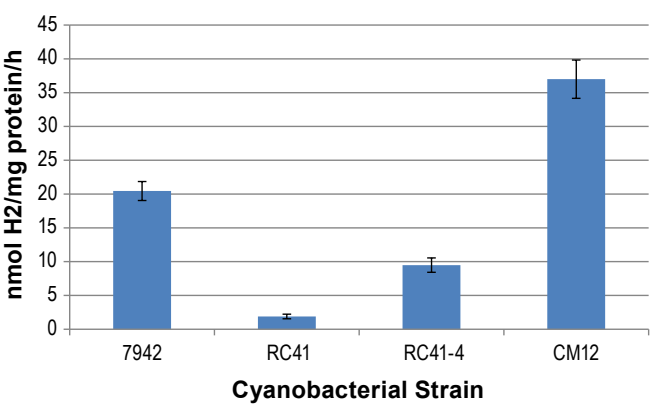

FIGURE 1. Comparison of hydrogenase activity of selected cyanobacterial strains. See text for strain details. Shown is the H_2-evolution activity assayed in an *in vitro* assay using reduced methyl viologen as the electron donor. Error bars describe one standard deviation from the mean of triplicate biological replicates.

Many of our strategies to engineer hydrogenase to function better in cyanobacteria involve substitutions of the amino acid residues composing the hydrogenase. To better study the effect of these substitutions, an easy method of protein purification is desirable so increases in activity can be directly correlated with changes to the protein. To facilitate protein purification, we designed an affinity-tagged version of our hydrogenase using the StrepII tag which binds tightly to the Streptactin chromatography resin. We achieved purification of the hydrogenase with increases in purification of over 100-fold using this technique (Table 1). Because we added the StrepII tag to the end of the hydrogenase small subunit, HynS, it also allowed us to visualize this protein on a western blot (Figure 2). Suprisingly, we did not purify an appreciable amount of the immature HynS, although this protein was observed in the crude extract. The large subunit (HynL) can also be examined using antisera available in our laboratory. As expected, only the mature, proteolytically cleaved version is obtained in the purified fraction (Figure 2).

TABLE 1. Comparison of affinity-tagged versions of the wild type environmentally derived hydrogenase (Construct 1) and the FeS cluster ligation substitution (Construct 2).

	Specific activity (nmole H_2 produced/ mg protein/h)	Fold purification
Construct 1 (crude)	369	
Construct 1 (purified)	41,450	112
Construct 2 (crude)	765	
Construct 2 (purified)	134,214	176

Previous results suggested that there is an optimal level of expression for the accessory proteins that mediate hydrogenase maturation. To find the optimal configuration, we generated 27 versions of our hydrogenase expression plasmids that contain combinations of three different promoters at three different sites. The three promoters have different strengths and include Rbc (low level expression), Trc (intermediate expression), and PsbA (high level expression). We have successfully created all 27 plasmids (Figure 3), and experiments to test activity in cyanobacteria are currently ongoing.

CONCLUSIONS AND FUTURE DIRECTIONS

- Using a combination of two different strategies, we have increased hydrogenase activity by 20-fold compared to our initial published activity levels.
- We have successfully designed a strategy for affinity purification of the hydrogenase and have used this strategy to obtain fractions with greater than 100-fold increased specific activity.

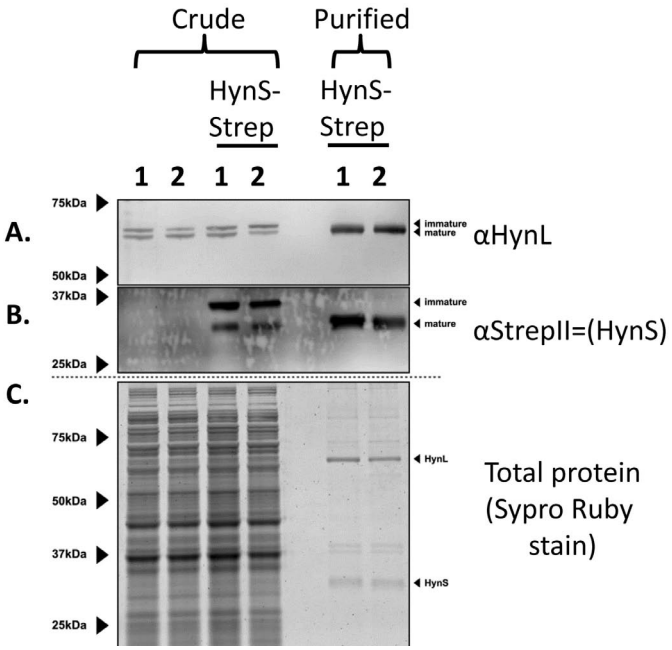

FIGURE 2. Affinity-tagging of HynS and purification of the hydrogenase complex. Samples include untagged and HynS-strep tagged versions of two constructs: the wild type environmentally derived hydrogenase (1) and the FeS cluster ligation mutant (2). A. Western blot with anti-HynL antisera. B. Western blot with anti-StrepII antisera to visualize HynS. C. Total protein visualized with Sypro Ruby.

- We have created a series of plasmids with promoters of different strengths to find the optimal levels of expression of the hydrogenase accessory proteins.

FY 2013 PUBLICATIONS/PRESENTATIONS

1. Weyman, PD. "Using synthetic biology to develop photosynthetic microorganisms into alternative energy factories", Nov. 2012, Swarthmore College. (Invited Speaker)

2. Weyman, PD. "Synthetic Biology Approaches to Develop Algae for Food Production." NASA Synthetic Biology Workshop on Food Production in Space, Ames Research Center, September 2012.

3. Weyman, PD. "An Expanded Role for Synthetic Genomic Approaches in Microbiology." Frontiers in Large Scale Organism and Pathway Engineering. DOE Joint Genome Institute. Walnut Creek, CA. April 29–30, 2013.

4. Weyman, PD. "Hydrogen from water in a novel recombinant oxygen-tolerant cyanobacterial system", EERE Fuel Cell Technologies Office, Annual Merit Review. May 17, 2013, Arlington, VA.

5. Yonemoto IY, Materri CM, Nguyen TA, Smith HO, Weyman PD. Dual organism design cycle reveals small subunit substitutions that improve [NiFe] hydrogenase hydrogen evolution. *Journal of Biological Engineering (*2013) 7:17.

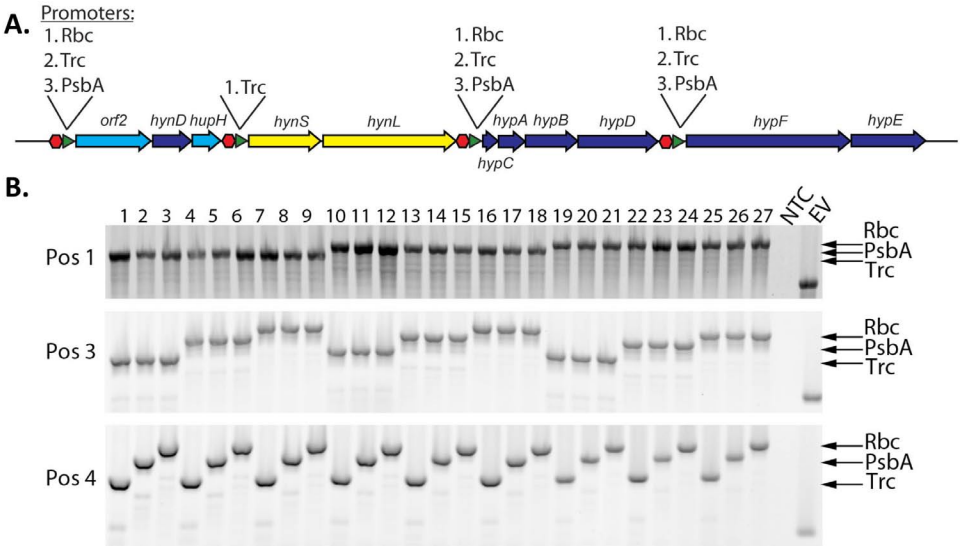

FIGURE 3. Promoter-modification plasmid design and confirmation. A. Three different promoters (Rbc, Trc, and PsbA) were inserted in all possible combinations at three different sites (positions 1, 3, and 4). B. Polymerase chain reaction results confirming correct assembly of the plasmids.

II.D.5 Probing O_2-Tolerant CBS Hydrogenase for Hydrogen Production

Pin-Ching Maness (Primary Contact), Scott Noble, and Jianping Yu
National Renewable Energy Laboratory (NREL)
15013 Denver West Parkway
Golden, CO 80401
Phone: (303) 381-6114
Email: pinching.maness@nrel.gov

DOE Manager
Katie Randolph
Phone: (720) 356-1759
Email: Katie.Randolph@go.doe.gov

Project Start Date: May 1, 2005
Project End Date: Continuation and direction determined annually by DOE

Overall Objectives

- Decipher the maturation machinery of the O_2-tolerant hydrogenase in *Rubrivivax gelatinosus* to transfer the correct number of genes to build an optimal cyanobacterial recombinant.
- Construct a cyanobacterial recombinant by expressing four hydrogenase genes and six maturation genes from *Rubrivivax gelatinosus* for sustained H_2 production.
- Demonstrate H_2 production in the cyanobacterial recombinant during photosynthesis for photolytic H_2 production.

Fiscal Year (FY) 2013 Objectives

Develop an O_2-tolerant cyanobacterial system for sustained and continuous light-driven H_2-production from water.

Technical Barriers

This project addresses the following technical barriers from the Hydrogen Production section (3.1.4) of the Fuel Cell Technologies Office Multi-Year Research, Development, and Demonstration Plan:

(AP) Oxygen Accumulation

Technical Targets

Characteristics	Units	2011 Target	2015 Target	2020 Target	Ultimate Target
Duration of continuous H_2 production at full sunlight intensity	Time units	2 min	30 min	4 h	8 h

FY 2013 Accomplishments

We sequenced the genome of *Rubrivivax gelatinosus* Casa Bonita strain (hereafter "CBS"), which uncovered a second set of hydrogenase maturation operon *hyp2*. We created *hypE* single and double mutant strains in *hyp1* and/or *hyp2* loci. Based on mutant analysis, we concluded that HypE proteins from the two loci can complement each other, and that no other gene in the CBS genome can substitute for the HypE function. Yet gene expression profiles based on quantitative reverse transcriptase-polymerase chain reaction (qRT-PCR) data suggest a role of *hyp1* to be consistent with assembling the CBS hydrogenase, which guides its expression in *Synechocystis*.

- We tested a strong *psbA* promoter to drive the expression of CBS hydrogenase genes in a *Synechocystis* recombinant. When compared to the original weaker *petE* promoter, hydrogenase protein levels increased by 16- to 44-fold with the strong *psbA* promoter. We have subsequently constructed a *Synechocystis* recombinant harboring nine CBS hydrogenase and related genes driven by the strong *psbA* and *psbA2* promoters. Work is underway to express *hypF1* in the recombinant driven by the *psbA* promoter.

✧ ✧ ✧ ✧ ✧

INTRODUCTION

Photobiological processes are attractive routes to renewable H_2 production. With the input of solar energy, photosynthetic microbes such as cyanobacteria and green algae carry out oxygenic photosynthesis using solar energy to extract reducing equivalents (electrons) from water. The resulting reducing equivalents can be fed to a hydrogenase system yielding H_2. However, one major barrier is that most hydrogen-evolving hydrogenases are inhibited by O_2, which is an inherent byproduct of oxygenic photosynthesis. The rate and duration of H_2 production is thus limited. Certain photosynthetic bacteria are reported to have an O_2-tolerant, H_2-evolving hydrogenase, yet these microbes do not split water and require other more expensive feedstocks.

To overcome these technical barriers, we propose to construct novel microbial hybrids by genetically transferring O_2-tolerant hydrogenases from other bacteria into cyanobacteria. These hybrids will use the photosynthetic machinery of the cyanobacterial hosts to perform the water-oxidation reaction with the input of solar energy, and couple the resulting reducing equivalents to the O_2-tolerant bacterial hydrogenase, all within the same microbe. By overcoming the sensitivity of the hydrogenase enzyme to O_2, we address one of the key technological hurdles (Barrier AP) to cost-effective photobiological H_2 production, which currently limits the production of H_2 in photolytic systems.

APPROACH

Our goal is to construct a novel microbial hybrid, taking advantage of the most desirable properties of both cyanobacteria and other bacteria, to serve as the basis for technology to produce renewable H_2 from water and solar energy. To achieve this goal, we will transfer the known O_2-tolerant hydrogenase from *Rubrivivax gelatinosus* CBS to the model cyanobacterium *Synechocystis* sp. PCC 6803.

RESULTS

Probing Hydrogenase Maturation Machinery in CBS

The overarching goal is to construct a cyanobacterial recombinant harboring the O_2-tolerant hydrogenase from *Rubrivivax gelatinosus* CBS using *Synechocystis* sp. PCC 6803 as a model host for sustained photolytic H_2 production. A prerequisite for success is to gain better understanding of the CBS hydrogenase and its underlying maturation machinery in CBS to ensure transfer of the correct genes into *Synechocystis* to confer hydrogenase activity. Annotation of the CBS genome revealed a complex picture of life using CO as the carbon and energy source, including CO sensor/transcriptional regulator and CO dehydrogenase, H_2-sensing hydrogenase, evolving hydrogenase (the "CBS hydrogenase"), and uptake hydrogenase. In addition to the set of hydrogenase maturation genes found earlier (*hyp1*), a second complete set of hydrogenase maturation genes (*hyp2*) was found within the uptake hydrogenase operon. This raises the question as to which set of maturation genes is responsible for building an active CBS hydrogenase and needs to be co-transformed along with the CBS hydrogenase into *Synechocystis*. Using qRT-PCR to probe gene expression, we found that *hyp1* genes (*A1, B1,* and *D1*) are specifically induced by CO (but not H_2), similar to that of the CBS hydrogenase, while *hyp2* genes (*C2, D2,* and *E2*) are specifically induced by H_2, but not CO (Figure 1). The data are consistent with a role of *hyp1* genes for the maturation of the evolving CBS hydrogenase, and a role of *hyp2* genes for the maturation of the uptake hydrogenase, which is not of interest to this project.

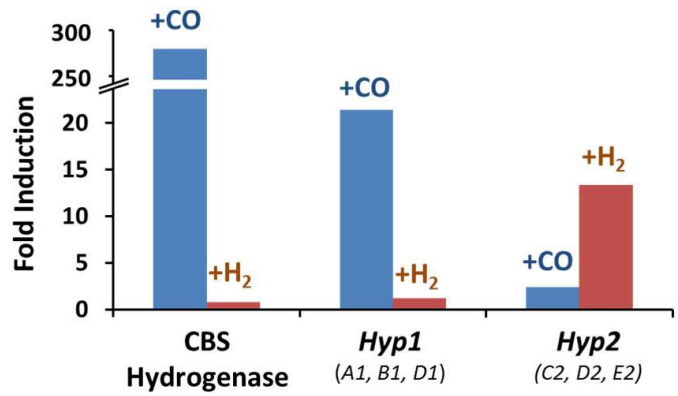

FIGURE 1. Quantitative RT-PCR of CBS maturation genes in various gas substrates. WT: wild type. Fold changes are based on control cultures grown in argon gas.

These gene expression data could not rule out the possibility that *hyp2* genes or any additional genes in the CBS genome are capable of assisting the maturation of the CBS hydrogenase. To address this question we took a genetic approach and created Δ*hypE1*, Δ*hypE2*, and Δ*hypE1*:Δ*hypE2* mutant strains. The double mutant has clearly lost the ability to utilize CO to support growth, indicating that it lacks a functional CBS hydrogenase and that there is no other gene in the CBS genome that can substitute for the HypE function. Interestingly, either Δ*hypE1* or Δ*hypE2* strains can grow in CO. This case study provides evidence that *hyp1* and *hyp2* genes are complementary—that either copy is able to mature the CBS O_2-tolerant hydrogenase. Yet based on the qRT-PCR evidence, initial work will focus on co-expressing only *hyp1* genes with the CBS hydrogenase in *Synechocystis* for photolytic H_2 production.

Expression of the CBS Hydrogenase in *Synechocystis*

Working toward building the cyanobacterial recombinant, we have used a weak *petE* promoter to drive the expression of CBS hydrogenase genes in *Synechocystis.* Lack of consistent H_2 production in the transgenic *Synechocystis* may have been resulted from low hydrogenase protein levels. To address this issue, we tested a strong *psbA* promoter to drive the hydrogenase genes *cooLXUH.* As shown in Figure 2, *psbA* promoter dramatically enhanced CBS hydrogenase protein expression in the cyanobacterium by 16- to 44-fold. Subsequently we have reconstructed a *Synechocystis* recombinant containing nine CBS hydrogenase and related genes, with *psbA* promoter driving the expression of *cooLXUH* (encoding CBS hydrogenase), and *PpsbA2* driving *hyp1ABCDE*. Work is ongoing to clone *hypF1* driven by *psbA* promoter to afford hydrogenase activity in *Synechocystis*.

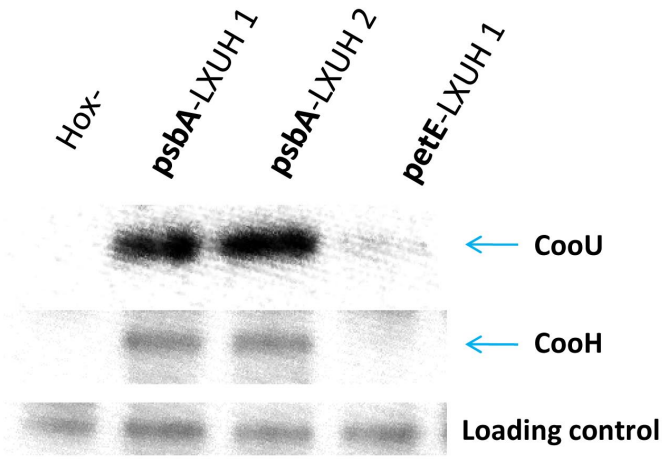

FIGURE 2. The strong *psbA* promoter enhanced the expression of CooLXUH in *Synechocystis*. Shown is a Western blot for CBS CooU and CooH subunits. Hox- is the background parent strain into which either the *psbA-LXUH* or *petE-LXUH* constructs were transformed. CooU and CooH were both expressed at higher levels from *psbA* promoter over *petE* promoter, with 16- and 44-fold increases, respectively.

CONCLUSIONS AND FUTURE DIRECTIONS

Conclusions

- Either *hyp1* or *hyp2* genes are capable of assembling the CBS O_2-tolerant hydrogenase based on mutant analysis. Yet qRT-PCR data are consistent with a role of *hyp1* in the maturation of CBS hydrogenase. Initial work will focus on expressing *hyp1* genes along with CBS hydrogenase in *Synechocystis*.
- Use of the strong *psbA* promoter dramatically enhanced CBS hydrogenase protein expression levels in *Synechocystis*. A *Synechocystis* recombinant has been constructed expressing nine CBS hydrogenase and related genes, driven by the strong *psbA* and *psbA2* promoters. Transformation of *hypF* is underway driven by *psbA* promoter in order to confer hydrogenase activity.

Future Directions

- We will further investigate the roles of CBS *hypE1* and *hypE2* in hydrogenase maturation by directly examining CO uptake and H_2 production in the single and double mutants.
- We will apply the strong *psbA* promoter to enhance expression of additional CBS hydrogenase genes in *Synechocystis* for consistent hydrogen production. We will optimize growth and induction conditions to boost CBS hydrogenase activity in the recombinant *Synechocystis*.

FY 2013 PUBLICATIONS/PRESENTATIONS

1. Eckert, C.; Boehm, M.; Carrieri, D.; Yu, J.; Dubini, A.; Nixon, P.J.; Maness, P.C. 2012. "Genetic analysis of the Hox hydrogenase in the cyanobacterium *Synechocystis* sp. PCC 6803 reveals subunit roles in association, assembly, maturation, and function." *J. Biol. Chem.* 287: 43502-43515.

2. Ghirardi, M.L.; King, P.W.; Mulder, D.W.; Eckert, C.; Dubini, A.; Maness, P.C.; Yu, J. 2013. "Hydrogen production by water photolysis." *Microbial Bioenergy*, Advances in Photosynthesis and Respiration series (Govindjee and T. Sharkey, eds.), in press.

3. Maness, P.C. 2012. "Genetic engineering in the cyanobacterium in *Synechocystis* sp. PCC 6803 for solar H_2 production." Presentation at the 14th International Symposium on Phototrophic Prokaryotes, August 5–10, 2012, Porto, Portugal.

4. Maness, P.C. 2013. "Probing O_2-tolerant CBS hydrogenase for hydrogen production." Presentation at the DOE Hydrogen and Fuel Cells Program Annual Merit Review, May 16, 2013, Arlington, VA (PD095).

II.E.1 Distributed Bio-Oil Reforming

Stefan Czernik (Primary Contact), Richard French, Michael Penev
National Renewable Energy Laboratory (NREL)
15013 Denver West Parkway
Golden, CO 80401
Phone: (303) 384-7703
Email: Stefan.Czernik@nrel.gov

DOE Manager
Sara Dillich
Phone: (202) 586-1623
Email: Sara.Dillich@ee.doe.gov

Project Start Date: October 1, 2004
Project End Date: September 30, 2013

Overall Objectives

- Develop the necessary understanding of process chemistry, catalyst deactivation and regeneration, and bio-oil compositional effects as a basis to define the process for distributed reforming.
- Demonstrate the technical feasibility for the process of producing hydrogen from biomass pyrolysis oils.

Fiscal Year (FY) 2013 Objectives

- Provide mass balances for auto-thermal reforming of three pyrolysis liquids.
- Show the relation between hydrogen yield and bio-oil composition and identify bio-oil that can deliver 10 g of hydrogen per 100 g of bio-oil.
- Update the H2A analysis based on the validated process performance results to assess the process energy efficiency and the cost of hydrogen.

Technical Barriers

This project addresses the following technical barriers from the production section of the Fuel Cell Technologies Office Multi-Year Research, Development, and Demonstration Plan:

(A) Reformer Capital Costs and Efficiency

(B) Operations and Maintenance

(C) Biomass Feedstock Issues

Technical Targets

Table 1 presents the technical targets for this project.

TABLE 1. Progress towards Meeting DOE Distributed Hydrogen Production Targets

Distributed Production of Hydrogen from Bio-Derived Renewable Liquids			
Process Characteristics	**Units**	**2015 DOE Targets**	**2013 NREL Status**
Production Energy Efficiency	%	70	70
Total Hydrogen Production Costs	$/gge	5.90	4.26+2.00*

*It was assumed that the allowance for compression, storage, and distribution will be $2.00/gge.
gge – gasoline gallon equivalent

FY 2013 Accomplishments

- Demonstrated hydrogen production by auto-thermal reforming of bio-oils generated from three feedstocks.
- Produced hydrogen from two bio-oils at a yield >10 g H_2/100 g bio-oil.
- Calculated a process energy efficiency of 70% and estimated the cost of production at $4.26/gge.

✧ ✧ ✧ ✧ ✧

INTRODUCTION

Renewable biomass is an attractive near-term alternative to fossil resources because it has near zero life-cycle carbon dioxide (CO_2) impact. The most recent assessment says that more than 1 billion tons of biomass could be available in the United States each year at less than $60/ton [1]. This cost may increase to $72/ton when transportation, drying, and grinding are included. This biomass could be converted to 100 million tons of hydrogen, enough to supply the light-duty transportation needs of the United States. This work addresses the challenge of distributed hydrogen production with a targeted total dispensed hydrogen cost of $2-$4/kg H_2 (produced, delivered and dispensed, but untaxed) [2]. Pyrolysis is used to convert biomass to a liquid that can be transported more efficiently and has the potential to be used in automated operation conversion systems [3,4]. "Bio-oil" can then be converted to hydrogen and CO_2 in a distributed manner at or near fueling stations.

The objective of this project is to develop a system that will provide distributed production of hydrogen from bio-oil.

To accomplish this we are developing a simple fixed-bed reactor suitable for unsupervised automated operation.

APPROACH

This research project is focused on developing a compact, low-capital-cost, low/no maintenance reforming system that will enable achievement of the cost and energy efficiency targets for distributed reforming of renewable liquids. In this project, we are evaluating the following steps in the process:

- **Bio-oil volatilization** using ultrasonic atomization. Blending with alcohol is being used to control the physical and chemical properties of the liquid, primarily to achieve an acceptable viscosity.
- **Heterogeneous auto-thermal reforming of bio-oil-derived gas and vapor.** Nickel and precious-metal reforming catalysts have been tested. Platinum has proven to be the most effective.

This year, a series of tests was conducted using an integrated bench-scale reactor system that was constructed in the previous year. As shown schematically in Figure 1, the system included the following operations: bio-oil atomization and evaporation, hot vapor filtration, partial-oxidation/steam reforming, water-gas shift, and hydrogen separation. Such a unit provided more complete and reliable assessment of the process performance results necessary for techno-economic evaluation. The operation of the unit was described in the FY 2012 annual progress report.

RESULTS

In FY 2012 we produced hydrogen from bio-oils produced by fast pyrolysis of oak and poplar wood. This year, in order to evaluate the relation between the hydrogen yield and the feed properties we prepared two more biomass-derived liquids—pine fast pyrolysis bio-oil and the lignin-free fraction of oak pyrolysis bio-oil—and used them in a similar series of reforming tests. We also characterized the physical and chemical properties that can affect hydrogen production for all of those liquids. The four biomass-derived liquids were analyzed to determine the following properties:

- Elemental composition (performed by Huffman Laboratories)
- Water content (Karl-Fischer titration)
- Lignin content (calculated from water content measurements for the whole oil and for the aqueous fraction produced by the water separation process)

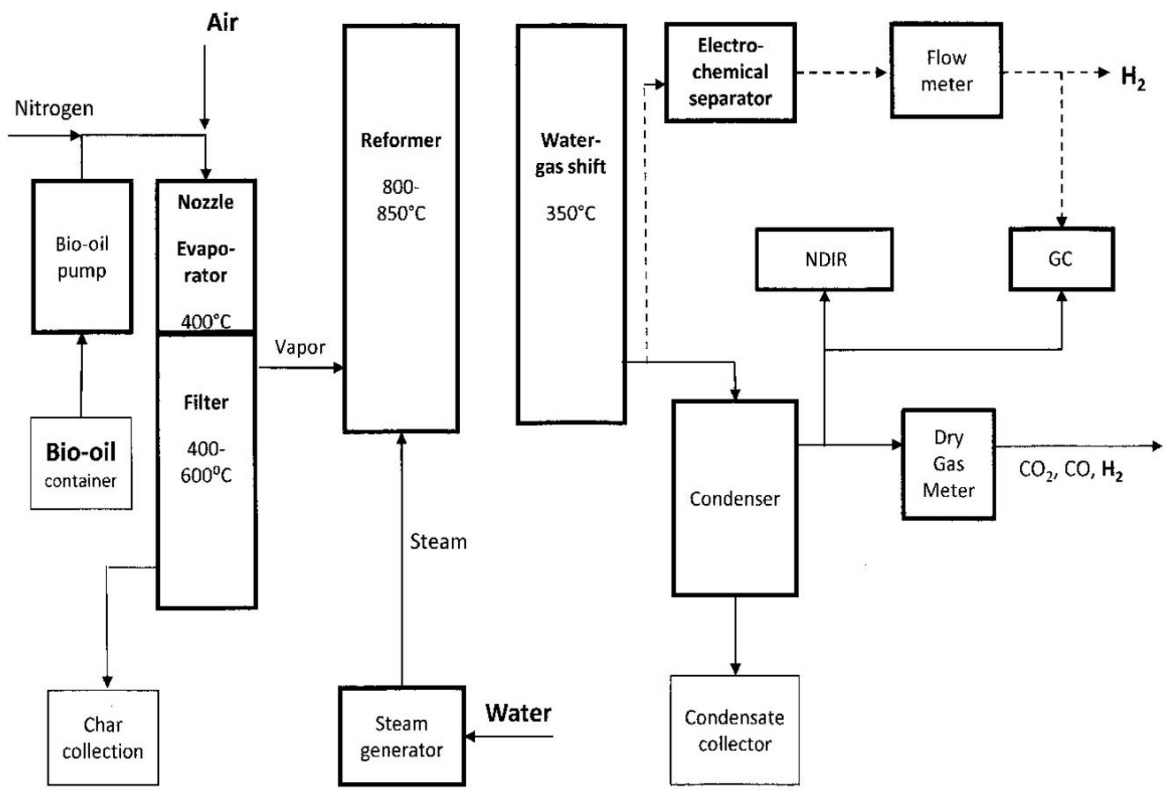

FIGURE 1. Schematic of the Integrated Bio-Oil to Hydrogen System

- Viscosity (rotary viscometer)
- Molecular weight distribution (size exclusion chromatography)
- Surface tension (performed by Kibron/PM Scientific)

Elemental composition of the feedstock sets a limit for a theoretical maximum yield of hydrogen (based on stoichiometric conversion). This yield will be greater for the materials with high carbon and hydrogen content and low oxygen content. Water content mostly affects (reduces) the viscosity of bio-oil and makes it easier to pump and atomize. Lignin, though it has theoretically higher potential for the production of hydrogen, is non-volatile and tends to form carbon deposits in the reactor. The average molecular weight is a measure of the amount of a high-molecular-weight fraction that is difficult to evaporate and, consequently, to convert to hydrogen. The high molecular weight of bio-oils indicates the presence of oligomeric lignin and possibly oligomeric carbohydrates originating from incomplete degradation during fast pyrolysis. Finally, surface tension affects the size of the droplets formed during liquid atomization; the average volume of a droplet is proportional to the surface tension of the liquid. Therefore, a high surface tension reduces the efficiency of liquid evaporation, which is an important stage of our process. Bio-oil characteristics are shown in Table 2.

TABLE 2. Bio-Oil Characteristics

	Oak Bio-Oil	Poplar Bio-Oil	Pine Bio-Oil	Lignin-Free Oak Bio-Oil
Elemental comp.				
C, wt%	44.9	47.4	48.2	12.5
H, wt%	7.2	7.5	7.4	10.0
O, wt%	47.8	45.1	44.3	77.5
Water, wt%	25.3	19.6	22.4	74.6
Lignin, wt%	32.9	38.0	31.2	0
Molecular weight,[a] Da	860	670	710	290
Viscosity, cP (25°C)	150	350	200	3.1
Surface tension, mN*m	43	20	30	37
Theoretical hydrogen yield, g/100 g feed	**12.6**	**13.8**	**13.5**	**3.8 (15.2)**[b]

[a] Weight average molecular weight
[b] Potential hydrogen yield on water-free basis

A series of experiments was carried out in the bench-scale reforming system using two biomass-derived liquids: pine pyrolysis bio-oil and a lignin-free fraction of oak pyrolysis bio-oil. Similar to the previously performed tests with oak and poplar bio-oils, the pine bio-oil was mixed with methanol at a 9:1 ratio, which stabilized the feed and reduced its viscosity. The lignin-free bio-oil fraction was used as is, without the addition of methanol. During these tests the bio-oil/methanol mixture was fed at a rate of 90 g/h and the lignin-free fraction was fed at 120 g/h. The reformer operated at a temperature of 850°C and the water-gas shift reactor at 350°C, with the atomic oxygen-to-carbon ratio (O/C) in the range of 0.85 to 1.0 and a steam-to-carbon molar ratio (S/C) of 3 to 4. The packed-bed reformer contained 200 g of 0.5% Pt/Al_2O_3 catalyst (BASF) and the water-gas shift reactor was packed with 200 g of a commercial Fe/Cr catalyst (Süd-Chemie). With a pine bio-oil feed rate of 90 g/h the system produced 107 L/h of hydrogen mixed with CO and CO_2 at the composition shown in Figure 2.

The process parameters and the yields of hydrogen produced from the two previously tested bio-oils and the two biomass-derived liquids processed in FY 2013 are summarized in Table 3.

These results show that reforming of poplar and pine bio-oils delivered >10 g H_2 per 100 g bio-oil, while reforming of oak bio-oil and of its lignin-free fraction produced less hydrogen. The lower hydrogen yield obtained from oak

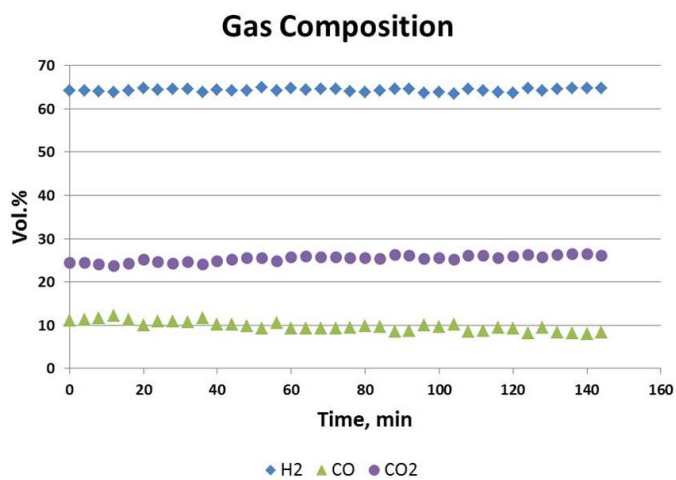

FIGURE 2. Product Gas Composition from Auto-Thermal Reforming with Water-Gas Shift of Pine Bio-Oil using BASF 0.5% Pt/Al_2O_3 Catalyst

TABLE 3. Process Parameters and Hydrogen Yields Produced by Reforming Bio-Oils

Feedstock	VHSV, h^{-1}	S/C	O/C	C conv, %	H_2 yield, g/100 g bio-oil
Oak bio-oil	2,100	3.5	1.0	84	**9.1**
Poplar bio-oil	2,100	3.0	0.9	89	**11.0**
Pine bio-oil	2,100	2.8	0.85	86	**10.5**
Oak lignin-free	1,100	4.0	1.5	89	**3.0 (12)**[a]

VHSV – methane-equivalent volumetric hourly space velocity
S/C – molar steam-to-carbon ratio
O/C – atomic oxygen-to-carbon ratio
C conv. – carbon conversion from bio-oil to gas
[a] Hydrogen yield on water-free basis (lignin-free oak bio-oil fraction contained only 25.6% organic compounds and 74.6% water)

bio-oil, compared to those from poplar and pine bio-oils, resulted from its lower carbon and higher oxygen content, which determined the maximum potential yield as shown in Table 2. In addition, the amount of carbon residue retained in the evaporator was greater for oak bio-oil than for the other liquids tested. This may have resulted from its higher molecular weight, which indicates higher non-volatile material content. Consequently, the carbon-to-gas conversion for the oak bio-oil was less than for the other liquids, which also negatively impacted the yield of hydrogen. The incomplete carbon-to-gas conversion—ranging from 84% to 89% for the different bio-oils—was due to the incomplete evaporation of non-volatile compounds (oligomeric lignin and carbohydrates) in the bio-oils, resulting in the solid residue in the evaporator. Because comparable amounts of the non-volatile material were found in all four bio-oils, the less-effective evaporation of oak bio-oil was most likely caused by its higher surface tension resulting in larger-sized bio-oil droplets generated by the ultrasonic nozzle.

Energy efficiency of the process is defined according to the following equation:

$$\text{Energy efficiency} = \frac{\text{LHV Hydrogen x 100\%}}{\text{LHVbio – oil + external process energy}}$$

where LHV is the lower heating value for hydrogen and for bio-oil used in the process. Because our bio-oil reforming process is auto-thermal, the only external energy needed is electricity to operate pumps and compressors; this is estimated at 2.92 kWh/kg H_2 or 10.5 MJ/kg H_2 (H2A analysis). For the lignin-free bio-oil fraction, external energy is needed to evaporate water added in the separation process; this is estimated at 10.0 MJ/kg H_2.

For the process energy efficiency calculation we assumed that the hydrogen yields in the full-scale system would be the same as those achieved in our bench-scale unit. With the LHV equal to 120.2 MJ/kg for hydrogen and 17.5 MJ/kg for the bio-oil/methanol feed (13.0 MJ/kg for the lignin-free fraction), the energy efficiency for the production of hydrogen from the bio-oils will range from 59% to 70% as shown in Table 4.

Costs of hydrogen production in a 1,500 kg/day plant were calculated for an nth plant in 2007 $ using the H2A v3 spreadsheet. According to the analysis performed by the NREL/Pacific Northwest National Laboratory techno-economic analysis group for DOE's Biomass Program, the cost of bio-oil was estimated at $236/ton. In our calculations we used that price for each bio-oil. The results are provided in Table 4.

The energy efficiency and production cost are strongly dependent on hydrogen yield and consequently are the most favorable for the poplar bio-oil and the least favorable for the lignin-free fraction. However, the production of the lignin-free fraction also delivers 6.6 kg of pyrolytic lignin per 1 kg of hydrogen. The market price of lignin from pulping processes is in the range of $200–$1,000/ton, thus the hydrogen production cost from the lignin-free fraction would be reduced by $1.32/kg to $3.74/kg. The pyrolytic lignin fraction potentially can have a much higher value, especially if it is applied as a phenol replacement for adhesive resin formulation—if it sells for half the price of phenol ($1.4/kg) it could bring a credit of up to $4.6/kg hydrogen. Considering this, we believe that the integrated production of hydrogen and co-products from bio-oil presents the most attractive scenario and should be thoroughly studied.

TABLE 4. Energy Efficiency and Costs of Hydrogen Production from Different Bio-Oils

Feedstock	Energy Efficiency, %	Hydrogen Production Cost, $/kg
Oak bio-oil	59.0	4.75
Poplar bio-oil	70.8	4.26
Pine bio-oil	67.8	4.37
Lignin-free oak bio-oil	62.0	5.06 3.74[a]

[a]This value was calculated assuming a $200/ton credit for the co-produced lignin fraction.

CONCLUSIONS AND FUTURE DIRECTIONS

- We identified optimum process parameters for the bio-oil auto-thermal reforming process: temperature 800–850°C, steam-to-carbon ratio 2.5–3.5, oxygen-to-carbon ratio 0.9–1.1, 0.5% Pt/Al_2O_3 catalyst, methane-equivalent space velocity about 2,000 h^{-1}.
- The hydrogen yields depended on both chemical composition and physical properties of bio-oils that were produced from different biomass feedstocks. The lower hydrogen yield obtained from oak bio-oil, compared to those from poplar and pine bio-oils, resulted from its lower carbon and higher oxygen content as well as the lower carbon-to-gas conversion.
- The incomplete carbon-to-gas conversion that ranged from 84% to 89% for the different bio-oils was due to the incomplete evaporation of non-volatile bio-oil compounds (oligomeric lignin and carbohydrates) that formed solid residue in the evaporator. The less-effective evaporation of oak bio-oil was most likely caused by its higher surface tension that resulted in larger-sized bio-oil droplets generated by the ultrasonic nozzle.
- Production of hydrogen from the lignin-free bio-oil fraction may be the most economically favorable process, but that strongly depends on the credit that can be obtained for the lignin fraction of bio-oil, which could be used for the production of adhesives or liquid fuels (by hydroprocessing).

FY 2013 PUBLICATIONS/PRESENTATIONS

1. Czernik, S. "Distributed Bio-Oil Reforming," 2013 DOE Hydrogen and Fuel Cells Program Annual Merit Review, May 15, 2013, Washington, DC.

REFERENCES

1. Perlack, R.; Stokes, B. (Leads). *U.S. Billion-Ton Update: Biomass Supply for a Bioenergy and Bioproducts Industry*, U.S. Department of Energy, ORNL/TM 2011/224, August 2011.

2. U.S. Department of Energy. *Fuel Cell Technologies Program Multi-Year Research, Development and Demonstration Plan*, Section 3.1 Hydrogen Production, July 2013, http://www1.eere.energy.gov/hydrogenandfuelcells/mypp/pdfs/production.pdf

3. Czernik, S.; Elam, C.; Evans, R.; Milne, T. "Thermochemical Routes to Hydrogen from Biomass−A Review," Bridgwater, A.V., Boocock, D.G.B., eds., *Science in Thermal and Chemical Biomass Conversion*, CPL Press: Newbury, UK, 2006, pp.1752−1761.

4. Evans, R.J.; Czernik, S.; French, R.; Marda, J. "Distributed Bio-Oil Reforming," *DOE Hydrogen Program FY2007 Annual Progress Report,* 2007.

II.E.2 Biomass-Derived Liquids Distributed Reforming

David King (Primary Contact), Yong Wang, Ayman Karim, James Rainbolt, Kurt Spies
Pacific Northwest National Laboratory (PNNL)
P.O. Box 999
Richland, WA 99354
Phone: (509) 375-3908
Email: david.king@pnnl.gov

DOE Manager
Sara Dillich
Phone: (202) 586-7925
Email: Sara.Dillich@ee.doe.gov

Project Start Date: October 1, 2004
Project End Date: September 30, 2013

Overall Objectives

- Identify catalyst, reactor, and operating conditions that maximize hydrogen selectivity and yield from biomass-derived liquids via a catalytic reforming approach
- Quantify hydrogen selectivity and yield requirements for aqueous phase reforming (APR) of biomass-derived liquids to meet the hydrogen 2015 cost target of <$5.90/gasoline gallon equivalent
- Demonstrate a viable pathway to produce hydrogen from biomass-derived liquids that meets the 2015 target

Fiscal Year (FY) 2013 Objectives

- Develop and demonstrate the feasibility of a two-step approach for the production of hydrogen from cellulose, combining cellulose deconstruction and APR
- Quantify selectivity, yield, and other requirement to enable this two-step approach to meet the 2015 target by H2A analysis
- Demonstrate experimentally the feasibility to meet these requirements in a set of catalytic reactions, generating hydrogen to meet the 2015 target
- Demonstrate the feasibility to apply this technology to the conversion of raw biomass to hydrogen

Technical Barriers

This project addresses the following technical barriers from the Hydrogen Production section of the Fuel Cell Technologies Office Multi-Year Research, Development, and Demonstration Plan:

(A) Reformer Capital Costs and Efficiency

(C) Biomass Feedstock Issues

(N) Feedstock Cost and Availability

Technical Targets

There is one primary technical target that we are addressing—H_2 production cost from bio-derived liquids reforming as shown in the following table:

Characteristics	Units	2011 Status	2015 Target	2020 Target
Hydrogen Levelized Cost (Production Only)	$/kg	6.6	5.9	2.3

Source: Fuel Cell Technologies Office Multi-Year Research, Development, and Demonstration Plan (MYRD&D Plan), Hydrogen Production Chapter, July,2013, http://www1.eere.energy.gov/hydrogenandfuelcells/mypp/pdfs/production.pdf

This multi-year project has examined the pathways for production of hydrogen from a variety of biomass-derived liquids. The cost of the starting feedstock has always proven to be a significant factor in the overall economics of hydrogen production. In FY 2013, this project focused on a pathway to convert cellulose to hydrogen, via an initial catalyzed "deconstruction" step to produce a polyol-rich product containing a high fraction of ethylene glycol, followed by APR of the ethylene glycol-rich product into hydrogen and CO_2. Ethylene glycol is one of the most facile molecules for production of hydrogen via APR and this two-step route should allow the use of cellulose, a less expensive feedstock than sugar/sugar alcohols we previously studied. H2A analysis is being used to establish performance targets as well as quantify the current production cost status of this route to meet the hydrogen cost target based on actual performance in catalytic tests. Beyond cellulose as a starting material, the final work on this project will focus on the replacement of cellulose by whole biomass via the same two-step approach. If this can be accomplished, this enables the use of a cheap biomass feedstock and should provide a path for further reducing the cost of hydrogen from biomass through a bio-liquid intermediary route.

✧ ✧ ✧ ✧ ✧

INTRODUCTION

Hydrogen production is a significant part of the Fuel Cell Technologies Office mission. It is most easily produced (and demonstrated to meet target cost) through the steam reforming of natural gas, which is seen as a transition fuel for hydrogen production. Natural gas reforming results in the co-production of the greenhouse gas CO_2. For this reason, there is a significant benefit in generating hydrogen from

renewable biomass, since the penalty for co-producing CO_2 is close to zero (the CO_2 co-production product does not need to be captured). Biomass gasification is one option; however this approach is limited by high capital costs. The cost of transporting raw biomass, and biomass availability, also places limits on the size of the gasifier, which results in loss of economies of scale. Steam reforming of some of the products of biomass processing is only possible for a few products (ethanol, methanol, glycerol, acetic acid), but many of the products, such as sugars, decompose on heating and are therefore not viable candidates for steam reforming.

One alternate approach for production of hydrogen from biomass-derived liquid phase (at ambient temperature) products is APR, which allows conversion of these less thermally stable compounds to hydrogen at modest temperatures and pressures without their decomposing or degrading in the reactor. The choice of feedstock with APR remains a consideration, as APR is not 100% selective toward hydrogen with most bio-derived liquid feedstocks, especially those with carbon numbers 5-6 or higher. This dictates that the approach for hydrogen production via APR requires highly active/selective catalysts and inexpensive feedstocks, preferably of low carbon number. Previously, we examined the aqueous fraction of bio-oil as a reactant; conversion of carboxylic acids present in this feedstock, notably acetic acid, was low and its presence in the feed appeared to deactivate the catalyst through a reversible poisoning mechanism. For this reason, in FY 2013 we revamped the program and examined an alternate feedstock and catalytic approach. Cellulose was selected for the initial primary investigation, and a two-step conversion pathway was employed. The first step was to facilitate the deconstruction of cellulose (according to literature precedents) to a mixture of polyols rich in ethylene glycol, followed by APR of this polyol mixture. We and others have established previously that ethylene glycol undergoes conversion to hydrogen with high yield via APR. Since we have focused previous work on the APR, the major focus of research in FY 2013 was on the cellulose deconstruction step. Successful deconstruction of cellulose can lead to a more ambitious effort to convert whole biomass (deconstructing the cellulose and hemi-cellulose fractions), followed by similar APR for hydrogen production with combustion of the unreacted lignin fraction for process heat.

APPROACH

The production of hydrogen from cellulose follows a two-step conversion process. The first step is described in the literature [1], and involves deconstruction of cellulose using bi-functional catalysis (acid plus metal under hydrogen pressure) to a mixture of oxygenates rich in polyols. In the most favorable cases, high yields of ethylene glycol have been reported. Since cellulose can be considered a polymer of glucose, it seems likely that glucose is the initial deconstruction product, as suggested by Liu et al. [1]. It is notable in that same work that sorbitol, the sugar alcohol derived from glucose, is unreactive, and therefore it is claimed that ethylene glycol is produced directly from glucose. However, the mechanisms for this transformation have not been fully developed. In the second step of the two-step process, the hydrogen overpressure is removed, and the polyol-rich mixture is converted to hydrogen via APR using a Pt-Re/ZrO_2 catalyst that we previously identified. The combining of these two steps has not been described in the literature prior to our proposing this approach for hydrogen production. The overall H_2 yield will very much depend upon the composition of the compounds that are produced during the cellulose deconstruction.

If we are successful with cellulose, we intend to move to whole biomass as a feedstock. We are expecting that the cellulose and hemicellulose portions of the biomass will be extracted and dissolved (as is cellulose by itself), leaving just the lignin fraction as a filterable by-product. APR will proceed to convert the products of deconstruction of both cellulose and hemicellulose to hydrogen and CO_2. The lignin fraction will be separated from the products of the first reactor by filtration, and can be combusted to provide process heat.

FY 2013 ACCOMPLISHMENTS

- Completed first pass H2A analysis for the two step process; identified key cost contributors to be feedstock cost and capital cost, including cost of processing waste water—indicating the need to demonstrate the ability to recycle the spent feed stream to the reactor and convert residual soluble carbon species to gaseous products to near extinction.
- Optimized the WO_3/Al_2O_3 (45 wt% WO_3) + 5%Ru/C catalyst system for the cellulose deconstruction at a 2:1 weight ratio, maximizing conversion and ethylene glycol yield.
- Obtained an ethylene glycol yield of 42% (carbon basis) at full conversion of cellulose, at 245°C and 180 minutes residence time (0.45 g catalyst and 4 g cellulose), equaling best literature values.

A summary of the key finding of our catalytic studies are provided in Table 1. We found that operation at 245°C provided the best performance compared to operation at lower temperatures (205°C and 225°C). Key points to be noted include:

- In the absence of the WO_3/Al_2O_3 catalyst component, the overall cellulose conversion from 5% Ru/C is low as is the selectivity to ethylene glycol (columns 1 and 2). The acidic function provided by WO_3/Al_2O_3 appears necessary to produce significant quantities of ethylene glycol via glucose.

- With increasing residence time, with the WO_3/Al_2O_3 + Ru/C catalyst, sorbitol decreases and ethylene glycol increases (columns 2 and 3). This is also shown more clearly in Figure 1, which includes data obtained at 60 minutes residence time as well. Although sorbitol may not be a primary intermediate in the production of ethylene glycol, neither is it unreactive as suggested by Liu [1]. At longer residence times, sorbitol appears to convert to ethylene glycol with this catalyst system. The long residence time data also suggest that ethylene glycol is stable under reaction conditions.
- The importance of the role of WO_3/Al_2O_3 is further supported by comparing performance of the combined catalysts at two different ratios (columns 3 and 4). The catalyst combination 0.17 g WO_3/Al_2O_3 + 0.28 g Ru/C performed poorly compared to the combination 0.28 g WO_3/Al_2O_3 + 0.17 g Ru/c (columns 3 and 4). Nevertheless, the presence of the 5% Ru/C catalyst component is clearly important in providing a hydrogenation function that generates terminal OH groups in the products.
- We also note that compared with direct APR of sorbitol, which we have described in earlier project work, it appears that this bifunctional catalyst system could provide a better route to hydrogen production from sorbitol via an ethylene glycol intermediate. This is because the direct APR of sorbitol produces a number of products in addition to hydrogen and CO_2. Nevertheless, based on the high cost of sorbitol as a feedstock, this new approach is not likely to be economically attractive as a route to hydrogen from bio-derived liquids.

TABLE 1. Comparative Performance of Ru/C and WO_3/Al_2O_3 + Ru/C at Two Different Ratios

Temperature (C)	245	245	245	245
Time (min)	30	30	180	180
Catalyst (g)				
Ru/C	0.17	0.17	0.17	0.28
WO_3/Al_2O_3		0.28	0.28	0.17
Conversion (%)	54.2	86.3	100.3	62.5
Yield (g/L)				
Ethylene Glycol	1.38	12.89	18.27	3.85
Sorbitol	4.08	7.51	1.42	4.58
Proplyene Glycol	1.75	0.87	2.44	1.23
Ethanol	1.5	0.75	0.99	1.06
1,2 Butanediol	0.36	0.74	1.22	0.67
Glycerol	1.67	0	0	0
Methanol	0	0.18	1.05	0
Acetic Acid	0	0	0.37	0

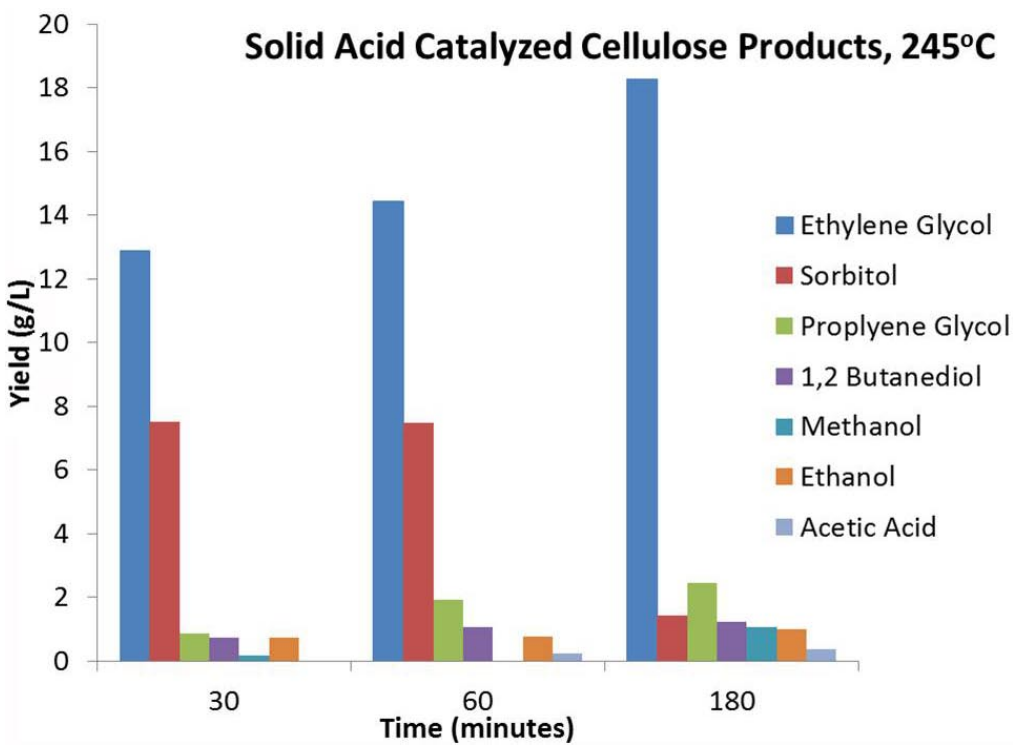

FIGURE 1. Yield of various products from the deconstruction of cellulose using a combination of WO_3/Al_2O_3 + Ru/C catalysts at 245°C.

FUTURE DIRECTIONS

The project will end with the end of FY 2013 funding. However, we point out the importance in any future work of determining the ability to recycle the catalyst and the waste water stream in subsequent cycles (cellulose deconstruction step) and as well APR catalyst longevity with the ethylene glycol-rich polyol feedstock.

FY 2013 PUBLICATIONS/PRESENTATIONS

1. A.M. Karim, C. Howard, B. Roberts, L. Kovarik, L. Zhang, D.L. King, Y. Wang "In situ XAFS studies on the effect of pH on Pt electronic density during aqueous phase reforming of glycerol", ACS Catalysis, 2, 2387–2394 (2012).

REFERENCES

1. Yue Liu, Chen Luo, and Haichao Liu, "Tungsten Trioxide Promoted Selective Conversion of Cellulose into Propylene Glycol and Ethylene Glycol on a Ruthenium Catalyst"; Angew. Chem. Int. Ed. 2012, 51, 3249 –3253.

III. HYDROGEN DELIVERY

III.0 Hydrogen Delivery Program Overview

INTRODUCTION

The Hydrogen Delivery program addresses all hydrogen distribution activities from the point of production to the point of dispensing. Research and development (R&D) activities address challenges to the widespread commercialization of hydrogen technologies in the near term through development of tube trailer and liquid tanker technologies as well as forecourt compressors, dispensers, and bulk storage; and in the mid- to long-term through development of pipeline and advanced compression technologies. Techno-economic analysis is used by the program to identify cost, performance, and market barriers to commercial deployment of hydrogen technologies, and to inform program planning and portfolio development.

GOAL

The goal of this program is to reduce the costs associated with delivering hydrogen to a point at which its use as an energy carrier in fuel cell applications is competitive with alternative transportation and power generation technologies.

OBJECTIVES[1]

The objective of the Hydrogen Delivery program is to reduce the cost of hydrogen dispensed at the pump to a cost that is competitive on a cents-per-mile basis with competing vehicle technologies. Based on current analysis, this translates to a hydrogen threshold cost of $2–$4 per gallon gasoline equivalent (gge) (produced, delivered and dispensed, but untaxed) by 2020[2], apportioned to $1-$2/gge for delivery only[3]. The program plans meet these objectives by developing low-cost, efficient, and safe technologies for delivering hydrogen from the point of production to the point of use, including stationary fuel cells and fuel cell electric vehicles. This objective applies to all of the possible delivery pathways. Interim and ultimate targets for various delivery components have been updated in the *Fuel Cell Technologies Program Multi-Year Research, Development, and Demonstration Plan (MYRD&D Plan)*.[4] Key objectives for specific delivery components include:

- **Tube Trailers:** Reduce the cost of compressed gas delivery via tube trailer by increasing vessel capacity and lowering trailer cost on a per-kilogram-of-hydrogen-transported basis.
- **Pipeline Technology:** Develop mitigation strategies for combined material fatigue and hydrogen-induced embrittlement in steel pipelines; advance the development and acceptance of alternative composite pipe materials that can reduce installed pipeline costs; and develop lower-cost, higher-reliability compression technology for hydrogen transmission by pipeline.
- **Liquid Delivery:** Reduce the capital and operating costs of hydrogen liquefiers and bulk liquid storage vessels.
- **Forecourt Technologies:**
  - Compression: Develop lower-cost, higher-reliability hydrogen compression technology for terminal and forecourt applications.
  - Storage: Develop lower capital cost off-board bulk storage technology.
  - Dispensers: Quantify and improve the safety and durability of 700 bar dispenser hose and nozzle assemblies.
- **Analysis:** Conduct comprehensive analyses on potential near- and longer-term hydrogen delivery options, comparing the relative advantages of each and examining possible transition scenarios between the two timeframes.

---

[1] Note: Targets and milestones were recently revised; therefore, individual project progress reports may reference prior targets.
[2] *Hydrogen Threshold Cost Calculation*, Program Record (Office of Fuel Cell Technologies) 11007, U.S. Department of Energy, 2012, http://www.hydrogen.energy.gov/pdfs/11007_h2_threshold_costs.pdf.
[3] *Hydrogen Production and Delivery Cost Apportionment*, Program Record (Office of Fuel Cell Technologies) 12001, U.S. Department of Energy, 2012.
[4] *Fuel Cell Technologies Program Multi-Year Research, Development, and Demonstration Plan* (MYRD&D Plan), Delivery Chapter, July, 2013, http://www1.eere.energy.gov/hydrogenandfuelcells/mypp/pdfs/delivery.pdf.

FISCAL YEAR (FY) 2013 STATUS AND PROGRESS

In FY 2013 the Hydrogen Delivery program focused on identifying the research, development and demonstration (RD&D) needs for materials and components for forecourt technologies to reduce capital costs and improve system reliability. In support of this effort two workshops were held to discuss the current status and challenges in these areas. The first workshop, *Polymer and Composite Materials Used in Hydrogen Service*, was held as a joint workshop with the Safety, Codes and Standards program.[5] Discussion centered on the knowledge gaps and data needed for the durable use of polymers and composite materials in high-pressure hydrogen service under the demanding duty cycles associated with 700 bar hydrogen fuel cell electric vehicle refueling; and on enabling lower-cost, higher-performance systems through attention to these knowledge gaps and revision of codes and standards. The participants identified material knowledge gaps in six key areas. The topical areas identified are shown in Table 1.

TABLE 1. Six key areas for RD&D were discussed for the reliable use of polymer and composite materials in high pressure hydrogen service at the workshop.

Polymer and Composite RD&D Areas Identified
Thermal performance of polymers at service conditions and impact of thermal excursions
Evaluation and minimization of gas permeation and absorption into polymers
Polymer performance characterization tests considering significant material variability
Characterization and performance of seals and o-rings
Liner buckling in pressure systems
Low-cost composite material systems

The second workshop, *Compression, Storage and Dispensing Cost Reduction*, was held at Argonne National Laboratory in March 2013. At this workshop information was shared by participants in order to identify the RD&D needs in the areas of compression, storage, and dispensing to enable cost reduction of hydrogen fuel at fueling stations (forecourt). The workshop was divided into sessions for three topic areas—compression, storage, and other forecourt issues. For each topic area, a panel of experts discussed the status of relevant technologies and identified the key issues and challenges in that topic area. The panel presentations were followed by a moderated discussion and breakout sessions to further clarify and explore the issues. Workshop participants discussed the key cost drivers, reliability issues, and high-impact RD&D activities to reduce the cost of hydrogen delivery at the forecourt. Following the workshop a report was issued along with a request for information (RFI) for public feedback.[6] The key areas discussed during the workshop and identified in the report are summarized in Tables 2-4. In addition to feedback on the workshop report, the RFI also solicited information on the current status of liquefaction technologies.

TABLE 2. Key Compression Challenges Discussed

	Issue	Relevant Activities
Compression	Lack of identified metallic materials for use in high-pressure hydrogen environments.	Standardize testing and qualification of metallic materials for use in high-pressure hydrogen environments, distinguishing between materials with high-fatigue cycle life and those without.
		Create metallic testing protocols that represent the use condition.
	Dynamic compressor seals have limited life in high-pressure hydrogen compressors due to thermal limitations of the seals (approximately 200°F).	Develop new polymer materials suitable for hydrogen in high-pressure and high-temperature applications (300°–400°F).
	Current compressor designs have low efficiencies and high capital and operating costs.	Develop innovative compression technologies.
		Target improved hydraulic efficiencies for current technology.
	The mean time between failures of the compressors in 700 bar hydrogen service is not well documented due to the lack of stations and historical data.	Continue to collect and analyze data from new and existing stations.

[5] The "Polymer and Composite Materials Used in Hydrogen Service" Workshop Proceedings are available here: http://www1.eere.energy.gov/hydrogenandfuelcells/mtg_poly_comp_materials.html

[6] The "Compression, Storage and Dispensing Cost Reduction" Workshop Proceedings are available here: http://www1.eere.energy.gov/hydrogenandfuelcells/wkshp_hydrogen_csd.html

TABLE 3. Stationary Storage Challenges Discussed

	Issue	Relevant Activities
Storage	Codes and standards are too conservative with regard to setback distances for both liquid and gaseous storage, resulting in a larger than necessary storage footprint and increased cost.	Determine why the current setback distances in the United States are twice those in Europe.
		Perform testing and analysis to find methods to reduce distances and work with the National Fire Protection Association to update the codes accordingly.
		Perform necessary analysis, testing, and demonstration to understand the feasibility and safety of underground storage at the forecourt.
	The cost of the carbon fiber used in high-pressure composite tanks is too high.	Develop low-cost carbon fiber for use in high-pressure applications.
		Improve batch-to-batch consistency of existing carbon fiber.
		Expand the supplier base for carbon fiber.
	The cycle life of carbon fiber tanks, particularly under partial cycles, is undefined.	Model and verify through testing tank life under typical station load conditions; in particular, quantify the life under both deep and shallow pressure cycles.
		Understand the failure modes associated with the decompression of saturated polymeric materials.
		Design non-destructive test methods for carbon fiber tanks to allow recertification and extend their service life beyond 15 years.
	The usable storage pressure is limited by component availability.	Initiate an R&D activity in the United States similar to the European Union's Smart Valve program to increase the usable storage pressure by developing high-pressure valves, fittings, and other balance of plant components.
	Focused development of hydrogen stations at existing gasoline stations limits the real estate available for installing storage to meet the current code requirements for setback distance.	Evaluate the feasibility of dedicated hydrogen filling stations (such as at large department stores/retail sites).

TABLE 4. Other Forecourt Issues Discussed

	Issue	Relevant Activities
Other Forecourt Issues	The optimal relationship between compressor throughput and compression ratio versus the storage pressure and volume to meet demand while minimizing cost is not well understood.	Statistical analysis to determine short-, mid-, and long-term station demand profiles.
		Optimize the cost trade-offs between compression and storage to meet short-, mid-, and long-term demand profiles at minimal cost.
	No devices exist that can test the quantity, quality, and performance of hydrogen delivery stations.	Develop devices that can test the rate and temperature at which hydrogen is delivered to a vehicle, the total mass of hydrogen delivered, and the quality of hydrogen delivered.
	Existing hydrogen flow meters are costly and only accurate to within 4% at the delivery conditions, while the existing standard requires 1-2% accuracy.	Develop a low-cost, high-accuracy hydrogen flow meter for measurement of hydrogen vehicle dispensing at 700 bar.
	Currently there are no welding standards for high-pressure applications.	Determine hydrogen embrittlement phenomena in traditional and friction stir welds.
		Engage ASME Section 12 to develop a clear and consistent inspection standard for high-pressure hydrogen welds.
	Current applicable code requires containerized storage to have explosion vents but does not indicate a test or qualification method for those vents. Containerized storage can also reduce station footprint and cost.	Develop explosion vent test standards and test methodology that would allow for containerized solutions, including underground storage.
		Develop modularized storage designs to reduce footprint at stations.
	Low-volume production, a small supplier base, and low equipment utilization leads to high costs.	Determine ways to better optimize station designs at early market, when there is low utilization.
		Develop better tools to forecast refueling demand over time.
		Develop small (<150 kg per day) modular station designs that can be moved and replaced with larger permanent stations as the market expands.
		Promote competition among the supplier base.
	Dispenser hose reliability is unknown and leads to frequent replacement.	Create and perform a test protocol that will determine the performance and degradation of dispenser hoses under application conditions and develop improved designs.

In FY 2013 the Hydrogen Delivery program released two new records (#12021 and #12022) to document the cost status of hydrogen delivery technologies for transport and distribution from central production facilities at an average cost of $4.00/kg, shown in Figure 1, and for compression, storage, and dispensing at forecourt production sites at an average of $2.45/kg.

A Small Business Innovation Research (SBIR) topic on hoses for hydrogen dispensing at 700 bar was also released and a Phase I award made to Nanosonic Inc. The project objective is to develop a low-cost hose for dispensing hydrogen which can operated reliably for more than 25,000 fuelings under the temperature and pressure cycles (-40°C and 875 bar) experienced during fueling of 700-bar tanks according to the SAE International Standard J2601 2010 fast-fill protocol. A second SBIR topic has also been released in collaboration with Office of Science on polymer and composite sealing materials for high-pressure hydrogen applications in order to address the poor reliability of polymer and composite seals in hydrogen applications identified at the workshops.

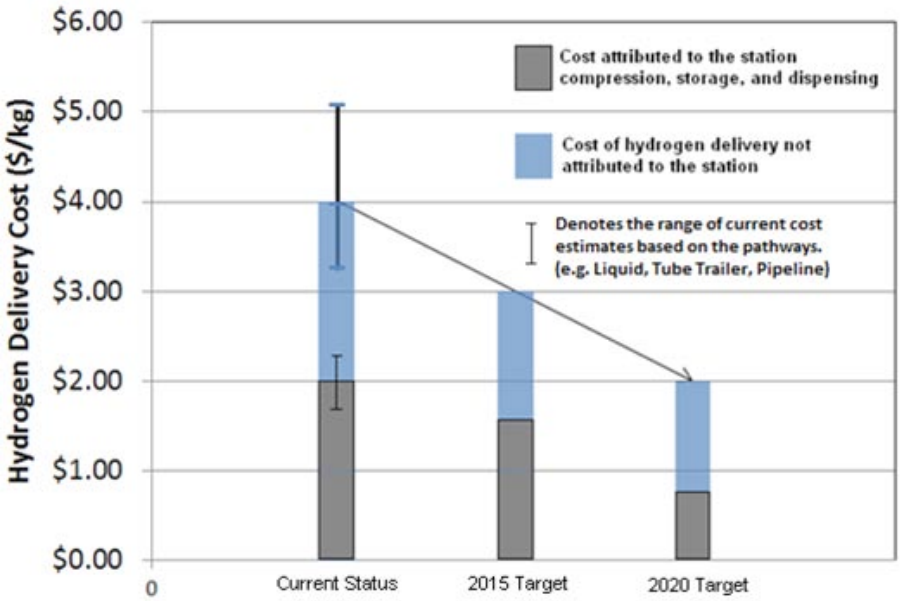

FIGURE 1. The average hydrogen delivery cost status based on nine 700 bar delivery scenarios including pipeline, tube trailer, and liquid delivery and 2015 and 2020 delivery targets are shown in the graph by the sum of the grey and the blue bars. The grey bars indicate the cost of the compression storage and dispensing at the fueling station. Data for these is available in the MYRD&D Plan and Record #12021 and Record #12022.

During FY 2013 progress was made in several key areas including:

Tube Trailers and Bulk Storage

Significant cost reduction at the forecourt can be achieved through the use of high-pressure tube trailers and low-cost on-site storage. Higher pressure tube trailers at the forecourt can move the gaseous compression upstream to the tube trailer terminals where economies of scale can reduce the cost of the compression. This year the following two projects have contributed to the cost reduction of the gaseous hydrogen delivery pathway.

- The TITAN™ module and TITAN™V integrated semitrailer configuration for hydrogen delivery were successfully extended to the TITAN™V Magnum configuration—increasing 3,600 psi hydrogen capacity to 800 kg (30% increase relative to the baseline TITAN™ module). Figure 2 shows the TITAN™V Magnum and the arrangement of large and small tanks within. (Hexagon Lincoln)
- The effectiveness of novel hydrogen mitigation technology to prevent hydrogen entering the structural steel layer was successfully demonstrated for concrete composite vessels designed for bulk hydrogen storage at 860 bar. A

FIGURE 2. The Hexagon Lincoln TITAN™V Magnum Composite Tube Trailer

more than 95% reduction in hydrogen uptake in the outer carbon steel layers was achieved when compared to the baseline case without using the mitigation technology. (Oak Ridge National Laboratory)

Pipeline Technologies

Pipelines are an attractive delivery pathway for large market scenarios. Advances in both pipeline compression and fiber reinforced polymer pipelines continue to improve the economics of the scenario, while work on hydrogen embrittlement of steel continues to improve our understanding of the performance of traditional pipeline materials in use in a hydrogen pipeline transmission and distribution network.

- A preliminary fatigue design curve for fiber-reinforced polymer pipelines was developed over the expanded pressure range of 750 to 3,000 psig. Data from this curve is necessary for the inclusion of fiber-reinforced polymer pipeline in ASME B31.12. A report documenting the findings will be submitted to ASME. (Savannah River National Laboratory)
- Reliable fatigue crack growth (da/dN vs ΔK) relationships were measured for pipeline steel in hydrogen environments. The crack growth rates were measured for the X65 weld heat-affected zone in 3,000 psi (21 MPa) hydrogen gas. These results show that the weld heat-affected zone is not more susceptible to hydrogen-accelerated fatigue crack growth compared to the base metal. These results are encouraging for the use of steel pipelines in hydrogen applications. (Sandia National Laboratories)
- Completed initial validation testing of single-stage oil-free centrifugal compressor system was performed in air and in helium at 60,000 rpm. Results confirmed a single-stage compression ratio of 1.10 and thermal stability. (Mohawk Innovative Technologies)

Forecourt Technologies

Forecourt technologies, in particular compression and onsite storage are a key area of focus for the program. Efforts in this area are focused on improving the reliability and reducing the cost of the technologies.

- Achieved 50% decrease in single production unit cost of an electrochemical compressor through reducing the cell part count by half, achieving a threefold increase in the current density and twofold increase in the cell active area to increase the production rate while lowering the total cells per stack. (Fuel Cell Energy)
- Performed analysis to show that high-pressure tube trailers delivering hydrogen at 350 bar can decrease the station cost by 20% when used for initial vehicle fill. (Argonne National Laboratory)

- Constructed a research cryo-compressed hydrogen delivery station. Results from testing will provide data on the footprint, efficiency, through-put and other valuable performance metrics. (Lawrence Livermore National Laboratory)

BUDGET

The FY 2013 appropriation provided $5.0 million for the Hydrogen Delivery program. The request for Production and Delivery in FY 2014 is $21 million, of which $9.4 million is planned for Delivery, with an emphasis on reducing near-term technology costs, increasing tube trailer capacity, and lowering the cost of pipeline delivery pathways.

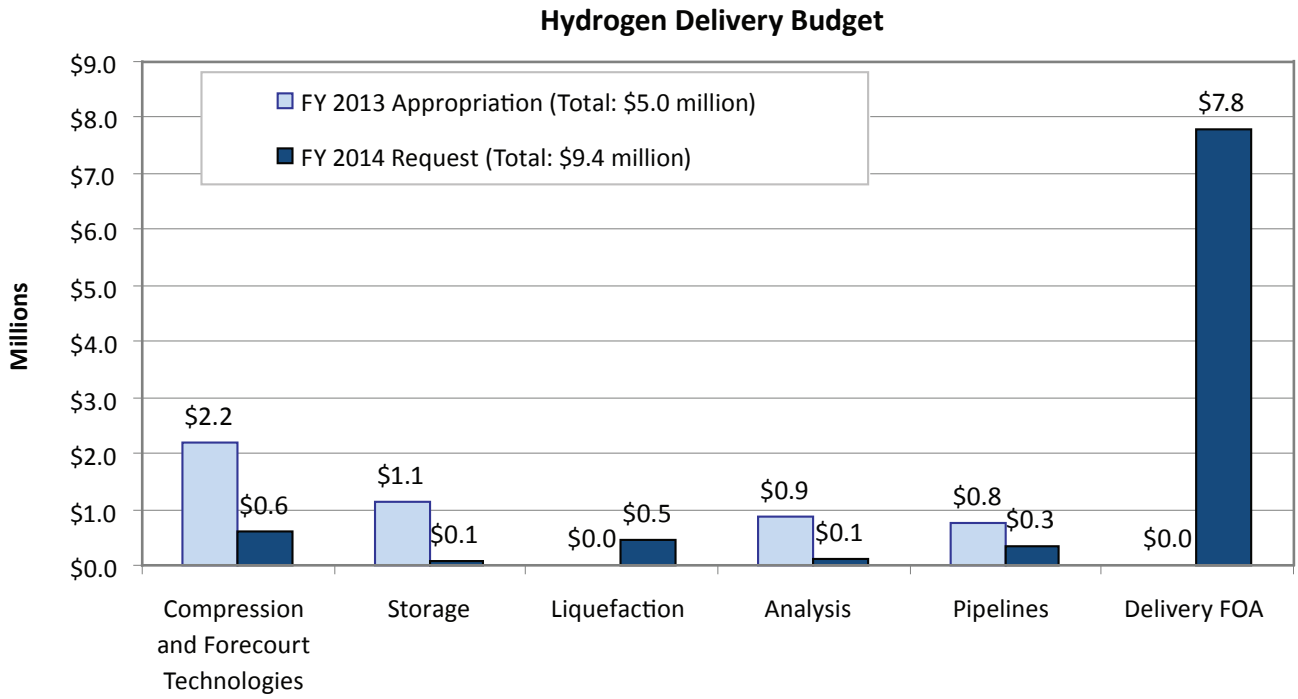

FOA – Funding Opportunity Announcement

FY 2014 PLANS

In FY 2014, the Hydrogen Delivery program will focus on several key efforts:

1. *Expanding the portfolios focus on forecourt and near term technologies.* To this end the program plans to release a funding opportunity for new RD&D projects for advanced technologies in the area of compression, storage, and dispensing. The program also plans to award a new SBIR project to address polymer and composite materials for durable high-pressure hydrogen seals to improve the reliability of forecourt technologies for 700 bar hydrogen dispensing. Additionally the program will be leveraging work in the Technology Validation program to facilitate a multi-laboratory effort in the 700 bar forecourt delivery technology.
2. *Identifying the key areas for hydrogen transport and distribution* through a workshop focused on RD&D needs for the transportation and distribution of hydrogen.
3. *Improving the analysis of hydrogen delivery pathways.* The completion of an independent panel review report on the current status of compression storage and dispensing technologies is expected in FY 2014. The results of this report will be used to revise and release an updated version of HDSAM. The updated version will also include an updated cryo-compressed hydrogen delivery scenario based on technology evaluation performed by Lawrence Livermore National Laboratory.

4. *Validation of cost reduction of forecourt delivery* through the completion of consolidation algorithms which will allow for significantly lower cost of compression at the forecourt when combined with high-pressure tube trailer delivery and the construction and testing of a steel-concrete composite vessel to verify the technology's performance and cost.

Erika Sutherland
Hydrogen Production and Delivery Team
Technology Development Manager
Fuel Cell Technologies Office
U.S. Department of Energy
1000 Independence Ave., SW
Washington, D.C. 20585-0121
Phone: (202) 586-3152
Email: Erika.Sutherland@ee.doe.gov

III.1 Hydrogen Delivery Infrastructure Analysis

Amgad Elgowainy (Primary Contact),
Krishna Reddi and Marianne Mintz
Argonne National Laboratory
9700 South Cass Avenue
Argonne, IL 60439
Phone: (630) 252-3074
Email: aelgowainy@anl.gov

DOE Manager
Erika Sutherland
Phone: (202) 586-3152
Email: Erika.Sutherland@ee.doe.gov

Project Start Date: October 2007
Project End Date: Project continuation and direction determined annually by DOE

Overall Objectives

Evaluate hydrogen delivery and refueling concepts that can reduce hydrogen delivery cost towards meeting the delivery cost targets.

Fiscal Year (FY) 2013 Objectives

- Incorporate SAE International (SAE) J2601 refueling protocol in the modeling of various hydrogen refueling station (HRS) configurations.
- Evaluate the role of high-pressure tube trailers in reducing hydrogen refueling station capital investment and operation cost.

Technical Barriers

This project directly addresses Technical Barriers A, B and E in the Hydrogen Delivery section of the Fuel Cell Technologies Office Multi-Year Research, Development, and Demonstration Plan. These barriers are:

(A) Lack of Hydrogen/Carrier and Infrastructure Options Analysis

(B) Reliability and Costs of Gaseous Hydrogen Compression

(E) Gaseous Hydrogen Storage and Tube Trailer Delivery Costs

Technical Targets

The project employs a simulation tool to investigate current and novel hydrogen delivery technologies and pathway options with the potential to meet the cost targets specified in the Fuel Cell Technologies Office Multi-Year Research, Development, and Demonstration Plan, and to assist with defining R&D areas that can bridge current and targeted performance and cost of major delivery and refueling components.

Contribution to Achievement of DOE Hydrogen Delivery Milestones

This project contributes to achievement of the following DOE milestone from the Hydrogen Delivery section of the Fuel Cell Technologies Office Multi-Year Research, Development, and Demonstration Plan:

- Task 2.2: Down-select two to three H2 pressurization and/or containment technologies that minimize delivery pathway cost for near-term markets. (2Q, 2013)

FY 2013 Accomplishments

- Developed a simulation tool that sizes HRS equipment according to SAE J2601 fueling protocol and tracks mass, temperature and pressure across delivery components. The tool's predictions were validated against measurement data published in the literature.
- Identified optimum cascade storage configurations for maximum storage utilization with lowest compression capacity and minimum combined storage and compression cost. The optimum configuration employs cascade buffer storage with capacity that equals 24% of the station daily dispensing capacity and compression throughput that equals 180% of the station average daily dispensing rate (as defined by the peak to average hourly demand ratio).
- Investigated the role of high-pressure tube trailers in reducing station capital investment. High-pressure tube trailers delivering hydrogen at 350 bar can decrease the station cost by 20% when used for initial vehicle fill.

✧ ✧ ✧ ✧ ✧

INTRODUCTION

Initiated as part of the H2A project, the Hydrogen Delivery Scenario Analysis Model (HDSAM) is an Excel-based tool that uses a design calculation approach to estimate the contribution of individual infrastructure components to hydrogen delivery cost, energy use, and greenhouse gas emissions. The model links individual components for specific market conditions to develop capacity/flow parameters for a complete hydrogen delivery infrastructure. HDSAM calculates the full, levelized cost (i.e., summed across all components) of hydrogen delivery, accounting for

losses and tradeoffs among the various component costs. The quality of the data and the direction of the analysis are vetted via presentations to experts in the Hydrogen Delivery Technical Team and other U.S. DRIVE partnership technical teams, and through formal interaction with independent consultants and researchers from other national laboratories.

From previous HDSAM analyses, the refueling station was found to contribute approximately half of the total delivery cost in a mature fuel cell electric vehicle (FCEV) market. Furthermore, the under-utilization of the HRS capital investment in early markets of FCEVs negatively impacts the economic viability of refueling infrastructure. It is suggested that delivery concepts that reduce refueling station capital investment may partially offset the adverse economics in early markets. Thus, the delivery analysis in FY 2013 was focused on identifying delivery concepts that can reduce HRS capital investment and operation cost. Compressing hydrogen to high pressures in tube trailers (at terminals upstream of the HRS) can reduce compression requirement at the station. Since compression and storage were shown to constitute the bulk of HRS capital cost, delivering high-pressure hydrogen in tube trailers to HRS can reduce the station's capital investment significantly.

APPROACH

Hydrogen refueling station components are sized to meet a specific demand profile while satisfying the SAE J2601 refueling protocol. A simulation tool was developed from first principles to model the physical laws of thermodynamics, mass, energy, momentum and heat transfer, and to solve for the temperature, pressure, and mass flow through hydrogen refueling components and FCEV onboard storage system. The simulation tool identifies the combination of compressor size and buffer storage capacity for minimum total capital and operation cost. The role of tube trailers in reducing HRS capital investment and operation cost was examined by simulating two possible operation scenarios in a typical hydrogen refueling station. In Scenario 1, the tube trailer is merely used to supply hydrogen to a compressor that replenishes a cascade buffer storage system. In Scenario 2, the high-pressure tube trailer directly fills the vehicle's tank during the early dispensing period, in addition to supplying hydrogen to a compressor for replenishing the cascade buffer storage system. Figure 1 shows the refueling station operation strategies for Scenarios 1 and 2.

RESULTS

Cascade Storage and Compression Optimization

The number of cascade pressure levels that ensures maximum back-to-back vehicle fills with lowest cost depends on the size of the vessel. The combination of compressor and cascade storage, when considered together, identify the potential lowest cost configuration at HRSs. Figure 2 shows the cascade system capital cost (shown on the left vertical axis), the hydrogen utilization (shown on the right vertical axis and defined as the ratio of total amount of hydrogen dispensed to the total amount hydrogen stored in the cascade system), and an economic index (shown on the left vertical axis and defined as the cascade system cost divided by the

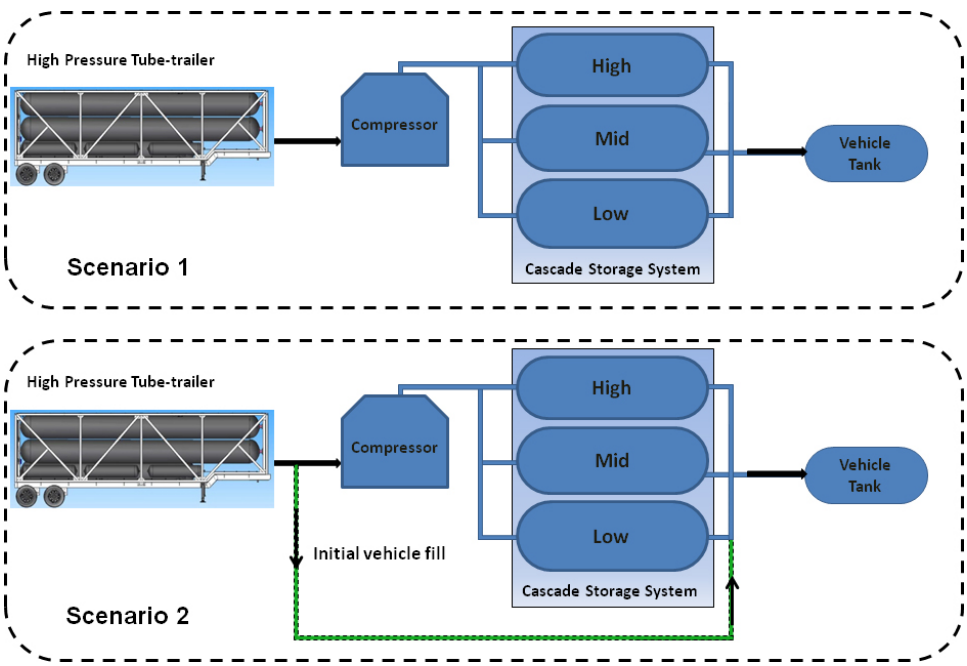

FIGURE 1. Operation Scenarios for High Pressure Tube Trailers at Refueling Stations

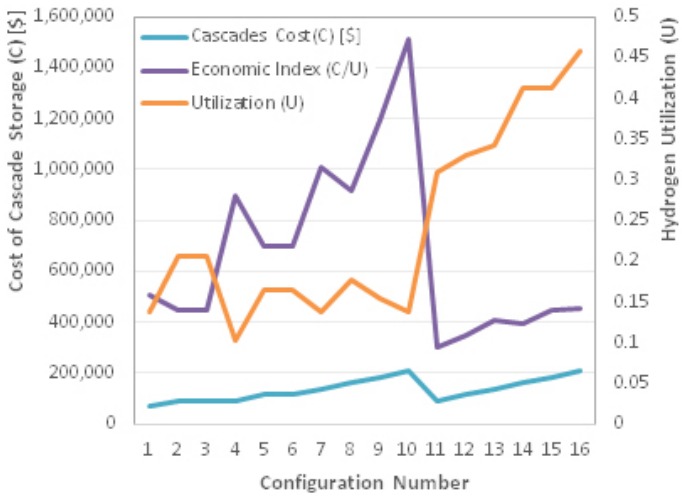

Configuration Number	Configuration (High-Medium-Low)
1	1-1-1
2	1-1-2
3	1-2-1
4	2-1-1
5	2-2-1
6	1-2-2
7	2-2-2
8	2-2-3
9	2-3-3
10	2-3-4
11	1-1-1-1
12	1-1-1-1-1
13	1-1-1-1-1-1(6)
14	1-1-1-1-1-1-1 (7)
15	1-1-1-1-1-1-1-1(8)
16	1-1-1-1-1-1-1-1-1 (9)

FIGURE 2. The Cost and Utilization of Different Cascade Configurations

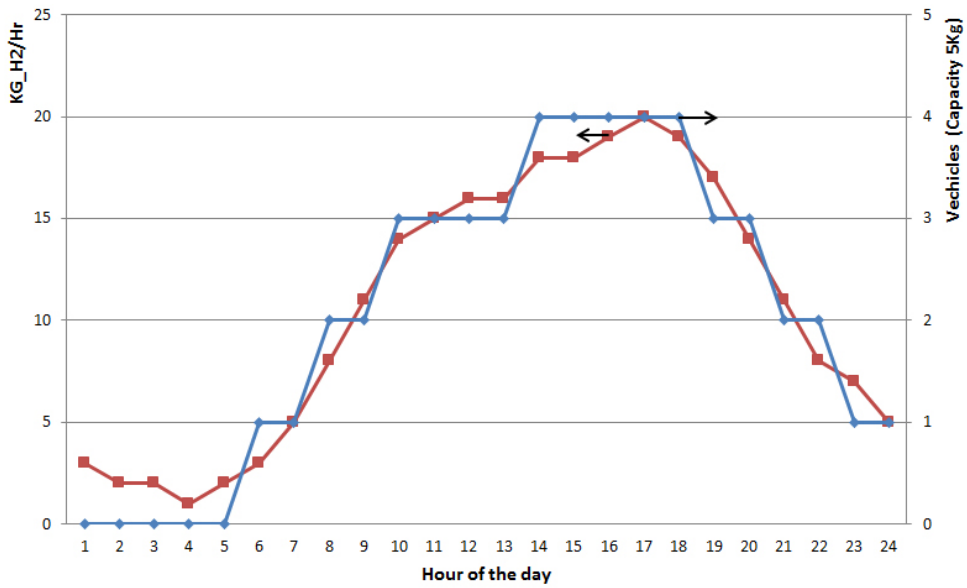

FIGURE 3. Hydrogen Demand (kg) and Number of Vehicles Per Hour

hydrogen utilization). The economic index is noteworthy since it represents the contribution of the cascade system to the cost of dispensed hydrogen. Since the primary goal is to achieve maximum back-to-back vehicle fills at lowest possible cost, it is desirable to minimize the economic index. The cost estimates reflect a 250 kg/day HRS with the hourly demand profile shown in Figure 3. Figure 2 shows that (for a vessel volume of 250 liters) the most economic option for this HRS is a cascade system with four pressure (i.e., cascade) levels (configuration# 11).

High-Pressure Tube Trailer Operation Strategy

Figure 4 shows the capital cost estimates for the combined compressor and cascade storage system (left vertical axis) and the required compressor capacity (right vertical axis) for different HRS operation scenarios. Using the tube trailer to initially fill the vehicle tank (Scenario 2) reduces the demand for compression and cascade storage at the refueling station. Furthermore, returning the tube trailer at a higher pressure further reduces the demand for compression at HRS, thereby reducing the initial capital investment and operation cost.

Cost Contribution of Station Components

The HRS compression and cascade buffer storage system was optimized for three sizes: 250, 500, and 1,000 kg/day. Figure 5 shows the total capital cost of the refueling station as a stacked bar of individual component cost (left vertical

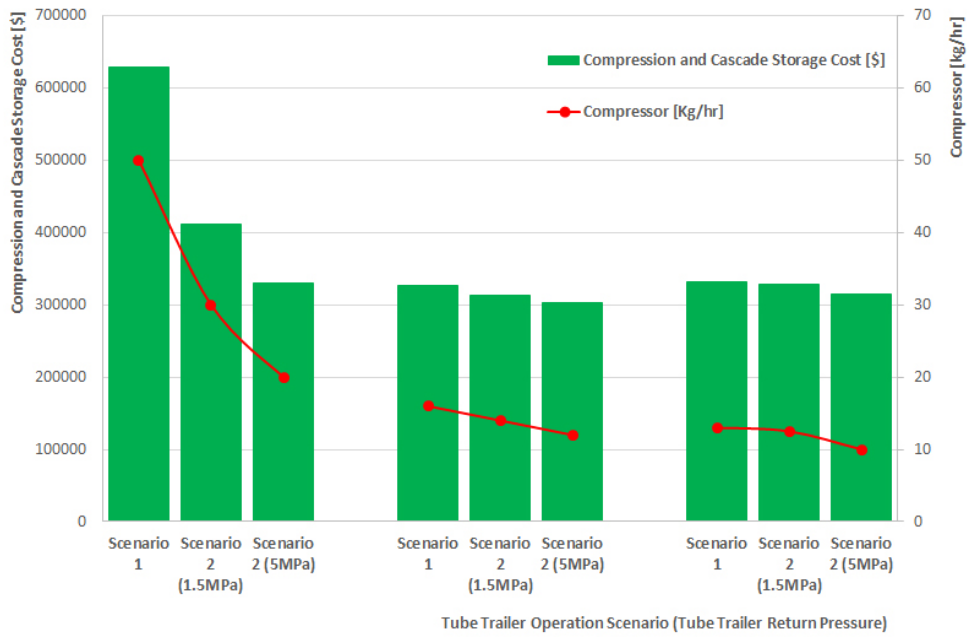

FIGURE 4. Combined Compression and Cascade Storage Cost along with Compressor Rating for a 250 kg/day Station

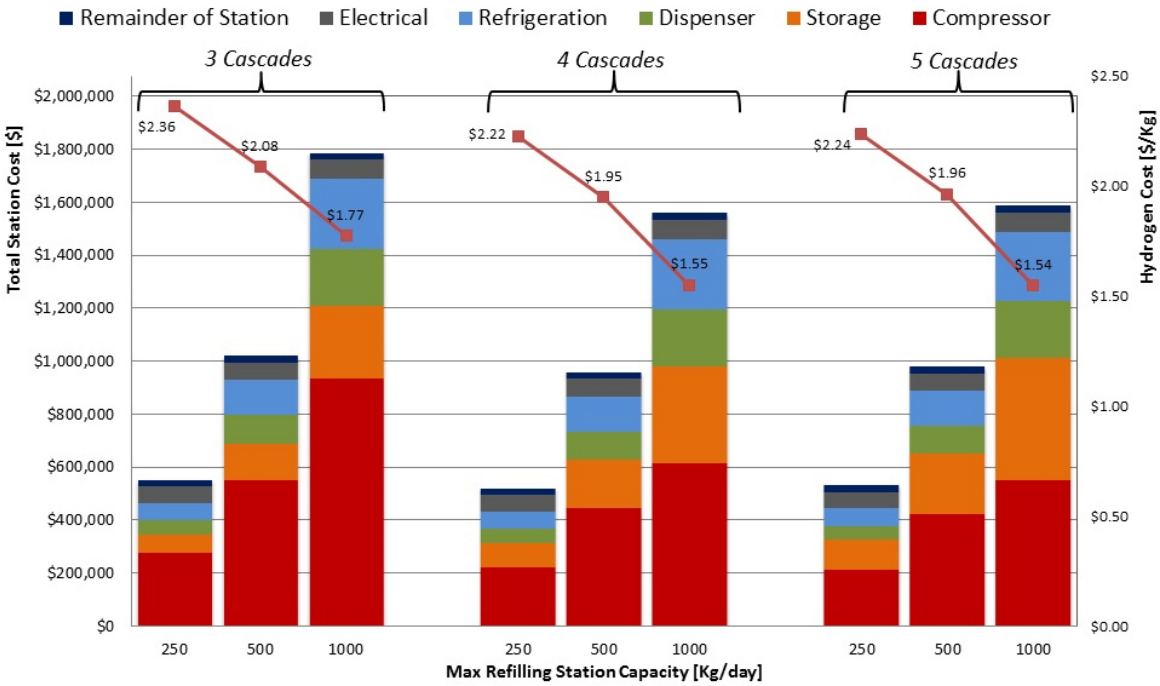

FIGURE 5. Capital Cost and Cost Contribution to Dispensed Hydrogen for Different Station Sizes and Configurations

axis). The figure also shows the contribution of the HRS capital cost toward the dispensed cost of hydrogen in $/kg (right vertical axis). The cost per kg of hydrogen for larger refueling stations is lower despite the larger capital cost due to the economies of scale associated with employing larger components. Figure 5 shows similar refueling hydrogen cost per kg for both 4-cascade and 5-cascade systems due to the tradeoff between lower capital cost for the 4-cascade system and lower operation cost for the 5-cascade system.

CONCLUSIONS AND FUTURE DIRECTIONS

FCEVs with 700 bar onboard storage systems require significant compression which is the single most significant contributor to HRS capital cost. High-pressure tube trailers can reduce the compression requirement at HRS when operated to initially fill the vehicle and returned at a higher pressure. The compression can further be reduced by optimizing the combined compressor capacity and cascade storage size for any particular hourly demand profile, station daily demand, cascade vessel size, and vehicle tank capacity.

For the remainder of FY 2013, effort will be directed at documenting and publishing the results and analysis, and at investigating other tube trailers operation strategies for further reduction of compression requirement at HRS.

III.2 Oil-Free Centrifugal Hydrogen Compression Technology Demonstration

Hooshang Heshmat
Mohawk Innovative Technology, Inc. (MiTi®)
1037 Watervliet Shaker Road
Albany, NY 12205
Phone: (518) 862-4290
Email: HHeshmat@miti.cc

DOE Managers
Erika Sutherland
Phone: (202) 586-3152
Email: Erika.Sutherland@ee.doe.gov
Katie Randolph
Phone: (720) 356-1759
Email: Katie.Randolph@go.doe.gov

Contract Number: DE-FG36-08GO18060

Subcontractor:
Mitsubishi Heavy Industries, Ltd, (MHI) Compressor Corporation, Hiroshima, Japan

Project Start Date: September 25, 2008
Project End Date: November 30, 2013

Overall Objectives

Design a reliable and cost-effective centrifugal compressor for hydrogen pipeline transport and delivery:

- Eliminate sources of oil/lubricant contamination
- Increase efficiency by using high rotational speeds
- Reduce system cost and increase reliability

Fiscal Year (FY) 2013 Objectives

- Validate performance of coupled oil-free motors
- Construct a dedicated test cell and install the required closed-loop piping
- Perform validation testing of single-stage compressor system in air and in helium

Technical Barriers

This project addresses the following technical barriers from the Hydrogen Delivery section of the Fuel Cell Technologies Office Multi-Year Research, Development and Demonstration Plan:

(B) Reliability and Costs of Gaseous Hydrogen Compression

(J) Hydrogen Leakage and Sensors

Technical Targets

This project is directed towards the design, fabrication and demonstration of the oil-free centrifugal compression technology for hydrogen delivery. This project will identify the key technological challenges for development and implementation of a full-scale hydrogen/natural gas centrifugal compressor. The project addresses the following DOE technical targets from the Hydrogen Delivery section of the Fuel Cell Technologies Office Multi-Year Research, Development and Demonstration Plan (see Table 1).

TABLE 1. Technical Targets for Hydrogen Compression

Category	2005 Status	FY 2012	FY 2017
Reliability	Low	Improved	High
Isentropic Efficiency	NA	NA	>88%
Capital Investment ($M) (based on 200,000 kg of H_2/day)	$15	$12	$9
Maintenance (% of Total Capital Investment)	10%	7%	3%
Contamination	Varies by Design		None

NA - not applicable

FY 2013 Accomplishments

- Completed validation testing of two coupled 100-kW oil-free motors.
- Completed installation of a dedicated test cell and required closed-loop piping for testing of the single-stage compressor.
- Performed initial validation testing of single-stage compressor system in air and in helium.

✧ ✧ ✧ ✧ ✧

INTRODUCTION

One of the key elements in realizing a hydrogen economy is the deployment of a safe, efficient hydrogen production and delivery infrastructure on a scale that can compete economically with current fuels. The challenge, however, is that hydrogen, the lightest and smallest of gases with a lower viscosity than natural gas, readily migrates through small spaces. While efficient and cost-effective compression technology is crucial to effective pipeline delivery of hydrogen, today's positive displacement hydrogen compression technology is very costly, and has poor reliability and durability, especially for components subjected

to wear (e.g., valves, rider bands and piston rings). Even so called "oil-free" machines use oil lubricants that migrate into and contaminate the gas path. Due to the poor reliability of compressors, current hydrogen producers often install duplicate units in order to maintain on-line times of 98-99%. Such machine redundancy adds substantially to system capital costs. Additionally, current hydrogen compression often requires energy well in excess of the DOE goal. As such, low capital cost, reliable, efficient and oil-free advanced compressor technologies are needed.

APPROACH

The MiTi® team will meet project objectives by conducting compressor, bearing and seal design studies; selecting components for validation testing; fabricating the selected centrifugal compressor stage and the corresponding oil-free bearings and seals; and conduct testing of the high-speed, full-scale centrifugal compressor stage and oil-free compliant foil bearings and seals under realistic pressures and flows in air and helium (used as a simulant gas for hydrogen). Specific tasks include: (1) compressor design analysis; (2) mechanical component detailed design; (3) detailed design and fabrication of a full-scale single-stage centrifugal compressor; (4) compressor performance testing wiith air and helium; (5) system design refinement; and (6) project management and reporting.

RESULTS

The MiTi® hydrogen compressor design consists of three frames operating at the same speed with a rotor tip velocity of 1,600 fps. The system capacity is 500,000 kg/day with a pressure ratio of approximately 2.4. A single-stage compressor system has been developed to verify aerodynamics of the MiTi® oil-free, high-speed, centrifugal compressor system. Fabrication, assembly and installation of the single-stage compressor has been completed (Figure 1) and initial performance verification testing has been conducted. The single-stage compressor system has been placed in a reinforced test cell and all instrumentations and controls have been completed. Key instrumentations and controls are located outside the cell in order to protect personnel and expensive instrumentations. The 200-kW motor drive system is fitted with seven pressure transducers and eight thermocouples positioned along the length of gas cooling path within the oil-free electric motors to monitor the performance of the foil bearings and electric motors. The compressor system is instrumented with nine proximity probes to monitor rotor vibration during operation. A high resolution video camera for remote monitoring and video recording is placed inside the cell. A custom command console has been completed for monitoring of all system data and simultaneous monitoring of the drive motor. A custom graphical user interface has been developed using LabVIEW®

FIGURE 1. Dedicated MiTi® test cell, 200-kW single-stage compressor and closed-loop gas system.

software (National Instruments). The new graphical user interface allows for direct command of motor speed control, monitoring of all pressure and temperature data, as well as high frequency spectral analysis of up to four proximity probes for vibration measurement. The command console has remote access capabilities to allow the operator control of all compressor and drive functions from a safe distance away from the cell. A closed-loop liquid cooling system for the motor drives has been installed that consists of a ¾-HP electric motor, solid particulate filter and liquid-to-air radiator. The system is capable of removing greater than 50 kW of heat load if necessary.

The single-stage compressor is driven with two oil-free, high-speed, 100-kW motors coupled together (Figure 2) using the MiTi® Coupling Technology. Using air as the test gas, the performance of each motor was successfully validated from 10,000 rpm to full speed of 60,000 rpm. Foil bearing temperatures were monitored during testing and stable bearing performance was confirmed. Bearing temperatures were less than 150°F at full speed. Rotor vibration was recorded using fiber-optic proximity probes. The maximum rotor motion measured at full speed was 0.0002 inch, which represents extremely low vibration, as it is approximately equivalent to the mechanical run-out of the rotor.

After successfully demonstrating stable, high-speed operation in air, the compressor was coupled to a closed-loop flow system for helium gas testing. The closed-loop, stainless steel flow system includes a large gas accumulator tank, particle filter, remotely actuated throttle valve and flow meter. The flow loop was constructed and instrumented according to the guidelines of American Society of Mechanical Engineers PTC-10.

Preliminary compressor testing in air (open-loop) and in helium (closed-loop) has been performed to verify the aerodynamics of the high-speed, oil-free, single-stage

FIGURE 2. MiTi® Single-stage compressor system with high speed oil-free motor drive.

compressor. A systematic testing plan was developed to approach the design point of the single-stage compressor with respect to the rotational speed. The test procedure began with pressurization of the flow loop with pure helium and purging of air until less than 1.0 % oxygen was detected. Proper safety measures were taken, including placement of "bomb-proof" Kevlar blankets over the test cell doors and evacuation of all personnel from the surrounding area. The compressor was then started with the speed increasing by 1-2 krpm increments, while rotordynamic behavior and foil bearing temperatures were monitored. The compressor speed was held constant at each speed increment for several minutes to observe the steady-state behavior at that speed. The compressor was then stopped for data analysis and reviewed with project management and the principle investigator.

Results from recent closed-loop compressor testing with helium are shown in Figure 3. The compressor flow was adjusted by position of the throttle valve. The figure shows a rise in pressure ratio and temperature ratio with increasing speed and flow restriction, indicating that significant compression work was being done of the test gas. Pressure ratio and temperature ratio are defined by the following relationships:

$$PR = \frac{P_{OUT-ABS}}{P_{IN-ABS}} \quad \text{and} \quad TR = \frac{T_{OUT-ABS}}{T_{IN-ABS}}$$

A maximum pressure ratio of approximately 1.10 was achieved in this test at 35 krpm with the throttle valve restriction set to 50%. Even though the compressor was operating at 35 krpm with helium gas, bearing temperatures did not exceed 130°F, which is more than 10°F lower than seen in air at 10 krpm. Because the helium gas was in a closed-loop system, the gas was reheated each time it passed through the compressor and, thus, much of the rise in temperature through the compressor system was due to reheating of the same gas volume.

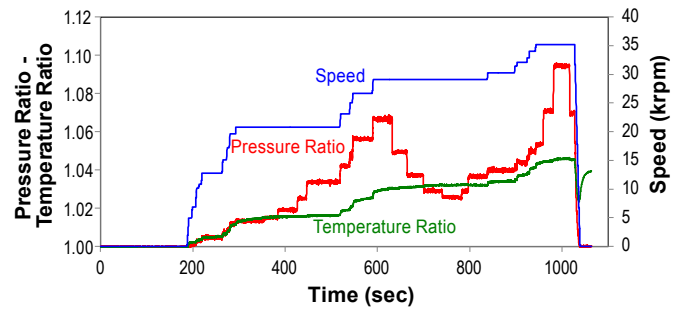

FIGURE 3. Experimental data of the single-stage compressor operating at speeds up to 35 krpm.

During helium testing, compressor flow was varied by partial closure of the remotely operated throttle valve, as discussed earlier. This procedure was performed at constant speeds of 20 krpm and 29 krpm in order to map compressor performance as a function of flow. The position of the throttle valve was used to approximate flow as a percentage of the maximum flow achieved when the valve was fully open. The compressor performance maps are shown in Figure 4 (a) for the 29 krpm speed condition. The results show that a peak experimental pressure ratio of 1.067 was achieved, which is only slightly lower than the predicted peak theoretical pressure ratio of 1.071 at this speed. These results show a good correlation between the theoretical estimates and measured performance. It is possible that with further flow restriction, an even higher experimental pressure ratio could be achieved. A high-accuracy inline flow meter has been ordered and will be installed next month. Compressor performance mapping will be repeated once accurate flow measurement is added to the flow loop.

Based on the preliminary compressor maps obtained along with temperature measurements of compressor inlet and discharge, compressor efficiency was calculated and experimental results were compared to the theoretical estimates based on mean-line analysis. The experimental adiabatic efficiency (total-to-static) was calculated using the following equation:

$$\eta_{T-S} = \frac{\left(P_{2s}/P_{1t}\right)^{(k-1)/k} - 1}{\left(T_{2t}/T_{1t}\right) - 1}$$

where subscripts 1 and 2 refer to the compressor inlet and discharge, respectively. Subscripts "s" and "t" refer to the static or total thermodynamic condition of the test fluid. The use of total-to-static adiabatic efficiency is the most appropriate for evaluation of a single stage compressor. A comparison of the theoretical and experimentally measured adiabatic compressor efficiencies is shown in Figure 4 (b). The experimentally measured efficiencies (the red curve) are higher than

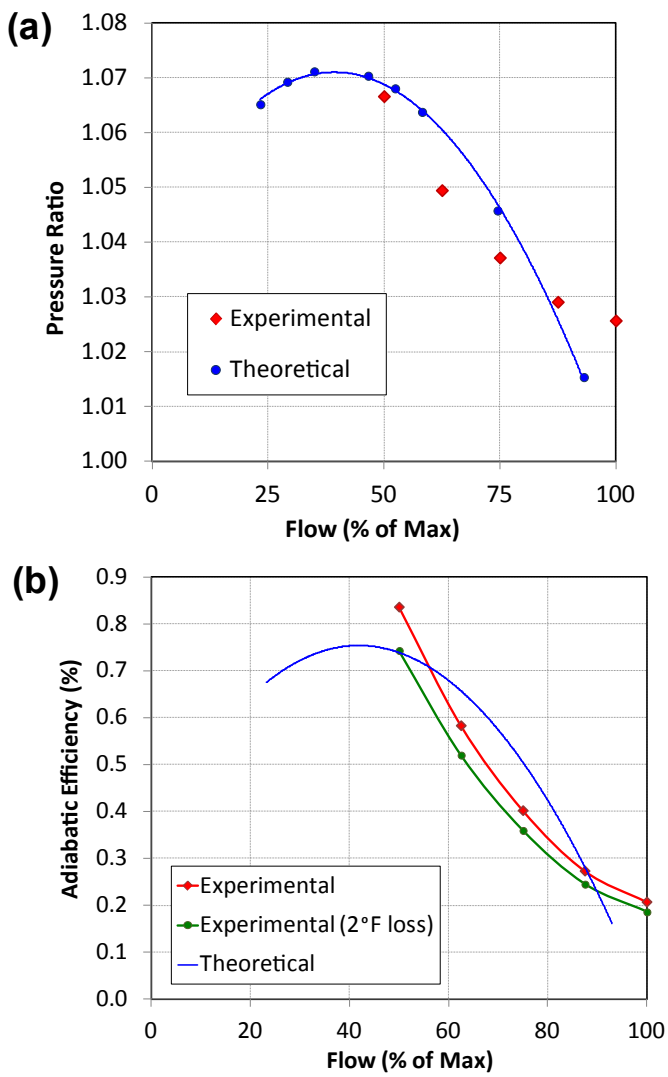

FIGURE 4. Comparison of theoretical and experimentally measured values for the single-stage compressor: (a) pressure ratio and (b) adiabatic efficiencies.

the theoretical prediction. This scenario is impossible and is due to the fact that experimentally measured discharge temperatures are lower than predicted. The lower than predicted compressor discharge temperature is due to the fact that the single-stage compressor is not thermally insulated from the environment and some heat of compression is lost to the surroundings through the piping and the motor housing. In order to account for this thermal loss, a constant value of 2.0°F was added to the compressor discharge temperature in the expression for adiabatic efficiency. This constitutes 11% of the total temperature rise due to compression and is a rather conservative assumption. The resulting calculated efficiency, plotted as the green curve, is closer to the theoretical prediction at the maximum adiabatic efficiency.

At the initiation of the project, it was planned to pursue two design approaches for the hydrogen compressor: a double-entry design by MiTi® and a single-entry design by MHI. During the design process, both companies held frequent conference calls and several site visits to exchange design information and coordinate the design process. The single-stage compressor based on MiTi®'s double-entry compressor design was designed and assembled for testing, as described above. During the design process, an aerodynamic compressor design software, computational flow dynamics, finite element analysis and rotordynamic analysis were performed to assure that the design met all the performance and safety requirements. The single-entry compressor, design by MHI, also followed the same comprehensive analyses but used different software packages available at MHI. During the design process, both MiTi® and MHI checked each other's analyses to ensure accuracy of the different software. Both designs meet the performance criteria for the hydrogen pipeline compressor; however, comparing the two designs with respect to performance, safety and economics, indicated that the double-entry design is superior for the hydrogen pipeline compressor. The safety margin for the single-entry design is less due to larger tip speeds required. Also, the analyses indicated that the single-entry compressor could be more costly due to the need for balance piston and thrust bearings. Therefore, it was decided to pursue the MiTi® double-entry design instead of the MHI single-entry compressor for performance verification testing.

CONCLUSIONS AND FUTURE DIRECTIONS

Installation of the single-stage centrifugal hydrogen compressor, dedicated test cell and closed-loop helium facility were completed and preliminary validation testing was performed. The single-stage compressor system includes two 100-kW, oil-free motors designed and fabricated at MiTi®. The two motors are coupled using MiTi®'s proprietary mechanical coupling technology. Initial validation testing of the motors indicated that each motor was capable of operating at the design speed of 60,000 rpm. Both motors independently evaluated, were thermally and dynamically stable. With proper safety precautions, the compressor system was evaluated in a reinforced test cell up to 35,000 rpm with air and helium used as a simulant gas for hydrogen. The following tasks are planned for the remainder of FY 2013:

- Single-stage performance testing in helium (as a simulant gas for hydrogen)
- Design refinements
- Final report

FY 2013 PUBLICATIONS/PRESENTATIONS

1. J.F. Walton, "Design of a Multi-Megawatt Oil-Free Centrifugal Compressor for Hydrogen Gas Transportation and Delivery," World Hydrogen Energy Conference, Toronto, Canada, June 6, 2012.

2. H. Heshmat, A. Hunsberger, Z. Ren, S. Jahanmir, and J.F. Walton, "Oil-Free Foil-Bearings for Centrifugal Hydrogen Compressor," Tribology Online, January 2013.

3. S. Jahanmir, "Oil-Free Compression for Hydrogen Delivery and Transportation," Hydrogen Delivery Technology Team Meeting, March 27, 2013, Golden, CO.

4. H. Heshmat, "Oil-Free Centrifugal Hydrogen Compression Technology Demonstration," DOE Hydrogen Program Annual Review and Peer Evaluation Meeting, May 15, 2013, Arlington, VA.

III.3 Development of High-Pressure Hydrogen Storage Tank for Storage and Gaseous Truck Delivery

Jon Knudsen, Don Baldwin
Hexagon Lincoln (formerly Lincoln Composites)
5117 N.W. 40th Street
Lincoln, NE 68524
Phone: (402) 470-5039
Email: jon.knudsen@hexagonlincoln.com, don.baldwin@hexagonlincoln.com

DOE Managers
Erika Sutherland
Phone: (202) 586-3152
Email: Erika.Sutherland@ee.doe.gov
Katie Randolph
Phone: (720) 356-1759
Email: Katie.Randolph@go.doe.gov

Contract Number: DE-FG36-08GO18062

Project Start Date: July 1, 2008
Project End Date: April 30, 2013

Overall Objectives

The objective of this project is to design and develop the most effective bulk hauling and storage solution for hydrogen in terms of:

- Cost
- Safety
- Weight
- Volumetric Efficiency

Fiscal Year (FY) 2013 Objectives

The objective in FY 2013 is to continue improvement of the baseline 3,600 psi bulk hauling and storage solutions for hydrogen in terms of

- Cost
- Safety
- Weight
- Volumetric Efficiency

Technical Barriers

This project addresses the following technical barriers from the Hydrogen Delivery section of the Fuel Cell Technologies Office Multi-Year Research, Development, and Demonstration Plan:

(E) Gaseous Hydrogen Storage and Tube Trailer Delivery Costs

Technical Targets

This project has focused primarily on the design and qualification of a 3,600 psi pressure vessel and International Organization for Standardization (ISO) frame system to yield a storage capacity solution of approximately 8,500 liters of water. The original scope of project was to increase working pressure in the current design. Together with DOE, the scope has been changed to work towards increasing available volume at the 3,600 psi working pressure.

TABLE 1. Progress towards Meeting Technical Targets for Hydrogen Storage

Characteristic	Units	2010 Target	2015 Target	2020 Target	Status	Comments
Storage Costs	$/kg	500	300		745	Primary driver is market price of carbon fiber. Potential to see $710/kg with 5,000 psi Titan V Magnum
Volumetric Capacity	kg/ liter (psi)	0.030 (6,815)	>0.035 (>8,265)		0.018 (3,600)	Trade studies indicate trailer cost optimization at 0.024 kg/liter (5,000 psi)
Delivery Capacity, Trailer	kg	700	700	940	800	Potential to see 1,050 kg with 5,000 psi Titan V Magnum

FY 2013 Accomplishments

- The TITAN™ module (see Figure 1) and TITAN™V integrated semitrailer configuration (see Figure 2) were successfully extended to the TITAN™V Magnum configuration, increasing 3,600 psi hydrogen capacity to 800 kg (30% increase relative to the baseline TITAN™ module). Figure 3 shows the TITAN™V Magnum and the arrangement of large and small tanks within.
- Hexagon Lincoln has also continued the design and evaluation of robust fire protection systems utilizing memory metal alloy as a trigger mechanism for de-pressurizing the tank in the case of a fire. Development will continue as improved components are aligned with required functionalities.

FIGURE 1. Assembled TITAN™ ISO Container (without outer panels) on Standard ISO Trailer

- The installation of a 100% hydrogen testing facility is complete. Candidate liner materials are being characterized and qualified as a means to ensure reliability and to reduce the permeation rates that are present in current Type 4 cylinders.
- Hexagon Lincoln was an active participant in the Hydrogen Compression-Storage-Delivery Workshop at Argonne National Laboratory on March 20, 2013.

INTRODUCTION

Successful commercialization of hydrogen fuel cell vehicles will depend upon the creation of a hydrogen delivery infrastructure that provides the same level of safety, ease, and functionality as the existing gasoline and diesel delivery infrastructure. Today, compressed hydrogen is shipped in tube trailers at pressures up to 3,000 psi (200 bar). However, the low hydrogen carrying capacity of these tube trailers results in high delivery costs. Hexagon Lincoln has developed large composite tanks and optimized hauling systems for the efficient and cost-effective storage and transportation of energy gasses, including compressed hydrogen gas.

The TITAN™ module is an ISO frame system that is currently in use worldwide to store and transport compressed natural gas over road, rail, or water. Hexagon Lincoln's TITAN™ module will not only provide a technically feasible method to transport compressed hydrogen over road, rail, and water, but a more cost and weight efficient means as well.

APPROACH

In Phase 1 of this project, Hexagon Lincoln will design and qualify a large composite pressure vessel and ISO frame that can be used for storage and transport of compressed hydrogen over road, rail, and water.

The baseline composite vessel will have a 3,600 psi service pressure, an outer diameter of 42.8 inches and a length of 38.3 feet. The weight of this tank will be

FIGURE 2. TITAN™V Trailer Concept and TITAN™V Trailer Prototype delivered in the First Quarter of 2012

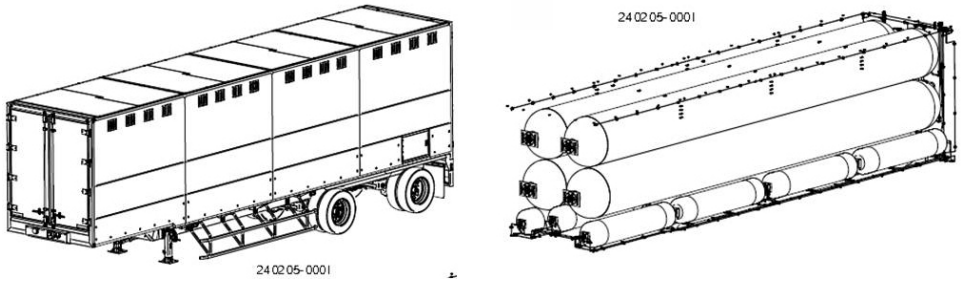

FIGURE 3. TITAN™V Magnum Trailer System with Arrangement of Tanks Shown at Right

approximately 2,485 kg. The internal volume is equal to 8,500 liters water capacity and will contain 154 kg of compressed hydrogen gas. The contained hydrogen will be approximately 6.0% of the tank weight (5.7% of the combined weight. Four of these tanks will be mounted in a custom-designed ISO frame, resulting in an assembly with a combined capacity of 616 kg of hydrogen. Installing the compressed hydrogen vessels into an ISO frame offers a benefit of having one solution for both transportable and stationary storage. This decreases research and development costs as well as the amount of infrastructure and equipment needed for both applications.

Phase 2 of the project was originally scoped to evaluate using the same approximate sized vessel(s) and ISO frame at elevated pressures. Trade studies completed in 2011 indicated that cost and volumetric efficiency of the TITAN™ module would be optimized at an operational pressure of 5,000 psi. In the next year however, Hexagon Lincoln identified concerns with moving forward with higher pressure delivery modules. The market is difficult to forecast at this time and the cost to fully qualify a higher pressure module is estimated at $5MM to complete. Based on this, it was determined that Hexagon Lincoln would work with our current product and move forward with increasing the potential volume per load as well as improvements in safety. Other projects include the evaluation, testing and qualification of improved fire protection systems, as well as development of a laboratory capability to investigate the effects of hydrogen on liner materials.

RESULTS

Proposed objectives for Phase 1 of this project were completed in the fourth quarter of 2009. This includes successful completion of a large 3,600 psi pressure vessel able to contain 8,500 liter water capacity. The successful qualification of an entire assembly into an ISO container was also completed. Figure 1 is a photograph of the TITAN™ module qualification test unit.

The design and analysis of a TITAN™V integrated semitrailer system was realized that adds an additional 18% capacity with respect to the baseline TITAN™ module. A prototype unit was delivered to Hexagon Lincoln in the first quarter of 2012, as shown in Figure 2. This configuration was successfully extended to the TITAN™ V Magnum configuration shown in Figure 3, increasing 3,600-psi hydrogen capacity to 800 kg (30% increase relative to the baseline TITAN™ module).

Trade studies completed in 2011 indicated that cost and volumetric efficiency of the TITAN™ module would be optimized at an operational pressure of 5,000 psi. However, Hexagon Lincoln has worked directly with DOE in determining that progression to the qualification of a 5,000 psi pressure vessel is not feasible at this time. This development is on hold pending solidification of a business case that justifies the high cost of qualification. Hexagon Lincoln is therefore concentrating efforts on the further development of our hauling equipment using the 3,600 psi TITAN™ pressure vessel, while continuing to evaluate all reasonable configuration options for operation with increased capacity and higher system pressures. Figure 4 shows a hydrogen payload and gross vehicle weight (GVW) comparison of feasible options vs. existing technology. (GVW includes the mass of an appropriate prime mover and a trailer chassis, if required.)

The three configurations at the left-hand side of Figure 4 are existing steel tube trailer configurations. The next two configurations are the TITAN™ module and TITAN™V Magnum™ trailer systems operating at 3,600 psi (250 bar). With these systems, an increased hydrogen payload can be achieved without exceeding the maximum allowed GVW for general use on the interstate system in the United States of 80,000 lb (36.3 tonne). Further increases in hydrogen payload can be achieved without exceeding the maximum GVW by extension of the TITAN™ equipment to higher operating pressures. As was identified in our previous trade studies, a 5,000 psi (350 bar) TITAN™V Magnum trailer system offers a particularly attractive option in terms of hydrogen hauling efficiency. However, qualification costs for this configuration are very high. In addition, higher level trade studies performed to determine the operating parameters of an optimized hydrogen delivery infrastructure may indicate that better overall efficiency will be achieved through operation of the bulk hauling equipment at pressures of 7,600 psi (525 bar) or higher. Consideration is therefore given to the extension of the SmartStore™ product line to hydrogen storage and transport, in particular during the critical phase of infrastructure development and deployment. SmartStore™ modules incorporate as many as 40 smaller diameter tanks in ISO-format containers. The options of operating 30-foot versions of the SmartStore™ system at 7,600 psi (525 bar) and 10,000 psi (700 bar) are also shown. The lower qualification costs and packaging flexibility of smaller diameter tanks facilitates SmartStore™ module optimization at these higher pressures.

Hexagon Lincoln has also continued the design and evaluation of robust fire protection systems utilizing memory metal alloy as a trigger mechanism for de-pressurizing the tank in the case of a fire. Development will continue as improved components are aligned with required functionalities.

The installation of a 100% hydrogen testing facility is complete. Candidate liner materials are being characterized and qualified as a means to ensure reliability and to reduce the permeation rates that are present in current Type 4 cylinders.

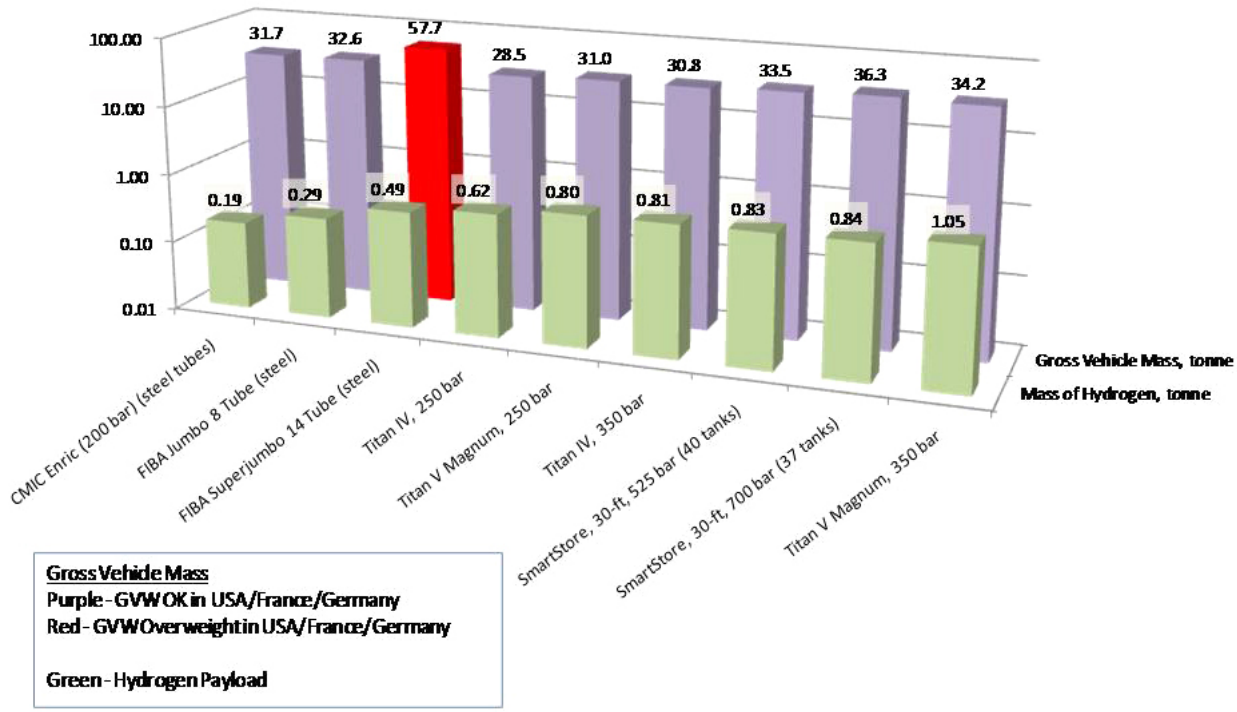

FIGURE 4. Comparison of GVW and H_2 Capacity for Current and Potential Bulk Hauling Configurations

CONCLUSIONS AND FUTURE DIRECTIONS

- The TITAN™V integrated semitrailer configuration was successfully extended to the TITAN™V Magnum configuration, increasing 3,600 psi hydrogen capacity to 800 kg (30% increase relative to the baseline TITAN™ module).
- Completion of the qualification and implementation of a safer and more reliable fire protection system. This includes integration of memory metal trigger mechanisms for distributed fire sensing and fast reacting dump system for safe evacuation of the hydrogen payload.
- Extreme low-temperature testing will be performed to ensure safe extension of the lower temperature operating limit of the TITAN™ tanks from the current -40°C to -50°C.
- Laboratory investigation of the short and long term effects of compressed hydrogen gas on pressure vessel liner materials will continue.

FY 2013 PUBLICATIONS/PRESENTATIONS

1. 2013 DOE Hydrogen Program Annual Merit Review, May 15, 2013

III.4 Fiber Reinforced Composite Pipeline

George Rawls
Savannah River National Laboratory (SRNL)
Materials Science & Technology
773-41A/173
Aiken, SC 29808
Phone: (803) 725-5658
Email: george.rawls@srnl.doe.gov

DOE Manager
Erika Sutherland
Phone: (202) 586-3152
Email: Erika.Sutherland@ee.doe.gov

Project Start Date: October 1, 2006
Project End Date: October 1, 2016

Overall Objectives

Successfully adapt spoolable fiber reinforced composite pipeline (FRP) currently used in the oil and natural gas industry for use in high-pressure hydrogen delivery systems and development of data needed for life management and codification fiber reinforced composite piping into the American Society of Mechanical Engineers (ASME) B31.12 Hydrogen Piping Code.

Fiscal Year (FY) 2013 Objectives

- Complete draft code section for FRP codification in ASME B31.12.
- Develop the fatigue design curve for unflawed FRP pipe over the range of design pressures from 750 psig to 3,000 psig.

Technical Barriers

This project addresses the following technical barriers from the Hydrogen Delivery section of the Fuel Cell Technologies Office Multi-Year Research, Development, and Demonstration Plan:

(D) High As-Installed Cost of Pipelines

(J) Hydrogen Leakage and Sensors

(K) Safety, Codes and Standards, Permitting

Technical Targets

This project is focused on the evaluation of FRP for hydrogen service applications. Assessment of the structural integrity of FRP piping and the individual manufacturing components in hydrogen will be performed. Insights gained will support qualifications of these materials for hydrogen service including:

- Transmission pipeline reliability: acceptable for hydrogen as a major energy carrier
- Transmission pipeline total capital cost $735k per mile (2015)
- Transmission pipeline total capital cost $715k, per mile (2020)
- H_2 delivery cost <$0.90/gasoline gallon equivalent
- H_2 pipeline leakage: <780 kg/mi/y (2020)

FY 2013 Accomplishments

In FY 2013, the SRNL project has focused on development of the technical basis needed for codification of FRP material into the ASME B31.12 Hydrogen Piping Code. The material testing in FY 2013 focused on the development of a fatigue curve for unflawed FRP piping. The fatigue tests were performed over a range of pressure between 750 psi and 3,000 psi. The tests were performed on an FRP product with a rated pressure of 1,500 psi. The results from the fatigue testing provided insight into specific failure modes of the FRP mechanical joint. A technical report was completed in collaboration with Oak Ridge National Laboratory (ORNL) to compile all the data from the DOE FRP H_2 testing effort. The report will serve as the baseline technical document for FRP codification into ASME B31.2

- **FRP Materials Testing**
  The fatigue tests were performed over a range of pressure between 750 psi and 3,000 psi and a preliminary design fatigue curve was developed.
- **FRP Codification into ASME B31.12**
  Technical baseline report for FRP codification was completed.

✧ ✧ ✧ ✧ ✧

INTRODUCTION

The goal of the overall project is to successfully adapt spoolable FRP currently used in the oil industry for use in high-pressure hydrogen pipelines. The use of FRP materials for hydrogen service will rely on the demonstrated compatibility of these materials for pipeline service environments and operating conditions. The ability of the polymer piping to withstand degradation while in service, and development of the tools and data required for life management are imperative for successful implementation of these materials for hydrogen pipelines.

APPROACH

To achieve the objective an FRP life management plan was developed. The plan was a joint document developed by SRNL and the ASME to guide generation of a technical basis for safe use of FRP in delivery applications. The plan addresses the needed material evaluations and also focuses on the needed information for codification of FRP into the ASME B31 Code of Pressure Piping. The B31.12 Hydrogen Piping Code is the existing code that provides a consensus standard for the safe and reliable implementation of the piping in hydrogen service. This plan is designed to provide the needed information to support the codification of FRP. The B31.12 Code addresses the initial construction of piping systems. The plan also identifies the tasks needed for the post construction management of FRP to insure structural integrity through end of life. The plan calls for detailed investigation of the following areas:

- System Design and Applicable Codes and Standards
- Service Degradation of FRP
- Flaw Tolerance and Flaw Detection
- Integrity Management Plan
- Leak Detection and Operational Controls Evaluation
- Repair Evaluation

RESULTS

Fatigue Testing

Fatigue testing of FRP was initiated at SRNL in FY 2012 and continued through FY 2013. The material testing in FY 2013 focused on the development of a fatigue curve for unflawed FRP piping. The fatigue tests were performed over a range of pressure between 750 psi and 3,000 psi. The tests were performed on an FRP product with a rated pressure of 1,500 psi. The range of test pressure was selected to provide sufficient data to understand the general shape of the FRP fatigue curve. Figure 1 shows the fatigue test data and the preliminary design fatigue curve.

The first fatigue test was performed at the rated pressure of the FRP product of 1,500 psi. During the test a seal failure of the mechanical connection was observed at 14,424 cycles. The O-ring seals were replaced and the test continued. The 1,500 psi test sample has been cycled to 20,127 cycles where a structural failure of the pressure boundary occurred in the center span of the test sample. The second fatigue test at the 1,500 psi rated product pressure was cycled to failure. The second test failed at 16,233 cycles. The second test failed at the end of the pipe and the initial visual evaluation indicated issues with the end joint preparation may be a contributing factor. Additional failure analysis is being conducted.

Two fatigue tests were performed at 3,000 psi which is twice the product rated pressure. Tests were performed above the rated product pressure to provide data and understanding of the available margins if overpressure events occur in-service. During the first 3,000 psi test, seal failures occurred at 447 cycles followed by a structural failure of the pressure boundary at 593 cycles. A second 3,000 psi fatigue test failed in the pressure boundary at 681 cycles. Inspection showed damage to the o-ring at completion of the second 3,000 psi fatigue test, but no seal failure occurred.

One fatigue test has been completed at 750 psi which is half the products rated pressure. The test sample has been cycled to 40,700 cycles without a structural failure where the test was terminated. Seal failure was observed at 23,071 cycles. The o-rings were replaced and the test was

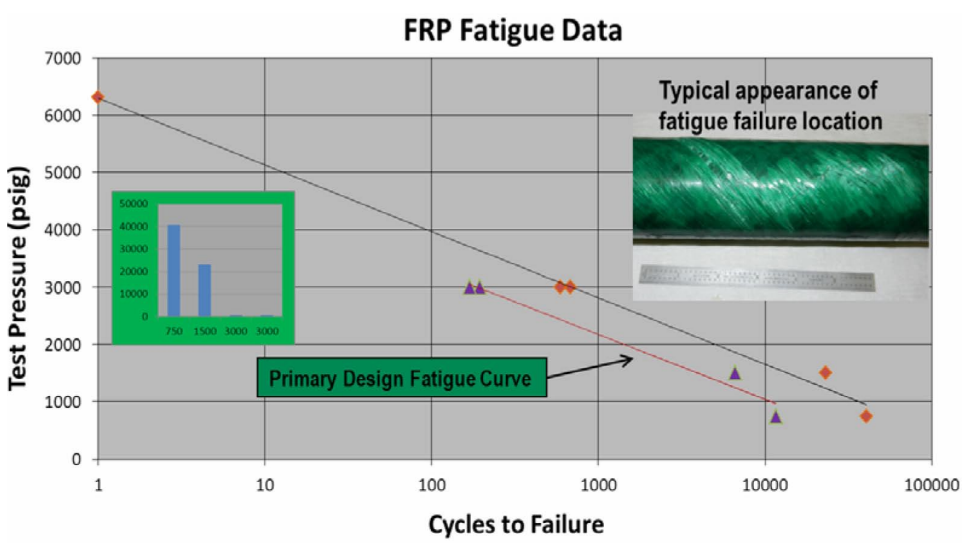

FIGURE 1. FRP Preliminary Fatigue Curve

completed. The o-ring damage was less severe than in the 1,500 and 3,000 psi tests.

The results from the fatigue testing provided insight into specific failure modes of the FRP mechanical joint as shown in Figure 2. The connectors are all metallic with elastomer o-ring seals. To form the connection the internal diameter of the polyethylene liner is machined to a specified diameter. The machined portion of the liner is where the o-rings in the metallic connector interface with the composite piping to form the fluid seal. The outer nut of the connector is tightened, mechanically compressing ferrules on the piping, resulting in compression of the seals.

O-ring failures occurred during the fatigue testing of the structural layer at all pressure levels. The o-ring failures show classic indication of extrusion from their retaining groove. The failure, shown in Figure 3, is a progressive distortion of the o-ring from the fatigue loading. The o-rings did not leak while testing with hydrogen or during burst testing.

Testing of the o-ring material showed that the material hardness (durometer level) was lower than the specified design value. Tested values showed that the rubber hardness was approximately 60 Durometer M. Values of 70 to 90 would be required based on literature data. Subsequent testing with high durometer o-rings (85 Durometer M) has resolved this issue. The o-ring data provides valuable insight into needed code examination.

ASME B31.12 Codification

A report summarizing the FRP testing by SRNL and ORNL has been completed. The report will become the basis for ASME Codification of FRP into the B31.12 Hydrogen Piping Code. Review comments from ASME, ORNL and Fiberspar (an FRP manufacturer) have been incorporated into the technical basis report. The report will be updated to include the 2013 fatigue testing data and the service experience data obtained from Fiberspar. The revised report will be provided to the ASME B31.12 Code Committee for peer review in September 2013.

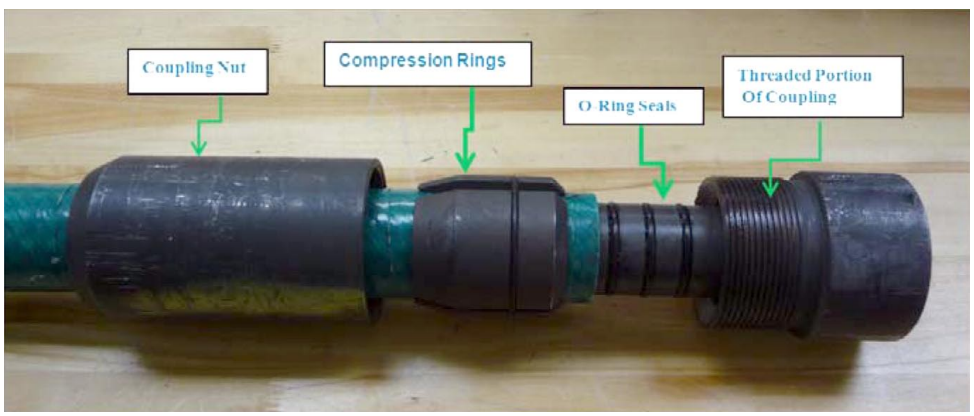

FIGURE 2. Components of FRP Compression Connector

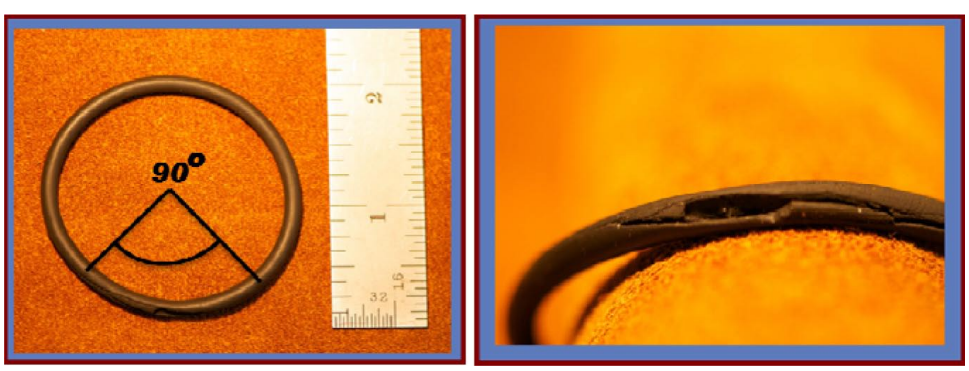

FIGURE 3. O-Ring Damage 3,000 psig Fatigue Test

CONCLUSIONS AND FUTURE DIRECTIONS

Conclusions

- FRP is an attractive technology with potential to support the DOE goal to reduce overall pipeline installation cost.
- Fatigue testing over the range of 750 psig to 3,000 psig has been completed. The data provide an initial indication on the fatigue life of FRP. The variability in the data still needs additional investigation. A preliminary design fatigue curve has been proposed based the current test data with a design margin applied based on literature review to estimate the variability.
- Fatigue testing of flaw FRP has been conducted. These tests have shown that a flaw will affect the fatigue life of FRP. These flawed fatigue test provide valuable information for installation and inspection requirements.
- The o-ring failures are a not structural failure of the pressure boundary, but still provide valuable data for the FRP codification process. The results of the o-ring failure analysis will be applied to specify attributes of the connector for examination, and types of examinations that need to be performed during fabrication and installation of the mechanical joint for the FRP pipeline.
- A report summarizing the FRP testing by SRNL and ORNL has been completed. The report will become the basis for ASME Codification of FRP. Review comments from ASME, ORNL and Fiberspar have been incorporated.

Future Work

- Perform additional fatigue testing in collaboration with Fiberspar to determine the variability in the fatigue data.
- Collect and document available service history data for FRP from literature and FRP manufacturers.
- Perform a long-term stress rupture test for flawed FRP samples.
- Evaluate non-mechanical joints for FRP application.
- Development inspection criteria for FRP joint based on conclusion from o-ring fatigue failures.
- Complete FRP Codification into ASME B31.12.

FY 2013 PUBLICATIONS/PRESENTATIONS

1. Gaseous Hydrogen Embrittlement of Materials in Energy Technologies, Chapter 1, Hydrogen Production and Containment, Woodhead Publishing, 2012.

2. SRNL FRP Piping Project, Presentation to Hydrogen Delivery Technology Team, Washington, DC, August 2012.

3. DOE Polymer and Composite Materials for Hydrogen Service Meeting, Washington, DC, October 2012.

4. Fiber Reinforced Composite Pipelines, Presentation to ASME B31.12 Committee Chairman, Phoenix, AZ, November 2012.

III.5 Hydrogen Embrittlement of Structural Steels

Brian Somerday
Sandia National Laboratories
P.O. Box 969
Livermore, CA 94550
Phone: (925) 294-3141
Email: bpsomer@sandia.gov

Sandia National Laboratories is a multi-program laboratory managed and operated by Sandia Corporation, a wholly owned subsidiary of Lockheed Martin Corporation, for the U.S. Department of Energy's National Nuclear Security Administration under contract DE-AC04-94AL85000

DOE Manager
Erika Sutherland
Phone: (202) 586-3152
Email: Erika.Sutherland@ee.doe.gov

Project Start Date: January 2007
Project End Date: Project continuation and direction determined annually by DOE

Overall Objectives

- Demonstrate the reliability/integrity of steel hydrogen pipelines subjected to cyclic pressure operating conditions
- Identify pathways for reducing the cost of steel hydrogen pipelines without compromising reliability/integrity

Fiscal Year (FY) 2013 Objectives

Establish reliable fatigue crack growth (da/dN vs ΔK) relationships for the fusion zone and heat-affected zone in X65 girth weld supplied by industry partner

Technical Barriers

This project addresses the following technical barriers from the Hydrogen Delivery section of the Fuel Cell Technologies Office Multi-Year Research, Development, and Demonstration Plan (Section 3.2.5):

(B) Reliability and Costs of Gaseous Hydrogen Compression

(D) High As-Installed Cost of Pipelines

(K) Safety, Codes and Standards, Permitting

Technical Targets

The principal targets addressed by this project are the following (Table 3.2.4 of the Fuel Cell Technologies Office Multi-Year Research, Development, and Demonstration Plan):

- Pipeline Reliability/Integrity

One salient reliability/integrity issue for steel hydrogen pipelines is hydrogen embrittlement. For steel pipelines, the central unresolved issue is the pipeline performance under extensive pressure cycling. One of the objectives of this project is to enable safety assessments of steel hydrogen pipelines subjected to pressure cycling through the use of structural integrity models in design codes, e.g., American Society of Mechanical Engineers (ASME) B31.12. This structural integrity analysis can determine limits on design and operating parameters such as the allowable number of pressure cycles and pipeline wall thickness. Efficiently specifying pipeline dimensions such as wall thickness also affects pipeline cost through the quantity of material required in the design.

FY 2013 Accomplishments

Reliable fatigue crack growth (da/dN vs ΔK) relationships were measured for the X65 weld heat-affected zone (HAZ) in 3,000 psi (21 MPa) hydrogen gas. These results show that the weld HAZ is not more susceptible to hydrogen-accelerated fatigue crack growth compared to the base metal.

✧ ✧ ✧ ✧ ✧

INTRODUCTION

Carbon-manganese steels are candidates for the structural materials in hydrogen gas pipelines; however, it is well known that these steels are susceptible to hydrogen embrittlement. Decades of research and industrial experience have established that hydrogen embrittlement compromises the structural integrity of steel components. This experience has also helped identify the failure modes that can operate in hydrogen containment structures. As a result, there are tangible ideas for managing hydrogen embrittlement in steels and quantifying safety margins for steel hydrogen containment structures. For example, fatigue crack growth aided by hydrogen embrittlement is a well-established failure mode for steel hydrogen containment structures subjected to pressure cycling. This pressure cycling represents one of the key differences in operating conditions between current hydrogen pipelines and those anticipated in a hydrogen delivery infrastructure. Applying structural integrity models in design codes coupled with measurement of relevant material properties allows quantification of the reliability/integrity of steel hydrogen pipelines subjected to pressure cycling. Furthermore, application of these structural integrity models is aided by the development of physics-based material models, which provide important insights such as the effects

of gas impurities (e.g., oxygen) on hydrogen-affected fracture properties. Successful implementation of these structural integrity and material models enhances confidence in the design codes and enables decisions about materials selection and operating conditions for reliable and efficient steel hydrogen pipelines.

APPROACH

The approach of this project is to apply specialized materials testing capabilities to measure the fatigue crack growth rates of technologically relevant pipeline steels in high-pressure hydrogen gas. These properties must be measured for the base materials but more importantly for the welds, which are likely to be most vulnerable to hydrogen embrittlement. Such measurements are necessary for enabling the application of structural integrity models in design codes. For example, the new ASME B31.12 code for hydrogen pipelines includes a fracture mechanics-based integrity management option, which requires material property inputs such as the fatigue crack growth relationship in hydrogen gas.

Following the establishment of reliable fatigue crack growth relationships for pipeline steel base metal, weld heat-affected zone, and weld fusion zone in hydrogen gas, a secondary approach of this project is to apply analytical techniques such as electron microscopy to define the mechanisms of hydrogen embrittlement for the purpose of proposing phenomenological models. These phenomenological models then serve as the foundation for developing analytical or numerical predictive models, which can provide quantitative insight into the effects of environmental, material, and mechanical variables on hydrogen embrittlement. Such predictive materials science models can enable the extrapolation of material data inputs required for structural integrity models.

RESULTS

The fatigue crack growth rate (da/dN) vs stress-intensity factor range (ΔK) relationship is a necessary material-property input into structural integrity models applied to steel hydrogen pipelines. One such integrity assessment methodology for steel hydrogen pipelines was recently published in the ASME B31.12 code. The measurements of crack propagation thresholds and fatigue crack growth relationships in this task support the objective of establishing the reliability/integrity of steel hydrogen pipelines.

Low-strength line pipe steels such as X52, X60, and X65 were selected for this task because of their stakeholder-recognized technological relevance for hydrogen pipelines. Generally, lower-strength steels are selected for hydrogen pipelines since these steels are less susceptible to hydrogen embrittlement. A section of X65 steel pipe containing a girth weld was provided by an industry partner. The emphasis in FY 2013 was to complete multiple measurements of the da/dN vs ΔK relationship for the weld fusion zone and heat-affected zone in 3,000 psi (21 MPa) hydrogen gas. An optical-microscope image revealing the base metal, weld fusion zone, and the HAZ is shown in Figure 1. This image demonstrates that the material regions have distinctly different metallurgical structures, particularly the base metal and fusion zone.

The hydrogen-affected fatigue crack growth relationship (da/dN vs ΔK) for the structural steel is the basic element in pipeline structural integrity models. The ASME B31.12 code requires measurement of the fatigue crack growth relationship for pipeline steels at the hydrogen gas operating pressure. Since the maximum pressure specified for hydrogen gas pipelines in the ASME B31.12 code is 3,000 psi (21 MPa), this upper-bound pressure was selected for the testing. As specified in ASME B31.12, the da/dN vs ΔK relationship was measured following ASTM Standard E647. Compact-tension crack-growth specimens were extracted from both the fusion zone and the HAZ such that the loading and crack propagation directions were in the longitudinal and circumferential orientations, respectively, relative to the pipe. In this way, the crack plane was fully contained in either the fusion zone or HAZ for the entire range of crack growth during the tests. Samples were extracted from the base metal for comparison. The load-cycle frequency selected for the testing was 1 Hz, consistent with previous testing on X52 line pipe steel in high-pressure hydrogen gas.

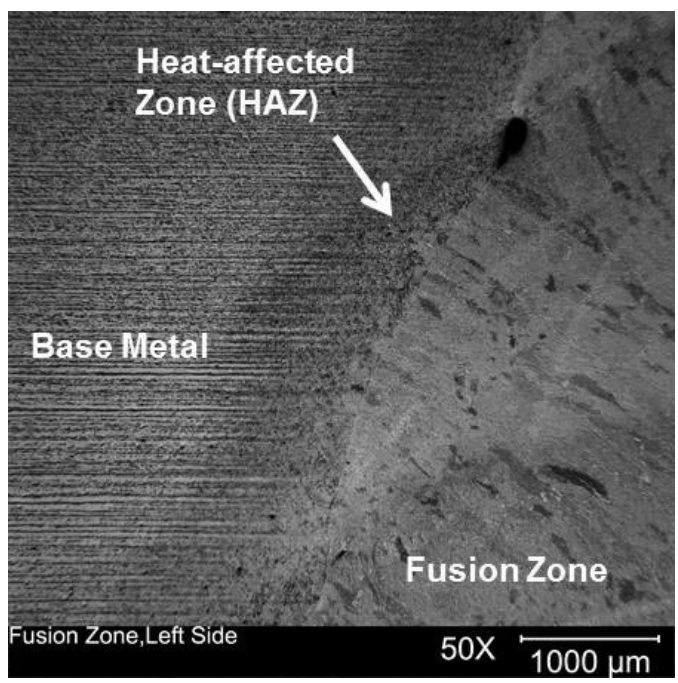

FIGURE 1. Optical-microscope image showing base metal, fusion zone, and HAZ of X65 weld.

Preliminary da/dN vs ΔK data for the X65 fusion zone and the HAZ revealed unexpectedly lower crack growth rates compared to X52 base metal in hydrogen gas at low ΔK values. Welds are expected to be more sensitive to hydrogen-assisted crack growth. Further analysis of the X65 weld fusion zone and the HAZ samples revealed that the pre-cracks deviated from their anticipated path, as shown for the fusion zone sample in Figure 2. The crack did not span the entire thickness of the specimen, instead exhibiting a non-uniform crack front, thus rendering the measured data unreliable. To mitigate the deviation of the crack front during pre-cracking, X65 fusion zone and HAZ compact tension samples were thinned from their original 13 mm (0.5 in) to 6 mm (0.25 in). Previous work has shown that thinner samples consistently exhibit more uniform crack fronts during pre-cracking while the change in sample geometry still conforms to ASTM E647 standard. In order to improve confidence in attaining a uniform crack front, side grooves were not machined and the specimen sides were polished to allow for observation of pre-cracks before initiating fatigue crack growth testing in hydrogen gas. The X65 HAZ specimen was observed to have uniform pre-crack fronts whereas the X65 fusion zone had non-uniform pre-crack fronts, e.g. significant crack growth on one side and negligible on the other.

The results from the X65 HAZ thinned specimen are shown in Figure 3 in comparison with X52 and X65 base metals. The data for the thinned specimen essentially overlay the original X65 HAZ data, both in 21 MPa H_2 gas. Both sets of data exhibit slightly lower crack growth rates at low ΔK values compared to the base metals, but all materials show similar trends at high ΔK values. The specimens were fractured after test completion and a side-by-side comparison of the two X65 HAZ specimens is shown in Figure 4. The optical images show that the thinned specimen exhibited a more uniform crack front during the pre-crack stage;

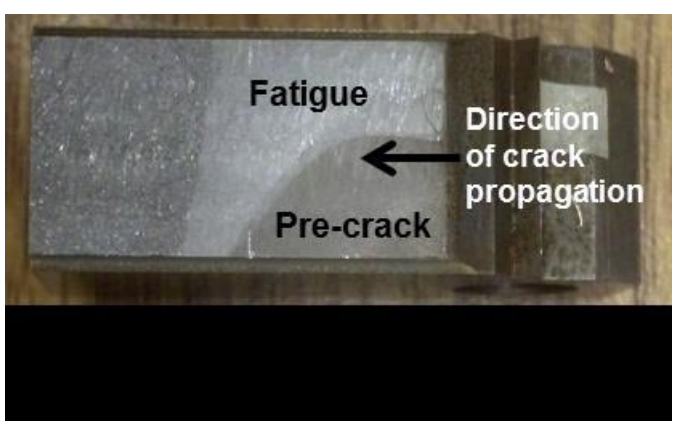

FIGURE 2. Optical-microscope image of fracture surface from compact tension specimen of X65 fusion zone showing a non-uniform pre-crack front (darker region, bottom right).

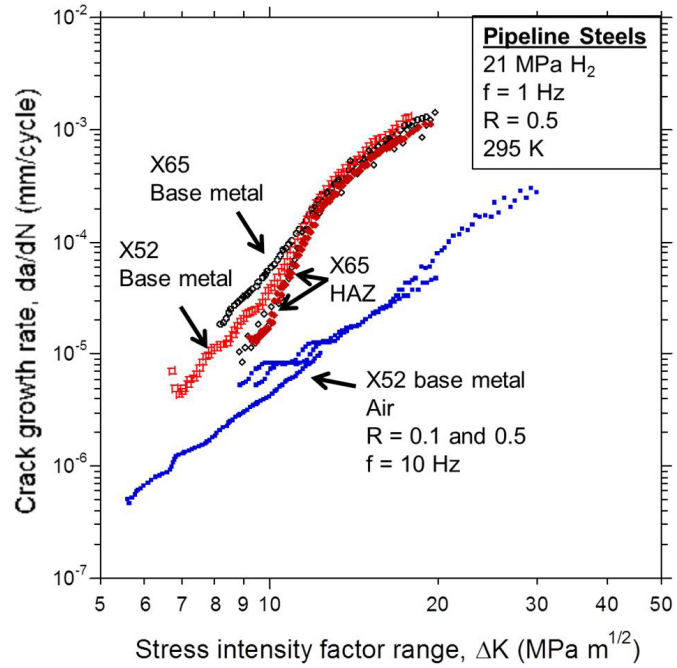

FIGURE 3. Fatigue crack growth relationships (da/dN vs ΔK) for X65 base metal and HAZ in 3,000 psi (21 MPa) hydrogen gas. The results are compared to measurements for X52 base metal in hydrogen gas and X52 base metal in air.

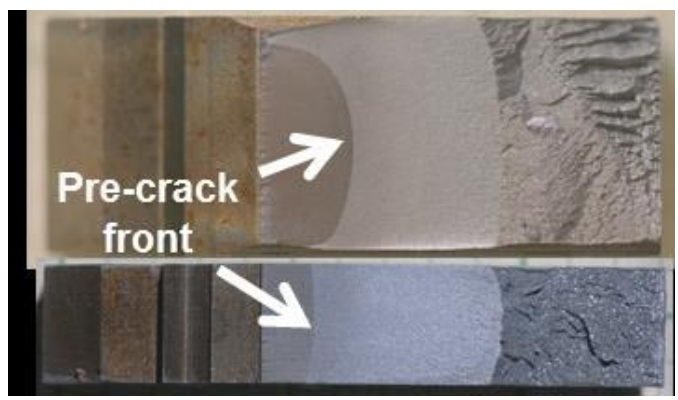

FIGURE 4. Optical-microscope images of fracture surfaces from compact tension specimens of X65 HAZ specimens comparing pre-crack fronts. The top specimen was the original geometry and the bottom was thinned to 6 mm (0.25 in).

however, both exhibited similar uniformity during fatigue crack growth in hydrogen.

Since the thinned X65 fusion zone specimen was observed to have a non-uniform pre-crack, this fatigue crack growth test has not been performed in hydrogen. Further testing on the X65 fusion zone will be conducted in the fourth quarter of FY 2013 on a modified specimen geometry and orientation. These specimen modifications are required to attain the goal of establishing reliable measurements of the da/dN vs ΔK relationships for the weld-fusion zone.

CONCLUSIONS AND FUTURE DIRECTIONS

- Reliable da/dN vs ΔK relationships were measured for the X65 weld HAZ in 3,000 psi (21 MPa) hydrogen gas. These results show that the weld HAZ is not more susceptible to hydrogen-accelerated fatigue crack growth compared to the base metal.
- (future) Develop an alternate specimen geometry and orientation for reliable measurements of the X65 weld fusion zone. Complete triplicate measurements of the da/dN vs ΔK relationships for the weld fusion zone and HAZ to establish reliable material-property inputs for structural integrity models.

FY 2013 PUBLICATIONS/PRESENTATIONS

1. "Elucidating the Variables Affecting Accelerated Fatigue Crack Growth of Steels in Hydrogen Gas with Low Oxygen Concentrations", B.P. Somerday, P. Sofronis, K.A. Nibur, C. San Marchi, and R. Kirchheim, *Acta Materialia*, 2013, doi: 10.1016/j.actamat.2013.07.001.

2. "Structural Materials Compatibility with Hydrogen", B.P. Somerday, I2CNER Annual Symposium, Kyushu University, Fukuoka, Japan, Jan. 2013.

III.6 Electrochemical Hydrogen Compressor

Ludwig Lipp (Primary Contact), Pinakin Patel
FuelCell Energy, Inc.
3 Great Pasture Road
Danbury, CT 06813
Phone: (203) 205-2492
Email: llipp@fce.com

DOE Managers
Erika Sutherland
Phone: (202) 586-3152
Email: Erika.Sutherland@ee.doe.gov
Dave Peterson
Phone: (720) 356-1747
Email: David.Peterson@go.doe.gov

Contract Number: DE-EE0003727

Subcontractor:
Sustainable Innovations, LLC, Glastonbury, CT

Start Date: July 15, 2010
End Date: October 14, 2014

Overall Objectives

- Demonstrate capability of electrochemical hydrogen compression (EHC) technology to meet the DOE targets for small compressors for refueling sites.
- Quantify EHC cell performance and durability.
- Reduce capital cost to demonstrate potential to meet DOE cost targets for hydrogen compression, storage, and delivery.

Fiscal Year (FY) 2013 Objectives

- Develop a solid-state EHC building block capable of compressing hydrogen from near-atmospheric pressure to 2,000-3,000 psi.
- Scale up the EHC active cell area by >100%.
- Increase compression efficiency (isentropic) to 73% (DOE 2015 target).

Technical Barriers

This project addresses the following technical barrier from the Hydrogen Delivery section (3.2) of the Fuel Cell Technologies Office Multi-Year Research, Development, and Demonstration Plan:

(B) Reliability and Costs of Gaseous Hydrogen Compression

Technical Targets

This project is directed at developing a solid-state EHC. The EHC is an enabling device for low-cost hydrogen delivery. Goals include the following:

- Single-stage compression of hydrogen from near-atmospheric pressure to 2,000-3,000 psi.
- Multi-stage compression of hydrogen from near-atmospheric pressure to 6,000-12,000 psi.
- Ensure no possibility of lubricant contamination of the hydrogen from compression (DOE 2020 target).
- Reduce EHC specific energy consumption.
- Scale up EHC to a capacity of 2 lb/day H_2.

The ultimate goal of the project is to meet the DOE targets for small compressors [1].

FY 2013 Accomplishments

- Design: Reduced EHC cell part count by >50% through design innovations.
- Hydrogen Flux: Increased operating current density (and therefore hydrogen flux) by ~3x over the 2010 baseline.
- EHC Scale-Up: Achieved >2x increase in cell active area by scaling up from 81 to 185 cm^2.
- Capital Cost: Achieved 50% decrease in single production unit cost through lowering part count and increasing the current density and active area to increase the production rate while lowering the total cells per stack.
- Efficiency: Reduced specific energy consumption at 3,000 psi to <5 kWh/kg H_2.
- Durability: Demonstrated 10,000 hour operation at >95% hydrogen recovery.

✧ ✧ ✧ ✧ ✧

INTRODUCTION

With the depletion of fossil fuel reserves and a global requirement for the development of a sustainable economy, hydrogen-based energy is becoming increasingly important. Production, purification, and compression of hydrogen represent key technical challenges for the widespread commercialization of hydrogen fuel cell technologies. In the transportation sector, onboard storage of pure hydrogen is required at pressures up to 10,000 psi and compression of the hydrogen fuel up to 12,000 psi.

The level of maturity of current hydrogen compressor technology is not adequate to meet projected infrastructure demands. Existing compressors are inefficient and have many moving parts, resulting in significant component wear and therefore excessive maintenance. New technologies that achieve higher operational efficiencies, are low in cost, safe and easy to operate are therefore required. This project addresses high-pressure hydrogen needs by developing a solid-state EHC.

APPROACH

The approach to address the project goals consists of the following major elements:

- Increase hydrogen recovery efficiency by improving flow field design.
- Reduce capital cost by increasing the hydrogen flux.
- Reduce operating cost by improving membrane and electrode design.
- Develop a multi-stage system concept for compression to 6,000-12,000 psi.

To this end, the approach includes the design, fabrication, and evaluation of improved cell architecture and the development and demonstration of critical sealing technology to contain the high-pressure hydrogen within the EHC.

RESULTS

A major focus of this year's efforts was to reduce the capital cost of the EHC building block design for 2,000-3,000 psi hydrogen product pressure. This was addressed by a multi-pronged approach of reduced cell part count, active area scale-up and increased current density. A number of design innovations were conceived, translated into a cell design, fabricated and individually tested in 81-cm^2 cells. The most successful changes were combined into the 2013 design, as shown in Figure 1. It features a >50% reduction compared to the baseline design. Mass manufacturability is an important criterion that was taken into account in the selection of the improved component designs. Simultaneously, the cell active area was scaled up by >100% from 81 cm^2 to 185 cm^2. The 185 cm^2 design has been validated for >1,000 hours of operation in a single cell. Validation at the stack level is planned for FY 2014.

The current density has been steadily increased in the project through improvements in cell design and materials. Figure 2 shows a 3-fold increase in current density over the 2010 baseline EHC. Since the hydrogen flux through the EHC is directly proportional to the current density, it enables higher hydrogen capacity from the same size EHC hardware. This equates to a proportional reduction in EHC capital cost.

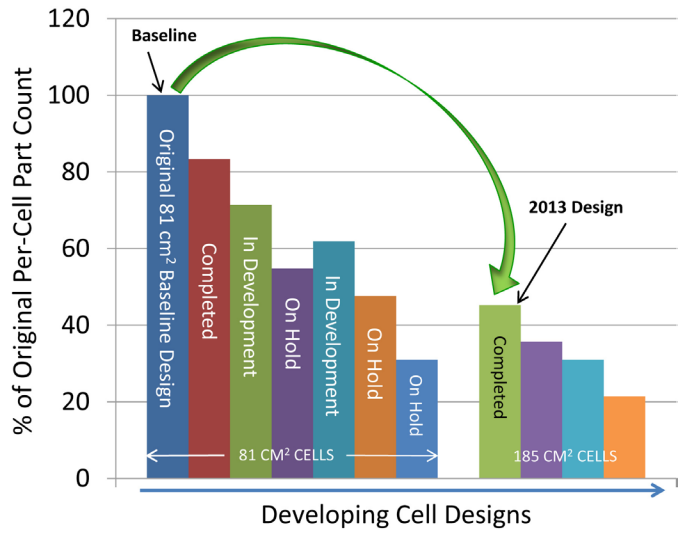

FIGURE 1. >50% Decrease in Cell Part Count for EHC Cost Reduction

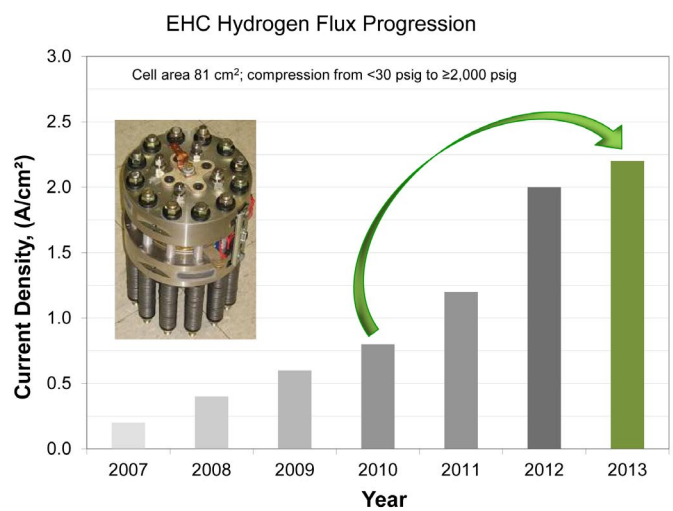

FIGURE 2. Increased Operating Current Density by ~3x over the 2010 Baseline

Overall, a >50% decrease in single production unit cost was achieved through the above improvements.

The EHC efficiency is measured by the hydrogen recovery as well as the specific energy consumption. Figure 3 shows the specific energy consumption of a number of recent EHC cells. In previous years efforts were centered at 2,000 psi. This year's focus was on reducing the specific energy consumption at a product pressure of 3,000 psi (with a hydrogen feed of 30 psi or less). Figure 3 shows a stepwise reduction in specific energy consumption at 3,000 psi from ~8 kWh/kg to <5 kWh/kg H_2. The reduction is attributed to improved cell design as well as refined operating procedures.

Durability and reliability are significant barriers for mechanical compressors, and major incentives for pursuing

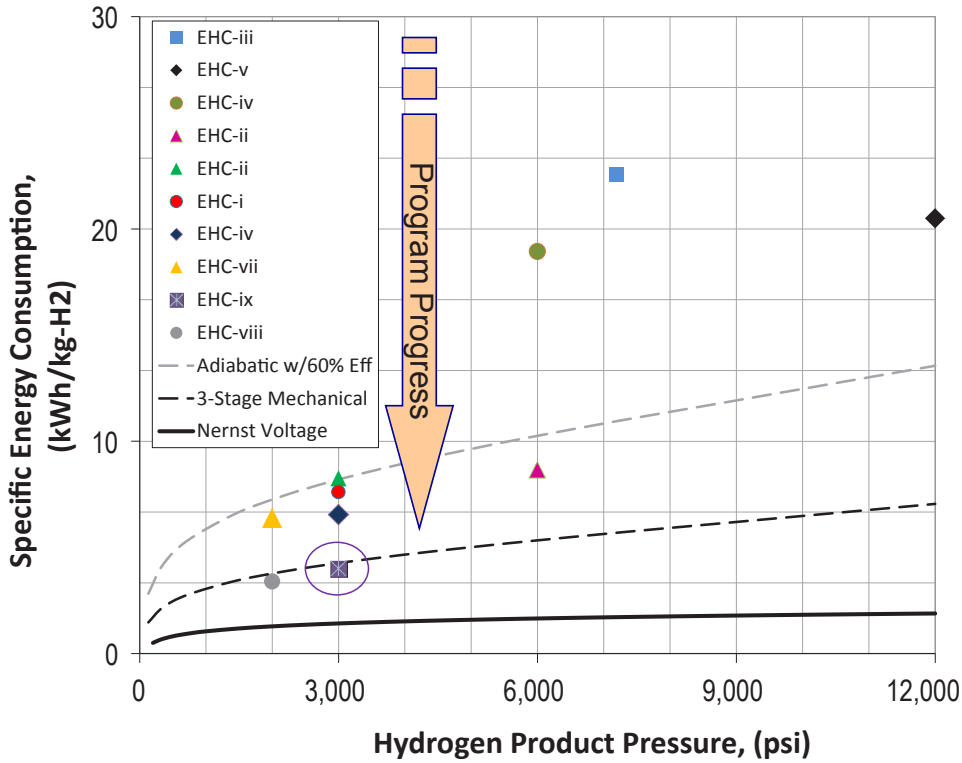

FIGURE 3. Reduced Specific Energy Consumption at 3,000 psi to <5 kWh/kg H_2

electrochemical compression. Therefore, emphasis was placed on endurance testing the EHC. A cell that began operation in FY 2012 continued to run in FY 2013, accumulating 10,000 hours of operation, as shown in Figure 4. Its hydrogen recovery was in excess of 95%. After initial fluctuations the cell performance was quite stable. Therefore, EHC is expected to be able to meet the DOE target for high compressor reliability.

CONCLUSIONS AND FUTURE DIRECTIONS

The EHC active area has been scaled up by >100%. Initial test data suggests the cell performance has been maintained in the scaled-up cell. The hydrogen flux through the EHC was increased by up to 3x, which translates to a lower capital cost. A >50% reduction in EHC cell part count also contributes to reduced cost. Durability of the EHC cell architecture has been demonstrated in a 10,000 hour test, confirming its robustness. The following summarizes critical performance parameters that were advanced during this reporting period:

Parameter	2012 Value	2013 Value
% of Original Part Count	80%	<50%
Current Density	1,200 mA/cm^2	2,200 mA/cm^2
Specific energy consumption at 3,000 psi	~8 kWh/kg	<5 kWh/kg
Endurance	6,000 hours	10,000 hours

Future efforts will include endurance testing of a 185-cm^2 EHC cell to fully validate successful active area scale-up. This will be followed by stack scale-up of the 185-cm^2 hardware to a short stack. This stack will be designed for a capacity of 2 lb/day H_2 at compression to 3,000 psi to meet the capacity objective of the project.

FY 2013 PUBLICATIONS/PRESENTATIONS

1. P. Patel and L. Lipp, "Electrochemical Hydrogen Compression (EHC)", DOE Hydrogen Compression, Storage and Dispensing Workshop, Argonne, IL, March 20, 2013.

2. L. Lipp, "Electrochemical Hydrogen Compressor", 2013 DOE Hydrogen Program Merit Review and Peer Evaluation Meeting, Arlington, VA, May 13–17, 2013.

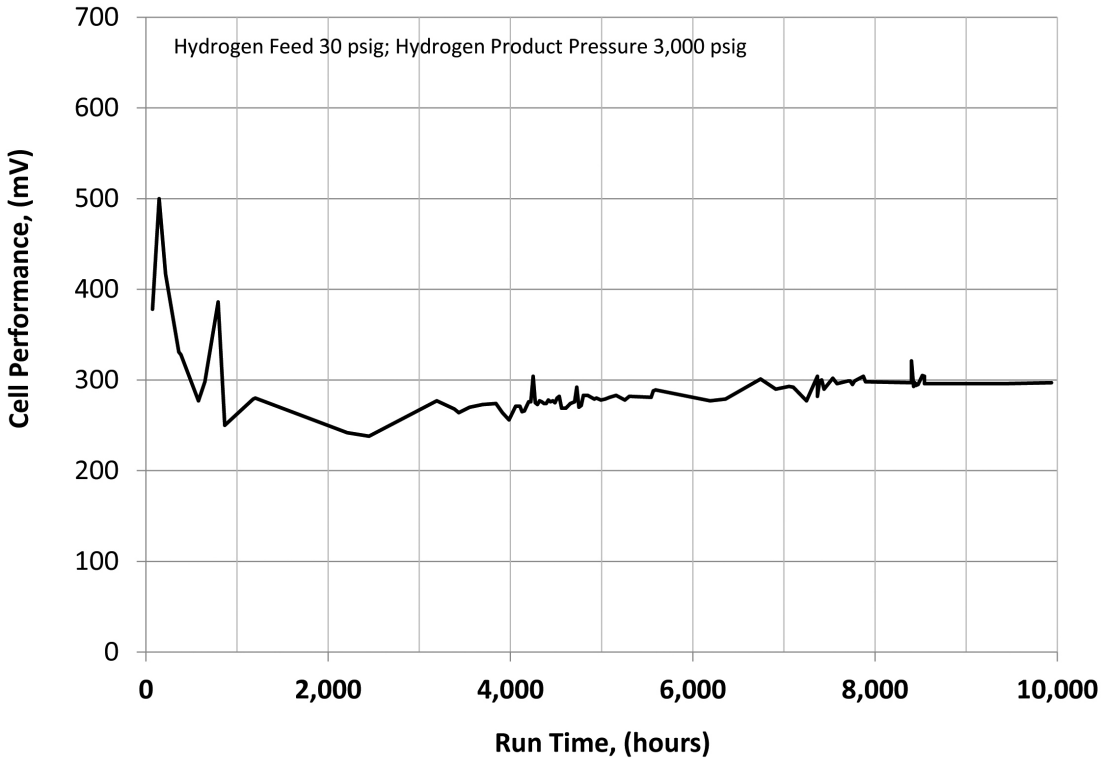

FIGURE 4. 10,000 Hour Endurance Demonstrated at >95% Hydrogen Recovery

REFERENCES

1. DOE Office of Energy Efficiency and Renewable Energy (EERE) Fuel Cell Technologies Office Multi-Year Research, Development and Demonstration (MYRD&D) Plan, Table 3.2.4 "Technical Targets for Hydrogen Delivery Components", section on Small Compressors, page 3.2-16.

III.7 Vessel Design and Fabrication Technology for Stationary High-Pressure Hydrogen Storage

Zhili Feng (Primary Contact), Fei Ren, Yanli Wang, Lawrence Anovitz and John Wang
Oak Ridge National Laboratory (ORNL)
1 Bethel Valley Rd, PO Box 2008, MS 6095
Oak Ridge, TN 37831
Phone: (865) 576-3797
Email: fengz@ornl.gov

DOE Manager
Erika Sutherland
Phone: (202) 586-3152
Email: Erika.Sutherland@ee.doe.gov

Subcontractors:
- Global Engineering and Technology LLC, Camas, WA
- Ben C. Gerwick Inc., Oakland, CA
- MegaStir Technologies LLC, Provo, UT
- University of Michigan, Ann Arbor, MI

Project Start Date: October 1, 2010
Project End Date: Project continuation and direction determined annually by DOE

Overall Objectives

- To address the significant safety and cost challenges in high-pressure stationary hydrogen storage technology
- To develop and demonstrate a novel steel/concrete composite vessel (SCCV) design and fabrication technology for stationary hydrogen storage systems

Fiscal Year (FY) 2013 Objectives

- Demonstrate the SCCV technology through design, engineering, analysis, and construction of a representative mock-up SCCV
- Determine the effectiveness of preventing hydrogen intake to mitigate hydrogen embrittlement of the layer steel vessel design
- Scale up the friction stir welding (FSW) process for thick-sectioned multiple layer vessel manufacturing

Technical Barriers

This project addresses the following technical barrier from the Hydrogen Delivery section (3.2.5) of the Fuel Cell Technologies Office Multi-Year Research, Development, and Demonstration Plan:

(E) Gaseous Hydrogen Storage and Tube Trailer Delivery cost

Technical Targets

This project aims at developing and demonstrating the novel design and fabrication technology for low-cost and high-safety SCCV for stationary gaseous hydrogen storage. The flexible and scalable composite vessel design can meet different stationary storage needs (e.g., capacity and pressure) at hydrogen fueling stations, renewable energy hydrogen production sites, and other non-transport storage sites. As shown in Table 1, the current generation composite vessel made using the existing design and manufacturing technology can readily exceed DOE's 2015 cost target. Moreover, with the successful development of advanced manufacturing technology such as the highly-automated FSW process, the next generation vessel has a high potential to meet DOE's 2020 capital cost target. Details of the cost analysis are given in [1].

TABLE 1. Progress towards Meeting Technical Targets for Stationary Gaseous H_2 Storage Tanks (for fueling sites, terminals, or other non-transport storage needs)

Pressure	DOE 2015 Target	Current SCCV	DOE 2020 Target	Next Generation SCCV
Low Pressure (160 bar) Purchased Capital Cost ($/kg of H2 stored)	$850	$681	$700	$652
Moderate Pressure (430 bar) Purchased Capital Cost ($/kg of H2 stored)	$900	$713	$750	$684
High Pressure (860 bar) Purchased Capital Cost ($/kg of H2 stored)	$1,200	$957	$1,000	$919

FY 2013 Accomplishments

- Completed detailed design and engineering of a ¼-sized mock-up composite SCCV capable of storing 90 kg gaseous hydrogen at 430 bar, and obtained vendors quotes from both steel vessel manufactures and concrete construction company.
- Demonstrated the effectiveness of the novel hydrogen mitigation technology to prevent hydrogen entering the structural steel layer. Achieved more than 95% reduction of hydrogen intake in the outer carbon steel layers when compared to the benchmark case without using the mitigation technology.

- Demonstrated superior mechanical properties with 0.6 inch thick multi-pass, multi-layer friction stir weld (MM-FSW) of A572 G50 steel. Multi-layered pipe structure was also fabricated by the MM-FSW technique. Scaling up MM-FSW to ASTM International (ASTM) SA724B steel intended for use in the ¼-sized mock-up is underway and expected to complete by the end of FY 2013.

✧ ✧ ✧ ✧ ✧

INTRODUCTION

Low-cost hydrogen delivery infrastructure is critical to successful market penetration of hydrogen-based transportation technologies, such as off-board bulk stationary hydrogen storage. Stationary storage is needed in many locations ranging from hydrogen production plants to refueling stations. The design capacity and pressure of the stationary storage vessel are expected to vary considerably depending on the intended usage, the location, and other economic and logistic considerations. For example, storage vessels at a hydrogen refueling station may have higher pressures but smaller storage capacity when compared to that at a renewable energy hydrogen production site. Therefore, it is important to make storage vessel design flexible and scalable in order to meet different storage needs. Moreover, as it provides the surge capacity to handle hourly, daily, and seasonal demand variations, the stationary storage vessel endures repeated charging/discharging cycles. Therefore, the hydrogen embrittlement in structural materials, especially the accelerated crack growth due to fatigue cycling, needs to be mitigated to ensure vessel safety. Therefore, safety and economics are two prevailing drivers behind the composite hydrogen storage technology.

In this project, ORNL leads a diverse multidisciplinary team consisting of industry and academia to develop and demonstrate an integrated design and fabrication technology for cost-effective high-pressure steel/concrete composite storage vessel that can meet different stationary hydrogen storage needs.

APPROACH

To address the cost and safety issues of current steel storage vessels, a SCCV concept is proposed, which features a multi-layer steel vessel surrounded by reinforced concrete. As illustrated in Figure 1, the shell section of the steel vessel is a layered structure. The innermost layer directly exposed to the high-pressure hydrogen is made of an austenitic stainless steel (e.g., AISI 316L or 304L), which excels as a hydrogen permeation barrier. The other layers are made of high-strength low alloy steel (e.g., ASTM SA724), which costs about four times less than stainless steel. The layered steel vessel technology is proven and accepted in industry standards and codes (e.g., American Society of Mechanical Engineers Boiler and Pressure Vessel Code). It has significant cost and safety advantages over the conventional single-section steel vessel. Moreover, the layered steel vessel is amiable to the advanced fabrication technology based on FSW for further reducing fabrication cost.

The steel vessel is encased in the pre-stressed concrete sleeve, which shares the structural loads with the steel inner vessel at an even lower cost when compared to structural steel. The optimal use of commodity materials (i.e., stainless steel, structural steel and concrete) is essential to the cost-effectiveness and safety of composite pressure vessel. Sensors will be embedded into both inner steel tanks and outer concrete sleeve to ensure the safe and reliable operation

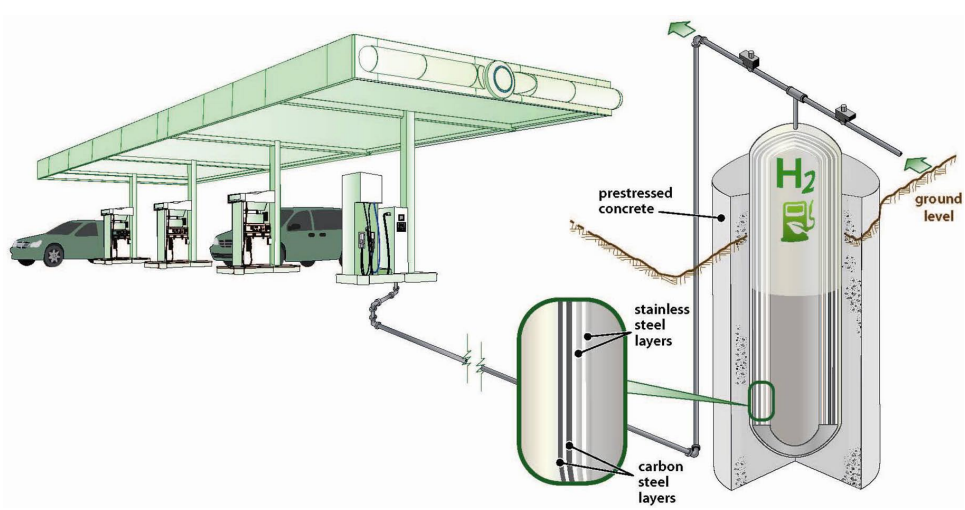

FIGURE 1. Schematic showing the design of a steel/concrete composite vessel comprising inner layered steel tanks and outer pre-stressed concrete confinement.

in field. The composite vessel shown in Figure 1 has the modular design with scalability and flexibility for meeting different storage pressure and capacity needs.

RESULTS

The major tasks in FY 2013 include: (1) engineering design of a 1/4 mock-up composite vessel and estimation of construction cost, (2) development of testing facility and evaluation of hydrogen permeation through multi-layered steel structures, and (3) demonstration of ORNL-patented MM-FSW for joining of thick steel sections. The key results from this year's substantial development are as follows.

Mock-up composite vessel design and construction:

The mock-up vessel has all the essential features and functionality of the full-size SCCV. It contains the inner steel vessel and the outer pre-stressed concrete reinforcement containment. The steel has a stainless steel inner layer as the hydrogen permeation barrier, hydrogen charging and discharging ports, and trunions for tank handling during the concrete construction and in-service installation. In addition, a manway on the top is added to the mock-up vessel, as it is an essential feature in the construction, inspection, and repair of the full-size steel vessel. The reinforcement skirt has a 6 inch-thick concrete layer and five layers of prestressing wires. This mock-up vessel is designed to store 89 kg of hydrogen compressed to 430 bar (6,250 psi, or 43 MPa), which is roughly ¼ of the full-scale vessel in terms of storage capacity (375 kg H_2 per tank at 430 bar). Figure 2 shows the completed engineering drawings of the mock-up vessel.

This mock-up SCCV will be constructed in two steps. The inner tank will be fabricated by a steel vessel manufacturer, and then transported to a construction company for concrete casting and reinforcing. The SCCV will then be transported and installed for testing. Initial manufacturing quotes have been received from vendors. Construction contracts will be released to the vendors in the fourth quarter of FY 2013.

Hydrogen permeation mitigation by multi-layered structure:

In order to evaluate the effectiveness of the hydrogen permeation mitigation concept, a special lab-scale high-pressure hydrogen permeation testing apparatus was designed and fabricated for this project. This apparatus made it possible to simulate the hydrogen permeation behavior through multi-layered steel structures under conditions similar to those expected in an SCCV. The testing system consisted of four layers of carbon steel. Each layer of the specimen was 3 mm in thickness. The specimen was placed inside a pressure vessel and maintained at a pressure about 2,000 psi. The diffusible hydrogen through these layers was measured using the technique described in [2] with 99.5%

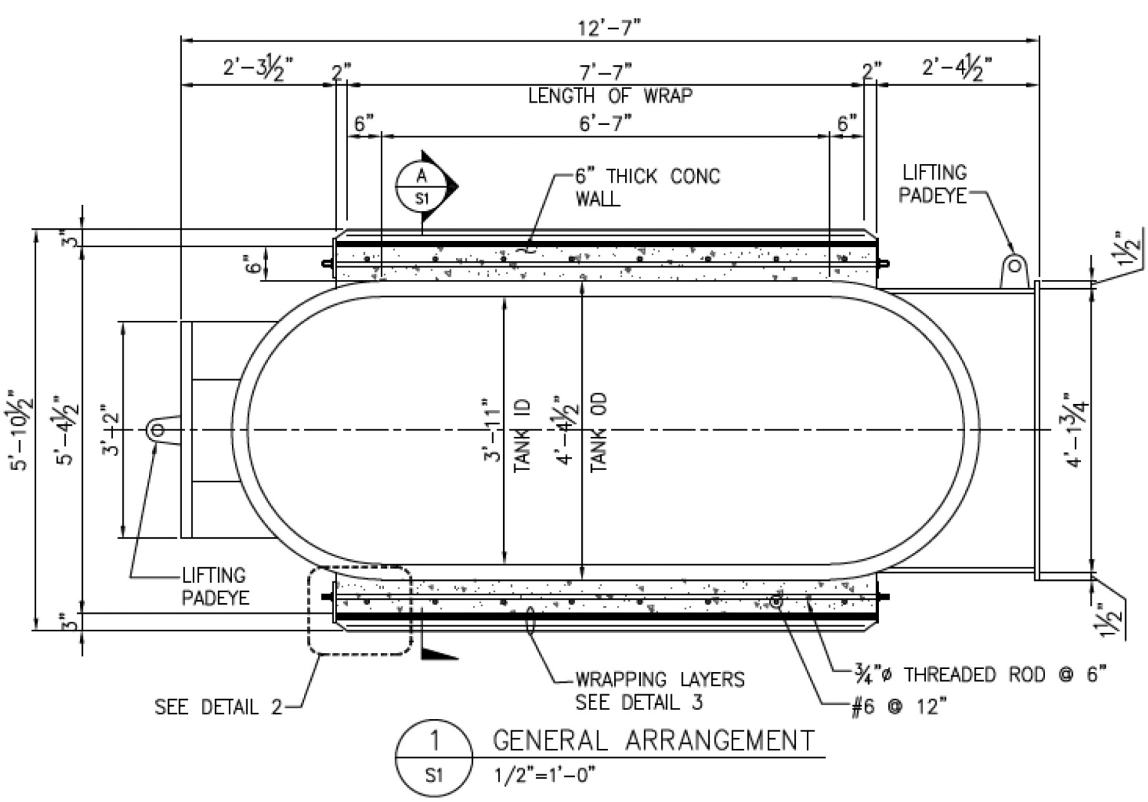

FIGURE 2. Engineering drawing of the ¼-sized mock-up SCCV.

pure glycerin. Initial testing at the ambient temperature (20°C) revealed that the hydrogen diffusion/permeation rate was extremely slow that meaningful experimental results would take months to obtain. In order to increase the hydrogen diffusion rate, a hot oil bath was used to heat up the entire experimental apparatus including the pressure vessel to 150°C.

The principle of the four-layer experimental design is shown in the insert of Figure 3. The high-pressure hydrogen (2,000 psi) permeating through the first layers (labeled as 1 and 4 in the insert) is recombined as H_2 molecules at the interface between the first layer and the second layer (which remains intimate contact under the high-pressure hydrogen) and escaped through the interface into the collecting points A and C. As in the case of the multi-layered vessel design, the collecting points effectively maintains at the pressure level of 1 atm (14.7 psi). As such, the second layers (labeled as 2 and 3 in the inset) are expected to experience a much reduced hydrogen pressure (thereby the amount of hydrogen permeated through) to avoid hydrogen embrittlement. The amount of hydrogen diffused through the second layer is measured at the collecting point B.

The quantitative measurement results along with the schematics of the specimen structure are shown in Figure 3. The hydrogen collection rate through the first layer was about 0.16-0.17 ml/in^2/hr at steady state. On the other hand, the collection rate significantly dropped to 0.0032-0.0058 ml/in^2/hr after the second layer, which is only about 3 percent of the permeation rate of the first layer. Therefore, we successfully demonstrated that the multi-layer steel vessel design is very effective in preventing the hydrogen permeation and mitigating hydrogen embrittlement.

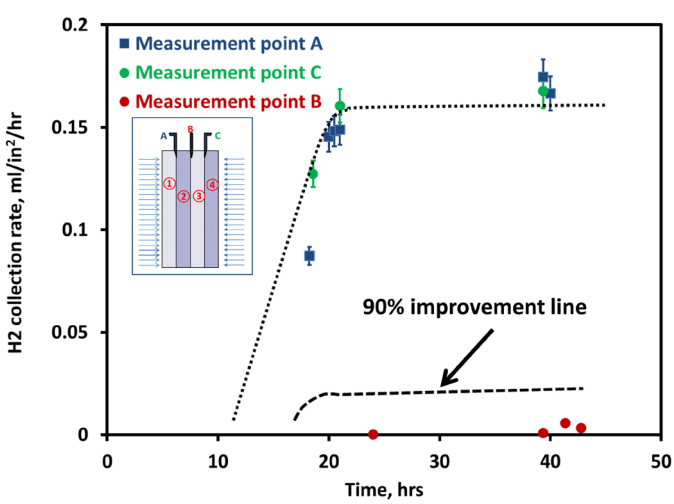

FIGURE 3. Measurements of the diffusible hydrogen through the layered structure (the insert schematic shows the layered experiment design)

Scale up demonstration of FSW technology:

A 15-mm-thick MM-FSW sample was fabricated using A572 G50 steel plates. Transverse tensile, Charpy V-impact toughness, and microhardness tests were performed. The details of the mechanical testing results and microstructure characterization are in Publication 2.

The average yield and ultimate tensile strengths of the weld material were 60 ksi and 76.3 ksi, respectively, which were comparable to the base metal. For all samples tested, the failure locations were in the base metal region of the transverse tensile specimen as shown in Figure 4, illustrated the superior strength of the weld region. Charpy V-impact test results show the toughness of the stir zone (SZ) and heat-affected zone (HAZ) were generally higher than the base metal, which can be related to the grain size of the SZ and HAZ. From scanning electron microscopy, the size of refined grains in SZ (ferrite and very small carbides inside ferrite) is less than 10 µm, while the grain size is more than 30 µm for the parent metal (mainly ferrite and small portion of pearlite). This grain refinement is typically observed in the SZ due to dynamic recrystallization during FSW. This observation can be related to the measured hardness of the SZ, HAZ, and base metal. Variations in hardness with grain size follow a Hall-Petch relationship [3]. With proven improvement in mechanical properties, MM-FSW technology is scaled up to fabricate 1.5 inch-thick multi-steel samples. Six layers of ¼-inch plates will be FSW and mechanical properties will be measured on this thick sample.

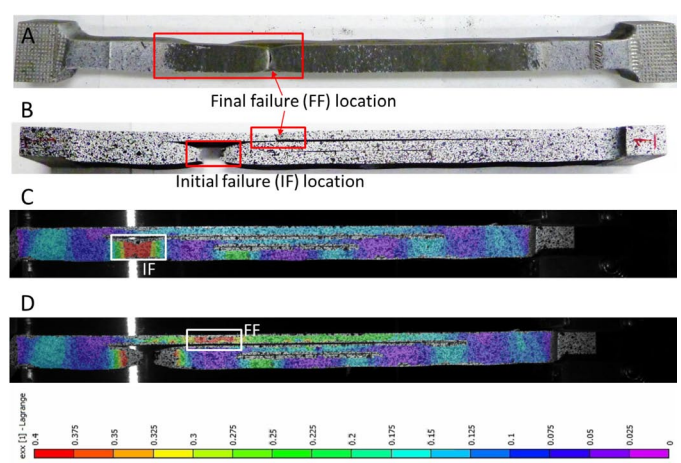

FIGURE 4. (a) Top view of the broken tensile specimen showing final failure location at top layer (b) Cross section view of tensile specimen showing initial and final failure locations after tensile test. (c) Digital image correlation image presenting strain level for the initial failure at middle and bottom layers. (d) Digital image correlation image displaying the strain map for the final failure at the top layer. Failure locations had high strain levels and both failure locations were found in the base metal.

CONCLUSIONS AND FUTURE DIRECTIONS

- A ¼-size mock-up composite vessel has been designed. Finite element analysis and design optimization are underway. Fabrication of the mock-up vessel is planned to start in FY 2014 and the completion date will be determined when the order is placed.
- The effectiveness of the hydrogen permeation mitigation using the multi-layered structure was experimentally shown to be more than 95%. The effectiveness of stainless steel inner layer as hydrogen permeation bearer will be performed in the future.
- Weld quality on the MM-FSW samples was proven to be superior to the base material. Multilayered pipe structure was manufactured by the MM-FSW technique. Thick MM-FSW samples are under fabrication and will be tested in the near future.

PATENTS ISSUED

1. US Patent No 8,453,515 "Apparatus and method for fatigue testing of a material specimen in a high-pressure fluid environment". Inventors: Jy-An Wang, Zhili Feng, Lawrence Anovitz, Ken Liu.

FY 2013 PUBLICATIONS/PRESENTATIONS

1. W. Zhang, F. Ren, Z. Feng, and J. Wang, "Design Analysis of Composite Vessel for High-Pressure Hydrogen Stationary Storage," Proceedings of the 2012 International Hydrogen Conference, Moran WY, Dec. 9–12, 2012.

2. Y.C. Lim, S. Sanderson, M. Mahoney, D. Qiao, Y. Wang, W. Zhang, and Z. Feng, "Mechanical properties and microstructure characterization of multilayered multipass friction stir steel weld," 2013 TMS Annual Meeting, San Antonio, TX, March 3–7, 2013.

3. W. Zhang, F. Ren, Z. Feng, and J. Wang, "Manufacturing Cost Analysis of Novel Steel/Concrete Composite Vessel for Stationary Storage of High-Pressure Hydrogen", Oak Ridge National Laboratory Report, ORNL/TM-2013/113, Oak Ridge National Laboratory, Oak Ridge, TN, Mar. 2013.

4. Z. Feng, F. Ren, W. Zhang, Y. Wang, Y.C. Lim, and J. Wang, 2013 DOE Annual Merit Review, Fuel Cell Technologies Program, Washington, DC, May 2013.

REFERENCES

1. W. Zhang, F. Ren, Z. Feng, and J. Wang, "Manufacturing Cost Analysis of Novel Steel/Concrete Composite Vessel for Stationary Storage of High-Pressure Hydrogen", Oak Ridge National Laboratory Report, ORNL/TM-2013/113, Oak Ridge National Laboratory, Oak Ridge, TN, Mar. 2013.

2. D.J. Ball, W. J. Gestal, Jr. and E.F. Nippes, "Determination of diffusible hydrogen in weldments by the RPR silicone-oil extraction method", *Welding Journal*, 1981, 50-s-56-s.

3. W.B. Lee, J.W. Kim, Y.M. Yeon, S.B. Jung, "Evaluation of the microstructure and mechanical properties of friction stir welded 6005 aluminum alloy," Mater. Sci. Technol. 19 (2003) 1513-1518.

III.8 Rapid High-Pressure Liquid Hydrogen Refueling for Maximum Range and Dormancy

Salvador M. Aceves (Primary Contact), Gene Berry, Francisco Espinosa-Loza, Guillaume Petitpas, Vernon Switzer
Lawrence Livermore National Laboratory (LLNL)
7000 East Avenue, L-792
Livermore, CA 94551
Phone: (925) 422-0864
Email: saceves@llnl.gov

DOE Manager
Erika Sutherland
Phone: (202) 586-3152
Email: Erika.Sutherland@ee.doe.gov

Subcontractors:
- Linde LLC, Hayward, CA
- Engineering, Procurement & Construction (EPC), Lakewood, CO

Start Date: October 1, 2009
Projected End Date: Project continuation and direction determined annually by DOE

Overall Objectives

- Demonstrate rapid refueling of cryogenic vessels
- Refuel cryogenic vessels even when warm and/or pressurized
- Refuel at high density (>80 kg H_2/m^3)

Fiscal Year (FY) 2013 Objectives

- Install liquid hydrogen pump
- Measure refuel performance

Technical Barriers

This project addresses the following technical barrier from the Hydrogen Delivery section of the Fuel Cell Technologies Office Multi-Year Research, Development, and Demonstration Plan:

(C) Reliability and Costs of Liquid Hydrogen Pumping

Technical Targets

The technical targets for this project are listed in Table 1.

FY 2013 Accomplishments

- Built and certified high-pressure fill hose
- Completed liquid hydrogen pump site construction and installation
- Operated pump and conducted 350 bar refuel experiments

✧ ✧ ✧ ✧ ✧

INTRODUCTION

Cryogenic pressure vessels have demonstrated the highest performance for automotive hydrogen storage, with density (43 g H_2/L), weight fraction (7.3%), cost ($11.3/kWh), and safety advantages (~8X lower expansion energy than compressed gas and secondary protection from vacuum jacket) [1,2]. Optimum refuel conditions are, however, still unknown. Today's hydrogen storage technologies (compressed and liquid hydrogen) operate at fixed temperature. Cryogenic pressure vessels, however, drift across the phase diagram depending on the level of use, cooling down and depressurizing when driven and heating up and pressurizing when parked. The challenge is demonstrating rapid, inexpensive refueling that maximizes driving range for typical utilization scenarios.

APPROACH

LLNL is researching a liquid hydrogen pump for cryogenic pressure vessel refueling. Manufactured by Linde, a leading supplier of cryogenic equipment, this pump takes liquid hydrogen at low pressure (near atmospheric) and delivers it at high pressure (up to 875 bar), high flow rate (100 kg/hour), low temperature (30-60 K), high density (>80 g/L), and low evaporative losses (less than 3% of

TABLE 1. Progress toward Meeting DOE Hydrogen Delivery Technical Targets for Liquid Hydrogen Pumps

Liquid hydrogen pumps				
DOE targets	FY 2011 status	FY 2015 target	FY 2020 target	LLNL Pressurized LH_2 pump
Uninstalled capital cost, $ (870 bar, 100 kg/hr)	-	150,000	150,000	1,300,000

LH_2 – liquid hydrogen

dispensed H_2). Pumped hydrogen can be directly dispensed into a cryogenic pressure vessel, even when warm and/or pressurized. In this project, LLNL has installed a liquid hydrogen pump and is planning to demonstrate its virtues for rapid and efficient cryogenic vessel refueling.

RESULTS

This year's LLNL effort was dedicated to installing and operating a high-pressure liquid hydrogen pump. The main activities necessary for pump construction and installation were as follows:

- Institutional permits—The initial phase of the work demanded obtaining institutional LLNL approvals. These approvals included environmental, facilities, and utilities.
- Utility planning—LLNL conducted a detailed study of different options to bring electric power to the site. It was finally decided that the most cost-effective option was an overhead power line into the site from a nearby (200 m) electric pole and a 500-kVA, 480-V transformer near the pump site. LLNL also analyzed options for bringing water and communication lines to the site and documented the best alternative in construction-ready drawings.
- Foundation calculations—In collaboration with Linde and EPC, LLNL calculated the necessary foundations for supporting both the pump and the Dewar. The resulting foundation design was documented into construction-ready drawings.
- Professional Engineer-stamped design package—In collaboration with EPC and Linde, LLNL produced a construction-ready design package consisting of about 30 drawings, including all the details for site construction (Figure 1).
- Foundation construction—Once the design package was complete, LLNL proceeded to build the foundation necessary for installing the pump and Dewar and for bringing the utilities. This was a major part of the construction effort, taking about two months.

FIGURE 1. Construction-ready liquid hydrogen pump site drawing including pictures of the main features and events leading to pump commissioning.

- Pump and Dewar installation—Once the foundation was built, the pump and Dewar were installed in place.
- Fencing and paving—The final stages of construction after pump installation included fencing around the pump and around the construction site as well as paving a 2,000 ft^2 access driveway enabling liquid hydrogen trucks to make site deliveries.
- High-pressure fill line design and construction—The LLNL contract with Linde does not include a dispenser. Instead, LLNL built a high-pressure flexible fill line rated for 875 bar for dispensing high-pressure hydrogen from the liquid hydrogen pump. This fill line is 3 meters long and was assembled by welding together three commercially available hose segments.
- High-pressure fill line qualification—The high-pressure flexible fill line was cryogenically pressure tested at liquid nitrogen temperature, demonstrating a safety factor greater than 4 (Figure 2) without bursting. Based on this experimental result and detailed documentation of strength calculations in a Lawrence Livermore Safety Note [3], the fill line was approved for operation at LLNL at pressures up to 875 bar.
- Installation of liquid hydrogen and cryogenic pressurized hydrogen tubes—Linde, in collaboration with LLNL, installed vacuum-jacketed tubes connecting the Dewar and the liquid hydrogen pump. They also installed the high-pressure pump outlet line up to the refuel point, as well as vent lines connecting all relief devices to the Dewar stack.
- Commissioning—In early July 2013, the pump was operated for the first time by Linde and LLNL. The pump demonstrated operation to 350 bar (the current pressure limit set by the existing LLNL experimental vessel).
- Authorities having jurisdiction authorization—TUV SUD, a nationally recognized test laboratory, reviewed and certified the pump electric system for safe operation. Based on this certification, LLNL electric authorities having jurisdiction authorized pump operation.
- High-pressure line insulation—The high-pressure pump outlet line was insulated with 5 cm of foam. Fittings remained uninsulated because these tend to loosen after several cold cycles. Full insulation will be applied in a few weeks after enough cold cycles are performed to avoid loosening of the fittings.

Once construction and commissioning was finalized, LLNL was able to start vessel refueling operations. LLNL has conducted 11 refuels at initial temperatures between 300 K and 20 K, dispensing around 70 kg of hydrogen into the existing 151-L, 350-bar cryogenic pressure vessel.

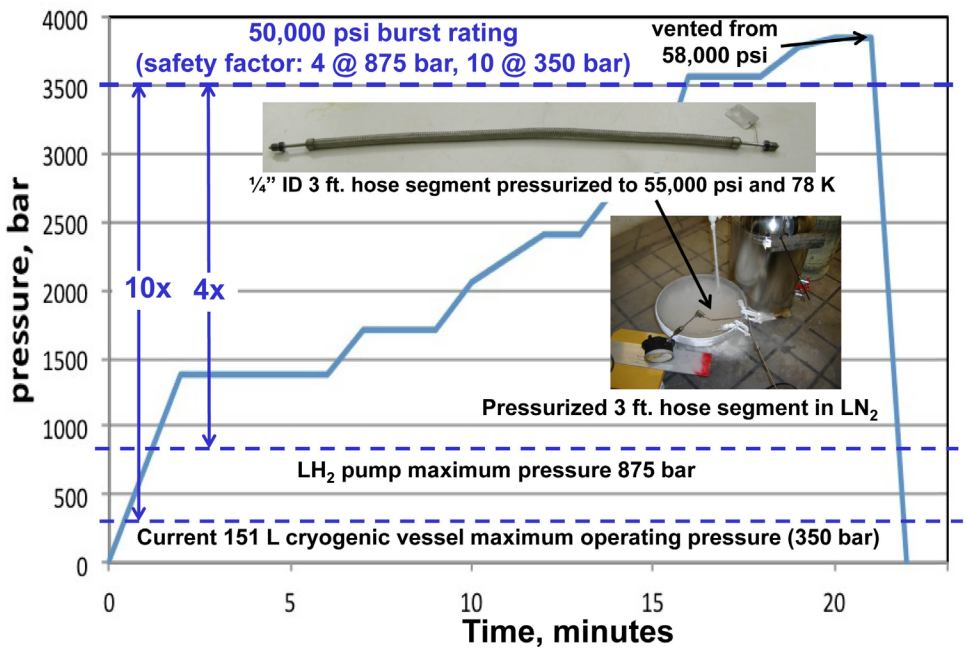

FIGURE 2. Pressure testing of cryogenic high-pressure fill line. A 3-ft long high-pressure line segment was tested while immersed in liquid nitrogen. The blue line shows pressure as a function of time during the 22-minute experiment. The target pressure (50,000 psi) was necessary for fill line certification at a safety factor of 4 over planned maximum working pressure of 875 bar. This safety factor was exceeded because the fill line was pressurized to 58,000 psi without failure.

The first step for conducting refueling experiments is precooling the high-pressure cryogenic pump outlet and flexible refuel line. Precooling was accomplished by running cryogenic hydrogen at a low flow rate for 12 minutes to reduce thermal shock and increase refuel density. This step would not be necessary in a fueling station where the line would remain cold due to frequent vehicle refuel operations.

Vessel refueling starts after precooling is concluded. Although the refueling time was quite short (~5 min), a waiting period was always held after each fill to make sure that vessel and hydrogen temperature equilibrated, thereby enabling accurate calculation of hydrogen refuel density. Including precooling, refueling, and equilibration time, each fill experiment takes about 90 minutes.

Analysis of pump refueling performance continues and demands calculation of the exact initial and final hydrogen density in the experimental 151-L cryogenic pressure vessel. Preliminary results (subject to change) indicate average total flow rate of at least 1.3 kg/min and electricity consumption between 1.3 and 1.5 kWh/kg. We anticipate that pump performance will improve when the high-pressure cryogenic pump outlet line is fully insulated.

CONCLUSIONS AND FUTURE DIRECTIONS

- Rapid, low-loss refueling of cryogenic vessels is possible through pressurized liquid hydrogen dispensing.
- LLNL installed a cryogenic high-pressure liquid hydrogen pump and Dewar and conducted preliminary refuel experiments to 350 bar.
- Further experiments are necessary to fully characterize pump performance to 350 bar with existing experimental vessel.
- Pump characterization to full pressure range (875 bar) will demand construction of a stronger experimental pressure vessel. This is planned for FY 2014-2015.

SPECIAL RECOGNITIONS & AWARDS/ PATENTS ISSUED

1. **Cryogenic Capable High Pressure Containers for Compact Storage of Hydrogen Onboard Vehicles,** Gene D. Berry, Salvador M. Aceves, Andrew H. Weisberg, Francisco J. Espinosa-Loza, Timothy O. Ross, European Patent EP 2,276,966, October 17, 2012.

FY 2013 PUBLICATIONS/PRESENTATIONS

1. Compact Hydrogen Storage in Cryogenic Pressure Vessels, Salvador M. Aceves, Francisco Espinosa-Loza, Elias Ledesma-Orozco, Guillaume Petitpas, in Handbook of Hydrogen Energy, Edited by S.A. Sherif, E.K. Stefanakos, and D.Y. Goswami, CRC Press, Taylor & Francis, ISBN-13: 978-1420054477, 2013.

2. **Hydrogen Storage in Pressure Vessels: Liquid, Cryogenic, and Compressed Gas**, Guillaume Petitpas and Salvador Aceves, in Hydrogen Storage Technology: Materials and Applications, Edited by Leonard E. Klebanoff, CRC Press, Taylor & Francis, Chapter 4, pp. 91-107, 2013.

3. **Cold Hydrogen Delivery in Glass Fiber Composite Pressure Vessels: Analysis, Manufacture, and Testing,** Andrew H. Weisberg, Salvador M. Aceves, Francisco Espinosa-Loza, Elias Ledesma-Orozco, Blake Myers, Brian Spencer, International Journal of Hydrogen Energy, Vol. 38, pp. 9271-9284, 2013.

4. **Modeling of sudden hydrogen expansion from cryogenic pressure vessel failure,** Petitpas, G. and Aceves, S.M., International Journal of Hydrogen Energy, Vol. 38, pp. 8190-8198, 2013**.**

5. **Web-Based Resources Enhance Hydrogen Safety Knowledge,** Weiner, S.C., Fassbender, L.L., Blake, C., Aceves, S.M., Somerday, B.P., and Ruiz, A., International Journal of Hydrogen Energy, Vol. 38, pp. 7583-7593, 2013.

6. **Safe, long range, inexpensive and rapidly refuelable hydrogen vehicles with cryogenic pressure vessels**, S.M. Aceves, G. Petitpas, F. Espinosa-Loza, M.J. Matthews, E. Ledesma-Orozco, International Journal of Hydrogen Energy, Vol. 38, pp. 2480-2489, 2013.

7. **Hydrogen Safety Training for Researchers and Technical Personnel,** Aceves, S.M., Espinosa-Loza, F., Petitpas, G., Ross, T.O., and Switzer, V.A., International Journal of Hydrogen Energy, Vol. 37, pp. 17497-17501, 2012.

8. **Vehicle refueling with liquid hydrogen thermal compression**, Guillaume Petitpas, Salvador M. Aceves, Nikunj Gupta, International Journal of Hydrogen Energy, Vol. 37, pp. 11448-11457, 2012.

REFERENCES

1. Aceves, S.M., Espinosa-Loza, F., Ledesma-Orozco, E., Ross, T.O., Weisberg, A.H., Brunner, T.C., Kircher, O., "High-density automotive hydrogen storage with cryogenic capable pressure vessels," International Journal of Hydrogen Energy, Vol. 35, pp. 1219-1226, 2010.

2. Ahluwalia, R.K., Hua, T.Q., Peng, J.-K., Lasher, S., McKenney, K., Sinha, J., Gardiner., M., "Technical assessment of cryo-compressed hydrogen storage tank systems for automotive applications," International Journal of Hydrogen Energy, Vol. 35, pp. 4171–4184, 2010.

3. Switzer, V., Aceves, S.M., "Cryogenic high pressure hydrogen refuel line," Mechanical Engineering Safety Note MESN 13-500008-AA, Lawrence Livermore National Laboratory, Livermore, CA, 2013.

III.9 Polymer and Composite Material Performance in Hydrogen

Christopher D. Moen
Sandia National Laboratories
P.O. Box 969
Livermore, CA 94551-0969
Phone: (925) 294-3709
Email: cmoen@sandia.gov

DOE Manager
Erika Sutherland
Phone: (202) 586-3152
Email: Erika.Sutherland@ee.doe.gov

Project Start Date: October 1, 2013
Project End Date: Project continuation and direction determined annually by DOE

Overall Objectives

- Identify knowledge gaps and data needs for using polymers and composite material systems in hydrogen service, particularly at high pressures (up to 100 MPa), demanding duty cycles, and long service life.
- Characterize failure mechanisms and discover mechanical behavior of polymer materials in high-pressure hydrogen gas at extreme temperature conditions.
- Place technical information in the hands of designers to positively impact performance, reliability, and safety.
- Participate in standards activities that concern the use of polymer materials and/or qualification of polymer materials.

Fiscal Year (FY) 2013 Objectives

Identify knowledge gaps and data needs for using polymers and composite material systems in hydrogen service, particularly at high pressures (up to 100 MPa), demanding duty cycles, and long service life.

Technical Barriers

This project addresses the following technical barriers from the Hydrogen Delivery section of the Fuel Cell Technologies Office Multi-Year Research, Development and Demonstration Plan:

(B) Reliability and Costs of Gaseous Hydrogen Compression

(E) Gaseous Hydrogen Storage and Tube Trailer Delivery Costs

(J) Hydrogen Leakage and Sensors

(K) Safety, Codes and Standards, Permitting

Technical Targets

This project is focused on improving the technical basis for selecting polymer materials for use in high-pressure hydrogen gas at extreme temperature conditions. Insights gained from these studies will be applied toward improving the performance, reliability, and safety of components that use polymer materials in compression, storage, dispensing, and vehicle fuel system applications, meeting the DOE 2015 hydrogen delivery targets:

- Aggregate fueling station cost: $1.60 gasoline gallon equivalent (centralized)
- Small compressor reliability: improved
- Small compressor maintenance: 2.5% of installed capital cost
- Uninstalled cost/dispenser: $40,000 at the design pressure specified, two hoses per dispenser (860 bar)

✧ ✧ ✧ ✧ ✧

APPROACH

While polymers and composites are currently used in fuel cell vehicle systems and fuel delivery and dispensing systems, designers and manufacturers continually look for ways to reduce costs through implementing new materials while improving safety, performance, and reliability. Designers and manufacturers typically seek chemical and mechanical characterization data for a material either to support direct implementation or to develop a more general performance-based standard that can then be used to qualify a class of materials.

This project supports the collection and generation of performance data for critical materials in hydrogen service and strives to fill knowledge gaps that would be most impactful. The learning that has been gained from similar DOE-sponsored research efforts is published in documents such as the Technical Reference on Hydrogen Compatibility of Materials, product standards, and peer-reviewed journal articles.

The first year of the project focused on knowledge gaps and data needs for understanding polymer behavior. Data needs were identified and validated through a series of information exchanges with industry stakeholders and literature survey.

ACCOMPLISHMENTS

The work product consists of a series of stakeholder meetings, literature reviews, and summary reports.

- Co-facilitated a panel session on *Assessing knowledge gaps for hydrogen vehicle and infrastructure codes and standards* at the August 2012 Composites Conference
- Facilitated an information-sharing meeting on the use of polymer and composite materials in hydrogen applications, October 17–18, 2012 [1]:
  - Identified knowledge gaps and data needs for using polymers and composite material systems in hydrogen service, particularly at high pressures (up to 100 MPa), demanding duty cycles, and long service life.
  - Provided important input to enable lower-cost, higher-performance systems through improved knowledge and revised codes and standards.
  - Informed testing needs to better enable near-term applications of polymers and composite systems in hydrogen service, including components at high pressure and extreme temperatures.
- Meeting participants identified material knowledge gaps in six different topical areas, motivated by safety, performance, and reliability concerns. The topical areas were:
  - Thermal performance of polymers at service conditions and impact of thermal excursions.
  - Evaluation and minimization of gas permeation and absorption into polymers.
  - Polymer performance characterization tests considering significant material variability.
  - Characterization and performance of seals and o-rings.
  - Liner buckling in pressure systems.
  - Low-cost composite material systems.
- Performed a literature review focused on the mechanical behavior (e.g. stress-strain, strength, ductility, fatigue resistance, failure) of polymer materials in hydrogen gas at extreme pressures and temperatures [2].
- Documented use-cases, available data, and data gaps for various polymer materials (to be completed by October 2013).

FUTURE DIRECTIONS

- Develop the capability to characterize mechanics and failure for polymers exposed to extreme conditions.
  - 100 MPa hydrogen exposure
  - -70°C to 120°C
- Execute characterization experiments for commonly used polymer materials that have insufficient performance data identified from FY 2013 and develop mathematical models of mechanical behavior.
- Disseminate research findings through publications and standards engagement.

FY 2013 PUBLICATIONS/PRESENTATIONS

1. "Polymer and composite materials used in hydrogen service", Polymer and Composite Materials Information Exchange Meeting Proceedings, SAND2012-10860P, Sandia National Laboratories, 2012.

2. Hecht, "Review on the effects of hydrogen pressure at extreme temperatures on polymer mechanics", SAND2013-2512, Sandia National Laboratories, 2013.

III.10 Development of a Centrifugal Hydrogen Pipeline Gas Compressor

Francis A. Di Bella, P.E.
Concepts ETI, Inc., d.b.a. Concepts NREC
285 Billerica Road, Suite 102
Chelmsford, MA 01824-4174
Phone: (781) 937-4718
Email: fdibella@conceptsnrec.com

DOE Managers
Erika Sutherland
Phone: (202) 586-3152
Email: Erika.Sutherland@ee.doe.gov
Katie Randolph
Phone: (720) 356-1759
Email: Katie.Randolph@go.doe.gov

Contract Number: DE-FG36-08GO18059

Subcontractors:
- Texas A&M University, College Station, TX
- HyGen Industries, Eureka, CA

Project Start Date: June 1, 2008
Project End Date: December 2013

Overall Project Objectives

- Develop and demonstrate an advanced centrifugal compressor system for high-pressure hydrogen pipeline transport to support DOE's strategic hydrogen economy infrastructure plan. Delivering 100,000 to 1,000,000 kg/day of 99.99% pure hydrogen gas from generation site(s) to forecourt stations at a compression ratio of 2.8 or greater. Reduce initial installed system equipment cost to less than $9 M (compressor package of $5.4 M) for 240,000 kg/day system.
- Reduce package footprint and improve packaging design.
- Reduce maintenance cost to below 3% of total capital investment. Increase system reliability to avoid purchasing redundant systems.

Fiscal Year (FY) 2013 Objectives

- Procure compressor components for one-stage prototype compressor
- Design control system and procure programmable logic controller and program
- Assemble prototype components
- Prepare test plan for prototype testing

Technical Barriers

This project addresses the following technical barriers from the Hydrogen Delivery (section 3.2) of the Fuel Cell Technologies Office Multi-Year Research, Development, and Demonstration Plan [1]:

(B) Reliability and Costs of Gaseous Hydrogen Compression

Technical Targets

The project has met the following targets as presented in DOE's 2007 Technical Plan for Hydrogen Delivery Projects [1] (Table 1).

In Summary: The original DOE proposal requirements were satisfied with the detailed design of a pipeline hydrogen compressor that utilizes all state-of-the-art and commercially available components, including high-speed centrifugal compressor, gearbox, intercooler, tilt-pad bearings, oil-free dry gas shaft seal, and controls. The testing of the prototype hydrogen compressor system will quantify these design objectives.

TABLE 1. Progress towards Meeting Technical Targets for Delivery of Hydrogen via Centrifugal Pipeline Compression

Characteristic	Units	DOE Target	Project Accomplishment	STATUS
Hydrogen Efficiency (f)	[btu/btu]	98%	98%	Objective Met
Hydrogen Capacity (g)	kg/day	100,000 to 1,000,000	240,000	Objective Met
Hydrogen Leakage (d)	%	< .5	0.2 (per Flowserve Shaft Seal Spec)	Objective Met
Hydrogen Purity (h)	%	99.99	99.99 (per Flowserve Shaft Seal Spec)	Objective Met
Discharge Pressure (g)	psig	>1000	1285	Objective Met
Comp. Package Cost (g)	$M	6.0 +/- 1	4.5 +/- 0.75	Objective Met
Main. Cost (Table 3.2.2)	$/kWhr	0.007	0.005 (per *CN* Analysis Model)	Objective Met
Package Size (g)	sq. ft.	350 (per HyGen Study)	260 (per *CN* Design)	Objective Met
Reliability (e)	# Sys.s Req.d	Eliminate redundent system	Modular sys.s with 240K kg/day with no redundency req.d	Objective Met

Note: Letters correspond to DOE's 2007 Technical Plan-Delivery Sec. 3.2-page 16

Results of Research Development: A pipeline-capacity, hydrogen centrifugal compressor can be made available now to meet the hydrogen economy needs of the future!

Accomplishments for Phases I and II (completed from 2008 to 2011) and Phase III (in progress)

Developed computer models to aid in analysis of hydrogen compressor:

- System Cost and Performance Model
  - Identifies hydrogen compressor package performance and component cost with respect to a variety of compressor-gearbox configurations
- System Reliability and Maintenance Cost Model
  - Estimates comparative reliabilities for piston and centrifugal compressors for pipeline compressors developed
    - Failure mode and effects analysis for component risk and reliability assessment
  - Estimates operation and maintenance costs for compressor system
    - Uses Federal Energy Regulatory Commission operation and maintenance database as the basis for determining the maintenance costs for a centrifugal compressor
- Anti-surge algorithm developed to assist in controls analysis and component selection of preliminary design (completed) and detailed design of pipeline compressor module (in progress), including:
  - Compressor design conditions confirmed by project collaborators
    - P_{inlet} = 350 psig, P_{outlet} = 1,250 psig; flow rate = 240,000 kg/day
    - A six-stage, 60,000 revolutions per minute (rpm), 3.6 (max) pressure ratio compressor with a mechanical assembly of integrally geared, overhung compressor impellers
    - Stress analysis completed
    - Volute (compressor housing) design in progress for two-stage prototype
    - Rotordynamics completed to verify shaft-seal-bearing integrity at operating speeds
- Completed critical component development (compressor rotor, shaft seal, bearings, gearing, safety systems) and specifications for near-term manufacturing availability
- Completed detailed design and cost analysis of a complete pipeline compressor and a laboratory-scale prototype for future performance lab verification testing
- Completed a one-stage laboratory prototype compressor system to verify mechanical integrity of major components at full power ratings per stage
- Procuring system components for one-stage prototype compressor

✧ ✧ ✧ ✧ ✧

INTRODUCTION

The DOE has prepared a Multi-Year Research, Development, and Demonstration Plan to provide hydrogen as a viable fuel for transportation after 2020, in order to reduce the consumption of limited fossil fuels in the transportation industry. Hydrogen fuel can be derived from a variety of renewable energy sources and has a very high energy content per kg, equivalent to the energy content in a gallon of gasoline. The switch to hydrogen-based fuel requires the development of an infrastructure to produce, deliver, store, and refuel vehicles. This technology development is the focus of the Hydrogen Production and Delivery sub-programs within the DOE. Pipeline transport of the hydrogen from the production sites to the population centers can reduce the costs of hydrogen delivery at market volumes. The cost to deliver the hydrogen resource to the refueling stations contributes to the cost per kg or per gasoline gallon equivalent (gge) that needs to be charged for the hydrogen fuel. Therefore, it is necessary that the cost to deliver the hydrogen be reducd, which implies that the cost of the compressor stations, their installation costs, and their efficiency in pumping the hydrogen fuel to the refueling stations must be reduced as well in order to meet the ultimate hydrogen delivery cost target of $2/gge (2040 goal).

The delivery cost target can be met if the compressor system can be made more reliable (to reduce maintenance costs), more efficient (to reduce operation costs), and be a smaller, more complete modular package (to reduce the compressor system equipment, shipment, and installation costs). To meet these goals, the DOE has commissioned Concepts NREC with the project entitled: The Development of a Centrifugal Hydrogen Pipeline Gas Compressor.

APPROACH

A three-phase approach has been programmed to implement the technical solutions required to complete a viable hydrogen compressor for pipeline delivery of hydrogen. The three phases include: Phase I-Preliminary Design, Phase II-Detailed Design of both a Full-Scale and Prototype Hydrogen Compressor, and Phase III-The Assembly and Testing of the Prototype Compressor.

The technical approach used by Concepts NREC to accomplish these goals is to utilize state-of-the-art aerodynamic/structural analyses to develop a high-

performance centrifugal compressor system for pipeline service. The centrifugal-type compressor is able to provide high pressure ratios under acceptable material stresses for relatively high capacities—flow rates that are higher than what a piston compressor can provide. Concepts NREC's technical approach also includes the decision to utilize commercially available, and thus proven, bearings, shaft seal technology, and high-speed gearing to reduce developmental risk and increase system reliability at a competitive cost.

The engineering challenge to implement this technical approach is to design a compressor stage that can achieve the highest compression ratio and thermodynamic efficiency, while also minimizing the number of stages and the impeller diameter. Ultimately, the major constraint is imposed by the limitations of the maximum stress capability of impeller material. This constraint is further aggravated by the need for the material selection to consider the effects of hydrogen embrittlement on the strength of the material. The selection of a rotor material that can enable the high tip speeds to be achieved while avoiding damage from hydrogen embrittlement was determined to be the major technical challenge for the project.

The Concepts NREC design is projected to meet all of these engineering challenges in order to provide a pipeline compressor system that meets DOE's specifications for near-term deployment.

The project team includes researchers at Texas A&M, led by Dr. Hong Liang, who are collaborating with Concepts NREC to confirm the viability of aluminum alloys for this compressor application. Also assisting with a collegial collaboration of suggestions are several national laboratories, including Sandia National Laboratories (fracture mechanics testing; Dr. Chris San Marchi), Savannah River National Laboratory (specimen "charging" with hydrogen plus tensile testing with H_2; Dr. Andrew Duncan and Dr. Thad Adams), and Argonne National Laboratory (Dr. George Fenske).

RESULTS

The engineering analysis has resulted in the design of the pipeline compressor package shown in Figure 1. The complete modular compressor package is 29 ft long x 10 ft tall x 6 ft wide at the base x 8 ft wide at the control panel, approximately one-half of the footprint of a piston-type hydrogen compressor.

The compressor selection uses six stages, each operating at 60,000 rpm, with a tip speed of less than 2,100 ft/s. Each compressor rotor and drive shaft is 8 inches in diameter and has an overall stage efficiency of between 79.5 and 80.5%, for an overall compressor isentropic efficiency of 80.3%. The first and last stages have a slightly different length, which helps to improve the rotordynamics for the

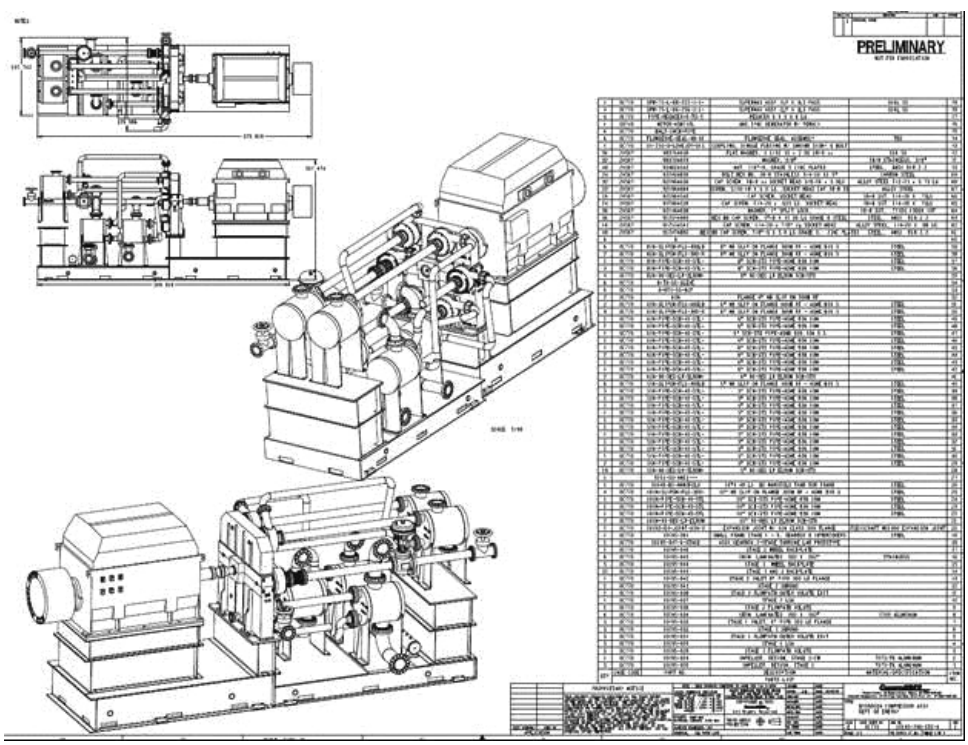

FIGURE 1. Pipeline Hydrogen Centrifugal Compressor: 240,000 kg/day; 350 to 1,285 psig

last stages. Each compressor impeller is a single, overhung (cantilevered) impeller attached to a drive shaft that includes a shaft seal, bearing, and drive pinion (Figure 2) integrated with the gearbox drive. The impeller rotor is designed without a bored hub, in order to reduce the hub "hoop" stresses. This requires the impeller to be mechanically attached to the high-strength steel alloy, a drive shaft with a patented design attachment system that enables the rotor to be removed from the gearbox without removing the drive shaft, so it does not disturb the shaft seal and bearings. A gas face seal will provide the isolation of the hydrogen from the lubricating oil. The 1,400 hp per stage can be sustained by using two tilting pad hydrodynamic bearings on either side of a 2.5-inch-long drive-pinion gear. The face seal and bearings are commercially available from Flowserve and KMC, respectively. The pinion and bull gear is part of a custom gearbox manufactured by Artec Machine Systems representing NOVAGEAR and utilizes commercially available gear materials that are subjected to stresses and pitch line speeds that meet acceptable engineering practice.

The material chosen for the compressor rotor and volute is an aluminum alloy: 7075-T6 alloy. The choice is based on its mechanical strength-to-density ratio or (S_{yield}/ρ), which can be shown to be a characteristic of the material's ability to withstand centrifugal forces. This aluminum alloy has a strength-to-density ratio that is similar to titanium and high-strength steels at the 140°F (max) operating temperatures that will be experienced by the hydrogen compressor. However, unlike titanium and most steels, aluminum is recognized by the industry as being very compatible with hydrogen.

Aluminum also helps to reduce the weight of the rotor, which leads to an improved rotordynamic stability at the 60,000 rpm operating speed. A rotor stability and critical speed analysis has confirmed that the overhung design is viable. The first stage compressor rotor has been manufactured and successfully spun to 110% of its 60,000 rpm operating speed. A subsequent fluorescent penetrant inspection and strain measurements of the rotor after the spin test indicated no creep or micro-crack design flaws as a result of the test.

The one-stage prototype compressor has been chosen for laboratory testing in Phase III of the project. The laboratory prototype is shown in Figures 3 and 4. The compressor components are being manufactured, and the balance of the system components are being purchased. The system will be assembled and tested starting in 2013 and will be completed in early 2014.

CONCLUSIONS AND FUTURE DIRECTIONS

The advanced, six-stage, intercooled, centrifugal compressor-based system can provide 240,000 kg/day of hydrogen from 350 to 1,280 psig (6,300 kWe) for pipeline-grade service. The original DOE proposal requirements were satisfied with the detailed design of a pipeline hydrogen compressor that utilizes all state-of-the-art and commercially available components, including high-speed centrifugal compressor, gearbox, intercooler, tilt-pad bearings, oil-free dry gas shaft seal, and controls. As a result of the sponsored research and development, a pipeline-capacity, hydrogen centrifugal compressor has been designed to meet the high volume hydrogen markets using commercially available, state-of-the-art components!

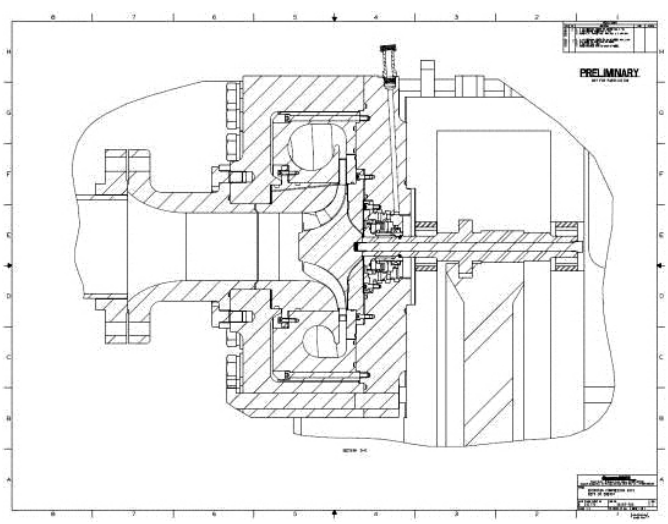

FIGURE 2. Mechanical Detailed Assembly of One-Stage, Prototype Compressor

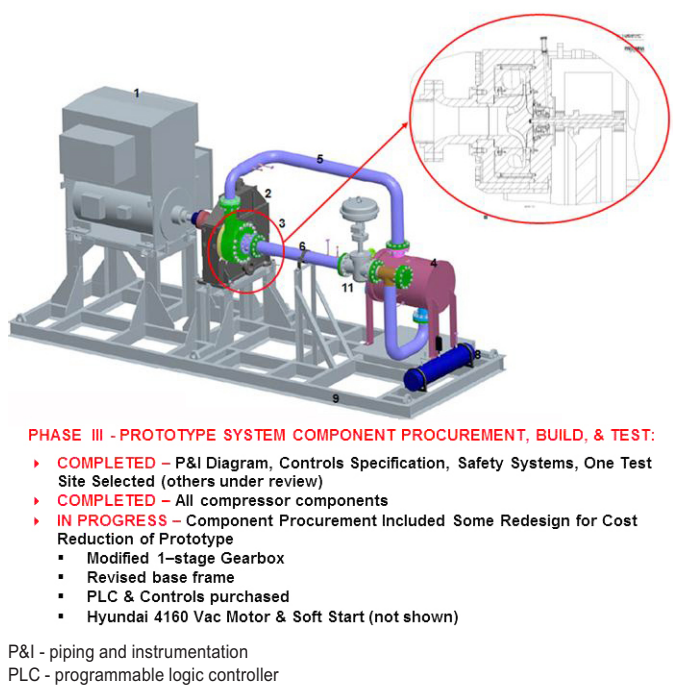

FIGURE 3. Detailed Specification for the One-Stage Prototype Compressor

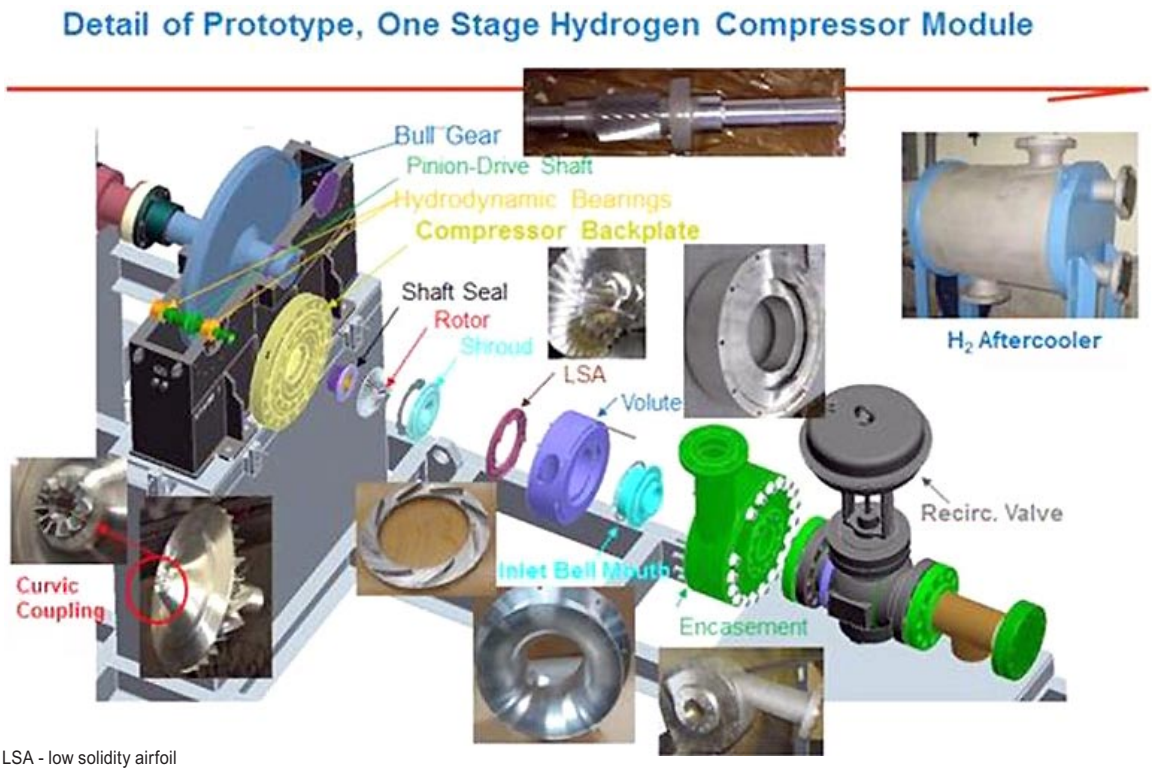

LSA - low solidity airfoil

FIGURE 4. Detail of Prototype, One-Stage Hydrogen Compressor Module

Objectives for This Year

Phase III System Component Procurement, Construction, and Validation Testing

- Continue component procurement for the one-stage prototype hydrogen compressor system
- Assemble the one-stage centrifugal compressor system
- Conduct aerodynamic testing and assessment of mechanical integrity of the compressor system
- Prepare a plan for placement of the prototype compressor for continued testing, including deployment at an industrial gas user or a university research laboratory

SPECIAL RECOGNITIONS AND AWARDS/ PATENTS ISSUED

Patent application filed on several innovations for centrifugal compressor design; filed March 2010 (provision file March 2009: SN 60/896985): "Centrifugal Compressor Design for Hydrogen Compression."

FY 2013 PUBLICATIONS/PRESENTATIONS

1. "Development of a 240,000 kg/day Hydrogen Pipeline Centrifugal Compressor for the Department of Energy's Hydrogen Delivery and Production Program," IMECE2012-88965.

REFERENCES

1. DOE Fuel Cell Technologies Office Multi-Year Research, Development, and Demonstration Plan.

III.11 Investigation of H_2 Diaphragm Compressors to Enable Low-Cost Long-Life Operation

Aashish Rohatgi (Primary Contact) and Ken Johnson
Pacific Northwest National Laboratory (PNNL)
902 Battelle Blvd.
Richland, WA 99352
Phone: (509) 372-6047
Email: aashish.rohatgi@pnnl.gov

DOE Manager
Erika Sutherland
Phone: (202) 586-3152
Email: Erika.Sutherland@ee.doe.gov

Project Start Date: June 1, 2013
Project End Date: September 30, 2013

Overall Objective

Reduce compressor operation and maintenance cost by reducing instances of diaphragm failure and the resulting need for repair of hydrogen gas compressors

Fiscal Year (FY) 2013 Objectives

- Identify the causes for the reduced lifetime of the diaphragm compressors operated under start-stop mode
- Develop material and compressor design solutions to enhance the lifetime of diaphragm compressors

Technical Barriers

This project addresses barriers "B" and "O" from the Hydrogen Delivery section of the Fuel Cell Technologies Office Multi-Year Research, Development, and Demonstration Plan:

(B) Reliability and Costs of Gaseous Hydrogen Compression

(O) Lack of Reliable Hydrogen Compressors

Technical Targets

This project is conducting research to decrease compressor operation and maintenance costs by improving the reliability of hydrogen compressors. Understandings gained from this work will be applied to future compressors to enable them to meet DOE 2015 compressor targets:

- 2.5% of installed capital cost for maintenance
- Improved reliability and life

INTRODUCTION

The goal of this project is to reduce the instances of diaphragm failures and the resulting need for repair of hydrogen gas compressors. Achieving this goal will help enable economical operation of hydrogen vending stations in support of DOE's goal of developing a hydrogen distribution network. For this project, PNNL has partnered with PDC Machines, Inc., a leader in hydrogen compressor technology, to develop materials and engineering solutions to the problem of repeated breakdown of hydrogen compressors. The team will investigate the diaphragm failures through materials characterization and modeling and identify diaphragm materials, compressor design, and operational procedures that will increase the life of diaphragms, especially under intermittent operation.

Short life of the diaphragms subjected to intermittent operation of the compressors is a key hurdle in developing an economical hydrogen distribution network. This hurdle exists because the repair costs and the downtime associated with repeated compressor breakdown may substantially increase the costs for fueling stations to serve as hydrogen vendors for hydrogen fuel cell vehicles. Consequently, there is a need to enhance the life of hydrogen compressors and enable a successful establishment of a wide-spread hydrogen distribution network via the existing gas stations and establishment of new stations.

APPROACH

PDC Machines, Inc. will share with PNNL its data and operation experience on compressor performance. Based on the data provided by PDC Machines, Inc., PNNL will perform an engineering analysis to systematically understand the diaphragm performance under different operating regimes. This analysis will include finite element models to understand the evolution of stresses and strains in the diaphragm leading to its final failure. Fatigue analysis will also be performed for the different operating cycles and the combined mechanical plus residual stress levels using the available fatigue curves for the alloys of interest. The microstructure of the diaphragm materials will be analyzed with special attention to the role of texture (anisotropy) and presence of residual stresses. Fractographic analysis of the failed diaphragms will be performed to help identify the failure mode, failure origin and eventually, the possible causes of the failure. Thus, the approach outlined in the preceeding will help us understand how the interplay

of the compressor design, operational procedures, and microstructure-dependent deformation behavior of the diaphragm may be controlled to enhance the diaphragm life.

ACCOMPLISHMENTS

This project was developed in conjunction with PDC Machines, Inc., a commercial supplier of diaphragm hydrogen compressors and has benefitted greatly from their assistance, both technical and material. The company provided detailed drawings of compressor designs (output H_2 pressures of 6,500 and 15,000 psi), diaphragm materials, as well as technical details that need to be considered when designing and operating diaphragm compressors. Using the compressor design and operational information provided by PDC Machines, Inc., PNNL developed a preliminary finite element model using ANSYS software to understand the diaphragm deformation and stresses as a function of gas compression. Materials characterization effort was also initiated using the diaphragm materials provided by PDC Machines. This involved surface characterization via roughness and residual stress measurements, microstructure characterization using optical and electron microscopy and fracture surface analysis using electron microscopy. On the basis of work performed to date and discussions with PDC Machines, Inc., the project accomplishments are:

- Contamination/debris in the H_2 gas and improper priming procedures when restarting a compressor after stopping have been identified as two important factors that adversely affect the life of the diaphragm. Figure 1 shows a picture of a used PDC diaphragm that was taken out of service owing to cracking. The diaphragm shows the ring of black deposit, suspected to be a cause in reducing the diaphragm life and generated by the impurities in the incoming H_2 gas.
- A finite element model of the diaphragm was developed and used to predict the location on the diaphragm where maximum contact sliding occurs relative to the compressor process head (see Figure 2). This location is close to the ring of black deposit in Figure 1, which could potentially be a site for fretting damage and subsequent failure, especially in the presence of any debris. It is pointed out that this result is consistent with the location of actual failures observed in the diaphragms of PDC's compressors.
- Initial examination of the cracked diaphragm showed the primary crack was approximately perpendicular to the radial direction, suggesting that radial stresses played a role in the diaphragm failure. Multiple cracks were also observed adjacent to the primary crack and at places the top surface of the diaphragm appeared to stretch across the primary crack, suggesting significant plastic deformation associated with the failure (see Figure 3).

Additional analysis of the diaphragm behavior via finite element modeling and microstructural examination is underway. Therefore, this project has enabled us to begin developing a fundamental understanding of design, materials and operational issues that affect the diaphragm life. We anticipate that this partnership and information and knowledge exchange between the industry and a national laboratory will be critical in helping DOE achieve its targets

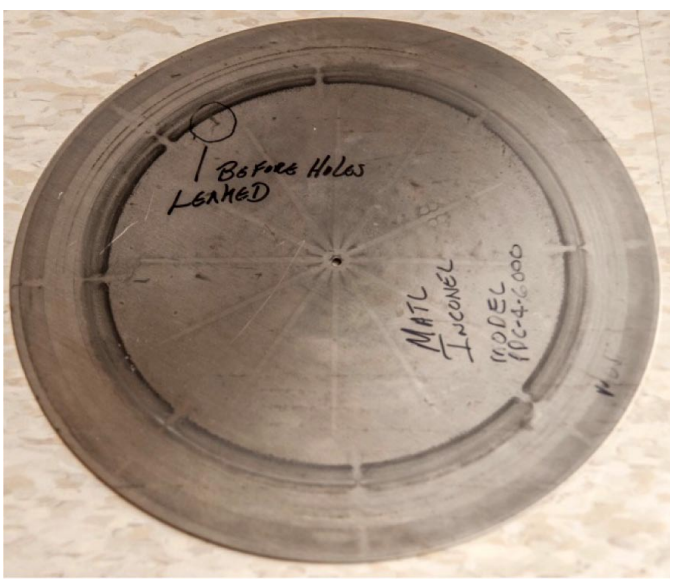

FIGURE 1. Picture of a PDC diaphragm taken out of service, showing the ring of black deposit suspected to be a cause in reduced diaphragm life. The location of the crack, where the diaphragm leaked, is circled with a black marker.

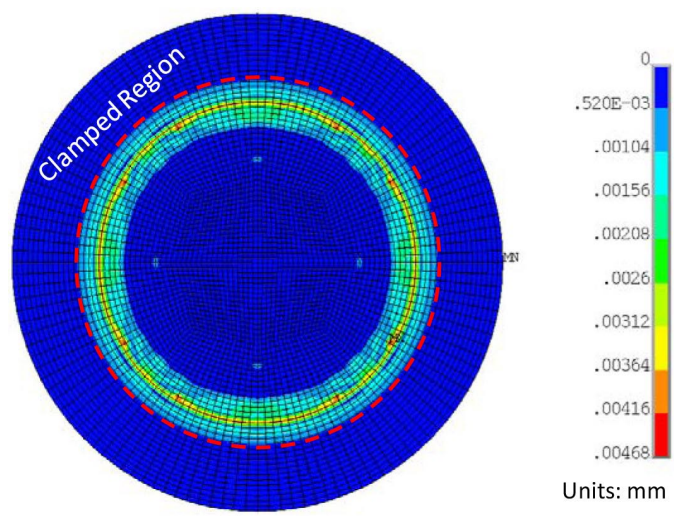

FIGURE 2. Finite element model predicted relative sliding between the diaphragm and the process head. The yellow contour band indicates the radial location of maximum sliding, which coincides with the ring of black deposit in Figure 1.

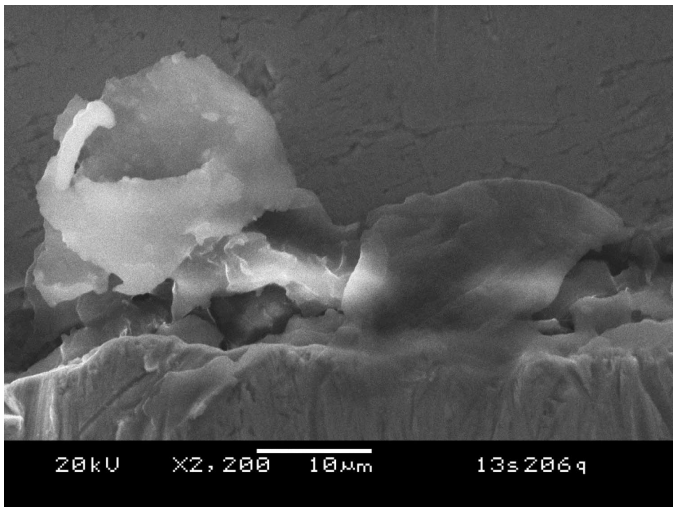

FIGURE 3. A scanning electron microscope image of a portion of the crack (from diaphragm shown in Figure 1) showing a thin layer of the diaphragm material "bridging" the primary crack, as well as numerous small surface cracks formed in the material adjacent to the crack.

for improving compressor reliability, increase diaphragm life and reduced maintenance costs.

FUTURE DIRECTIONS

The following are three potential areas for further research to enable long life for H_2 compressors:

- Understanding the role of diaphragm microstructure in controlling its operational life.
- Design tools for evaluating interactions between compressor design, fluid flow, and diaphragm response.
- Effect of impurities and debris on fatigue life of the diaphragm.

FY 2013 PUBLICATIONS/PRESENTATIONS

1. DOE July 2013 Milestone Report
2. DOE August 2013 Milestone Report
3. Project Review technical presentation to PDC Machines, Inc.
4. Project Review technical presentation to Fuel Cell Technology office, DOE

IV. HYDROGEN STORAGE

IV.0 Hydrogen Storage Program Overview

INTRODUCTION

The Hydrogen Storage program supports research and development (R&D) of materials and technologies for compact, lightweight, and inexpensive storage of hydrogen for automotive, portable, and material handling equipment (MHE) applications. The Hydrogen Storage program has developed a two-prong strategy, with a near-term focus on improving performance and lowering the cost of high-pressure compressed hydrogen storage systems and a long-term focus on developing advanced cold/cryo-compressed hydrogen storage systems and materials-based technologies for hydrogen storage.

In Fiscal Year (FY) 2013, the program focused on development of lower cost precursors and fillers for carbon fiber composites to lower the cost of high-pressure compressed hydrogen systems, system engineering for transportation applications, and continued R&D efforts in materials-based storage including metal hydrides, chemical hydrogen storage materials, and hydrogen sorbents.

GOAL

The program's goal is to develop and demonstrate commercially viable hydrogen storage technologies for transportation, portable power, and MHE applications.

OBJECTIVES[1]

The Hydrogen Storage program's objective regarding light-duty vehicles is to provide sufficient onboard hydrogen storage to allow for a driving range of more than 300 miles (500 km), while meeting packaging, cost, safety, and performance requirements to be competitive with current vehicles. Although some fuel cell electric vehicles (FCEVs) have been demonstrated to travel more than 300 miles on a single fill using high-pressure tanks, this driving range must be achievable across the full range of vehicle models without compromising space, performance, or cost.

By 2017, the program aims to develop and verify onboard automotive hydrogen storage systems achieving the following targets that will allow some hydrogen-fueled vehicle platforms to meet customer performance expectations:

- 1.8 kWh/kg system (5.5 wt%),
- 1.3 kWh/L system (0.040 kg hydrogen/L), and
- $12/kWh ($400/kg stored hydrogen capacity)

The following ultimate targets are intended to facilitate the introduction of hydrogen-fueled propulsion systems across the majority of vehicle classes and models. Advanced storage materials and concepts will be needed to meet the 2017 and ultimate targets.

- 2.5 kWh/kg system (7.5 wt%),
- 2.3 kWh/L system (0.070 kg hydrogen/L), and
- $8/kWh ($266/kg stored hydrogen capacity)

[1] Note: Targets and milestones were recently revised; therefore, individual project progress reports may reference prior targets.

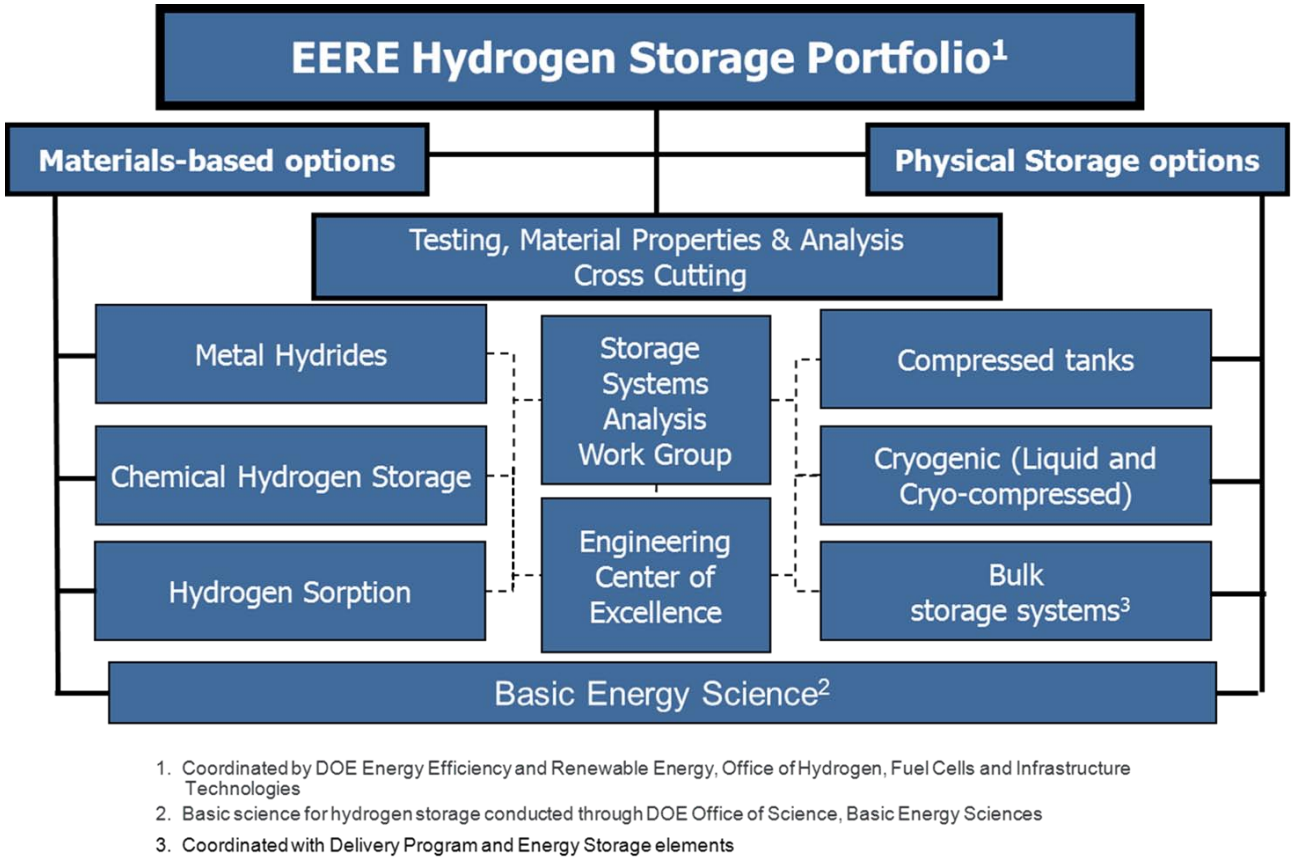

FIGURE 1. The EERE Hydrogen Storage Portfolio of Technologies and their Interrelationships

FY 2013 STATUS

The Hydrogen Storage program has developed comprehensive sets of hydrogen storage targets for onboard automotive, portable power, and MHE targets. The targets can be found in the *Multi-Year Research Development and Deployment Plan* (MYRD&DP). The status of the various storage technologies pursued is evaluated through analysis within individual projects, but also through independent analysis carried out through the program.

In the near-term, automotive companies plan to commercialize FCEVs that use compressed hydrogen systems onboard, with system cost being one of the most important challenges to commercialization. The program, working with automotive original equipment manufacturers through the U.S. DRIVE Partnership, established onboard automotive hydrogen storage system cost targets of $12/kWh of usable stored hydrogen to be reached by 2017, with $8/kWh of usable storage hydrogen as an Ultimate Full Fleet target. In 2013 Strategic Analysis Inc. (SA), working with Argonne National Laboratory (ANL) and the National Renewable Energy Laboratory (NREL), completed a thorough cost analysis for baseline Type IV 350 and 700 bar compressed hydrogen storage systems, for both single- and multi-tank configurations. The cost analysis used a Design for Manufacturing and Assembly (DFMA®) methodology and included considerable input from appropriate stakeholders. A complete description of the methodology, key assumptions and results, along with a performance analysis by ANL, has been published in program data record 13010: *Onboard Type IV Compressed Hydrogen Storage Systems – Current Performance and Cost*.[2] Figure 2 shows the projected variable volume manufacturing costs for 700 bar, Type IV onboard system with a 5.6 kg hydrogen usable capacity and includes the component breakdown costs. Current high volume costs are projected to be approximately 50% and 100% higher than the 2017 and Ultimate Full Fleet targets, respectively.

2 DOE Fuel Cell Technologies Office Record 13010: *Onboard Type IV Compressed Hydrogen Storage Systems – Current Performance and Cost* [http://hydrogen.energy.gov/pdfs/13010_onboard_storage_performance_cost.pdf].

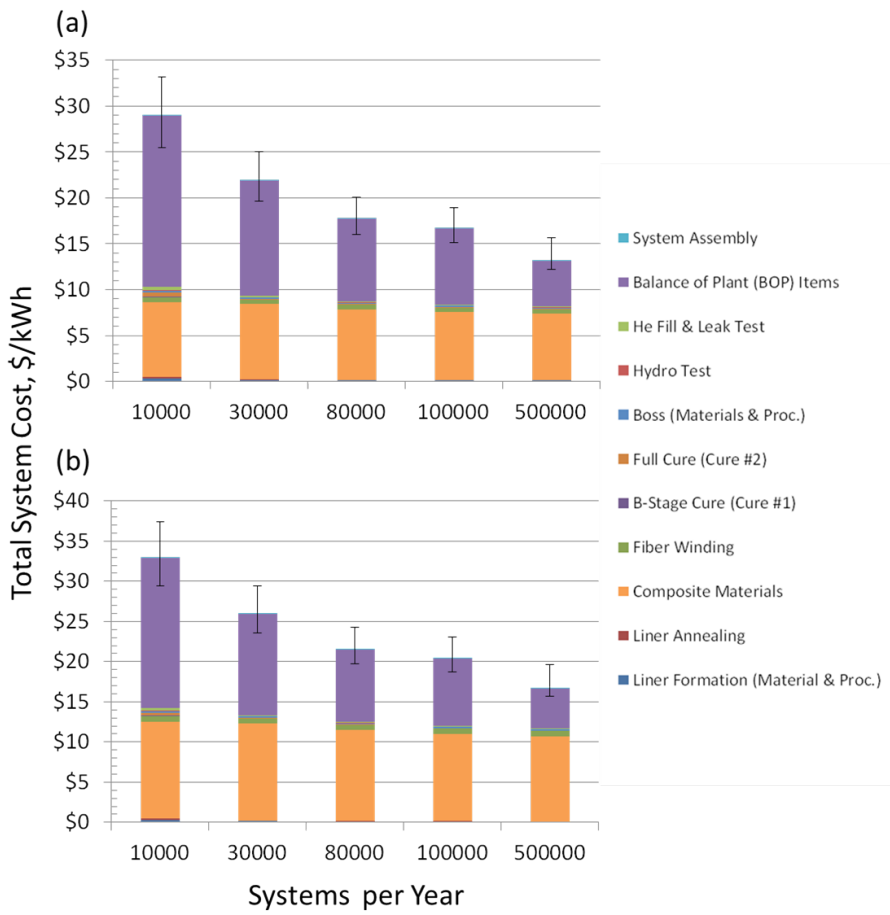

FIGURE 2. Projected costs in 2007$, at various annual manufacturing volumes, for (a) 350 bar and (b) 700 bar compressed hydrogen storage systems, sized to deliver 5.6 kg of hydrogen to the vehicle fuel cell powerplant. Cost analysis performed by SA in 2013.

As a longer-term strategy, the Hydrogen Storage program continues to pursue less mature hydrogen storage technologies that have the potential to satisfy all onboard hydrogen storage targets. These technologies include cold (temperatures as low as ~150-200 K) and cryo–compressed (temperatures <150 K) hydrogen and materials-based storage technologies. The materials-based efforts include total systems engineering and hydrogen storage materials discovery, including adsorbents, metal hydrides, and chemical hydrogen storage materials. A major effort in this area the last several years has been through the Hydrogen Storage Engineering Center of Excellence (HSECoE). In 2013 the HSECoE completed Phase II and is transitioning into Phase III – sub-scale system prototype development and evaluation. As part of the Phase II-III transition decisions, a thorough review of the projected status of both system performance and material availability was carried out. Figure 3 compares the modeled systems performance at the end of Phase I and Phase II for the sorbent and chemical systems, respectively. Neither system is projected to meet the program targets for onboard hydrogen storage with currently available materials. However, these efforts are able to help define the material properties that are needed for a complete system to meet the targets. The results will be used to help guide future hydrogen storage material development efforts. For Phase III of the HSECoE efforts, the decision was made to continue only with the sorbent system prototypes. This decision was partially based on the fact that neither of the two primary chemical hydrogen storage materials investigated by the HSECoE, namely ammonia borane (NH_3BH_3) and alane (AlH_3), are widely available in bulk nor is there a low-cost, energy-efficient process available for their regeneration. Therefore, it was decided to not continue towards sub-scale system prototype evaluation until materials are available that are projected to be low-cost and are able to be efficiently regenerated.

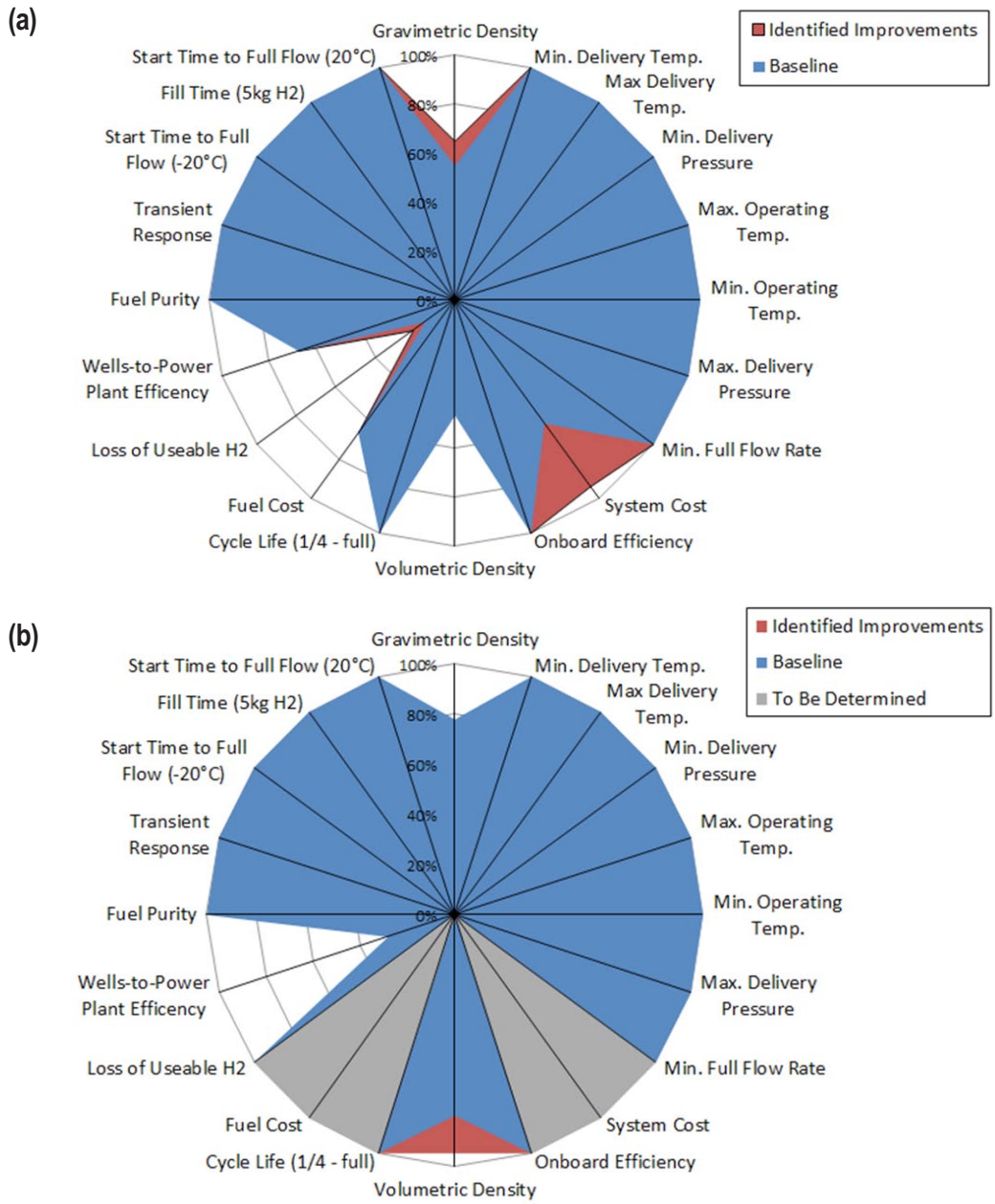

FIGURES 3a and 3b. Status of projected sorbent (3a) and chemical hydrogen storage (3b) system performance versus 2017 onboard system targets. Note that the systems were sized to provide 5.6 kg of usable hydrogen. Blue areas indicate projected status at end of Phase I, red areas indicate identified improvements as of the end of Phase II, and the grey areas indicates performance metrics which still must be determined.

Advanced Materials Development

In FY 2013 the program continued efforts in developing and improving hydrogen storage materials with potential to meet the 2017 onboard storage targets in addition to the 2015 portable power and MHE targets. In the area of metal hydrides, efforts emphasized material discovery coupled with reducing desorption temperatures and improving kinetics. For chemical hydrogen storage materials, much of the focus was on developing reversible or regenerable liquid phase materials, such as slurries or solutions, and also increasing efficiency of regeneration routes for solid-phase materials. For hydrogen sorbents, efforts were focused on increasing the isosteric heat of adsorption mainly through metallization to increase the adsorbed capacity at higher temperatures and improving standard measurement practices for hydrogen capacity. Also in FY 2013, the Hydrogen Storage program maintained efforts to collect and

disseminate materials data on advanced hydrogen storage materials that comprise the hydrogen storage materials database (http://hydrogenmaterialssearch.govtools.us/).

- Developed an ad hoc working standard of an activated-carbon material to test instrumentation and measurement protocols for hydrogen capacity. (NREL)
- Demonstrated direct spectroscopic evidence of a reversible room temperature sorption/desorption from a unique C-H interaction via diffuse reflectance infrared Fourier transform spectroscopy and neutron scattering. (NREL)
- Identification of a higher performance Liquid Organic Carrier, butylperhydropyrolidine, that undergoes pincer complex catalyzed dehydrogenation at practical turnover rates at 140ºC (Hawaii Hydrogen Carriers, LLC)
- Demonstrated regeneration of $LiAlH_4$ electrolyte material for electrochemical formation of alane and identified diglyme as an inexpensive additive to increase rate (3X) and efficiency of alane production (Savannah River National Laboratory, SRNL)

Engineering

In FY 2013, the HSECoE completed assessment of hydrogen storage systems for cryo-sorbents and liquid-phase off-board regenerable chemical hydrogen storage material systems which allowed the HSECoE to successfully transition from Phase II into Phase III. Assessments included model validation through component level testing and tradeoff analyses that compared novel system designs and candidate storage materials. Based on these results, the center chose to terminate work on chemical hydrogen storage material systems and focus Phase III efforts on cryo-sorbent systems based on a metal organic framework (MOF)-5 material. The Phase III evaluations will include designing, constructing, and testing subscale prototype concepts such as the Hexcel and modular adsorbent tank insert heat exchanger designs.

- Completed assessment of chemical hydrogen storage materials and systems and will terminate work on these systems due to low probability of identifying materials that meet 8.5 wt% fluid gravimetric requirements and regeneration efficiencies. Developed a 6 wt% H_2 liquid phase chemical hydrogen storage media having a viscosity before and after dehydrogenation below 1,500 cP. (HSECoE)
- Developed an ammonia scrubber resulting in a minimum ammonia outlet concentration of 0.1 ppm/v (inlet concentration = 500 ppm/v) having a maximum mass of 1.2 kg and a maximum volume of 1.6 liters. (HSECoE)
- Completed assessment of adsorbent system and downselected both the Hexcel and modular adsorbent tank insert heat exchanger designs for subscale prototype adsorbents systems to be evaluated in Phase III. (HSECoE)
- Completed cryogenic pressure vessel burst testing of Type I (all metal) and IV (composite overwrapped) tanks. Tanks burst at 77 K and pressures above the design limits, proving the efficacy of both types of tanks at cryogenic temperatures. (Hexagon Lincoln)
- Demonstrated an internal flow-through heat exchanger system based on compacted media capable of allowing less than 3-minute scaled refueling time and hydrogen release rate of 0.02 $g_{hydrogen}$/(sec-kW) with a mass less than 6.5 kg and a volume less than 6 liters. (SRNL)
- Developed an adsorbent acceptability envelope that identifies coupled material properties and system dimensions that affect gravimetric and volumetric capacity, charging, and discharging rates. (SRNL)
- Completed costing of 135 cryo-sorbent tanks configurations and identified a 100-bar, Type I vessel with MOF-5 as the lowest cost option. (Pacific Northwest National Laboratory, PNNL)
- Identified balance-of-plant components for a cryo-sorbent hydrogen storage system with a total mass of less than 9.4 kg and volume of less than 11.6 L exceeding the system targets of 17 kg and 18.5 L (PNNL)
- Completed fabrication and testing of a microchannel combustor/heat exchanger to provide hydrogen preheating in an adsorption hydrogen storage system. (Oregon State University)

Advanced Physical Storage

In FY 2013, the program continued to reduce the cost of compressed hydrogen gas storage tanks with efforts focused on low-cost, high-strength carbon fiber and advanced tank designs. Lightweight compressed gas storage vessels requiring a composite overwrap to contain hydrogen gas are considered the most likely near-term hydrogen storage solution for the initial commercialization of FCEVs, as well as for other early market applications. Carbon

fiber composite overwraps can currently contribute as much as 75% or more to the overall cost of advanced Type IV tanks. The Hydrogen Storage program supported efforts at Oak Ridge National Laboratory (ORNL) to reduce the cost of polyacrylonitrile-based (PAN) fibers used as precursors to produce high-strength carbon fibers. The ORNL efforts focused on advanced precursor materials and processing since precursors have been shown to contribute approximately 50% of the total cost of high-strength carbon fibers. The team investigated the use of low-cost textile-grade fibers made from PAN blended with a methyl acrylate comonomer (PAN-MA) as lower cost precursors and continued to improve on the development of melt-spinnable PAN precursors and processing techniques to replace the current more costly wet processing methods. Additionally, a team lead by PNNL, focused on reducing the cost of a Type IV tank system by developing novel alternative resins and resins matrix modification, modifying the carbon fiber surface to improve composite translational efficiency, developing methods for alternative fiber placement and enhanced operating conditions that demonstrated routes to increase carbon fiber usage efficiency. Two new Small Business Innovation Research (SBIR) Phase I awards were made that focused on alternative fiber placement and novel resin modifications to reduce the usage of carbon fiber in Type IV tanks. Through an SBIR Phase II project, Applied Nanotech, Inc. continued the development of lightweight, high-strength carbon nanotube reinforced composite overwraps to reduce the cost of tanks.

- Downselected to a single PAN-MA precursor fiber composition and refined the conversion protocol to achieve a 35% improvement in tensile strength (405 ksi) and 10% improvement in tensile modulus (33 Msi) compared to 2012 results. (ORNL)
- Improved spinning and drawing equipment and developed and implemented processes for producing sample quantities of melt-spun PAN-MA precursor that achieved the Go/No-Go milestone of 150 ksi tensile strength and 15 Msi tensile modulus. (ORNL)
- Demonstrated strategies to reduce the cost of pressure vessels by 15% through modeling and material testing consisting of:
  - Testing properties of low-cost resins (4% cost reduction)
  - Testing properties of additives to enhance resin properties (5% cost reduction)
  - Modeling to demonstrate alternative fiber placement and fiber types (6% cost reduction) (PNNL)

Testing & Analysis

In FY 2013, the Hydrogen Storage program continued carrying out assessments of hydrogen storage technologies and to disseminate proper hydrogen storage material testing and characterization procedures to evaluate material/system performance against requirements of hydrogen fuel cell applications. Technical analysis and cost modeling of Type IV pressure vessel systems remained a critical focus during FY 2013, with a baseline cost and validation of the performance costs with tank manufacturers' data.

- Refined the ABAQUS finite-element model of carbon fiber filament wound Type IV vessel for hydrogen storage at 350 and 700 bar. Calibrated and validated the ABAQUS model against other models based on modified netting analysis and transfer functions derived from data supplied by tank manufacturers. (ANL)
- Formulated models and performed reverse engineering to determine thermodynamic and kinetic properties of metal hydride materials needed to meet system targets and compared to metal hydride acceptability envelope developed by the HSECoE. (ANL)
- Updated DFMA® cost analysis and validated key performance parameters for pressure vessels based on discussions with industry, the U.S. DRIVE Partnership Hydrogen Storage Tech Team, the Storage System Analysis Working Group, ANL, PNNL, HSECoE, and project collaborators where the key parameters included (1) the composite fiber and resin masses as a function of tank capacity, (2) fiber and resin material costs, and (3) cost of the balance-of-plant components. (SA)
- Completed cost analysis of the off-board regeneration of spent ammonia borane and alane slurries for use by the HSECoE. (SA)
- Updated, completed, and posted online Section 6: Thermal Properties of the Best-Practices Document on the Characterization of Hydrogen Storage Materials[3]. (Hydrogen Technology Consulting through NREL)

[3] http://www1.eere.energy.gov/hydrogenandfuelcells/hydrogen_publications.html#h2_storage

BUDGET

$17.5 million from the President's FY 2014 budget request is planned for hydrogen storage—compared with $16.2 million from the FY 2013 congressional appropriation. In FY 2014, the Hydrogen Storage program will continue to focus on nearer-term R&D to lower the cost of high-pressure storage systems and longer-term technology development including cold/cryo-compressed hydrogen and materials discovery and system engineering for materials-based storage technologies. The program will also continue to carry out systems analyses. The program plans to initiate new activities in these areas for onboard automotive and non-automotive applications.

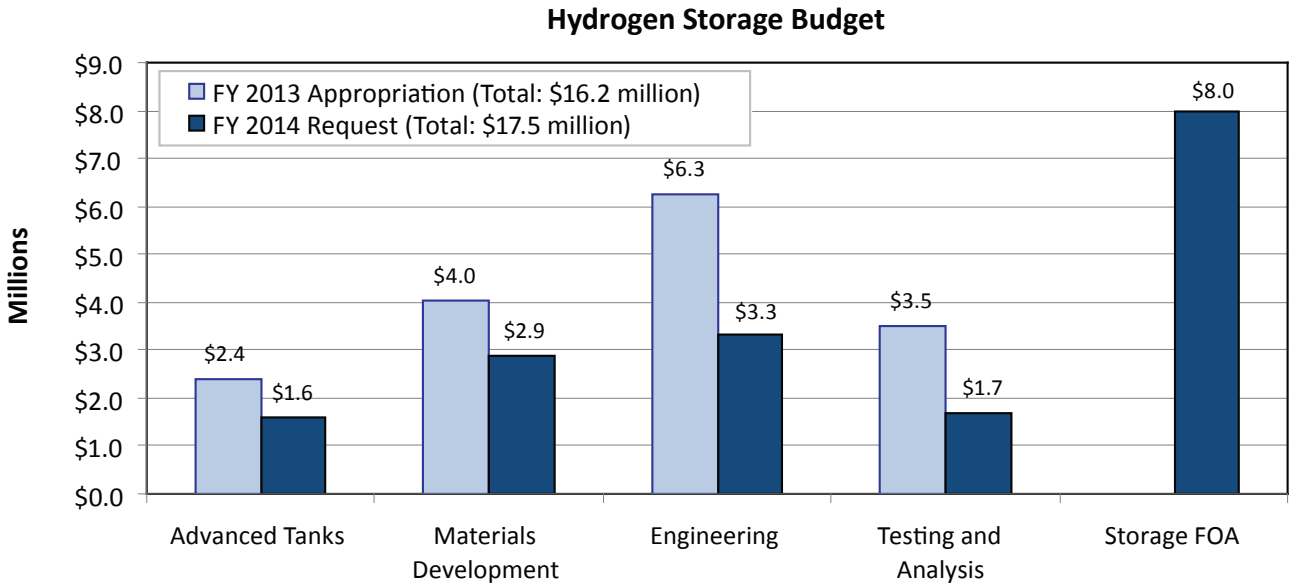

FY 2014 PLANS

The technology portfolio for Hydrogen Storage emphasizes materials R&D to meet system targets for onboard automotive and non-automotive applications. While a focus on light-duty vehicle applications will continue, increased emphasis will be placed on new materials and novel concepts to meet performance requirements for portable power and material handling equipment applications. The increased emphasis on developing lower-cost physical storage technologies will continue to be expanded. Specifically, the program will coordinate with and leverage other efforts (e.g., Advanced Manufacturing, Vehicle Technologies, DARPA, etc.) to develop approaches to produce low-cost carbon fiber for composite cylinders. System engineering and analysis will continue through the HSECoE, ANL, and SA. Coordination with basic science efforts, including theory, characterization, and novel concepts, will continue during FY 2014.

Ned Stetson
Hydrogen Storage Team Lead
Fuel Cell Technologies Program
U.S. Department of Energy
1000 Independence Ave., SW
Washington, D.C. 20585-0121
Phone: (202) 586-9995
Email: Ned.Stetson@ee.doe.gov

IV.A.1 System Analysis of Physical and Materials-Based Hydrogen Storage Options

Rajesh K. Ahluwalia (Primary Contact),
Thanh Q. Hua, J-K Peng, and Hee Seok Roh
Argonne National Laboratory
9700 South Cass Avenue
Argonne, IL 60439
Phone: (630) 252-5979
Email: walia@anl.gov

DOE Managers
Grace Ordaz
Phone: (202) 586-8350
Email: Grace.Ordaz@ee.doe.gov
Ned Stetson
Phone: (202) 586-9995
Email: Ned.Stetson@ee.doe.gov

Start Date: October 1, 2009
Projected End Date: September 30, 2016

Overall Objectives

- Support DOE with independent system level analyses of various hydrogen storage approaches and determine the feasibility of meeting DOE targets.
- Model various developmental hydrogen storage systems.
- Provide results to the Hydrogen Storage Engineering Center of Excellence for assessment of performance targets and goals.
- Develop models to "reverse-engineer" particular approaches.
- Identify interface issues, opportunities, and data needs for technology development.

Fiscal Year (FY) 2013 Objectives

- Estimate the CF requirements for Type 4 compressed hydrogen tanks.
- Update the gravimetric and volumetric capacities of 350- and 700-bar hydrogen storage systems.
- Determine the material properties needed to satisfy the system level targets for hydrogen storage in metal hydrides.
- Construct flowsheets to estimate the fuel cycle efficiency of carbon-boron-nitrogen (CBN) regeneration.

Technical Barriers

This project addresses the following technical barriers from the Hydrogen Storage section of the Fuel Cell Technologies Office Multi-Year Research, Development, and Demonstration Plan:

(A) System Weight and Volume

(B) System Cost

(C) Efficiency

(E) Charging/Discharging Rates

(J) Thermal Management

(K) System Life Cycle Assessments

Technical Targets

This project is conducting system level analyses to address the DOE 2017 technical targets for onboard hydrogen storage systems:

- System gravimetric capacity: 1.8 kWh/kg
- System volumetric capacity: 1.3 kWh/L
- Minimum hydrogen delivery pressure: 5 bar
- Refueling rate: 1.5 kg/min
- Minimum full flow rate of hydrogen: 0.02 g/s/kW

FY 2013 Accomplishments

- Refined the ABAQUS finite-element model of carbon fiber (CF) wound Type 4 vessel for hydrogen storage at 350 and 700 bar. Calibrated and validated the ABAQUS model against other models based on modified netting analysis and transfer functions derived from data supplied by a tank manufacturer.
- Updated CF requirements and component data for single-tank and multi-tank 350- and 700-bar storage systems.
- Proposed and evaluated different methods of reducing CF composite usage: winding doilies to reduce stresses in shoulder and boss areas, varying hoop angles for more uniform sharing of loads, integrated end cap, and increasing stress ratio to reduce helical windings.
- Formulated models and performed reverse engineering to determine thermodynamic and kinetic properties of metal hydride materials needed to meet system targets.
- Performed off-board analysis of CBN regeneration using two different schemes: one by digestion of spent fuel with formic acid and another with methanol.

✧ ✧ ✧ ✧ ✧

INTRODUCTION

Several different approaches are being pursued to develop onboard hydrogen storage systems with the goal of meeting the DOE targets for light-duty vehicle applications. Each approach has unique characteristics, such as the thermal energy and temperature of charge and discharge, kinetics of the physical and chemical process steps involved, and requirements for the materials and energy interfaces between the storage system and the fuel supply system on the one hand, and the fuel user on the other. Other storage system design and operating parameters influence the projected system costs as well. We are developing models to understand the characteristics of storage systems based on the various approaches, and to evaluate their potential to meet the DOE targets for onboard applications, including the off-board targets for energy efficiency.

APPROACH

Our approach is to develop thermodynamic, kinetic, and engineering models of the various hydrogen storage systems being developed under DOE sponsorship. We then use these models to identify significant component and performance issues, and to assist DOE and its contractors in evaluating alternative system configurations and design and operating parameters. We establish performance criteria that may be used, for example, in developing storage system cost models. We refine and validate the models as data become available from the various developers. We work with the Hydrogen Storage Systems Analysis Working Group to coordinate our research activities with other analysis projects to assure consistency and to avoid duplication. An important aspect of our work is to develop overall systems models that include the interfaces between hydrogen production and delivery, hydrogen storage, and the fuel cell or internal combustion engine hydrogen user.

RESULTS

Physical Storage

We used ABAQUS to analyze the performance of four 70-MPa Type 4 compressed hydrogen storage tanks under different fiber winding and placement scenarios. The tanks have an external length to diameter ratio of 3 and hold 5.6 kg of usable hydrogen. The first tank is modeled with conventional helical and hoop windings with 90° hoop winding angle. No special features are incorporated in the dome. To meet the safety factor of 2.25, this tank requires 107.4 kg of CF composite with 60% T700S fiber by volume. The second tank is similar to the first, with the exception that the hoop winding angle varies layer by layer, increasing from 75° in the innermost hoop layer to ~90° in the outermost layer. Varying the hoop winding angle has the effect of transferring part of the load from the inner layers to the outer layers. The stress distribution across the thickness of the composite becomes more uniform, and the total amount of CF composite needed is reduced to 102 kg. The third tank has variable winding angles as in the second tank, and also has "doilies" strategically added in the dome. The use of doilies for local reinforcement reduces the number of helical windings needed. The thickness of the helical windings in the cylindrical section of the tank reduces from 18.5 mm in Tank 1 to 14.3 mm in Tank 3. The total weight of CF composite is similarly reduced to just 91 kg. The fourth tank is based on the Integrated End-Cap Vessel concept. The domes are reinforced with end caps made by resin transfer molding. We assume that the tensile strength of the composite in the end caps is 30% lower than that of the composite used for filament winding. The total composite weight, including the end caps is, then, 92.6 kg. While the weight is slightly higher for Tank 4 than Tank 3, Tank 4 may have a cost advantage, in that it may be easier to manufacture the end caps than to wind doilies on the dome.

We also evaluated the potential to achieve a greater than 10% reduction in CF composite usage. This can be accomplished by increasing the stress ratio, which is defined as the ratio of helical to hoop stresses in the cylindrical section of the tank. Stress ratio is generally limited so as to prevent end-dome rupture and/or boss blow out, particularly for very high-pressure tanks. The stress ratios in our baseline cases were ~0.45 for the 700-bar tanks with doilies, ~0.42 for the 700-bar tanks with end caps, and ~0.51 for the 350-bar tanks with doilies. Some of the results were calibrated with a manufacturer's tank that has extra helical winding to help pass the 45° drop test. We examined scenarios without the extra built-in helical winding and allow the stress ratio to increase, while still meeting all safety requirements. For 700-bar tanks, our analysis showed that stress concentration in the shoulder and boss areas limits the maximum allowable stress ratio to 0.53-0.55 for filament-wound-only tanks with doilies, and to 0.61 for tanks using end caps. The stress ratio can also be increased to 0.63 for 350-bar tanks with doilies. With the higher stress ratios, the composite weight is reduced by 10-12% in the 700-bar tanks with doilies, and by 12-14% in the 350-bar tanks with doilies. Figure 1 shows the stress distribution in a 700-bar tank with end caps for two stress ratios. The stress ratio is higher than the comparable tank with doilies due to the reduced stress concentration in the shoulder and boss areas as a result of improved stiffness continuity in the end cap design. With the higher stress ratio, the weight of the needed composite is 17% lower than in the corresponding baseline design with end caps.

We modeled a tank with combined high- and low-grade CF. High-grade CF (T700S) was used in the more highly stressed inner hoop layers, while the lower grade T300

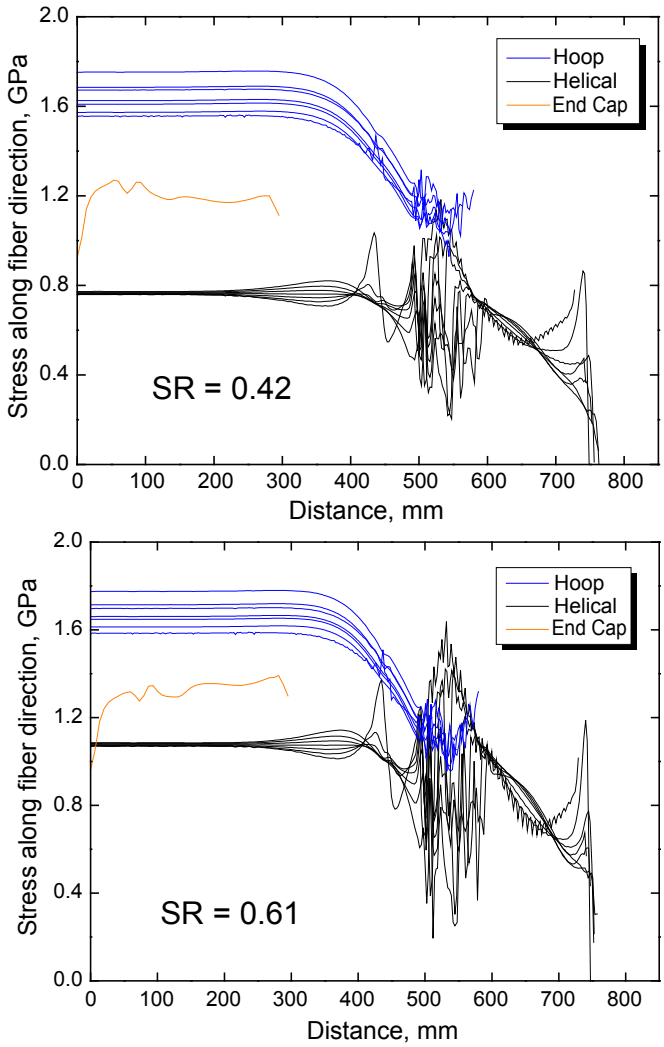

FIGURE 1. Stress along the Fiber Direction for Hoop, Helical, and End Cap Fibers for SR = 0.42 (top) and SR = 0.61 (bottom)

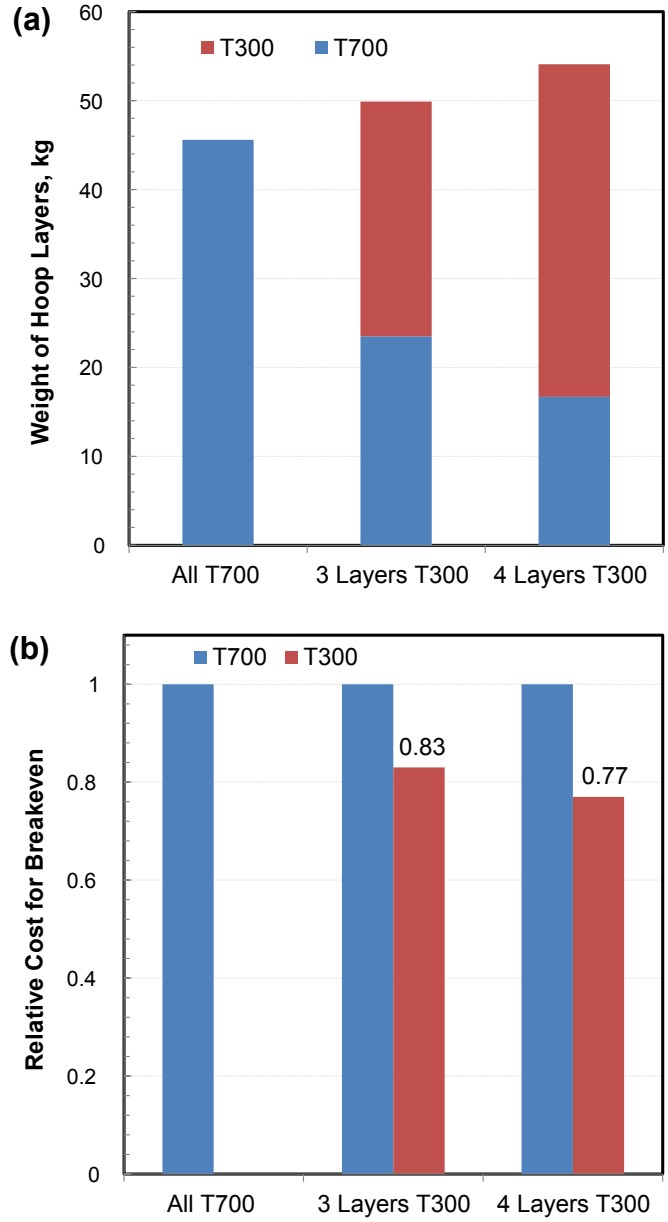

FIGURE 2. (a). Changes in the Mass of Hoop Layers when Three or Four Outer Layers are Replaced with T300; (b). Maximum Relative Cost of T300 for Breakeven in Total CF Material Cost

(presumably less expensive) CF was used in outer layers where stresses are lower. All helical layers were T700S. Because the tensile strength of T300 CF is 28% lower than that of T700S, a larger amount of CF was needed to absorb the same load. Figure 2a shows the increase in the mass of hoop layers when three or four outer hoop layers were wrapped with T300 CF composite. The potential cost savings can be deduced from Figure 2b, where the maximum relative unit cost of T300 material (as a fraction of T700 unit cost) is calculated for breakeven in total CF composite material cost.

We updated the system gravimetric and volumetric capacities for the 350- and 700-bar one- and two-tank systems. The ABAQUS results for composite weight were initially calibrated against selective data obtained from a tank manufacturer and further benchmarked against the "Tank Attribute Estimator" tool [1]. The tool consists of empirical correlations which were constructed using a wider set of design data provided by the same tank manufacturer.

Additionally, the system balance-of-plant equipment has been updated, based on detailed discussions with automotive manufacturer experts and feedback from members of the Hydrogen Storage Tech Team. For 700-bar storage, the updated gravimetric capacities are 4.4 wt% for one-tank and 4.1 wt% for two-tank systems. The corresponding volumetric capacities are 25.0 g-H_2/L and 24.2 g-H_2/L, respectively. For comparison, the 2010 [2] system gravimetric capacities were 5.2 and 4.8 wt% for one- and two-tank systems and the volumetric capacities were 26.3 and 25.6 g-H_2/L, respectively. The updated capacities are lower mainly because of the

higher CF composite weight and volume, partially offset by the absence of the glass fiber that was incorporated in the 2010 systems. The outer 3-mm glass fiber was intended for cosmetic purposes but had no structural function, and was omitted in the updated analyses. For 350-bar storage pressure, the updated gravimetric capacities for one- and two-tank systems are 5.4 and 4.7 wt%, and the volumetric capacities are 17.7 and 17.2 g-H_2/L, respectively. The 2010 system gravimetric capacities were 5.5 and 5.0 wt% for one- and two-tank systems and the volumetric capacities were 17.6 and 17.2 g-H_2/L, respectively.

Hydrogen Storage in Metal-Hydrides

We conducted a "reverse engineering" systems analysis to determine the minimal material requirements of a low-temperature metal hydride (MH) storage system to meet the DOE 2017 performance targets. Figure 3 shows a schematic of a low-temperature MH system that is thermally integrated with the fuel cell system. For such a hydrogen storage system, a buffer tank would be needed for system startup from –40°C ambient temperature. Expanded natural graphite is dispersed in the MH bed to enhance the bed's thermal conductivity. The MH material is compacted to improve the bulk density, and it must have sufficiently fast kinetics to allow complete refueling (5.6 kg usable hydrogen) in 3.7 minutes. The MH bed should be able to supply the minimum full flow rate of 1.6 g/s. The Type 3 MH storage tank has an Al 6061-T6 alloy liner and it is wrapped with T700S CF composite. The liner and CF thicknesses are sized to meet the 2.25 safety factor and 5,500 lifetime pressure cycles. We assume 100% onboard storage system efficiency with no requirement for an onboard hydrogen burner.

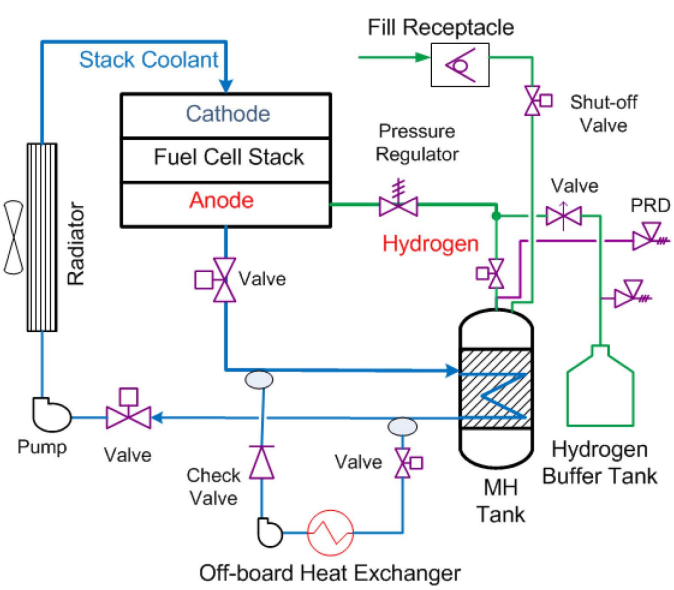

FIGURE 3. Low-Temperature MH Hydrogen Storage System

The usable storage capacity of the MH is related to the intrinsic material capacity, the minimum state-of-charge, X_{min} (SOC, 10% nominal), and the maximum SOC, X_{max} (90% nominal). The minimum and maximum SOC are determined by the kinetic requirement that the bed should be able to supply the minimum full flow rate of 1.6 g/s. Figure 4a shows the kinetic time for isothermal discharging from 100% SOC to X_{min} at the minimum fuel cell stack coolant temperature of 60°C and 5-atm back pressure. For charging, results from our analysis show that for given thermodynamics, activation energy and charge pressure, there is an optimum temperature (Figure 4b) at which the charge rate is the fastest.

Table 1 summarizes the preliminary results of the reverse engineering analysis. The bed consists of 51.2 kg MH with 5.1 kg expanded natural graphite, and it stores 5.6 kg of recoverable hydrogen. The MH needs a minimum material capacity of 13.6 wt% hydrogen to meet the 5.5 wt% target for the system gravimetric capacity. The MH material needs a minimum bulk density of 589 kg/m^3 and a bed porosity of 24.7% to meet the 40 g/L target for the system volumetric capacity. With a bed thermal conductivity of 8.4 W/m.K and

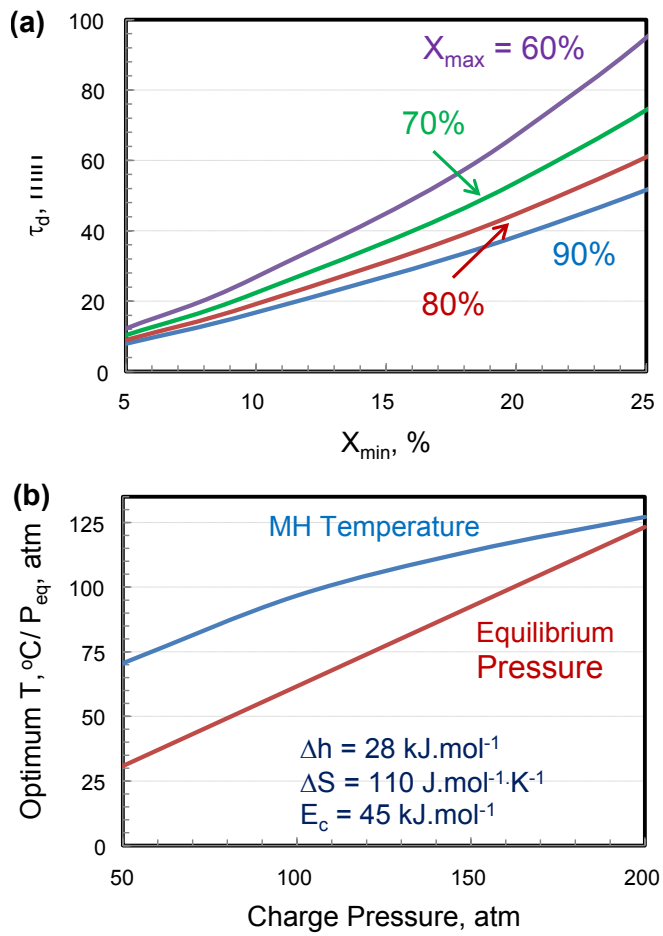

FIGURE 4. (a) Kinetic time for Isothermal Dehydriding from 100% SOC to X_{min} (b) Optimum Temperature for Fastest Charge Rate

TABLE 1. Reference Values for Meeting Onboard Targets

Independent Variables	Related Variables	Reference Values	Constraints
MH Intrinsic Capacity		13.6% H capacity	5.5 wt% gravimetric capacity
Fill Ratio	Bulk Density	24.7% bed porosity	40 g/L volumetric capacity
	Thermal Conductivity	589 kg/m^3 MH bulk density	
		8.4 W/m.K bed conductivity	
HX Tube Spacing	Number of HX Tubes	r_2/r_1 = 3.1	1.5 kg/min refueling rate
		85 U tubes	
Mass of MH	Mass of Expanded	51.2 kg MH	5.6 kg usable H_2
	Natural Graphite	5.1 kg ENG	
Buffer Tank Capacity	Weight of Al tank	11.1 kg buffer tank weight	Startup from -40°C
		33.7 L buffer tank volume	
Discharge Kinetics	X_{min} = 10%	τ_d = 16.8 min	1.6 g/s min full flow rate
Charge Kinetics	X_{max} = 90%	k_c = 4.2 g/kg$_{MH}$/min/atm	X_{min} to X_{max} in 1.85 min at T_{opt}

ENG - enhanced natural graphite

85 Utubes for heat transfer, the bed can be charged fully at the rate of 1.5 kg-H_2/min. A kinetic time of 16.8 min is needed for the system to discharge from 90% SOC to the minimum 10% SOC while delivering 1.6 g/s full flow rate to the fuel cell. Finally, a 33.7-L buffer tank weighing 11.1 kg is needed to meet the requirements for system startup at an ambient temperature of –40°C.

Off-Board Regeneration of CBN

We developed engineering flowsheets (Figure 5) and analyzed the off-board regeneration process for CBN materials using two different schemes proposed by the University of Oregon [3]. In the first scheme, the spent fuel trimer is treated with formic acid to form a digested intermediate product. The reaction is expected to occur favorably at ambient conditions. In a typical experiment using a model substrate (6-membered ring instead of 5-membered ring), the digested product formed nicely. The intermediate product is then decarboxylated to yield fresh CBN fuel and CO_2. While the decarboxylation reaction has not been demonstrated, computation of reaction thermodynamics shows that it is an endothermic process. To complete the regeneration cycle, formic acid is produced by reforming CO_2 and hydrogen. In our flowsheet, we assumed that hydrogen is produced by steam methane reformation and formic acid is produced by an integrated process developed by BP Chemicals [4]. In the second scheme, the spent fuel is first digested with methanol (MeOH). The digested intermediate product is reduced using sodium alanate ($NaAlH_4$) to form fresh CBN fuel and $NaAl(OMe)_4$. The fresh CBN fuel is filtered out from the solution which is subsequently hydrolyzed to form alumina, methanol, sodium hydroxide and water. Methanol is distilled off and returned to the digestion reactor. Alumina is recovered to produce aluminum by the well-established industrial Hall-Heroult process. Sodium hydroxide and water are electrolyzed to produce sodium metal by hydrogen-assisted electrolysis, a technique that has been demonstrated by Millennium Cell [5]. Sodium hydride is produced by the direct reaction of hydrogen with liquid sodium. To complete the regeneration cycle, sodium alanate is produced by mechanical ball milling of NaH and aluminum in hydrogen under pressure.

The amount of electricity consumed to produce aluminum accounts for nearly two-thirds of the total primary energy in the MeOH/$NaAlH_4$ scheme and resulted in a low well-to-tank efficiency of 15.5%. The well-to-tank efficiency is estimated at 30.5% for the formic acid scheme of regeneration but still falls far short of the DOE target of 60%.

CONCLUSIONS AND FUTURE DIRECTIONS

- We estimated that the composite weight for a Type 4 tank holding 5.6 kg usable hydrogen is 91 kg and can be reduced by 10-12% if the stress ratio is raised from 0.45 to 0.55. We estimated that, with end caps, the composite weight is 92 kg and can be reduced by 17% if the stress ratio is raised from 0.42 to 0.61.
- We updated the system gravimetric and volumetric capacities for the 350- and 700-bar one- and two-tank systems. For the 700-bar systems, the system gravimetric capacities were 4.1 to 4.4 wt% and volumetric capacities were 24.2 to 25.0 g-H_2/L. For the 350-bar systems, the calculated system gravimetric capacities were 4.7 to 5.4 wt% and the volumetric capacities were 17.1 to 17.7 g-H_2/L.
- We estimated that a metal hydride needs a minimum hydrogen material capacity of 13.6 wt% to meet the 5.5 wt% target for the system gravimetric capacity. The MH material needs a minimum bulk density of

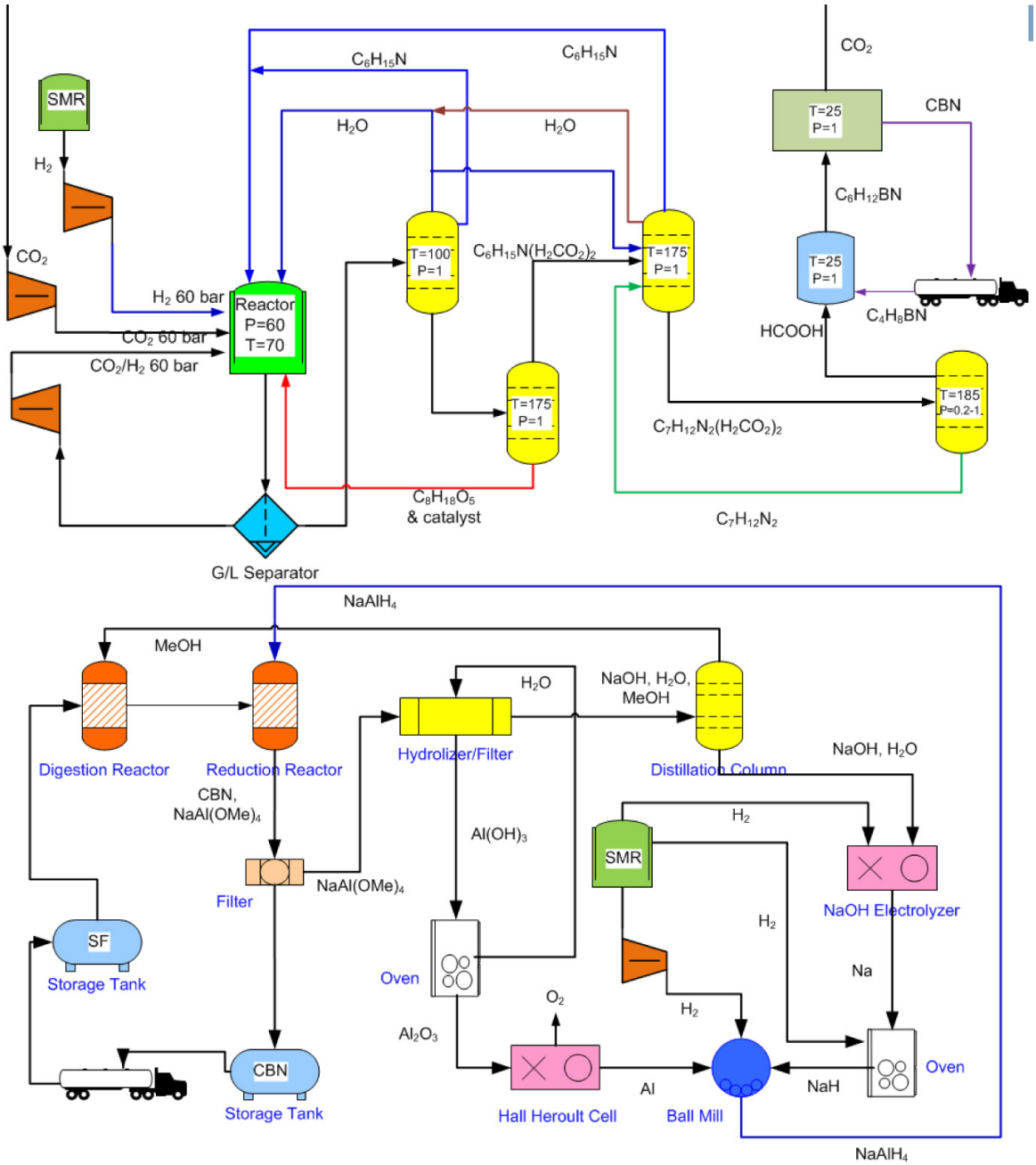

FIGURE 5. Flowsheets for CBN Regeneration using Formic Acid (top) and MeOH/$NaAlH_4$ (bottom)

589 kg/m^3 and a bed porosity of 24.7% to meet the 40 g/L target for the system volumetric capacity. We estimated that a 33.7-L buffer tank weighing 11.1 kg is needed to meet the requirements for system startup from –40°C ambient temperature.

- We estimated a well-to-tank efficiency of ~15.5% for regenerating CBN using MeOH/$NaAlH_4$. The well-to-tank efficiency improves to ~30.5% using formic acid to digest the spent fuel.
- In FY 2014, we will continue to run ABAQUS simulations to analyze hydrogen storage in near-term, Type 4, 350-bar and 700-bar CF wound pressure vessels and update the system performance with respect to gravimetric capacity, volumetric capacity and CF requirements. We will investigate methods of simplifying the system layout by combining functionalities to eliminate components.
- In FY 2014, we will work with Small Business Innovation Reseach and other projects, run MultiMech

and ABAQUS simulations to analyze and evaluate methods of reducing CF usage by employing advanced materials (e.g., nano-composites, cheaper resins), advanced fabrication techniques (e.g., doilies, varying hoop angles), integrated end caps, and hybrid CFs of different grades (strengths).

- In FY 2014, we will perform independent analyses to determine the material requirements for hydrogen storage in adsorbents and in off-board reversible chemicals, considering both the onboard system and off-board energy consumption. The primary goal of the analyses will be to determine the range of materials properties that are needed for the systems to meet the DOE onboard and off-board performance targets.
- Also, in FY 2014, we will evaluate the viability of storing hydrogen in unstable complex hydrides such as $Ti(AlH_4)_4$. If viable, we will perform system analysis to determine attributes of this new class of materials needed to satisfy requirements for vehicular systems

FY 2013 PUBLICATIONS/PRESENTATIONS

1. T.Q. Hua and R.K. Ahluwalia, "Hydrogen Storage in Ammonia Borane – Off-board Regeneration Processes and Efficiencies," International Journal of Hydrogen Energy, 37 (2012) 14382-14392.

2. H.S. Roh, T.Q. Hua, and R.K. Ahluwalia, "Optimization of Carbon Fiber Usage in Type-4 Hydrogen Storage Tanks for Fuel Cell Automobiles," International Journal of Hydrogen Energy, 38 (2013) 12795-12802.

3. T.Q. Hua, H.S. Roh, and R.K. Ahluwalia, "Analysis Methodology and Parameters for Type-4 Hydrogen Storage Tanks," Storage System Analysis Working Group Meeting, Southfield, MI, November 2012.

4. R.K. Ahluwalia, T.Q. Hua, J-K. Peng, and H.S. Roh, "System Level Analysis of Hydrogen Storage Options," Hydrogen Storage Tech Team Meeting, Southfield, MI, November 2012

5. T.Q. Hua, H.S. Roh, and R.K. Ahluwalia, "Optimization of Carbon Fiber Usage in Type-4 Hydrogen Storage Tanks for Fuel Cell Automobiles," AIChE 5th Annual Midwest Regional Conference, Illinois Institute of Technology, Chicago, January 2013.

REFERENCES

1. K. Simmons, "Comparison of Methods to Estimate the Mass and Cost of Hydrogen Storage Tanks," Storage System Analysis Working Group Meeting, Southfield, MI, November 2012.

2. R.K. Ahluwalia, T.Q. Hua, J.K. Peng, D. Papadias, and R. Kumar, "System Level Analysis of Hydrogen Storage Options," 2011 DOE Hydrogen Program review, Washington DC, May 2011.

3. S-Y Liu, University of Oregon, Personal Communication, 2012.

4. J. Anderson, D. Drury, J. Hamlin, and A. Kent. Process for the Preparation of Formic Acid. US Patent 4855496, August 9, 1989.

5. O. Moreno, M. Kelly, J. Ortega, and R. Mohring, "Process for the Regeneration of Sodium Borate to Sodium Borohydride," 2007 DOE Independent Project – Go/No-Go Decision, Argonne, IL 2007.

IV.A.2 Hydrogen Storage Cost Analysis

Brian D. James (Primary Contact),
Whitney G. Colella, Jennie M. Moton
Strategic Analysis, Inc. (SA)
4075 Wilson Blvd. Suite 200
Arlington VA 22203
Phone: (703) 778-7114
Email: bjames@sainc.com

DOE Managers
Grace Ordaz
Phone: (202) 586-8350
Email: Grace.Ordaz@ee.doe.gov
Katie Randolph
Phone: (720) 356-1759
Email: Katie.Randolph@go.doe.gov

Contract Number: DE-EE0005253

Project Start Date: September 30, 2012
Project End Date: September 29, 2016

Overall Objectives

- Identify and/or update the configuration and performance of a variety of H_2 storage systems for both vehicular and stationary applications.
- Conduct rigorous cost estimates of multiple H_2 storage systems to reflect optimized components for the specific application and manufacturing processes at various rates of production.
- Explore cost parameter sensitivity to gain understanding of system cost drivers and future pathways to lower system cost.

Fiscal Year (FY) 2013 Objectives

- Update and expand the cost analysis of onboard H_2 storage in pressurized carbon composite (fiber and resin) pressure vessels.
- Validate the cost analysis methodology and results as a function of manufacturing rate against industry estimates, and thereby increase confidence in these estimates.
- Develop a sensitivity analysis of H_2 pressure vessel cost as a function of tank size (4 to 8 kg of H_2/vessel), pressure (350 to 700 bar), and number of pressure vessels within the system (1, 2, or 3).
- Assess the costs of two off-board chemical hydride recycle systems: recycle for the ammonia borane (AB) and alane storage systems.
- Identify cost drivers and future pathways to lower cost.
- Document all analysis results and assumptions.

Technical Barriers

This project addresses the following technical barriers from the Hydrogen Storage section of the Fuel Cell Technologies Office Multi-Year Research, Development, and Demonstration Plan:

(B) System Cost

(H) Balance-of-Plant (BOP) Components

(K) System Life-Cycle Assessments

Technical Targets

This project conducts cost modeling to attain realistic, process-based system costs for a variety of H_2 storage systems. These values can inform future technical targets for system storage cost.

- Onboard System Hydrogen Storage Cost: $12/kWh net (2017 target)

FY 2013 Accomplishments

Accomplishments relating to onboard compressed H_2 storage systems:

- Developed pressure vessel system definitions and bills of materials for various tank capacities (4 to 8 kg of H_2/vessel usable H_2) and pressure ratings (350 and 700 bar).
- Worked with Argonne National Laboratory (ANL), the DOE Hydrogen Storage Tech Team, and Ford Motor Company to select tank system specifications for nine configurations (number of tanks, length-to-diameter ratio, geometric parameters, carbon fiber requirements, gravimetric and volumetric capacities, composite efficiency, fiber strength variability, winding efficiency, safety factors, service life, material properties, multi-tank configurations, BOP, etc.) to be used as the basis of comparison with current or projected industry data.
- Worked with ANL to take their ABAQUS model tank results and appropriately include those fiber and resin masses (and dimensions) into the SA Design for Manufacturing and Assembly (DFMA®) cost analysis.
- Updated BOP cost estimates based on original equipment manufacturer (OEM) price quotations and learning curves for production rates outside the quotation range.

- Updated the DFMA cost analysis for five annual production rates, for five tank configurations. Analyzed manufacturing methods. Conducted sensitivity studies.
- Validated key performance parameters for pressure vessels based on discussions with industry, the DOE H2 Storage Tech Team, the Storage System Analysis Working Group, ANL, Pacific Northwest National Laboratory (PNNL), the H2 Storage Engineering Center of Excellence (HSECoE), and project collaborators. Key parameters include (1) the composite fiber and resin masses as a function of tank capacity, (2) fiber and resin material cost, and (3) cost of the BOP components. These are key cost drivers.
- Refined assumptions, models, and analysis based on expert feedback.
- Analyzed the sensitivity of H_2 storage cost to usable H_2 tank capacity (4 to 8 kg H_2), number of tanks (1-3) per system, design pressure (350 and 700 bar), and manufacturing rate (10,000 to 500,000 tank systems/year [sys/yr]).

Accomplishments relating to off-board regeneration of H_2 storage media:

- Completed cost analysis of the off-board regeneration of spent AB (BNH_2) back into an AB (AB or BH_3NH_3) slurry suitable for use in a vehicular onboard H_2 storage system.
- Completed cost analysis of the off-board regeneration of aluminum (spent alane) back into an alane slurry suitable for use in an onboard alane (AlH_3) H_2 storage system.

✧ ✧ ✧ ✧ ✧

INTRODUCTION

The Fuel Cell Technologies Office (FCTO) states that H_2 storage is a key enabling technology for the advancement of H_2 and fuel cell power technologies in transportation, stationary, and portable applications. Consequently, the FCTO has established a goal of developing and demonstrating viable H_2 storage technologies for transportation and stationary applications. This cost assessment project supports the overall FCTO goals by identifying the current technology system components, performance levels, and manufacturing/assembly techniques most likely to lead to the lowest system storage cost. Furthermore, the project is forecasting the cost of these systems at a variety of annual manufacturing rates to allow comparison to the overall 2017 and "Ultimate" DOE cost targets. The cost breakdown of the system components and manufacturing steps can then be used to guide future research and development decisions.

During the second year of the project, onboard H_2 storage in pressurized carbon composite pressure vessels was selected for analysis. While this system has been previously analyzed by DOE, the objective is to update and expand the cost analysis while also validating the cost analysis methodology and results against industry estimates, thereby increasing confidence for future cost analysis projects. Additionally, two off-board chemical hydride recycle systems were selected for cost analysis: recycle for the AB and alane storage systems. The vehicular onboard components of these systems have been previously analyzed. However, an assessment of the off-board recycle costs is needed to allow DOE to assess the full cost of the storage method.

APPROACH

To generate cost estimates for the compressed H_2 pressure vessel system, a DFMA®-style analysis was conducted. Key system design parameters and an engineering system diagram describing process flows were obtained from a combination of industry partners, ANL, and members of the HSECoE [1]. From this system design, the physical embodiment of the system was developed, including materials, scaling, dimensions, and design. Based on this physical embodiment, the manufacturing process train was modeled to attain the cost to manufacture each part. Industry partners were consulted to assess current and future manufacturing procedures and parameters. Cost was based on the capital cost of the manufacturing equipment, machine rate of the equipment, equipment tooling amortization, part material costs, and other financial assumptions. Once the cost model was complete for the system design, sensitivity data for the modeled technology was obtained by varying the key parameters. These results were shared with ANL, the National Renewable Energy Laboratory (NREL), and industry partners to obtain feedback and further refine the model.

The analysis explicitly includes fixed factory expenses such as equipment depreciation, tooling amortization, utilities, and maintenance as well as variable direct costs such as materials and labor. However, because this analysis is intended to model manufacturing costs, a number of components that usually contribute to the OEM price are explicitly not included in the modeling. These costs are excluded from this analysis: profit and markup; one-time costs such as non-recurring research/design/engineering; and general expenses such as general and administrative costs, warranties, advertising, and sales taxes.

The off-board regeneration cost analysis for the alane and AB systems is based on a less-detailed cost analysis methodology. For each of the systems, a process flow diagram is developed based on input from ANL. The AB regeneration system is based on the Los Alamos National Laboratory (LANL) one-pot process using hydrazine (N_2H_4) to recycle spent AB (BNH_2) back into AB (BH_3NH_3) [2-4]. Since hydrazine is a major cost contributor in the

regeneration process, hydrazine cost is independently analyzed based on the benzophenone process, which converts ammonia, oxygen, and water into hydrazine [5]. The alane regeneration system is based on the dimethylethylamine (DMEA) process [6]. Both regeneration systems are nominally sized for a central plant with an equivalent capacity of 100 metric tons per day of H_2. A modified form of the H2A H_2 production cost analysis spreadsheet [7] is used to assess regeneration cost. While we do not seek to compute H_2 production costs, the H2A model is based on a discounted cash flow tool that applies to this regeneration analysis. Furthermore, the H2A model is a transparent and familiar tool to the H_2 community. Regeneration costs are computed per kg of H_2 eventually releasable onboard the vehicle. Capital costs of the systems are estimated by a summation of major subsystems identified on the process flow diagram, and are based on handbook [8] capital cost correlations for the type of subsystem and pertinent scaling factors (such as flow rate, pressure, temperature, etc.).

RESULTS

The results from sensitivity studies on compressed H_2 pressure vessel storage systems demonstrate the effects of varying tank design parameters and annual production rates. Figure 1 shows the cost breakdown for single-tank H_2 storage systems holding 5.6 kg of usable H_2 and operating at up to 70 Megapascals (MPa) (i.e., 700 bar), as a function of manufacturing rate. H_2 storage costs range from ~$33/kWh (at 10,000 sys/year) to ~$17/kWh (at 500,000 sys/year). Projected costs are based on year 2007 U.S. dollars with H_2 energy based on the lower heating value (33.3 kWh/kgH_2). Error bars represent plus and minus two standard deviations (middle 95.4% of expected costs assuming a normal distribution). The H_2 storage cost per unit energy decreases significantly with increased annual production rate. Results indicate that the two most significant cost drivers are (1) the composite materials costs (primarily the carbon fiber cost) and (2) the cost of BOP components. Further analyses show that these remain the two key cost drivers for the range of operating pressures, tank configurations, and manufacturing rates evaluated in this project so far. BOP components are revised from previous analyses and incorporate recommendations from industry for enhanced functionality and safety.

As shown in Figure 1, the materials costs decline only moderately with manufacturing rate (~12% over a production increase from 10,000 to 500,000 sys/yr) while the BOP cost declines significantly (~73%) over the same range. BOP costs scale down significantly in moving to higher annual production volumes due to both manufacturing economies of scale and projected design improvements made economical by high production. As a result, the composite materials costs become a higher percentage of total system costs in moving to higher annual production volumes.

Figure 2 shows the cost breakdown for dual-tank H_2 storage systems holding 5.6 kg of usable H_2 and operating at up to 35 MPa (i.e., 350 bar), as a function of manufacturing rate. In contrast to Figure 1, at all but the highest production levels, the key cost driver is the BOP. BOP costs are greatly impacted by economies of scale in mass production, whereas composite materials costs benefit less so. As shown in the figure, the materials costs decline only moderately with manufacturing rate (~12% over a production increase from 10,000 to 500,000 sys/year) while the BOP cost declines significantly (~74%) over the same range. H_2 storage costs range from ~$37/kWh (at 10,000 sys/year) to ~$15/kWh (at 500,000 sys/year).

Based on techno-economic modeling of the LANL one-pot, hydrazine-based, AB recycle system, the AB regeneration cost is estimated at about $10 per kg of H_2 releasable on the vehicle, even assuming a future hydrazine market price of $1/kg N_2H_4. This is a prohibitively high cost and suggests that alternative AB regeneration routes may be more promising. A sensitivity analysis indicates that the AB regeneration cost is highly sensitive to hydrazine price, which, in turn, is most sensitive to 1) ammonia costs and 2) hydrazine plant capital costs. Hypothetically speaking, if the hydrazine cost were zero, the AB regeneration cost would be about $2.28/kg H_2, which is still higher than the competitive H_2 target of $2/kg H_2. Thus, according to this analysis, it appears quite financially challenging to try

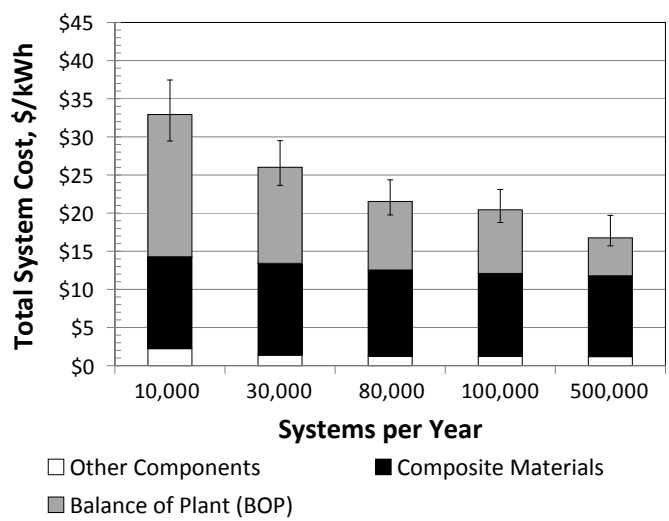

Other Components Include:

System Assembly	B-Stage Cure (Cure #1)
He Fill and Leak Test	Fiber Winding
HydroTest	Linear Annealing
Boss (Materials and Processing)	Linear Formation (Materials and Processing)
Full Cure (Cure #2)	

FIGURE 1. System Cost Results for Compressed H_2 Storage: 70 MPa, Single Tank, 5.6 kg H_2 Usable Capacity

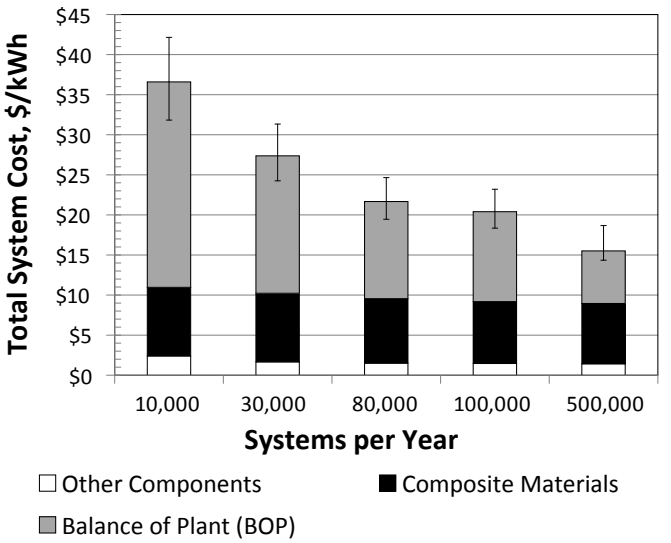

Other Components Include:	
System Assembly	B-Stage Cure (Cure #1)
He Fill and Leak Test	Fiber Winding
HydroTest	Linear Annealing
Boss (Materials and Processing)	Linear Formation (Materials and Processing)
Full Cure (Cure #2)	

FIGURE 2. System Cost Results for Compressed H_2 Storage: 35 MPa, Dual Tank, 5.6 kg H_2 Usable Capacity

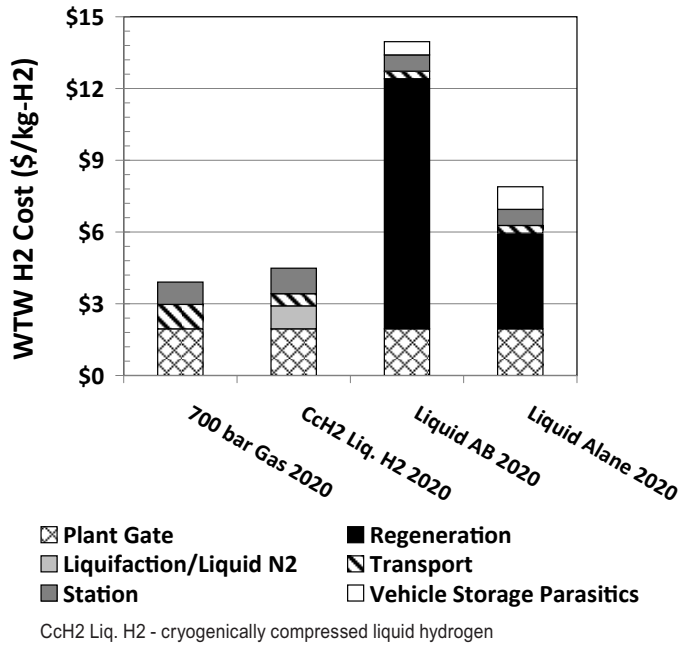

FIGURE 3. Well-to-wheel (WTW) Cost of H_2 Delivered to the Vehicle

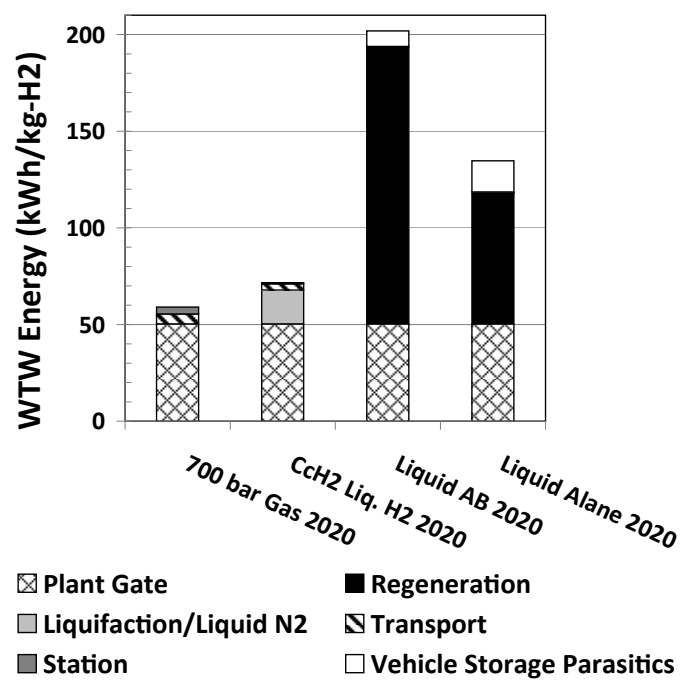

FIGURE 4. WTW Energy Consumption for H_2 Delivered to the Vehicle

to regenerate spent AB based on the hydrazine method. Preliminary results from the alane regeneration process (DMEA pathway) indicate that this approach may be more cost competitive than the AB regeneration process, although still expensive. The alane off-board regeneration cost is estimated at \$4/kg H_2. At the same time, capital cost estimates for the AB and alane off-board regeneration processes are uncertain due to a lack of optimized process conditions, particularly reactor residence times.

Figure 3 shows that the off-board regeneration cost for either AB or alane is a significant cost driver to the overall well-to-wheel (WTW) cost of H_2 delivered to the vehicle. The off-board regeneration cost makes the WTW costs of both AB and alane scenarios more expensive than either compressed gas or liquid H_2 scenarios. Figure 4 shows similar results, but for energy use. The off-board regeneration energy consumption for either AB or alane is a significant contributor to the overall WTW energy consumption of H_2 delivered to the vehicle. The off-board regeneration energy consumption makes the WTW energy consumption of both AB and alane scenarios less efficient than either compressed gas or liquid H_2 scenarios.

CONCLUSIONS AND FUTURE DIRECTIONS

Based upon work from this year, the following conclusions and future directions are revealed:

- Key cost drivers for carbon fiber pressure vessel systems are (1) the carbon fiber materials cost and (2) the BOP component costs. Thus, accurate estimation of the carbon fiber price and the mass of fiber required in each vessel is very important, as are efforts to simplify and reduce the size and extent of the BOP.

Costs for compressed H_2 storage systems holding 5.6 kg H_2 usable are estimated at:

- Single-tank system at 700 bar:
  - ~$33/kWh at 10,000 systems/year
  - ~$17/kWh at 500,000 systems/year
- Single-tank system at 350 bar:
  - ~$29/kWh at 10,000 systems/year
  - ~$13/kWh at 500,000 systems/year
- Dual-tank system at 700 bar:
  - ~$40/kWh at 10,000 systems/year
  - ~$19/kWh at 500,000 systems/year
- Dual-tank system at 350 bar:
  - ~$37/kWh at 10,000 systems/year
  - ~$15/kWh at 500,000 systems/year
- The AB (hydrazine regeneration pathway) and alane (DMEA regeneration pathway) off-board regeneration costs are estimated at ~$10/kg H_2 and $4/kg H_2, respectively. These costs are prohibitively high and result in life cycle costs two to four times higher than compressed or liquefied H_2 life cycle costs. Other regeneration pathways may result in lower cost.

Future work will:

- Continue to refine the H_2 pressure vessel cost analysis.
- Gather further OEM data on BOP component costs.
- Explore BOP component simplification and combined functionality as a pathway to lower cost.
- Redesign and re-cost the tank mounting mechanisms from complex frame-mounted systems to less equipment-intensive approaches.
- Assess the cost impact of advanced tankage concepts such as use of strength-graded fibers, carbon nanotube addition between fiber layers to increase translational strength, and cold H_2 storage (200 Kelvin).

FY 2013 PUBLICATIONS/PRESENTATIONS

1. James, B.D., Spisak, A.B., Colella, W.G., *Hydrogen Storage Cost Analysis,* annual report for the U.S. DOE EERE FCT program, July 2012.

2. James, B.D., Colella, W.G., *Alane and Ammonia Borane Off-Board Recycle Analysis Status,* presentation to U.S. DOE EERE FCT Headquarters, Forrestal Building, Washington, D.C., Sept. 25th, 2012.

3. James, B.D., Colella, W.G., *Analysis of Recycling Alane and Ammonia Borane Off-Board Vehicles,* presentation to U.S. DOE Hydrogen Storage Engineering Center of Excellence, delivered remotely, Arlington, VA, Oct. 11th, 2012.

4. James, B.D., Colella, W.G., Paster, M., *Energy, Emissions, and Economic Analysis of Off-board Recycling of Alane and Ammonia Borane for Hydrogen Fuel Cell Vehicles,* presentation to U.S. DOE EERE Fuel Pathway Integration Technical Team (FPITT), delivered remotely, Arlington, VA, Oct. 24th, 2012.

5. James, B.D., Spisak, A.B., *Pressure Vessel Cost Analysis*, presentation to Storage Systems Analysis Working Group (SSAWG) & H2 Storage Tech Team, delivered remotely, Arlington, VA, Nov. 14th, 2012.

6. James, B.D., Spisak, A.B., *Pressure Vessel Cost Analysis*, presentation to DOE Storage Principal Investigator Meeting, Washington, DC (ARPA-E offices), Nov. 28th, 2012.

7. James, B.D., Moton, J.M., "Updated Pressure Vessel Balance of Plant and System Costs," update to DOE Storage Team, Arlington, VA, March 12th, 2013.

8. Colella, W.G., "Advanced Electrochemical Systems," *California Renewable Energy and Storage Technology Conference*, California State University Northridge, Northridge, CA, May 4th, 2013.

9. James, B.D., Moton, J.M., Colella, W.G., "Hydrogen Storage Cost Analysis, Preliminary Results," presentation at the 2012 DOE Hydrogen and Fuel Cells Program Review, Arlington, VA, May 15th, 2013.

10. James, B.D., Moton, J.M., Colella, W.G., "Advanced Hydrogen Compression Systems for Serving a Hydrogen Vehicle Refueling Infrastructure," *American Society of Mechanical Engineers (ASME) 2013 7th International Conference on Energy Sustainability*, Minneapolis, MN, July 14–19th, 2013 (in preparation).

11. James, B.D., Colella, W.G., Moton, J.M., *Hydrogen Storage Cost Analysis*, annual report for the U.S. DOE EERE FCT program, July 2013.

REFERENCES

1. "Technical assessment of compressed hydrogen storage tank systems for automotive applications," T.Q. Hua, R.K. Ahluwalia, J.-K. Peng, M. Kromer, S. Lasher, K. McKenney, K. Law, J. Sinha, International Journal of Hydrogen Energy 36 (2011) 3037-3049. (doi:10.1016/j.ijhydene.2010.11.090)

2. Sutton, A.D., "Efficient Regeneration of Ammonia Borane," ACS Meeting, Aug. 20, 2009.

3. Sutton et al., "Regeneration of Ammonia Borane Polyborazylene," U.S. Patent Application 2010/0272622 A1, October 28, 2010.

4. "Off-board Regeneration of Ammonia Borane for Use as a Hydrogen Carrier for Automotive Fuel Cells," Thanh Hua, Rajesh Ahluwalia, submission for publication in the International Journal of Hydrogen Energy, April 2, 2012.

5. "Hydrazine Production from Ammonia via Azine," Hiromu Hayashi et. al., Industrial and Engineering Chemistry Product Research and Development, Vol. 15 No. 4 (1976) 299-303.

6. "Alane hydrogen storage for automotive fuel cells - Off-board regeneration processes and efficiencies," Thanh Q. Hua, Rajesh K. Ahluwalia, International Journal of Hydrogen Energy, Volume 36, Issue 23, November 2011, Pages 15259–15265. (doi:10.1016/j.ijhydene.2011.08.081)

7. "H2A Hydrogen Production Analysis Model Version 3," Darlene Steward, National Renewable Energy Laboratory, presented at 2012 DOE Hydrogen and Fuel Cells Program Review, Washington, DC, May 15, 2012.

8. Peters, Max S., Timmerhaus, Klaus D., West, Ronald E., Equipment Costs Plant Design and Economics for Chemical Engineers – 5th Edition, (New York, NY: McGraw-Hill, 2002). http://www.mhhe.com/engcs/chemical/peters/data/ce.html

9. "Low-Cost Precursors to Novel Hydrogen Storage Materials," Final Report, Suzanne W. Linehan, Arthur A. Chin, Nathan T. Allen, Robert Butterick, Nathan T. Kendall, I. Leo Klawiter, Francis J. Lipiecki, Dean M. Millar, David C. Molzahn, Samuel J. November, Puja Jain, Sara Nadeau, Scott Mancroni, The Dow Chemical Company, December 31, 2010, Prepared for U.S. Department of Energy, Office of Energy Efficiency and Renewable Energy Hydrogen Program, Hydrogen Storage, Under Contract DE-FC36-05GO15053.

IV.A.3 Best Practices for Characterizing Engineering Properties of Hydrogen Storage Materials

Karl J. Gross (Primary Contact), Russell Carrington[1], Steven Barcelo[1], Abhi Karkamkar[2], Justin Purewal[3], Pierre Dantzer[4], Shengqian Ma and Hong-Cai Zhou[5], Kevin Ott, Tony Burrell and Troy Semeslberger[6], Yevheniy Pivak and Bernard Dam[7], Dhanesh Chandra[8], Bruce Hardy[9]

H2 Technology Consulting LLC
PO Box 1302
Alamo, CA 94507
Phone: (510) 468-7515
Email: kgross@h2techconsulting.com

[1] University of California, Berkeley
[2] Pacific Northwest National Laboratory
[3] California Institute of Technology
[4] Université Paris-Sud
[5] Texas A&M University
[6] Los Alamos National Laboratory
[7] VU University Amsterdam and the Delft University of Technology
[8] University of Nevada, Reno
[9] Savannah River National Laboratory

DOE Managers
Jesse Adams
Phone: (720) 356-1421
Email: Jesse.Adams@go.doe.gov
Channing Ahn
Phone: (202) 586-9490
Email: Channing.Ahn@ee.doe.gov

Project Start Date: February 7, 2007
Project End Date: Project continuation and direction determined annually by DOE

Overall Objectives

- To prepare reference documents detailing best practices and limitations in measuring hydrogen storage and engineering properties of materials.
  - The documents are reviewed by experts in the field.
  - The final documents will be made available to researchers at all levels in the DOE hydrogen storage sub-program.

Fiscal Year (FY) 2013 Objectives

- To complete document section 6: "Measurements of Engineering Thermal Properties of Hydrogen Storage Materials"
- To complete document section 7: "Measurements of Engineering Mechanical Properties of Hydrogen Storage Materials"

Technical Barriers

This project addresses the following technical barriers from the Hydrogen Storage section of the Fuel Technologies Office Multi-Year Research, Development, and Demonstration Plan:

(A) System Weight and Volume

(C) Efficiency

(D) Durability/Operability

(E) Charging/Discharging Rates

(J) Thermal Management

(P) Reproducibility of Performance

Technical Targets

The goal of this project is to prepare reference documents detailing the recommended best practices and limitations in making critical performance and engineering properties measurements on hydrogen storage materials. These reference documents will provide a resource to improve the accuracy and efficiency of critical measurements to aid the projects and ultimately the entire program to achieve or exceed the technical storage targets.

In particular this project is focused on the following target-related performance measurements:

- Kinetics: System fill time for 5-kg hydrogen, minimum full-flow rate and start time to full-flow
- Capacity: gravimetric and volumetric capacity
- Thermodynamic Stability: maximum/minimum delivery pressure of H_2 from tank and impact on capacity and kinetic-related targets
- Cycle-Life Properties: cycle life and cycle life variation
- Heat Transfer Properties: system fill time for 5-kg hydrogen, minimum full-flow rate and start time to full-flow

FY 2013 Accomplishments

- Contributions to this project from world experts have been received including written materials, examples, presentation or editorial review of draft documents.
- External contributions and review of Engineering Thermal Properties section completed through collaborations with:
  - Dr. Maximilian Fichtner, Karlsruher Institute for Technology, Germany
  - Dr. Robert Bowman Jr., Consultant to U.S. Department of Energy
  - Dr. Ewa Rönnebro, Pacific Northwest National Laboratories
  - Dr. Bart van Hassel, United Technologies Research Center, USA
  - Dr. Lars Röntzsch, Fraunhofer Institute for Manufacturing Technology and Advanced Materials, Dresden, Germany
  - Dr. Michel Latroche, Institut de Chimie et des Matériaux de Paris Est CNRS, France
  - Dr. Patricia De Rango, Institut Néel CNRS, Grenoble, France
  - Dr. Mike Veenstra, Dr. Jun Yang, and Dr. Andrea Sudik, Ford Motor Co.
  - Dr. Bruce Hardy, Savannah River National Laboratory
  - Professor David Grant and Dr. Alastair Stuart, of the University of Nottingham, United Kingdom
- Sections 1-5 (Introduction, Kinetics, Capacity, Thermodynamic, and Cycle-Life Properties sections 100% complete.
- "Recommended Best Practices for the Characterization of Storage Properties of Hydrogen Storage Materials" sections 1-5 posted on DOE website for world-wide access. Please download the current document from: http://www1.eere.energy.gov/hydrogenandfuelcells/pdfs/best_practices_hydrogen_storage.pdf
- Thermal Properties section 6, 100% complete and posted on DOE website for world-wide access. Please download the current document from: http://www1.eere.energy.gov/hydrogenandfuelcells/pdfs/best_practices_hydrogen_storage_section_6.pdf
- Mechanical Properties section currently in progress.

✧ ✧ ✧ ✧ ✧

INTRODUCTION

The Hydrogen Storage sub-program goal is the development of hydrogen storage materials that meet or exceed the DOE's targets for the onboard hydrogen storage in a hydrogen-powered vehicle. The growth of research efforts in this field and new approaches to solving storage issues has brought the talents of a wide-range of researchers to bear in solving the grand challenge of hydrogen storage. There is a need to have common metrics and best practices for measuring the practical hydrogen storage properties of new materials that are being developed within the DOE Hydrogen Storage Program as well as at an international level. H2 Technology Consulting is tasked with creating clear and comprehensive resources that will provide detailed knowledge and recommendations for best practices in the measurements of these properties.

APPROACH

This project is a combined approach of documenting the experience the primary contact and other experts in the field have with these measurement, incorporating examples from the literature, performing experimental measurements to demonstrate important issues, and finally, condensing key information into concise reference guides. Each section covers such topics as the overall purpose of the measurements, some basic theory, experimental consideration, methods of measurement, and many details on both material properties and experimental factors that may strongly influence the final results and conclusions. Participation from other experts in the field is being sought out for input, relevant examples, and critical review at all levels.

RESULTS

This year work was completed on the "Best Practices for Characterizing Engineering Properties of Hydrogen Storage Materials" document section 6 covering the measurement of Thermal Properties of hydrogen storage materials and it is now posted on the DOE website.

For this work collaborations were established with the following international experts in the field: Ewa Rönnebro, Pacific Northwest National Laboratory; Bart van Hassel, United Technologies Research Center; Lars Röntzsch, Fraunhofer Institute for Manufacturing Technology and Advanced Materials, Dresden, Germany; Michel Latroche, Institut de Chimie et des Matériaux de Paris Est CNRS, France; Patricia De Rango, Institut Néel CNRS, Grenoble, France; Mike Veenstra and Jun Yang of Ford Motor Co.; Bruce Hardy, of Savannah River National Laboratory; and David Grant, of the University of Nottingham, United Kingdom. In addition, the work has been coordinated and has received important scientific input through our contract

monitor Phil Parilla at the National Renewable Energy Laboratory.

This year's second task is on section 7: Engineering Mechanical Properties measurements. It includes:

1. The examination of benefits and limitations of methods for measuring porosity, skeletal, apparent, and packing densities.
2. The validity of translating measurements on small samples to full systems scale performance.
3. Currently used and alternative methods for measuring material expansion forces will also be presented.

The objective of this subtask is to review measurement techniques currently being used for measuring mechanical properties of hydrogen storage materials. As this has not been done extensively in this field, the task will include an evaluation of common mechanical properties measurement methods used in other applied materials fields that may be appropriate for hydrogen storage materials. A focus will be on clarifying problem areas in these measurements and to establish some common methods.

The following are some examples of the content of the work performed in FY 2013 on these two engineering properties sections.

Section 6: Measurements of Engineering Thermal Properties of Hydrogen Storage Materials

Thermal Conductivity: Thermal conductivity is a property of a conducting medium and, like the viscosity, is primarily a function of temperature [1]. Thermal conductivity k (sometimes given by the symbol λ), in ($W \cdot K^{-1} \cdot m^{-1}$), describes the ability of a material to transfer heat. This transfer of heat is defined by Equation 1 (called Fourier's law):

Equation 1

$$Q_x = -kA\frac{dT}{dx}$$

where Q_x is the heat transfer rate in the x direction, in W; A is the area normal to direction of heat flux, in m^2; dT/dx is the temperature gradient in the x direction, in $K^{-1} \cdot m^{-1}$, and k is the thermal conductivity, in $W \cdot K^{-1} \cdot m^{-1}$. The negative sign indicates that the flux is down the gradient, and it can be shown from irreversible thermodynamics that the coefficient k is always positive.

There are many different methods to measure thermal conductivity and there are a number of considerations in selecting an appropriate measurement method beginning with the form of the material (gas, liquids, solids, powders) and the temperature range for which the material will be used. Section 6 of the Best Practices document describes in detail a wide range of methods and the criteria for selecting the most appropriate technique for hydrogen storage materials measurements. One example is the "Guarded Hot Plate" measurement method. Figure 1 presents a schematic representation of a guarded hot plate instrument for measuring thermal conductivities of powdered hydrogen storage materials.

The Guarded Hot Plate method uses unidirectional heat transfer through a pair of identical samples. A temperature gradient within each sample is formed by producing a known heat flux to a hot plate between the samples while providing a heat sink at a cold plate on the opposite side of each sample. The temperatures at each side of the samples are measured when the system reaches steady state. Using the heat flux, sample thickness and surface areas, and temperature measurements, Fourier's unidirectional heat conduction equation can then be applied to easily calculate an effective thermal conductivity for the samples.

Another example is the in situ measurement of effective thermal conductivity using the Thermal Probe method. The thermal conductivity of sodium-alanates was measured under a variety of charged and discharged condition by Dedrick et al. using the thermal probe method and finite element modeling. The apparatus developed for those measurements is shown in Figure 2.

The accurate determination of the effective thermal conductivity and heat capacity of storage materials, additives, and system components is critical for modeling and design of advanced systems. An example of materials and system modeling is given below for an advanced complex-

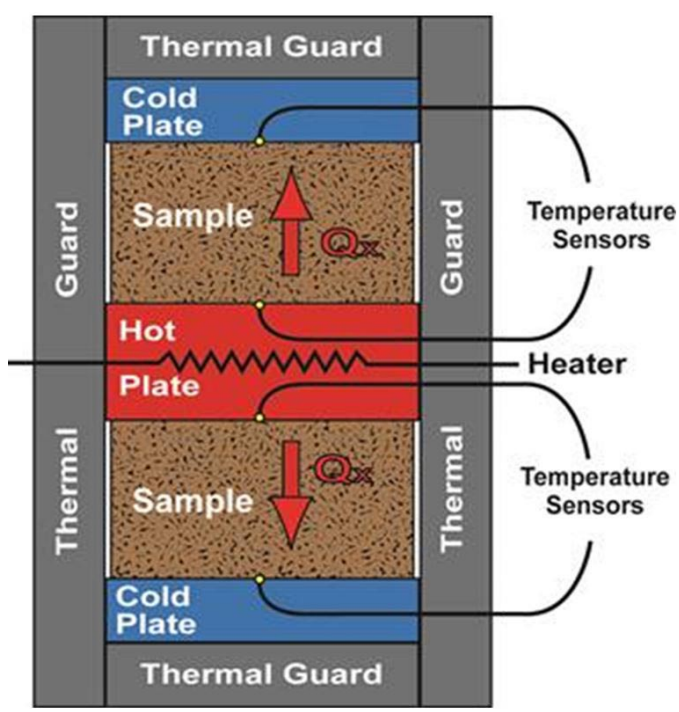

FIGURE 1. Schematic of Basic Guarded Hot Plate Design

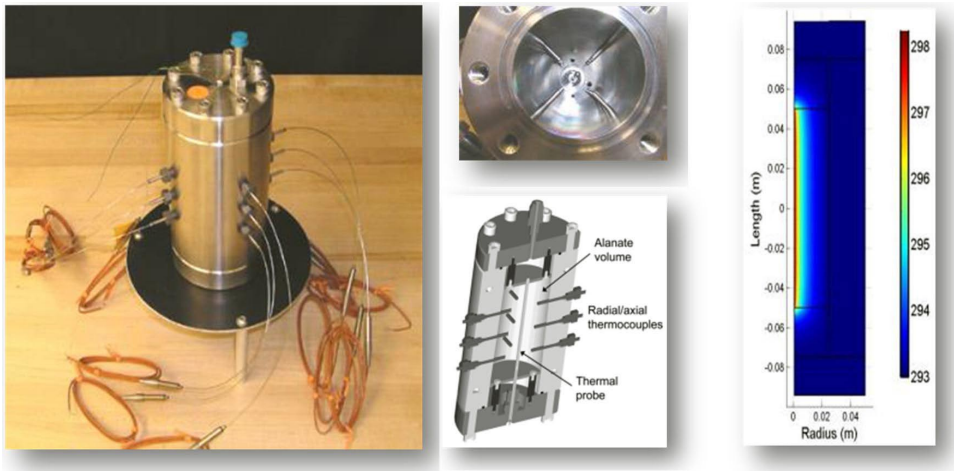

FIGURE 2. Instrumented Chamber and Modeling Results to Measure Thermal Conductivity and Wall Resistance as a Function of Phase, Temperature, Cycle, Morphology, and Pressure [2,3]

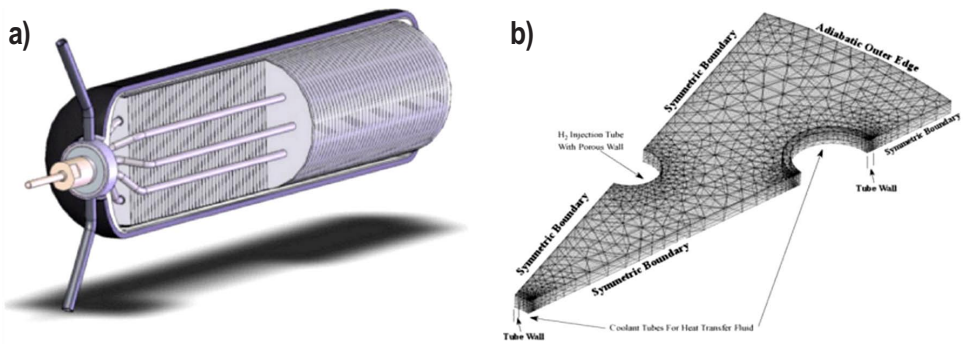

FIGURE 3. a) Example of a Shell, Tube and Fin Complex Hydride Bed Configuration [5]; **b)** Geometry for a Three-Dimensional Shell, Tube and Fin Computations Model [4]

hydride ($TiCl_3$ doped sodium alanate) system that includes a shell and tube heat transfer solution. The low thermal conductivity of the alanate necessitated design features that maintained a relatively short length scale for heat transfer within the bed. A schematic rendition of a prototype system (United Technologies Research Center) and the geometric configuration of the finite element model (Savannah River National Laboratory) are shown in Figure 3. Computational modeling was used to be able to simulate the behavior of complex metal hydride tanks [4].

Simulation results for charging the bed are shown in Figure 4. The image (left) shows the reduction in temperature from the mid-plane of the hydride layer to the mid-plane of the fin. The plan view (right) shows the temperature profile over the mid-plane of the hydride layer. Such modeling aids in understanding and designing for large temperature gradients in complex hydride-based storage beds. A critical requirement is the input of accurately measured parametric data such as the effective thermal conductivity and heat capacity of the storage material and components.

The Section 7: Measurements of Engineering Mechanical Properties of Hydrogen Storage Materials

Lattice volume expansion on hydriding has a significant impact on the mechanical properties of hydride storage materials. Hydrogen absorption causes varying degrees of decrepitation in metal hydrides. Cycling and vibration in normal hydrogen storage applications can cause segregation and interlocking of microscopic particles which, by expansion during hydriding, can impart enormous forces on a containment vessel, change material storage properties, and affect the long-term stability of the storage materials. Figure 5 is a schematic representation of an example of the process and potential impact (material-based mechanical failure of a hydride storage tank) of the mechanical properties of hydrogen storage materials.

Lattice expansion, decrepitation, particle size distribution, and expansion forces are some of the many important mechanical properties of hydrogen storage

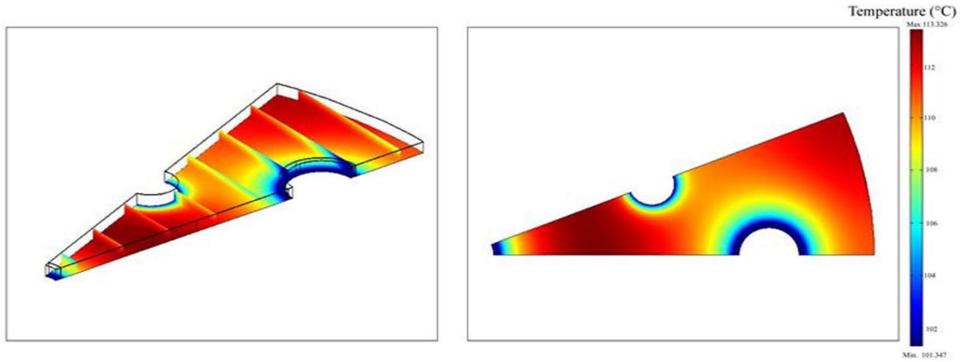

FIGURE 4. Isometric and Plan Views of Temperature Profile for Three-Dimensional Model at 40 Seconds; Base of Isometric Figure is at Bed Mid-Plane (center of the hydride bed layer between fins) [4]

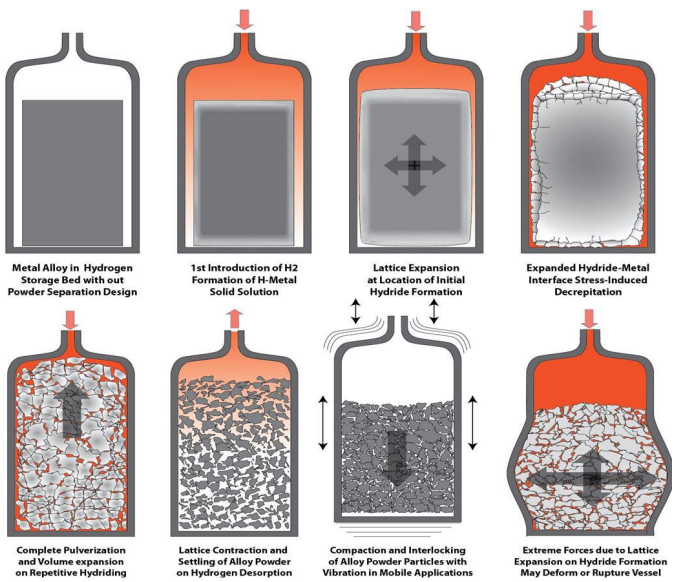

FIGURE 5. Schematic Illustration of Hydride Expansion in Confined Storage Vessel

materials that must be measured and evaluated in the process of developing advanced hydrogen storage systems.

CONCLUSIONS AND FUTURE DIRECTIONS

In FY 2013 we were able to establish important collaborations and technical assistance from experts in the field. We finalized section 6: "Measurements of Engineering Thermal Properties of Hydrogen Storage Materials." in a timely manner. We are currently working on completing the final version of the Engineering Mechanical Properties measurement section (7) of the document.

FY 2013 PUBLICATIONS/PRESENTATIONS

1. "Recommended Best Practices for the Characterization of Storage Properties of Hydrogen Storage Materials" sections 1-5 posted on DOE website for world-wide access. Please download the current document from: http://www1.eere.energy.gov/hydrogenandfuelcells/pdfs/best_practices_hydrogen_storage.pdf

2. Thermal Properties section 6, 100% complete and posted on DOE website for world-wide access. Please download the current document from: http://www1.eere.energy.gov/hydrogenandfuelcells/pdfs/best_practices_hydrogen_storage_section_6.pdf

SPECIAL RECOGNITIONS & AWARDS

1. 2013 DOE Hydrogen and Fuel Cells Program; Hydrogen Storage Sub-Program Award recognizing outstanding technical contributions http://www.hydrogen.energy.gov/annual_review13_awards.html

REFERENCES

1. Welty, J.R. and Wicks, C.E., "*Fundamentals of momentum, heat, and mass transfer*", Ed. John Wiley, 4th ed. (2001), New York, U.S.A.

2. Dedrick, D.E., Kanouff, M.P., Replogle, B.C. and Gross, K.J., "*Thermal properties characterization of sodium alanates*", J. Alloys and Compounds, Vol. 389, (2005) p. 299–305.

3. K. Gross et al. "*Hydride Development for Hydrogen Storage*", DOE Hydrogen and Fuel Cells Annual Merit Review, Berkeley, CA May 19–22, 2003.

4. Hardy, B.J., Anton, D.L. "*Hierarchical methodology for modeling hydrogen storage systems. Part II: Detailed models*". Int. J. of Hydrogen Energy, 34 (2009), p. 2992-3004.

5. Mosher, D., Tang, X., Arsenault, S., Laube, B., Cao, M., Brown, R. and Saitta, S. "*High Density Hydrogen Storage System Demonstration Using $NaAlH_4$ Complex Compound Hydrides*". DOE Hydrogen Program Annual Peer Review, Arlington, VA, 2007.

IV.B.1 Hydrogen Storage Engineering Center of Excellence

Donald L. Anton (Primary Contact),
Theodore Motyka, Bruce J. Hardy,
David A. Tamburello and Claudio Corgnale
Savannah River National Laboratory (SRNL)
Bldg. 999-2W
Aiken, SC 29808
Phone: (803) 507-8551
Email: DONALD.ANTON@SRNL.DOE.GOV

DOE Managers
Ned Stetson
Phone: (202) 586-9995
Email: Ned.Stetson@ee.doe.gov
Jesse Adams
Phone: (720) 356-1421
Email: Jesse.Adams@go.doe.gov

Technical Advisor
Robert Bowman
Phone: (818) 354-7941
Email: rcbjr1967@gmail.com

Subcontractors:

- Pacific Northwest National Laboratory (PNNL), Richland, WA
- United Technologies Research Center (UTRC), E. Hartford, CT
- General Motors (GM), Detroit, MI
- Ford Motor Company. (FMC), Dearborn, MI
- The National Renewable Energy Laboratory (NREL), Golden, CO
- Los Alamos National Laboratory (LANL), Los Almaos, NM
- The Jet Propulsion Laboratory (JPL), Pasadena, CA
- The University of Michigan (UM), Ann Arbor, MI
- The California Institute of Technology (Cal Tech), Pasadena, CA
- Oregon State University (OSU), Corvallis, OR
- Hexagon Lincoln LLC, Lincoln, NB
- University of Québec, Trios Rivieres (UQTR), Trois Rivieres, QC, Canada

Project Start Date: February 1, 2009
Project End Date: March 31, 2015

Overall Objectives

- Develop system models that will lend insight into overall fuel cycle efficiency.
- Compile all relevant materials data for candidate storage media and define future data requirements.
- Develop engineering and design models to further the understanding of onboard storage energy management requirements.
- Develop innovative onboard system concepts for metal hydride, chemical hydrogen storage, and adsorption hydride materials-based storage technologies.
- Design components and experimental test fixtures to evaluate the innovative storage devices and subsystem design concepts, validate model predictions, and improve both component design and predictive capability.
- Design, fabricate, test, and decommission the subscale prototype components and systems of each materials-based technology (adsorbents, metal hydrides, and chemical hydrogen storage materials).

Fiscal Year (FY) 2013 Objectives

Hydrogen Storage Engineering Center of Excellence (HSECoE) Management

- Coordination and facilitation of partner's activities
  - Organize and conduct one F2F Center Technical Meeting.
  - Publish two metal hydride models on the HSECoE website.
  - Complete Phase 3 Go/No-Go requirements.
- Complete balance of plant (BOP) and cost analysis for adsorbent system (performance and cost analysis).
- Complete balance of plant and cost analysis for chemical hydride system (performance and cost analysis).
- Complete prototype system testing plan for both adsorbent and chemical hydride systems (integrated power plant and storage system modeling).
- Demonstrate adsorbent system heating (transport phenomena).
- Demonstrate stable flow-through reactor design for slurry ammonia borane (AB) (transport phenomena).
- Identify scale-up methods for slurry AB (materials operating requirements).
- Identify optimum adsorbent packing strategies (materials operating requirements).
- Submit for publication two peer reviewed journal articles outlining the required materials properties needed to meet the DOE System Technical Targets for adsorbents and chemical hydrides (materials operating requirements).

- Demonstrate stable gas liquid separator design (enabling technologies).
- Complete manufacturing analysis to determine adsorbent system down-select priority (enabling technologies).
- Identify and design one adsorbent system to go forward with in Phase 3.
- Identify and design one chemical hydride system to go forward with in Phase 3.

SRNL HSECoE Technical Work Scope

- Design apparatus for heating the adsorbent to yield H2 discharge on an appropriate time scale and compatible with flow-through cooling.
- Identify form of MOF-5 to be used in prototype and sub-scale prototype tests.
- Apply/develop system models to:
  - Determine best performing metal-organic framework (MOF) form.
  - Determine consumption of stored hydrogen for heating and other processes.
  - Identify optimal system design concepts.
  - Evaluate cooling processes other than flow-through cooling.
- Develop concept of cooled tank wall to reduce exhaust H2 required for flow-through cooling.
- Evaluate alternative methods to flow-through cooling:
- Determine minimally acceptable adsorbent material properties to meet the 2017 and ultimate system targets.

Technical Barriers

This project addresses the following technical barriers from the Hydrogen Storage section of the Fuel Cell Technologies Office Multi-Year Research, Development, and Demonstration Plan:

(A) System Weight and Volume

(B) System Cost

(C) Efficiency

(D) Durability/Operability

(E) Charging/Discharging Rates

(G) Materials of Construction

(H) Balance-of-Plant (BOP) Components

(J) Thermal Management

(K) System Life Cycle Assessments

(L) Lack of Tank Performance Data and Understanding of Failure Mechanisms

(O) Lack of Understanding of Hydrogen Physisorption and Chemisorption

(R) By-Product/Spent Material Removal

Technical Targets

This project directs the modeling, design, build, and demonstration of prototype hydrogen storage systems for each metal hydride, chemical hydrogen storage, and hydrogen adsorption material meeting as many of the DOE Technical Targets for light-duty vehicular hydrogen storage. The current status of these systems versus the onboard hydrogen storage system technical targets as of the end of Phase 2 is given in Table 1.

FY 2013 Accomplishments

Center Wide Accomplishments

- Completed Phase 3 Go/No-Go requirements.
- Completed assessment of chemical hydrogen storage materials and systems. Will terminate work on these systems due to low probability of identifying materials that meet 8.5 wt% fluid gravimetric requirements and regeneration efficiencies.
- Developed a 6 wt% H2 liquid phase chemical hydrogen storage media having a viscosity before and after dehydrogenation below 1,500 cP.
- Developed a 45 wt% AB slurry having a viscosity less than 1,500 cP.
- Developed a flow-through reactor capable of discharging 0.8 g/s H2 from a 40 wt% AB fluid-phase composition having a mass of no more than 2 kg and a volume of no more than 1 liter.
- Developed an ammonia scrubber resulting in a minimum ammonia outlet concentration of 0.1 ppm (inlet concentration = 500 ppm) having a maximum mass of 1.2 kg and a maximum volume of 1.6 liters.
- Designed a chemical hydrogen storage system based on 50% AB/Si oil having a mass of 137 kg and a volume of 147 liters.
- Demonstrated a composite MOF-5 adsorbent monoliths having H2 effective kinetics equivalent to 5.6 kg usable H2 over three minutes and permeation in packed and powder particle beds with flow rate of 1 m/s superficial velocity and pressure drop of 5 bar.
- Completed assessment of adsorbent storage system. Down-selected both the Hexcel and modular adsorbent tank insert (MATI) heat exchanger designs for subscale prototype adsorbent systems to be evaluated in Phase 3.
- Completed composite MOF-5 adsorbent monoliths were demonstrated having H2 effective kinetics equivalent to

TABLE 1. System Status vs. Technical Targets

			Adsorbent System			Chemical Systyem		
			Phase 2 *Actual (automotive scale)*			Projected System HSECoE Go/No-Go*What could be built in the future (full scale)*		
Target	Units	2017 DOE Goal (System)	Phase 2 HSECoE Targets (Material)	Phase 2 HSECoE Targets (BOP only)	Phase 2 HSECoE Targets (System)	Phase 2 HSECoE Targets (Material)	Phase 2 HSECoE Targets (BOP only)	Phase 2 HSECoE Targets (System)
Gravametric Capacity	kg H2/kg system	0.055	0.187	0.10	0.0352	0.0872	0.15	0.055
mass	*kg*	*102*		*16.1*	159			*102*
Volumetric Capacity	kg H2/L system	0.04	0.03	0.053	0.0175	0.078	0.132	0.049
Volumetric	*liters*	*140*		*16.9*	320			*114*
System Cost	$/kWh net	6	3.5	5.62	12.74			
	$	*1,119*		*1048*	2376			
Fuel Cost	$/gge at pump	2-6			4.89			
Min Operating Temp	°C	-40			-40			-20
Max Operating Temp	°C	60			60			60
Min Delivery Temp	°C	-40			-40			-20
Max Delivery Temp	°C	85			85			85
Cycle Life	Cycles	1500			1500			1000
Min Delivery Pressure	bar	5			5			5
Max Delivery Pressure	bar	12			12			12
Onboard Efficiency	%	90			92			95
Well to Power Plant Efficiency	%	60			39.2			37
System Fill Time	min	3.3			3.3			2.9
Min Full Flow Rate	(g/s/kW)	0.02			0.02			0.02
	g/s	*1.6*			*1.6*			*1.6*
Start Time to Full Flow (20°C)	sec	5			5			1
Start Time to Full Flow (-20°C)	sec	15			15			1
Transient Response	sec	0.75			0.75			0.5
Fuel Purity	% H2	99.97			99.99			99.97
Permeation, Toxicity, Safety	Scc/h	Meets or Exceeds Standards			s			s
Loss of Useable Hydrogen	(g/h)/kg H2 stored	0.05			0.44			0.05

5.6 kg usable H2 over three minutes and permeation in packed and powder particle beds with flow rate of 1 m/s superficial velocity and pressure drop of 5 bar.

- Completed cryogenic pressure vessel burst testing of both Type I and IV composites tanks at 77 K and pressures exceeding design limits, proving the efficacy of composite cryogenic/composite pressure vessels.
- Demonstrated an internal flow-through the heat exchanger system based on compacted media was demonstrated capable of allowing less than three minute scaled refueling time and H2 release rate of 0.02 g H2/(sec. kW) with a mass less than 6.5 kg and a volume less than 6 liters.
- Identified system concepts have been identified having a mass less than 137 kg and a volume less than 279 liters meeting all of the HSECoE drive cycles.
- Achieved a well-to-power plant efficiency of 39.9% for the 80 K/60-bar system which is 65% of the ultimate target of 60% efficiency.

SRNL Technical Accomplishments

- Demonstrated a demonstration of a flow-through cooling system and validated detailed models for both powder MOF-5 and compacted MOF-5 pellets.
- Developed an adsorbent acceptability envelope (AAE) that identifies coupled material properties and system dimensions that affect gravimetric capacity, volumetric capacity, charging rates, and charging/discharging rates.
- Designed, evaluated, and demonstrated heat transfer technologies for cooling the adsorbent during the charge phase and heating it during the discharge phase.
  - Charging is best achieved using LN_2-assisted flow-through cooling.
  - While pelletized MOF-5 offers some improvement in volumetric capacity, the time to charge and the mass of the system both increase compared to powder MOF-5 systems.
- Down-selected powder MOF-5 after detailed component and system level performance for modified forms including pellets at different levels of compaction and amended MOF-5 containing additives to enhance thermal conductivity.
- Developed a fully customizable cryo-adsorbent system model to compare possible full-scale systems.
  - Parametric study: reduced over ½ billion possible adsorbent system models down to two adsorbent systems that will be evaluated as prototypes in Phase 3.

– Projected future system designs assuming possible system, component, and/or material improvements to identify systems that could meet or surpass the DOE 2017 Technical Targets.

✧ ✧ ✧ ✧ ✧

INTRODUCTION

The HSECoE brings together all of the materials and hydrogen storage technology efforts to address onboard hydrogen storage in light-duty vehicle applications. The effort began with a heavy emphasis on modeling and data gathering to determine the state of the art in hydrogen storage systems. This effort spanned the design space of vehicle requirements, power plant and BOP requirements, storage system components, and materials engineering efforts. These data and models will then be used to design components and sub-scale prototypes of hydrogen storage systems which will be evaluated and tested to determine the status of potential system against the DOE 2017 light-duty vehicle technical targets for hydrogen storage systems.

APPROACH

A team of leading North American national laboratories, universities, and industrial laboratories, each with a high degree of hydrogen storage engineering expertise cultivated through prior DOE, international, and privately sponsored programs, has been assembled to study and analyze the engineering aspects of condensed phase hydrogen storage as applied to automotive applications. The technical activities of the Center are divided into three system architectures; adsorbent, chemical hydrogen storage, and metal hydride, and are matrixed with six technologies areas: Performance Analysis, Integrated Power Plant/Storage System Analysis, Materials Operating Requirements, Transport Phenomena, Enabling Technologies and Subscale Prototype Construction, Testing and Evaluation. The project is divided into three phases: Phase 1: System Requirements and Novel Concepts; Phase 2: Novel Concept Modeling Design and Evaluation Phase; 3: Subscale System Design, Testing and Evaluation.

RESULTS

SRNL and its subrecipient UQTR to date have met and or exceeded their FY 2013 objectives for all of their major technical goals within the HSECoE. These objectives fall within the areas of Transport Phenomena, Adsorbent System Level Modeling, Material Operating Requirements and System Architecture. Transport Phenomena and Adsorbent System Modeling results are shown below for adsorbent systems.

Transport Phenomena

- Developed an AAE that identifies coupled material properties and system dimensions that affect gravimetric capacity, volumetric capacity, charging rates, and discharging rates. Figure 1 provides a functional diagram of the AAE.

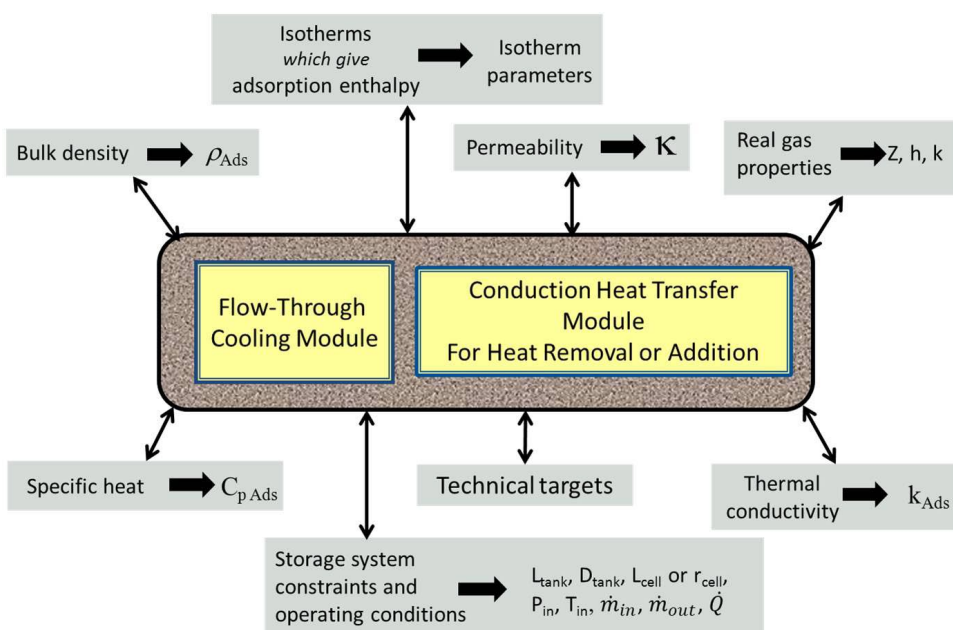

FIGURE 1. Functional diagram of the AAE.

  - The AAE utilizes coupled, lumped parameter, transient energy, and mass balances that are solved numerically, accounting for the adsorbent material properties, the heat of adsorption, internal heat exchanger concepts, storage vessel designs, and the assumed BOP.
  - The AAE can be used to either evaluate adsorbents with known properties (isotherms, thermal conductivity, specific heat, etc.) or to determine the adsorbent properties required to meet performance targets.
- Carried out experiments for different flow-through cooling adsorbent systems, with experimental conditions and data measured. The flow-through cooling concept, which applies to both powder and pellet based systems, was tested using a specially designed reservoir with an internal diameter of 0.05 m and a length of 0.3 m. A two-dimensional sketch of the reservoir is reported in Figure 2.
- Detailed numerical models were validated against data for several flow-through cooling experimental configurations. Figure 3 provides an example of these experimental and computational comparisons.
  - MOF-5 powder with no internal heat exchanger.
  - MOF-5 pellets within a Hexcel internal heat exchanger, using MaxSorb powder as filler in the void spaces around the pellets.
  - MOF-5 powder within a Hexcel internal heat exchanger.
- Both experimental measurements and numerical models of the flow-through cooling technique showed that the performance of powder-form adsorbents was superior to that of pellet-form, as shown in Figure 4.

Adsorbent System Level Modeling

- The MatLAB® version of the cryo-adsorbent system models has been updated to reflect the latest input from all HSECoE partners for both of the primary designs. Figure 5 shows the latest version of the flow-through cooling with a Hexcel resistance heater design, while Figure 6 shows the latest version of the MATI-isolated LN_2/H_2 heat exchanger design.
- Created cryo-adsorbent system model improvement projections (using the MatLAB® versions) based on altered versions of "powder MOF-5" (changed the Dubinin-Astakhov parameters and/or material properties in "what if" scenarios). Figure 7 shows examples of these projections.
- Both the Simulink® and MatLAB® versions of the cryo-adsorbent system models have been updated to include the following options, with additional testing, debugging, and updates ongoing. Note that all subroutines have expansion abilities should additional options/improvements be available/desirable:
  - First order system and individual component cost estimates.

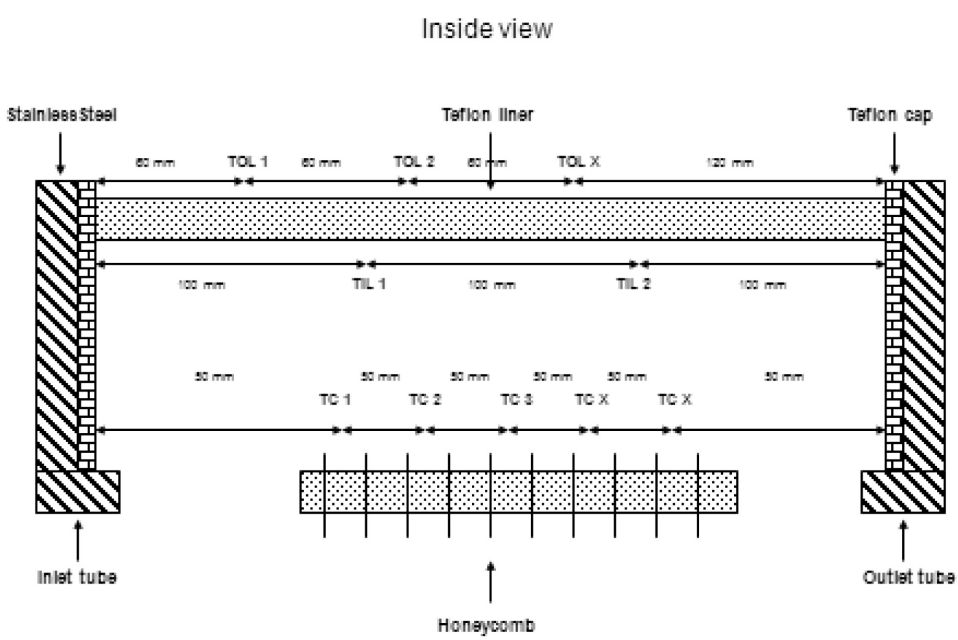

Teflon is a registered trademark of E. I. du Pont de Nemours and Company

FIGURE 2. Inside view of the reservoir used for pellet and powder-form experiments.

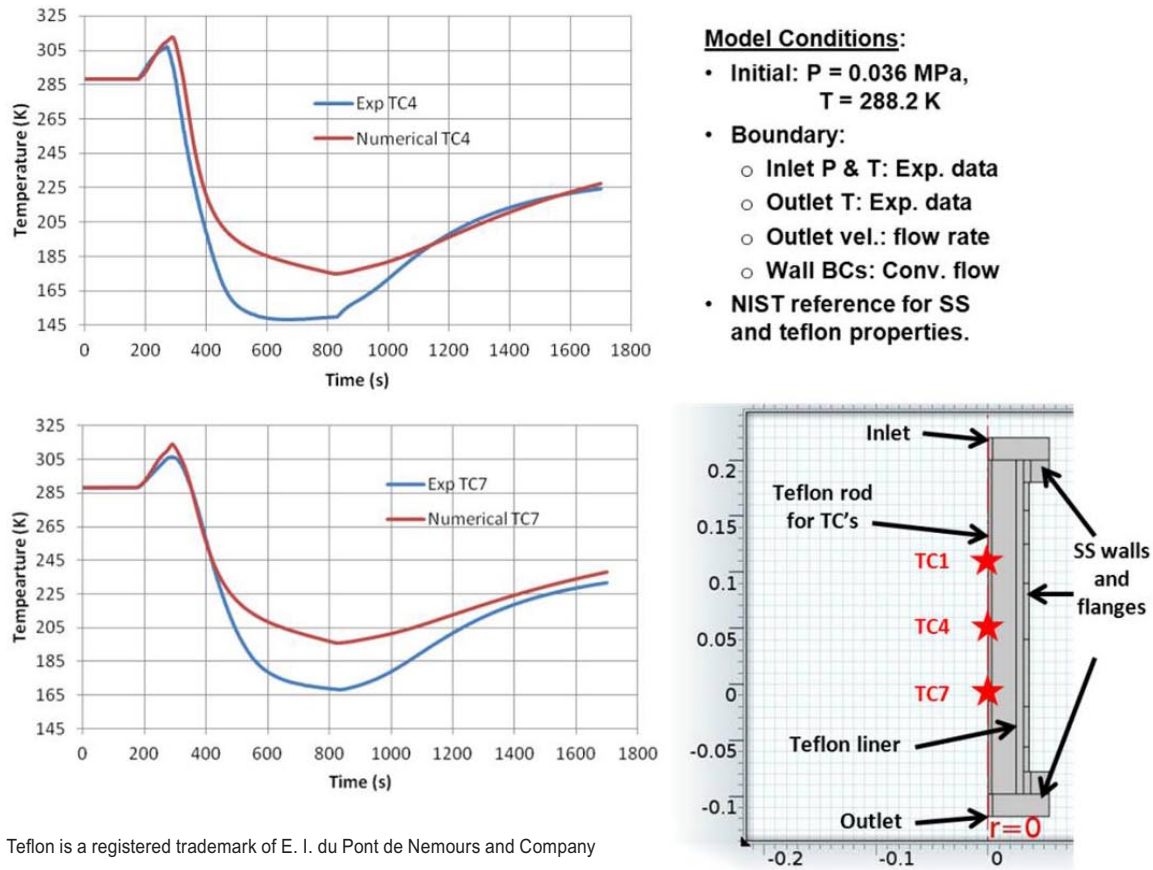

Teflon is a registered trademark of E. I. du Pont de Nemours and Company

FIGURE 3. Experimental data versus numerical simulations of MOF-5 powder with no internal heat exchanger.

- Overall system ranks based on a value algorithm developed by Ford that incorporates the system cost, gravimetric capacity, and volumetric capacity.
- Dubinin-Astakhov parameters for hydrogen storage within several cryo-adsorbents (single and multi-component versions are available).
- Internal tank heat exchanger concepts, where the mass and volume of the heat exchanger is adaptable based on the properties (and amount) of the cryo-adsorbent.
- A tank design algorithm, with a wide variety of material and dimensional options, which was developed by PNNL with input from SRNL and Hexagon Lincoln.

CONCLUSIONS AND FUTURE DIRECTIONS

Chemical hydride efforts were centered on slurry/solvent materials utilizing flow through reactor development with dynamic temperature control, high-flow gas liquid separation and impurity trapping. Studies were continued on endothermic and exothermic chemical. Ultimately, the chemical hydride efforts were terminated based on the regeneration costs and other associated technology factors outside of the HSECoE scope.

Adsorbent system efforts concentrated on material, subcomponent, and system characterization and validation leading up to the system selection for prototype testing in Phase 3. Two prevailing designs were identified: 1) powder MOF-5 in a hexagonal structure (Hexcel) that utilizes flow-through cooling during refueling and resistance heating during discharge, and 2) compacted MOF-5 in a MATI utilizing isolated-LN_2 during refueling and isolated-H2 during discharge. Several factors affected this selection, including the detailed model analyses with experimental validation, the overall system performance projections, the projected costs, the projected interaction with the forecourt, and the future direction of adsorbent material research.

Future technical work by SRNL in the adsorbent area will include:

- Validating, tuning, and refining the system model estimates of the prototype adsorbent systems in Phase 3.
- Validating, tuning, and refining the detailed models of the Phase 3 Hexcel prototype design, which uses powder MOF-5 in an aluminum hexagon with flow-through

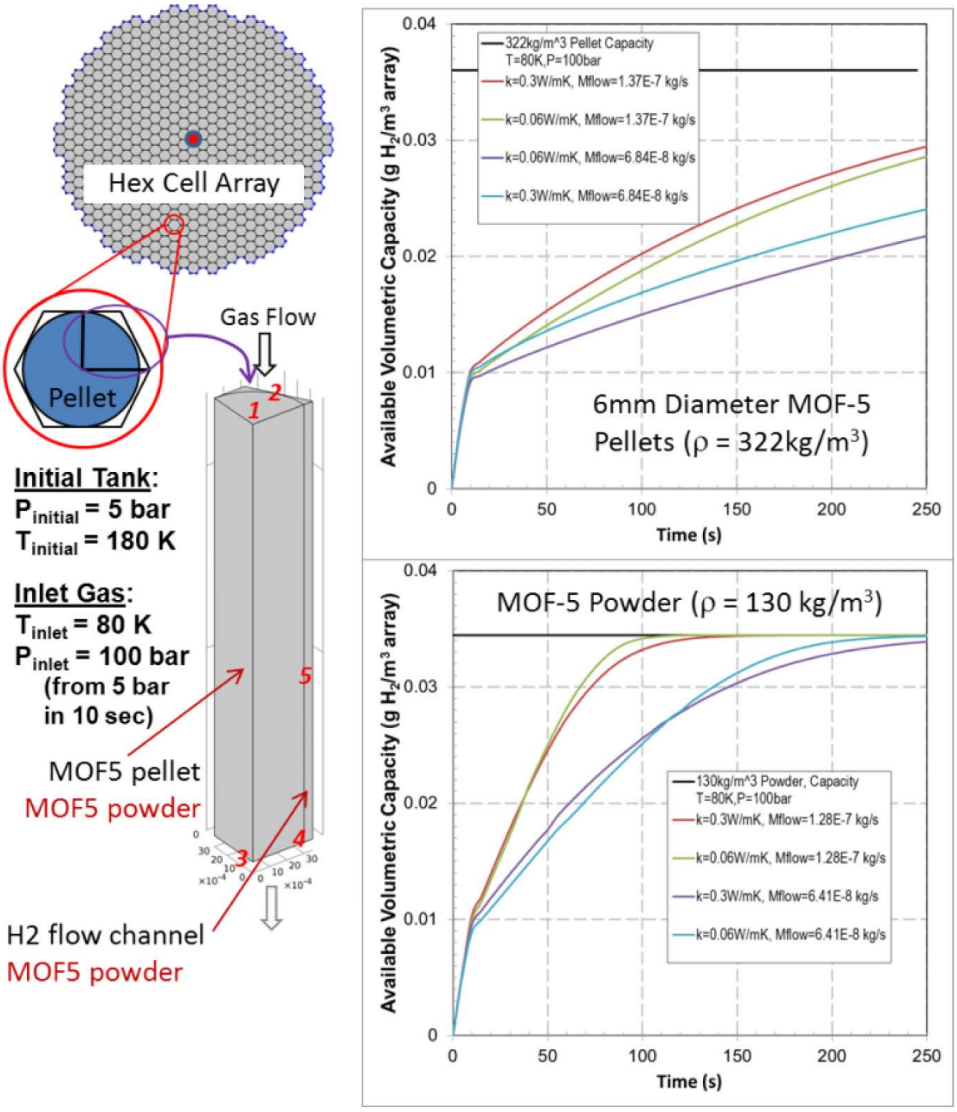

FIGURE 4. Computational analysis of MOF-5 pellet flow-over cooling versus MOF-5 powder flow-through cooling.

cooling during refueling and resistance heating during discharge.

- Building an experimental testing facility, designing, fabricating and evaluating a subscale prototype flow though adsorption system utilizing the Hexcel design.
- Building an experimental testing facility and testing the Phase 3 MATI prototype design, which uses compacted MOF-5 in the MATI with isolated-LN_2 cooling during refueling and isolated-H2 during discharge.

FY 2013 PUBLICATIONS/PRESENTATIONS

1. Corgnale C, Hardy B, Anton D. Structural Analysis of Metal Hydride-Based Hybrid Hydrogen Storage Systems. International Journal of Hydrogen Energy, Vol. 37, Issue 19, 2012, Pages 14223-14233.

2. Gross K, Hardy B. Recommended Best Practices for Characterizing Engineering Properties of Hydrogen Storage Materials. V148: November 20, 2012. National Renewable Energy Laboratory Contract No. 147388.

3. Hardy B, Corgnale C. Adsorbent Based Hydrogen Storage System Models. Invited paper at the 2012 World Hydrogen Energy Conference Toronto, Ontario, Canada.

4. Anton D, Hardy B, Motyka T, Pasini JM, Van Hassel B, Corgnale C, Kumar S, Simmons K. Metal Hydride Hydrogen Storage for Automotive Applications: Materials and System Challenges. 2012 World Hydrogen Energy Conference, Toronto, Ontario, Canada.

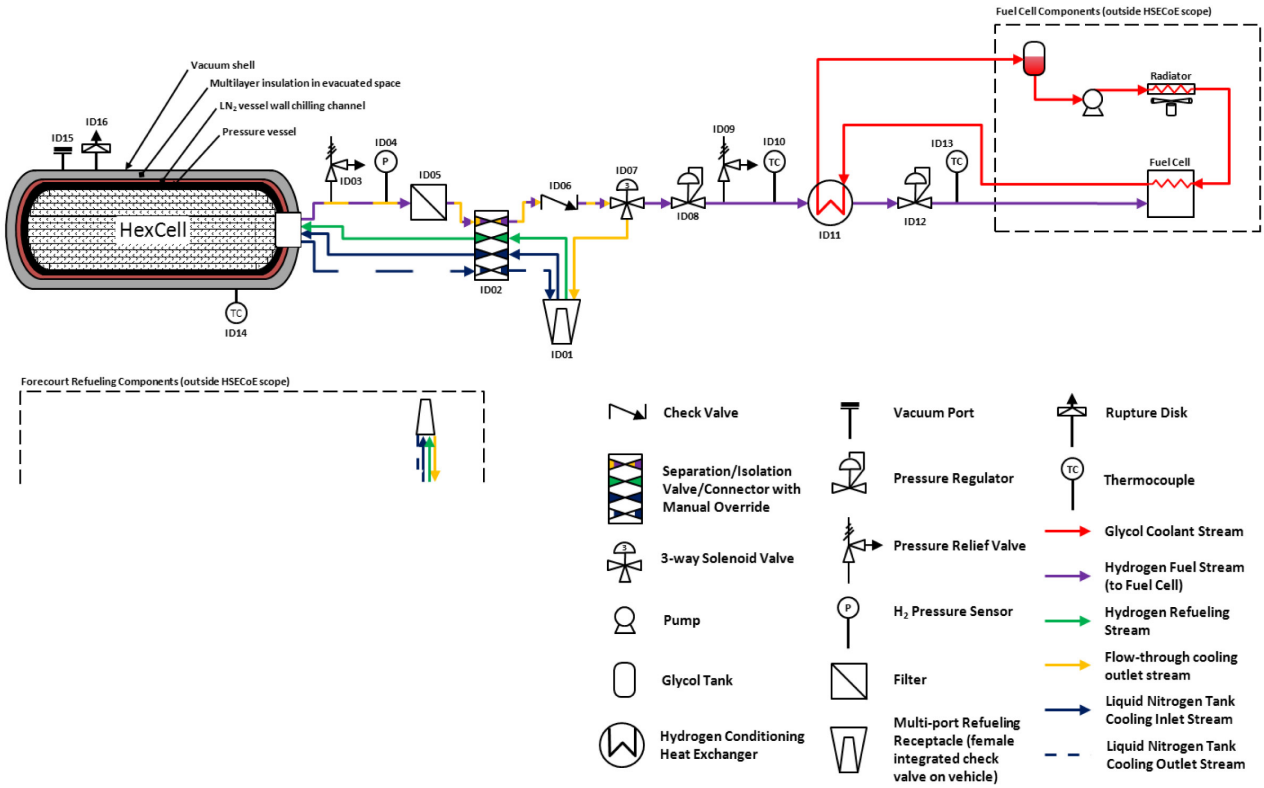

FIGURE 5. Overall system diagram for the flow-through cooling with a Hexcel resistance heater design.

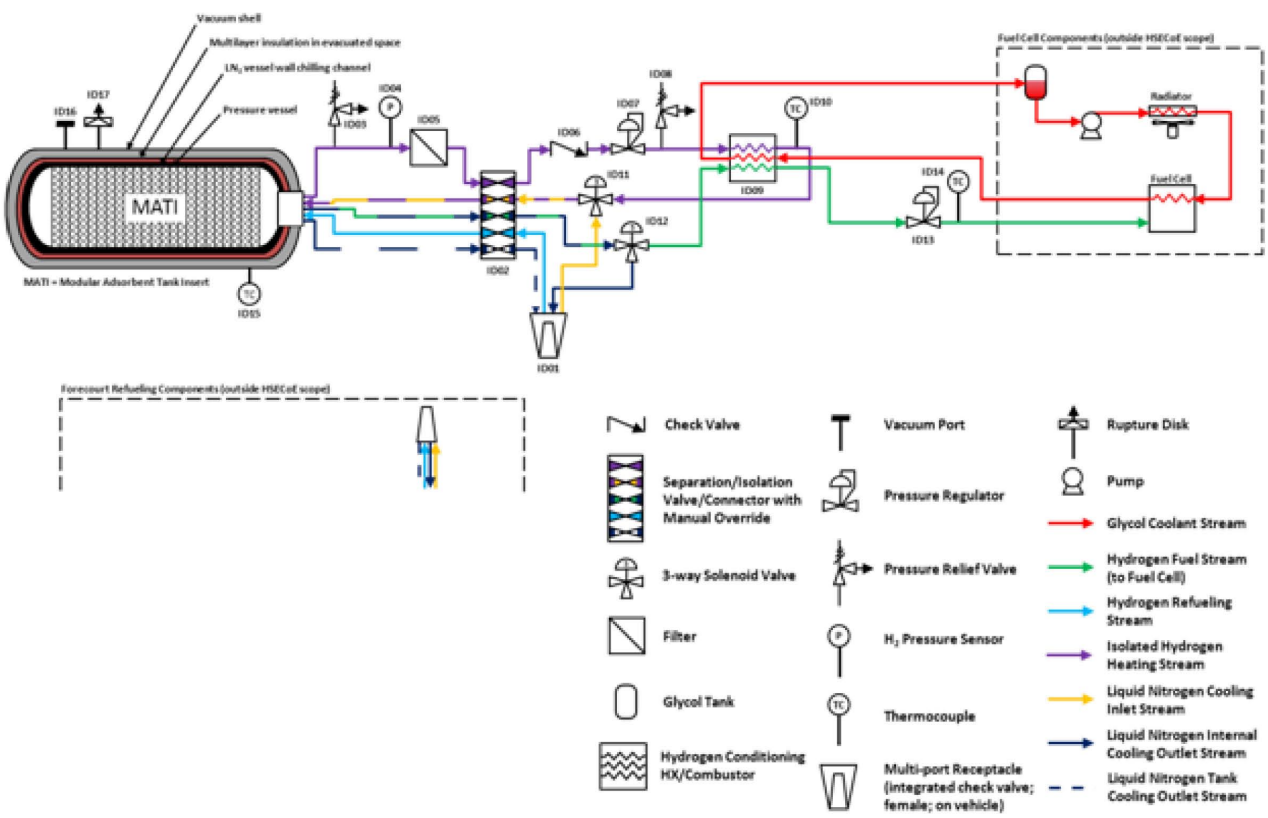

FIGURE 6. Overall system diagram for the MATI isolated-LN_2/H_2 heater design.

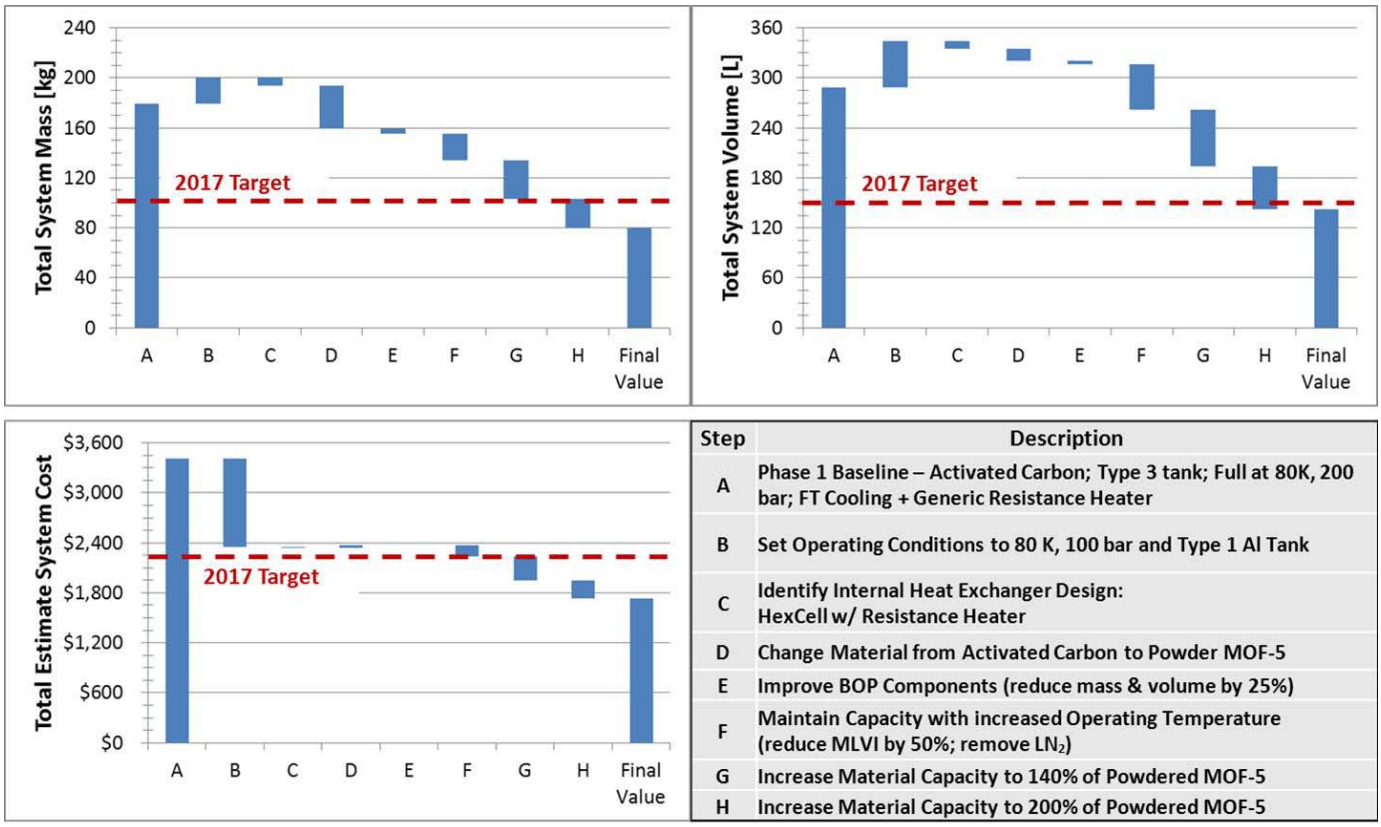

Step	Description
A	Phase 1 Baseline – Activated Carbon; Type 3 tank; Full at 80K, 200 bar; FT Cooling + Generic Resistance Heater
B	Set Operating Conditions to 80 K, 100 bar and Type 1 Al Tank
C	Identify Internal Heat Exchanger Design: HexCell w/ Resistance Heater
D	Change Material from Activated Carbon to Powder MOF-5
E	Improve BOP Components (reduce mass & volume by 25%)
F	Maintain Capacity with increased Operating Temperature (reduce MLVI by 50%; remove LN_2)
G	Increase Material Capacity to 140% of Powdered MOF-5
H	Increase Material Capacity to 200% of Powdered MOF-5

FIGURE 7. Possible changes/improvements in the total system mass, total system volume, and estimated total system cost for an 80 K, 100 bar, Hexcel cryo-adsorbent system.

IV.B.2 Systems Engineering of Chemical Hydrogen Storage, Pressure Vessel, and Balance of Plant for Onboard Hydrogen Storage

Jamie D. Holladay (Primary Contact),
Kriston P. Brooks, Kevin L. Simmons,
Ewa C.E. Rönnebro and Mark R. Weimar
Pacific Northwest National Laboratory (PNNL)
PO Box 999/ K2-12
Richland, WA 99352
Phone: (509) 371-6692
Email: Jamie.Holladay@pnnl.gov

DOE Managers
Ned Stetson
Phone: (202) 586-9995
Email: Ned.Stetson@ee.doe.gov
Jesse Adams
Phone: (720) 356-1421
Email: Jesse.Adams@go.doe.gov

Contract Number: DE-AC05-76RL01830

Project Start Date: February 1, 2009
Project End Date: January 31, 2014

Overall Objectives

- Develop engineering and design models to further the understanding of onboard storage energy management requirements.
- Develop innovative onboard system concepts for chemical hydrogen storage and cryogenic adsorption materials-based storage technologies.
- Develop and validate models for a chemical hydrogen storage system.
- Work with our partners to integrate our validated models into system framework that will lend insight into overall fuel cycle efficiency.
- Develop materials characteristic performance envelope for chemical hydrogen storage systems.
- Demonstrate key components for chemical hydrogen and cryo-sorbent-based materials.
- Reduce system volume and mass while optimizing system storage capability and performance through value engineering of heat exchangers and balance-of-plant (BOP) components.
- Mitigate materials incompatibility issues associated with hydrogen embrittlement, corrosion, and permeability through suitable materials selection for vessel materials, heat exchangers, plumbing and BOP components.
- Project the cost of chemical and cryo-sorbent materials-based hydrogen storage systems.

Fiscal Year (FY) 2013 Objectives

- Chemical Hydrogen Storage Design
  - Validate models and concepts via experiments
  - Scale up slurry production
  - Assess feasibility of liquid-slurry chemical hydrogen storage
  - Assess feasibility of volume-exchange tank
  - Assess feasibility of slurry use with heat exchanger, pump, valves
  - Project system efficiency, mass, and volume
- Pressure Vessel for Cryo-Adsorbent Hydrogen Storage
  - Exercise "tankinator" model to assess materials and design options for Type I, III, and IV vessels
  - Optimize vessel design in terms of cost
  - Assess vessel cost as function of pressure and temperature
  - Project system mass and volume
- BOP
  - Maintain BOP library
  - Size components (heat exchangers, valves, pumps, etc.)
  - Determine material compatibility
  - Identify where improvements can be made
- Cost Modeling to project the systems cost at various production levels

Technical Barriers

This project addresses the following technical barriers for Hydrogen Storage from the Fuel Cell Technologies Office Multi-Year Research, Development, and Demonstration Plan:

General to all storage approaches:

(A) System Weight and Volume

(B) System Cost

(C) Efficiency

(D) Durability/Operability

(E) Charging/Discharging Rates

(G) Materials of Construction

(H) Balance of Plant (BOP) Components:

(I) Dispensing Technology

(J) Thermal Management

(K) System Life-Cycle Assessments

(N) Hydrogen Venting

Off-Board regenerable specific

(R) By-Product/Spent Material Removal

Technical Targets

The technical targets for this project are presented in Table 1.

FY 2013 Accomplishments

- Completed testing of eight materials for use in Type IV pressure vessels determining tensile strength, storage modulus, elongation, and glass transition temperatures under cryogenic conditions.
- Identified BOP components for a cryo-sorbent hydrogen storage system with a total mass less than 9.4 kg and volume less than 11.6 L exceeding our targets of 17 kg and 18.5 L.
- Developed manufacturing approaches for Type I and III cryo-sorbent pressures.
- Completed a tradeoff study on joining techniques and identified friction stir welding as the most likely candidate to be able to join the tanks during the manufacturing process without damaging the sorbent materials.
- Developed the thermos bottle concept to enable fast tank cooling with liquid nitrogen rather than cryogenic hydrogen. This concept would potentially reduce the excess hydrogen required for a 5.6-kg fill from over 11 kg to ~1.1 kg depending on initial tank pressure.

TABLE 1. Progress towards Meeting Technical Targets for Hydrogen Storage

Hydrogen Storage Enginering Center of Excellence

Phase 2 System Status

6/30/2013

			Adsorbent System			Chemical Systyem		
			Phase 2 *Actual (automotive scale)*			Projected System HSECoE Go/No-Go*What could be built in the future (full scale)*		
Target	Units	2017 DOE Goal (System)	Phase 2 HSECoE Targets (Material)	Phase 2 HSECoE Targets (BOP only)	Phase 2 HSECoE Targets (System)	Phase 2 HSECoE Targets (Material)	Phase 2 HSECoE Targets (BOP only)	Phase 2 HSECoE Targets (System)
Gravametric Capacity	kg H2/kg system	0.055	0.187	0.10	0.0352	0.0872	0.15	0.055
mass	*kg*	*102*		*16.1*	159			*102*
Volumetric Capacity	kg H2/L system	0.04	0.03	0.053	0.0175	0.078	0.132	0.049
Volumetric	*liters*	*140*		*16.9*	320			*114*
System Cost	$/kWh net	6	3.5	5.62	12.74			
	$	*1,119*		*1048*	2376			
Fuel Cost	$/gge at pump	2-6			4.89			
Min Operating Temp	°C	-40			-40			-20
Max Operating Temp	°C	60			60			60
Min Delivery Temp	°C	-40			-40			-20
Max Delivery Temp	°C	85			85			85
Cycle Life	Cycles	1500			1500			1000
Min Delivery Pressure	bar	5			5			5
Max Delivery Pressure	bar	12			12			12
Onboard Efficiency	%	90			92			95
Well to Power Plant Efficiency	%	60			39.2			37
System Fill Time	min	3.3			3.3			2.9
Min Full Flow Rate	(g/s/kW)	0.02			0.02			0.02
	g/s	*1.6*			*1.6*			*1.6*
Start Time to Full Flow (20°C)	sec	5			5			1
Start Time to Full Flow (-20°C)	sec	15			15			1
Transient Response	sec	0.75			0.75			0.5
Fuel Purity	%H2	99.97			99.99			99.97
Permeation, Toxicity, Safety	Scc/h	Meets or Exceeds Standards			s			s
Loss of Useable Hydrogen	(g/h)/kg H2 stored	0.05			0.44			0.05

- Completed the development of the "tankanator" model and provided it to Savannah River National Laboratory (SRNL) for insertion into their models.
- Completed costing of 135 cryo-sorbent tank configurations and identified a 100-bar, Type I vessel with MOF-5 as the lowest cost option.
- Reduced projected cost of the cryo-sorbent hydrogen storage system from >$3,000/system in FY 2012 to less than $2,500/system in FY 2013.
- Terminated work on Type IV pressure vessels for 40 K cryogenic operation due to liner separation from the shell at pressures less than 35 bar and limitations on low-cost liner materials.
- Validated reactor model for an exothermic (slurry ammonia borane, AB) and endothermic (slurry alane as simulant) chemical hydrogen systems.
- Developed chemical hydrogen storage system model which included instrumentation, controls, controls logic, and engineering improvements increase the parts in the system from 12 in FY 2012 to 47 in FY 2013. This was used for cost, mass and volume calculations.
- Developed a feasible pathway to achieve DOE gravimetric and volumetric hydrogen storage targets using exothermic chemical hydrogen materials.
- Reduced projected costs from ~$4,700/system to ~$3,000/system by moving from a solid chemical hydrogen system to a slurry chemical hydrogen system.
- Validated the slurry flow-through reactor, heat exchangers, and volume exchange tanks.
- Demonstrated that the slurry could successfully flow at -20°C.
- Identified the need for pump development for size and mass reduction for fresh AB.
- Demonstrated that a pleated membrane could be used in a volume exchange tank for chemical hydrogen slurries.
- Demonstrated fluidization of settled solids and removal of slurry from a volume exchange tank such that a hydrogen storage system based on this concept could be drained and filled within 5 minutes, meeting the DOE targets.
- Demonstrated a 50 wt% AB slurry with a viscosity less than 1,500 cP meeting DOE targets.
- Measured settling and flocculation rates of spent and fresh AB.
- Demonstrated that Triton X-15 significantly reduces foaming at low weight percent loadings (1-3%) in AB slurries.
- Scaled up slurry production process from <150 mL batches to >750 mL batches.

✧ ✧ ✧ ✧ ✧

INTRODUCTION

Multiple onboard vehicle-scale hydrogen storage demonstrations have been done, including several studies to examine characteristics that impact systems engineering. However, none of these demonstrations have simultaneously met all of the DOE hydrogen storage sub-program goals. Additionally, engineering of new chemical hydrogen storage approaches is in its infancy, with ample opportunity to develop novel systems capable of reaching the DOE targets for storage capacity. The goal of the Hydrogen Storage Engineering Center of Excellence (HSECoE), led by SRNL, is to develop and demonstrate low-cost, high-performing, onboard hydrogen storage through a fully integrated systems design and engineering approach. Toward this end, PNNL is working with HSECoE partners to design and fabricate a system based on slurry chemical hydrogen storage media.

APPROACH

As part of the HSECoE, PNNL actively contributes to all five technology areas and targets six key objectives to optimize performance characteristics and reduce the size, weight, and cost of a H_2 storage system. This is being accomplished through engineering and integrated design approach, including application of advanced materials (structural and H_2 storage), and assessments of manufacturing and cost impact based on established models/approaches for technology tradeoff or "viability" studies.

PNNL serves multiple leadership roles within the HSECoE technology area structure to help facilitate collaboration across the center partnership and to feed technical results to other HSECoE partners. Achieving the objectives enables PNNL, SRNL, and other HSECoE partners to demonstrate onboard hydrogen storage with the potential to meet DOE technical targets. This technology and design knowledge will be transferred to the participating automotive original equipment manufacturers, thus advancing the hydrogen market sector and production of future hydrogen-powered vehicles. As appropriate, the models, catalogues, and lessons learned will be made available to the fuel cell community to accelerate fuel cell technology commercialization.

RESULTS

Cryo-Sorbent Hydrogen Storage

The cryo-sorbent hydrogen storage system work completed in FY 2013 was focused on: Type IV pressure vessel evaluation, optimal vessel type selection, cost projection, BOP identification to meet mass and volume targets, and hydrogen filling optimization.

Analysis completed in Phase I of the project (FY 2012) indicated that the pressure vessel accounted for the majority of cost, and BOP mass and volume. Therefore we began a systemic study with our partners to identify the optimal conditions and vessel type to minimize cost while increasing the volumetric and gravimetric hydrogen content. Therefore we evaluated Type I, III, and IV pressure vessels in various system configurations. Type IV pressure vessels use a polymer liner with carbon fiber outer layers. They offer a light-weight solution compared to the other pressure vessel types. Through computer modeling, we determined that the polymer liner needed to be limited to 2.55 mm in order to meet the volumetric and gravimetric BOP targets. We tested eight materials for hydrogen permeation, tensile strength, fatigue, coefficient of thermal expansion, elongation, and storage modulus in cryo-genic conditions, and we measured their glass transition temperatures. Hexagon Lincoln tested the materials for weld strength and impact. Halar and high-density polyethylene had the best properties. However, we found that even the best materials, when used as a liner, would separate from the shell when the hydrogen pressure was less than 35 bar. This would mean that the hydrogen pressure would always need to remain >35 bar, severely limiting the usable hydrogen. Therefore, the Type IV pressure vessels were out-selected.

PNNL developed the "tankinator" model which combined the predictive performance and sizing models with costs to be able to predict tank costs at different pressures and temperatures. Specifically, the tankinator code estimated the necessary wall thickness for pressure vessels given a Type (I, II, or III), operating pressure, cost, and two out of the following three: storage volume, diameter, or length. Its ability to estimate reasonable wall thickness and pressure vessel mass was validated against tank geometry designs available in the open literature and some proprietary tank design information. It includes a winding model that evaluated the amount of fiber and resin required. For manufacturing, it included the winding time. We adapted a model that Thiokol used to estimate the costs of Type II and Type IV tanks to evaluate the costs. We added Type III pressure vessels and a manufacturing process flow model that examined the steps in the manufacturing process, identifying equipment and costs, cycle times, and labor required. The cost estimation component of the analysis was validated against a proprietary database of existing tank designs. The cost estimation was also validated through cross comparison of the PNNL cost model to a third-party manufacturing process flow cost model. Figure 1 has a snapshot of the model inputs, Type I pressure vessel. The model predicts the total system cost, amount of fiber used, materials costs, manufacturing costs, and BOP costs. This model was used to predict the costs of 135 different cases and identified 100-bar Type I system with MOF-5 as the lowest cost option. The Center developed a detailed system schematic which included BOP instrumentation, controls, control logic, etc. The BOP was optimized using the 100-bar Type I system. PNNL optimized the system BOP to minimize mass and volume and identified a system with BOP having a mass of 9.4 kg and volume of 11.6 L which was under our targets of 17 kg and 18.5 L. This was a bottom-up design.

Finally, the Center examined the challenge of cooling the pressure vessel during filling. An "empty" tank may have a temperature of 180 K and needs to be cooled to 80 K for a complete fill. The conventional approach for filling the cryo-sorbent tanks is to cool the tank by flowing cryo-compressed hydrogen. The hydrogen would cool the sorbent media, tank walls, etc., to the desired operating temperature. This process is highly inefficient and is particularly poor at cooling the tank walls. SRNL determined that it is nearly impossible meet the DOE fill time target using only flow-through hydrogen to cool and fill a cryo-sorbent tank at 100 bar, assuming temperatures above 180 K. Lowering tank pressure would make it even less likely to meet the fill time target. Furthermore, we determined that flow-through hydrogen to

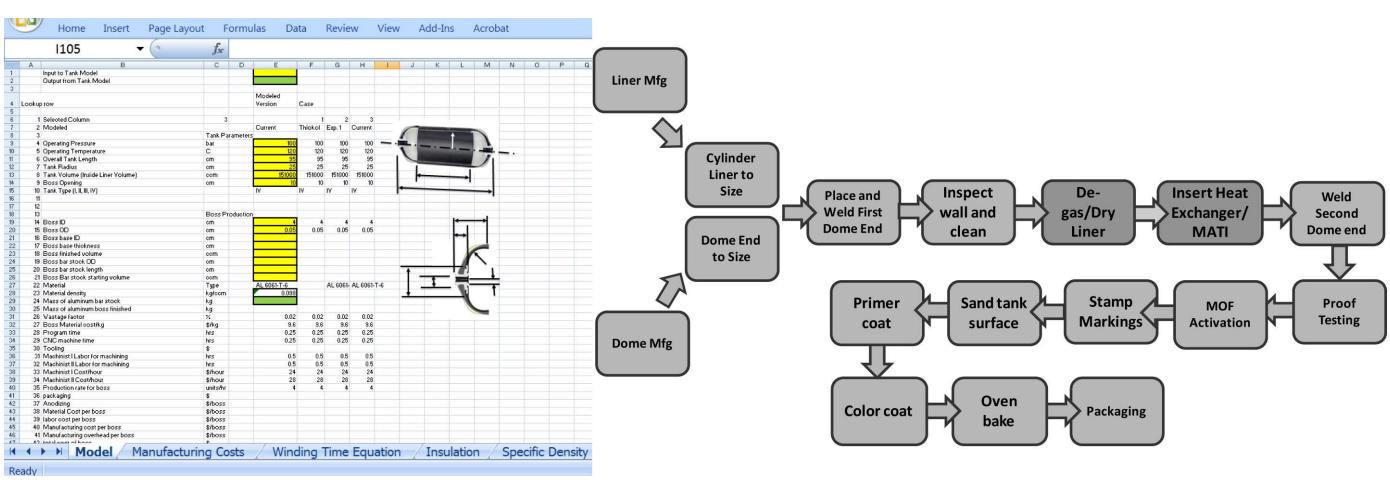

FIGURE 1. Tankinator Model Inputs and Example Manufacturing Flow Chart

cool the tank requires a loss of up to 11 kg of H_2 for a 5-6 kg H_2 fill. While the excess hydrogen can be recompressed and cooled, this additional processing would increase costs. SRNL's analysis indicated that the sorbent media is relatively quickly cooled by the hydrogen, but the pressure vessel and insulation required the majority of the excess hydrogen to reach the desired temperatures. PNNL developed a thermos concept (Figure 2) which would utilize liquid nitrogen to cool the pressure vessel outer surface. SRNL projected that using liquid nitrogen as a pre-fueling coolant can reduce the waste of hydrogen fuel from 11 kg/fill to 1.1-2.4 kg depending on tank pressure. Coupling the Modular Adsorption Tank Insert design being developed by Oregon State University with the thermos concept would virtually eliminate excess hydrogen. With or without the Modular Adsorption Tank Insert, the thermos concept would enable an empty tank to fill within the 5 minute DOE Target.

Chemical Hydrogen Storage

PNNL's chemical hydrogen storage work in the Center was focused on: model validation, BOP identification, key part validation, and AB slurry production and characterization. Developing and validating system models is a key objective of this project. Los Alamos National Laboratory (LANL) provided PNNL data from their flow reactor for both an exothermic chemical hydrogen material (AB slurry) and an endothermic chemical hydrogen material (alane slurry). The model fit the AB slurry experimental data without any need for modification. However, the alane experimental results did not fit the model. This was because the model used reaction kinetics for an "active" alane developed by Graetz [1]. The alane used in LANL's experiments was not activated. Therefore we used data from one of the experimental runs to fit the data for the less active alane. The new kinetic equation was put into the model. Other experimental runs at different flow rates were compared to the model and found to have a good fit. Figure 3 contains the results of the AB slurry experimental and model data and the fixed alane experimental and model data.

Previously, PNNL worked with United Technologies Research Center, and LANL to develop a chemical hydrogen storage system schematic. In FY 2013, we added instrumentation, controls, and control logic to the schematic. This increased the part count from 12 to over 47 and was used to predict the mass, volume and cost of the system. PNNL identified off-the-shelf parts that could be used to build the design. We believe that the part count can be reduced to ~34. The system mass was 137 kg with the BOP accounting for approximately 54 kg. We then identified a pathway to reduce the BOP mass to 38 kg meeting our 41 kg target. We proposed that the pump, radiator, and valves mass could be reduced by 25%; the mass of the mixers for the tank could be reduced by 50%; and the clean-up system mass could be reduced by 75% by using a material that did not produce as much impurities. In order to achieve the 5.5 wt% gravimetric target, these BOP improvements would be required, plus the hydrogen content would need to be increased to ~8 wt%. However, if a liquid chemical hydrogen material that did not require mixing and had minimal

FIGURE 2. Conceptual Design for the Thermos Bottle Concept to Reduce Cooling Time and Excess Hydrogen Requirements during Filling

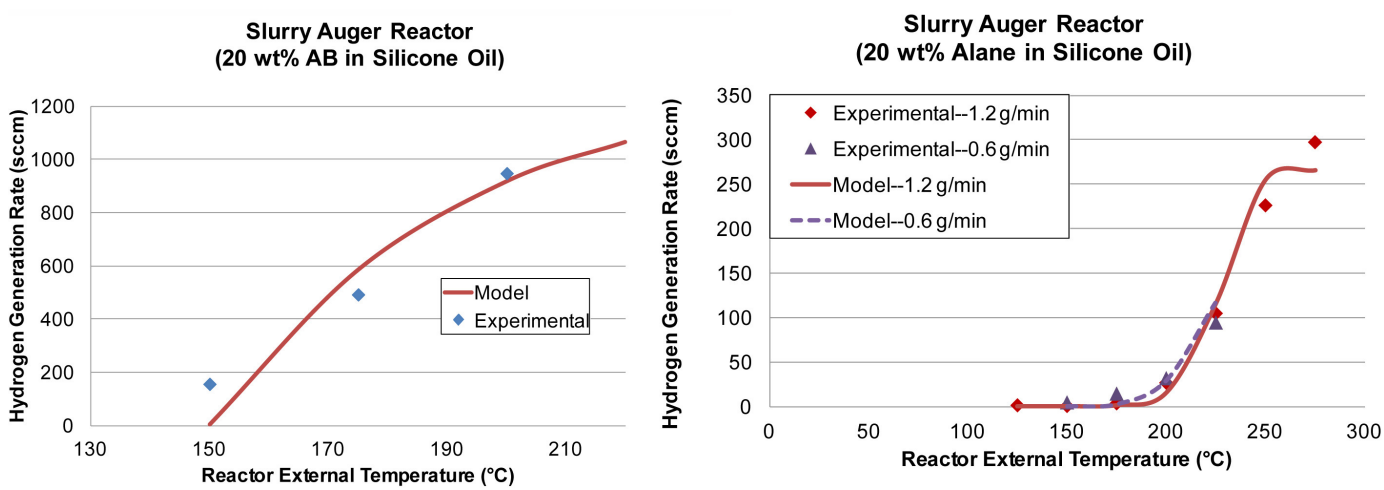

FIGURE 3. Model Validation for Slurry AB and Slurry Alane

hydrogen clean-up was used, the required gravimetric capacity to meet the DOE targets could be reduced to 7.8 wt%.

The proposed schematic's key components were the reactor, gas-liquid phase separator, pumps, valves, heat exchangers, volume displacement tank, and hydrogen cleanup system. PNNL validated the heat exchangers (FY 2012), volume displacement tanks (FY 2013), and pumps (FY 2013). The gear pump identified in FY 2012 worked well with the simulant and spent AB. However, with fresh AB slurry the pump seized. Syringe and peristaltic pumps could successfully pump the fresh AB slurry. Unfortunately, syringe and peristalitic pumps are not suitable options for a vehicle, so future work would be needed to develop a suitable pump for slurry AB should the DOE or others move forward with it. In FY 2013 we assembled a simple system composed of a prototypical heat exchanger, pump, Swagelok® fittings, and valves to study the impact of slurry setting and to validate the heat exchanger model. We used simulant for the majority of the tests, although spent AB slurry was also used. We operated the system with the simulant for several hours and then turned off the pump. The slurry was allowed to settle overnight. The system successfully re-started the next day. We did this cycle several times and then pulled apart the system looking for deposits of material. We found a slight deposit in the 90 degree elbows. By removing the 90 degree elbow this problem can be resolved. In addition, we decreased the system temperature to -20°C and tested the system in the same way. The system with the settled slurry was able to start and operate at the low temperatures.

For a liquid chemical hydrogen system, both the fresh and spent fuel must be stored onboard. Rather than use separate tanks for fresh and spent fuel, we proposed a volume exchange tank. We ran chemical compatibility tests on various materials, ethylene propylene diene monomer, Viton®, and Buna-N, to ensure that the materials can work well with AB and spent AB. None of the materials showed significant changes in tensile strength or elongation. Viton® had the lowest mass and length change. To minimize the stress on the membrane we developed a pleated membrane which rather than stretch, unfolds to the desired shape (Figure 4a). We also examined ways to homogenize a settled slurry and flocculated slurry by using an ultrasound, impeller mixer, French press, jet mixing, and vibration. French press was identified as the best candidate. Using 11 kg of simulant slurry, we demonstrated that a volume exchange tank with a French press can homogenize a fully settled slurry and remove 98% of it within 1.7 minutes (Figure 4b). This rate would meet the DOE targets in a full-scale device.

In FY 2013 we completed our AB slurry work. We measured the flocculation and settling rate of a 45 wt% AB slurry (Table 2) and scaled up slurry manufacturing from 100-ml to 750-ml batches. In addition, we completed our investigation into additives for the slurry by examining DOW's Triton™ X-15, X-35, and X-45. When added to a 35-wt% AB slurry at 1-wt% mass, the X-15 reduced foaming during reaction and increased slurry stability (decreased the slurry's tendency to solidify). The additive X-35 reduced the foaming but not as much as X-15, and X-45 had no visible effect. Therefore, we added the X-15 to all future slurries developed and tested. We demonstrated this slurry in a flow-through reactor equipped with a mixer. At a set point of 200°C, 300 rpm mixing, and 1.75 min residence time (same order of magnitude as a full-scale system), no plugging of

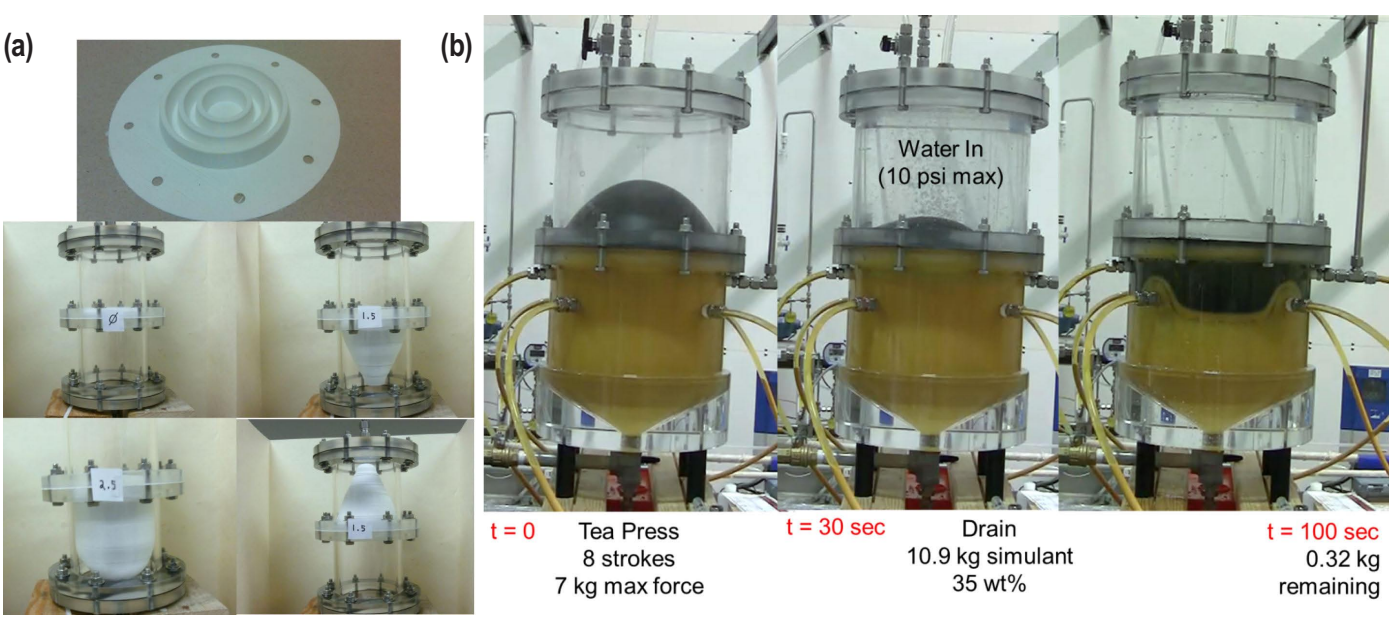

FIGURE 4. Volume Exchange Tank (a) Pleated Membrane (b) Mixing and Removal of Spent AB Slurry

TABLE 2. Flocculation Rate and Settling Rate of 45 wt% AB Slurry

Time	Fresh AB Flocculation	Spent AB Settling
0 min	-	-
5 min	10.4%	21.1%
10 min	21.1.%	26.3%
1h	21.1%	26.3%
2 h	26.3%	36.8%
3 h	26.3%	36.8%
24 h	26.3%	36.8%

the reactor was observed. The product was a foam which reformed a slurry with slight mixing. Nuclear magnetic resonance testing revealed that over 2 equivalents of hydrogen had been released from the AB. LANL continued the flow reactor testing and quantifying the hydrogen production rate and impurities. LANL's data was used to validate the model.

Finally, a 50 wt% AB slurry has been developed. The fresh slurry had a viscosity of 966 cP, significantly higher than that of a 45 wt% slurry (270 cP). This indicates that the liquid carrier (silicon oil) was almost fully loaded and that higher solid loadings would be difficult.

Cost Analysis

In FY 2013 we completed the cost analysis for the more detailed schematics described previously. Vender quotes were used for the off-the-shelf components such as valves, fittings, insulations, and heat exchangers. For specialty components, cost quotes were done following procedures described in previous annual reports. In addition, we included estimates for manufacturing and system assembly as well as applied standard learning curves. System costs were calculated for yearly productions ranging from 10,000 to 500,000 units per year. We worked with our partners to identify lower cost parts and improved manufacturing compared to previous years. This resulted in cost reduction for the cryo-sorbent-based storage system from $3,000/unit to ~$2,500/unit. For the chemical hydrogen system, we previously had priced the solid- rather than a slurry-based system. Changes to a liquid-based system significantly reduced cost from ~$4,600/unit to ~$3,000/unit. Much of the cost reduction is in lower BOP cost due to the reduction in the number of valves. Comparing these costs to those reported by TIAX for 350-bar, 700-bar and cryo-compressed hydrogen all with carbon fiber tanks revealed that both the slurry AB and the sorbent were the same as or less expensive than the compressed gas storage and that the cryo-sorbent was competitive with cryo-compressed (Figure 5).

CONCLUSIONS AND FUTURE DIRECTIONS

PNNL's cryo-sorbent-based storage system efforts resulted in down-selection to a relatively low-cost storage system. We out-selected the Type IV pressure vessels. We also were able to identify BOP components that meet the Center's BOP targets for mass and volume. We developed manufacturing schemes for systems using Types I, III, and

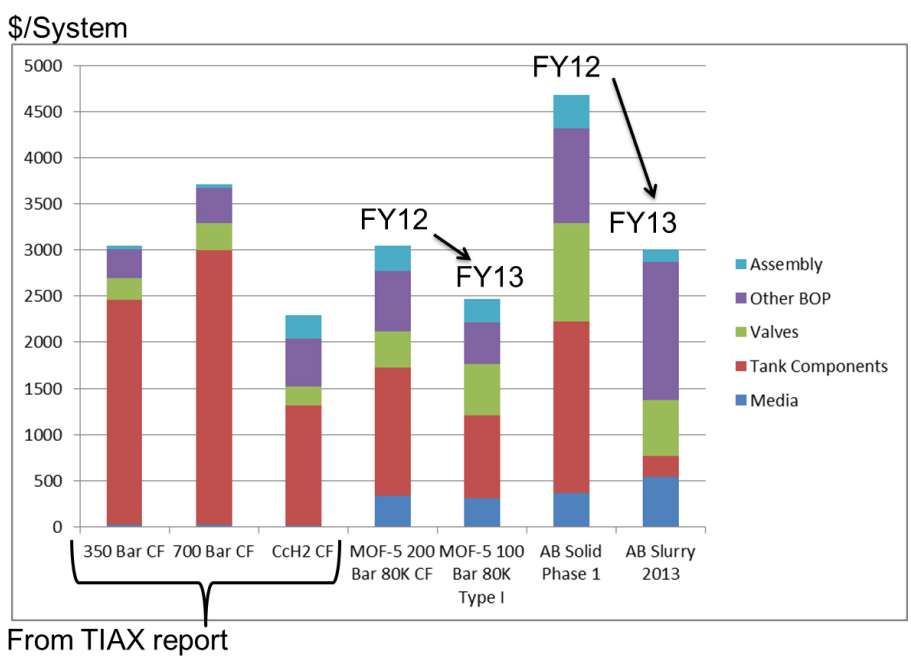

FIGURE 5. Projected Hydrogen Storage System Costs

IV pressure vessels. We completed our tankinator model and provided it to SRNL for inclusion in their models. We invented the thermos bottle concept to decrease the fill time and drastically reduced the excess hydrogen required for tank cooling. Finally, we showed a projected cost reduction for the sorbent based systems.

PNNL's chemical hydrogen efforts in FY 2013 were on validating the model and key components. We developed a pathway to achieve the DOE's gravimetric targets. Our analysis showed that if the gravimetric targets were achieved the volumetric targets would also be realized. We validated the heat exchangers and volume exchange tank. We developed the pleated membrane for the volume exchange tank and French press for mixing. We demonstrated that off-boarding/onboarding could be done at rates sufficient for a 5-minute fill. We showed that the settled slurry would not necessarily clog the system and that the slurry was flowable at temperatures as low as -20°C, meeting the DOE targets. Finally, we projected a 35% cost reduction by changing from the solid-based AB system to the liquid-based system.

FUTURE WORK

- Design sub-scale cryo-adsorbent system prototype (joint with partners)
- Complete chemical hydrogen model verification:
  - Compare model to additional reactor data provided by LANL
  - Refine model if necessary
  - Materials requirements
- Demonstrate advanced pressure vessel system for dormancy, etc. (with Hexagon Lincoln)
- Elevated design concepts
  - Sorbent: reduce part count by up to 30%
- Refine cost model
  - Update BOP
  - Improve manufacturing estimates

FY 2013 PUBLICATIONS/PRESENTATIONS

Publications

1. Devarakonda MN, KP Brooks, E Ronnebro, SD Rassat, and JD Holladay. 2012. "Chemical Hydrides for Hydrogen Storage in Fuel Cell Applications." In *SAE World Congress and Exhibition, April 24-26, 2012, Detroit, Michigan*, pp. SAE Technical Paper 2012-01-1229. SAE International, Warrendale, PA. doi:10.4271/2012-01-1229

2. Devarakonda MN, KP Brooks, E Ronnebro, and SD Rassat. 2012. "Systems Modeling, Simulation and Material Operating Requirements for Chemical Hydride Based Hydrogen Storage." *International Journal of Hydrogen Energy* 37(3):2779-2793. doi:10.1016/j.ijhydene.2011.06.121

3. Nguyen BN, and KL Simmons. 2012. "A Multiscale Modeling Approach to Analyze Filament-Wound Composite Pressure Vessels." *Journal of Composite Materials*. doi:10.1177/0021998312454508

4. Brooks KP, MN Devarakonda, SD Rassat, and JD Holladay. 2011. "Systems Modeling of Chemical Hydride Hydrogen Storage Materials for Fuel Cell Applications." *Journal of Fuel Cell Science and Technology* 8(6):Article No. 061021. doi:10.1115/1.4004477

5. Choi YJ, Y Xu, WJ Shaw, and E Ronnebro. 2012. "Hydrogen Storage Properties of New Hydrogen-Rich BH3NH3-Metal Hydride (TiH2, ZrH2, MgH2, and/or CaH2) Composite Systems." *Journal of Physical Chemistry C* C116(15):8349-8358. doi:10.1021/jp210460w

6. Majzoub EH, and E Ronnebro. 2012. "Methodology of Materials Discovery in Complex Metal Hydrides Using Experimental and Computational Tools." *Materials Science and Engineering R: Reports* 73(2):15-26. doi:10.1016/j.mser.2012.01.001

Presentations

1. Ronnebro E. 2012. "Fluid Phase Chemical Hydrogen Storage - Materials Operating Requirements." Presented by Ewa Ronnebro (Invited Speaker) at Hydrogen Storage Engineering Center of Excellence face to face meeting, Mystic, CT on October 11, 2012. PNNL-SA-91205.

2. Holladay JD, KP Brooks, E Ronnebro, and AJ Karkamkar. 2012. "Chemical Hydrogen for On-Board Vehicle Hydrogen Storage." Presented by Jamie Holladay at Fuel Cell Seminar and Energy Exposition, Uncasville, CT on November 9, 2012. PNNL-SA-91871.

3. Ronnebro E, MP Westman, J Chun, AJ Karkamkar, and KP Brooks. 2013. "HSECoE TTR Materials Operating Requirements - Chemical Hydrogen Storage." Presented by Ewa Ronnebro (Invited Speaker) at US Drive - Hydrogen Storage Tech Team Meeting, Detroit, MI on March 21, 2013. PNNL-SA-94267.

4. Simmons KL, KP Brooks, E Ronnebro, and JD Holladay. 2013. "System Modeling and Balance of Plant for the Chemical Hydrogen Storage Systems." Presented by Kriston Brooks (Invited Speaker) at Hydrogen Storage Technical Team Meeting, Southfield, MI on March 21, 2013. PNNL-SA-94281.

5. Simmons KL, MR Weimar, KP Brooks, BA Van Hassel, and M Veenstra. 2013. "HSECoE 2013 Tech Team Meeting Chemical Hydrogen BOP/Cost." Presented by Kevin L Simmons, Mark Weimar at Hydrogen Storage Engineering Center of Excellence Tech Team Review, Southfield, MI on March 21, 2013. PNNL-SA-94408.

REFERENCES

1. Graetz J and JJ Reilly. JChemPhysB 109 (2005) 22181-85.

IV.B.3 Advancement of Systems Designs and Key Engineering Technologies for Materials-Based Hydrogen Storage

Bart van Hassel (Primary Contact),
Jose Miguel Pasini, Igor Fedchenia, David Gerlach,
John Khalil, Reddy Karra, Jose Santana,
Ron Brown, Randy McGee and Allen Murray
United Technologies Research Center (UTRC)
411 Silver Lane
East Hartford, CT 06108
Phone: (860) 610-7701
Email: vanhasba@utrc.utc.com

DOE Managers
Ned T. Stetson
Phone: (202) 586-9995
Email: Ned.Stetson@ee.doe.gov
Jesse Adams
Phone: (720) 356-1421
Email: Jesse.Adams@go.doe.gov

Contract Number: DE-FC36-09GO19006

Project Start Date: February 1, 2009
Project End Date: June 30, 2015 (including 1 year no-cost extension)

Overall Objectives

UTRC's overall objectives mirror those of the Hydrogen Storage Engineering Center of Excellence (HSECoE) to advance hydrogen storage system technologies toward the DOE Hydrogen Program's 2017 storage targets. Outcomes of this project will include:

- A more detailed understanding of storage system requirements.
- Development of higher performance and enabling technologies such as novel approaches to heat exchange, onboard purification and compacted storage material structures.
- Component/system design optimization for prototype demonstration.

Fiscal Year (FY) 2013 Objectives

- Develop vehicle/powerplant/storage system integrated system modeling elements to improve specification of storage system requirements and to predict performance for candidate designs.
- Engineer and test specialty components for H_2 storage systems.
- Assess the viability of onboard purification for various storage material classes and purification approaches.
- Conduct risk assessments during the progression of the phased HSECoE efforts.
- Collaborate closely with HSECoE partners to advance materials-based hydrogen storage system technologies.

Technical Barriers

This project addresses the following technical barriers from the Storage section (3.3.5) of the Fuel Cell Technologies Office Multi-Year Research, Development and Demonstration Plan:

(A) System Weight and Volume

(C) Efficiency

(D) Durability/Operability

(E) Charging/Discharging Rates

(H) Balance-of-Plant (BOP) Components

(J) Thermal Management

Technical Targets

The goals of this project mirror those of the HSECoE to advance hydrogen storage system technologies toward the DOE Hydrogen Program's 2017 storage targets in Table 1 [1].

TABLE 1. Status of UTRC's S*M*A*R*T Milestones

Characteristic	Units	S*M*A*R*T Targets	Storage System Type	UTRC 2013 Status
Gas/Liquid Separator	kg	<5.4	Chemical Hydrogen Storage System	5.8
	L	<19		2.7
	ppm	<100		800±200
Ammonia Filter	kg	<1.2	Chemical Hydrogen Storage System	1.1
	L	<1.6		1.6

FY 2013 Accomplishments

Accomplishments during the current project period comprise:

- Developed the architecture of a graphical user interface (GUI) for the Simulink framework. Obtained feedback through a beta-test with Sandia National Laboratories (SNL), Oak Ridge National Laboratory (ORNL) and the National Renewable Energy Laboratory (NREL).
- Built gas/liquid separator (GLS) test facility for chemical hydrogen storage system.

- Collaborated with vendor on the design of an axial GLS with a low profile that is capable of meeting the S*M*A*R*T milestone targets.
- Quantified the performance of the GLS as a function of flow rate, pressure, and temperature.
- Developed computational fluid dynamics (CFD) model of the GLS and modified experimental setup to validate the model by measuring the droplet size distribution in the outlet of the GLS.
- Optimized $MnCl_2$ loading on super-activated carbon (SAC) IRH-33 for a high capacity and regenerable NH_3 sorbent material in order to minimize weight, volume, and pressure drop of the filter in the chemical hydrogen storage system.
- Delivered optimized filter to Los Alamos National Laboratory (LANL) for competitive adsorption assessment with borazine. Fuel cell grade H_2 was demonstrated with the combined filter assembly.
- Performed qualitative risk analysis of HSECoE designs/materials by performing flammability tests of ammonia borane (AB) in powder and slurry form and by developing a metal-organic framework (MOF)-5 dust explosion test plan for Ford/BASF.

✧ ✧ ✧ ✧ ✧

INTRODUCTION

Physical storage of hydrogen through compressed gas and cryogenic liquid approaches is well established, but has drawbacks regarding weight, volume, cost, and efficiency which motivate the development of alternative, materials-based methods of hydrogen storage. Recent worldwide research efforts for improved storage materials have produced novel candidates and continue in the pursuit of materials with overall viability. While the characteristics of the storage materials are of primary importance, the additional system components required for the materials to function as desired can have a significant impact on the overall performance and cost. Definition, analysis and improvement of such systems components and architectures, both for specific materials and for generalized material classes, are important technical elements to advance in the development of superior methods of hydrogen storage.

APPROACH

UTRC's approach is to leverage in-house expertise in various engineering disciplines and prior experience with metal hydride system prototyping to advance materials-based H_2 storage for automotive applications. During the fourth year of the HSECoE project, UTRC continued the development of the Simulink framework for comparing H_2 storage systems on a common basis. A GUI was developed in order to facilitate the use of this Simulink framework by a wider audience. UTRC downsized a GLS design to the scale that is required for an automotive application of the chemical hydrogen storage system. UTRC built an experimental test facility for testing this GLS and validated the design concept by demonstrating the S*M*A*R*T milestone. UTRC developed a CFD model of the GLS and performed test facility modifications in order to enable model validation. UTRC's approach to H_2 purity for the chemical hydrogen storage system was to optimize the composition of the NH_3 sorbent material in order to minimize weight, volume and pressure drop while demonstrating the SAE International (SAE) purity target [2]. UTRC developed and validated a dynamic breakthrough model of the NH_3 sorbent bed. UTRC's approach to H_2 purity for the cryo-adsorption system was to evaluate different types of particulate filters.

RESULTS

UTRC designed the architecture of a GUI of the Simulink framework in which different H_2 storage systems are compared on a common basis, as illustrated in Figure 1. The GUI was subsequently beta-tested with SNL, ORNL and NREL in order to obtain valuable feedback before making it available on the HSECoE website.

Safety and risk assessment has a central place in all the work that is performed at UTRC and within the HSECoE. UTRC developed a MOF-5 dust explosion test plan for Ford/BASF, and the initial results were reported by Ford/BASF at the tech team review in March 2013 and during the 2013 Annual Merit Review. UTRC assessed the ignition properties of AB as slurry in silicone oil and as a powder. The results of these tests are shown in Figure 2. The ignition properties of AB were similar in both tests. However, ignition of H_2 (generated during the exothermic AB thermolysis) can ignite the silicone oil slurrying agent while in air.

UTRC optimized an ammonia sorbent for the chemical hydrogen storage system in collaboration with the Université du Québec à Trois-Rivières, Canada. The sorbent makes it possible to scrub NH_3 down to 0.1 ppm with a replacement\ regeneration interval of 1,800 miles of driving at an inlet NH_3 concentration of 500 ppm while having a mass and volume of 1.2 kg and 1.6 liters, respectively, which is an important S*M*A*R*T milestone for the chemical hydrogen storage system development within the HSECoE. The results of the optimization study are shown in Figure 3. Fifty wt% $MnCl_2$ on SAC IRH-33 resulted in the most compact filter. This also resulted in a full-size filter with the lowest pressure drop, as shown in Figure 4. The dynamic breakthrough capacity of UTRC's sorbent filter was shown to be a factor of 6 higher than commercially available NH_3 sorbent materials. UTRC's NH_3 sorbent is regenerable, as discussed in the previous annual report [3]. UTRC characterized the sorbent material

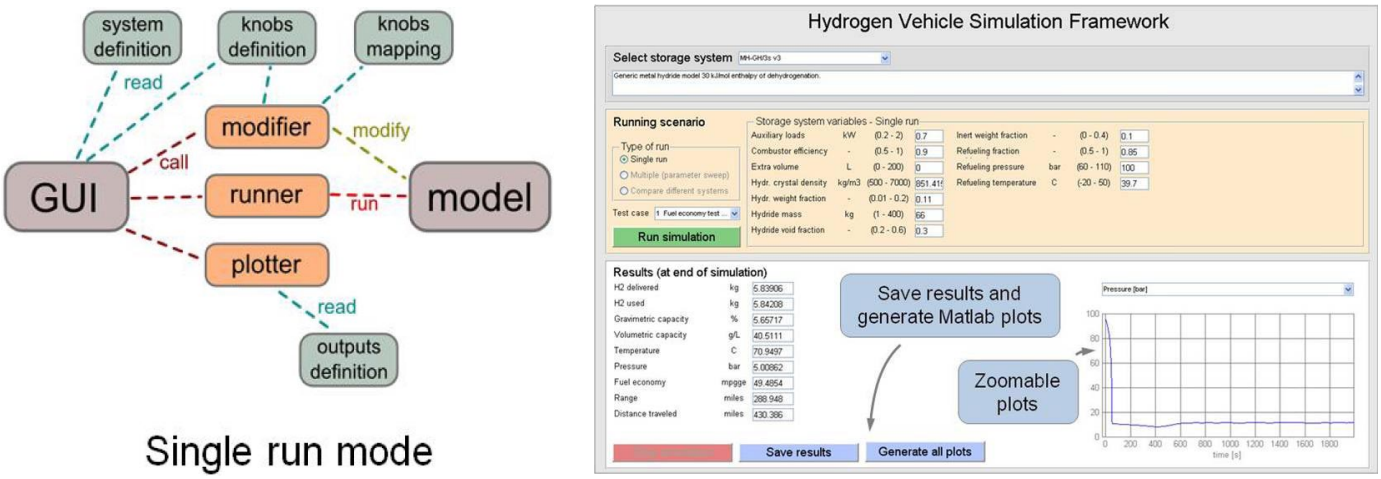

FIGURE 1. Architecture of GUI for Simulink framework.

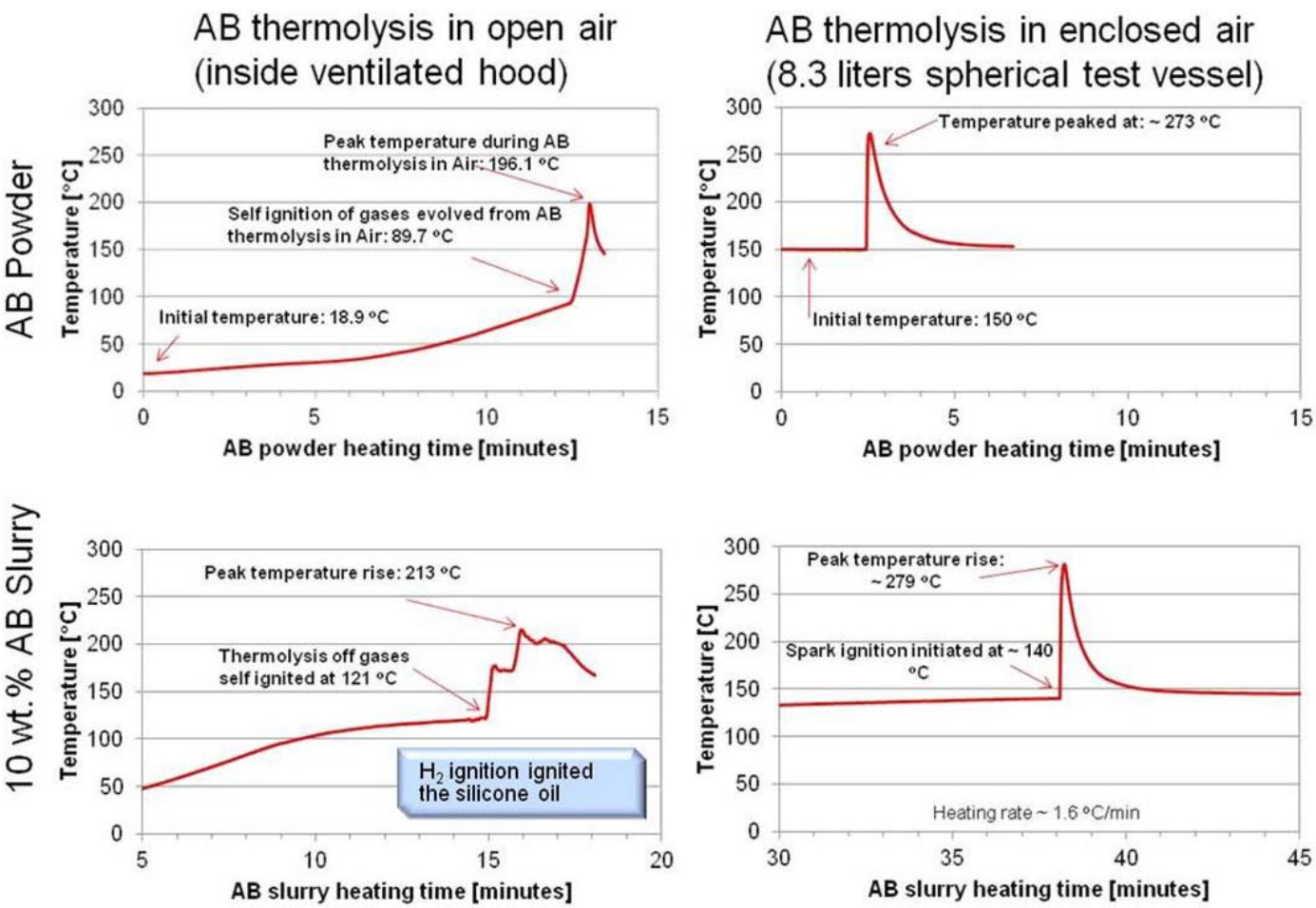

FIGURE 2. Comparison of ignition properties of AB in a silicone oil slurry and in powder form. One series of experiments was performed in open air while a second series of experiments was performed in a closed vessel.

by measuring the NH_3 adsorption isotherm over a wide range of temperature, as shown in Figure 5. A model was developed in order to explain the shape of the adsorption isotherm [4]. The isotherm data were used as input to a COMSOL model of the dynamic impurity breakthrough of a sorbent bed [5]. The model is getting validated with dynamic sorption capacity

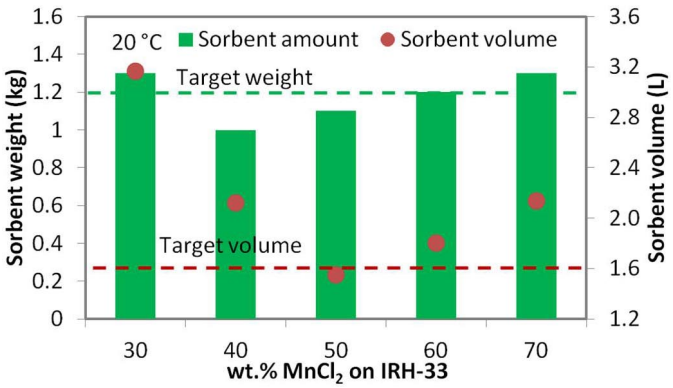

FIGURE 3. Optimization of $MnCl_2$ loading on SAC IRH-33 for NH_3 filter.

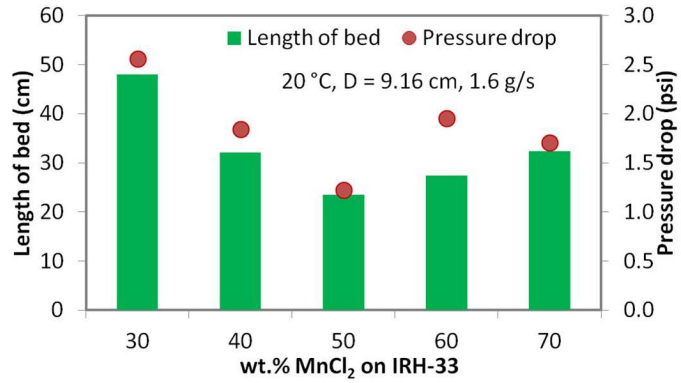

FIGURE 4. Bed length and pressure drop of NH_3 filter.

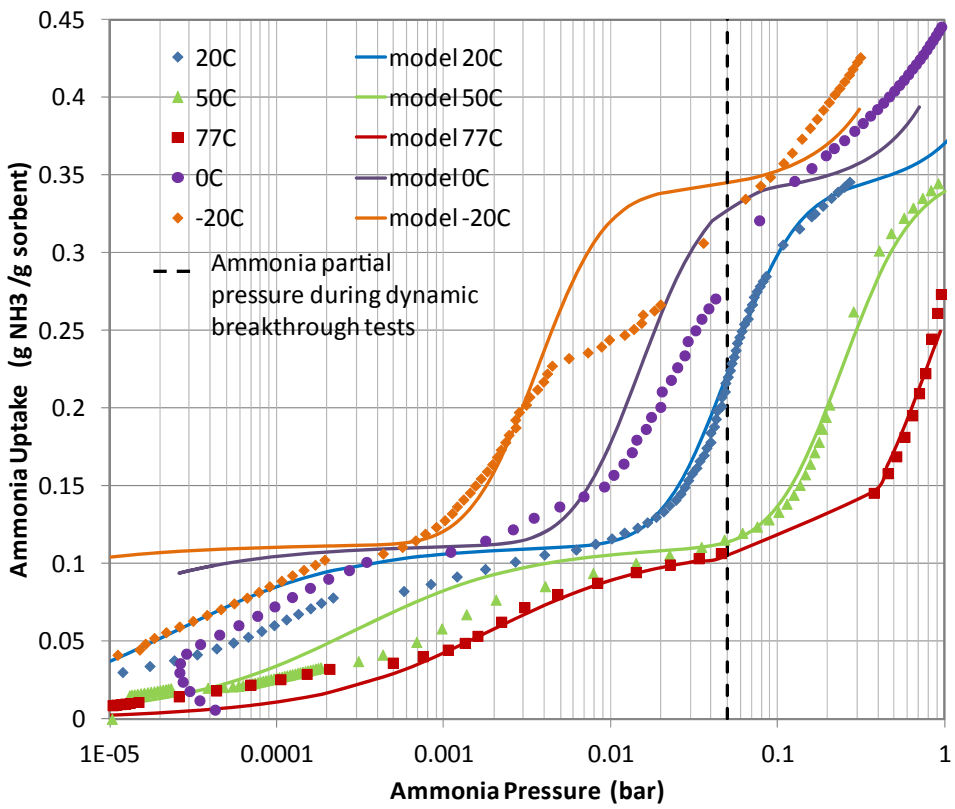

FIGURE 5. NH_3 adsorption isotherms of 40 wt% $MnCl_2$ on SAC IRH-33.

data as a function of flow rate, pressure and temperature and some initial results are shown in Figure 6.

H_2 quality from cryo-adsorption systems is impacted by particulates that get entrained into the hydrogen that is supplied to the fuel cell system. UTRC evaluated the performance of porous metal particulate filters to mitigate particulates and for containing the adsorbent material in its storage tank. The particulate concentration was measured by means of an engine exhaust particle sizer spectrometer downstream of a particulate filter in a packed bed of Maxsorb* and MOF-5 powder at room temperature. Measurements at high flow rates showed the formation of a filter cake and a corresponding increase in pressure drop. The results indicate that a 0.5 micrometer porous metal filter is capable of reducing the particulate concentration to a level of 400 $\mu g/m^3$, which is below the SAE J2719 guideline [3] of 1,000 $\mu g/m^3$. Filter type and size need to be carefully selected for cryogenic and flow-through cooling operating conditions.

A fluid-based chemical hydrogen storage system, such as for instance AB dissolved in ionic liquids (as being developed by LANL) or suspended in a slurry (as being developed by the Pacific Northwest National Laboratory, PNNL),

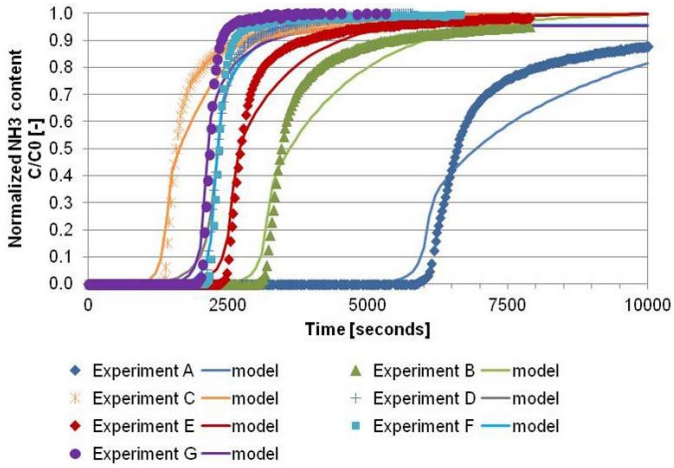

FIGURE 6. Dynamic breakthrough modeling of NH_3 through a filter with 40 wt% $MnCl_2$ on IRH-33 under various operating conditions (flow rate, pressure and temperature).

requires a GLS. It separates hydrogen gas produced during AB thermolysis from the fluid that will also contain the AB thermolysis byproducts (e.g. BNH_x). UTRC collaborated with a vendor on downsizing a passive GLS design with a low profile and no moving parts that deploys three different separation mechanisms: coalescence, gravity and centrifugal action. UTRC built a GLS facility for testing the GLS performance under the S*M*A*R*T milestone conditions, as shown in Figure 7. The key components were discussed in the previous quarterly report [2].

UTRC quantified the performance of the GLS with a three-factor two-level factorial design of experiment with the following factors: 1) gas and liquid flow rate N_2: 300 slpm (oil: 360 ml/min) and N_2: 600 slpm (oil: 720 ml/min); 2) pressure (6 and 12 bar); and 3) temperature (70 and 170°C). N_2 gas was used instead of H_2 gas and the liquid phase was silicone oil AR-20 (viscosity: 20 mPa·s at 25°C), as used by PNNL and LANL in their AB slurries. The temperature was shown to have a large effect on the efficiency of the gas/liquid separator, prompting the need to cool down the two-phase mixture before separation when such a silicone oil would be used as a slurrying agent. UTRC demonstrated that the silicone oil could be separated from N_2 gas with a 99.99% efficiency (100 ppm carry-over) at 70°C and 12 bar (abs) pressure under reduced flow conditions (i.e. 360-720 ml/min of liquid phase and 300 slpm of N_2 gas instead of 720 mL/min liquid phase and 600 slpm of N_2 gas for the S*M*A*R*T milestone), as shown in Figure 8. The experimental results clearly show a critical N_2 gas flow rate above which the liquid carry-over starts to increase. The GLS had a mass and volume of 5.8 kg and 2.7 liters, respectively, which was slightly above the 5.4 kg weight target but well below the 19 liters volume target.

An axi-symmetric CFD model was developed of the GLS. The model predicts that droplets smaller than

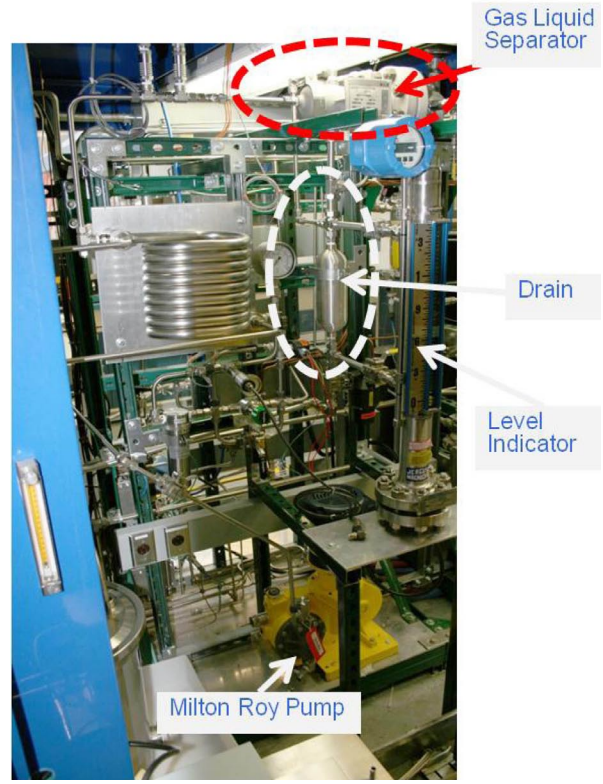

FIGURE 7. GLS test facility at UTRC.

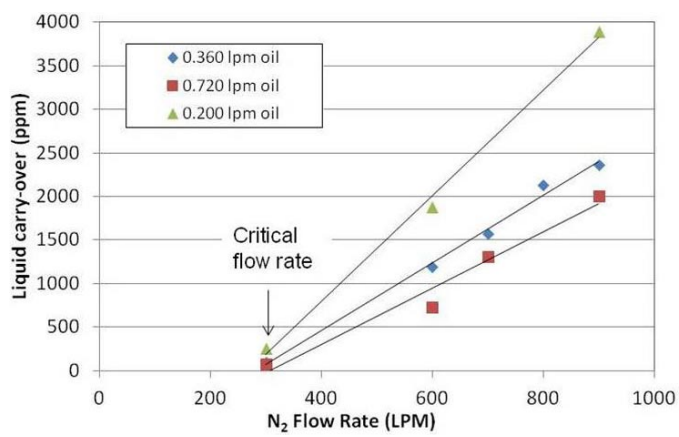

FIGURE 8. Liquid carry-over results of GLS at 12 bar and 70°C. The liquid carry-over in ppm is defined as the ratio of the silicone oil mass that was separated out of the N_2 gas by a coalescence filter downstream of the GLS and the silicone oil mass that was co-injected with N_2 at the inlet of the GLS.

50 micrometers cannot be separated as these tiny droplets will simply follow the streamlines of the gas and carryover into the vortex finder and out of the GLS. Two phase flow correlations were used to determine design parameters that can be used for minimizing the formation of such small droplets. An optical high-pressure side glass assembly was installed downstream of the GLS in order to measure the outlet droplet size distribution in support of model validation,

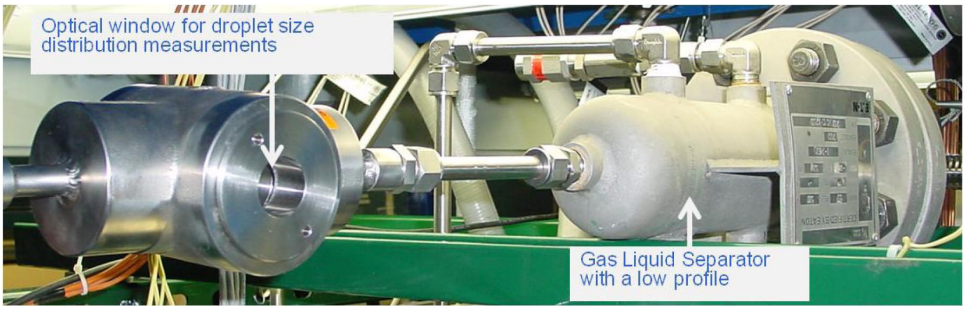

FIGURE 9. Side-glass assembly for droplet size distribution measurements at outlet of GLS.

as shown in Figure 9. Such measurements will be part of the orderly completion of the chemical hydrogen storage system development work in calendar year 2013, as the DOE elected to discontinue the chemical hydrogen storage system development at the end of Phase 2 of the HSECoE project.

CONCLUSIONS AND FUTURE DIRECTIONS

Conclusions derived from the work in FY 2013 are:

- The Simulink framework is critical for comparing the performance of different H_2 storage systems on a common basis and can be made more user-friendly through the development of a graphical user interface.
- AB as a slurry in silicone oil has similar ignition properties as AB in powder-form but the silicone oil acts as an additional fuel source.
- Fifty wt% $MnCl_2$ on super-activated carbon IRH-33 is an effective and regenerable sorbent to scrub ammonia from H_2 produced during the thermolysis of AB.
- A procedure needs to be developed for sizing the particulate filter area in cryo-adsorption systems in order to contain sorbent and meet SAE purity standards.
- The efficiency of the GLS was shown to be strongly dependent on flow rate, pressure and temperature. Operating conditions were determined that minimized liquid carry-over to <100 ppm of the inlet oil mass.

Future work in Phase 3 will comprise:

- Lead integrated power plant/storage system modeling technical area.
- Collaborate with SRNL and NREL on making the Simulink framework available on the HSECoE website.
- Update high level models to reflect the as-fabricated behavior of the cryo-adsorption system and assess its impact on the power plant performance.
- Incorporate updated chemical hydrogen storage system model in Simulink framework after LANL/PNNL have collected and analyzed their latest kinetic data.
- Collaborate with Ford/BASF on qualitative risk assessments of cryo-adsorption system.
- Engineering and testing of specialty components for H_2 storage systems and their experimental evaluation, such as the particulate filter in the cryo-adsorption system.
- Orderly completion of the GLS and ammonia filter development for the chemical hydrogen storage system, with an emphasis on collecting data for model validation.
- Publish results in peer reviewed journals.

FY 2013 PUBLICATIONS/PRESENTATIONS

1. José Miguel Pasini and Bart A. van Hassel, Vehicle Simulation Framework: Graphical User Interface, Face-To-Face 9 Meeting HSECoE, Mystic, CT, October 9–11, 2012.

2. Bart Van Hassel, Allen Murray, Randy C. McGee, Gas Liquid Separator Development, Face-To-Face 9 Meeting HSECoE, Mystic, CT, October 9–11, 2012.

3. Jagadeswara Reddy Karra and Bart A. van Hassel, H_2 Quality, Face-To-Face 9 Meeting HSECoE, Mystic, CT, October 9–11, 2012.

4. John Khalil, MOF-5 Safety Testing, Face-To-Face 9 Meeting HSECoE, Mystic, CT, October 9–11, 2012.

5. Bart A. van Hassel, M. Gorbounov, J. Holowczak, I. Fedchenia, X. Tang, R. Brown and Jose Miguel Pasini, Advancement of System Designs and Key Engineering Technologies for Materials-Based Hydrogen Storage, International Symposium on Metal-Hydrogen Systems 2012, Kyoto, Japan, October 23, 2012.

6. B.A. van Hassel, R. McGee, R. Karra, J. Khalil, R. Brown, A. Murray, Engineering Aspects of Materials Based Hydrogen Storage Systems, IEA Task 32 Kyoto, Japan, October 26–27, 2012.

7. Randy C. McGee, Allen Murray, Joe Rampone, Lou Chiappetta, Reddy J. Karra, David Gerlach, Igor Fedchenia and Bart A. van Hassel, Gas Liquid Separator and H_2 Quality, March 20-22, 2013, Tech Team Review HSECoE Project, Southfield, MI.

8. B.A. van Hassel, R. McGee, R. Karra, A. Murray, I. Fedchenia, D. Gerlach, and Jose Miguel Pasini, Engineering Aspects of Materials Based Hydrogen Storage Systems, April 20–25, 2013, IEA Task 32 Meeting, Heraklion, Greece.

9. Bart A. van Hassel , J.M. Pasini, R.C. McGee, L. Chiappetta, A. Murray, J.C. Rampone, J.R. Karra, D. Gerlach, I. Fedchenia, J. Khalil, and R. Brown, Advancement of Systems Designs and Key Engineering Technologies for Materials Based Hydrogen Storage, Annual Merit Review, May 14, 2013, Crystal City, VA.

10. Bart A. van Hassel, Jagadeswara. R. Karra, Jose Santana, Salvatore Saita, Allen Murray, Daniel Goberman, Richard Chahine and Daniel Cossement, Ammonia Sorbent Development for On-Board H_2 Purification, submitted to Separation and Purification Technology.

11. Igor I. Fedchenia, Bart A. van Hassel and Ron Brown, Solution of Inverse Thermal Problem for Assessment of Thermal Parameters of Engineered H_2 Storage Materials, submitted to Inverse Problems in Science and Engineering.

12. José Miguel Pasini, Claudio Corgnale, Bart A. van Hassel, Theodore Motyka, Sudarshan Kumar, and Kevin L. Simmons, "Metal hydride material requirements for automotive hydrogen storage systems," Accepted by Int. J. Hydrogen Energy, vol. **38**, pp. 9755-9765 (2013).

13. Bart A. van Hassel, Jagadeswara. R. Karra , David Gerlach, and Igor I. Fedchenia, Dynamics of fixed-bed adsorption of ammonia on impregnated activated carbon for hydrogen purification, to be submitted to Separation and Purification Technology.

REFERENCES

1. http://www1.eere.energy.gov/hydrogenandfuelcells/mypp/pdfs/storage.pdf

2. Information Report on the Development of a Hydrogen Quality Guideline for Fuel Cell Vehicles, SAE International Surface Vehicle Information Report, J2719 APR2008, Revised 2008-04.

3. Bart van Hassel, Jose Miguel Pasini, Andi Limarga, John Holowczak, Igor Fedchenia, John Khalil, Reddy Karra, Ron Brown, Randy McGee, Advancement of Systems Designs and Key Engineering Technologies for Materials Based Hydrogen Storage, Annual Report of UTRC's contribution to HSECoE project, July, 2012.

4. Bart A. van Hassel, Jagadeswara. R. Karra, Jose Santana, Salvatore Saita, Allen Murray, Daniel Goberman, Richard Chahine and Daniel Cossement, Ammonia Sorbent Development for On-Board H_2 Purification, submitted to Separation and Purification Technology.

5. Bart A. van Hassel, Jagadeswara. R. Karra , David Gerlach, and Igor I. Fedchenia, Dynamics of fixed-bed adsorption of ammonia on impregnated activated carbon for hydrogen purification, to be submitted to Separation and Purification Technology.

IV.B.4 Chemical Hydride Rate Modeling, Validation, and System Demonstration

Troy A. Semelsberger (Principal Investigator), Biswajit Paik, Brian Rekken, Ben Davis, and Jose I. Tafoya
Los Alamos National Laboratory (LANL)
MS J579, P.O. Box 1663
Los Alamos, NM 87545
Phone: (505) 665-4766
Email: troy@lanl.gov

DOE Managers
Ned Stetson
Phone: (202) 586-9995
Email: Ned.Stetson@ee.doe.gov
Jesse Adams
Phone: (720) 356-1421
Email: Jesse.Adams@go.doe.gov

Project Start Date: February 2009
Project End Date: February 2015

Overall Objectives

- Develop an automotive chemical hydrogen storage system capable of meeting all of the 2017 DOE targets simultaneously
- Develop and validate chemical hydrogen storage system models
- Quantify viable chemical hydrogen storage material properties that will meet DOE 2017 technical targets with our current system
- Develop and demonstrate "advanced" (non-prototypical) engineering concepts

Fiscal Year (FY) 2013 Objectives

- Quantify reaction characteristics of liquid exothermic media (methoxy propylamineborane), slurry endothermic media (alane), and slurry exothermic media (ammonia borane)
- Design, build, and demonstrate advanced dehydrogenation reactors
- Develop an onboard fluid-phase chemical hydrogen storage system; system designer

Technical Barriers

This project addresses the following technical barriers from the Technical Plan - Storage section of the Fuel Cell Technologies Office Multi-Year Research, Development, and Demonstration Plan:

(A) System Weight and Volume

(B) System Cost

(C) Efficiency

(D) Durability/Operability

(E) Charging/Discharging Rate

(F) Codes and Standards

(G) Materials of Construction

(H) Balance-of-Plant (BOP) Components

(J) Thermal Management

(K) System Life-Cycle Assessment

(R) By-product/Spent Material Removal

Technical Targets

The summary of our progress in relation to the DOE 2017 technical targets for both ammonia borane and alane can be seen in Figure 1. The cost target was assumed to be $7/kg of hydrogen. The estimated values are based on the Hydrogen Storage Engineering Center of Excellence's chemical hydrogen storage system design. Both systems assume 50 wt% slurry loadings for ammonia borane and alane.

Accomplishments

- Designed, built and tested novel auger reactor
- LANL was the first to demonstrate and characterize flow through reactor studies on 20 wt% alane slurry and 20 wt% ammonia borane slurry
- Identified reactor operating limits for various fluid-phase chemical hydrogen storage media
- Quantified impurities generated from ammonia borane slurries, alane slurries, and methoxy propylamine borane
- LANL developed the first empirical rate expression describing slurry alane dehydrogenation from flow reactor data

✧ ✧ ✧ ✧ ✧

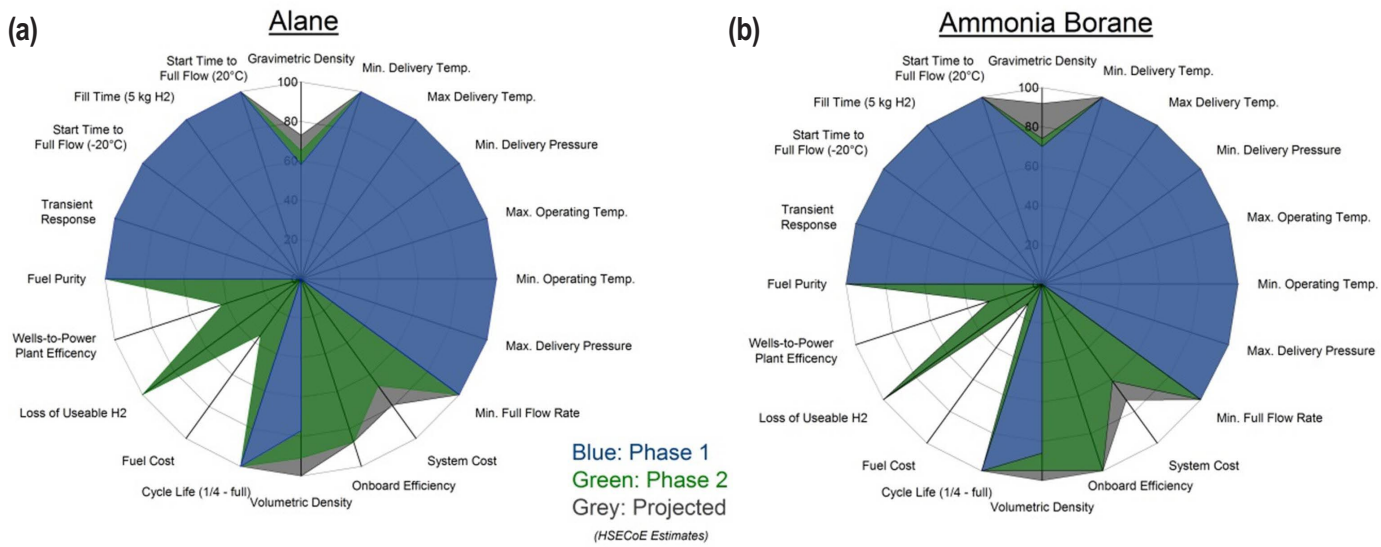

FIGURE 1. Spider chart summarizing our progress in meeting the DOE 2017 technical targets for (a) 50 wt% alane slurry and (b) 50 wt% ammonia borane slurry.

INTRODUCTION

Hydrogen storage systems based on chemical hydrogen storage materials require a chemical reactor to release the hydrogen from the storage media, which is a fundamental difference from the other modes of hydrogen storage, adsorbents and metal hydrides. This hydrogen-release reactor is crucial to the performance of the overall storage system, especially in meeting the DOE targets for hydrogen generation rate, transient operation, and startup times. The reactor must be designed to achieve these targets while meeting the constraints of the overall system volume and weight targets.

LANL will also address the unique requirements of onboard automotive hydrogen storage systems. For example, these systems require fast startup, operation over a wide dynamic range (10:1 turndown or greater), and fast transient response to meet the demands of a drive cycle. The LANL team will develop novel reactor designs and operation strategies to meet these transient demands. In addition, the shelf life and stability of the hydrogen storage media is crucial for an automotive system, especially pertaining to safety and cost. Starting with the kinetics models, the LANL team will develop mathematical models for the aging characteristics of candidate hydrogen storage media (for example, complex metal hydrides or chemical hydrogen storage materials) subjected to a range of environmental factors. These models can be incorporated into system-level models of performance and cost and also used for the development of accelerated aging protocols necessary for later testing.

RESULTS

Reaction Characteristics of Slurry Alane and Slurry Ammonia Borane with Auger Reactor

Experiments were performed using our novel in-house built auger reactor to determine the reaction characteristics of 20 wt% "uncatalyzed" alane slurry, and 20 wt% ammonia borane slurry. The reaction characteristics of interest are reaction selectivity (i.e., impurities), conversion, and hydrogen production. Reactor durability and operability are also important performance characteristics. Typical operating conditions for ammonia borane slurries consisted of feed flow rates ranging from 0.5–3.12 mL/min and reactor temperatures ranging from 150–225°C. All reaction runs used 20 wt% ammonia borane slurry. Although this is not the highest ammonia loading achievable, it is however the loading that was used to screen potential reactor designs without exhausted our ammonia borane supply. The products observed from ammonia borane dehydrogenation as a function of temperature are shown in Figure 2. The identified fuel cell impurities include ammonia, borazine and diborane. Low-temperature dehydrogenation favors ammonia formation while high temperature operation favors borazine and diborane. The most favorable reactor temperatures for producing the least amount of fuel cell impurities are around 150°C. Lower reactor temperatures, however, demonstrate slower kinetics. Slower reaction kinetics result in larger reactors in order to generate the necessary hydrogen flow rates. The auger reactor demonstrated significant improvements in durability and operability as compared to the typical flow through reactor, evidenced by continued reactor operation without fouling during reactor testing.

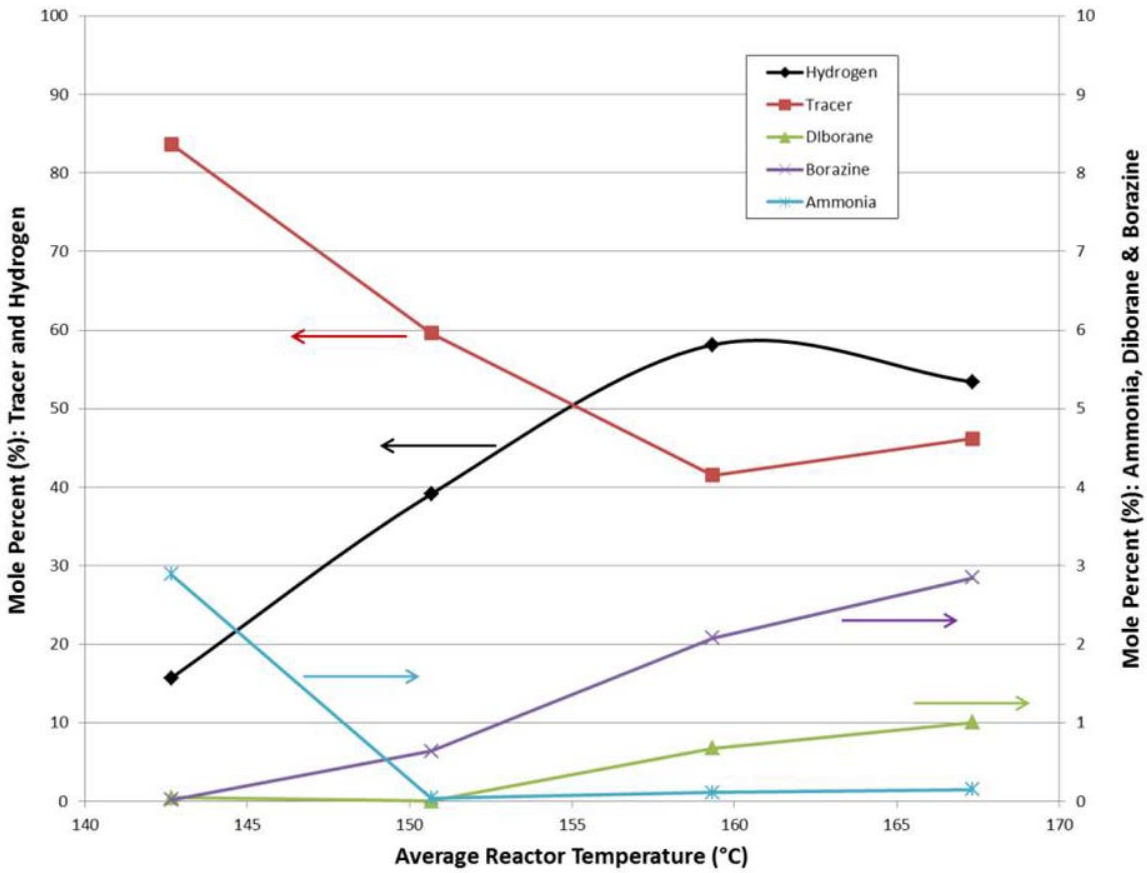

FIGURE 2. Effluent mole percentages observed during dehydrogenation of 20 wt% ammonia borane slurry as a function of temperature (auger reactor operating at 40 rpm).

Dehydrogenation of alane slurry was also investigated using our novel in-house built auger reactor. The alane slurries consisted of as-received, "uncatalyzed" alane from ATK. Typical operating conditions for alane slurries consisted of feed flow rates ranging from 0.5–2.0 mL/min and reactor temperatures ranging from 150–275°C. The auger speed was maintained at 40 rpm for all runs. Alane conversions of one were observed for reaction temperatures around 260°C and a space-time of 6.8 min. The elevated reactor temperatures required for complete alane conversion is directly attributed to the fact that alane was not "catalyzed" or "pre-activated." Lower dehydrogenation temperatures can be achieved by doping and/or "pre-activating" alane. These approaches will likely be required for on-board automotive applications because of the increased energy efficiency, decreased start-up time, and decreased system mass and volume (e.g., radiator, reactor, etc,). Alane is attractive not only because of its relatively high hydrogen content (10.1 wt% H_2), but also due to its high hydrogen selectivity. No impurities were observed during the dehydrogenation of alane for temperatures lower than 210°C. Reaction temperatures greater than 210°C resulted in undesired side reactions of alane with silicon oil. Consequently, trace amounts of gas phase impurities were observed for reactor temperatures greater than 210°C. Reactor fouling was not observed during 10 hours of continuous reactor operation with alane slurries. Data collected was regressed using a power rate law. The fitted rate expression for alane dehydrogenation with our novel in-house built auger reactor is

$$-r_{Alane}\Big|_{apparent} = kC_{alane}^{0.5}$$

$$k(T) = Ae^{\left(\frac{-E_a}{RT}\right)}, \quad A = 3.7x10^6, \quad E_a = 90.75\frac{kJ}{mol}$$

The fitted rate expression can be seen in the alane conversion parity plot shown in Figure 3. The parity plot shows good agreement in comparing the model predicted alane conversion to the experimentally observed alane conversion.

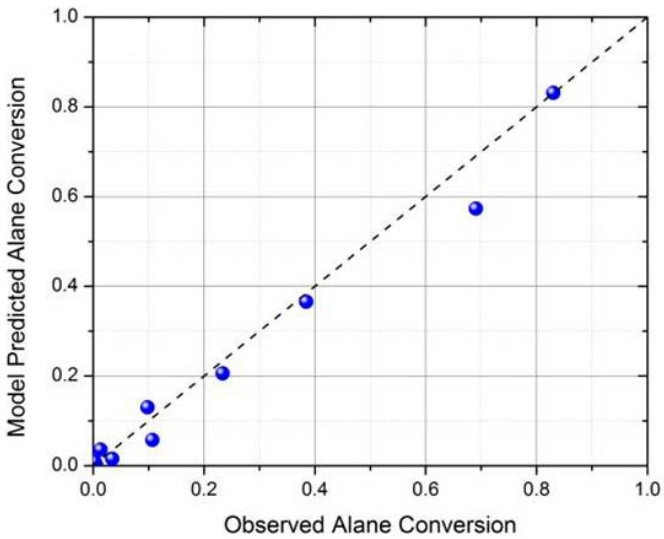

FIGURE 3. Parity plot comparing model predicted alane conversions to experimentally observed alane conversions collected with LANL in-house built auger reactor.

SUMMARY

- Successfully designed and built novel fluid-phase reactors
- Performed flow reactor studies with methoxy propylamineborane, alane slurries, and ammonia borane slurries without reactor fouling or reactor slugging
- Quantified gas phase impurities produced alane and ammonia borane slurries

FUTURE DIRECTIONS

Material Properties

- Develop viable material property guidelines for chemical hydrogen storage media that will meet the DOE 2013 technical targets.

Reactor Testing

- Perform reaction studies with 30 and 50 wt% alane slurry loadings and 30 and 50 wt% ammonia borane slurry loadings.

Borazine Scrubber

- Perform additional borazine scrubbing experiments to determine pressure effects on borazine adsorption capacities with activated carbon.

FY 2013 PUBLICATIONS AND PRESENTATIONS

1. "Overview of LANL's Engineering Research Efforts for Chemical Hydrogen Storage" WHEC 2012, Toronto, CA, *Invited Speaker.*

2. "Chemical Hydride Rate Modeling, Validation, and System Demonstration" 2013 Annual Merit Review, Washington, D.C., May 2013.

IV.B.5 System Design, Analysis, Modeling, and Media Engineering Properties for Hydrogen Energy Storage

Matthew Thornton (Primary Contact), Lin Simpson, Aaron Brooker, and Jonathon Cosgrove
National Renewable Energy Laboratory (NREL)
1617 Cole Boulevard
Golden, CO 80401
Phone: (303) 275-4273
Email: Matthew.Thornton@nrel.gov

DOE Managers
Ned Stetson
Phone: (202) 586-9995
Email: Ned.Stetson@ee.doe.gov
Jesse Adams
Phone: (720) 356-1421
Email: Jesse.Adams@go.doe.gov

Subcontractors:
- Strategic Analysis Inc., Arlington, VA
- Mark Paster, Annapolis, MD

Project Start Date: February 2, 2009
Project End Date: June 30, 2015

Overall and Fiscal Year (FY) 2013 Objectives

- Perform vehicle-level modeling and simulations of various storage system configurations.
- Lead the storage system energy analysis and provide results.
- Compile and obtain media engineering properties for adsorbent materials.

Technical Barriers

This project addresses the following technical barriers from the Hydrogen Storage section of the Fuel Cell Technologies Office Multi-Year Research, Development, and Demonstration Plan:

(A) System Weight and Volume

(B) System Cost

(C) Efficiency

(E) Charging/Discharging Rates

(I) Dispensing Technology

(K) System Life-Cycle Assessments

Technical Targets

This project is conducting simulation and modeling studies of advanced onboard materials-based hydrogen storage technologies. Insights gleaned from these studies are being applied toward the design and synthesis of hydrogen storage vessels that meet the following DOE 2015 hydrogen storage for light-duty vehicle targets:

- Cost: to be determined
- Specific energy: 0.055 kg H_2/kg system
- Energy density: 0.040 kg H_2/L system
- Charging/discharging rates: 3.3 min
- Well to power plant efficiency: 60%

FY 2013 Accomplishments

- Used the vehicle model and the center modeling framework, developed in previous years, to evaluate the performance of specific storage system designs across all material classes and assess the design impacts on vehicle performance to help guide specific system designs and focus engineering solutions that will overcome barriers to meeting technical targets.
- Performed vehicle-level tradeoff analyses to better understand the impact of key engineering designs, for example, the tradeoff between mass, onboard hydrogen storage capacity, and vehicle range.
- Used Hydrogen Delivery Scenario Analysis Model (HDSAM) to calculate preliminary greenhouse gas (GHG) emissions and well-to-power plant (WTPP) efficiency figures for baseline physical storage systems and candidate materials-based storage systems for each material class.
- Applied an array of measurement techniques to provide engineering properties of sorbent materials.

✧ ✧ ✧ ✧ ✧

INTRODUCTION

Overcoming challenges associated with onboard hydrogen storage is critical to the widespread adoption of hydrogen-fueled vehicles. The overarching challenge is identifying a means to store enough hydrogen onboard to enable a driving range greater than 300 miles within vehicle-related packaging, cost, safety, and performance constraints. By means of systems analysis and modeling, hydrogen

storage system requirements for light-duty vehicles can be assessed. With these findings and through collaboration with our Hydrogen Storage Engineering Center of Excellence (HSECoE) partners, optimal pathways for successful hydrogen storage system technology can be identified to enable future commercialization of hydrogen-fueled vehicles.

APPROACH

An array of tools and experience at NREL are being used to meet the objectives of the HSECoE. Specifically, extensive knowledge of multiple vehicle simulations, well-to-wheels (WTW) analysis, and optimization are being employed and integrated with fuel cell and material-based hydrogen storage system models developed by other HSECoE partners. This integrated model framework allows for the evaluation of various hydrogen storage options on a common basis. Engineering requirements are defined from these studies, thus enabling the design of hydrogen storage vessels that could meet DOE performance and cost targets in a vehicle system context.

In the area of media engineering, attaining the objectives of the HSECoE relies on NREL's leadership in developing custom analytical instrumentation for hydrogen adsorption analysis. These tools are used to thoroughly characterize hydrogen storage adsorbents so that an optimized storage vessel specific to the adsorption material may be efficiently engineered. NREL uses these methods to analyze adsorption materials identified by the HSECoE as holding promise for application in commercial on-vehicle refuelable hydrogen storage systems capable of meeting DOE targets.

RESULTS

The following will provide results from work completed this year to support the HSECoE with a focus on three main tasks. In collaboration with our original equipment manufacturer (OEM) partners, NREL (1) worked with the system architects to perform simulations and tradeoff studies to help with the high-level storage system designs and engineering, including mass and volume trade-offs; (2) performed energy analysis on specific system designs being considered by the HSECoE; and (3) continued work in the area of adsorbent materials characterization and analysis.

To gain a better understanding of the interactions that exist between various materials-based hydrogen storage systems and the vehicle system as well as the engineering challenges that exist when integrating one of these systems with a vehicle, NREL developed a vehicle-level model designed to be sensitive to these issues. In previous work under the HSECoE, the Hydrogen Storage SIMulator (HSSIM) was developed as a specialized tool that could be used to assist in the design and engineering of materials-based hydrogen storage systems being considered by the HSECoE. This tool was designed to not only allow for understanding key trade-offs, but also to have a seamless integration with the HSECoE fuel cell and detailed hydrogen storage system models and to evaluate progress towards the U.S. Department of Energy's hydrogen storage technical targets. This model has been integrated with a fuel cell model developed by Ford Motor Company in a HSECoE common modeling framework developed by United Technologies Research Center and other HSECoE partners (Figure 1).

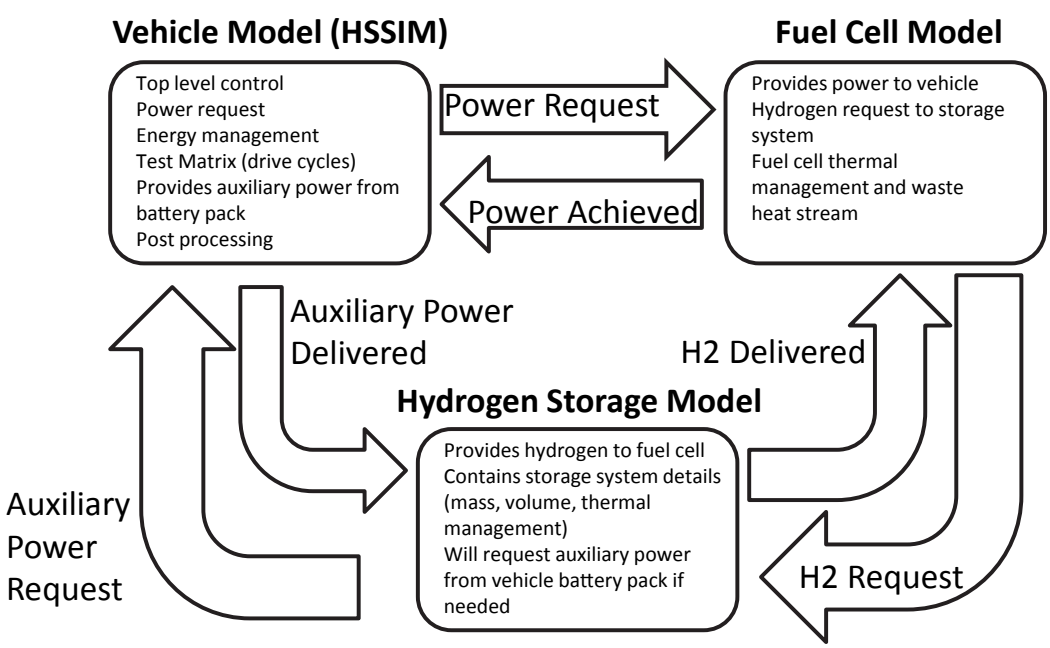

FIGURE 1. HSECoE Integrated Modeling Framework

The HSSIM vehicle model is designed to evaluate high-level attribute improvements. To accomplish this, the inputs, such as the glider and powertrain components, are also defined at a high level. The vehicle glider is defined with a specific frontal area, drag coefficient, mass, center of gravity, front axle weight fraction, and wheelbase. The wheels are defined by inertia, a rolling resistance coefficient, coefficient of friction, and radius. The inputs for the motor are power, peak efficiency, mass per unit of power, cost per unit of power, and time to full power. The battery inputs include power, energy, mass per unit of energy, and round trip efficiency. Auxiliary loads are assumed to be a specified constant plus an amount required for the fuel cell and hydrogen storage systems. These inputs match the DOE's technical target units, such as battery kilograms per kilowatt hour, so that the impact of improvements can be evaluated over time as the targets change.

A key part of developing the vehicle model was working with the center OEMs on developing a test matrix that will be used to evaluate all the storage systems being considered across the center on a common basis. The test matrix was structured to evaluate the performance of the storage systems against the technical targets under standard and realistic transient driving conditions. The matrix was also designed to exercise a given system from full to empty to provide an understanding of its performance over the entire range of fill conditions. Therefore, the test cases were designed to repeat a drive cycle or set of drive cycles until the storage system being evaluated was empty. Standard drive cycles are typically not long enough to achieve this and would not even deplete a buffer tank in some systems. The important point here is that when evaluating the complex dynamics of hydrogen storage systems, this approach of repeating drive cycles to create test cases is critical to gaining the feedback necessary to refine and improve the systems.

As shown in Table 1, the center test matrix includes five test cases:

The first case combines repeats of the urban dynamometer driving schedule (UDDS) and the highway fuel economy test (HWFET) until the storage system is depleted. This is used to determine the vehicle-level fuel economy (FE) and, from that, figure the vehicle range. The fuel economy is calculated using the current Environmental Protection Agency (EPA) five-cycle procedure of adjusting and weighting the UDDS and HWFET to provide one fuel economy figure that represents real-world use—it is not the raw figures that come directly from running the cycles. Similarly, the range is then calculated from the adjusted and weighted UDDS and HWFET figures and not simply the cycles' miles traveled until the storage system is empty. Again, this test matrix is key to providing a means to evaluate the fuel economy, range, and other vehicle-level

TABLE 1. Test Matrix Used across the Center to Evaluate the Performance of All the Storage Systems

Case	Test Schedule	Cycles	Description	Test Temp (°F)	Distance per cycle (miles)	Duration per cycle (minutes)	Top Speed (mph)	Average Speed (mph)	Max. Acc. (mph /sec)	Stops	Idle	Avg. H2 Flow (g/s)*	Peak H2 Flow (g/s)*	Expected Usage
1	Ambient Drive Cycle - Repeat the EPA FE cycles from full to empty and adjust for 5 cycle post-2008	UDDS	Low speeds in stop-and-go urban traffic	75 (24 C)	7.5	22.8	56.7	19.6	3.3	17	19%	0.09	0.69	1. Establish baseline fuel economy (adjust for the 5 cycle based on the average from the cycles) 2. Establish vehicle attributes 3. Utilize for storage sizing
		HWFET	Free-flow traffic at highway speeds	75 (24 C)	10.26	12.75	60	48.3	3.2	0	0%	0.15	0.56	
2	Aggressive Drive Cycle - Repeat from full to empty	US06	Higher speeds; harder acceleration & braking	75 (24 C)	8	9.9	80	48.4	8.46	4	7%	0.20	1.60	Confirm fast transient response capability – adjust if system does not perform function
3	Cold Drive Cycle - Repeat from full to empty	FTP-75 (cold)	FTP-75 at colder ambient temperature	-4 (-20 C)	11.04	31.2	56	21.1	3.3	23	18%	0.07	0.66	1. Cold start criteria 2. Confirm cold ambient capability – adjust if system does not perform function
4	Hot Drive Cycle - Repeat from full to empty	SC03	AC use under hot ambient conditions	95 (35 C)	3.6	9.9	54.8	21.2	5.1	5	19%	0.09	0.97	Confirm hot ambient capability - adjust if system does not perform function
5	Dormancy Test	n/a	Static test to evaluate the stability of the storage system	95 (35 C)	0	31 days	0	0	0	100%	100%			Confirm loss of useable H2 target

performance features of the storage systems on a common and comparable basis.

NREL used these model outputs from the framework to evaluate the current status of various adsorbent and chemical hydrogen storage material-based systems being evaluated by the HSECoE. Because this work is in progress, the results presented here are preliminary and may change over time as the storage systems are refined and the models are adjusted accordingly. That is, the intent is to show how the model outputs can be used to evaluate and compare different storage systems and support engineering solutions to particular barriers. The intent, at least at this time, is not to develop an argument for which system or materials class has the most promise for actual vehicle application. Vehicle-level results will be presented for a select group of these systems (i.e., this is not a comprehensive set of systems being evaluated under the HSECoE, nor is it a complete set of storage models included in the framework). For the model application, example results discussed in this section's simulations were run with several adsorbent and chemical hydrogen storage material systems being evaluated for phase III of the project and include HexCell powder MOF-5 and MATI Puck MOF-5 (0.32 g/cc) adsorbent systems and the ammonia-borane slurry and alane slurry chemical hydrogen storage material systems. In addition, a 700-bar compressed gas system was included for comparison to the materials-based systems.

For the following discussion, model applications and results reported are based on Test Case 1 of the framework exclusively (i.e., UDDS and HWFET combined test cycles). In addition, a midsize car class was selected for the initial baseline simulations within the framework. The intent was to be representative of a high-sales-volume midsize car, such as the Ford Fusion, Chevrolet Malibu, or Toyota Camry. The attributes associated with this size vehicle are a frontal area of 2.2 m^2, drag coefficient of 0.29, and tire size of P195/65R15. The electric motor was sized to 100 kW with 85% efficiency from the motor to the road. Consistent with most fuel cell vehicles, the vehicle includes a 20-kW/1-kWh battery pack for hybridization for capturing regenerative braking and assistance with propulsion. The state of charge of the battery is maintained between 40% and 80%, with the target state of charge varying throughout the cycle depending on driving conditions. The vehicle glider weight (excluding the hydrogen storage system and other drive components) is 1,104 kg. The motor and power electronics combined weight is 105 kg, the battery system weight is 51 kg, the fuel cell system with cooling weight is 214 kg, and the hydrogen storage system weight varied. All of the following results are based on the vehicle configuration above, but the model is capable of simulating both larger and smaller vehicle classes and configurations.

For the example systems included in Table 2, the fuel economy for materials-based systems ranged from 49/48 miles per gasoline gallon equivalent (mpgge) for the MOF-5 systems to 44 mpgge for the alane slurry system. The alane slurry system performed the worst in terms of fuel economy due to its onboard endothermic nature. The system burns hydrogen to create the needed temperatures for the storage system hydrogen release and storage system thermal management. The use of hydrogen for system thermal management results in poor onboard efficiency and, subsequently, poor fuel economy. The ammonia-borane slurry and MOF-5 systems performed better in this example due to their high gravimetric efficiency, resulting in lower overall system and vehicle mass and therefore better fuel economy. As a result, the MOF-5 systems also offer the best range results of 274/269 miles based on the above vehicle configuration and 5.6 kg nominal usable hydrogen storage capacity. The compressed gas systems demonstrated slightly better, but comparable fuel economy and range relative to these example material-based systems.

The ammonia-borane slurry chemical hydrogen storage material system had a gravimetric density of 4.2 weight percent (i.e., the percent of hydrogen mass to the overall storage system mass; the DOE 2017 technical target for gravimetric density is 5.5 weight percent). This was the best-performing materials-based system and was comparable to the compressed gas system, which had a gravimetric density of 4.7 weight percent. That said, the ammonia-borane slurry system outperformed the compressed gas systems and all of the other materials-based systems in terms of volumetric density with nearly 37 g of hydrogen per system liter. The

TABLE 2. Vehicle-Level Performance Summary

Hydrogen Storage System	Adjusted Fuel Economy (mpgge)	Range (mi)	Onboard Efficiency (%) UDDS/HFET	Gravimetric Density (wt%)	Volumetric Density (g/l)	System Mass (kg)
Exothermic Ammonia-Borane Slurry	47	264	97	4.2	36.8	137.1
Endothermic Alane Slurry	44	244	93	3.4	34.3	185.1
HexCell Powder MOF-5	49*	274*	92**	3.5	17.5	137.6
MATI Puck MOF-5 (0.32 g/cc)	48*	269*	97**	3.4	20.7	149.3
700-bar Compressed Gas	50	279	100	4.7	25.0	119.0

*Preliminary Model Results **Off Model Calculations

DOE's 2017 technical target for volumetric density is 40 g/L. For all the example materials-based systems included here, the HexCell powder MOF-5 system performed the best in terms of fuel economy, range, and gravimetric density and was comparable to the compressed gas systems. As noted, the ammonia-borane slurry system performed best in terms of volumetric density, but it is important to remember that the ammonia-borane slurry system is an off-board regenerable system that is accompanied by unique refilling challenges, logistics, and costs that are not captured in the above analysis.

NREL also continued to support the HSECoE by performing energy analyses on various storage system designs being evaluated for phase III of the project. These analyses provide the center system architects and other partners with high-level estimates about the overall energy inputs required by a given system, including WTPP efficiency (%), hydrogen cost ($/kg), and GHG emissions (carbon dioxide equivalent) on a gram per mile basis for future 2020 scenarios.

HDSAM was used to estimate the above parameters for each system. To date, the HDSAM model has been run for the HexCell powder MOF-5, MATI Puck MOF-5 (0.32 g/cc) and 60-bar 80 K gas adsorbent systems, and the ammonia-borane slurry and alane slurry chemical hydrogen storage material systems to produce preliminary WTPP efficiency, GHG emissions, and hydrogen cost figures. In addition, model runs were performed on a 700-bar compressed gas system and a cryogenic-compressed liquid hydrogen system (CcH_2, <200 K) for comparison to the materials-based systems.

Table 3 shows the storage system results (i.e., WTW cost breakdown, WTW energy breakdown, WTW GHG breakdown, and volumetric efficiency) for the two chemical hydrogen storage systems and the three adsorbent system, as well as the 700-bar compressed gas and cold gas cryogenic-compressed liquid hydrogen systems. The ammonia-borane system, which offers several onboard advantages over the alane system—an exothermic onboard reaction leads to higher onboard efficiency (96% vs. 88%)—has higher regeneration cycle costs and energy inputs. Both materials showed a higher cost and lower efficiency than the adsorbent systems and the two physical storage systems. This indicates a need for advancements and cost reductions for chemical hydrogen storage material systems in general. This analysis supports the need for additional research focused on reducing the cost of chemical hydrogen storage material off-board regeneration cycles in order for these systems to be viable. The adsorbent systems performed better than the chemical hydrogen storage material systems in terms of cost, energy, and GHG emissions, but were still higher in all of these areas then the physical storage systems and also require additional advancements in order to compete with the incumbent systems.

NREL wrapped up the media engineering support component of the work early in the year. This work primarily involved completing an initial analysis of MOF-5 at temperatures below 77 K. The initial results suggest that the present model predictions for the hydrogen storage properties as a function of pressure of MOF-5 at these temperatures are reasonable. Based on this initial assessment, the effort was stopped to enable more focus on model transfer for public access. A set of plans for improving the cryostat-based low-temperature measurements and improving overall accuracy was developed and can be implemented in the future should measurements with temperatures below 77 K be needed in the future for advanced sorbent materials.

FUTURE DIRECTIONS

- Continue to run vehicle simulations to support engineering design and support the center modeling framework refinements and enhancements:
  - Run vehicle simulations to support high-level storage system design and engineering tradeoffs.
  - Run vehicle simulations to support storage system sizing analyses.

TABLE 3. WTW Results Summary

	WTW H_2 Cost ($/kg-$H_2$)	WTW Energy Efficiency (%)	WTW GHG Emissions (g/mile)	Volumetric Efficiency (gms-H_2/L)
2020 700-bar Gas - T520*	3.91	56.4	230	25.6
2020 CcH_2 - Liquid H_2 Truck	4.49	46.5	289	41.8
2020 Liquid Ammonia-Borane	13.96	16.5	915	41.4
2020 Liquid Alane	7.89	24.7	642	32.2
2020 Absorbent 1 60-bar 80 K Gas-T340	5.92	40.4	401	24.1
2020 Absorbent HexCell 100-bar 80 K Gas-T340**	6.16	39.2	412	17.5
2020 Absorbent MATI 100-bar 80 K Gas-T340**	5.69	42.1	391	20.7

*T520, 520 Bar Insulated Tube Truck; **T340, 340 Bar Insulated Tube Truck

- Evaluate storage system impacts on vehicle performance (e.g., fuel economy, range).
- Work with HSECoE partners to make center-developed models available and accessible to the broader research and academic community through a controlled web-based access portal.

FY 2013 PUBLICATIONS/PRESENTATIONS

1. System Design, Analysis, Modeling, and Media Engineering Properties for Hydrogen Energy Storage, Matthew Thornton, DOE Annual Merit Review Meeting, May 14, 2013, Washington, D.C.

IV.B.6 Thermal Management of Onboard Cryogenic Hydrogen Storage Systems

Mei Cai (Primary Contact), Peter Hou,
Jerome P. Ortmann, and Martin Sulic
General Motors (GM) R&D Center
30500 Mound Road
Warren, MI 48090
Phone: (586) 596-4392
Email: mei.cai@gm.com

DOE Managers
Ned Stetson
Phone: (202) 586-9995
Email: Ned.Stetson@ee.doe.gov
Jesse Adams
Phone: (720) 356-1421
Email: Jesse.Adams@go.doe.gov

Contract Number: DE-FC36-09GO19003

Project Start Date: March 1, 2009
Project End Date: June 30, 2015

Overall Objectives

Main objectives of this project are:

- Develop system simulation models and detailed transport models for onboard hydrogen storage systems using adsorbent materials, and to determine system compliance with the DOE technical targets
- Design, build, and test an experimental vessel for validation of cryo-adsorption models and determine the fast fill and discharge dynamics of cryo-adsorbent storage systems

Fiscal Year (FY) 2013 Objectives

- Demonstrate 3-minute scaled refueling by an internal flow-through cooling system based on powder media
- Validate metal-organic framework (MOF)-5 powder bed capable of 0.15 g H_2/(g MOF) and 20 g H_2/(liter MOF)
- Demonstrate scaled H_2 release rate of 0.02 (g H_2/s)/kW by an internal heating system (<6.5 kg and 6 L)

Technical Barriers

This project addresses the following technical barriers from the Hydrogen Storage section of the Fuel Cell Technologies Office Multi-Year Research, Development, and Demonstration Plan:

(A) System Weight and Volume

(C) Efficiency

(E) Charging/Discharging Rates

(J) Thermal Management

Technical Targets

In this project, studies are being conducted to develop MOF-5-based storage media with optimized engineering properties. This material has the potential to meet the 2017 technical targets for onboard hydrogen storage as shown in the following table:

Storage Parameter	2017 Target (system)	MOF-5 (material)
System Gravimetric Capacity	0.055	0.187
System Volumetric Capacity	0.040	0.028

FY 2013 Accomplishments

- Completed the installation and testing of the cryo-vessel with automated control instrumentation
- Obtained performance and operational data of MOF-5 powder/heat exchanger system
- Installed and tested helical coil heat exchanger in the cryo-vessel, reaching targeted H_2 release rate
- Validated adsorption and desorption models with cryo-vessel experiments

✧ ✧ ✧ ✧ ✧

INTRODUCTION

The DOE is supporting research to demonstrate viable materials for onboard hydrogen storage. Onboard hydrogen storage systems based on cryo-adsorbents are of particular interest due to the high gravimetric hydrogen capacity and fast kinetics of the sorbent materials at low temperatures and moderate pressure. However, cryo-adsorbents are generally characterized by low density and unsatisfactory thermal properties. As part of the Hydrogen Storage Engineering Center of Excellence (HSECoE) team, the GM team is building system models and detailed transport models to optimize a cryo-absorbent fuel tank. A laboratory-scale cryogenic vessel was designed, built, and tested to determine the charging and discharging capabilities of an actual, operational system.

APPROACH

The 3-liter stainless steel cryogenic test vessel (Figure 1) is sealed in an evacuated chamber that is temperature controlled down to cryogenic temperatures to best establish adiabatic conditions. Approximately 525 g of pure MOF-5 powder is packed into the 3-liter test vessel resulting in an adsorbent bed density of 0.18 g/cm^3. Mass flow rates in and out of the adsorption vessel are measured with a number of selectable orifice meters to allow accurate measurement over a large range of flow rates (0.005 to 0.75 g/s). A GM-designed helical coil heater with a center heating element is installed in the vessel to supply heat to the adsorbent bed during discharge. The vessel can be pressurized by either controlling the outlet flow rate or closing the outlet. A total of 32 high-precision resistive temperature devices (RTDs) and associated data acquisition channels are used to measure temperatures throughout the system and in the adsorption bed. Twenty-two of the RTDs are devoted to measuring temperatures throughout the bed and at the inlet and outlet ports. The remaining ten are associated with monitoring thermal conditions of hydrogen gas flow throughout the apparatus.

Three-dimensional adsorption and desorption models of the 3-liter cryogenic test vessel were developed using COMSOL Multiphysics® software. COMSOL Multiphysics® contains application modes allowing for fluid flow through a porous media. The porous and fluid media are treated as a single medium having volume-averaged variables such as the flow velocity, pressure, and density. The gas and the solid bed are assumed to be in thermal equilibrium. Real gas properties of hydrogen are calculated using equations for a compressibility factor. Properties that are temperature or pressure dependent (and time-varying), such as the heat capacity of the MOF-5 bed and the heat of adsorption, are calculated at each time step. The amount of adsorbed hydrogen was quantified by employing a Dubinin-Astakhov isotherm. Model simulations were performed for the charging and discharging processes for the 3-liter cryogenic vessel. The flow in the system was modeled with Free and Porous Media Flow physics, and the heat transfer process was modeled with Heat Transfer with Porous Media. Pressure drop and flow velocity fields can be calculated with the former physics, and the process of heat transfer in the solids, fluids, and porous media can be investigated with the latter one.

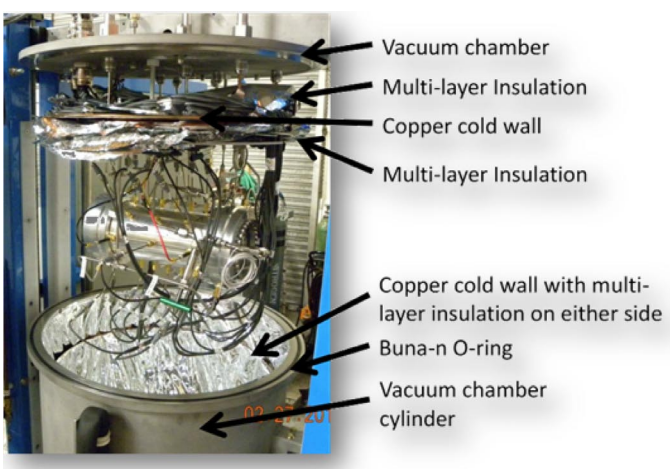

FIGURE 1. 3-liter vessel mounted to instrument with RTDs attached prior to closing vacuum chamber.

RESULTS

A. Cryogenic Test Vessel – Charging Tests

Various adsorptions were performed on the MOF-5 powder bed to examine our 3-minute refueling milestone within the parameters of 5–60 bar and 150–80 K. A pressure of 60 bar can be reached within one minute, thus leaving more than 2 minutes for flow-through cooling. However, with an initial bed temperature of 150 K, the lowest bed temperature at 3 minutes during our testing was still above 100 K. The slow cooling effect seen in the MOF-5 powder bed is attributed to the test vessel itself and the interaction of the incoming cold gas with the warm gas inside the vessel. The large thermal mass of the stainless steel pressure vessel, approximately 25 lbs, coupled with the limited intimate contact the cold hydrogen gas has with the internal vessel wall result in only a small decrease in vessel body temperature. The body temperature has a significant effect on the overall bed temperature. When flow-through cooling is halted, the bed and vessel wall quickly reach a temperature equilibrium close to that of the vessel wall's initial state. To drive the vessel temperature down during an adsorption, external cooling would be required. Unfortunately, while our apparatus does have liquid nitrogen flow control to the vessel end caps, it was not designed for a rapid cooling process. The larger factor for the slow flow-through cooling is the mixing of the incoming cold hydrogen with the warm bed hydrogen. In an ideal case, the cold gas would move through the bed while pushing the warm gas out like two immiscible liquids. This would allow for higher inlet flow rates compared to the outlet due to the higher density of the incoming gas. Unfortunately this is not the case. The cold gas moves throughout the vessel, therefore the hydrogen gas that is removed is not necessarily the warmest gas within the bed. This is apparent in Figure 2. The temperature profiles shown are center points moving away from the inlet as they get closer to the outlet. While it is expected that the exothermic heat of adsorption onset should be a progression from inlet to outlet, it is clear from Figure 2 that the further a point is away from the inlet the slower is the cooling effect, indicating that the incoming cold hydrogen is not progressing through the bed by pushing the warm gas out. A vessel design to improve

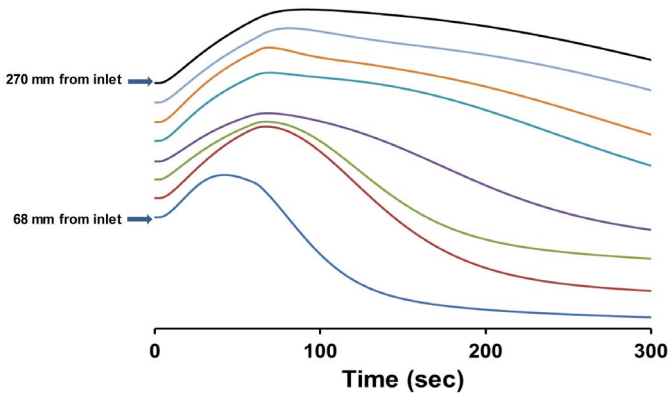

FIGURE 2. Experimental temperature profiles shown are center points moving away from the inlet as they get closer to the outlet. The further a point is away from the inlet the slower is the cooling effect.

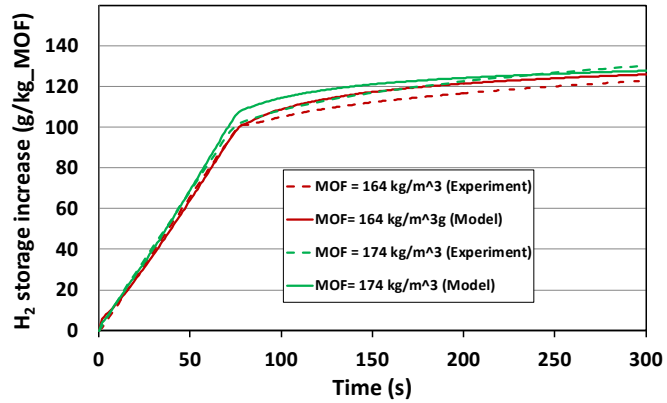

FIGURE 3. Effect of MOF density on H_2 storage increase rate.

flow-through cooling would require directional channels for the gas.

To decrease the mixing of the gases we added more adsorbent to the inlet side of the test vessel. Prior to adding more adsorbent the existing bed was compacted as much as possible. The new MOF-5 powder (7.78 g), was also compacted before the vessel was sealed. By compacting and adding more powder to the inlet side of the test vessel it was our intention to slow down diffusion of the incoming cryogenic hydrogen through the initial section of the bed, thereby displacing the warm gas more effectively. The compaction increased the bed density of MOF in the system from 164 kg/m^3 to 174 kg/m^3. Experimental and modeling results from the two cases are shown in Figure 3. The data in Figure 3 indicates that the density of MOF has an effect on the H_2 charging rate per unit mass of MOF. The H_2 charging rate per unit mass of MOF increases with the density of MOF in the vessel. The key factor for successful fast H_2 charging is to remove the heat from the vessel as soon as possible. To optimize the fast removal of heat from the system, preventing the back mixing of cold H_2 and hot H_2 is crucial. As the density of MOF in the system increases, the intensity of back mixing among hot and cold H_2 in the system can be reduced. Therefore, the heat removal efficiency can increase, which leads to lower average bed temperatures and higher efficiency of H_2 charging. The improved efficiency due to the compacted MOF was not sufficient to counteract the heat of adsorption and attain the target refueling time of 3 minutes.

B. Modeling of the Ideal Charging Process

During charging, the adsorbent vessel and the bed must be cooled for effective hydrogen adsorption. In addition, since hydrogen adsorption is an exothermic process, the heat of adsorption must also be removed. An ideal charging case was modeled that aimed to cool the system within 3 minutes without considering the limits on peak mass flow rate inherent in the 3-liter cryogenic vessel's equipment configuration. For the ideal case, the pressure was ramped from 5 bar to 60 bar within 1 minute, and the outlet was opened gradually at the beginning of the pressure ramp and fully opened in 20 seconds. The inlet H_2 temperature was set to 80 K. Operations with two different initial system temperatures (150 K and 80 K) were investigated. Due to the impact of the initial system temperature, profiles of both the inlet and outlet mass flow rates and the amount of H_2 accumulation in the vessel were different in the two cases, even though the outlet velocity profiles were set to the same value. For the 150 K case, the inlet mass flow rate was approximately 0.4 g/s after the pressure ramp and the outlet mass flow rate was about 0.18 g/s. At the end of 3 minutes of charging, slightly more than 40 grams of H_2 was accumulated in the vessel. The final average bed temperature was 137 K. With this outlet velocity, the vessel could not be refueled within 3 minutes. For the case with an initial system temperature of 80 K, a lot more H_2 can be added into the vessel during the first 60 seconds. At the end of 3 minutes of charging, around 87 grams of H_2 was accumulated in the vessel and the final average bed temperature was 82 K, very close to the desired value. It is more difficult to flow a high volume of cold H_2 into a hot vessel than into a cold vessel. The impact of initial temperature on the process of charging is twofold. The hot system needs a larger quantity of cold H_2 to cool down, and it also results in having a lower inlet mass flow rate than the cooler system.

C. Modeling of the Experimental Discharging Experiments

The objective of the discharge experiments is to demonstrate that an internal heating element is capable of supplying the heat required to desorb enough H_2 to maintain a desired release rate (0.02 g H_2/sec). The adsorbent bed initially contained a total of 96 g of H_2 at a temperature of approximately 80 K and a pressure of 60 bar. In order to fully discharge the usable H_2, the final state of the bed should be 150 K and 5 bar. Two levels of power (39 W and 58 W)

for the helical coil heater were used in the experiments and modeled with COMSOL. For the first experiment 39 W was supplied to the heater, and the resulting heat flux of 678 W/m^2 raised the average bed temperature to only 123 K at the end of the experiment. The H_2 in the bed was not fully desorbed, which resulted in a total of 11 grams of H_2 (adsorbed plus gas) remaining in the vessel. Increasing the supplied power to 58 W for the second experiment produced a heat flux of 978 W/m^2 from the heating element surface and raised the bed's average temperature to a final value of 150 K. Figure 4 shows the amount of H_2 remaining in the bed during the course of this experiment and the modeling simulation. The initial amount of adsorbed H_2 was calculated using the Dubinin-Asthakov model with a temperature of 84 K and pressure of 61 bar. The experimental value for the total amount of adsorbed plus gaseous H_2 (ntotal) was estimated using the outlet flow rate of 0.02 grams/sec. The temperatures in the vessel at the end of discharging were not uniform. Therefore, to estimate the total amount of H_2 remaining in the bed (ntotal) at the end of discharging, the temperature of the system was equilibrated after closing the outlet. The revised value of ntotal in Figure 4 was then calculated by using the Dubinin-Asthakov model with the equilibrated temperature and pressure. As the revised ntotal value of 6 grams of H_2 is close to the modeled value, the prediction of the Dubinin-Asthakov model over the experimental range, i.e., 4 bar, 150 K to 60 bar, 80 K, appears to be consistent. The discharge experiment with the cryogenic vessel shows that the helical coil heater supplies adequate heat to maintain desorption and release H_2 at the desired target rate. However, the heater's weight and volume targets could not be met.

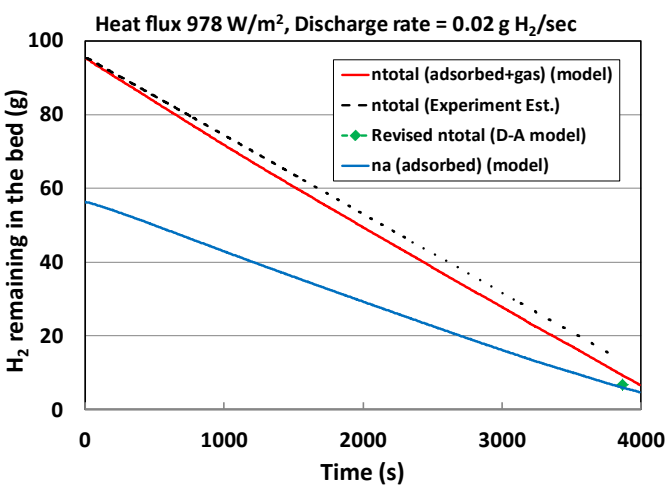

FIGURE 4. Total and adsorbed hydrogen in the bed for desorption run.

While the discharge experiments validate the accuracy of the model in simulating the desorption process, some differences between experimental and modeled results should be noted. For the discharge process there was a brief pressure increase in the vessel near the beginning of the experiments which was not captured in the model simulations. This may be attributed to the possibility that the intensity of convection in the experiment is better than that in the model. Therefore, the gas in the real system can be heated up faster than that in the model and the pressure increase is more evident in the real system. As mass transport in the real system is better than that in the model, gases could be released more easily and the pressure then drops faster in the real system. Temperature comparisons between the experiments and the model simulations are useful, but they are limited by the fact that the RTDs measure temperatures at a finite set of points, whereas the model can integrate the temperatures over the entire volume of the storage bed. However, we found that the average temperatures of the RTD measurements agreed reasonably well with the model's values.

FUTURE DIRECTION

GM will participate in Phase 3 as an advisor to the HSECoE team. No experimental work is planned for Phase 3.

FY 2013 PUBLICATIONS/PRESENTATIONS

1. M. Cai, et al. (2013), Thermal Management of On-Board Cryogenic Hydrogen Storage Systems, presented at the 2013 DOE Hydrogen Program Annual Merit Review Meeting, Washington, D.C.

2. J.P. Ortmann, and N.S. Kaisare, Modeling of Cryo-adsorption of Hydrogen on MOF-5 pellets: Effect of pellet properties on moderate pressure refueling, International Journal of Hydrogen Energy, manuscript submitted, 2013.

3. P. Hou, J.P. Ortmann, M. Sulic, M. Cai, Experimental and numerical study of the discharging process of a MOF-5 hydrogen storage system, GM Internal Report, 2013.

4. P. Hou, J.P. Ortmann, M. Sulic, M. Cai, Experimental and numerical study of the charging process of a MOF-5 hydrogen storage system, GM Internal Report, 2013.

IV.B.7 Ford/BASF SE/UM Activities in Support of the Hydrogen Storage Engineering Center of Excellence

Michael Veenstra (Primary Contact, Ford),
Jun Yang (Ford), Chunchuan Xu (Ford),
Donald Siegel (University of Michigan),
Yang Ming (University of Michigan)
Ford Motor Company
2101 Village Road
Dearborn, MI 48121
Phone: (313) 322-3148
Email: mveenstr@ford.com

DOE Managers
Ned Stetson
Phone: (202) 586-9995
Email: Ned.Stetson@ee.doe.gov
Jesse Adams
Phone: (720) 356-1421
Email: Jesse.Adams@go.doe.gov

Contract Number: DE-FC36-GO19002

Subcontractor:
University of Michigan (UM), Ann Arbor, MI

Project Start Date: February 1, 2009
Project End Date: June 30, 2015

Overall Objectives

This project addresses three of the key technical obstacles associated with the development of a viable hydrogen storage system for automotive applications:

- (Task 1) Create accurate system models that account for realistic interactions between the fuel system and the vehicle powerplant.
- (Task 2) Develop robust cost projections for various hydrogen storage system configurations.
- (Task 3) Assess and optimize the effective engineering properties of framework-based hydrogen storage media (such as metal-organic frameworks [MOFs]).

Fiscal Year (FY) 2013 Objectives

The project focus during FY 2013 was to complete the following objectives to achieve a Phase 2 to Phase 3 Go/No-Go decision milestone in support of the Hydrogen Storage Engineering Center of Excellence (HSECoE):

- Report on ability to develop compacted MOF-5 adsorbent media having a total hydrogen material density of greater than or equal to 0.3 g/L, hydrogen density of 11 wt% and 33 g/liter, and thermal conductivity of 0.5 W/m-K at P = 60-5 bar and T = 80-160 K.
- Report on ability to demonstrate composite MOF-5 adsorbent monoliths having hydrogen uptake kinetics allowing for 5.6 kg usable hydrogen storage over a 3-minute fill time, and permeation in packed and powder forms sufficient for a flow rate of 1 m/s superficial velocity and pressure drop of 5 bar.

Technical Barriers

This project addresses the following technical barriers from the Hydrogen Storage section of the Fuel Cell Technologies Office Multi-Year Research, Development, and Demonstration Plan:

(A) System Weight and Volume

(B) System Cost

(C) Efficiency

(D) Durability/Operability

(E) Charging/Discharging Rates

(H) Balance of Plant (BOP) Components

(J) Thermal Management

Technical Targets

The outcomes of this project impact vehicle and system level models, cost analysis, and materials property assessment and optimization. Insights gained from these studies are applied towards the engineering of hydrogen storage systems that meet the DOE 2017 and ultimate hydrogen storage targets (Table 1).

TABLE 1. Technical Targets

Storage Parameter	Units	2017	Ultimate
System Gravimetric Capacity	$kg \cdot H_2/kg$	0.055	0.075
System Volumetric Capacity	$kg \cdot H_2/L$	0.040	0.070
Storage System Cost	$\$/kWh_{net}$	12	8
System Fill Time (for 5 kg H_2)	min	3.3	2.5
Minimum Full Flow Rate	(g/s)/kW	0.02	0.02
Min/Max Delivery Temperature	°C	-40/85	-40/85
Min. Delivery Pressure (Fuel Cell)	atm	5	3

FY 2013 Accomplishments

- Task 1. System Modeling
  - Performed the adsorbent system architect role in the HSECoE which coordinated the down-selection of MOF-5 and conducted various design and performance trade-offs.
  - Refined the failure mode and effects analysis (FMEA) for the adsorbent hydrogen storage systems based on the HSECoE team design actions.
- Task 2. Cost Analysis
  - Participated with the HSECoE partners in providing cost projection of the material-based hydrogen storage systems, utilizing the high volume automotive estimating background.
- Task 3. Assessment/Optimization of Framework-Based Storage Media
  - Demonstrated a theoretical total capability of ≥33 g/l for densities of ≥0.3 g/cc and potential for 11 wt% and thermal conductivity of ≥0.5 W/m-K can be approached with 10% enhanced natural graphite (ENG) at ~100 to 150 K.
  - Conducted sub-scale cycle test that provided effective kinetics with the potential for a 3-minute fill. Provided permeation data that indicates a projected pressure drop of 3.6 bar at 77 K for 0.3 g/cc MOF compact.
  - Completed microscopy characterization and assessed the potential to exploit anisotropic properties of densified pellets/pucks. Initiated a design of experiments-based study to quantify effects of humidity exposure. Conducted cycle testing, particle ignition evaluation, internal pressure analysis, and neutron imaging of MOF-5 powders and compacts.

✧ ✧ ✧ ✧ ✧

INTRODUCTION

Widespread adoption of hydrogen as a vehicular fuel depends critically on the development of low-cost, onboard hydrogen storage technologies capable of achieving high energy densities and fast kinetics for hydrogen uptake and release. Since present-day technologies based on compression and liquefaction are unlikely to attain established DOE targets, development in materials-based approaches have garnered increasing attention. To hasten development of these 'hydride' materials, the DOE previously established three centers of excellence for materials-based hydrogen storage research. While the centers have made substantial progress in developing new storage materials, challenges associated with the engineering of the storage system around a candidate storage material have received much less attention.

APPROACH

Ford-UM-BASF is conducting a multi-faceted research project that addresses three of the key challenges associated with the development of materials-based hydrogen storage systems.

Systems Modeling (Task 1): We are evaluating and developing hydrogen storage system operating models to optimize the storage system operation as it interacts with the fuel cell system.

Cost Analysis (Task 2): We are performing hydrogen storage manufacturing cost analyses for various candidate system configurations and strategies to facilitate potential cost reductions.

Sorbent Media Assessment & Optimization (Task 3): We are characterizing the "effective engineering properties" for MOFs in order to devise optimal strategies for their use in an adsorbent system.

RESULTS

Following is a description of our technical results for each task and how these results relate to achieving the DOE targets.

Task 1. System Modeling

During this past year, the system modeling effort resulted in a utility function for the adsorbent team to utilize in their trade-off studies to optimize the system configuration. The utility function was developed based on the HSECoE Simulink® framework to evaluate the changes in the vehicle attributes due to modifying the 2017 targets by +/- 10% increments. The key system targets that were analyzed were the gravimetric density, volumetric density, and system cost. The vehicle attribute (i.e. driving range, fuel economy, etc.) effects were analyzed while varying the system from the specified target values. Since this was a theoretical exercise rather than based on a particular system, it was assumed that only the specific target being analyzed was changing while the other target value remained consistent, such as for the gravimetric case which assumed volumetric remained constant. The resulting function was an expression that utilized the percent change from the target values, the customer importance factor, and the correlation slope from the models to provide a normalized system ranking and facilitate trade-offs between the key system targets. The modeling team also prepared the HSECoE model framework for a public release using a graphical user interface and conducted a beta trial. In addition, an initial FMEA update was conducted to evaluate the effects of the Phase 2 actions and activities. The potential change is shown

in Figure 1 which indicates the original risk priority number in red and revised values in blue.

Task 2. Cost Analysis

The cost analysis effort during this past year produced several key results that assisted in significant progress of the system cost assessment. First, the team established baseline raw material cost values and aligned these assumptions with other related projects within the DOE portfolio through a benchmarking effort. Second, the cost projections in conjunction with PNNL included a sensitivity assessment of adsorbent systems with different types of tank technologies (I, III, IV), MOF-5 densities (powder, 0.32 g/cc, 0.52 g/cc), ENG levels (neat, 5%, 10%) along with a combination of MOF-5 pellets and AX-21 powders. Based on this analysis, the system cost for the adsorbent system was reduced due to the decrease in operating pressure from 200 bar to 100 bar and use of a Type I tank. Finally, deep-dive design reviews provided an effective method to determine the required components within the system and further reduce cost.

Task 3. Sorbent Media Assessment and Optimization

Isotherm data was collected to evaluate the working capacity of the MOF-5 material between 5 and 60 bar. For gravimetric density, the performance decreased from 12 wt% (total) for a powder form (80 K) to 7% for a 0.3 g/cc compact. This value can be increased to 9 wt% and then 12 wt% when both temperature swing and a 60% packing efficiency is included. For volumetric density, a similar assessment was made but the performance increases from 20 g/l for a powder (80 K) to 22 g/l for a 0.3 g/cc compact (5% ENG) and further increase to 34 g/l for a 0.5 g/cc compact (5% ENG) with a temperature swing but will be reduced if a packing efficiency (60%) is included.

MOF-5 has an extremely low thermal conductivity and will likely require enhancement of its thermal transport properties to allow for efficient heat exchange designs at the system level. ENG at 10 wt% loading has been shown to significantly improve (~4x to 6x) the thermal conductivity of MOF-5, achieving ≥0.5 W/m-K at ~100 to 150 K. Figure 2 provides images of MOF-5 pellets containing 5% ENG. The single pellet image in Figure 2 appears to have an ENG gradient from top to bottom.

Microscopy analysis confirmed that the ENG gradient was superficial. However, this analysis also revealed a preferred or anisotropic orientation of the ENG within the material. Figure 2 (right) demonstrates this anisotropic orientation of the ENG as highlighted with yellow lines from the imaging analyzer. Based on this discovery, we proceeded to characterize the anisotropic performance of the MOF-5 to pursue potential optimization of the cross-compression oriented ENG particles and crystallites within the pellets. The alignment of ENG leads to an improved thermal conductivity in the radial direction, Figure 3. In other words, thermal conductivity is improved (~3x) in the cross-compression direction (red line), which is perpendicular to the press direction, compared to that along the press direction (blue line). Permeation was also slightly higher in the cross-compression direction (~2x) due to the ENG channels formed within the MOF compacts. As shown in Figure 3, a unique pellet was developed to evaluate the cross-compression anisotropic properties.

A key concern regarding the use of MOF-5 in onboard storage applications is the potential sensitivity to air and/or impurities in the hydrogen stream. During this past

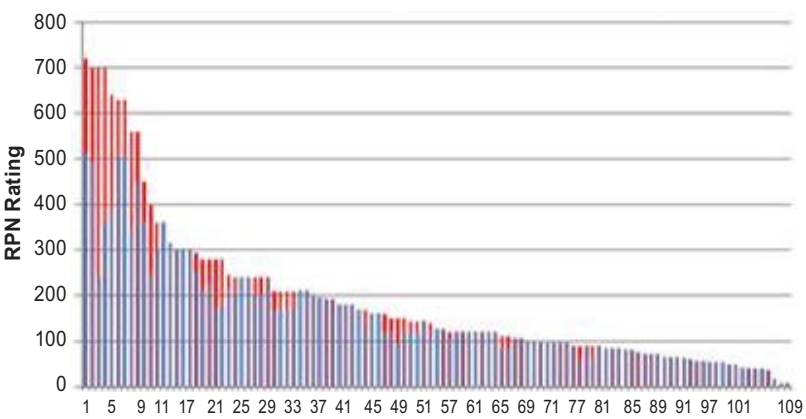

FIGURE 1. Updated Adsorbent FMEA Pareto Chart of Risk Priority Numbers with Phase 2 Results

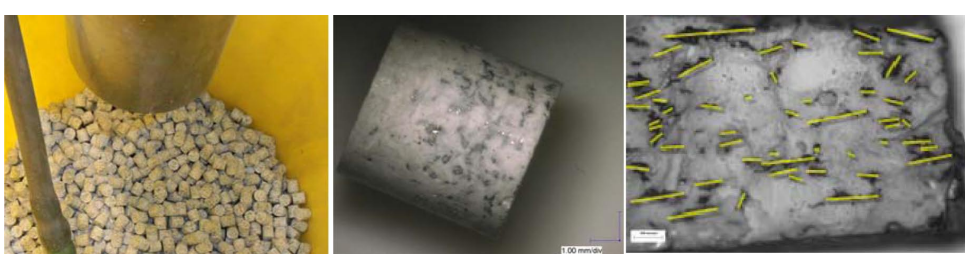

FIGURE 2. Images of MOF-5 Pellets with 5% ENG and Anisotropic Imaging Analysis

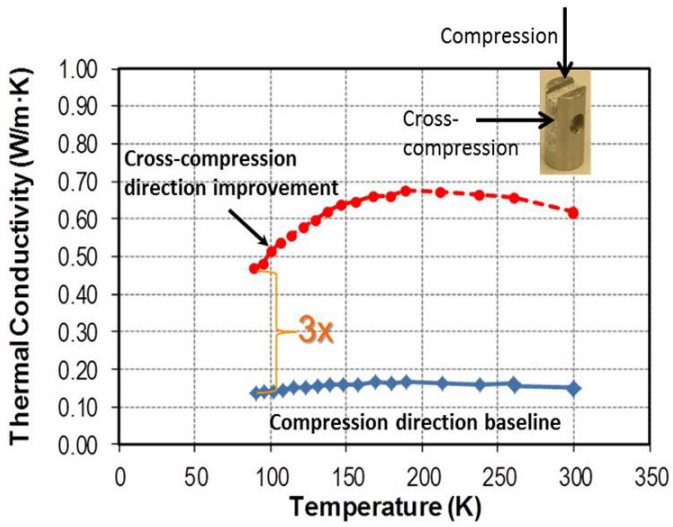

FIGURE 3. Thermal Conductivity Test Results to Compare the Anisotropic Effects

year, we have conducted tests to assess the impact of exposing MOF-5 powders to humidified air. Initial testing was conducted in the lab with approximately 45% relative humidity and a temperature of ~22°C. A 12 minute exposure was found to result in a 1.2% to 1.5% decrease in hydrogen uptake capacity. A 1.5 hour exposure had an additional, yet small, decrease to 3.5% to 3.7% compared to the unexposed sample. X-ray diffraction patterns were measured for samples exposed for different durations and were found to be in agreement with the update data. We also completed Hartman tube and 20-L sphere dust ignition tests on MOF-5, along with degradation cycle testing (>390 cycles) to confirm the robustness of the MOF-5 for practical onboard storage systems.

CONCLUSIONS AND FUTURE DIRECTIONS

- Task 1. System Modeling
  - Update the cryo-adsorbent system model with Phase 3 performance data, validate alignment within +/- 10%, integrate into the framework; document and release models to the public.
  - Complete the FMEA associated with real-world operating conditions for a MOF-5-based system, for both Hexcel and Modular Adsorption Tank Insert concepts based on the Phase 3 test results. Report on the ability to reduce the risk priority numbers from the Phase 2 peak/mean and identify key failure modes.
- Task 2. Cost Analysis
  - Conduct analysis of various adsorbed hydrogen storage systems in order to recommend design revisions and direction based on high volume automotive cost projections.
  - Provide hydrogen storage cost reductions for achieving the DOE targets with the other HSECoE project partners (with a focus on part integration and reduction).
- Task 3. Sorbent Media Assessment and Optimization
  - Conduct a scale-up of the MOF-5 manufacturing process to deliver >9 kg of material while maintaining performance, as measured by surface area and particle size, to within 10% of lab-scale procedure.
  - Based on the scaled-up material, characterize practical media-level properties via microscopy, imaging, and other empirical studies to improve performance of adsorbent materials within the prototype systems.
  - Evaluate MOF-5 degradation beyond 300 cycles based on maximum allowable impurity levels as stated in SAE J2719 and report on the ability to mitigate to less than 10%.

SPECIAL RECOGNITIONS & AWARDS/ PATENTS ISSUED

1. Michael Veenstra was a recipient of a United States Council for Automotive Research special recognition award on May 8, 2013 for his work on the Hydrogen Storage Tech Team and for his guidance with system design requirements for sorbent-based storage systems in the HSECoE. DOE Leadership recognized that his contributions will translate to improved solicitations and research direction in the future.

FY 2013 PUBLICATIONS/PRESENTATIONS

1. J.J. Purewal, D. Liu, J. Yang, A. Sudik, M. Veenstra, J. Yang, S. Maurer, U. Müller, and D.J. Siegel "Improved Hydrogen Storage and Thermal Conductivity in High-Density MOF-5 Composites," Journal of Physical Chemistry C, 116 (38), pp 20199–20212, September 2012.

2. C. Xu, J. Yang, M. Veenstra, A, Sudik, J.J. Purewal, B.J. Hardy, J. Warner, S. Maurer, U. Müller, and D.J. Siegel "Hydrogen Permeation and Diffusion in Densified MOF-5 Pellets," International Journal of Hydrogen Energy, 2012, February 2013.

3. M. Veenstra. "MOF-5 Development in Support of the Hydrogen Storage Engineering Center of Excellence," USDRIVE Hydrogen Storage Technical Team, March 20, 2013.

4. D.J. Siegel. "Adsorbent System Go/No-Go Discussion," Phase 3 Go/No-Go Milestone Review, March 22, 2013.

5. M. Veenstra, "Ford/BASF/UM Activities in Support of the Hydrogen Storage Engineering Center of Excellence", 2013 DOE Hydrogen Program Annual Merit Review Meeting, Arlington, VA, May 14, 2013.

IV.B.8 Microscale Enhancement of Heat and Mass Transfer for Hydrogen Energy Storage

Kevin Drost (Primary Contact), Goran Jovanovic, Vinod Narayanan, Brian Paul, Christopher Loeb, Mohammad Ghazvini, Agnieszka Truszkowska, Hailei Wang
School of Mechanical, Industrial and Manufacturing Engineering
Rogers Hall
Oregon State University
Corvallis, OR 97331
Phone: (541) 713-1344
Email: Kevin.Drost@oregonstate.edu

DOE Managers
Ned Stetson
Phone: (202) 586-9995
Email: Ned.Stetson@ee.doe.gov
Jesse Adams
Phone: (720) 356-1421
Email: Jesse.Adams@go.doe.gov

Contract Number: DE-FC36-08GO19005

Project Start Date: February 1, 2009
Project End Date: June 30, 2015

Overall Objectives

Use microchannel processing techniques to:

- Demonstrate reduction in size and weight of hydrogen storage systems
- Improve charge and discharge rates of hydrogen storage systems
- Reduce size and weight and increase performance of thermal balance-of-plant components

Fiscal Year (FY) 2013 Objectives

- Demonstrate ability to develop and demonstrate a modular absorption task insert (MATI) designed for a system consisting of 100% densified media and capable of allowing less than 3 min. refueling time and H_2 release rate of 0.02 g H_2/(sec. kW) with a mass less than 9.4 kg and a volume less than 4.2 liters (Barriers A and E).
- Demonstrate a 1-kW catalytic combustor to augment partial hydrogen preconditioning by an existing fuel cell radiator with >90% efficiency having a mass less than 0.5 kg and volume less than 0.5 liters.

Technical Barriers

This project addresses the following technical barriers from the Storage section (3.3.5) of the Fuel Cell Technologies Office Multi-Year Research, Development, and Demonstration Plan:

(A) System Weight and Volume

(E) Charging/Discharging Rates

(H) Balance-of-Plant (BOP) Components

Technical Targets

The Phase II technical targets for the Microscale Enhancement of Heat and Mass Transfer for Hydrogen Energy Storage project are shown in Table 1.

TABLE 1. Phase II Technical Targets

Characteristic	Units	2013 Smart Goals	Status
MATI Weight	Kg	9.4	6.0
MATI Volume	Liter	4.2	3.0
Microcombustor Weight	Kg	0.9	0.29
Microcombustor Volume	Liter	0.65	0.15
Microcombustor Efficiency	%	85	86

FY 2013 Accomplishments

Key developments and technical accomplishments for the reporting period are:

- Completed separate effects and integrated testing of the MATI (Barriers A and E).
- Completed model validation for adsorption and desorption with a single MOF-5 puck (Barriers A and E).
- Completed modeling of the charge and discharge cycle for a full-scale MATI to support the development of conduction enhancements for adsorbing media (Barriers A and E).
- Updated the design and production cost estimate for the MATI (Barriers A and E).
- Completed fabrication and testing of a microchannel combustor/heat exchanger to provide hydrogen preheating in an adsorption hydrogen storage system (Barrier H).

✧ ✧ ✧ ✧ ✧

INTRODUCTION

Hydrogen storage involves coupled heat and mass transfer processes that are significantly impacted the by size, weight, cost, and performance of system components. Micro-technology devices that contain channels of 10-500 microns in characteristic length offer substantial heat and mass transfer enhancements by greatly increasing the surface-to-volume ratio and by reducing the distance that heat or molecules must traverse. These enhancements often result in a reduction in the size of energy and chemical systems by a factor of 5-10 over conventional designs, while attaining substantially higher heat and mass transfer efficiency. We are developing 1) advanced tank inserts for enhanced heat and mass transfer during charge and discharge of adsorbent hydrogen storage systems; and 2) microchannel-based thermal balance of plant components such as combustors, heat exchangers, and chemical reactors.

APPROACH

Our technical approach to meet the Phase II goals is that for each high-priority component, we will use microchannel technology to reduce the relevant barriers to heat and mass transfer. Our approach involves the optimizing the performance of a single unit cell and then "Numbering Up" using appropriate simulation tools that we then validate by experimental investigation.

RESULTS

We identified two high-value applications of microchannel technology. The first is the development of a MATI for cooling during charging, heating during discharging, and hydrogen distribution. The second application is the development of an integrated microchannel combustor and heat exchanger that can be used for preheating hydrogen that can be used with fuel cell waste heat to preheat hydrogen that is used discharge storage.

MATI—A tank insert that integrates storage media, microchannel heat exchangers, and microchannel hydrogen distribution plates allows convenient use of densified adsorption media with in-excess-of 94% of the tank volume being densified media. The concept separates the cooling process from the charging process, allowing flexibility in cooling strategies, and the MATI can provide heating during discharge, avoiding the need to use electric energy for discharge heating. A schematic of a single cell is presented in Figure 1. The full-sized MATI would consist of a number of cells along with headers for cooling fluid and distributing hydrogen. Progress to date on the development of the microchannel-based tank insert includes:

- *Completed separate effects and integrated testing of the MATI*—Cryogenic test apparati have been assembled for experimental investigations of charging and discharging a MATI. Integrated testing involves experimental investigations of the complete charging and discharge cycles including hydrogen distribution and adsorption and the removal of the heat of adsorption using liquid nitrogen. Integrated tests were completed in FY 2013. Separate effects testing determined the heat transfer coefficient in the MATI cooling plate for both single- and two-phase flow. The integrated testing initially focused on investigating the absorption and desorption of nitrogen and hydrogen in single pucks of activated carbon and MOF-5. Integrated testing then focused on testing a multi-puck MATI with three cooling plates, two hydrogen distribution plates, and four 1.5-cm thick pucks of MOF-5.
- *Completed model validation for adsorption and desorption with a single MOF-5 puck*—Simulation models have been developed to model all relevant phenomena associated with the charging and discharging of the MATI. During the reporting period the models were validated against the experimental results of our integrated testing. Figure 2 shows typical comparisons of experimental and simulated results for the temperature distribution in a MOF-5 puck. Overall, the average error between experiment and simulation results was between 4% and 5% with the maximum error being between 8% and 9%. Based on these results we are confident that we can accurately model the adsorption and desorption behavior of a single puck, giving confidence that our predictions of system level charging and discharging are valid.

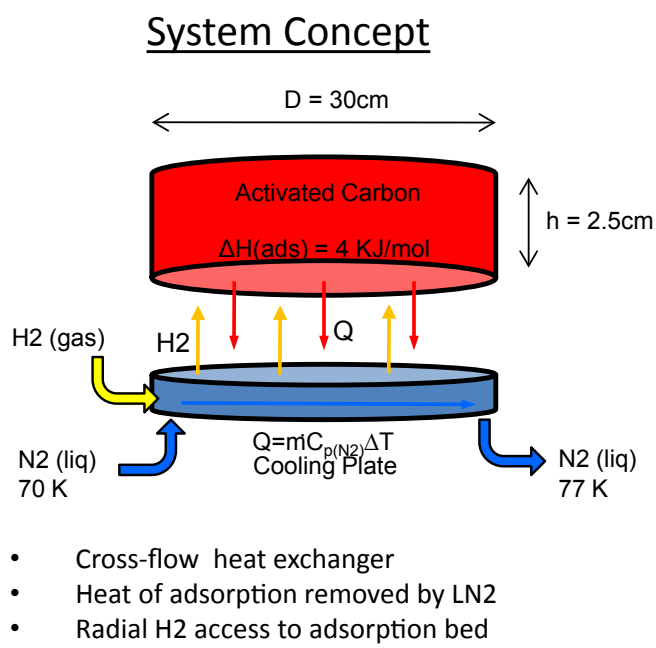

FIGURE 1. MATI Concept

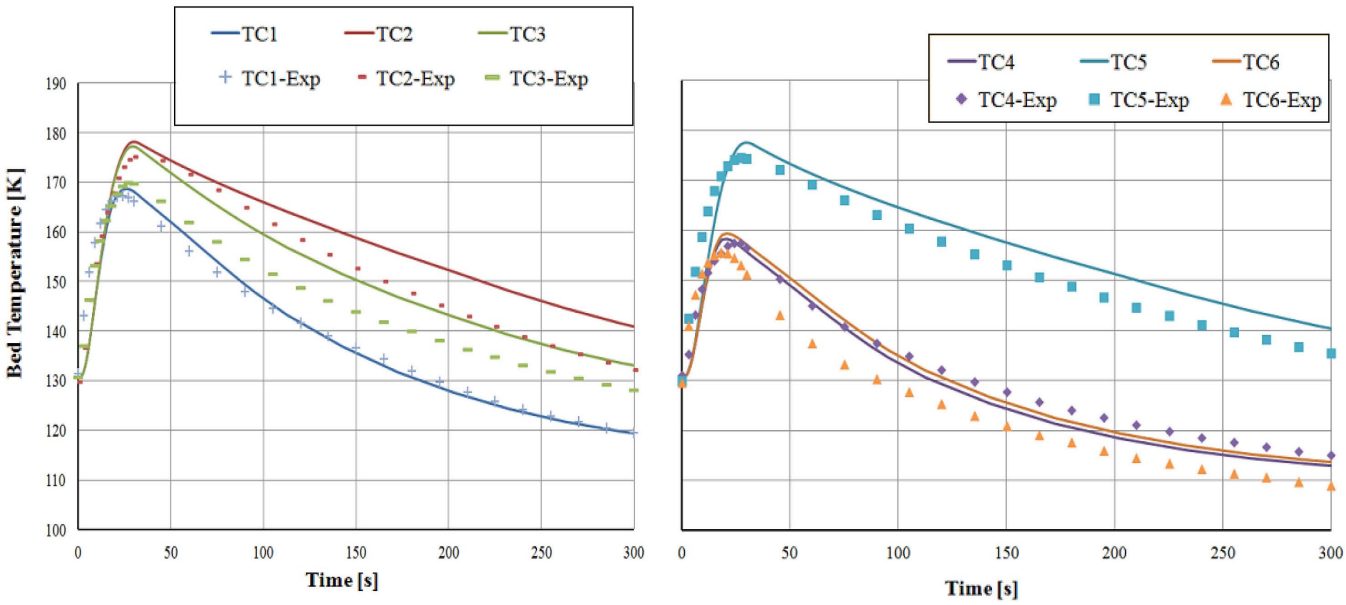

FIGURE 2. LN_2-Cooled Adsorption on MOF-5; Experimental and Modeling Results

- *Completed system modeling of the charge and discharge cycle for a full-scale MATI*—A two-dimensional version of the model has been used to evaluate the required conductivity enhancement of the adsorbent bed, so that we can use 5-cm spacing between cooling plates. The modeling results show that the average bed conductivity needs to be increased to 3.0 W/mK and that this can be accomplished with the use of embedded aluminum fins in the adsorbing media. With this level of conduction enhancement, simulation of the charging cycle showed that the bed could be fully charged with hydrogen in three minutes. Modeling of the discharge cycle showed that the use of fuel cell waste heat for discharge was feasible. In this case the hydrogen from storage is heated using fuel cell heat and returned to the storage system where the hot hydrogen provides the required heating for discharge.
- *Completed demonstration of aluminum fabrication*—Our cost and weight targets require that aluminum be used as our material of construction. During the reporting period we successfully demonstrated our ability to pattern and bond aluminum cooling plates.
- *Updated MATI fabrication, weight, and cost analysis*—Our MATI system design and cost estimates were modified to reflect two key design changes: the use of stamping for the patterning process and the use of micro-pyramidal truss networks to provide the flow structure in the cooling plates and the hydrogen distribution plates. Our current weight and cost estimates are shown in Figure 3.

Integrated Microscale Combustor/Heat Exchanger (µCHX)—The µCHX, shown in Figure 4, will be used to safely and efficiently preheat hydrogen discharged from the adsorption hydrogen storage system before it enters the fuel cell. In cold conditions, the fuel cell produces insufficient heat to heat the hydrogen to the required inlet temperature for the fuel cell. In these cases a small fraction of the hydrogen will be combusted to preheat the balance of the hydrogen to a temperature appropriate for fuel cell operation. During the current reporting period we:

- *Completed design and testing of the µCHX for adsorption system hydrogen preheating*—We have modified the design of the µCHX for the hydrogen preheating application. The significant changes are in heating load (<0.5 kW) and application (heating hydrogen initially at cryogenic temperatures). The key design issue was to avoid freezing of the products of combustion (water) in the recuperation section of the device. The device has been fabricated and tested. Testing results confirm modeling predictions of performance. The new design is slightly less efficient (90%) and much smaller than the oil heating application described above. This combustor design is shown in Figure 4.
- *Filed a patent on the this concept for automotive and space heating applications*

CONCLUSIONS AND FUTURE DIRECTIONS

Key conclusions resulting from our research include:

- The use of the modular adsorption tank insert allows convenient use of densified adsorption media with in excess of 94% of the tank volume being densified

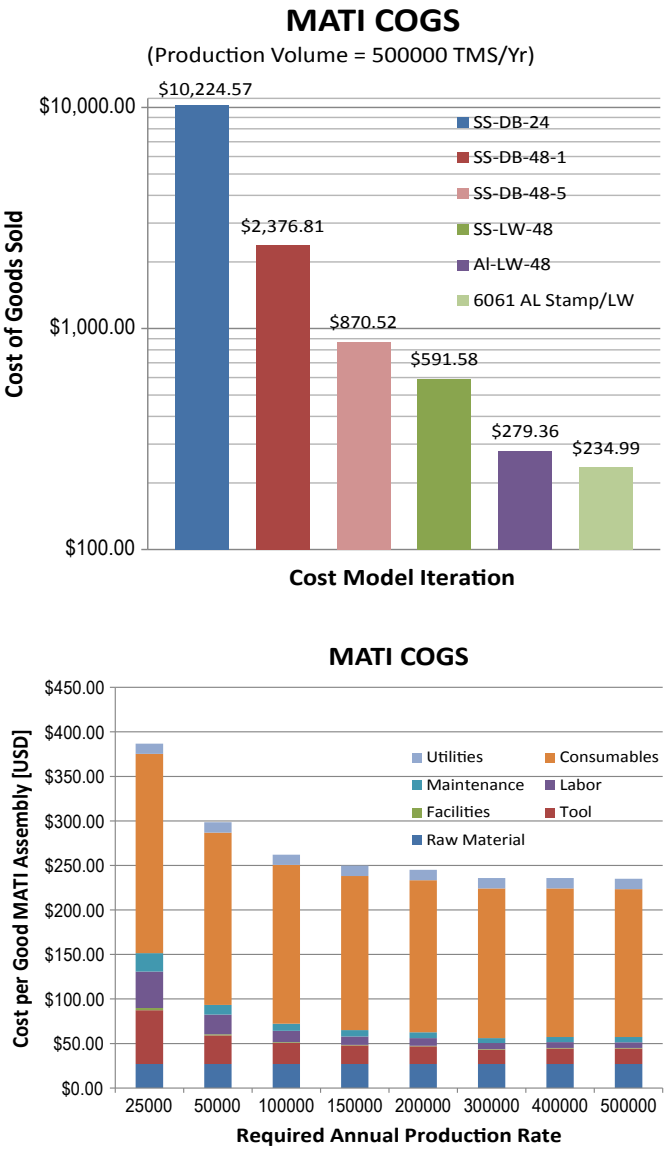

FIGURE 3. Cost of Goods Sold (COGS) of the MATI as a Function of Production Volume

media. The concept separates the cooling process from the charging process, allowing flexibility in cooling strategies, and the MATI can provide both cooling during charging and heating during discharge with a weight under 9.5 kg for a hydrogen storage system containing 5.6 kg of hydrogen.

- The µCHX, can provide hydrogen preheating, increasing the flexibility of the storage system with a minimal impact on system weight and size.

The MATI has been selected for inclusion in the third phase of the Hydrogen Storage Engineering Center of Excellence. Our research will focus on the demonstration of the MATI and include completion of the design, assembly,

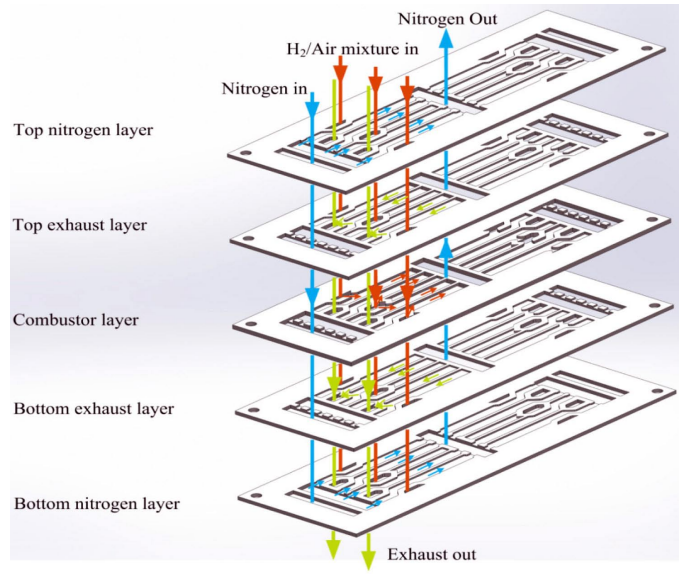

FIGURE 4. Microchannel Integrated Combustor/Heat Exchanger for Hydrogen Heating

and testing of a multi-cell MATI. Testing will measure heat removal rates, hydrogen distribution, and durability. After testing at Oregon State University, the MATI will be supplied to Savannah River National Laboratory for independent testing.

FY 2013 PUBLICATIONS/PRESENTATIONS

1. E.D. Truong, E. Rasouli, and V. Narayanan, "Cryogenic single-phase heat transfer in a microscale pin fin heat sink," Proceeding of SHTC 2013-17660, ASME summer heat transfer conference, Minneapolis, Minnesota, 2013.

2. E. Rasouli, E.D. Truong, and V. Narayanan, "Cryogenic single phase and phase change heat transfer in a microscale pin fin heat sink," Presentation only in ICNMM 2013-73151, 11th International Conference on Nanochannels, Microchannels and Minichannels, Sapporo, Japan, 2013.

3. L.J. Steigleder, "A microchannel-based thermal Management System for Hydrogen Storage Adsorptent Beds," M.S. Thesis, Oregon State University, June 14th, 2013.

4. S.V. Pawar, "Fabrication of Precipitation-Hardened Aluminum Microchannel Cooling Plates for Adsorption-based Hydrogen Storage Systems," M.S. Thesis, Oregon State University, Corvallis, Oregon, March 21st, 2013.

5. M. Ghazvini and V. Narayanan, "Design of A microscale Combustor- Heat Exchanger for Low Temperature Applications," Accepted for *ASME 2013 Summer Conference* (HT2013), July 14–19, 2013, Minneapolis, Minnesota.

6. M.M. Ghazvini and V. Narayanan, "A Microscale Combustor-Heat Exchanger for Low Temperature Applications- Experimental Results," Oral presentation, *ASME 11th International Conference on Nanochannels, Microchannels and Minichannels* (ICNMM2013), June 16–19, 2013, Sapporo, Japan.

7. M. Ghazvini and V. Narayanan, "A microscale combustor recuperator and oil heat exchanger – design and thermofluidic characterization," *Int J of Heat and Mass Trans,* Vol. 64, pp. 988-1002, 2013.

8. C. Loeb and G. Jovanovic, 2013 "*Cryogenic Hydrogen Adsorption On MOF-5 With Novel Microchannel Thermal Management System - Experiment and Simulation,*" American Institute of Chemical Engineers, San Francisco, CA, USA, 2013 (*in review*).

9. C. Loeb, "*Enhancement and Modeling of Cryogenic Solid-State Hydrogen Storage Systems with a Novel Microchannel Thermal Management Device,* " Ph.D. Thesis Oregon State University, Corvallis, OR, June 2013 (http://hdl.handle.net/1957/39687)

10. C. Loeb, A. Truszkowska, and G. Jovanovic, "Increasing hydrogen storage in compressed MOF-5 system using a microchannel thermal management device: experiment and simulation," Advances in Chemical Engineering and Science, 2013 (*in review*).

IV.B.9 Development of Improved Composite Pressure Vessels for Hydrogen Storage

Norman Newhouse (Primary Contact), Jon Knudsen, John Makinson
Hexagon Lincoln Inc. (formerly Lincoln Composites, Inc.)
5117 NW 40th Street
Lincoln, NE 68524
Phone: (402) 470-5035
Email: norman.newhouse@hexagonlincoln.com

DOE Managers
Ned Stetson
Phone: (202) 586-9995
Email: Ned.Stetson@ee.doe.gov
Jesse Adams
Phone: (720) 356-1421
Email: Jesse.Adams@go.doe.gov

Contract Number: DE-FC36-09GO19004

Project Start Date: February 1, 2009
Project End Date: September 30, 2015

Overall Objectives

- Improve the performance characteristics, including weight, volumetric efficiency, and cost, of composite pressure vessels used to contain hydrogen in adsorbants.
- Evaluate design, materials, or manufacturing process improvements necessary for containing adsorbants.
- Demonstrate these improvements in prototype systems through fabrication, testing, and evaluation.

Fiscal Year (FY) 2013 Objectives

- Confirm operating conditions chosen for adsorbent technology-based hydrogen storage system.
- Evaluate design options for Type 1, Type 3, and Type 4 tanks to meet system requirements for demonstrating adsorbent technology-based hydrogen storage system.
- Fabricate and test leading candidate designs to confirm suitability for Phase 3 use.

Technical Barriers

This project addresses the following technical barriers from the Hydrogen Storage section of the Fuel Cell Technologies Office Multi-Year Research, Development, and Demonstration Plan:

(A) System Weight and Volume

(B) System Cost

(G) Materials of Construction

Technical Targets

This project is conducting fundamental studies for the development of improved composite pressure vessels for hydrogen storage, and developing an optimized vessel for use by Hydrogen Storage Engineering Center of Excellence (HSECoE) partners in demonstrating a functioning vehicle storage system using adsorbant materials. The targets apply to the storage system, of which the vessel is a part. Insights gained from these studies will be applied toward the design and manufacturing of hydrogen storage vessels that meet the following DOE hydrogen storage targets:

	2017	Ultimate
• Gravimetric capacity:	5.5 wt%	7.5 wt%
• Volumetric capacity:	40 g/L	70 g/L
• Storage system cost:	$12/kWh	$8/kWh

FY 2013 Accomplishments

- HSECoE partners confirmed operating requirements for the Phase 2 test vessel, including a reduction in operating pressure from 200 bar to 100 bar, which will reduce the cost and weight of the vessel while essentially maintaining system performance.
- The Phase 1 test vessel, of Type 4 construction, was subjected to a burst test at cryogenic temperatures to confirm composite strength is not degraded at cryogenic temperatures reflecting operating conditions. Two units were tested. The liner cracked in both tests due to high stresses in the liner. There was no evidence of strength loss in the composite.
- The Phase 2 test vessel, of Type 1 construction, was designed and manufactured. It was subjected to a burst test at ambient temperature, achieving 370 bar, which confirmed the design and safety for use. The Type 1 vessel is heavier than Type 4, but about 30% to 50% lower cost.
- Phase 2 test vessels were distributed to HSECoE partners as requested.
- The Phase 2 test vessel was subjected to 200 pressure cycles followed by a burst test at cryogenic temperatures to confirm strength at expected operating conditions. The burst pressure of 460 bar exceeded requirements, and as expected was greater than the ambient temperature burst.

- Full-scale designs for Type 1 and Type 4 tanks were evaluated. If Type 4 liner performance at cryogenic temperatures was acceptable, the DOE SMART milestones for weight could be met.
- A patent is being pursued for an external vacuum insulating shell, with Hexagon Lincoln and Pacific Northwest National Laboratory engineers as inventors. The vacuum shell insulates the tank during service, and additionally improves system performance as it permits pre-cooling of the tank using liquid nitrogen during the filling operation, and venting of any gas that permeates or leaks from the tank without compromising the vacuum insulation.

✧ ✧ ✧ ✧ ✧

INTRODUCTION

Hexagon Lincoln is conducting research to meet DOE 2017 Hydrogen Storage goals for a storage system by identifying appropriate materials and design approaches for the hydrogen container. At the same time, the pressure vessels must continue to maintain durability, operability and safety characteristics that already meet DOE guidelines for 2017. There is a continuation of work with HSECoE partners to identify pressure vessel characteristics and opportunities for performance improvement. Hexagon Lincoln is working to develop high-pressure vessels as are required to enable tank design approaches to meet weight and volume goals and to allow adsorbant materials that operate at cryogenic temperatures to operate efficiently.

APPROACH

Hexagon Lincoln established a baseline design for full scale and test tank using HSECoE team operating criteria as a means to compare and evaluate potential improvements in design, materials and process to achieve cylinder performance improvements for weight, volume and cost. Hexagon Lincoln selected the most promising engineering concepts to meet Go/No-Go requirements for moving forward. The emphasis was on demonstrated technology to ensure ability of HSECoE partners to test their system components.

During Phase 2, operating conditions were updated and confirmed, and new baselines were developed. Testing of bench-top test vessels was conducted to confirm their safety for use. Alternate designs and materials were evaluated to assess ability to meet established targets for weight and volume.

RESULTS

HSECoE partners established updated criteria for operation at 100-bar service pressure, with an operating temperature range from 80 K to 373 K. A test vessel configuration with Type 1 construction and a 2-liter volume was also established to demonstrate component technology. Test vessels were designed, manufactured, tested, and distributed to HSECoE partners to facilitate testing of prototype components.

A concept for insulating the tank during operating, and providing the means for cooling the tank prior to refueling, was further developed. A patent application was filed during the past year, with Hexagon Lincoln and Pacific Northwest National Laboratory engineers listed as authors.

The test vessel developed during Phase 1 had previously been burst tested to confirm safety for use. Another Type 4 vessel design had been successfully exposed to liquid nitrogen and subsequently burst at ambient temperature to assess capability for the liner and composite to tolerate exposure to cold temperatures. Two Phase 1 test vessels were pressurized with liquid nitrogen with the intent to burst (Figure 1). Both leaked due to a cracked liner, one at 285 bar, the other at 230 bar. The liner was analyzed, and it was determined the crack was likely the result of a high stress at the boss/liner interface that was exacerbated by the cold temperature. However, the test confirmed the liner would remain intact to strains representative of operating pressure

FIGURE 1. Type 4 Tank Test

and temperature, and there was no indication of strength loss in the carbon fiber composite.

The Phase 2 Type 4 test vessel was designed using aluminum 6061-T6 and a three-piece construction (Figures 2 and 3). The three-piece construction allowed HSECoE partners to remove and replace components in the vessel between tests. A Type 1 vessel would be higher weight than Type 4 construction, but would be 30% to 50% lower cost. A burst test to 370 bar confirmed safety. The test vessel was subjected to 200 cycles to service pressure at 80 K, then burst at 460 bar. This test confirmed safety for use by HSECoE partners in laboratory testing.

A study was conducted comparing Type 1 and Type 4 vessels that would meet HSECoE design requirements for a full-scale vessel. A Type 1 vessel made with AA 6061-T6 would have no problem with the low temperature of 80 K. The Type 4 vessel appears to have no problem with composite operating at lower temperatures, but an high-density polyethylene (HDPE) liner has some sensitivity to the low temperature.

FIGURE 2. Type 1 Tank Assembly

FIGURE 3. Type 1 Tank Components

The American Society of Mechanical Engineers pressure vessel code was referenced as a goal to meet. It was practical to meet Section X Class III requirements when the service pressure was >210 bar, but below that, Class I requirements would apply, and the resulting design would be overly conservative. The federal requirements for this application would be under the jurisdiction of the Department of Transportation, National Highway Traffic Safety Administration. The requirements of Department of Transportation/National Highway Traffic Safety Administration would be met by the full-scale tank design.

Calculations were made for Type 1 and Type 4 tanks. The goal was for tank mass to be less than 10 kg for a volume of 120 liters and an operating pressure of 60 bar. The results of calculations are provided in Table 1. One design change that enables the weight goal to be met is to reduce the thickness of the liner in the Type 4 tank, possibly by using a high elongation resin layer to prevent leakage. Permeation is not a significant issue for the given operating conditions, because permeation is significantly reduced by virtue of operating at the cold temperature.

TABLE 1. Type 1 and Type 4 Tank Calculations

Material	Dia (mm)	L (mm)	Wt (kg)
AA6061-T6	440	950	30.00
Carbon/HDPE	440	950	11.35
Carbon/tbd	434	950	8.61

Dia – diameter; L – length; Wt – weight; tbd – to be determined

CONCLUSIONS AND FUTURE DIRECTIONS

- A Type 1 tank can meet the pressure and temperature requirements for Phase 3 testing and component development, and has the lowest project risk. A revised design of lighter weight will be developed and tested.
- The Type 4 tank that was tested was marginal in terms of ability to meet project requirements due to the liner sensitivity to low temperature. The composite is believed to be suitable for cold temperature. A Type 4 tank has the potential to significantly reduce weight if a suitable liner is developed. Efforts will be made in Phase 3 to develop a suitable liner and conduct additional testing.
- Type 1, Type 3, and Type 4 tank full-scale designs will be developed and evaluated for suitability.
- The concept for insulating and pre-cooling the tank appears to be useful to the project. A full-scale component will be designed and modeled. A subscale unit will be manufactured and tested.

SPECIAL RECOGNITIONS & AWARDS/ PATENTS ISSUED

1. A patent application was filed on the concept for a thermal insulation shell system that would also allow cooling of the tank prior to refilling.

FY 2013 PUBLICATIONS/PRESENTATIONS

1. 2013 DOE Hydrogen Program Annual Merit Review, May 14, 2013.

IV.C.1 Hydrogen Sorbent Measurement Qualification and Characterization

Philip A. Parilla (Primary Contact), Lin Simpson, Jeffrey Blackburn, Katherine Hurst, Chaiwait Engtrakul, Thomas Gennett
National Renewable Energy Laboratory (NREL)
15013 Denver West Pkwy
MS 3211
Golden, CO 80228
Phone: (303) 384-6506
Email: Philip.Parilla@nrel.gov

DOE Managers
Jesse Adams
Phone: (720) 356-1421
Email: Jesse.Adams@go.doe.gov
Channing Ahn
Phone: (202) 586-9490
Email: Channing.Ahn@ee.doe.gov

Subcontractor:
H2 Technology Consulting LLC, Alamo, CA

Collaborators:
- University of Missouri – Peter Pfeifer group
- National Institute of Standards and Technology, Facility for Adsorbent Characterization and Testing (FACT) – ARPA-E Project
- National Institute of Standards and Technology – Laura Espinal group
- Oak Ridge National Laboratory – Raina Olsen group

Project Start Date: October 1, 2012
Project End Date: Project continuation and direction determined annually by DOE

Overall Objectives

- Provide validation measurements for the hydrogen capacity of storage materials.
- Assist research groups within the hydrogen storage community to perform robust and accurate measurements of the hydrogen storage capacity.
- Analyze for, identify, and recommend corrective actions for major sources of measurement error in volumetric and temperature programmed desorption (TPD) systems.

Fiscal Year (FY) 2013 Objectives

- Assist materials-research groups to characterize and qualify their samples for hydrogen-storage properties:
  - Measure external samples at NREL to compare results with source group's and/or third-party's results.
  - Discover sources of measurement discrepancies and advise on corrective actions, if needed, for source group.
- Analyze for, identify, and recommend corrective actions for major sources of measurement error in volumetric and TPD systems:
  - Analyze *realistic* models for random and systematic errors.
  - Develop ad hoc working standards to assist in diagnosing and testing hydrogen capacity measurement instrumentation.
  - Identify the major error sources that will dominate the measurement.
  - Recommend improved instrumentation and procedures to minimize such errors.

Technical Barriers

This project addresses the following technical barriers from the Hydrogen Storage section of the Fuel Cell Technologies Office Multi-Year Research, Development, and Demonstration Plan:

(A) System Weight and Volume

(B) System Cost

(C) Efficiency

(E) Charging/Discharging Rates

(K) System Life-Cycle Assessments

(O) Lack of Understanding of Hydrogen Physisorption and Chemisorption

(P) Reproducibility of Performance

Technical Targets

This project supports the following overall DOE objective: "Capacity measurements for hydrogen-storage materials must be based on valid and accurate results to ensure proper identification of promising materials for DOE support." This project focuses on this through the FY 2013 objectives as listed above. Insights gained from these studies will be applied toward the design and synthesis of hydrogen storage materials that meet the following DOE hydrogen storage targets:

- Cost: $4/kWh net
- Specific energy: 1.5 kWh/kg

- Energy density: 0.9 kWh/L
- The specific technical objectives include:
  - Disseminate measurements qualification and validation improvements to the hydrogen community.
  - Work with hydrogen-storage material-synthesis researchers to measure, at least, two external samples.

FY 2013 Accomplishments

- Developed an ad hoc working standard of an activated-carbon material to test instrumentation and measurement protocols for hydrogen capacity.
- Measured three external samples from outside laboratories. This surpasses the milestone of measuring two external samples.
- Collaborated with outside labs to investigate and verify operation of their hydrogen capacity equipment.
- Continued to develop realistic models for the data analysis for volumetric systems, both for isothermal and non-isothermal conditions. Used models to understand both systematic and random error sensitivities.
- Discussed the major error sources that dominate the measurement; the most dominant errors are still systematic errors.
- Reported detailed findings and recommendations on hydrogen capacity measurements.
- Continued to manage and collaborate on the Best Practices project with its seven sections: Introduction, Capacity, Kinetics, Thermodynamics, Cycle-Life, Thermal Properties, and Mechanical Properties Measurements.

✧ ✧ ✧ ✧ ✧

INTRODUCTION

The ultimate goal of the Hydrogen Storage sub-program is the development of hydrogen storage systems that meet or exceed the DOE's goals for onboard storage in hydrogen-powered vehicles. In order to develop new materials to meet these goals, it is extremely critical to *accurately and precisely* measure the materials' properties relevant to the specific goals; otherwise the metrics are meaningless and achieving of goals, uncertain. In particular, capacity measurements for hydrogen-storage materials must be based on valid and accurate results to ensure proper identification of promising materials for DOE support. A previous round-robin study had discovered major discrepancies among the different participating laboratories for capacity measurements on a standard material, both for room-temperature and liquid-nitrogen capacity determinations [1]. This study emphasizes the importance of maintaining a quality assurance effort within the hydrogen storage community. This project focuses on maintaining a world-class measurement facility for determining hydrogen storage capacities of novel research materials, understanding the experimental issues, procedures, and analysis to ensure accurate measurements, and assisting the hydrogen storage community in performing and understanding these measurements. NREL's main focus is on the volumetric capacity measurement technique; this is also known as the manometric and Sieverts technique. NREL also has extensive experience in the TPD (or thermal desorption spectroscopy) technique.

APPROACH

NREL continues with a multiyear intensive effort to improve measurement quality and accuracy, understand the sources of and correct for measurement error, work with external groups to provide measurements and verify results, collaborate with the hydrogen community to improve measurements, and manage and coordinate with the "Best Practices" Project to disseminate recommended practices and procedures. In previous FYs, this effort was folded into the main materials-development program. This effort has its roots even before the Hydrogen Sorption Center of Excellence, but the effort accelerated during its existence as NREL was the main measurement resource for the Hydrogen Sorption Center of Excellence. The approach can be divided into two components: 1) work with external groups to measure samples and to examine their measurement techniques and procedures; and 2) in general analyze for, identify, and recommend corrective actions for major sources of measurement error in volumetric systems.

With respect to working with external groups, NREL actively seeks out collaborations for comparison studies, helps out with DOE projects to ensure robust measurements, and tests very promising results for verification. Additionally, NREL works with external groups to discover sources of measurement discrepancies and advise on corrective actions, if needed. This entails sending standardized samples to external labs to test instrumentation and experimental procedures, examining data and data analysis protocols to discover possible avenues to improve measurement techniques, and making recommendations to labs for improvements. In this FY, NREL has looked at several commercially available activated carbons to be used as standardized samples. With respect to measurement error, NREL analyzes *realistic* models for random and systematic errors, identifies the major error sources that will dominate the measurement, and recommends improved instrumentation, protocols and data analysis to minimize such errors.

RESULTS

1. Developed an ad hoc working standard of an activated-carbon material to test instrumentation and measurement protocols for hydrogen capacity. This standard will be for both room temperature and liquid-nitrogen temperature measurements. The room-temperature work has been completed and the liquid-nitrogen work is still progressing at the time of this report. It is expected that the latter will be completed by September 2013. Five activated carbons were obtained from well-known commercial chemical supply companies and each went through a series of tests to determine their suitability as a standard material. Some of the criteria that are desirable for a standard material are: 1) commercially available, 2) easily handled, 3) non-hazardous, 4) little or no contaminants, 5) a reasonable hydrogen capacity but not too easy, 6) reproducible results, 7) air stable, 8) long shelf life, and 9) degassing protocol should be reasonable and not extreme. During an initial degassing procedure, it became apparent that several samples contained impurities that are commonly associated with activated carbons: sulfur. Both Brunauer-Emmett-Teller (BET) and pressure-concentration-temperature (PCT) measurements were performed. Figure 1 shows the PCT results for a survey of five different activated carbon samples in the initial screening to find the standardized material. Sample #2 showed the best PCT isotherm, had a reasonable BET value (1,234 m^2/g), and had no detectable impurities; therefore, it is the leading candidate for the standard material.

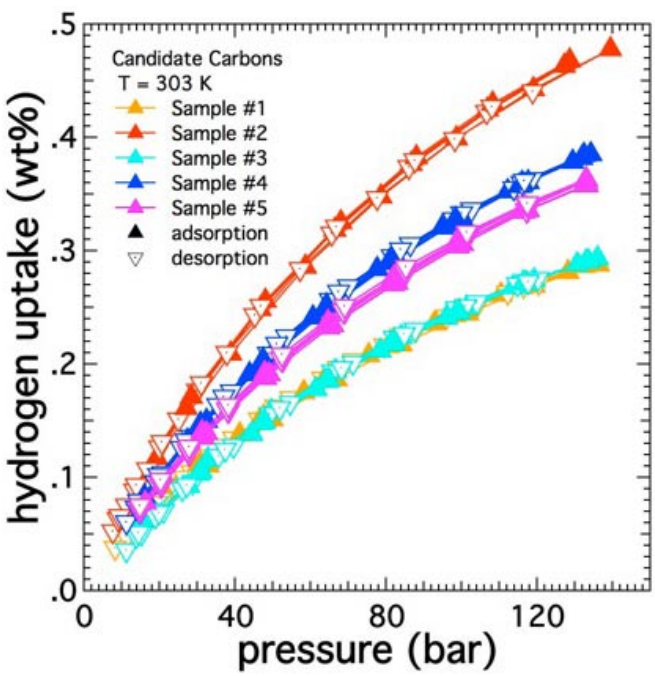

FIGURE 1. PCT measurements (hydrogen capacity versus pressure) to find an ad hoc standard sample for room temperature measurements. Sample #2 has the highest capacity among the materials examined.

2. Measured three external samples from outside laboratories. This surpasses the milestone of measuring two external samples. Each sample typically undergoes approximately five measurements using different techniques in the course of a typical analysis. Techniques include multiple PCT isotherms, BET, TPD during degas, TPD after PCT, density and cycle-life PCT. Sample material types included templated carbon with and without catalysts, BC_x (a boron substituted carbon material formed by the pyrolization of triethylborane) with and without catalysts, and metal-organic frameworks. Data from these external samples are considered proprietary and cannot be shown here.

3. Collaborated with outside labs to investigate and verify operation of their hydrogen capacity equipment. When discrepancies were found, we worked with the lab to discover source of the discrepancy and made suggestions to remedy it.

4. Continued to develop realistic models for the data analysis for volumetric systems, both for isothermal and non-isothermal conditions. The importance of using realistic models should not be underestimated. Volumetric mass-balance models in the scientific literature, although ideally correct, typically do not account for real-world measurement situations. Most volumetric systems contain many more moles in the gas phase than the moles sorbed onto the sample thus requiring very accurate mass-balance accounting. Examples of real-world issues absent in the models include valves that change volume with operation and can transport gas between volumes, assumptions of non-measured pressure values, and the absence of temperature gradients or unrealistic temperature gradients. We conclude that the most dominant errors are systematic errors! The main sources of systematic error are improper "null" calibration, inadequate data analysis models (mass-balance models), ignorance of the large error associated with non-uniform temperature fluctuations, and ignorance of the importance of having adequate sample mass. The null calibration is the main factor in determining the accuracy of the mass-balance accounting. An example of the importance of the null calibration constant is demonstrated in Figure 2. It shows several PCT curves that all come from the same raw data but use different null calibration constants to calculate the hydrogen capacity; the black curve is the correct data. This clearly demonstrates how important it is to determine the correct null calibration constant. How sensitive the influence of an error in the null calibration is on the resulting PCT data depends on several factors,

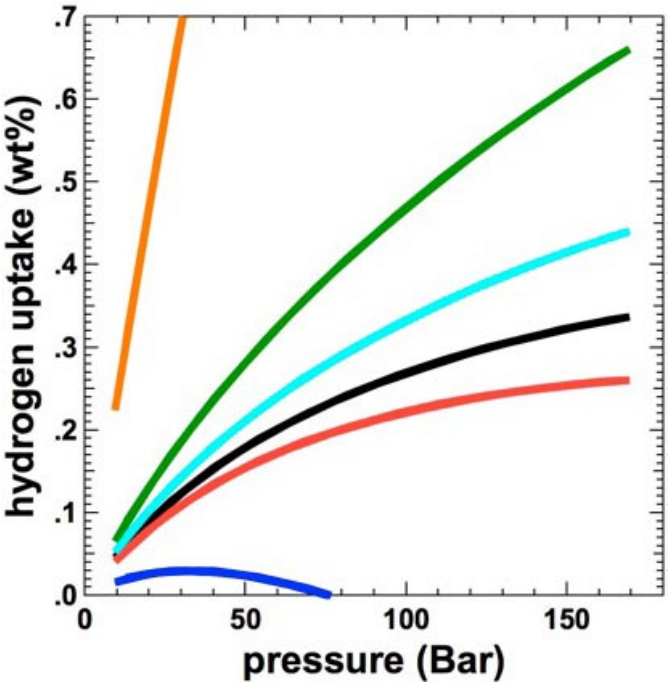

FIGURE 2. PCT curves that all come from the same raw data, but use different null calibration constants to calculate the hydrogen capacity; the black curve is the correct data. This clearly demonstrates how important it is to determine the correct null calibration constant.

but the most important are: the magnitude of the error, the specific capacity of the sample and the mass of the sample.

CONCLUSIONS AND FUTURE DIRECTIONS

- The hydrogen-storage community will benefit from efforts to ensure accurate capacity measurements. Increased quality-control efforts will ensure that the proper emphasis will be placed on new hydrogen-storage materials. There is sufficient cause to believe that inaccurate measurements may have misdirected emphasis.
- Direct collaboration among the laboratories performing capacity measurements has improved measurement accuracy and the quality of published results thereby allowing for more effective utilization of the available research and development resources. An ad hoc standard material will facilitate in determining proper instrument calibration and measurement protocols.
- Several key aspects of the measurement equipment and protocols have been identified to minimize experimental error. Recommendations addressing these issues have been made to improve measurement quality.
- The hydrogen-storage community will continue to benefit from these efforts in the future and help ensure high quality research. NREL will continue to assist in these efforts and provide expertise for the hydrogen-storage community. NREL will adjust its measurement program to meet the needs for the DOE program, such as expanding its capabilities towards a wider range of temperature and/or pressure or facilitating new materials.
- With the recent advances in developing prototype systems within the Hydrogen Storage Engineering Center of Excellence, it has become clear that hydrogen capacities based on a volumetric basis are equally, if not more, important for material comparison. Since previously this reporting practice has not been as emphasized, there is perhaps even more ambiguity and confusion regarding the proper measurement procedures, data analysis and reporting for the volumetric capacities of materials. We feel the need exists to explore and discuss the various options within the hydrogen storage community, both domestically and internationally.

SPECIAL RECOGNITIONS & AWARDS/ PATENTS ISSUED

1. 2013 DOE Hydrogen and Fuel Cell Program R&D Award, "In recognition of outstanding achievements in the establishment of best practices for characterizing hydrogen storage materials", awarded to Karl Gross ("Best Practices" document) and Philip Parilla (NREL measurement science efforts and technical monitor for "Best Practices").

FY 2013 PUBLICATIONS/PRESENTATIONS

1. "A dynamic calibration technique for temperature programmed desorption spectroscopy", Hurst, K.E., Heben, M.J., Blackburn, J.L., Gennett, T., Dillon, A.C., Parilla, P.A., Review of Scientific Instruments **84** 025103 (2013).

2. "Realistic modeling and error analysis for non-isothermal volumetric apparatus" in preparation, P.A. Parilla et al.

3. "Modeling and error analysis for a differential Sieverts apparatus" in preparation, P.A. Parilla et al.

4. Invited Talk Oct. 2012, FACT Meeting– P.A. Parilla *"Lessons Learned from the DOE Hydrogen Program: Adsorption Measurements."*

5. Invited Talk May 2013, 2013 U.S. DOE Hydrogen And Fuel Cells Program Annual Merit Review And Peer Evaluation Meeting – P.A. Parilla *"Hydrogen Sorbent Measurement Qualification and Characterization."*

REFERENCES

1. Zlotea et. al., International Journal of Hydrogen Energy 34 (2009) 3044.

IV.C.2 Room Temperature Hydrogen Storage in Nano-Confined Liquids

John J. Vajo
HRL Laboratories, LLC
3011 Malibu Canyon Road
Malibu, CA 90265
Phone: (310) 317-5745
Email: jjvajo@hrl.com

DOE Managers
Katie Randolph
Phone: (720) 356-1759
Email: Katie.Randolph@go.doe.gov
Grace Ordaz
Phone: (202) 586-8350
Email: Grace.Ordaz@ee.doe.gov

Contract Number: DE-EE0005659

Project Start Date: March 05, 2012
Project End Date: March 14, 2015

Overall Objectives

- Characterize the enhanced solubility of hydrogen in nano-confined liquids
- Optimize the confining scaffold and solvent liquid for room temperature hydrogen storage
- Understand the effect of nano-confinement on solvent properties and the mechanism of solubility enhancement

Fiscal Year (FY) 2013 Objectives

- Extend solubility measurements from bulk liquids to nano-confined liquid/scaffold composites
- Validate the reported enhanced solubility for hydrogen in nano-confined hexane/mobile crystalline material (MCM)-41 composite
- Develop molecular dynamics simulations for nanoscale scaffold pore and bulk solvent liquids

Technical Barriers

This project addresses the following technical barriers from the Hydrogen Storage section (3.3.5) of the Fuel Cell Technologies Office Multi-Year Research, Development and Demonstration Plan:

(A) System Weight and Volume

(C) Efficiency

(E) Charging/Discharging Rates

Technical Targets

This project is conducting initial studies of enhanced hydrogen solubility in nano-confined liquid solvents. Results from these studies will be applied to developing nano-confined liquid/nanoporous scaffold composite hydrogen storage materials that meet the following DOE targets:

- Specific energy: 6 wt% hydrogen (material basis)
- Energy density: 50 g/L hydrogen (material basis)

FY 2013 Accomplishments

- Developed technique for measuring hydrogen solubility in bulk and nano-confined liquids using helium purging with freeze/pump/thaw cycles for degasing and ultrasonic agitation to achieve equilibration.
- Developed methods for preparing nano-confined solvent/scaffold composites with specific and homogeneous compositions.
- Measured hydrogen solubility in nano-confined hexane/mesoporous silica (MCM-41) composite. No solubility enhancement was observed, contrary to published results.
- Developed molecular dynamics simulations of a nanoscale silica pore and bulk liquid hexane that give accurate Si-O bond lengths and hexane densities and heat capacities.

✧ ✧ ✧ ✧ ✧

INTRODUCTION

The prospect of storing hydrogen by dissolving molecular H_2 in a liquid solvent is compelling because dissolution is a chemically simple, readily reversible, room temperature process that occurs with low enthalpy. Despite these attractive attributes, the solubility of hydrogen in bulk liquid solvents is much too low to be technologically useful. For example, hexane, which has a relatively high hydrogen solubility, dissolves <0.2 wt% H_2 at 100 bar and <1 wt% at 700 bar. These solubilities are at least 10x too low for storage applications.

However, the solubilities of gases in liquids have been reported to be greatly enhanced when the liquid is confined within the pores of nanoporous scaffolds [1]. For example, a 16x enhancement was reported for H_2 dissolved in hexane that was confined within nanoporous silica with 3.4 nm pores while a 50x enhancement was claimed for a silica gel with 8.7 nm pores.

These enhanced solubilities are sufficiently high for practical applications. Specifically, we estimate that if an enhancement for hexane of 25x was achieved at 350 bar, then using a scaffold with a pore volume of 4 cm^3/g could enable material basis storage densities of 6 wt% and 50 g/L at room temperature. An enhancement of 25x is high but within the reported range. Attaining this enhancement at 350 bar is an extrapolation that must be tested because previous measurements have been conducted only up to 60 bar. A scaffold with a pore volume of 4 cm^3/g is very high but such pore volumes have been demonstrated.

Because of the similarity and compatibility with compress gas storage, hydrogen storage in nano-confined liquids could significantly improve compressed gas systems with minimal changes to compressed gas vehicle designs and delivery infrastructure, thus facilitating technology transition. Operation at room temperature also addresses current limitations of high capacity metal hydride materials, which require elevated temperatures, and adsorbents, which require cryogenic cooling.

APPROACH

Our approach is to study composites consisting of a liquid solvent for molecular hydrogen that is infiltrated into and confined within a nanoporous scaffold. We will investigate a variety of liquid solvents and scaffold materials. The solvents will include linear, branched, and cyclic molecules while the nanoporous scaffolds will include aluminosilicates, e.g., silica gels and zeolites, and carbon, e.g., activated carbon and carbon aerogel. Volumetric hydrogen storage measurements will be used to determine hydrogen storage capacities and explore the effects of pairing different scaffold-pore and solvent-molecule sizes, shapes, and chemistries. In addition, computational simulations will be performed to understand the mechanism of solubility enhancement by evaluating the effects of nano-confinement on liquid structure, e.g., excess molar volume, pair correlation distributions, and local ordering. Storage capacity measurements together with the simulations will be used to optimize performance and assess the possibility for hydrogen storage via enhanced solubility to meet the DOE goals.

RESULTS

To enable accurate comparison of the solubility of hydrogen in bulk and nano-confined liquids, work began by developing volumetric techniques that could be used for both types of liquids. Solubility measurements of gases in liquids, including hydrogen, have been made for more than 100 years by a variety of techniques including volumetric methods. While these techniques have been optimized for bulk liquid samples, most would not also work well for samples where the liquid is confined within the pore volume of a nanoporous scaffold. For example, bulk liquids are often mechanically stirred to achieve equilibrium solubility and evaporated under vacuum to remove dissolved gases. In contrast, nano-confined liquid/scaffold composites are often dry powders or granules, which cannot be effectively stirred, even when the scaffold pores are completely or nearly completely filled with liquid. In addition, loss of an undetermined amount of the confined liquid through evaporation during degasing is unacceptable if the composite composition is to be controlled and homogeneous. To address these issues for both bulk and nano-confined liquids, we used ultrasonic agitation and helium purging. We modified our sample fixtures to include a thin extension tube, which enabled the sample vessel to vibrate slightly and couple to the ultrasonic energy from a standard ultrasonic bath. Vibration from the bath promoted hydrogen dissolution without bulk stirring. Samples were also prepared under helium with solvent liquid that was thoroughly purged with helium to remove condensable gases such as nitrogen, oxygen, argon, carbon dioxide, and water. After loading, any dissolved helium was removed by using at least three liquid nitrogen freeze/pump/thaw cycles. This procedure yielded degased samples while preventing any loss of volatile solvent.

Figure 1 shows an example solubility measurement. Hydrogen is expanded from a reservoir into contact with a sample of bulk liquid hexane at ~1.7 hr. Over the next 0.5 hr hydrogen dissolution occurs very slowly as indicated by the slow decrease in pressure. At ~2.2 hr an ultrasonic cleaner, in which the sample vessel was immersed, was turned on for 5 min. During this interval a rapid decrease in the pressure occurred resulting from dissolution of hydrogen. At ~2.9 hr the treatment was repeated but, this time, no noticeable change occurred indicating that the dissolution of hydrogen

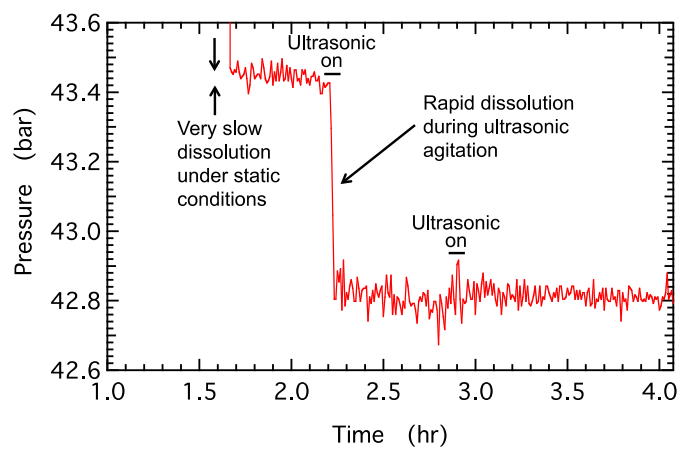

FIGURE 1. Hydrogen solubility measurement using ultrasonic agitation. The system pressure versus time is shown after exposing a bulk sample of hexane to hydrogen at ~43 bar. Under static conditions, from 1.7 hr to 2.2 hr, hydrogen uptake (dissolution) is very slow. During 5 min with ultrasonic agitation, indicated by the line segment under the "Ultrasonic on" label, rapid dissolution occurs. A second ultrasonic treatment at 2.9 hr shows no effect indicating that dissolution had reached equilibrium.

in the hexane was already at equilibrium. From the difference between the moles of hydrogen initially in the reservoir and the final moles of hydrogen in the gas phase, determined by calibrating the system volumes and measuring the initial and final pressures, the moles of dissolved hydrogen and, thereby, the hydrogen solubility was determined. This technique is applicable to both bulk and nano-confined liquid materials.

Using this procedure, the solubility of hydrogen in bulk hexane was measured as a function of pressure using two HRL Sieverts apparatus. The results are shown in Figure 2 and compared with published state-of-the-art results [2]. The error bars for the HRL data originate from uncertainty in accounting for the vapor pressure of the hexane. The positive error direction gives the solubility assuming that the hexane vapor pressure was equal to its equilibrium value, while the negative direction assumes zero vapor pressure. Thus far, we have been unable to convincingly determine the actual hexane pressure during the hydrogen solubility measurements. The solubilities from both apparatus agree with each other and with published values to within ~15%.

After establishing measurements on bulk liquids, nano-confined liquid/porous scaffold composites were carefully prepared. Scaffolds were first thoroughly dried by heating at ~250°C under dynamic vacuum for ~10 hr. The scaffolds were then backfilled with helium and infiltrated with helium-purged solvent under a helium atmosphere. Scaffold filling was expressed as vol%, i.e., the fraction of the scaffold pore volume that was filled with solvent. This filling was determined by weight using the accepted bulk liquid density and the scaffold pore volume, determined separately by nitrogen adsorption. To ensure that the solvent was

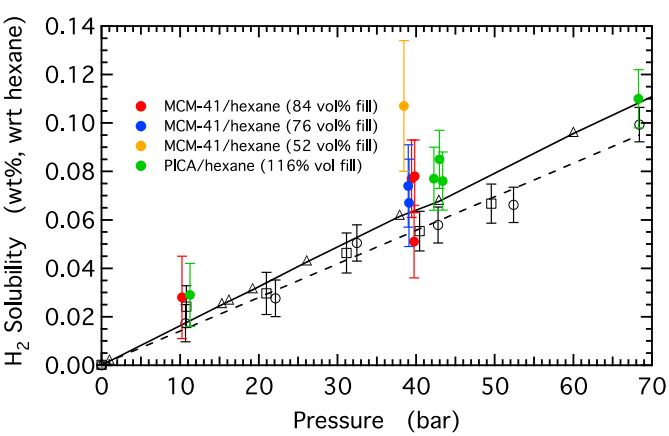

FIGURE 2. Hydrogen solubility in bulk and nano-confined hexane. Open symbols show hydrogen solubility in bulk hexane from reference 2 (open triangles) and two HRL Sieverts apparatus (open circles and squares). The Henry's law constants, proportional to the slope of the linear fits, are equal for the HRL data (dashed line) and ~15% lower than the published data (solid line). The error bars for the HRL data reflect the uncertainty introduced by the vapor pressure of hexane as described in the text. Several nano-confined hexane composites are shown, as indicated (filled circles) with varying volume fillings for hexane/MCM-41 and for hexane/PICA activated carbon.

homogeneously distributed throughout the scaffold, liquid/scaffold composites were place in a sealed volumes and heated to ~85°C for several days. Homogenized composites were connected to a Sieverts apparatus and degased using freeze/pump/thaw cycles with liquid nitrogen.

Hydrogen solubilities for nano-confined hexane/scaffold composites are shown in Figure 2. The solubility is expressed as wt% hydrogen with respect to the mass of hexane to facilitate comparison to bulk hexane. The first composite studied was hexane/mesoporous silica (MCM-41). This composite was chosen because a 16x hydrogen solubility enhancement was reported for this system [1]. In addition, MCM-41 mesoporous silica is commercially available and has a well characterized and controlled structure consisting of hexagonally close-packed 1-dimensional pores with 3.4 nm diameter hexagonal cross sections [3]. Composites with volume fillings of 52%, 76%, and 84% showed no enhancement in hydrogen solubility within the uncertainty given by the hexane vapor pressure. In addition, a hexane/PICA activated carbon composite was tested as a function of pressure. PICA activated carbon is a microporous carbon with <2 nm slit-shaped pores. Again, no enhancement was observed.

The lack of enhancement for the hexane/MCM-41 composite is in contrast to published results, which claim a 16x enhancement. A comparison is shown in Table 1. Hydrogen capacities for the empty MCM-41 scaffold and bulk hexane are roughly similar, within ~2x. However, the capacities for the hexane/MCM-41 composites and the enhancement factors relative to both the bulk hexane and the empty scaffold differ considerably. While a 15.9x enhancement is reported with respect to bulk hexane, our measurement gives 1x. With respect to the empty scaffold a 3x increase was claimed whereas our measurements show a decrease, ~0.5x. The origin of this discrepancy is not clear. However, preparation of the composite in the published results was reported to include evacuation at room temperature. This procedure seems questionable considering the volatility of hexane.

An effort was made to resolve these discrepancies with the published results by contacting the Le Centre National de la Recherche Scientifique (CNRS) group. Through email exchanges, the difficulty of these measurements was stressed and alternative solvents and scaffolds were suggested. However, no specific, actionable advice regarding the hexane/MCM-41 composite was received. At this point we plan move beyond this system and screen a variety of solvent/scaffold composites to experimentally verify an enhanced solubility effect.

In parallel with the experiments described above, computational verification of an enhanced solubility effect was studied using molecular dynamics simulations. To begin, simulations of an empty scaffold and a bulk solvent were conducted separately. These simulations will eventually be

TABLE 1. Comparison of Hydrogen Capacities for Hexane/MCM-41 Composite

Hydrogen Capacity	Bulk n-Hexane (mmol/cm³)	Empty MCM-41 (mmol/cm³)	Composite Hexane/MCM-41 (mmol/cm³)	Capacity ratio wrt bulk hexane	Capacity ratio wrt empty MCM-41
CNRS Chem Phys Lett 2010 JACS 2012	0.17	0.87	2.7 (60 vol%)	15.9 x large enhancement	3.1 x large enhancement
HRL	0.185	0.4 ± 0.1	0.19 (52 vol%) 0.18 (76 vol%) 0.18 (84 vol%)	1.03 x 0.97 x 0.97 x no enhancement	0.48 x 0.45 x 0.45 x lower

CNRS - Le Centre National de la Recherche Scientifique; wrt - with respect to

combined, and the solvent will be simulated confined within the scaffold with an ultimate plan to also include dissolved H_2. All simulations were performed using the large-scale atomic/molecular, massively parallel, molecular dynamics simulator, developed by Sandia National Laboratories, with chemistry at Harvard macromolecular mechanics force fields. These force fields are Lennard-Jones potentials with variable cutoff distances and widths.

Simulation of the scaffold began with bulk silica followed by simulations of a nanoscale silica pore. The initial and final configurations of a ~2-nm diameter silica nanopore are shown in Figure 3. The final Si-O bond length is 0.1626 +-0.0027 nm, which agrees well with experimental values of 0.1600 nm to 0.1615 nm. After running the simulation for 2,000 ps, more disorder is seen near the pore, reflecting relaxation to minimize the pore energy. This simulation of a silica scaffold is now ready for inclusion of a liquid solvent, such as hexane.

Simulation of bulk liquid hexane is shown in Figure 4. Over the course of the simulation at 300 K, the density rises as the periodic volume contracts from an intentionally chosen dilute initial state. The final simulated density of 0.662 g/cm^3 agrees well with the experimental density of 0.659 g/cm^3. The heat capacity was also determined by performing simulations and monitoring the enthalpy at several temperatures, from 250°C to 300°C. The heat capacity was found to be extremely sensitive to the Lennard-Jones potential cutoff distance and cutoff length. When optimized, a heat capacity of 216 J/mol-K was obtained, ~9% larger than the experimental value of 198 J/mol-K. This simulated hexane will next be used in a confined configuration formed with perfectly reflective smooth walls in two dimensions while retaining a periodic boundary in one direction.

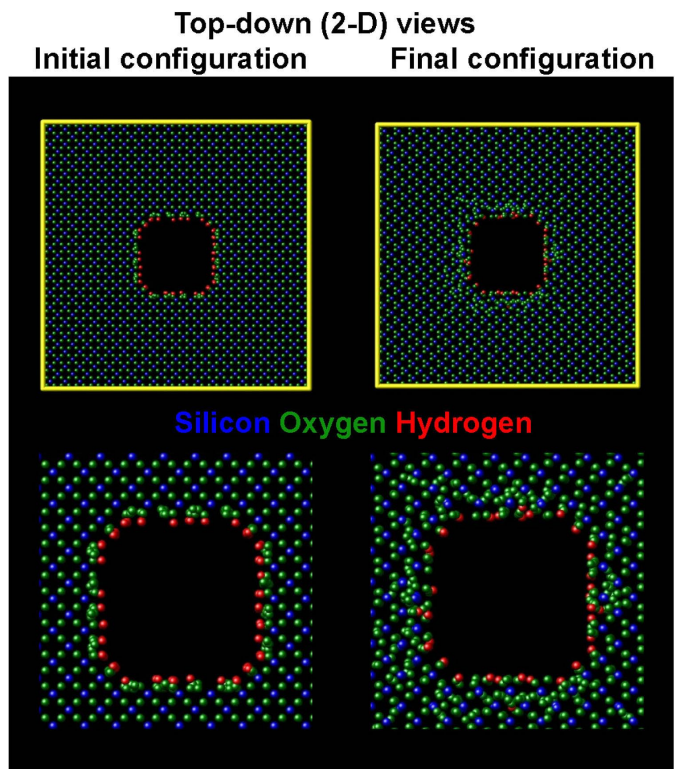

FIGURE 3. Molecular dynamics simulation of silica nanopore. Top-down 2-dimensional views are shown of the initial configuration (left) and final configuration (right); (top) full view and (bottom) close-up of pore. The overall volume with periodic boundary conditions is ~6.5 x 6.5 x 6.5 nm^3 containing ~16,000 atoms with an ~2-nm diameter pore. The surface of the pore contains Si-O-Si and Si-OH surface terminations. The simulation temperature is 300 K.

SUMMARY

Techniques have been developed for accurate measurements of hydrogen solubility in both bulk and nano-confined liquids. An attempt to verify the enhanced solubility reported for hydrogen in the nano-confined liquid/porous scaffold composite, hexane/MCM-41, was unsuccessful. Work is continuing to test for enhanced solubility in a variety of liquid/scaffold composites. Molecular dynamics simulations have also been developed for a silica nanopore and bulk liquid hexane. These simulations will next be combined to look for changes in the structure of nano-confined hexane.

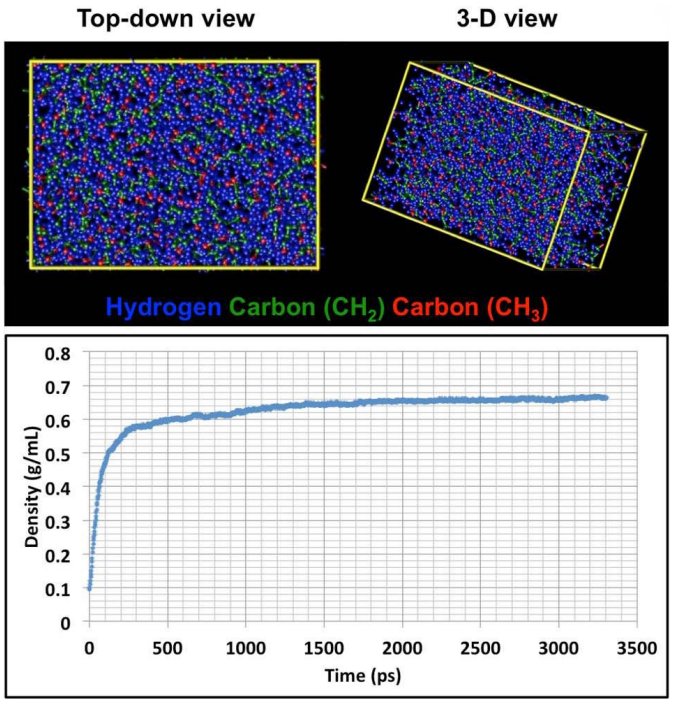

FIGURE 4. Molecular dynamics simulation of bulk liquid hexane. (top) Top-down and 3-dimensional views. (bottom) Hexane density during simulation. 250 hexane molecules were simulated at 300 K. The final volume was 4.5 x 3.25 x 3.7 nm^3 with periodic boundary conditions.

FY 2013 PUBLICATIONS/PRESENTATIONS

1. Room temperature hydrogen storage in nano-confined liquids, Presentation to the Hydrogen Storage Tech Team, Southfield, MI, September 20, 2012.

2. Room temperature hydrogen storage in nano-confined liquids, Presentation at the Hydrogen Storage PI Meeting, Washington, DC, November 27, 2012.

3. Room temperature hydrogen storage in nano-confined liquids, Presentation at the 2013 DOE Fuel Cell Technologies Program Annual Merit review, Crystal City, Virginia, May 2013.

REFERENCES

1. V. Rakotovao, R. Ammar, S. Miachon, M. Pera-Titus, "Influence of the mesoconfining solid on gas oversolubility in nanoliquids", *Chem. Phys. Lett.*, **485**, 299-303 (2010).

2. E. Brunner, "Solubility of Hydrogen in 10 Organic Solvents at 298.15, 323.15, and 373.15 K", *J. Chem. Eng. Data*, **30**, 269-273 (1985).

3. http://www.zeolite.utm.my/images/mcm41.gif.

IV.C.3 Hydrogen Storage in Metal-Organic Frameworks

Jeffrey Long
Lawrence Berkeley National Laboratory (LBNL)
1 Cyclotron Road
Berkeley, CA 95720
Phone: (510) 642-0860
Email: jrlong@berkeley.edu

DOE Managers
Jesse Adams
Phone: (720) 356-1421
Email: Jesse.Adams@go.doe.gov
Channing Ahn
Phone: (202) 586-9490
Email: Channing.Ahn@ee.doe.gov

Subcontractors:
- National Institute of Standards and Technology (NIST), Gaithersburg, MD (Craig Brown)
- General Motors Corporation (GM), Warren, MI (Anne Dailly)

Project Start Date: April 1, 2012
Project End Date: March 31, 2015

Overall Objectives

- Research and development of onboard systems that allow for a driving range greater than 300 miles.
- Materials sought with the potential for meeting the DOE targets of reversible uptake:
  - 2017 targets: 5.5% H_2 by mass, volumetric capacity of 40 g/L
  - "Ultimate full fleet" targets: 7.5% H_2 by mass, 70 g/L
- Synthesize new metal-organic frameworks (MOFs) capable of achieving the -20 kJ/mol adsorption enthalpy required for use as hydrogen storage materials operating 100 bar at ambient temperatures.

Fiscal Year (FY) 2013 Objectives

- Synthesize MOFs exhibiting reversible H_2 uptake greater than 2.5 wt%.
- Prepare a high-valent MOF with an initial adsorption enthalpy greater than 12 kJ/mol (at 298 K and 300 bar).
- Synthesize new MOFs with the multifunctional ligands prepared in year one.
- Prepare at least two MOFs with the optimal 7 Å between opposing pore surfaces as predicted with *in silico* screening techniques.
- Demonstrate that improved understanding of MOF-H_2 interactions through inelastic neutron scattering experiments and new approaches to calculate observed spectra provide new insight into the governing physics of adsorption in porous media.
- Demonstrate the ability to determine H_2-metal interactions in realistic systems containing low-coordinate metal cations.
- Demonstrate the correlation between high-pressure measurements and theoretical and spectroscopic predictions.
- Demonstrate the ability to measure H_2 adsorption in a test material up to 10 cycles at 298 K.
- Demonstrate the ability to measure H_2 adsorption in a test material up to 10 cycles at temperatures relevant to use in onboard vehicle applications.

Technical Barriers

This project addresses the following technical barriers from the Hydrogen Storage section of the Fuel Cell Technologies Office Multi-Year Research, Development and Demonstration Plan:

(A) System Weight and Volume

Technical Targets

Specific efforts are focused on the research and development of onboard systems that allow for a driving range greater than 300 miles. Materials are sought with the potential for meeting the 2017 DOE targets of reversible uptake and, subsequently, the "ultimate full fleet" targets (see Table 1).

FY 2013 Accomplishments

- Published joint theory/experiment paper in *J. Am. Chem. Soc.* on the hydrogen storage properties of M-BTT (M = Cu, Mn, Fe, Zn), a MOF with open M^{2+} cation sites.
- Synthesized five new MOFs with ligands prepared in year one.
- A new isostructural MOF series (M_2dobdc') has been synthesized and characterized.
- The structure of M_2(dobdc') and D_2 binding sites were elucidated via powder neutron diffraction.

TABLE 1. Progress towards Meeting Technical Targets for Onboard Hydrogen Storage for Light-Duty Vehicles

Storage Parameter	Units	2017 Target	Ultimate Target	2013 Status†
System Gravimetric Capacity: Usable, specific-energy from H_2 (net useful energy/max system mass)*	kWh/kg (kg H_2/kg system)	1.8 (0.055)	2.5 (0.075)	(0.016 kg H_2/kg adsorbent)
System Volumetric Capacity: Usable, energy density from H_2 (net useful energy/max system volume)	kWh/L (kg H_2/L system)	1.3 (0.040)	2.3 (0.070)	(0.011 kg H_2/L adsorbent)

* Generally the full mass (including hydrogen) is used; for systems that gain weight, the highest mass during discharge is used. All capacities are net useable capacity able to be delivered to the power plant. Capacities must be met at end of service life.
† Since the project deals with the development of storage materials, the performance status is given in terms of storage capacity for storage materials, not the whole storage system.

INTRODUCTION

MOFs are promising solid sorbents for storage of H_2 at room temperature. They can be tailored to incorporate a large number of selected metal ions, thereby tuning the H_2 binding energy. The overall aim of the project is to synthesize new MOFs capable of achieving the –20 kJ/mol adsorption enthalpy required for use as hydrogen storage materials operating under 100 bar at ambient temperatures.

APPROACH

This research involves investigators with a range of capabilities—including synthesis and characterization of new materials, electronic structure calculations, neutron diffraction and scattering studies, and high-pressure gas sorption measurements. The team performs work in four areas: Task 1) Synthesis of Metal-Organic Frameworks (Long-LBNL), Task 2) Characterization of Framework-H_2 Interactions (Brown-NIST), Task 3) First-Principles Calculations of Hydrogen Binding Enthalpies (Head-Gordon-LBNL), and Task 4) High-Pressure H_2 Adsorption Measurements (Dailly-GM).

RESULTS

In order to address the system weight and volume technical barriers from the Hydrogen Storage section of the Fuel Cell Technologies Office Multi-Year Research, Development, and Demonstration Plan we are synthesizing a number of new metal-organic frameworks with the potential to reversibly adsorb large quantities of H_2 at modest pressures and temperatures. To reach these goals two separate approaches are being used. The first is maximizing H_2 uptake by preparing MOFs with optimal opposing pore surface distances. Theoretical calculations have shown that to maximize H_2 uptake materials with opposing surfaces 7 Å apart are needed. In order to rapidly screen the pore size of a large number of MOF structures for this optimal 7 Å distance we have developed an *in silico* screening tool that calculates opposing surface distances as a function of surface area from crystallographic information files. MOF-5, for example, features a large fraction of surface area outside the 7 Å distance (Figure 1).

In addition to maximizing pore size and opposing pore distances, we are currently rigorously investigating MOFs with coordinatively unsaturated metal cation sites. The majority of work thus far has been devoted to the synthesis and characterization of the M_2(dobdc') (M = Mg^{2+}, Mn^{2+}, Fe^{2+}, Co^{2+}, Ni^{2+}) (dobdc'$^{4-}$ = 2,4-dioxido-1,5-benzenedicarboxylate) ("dobdc-prime") metal-organic framework series as well as other MOF-74 analogs (Figure 2). These materials are similar in structure to the already reported, and well studied, M_2(dobdc) (M = Mg^{2+}, Mn^{2+}, Fe^{2+}, Co^{2+}, Ni^{2+}, Zn^{2+}) (dobdc^{4-} = 2,5-dioxido-1,4-benzenedicarboxylate) or MOF-74 structure. The synthesis of H_4dobdc' is extremely simple compared to H_4dobdc and can be realized by the direct carboxylation of resorcinol with CO_2 in the presence of potassium carbonate. An analogous synthesis with hydroquinone to produce H_4dobdc is not possible thus more expensive, solvent

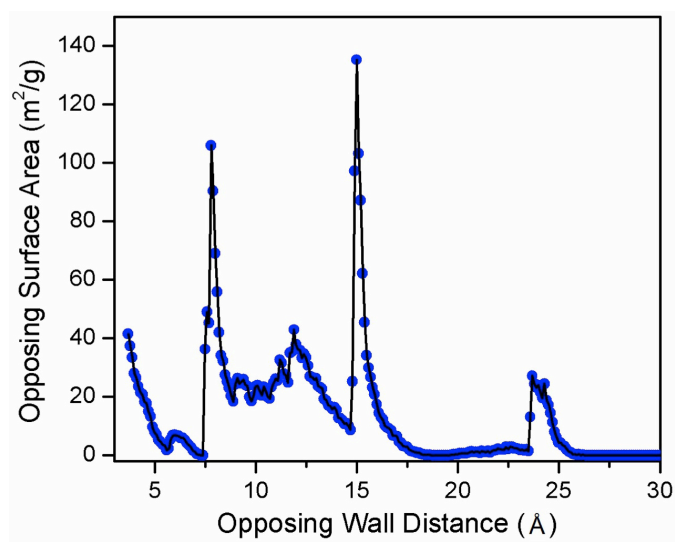

FIGURE 1. Opposing surface area distribution for $Zn_4O(BDC)_3$ as calculated with a 3.68-Å probe molecule diameter and a 0.1-Å step size.

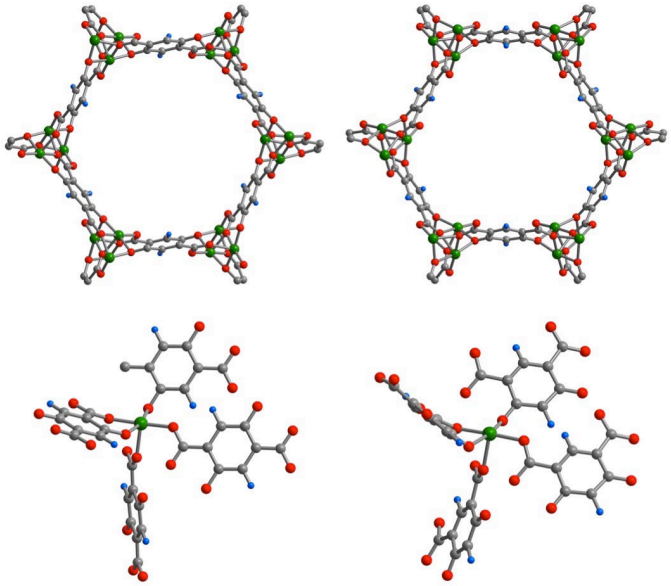

FIGURE 2. (upper) Crystal structures of Ni_2(dobdc) (left) and Ni_2(dobdc') (right) as viewed down the (0,0,1) direction. Green, red, gray, and blue represent nickel, oxygen, carbon, and hydrogen atoms, respectively. (lower) Close up of the coordination environment of Ni^{2+} in Ni_2(dobdc) (left) and Ni_2(dobdc')(right).

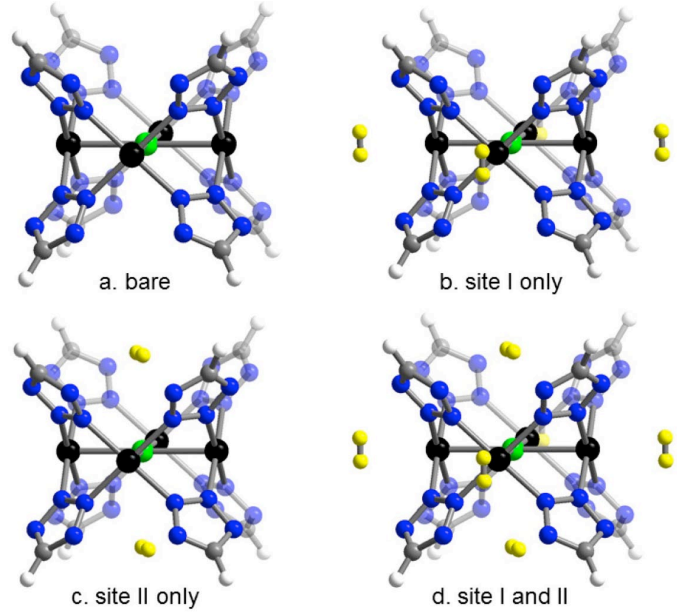

FIGURE 3. Representative density functional theory structural models of the hypothetical $[M_4Cl(tz)_8]^-$ (M = Mn, Cu, Zn; tz^- = 5-*H*-tetrazolate) molecule and its H_2-bound variants calculated for assessment of the H_2 binding energies. For each of the metals surveyed, four structures were calculated. Starting with the parent molecule shown in (a), H_2 molecules were introduced to (b) site I, (c) site II, or (d) site I and II. Black, green, white, gray and blue spheres represent M, Cl, H, C, and N atoms, respectively, while the H atoms of the bound H_2 molecules are displayed as yellow spheres for clarity.

intensive synthetic techniques are required. It was our hope that the MOF-74 structure type could be synthesized with this new ligand as the synthesis of large amounts of MOF based on it would be significantly cheaper and have far less environmental impact than the synthesis of H_4dobdc, which is currently made via far less green methods. Furthermore, both Ni_2(dobdc') and Co_2(dobdc') exhibit low coverage isosteric heats of H_2 adsorption of approximately -12.0 kJ/mol, on track with the FY 2013 target. Future work with these materials will focus on further characterization of M-D_2 and M-H_2 interactions via neutron scattering techniques and theoretical calculations.

We have also recently published work on combined theoretical/experiment work with metals of the $M_3[(M_4Cl)_3(BTT)_8]_2$ (M-BTT; BTT^{3-} = 1,3,5-benzenetristetrazolate, M = Cu, Mn, Fe, Zn) structure type (Figure 3). Variable-temperature infrared spectroscopy studies of Mn-BTT, Fe-BTT and Cu-BTT, for which the thermodynamics of H_2 adsorption is experimentally probed was complemented by a detailed density functional theory study, in which molecular fragments representing the metal clusters within the extended solid are simulated to obtain a more thorough description of the structural and thermodynamic aspects of H_2 adsorption at the strongest binding sites. The close agreement between the theoretical and experimental data confirmed that the theoretical model is able to accurately describe the binding environments for H_2 within the M-BTT structure type. The effect of substitutions at the metal cluster, namely the identity of the metal ion or the anion within the tetranuclear cluster showed that the configuration of this unit indeed plays an important role in determining the affinity of the framework towards H_2. Interestingly, the theoretical study has identified that the Zn-based analog would be expected to facilitate an adsorption profile that is enhanced over the compounds that have been synthesized experimentally to date, highlighting the importance of a combined experimental and theoretical approach to the design and synthesis of new MOFs for H_2 storage applications.

CONCLUSIONS AND FUTURE DIRECTIONS

- The recently completed opposing surface area distribution program will be used to down select MOFs for room-temperature H_2 storage.
- We have shown excellent agreement between experimental data and theoretical calculations; this will further be used to inform the synthesis of new MOF materials.
- Fruitful collaboration between researchers at NIST and LBNL has led to a better understanding of metal-hydrogen interactions in a number of new frameworks.
- Promising samples will be sent to GM for high-pressure hydrogen adsorption and cycling measurements.

FY 2013 PUBLICATIONS/PRESENTATIONS

1. "Opposing Surface Area Distribution (OSAD) as a Characterization Tool for Microporous Metal-Organic Frameworks" Sumida, K.; Rogow, D.L.; Herm, Z.R.; Long, J.R. *Langmuir* submitted.

2. "Impact of Metal and Anion Substitutions on the Hydrogen Storage Properties of M-BTT Metal-Oroganic Frameworks" Sumida, K.; Stuck, D.; Mino, L.; Chai, J.-D.; Bloch, E.D.; Zavorotynska, O.; Murray, L.J.; Dinca, M.; Chavan, S.; Bordiga, S.; Head-Gordon, M.; Long, J.R. *J. Am. Chem. Soc.* **2013**, *135*, 1083-1091.

IV.C.4 The Quantum Effects of Pore Structure on Hydrogen Adsorption

Raina Olsen
Oak Ridge National Laboratory
One Bethel Valley Road
P.O. Box 2008, MS-6115
Oak Ridge, TN 37831-6115
Phone: (573) 999-2371
Email: olsenrj@ornl.gov

DOE Managers
Channing Ahn
Phone: (202) 586-9490
Email: Channing.Ahn@ee.doe.gov
Ned Stetson
Phone: (202) 586-9995
Email: Ned.Stetson@ee.doe.gov

Technical Advisor
James Morris
Phone: (865) 630-0020
Email: morrisj@ornl.gov

Project Start Date: October 31, 2011
Project End Date: October 30, 2013

Overall Objectives

- Understand how quantum effects may be used to increase hydrogen storage
- Measure properties of a sample with unusually high volumetric hydrogen storage

Fiscal Year (FY) 2013 Objectives

- Materials characterization
- Analysis of inelastic neutron scattering data
- Theoretical solution of quantum states of hydrogen adsorbed in expanded graphite pores

Technical Barriers

This project addresses the following technical barrier from the Hydrogen Storage section (3.3.5) of the Fuel Cell Technologies Office Multi-Year Research, Development, and Demonstration Plan:

(A) System Weight and Volume

Technical Targets

This project studies a class of Saran carbon adsorbents with unusually high volumetric storage (Table 1) compared to similar carbons. The samples were synthesized and measured by the Alliance for Collaborative Research in Alternative Fuel Technology (ALL-CRAFT) group at the University of Missouri [1-3] during preliminary work.

FY 2013 Accomplishments

- Characterization of the samples of interest with X-ray diffraction (XRD), Raman spectroscopy, transmission electron microscopy (TEM), and CO_2 adsorption, which shows evidence for narrow graphitic pores [4]
- Discovery of a temperature dependent phase transition to an exceptionally high density phase in the samples of interest, based on evidence from hydrogen isotherms and small angle neutron scattering (SANS) spectra
- Proposed theoretical model of a significant, highly novel quantum effect for H_2 adsorbed in a model pore consistent with the experimental properties of the samples of interest [5]
- Analysis of experimental inelastic neutron scattering data [6,7] and calculation of the quantum states of H_2 adsorbed in graphene slit-pores, resulting in better understanding of the quantum behavior of adsorbed H_2

✧ ✧ ✧ ✧ ✧

TABLE 1. Volumetric and gravimetric performance of a representative Saran carbon (HS;0B) compared with an industry standard activated carbon (MSC-30).

Characteristic	Units	2017 Target (System)	2017 Target (Material)	HS;0B		MSC-30	
				300 K 90 bar	80 K 90 bar	300 K 90 bar	80 K 90 bar
Volumetric Storage	g H_2/L sample	40	~80	14.7	58.4	8.50	41.6
Gravimetric Storage	wt% (g H_2/g system *100)	5.5	~11	1.22	4.68	2.21	9.90

INTRODUCTION

No current hydrogen storage method is able to simultaneously meet the 2017 gravimetric and volumetric system targets. There are two competing types of material solutions. Chemical systems hold the H_2 in a much smaller volume with strong bonds, but their weight is generally too large. Adsorbents hold the H_2 on a lighter high surface area material with weaker forces which are not able to squeeze the molecules much closer together than they are in liquid H_2, but this density is not high enough to meet volumetric targets. It seems unlikely that either the 2017 or ultimate targets will be met without a radically different approach to the problem.

The ALL-CRAFT group at the University of Missouri has produced a class of Saran nano-porous carbon adsorbents with several unusual and desirable characteristics [1-4]. In particular, their volumetric storage is 40-75% higher than the best alternative carbons (Table 1). While the gravimetric performance is 45-55% smaller than other carbons, it is notable that these values are achieved with sample surface areas of ~700 m^2/g, nearly a quarter of typical high-performing carbons. The high adsorption per unit surface area originates from the apparent ability of the material to store the adsorbed H_2 at approximately twice the density of liquid H_2, which is theoretically impossible according to classical adsorption models. If a higher surface area material with the same performance samples could be synthesized, it could simultaneously meet gravimetric and volumetric system targets at cryogenic temperature, while possessing all of the other advantageous properties of a carbon adsorbent which are helpful in meeting and exceeding targets for system cost, durability, safety, refueling time, and thermal management.

APPROACH

Two assumptions provide the foundation of this project. The first is that preliminary data on the samples of interest [1-3] is reasonably correct and there are indeed novel physical mechanism(s) at work in these materials which can be utilized to increase hydrogen storage performance. The second is that there is a link between the unique properties of the samples which were observed during preliminary work. These include the high magnitude of cryogenic H_2 adsorption as well as the shape of the isotherms, the structural properties of the samples such as their narrow distribution of small pores, and the measured differences between quantum states for H_2 adsorbed in one of the samples of interest compared to H_2 adsorbed in three other carbon materials [2,7].

Rather than making new materials, hoping for slight improvements, the focus of this project has been on understanding these samples so that significantly better materials can be intelligently designed. The initial assumptions led to a hypothesis that there are some significant quantum effect(s) which are highly dependent on pore structure and able to significantly increase hydrogen adsorption. A combination of theory and experiment has been used to explore this hypothesis, seeking insight into the sample structure, verifying that there are indeed unique and desirable mechanism(s) at work, probing their properties, and exploring their theoretical basis.

RESULTS

Characterization of the sample of interest [4] shows it is highly graphitic. XRD spectra, shown in Figure 1(a), show a large graphite 002 peak, though its broadness indicates significant disorder. Pore size distributions were calculated from CO_2 isotherms (Figure 1(b)) and show mainly pores <1 nm. TEM images show a significant amount of disordered graphite, and pores which form where graphene layers split apart [4]. But the pore shown in Figure 1(c) was the smallest observed; most were >1 nm in width. One may hypothesize that the unseen <1 nm pores lie parallel to the planar dimension of the flaky sample grains [2,4] and thus parallel to the TEM field of view. If these pores are similarly formed where graphene layers split apart, they might likely be constrained by the thinness of the flake to be narrower and flatter than observed pores. Thus the sample is graphitic with narrow pores, and graphene slit-pores are a plausible model.

It is important to validate the H_2 isotherms (Figure 2) originally measured by ALL-CRAFT at 80 and 90 K [1-3]. The unusual behavior has been observed in three Saran samples synthesized with similar procedures measured by ALL-CRAFT. However, these unusual properties (lack of a peak in the cryogenic gravimetric excess and high overall amounts) can easily be the result of "null" calibration errors in volumetric measurements [8]. A sample of HS;0B-20 was sent to the National Renewable Energy Laboratory (NREL) for measurement of a H_2 isotherm at ~76 K in a liquid N_2 bath. The NREL isotherm (Figure 2, bottom) is typical in magnitude and shape for a low surface area carbon with narrow pores. ALL-CRAFT also measured this sample in a liquid N_2 bath, finding very good agreement with the NREL data. There are two possible explanations for these results. The first is that the original measurements were wrong and the new measurements are correct. The second is that all isotherms are reasonably correct, and there is a temperature dependent phase change between a classical adsorbed phase and a novel high density phase. This hypothesis is supported by the original measurements of HS;2B, which showed a typical isotherm at 80 K and the unusually high adsorption at 90 K. Additionally, HS;0B and HS;2B were measured sequentially with the same calibration, but no single value for the calibration error [8] at 80 K results in good agreement between the corrected isotherms of these otherwise similar samples. The instrument was also validated near the time of these measurements by comparison of NREL and ALL-CRAFT isotherms for two activated carbons [1].

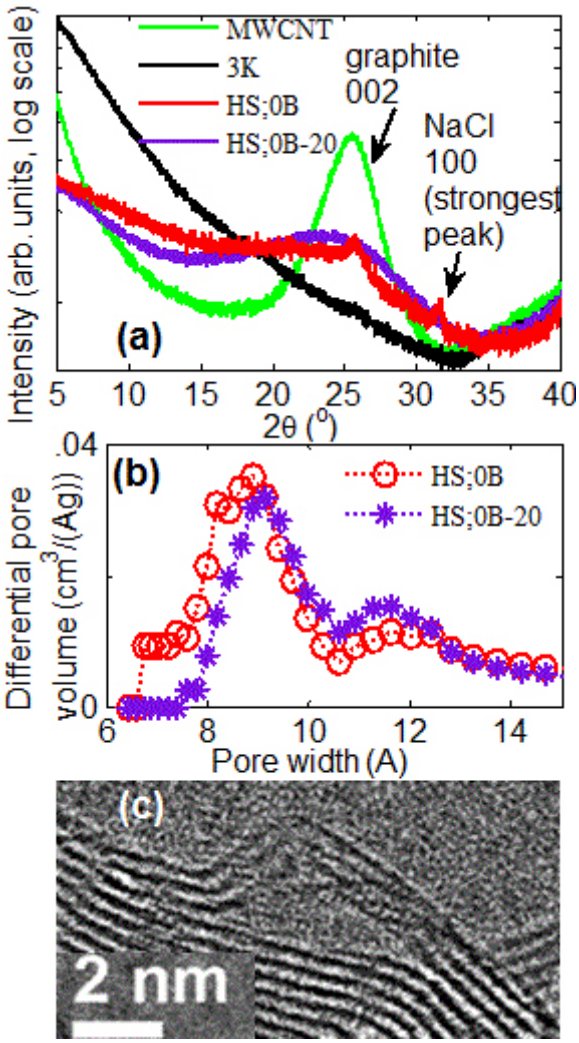

FIGURE 1. Materials characterization of Saran carbon HS;0B and variants, activated carbon 3K, and multi-walled carbon nanotubes (MWCNTs). (a) XRD spectra (b) Pore size distributions calculated from CO_2 adsorption isotherms. (c) Bright field TEM image of HS;0B.

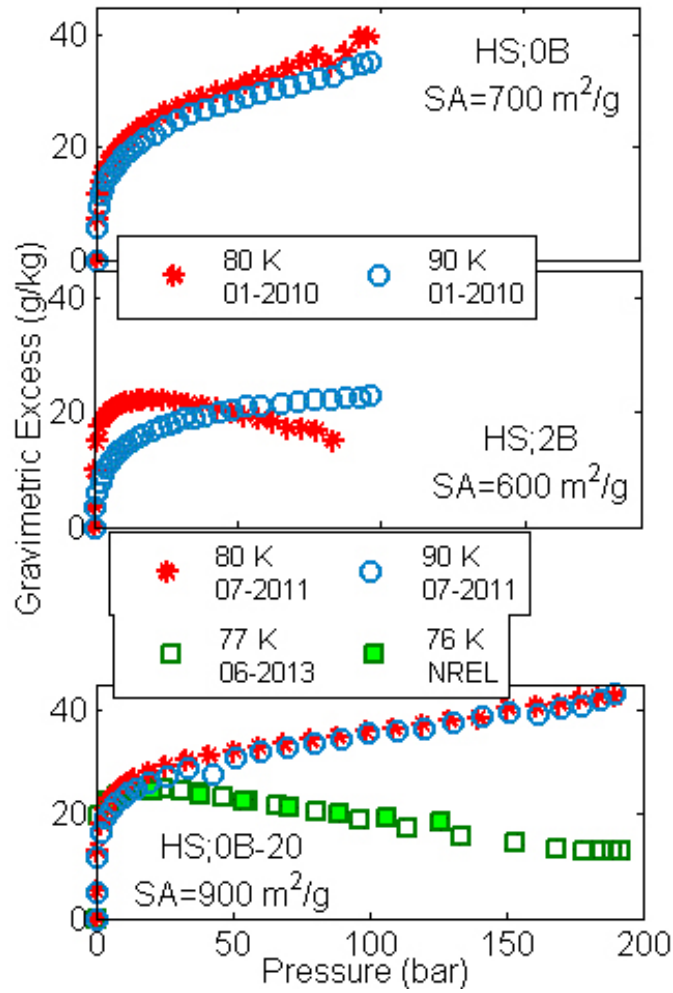

FIGURE 2. Gravimetric excess hydrogen adsorption, in grams H_2 per kilogram of sample, for three variants of a Saran carbon. Except where noted, all isotherms were collected by the ALL-CRAFT group using a Hiden HTP1 volumetric analyzer, with the month and year of the measurement noted in the captions. The NREL measurement was done in 06-2013.

SANS was used to look for evidence of the proposed phase transition. SANS is sensitive to surfaces or interfaces between different materials and has previously been used to study the amount of H_2 in carbon adsorbents [9]. Because the coherent scattering length is positive for C and negative for H, the surface contrast and thus the SANS intensity increases monotonically as hydrogen is adsorbed in carbon pores. Collected spectra also contain an incoherent component linearly proportional to the amount of hydrogen in the sample cell. Spectra are shown in Figure 3(b) for H_2 adsorbed in HS;0B and 3K, an activated carbon with typical properties. Hydrogen pressure was held fixed at ~104 bar while the temperature was varied between ~55-115 K. For a classical system, the amount of hydrogen in the cell (including the adsorbed and gas phases) and thus the scattering intensity should drop monotonically as the temperature rises. For sample 3K, the expected result is obtained. But for HS;0B, the SANS intensity increases between 80 K and 90 K, the same approximate temperature range over which the measured H_2 isotherms show evidence of a transition to a high density phase (Figure 2).

Theoretical work has explored the many-body quantum problem of H_2 in narrow graphene slit-pores [5]. In these pores, there is a special "staggered" quantum state in which the H_2 hops back and forth between the top and bottom of the pore as it travels along the surface (Figure 4(a)). This state has a pair-correlation function (Figure 4(b)) similar to liquid H_2 [10]. Thus, this quantum state mimics the natural form taken by H_2 at high density to minimize its inter-molecular interactions, but in a single delocalized quantum state that extends over the entire pore rather than in many individual

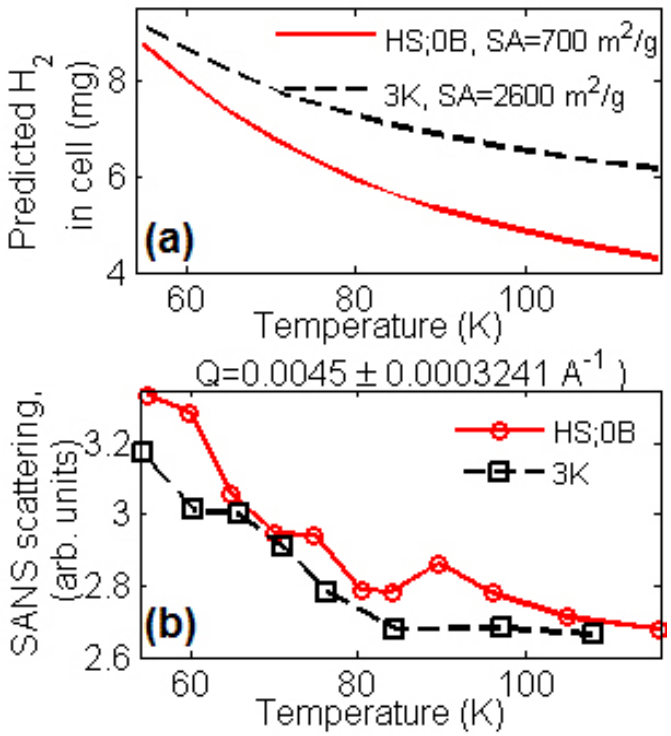

FIGURE 3. SANS measurements of H_2 adsorbed in two porous materials: Saran carbon HS;0B and activated carbon 3K. Temperature was varied as pressure was held constant at 105.1 ± 0.4 bar for HS;0B and 102.7 ± 0.1 bar for 3K. (a) Estimated amount of H_2 in the sample cell, calculated by assuming that because of the high pressure and low temperature, the adsorption surfaces hold a full monolayer of H_2 at all temperatures studied while the gas density drops as the temperature rises. (b) SANS intensity at a neutron momentum transfer Q=0.0045 $Å^{-1}$ for H_2 adsorbed in each sample. Error bars are the size of the symbols. A small value of Q, corresponding to a large wavelength, was used to reduce the effect of Å-scale variations in the H_2 density inside the pores.

quantum states localized at different positions. Due to the hopping motion, the staggered state has non-zero kinetic energy (Figure 4(c)). But as coverage increases, the ability of this state to minimize the interaction energy makes it much lower in energy than any other state (Figure 4(d)). Preliminary calculations show this energy difference is large enough to form a Bose-Einstein condensate (BEC) at temperatures up to 60 K in narrow pores with widths from 7.3-8.9 Å. A BEC is a unique quantum form of matter in which many particles occupy the same quantum state, and has never been observed above 2.2 K. Thus this work [5] predicts a highly novel quantum effect in pores consistent with the measured properties of the samples of interest. However, conventional quantum methods are not able to accurately describe this system at the very high densities of interest and thus still cannot explain the high performance of the samples.

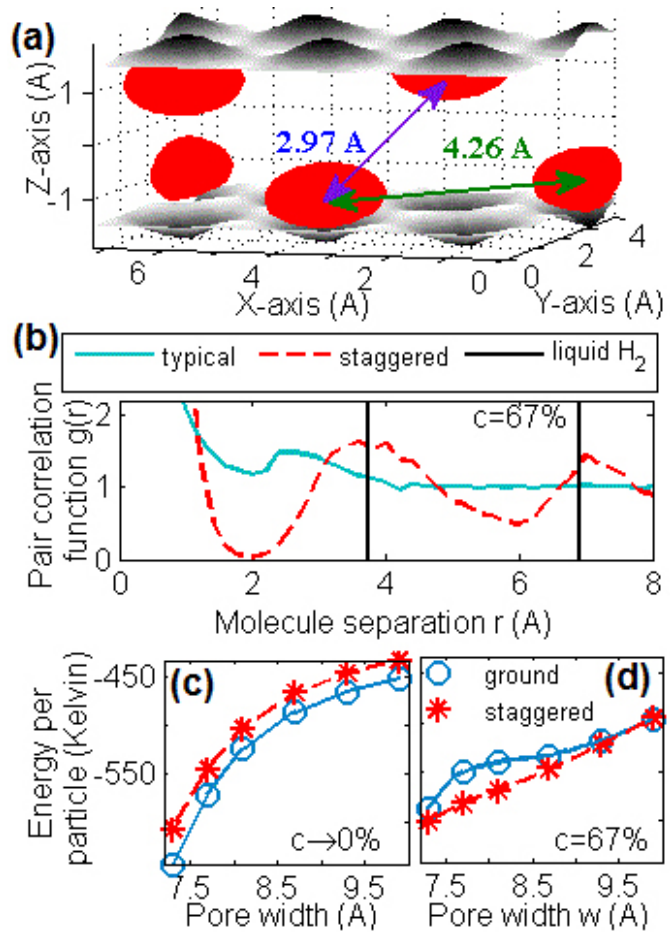

FIGURE 4. (a) Depiction of a "staggered" quantum state for H_2 adsorbed in a potential formed by two parallel layers of graphene, with 7.7 Å separation. The corrugated V=0 potential energy surfaces which enclose the adsorption volume are shown in gray. The red ovals within the pore show the regions of most concentrated probability density, where the H_2 is most likely to be found. Nearest neighbor distances between peaks in the probability density are also shown. (b) Pair correlation function for the staggered quantum state compared to a typical quantum state in the same pore. The pair correlation function gives the likelihood to find an H_2 a distance *r* away from another H_2, and is normalized to be equal to 1 for an ideal gas. The location of peaks in the pair correlation function for liquid H_2 are also marked [10]. (c) Energy of the staggered quantum state compared to the ground state (with zero kinetic energy) as a function of pore width for a coverage of c=0% and (d) c=67% of a full monolayer of adsorbed H_2.

CONCLUSIONS AND FUTURE DIRECTIONS

Because this project is nearly complete, there is not enough time to prove that H_2 storage targets can be met by utilizing the proposed quantum effect and understand its properties well enough to design new materials. Nevertheless, the necessary tasks to meet these goals are as follows,

- Typical BECs can be observed using deep-inelastic neutron scattering [11]. Preliminary deep-inelastic neutron scattering with the sample of interest is

consistent with the proposed BEC [4]. Specific heat measurements can also be done to prove the presence of a quantum effect.

- Probe the new physics of the system. In this novel BEC, particles condense into a state with non-zero kinetic energy, thus diffusion measurements of adsorbed H_2 [12] in the samples of interest using quasi-elastic neutron scattering may reveal how condensed particles move. Neutron diffraction measurements can also probe the positions of condensed particles relative to one another in the high density phase.
- Theoretically examine the link between the proposed BEC condensation and the observed high H_2 density. Classically, if we imagine the H_2 particles as hard spheres with a diameter of ~3.5 Å, there is an upper limit on their maximum density which is near the density of liquid H_2, and conventional quantum mechanics does not explain how this density can be exceeded. But the samples of interest do appear to exceed this upper limit. One may postulate that if the particles in this new BEC move relative to one another, and if they interact on a discrete time scale, then the system may achieve seemingly impossible high densities when any given pair of particles have a relative motion such that they only interact when they are farther apart than 3.5 Å, even though they may be closer together at other times. It is clearly possible for particles in this new BEC to move relative to one another, since they condense into a state with non-zero kinetic energy. Recent experimental work [13] has shown that electrons interact with their environment on a discrete time scale; this theory must now be extended to other particles, such as H_2 and particles in a BEC, and applied to the current system.

FY 2013 PUBLICATIONS

1. R.J. Olsen, M. Beckner, P. Pfeifer, M.B. Stone, C. Wexler, and H. Taub, "Quantum excitation spectrum of adsorbed hydrogen observed by inelastic neutron scattering," *Carbon*, **58** 46-58 (2013).

2. C. Contescu, H. Zhang, R.J. Olsen, E. Mamontov, J.R. Morris & N. Gallego, "Isotope effect on adsorbed quantum phases: diffusion of H_2 and D_2 in nanoporous carbon," *Physical Review Letters*, **110**, 236102 (2013).

3. J.R. Morris, C.I. Contescu, M.F. Chisholm, V.R. Cooper, J. Guo, L. He, Y. Ihm, E. Mamontov, Y.B. Melnichenko, R.J. Olsen, S.J. Pennycook, M. B. Stone, H. Zhang & N. C. Gallego, "Modern approaches to studying gas adsorption in nanoporous carbons," *Journal of Materials Chemistry A*, DOI 10.1039/C3TA10701A (2013).

4. R.J. Olsen, "High temperature Bose condensation into an excited state at equilibrium," *Physical Review Letters*, under review.

5. R.J. Olsen, M.B. Stone, "Coupling of rotational and vibrational motion to translational motion for H_2 adsorbed on corrugated graphite surfaces" *Physical Review B*, under review.

FY 2013 PRESENTATIONS

1. R.J. Olsen, "A high temperature Bose condensate of hydrogen molecules adsorbed in a narrow graphene pore" Carbon 2013 Conference, Rio de Janerio Brazil, July 2013.

2. R.J. Olsen, "The quantum effects of pore structure on hydrogen adsorption," 2013 Annual Merit Review, Washington, D.C., May 2013.

3. R.J. Olsen, DOE EERE Postdoctoral Research Awards Annual Meeting, "The quantum effects of pore structure on hydrogen adsorption," Golden, CO, April 2013.

4. R.J. Olsen, "Quantum mechanics of hydrogen adsorption studied by neutron scattering", University of Tennessee, Materials Science and Engineering, Knoxville TN, Nov. 2012.

REFERENCES

1. P. Pfeifer et al., 2010 DOE EERE Annual Merit Review Presentation, "multiply surface-functionalized nanoporous carbon for vehicular hydrogen storage," (http://www.hydrogen.energy.gov/pdfs/review10/st019_pfeifer_2010_o_web.pdf).

2. R.J. Olsen, *Investigations of Novel Hydrogen Adsorption Phenomena* (PhD thesis), University of Missouri Columbia (2011).

3. P. Pfeifer et al., 2012 DOE BES Annual Progress Report, "New pathways and metrics for enhanced, reversible hydrogen storage in boron-doped carbon nanospaces," (http://www.hydrogen.energy.gov/pdfs/progress12/iv_h_7_pfeifer_2012.pdf).

4. R.J. Olsen, 2013 DOE EERE Annual Merit Review Presentation, "The quantum effects of pore structure on hydrogen adsorption," (http://www.hydrogen.energy.gov/pdfs/review13/st107_olsen_2013_o.pdf).

5. R.J. Olsen, "High temperature Bose condensation into an excited state at equilibrium," *Physical Review Letters*, under review.

6. R.J. Olsen & M.B. Stone, "Coupling of rotational and vibrational motion to translational motion for H_2 adsorbed on corrugated graphite surfaces" *Physical Review B*, under review.

7. R.J. Olsen et al., "Quantum excitation spectrum of adsorbed hydrogen observed by inelastic neutron scattering," *Carbon*, **58**, 46-58 (2013).

8. P. Parilla et al., 2012 DOE EERE Annual Merit Review Presentation, "Hydrogen sorbent measurement qualification and characterization," (http://www.hydrogen.energy.gov/pdfs/review12/st014_parilla_2012_o.pdf).

9. N. Gallego et al., "Hydrogen confinement in carbon nanopores: extreme densification at ambient temperature," *Journal of the American Chemical Society* **133**, 13794 (2011).

10. M. Celli et al., "Microscopic structure factor of liquid hydrogen by neutron-diffraction measurements," *Physical Review B* **71**, 014205 (2005).

11. S.O. Diallo et al., "Bose-Einstein Condensate in solid helium," *Physical Review Letters* **98**, 205301 (2007).

12. C. Contescu et al., "Isotope effect on adsorbed quantum phases: diffusion of H_2 and D_2 in nanoporous carbon," *Physical Review Letters*, **110**, 236102 (2013).

13. P. Catillon et al., "A search for the de Broglie particle internal clock by means of electron channeling," *Foundations of Physics* **38**, 659 (2008).

IV.C.5 Metallation of Metal–Organic Frameworks: En Route to Ambient Temperature Storage of Molecular Hydrogen

Joseph E. Mondloch (Primary Contact),
Joseph T. Hupp, Omar K. Farha
Northwestern University
2145 Sheridan Road
Evanston, IL 60208
Phone: (847) 467-4932
Email: mojo0001@gmail.com

DOE Managers
Channing Ahn
Phone: (202) 586-9490
Email: Channing.Ahn@ee.doe.gov
Ned Stetson
Phone: (202) 586-9995
Email: Ned.Stetson@ee.doe.gov

Technical Advisor
Joseph T. Hupp
Phone: (847) 491-3504
Email: j-hupp@northwestern.edu

Contract Number: AC05-06OR23100.

Project Start Date: November 1, 2011
Project End Date: November 1, 2013

Overall Objectives

- Synthesis of robust –OH or $–NH_2$ functionalized sorbents
- Develop synthetic strategies to incorporate metal cations and clusters into functionalized sorbents
- Materials characterization and performance for room temperature physisorption-based storage (isosteric heat of adsorption [Q_{st}] between 15 and 25 kJ/mol)

Fiscal Year (FY) 2013 Objectives

- Synthesis of –OH functionalized sorbent platform for routine metallation
- Solution and vapor-phase metallation of –OH functionalized sorbents
- Materials characterization and performance analysis

Technical Barriers

This project addresses the following technical barriers from the Hydrogen Storage section of the Fuel Cell Technologies Office Multi-Year Research, Development and Demonstration Plan:

(A) System Weight and Volume

(E) Charging/Discharging Rates

(O) Lack of Understanding of Hydrogen Physisorption and Chemisorption

Technical Targets

This project consists of developing high-area sorbents capable of being modified with divalent metal cations. These materials aim to meet the DOEs 2017 hydrogen storage targets:

- System Gravimetric Capacity:
  - 1.8 kWh/kg (0.055 kg H_2/kg system)
- System Volumetric Capacity:
  - 1.3 kWh/L (0.040 kg H_2/L system)

FY 2013 Accomplishments

- Synthesis of a robust and functionalized high-area sorbent platform for metallation
- Solution and vapor-phase (atomic layer deposition, ALD) metallation of functionalized high-area sorbents
- Materials performance analysis (quantify Q_{st})

✧ ✧ ✧ ✧ ✧

INTRODUCTION

Physisorption-based sorbents such as metal-organic frameworks (MOFs) are attractive candidates for the storage of molecular hydrogen (H_2). MOFs are built up from well-defined molecular components and key functional material properties, such as pore size and functionality, can be readily controlled. On a materials basis, some of these sorbents meet the DOE's technical targets for both gravimetric and volumetric capacity, albeit at cryogenic temperatures. A crucial challenge for physisorption-based sorbents has therefore been storage of H_2 at or near room temperature. Storing H_2 at or near room temperature will require sorbents that can bind H_2 more effectively.

APPROACH

Our approach relies on introducing coordinatively unsaturated metal cation sites into (–OH or $–NH_2$)

functionalized high-area physisorption-based MOFs. Recent computational evidence has suggested that divalent metal cations are capable of achieving the binding energies (Q_{st} ~15-25 kJ/mol) necessary to store H_2 at room temperature [1]. Most often coordinatively unsaturated metal sites are introduced from the condensed phase (i.e., from solution). While we are pursuing solution-based metallation as well, our focus has shifted towards utilizing a vapor-phase metallation technique—ALD.

ALD is capable of depositing mono-, di-, tri- and tetra-valent metal cations, as well as small metal-oxo(hydroxy) clusters, into ultra-high aspect ratio structures such as MOFs [2]. The unique feature of ALD is that it relies on self-limiting chemical surface reactions, allowing precise, atomic level control over both the location and number of metal (and –oxo(hydroxy)) species deposited. This in turn will allow precise tuning of the H_2 binding energies within metallated MOF sorbents. Furthermore, because deposition occurs in the vapor-phase, we avoid purification and activation steps and circumvent problems associated with (H_2 sorption) site blocking solvent molecules [3].

RESULTS

We employed a new synthetic strategy capable of metallating MOFs from the vapor-phase: ALD. The key to enabling metallation by ALD in MOFs (AIM) was the synthesis of a new MOF, NU-1000 (Figure 1). NU-1000 is a Zr-based MOF that is thermally and hydrothermally stable (~500ºC) and contains large one-dimensional mesopores and apertures (required for diffusion of vapor-phase precursors). The structure is built up from $Zr_6(\mu_3\text{–OH})_8(\text{–OH})_8$ nodes and TBApy linkers. Four of the eight terminal –OH groups point into large 3.1 Å mesoporous channels, while the remainng terminal –OH groups lie in between sheets of the Zr_6 nodes. NU-1000 has a Brunauer-Emmett-Teller surface area of 2,300 $m^2\ g^{-1}$ and a total pore volume of 1.4 $cm^3\ g^{-1}$. In short, NU-1000 is an ideal platform for readily metallating a MOF via ALD and solution-based techniques.

NU-1000 was placed in an ALD reactor and exposed to $Al(Me)_3$ and $Zn(Et)_2$. Metallation was confirmed by inductively coupled plasma optical emission spectroscopy; on average eight Al and four Zn atoms per $Zr_6(\mu_3\text{–OH})_8(\text{–OH})_8$ node were incorporated into NU-1000. The resultant materials have been termed Zn-AIM and Al-AIM. Very similar metal loadings can also be obtained by depositing $Al(Me)_3$ and $Zn(Et)_2$ from solution. Powder X-ray diffraction (PXRD) (Figure 2a), N_2 adsorption isotherms (Figure 2b), diffuse reflectance infrared Fourier transform spectroscopy

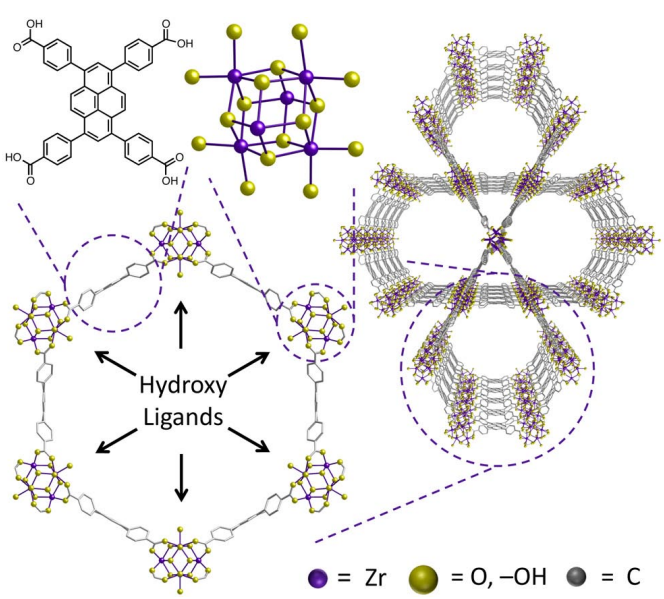

FIGURE 1. Relevant structural features and representation of NU-1000. For simplicity hydrogen atoms are not shown.

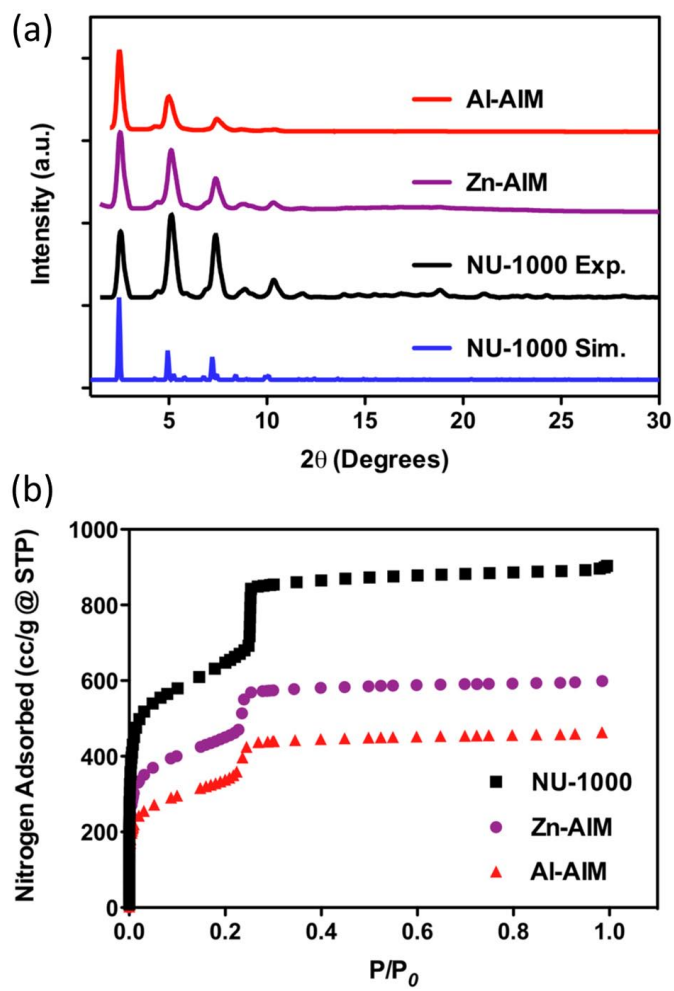

STP - standard temperature and pressure

FIGURE 2. (a) PXRD patterns of NU-1000 simulated (Sim.) from the crystallographically solved structure, NU-1000 experimental (Exp.), Zn-AIM, and Al-AIM. (b) Pore size distributions and N_2 adsorption isotherms for NU-1000, Zn-AIM and Al-AIM.

and scanning electron microscopy-energy dispersive X-ray characterization confirmed that metallation occurs at the $Zr_6(\mu_3–OH)_8(–OH)_8$ node and that the NU-1000 framework is robust to the ALD treatment. These are extremely high metal loadings in the context of typical metal loadings within MOFs and in principle should lead to higher H_2 storage capacities at or close to room temperature.

Next we moved to utilizing ALD to deposit Cu cations within NU-1000, on average we observe eight Cu atoms per $Zr_6(\mu_3–OH)_8(–OH)_8$ node. PXRD, N_2 adsorption isotherms and diffuse reflectance infrared Fourier transform spectroscopy again confirmed the integrity of the material. The surface area normalized H_2 uptake is shown in Figure 3a, the Cu-AIM sample uptakes more H_2 at 77 K, per unit surface area, than the parent MOF NU-1000. Temperature-dependent H_2 isotherms were collected (Figure 3b) and Q_{st} were extracted utilizing either single- or dual-site Langmuir adsorption isotherm models followed by Clausius-Clapeyron analysis. The Cu-AIM sample shows a 60% increase in Q_{st} over the parent MOF (Figure 3c), albeit at only ~7 kJ/mol. The results demonstrate the ability of ALD to incorporate metal sites capable of more strongly binding molecular H_2 and without having to remove solvent or other ligated molecules.

CONCLUSIONS AND FUTURE DIRECTIONS

Conclusions

- A robust –OH functionalized Zr_6-based sorbent, NU-1000, has been synthesized and characterized
- NU-1000 has been metallated via ALD and solution
- A 60% increase in Q_{st} is observed

Future Directions

- Optimize ALD metallations
- Explore additional ALD chemistry, including metal-oxide/hydroxide clusters
- Materials characterization and performance

SPECIAL RECOGNITIONS & AWARDS/ PATENTS ISSUED

1. Mondloch, J.E.; Bury, W.; Farha, O.K.; Hupp, J.T. "*Gas-Phase Deposition by Atomic Layer Deposition in Metal–Organic Frameworks*" Invention disclosure, submitted.

FY 2013 PUBLICATIONS/PRESENTATIONS

1. Mondloch, J.E.; Bury, W.; Fairen-Jimenez, D.; Kwon, S.; DeMarco, E.J.; Weston, M.H.; Sarjeant, A.A.; Nguyen, S.T.; Stair, P.C.; Snurr, R.Q.; Farha, O.K.; Hupp, J.T. "*Vapor-Phase Metalation by Atomic Layer Deposition in a Metal–Organic Framework*" *J. Am. Chem. Soc.* **2013,** *135,* 10294.

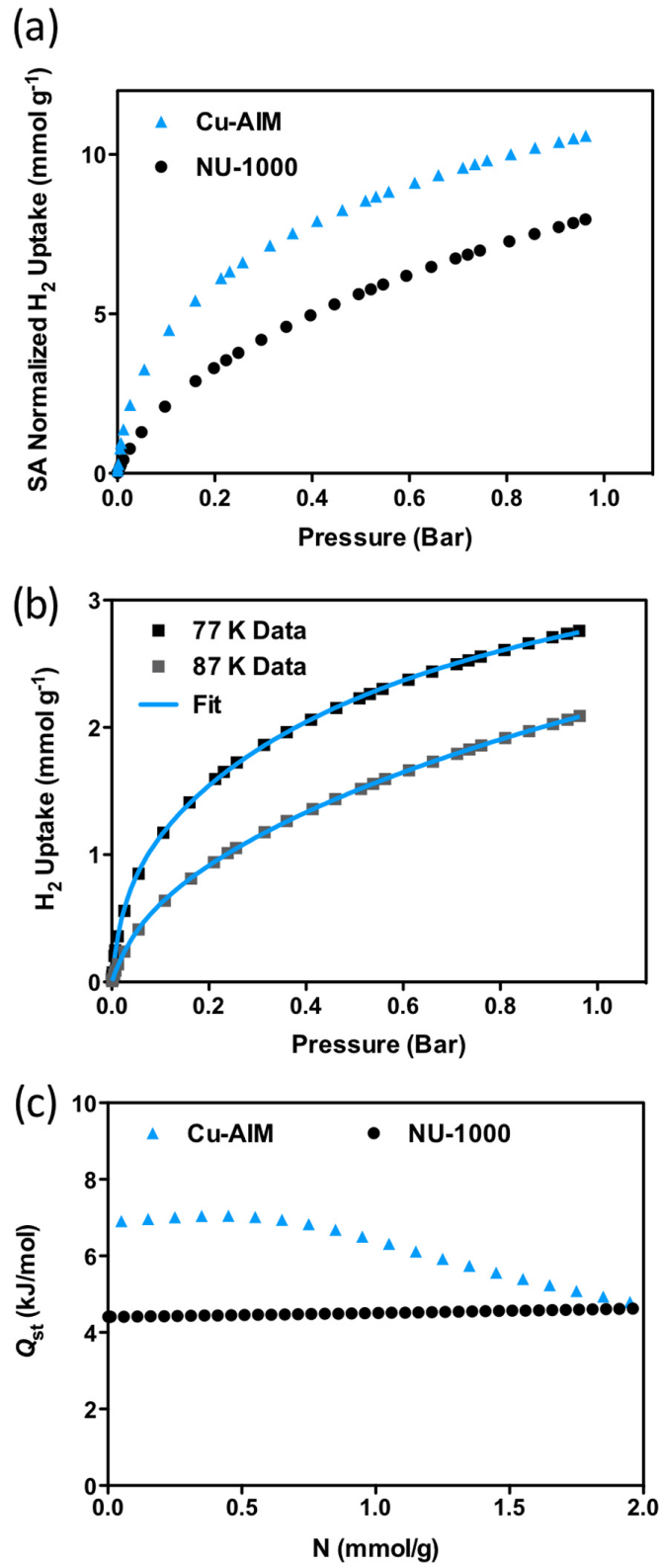

FIGURE 3. (a) Surface area normalized H_2 adsorption of NU-1000 and Cu-AIM. (b) Temperature-dependent H_2 sorption for Cu-AIM and fits to a dual-site Langmuir model. (c) Q_{st} for NU-1000 and Cu-AIM.

2. Mondloch, J.E.; Farha, Bury, W.; Farha, O.K.; Hupp, J.T. "*Metal- and Cluster-Modified Sorbents for the Ambient Temperature Storage of Molecular Hydrogen*" Presented at Annual DOE EERE Postdoctoral Research Award Meeting, Golden, CO, 2013.

3. Mondloch, J.E.; Bury, W.; Farha, O.K.; Hupp, J.T. "*Metallation by Atomic Layer Deposition In A Metal–Organic Framework (AIM)*" ALD-AVS 2013, San Diego, CA, 2013.

REFERENCES

1. Getman, R.; Miller, J.; Wang, K.; Snurr, R. "Metal Alkoxide Functionalization in Metal-Organic Frameworks for Enhanced Ambient-Temperature H_2 Storage" *J. Phys. Chem. C* **2011,** *115,* 2066.

2. Mondloch, J.E.; Bury, W.; Fairen-Jimenez, D.; Kwon, S.; DeMarco, E.J.; Weston, M.H.; Sarjeant, A.A.; Nguyen, S.T.; Stair, P.C.; Snurr, R.Q.; Farha, O.K.; Hupp, J.T. *J. Am. Chem. Soc.* **2013,** *135,* 10294.

3. Sumida, K; Stück, D.; Mino, L.; Chai, J.-D.; Bloch, E.D.; Zavorotynska, O.; Murray, L,J.; Dincă, M.; Chavan, S.; Bordiga, S.; Head-Gordon, M.; Long, J.R. *J. Am. Chem. Soc.* **2012,** *135,* 1083.

IV.C.6 Weak Chemisorption Validation

Thomas Gennett (Primary Contact),
Jeffrey Blackburn, Katherine Hurst, Philip Parilla,
Chaiwat Engtrakul, Steve Christensen, Yufeng Zhao
National Renewable Energy Laboratory (NREL)
1617 Cole Blvd.
Golden, CO 80401-3393
Phone: (303) 384-6628
Email: thomas.gennett@nrel.gov

DOE Managers
Jesse Adams
Phone: (720) 356-1421
Email: Jesse.Adams@go.doe.gov
Channing Ahn
Phone: (202) 586-9490
Email: Channing.Ahn@ee.doe.gov

Subcontractor:
Craig M. Jensen, University of Hawaii, Honolulu, HI

Project Start Date: October 1, 2011
Project End Date: Project continuation and direction determined annually by DOE

Overall Objectives

Evaluate the weak chemisorption/spillover process as a means to achieve DOE 2017 hydrogen storage goals.

Fiscal Year (FY) 2013 Objectives

- Evaluate universal reproducibility of enhanced adsorption weak chemisorption/spillover effects.
- Determine type of interaction of the support with the spilt-over hydrogen via diffuse reflectance infrared Fourier transform spectroscopy (DRIFTS) and nuclear magnetic resonance (NMR).
- Determine the theoretical, idealized upper limit of gravimetric sorption capacity from hydrogen spillover onto a carbon substrate.
- Communicate validated results to the community at large.

Technical Barriers

This project addresses the following technical barriers from the Hydrogen Storage section of the Fuel Cell Technologies Office Multi-Year Research, Development, and Demonstration Plan:

(A) System Weight and Volume

(B) System Cost

(C) Efficiency

(E) Charging/Discharging Rates

(O) Lack of Understanding of Hydrogen Physisorption and Chemisorption

Technical Targets

This project is validating experimentally observed weak chemisorption. Insights gained from this work may be applied toward the future design and synthesis of hydrogen storage materials that meet the following DOE 2017 hydrogen storage targets:

- Specific energy: 1.8 kWh/kg
- Energy density: 1.3 kWh/L

The specific technical objectives include:

- Conduct and correlate high-pressure NMR spectroscopy results with NREL DRIFTS to determine the specific C-H interactions involved in weak chemisorption-based hydrogen storage material.
- Determine the upper limit of percent by weight hydrogen uptake due to spillover in an optimized substrate matrix.
- Incorporate atomic level metal, (possibilities include Fe, Zn, Al, Ti, Ni, Co, etc.) into two distinct covalent-organic framework (COF) structures with pore diameters that may range of 30-100 angstroms via modified atomic layer deposition. The validation of the extent of metal incorporation within the final materials' matrix will be characterized by the appropriate X-ray, neutron scattering, Brunauer-Emmett-Teller, and/or spectroscopic techniques.

FY 2013 Accomplishments

- We completed the initial series of variable temperature ^{1}H-NMR experiments on the templated carbon (TC) and palladium-decorated TC samples. The results are shown in Figure 1:
  - TC shows a single peak, so we are getting rapid exchange at the substrate surface on the timeframe of NMR and it is shifted upfield to approximately 5.6 ppm (Figure 1a).
  - For the Pd-TC carbon samples both the free H2 (7.2 ppm) and carbon substrate (5.6 ppm) hydrogen gas peaks being present indicates H2 is persisting longer in each environment, possible due to a stronger-spillover type interaction (Figure 1b).

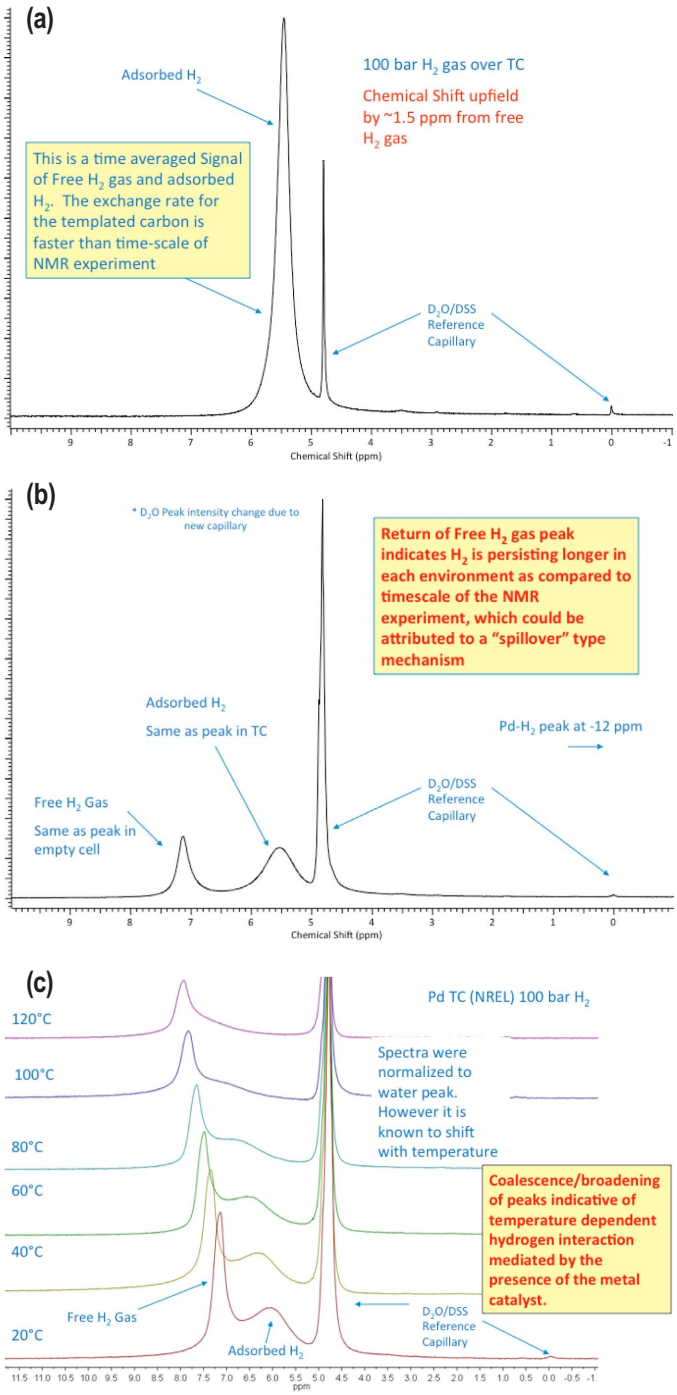

FIGURE 1. ^{1}H NMR data of PdTC material that illustrates the appearance of a new C-H interaction upon exposure of the sample to hydrogen overpressures at room temperature.

  - Coalescence of peaks indicates temperature dependence of the peaks and that the process is indeed a rapid exchange (Figure 1c).
- Demonstrated direct spectroscopic evidence of a reversible room temperature sorption/desorption apparently from a unique C-H interaction via DRIFTS and neutron scattering:
  - DRIFTS measurements up to 100 bar hydrogen overpressure for Pd/TC showed a unique reversible infrared stretch that was tentatively assigned to spilt-over hydrogen (Figure 2).
- Series of X-ray raman experiments completed at Stanford National Accelerator Laboratory.
- Five articles published, three separate peer-review journal articles related to our efforts are in preparation.

✧ ✧ ✧ ✧ ✧

INTRODUCTION

The ultimate goal of the Hydrogen Storage sub-program is the development of hydrogen storage systems that meet or exceed the DOE's goals for the onboard hydrogen storage in hydrogen-powered vehicles. With the tremendous interest in weak chemisorption materials for hydrogen storage, NREL and DOE have dedicated considerable resources working with partner institutions to synthesize specific materials and to develop/perform the requisite measurements in order to establish the capacity, kinetics and overall performance of these materials. The key critical issues that must be resolved for these materials include reproducibility of material synthesis, understanding the kinetics of H transport on receptor surfaces, and which chemical reactions are desired and which are not. In addition, weak chemisorption properties are intricately linked to more standard H_2 storage mechanisms, so information gained on the hydrogen-substrate interactions should help accelerate viable sorbent development.

APPROACH

Our approach included the synthesis and characterization of TC and Pd/TC materials with an unexplained enhancement of hydrogen sorption in the presence of catalysts that has been attributed in the past to hydrogen spillover. These materials were synthesized at NREL and through spectroscopic evaluation of the materials with DRIFTS and NMR we determined peak assignments in order to determine if spilt-over hydrogen spectroscopic modes are in regions expected for room temperature hydrogen desorption.

RESULTS

1. **^{1}H NMR evidence for spilt-over hydrogen on a Pd-TC material.** NREL synthesized multiple batch samples of Pd-TC for both DRIFTS and NMR experiments were performed. The results are shown in Figures 1 a-c.
2. **DRIFTS determination of new hydrogen-substrate interactions for an apparent spillover material.** Using infrared spectroscopy to identify distinct substrate-

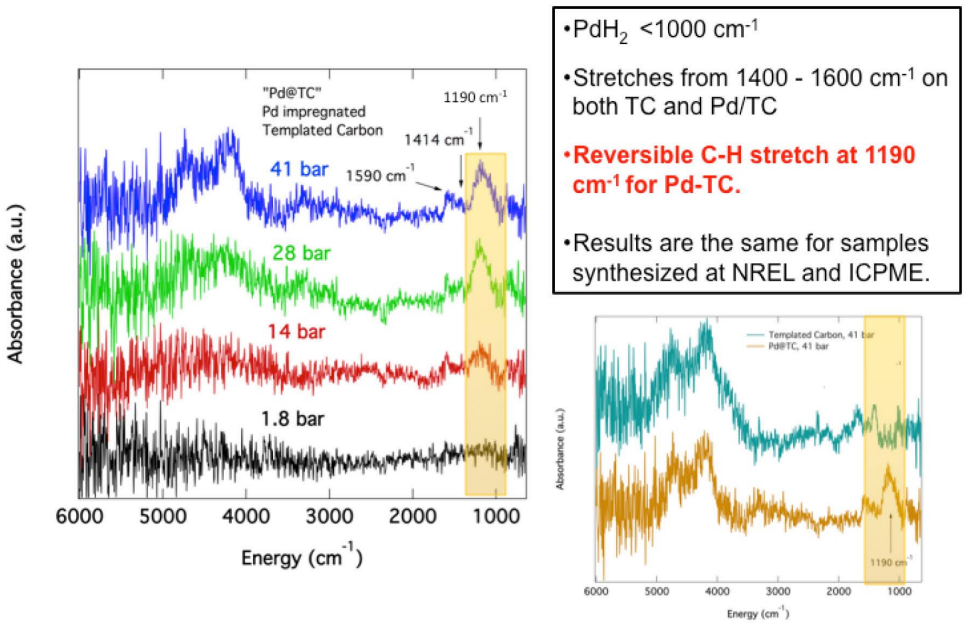

FIGURE 2. DRIFTS spectra for PdTC sample which illustrates the reversibility of the new C-H peaks that appear in the infrared spectrum.

hydrogen interactions is an essential component of our work as we look to establish the energetics associated with the spiltover hydrogen. Figure 2 shows DRIFTS spectra for several samples charged with D_2 and treated at various temperatures.

3. We completed the synchrotron spectroscopic investigation of hydrogen-matrix interactions on the sorbents.
4. Determined the upper limit of hydrogen uptake (weight percent) due to spillover in an optimized substrate matrix.

We performed, thorough density functional theory-based modeling of the whole process of hydrogen spillover in flat graphene sheets (2 nm by 3 nm) catalyzed by Pd particles (0.5 nm by 0.8 nm by 0.8 nm), addressing the issues of nucleation, growth patterns, and mechanism of H migration.

Our theoretical study revealed:

- The only sustainable hydrogen storage in graphitic material is through chemisorbed H pairs with the two H atoms bound to the adjacent C atoms in alternative sides of a graphene sheet.
- Nucleation of stable H chemisorptions starts with formation of compact, hexagonal H patches. The smallest stable patch contains 16 H atoms, with the average binding energy of 12 kJ/mol-H_2. As the patch size increases, the binding energy increases and reaches to the maximum value of 40 kJ/mol at infinite size.
- Cooperative migration of the H pairs is required by the energetics and kinetically water can mediate the cooperative migration by reducing the kinetic barrier to ~1.0 eV. This indicates that moisture is important for improving kinetics of hydrogen spillover.
- Once the catalytic center is fully surrounded by chemisorbed H atoms, the H migration from the catalysts to carbon stops. This determines the maximum distance that H atoms can reach out from a catalytic center. If one assumes hexagonal patches, then ideally, six such patches with a size similar to the catalytic particle roughly fills the 360-degree angular space, which terminates the spillover around that catalytic particle. That gives a maximum area ratio of 6:1 of H covered graphene over that of metal-covered graphene. Based on this ratio and the lattice parameters and the standard atomic weight (12.011 for C, 106.45 for Pd), homogeneous distribution of Pd nanoparticles (3 atomic layer thickness, 2-nm diameter) on graphene, with optimum interdistance of 5-6 nm, the maximum H capacity is derived as 2.75 ± 0.25% wt%.
- Stable topological defects (e.g. Stone-Walse defects) and boron dopants can improve both the kinetics and possibly the hydrogen capacity.

5. NREL will investigate application of "modified" atomic layer deposition techniques to incorporate various metal dopants into framework-type materials and the effect on the isosteric heat of adsorption for hydrogen.
   – COFs are porous materials in which organic building blocks are linked by covalent bonds. These crystalline extended structures exhibit high thermal stability and have pore sizes ranging

from 9-32 Å. A co-condensation reaction between 2,3,6,7,10,11-hexahydroxytriphenylene and 4,4'-biphenyldiboronic acid was utilized to produce COF-10 (32 Å). Reactions were carried out following a previously described method (see J. Am. Chem. Soc. 2007, 129, 12914-12915). In addition, COF-1 (15 Å) was produced using a simplified, one-step condensation reaction of 1,4-diboronic acid. The COFs above were produced in gram quantities allowing for more accurate analysis before and after metallation by atomic layer deposition. Atomic layer deposition experiments will proceed in the fourth quarter of FY 2013.

CONCLUSIONS AND FUTURE DIRECTION

- Reconcile spillover propagation mechanisms:
  - Reconciled mechanism with metal-mediated processes and theoretically established maximum capacity for spilt-over hydrogen on a graphene surface.
  - Observed a reversible C-H interaction on Pd-TC via DRIFTS, NMR and neutron scattering.
- Determine ultimate spillover capacity possible with optimized interactions and substrate chemistry:
  - Theory predicts a "wet" gas composition to enhance diffusion (mediate) across substrate surface away from metal sites.
  - Determined a maximum hydrogen sorption for graphene at 2.75% w/w assuming both sides hydrogenated. For common carbon surfaces the capacity is expected to be much less.
- Stanford National Accelerator Laboratory Work:
  - X-ray raman spectroscopy technique should be able to detect hydrogen strongly bound to the carbon when the sp^2 bonds are converted to sp^3.
  - We did not observe changes in the spectra that would support strong sp^3 C-H bonding orbital which may be the result of:
    - We do not form a true sp^3 for the C-H interaction did not occur for the Pd-TC material.
    - We may be below the detection limits because of the small number of C-H bonds formed are below the detection limits of the technique.
- Report detailing findings and recommendations at: Tech Team update, (September 2013); final analysis and recommendations were presented at the annual DOE Annual Merit Review, May 2013, and within a position paper submitted July 2013.

FY 2013 PUBLICATIONS/PRESENTATIONS

Publications

1. *Hydrogen adsorption properties of platinum decorated hierarchically structured templated carbons*, Hyunchul Oh, Thomas Gennett, Plamen Atanassov, Mert Kurttepeli, Sara Bals, Katherine E. Hurst, Michael Hirscher, Microporous and Mesoporous Materials 177 (2013) 66–74.

2. *A Dynamic Calibration Technique for Temperature Programmed Desorption Spectroscopy,* K.E. Hurst, M.J. Heben, J.L. Blackburn, T. Gennett, A.C. Dillon and P.A. Parilla. Review of Scientific Instruments (2013) 84(2), 025103/1-025103/9.

3. *Spectroscopic Identification of Hydrogen Spillover Species in Ruthenium-modified High Surface Area Carbons by Diffuse Reflectance Infrared Fourier Transform Spectroscopy*, Jeffrey L. Blackburn, Chaiwat Engtrakul, Justin B. Bult, Katherine E. Hurst, Yufeng Zhao, Qiang Xu, Philip A. Parilla, Lin J. Simpson, Craig Brown, Thomas Gennett, J. Phys. Chem. C, 2012, 116 (51), pp 26744–26755.

4. *Reactions and reversible hydrogenation of single-walled carbon nanotube anions,* C. Engtrakul, C.J. Curtis, L.M. Gedvilas, L.J. Simpson, P. A. Parilla, M. J. Heben, T. Gennett, Journal of Materials Research (2012), 27(21), 2806-2811.

5. *Manipulation of Hydrogen Binding Energy and Desorption Kinetics by Boron Doping of High Surface Area Carbon*, Justin B. Bult, Justin Lee, Kevin O'Neill, Chaiwat Engtrakul, Katherine E. Hurst, Yufeng Zhao, Lin Simpson, Phillip Parilla, Thomas Gennett, Jeffrey L. Blackburn, J. Phys. Chem. C, 2012, 116 (50), pp 26138–26143.

6. *Synthesis of Novel Lithiated BC_6 Materials with Enhanced H_2 Binding Sites,* C. Engtrakul, J.L. Blackburn, J.B. Bult, K.J. O'Neill, P.A. Parilla, T. Gennett, L.J. Simpson, in preparation.

7. *Multi-Institutional Comparison of Volumetric H_2 Adsorption Measurements on Carbon Sorbents*, K.E. Hurst, K.J. O'Neill, J.L. Blackburn, T. Gennett, and P.A. Parilla, in preparation.

Presentations

1. NREL Hydrogen Storage Efforts-Task 32, Thomas Gennett (et.al) IEA-HIA Task 32 Kickoff meeting, Heraklion, Crete, Greece 21-25 April 2013.

2. Invited Talk; Weak hydrogen chemisorption validation, Thomas Gennett, DOE Fuel Cell Technologies Program Annual Merit Review, May, 2013, Washington, D.C.

IV.C.7 Hydrogen Trapping through Designer Hydrogen Spillover Molecules with Reversible Temperature and Pressure-Induced Switching

Angela D. Lueking (Primary Contact), Jing Li, Sarmishtha Sircar, Cheng-Yu Wang, Yonggang Zhao, Haohan Wu, Qihan Gong, Zhijuan Zhang
The Pennsylvania State University
120 Hosler
University Park, PA 16802
Phone: (814) 863-6256
Email: adl11@psu.edu

DOE Managers
Jesse Adams
Phone: (720) 356-1421
Email: Jesse.Adams@go.doe.gov
Channing Ahn
Phone: (202) 586-9490
Email: Channing.Ahn@ee.doe.gov

Contract Number: DE-FG36-08GO18139

Subcontractor:
Rutgers University, Piscataway, NJ

Project Start Date: January 1, 2009
Project End Date: June 30, 2014

Overall Objectives

- Synthesize designer microporous metal-organic frameworks (MMOFs) mixed with catalysts to enable H-spillover for H_2 storage at 300 K-400 K and moderate pressures
- Reproducibly introduce catalysts into MMOF without degrading MMOF structure
- Explore MMOF structural changes induced by pressure and hydrogen spillover
- Ensure spillover reproducibility with spectroscopic characterization and validation of measurement techniques

Fiscal Year (FY) 2013 Objectives

- Optimize synthesis procedure and hydrogen uptake of one catalyst-doped MMOF, using CuTDPAT (or $[Cu_3(TDPAT)(H_2O)_3]\bullet 10H_2O\bullet 5DMA$, H_6TDPAT = 2,4,6-tris(3,5-dicarboxylphenylamino)-1,3,5-triazine)
- After doping, compare uptake of CuTDPAT to CuBTC with similar paddle wheel structure and IRMOF8, which has the highest reported uptake for a catalytically-doped MMOF
- Determine and compare stability after various catalytic doping techniques and gas exposures
- Calculate theoretical capacity for hydrogenation of CuTDPAT using density functional theory
- Identify kinetic barriers to reach thermodynamic predicted capacity of doped CuTDPAT
- Spectroscopic verification of hydrogenation of CuTDPAT, before and after pre-bridging technique

Technical Barriers

This project addresses the following technical barriers from the Hydrogen Storage section of the Fuel Cell Technologies Office Multi-Year Research, Development, and Demonstration Plan:

(A) System Weight and Volume

(D) Durability/Operability: Min/max temperature/maximum pressure

(E) Charging/Discharging Rates

(O) Lack of Understanding of Hydrogen Physisorption and Chemisorption

(P) Reproducibility of Performance

Technical Targets

Technical targets for this project are listed in Table 1.

FY 2013 Accomplishments

- CuTDPAT MMOF (Figure 1) was selected for detailed studies due to favorable pore structure; high surface area; stability with time, temperature, and moisture exposure; and surface chemistry that facilitates multiple catalytic doping methods.
- Preliminary density-functional calculations suggest reversible hydrogenation of CuTDPAT is possible up to 3.25 wt%, with a binding energy that is favorable for reversible room temperature hydrogenation (ΔE_{avg}= -0.55 eV; target is -0.6 < dE < -0.2 eV, as calculated by Yakobson et al. [1]).
- In addition to CuTDPAT, Cu-BTC and IRMOF8 were selected for comparison. The former has a similar Cu paddlewheel structure, whereas IRMOF8 has the highest reported uptake via spillover, to date.

TABLE 1. System Gravimetric Capacity 2017/Ultimate Target (5.5/7.5 wt%) of Metal-Doped "Spillover" Materials

Sample	Hydrogen in excess of He at 298 K (wt%)	
	1 bar	70 bar [or 20 bar]
Activated carbon (AC) used for catalyst support	0.0185	0.646
Catalyst used in pre-bridging technique: Pt/AC	0.0362	0.791
Pt/AC (prior FY 2012 results; six + samples tested)	0.01-0.03	0.79-0.91
a: IRMOF8 (as-received)	0.0118	0.357 0.337
b: PB-IRMOF8 (pre-bridge doping with Pt/AC catalyst)	0.0247	0.317
c: CuTDPAT (as-received)	0.00568	0.351
d: PB-CuTDPAT (pre-bridge doping with Pt/AC catalyst); three batches, multiple replicates	0.0441	0.30-0.56 (24 hours) ~1.0 (80 hours) kinetic limitations observed
e: CuBTC (as-received)	0.0179	[0.17, at 20 bar]
f: PB-CuBTC (pre-bridge doping with Pt/AC catalyst)	0.0186	[0.61, at 20 bar]

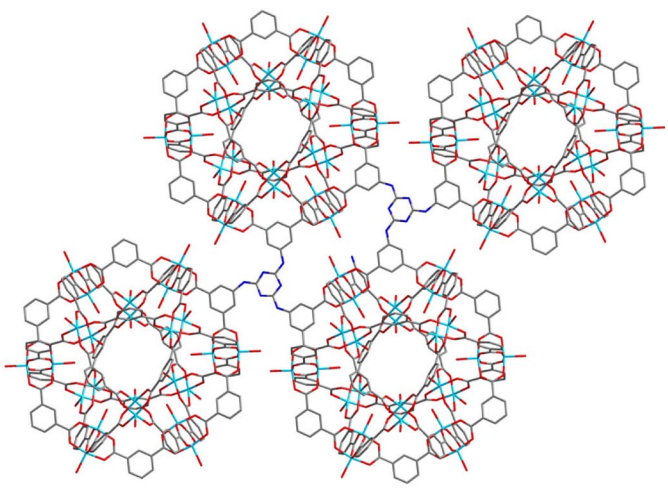

FIGURE 1. CuTDPAT structure, in which copper paddlewheel metal cluster is connected via the TDPAT organic ligand to form the long-range crystalline order. TDPAT contains N in the center rings as well as three branches stretching from the center ring, similar to melamine. (Gray: C, Blue: N, Red: O, Cyan: Cu)

- Extending the FY 2012 doping studies, the pre-bridge catalytic doping technique retains surface area (97-107%) and structure (X-ray diffraction [XRD] remains intact) for CuTDPAT, CuBTC, and IRMOF8, comparing 'as received MMOFs' to samples after this doping technique. In contrast, direct-doping reduced the surface area to 30-49% relative to the precursor.

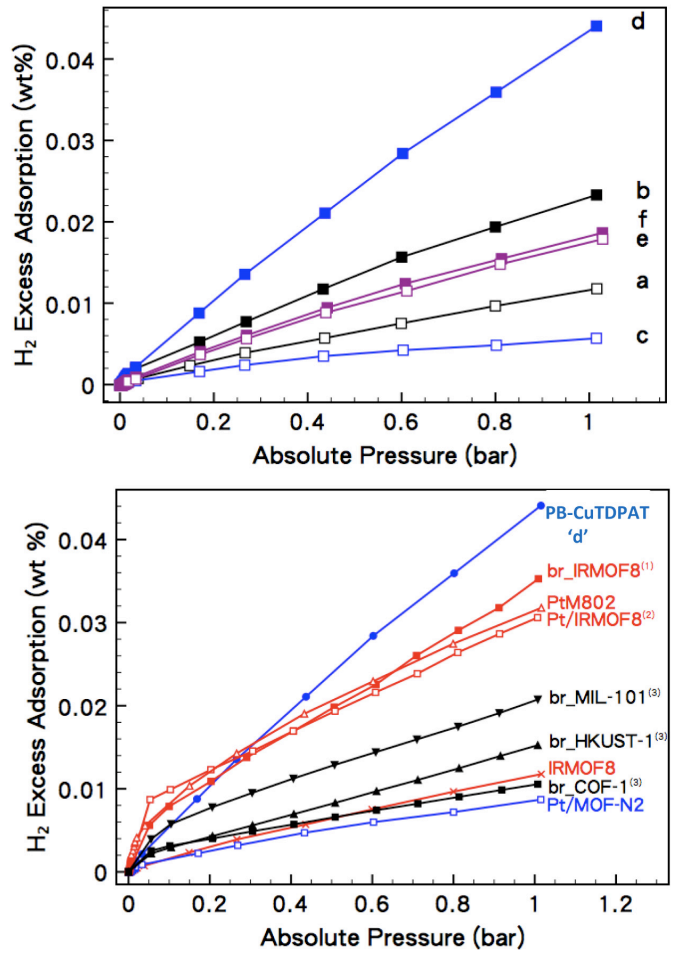

FIGURE 2. Top: low-pressure H_2 isotherms at 298 K for the three MMOF samples doped via the pre-bridge doping technique to introduce ~10% Pt/AC catalyst. Labels correspond to samples in Table 1. Bottom: comparison of data for 'd' (PB-CuTDPAT) relative to other published literature for catalyst-doped MMOFs. Data taken from: (1) *J. Am. Chem. Soc.* 2006, 128, 8136-8137; (2) *J. Phys. Chem. C.* 2011, 115, 4793-4799; (3) *AIChE Journal.* 2008, 54, 269-279.

- Good reproducibility of hydrogen uptake was demonstrated for four batches of PB-CuTDPAT sample on three different measurement techniques (gravimetric, low-pressure, and high-pressure volumetric).
- PB-CuTDPAT has 7.8-fold enhancement relative to CuTDPAT, which is the highest of the three selected MMOFs and highest of published low-pressure H_2 uptake data for catalytically-doped MMOFs (Figure 2).
- Kinetic limitations were identified as the main hurdle to achieve theoretically predicted hydrogen uptake at high pressure for PB-CuTDPAT. (Experimentally, the 70 bar H_2 uptake was not complete after 24+ hours, Figure 3.) Preliminary (as well as on-going) stability studies of the 'as-received' CuTDPAT with high-pressure H_2 exposure show loss of surface area despite retention of the XRD pattern.

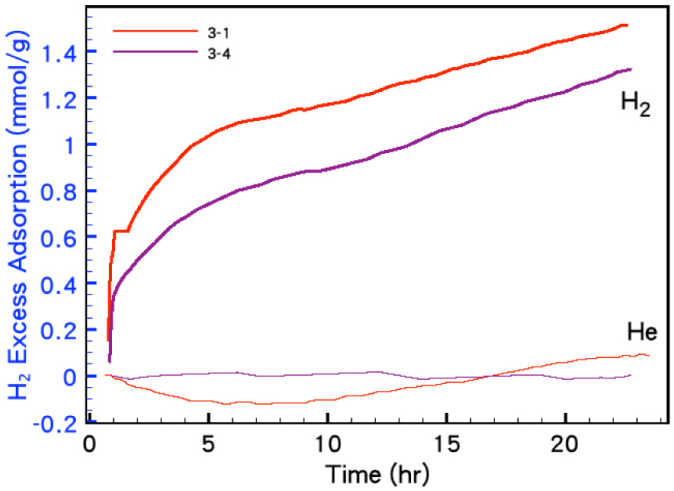

FIGURE 3. Select high-pressure (70 bar, 298 K) hydrogen uptake for PB-CuTDPAT for two replicates. Kinetic limitations are observed at high pressure that were not evident for the 1-bar data shown in Figure 1.

- Spectroscopic evidence for hydrogenation of the nitrogen sites was identified for PB-CuTDPAT (and not found for as-received CuTDPAT) via X-ray photoelectron spectroscopy (XPS) (Figure 4). Combined with density-functional calculations, N-hydrogenation should help to further elucidate the mechanism of hydrogen spillover.
- A paper was published on the accuracy of improved differential volumetric methods.

✧ ✧ ✧ ✧ ✧

INTRODUCTION

The term *hydrogen spillover* has been used to describe a synergistic effect between high-surface area adsorbents and associated catalysts. The associated catalyst dissociates molecular H_2 into atomic H species, which may then diffuse to and chemisorb to the support. This process occurs at moderate temperature (i.e., 300 K) and generally leads to a much higher uptake than expected for the metal catalyst or high-surface area adsorbent alone under comparable conditions. Spillover materials using MMOFs have been reported to have high uptake at ambient temperature: bridged ('br') PtC/IRMOF8 achieved 4 wt% excess adsorption at 100 bar and 298 K [2]. Independent groups have demonstrated up to 4.2 wt% at 6.9 MPa after extended equilibration for brPtC/IRMOF8 [3]. Subsequent reports on spillover materials at room temperature have varied from less than physisorption to almost 9 wt%, demonstrating difficulties in reproducibility and invoking controversy. These uptakes approach DOE goals; however, as the process is highly dependent upon synthesis, measurement, and catalytic particle size [4,5], the process remains poorly understood. It is anticipated that optimization of

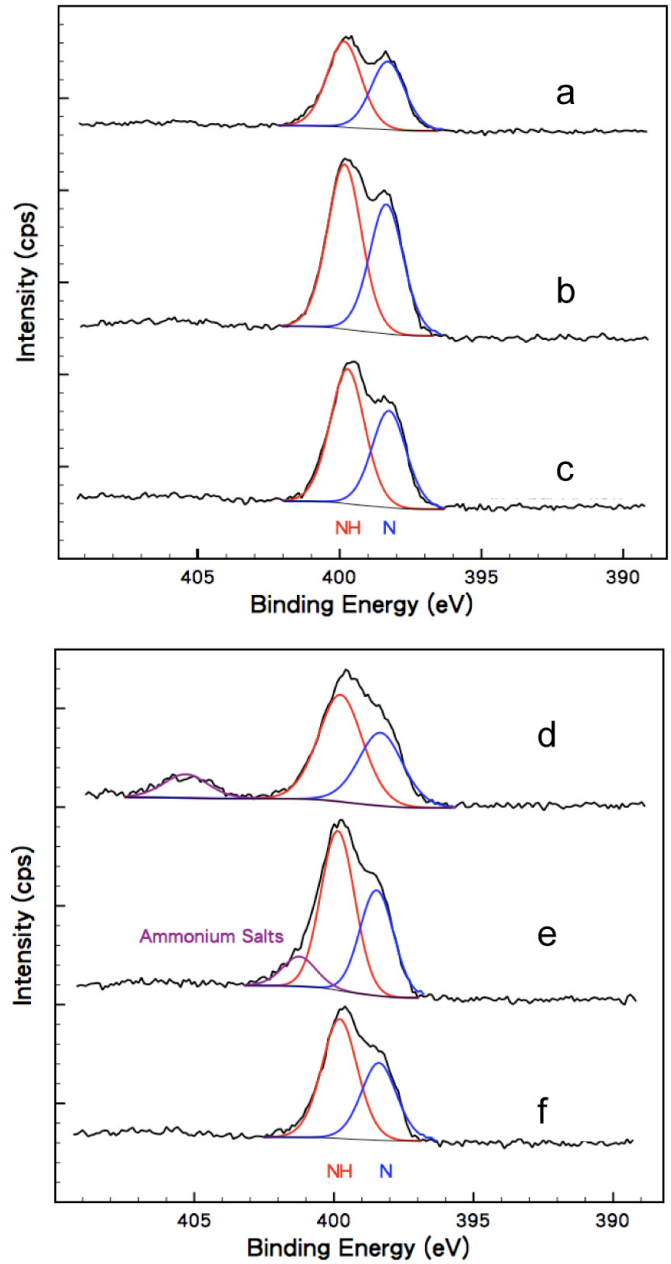

FIGURE 4. The XPS N 1s spectra of (a) as-received CuTDPAT, (b) CuTDPAT after H_2 exposure at 300 K and 70 bar, (c) sample 'b' after subsequent desorption at 120°C in flowing Ar; (d) PB-CuTDPAT after H_2 exposure at 300 K and 70 bar, (e) PB-CuTDPAT after H_2 exposure at 150°C and 1 bar, and (f) sample 'd' after a subsequent treatment at 120°C in flowing Ar. The two N peaks in CuTDPAT are attributed to the two types of N groups (aromatic and NH in the melamine-like branches) in the TDPAT ligand. The undoped CuTDPAT has negligible changes in the N 1s spectra after the various treatments, whereas PB-CuTDPAT shows evidence for nitrogen hydrogenation (matching 'ammonium salt' reference spectra), which is reversible after the 150°C Ar desorption treatment.

the MMOF structure, surface chemistry, and porosity will further increase uptake via spillover. Meeting DOE hydrogen storage targets at moderate temperature will have

significant engineering advantages for mobile applications, as temperature of operation has implications for system weight.

APPROACH

The project relates to materials development and optimization of catalyst, surface chemistry, crystal and pore structure, and system parameters for the hydrogen spillover phenomenon. For surface chemistry, different MMOFs were doped with catalyst to test hydrogen storage and the effect of functional groups. Novel methods to incorporate a hydrogen dissociation catalyst into MMOFs were evaluated by focusing on methods that lead to well-dispersed catalytic entities without compromising the original pore structure and surface area of the MMOF. The current 'pre-bridge' technique is adapted from methods published previously [6,7], with adaptation to use an optimized hydrogenation catalyst and MMOFs with various structures and surface chemistry. Hydrogen uptake is quantified utilizing both gravimetric and differential volumetric adsorption methods; the former allows for precise catalyst activation whereas the latter allows for high-pressure measurements and is more accurate than conventional volumetric techniques. Complementary spectroscopic techniques are being used to identify the active sites that bind with spilled-over hydrogen.

RESULTS

In prior years of this project, we have developed and tested some 20 new metal-organic framework (MOF) structures; worked to reproducibly optimize the uptake of carbon-based PtAC catalysts; developed techniques to verify spillover to specific surface sites on MMOFs with spectroscopy; conducted extensive reproducibility tests on standard samples, including the effect of measurement, synthesis, and pretreatment conditions; and quantitatively validated our differential adsorption measurement. After testing four techniques to incorporate catalysts into the MMOF (in FY 2012), the 'pre-bridge' technique was selected due to its high retention of surface area and MOF structure, combined with the resulting high dispersion of the introduced Pt/AC catalyst. For three MMOFs, the 'pre-bridge' technique maintained 90-110% of the surface area of the original MOF while retaining structure (as measured by XRD). In contrast, common catalyst doping techniques, when applied to MOFs, may degrade surface area by as much as 20-70% and may lead to complete amorphitization of structure.

In FY 2013, CuTDPAT (Figure 1) was selected for more extensive studies due to its structure and stability. CuTDPAT is the smallest member of (3,24)-connect nets of *rht* topology made of a three-armed hexacarboxylate ligand and 24 $M_2(COO)_4$ paddle wheel based supramolecular building blocks. The CuTDPAT framework is highly porous and contains three different types of cages; cuboctahedron, truncated tetrahedron, and truncated octahedron. The pore volume, Brunauer-Emmett-Teller and Langmuir surface areas are estimated to be 0.93 cc/g, 1,938 and 2,608 m^2/g, respectively, calculated from N_2 adsorption isotherms (77 K). CuTDPAT is featured with a high density of both open metal sites (1.76/nm^3) and Lewis basic sites (3.52/nm^3), as well as high thermal and water stability. At 77 K and 67 bar, CuTDPAT takes up 4.83 (excess) and 6.77 (total) wt% of H_2, respectively. At 298 K and 60.9 bar, the uptake of the as-received CuTDPAT is 0.61 (excess) and 1.04 (total) wt%, respectively, as measured by Rutgers University.

A hydrogen dissociation catalyst, PtAC, was successfully incorporated into the CuTDPAT structure via the pre-bridge technique, with almost complete surface area retention for four preparations. At low pressure and 298 K, the hydrogen uptake of PB-CuTDPAT was enhanced 7.8-fold relative to the 'as-received' CuTDPAT (Figure 2). The enhancement of CuTDPAT is greater than that for either IRMOF8 or CuBTC using the same doping technique (Figure 2, top), and shows the highest uptake to date of any published data for catalyst-doped MMOFs (Figure 2, bottom). The slope of the low-pressure isotherm is high, suggesting that increasing the pressure should further enhance the capacity. However, high-pressure measurements demonstrate severe kinetic limitations at 80 bar (Figure 3), and analysis of the PB-CuTDPAT after this high-pressure H_2 exposure demonstrates almost complete degradation of N_2 surface area, despite the XRD pattern remaining intact. Alternate methods to introduce H_2 into PB-CuTDPAT are being tested, and tests to confirm the stability of as-received CuTDPAT in high-pressure He and H_2 are underway. X-ray photoelectron spectroscopy demonstrates reversible hydrogenation/dehydrogenation of N surface sites after the pre-bridge doping technique, and similar results are not found for the as-received CuTDPAT (Figure 4). Infrared spectroscopy was used to confirm the XPS results and further elucidate the mechanism of hydrogen spillover in this structure.

CONCLUSIONS AND FUTURE DIRECTIONS

- The pre-bridge doping technique successfully introduces well-dispersed hydrogenation catalysts into three MMOFs, while retaining surface area (97-107%) and structure (as determined with XRD).
- Although the low-pressure hydrogen uptake (1 bar, 298 K) for PB-CuTDPAT was extremely promising (7.8-fold enhancement relative to CuTDPAT; highest reported uptake at 1 bar and 298 K relative to other literature reports), high-pressure measurements are plagued by kinetic limitations.
- Stability of as-received CuTDPAT after high-pressure H_2 exposure is being investigated.
- Hydrogen spillover is verified with spectroscopic measurements. Specifically, XPS of PB-CuTDPAT shows

evidence of nitrogen hydrogenation, whereas as-received CuTDPAT does not.

SPECIAL RECOGNITIONS & AWARDS/ PATENTS ISSUED

1. A. Lueking completed an Incoming Marie Curie Fellowship for her work related to spillover.

FY 2013 PUBLICATIONS/PRESENTATIONS

1. Liu, X.M.; Tang, Y.; Xu, E.S.; Fitzgibbons, T.C.; Gutierrez, H.R.; Tseng, H.H.; Yu, M.S.; Tsao, C.S.; Badding, J.V.; Crespi, V.H.; Lueking, A.D. Evidence for Ambient-Temperature Reversible Catalytic Hydrogenation in Pt-doped Carbons, *Nano Letters,* 13, 137-141, 2013.

2. Gong, Q.H.; Zhang, R.; Emge, T.J.; Li, J. "Systematic Design and Synthesis of New Metal Organic Framework Structures", *Chimia*, 67, 393-396, 2013.

3. Sircar, S.; Wang, C.Y.; Lueking, A.D. "Design of High Pressure Differential Volumetric Adsorption Measurements with Increased Accuracy", *Adsorption*, In Press, Available On-Line (http://link.springer.com/article/10.1007/s10450-013-9558-8), July 2013.

4. Li, J. (Invited speaker), "MOFs: Structures, Functions, and Applications", Wuhan University, Wuhan, China, October 11, 2012.

5. Li, J. (Invited speaker), "Metal Organic Frameworks: Microporosity, Multifunctionality, and Adsorption Based Applications", ExxonMobil Research and Engineering Company, Annandale, NJ, November 28, 2012.

6. Li, J. (Invited speaker), "Microporous Metal Organic Frameworks: Solvothermal Synthesis, Structure-Pore Functionalization, and Potential Applications", The 3rd International Solvothermal and Hydrothermal Association Conference, Austin, Texas, January 13–17, 2013.

7. Lueking, A.D. (Invited speaker), "Hydrogen Storage via Spillover through a Combined Experimental and Modeling Approach", Marie Curie Fellow Seminar, University of Crete, Heraklion, April 4, 2013.

8. Li, J. (Invited Speaker), "Engineering Structure and Porosity of Microporous MOFs for Enhanced Functionality and Performance", 3rd International Conference on Multifunctional, Hybrid and Nanomaterials, Sorrento, Italy, March 3–7, 2013.

REFERENCES

1. Singh, A.K.; Ribas, M.A.; Yakobson, B.I. *Acs Nano* **2009**, *3*, 1657.

2. Li, Y. and Yang, R.T. *J. Am. Chem. Soc.* 2006, 128, 8136-8137.

3. Tsao, C.S.; Yu, M.S.; Wang, C.Y.; Liao, P.Y.; Chen, H.L.; Jeng, U.S.; Tzeng, Y.R.; Chung, T.Y.; and Wu, H.C. *J. Am. Chem. Soc.* 2009, 131, 1404-1406.

4. Stadie, N.P.; Purewal, J.J.; Ahn, C.C.; and Fultz, B. *Langmuir.* 2010, 26, 15481-15485.

5. Stuckert, N.R.; Wang, L.; and Yang, R.T. *Langmuir.* 2010, *26*, 11963-11971.

6. Yang, S.J.; Cho, J.H.; Nahm, K.S.; and Park, C.R. *Int J Hydrogen Energ.* 2010, 35, 13062-13067.

7. Lee, S.Y. and Park, S.J. *Int J Hydrogen Energ.* 2011, 36, 8381-8387.

IV.D.1 Design of Novel Multi-Component Metal Hydride-Based Mixtures for Hydrogen Storage

Christopher Wolverton (Primary Contact), Vidvuds Ozolins (University of California, Los Angeles), Harold H. Kung
Department of Materials Science & Engineering
Northwestern University
Evanston, IL 60208
Phone: (847) 467-0593
Email: c-wolverton@northwestern.edu

DOE Managers
Katie Randolph
Phone: (720) 356-1759
Email: Katie.Randolph@go.doe.gov
Ned Stetson
Phone: (202) 586-9995
Email: Ned.Stetson@ee.doe.gov

Subcontractors:
- Jun Yang, Ford Motor Company, Dearborn, MI
- Sheldon Shore, Ohio State University, Columbus, OH
- Sonjong Hwang, Caltech, Pasadena, CA

Contract Number: DE-FC36-08GO18136

Project Start Date: September 1, 2008
Project End Date: August 31, 2013

Overall Objectives

- Discover novel mixed hydrides for hydrogen storage which enable the DOE 2017 system-level goals.
- Discover a material that desorbs 8.5 wt% H_2 or more at temperatures below 85°C.
- Via the combination of first-principles calculations of reaction thermodynamics and kinetics with material and catalyst synthesis, testing, and characterization, search for combinations of materials from distinct categories to form novel multicomponent reactions.

Fiscal Year (FY) 2013 Objectives

- Determine storage capacities, kinetics, and reversibility for reactions predicted to have high capacity and suitable thermodynamics for H_2 storage applications, i.e., $2LiBH_4 + 5Mg(BH_4)_2$ and $B_{20}H_{16}$.
- Use combined theory and experiment to characterize reaction products from $2LiBH_4 + 5Mg(BH_4)_2$.
- Synthesize $B_{20}H_{16}$ and determine hydrogen desorption properties and reaction products.
- Develop computational methods to extend calculation of kinetics beyond mass transport to predict dissociation, surface diffusion, and other kinetic barriers.

Technical Barriers

This project addresses the following technical barriers from the Hydrogen Storage section of the Fuel Cell Technologies Office Multi-Year Research, Development, and Demonstration Plan:

(O) Lack of Understanding of Hydrogen Physisorption and Chemisorption

(A) System Weight and Volume

(E) Charging/Discharging Rates

Technical Targets

This study is aimed at fundamental insights into new materials and the thermodynamic and kinetic aspects of H_2 release and reabsorption from them. Insights gained from these studies will be applied toward the design and synthesis of hydrogen storage materials that meet the following DOE 2017 hydrogen storage targets:

- Specific energy: 1.8 kWh/kg
- Energy density: 1.3 kWh/L

FY 2013 Accomplishments

- Focused efforts on two main reactions, predicted to have high capacity and suitable thermodynamics for H_2 storage applications: $2LiBH_4 + 5Mg(BH_4)_2$ and $B_{20}H_{16}$.
- $B_{20}H_{16}$ extremely promising – first known H_2 storage reaction with high capacity, good thermodynamics, and computational predicted fast mass transport kinetics.
- Theoretically predicted that mass transport in $B_{20}H_{16}$ is fast. Subcontract at Ohio State University focused on synthesis of $B_{20}H_{16}$ compound (future plans will focus on desorption, nuclear magnetic resonance [NMR], kinetics, and reaction products – full characterization of this material).
- H_2 desorption and decomposition pathways have been studied in $2LiBH_4 + 5Mg(BH_4)_2$ using NMR; reaction products consistent with theoretically predicted B_2H_6 anion; still much to explore in this system in terms of reversibility of reaction products (see Future Plans).
- Low-temperature hydrogen desorption observed for $LiBH_4$-carbon composite. Stable cycling can be attained after a few cycles.

- Using the predictive models of kinetics of mass transport, the Al mass transport in $B_{20}H_{16}$ is quite high (important for H_2 release from AlB_4H_{11}), but the mass transport in $LiBH_4$ is very low (much lower than that in $NaAlH_4$); potential avenue for borohydrides – low-lying eutectics (see Future Plans).
- Computational survey of dopants that lower surface dissociation or diffusion for MgB_2 rehydrogenation.

✧ ✧ ✧ ✧ ✧

INTRODUCTION

The long-term DOE targets for hydrogen storage systems are very challenging, and cannot be met with existing materials. The vast majority of the work to date has delineated materials into various classes, e.g., complex and metal hydrides, chemical hydrides, and sorbents. However, very recent studies indicate that mixtures of storage materials, particularly mixtures between various classes, hold promise to achieve technological attributes that materials within an individual class cannot reach. Our project involves a systematic, rational approach to designing novel multicomponent mixtures of materials with fast hydrogenation/dehydrogenation kinetics and favorable thermodynamics using a combination of state-of-the-art scientific computing and experimentation. Specifically, we focus on combinations of materials from distinct categories to form novel multicomponent reactions.

APPROACH

We use the accurate predictive power of first-principles modeling to understand the thermodynamic and microscopic kinetic processes involved in hydrogen release and uptake and to design new material/catalyst systems with improved properties. Detailed characterization and atomic-scale catalysis experiments elucidate the effect of dopants, and nanoscale catalysts in achieving fast kinetics and reversibility. And, state-of-the-art storage experiments give key storage attributes of the investigated reactions, validate computational predictions, and help guide and improve computational methods. In sum, our approach involves an effective blend of 1) H_2 storage measurements and characterization, 2) state-of-the-art computational modeling, 3) detailed catalysis experiments, and 4) an in-depth automotive perspective.

RESULTS (SELECTED EXAMPLES)

Fast Mass Transport Kinetics in $B_{20}H_{16}$: A High-Capacity Hydrogen Storage Material

The storage of hydrogen in an economical and practical way remains a significant challenge in the development of hydrogen fuel cell vehicles. Reversible storage in the solid state (such as in complex metal hydrides) has gained much interest due to the favorable storage densities that can be achieved. A candidate material must release hydrogen at a few bar and operate using the waste heat from the proton exchange membrane fuel cell. Well-established methods such as the grand canonical linear programming method have been used to screen hydrogen storage reactions using energetics obtained from first-principles calculations in order to determine those that are thermodynamically allowable. Besides releasing and absorbing hydrogen in the target range of temperatures and pressures, these reactions should occur rapidly where the targeted rehydrogenation rate proposed by the DOE is 2.0 kg H_2/min. Of the known hydrogen storage reactions that have thermodynamic properties and storage capacities that meet the DOE targets, all suffer from unacceptably slow reaction rates.

There are many processes that may limit the dehydrogenation or rehydrogenation rates of metal hydrides such as nucleation, growth, and H_2 dissociation and recombination at surfaces. In particular, many studies have focused on the kinetics of long-range mass transport during the growth stage. There are both experimental and theoretical evidence that this mass transport step occurs via the diffusion of point defects through bulk phases and that it may be rate limiting in many reactions. This provides motivation to determine the mass transport barrier for proposed reactions. Those reactions with high mass transport barriers can be disregarded for practical applications since their kinetics will be unacceptably slow, unless a suitable catalyst can be found.

Recently, the decomposition of $B_{20}H_{16}$ (Figure 1) has been predicted to occur via a single-step reaction:

$$B_{20}H_{16} \rightarrow 20B + 8H_2$$

The enthalpy change of reaction is equal to 33 kJ/mol H_2 with a calculated equilibrium temperature of 20°C (at a pressure of 1 bar H_2), releasing 6.9 wt% H_2 with a volumetric density of 64.1 g H_2/L. These thermodynamic properties and large storage capacity makes this reaction attractive for applications in passenger vehicles. We focus on the kinetics of mass transport in reaction.

Free energies of formation for defects are plotted versus temperature in Figure 2 at both of the interfaces inserted in Figure 2. Of the defects in $B_{20}H_{16}$, we find that interstitial H_2 has the lowest free energy of formation under all assumed conditions; it is equal to 0.55 eV/defect at the $B/B_{20}H_{16}$ interface and increases from 0.28 to 0.63 eV/defect at the $B_{20}H_{16}/H_2$ interface as the temperature is increased from 250 to 500 K. This temperature dependence of the free energy of formation is due to the chemical potential of hydrogen gas, which decreases with increasing temperature. Of the remaining defects, the formation energy of neutral BH vacancies is several hundred meV above that of interstitial

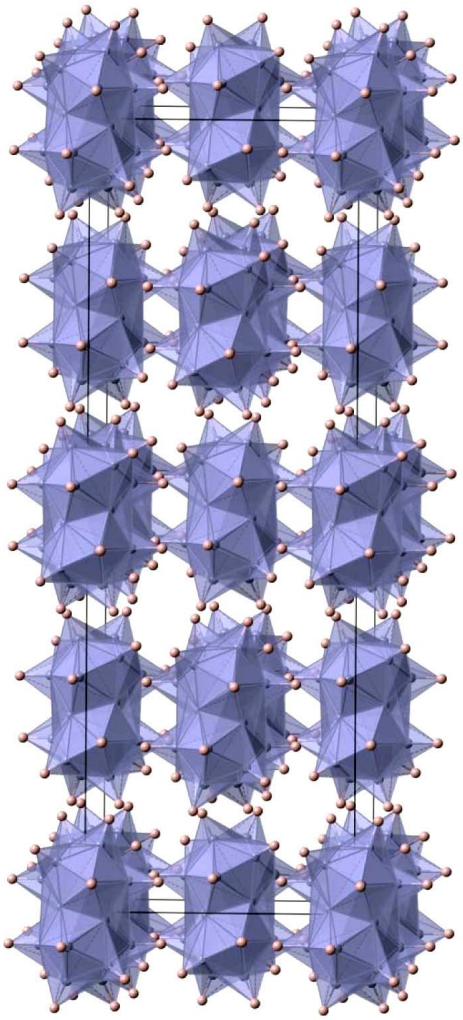

FIGURE 1. Structure of $B_{20}H_{16}$ with B atoms represented by purple spheres, H atoms by pink spheres, and $B_{20}H_{16}$ clusters by polyhedra.

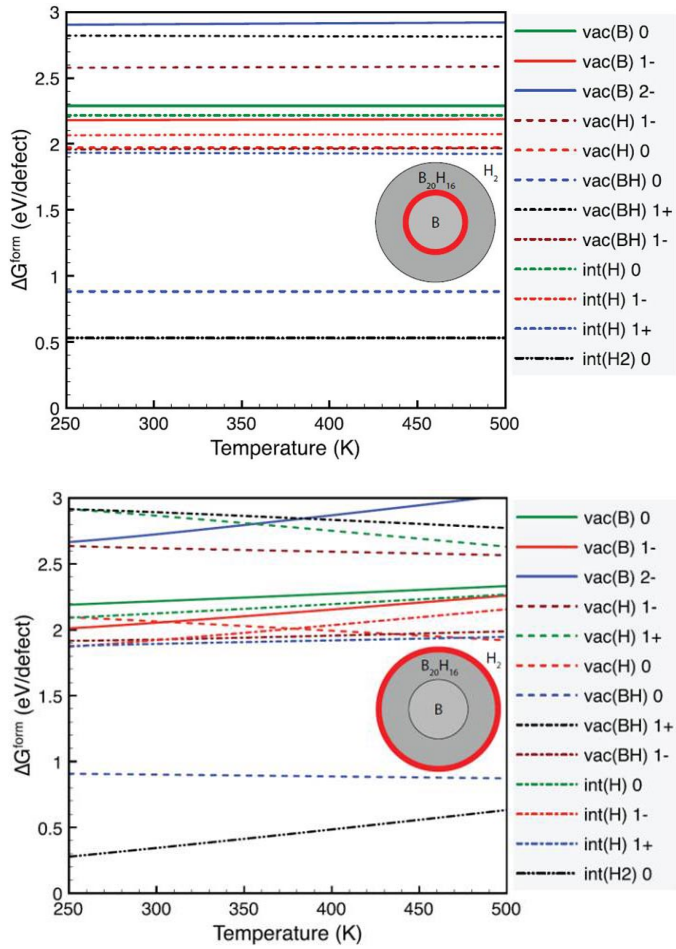

FIGURE 2. Free energies of formation for defects in $B_{20}H_{16}$. Only those defects with formation energies of less than 3 eV are shown. The bold red lines on the inset morphologies show the interfaces at which each set of formation energies is calculated.

H_2 and all other defect formation energies are still higher by at least 1 eV. From steric arguments used in most crystals, it is somewhat surprising that an H_2 dimer, instead of some other monatomic type, is the lowest-energy interstitial defect. However, since $B_{20}H_{16}$ is a molecular crystal, there exist large voids in the structure in which it is possible that both atoms in an H_2 dimer can each be more than 1.5 Å from any other atom in the crystal. This large distance between the H_2 dimer and the host $B_{20}H_{16}$ clusters allows the formation energy of this interstitial defect to remain relatively low.

Having established that interstitial H_2 forms with the lowest energy of all defects, we now turn to the diffusion of this type. From Kinetic Monte Carlo (KMC) simulations, we find that the energy landscape between interstitial H_2 sites in $B_{20}H_{16}$ is relatively flat and that the largest barrier for diffusion is only 116 meV. Using the concentration gradients obtained from the energies shown in Figure 2, and the diffusivities obtained from KMC simulations, the overall flux of interstitial H_2 is shown on an Arrhenius plot in Figure 3. Since the flux depends on the length of the region over which the concentration gradient is calculated, we have made the arbitrary choice to show the results when the length of the $B_{20}H_{16}$ region is 1 µm; however, such a choice will have no effect on the calculated activation energy since this distance does not depend on temperature. The vertical, dashed line in this figure shows the location of the equilibrium temperature for $B_{20}H_{16} \rightarrow 20B + 8H_2$, where the concentration gradient, and thus flux, decreases to zero since the chemical potential of hydrogen is exactly equal at both interfaces at this temperature. Taking the slopes above and below the critical temperature in Figure 3, we find that the activation energies for dehydrogenation and rehydrogenation are 70 and 6 kJ/mol, respectively. We note that the activation energy, especially for dehydrogenation, is lower than the free energies of formation shown in Figure 2. Therefore, the mass transport rates in reaction should be sufficiently fast for practical applications. It must be emphasized that rapid

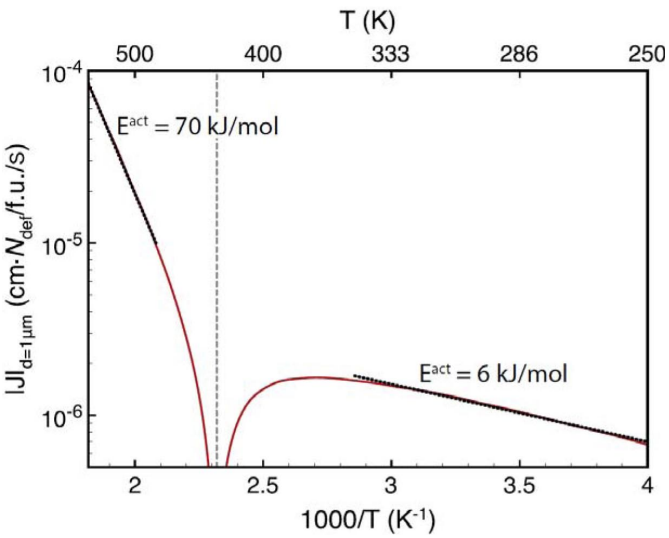

FIGURE 3. Calculated flux of interstitial H_2 across a 1-μm region of $B_{20}H_{16}$. The vertical dashed line shows the equilibrium temperature for the reaction. Separate linear fits to high- and low-temperature regions are shown as dotted black lines along with the associated activation energy.

mass transport is a necessary, but not sufficient, condition for reaction kinetics that are acceptably fast. Other processes such as nucleation and H_2 dissociation may also limit the reaction rate. However, methods for catalyzing these processes in particular have already been demonstrated in other hydrogen storage systems. With this, the combination of fast mast transport kinetics and large hydrogen content in $B_{20}H_{16}$ makes this material promising for the vehicular storage of hydrogen.

The Synthesis of Icosaborane-16 ($B_{20}H_{16}$)

Several methods have been reported for the preparation of icosaborane-16 ($B_{20}H_{16}$) but all were carried out under extreme condition and with as low as 9 to 15% yield. No commercial source is available. The method we plan to use in this project is a modified catalytic pyrolysis of decaborane-14 ($B_{10}H_{14}$). The reported yields for the original procedure range from 10 to 15%.

The synthesis of catalyst, methylaminodimethylborane

A 1:1 molar ratio of methylamine and trimethylborne were condensed in a container and then the mixture was heated 2 hours at 310ºC. The formed products after heating were then opened to traps maintained at -95°C and -196°C. The contents of the -95°C trap were distilled to produce methylaminodimethylborane. The overall procedure includes the following two reactions.

$$MeNH_2 + BMe_3 \rightarrow MeNH_2BMe_3 \quad (1)$$

$$MeNH_2BMe_3 \rightarrow MeNHBMe_2 + CH_4 \quad (2)$$

The synthesis of icosaborane-16

Decaborane-14 was charged in a container which is connected to a tube. In another container, catalyst of methylaminodimethylborane was charged and also connected to the tube. The flow rate of both chemicals can be adjusted. Daceborane-14 will be heated at 100°C and methylaminodimethylborane will kept at 0°C. Both staring materials are passed through the tube whose middle part will be heated at 350°C under dynamic vacuum. The other end of the tube connected to pump through a liquid nitrogen trap. The product will deposit just outside the hot zone of the pyrolysis tube. The raw product was purified by repeated sublimation.

Characterizing Carbon Catalysts for Mixed $LiBH_4$-$Mg(BH_4)_2$ Dehydrogenation/Rehydrogenation

We had observed better cyclability in complex metal hydride-carbon composite (~40% metal hydride loading and prepared by room temperature liquid infusion) when the hydride was $LiBH_4$as compared with the mixed $LiBH_4$-$Mg(BH_4)_2$.

Although the mixed hydride $LiBH_4$-$Mg(BH_4)_2$ had better dehydriding property than $LiBH_4$, the poor reversibility is problematic. We set out to determine whether the single hydride, $Mg(BH_4)_2$, on carbon can be rehydrided. Figure 4 shows several cycles of hydrogenation and dehydrogenation of $Mg(BH_4)_2$-carbon composite. H_2 released is expressed as wt% of the total composite and should be higher if only $Mg(BH_4)_2$was considered. The hydriding was performed at 300°C at 50-bar H_2 pressure for 15 h. The extent of rehydriding was poor compared with $LiBH_4$-carbon composite rehydrided at only 11 bar pressure for 1 h and it appeared that the amount of hydrogen released decreased with each cycle. This data seemed in line with literature reports indicating that $Mg(BH_4)_2$ can only be rehydrided under harsh conditions. The proposed cause for the continuous erosion in hydrogen storage property was the formation of $MgB_{12}H_{12}$. Stavilahas reported that $Li_2B_{12}H_{12}$ and $Na_2B_{12}H_{12}$ can be rehydrogenated at conditions that $Ca_2B_{12}H_{12}$ show no rehydrogenation. We propose that the observed difference in the reversibility of composites of carbon-$LiBH_4$ and carbon-$Mg(BH_4)_2$ is due to the difference in the ease of rehydrogenation of the products $Li_2B_{12}H_{12}$ and $MgB_{12}H_{12}$. It has been reported that the H_2 desorption pressure at 300°C in a $LiBH_4$-carbon composite prepared by melt infusion can greatly exceed that dictated by thermodynamics for the decomposition pathway of $LiBH_4$ to LiH+ B +1.5 H_2. However, if a significant fraction of $LiBH_4$ decomposed through the $Li_2B_{12}H_{12}$ ($LiBH_4 \rightarrow 10/12$ LiH + $1/12 Li_2B_{12}H_{12}$ + 13/12 H_2) pathway then higher pressure is possible. The observed pressures from some of our experiments also suggest that a portion of $LiBH_4$ in the composite may decompose through the $Li_2B_{12}H_{12}$ pathway. It is not surprising

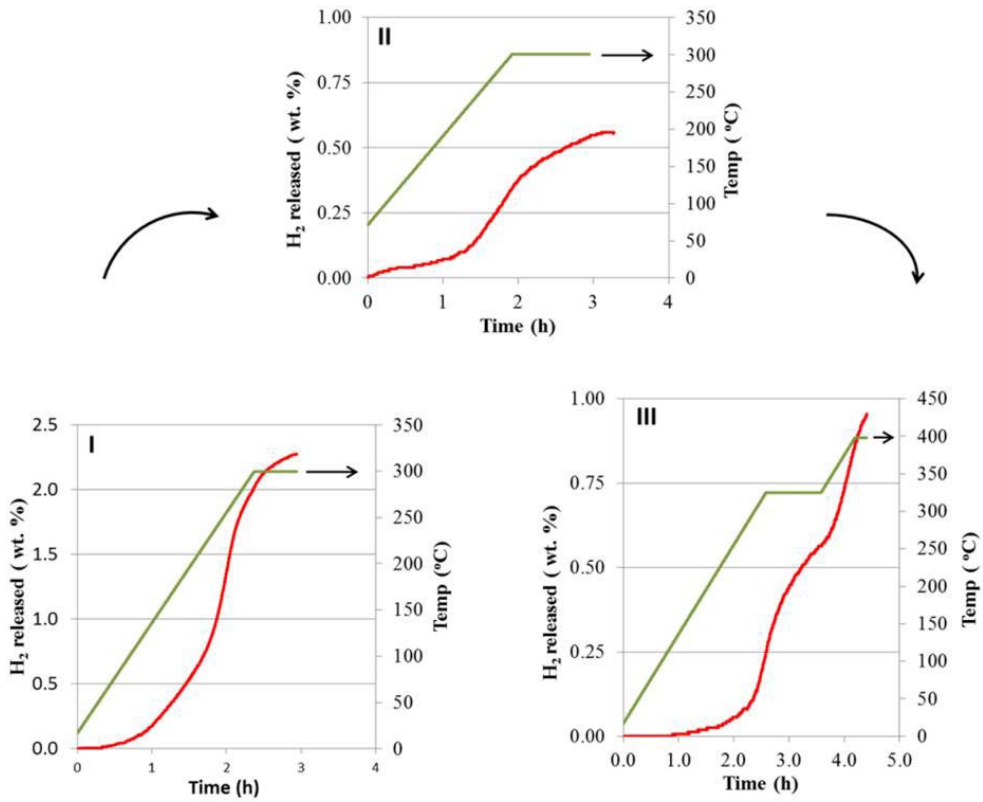

FIGURE 4. Three dehydriding cycles of $Mg(BH_4)_2$-carbon composite (hydride loading is 34.8 wt%). After each dehyriding, the sample was rehydrided for 15 h at 50-bar H_2.

that in a confined space, clustering of BH_4^- to generate $B_{12}H_{12}^=$ may be facilitated. Thus, the combined facts that decomposition through $Li_2B_{12}H_{12}$ could result in H_2 pressure of practical interest and the fact that rehydrogenation of $Li_2B_{12}H_{12}$ is feasible suggest that the new phase of our research should be focused on the synthesis of $Li_2B_{12}H_{12}$ and its infusion into carbon to test whether $Li_2B_{12}H_{12}$ is formed in the dehydrogenation and can be rehyrogenated in a $LiBH_4$-carbon composite.

In Figure 5a, dehydriding of $LiBH_4$-carbon composite from room temperature to 300°C (1) as prepared composite, (2) second cycle of dehydriding after rehydriding at 300°C; 2,200 psig H_2 pressure; and (3) third cycle of dehydriding after rehydriding as in (2). The Y axis is with respect to total weight of the sample. The lack of low-temperature H_2 for Cycle 1 is possibly because of oxygen and moisture leakage into the sample during shipping. Although the increases in H_2 pressure in the region below 280°C were similar for the second and third cycle, there was evidence of some degradation in the storage property with further cycling as the pressure achieved at 300°C decreased noticeably in the third cycle. The low-temperature features in Cycles 2 and 3 are real because any solvent contaminant would have been pumped away after the first cycle.

After the third cycle at 300°C, the sample was subjected to two more dehydriding/rehydriding cycles in which the dehydriding was carried out to 350°C (at the end of this series, the sample would have been subjected to a total of five cycles, Figure 5b), and the rehydriding was also conducted at this temperature. The first dehydriding profile is shown in curve 4, and it appears to be quite similar to curve 3 of the previous slide. However, the dehydriding profile of the second cycle (curve 5) indicated further degradation of the H_2 storage property. After this series of experiments, the sample was subjected to four additional cycles of dehydriding/rehydriding with a temperature limit of 450°C. Within experimental error, all the dehydriding profiles (Figure 5b, curves 6-9) were the same and similar to curve 5. Steady and reversible performance has been attained.

Gao, et al., [1] proposed that a major reason for the loss in the reversibility in the hydrogen cycle for hydrides confined in carbon nanopores was due to the loss of alkali metals through reactions with carbon. They observed improved reversibility through the addition of alkali metals to the composite. Our data appear to support their proposal. After the third cycle at 300°C, the impurities on carbon that could react with the hydride at that temperature was depleted. Therefore, up to 300°C, the dehydriding profile of Cycle 4 did not deviate from that of Cycle 3 in any significant manner

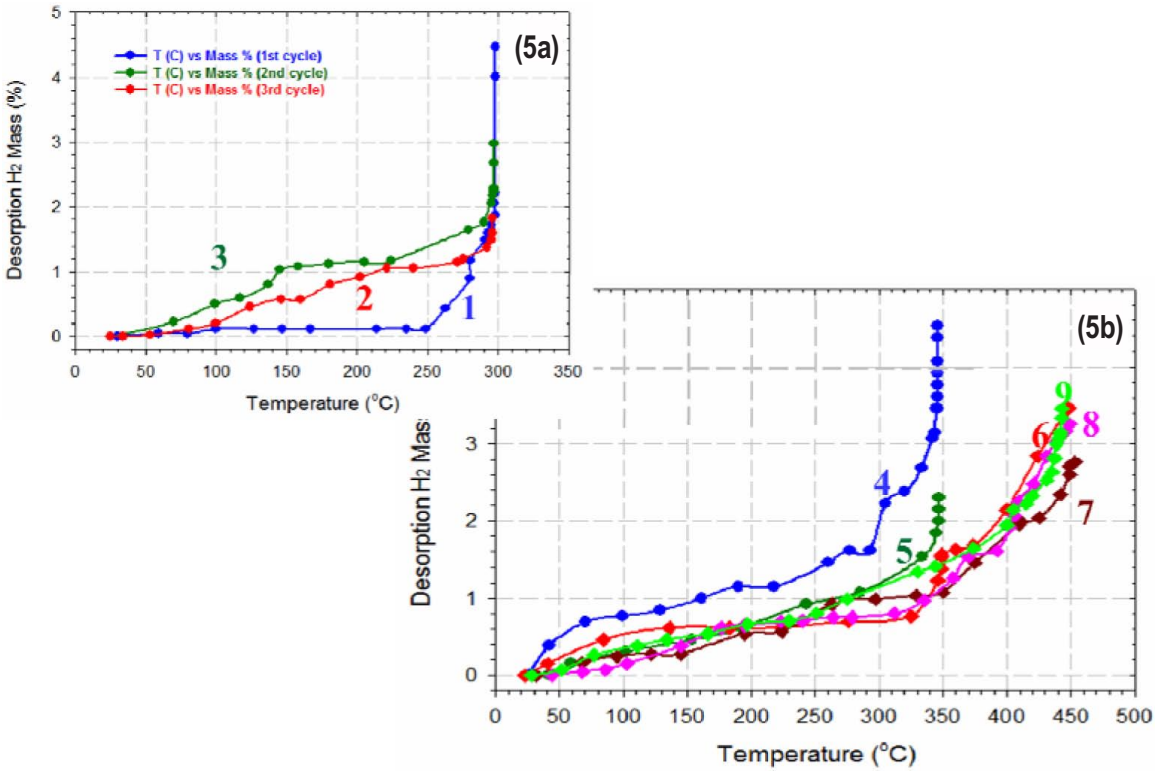

FIGURE 5. H_2 desorption of $LiBH_4$-carbon composite. The numbers indicate the cycle number of desorption. Hydrogenation temperature before desorption was 300°C for cycles 2-4; 350°C for cycle 5 and 450°C for cycles 6-9; pressure was at 2,200 psig.

(compare curve 4 and curve 3). However, cycle 4 terminated at 350°C, a temperature higher than any of the previous cycles, and as a result further reaction between the hydride and residual carbon impurities took place. This caused additional degradation in the amount of hydrogen released (curve 5). At this time, all reactive impurities on the carbon were depleted, and repeatable dehydriding profiles could be obtained, which were the last four cycles at 450°C. That reversible behavior can be obtained suggests that, indeed, the physical constraint of the carbon pores can suppress sintering.

NMR Studies of the Decomposition Products of $2LiBH_4+5Mg(BH_4)_2$

Multinuclear and high resolution magic angle spinning (MAS) solid-state NMR experiments were performed using a Bruker 500-MHz spectrometer and a Bruker 4-mm MAS probe (^{11}B background free). Samples include the as-milled mixture of 2:5 borohydrides and solid residue after H_2 desorption at lower temperatures. The ex situ ^1H and ^{11}B NMR spectra (Figure 6) showed eminent decrease of BH_4 (~ -41 ppm peak for both $LiBH_4$ and $Mg(BH_4)_2$) units and their transformation to other boron species. There was no single borane species (B_nH_m) that was identified unambiguously. The borane species were mainly characterized by a broad -26 ppm peak (see Figure 7) after thermal heating above 280°C. Note that -26 ppm peak cannot be due to $Li_2B_{12}H_{12}$ of which resonance is expected at -15 ppm.

Besides the sharp -17.7 ppm and a broad peak at -1 ppm (amorphous boron), the main -26 ppm peak represents the major boron species. Considering all possible different boron bonding environments in B_nH_m, it is quite encouraging to see a single resonance to represent the desorption product.

Before the main -26 ppm peak, an ^{11}B peak at -30.5 ppm appeared upon heating at lower temperature (200°C). The peak could possibly be assigned to B_3H_8 formation. However, its formation was not in significant quantity, and other sharp peaks at -48.6 ppm and -17.8 ppm were accompanied. After heating at 200°C, the deduction in hydrogen content measured by ^1H NMR was less than 10% (Figure 8, [H] plot). [H] plot for the new batch showed noticeable difference from the first batch that contains boron oxide in large fraction.

The -48.6 ppm peak which might be transient, disappeared at higher temperatures. Such peaks at the high field are due to higher B coordination with more 3-center-2 electron bonds around B. Identifying such moiety could be valuable information in the early stage of the dehydrogenation reaction. The -17.7 ppm peak also formed at low-temperature heating, and remained unchanged up to 320°C. The -17.7 ppm peak can be associated with a stable boron species, such as closoborane, -15.5 ppm for $B_{12}H_{12}$. The

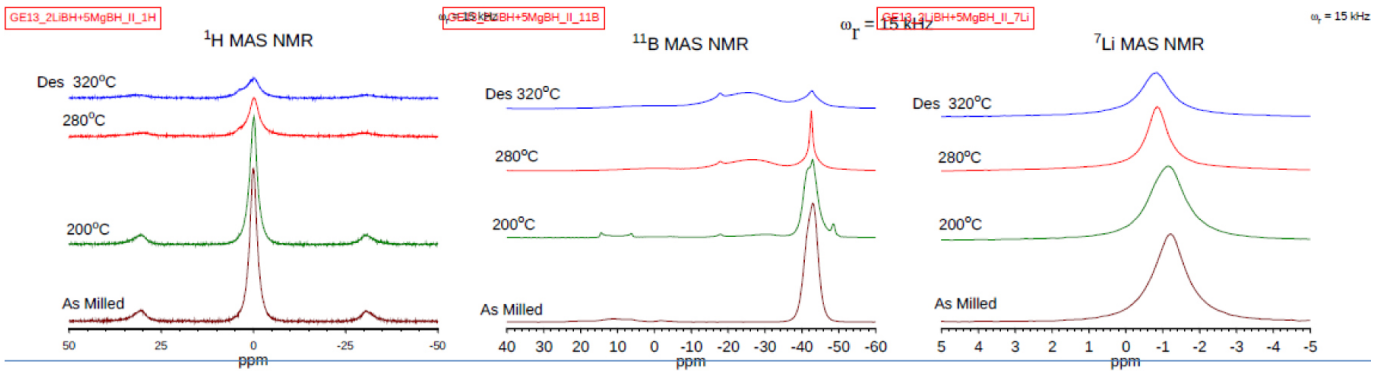

FIGURE 6. Solid-state NMR ^{1}H (left panel), ^{11}B (middle panel) and ^{7}Li (right panel) spectra upon H_2 desorption reactions.

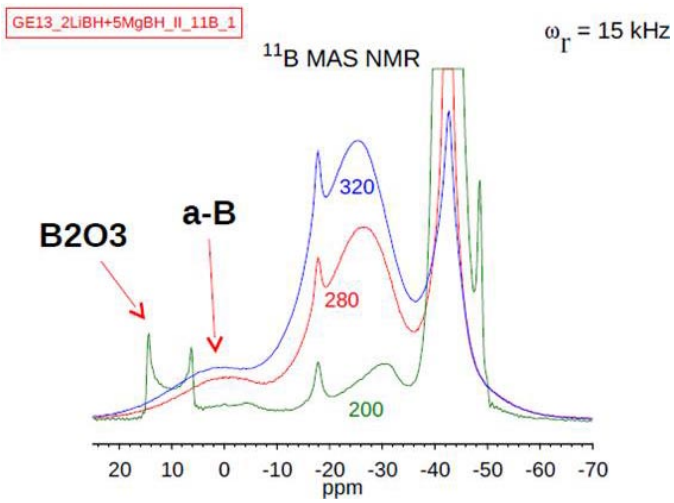

FIGURE 7. ^{11}B MAS NMR Spectra

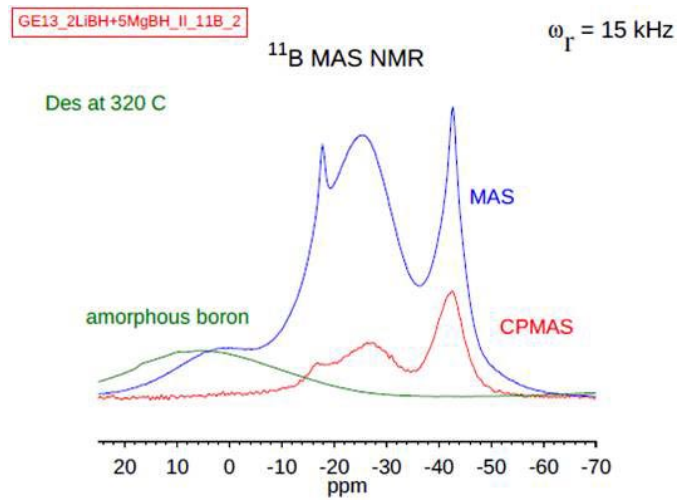

FIGURE 9. ^{11}B MAS NMR Spectra

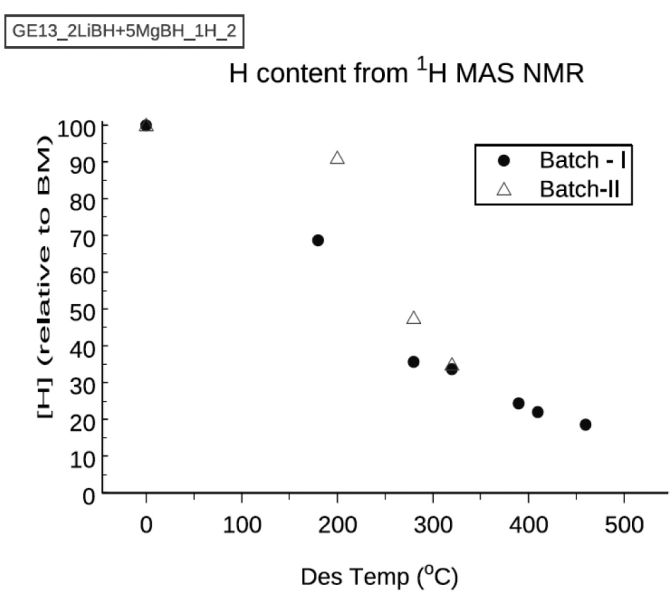

FIGURE 8. ^{1}H MAS NMR Using Two Batches

-26 ppm peak cannot be assigned to any known closo-borane structure although observing the single resonance is highly encouraging.

The peak near 0 ppm is assigned as amorphous boron at the moment. The peak appears at nearly the same position of the ^{11}B spectrum of neat amorphous boron (Aldrich). ^{1}H-^{11}B cross-polarization MAS NMR also supports the nature of the boron species which bears no direct B-H chemical bonds. It is surprising to see the formation of amorphous boron, because amorphous boron is not expected from the calculation (Figure 9).

Mass Transport in $Mg(BH_4)_2$ and $LiBH_4$

We have continued our study of mass transport in lithium borohydride ($LiBH_4$) and magnesium borohydride, $Mg(BH_4)_2$. Both materials exhibit high volumetric and gravimetric hydrogen densities and predicted thermodynamic properties that are promising for reversible onboard hydrogen storage, especially when used in destabilized reactions.

Thermodynamically, the dehydrogenation reactions in the pure compounds are predicted to take place as:

$$Mg(BH_4)_2 \rightarrow 1/6\ MgB_{12}H_{12} + 5/6\ MgH_2 + 13/6\ H_2 \quad (3)$$

$$LiBH_4 \rightarrow 1/12\ Li_2B_{12}H_{12} + 5/6\ LiH + 13/6\ H_2 \quad (4)$$

We have applied the model of mass transport to the reactions (3) and (4). This formalism is based on local equilibrium assumptions at interfaces where diffusion is driven by concentration gradients across the phases participating in the reactions. Defect formation energies are calculated from density-functional theory, and both charged and neutral defects are taken into account. Our results reported in the previous quarter show that neutral BH_3 vacancies in magnesium borohydride (BH_3) have the highest concentration gradient, while all other concentration gradients are several orders of magnitudes smaller. The structure of the neutral BH_3 vacancy is shown in Figure 10. It shows that removing a neutral BH_3 complex leaves behind a negatively charged H^- anion occupying the vacant site. The preferred diffusion mechanism involves an exchange of a neutral BH_3 complex with a near-neighbor BH_4^- anion as shown in Figures 10 and 11. Our density-functional theory results demonstrate that the calculated activation barrier is approximately 2 eV for $Mg(BH_4)_2$ and 1.6 eV for $LiBH_4$; both these values are significantly higher than the calculated migration barrier for AlH_3 vacancies in $NaAlH_4$ (0.34 eV). Together with the significantly lower (by several orders of magnitude) values of the vacancy concentration gradients when compared with those calculated by us for $NaAlH_4$; these results demonstrate that the intrinsic mass transport rates in magnesium borohydride and lithium borohydride are very slow due to the high energy barrier involved in forming the transition state structure with the doubly negatively charged BH_5 complex.

We will explore the effect of mixing Mg and Li borohydrides and the associated changes in diffusion rates due to the introduction of anion vacancies as a result of Mg^{2+}/Li^+ substitution in magnesium borohydride. This represents a promising strategy for accelerating mass transport and reaction kinetics in borohydrides.

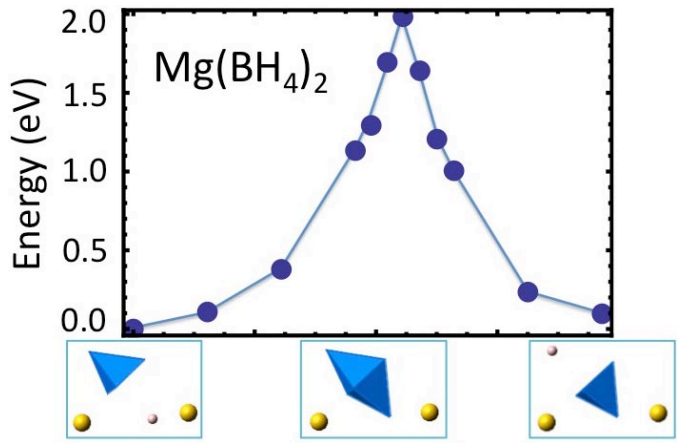

FIGURE 10. Calculated activation barrier for the diffusion of BH_3 vacancies in $Mg(BH_4)_2$. The H^- anion is colored pink, Mg^{2+} cations are yellow, and BH_n complexes are blue. Left panel shows the initial state with BH_3 vacancy on the lower left, the middle panel is the transition state, and the right panel shows the final state after BH_3 is exchanged between H^- and a neighboring BH_4^-.

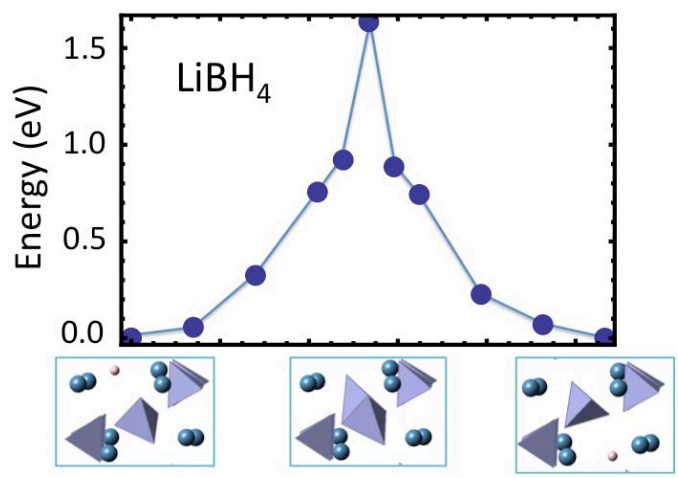

FIGURE 11. Calculated activation barrier for the diffusion of BH_3 vacancies in $LiBH_4$. Same convention as Figure 10, except Li^+ cations are blue.

FUTURE DIRECTIONS

- Complete synthesis of $B_{20}H_{16}$ (subcontract); perform desorption experiments for this compound; and extend NMR experiments to determine reaction products (if non-crystalline). Perform computations of observed reaction products to confirm results and provide predictions of thermodynamics/kinetics.
- Extend NMR experiments to "recharged" $2LiBH_4 + 5Mg(BH_4)_2$ samples, to determine portion(s) of the reaction that are reversible.
- Computational efforts to continue on kinetics, defects, diffusion/mass transport in promising predicted reactions (mass transport nearly complete; focusing on other barriers now – surface reactions, nucleation).
- Potentially promising avenue for "fast kinetics" borohydrides: low melting point combinations (i.e., low-lying eutectics). Direct some computational effort to finding these low-lying eutectics (*ab-initio* molecular dynamics and l-integration).
- Investigate the inclusion of various additives to $LiBH_4$-carbon composites 1) to improve the kinetics of the hydrogen cycle, 2) to ameliorate the initial degradation in cyclability, and 3) to influence the decomposition pathway so that $LiBH_4$ will decompose to more reversible reaction products.

REFERENCES

1. Gao, J.; Ngene, P.; Lindemann, I.; Gutfleisch, O.; de Jong, K.P.; de Jongh, P.E., Enhanced reversibility of H2 sorption in nanoconfined complex metal hydrides by alkali metal addition. *Journal of Materials Chemistry* **2012**,*22* (26), 13209-13215.

IV.D.2 Hydrogen Storage Materials for Fuel Cell-Powered Vehicles

Andrew Goudy
Delaware State University
1200 N. Dupont Highway
Dover, DE 19901
Phone: (302) 857-6534
Email: agoudy@desu.edu

DOE Managers
Ned Stetson
Phone: (202) 586-9995
Email: Ned.Stetson@ee.doe.gov.
Katie Randolph
Phone: (303) 275-4901
Email: Katie.Randolph@go.doe.gov

Contract Number: DE-FC36-06GO86046

Subcontractor:
University of Delaware, Newark, DE

Start Date: July 1, 2006
Projected End Date: September 30, 2014

Overall Objectives

The objectives of this project are to:

- Identify complex hydrides that have great hydrogen storage potential.
- Develop new catalysts and engineering techniques for increasing reaction rates and lowering reaction temperatures.
- Perform kinetic modeling studies that will identify the rate-controlling processes in the hydrogen desorption reactions.
- Develop techniques for improving the sorption capabilities of metal-organic frameworks (MOFs).

Fiscal Year (FY) 2013 Objectives

- Develop a new catalyst for the $LiNH_2/MgH_2$ system that will increase reaction rates and lower reaction temperatures.
- Perform kinetic modeling studies that will identify the rate-controlling processes in the $LiNH_2/MgH_2$ system.
- Determine the effects of nitro-functionalization on the gas sorption capability of isoreticular metal-organic framework (IRMOF)-8.

Technical Barriers

This project addresses the following technical barriers from the Hydrogen Storage section of the Fuel Cell Technologies Office Multi-Year Research, Development, and Demonstration Plan:

(A) System Weight and Volume

(D) Durability/Operability

(E) Charging/Discharging Rates

(O) Lack of Understanding of Hydrogen Physisorption and Chemisorption

Technical Targets

This project is conducting fundamental studies of complex amide materials and other promising hydrogen storage materials. Insights gained from these studies will be applied toward the design and synthesis of hydrogen storage materials that meet DOE's 2015 gravimetric goal of 5.5 weight percent hydrogen storage for the system. Table 1 summarizes the targets.

TABLE 1. Project Technical Targets

Storage Parameter	Target	$LiNH_2/MgH_2$
System Gravimetric Capacity	0.055 kg H_2/kg System	To be determined
System Volumetric Capacity	0.040 kg H_2/L System	To be determined

FY 2013 Accomplishments

- The $LiNH_2/MgH_2$ system has been kinetically modeled, and the rate controlling process has been identified.
- Have compared the dehydriding kinetics of the $LiNH_2/MgH_2$ system at constant pressure driving forces and found that the rates of hydrogen release from the catalyzed and un-catalyzed mixtures are in the order RbH > KH > un-catalyzed.
- Have shown that the nitro-functionalization of IRMOF-8 leads to a reduction in the surface area and a decreased pore volume. However, the decrease is not as great as one would expect based solely on the change in surface area and pore volume.
- A novel concept called the sticking factor was determined for comparison of the adsorption of H_2, CH_4, and CO_2 on the surfaces of IRMOF-8 and IRMOF-8-NO_2 at various temperatures. Since the sticking factors for gases adsorbed on the IRMOF-8-NO_2 were greater than those for gases adsorbed on the IRMOF-8, this indicated that nitro-functionalization of IRMOF-8 increases the sticking efficiency of gases.

INTRODUCTION

The U.S. Department of Energy Metal Hydride Center of Excellence has described $2LiNH_2$+MgH_2 as an important "near-term" system for hydrogen storage. This is because of its good long-term cycling behavior and high hydrogen capacity. Current efforts in our research lab are focused on performing hydrogen storage studies on this system. We have developed methods for the synthesis, characterization, and modeling of this system as well as developing new catalysts and engineering techniques for increasing reaction rates and lowering reaction temperatures. We have also extended these studies to include carbon materials, MOFs, and possibly other nanostructured and porous materials as potential hydrogen storage materials. Once a suitable material has been identified for hydrogen storage, it will be necessary to design, fabricate, and test a hydride-based hydrogen storage system for fuel cell applications.

APPROACH

To achieve the project objectives, it was first necessary to design suitable methods for synthesizing, characterizing, and testing the materials. These methods included synthesis of new materials by mechanical alloying using ball milling, determining thermal stability using thermal gravimetric analysis or thermally programmed desorption (TPD), using X-ray diffraction to determine phase purity and crystal structure, using pressure-composition isotherm (PCI) analyses to determine thermodynamic stability, finding catalysts for making the hydriding faster and reversible, determining kinetic rate curves using constant pressure driving forces, and performing modeling to gain understanding of the mechanism.

RESULTS

The $2LiNH_2/MgH_2$ system releases hydrogen according to the following equations:

$$MgH_2 + 2LiNH_2 \rightarrow Mg(NH)_2 + 2LiH \quad (1)$$

$$Mg(NH)_2 + 2LiH \leftrightarrow Li_2Mg(NH)_2 + 2H_2 \quad (2)$$

TPD curves were constructed for the $2LiNH_2/MgH_2$ system to determine the relative desorption temperatures. The curves shown in Figure 1 indicate that the catalyzed mixtures release hydrogen at a lower temperature than un-catalyzed (pristine) mixture. This is believed to be largely due to the fact that both Rb and K have the same electronegativity and thus similar destabilizing effect on the N-H bond. Figure 2 contains PCI curves for the RbH catalyzed mixtures. Also shown in Figure 2 are the van't

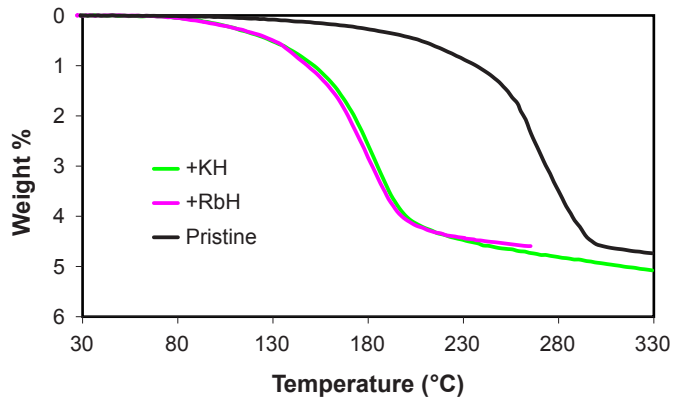

FIGURE 1. TPD curves for the $LiNH_2/MgH_2$ system. The mixtures doped with "catalytic additives" desorb H_2 at ~90°C lower than the un-catalyzed (pristine) mixture. Scans were done at 4°C per minute.

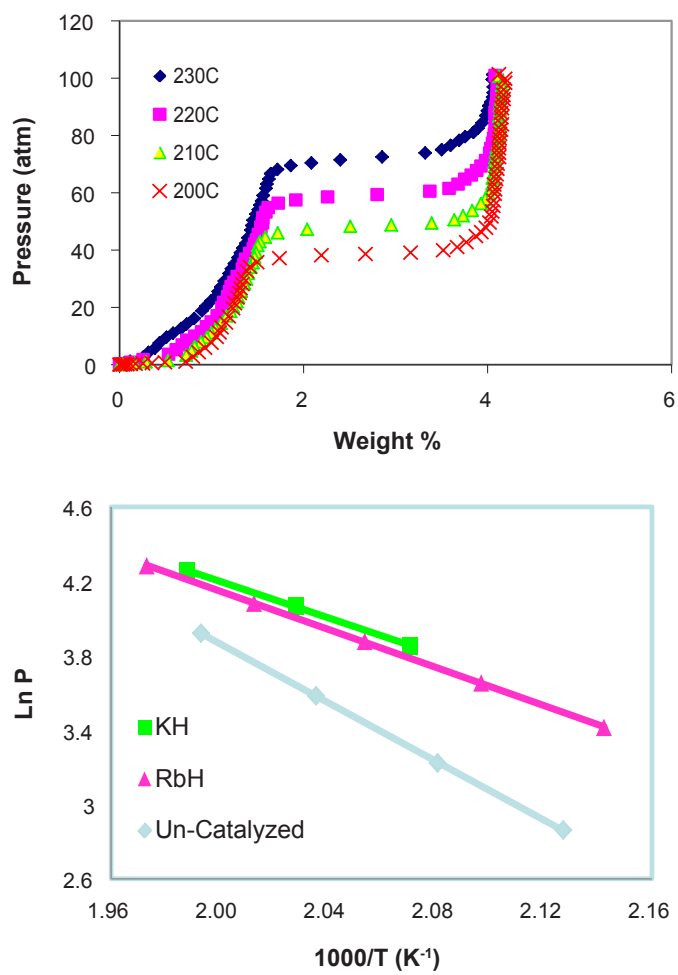

FIGURE 2. Thermodynamics for the $LiNH_2/MgH_2$ system. The graph on the top contains PCI curves for $2LiNH_2/MgH_2$ doped with RbH, which is typical of these systems. The graph on the bottom contains van't Hoff plots for $2LiNH_2/MgH_2$ doped and un-catalyzed mixtures.

Hoff curves that were used to determine the enthalpies of desorption for the catalyzed and un-catalyzed mixtures. The desorption enthalpies for the catalyzed mixtures are ~42 kJ/mol, whereas the enthalpy for the un-catalyzed mixture is 65 kJ/mol. The fact that the desorption enthalpy for hydrogen release from the un-catalyzed mixture was much higher than that from the catalyzed mixtures is consistent with the TPD findings.

The kinetics of hydrogen release from the $2LiNH_2/MgH_2$ system was also measured. The dehydrogenation kinetics of the catalyzed and un-catalyzed mixtures was compared at 210°C. In each case, a constant pressure thermodynamic driving force was applied in which the ratio of the plateau pressure to the applied hydrogen pressure was set at 10. Figure 3 contains plots for the rate of hydrogen release from the catalyzed and un-catalyzed mixtures. Kinetics was done in the two-phase region. Results show that the RbH catalyzed mixture desorbs H_2 approximately twice as fast as the KH catalyzed mixture and 60 times faster than the un-catalyzed mixture.

An attempt was also made to determine the rate-controlling process in these samples by doing kinetic modeling. The theoretical equations that were used are shown below:

$$\frac{t}{\tau} = 1 - (1 - X_B)^{1/3} \quad (3)$$

$$\frac{t}{\tau} = 1 - 3(1 - X_B)^{2/3} + 2(1 - X_B) \quad (4)$$

where τ is a constant that depends on several parameters such as the initial radius of the hydride particles, the gas phase concentration of reactant, the density of the metal hydride, etc.

The model based on Eq. (3) will have chemical reaction at the phase boundary controlling the reaction rate, whereas the model based on Eq. (4) is one in which diffusion controls the overall reaction rate. Both equations were fitted to the kinetic data for the $LiNH_2/MgH_2$ system. Figure 3 contains modeling plots for the $2LiNH_2/MgH_2$ system catalyzed by RbH. In the graph, one curve is an experimental curve, a second curve is based on the overall rate being controlled by diffusion, and a third curve is calculated based on chemical reaction controlling the rate. The plots show a good fit for a diffusion controlled model up to 70% of the reaction but not beyond. This means that the process controlling hydrogen desorption at the later stage of the reaction is different from that at the beginning. The kinetic modeling plots for the KH catalyzed and the un-catalyzed systems showed that diffusion was the rate-controlling process.

We have also developed a rapid solvothermal method for synthesizing IRMOF-8 and have functionalized it by adding $–NO_2$ groups to the linker. It was found that functionalization decreased the surface area and decreased the amount of gas adsorption. However, functionalization increased the

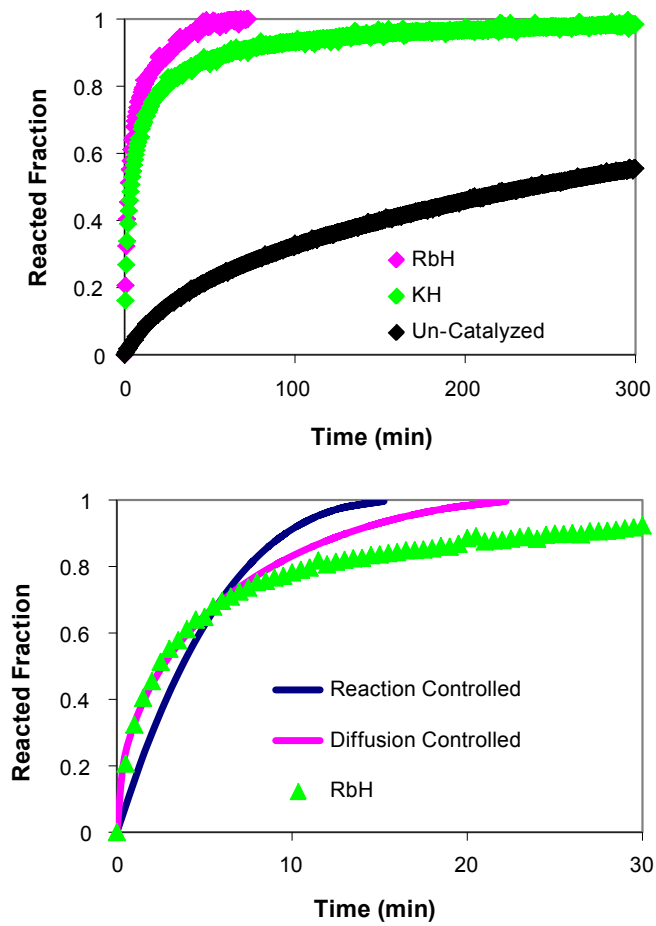

FIGURE 3. Kinetics and modeling plots for the $LiNH_2/MgH_2$ system. Measurements were done at 210°C and N = 10 (where N = plateau pressure/applied pressure).

enthalpy for adsorption of H_2, CH_4, and CO_2 on IRMOF-8. Sticking efficiencies of the various gases were increased as a result of NO_2 functionalization. Sticking efficiencies were determined based on a newly developed parameter called the sticking factor (θ). The sticking factor is defined by:

$$\theta = \frac{\%\ \text{Hydrogen Adsorbed}}{\text{Surface Area}\ (\frac{m^2}{g})} \quad (5)$$

Results showed that θ increases with ΔH and molecular weight. Also, θ decreases with increasing temperature. Results are given in Figure 4.

CONCLUSIONS AND FUTURE DIRECTIONS

- The results of this study show that the new catalytic additive, RbH, is significantly better than KH for enhancing hydrogen desorption from the $2LiNH_2/MgH_2$ system, but the RbH and KH additives have nearly the same capability for lowering the hydrogen desorption temperature of the $2LiNH_2/MgH_2$ mixture.

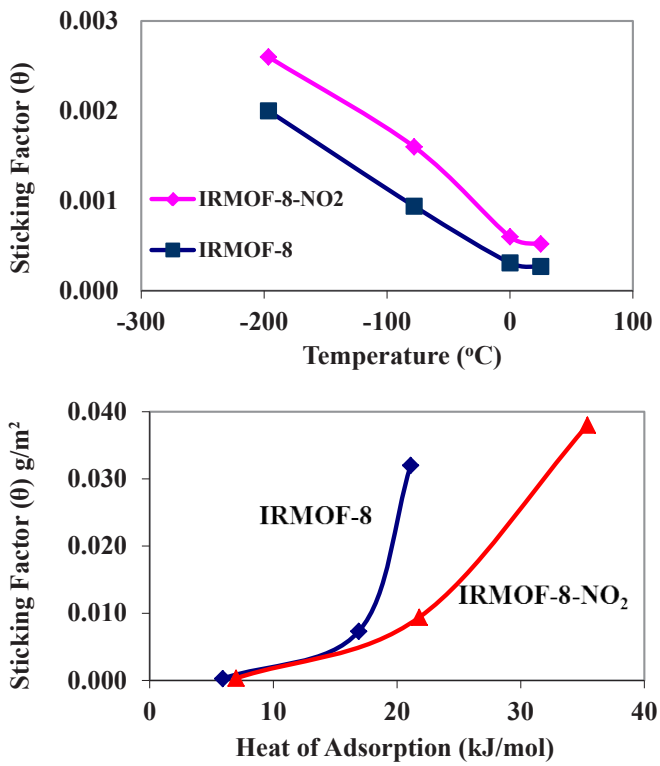

FIGURE 4. Sticking efficiencies and adsorption enthalpies for MOFs. The graph at the top shows sticking factor (θ) vs. temperature for H_2 on the MOFs. The graph at the bottom is θ vs. ΔH of H_2, CH_4, or CO_2 for the MOFs.

- The modeling studies using the shrinking core model and a method developed by Hancock and Sharp both indicated that the reaction rates are controlled by diffusion in the two-phase plateau region. The faster kinetics in the RbH doped mixture is attributed to the fact that Rb has a larger radius and is thereby able to expand the lattice, thus facilitating the diffusion process.
- Results have shown that the nitro-functionalization of IRMOF-8 leads to a reduction in the surface area and a decreased pore volume. However, the decrease is not as great as one would expect based solely on the change in surface area and pore volume.
- A novel concept called the sticking factor was determined for comparison purposes. Since the sticking factors for gases adsorbed on the IRMOF-8-NO_2 were greater than those for gases adsorbed on the IRMOF-8, this indicated that nitro-functionalization of IRMOF-8 increases the sticking efficiency of gases.
- In FY 2013-2014, the following work is planned:
  - Continue to perform kinetics and modeling studies on the $LiNH_2/MgH_2$ system based destabilized systems using our newly developed RbH catalytic additive. We will focus on absorption studies, including modeling work, since most of the work to date has been on desorption kinetics.
  - Continue the cycling studies on the RbH catalyzed $MgH_2/LiNH_2$ system.
  - Use techniques such as residual gas analysis to determine if dehydrogenation is accompanied by the release of other gaseous byproducts such as ammonia.
  - Continue to study the effect of functionalization on MOFs. The goal is to increase ΔH for gas adsorption and thus increase the desorption temperatures.

PATENTS ISSUED

1. A Rubidium Hydride Catalyzed Lithium Amide/Magnesium Hydride System for Hydrogen Storage Applications, (Patent pending).

FY 2013 PUBLICATIONS/PRESENTATIONS

1. Durojaiye T, Hayes J, and Goudy A, "Rubidium Hydride – A Highly Effective Dehydrogenation Catalyst for the lithium amide/magnesium hydride system" J. Phys Chem C, 117 (2013) 6554 – 6560.

2. Samuel Orefuwa, Esosa Iriowen, Hongwei Yang, Bryan Wakefield, and Andrew Goudy, "Effects of Nitro-Functionalization on the Gas Sorption Properties of Isoreticular Metal-Organic Framework-Eight (IRMOF-8)", Micropor. Mesopor. Mater., 177 (2013) 82-90.

3. A.A. Ibikunle, S.T. Sabitu, A.J. Goudy, "Kinetics and Modeling Studies of the $CaH_2/LiBH_4$, $MgH_2/LiBH_4$, $Ca(BH_4)_2$ and $Mg(BH_4)_2$ Systems" J. Alloys Compds, 556 (2013) 45–50.

4. Andrew Goudy, Adeola Ibikunle, Saidi Sabitu, and Tolulope Durojaiye, "Thermodynamics and Kinetics of Complex Borohydride and Amide Hydrogen Storage Materials" Materials Challenges in Alternative and Renewable Energy II, in Ceramic Transactions, Vol 239, Edited by George Wicks, Wiley, 2013, ISBN: 978-1-118-58098-1.

5. Saidi Temitope Sabitu and Andrew Goudy, "Dehydrogenation kinetics and modeling studies of MgH_2 enhanced by transition metal oxides catalysts using constant pressure thermodynamic driving forces", Metals 2012, *2*, 219-228; doi:10.3390/met2030219.

6. Saidi Sabitu and Andrew Goudy, "Dehydrogenation kinetics and modeling studies of $2LiBH_4 + MgH_2$ enhanced by NbF_5 catalyst" J. Phys. Chem. C 116 (2012) 13545−13550.

7. Adeola Ibikunle and Andrew Goudy, "Kinetics and Modeling Study of a $Mg(BH_4)_2/Ca(BH_4)_2$ Destabilized System" Int. J. Hyd. Energy 37 (2012) 12420–12424.

8. Saidi Sabitu and Andrew Goudy, "Dehydrogenation kinetics and modeling studies of MgH_2 enhanced by NbF_5 catalyst using constant pressure thermodynamic forces" Int. J. Hyd. Energy 37 (2012) 12301–12306.

9. T. Durojaiye and A.J. Goudy, "Desorption kinetics of lithium amide/magnesium hydride systems at constant pressure thermodynamic driving forces", Int. J. Hyd. Energy, 37 (2012) 3298-3304.

10. Samuel A. Orefuwa, Hongwei Yang, and Andrew J. Goudy, "Rapid Solvothermal Synthesis of an Isoreticular Metal Organic Framework with Permanent Porosity for Hydrogen Storage", Micropor. Mesopor. Mater., 153 (2012) 88–93.

11. Adeola Ibikunle, Saidi Sabitu, and Andrew Goudy, "Kinetics and Modeling Studies of Some Alkaline Earth Borohydrides at Constant Pressure Thermodynamic Forces", ACS National Meeting, Philadelphia, PA, August, 2012.

12. Andrew Goudy, Saidi Sabitu, Adeola Ibikunle, Tolulope Durojaiye, "Kinetics Studies on Some Complex Borohydride and Amide Hydrogen Storage Materials", NanoSciences & Technologies Conference, Qingdao, China, October, 2012.

IV.D.3 Neutron Characterization in Support of the DOE Hydrogen Storage Sub-Program

Terrence J. Udovic (Primary Contact),
Craig M. Brown, Dan A. Neumann
NIST Center for Neutron Research
National Institute of Standards & Technology (NIST)
100 Bureau Dr., MS 6102
Gaithersburg, MD 20899-6102
Phone: (301) 975-6241
Email: udovic@nist.gov

DOE Managers
Ned Stetson
Phone: (202) 586-9995
Email: Ned.Stetson@ee.doe.gov
Channing Ahn
Phone: (202) 586-9490
Email: Channing.Ahn@ee.doe.gov

Project Start Date: June 2010
Project End Date: Project continuation and direction determined annually by DOE

Overall Objectives

- Support the DOE-funded hydrogen-storage projects by providing timely, comprehensive characterization of materials and storage systems using state-of-the-art neutron methods.
- Direct partner synthesis efforts based on the understanding gained through the use of these methods.
- Demonstrate the fundamental characteristics of useful hydrogen-storage materials.

Fiscal Year (FY) 2013 Objectives

- Complete our investigations and publish results concerning how $LiBH_4$ nanosequestration in various carbon scaffolds affects the nature of tetrahydroborate (BH_4^-) anion mobilities.
- Complete our investigations and publish results concerning how iodide substitution in $LiBH_4$ perturbs the parent structure and BH_4^- anion mobilities.
- Elucidate the nature of the mobile hydrogenous species previously observed in $NaAlH_4$ using neutron spectroscopic techniques.

Technical Barriers

This project addresses the following technical barriers from the Hydrogen Storage section of the Fuel Cell Technologies Office Multi-Year Research, Development, and Demonstration Plan:

(A) System Weight and Volume

(O) Lack of Understanding of Hydrogen Physisorption and Chemisorption

Technical Targets

NIST provides important materials metrologies for DOE-funded projects using neutron-scattering measurements to understand and characterize hydrogen-substrate interactions of interest in a variety of materials ranging from H_2 adsorbed in nanoporous materials to H chemically bonded in complex hydride materials. Insights gained from these studies will be applied toward the design and synthesis of hydrogen-storage materials that meet the following DOE 2017 storage targets:

- Specific energy: 1.8 kWh/kg
- Energy density: 1.3 kWh/L
- Cost: $12/kWh

FY 2013 Accomplishments

- Manuscript published concerning the utility of neutron scattering fixed-window scans for characterizing the relative reorientational mobilities of BH_4^- anions in various environments.
- Two manuscripts published concerning the nature of the subtle order-disorder phase transitions of some heavier alkali-metal borohydrides.
- Manuscript published on joint nuclear magnetic resonance (NMR)/quasielastic neutron scattering (QENS) study of BH_4^- translational/reorientational dynamics in $LiBH_4$ infiltrated in 4-nm pore size ordered-pore carbon.
- Manuscript submitted on detailed QENS study of confinement effects on $LiBH_4$ nanosequestered in both ordered (columnar-pore) carbon frameworks and carbon aerogels.
- Manuscript published on BH_4^- reorientational mechanism in a hexagonal $LiBH_4$-LiI solid solution.
- Manuscript published concerning the nature of the mobile Al-containing species previously observed in $NaAlH_4$.

INTRODUCTION

To obtain the DOE levels of hydrogen storage in a timely manner, it is imperative that trial-and-error testing of materials be avoided. Thus, the focus must be upon the rational design of new systems. From a thorough understanding of the physics and chemistry that govern the hydrogen-substrate interactions, we will be able to make a more concerted effort to push the frontiers of new materials. The key to improving materials is a detailed understanding of the atomic-scale locations of the hydrogen and determining how it gets there and how it gets out. Neutron scattering is perhaps the premier technique for studying hydrogen, and the NIST Center for Neutron Research is currently the leading facility in the U.S. for studying these materials.

APPROACH

NIST provides important materials characterization for DOE-funded hydrogen storage projects using neutron-scattering measurements to probe the amount, location, bonding states, dynamics, and morphological aspects of (i) molecular hydrogen in carbon-based materials such as polymers, metal organic frameworks (MOFs), and carbonaceous materials such as carbon nanohorns, and (ii) atomic hydrogen in a variety of complex hydride materials including those containing boron and nitrogen, as well as their intermediates and by-products. NIST works directly with DOE and other partners that produce novel hydrogen-storage materials to analyze the most promising samples and to help determine and resolve the fundamental issues that need to be addressed.

RESULTS

In collaboration with University of Maryland, University of Pennsylvania, and General Motors, the phonon density of states of the recently synthesized metal hydrazinoborane, $LiN_2H_3BH_3$, was measured by neutron vibrational spectroscopy (NVS). Agreement with the simulated spectrum from density functional theory (DFT) phonon calculations (Figure 1) corroborated the proposed structure based on X-ray diffraction results.

In collaboration with University of Maryland, University of Michigan, Delft University of Technology, HRL Laboratories, and the Institute of Metal Physics-Ekaterinburg, the reorientational dynamics of BH_4^- anions in a variety of environments were measured as a function of temperature via neutron scattering fixed-window scans (FWSs) at zero energy transfer using a neutron backscattering spectrometer [1]. The temperature dependence of the FWS was found to be a useful indicator of the relative reorientational mobilities of BH_4^- anions in the various alkali-metal borohydride compounds MBH_4 (M=Li, Na, K, Rb, Cs), $LiBH_4$ nanoconfined in carbon scaffolds, and $LiBH_4$-LiI solid solutions. Figure 2 displays the FWSs for the family of alkali-metal borohydrides between 4 K and 300 K. Although in this temperature range, the orthorhombic structure for $LiBH_4$ is atypical of the face-centered-cubic structure observed for $NaBH_4$, KBH_4, $RbBH_4$, and $CsBH_4$, its FWS indicates that it possesses the least rotationally-mobile BH_4^- anions of all alkali-metal analogs, which is in line with the overall observed trend that mobility increases with cation size. The onset temperatures of observable motion (on the order of 10^8 jumps/s) are approximately 150 K for $LiBH_4$, 120 K for $NaBH_4$ and KBH_4, 100 K for $RbBH_4$, and 80 K for $CsBH_4$. Likewise, the temperatures where motion starts becoming too rapid (surpassing 10^{10} jumps/s) to be easily observed are approximately 270 K for $LiBH_4$, 200 K for $NaBH_4$ and KBH_4, 190 K for $RbBH_4$, and 170 K for $CsBH_4$.

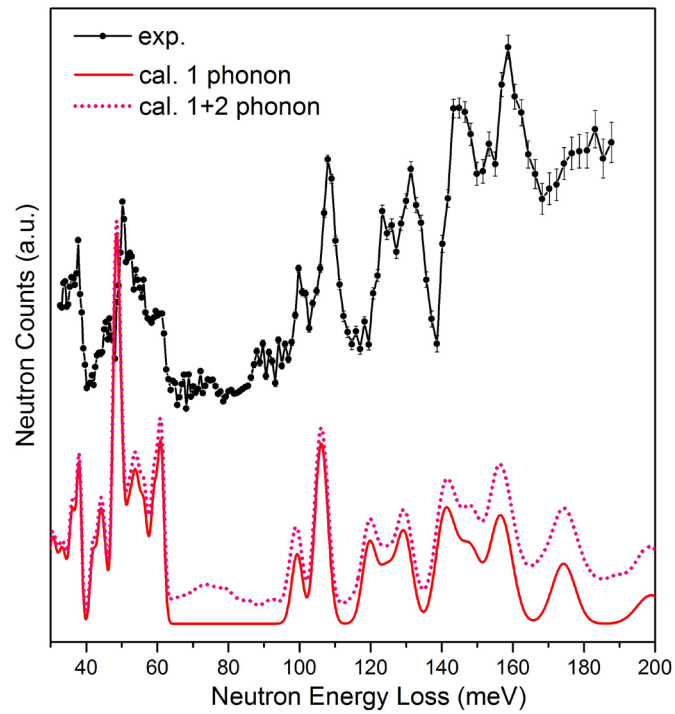

FIGURE 1. The NVS-measured (4 K) and DFT-calculated vibrational spectra for $LiN_2H_3BH_3$.

In collaboration with University of Maryland, University of Michigan, and Delft University of Technology, neutron vibrational spectra were measured for the alkali borohydrides KBH_4, $RbBH_4$, and $CsBH_4$ to probe the low-temperature phase transitions previously identified using thermodynamic and/or crystallographic techniques [2]. The BH_4^- torsional band for each compound changed noticeably across its corresponding phase transition. Previous neutron powder diffraction (NPD) measurements showed that the transitions for both $NaBH_4$ and KBH_4 are order-disorder transitions involving the relative orientations of the BH_4^- anions.

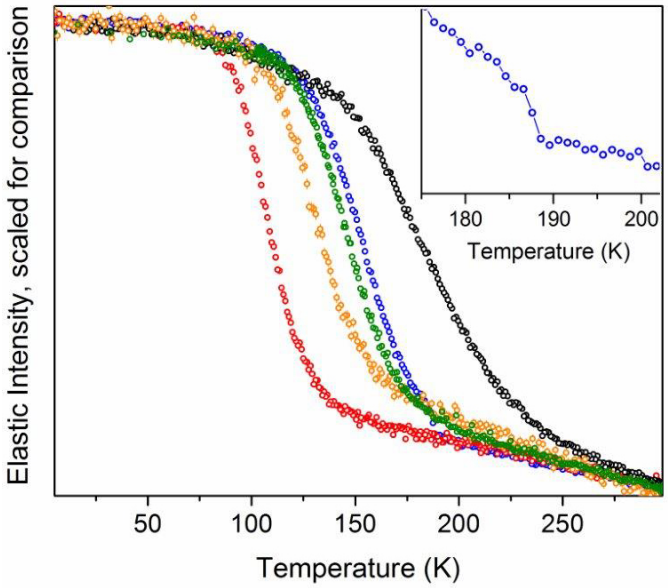

FIGURE 2. FWSs for BH_4^- anions in MBH_4 compounds (from right to left, M = Li, Na, K, Rb, and Cs) as a function of temperature. The inset shows evidence of the order–disorder phase transition of $NaBH_4$ just below 190 K.

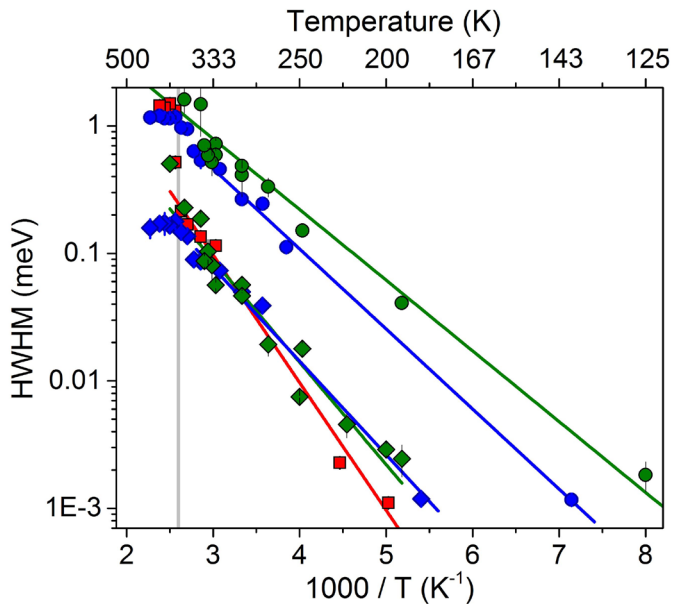

FIGURE 3. Comparison of the temperature dependencies of the QENS linewidths for bulk $LiBH_4$ (red), $LiBH_4$ in a 4-nm NPC (green), and $LiBH_4$ in a 13-nm carbon aerogel (blue). Vertical gray line marks the 385 K bulk phase transition temperature.

However, diffraction measurements for both $RbBH_4$ and $CsBH_4$ failed to unequivocally identify long-range-ordered phases below their transitions [3]. The NVS measurements of BH_4^- torsional as well as translational optic bands across the transitions, corroborated by DFT phonon calculations, suggested that the subtle $RbBH_4$ and $CsBH_4$ transitions are indeed analogous to those observed for $NaBH_4$ and KBH_4, but of shorter range.

Continuing a collaboration with University of Missouri-St. Louis, Washington University-St. Louis, Sandia National Laboratories, and California Institute of Technology, a further dynamical comparison was made between bulk $LiBH_4$ and $LiBH_4$ sequestered inside both ordered-nanopore carbon (NPC) scaffolds and carbon aerogels. QENS measurements of $LiBH_4$ sequestered in either ordered NPCs (with either 2-nm or 4-nm pore sizes) or carbon aerogels (with 13-nm average pore size) indicated similar dynamical results: i.e., BH_4^- anions in the core regions of the pores undergo slower, bulk-like reorientations, and BH_4^- anions near the pore walls undergo order-of-magnitude faster reorientations. The data for the NPCs suggest that both types of dynamically distinct anions undergo single C_2 or C_3 axis reorientational jumps below 330 K. By 400 K (which is above the bulk phase transition temperature), both reorient more diffusively around multiple axes. Figure 3 compares the Arrhenius-like temperature dependence of the QENS linewidths for bulk $LiBH_4$, $LiBH_4$ in a 4-nm NPC, and $LiBH_4$ in a 13-nm carbon aerogel.

In collaboration with University of Maryland and the Institute of Metal Physics-Ekaterinburg, the reorientational dynamics of BH_4^- anions in the hexagonal 1:1 $LiBH_4$–LiI solid solution were characterized by QENS with results extended to high momentum transfers [4]. The high reorientational mobility compared to that for BH_4^- in other solid-state environments reflected a synergistic combination of the underlying hexagonal close-packed lattice and the unusually large BH_4^- crystallographic site stabilized by the presence of the I^- anions throughout the structure. Elastic incoherent structure factor (EISF) data (Figure 4) at 125 K revealed a dominant uniaxial reorientation mechanism consisting of rapid BH_4^- diffusive-like rotational motions of three H atoms in a ring around the *c*-directed trigonal B-H axis, with the fourth axial H atom remaining stationary (orbit model). By 200 K, this diffusive ring of three H atoms underwent additional noticeable jump exchanges with the axial H atom (orbit-exchange model), identical to what had been observed for BH_4^- reorientations in hexagonal $LiBH_4$ at much higher temperature. The two separate mechanisms were consistent with the two reorientational motions revealed recently by NMR measurements. An average rotational activation energy of 36 meV ± 1 meV was derived over a wide temperature range.

In collaboration with Washington University-St. Louis, RCB Hydrides, University of Missouri-St. Louis, and Radboud University, we further investigated the newly discovered, mobile, Al-containing species termed S105 that was found to be present in certain $NaAlH_4$ samples, with S105 a likely facilitator of Al-atom transport [5]. We found that hydroxide impurities played a crucial role in the formation of the species. Specifically, in bare $NaAlH_4$,

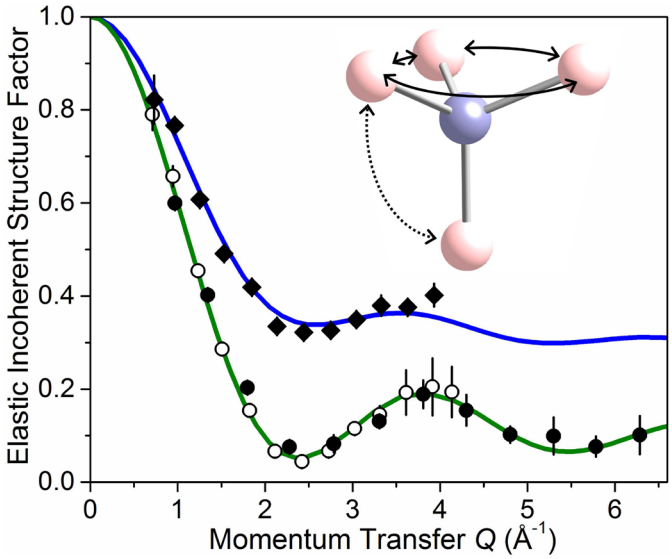

FIGURE 4. EISFs derived from QENS measurements for $LiBH_4$-LiI at 125 K (black diamonds) and 250 K (black circles), compared with the orbit model (blue line) and the orbit-exchange model (green line). A schematic of BH_4^- reorientational jumps is depicted in the inset. The observed EISFs for hexagonal $LiBH_4$ at 400 K (open circles) are shown for comparison.

S105 was present after melting (under sufficient hydrogen pressure to block the dehydriding reaction) only in samples either exposed to H_2O vapor or mixed with metal hydroxides. Moreover, both in situ NMR and NVS measurements indicated that S105 likely involved very (rotationally and translationally) mobile AlH_4^- tetrahedra. We proposed that hydroxide impurities promoted fast diffusion of nearby AlH_4^- units, similar to enhanced motions seen in NaH; the hydroxides also reacted with $NaAlH_4$ to form NaH and subsequently produce Na_3AlH_6, which was always found to accompany S105. Our measurements revealed that the only chemical components of S105-containing alanate apart from hydroxides were $NaAlH_4$ and Na_3AlH_6. Presence of the S105 species in $NaAlH_4$ samples also led to faster dehydriding in hot, undoped $NaAlH_4$ solid, pointing to an enhancement of the hydrogen reaction kinetics by S105.

CONCLUSIONS AND FUTURE DIRECTIONS

- Neutron methods have provided crucial, non-destructive characterization tools for the DOE Hydrogen Storage Sub-Program.
- Agreement between NVS and DFT corroborates the recently-synthesized-$LiN_2H_3BH_3$ structure that was determined by diffraction methods.
- Neutron-scattering fixed-window scans are shown to be a valuable technique for making relative comparisons of BH_4^- anion rotational mobilities in a host of solid-state environments.
- NVS, NPD, and DFT indicate that the anion-ordered phases in $RbBH_4$ and $CsBH_4$ do exist but are short-ranged, unlike the long-range order observed for the lighter $NaBH_4$ and KBH_4 compounds.
- QENS measurements of $LiBH_4$ sequestered in either ordered nanoporous carbons or carbon aerogels indicate similar dynamical results: core BH_4^- anions undergo slower, bulk-like, jump reorientations, and interface BH_4^- anions undergo order-of-magnitude faster, more diffusive reorientations.
- QENS measurements of BH_4^- anions in a 1:1 hexagonal $LiBH_4$-LiI alloy indicate BH_4^- reorientations predominantly around the *c*-directed B-H bond at 125 K with additional jump exchanges between the axial H and other three trigonal Hs occurring above this temperature, similar to what occurs for hexagonal $LiBH_4$ at 400 K.
- Neutron vibrational spectra are consistent with NMR results suggesting that the unusual S105 species found in some pretreated $NaAlH_4$ samples involves mobile AlH_4^- tetrahedral anions whose formation is promoted by hydroxide impurities.
- We will continue to support the DOE Hydrogen Storage Sub-Program where needed.

FY 2013 PUBLICATIONS/PRESENTATIONS

1. X. Chen, Y. Zhang, Y. Wang, W. Zhou, D.A. Knight, T.B. Yisgedu, Z. Huang, H.K. Lingam, B. Billet, T.J. Udovic, G.M. Brown, S.G. Shore, C.M. Wolverton, and J.-C. Zhao, "Structure Determination of an Amorphous Compound AlB_4H_{11}," Chem. Sci. 3, 3183 (2012).

2. K.J. Alvine, M. Tyagi, C.M. Brown, T.J. Udovic, T. Jenkins, M.E. Bowden, A.L. Schemer-Kohrn, and S. G. Pitman, "Hydrogen Species Motion in Piezoelectrics: A Quasi-Elastic Neutron Scattering Study," J. Appl. Phys. 111, 053505 (2012).

3. J.L. Blackburn, C. Engtrakul, J. Bult, K. Hurst, Y. Zhao, Q. Xu, P. Parilla, L. Simpson, M.R. Hudson, C. M. Brown, T. Gennett, "Spectroscopic Identification of Hydrogen Spillover Species in Ruthenium-modified High Surface Area Carbons by Diffuse Reflectance Infrared Fourier Transform Spectroscopy," J. Phys. Chem. C 116, 26744 (2012).

4. J. Purewal, J.B. Keith, C.C. Ahn, B. Fultz, C.M. Brown, and M. Tyagi, "Hydrogen Diffusion in Potassium Intercalated Graphite Studied by Quasielastic Neutron Scattering", J. Chem. Phys. 137, 224704 (2012).

5. N. Verdal, T.J. Udovic, W. Zhou, J.J. Rush, D.J. De Vries, and M.R. Hartman, "Vibrational Spectroscopic Study of Subtle Phase Transitions in Alkali Borohydrides: Comparison with First-Principles Calculations," J. Phys. Chem. C 117, 876 (2013).

6. E.G. Sorte, R.C. Bowman, Jr., E.H. Majzoub, M. H.W. Verkuijlen, T. J. Udovic, and M. S. Conradi, "Mobile Species in $NaAlH_4$," J. Phys. Chem. C 117, 8105 (2013).

7. B.B. Kitchen, N. Verdal, T.J. Udovic, J.J. Rush, M.R. Hartman, and D.J. DeVries, "Investigation of an Unusual Low-Temperature Phase Transformation in $RbBH_4$ by Neutron Diffraction," J. Solid State Chem. 203, 51 (2013).

8. A. Qajar, M. Peer, R. Rajagopalan, Y. Liu, C. Brown, and H.C. Foley, "Surface Compression of Light Adsorbates inside Microporous PFA-derived Carbons," Carbon 60, 538 (2013).

9. N. Verdal, T.J. Udovic, J.J. Rush, H. Wu, and A.V. Skripov, "Evolution of the Reorientational Motions of the Tetrahydroborate Anions in Hexagonal $LiBH_4$–LiI Solid Solution by High-Q Quasielastic Neutron Scattering," J. Phys. Chem. C 117, 12010 (2013).

10. X. Liu, E.H. Majzoub, V. Stavila, R. Bhakta, M. Allendorf, D.T. Shane, M.S. Conradi, N. Verdal, T.J. Udovic, and S.-J. Hwang, "Probing the Unusual Proton and Anion Mobility of $LiBH_4$ Confined in Highly Ordered Nanoporous Carbon Frameworks via Solid State NMR and Quasielastic Neutron Scattering," J. Mater. Chem. A (in press); dx.doi.org/10.1039/c3ta12051a.

11. T.J. Udovic, N. Verdal, J.J. Rush, D.J. De Vries, M.R. Hartman, J.J. Vajo, A.F. Gross, and A.V. Skripov, "Mapping Trends in the Reorientational Mobilities of Tetrahydroborate Anions via Neutron-Scattering Fixed-Window Scans," J. Alloys Compds. (in press); dx.doi.org/10.1016/j.jallcom.2013.02.025.

12. H. Wu, W. Zhou, F.E. Pinkerton, T.J. Udovic, T. Yildirim, and J. J. Rush, "Metal Hydrazinoboranes: Crystal Structures and High-Extent Dehydrogenation," American Chemical Society National Meeting, Philadelphia, PA, Aug. 2012.

13. C.M. Brown, "Understanding Adsorption through Structure and Spectroscopy," American Chemical Society National Meeting, Philadelphia, PA, Aug. 2012. (invited)

14. C.M. Brown, "A View from the Inside: What We Understand about Adsorption in Porous Materials through Structure and Spectroscopy," Chemistry Seminar, Clemson University, SC, Sep. 2012. (invited)

15. T.J. Udovic, N. Verdal, J.J. Rush, and V. Stavila, "Reorientational Dynamics Studies of Various Hydroborate Anions using Quasielastic Neutron Scattering," International Symposium on Metal-Hydrogen Systems--Fundamentals and Applications, Kyoto, Japan, Oct. 2012. (invited)

16. T.J. Udovic, "NIST Center for Neutron Research Plans for International Collaborations in Task 32: Hydrogen-Based Energy Storage," IEA HIA Expert Meeting of Task 22 – Fundamental and Applied Hydrogen Storage Materials Development, Kyoto, Japan, Oct. 2012. (invited)

17. C.M. Brown, "A View from the Inside: What We Understand about Adsorption in Porous Materials through Structure and Spectroscopy," Physics Seminar, University of Missouri-Columbia, Oct. 2012. (invited)

18. C.M. Brown, "Understanding Adsorption in Porous Materials through Structure and Dynamics," Frontiers in Chemical Spectroscopy, Abingdon, Oxford, UK, Nov. 2012. (invited)

19. C.M. Brown, "Neutron Diffraction," 600 Seminar Series Lecture, University of Delaware, Wilmington, DE, Nov. 2012. (invited)

20. C.M. Brown, "Neutron Scattering," 600 Seminar Series Lecture, University of Delaware, Wilmington, DE, Dec. 2012. (invited)

21. H. Wu, "Novel Hydrogen Storage Materials and Related Structural Studies," Department of Materials Science and Engineering Seminar, University of Maryland, College Park, MD, Mar. 2013. (invited)

22. N. Verdal, T.J. Udovic, J.J. Rush, and A.V. Skripov, "Neutron Scattering Studies of Destabilized Lithium Borohydride," American Physical Society March Meeting, Baltimore, MD, Mar. 2013.

23. T.J. Udovic, "Neutron Metrology of Hydrogen in Bulk and Nanoconfined Metal-Hydride and Complex-Hydride Systems," IEA HIA Kickoff Expert Meeting of Task 32 – Hydrogen-Based Energy Storage, Heraklion, Crete, Greece, Apr. 2013. (invited)

24. C.M. Brown, "Understanding Adsorption in Porous Materials through Structure and Spectroscopy," American Chemical Society National Meeting, New Orleans, LA, Apr. 2013. (invited)

25. T.J. Udovic, C.M. Brown, D.A. Neumann, "Neutron Characterization in Support of the DOE Hydrogen Storage Sub-Program," DOE EERE Annual Merit Review, Arlington, VA, May 2013. (invited)

26. C.M. Brown, "Hydrogen Storage in Metal Organic Frameworks," DOE EERE Annual Merit Review, Arlington, VA, May 2013. (invited)

27. H. Wu, "Novel Hydride Materials for Hydrogen Storage," Gordon Research Conference on Hydrogen-Metal Systems, Lucca (Barga), Italy, Jul. 2013.

28. N. Verdal, T.J. Udovic, J.J. Rush, A.V. Skripov, X. Liu, E.H. Majzoub, J.J. Vajo, and A.F. Gross, "Reorientational Mobilities and Mechanisms of BH_4^- Anions in $LiBH_4$: Effects of Iodide Substitution and Nanoconfinement," Gordon Research Conference on Hydrogen-Metal Systems, Lucca (Barga), Italy, Jul. 2013.

29. O.A. Babanova, A.V. Soloninin, A.V. Skripov, V. Stavila, N. Verdal, T.J. Udovic, and J.J. Rush, "Nuclear Magnetic Resonance Studies of Reorientational Motion in $A_2B_{12}H_{12}$ (A = Na, K, Rb, Cs)," Gordon Research Conference on Hydrogen-Metal Systems, Lucca (Barga), Italy, Jul. 2013.

REFERENCES

1. T. J. Udovic *et al.*, J. Alloys Compds. (in press): dx.doi.org/10.1016/j.jallcom.2013.02.025.

2. N. Verdal *et al.*, J. Phys. Chem. C **117**, 876 (2013).

3. B. B. Kitchen *et al.*, J. Solid State Chem. **203**, 51 (2013).

4. N. Verdal *et al.*, J. Phys. Chem. C **117**, 12010 (2013).

5. E. G. Sorte *et al.*, J. Phys. Chem. C **117**, 8105 (2013).

IV.E.1 Fluid Phase Chemical Hydrogen Storage Materials

Benjamin L. Davis (Primary Contact),
Brian D. Rekken, and Troy A. Semelsberger
Materials Physics and Applications, Materials Synthesis and Integrated Devices
Los Alamos National Laboratory (LANL), MS J514
P.O. Box 1663
Los Alamos, NM 87545
Phone: (505) 500-2463
Email: bldavis@lanl.gov

DOE Managers
Grace Ordaz
Phone: (202) 586-8350
Email: Grace.Ordaz@hq.doe.gov
Ned Stetson
Phone: (202) 586-9995
Email: Ned.Stetson@ee.doe.gov

Partner
Tom Baker, University of Ottawa, Ontario, Canada

Project Start Date: October 1, 2010
Project End Date: January 1, 2014

Overall Objective

Develop fluid, pumpable ammonia-borane (AB)-based fuels using ionic liquids that have sufficient H_2 content, release kinetics, and stability for use by the Hydrogen Storage Engineering Center of Excellence (HSECoE) for vehicular applications.

Fiscal Year (FY) 2013 Objectives

Further refine additives that incorporate neutral and ionic functionalities, that react with AB to yield fluid phase pumpable products.

Technical Barriers

This project addresses the following technical barriers from the Storage section of the Fuel Cell Technologies Office Multi-Year Research, Development, and Demonstration Plan:

(A) System Weight and Volume

(D) Durability/Operability

(E) Charging/Discharging Rates

Technical Targets

A significant barrier to the application of off-board regenerable hydrogen storage materials is on- and off-boarding of the fuel and spent fuel, respectively. A fluid, pumpable fuel that remains liquid through dehydrogenation to the spent fuel form is desired for readily engineered fueling concepts. This project is exploring other compositions of AB/room temperature ionic liquid (RTIL) systems; the original concept was developed within Center of Excellence in Chemical Hydrogen Storage by Professor Larry Sneddon of the University of Pennsylvania. This work showed great promise with excellence gravimetric and volumetric capacities as well as discharging rates. Subsequent work at LANL has shown that these RTIL-based fuels could also be regenerated off-board without separating the spent fuel from the RTIL. Successful development of fluid systems should meet the following DOE 2017 and HSECoE targets:

- Gravimetric capacity (1.8 kWh/kg)
- Volumetric capacity (1.3 kWh/L)
- H_2 discharge rate (minimum full flow rate 1.5 kg H_2/min)
- H_2 purity (99.97% H_2)
- Start-up time to full flow (5 s @ 20°C, 5 s @ -20°C)
- Shelf life: loss of usable H_2 (0.05 g/hr-kg H_2 stored)
- HSECoE: 40 wt% AB dissolved or slurried

FY 2013 Accomplishments

- Designed and synthesized ionic liquids tethered to amineboranes (ILTA).
- Demonstrated several examples of ILTA that remain a liquid after H_2 release and cooling to room temperature (RT).
- Initial examples of ILTA/AB mixtures yield liquid products after H_2 release and cooling to RT.
- A survey of neutral functionalities tethered to aminboranes was completed, with an additional candidate (benzylamineborane) evaluated. Currently none of the surveyed additives incorporating neutral functionalities are able to form slurries with AB that exceed the stored H_2 wt% demonstrated by hexylAB/AB described last year.
- Quantitatively observed that H_2 impurities are a function of AB particle size. A method for generating very small AB particles is detailed.

✧ ✧ ✧ ✧ ✧

INTRODUCTION

Chemical hydrogen storage (CHS) involves storing H_2 in molecular chemical bonds where an onboard chemical reaction is used to release H_2. Currently the resulting spent fuel may be regenerated off-board using chemical processing. CHS provides a diversity of options to enable H_2 for transportation as well as other niche and stationary applications. Especially attractive, CHS offers the potential for no direct H_2 handling by the consumer, as well as low pressure storage concepts.

Researchers at LANL and the University of Ottawa are focused on the development of liquid AB fuels that integrate with the HSECoE. We are currently studying the formation, stability, and catalytic release of H_2 from these materials.

APPROACH

A serious drawback of AB-based pumpable fuels is product precipitation during H_2 removal. To address this concern, we are developing functionalized amineborane additives which react with AB to generate fluid products. The functionalities have the additional benefit of preventing the formation of gaseous impurities such as ammonia or borazine. Two classes of functionalities are being explored—inexpensive, off-the-shelf, neutral organic components and ionic liquid moieties that covalently attached to an amine. Currently fuel mixtures are heated for an extended period and their final phase assessed at the end of the experiment. Future experimental apparatus will assess the point in which the fuel's viscosity sharply increases, allowing us to identify which functionalities have the greatest impact on phase properties.

RESULTS

Building on FY 2012's results with functionalized amineborane additives, Ottawa surveyed available amines that are inexpensive yet may generate fluid phase properties in the AB slurry. A group of hydrophobic amines incorporating a phenyl functional group were chosen because of the possible pi-pi interactions with imidazolium-based ionic liquids. A list of the amineboranes synthesized along with their initial/final states after heating to 130°C is shown (Table 1).

TABLE 1. Amineboranes Synthesized along with their Initial/Final States after Heating to 130°C

Amine-Borane	H_2 Charged State at RT	H_2 spent State at RT
benylamine-borane	Solid (m.p. 57°C)	Solid
o-methylbenzylamine-borane	Solid (m.p. 110°C)	Solid
3-phenylpropylamine-borane (3-PPAB)	Liquid	Liquid

m.p. – melting point

Previous experience with AB and ionic liquids has shown that two solids may deliquesce, and as such mixtures of the above amineboranes with AB were examined. Only the liquid 3-PPAB formed a slurry with AB (1:1 molar), which became a homogenous liquid after H_2 release like hexylamineborane [1]. Although we did not determine the upper bound of AB that could be slurried with 3-PPAB, the 4.8 wt% of stored H_2 does not meet the HSECoE target for a slurry and thus this avenue of pursuit was suspended.

In conjuction with our HSECoE partners, an amineborane described last year was up scaled to use in reactor evaluations. Although 3-methoxypropylamineborane (3-MPAB) only stores 3.9 wt% H_2 neat, this amineborane readily forms slurries with AB (for instance a 1:1 molar slurry is 6.5 wt% H_2), and thus could meet the HSECoE target of 40 wt% AB or 6 wt% H_2 stored overall. H_2 measurements indicated 3-MPAB only released a portion of its stored H_2 [2] and ^{11}B NMR of the spent fuel indicated the presence of 3-MPAB and intermediate borazanes (Figure 1). One reason for the incomplete H_2 release from 3-MPAB could be the volatility of the 3-methoxypropyl functional group which allows the fuel and its intermediates to leave the reactor (parent amine boiling point ~120°C).

To avoid issues of volatility and possibly avoid the use of a pure ionic liquid entirely, amineboranes were covalently attached to an ionic liquid. Using a four step synthetic pathway multiple derivatives were formed (Figure 2), only a couple of which are liquid at room temperature (F, G).

Although the ILTAs made to date are insufficient to meet DOE targets in pure form, blends with AB were evaluated to increase stored H_2 density. ILTA "G" can be slurried with 2 equivalent of AB, yielding a material with 2.8 wt% H_2 that still remains liquid after H_2 release. Unfortunately the stored H_2 density can't be increased further; somewhere between 2 and 5 equivalent of AB, the products of H_2 release become solid.

The HSECoE has previously noted that the size of their AB particles was critical to forming slurries with silicon oil [3]; while releasing H_2 from the AB/ILTA fuel blends, it became evident that the size of AB may also affect the amount of impurities with the H_2 stream as well. By dissolving AB in dry tetrahydrofuran and rapidly adding hexanes, very small AB particles were produced (Figure 3). Evaluating the impurities in the H_2 release stream, not surprisingly, showed fewer impurities associated with AB using the smaller particles. We attribute this to the better mixing of the ILTA and AB, where there is a better chance to co-oligomerize/polymerize.

CONCLUSIONS AND FUTURE DIRECTIONS

- A survey of neutral functionalities tethered to AB is complete; 3-phenylpropyl was found to perform in

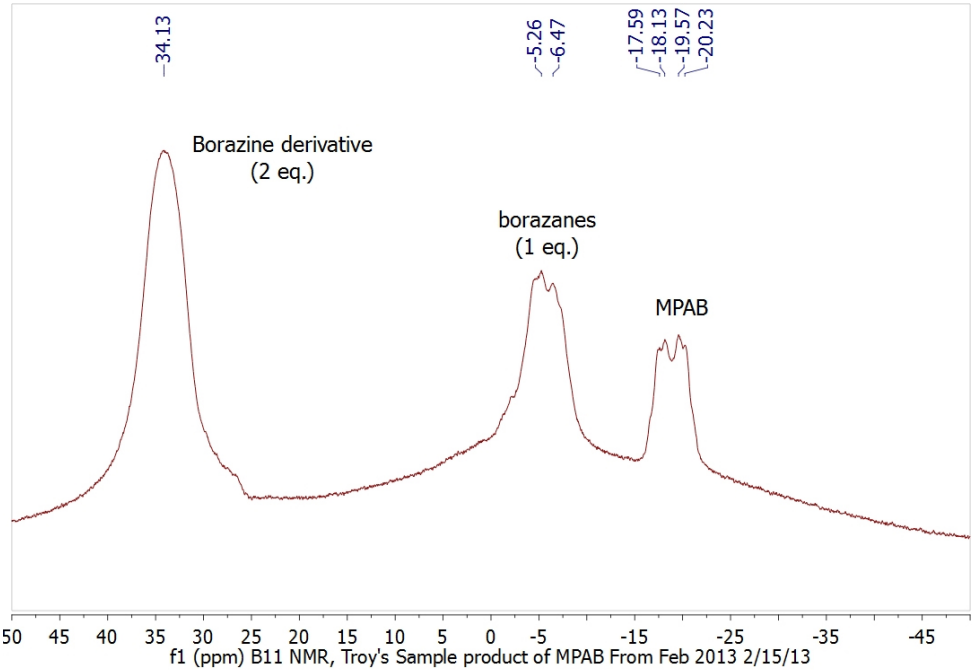

FIGURE 1. ^{11}B NMR of Spent 3-MPAB Fuel after Flowing thru the HSECoE Reactor

Additive	Identifier	Initial State(20 °C)	Spent State (20 °C)	Wt. % H_2
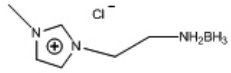	A	Solid	Solid	2.5
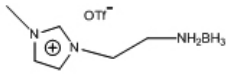	B	Solid	Solid	1.5
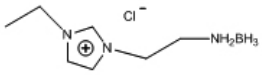	C	Solid	Solid	2.3
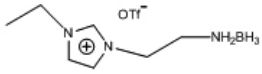	D	Oily Wax	Solid	1.4
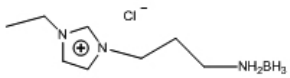	E	Solid	Solid	2.1
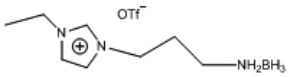	F	Liquid	Viscous liquid	1.4
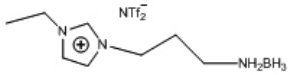	G	Liquid	Liquid	1.0

FIGURE 2. List of ILTA Synthesized, wt% H_2, and Room Temperature State before and after H_2 Release

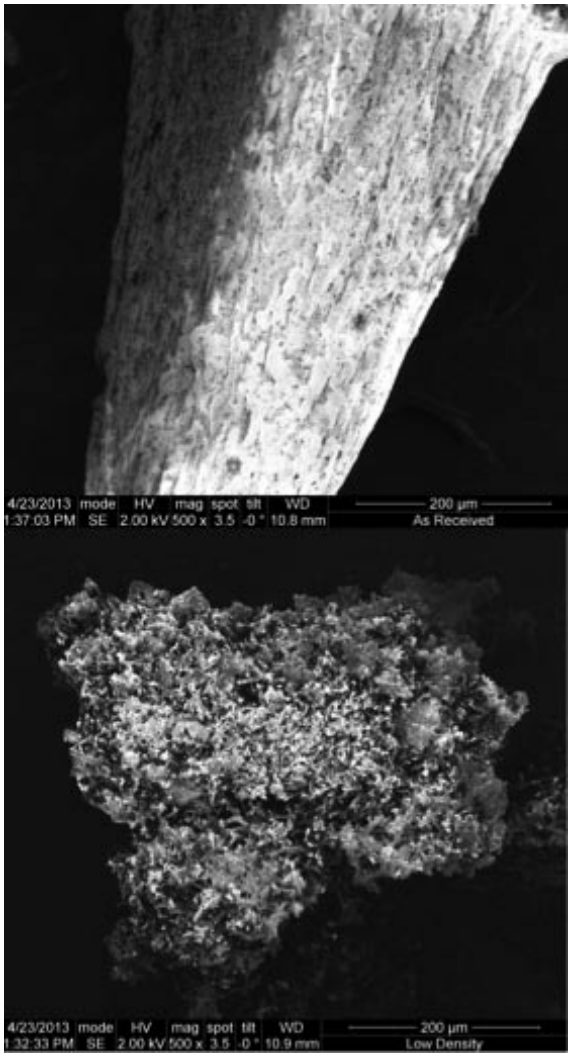

FIGURE 3. Scanning Electron Microscope Images of AB, as Received from JSC Aviobor (top), and Precipitated AB (bottom)

fashion similar to the hexyl moiety described last year. None of the neutral additives appear able to dissolve AB.

- Up scale and evaluation of 3-methoxypropylamineborane for HSECoE reactor testing suggests that neutral functionalities require higher boiling points than 120°C for the parent amine.
- Ionic liquids tethered to amineboranes were successfully synthesized and evaluated. Current derivatives store H_2 insufficiently and have limited ability to form slurries with AB that form fluid phase products and meet HSECoE material targets.
- Fine particle AB was produced that yields less impurities from AB/additive blends.

SPECIAL RECOGNITIONS & AWARDS/ PATENTS ISSUED

1. Nonprovisional patent application submitted for functionalized amineborane/AB fuel blends (13850959).

FY 2013 PUBLICATIONS/PRESENTATIONS

1. "Possible Gasoline Substitute: Storing H_2 Chemically for Automotive Applications" Bowdoin College, Sept 2012.

2. Benjamin L. Davis, Brian Rekken, Ryszard Michalczyk, Edward B. Garner, III, David A. Dixon, Hassan Kalviri, R. Tom Baker, and David L. Thorn. "Lewis Base Assisted B-H Bond Redistribution in Borazine and Polyborazylene" *Chem. Comm.*, **2013**, DOI:10.1039/C3CC44748K.

REFERENCES

1. IV.B.2 Fluid Phase Chemical Hydrogen Storage Materials, FY 2012 Annual Progress Report, DOE Hydrogen and Fuel Cells Program.

2. IV.B.4 Hydrogen Storage Engineering Center of Excellence: Chemical Hydrogen Rate Modeling, Validation, and System Demonstration, FY2013 Annual Progress Report, DOE Hydrogen and Fuel Cells Program.

3. Materials Operating Requirements, Chemical Hydrogen Storage. FY2013 Hydrogen Storage Engineering Technical Team Review, Ronnebro, E.; Westman, M.; Chun J.; Karkamkar, A. March 20–21, 2013, Southfield MI.

IV.E.2 Development of a Practical Hydrogen Storage System Based on Liquid Organic Hydrogen Carriers and a Homogeneous Catalyst

Craig Jensen[1] (Primary Contact), Daniel Brayton[1], and Scott Jorgensen[2]
[1]Hawaii Hydrogen Carriers, LLC
531 Cooke Street
Honolulu, HI 96813
Phone: (808) 339-1333
Email: hhcllc@hotmail.com

DOE Managers
Ned Stetson
Phone: (202) 586-9995
Email: Ned.Stetson@ee.doe.gov
Katie Randolph
Phone: (720) 356-1759
Email: Katie.Randolph@go.doe.gov

Subcontractor:
[2]General Motors Technical Center, Warren, MI

Contract Number: DE-EE0005020

Project Start Date: July 1, 2011
Project End Date: November 31, 2013

Objectives

The objective of this project is to optimize a hydrogen storage media based on a liquid organic hydrogen carrier (LOC) and design a commercially viable hydrogen delivery system based on this LOC media. The project consists of two parts: Part 1 (conducted at Hawaii Hydrogen Carriers, LLC has the objective to develop an optimized catalyst/organic carrier combination; and Part 2 (conducted at General Motor Research Center) has the objective of designing of a space, mass and energy efficient tank and reactor system to house the carrier and release hydrogen.

Fiscal Year (FY) 2013 Objectives

- Identify an LOC that undergoes pincer complex catalyzed, selective dehydrogenation at higher rates and with higher hydrogen cycling capacity than methylperhydroindole.
- Determine if the activity of economically viable, low (100 ppm) PCP pincer catalyst loadings are adequate to meet the demands of an automotive fuel cell.
- Initiate long-term, scale-up, dehydrogenation/re-hydrogenation cycling studies.

Technical Barriers

This project addresses the following technical barriers from the Hydrogen Storage section of the Fuel Cell Technologies Office Multi-Year Research, Development, and Demonstration Plan:

(A) System Weight and Volume

(B) System Cost

(C) Efficiency

(E) Charging/Discharging Rates

(H) Balance-of-Plant (BOP) Components

(J) Thermal management

(Q) Regeneration Processes

Technical Targets

1. Identification of a low-cost LOC that, in the presence of low loading of a homogeneous pincer catalyst, will release >7 wt% H_2 at sufficiently high rates and low temperatures in a practical, onboard dehydrogenation reactor to meet the demands of an onboard fuel cell.
2. Identification of a LOC/pincer catalyst combination of sufficiently high hydrogen cycling capacity that rapidly dehydrogenates without also undergoing LOC degradation upon cycling.
3. Utilization of the advantages of the liquid hydrogen storage medium to eliminate thermal management problems associated with solid-state hydrogen absorbing materials.
4. Design of a space-, mass- and energy-efficient tank and reactor system to house the LOC and facilitate hydrogen release that can be easily interfaced with a fuel cell.

FY 2013 Accomplishments

- Identification of a higher performance LOC, butylperhydropyrolidine (BHP) that undergoes pincer complex catalyzed dehydrogenation at practical rates at 140ºC.
- Demonstration of the dehydrogenation of LOCs at practical rates at low, economically viable, 100-ppm catalyst loadings.
- Demonstration that the reversible dehydrogenation of both BHP and methylperhydroindole, (MHI) can be subjected to at least 25 cycles of dehydrogenation and re-hydrogenation with virtually no degradation of the

LOC or the phosphorus-carbon-phosphorus (PCP) pincer catalyst.

- Determination that while a double helical reactor would provide a significant saving of space, it would not improve heating efficiency and would be prohibitively costly.

✧ ✧ ✧ ✧ ✧

INTRODUCTION

For decades, hydrogen has been targeted as the utopian fuel of the future on account of its abundance and environmental friendliness. However, a major difficulty in the utilization of hydrogen as a fuel for vehicles is the problem of onboard storage because hydrogen is problematic to store at high density. While this is a major problem for vehicles, it is also a significant problem for portable power as it adds to both the cost and inconvenience of frequent delivery and change-over of hydrogen supply for all fuel cell applications. Thus a high density, high stability method for storing hydrogen is essential to the implementation of fuel cells in all but a few niche applications. Another major concern about hydrogen is putting an infrastructure in place. While this could be done for any form of hydrogen carrier, the barrier to implementing an LOC would be significantly lower than others because it is a similar type of chemical to the current distribution system. The tanks, piping and refinery systems used to make and deliver gasoline are appropriate for LOCs. In addition to the easy adaption to existing infrastructure, LOCs have many other enormous practical advantages. Cheap, abundant LOCs can reversibly release 7-8 wt% hydrogen. They can be economically manufactured in the massive quantities required to meet the anticipated demand and would eliminate the thermal management problems commonly associated with the systems based on solid-state hydrogen absorbing materials. The technology has the potential to exceed the performance of carbon-emitting technologies such as direct methanol fuel cell. We have recently discovered catalysts that enable this technology that has remained a tantalizing but impractical possibility over the last 60 years. This project targets the development of a commercially viable LOC-based hydrogen storage and delivery system. The project consists of two parts: 1) development of an optimized catalyst/carrier combination; and 2) the design if a space, mass, energy efficient tank and reactor system to house the carrier and release the hydrogen.

Although promising hydrogen cycling performances have been demonstrated, these previous LOC studies utilized very high loadings of heterogeneous and precious metal catalysts in order to achieve acceptable dehydrogenation kinetics at temperatures that are near the operating temperatures of proton exchange membrane (PEM) fuel cells (≤150ºC). The high cost of the massive quantities of precious metals precludes the commercialization of these systems.

In order to overcome the barrier to practicality that is imposed by the heterogeneous catalysts, we have developed alternative homogeneous catalysts. Homogenous catalytic systems typically operate at significantly lower temperatures and show much greater product specificity than their heterogeneous counterparts. In 1997, we discovered that the "pincer" complex, $IrH_2\{2,6\text{-}C_6H_3\text{-}CH_2PBu^t{}_2\}_2$ (1), catalyzes the dehydrogenation of cycloalkanes to arenes. This was the first report of a homogenous catalyst for this reaction. The unique reactivity of this especially robust and active catalyst can be ascribed to the tridentate "PCP pincer" ligands which contain two coordinating, neutral phosphorus centers as well as an anionic, coordinating carbon site. It has been found that electronic environment of the catalytic metal center of the pincer complex is highly sensitive to minor changes in the PCP pincer ligand. Following our report that 1 catalyzes the dehydrogenation of aliphatic groups, the related PCP pincer complexes, $IrH_2\{2,6\text{-}C_6H_3\text{-}CH_2PPr^i{}_2\}_2$ (2) and $IrH_2\{C_6H_3\text{-}2,6\text{-}(OPBu^t{}_2)_2\}$ (3) were shown to shown to have incremental improvement in catalytic efficiency. It is now well established that dihydro PCP pincer iridium complexes can selectively dehydrogenate aliphatic groups under much milder conditions than those required for the corresponding heterogeneous catalysts, such as platinum on alumina without harm to other functional groups of an organic molecule.

More recently, we found 1 and the related complexes, 2 and 3, to be highly to be active catalysts for the dehydrogenation of amines, ethylperhydrocarbazole (EHC) and other heterocyclic LOCs.

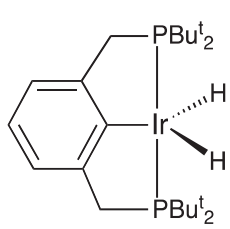

$IrH_2\{2,6\text{-}C_6H_3\text{-}CH_2PBu^t{}_2\}_2$ (1)

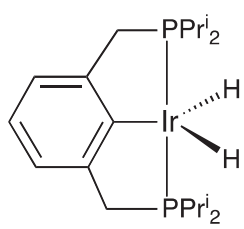

$IrH_2\{C_6H_3\text{-}2,6\text{-}(CH_2PPr^i{}_2)_2$ (2)

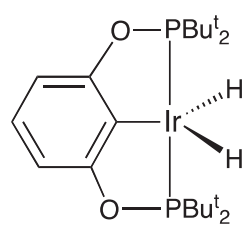

$IrH_2\{C_6H_3\text{-}2,6\text{-}(OPBu^t{}_2)_2$ (3)

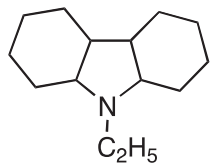

N-ethylperhydroethylcarbazole (EHC)

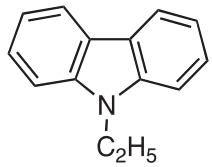

N-ethylcarbazole (EC)

Recently, we synthesized the novel AsCAs pincer complex, $IrH_2\{C_6H_3\text{-}2,6\text{-}(OAsBu^t_2)_2\}$ (4), and found it to be a highly active dehydrogenation catalyst for LOCs. At 150°C, 4 catalyzes the dehydrogenation of EHC at rates that are nearly double those achieved with 3. Furthermore, it exhibited acceptable activity at 125ºC, a temperature at which the PCP catalysts are completely inactive.

APPROACH

Clearly, our studies of the LOC/pincer catalyst systems have demonstrated the potential of these systems to serve as the basis of a practical hydrogen storage system. However, further studies must be conducted to find the system and conditions that gives the best combination of high cycling capacity, rapid dehydrogenation kinetics, and lack of LOC degradation upon cycling. In order to accomplish this we are conducting the following four tasks:

Task 1.1 Isothermal kinetic studies of the pincer complex catalyzed dehydrogenation of the candidate LOCs, N-EHC, N-MHI, perhydro-indolizidine (HIZ), and aminomethyl-cyclohexane.

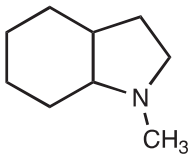

perhydro-methylindole

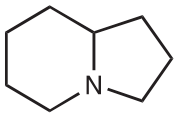

perhydro-indolizidine (HIZ)

Task 1.2 In cases where incomplete dehydrogenation of the LOC is observed, studies of the dehydrogenation reaction in the presence of a hydrogen acceptor (transfer dehydrogenation) are being carried out to determine if the reaction is limited by kinetic or thermodynamic constraints.

Task 1.3 Studies to determine if the formation of unwanted side products that arise in some LOC systems can be controlled by the addition of additives.

Task 1.4 Cycling studies to determination if LOC/catalyst combinations that have acceptable dehydrogenation kinetics and capacity will undergo cycling without degradation of LOC and/or catalyst.

Additionally, the practical advance of LOC systems also requires the design of a deployable reactor to house the LOC and facilitate the hydrogen release that can be easily interfaced with a fuel cell. The U.S. DRIVE Hydrogen Storage Tech Team and the reviewers at the Annual Merit Review concluded that much of the value of the engineering portion of the project had already been harvested by the general case analysis. Both sets of reviewers advised us that the engineering portion of the project should be curtailed and that a significantly increased portion of the remaining resources should be used to try to identify an LOC with higher practically available hydrogen. During the past year have taken heed of this advice and reduced the scope of our engineering efforts as detailed in the following.

2.1 Model Development The sub-task is divided into four parts. The first part is to devise a notional model of the entire system. In Part 2, one or more reactor model(s) are developed in detail using COMSOL. As the model or models are completed, they are validated in Part 3 to be certain the fluid mechanics, heat transfer, and reaction proceed as would be expected based on the standard engineering concepts. Part 4 entails a basic estimate of the cost of the system.

2.2 Function Evaluation Our experience indicates that the system function and cost is often fixed by the full flow condition. To ensure efficient use of resources, we will evaluate this functionality first. Once the reactor "runs" at the full-flow condition it will be evaluated at idle. Once these extremes have been evaluated, the mid-speed/mid-load condition will be evaluated and finally transient performance is then evaluated.

2.3 System Optimization This task is centered on improving the storage materials. Based on what we have learned about the system function, we will look for both reactor and BOP aspects where cost-effective change is possible. However, we are focusing on aspects of the LOC enable that can lead to significant improvements in the overall system.

2.4 Final Simulations Steady-state and transient simulations are being carried out.

RESULTS

Catalyst and LOC Optimization

Task 1.1 Isothermal Kinetic Studies

During the past year, we obtained improved kinetic data that allowed us to derive more reliable values for the activation energies (MHI, 132 kJ/mol; EHC 107 kJ/mol) and frequency factors (MHI, 7.23×10^9 $M^{-1}s^{-1}$, EHC 4.53×10^7 $M^{-1}s^{-1}$). We also determined that contrary to the indications of preliminary studies we reported last year, higher initial rates of LOC dehydrogenation are achieved with the AsCAs pincer complex, $IrH_2\{C_6H_3\text{-}2,6\text{-}(OAsBu^t_2)_2\}$. However, the AsCAs pincer complex has much lower thermal stability than the PCP and begins to undergo significant decomposition

within a few hours at the temperatures required for the dehydrogenation reaction.

We have previously determined that the iridium PCP pincer catalyst, $IrH_2\{C_6H_3\text{-}2,6\text{-}(OPBu^t_2)_2\}$ catalyzes the dehydrogenation of the nitrogen-containing 5-membered ring of MHI and EHC at rates that are adequate for PEM fuel cell applications in the 150-200ºC temperature range. These findings led us to explore the dehydrogenation of butyl perhydropyrolidene (BHP).

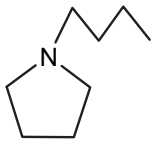

Butyl perhydropyrolidine (BHP)

During the past year, we found that the 5-member ring of BHP undergoes dehydrogenation at significantly higher rates than that of MHI. For example, virtually quantitative dehydrogenation was found to occur at 140ºC in 18 h. Although isothermal kinetic studies of BHP indicate the activation energy for the dehydrogenation of BHP (166 kJ/mol) is actually higher than for MHI, the frequency factor is 4 orders of magnitude higher (2.17×10^{14} $M^{-1}s^{-1}$). Thus the higher rates of dehydrogenation are apparently due to BHP having much less steric constraint than MHI in accessing the metal center of the pincer catalyst.

The FY 2012 Annual Merit Review reviewers were concerned that the PCP pincer catalyst is based on a precious metal and therefore might be prohibitively expensive for utilization in a commercially affordable hydrogen storage system. The high cost of iridium is indeed a very significant consideration. According to our calculations, the cost of the catalyst would be acceptable only if extremely low catalyst loadings were able to effect the dehydrogenation LOCs at rates that could meet the operational demands of an onboard PEM fuel cell. According to our calculations, an acceptable cost of $5/liter would allow a catalyst loading of only 100 ppm as opposed to the much higher, 1 mol% catalyst concentrations that were used in our previous studies. We have found that acceptable rates of dehydrogenation can be achieved the low, 100-ppm catalyst concentrations. These finding suggest the iridium-based catalyst could indeed be economically viable.

Surprisingly, we found that the pincer complex exhibits higher catalytic activities at the lower level loadings (rate constants of 1.37×10^{-3} and 2.75×10^{-4} s^{-1} for BHP and MHI respectively). We believe this is an experimental artifact due to the deposition of significants amounts of catalyst on the walls of our reactors when they are loaded with 1 mol% catalyst solutions. Therefore, we feel that the kinetic values obtained at the 100-ppm catalyst loadings are the more accurate than those based on the 1 mol% solutions.

Task 1.2 Differentiation of Thermodynamic vs. Kinetic Limitations

We have previously determined that, as seen in Equation 1, the iridium PCP pincer complex, $IrH_2\{C_6H_3\text{-}2,6\text{-}(OPBu^t_2)_2\}$ efficiently catalyzes the dehydrogenation of the nitrogen-containing 5-membered ring of MHI but exhibits only modest activity with the 6-membered ring. This was also found to be the case for HIZ and EHC. In order to differentiate whether this due a high kinetic barrier to the dehydrogenation of the 6-member rings, or high C-H bond strengths in the saturated 6-membered rings, and thus unfavorable free energies of dehydrogenation in the

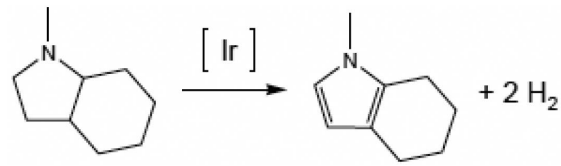

(1)

160-200°C temperature range, we carried out studies of the dehydrogenation of MHI and EHC in the presence of the hydrogen acceptor, t-butylethylene. In all cases, gas chromatograph-mass spectrometry (GCMS) analysis of the product mixture contained less than 5% conversion to the fully dehydrogenated products, N-methylindole and N-ethylcarbozole while the partially dehydrogenated products, N-methyl-tetrahydroindolizidine and N-ethyloctahydrocarbazole were obtained in >95% yield. Thus the more favorable thermodynamics of the transfer dehydrogenation reactions did not result in the production of the fully dehydrogenated products. We conclude that resistance to the dehydrogenation of the 6-membered rings is due to kinetic constraints.

Task 1.3 Additive Intervention of Side Reactions

Work on this task was completed last year.

Task 1.4 Cycling Studies

During the past year, we constructed and tested two reactors for our scale-up cycling studies. Initial cycling experiments were run with the homogenous PCP pincer complex serving as both the dehydrogenation and re-hydrogenation catalyst. MHI was dehydrogenated and re-hydrogenated 10 times and GCMS and nuclear magnetic resonance (NMR) analysis was carried out after each half cycle. No traces of LOC or catalyst decomposition products were detected. However, only 89% re-hydrogenation was achieved in these experiments. In order to achieve 100% re-hydrogenation, second set of cycling studies have been initiated in which 100 ppm of Pd on carbon black was included with the solution of pincer complex and LOC. Studies are currently being carried out on both MHI and BHP. To date, 25 cycles of dehydrogenation and re-hydrogen have been preformed. GCMS and NMR analysis confirmed that there has been virtually no degradation of the LOC or

catalyst during 1 million catalytic turnovers that the pincer catalyst has performed to date.

Reactor Design and Modeling Tasks

As mentioned before, the engineering portion of the project was curtailed in accordance with the recommendation of two sets of project reviewers.

Task 2.1 Model Development Our previous modeling studies have shown that helical reactors reduce heat loss in the system and that the mass and volume of the reactor can be significantly reduced by use of micro-channel heat exchangers. During the past year we have designed a double helical reactor that would provide a further significant saving of space.

Task 2.2 Function Evaluation While the double helical reactor provides a significant savings of space. It does not improve the heating efficiency and is prohibitively costly.

Task 2.3 System Optimization Modeling studies show that heat transfer is most effective in a helical reactor. Better heat transfer allows a short, easy to package reactor that reduces heat loss.

Task 2.4 Final Simulations Simulations have been carried out using the rate constants and activation energies that were determined in our isothermal kinetic studies. These studies indicate that if the dehydrogenation kinetics could be improved by a factor of 10, hydrogen could be evolved from a helical reactor containing 100 L of BHP at a rate adequate to meet the requirements of an onboard automotive PEM fuel cell.

CONCLUSIONS

Our previous studies have shown that the PCP pincer complexes effectively catalyze the rapid dehydrogenation of saturated 5-membered, nitrogen-containing rings. During the past year we have determined that higher initial rates of LOC dehydrogenation are obtained with the AsCAs pincer complex, $IrH_2\{C_6H_3\text{-}2,6\text{-}(OAsBu^t_2)_2\}$. However, the AsCAs pincer complex has much low thermal stability than the PCP and begins to undergo significant decomposition within a few hours at the temperatures required for the dehydrogenation reaction. During the past year, we have also found that BHP undergoes quantitative dehydrogenation at 140ºC in 18 h. This is significantly lower than the 160 and 180ºC temperatures that we previously found to be required to achieve the same rates for MHI and EHC, respectively. Thus the best LOC/catalyst combination that identified in our studies is BHP/$IrH_2\{C_6H_3\text{-}2,6\text{-}(OPBu^t_2)_2\}$.

We have found that acceptable rates of LOC dehydrogenation can be achieved at 200°C in the presence of only 100 ppm of the pincer catalyst. This translates to an acceptable catalyst cost of ~$5/L. Thus, effective loadings of the iridium-containing catalyst would not be cost prohibitive for an onboard, LOC-based hydrogen storage system. We have also carried out scale-up cycling studies with both MHI and BHP solutions containing low concentrations of the pincer catalyst. To date, 25 cycles of dehydrogenation and re-hydrogen have been carried out. GCMS and NMR analysis has verified that virtually no degradation of the LOC or catalyst occurred during the 1 million catalytic turnovers that the pincer catalyst has performed to date. This finding also indicates the PCP pincer catalyst could be in a practical LOC-based hydrogen storage system.

Our previous modeling studies have shown that helical reactors reduce heat loss in the system and that the mass and volume of the reactor can be significantly reduced by use of micro-channel heat exchangers. During the past year we have found that while a double helical reactor provides a significant saving of space, it does not improve the heating efficiency and is prohibitively costly.

FUTURE DIRECTIONS

LOC Screening and Evaluation

We plan to extend our scale-up, long-term cycling studies of BHP and MHI to 100 cycles of dehydrogenation/re-hydrogenation.

Reactor Design

We plan to carry out a final simulation modeling of our best helical reactor design using the final higher rate constants that were derived from our studies of solutions of BHP and MHI containing low concentrations of the PCP pincer catalysts. The results of the modeling study will be evaluated in order to determine if the operation of the system with our best combination of LOC and pincer catalyst is practically viable.

FY 2013 PRESENTATIONS

1. "Development of Liquid, High Capacity Hydrogen Carriers", C.M. Jensen, D. Brayton, S. Jorgensen, G. Severa, E. Rönnebro, M. Chong, T. Autrey, A. Karkamkar, and S. Orimo, Materials for Hydrogen Storage – Future Perspectives, Kirkenes, Norway, 06/20/12.

2. "Development of Liquid, High Capacity Hydrogen Carriers", C.M. Jensen, D. Brayton, S. Jorgensen, G. Severa, E. Rönnebro, M. Chong, T. Autrey, A. Karkamkar, and S. Orimo, International Symposium on Metal-Hydrogen Systems; Kyoto, Japan,10/06/12.

3. "Development of Liquid, High Capacity Hydrogen Carriers", C.M. Jensen, D. Brayton, S. Jorgensen, M. Chong, J. Wang and S. Orimo, 7th EMPA Hydrogen and Energy Symposium, Stoos, Switzerland 01/22/13.

IV.E.3 Novel Carbon(C)-Boron(B)-Nitrogen(N)-Containing H_2 Storage Materials

Shih-Yuan Liu
University of Oregon
Department of Chemistry
1253 University of Oregon
Eugene, OR 97403-1253
Phone: (541) 346-5573
Email: lsy@uoregon.edu

In collaboration with:

- Dr. Tom Autrey, Dr. Abhi Karkamkar, and Mr. Jamie Holladay
  Pacific Northwest National Laboratory
- Dr. David Dixon
  The University of Alabama
- Dr. Paul Osenar
  Protonex Technology Corporation

DOE Managers
Grace Ordaz
Phone: (202) 586-8350
Email: Grace.Ordaz@ee.doe.gov
Katie Randolph
Phone: (720) 356-1759
Email: Katie.Randolph@go.doe.gov

Contract Number: DE-EE0005658

Project Start Date: March 5, 2012
Project End Date: March 14, 2015

Overall Objective

Develop new CBN-based chemical hydrogen storage materials that have the potential to meet the DOE technical targets for automotive applications.

Fiscal Year (FY) 2013 Objectives

- Synthesize Compound **E** and its derivatives
- Develop catalysts that can achieve H_2 desorption from the carbon portions of the CBN compounds to achieve higher storage capacity of these materials
- Determine the thermodynamics and kinetics for the desorption of Compound **H**
- Characterize the viscosity of spent fuel of Compound **B** and its fuel blends
- Complete the potential energy surface calculations for the potential diverse pathways of H_2 desorption from Compound **B**

Technical Barriers

This project addresses the following technical barriers from the Hydrogen Storage section of the Fuel Cell Technologies Office Multi-Year Research, Development, and Demonstration Plan:

(A) System Weight and Volume

(C) Efficiency

(E) Charging/Discharging Rates

Technical Targets

This project is developing and characterizing new CBN materials for hydrogen storage. Insights gained from these studies will be applied toward the design and synthesis of hydrogen storage materials that meet the following DOE 2017 hydrogen storage system targets:

- Specific energy: 1.8 kWh/kg (5.5 wt%)
- Energy density: 1.3 kWh/L (4.0 vol%)

FY 2013 Accomplishments

- Synthesized 9 out of 12 proposed CBN materials
- Characterized all synthesized materials in terms of capacity, melting point, and density
- Characterized Compound **B** with regard to: viscosity, polarity, enthalpy of H_2 desorption, H_2 purity, thermal stability
- Characterized properties of fuel blends with **B** as the "solvent"
- Calculated important thermodynamic and kinetic parameters for select CBN compounds and developed a preliminary understanding of the desorption mechanism for CBN material **B**
- Demonstrated stable fuel cell operation with Compound **B**

✧ ✧ ✧ ✧ ✧

INTRODUCTION

Approaches to store H_2 in chemical bonds provide a means for attaining high energy densities. Molecular complexes containing protic and hydridic hydrogen such as ammonia-borane (AB) provide between 8 to 16 wt% H_2 at acceptable temperatures in a kinetically controlled decomposition. AB shows promise to meet a number of

important technological targets such as high volumetric and gravimetric density of H_2, fast kinetics, thermal stability, facile synthesis at large scale, and safe handling under atmospheric conditions. Some of the challenges involving AB include: volatile impurities (e.g., ammonia, diborane, borazine), handling of solids, and the economics of spent fuel regeneration [1-4].

This project is developing hydrogen storage materials that contain the element carbon in addition to boron and nitrogen. The inclusion of carbon can be advantageous for developing chemical H_2 storage materials that are structurally well defined (thus have good potential to be liquid phase), exhibit thermodynamic properties conducive to reversibility, and demonstrate good storage capacities.

APPROACH

This project will develop new CBN H_2 storage materials that have the potential to meet the DOE targets for motive and non-motive applications. Specifically, we will be focusing on three basic systems: 1) liquid-phase systems that release H_2 in a well-defined and high-yield fashion, minimizing the formation of NH_3 and $B_3N_3H_6$; 2) reversible storage systems that could potentially be regenerated onboard; and 3) high H_2-content storage systems that can be used in slurries and regenerated off-board (see Figure 1). Computational chemistry studies will help direct our research. Finally, we will demonstrate the developed material with a fuel cell. These new materials will be prepared and characterized by our interdisciplinary team comprised of the University of Oregon, The University of Alabama, Pacific Northwest National Laboratory, and Protonex Technology Corporation (Southborough, MA, a small business fuel cell manufacturer).

RESULTS

Characterization of the Liquid Carrier B and its Fuel Blends

In FY 2012, we synthesized a liquid carrier Compound **B** and developed catalytic conditions for the release of H_2 from this compound at 80°C. This year, we performed additional characterization studies of Compound **B** that are relevant to H_2 storage applications.

The thermal stability of liquid carrier **B** was investigated using thermal gravimetric analysis/mass spectrometry (TGA/MS). We did not detect any volatile materials (H_2, Et_2O, tetrahydrofuran [THF], pentane, etc.) in the mass spectrometer at 30°C. However, slight H_2 evolution can be observed starting at 50°C (Figure 2a, green trace; t = 360 min). Similarly, escape of residual diethyl ether (Figure 2a, black trace) and THF (Figure 2a, red trace) from the liquid carrier **B** can be observed starting at 50°C. Also, the thermal decomposition of Compound **B** was monitored using ^{11}B nuclear magnetic resonance spectroscopy, which corroborates the TGA/MS data and indicates that the liquid carrier **B** decomposes slowly at 50°C.

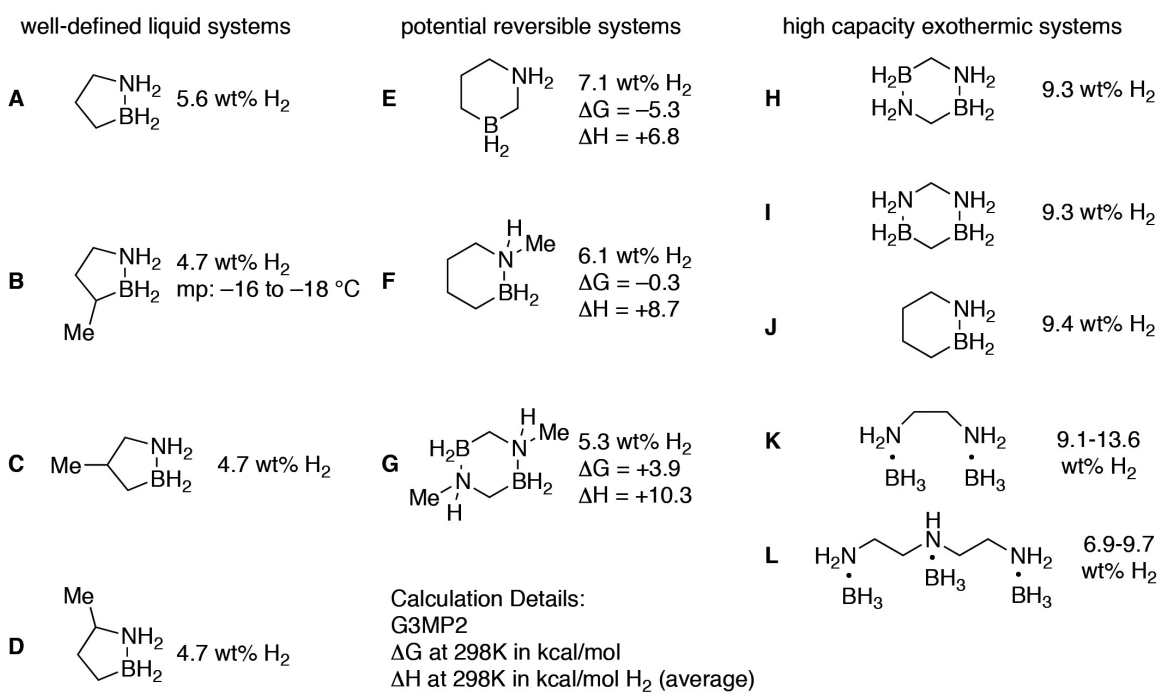

FIGURE 1. Selected synthetic targets and their potential storage capacities and predicted thermodynamic parameters.

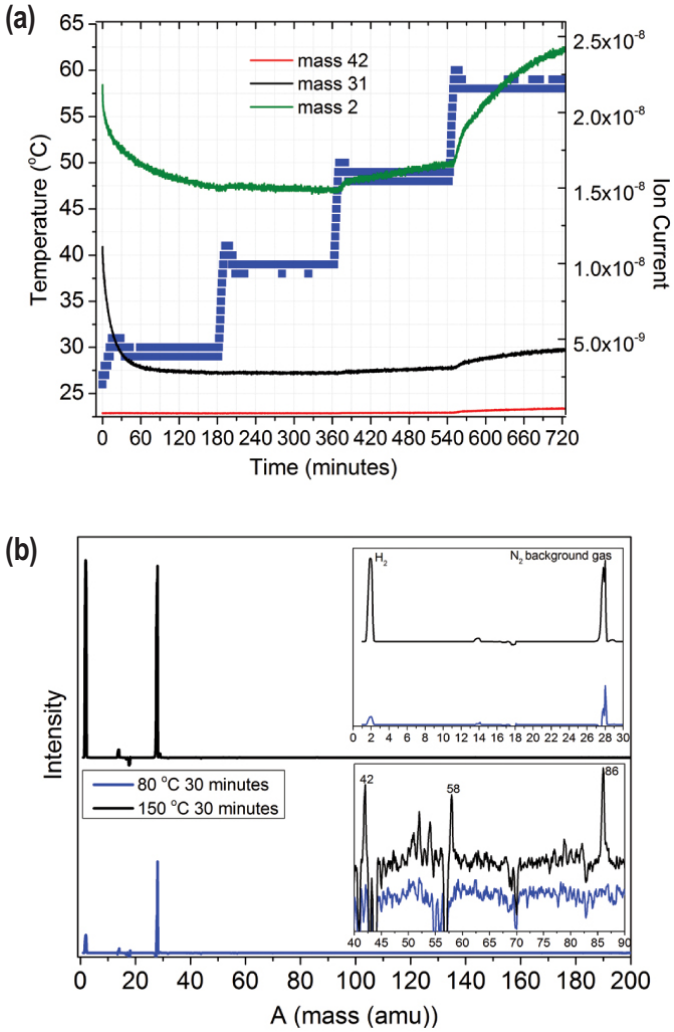

FIGURE 2. (a) MS coupled TGA: monitoring of volatile materials via mass spectrometry (green: hydrogen; black: diethyl ether; red: THF). (b) RGA data for liquid carrier **B** at 150°C (black trace) and at 80°C (blue trace). Top right inset: zoomed-in region below 30 amu. Bottom right inset: zoomed-in region from 40–90 amu.

The purity of generated H_2 gas is an important factor to evaluate the hydrogen storage material. We carried out residual gas analysis (RGA) of the volatile components when **B** was heated at 150°C, (Figure 2b, black trace) and at 80°C (Figure 2b, blue trace) to monitor the purity of H_2 generated from the desorption of **B**. As can be seen from the data, with the exception of some N_2 background gas, H_2 is the major detectable species both at 80 and 150°C. At 150°C, a trace amount of Compound **B** (amu = 86) can be detected in the gas stream (Figure 2b, bottom right inset). The data indicate that (1) both the starting material carrier **B** and its spent fuel trimer are not very volatile at an operating temperature of 80°C, and (2) the thermal hydrogen desorption from **B** does not lead to appreciable impurities in the H_2 gas stream. Some residual ether (THF, diethyl ether) from the synthesis was detected in some experiments, but notably no parent borazine $B_3N_3H_6$ was detected.

Another important characteristic of a liquid H_2 storage carrier is its viscosity. A viscosity value smaller than 500 cP is considered to be suitable for pumping [5]. We measured the viscosity of Compound **B** using a dynamic mechanical rheometer and found it to be 25 ± 5 cP at room temperature, which is comparable to that of ethylene glycol. Temperature dependent viscosity studies in the range of 15–50°C did not show significant changes.

We determined that AB is relatively soluble in the liquid Compound **B**. The resulting fuel blend (**B**: AB = 2:1 molar ratio) exhibits improved H_2 capacity (5.6 wt% H_2 vs. 4.7 wt% H_2 for pure **B**), faster kinetics (relative to thermal H_2 desorption for either pure B or AB), and produces a spent fuel that is a liquid at room temperature. RGA analysis of the volatiles that were released upon thermal decomposition shows no detection of borazine, ammonia, or diborane.

Synthesis and Characterization of New Targets D, G, and B-Methyl Substituted Amine-Boranes

With respect to new targets, we successfully synthesized targets **D, G,** and **H** and performed measurements of the dehydrogenation reaction of some of these compounds using the automated gas burette. At a concentration of 0.59 M in diglyme, we dehydrogenated Compound **D** using $CoCl_2$ and found that it took about 100 minutes to dehydrogenate two equivalents hydrogen at 80°C, which is much slower than any of the BN-cyclopentyl series, i.e., compounds **A-C**. As for Compound **G**, two equivalents of H_2 could also be released as expected at 0.17 M using Pd/C at 120°C.

In addition to the compounds listed in Figure 1, we synthesized *B*-methyl substituted amine-boranes for potential use in chemical hydrogen storage. Though many *N*-substituted amine-boranes have been studied, a relatively small number of *B*-substituted amine-boranes have been investigated. We synthesized *B*-methyl AB derivatives by mixing ammonium chloride or methylamine hydrochloride and lithium methylborohydride in ether solution to give NH_3BH_2Me and $MeNH_2BH_2Me$, respectively. We dehydrogenated both of these two compounds under Co(II) chloride catalysis at 80°C, the same as for Compound **B**. Two equivalents of hydrogen can be released from both *B*-methyl AB derivatives (Figure 3). The spent fuel product of $MeNH_2BH_2Me$ can be regenerated to the charged form with formic acid and lithium aluminum hydride.

Investigation of CBN Systems with Computational Chemistry

We have predicted the boiling points and many thermodynamic parameters (heats of formation, heats of dehydrogenation, etc.) of the target CBN compounds using computational chemistry. We have also been investigating possible mechanisms for the dehydrogenation of **B**. We began our work first using density functional theory at the B3LYP/DZVP2 level and then refined the calculations using the

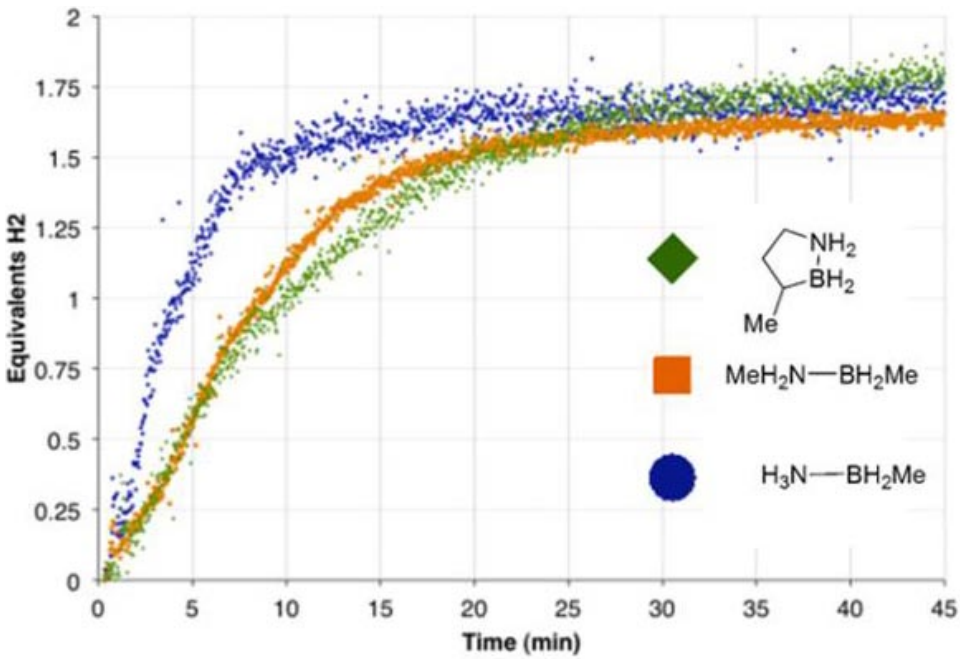

FIGURE 3. Synthesis and dehydrogenation of *B*-methyl AB derivatives

higher correlated molecular orbital theory G3MP2 level, all at 298 K. The potential energy surface for our current working mechanistic hypothesis for the dehydrogenation of **B** is shown in Figure 4. Compound **B** first forms a dehydrodimer with release of 2 equivalent of H_2 (Figure 4a). This dehydrodimer is in equilibrium with its dehydromonomer. This dehydromonomer of **B** can react with the dehydrodimer (Figure 4b) to generate a cyclotriborazane. The sequential release of hydrogen from the cyclotriborazane intermediate is exothermic by 24 kcal/mol to form the final spent fuel material (Figure 4c). The stepwise dehydrogenation reactions have barriers that decrease as each equivalent of hydrogen is released.

Scale-Up Synthesis and Fuel Cell Operation of Compound B

With preliminary RGA studies showing the purity of the hydrogen stream, we set out to test the hydrogen produced from **B** in a working fuel cell. However, this required the use of large quantities of material. In order to access larger quantities (~40 g), we had to modify the existing protocols to use techniques such as distillation and filtration that allow for greater scalability. Previously, we reported the isolation of less than 1 g at a time. Using the current system, we can isolate >10 g at a time. About 45 g of **B** have been produced in this manner. Additional compound **B** was obtained from recycling of its spent fuel according to our published procedures [6].

Initial fuel cell tests using Compound **B** showed the presence of some volatiles in the gas stream; the fuel cell stack performance decreased rapidly when its hydrogen source was switched from Protonex facility hydrogen to the hydrogen generated by the dehydrogenation of **B** using an iron(II) chloride catalyst. Upon investigation, we found that the gas stream contained miniscule amounts of THF, which was used in the preparation of **B**. We used a cold trap (dry ice/methanol) to collect volatiles when we tested **B** on the largest scale to date (17.4 g) and were pleased to find virtually identical fuel cell stack operation for this test versus using facility hydrogen. We were able to operate the stack for 6.75 minutes with a load of 4 A and 8.5 V. After switching the stack back to facility hydrogen, we observed no decrease in stack performance.

CONCLUSIONS AND FUTURE DIRECTIONS

This year, we were able to synthesize all target compounds in Figure 1 with the exception of **E**, **I**, and **L**. Additionally, we synthesized new *B*-methyl AB derivatives and characterized their hydrogen release and recyclability. We investigated the hydrogen release characteristics of pure and blended CBN compounds. Mechanistic studies were initiated by the use of computational chemistry. Finally, we operated a fuel cell stack using the hydrogen generated from liquid carrier **B**. Next year, we will try to:

- Synthesize derivatives of **E** and investigate reversible H_2 activation.
- Develop catalysts to achieve H_2 desorption from the carbon portions of the CBN compounds.

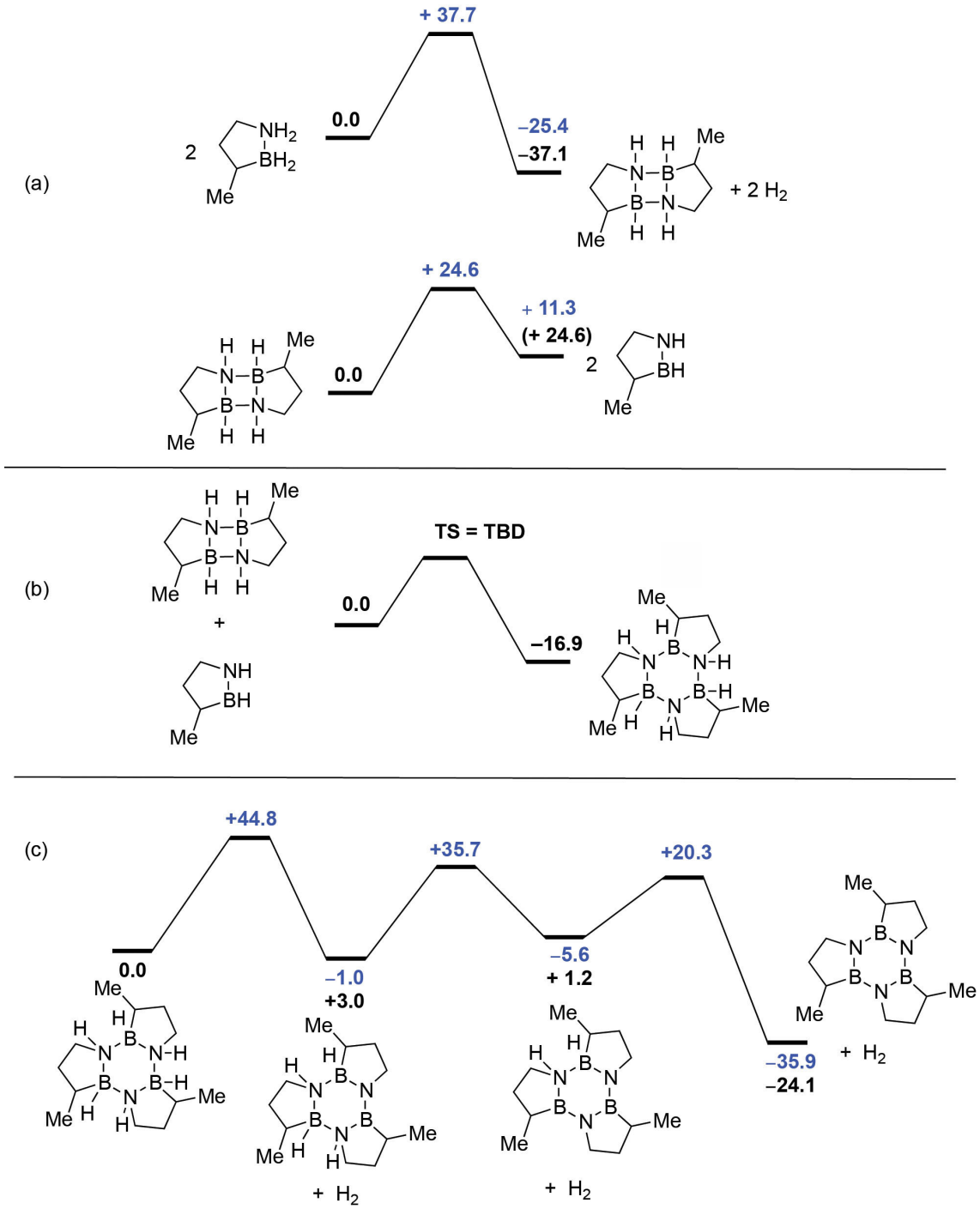

FIGURE 4. Potential energy surface in kcal/mol for the current working mechanistic hypothesis. a) dehydrogenation of **B** to form dehydromonomer and dissociation of the dehydrodimer to form the dehydromomoner. b) reaction of the dehydrodimer with the dehydromonomer to form a cycloborazane derivative. c) Sequential dehydrogenation of cyclotriborazane to the final spent fuel material. Blue values are B3LYP/DZVP2 and black values are G3MP2.

- Achieve 4-5 equivalent of H_2 release for Compound **H** (9.3 wt% to 11.6 wt%).
- Determine the thermodynamics and kinetics for the desorption of Compound **H**.
- Characterize viscosity of spent fuel of Compound **B** and its fuel blends.
- Continue to optimize fuel blends with respect to capacity, melting point, stability.

- Continue computational investigation of dehydrogenation mechanisms. Complete the potential energy surface for direct comparison of different pathways for the H_2 desorption from **B**.

SPECIAL RECOGNITIONS & AWARDS/ PATENTS ISSUED

1. Liu, S.-Y.; Chen, G. 2013. 1,4-Diazonia-2,5-diboratacyclohexanes and 1,4,2,5-Diazadiborines. U.S. Provisional Patent Application No. 61/755,869, January 23, 2013. Patent Pending.

2. Liu, S.-Y.; Campbell, P. 2012. B-Alkyl-Substituted Ammonia Boranes. U.S. Provisional Patent Application No. 61/683,073, August 14, 2012. Patent Pending.

FY 2013 PUBLICATIONS/PRESENTATIONS

1. Luo, W.; Neiner, D.; Karkamkar, A.; Parab, K.; Garner, E. B., III; Dixon, D. A.; Matson, D.; Autrey, T.; Liu, S.-Y. *Dalton Trans.* **2013**, *42*, 611–614.

2. Campbell, P.G.; Ishibashi, J.S.A.; Zakharov, L.N.; Liu, S.-Y. *Aust. J. Chem.* **2013**. http://dx.doi.org/10.1071/CH13198.

REFERENCES

1. McWhorter, S.C. Read, G. Ordaz, N. Stetson. "Materials-Based Hydrogen Storage: Attributes for Near-Term, Early Market PEM Fuel Cells" *Current Opin. Sol. State Mat. Sci.* **2011**, *15*, 29.

2. A. Staubitz, A.P. Robertson, I. Manners. "Ammonia-borane and related compounds as dihydrogen sources" *Chem. Rev.* **2010**, *110*, 4079.

3. C.L. Aardahl, D. Rassat. "Overview of systems considerations for on-board chemical hydrogen storage" *Int. J. Hydrogen. Energy.* **2009**, *34*, 6676.

4. A.D. Sutton, A.K. Burrell, D.A. Dixon, E.B. Garner, III, J.C. Gordon, T. Nakagawa, K.C. Ott, J.P. Robinson, and M. Vasiliu. "Regeneration of Ammonia Borane Spent Fuel by Direct Reaction with Hydrazine and Liquid Ammonia" *Science,* **2011**, *331*, 1426.

5. Effects of Liquid Viscosity on Rotodynamic (Centrifugal and Vertical) Pump Performance (ANSI/HI 9.6.7, 2004).

6. W. Luo, P.G. Campbell, L.N. Zakharov, S.-Y. Liu, "A Single-Component Liquid-Phase Hydrogen Storage Material" *J. Am. Chem. Soc.* **2011**, 133, 19326.

IV.E.4 Aluminum Hydride: the Organic-Metallic Approach

James Wegrzyn (Primary Contact), Chengbao Ni, Wei Min Zhou
Brookhaven National Laboratory (BNL)
Building 815
Upton, NY 11973
Phone: (631) 344-7917
Email: wegrzyn@bnl.gov

DOE Managers
Ned Stetson
Phone: (202) 586-9995
Email: Ned.Stetson@ee.doe.gov
Channing Ahn
Phone: (202) 586-9490
Email: Channing.Ahn@ee.doe.gov

Project Start Date: October 1, 2011
Project End Date: September 30, 2013

Overall Objectives

Develop onboard vehicle storage systems using aluminum hydride that meets all of DOE's targets for the proton exchange membrane fuel cell vehicle.

- Produce aluminum hydride material with a hydrogen gravimetric storage capacity greater than 9.7% (kg-H_2/kg) and volumetric storage capacity of 0.13 kg-H_2/L.
- Assist in developing aluminum hydride slurry storage systems for better than 6% hydrogen gravimetric material density, 0.07 kg-H_2/L volumetric hydrogen storage capacity, and well-to-wheels efficiencies greater than 60%.

Fiscal Year (FY) 2013 Objectives

Develop practical and economical processes for regenerating aluminum hydride.

Technical Barriers

This project addresses the following technical barriers from the Hydrogen Storage section of the Fuel Cell Technologies Office Multi-Year Research, Development, and Demonstration Plan:

(A) System Weight and Volume

(B) System Cost

(E) Charging/Discharging Rates

Technical Targets

Table 1 is a listing of the 2015 DOE hydrogen storage targets along with BNL's current 2013 aluminum hydride project status. The well-to-wheels efficiency listed in the table under the column for 2013 Status was taken from an independent analysis by Argonne National Laboratory on the alane adduct (AlH_3:TEA) storage system. The 0.0582 gravimetric storage parameter listed in Table 1 was a measured value obtained by decomposing 60 wt% alane slurries. The slurries consisted of aluminum hydride particles having a hydrogen content of 9.7 wt% that were suspended in liquid glycol. The gravimetric storage parameter was hydrogen material weight only, and did not take into account the balance of plant weight.

TABLE 1. Progress in Meeting Technical Hydrogen Storage Targets for Aluminum Hydride Regeneration

Storage Parameter	Units	2015 Target	2013 Status
Gravimetric	wt% H_2	0.055	0.0582
Volumetric	kg H_2/L	0.040	0.070
Fuel Flow Rate (temperature)	(g/s)/kW °C	0.02 80	0.02 80
Well-to-Wheels Efficiency	kW-H_2/kW	60%	>55%
Refueling Time	min	3.3	To Be Determined

FY 2013 Accomplishments

- Demonstrated direct synthesis of alane tertiary amines by reacting γ-AlH_3 in a diethylether solution with various tertiary amines, resulting in high yields of N-alkylpiperidine:alane, N-alkylmorpholine:alane, and N-alkylpyrrolidine:alane.
- Identified the N-ethylpiperidine:alane and N-ethylmorpholine:alane as being two compounds that improved yields, controllability and energy efficiency for recovering donor free aluminum hydride as compared to the previous 55% wells-to-wheels efficiency for recovering aluminum hydride from the triethylene:alane compound.

✧ ✧ ✧ ✧ ✧

INTRODUCTION

AlH_3 (alane) is a promising hydrogen storage material because of its high hydrogen capacity (10.1 wt% and 1.48 g/mL) and its low decomposition temperature

(<100ºC). The main challenge of using alane as a storage medium is finding methods for the cost- and energy-effective hydrogenation of aluminum back to donor-free AlH_3. Several synthetic methods that include reaction of $AlCl_3$ with alkali alanates, electrochemical synthesis from $LiAlH_4$ and $NaAlH_4$, and direct hydrogenation of Al metal all involve either expensive materials or very high H_2 pressures. These methods are therefore not practical for large-scale commercial manufacturing of aluminum hydride. Previous work at Brookhaven has shown a three-step alane regeneration pathway involving titanium catalyzed aluminum metal, hydrogen, and tertiary amines (Figure 1). In such a process a 2:1 adduct $(amine)_2$:AlH_3 (amine = Me_3N or $EtMe_2N$) is formed by hydrogenation of Al in a chemical reactor with an organic solvent at moderate temperatures and pressures. The 2:1 adduct is then transaminated with a second amine (nominally Et_3N) to yield the less stable Et_3N:AlH_3 compound. This compound is then decomposed under moderate heat and vacuum distillation to leave donor-free α-AlH_3. This additional chemical step of converting the 2:1 to a 1:1 adduct is necessary, since the 2:1 adducts directly decompose to aluminum metal. Although donor-free alane was identified in the product, the ($Et_3N{\cdot}AlH_3$) decomposition step suffered from several drawbacks, including low yields of AlH_3, low energy efficiency, slow kinetics, and contamination of the product by varying amounts of Al metal.

APPROACH

For this year the approach was to improve the well-to-wheels efficiency by studying the structures of 1:1 and 2:1 Lewis base stabilized alane tertiary amine adducts. In particular the project investigated the synthesis, characterization and thermal decomposition of various N-alkylpiperidine:alane, N-alkylmorpholine:alane and N-alkylpyrrolidine:alane compounds. The purpose of the study was to identify new energy efficient pathways for synthesizing alane. Alane tertiary amine adducts have a rich chemistry by possessing three types of structures (Figure 2). The type of structure depends on the steric hindrance of

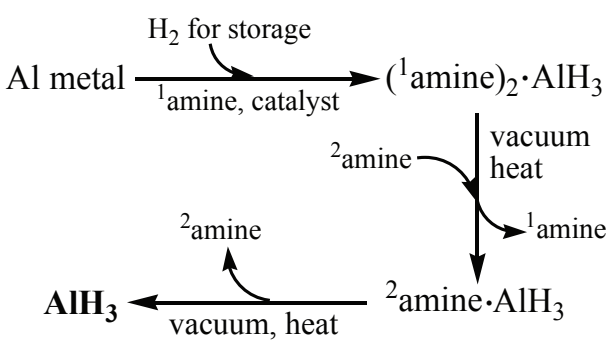

FIGURE 1. Three-step process for recovering aluminum hydride from amine:AlH_3.

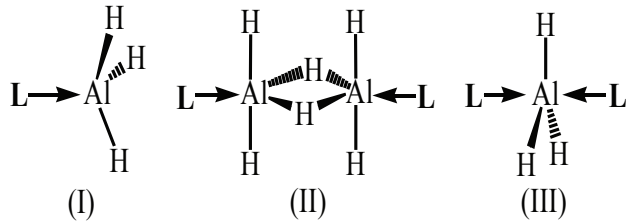

FIGURE 2. The three structure types of mono-dentate Lewis base alane compounds; (I) mono, (II) dimer, (III) bis.

the mono-dentate tertiary amine. These three structures are labeled the 1:1 mono-compound, the 1:1dimer compound, and the 2:1 bis-compound. It is generally accepted that less steric hindered Lewis bases will form either 1:1 or 2:1 complexes with alane, but the bulkier hindered bases will yield only 1:1 compounds. These observations are relevant to the recovery of donor-free AlH_3, since only the 1:1 bulky ethyl bases such as the 1:1 triethylene:alane (Et_3N:AlH_3), the 1:1 N-ethylmorpholine:alane (NEM:AlH_3), as well as the 1:1 N-ethylpiperidine:alane (NEPi:AlH_3) have thus far afforded α-AlH_3 recovery under moderate heat and vacuum distillation removal of the tertiary amine.

RESULTS

Nuclear Magnetic Resonance (NMR) and Infrared (IR) Spectroscopy

At room temperature, both N-methylpiperidine:alane (NMPi:AlH_3) and NEPi:AlH_3 are viscous liquid; their identities were established by NMR and IR spectroscopy. The 1H NMR spectra confirmed that each adduct has one NMPi (or NEPi) molecule per AlH_3 moiety. In the IR spectra (Figure 3a), the Al-H absorptions are centered at 1,775 cm^{-1} for NMPi:AlH_3 and at 1,777 cm^{-1} for NEPi:AlH_3. It can be noted that the small difference in Al-H stretching frequencies between NMPi:AlH_3 and NEPi:AlH_3 may reflect the differences in the relative Lewis basicity of NMPi and NEPi. Although the 2:1 adducts L_2:AlH_3 (L = NMPi or NEPi) were not isolated, in situ studies were performed to probe interactions between AlH_3 and N-alkylpiperidine. As shown in Figure 3a, addition of eight equivalent of NMPi into a solution of NMPi:AlH_3 (1 equivalent) caused the Al-H absorption to shift from 1,775 cm^{-1} to 1,712 cm^{-1}. This indicates the formation of $(NMPi)_2$:AlH_3. In contrast, NEPi:AlH_3 did not show any such changes, suggesting no or a negligible amount of $(NEPi)_2$:AlH_3 were formed under similar conditions. Such dramatic difference is due primarily to the steric effects from the ethyl group in NEPi. Similar difference was also observed for the N-alkylpyrrolidine:alane compounds. To further study the elusive nature of $(NMPi)_2$:AlH_3, a series of IR spectra of NMPi:alane under different conditions were recorded. As illustrated in Figure 3b, upon on addition of four equivalent

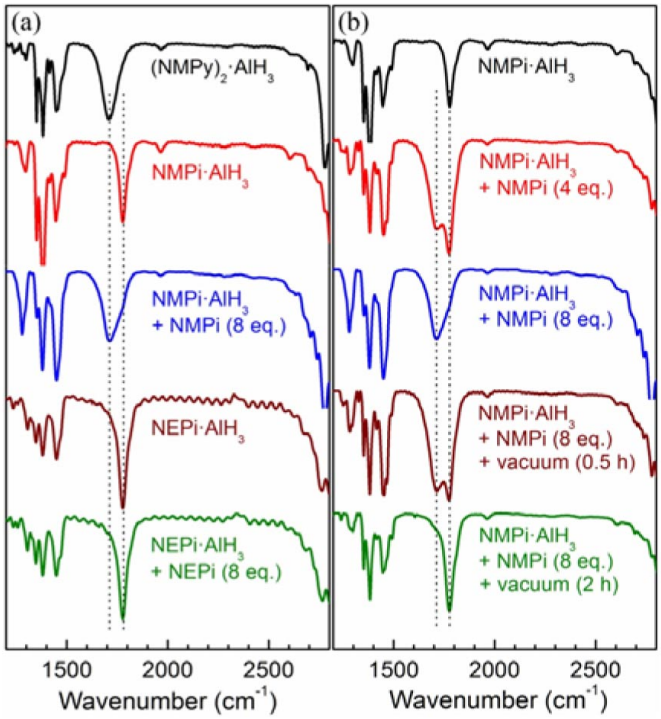

FIGURE 3. (a) IR spectra of NMPi:AlH_3 and NEPi:AlH_3 adducts in Et_2O; (b) IR spectra of NMPi:AlH_3 under different conditions of excess N-methylpiperidine.

of NMPi into NMPi:AlH_3 (1 equivalent), a new peak at 1,712 cm^{-1} appeared. Further addition of NMPi (up to eight equivalent) generated more $(NMPi)_2$:AlH_3, as evidenced by the disappearance of NMPi:AlH_3 at 1,775 cm^{-1}. When this mixture was held under vacuum, the $(NMPi)_2$:AlH_3 absorption peak (1,712 cm^{-1}) decreased gradually with concurrent appearance of the NMPi:AlH_3 absorption peak. Thus, in the presence of excess NMPi, $(NMPi)_2$:AlH_3 is formed and exists in equilibrium with NMPi:AlH_3; however, it is not isolable because it readily loses under vacuum one NMPi molecule to form NMPi:AlH_3. Compared to more stable 2:1 adducts, such as $(EtMe_2N)_2$:AlH_3 and $(NMPy)_2$:AlH_3, the labile nature of the first NMPi molecule in $(NMPi)_2$:AlH_3 can be attributed to the increased steric hindrance of NMPi:

Thermal Decomposition

This year the project focused on studying the thermal properties (or decomposition pathways) of the 1:1 N-methylmorpholine:alane (NMM:AlH_3), NEM:AlH_3 and NEPi:AlH_3 compounds in order to replace the 1:1 Et_3N:AlH_3 compound in the recovery step for AlH_3. This replacement is beneficial because the separation of AlH_3 from Et_3N:AlH_3 is associated with several undesired processes, including evaporation loss of Et_3N:AlH_3 and formation of aluminum metal. Also it is worth recalling that all 2:1 amine:alane adducts previously studied in this project always decomposed directly to aluminum metal upon heating. This fact suggests limiting the scope of the investigation to only 1:1 compounds. It was found that the 1:1 NMM:AlH_3 (solid) is stable up to 80°C, and no reaction was observed below 80°C. However at 85°C, NMM:AlH_3 gradually decomposed to a grey solid, which was confirmed to be aluminum metal by X-ray diffraction (XRD) analysis. Thus, NMM:AlH_3 is not suitable for the separation and recovery of donor free AlH_3. Decomposition of NEM:AlH_3 was also studied in a similar manner. In the temperature range of 20 to 55°C, no reaction occurred. Between 60 and 70°C and under reduced pressures (~20 mm Hg), NEM:AlH_3 readily changed to a grey solid with significant loss of mass. XRD analyses showed the formation of α-AlH_3 with a small amount of Al metal (Figure 4). Compared to that of NMM:AlH_3, the decomposition of NEM:AlH_3 to give alane could be attributed to the greater steric hindrance and the decreased Lewis basicity of NEM. Further increasing the reaction temperature (>75°C) of NEM:AlH_3 gave mostly Al metal with a trace amount of (or no) α-AlH_3. Thus, the ideal temperature range for the separation of AlH_3 from NEM:AlH_3 is between 60 and 70°C. As a result, unlike Et_3N:AlH_3, which requires a metal hydride additive (such as LiH or $LiAlH_4$) as catalyst or seed for the decomposition, NEM:AlH_3 and NEPi:AlH_3 do not require any catalyst in the alane recovery process. Thus, no external hydride impurities are introduced into the product for the NEM:AlH_3 and NEPi:AlH_3 reactions. Although a small amount of α-AlH_3

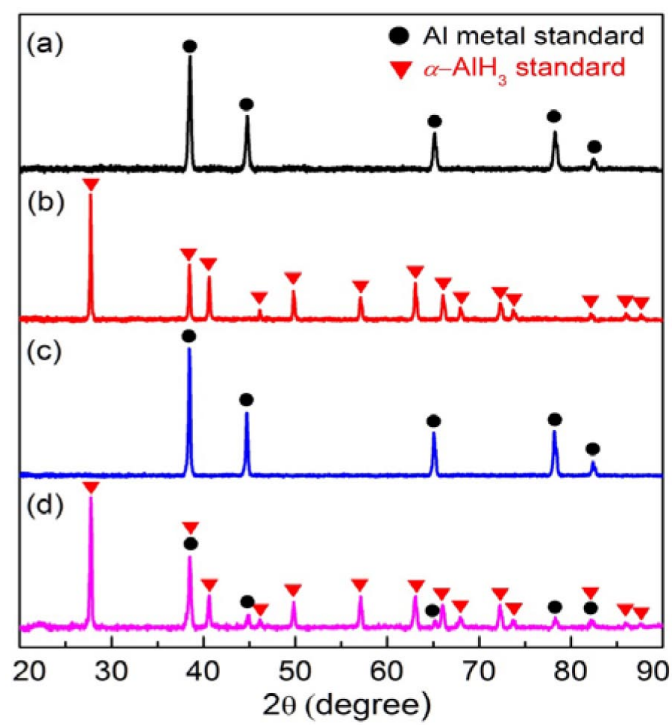

FIGURE 4. XRD patterns of the decomposition products of NMM·AlH_3 and NEM·AlH_3: (a) Al metal (standard); (b) α-AlH_3 (standard); (c) the NMM:AlH_3 decomposition product; (d) the NEM:AlH_3 decomposition products.

(as seed/catalyst) can hasten the reaction to some extent. We note that the alane product from NEM:AlH_3 and NEPi:AlH_3 may contain a small amount of Al metal; however, the yield and selectivity of these two reactions are significantly improved compared to Et_3N:AlH_3. Thus, NEM:AlH_3 and NEPi:AlH_3 are both better intermediates than Et_3N:AlH_3 for the separation and recovery of alane.

CONCLUSIONS

The thermal decomposition pathways of NMM:AlH_3, NEM:AlH_3 and NEPi:AlH_3 have been elucidated this year. It was shown that the efficiency for recovering AlH_3 from tertiary amine alanes greatly improves when incorporating either the NEM:AlH_3 or NEPi:AlH_3 compounds into the synthesis process, rather than using the TEA:AlH_3 compound. The main conclusion reached was that the 1:1 NMM:AlH_3 compound decomposes directly to aluminum metal, while the 1:1 NEM:AlH_3 and 1:1 NEPi:AlH_3 compounds can be selectively transformed to donor free AlH_3. Therefore by combining the transamination of $(DMEA)_2$:AlH_3 with either NEM:AlH_3 or NEPi:AlH_3, we have established a new separation pathway for the recovery of donor free AlH_3. This new pathway has improved yields, selectivity, and energy efficiency. More importantly, because of the fast reaction kinetics (even at room temperature), the new pathway can be combined with hydrogenation of Al metal to prepare donor-free AlH_3. The process still involves multiple chemical steps, but requires only a one-pot reactor. Achieving the synthesis of donor-free AlH_3 in a single pot reactor would significantly reduce cost. However, whether aluminum hydride would meet DOE's hydrogen fuel cost target awaits further validation testing.

FY 2013 PEER-REVIEWED PUBLICATIONS

1. Ni, Chengbao; Yang L.; Muckerman J.T.; Graetz J.; N-Alkylpyrrolidine Alane Compounds for Energy Applications, *J. Phys. Chem. C.*, Jan. (2013) 117, p2628.

2. Ni, Chengbao; Wegrzyn J.; Zhou W-M; Celebi Y.; N-Alkylpiperidine Alane Compounds and Their Applications in Alane Regeneration, *Int. J Hydrogen Energy*, Aug. (2013).

3. Ni, Chengbao; Yang L.; Muckerman J.T.; Graetz J.; Aluminum Hydride Separation Using N-Alkylmorpholine, *J. Phys. Chem. C.*, June (2013) 117, p14983.

IV.E.5 Electrochemical Reversible Formation of Alane

Ragaiy Zidan (Primary Contact)[1], Joe Teprovich[1], Doug Knight[2], Scott Greenway[2]
[1]Savannah River National Laboratory (SRNL)
999-2W Room 121
Savannah River Site
Aiken, SC 29808
Phone: (803) 646-8876
Email: ragaiy.zidan@srnl.doe.gov
[2]Greenway Energy, LLC

DOE Managers
Ned Stetson
Phone: (202) 586-9995
Email: Ned.Stetson@ee.doe.gov
Channing Ahn
Phone: (202) 586-9490
Email: Channing.Ahn@ee.doe.gov

Project Start Date: October 1, 2011
Project End Date: Project continuation and direction determined annually by DOE

Overall Objectives

- Develop methods of alane production and regeneration that lower the cost of alane production to less than $10/kg
- Demonstrate and characterize alane production system that lowers the cost of alane production with the lowest possible capital and operating costs
- Identify and quantify fundamental properties of alane production chemistry and physics that will lead to improved design and modeling of systems for alane production and use

Fiscal Year (FY) 2013 Objectives

- Demonstrate regeneration of the electrolyte for the electrochemical production of alane from spent alane, hydrogen, and electrochemical cell byproducts
- Improve electrochemical cell design to allow collection of individual electrode products that will enable electrolyte regeneration
- Identify methods to increase the efficiency of electrochemical alane production

Technical Barriers

This project addresses the following technical barriers from the Technical Plan - Storage section of the Fuel Cell Technologies Office Multi-Year Research, Development, and Demonstration Plan:

(A) System Weight and Volume

(B) System Cost

(C) Efficiency

(Q) Regeneration Processes

Technical Targets

In this project, studies are being conducted to lower cost and improve efficiency of the electrochemical method to form AlH_3. This material has the potential to meet long-term and near-term targets for automotive and portable power applications [1,2]. The research performed as part of this contract is equally applicable to both areas.

- By 2015, develop and verify a single-use hydrogen storage system for portable power applications achieving 0.7 kWh/kg system (2.0 wt% hydrogen) and 1.0 kWh/L system (0.030 kg hydrogen/L) at a cost of $0.09/Whnet ($3/g H2 stored).
- By 2017, develop and verify onboard automotive hydrogen storage systems achieving 1.8 kWh/kg system (5.5 wt% hydrogen) and 1.3 kWh/L system (0.040 kg hydrogen/L) at a cost of $12/kWh ($400/kg H2 stored).

FY 2013 Accomplishments

- Demonstrated regeneration of $LiAlH_4$ electrolyte for electrochemical charging
- Identified a commercially available, low-cost catalyst that can be used in reasonable quantities to accomplish electrolyte recharging
- Demonstrated electrochemically active compounds and used electrochemical impedance spectroscopy to show that kinetic improvements were due to more than increased ionic conductivity
- Demonstrated a divided cell for alane electrochemistry that was able to isolate alane and Li products from the electrolysis of $LiAlH_4$
- Signed a Cooperative Research and Development Agreement with Ardica Technologies, Inc., to develop commercial alane production methods

✧ ✧ ✧ ✧ ✧

INTRODUCTION

The DOE is supporting research to demonstrate viable materials for onboard hydrogen storage. Aluminum hydride (alane - AlH_3), having a gravimetric capacity of 10 wt% and volumetric capacity of 149 g H_2/L and a desorption temperature of ~60°C to 175°C (depending on particle size and the addition of catalysts) has the potential to meet the 2015 and 2017 DOE targets for portable power and automotive applications. The main drawback for using alane as a hydrogen storage material is unfavorable thermodynamics towards hydrogenation. Zidan et al. [3] were the first to show a reversible cycle utilizing electrochemistry and direct hydrogenation, where gram quantities of alane were produced, isolated, and characterized. This regeneration method is based on a complete cycle that uses electrolysis and catalytic hydrogenation of spent Al(s). This cycle avoids the impractical high pressure needed to form AlH_3 and the chemical reaction route of AlH_3 that leads to the formation of alkali halide salts, such as LiCl or NaCl, which become a thermodynamic sink because of their stability.

During FY 2013, research has continued to demonstrate critical steps to the overall cycle and to improve the electrolysis cells for alane generation. Efforts to demonstrate the other parts of the alane fueling cycle include the demonstration of a method to regenerate $LiAlH_4$ from the products of the electrolysis reaction and identification of catalysts for the regeneration. Improvements in the electrochemical cell design were made for product isolation and to limit transport between the sides of the cell to a single ion. Collaborative research with Ardica has also started under a Cooperative Research and Development Agreement on methods to reduce the cost of alane production for use in commercial devices.

APPROACH

The electrochemical generation of alane has been shown by Zidan et al. [3,4] to be capable of generating high purity material using methods that can be developed into a fueling cycle for hydrogen vehicles, portable power systems, or other applications. This research has demonstrated the system electrochemistry and improvements have been made to improve the efficiency of the electrochemical alane production reactions. The regeneration of the electrolyte from spent materials and improvements in the separations process are equally as important in developing overall alane production and reprocessing schemes. SRNL has developed and demonstrated a method to regenerate the electrolyte for the electrochemical cell with materials present in electrochemical cell cathode, dehydrogenated alane, and hydrogen gas. Improvements to the electrochemical cell design have also been realized to allow improved separation of the cell products to enable electrolyte generation and separation of alane.

RESULTS

Figure 1 shows the reactor for regenerating the electrolyte for the electrochemical cell. The regeneration of the electrolyte for electrochemical alane production was performed in a Parr™ reactor that can operate at elevated temperatures and pressures. The reactants for the regeneration method are lithium hydride, activated aluminum, hydrogen gas and Ti-based catalyst. These reactants simulate using the cathode product from electrochemical alane synthesis, dehydrogenated alane from a hydrogen storage application, and hydrogen for refueling. The reactants are combined with an inexpensive heterogeneous catalyst and tetrahydrofuran (THF) in the reactor. The reactor is heated to 75°C with stirring to carry out the reaction. The solids are filtered and the electrolyte is used to for the electrochemical regeneration of alane.

The $LiAlH_4$ yield for the electrolyte regeneration was above 75% with only minor adjustments to the catalyst loading of the reactor and no optimization of the reaction conditions. The reaction product contained mostly alane with other minor by-products including Al and Li_3AlH_6. Figure 2 shows an X-ray diffraction of the reaction product isolated from the solvent showing strong signals from $LiAlH_4$ with minor peaks from by-products. Previous experience with similar systems has shown that the reaction product distribution can be shifted through changes in temperature, pressure, and catalyst loading. Future work on the regeneration of the electrolyte will include increasing the yield of $LiAlH_4$ and selectivity over byproducts.

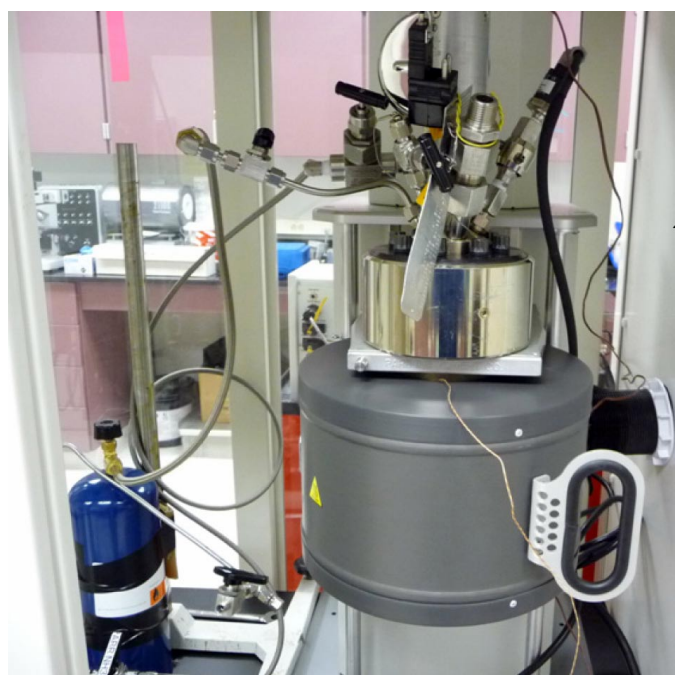

FIGURE 1. Reactor setup for electrolyte regeneration experiments.

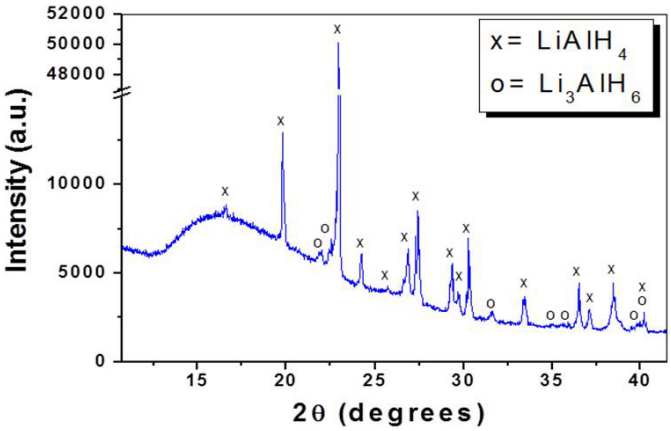

FIGURE 2. X-ray diffraction of the regenerated $LiAlH_4$ from Al, LiH, and H_2 in THF. The product was isolated by vacuum distillation of the solvent. The minor Li_3AlH_6 phase observed is likely due to the solvent removal process.

New electrochemical cell designs were fabricated to allow easier precipitation and collection of pure alane along with isolating the cathode product for regeneration reactions. Figure 3 shows one of the new divided cell designs. The anolyte was concentrated $LiAlH_4$ in THF and the catholyte was concentrated LiCl in THF. A Nafion® 117 membrane that had been ion-exchanged to the lithium form and dehydrated was used as the divider for the cell. Modifications to the electrode design were also made to minimize the distance of the electrodes from the membrane so that ohmic losses in the cell are reduced. There were no indications of leaking between the compartments of the cell even after five days of continuous operation.

Testing was also conducted to see how the addition of co-solvents could decrease ohmic losses in the electrochemical cell. Figure 4 shows a characterization of the ionic conductivity of 1.0 M $LiAlH_4$ as diglyme is added to the solution in small aliquots. Addition of less than 2.5 vol% diglyme caused an increase of nearly 300% in the conductivity of the electrolyte. A possible explanation for this phenomenon is the increased ionic mobility of the ions as they are complexed by the diglyme in the solution. Diglyme contains three oxygen atoms which allow it to chelate and bind to the Li^+ in solution leading to the enhanced conductivity. Addition of diglyme above 2.5% did not yield increased conductivity and a significant decrease in the solution conductivity was seen when the solution separated into two phases above 3.5 vol% diglyme.

CONCLUSIONS AND FUTURE DIRECTIONS

- Demonstrated the regeneration of the electrolyte in a Parr™ reactor with temperature and pressure
- Produced $LiAlH_4$ during regeneration with 75% yield

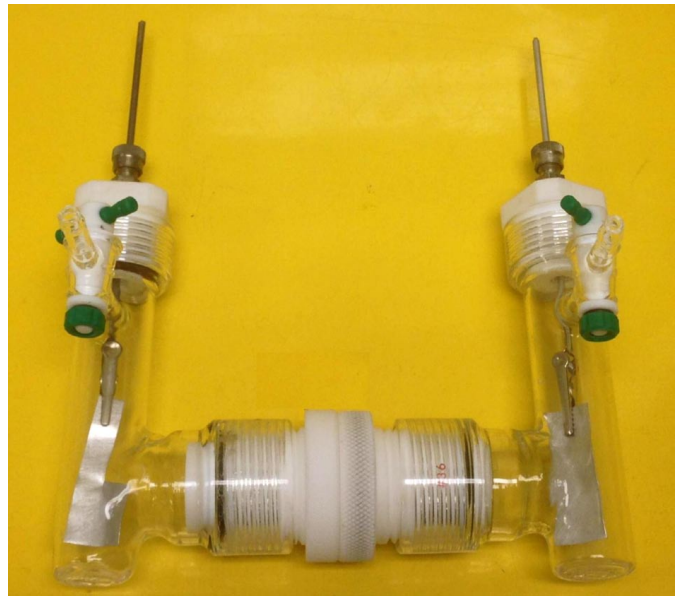

FIGURE 3. Divided electrochemical cell design for alane production. The cell yielded pure alane and lithium metal in two separate electrodes with different electrolyte solutions.

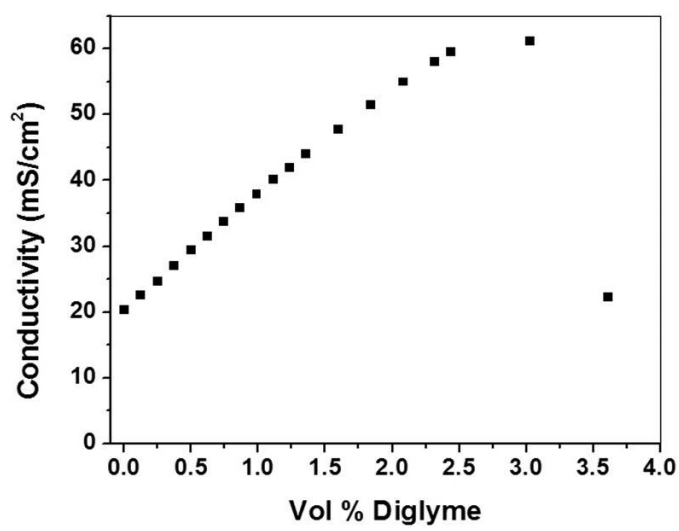

FIGURE 4. Plot of conductivity of the solution versus volume percent of added diglyme. The addition of small amounts of diglyme shows a significant improvement in the cell conductivity.

- Identified an inexpensive catalyst for the electrolyte regeneration
- Designed and tested divided electrochemical cells for alane production
- Demonstrated the effectiveness of co-solvents to significantly increase the conductivity of the electrolyte solution for alane production

SPECIAL RECOGNITIONS & AWARDS/ PATENTS ISSUED

1. Ragaiy Zidan, Douglas A. Knight, Long V. Dinh; Novel Methods for Synthesizing Alane without the Formation of Adducts and Free of Halides US20120141363 Feb 2013.

2. Ragaiy Zidan; Electrochemical Process and Production of Novel Complex Hydrides US8,470,156B2 Jun 2013.

FY 2013 PUBLICATIONS/PRESENTATIONS

1. Long V. Dinh, Douglas A. Knight, Mark Paskevicius, Craig E. Buckley and Ragaiy Zidan, "Novel methods for synthesizing halide-free alane without the formation of adducts," Applied Physics A, 2012 Vol. 107, No. 1, 173-181. [PB]

2. Joseph A. Teprovich Jr., Theodore Motyka, Ragaiy Zidan, "Hydrogen system using novel additives to catalyze hydrogen release from the hydrolysis of alane and activated aluminum," Int. J. of Hydrogen Energy 2012 Vol. 3, Issue 2, 1594-1603. [PB]

3. Ragaiy Zidan, "Development and characterization of novel hydrogen storage materials", Oct 27, 2012, International Energy Agency (IEA) HIA Task 22 Meeting Kyoto Japan. [PR]

4. "Novel Materials and New Methods for Hydrogen Storage," International Symposium on Metal-Hydrogen Systems 2012, Oct 21, Kyoto, Japan Invited Speaker. [PR]

REFERENCES

1. Teprovich, J.A., T. Motyka, and R. Zidan, International Journal of Hydrogen Energy, 2012. **37**(2): p. 1594-1603.

2. Graetz, J. and J.J. Reilly, J. Phys. Chem. B, 2005. **109**(47): p. 22181-22185.

3. Zidan, R., et al., Chemical Communications, 2009(25): p. 3717-3719.

4. Martinez-Rodriguez, M.J., et al., Appl. Phys. A-Mater. Sci. Process., 2012. **106**(3): p. 545-550.

IV.F.1 Lifecycle Verification of Polymeric Storage Liners

Barton Smith (Primary Contact) and
Lawrence M. Anovitz
Oak Ridge National Laboratory
P. O. Box 2008
Oak Ridge, TN 37831
Phone: (865) 574-2196
Email: smithdb@ornl.gov

DOE Managers
Grace Ordaz
Phone: (202) 586-8350
Email: Grace.Ordaz@ee.doe.gov
Ned Stetson
Phone: (202) 586-9995
Email: Ned.Stetson@ee.doe.gov

Project Start Date: June 2008
Project End Date: September 2013

Overall Objectives

Perform durability qualification measurements on specimens of Type IV storage tank liners (polymers) at the nominal working pressure using thermal cycling commensurate with the design lifetime, followed by permeation measurements to determine if the steady-state leakage rate in the tank could potentially exceed the specification for hydrogen fuel cell passenger vehicles.

Fiscal Year (FY) 2013 Objectives

Continue durability qualification measurements on specimens of novel polymers proposed for use as storage tank liners and hydrogen barrier materials.

Technical Barriers

This project addresses the following technical barriers from the Fuel Cell Technologies Office Multi-Year Research, Development, and Demonstration Plan, section 3.3.5 - Hydrogen Storage:

(D) Durability/Operability (of on-board storage systems – lifetime of at least 1,500 cycles)

(G) Materials of Construction (vessel containment that is resistant to hydrogen permeation)

(L) Lack of Tank Performance Data and Understanding of Failure Mechanisms

Technical Targets

This project addresses the following technical targets for onboard hydrogen storage systems R&D [1]:

- Operational cycle life (1/4 tank to full):
  - FY 2017: 1,500 cycles; ultimate: 1,500 cycles
- Environmental health and safety:
  - Permeation and leakage: meets or exceeds applicable standards
  - Loss of useable H_2: FY 2017: 0.05 g/h/kg H_2; ultimate: 0.05 g/h/kg H_2

FY 2013 Accomplishments

- Temperature cycling and permeation measurements are in progress for four tank liner polymers.
- Demonstrated that permeation in polymers is not linearly dependent on pressure and is influenced by the compressibility of the polymers.

✧ ✧ ✧ ✧ ✧

INTRODUCTION

Type IV high-pressure hydrogen storage tanks employ polymeric liners as permeation barriers to hydrogen. The tank liners can be stressed by cyclical excursions between temperature extremes, and the cumulative effects of repeated cyclical stress could harm the tank's durability, i.e., its ability to maintain an acceptably low leakage rate. Furthermore, ultra-high environmental temperatures can promote large hydrogen permeation rates and hydrogen saturation in the liner material, while ultra-low environmental temperatures can severely reduce the elasticity of liner materials and induce microcracking. The rapid pressurization of hydrogen in the tank during filling operations raises the temperature of the gas, the liner, and the carbon fiber matrix reinforcement shell. Minimum temperatures during winter months in northern latitudes may reach -40°C, and maximum temperatures after filling during summer months may reach 125°C.

The hundreds or thousands of thermal cycles that occur during fill cycles over the operational lifetime of the tank could thus affect the permeability characteristics of the liner. Failure modes for the liner's performance—based on the interaction of high pressure and extreme temperature—must be considered and investigated. Hydrogen leakage through a liner microcracked by extreme temperature cycling could accelerate under sustained high temperature and pressure,

or hydrogen saturation of the reinforcement layers external to the liner could put backpressure on the liner as the tank pressure decreases during vehicle operation, thereby causing the liner to separate from the reinforcement layers. The objective of this project is to evaluate the durability of polymer tank liners by cycling tank liner specimens between temperature extremes while monitoring the hydrogen permeabilities. Significant changes in permeability are expected to be prime indicators of whether such degradation occurs.

APPROACH

Hydrogen permeation verification measurements for storage tank liner materials are being carried out in a high-pressure permeation test vessel designed to measure hydrogen permeation in polymer materials at select intervals in the temperature cycling process. The pressure vessel (see Figure 1) is comprised of two stainless steel Type 316 flanges that are bolted together in a configuration designed to withstand working pressures up to 860 bar without leaking. The polymer specimen being evaluated is sealed by compression in an annular ring between pressure vessel flanges (10 cm^2 sealing area). The vessel is immersed in a chilled bath (reservoir) of ethylene glycol and distilled water at a temperature that varies from -30 to -50ºC during the thermal cycle. The reservoir is the low-temperature heat sink for the temperature-cycling process and its temperature fluctuates as it absorbs heat from the vessel during the cooling interval. The vessel is internally heated with six 300-W (1,800-W total) cartridge heaters to accomplish the heating portion of the temperature cycle. The temperature cycling/permeation measurement apparatus is shown in Figure 2. The specimen is continuously differentially pressurized during temperature cycling, with the high-pressure hydrogen on one side of the specimen and a sub-atmospheric pressure maintained on other side. The permeation measurements are performed with the specimen in the pressure vessel by calculating a gas transfer rate from the pressure rise rate in the fixed downstream volume.

The polymer specimens are prepared from liners provided by multiple manufacturers of Type IV storage tanks. The tank liners are too thick to use for lab-timeframe permeation measurements and are typically curvilinear in shape, so we prepare specimens by lathe-turning small sections of the liner to thicknesses of approximately 1 mm. The turning is done on the exterior (lower pressure) side of the liner. The thinned liner is then punched into a 5.7-cm diameter disc. The disc is then wet sanded with a succession of progressively finer grits through International Organization for Standardization P1200. The specimen disc is oriented in the pressure vessel so the liner interior (pristine surface) is exposed to the high-pressure hydrogen. A 4.5-cm

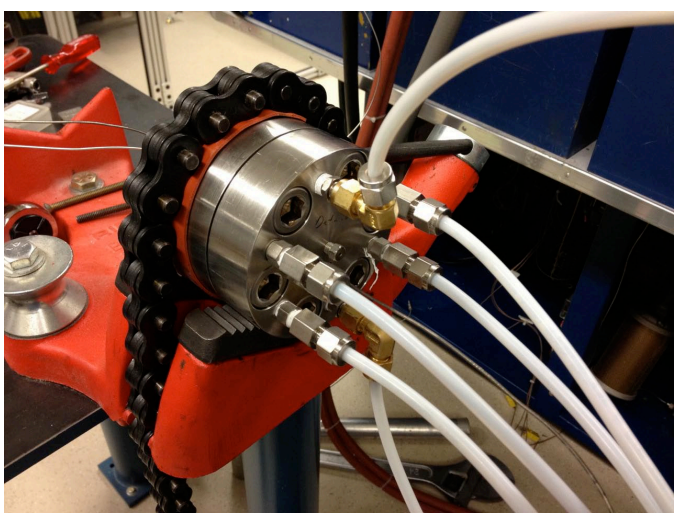

FIGURE 1. Assembled pressure vessel showing water-tight electrical connections to cartridge heaters and bolt configuration.

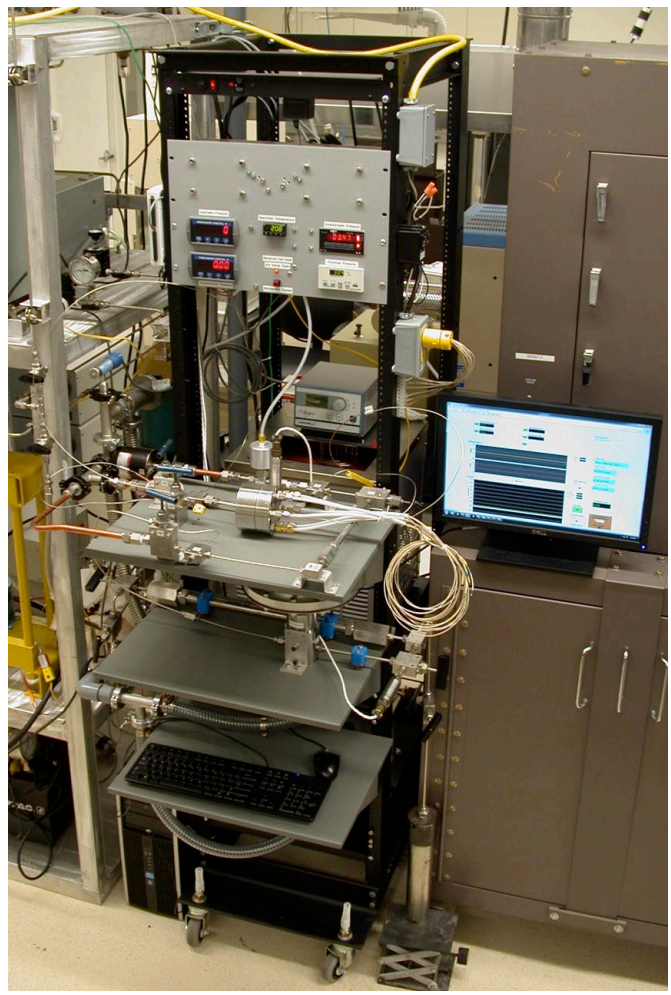

FIGURE 2. Temperature cycling and high-pressure permeation measurement apparatus.

diameter circular area is directly exposed to high-pressure H_2, and this is the area over which the gas transfer rate is determined.

Our temperature cycling protocol and methodology is based on the tank liner durability test protocol specified in SAE International J2579 [2]. The J2579 test protocol for compressed hydrogen storage systems prescribes long-term thermal cycling at the maximum allowable pressure of the storage tanks. We subject the tank liner specimens to 1,500 thermal cycles over the temperature range 40 to 85°C at constant hydrogen pressurizations of 350 bar (5,000 psia) and 700 bar (10,000 psia). Testing at these pressures, with cycling between 40 and 85°C, requires an automated temperature control strategy. Our heating rate replicates the rapid temperature rise in the tank liner during fill cycles (heating rate of approximately 20°C per minute). After heating, the low-temperature reservoir removes the heat from the pressure vessel until it reaches the low end of approximately 40°C. Process control software provides automated and unattended operation, and the test progress can be remotely monitored and controlled via the Web. A complete heating and cooling cycle requires approximately 20 minutes, and the completion of 1,500 thermal cycles with permeation measurements, at a single pressure, requires approximately one month to complete.

The permeation measurements are performed at regular intervals during the 1,500 temperature cycles. The permeation coefficients are measured at four temperatures (-40, -10, 30, and 85°C) at intervals of 0, 750, and 1,500 cycles. The coefficients are measured at the temperature extremes (40 and 85°C) at intervals of 250, 500, 1,000, and 1,250 cycles.

Our progress this year was slowed by numerous unexpected difficulties related to below-expected performance of components in the temperature cycling apparatus. The cartridge heaters produced less heat than specified by the manufacturer and it was necessary to modify the heating control and algorithm through extensive trials to compensate for the lower-than-expected heat output. We also found that it was necessary to cool the reservoir bath with a secondary, ultra-low-temperature recirculating bath to increase heat capacity and cooling power in the reservoir. We evaluated several candidate heat transfer fluids for the ultra-low temperature bath (ethylene glycol-water mixtures being far too viscous at temperatures below -40°C) and found that a specialty blend of a terpene hydrocarbon met our requirements for low viscosity, low freezing temperature, and non-flammable characteristics. The result was a decrease in the cycle time from approximately one hour to about 25 minutes. Additionally, we discovered that a significant amount of trial and error is required to perfect the procedure for sealing each type of polymer. Differences between thermal expansion of the polymer and the stainless steel vessel introduce numerous opportunities for gas leaks. The variations in polymer hardness, modulus, and surface texture require a systematic approach to achieving a durable seal.

RESULTS

The liner materials available for evaluation during FY 2013 are:

- Extrusion-molded high-density polyethylene (HDPE)
- Injection-molded HDPE
- Rotationally-molded HDPE
- Extrusion-molded polyamide-6 (PA-6)
- Blow-molded polyethylene terephthalate (PET)
- Extrusion-molded PA-6, with carbon black additive
- Injection-molded HDPE with nano-clay additive

We completed a durability characterization of liner Material 1, extruded HDPE, in a previous project year, and results from this characterization are available in previous annual progress reports. The four highest-priority measurements are for liner Materials 2, 3, 4, and 6 because they are currently being used in Type IV tanks. Polymers 5 and 7 are being considered for use as liner materials.

Results on our evaluations of Materials 2, 3, 4, and 6 were not ready for publication at the time of this progress report. We intend to publish the results of these evaluations in the archival literature so they will be available to a wide audience.

In addition to the temperature cycling measurements we conducted an extensive series of hydrogen diffusion and permeation measurements on tank liner polymers to characterize the relative hydrogen-barrier capabilities of the polymers and the pressure-dependence of the permeability coefficients. Presentation of the entirety of the results of these measurements is beyond the scope of this report and they will be published in the near future in the archival literature. In this report we present highlights of the permeability measurements that we expect will be of use to researchers and technologists who are investigating the use of polymeric materials in hydrogen storage and delivery systems.

Figure 3 shows the temperature dependence of the hydrogen permeability coefficients for four polymers being evaluated for durability in the temperature cycling experiments, as well as the coefficients for a thermotropic liquid crystal polymer (TLCP). TLCPs have been proposed for use as a hydrogen barrier material due to their lower permeabilities. The TLCP evaluated was compression-molded DuPont HX 3000. The other polymers were proprietary formulations provided by storage tank manufacturers. The measurements shown were made at temperatures ranging from 30 to 85°C at a differential pressurization of approximately 135 bar (2,000 psia) with the

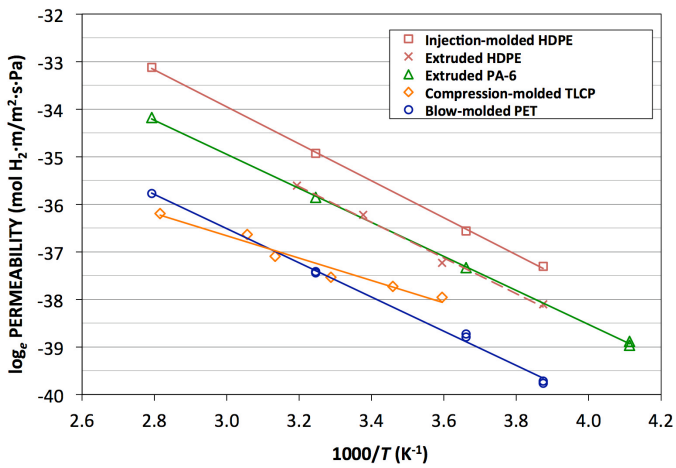

FIGURE 3. Temperature dependence of the hydrogen permeability for four tank liner polymer specimens and an additional specimen of TLCP. All measurements were made using a differential hydrogen pressure of 134 bar (13,400 kPa) with the exception of the roto-molded HDPE, which was measured at 345 bar (34,500 kPa).

exception of the rotationally-molded (roto-molded) HDPE, which was done at 345 bar (5,000 psia). Measurements of the permeability coefficient values were extremely reproducible for HDPE, PA-6 and PET polymers. Measurements of the TLCP permeability coefficients were much less reproducible, and reliable measurements could not be made at temperatures below 10°C. It was difficult to prepare specimens from the TLCP due to its brittleness and tendency to become friable at cut edges, and TLCP specimens exhibited a substantial amount of creep and deformation following pressurization at temperatures substantially above room temperature.

There were no statistically significant differences between the permeabilities of the HDPE produced by extrusion molding, rotational molding, and injection molding manufacturing processes. The permeability of PET was about an order of magnitude less than that of HDPE. The permeability of TLCP is comparable to that of blow-molded PET.

The temperature dependence of the permeability coefficients for a particular polymer at a specified hydrogen pressure can be modeled very accurately by the Arrhenius equation for an activated process, i.e.,

$$P = P_0 \, exp(E_A/RT) \qquad \text{Eq. 1}$$

where E_A is the activation energy for permeation in J/mole, R is the gas constant, T is the temperature in Kelvin, and P_0 is a pre-exponential scaling factor in mol H_2·m/m^2·s. Table 1 lists the E_A and P_0 coefficients determined by a least-squares fit to the permeation measurements. The TLCP has activation energy and pre-exponential factor that are unusually low and high, respectively, when compared to the other polymers.

TABLE 1. Activation energies and pre-exponential scaling factors for calculating hydrogen permeability coefficients for select polymers using Eq. 1. The standard error for the E_A value is shown in square brackets.

Polymer	Pressure bar	E_A kJ/mol H_2	P_0 mol H_2·m/m^2·s
Injection-molded HDPE	134	32.3 [0.5]	2.08×10^{-10}
Extrusion-molded HDPE	104	31.2 [1.7]	5.51×10^{-11}
Rotomolded HDPE	345	32.1 [0.8]	2.58×10^{-10}
Extrusion-molded PA-6	137	30.0 [0.2]	3.38×10^{-11}
Compression-molded TLCP	136	19.5 [2.0]	7.09×10^{-13}
Blow-molded PET	137	29.9 [0.9]	6.71×10^{-12}

Hydrogen transport in polymers differs from that in metals in one important aspect: it is not necessary for the hydrogen molecule to dissociate prior to dissolution in polymers. Sieverts' Law, which predicts that the solubility of hydrogen gas in metals will be proportional to the square root of the partial pressure of the gas in thermodynamic equilibrium, is not applicable to polymers. Thus the concentration of hydrogen dissolved in a polymer should be linearly proportional to applied pressure rather than proportional to the square root of the applied pressure. The permeability is directly proportional to the solubility, and thus the permeability of hydrogen in polymers should likewise be linearly proportional to the pressure.

Figure 4 shows the dependence of the specific permeabilities P_{sp} of several tank liner polymers on hydrogen pressure (mechanical pressure, which translates into an applied force to the polymer). We observed slight deviations from a linear dependence of P_{sp} on pressures in the range 100 to 14,000 kPa. The amount of deviation roughly follows the Young's modulus of the polymer—the larger the modulus, the more compressible the polymer, and the less linear the dependence of P_{sp} on pressure. This deviation

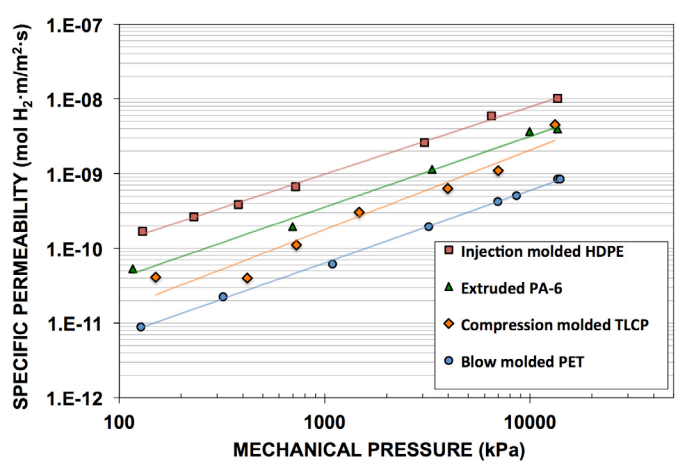

FIGURE 4. Pressure dependencies of the specific permeabilities of four polymers.

from linear pressure dependence is evidenced by the data shown in Table 4. The slope of the P_{sp} versus pressure curves increases as the modulus E increases. It follows that the polymer is being elastically compressed by the hydrogen pressure, and the compression reduces the free volume in the polymer. Polymers with larger moduli are more resistant to compression and therefore have P_{sp} values that are more linear with pressure.

TABLE 4. Dependence of specific permeability of polymers on hydrogen pressure, correlated to approximate values of their moduli. The standard error for each dependency is shown in square brackets.

Polymer	Pressure dependence of P_{sp} (mol H_2·m/m^2·s/kPa)	E (MPa)
Injection-molded HDPE	0.89 [0.02]	1,000
Extrusion-molded PA-6	0.95 [0.05]	2,400
Blow-molded PET	0.95 [0.01]	3,100
Compression-molded TLCP	1.06 [0.11]	>8,000

This compressibility effect is likewise evident in the case where the pressure dependence of P_{sp} for a single polymer is measured as a function of temperature, as shown in Figure 5. The modulus increases as the temperature decreases, making the polymer progressively less compressive and therefore having less free volume. The dependence of P_{sp} on pressure becomes more linear as the temperature decreases, as evidenced by the P_{sp} values

TABLE 5. Dependence of specific permeability on temperature for extrusion molded HDPE. The standard error for each dependency is shown in square brackets.

Temperature (°C)	Pressure dependence of P_{sp} (mol H_2·m/m^2·s/kPa)
85	0.89 [0.03]
23	0.90 [0.04]
5	0.92 [0.05]
-15	0.96 [0.06]

CONCLUSIONS AND FUTURE DIRECTIONS

The measurements of hydrogen permeabilities for several polymers in current use as tank liners—or being proposed for future use for such applications—show that the polymers have permeabilities that differ by an order of magnitude or less. The activation energies measured over the temperature range 30 to 85°C were very closely grouped around 31 kJ/mol, the exception being the specimen of compression-molded TLCP which had an activation energy of 19.5 kJ/mol. All the polymers show promise as good hydrogen barrier materials, based on their permeability coefficient values. The TLCP exhibited a significant amount of pressure-induced creep when subjected to prolonged temperatures above room

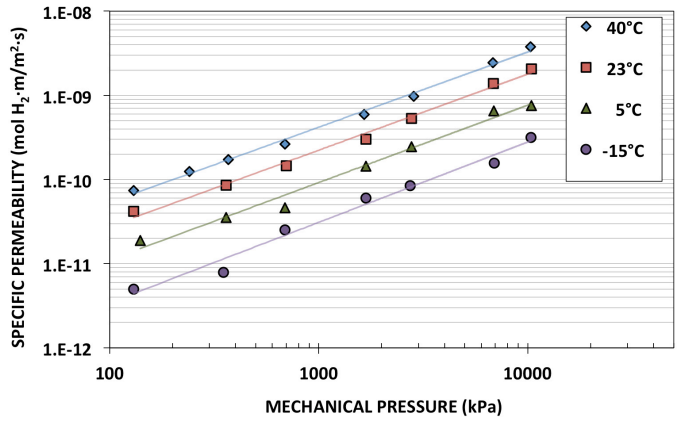

FIGURE 5. Pressure dependencies of a specimen of extrusion-molded HDPE, measured at multiple temperatures.

temperature. Additional evaluation of the high-pressure stress behavior of TLCP is in order before it can be qualified as a realistic barrier material candidate.

Unforeseen delays brought about by instrumentation problems in the temperature cycling apparatus delayed completion of the lifecycle durability measurements. Our intent is to complete measurements on as many polymers as possible this year and to publish the test procedure along with the durability measurements early next year.

The use of disc specimens for the durability measurements is a useful screening method, but this methodology might not be sufficient for predicting the performance of polymer liners in actual systems. Liners in tank systems will be exposed to flexural and tensile conditions in addition to those brought about by thermal cycling, and interactions of the liner with the surrounding walls will add to the complexity of a real-world evaluation of the liner's durability.

A test methodology that incorporates an *in toto* temperature cycling evaluation of tank liner in contact with the composite reinforcement would:

- Provide a fuller understanding of how liners function when situated in proximity to the composite reinforcement.
- Address the issue of absorption of H_2 in the liner and the subsequent volumetric expansion of the liner or pressurization of the void between the liner and reinforcement layers, and how these conditions could pose a concern for delamination during rapid depressurization of the tank.
- Provide a direct measurement of tank liner leakage as a function of cycle life.

Additional future work, which is also beyond the scope of the current project, should address the impact of rapid depressurization on the liner and perform a number of

temperature cycling and permeation measurements using H_2 incorporating concentrations of likely contaminants.

FY 2013 PUBLICATIONS/PRESENTATIONS

1. 2013 DOE Hydrogen Program Annual Merit Review – Crystal City, Virginia – May 15, 2013, oral presentation ST053.

2. Progress Update, "Lifecycle verification of polymer liners in storage tanks," Hydrogen Storage Tech Team Meeting, USCAR, Southfield, Michigan, April 18, 2013.

REFERENCES

1. Fuel Cell Technologies Program MYRDD Plan, Section 3.4 - Hydrogen Storage, September 2011 interim update.

2. SAE J2579, "Technical Information Report for Fuel Cell and Other Hydrogen Vehicles (January 2009)," Fuel Cell Standards Committee, SAE International.

IV.F.2 Melt Processable PAN Precursor for High-Strength, Low-Cost Carbon Fibers

Felix L. Paulauskas, Bob Norris (Primary Contact), Hippolyte Grappe, Amit Naskar, Ken Yarborough, and Fue Xiong
Oak Ridge National Laboratory (ORNL)
MS 6053
Oak Ridge, TN 37831-6053
Phone: (865) 576-1179
Email: norrisrejr@ornl.gov

DOE Managers
Ned Stetson
Phone: (202) 586-9995
Email: Ned.Stetson@ee.doe.gov
Grace Ordaz
Phone: (202) 586-8350
Email: Grace.Ordaz@ee.doe.gov

Subcontractor:
Donald G. Baird, James E. McGrath, Jianhua Huang
Virginia Polytechnic Institute and State University, Blacksburg, VA

Project Start Date: November 2006
Project End Date: Project continuation and direction determined annually by DOE

Overall Objectives

- Demonstrate means to achieve cost reduction of ≥25% in manufacture of carbon fiber meeting properties of industry baseline carbon fiber utilized in fabrication of composite vessels for hydrogen storage.
- Develop and demonstrate new chemistry and spinning techniques and assess capability for advanced conversion technologies to meet needs in reducing carbon fiber manufacturing costs for fiber meeting project performance goals.

Fiscal Year (FY) 2013 Objectives

- Demonstrate spinning of a sample tow of ~10-12 micron fibers from high molecular weight (>200,000 MW) dope that can be easily spooled and de-spooled for conversion at ORNL's Precursor Development System and yielding 15 Msi modulus and 150 ksi strength.
- Demonstrate spinning of a sample tow of ~10-12 micron fibers from high MW (>200,000) dope for conversion at ORNL's Precursor Development System and yielding 20 Msi modulus and 200 ksi strength.

Technical Barriers

High-strength carbon fibers account for approximately 65% of the cost of the high-pressure storage tanks. This project addresses the following technical barriers from the Hydrogen Storage section of the Fuel Cell Technologies Office Multi-Year Research, Development, and Demonstration Plan:

(A) System Weight and Volume

(B) System Cost

(D) Durability/Operability

(G) Materials of Construction

High strength carbon fiber enables the manufacture of durable, lightweight, compressed hydrogen storage vessels for use in high-pressure storage. Unfortunately, current high strength carbon fiber products are far too expensive to meet DOE goals for storage system costs.

Technical Targets

Working targets are approximate equivalence with Toray T-700 at substantially reduced production costs:

- 700 ksi ultimate tensile strength
- 33 Msi tensile modulus
- Production cost reduction of at least 25% versus baseline

FY 2013 Accomplishments

- Improved spinning and drawing equipment and processes have been developed and implemented for producing initial sample quantities of melt-spun polyacrylonitrile (PAN) precursor adequate to meet feasibility demonstration milestones. Appropriate conversion recipes were developed to match the precursor characteristics. The Go/No-Go milestone of 15 Msi modulus and 150 ksi strength was achieved with converted carbon fiber demonstrating basic feasibility of this approach.
- A number of "engineering" obstacles associated with this approach have been resolved and approaches for further scaling up to the next level of development have been identified. Properties projected to be met in FY 2014 of 25 Msi modulus and 250 ksi strength were actually achieved with one sample during this period, but

larger scale precursor processing, enhanced chemistry, and more optimized conversion processes are required to meet ultimate project objectives. Based on success to date, a roadmap to achieve these goals has been outlined for execution in the following reporting periods.

✧ ✧ ✧ ✧ ✧

INTRODUCTION

The exceptional strength-to-weight ratio of carbon fiber composite tanks makes them prime candidates for use with materials-based, cryogenic, or high-pressure gas for both vehicular and stationary storage applications. Cost is the primary issue with composite tank technology. A critical challenge lies in the cost of the fiber and the manufacture of composite tanks. Current projections of the manufactured cost per unit for high production volumes are about a factor of nine above storage system targets, and it is estimated that about 40-70% of the unit cost is due to the base cost of the carbon fiber (approximately 40% of the fiber cost is due to the precursor and the remainder due to thermal processing). Research and development (R&D) is needed as composite storage technology is most likely to be employed in the near term for transportation applications and will be needed for most materials-based approaches for hydrogen storage.

Currently, composite tanks require high-strength fiber made from carbon-fiber grade PAN precursor. Manufacturing R&D is needed to develop lower cost, high quality PAN or alternate precursors and reduced energy or faster conversion processes for carbon fiber, such as microwave and/or plasma processing. Developing and implementing advanced fiber processing methods has the potential to reduce cost by 50% as well as provide the technology basis to expand U.S. competitiveness in high-strength fiber manufacturing [1]. This project will leverage previous and ongoing work of the FreedomCAR's program to develop a low-cost, high-strength carbon fiber. Analysis is ongoing in related DOE projects to determine appropriate targets for storage systems as a function of construction materials and fabrication costs. Until targets are definitively established, this project will seek to develop carbon fibers with properties equivalent to Toray's T700/24k fiber (24k tow, 700 ksi ultimate tensile strength, 33 Msi tensile modulus), and reduce production costs of the fiber by at least 25%.

APPROACH

This project is structured into tasks focused on precursor development and conversion process improvements. Development and demonstration of melt-spinnable PAN is the project's primary precursor option. If successful, melt spinning is projected to be significantly less costly than wet spinning with capability to produce high quality, relatively defect-free precursor. This requires concurrent activities in both development of melt-stable PAN copolymer and blends as well as the processes necessary to successfully spin the formulations into filamentary tows. Melt processing of PAN is a difficult issue, although Virginia Tech and others have made modest progress over the last decade [2-6]. One of the principal problems is that PAN degrades (cross-links) even without main chain scission or weight loss, and this essentially precludes melt processing. Reactions of the side groups have been discussed in many reports [7-10]. These degradative reactions can take place both in an intra-molecular manner, but also via inter-molecular branching and gelation, which quickly alters the capacity for these materials to be melt-fabricated. At 200-220°C, the material can quickly increase in viscosity, thus rendering an intractable material in a very short time. Ideally, one would like to maintain constant viscosity for a required period, and practical considerations suggest that this should be at least 30 minutes or longer. Backup options include other precursor alternatives such as textile PAN, polyolefins, and incorporation of nanomaterials.

Demonstrating and down-selecting a precursor capable of meeting performance targets utilizing conventional conversion processing defines the pathway for the balance of project activities. In conversion, critical processability parameters include: (i) highly controlled temperature and stretching, especially during pre-treatment and stabilization; (ii) residence time in various conversion modules; (iii) optimal graphitization for maximum strength; (iv) uniform treatment of fibers throughout the tow; and (v) strict control of each of these parameter through all of the various stages of conversion operation. Related ORNL work in advanced processing technologies address these issues, with a focus on increasing line speed in a reduced footprint, with reduced energy consumption. Means to adapt these emerging processes will be developed and evaluated for applicability to meeting requirements of this program area. As the alternative approaches are demonstrated, the energy efficiency and overall economics of the complete system will be evaluated and forecast for production scale up.

RESULTS

During this period, the project team with sponsor encouragement decided to put precursor chemistry development work on hold in order to focus limited resources on demonstrating feasibility of the melt-spinning approach. For this demonstration effort, some baseline high MW PAN-based formulations are being utilized that, while representative of the processing requirements ultimately required to meet project goals, probably cannot be converted themselves into carbon fiber meeting those performance goals. Significant "engineering" obstacles have been encountered in utilizing the very simple experimental

equipment available in this project; a number of these hurdles have been overcome during this period and we have identified solutions for resolving others we expect to encounter on the pathway to our goals. Examples already implemented include improved spinneret design and construction, improved filtration, means for maximizing small sample utilization with integration of purging materials for maintaining open holes as the sample is expended, enhanced extrusion barrel heating, larger spinning pressure chamber, indexed take-up winding patterns, etc. Most recently, capability for precursor fiber drawing in a separate process between spinning and conversion has been incorporated. As we continue to resolve these issues, we have gained confidence that the approaches we have proposed do have great potential for meeting program goals given appropriate levels of resources.

A batch fiber drawing system was built to stretch as-spun PAN fibers. The system is good for trying and determining the drawing conditions for a specific fiber sample, but it is not good for generating long and continuous filaments. So a new continuous fiber drawing system was designed and built this year (see Figure 1). The system can use a steam bath, water bath or electric oven to heat the fibers, but the steam bath seems to work the best for PAN fibers.

The as-spun fibers were de-spooled and wound on an aluminum bobbin after passing through a water bath containing an antistatic agent, which made further handling of the fibers easier (Figure 2). The filaments were then put in a convection oven at 150°C for about five minutes for pre-conditioning. This was to remove the residual plasticizers from the fibers and reduce the voids in the fibers. The bobbin of annealed fibers was mounted onto the fiber drawing system and the fibers were drawn under saturated steam where up to a 600% draw ratio was reached so far with the diameter of drawn fiber reaching about 13 microns (see Table 1 and Figure 3). The drawn fibers (both sample #1 and #2) from Virginia Tech (VT) were sent to ORNL for evaluation.

The drawn PAN/VT fibers have been successfully converted to carbon fibers. The tensile strength and modulus

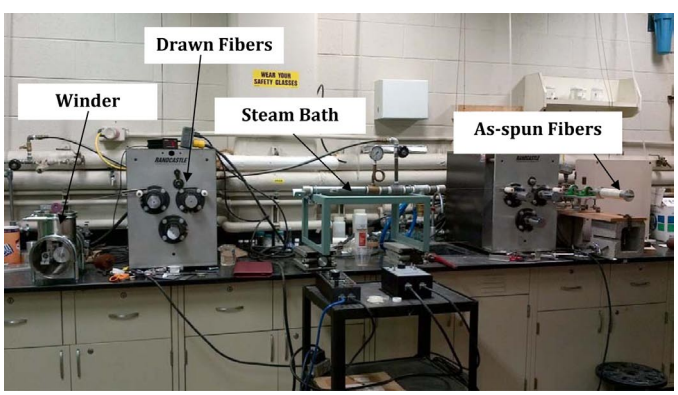

FIGURE 1. New Continuous Fiber Drawing System with Steam Bath

FIGURE 2. Drawn PAN/VT Fibers Generated with Water and Acetonitrile

TABLE 1. Spinning and Drawing Conditions for PAN/VT Fibers

As-spun fibers	Polymer	PAN/VT with 93 mol% PAN
	Plasticizer and content	Water 14 wt%, acetonitrile 14 wt%
	Spinning temperature	165°C
	Fiber formation zone P	170 psi, N_2
	Number of spinneret holes	18
	Diameter of holes	55 µm
	Diameter of as-spun fibers	~35 µm
Drawn fibers #1	Heating media	Saturated Steam
	Steam pressure	18 psi
	Steam temperature	124°C
	Draw ratio (second stretch)	4
	Filament number	8
	Filament diameter	18 microns (to be confirmed)
Drawn fibers #2	Heating media	Saturated Steam
	Steam pressure	18 psi
	Steam temperature	124°C
	Draw ratio (second stretch)	6
	Filament number	8
	Filament diameter	13 microns (to be confirmed)

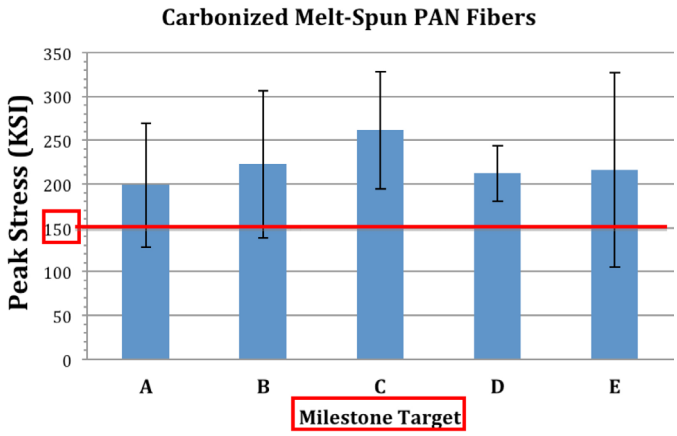

FIGURE 3. Tensile Strength of Carbonized Melt-Spun PAN Fibers—March 2013's Milestone is 150 ksi

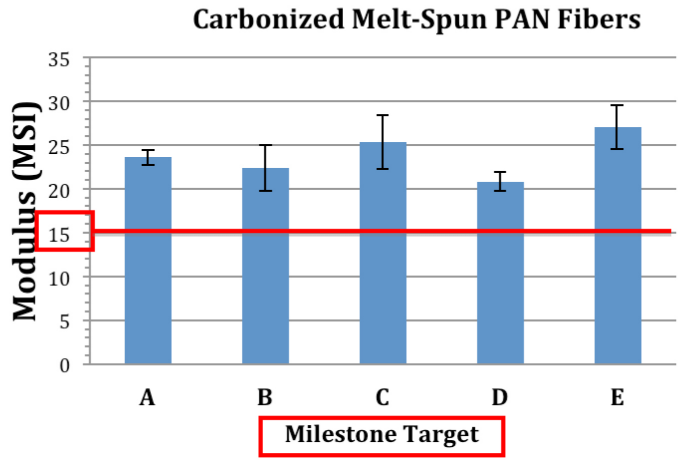

FIGURE 4. Tensile Modulus of Carbonized Melt-Spun PAN Fibers—March 2013's Milestone is 15 Msi

of the carbonized fibers is shown in Figures 3 and 4, respectively. The strength over 150 ksi and modulus higher than 15 Msi for the carbonized fibers meets the goal of the critical Go/No-Go milestone for feasibility demonstration. Other samples significantly exceeded this critical milestone target including one sample with properties over 250 ksi and 25 Msi.

CONCLUSIONS AND FUTURE DIRECTIONS

The critical Go/No-Go milestone chosen by the project and program management team of 15 Msi modulus and 150 ksi strength for converted carbon fiber was achieved during this period. This milestone was chosen to establish a baseline indicative of technical feasibility for this project approach. Several samples processed during this period significantly exceeded this baseline property level.

Significant progress has been made in demonstrating melt spinning processes and producing precursor fiber in sufficient quality and quantity to begin carbon fiber conversion investigations. Mechanical properties of the melt spun precursor fiber are approaching those are commercially produced fibers. Initial conversion protocols have been developed and demonstrated indicating that we are indeed taking an effective approach and making progress beyond the stage-gate milestone established for taking this initiative to the next level of development.

Near-term objectives are for Virginia Tech to produce longer and more uniform tows that are then drawn in a secondary step as previously described. ORNL will characterize fiber and conduct more extensive conversion trials on precursor filaments generated using its precursor evaluation system. In this next stage of development, we will resume working the precursor chemistry we believe necessary to enhance baseline properties and move towards the ultimate goals of 33 Msi modulus and 700 ksi strength. We will need to scale the spinning processes up so that we can work with larger tow sizes and more continuous tows in further enhancing the conversion processes and providing feedback to the chemistry and fiber forming development. The filaments at various steps of the conversion process will be fully characterized and the data used to commence optimization of precursor chemistry and the filament generation process. In order to fully address application requirements, we will also need to evaluate and implement appropriate post treatment operations including surface treatment and sizing for the fiber. We will also evaluate whether advanced plasma-based conversion processes (oxidative stabilization and carbonization) under development at ORNL are appropriate for these fibers in reducing costs while meeting performance goals. As the technology is being successfully demonstrated at the Carbon Fiber Technology Facility in Oak Ridge, ORNL will concentrate on the commercialization strategy for technology transfer and implementation.

FY 2013 PUBLICATIONS/PRESENTATIONS

1. Felix L. Paulaukas, "High Strength Carbon Fibers", presentation at 2013 DOE Hydrogen Program and Vehicle Technologies Annual Merit Review and Peer Evaluation Meeting, May 13–17, 2013.

2. Felix L. Paulauskas, "High Strength Carbon Fibers and Status Report", presentation at Hydrogen Storage Tech Team Meeting, April 18, 2013.

REFERENCES

1. Hydrogen, Fuel Cells and Infrastructure Technologies Program Multi-Year Research, Development and Demonstration Plan Planned program activities for 2005-2015, October 2007 update.

2. Wiles, K.B., V.A. Bhanu, A.J. Pasquale, T.E. Long, and J.E. McGrath, Journal of Polymer Science: Part A: Polymer Chemistry, Vol. 42, 2994-3001 (2004).

3. Bhanu, V.A., P. Rangarajan, K. Wiles, M. Bortner, S. Sankarapandian, D. Godshall, T.E. Glass, A.K. Banthia, J. Yang, G. Wilkes, D. Baird, and J.E. McGrath, Polymer, 43, 4841-4850, (2002).

4. Godshall, D., P. Rangarajan, D.G. Baird, G.L. Wilkes, V.A. Bhanu, and J.E. McGrath, "Polymer 44 (2003), 4221-4228.

5. Rangarajan, P., V.A. Bhanu, D. Godshall, G.L. Wilkes, J.E. McGrath, and D.G. Baird, Polymer 43, 2699-2709 (2002).

6. Bortner, Michael J., Vinayak Bhanu, James E. McGrath, and Donald G. Baird, Journal of Applied Polymer Science, 93(6), 2856-2865 (2004).

7. Peng, Fred M., "Acrylonitrile Polymers," in Mark, Herman F.; Bikales, Norbert M.; Overberger, Charles G.; Menges, Georg; Editors. Encyclopedia of Polymer Science and Engineering, Vol. 1: A to Amorphous Polymers. (1986), 843 pp, pages 426-470, and references therein.

8. Back, Hartwig, C, and Knorr, Raymond S. "Acrylic Fibers," in Mark, Herman F.; Bikales, Norbert M.; Overberger, Charles G.; Menges, Georg; Editors. Encyclopedia of Polymer Science and Engineering, Vol. 1: A to Amorphous Polymers. (1986), 843 pp, pages 334-388, and references therein.

9. Capone, Gary J.; Masson, James C. Fibers, acrylic. Kirk-Othmer Encyclopedia of Chemical Technology (5th Edition) (2005), 11 188-224

10. Frushour, Bruce G.; Knorr, Raymond S. Acrylic fibers. International Fiber Science and Technology Series (2007), 16(Handbook of Fiber Chemistry (3rd Edition)), 811-973.

IV.F.3 Development of Low-Cost, High-Strength Commercial Textile Precursor (PAN-MA)

C. D. Warren (Primary Contact),
Felix L. Paulauskas, Hippolyte Grappe, Fue Xiong,
Ken Yarborough, Ana Paula Vidigal
Oak Ridge National Laboratory (ORNL)
1 Bethel Valley Road
Oak Ridge, TN 37831
(865) 574-9693
Email: warrencd@ornl.gov
Email: paulauskasfl@ornl.gov

DOE Managers
Grace Ordaz
Phone: (202) 586-8350
Email: Grace.Ordaz@ee.doe.gov
Ned Stetson
Phone: (202) 586-9995
Email: Ned.Stetson@ee.doe.gov

Project Start Date: April 21, 2011
Project End Date: November 30, 2014

Overall Objectives

- Down-select from 11 candidate polymer compositions to three for spinning fibers.
- Evaluate three fiber compositions to yield guidance for selecting the best fiber composition.
- Demonstrate at least 300 KSI breaking strength and 30 MSI modulus by mid project. (Gate Milestone)
- Optimize the conversion protocol to achieve at least a 650 KSI ultimate strength fiber.
- Develop a new precursor with carbonized fiber property strengths approaching that of aerospace grade carbon fibers but at costs comparable to industrial grade carbon fibers.

Fiscal Year (FY 2013) Objectives

- Down-select to one fiber composition for property optimization.
- Begin optimization of selected fiber composition.
- Increase finished carbon fiber tensile strength from 300 KSI to 405 KSI.
- Increase finished carbon fiber tensile modulus from 30 MSI to 33 MSI.
- Establish a firm commercialization commitment if final target properties are met at the end of the project.

Technical Barriers

This project addresses the following technical barriers from the Hydrogen Storage section of the Fuel Cell Technologies Office Multi-Year Research, Development, and Demonstration Plan:

(B) System Cost

(A) System Weight and Volume

Technical Targets

The cost of the carbon fiber in hydrogen storage systems is 60-80% of the total system cost (Figure 1). Precursors account for 55% of the total cost of the carbon fiber (Figure 2). The precursor alone can account for 33-44% of the cost of the tank. The hydrogen storage team has been conducting projects to develop lower-cost carbon fiber precursors to reduce the cost of carbon fiber for hydrogen storage tanks. This effort is to develop a solution spun textile grade polyacrylonitrile with methyl acrylate (PAN-MA) precursor with strengths in the range of 650-700 KSI (Table 1). This project is a shorter-term, lower-risk approach to addressing the same issue as is being addressed by the melt-spun polyacrylonitrile (PAN) project. Ideally, the fiber developed in this project could be ready for commercialization within one to two years to meet programmatic needs. The melt-spun PAN when developed could be ready for market introduction a few years later. Both

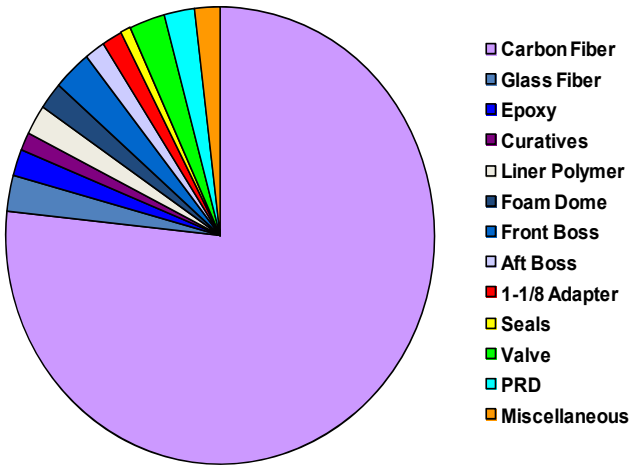

FIGURE 1. Cost of Hydrogen Storage System Broken Out by Major Components and Materials

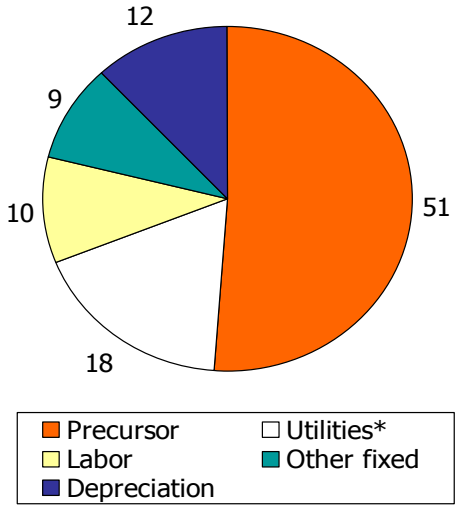

FIGURE 2. Carbon Fiber Production Costs

precursors would be suitable for applications in a wide range of other industries.

TABLE 1. Progress towards Meeting Technical Targets for PAN-MA Based Lower Cost Carbon Fiber for Hydrogen Storage Tanks

	Strength (KSI)	Modulus (MSI)	Estimated Production Costs
Current Market Fibers	750	38	$15-20/lb
Target	650-750	35-38	$10-12/lb
Current Status of Candidate Precursors	402	36	$10-12/lb

KSI--kilopounds per square inch; MSI--megapounds per square inch

FY 2013 Accomplishments (as of 1 July 2013)

- Down-selected to one fiber composition for property optimization.
- Optimized selected fiber composition.
- Increased finished carbon fiber tensile strength from 300 KSI to 405 KSI.
- Increased finished carbon fiber tensile modulus from 30 MSI to 33 MSI.
- Refined the conversion protocol for the first three of four oxidation stages, achieving fiber properties of 402 KSI breaking strength and 36 MSI modulus.
- Received commitment from the director of research from our partner company that the precursor will go into commercial production if minimum project property goals are achieved (i.e., 650 KSI strength and 35 MSI modulus).

✧ ✧ ✧ ✧ ✧

INTRODUCTION

In previous years, the Vehicle Technologies Program developed technologies for the production of lower-cost carbon fiber for use in body and chassis applications in automobiles. Program goals target materials that have tensile strengths in excess of 250 KSI and modulus of at least 25 MSI. Past work included the development of a vinyl-acetate co-monomered, lower-cost precursor and methods for manufacturing precursors into finished carbon fiber. The basic premise of the project was to be able to use PAN material produced in a high volume textile production process for a carbon fiber precursor rather than the specialty material that is typically used for carbon fiber precursors. A textile line that formerly made knitting yarn has been retrofitted and that precursor is being commercialized.

The previously developed fiber had strengths slightly below 500 KSI, which is far above strengths suitable for automotive structural applications but insufficient for many higher demanding applications with higher performance requirements such as the manufacture of hydrogen storage tanks. In order to preserve the cost advantages of using a high-volume PAN fiber, and simultaneously meet the needs of higher performance applications, it was proposed to develop the capability to use methyl-acrylate based, textile grade, PAN as a carbon fiber precursor and to manufacture that precursor on a textile line.

The purpose of this current project is to take one precursor technology, textile-based PAN, while using a higher performance chemical formulation, from the technical feasibility stage and scale up to technology demonstration. This project will result in the determination of the best polymer formulation and conversion protocol (time-temperature-tension profiles) to produce the best carbon fiber while the precursor is readily and inexpensively manufacturable in existing textile PAN plants. Successful completion of this project will result in defining the precursor formulation and manufacturing methods to produce carbon fiber. SGL Carbon Fibers is the partner for this work and has both the commitment and ability to commercialize the technology. SGL purchased FISIPE after FISIPE's involvement in the development of the first precursor. Therefore the team that developed the first textile-based precursor is involved in this work but now under the name SGL rather than FISIPE. Deliverables include spools of fully carbonized, surface-treated and sized carbon fiber. This project is on the critical path for the development of lower-cost carbon fiber.

APPROACH

The first step to developing a new precursor is to define and analyze candidate precursor formulations. Those are then down-selected and multiple candidate polymer formulations are produced. For this project, SGL/FISIPE down-selected

to 11 candidate formulations. Those polymer formulations were sent to ORNL for evaluation from which three polymer formulations were selected to be spun into precursor fiber for attempted conversion into carbon fiber. SGL/FISIPE worked to determine how to spin each of those three formulations into precursor fiber tows and sent them to ORNL for conversion trials. Developing uniformly round fibers and maintaining fiber consistency from fiber to fiber and along the length of each fiber were critical parameters.

Upon receipt of the precursor spools, ORNL began the thermal evaluations to pinpoint conversion temperatures of the precursor, particularly the temperatures to be used for oxidative stabilization. The next step was to determine the limits of fiber stretching that can be achieved in each of the oxidative stabilization stages. As a general rule, higher levels of tension (i.e., percentage of stretching) will promote better polymer chain alignment along the axis of the fiber and will result in higher breaking strengths of the fiber. It is therefore necessary to apply the maximum tension to the fiber, especially during the early stages of oxidative stabilization, without breaking the filaments and without damaging the filaments.

The amount of stretching in each stage of conversion, the optimum temperatures for conversion and the time that the precursor is exposed to those conditions must be developed for each of the seven stages (Prestretching, Oxidation 1, Oxidation 2, Oxidation 3, Oxidation 4, Low-Temperature Carbonization and High-Temperature Carbonization) of processing. These must be done sequentially, completing each processing step before proceeding to the next. Only after completing all of these steps, can the final properties of the fiber be determined. The plan was to evaluate the three formulations, pinpointing processing parameters in approximate ranges and then down-select to one final formulation. For that formulation, all spinning and conversion parameters are now being optimized. That down-selection has been made to the F2000 formulation.

The main challenges to be addressed in optimizing the performance of the selected precursor are:

- Adapting high-speed processes for producing fiber containing higher acrylonitrile (AN) concentrations.
- Adapting high-speed processes for producing fiber containing methyl-acrylate (MA) co-monomers.
- Adapting high-speed processes for producing fiber with increased chemical purity in order to minimize defects.
- Spinning of round fibers rather than the kidney-shaped fibers that are typically produced during textile fiber production.
- Improving the fiber consistency from fiber to fiber and along the fiber length without sacrificing production speed and throughput.
- Determining the optimal conversion protocol by balancing residence time, temperature, and applied tension during each of the multiple steps in precursor conversion to carbon fiber.

RESULTS

The down-selection of chemical compositions and fiber formulations started in April of 2011. The main issue related to achieving the proper formulation was the generation of the PAN-polymer with a higher AN content and with an MA co-monomer. Dealing with MA co-monomered polymer required some changes to SGL/FISIPE's equipment and standard practices which required three months. SGL/FISIPE generated 11 candidate compositions. Those 11 compositions were sent to ORNL for evaluation. Differential scanning calorimetry (DSC) curves and other technical data for those compositions were generated for comparison to each other and to known aerospace and industrial grade precursors. The research team then selected three fiber compositions from the first 11 formulations for fiber spinning and preliminary evaluation trials (Figure 3).

Upon receipt of the three fiber candidates, ORNL began the thermal evaluations to pinpoint conversion temperatures of the precursor, particularly the temperatures to be used for oxidative stabilization. Two features are prominent and were expected from the thermal evaluations: (1) the onset of the exotherm occurs at a slightly different temperature from traditional precursors indicating a different starting temperature for oxidative stabilization; (2) the exothermic curve is steeper for the PAN-MA precursors than it is for the polyacrylonitrile with a vinyl acetate comonomer precursors indicating a slower temperature ramp up being necessary during oxidative stabilization.

The next step was to determine the limits of fiber stretching that can be achieved in each of the stages during oxidative stabilization. As a general rule, higher levels of tension (i.e., percentage of stretching) will promote better polymer chain alignment along the axis of the fiber and will result in high breaking strength of the fiber. It is therefore necessary to apply the maximum tension to the fiber, especially during the early stages of oxidative stabilization, without breaking the filaments. Damage to the filaments that is hidden can also be induced by the tensioning. That damage many not show up until later processing stages. After determining the temperature and tension limits for processing, precursor conversion trials were conducted for those three fiber formulations. The results of those trials are shown below in Table 2. The F2000 formulation was selected for full development. Filament diameters for the new precursor were measured at 11.7 microns which is within the desired range for an oxidized precursor. Normal ranges are 11-12 microns which, after carbonization, produce ~7-micron diameter carbonized fiber.

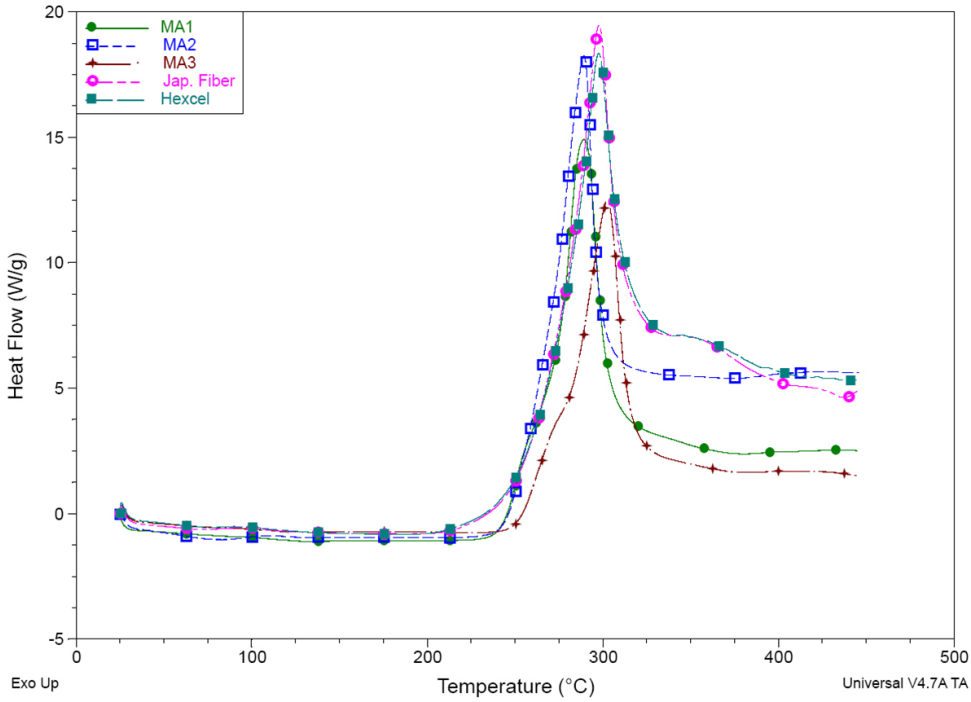

FIGURE 3. DSC Scans of the Three Fiber Compositions Compared to Aerospace and Industrial Grade Precursors

Table 2. Final Fiber Properties for Three Candidate Precursor Systems

Fiber Designation	Tensile Strength (KSI)	Tensile Modulus (MSI)
F1921	324.7	26.9
F2000	372.8	36.0
F2027	252.7	27.2

At this point precursor optimization began. Using the three spools of laboratory-produced F2000 that ORNL had, temperature profiles during oxidation were then determined. The temperature profiles are the temperature setting of each of the oxidation ovens and dwell times before significant polymer stretching (tensioning) is applied. Figure 4 shows the DSC curves used for that evaluation. Axis data labels are intentionally omitted for this and all DSC curves in this report due to export control restrictions. The closeness of the Stage 1 and Stage 2 curves is indicative of further improvements that can still be made in the oxidation temperature profile.

The processing parameters (temperature, time at that temperature and tension applied during oxidative stabilization) during oxidation are interdependent. If any one of the processing conditions in the first stage of oxidation is changed, then the processing conditions that will be optimal in Stage 2 are altered. If Stage 2 parameters are changed then Stage 3 will be altered, etc. As a result, it is critical when optimizing a precursor to finish each processing stage in series rather than in parallel. As an example, if the

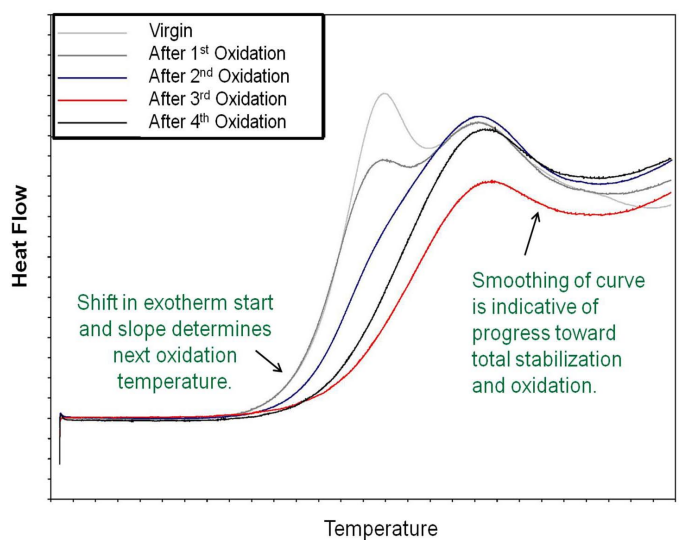

FIGURE 4. DSC Curves for the F2000 Precursor after Various Stages of Oxidative Stabilization

temperature is increased during one stage of oxidation, or the residence time at temperature is increased then the resulting material will be more highly crosslinked and the amount of oxygen diffusion into the fiber will have increased as will the degree of polymer crosslinking. Likewise, if the fiber is more highly stretched, then the fiber diameter will have decreased, affecting oxygen diffusion into the fiber. For each of these

parameters (time, tension, and degree of stretch) there is an optimal processing condition for each production step. Too little of each of these and the fiber's final properties are compromised. Too much of each of these and the fibers are damaged. Fortunately, once these conditions are optimized, as long as the precursor chemistry is not changed, the processing conditions will not change either.

After determining these beginning temperatures, the amount of stretch that can be given to the precursors during each stage of processing had to be determined. This is done by systematically adding tension to precursors that have been processed through all earlier stages until the breaking point of the precursor at the next temperature is achieved. Figure 5 shows the tension and percent stretching for fibers after exposure to the temperatures determined in the previous step. Of particular interest are the ends of each curve which indicate the upper tension limit of the processing window for these precursors. The closeness of the first and second stage curves indicates that not much progress was being made during the first stage oxidation so either the temperature or the residence time will have to be increased. Since the goal of this effort is to develop a lower-cost carbon fiber, a temperature increase of just a few degrees Celsius was used to combat this problem. The closeness of data and the magnitude of the data after the third and fourth stages are indicative of damage during earlier stages, likely due to over stretching the fibers. Export control restrictions require that all tension loads, stretching percentages, oven temperatures, and residence times not be publicly disclosed, therefore axis values are intentionally left off of these charts.

One issue that had to be dealt with for these precursors was "fuzzing" of the fiber tow during processing. Figure 6 shows an example of this. Fiber fuzzing is typically due to small, not fully developed "baby" fibers present in the precursor. Upon tensioning, these fibers see a higher than average stress, exceed their strength and break. This issue has been resolved.

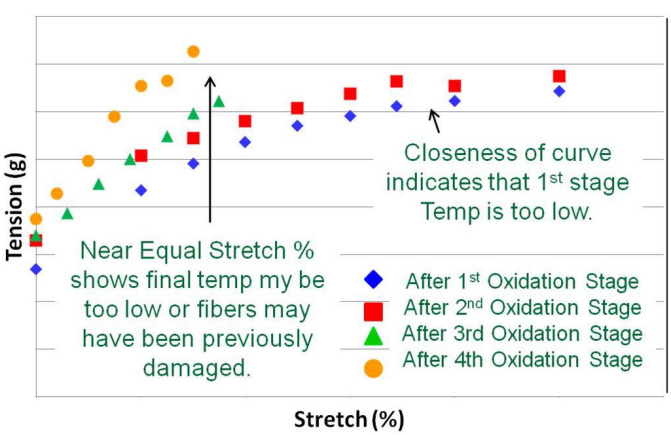

FIGURE 5. Stretch–Break Curves for F2000 Precursor

As second issue that had to be dealt with was the cross-sectional geometry of the fibers. Typical textile production processes yield fibers that are kidney bean in shape (Figure 7A). These are fine and even preferable for making carpet fiber or knitting yarn but not for carbon fiber. Carbon fiber properties are enhanced by having uniformly round fibers (Figure 7B). To solve this problem a slightly different configuration for spinning the precursor into the solvent bath during solution spinning of the precursor had to be adopted. The details are proprietary.

Figures 8 and 9 show tensile strength and tensile modulus as a function of time for tracking precursor progress. Each data point is the average of 18 tests.

While we have not yet achieved Hydrogen Storage sub-program goals, the properties achieved thus far are sufficient for this precursor to go into production for lower performance applications. As a result, SGL/FISIPE is now moving to produce the precursor that they are supplying for this work on their full-scale production line. The production material is scheduled to arrive in early August 2013.

FIGURE 6. Top: "Fuzzing" of Filament Tow during Oxidative Stabilization. Bottom: Tow not exhibiting "Fuzzing"

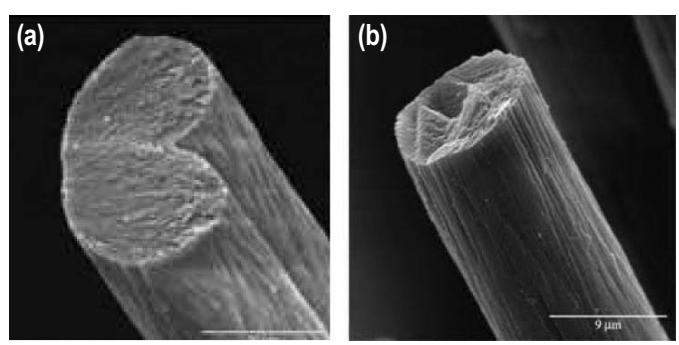

FIGURE 7. (A) Typical Textile-Produced PAN Fibers (B) Carbon Fiber-Grade PAN Fibers

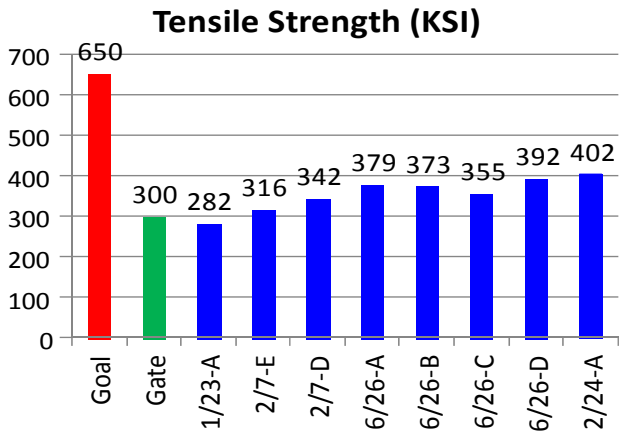

FIGURE 8. Tensile Strength as a Function of Time for the F2000 Precursor

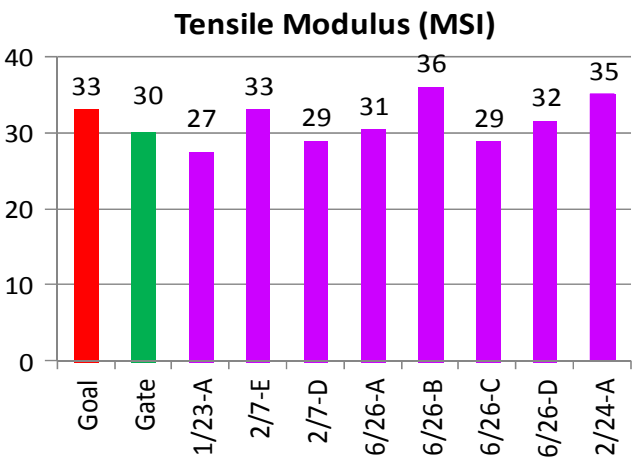

FIGURE 9. Tensile Modulus as a Function of Time for the F2000 Precursor

CONCLUSIONS AND FUTURE DIRECTIONS

The Gate milestone for project continuation has been met. The original 11 polymer compositions have now been selected down to one final composition. That material is being produced on full-scale production lines while optimization of the conversion protocol is occurring. To date, we are approximately half way through the conversion protocol optimization phase. Work to improve fiber consistency from filament to filament and along the lengths of the filaments has mostly been completed. This is a task that manufacturers will continue throughout the production life of the precursor since it is critical to pushing the final carbon fiber properties higher.

SPECIAL RECOGNITIONS & AWARDS/ PATENTS ISSUED

1. The Carbon Fiber Team won the Oak Ridge National Laboratory award for Most Outstanding Research team for 2012.

2. Dr. Felix Paulauskas won the Oak Ridge National Laboratory award for Most Outstanding Researcher for 2012.

FY 2013 PUBLICATIONS/PRESENTATIONS

1. Warren, C.D., Wheatley, A. and Das S., "Low Cost Carbon Fibre for Automotive Applications Part 1: Low Cost Carbon Fibre Development", Chapter 3 in Advanced Composite Materials for Automotive Applications: Structural Integrity and Crashworthiness, (in final editing) Publisher: Wiley, Edited by: Ahmed Elmarkbi. (2013).

2. Warren, C.D., Wheatley, A. and Das S., "Low Cost Carbon Fibre for Automotive Applications Part 2: Applications, Performance and Cost Reduction Models" Chapter 17 in Advanced Composite Materials for Automotive Applications: Structural Integrity and Crashworthiness, (in final editing) Publisher: Wiley, Edited by: Ahmed Elmarkbi. (2013).

IV.F.4 Synergistically Enhanced Materials and Design Parameters for Reducing the Cost of Hydrogen Storage Tanks

Kevin L. Simmons
Pacific Northwest National Laboratory (PNNL)
PO Box 999, MSIN K2-44
Richland, WA 99352
Phone: (509) 376-3651
Email: kevin.simmons@pnnl.gov

DOE Managers
Ned Stetson
Phone: (202) 586-9995
Email: Ned.Stetson@ee.doe.gov
Grace Ordaz
Phone: (202) 586-8350
Email: Grace.Ordaz@ee.doe.gov

Subcontractors:
- Hexagon Lincoln, Lincoln, NE
- Ford Motor Company, Dearborn, MI
- Toray Composites America, Decatur, AL
- AOC, LLC, Collierville, TN

Project Start Date: January 18, 2012
Project End Date: September 30, 2015

Overall Objectives

- Reduce carbon fiber (CF) usage and associated compressed hydrogen tank cost through a series of combined material and design approaches for a cumulative 37% cost savings.
- Improve the tank cost performance using the following techniques in a holistic design approach: (A) resin matrix modifications and alternatives, (B) load translational efficiency improvements by CF surface modification, (C) alternate fiber placement and materials, and (D) enhanced operating conditions to increase the energy density.
- Demonstrate the combined costs reductions through modeling, materials, and burst testing.

Fiscal Year (FY) 2013 Objectives

- Develop a feasible pathway to achieve at least a 10% ($1.5/kWh) cost reduction, compared to a 2010 projected high-volume baseline cost of $15/kWh for 70-MPa Type IV pressure vessels
- Conduct material testing of resin modifications with higher filler concentrations
- Evaluate tank dormancy for cold gas storage
- Establish tank modeling for resizing of cold gas storage
- Complete tooling for producing liners for baseline tanks
- Fabricate baseline sub-scale prototype tank
- Accomplish burst testing of baseline sub-scale tank

Technical Barrier

This project addresses the following technical barriers from the Hydrogen Storage section of the Fuel Cell Technologies Office Multi-Year Research, Development, and Demonstration Plan:

(A) System Weight and Volume

(B) System Cost

(G) Materials of Construction

(H) Balance-of-Plant (BOP) Components

Technical Targets

This project contributes to achieving the following DOE milestone from the Hydrogen Storage R&D section of the Fuel Cell Technologies Office Multi-Year Research, Development, and Demonstration Plan:

- By 2017, develop and verify onboard automotive hydrogen storage systems achieving 1.8 kWh/kg system (5.5 wt% hydrogen) and 1.3 kWh/L system (0.040 kg hydrogen/L) at a cost of $12/kWh ($400/kg $H_{2\ stored}$).

TABLE 1. Progress towards Meeting Technical Targets for Onboard Hydrogen Storage for Light-Duty Fuel Cell Vehicles

Technical System Targets: Onboard Hydrogen Storage for Light-Duty Fuel Cell Vehicles			
Storage Parameter	**Units**	**2017 Targets**	**PNNL 2013 Status**
System Gravimetric Capacity	kg H_2/kg system	0.055	0.051
System Volumetric Capacity	kg H_2/L system	0.040	.027
Storage System Cost	$/kWh net	12	15.37

FY 2013 Accomplishments

- Developed and validated simplified estimator model for predicting tank parameters within +/- 5% of existing tank hardware.

- Completed extensive cost estimating comparison with Argonne National Laboratory and Strategic Analysis, resulting in consistent values.
- Identified 15% tank cost reduction opportunities and projected path toward a 37% target reduction.
- Accomplished modeling and material testing to identify the following potential cost savings:
  - Low cost resins (4% cost reduction)
  - Resin additive/modification improvements (5% cost reduction)
  - Alternative fiber placement and fiber types (6% cost reduction)
- Total savings after cost model analysis is 15%.

✧ ✧ ✧ ✧ ✧

INTRODUCTION

The ultimate DOE goal of this research is to reduce the cost of compressed hydrogen storage vessels by at least 50% from the current high volume projections of $17/kWh for commercialization in early-market and light-duty hydrogen fuel cell vehicles. The cost and performance baseline comparisons are the current 70-MPa , high-pressure storage vessels primarily constructed of standard-modulus, high-strength CF in an epoxy matrix that is overwrapped on a high density polyethylene liner (Type IV pressure vessel). The high-strength CF composite can account for nearly70-80% of the overall tank costs.

Since the composite is the dominate cost, the objective of this research is to reduce CF usage and associated tank cost through a series of combined material and design improvements that are estimated to total nearly 37% in overall cost savings. The project has identified, through modeling a series of material design requirements and experiments, the cost savings necessary to achieve the project goal. It is probable that these cost savings, combined with future reductions in CF cost, could lead to the 50% ultimate DOE target.

APPROACH

The project takes a holistic approach to improve performance by lowering the required gas pressure at lower operating temperature, refining the tank composite design with local reinforcement and hybrid layups, plus increasing the composite translation efficiency with material modifications at the composite constituent level. The project team includes industry experts in each of the following focus areas of improvement: enhanced operating conditions to improve energy density/pressure ratios, load translational efficiency improvements by CF surface modification, resin matrix modifications and alternatives, and alternate fiber placement and materials. We expect these savings approaches to be compatible and additive.

RESULTS

The project milestone, "to develop a feasible pathway to achieve at least a 10% ($1.5/kWh) cost reduction, compared to a 2010 projected high-volume baseline cost of $15/kWh for 70-MPa Type IV pressure vessels through detailed cost modeling and specific individual technical approaches," has been exceeded with an estimated 15% cost reduction in the first year based on detailed cost modeling and specific individual approaches to cost reductions. A thorough baseline performance and cost analysis was shown to compare within 5% of existing tank hardware predictions and 10% of tank costs estimated by two other independent cost models. The waterfall diagram in Figure 1 illustrates the progress of the individual technical approaches (described in the following) with estimates of future savings of nearly 40%. Each of the cost saving measures described are cumulative.

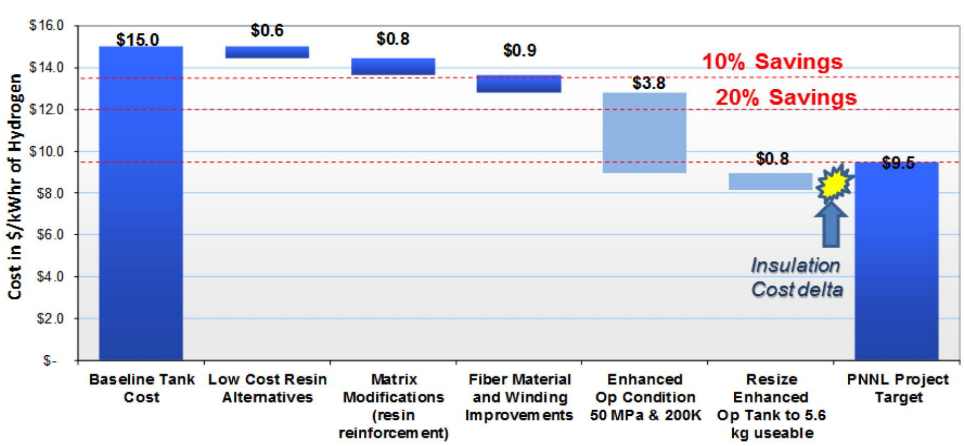

FIGURE 1. Waterfall Plot of Costs Savings

Low-Cost Resin Systems

When changing resin chemistry, the most critical element in composites is the interfacial adhesion. Fiber surface chemistries must be compatible with the resin system in use or the results will be poor-performing composite properties. The results of poor fiber wetting from incompatible surfaces of CF can be dry fiber bundles, low interfacial shear strength, and low translational efficiency in the tank windings.

Toray has developed several surface treatments for T700 fibers that have been tested with four AOC resin systems. The AOC vinyl-ester resins are lower in cost than the standard epoxies used in filament winding. Short-beam shear tests were performed to confirm that interfacial adhesion between the AOC resins and Toray fibers is similar to short-beam shear performance of the current epoxy resin system. Toray fabricated and tested short-beam shear specimens, with Ford testing a second set to confirm the test results. The tests identified fiber surface treatments that exceeded the shear strength of the CF epoxy baseline materials which confirmed vinyl-ester as a low resin replacement resulting in 4% lower tank cost.

Resin Matrix Modifications

Resin fillers or additives can improve load translation in the composite by increasing the resin modulus and strength to be more compatible with the fiber transverse modulus, as well as some improvement in matrix elongation at break. Detailed finite element calculations, including elastic/plastic matrix deformation with damage, were performed for a composite tank cylinder to estimate the effect of nano-additives on composite strength and burst pressure. Tensile test models of the matrix alone agreed within 5% of particle strengthening effects reported in the literature. Based on these calculations, we estimate that a 15% improvement in matrix modulus with an accompanying 12% increase in strength can be achieved to an increased burst pressure of approximately 8%. This is equivalent to an 8% reduction in CF usage. Because this is direct modification of the resin matrix properties and not the fiber, we expect additional strength improvement with the CF modification for a combined savings. Figure 2 illustrates the various morphologies being under evaluation and Figure 3 is the results of the various morphologies in the low-cost resin.

Composite Layup Optimization Study

A modeling study was conducted to evaluate alternative fibers, fiber combinations, and alternative laminate designs in the construction of 70-MPa all-composite pressure vessels. The primary and secondary evaluation parameters were vessel cost and mass, respectively. A finite element model was constructed of an axisymmetric cylindrical vessel wall. The model was loaded with pressure on the inner radius and axially with the appropriate closed end axial load.

The single fiber design comparison demonstrated that the industry standard T700 fiber provides the best strength vs. cost price point of the fibers that were evaluated. The hybrid combinations of the currently available commercial fibers did not show a significant cost reduction, however, several layup combinations did show a significant reduction in the tank mass. In particular, the combination of 51% T720 inside and 49% T700 outside predicted a mass reduction of 23% without impacting the tank cost.

Altering the typical layup design approach for wind angle and sequencing showed the most significant potential for reducing both tank cost and mass. In addition, the benefit of these alternate layup designs would apply to any fiber and they are not limited to the T700 fiber used for the study. Tailoring the wind angles has the potential to reduce cost

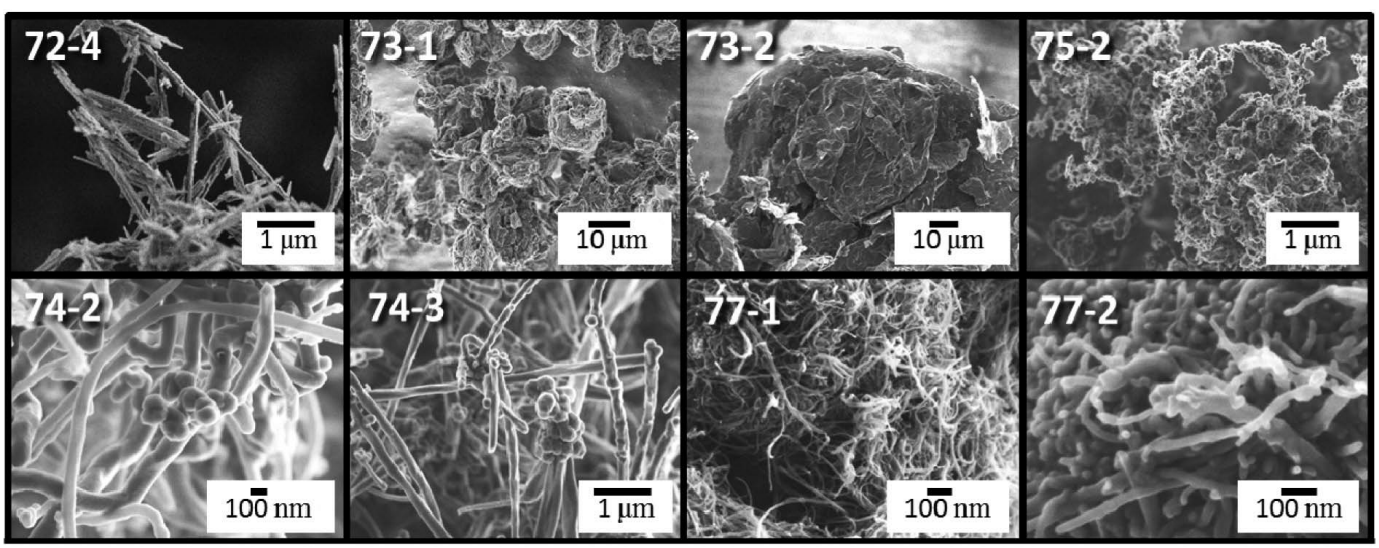

FIGURE 2. Scanning Electron Microscope Images of Nano-Scale Material Morphology

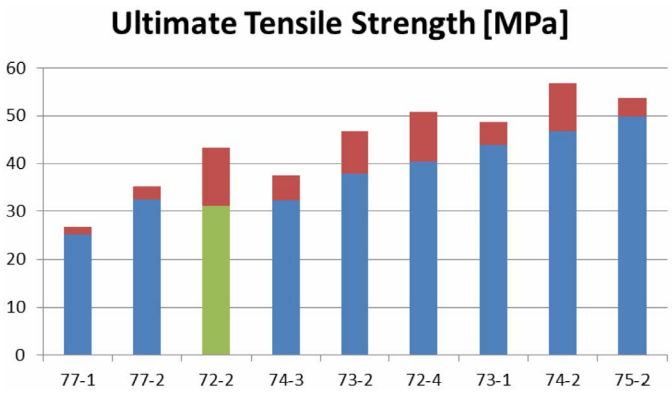

FIGURE3. Nano-Scale Material Tensile Strength Results of Various Morphologies

and mass by 3% to 14%. Increasing the stresses in the low angle helical (near axial) fibers could potentially reduce cost and mass by 7% to 16%. Implementing these alternate layup designs will require more detailed composites analysis of the tank, including the need for local reinforcement in the dome. Therefore, a low- to mid-range composite cost savings of 6% was assumed in the FY 2013 cost analysis. Detailed tank design analysis and testing will be performed during the ongoing tasks of this project to validate and likely increase this number.

CONCLUSIONS AND FUTURE DIRECTIONS

The conclusions from FY 2013 have demonstrated that there are several routes in cost reduction through combined material improvements and design. The work in FY 2013 has exceeded the target of a 10% cost savings by nearly 5% through material improvements. It is expected that future work will demonstrate these improvements in tank design and through the use of alternative materials and their improved properties.

FY 2014 FUTURE WORK

- Perform thermal and cost modeling to show the feasibility of 20% cost savings using tank insulation concepts for cold gas enhanced operation.
- Fabricate and burst test prototype baseline T700S CF plus epoxy tanks rated for 50 MPa and 70 MPa.
- Perform material testing of T700S fiber treatments and alternate filled resins at room temperature and cold gas operating temperature for comparison with T700S CF and epoxy composite used in the baseline prototype tank.
- Fabricate and burst test prototype 50-MPa prototype tanks using the standard T700S CF plus AOC alternate resins reinforced with nano-particle additives.
- Report project results of modeling, material testing, and tank fabrication and burst testing.

FY 2013 PUBLICATIONS/PRESENTATIONS

1. K.L. Simmons. 2013. "Enhanced Materials and Design Parameters for Reducing the Cost of Hydrogen Storage Tanks." Project ID# ST101. DOE Fuel Cells Office Annual Merit Review, May 13–17, 2013, Arlington, VA. Pacific Northwest National Laboratory, Richland, WA.

V. FUEL CELLS

V.0 Fuel Cells Program Overview

INTRODUCTION

The Fuel Cells program supports research, development, and demonstration of fuel cell technologies for a variety of transportation, stationary, and portable applications, with a primary focus on reducing cost and improving durability. These efforts include research and development (R&D) of fuel cell stack components, system balance-of-plant (BOP) components, and subsystems, as well as system integration. The program seeks a balanced, comprehensive approach to fuel cells for near-, mid-, and longer-term applications. Existing early markets and near-term markets include portable power, backup power, auxiliary power units, and specialty applications such as material handling equipment. In the mid- to long-term, development of fuel cells for transportation applications is a primary goal due to the significant reduction in the nation's energy and petroleum requirements that would result from market availability of high-efficiency fuel cell electric vehicles. Development of fuel cells for distributed power generation (e.g., combined heat and power (CHP) for residential and commercial applications) is also underway. The program's portfolio of projects covers a broad range of technologies, including polymer electrolyte membrane (PEM) fuel cells, direct methanol fuel cells, alkaline membrane fuel cells, and solid oxide fuel cells.

The program's fuel cell tasks in the *Fuel Cell Technologies Office Multi-Year Research, Development and Demonstration Plan* are organized around development of components, stacks, sub-systems, and systems; supporting analysis; and testing, technical assessment, and characterization activities. Task areas for fuel cell system and fuel processor sub-system development for stationary power generation applications are included, as are those for early market fuel cell applications, such as portable power, and for the development of innovative concepts for fuel cell systems.

GOAL

The program's goal is to advance fuel cell technologies for transportation, stationary, and portable applications to make them competitive in the marketplace in terms of cost, durability, and performance, while ensuring maximum environmental and energy-security benefits.

OBJECTIVES[1]

The program's key objectives include:

- Develop a 60% peak-efficient, direct-hydrogen fuel cell power system for transportation, with 5,000-hour durability, that can be mass-produced at a cost of $30/kW ($40/kW by 2020).
- By 2020, develop distributed generation and micro-CHP fuel cell systems (5 kW) operating on natural gas or liquid petroleum gas that achieve 45% electrical efficiency and 60,000-hour durability at an equipment cost of $1,500/kW.
- By 2020, develop medium-scale CHP fuel cell systems (100 kW–3 MW) that achieve 50% electrical efficiency, 90% CHP efficiency, and 80,000-hour durability at a cost of $1,500/kW for operation on natural gas and $2,100/kW when configured for operation on biogas.
- By 2020, develop a fuel cell system for auxiliary power units (1–10 kW) with a specific power of 45 W/kg and a power density of 40 W/L at a cost of $1,000/kW.

FISCAL YEAR (FY) 2013 STATUS AND PROGRESS

Cost reductions and improvements in durability continue to be the key challenges facing fuel cell technologies. In addition, advances in air, thermal, and water management are necessary for improving fuel cell performance; some stationary applications would benefit from increased fuel flexibility; and, while fuel cells are approaching their targets for power density and specific power, further progress is required to achieve system packaging requirements necessary for commercialization.

[1] Note: Targets and milestones were recently revised; therefore, individual project progress reports may reference prior targets.

One of the most important metrics is the projected high-volume manufacturing cost for automotive fuel cells, which the program tracks on an annual basis. In 2013, the program introduced several changes in the cost projection assumptions, including an increase in platinum price and an added requirement that the model system must meet the heat rejection target. These changes resulted in an increase in the projected cost status to $55/kW in 2013. However, if previous year status numbers are updated to include the new assumptions and requirements made in the 2013 analysis, the 2013 cost status still represents a more than 50% decrease from the 2006 status, as depicted in Figure 1. This decrease stems in part from a reduction in platinum group metal (PGM) loading and an increase in cell power density, allowing the design of smaller and less expensive stacks.

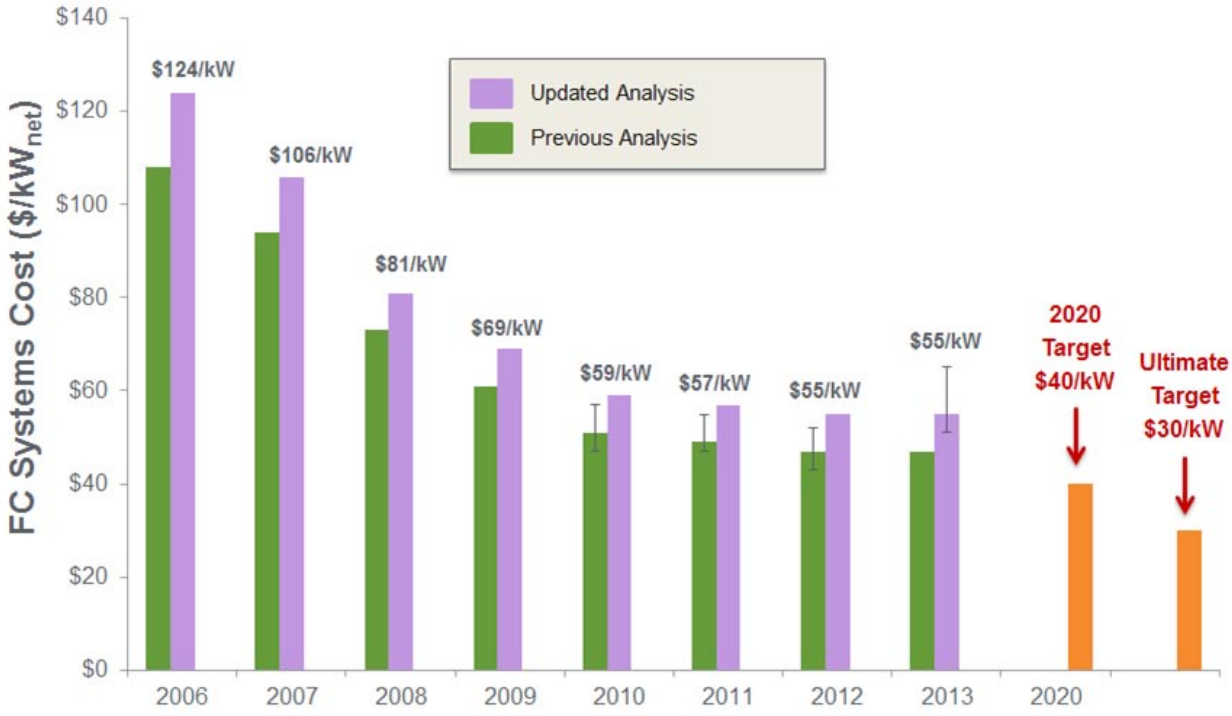

Figure 1. Modeled cost of an 80-kW automotive fuel cell system based on projection to high-volume manufacturing (500,000 units/year).[2]

To enable vehicle commercialization, the program is targeting cost reduction to $40/kW by 2020. Long-term competitiveness with alternative powertrains is expected to require further cost reduction to $30/kW, which represents the program's ultimate cost target. The $40/kW target, which represents a new target introduced in 2013, was selected with input from the U.S. DRIVE Partnership and from a Request for Information (RFI).

The program sponsors technical working groups on the topics of durability, transport modeling, and catalysis. These working groups, comprised of representatives from DOE-funded R&D projects, met in 2013 to exchange information, create synergies, share experimental and computational results, and collaboratively develop methodologies for and understanding of further R&D needs in the topical areas. Additional R&D needs examined in 2013 include the requirement for improved and standardized rotating disk electrode (RDE) testing techniques for ex situ catalyst screening. This need was addressed by issuing a RFI seeking input from the research community on proposed standards for RDE testing. Input from the RFI process will be used to issue a standard protocol and list of best practices, which will enable the RDE technique to provide more value and will make cross-laboratory comparison of RDE results possible.

[2] DOE Hydrogen and Fuel Cells Program Record #13012, http://hydrogen.energy.gov/pdfs/13012_fuel_cell_system_cost.pdf.

Catalysts

- **Developed dealloyed catalysts that meet mass activity target and show high performance in high current fuel cell testing (General Motors):** Dealloyed platinum-nickel (PtNi) and platinum-cobalt (PtCo) catalysts developed in a project led by General Motors have high oxygen reduction reaction (ORR) mass activity, 0.6 A/mg_{PGM} for PtCo and up to 0.75 A/mg_{PGM} for PtNi, exceeding the 2017 mass activity target of 0.44 A/mg_{PGM}. Both catalysts also meet the voltage cycling durability target, maintaining a mass activity greater than 0.26 A/mg_{PGM} after 30,000 voltage cycles (Figure 2). In addition to their high mass activity, both catalysts have demonstrated high performance operation at high current in membrane electrode assemblies (MEAs). At 1.5 A/cm^2, the $PtNi_3$ and $PtCo_3$ MEAs both met the 0.56 V project milestone (Figure 3).

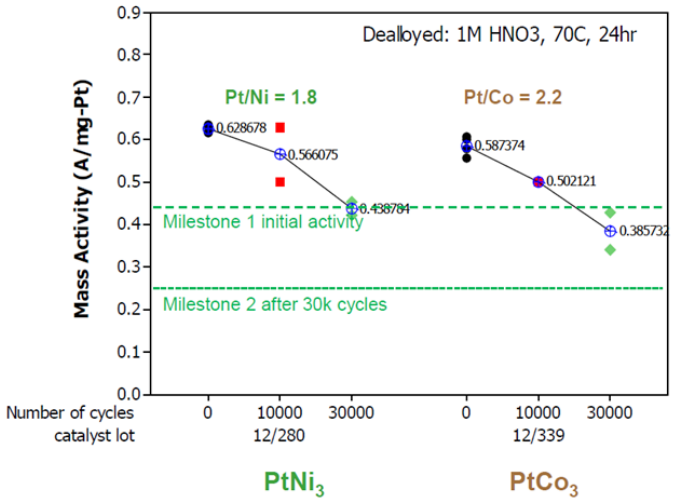

FIGURE 2. Mass activity of dealloyed PtNi and PtCo cathode catalysts measured in MEAs at beginning of life and after 10,000 and 30,000 cycles between 0.6 and 1.0 V.

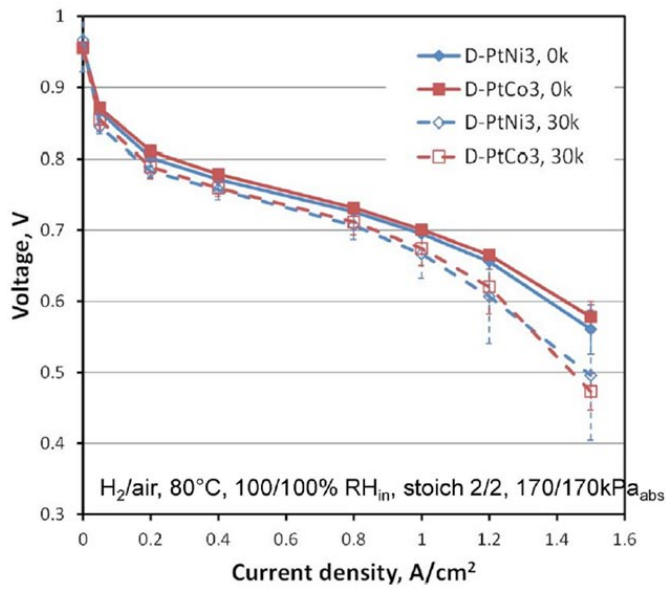

FIGURE 3. MEA performance of PtNi and PtCo dealloyed catalysts.

- **Developed meso-structured catalysts with specific activity 8X that of platinum (Argonne National Laboratory):** A new annealing process has enabled Argonne National Laboratory to modify PtNi nanostructured thin film (NSTF) catalysts to achieve greatly enhanced ORR activity. The annealing process decreases the surface roughness of the nanowhiskers and increases crystallite grain size through coalescence, producing a surface with predominantly (111) facets. Testing of the resulting meso-structured thin film (MSTF) catalysts using the RDE technique has demonstrated an 8X increase in specific activity over polycrystalline Pt, and a 2X increase over PtNi NSTF.
- **Developed scaled-up production procedure for non-precious cathode catalysts, up to 30 g batches (Northeastern University):** A project led by Northeastern University has developed multiple high-performance catalysts free of platinum group metals. MEAs containing an iron charge-transfer-salt (Fe-CTS) catalyst developed at the University of New Mexico have demonstrated current densities of over 100 mA/cm^2 at 0.8 V internal resistance-free. The catalyst experienced almost no degradation when subjected to the Nissan catalyst durability voltage cycling protocol. Scale up of the synthesis procedure by Pajarito Powders has enabled production of 30 g batches, with performance approaching that of the lab-scale produced catalyst.

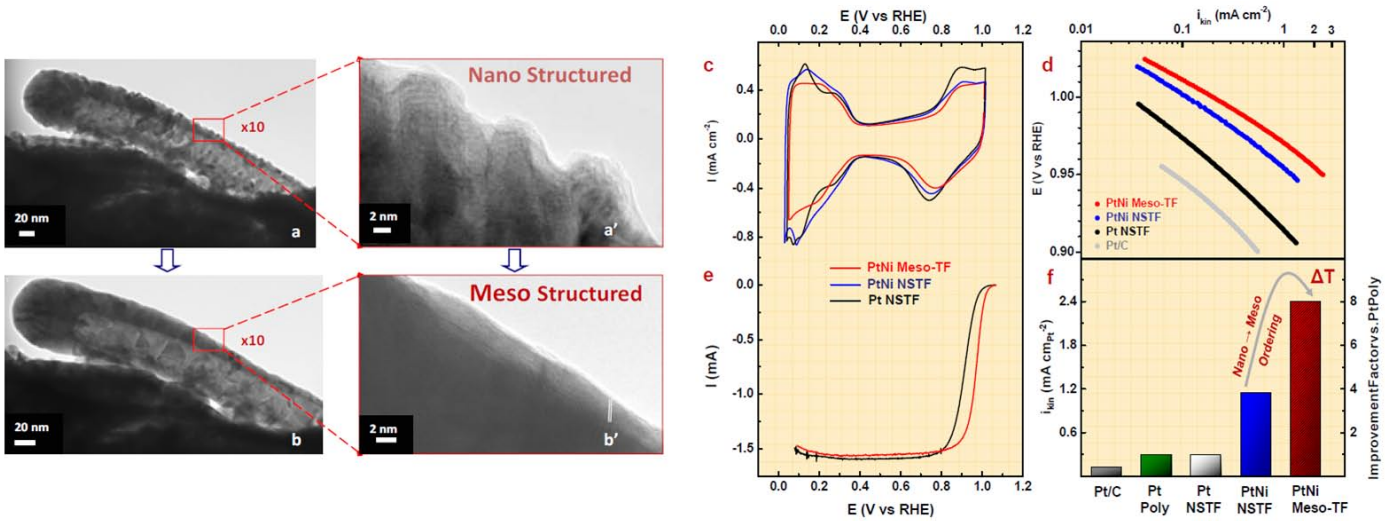

FIGURE 4. In situ transmission electron microscopy transition from nanostructured into mesostructured thin film: (a)-(b) annealing between room temperature and 400°C on a single whisker that induce the ordering from randomly oriented to a homogeneous structure with crystalline domains; cyclic voltammetry on the thin-film-based catalysts: (c) Pt-NSTF, PtNi-NSTF, and PtNi-MSTF; (e) the ORR polarization curves; (d) Tafel plots; and (f) specific activities at 0.95 V and improvement factor versus Pt-Poly (and Pt-NSTF).

Membranes

Developed low-cost fabrication methods for dimensionally-stabilized membranes (Giner, Inc.): Development of an improved fabrication procedure has enabled Giner to produce high-performance mechanically-supported membranes based on their dimensional stabilization technology. In 2013, Giner's mechanical deformation technique for support fabrication was down-selected for further development. Improvements in the release process from the micromolds enabled achievement of porosity up to 60% with stable, high-modulus polysulfone. Dimensionally stabilized membranes have already demonstrated excellent mechanical properties, but the laser-drilling technique previously used for fabrication is not suitable for low-cost manufacturing. Current low-volume production cost of the membrane supports using the new mechanical deformation technique is \$50-100/m^2. The technique is compatible with roll-to-roll processing methods, and is projected to be capable of approaching \$10/m^2 at high volume, which would enable achievement of the program's target of \$20/m^2 for complete membrane production (support plus ionomer) at high volume.

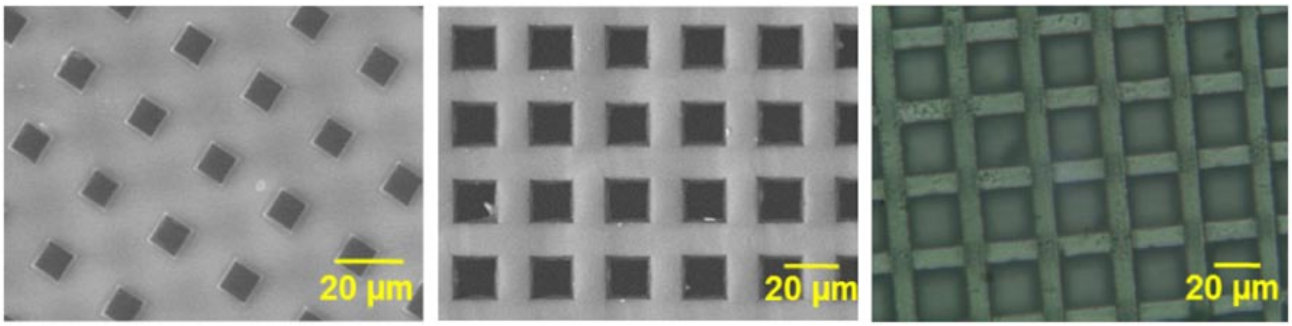

FIGURE 5. Progress in membrane supports generated by mechanical deformation—left: 11-µm pores, 15% porosity; center: 16-µm pores, 33% porosity; right: 22-µm pores, 62% porosity.

MEA Integration

Achieved PGM total content of 0.17 g/kW while meeting heat rejection target (3M Company): Improvements in MEAs containing PtNi NSTF catalysts have enabled performance improvement at high current densities, resulting in PGM total content levels as low as 0.17 g/kW at 150 kPa_{abs} (Figure 6). While the program has demonstrated similar PGM total content levels in previous year, this year's results mark a major improvement since they were achieved for the first time at a high operating temperature of 90°C and voltage of 0.69 V, conditions that satisfy the DOE heat rejection target, Q/ΔT ≤1.45. When compared to PGM total content measured at 0.69 V in 2012, this year's results mark a 20% improvement. Further development is required to achieve DOE's target level of 0.125 g/kW, and to simultaneously meet durability targets.

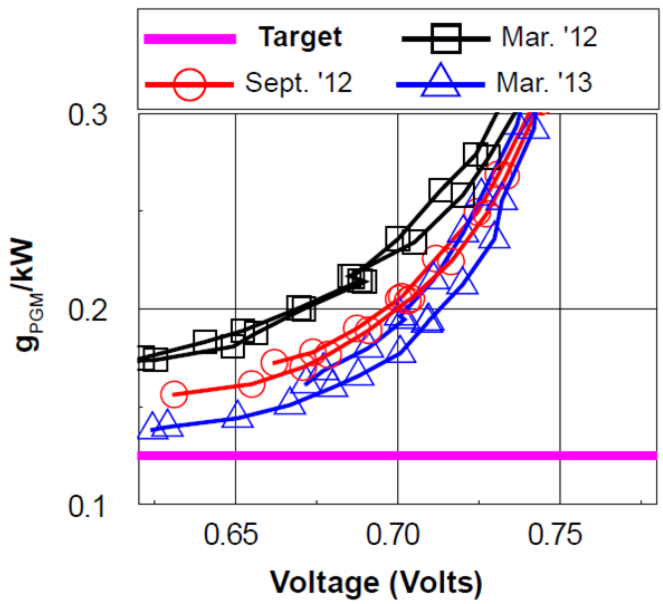

FIGURE 6. PGM total content of MEAs containing NSTF catalysts.

BUDGET

The President's FY 2014 budget request calls for approximately $37.5 million for the Fuel Cells program. Figure 7 shows the budget breakdown by R&D area for the FY 2013 congressional appropriation of $42.4 million and the FY 2014 budget request. The program continues to focus on reducing costs and improving durability with an emphasis on fuel cell stack components. In the budget breakdown, the systems and BOP categories include projects related to portable and stationary power. New projects were awarded in FY 2013 for non-precious catalysts, membranes, and MEA integration. Funding Opportunity Announcement (FOA) funds allocated in FY 2014 will be spent on expected alternate awards from the previous R&D solicitation. The Fuel Cells program does not plan to have a FOA issued for awards funded in FY 2014.

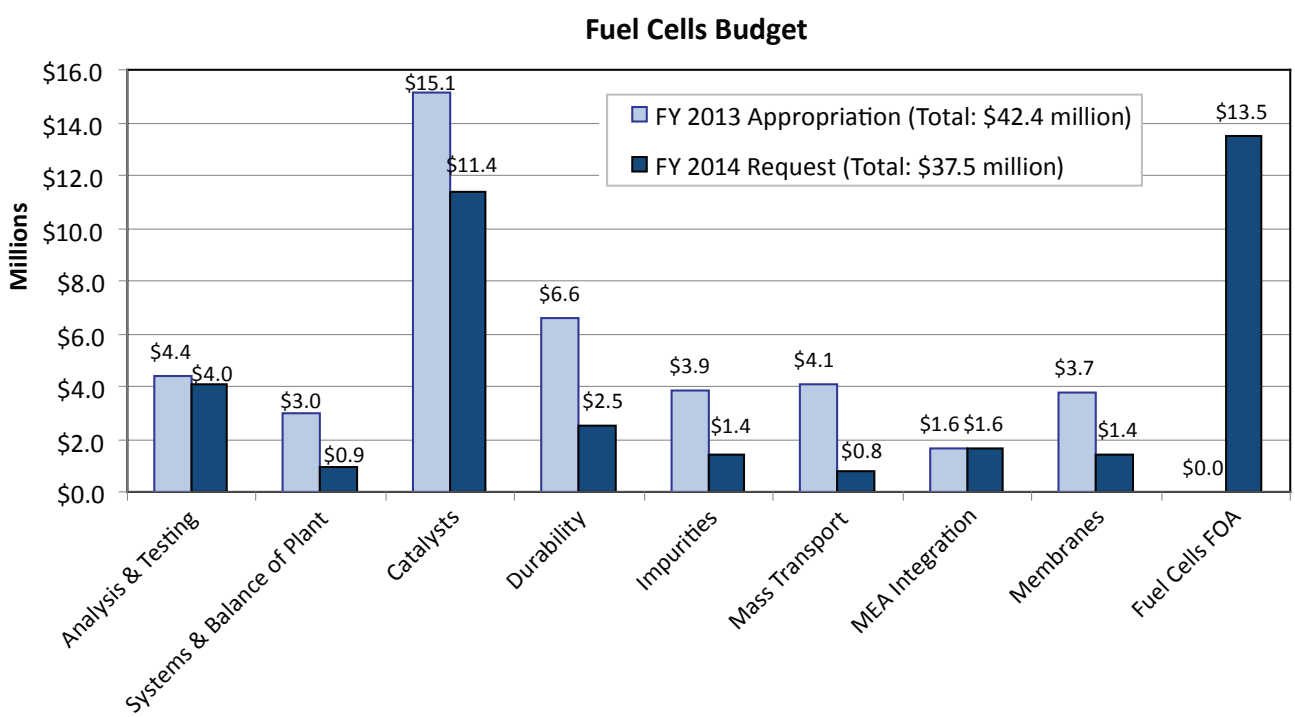

FIGURE 7. Fuel Cells program budgets in 2013 and 2014. FOA funds allocated in FY 2014 will be spent on expected alternate awards from previous R&D solicitation.

FY 2014 PLANS

In FY 2014, the Fuel Cells program will continue R&D efforts on fuel cells and fuel cell systems for diverse applications, using a variety of technologies (including PEM, solid oxide, and alkaline membrane fuel cells) and a range of fuels (including hydrogen, natural gas, and bio-derived renewable fuels). A workshop in February will provide a forum to exchange information and discuss R&D needs to reduce the cost and complexity of removing impurities from natural gas, LPG, biogas, associated petroleum gas, diesel, and biodiesel for fuel cell applications. Support will continue for R&D that addresses critical issues with electrolytes, catalysts, electrodes, and modes of operation, with an emphasis on durability improvement. The program will also continue its emphasis on science and engineering with a focus on component integration at the cell and stack level, as well as on integration and component interactions at the system level. Emphasis will continue to be placed on BOP component R&D, such as air compressors that can lead to lower cost and lower parasitic losses. Ongoing support of modeling will guide component R&D, benchmarking complete systems before they are built and enabling exploration of alternate system components and configurations. Cost analysis efforts have been expanded beyond transportation applications to also include distributed power generation systems (including CHP) and systems for emerging markets for a variety of fuel cell technologies; further detailed results of these analyses are expected in FY 2014. Updates to target values will be released in a revision of the *Multi-Year Research, Development and Demonstration Plan*, which is scheduled for release in FY 2014.

Dr. Dimitrios Papageorgopoulos
Fuel Cells Team Lead
Fuel Cell Technologies Office
U.S. Department of Energy
1000 Independence Ave., SW
Washington, D.C. 20585-0121
Phone: (202) 586-5463
Email: Dimitrios.Papageorgopoulos@ee.doe.gov

V.A.1 Durable Catalysts for Fuel Cell Protection during Transient Conditions

Radoslav T. Atanasoski (Primary Contact), George D. Vernstrom, Gregory M. Haugen, Jimmy Wong, Theresa M. Watschke, Ljiljana L. Atanasoska, Amy E. Hester
Fuel Cell Components Program, 3M Company
3M Center, Building 201-2N-05
St. Paul, MN 55144-1000
Phone: (651) 733-9441
Email: rtatanasoski@mmm.com

Timothy C. Crowtz, Jessie E. Harlow, Robbie J. Sanderson, David A. Stevens, Jeff R. Dahn
Dalhousie University, Halifax, Nova Scotia, Canada

David A. Cullen, Karren L. More, Shawn Reeves
Oak Ridge National Laboratory, Oak Ridge, TN

Deborah J. Myers, Vojislav R. Stamenkovic, Nenad M. Markovic
Argonne National Laboratory, LeMont, IL

Hao Zhang, Sumit Kundu, Wendy Lee
AFCC Automotive Fuel Cell Cooperation, Burnaby, BC, Canada

DOE Managers
Kathi Epping Martin
Phone: (202) 586-7425
Email: Kathi.Epping@ee.doe.gov
David Peterson
Phone: (720) 356-1747
Email: David.Peterson@go.doe.gov

Technical Advisors
Thomas Benjamin
Phone: (630) 252-1632
Email: Benjamin@cmt.anl.gov
John P. Kopasz
Phone: (630) 252-7531
Email: kopasz@anl.gov

Contract Number: DE-EE0000456

Subcontractors and Federally Funded Research and Development Centers:
- Dalhousie University, Halifax, Nova Scotia, Canada
- Oak Ridge National Laboratory, Oak Ridge, TN
- AFCC Automotive Fuel Cell Cooperation, Burnaby, BC, Canada

Project Start Date: August 1, 2009
Projected End Date: December 31, 2013

Overall Objectives

- Develop catalysts that will enable proton exchange membrane (PEM) fuel cell systems to weather the damaging conditions in the fuel cell at voltages beyond the thermodynamic stability of water during the transient periods of fuel starvation.
- Demonstrate that these catalysts will not substantially interfere with the performance of nor add much to the cost of the existing catalysts.

Fiscal Year (FY) 2013 Objectives

- Start-up/shut-down: 5,000 cycles/pulses with loading of 0.088 mg/cm^2 precious-grade metal (PGM) total on the cathode, 1.45 V upper limit and >90% surface area retention.
- Cell Reversal: 200 high current density pulses of 200 mA/cm^2 with loading of 0.037 mg/cm^2 PGM total on the anode and upper voltage limit <1.7 V.
- Oxygen reduction reaction (ORR) inhibition on the anode: factor of >100 in the kinetic region.
- Catalyst scale up: short stacks testing for 'real life' application.

Technical Barriers

This project addresses the following technical barriers from the Fuel Cells section of the Fuel Cell Technologies Office Multi-Year Research, Development and Demonstration Plan:

(A) Durability

Technical Targets

While the number of start-up and shut-down (SU/SD) cycles for an automotive fuel cell has been projected to be over 30,000, the number of these events when the cathode electrochemical potential exceeds 1.23 V has been estimated at ~5,000. The number of complete fuel starvation events when a cell experiences a voltage reversal has been anticipated at ~200 [1].

In Table 1, DOE approved technical targets of the project are listed along with the dates when they were accomplished.

FY 2013 Accomplishments

The final year project milestones have been achieved:

- 200 cycles of 200 mA/cm^2 for cell reversal with 0.037 mg/cm^2 total PGM on the anode with 1.7 V upper limit.

TABLE 1. The Technical Targets

Task 1: OER Active Catalyst	# of Cycles	PGM (mg/cm^2)	End Voltage	ECSA Loss	Status/Comments
SU/SD (Cathode)	(>)	(<)	(<)	(<)	
2011	5,000	0.095	1.60 V	12%	Achieved 09/2011
Go/No-Go	5,000	0.090	1.60 V	10%	Achieved 01/2012
2013	5,000	0.088	1.45 V	10%	Achieved 03/2013
Cell Reversal (Anode)					
2011	200	0.050	2.00 V	10%	Achieved 09/2011
Go/No-Go	200	0.045	1.80 V	10%	Achieved 01/2012
2013	200	0.037	1.70 V	10%	Achieved 03/2013
Task 2: Suppression of ORR (Anode)					
Go/No-Go	Factor of 10 in the kinetic region				Achieved 01/2012
2013	Factor of >100 in the kinetic region				Achieved 02/2013
Task 3: Scale-Up					
2013	'Real life' evaluation readiness				12/2013; ~11 stacks

OER - oxygen evolution reaction; ECSA - electrochemically active surface area

- 5,000 start-up cycles with upper voltage limit of 1.45 V and with 0.088 mg/cm^2 total PGM on the cathode with ECSA loss of <10%.
- Reduced ORR current on the anode by a factor >1,000.
- Fundamentals of the high specific and mass OER activity of RuIr-Pt/nanostructured thin film (NSTF) were explored and potential explanations elaborated.
- Full-size catalyst-coated membranes (CCMs) for three short stacks were produced at 3M and were evaluated by AFCC.
- Fuel cell performance of low-loading Pt on OER-able anode was the same as on higher Pt loading anodes, for both NSTF and dispersed-based catalysts.
- Shortcomings identified during the stack testing were addressed and preliminary solutions were successfully introduced.
- Second fuel cell manufacturer tested and confirmed the 3M lab results.

✧ ✧ ✧ ✧ ✧

INTRODUCTION

The project addresses a key issue of importance for successful transition of PEM fuel cell technology from development to pre-commercial phase (2010-2015). This issue is the failure of the catalyst and the other thermodynamically unstable membrane electrode assembly (MEA) components during SU/SD and local fuel starvation at the anode, commonly referred to as transient conditions. During these periods the electrodes can reach potentials up to 2 V. One way to minimize the damage from such transient events is to lower the potential seen by the electrodes. At lower positive potentials, increased stability of the catalysts themselves and reduced degradation of the other MEA components is expected.

APPROACH

This project tries to alleviate the damaging effects during transient conditions from within the fuel cells via improvements to the existing catalyst materials. We are modifying both the anode and the cathode catalysts to favor the oxidation of water over carbon corrosion by maintaining the cathode potential close to the onset potential for water oxidation. The presence of a highly active OER catalyst on the cathode reduces the overpotential for a given current demand thus reducing the driving force for carbon and platinum dissolution. In addition, inhibition of the ORR on the anode side lowers the ORR current through reduced proton demand which in turn decreases the OER current on the cathode resulting in reduced cathode potential.

Key requirements for both concepts are to implement the added catalyst with negligible inhibition of the fuel cell performance and with minimal increment of PGM.

RESULTS

Efficient Oxygen Evolution Reaction Catalysts

The activity during the fourth year of the project continued to revolve around making a more efficient and durable OER catalyst while decreasing the total PGM content towards the 2017 DOE target of 0.125 mg/cm^2. Most of the OER catalysts tested during this reporting period were nominally 90% at Ir and 10% at Ru. All the catalysts were tested in a 50-cm^2 PEM fuel cell, with the working electrode under nitrogen and the reference/counter electrode under either 1% or 100% hydrogen.

SU/SD Test

The generic electrochemical test mimicking the real SU/SD events remained the same as in 2012 [1,2]. Two modifications were made to explore the impact of the upper level potential and frequency of potential excursions to the lower level on the Pt surface area loss. The modifications were:

- 1.6 V upper limit at every cycle, rather than to 1.45 V.
- 0.65 V lower limit at every cycle rather than at every 10 cycles.

This study was performed on a series of samples with 0.085 mg/cm^2 of Pt/NSTF. The added OER catalyst was

varied from 1–10 μg/cm^2 of IrRu. The results for the ECSA retention after 5,000 cycles are presented in Figure 1. In comparison with the usual cycles to 1.45 V with 0.65 V lower limit excursions at every 10 cycles, both cycling modifications have a significant impact on the ECSA losses. Excursions to 650 mV at every cycle show a much larger surface area loss than with any of the previous test procedures. 150 mV increase in the upper voltage limit, to 1.6 V, results in 26% additional Pt surface area loss. By the end of the 5,000 cycles, the OER activities of 1 μg/cm² IrRu have fallen into the range of Pt samples. However, 10 μg/cm² of IrRu has more than enough OER catalyst to still protect the platinum. The two implications for the future work are:

(i) Pt dissolution is strongly determined by the frequency of the lower voltage limit and by the level of the upper voltage limits.

(ii) The question why Pt exposed to the same potential regime dissolves less when OER catalyst is present should be addressed.

Cell Reversal Test

In electrochemical terms, the cell reversal test procedure remained the same as in the previous year [2]. However, the total PGM loading target was decreased from 45 μg/cm^2 to 37 μg/cm^2. The upper voltage limit requirement of 1.8 V for FY 2012 was lowered to 1.7 V for 2013. In Figure 2 the end voltage of 200th 0.2 A/cm^2 cycle and ECSA estimate are presented for two series of catalysts: 25 μg/cm^2 and 30 μg/cm^2 Pt/NSTF as substrates with 6–12 μg/cm^2 added IrRu. All the catalysts with >8 μg/cm^2 IrRu samples fulfilled the 1.7 V milestones. However, the H-pump value as an expression of the hydrogen oxidation reaction activity for the 25 μg/cm^2 Pt/NSTF with 8 μg/cm^2 IrRu was by a factor of 3 higher than the 30 μg/cm^2 Pt/NSTF with the same amount IrRu. Therefore, to fully satisfy the milestone PGM loading of 37 μg/cm^2, a new series of samples was made with 29 μg/cm^2 Pt/NSTF with 8 μg/cm^2 IrRu. The H-pump value for this sample was satisfactory and so were the cell reversal characteristics as presented by the triangles in Figure 2.

Scale-Up and Short-Stack Evaluation

In 2013, the scale-up and the full-size short stack evaluation continued to be the focus of the project. The 2013 milestone for the scale-up called for evaluation of three short stacks. The CCM compositions were as follows:

Anodes:

1. Dispersed: 50 μg/cm^2 Pt (commercial catalyst; 3M produced)
2. NSTF: 50 μg/cm^2 Pt + 15 μg/cm^2 IrRu (NSTF baseline; historical)
3. NSTF: 29 μg/cm^2 Pt + 8 μg/cm^2 IrRu (NSTF 2013 milestone)

All the CCMs were made by 3M with the same 3M-coated dispersed cathode (0.4 mg/cm^2 Pt) and 3M 12 μm reinforced membrane, 725 equivalent weight (surface area >300 cm^2). The final MEA and stack assembly and testing was done by AFCC.

As illustrated in Figure 3, performance-wise all three stacks came very close to each other. Actually, the 2013

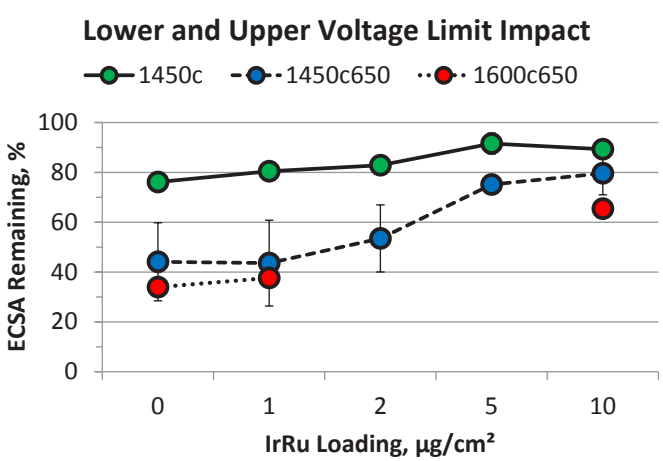

Green (top line): 1.45 V upper limit with lower limit of 0.65 V at every cycle 10th cycle
Blue (middle line): 1.45 V upper limit with lower limit of 0.65 V at every cycle
Red (bottom line):1.6 V upper limit with lower limit of 0.65 V at every cycle.
2012 SU/SD test protocol (see text); 0.085 mg/cm^2 of Pt/NSTF; OER catalyst loading 1–10 μg/cm^2 of IrRu. 50-cm^2 MEA under nitrogen/1% hydrogen, 70°C, fully saturated. 5,000 SU/SD cycles; IrRu loading indicated on the graph.

FIGURE 1. The Impact of the Upper Level Potential and the Frequency of Potential Excursions to the Lower Level on the Pt Surface Area Loss

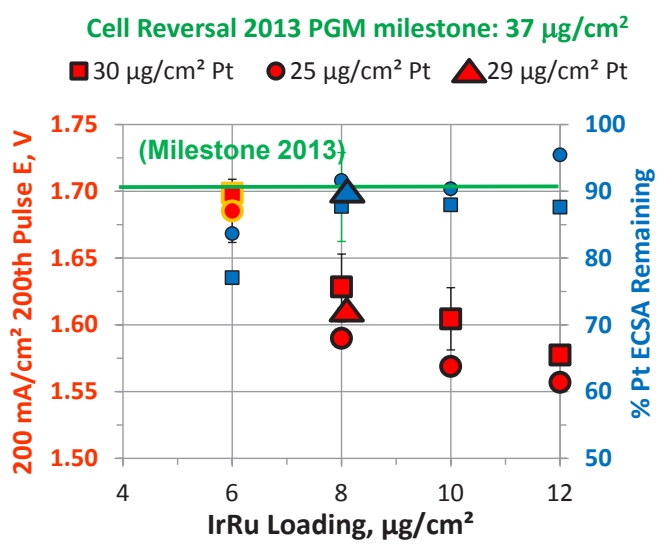

FIGURE 2. Cell reversal testing for two series of OER catalysts: 25 μg/cm^2 and 30 μg/cm^2 Pt/NSTF as substrates with 6–12 μg/cm^2 added IrRu. The end voltage of 200th 15 sec. 200 mA/cm^2 cycle (red) and ECSA estimate (blue) are presented. The big triangle represents the 2013 milestone sample with 8 μg/cm^2 on 29 μg/cm^2 Pt/NSTF. Note: Samples with 6 μg/cm^2 added IrRu did not fulfill the end voltage requirement

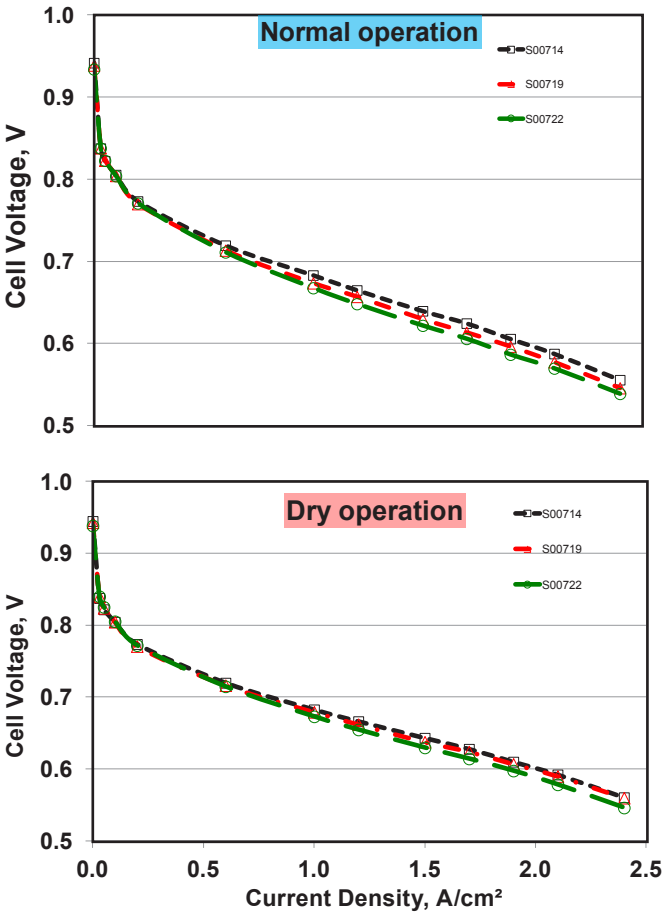

Black: Dispersed: 50 μg/cm^2 Pt (baseline commercial catalyst)
Green: NSTF: 50 μg/cm^2 Pt + 15 μg/cm^2 IrRu (2012 NSTF baseline)
Red: NSTF: 29 μg/cm^2 Pt + 8 μg/cm^2 IrRu (NSTF 2013 milestone)
3M-coated dispersed cathode (0.4 mg/cm^2 Pt) and 3M 12 mm reinforced, membrane, 725 equivalent weight (surface area >300 cm^2). Final MEA and stack assembly and testing done by AFCC.

FIGURE 3. Short Stacks Full Cell Architecture Evaluation of OER Modified Pt/NSTF Anodes: Performance under Normal and Dry Conditions

milestone NSTF with 29 μg/cm^2 Pt with 58% of baseline 50 μg/cm^2 Pt did even slightly better. However, due to the much lower OER catalyst content, 8 μg/cm^2 IrRu vs. 15 μg/cm^2 IrRu, the cell reversal durability for the 2013 milestone NSTF did suffer. A proper balance between the Pt and IrRu contents should be able to remedy this drawback while keeping the performance benefits as presented in Figure 3.

FUTURE WORK

The remainder of the final year will be focused on three major areas:

- OER-Pt NSTF catalysts evaluation readiness for "real life" automotive applications:
  - Continue the short stack evaluation with AFCC with new/modified OER catalysts.
  - Assess the boundaries of the OER–Pt/NSTF application.
  - Assess the lowest Pt loading limit with respect to performance.
- Research and development of the OER catalyst with respect to durability in 'real life':
  - Fundamental materials studies to further the understanding and the paths to improvement of the stability of the OER-Pt NSTF catalysts.
- Fundamental engineering studies of the OER-Pt NSTF catalysts:
  - Understand the impact of processing, integration and interaction with other MEA components.

FY 2013 PUBLICATIONS/PRESENTATIONS

Papers

1. RT Atanasoski, LL Atanasoska, DA Cullen: "Efficient Oxygen Evolution Reaction Catalysts for Cell Reversal and Start/Stop Tolerance" in M. Shao ed., "*Electrocatalysis in Fuel Cells: A Non and Low Platinum Approach*", Chapter 22, Springer, March, 2013.

2. RT Atanasoski, DA Cullen, GD Vernstrom, GM Haugen LL Atanasoska:"A Materials-Based Mitigation Strategy for SU/SD in PEM Fuel Cells: Properties and Performance-Specific Testing of IrRu OER Catalysts", *ECS Electrochem. Lett.*, 2 (3) F25-F28, 2013.

3. RT Atanasoski, LL Atanasoska, DA Cullen, GM Haugen, KL More, GD Vernstrom: "Fuel Cells Catalyst for Start-up and Shutdown Conditions: Electrochemical, XPS, and TEM Evaluation of Sputter-Deposited Ru, Ir, and Ti on Pt-Nano-Structured Thin Film (NSTF) Support", *Electrocatalysis*, 3, 284–297, 2012.

4. LL Atanasoska, DA Cullen, AE Hester, RT Atanasoski: "XPS and STEM of the interface formation between ultra-thin Ru, Ir and Pt layers and perylene red catalyst support whiskers", *ECS Transactions* (Abs# 3748, PRiME 2012, Honolulu, Hawaii).

Presentations

1. R.T. Atanasoski, L.L. Atanasoska, D.A. Cullen, A. Hester: *"Oxygen Evolution Reaction on Minute Amounts of Ru and Ir Catalyst for Application in Fuel Cell Protection", Symposium* I4 - *Electrocatalysis 6*, PRiME 2012, Honolulu, Hawaii, Oct. 08, 2012 (Invited, opening talk; # 3737).

2. L.L. Atanasoska, DA Cullen, A. Hester, RT Atanasoski: "*XPS and STEM of the Interface Formation between Ultra-Thin Ru, Ir and Pt Layers and Perylene Red Catalyst Support Whiskers"* (Abstract #3748, Honolulu PRiME 2012).

3. D. Stevens, J. Harlow, R. Sanderson, T. Crowtz, J. Dahn, G. Vernstrom, L. Atanasoska, G. Haugen, and R. Atanasoski: "*Rotating Disk Electrode Techniques Designed to Simulate Fuel Cell Startup/Shut-Down Transient Conditions"* (Abstract #1319, Honolulu PRiME 2012).

4. J. Harlow, D. Stevens, R. Sanderson, T. Crowtz, J. Dahn, G. Haugen, L. Atanasoska, G. Vernstrom, and R. Atanasoski:

"*Durable, OER-Active Compositions of Pt, Ir, and Ru for PEM Fuel Cell Start-Stop Protection*" (Abstract #1365, Honolulu PRiME 2012).

Presentations to DOE

1. "Durable Catalysts for Fuel Cell Protection during Transient Conditions" Project progress Review, presented to DOE (internal), September, 2012, St. Paul, Minnesota.

2. "Durable Catalysts for Fuel Cell Protection during Transient Conditions" Project progress Review, presented to DOE (internal), April, 2012, Vancouver, Canada.

3. "Durable Catalysts for Fuel Cell Protection during Transient Conditions" presented at the FC Tech Team, Detroit, April, 2013.

4. "Durable Catalysts for Fuel Cell Protection during Transient Conditions" presented at the DOE 2013 AMR, May, 2013, Washington, D.C.

REFERENCES

1. RT Atanasoski, DA Cullen, GD Vernstrom, GM Haugen LL Atanasoska:"A Materials-Based Mitigation Strategy for SU/SD in PEM Fuel Cells: Properties and Performance-Specific Testing of IrRu OER Catalysts", *ECS Electrochem. Lett*., 2 (3) F25-F28, 2013.

2. R.T. Atanasoski, Project review at the DOE 2010 Vehicle Technologies and Hydrogen Programs Annual Merit Review, May 2012, Washington, D.C., FC# 003.

V.A.2 Extended, Continuous Pt Nanostructures in Thick, Dispersed Electrodes

Bryan Pivovar (Primary Contact), Shyam Kocha, KC Neyerlin, Jason Zack, Shaun Alia, Arrelaine Dameron, Svitlana Pylypenko, Justin Bult, Brian Larsen, Jeremy Leong
National Renewable Energy Laboratory (NREL)
15013 Denver West Parkway
Golden, CO 80401
Phone: (303) 275-3809
Email: Bryan.Pivovar@nrel.gov

DOE Manager
Kathi Epping Martin
Phone: (202) 586-7425
Email: Kathi.Epping@ee.doe.gov

Subcontractors:
- Dave Cullen, Oak Ridge National Laboratory (ORNL), Oak Ridge, TN
- Rod Borup, Los Alamos National Laboratory, Los Alamos, NM
- Yushan Yan, University of Delaware, Newark, DE
- Eric Eisenbraun, State University of New York – Albany, Albany, NY
- Stacey Bent, Han-Bo-Ram Lee, Stanford University, Stanford, CA
- Tom Zawodzinski, Alex Papendrew, University of Tennessee, Knoxville, TN
- Svitlana Pylypenko, Dave Diercks, Colorado School of Mines (CSM), Golden, CO
- Kev Adjemian, (In-kind) Nissan Technical Center North America, Farmington Hills, MI
- Fumiaki Ogura, (In-kind) Tanaka Kikinzoku Kogyo, Hiratsuka, Japan

Project Start Date: July 20, 2009
Project End Date: September 30, 2014

Overall Objectives

- Increasing mass activity and durability of Pt-based electrocatalysts through the implementation of high-surface-area, extended-surface electrocatalysts.
- Optimize fuel cell performance of extended-surface electrocatalysts.
- Demonstrate DOE 2020 target performance and durability in fuel cell tests.

Fiscal Year (FY) 2013 Objectives

- Produce novel extended thin-film electrocatalyst structures (ETFECS) with increased activity and durability, moving towards meeting all 2020 DOE catalyst targets.
- Further increase electrochemically available surface area (ECA) and mass activity of extended surface catalysts.
- Down-select and incorporate ETFECS into membrane electrode assemblies (MEAs) for fuel cell testing of performance and durability.
- Demonstrate <40% mass activity loss in initial catalytic activity (DOE 2020 target).
- Go/No-Go decision for catalyst synthesis. No-Go all catalyst synthesis routes that have not demonstrated mass activities above 0.44 A/mg Pt @ 900 mV (internal resistance-free).

Technical Barriers

This project addresses the following technical barriers from the Fuel Cells section (3.4.5) of the Fuel Cell Technologies Office Multi-Year Research, Development, and Demonstration Plan:

(A) Durability (of catalysts and MEAs)

(B) Cost (of catalysts and MEAs)

(C) Performance (of catalysts and MEAs)

Technical Targets

This project synthesizes novel ETFECS and incorporates these catalysts into electrodes with and without carbon for further study. The project has targets outlined in the Multi-Year Research, Development, and Demonstration Plan for both electrocatalysts for transportation applications (Table 3.4.13) and MEAs (Table 3.4.14). The specific targets and status of highest relevance are presented in Table 1.

FY 2013 Accomplishments

- Go decision for electrocatalysts synthesized by galvanic displacement; atomic layer deposition, chemical vapor deposition and sputtering were decided to be No-Go.
- Developed Pt nanotube catalysts by galvanic displacement based on Ni and Co nanowire templates.
- Demonstrated mass activities of ETFECS as high as 900 mA/mg-Pt @ 900 mV in RDE tests.

TABLE 1. Technical Targets for Electrocatalysts for Transportation Applications

Characteristic	Units	2017/2020 Targets	Status
Mass Activity (150 kPa H_2/O_2, 80°C, 100% relative humidity)	A/mg-Pt @ 900 mV	0.44/0.44	0.45
Electro catalyst support stability	% mass activity loss	<10/<10	<10*
Loss in initial catalytic activity	% mass activity loss	<40/<40	<10*

*measured in rotating disk electrode (RDE), following 30,000 cycles between 0.6 and 1 V.

- Demonstrated surface areas as high as 90 m^2/g.
- Demonstrated specific activities as high as 3.0 mA/cm^2 Pt @ 900 mV.
- Demonstrated high durability of ETFECS in potential cycling between 0.6 and 1 V for 30,000 cycles, including ability to maintain mass activity in MEAs for select non-alloyed ETFECS.
- Demonstrated mass activity of ETFECS as high as 150 mA/mg-Pt @ 900 mV in fuel cell tests.

✧ ✧ ✧ ✧ ✧

INTRODUCTION

Conventional nanoparticle Pt/C electrocatalysts (2–5 nm) used in automotive fuel cells appear to have plateaued in terms of electrochemical area and catalytic activity. ETFECS offer the possibility of higher specific activities comparable to that of bulk poly-Pt. ETFECS typically exhibit lower ECAs and consequently lower mass activities. By investigating a number of alternative synthesis techniques, we expect to raise the ECA to deliver the benefits of both a high specific and mass activity. An additional benefit of ETFECS is that larger Pt structures are less susceptible to oxidation and dissolution thus leading to a highly active, durable and low-cost electrocatalyst system.

APPROACH

Our overall approach towards developing extended-surface Pt catalysts for their high mass activity and durability, and incorporating these structures into robust, high-efficiency MEAs has focused on two areas. (1) Synthesis of novel ETFECS: Pt nanoparticles with continuity over tens of nanometers or more have demonstrated enhanced specific activity and exceptional durability (3M [1], others [2]). In our work we examine vapor deposition including sputtering, chemical vapor deposition and atomic layer deposition as well as wet chemistry methods that include spontaneous galvanic displacement (SGD). We have focused on increased Pt mass activity. Low-Pt ECAs, typically around 10 m^2/gPt, have resulted in limited mass activity in the past and further gains in specific activity (due to alloying effects) are possible. (2) Electrode studies involving ETFECS: effective incorporation of extended-Pt catalysts into high-performance electrodes remains a challenge due to the unique structure and properties of these materials. We have incorporated ETFECS into electrodes for fuel cell and RDE testing and evaluated their performance and durability.

RESULTS

In the area of Pt deposition, we have continued our focus on chemical vapor deposition, atomic layer deposition, and SGD. A summary highlighting our highest performing results to date is shown in Figure 1. Based on this figure, we have only met the DOE mass activity target using SGD and we have down-selected our catalyst synthesis efforts to focus only on SGD materials synthesized from Ni and Co (May 2013). While Ag and Cu have met the DOE target, we included these materials in the No-Go category due to anode contamination concerns and the higher performances of the Ni and Co systems.

We have performed detailed studies on the galvanic displacement of both Ni and Co displaced Pt nanowires. The impact that Pt displacement level had on performance of both of these systems is highlighted in Figure 2. Figure 2 shows that Pt-Ni nanowires (NWs) have reached mass activities up to 900 mA/mg Pt and Pt-Co NWs have reached 800 mA/mg Pt, values significantly higher than the DOE 2020 mass activity target (440 mA/mg Pt). These two systems both exhibit the highest mass activity at low Pt displacement percentages, but achieve their high mass activities in different ways. The Ni system shows exceptionally high ECA, reaching a value as high as 90 m^2/g Pt at low displacement percentages. This high ECA is similar to Pt-C nanoparticle catalyst and significantly higher than other

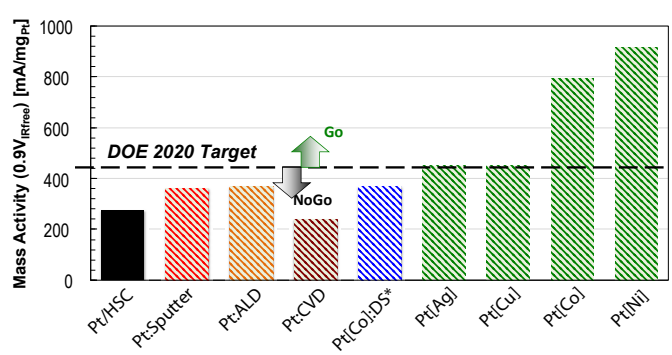

FIGURE 1. Summary of Highest Mass Activity Performance by Synthesis Technique

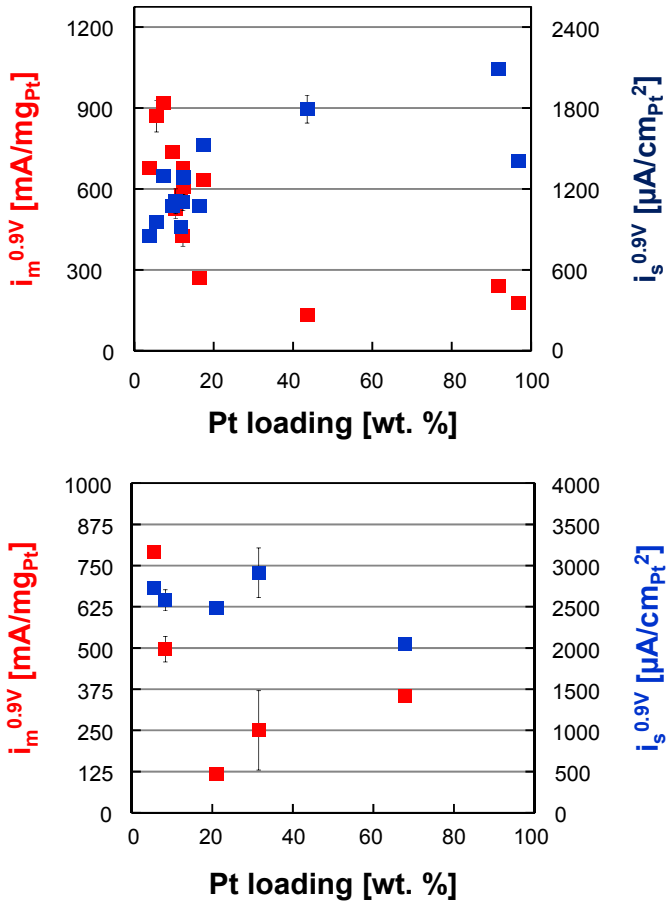

FIGURE 2. Mass and Specific Activity of Pt-Ni NWs and Pt-Co NWs as a Function of Displacement

extended surface electrocatalysts demonstrated to date. The Co system achieves its high activity through gains in specific activity rather than in surface area. The ECA of this system has been limited to ~30 m^2/g Pt, but has specific activities significantly higher than the Ni-based system. Future work will focus on increasing the specific activity of the Ni system and the surface area of the Co system.

The durability of these systems has also been investigated in RDE tests. Both the Pt-Ni NWs and the Pt-Co NWs have shown the ability to maintain the DOE 2020 mass activity target following 30,000 potential cycles. The two systems show strong differences in their compositions pre- and post- electrochemical testing. The Pt-Ni NWs have shown consistent composition as a function of test conditions where exposure to acid and 30,000 potential cycles have resulted in roughly invariant Pt:Ni compositions of 17:83. Pt-Co NWs, on the other hand, have shown extreme changes in composition on exposure to acid, with a starting material with a Pt:Co composition of 75:25 transforming into a Pt:Co material with 95:5 composition due to leaching out of the Co core of the material. These dramatic differences in behavior between Ni and Co were unexpected and give hope

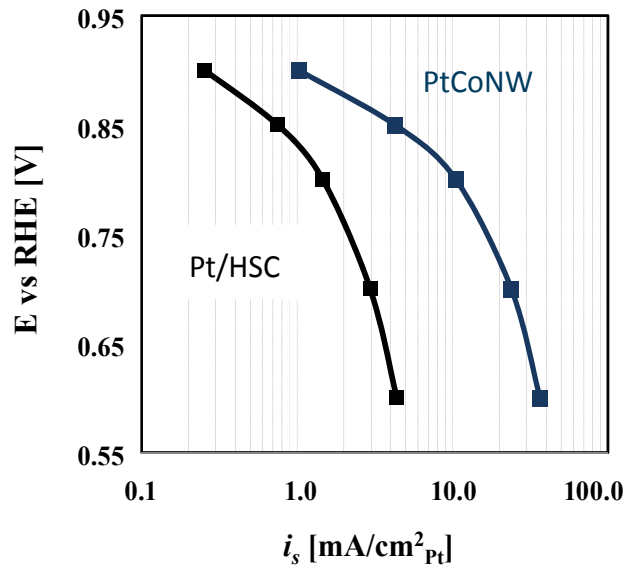

FIGURE 3. Fuel Cell Performance of Pt-Co NWs

that specific features of these systems can be leveraged into producing target materials and properties.

We have significantly increased our efforts in MEA fabrication and fuel cell testing of ETFECS materials. Figure 3 shows our top fuel cell performance to date using an ETFECS catalyst, Pt-Co NWs. Figure 3 is plotted on a surface area normalized basis and shows the significant increase in specific activity of the ETFECS sample compared to traditional Pt-C. These Pt-Co NWs exhibited surface areas in the MEA approaching those of RDE tests and had well defined Pt voltammograms. The specific activity in fuel cell was about half of that of RDE, and the resulting fuel cell mass activity was competitive with Pt/high surface carbon baseline.

Our fuel cell testing efforts with Pt-Ni NWs showed a high specific activity at high current after acid washing. These studies point to a number of concerns for this system that we still need to address, including: Ni dissolution (not apparent in RDE), lack of Pt features in initial cyclic voltammatry; decreased surface areas (relative to RDE); and low-Pt loading during tests (Ni as a magnetic element impacted MEA fabrication and limited our tests to low loading levels).

Fabrication methods investigated to date include direct spraying, decal spray with transfer, filtering with transfer, and direct painting. Beyond fabrications methods we have also focused on issues involving ink formulation, including: difficulties involving support-less electrocatalysts that behave differently than traditional Pt/C catalysts and Pt blacks; the catalyst dispersions (inks) created and MEA fabrication process is significantly more complicated. Preliminary investigations suggest, solvent choices can aid in improving dispersions.

CONCLUSIONS AND FUTURE DIRECTIONS

The project has synthesized many novel catalysts using materials, geometries, and approaches not previously demonstrated. We have down-selected a catalyst synthesis route to focus on galvanic displacement of Co and Ni samples due to the high mass activities achieved (up to 900 mA/g Pt). We have demonstrated exceptionally high surface areas of ETFECS, up to 90 m^2/g Pt. We have tested ETFECS in fuel cells and have achieved mass activities as high as 150 mA/g Pt. Our efforts going forward will seek to further increase catalyst activity and optimize MEA performance in order to maintain RDE activity in fuel cell tests by focusing on:

- Electrocatalyst synthesis:
  - Focus on galvanic displacement (NREL, University of Delaware), all other synthesis routes were determined to be No-Go within project. Focus on Pt-Ni, Pt-Co.
  - Pt-Ni: Focus on oxide passivating layer, effects of annealing and attempting to further increase specific activity.
  - Pt-Co: Focus on increasing surface area, leaching of excess Co.
  - Advanced characterization of materials (Colorado School of Mines, ORNL).
- Fuel cell studies:
  - Improve catalyst performance in MEAs with a focus on MEA fabrication using down-selected electrocatalysts.
  - Explore factors impacting observed ECAs, activity, and durability.

SPECIAL RECOGNITIONS & AWARDS/ PATENTS ISSUED

1. Principal Investigator, Bryan Pivovar, was presented the 2012 Charles Tobias Young Investigator Award (Electrochemical Society) at the Fall 2012 Electrochemical Society Meeting, October 2012, Honolulu, HI.

FY 2013 PUBLICATIONS/PRESENTATIONS

1. Alexander B. Papandrew, Rob W. Atkinson, Gabriel A. Goenaga, Shyam S. Kocha, Jason W Zack, Bryan S. Pivovar, and Thomas A. Zawodzinski, "Oxygen Reduction Activity of Vapor-Grown Platinum Nanotubes," *JECS*, 160(8), F848-F852, (2013).

2. Shaun M. Alia, Kurt O. Jensen, Christian Contreras, Fernando Garzon, Bryan Pivovar, and Yushan Yan, "Platinum-Coated Copper Nanowires and Platinum Nanotubes as Oxygen Reduction Electrocatalysts," *ACS Catal*., 2013, 3, 358-362.

3. K.C. Neyerlin, Brian A. Larsen, Svitlana Pylypenko, Shyam S. Kocha, and Bryan S. Pivovar, "Activity of Pt Extended Network Electrocatalyst Structures Made from Spontaneous Galvanic Displacement," *ECS Trans. 2013 50(2): 1405-1413.*

4. Alexander B. Papandrew, Rob W. Atkinson, Gabriel A. Goenaga, David L. Wilson, Shyam S. Kocha, K.C. Neyerlin, Jason W Zack, Bryan S. Pivovar, and Thomas A. Zawodzinski, "Oxygen Reduction Activity of Vapor-Grown Platinum Nanotubes," *ECS Trans. 2013 50(2): 1397-1403.*

5. Justin Bult, K.C. Neyerlin, Steven Christensen, Arrelaine Dameron, Shyam S. Kocha, Jason W Zack, Bryan S. Pivovar, and Katherine Hurst, "Synthesis and Electrochemical Characterization of Carbon Supported Platinum Grown by Template Assisted Gas Phase Deposition," ECS Trans. 2013 50(2): 1723-1727.

6. Brian A. Larsen, K.C. Neyerlin, Justin Bult, Christopher Bochert, Jeffrey L. Blackburn, Shyam Kocha, Bryan Pivovar, "Platinum nanoplates as novel oxygen reduction reaction electrocatalysts" *Journal of The Electrochemical Society*, 159 (10) F1-F5 (2012).

7. Kazuma Shinozaki, Bryan S Pivovar, and Shyam S Kocha, "Influence of Film Morphology On the Oxygen Reduction Reaction Activity in Rotating Disk Electrode Studies," October 7–12, Honolulu, Hawaii, PRiME 2012, Abstract 1239.

8. Bryan S Pivovar, K.C. Neyerlin, Shaun M Alia, Brian A Larsen, Svitlana Pylypenko, David A Cullen, David R Diercks, and Shyam S Kocha, "Extended Surface Pt Electrocatalysts: Synthesis and Challenges in Fuel Cell Applications," October 7–12, Honolulu, Hawaii, PRiME 2012, Abstract 1245.

9. Shyam S. Kocha, Jason Zack, K.C. Neyerlin, and Bryan S. Pivovar "Influence of Nafion on the Electrochemical Activity of Pt-based Electrocatalysts," October 7–12, Honolulu, Hawaii, PRiME 2012, Abstract 1269.

10. Kelly A. Perry, Brian Larsen, K.C. Neyerlin, Bryan S. Pivovar, and Karren L. More, "Elemental and Morphological Analysis of Novel Pt Catalysts Synthesized by Galvanic Displacement," October 7–12, Honolulu, Hawaii, PRiME 2012, Abstract 1273.

11. Shaun M Alia, Brian A Larsen, Svitlana Pylypenko, David A Cullen, David R Diercks, K.C. Neyerlin, Shyam S Kocha, and Bryan S Pivovar "Platinum Coated Nickel Nanowires As Oxygen Reducing Electrocatalysts," October 7–12, Honolulu, Hawaii, PRiME 2012, Abstract 1308.

12. K.C. Neyerlin, Brian Larsen, Shyam S. Kocha, and Bryan S. Pivovar "Electrochemical Performance of Pt Extended Network Catalysts from Spontaneous Galvanic Displacement in MEAs," October 7-12, Honolulu, Hawaii, PRiME 2012, Abstract 1377

13. Justin Bult, K.C. Neyerlin, Steven Christensen, Arrelaine Dameron, Bryan S. Pivovar, and Katherine Hurst "Controlled Pt Coverage for Extended Thin Film Catalyst ORR Studies via Templated Gas Phase Synthesis," October 7–12, Honolulu, Hawaii, PRiME 2012, Abstract 1426.

14. Alexander B. Papandrew, Rob Atkinson, Gabriel A. Goenaga, David Wilson, Shyam S. Kocha, K.C. Neyerlin, Jason Zack, Bryan S. Pivovar, and Thomas A. Zawodzinski, Jr. "Oxygen Reduction Activity of Vapor-Grown Platinum Nanotubes," October 7–12, Honolulu, Hawaii, PRiME 2012, Abstract 1564.

15. K.C. Neyerlin, Brian Larsen, Shyam S. Kocha, and Bryan S. Pivovar "Activity and Durability of Pt Extended Network Electrocatalyst Structures Made from Spontaneous Galvanic Displacement," October 7–12, Honolulu, Hawaii, PRiME 2012, Abstract 1565.

REFERENCES

1. http://www.hydrogen.energy.gov/pdfs/review08/fc_1_debe.pdf.

2. Z. Chen, W. Li, M. Waje, Y.S. Yan, *Angew. Chem. Int. Ed.* 2007, 46:4060-4063.

V.A.3 Nanosegregated Cathode Alloy Catalysts with Ultra-Low Platinum Loading

Nenad M. Markovic (Primary Contact) and
Vojislav R. Stamenkovic
Argonne National Laboratory
Argonne, IL 60439
Phone: (630) 252-5181
Email: nmmarkovic@anl.gov; vrstamenkovic@anl.gov

DOE Manager
Nancy Garland
Phone: (202) 586-5673
Email:Nancy.Garland@ee.doe.gov

Contributors:
- Karren More, Oak Ridge National Laboratory
- Shuoheng Sun, Brown University, Rhode Island
- Guofeng Wang, University of Pittsburgh
- Charles Hays, Jet Propulsion Laboratory
- Radoslav Atanasoski, 3M Company

Project Start Date: September 2009
Project End Date: September 2014

Overall Objectives

- Fundamental understanding of the oxygen reduction reaction on multimetallic PtM (M = Co, Ni, Fe, Mn, Cr, V, and Ti) and PtM_1N_2 (M_1 = Co or Ni; N_2 = Fe, Mn, Cr, V, and Ti) materials.
- Develop highly-efficient, durable, nanosegregated Pt-skin PtM and PtM_1N_2 catalysts with ultra-low Pt content.
- Develop highly-active and durable Au/PtM_3 nanoparticles with ultra-low Pt content.
- Find relationships between activity/stability of well-characterized bulk alloys and real nanoparticles.
- Develop novel chemical and physical methods for synthesis of monodispersed PtM and PtM_1N_2 alloy nanoparticles and thin metal films.
- Resolve electronic/atomic structure and segregation profile of PtM and PtM_1N_2 systems.
- Resolve composition effects of PtM and PtM_1N_2 systems.
- Demonstrate mass activity and stability improvement of PtM and PtM_1N_2 alloy nanoparticles in rotating disk electrodes and membrane electrode assemblies (MEAs).
- Use computational methods as the basis to form any predictive ability in tailor-making binary and ternary systems to have desirable reactivity and durability properties.
- Develop and synthesize highly active and durable practical catalyst with ultra-low content of precious metals.

Fiscal Year (FY) 2013 Objectives

- Optimization of synthesis methods to produce larger volumes of catalysts in a single batch.
- Evaluation of the existing protocols for surfactant removal after colloidal synthesis.
- Synthesis and characterization of the PtM_1N_2 ternary alloy nanoparticles with controlled particle size and elemental distribution.
- Evaluation of the nanosegregated compositional profile in ternary systems.
- Utilization of highly crystalline practical catalysts in the form of nanowires and thin metal films.
- Design and synthesis of multimetallic nanowires with controlled length, width, and composition.
- Utilization of highly crystalline thin metal films as practical catalysts.
- Evaluation of catalyst properties in MEA.

Technical Barriers

This project addresses the following technical barriers from the Fuel Cells section of the Fuel Cell Technologies Office Multi-Year Research, Development, and Demonstration Plan:

(A) Durability

(B) Cost

(C) Performance

Technical Targets

This project is conducting fundamental studies of the oxygen reduction reaction on Pt-based PtM (M = Ni, Co, Fe, Cr, V, and Ti) binary and PtM_1N_2 (NM = Fe, Co, and/or Ni) catalysts as well as on Au/Pt_3M ternary nanoparticles. Insights gained from these studies will be applied toward the design and synthesis of highly-efficient, durable, nanosegregated Pt-skin catalysts with ultra-low Pt content that meet or exceed the following DOE 2015 targets:

Specific activity at 0.9 ViR-free: 720 mA/cm^2	PGM total content: 0.2 g/kW
Mass activity at 0.9 V: 0.44 A/mg$_{Pt}$	Total loading: 0.2 mg/cm^2
Catalyst support loss: <30%	Durability w/cycling (80°C): 5,000 hrs

PGM – precious-grade metal

FY 2013 Accomplishments

- Synthesized wide range of bi/multi metallic nanoparticles with controlled size and composition by colloidal organic solvo-thermal approach.
- Developed vapor deposition/annealing methods to make stable and active Pt thin metal film (1-7 atomic layers) on Pt_3Ni substrate.
- Established relationships between the morphology/thickness of Pt atoms in skeleton structure and stability/activity of the catalysts: Pt film can both effectively protect Ni from dissolution and provide superior catalytic activity (x6 vs. Pt).
- Developed experimental protocol to synthesize PtNi/C nanoparticles with Pt multilayered "skin" (2-3 ML) that are mimicking stability/activity of thin metal film systems.
- In MEAs, for PtNi/C multilayered skin confirmed: (i) three times higher specific activity (SA ~0.8 mA/cm^2) than benchmark Pt/C catalysts and mass activity of ~035 A/mg$_{Pt}$; (ii) high durability, e.g., after 20K cycles activity, surface area loss was only 12% compared to ~40% for Pt/C.
- Established accurate surface area determination for the nanoscale catalyst with Pt-skin surfaces.
- Performed extended X-ray absorption fine structure analysis characterization in MEAs on PtNi multilayered skin catalysts, which revealed that catalyst did not suffer structural/composition changes after 20K cycles in the MEA.
- Developed magnetron sputtering deposition methods and annealing protocol to make reproducible ternary Pt-alloy thin-metal films.
- Performed composition optimization of ternary $Pt_3M_1N_2$ catalysts.
- Developed synthetic routes and characterized monodisperse, highly homogeneous ternary alloy nanoparticles.
- Performed modeling related to the existence of Pt-Skin structure in ternary alloy catalysts for extended and nanoscale systems.
- Establish activity trend for ternary Pt_3MN nanoparticles.
- Synthesis and characterization of the core/shell Au/$CoPt_3$ nanoparticles
- Demonstrated that ternary alloys could provide additional activity gain vs. binaries (4-fold vs. Pt-poly).
- Established procedure for efficient removal of surfactants after colloidal synthesis.
- Developed synthetic routes and characterized monodisperse, highly homogeneous multimetallic nanoparticles with inner gold shell.
- Developed synthetic routes and characterized highly homogeneous multimetallic nanowires.
- Developed annealing protocols for multimetallic nanowires with Pt-skin surfaces.
- Developed thin-film-based mesoscale electrocatalysts with tunable composition and surface structure.
- Mesostructured thin-film-based materials acheived the highest specific activity for the oxygen reduction reaction (ORR) ever measured for practical electrocatalysts.

✧ ✧ ✧ ✧ ✧

INTRODUCTION

In the quest to make the polymer electrolyte membrane a competitive force, one of the major limitations is to reduce the significant overpotential for the ORR and minimize dissolution of the cathode catalysts. Here, we report a progress for FY 2013 in experimental and theoretical studies to addressing the importance of alloying Pt with 3d elements (M = Ni, Co, Fe etc.) in order to form catalytically active materials with so-called *nanosegregated profile* [1]. In our previous work we have identified that the nanosegregated surfaces are superior in both exceptional catalytic activity for the ORR and improved stability of Pt surface atoms.

APPROACH

In order to address the challenges that are listed as the DOE targets for the Hydrogen and Fuel Cells Program we rely on our materials-by-design approach [1-9]. This involves four major steps: (i*)* advanced chemical and physical methods for synthesis of novel nano/mesoscale materials, which enables control of their size, composition, morphology and structure; (ii) characterization of atomic and electronic properties by ex situ and in situ surface specific tools and theoretical methods; (iii) resolving the surface electronic and crystal structures at atomic/molecular level that govern efficient kinetics of the ORR; and (iv*)* synthesis/fabrication (scale up) of the highly efficient practical catalysts, which are guided by the fundamental understanding of structure-function relationships.

RESULTS

Surfactant Removal from Nanoparticles Prepared by Solvo-Thermal Synthesis

During the solvo-thermal synthesis, Pt and Pt-alloy surfaces of nanoparticles have been covered by surfactant molecules, oleylamine and oleic acid. If not removed, these molecules can tremendously affect catalytic properties by blocking active sites for adsorption of reactants. Pt and Pt-alloy nanoparticles were subject to different treatments in order to evaluate their efficiency in removing the surfactant molecules that are strongly attached to the Pt surface atoms. The surface cleanness of differently treated particles was characterized by thermogravimetric analysis, infrared absorption spectroscopy and cyclic voltammetry. Obtained results revealed that thermal annealing is the most effective method to clean the surface of the Pt-based nanoparticles. In addition, these findings provide a direct correlation between the surface cleanness and functional properties of differently treated Pt nanoparticles, and point out the importance of efficient surfactant removal in catalytic applications. Figure 1a displays transmission electron microscope (TEM) images of as-synthesized Pt nanoparticles with surfactant molecules, in which the average particle size is around 3 nm. Figure 1b and 1c illustrate that after the nanoparticles were loaded on a high surface area carbon support and subsequently annealed at 185ºC, no significant change of particle size and/or shape was observed. Other surfactant removal treatments of Pt nanoparticles with carbon were detailed in a full article ACS Catalysis, 2(2012)1358. Briefly, the results display the order of activity as: annealed > HAc > UV-O_3 > untreated > TMAOH. Based on the shape of cyclic voltammograms and the ORR current densities, thermal annealing method is established to be the most effective approach in cleaning the surface of the catalysts.

Highly Homogeneous and Efficient Ternary Alloy Nanoparticles

In order to approach multimetallic electrocatalysts at nanoscale and to have surface chemistry under control [8], it is of paramount importance to have highly homogeneous distribution of constituents among the entire volume of a single nanoparticle. Our focus in the previous report has been on Pt-skin formation over ternary alloys by annealing treatment only. Here, we proceed towards monodisperse nanoparticles with homogeneous elemental distribution and hence surface chemistry that can lead to formation of multilayered Pt-skin surfaces. Our solvo-thermal approach was used to obtain nanoparticles that went through a mild annealing treatment in order to remove surfactants. Figure 2 summarizes structural and electrochemical characterizations of ternary alloy nanoparticles. TEM images in Figure 2 confirm that nanoparticles are monodisperse particles with an average particle size of ~6 nm, which is close to the optimal size for Pt-alloy catalysts established before [5]. Distribution of elements in the ternary nanoparticles was mapped by energy dispersive X-rays based on high angle annular dark field–scanning transmission electron microscopy. Figures 2b-e show overlapped and separate maps of the elements in a typical $Pt_3(CoNi)_1$ particle. It is obvious that all of the constituents, Pt, Co and Ni, are uniformly distributed across the particle, and well intermixed in the overlapping map (Figure 2b). The observations here are consistent with our recent findings on Pt-bimetallic nanoparticles prepared by similar approach [9], confirming the highly homogeneous nature of the ternary alloy nanoparticles obtained by organic solution synthesis. Previously established protocol for thermal treatment was applied to remove the surfactants and induce beneficial surface segregation for best catalytic performance. TEM images in Figures 2f and 2g show that no significant size or morphology change happened after these treatments. A catalyst suspension was prepared by sonication of the catalyst in deionized water, and a drop of that suspension was deposited on a polished glassy carbon disk (6 mm in diameter) electrode. The content of Pt in the catalyst was adjusted to ~25%, and the loading of Pt on the glassy carbon electrode was ~12 $\mu g/cm^2_{disk}$. Figures 2 h, i, and j summarizes electrochemical results for the $Pt_3(CoNi)_1$ nanocatalysts and commercial Pt/carbon of a similar size (6 nm, Tanaka), that was used as a reference. The measured cyclic voltammograms (CVs) have H_{upd} peaks at E <0.4 V and Pt oxidation/reduction peaks at 0.8 ~ 0.9 V. The onset of Pt-OH_{ad} on the ternary catalyst shifted positively for >25 mV vs. Pt/C (Figure 2h), confirming altered electronic structures and surface adsorption properties of ternary alloy nanoparticles. Consequently, corresponding polarization curves exhibit similar shifts in half-wave potentials, and show substantially enhanced catalytic activities (Figure 2j). At 0.95 V, the as-prepared and annealed $Pt_3(CoNi)_1$/C catalysts have achieved improvement factors of 2.3 and 4.2 in specific activity versus Pt/C, with the annealed catalyst reaching 0.55 mA/cm^2 (versus 0.13 mA/cm^2 for Pt/C). The level of catalytic activity improvement is consistent with the trend established on extended thin-film surfaces reported previously. Similar improvement factors were also present in mass activity, with the annealed $Pt_3(CoNi)_1$/C achieving 183 A/g in comparison to 49 A/g for Pt/C.

Mesostructured Thin Films as Electrocatalysts

We developed a new class of catalysts based on mesostructured multimetallic thin films with adjustable structure and composition, which have been tailored to emulate the distinctive properties of the Pt(111)-skin. We aimed towards materials that can bridge the world of extended surfaces with superior activity and nanoscale systems with high utilization of precious metals. Such synergy is present at the mesoscale, which does not only imply a specific length scale, but also a principle of operating "in between" different physical regimes that exhibit

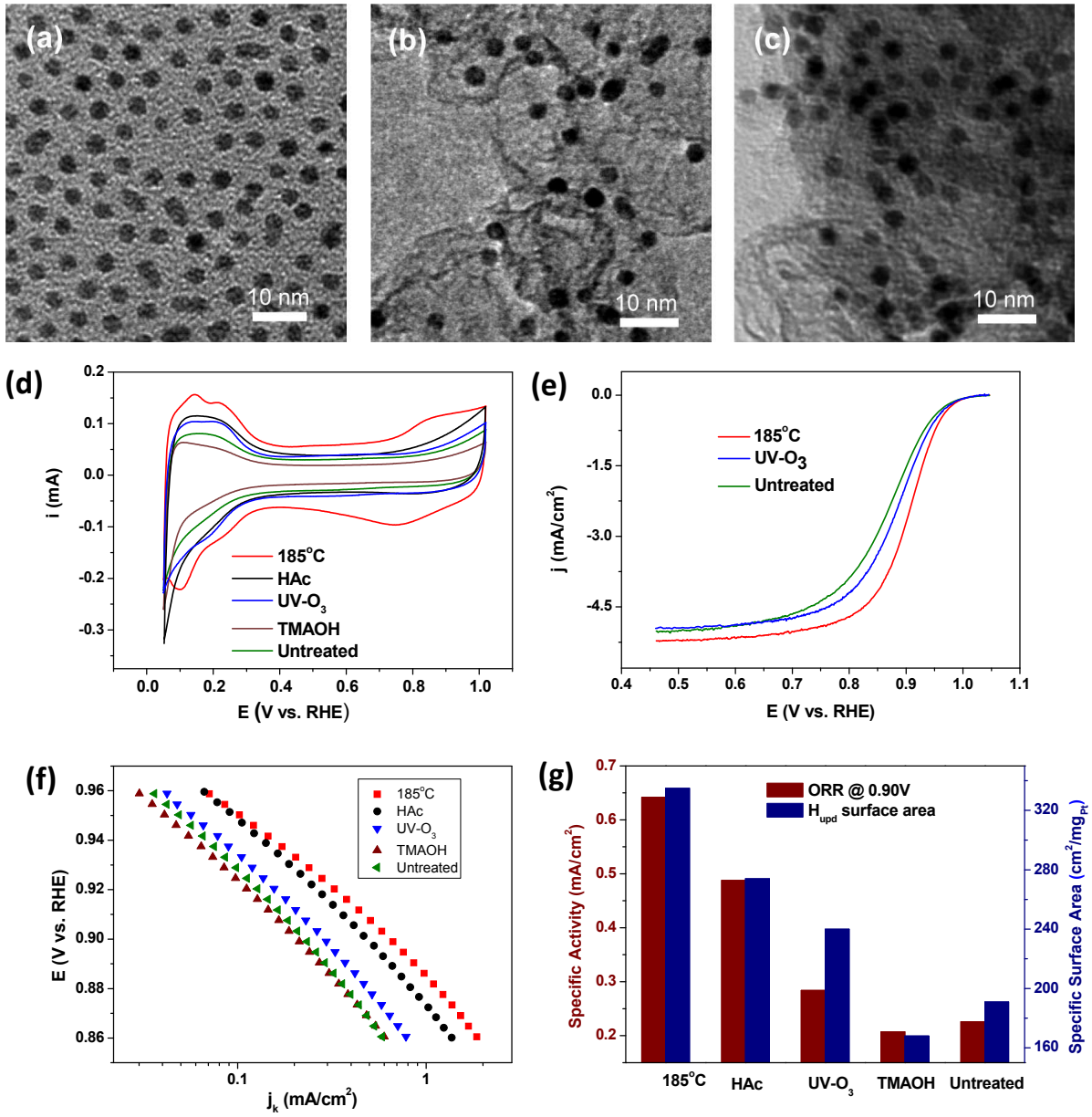

FIGURE 1. TEM images of (a) as-synthesized Pt nanoparticles, (b) Pt nanoparticles loaded on carbon black, (c) Pt nanoparticles on carbon black after annealing, (d) cyclic voltammograms of Pt/C of after different treatments with respect to the untreated sample, (e) ORR polarization curves of annealed, ultraviolet ozone treated versus untreated sample, (f) Tafel plots of Pt/C at 20 mVs^{-1}, 1,600 rpm, 20˚C, and (g) specific activity at 0.90 V and specific surface area.

distinct functional behavior. Continuous Pt and Pt-alloy nanostructured thin films (NSTF) [9] were deposited by planar magnetron sputter deposition. It is well known that NSTF catalysts provide good surface area utilization and eliminate issues related to carbon support corrosion and contact resistance at the carbon-metal interface that lead to poor utilization and degradation of the catalyst. Ability to control the deposition rate, as well as the combination and order of constituents, established sputter deposition as an effective tool to form thin films with desirable thickness, composition profile and surface roughness. However, the surface structure of a thin film, an important catalytic parameter, cannot be altered by this method to match those established on single crystalline systems. For that reason, we attempted a thorough examination of thin film properties on extended, flat, non-crystalline and chemically-inert substrates such as a mirror polished glassy carbon surface. This approach brings an additional level of control in terms of defined geometric surface area and surface roughness factor that is unattainable in the case of nanoscale substrates. Consequently, our efforts have been directed toward exploring structural transitions in polycrystalline thin films,

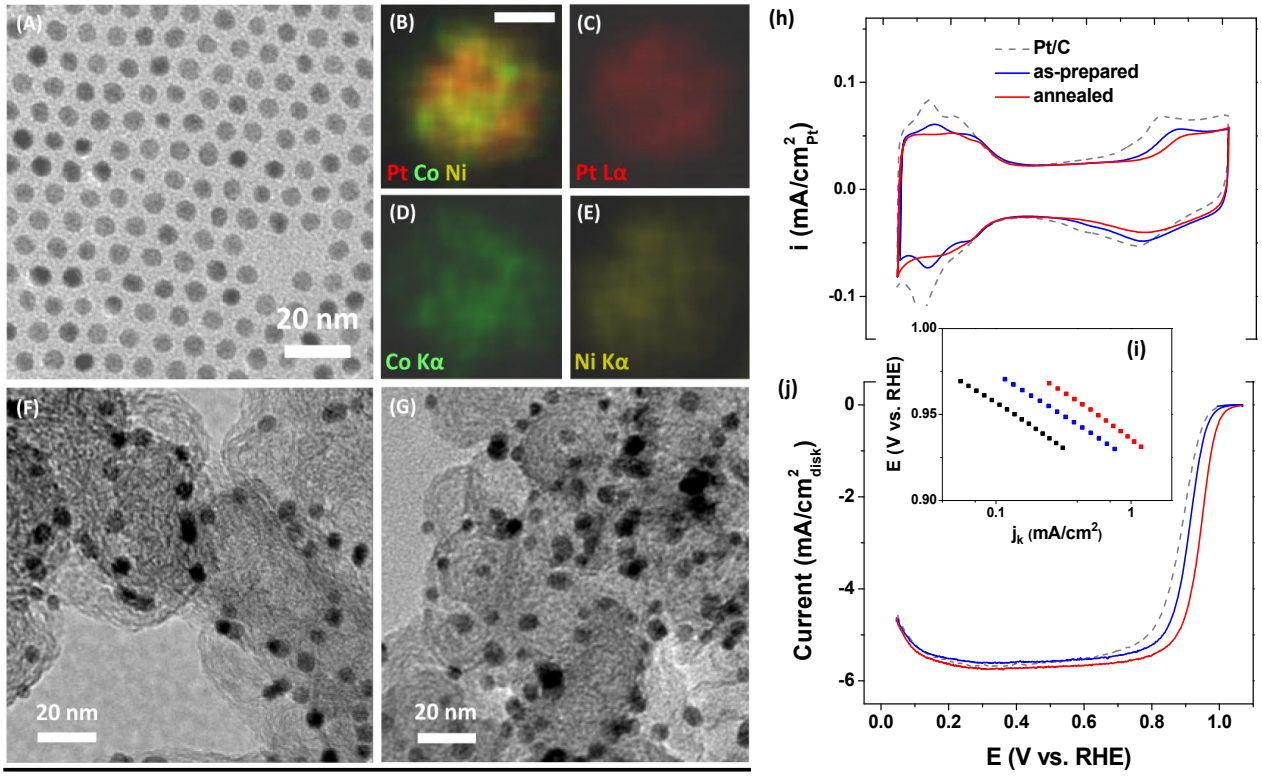

FIGURE 2. TEM image of (a) as-synthesized $Pt_3(CoNi)_1$ alloy nanoparticles; (b-e) representative elemental maps from energy dispersive X-ray spectroscopy analysis based on scanning transmission electron microscopy for (b) overlapping of Pt, Co and Ni, (c) Pt, (d) Co, and (e) Ni: the scale bar in (b) is equal to 2 nm and it also applies for (c) – (e); (f) and (g) show TEM images of the ternary catalyst before (f) and after (g) surfactant removal and thermal treatment; (h) CVs recorded at 50 mV/s in Ar saturated 0.1 M $HClO_4$; (i) Tafel plots of the kinetic current densities depending on electrode potentials; (j) polarization curves for the ORR with iR drop correction recorded in O_2 saturated 0.1 M $HClO_4$.

and we found that as-deposited Pt film with corrugated nanostructured three-dimensional surface morphology has been transformed into a smooth two-dimensional surface with large 20x100 nm (111) facets. The characteristic surface features are confirmed by both scanning tunneling microscopy and electrochemical cyclic voltammetry to be predominantly (111) facets encompassing the entire surface. The synergy between the surface structure, domain size, and functionality defines that the thin-film surface has a distinct mesostructred morphology. These findings clearly demonstrate the feasibility of controlling surface ordering of extended Pt thin films deposited over a non-crystalline substrate, i.e., without use of templates for epitaxial growth. Instead of building the crystal lattice from a seed or underlying crystalline substrate, individual randomly oriented nanoscale grains coalesce and form large well-ordered (111) facets. All of that greatly expands the potential for utilization of thin-film materials and introduces thermal annealing in a controlled atmosphere as a compelling tool in the fine tuning of a thin film's structure and hence electrocatalytic properties. Figure 3 depicts this thermodynamically driven transition that releases stress and strain of the as-deposited thin film and leads towards the state with minimum surface energy without compromising the overall shape and dimension of the whisker. Similar to Pt thin films on glassy carbon, the initial nanostructured surface morphology that originated from the closely bonded whiskerettes' tips is transformed into a smooth continuous film with large crystalline domains (20-40 nm). Specifically, randomly oriented nanoscale grains coalesce and give rise to a mesostructured thin film with unique physiochemical properties, therefore, the materials after this treatment will be referred to as mesostructured thin films (MSTF). Close inspection of high-resolution TEM micrographs after applied thermal treatment confirms that emerged facets with (111) structure prevail on the surface while under-coordinated sites are diminished, which also has important implications towards improved stability. Figure 3 also summarizes the electrochemical signature and compares adsorption and catalytic properties between different classes of thin-film materials and state-of-the-art Pt/C by rotating disk electrode. From CV it is obvious that the onset of surface oxide formation is shifted positively in the following order: Pt-NSTF < PtNi-NSTF < PtNi Meso-TF and consequently, the ORR polarization curves, follow the same trend in activity. Figures 3d and 3f summarize kinetic current densities (specific activities per electrochemically active surface area of Pt) as Tafel plots and a bar graph. Usually we report values

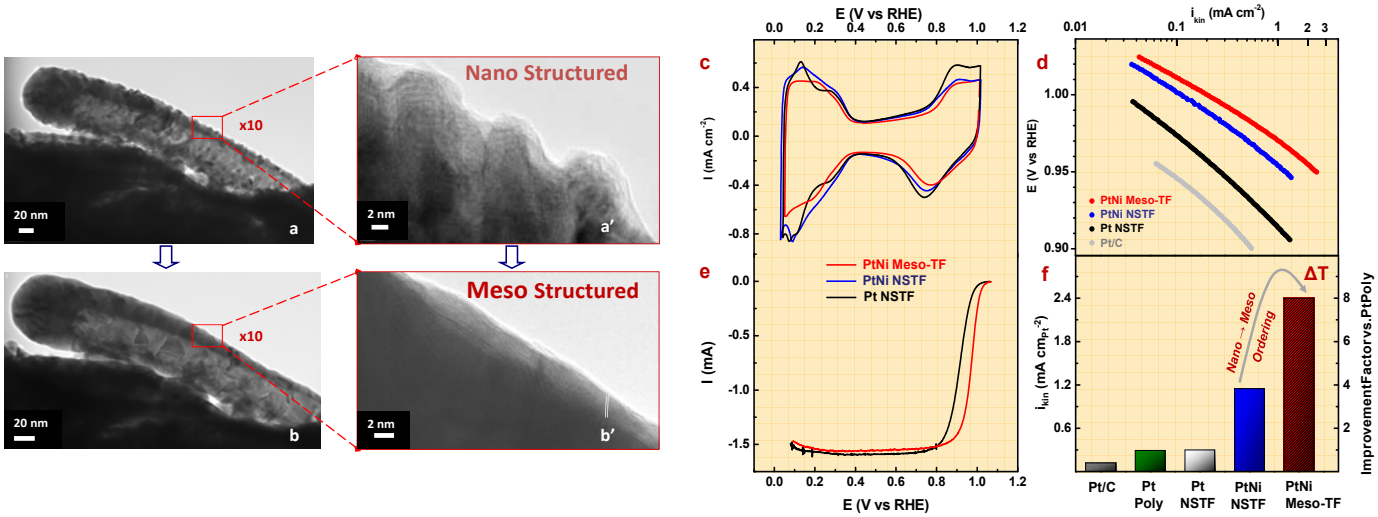

FIGURE 3. In situ TEM transition from nanostructured into mesostructured thin film: (a)-(b) annealing between room temperature and 400°C on a single whisker that induce the ordering from randomly oriented to a homogeneous structure with crystalline domains; cyclic voltammetry on the thin-film-based catalysts: (c) Pt-NSTF, PtNi-NSTF and PtNi-MSTF; (e) the ORR polarization curves; (d) Tafel plots and (f) specific activities at 0.95 V and improvement factor versus Pt-Poly (and Pt-NSTF).

measured at 0.95 V to avoid diffusion-induced errors in kinetic current densities. The activity of PtNi MSTF exhibits an improvement factor of over 8 versus Pt-poly and Pt-NSTF, and when compared to the conventional Pt/C catalyst, the specific activity of the PtNi MSTF has 20-fold improvement. Even though optimal film thickness, alloy composition and total Pt loading will be extensively studied in the future, the measured improvement expressed in A/mg_{Pt} corresponds to a mass activity that is already three times higher than the DOE technical target. The CV curves, trend in specific activity, low Tafel slope, and the structural characterizations strongly suggest that the annealed PtNi Meso-TF has a nanosegregated Pt(111)-skin type of near-surface structure. The developed approach will be applied to generate a wide range of electrocatalysts with tailored structure/composition, ultra-low precious metal content as well as high activity and durability.

CONCLUSIONS AND FUTURE DIRECTIONS

- PtM and $Pt_3M_1N_2$ nanoparticles cathode catalysts obtained from the organic solvo-thermal synthesis exhibit superior activity and stability than those prepared by the conventional methods. The method to synthesize of Pt_3MN nanoparticles with highly active Pt-skin morphology is established.
- Specific and mass activity improvements are obtained for Pt-skin Pt_3MN/C nanoparticles in rotating disk electrode measurements. Advanced theoretical modeling methods predicted and confirmed Pt-skin type of nanosegregated structures in ternary alloys.
- Ternary systems operate through the same mode of action of improving the catalytic properties of the topmost Pt atoms as binary alloys.
- Ex situ characterization in MEA of the most promising nanoscale catalyst confirmed that the structure and composition of the catalyst was not changed after 20K cycles.
- Future effort will be dedicated to the scale up synthesis of the most promising catalysts and MEA evaluation.
- Further decrease of the non-precious metal content will be pursued for different classes of catalysts based on thin films, nanowires and nanoparticles.

FY 2013 PUBLICATIONS/PRESENTATIONS

1. D. Li, C. Wang, D. Tripkovic, S. Sun, N.M. Markovic, V.R.Stamenkovic *Surfactant Removal from Nanoparticles Prepared by Solvo Thermal Colloidal Synthesis* **ACS Catalysis, *2(2012)1358.***

2. C. Wang, N.M. Markovic and V.R. Stamenkovic *Advanced Platinum Alloy Electrocatalysts for the Oxygen Reduction Reaction* **ACS Catalysis, *2(2012)891.***

3. C. Wang, D. Li, M.Chi, J. Pearson, R.B.Rankin, J.Greeley, Z.Duan,G.Wang, D.van derVliet, K.L. More, N.M.Markovic, V.R.Stamenkovic *Rational Development of Ternary Electrocatalysts* **Journal of Physical Chemistry Letters, 3(2012)1668.**

4. D. van derVliet, C. Wang, D. Tripkovic, D. Strmcnik, X.F. Zhang, M.K. Debe, R.T. Atanasoski, N.M. Markovic, V.R. Stamenkovic *Mesostructured Thin Films as Electrocatalysts with Tunable Composition and Surface Morphology* **Nature Materials, 11(2012)1051.**

5. C. Wang, D. Strmcnik, D. van der Vliet, N. Markovic, V. Stamenkovic *Materials for Energy Conversion at Solid-Liquid Inetrfaces* **2012 Materials Research Society Spring Meeting, April 2012, San Francisco, CA.**

6. D. van der Vliet, C. Wang, D. Li, N. Markovic, V. Stamenkovic *Towards Nano-engineered Pt-Skin High Surface Area Catalysts* **221th Int. Meeting of the Electrochemical Society, May 2012, Seattle, WA.**

7. D. van der Vliet, C. Wang, D. Li, N. Markovic, V. Stamenkovic *The Effect of Annealing on the Electrocatalytic Properties of Multimetallic Platinum Alloy Catalysts* **221th Int. Meeting of the Electrochemical Society, May 2012, Seattle, WA.**

8. C. Wang, D. van der Vliet, D. Tripkovic, Datrmcnik, N. Markovic, V. Stamenkovic *Synthesis of Nanocatalysts with Tailored Structures* **244th American Chemical Society National Meeting, August 2012, Philadelphia, PA.**

9. C. Wang, D. van der Vliet, D. Tripkovic, D. Strmcnik, D. Li N. Markovic, V. Stamenkovic *Advanced Electrocatalysts for PEM Fuel Cells* **222th Electrochemical Society Meeting, October 2012, Honolulu, HI.**

REFERENCES

1. V. Stamenkovic, B. Fowler, B.S. Mun, G. Wang, P.N. Ross, C. Lucas, and N.M. Markovic, "Improved Oxygen Reduction Activity on $Pt_3Ni(111)$ via Increased Surface Site Availability", *Science.*, **315** (2007) 493-497.

2. N.M. Markovic and P.N. Ross, "Surface Science Studies of Model Fuel Cell Electrocatalysts", *Surface Science Report*, **45** (2002) 121-229.

3. V. Stamenkovic and N.M. Markovic, "Electrocatalysis on Model Metallic and Bimetallic Single Crystal Surfaces, Model Systems in Catalysis: From Single Crystals and Size Selected Clusters", Editor: Robert M. Rioux, Harvard University, USA,; Publisher: Elsevier Science, Amsterdam, The Netherlands, *2009.*

4. K.J.J. Mayrhofer, B.B. Blizanac, M. Arenz, V. Stamenkovic, P.N. Ross and N.M. Markovic, "The Impact of Geometric and Surface Electronic Properties of Ptcatalysts on the Particle Size Effect in Electrocatalysis", *J. Phys. Chem, B*, **109** (2005) 14433-14440.

5. C. Wang, D. van der Vliet, K.C. Chang, H. You, D. Strmcnik, J.A. Schlueter, N.M. Markovic, V.R. Stamenkovic, "Monodisperse Pt_3Co Nanoparticles as a Catalyst for the Oxygen Reduction Reaction: Size Dependent Activity", *J. Phys. Chem. C.,* **113**(2009)19365.

6. C. Wang, D. van der Vliet, K.C. Chang, N.M. Markovic, V.R. Stamenkovic, "Monodisperse Pt_3Co Nanoparticles as Electrocatlyst: the Effect of Particle Size and Pretreatment on Electrocatalytic Reduction of Oxygen", *Phys.Chem.Chem.Phys*., **12**(2010)6933-6939; ***COVER Article***.

7. V. Stamenkovic, B.S. Mun, M. Arenz, K.J.J.Mayrhofer, C. lucas, G. Wang, P.N. Ross, and N.M. Markovic, " Trends in Electrocatalysis on Extended and Nanoscale Ptbimetallic Alloy Surfaces ", *Nature Materials.*, **6** (2007) 241-247.

8. C. Wang, M.Chi, D. Li, D. Strmcnik, D.van derVliet, G. Wang, V. Komanicky, K.-C. Chang, A.P. Paulikas, D. Tripkovic, J. Pearson, K.L. More, N.M.Markovic and V.R.Stamenkovic, "Design and Synthesis of Bimetallic Electrocatalyst with Multilayered Pt-Skin Surfaces" , *Journal of American Chemical Society*, **133**(2011)14396.

9. C. Wang, M. Chi, D. Li, D. van derVliet, G. Wang, Q. lin, J.F. Mitchell, K.L. More, N.M.Markovic, V.R.Stamenkovic, "Synthesis of Homogenious Pt-Bimetallic Nanoparticles as Highly Efficient Electrocatalysts", ACS Catalysis, **1**(2011)1355.

10. D. van derVliet, C. Wang, M.K. Debe, R.T. Atanasoski, N.M.Markovic, V.R.Stamenkovic, "Platinum Alloy Nanostructured Thin Film Catalysts for the Oxygen Reduction Reaction", *Electrochimica Acta*, 56,24(2011)8695.

V.A.4 Contiguous Platinum Monolayer Oxygen Reduction Electrocatalysts on High-Stability Low-Cost Supports

Radoslav Adzic (Primary Contact), Jia Wang, Miomir Vukmirovic, Kotaro Sasaki, Yang Shao-Horn[1], Rachel O'Malley[2]
Brookhaven National Laboratory (BNL), Bldg. 555
Upton, NY 11973-5000
Phone: (631) 344-4522
Email: adzic@bnl.gov

DOE Manager
Nancy Garland
Phone: (202) 586-5673
Email: Nancy.Garland@ee.doe.gov

Subcontractors:
- Massachusetts Institute of Technology (MIT), Cambridge, MA
- Johnson Matthey Fuel Cells (JMFC), London, England

Project Start Date: July 1, 2009
Project End Date: September 30, 2013

Overall Objectives

- Synthesizing high-performance Pt monolayer (ML) on stable, inexpensive metal or alloy nanostructured fuel cell electrocatalysts for the oxygen reduction reaction (ORR).
- Increasing activity and stability of Pt ML shell and stability of supporting cores, while reducing noble metal contents.

Fiscal Year (FY) 2013 Objectives

Scale up of syntheses to produce multi-gram quantities of following three catalysts:

- Pt ML on Pd hollow nano-particles using a microemulsion or similar method
- Pt ML on ultra-thin Pd alloy nanowires (NWs)
- Pt ML on WNi and Pd_9Au_1 alloys obtained by electrodeposition
  - Delivering a 450-cm^2 membrane electrode assembly (MEA) for testing at United Technologies Corporation
  - Achieving a 100% utilization of Pt

Technical Barriers

This project addresses the following technical barriers from the Fuel Cells section of the Fuel Cell Technologies Office Multi-Year Research, Development, and Demonstration Plan:

(A) Durability

(B) Cost

(C) Performance

Technical Targets

We are focusing on simplifying synthetic processes to obtain better catalysts' activity, higher Pt utilization, lower content of platinum-group metal (PGM) and more simple MEAs formation (Table 1).

TABLE 1. Progress toward Meeting DOE Fuel Cell Electrocatalysts Technical Targets

Characteristic	Units	Target 2017	Achieved 2013
PGM total loading	mg PGM/cm^2 electrode area	0.125	0.05 (Pt/PdAu, Pt/PdWNi/GDL)
Mass activity	A/mg Pt @ 900 $mV_{iR\text{-}free}$	0.44	1.7 (Pt/PdAu NWs)
Specific activity	mA/cm^2 @ 900 $mV_{iR\text{-}free}$		1.4 (Pt/hollow Pd)
PGM mass activity			0.5 (Pt/hollow Pd)
Loss in initial catalytic activity	% mass activity loss	<48	No loss in activity in 200,000 cycles (Pt/PdAu)

GDL - gas difussion layer

FY 2013 Accomplishments

- Demonstrated synthesis and high performance of hollow Pd nano-particles and $Pt_{ML}/Pd_{hollow}/C$ catalyst. The synthesis methods are readily scalable to multi-gram quantities.
- Synthesis of ultra-thin bimetallic PdAu NWs has been developed to provide an excellent support for Pt_{ML}.
- Developed a method for electrochemical deposition of NW cores on GDLs.
- Developed a method for electrodeposition of metal, alloy and refractory metal alloy nano-particles on GDLs. Highly active and durable Pt_{ML}/Pd_9Au_1 NW/GDL and Pt_{ML}/Pd/WNi/GDL electrocatalysts have been obtained.
- Pt utilization close to 100% has also been demonstrated.

- Developed electrochemical cell for production of electrodes of 440 cm^2 (industrial size).

✧ ✧ ✧ ✧ ✧

INTRODUCTION

Further developments of oxygen reduction electrocatalysts are inevitable to lessen the remaining technological difficulties that hamper automotive applications of fuel cells, and we thus have focused on reducing Pt, or PGM contents in our Pt ML electrocatalysts, while increasing their stability and activity. The understanding of the properties of Pt ML electrocatalysts, and of a broader class of core-shell electrocatalysts, has considerably grown up. Optimizing the properties of nanostructured cores such as the composition, size and shape makes it possible to facilitate the Pt ML catalysts ready for the applications.

APPROACH

The properties of Pt ML, particularly such as the ORR activity and stability, can be improved by core-shell interaction using appropriate cores, which reduces oxygen binding energy through the following measures [1]: (i) compression of Pt ML atoms induced by core, hollow core, subsurface ML, (ii) electronic effects of cores, (iii) decreasing the number of low-coordination atoms, and (iv) increasing stability of cores with specific structure, composition and shape. We have also performed electrodeposition of cores such as metal and alloy nano-particles, nano-rods, and NWs to optimize their shapes and composition and maximize catalyst utilization. Refractory metal alloys electrodeposited by co-deposition of Ni and W, are also used as cores to further reduce the PGM content.

RESULTS

Synthesis and Performance of Hollow Pd Nano-Particles and $Pt_{ML}/Pd_{hollow}/C$ Catalyst

Three different syntheses of hollow Pd nano-particles have been developed, i.e., (i) by microemulsion, (ii) reduction in water with citrate, and (iii) galvanic replacement of Cu as a sacrificial metal with no surfactant. These methods are scalable to multi-gram quantities. The formation of the hollow structure from these Pd nano-particles was verified by transmission electron microscopy. The activity and stability of the $Pt_{ML}/Pd_{hollow}/C$ catalysts have been examined by rotating disk electrode and MEA tests. The catalyst synthesized by the method (iii) showed the most enhanced activity and stability for the ORR among there catalysts. The PGM loading in cathode was 70 μg/cm^2. In the MEA tests, the Pt and PGM mass activity was 1.2 A/mg and 0.53 A/mg (at 0.9 V), respectively (Figure 1), and the specific activity was 1.4 mA/cm^2 (at 0.9 V). There was no change in polarization curves with O_2 and air in 1,000 potential cycle stability tests.

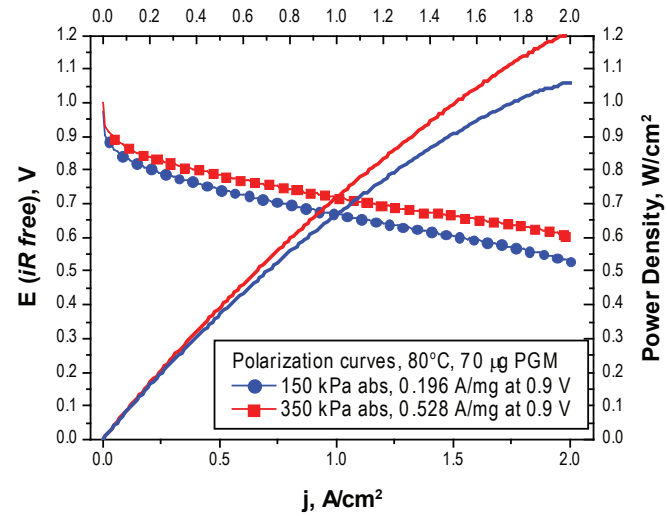

FIGURE 1. Polarization curves and power density curves of MEA tests from $Pt_{ML}/Pd_{hollow}/C$ catalyst operating at 80°C. Cathode PGM loading: 70 μg/cm^2; electrode area: 5 cm^2.

We note that hollow Pt nano-particles were also prepared by the replacement of Cu. In rotating disk electrode tests, the PGM mass activity was 0.32 A/mg, and the specific activity was 2.06 mA/cm^2. No loss in ORR was observed after 10,000 potential cycles.

Pt_{ML}/Pd/C Catalyst Synthesized in Ethanol

We have developed a new Pt ML synthesis method on Pd nano-particles in ethanol. Galvanic displacement of Pd by Pt takes place, while Pd^{2+} ions are reduced by ethanol at elevated temperatures. High-angle annular dark field–scanning transmission electron microscope and electron energy loss spectroscopy measurements confirmed the core-shell structure. The PGM loading in the cathode was 150 μg/cm^2. The Pt and PGM mass activity in the MEA tests was 0.9 A/mg and 0.4 A/mg, respectively (Figure 2), and the activity with O_2 and air did not change after 2,000 potential cycle tests.

Pt_{ML} on Ultra-Thin Bimetallic PdAu NWs

The ultra-thin $Pd_{1-x}Au_x$ NWs are prepared by a solution-based method wherein the chemical composition can be readily and predictably controlled. The composition and size-dependent performance in hierarchical $Pd_{1-x}Au_x$ NWs encapsulated with a Pt_{ML} shell ($Pt/Pd_{1-x}Au_x$) was observed. After the deposition of a Pt_{ML}, a volcano-type composition dependence is observed in the ORR activity of the $Pt/Pd_{1-x}Au_x$ NWs as the Au content is increased from 0 to 30% with the highest activity of the Pt/Pd_9Au_1 NWs, representing the optimum performance. In the MEA tests,

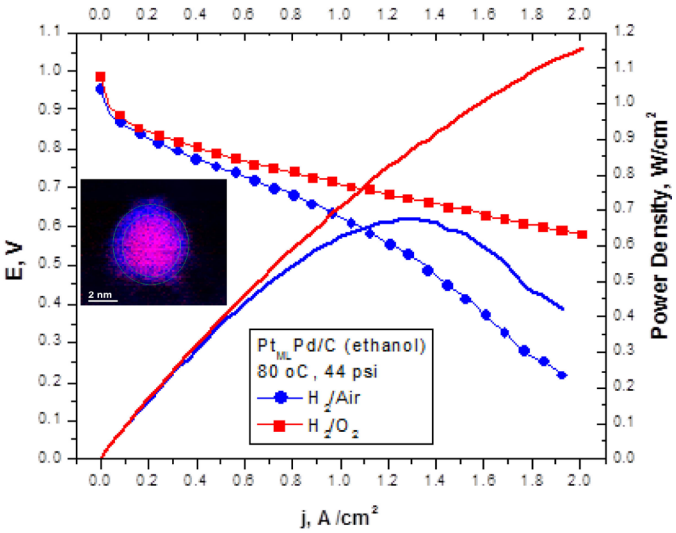

FIGURE 2. Polarization curves and power density curves of MEA tests from Pt_{ML}/Pd/C catalyst synthesized in ethanol, operating at 80°C. The inset shows a two-dimensional image of Pd (red) and Pt (blue) electron energy loss spectroscopy signals from a Pt_{ML}/Pd/C nano-particle. Cathode PGM loading: 150 µg/cm^2 (70 µg/cm^2 Pt); electrode area: 5 cm^2.

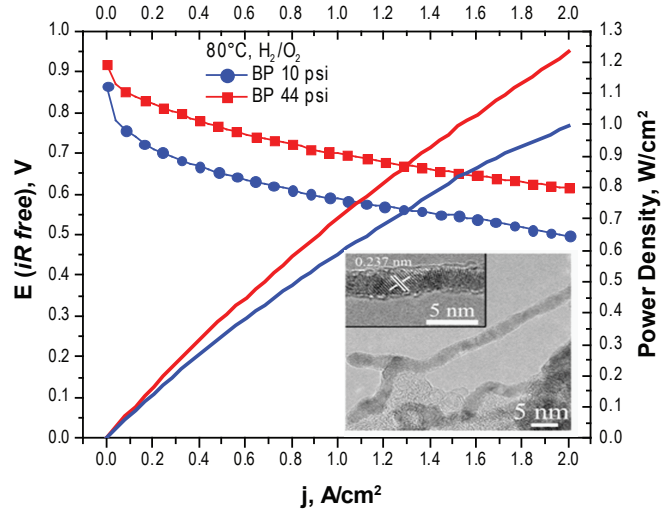

FIGURE 3. Polarization curves and power density curves of MEA tests from Pt_{ML} on ultra-thin PdAu NW catalyst operating at 80°C. The inset shows transmission electron microscope images of PdAu naniwires. Cathode PGM loading: 70 µg/cm^2; electrode area: 5 cm^2.

the Pt and PGM mass activity was 1.7 A/mg and 0.72 A/mg at 0.9 V (Figure 3), respectively. The specific activity was 0.72 mA/cm^2.

Electrochemical Deposition of NW Cores, Refractory Metal Alloys and 100% Pt Utilization

We have developed the scale up in electrodeposition of catalysts directly on GDLs, with three electrochemical cells of electrode areas of 5, 25, and 450 cm^2. Potential pulse deposition protocol was tailored to optimize the deposition processes on GDLs. The unique feature of the electrodeposited PtML catalysts on electrodeposited cores on GDLs is that all Pt atoms are accessible to both electrons and protons and thus, they have a 100% utilization. In comparison with 15-20% Pt utilization in a conventional Pt/C catalyst (4-5 nm diameter) and about 50% in PtML catalysts obtained in conventional preparation of the MEA.

Pt_{ML}/Pd_9Au_1 NW/GDL

Similar ORR activity in MEA tests was obtained for 5- and 25-cm^2 electrode cells; the Pt and PGM mass activity was 1.2 A/mg and 0.5 A/mg, respectively, and the specific activity was 0.4 mA/cm^2. Lower activity for 450 cm^2 may be caused by the ambient pressure applied and low open circuit potential indicating inadequate state of the surface.

Pt_{ML}/Pd/WNi/GDL

We demonstrated the electrodeposition of refractory metal alloy from aqueous solutions on GDLs. A co-deposition of W and Ni can take place, although W cannot

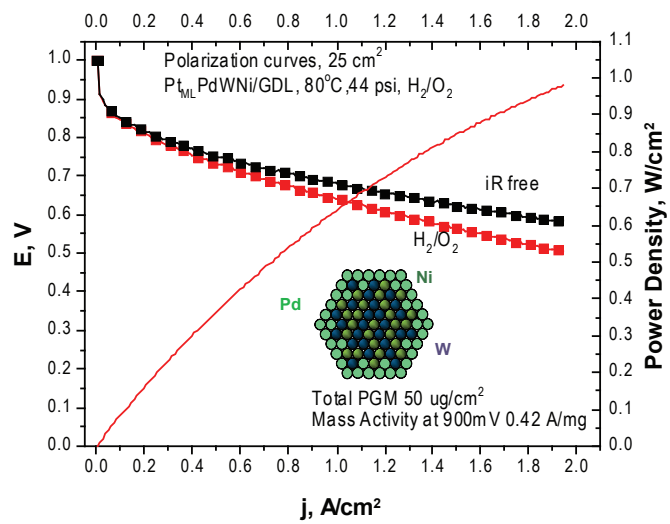

FIGURE 4. Polarization curves and power density curves of MEA tests from Pt_{ML} on Pd/NiW/GDL operating at 80°C. The inset shows a schematic model of NiW nano-particle core with a partially displaced by Pd. Cathode PGM loading: 50 µg/cm^2; electrode area: 25 cm^2.

separately be deposited from aqueous solutions. These particles provide a stable and inexpensive support as cores. We then deposited Pd on NiW cores through the galvanic displacement of Ni, followed by Pt ML deposition by the Cu underpotentially deposited method. The PGM loading in cathode was 50 µg/cm^2. The Pt and PGM mass activity was 1.1 A/mg and 0.42 A/mg, respectively (Figure 4). We note that the performance even increased after 5,000 (5 cm^2) and 15,000 (25 cm^2) potential tests.

MEA Tests of Pt_{ML}/Pd/C at 3M

The MEA test under potential cycles between 0.6 V and 1.2 V at 70°C at 100% relative humidity demonstrated that the mass activity almost doubled and the specific activity increased ~3-4 times with an increase in the number of potential cycles, supporting the self-healing mechanism, in which we have proposed.

CONCLUSIONS AND FUTURE DIRECTIONS

- Further improvements of Pt ML catalyst aimed at reducing the cost of the Pd core, increasing stability and improving syntheses efficiency have been achieved.
- These include several syntheses of hollow Pd cores, Pd alloys with refractory metals, Pd_9Au_1 alloy, Pt ML on ultra-thin Pd NWs and electrodeposited Pd nanostructures, verified in scale up syntheses and the MEA tests.
- The unique features of Pt ML catalysts with electrodeposited cores including Pt utilization of 100% have been demonstrated. Technology based on electrodeposition of catalysts on GDLs appears promising.
- The mechanism of stability of core-shell electrocatalysts, including the self-healing mechanism, has been verified in tests involving potential cycling to 1.2 V at 3M.

Future work will focus on:

- Syntheses of hollow Pd and Pt to maximize the hollow and to optimize the particle size in relation to the degree of atom's contraction and activity.
- Tuning the effect of core on a Pt ML shell by hetero-layered core structure. Graphene oxide as support.
- Electrodeposition of selected alloys as stable, inexpensive cores with known segregation properties. Optimization of the cores shapes.
- Using non-aqueous solvents for electrodeposition of reactive metal cores, underpotentially deposited of various MLs for Pt ML deposition on reactive metals and alloys.

SPECIAL RECOGNITIONS & AWARDS/ PATENTS ISSUED

1. A special issue of the journal "*Electrocatalysis*" published to tribute R. Adzic's outstanding achievements in the areas of electrochemistry and electrocatalysis (volume 3, 2012).

2. R. Adzic, J. Wang, M. Vukmirovic, K. Sasaki received an R&D Award.

3. Four patent applications have been submitted in 2012-2013.

FY 2013 PUBLICATIONS/PRESENTATIONS

1. K.A. Kuttiyiel, K. Sasaki, D. Su, M.B. Vukmirovic, N.S. Marinkovic, R.R. Adzic, "Pt Monolayer on Au-Stabilized PdNi Core-Shell Nanoparticles for Oxygen Reduction Reaction", Electrochimica Acta, in press.

2. L. Yang, M.B. Vukmirovic, D. Su, K. Sasaki, J. Herron, M. Mavrikakis, S. Liao, R.R. Adzic, "Tuning the Catalytic Activity of Ru@Pt Core-Shell Nanoparticles for the Oxygen Reduction Reaction by Varying the Shell Thickness", Journal of Physical Chemistry C, in press.

3. K. Sasaki, H. Naohara, Y-M. Choi, J. X. Wang, M.B. Vukmirovic, P. Liu, R.R. Adzic, "Recent Advances in Platinum Monolayer Fuel Cell Electrocatalysts for the Oxygen Reduction Reaction", The Journal of Fuel Cell Technology, 12(3) (2013) 58-64.

4. Y. Zhang, C. Ma, Y. Zhu, R. Si, Yun Cai, J.X. Wang, R.R. Adzic, "Hollow Core Supported Pt Monolayer Catalysts for Oxygen Reduction", Catalysis Today, 202 (2013) 50-54.

5. K.A. Kuttiyiel, K. Sasaki, Y. Choi, D. Su, P. Liu, R.R. Adzic, "Nitride Stabilized PtNi Core−Shell Nanocatalyst for High Oxygen Reduction Activity", Nano Letters, 12(12) (2012) 6266–6271.

6. K. Sasaki, H. Naohara, Y.M. Choi, Y. Cai, W.-F. Chen, P. Liu, R.R. Adzic, "Highly Stable Pt Monolayer on PdAu Nanoparticle Electrocatalysts for the Oxygen Reduction Reaction", Nature Communications, (2012) DOI:10.1038/ncomms2124.

7. R.R. Adzic, "Platinum Monolayer Electrocatalysts: Tunable Activity, Stability, and Self-Healing Properties", Electrocatalysis, 3(3-4) (2012) 163-169.

8. H.I. Karan, K. Sasaki, K.A. Kuttiyiel, C.A. Farberow, M. Mavrikakis, R.R. Adzic, "Catalytic Activity of Platinum Monolayer on Iridium and Rhenium Alloy Nanoparticles for the Oxygen Reduction Reaction", ACS Catalysis, 2(5) (2012) 817-824.

9. K.A. Kuttiyiel, K. Sasaki, Y-M. Choi, D. Su, P. Liu, R.R. Adzic, "Bimetallic IrNi Core Platinum Monolayer Shell Electrocatalysts for the Oxygen Reduction Reaction", Energy & Environmental Science, 5(1) (2012) 5297-5304.

10. M.B. Vukmirovic, Y. Cai, S.T. Bliznakov, K. Sasaki, J.X. Wang and R.R. Adzic, "Platinum Monolayer Electrocatalysts for the Oxygen Reduction Reaction", ECS Transaction, doi: 10.1149/1.3701965 ECS Trans. 2012 volume 45, issue 2, 15-23.

11. C. Koenigsmann, E. Sutter, T.A. Chiesa, R.R. Adzic, S.S. Wong, "Highly Enhanced Electrocatalytic Oxygen Reduction Performance Observed in Bimetallic Palladium-Based Nanowires Prepared under Ambient, Surfactantless Conditions", Nano Letters, 12(4) (2012) 2013-2020.

12. K.P. Gong, Y. Cho, M.B. Vukmirovic, P. Liu, C. Ma, D. Su, R.R. Adzic, "Tetrahedral Palladium Nanocrystals: A New Support for Platinum Monolayer Electrocatalysts with High Activity and Stability in the Oxygen Reduction Reaction", Zeitschrift für Physikalische Chemie, 226(9-10) (2012) 1025-1038.

13. S.T. Bliznakov, M.B. Vukmirovic, L. Yang, E.A. Sutter, R.R. Adzic, "Pt Monolayer on Electrodeposited Pd Nanostructures: Advanced Cathode Catalysts for PEM Fuel Cells", Journal of the Electrochemical Society, 159(9) (2012) F501-F506.

REFERENCES

1. R.R. Adzic, "Platinum Monolayer Electrocatalysts: Tunable Activity, Stability, and Self-Healing Properties", Electrocatalysis, 3(3-4) (2012) 163-169.

V.A.5 The Science and Engineering of Durable Ultra-Low PGM Catalysts

Fernando H. Garzon (Primary Contact),
Jose-Maria Sansiñena, Mahlon Wilson,
Jerzy Chlistunoff, Ivana Matanovic, Neil Henson,
and Eric L. Brosha
Los Alamos National Laboratory (LANL)
MPA-11, MS. D429
Los Alamos, NM 87545
Phone: (505) 667-6643
Email: garzon@lanl.gov

DOE Manager
Nancy Garland
Phone: (202) 586-5673
Email: Nancy.Garland@ee.doe.gov

Subcontractors:
- Yushan Yan, University of California, Riverside, CA/University of Delaware, Newark, DE
- Abhaya Datye and S. Michael Stewart, University of New Mexico, Albuquerque, NM
- Siyu Ye and David Harvey, Ballard Fuel Cells, Burnaby, BC, Canada

Project Start Date: October 2009
Project End Date: October 2014

Overall Objectives

- Development of durable, high mass activity platinum-group metal (PGM) cathode catalysts enabling lower cost fuel cells
- Elucidation of the fundamental relationships between PGM catalyst shape, particle size, and activity to help design better catalysts
- Optimization of the cathode electrode layer to maximize the performance of PGM catalysts, improving fuel cell performance and lowering cost
- Understanding the performance degradation mechanisms of high mass activity cathode catalysts to provide insights to better catalyst design
- Development and testing of fuel cells using ultra-low loading of high-activity PGM catalysts to validate advanced concepts

Fiscal Year (FY) 2013 Objectives

- Incorporation of Pt supported on pyrolyzed polypyrrole (PPy) nanowire catalysts into fuel cells
- Optimization of ceria particle size for high-performance, low free radical generation cathode catalysts
- Accelerated stress testing of fuel cells incorporating ceria-free radical scavengers
- Extensive materials characterization of fuel cell components after accelerated stress testing
- Completion of theoretical modeling of the effect of size and geometry on Pt nanowire catalyst performance
- Completion of theoretical modeling of ceria particle-free radical scavenging mechanism

Technical Barriers

- PGM catalysts are difficult to synthesize in configurations other than quasi-spherical particles
- PGM area specific activity may decrease with decreasing particle size
- Durability may decrease with greater PGM surface area to volume ratios

Technical Targets

The technical targets for catalyst loading are indicated in Table 1. These targets were formulated with the assumption that fuel cell durability and impurity tolerance would not be impacted by the decreased Pt loadings used in the fuel cells.

TABLE 1. Technical Targets: Electrocatalysts for Transportation Applications (Extracted from Table 3.4.12. Technical Plan, April 27, 2007)

Characteristic	Units	2005 Status		Stack Targets	
		Cell	Stack	2010	2015
PGM total content (both electrodes)	g/kW (rated)	0.6	1.1	0.3	0.2
PGM total loading	mg PGM/cm^2 electrode area	0.45	0.8	0.3	0.2

FY 2013 Accomplishments

- Achieved preparation of fuel cells with novel nanowire PGM catalyst layers <25 µm thick with <0.1 mg Pt/cm^2 and an electrochemical surface area >70 m^2/g.
- Optimized Pt-ceria ratios for low free radical generation catalysts with less than 10% difference in fuel cell performance at 0.6 V from non-ceria catalysts.
- Completed high-resolution transmission electron microscopy (HRTEM) imaging of novel PPy nanowire PGM catalysts.
- Completed optimization of fuel cell components using novel nanowire PGM catalysts to demonstrate 5-cm^2 single-cell performance with <<0.1 mg Pt/cm^2 that equal

or exceed conventional membrane electrode assemblies (MEAs) with 0.2 mg Pt/cm^2.

- Accelerated stress testing of fuel cells incorporating free-radical scavengers commenced with first cycle completed.
- Completed characterization of accelerated stress testing samples.
- Completed the extension of theoretical modeling to larger structures that better approximate the dimensions of experimental nanowire materials.

✧ ✧ ✧ ✧ ✧

INTRODUCTION

Minimizing the quantity of Pt-group metals used in polymer electrolyte membrane fuel cells (PEMFCs) is one of the remaining challenges for fuel cell commercialization. Tremendous progress has been achieved over the last two decades in decreasing the Pt loading required for efficient fuel cell performance. Unfortunately, the fluctuations in the price of Pt represent a substantial barrier to the economics of widespread fuel cell use. Durability and impurity tolerance are also challenges that are tightly coupled to fuel cell Pt electrode loading. Traditional approaches to decreasing the amount of Pt required for good performance include:

- Increasing mass activity by decreasing Pt particle size by supporting on carbon
- Formulating Pt-Co, Pt-Cr alloys to improve mass activity
- Increasing Pt utilization by optimization of electronic and ionic contact of the Pt particles
- Improving conductivity of the electronic and ionic conducting constituents of the MEA
- Improving reactant to and product mass transport away from the electroactive sites

Recent novel approaches include the nanoengineering of core shell catalysts and Pt particles of unusual geometries such as nanowires/whiskers.

The success of the aforementioned approaches has been great; however, further advances using such approaches have been hampered by a lack of underlying scientific understanding of the catalyst activity, particle growth mechanisms, and optimization strategies for designing composite electrodes.

APPROACH

Our approach to new PGM catalyst design is multi-tiered**.** We are designing new low-platinum loading catalysts on novel support materials to improve fuel cell performance. Novel shapes—nanoparticles, nanotubes, and nanowires—are being synthesized in a variety of sizes. We are using contemporary theoretical modeling and advanced computational methods to understand and engineer the new catalysts. We are also modeling and designing appropriate catalyst architectures to maximize the performance of our novel catalysts. Catalyst-support interactions and their effects on durability and mass activity are also investigated. New methods to reduce the free radical attack on fuel cell components are being studied. We study and test the performance of the catalysts in electrochemical cells, single-cell fuel cells, and fuel cell stacks. The new catalysts are being extensively characterized before and after fuel cell operation.

RESULTS

During normal operation of PEMFCs, free radicals ($OH^{\cdot}$, $OOH^{\cdot}$, $H^{\cdot}$) are formed which attack the catalyst layer ionomer, catalyst support, and membrane, leading to significant performance loss and eventual membrane failure due to pinhole and/or crack formation [1-2]. In an effort to reduce this commonly observed mode of membrane degradation, the addition of free radical scavengers into the anode catalyst layer, cathode catalyst layer (CCL), and/or the membrane has been investigated. These free radical scavengers are typically salts (such as Mn^{2+} or Ce^{3+}) or oxides (such as CeO_2). Through accelerated stress testing (designed to greatly amplify the degradation of the membrane), it has been demonstrated that these additives can greatly increase membrane lifetime by consuming free radicals before they are able to attack the membrane.

While these antioxidants greatly improve membrane lifetime, they have a deleterious impact on performance, particularly when the cathode is degraded. Specifically, the antioxidant cations (released as Ce^{3+}/Ce^{4+} through dissolution in the case of CeO_x) will accumulate in the CCL through strong interactions with the sulfonate in the ionomer. These cations then compete with protons for sulfonate sites in the CCL, leading to increased CCL ionic resistance and a subsequent loss in performance. This effect is more evident once the cathode has degraded as the reaction distribution shifts towards the cathode-gas diffusion layer interface. Controlling the rate of CeO_x dissolution is therefore of great importance, as it may be possible to maintain sufficient cerium oxide for free radical scavenging while minimizing the impact of the dissolved cations on the CCL. Therefore, our work focuses on the impact of CeO_x crystallite size on dissolution rate. Three different CeO_x samples (6 nm–30 nm particle size) were synthesized and were characterized using X-ray diffraction and gas sorption measurements.

The chemical stabilities of these CeO_x samples were investigated in 1 M H_2SO_4 using ultraviolet-visible spectroscopy to monitor the concentration of Ce^{3+}/Ce^{4+} cations. The trend in chemical stability was found to be:

CeO_x 25 nm > CeO_x 13 nm > commercial 30 nm > CeO_x 6 nm. Interestingly, two of the LANL materials showed higher stability than the larger particle size commercial control sample.

In situ testing was then performed by incorporating the CeO_x additives into the anode catalyst layer of an MEA. Accelerated stress testing was then performed on each MEA (1.3 V upper potential limit, 0.6 V lower potential limit for 4,700 cycles) to evaluate the impact of the CeO_x additives on end-of-life (EOL) performance. Significantly, despite the clear differences in chemical stability found through ex situ testing, no difference in EOL performance was observed among the MEAs prepared using the four different CeO_x additives. This may suggest that at the loadings used for this study, the CCL becomes saturated with Ce cations even with the most stable 25-nm CeO_x, prepared at 800°C. Finally, the impact of relative humidity (RH) was also investigated. By varying the anode RH between 50 and 100%, it was determined that anode RH has a large impact on EOL performance of the MEAs containing CeO_x. The effect is believed to be related to the dissolution rate of CeO_x and the transport of cations in the relatively larger water fluxes.

In order to enhance the catalytic properties of cerium oxides, dopants such as praseodymium and gadolinium have been used to increase the electrical and/or ionic conductivity of cerium oxide. Our recent ex situ experiments show an enhancement of selectivity for free radical elimination upon the substitution doping of ceria. While many groups have reported on the synthesis of these mixed-metal oxides, there is little known about where these dopants are incorporated into the cerium oxide lattice. Our recent work represents the first direct evidence of praseodymium phase separation in mixed cerium-praseodymium oxides. X-ray diffraction and HRTEM were used to verify the presence of a single cubic phase with no amorphous coating. X-ray photoemission spectroscopy showed a strong decrease in surface Ce^{+3}, and that increasing the bulk composition of praseodymium results in a shift towards the Pr^{+4} oxidation state for surface praseodymium atoms, suggesting the formation of a PrO_2 shell. From HRTEM paired with energy dispersive X-ray spectroscopy, we have determined that the concentration of praseodymium does not increase in proportion with cerium, demonstrating a core shell structure. Regardless of particle size and method of synthesis, praseodymium preferentially incorporates into or onto the surface of a cerium oxide core. Further research will be performed to better understand why these materials show enhanced selectivity for oxygen-free radical destruction.

Previously in this project, nanowire catalyst supports were prepared by electropolymerizing pyrrole to PPy onto conductive substrates and even gas diffusion layers. While desirable morphologies were obtained, difficulties were encountered in achieving high Pt catalyst dispersions and utilizations, and the "thin-film" style of electrode easily flooded. Consequently, the approach was redirected to investigating bulk, chemically polymerized nanowires that are catalyzed and fabricated into MEAs as a powder, thus using conventional processes. The advantages over standard carbon blacks, such as higher porosities and connectivity, are retained as with the electro-polymerized structures.

While going to chemical polymerization conceivably enables the introduction of other nanowire fabrication processes, pyrrole is still preferable over, for example, aniline, because the pyrolysis of the former has a much higher yield and better retention of the original structure than the latter. While it is not as easy to synthesize nanofibers as with aniline, there are a number of "soft" template processes for synthesizing PPy nanofibers. Of the simpler methods explored, one particular process provided high yields, good product uniformity, and a desirable "branched" morphology that serves to maintain open porosity and resist fibers from aligning or bundling. The soft template in this case consists of heparin and methylene blue [3], and a micrograph of nanowires synthesized by a generally similar procedure to the literature is shown in Figure 1a. A benefit of this process is that the ratio of heparin to methylene blue can be used to provide some control over fiber diameter. On the other hand, heparin is too expensive to be practical as a precursor. Coincidentally, heparin was originally used as a template in our earlier electropolymerization efforts, but starch served as a satisfactory replacement. When the heparin was replaced with starch in the methylene blue soft template process, however, PPy globules instead of nanofibers were obtained, as shown in Figure 1b.

The failure of the starch to form nanofibers is likely due to an inability to ionically pair with the two tertiary amine ligands on methylene blue because of the lack of anionic functional groups, whereas heparin has a pair of anionic functional groups per ring. In order to effectively replace heparin with its $2^{(-)}$ groups per saccharide ring, several common carbohydrates with anionic functionality were investigated. These were pectin ($<1^{(-)}$/ring), sodium alginate ($1^{(-)}$/ring) and the ι (iota) and λ (lambda) carrageenans (1 and $1.5^{(-)}$/ring, respectively). Since purified carbohydrates can be quite expensive, very low-cost food grade supplies were tested. Interestingly, only the alginate failed to form nanofibers, while even the pectin, with lower functionality due to partially methoxylated carboxylate groups, provided nanofibers. However, the linked globules formed with the alginate indicated some inclination to form fibers. Not surprisingly, the best results were obtained with the highest functionality saccharide, the λ–carrageenan, which became the basis for further efforts.

Transmission electron micrographs of PPy synthesizied using a methylene blue plus λ–carrageenan template are shown in Figure 2. The fibers in this sample are approximately 60 nm in diameter with no discernable structure or interface between the template and PPy

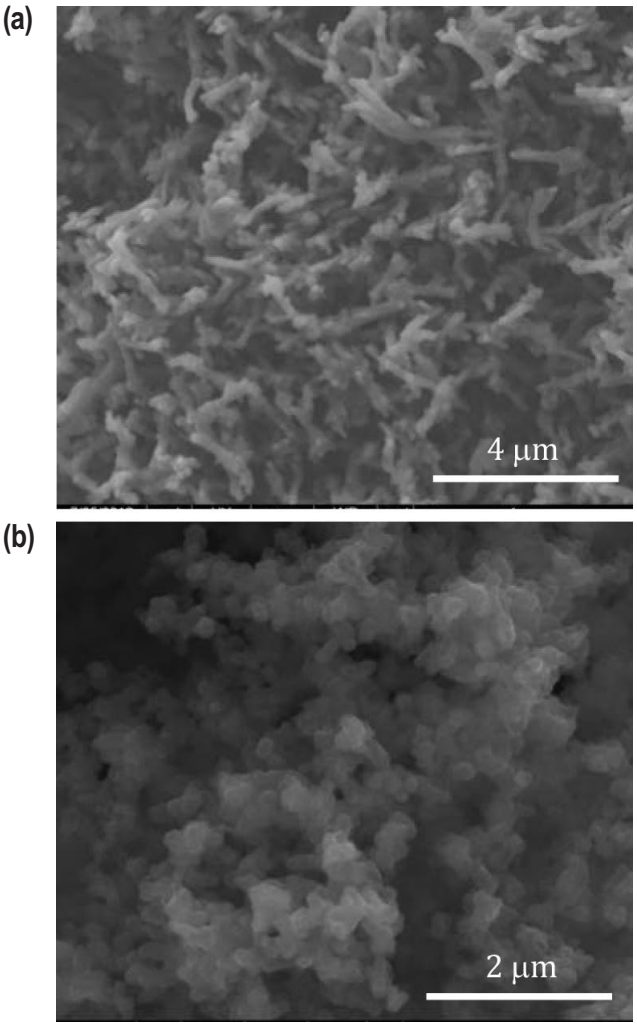

FIGURE 1. Scanning electron micrographs of PPy structures formed using templates of methylene blue combined with a) heparin and b) starch.

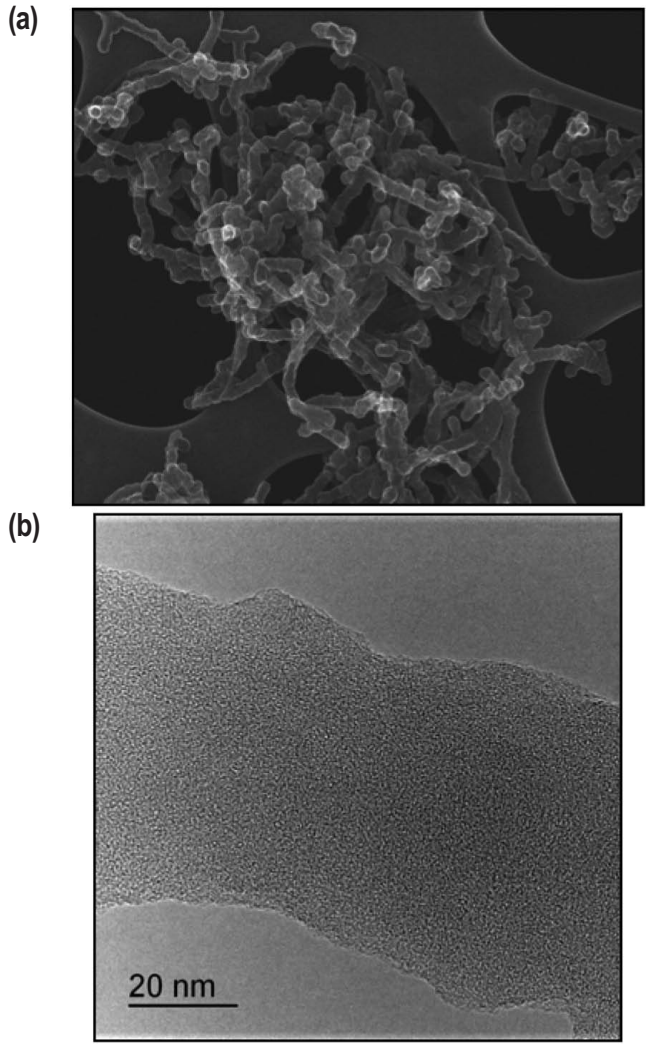

FIGURE 2. Micrographs of a) PPy nanowires (supported on a microgrid) and b) an individual PPy nanowire.

components. Further, the fibers are clearly solid (as preferred), unlike the tubes that are often obtained. To a large extent, the components are intermingled, as evidenced by the change in solution color that occurs as the methylene blue is taken up during the polymerization process.

Pyrolysis at 1,000ºC for 1 h in nitrogen or argon retains the general morphological features of the precursor, but a highly graphitic, yet convoluted, structure evolves, as seen in Figure 3a. After a pyrolysis heat treatment, about 10% (atomic) of the graphitic material remains as nitrogen. Despite the relatively modest pyrolysis temperature and the high nitrogen content, the nanowires are highly graphitic as measured by X-ray and electron beam diffraction.

The highly convoluted surface of the nanowires, evident in the Figure 3 micrographs, as well as the high nitrogen content, might be expected to provide a high density of nucleation and anchor sites for Pt catalyzation. Indeed, platinization by the polyol process provided highly dispersed Pt despite a relatively high catalyst surface loading (13.5 wt% Pt on a 70 m^2/g support). The Pt crystallites are about 2 nm by X-ray diffraction peak broadening, and the particles average about 2.2 nm by transmission electron microscope analysis and provide an electrochemical surface area of 91 m^2/g Pt (loading determined by X-ray fluorescence spectroscopy). As can be seen in Figure 3, many of the Pt particles are oriented in strings, primarily along interfaces between graphitic features.

Because of the unusual nature of the porous nanowire powders, some difficulties were encountered in formulating inks for fabricating MEAs, but the polarization and resistance curves for one with a very low 0.03 mg Pt/cm^2/electrode loading that provided good fuel cell performance and behavior are shown in Figure 4. Operation of the cell for 250 h under various operating conditions resulted in no loss of performance except for the hysteresis observed, reflecting

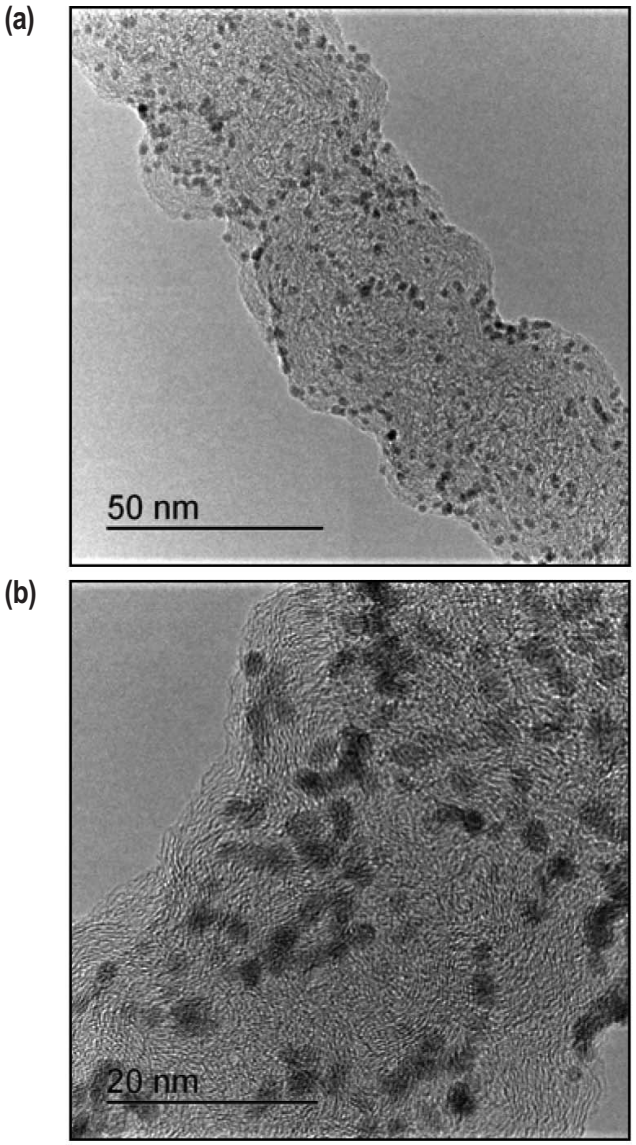

FIGURE 3. Transmission electron micrographs of pyrolyzed and platinized PPy nanowires at a) lower and b) higher magnifications.

a bit of flooding at high-current density operation. Carbon corrosion of the nanowires was not visually evident, but while the 250 h test does not constitute a very long-term carbon durability test, it is at least promising that the nitrogen-rich and convoluted nanowire surface is not unusually susceptible to corrosion.

FUTURE DIRECTIONS

Modeling

- Density functional theory modeling of nanotubes/wires:
  - Complete computations on larger Pt tubes/wires

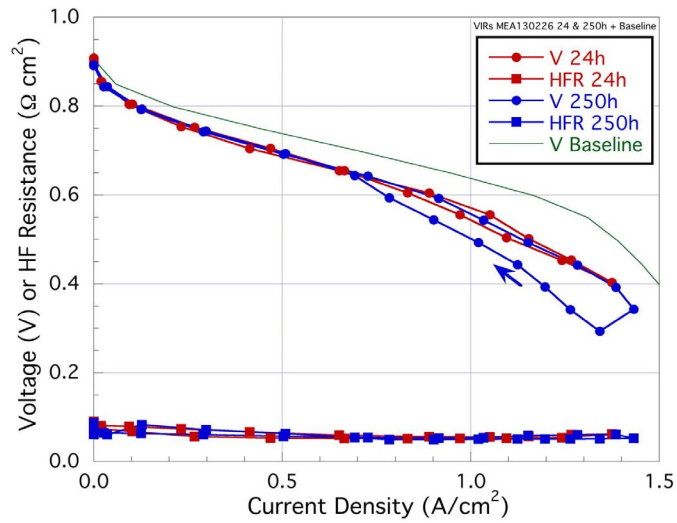

FIGURE 4. Polarization and resistance curves of a 0.03 mg Pt/cm^2/electrode fuel cell operating at 30 psig and 80˚C after 24 and 250 h of operation. Compared to a "baseline" cell (green) fabricated in a similar manner with identical membrane and gas diffusion layers but with 0.19 mg Pt/cm^2/electrode of 20 wt% Pt-C catalyst.

- Catalyst layer microstructural calculations:
  - Transient simulations
  - Incorporate water transport
  - Investigate nanowire supports

Ceria Free Radical Scavenger Additives

- Free radical and peroxide decomposition studies of doped cerias
- Fuel cell lifetime testing with differing ceria particle sizes, dopants
- Accelerated stress test studies of prime candidates

Pyrolyzed PPy Nanowire Supports

- Synthesize finer nanowires
- Characterize PPy nanowire functionality and durability
  - Tailor pyrolyzed nanowire composition
- Catalyst layer composition and processing optimization
- Comprehensive fuel cell and accelerated stress test testing
  - Synthesize large Pt-PPy batches

FY 2013 PUBLICATIONS

1. Sansiñena, J.-M.; Wilson, M.S.; Garzon, F.H., Conductive Nanostructured Materials for Supported Metal Catalysts. *ECS Transactions* **2013,** *50* (2), 1693-1699.

2. Matanovic, I.; Kent, P.R.C.; Garzon, F.H.; Henson, N.J., Theoretical Study of the Structure, Stability and Oxygen Reduction Activity of Ultrathin Platinum Nanowires. *ECS Transactions* **2013,** *50* (2), 1385-1395.

3. Matanovic, I.; Kent, P.R.C.; Garzon, F.H.; Henson, N.J., Density Functional Study of the Structure, Stability and Oxygen Reduction Activity of Ultrathin Platinum Nanowires. *Journal of the Electrochemical Society* **2013,** *160* (6), F548-F553.

4. Matanovic, I.; Kent, P.R.C.; Garzon, F.H.; Henson, N.J., Density functional theory study of oxygen reduction activity on ultrathin platinum nanotubes. *Journal Of Physical Chemistry C* **2012,** *116* (31), 16499-16510.

5. Alia, S.M.; Jensen, K.; Contreras, C.; Garzon, F.; Pivovar, B.; Yan, Y., Platinum Coated Copper Nanowires and Platinum Nanotubes as Oxygen Reduction Electrocatalysts. *ACS Catalysis* **2013,** *3* (3), 358-362.

6. Ogumi, Z.; Matsuoka, H.; Garzon, F.; Kim, H.; Wan, L.-J.; Tamao, K.; Nakamura, M., Electrochemistry 80th Anniversary Special Issue. *Electrochemistry* **2013,** *81* (3), 140-197.

FY 2013 PRESENTATIONS

1. Matanovic, I.; Garzon, F.H.; Kent, P.R.; Henson, N.J., Theoretical Study of the Structure, Stability and Oxygen Reduction Activity of Ultrathin Platinum Nanotubes. *ECS Meeting Abstracts* 2012, *1202* (13), 1563-1563.

2. Sansinena, J.-M.; Wilson, M.S.; Garzon, F.H., Conductive Nanostructured Materials for Supported Metal Catalysts. *ECS Meeting Abstracts* 2012, *1202* (13), 1688-1688.

3. Sansinena, J.-M.; Nelson, M.; Wilson, M.S.; Garzon, F., Electrochemical Synthesis of Oxygen Reduction Catalysts Based on Pt Coated Polypyrrole Nanowires Using Starch as Template Molecule. ECS Meeting Abstracts 2010, 1002 (6), 356-356.

4. Matanovic, I.; Garzon, F.; Henson, N., Theoretical Study of Electrochemical Processes on Novel Platinum Group Metal Catalysts. ECS Meeting Abstracts 2011, 1101 (41), 1894-1894.

5. Berliba-Vera, E.K.; Delariva, A.; Atanassov, P.; Datye, A.; Garzon, F., Nucleation of Platinum on Carbon Blacks. ECS Meeting Abstracts 2010, 1002 (10), 640-640.

REFERENCES

1. L. Gubler, S. Dockheer, W. Koppenol, *J. Electrochem. Soc.*, 2011, **158** (7), B755-B769.

2. L. Gubler, W. Koppenol, *J. Electrochem. Soc.*, 2012, **159** (2), B211-B218.

3. Wei, M., T. Dai, and Y. Lu, Synthetic Metals, 2010. **160**(9–10): p. 849-854.

V.A.6 Engineered Nano-Scale Ceramic Supports for PEM Fuel Cells

Eric L. Brosha (Primary Contact)[1], Lior Elbaz[1], Tommy Rockward[1], Neil J. Henson[1], Karren More[2], Aaron Roy[3], Kateryna Artyushkova[3], Alexey Serov[3], Plamen Atanassov[3], and Timothy Ward[3]
[1]Los Alamos National Laboratory (LANL)
MS D429, P.O. Box 1663
Los Alamos, NM 87545
Phone: (505) 665-4008
Email: brosha@lanl.gov

DOE Manager
Nancy Garland
Phone: (202) 586-5673
Email: Nancy.Garland@ee.doe.gov

Subcontractors:
[2]Oak Ridge National Laboratory (ORNL), Oak Ridge, TN
[3]University of New Mexico (UNM), Albuquerque, NM

Project Start Date: September 2009
Project End Date: 2013

Overall Objectives

- Develop a ceramic alternative to carbon material supports for a polymer electrolyte fuel cell cathode.
- Ceramic support replacement for carbon must:
  - Have enhanced resistance to corrosion and Pt coalescence.
  - Preserve positive attributes of carbon such as cost, surface area, and conductivity.
  - Be compatible with present membrane electrode assembly (MEA) architecture and preparation methods.
- Ceramic properties goals:
  - Surface area suitable for high fuel cell performance.
  - High Pt utilization with enhanced Pt-support interaction to resist Pt loss.
  - Adequate electronic conductivity.
  - Corrosion resistance.
  - Synthetic methods amenable to scale up.
  - Reasonable synthesis costs.

Fiscal Year (FY) 2013 Objectives

- Perform accelerated stress test (AST) ½ cell electrochemical experiments on ceramic support candidates.
- Fabricate 5-cm^2 MEAs and test in fuel cell.
- Perform fuel cell durability tests on MEAs using ceramic support on cathode.
- Validate ceramic support fuel cell AST in ½ cell and fuel cell against commercial Pt-carbon catalyst.

Technical Barriers

This project addresses the following technical barriers from the Fuel Cells section of the Fuel Cell Technologies Office Multi-Year Research, Development and Demonstration Plan:

(A) Durability: Pt sintering, corrosion loss, effects from load-cycling and high potential.

(B) Cost: Better Pt utilization balanced by cost difference of new support vs. carbon.

(C) Performance: Pt sintering, corrosion loss, and loss of electro-active surface area.

Technical Targets

- Precious metal loading (0.2 mg/cm^2)
- Cost (<$3/kW)
- Activity (0.44 A/mg_{Pt} @ 0.9 $V_{iR\text{-}free}$)
- Electrocatalysis support loss (<30 mV after 100 hrs @ 1.2 V)
- Electrochemical surface area loss (<40%)

FY 2013 Accomplishments

- Ceramic supports for proton exchange membrane fuel cell (PEMFC) cathode catalysts have been identified in this project and tested for enhanced ½-cell durability compared to commercial Pt/XC-72 catalysts.
- A novel Mo_2C support utilizing Pt nano-raft structures shows both enhanced activity and durability compared to commercially sourced Pt/XC-72 catalysts.
- Pt imbedded into/onto the support during the synthesis process makes the catalyst more durable and active for the oxygen reduction reaction (ORR) compared to catalysts prepared by post-synthesis Pt disposition.
- Fuel cell testing for durability has started in FY 2013.

- Initial performance indicates optimization of catalyst and method of MEA fabrication will require further development work.
- Initial loading levels lead to cathode microstructures that impedance analysis indicates impacting performance.
  - Obvious mass transport issues identified, and cross-over, but not loss of kinetics.
- Focus made on understanding results from first fuel cell test.
- Remainder of project will concentrate on application of AST protocols to fuel cells to validate that durability seen in ½ cell measurements carries over to fuel cell.

✧ ✧ ✧ ✧ ✧

INTRODUCTION

Development of electronically conductive ceramic materials is of fundamental importance to a wide variety of applications [1-4]. One application of particular interest is PEMFCs [5], where strong oxidizing conditions exist, especially in the cathode [6-8]. The reaction that takes place on the cathodic side of PEMFCs is the ORR which is considered to be kinetically sluggish [9] and thus, it is catalyzed, usually with platinum nano-particles [10]. Due to the high cost of such catalysts [11], and in order to maintain their optimized nano-crystallite structure, they are normally supported on a relatively cheap, electronically conductive, porous, high surface area support. Most of the electrode support materials used in fuel cells today are carbon-based [12] which are highly sensitive to corrosive conditions and thus corrode under normal fuel cell operating conditions [7]. This leads to processes that can be detrimental to the fuel cell and is manifested in the form of loss of surface area, impediment of mass transport and loss of catalyst activity due to sintering or dissolution. The direct consequence of these effects is the loss of the overall fuel cell power output overtime and shortening their lifetime; both make this technology less attractive to industry. In order to make PEMFCs more viable, it is necessary to extend their lifetime and reliability by improving the catalyst support.

New materials, which are electronically conductive and are corrosion resistant, are also important to other technologies such as metal-air batteries.

Various ceramic materials have been proposed over the years as a replacement for the commonly used carbon supports. These include titanium oxides [13], molybdenum nitride [14,15], and tungsten oxide [16]. While there are numerous studies investigating the catalytic activity of molybdenum carbide, the performance and durability of this material as a catalyst support has not been extensively studied. In this work, several support candidates have been investigated as potential non-carbon supports. In this final year for this particular project, molybdenum nitride and molybdenum carbide show promise. However, one Pt-molybdenum carbide system was identified in this work that exhibits exceptional stability and potential for high activity and performance and all of the FY 2013 work was concentrated on this non-carbon support catalyst. We propose the use of molybdenum carbide supporting Pt nano-raft structures as a possible support for catalysts for use in fuel cell cathodes.

APPROACH

At the end of FY 2012, ½-cell testing using an AST indicated that samples prepared using polymer-assisted deposition (PAD) exhibited compromised durability because of the significant amount of residual carbon remaining in the sample post synthesis. Since we showed in ½ cell characterization in FY 2012 that the Pt/Mo_2C/C exhibited activity that was actually better than commercial Pt/XC-72 catalysts of the same Pt loading, we looked at new synthetic approaches to eliminate excess C contamination in the catalyst. Two new approaches were investigated to prepare the Pt/Mo_2C. A novel catalytic synthesis of Pt/Mo_2C, from a physical mixture of precursors, led to the production of unique platinum structures: nano-rafts, containing less than six atoms of Pt on a molybdenum carbide support. The Materials Foundry of Monterrey, CA invented this particular synthetic approach. A second approach was investigated in parallel at the University of New Mexico using a novel synthesis method, which focuses on the controlled decomposition of magnesium containing precursors under syngas to yield a high surface β-Mo_2C phase. A newly developed Pt-Mo salt has been prepared by adding chloroplatinic acid hydrate to a solution of $(NH_4)_2Mg(MoO_4)_2$. A precipitate is formed from the solution by using ammonium hydroxide, which produces an insoluble salt containing platinum, magnesium, and molybdenum. The molybdenum salt is then reacted in syngas at elevated temperature producing a solid solution of Pt and β-Mo_2C as well as MgO, which serves as a sacrificial support.

RESULTS

Transmission electron microscope (TEM) was used to further characterize the Pt imbedded Mo_2C prepared by the Materials Foundry. The sample was composed of two agglomerate morphologies (1) spongy-porous and (2) sheet-like. The spongy-porous agglomerates are comprised of a 'skeleton' of nano-crystalline Mo_2C that forms interlocking flat-sheets (Figure 1a) and nanowires (Figures 1b and c) and large sheets (Figure 1d) that are thin and comprised of densely packed nano-crystalline Mo_2C. The Pt is homogenously dispersed throughout the Mo_2C support and could be seen in the high-angle annular dark field (HAADF)

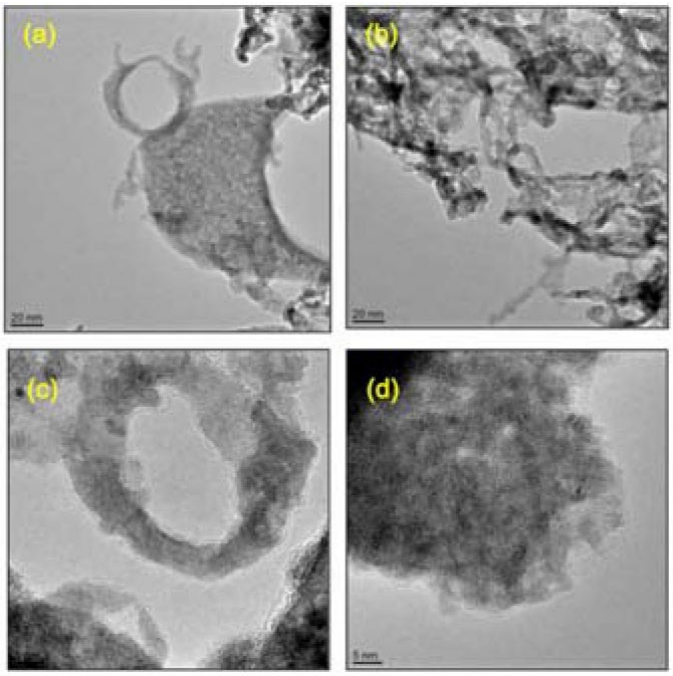

FIGURE 1. TEM images of (a) sheets of nano-crystalline Mo_2C, (b and c) nano-wires of Mo_2C, and (d) large sheets of densely packed Mo_2C.

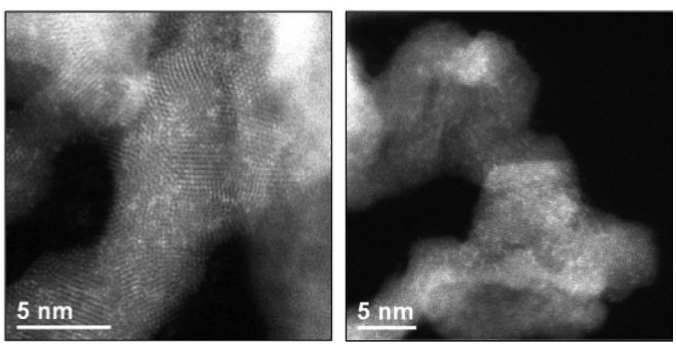

FIGURE 2. HAADF transmission electron microscopy images taken at Oak Ridge National Laboratory of Pt nano-raft structures created on Mo_2C support in situ.

scanning transmission electron microscope (STEM) image (Figure 2), where the brighter "islands" distributed on the Mo_2C surface are small clusters (nano-rafts) of Pt atoms. These nano-rafts are composed of three to six atoms of Pt. These structures are not Pt nanoparticles and are not crystalline. This supports the previous observation made using X-ray diffraction (XRD), where Pt was not detected once it was imbedded in the Mo_2C.

Suspensions of nano-rafts and a commercially available Pt/XC-72 in 0.05%$_{wt}$ Nafion® in isopropanol were prepared and 30 µl were deposited on the glassy carbon disk of an rotating ring disc electrode (RRDE) electrode and were let to dry overnight. Figure 3 shows the rotating disk electrode (RDE) results obtained with nano-rafts and Pt/XC-72 at

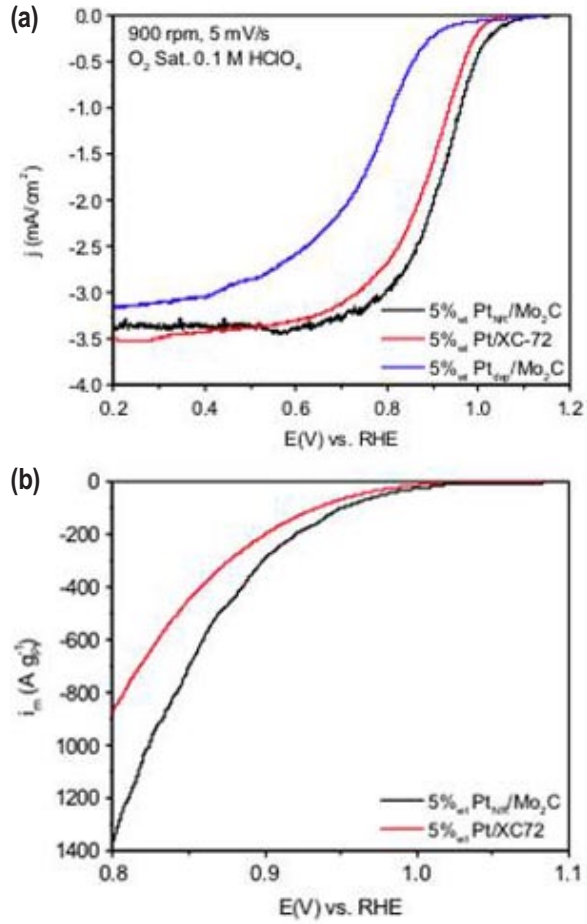

FIGURE 3. RDE electrochemical ½ cell characterization of Pt nano-raft/Mo_2C (black curve) compared to commercial Pt/XC-72 (red curve) and to Pt-Mo_2C prepared by an incipient wetness approach (blue curve).

900 rpm and 5 mV s^{-1}. From these results, the half wave potential for ORR with nano-rafts is 0.92 V vs. the reference hydrogen electrode (RHE), whereas with the carbon supported Pt, the measured half wave potential is 0.89 V vs. RHE. A difference in onset potentials was also observed and was found to be 1.11 V and 1.04 V vs. RHE for the nano-rafts and Pt/XC-72, respectively. The reaction seems to be predominantly a four-electron reduction of oxygen to water in both cases, as insignificant amounts of peroxide were formed and detected by the Pt ring on the RRDE electrode (not shown). The limiting current correlates to a 3.6 electron process according to the value obtained from the Levich equation. This is in agreement with the peroxide detected on the ring. The activity per mass unit of Pt was calculated from the RRDE data. The mass activity of the nano-rafts and Pt/XC-72 was plotted versus the potential (Figure 3b). It is apparent that the nano-rafts are superior to the commercially available platinum on carbon per mass unit as the mass activity of the nano-rafts reaches 290 A g_{Pt}^{-1} whereas the Pt/XC-72 is only 190 A g_{Pt}^{-1} at 0.9 V vs. RHE. These results can be interpreted in two ways. First, the utilization of the

Pt on in the nano-rafts is higher than on carbon, due to the simple sheet-like morphology of the rafts, which leaves all Pt atoms exposed (100% dispersion) in contrast on carbon particles form and the dispersion is generally not more than 10%. And second, the Pt in nano-rafts is chemically modified due to strong interaction with the Mo_2C. This chemical modification increases the ORR of Pt in nano-rafts relative to Pt on carbon. These are not mutually exclusive explanations, so both may play a role in the enhanced activity of Pt in nano-rafts.

In order to evaluate the Pt-ceramic support catalysts prepared in this work, a ½ cell AST was designed and shown to significantly degrade commercial Pt/XC-72 catalysts in a reasonable amount of time (e.g. <24 hrs and 5,000 cycles). This protocol proved to be a useful tool to test more durable ceramic supports as well. The AST was conducted at 23°C in de-aerated 0.1 M $HClO_4$ cycling between 0.6 V vs. RHE to 1.3 V vs. RHE in 14 s for 5,000 cycles. Figure 4 shows the results of applying this AST to Pt/C and several supports prepared in this project over the past four years. The two most durable supports are Pt nano-raft/Mo_2C and the carbon-free Mo_2N with Pt deposited onto the support post synthesis. Note that the nano-raft Pt Mo_2C is superior to the Mo_2C with Pt applied post support synthesis losing less than 10% of initial electrochemically active surface area over 5,000 cycles.

XPS analysis on the nano-raft Pt/Mo_2C sample supports the results from this durability AST experiment. The interactions of the platinum nano-rafts with the Mo_2C support were studied at UNM using X-ray photoelectron spectroscopy (XPS) and were compared to those of platinum

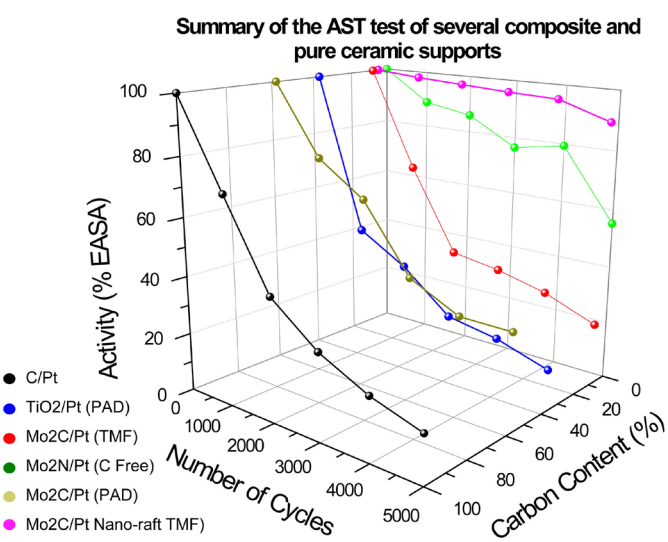

FIGURE 4. Results of the application of LANL ceramic support durability AST for: a commercial Pt/XC-72 fuel cell catalyst, PAD-prepared TiO_2/C and Mo_2C/C, Mo_2N prepared by conventional solid-state synthesis, and Pt-Mo_2C (Pt applied to support post support synthesis) and nano-raft Pt/Mo_2C prepared by The Materials Foundry.

on carbon electro-catalyst such as XC-72. Conventional Pt on C have three types of Pt present with metallic Pt being the dominant. In comparison, the Pt nano-raft Mo_2C showed no metallic Pt that is not interacting with the carbide support. There were some small amounts of oxidized Pt (approximately 18.6%) but the major species observed were Pt associated with carbon. The Mo 3d spectra showed binding energies of Mo mostly (e.g. 70%) associated with carbide indicating small amounts of surface oxidation (e.g. 30%). The Pt 4f and C 1s spectra for Pt nano-rafts on Mo_2C reveals the electronic structure of platinum is significantly impacted by the support. On Mo_2C the bond between Pt and C was found to be of a complexing type that is generally associated with organometallic compounds. These results will be presented in more detail in a publication that is currently nearing completing.

The difference in bond types between Pt on XC-72 and Pt on Mo_2C would suggest durability differences and these data are in agreement with the results from the AST experiments and Figure 4. On XC-72, 23% of the Pt is bound to a mixture of graphitic and amorphous carbon. Durability studies suggest this bond is weak and allows platinum to migrate and sinter [17]. In contrast, as confirmed by XPS, on Mo_2C there is no 'free' Pt that is not interacting with the support. Thus XPS measurements determined that Pt on Mo_2C is stabilized against sintering due to interaction between platinum and carbon in the crystalline lattice in the support.

New, larger quantity samples were provided by the The Materials Foundry to prepare electrode inks for fuel cell investigations. Standard 5-cm^2 decals were prepared using ink methods commonly employed in the preparation of fuel cells using conventional, commercial Pt/C catalysts. XL100 membranes were used and loadings were adjusted at 0.2 mg_{Pt}/cm^2 on the cathode using the Pt nano-raft Mo_2C catalyst (5 wt% Pt); excessively thick cathodes were required (areas as thick as 70–100 µm were observed in cross-section SEM analysis). Electrode thicknesses of such magnitude may induce mass transport problems. Another area of concern was that the hot pressing, decal transfer methods may not be suitable due to the hardness of the support and membrane piercing was a concern. This last concern may have been realized because several of the initial membranes quickly formed holes during initial fuel cell testing. The initial MEA exhibited crossover issues and local membrane thinning that lead to hole formation and failure. Figure 5a shows the initial results of testing the second membrane and after three consecutive 1.2 V holds for 24 hr each. Figures 5b and c show the impedance data for this fuel cell after initial break-in and after the three 24-hr 1.2 V holds. These data show that initially the charge transfer region decreased as did the voltage but after 190 hr of operation and three consecutive 24-hr voltage holds, the charge transfer region remained unchanged while the onset of mass transport became more pronounced. This indicated the electrode kinetics were

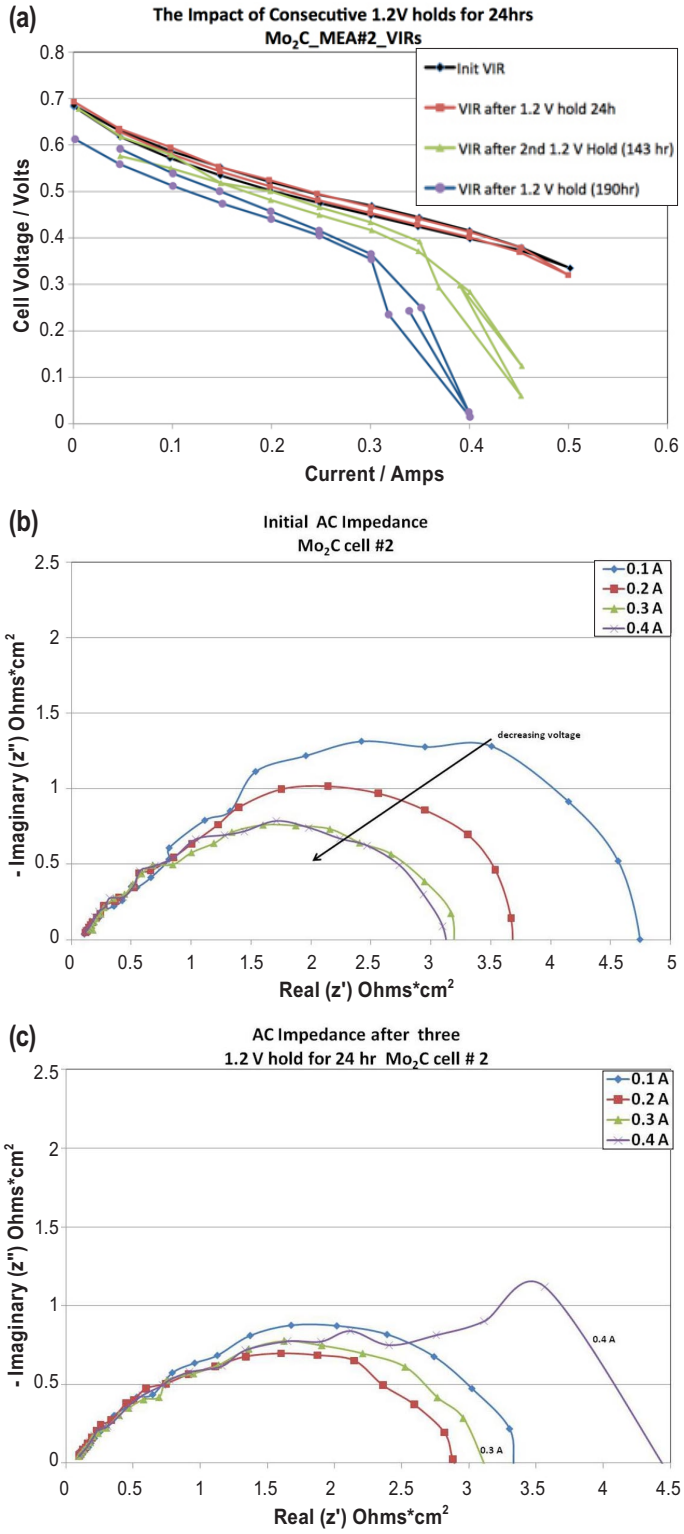

FIGURE 5. Figure 5. First fuel cell testing results using MEAs prepared with Pt/Mo_2C cathode catalyst synthesized using materials provided by The Materials Foundry. 5 cm^2; Cathode: 5% Pt/Mo_2C 0.2 mg_{Pt}/cm^2; Anode 20% Pt/XC-72 0.2 mg_{Pt}/cm^2; relative humidity 100%, 30 psig H_2/air 160/550 sccm: (a) voltage-current-resistance curves (initial, and after 1st, 2nd, and 3rd 1.2 V holds ea. 24 hours), (b) initial AC impedance response at 0.1–0.4 A, and (c) AC impedance response 0.1–0.4 A after 1st 1.2 V 24-hour hold.

stable to the voltage holds. The lower open-circuit voltage was attributed to higher hydrogen crossover consistent with evidence of membrane thinning from SEM cross-section imaging. Post mortem investigations using XRD analysis of cathode catalyst showed no evidence of Pt coalescence—in fact, no diffraction peaks associated with Pt were observed at all—however, some molybdenum oxide was evident in the XRD pattern. More fuel cell testing and optimization of the ink, Pt/Mo_2C catalyst, and study of break-in procedure optimization, and fuel cell durability testing will be required.

The new synthetic approach invented by The Materials Foundry is limited in control over support surface area, which may impact catalyst optimization. Moreover, intellectual property considerations limit information that may be shared by this company with LANL and the fuel cell community. The University of New Mexico has been working on non-carbo thermal moly carbide synthetic approaches to prepare nano-raft structures (confirmation through TEM and XPS analysis) without excess, residual carbon. Their task will enable greater scientific investigation and optimization of this unique and desirable catalyst system. One approach, using a sacrificial anode support uses a specially prepared Mg-molybdate precursor that when reacted with CO and H_2 leads to the formation of MgO and Mo_2C. The MgO serves to prevent agglomeration and sintering of the carbide and may be easily removed by an HCl etch post synthesis. Particle sizes between 25 and 100 nm have been prepared and surface areas higher than 50 m^2/g have been prepared with no excess, residual C. Several approaches to Pt incorporation have been tested and high Pt dispersions (confirmed by XRD and TEM in the near future) have been achieved. Electrochemical ½ cell and fuel cell testing have commenced at the time of this report's preparation and initial electrochemical results strongly suggest that the at least some characteristics of the nano-raft Pt structures have been prepared using these approaches however, TEM characterization at ORNL will be necessary.

Last, the computational work produced results that are supportive of the evidence of enhanced durability seen in the data above. A (100) $MoC_{0.5}$ surface model was created and a layer of Pt atoms were placed on the surface using a simple structural model. The Pt-Pt bond distance on the carbide surface was calculated to be 3.0Å and this value indicates a forced registry is taking place on the surface of the support. The Pt-Pt bond distance on a Pt/C is typically in the range of 2.80Å on a Pt(111) surface for comparison. The d-band center energy of Pt atoms on the moly carbide surface was calculated to be -2.42 eV and this value is lower when compared to -1.88 eV from recent computations performed for Pt(111) surfaces. In the remaining time for this project, we hope to calculate over-potentials and effect of support on Pt solubility. In summary, the modeling results, XPS spectra, and electrochemical characterization are all in agreement.

CONCLUSIONS

- Molybdenum carbide-carbon composite was successfully synthesized using the LANL PAD technique:
  - The resulting $MoC_{0.56}$/C was predominately composed of 1-nm crystallites of cubic phase $MoC_{0.56}$ (56.1%) and amorphous carbon (40.7%).
  - Platinum was deposited on the $MoC_{0.56}$/C and confirmed to be uniformly distributed by the small and uniform crystallite size measured with XRD.
- The Pt on $MoC_{0.56}$/C composite support showed enhanced ORR catalytic activity when compared to Pt on carbon.
- A ½-cell AST was developed and tested to ascertain effectiveness as a measure to test a Pt/ceramic support's resistance to corrosion and Pt loss:
  - AST shown to effectively kill commercial Pt/XC-72 catalysts in a reasonable amount of time (e.g. 5,000 cycles in less than 24 hours). Complete loss of ECSA in a commercial Pt/XC-72 demonstrated in 10,000 cycles.
- Presence of carbon in PAD prepared samples impacted durability and offsets benefits of enhanced activity.
- New methods were explored to prepare Pt deposited, carbon free Mo_2C catalysts that lead to discovery of unique properties of Pt nano-raft structures placed onto Mo_2C surfaces:
  - Presence of Pt nano-raft structures confimed using ORNL HAADF STEM imaging.
- The Pt nano-raft structures supported on Mo_2C show enhanced catalytic activity when compared to Pt on carbon or Pt deposited onto Mo_2C post synthesis of the ceramic support. E½ is 0.92 V vs. RHE and the onset potential is 1.11 V vs. RHE compared to 0.89 V and 1.04 V, respectively for commercial Pt/XC-72:
  - Mass activity for new Pt nano-raft/Mo_2C at 0.9 V vs. RHE is 290 A/g_{Pt} compared to 190 A/g_{Pt} for commercial Pt/XC-72.
- AST ½-cell testing performed on a Pt nano-raft/Mo_2C catalyst shows that this catalyst is significantly more durable than the commercially available Pt/XC-72 catalyst:
  - Pt/XC-72 losses approximately 90% of ECSA after 5,000 cycles compared to approximately 10% loss for Pt nano-raft/Mo_2C catalyst.
  - AST also showed that Pt nano-raft/Mo_2C is also significantly more durable than Pt/Mo_2C catalysts prepared when Pt disposition occurs post support synthesis.
  - These data indicate unique properties associated with the Pt and its interaction with the support with synthesis that forms nano-raft structures.
- XPS investigations combined with modeling results support enhanced Pt-support interactions, which was one of the objectives of the project:
  - XPS data were collected at UNM and compared to Pt/XC-72.
  - XPS data clearly shows different Pt spectra than for Pt on carbon and suggest enhanced Pt-support interaction compared to Pt/XC-72.
  - Pt binding energy is shifted to higher energies for the Mo_2C support compared to XC-72.
  - Pt on Mo_2C shows no metallic Pt that is not interacting with the support. Major Pt species associated with carbon.
- Initial fuel cell testing with nano-raft catalysts combined with fuel cell AST protocol immediately suggested stable electrode kinetics but un-optimized Pt loadings lead to overly thick cathodes that created mass transport limitations:
  - No evidence in XRD of Pt coalescence and particle growth post AST.

FUTURE DIRECTIONS

- Understand source of activity and origin of enhanced durability of the Pt nano-raft structures.
- Optimize ink and method of the MEA preparation.
- In conjunction with increased fuel cell testing activity, improve initial performance and perform more durability testing.
- Scale up of batch size and optimization of support surface area.
- Correlate studies of ½ cell, fuel cell, and XPS results with increase number of samples and optimize Pt loading.
- Scale up for Pt nano-raft/Mo_2C catalysts produced numerous samples with varying activity, surface properties. Correlate activity data to surface properties.
- Understand degradation mechanisms through durability testing/bulk quantities and recovery of fuel cell materials.

COLLABORATION AND COORDINATION WITH OTHER INSTITUTIONS

- Los Alamos National Laboratory (LANL)
- Oak Ridge National Laboratory (ORNL)

- University of New Mexico (UNM)
- The Materials Foundry (TMF)

FY 2013 PUBLICATIONS/PRESENTATIONS

1. K. Blackmore, L. Elbaz, E. Brosha, A. Burrell, and T.M. McCleskey, "Nano-scale Titania Ceramic Supports for PEM Fuel Cells," *J. Mater. Res.* **27** no. 15 (2012).

2. L. Elbaz, C. Kreller, N. Henson and E.L. Brosha, "Molybdenum Carbide-Carbon Composite Support for Oxygen Reduction Catalysts", submitted to the Journal of Power Sources.

3. L. Elbaz and E.L. Brosha, "Accelerated Stress Tests in Half-Cell for Catalysts Supports for Polymer-Electrolyte-Membrane Fuel Cells", in preparation.

4. L. Elbaz, K. More, K. Artyushkova, N. Henson, Jonathan Phillips and E. L. Brosha, "Evidence of Enhanced Electrocatalytic Activity of Molybdenum Carbide Supported Platinun Nano-Rafts", in preparation.

5. A. Roy, A. Serov, E. Brosha, P. Atanassov, and T. Ward, "Synthesis and Characterization of High Surface Area Mo_2N as a Durable Support for Electrocatalysts, in preparation, *Am. Chem. Soc., Div. Energy Fuels*, 2013.

6. A. Roy, U. Martinez, P. Atanassov, E. Brosha, and T. Ward, "Highly Dispersed Pt on Mo2C: Durable Catalyst for Oxygen Reduction Reaction," 224th Meeting of the ECS, San Francisco, CA, October 2013.

7. L. Elbaz and E.L. Brosha," Development of Ceramic Supports for Polymer Membrane-Electrolyte Fuel Cells," Electrochemistry Israel, Ben Ilam University, June 2013.

8. L. Elbaz, J. Phillips, N. Henson, and E. Brosha, "Molybdenum Carbide as Support for Platinum Catalysts for Oxygen Reduction in Fuel Cells," PRIME 222nd Meeting of the Electrochemical Society, Honolulu, HI, October, 2012.

9. M. Sykora, A. Mueller, C. Kreller, E. Brosha, and F. Garzon, "Synthesis and Characterization of Molybdenum Nitride for Electrosynthesis Applications" PRIME 222nd Meeting of the Electrochemical Society, Honolulu, HI, October, 2012.

10. L. Elbaz, T. Rockward, N.J. Henson, K. Artyushkova, K. More, J. Phillips, and E.L. Brosha," Evidence of Enhanced Activity on In-situ Formed Pt Nano-rafts on Molybdenum Carbide Support," 224th Meeting of the ECS, October 2013.

REFERENCES

1. Buessem, W.R. *Miner. Ind., Pa. State Univ.***1967**, *36*, 1.

2. Cihlar, J.; Trunec, M. *Sklar Keram.***2006**, *56*, 327.

3. Herrmann, R. *CFI, Ceram. Forum Int.***2010**, *87*, E15.

4. Tong, J.; O'Hayre, R.; John Wiley & Sons Ltd.: 2011, p 169.

5. Armstrong, K.J.; Elbaz, L.; Bauer, E.; Burrell, A.K.; McCleskey, T.M.; Brosha, E.L. *J. Mater. Res.***2012**, *27*, 2046.

6. Chizawa, H.; Ogami, Y.; Naka, H.; Matsunaga, A.; Aoki, N.; Aoki, T.; Tanaka, K. *ECS Trans.***2007**, *11*, 981.

7. Linse, N.; Scherer, G.G.; Wokaun, A.; Gubler, L. *J Power Sources***2012**, *219*, 240.

8. Shao, Y.; Wang, J.; Kou, R.; Engelhard, M.; Liu, J.; Wang, Y.; Lin, Y. *Electrochim Acta***2009**, *54*, 3109.

9. Yuan, X.; Xia, X.; Zeng, X.; Zhang, H.; Ma, Z. *Huaxue Jinzhan***2010**, *22*, 19.

10. Gottesfeld, S. *ECS Trans.***2008**, *6*, 51.

11. Sun, Y.; Delucchi, M.; Ogden, J. *Int. J. Hydrogen Energy***2011**, *36*, 11116.

12. Antolini, E. *Appl. Catal., B***2009**, *88*, 1.

13. Blackmore, K.J.; Bauer, E.; Elbaz, L.; Brosha, E.L.; McCleskey, T.M.; Burrell, A.K. *ECS Trans.***2011**, *30*, 83.

14. Blackmore, K.J.; Elbaz, L.; Bauer, E.; Brosha, E.L.; More, K.; McCleskey, T.M.; Burrell, A.K. *Journal of the Electrochemical Society***2011**, *158*, B1255.

15. Hobbs, B.S.; Tseung, A.C.C. *Nature***1969**, *222*, 556.

16. Alexander, A.M.; Hargreaves, J.S. *Chem Soc Rev* **2010**, *39*, 4388.

17. Patel, A.; Artyushkova, K.; Atanassov, P.; Colbow, V.; Dutta, M.; Harvey, D.; Wessel, S. *Journal of Vacuum Science & Technology A* **2012**, *30*.

V.A.7 Tungsten Oxide and Heteropoly Acid-Based Systems for Ultra-High Activity and Stability of Pt Catalysts in PEM Fuel Cell Cathodes

John Turner (Primary Contact), Jason Zack, Katherine Hurst, Kelly Mason, Virginia Anderson, KC Neyerlin, Anne Dillon, Bryan Pivovar, and Shyam Kocha
National Renewable Energy Laboratory (NREL)
15013 Denver West Pkwy
Golden, CO 80401
Phone: (303) 275-4270
Email: John.Turner@nrel.gov

DOE Manager
Kathi Epping Martin
Phone: (202) 586-7425
Email: Kathi.Epping@ee.doe.gov

Subcontractors:
- University of Colorado Boulder (UC-Boulder), Boulder, CO
- Colorado School of Mines (CSM), Golden, CO

Project Start Date: May 2010
Project End Date: April 2014

Overall Objectives

Improve electrocatalyst and membrane electrode assembly (MEA) durability and activity through the use of Pt/WO_X (tungsten oxide) and Pt/HPA-C (heteropoly acid) modifications to approach automotive proton exchange membrane (PEM) fuel cell activity targets (0.44 mA/mg Pt) and durability targets (5,000 h/10 y).

- Optimize Pt anchoring to support:
  - To suppress loss in Pt electrochemical area (ECA) under start-stop and load cycling operations
  - Enhance electrocatalytic activity
- To demonstrate lower support corrosion:
  - Suppress Pt agglomeration/electrode degradation
  - Increase durability under automotive start-up/shut-down operation

Fiscal Year (FY) 2013 Objectives

- Determine viability of scaling up hot-wire chemical vapor deposition (HWCVD) WOx synthesis and atomic layer deposition (ALD) of Pt to gram quantities
- Optimize the Pt in WOx system and make a Go/No-Go decision based on its performance vs. PtC

Technical Barriers

This project addresses the following technical barriers from the Fuel Cells section of the Fuel Cell Technologies Office Multi-Year Research, Development, and Demonstration Plan:

(A) Durability

(B) Cost

(C) Performance

Technical Targets

This project addresses the activity and durability of Pt-supported catalysts in automotive applications during start-up and shut-down. This regime is where corrosion and electrode degradation take place in PEM fuel cells and can ultimately limit the lifetime. Our target is to synthesize alternative supports such as WO_X and HPA-functionalized carbon blacks and to evaluate them for improved corrosion resistance while maintaining or improving activity in comparison to conventional Pt/C supports. Studies are first being conducted in rotating disk electrode (RDE) setups due to the small quantity of materials synthesized and will be followed by testing in fuel cells. The following targets are being addressed:

- Mass activity: >275 mA/mg_{Pt}
- Durability under start-up/shut-down cycling: ECA loss <40%

FY 2013 Accomplishments

- Synthesized well-distributed and high-wt% Pt/WO_X using ALD for Pt and HWCVD for tungsten oxide.
- Scaled up WO_X preparation to gram levels for ALD platinum deposition.
- Deposited ALD Pt/WO_X (UC-Boulder) that was scaled up to g quantity. However, mass activity of scaled-up ALD Pt/WO_X was low.
- Prepared Pt colloids (CSM) that were subsequently deposited on HPA-functionalized carbons. These were scaled up to generate 1 g quantity.
- Obtained gram quantities of Pt/SnO_2 from a commercial catalyst supplier (TKK), and evaluated Pt/SnO_2 in RDE with and without Nafion®.
- Prepared Pt/SnO_2 catalyst-coated membranes and began subscale testing.

- Studied alternative support materials for conductivity and corrosion resistance.
- Performed a subscale test run comparing Pt/C MEA to a Pt/HPA-C MEA.

✧ ✧ ✧ ✧ ✧

INTRODUCTION

Start-up and shut-down operations in automotive fuel cells can cause significant degradation in conventional Pt/C nanoparticle electrocatalysts. Potentials at the cathode approaching ~1.6 V for short times lead to carbon corrosion and subsequent loss of Pt activity. For this project we are evaluating alternative supports for Pt for greater stability and corrosion resistance than conventional carbon blacks. These alternative supports could allow the fuel cell system balance of plant to be simplified, lowering the costs while simultaneously increasing the durability and leading to a more commercially viable product.

APPROACH

Oxide supports such as WO_X are grown using a HWCVD method, and then ALD or wet-chemistry is used to deposit Pt nanoparticles on the support. These oxide supports are inherently more stable than carbon blacks but have drawbacks in terms of lower surface area and lower electronic conductivity as compared to carbon blacks. Therefore, the electronic conductivity and the electrochemical activity as a function of adding small quantities of highly graphitized carbon blacks/fibers are being studied. The added graphitized carbon is not susceptible to corrosion because the Pt nanoparticles have a closer interaction with the WO_X or HPA-C. Durability cycling protocols that simulate start-up/shut-down were developed to quantify the suppression of degradation with the alternative corrosion resistant supports.

RESULTS

Synthesis

HPA functionalization of carbon was carried out to: i) shield carbon against corrosion; ii) stabilize nano-metallic particles; iii) decompose peroxide; iv) alter electrochemistry on the Pt surface; and v) conduct protons. These functionalized carbons were used as supports for depositing Pt nanoparticles that were synthesized using a colloidal preparation. A literature recipe [1] was modified significantly to synthesize small controlled Pt nanoparticles with controlled sizes by: decreasing the temperature to 80°C; bubbling dilute CO into solution; and gradually adding 0.25 M NaOH over 3 h. This method was used to scale up the catalyst synthesis to g quantities in order to prepare MEAs for testing in subscale fuel cells. Transmission electron microscopy (TEM) and scanning transmission electron microscopy (STEM) images of the synthesized catalysts are shown in Figure 1. Pt/WO_X was scaled up to g quantities using ALD deposition on HWCVD WO_X. Figure 2 illustrates the NREL Rotary ALD system for uniform scalable Pt deposition on WO_X powders.

Conductivity and Corrosion Measurements

Conductivity and corrosion measurements were carried out on non-carbon support materials that showed promise as a substitute for the conventional carbon blacks. Conductivity measurements were carried out in an in-house experimental setup that consisted of Au-coated Cu plates. The density and conductivity of various support materials as well as supports mixed with various amounts of a graphitized carbon were determined at various loads and were reported previously.

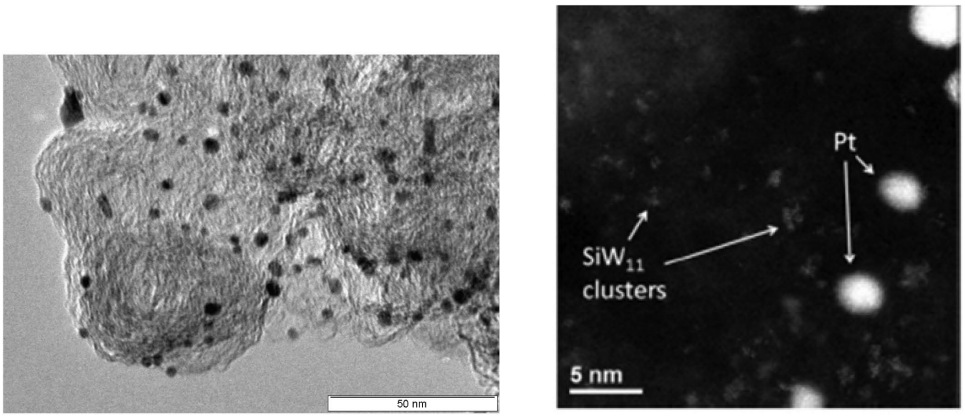

FIGURE 1. TEM and Z-contrast STEM image of Pt/SiW_{11}-C showing spatial distribution of Pt (~3–5 nm bright white spots) and SiW_{11} (~1 nm dull gray spots). Catalysts synthesized by wet-chemistry from Pt precursors and HPA-functionalized carbon black.

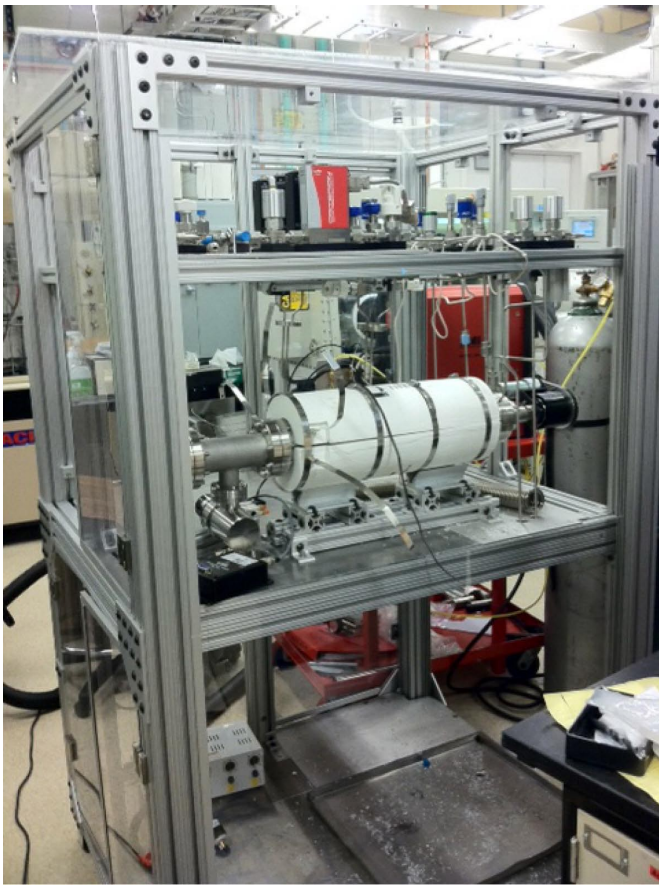

FIGURE 2. NREL Rotary ALD system for uniform scalable Pt deposition on WO_x powders.

The challenges that result from the lower conductivity of alternative supports are illustrated in Figure 3.

Corrosion of Supports

Corrosion studies were carried out in RDE cells, and the working electrodes were subjected to high anodic potentials to estimate the onset of corrosion currents. Figure 4 (a and b) depicts the conductivity and corrosion currents for the support materials that were evaluated. TiO_2, TaC, and WO_3 showed the highest corrosion resistances, while TiC had the lowest corrosion resistance.

Durability Protocols

Durability protocols were established for evaluating the corrosion resistance of alternate supports in collaboration with the DOE Durability Working Group [2]. Figure 5 depicts the durability protocol that simulated start-stop degradation in the voltage range 1–1.6 V. The measurements are designed to be conducted at room temperature and atmospheric pressure in RDE setups.

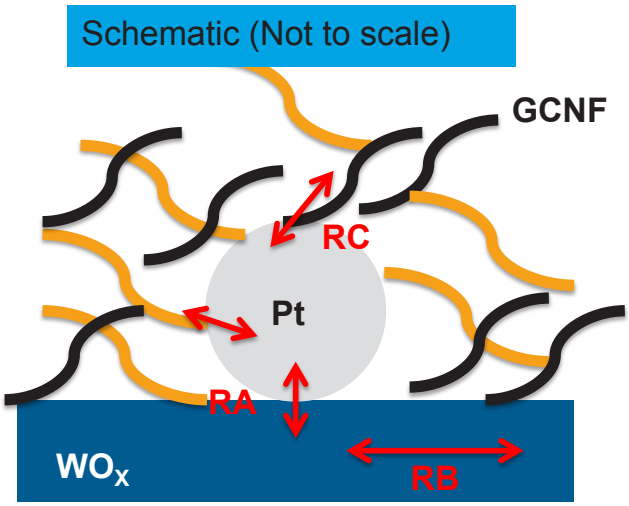

FIGURE 3. Illustration of the challenges that result from the lower conductivity of alternative supports. Shown are the electron pathways that impact conductivity. Contact point between Pt and support: RA. Electronic conductivity through the support: RB. Electronic conductivity through the added carbon matrix: RC. Coating of Nafion® ionomer on Pt and WO_x and C not shown: (RNafion). Addition of carbon matrix such as graphitized carbon black nano-fibers (GCNFs) enhances the overall conductivity, but does not address RA and RB.

Electrochemical Characterization

Pt Black-WO_x Mixtures: We completed a study that evaluated Pt black mixed with various amounts of a graphitized carbon black nano-fiber (GCNF). For very thin films (low loadings) with the addition of carbon black, it was possible to meet the baseline Pt/C oxygen reduction reaction activity values. The results verify that electronic conductivity issues will be encountered when WO_x or other low conductivity, corrosion-resistant oxide supports are used. Utilizing the established DOE protocols, durability tests of these materials with and without the addition of GCNF were also conducted and the results are summarized in Figure 6. The mixed Pt black-GCNF materials show activity and durability that are better than that of the conventional Pt/C baseline materials from TKK.

Pt/WO_x: The mass activity of ALD-deposited Pt/WO_x improved to ~175 mA/mg when measured in RDE half-cells (Figure 7). This activity is a significant improvement but falls short of the activity of baseline Pt/C. Pt/WO_x was scaled up to g quantities using ALD deposition on HWD WO_x; however, the scaled-up Pt/WO_x-C did not show these improvements. The lower activity of Pt/WO_x is primarily due to the low electronic conductivity of the WO_x as seen by the doubling in activity with the addition of 50 wt% carbon black. Based on these results, further work on Pt/WO_x has been given a No-Go and alternative paths are being pursued.

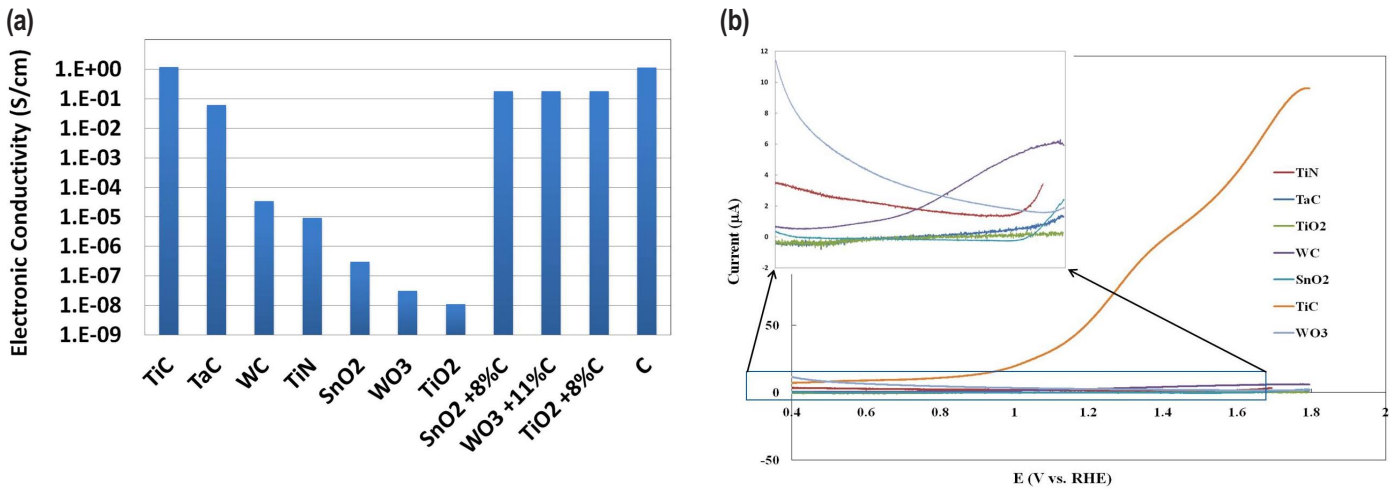

FIGURE 4. a) Conductivity of alternative supports. b) Corrosion currents (corrected) of alternative support materials. Gold disk used.

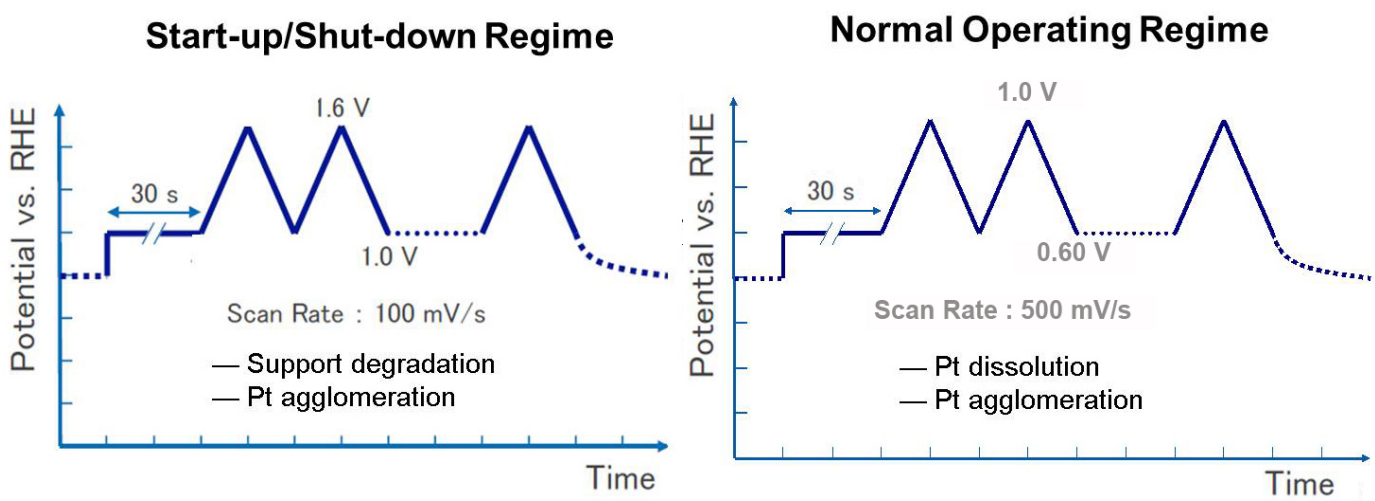

FIGURE 5. Durability protocols simulating start-stop degradation in the voltage range 1–1.6 V as well as the normal operating regime.

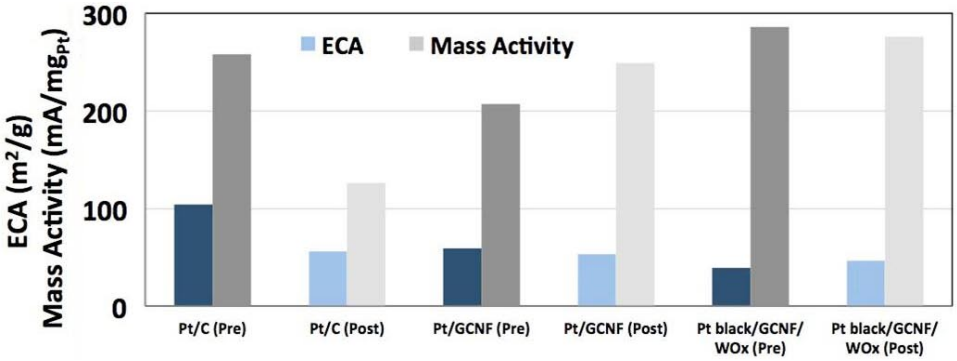

FIGURE 6. Durability comparisons for Pt black + GCNF + WO_X systems. Pt and GCNF from TKK, WO_X from NREL (1.0–1.6 V protocol).

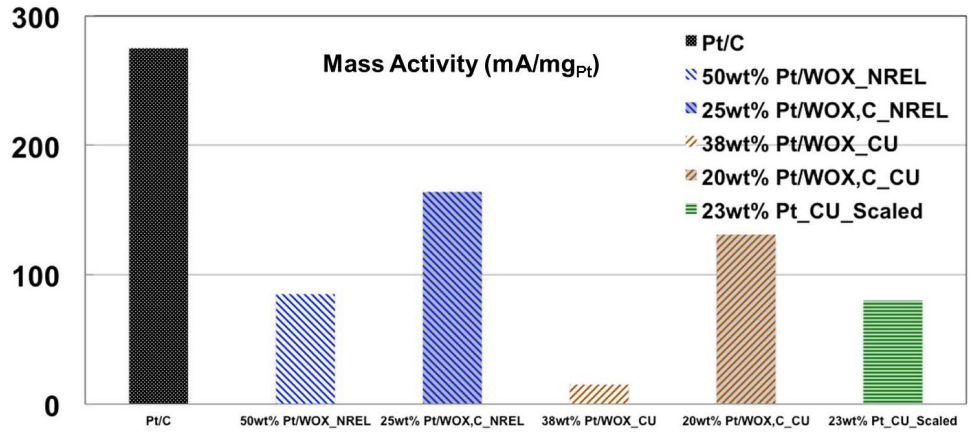

FIGURE 7. Mass activity of Pt/WO_x synthesized using various techniques measured in RDE half-cells.

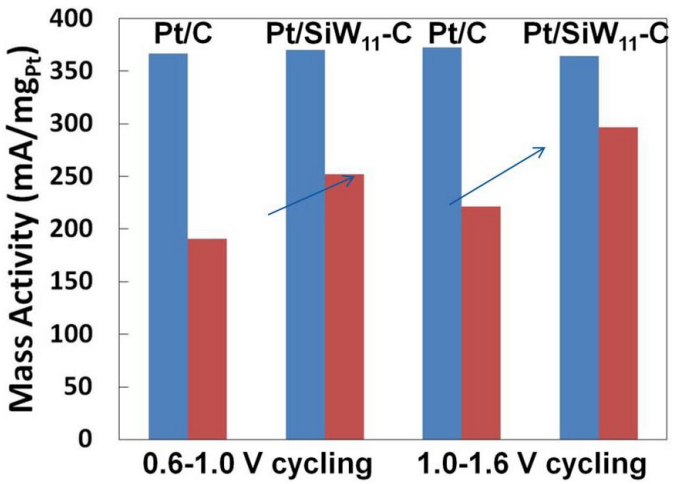

FIGURE 8. Durability results for Pt/HPA-C conducted using previously developed protocols. HPA loading was chosen such that initial activity was near equal to that of Pt/C. (0.6–1.0 V cycling, 30,000 cycles, 500 mV/s; 1.0–1.6 V cycling, 6,000 cycles, 100 mV/s)

Pt/HPA-C: Durability results on Pt/HPA-C were conducted using the previously developed DOE protocols. Results of durability tests are shown in Figure 8. The 0.6–1.0 V cycling (30,000 cycles, 500 mV/s) was used to evaluate Pt dissolution, while 1.0–1.6 V cycling (6,000 cycles, 100 mV/s) was used to evaluate support corrosion. HPA loading was chosen such that initial activity was nearly equal to that of Pt/C. In both cases, HPA helped maintain catalyst activity by slowing particle growth. MEAs were also prepared with scaled-up catalyst and tested in subscale fuel cells for initial activity.

Pt/SnO_2: The performance of a Pt/SnO_2 electrocatalyst produced by a commercial catalyst manufacturer (TKK) was evaluated in RDE studies. For this catalyst, with the addition of a graphitized carbon black to enhance conductivity, values close to the benchmark Pt/C activity of 275 mA/mg_{Pt} were achieved. These activities were found to be even higher for ink formulations that were Nafion®-free. The catalyst was spray-coated onto Nafion® membranes and evaluated in subscale fuel cells. Initial results were lower than what we found in RDE studies, and ink optimization and modification will be necessary to achieve higher activity values in fuel cells.

CONCLUSIONS AND FUTURE DIRECTIONS

The following conclusions summarize the work conducted in FY 2013:

- Pt/WO_x was scaled up to gram quantities using the ALD technique and evaluated for activity in RDE setups.
- Pt/HPA-C was synthesized in larger quantities and spray-coated onto a membrane to form MEAs that were tested in subscale fuel cells.
- Pt/HPA-various carbon blacks were synthesized in larger quantities and evaluated for activity in RDE setups.
- Pt/SnO_2 was obtained in larger quantities and spray-coated onto a membrane to form MEAs that were tested in subscale fuel cells.
- Various alternative supports were evaluated for conductivity and corrosion resistance.
- Pt was deposited onto TiN support and electrochemically characterized in RDE half-cells

Due to the low electronic conductivity of WO_x and consequent low activity of Pt/WO_x catalysts, no further work will be conducted in this area. Future work will use alternative nitride and carbide supports as well as the HPA-modified graphitized carbons in an attempt to meet the DOE targets.

FY 2013 PUBLICATIONS/PRESENTATIONS

1. Kocha, S.S., et al. "Influence of Ink Composition on the Electrochemical Properties of Pt/C Electrocatalysts." Presentation at the Fall ECS Meeting, Honolulu, HI, 2012.

2. Kocha, S.S., et al. "Influence of Ink Composition on the Electrochemical Properties of Pt/C Electrocatalysts." *ECS Transactions* 50.2 (2013): 1475-1485.

3. Kocha, S.; Garsany, Y.; Myers, D. "Testing Oxygen Reduction Reaction Activity with the Rotating Disc Electrode Technique." Webinar, March 12, 2013. http://www1.eere.energy.gov/hydrogenandfuelcells/pdfs/webinarslides_rde_technique_031213.pdf.

4. Mason, K.S.; Neyerlin, K.; Kuo, M.; Horning, K.; Kocha, S.S.; Turner, J.A.; Herring, A. "Durability Enhancement of Pt/C Catalysts via Support Functionalization with Silicotungstic Acid." Poster presentation at the 222nd ECS Meeting, Honolulu, HI, October 2012.

5. Hurst, K.; Parilla, P.; Kocha, S.; Zack, J.; Neyerlin, K.C.; Turner, J. "Tungsten oxide nanowire supports for PEM cathode catalysts." Presentation at the Spring MRS Meeting, San Francisco, CA, April 3, 2013.

REFERENCES

1. Wang, Y.; Ren, J.; Deng, K.; Gui, L.; Tang, Y. *Chem. Mater.* **2000**, *12*, 1622.

2. Kocha, S.; Myers, D.; Borup, R. *Accelerated stress tests for oxide supports*, DOE-EERE Durability Working Group Meeting, Boston, MA, 2011.

V.A.8 Synthesis and Characterization of Mixed-Conducting Corrosion Resistant Oxide Supports

Vijay K. Ramani (Primary Contact), Jai Prakash
Illinois Institute of Technology (IIT)
10 W 33rd Street 127
Chicago, IL 60616
Phone: (312) 567-3064
Email: ramani@iit.edu

DOE Managers
Kathi Epping Martin
Phone: (202) 586-7425
Email: Kathi.Epping@ee.doe.gov
Gregory Kleen
Phone: (720) 356-1672
Email: Gregory.Kleen@go.doe.gov

Contract Number: DE-EE0000461

Subcontractors:
Nissan Technical Center, North America (NTCNA)
Farmington Hills, MI

Project Start Date: September 1, 2010
Project End Date: December 31, 2013

Overall Objectives

- <40% electrochemical area (ECA) loss in electrocatalysts using the synthesized supports tested per the General Motors (GM) protocol.
- <30 mV electrocatalyst support loss in the synthesized supports after 100 h at 1.2 mV; tested using the GM protocol.
- These targets are taken from the 2007 Multi-Year Research, Development, and Demonstration Plan.

Fiscal Year (FY) 2013 Objectives

- Evaluate the suitability of titanium dioxide-ruthenium dioxide (RTO), indium tin oxide (ITO) and zirconium-doped indium oxide (ZIO) (mixed metal oxides) as conducting catalyst supports for proton exchange membrane fuel cells (PEMFCs).
- Optimize the Pt deposition method on the above catalyst supports to improve PEM fuel cell performance and durability.
- Demonstrate the performance and durability (under start-stop and load cycling protocols) of Pt deposited on RTO, ITO in a PEMFC.
- Prepare a preliminary cost model for new supports.

Technical Barriers

This project addresses the following technical barriers from the Fuel Cells section of the Fuel Cell Technologies Office Multi-Year Research, Development, and Demonstration Plan:

(A) Durability

Technical Targets

The specific technical targets that we were trying to address during this year in this project were the following:

- Synthesis of non-carbon catalysts supports and Pt catalysts (supported on those supports) that lead to less than 40% ECA loss during potential cycling following the GM protocol.
- Synthesis of non-carbon supports that result in less than 30 mV polarization losses after 100 h at 1.2 V (tested per the GM protocol).
- These targets were taken from the 2007 Multi-Year Research, Development, and Demonstration Plan.

FY 2013 Accomplishments

- We have demonstrated that ITO synthesized using the co-precipitation method possessed the following properties: 1) high electrical conductivity (1-3 S/cm); 2) better electrochemical stability than carbon; and 3) better catalyst stability than Pt/C catalysts when subject to potential cycling (10,000 cycles from 0.6 to 0.95 V).
- ITO was also synthesized using two other strategies (epoxide initiator and supercritical CO_2 methods) in order to get materials with higher surface area, and both showed similar electrochemical stability as ITO synthesized using the co-precipitation method.
- ZIOs have shown better electrochemical stability than carbon (start-stop stability test). The conductivity (around 0.1 S/cm) and Brunauer-Emmett-Teller (BET) surface area were still low but efforts are in progress to improve these properties.
- A cost model for RTO supports has been developed and their durability benefits have been considered.

✧ ✧ ✧ ✧ ✧

INTRODUCTION

In recent years, fuel cells have been demonstrated as feasible devices to convert chemical energy to electrical energy with high power density, high efficiency, and zero carbon dioxide emissions. However, one of the main issues delaying its commercialization is the durability of the electrocatalysts. The commercial carbon black currently used as support material for the Pt in the electrocatalyst can undergo corrosion under fuel cell operational conditions [1]:

$C+2H_2O \rightarrow CO_2+4H^+ +4e^-$ E_o^0= 0.207 V vs. standard hydrogen electrode

This thermodynamically favorable reaction is very slow under normal operating conditions but can be accelerated during voltage transients occurring during start-stop and fuel starvation. This causes reverse currents in the fuel cell, which drives the potential at the cathode to as high as 1.5 volts [2,3]. The irreversible carbon corrosion leads to the aggregation of Pt, which results in a loss of electrochemical active surface area (ECSA). This contributes to significant and irreversible losses in fuel cell performance. This is a critical factor in delaying the adoption of fuel cell technologies by the automobile industry. In order to overcome these obstacles, it is necessary to replace the carbon support with a high electronic conductivity, high surface area, porous material, with high corrosion resistance under fuel cell operating conditions. In this project, we are working on the synthesis and characterization of the electrochemical stability of non-carbon supports.

APPROACH

To solve the problems discussed in the previous section, we have synthesized and evaluated two kinds of non-carbon supports. The first was ITO which possesses good electrical conductivity for a PEMFC catalyst support. We have used three methods to synthesize high surface area and electrochemically stable ITO: co-precipitation, epoxide initiator, and supercritical CO_2 drying methods. Each support was evaluated for electrochemical stability using start-stop transient (cycling from 1 to 1.5 volts at 0.5 V/s for 10,000 cycles) protocols. Pt was deposited onto the supports that showed good stability during start-stop cycling protocol. Start-stop protocol and load cycling protocol (changing the electrode potential using a rectanglular wave between 0.6 and 0.95 volts with a hold of 3 seconds at each potential for 10,000 cycles) were used to examine the stability of the catalyzed supports. The second non-carbon support evaluated during this year was ZIO. So far, the biggest criticism for metal oxide-based supports is the cost of the material compared to conventional carbon support, which is very inexpensive. To address this concern, a cost model for RTO was developed. NTCNA has prepared a preliminary cost model for these non-carbon support materials considering their durability benefits.

RESULTS

ITO was synthesized using three different procedures: co-precipitation, supercritical CO_2, and epoxide initiator methods. Those methods were intentionally selected to get metal oxides with high surface area, a key characteristic needed for a catalyst support when depositing Pt onto it. The electrical conductivity and BET surface areas are shown in Table 1.

The pseudo capacitance loss for ITO prepared by these three different methods was less than 10% over 10,000 cycles compared with the 230% change observed for Vulcan XC-72 carbon. These results (see Figure 1) are promising and suggest that ITO is a very resistant and durable catalyst support and does not degrade during start-up/shut-down transients in PEMFCs. Catalyst stability for 40% Pt/ITO (co-precipitation) was also evaluated following the same protocol (1.0 to 1.5 V potential cycling). The loss in the ECSA was less than 20% after 10,000 cycles, whereas it was 40% for commercial Pt/C (Tanaka 46% Pt) after the same number of cycles (see Figure 2a). The Pt/ITO was also tested using load cycling protocol (0.6 to 0.95 V) and this result showed similar loss in the ECSA to commercial Pt/C (Tanaka, 46%) after 10,000 cycles (Figure 2b).

ZIOs were synthesized by co-precipitation, using silica-templates, and epoxide initiator methods. The materials were annealed at 400 or 800°C in air for three hours to allow zirconium atoms to dope the indium oxide lattice. The BET surface area and electronic conductivity of zirconium doped indium oxide were 40-50 m^2/g and around 0.1 S/cm (see Table 2). The BET surface areas are still low but we are currently working to improve the surface area of the materials by making them into aerogels (alcogels dried using supercritical CO_2 to maintain the porous structure). Figure 3 shows the results of the stability test for the supports subjected to start-stop protocol and its comparison with Vulcan carbon, zirconium indium oxide, 10% ZrO_2 and 90% In_2O_3 by molar ratio, annealed at 800°C (ZIO [1:9 mol]/800°C/co-precipitation) was the most stable among the materials assayed.

TABLE 1. Properties of ITO Catalyst Supports

	Vulcan XC-72	Commercial ITO	ITO 1 co-precipitation	ITO 2 supercritical drying	ITO 3 epoxide initiator
BET (m^2/g)	207 ± 4	30 ± 2	45 ± 2	72 ± 2	41 ± 1
Conductivity (S/cm)	31 ± 5	0.6 ± 0.1	1.3 ± 0.1	1.2 ± 0.1	1.9 ± 0.1

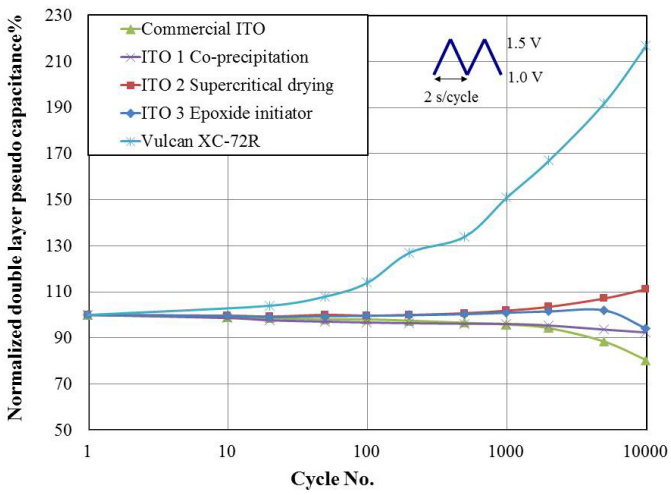

FIGURE 1. Electrochemical stability under start-stop cycling protocol for ITO catalyst supports.

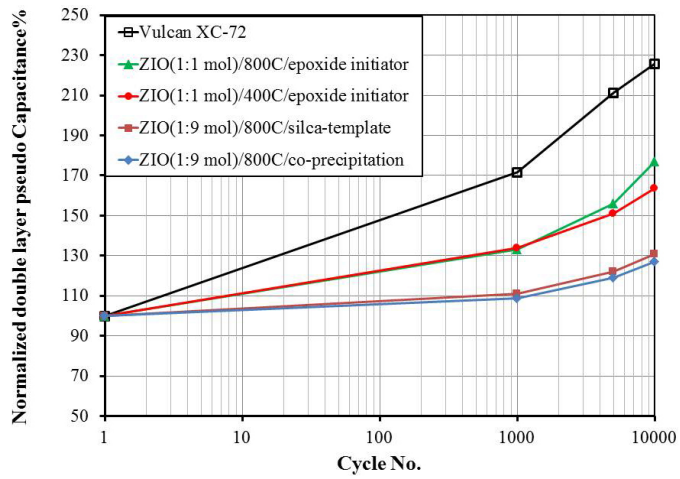

FIGURE 3. Electrochemical stability under start-stop cycling protocol for ZrO_2-In_2O_3 mixed oxides.

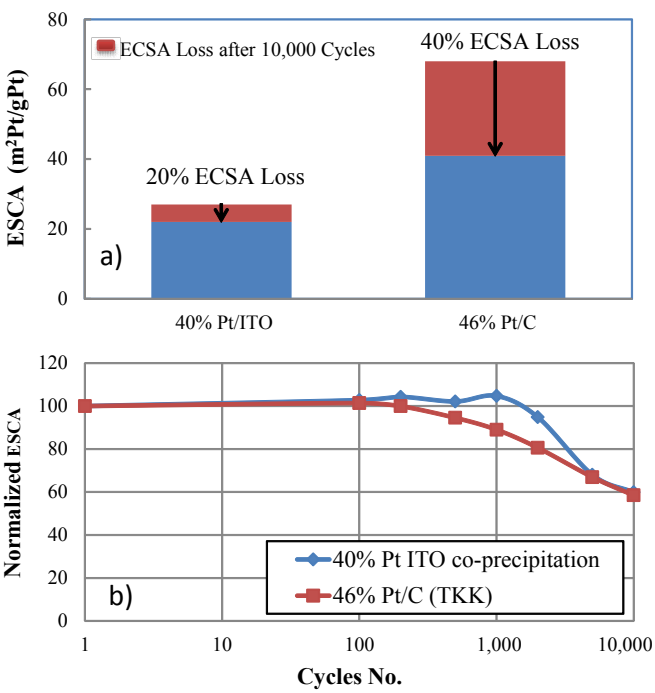

FIGURE 2. Comparison of the electrochemical stability of ITO (co-precipitation) and commercial Pt/C (loss of ECSA) under a) start-stop and b) load cycling protocols.

Cost Model for RuO_2-TiO_2: Though the RTO support is more expensive compared with carbon, the total catalyst cost is still dominated by platinum. Material costs of the carbon and non-carbon-based catalysts are compared as shown in Figure 4. It should also be noted that ruthenium only makes up 38% of the mass of the support, while the rest is relatively inexpensive TiO_2. The major advantage of using metal oxide support at the cathode is its excellent resistance

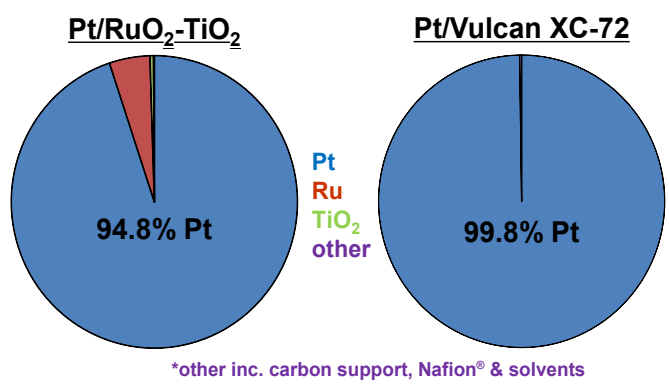

FIGURE 4. Cathode material cost comparison between Pt/non-carbon and Pt/Vulcan XC-72.

TABLE 2. Properties of ZIO Catalyst Supports

	BET Surface Area (m^2/g)		Electrical Conductivity (S/cm)	
Material	Annealed at 400°C	Annealed at 800°C	Annealed at400°C	Annealed at 800°C
ZIO (1:9 mol)/co-precipitation	37	17	0.07± 0.01	0.09± 0.01
ZIO (1:9 mol)/silica-template	38	18	N/A	N/A
ZIO (1:1 mol)/epoxide initiator	50	7	N/A	N/A

N/A – not available

to degradation under start-stop cycling. This durability needs to be considered while doing the cost analysis. Based on the data obtained for these two cathode materials, Pt/RTO and Pt/Vulcan XC-72 under the start-stop durability cycling test, a "durability factor" was calculated using following equation:

$$\text{Durability factor} = \frac{\text{Mass Activity Retention of the Catalyst}}{\text{Mass Activity Retention of Pt/RuO}_2\text{ - TiO}_2}$$

Pt/RTO retained 86% of its mass activity while Pt/Vulcan XC-72 retained only 66% of its initial mass activity under start-stop durability cycling. Based on this protocol, Pt/Vulcan XC-72 is only 69% as durable as the Pt/RTO. When this factor is taken into account, and given the fact that the platinum costs dominate overall catalyst cost, there was minimal difference in electrocatalyst costs between Pt/C and Pt/RTO.

CONCLUSIONS AND FUTURE DIRECTIONS

- We have shown that ITO and ZIO had better electrochemical stability than carbon under start-up and shut-down potential cycling protocol.
- After considering the durability advantages of Pt/RTO, the preliminary cost model shows that Pt/RTO is only slightly more expensive than Pt/Vulcan XC-72.

The future directions for the next FY are:

- Optimize the deposition of Pt on non-carbon supports to get higher ESCA and oxygen reduction reaction activities.
- Synthesize high surface area metal oxides by drying of alcogels using supercritical CO_2.
- Evaluate the conductivity and electrochemical stability of hafnium-doped indium oxide.
- Synthesize functionalized mixed metal oxides with proton conductivity.
- Complete the cost model.
- Prepare membrane electrode assemblies with best supports (catalyzed) to deliver to DOE.

FY 2013 PUBLICATIONS/PRESENTATIONS

1. Chih-Ping Lo, Guanxiong Wang, Amod Kumar, Vijay Ramani, "TiO_2–RuO_2 electrocatalyst supports exhibit exceptional electrochemical stability" Applied Catalysis B: Environmental **140–141** (2013) 133–140.

2. Chih-Ping Lo, and Vijay Ramani, "SiO_2-RuO_2: A Stable Electrocatalyst Support" ACS Applied Materials and Interfaces, **4**, (2012) 6109–6116.

3. Guanxiong Wang "Ruthenium Titanium Oxide (RTO) electrocatalyst supports exhibit exceptional start-stop durability" 223rd ECS Meeting, Toronto, Ontario, Canada. May 2013.

REFERENCES

1. N. Takeuchi; T.F. Fuller, J. Electrochemical Society, 155 (2008) B770-B775.

2. Reiser, L. Bregoli, T.W. Patterson, J.S. Yi, J.D. Yang, M.L. Perry, T.D. Jarvi, Electrochem. Solid-State Lett. 8 (2005) A273-A276.

3. H. Tang, Z. Qi, M. Ramani, J.F. Elter, J. Power Sources 158 (2006) 1306-1312.

V.A.9 Development of Novel Non-PGM Electrocatalysts for Proton Exchange Membrane Fuel Cell Applications

Sanjeev Mukerjee
Department of Chemistry and Chemical Biology
Northeastern University (NEU)
Boston, MA 02115
Phone: (617) 373-2382
Email: S.mukerjee@neu.edu

DOE Managers
Kathi Epping Martin
Phone: (202) 586-7425
Email: Kathi.Epping@ee.doe.gov
David Peterson
Phone: (720) 356-1747
Email: David.Peterson@go.doe.gov

Contract Number: DE-EE0000459

Subcontractors:
- University of New Mexico, Albuquerque, NM (UNM) (Prof. Plamen Atanassov)
- Michigan State University, East Lansing, MI (MSU) (Prof. Scott Barton)
- University of Tennessee, Knoxville, TN (UTK) (Prof. Thomas Zawodzinski)
- Nissan Technical Center, North America (NTCNA), Detroit, MI (Dr. Nilesh Dale)
- Pajarito Powder, Albuquerque, NM (Dr. Bar Halevi)
- Los Alamos National Laboratory, Los Alamos, NM (LANL) (Dr. Piotr Zelenay)

Project Start Date: August 1, 2010
Project End Date: August 1, 2014

Overall Objectives and Objectives for Fiscal Year (FY) 2013

The objective of this project is to design non-platinum group metal (PGM)-based catalysts and supporting gas transport layer, both in the interfacial reaction layer between the electrode and membrane as well as in the underlying gas diffusion medium, for meeting and exceeding DOE goals for application in solid polymer electrolyte fuel cells. This project is focused on materials development and is assisted by advanced analytical tools, computation, and testing for improving the design via critical understanding of electrocatalysis in these novel structures. The principle target for the reporting fiscal year was to reach the project's Go/No-Go milestone of 100 mA/cm^2 at 0.8 V (internal resistance-free, iR-free) at 80°C, pure H_2/O_2, with 1.5 bar total pressure. In addition, the project also will demonstrate scale-up capability for the down-selected catalyst in the range of 10-20 gm.

Technical Barriers

This project addresses the following technical barriers from the Fuel Cells section of the Fuel Cell Technologies Office Multi-Year Research, Development, and Demonstration Plan:

(B) Cost (eliminate precious metal loading of catalysts)

(C) Performance (increase the specific and mass activities of catalysts)

(A) Durability (increase the durability/stability of catalysts with cycling)

Technical Targets

The technical targets for this project are listed in Table 1.

TABLE 1. Progress towards Meeting Technical Targets for Non-PGM Electrocatalysts for Transportation Applications

Characteristic	Units	2015 Target	NEU 2012 status
Specific Activity @ 80°C, 150 kPa, H_2/O_2, 100% relative humidity (RH)	A/cm^3 A/cm^2	300 A/cm^3 (iR-free) 100 mA/cm^2 (iR-free)	130 A/cm^3 85 mA/cm^2
Durability at 80°C Cycling: Catalyst Durability	% loss of activity	5%	<1%
Durability at 80°C Cycling: Carbon Corrosion Durability	% loss of activity	10%	<50% Partially recoverable

FY 2013 Accomplishments

1. Cross-laboratory rotating disk electrode (RDE) measurement of a wide variety of samples emanating from diverse choice of polymer precursors at MSU, NEU, a UNM indicates a confluence in terms of performance; measured values are very close (within the errors inherent in these measurements) to those of the current state-of-the-art materials recently reported by our partners at LANL [1]. Two catalysts were down-selected based on these results, the first referred to as UNM-CTS catalyst (from UNM) and the second referred to as NEU-Fe MOF (from NEU).
2. Extrapolation of fuel cell-derived iR corrected data obtained using UNM-Fe-CTS electrocatalysts currently

indicates volumetric performance in the range of 150-400 A/cm^3. This performance is beyond the DOE 2015 target of 300 A/cm^3. All measurements and conducted with pure H_2/O_2, 1.5 bar total pressure, 100% humidification using a 212 Nafion® membrane. Geometric area activity measurement conducted on the same electrocatalyst under the conditions mentioned above show 100 mA/cm^2 at 0.8 V (iR-free). These measurements were conducted independently at NEU as well as at the NTCNA using three separate membrane electrode assemblies (MEAs) from two different electrocatalyst batches (iR-free is currently 105 mA/cm^2).

3. Durability measurements conducted on the down-selected UNM-Fe-CTS catalysts show excellent tolerance to catalyst stability tests (based on Nissan protocol, similar to DOE). Carbon corrosion tests, which involve load cycling to 1.5 V vs. the reference hydrogen electrode, however, indicated significant losses, which followed along similar lines to the losses with a PGM cathode.
4. Understanding of the nature of the active site was significantly advanced in this reporting period with identification of a dual site mechanism wherein the N_{2+2} site was responsible for the initial adsorption and reduction of oxygen to peroxide moieties followed a second cascade step of further reduction of the peroxide in closely surrounding Fe-N_2 sites. Such formulation of the mechanism was supported with in situ X-ray absorption spectroscopy (XAS) and targeted electrochemical probe measurements.

✧ ✧ ✧ ✧ ✧

INTRODUCTION

Recent reports [1,2] have clearly demonstrated the significant advancements made in enabling good oxygen reduction activity by Fe-based non-PGM catalysts. These so called Fe-N_x-based systems have evolved over several decades of intense work leading up to the current state of the art, reported recently in references [1,2]. This report provides for the first time a comprehensive view of (a) confluence of oxygen reduction reaction (ORR) activity derived from materials prepared using a variety of polymeric precursor materials viz. the current state of the art by three different university groups, (b) excellent durability in terms of catalyst stability (*vide* DOE and Nissan protocols) and recovery of losses incurred during carbon corrosion measurement when placed under load, and (c) detailed understanding of the nature of active site and electrocatalytic pathways as distinct from the parallel pathway in alkaline electrolytes.

APPROACH

The approach adopted in this reporting period involved (a) material preparation using a wide variety of precursor materials in conjunction with Fe-containing salts pyrolyzed at temperatures of 700-800°C under inert atmosphere followed with repeated steps (up to three) of etching (in acid) and repyrolysis, (b) rotating ring disc electrode and fuel cell tests using well-established protocols for cross-laboratory performance comparison and extrapolation of volumetric activity (from iR-corrected fuel cell data), (c) durability measurements using two well-established protocols (catalyst durability) and carbon corrosion tests (both DOE protocols), and (d) investigation of the nature of active site and ORR electrocatalysis steps as measured using in situ synchrotron spectroscopy at the Fe-K edge under actual cell *operando* conditions.

RESULTS

Following intensive work aiming to develop an alternative to precious metal-based catalysts for ORR cathodes, the most promising catalysts are materials synthesized using the sacrificial support method (SSM) originating at UNM. Based on consistent studies, a few SSM-based catalysts (Fe-AAPyr [Fe-amino-antipyrene], Fe-CTS [Fe-charge transfer salt], and Fe-CBDZ [Fe-carbandazim]) were selected for further testing to validate activity and stability in a fuel cell environment. As shown in the later sections, the catalysts based on a CTS precursor have shown the most promising results. Fe-CTS catalysts were prepared by modified SSM (Figure 1). The detailed synthesis approach is delineated in the July 2013 interim report. Briefly, the precursor material was a CTS (nicarbazin, NCB - Nicarbazin, Sigma-Aldrich), and the Fe salt chosen was iron nitrate ($Fe(NO_3)_3*9H_2O$, Sigma-Aldrich); this was in conjunction with the UNM silica templating approach to fabricating electrocatalysts. Figure 2 shows the ORR-iV curves of catalysts at 1,600 RPM in O_2-saturated 0.5 M H_2SO_4 solution measured at the NTCNA. Table 2 lists the $E_{1/2}$, the kinetic currents at 0.8 V, and the Tafel slope of catalysts. The iV curves and ORR activities were compared with those of a TKK 20% Pt on a high surface area carbon catalyst. Fe-CTS presented the highest kinetic current density of 4.6 mA cm^{-2} with a Tafel slope of 52 mV/decade. This kinetic current density achieved 50% of the kinetic current of 20% Pt-based catalyst. In the iV curves, Fe-CTS showed an active reduction peak around 0.75 V, which might be associated with the active site of the catalyst. Based on the results summarized in Table 2 and shown in Figure 2, Fe-CTS showed the highest activity among the tested catalysts, so Fe-CTS was chosen for MEA tests and further optimization.

Figures 3a and 3b represent linear polarization results with pure H_2/O_2, fully humidified at 80°C with 1.5 bar total

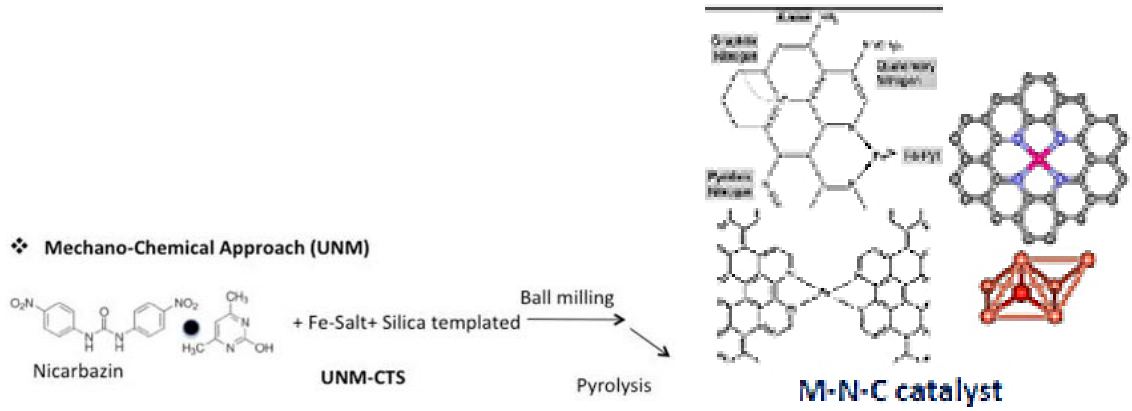

FIGURE 1. Representation of chemistry and pyrolysis conditions used for the down-selected electrocatalysts by cross-laboratory partners, UNM and NEU.

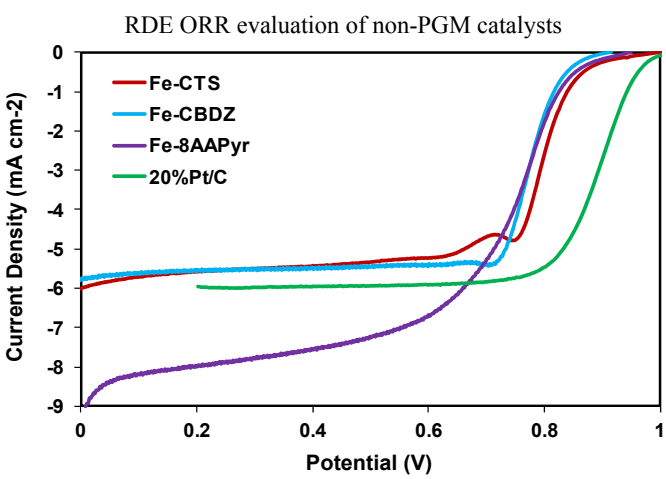

FIGURE 2. Cross-laboratory comparison of ORR activity measured using rotating ring disk electrode technique, performance comparison shown at 900 rpm. Electrolyte is 0.1 M $HClO_4$, room temperature with standard catalyst loading of ~600 μg/cm^2.

TABLE 2.

Catalyst	$E_{1/2}$ mV	Kinetic Current* mA cm^{-2}	Tafel Slope mV/decade
Fe-CTS	796	4.6	52
Fe-CBDZ	776	2.31	50
Fe-8AAPyr	747	2.32	90
20%Pt/C	894	8.3	57

pressure. The membrane used in these tests at NEU was Nafion® (212), with cathode catalyst loading at 2 mg/cm^2 and the choice of anode reference electrode as Pt/C, 0.4 mg/cm^2 (common electrode used as reference by NTCNA and NEU, sourced from Johnson Mathey Fuel Cells, Inc.) The substrate used on the cathode side for spray addition of non-PGM catalysts was from SGL Carbon (25 BCH). Linear polarization measurements were conducted using 18 MEAs prepared from three separate batches of UNM-CTS catalysts with groups containing variations of relative ratios of Nafion® (between 35% and 50% based on total carbon content of the catalyst layer). The best results (Figure 3a) were obtained with total Nafion® content of 50% with a group of three separate MEAs prepared using catalysts from two separate batches. Since a standard conventional anode electrode is used with pure H_2, the fuel cell polarization measurements amount to a quasi half-cell measurement of the cathode polarization losses.

Corrections for iR were conducted according to the methodology described in detail earlier [3-5], with the aid of a non-linear regression analysis of the overall polarization behavior which can be described using the equation $E = E^{\circ}_{OCV} - (\eta_{act,a} + \eta_{act,c}) - \eta_{ohmic} - (\eta_{conc,a} + \eta_{conc,c})$. Experimental fitting results gave reproducible values of η_{ohmic}, which was used for iR correction of the polarization data shown in Figure 3b. All three MEAs based on two separate batches of UNM-CTS catalysts passed the metrics. The iR correction conducted using the regression method was independently verified using electrochemical impedance measurements conducted as a function of current density.

In addition volumetric projection of the data of the areal activity was calculated using the procedure described earlier [6]. In order to use the fuel cell data in the context of volumetric activity, the well-known relationship:

$$I_{vol}(E) = \frac{I_{areal}(E) \times \rho}{loading}$$

was used with projection conducted from a range of current densities measured close to the ORR onset potential (0.1 to 10 mA/cm^2) to 0.8 $V_{iR\text{-}free}$ (reported in this case for a total pressure of 1.5 bar) and a catalyst layer density of 0.4 g/cm^3. Such a projection over decades of current density was designed to obtain volumetric activity values without the concomitant effects of ohmic and mass transport losses and has been reported as standard practice in earlier references [1,2]. Figure 3c shows the results of our projection and the resultant volumetric activity, and we used the exact procedures reported earlier [1,2] for this projection. It is important to note that the data obtained for this projection was acquired using a more sensitive potentiostat with higher current resolution (nano-amps) as compared to those reported in Figures 3a and 3b where a standard electronic load box was employed for its higher current range. The iR-corrected Tafel plot shown in terms of area activity in 3b clearly meets the project's Go/No-Go criterion. The plot in Figure 3b is an average of the performance from the three best MEAs with concomitant error bars showing variation in the data. In each volumetric projection (Figure 3c) more than 15 points were used within a current range of 0.1 to 10 mA/cm^2. In two of the MEAs reported for their areal activity (Figures 3a-b) the concurrent volumetric activity (measured separately, Figure 3c) exceeded 400 A/cm^3 at 0.8 $V_{iR\text{-}free}$, pure H_2/O_2 with 1.5 bar total pressure, a value above the DOE target for 2017. However, it is important to note that this volumetric activity should be used with great caution as it is a projected number.

Validation of the fuel cell results measured at NEU was independently conducted at NTCNA. Measurements conducted at the NTCNA are shown in Figure 4. The UNM Fe-CTS down-selected catalysts were made into MEAs using an NRE211 membrane. In making the ink, the Fe-CTS catalyst was mixed with deionized water, ethanol, and 20% Nafion® dispersion (Ion Power DE2020). We aimed to optimize the ionomer-to-catalyst (I/C) ratio in the catalyst ink recipe. Three I/C ratios of 0.54, 0.82, and 1.2, corresponding to 35, 45, and 55 wt% Nafion®, respectively, were investigated. The amount of Nafion® was adjusted to make the catalyst ink corresponding to the three I/C ratios.

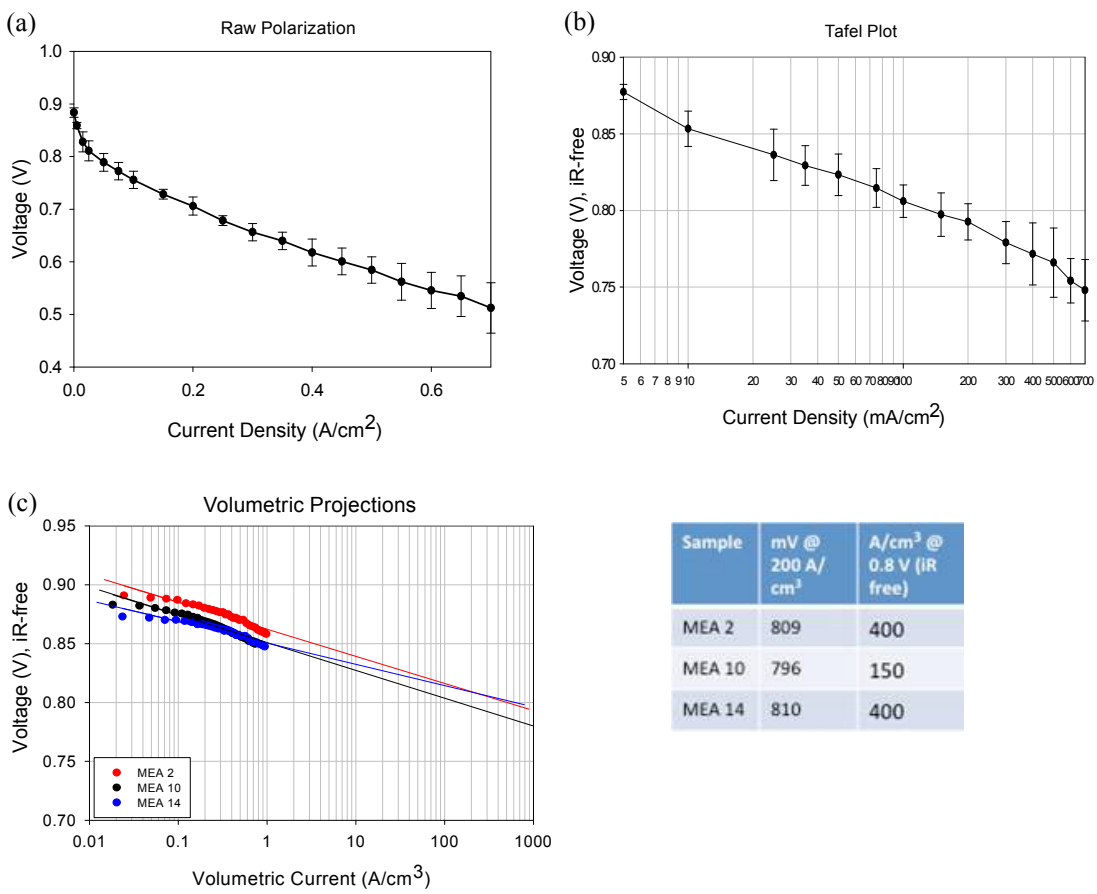

Sample	mV @ 200 A/cm^3	A/cm^3 @ 0.8 V (iR free)
MEA 2	809	400
MEA 10	796	150
MEA 14	810	400

FIGURE 3. Fuel cell polarization results from UNM-Fe-CTS catalysts measured using a 5-cm^2 single cell conducted at NEU using DOE-recommended operating conditions of 80°C, 100% humidification, pure H_2/O_2, 1.5 bar total pressure. Error bars in the fuel cell data indicate average of results from three different MEAs sourced from two separate batches of electrocatalysts. Cathode loading used was 2 mg/cm^2, 50% Nafion®. (a) Raw polarization results, (b) iR-corrected Tafel plot showing the results meeting the DOE Go/No-Go metrics, and (c) volumetric projection of the data measured at low current densities projected to 0.8 V (iR-free).

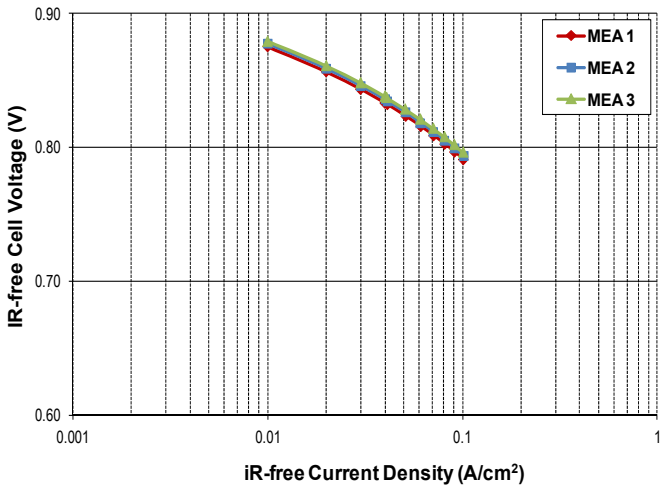

FIGURE 4. Fuel cell polarization results from UNM-Fe-CTS catalysts measured using a 25-cm^2 single cell conducted at NTCNA using DOE-recommended operating conditions of 80°C, 100% humidification, pure H_2/O_2, 1.5 bar total pressure. Results from three different MEAs sourced from two separate batches of electrocatalysts are shown. Cathode loading used was 4 mg/cm^2, 55% Nafion®.

The homogenized catalyst ink was sprayed onto SGL 25BCH gas diffusion layers (GDLs) using the in-house spray system at NTCNA. The system is an automated spray deposition machine capable of preparing reproducible, uniformly-sprayed gas diffusion electrodes (GDEs) with accurate loading. For each GDE, the catalyst loading was kept constant at 4 mg/cm^2, regardless of the Nafion® content of the ink (35, 45, or 55 wt%).

MEAs (25 cm^2) were assembled by hot-pressing a JMFC GDE (0.4 mg Pt/cm^2) anode, an NRE211 membrane, and an UNM Fe-CTS-based GDE cathode (4 $mg_{catalyst}/cm^2$). The MEAs were tested using custom-designed 25-cm^2 cell hardware on a Hydrogenics fuel cell test station. In order to verify the absence of Pt contamination on the non-PGM catalyst cathode, cyclic voltammograms (CVs) of all the MEAs tested at different Nafion® loadings were obtained. The CV profiles of all the MEAs did not exhibit any peaks that could be attributed to Pt contamination.

As shown in Figure 4, the MEA containing the Fe-CTS catalyst with 55% Nafion® gave 100 mA cm^{-2} at 0.8 $V_{iR\text{-}free}$, the first report of fuel cell performance that meets the current DOE design target for non-PGM cathode proton exchange membrane fuel cell catalysts for potential future automotive applications. This result was reproduced using three MEAs from two different catalyst batches. The reproducibility of the high current densities obtained with this catalyst is confirmed by the overlapping Tafel plots.

Durability measurements of the UNM-Fe-CTS catalyst were also independently conducted at NTCNA. The

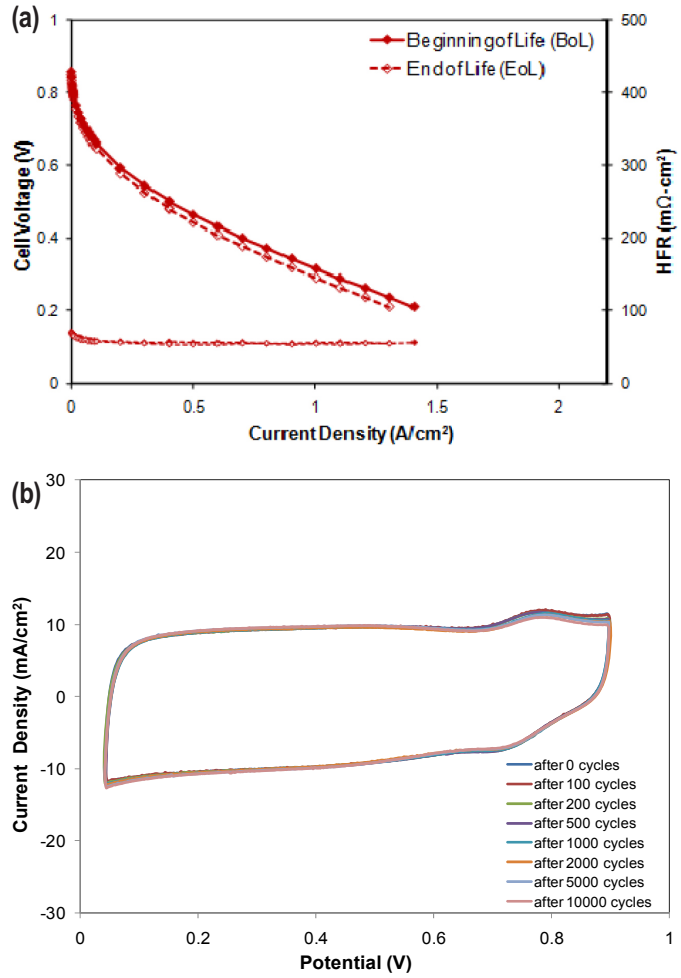

FIGURE 5. Durability measurements conducted at the NTCNA using DOE protocols for catalyst stability are shown for the UNM-Fe-CTS catalyst. As shown, this sample showed excellent durability for catalyst stability test.

durability evaluation used automotive accelerated stress tests, which simulate the actual stack conditions under fuel cell electric vehicle operating conditions. The catalyst showed excellent durability under the Nissan load cycling protocol (Table 2), with polarization performance undergoing minimal change after 10,000 potential cycles (shown in Figure 5a for the Nafion® 45% sample). All MEAs that were tested under the load cycling protocol showed the same durability regardless of Nafion® content.

The corresponding CV profile, as shown in Figure 5b, also did not change significantly after 10,000 potential cycles. The beginning-of-life CV shows a clean profile with no peaks that can be attributed to Pt contamination, and the end-of-life CV (CV after 10,000 potential cycles) also does not show any peaks due to Pt. This is good evidence that no Pt particles migrated from the anode to the cathode during the potential cycling durability test.

Scale-Up Efforts at Pajarito Powders

Pajarito Powder has begun an initial scale-up of the CTS catalyst developed by UNM in anticipation of a successful continuation of the DOE contract. Pajarito Powder's initial statement of work included scaling up the best-performing catalyst at the time, which was the MSU Fe-Melamine catalyst that was the previous best-performing catalyst. Pajarito successfully scaled the Fe-Melamine catalyst according to the statement of work by the time of the Go/No-Go decision in late June. However, by this time the newly developed UNM-Fe-CTS catalyst had emerged as the leading catalyst, meeting the Go/No-Go criteria. It was far too late to change catalysts for scale-up by the time the CTS had been initially tested.

Nevertheless, Pajarito Powder began initial scale-up investigations of UNM-Fe-CTS catalyst in anticipation of Phase 2 of the DOE project. The results of the initial scale-up efforts for the Fe-CTS catalysts are reported here. This was conducted as an additional effort funded internally by Pajarito to assist in initial phase of the DOE project.

The Fe-CTS catalyst is made using an SSM developed at UNM where C/N precursors are mixed with iron metal salts and silica. The mixture is then pyrolized at ambient pressure, the silica and excess iron are etched and leached, and the compound is then pyrolyzed again to achieve better performance and stability. This chemically intensive approach has several key steps requiring optimization in the scale-up effort. The initial scale-up effort is focused on a 10-20 gram batch, with the goal that the methods developed can be applied towards 30-50 gram batches immediately, and 100-200 gram batches in the near future, while further demonstrating a technology trajectory to 1-kg batches.

The synthesis process is readily divided into five major steps: a) mixing of precursors and silica, b) first pyrolysis, c) etching of silica and leaching of excess iron, d) washing catalyst after etch/leach, and e) second pyrolysis. Each of these steps was analyzed for ease of scale-up, and appropriate scale-up equipment was purchased and installed. For example, the mixing of dry precursors was done at UNM in 100 mL planetary mill jars. This can be readily scaled up using a ball-mill with 4x1 L jars, so that 4x200+ grams of precursor mixture can be made in a single processing step, yielding 4x50 grams of catalyst. Other methods of mixing, such as dry and wet shear mixers as well as continuous slurry homogenizers, are also being examined.

The pyrolysis step was initially scaled from 15-ml alumina boats used at UNM to 150-mL alumina boats, where each 150-mL boat yields ~7 grams of finished catalyst. 25 grams of finished catalyst therefore requires 500 mL of precursor mix, so that four 150-mL alumina boats yield 30-gram batches. Pyrolysis of multiple 150-mL boats in parallel in a 3-inch inside diameter tube furnace with 30-inch heated zone therefore allows 25-gram+ batches to be made. Further, custom-made shallow pans with 2,000-mL+ precursor capacity will allow for 200+ gram-per-batch pyrolysis in the same system, and installation of a 6-inch pyrolysis processing tube will allow for 400+ gram-per-batch pyrolysis. The pyrolysis conditions, including sweep rate, temperature ramp and dwell, and oxygen scrubbing, had to be adjusted to account for the increase in scale of processing tube.

The etching step has been scaled up as well with 25+ grams of finished catalyst etched in a single batch. Etching scale-up required proportional increases in etchant and processing vessel volumes, as well as several modifications to the procedure, since the larger batch sizes create slower diffusion of etchants and etching products in the larger volume slurry of the catalyst/silica mix for a 25-gram batch. The increase in hydrofluorhydric acid (HF) use also required installation of an HF vapor-scrubbing hood. Post-etching washing done in the lab scale using repeated centrifugation/decanting cycles was streamlined to culminate in filtration using HF-compatible washing and filtration equipment. Powder drying using vacuum heating allows for quick drying and reduction in processing time.

The second pyrolysis conditions had to be similarly adjusted; sweep rate, temperature ramp and dwell, and oxygen scrubbing had to be adjusted to account for the increase in scale of processing tube.

As expected, the lab-scale synthesis for Fe-CTS had to be modified in several stages, with steady improvements made in the very brief three months that the Fe-CTS formulation has existed and been available for scale-up. The performance of the 30+ gram batches produced at Pajarito Powder is approaching the performance of the UNM-Fe-CTS catalyst measured at both NEU and NTCNA. The performance data show that Pajarito Powder has demonstrated the ability to produce 30+ gram batches of the UNM-Fe-CTS catalyst, and therefore also demonstrate the scalability of the UNM-Fe-CTS catalyst (Figure 6).

CONCLUSIONS

1. Cross-laboratory studies of materials emanating from the pyrolysis of diverse polymer precursors in conjunction with Fe and Co salts indicate a common evolution of active sites for ORR reduction. Down-selected catalysts referred to as UNM-Fe-CTS have successfully met the Go/No-Go milestones with independent measurements at NEU and NTCNA with a statistically significant number of MEAs and batches of catalysts.
2. Detailed durability studies indicate excellent tolerance to catalyst stability tests, and relatively poor resistance to carbon corrosion test protocols; the latter, however, is at par with those observed for PGM catalysts.

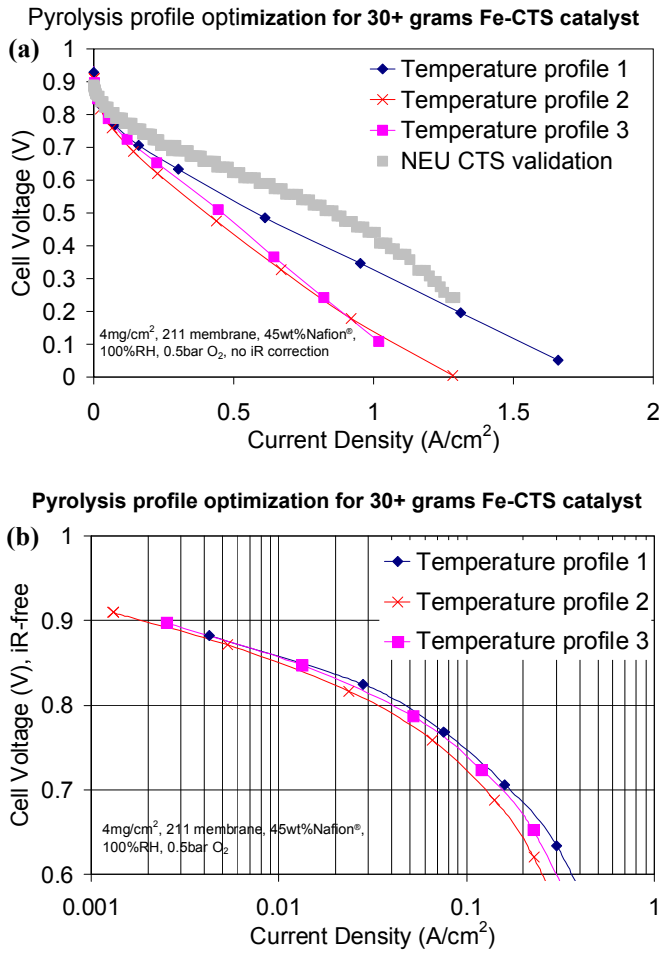

FIGURE 6. (a) Pyrolysis thermal profile effects on 30+ grams batch-scale Fe-CTS performance. Performance validation from NEU is shown for comparison measured under similar conditions. (b) Corresponding Tafel plots for the 30+ gm scaled-up samples.

3. Scale-up of 30+ gms batch size has been demonstrated using the down-selected electrocatalyst.

FUTURE DIRECTIONS

1. The principle focus of the group will be to transition the team to Phase II of this effort, where the focus will be to significantly improve the mass transport in the GDL for enabling transition from operation in pure O_2 to air.
2. Optimize scale-up and MEA fabrication for meeting DOE Phase 1 metrics with the scaled-up batches in a consistent way.
3. Further test the validity of the proposed mechanism using a final set of in situ and *operando* synchrotron XAS data in conjunction with density functional theory calculations. In addition, use the in situ spectroscopy to probe degradation pathways.

FY 2013 PUBLICATIONS/PRESENTATIONS

1. 'Fundamental Mechanistic Understanding of Electrocatalysis of Oxygen Reduction on Pt and Non Pt Surfaces: Acid vs. Alkaline Medium', N. Ramaswamy, and S. Mukerjee, Advances in Physical Chemistry, Vol. 2012, Article ID 491604, (2012).

2. 'Structure of the catalytic sites in Fe/N/C-catalysts for O_2-reduction in PEM fuel cells', Ulrike I. Kramm, Juan Herranz, Nicholas Larouche, Thomas M. Arruda, Michel Lefèvre, Frédéric Jaouen, Peter Bogdanoff, Sebastian Fiechter, Irmgard Abs-Wurmbach, Sanjeev Mukerjee, and Jean-Pol Dodelet, *Phys. Chem. Chem. Phys.*, 2012, **14**, 11673–11688.

3. 'Highly active and durable templated non-PGM cathode catalysts derived from iron and aminoantipyrine', A. Serov, M. H. Robson, B. Halevi, K. Artyushkova, and P. Atanassov, *Electrochimica Acta,* Volume 22, August 2012, Pages 53–56.

4. 'Templated non-PGM cathode catalysts derived from iron and poly(ethyleneimine) precursors', A. Serov, M. H. Robson, K. Artyushkova, and P. Atanassov, Applied Catalysis B: Environmental, Volume 127, 30 October 2012, Pages 300–306.

5. 'Density functional theory calculations of XPS binding energy shift for nitrogen-containing graphene-like structures', K. Artyushkova, B. Kiefer, B. Halevi, A. Knop-Gericke, R. Schlogl, and P. Atanassov, *Chem. Commun.*, 2013, 49, 2539.

REFERENCES

1. Wu, G.; More, K.L.; Johnston, C.M.; Zelenay, P. *Science* 2011, *332*, 443.

2. Lefèvre, M.; Proietti, E.; Jaouen, F.; Dodelet, J.-P. *Science* 2009, *324*, 71.

3. Saha, M.S.; Gullá, A.F.; Allen, R.J.; Mukerjee, S. *Electrochimica acta* 2006, *51*, 4680.

4. Haji, S. *Renewable Energy* 2011, *36*, 451.

5. Zhang, J.; Zhang, L.; Bezerra, C.W.; Li, H.; Xia, Z.; Zhang, J.; Marques, A.L.; Marques, E.P. *Electrochimica Acta* 2009, *54*, 1737.

6. Gasteiger, H.A.; Kocha, S.S.; Sompalli, B.; Wagner, F.T. *Applied Catalysis B: Environmental* 2005, *56*, 9.

V.A.10 High-Activity Dealloyed Catalysts

Anusorn Kongkanand
General Motors, LLC (GM)
895 Joslyn Ave
Pontiac, MI 48340-2920
Phone: (585) 953-5538
Email: anusorn.kongkanand@gm.com

DOE Managers
Dimitrios Papageorgopoulos
Phone: (202) 586-5463
Email: Dimitrios.Papageorgopoulos@ee.doe.gov
Gregory Kleen
Phone: (720) 356-1672
Email: Gregory.Kleen@go.doe.gov

Contract Number: DE-EE0000458

Subcontractors:
- David Ramaker, George Washington University (GWU), Washington, DC
- Rachel O'Malley, Johnson Matthey Fuel Cells (JMFC), Sonning Common, UK
- Yang Shao-Horn, Massachusetts Institute of Technology (MIT), Cambridge, MA
- Sanjeev Mukerjee, Northeastern University (NEU), Boston, MA
- Peter Strasser, Technical University Berlin (TUB), Berlin, Germany

Project Start Date: August 1, 2010
Project End Date: November 30, 2013

Overall Objectives

- Demonstrate, in 50-cm^2 membrane electrode assemblies (MEAs) in fuel cells using catalyst precursors prepared in large batch size, a dealloyed catalyst that satisfies DOE 2017 catalyst goals.
- Determine, at the atomic scale, where alloying-element atoms should reside with respect to the surface of the catalyst particle for simultaneously good activity, durability, and high-current density performance in air.
- Develop and demonstrate electrodes giving high current density performance in air adequate to meet the DOE platinum group metal (PGM) loading targets of <0.125 g_{PGM}/kW_{rated} and <0.125 mg_{Pt}/cm^2_{geo}.
- Scale up of synthesis and dealloying. Test durability of activity and power density in full-active-area cells.

Fiscal Year (FY) 2013 Objectives

- Optimize manufacturable procedures for precursor synthesis and dealloying of the catalyst powders.
- Demonstrate electrodes made from dealloyed catalysts that give good high current density performance using air as the oxidant: >0.56 V at 1.5 A/cm^2 when tested with the DOE-targeted cathode loadings ≤0.1 mg_{PGM}/cm^2.
- Improve understanding of where alloying-element atoms should reside with respect to the surface of the catalyst particle for simultaneously good activity, durability, and high-current-density performance in air.

Technical Barriers

This project addresses the following technical barriers from the Fuel Cells section of the Fuel Cell Technologies Office Multi-Year Research, Development, and Demonstration Plan:

(B) Cost

(A) Durability

(C) Performance

Technical Targets

TABLE 1. Progress towards Meeting Technical Targets for Electrocatalysts for Transportation Applications

Characteristic	Units	2017 DOE Stack Targets	Project 2013 Status (50 cm^2 at GM)
Mass activity	A/mg_{PGM} @ 900 $mV_{iR\text{-}free}$	≥0.44	0.6-0.75 (PtNi&PtCo)
Loss in catalytic (mass) activity	% lost after 30k cycles 0.6-1.0 V	≤40%	0-40% (PtNi&PtCo)
PGM Total Content	g_{PGM}/kW_{rated}	≤0.125	0.16 @1.5 A/cm^2 in H_2/air
PGM Total Loading	mg_{PGM}/cm^2_{geo}	≤0.125	0.15 (still 0.05 on anode)
Performance @ rated power	mW/cm^2	1,000	945
Performance @ 0.8 V	mA/cm^2	300	240

FY 2013 Accomplishments

- Developed several catalysts derived from large-batch $PtNi_3$ and $PtCo_3$ achieving initial mass activities of 0.60-0.75 A/mg_{PGM}, substantially exceeding the target of 0.44 A/mg_{PGM}.

- The above catalysts, demonstrated in two labs, lost only 0-40% of its initial activity after 30,000 cycles (0.6-1.0 V), bettering the target of <40% loss.
- MEAs made with large-batch catalysts at 0.1 mg_{PGM}/cm^2 gave 0.58 V at 1.5 A/cm^2. Although higher than the project milestone of 0.56 V, there is still some room for improvement. Voltage after 30,000 cycles (0.6-1.0 V) was still lower than the target of 0.56 V.

✧ ✧ ✧ ✧ ✧

INTRODUCTION

The amount of expensive platinum used as the oxygen reduction catalyst in fuel cells must be reduced about 4-fold to make proton exchange membrane fuel cells cost-competitive with other power sources. Pt-alloy catalysts, typically prepared with a composition of Pt_3M (M being a non-precious metal) have historically provided about half of the necessary activity gain vs. state-of-the-art pure-Pt/carbon catalysts. Prior to this project, team member Peter Strasser's group had shown, in small-scale laboratory experiments, that additional activity gains could be obtained by first synthesizing alloys with excess M and then removing most of the M by an electrochemical treatment [1]. They hypothesized that this treatment leaves the surface Pt atoms closer to one another than they are in pure Pt, causing electronic structure changes that accelerate the reduction of oxygen [2]. This project has developed manufacturable means of scaling up these dealloyed catalysts, confirming that most of the activity gains seen in ex situ laboratory experiments can also be achieved in practical fuel cells at GM, which satisfy the DOE catalyst activity target. However, we identified severe problems: (1) lack of durability and (2) poor performance in hydrogen/air fuel cells at high current density, associated with the use of the alloying element, copper, which had seemed most attractive in ex situ experiments. In FY 2012 we successfully shifted to other alloying elements, cobalt and nickel, which avoid one of the mechanisms whereby copper caused problems. We continue to pursue ideas to solve the durability shortfall that we have seen to date for the large-scale dealloyed $PtNi_3$ and $PtCo_3$ materials.

APPROACH

Because of the poor durability of D-$PtCu_3$ and anode poisoning due to dissolved Cu crossing over and plating, last year we shifted our efforts to other alloying elements, cobalt and nickel. Small-batch GM-made D-$PtCo_3$ and D-PtCo catalysts met, in 50-cm^2 fuel cells at GM, both the initial activity and the durability DOE 2017 targets, however, large-batch JMFC-made D-$PtNi_3$ catalysts met only the initial activity target. To understand this discrepancy, this year, advanced electron microscopy and synchrotron X-ray techniques were applied to tested and aged electrodes to correlate atomic-scale structure and composition with differences in activity and durability between individual catalysts, thereby guiding further catalyst development. Extensive work was done modifying catalyst precursor synthesis and dealloying procedure to generate durably active dealloyed catalysts. Demonstrated at two labs, several catalysts made from at least two large-batches of $PtNi_3$ and $PtCo_3$ precursors simultaneously satisfied both DOE 2017 initial activity and durability targets, and therefore we passed the Go/No-Go gate in October 2012.

RESULTS

To resolve the discrepancy in the durability observed between GM-made small-batch D-$PtCo_3$ and JMFC-made large-batch D-$PtNi_3$, in situ extended X-ray absorption fine structure was employed by NEU and GWU. The findings are summarized in Table 2. It was found that while GM D-$PtCo_3$ and D-PtCo show a large fraction of single-core with a shell structure, the JMFC D-$PtNi_3$ show mostly multi-core with porous-shell structure. With voltage cycling, Pt-Ni interaction decreases indicating loss of Ni from the shell. Pt-Pt distance was also seen to increase approaching that of pure Pt. Losses of Ni and Pt strain explain the loss of oxygen reduction reaction (ORR) activity after voltage cycling for JM D-$PtNi_3$. Transmission electron microscopy (TEM) analyses by MIT on these catalysts confirmed these findings.

TABLE 2. Structure and Composition Determined by Extended X-Ray Absorption Fine Structure Measurement of Different Catalysts at Different Number of Cycles

Precursor	d (nm)	Cycles	R_{Pt-Pt} (Å)	Microstructure
GM small-batch D-PtCo/HSC	4.0	~100	2.70	Mostly SC-S
GM small-batch D-$PtCo_3$/HSC	4.0	~100	2.71	50% SC-S, 50% MC-PS
D-$PtNi_3$/HSC	4.5	~100	2.72	MC-PS w M in PS
D-$PtNi_3$/HSC	5.5	10k	2.73	MC-PS w < M in PS
D-$PtNi_3$/HSC	6.5	30k	2.74	MC-PS w << M in PS
Pt/VC	3-5	~100	2.75	Nanoparticle

Single Core (SC), Shell (S), Multiple-Core (MC), Porous Shell (PS)

It is reported by several groups that the morphology of a catalyst can be affected by many factors such as precursor composition, size, and dealloying condition [3-5]. On a flat system, Erlebacher showed that morphology can be governed by the relative rate of nonnoble-element dissolution and noble atom surface diffusion [5]. TUB attempted to tune this rate by conducting acid treatment in sulfuric acid in presence of air or nitrogen gas (Figure 1). In air, O_2 creates a corrosion potential of ~1 V (higher than ~0.6 V in the N_2 case) and enhances Ni dissolution, and therefore removes more Ni. Large numbers of porous particles were observed

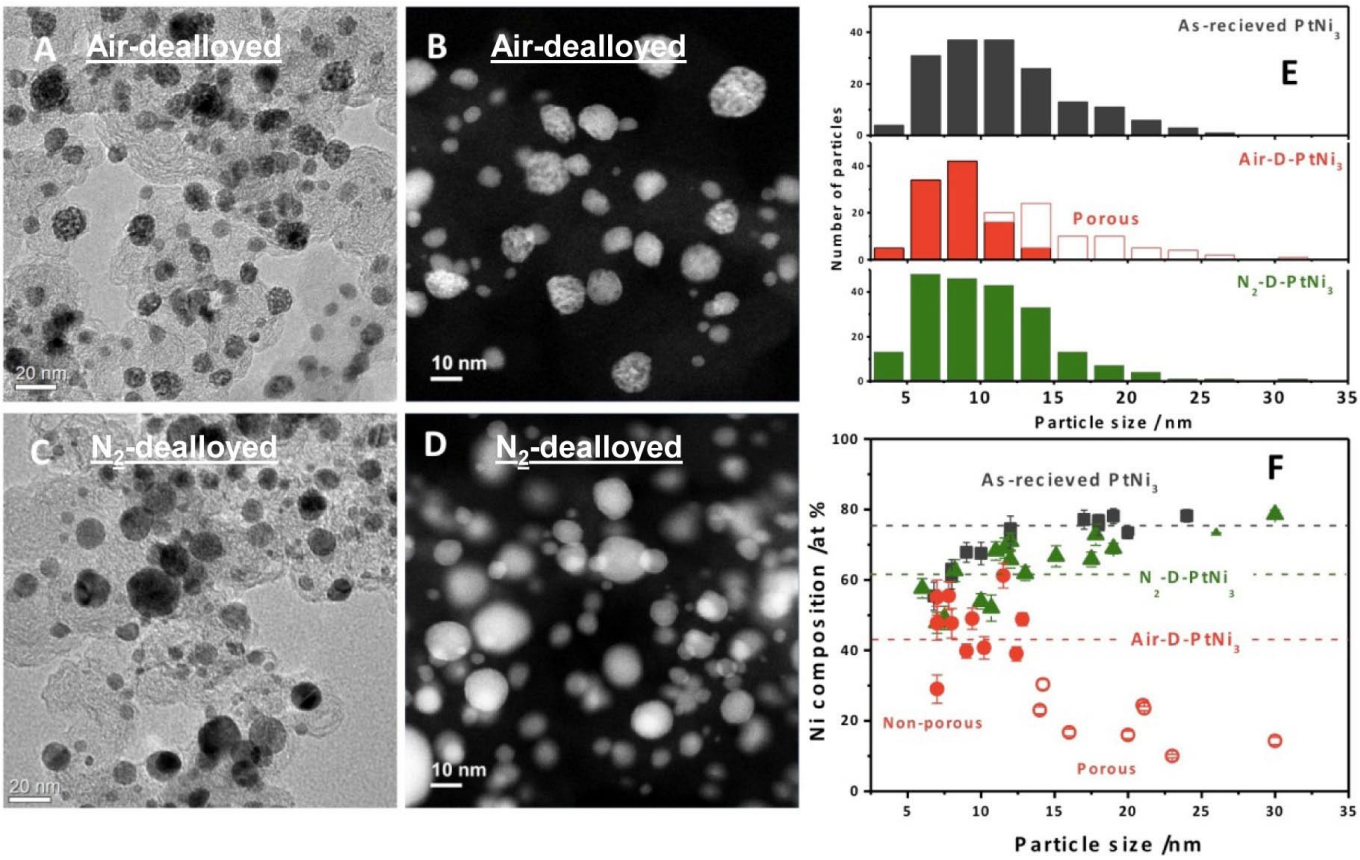

FIGURE 1. (A) TEM image and (B) High-angle annular dark-field (HAADF)-Scanning TEM (STEM) image of air-dealloyed-$PtNi_3$ 11/176 catalyst. (C) TEM image and (D) HAADF-STEM image of N_2-dealloyed-$PtNi_3$ catalyst. (E) Particle size distributions. (F) Size-composition-porosity relationships, where the horizontal dash lines represent the average compositions. It is shown that porous particles begins to form at particle larger than 13 nm and shows less residual Ni in air-dealloyed-$PtNi_3$ catalyst.

when dealloyed in air. Interestingly, only particles with its size larger than about 13 nm were seen to be porous. Smaller particles were solid and retained more Ni. These results indicate that particle size plays a significant role in determining the particle morphology and perhaps smaller particles are more stable than larger ones.

JMFC studied more than eight different preparation paths in order to improve the particle size distribution of its precursors. Figure 2 compares TEM images of JMFC old and new precursors. The particle size distribution is clearly improved in the new precursor. However, the new precursor is no longer single phase, showing some amount of pure Ni phase. Although our original approach was to make a single-phase alloy which was thought to give a more uniform dealloying process, it was very challenging to achieve acceptable particle size distribution with a single phase. JMFC now also made progress in eliminating the pure Ni phase which may induce complication during MEA fabrication.

The improved JMFC precursor was then dealloyed and treated under a series of conditions at GM. The $PtNi_3$ precursor was either leached in 1M nitric acid under air or 0.5M sulfuric acid under nitrogen. The acid-leaching temperature and time were also changed to obtain the Pt/Ni atomic ratio in the range suitable for fuel cell testing (Pt/Ni ~0.8-3). Post-dealloying thermal annealing was shown in rotating-disk experiment that could improve activity and stability [6]. A similar procedure was also applied to the catalysts in this study. Figure 3 shows the mass activities of the resultant catalysts as a function of voltage cycle. Nitric-acid/air 70°C, 24 hours (second triad from the right) was the same dealloying condition that was applied to the old precursors (11/176) last year that showed mass activity of 0.17 A/mg_{PGM} after 30,000 cycles. The catalyst prepared from the new precursor showed excellent activity and durability, fulfilling Milestone 1 (initial activity ≥0.44 A/mg_{PGM}), Milestone 2 (activity after 30k cycles ≥0.26 A/mg_{PGM}), and the DOE target of ≤40% loss of initial activity after 30k cycles. In fact, all of the catalysts in Figure 3 (save the one leached at 50°C) fulfilled the same. Sulfuric-acid/N_2 dealloying is a less oxidative condition than nitric-acid/air and therefore requires higher acid-leaching temperature to remove sufficient Ni. However, still higher Ni was retained in the particles. High resolution-TEM analyses by MIT on these particles showed a formation of Pt shell that might stabilize

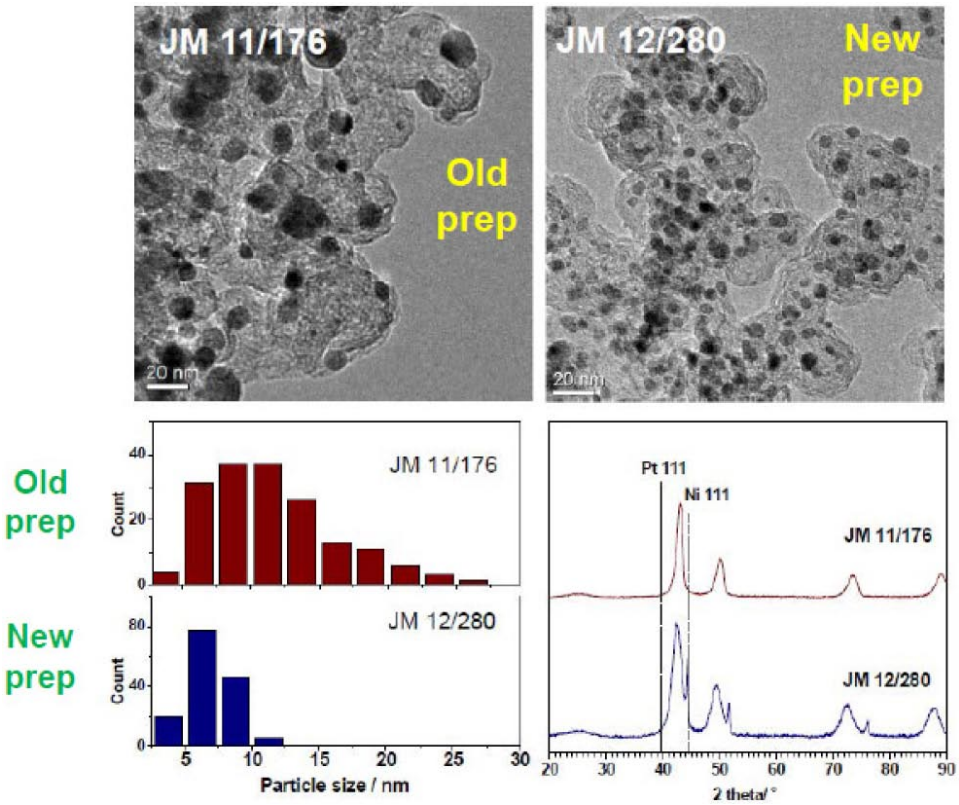

FIGURE 2. TEM images, particle-size histograms, and powder X-ray diffractogram of JMFC's old and new $PtNi_3$ precursors. The vertical lines in the diffractogram show the diffractions of Pt and Ni phases.

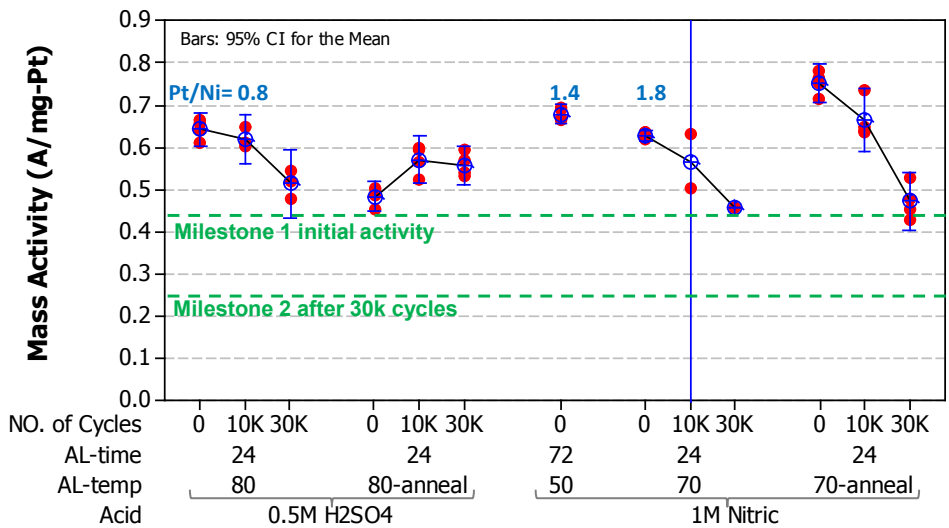

FIGURE 3. GM 50-cm^2 MEA mass-activity data for JMFC $PtNi_3$ new precursor (12/280) dealloyed under different times/temperatures/acid-types, with and without a post-dealloying anneal of the powder (4 h 400°C in 5% H_2/N_2). Blue error bars showing 95% confidence interval for the mean are large when only two samples have been completed due to large multiplier of standard deviation for only two samples.

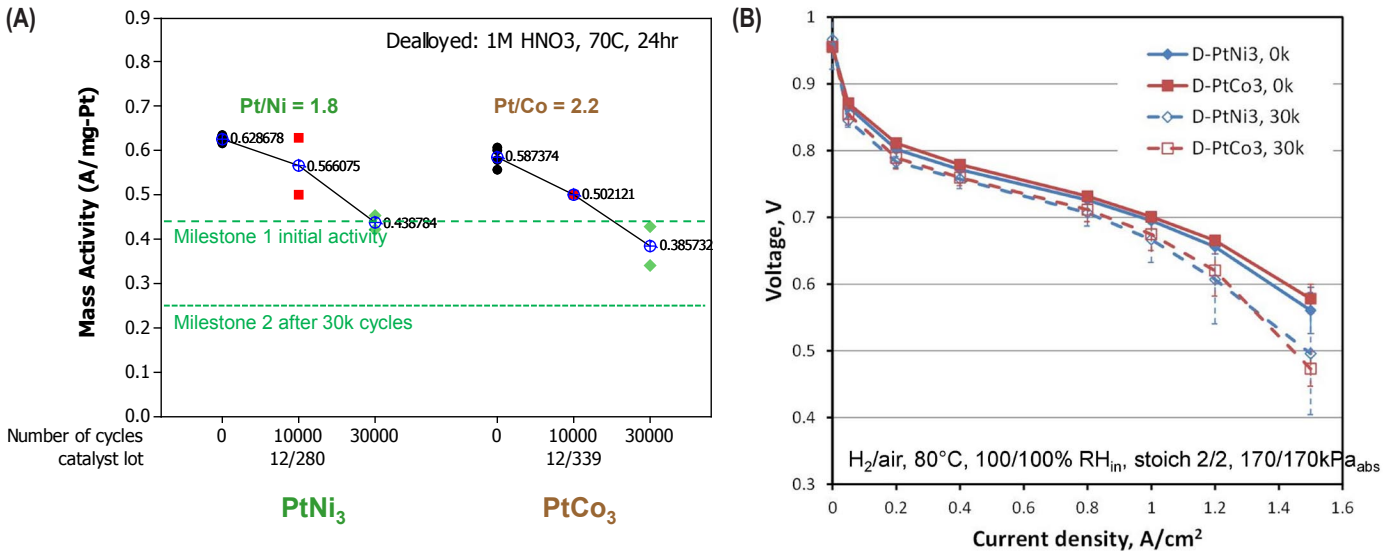

FIGURE 4. GM 50-cm^2 MEA (A) mass-activities and (B) H_2/air polarization curves of D-PtNi$_3$ and D-PtCo$_3$ catalysts as a function of voltage cycles. Both were dealloyed using the same condition (1M HNO_3, air, 70°C, 24 h).

Ni. The post-dealloying thermal annealing appeared to improve the stability when the precursors were sulfuric-acid/N_2-dealloyed, although it is unclear whether it offered any advantage when the precursors were nitric-acid/air-dealloyed.

To compare the activity and durability of PtNi and PtCo catalysts, JMFC prepared PtCo$_3$ precursor using the same synthetic path as the PtNi$_3$ new precursor (12/280) and then GM applied the same dealloying treatment to both precursors and evaluated them in 50-cm^2 MEAs. Figure 4 compares the durability of the ORR activity and H_2/air performance of these two catalysts. It is obvious that both catalysts perform very similarly over the course of testing. This is consistent with our original expectations based on the similarities of their known corrosion properties and heats of mixing between the two systems.

Two trips to the synchrotron beamlines (eight days at the National Synchrotron Light Source at Brookhaven National Laboratory, four days at the APS) were made in April this year to conduct X-ray absorption measurements by GWU and NEU on the above-tested and aged D-PtNi$_3$ catalysts, to correlate atomic-scale structure and composition with differences in activity and durability, to guide the further catalyst development. The analyses are underway.

CONCLUSIONS AND FUTURE DIRECTIONS

- The initial activity and durability criteria were met with multiple, large-batch, dealloyed catalysts thereby passing the gate decision.
- The particle size of the precursors was the dominant factor influencing durability. Catalysts prepared from smaller particle-size precursors resulted in Pt-shell over alloy-core morphology which appeared to have greater durability over the porous analogues.
- Both D-PtNi$_3$ and D-PtCo$_3$ showed very similar initial activity and retention of activity.
- In FY 2014, we will focus our effort to
  - Optimize manufacturable syntheses/treatments for uniform particle size and high surface area to maximize H_2/air fuel cell performance with low-Pt-loaded electrodes.
  - Perform durability testing on full-active-area cells and deliver to DOE for validation.
  - Perform advanced characterization to correlate atomic-scale structure and composition with activity and durability.

PATENTS ISSUED

1. U.S. Provisional Application No. 61/823,032, "Ternary dealloyed catalyst" Joint patent JMFC-GM.

FY 2013 PUBLICATIONS/PRESENTATIONS

Presentations and Published Abstracts

1. Strasser, P., "Materials for Fuel Cell Catalysts", American Chemical Society, San Diego, CA, March 26, 2012.

2. Strasser, P., "Core-Shell Nanoparticle Catalyst Concepts for High Performance Polymer Electrolyte Membrane Fuel Cells", keynote presentation at the Grove Fuel Cells 2012 Science & Technology Conference, Berlin, Germany, April 11, 2012.

3. Gan, L.; Heggen, M.; Rudi, S.; and Strasser, P., "Core-Shell Compositional Fine Structures of Dealloyed $Pt_{1-x}Ni_x$ Nanoparticles and their Impact on Oxygen Reduction Catalysis",Goettingen ETEM Workshop on Heterogeneous Catalysis, Surface Science and Energy Research, July 9–11, 2012, Goettingen, Germany.

4. Strasser, P., "Oxygen Electrocatalysis on Nanostructured Metal and Oxide Nanoparticles", Summer School on Electrocatalysis on Nanoparticles, August 5–9, 2012, Copenhagen, Denmark.

5. Ramaker, D.E., Caldwell, K., Mukerjee, S., Jia, Q., and Ziegelbauer, J.M. "Investigations on High Activity De-alloyed Pt_3Co Cathodic Catalysts using XAS", 53rd Annual Meeting of the International Society of Electrochemistry, Aug. 19–20, 2012, Prague, CZ, ISE#120638.

6. Strasser, P., "Nanostructured Electrocatalysts Based on Dealloyed Pt Bimetallic Alloys", International Society of Electrochemistry, August 19–24, Prague, Czech Republic.

7. Wagner, F.T.; Kongkanand, A.; Ziegelbauer, J.M.; Thompson, E.L.; Owejan, J.O.; and Liu, Z.Q., "High Activity Dealloyed Catalysts: Review of Progress against Milestones", review of project with DOE personnel, Honeoye Falls, NY, Sept. 19, 2012.

8. Ramaker, DE; Caldwell, K.; Mukerjee, S.; Jia, Q.; and Ziegelbauer, J.M., "High Activity De-alloyed PtM_n (M = Co and Ni) Cathodic Catalysts showing OO(H) or O(H) coverage on Pt Consistent with the Sabatier Model", Pacific Rim Meeting on Electrochemical and Solid-State Science, Honolulu, HI, Oct. 7–12, 2012.

9. Wagner, F.T.; Kongkanand, A.; Ziegelbauer, J.M.; Thompson, E.L.; Owejan, J.O.; and Liu, Z.Q., "High Activity Dealloyed Catalysts: Review of Progress against Milestones", review of project with DOE personnel, Honeoye Falls, NY, Nov. 8, 2012.

10. Binghong Han, Christopher Earl Carlton, Jin Suntivich, Zhichuan Xu, Yang Shao-Horn, "Roles of Transition Metal Chemistry on the Activity and Stability of Pt-alloy Nanoparticles," MRS Fall, 2012.

11. L Gan, M Heggen, S Rudi, P Strasser. Subsurface Enrichment in Highly Active Dealloyed PtxNi1-x Catalysts for Oxygen Reduction. Pacific Rim Meeting on Electrochemical and Solid-State Science (PRiME2012), Joint 222nd ECS Meeting, October 7–12, 2012. Hawaii, US.

12. D.E. Ramaker, X-ray Absorption Spectroscopy, an in operando probe of reactions in fuel cells and batteries, 245th ACS meeting, April 7–11, 2013, Ne Orleans, LA.

Publications

1. H.L. Xin, J.A. Mundy, Z. Liu, R. Cabezas, R. Hovden, L.F. Kourkoutis, J. Zhang, N.P. Subramanian, R. Makharia, F.T. Wagner, D.A. Muller, Atomic-resolution spectroscopic imaging of ensembles of nanocatalyst particles across the life of a fuel cell, Nano Letters, 12 (2012) 490-497.

2. Z.Y. Liu, H.L. Xin, Z.Q. Yu, Y. Zhu, J.L. Zhang, J.A. Mundy, D.A. Muller, F.T. Wagner, Atomic-Scale Compositional Mapping and 3-Dimensional Electron Microscopy of Dealloyed $PtCo_3$ Catalyst Nanoparticles with Spongy Multi-Core/Shell Structures, Journal of the Electrochemical Society, 159 (2012) F554-F559.

3. Z. Yu, J. Zhang, Z. Liu, J.M. Ziegelbauer, H. Xin, I. Dutta, D.A. Muller, F.T. Wagner, Comparison between dealloyed $PtCo_3$ and $PtCu_3$ cathode catalysts for proton exchange membrane fuel cells, Journal of Physical Chemistry C, 116 (2012) 19877-19885.

4. L. Gan, M. Heggen, R. O'Malley, B. Theobald, P. Strasser, Understanding and Controlling Nanoporosity Formation for Improving the Stability of Bimetallic Fuel Cell Catalysts, Nano Letters, 13 (2013) 1131-1138.

5. L. Gan, M. Heggen, S. Rudi, P. Strasser, Core–Shell Compositional Fine Structures of Dealloyed PtxNi1–x Nanoparticles and Their Impact on Oxygen Reduction Catalysis, Nano Letters, 12 (2012) 5423-5430.

6. C. Cui, L. Gan, H.H. Li, S.H. Yu, M. Heggen, P. Strasser, Octahedral PtNi nanoparticle catalysts: Exceptional oxygen reduction activity by tuning the alloy particle surface composition, Nano Letters, 12 (2012) 5885-5889.

7. A. Kongkanand, W. Gu, F.T. Wagner, Electrocatalyst Design in Proton Exchange Membrane Fuel Cells for Automotive Application, in: F. Tao, W. Schneider, P. Kamat (Eds.) Heterogeneous Catalysis at the Nanoscale for Energy Applications, Wiley-VCH, 2013. (one section on dealloyed catalyst)

8. Q. Jia, D.E. Ramaker, J.M. Ziegelbauer, N. Ramaswamy, A. Halder, S. Mukerjee, Fundamental Aspects of ad-Metal Dissolution and Contamination in Low and Medium Temperature Fuel Cell Electrocatalysis: A Cu Based Case Study Using In Situ Electrochemical X-ray Absorption Spectroscopy, The Journal of Physical Chemistry C, 117 (2013) 4585-4596.

9. Chunhua Cui, Lin Gan, Hui-Hui Li, Shu-Hong Yu, Marc Heggen and Peter Strasser, Octahedral PtNi nanoparticle catalysts: exceptional oxygen reduction activity by tuning the alloy particle surface composition. Nano Lett. 2012, 12 (11), 5885–5889.

10. Chunhua Cui, Mahdi Ahmadi, Farzad Behafarid, Lin Gan, Max Neumann, Marc Heggen, Beatriz Roldán Cuenya and Peter Strasser*, Shape-selective bimetallic nanoparticle electrocatalysts: evolution of their atomic-scale structure, chemical composition, and electrochemical reactivity under various chemical environments. Faraday Discuss., 2013, DOI: 10.1039/C3FD20159G.

11. Chunhua Cui, Lin Gan, Marc Heggen, Stefan Rudi and Peter Strasser*, Compositional segregation in shaped Pt alloy nanoparticles and their structural behavior during electrocatalysis. Nature Mater. 2013, accepted.

12. Gan L; Heggen M; O'Malley R; Theobald B; Strasser P (2013) Understanding and controlling nanoporosity formation for improving the stability of bimetallic fuel cell catalysts. Nano Lett 13:1131-1138.

13. Gan L; Heggen M; Rudi S; Strasser P (2012) Core-shell Compositional Fine Structures of Dealloyed PtxNi1-x Nanoparticles and their Impact on Oxygen Reduction Catalysis. Nano Lett 12:5423-5430.

14. Gan L; Rudi S; Cui CH; Strasser P (2013) Ni-catalyzed Growth of Graphene Layers During Thermal Annealing: Implications for the Synthesis of Carbon-supported Pt-Ni Fuel Cell Catalysts. ChemcatChem. (Submitted)

15. Gan L; Cui CH; Rudi S; Strasser P (2013) Core-shell and nanoporous particle architectures and their effect on the activity and stability of Pt ORR electrocatalysts. Top Catal (Submitted)

REFERENCES

1. Koh, S. and P. Strasser, *Electrocatalysis on bimetallic surfaces: Modifying catalytic reactivity for oxygen reduction by voltammetric surface dealloying.* Journal of the American Chemical Society, 2007. **129**(42): p. 12624-12625.

2. Strasser, P., et al., *Lattice-strain control of the activity in dealloyed core-shell fuel cell catalysts.* Nature Chemistry, 2010. **2**(6): p. 454-460.

3. Chen, S., et al., *Platinum-alloy cathode catalyst degradation in proton exchange membrane fuel cells: Nanometer-scale compositional and morphological changes.* Journal of the Electrochemical Society, 2010. **157**(1): p. A82-A97.

4. Oezaslan, M., M. Heggen, and P. Strasser, *Size-Dependent morphology of dealloyed bimetallic catalysts: Linking the nano to the macro scale.* Journal of the American Chemical Society, 2012. **134**(1): p. 514-524.

5. Erlebacher, J., et al., *Evolution of nanoporosity in dealloying.* Nature, 2001. **410**(6827): p. 450-453.

6. Wang, C., et al., *Design and synthesis of bimetallic electrocatalyst with multilayered Pt-skin surfaces.* Journal of the American Chemical Society, 2011. **133**(36): p. 14396-14403.

V.A.11 Development of Ultra-Low Platinum Alloy Cathode Catalysts for Polymer Electrolyte Membrane Fuel Cells

Branko N. Popov
University of South Carolina (USC)
301 Main Street
Columbia, SC 29208
Phone: (803) 777-7314
Email: popov@cec.sc.edu

DOE Managers
Donna Lee Ho
Phone: (202) 586-8000
Email: Donna.Ho@ee.doe.gov
Reg Tyler
Phone: (720) 356-1805
Email: Reginald.Tyler@go.doe.gov

Technical Advisor
Thomas Benjamin
Phone: (630) 252-1632
Email: benjamin@anl.gov

Contract Number: DE-EE0000460

Subcontractor:
Dr. Hansung Kim (Co-PI) Yonsei University, S. Korea.

Project Start Date: September 1, 2010
Project End Date: May 31, 2014

Overall Objectives

- Synthesize carbon composite catalyst (CCC) support and optimize the parameters that control the number of catalytic sites.
- Develop low cost and durable hybrid cathode catalyst (HCC).
- Develop Pt and Pt-alloy/activated graphitic carbon catalyst.
- Optimize the procedures for the formation of more active Pt-alloy catalysts.
- Develop facile scale up catalyst synthesis procedure (at least 100 g).
- Demonstrate kinetic mass activity in H_2/O_2 fuel cell higher than DOE target of 0.44 A mg_{PGM}^{-1} and durability of the mass activity (≤40% loss of initial mass activity).
- Demonstrate high current performance in H_2/air fuel cell that meets DOE targets and durability of high current performance in H_2/air under potential cycling (0.6-1.0 V) and potential holding (1.2 V) experimental conditions (≤30 mV loss at 0.8 A cm^{-2}).
- Construct short stack (50 cm^2 up to 10 cells) and evaluate the performance under simulated automotive conditions.

Fiscal Year (FY) 2013 Objectives

- Evaluation of different strategies for the optimization of HCC with total loadings of 0.2 mg_{Pt} cm^{-2} /membrane electrode assembly (MEA):
  - Initial and durability of kinetic mass activities.
  - Catalyst and support durability under potential cycling and potential holding experimental conditions, respectively.
- Synthesis and performance evaluation of Pt/USC-activated graphitic carbon (AGC) catalyst with total loadings of 0.2 mg_{Pt} cm^{-2}/MEA:
  - Initial and durability of kinetic mass activities.
  - Catalyst and support durability under potential cycling and potential holding experimental conditions, respectively.

Technical Barriers

This project addresses the following technical barriers from the Fuel Cells section of the Fuel Cell Technologies Office Multi-Year Research, Development, and Demonstration Plan:

(A) Durability

(B) Cost

(C) Performance

Technical Targets

In this project, studies are being conducted to develop highly active and stable ultra-low Pt loading cathode catalysts for polymer electrolyte membrane fuel cells. This includes HCC and Pt/USC-AGC catalysts using procedures developed at USC. These catalysts have the potential to meet the 2017 DOE technical target for electrocatalysts for transport applications as shown in Table 1.

FY 2013 Accomplishments

- Achieved initial mass activity of 0.38 A mg_{Pt}^{-1} and 0.2 A mg_{Pt}^{-1} after 30k cycles, and 0.19 A mg_{Pt}^{-1} (after 400 h potential holding) for the HCC catalyst.

TABLE1. Progress towards Meeting Technical Targets for Electrocatalysts for Transport Applications

Characteristic	Units	2017 Targets	Status
PGM total content	g/kW (rated)	0.125	0.32 Pt/USC-AGC 0.34 Pt/CCC
PGM total loading	mg cm^{-2}	0.125	0.2
Mass activity (80°C, 100% RH, 150 kPa_{abs}.)	A/mg_{Pt} @ 0.9 $V_{iR\text{-}free}$	0.44	0.38 A/mg_{Pt} HCC 0.25 A/mg_{Pt} Pt/USC-AGC
Catalyst durability (30,000 cycles, 0.6-1.0 V, 50 mV/s, 80/80/80, 100 kPa_{abs}., H_2/N_2)	% Mass activity loss % ECSA loss mV loss @ 0.8 A cm^{-2}	≤40% ≤40% ≤30 @ 0.8 A cm^{-2}	HCC 47% loss (MA) 15% loss (ECSA) 46 mV loss (H_2-air) Pt/USC-AGC 52% loss (MA) 51% loss (ECSA) 78 mV loss (H_2-air)
Support durability (1.2 V for 400 h at 80°C, H_2-$N_{2,\ 150}$ $kPa_{abs.}$ 100% RH)	% Mass activity loss % ECSA loss	≤40% ≤40% ≤30 mV @ 0.8 A cm^{-2}	HCC 50% loss (MA) 24% loss (ECSA) 29 mV loss (H_2-air) Pt/USC-AGC 32% loss (MA) 6% loss (ECSA) 18 mV loss (H_2-air)

PGM – platinum-group metal; iR – internal resistance; RH – relative humidity; ECSA – electrochemical surface area; MA – mass activity

- Accomplished potential losses (iR-corrected) of 46 and 29 mV after 30k cycles and 400 h potential holding, respectively for the HCC catalyst.
- Achieved initial mass activity of 0.25 A mg_{Pt}^{-1} and 0.12 A mg_{Pt}^{-1} after 30k cycles, and 0.17 A mg_{Pt}^{-1} (after 400 h potential holding) for the Pt/USC-AGC catalyst.
- Accomplished potential losses (iR-corrected) of 78 mV and 18 mV after 30 k cycles and 400 h potential holding, respectively for the Pt/USC-AGC catalyst.

✧ ✧ ✧ ✧ ✧

INTRODUCTION

Stable, highly active Pt/CCC and HCCs were developed that show higher performance than the commercial Pt/C at low loadings (≤0.1 mg cm^{-2}). The hybrid cathode catalyst is a combination of nitrogen-containing CCC and platinum, which shows higher activity for the oxygen reduction reaction (ORR) [1-12]. Pt catalyst deposited on USC activated graphitic carbon (Pt/USC-AGC) support with high activity towards oxygen reduction was synthesized and its catalytic activity was evaluated.

APPROACH

Currently, the main strategies to decrease the platinum loading in cathode electrodes are based on the optimization of electrode structures and implementation of more active Pt-alloy catalysts. The new approach used in this work consists of development of a hybrid cathode catalyst through a patented process. In brief, in-house developed procedures were used for the HCC synthesis including (a) CCC support synthesis using transition metal-assisted low temperature graphitization process, (b) surface modification of the CCC support for uniform Pt deposition, (c) platinum deposition on CCC support (Pt/CCC) using a modified polyol process, and (d) high temperature annealing process to control the catalyst particles size of the HCC catalyst. The goal of our second strategy is the synthesis of Pt catalyst deposited on activated graphitic carbon support developed at USC (Pt/USC-AGC).

RESULTS

In this reporting period (FY 2013), procedures for the synthesis of CCC and USC-AGC were optimized and used as catalyst supports for the preparation of Pt/CCC, HCC and Pt/USC-AGC catalysts. The performance of these catalysts was studied in 25-cm^2 single fuel cells according to the testing protocol suggested by the U.S. DRIVE Partnership/ Fuel Cell Technical Team. The catalyst durability was evaluated by cycling the cathode potential between 0.6 and 1.0 V under H_2/N_2 (200/75 cc min^{-1}) in the anode and cathode compartments, respectively at a cell temperature of 80°C and 100% RH. The support durability was evaluated by holding the potential at 1.2 V (vs. anode) under H_2/N_2 in the anode and cathode compartments, respectively at a cell temperature of 80°C, 100% RH and 150 kPa back pressure. The mass activity was evaluated under the following conditions: H_2/O_2

(stoic. 2/9.5); 100% RH; 80°C; and 150 kPa_{abs} back pressure. The H_2/air fuel cell performance was evaluated under the following conditions: H_2/air (stoic. 1.5/1.8); 40% RH; 80°C; and 150 kPa_{abs} back pressure.

Platinum was deposited on CCC support by a polyol method [13]. The initial fuel cell performances of 35 and 40% Pt/CCC under H_2/O_2 (constant flow, 750/750 sccm) and H_2/air (40% RH, 80°C, and 150 kPa_{abs} back pressure) are shown in Figure 1(a) and Figure 1(b), respectively. Figure 1(a) shows that both 35% and 40% Pt/CCC catalysts exhibit ~2.1 A cm^{-2} at 0.7 $V_{iR\text{-}free}$. The H_2/air fuel cell testing (Figure 1b) shows 1.25 A cm^{-2} for both the catalysts at 0.58 $V_{iR\text{-}free}$ (1.5/1.8 stoic.) and 1.35 A cm^{-2} at 0.58 $V_{iR\text{-}free}$ (1.5/2.0 stoichiometry). This high fuel cell performance is due to the synergistic effect between the Pt and CCC support, which itself possesses catalytic active sites for ORR.

The HCC catalyst was prepared by impregnating a transition metal salt in Pt/CCC, followed by the application of a protective coating and high temperature pyrolysis developed at USC. The protective coating prevented the Pt-alloy particle growth and uniform Pt-alloy particles of ~4.0 nm could be distributed on the CCC support. The HCC catalyst was subjected to both catalyst and support durability studies in a 25-cm^2 area MEA and the results are summarized and compared with that of a commercial 46% Pt/C catalyst in Table 2. The stability of mass activity of HCC and commercial 46% Pt/C catalysts are compared in Figure 2 which shows an initial mass activity of 0.38 A mg_{Pt}^{-1} and mass activity of 0.20 A mg_{Pt}^{-1} after 30k cycles in H_2/O_2, corresponding to a loss of 47% for the HCC catalyst. The commercial 46% Pt/C catalyst showed an initial and final (after 30k cycles) mass activities of 0.18 and 0.06 A mg_{Pt}^{-1}, respectively (67% loss). The ECSA of HCC

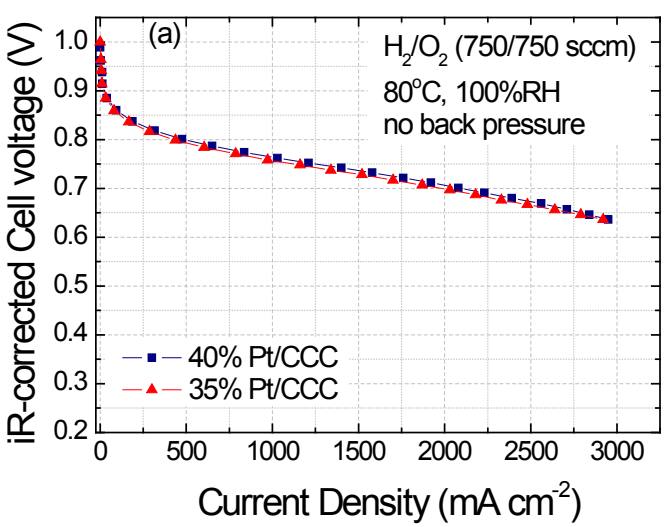

FIGURE 1(a). H_2/O_2 fuel cell performance of 35% and 40% Pt/CCC catalysts. The fuel cell operating conditions are: H_2/O_2 (750/750 sccm), 80°C, 100% RH, no back pressure. Nafion® NRE 212 membrane was used as the electrolyte.

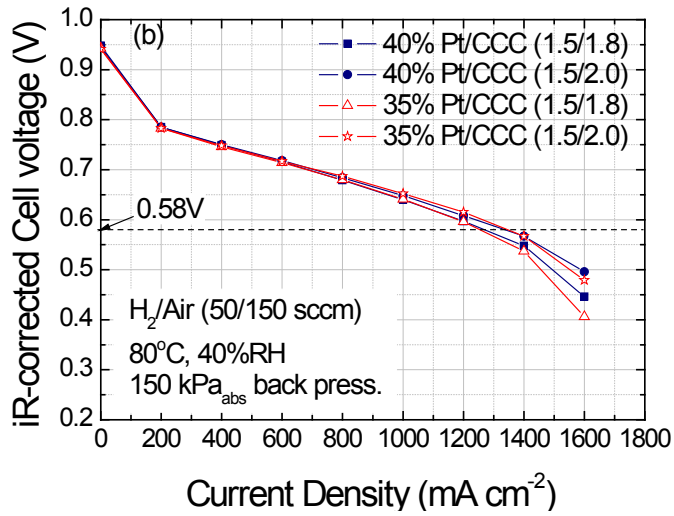

FIGURE 1(b). H_2/air fuel cell performance of 35% and 40% Pt/CCC catalysts. The fuel cell operating conditions are: H_2/air (1.5/1.8), 59°C, 40% RH, 150 kPa back pressure. Nafion® NRE 212 membrane was used as the electrolyte.

catalyst decreased from 23.2 to 19.8 m^2 g^{-1} after 30k cycles (15% loss). The H_2/air fuel cell polarization curves showed an initial H_2/air performance of 800 mA cm^{-2} at 0.607 $V_{iR\text{-}free}$ and 0.561 $V_{iR\text{-}free}$ after 30k cycles (iR-corrected voltage loss is 46 mV). The corresponding cell potential loss is 53 mV after 30k cycles. The loss in cell voltage is slightly higher than the 2017 DOE target (≤30 mV loss after 30k cycles). The cell potential loss of 53 mV after 30k cycles is much lower than that observed for the commercial 46% Pt/C catalyst (149 mV loss after 30k cycles) as shown in Table 2.

The results of support durability for the HCC catalyst are summarized in Table 2. The HCC catalyst showed an initial mass activity of 0.38 A mg_{Pt}^{-1}, which decreased to 0.19 A mg_{Pt}^{-1} after 400 h potential holding at 1.2 V. The HCC catalyst exhibited an initial H_2/air performance of 800 mA cm^{-2} at 0.644 $V_{iR\text{-}free}$ and decreased to 0.615 $V_{iR\text{-}free}$ after 400 h (iR-correcetd voltage loss is 29 mV). The cell voltage loss is also 29 mV after 400 h holding. The DOE 2017 target is ≤30 mV loss after 400 h potential holding. The ECSA decreased from 21.3 to 16.2 m^2 g^{-1} after 400 h (24% loss). These results indicate that the HCC catalyst is stable at high potentials due to the highly graphitized nature of the CCC support.

Platinum was deposited on USC-AGC support by a polyol method [13] with a particle size of ~3.1 nm. The catalyst durability test was performed by cycling the cathode between 0.6 and 1.0 V under H_2/N_2 and the results are summarized in Table 3. The Pt/USC-AGC catalyst shows an initial mass activity of 0.25 A mg_{Pt}^{-1}, which decreased to 0.12 A mg_{Pt}^{-1} after 30k cycles (52% loss). The ECSA decreased from 31.4 m^2 g^{-1} to 15.3 m^2 g^{-1}, corresponding to a loss of 51% after 30k cycles.

TABLE 2. Summary of Catalyst Stability Test (30k Potential Cycling between 0.6 and 1.0 V) and Support Stability Test (Potential Holding at 1.2 V for 400 h) for the HCC Catalyst

HCC	Particle size (nm)	Mass activity ($A\ mg_{Pt}^{-1}$)		ECSA ($m^2\ g^{-1}$)		Cell voltage loss at 800 mA cm^{-2} (mV)	
		Initial	Final	Initial	Final	V_{Cell}	$V_{iR\text{-}free}$
Catalyst Durability	4.0	**0.38**	0.2 (47% loss) (30k cycles)	23.2	19.8 (**15% loss**) (30k cycles)	**53** (30k cycles)	**46** (30k cycles)
Support Durability	4.0	0.38	0.19 (50% loss) (400 h)	21.3	16.2 (24% loss) (400 h)	29 (400 h)	29 (400 h)
Pt/C Catalyst Durability	2.2	**0.18**	0.06 (67% loss) (30k cycles)	67.8	11.8 (**82.6% loss**) (30k cycles)	**149** (30k cycles)	**142** (30k cycles)

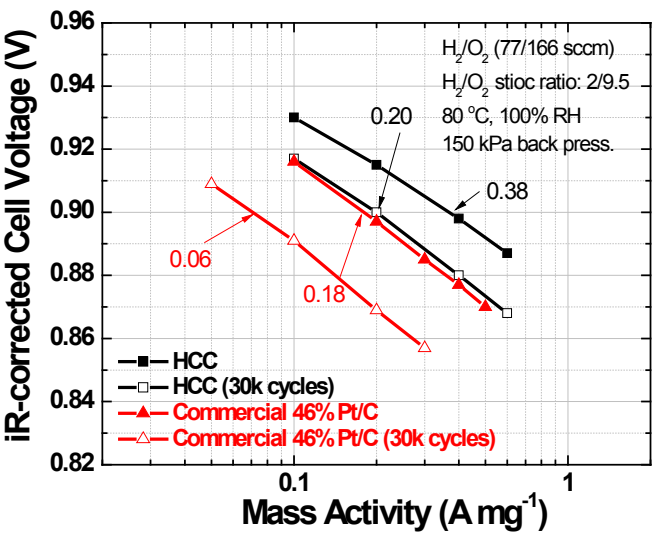

FIGURE 2. Comparison of mass activities of HCC and commercial 46% Pt/C catalysts before and after 30k potential cycling between 0.6 and 1.0 V. The fuel cell operating conditions are: H_2/O_2 (2.0/9.5), 80°C, 100% RH, 150 kPa_{abs} back pressure. Nafion® NRE 212 membrane was used as the electrolyte.

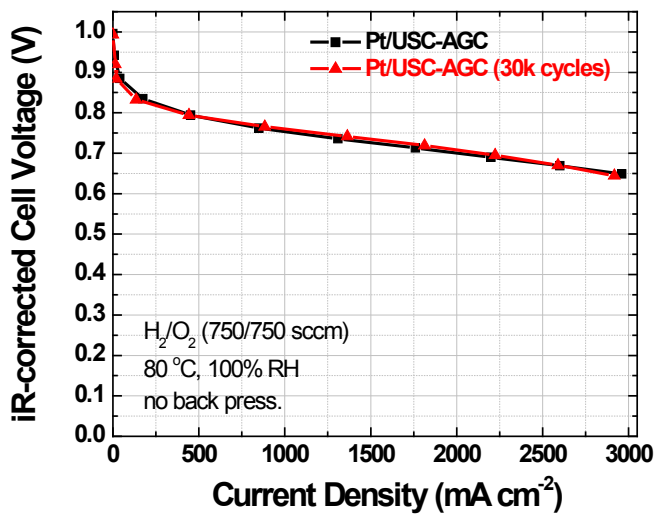

FIGURE 3. Comparison of H_2/O_2 fuel cell performance of Pt/USC-AGC catalyst before and after 30k potential cycling between 0.6 and 1.0 V. The fuel cell operating conditions are: H_2/O_2 (750/750 sccm), 80°C, 100% RH, no back pressure. Nafion® NRE 212 membrane was used as the electrolyte.

Table 3 also shows that the Pt/USC-AGC catalyst exhibits an initial H_2/air performance of 800 mA cm^{-2} at 0.668 $V_{iR\text{-}free}$ which decreased to 0.590 $V_{iR\text{-}free}$ after 30k cycles. The Pt/USC-AGC catalyst showed iR-corrected voltage loss of 78 mV and cell voltage loss of 82 mV after 30k cycles which are higher than the 2017 DOE targets (≤30 mV loss after 30k cycles). The cell potential loss of 82 mV after 30k cycles is much lower than that observed for the commercial 46% Pt/C catalyst (149 mV loss after 30k cycles) as shown in Table 2.

Additionally, the initial and final (after 30k cycles) H_2/O_2 (750/750 sccm) fuel cell performances of Pt/USC-AGC are compared in Figure 3. The initial and final fuel cell performances are identical at high- and low-potential regions for the Pt/USC-AGC catalyst. This result indicates that the catalyst activity of Pt/USC-AGC catalyst is stable during the potential cycling experiment.

The support durability test for the Pt/USC-AGC catalyst was evaluated in 25-cm^2 area MEAs. The mass activity and H_2/air fuel cell performance was measured at regular intervals and the results are summarized in Table 3. The Pt/USC-AGC catalyst shows an initial mass activity of 0.25 A mg_{Pt}^{-1}, which decreased to 0.17 A mg_{Pt}^{-1} after 400 h potential holding at 1.2 V. The observed mass activity loss of 32% and ECSA loss of 6% are much lower than the 2017 DOE target of ≤40% loss after 400 h potential holding.

The initial and final (400 h) H_2/air fuel cell polarization curves are compared in Figure 4. The Pt/USC-AGC catalyst exhibits an initial H_2/air performance of 800 mA cm^{-2} at 0.671 $V_{iR\text{-}free}$ and decreased to 0.653 $V_{iR\text{-}free}$ after 400 h potential holding at 1.2 V. The voltage losses are 18 (iR-free)

TABLE 3. Summary of Catalyst Stability Test (30k Potential Cycling between 0.6 and 1.0V) and Support Stability Test (Potential Holding at 1.2 V for 400 h) for the Pt/USC-AGC Catalyst

Pt/AGC	Particle size (nm)	Mass activity (A mg_{Pt}^{-1})		ECSA (m^2 g^{-1})		Cell voltage loss at 800 mA cm^{-2} (mV)	
		Initial	Final	Initial	Final	V_{Cell}	$V_{iR\text{-}free}$
Catalyst Durability	3.1	0.25	0.12 (52% loss) (30k cycles)	31.4	15.3 (51% loss) (30k cycles)	82 (30k cycles)	78 (30k cycles)
Support Durability	3.1	0.25	0.17 (32% loss) (400 h)	31.4	29.5 (6% loss) (400 h)	29 (400 h)	18 (400 h)

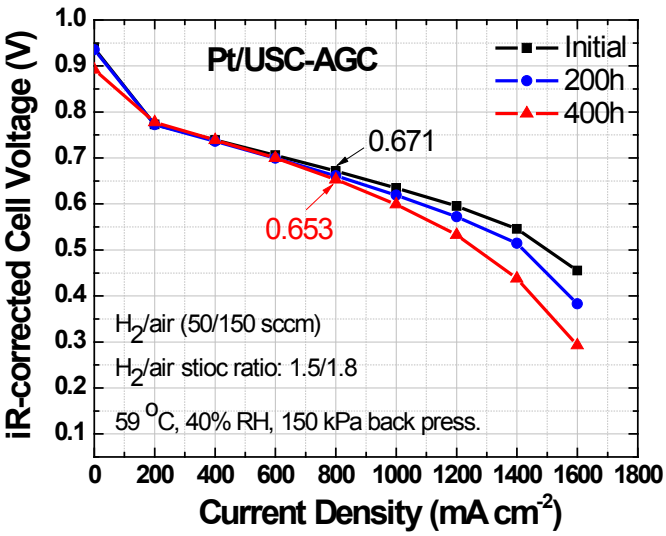

FIGURE 4. H_2/air fuel cell performance of Pt/AGC before and after 400 h potential holding at 1.2 V. The fuel cell operating conditions are: H_2/air (1.5/1.8), 59°C, 40% RH, 150 kPa back pressure. Nafion® NRE 212 membrane was used as the electrolyte.

and 29 mV (cell voltage) after 400 h cycles. The DOE 2017 target is ≤30 mV loss after 400 h potential holding. These results indicate that the Pt/USC-AGC catalyst is stable at high potentials due to the highly graphitized nature of the USC-AGC support.

Further catalyst and MEA optimization studies are in progress in order to increase the high current density performance of the HCC and Pt/USC-AGC catalysts to meet the 2017 DOE targets.

CONCLUSIONS AND FUTURE DIRECTIONS

Conclusions

- Achieved initial mass activity of 0.38 A mg_{Pt}^{-1} and 0.2 A mg_{Pt}^{-1} after 30k cycles (47% loss) and 0.19 A mg_{Pt}^{-1} (50% loss after 400 h potential holding) for the HCC catalyst.
- Accomplished iR-corrected potential losses of 46 mV and 29 mV after 30k cycles and 400 h potential holding experiments, respectively for the HCC catalyst.
- Accomplished ECSA losses of 15% and 24% after 30k cycles and 400 h potential holding experiments, respectively for the HCC catalyst.
- Achieved initial mass activity of 0.25 A mg_{Pt}^{-1} and 0.12 A mg_{Pt}^{-1} after 30k cycles (52% loss) and 0.17 A mg_{Pt}^{-1} (32% loss after 400 h potential holding) for the Pt/USC-AGC catalyst.
- Accomplished iR-corrected potential losses of 78 mV and 18 mV after 30k cycles and 400 h potential holding, respectively for the Pt/USC-AGC catalyst.
- Accomplished ECSA losses of 51% and 6% after 30k cycles and 400 h potential holding experiments, respectively for the Pt/USC-AGC catalyst.

Future Anticipated Accomplishments

- Synthesis of highly stable and highly graphitized CCC and AGC supports with Brunauer-Emmett-Teller surface area of 150-200 m^2/g.
- Transition metal content optimization studies and synthesis of HCC and Pt-alloy/USC-AGC catalysts containing low transition metal content (<8 wt%) in the alloy.
- Optimizing the procedures to purify the high temperature treated CCC and USC-AGC.

The goal is to select a best performing catalyst which satisfies the 2017 DOE requirements of ≤40% loss of mass activity, ≤40% loss of ECSA and ≤30 mV loss at 0.8 A/cm^2 under H_2-air after 30k potential cycling (between 0.6 and 1.0 V) and potential holding (at 1.2 V for 400 h) experiments.

FY 2013 PUBLICATIONS/PRESENTATIONS

Publications

1. Ákos Kriston, Tianyuan Xie, David Gamliel, Prabhu Ganesan, Branko N. Popov, "Effect of Ultra-Low Pt Loading on Mass Activity of PEM Fuel Cells," *J. Power Sources*, **243** (2013) 958-963.

2. Akos Kriston, Tianyuan Xie, Prabhu Ganesan, Branko N. Popov, "Effect of Pt Loading on Mass and Specific Activity in PEM Fuel Cells," *J. Electrochem. Soc*., **160** (2013) F406-F412.

3. Branko N. Popov, Tianyuan Xie, Taekeun Kim, Won-suk Jung, Akos Kriston Brian Murphy and Prabhu Ganesan, "Development of Ultra-Low Pt Alloy Cathode Catalyst for PEM Fuel Cells," *ECS Transactions*, **50** (2) (2013) 773-785.

4. Tianyuan Xie, Taekeun Kim, Won Suk Jung, Kriston Akos Prabhu Ganesan and Branko N. Popov, "Development of Highly Active Pt_2Ni/C Catalyst for PEM Fuel Cell," *ECS Transactions*, **50** (2) (2013) 1615-1626.

5. Taekeun Kim, Won Suk Jung, Tianyuan Xie, Akos Kriston, Prabhu Ganesan, David Gamliel, Brian Murphy and Branko N. Popov, "Development of Hybrid Cathode Catalyst for PEM Fuel Cells," *ECS Transactions*, **50** (2) (2013) 1875-1885.

6. Akos Kriston, Tianyuan Xie, Taekeun Kim, Won Suk Jung, David Gamliel, Brian Murphy Prabhu Ganesan, Branko N. Popov, "Analyzing the effect of Ultra-Low Pt Loading on Mass and Specific Activity of PEM Fuel Cells," *ECS Transactions*, **50**, (2013) 1427-1438.

Presentations

1. Akos Kriston, Tianyuan Xie, Taekeun Kim, Won Suk Jung, David Gamliel, Brian Murphy Prabhu Ganesan, Branko N. Popov, Analyzing the effect of Ultra-Low Pt Loading on Mass and Specific Activity of PEM Fuel Cells, *222nd ECS Meeting*, Honolulu, HI, October 7–12, 2012.

2. Branko N. Popov, Tianyuan Xie, Taekeun Kim, Won-suk Jung, Akos Kriston Brian Murphy, David Gamliel and Prabhu Ganesan, Development of Ultra-Low Pt Alloy Cathode Catalyst for PEM Fuel Cells, *222nd ECS Meeting*, Honolulu, HI, October 7–12, 2012.

3. Tianyuan Xie, Won Suk Jung, Taekeun Kim, Kriston Akos Prabhu Ganesan and Branko N. Popov, Development of Highly Active Pt_2Ni/CCC Catalyst for PEM Fuel Cell, *222nd ECS Meeting*, Honolulu, HI, October 7–12, 2012.

4. Taekeun Kim, Won Suk Jung, Tianyuan Xie, Akos Kriston, Prabhu Ganesan, David Gamliel, Brian Murphy and Branko N. Popov, Development of Hybrid Cathode Catalyst for PEM Fuel Cells, *222nd ECS Meeting*, Honolulu, HI, October 7–12, 2012.

REFERENCES

1. N.P. Subramanian, S.P. Kumaraguru, H.R. Colon-Mercado, H. Kim, B.N. Popov, T. Black and D.A. Chen, "Studies on Co-Based Catalysts Supported on Modified Carbon Substrates for PEMFC Cathodes," *J. Power Sources*, **157** (2006) 56-63.

2. R.A. Sidik, A.B. Anderson, N.P. Subramanian, S.P. Kumaraguru and B.N. Popov, "O_2 Reduction on Graphite and Nitrogen-Doped Graphite: Experiment and Theory," *J. Phys. Chem. B*, **110** (2006) 1787-1793.

3. X. Li, H.R. Colon-Mercado, G. Wu, J.-W. Lee, B.N. Popov, "Development of Method for Synthesis of Pt-Co Cathode Catalysts for PEM Fuel Cells," *Electrochem. Solid-State Lett.*, **10** (2007) B201-B205.

4. Nallathambi, Vijayadurga; Lee, Jong-Won; Kumaraguru, Swaminatha P, Wu, Gang; Popov, Branko N, "Development of high performance carbon composite catalyst for oxygen reduction reaction in PEM Proton Exchange Membrane fuel cells," *J. Power Sources*, **183** (2008) 34-42.

5. Subramanian, Nalini P, Li, Xuguang, Nallathambi, Vijayadurda, Kumaraguru, Swaminatha P, Colon-Mercado, Hector, Wu, Gang, Lee, Jong-Won, Popov, Branko N, "Nitrogen-modified carbon-based catalysts for oxygen reduction reaction in polymer electrolyte membrane fuel cells," *J. Power Sources*, **188** (2009) 38-44.

6. Liu, Gang, Li, Xuguang, Ganesan, Prabhu, Popov, Branko N, Development of non-precious metal oxygen-reduction catalysts for PEM fuel cells based on N-doped ordered porous carbon," *Appl. Catal. B: Environmental,* **93** (2009) 156-165.

7. Liu, Gang, Li, Xuguang, Ganesan, Prabhu, Popov, Branko N, "Studies of oxygen reduction reaction active sites and stability of nitrogen-modified carbon composite catalysts for PEM fuel cells," *Electrochim. Acta*, **55** (2010) 2853-2858.

8. Li, Xuguang, Park, Sehkyu, Popov, Branko N, "Highly stable Pt and PtPd hybrid catalysts supported on a nitrogen-modified carbon composite for fuel cell application," *J. Power Sources*, **195** (2010) 445-452.

9. Xuguang Li, Gang Liu, Branko N. Popov, "Activity and stability of non-precious metal catalysts for oxygen reduction in acid and alkaline electrolytes," *J. Power Sources*, **195** (2010) 6373-6378.

10. B.N. Popov, X. Li and J.W. Lee, "Power source research at USC: Development of advanced electrocatalysts for polymer electrolyte membrane fuel cells," *Int. J. Hyd. Energy*, **36** (2011) 1794-1802.

11. Xuguang Li, Branko N. Popov, Takeo Kawahara, Hiroyuki Yanagi, "Non-precious metal catalysts synthesized from precursors of carbon, nitrogen, and transition metal for oxygen reduction in alkaline fuel cells," *J. Power Sources*, 196 (2011), 1717-1722.

12. Gang Liu, Xuguang Li, Jong-Won Lee and Branko Popov, "A Review of the Development of Nitrogen Modified Carbon-based catalyst for Oxygen Reduction at USC," *Catalysis Science & Technology,* 1, (2011) 207-217.

13. N. Long, N. Chien, T. Hayakawa, H. Hirata, G. Lakshminarayana, M. Nogami, "The synthesis and characterization of platinum nanoparticles: a method of controlling the size and morphology," *Nanotechnology* **21** (2010) 035605/1~035605/16.

V.A.12 Non-Precious Metal Fuel Cell Cathodes: Catalyst Development and Electrode Structure Design

Piotr Zelenay (Primary Contact), R. Borup, H. Chung, D. Langlois, Q. Li, G. Wu
Materials Physics and Applications Division
Los Alamos National Laboratory (LANL)
Los Alamos, NM 87545
Phone: (505) 667-0197
Email: zelenay@lanl.gov

DOE Manager
Nancy Garland
Phone: (202) 586-5673
Email: Nancy.Garland@ee.doe.gov

Subcontractors:
- J. Ziegelbauer, General Motors, Honeoye Falls, NY
- M. Odgaard, IRD Fuel Cells, Albuquerque, NM
- S. Litster, Carnegie Mellon University, Pittsburgh, PA
- M. Neidig, University of Rochester, Rochester, NY
- Z. Chen, University of Waterloo, Waterloo, Canada
- K. L. More, Oak Ridge National Laboratory, Oak Ridge, TN

Project Start Date: April 1, 2013
Project End Date: March 31, 2016

Overall Objectives

Advance non-platinum-group metal (non-PGM) cathode technology through the development and implementation of novel materials and concepts for oxygen reduction catalysts and electrode layers with:

- Oxygen reduction reaction (ORR) activity viable for practical fuel cell systems
- Much improved durability
- Sufficient ionic/electronic conductivity within the catalyst layer
- Adequate oxygen mass transport
- Effective removal of the product water

Fiscal Year (FY) 2013 Objectives

- Optimize the most active LANL catalysts by the heat-treatment approach for maximum hydrogen-air performance
- Synthesize non-pyrolyzed phthalocyanine-derived catalysts
- Develop testing protocols for the evaluation of the performance durability of non-PGM catalysts

Technical Barriers

This project addresses the following technical barriers from the Fuel Cells section of the Fuel Cell Technologies Office Multi-Year Research, Development, and Demonstration Plan [1]:

(A) Durability (catalysts, electrode layers)

(B) Cost (catalyst, membrane electrode assemblies [MEAs])

(C) Performance (catalysts, electrodes, MEAs)

Technical Targets

Non-PGM fuel cell catalyst research in this project focuses on the DOE technical targets in Table 3.4.13 in Section 3.4.4 (Technical Challenges) of the Multi-Year Research, Development, and Demonstration Plan [1]. The main DOE performance target for non-Pt (more precisely, non-PGM) ORR catalysts is listed in Table 1.

The ultimate technical targets of the project are:

- Volumetric catalyst activity in MEA at 0.80 V (*i*R-free), 80°C: ≥300 A cm^{-3}
- Four-electron selectivity (rotating ring-disk electrode): ≥99%; H_2O_2 ≤ 1%
- MEA maximum power density at 80°C: ≥1.0 W cm^{-2}
- Performance loss at 0.80 A cm^{-2} after 30,000 cycles in N_2: ≤30 mV

TABLE 1. Project Technical Targets

Table 3.4.13 Technical Targets: Electrocatalysts for Transportation Applications				
Characteristic	Unit	2011 Status	Targets	
			2017	2020
Non-Pt catalyst activity per volume of supported catalyst	A/cm^3 @ 800 $mV_{IR\text{-}free}$	60 (measured at 0.8 V) 165 (extrapolated from >0.85 V)	300	300

IR-free – internal resistance free

APPROACH

Materials development, which represents the core of this research effort, focuses on the following four groups of catalysts and supports: (1) heat-treated catalysts obtained using multiple nitrogen precursors; (2) alternative supports for heat-treated catalysts; (3) non-pyrolyzed phthalocyanine-derived catalysts; and (4) metal-free catalysts based on nitrogen-doped nanostructures.

In FY 2013, we have concentrated on the optimization of heat-treated metal-nitrogen-carbon catalysts. A new Fe-based catalyst derived from polyaniline (PANI) has been synthesized and characterized (Figure 1). The surface area of this catalyst is ca. 1,100 m^2/g, significantly more than the surface area of non-PGM catalysts prepared previously. This new catalyst exhibits improved fuel cell performance, reaching a current density of more than 100 mA/cm^2 at 0.8 V (*i*R-free) in fuel cell testing (Figure 2). The latter performance already matches the state of the art in non-PGM electrocatalysis of oxygen reduction in an operating MEA.

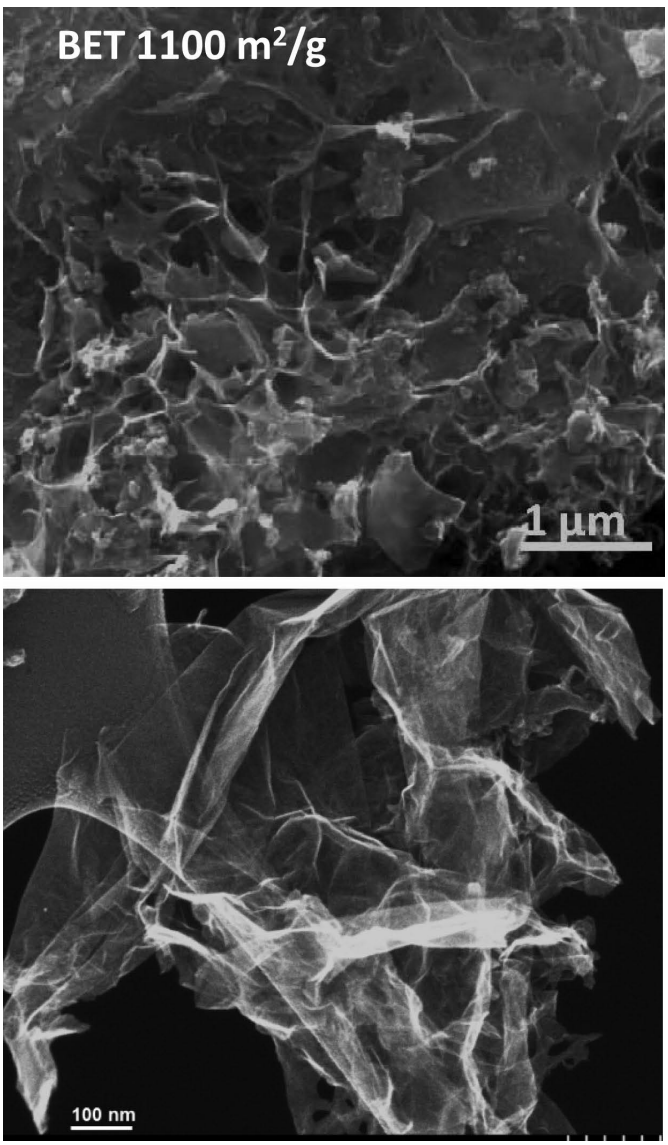

FIGURE1. Morphology of the high surface-area PANI-Fe-C catalyst.

In another part of the catalyst development effort, nitrogen-doped carbon nanotubes were prepared with strictly controlled tube diameter and nitrogen functionalities by varying transition metals precursors (Figure 3). Given the commonly accepted hypothesis that ORR active sites species are embedded into the graphitized carbon structures [2], the highly graphitic nanotubes can offer a potentially attractive host for the ORR active sites in non-PGM catalysts under the development in this project by enhancing catalytic activity. Improvements to the catalyst performance durability and even mass transfer are also possible.

Extensive catalyst characterization effort has begun with the purpose of evaluating the performance and understanding the nature of the ORR active site(s). In particular, a new characterization technique of nuclear resonance vibrational spectroscopy (NRVS) is being combined with density functional theory (DFT) to study the surface active Fe species and to elucidate the nature of active site(s) (Figure 4, left). In the part of the project that concentrates on the electrode layer design and characterization, microstructered electrode scaffold (MES) diagnostics has been used to measure spatiotemporal, through-plane distribution of potential, conductivity, and reaction rate (Figure 4, right). The ultramicroelectrode measurements of O_2 concentration in the electrode have been realized by flux-interrupt method. The newly developed in situ current-probe technique allows for accurate conductivity determination.

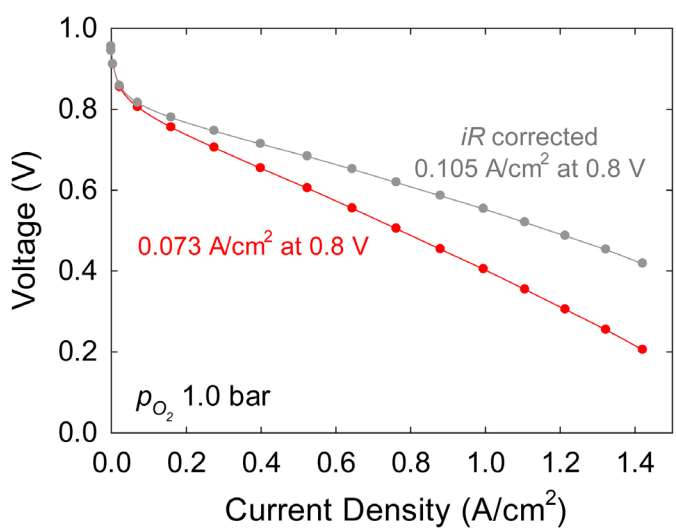

FIGURE 2. Fuel cell performance of the high surface-area PANI-Fe-C catalyst. Anode: 2.0 mg/cm^2 Pt; cathode: 4.1 mg/cm^2; cell temperature: 80°C; 100% relative humidity; membrane: two Nafion® 212 layers.

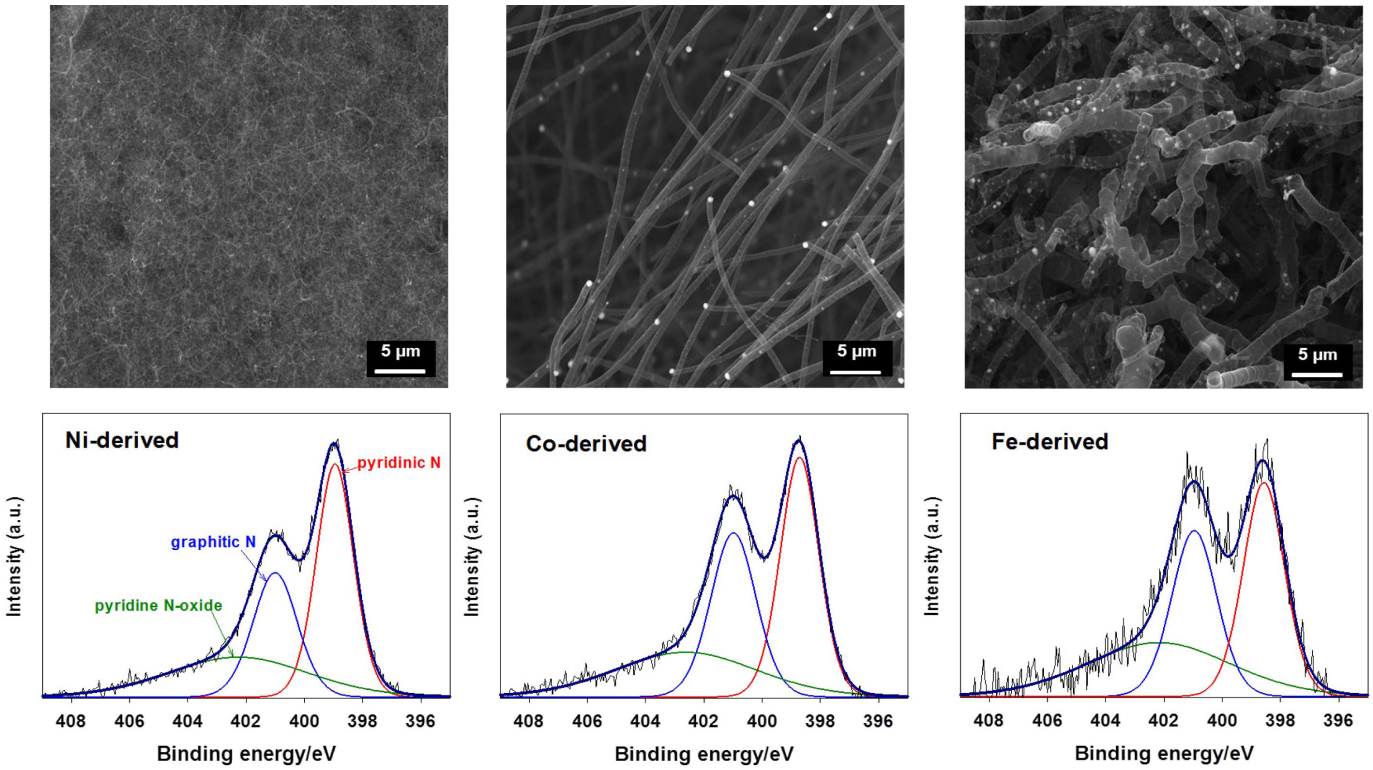

FIGURE 3. Nitrogen-doped carbon micro- and nano-tubes with the diameter and nitrogen functionalities controlled by the transition metal used in the synthesis. Top: scanning electron microscopy images; bottom: corresponding N1s X-ray photoelectron spectroscopy data.

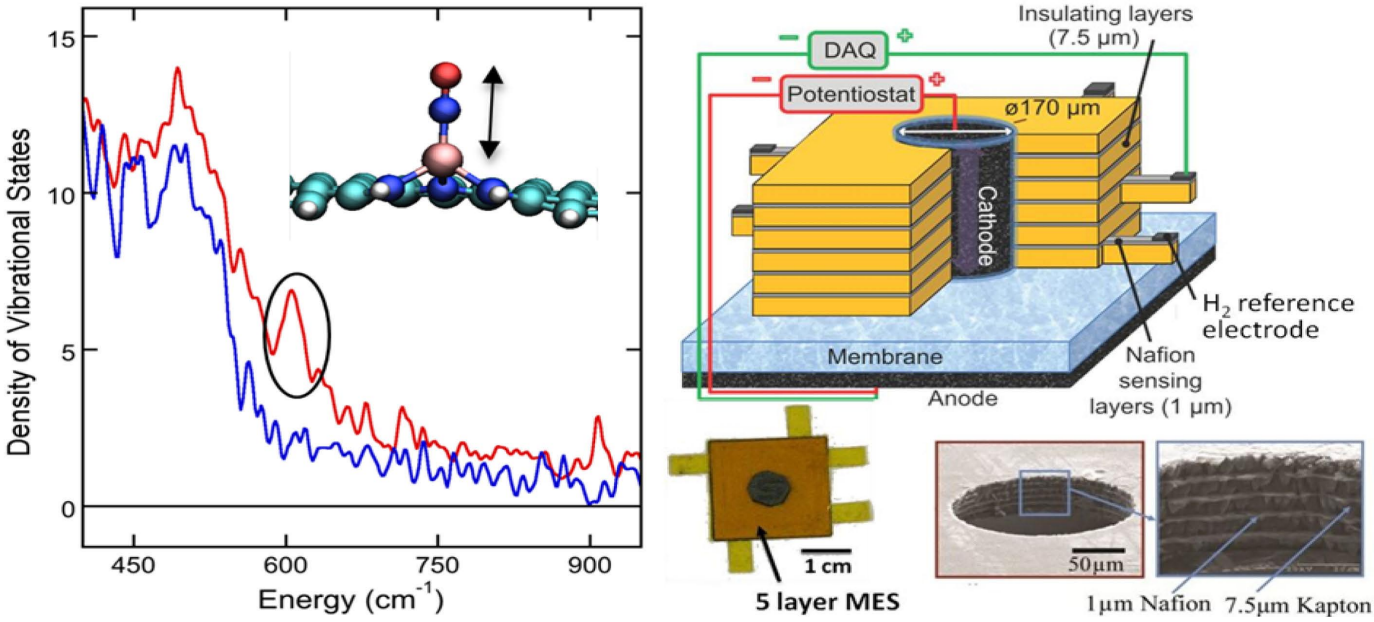

Nafion is a registered trademark of E. I. du Pont de Nemours and Company

FIGURE 4. Selected catalyst and electrode characterization methods. Left: NRVS spectra with DFT-assigned vibrational mode of the NO probe molecule; right: MES diagnostics.

A careful cathode design is required to (1) enhance the mass transport of oxygen, (2) assure sufficient protonic conductivity, (3) prevent catalyst layer flooding, and (4) make non-PGM catalysts potentially viable for automotive applications. Once optimized, the cathodes will undergo a scale-up, necessary for obtaining the project deliverable, a 50-cm^2 MEA (Figure 5).

FY 2013 ACCOMPLISHMENTS

- High-surface-area, graphene-rich, PANI-derived catalyst was synthesized and tested in a fuel cell, reaching current density in excess of 0.1 A/cm^2 at 0.8 V (already matching the state of the art in non-PGM cathode performance).
- Carbon nano/micro tubes were synthesized using a one-step, simple synthesis method that assures high yields and requires no further purification; the control over the tube diameter and the nature of nitrogen functionalities was achieved via proper selection of a transition metal.
- Three-dimensional graphene-based nanostructures were synthesized in order to enhance non-PGM catalyst utilization while maintaining high electron conductivity; methodology possibly adaptable to heat-treated non-PGM ORR catalysts under development at LANL.
- Electrospinning was successfully used in the preparation of three-dimensional non-PGM electrodes.
- NRVS was demonstrated to be a surface-specific technique, of considerable value to the ORR active site studies with Fe-based non-PGM catalysts.

FUTURE DIRECTIONS

Catalyst Development:

- Development and optimization of multi-nitrogen-precursor, heat-treated ORR catalysts with high activity and four-electron selectivity.
- Synthesis of non-PGM catalysts supported on highly-graphitic carbon(s) as a way of enhancing active-site density and improving performance durability.
- Validation of the metal-free approach in ORR electrocatalysis.
- Development of the durability and stress-test cycling protocols specific to non-PGM catalysts, (including a realistic potential/voltage window under specific environmental conditions of humidity, reagent stoichiometry, etc.).

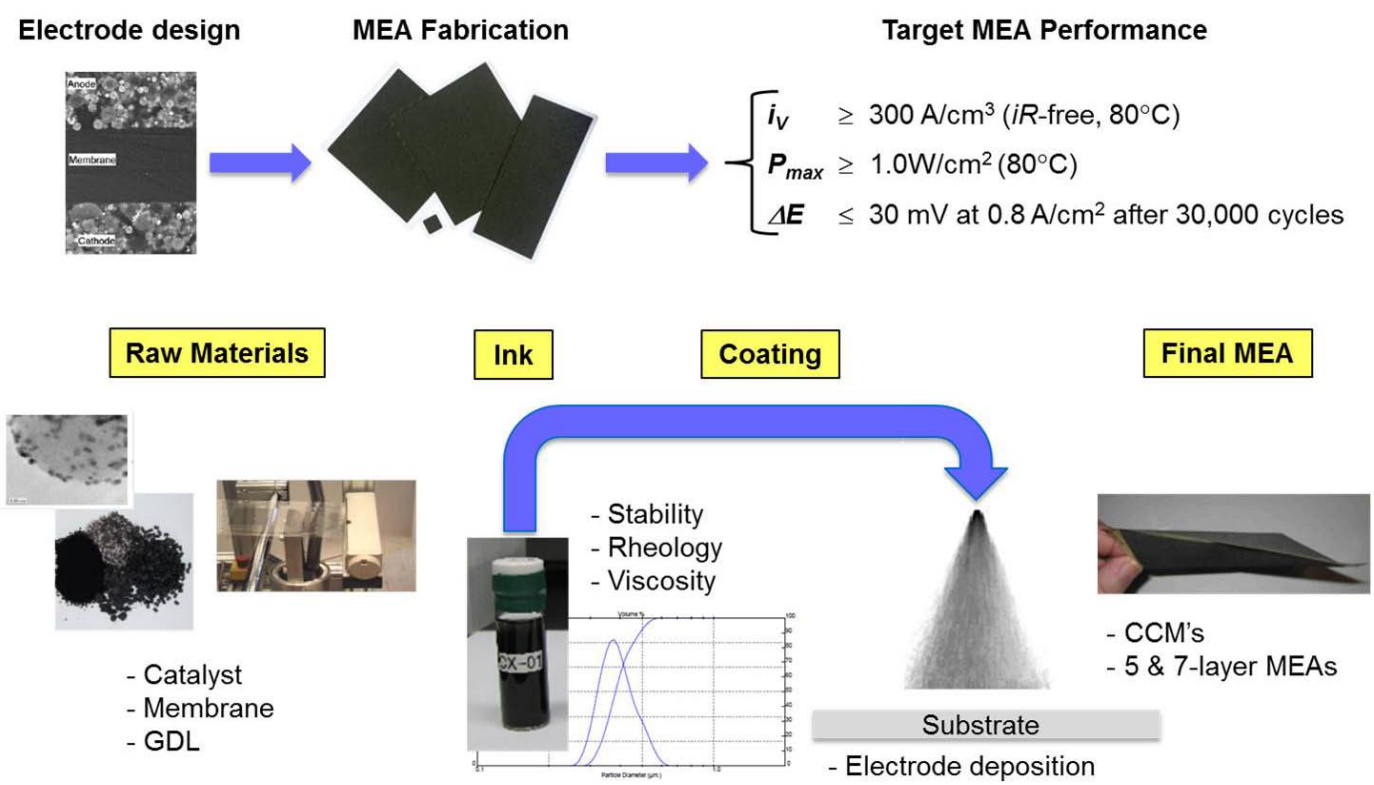

FIGURE 5. A scheme of MEA fabrication with targets.

Characterization:

- Validation of the surface-probe approach for the ORR active-site identification.
- Full implementation of advanced catalyst characterization methods (NRVS, magnetic circular dichroism, Mößbauer, MES, low-voltage aberration-corrected scanning transmission electron microscopy, high-resolution scanning electron microscopy/scanning transmission electron microscopy, inductively coupled plasma, X-ray fluorescence, nano-X-ray computer tomography, X-ray absorption, thermogravimetric analysis, porosimetry, etc.) in non-PGM catalysis studies.

Electrode Design and Modeling:

- Initiation of the predictive model for non-PGM catalyst layers (ORR activity, conductivity, and O_2 transport); validation of the preliminary model.
- Adoption of the agglomerate model to non-PGM cathodes.
- Complete implementation of the pore-scale model.
- Fabrication of MEAs with optimized microstructure and morphology.
- Demonstration of Generation-1 spray-coated MEA with non-PGM cathode.

SPECIAL RECOGNITIONS & AWARDS/ PATENTS ISSUED

1. Piotr Zelenay, The Electrochemical Society Energy Technology Division Research Award, The Electrochemical Society Meeting, Toronto, Canada, May 2013.

FY 2013 PUBLICATIONS (SINCE APRIL 2013)

1. G. Wu, K.L. More, P. Xu, H.-L.Wang, M. Ferrandon, A.J. Kropf, D.J. Myers, S. Ma, C.M. Johnston, P. Zelenay, A Carbon-Nanotube-Supported Graphene-Rich Non-Precious Metal Oxygen Reduction Catalyst with Enhanced Performance Durability, *Chem. Commun.*, **49**, 3291-3293, 2013.

2. G. Wu, P. Zelenay, Nanostructured Non-Precious Metal Catalysts for Oxygen Reduction Reaction., *Acc. Chem. Res.*, doi:10.1021/ar400011z, 2013.

3. H.T. Chung, J.H. Won, P. Zelenay, Active and Stable Carbon Nanotube/Nanoparticle Composite Electrocatalyst for Oxygen Reduction. *Nat. Commun.*, doi:10.1038/ncomms2944, 2013.

FY 2013 PRESENTATIONS (SINCE APRIL 2013)

1. Hydrogen and Fuel Cells Zing Conference 2013, Silverado Resort and Spa, Napa, California, July 12–15, 2013. Title: "Nanostructure *vs.* Reactivity of Non-Precious Metal Oxygen Reduction Catalysts;" H. T. Chung, G. Wu and P. Zelenay (invited lecture).

2. First International Conference on Electrochemical Materials and Technologies for Clean Sustainable Energy, Guangzhou, China, July 5–9, 2013. Title: "The Effect of Carbon Derived from Different Nitrogen Precursors on Oxygen Reduction Activity of Non-Precious Metal ORR Catalysts;" P. Zelenay, G. Wu, Q. Li, H.T. Chung (invited keynote lecture).

3. U.S. Department of Energy, Energy Efficiency and Renewable Energy, Fuel Cell Technologies Program, 2013 Merit Review and Peer Evaluation Meeting, Arlington, VA, May 13–17, 2013. Title: " Non-Precious Metal Fuel Cell Cathodes: Catalyst Development and Electrode Structure Design;" P. Zelenay (delivered by R. Borup) (DOE invited poster presentation).

REFERENCES

1. *Multi-Year Research, Development and Demonstration Plan: Section 3.4 Fuel Cells*, Fuel Cell Technologies Program, 2011. http://www1.eere.energy.gov/hydrogenandfuelcells/mypp/pdfs/fuel_cells.pdf

2. G. Wu, P. Zelenay, Nanostructured Non-Precious Metal Catalysts for Oxygen Reduction Reaction, *Acc. Chem. Res.*, doi:10.1021/ar400011z, 2013.

V.B.1 Dimensionally Stable High Performance Membrane

Cortney Mittelsteadt (Primary Contact),
Avni A. Argun, Castro Laicer
Giner, Inc./Giner Electrochemical Systems (GES), LLC
89 Rumford Avenue
Newton, MA 02466
Phone: (781) 529-0529
Email: cmittelsteadt@ginerinc.com

DOE Manager
Donna Ho
Phone: (202) 586-8000
Email: Donna.Ho@ee.doe.gov

Technical Advisor
John Kopasz
Phone: (630) 252-7531
Email: Kopasz@anl.gov

Contract Number: DE-EE0004533

Project Start Date: October 1, 2010
Project End Date: June 30, 2014

Overall Objectives

- Achieve mechanically supported, low equivalent-weight (EW) thin film ionomers that meet the DOE performance and cost targets for fuel cell membranes
- Demonstration of a cost-effective, roll-to-roll adaptable membrane electrode assembly (MEA) fabrication method
- Commercialization of Dimensionally Stable Membranes (DSM™) for highly reliable fuel cell systems

Fiscal Year (FY) 2013 Objectives

- Develop a robust, scalable process to fabricate 5- to 12-µm thick microporous DSM™ substrates with 50% pore density
- Optimize DSM™ support materials to yield favorable mechanical properties and negligible dimensional changes in water at 80°C
- Develop and characterize MEAs using the developed DSM™ substrates

Technical Barriers

This project addresses the following technical barriers from the Fuel Cells and Manufacturing R&D sections of the Fuel Cell Technologies Office Multi-Year Research, Development, and Demonstration Plan:

Fuel Cells

(A) Durability

(B) Cost

(C) Performance

Manufacturing R&D

(A) Lack of High-Volume Membrane Electrode Assembly Processes

Technical Targets

Progress has been made in achieving the DOE targets listed in the Multi-Year Research, Development, and Demonstration Plan. Table 1 lists the DOE's technical targets and where our research and development efforts stand to date.

TABLE 1. DOE Technical Targets and GINER/GES Status

Characteristic	Unit	2017 Target	DSM™ Status
Oxygen crossover	mA/cm^2	2	1.5[a]
Hydrogen crossover	mA/cm^2	2	1.8[a]
Membrane Conductivity Operating Temperature 20°C -20°C	S/cm	 0.10 0.07 0.01	 0.093[b] 0.083 Not tested
Operating Temperature	°C	≤120°C	95°C
Area Resistance	$Ohm \cdot cm^2$	0.02	0.03
Cost	$\$/m^2$	20	~$50
Lifetime	hours	5,000	Untested
Durability with cycling <80°C	cycles	20,000	20,000
Unassisted Start from low temperature	°C	-40	Untested
Thermal cyclability in presence of condensed water		Yes	Yes

[a]Crossover measured for 1 atm of pure H_2 and pure O_2 at 95°C and 50% relative humidity
[b]For 1-mil DSM™ operating at 95°C with H_2/air at 20 psi. H_2/air stoichiometry of 1.1/2.0

This project pursued three DSM™ fabrication processes based on the criteria of performance optimization and cost reduction. All three processes (phase inversion, ultraviolet (UV) microreplication, and mechanical deformation) are based on the use of molding technology and are favorably scalable for high-volume production. After evaluation of these processes, the mechanical deformation method was down-selected to prepare fuel cell membranes capable of achieving the following DOE targets:

- Area resistance: <0.02 $\Omega.cm^2$

- Cost: <20 $/m^2
- Lifetime: >5,000 hours
- Durability at 80°C: >20,000 cycles

FY 2013 Accomplishments

- Comprehensive work on material development for the UV microreplication process yielded a number of polymers that achieved high tensile strength (>10 MPa), high elastic modulus (>100 MPa), and long elongations (>5% at break) while retaining dimensional stability and resistance to acid hydrolysis.
- Preliminary use of the roll-to-roll setup at UMass-Amherst facilities has shown that using a 6" roll, seamless formation of DSM™ supports with dimensions of up to 6" x 19" (~730 cm^2) can be prepared at web speeds of 8 inch/min.
- By improving the release process of polysulfone from micromolds, a film porosity of over 60% has been demonstrated using a mold-assisted mechanical deformation route. This method is projected to yield <$20/m^2 DSM™ cost when adapted to a roll-to-roll process.

✧ ✧ ✧ ✧ ✧

INTRODUCTION

In proton exchange membrane fuel cells, attaining and maintaining high membrane conductivity at various operating conditions is crucial for the fuel cell performance and efficiency. Lowering the EW of perfluorinated ionomers is one of the few options available to improve membrane conductivity, especially in the low relative humidity regime. However, excessive changes in membrane dimensions upon application of wet/dry or freeze/thaw cycles yield catastrophic losses in membrane integrity, thus hindering their long-term durability. This is especially of concern when low-EW ionomers are used in thin membrane configurations to minimize resistive losses. Incorporating perfluorinated ionomers of low EW within highly porous, dimensionally stable support materials is an optimal method to achieve the DOE membrane metrics for conductivity and durability. A scalable, cost-effective method to fabricate these composite membranes is also necessary to achieve the DOE target of <$20/m^2. Giner/GES has developed DSM™ technology to provide mechanical support for the conductive ionomer. These composite membranes include a highly conductive and high-acid-content ionomer within a thin and durable polymer support with well-defined pores and high (50%) porosity. Utilizing high-strength engineering polymers, the DSM™ approach completely restrains the in-plane swelling of the ionomer. Providing a non-tortuous, through-plane path for ionic transport minimizes the conductivity penalty due to the support structure. Additionally, when filled with low-EW perfluorinated sulfonic acid (PFSA) ionomers, the DSM™ meets nearly all of the DOE's 2017 durability and performance targets, including those for freeze/thaw cycling and wet/dry cycling operation.

As currently manufactured, DSM™ is far too expensive (~$100 to 1,000/m^2) for automotive and stationary applications. A scalable, continuous fabrication method is needed to reduce the cost down to or below the DOE's 2017 cost target of $20/m^2.

APPROACH

A major goal for this project is the optimization of materials and processes for cost-effective manufacturing of DSMs™ consisting of a low-EW PFSA ionomer embedded in a 5- to 12-µm-thick microporous support film with 20-µm pore diameter and 50% pore density. The project has investigated three micromolding processes (phase inversion, UV microreplication, and mechanical deformation) and evaluated their feasibility for scaled fabrication at low cost. The *Phase Inversion* process involves casting a polymer solution on a micromold followed by rapid precipitation of the polymer in a non-solvent to yield porous films. First used during Phase II of this project, this method aims to develop a DSM™ support that is less expensive and easier to scale up compared to laser micromachining. The *UV Microreplication* method is a soft lithography approach that uses imprint lithography principles and involves the use of a low-viscosity, UV-crosslinkable monomer solution placed between a low-surface-energy mold (pillars) and a backing layer. This is a highly scalable process that generates materials at low cost and high volume. The *Mechanical Deformation* method relies on puncturing commodity plastics. This process is also readily scalable to generate a proven DSM™ support with proven materials at low cost.

The initial stage of the project involved fabrication of electroformed nickel "pillar" molds by NIL Technology (NILT, Denmark) to be used for generation of the DSM™ supports using all three methods. Figure 1 shows tilted and cross-sectional SEM micrographs of a representative nickel micromold with 10-µm pillar height and 50% area coverage. Upon elimination of the *Phase Inversion* process due to complications with solvent waste and inferior material properties, Giner has continued to investigate both *UV Microreplication* and *Mechanical Deformation* methods.

RESULTS

During FY 2013, Giner/GES investigated two micromold-assisted DSM™ fabrication methods: *UV Microreplication* and *Mechanical Deformation*. Based on the results shown in this section, the *Mechanical Deformation* has been selected as the most viable method and is being

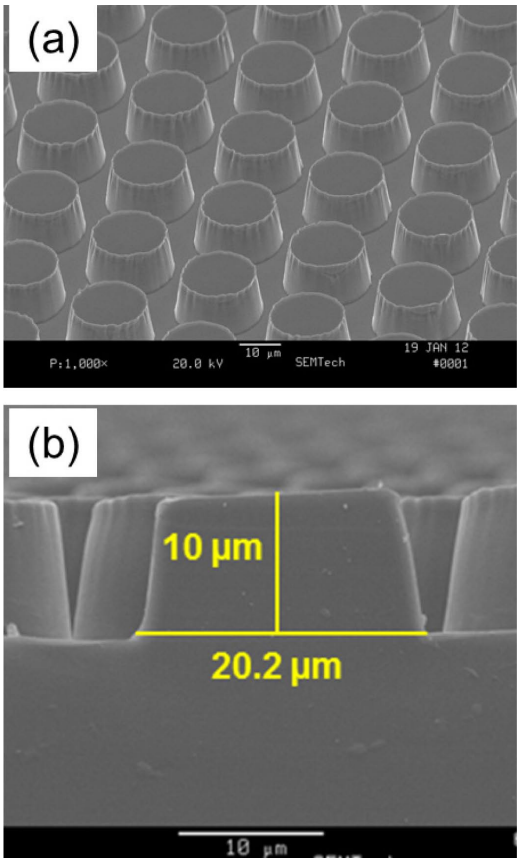

FIGURE 1. Scanning Electron Micrographs of Micromold Pillars (a) Tilted View (b) Cross-Sectional View with Dimensions

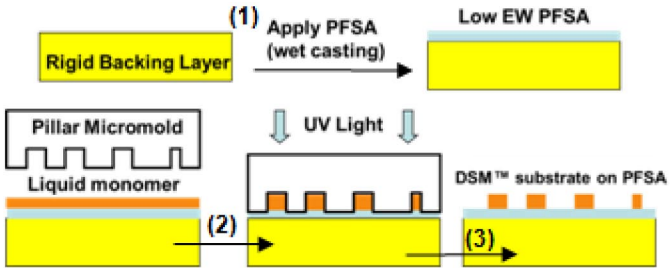

FIGURE 2. UV Microreplication Process Showing the Fabrication of DSM™ Substrates on a PFSA Ionomer Layer

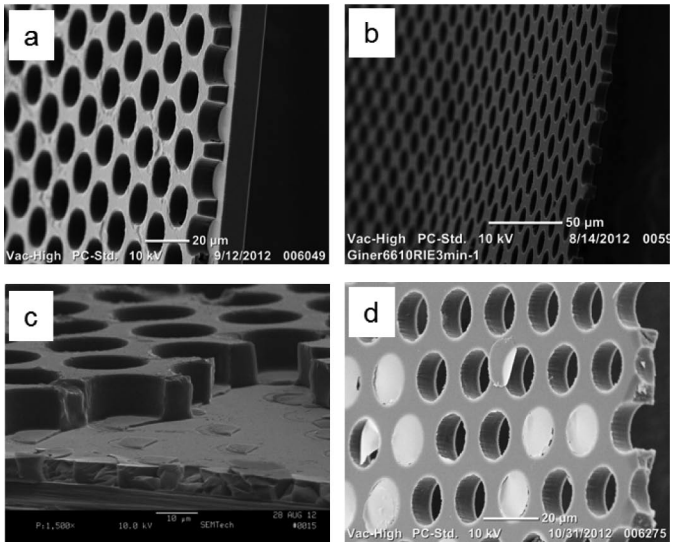

FIGURE 3. Scanning Electron Micrographs of the Porous DSM™ Substrates — Substrate bound (a) and free-standing (b) films free of residual layers. Films with minimal residual layers are shown in (c) and (d)

actively pursued by Giner/GES to achieve the DOE's 2017 targets for cost, performance, and durability.

UV Microreplication. This process flow involves the use of a low-viscosity, UV-crosslinkable monomer solution placed between a low-surface-energy mold and a backing layer followed by UV exposure and removal of the crosslinked polymer film to yield a DSM™ support with well-defined cylindrical pores as shown in Figure 2. This process was investigated at UMass-Amherst in collaboration with the Carter Research Group. A state-of-the-art Nanonex NX-200 Universal Imprinter was utilized to investigate microreplication of polymers by imprint lithography. Using low-surface-energy micromolds, 10-µm-thick, 4" wide DSM™ substrates were formed using the process shown in Figure 2. During the imprint process, the precursor monomer fills the mold under an applied pressure and is rapidly crosslinked with UV light to yield porous polymer films. The resulting films showed high tensile strength and were sufficient flexibility for roll-to-roll adaption. Upon optimization of the processing conditions such as wet precursor thickness, applied pressure, and imprint duration, it was possible to obtain porous films with minimal residual layers after releasing from the micromolds. Figure 3, which shows SEM micrographs of processed films, demonstrates the effect of process parameters on the film quality, uniformity, and the extent of residual layers. The wet monomer thickness, surface treatment, and the rigidity of the backing layer were important parameters that affected the quality of the porous films and the thickness of residual layers. Figures 3a, 3b show examples of a porous film produced on a corona-treated, rigid backing layer that is free of residual layers (completely open pores, shown both as a substrate-bound and a free-standing film). However, the use of a plastic (Mylar) backing layer caused residual layers of 0.5-0.8 µm as shown in Figures 3c, 3d. We note that the residual layers are not continuous and appear to stick on the backing layer (Figure 3c), thus leaving the pores partially open for the free-standing film of the DSM™ substrate (Figure 3d). Finally, when spin casting was used to apply the monomer layers, faster spin rates translated into thinner wet monomer thickness to minimize the residual layer thickness (not shown).

Mechanical Deformation. This method is attractive because it uses materials already qualified by laser-drilled DSM™ substrates. This method can utilize commodity thermoplastics with very fast processing times allowing for roll-to-roll production. Preliminary perforation trials conducted with polysulfone have yielded films with 10- to 15-µm-wide pores and ~15-33% porosity as shown in Figure 4 top and center (less than the targeted 50% porosity). This was mainly due to excessive tearing of polysulfone during the mold release step. By improving the release properties of polysulfone from micromolds, a film porosity of over 60% has been demonstrated using a square pattern as shown in Figure 4 bottom.

CONCLUSIONS

The goal by the end of FY 2013 was to select and optimize a scalable process for cost-effective manufacturing of DSMs™ for fuel cells. Giner's formulation and process development effort for the *UV Microreplication* method has yielded materials with substantial improvements in mechanical properties over the ionomers used in fuel cells. A comprehensive work on material development yielded a number of polymers that achieved high tensile strength (>10 MPa), high elastic modulus (~200 MPa), and good elongation (>10% at break) while retaining dimensional stability and resistance to acid hydrolysis. However, these materials still fail to yield the desired mechanical properties at elevated (~80°C) temperatures. Despite the successes in material and process development, the UV-curable polymers are still not adequate mechanically for use in fuel cells. The *Mechanical Deformation* route was explored to produce prototype polysulfone DSM™ supports with over ~60% porosity. This represents the ideal support geometry with an engineering thermoplastic. The potential of this method is due to its very low material risk and high roll-to-roll adaptability. Upon qualification of these DSM™ supports for fuel cells, the focus of the project will be to scale up this method to fabricate larger (12") micromolds and transfer the batch process to a pilot-size roll-to-roll setup to continuously produce DSMs™.

SPECIAL RECOGNITIONS & AWARDS/ PATENTS ISSUED

1. Mittelsteadt C.K.; Argun, A.A.; Laicer, C.; Willey, J. "*Dimensionally Stable Membrane Substrate and Method of Fabrication Thereof*" US provisional patent application, 2013.

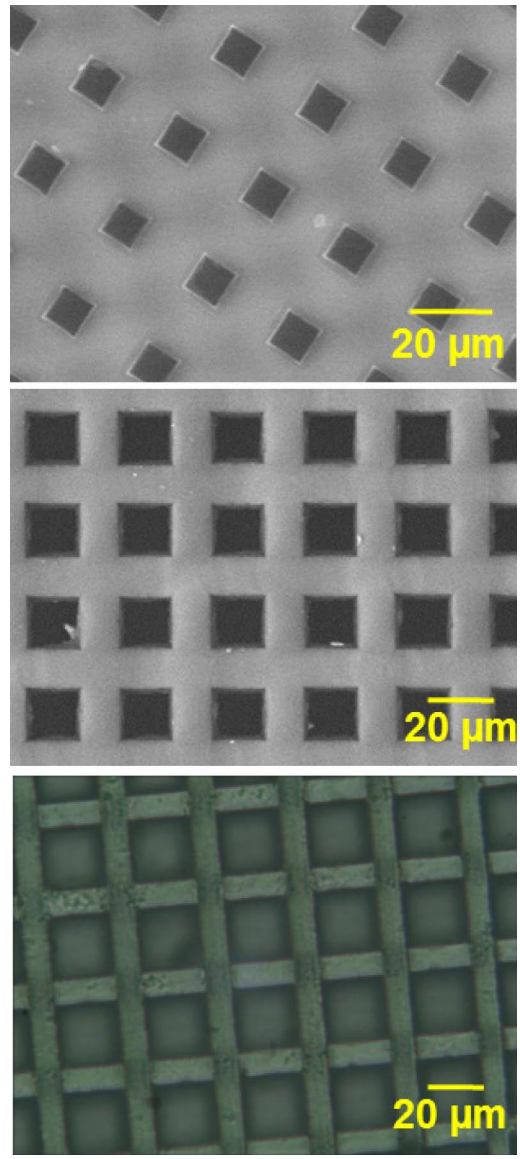

FIGURE 4. Progress in DSM™ Substrates Generated with *Mechanical Deformation* — Top: 11-µm pores, 15% porosity; Center: 16-µm pores, 33% porosity; Bottom: 22-µm pores, 62% porosity

FY 2013 PUBLICATIONS/PRESENTATIONS

1. Mittelsteadt, C.K., A. Argun, C. Laicer, J. Willey, P. Maxwell. "*2013 Fuel Cells Tech Team*" March 2013.

2. Mittelsteadt, C.K., A. Argun, C. Laicer, J. Willey, P. Maxwell. "*2013 Annual Merit Review Proceedings– Fuel Cells*" May 2013.

V.B.2 High-Temperature Membrane with Humidification-Independent Cluster Structure

Ludwig Lipp (Primary Contact), Pinakin Patel, Ray Kopp
FuelCell Energy (FCE), Inc.
3 Great Pasture Road
Danbury, CT 06813
Phone: (203) 205-2492
Email: llipp@fce.com

DOE Managers
Donna Ho
Phone: (202) 586-8000
Email: Donna.Ho@ee.doe.gov
Greg Kleen
Phone: (720) 356-1672
Email: Greg.Kleen@go.doe.gov

Technical Advisor
Thomas Benjamin
Phone: (630) 252-1632
Email: benjamin@anl.gov

Contract Number: 36-06GO16033

Subcontractor:
Giner, Inc., Newton, MA

Start Date: June 1, 2006
Projected End Date: December 31, 2013

Overall Objectives

- Develop membranes that are capable of operation at up to 120°C for automotive applications.
- Demonstrate improved mechanical properties leading to increased durability.
- Quantify performance and life improvements at conditions relevant to automotive fuel cells.

Fiscal Year (FY) 2013 Objectives

- Design composite membrane with polymer support structure to increase durability at automotive cycling conditions at operating temperatures up to 120°C (overall goal: meet DOE 2020 targets).
- Characterize chemical and mechanical stability using accelerated stress tests.
- Fabricate membrane electrode assemblies (MEAs) to assess in-cell durability at 95°C.

Technical Barriers

This project addresses the following technical barriers from the Fuel Cells section of the DOE Fuel Cell Technologies Office Multi-Year Research, Development, and Demonstration Plan [1]:

(A) Durability

(B) Cost

(C) Performance

Technical Targets

This project is developing a multi-component composite (mC^2) membrane to meet the following DOE 2020 technical targets for membranes:

- Membrane area specific resistance: 0.02 Ωcm^2
- Membrane durability:
  - Mechanical: 20,000 relative humidity (RH) cycles (from 0% RH to 90°C dewpoint) with <10 sccm crossover
  - Chemical: >500 hours at steady-state open circuit voltage

FY 2013 Accomplishments

- Supported membrane: Fabricated supported membrane using advanced ionomers and Giner Inc.'s 2DSM™ polymer support materials.
- Swelling: Demonstrated negligible in-plane swelling of the supported membrane.
- Conductivity: Increased in-plane conductivity to three times that of conventional Nafion®.

✧ ✧ ✧ ✧ ✧

INTRODUCTION

This project is focused on the development of composite polymer electrolyte membranes (PEMs) that can operate at low RH and over a wide temperature range (-20 to 120°C). Their main application is in transportation fuel cells. In addition, FCE is considering use of these membranes for co-production of hydrogen from high-temperature fuel cells. The higher operating temperature imparts improved tolerance to impurities, such as carbon monoxide, thereby increasing the co-production efficiency and simplifying the system.

The goal is to develop a structure in which ion-conducting clusters remain intact at low RH. A major challenge is that current proton conducting polymers cannot sufficiently hold on to water under these conditions. Since the conduction mechanism relies on movement of hydrated species, the conducting path is compromised, resulting in low performance. Membranes that can operate at lower RH at elevated temperatures up to 120°C will reduce the fuel cell system complexity and cost by reducing or eliminating the need for a humidifier in the system. This project is developing a composite membrane, in which both the ionic conductivity and mechanical properties are enhanced to meet DOE's 2017 and 2020 goals for transportation fuel cells.

APPROACH

The overall concept for mC^2 is shown in Figure 1. The emphasis in the past year has been to incorporate a polymer support for a mechanically stronger membrane with reduced in-plane swelling for improved durability throughout the range of operating conditions expected in automotive applications. The detailed approach to address the DOE target parameters is summarized in Table 1.

TABLE 1. Approach for the Composite Membrane

Target Parameter	DOE Target (2017)	Approach
Area specific proton resistance at: 120°C and 40-80 kPa water partial pressure	0.02 Ω cm^2	Multi-component composite structure, lower equivalent weight, polymer support for thinner membrane
80°C and 25-45 kPa water partial pressure	0.02 Ω cm^2	Higher number of functional groups
Hydrogen and oxygen cross-over at 1 atm	2 mA/cm^2	Support polymer for mechanically stronger membrane structure
Minimum electrical resistance	1,000 Ω cm^2	Improved membrane thickness tolerance and additive dispersion
Cost	$20/$m^2$	Simplify polymer processing
Durability Mechanical (Cycles with <10 sccm crossover)	>20,000	Mechanically strong support polymer for reduced swelling
Durability Chemical (Hours at steady-state open circuit voltage)	>500	Chemically stabilized ionomer

RESULTS

This year's efforts were focused on incorporating a durable support polymer material into the mC^2 membrane. Micrograph pictures of the 2DSM™ support polymer and a composite membrane incorporating the support polymer at its center are shown in Figure 2. The selected support polymer has very high mechanical strength, temperature stability well beyond the expected membrane operating temperature and excellent chemical resistance in the ionomer and fuel cell environment. It is optimized to provide the largest possible void volume while ensuring excellent mechanical support.

Two grades of advanced ionomer were used, with different equivalent weights. In all cases, the introduction of the 2DSM™ support prevented in-plane swelling, as shown in Figure 3. The water uptake with increasing temperature

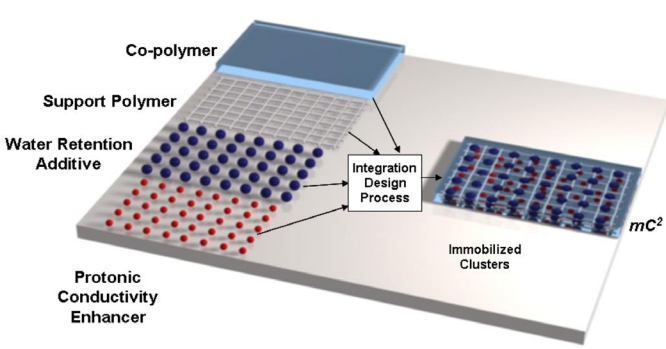

FIGURE 1. Multi-Component Composite Membrane (mC^2) Concept

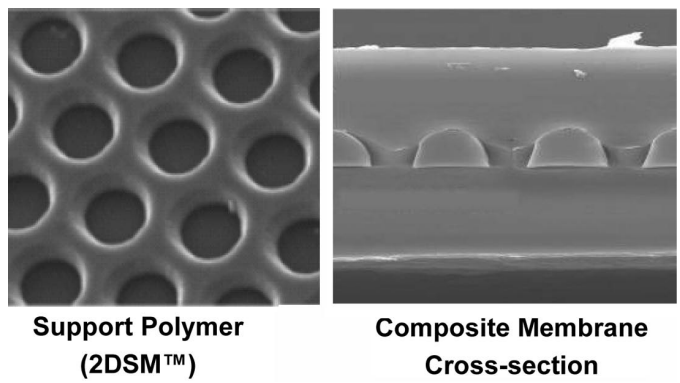

FIGURE 2. 2DSM™ Support Polymer and Cross-Section of Supported Membrane Incorporating It

and therefore humidity resulted in swelling only in the thickness direction of the membrane. This swelling is much more easily tolerated by the fuel cell hardware and is not expected to cause issues due to mechanical failure, electrode delamination and contact loss, as is often experienced with significant in-plane swelling. The data points shown in Figure 3 are the average data from three samples. The error bars represent the range of dimensional change obtained at each temperature. They show that an adequate level of confidence was achieved with the measurement setup.

Figure 4 shows the in-plane conductivity of one of the first 2DSM™ samples fabricated. The curve exhibits the expected shape, indicating good stability of the membrane throughout the range of relative humidity. The conductivity of the 25-µm thick sample is >60% higher than a Nafion®

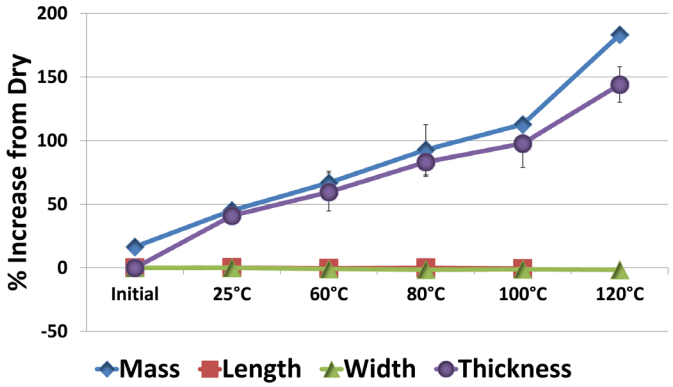

FIGURE 3. Dimensional Stability Measurements Show No Swelling in Length and Width as a Function of Water Uptake

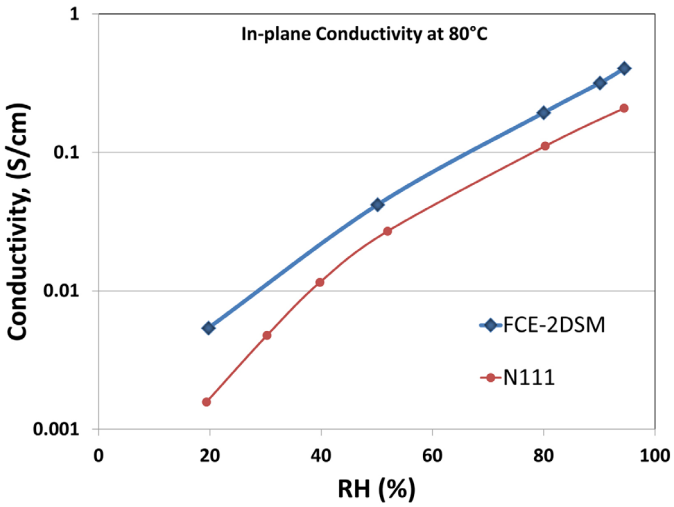

FIGURE 4. Conductivity of the Supported Membrane as a Function of RH is Significantly Improved Compared to a Conventional Nafion® Membrane

membrane of the same thickness. Improvements in the membrane fabrication process and use of the lower equivalent weight ionomer resulted in higher conductivities, up to 3x higher than a 25-µm thick Nafion® membrane, as shown in Table 2.

CONCLUSIONS AND FUTURE DIRECTION

An mC^2 membrane design with a 2DSM™ support polymer for high-temperature and low-RH operation has been implemented to fabricate membranes with enhanced durability at the DOE target conditions (Table 1). Accomplishments include:

- Successfully incorporated support polymer into advanced ionomer system, resulting in a thin (~25-µm thick) membrane with good handling properties.

TABLE 2. Progressively Increased In-Plane Conductivity up to 3x Higher Compared to Nafion®

Sample	Thickness (mm)	In-plane Conductivity (S/cm at 80°C, 50% RH)
N111 (conventional)	25	0.018
DSM-1	25	0.027
DSM-2	20	0.040
DSM-3	25	0.054

Progress

- Demonstrated mC^2 with no in-plane dimensional change (swelling) as a function of water content.
- Achieved up to 3x higher conductivity compared to a conventional membrane.

The remainder of the project will focus on fabrication of MEAs and their testing. The tests will include accelerated stress tests to assess membrane durability. Specifically, RH cycling tests to determine the mechanical durability and open circuit voltage tests to assess chemical stability. Testing will also entail fuel cell endurance testing at elevated temperature (95°C) in 25- to 50-cm^2 single cells up to 1,000 hours.

FY 2013 PUBLICATIONS/PRESENTATIONS

1. L. Lipp, "High Temperature Membrane With Humidification-Independent Cluster Structure", 2013 DOE Hydrogen Program and Vehicle Technologies Program Annual Merit Review and Peer Evaluation Meeting, Washington, D.C., May 13–17, 2013.

REFERENCES

1. DOE Office of Energy Efficiency and Renewable Energy (EERE) Fuel Cell Technologies Office Multi-Year Research, Development and Demonstration (MYRD&D) Plan, Section 3.4 "Fuel Cells", http://www1.eere.energy.gov/hydrogenandfuelcells/mypp/pdfs/fuel_cells.pdf.

V.B.3 Corrugated Membrane Fuel Cell Structures

Stephen Grot
Ion Power Incorporated
720 Governor Lea Rd.
New Castle, DE 19720-5501
Phone: (302) 832-9550
Email: s.grot@ion-power.com

DOE Managers
Donna Ho
Phone: (202) 586-8000
Email: Donna.Ho@ee.doe.gov
Reginald Tyler
Phone: (720) 356-1805
Email: Reginald.Tyler@go.doe.gov

Technical Advisor
Thomas Benjamin
Phone: (630) 252-1632
Email: benjamin@anl.gov

Contract Number: DE-EE0000462

Subcontractors:
- Graftech International Holdings Inc., Parma, OH
- General Motors Corporation, Flint, MI

Project Start Date: September 1, 2010
Project End Date: August 31, 2013 (Discontinued)

Overall Objectives

- Achieve a platinum catalyst utilization target of 0.2 g Pt/kWe
- Demonstrate target properties <10 mOhm-cm^2 electrical resistance at >20 psi compressive strength
- Offer at least 80% of the power density that can be achieved by using the same membrane electrode assembly (MEA) in a flat plate structure
- Successfully test a corrugated fuel cell single cell, meeting a minimum power density of 70 mW/cm^2 at 0.8 V

Fiscal Year (FY) 2013 Objectives

- Develop cell fixturing equipment
- Test electrical resistance of the convoluted single-cell structure
- Develop a new gas diffusion layer (GDL) that can be corrugated for the fuel cell

Technical Barriers

This project addresses the following technical barriers from the Fuel Cells section of the Fuel Cell Technologies Office Multi-Year Research, Development, and Demonstration Plan:

(B) System Cost (GDL, lower plate/GDL, manufacturing costs)

(C) Performance (high power density with low Pt-loaded MEAs)

Technical Targets

In this project, corrugated membrane fuel cell structures are being constructed to assist the Fuel Cell Technologies Office in making progress toward meeting the important DOE objectives of power density (650 W/L) and platinum utilization (0.125 g/kW) by 2017 [1]. Ion Power has tested many fuel cell configurations with a wide variety of GDLs with varying pore sizes to determine the configuration with the greatest ability to meet power density needs when used in a corrugated structure.

FY 2013 Accomplishments

- Performed a finite element analysis of the convoluted cell structure to anticipate expected voltage drops and temperature profiles in the fuel cell
- Demonstrated a new wire screen-based GDL that exceeds the performance of traditional graphite fiber paper-based GDLs
- Developed a method for incorporating the membrane into the corrugated fuel cell structure
- Met target for areal resistance under compression for a fuel cell with corrugated membrane structure

✧ ✧ ✧ ✧ ✧

INTRODUCTION

The DOE supports research to overcome critical technical barriers in fuel cell technology. Corrugated membrane fuel cell structures possess the potential to meet the targets of the DOE power density targets, by essentially packaging more membrane area into the same fuel cell volume as compared to conventional stack constructions. Ion Power's targets consist of meeting a power density measurement of 1 W/cm^2 while simultaneously achieving a platinum utilization of 0.2 g Pt/kW.

In order to meet the DOE's goal of reducing the use of platinum in fuel cell cathodes, Ion Power has proposed a novel concept of a corrugated membrane fuel cell structure with a two-fold increase in the membrane active area over the geometric area of the cell. A comparison of the corrugated geometry and traditional flat fuel cell geometry can be found in Figure 1.

APPROACH

For the development of the corrugated membrane electrode structure, Ion Power's approach will consist of compressing additional membrane area into the same geometric plate footprint. A fuel cell consisting of a 50-cm^2 single-cell test jig will be designed and fabricated to allow testing of both conventional, flat MEAs possessing standard flow fields and the corrugated single-cell assemblies. This test jig will also allow the hand assembly of each of the individual components. Inserts will be created to generate both straight through flow and serpentine flow in both the flat and corrugated MEAs. Water, thermal, and gas flow management issues will be investigated.

RESULTS

Early in FY 2013, a three-dimensional finite element analysis of the cell was performed to examine the expected voltage drops in the convoluted fuel cell and to look at the expected temperature and stress profiles in the cell. The results of the structural and thermal analyses can be seen in Figure 2.

The stresses in the cell were found to fall well within the strength capabilities of the materials and should provide sufficient contact pressure for the cell to function properly. However, the thermal analysis displayed one potential issue: the temperature differential between the coolant and the membrane at the center of the convolution is 9-11°C at full power. This high temperature is a result of the longer thermal path of this area of the membrane to the coolant cavity of the cell stack. These high temperatures may be problematic for the membrane. We propose to address this issue by slightly lowering the operating current density, thereby reducing the amount of heat generated.

As a result of the General Motors recent re-organization and the consequent limit on GM's fuel cell-dedicated resources, they are no longer able to support this project. The loss of GM as a partner and key manufacturer subcontractor has delayed the project's progress.

Dozens of fuel cell configurations have been tested during FY 2013 with significant improvements in the microporous layer integration into the coated-wire screen GDL. Traditional Teflon®/carbon black microporous layers were integrated onto the wire screen in order to allow for proper water management of the GDL. Figure 3 shows the dramatic differences in performance of various microporous layer application methods to the wire-screen GDL. The microporous layer optimization work shown in Figure 3 was performed in flat cell configurations at a cell temperature of 65°C. The wire screen enables the GDL to be corrugated and improves microporous layer functionality.

Once a suitable wire-screen GDL was developed, the next challenge of integrating a catalyzed membrane into the structure was addressed using two approaches. The first approach involved applying a catalyst/membrane coating to each of the GDLs and then bringing the two GDL halves together. The second approach involved forming a full

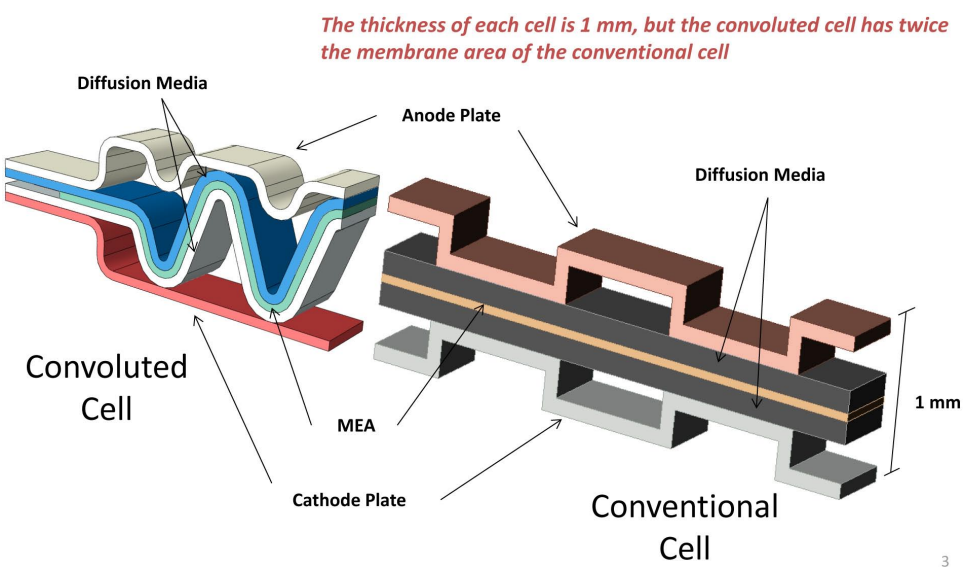

FIGURE 1. Comparison of Convoluted Cell and Conventional Cell

How much mechanical and thermal stress is the structure under?

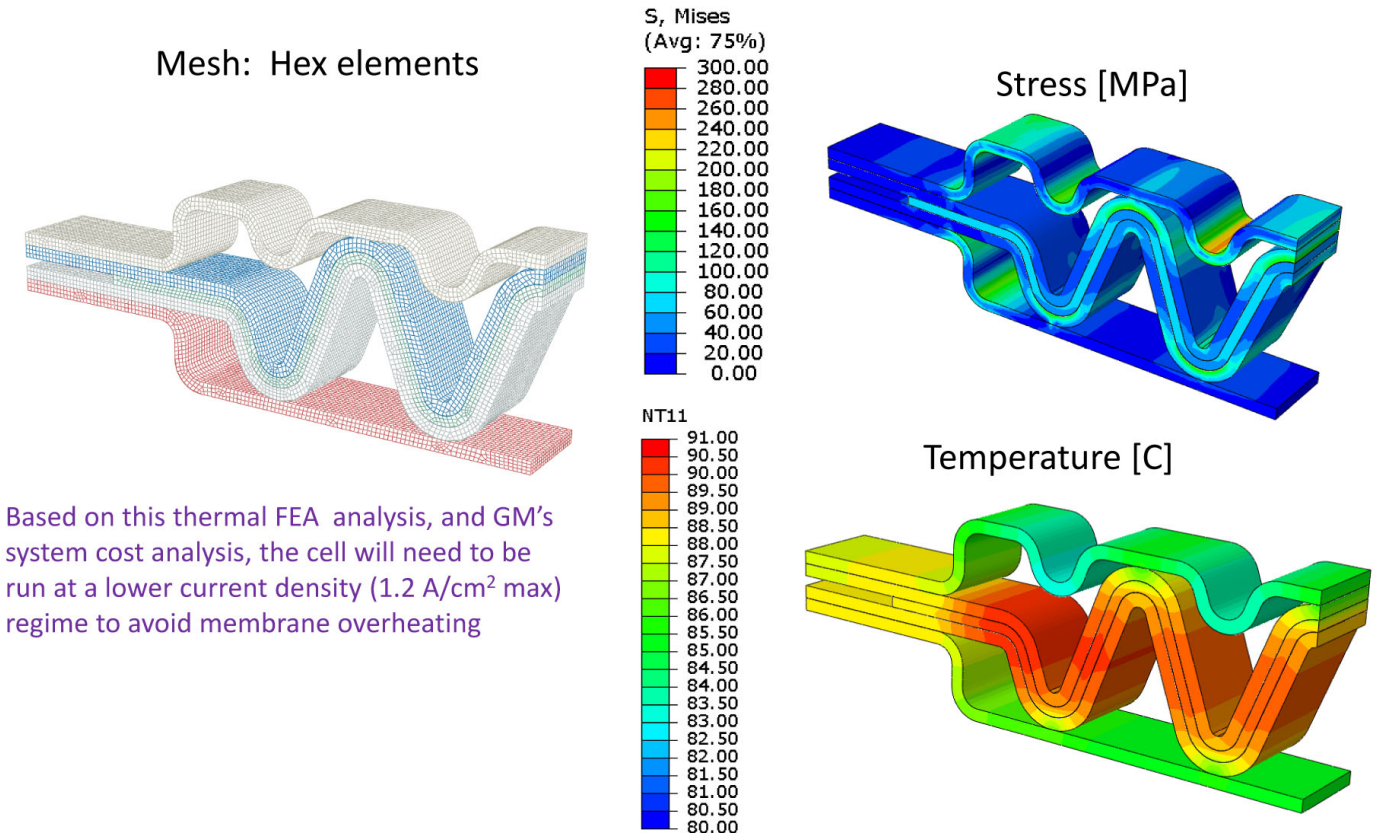

Based on this thermal FEA analysis, and GM's system cost analysis, the cell will need to be run at a lower current density (1.2 A/cm^2 max) regime to avoid membrane overheating

FIGURE 2. FEA Structural and Thermal Results

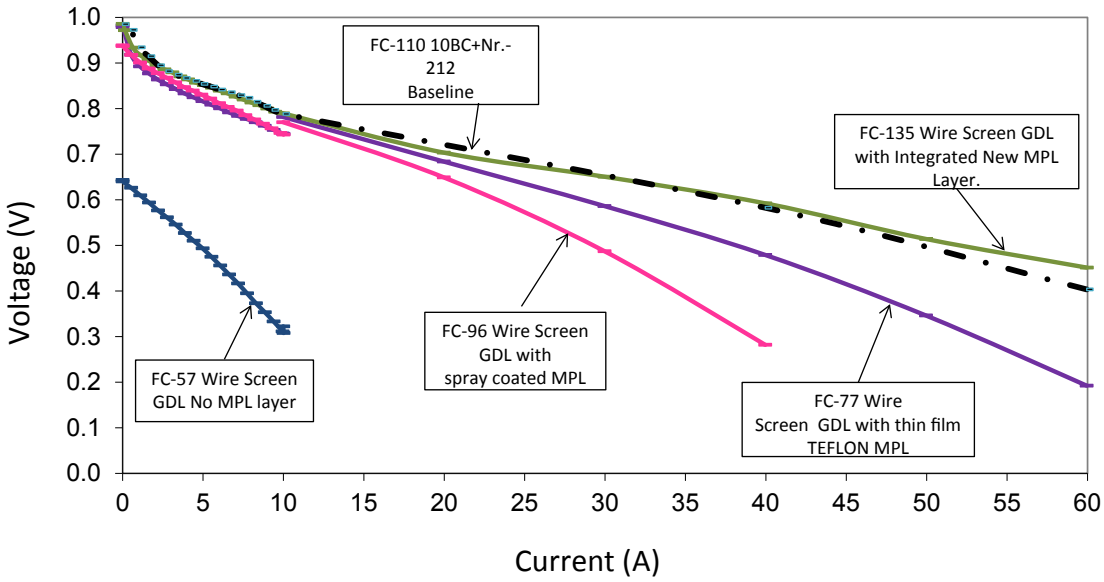

FIGURE 3. Improvements in Performance of Wire-Screen GDLs by the Incorporation of Various Microporous Layers

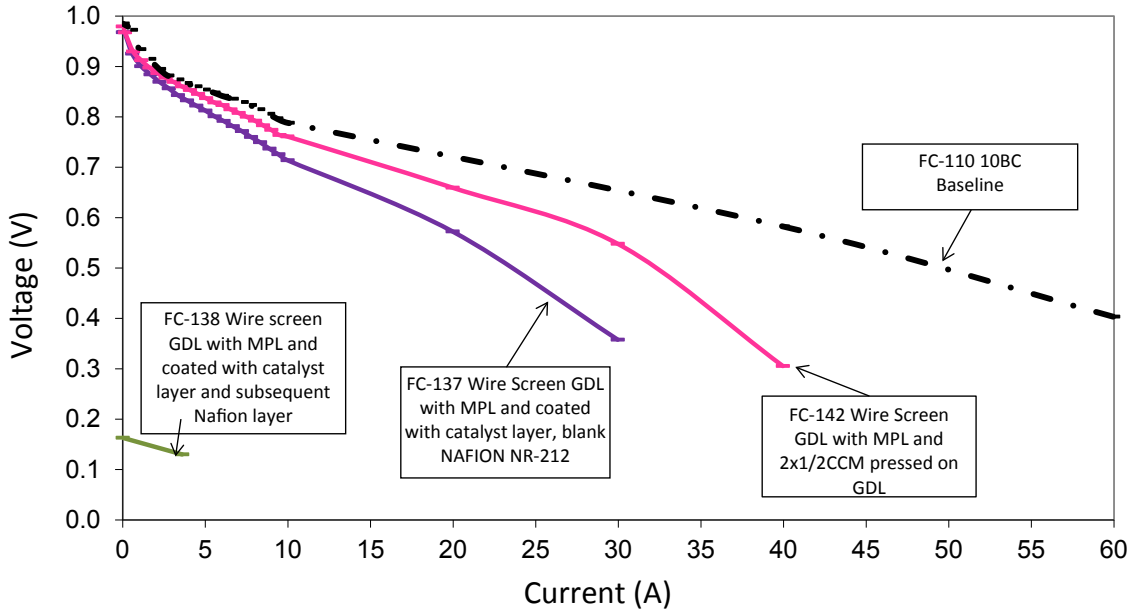

FIGURE 4. Membrane Incorporation into Wire-Screen GDL

catalyst-coated membrane into a corrugated form and then placing it on the corrugated GDL during cell assembly. In order to demonstrate the feasibility of using two membrane halves as the membrane component in the fuel cell, Ion Power compared several flat fuel cell configuration tests to the performance of a single, 50-micron Nafion® NR 212 membrane baseline. The following configurations were tested at 65°C and the results can be seen in Figure 4:

- Wire-screen GDL coated with catalyst on the microporous layer, using blank membrane
- Wire-screen GDL coated with catalyst and ionomer, no separate membrane necessary
- Wire-screen GDL with microporous layer and one-half catalyst-coated membrane pressed on both GDLs

The results shown in Figure 4 demonstrate that challenges remain in using the first approach for integrating the catalyst/membrane coating onto the GDL.

By August 2013, Ion Power was able to demonstrate a power density of 40 mW/cm^2 on a corrugated fuel cell, which reaches 60 percent that of the Go/No-Go decision criteria of 70 mW/cm^2. This result was achieved on a fuel cell single cell with a silicon seal material utilizing the second approach, whereby the catalyst-coated membrane was formed using the membrane corrugation tool. Ion Power saw improvement in this area throughout July and August on corrugated fuel cells, while working through obstacles related to the corrugation, lamination, and sealing of the cell. However, Ion Power was not able to meet the Go/No-Go decision performance target by the deadline of August 31.

CONCLUSIONS/FUTURE DIRECTIONS

- As Ion Power was unable to meet the Go/No-Go decision criteria of achieving a minimum power density of 70 mW/cm^2 on a corrugated fuel cell single cell, this project was discontinued by the DOE effective August 31, 2013. Ion Power is pleased with its work on this project, and its contributions to fuel cell industry, as well as having laid the groundwork for the field of corrugated fuel cells.
- One major accomplishment of this project is that we demonstrated a new type of metal-based GDL that has the potential to reduce the costs associated with the traditional fiber-based GDLs.
- While nothing in this project has shown that the concept of corrugated fuel cells lacks merit, technical challenges remain in order to properly build the structures. Ion Power believes that further development work in the field of corrugated fuel cell structures will be able to reach the power density target of 70 mW/cm^2 in the future.

FY 2013 PUBLICATIONS/PRESENTATIONS

1. 2013 Hydrogen and Fuel Cells Program Annual Merit Review Presentation

REFERENCES

1. U.S. Department of Energy. *Multi-Year Research, Development, and Demonstration Plan*. Fuel Cell Technologies Office. July, 2013. <http://www1.eere.energy.gov/hydrogenandfuelcells/mypp/pdfs/fuel_cells.pdf>

V.C.1 High Performance, Durable, Low Cost Membrane Electrode Assemblies for Transportation Applications

Andrew Steinbach (Primary Contact),
Dennis van der Vliet, Andrei Komlev,
Darren Miller, Sean Luopa, Amy Hester,
James Sieracki, Mike Yandrasits, and Matthew Pejsa
3M Company, Fuel Cell Components Program
3M Center, Building 201-2N-19
St. Paul, MN 55144-1000
Phone: (651) 737-0103
Email: ajsteinbach2@mmm.com

DOE Managers
Kathi Epping Martin
Phone: (202) 586-7425
Email: Kathi.Epping@ee.doe.gov
Gregory Kleen
Phone: (720) 356-1672
Email: Gregory.Kleen@go.doe.gov

Technical Advisor
John Kopasz
Phone: (630) 252-7531
Email: kopasz@anl.gov

Contract Number: DE-EE0005667

Subcontractors:
- Johns Hopkins University, Baltimore, MD
- Michigan Technological University, Houghton, MI
- Lawrence Berkeley National Laboratory, Berkeley, CA
- General Motors Co., Pontiac, MI (in negotiation)
- Argonne National Laboratory, Argonne, IL (collaborator)

Project Start Date: September 1, 2012
Project End Date: August 31, 2015

Overall Objectives

- Demonstrate a durable, low-cost, and high-performance membrane electrode assembly (MEA) for transportation applications, characterized by:
  - total platinum (Pt) group metal loadings of ≤0.125 mg/cm^2 of MEA area
  - performance at rated power of ≥1,000 mW/cm^2
  - performance at ¼ power (0.8 V) of ≥0.3 A/cm^2
  - durability of ≥5,000 hours under cycling conditions
  - Q/ΔT of ≤1.45 kW/°C
  - cost of $5-$9/kW, projected at high volume
- Improve operational robustness to allow achievement of transient response, cold-startup, and freeze-startup system targets.

Fiscal Year (FY) 2013 Objectives

- Optimize post-processing of 3M Pt_3Ni_7/nanostructured thin film (NSTF) oxygen reduction reaction (ORR) cathode electrodes for improved MEA activity, durability, and rated-power capability.
- Integrate ultra-low platinum-group metal (PGM) NSTF anode catalysts, NSTF cathode catalysts, and next-generation supported 3M polymer electrolyte membranes (PEMs) for improved MEA performance, durability, and cost.
- Identify key factors influencing NSTF MEA durability, including Pt_3Ni_7/NSTF electrocatalyst durability and maintenance of rated power.
- Improve operational robustness via anode gas diffusion layer optimization.

Technical Barriers

(A) Durability

(B) Cost

(C) Performance

Technical Targets

This project is focused on development of a durable, high-performance, low-cost, and robust MEA for transportation applications. Table 1 lists current project status against the DOE Technical Targets for Membrane Electrode Assemblies (Table 3.4.14) and a subset of Electrocatalyst Targets (Table 3.4.13) from the 2012 Multi-Year Research, Development and Demonstration Plan. The project status values are provided by results from the 2013 (March) Best of Class (BOC) MEA, tested in duplicate and described at the bottom of Table 1. This MEA has achieved 84% of the performance at rated power and 68% of the performance at 0.8 V characteristics, and PGM total content and Q/ΔT are higher than the allowable target by 31 and 5.5%, respectively. An estimate of total MEA cost is not available, but the PGM catalyst cost is estimated to be $6/kW. Durability with cycling status is not available.

TABLE 1. Status against Technical Targets

Characteristic	Units	2017 Targets	3M 2013 Status*
Q/ΔT	kW/°C	1.45	1.53
Cost	$/kW	9	6 (PGM only @ $35/$g_{Pt}$)
Durability with cycling	hours	5,000	NA
Performance @ 0.8 V	mA/cm^2	300	203
Performance @ rated power	mW/cm^2	1,000	837
PGM total content (both electrodes)	g/kW (rated)	0.125	0.164
PGM total loading	mg PGM/cm^2 electrode area	0.125	0.137

*3M Status with 2013(March) Best of Class MEA:

- 0.02 mg_{PGM}/cm^2 PtCoMn/NSTF anode, 0.117 mg_{PGM}/cm^2 Pt_3Ni_7(TREATED)/NSTF cathode, 24μ 825 equivalent weight 3M PEM, 3M 2979 gas diffusion layers, optimized flow fields.
- 90°C, 150 kPa H_2/air, 84°C dewpoints, 2.0/2.5 H_2/air stoichiometry.
- Performance at rated power, Q/ΔT characteristics calculated at 1.24 A/cm^2, 0.675 V.

NA - not available

FY 2013 Accomplishments

- Demonstrated a 25% increase in rated power output per unit PGM over 2012 pre-project status with the 3M 2013 (March) BOC MEA, directly reducing cost.
- Demonstrated annealed Pt_3Ni_7/NSTF cathode catalyst with ORR mass activity of 0.52 A/mg (30% increase over unannealed), and dealloyed Pt_3Ni_7/NSTF catalyst with peak power of 1 W/cm^2 at 0.60 V, (41% gain over 2012 status), potentially leading to improved cost, performance at 0.80 V, and performance at rated power.
- Completed multi-month PEM-cathode catalyst integration study which identified two performance-influencing factors caused by PEM-catalyst interactions.
- Demonstrated anode catalyst PGM reduction of 33% from 2012 status, and identified possible pathways for further PGM and cost reduction.
- Improved cold-startup robustness via development of an improved anode gas diffusion layer (GDL), leading to an 88% gain in 40°C performance compared to the 2012 baseline.
- Initiated substantial project to evaluate and improve component and MEA durability.

✧ ✧ ✧ ✧ ✧

INTRODUCTION

While significant progress has been made, state-of-the-art PEM fuel cell MEAs utilized in today's prototype automotive traction fuel cell systems continue to suffer from significant limitations due to high cost, insufficient durability, and low robustness to off-nominal operating conditions. State-of-the art MEAs based on conventional carbon-supported Pt nanoparticle catalysts currently incorporate precious metal loadings which are significantly above those needed to achieve MEA cost targets; performance, durability and/or robustness decrease significantly as loadings are reduced. This project focuses on integration of 3M's state-of-the-art NSTF anode and cathode catalysts with 3M's state-of-the-art PEMs, advanced and low-cost GDLs, and robustness-enhancing interfacial layers. At significantly lower precious metal content, the NSTF catalyst technology platform has several significant demonstrated benefits in performance, durability, and cost over conventional catalysts.

APPROACH

Optimize integration of advanced anode and cathode catalysts with next generation PFSA PEMs, gas diffusion media, and flow fields for best overall MEA performance, durability, robustness, and cost by using a combined experimental and modeling approach.

RESULTS

Significant work has been conducted to improve rated-power performance coincident with anode and cathode PGM loading reduction. Figure 1(A) shows measured polarization curves and Figure 1(B) shows PGM content per unit power output for the pre-project baseline MEA (March 2012), an improved MEA just after project commencement (Sept. 2012), and a further improved March 2013 BOC MEA. Compared to the pre-project baseline MEA, the March 2013 BOC MEA achieved a 49 mV gain in cell voltage at 1.41 A/cm^2 and reduced PGM content 10%, resulting in a 25% gain in power output per unit PGM at 0.675 V.

We have previously reported many of the unique properties of the highly active Pt_3Ni_7/NSTF ORR cathode catalyst [1], the benefit of annealing for further improved activity [2] and the requirement of dealloying for improved rated power [1]. In current annealing optimization work, mass activity was increased from 0.40 (unannealed) to 0.52 A/mg, a 30% increase, and also identified that the activity gain is sensitive to annealing process variables and correlates with a measured catalyst structure parameter. Development of an optimized dealloying method is occurring at Johns Hopkins University (JHU). After application of a JHU electrochemical dealloying method, the Pt_3Ni_7/NSTF MEA's current density at 0.60 V increased 80% compared to non-dealloyed and 42% compared to 3M best-practice

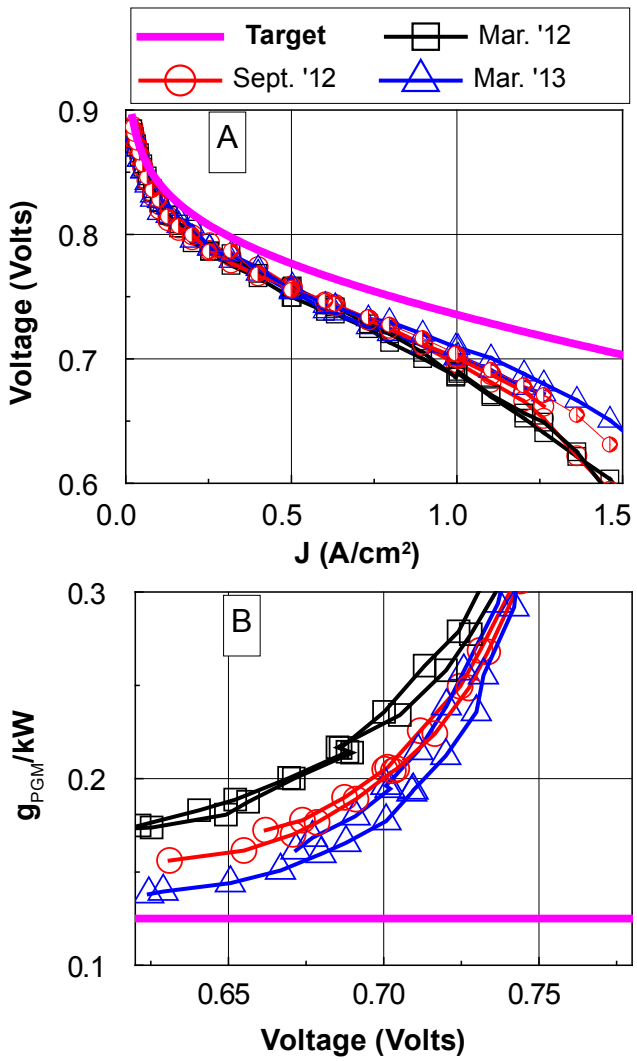

FIGURE 1. Performance Progression during FY 2013 for Integrated Project MEAs. (A): Measured Polarization Curves. (B): PGM Content per Unit Power Output. Conditions: 90/84/84°C Cell/Anode/Cathode, 150/150 kPa H_2/Air, Stoichiometry 2.0/2.5.

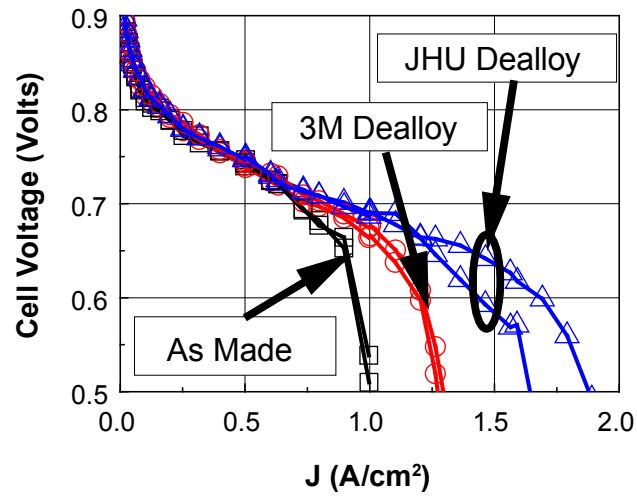

FIGURE 2. Pt_3Ni_7/NSTF Dealloying Development during FY 2013. Conditions: 80/68/68°C Cell/Anode/Cathode, 150/150 kPa H_2/Air, Stoichiometry 2.0/2.5.

dealloying (Figure 2), and exhibited an ORR mass activity of 0.4 A/mg. The JHU electrochemical dealloying method used is not amenable to high volume production, but provides a near-term entitlement result and a structural/compositional target for volume-capable dealloying process development. High-angle annular dark-field scanning transmission electron microscopy characterization of annealed and/or dealloyed materials is occurring at Oak Ridge National Laboratory, and has revealed that a significant portion of the high mass activity of the Pt_3Ni_7/NSTF cathode is due to substantial porosity development during MEA conditioning.

In an integration study, we evaluated the influence of basic PFSA PEM variables (equivalent weight [EW], thickness, support) on performance with MEAs containing either the 2013 (March) BOC cathode or a 0.10 mg_{PGM}/cm^2 PtCoMn/NSTF cathode [3]. PEM integration work with the BOC cathode revealed that the MEA limiting current density decreased as the PEM effective EW increased above ca. 900, and results with the PtCoMn/NSTF cathode suggested that the observed performance variation was consistent with PEM-induced decreased MEA areal-utilization [4].

Significant work to reduce MEA cost via PGM-content minimization of the NSTF hydrogen oxidation reaction anode catalyst revealed that sufficient performance was maintained with as little as 20 $\mu g_{PGM}/cm^2$, and possible further reduction is possible with NSTF support optimization [3]. In a study with Argonne National Laboratory, the surface-specific hydrogen oxidation reaction activity of a fully-conditioned PtCoMn/NSTF anode was found to be ca. 10x higher than Pt/C [5].

Significant improvement in NSTF MEA operational robustness was also demonstrated. Figure 3 shows the performance sensitivity to operating temperature of a representative 3M NSTF MEA was dramatically improved when the baseline anode GDL was replaced with a newly-developed anode GDL. With the new GDL, the current density at 40°C was 88% higher than with the baseline anode GDL. Work conducted at Michigan Technological University (MTU) and Lawrence Berkeley National Laboratory has focused on understanding the mechanism(s) by which the anode GDL influences NSTF MEA low-temperature performance via a combined materials characterization and modeling approach. Characterization of three different 3M anode GDLs, which induce a ca. three-fold variation in NSTF MEA low-temperature performance, is nearly complete and included evaluation of capillary pressure, static and dynamic contact angles, and studies of material structure by X-ray tomography. In addition, MTU has conducted pore network modeling studies to determine the transient thermal and mass

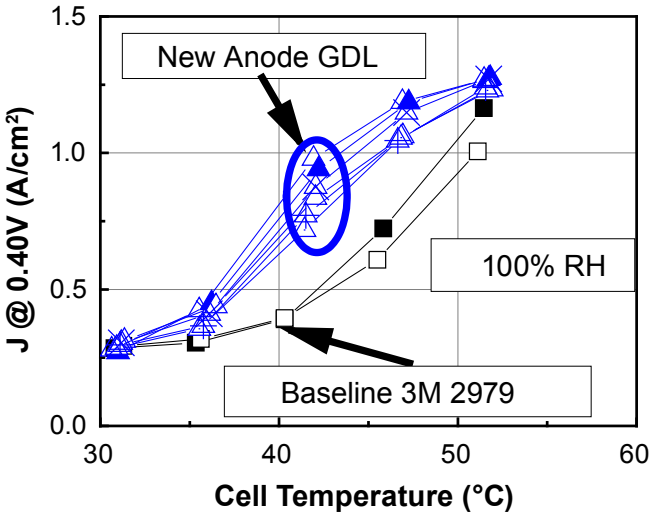

FIGURE 3. Performance Sensitivity to Operating Temperature as a Function of Anode GDL. Conditions: 100/100% Anode/Cathode Relative Humidity (RH), 100/150 kPa H_2/Air, 800/1800 SCCM, Potentiostatic Hold at 0.40 V.

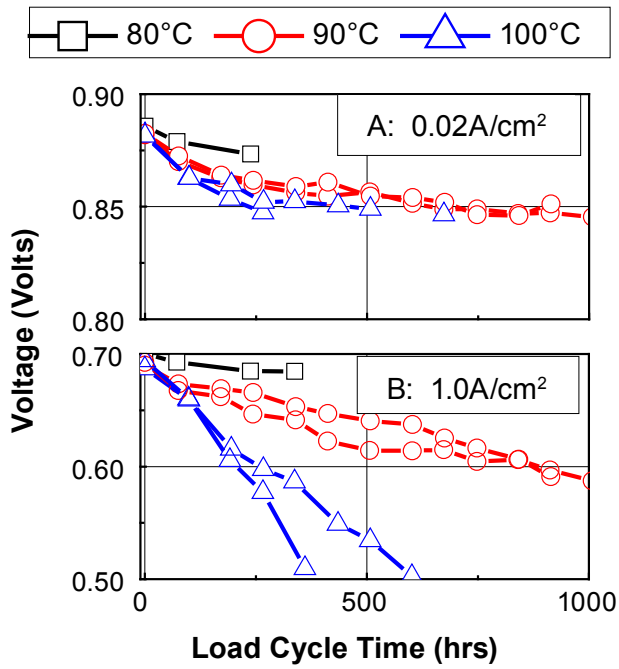

FIGURE 4. Influence of Load Cycle Operating Temperature on MEA Performance Durability. MEA Construction: 0.05/0.15 mg_{PGM}/cm^2 PtCoMn/NSTF Anode/Cathode, 3M 24μ 825EW PEM, and 3M 2979 GDLs. Performance Check Conditions: 80/68/68°C Cell/Anode/Cathode, 150/150 kPa H_2/Air, Stoichiometry 2.0/2.5. (A) 0.02 A/cm^2 and (B) 1.0 A/cm^2.

transport characteristics which occur during cold-startup and sensitivity studies to GDL solid phase distributions, both done in preparation for model incorporation of project material sets.

Extensive evaluation of MEA and component durability has also been conducted. The March 2013 BOC MEA passed the 500-hour MEA chemical durability [6] test with only 2% voltage loss, as compared to the 20% target-allowable loss. Evaluation of the March 2013 BOC MEA's cathode under a electrocatalyst durability test [6] indicated a severe 66% loss in mass activity, larger than the allowable 40% target and also much larger than the 38% loss exhibited by our previous baseline PtCoMn/NSTF cathode [7]. Substantial efforts were also initiated to improve the maintenance of MEA rated-power performance after the MEA is degraded by load cycling, starting with experiments aimed at mechanism determination via sensitivity studies. We have confirmed strong sensitivities to load cycle operating temperature, PFSA PEM type, and NSTF cathode alloy type. Figure 4 shows that as the load cycling temperature increased from 80 to 100°C, the performance loss rate increased modestly at 0.02 A/cm^2 but substantially at 1.0 A/cm^2.

CONCLUSIONS AND FUTURE DIRECTIONS

While significant progress has been made, considerable additional work is needed to achieve project performance, cost and durability targets and to improve operational robustness of NSTF MEAs. Primary future directions include:

- Continue cathode annealing and dealloying development for further performance improvement and PGM reduction, with a significant focus on scalable dealloying processes.
- Increase focus towards improving NSTF MEA operational robustness, including materials optimization, characterization, and modeling of the anode GDL.
- Develop mechanistic understanding of rated-power degradation via continued sensitivity and diagnostic studies, followed by materials-based mitigation development.
- Improve the 2013 BOC MEA cathode electrocatalyst durability via evaluation of various proprietary approaches (developed outside this project).

FY 2013 PUBLICATIONS/PRESENTATIONS

1. Andrew Steinbach, Project Kickoff Presentation to DOE, Sept. 2012, St. Paul, MN.

2. X. Wang, R.K. Ahluwalia, and A.J. Steinbach, "Kinetics of Hydrogen Oxidation and Hydrogen Evolution Reactions on Nanostructured Thin-Film Platinum Alloy Catalyst", *J. Electrochem. Soc.,* **160**(3) F251-F261 (2013).

3. Project Update Presentation to DOE, Feb. 2013, Golden, CO.

4. Andrew Steinbach, "High Performance, Durable, Low Cost Membrane Electrode Assemblies for Transportation Applications", Presentation FC104, 2013 DOE Annual Merit Review, May 2013, Washington, D.C.

REFERENCES

1. Debe et al., "Extraordinary Oxygen Reduction Activity of Pt_3Ni_7", *J. Electrochem. Soc.*, **158** B910 (2011).

2. Mark K. Debe, Presentation FC001, 2011 Annual Merit Review, DOE Hydrogen and Fuel Cell Vehicles Technology Programs, May 2011, Washington, D.C.

3. Andrew J. Steinbach, Presentation FC104, 2013 Annual Merit Review, DOE Hydrogen and Fuel Cell Vehicles Technology Programs, May 2013, Washington, D.C.

4. Steinbach et al., "Polymer Electrolyte Membrane Fuel Cell Active Area Utilization Dependence on Relative Humidity Measured via AC Impedance High Frequency Resistance", *ECS Trans.*, Submitted.

5. Wang et al., "Kinetics of Hydrogen Oxidation and Hydrogen Evolution Reactions on a Nanostructured Thin-Film Platinum Alloy Catalyst", *J. Electrochem. Soc.,* **160**(3) F251 (2013).

6. U.S. Drive Partnership, Fuel Cell Technical Team, "Cell Component Accelerated Stress Test and Polarization Curve Protocols for Polymer Electrolyte Membrane Fuel Cells", Rev. Dec. 16th, 2010. http://www.uscar.org/commands/files_download.php?files_id=267.

7. Mark K. Debe, Presentation FC001, 2012 Annual Merit Review, DOE Hydrogen and Fuel Cell Vehicles Technology Programs, May 2012, Washington, D.C.

V.C.2 Rationally Designed Catalyst Layers for PEMFC Performance Optimization

Deborah J. Myers (Primary Contact),
Nancy N. Kariuki, Xiaoping Wang, and Di-Jia Liu
Argonne National Laboratory
9700 S. Cass Avenue
Lemont, IL 60439
Phone: (630) 252-4261
Email: dmyers@anl.gov

DOE Manager
Nancy Garland
Phone: (202) 586-5673
Email: Nancy.Garland@ee.doe.gov

Subcontractors:
- Johnson Matthey Fuel Cells, Sonning Common, United Kingdom
  Alex Martinez, Jonathan Sharman, and Graham Hards
- United Technologies Research Center, East Hartford, CT
  Zhiwei Yang and Michael Perry
- University of Texas at Austin, Austin, TX
  Paulo Ferreira
- Indiana University Purdue University Indianapolis, Indianapolis, IN
  Jian Xie

Project Start Date: May 1, 2013
Project End Date: April 30, 2016

Overall Objectives

Realize the oxygen reduction reaction (ORR) mass activity benefits of advanced Pt alloy cathode electrocatalysts observed at low current densities and on oxygen and in rotating-disk electrode (RDE) measurements in membrane electrode assemblies (MEAs) and stacks operating at high current densities (>1 A/cm²) and on air.

Fiscal Year (FY) 2013 Objectives

- Identify the sources of the performance loss of cathodes based on an advanced cathode catalyst.
- Establish the correlations between agglomerate structure in the advanced cathode catalyst and platinum catalyst inks and electrode layer structure using, for example, X-ray and microscopic techniques.
- Determine the effects of ink composition (e.g., catalyst to ionomer ratio) and catalyst type (i.e., advanced alloy versus Pt of similar particle size) on electrode properties and performance.
- Develop a method and an algorithm to map electrode structure from imaging data.

Technical Barriers

This project addresses the following technical barriers from the Fuel Cells section of the Fuel Cell Technologies Office Multi-Year Research, Development, and Demonstration Plan:

(C) Performance

(B) Cost

(A) Durability

Technical Targets

Meeting the project objectives will enable proton exchange membrane fuel cells (PEMFCs) to achieve the DOE 2017 fuel cell technical targets:

- Performance: >300 mA/cm^2 at 800 mV and >1,000 mW/cm^2 at rated power
- Cost: $5-9/kWe catalyst and <$30 kWe system
- Durability with cycling: 5,000 hours (<80ºC) and 2,000 hours (>80ºC), <40% loss of initial catalytic mass activity at 900 mV on O_2; <30 mV loss at 0.8 A/cm²

FY 2013 Accomplishments

- Identified advanced cathode catalyst to be studied in this project. Synthesis of this catalyst has been scaled up to hundred gram quantities.
- Performed ultra-small angle X-ray scattering (USAXS) and cryogenic transmission electron microscopy (TEM) on catalyst-ionomer-solvent inks containing the advanced alloy catalyst, a standard Pt/C, and Pt/C with particle size comparable to that of the advanced alloy catalyst to determine the catalyst and ionomer primary particle and agglomerate size and size distribution.
- Developed a Monte-Carlo simulation model to determine the structure of the catalyst layer knowing the catalyst ink composition with inputs of the size distributions of Pt or alloy particles, primary carbon particles and carbon agglomerates, and primary ionomer and ionomer agglomerates being determined using USAXS and TEM.
- Fabricated catalyst-coated membranes containing the advanced alloy catalyst and platinum catalysts of two particle sizes and initiated electrochemical measurements to determine the sources of voltage losses.

INTRODUCTION

One of the major cost contributors to PEMFC systems for automotive and stationary power applications is the platinum-group metal (PGM) cathode electrocatalyst [1]. The high cost of the cathode electrocatalyst results from the high loadings of catalyst necessary to overcome the limitations of low ORR activity, low utilization of PGM, and loss of activity with operating time. Alloying platinum with base metals (e.g., cobalt, iron, and nickel) is well-known to improve its intrinsic ORR activity [2]. While ORR activities exceeding the DOE 2017 targets (>0.44 A/mg PGM and 720 µA/cm² @ 900 mV) have been demonstrated for high-surface-area-carbon-supported Pt alloy and core-shell nanoparticle catalysts in aqueous cell RDE tests [3], some as high as 2 A/mg Pt [4], the full activities and performance of these promising catalysts have yet to be achieved in MEAs, especially when operating at realistic current densities and on air rather than oxygen. Figure 1 illustrates that PEMFC cathodes containing alloy catalysts outperform cathodes containing Pt catalysts at all current densities when operating with oxygen as the cathode gas and at current densities <1,000 mA/cm² when operating with air as the cathode gas.

There are several possible reasons the full potentials of the advanced alloy, de-alloyed, and core-shell materials have not been realized in MEAs operating on air and at current densities >1 A/cm^2. One may arise from the complex requirements for full utilization of the electrocatalytic sites and for adequate reactant transport in the MEA cathode layer. These requirements are easily fulfilled in the RDE environment by virtue of the thinness of the catalysts film, its intimate contact with a glassy carbon substrate, flooding of the film with an oxygen-saturated proton-conducting electrolyte, and efficient transport of reactants to the film by electrode rotation. These requirements are also easily

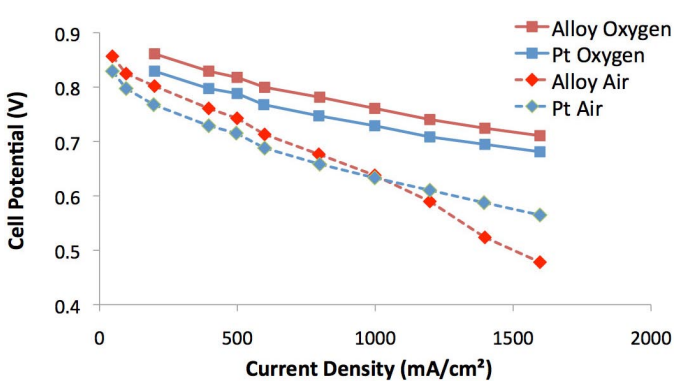

FIGURE 1. Example of lack of performance benefit of a Pt alloy over Pt when operating at >1,000 mA/cm² on air (cathode loading 0.2 mg Pt/cm², 80°C, 50/50 kPa gauge).

met in the fuel cell at low current densities in an oxygen environment where the electrocatalytic reaction rate dominates the voltage losses and demands on transport to the reactive sites are easily filled. Fulfillment of these requirements at high current densities in an MEA cathode relies on optimization of the electrode composition and structure to balance the structure of the proton-conducting phase, the electron-conducting phase, and the distribution and size of pores for reactant/product diffusion. This optimization is a lengthy, trial-and-error process and has taken several years for the traditional Pt-only cathode layers. The goal of this project is to optimize the electrode layer composition, structure, and materials properties of cathodes based on advanced alloy cathodes so they can achieve their entitled performance at high current densities and on air and exceed the DOE performance and durability targets for PEMFCs for automotive applications.

APPROACH

This project is following a new and comprehensive approach to achieving the goals: (1) determination of the agglomerate, particle, and pore structure of the advanced Pt alloy/C-based electrodes; (2) using this information and electrochemical diagnostic techniques to determine the performance-limiting property of the current electrode structure; (3) rational design of the catalyst layer/MEA structure guided by computational modeling; (4) development of the catalyst support morphology, surface functionality, and catalyst ink composition to be used for making the performance-optimizing cathode layer, guided by the modeling results; (5) study of the dispersion of Pt alloy/C catalyst aggregates and the perfluorosulfonic acid ionomer particles in liquid media and the agglomeration of these aggregates/particles during the evaporation process; and (6) development of a solvent removal process that maintains the dispersion and agglomerate structure of the ink.

The advanced Pt alloy is a state-of-the-art de-alloyed Pt/Ni catalyst developed in the on-going General Motors-led project entitled "High-Activity Dealloyed Catalysts." The key characteristics and metrics of this catalyst are:

- Catalyst deposited as nanoparticles onto conventional carbon black supports, identical to those used for standard Pt/C reference catalysts.
- Catalyst deposition chemistry is proven and via methods scalable to commercial levels.
- Nominal initial atomic composition prior to de-alloying is $Pt_{25}Ni_{75}$.
- Mass activity (O_2 @ 0.9 V) is >0.60 A/mg Pt (exceeds DOE 2017 target).
- Mass activity loss after 30,000 0.60 to 1.0 V cycles is <40% (exceeds DOE kinetic stability target).

RESULTS

The advanced cathode catalyst to be studied in this project has been identified. It has oxygen reduction activity and kinetic stability in an MEA that exceeds DOE 2017 target and has been scaled up by Johnson Matthey Fuel Cells. USAXS and TEM have been performed on catalyst-ionomer-solvent inks. These inks contain the standard Pt/C catalyst (Pt particle size of 2-3 nm), a Pt/C catalyst that has been heat-treated to grow the particle size to be comparable to that of the advanced alloy catalyst (>5 nm), or the advanced alloy catalyst. The ionomer to catalyst ratio and type and amount of solvent used in the inks was varied to determine how they affect the ink and electrode layer structure and, ultimately, performance. Analysis of these USAXS and TEM data is providing the ionomer and catalyst/carbon primary and aggolomerate structure in the ink. A Monte Carlo simulation model has been developed to determine the structure of the catalyst layer knowing the catalyst ink composition. The model inputs include the size distributions of Pt particles, primary carbon particles and carbon agglomerates, and primary ionomer particles and ionomer agglomerates, as determined from the USAXS and TEM measurements. Catalyst-coated membranes using the advanced alloy catalyst in the cathode layer and platinum catalysts, for comparison, have been fabricated by Johnson Matthey Technology Center and are now being tested at United Technologies Research Center to determine their overall performance and the sources of voltage losses using a variety of electrochemical techniques, such as electrochemical impedance spectroscopy and limiting current using a variety of cathode gas compositions.

CONCLUSIONS AND FUTURE DIRECTIONS

As this project is relatively new, no major conclusions are available at this point. Future directions will be to determine the sources of the voltage losses that are unique to the advanced alloy catalysts operating at high current densities and on air and to mitigate these losses. The approaches to mitigating these losses will be to alter the catalyst layer structure and composition and the intrinsic materials properties, such as proton conductivity of the carbon support. Other approaches will be developed, if necessary, when the sources of these voltage losses are known.

FY 2013 PUBLICATIONS/PRESENTATIONS

1. Myers, D., "Rationally Designed Catalyst Layers for PEMFC Performance Optimization", 2013 DOE Hydrogen and Fuel Cells Program and Vehicle Technologies Program Annual Merit Review and Peer Evaluation Meeting, Washington D.C., May 13–17, 2013. (Poster)

REFERENCES

1. Papageorgopoulos, D.; "Fuel Cells-Session Introduction", 2013 DOE Hydrogen and Fuel Cells Program and Vehicle Technologies Program Annual Merit Review and Peer Evaluation Meeting, Washington D.C., May 13–17, 2013.

2. (a) Gasteiger, H.A.; Kocha, S.S.; Sompalli, B.; Wagner, F.T., Activity benchmarks and requirements for Pt, Pt-alloy, and non-Pt oxygen reduction catalysts for PEMFCs. Appl Catal B-Environ 2005, 56 (1-2), 9-35; (b) Thompsett, D., Pt Alloys as Oxygen Reduction Catalysts. In Handbook of Fuel Cells: Fundamentals, Technology and Applications; Vol 3, Vielstich, W.; Lamm, A.; Gasteiger, H. A., Eds. John Wiley & Sons: Chichester, 2003; p 467.

3. (a) Zhang, J.; Lima, F.H.B.; Shao, M.H.; Sasaki, K.; Wang, J.X.; Hanson, J.; Adzic, R.R., "Platinum monolayer on non-noble metal-noble metal core-shell nanoparticle electrocatalysts for O_2 reduction", J Phys Chem B 2005, 109 (48), 22701-22704; (b) Wang, C.; van der Vilet, D.; Chang, K.C.; You, H.D.; Strmcnik, D.; Schlueter, J.A.; Markovic, N.M.; Stamenkovic, V.R., "Monodisperse Pt_3Co Nanoparticles as a Catalyst for the Oxygen Reduction Reaction: Size-Dependent Activity", J Phys Chem C 2009, 113 (45), 19365-19368; (c) Wang, C.; Wang, G.F.; van der Vliet, D.; Chang, K.C.; Markovic, N.M.; Stamenkovic, V.R., "Monodisperse Pt3Co nanoparticles as electrocatalyst: the effects of particle size and pretreatment on electrocatalytic reduction of oxygen.", Phys Chem Chem Phys 2010, 12 (26), 6933-6939; (d) Markovic, N.; Stamenkovic, V., Nanosegregated Cathode Alloy Catalysts with Ultra-Low Platinum Loading. DOE Hydrogen Program 2012 Annual Report 2012.; (f) Debe, M.K.; Steinbach, A.J.; Hendricks, S.M.; Kurkowski, M.J.; Vernstrom, G.D.; Atanasoski, R.T.; Hester, A.E.; Haug, A.T.; Lewinski, K.A.; Deppe, S.K., "Advanced Cathode Catalysts and Supports for PEM Fuel Cells", DOE Hydrogen Program 2012 Annual Report 2012; (g) Mani, P.; Srivastava, R.; Strasser, P., "Dealloyed Pt-Cu core-shell nanoparticle electrocatalysts for use in PEM fuel cell cathodes", J Phys Chem C 2008, 112 (7), 2770-2778.

4. Markovic, N.; Stamenkovic, V., "Nanosegregated Cathode Alloy Catalysts with Ultra-Low Platinum Loading", DOE Hydrogen Program 2012 Annual Report 2012.

V.D.1 Durability Improvements Through Degradation Mechanism Studies

Rod Borup[1] (Primary Contact),
Rangachary Mukundan[1], Yu Seung Kim[1],
Dusan Spernjak[1], Joe Fairweather[1], John Davey[1],
Roger Lujan[1], D. Langlois[1], Nathan Mack[1],
Rajesh Ahluwalia[2], Xiaohua Wang[2], Adam Weber[3],
Ahmet Kusoglu[3], Karren More[4], Mike Brady[4],
Paul Beattie[5], Warren Williams[5], Steve Grot[6],
Kateryna Artyushkova[7], Plamen Atanassov[7],
Dan Hussey[8], David Jacobson[8]

[1]Los Alamos National Laboratory (LANL)
MS D429, P.O. Box 1663
Los Alamos, NM 87545
Phone: (505) 667-2823
Email: Borup@lanl.gov

DOE Manager
Nancy Garland
Phone: (202) 586-5673
Email: Nancy.Garland@ee.doe.gov

Subcontractors and Collaborators:
[2] Argonne National Laboratory, Argonne, IL
[3] Lawrence Berkeley National Laboratory, Berkeley, CA
[4] Oak Ridge National Laboratory, Oak Ridge, TN
[5] Ballard Power Systems, Burnaby, BC, Canada
[6] Ion Power, New Castle, DE
[7] University of New Mexico, Albuquerque, NM
[8] National Institute of Standards and Technology, Gaithersburg, MD

Start Date: October 2009
Project End Date: 2013

Overall Objectives

- Identify and Quantify Degradation Mechanisms
  - Degradation measurements of components and component interfaces
  - Elucidation of component interactions, interfaces, operation leading to degradation
  - Development of advanced in situ and ex situ characterization techniques
  - Quantify the influence of inter-relational operation between different components
  - Identification and delineation of individual component degradation mechanisms
- Understand Electrode Structure Impact—Applied Science Subtask
  - Better understand the electrode structural and chemical effects on durability
  - Understand impact of electrode structure on durability and performance
  - Correlate different electrode structures to fuel cell performance and durability
  - Define different fabrication effects (esp. solvents) for high-durability electrode structures
- Develop Models Relating Components and Operating Conditions to Fuel Cell Durability
  - Individual degradation models of individual fuel cell components
  - Development and dissemination of an integrated comprehensive model of cell degradation
- Methods to Mitigate Degradation of Components
  - New components/properties, designs, operating conditions

Fiscal Year (FY) 2013 Objectives

- Refine Degradation Model
  - Incorporate carbon corrosion effects
  - Incorporate membrane and catalyst layer ionomer effects
  - Model metal bipolar plate corrosion and contact resistance
- Characterize Degradation Mechanisms of Components
  - Carbon corrosion and effects on catalyst layer structural changes
  - Membrane degradation by measuring changes to water uptake and membrane structure
  - Metal bipolar plate corrosion

Technical Barriers

This project addresses the following technical barriers from the Fuel Cells section of the Fuel Cell Technologies Office Multi-Year Research, Development, and Demonstration Plan:

(A) Durability

(B) Cost

Technical Targets

- Transportation Durability: 5,000 hours (with cycling)
  - Estimated start/stop cycles: 17,000
  - Estimated frozen cycles: 1,650
  - Estimated load cycles: 1,200,000
- Stationary Durability: 40,000 hours
  - Survivability: stationary -35°C to 40°C
  - Cost ($25/kW$_e$)

FY 2013 Accomplishments

- Measured carbon corrosion and completed initial development of carbon corrosion model:
  - Measured carbon corrosion rates for Pt-catalyzed corrosion of Ketjen® black (E-type), Vulcan® XC72 (V-type), and graphitized carbon (EA-type) supports
  - Examined mixing more stable catalyst supports and showed mixture retains more of the pore structures and maintains transport properties better during a carbon corrosion accelerated stress test (AST)
  - Post-characterization revealed increasing graphitic content and increasing oxygen concentration in the catalyst layer
  - Modified catalyst durability model to account for changes due to carbon corrosion
  - Determined the effect of aging on the specific surface area of carbon (S_C, m^2-C/g-C)
  - Characterized the percent change in Pt particle size to be much greater for Pt supported on E-carbon in surface layer than Pt particles supported on EA-carbon in inner layer
- Measured and modeled membrane and ionomer degradation, including gas crossover during membrane degradation:
  - Modeled open-circuit voltage (OCV) data to show Pt particles deposited in aged membrane promote reaction between H_2 crossing over from anode and O_2 crossing over from cathode
  - Demonstrated that Pt particle migration affects the membrane H_2 crossover
  - Developed a component model for chemical/mechanical membrane durability and validated prediction of changing H_2O uptake based on nanostructure degradation
  - Modeled catalyst layer ionomer degradation as contributing cause to electrochemical surface area (ECSA) loss
- Measured corrosion properties of metal bipolar plates, contact resistance and corrosion products:
  - Developed model for SS 316L and G35 metal bipolar plates
- Characterized membrane electrode assembly (MEA) structure degradation:
  - Demonstrated that the durability response of low-loaded cathodes (0.05 mg/cm^2) is significantly different than that of higher-loaded cathodes (>0.10 mg/cm^2)
  - Attributed differences in catalyst layer degradation from different casting solvents to Nafion® relaxation in catalyst layer

✧ ✧ ✧ ✧ ✧

INTRODUCTION

The durability of polymer electrolyte membrane (PEM) fuel cells is a major barrier to the commercialization of these systems for stationary and transportation power applications. By investigating component and cell degradation modes, defining the fundamental degradation mechanisms of components and component interactions, new materials can be designed to improve durability. To achieve a deeper understanding of PEM fuel cell durability and component degradation mechanisms, we have assembled a multi-institutional and multi-disciplinary team with significant experience investigating these phenomena.

APPROACH

Our approach to understanding durability and degradation mechanisms within fuel cells is structured in three areas: fuel cell testing (life testing, ASTs, ex situ aging), characterization of component properties as a function of aging time, and modeling (component aging and integrated degradation modeling). The modeling studies tie together what is learned during component characterization and allow better interpretation of the fuel cell studies. This approach and our team give us the greatest chance to increase the understanding of fuel cell degradation and to develop and employ materials that will overcome durability limitations in fuel cell systems. This work is also being coordinated with other funded projects examining durability through a DOE Durability Working Group.

RESULTS

Electrode Structural Changes and Carbon Corrosion

The structural change of the catalyst layer can cause changes in the PEM fuel cell performance due to loss of

catalyst utilization, electronic/protonic conductivity, and changes in the mass transport of the gases. A primary cause for changes in the structure of the catalyst layer is the corrosion of carbonaceous electrode supports leading to electrode collapse, reduced active catalyst area, and increased surface hydrophilicity. Figure 1 shows comparisons of cathode catalyst layers after 389 hours of the DOE/U.S. DRIVE Durability Drive Cycle Test (including wet/dry cycles). The fresh catalyst layer (Figure 1a) shows a non-compacted catalyst layer of about 7-8 microns thick, while after testing (Figure 1b) the catalyst layer shows about 30% compression/thinning due to either loss of carbon or due to loss of the pore structure of the catalyst layer.

Catalyst layer thinning is regularly observed due to carbon corrosion, which is accelerated at high potentials that are produced during shut-down/start-up transients. Carbon corrosion measurements were made for three different types of carbon, E-carbon (high surface area carbon), V-carbon (Vulcan) and EA-carbon (graphitized carbon). Figure 2 shows scanning transmission electron microscopy (STEM) images of the cathode catalyst layer as a function of time during 1.2 V holds for E-Carbon. The fresh catalyst layer had a catalyst layer thickness of 25 microns, whereas after only 20 hours of potential hold, the catalyst layer thickness was reduced to about 15 microns, 8 microns at 40 hours, and 5 microns at 100 hours. Mass transport losses associated with significant cathode "thinning" >50% after only 20 hours at 1.2 V were observed. Post characterization (X-ray photoelectron spectroscopy) after the carbon corrosion AST shows that both graphitic content (as percent) and oxygen content increases. The graphitic content increase is likely due to a decrease of amorphous carbon due to corrosion, while the increasing oxygen content is likely on the carbon surface and has the tendency to change the hydrophobic properties of the catalyst layer and can affect the mass transport due to changing catalyst layer water content.

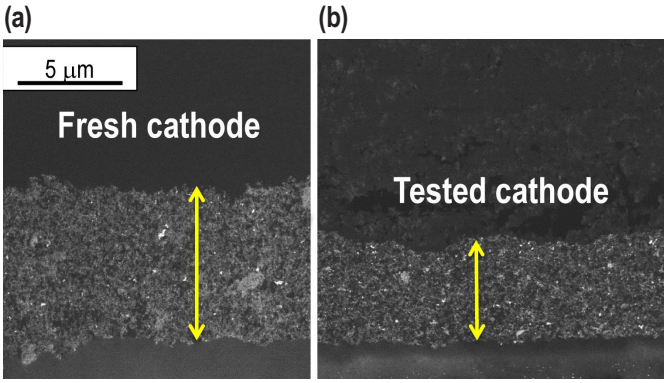

FIGURE 1. STEM images of the cathode catalyst layer with HSAC (high surface area carbon) (a) fresh, and (b) after 389 hours of testing using the U.S. DRIVE Durability Drive Cycle Test.

Measurements indicate that the performance loss is due to both kinetic losses arising from loss of active surface area and due to increases in mass transport resistance. To minimize the losses due to mass transport resistance, mixtures of E and EA carbon were made to measure the effect on mass transport resistance, to determine if by stabilizing the catalyst layer void volume, a portion of the performance loss can be prevented. Figure 3 shows a bar plot of mass activity and ECSA (Figure 3a) and associated polarization performance (Figure 3b) for E-carbon, EA-carbon, V-carbon, and an MEA made of a mixture of E- (60%) and EA- (40%) carbon. Figure 3c shows impedance spectra for the samples measured at 1 A/cm^2. The post-aging transport losses of the E-carbon are very large (blue squares), whereas when mixed with the EA-carbon, the transport losses were minimized (green squares). However, the overall performance of the EA-carbon after 400 hours of the AST was the highest.

Nanostructure of Degraded Membrane

We have previously observed that the membrane structure changes during aging, with the crystallinity of the membrane being more pronounced (transmission electron microscopy [TEM] inserts in Figure 4b). In FY 2013, small angle X-ray scattering (SAXS) was used to quantify these changes for Nafion® 212 (Figure 4a). The results for the Nafion® 212 membrane show that upon aging, the SAXS

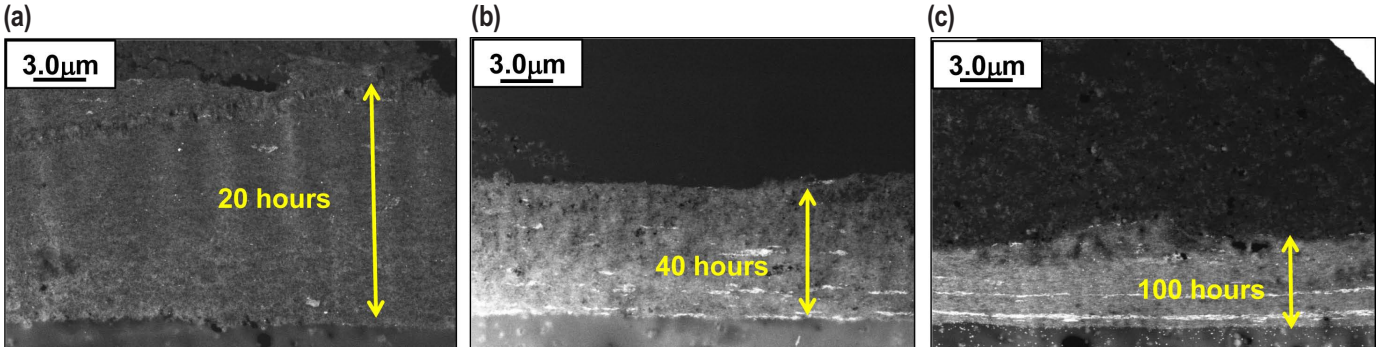

FIGURE 2. STEM images of the cathode catalyst layer with HSAC after carbon corrosion AST hold at 1.2 V for (a) 20 hours, (b) 40 hours and (c) 100 hours.

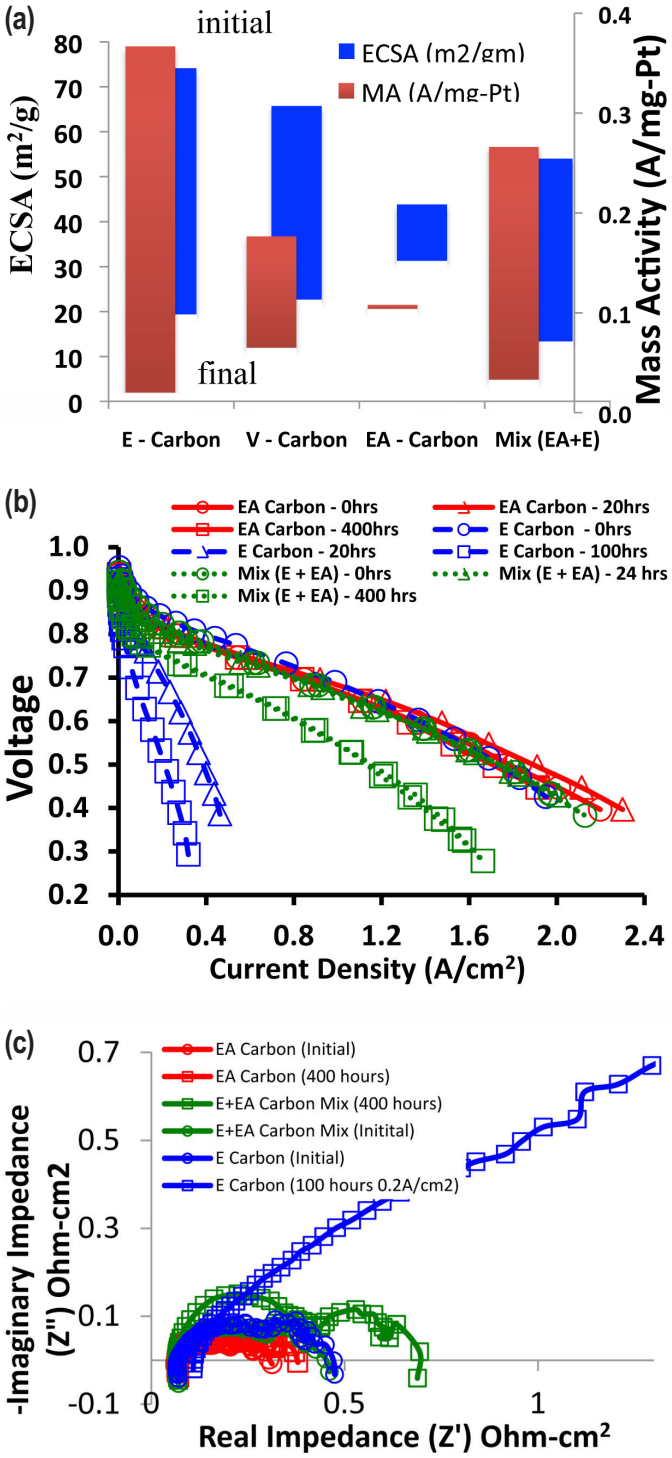

FIGURE 3. For catalyst layers comprised of Pt supported on carbon, with E-carbon (HSAC), Vulcan carbon, EA-carbon (graphitized), and a catalyst layer with a mixture of EA+E carbon: (a) bar plot with initial and final ECSA and mass activities, (b) polarization curves as a function of time during a 1.2 V carbon corrosion AST hold, and (c) impedance spectra at 1.0 A/cm^2. Note: MEA Pt loadings were 0.15 mg/cm^2 (E)/0.15 mg/cm^2 (EA+E)/0.25 mg/cm^2 (EA).

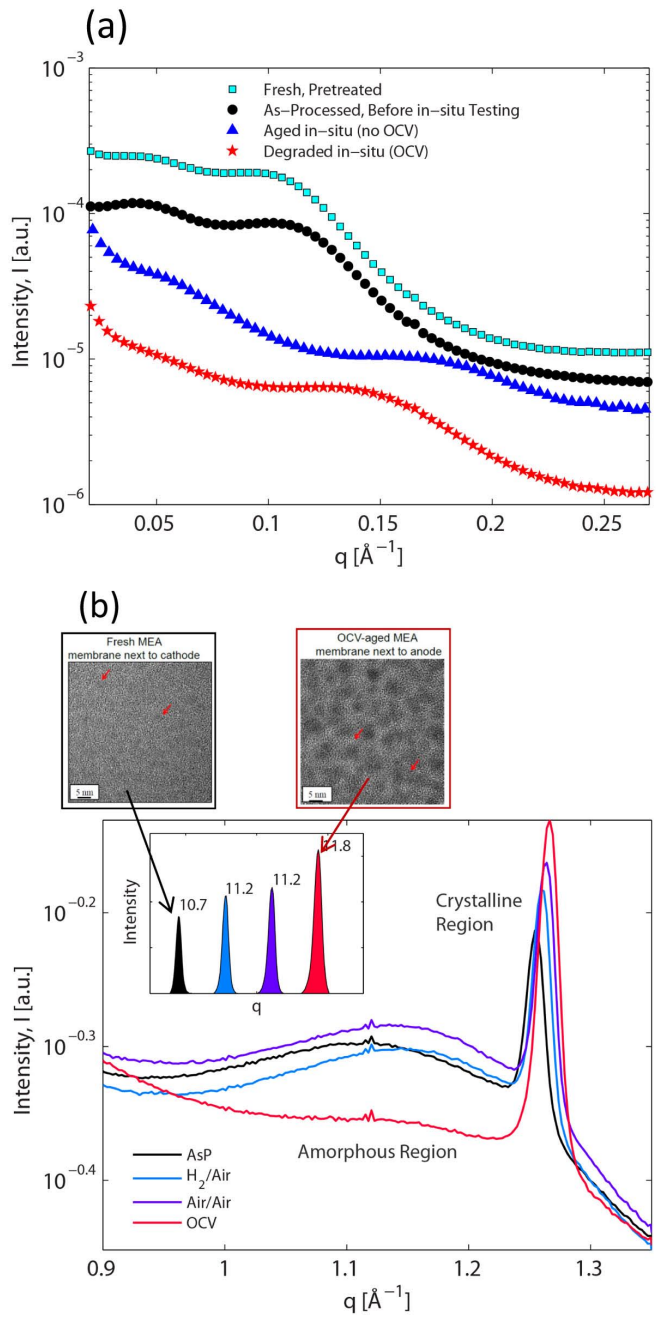

FIGURE 4. Characterization of Nafion® 212 membrane fresh and with different aging treatments by (a) SAXS and (b) WAXS.

peak indicative of membrane/water structure occurs at a much larger scattering vector (q - 0.18 vs. 0.1 for fresh); upon boiling of the aged membrane, d-spacing increases. However, this is still lower than fresh membrane. Increased crystallinity of the membrane was measured by wide angle X-ray scattering (WAXS) and is shown in Figure 4b. The crystallinity of the membrane was lowest in the fresh sample (AsP), and increased with aging treatment, with the highest crystallinity observed after OCV testing. These higher

crystallinity/aging measurements correspond to lower water uptake in the membrane.

CONCLUSIONS

Testing and advanced characterization were conducted to determine component degradation; testing included drive-cycle tests, start-up/shut-down tests, and available ASTs, with varying conditions and materials. Advanced characterization techniques included a) TEM and scanning electron microscopy (SEM) measurements that identified the corrosion of different types of carbons during AST and fuel cell operation and its effect on catalyst layer structure; b) SAXS and WAXS characterization of the changes to membrane structure and crystallinity and correlating nanostructural changes to membrane water-uptake; c) advanced electrochemical impedance spectroscopy that measured the effect of metal bipolar plate corrosion and changes to internal contact resistance, and delineated mass transport losses from electrode structure changes; and d) atomic force microscopy studies that revealed changes to catalyst layer ionomer relaxation with different solvent manufacturing techniques and their effect on mass transport properties.

The degradation modeling was refined to include advanced component models. These included a) incorporation of a carbon corrosion model into the catalyst durability model; b) development of a membrane degradation model for combined chemical/mechanical membrane durability and validating the prediction of changing H_2O uptake based on nanostructure degradation; c) modeling the effect of Pt incorporation into the membrane on gas crossover and membrane/ionomer degradation, and quantifying ionomer degradation contributions to ECSA loss; and d) modeling metal bipolar plate corrosion and contact resistance increase during aging.

FUTURE DIRECTIONS

Component Interactions

- Measure transport of dissolved cations through catalyst ionomer and membrane
- Further quantitate relationship between ionomer relaxation, carbon corrosion, and resulting changes in carbon catalyst layer structure (Pt/pore distributions, Pt utilization, ECSA, catalyst supports and mixtures)
- Incorporate component membrane model into integrated model
- Model refinement incorporating data on advanced materials and better delineated degradation mechanisms; incorporate transport of dissolved cations through catalyst ionomer and membrane from carbon plates, seals, and metal bipolar plates

Understand Carbon/Nafion®/Catalyst Structure and Durability Effects

- Understand the effect of catalyst layer structure on durability, different methods of forming catalyst layers
- Improve durability/performance of low-loaded MEAs (0.05 mg/cm^2)
- Identify ionomer degradation source for fluoride emission rate (catalyst layer vs. membrane)

Define Effect of Carbon Corrosion on Catalyst Layer Structure and Transport Losses

- Quantify relationship between carbon corrosion and changes in catalyst layer structure
- Identify uniform methodology for measuring real durability impact of start-up/shut-down, air cycling
- Spatial/areal performance variations over aging remain largely undetermined

Catalyst Durability

- Reduce solubility of Pt via increasing support interactions, alloying
- Understand/model dissolution of Pt at elevated temperatures and in oxygen
- Understand effect of Pt transport and band formation

Component Surface Properties

- Understand effects of changing surface chemistry on bipolar plates, catalysts, gas diffusion layers

Mitigation of Degradation

- Increase catalyst transport, stability through use of stable structures and stable materials

ISSUED PATENTS

1. Advanced membrane electrode assemblies for fuel cells, USP 8,227,147 (2012).

2. Non-Aqueous liquid composition of ion exchange polymers, USP 7,981,319 B2 (2011), USP 8,236,207 B2 (2012), USP 8,394,298 (2013).

FY 2013 PUBLICATIONS/PRESENTATIONS

Publications

1. Hussey, D.S.; Spernjak, D.; Weber, A.Z.; Mukundan, R.; Fairweather, J.; Brosha, E.L.; Davey, J.; Spendelow, J.S.; Jacobson, D.L.; Borup, R.L. **Accurate measurement of the through-plane water content of proton-exchange membranes using neutron radiography,** Journal of Applied Physics (2012), 112(10).

2. Spernjak, Dusan; Fairweather, Joseph; Mukundan, Rangachary; Rockward, Tommy; Borup, Rodney L., **Influence of the microporous layer on carbon corrosion in the catalyst layer of a polymer electrolyte membrane fuel cell,** Journal of Power Sources (2012), 214, 386-398.

3. Mishler, Jeffrey; Wang, Yun; Mukundan, Rangachary; Spendelow, Jacob; Hussey, Daniel S.; Jacobson, David L.; Borup, Rodney L., **Probing the water content in polymer electrolyte fuel cells using neutron radiography,** Electrochimica Acta (2012), 75, 1-10.

4. J. Chlistunoff, J.R. Davey, K.C. Rau, R. Mukundan, and R.L. Borup, **PEMFC Gas Diffusion Media Degradation Determined by Acid-Base Titrations,** ECS Transactions (2012).

5. Rangachary Mukundan, Greg James, Dana Ayotte, John Davey, David Langlois, Dusan Spernjak, Dennis Torraco, Sivagaminathan Balasubramanian, Adam Z Weber, Karren More, and Rodney L. Borup, **Accelerated testing of carbon corrosion and membrane degradation in PEM fuel cells,** ECS Transactions (2012).

6. J.D. Fairweather, D. Spernjak, R. Mukundan, R.K. Ahluwalia, S. Arisetty, R.L. Borup, **Time Resolved Corrosion of Electrode Supports in PEM Fuel Cells,** ECS Transactions (2012).

7. Joseph Fairweather, Dusan Spernjak, Adam Z. Weber, David Harvey, Silvia Wessel, Daniel S. Hussey, David L. Jacobson, Kateryna Artyushkova, Rangachary Mukundan, and Rodney L. Borup, **Effects of Cathode Corrosion on Through-Plane Water Transport in Proton Exchange Membrane Fuel Cells,** Journal of the Electrochemical Society, **160** (9) F980-F993 (2013).

8. Gi Suk Hwang, Hyoungchul Kim, Roger Lujan, Rangachary Mukundan, Dusan Spernjak, Rodney L. Borup, Massoud Kaviany, Moo Hwan Kim, and Adam Z. Weber, **Phase-Change-Related Degradation of Catalyst Layers in Proton-Exchange-Membrane Fuel Cells**, Electrochimica Acta, Volume 95, pp 29-37 (2013).

9. Arisetty, S.; Wang, X.; Ahluwalia, R. K.; Mukundan, R.; Borup, R.; Davey, J.; Langlois, D.; Gambini, F.; Polevaya, O.; Blanchet, S., **Catalyst Durability in PEM Fuel Cells with Low Platinum Loading,** Journal of the Electrochemical Society (2012), 159(5), B455-B462.

10. Mishler, Jeffrey; Wang, Yun; Mukherjee, Partha P.; Mukundan, Rangachary; Borup, Rodney L., **Subfreezing operation of polymer electrolyte fuel cells: Ice formation and cell performance loss,** Electrochimica Acta (2012), 65, 127-133.

11. C. Welch, A. Labouriau, R. Hjelm, B. Orler, C. Johnston, Y.S. Kim, **Nafion in Dilute Solvent Systems: Dispersion or Solution?** *ACS Macro Letters*, 1, 1403-1407 (2012).

12. J. Dillet, D. Spernjak, A. Lamibrac, G. Maranzana, R. Mukundan, J. Fairweather, S. Didierjean, R.L. Borup, O. Lottin, **Impact of flow rates, Pt loading, and carbon support on performance, CO_2 evolution, and active surface area during repeated startups and shutdowns in polymer-electrolyte membrane fuel cells**, submitted to J. Electrochem. Soc.

Invited Presentations

1. R.L. Borup, R.K. Ahluwalia, K.L. More, C.J. Johnston, and R. Mukundan, **Degradation Mechanisms in PEM Fuel Cells,** 222th ECS Meeting – Honolulu, Hawaii, October 7 – October 12, 2012.

2. Rod Borup, **PEM Fuel Cells: Microstructural Design and Durability at the Microstructural Level,** Materials by Design Workshop, 2013 Los Alamos National Laboratory Materials Summer Research Group (SRG).

3. Borup, Rod et al., **Durability Improvements Through Degradation Mechanism Studies,** FC Tech Team, Detroit MI, September 12, 2012.

Contributed Presentations

1. A. Lamibrac, J. Durst, D. Spernjak, G. Maranzana, J. Dillet, S. Didierjean, O. Lottin, F. Maillard, L. Dubau, M. Chatenet, R. Mukundan, and R.L. Borup, **Internal Currents, CO_2 Emissions and Decrease of the Pt Electrochemical Surface Area during Fuel Cell Start-Up and Shut-Down,** 222th ECS Meeting – Honolulu, Hawaii, October 7 – October 12, 2012.

2. J.D. Fairweather, D. Spernjak, R. Mukundan, R.K. Ahluwalia, S. Arisetty, and R.L. Borup, **Time Resolved Corrosion of Electrode Supports in PEM Fuel Cells,** 222th ECS Meeting – Honolulu, Hawaii, October 7 – October 12, 2012.

3. D.S. Hussey, D. Jacobson, B. Khaykovich, M.V. Gubarev, D. Spernjak, J.D. Fairweather, R. Mukundan, R. Lujan, and R.L. Borup, **Neutron Imaging PEMFCs with ~1 µm Spatial Resolution,** 222th ECS Meeting – Honolulu, Hawaii, October 7 – October 12, 2012.

4. R. Mukundan, G. James, D. Ayotte, J. Davey, D. Langlois, D. Spernjak, D. Torraco, S. Balasubramanian, A. Weber, K.L. More, and R.L. Borup, **Accelerated Testing of Carbon Corrosion and Membrane Degradation in PEM Fuel Cells,** 222th ECS Meeting – Honolulu, Hawaii, October 7 – October 12, 2012.

5. J. Chlistunoff, K.C. Rau, R. Mukundan, and R.L. Borup, **PEMFC Gas Diffusion Media Degradation Determined by Acid-Base Titrations,** 222th ECS Meeting – Honolulu, Hawaii, October 7 – October 12, 2012.

6. D. Spernjak, J.D. Fairweather, T. Rockward, K.C. Rau, R.L. Borup, and R. Mukundan, **Influence of In Situ and Ex Situ Aging of Gas Diffusion Layers on Fuel Cell Performance Degradation**, 222th ECS Meeting – Honolulu, Hawaii, October 7 – October 12, 2012.

7. D. Spernjak, R. Mukundan, P. Wilde, R. Schweiss, K.L. More, D. Langlois, J.D. Fairweather, and R.L. Borup, **PEM Fuel Cell Performance and Durability with Different Treatments of Microporous Layer,** 222th ECS Meeting – Honolulu, Hawaii, October 7 – October 12, 2012.

8. Borup, Rod et al., **Durability Improvements Through Degradation Mechanism Studies,** DOE Fuel Cell Technologies Annual Merit Review, Arlington, VA, May 13–17, 2013.

V.D.2 Durability of Low-Platinum Fuel Cells Operating at High Power Density

Scott Blanchet (Primary Contact), Olga Polevaya, May Tan
Nuvera Fuel Cells Inc.
Building 1, 129 Concord Rd.
Billerica, MA 01821
Phone: (617) 245-7667
Email: blanchet.s@nuvera.com

DOE Managers
Kathi Epping Martin
Phone: (202) 586-7425
Email: Kathi.Epping@ee.doe.gov
Gregory Kleen
Phone: (720) 356-1672
Email: Gregory.Kleen@go.doe.gov

Technical Advisor
Thomas G. Benjamin
Phone: (630) 252-1632
Email: Benjamin@anl.gov

Contract Number: DE-EE0000469

Subcontractors:
- Los Alamos National Laboratory (LANL) Los Alamos, NM
- Argonne National Laboratory (ANL), Argonne, IL

Project Start Date: September 1, 2009
Project End Date: August 31, 2013

Overall Objectives

- The objective of this project is to study and identify strategies to assure durability of fuel cells designed to meet DOE 2015 cost targets.
- Develop a practical understanding of the degradation mechanisms impacting durability of fuel cells with low-Pt loading (≤0.2 mg/cm^2) operating at high power density (≥1.0 W/cm^2).
- Develop approaches for improving the durability of low-loaded, high-power stack designs.

Fiscal Year (FY) 2013 Objectives

- Complete comparative study of voltage degradation in single cells with the different flowfield architecture under load cycle protocols.
- Complete durability model of the cathode with the focus on Pt ageing and the cathode electrode performance variations under designed operating conditions.
- Validate the durability model against load cycle tests in short stacks.

Technical Barriers

This project addresses the following technical barriers from the Fuel Cells section of the Fuel Cell Technologies Office Multi-Year Research, Development, and Demonstration Plan:

(A) Durability

(B) Cost

Technical Targets

The technical targets for this project are listed in Table 1.

TABLE 1. Progress towards Meeting Technical Targets for Transportation Fuel Cell Stacks Operating on Direct Hydrogen for the Transportation Applications

Characteristics	Units	2010/2017 Stack Targets	Nuvera 2013 Status
Cost	$/kWe	25/15	~22 estimated[1]
Durability with Cycling	Hours	5,000	12,000 hrs[2]; 5,500 hrs in automotive cycle conditions[3]
Performance at Rated Power	mW/cm^2	1,000	1,250[4] and 1,375[5]

[1] Cost assessment of Nuvera's architecture by Directed Technologies Inc. based on their DOE-sponsored Design for Manufacturing and Assembly model [1].
[2] Demonstrated under power profile specific to fork truck applications in material handling market at total Pt loading of 0.5 mg/cm^2.
[3] Demonstrated in 20-cell stack of 360-cm^2 cell active area by Nuvera customer in automotive load profile, total loading 0.5 mg/cm^2.
[4] Demonstrated in 250-cm^2 Orion stack by Nuvera at Pt loading of 0.096 mg/cm^2.
[5] Demonstrated in 50-cm^2 single cell with open flowfield (SCOF) at 2.5 A/cm^2 by Nuvera at Pt loading 0.2 mg/cm^2.

FY 2013 Accomplishments

- ANL completed development of Pt dissolution and catalyst performance degradation models, representing the building blocks of the full cathode durability model and establishing relations between changes in overpotentials, electrocatalyst surface area (ECSA), and oxygen mass transport, calibrating coefficients against the experimental values obtained in single-cell durability tests.
- The project milestone #4, completed on schedule, validated the durability model against load cycle tests in short stacks with membrane electrode assemblies (MEAs) of 250-cm^2 active area.
- Benchmarking of Rochester Institute of Technology land-channel cell architecture against Nuvera single cell with open flowfield (RIT vs. SCOF) under the new stress test (NST) N1A concluded independence of the

ECSA loss of the cell architecture and resulted in higher degradation of the RIT cell due to the larger increase in mass transport overpotentials. Results were reported on the MEAs with 0.4- and 0.15-mg_{Pt}/cm^2 cathode loadings.

- Performance loss of 0.002%/hour at the rated current density (RCD) of 1.5 A/cm^2 (0.9 W/cm^2 at the beginning of life), demonstrated on the low-Pt MEAs (total loading 0.2 mg/cm^2) in the open flowfield architecture under the accelerated load cycle test, was related to the 0.0018%/hour performance loss of normal Pt-loaded MEAs (total loading 0.45 mg/cm^2) in Nuvera short stack over 5,500-hr simulated drive cycle test; therefore, proving the feasibility of low-Pt MEAs to achieve 5,000-hr lifetime target at the moderate RCD.
- Dissemination of the cathode durability model was started with the first publication of the Pt dissolution block and will continue in the next months for the catalyst performance degradation.

✧ ✧ ✧ ✧ ✧

INTRODUCTION

Understanding and improving the durability of cost-competitive fuel cell stacks is imperative to successful deployment of the technology. Stacks will need to operate well beyond today's state-of-the-art rated power density with very low Pt loading in order to achieve the cost targets set forth by DOE ($15/kW) and ultimately be competitive with incumbent technologies. Little to no study of durability factors has been carried out in this area of design and operation. The industry today is focusing mostly on reduced Pt loading as it heads for the DOE target point of 0.2 mg/cm^2 Pt and 1.0 W/cm^2 power density. As demonstrated through DOE-sponsored cost modeling, this point falls short of the corresponding $15/kW stack cost target for 2015.

APPROACH

Nuvera proposes an accelerated cost-reduction path focused on substantially increasing power density to address non-platinum-group metal material costs as well as Pt. Understanding the largely unstudied factors affecting stack durability under these high power conditions is the focus of the present project. Of specific interest is the impact of combining low Pt loading with high power density operation, as this offers the best chance of achieving long-term cost targets. The team effort is divided into two activities: modeling and experimentation.

RESULTS

Development of the durability model by ANL was completed, finalizing the catalyst performance degradation model in addition to the earlier-developed Pt dissolution part of the model, therefore, completing the full cathode durability model and establishing relations between changes in overpotentials, ECSA, and oxygen mass transport. The model, independent of the cell architecture, utilized inputs from the single-cell accelerated stress tests (ASTs) and NSTs, beginning-of-life properties of the studied material set, and prescribed use cycles to output cathode ECSA, particle size distribution, overpotentials, and cell voltage as a function of cycle time and the current density.

The Pt dissolution model included generic dissolution and oxide growth thermodynamics and kinetics, accounting for the ECSA loss and particle growth dependence on the cycle, determined primarily by the coalescence mechanism. Predictability of the Pt dissolution model specific to the ECSA under load cycling is shown in Figure 1 for the serpentine cell and the open flowfields architecture (SCOF and short stacks). Modeled ECSA loss was similar for both

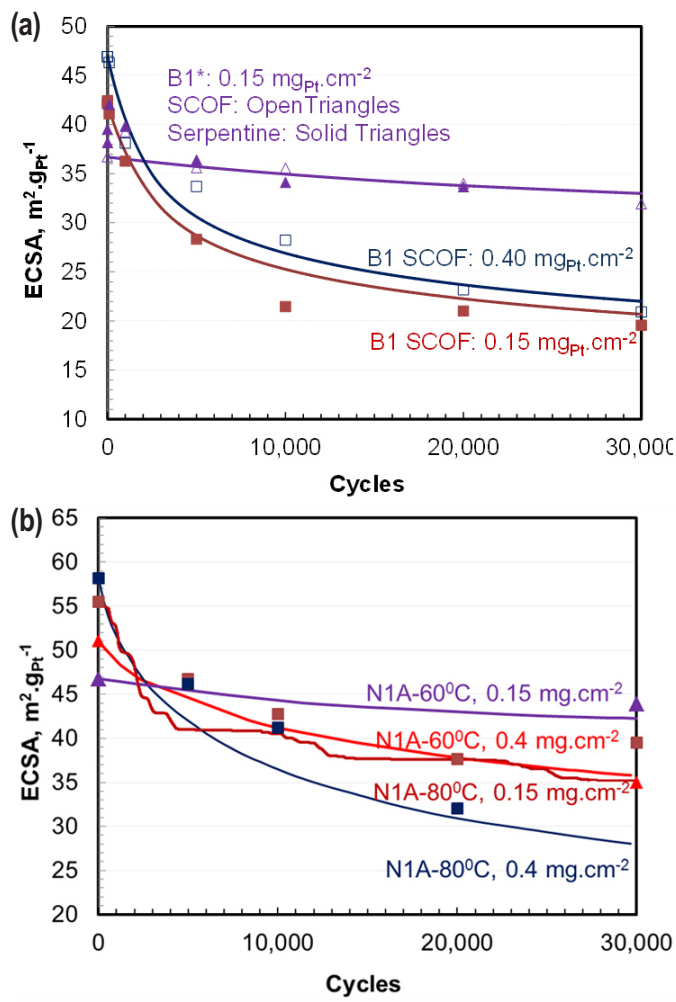

FIGURE 1. Validation of Pt dissolution model specific to cathode ECSA in a) SCOF and serpentine single cells under catalyst cycling ASTs, and b) SCOF and stack cells under N1A load cycle tests. Symbols are experimental data, lines show results of the modeling.

flowfields and not affected by the loading but, rather, upper cycle potential. Rapid fluctuations of the upper potential limits during one of the tests in Figure 1b are well simulated by the irregular shape of the modeling curve. As resulted from the aqueous studies, the dissolution rates at 80°C were higher than at 60°C, explaining higher ECSA decrease in the higher temperature N1A tests.

Platinum migration out of the cathode and re-deposition in the membrane, occurring with MEA ageing under load cycling, were studied by transmission electron microscope imaging and quantified by the direct particle counting methods developed at Oak Ridge National Laboratory [2]. Although an insignificant loss of Pt mass from the cathode to the membrane was concluded and, therefore, omitted from the model, imaging of the cathode-membrane interface showed great differences in Pt propagation into the membrane in the MEAs after NSTs. After the ASTs with no current draw from the cell, Pt particles grew to the larger sizes and remained at the interface without moving into the membrane.

The innovative multi-nodal reaction-diffusion model of the proton exchange membrane fuel cell cathode developed in the past year targeted characterizing mass transport overpotentials specific to the gas diffusion layer, catalyst, and ionomer in the electrode interface. The transport coefficients of the model were derived from the comprehensive analysis of the alternating current impedance spectra, using resistances of the equivalent transmission circuits. Variations in the transport coefficients with ageing under potential cycling were studied to formulate the correlations of the transport overpotentials as a function of current density and time. The transport coefficients were correlated to the cathode ECSA, Pt particle size, catalyst layer thickness, and operating conditions. The parity plots in Figure 2 show good fit between modeling and experiments as well as the dominating role of oxygen transport through the electrode ionomer in total overpotentials under studied conditions. Validation of the cathode performance degradation model applied to the MEAs with 0.4- and 0.15-mg_{Pt}/cm^2 cathode loadings is shown in Figure 3 under load cycle N1A and

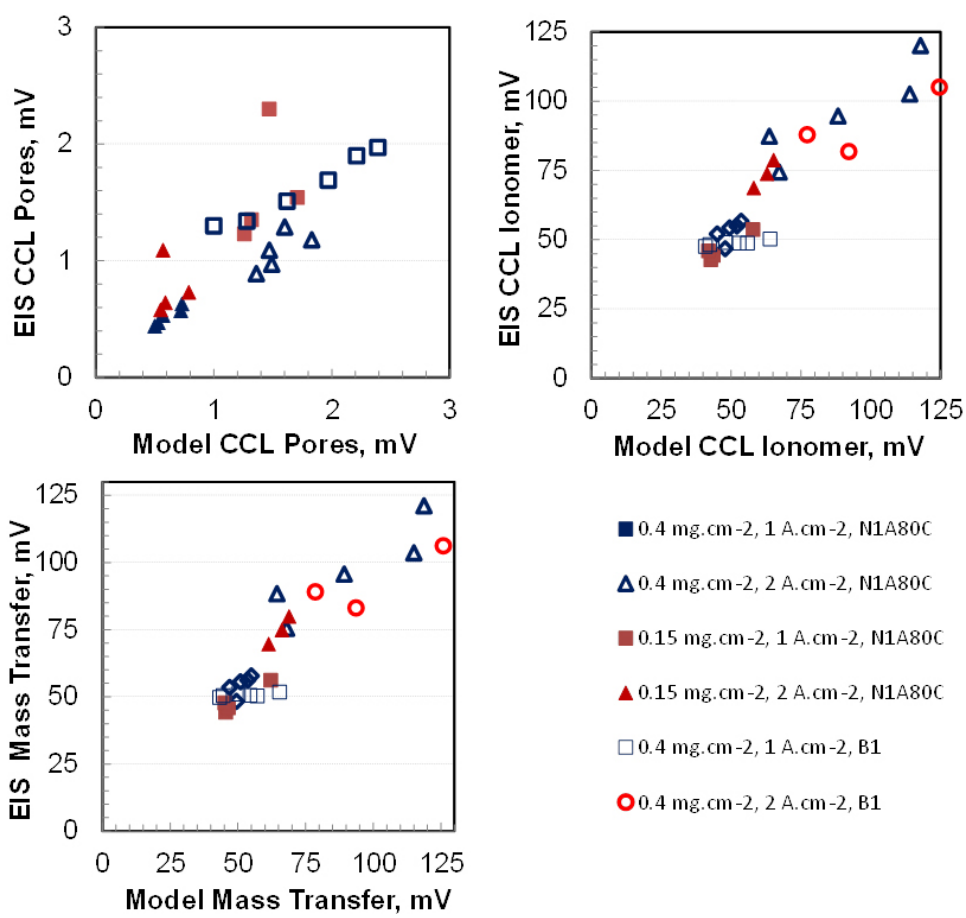

CCL – cathode catalyst layer; EIS - electrochemical impedance spectroscopy

FIGURE 2. Parity plots of mass transport overpotentials (through the cathode catalyst layer, ionomer, and overall) derived from the model against experimental electrochemical impedance spectroscopy data in N1A and B1 tests.

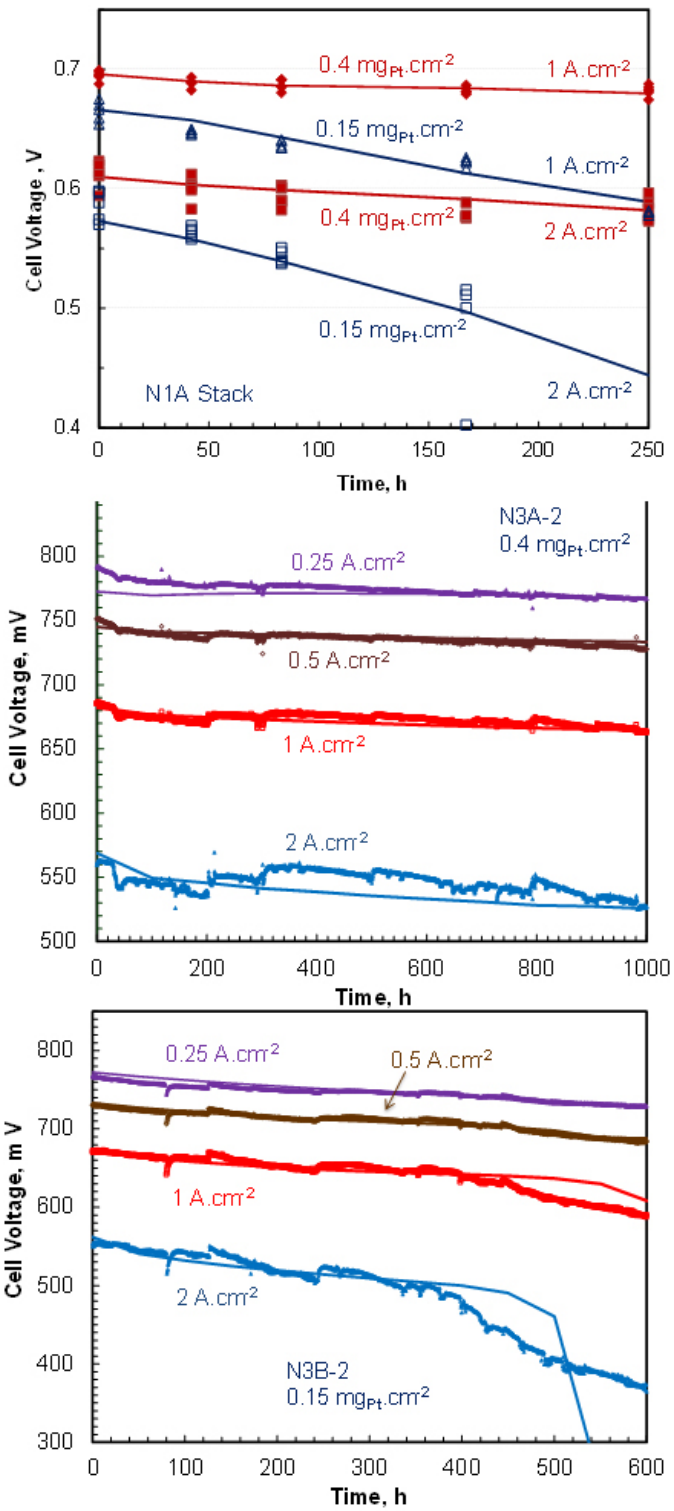

FIGURE 3. Validation of performance degradation model in stacks at the RCD = 2.0 A/cm^2 under N1A load cycle test (upper chart); N3 simulated drive cycle test, total loading 0.45 mg$_{Pt}$/cm^2 (middle chart); N3 test, total loading 0.2 mg$_{Pt}$/cm^2 (lower chart).

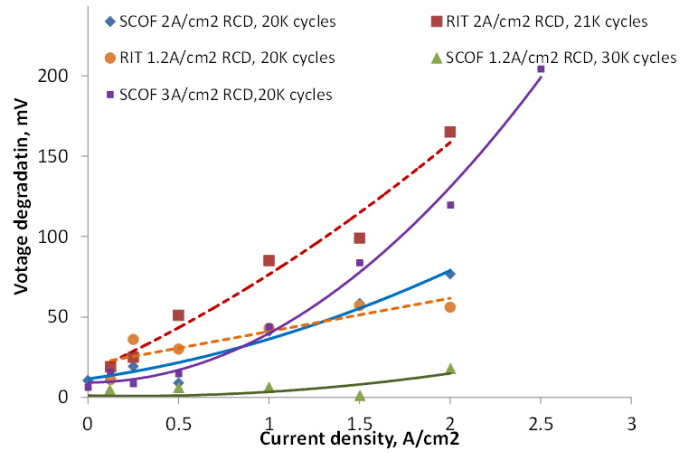

FIGURE 4. Voltage degradation in SCOF and RIT cells under N1A load cycle tests. RCD varied from 1.2 to 3.0 A/cm^2. Total loading is 0.2 mg$_{Pt}$/cm^2.

simulated drive cycle N3—both tested in short Orion stacks. Validation of the degradation model in full active area stack cells concluded the fourth milestone of this project.

Durability testing in 50-cm^2 SCOFs and land-channel (RIT) architecture supported modeling and allowed comparing cell architectures for voltage degradation under load cycling. Testing was conducted under N1A protocol at two levels of cathode Pt loading (0.40- and 0.15-mg$_{Pt}$/cm^2) and RCD (1.2 and 2.0 A/cm^2). N1A test in SCOF was also conducted at 3 A/cm^2 RCD, expectedly resulting in higher voltage degradation at the RCD and lower degradation at the upper cycle potential. N1A test was designed to mimic catalyst cycling AST B1 protocol, defined by the DOE, with the addition of the current draw, cycled between two levels of the current density. The upper potential in N1A is lower than in the B1 AST, and consistent with the simulated drive cycle N3 previously tested on Orion short stacks. Aggregated assessment of the performance metrics for N1A durability testing concluded similar ageing of Pt in both cell architectures and higher voltage degradation in the RIT cell as a function of the current density, shown in Figure 4 and attributed to the larger increase in mass transport overpotentials in the RIT architecture.

Low-Pt MEAs exhibited increasing decay as the current increased, while the decay for the higher loaded MEAs remained relatively constant. This result was reproduced at the different test conditions, both in single cells and in short stacks. The voltage degradation of low-Pt MEAs in the open flowfield single cells remained low at 0.002%/hour at the RCD, not exceeding 1.2 A/cm^2, therefore promising to achieve automotive lifetime target of 5,000 hours with 10% performance loss.

Durability testing in short stacks under simulated combined city and highway driving cycle NST N3 protocol continued at the RCD of 2.5 A/cm^2 on 0.45 mg$_{Pt}$/cm^2 MEAs.

In this NST, the cathode pressure and flow conditions vary with the current density, following the operating map of the air compressor in the automotive system.

CONCLUSIONS AND FUTURE DIRECTION

- A complete durability model of the cathode was developed at ANL with the focus on Pt ageing and the cathode electrode performance variations under designed operating conditions.
- The model was calibrated using inputs from the ASTs and NSTs in single cells and then validated against durability tests in short stacks with 250-cm^2 active area cells.
- Durability testing under NST protocols has been completed on all studied single cells at LANL and Nuvera and on short stacks at Nuvera, yielding valuable data inputs to the durability model.
- The feasibility of low-Pt MEAs to achieve the 5,000-hr lifetime target at the moderate RCD below 1.2 A/cm^2 was demonstrated by relating the degradation rate under the accelerated load-cycle test to the degradation rate in the 5,500-hr drive-cycle test completed on Nuvera short stack (360-cm^2 active cell area, 0.45 mg_{Pt}/cm^2 loading).
- Dissemination of the cathode durability model was started with the first publication of the Pt dissolution block and will continue in the next months for the catalyst performance degradation, concluding the final program milestone.

SPECIAL RECOGNITIONS & AWARDS/ PATENTS ISSUED

1. Poster presentation at the Fuel Cell Seminar 2012, November 5–8, Mohegan Sun, CT was awarded the 2nd prize.

FY 2013 PUBLICATIONS/PRESENTATIONS

1. O. Polevaya, Durability of Low Pt Fuel Cells Operating at High Power Density, 2013 DOE Annual Merit Review, Washington, DC, May 14, 2013.

2. R.K. Ahluwalia et al., Thermodynamics and Kinetics of Platinum Dissolution from Carbon-Supported Electrocatalysts in Aqueous Media under Potentiostatic and Potentiodynamic Conditions Fuel Cells, Electrolyzers, and Energy Conversion, J. Electrochem. Soc. 2013 160(4): F447-F455.

3. O. Polevaya, Presentation at the Durability Working Group Meeting 2013, February 28, Washington, DC.

4. O. Polevaya, Presentation at the USCAR Fuel Cell Technical Team Meeting, January 16, Detroit, MI.

5. O. Polevaya et al., Fuel Cell Durability at High Power Density from Subscale Single Cells to the Full Area Stacks, Poster presentation at the Fuel Cell Seminar 2012, November 5–8, Mohegan Sun, CT.

6. R.K. Ahluwalia, Modeling Durability of ORR Catalysts in Polymer Electrolyte Fuel Cells, Fuel Cell Tech Team Meeting, Southfield, MI, September 12, 2012.

REFERENCES

1. B. James et al., Mass Production Cost Estimation for Direct H_2 PEM Fuel Cell Systems for Automotive Applications, 2012 Update, October 18, 2012.

2. K.L. More, Characterization of fuel cell materials, 2012 DOE Annual Merit Review, Washington, DC, May 14–18, 2012.

V.D.3 Accelerated Testing Validation

Rangachary Mukundan[1] (Primary Contact),
Rod Borup[1], John Davey[1], Roger Lujan[1],
Dennis Torraco[1], David Langlois[1], Fernando Garzon[1],
Dusan Spernjak[1], Joe Fairweather[1],
Sivagaminathan Balasubramanian[2], Adam Weber[2],
Mike Brady[3], Karren More[3], Greg James[4],
Dana Ayotte[4], Paul Beattie[4], Steve Grot[5],
Gaël Maranzana[6], Adrien Lamibrac[6], Jérôme Dillet[6],
Olivier Lottin[6], and Kateryna Artyushkova[7]

[1]Los Alamos National Laboratory
MS D429, P.O. Box 1663
Los Alamos, NM 87545
Phone: (505) 665-8523
Email: Mukundan@lanl.gov

DOE Manager
Nancy Garland
Phone: (202) 586-5673
Email: Nancy.Garland@ee.doe.gov

Subcontractors:
[2] Lawrence Berkeley National Lab, Berkeley, CA
[3] Oak Ridge National Laboratory, Oak Ridge, TN
[4] Ballard Power Systems, Burnaby, BC, Canada
[5] Ion Power, New Castle, DE
[6] LEMTA, Université de Lorraine, Vandoeuvre-lès-Nancy, France
[7] University of New Mexico, Albuquerque, NM

Project Start Date: October 2009
Project End Date: 2013

Overall Objectives

- Correlation of the component lifetimes measured in an accelerated stress test (AST) to "real-world" behavior of that component
- Validation of existing component-specific ASTs for electrocatalysts, catalyst supports, and membranes (mechanical and chemical degradation)
- Development of new ASTs for gas diffusion layers (GDLs) and bipolar plates
- Coordination of effort with the Fuel Cell Technical Team and the Durability Working Group

Fiscal Year (FY) 2013 Objectives

- Correlation of the component lifetimes measured in an AST to those measured during U.S. DRIVE "Protocol for Determining Cell/Stack Durability"
- Validation of existing component-specific ASTs for catalyst and membrane degradation against U.S. DRIVE "Protocol for Determining Cell/Stack Durability"
- Development and validation of new AST for GDL materials

Technical Barriers

This project addresses the following technical barriers from the Fuel Cells section (3.4.5) of the Fuel Cell Technologies Office Multi-Year Research, Development, and Demonstration Plan:

(A) Durability

(B) Cost

Technical Targets

Cost and durability are the major challenges to fuel cell commercialization. ASTs enable rapid screening of fuel cell materials and are critical in meeting the long lifetimes required for stationary and automotive environments. Moreover, these ASTs can also help predict the lifetimes of the various components in "real-world" applications.

- Transportation Durability: 5,000 hours (with cycling)
  - Estimated start/stop cycles: 17,000
  - Estimated Frozen cycles: 1650
  - Estimated Load cycles: 1,200,000
  - Cost (30 $/kWe)
- Stationary Durability: 40,000 hours (2015); 60,000 hours (2020)
  - Survivability: Stationary -35°C to 40°C
- Bus Durability: 12 years/500,000 miles (2016 and ultimate)
  - Power plant lifetime: 18,000 hours (2016), 25,000 hours (ultimate)
  - Power plant cost: $450,000 (2016), $200,000 (ultimate)
  - Range: 300 miles
  - Fuel economy: 8 miles/gallon diesel equivalent

FY 2013 Accomplishments

- Completed U.S. DRIVE recommended drive cycle test on four different membrane electrode assemblies (MEAs) utilizing three different membranes and three different catalyst layers

- Completed failure analysis of MEAs and derived correlation between AST and drive cycle data
- Identified correlations between electro-catalyst AST and drive cycle operations and identified carbon corrosion during drive cycle operation
- Identified mechanical degradation as main membrane failure mode during drive cycle operation
- Identified GDL degradation during drive cycle operation at high humidities
- Identified previously proposed GDL AST as too severe to correlate with in situ fuel cell testing and initiated development of a new AST based on drive cycle degradation data
- Modeled voltage loss breakdown with assignment of voltage losses to specific degradation mechanisms

✧ ✧ ✧ ✧ ✧

INTRODUCTION

The durability of polymer electrolyte membrane (PEM) fuel cells is a major barrier to the commercialization of these systems for stationary and transportation power applications [1]. Commercial viability depends on improving the durability of fuel cell components to increase the system reliability and to reduce system lifetime costs by reducing the stack replacement frequency. The need for ASTs can be quickly understood given the target lives for fuel cell systems: 5,000 hours (~7 months) for automotive, and 40,000 hrs (~4.6 years) for stationary systems. Thus, testing methods that enable more rapid screening of individual components to determine their durability characteristics, such as off-line environmental testing, are needed for evaluating new component durability with a rapid turn-around time. This allows proposed improvements in a component to be evaluated rapidly and independently, subsequently allowing rapid advancement in PEM fuel cell durability. These tests are also crucial to developers in order to verify that durability is not sacrificed while making improvements in costs (e.g., lower platinum-group metal [PGM] loading) and performance (e.g., thinner membrane or a GDL with better water management properties).

DOE has suggested AST protocols for use in evaluating materials, but only for the catalyst layer components (electrocatalyst and support) and for the membrane [2,3]. The US Fuel Cell Council has also suggested AST protocols for the same materials [4]. While these protocols have concentrated on the catalyst, catalyst support, and membrane materials, to date, no accelerated degradation protocols have been suggested for GDL materials or micro-porous layers (MPLs), bipolar plates, or seals. In spite of recent advances in AST development, a main portion, which is deficient, is the quantitative correlation between the results of a given fuel cell AST and the degradation rate or life in an operating fuel cell.

APPROACH

A main desired outcome of this task is the correlation of the component lifetime measured in an AST to in situ behavior of that component in "real-world" situations. This requires testing of components via ASTs and in operating fuel cells, and delineating the various component contributions to the overall cell degradation. This will primarily be performed by using a simplified one-dimensional model that takes into account the different component contributions like membrane ionic conductivity, cathode catalyst layer kinetic losses, and mass transport losses (catalyst layer and GDL) to the overall losses observed in operating cells [5]. This project will then attempt to correlate the performance losses observed due to a particular component in "real-world" situations with the degradation in AST metrics of that component. The correlation between AST and life data if state-of-the-art materials are used, in essence, gives one data point. Thus, for a reasonable correlation to be made, materials with different life spans are utilized in this project. Providing the variable material durability relies on the expertise of the suppliers as partners in this project. This work is also being coordinated with other funded projects examining durability through the DOE Durability Working Group.

RESULTS

The U.S. DRIVE Fuel Cell Technical Team recommended protocol for determining cell/stack durability [6] was performed on various MEA/GDLs using 50-cm^2 quad-serpentine hardware purchased from Fuel Cell Technologies Inc. An example of this drive cycle is demonstrated in Figure 1a, where two cycles are shown for clarity. We have termed this drive cycle as the "Wet/Dry Drive Cycle" since it involves both current cycling and relative humidity (RH) cycling. A modified drive cycle was used in some of these tests where only the high RH portion of the test was repeated. We have termed this test the "Wet Drive Cycle," and it consists of current cycling from 0.02 A/cm^2 to 1.2 A/cm^2 for 30 seconds each at a cell temperature of 80°C with anode and cathode dew points at 83°C. MEAs were also subjected to the start/stop protocol recommended by the Durability Working Group, as illustrated in Figure 1b. Here the cell was operated at a current density of 1.2 A/cm^2 for 5 minutes and then shut down with air at the anode for 200 secs, followed by the next start-up in H_2 and operation for a further 5 minutes. To distinguish the effect of just the start-up (shut-down), the air (H_2) used during the shut-down (start-up) was replaced with N_2.

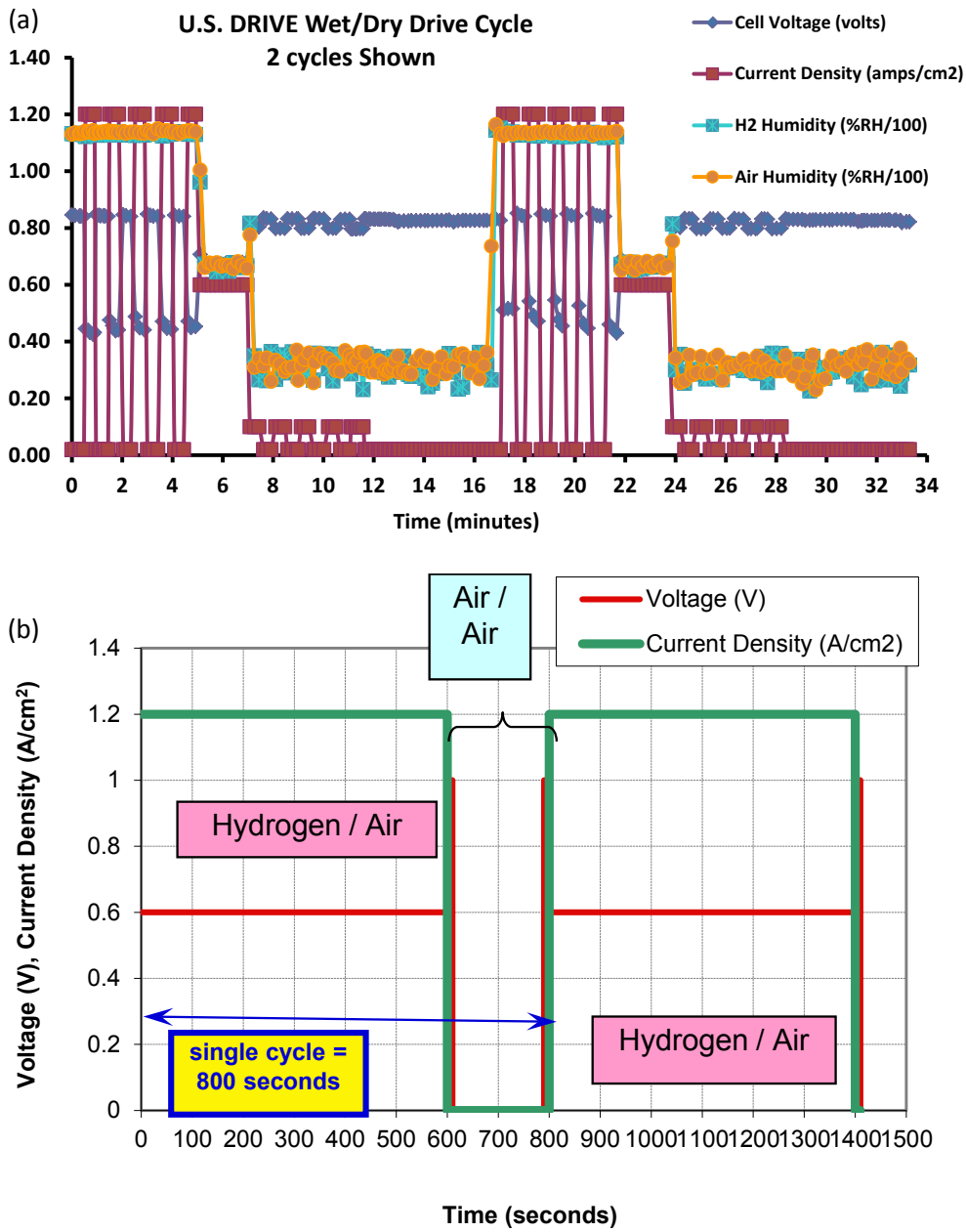

FIGURE 1. a) Voltage, current density, flow rates, and RHs as a function of time during the Wet/Dry Drive Cycle testing protocol. b) Voltage and current density as a function of time during the start/stop protocol.

Catalyst Degradation

The electro-catalyst degradation observed in the Wet/Dry Drive Cycle test showed a direct correlation with the electro-catalyst AST performed on an identical catalyst. For example, the percent electrochemical surface area (ECSA) loss observed in the Wet/Dry Drive Cycle and the 0.6 to 1.0 V cycling AST is plotted in Figure 2a and shows excellent agreement in terms of ECSA loss with potential cycles. Similar results were also obtained for the Wet Drive Cycle testing, where the ECSA loss was similar during the first 20,000 cycles. The wet cycling, however, showed increased loss in ECSA compared to the AST (at >20,000 cycles), which is probably due to the higher RH (114%) used in the Wet Drive Cycle. Post-mortem testing illustrated an increase in Pt crystallite size with decreasing ECSA consistent with field test data from buses reported in FY 2012. In addition to the Pt growth, significant electrode thinning was also observed after long-term drive cycle testing, especially in high surface area carbon (HSAC)-based MEAs. This is consistent with non-dispersive infrared measurements showing evolved CO_2

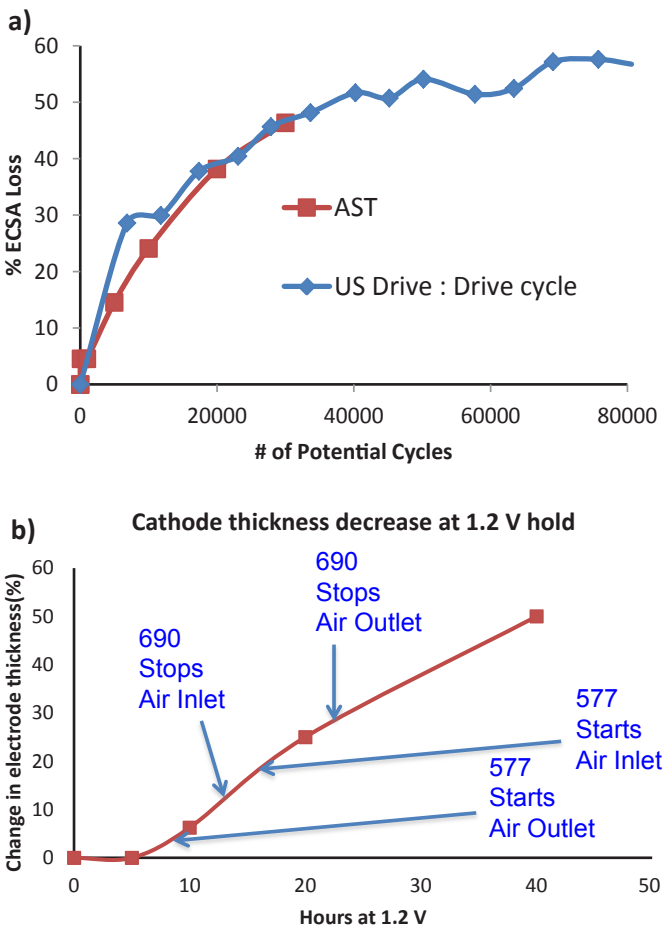

FIGURE 2. a) ECSA loss (%) of HSAC-based catalyst layer during Wet/Dry Drive Cycle testing and during 0.6 to 1.0 V cycling electro-catalyst AST. b) Change in electrode thickness (%) as a function of duration during the 1.2 V carbon corrosion AST. Data from start and stop tests of a similar MEA is also presented for comparison.

from carbon corrosion of the cathode at voltages as low as 0.9 V.

The effect of start/stops on a HSAC-based electrode was evaluated at University of Lorraine (Nancy, France) in a counter-flow configuration on a 5 parallel channel 1 cm x 30 cm segmented cell. These results indicate that start-ups are more damaging than shut-downs, and those segments exposed to air/air potentials for the longest time show the most degradation. The degradation results in both a decrease in catalyst layer thickness and an increase in the Pt particle size. These changes result in a loss in both the kinetic and mass transport performance of the MEAs. The catalyst layer thickness for an HSAC-based MEA observed during the start/stop tests is compared to that observed during the 1.2 V AST test in Figure 2b. Approximately 15 hours of the AST corresponds to ≈300 start/stop operations, implying that 400 hours of testing will correspond to ≈8,000 start/stop operations. Further experimentation is underway with higher durability carbons and longer hold-times to quantify this effect. Moreover, the U.S. DRIVE Fuel Cell Technical Team has recommended a new AST for carbon corrosion (cycling from 1.0 to 1.5 V), which will be evaluated in the future.

Membrane Degradation

The drive cycle results showed membrane degradation in addition to the catalyst degradation reported in the previous section. This membrane degradation resulted in increased crossover and eventual failure of the cells. This is illustrated in Figure 3a, where the crossover of various MEAs tested under both the Wet and Wet/Dry Drive Cycles is plotted. The Wet/Dry Drive Cycle resulted in faster failure than the Wet Drive Cycle, and the non-stabilized (Sample A) membrane resulted in faster failure than the chemically and mechanically stabilized membrane (Sample B). Ex situ characterization of beginning-of-life (BOL) and end-of-life (EOL) MEAs revealed little change in thickness of the membrane (Figure 3b) up to 2,500 hours of the drive cycle testing. The failure of the MEAs was due to local thinning of the membrane probably caused by membrane mechanical degradation accelerated by chemical degradation, rather than purely membrane chemical degradation. These results are consistent with the field data from buses reported in FY 2012, where no membrane thinning was observed in the field at EOL and failure was due to cracks in the membrane mainly at the inlet and outlet of cells. Thus, drive cycle testing confirms that the open-circuit voltage AST is too severe and the RH cycling AST too benign when compared to the degradation observed in real-world applications. A combined mechanical/chemical AST which involves RH cycling under open-circuit voltage at 80°C was able to reproduce the failure mode observed in the field data and will be studied further to serve as a membrane AST capable of predicting lifetimes. Further testing is ongoing and has revealed that mechanically and chemically stabilized membranes (Gore-Select® M720.18 and Dupont™ Nafion® XL) last over 3,000 hours of Wet/Dry Drive Cycle testing without any observable increase in crossover.

GDL Degradation

The durability of two different GDL materials provided by SGL Carbon was evaluated. The standard GDL material was Sigracet® 25BC with 5% poly-tetrafluoroethylene in the substrate and 23% poly-tetrafluoroethylene in the MPL. A new GDL material (25BN) that contained 25% multi-walled carbon nano-tubes in the MPL was also evaluated [7]. The cells with BC and BN cathode GDLs were subjected to either the Wet/Dry Drive Cycle or Wet Drive Cycle. Extensive in situ characterization including cyclic voltammetry, alternating current impedance, and polarization curves in air/oxygen/HelOx were performed periodically during the drive cycle ageing. Ex situ characterization including scanning electron microscope cross-sections, X-ray photoelectron spectroscopy (XPS), and transmission electron microscopy were performed on MEAs at BOL and

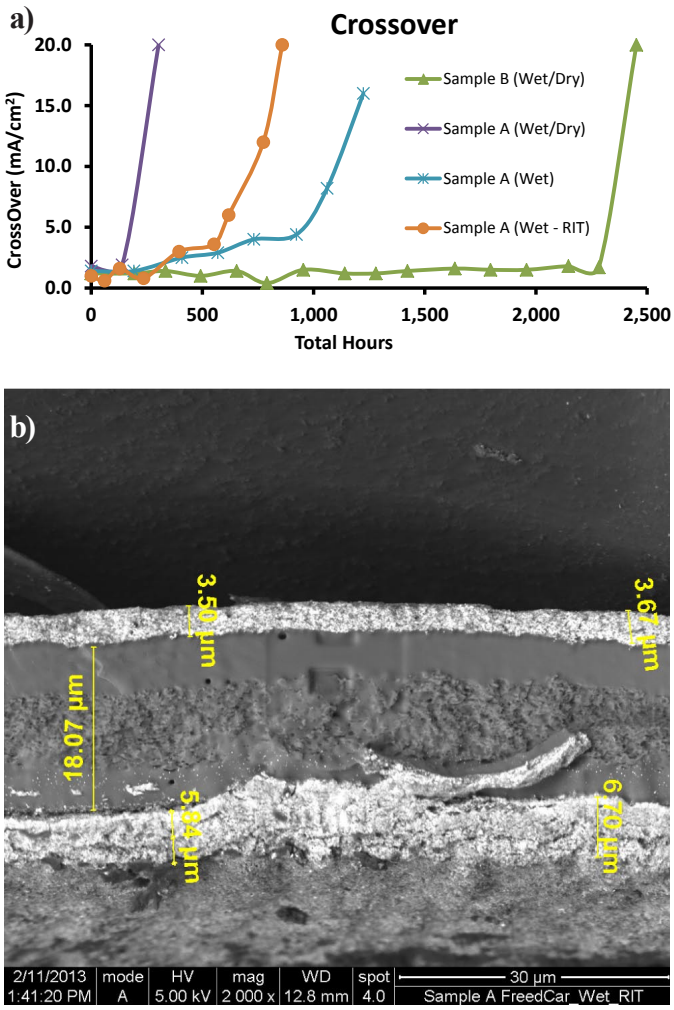

FIGURE 3. a) Crossover of various non-stabilized membranes (Sample A) and mechanically/chemically stabilized (Sample B) during both Wet/Dry and Wet Drive Cycle testing. b) Cross section of a non-stabilized MEA subjected to 850 hours of Wet Drive Cycle testing.

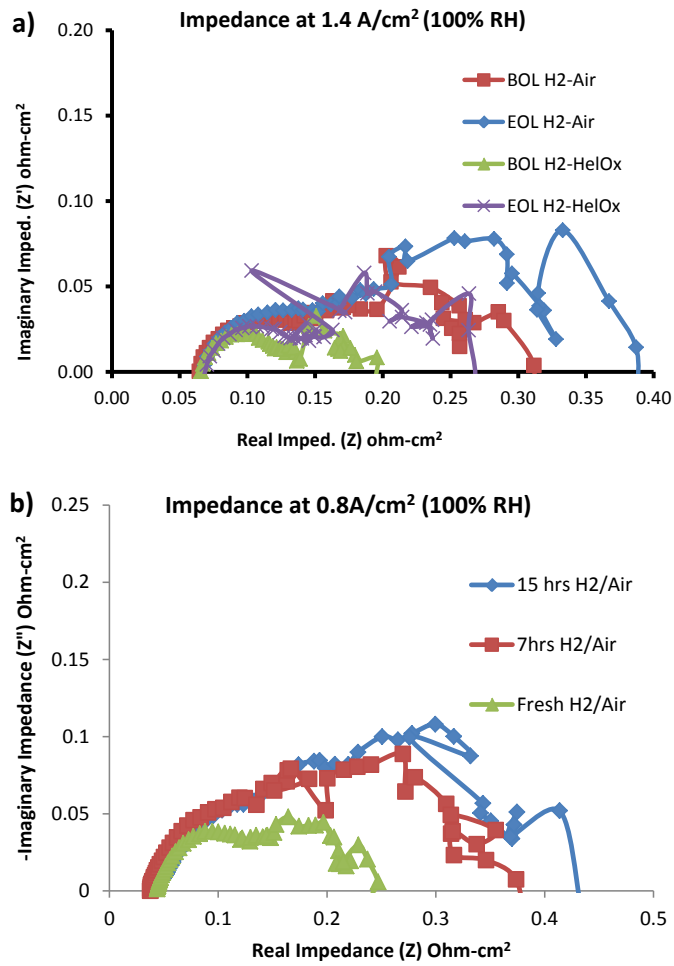

FIGURE 4. a) Alternating current impedance at high current density of MEAs with a) in situ and b) ex situ aged GDLs.

at EOL. The GDL materials were also subjected to an ex situ AST ageing protocol and subsequently tested in situ with fresh commercial Gore® Primea® MEAs to illustrate the effect of GDL AST-ageing on fuel cell performance. The ex situ ageing of GDLs was achieved by submerging them in a boiling solution of 30% hydrogen peroxide at 95°C for prolonged intervals up to 15 hours (this protocol was first reported by SGL as their part of the DECODE project). The GDLs were removed periodically at different time intervals, and XPS and contact angle measurements were performed to quantify any changes to the GDL material as a function of ageing time.

The drive cycle testing of the MEA/GDLs resulted in voltage degradation as a function of time. The MEA with the low surface area carbon (LSAC)-based cathode-catalyst showed little change in the kinetic region and <20% ECSA loss after approximately 125 hours of ageing. However, this MEA showed up to 100 mV loss at a current density of 2 A/cm^2. The catalyst layer thickness of the EOL MEAs indicates no change in the catalyst layer thickness of this TEC10EA40E catalyst-based MEA. These results indicate that while there is little catalyst degradation in the LSAC-based MEA, there is still voltage degradation at high current densities. Alternating current impedance data were obtained to delineate the voltage losses observed in the polarization curves. The impedance at high current densities for this MEA is illustrated in Figure 4a, showing an increase in the low frequency region of the impedance. Moreover, this increase in resistance was greater when measured with air at the cathode than when measured with HelOx at the cathode (Figure 4a). These results, when combined with the ex situ examination of the catalyst layer, confirm that the LSAC catalyst layer itself does not degrade much and does not contribute significantly to voltage loss while ageing. These results also indicate that the mass transport losses are probably arising from changes to other components in the system, namely the GDL. The high current impedance shown in Figure 4b clearly illustrates increase in the mass transport

resistance (low frequency arc) of the cells using the ex situ aged GDL when compared to the cell using the fresh GDL. The impedance and voltage-current-resistance characteristics obtained from the ex situ aged GDLs were similar to those observed in the in situ drive cycle-aged GDLs. This provides further evidence of GDL degradation during drive cycle operation of fuel cells and suggests that the ex situ ageing can be used as an AST for probing the durability of GDL materials. Finally, the use of the improved 25 BN GDL showed remarkable improvement in the drive cycle durability performance, further confirming GDL degradation as the major degradation mechanism in these MEAs. XPS results from the ex situ aged GDLs confirmed GDL oxidation consistent with loss of hydrophobicity and observed decreases in contact angle. The XPS and polarization results also indicate that most of the changes in the GDL happen during the first few hours of the ex situ ageing. Further tests using lower peroxide concentrations and lower temperatures are underway in order to design an improved GDL AST that can simulate in situ GDL degradation.

CONCLUSIONS AND FUTURE DIRECTIONS

The electro-catalyst AST was found to accurately capture the Pt ECSA loss occurring during Wet/Dry Drive Cycle testing. While the 1.2 V hold AST was able to simulate the carbon corrosion occurring during unmitigated start/stops, the duration of the AST was long (400 hours). The Fuel Cell Technical Team has recommended a new AST (1.0 to 1.5 V cycling) for carbon corrosion, which will be performed in FY 2014. Significant carbon corrosion was observed during drive cycle testing of a HSAC-based MEA, while negligible catalyst thinning (corrosion) was observed on a LSAC-based MEA. GDL degradation was found to be the limiting factor during the Wet/Dry Drive Cycle testing (at high current densities) of low-loaded LSAC-based MEAs. This GDL degradation can be mitigated using an advanced GDL that incorporates 25% multi-walled carbon nanotubes in the MPL. Membrane mechanical degradation was found to be the limiting factor during the Wet/Dry Drive Cycle testing of high-loaded MEAs.

AST Testing

- Conduct tests on LSAC, HSAC, and Vulcan carbon-based MEAs using the 1.0 to 1.5 V cycling carbon corrosion AST
- Develop ASTs for metal bipolar plate materials
- Refine GDL AST to better simulate GDL degradation observed during drive-cycle testing

"Real-World" Testing

- Complete Wet/Dry Drive Cycle testing (up to 5,000 hours) on chemically and mechanically stabilized membranes (Dupont™ Nafion® XL)
- Obtain "real-world" data from materials handling applications

Characterization of Materials

- Complete ex situ characterization of catalyst particle size distribution, layer thickness, membrane thickness, and GDL hydrophobicity as a function of drive cycle test time

Correlation of AST to "Real-World" Data

- Complete statistical correlation of performance degradation with physical properties in both AST and "real-world" data

FY 2013 PUBLICATIONS/PRESENTATIONS

1. S. Arisetty, X. Wang, R.K. Ahluwalia, R. Mukundan, R. Borup, J. Davey, D. Langlois, F. Gambini, O. Polevaya, S. Blanchet, "Catalyst Durability in PEM Fuel Cells with Low Platinum Loading", Journal of the Electrochemical Society (2012), 159(5), B455-B462.

2. J.D. Fairweather, D. Spernjak, A.Z. Weber, D. Harvey, S. Wessel, D.S. Hussey, D.L. Jacobson, K. Artyushkova, R. Mukundan, and R.L. Borup, "Effects of Cathode Corrosion on Through-Plane Water Transport in Proton Exchange Membrane Fuel Cells", *J. Electrochem. Soc.*, **160 (9),** p. F980-F993 (2013).

3. R. Mukundan, G. James, D. Ayotte, J. Davey, D. Langlois, D. Spernjak, D. Torraco, S. Balasubramanian, A. Weber, K. More, and R. Borup, "Accelerated testing of carbon corrosion and membrane degradation in PEM fuel cells", *ECS Trans.*, **V. 50 No. 2**, 1003-1010 (2013).

4. R. Mukundan, J. Davey, K. Rau, D. Langlois, D. Spernjak, J. Fairweather, K. Artyushkova, R. Schweiss, and R. Borup, "Degradation of Gas Diffusion Layers in PEM fuel cells during drive cycle operation", *Abstract Accepted, 224th ECS Meeting, San Franciso* (2013).

5. R. Mukundan, et. al., "Accelerated Testing Validation", FC Tech Team, Detroit, MI, February 12, 2013 (Invited Presentation).

6. R. Mukundan, et. al., "Durability of Polymer Electrolyte Membrane Fuel Cells", The 19th International Conference on Solid State Ionics, Kyoto, Japan 2013 (Invited Presentation).

7. R. Mukundan, et. al., "Durability of Polymer Electrolyte Membrane Fuel Cells", University of Lorraine, Nancy, France, June 2013 (Invited Presentation).

8. R. Mukundan, et. al., "Durability of Polymer Electrolyte Membrane Fuel Cells", CEA, Grenoble, France, June 2013 (Invited Presentation).

REFERENCES

1. R. Borup, J. Meyers, B. Pivovar, et al., *Chemical Reviews*; **107(10)**, 3904 (2007).

2. T.G. Benjamin, Abstracts of the International Workshop on Degradation Issues in Fuel Cells, Hersonessos, Crete, Greece, (2007).

3. N.L. Garland, T.G. Benjamin, J.P. Kopasz, *ECS Trans.*, **V. 11 No. 1**, 923 (2007).

4. S. Knight, G. Escobedo, *Meeting Abstracts of 2006 Fuel Cell Seminar*, Honolulu, HI (2006).

5. A.Z. Weber, J. Newman, "Modeling Transport in Polymer-Electrolyte Fuel cells" *Chemical Reviews*, **V. 104**, 4679-4726 (2004).

6. FreedomCAR Fuel Cell Tech Team Cell Component AST and polarization curve Protocols for PEM Fuel Cells (Electrocatalysts, Supports, Membranes and MEAs), Revised December 16, 2010.

7. R. Schweiss, M. Steeb, P. M. Wilde, and T. Schubert, *J. Power Sources*, **220**, 79-83 (2012).

V.D.4 Analysis of Laboratory Fuel Cell Technology Status – Voltage Degradation

Jennifer Kurtz (Primary Contact), Huyen Dinh, Sam Sprik, Genevieve Saur, Chris Ainscough, and Mike Peters
National Renewable Energy Laboratory
15013 Denver West Parkway
Golden, CO 80401-3305
Phone: (303) 275-4061
Email: jennifer.kurtz@nrel.gov

DOE Manager
Kathi Epping Martin
Phone: (202) 586-7425
Email: Kathi.Epping@ee.dog.gov

Project Start Date: July 1, 2009
Project End Date: Project continuation and direction determined annually by DOE

Overall Objectives

- Conduct an independent assessment to benchmark state-of-the-art fuel cell durability in a non-proprietary method
- Leverage analysis experience from the Fuel Cell Electric Vehicle Learning Demonstration project
- Collaborate with key fuel cell developers on the analysis

Fiscal Year (FY) 2013 Objectives

- Complete the annual update on status of the voltage degradation analysis for publication, including new data sets and partners since the FY 2012 update
- Establish price data templates and pursue gathering current price data for fuel cell developer products

Technical Barriers

This project addresses the technical barrier of understanding the durability of state-of-the-art fuel cell stacks and systems currently developed in a laboratory setting, as well as a lack of consistent reporting on the durability of these systems. This project addresses the following technical barrier from the Fuel Cells section of the Fuel Cell Technologies Office Multi-Year Research, Development, and Demonstration Plan:

(A) Durability

Technical Targets

This project is conducting an independent assessment of the durability of current laboratory fuel cell stacks and systems. The analysis, applied uniformly on all data sets, studies the projected operation time to 10% voltage drop. All results are aggregated to protect proprietary information and reported on by the expected application.

FY 2013 Accomplishments

- Analyzed fuel cell stack and system data in six application categories (backup, automotive, bus, forklift, portable, and stationary) and from 15 fuel cell developers (U.S. and international developers)
- Published 14 composite data products (CDPs) [1] on:
  - Operation time and projected operation time to 10% voltage drop
  - Projected operation time sensitivity to voltage drop levels (Table 1)
  - Comparison of automotive and material handling equipment laboratory and field durability projections
  - Power capability
  - Data sets operated beyond 10% voltage drop
  - Durability projections by configuration and test condition
  - Test configuration and condition breakdowns
  - Time series variation of results

TABLE 1. Projected Operation Time to 10% Voltage Drop Summary by Application

Application	Average Projected Time to 10% Voltage Drop (Hours)	Average Operation (Hours)
Backup power	2,500	1,100
Automotive	3,600	2,200
Bus	6,200	3,800
Forklift	14,600	4,400
Prime	9,300	5,600

- Included data on proton exchange membrane, direct methanol, and solid oxide fuel cell of full active area short stacks and full stacks with systems
- Shared all detailed data analysis results with data providers

✧ ✧ ✧ ✧ ✧

INTRODUCTION

The U.S. Department of Energy (DOE) has funded significant research and development activity with universities, national laboratories, and the fuel cell industry to improve the market competitiveness of fuel cells. Most of the validation tests to confirm improved fuel cell stack performance and durability (indicators of market competitiveness) are completed by the research organizations themselves. Although this allows the tests to be conducted by the developers most familiar with their specific technology, it also presents a number of challenges in sharing progress publicly because test conditions and data analysis take many forms and data collected during testing are often considered proprietary.

The National Renewable Energy Laboratory (NREL) is benchmarking the state-of-the-art fuel cell performance, specifically focusing on durability, through independent assessment of current laboratory data sets. NREL's data processing, analysis, and reporting capitalize on capabilities developed in DOE's Fuel Cell Electric Vehicle Learning Demonstration. Fuel cell stack durability status is reported annually and includes a breakdown of status for different applications. A key component of this project is the collaborative effort with key fuel cell developers to understand what is being tested in the laboratory, study analysis results, and expand the included data sets.

APPROACH

The project involves voluntary submission of data from relevant fuel cell developers. NREL is contacting fuel cell developers for multiple fuel cell types to either continue or begin a data sharing collaboration. A continuing effort is to include more data sets, types of fuel cells, and developers.

Raw and processed data are stored in NREL's Hydrogen Secure Data Center. Processing capabilities are developed or modified for new data sets and then included in the analytical processing of NREL's Fleet Analysis Toolkit. The incoming raw data may be new stack test data or they may be a continuation of data that have already been supplied to NREL. After the raw data are processed, the results are analyzed with particular attention to durability and operating conditions. Each individual data set has a set of data figures that are shared with the data provider and used to create the CDPs. CDPs are designed to report on the technology status without revealing proprietary information.

RESULTS

This fuel cell stack durability analysis expanded the number of data sets analyzed, applications and fuel cell types studied, and amount of details published. Results published in April 2013 were the fifth update for this analysis effort. The annual voltage degradation analysis of state-of-the-art laboratory durability was completed in advance of the milestone to provide an update that could be presented at the DOE's Annual Merit Review. In the current published data set, six applications were covered, 15 fuel cell developers supplied data (more than one data set in many cases), and the data sets covered proton exchange membrane, direct methanol, and solid oxide fuel cell stack testing. A total of 98 data sets have been analyzed. Note that a data set represents a short stack, full stack, or system test data. Of the total data sets, 78% have been retired (Figure 1), meaning the system or stack is not accumulating any new operation hours either because of test completion, technology upgrades, or failures. The published data results include eight CDPs. The power capability illustrates the range of fuel cell power for the data sets by application from <2 kW to >50 kW. Most of the analyzed data sets are laboratory systems at less than 14 kW power.

The analyzed data sets are from laboratory testing of full active area short stacks (e.g., stacks with fewer cells than the expected full power stack) and test systems with full power stacks. The data sets also vary from one to the other in how the stack/system was tested. Data were generated between 2004 and late 2012 from different testing methods that included constant load, transient load, and accelerated testing. The variability in test conditions and test setups created a group of data that can be difficult to compare. Additional breakdown of the data sets is an important aspect of future work and is dependent on the accumulation of more data sets in order to not reveal an individual data supplier's contribution to the results or proprietary data.

Fuel cell durability is studied at a design-specific current point and measured against a target of 10% voltage drop from beginning of life. The 10% voltage drop metric is used for assessing voltage degradation with a common measurement, but the metric may not be the same as end-of-life criteria and does not address catastrophic failure modes. Figure 2 is an aggregated set of results separated by application and identifies the percentage of short stacks and how many data sets are still operating (at the time of the results) for each application. Each application has the average, maximum, and 25th and 75th percentile values identified for the operation hours and the projected hours to 10% voltage drop.

The 10% voltage drop level is not necessarily a measurement for end of life or even a significant reduction in performance. Many data sets have not passed (or did not pass) the metric of 10% voltage degradation. The reason data sets operated beyond 10% voltage degradation could be because end-of-life criteria may be greater than 10% voltage degradation or because the test was designed to operate until a failure occurred. The stack configuration and test conditions can have a significant impact on the projected time to 10% voltage degradation within an application. In general,

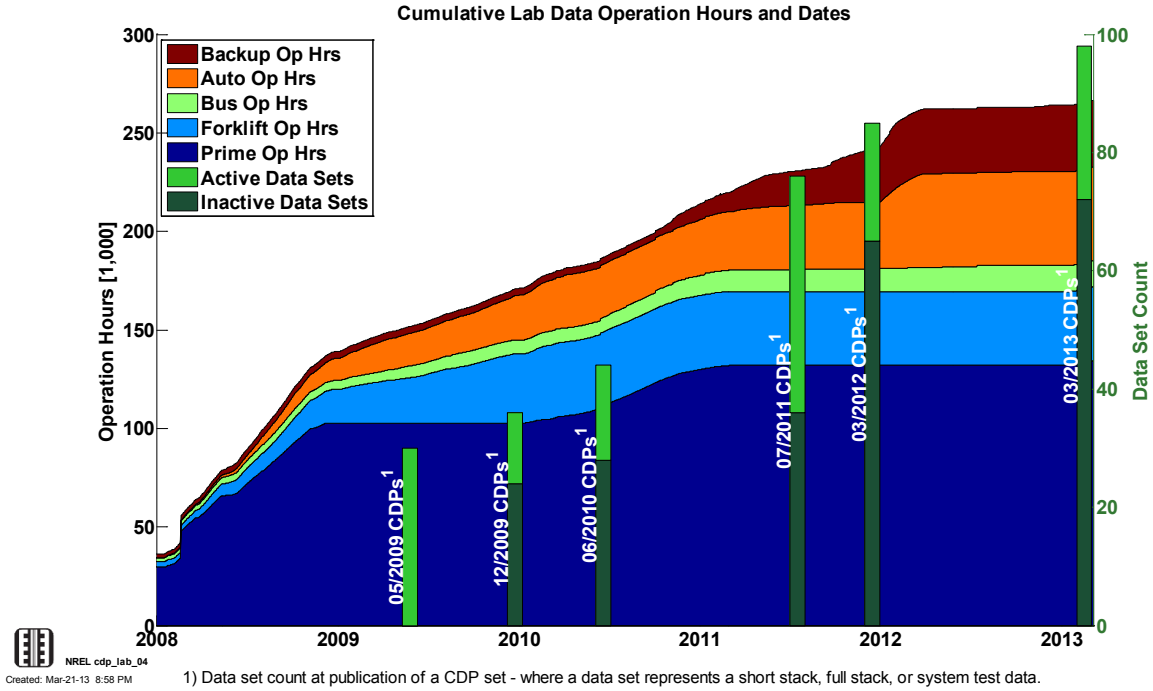

FIGURE 1. Cumulative Lab Data Operation Hours and Dates

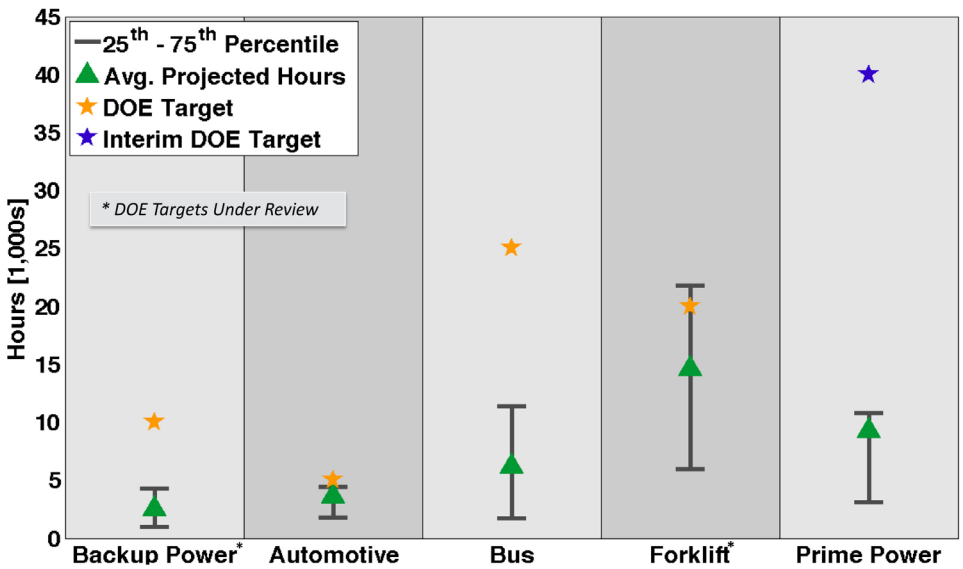

FIGURE 2. Operation Hours and Projected Hours to 10% Voltage Drop by Application Category

the average projection decreases with more aggressive test conditions and full systems (Figure 3). Not all applications have data sets in each configuration or test condition group. The test condition groups include:

- Steady – little or no change to load profile
- Duty Cycle – load profile mimics real-world operating conditions
- Accelerated – test profile is more aggressive than real-world operating conditions.

Most applications have seen an increase in average time to 10% voltage degradation over the last three years (Figure 4). Averages may decrease from year to year based on new data sets added and varied test conditions and configurations. Another possible reason for changes year-

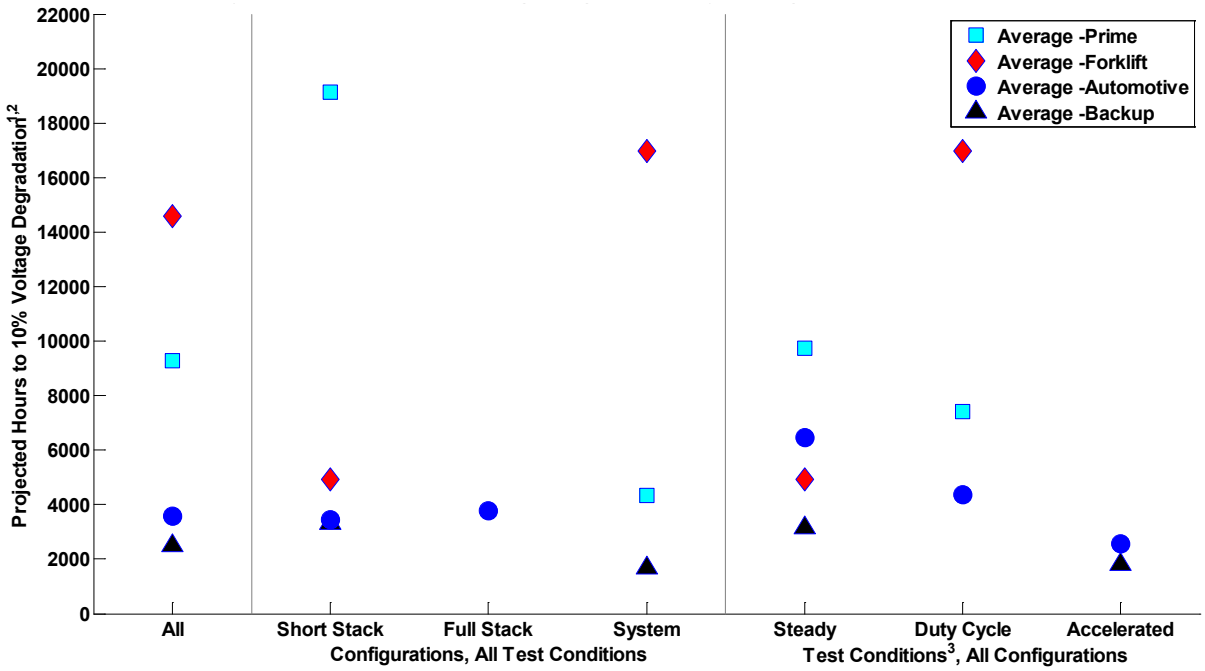

1) The DOE 10% voltage degradation metric is used for assessing voltage degradation; it may not be the same as end-of-life criteria and does not address catastrophic failure modes.
2) Not all applications have data sets in each configuration or test condition group.
3) Steady - little or no change to load profile
Duty Cycle - load profile mimics real-world operating conditions
Accelerated - test profile is more aggressive than real-world operating conditions

NREL cdp_lab_08
Created: Apr-01-13 1:42 PM

FIGURE 3. Projected Hours to 10% Voltage Drop by Configuration and Test Condition

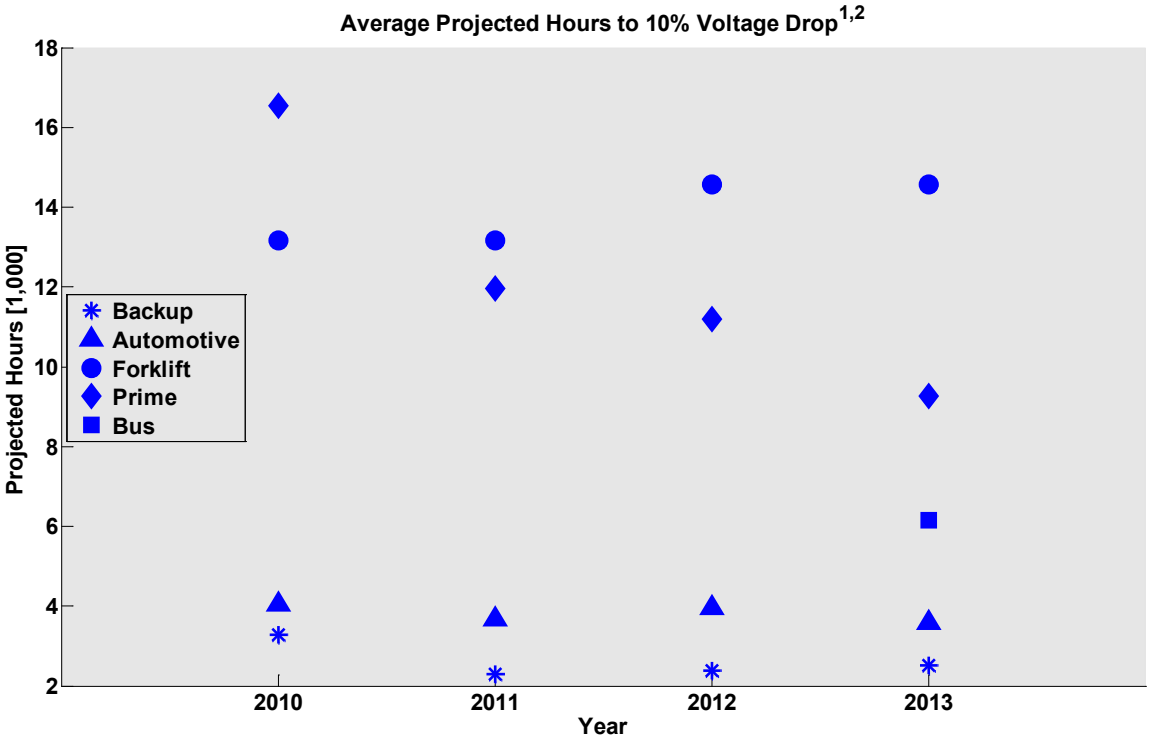

(1) The DOE 10% voltage degradation metric is used for assessing voltage degradation; it may not be the same as end-of-life criteria and does not address catastrophic failure modes.
(2) At least 13 fuel cell developers supplied data, including international. Analysis is updated periodically.

NREL cdp_lab_10
Created: Apr-01-13 2:32 PM

FIGURE 4. Average Projected Hours to 10% Voltage Degradation by Year and Application Group

to-year (particularly when the average decreases) is fuel cell development is focusing on multiple performance metrics that include durability, cost reduction, and efficiency. A test configuration may have been based on improvements in an area other than durability, with a small negative impact on durability. Development that focuses on more than one area (such as durability and cost reduction) is actually a statement on how far the technology has progressed. The research is not just focused on durability solutions. An up and down trend of average durability in an application from the past few years represents the degree of integration amongst the highest priority research topics. In addition, there are continued needs for the technology that is capable of meeting both cost and durability targets.

CONCLUSIONS AND FUTURE DIRECTIONS

This project has leveraged other technology validation projects and existing industry relationships to steadily increase the quantity and depth of reporting on the state-of-the-art fuel cell durability status with a relatively low investment from DOE. U.S. and international developers have voluntarily supplied at least one data set, and it is an ongoing effort to include new data sets, update data sets already included (if applicable), and include new fuel cell developers, applications, and types. The voluntary participation of leading fuel cell developers showcases the fuel cell durability improvements with the current technology and provides an overall technology benchmark (with the published aggregated data) and an individual developer benchmark (with the detailed data products). The data are fully integrated into Fleet Analysis Toolkit, and an online interface provides information on the project, contact information for interested collaborators, and all publications. The published results from April 2013 are the fifth update and were completed ahead of the milestone requirement with many new data sets and results. Future work includes the following:

- Continue cultivating existing collaboration and developing new collaborations with fuel cell developers
- Gathering, processing, and reporting on current fuel cell product cost and/or price

FY 2013 PUBLICATIONS/PRESENTATIONS

1. Kurtz, J., Dinh, H., "Fuel Cell Technology Status Analysis Project: Partnership Opportunities," Fact sheet describing opportunities for industry to participate in NREL's fuel cell technology performance, durability, and price analysis. (June 2013)

2. Kurtz, J., Dinh, H., Sprik, S., Saur, G., Ainscough, C., Peters, M., "Fuel Cell Technology Status – Voltage Degradation," Presented at the 2013 Annual Merit Review and Peer Evaluation Meeting, Washington, D.C. (May 2013)

3. Kurtz, J., Dinh, H., Sprik, S., Saur, G., Ainscough, C., Peters, M., "State-of-the-Art Fuel Cell Voltage Durability Status: Spring 2013 Composite Data Products." (May 2013)

REFERENCES

1. http://www.nrel.gov/hydrogen/proj_fc_analysis.html

V.D.5 Development of Micro-Structural Mitigation Strategies for PEM Fuel Cells: Morphological Simulations and Experimental Approaches

Dr. Silvia Wessel (Primary Contact), David Harvey
Ballard Power Systems
9000 Glenlyon Parkway
Burnaby, B.C. V5J 5J8
Phone: (604) 453-3668
Email: silvia.wessel@ballard.com

DOE Managers
Kathi Epping Martin
Phone: (202) 586-7425
Email: Kathi.Epping@ee.doe.gov
David Peterson
Phone: (720) 356-1747
Email: David.Peterson@go.doe.gov

Technical Advisor
John Kopasz
Phone: (630) 252-7531
Email: kopasz@anl.gov

Contract Number: DE-EE0000466

Subcontractors:
- Georgia Institute of Technology, Atlanta, GA (Dr. S.S. Yang)
- Los Alamos National Laboratory, Los Alamos, NM (Dr. R. Borup)
- Michigan Technological University, Houghton, MI (Dr. J. Allen)
- Queen's University, Kingston, Ontario, Canada (Drs. K. Karan, J. Pharoah)
- University of New Mexico, Albuquerque, NM (Dr. P. Atanassov)

Project Start Date: January 1, 2010
Project End Date: March 31, 2013

Overall Objectives

- Identify/verify catalyst degradation mechanisms
- Correlate catalyst performance/catalyst structural change as a function of unit cell operational conditions and catalyst layer morphology/composition
- Develop kinetic and material models for catalyst layer aging, i.e., macro-level unit cell degradation model, micro-scale catalyst layer degradation model, and molecular dynamics degradation model of the platinum/carbon/ionomer interface
- Develop durability windows and mitigation strategies for catalyst degradation through modification of operational conditions and component structural morphologies/compositions

Fiscal Year (FY) 2013 Objectives

- Simulate Pt dissolution and transport of Pt species in the ionomer using the developed Molecular Dynamics Model
- Complete the 2-phase flow transient micro-structural catalyst model and simulation of effective properties
- Recode the one-dimensional unit cell performance model in OpenFOAM© and include degradation
- Develop correlations linking the catalyst layer structure with membrane electrode assembly (MEA) performance and degradation
- Develop Durability Windows

Technical Barriers

This project addresses the following technical barriers of the DOE Fuel Cell Technologies Office Multi-Year Research, Development, and Demonstration Plan [1].

(A) Durability (of the Pt catalyst and Pt cathode catalyst layer)

(B) Performance

(C) Cost (indirect)

Technical Targets

In this project fundamental studies of the Pt/carbon catalyst degradation mechanisms and degradation rates are conducted and correlated with unit cell operational conditions and catalyst layer structure and composition. Furthermore, forward predictive micro and macro models for cathode performance and degradation are being developed. Design curves, generated both through model simulations and experimental work, will enable MEA designers to optimize performance, durability, and cost towards the 2020 targets for fuel cell commercialization [1]:

- System Durability (10% performance loss)
  - Transportation applications: 5,000 hours
  - Stationary applications (1-10 kW_e): 60,000 hours
- Electrocatalyst (transportation applications)
  - Support Stability: <10% mass activity loss after 400 hrs @ 1.2 V in H_2/N_2
  - Effective catalyst surface area (ECSA) loss <40%
  - Platinum-grade metal total loading: 0.125 mg/cm^2

FY 2013 Accomplishments

- Identified the preferred Pt dissolution site on a Pt crystal anchored on a carbon surface and extracted the transport/diffusion rates of Pt species in the ionomer
- Predicted the local distribution of effective properties and identified oxygen "storage" aspects of ionomeric films through transient micro-structural catalyst model simulations
- Developed a Pt dissolution model for mixed Pt oxide formation from water and air for performance and degradation prediction
- Built the Unit Cell Model in an open-source platform that allows for continued improvement of the model in the public domain.
- Developed correlations of beginning of test (BOT) and end of test (EOT) performance loss breakdown with cathode catalyst layer composition, morphology, material properties, and operational conditions
- Identified design windows and parameters which are key MEA design levers
- Identified a design flow path of interactions from materials properties and catalyst layer effective properties to performance loss breakdown for conditioned and degraded catalyst layers

✧ ✧ ✧ ✧ ✧

INTRODUCTION

Catalyst/catalyst layer degradation has been identified as a substantial contributor to fuel cell performance degradation and this contribution is expected to increase as MEAs are driven to lower Pt loadings in order to meet the cost targets for full-scale commercialization. Prior to the start of this project significant progress was made in identifying catalyst degradation mechanisms [2,3] and several key parameters that greatly influence the degradation rates, including electrode potentials, potential cycling, temperature, humidity, and reactant gas composition [2,4,5,6]. Despite these advancements, many gaps with respect to catalyst layer degradation and an understanding of its driving mechanisms still existed. In particular, acceleration of the mechanisms under different fuel cell operating conditions, due to different structural compositions, and as a function of the drive to lower Pt loadings was an area not well understood. In order to close these gaps, this project focused on understanding of the effect of operating conditions and cathode catalyst layer structure and composition on catalyst degradation mechanisms and degradation rates.

The project objective was to develop forward predictive models and to conduct systematic cell degradation studies that enable quantification of the cathode catalyst layer degradation mechanisms and rates and correlation of materials properties as a function of key operational and structural parameters.

APPROACH

Models have been developed at the molecular, micro-structural, and macro-homogeneous scales that include degradation effects related to platinum dissolution, transport and plating, carbon surface oxidation and corrosion, and ionomer thinning/conductivity loss. The models provide the ability to study the effects of composition, the morphological design, and the operational window on catalyst degradation via simulated accelerated stress testing. The design curves generated in each scale of the modeling work enable the development of mitigation strategies through trade-off analysis.

Accelerated stress testing coupled with state-of-the-art in situ/ex situ characterization techniques have been used to correlate MEA performance loss with structural changes measured within the Pt cathode, as well as to develop key operational and catalyst/catalyst layer structural degradation design curves. The experimental results also served to provide model validation.

RESULTS

Model Development

Efforts within this fiscal year were focussed on the open-source integration into OpenFOAM©, development of the graphical user interface, the completion of work on the platinum oxide model, and the investigation of the effect of platinum loading mass transport limitations in the microstructural catalyst model.

In order to simulate platinum dissolution and plating, a platinum oxide model capable of predicting the oxide coverage under air and hydrated conditions was required. As noted previously, literature models for the prediction of oxides under air and hydrated conditions were readily available, but were only validated for voltages below the equilibrium open-circuit voltage (OCV) potential of the cell. Upon investigation it was found that these models were not capable of capturing the growth of oxides on the platinum surface for potentials above the OCV. A re-derivation and modification of the existing models was undertaken such that key changes were made in the behavior of oxide growth and the description for the availability of active platinum sites. The modified and improved oxide model (Figure 1B) shows substantially better predictive capability as compared to the original (Figure 1A) model. In particular, the ability of the model to capture the oxidation peak has been dramatically improved while the reduction peak still shows some room for improvement around the location of the onset

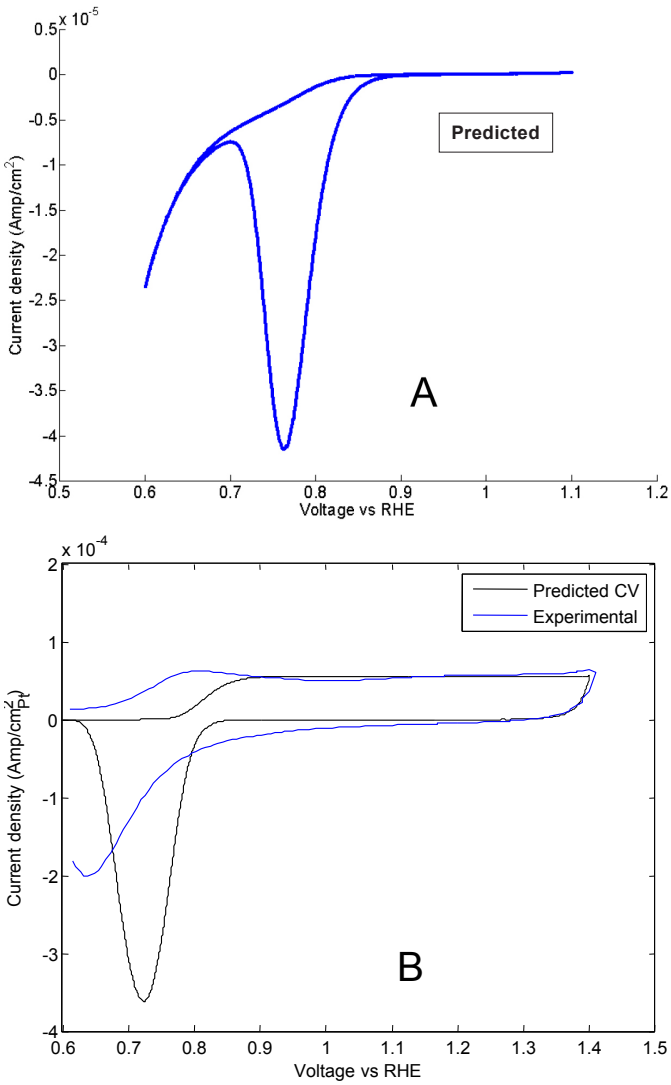

FIGURE 1. Cyclic voltammogram predictions using (A) the literature Pt-oxide model and (B) a re-derived, modified Pt-oxide model.

potential. Coupling the modified Pt oxide model to transport and oxygen reduction reaction kinetic parameters in the integrated MEA Degradation Model will properly capture the performance in the operating range of the fuel cell.

The effect of platinum loading was studied in the micro-structural model by systematically increasing the overall loading and probing the specific transport phenomena within the catalyst morphology. In each case the local Knudsen effects (Figure 2A) were accounted for, in addition to transport across and within the ionomeric films. It was found that the oxygen concentration dropped substantially as a function of the increased catalyst layer thickness (Figure 2B) such that gas phase transport worsens as the thickness increases. The effect of this thickness change is contrary to what is seen in regards to the polarization predictions (Figure 2C) in which there are additional losses related to the gas phase transport. These polarization curves show a distinct loss due to a reduction in platinum surface area, but the loss of this area also incurs a secondary effect related to the interfacial areas between ionomer and platinum. This change in the interfacial area produces an effect which can be described via a shape factor correction in the local diffusion and resulting concentration (Figure 2D). This shape factor is a predicted plot from the microstructural simulations and shows clearly that the localized species transport resistance increases significantly as the platinum loading is reduced.

The open-source model integration has been completed in OpenFOAM© and will be fully released as the FC-PEM Simulation Package. The model has been implemented in a flexible dimensional format such that one-, two-, and three-dimensional simulations are possible. Further, the package has a graphical user interface in order to manage case files, runs, and modification of various required user input data. The model uses front end mesh generators, calculation packages, and post-processing that is freely available in the open-source domain.

Experimental Parametric Studies

Efforts within this fiscal year were focused on developing (1) correlations that link MEA performance and degradation to catalyst layer composition, structure, component properties, and effective properties and (2) design windows. The overall motivation was to identify parameters which are key levers for the MEA designer, and that would allow the catalyst manufacturer to optimize catalyst parameters for enhanced MEA performance and durability. Figure 3A shows the approach taken in linking the catalyst carbon support and catalyst powder structure to the catalyst layer structure, effective properties, and performance of the MEA. This approach addresses both BOT and EOT performance; the latter being captured via changes in the catalyst layer structure and effective properties with degradation. The detailed interactions of the different measurables is shown on Figure 3B. While most of the parameters were quantified (green boxes), the yellow and pale blue colors highlight the gaps in quantification methods, and these are subsequently calculated by the Unit Cell Model.

The reaction distribution in the catalyst layer is affected through balancing of the different over-potentials in order to minimize the total polarization losses. Thus, changes to one catalyst layer property can have an affect on each of the different over-potentials that are inherent in the polarization characteristics. For example, mass transport limitations, caused by reduced diffusivity or increased catalyst layer thickness, will reduce the local oxygen concentration at the catalyst surface causing an increase in kinetic losses. This results in a shift of the reaction distribution in the catalyst layer to access more oxygen, thus causing a reduction in mass transport losses and an associated increase in catalyst layer ionic loss. Similarly, proton conductivity, intrinsic kinetic

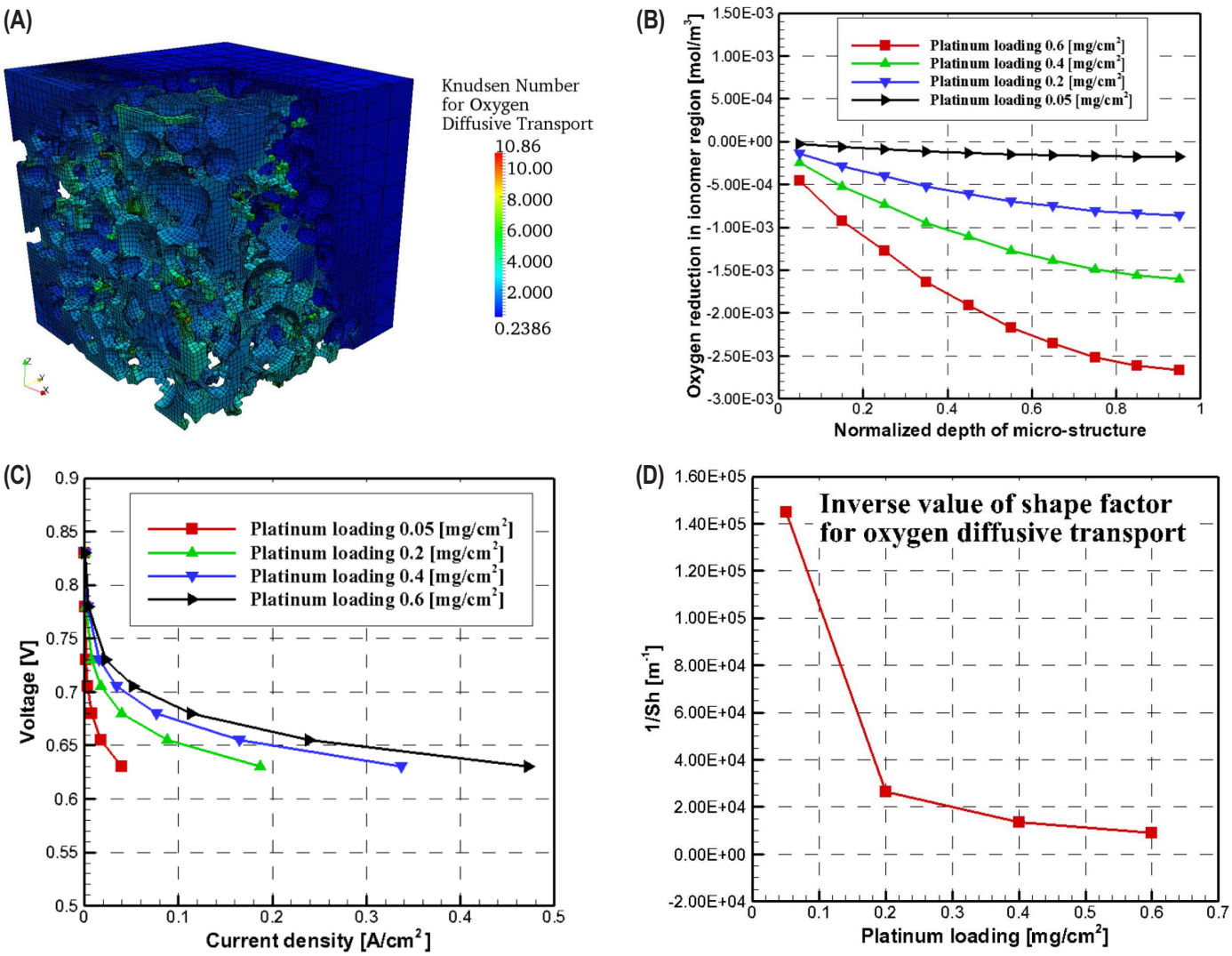

FIGURE 2. (A) Knudsen number for a catalyst morphology; platinum loading effect on (B) oxygen transport normalized depth profile, (C) catalyst polarization, and (D) the effective shape factor for oxygen transport.

activity, and catalyst surface area can also affect the reaction distribution and polarization losses. An example of the effect of catalyst layer thickness is shown in Figure 4.

While an increase in catalyst layer thickness affects mass transport losses due to oxygen depletion effects, catalyst layer ionic loss, caused by an increase in ionic resistance, was observed to be the dominant loss mechanism (Figure 4a). In this example, the Pt loading was held constant, and the thickness increase was due to a lower Pt/C ratio within the catalyst layer. For the thicker catalyst layers the current distribution is forced further into the catalyst layer to access the same amount of ECSA as the thinner catalyst layer. As a result, the thicker catalyst layer exhibits a higher ionic loss. With degradation (Figure 4A), the catalyst layer ionic loss increases due to Pt depletion at the membrane/catalyst interface (Figure 4C) which shifts the reaction penetration further into the catalyst layer. An effective thickness (Figure 4B) calculated from the catalyst layer ionic losses and the ionic resistivity shows that the increase in effective thickness (reaction penetration) agrees with the thickness of the Pt depleted region (~3 μm Pt depletion for the 9 μm layer and 6-8 μm Pt depletion for the 31 μm layer).

Durability windows were developed for both the catalyst layer structural design levers and operational conditions. Table 1 summarizes the time at the upper AST potential to reach 15% performance loss at a current density of 1.0 A/cm^2 for a variety of operational parameters. As shown before, the impact of the upper potential limit is most severe; under 100% relative humidity (RH) conditions, the operational time is increased ~34 times by reducing the upper potential limit from 1.4 V to 1.0 V. The effect of temperature is less severe and in fact at lower potentials (≤1.2 V) when Pt dissolution is the dominant degradation mechanism, the effect of temperature in the range from 60 to 90°C is

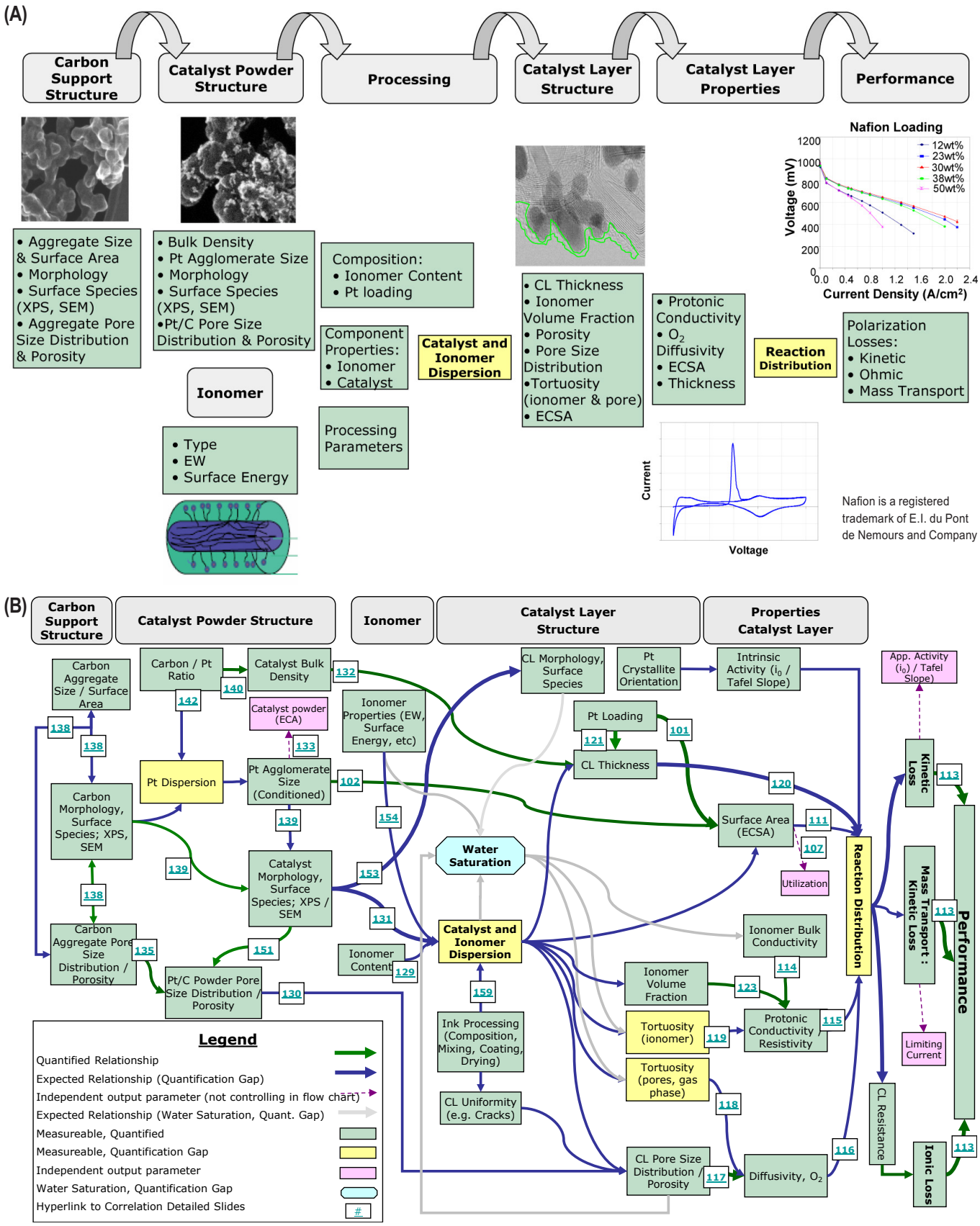

FIGURE 3. (A) Correlations approach flow chart. (B) Interactions and linkage of catalyst layer component characteristics, catalyst layer composition, structure, and effective properties and performance.

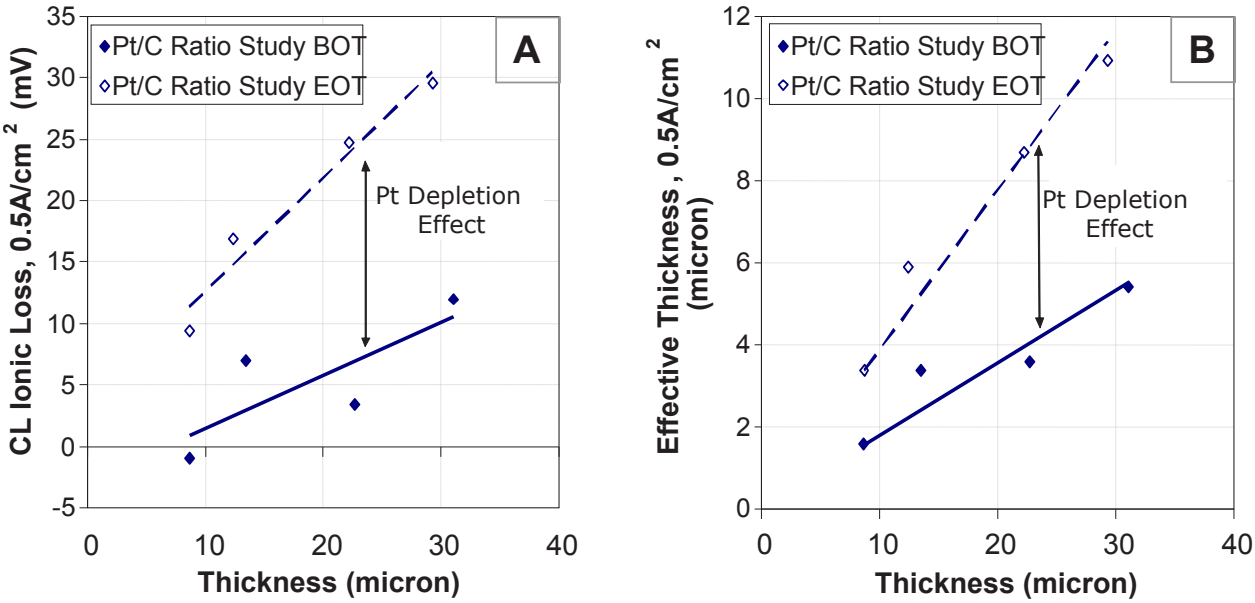

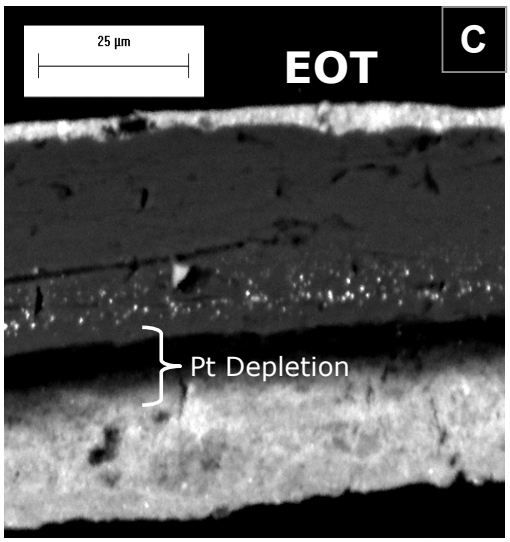

FIGURE 4. Catalyst layer ionic loss as a function of (A) measured catalyst layer thickness and (B) effective catalyst layer thickness (reaction penetration), (C) scanning electron micrograph of a degraded catalyst layer.

TABLE 1. Operational Durability Windows for the Baseline MEA (Pt50LSAC, 0.4 mg/cm^2 cathode loading)

Operational Parameter	Lower Level	Lower Level Time to 15% Performance Loss	Upper Level	Upper Level Time to 15% Performance Loss
UPL (100% RH, 80°C)	1.0 V	243 hours	1.4 V	7 hours
Temperature (100% RH, 1.4 V UPL)	60°C	46 hours	90°C	2.5 hours
Temperature (50% RH, 1.4 V UPL)	60°C	70 hours	90°C	5 hours
RH, cathode (1.4 V UPL, 80°C)	60% RH	11 hours	100% RH	8 hours
RH, cathode (1.2 V UPL, 80°C)	60% RH	1,500 hours	100% RH	200 hours

UPL - upper potential limit

insignificant. However, carbon corrosion is substantially affected by temperature and at an upper potential limit of 1.4 V, an increase in temperature from 60 to 90°C reduces the operational time ~18 times at 100% RH and 14% at 50% RH. Furthermore, changing the RH from 100% to 50% at constant temperature will approximately double the operational time to reach 15% performance loss. The effect of RH was found to be more significant for the Pt dissolution mechanism; a 7.5x increase in time to 15% voltage loss can be achieved by reducing the cathode RH from 100% to 60%.

CONCLUSIONS

The overall conclusions are:

- The lower corner and lower edge Pt atoms at the carbon interface were found to be the least stable and as such most likely to dissolve.
- The diffusion rates for PtO_2 and $Pt(OH)_2$ species were found to be very similar due to their similar size (activation energy of diffusion: -13 kJ/mol for $Pt(OH)_2$, -11 kJ/mol for PtO_2.
- Oxygen dissolution modeled within the catalyst structure showed that the ionomer films tend to be thin with little resistance.
- The effect of catalyst layer composition on local conditions is observed through the variation in transport parameters, with decreasing platinum loading, the transport resistance increases due to an increased 'localized' current demand and reduced ionomeric contact area.
- The correlations between materials properties, composition, structure, and effective properties of cathode components show similar trends for BOT and EOT MEAs.
- Design windows reveal durability acceleration factors for various operational conditions.

Overall, this work has provided significant advancements in the ability to model and design durable fuel cell products and to understand the role of catalyst layer morphology and structure on the durability of the MEA. The outcome of this project is subsequently assisting in reducing the iterative design/test cycle process for next generation fuel cell products via model simulations.

FY 2013 PUBLICATIONS/PRESENTATIONS

1. G. Brunello, J.I. Choi, S.S Jang, "Multi-scale First Principle Modeling of Three-Phase System of Polymer Electrolyte membrane Fuel cell", submitted abstract 222nd ECS Meeting, Honolulu, Hawai'i, October 7–12, 2012.

2. G. Brunello, J.I. Choi, S.S Jang, "Density Funcional Theory Study and Model development on Pt-Nano-particles", submitted abstract 222nd ECS Meeting, Honolulu, Hawai'i, October 7–12, 2012.

3. G. Brunello, J.I. Choi, S.S Jang, "Density Functional Theory Study of Pt Dissolution at Water-Pt Interface", submitted abstract 222nd ECS Meeting, Honolulu, Hawai'i, October 7–12, 2012.

4. V. Colbow, M. Dutta, A. Young, Z. Ahmad, D. Harvey, S. Wessel, "Performance Degradation and Structural Changes with Pt Cathode Catalyst layer Design", submitted abstract 222nd ECS Meeting, Honolulu, Hawai'i, October 7–12, 2012.

5. D.Harvey, A. Bellemare-Davis,K. Kunal, B. Jayansankar, J. Pharoah, V. Colbow, A. Young, S. Wessel, "Statistical Simulation of the Performance Degradation of a PEMFC Electrode Assembly" submitted abstract 222nd ECS Meeting, Honolulu, Hawai'i, October 7–12, 2012.

6. K. Artyushkova, P. Atanassov, M. Dutta, V. Colbow, S. Wessel, "Ex-situ Characterization of Degradation Mechanism of MEAs by iImaging XPS and SEM", submitted abstract 222nd ECS Meeting, Honolulu, Hawai'i, October 7–12, 2012

7. S.A. Stacy, J.S. Allen, Percolation in Catalyst Layer of PEMFC", submitted abstract 222nd ECS Meeting, Honolulu, Hawai'i, October 7–12, 2012.

8. R. Shahbazian-Yassar, "Membrane Electrode Assembly Degradation in Proton Exchange Membrane Fuel Cells: A View From Nanoscale", International Conferences of Young Researchers on Advanced Materials, July 1–6, 2012, Singapore.

9. M. Khakaz-Baboli, D.A. Harvey, J.G.Pharoah, "Investigating the performance of catalyst layer micro-structures with different platinum loadings", submitted abstract 222nd ECS Meeting, Honolulu, Hawai'i, October 7–12, 2012.

10. S. Wessel, V.Colbow, M. Dutta, A. Young, D. Harvey, "The impact of Materials Properties and Cathode Catalyst Structure/ Composition on MEA Performance and Durability", Hydrogen and Fuel Cells 2013, Vancouver B.C., June 16–19, 2013.

11. D. Harvey, A. Bellemare-Davis, B. Jayasankar, K. Karan, J. Pharoah, A. Young, M. Dutta, V. Colbow, S. Wessel, "Simulation of the ORR Multi-pathway and Catalyst Dissolution for a PEMFC: The Effect of Surface Coverage and AST cycling", Hydrogen and Fuel Cells 2013, Vancouver B.C.,June 16–19, 2013.

12. S. Wessel, "Water management in Low Temperature PEM Fuel Cells, Industrieworkshop: Wassermanagement in PEM-Brennstoffzellen, Freiburg (Germany), 31 January 2013.

13. K. Artyushkova, P. Atanassov, M. Dutta, D. Harvey, V. Colbow, and S. Wessel, "Structural Correlations: Design Levers for Performance and Durability of Catalyst Layers" submitted abstract 224th ECS Meeting, San Francisco, CA, October 27 – November 1, 2013.

REFERENCES

1. Hydrogen, Fuel Cells & Infrastructure Technologies Program: Multi-Year Research, Development and Demonstration Plan, U.S. Department of Energy, Energy Efficiency and Renewable Energy, 2011 revision. http://www.eere.energy.gov/hydrogenandfuelcells/mypp/

2. J. Wu, X.Z. Yuan, J.J. Martin, H. Wang, J. Zhang, J. Shen, S. Wu, W. Merida, A Review of PEM Fuel Cell Durability: Degradation Mechanisms and Mitigation Strategies. Journal of Power Sources 184, 104-119.

3. R. Borup, J.P. Meyers, B. Pivovar, Y.S. Kim, R. Mukundan, N. Garland, D. Myers, M. Wilson, F. Garzon, D. Wood, P. Zelenay, K. More, K. Stroh, T. Zawodinski, J. Boncella, J.E. McGarth, M. Inaba, K. Miyatake, M. Hori, K. Ota, Z. Ogumi, S. Miyata, A. Nishikata, Z. Siroma, Y. Uchimoto, K. Yasuda, K. Kimijima, N. Iwashita, Scientific Aspects of Polymer Electrolyte Fuel Cell Durability and Degradation. Chemical Reviews 2007, 107, 3904-3951.

4. Y. Shao, G. Yin, Y. Gao, Understanding and Approaches for the Durability Issues of Pt-Based Catalysts for PEM Fuel Cell. Journal of Power Sources 2007, 171, 558-566.

5. M.S. Wilson, F. Garzon, K.E. Sickafus, S. Gottesfeld, Surface Area Loss of Supported Platinum in Polymer Electrolyte Fuel Cells. Journal of the Electrochemical Society 1993, 140, 2872-2876.

6. P.J. Ferreira, G.J. Ia O', Y. Shao-Horn, D. Morgan, R. Makharia, S. Kocha, H. Gasteiger, Instability of Pt/C Electrocatalysts Membrane Fuel Cells A Mechanistic Investigation. Journal of the Electrochemical Society 2005, 152, A2256-A2271.

V.E.1 Effect of System Contaminants on PEMFC Performance and Durability

Huyen N. Dinh (Primary Contact), Guido Bender, Clay Macomber, Heli Wang, Bryan Pivovar
National Renewable Energy Laboratory (NREL)
15013 Denver West Parkway
Golden, CO 80401-3305
Phone: (303) 275-3605
Email: Huyen.Dinh@nrel.gov

DOE Manager
Kathi Epping Martin
Phone: (202) 586-7425
Email: Kathi.Epping@ee.doe.gov

Subcontractors:
- Kelly O'Leary, Paul Yu, Balsu Lakshmanan, General Motors LLC, Honeoye Falls, NY
- John Van Zee, John Weidner, Masato Ohashi, University of South Carolina, Columbia, SC
- Tommy Rockward, Los Alamos National Laboratory, Los Alamos, NM
- Jean St-Pierre, University of Hawaii, Honolulu, HI
- Ryan Richards and Jason Christ, Colorado School of Mines, Golden CO
- Steve Hamrock (in-kind partner), 3M, St. Paul, MN
- Paul Beattie (in-kind partner), Ballard Power Systems, Vancouver, BC, CANADA
- Olga Polevaya (in-kind partner), Nuvera Fuel Cells Inc., Billerica, MA

Project Start Date: July 20, 2009
Project End Date: September 2013

Overall Objectives

Our overall objective is to decrease the cost associated with system components without compromising function, fuel cell performance, or durability. Our specific project objectives are to:

- Identify and quantify system-derived contaminants
- Develop ex situ and in situ test methods to study system components
- Identify severity of system contaminants and impact of operating conditions
- Identify contamination mechanisms
- Develop models/predictive capability
- Guide system developers on future material selection
- Disseminate knowledge gained to the community

Fiscal Year (FY) 2013 Objectives

- Identify impact of operating conditions
- Identify contamination mechanism(s) for system contaminants
- Develop a model for contamination mechanism
- Disseminate project information to the fuel cell community

Technical Barriers

This project addresses the following technical barriers from the Fuel Cells section (3.4.4) of the Fuel Cell Technologies Office Multi-Year Research, Development, and Demonstration Plan:

(A) Durability

(B) Cost

Technical Targets

This project focuses on quantifying the impact of system contaminants on fuel cell performance and durability. Insights gained from these studies will increase performance and durability by limiting contamination-related losses and decrease overall fuel cell system costs by lowering balance-of-plant (BOP) material costs. Proper selection of BOP materials will help meet the following DOE 2020 targets:

- Cost: $30/kW for transportation; $1,000–1,700/kW for stationary
- Lifetime: 5,000 hours for transportation; 60,000 hours for stationary

FY 2013 Accomplishments

- Screened seven additional, relevant, commercially available BOP materials, as recommended by Ballard and Nuvera, for fuel cell contamination (62 BOP materials screened total).
- Identified contamination mechanism(s) of organic compounds: adsorption on catalyst, redox reaction, reaction and absorption with ionomer, and membrane poisoning.
- Determined that functional groups of organic compounds are important in understanding system contaminants and that performance loss may contain reversible, recoverable, and non-recoverable contributions. This knowledge can help identify future mitigation strategies for contaminants.

- Performed in-depth parametric studies to determine the impact of various fuel cell operating conditions (cell temperature, contaminant concentration, relative humidity [RH], current density, and catalyst loading) on fuel cell performance for selected extracts and organic compounds.
- Developed a model on the effect of organic compounds on fuel cell performance.
- Disseminated project information to the fuel cell community via the NREL website (www.nrel.gov/hydrogen/contaminants.html), publications, and presentations. The NREL website also includes an interactive material-selection tool that enables viewers to quickly find relevant and revealing information for a specific material relative to other materials in the same family class (www.nrel.gov/hydrogen/system_contaminants_data/).

✧ ✧ ✧ ✧ ✧

INTRODUCTION

Cost and durability issues of polymer electrolyte membrane fuel cell (PEMFC) systems have been challenging for the fuel cell industry. The projected BOP system cost (over $25/kW in 2012 [1]) has risen in importance as projected fuel cell stack cost has decreased (approximately $20/kW in 2012 [1] compared to $65/kW in 2006 [2]). Lowering the cost of PEMFC system components requires understanding of the materials used in these components and the contaminants that are derived from them, which have been shown to affect the performance and durability of fuel cell systems. Unfortunately, there are many possible contamination sources from system components [3-5]. Currently deployed, high-cost, limited-production systems use expensive materials for system components. In order to make fuel cell systems commercially competitive, the cost of BOP components needs to be lowered without sacrificing performance and durability. Fuel cell durability requirements limit the performance loss attributable to contaminants to at most a few mV over required lifetimes (thousands of hours), which means system contaminants must have a near-zero impact.

As catalyst loadings decrease and membranes are made thinner (both are current trends in automotive fuel cell R&D), operation of fuel cells becomes even more susceptible to contaminants. In consumer automotive markets, low-cost materials are usually required, but lower cost typically implies higher contamination potential. The results of this project will provide the information necessary to help the fuel cell industry make informed decisions regarding the cost of specific materials versus the potential contaminant impact on fuel cell performance and durability.

APPROACH

Our goal is to provide an increased understanding of fuel cell system contaminants and to help guide the implementation and, where necessary, development of system materials to support fuel cell commercialization. While much attention has been paid to air and fuel contaminants, system contaminants have received limited public attention and very little research has been publicly reported [6-9]. Our approach is to perform parametric studies to characterize the effects of system contaminants on fuel cell performance and durability, as well as to identify the severity of contamination, identify contamination mechanisms, develop a model, and disseminate information about material contamination potential that would benefit the fuel cell industry in making cost-benefit analyses for system components.

Last year, we identified and quantified potential contaminants derived from system component materials and screened the impact of leachants on the fuel cell catalyst, ionomer, and membrane via ex situ and in situ tests. Model compounds capable of replicating the deleterious impact of system-based contaminants were also studied.

The majority of our effort is focused on the liquid-based contaminants derived from structural plastics and assembly aid materials (lubricant, grease, adhesive, and seal). A minor part of our efforts is focused on an in situ durability study of gas-based contaminants (siloxane focus) and an ex situ electrochemical study of the effect of membrane degradation by-products on catalysis. The BOP materials selected for this study are commercially available commodity materials and are generally developed for other applications for which common additives/processing aids may not be a concern, but they may present problems for fuel cells.

RESULTS

We completed screening of 62 BOP materials total—from 14 different manufacturers, comprising different chemistries, and used for different functions—using multiple screening methods, totaling more than 740 experiments and over 1,000 h of in situ testing. Because there is a tremendous amount of data and knowledge generated from this project, we developed an NREL website (www.nrel.gov/hydrogen/system_contaminants_data/) to share the data with the public, including the screening results. For this report, we highlight some key accomplishments that emerged from our work, including the contamination mechanisms identified and the effect of fuel cell operating parameters.

We performed fundamental/mechanistic studies on selected organic model compounds and mixtures of compounds to understand their poisoning mechanisms and how they affect voltage loss, in both in situ fuel cell and ex situ electrochemical testing. Figure 1 shows an example data set that includes the performance effect of an extract

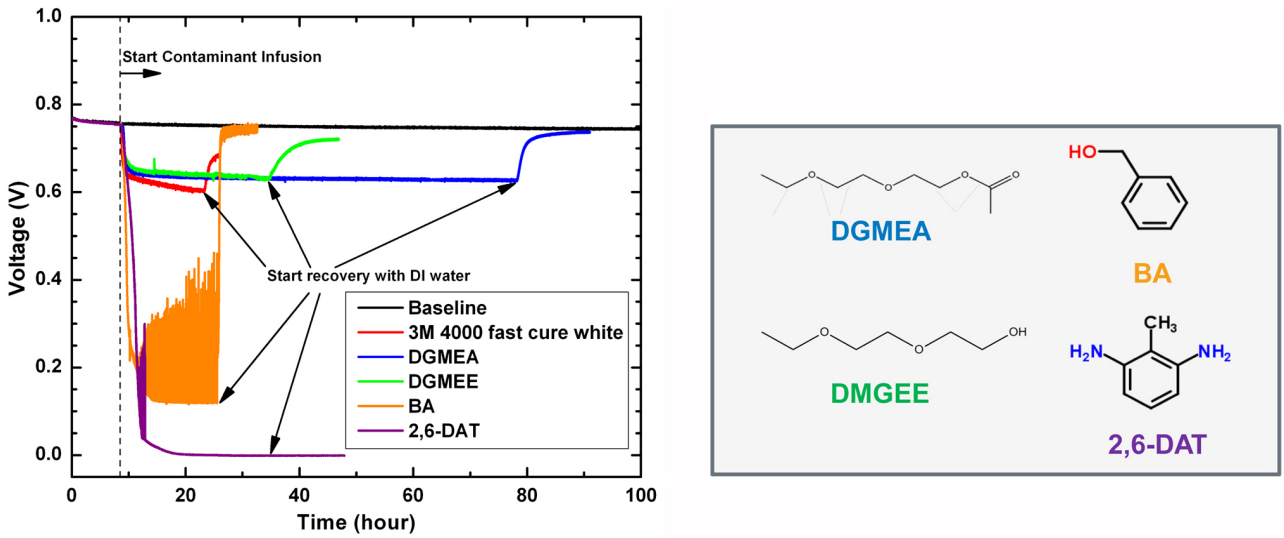

FIGURE 1. Total in situ cell voltage loss due to contamination of the fuel cell cathode by the individual organic model compounds (2-(2-ethoxyethoxy)-ethanol acetate, 2-(2-ethoxyethoxy)-ethanol, benzyl alcohol, and 2,6-DAT; total organic carbon = 1,280 ppm each). The black curve is the baseline curve where no contaminants were infused into the cathode. The red curve is the voltage loss resulting from infusing the 3M™ 4000 Fast Cure white extract (total organic carbon = 1,280 ppm). Standard operating conditions: cell temperature = 80°C, RH = 32%/32%, H_2 and air stoichiometry = 2/2, back pressure = 150/150 kPa, i = 0.2 A/cm^2.

as well as that of individual model compounds that were found in the extract. The extract was created by aging the urethane material 3M™ 4000 Fast Cure white in de-ionized water at elevated temperature. The four individual organic compounds, shown in Figure 1, were model compounds. Note that the experiment was designed such that all compounds or compound mixtures had the same total organic compound value. Voltage losses for the individual aliphatic compounds (2-[2-ethoxyethoxy]-ethanol acetate and 2-[2-ethoxyethoxy]-ethanol) reached steady state while the voltage loss for the extract continued to decrease. Voltage losses for the aliphatic and benzyl alcohol compounds were mostly reversible, indicating that these organic compounds were likely contaminated by reversible processes like physisorption onto the Pt surface and/or absorption into the membrane and ionomer. The voltage loss for 2,6-methyl benzenediamine (2,6-DAT) was irreversible, indicating that it may have chemisorbed and/or reacted with the membrane and ionomer. In summary, model compounds result in different contamination effects (voltage loss, high frequency resistance [HFR], and recoverability) than that observed for the multi-component extract.

Our studies show that mixtures of organic compounds may have different contamination and recovery effects than individual compounds, indicating that compound concentration is very important and further suggesting that interaction between organic compounds may occur. Figure 2 shows that the voltage loss and HFR for mixtures of aliphatics and benzyl alcohol reached steady state and were reversible (green curve), indicating minimal interaction between these three model compounds. Voltage loss and HFR for mixtures containing 2,6-DAT continued to change with time and were not reversible (magenta and grey curves), suggesting that 2,6-DAT dominated the contamination and recovery responses. The resistance data also indicated that organic contaminants can impact kinetic performance by either eliminating proton pathways to catalyst reaction sites or increasing the resistance of the ionomer in the catalyst layer. This process appeared to be slow and was associated with the 2,6-DAT compound. Voltage and HFR responses for 3M™ 4000 Fast Cure white showed the combined effect of the four individual organic compounds. Although the extract contained many components (organics, inorganics, and ions), these studies indicated that organic compounds can dominate the contamination and recovery effects. The table in Figure 2 is an example of the comprehensive quantitative analysis that we will be doing to quantify and understand the contamination effects.

From the 62 BOP materials screened, three structural materials and two assembly aid materials were selected for parametric studies. In situ infusion experiments were carried out on selected extracts and organic compounds to understand the effect of different operating conditions (contaminant concentration, RH, cell temperature, current density, and catalyst loading) on fuel cell performance and recovery. The parameters studied reflect 80% of typical fuel cell operation. Figure 3 shows the effect of concentration and RH on fuel cell performance in the presence of 2,6-DAT contaminant in the feed stream. The data confirmed that concentration was an important driver for cell performance loss. In addition, the data suggested that liquid water content may have impacted performance and recovery effects. This

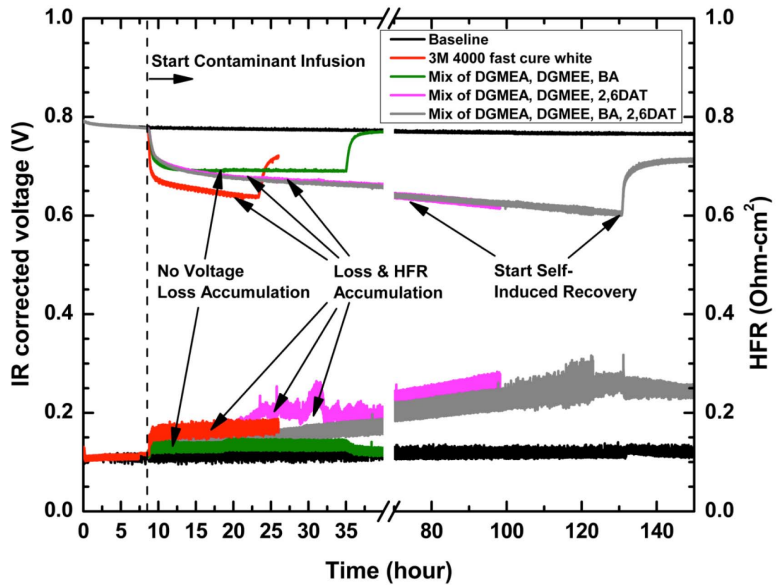

Material Extract	Immediate Voltage Loss [mV]	Immediate Voltage Degradation Rate [mV/h]	Voltage Loss Accumulation Rate [mV/h]	HFR Accumulation Rate [mΩcm²/h]	Reversible Performance Loss [%]	ECA Loss after self-induced Recovery [%]
3M™ 4000 Fast Cure white	121	251	2.3	1.02	56	36

Example data (fraction) from comprehensive quantitative analysis for characterization of performance effect.

FIGURE 2. In situ cell voltage loss (internal resistance-corrected) and HFR change due to contamination of the fuel cell cathode by different organic compound mixtures. The total concentration for all mixtures were the same (total organic carbon = 1,280 ppm). Standard operating conditions were used.

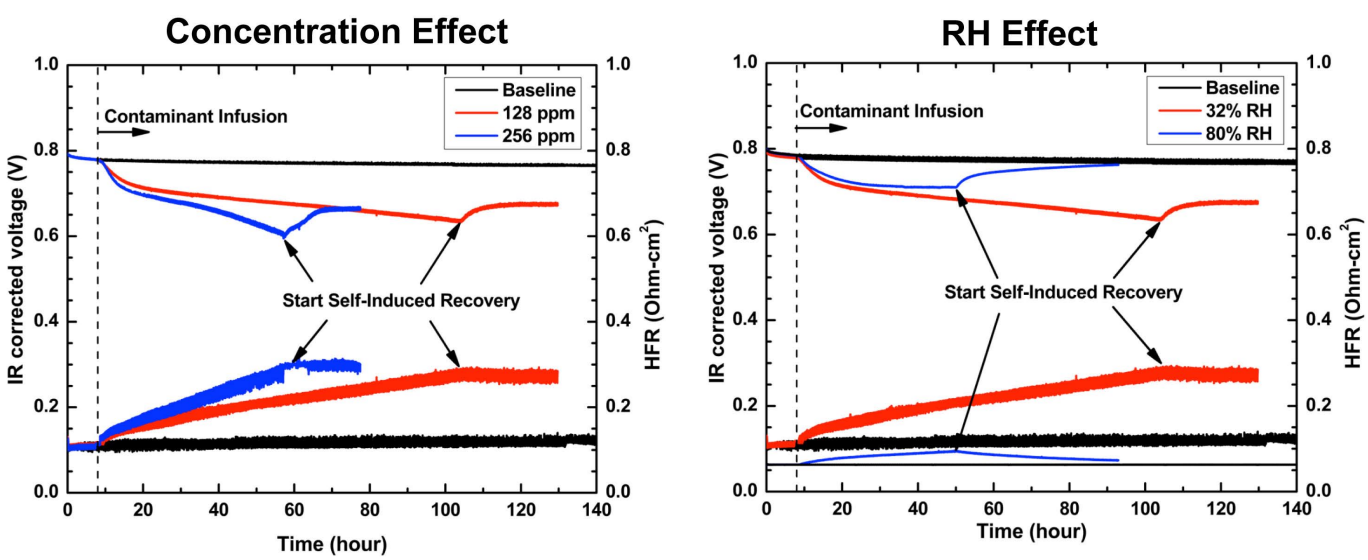

FIGURE 3. Example data from parametric study of organic compound: 2,6-DAT. The left plot shows the effect of contaminant concentration and the right plot shows the RH effect on fuel cell performance and recovery. Standard operating conditions were used.

information may be useful for mitigating the effect of specific contaminants. The plot and table in Figure 4 show that lower catalyst loading resulted in a stronger response to an identical contaminant (2,6-DAT). This response was indicated by a higher immediate performance loss, which was likely due to contaminant adsorption onto the catalyst surface. A larger

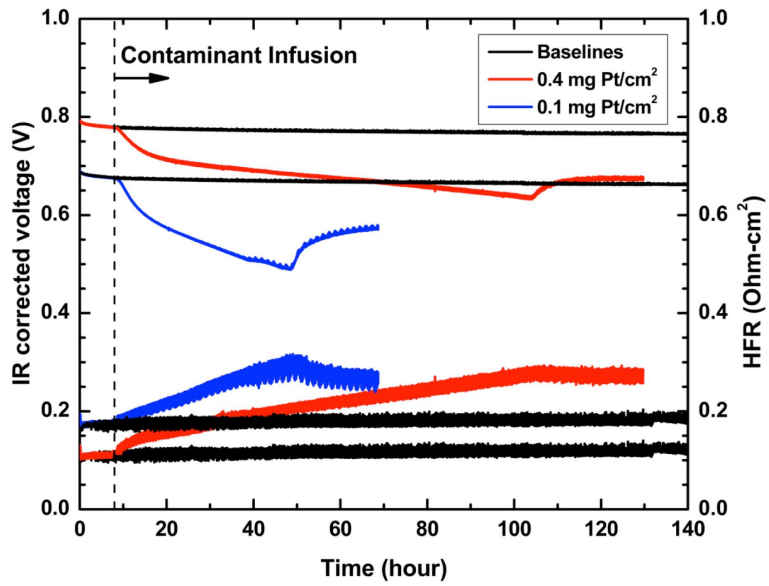

Anode/Cathode Catalyst Loading [mg Pt/cm^2]	Immediate Voltage Loss [mV]	Immediate Voltage Degradation Rate [mV/h]	Voltage Loss Accumulation Rate [mV/h]	HFR Accumulation Rate [mΩcm^2/h]	Reversible Performance Loss [%]	ECA Loss after self-induced Recovery [%]
0.05/0.4	77	11	1	1.7	24	38
0.05/0.1	104	15	4	3.2	45	47

FIGURE 4. The effect of catalyst loading on fuel cell performance and recovery in the presence of 2,6-DAT contaminant. Standard operating conditions were used.

performance loss accumulation was also observed for the lower catalyst loading and this loss may be related to the contaminant reacting with ionomer and membrane.

The experimental work for the project is complete, and in-depth analysis of in situ parametric data will be performed for the remainder of the project. Furthermore, we have developed and are finalizing the isothermal time-dependent two-dimensional model for characterizing the effects of contaminants at various operating conditions and for selected model compounds. The model has been validated with experimental data.

CONCLUSIONS AND FUTURE DIRECTIONS

- We found that functional groups of organic compounds are important in understanding system contaminant effects.
- We found that performance loss may contain reversible, recoverable, and non-recoverable contributions.
- We identified several contamination mechanisms: adsorption on catalyst, redox reaction, and reaction/absorption processes with ionomer and membrane, resulting in ohmic and kinetic loss.
- We found that the feed rate, RH, and current density strongly affected contamination while cell temperature changes (80°C and 50°C) showed some impact on performance loss and recovery. We also found that liquid water content may impact performance and recovery and that lower Pt catalyst loading resulted in higher performance loss.
- We modeled the effects of operating conditions on fuel cell performance for specific contaminating species and model compounds.
- We will continue to perform comprehensive quantitative analysis of in situ parametric data to characterize the contamination effects.
- We will disseminate project information via the NREL website, publications, reports, and presentations.

FY 2013 PUBLICATIONS/PRESENTATIONS

1. Macomber, C.S.; Christ, J.; Wang, H.; Pivovar, B.S.; Dinh, H.N. "Characterizing Leachant Contaminants from Fuel Cell Assembly Aids, a Prelude to Effects on Performance." *ECS Transactions* **2012,** *50* (2), 603-618.

2. Opu, M.S.; Ohashi, M.; Cho, H.-S.; Macomber, C.S.; Dinh, H.N.; Van Zee, J.W. "Understanding the Effects of Contaminants from Balance of Plant Assembly Aid Materials on PEMFCs In-Situ Studies." *ECS Transactions* **2012,** *50* (2), 619-634.

3. Wang, H.; Macomber, C.S.; Dinh, H.N. "Evaluation of PEMFC System Contaminants on the Performance of Pt Catalyst via Cyclic Voltammetry." *ECS Transactions*, **2012**, 50(2), 659-669.

4. Christ, J.M.; Neyerlin, K.C.; Wang, H.; Richards, R.; Dinh, H.N. "Impact of Polymer Electrolyte Membrane Degradation Products on the Activity of the Oxygen Reduction Reaction for Platinum Catalysts." *ECS Transactions*, **2012,** *50* (2), 691-700.

5. Dinh, H. "Effect of System Contaminants on PEMFC Performance and Durability." Section V.B.1. *2012 DOE Hydrogen and Fuel Cells Program Annual Progress Report*; pp. V57-V62.

6. H. Cho and J.W. Van Zee, "An isothermal model for predicting performance loss in PEMFCs from BOP leachates", *J. Electrochem. Soc*., submitted (2013).

7. H. Cho, M. Ohashi, and J.W. Van Zee, "Understanding the contamination mechanisms for PEMFCs resulting from aniline leachate", *Electrochim. Acta*, submitted (2013).

8. C.S. Macomber, J. Christ, H. Wang, B. Pivovar, H.N. Dinh. "Characterizing Leachant Contaminants from Fuel Cell Assembly Aids, a Prelude to Effects on Performance." 222nd ECS Meeting, Honolulu, HI, Oct. 7–12, 2012.

9. Md. Opu, M. Ohashi, H.S. Cho, C.S. Macomber, H.N. Dinh, J.W. Van Zee. "Understanding the Effects of Contaminants from Balance of Plant Assembly Aid Materials on PEMFCs In-situ Studies." 222nd ECS Meeting, Honolulu, HI, Oct. 7–12, 2012.

10. Hyun-Seok Cho, Md. S. Opu, Masato Ohashi, J.W. Van Zee. "The Contamination Behavior of Organic Compounds on PEMFC." 222nd ECS Meeting, Honolulu, HI, Oct. 7–12, 2012.

11. H. Wang, C.S. Macomber, H.N. Dinh. "Evaluation of PEMFC System Contaminants on the Performance of Pt Catalyst via Cyclic Voltammetry." 222nd ECS Meeting, Honolulu, HI, Oct. 7–12, 2012.

12. J.M. Christ, K.C. Neyerlin, H. Wang, R. Richards, H.N. Dinh. "Utilizing a Rotating Ring Disk Electrode to Simultaneously Measure Contaminate Species Adsorption Effects on Two Different Catalyst Surfaces." 222nd ECS Meeting, Honolulu, HI, Oct. 7–12, 2012.

13. J.M. Christ, K.C. Neyerlin, H. Wang, R. Richards, H.N. Dinh. "Impact of Polymer Electrolyte Membrane Degradation Products on the Activity of the Oxygen Reduction Reaction for Platinum Catalysts." 222nd ECS Meeting, Honolulu, HI, Oct. 7–12, 2012.

14. H.N. Dinh, M. Das, K.C. Neyerlin, Md. Opu, H. Wang, C.S. Macomber, M. Ohashi, J.W. Van Zee. "Screening Balance of Plant Materials to Understand Their Effect on Fuel Cell Performance." 222nd ECS Meeting, Honolulu, HI, Oct. 7–12, 2012.

15. H.N. Dinh, B. Lakshmanan. "Effect of System Contaminants on PEMFC Performance and Durability." Fuel Cell Tech Team Presentation, Nov. 14, 2012.

16. H.N. Dinh, G. Bender. "Effect of System Contaminants on PEMFC Performance and Durability." DOE Mid-Year Review, Golden, CO, Feb. 21, 2013.

17. J.M. Christ, K.C. Neyerlin, R. Richards, H.N. Dinh. "Impact of Polymer Electrolyte Membrane Chemical Degradation Products on Oxygen Reduction Reaction Activity for Platinum Catalysts." Conference on Earth and Energy Research, Golden, CO, Feb. 22, 2013.

18. H.N. Dinh, G. Bender. "Effect of System Contaminants on PEMFC Performance and Durability." DOE Durability Working Group Meeting, Crystal City, VA, Feb. 28, 2013.

19. H.N. Dinh, C.S. Macomber, M. Das, Md. Opu, H-S Cho, K.C. Neyerlin, H. Wang, G. Bender, M. Ohashi, J.W. Van Zee. "Understanding the Effects of Contaminants from Balance of Plant Materials on Fuel Cell Performance." 2013 MRS Spring Meeting (Invited), San Francisco, CA, Apr. 4, 2013.

20. H.N. Dinh. "Effect of System Contaminants on PEMFC Performance and Durability." DOE Fuel Cell Technologies Office Annual Merit Review, Washington, DC, May 2013.

REFERENCES

1. B. James, A. Spisak. "Mass Production Cost Estimation of Direct H_2 PEM Fuel Cell Systems for Transportation Applications: 2012 Update." October 18, 2012.

2. R. Farmer. Presentation on "Fuel Cell Technologies: FY 2011 Budget Request Briefing." February 12, 2010.

3. D. Gerard. "Powertrain Plastic Materials." SAE Mid-Michigan Conference, February 11, 2008.

4. D. Gerard. "Materials and Materials Challenges for Advanced Automotive Technologies Being Developed to Reduce Global Petroleum Consumption." 2007 Materials Science and Technology (Invited), Detroit, MI, September 16–20, 2007.

5. D.A. Masten, A.B. Bosco. *Handbook of Fuel Cells* (eds.: W. Vielstich, A. Lamm, H.A. Gasteiger), Wiley (2003): Vol. 4, Chapter 53, p. 714.

6. Q. Guo, R. Pollard, J. Ruby, T. Bendon, P. Graney, J. Elter. *ECS Trans*., Vol. 5(1), p. 187 (2007).

7. G.A. James, et. al. "Prevention of Membrane Contamination in Electrochemical Fuel Cells." U.S. Patent Application US2005089746A.

8. R. Moses. "Materials Effects on Fuel Cell Performance." National Research Council Canada Institute for Fuel Cell Innovation, International Fuel Cell Testing Workshop, September 20-21, 2006.

9. K. O'Leary, B. Lakshmanan, M. Budinski. "Methodologies for Evaluating Automotive PEM Fuel Cell System Contaminants." 2009 Canada-USA PEM Network Research Workshop, February 16, 2009.

V.E.2 The Effect of Airborne Contaminants on Fuel Cell Performance and Durability

Jean St-Pierre (Primary Contact), Yunfeng Zhai, Junjie Ge, Michael Angelo, Tatyana Reshetenko, Trent Molter[1], Leonard Bonville[1], Ugur Pasaogullari[1], William Collins[2], Silvia Wessel[3]
Hawaii Natural Energy Institute
1680 East-West Road
Honolulu, HI 96822
Phone: (808) 956-3909
Email: jsp7@hawaii.edu

DOE Managers
Nancy Garland
Phone: (202) 586-5673
Email: Nancy.Garland@ee.doe.gov
Reg Tyler
Phone: (720) 356-1805
Email: Reginald.Tyler@go.doe.gov

Technical Advisor
Walter Podolski
Phone: (630) 252-7558
Email: podolski@anl.gov

Contract Number: DE-EE0000467

Subcontractors:
[1] University of Connecticut, Storrs, CT
[2] UTC Power, South Windsor, CT
[3] Ballard Power Systems, Burnaby, BC, Canada

Project Start Date: April 1, 2010
Project End Date: March 31, 2014

Overall Objectives

- Identify and mitigate the adverse effects of airborne contaminants on fuel cell system performance and durability
- Provide contaminants and tolerance limits for filter specifications (preventive measure)
- Identify fuel cell stack's material, design, operation or maintenance changes to remove contaminant species and recover performance (recovery measure)

Fiscal Year (FY) 2013 Objectives

- Quantify performance loss for at least four different contaminants under various operating conditions
- Quantify spatial variability of performance loss and identify principal poisoning mechanism for at least four different contaminants

Technical Barriers

This project addresses the following technical barriers from the Fuel Cells section of the Fuel Cell Technologies Office Multi-Year Research, Development, and Demonstration Plan:

(A) Durability

(B) Cost

(C) Performance

Technical Targets

The following 2017 technical targets for automotive applications, 80-kW_e (net) integrated transportation fuel cell power systems operating on direct hydrogen, are considered:

- Durability: 5,000 hours in automotive drive cycle
- Cost: \$30 kW_e^{-1}
- Performance: 60% energy efficiency at 25% of rated power

The effects of specific airborne contaminants are studied and the resulting information will be used to impact both preventive measures and recovery procedures:

- Airborne contaminant tolerance limits to support the development of filtering system component specifications and ensure negligible fuel cell performance losses
- Fuel cell stack material, design, operation, or maintenance changes to recover performance losses derived from contamination mechanisms

FY 2013 Accomplishments

- Documented the unknown effects of seven airborne contaminants and one foreign cation on fuel cell performance and energy efficiency losses for key operating conditions (contaminant concentration, current density and temperature)
- Established tolerance limits for seven airborne contaminants and one foreign cation and 0.5, 1 and 5% performance loss levels over the target automotive fuel cell system life of 5,000 hours that offer guidance for filtering system design and cost
- Separated contaminant effects into three types of resistance losses for seven airborne species to facilitate

the selection of ex situ and in situ diagnostic techniques for mechanism determination

- Built ex situ and in situ diagnostic techniques database for seven airborne contaminants and one foreign cation to support the development of contamination mechanisms and recovery procedures that diminish the contamination impact on system durability, cost, and performance

✧ ✧ ✧ ✧ ✧

INTRODUCTION

The composition of atmospheric air cannot be controlled and typically includes contaminants, volatile compounds, as well as ions entrained by liquid water drops in the form of rain, mist, etc., especially near marine environments. Proton exchange membrane fuel cells operated with ambient air are therefore susceptible to deleterious effects which include decreased cell performance and durability [1]. Numerous air contaminants have not yet been tested in fuel cells and consequently their effects as well as recovery methods are unknown [2]. Furthermore, prevention is difficult to achieve because tolerance limits are also missing in most cases. This increases the risk of failure for fuel cell systems and thus jeopardizes their introduction into the market.

Airborne contaminants and foreign ions have previously been selected using a cost-effective two-tiered approach combining qualitative and quantitative criteria [2]. Automotive fuel cells are used under a wide range of operating conditions resulting from changes in power demands (drive cycle). Temperature and current density impact fuel cell contamination the most [2,3]. The effect of contaminant concentration is also particularly important to assess contaminant threshold concentrations for pre-determined fuel cell performance losses and define air filtering system tolerances (prevention) [2,3]. It is likely that prevention will be insufficient to avert all contaminant effects. Therefore, recovery procedures will also be needed, and these are more easily devised by understanding the origins of the contaminant effects (mechanisms).

APPROACH

The effects of contaminants on fuel cell performance were investigated by varying operating conditions over the widest ranges possible within design specifications. Temperature was kept above 0°C, from 10 to 80°C, to avoid significant experimental complications under freezing conditions. Current density was maintained between 0.2 and 1 A cm^{-2}. The lower end of this range was sufficiently large to ensure losses are observable. Contaminant concentration was larger than the actual concentration in the atmosphere but still at trace levels to guarantee a steady state was reached relatively rapidly and a significant performance loss was perceived. The initial contaminant concentration was guessed and subsequently other contaminant concentrations were adapted based on the initial guess results. Two empirical relations were used to estimate tolerance limits from contaminant concentration dependent data and were inspired from a carbon monoxide contamination mathematical model [4].

Impedance spectroscopy was first used to classify airborne contaminant effects into different resistance losses to focus subsequent activities. As a second step, additional, more detailed information was obtained using other diagnostics methods to unravel contamination mechanisms: rotating/ring disc electrode, membrane conductivity cell, tracer method for residence time distribution measurements, segmented fuel cell for current/cell voltage distributions over the active area, and gas chromatography. Because many of these diagnostics methods are not applicable or are irrelevant to foreign ions partly due to their different state (in a liquid rather than a gaseous state) and behavior (salt precipitation within the fuel cell), other diagnostic methods were employed including photography, scanning electron microscopy and energy dispersive X-ray spectroscopy. Mathematical modeling was also exploited as experimental data obtained with many in situ diagnostic methods are subject to misinterpretations because the presence of foreign ions in the membrane and ionomer affects fuel cell resistance losses that invalidate assumptions needed to separate individual performance loss contributions [5].

RESULTS

Figure 1 summarizes the effects of temperature, current density and contaminant concentration on steady state fuel cell voltage losses for all seven airborne contaminants and one foreign cation. Cation tests were limited to 100 h for practical purposes and did not reach a steady state during this period. By contrast, airborne contaminant effects were tested for variable durations. Generally, the effect of current density was observed to be either small or more moderate than for temperature and contaminant concentration. Two outlier contaminants were noted. Bromomethane contamination was weakly affected by all operating conditions hinting at a different mechanism. The Ca^{2+} ion precipitates at a low current density of 0.2 A cm^{-2} and with operating conditions favoring cation uptake by the membrane, leading to a large performance effect.

Contaminant tolerance limits were estimated based on Figure 1c data obtained under nominal operating conditions (80°C, 1 A cm^{-2}) and using the following two empirical equations with limits of, respectively, $V_{ss,c}/V_{ss,0}$=1 and 0 for $c \rightarrow 0$ and ∞:

$$\frac{V_{ss,c}}{V_{ss,0}} = 1 - \frac{1}{1 + \frac{a}{c^b}} \quad (1)$$

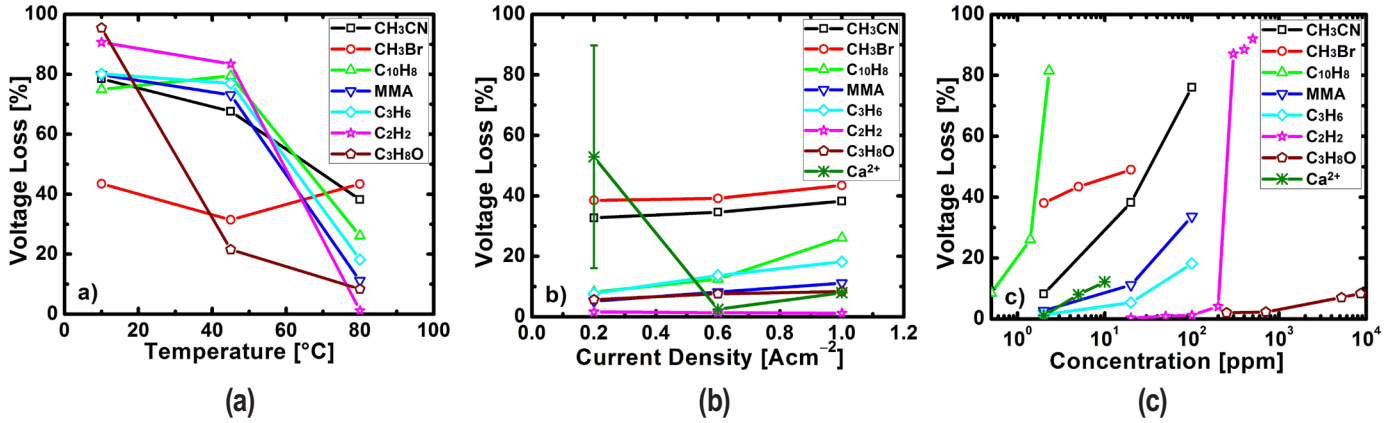

FIGURE 1. Effect of temperature (a), current density (b) and contaminant concentration (c) on fuel cell performance losses resulting from an exposure to seven airborne contaminants (at steady state) and one foreign cation (≤100 h exposure). CH_3CN: acetonitrile, CH_3Br: bromomethane, $C_{10}H_8$: naphthalene, MMA: methyl methacrylate, C_3H_6: propylene, C_2H_2: acetylene, C_3H_8O: iso-propanol.

$$\frac{V_{ss,c}}{V_{ss,0}} = 1 - \frac{1}{1 + \frac{a}{e^{bc} - 1}} \qquad (2)$$

where $V_{ss,c}$ is the steady-state cell voltage during contamination (100 h value for Ca^{2+}), $V_{ss,0}$ is the steady-state cell voltage before contamination, c is the contaminant concentration and, a and b are fitted parameters. Equation 2 was used for most contaminants whereas Equation 1 was employed for bromomethane because it leads to a more gradual change with concentration. All contaminant tolerance limits and equation parameters are given in Table 1 with r^2 representing the curve fit correlation coefficient. It is implied that a steady state is reached within the 5,000 hours automotive system life. The confidence level in these contaminant tolerance limits is color coded: high in green (located within the experimental contaminant concentration range), medium in yellow (smaller than the lower end of the experimental contaminant concentration range by a factor approximately less than 10) and low in red (much smaller than the lower end of the experimental contaminant concentration range). A tolerance limit of 380 ppm has already been deduced for Ca^{2+} by a mathematical model [5], which is significantly larger than the corresponding value of 0.71 ppm based on experimental data (Table 1). The difference is expected because the model only takes into account a single mechanism for the performance loss (membrane resistance) whereas experimental data include all sources of performance loss.

A validated SO_2 contamination equivalent electrical circuit model was used [6] to extract key resistance losses from impedance spectra obtained with all seven airborne contaminants (Figure 2). Generally, changes in both kinetic (oxygen reduction reaction, R_c) and mass transfer resistances (R_d) are observed. By contrast, only acetonitrile leads to ohmic resistance R losses (membrane, ionomer). These findings indicate that multiple steps in recovery procedures may be needed as more than one type of resistance loss for

TABLE 1. Contaminant Tolerance Limits for 5, 1 and 0.5 % Fuel Cell Performance Losses

Contaminant	Predicted contaminant tolerance (ppm)			Experimental contaminant concentration range (ppm)	Empirical correlation parameters		
	$V_{ss,c}/V_{ss,0}$=0.95	$V_{ss,c}/V_{ss,0}$=0.99	$V_{ss,c}/V_{ss,0}$=0.995		*a*	*b*	r^2
Acetonitrile	1.7	0.33	0.16	2-100	9.03×10^{-5}	2.80×10^{-6}	0.995
Acetylene	210	170	158	20-500	611,000	0.0507	0.994
Bromomethane	5.7×10^{-6}	1.1×10^{-9}	3.0×10^{-11}	2-20	1.84	0.193	0.995
Iso-propanol	4,200	800	400	250-8,600	8.53×10^{-5}	1.07×10^{-9}	0.857
Methyl methacrylate	9.9	1.9	0.95	2-100	4.03×10^{-6}	2.13×10^{-8}	0.988
Naphthalene	0.63	0.21	0.12	0.5-2.4	59.2	2.26	0.987
Propene	23	4.5	2.2	2-100	6.86×10^{-6}	1.56×10^{-8}	0.978
Ca^{2+}	3.7	0.71	0.35	2-10	2.13×10^{-7}	3.05×10^{-9}	0.925

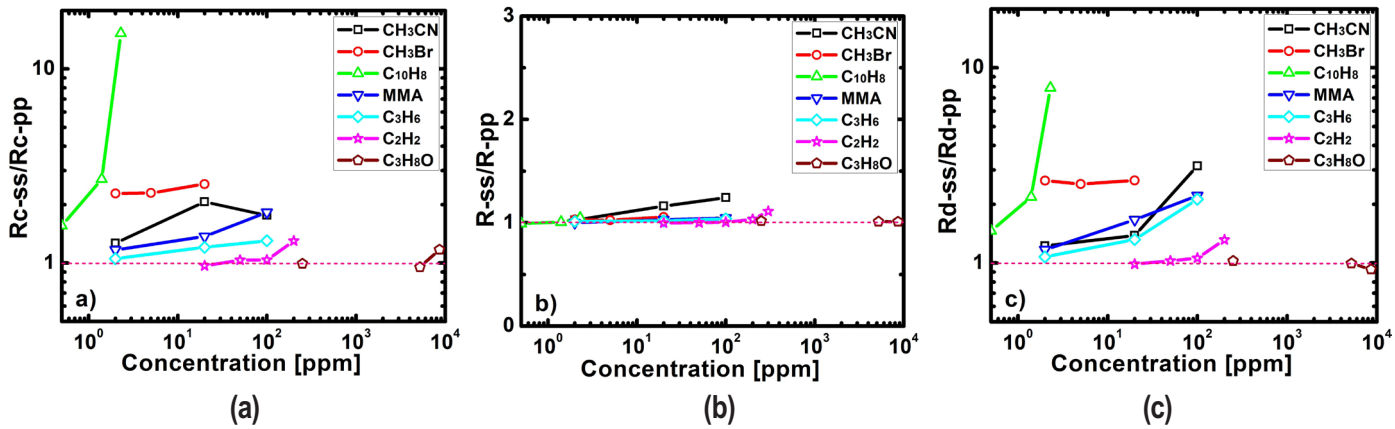

FIGURE 2. Dimensionless ratios of steady-state equivalent circuit model resistances during contamination (ss subscript) to pre-poisoning (pp subscript) values. Oxygen reduction reaction resistance R_c (a), membrane resistance R (b) and generalized finite length Warburg element resistance R_d (c). CH_3CN: acetonitrile, CH_3Br: bromomethane, $C_{10}H_8$: naphthalene, MMA: methyl methacrylate, C_3H_6: propylene, C_2H_2: acetylene, C_3H_8O: iso-propanol.

each contaminant is common. Furthermore, kinetic and mass transfer resistance changes are linked because their behaviors are quite similar as a function of contaminant concentration. It is hypothesized that contaminant adsorption on the catalyst surface decreases the active area and lengthens the oxygen mass transfer path to reach uncovered catalyst sites.

Additional data to resolve contamination mechanisms were obtained using other diagnostic methods for all seven airborne contaminants and one foreign cation. Results are summarized in Table 2. From a kinetic resistance standpoint, rotating ring/disc electrode results generally reveal that airborne contaminants decrease the catalyst active area (electrochemical catalyst area) and also modify the oxygen reduction reaction mechanism with an increase in the peroxide production side reaction (H_2O_2 current). The net effect of these changes is a poorer catalyst performance (kinetic current) and a greater risk of ionomer or membrane degradation by radical attack. The rotating ring/disc electrode is not directly applicable to the Ca^{2+} contaminant. The relatively high acid concentration needed to minimize the ohmic drop correction disturbs the Ca^{2+}/H^+ exchange process between the aqueous solution and the catalyst layer ionomer. Therefore, in situ polarization curve and cyclic voltammetry data were used as surrogate values for Ca^{2+}. From an ohmic resistance point of view, airborne contaminants do not affect the membrane conductivity. However, the Figure 2b acetonitrile result suggests that a decomposition product is responsible for the change. As for Ca^{2+}, the membrane conductivity is moderately affected at the 5 ppm level. The measurement of the liquid water content inside gas diffusion electrodes is planned and are expected to provide insight into the effect of airborne contaminants' adsorption on their hydrophobic properties. This measurement will not be completed for the foreign cation case as salt precipitation is not expected under automotive conditions (relative humidity <100 %). All contaminants create current redistributions induced by an uneven contaminant concentration distribution over the electrode active area, thus increase risks of local membrane failures in the long term by an increased peroxide generation rate for airborne contaminants or greater pinhole formation probability due to the presence of the foreign ion expulsing water from the membrane and increasing its brittleness. Acetylene, methyl methacrylate and propene are partly or fully oxidized to CO_2 or CO within the fuel cell and cell voltage operating range. This situation explains the gradual and complete performance recovery after the contaminant injection is interrupted and provides an avenue to further accelerate the revival process. The Ca^{2+} ion may precipitate as a salt blocking pores in the gas diffusion electrode and flow field channels, Figure 1b, therefore Ca^{2+} removal in this case is better achieved by keeping and transferring the foreign cation into the aqueous phase.

CONCLUSIONS AND FUTURE DIRECTIONS

- Generally, temperature and contaminant concentration significantly affected fuel cell contamination whereas the current density effect was relatively smaller
- Fuel cell contamination by bromomethane was hardly affected by any operating condition whereas Ca^{2+} widely influenced fuel cell losses with current density
- Contaminant tolerance limits for seven airborne contaminants and one foreign cation, and a fuel cell performance loss of 1% fluctuate from ~0.2 ppm to 800 ppm with the exception of bromomethane
- Complete planned diagnostic tests to support the development of contamination mechanisms and recovery strategies
- Complete long-term tests to assess the impact of increased peroxide production with airborne

TABLE 2. Summary of Ex Situ and In Situ Diagnostic Methods' Results for Seven Airborne Contaminants and One Foreign Cation

Contaminant	Kinetic current (% loss in air at 30°C and 0.9 V vs RHE)	Electrochemical catalyst area (% loss in N_2 at 30°C)	H_2O_2 current (% gain in air at 30°C and 0.5 V vs RHE)[a]	Membrane conductivity (% loss at 80°C and 50 % relative humidity)	GDE water content	Dimensionless local current (maximum % loss and gain in air at 80°C)	Contaminant conversion (% in air at 80°C)[b]
Acetonitrile	85 (16.9 mM)	>60 (16.9 mM)	130 (16.9 mM)	0 (100 ppm)	TBD	TBD	Test completed (analysis ongoing)
Acetylene	100 (4,030 ppm)	>90 (4,040 ppm)	601 to 1027 (4,030 ppm)	1-2 (500 ppm)	TBD	–99 to 100 after 30 min, –17 to 18 at steady state (300 ppm)	0.8 to 100 for 0.55 to 0.85 V (300 ppm)
Bromomethane	54 (400 ppm)	43 (400 ppm)	56 (400 ppm)	-	TBD	–19 to 12 (5 ppm)[c]	TBD
Iso-propanol	12 (1 mM)	7 (1 mM)	18 (1 mM)	-	TBD	TBD	TBD
Methyl methacrylate	72 (1 mM)	65 (1 mM)	350 to 491 (1 mM)	-	TBD	–7 to 6 (20 ppm)	49 to 57 for 0.55 to 0.68 V (20 ppm)
Naphthalene	77 (sat soln)[d]	>90 (sat soln)[d]	171 (sat soln)[d]	-	TBD	TBD	TBD
Propene	53 (1,010 ppm)	38 (1,010 ppm)	604 (1,010 ppm)	-	TBD	–8 to 6 (100 ppm)	43 to 89 for 0.55 to 0.85 V (100 ppm)
Ca^{2+}	21 (5 ppm)[e]	16-46 (5 ppm)[e]	-	1.1-11 (5 ppm)[f]	-	–50 to 20 (5 ppm)[g]	-

[a] The total current is still mostly due to oxygen reduction in spite of a large peroxide production rate increase.
[b] In all cases, observed products include the unaltered contaminant, CO and CO_2.
[c] A steady state was not attained at the end of the contamination period.
[d] 0.25 mM solubility at 25°C.
[e] Derived from in situ polarization curve and cyclic voltammetry tests.
[f] In situ result by current interrupt for 0.6-1 A cm^{-2} and 125 % relative humidity before a steady state is reached at 100 h.
[g] 0.6 rather than 1 A cm^{-2} before a steady state is reached at 100 h.
RHE – reversible hydrogen electrode; GDE – gas diffusion electrode; TBD – to be determined

contaminants and increased membrane brittleness with a foreign cation on fuel cell durability

- Disseminate the large fuel cell contamination database

FY 2013 PUBLICATIONS/PRESENTATIONS

1. J. Qi, X. Wang, U. Pasaogullari, L. Bonville, T. Molter, 'Effect of Al^{3+} Contaminant on Polymer Electrolyte Fuel Cell Performance', *J. Electrochem. Soc.*, **160** (2013) F916.

2. M.A. Uddin, X. Wang, J. Qi, M.O. Ozdemir, L. Bonville, U. Pasaogullari, T. Molter, 'Effects of Chloride Contamination on PEFCs', *Electrochem. Soc. Trans.*, accepted.

3. J. Qi, X. Wang, M.O. Ozdemir, M.A. Uddin, L. Bonville, U. Pasaogullari, T. Molter, 'Effect of Cationic Contaminants on Polymer Electrolyte Fuel Cell Performance', *Electrochem. Soc. Trans.*, accepted.

4. X. Wang, J. Qi, O. Ozdemir, U. Pasaogullari, L.J. Bonville, T. Molter, 'Effect of Ca^{2+} as an Air Impurity on Polymer Electrolyte Fuel Cells', *Electrochem. Soc. Trans.*, accepted.

5. J. St-Pierre, J. Ge, Y. Zhai, T.V. Reshetenko, M. Angelo, 'PEMFC Cathode Contamination Mechanisms for Several VOCs - Acetonitrile, Acetylene, Bromomethane, Iso-propanol, Methyl Methacrylate, Naphthalene and Propene', *Electrochem. Soc. Trans.*, accepted.

6. Y. Zhai, J. St-Pierre, J. Ge, 'PEMFC Cathode Contamination with Acetylene - Potential Dependency', *Electrochem. Soc. Trans.*, accepted.

7. M.A. Uddin, X. Wang, J. Qi, M.O. Ozdemir, L. Bonville, U. Pasaogullari, T. Molter, 'Effects of Chloride Contamination on PEFCs', in *Meeting Abstracts*, Electrochemical Society volume 2013-2, The Electrochemical Society, Pennington, NJ, 2013, abstract 1334 (224th Electrochemical Society meeting oral presentation).

8. J. Qi, X. Wang, M.O. Ozdemir, M.A. Uddin, L. Bonville, U. Pasaogullari, T. Molter, 'Effect of Cationic Contaminants on Polymer Electrolyte Fuel Cell Performance', in *Meeting Abstracts*, Electrochemical Society volume 2013-2, The Electrochemical Society, Pennington, NJ, 2013, abstract 1333 (224th Electrochemical Society meeting oral presentation).

9. X. Wang, J. Qi, O. Ozdemir, U. Pasaogullari, L.J. Bonville, T. Molter, 'Effect of Ca^{2+} as an Air Impurity on Polymer Electrolyte Fuel Cells', in *Meeting Abstracts*, Electrochemical Society volume 2013-2, The Electrochemical Society, Pennington, NJ, 2013, abstract 1332 (224th Electrochemical Society meeting oral presentation).

10. J. St-Pierre, J. Ge, Y. Zhai, T. Reshetenko, M. Angelo, 'PEMFC Cathode Contamination Mechanisms for Several VOCs - Acetonitrile, Acetylene, Bromomethane, Iso-Propanol, Methyl Methacrylate, Naphthalene and Propene', in *Meeting Abstracts*, Electrochemical Society volume 2013-2, The Electrochemical Society, Pennington, NJ, 2013, abstract 1330 (224th Electrochemical Society meeting oral presentation).

11. Y. Zhai, J. St-Pierre, J. Ge, 'PEMFC Cathode Contamination with Acetylene - Potential Dependency', in *Meeting Abstracts*, Electrochemical Society volume 2013-2, The Electrochemical Society, Pennington, NJ, 2013, abstract 1329 (224th Electrochemical Society meeting oral presentation).

12. T. Reshetenko, J. St-Pierre, 'The Impact of Selected Air Pollutants on Spatial PEMFC Performance', in *Meeting Abstracts*, Electrochemical Society volume 2013-2, The Electrochemical Society, Pennington, NJ, 2013, abstract 1328 (224th Electrochemical Society meeting oral presentation).

13. J. Ge, Y. Zhai, J. St-Pierre, 'An RRDE Evaluation of the C_2H_2 Effect on the ORR', in *Meeting Abstracts*, Electrochemical Society volume 2013-2, The Electrochemical Society, Pennington, NJ, 2013, abstract 1302 (224th Electrochemical Society meeting oral presentation).

14. J. St-Pierre, M. Angelo, 'The Effect of Airborne Contaminants on Fuel Cell Performance and Durability', United States Department of Energy 2013 Annual Merit Review meeting, Washington, DC, May 14, 2013.

15. J. St-Pierre, 'The Effect of Airborne Contaminants on Fuel Cell Performance and Durability', US DRIVE Fuel Cell Tech Team meeting, Southfield, MI, November 14, 2012.

REFERENCES

1. J. St-Pierre, 'Air Impurities', in *Polymer Electrolyte Fuel Cell Durability*, Edited by F.N. Büchi, M. Inaba, T.J. Schmidt, Springer, 2009, p. 289.

2. J. St-Pierre, Y. Zhai, M. Angelo, *Int. J. Hydrogen Energy*, **37** (2012) 6784.

3. Y. Zhai, J. St-Pierre, M. Angelo, *Electrochem. Soc. Trans.*, **50**(2) (2012) 635.

4. J. St-Pierre, *Electrochim. Acta*, **55** (2010) 4208.

5. J. St-Pierre, *Int. J. Hydrogen Energy*, **36** (2011) 5527.

6. Y. Zhai, K. Bethune, G. Bender, R. Rocheleau, *J. Electrochem. Soc.*, **159** (2012) B524.

V.F.1 Fuel Cell Fundamentals at Low and Subzero Temperatures

Adam Z. Weber
Lawrence Berkeley National Laboratory
1 Cyclotron Rd, MS 70-108B
Berkeley, CA 94720
Phone: (510) 486-6308
Email: azweber@lbl.gov

DOE Manager
Donna Ho
Phone: (202) 586-8000
Email: Donna.Ho@ee.doe.gov

Subcontractors:
- Los Alamos National Laboratory, Los Alamos, NM
- United Technologies Research Center, East Hartford, CT
- 3M Company, St Paul, MN
- The Pennsylvania State University, State College, PA

Project Start Date: September 21, 2009
Project End Date: September 30, 2014

Overall Objectives

- Fundamentally understand transport phenomena and water and thermal management at low and subzero temperatures
- Examine water (liquid and ice) management with nano-structured thin-film (NSTF) catalyst layers (CLs)
- Develop diagnostic methods for critical properties for operation with liquid water
- Elucidate the associated degradation mechanisms due to subzero operation and enable mitigation strategies to be developed

Fiscal Year (FY) 2013 Objectives

- Develop and validate model for NSTF CLs showing impact of different diffusion media and temperature
- Quantify performance changes with NSTF at different temperatures, material sets, and compression
- Develop diagnostic methods for critical properties for operation with liquid water
- Examine freeze kinetics and ionomer morphology in traditional CLs and thin-film model systems

Technical Barriers

This project addresses the following technical barriers from the fuel cell section of the Fuel Cell Technologies Office Multi-Year Research, Development, and Demonstration Plan:

(A) Durability

(C) Performance
- Cell Issues
- Stack Water Management
- System Thermal and Water Management
- System Start-up and Shut-down Time and Energy/ Transient Operation

Technical Targets

This project is conducting fundamental investigations into fuel cell operation at low and subzero temperatures. The knowledge gained will provide valuable insight necessary to devise material and mitigation strategies to meet DOE targets. These include those related to durability, performance, and cost. Specially:

- Durability
  - 5,000 hr (automotive) and 40,000 hr (stationary)
  - Thermal cycling ability with liquid water
- Performance
  - Unassisted start from -40°C
  - Cold start to 50% power in 30 seconds and with 5 MJ or less energy
  - Efficiency of 65% and 55% for 25% and 100% rated power, respectively
  - Stack power density of 2 kW/kg
  - Platinum-grade metal loading of 0.2 g/kW
- Cost: $15/kW$_e$

FY 2013 Accomplishments

- Elucidated impact of anode gas-diffusion layer (GDL) on low-temperature performance utilizing both modeling and experiments, which showed increased performance with GDLs that promoted more water movement out of the anode side of the cell with less flooding.
- Examined in-depth the underlying membrane structure/ function relationships including direct visualization of water profiles demonstrating importance of membrane interface on transport phenomena.
- Analyzed polarization curves showing perhaps significant ionic-conduction limitations in NSTF CLs at low-temperature operation.
- Developed mechanical stress model.

- Studied ionomer thin films on different substrates showing impact of film thickness, thermal history, and substrate interactions.
- Measured effective gas diffusivities in partially saturated gas-diffusion layers.

✧ ✧ ✧ ✧ ✧

INTRODUCTION

Polymer electrolyte fuel cells experience a range of different operating conditions. As part of that range, they are expected to be able to survive and start at low and subzero temperatures. Under these conditions, there is a large amount of liquid and perhaps frozen water due to the low vapor pressure of water. Thus, water and thermal management become critical to understand and eventually optimize operation at these conditions. Similarly, durability aspects due to freezing and low temperatures are somewhat unknown and need further study in order to identify mechanisms and mitigation strategies. In addition, it is known that thin-film CLs such as the NSTF developed by 3M Company have issues with large amounts of liquid water due to their thinness. These layers provide routes towards meeting the DOE cost targets due to their high catalytic activities at low precious metal loadings. This project directly focuses on the above aspects of operation at lower temperatures with both NSTF and traditional CLs with the goal that improved understanding will allow for the DOE targets to be met with regard to cold start, survivability, performance, and cost.

APPROACH

The overall approach is to use a synergistic combination of cell, stack, and component diagnostic studies with advanced mathematical modeling conducted at various locations (national laboratories, industry, and academia). Ex situ diagnostics are used to quantify transport properties and to delineate phenomena that are used in the modeling. The two-dimensional (2-D) cell model is developed and validated by comparison of measured in situ cell performance in single cells under a variety of cell assemblies and architectures in order to highlight specific controlling phenomena. Durability is probed by doing cycling and other stress tests as well as taking failed cells from the in situ testing and duplicating their failure ex situ. To understand controlling phenomena and the impact of various layers, a systematic investigation at the component scale is accomplished including the development of a suite of advanced ex situ diagnostics that measure and evaluate the various critical material properties and transport-related phenomena.

RESULTS

As fuel cells operate at low and subzero conditions, liquid water and water management become more important. Thus, there is a need to study properties of the porous fuel cell layers in the presence of liquid water. It is also expected that this is probably exacerbated in thin-film CLs such as NSTF CLs. As an example of this, Figure 1 shows the impact of temperature on baseline NSTF cells (3M 2009 "Best in Class"). As the cell temperature decreases such that vapor-phase removal is not sufficient and liquid water forms, the performance drastically decreases. This change in performance is also captured in the developed, physics-based 2-D mathematical model for this cell that utilized findings and properties from the advanced diagnostics developed in this project.

In Figure 2a, possible routes to performance increase are shown by use of the model. It is clear that development of schemes in which water is moved out the anode and hence minimize flooding of the cathode should increase performance. Indeed, removal of the MPL from the anode GDL should show significant performance increases. In Figure 2b, it is seen that the experimental data justify this supposition in that the lower temperature performance increases as the MPL thickness is decreased. However, one must be cognizant that thinner or no MPLs can promote shorting of the cell during assembly due to carbon fiber penetration into the GDLs, thus a minimum thickness is probably required. Beyond just the MPL, another possible route for low-temperature performance increase is using different anode GDLs. This possibility is shown in Figure 3, where it is clear that some anode GDLs perform significantly

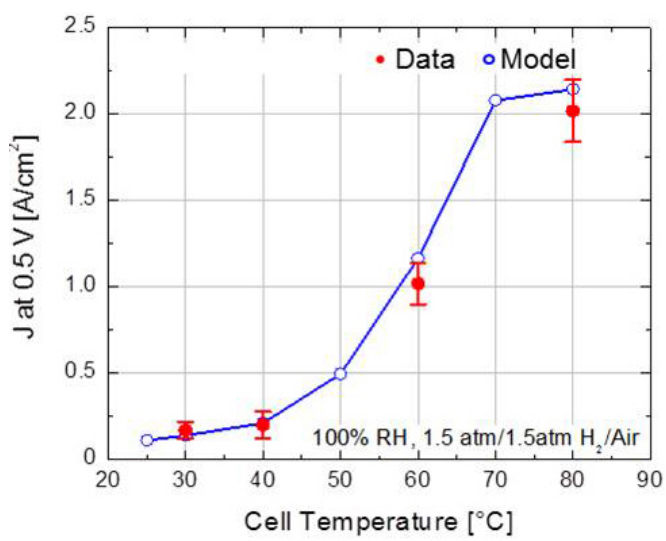

RH - relative humidity

FIGURE 1. Current density at 0.5 V cell potential from data and model predictions of an NSTF cell as a function of cell temperature with fully humidified feeds.

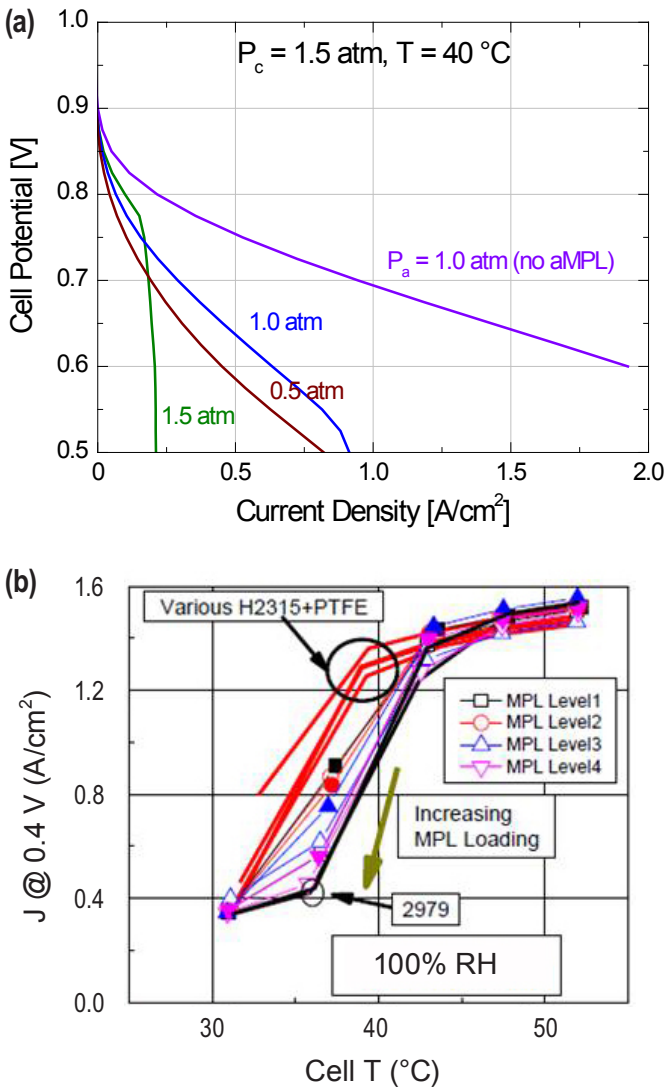

FIGURE 2. (a) Predicted polarization curves using the mathematical model and different anode diffusion media and pressure conditions. (b) Experimental data showing impact of MPL thickness (loading) on cell current density at 0.4 V as a function of cell temperature.

better at lower temperatures than others. To investigate this in more detail, neutron imaging results, shown in Figure 3b, demonstrate that the better performing GDLs seem to reduce the anode and cathode water contents, perhaps by providing routes for water to leave the cell and promoting water transport from cathode to anode. The exact reasons for this behavior are currently under investigation. Finally, Figure 3a also shows the impact of cell compression on performance. As the GDL becomes compressed, the contact resistance between the GDL and bipolar plate is decreased, resulting in better performance. However, continued compression reduces the GDL porosity and causes mass-transport limitations and increased heterogeneity of GDLs under lands and channels. From this study, it appears that 5-10% compression is optimal.

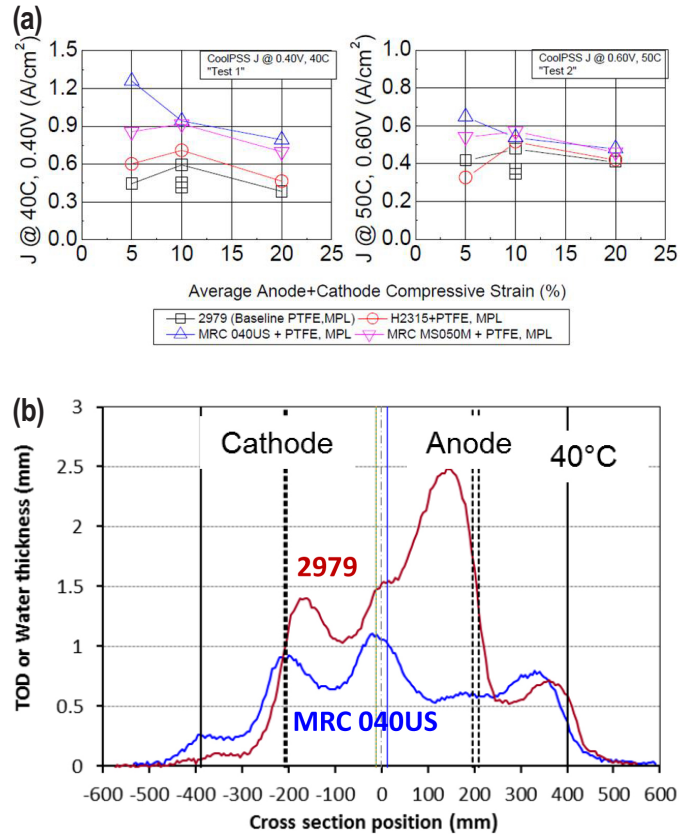

FIGURE 3. (a) Impact of cell compression and different GDLs on cell current density at two different temperatures and potentials. (b) Neutron-imaging water content for NSTF cells at 0.3 V with different GDLs; the lines in the middle denote the MEA.

A key issue in operating at lower temperatures is water removal from and build-up in the cell. This accumulation of water in the porous diffusion media will impede the transport of reactant gases from the channels to the active sites. Previously, it was unknown how the saturation, the volume fraction of water in the pore space, impacts the gas diffusion coefficient. This year, we developed a hydrogen pump limiting current setup to measure this relationship. The results, as shown in Figure 4, demonstrate an almost cubic dependence of the gas diffusion coefficient on both the porosity and liquid saturation for a carbon-paper GDL, where the effective gas diffusion coefficient is a product of the two expressions: $\frac{\langle D \rangle}{D} = f(\varepsilon) f(S_L)$. This cubic dependence is quite different than the often assumed 1.5 power (so-called Bruggemann expression), and incorporation of these results into the model enabled the good agreement shown in Figure 1. This diagnostic will further increase understanding of transport phenomena at low temperatures and is being refined and utilized for more fuel cell layers and prospective materials.

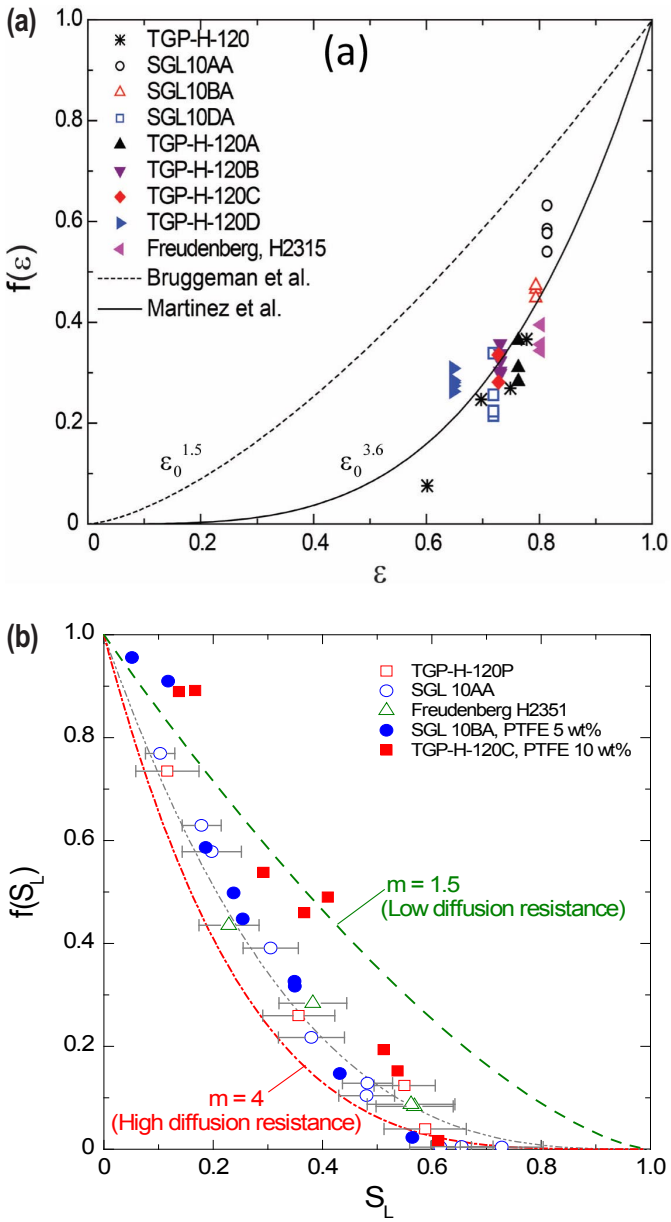

FIGURE 4. Measured effective diffusivity of hydrogen as a function of porosity (a) (normalized to bulk diffusivity) and saturation (b) (normalized to effective dry diffusivity) for different GDL papers.

CONCLUSIONS AND FUTURE DIRECTIONS

The project focus this year was on developing and utilizing diagnostic methods for fuel cell components at low temperatures and incorporating them into a performance model that can describe observed changes. To this end, several novel methods were developed, and measurements for membranes, GDLs, and CL ionomer were made. The results allow for a better understanding of liquid and ice formation and movement within the cell, as well as limitations due to ionomer films at low catalyst loadings. In addition, single-cell testing of NSTF cells was accomplished with the model able to replicate performance decrease as a function of anode GDL and temperature.

In terms of future work, this can be summarized as:

- Cell Performance
  - United Technologies Research Center to run cool and cold starts including adiabatic and temperature transients:
    - NSTF and low-loaded traditional CLs
    - Run hybrid water transport plate cells
  - Los Alamos National Laboratory to run NSTF cells including various tests:
    - Segmented cell
    - Power transients
    - National Institute of Standards and Technology high and higher resolution neutron imaging
  - 3M to run cells to determine water balance and impact of NSTF structure
- Component characterization
  - Traditional CLs
    - Examine thin-film membrane morphology
  - NSTF CLs
    - Proton migration on platinum
  - GDLs
    - Liquid-water movement out of the GDLs by droplets
    - Measurement of effective diffusivities, thermal conductivities, and relative permeabilities
  - MPLs: how do they work with liquid water?
  - Membrane
    - Interfacial resistance and membrane morphology with different environments
- Modeling
  - Use data from all partners to understand the anode GDL and water-out-the-anode scheme for NSTF CLs
  - Develop transient model and examine CL water capacity versus water removal fluxes as a function of CL thickness
  - Optimize schemes and structures to increase low-temperature performance
- Examine failed MEAs and cyclical isothermal cold starts for durability concerns
- Understand and increase the operating window with thin-film CLs

FY 2013 PUBLICATIONS

1. Miguel A. Modestino, Ahmet Kusoglu, Alexander Hexemer, Adam Z. Weber, and Rachel A. Segalman, 'Controlling Nafion Structure and Properties via Wetting Interactions,' *Macromolecules*, **45** (11), 4681-4688 (2012).

2. Ahmet Kusoglu, Anthony Kwong, Kyle T. Clark, Haluna P. Gunterman, and Adam Z. Weber, 'Water Uptake of Fuel-Cell Catalyst Layers,' *Journal of the Electrochemical Society*, **159** (9), F530-F535 (2012).

3. Ahmet Kusoglu, Alexander Hexemer, Ruichun Jiang, Craig S Gittleman, and Adam Z. Weber, 'Effect of Compression on Conductivity and Morphology of PFSA Ionomers,' *J. Membrane Science*, **421-422**, 283-291 (2012). doi:10.1016/j.memsci.2012.07.027.

4. Gi-suk Hwang and Adam Z. Weber, 'Effective-Diffusivity Measurement of Partially-Saturated Fuel-Cell Gas-Diffusion Layers,' *Journal of the Electrochemical Society*, **159** (11), F683-F692 (2012).

5. Ahmet Kusoglu, Suchol Savagatrup, Kyle T. Clark, and Adam Z. Weber, 'Role of Mechanical Factors in Controlling the Structure/Function Relationship of PFSA Ionomers,' *Macromolecules*, **45** (18), 7467-7476 (2012). doi: 10.1021/ma301419s.

6. Daniel S. Hussey, Dusan Spernjak, Adam Z. Weber, Rangachary Mukundan, Joseph Fairweather, Eric L. Brosha, John Davey, Jacob S. Spendelow, David L. Jacobson, and Rodney L. Borup, 'Accurate measurement of the through-plane water content of proton-exchange membranes using neutron radiography,' *J. Appl. Phys.*, **112**, 104906 (2012).

7. Thomas J. Dursch, Monica A. Ciontea, Greg J. Trigub, Clayton J. Radke, and Adam Z. Weber, 'Pseudo-isothermal Ice-Crystallization Kinetics in the Gas-Diffusion Layer of a Fuel Cell from Differential Scanning Calorimetry,' *International Journal of Heat and Mass Transfer*, **60**, 450-458 (2013).

8. Miguel A. Modestino, Devproshad K. Paul, Shudipto Dishari, Stephanie A. Petrina, Frances I. Allen, Michael A. Hickner, Kunal Karan, Rachel A. Segalman, and Adam Z. Weber, 'Self-assembly and transport limitations in confined Nafion films,' *Macromolecules*, **46** (3), 867-873 (2013).

9. Gi Suk Hwang, Hyoungchul Kim, Roger Lujan, Rangachary Mukundan, Dusan Spernjak, Rodney L. Borup, Massoud Kaviany, Moo Hwan Kim, and Adam Z. Weber, 'Phase-Change-Related Degradation of Catalyst Layers in Proton-Exchange-Membrane Fuel Cells,' *Electrochimica Acta*, **95**, 29-37 (2013).

10. Adam Z. Weber, Sivagaminathan Balasubramanian, and Prodip K. Das, 'Proton Exchange Membrane Fuel Cells,' in *Advances in Chemical Engineering: Fuel Cell Engineering: Model-based Approaches for Analysis, Control and Optimization*, Kai Sundmacher, Editor, Vol. 41, Elsevier, 65-144 (2012).

11. Thomas J. Dursch, Monica A. Ciontea, Gregory J. Trigub, Clayton J. Radke, and Adam Z. Weber, 'Ice-Crystallization Kinetics and Water Movement in Gas-Diffusion and Catalyst Layers', *ECS Transactions*, **50** (2), 429-435 (2012).

12. Ahmet Kusoglu and Adam Weber, 'Role of Chemical-Mechanical Energies in Understanding Structure and Properties of Aged and Degraded Membranes', *ECS Transactions*, **50** (2), 961-965 (2012).

FY 2013 PRESENTATIONS

1. T.J. Dursch, G.J. Trigub, C.J. Radke, A.Z. Weber, 'Isothermal Ice-Crystallization Kinetics in Catalyst Layers of Proton-Exchange-Membrane Fuel Cells,' *86th Colloid and Surface Science Symposium*, Montreal, Canada, June 2012.

2. Ahmet Kusoglu, Adam Z. Weber, Michael Hickner, Kunal Karan 'Understanding Confinement Effects on PFSA Ionomer,' ACS Materials in Fuel Cells, Asilomar, California, February 2013.

3. Ahmet Kusoglu, Adam Z. Weber, Michael Hickner, Kunal Karan 'Water Uptake and Transport in Nafion,' ACS Materials in Fuel Cells, Asilomar, February 2013. (invited talk)

4. Gi Suk Hwang, Dilworth Y. Parkinson, Ahmet Kusoglu, Alastair A. MacDowell, and Adam Z. Weber, 'Understanding Water Uptake and Transport in Polymer-Electrolyte Membrane Fuel Cells Using X-Ray Micro-tomography,' *245th ACS National Meeting & Exposition,* New Orleans, Louisiana, April 2013.

5. Prodip K Das and Adam Z. Weber, 'Understanding Water Management as a Function of Catalyst-Layer Thickness,' *222nd Meeting of the Electrochemical Society*, Honolulu, Hawaii, October 2012.

6. G.S. Hwang, D. Parkinson, A. Kusoglu, A. MacDowell, and A. Z. Weber, 'Water Uptake and Transport in Nafion,' *222nd Meeting of the Electrochemical Society*, Honolulu, Hawaii, October 2012.

7. T.J. Dursch, M.A. Ciontea, G.J. Trigub, C.J. Radke, A. Z. Weber, 'Ice-Crystallization Kinetics and Water Movement in the Gas-Diffusion and Catalyst Layers of a Proton-Exchange-Membrane Fuel Cell,' *222nd Meeting of the Electrochemical Society*, Honolulu, Hawaii, October 2012.

8. Jeff T. Gostick, Gisuk Hwang, and Adam Z. Weber, 'Understanding Invasion Mechanisms in Fibrous Gas Diffusion Media: Direct Comparison of Simulations with Tomographic Visualization,' *223rd Meeting of the Electrochemical Society*, Toronto, Canada, April 2013.

9. Rachid Zaffou, Mike L. Perry, Zhongfen Ding, 'Performance of PEFCs with Ultra-Low Catalyst Loadings under Low Temperature Operation,' *223rd Meeting of the Electrochemical Society*, Toronto, Canada, April 2013.

10. Adam Z. Weber, 'Water Uptake in PFSA Membranes,' *223rd Meeting of the Electrochemical Society*, Toronto, Canada, April 2013. (invited tutorial talk)

11. Ahmet Kusoglu, and Adam Z Weber, 'Structure-Property Relationship of Perfluorinated Sulfonic Acid (PFSA) Membranes,' *APS March Meeting,* Baltimore, Maryland, March 2013.

12. Adam Z. Weber, 'Understanding Ionomer-Related Transport and Morphology in Polymer-Electrolyte Fuel Cells,' *Princeton Chemical Engineering Colloquium*, October, 2012.

13. Anthony Kwong, Haluna P. Gunterman, Adam Z. Weber 'Impact of Temperature on PEMFC Gas-Diffusion Layer Properties,' *AIChE Annual Meeting*, November, 2012.

14. Ahmet Kusoglu, and Adam Z Weber, 'Mechanical/Chemical Energy Balance in Perfluorinated Sulfonic Acid Membranes,' *SSPC13 Meeting,* Grenoble, France, September 2012. (invited talk)

15. Prodip Das and Adam Z. Weber, 'Understanding Water Management as a Function of Fuel-Cell Catalyst-Layer Thickness,' *International Society of Electrochemistry Annual Meeting*, Prague, Czech Republic, August 2012.

16. Prodip K. Das, Sophia E.M. Haussener, Anthony Kwong, Gi-suk Hwang, Haluna P. Gunterman, Adam Z. Weber, 'Physicochemical Characterization of Fuel-Cell Diffusion Media,' *ASME 2012 10th International Conference on Nanochannels, Microchannels and Minichannels,* Puerto Rico, July 2012.

17. Prodip K. Das and Adam Z. Weber, 'Water-Droplet Adhesion Force on Fuel-Cell Gas-Diffusion Layers: Beyond Contact-Angle Measurements,' *ASME 2012 10th International Conference on Nanochannels, Microchannels and Minichannels,* Puerto Rico, July 2012.

V.F.2 Transport in PEMFCs

Cortney Mittelsteadt (Primary Contact), Hui Xu, Shelly Brawn (Giner)
Sirivatch Shimpalee, Visarn Lilavivat (University of South Carolina)
James E. McGrath, Jarrett Rowler (Virginia Polytechnic and State University [VA Tech])
Don Conners, Guy Ebbrell (AvCarb)
Kevin Russell (Tech-Etch)
John W Van Zee (University of Alabama)
Giner, Inc./Giner Electrochemical Systems, LLC
89 Rumford Ave.
Newton, MA 02466
Phone: (781) 529-0529
Email: cmittelsteadt@ginerinc.com

DOE Managers
Donna Ho
Phone: (202) 586-8000
Email: Donna.Ho@ee.doe.gov
Gregory Kleen
Phone: (720) 356-1672
Email: Gregory.Kleen@go.doe.gov

Technical Advisor
John Kopasz
Phone: (630) 252-7531
Email: kopasz@anl.gov

Contract Number: DE-EE0000471

Subcontractors:
- Tech-Etch, Plymouth, MA
- Ballard Material Products, Inc., Lowell, MA
- Virginia Polytechnic and State University (VA Tech), Blacksburg, VA
- University of South Carolina (USC), Columbia, SC

Project Start Date: November 1, 2009
Project End Date: April 30, 2014

Overall Objectives

- Design fuel cell components (membranes, gas diffusion layers [GDLs], bipolar plates, and flow fields) that possess specific transport properties
- Establish a computational fluid dynamics (CFD) model to elucidate the effect of component variables on these transport properties
- Determine sensitivity of fuel cell performance to these component properties to identify limiting components for fuel cell transport loss

Fiscal Year (FY) 2013 Objectives

- Design block copolymers with various structure and chemistry
- Determine bulk membrane properties of block copolymers and correlate to their structure and chemistry:
  - Water uptake and diffusivity
  - Electro-osmotic drag
- Evaluate fuel cell performance on block copolymer membranes
- Perform transient, three-dimensional modeling of fuel cell operation on block copolymer membranes

Technical Barriers

This project addresses the following technical barriers from the Fuel Cells section of the Fuel Cell Technologies Office Multi-Year Research, Development, and Demonstration Plan:

(A) Durability

(C) Performance

Technical Targets

The goal of this project is to determine sensitivity of fuel cell performance to component properties to determine limiting components and guide research. This project aims to develop fuel cell components (i.e., membranes, GDLs, bi-polar plates and flow fields), not with the goal of reaching DOE specific technical targets such as catalyst loading and cost targets, but rather that possess specific properties (i.e., water transport and conductivity). A CFD model will then be developed to elucidate the effect of certain parameters on these specific properties (i.e., the effect of membrane type and thickness on membrane water transport). Ultimately, the model will be used to determine the sensitivity of fuel cell performance to component properties to determine limiting components and guide research.

FY 2013 Accomplishments

- Designed two sets of hydrocarbon block polymers with one varying oligomer and the other varying block length, annealing temperature and ion-exchange capacity (IEC)
- Characterized the water uptake/diffusivity of the above block copolymers and obtained diffusivity at temperatures lower than 80°C

- Characterized electro-osmotic drag coefficients (EODCs) of the above block copolymers and correlated to their chemistry and structure
- Evaluated fuel cell performance of membrane electrode assemblies (MEAs) based on hydrocarbon block copolymer membrane and compared to Nafion® membranes
- Simulated cell performance, current distribution, water distribution of MEAs based on hydrocarbon block polymer membranes
- Performed electrode flooding to evaluate the mitigation effects of hydrocarbon membranes compared to Nafion® membranes

✧ ✧ ✧ ✧ ✧

INTRODUCTION

Many fuel cell component properties that influence water transport and thermal management are not well-understood [1,2]. A better understanding of how water transport and thermal management can be controlled would represent a significant step forward in meeting the DOE's stated 2015 targets. This project aims for a better understanding of water transport and thermal management by tailoring fuel cell components to exhibit specific measurable transport properties. These transport properties are then used in a model, which will enable the prediction of the effect of changing component parameters on transport properties.

APPROACH

This project seeks to develop fuel cell components possessing specific transport properties. Membranes will be developed to achieve different ratios of water transport and conductivity. Bulk membrane properties (i.e., diffusivity, water uptake, conductivity) will be evaluated and modeled. Also, GDLs, bipolar plates, and flow fields will be developed and tailored to illustrate specific differences in porosity, tortuosity and hydrophobicity. The fuel cell performance will be evaluated using these components and compared with the model. The model will be used to predict the effect of changing component parameters (i.e., changing membrane type and thickness, changing flow field configuration) on component transport properties and fuel cell performance.

RESULTS

Two sets of hydrocarbon block copolymer membranes were designed and synthesized at VA Tech providing design guidelines for polymer electrolyte membranes (PEMs) beyond Nafion® membranes, as the structure, chemistry, and phase separation of copolymer blocks largely impact the transport properties in PEM fuel cells. Matrix 1 membranes (see Table 1) are based on block copolymer 6FPAEB-BPSH with various block length (7k-7k, 15k-15k, and 10k-18k), IEC (1.55 and 2.01 meq/g), annealing temperature (110 and 220°C). Matrix 2 membranes (see Table 2) contain the same hydrophilic oligomer, BPSH, but a different hydrophobic oligomer, 6FK, 6FPAEB or 6FBPS0. Water uptake, conductivity, diffusivity, and EODC of these block copolymer membranes were characterized at Giner. The properties of these membranes were used by USC to simulate the fuel cell performance, water distribution, and current distribution, which were compared with experimental results of MEAs made from selected block copolymer membranes.

As expected, changing the chain length, IEC and annealing has little effect on the water uptake isotherms (data not shown). Transmission electron microscopy shows clear phase separation for both the 7k-7k and 15k-15k block copolymers. Though there is little difference in water uptake, the smaller block polymers have lower water diffusivity as seen in Figure 1. The figure also shows that

TABLE 1. Hydrocarbon Block Copolymer Matrix 1: Varied Block Length, IEC, Annealing Temperature

	Polymer	Thermal Treatment Temperature (°C)	IEC (meq/g)
1	6FPAEB-BPSH100 7k-7k	110	1.55
2	6FPAEB-BPSH100 15k-15k	110	1.55
3	6FPAEB-BPSH100 10k-18k	110	2.01
4	6FPAEB-BPSH100 7k-7k	220	1.55
5	6FPAEB-BPSH100 15k-15k	220	1.55
6	6FPAEB-BPSH100 10k-18k	220	2.01

6FPAEB - hexafluoro bisphenol a benzonitrile
BPSH - block polysulfone ether polymer

TABLE 2. Hydrocarbon Block Copolymer Matrix 2: Varied Oligomer

Sample	Block Copolymer	Block Length	IEC (meq/g)[a]	Water Uptake (%)[b]	Conductivity (S/cm)[c]
JR-143-2	6FK-BPSH	8K – 8K	1.45	21	0.10
JR-143-3	6FPAEB-BPSH	13K – 13K	1.63	37	0.14
JR-143-4	6FBPS0-BPSH	10K – 10K	1.47	35	0.10

6FK - hexafluoro ketone
6FBPS0 - hexafluoro biphenol sulfone
6FPAEB - hexafluoro bisphenol a benzonitrile

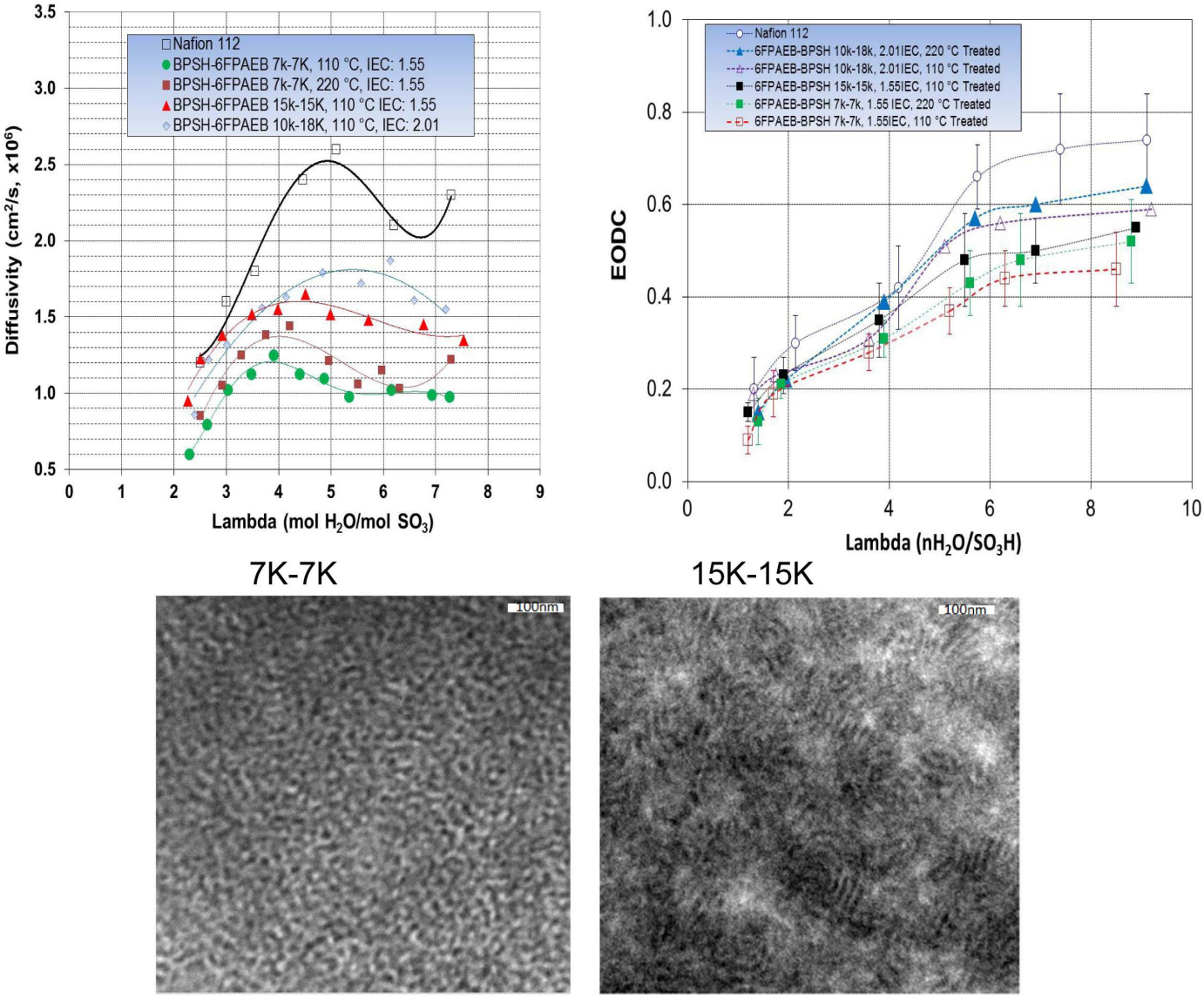

FIGURE 1. Diffusivity and EODC of Matrix 1 Membranes: Varied Block Length, IEC, Annealing Temperature

higher annealing temperature increases the water diffusivity likely due to improved phase separation. The diffusivity of all of the hydrocarbon-based ionomers was significantly lower than that of Nafion®. This is expected as the chain length increases, the scale of phase separation increases, and the water behaves more like "bulk water". The EODC of the hydrocarbon membranes with different chain lengths followed the same pattern as diffusivity. EODC also appears

to decrease with chain length as seen in Figure 1, though the results are within measurement error. All the hydrocarbon copolymers were lower than Nafion®. This is again attributed to the "tighter" water structure of the short-chain polymers. Under such confinement, it is reasonable that the acid will be more tightly coordinated with the surrounding waters, favoring Grotthus hopping and thereby decreasing the EODC.

Hydrophobicity of the inactive chain may also have a minor effect on EODS as seen in Figure 2. The trend for EODC is in the same order as hydrophobicity of the three inactive blocks (6FPAEB<6FK<6FBPS0). It was not possible to generate polymers with the exact same block length and IEC for this comparison, however, and these polymers also follow the same pattern of block length mentioned above and it is not possible to divorce these effects.

A selected hydrocarbon block copolymer membrane 6FPAEB-BPSH 1000 (13k-13k, IEC=1.7, annealed at 210°C, 30-µm thick) was made into MEAs, which were tested for fuel cell performance (see Figure 3). It can be seen that at higher humidity, the hydrocarbon membrane gives higher performance than Nafion® 112 membrane; however, at lower humidity, Nafion® 112 membrane demonstrates better performance. CFD simulations predict similar trends using different properties of these two categories of membranes (hydrocarbon membrane possess lower EODC coefficient and water diffusivity than Nafion® 112 membrane). Using the water transport numbers from the external characterizations of the membranes the CFD model predicts a higher rate of water transport to the cathode, and a subsequently thicker water film at the Nafion® MEA cathode, resulting in flooding at lower current densities.

Local distributions of water content in the membrane (Nafion® vs. hydrocarbon) and liquid water on the cathode MEA/GDL interface at 95% relative humidity and 0.6 A/cm^2 were simulated and are shown in Figure 4. Though water contents for both membranes are similar, the higher EODC of Nafion® leads to greater flooding at the cathode, predicted in the CFD model and seen in the polarization curves.

CONCLUSIONS AND FUTURE DIRECTIONS

- Two sets of hydrocarbon block polymers have been successfully synthesized with one varying oligomer and the other varying block length, annealing temperature and IEC.
- Diffusivity of the above hydrocarbon membranes have been characterized using Giner's dynamic water uptake system:
  - All hydrocarbon membranes show lower diffusivity than Nafion® membranes.

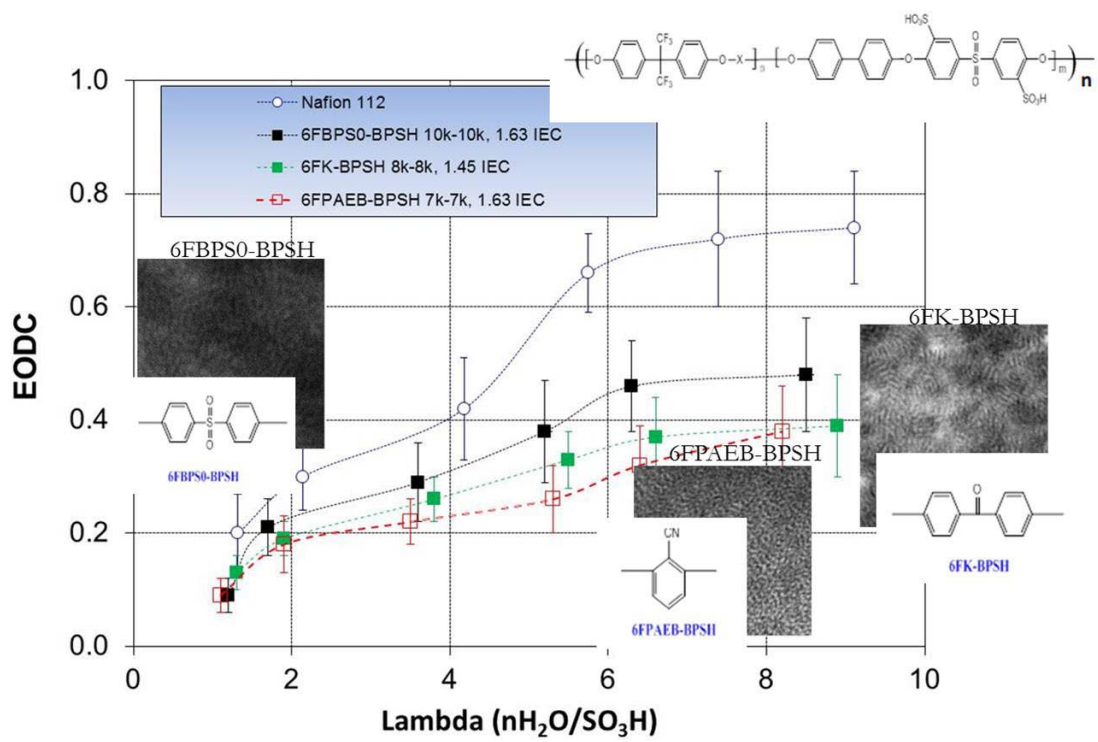

FIGURE 2. EODC of Matrix 2 Membranes: Varied Hydrophobicity of Inactive Oligomer

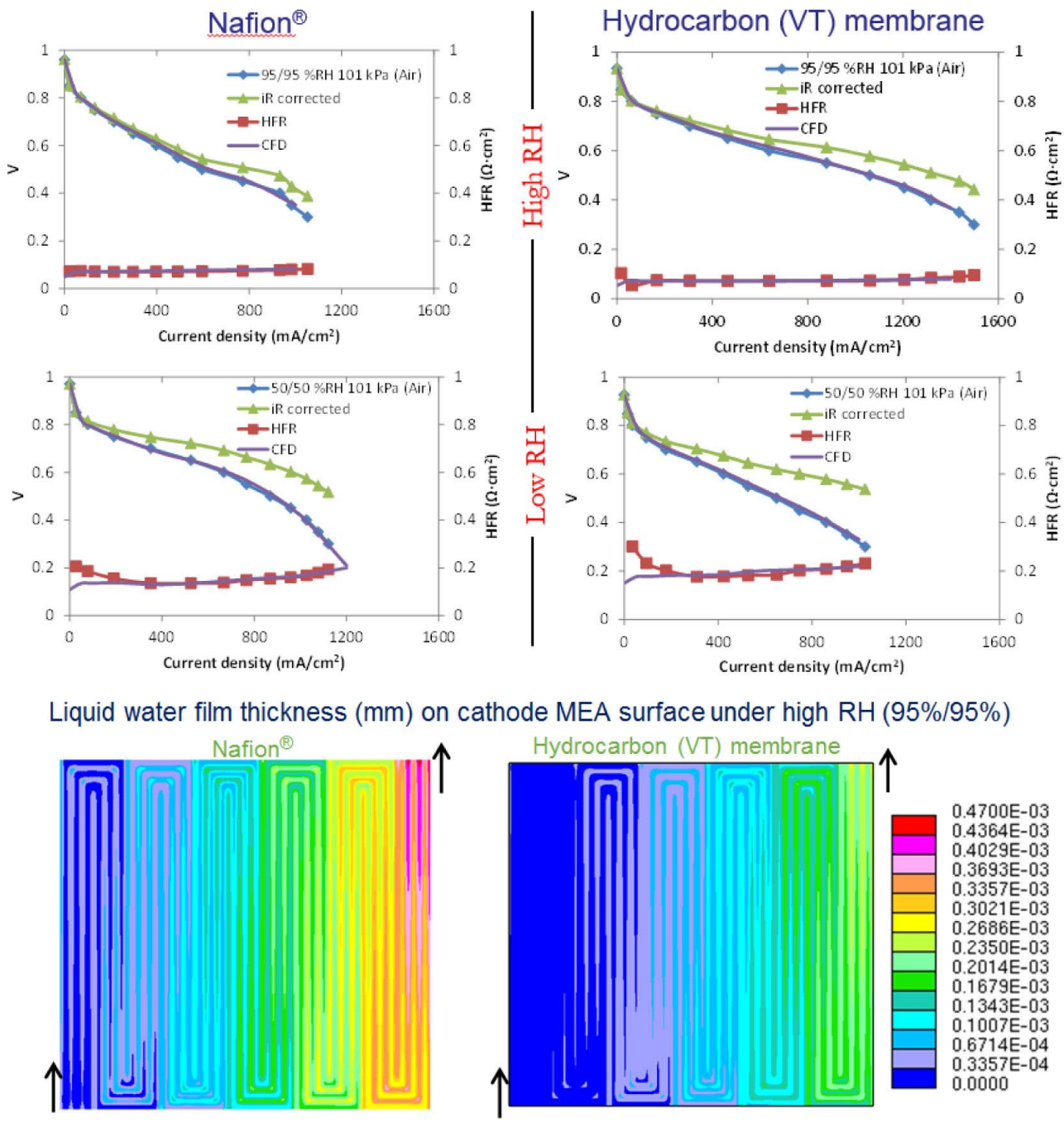

FIGURE 3. Fuel Cell Performance Comparison of Hydrocarbon Membranes with Nafion® Membranes

- Larger block lengths lead to higher water diffusivity. This appears to be due to the longer lengths of order as seen in transmission electron microscope images.

- EODC of the above hydrocarbon membranes have been characterized using Giner's dead-end hydrogen pump system:
  - All hydrocarbon membranes show lower EODC than Nafion® membranes.
  - Differences amongst hydrocarbon materials are less than between those membranes and Nafion®, however they appear to trend towards larger degrees of separation lead to higher EODC.

- Fuel cell performance of MEAs based on hydrocarbon membranes were evaluated and compared to that of Nafion® membranes:

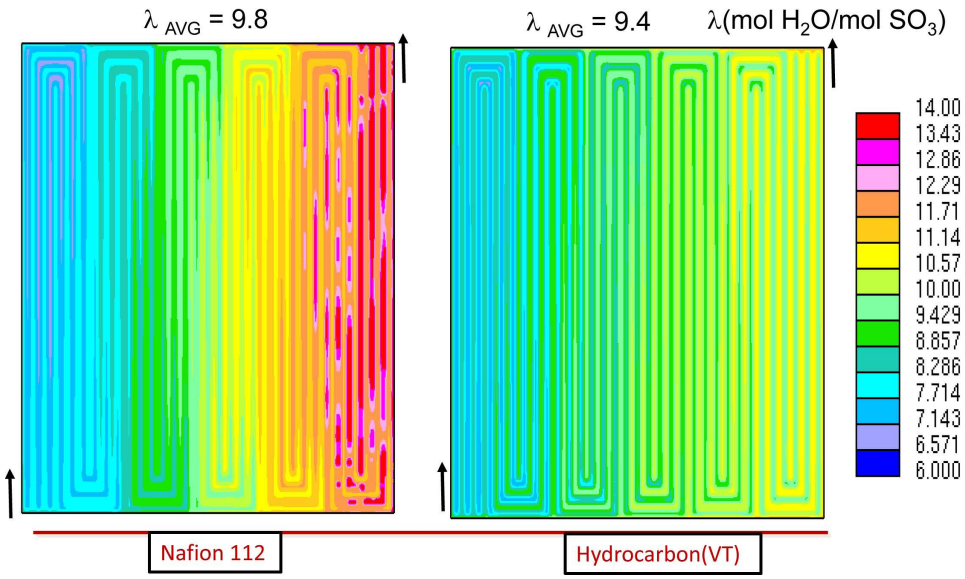

FIGURE 4. Local Distributions of Water Content in Membrane (Nafion® vs. Hydrocarbon) at 95% Relative Humidity

  - At higher humidity, hydrocarbon membranes show better performance than Nafion® membranes and vice versa.
- Local distributions of water content in hydrocarbon membranes and liquid have been simulated and compared with Nafion® membranes.
- Develop a new method for measuring diffusion within the diffusion media, while concentrating on the flooded region.

FY 2013 PUBLICATIONS/PRESENTATIONS

1. "Novel System for Characterizing Electro-Osmotic Drag Coefficient of Proton Exchange Membranes," presented in 220th Meeting of ECS, Abstract #1304, Honolulu, October 2012.

2. M. Martinez, S. Shimpalee, T. Cui, B. Duong, S. Seraphin, J.W. Van Zee, "Effect of microporous layer on MacMullin number of carbon paper gas diffusion layer," *J. of Power Sources*, **207**(1), 91-100 (2012).

3. "Using a novel current distribution board to understand local transport in PEMFCs" , presented in 220th Meeting of ECS, Abstract #1545, Honolulu, October 2012.

4. Chen, Yu; Lee, Chang Hyun; Rowlett, Jarrett R.; McGrath, James E., "Synthesis and characterization of multiblock semi-crystalline hydrophobic poly(ether ether ketone)-hydrophilic disulfonated poly(arylene ether sulfone) copolymers for proton exchange membranes," *Polymer*, **53**(15), 3143-3153 (2012).

5. Chen, Yu; Guo, Ruilan; Lee, Chang Hyun; Lee, Myoungbae; McGrath, James E, "Partly fluorinated poly(arylene ether ketone sulfone) hydrophilic-hydrophobic multiblock copolymers for fuel cell membranes," *International Journal of Hydrogen Energy*, **37**(7), 6132-6139 (2012).

6. "Transport in PEMFC Stacks," Presented in DOE Hydrogen and Fuel Cell Merit Review Meeting, Arlington, VA, May 2013.

7. V. Lilavivat, S. Shimpalee, H. Xu, J.W. Van Zee, and C.K. Mittelsteadt, "Novel current distribution board for PEMFC," submitted to *Intl J. of Hydrogen Energy* (2013).

8. V. Lilavivat, S. Shimpalee, H McCrabb, and J. W. Van Zee, "Fundamental Analyses, Observations, and Predictions of Liquid Droplet Movement on Etched-Metal Surfaces for PEMFC," submitted to *Electrochimica Acta* (2013).

9. Chen, Yu; Rowlett, Jarrett R.; Lee, Chang Hyun; Lane, Ozma R.; Van Houten, Desmond J.; Zhang, Mingqiang; Moore, Robert B.; McGrath, James E., "Synthesis and characterization of multiblock partially fluorinated hydrophobic poly(arylene ether sulfone)-hydrophilic disulfonated poly(arylene ether sulfone) copolymers for proton exchange membranes," *Journal of Polymer Science, Part A: Polymer Chemistry* (2013), published online: DOI: 10.1002/pola.26618.

10. The effect of block length upon structure, physical properties, and transport within a series of sulfonated poly(arylene ether sulfone)s, Y. Fan, C.J. Cornelius, H.S. Lee, J.E. McGrath, M. Zhang, R.B. Moore and C.L. Staiger, *Journal of Membrane Science*, **430**, 106-112 (2013).

REFERENCES

1. T.A. Zawodzinski, C. Derouin, S. Radzinski, R.J. Sherman, V.T. Smith, T.E. Springer and S. Gottesfeld, *J. Electrochem. Soc.*, **140**, 1041 (1993).

2. T.V. Nguyen and R.E. White, *J. Electrochem. Soc.*, **140**, 2178 (1993).

V.F.3 Investigation of Micro- and Macro-Scale Transport Processes for Improved Fuel Cell Performance

Jon P. Owejan, Wenbin Gu (Primary Contact), Matthew Mench, Michael Hickner, Satish Kandlikar, Thomas Trabold, Jeffrey Gagliardo, Anusorn Kongkanand, Vinod Kumar
General Motors
895 Joslyn Ave
Pontiac, MI 48340
Phone: (585) 953-5552
Email: wenbin.gu@gm.com

DOE Managers
Donna Ho
Phone: (202) 586-8000
Email: Donna.Ho@ee.doe.gov
David Peterson
Phone: (720) 356-1747
Email: David.Peterson@go.doe.gov

Technical Advisor
John Kopasz
Phone: (630) 252-7531
Email: kopasz@anl.gov

Contract Number: DE-EE0000470

Subcontractors:
- Penn State University, University Park, PA
- University of Tennessee, Knoxville, TN
- Rochester Institute of Technology, Rochester, NY
- University of Rochester, Rochester, NY

Project Start Date: June 1, 2010
Project End Date: November 30, 2013

Overall Objectives

Investigate and synthesize fundamental understanding of transport phenomena at both the macro- and micro-scales for the development of a down-the-channel model that accounts for all transport domains in a broad operating space.

Fiscal Year (FY) 2013 Objectives

- Characterize saturated relationships in state-of-the-art fuel cell materials.
- Obtain a comprehensive down-the-channel validation dataset for an auto-competitive material set.
- Develop multidimensional component models to output bulk and interfacial transport resistances.
- Demonstrate integrated transport resistances with a one plus one-dimension (1+1D) fuel cell model solved along a straight gas flow path.
- Identify critical parameters for low-cost material development.

Technical Barriers

This project addresses the following technical barriers from the Fuel Cells section of the Fuel Cell Technologies Office Multi-Year Research, Development, and Demonstration Plan:

(B) Cost

(C) Performance

Technical Targets

This project supports fundamental studies of fluid, proton, and electron transport with a focus on saturated operating conditions. Insights gained from these studies are being used to develop modeling tools that capture fundamental transport physics under single- and two-phase conditions. The primary deliverables are:

- Validated cell model including all component physical and chemical properties.
- Public dissemination of the model and instructions for exercise of the model.
- Compilation of the data generated in the course of model development and validation.
- Identification of rate-limiting steps and recommendations for improvements to the plate-to-plate fuel cell package.

FY 2013 Accomplishments

- Auto-competitive validation data set is complete with 95% confidence intervals.
- Several one-dimensional relationships have been established or refined based on parametric and characterization methods developed within the project.
- Demonstrated improved down-the-channel 1+1D model prediction with new relationships integrated.
- Published validation, parametric studies, and characterization data to a project website at: www.pemfcdata.org.

✧ ✧ ✧ ✧ ✧

INTRODUCTION

The transport physics associated with fuel cell operation are widely debated amongst researchers because comprehensive micro/nano-scale process validation is very difficult. Furthermore, fuel cell operation has a strong interdependence between components, making it difficult to separate the key relationships required for predictive models with ex situ methods. Generally, a validated model that predicts operation based on known design parameters for fuel cell hardware and materials is highly desired by developers. Such a model has been proposed by many research groups for dry (less than 100% relative humidity exhaust) operation with moderate success; however, these modelers unanimously assert that their ability to predict wet operation is limited by two-phase component-level understanding of transport processes. Additionally, as two-phase models continue to be refined benchmarking progress is difficult due to incomplete validation datasets.

In the current work, our team is developing characterization tools for saturated relationships based on the evolution of a dry 1+1D model for accurate wet prediction [1]. To complement this work we are also developing a comprehensive validation dataset based on a wide proton exchange membrane fuel cell (PEMFC) operating space. As data and modeling reach a final form, these are uploaded to a project website at www.pemfcdata.org. All characterization and validation work is conducted with common material sets that represent current and next generations of PEMFC design.

APPROACH

This project is organized around baseline and next-generation material sets. These materials define parametric bounds for component and integrated down-the-channel modeling efforts. The baseline material set was chosen based on the commercial state-of-the-art that exists today. The next-generation material set consists of transport impacting parametric changes that are in-line with the DOE 2015 targets for reduced cost while improving durability and performance. For characterization and validation experiments, a standard protocol was also developed to enable the team to conduct experiments with the same boundary conditions.

The first phase of this project was experimentally focused on characterization work that is organized by transport domain, comprising thin film ionomers, bulk membranes, porous electrodes, gas diffusion layers (GDLs), and flow distribution channels. The specifics of these relationships were outlined previously [2]. In anticipation of this integrated model, validation data sets are being collected in parallel with small-scale hardware specifically designed to include automotive stack constraints [3]. Currently, with these experimental methods established, work becomes more modeling focused as the physical mechanisms that govern the observed transport phenomenon are described multi-dimensionally at the component level and evaluated with a 1+1D fully integrated model. This work continuously guides parametric studies with novel material changes.

RESULTS

Validation Data

Compared to the baseline material set, the auto-competitive material set has a thinner membrane, lower cathode catalyst loading and ionomer-to-carbon ratio, advanced flowfield (with shallower channels, narrower lands, and modified exit headers), and notably, a novel anode GDL that is highly tortuous. Using the project protocol that varies outlet temperature, inlet relative humidity, outlet pressures, and current density [4], the auto-competitive validation data set is complete with 95% confidence intervals for the mean established for performance metrics by three separate experimental runs. The lower loaded auto-competitive cell generally shows a lower performance and a higher level of uncertainty, and would require an increased sample size to further reduce the confidence intervals. The auto-competitive cell shows on average 16% more of the reaction water staying on the cathode as a result of the high mass transport resistance anode GDL. Figure 1 compares the measured liquid water distribution, overall water balance, current and high-frequency resistance (HFR) distributions from the auto-competitive materials test to those from the baseline materials test. The water balance value represents the amount of product water moving to the cathode flow-

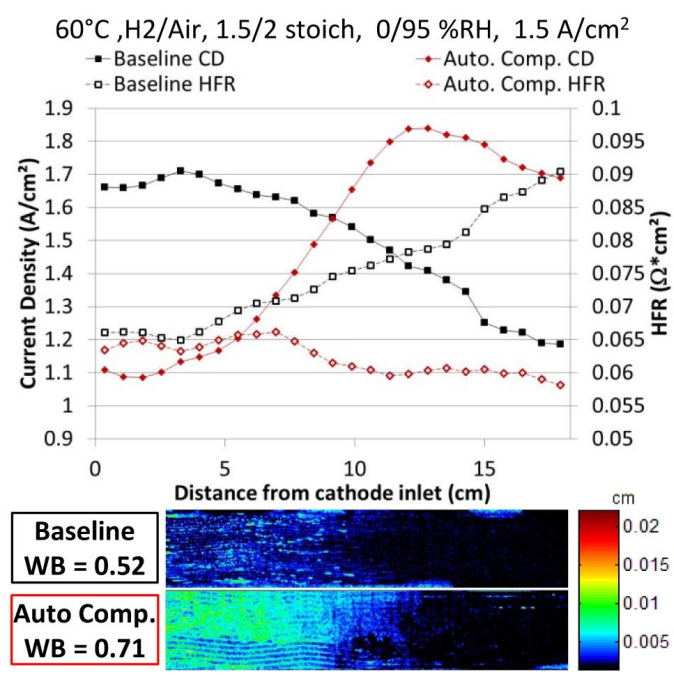

FIGURE 1. Liquid water distribution, overall water balance (WB), current and HFR distribution data: auto-competitive materials vs. baseline materials.

field. The higher diffusion resistance anode GDL drives more product water towards the cathode flow-field, and membrane hydration uniformity down the channel is improved. While similar behavior was observed at 80°C (not shown) for both auto-competitive and baseline materials, an opposite trend in current distribution is clearly seen at 60°C, indicating that the auto-competitive material set yields a higher risk of flooding the catalyst layer at a lower temperature. More liquid water accumulates near the cathode inlet, which overshadows the effect of higher oxygen pressure there on the reaction current.

Transport in Thin Ionomer Films

Platinum loading has to be reduced to meet the DOE cost target of $30/kWe for hydrogen fuel cell power systems for transportation. The local oxygen transport resistance measured by the limiting current method can be used to predict the voltage loss associated with low loaded electrode [5]. Recent experiments from this project have yielded an engineering approach to account for the effect of Pt dispersion on local oxygen transport resistance [6]. To understand the origin of the observed local resistance and develop mitigation methods accordingly, we use a flat model electrode to measure intrinsic transport properties of ionomer without convolution of a porous medium. Successful measurements made for a 100-nm thin ionomer film showed comparable bulk oxygen transport resistance to that of thick (>10 µm) membranes. In collaboration with Lawrence Berkeley National Laboratory and University of Calgary [7], we have measured the ionic domain structure and water uptake of thin films with thickness varying from 50 to 4 nm on Si- and Au-coated wafers. Ionic domain structure is altered in thin films, which will lead to different transport properties. Small domains in thin films decrease the proton conductivity and may change the nature of the catalyst particle/ionomer interface. Figure 2 shows film thickness increase with water uptake at various relative humidity levels with respect to film thickness. Thin films show much higher swelling on Si surfaces, which may be due to less hydrophobic reinforcement because of limited/no ion domain structure. Now that some of the physics of thin films are clarified, we are working on repeating this study on Pt and carbon surfaces, which are relevant to real electrodes, and measuring specific interactions between the ionomer and the Pt/carbon surfaces that may lead to altered thin film properties compared to what we know from bulk membrane measurements.

Transport in Diffusion Materials

GDL gas diffusivity and thermal conductivity are two key transport parameters that determine heat and mass transfer within a cell and thus the cell performance at given operating conditions. The presence of liquid water in porous media enhances heat transfer but impedes mass transport. We have designed and built a Loschmidt diffusion cell to measure the effective diffusion coefficients of partially

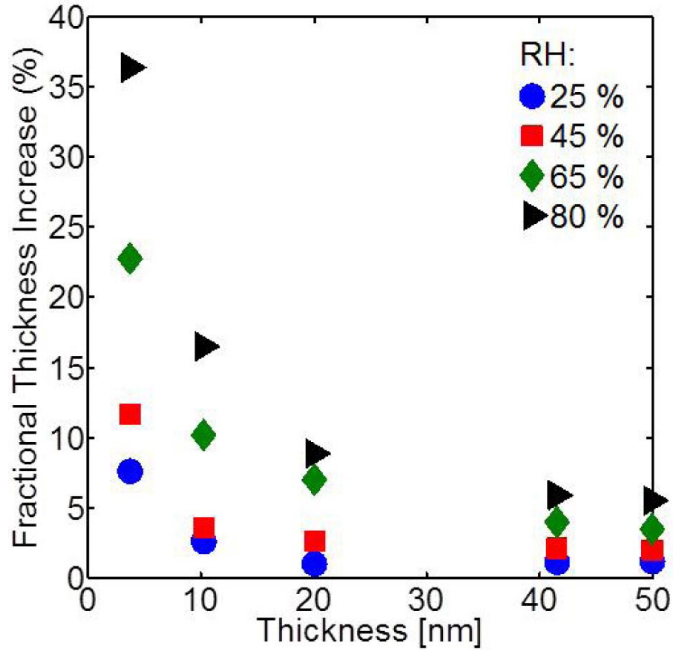

FIGURE 2. Thin-film swelling on Si wafers measured by ellipsometry showing higher water uptake with thinner film.

saturated porous samples. A new analytical solution method has been developed that simplifies diffusion cell design and enables a much more compact design with high precision [8]. We measured GDL thermal conductivity as a function of water saturation as well as compression. It is found that compression has significant impact on auto-competitive material sets but not on baseline materials. Figure 3 shows the measured thermal conductivity for both baseline and auto-competitive material sets in comparison with their theoretical maximum values based on completely connected pores. The departure from this maximum value represents liquid that is non-aligned/connected. At low saturation, the departure from the maximum is greater, indicating that more liquid is present as isolated droplets, as expected from condensation processes.

A two-dimensional component level model was developed for the numerical simulations of the GDL component using the measured transport properties and capillary flow. It considers the effect of compression variation over land and channel on the GDL structure and will allow integration with direct X-ray micro-tomography scans underway, in addition to coupled heat and mass transfer. The simulated liquid water accumulation over land and channel is useful in justifying the one-dimensional simplification of the two-phase 1+1D model and further providing an average value of liquid water saturation for model validation.

Transport in Flow Distributor Channels

Water coverage in the PEMFC gas channel is an important variable within the down-the-channel 1+1D model.

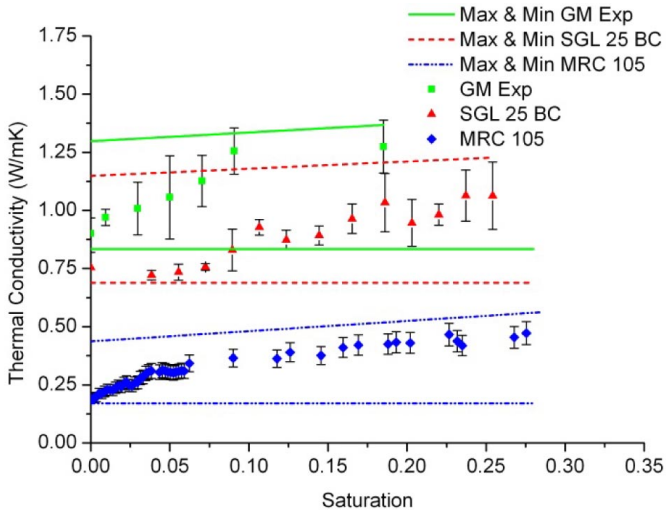

FIGURE 3. Measured GDL thermal conductivity as a function of liquid water saturation in comparison with the theoretical maximum value. The minimum value corresponds to a dry GDL.

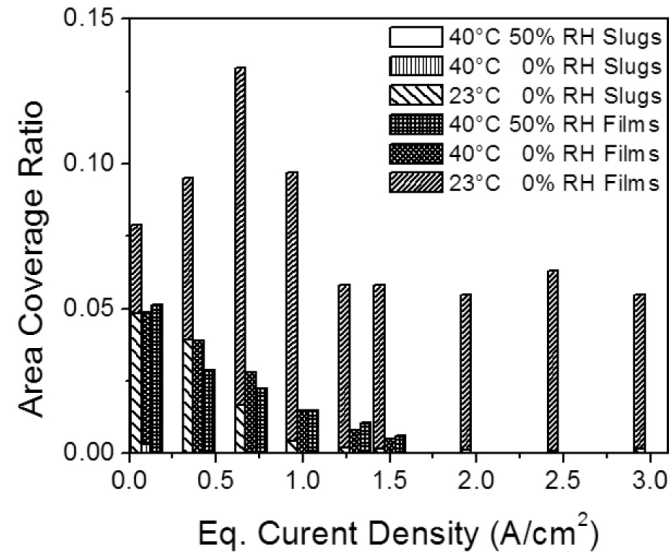

FIGURE 4. The area coverage ratio measured at 40 and 23°C for 0 and 50% inlet humidity conditions.

Multi-channel visualization was performed to quantify the area coverage ratio (ACR), defined as the area of liquid water blocking the reactant channels over the total projected channel area. A flow pattern identification algorithm was developed to distinguish between slug flow and film flow regime within the segmented liquid water. Figure 4 compares the obtained ACR for the different conditions of inlet humidification and temperature under slug and film flow regimes. It can be concluded that the ACR decreases at higher current densities and with increasing temperatures. Higher temperature leads to less liquid water presence in the channels and increased air velocity, which reduces the residence time of the water features within the reactant channels. With increased temperature, no slug flow was observed. Higher current densities and higher temperatures both favored the transition to film flow regime. Slug flow was found to be dominant at the lower current densities at ambient conditions. Oxygen transport resistance at the air flow channel and GDL interface has been further investigated via a numerical approach in the presence of either multiple liquid water droplets [9] or a single film as typical conditions in a PEMFC air flow channel. The interfacial transport resistance, expressed through the non-dimensional Sherwood number (Sh), was found to increase significantly above the fully developed value (Sh = 3.349) in the droplet wake region. The average Sh number in between two neighboring droplets increases with the number of droplets, droplet size, and superficial mean air velocity, with the highest value corresponding to an increase of 122% with respect to the fully developed Sh. A single film was found to decrease the effective Sh at the side region and also affect the downstream region similarly for a comparable length of the film. An elemental modeling scheme has been developed to predict the two-phase pressure drop in the reactant channels. The scheme takes into account the gas consumption down the channel, local water saturation, changing mass quality, and the effect of saturation pressure on water removal from the gas channels in the gas phase. The two-phase pressure drop predictions use the modified English–Kandlikar model within the elemental scheme.

In situ neutron imaging experiments were conducted at low cell temperature (20~35°C) to study active and non-active area water volumes as a function of cell temperature and current density [10]. The newly developed MATLAB®-based image analysis software allows for water thickness quantification for different areas within the cell, so water progression is able to be studied through the flow fields, anode, and cathode independently. The software has the capability to compare changes in water thickness for images taken in succession, so we may get a more accurate understanding of the flow of water through the fuel cell via analyzing multiple images together. Our in situ neutron imaging experiments demonstrated severe flow misdistribution resulting from water accumulation in non-active transitions and water build-up around the edge of the manifold. The extracted pressure drop data suggests that the water mitigation strategy should focus specifically on anode, where most of the reactant is consumed, resulting in an insufficient driving force for water to exit that area.

Modeling

The relationships described above for the various components are summarized with a down-the-channel 1+1D model. More accurately accounting for the transport relationships elucidated in this project has improved predictions of the performance and water balance response to key changes in material and operating parameters. The model

agrees reasonably well with baseline material set validation data. Better agreement in HFR distribution was achieved by considering a parabolic distributed compression load down the channel that results from the printed circuit board used for distributed measurements. For the auto-competitive material set, the model agrees with the data at 80°C and is predictive for overall water balance, but shows large discrepancy in current distribution at a lower temperature. It is hypothesized that the auto-competitive material set yields a more flooded catalyst layer and thus results in an opposite trend in current distribution compared to that shown in Figure 1. The model needs to address the liquid water saturation issue in the electrode.

CONCLUSIONS AND FUTURE DIRECTIONS

A well-organized characterization, modeling, and validation framework was developed early in this project. The first phase (FY 2011) of execution was largely focused on experimental development. The focus gradually shifted to model development while continuing to complete validation data. During the current phase of the project (FY 2013), results from these methods were described with multidimensional component models and summarized in a down-the-channel model that is compared to a comprehensive validation database. Specific highlights from FY 2013:

- Auto-competitive validation data set with 95% confidence intervals established.
- Channel-to-manifold two-phase pressure drop measured as a function of water volume.
- GDL/channel interfacial oxygen transport resistance related to ACR and two-phase channel pressure drop.
- GDL transport resistance transition from dry to wet and thermal conductivity as a function of saturation measured.
- Local oxygen transport resistance correlated to both Pt surface area and the surface area of ionomer film that covers Pt/C catalyst.
- Down-the-channel 1+1D model improved with new relationships integrated, and the need for model refinement identified.

The final phase of this project will be focused on finalizing the two-phase down-the-channel model, wrapping up component characterization and modeling, and reporting. In particular, a better catalyst layer liquid water model will be incorporated to improve current distribution prediction of the auto-competitive material set. Using this model as a guide, the project will be completed with parametric studies focused on rate limiting material constraints for transport within a PEMFC.

FY 2013 PUBLICATIONS/PRESENTATIONS

1. Dishari, S.K., Hickner, M.A., "Confinement and Proton Transfer in NAFION® Thin Films," *Macromolecules*, 46(2), 413-421 (2013).

2. Gopalan, P. and Kandlikar, S.G., "Droplet-Sidewall Dynamic Interactions in PEMFC Gas Channels," *Journal of the Electrochemical Society*, 159(8), F1-F8 (2012).

3. Grimm, M., See, E.J., and Kandlikar, S.G., "Modeling gas flow in PEMFC channels: Part I-Flow pattern transitions and pressure drop in a simulated ex situ channel with uniform water injection through the GDL," *International Journal of Hydrogen Energy*, 37(17), 12489-12503 (2012).

4. Gopalan, P. and Kandlikar, S.G., "Effect of Channel Material on Water Droplet Dynamics in a PEMFC Gas Channel," *Journal of the Electrochemical Society*, 160(6), F487-F495 (2013).

5. Kandlikar, S.G., See, E.J., Gopalan, P., Koz, M., and Banerjee, R., "Two-phase Flow in GDL and Reactant Channels of a Proton Exchange Membrane Fuel Cell," *8th Int. Conference on Multiphase Flow (ICMF 2013)*, May 26–31, 2013.

6. Liu, X., Lin, J., McConnaghy, K.M., Trabold, T.A., Gagliardo, J.J., and Owejan, J.P., "Investigation of channel-to-manifold water transport in proton exchange membrane fuel cells," *Proceedings of the ASME 6th International Conference on Energy Sustainability & 10th International Fuel Cell Science, Engineering and Technology Conference,* Paper ESFuelCell2012-91093, San Diego, CA, July 23–26, 2012.

7. Liu, X., Trabold, T.A., Gagliardo, J.J., Jacobson, D.L., and Hussey, D.S., "Neutron imaging of water accumulation in the active area and channel-to-manifold transitions of a PEMFC," *Proceedings of the ASME 7th International Conference on Energy Sustainability & 11th International Fuel Cell Science, Engineering and Technology Conference,* Paper ESFuelCell2013-18183, Minneapolis, MN, July 14–19, 2013.

8. Modestino, M.A., Allen, F.I., Paul, D.K., Dishari, S.K., Petrina, S.A., Hickner, M.A., Karan, K., Minor, A.M., Segalman, R.A., Weber, A.Z., "Self-assembly and transport limitations in confined Nafion films," *Macromolecules*, 46(3), 867–873 (2013).

9. Koz, M. and Kandlikar, S.G., "Numerical investigation of interfacial transport resistance due to water droplets in proton exchange membrane fuel cell air channels," *Journal of Power Sources*, 243, 946-957 (2013).

10. Cekmer, O., LaManna, J.M., and Mench, M.M., "Alternative analytical analysis for improved Loschmidt diffusion cell," International Journal of Heat and Mass Transfer, 65(10), 883-892 (2013).

11. Owejan, J.P., Owejan, J.E., and Gu, W., "Impact of Platinum Loading and Catalyst Layer Structure on PEMFC Performance," *Journal of The Electrochemical Society*, 160 (8), F824-F833 (2013).

12. Jiang, R. and Gu, W., "Fuel cell membranes with expanded polytetrafluoroethylene (ePTFE) reinforcement: morphology, performance and durability," Paper#L5-3, Electromembrane processes and materials, Satellite Meeting of The 63rd ISE Annual Meeting, Ceský Krumlov, Czech Republic, August 26–29, 2012.

13. Koz, M. and Kandlikar, S.G., "A Preliminary Study for 3D Numerical Simulation of a Through-Plane Temperature Profile in a PEMFC Incorporating Coolant Channels," 10th International Conference on Nanochannels, Microchannels, and Minichannels, Rio Grande, Puerto Rico, July 8–12, 2012.

14. LaManna, J.M., Chakraborty, S., Xu, G., Bothe, J., Zhang, F.Y., Gagliardo, J.J., Owejan, J., and Mench, M.M., "Gas Diffusion Layer Through-Plane Transport Studies," 2012 Electrochemical Energy Storage and Conversion Forum. Knoxville, Tennessee, April 2012. *Jacob LaManna won first place in the 2012 Electrochemical Energy Storage and Conversion Forum Poster Competition.

15. Owejan, J.P., "Neutron metrology methods for in situ diagnostics of transport in electrochemical systems," invited talk at the spring meeting of the Materials Research Society, San Francisco, California, April 2012.

16. Owejan, J.P., "Neutron diagnostics for fuel cells and batteries," invited talk at the Electrochemical Energy Storage and Conversion Forum, Knoxville, Tennessee, April 2012.

17. Owejan, J.P., Owejan, J.E., and Gu, W., "Impact of Platinum Loading and Catalyst Layer Structure on PEMFC Performance," ECS 222nd Meeting, Honolulu, Hawaii, October 7–12, 2012.

18. Gopalan, P. and Kandlikar, S.G., "Effect of Channel Material on the Behavior of Water Droplet Emerging from the GDL into the PEMFC Gas Channels," ECS 222nd Meeting, Honolulu, Hawaii, October 7–12, 2012.

19. Koz, M. and Kandlikar, S.G., "Numerical Simulation of the Interfacial Oxygen Transport Resistance for a PEMFC Cathode Incorporating Water Droplet Coverage," ECS 222nd Meeting, Honolulu, Hawaii, October 7–12, 2012.

20. See, E.J. and Kandlikar, S.G., 2012, "A Two-Phase Pressure Drop Model Incorporating Local Water Balance in PEM Fuel Cell Gas Channels," ECS 222nd Meeting, Honolulu, Hawaii, October 7–12, 2012.

REFERENCES

1. Gu, W., Baker, D.R., Liu, Y., Gasteiger, H.A., "Proton exchange membrane fuel cell (PEMFC) down-the-channel performance model," Handbook of Fuel Cells - Volume 5, Prof. Dr. W. Vielstich *et al*. (Eds.), John Wiley & Sons Ltd. (2009).

2. Owejan, J.P., 2011 Annual Progress Report for the DOE Hydrogen and Fuel Cells Program (2011).

3. Owejan, J.P., Gagliardo, J.J., Sergi, J.M., Kandlikar, S.G., Trabold, T.A., "Water management studies in PEM fuel cells, Part I: Fuel cell design and in situ water distributions," *International Journal of Hydrogen Energy*, 34 (8), 3436-3444 (2009).

4. http://www.pemfcdata.org/data/Standard_Protocol.xls.

5. Greszler, T.A., Caulk, D., and Sinha, P., "The Impact of Platinum Loading on Oxygen Transport Resistance," *Journal of the Electrochemical Society*, 159 (12), F831-F840 (2012).

6. Owejan, J.P., Owejan, J.E., and Gu, W., "Impact of Platinum Loading and Catalyst Layer Structure on PEMFC Performance," *Journal of the Electrochemical Society*, 160(8), F824-F833 (2013).

7. Modestino, M.A., Allen, F.I., Paul, D.K., Dishari, S.K., Petrina, S.A., Hickner, M.A., Karan, K., Minor, A.M., Segalman, R.A., Weber, A.Z., "Self-assembly and transport limitations in confined Nafion films," *Macromolecules*, 46(3), 867–873 (2013).

8. Cekmer, O., LaManna, J.M., and Mench, M.M., "Alternative analytical analysis for improved Loschmidt diffusion cell," *International Journal of Heat and Mass Transfer*, 65(10), 883-892 (2013).

9. Koz, M. and Kandlikar, S.G., "Numerical investigation of interfacial transport resistance due to water droplets in proton exchange membrane fuel cell air channels," *Journal of Power Sources*, 243, 946-957 (2013).

10. Liu, X., Trabold, T.A., Gagliardo, J.J., Jacobson, D.L., and Hussey, D.S., "Neutron imaging of water accumulation in the active area and channel-to-manifold transitions of a PEMFC," *Proceedings of the ASME 7th International Conference on Energy Sustainability & 11th International Fuel Cell Science, Engineering and Technology Conference,* Paper ESFuelCell2013-18183, Minneapolis, MN, July 14–19, 2013.

V.F.4 Transport Studies Enabling Efficiency Optimization of Cost-Competitive Fuel Cell Stacks

Amedeo Conti (Primary Contact), Robert Dross
Nuvera Fuel Cells
129 Concord Road
Billerica, MA 01821
Phone: (617) 245-7605
Email: aconti@nuvera.com
Email: rdross@nuvera.com

DOE Managers
Kathi Epping Martin
Phone: (202) 586-7425
Email: Kathi.Epping@ee.doe.gov
Gregory Kleen
Phone: (720) 356-1672
Email: Gregory.Kleen@go.doe.gov

Technical Advisors
Thomas Benjamin
Phone: (630) 252-1632
Email: benjamin@anl.gov
John Kopasz
Phone: (630) 252-7531
Email: kopasz@anl.gov

Contract Number: DE-EE0000472

Subcontractors:
- Johnson Matthey Fuel Cell Ltd. (JM), England
- Lawrence Berkeley National Laboratory, Berkeley, CA
- Pennsylvania State University, State College, PA

Project Start Date: September 1, 2009
Project End Date: November 30, 2012

Overall Objectives

- Optimize the efficiency (electric potential at rated current) of a stack technology that meets DOE cost targets.
- Develop and publish a validated predictive transport model that enables efficiency maximization at conditions that meet DOE cost targets.
- Demonstrate stable and repeatable high performance on a full-format fuel cell stack, namely 7.5 W/mg-Pt.

Fiscal Year (FY) 2013 Objectives

- Validate the predictive transport model with varied operating conditions, membrane electrode assembly (MEA) Pt loadings, and flowfield architectures.
- Publish the predictive model in format agreed to by the DOE.

Technical Barriers

This project addresses the following technical barriers from the Fuel Cells section of the Fuel Cell Technologies Office Multi-Year Research, Development, and Demonstration Plan:

(B) Cost

(C) Performance

Technical Targets

This project is primarily focused on reducing stack cost and improving efficiency by modeling and optimizing transport properties of the MEA. Stack cost is reduced through a combination of increased power density and decreased noble metal content. The performance target of 7.5 W/mg-Pt at 500 mV was selected based on cost modeling results, as the performance required to achieve the 2015 DOE cost target of $15/kW$_e$. Efficiency (electric potential at rated current) of the stack technology will be optimized with the ultimate goal of approaching the 2015 DOE efficiency targets (as defined in the 2007 DOE Multi-Year Research, Development, and Demonstration Plan):

- Stack efficiency at rated power: 55%
- Stack efficiency at 25% of rated: 65%

FY 2013 Accomplishments

- Exceeded the technical target for the project by 66% demonstrating performance of 12.5 W/mg-Pt at 500 mV on a full format stack.
- Optimized the efficiency of the stack, demonstrating over 50% stack efficiency (635 mV) at a specific power of 7.9 W/mg Pt.
- Validated the predictive transport model with varied operating conditions, MEA Pt loadings, and flowfield architectures.
- Published the predictive model as an executable file at http://ecpower.utk.edu.

✧ ✧ ✧ ✧ ✧

INTRODUCTION

Hydrogen fuel cells are recognized as one of the most viable solutions for mobility in the 21st century; however, there are technical challenges that must be addressed before the technology can become available for mass production. One of the most demanding aspects is the costs of present-day fuel cells which are prohibitively high for the majority of envisioned markets. The fuel cell community recognizes two major drivers to an effective cost reduction: (1) decreasing the noble metals content, and (2) increasing the power density in order to reduce the number of cells needed to achieve a specified power level. Nuvera's technology exhibits great promise for increasing power density on account of its proven ability to operate stably at high current densities (>1.5 A/cm^2). However doing so compromises efficiency, increases the heat rejection duty, and is thus more demanding on the cooling system. These competing aspects are being assessed in order to identify the proper tradeoffs, and ensure the modeling and experimental activities of the AURORA Program with respect to system-level constraints for automotive applications. This project will develop a predictive transport model to identify and help us reduce losses and increase efficiency for high current density operation.

APPROACH

Nuvera structured the activities in the scope of the project to orbit around a focal point consisting of the fuel cell predictive model. Cost and system analyses were performed in order to define the boundaries of the design space that the model should represent. This analytical work will inform the experimental tests on a new single-cell fixture to illuminate the physics and the parameters composing the backbone of the fuel cell model. The predictions generated by the model drive both the process of optimization of the fuel cell operating conditions and the material development. The combined results of these two activities are verified on single-cell fixtures as well as on full active area hardware, and the experimental data obtained is used to validate and calibrate the model through multiple iterations.

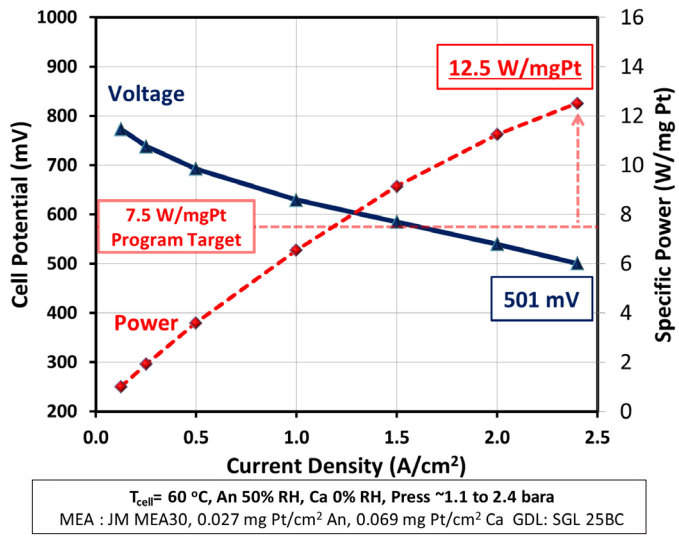

GDL - gas diffusion layer

FIGURE 1. Polarization Curve for JM MEA#30 – Optimized for Maximum Specific Power

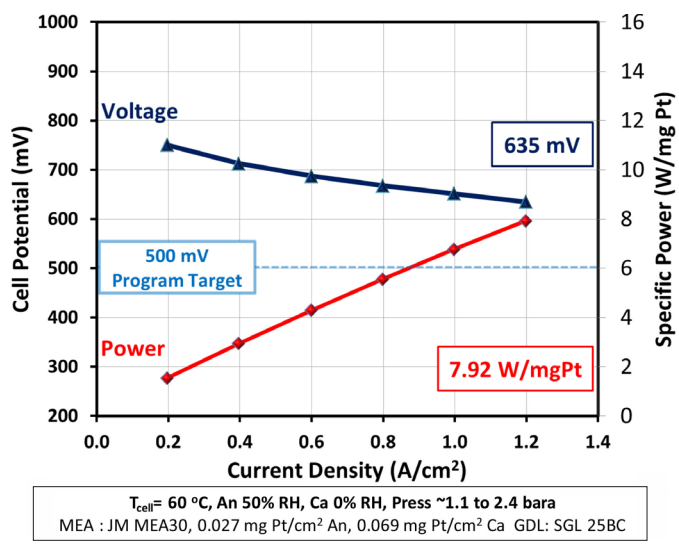

FIGURE 2. Polarization Curve for JM MEA#30 – Optimized for Maximum Efficiency

RESULTS

In FY 2013 Nuvera completed the evaluation of low Pt loaded MEAs from JM with the goal of demonstrating even higher performance in terms of specific power and efficiency. As shown in Figure 1, Nuvera tested a JM MEA 30 with a total Pt loading of 0.096 mg Pt/cm² in a 4-cell full-format stack. This stack demonstrated a significant improvement in specific power reaching 12.5 W/mg Pt at 501 mV and 2.4 A/cm^2 thus exceeding the project target by 5 W/mg Pt! The polarization curve was also optimized for efficiency and, as shown in Figure 2, the stack achieved an average voltage of 635 mV at 7.92 W/mg Pt and 1.2 A/cm^2 thus exceeding the efficiency target for the project by 135 mV.

The University of Tennessee, Knoxville team completed an extensive validation test matrix of the predictive transport model. The model was validated under a wide range of conditions including current densities of 1 and 2 A/cm^2, coolant inlet temperatures from 60°C to 90°C, low and high coolant flowrates, reactant humidification from 0 to 100%, reactant pressures of 1.8 and 2.4 bara, and cathode reactants of air and heliox. Two different architectures (channel/land and open-flowfield) and two different MEA designs (total Pt loadings of 0.55 and 0.20 mg Pt/cm^2) were also

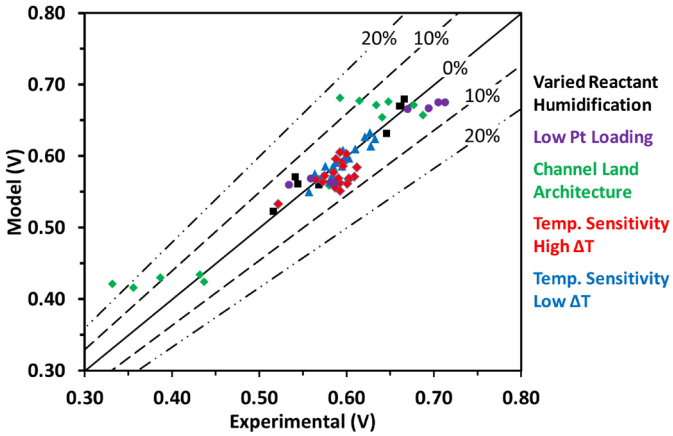

FIGURE 3. Predictive Model Validation Summary for Performance

used to validate the model. For each of these conditions cell performance, high frequency resistance and net water drag were measured on a 50-cm^2 cell and compared with model predictions. In Figure 3 the voltage obtained experimentally is plotted vs. the model prediction for each of the 67 different conditions validated. Ninety-eight percent of the points were within ±20% error and 92% of the points were within ±10% error. The model validation studies conducted by the University of Tennessee, Knoxville provide a high level of confidence that the model is valid through a wide range of reactant and cell conditions.

CONCLUSIONS AND FUTURE DIRECTIONS

The project has ended, successfully meeting all objectives and technical targets.

FY 2013 PUBLICATIONS/PRESENTATIONS

1. Srouji A.K., Zheng L.J., Dross R., Turhan A., Mench M.M., "Oxygen transport in PEFC with ultra-low loading electrodes," in preparation.

2. Srouji A.K., Zheng L.J., Dross, R., Turhan A., Mench M.M., "Water management in PEFC with porous metallic flow field at ultra-high current density," Journal of Power Sources, in press.

3. Zheng L.J., Srouji A.K., Dross, R., Turhan A., Mench M.M., "Computational engineering of porous flow field PEFCs to enable high temperature high power density operation," *Journal of the Electrochemical Society*, **160**, F119 (2013).

4. (Invited) M.M. Mench, "Progress in Ultra-High Current Fuel Cell Designs and Emerging Research Challenges in Polymer Electrolyte Fuel Cells," *University of Toronto Mechanical and Industrial Engineering Distinguished Seminar Series*, University of Toronto, March 9, 2012.

5. (Invited) M.M. Mench, "Progress in Ultra-High Current Fuel Cell Designs in Polymer Electrolyte Fuel Cells and Pathway to Greatly Enhanced Power Density in All-Vanadium Flow Batteries," *University of Padova*, Italy, June 12, 2012.

6. (Keynote Speaker), Mench, M. M., "Pathways to Achieve Ultra-High Power, Low Cost Polymer Electrolyte Fuel Cells Through Heat and Water Management," *The International Workshop on Fuel Cell and Hydrogen Energy,* KAIST University, Republic of Korea, on February 16th, 2012.

7. (Keynote Speaker), Mench, M. M., "Progress and Emerging Research Challenges in Polymer Electrolyte Fuel Cells," *HYFUSEN2 Conference*, Mar del Plata Argentina, June 6–11, 2011.

8. Srouji A.K., Zheng L.J, Turhan A, Mench M.M., "Eliminating the Channel/Land Paradigm: Ultra-high Current Density Operation of PEFC with Open Metallic Element Flow Field," *1st International Educational Forum on Environment and Energy Science*, Kona, Hawaii Dec. 2012.

9. (poster) Zheng L.J., Srouji A.K., Mench M.M., "Combined Study of Porous-Flow-Field PEFC Under Ultra-High Current Density Operation," *Gordon Research Conference Fuel Cells*, Smithfield, Aug. 2012.

10. Srouji A.K., Zheng L.J., Mench M.M., "Study of Water Transport in a PEFC with an Open Metallic Element Flow Field at Ultra-High Current Density," *221st ECS Meeting*, Seattle, May 2012.

V.G.1 Large-Scale Testing, Demonstration and Commercialization of the Nanoparticle-Based Fuel Cell Coolant (SBIR Phase III)

Satish Mohapatra (Primary Contact), Sreya Dutta, David Schiemer, Patrick McMullen and Kevin Coscia
Dynalene Inc.
5250 W. Coplay Rd.
Whitehall, PA 18052
Phone: (610) 262-9686
Email: satishm@dynalene.com

DOE Manager
Kathi Epping Martin
Phone: (202) 586-5463
Email: Kathi.Epping@ee.doe.gov

Contract Number: EE00004532

Subcontractors:
- University of Tennessee, Knoxville (UTK), TN
- Protonex Inc., MA

Project Start Date: October 1, 2010
Project End Date: September 30, 2013

Overall Objectives

- Understand coolant durability requirements by working with different fuel cell companies.
- Optimize coolant property in order to maintain low electrical conductivity and other thermo-physical properties for over 5,000 operating hours.
- Demonstrate materials compatibility of the fuel cell components with the coolant.
- Develop a system for long-term durability and diagnostics testing of nano-particle fuel cell coolant.

Fiscal Year (FY) 2013 Objectives

- Increase the nano-particle surface charge to >500 μeq/g for both cationic and anionic particles.
- Examine the compatibility of different coolants with the components of a typical fuel cell system over the course of 5,000 hours.
- Validate efficiency of corrosion inhibition abilities of Dynalene coolants at high temperature.
- Determine the effect of nano-particles on the surface of fuel cell components through various testing.
- Perform and compare short-term (100 hrs) and long-term (1,000 hrs) performance of coolants in the fuel cell (with or without applied voltage) in order to determine optimal coolant configuration.
- Achieve successful commercialization of the Dynalene Fuel Cell (Dynalene FC) coolant.

Technical Barriers

This project addresses the following technical barriers from the Fuel Cells section of the Fuel Cell Technologies Office Multi-Year Research, Development, and Demonstration Plan:

(A) Durability

(B) Cost

(C) Performance

Technical Targets

Dynalene FC is expected to help the fuel cell industry achieve the durability, cost, and performance targets. The current findings can be summarized as:

- Durability: coolant designed to have shelf life of 5,000 hrs. Immersion testing demonstrated minimal corrosion, and superior compatibility with system materials thereby extending the durability of the fuel cell system components such as the pump, the radiator, valves, seals/gaskets, and any other components coming in contact with the coolant.
- Cost: the projected selling price of coolant as production scales up (>100,000 gal/year) is about $10 per gallon, which is close to the price of the current automotive coolants.
- Performance: Dynalene LC and FC showed low electrical conductivity (<2 μS/cm) with high boiling point (>100°C), high thermal conductivity and low viscosity. The fluid is freeze tolerant under extremely cold conditions (<-40°C) which will assist both transportation and stationary fuel cells to quickly warm up during cold starts.

FY 2013 Accomplishments

Following are the accomplishments from July 1, 2012 to June 30, 2013:

- Surface charge of reformulated nano-particle has been increased to 890 μeq/g.

- Compatibility and thermal degradation studies of polymers and metals have been performed at 80°C for 5,000 hours.
- Corrosion inhibitors have been validated for metals at 80°C using electrochemical set-up.
- Coolants have been tested in working fuel cell in 100-hour tests with or without applied voltage.
- Freeze/thaw tests completed and confirmed that particles remain stable in coolant.
- More than 10 companies testing and some of them purchasing Dynalene FC and LC coolants.

✧ ✧ ✧ ✧ ✧

INTRODUCTION

This project addresses the goals of the Fuel Cell Technologies Office of the DOE to have a better thermal management system for fuel cells. Proper thermal management is crucial to the reliable and safe operation of fuel cells. A coolant with excellent thermo-physical properties, non-toxicity, and low electrical conductivity is desired for this application.

An ideal coolant must be durable for >5,000 hrs of operation, and therefore, the coolant must be tested for such duration. Electrical conductivity of the coolant should be less than 10 µS/cm throughout the testing period and the coolant must be compatible with all the materials (metals, plastics, rubbers, and composites) at the highest operating temperature (up to 120°C). Current automotive coolants do not satisfy the electrical conductivity criteria due to the presence of ionic corrosion inhibitors in them. Water/glycol solutions without inhibitors can have low starting electrical conductivity, but it can increase rapidly due to corrosion of metal components leading to build-up of ions in the coolant. Fuel cell developers are using water or water/glycol mixtures with a de-ionizing filter in the coolant loop. The filter needs to be replaced frequently to maintain the low electrical conductivity of the coolant. This method significantly increases the operating cost and also adds extra weight/volume to the system. Dynalene Inc. has developed and patented a fuel cell coolant with the help of DOE Small Business Innovation Research Phase I and Phase II funding (Project # DE-FG02-04ER83884). This technology has been patented in the U.S., Canada, and Europe. The technical feasibility of this coolant was demonstrated in short-term tests using a dynamic re-circulating loop.

APPROACH

Conductivity of the reformulated nano-particles dispersed in bioglycol-distilled water was measured as NaCl solution was gradually added to it. Corrosion inhibitors for metals and polymers validated via immersion testing in different formulations of Dynalene coolants at 80°C for 5,000 hours. Coolant properties were monitored at regular intervals and the components were characterized using scanning electron microscopy and energy dispersive X-ray spectroscopy for any signs of degradation and inhibition. High-temperature electrochemical testing on metals was done to study the corrosion inhibitive properties of the coolants. UTK researchers performed 100 hrs testing of Dynalene coolants in their fuel cell systems at 70°C with applied voltage varying between 0-35 V.

RESULTS

Dynalene reformulated the nano-particles and achieved a surface charge of 890 µeq/g, which further helped in scavenging the stray ions in the system. Figure 1 shows the change in conductivity on addition of NaCl solution. The particles exhibited very low electrical conductivity till they were saturated with the salt solution.

Change in the electrical conductivity of the fluids in presence of metals and polymers is an important deciding factor for materials selection for fuel cells, as a considerable increase in the conductivity might indicate that ions might be leaching from the immersed materials and contaminating the fluids. Based on the 5,000 hr-80°C immersion studies, a list of materials have been recommended for Dynalene LC as shown in Figure 2. Scanning electron microscopy and energy dispersive X-ray spectroscopy studies on the metal samples showed presence of inhibitive surface layer in presence of the inhibited coolants. Surface cracks and swelling on the polymers were much less in the inhibited coolants compared to the uninhibited fluid.

Electrochemical corrosion studies of aluminum at 50°C and 80°C showed that in presence of the inhibitors the corrosion resistance improved due the formation of the inhibitive layer. For the coolants with inhibitor, on increasing the incubation period from two hours to four days, the corrosion rate dropped further. The electrochemical corrosion rate for Al in Dynalene LC at 50°C is shown in Figure 3.

UTK researchers tested different formulations of Dynalene coolants in their fuel cell stack at 70°C. The electrical conductivity of the fluid did not show any appreciable fluctuation. When the applied voltage was as high as 35 V, a slight decrease in the electrical conductivity was seen, it is postulated that the fuel cell was acting as a deionizer and pulling the ions from the fluid. Separately, inductively coupled plasma analysis performed on the tested coolants showed negligible leaching of ions in to the coolants from the fuel cell components.

To see the effect of nano-particles on the fuel cell, a high concentration of nano-particles and surfactant was deliberately added to one of the coolants, which caused

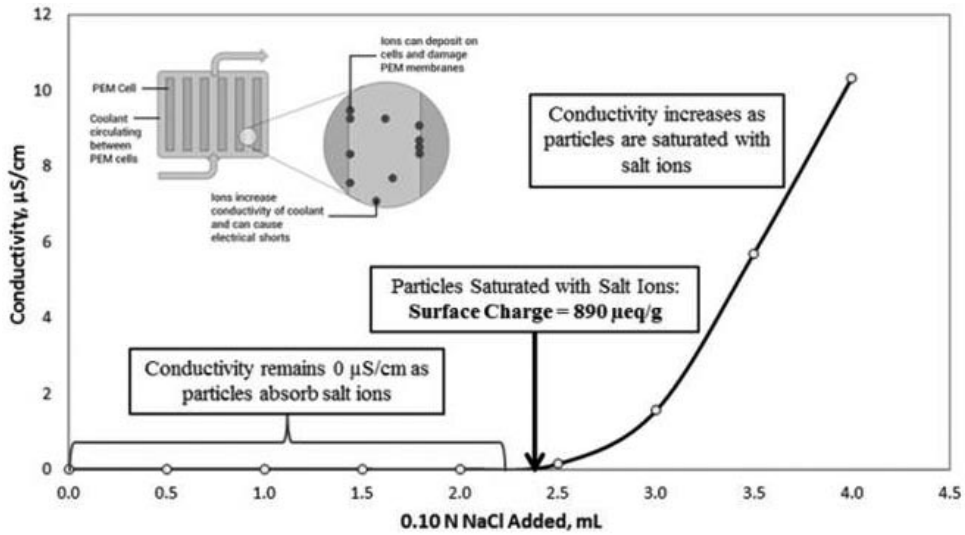

FIGURE 1. Change in electrical conductivity of reformulated nano-particle containing bioglycol-distilled water on addition of 0.10 N NaCl solution.

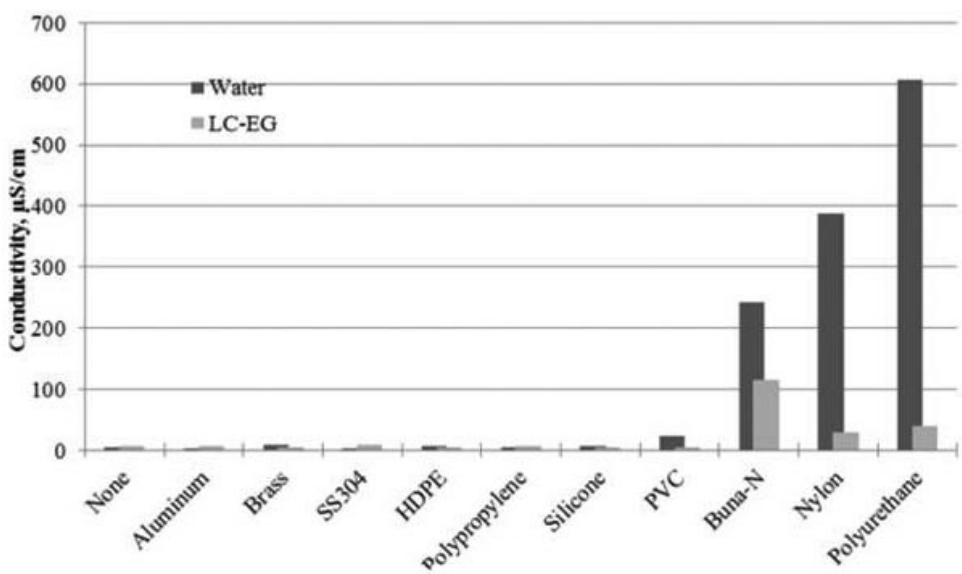

HDPE - high-density polyethylene; PVC - polyvinyl chloride

FIGURE 2. Change in electrical conductivity of materials subjected to 5,000 hour immersion testing in LC at 80°C.

bursting of pipes and blocked the coolants channels. On the other hand, Dynalene FC with an optimized concentration of nano-particles and surfactant was successfully circulated in the fuel cell stack.

CONCLUSIONS AND FUTURE DIRECTIONS

- Surface charge of the nano-particles increased to 890 µeq/g which surpassed the target of 500 µeq/g.
- Long-term material compatibility testing (5,000 hours) was completed for control glycol water, Dynalene LC, Dynalene FC and glycol water containing the individual components.
- The corrosion inhibitors were validated for both accelerated (electrochemical) and long-term (immersion) testing.
- UTK researchers completed and compared 100 hrs of testing of Dynalene fuel cell coolants in their working fuel cell with or without voltage application.
- The coolants showed a small change in electrical conductivity in the UTK fuel cell. Inductively coupled

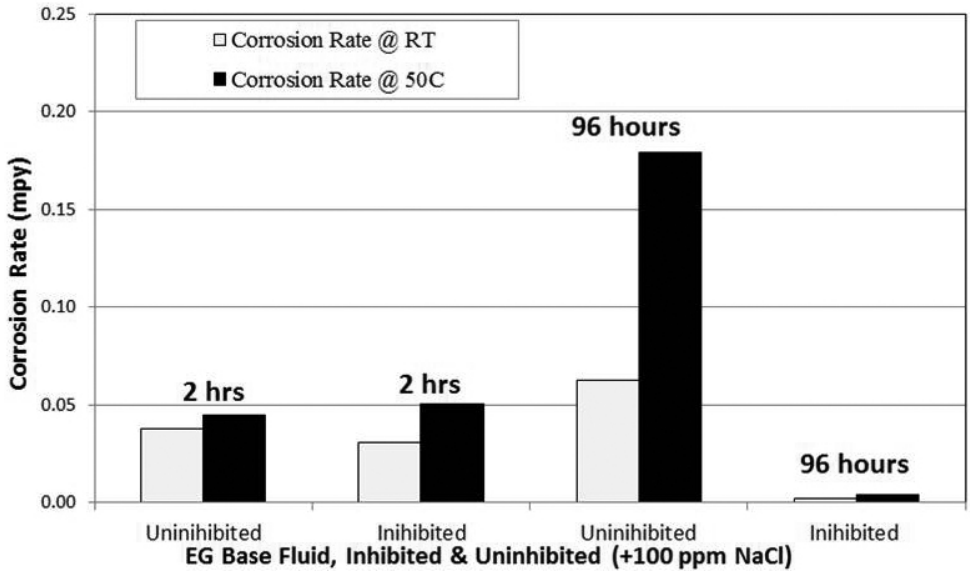

FIGURE 3. Effect of immersion time and temperature on the electrochemical behavior of Al alloy in inhibited and control glycol-water solution.

plasma analysis confirmed minimum leaching of ions in to the coolants.

- Dynalene is producing and selling Dynalene FC and LC to fuel cell companies.

Future work planned for the rest of the fiscal year:

- Continue surface and elemental characterization of the multiple fuel cell components that completed 5,000 hrs of testing.
- Continue high performance liquid chromatography and ion chromatography studies on the high-temperature treated glycol-water coolants to understand the degradation and breakdown of the glycols in to the component acids.
- On-going high-temperature testing of the nano-particles and surfactant at 110°C for 1,000 hrs to study their thermo-physical and degradation properties.
- Continue voltage testing with metal plates in nano-particles containing coolants to understand the coating effect of the nano-particles on the fuel cell plates.
- Perform 1,000 hrs of long-term testing with the coolants in the UTK fuel cell system.

FY 2013 PUBLICATIONS/PRESENTATIONS

1. Y. Garsany, S. Dutta and K.E. Swider-Lyons,"The Poisoning and Recovery of Pt/VC Electrocatalysts Contaminated with Glycol-Based Coolant Formulations" oral presentation at Pacific RIM Meeting, Honolulu, Hawaii, Oct. 7–12th 2012.

2. S. Dutta, K. Coscia, S. Mohapatra and P. McMullen, "Materials Compatibility and Corrosion in Glycol-Based Fuel Cell Coolants for Automotive Applications" poster and Symposium paper for Fuel Cell Seminar & Exposition 5–8th Nov. 2012, Uncasville, CT.

3. B.D. Gould, Y. Garsany, S. Dutta and K. Swider-Lyons, "Deactivation and recovery of polymer electrolyte fuel cells with commercial glycol-based coolants" paper submitted to 23rd North American Catalysis Society Meeting, June 2nd–7th, 2013, Louisville, Kentucky.

V.G.2 New High-Performance Water Vapor Membranes To Improve Fuel Cell Balance-of-Plant Efficiency and Lower Costs (SBIR Phase II)

Earl H. Wagener (Primary Contact), Brad P. Morgan
Tetramer Technologies L.L.C.
657 S. Mechanic St.
Pendleton, SC 29670
Phone: (864) 646-6282
Email: earl.wagener@tetramertechnologies.com

DOE Manager
Nancy L. Garland
Phone: (202) 586-5673
Email: Nancy.Garland@ee.doe.gov

Contract Number: DE-SC0006172

Project Start Date: September 17, 2012
Project End Date: September 16, 2014

Overall Objectives

- Develop improved low-cost water vapor membranes for cathode humidification modules in fuel cells.
- Synthesize new polymer molecular architectures, which avoid chemical degradation, increase water vapor transport and exhibit good mechanical durability at lower cost.
- Determine long-term stability of membranes through chemical resistance tests. In parallel, continue the synthesis of higher permeability polymer architectures.
- Down-select best candidates for scale up and provide prototypes to collaborators.

Fiscal Year (FY) 2013 Objectives

- Consistently produce membranes with permeance of 18,000 gas permeation units (GPU) at 85°C with no chemical degradation over 2,000 hours
- Durability of 2,000 hours with <20% drop in performance
- Crossover leak rate of <150 GPU
- Temperature durability of 90°C with excursions to 100°C
- Cost of <$10/m^2 at volumes of 2,500 kg/yr

Technical Barriers

This project addresses the following technical barriers from the Fuel Cell section (3.4) of the Fuel Cell Technologies Office Multi-Year Research, Development, and Demonstration Plan:

(A) Durability

(B) Cost

(C) Performance

Technical Targets

- Ionomer membrane performance optimization through improvements in molecular architecture.
- Durability improvement.
- Scale up of high performance materials to lower cost.

FY 2013 Accomplishments

- Synthesis of six new monomer and 12 new film forming polymer structures with key design elements.
- Extensive optimization of reaction conditions and purification methods resulting in higher yields and greater purity monomers and polymers.
- Characterization (nuclear magnetic resonance, mass spectrometry, elemental analysis, Fourier transform infrared spectroscopy and gel permeation chromatography) of these materials has been defined.
- New methods to prepare membranes with improved transport performance and durability have been identified.
- Determined that previous polymer structures would not reach the target water vapor permeation or mechanical stability goals.
- Demonstrated the ability to improve structures towards long-term stability through various means.
- Consistently met the target goal of crossover leak rate less than 150 GPU.
- Passed the 20,000-cycle hours durability test.
- Scaled up the down-selected polymer to 100 grams to verify cost projections.

✧ ✧ ✧ ✧ ✧

INTRODUCTION

Hydrogen fuel cells are one of the more promising alternative energy and propulsion systems with the most promising type of fuel cell for automotive and stationary power applications being the proton exchange membrane (PEM) fuel cell. PEMs have the advantage of high power density at the low operating temperatures required for

systems that will see frequent on/off cycling. One of the biggest challenges for PEM systems is the fact that PEMs perform much better with higher water environments to effectively conduct protons from the anode to the cathode of the cell. The design of a membrane humidifier unit as part of the balance of plant has been proposed and has been emphasized by DOE in the Multi-Year Research, Development, and Demonstration Plan in Table 3.4.9 and Table 3.4.10 to utilize the water produced as a byproduct of the oxygen reduction reaction to humidify the inlet air to the fuel cell [1].

The use of membrane humidifiers for fuel cell applications represents a reasonable value proposition; however, expanding the accessible markets for these membranes to increase volumes and lower manufacturing cost is also beneficial, particularly when the new applications satisfy the overall DOE objectives of saving energy. Dehumidification of feed air to heating, ventilation and cooling systems using these membranes can save as much as 40% of the energy required to condition air [2]. The membranes currently being commercialized do not meeting the desired size, weight and pressure drop requirements for automotive applications. More importantly the durability of current membranes has not been found to maintain performance due to degradation mechanisms of the membrane. In 2012, Gore reported that both their new perfluorosulfonic acid (PFSA) and hydrocarbon membranes suffered from detrimental loss in performance with a loss in permeance of up to 60% within 500 hours [3]. This loss in performance was attributed to the potential for anhydride formation and was confirmed using methods developed by Collette for PFSAs [4,5]. Gore also addressed a loss in performance from salt contamination where the membrane lost more than 70% of permeance after being converted to the corresponding sodium salt [3]. These possible means for loss in performance drove us to develop a more robust system, which alleviates these degradation mechanisms.

APPROACH

Nafion® has been found widely useful as an ion exchange membrane for chloroalkali cells, which has become a very profitable market and has kept the cost of the current PFSAs much higher than what would be needed for membranes within the fuel cell market. The demand for a cheaper membrane material that does not undergo detrimental side processes has been the inspiration for Tetramer's membrane development work. The evolution of Tetramer's basic ionomer technology with polymers designed for hydrogen ion transport in PEM fuel cells has led to a semifluorinated ionomer, whose identity will be released after intellectual property is established, that has equaled or exceeded the incumbent PFSA with significant (>50%) cost and processing advantages.

The development of water vapor transfer membranes at Tetramer during this project has met the initial target of reproducibly producing 18,000 GPU for water vapor permeance. Since thin, unsupported membranes have been found to possess mechanical deficiencies, a supported configuration that increases the mechanical durability of the membrane with minimal detriment to overall flux has been implemented. New membranes with unique polymer design elements that emphasize high water transport while alleviating possible means of performance degradation have been proposed and are the driving force for this contract. The synthesis of these new monomers and polymers has been demonstrated; optimization of polymer architecture is in progress and characterization of long-term water vapor transport by both Tetramer and industry partners are currently being explored.

RESULTS

The design and development of high-performance low-cost water vapor membranes for cathode humidification through unique polymer structures is being explored. The commercially available 25-µm (N111) and 50-µm (N112) Nafion® membranes do not meet the 18,000 GPU performance target herein, and neither does a Perma Pure™ device made with Nafion® hollow tube membranes. The water transfer permeance target of 18,000 GPU (gas permeation units, 1 GPU=1 x 10^{-6} cm^3(standard temperature and pressure)/(cm^2·s·cmHg) is a 50% increase over the 25-µm Nafion® N111. Tetramer membranes have been found to achieve the 18,000 GPU target consistently and are currently being explored to meet the need for minimal crossover, loss in performance over time, highest durability temperatures and lowest cost.

The need for unique polymer design for water vapor membranes has been addressed by Tetramer through a systematic approach in which four key polymer design elements were explored. These polymer design elements are summarized in Figure 1. The first and most critical parameter was to design a water permeability unit that consists of hydrophilic groups with ionic or intermolecular attractions. The selected polymer structures have potential for water transport without the possible side effects of anhydride formation. The need for mechanical strength has been addressed in our polymer design by incorporating rigid, hydrophobic structures that impart toughness and keep the material from becoming water-soluble. Synthetic chemistry groups such as McGrath's at Virginia Tech have explored this key parameter with critical design elements including the need for block copolymers with hard/soft segments [6]. This concept has inspired some of the current materials being explored, which have shown promise. The need for processability has received a great deal of attention especially within the membrane world. To make high quality uniform thin films, the need to either melt process or solution cast the

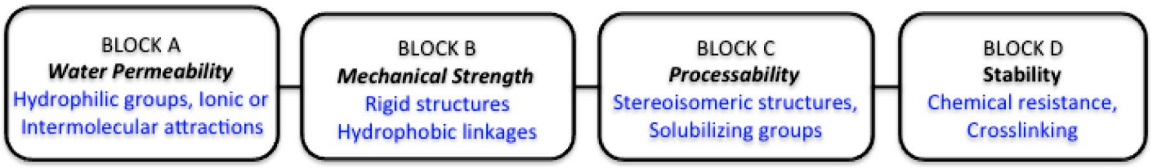

FIGURE 1. Water Vapor Membrane Polymer Design Elements

polymer can be addressed by the inclusion of stereoisomeric structures to disrupt packing as well as solubilizing groups. The last parameter addressed has been stability in which specific synthons have been chosen to ensure chemical resistance, as well as chemical groups that allow for crosslinking have been incorporated into the polymer design to impart an additional robustness for the material.

To evaluate membranes for water vapor transport quickly without the need of assembling a full-scale fuel cell system, we have acquired a testing unit from one of our collaborators, MTR and have duplicated the testing conditions that General Motors (GM) used during automotive applications. GM will continue to test our membranes in parallel, which will help speed up our evaluations. GM's testing system is projected to be operational by mid-August. These parameters are summarized in Figure 2 and are currently being explored for all membranes prepared as an initial screening method to evaluate the membranes. For the new structures synthesized to date, five of these new polymer structures have achieved between 17,000 and 20,000 GPU, as seen in Figure 3. The membranes from these were then tested for anhydride formation using the methods developed by Collette [4,5]. These membranes have been exposed to 80°C for 240 hours and 140°C for 4 hours, after which no anhydride formation was observed as seen in Figure 4 [7,8].

The development of these membranes is still being pursued and increasing the permeance of the current materials while maintaining these transport properties over long-term durability studies is critical to the success of the project. The testing of these polymers for any signs of degradation will be critical followed by an increase in operation temperatures. The down-selected materials from this study will be tested by our industry partners under their conditions to ensure we meet the design demands for today's humidification technology needs.

FUTURE DIRECTIONS

- Continue durability tests at higher temperatures (95°C) and longer times to assure chemical resistance. In parallel, continue synthesis of new polymer architectures to increase water vapor transport from 20,000 GPU to 30,000 GPU.
- Utilize initial results to optimize membrane durability to less than 20% loss in performance after 2,000 hours.

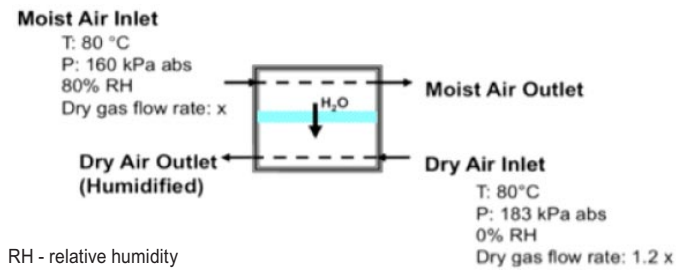

FIGURE 2. Test Conditions for Water Vapor Transport Membranes

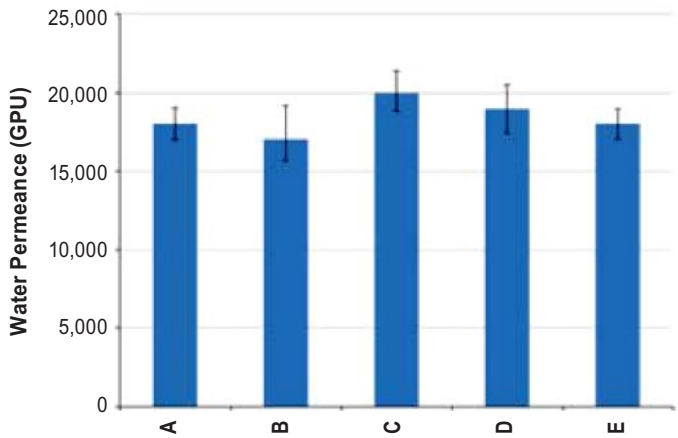

FIGURE 3. New Membranes Initial Performance

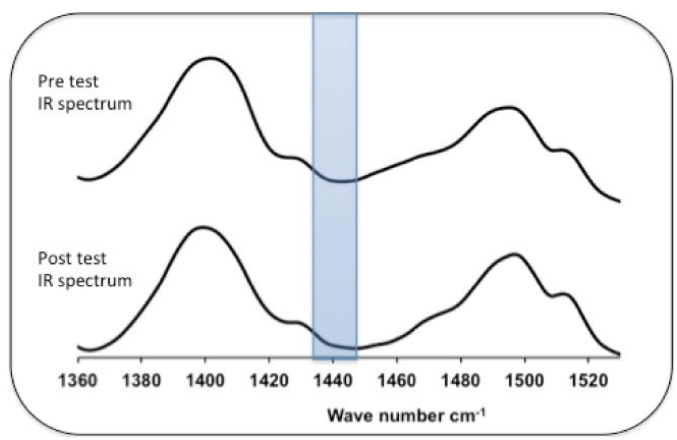

FIGURE 4. Fourier Transform Infrared Spectroscopy of Membrane Pre-Heat Treatment and Post-Heat Treatment at 80°C for 240 Hours

- Use these new molecular architectures to increase temperature durability from 80°C to 90°C with excursions of 100°C.
- Automotive prototype membrane performance testing.
- Down-selected membranes will be tested for non-automotive prototype membrane performance using module prototype production.

FY 2013 PUBLICATIONS/PRESENTATIONS

1. Wagener, Earl H.; Morgan, Brad P. "New High Performance Water Vapor Membranes To Improve Fuel Cell Balance of Plant Efficiency and Lower Costs", DOE Annual Merit Review, Crystal City, VA, May 14, 2013, Oral Presentation fc102, available from www.hydrogen.energy.gov.

REFERENCES

1. Fuel Cell Technologies Office Multi-Year Research, Development and Demonstration Plan, Department of Energy Office of Energy Efficiency and Renewable Energy 3.4 – 24 (2012).

2. Zhang, Yinping; Jiang, Yi; Zhang, Li Zhi; Deng, Yuchun; Jin, Zhaofen "Analysis of thermal performance and energy savings of membrane based heat recovery ventilator", Energy, 25, 515-527 (2000).

3. Johnson, William. B. "Materials and Modules for Low-Cost, High Performance Fuel Cell Humidifiers", DOE Annual Merit Review, Crystal City, VA, May 17, 2012, Oral Presentation fc067, available from www.hydrogen.evergy.gov.

4. Collette, Floraine M.; Lorentz, Chantal; Gebel, Gerard; Thominette, Francette, "Hygrothermal aging of Nafion", Journal of Membrane Science, 330(1-2), 21-29 (2009).

5. Collette, Floraine M.; Thominette, Francette; Escribano, Sylvie; Ravachol, Angèle; Morin, Arnaud; Gebel, G., "Fuel cell rejuvenation of hygrothermally aged Nafion", Journal of Power Sources, 202, 126-133 (2012).

6. Hickner, Michael A.; Ghassemi, Hossein; Kim, Yu Seung; Einsla, Brian R.; McGrath, James E. "Alternative Polymer Systems for Proton Exchange Membranes (PEMs)", Chem. Rev., 104, 4587-4612 (2004).

7. Wagener, Earl H.; Morgan, Brad P. "New High Performance Water Vapor Membranes To Improve Fuel Cell Balance of Plant Efficiency and Lower Costs", DOE Annual Merit Review, Crystal City, VA, May 14, 2013, Oral Presentation fc102, available from www.hydrogen.energy.gov.

8. Wagener, Earl H.; Morgan, Brad P. "New High Performance Water Vapor Membranes To Improve Fuel Cell Balance of Plant Efficiency and Lower Costs", DOE Annual Merit Review, Crystal City, VA, May 15, 2012, Poster Presentation fc102, available from www.hydrogen.energy.gov.

V.G.3 Roots Air Management System with Integrated Expander

Dale Stretch (Primary Contact), William Eybergen, Brad Wright
Eaton Corporation
W126N7250 Flint Drive
Menomonee Falls, WI 53051-4404
Phone: (248) 226-6799
Email: DaleAStretch@Eaton.com

DOE Manager
Jason Marcinkoski
Phone: (202) 586-7466
Email: Jason.Marcinkoski@ee.doe.gov

Contract Number: DE-EE0005665

Subcontractors:
- Ballard Power Systems, Burnaby, BC, Canada
- Kettering University, Flint, MI
- Electricore, Inc., Valencia, CA

Project Start Date: July 5, 2012
Project End Date: July 4, 2015

Overall Objectives

Primary Objectives

- 62/64% (baseline 2011), >65/70% (target 2017), compressor/expander efficiency at 25% of full flow
- 80% (baseline 2011), >90% (target 2017), combined motor/motor controller efficiency full flow
- 11.0/17.3 kW (baseline2011), <8/14 kW (target2017), compressor/expander input power at 100% of full flow

Secondary Objectives

- Meeting all 2017 project target objectives in Table 1
- Conduct a cost reduction analysis to identify areas for additional possible cost reductions

A fully tested and validated TRL 7 air management system hardware capable of meeting the 2017 project targets in Table 1 will be delivered at the conclusion of this project.

Fiscal Year (FY) 2013 Objectives

- Tune the peak efficiency island of the compressor to best fit the primary objective of 14.0-kW input power @ 100% of full flow and 2.0-kW input power @ 25% of full flow.
- Design rotor configuration of the expander to optimize output power of the expander to best fit the primary objective of 6.0-kW input power @ 100% of full flow and 1.0-kW input power @ 25% of full flow.
- Develop compressor/expander and motor concept to meet the primary objective of 8.0-kW input power @ 100% of full flow and 1.0-kW input power @ 25% of full flow.
- Develop compressor and expander computational fluid dynamics (CFD) capability (demonstrate ability to model compressor case clearances of 40 µm and rotor clearance of 80 µm) and optimize the roots compressor and expander inlet, outlet and rotor geometry to position peak efficiency islands to maximize the performance of the cathode air system.
- Develop expander plastic rotors that meet the application requirements.
- Supply compressor and expander performance data and maps, Ballard 75-kW module data to Argon National Laboratory. The models will be used to determine the optimal compressor expander combination to maximize the Ballard FC module performance.

Technical Barriers

This project addresses the following technical barriers from the Fuel Cells section of the Fuel Cell Technologies Office Multi-Year Research, Development, and Demonstration Plan:

(B) Cost: Reduce by ~50%

(C) Performance
- Reduce power by ~30%
- Motor efficiency: increase by ~40%
- Compressor efficiency: increase by ~5%
- Expander efficiency: increase by ~9%

Technical Targets

A fully tested and validated TRL 6 air management system hardware capable of meeting the 2017 project targets in Table 1 delivered at project conclusion.

FY 2013 Accomplishments

Optimize Compressor

- Improved the compressor/expander test rig by adding relative humidity and inlet temperature control.
- Reduced the compressor power consumption on tested hardware from 15.6 kW to 14.7 kW by increasing the rotor helix angle.

TABLE 1. 2015 and 2017 Project Targets

Characteristic	Units	Current Status	Project Target 2015	DOE Target 2017
Input power[a] at full flow[b] (with expander/without expander)	kWe	9.9/13.8	8/14	8/14
Combined motor and motor controller efficiency at full flow[b]	%	90	90	90
Compressor/expander efficiency at full flow (compressor/ expander only)[b]	%	68/64	75/75	75/80
Input power at 25% flow[c] (with expander/without expander)	kWe	1.3/1.7	1.0/2.0	1.0/2.0
Combined motor and motor controller efficiency at 25% flow[c]	%	70	80	80
Compressor/expander efficiency at 25% flow[c]	%	61/70	65/70	65/70
Input power at idle[d] (with/without expander)	We	TBD/270	200/200	200/200
Combined motor/motor controller efficiency at idle[d]	%	TBD	?	70
Compressor/expander efficiency at idle[d]	%	TBD	60/60	60/60
Turndown ratio (max/min flow rate)		20	20	20
Noise at maximum flow (excluding air flow noise at air inlet and exhaust)	dB(A) at 1 meter	65 (with enclosure and suppression)	65 (with enclosure and suppression)	65
Transient time for 10-90% of maximum airflow	sec	1	1	1
System volume[e]	liters	15	15	15
System weight[e]	kg	16	15	15
System cost[f]	$	TBD	500	500

[a] Electrical input power to motor controller when bench testing fully integrated system. Fully integrated system includes control system electronics, air filter, and any additional air flow that may be used for cooling.
[b] Compressor: 92 g/s flow rate, 2.5 bar (absolute) discharge pressure; 40°C, 25% relative humidity (RH) inlet conditions. Expander: 88 g/s flow rate, 2.2 bar (absolute) inlet pressure, 70°C, 100% RH inlet conditions.
[c] Compressor: 23 g/s flow rate, minimum 1.5 bar (absolute) discharge pressure; 40°C, 25% RH inlet conditions. Expander: 23 g/s flow rate, 1.4 bar (absolute) inlet pressure, 70°C, 100% RH inlet conditions.
[d] Compressor: 4.6 g/s flow rate, minimum 1.2 bar (absolute) discharge pressure; 40°C, 25% RH inlet conditions. Expander: 4.6 g/s flow rate, <compressor discharge pressure, 70°C, 20% RH inlet conditions.
[e] Weight and volume include the motor, motor controller and system enclosure.
[f] Cost target based on a manufacturing volume of 500,000 units per year.
[g] DTI cost model of the Honeywell 100,000 rpm machine, 2.5 bar (absolute), 92 g/s, dry air, 40°C: $960 including markup. TIAX 2009 estimate of Honeywell technology (compressor, expander, motor, motor controller) presented at 2010 Annual Merit Review and Peer Evaluation: $790 including 15% markup.
TBD – to be determined

- Increased the compressor pressure ratio on tested hardware from 2.4 to 2.6 by increasing the rotor helix angle.
- Theoretically estimated the final compressor design to have a power consumption of 13.8 kW. This compressor is 38% smaller than the compressor tested where 14.7 kW was achieved.

Optimize Expander

- Increased the expander power production on tested hardware from 3.2 kW to 3.5 kW by the addition of a diverter on the inlet port.
- Determined the optimal inlet port angle, for power production, on the tested expander. The 60 deg inlet angle had a 0.3 kW greater power than the 90 deg (which was the worst performer).
- Increased the expander pressure ratio on tested hardware from 1.6 to 1.75 by optimizing the inlet port diverter shape.
- Theoretically estimated the final expander design to have a power production of 3.9 kW.

Develop Compressor/Expander Assembly with Integrated Motor

- Created layout of expander, compressor and motor integrated system that optimized the system performance but minimized bearing and gear part count. Current part count of major components is 35 which include 10 bearings and seven gears.
- Designed and analytically optimized plastic rotors to meet speed and load requirement. Final design with aluminum insert can spin up to 20,000 rpm @ 150ºC. This is sufficient for all operating conditions the expander will experience.
- Designed plastic rotor mold and determined porting that would optimize the root fiber content.
- Worked with Argonne National Laboratory to develop roots compressor and expander models for Period 2 fuel cell system modeling optimization. Validated their models with empirical data.

Modeling

- Improved the ability to more accurately model Roots expanders and compressors by reducing the model tip to root and tip to wall clearances. Clearances were reduced from 600 µm to <100 µm, a six-fold reduction. This will provide a more accurate optimization tool for optimizing the compressor and expander inlet and outlet and root geometries.

✧ ✧ ✧ ✧ ✧

INTRODUCTION

Proton exchange membrane (PEM) fuel cells remain an emerging technology in the vehicle market with several cost and reliability challenges that must be overcome in order to increase market penetration and acceptance. The DOE has identified the lack of a cost-effective, reliable, and efficient air supply system that meet the operational requirements of a pressurized PEM 80-kW fuel cell are some of the major technological barriers that must be overcome. This project will leverage roots blower advancements and develop and demonstrate an efficient and low-cost fuel cell air management system. Eaton will build upon our newly developed P-Series roots blower and shift the peak efficiency making it ideal for use on an 80-kW PEM module. Advantages to this solution include:

- Lower speed of the roots blower eliminates complex air bearings present on other systems.
- Broad efficiency map of roots systems provide an overall higher drive cycle fuel economy.
- Core roots machine technology has been developed and validated for other transportation applications.

Eaton will modify their novel R340 Twin Vortices Series (TVS) roots-type supercharger for this application. The TVS delivers more power and better fuel economy in a smaller package as compared to other supercharger technologies. By properly matching the helix angle with the rotor's physical aspect ratio the supercharger's peak efficiency can be moved to the operating range where it is most beneficial for the application. The compressor will be designed to meet the 92 g/s flow at a pressure ratio of 2.5, similar in design to the R-Series 340. A net shape plastic expander housing with integrated motor and compressor will significantly reduce the cost of the system.

APPROACH

The approach will be to leverage recent advancements to and further develop roots compressor and expander technology by leveraging the broad efficiency map of Eaton's TVS compressor to improve the overall fuel cell drive cycle fuel economy. In Period 1, the project will optimize the expander and compressor individually at the specified requirements, with an integrated expander, compressor and motor concept as the final deliverable. The primary goal will be meet the power and efficiency objects. The secondary objective is to reduce subsystem cost by keeping part count low by developing a net shape plastic expander housing and rotor. This work will be supplemented with CFD analysis to help optimize the expander and compressor performance and system analysis which will help optimize the integrated system

Period 2 will finalize the integrated concept, then build and test the integrated system and individual subsystems. The last phase (3) will be to incorporate the roots air management system with integrated expander into an overall hydrogen and fuel cells application. This will include designing, building and testing the complete system.

RESULTS

The team continued to development the compressor, expander and finalized the system concept using both experimental and analytical methods in the last three months.

Inlet Outlet Expander CFD

This last quarter improvements were made on the CFD modeling capability. CFD analysis of the supercharger-expander with 300-µm gap width clearances using the STAR-CCM+ software were achieved in the first quarter of this year, but calculations of torque did not correlate very well with the experimental data so refinement to the gap clearances was pursued. This pursuit proved to be difficult because the smaller gap width need for better accuracy cause the "off the shelf" available software to crash during the mesh generation process. Hence, it was decided to acquire specialized software that would generate a refined mesh and not crash during analysis. Results show that the rotor torque correlation is more accurate. Additional work is needed on the flow correlation, but this is believed to be a much easier problem to solve by using a more refined mesh and by adjusting some of the input parameters.

Expander Test Stand

Inlet air temperature control was added to the test stand, by using an air-to-liquid heat exchanger and by incorporating controlled temperature conditioning equipment. Relative humidity control was added to the airflow stream via pulse width modulated solenoid injector and a high-pressure pump.

Expander Test Results

An expander with the highest efficiency possible and meet DOE power and efficiency targets, lessons learned from testing were as follows. The direction of rotation has been

determined through testing existing compressor designs as expanders with forward and reverse rotations. Reverse rotation, opposite of compressor rotation, consistently produces 5-10% improvement over a standard rotation arrangement. A multitude of inlet variations have been tested with a 60°, measured from perpendicular to rotor axis, inlet produces the best results. The 60° inlet will also contain optimized diverter geometry to shift the peak efficiency island toward the expander's operating targets. The inlet must be a minimum of 45-mm inside diameter to support a 250 cc expander displacement. The V250 Gen 2 rotors feature an increased root radius and provide increased efficiency over the Gen 1 rotors by eliminating a leak path from the rotor's root to the bearing bore. The optimized V250 expander will incorporate these parameters with input from the CFD model to create the V250 optimized expander. Performance estimates for the V250, optimized to DOE specifications, are 0.38 kW @ 25% full flow and 3.98 kW @ 100% full flow.

Compressor Test Results

The optimized compressor will leverage both P400 and R340 designs to create a reduced displacement, high helix angle compressor capable of 2.5 pressure ratio with power consumption under the DOE target of 14 kW. The increased helix angle of the P400 allowed the unit to reach pressure ratios over 2.6 without exceeding the temperature limits of the compressor. The increased helix angle of the P400 rotor, when applied to the R340 rotor, will reduce its overall length and displacement creating a high helix angle compressor with a displacement of 260cc/rev named P260. This change will increase the operating speed of the compressor and shift the 25% full flow and 100% full flow operating points towards the peak efficiency island. Performance estimates for the P260 compressor, at DOE specified conditions, should be 1.7 kW @ 25% full flow and 13.8 kW @ 100% full flow.

Develop Compressor/Expander with Integrated Motor

The system concept design, Figure 1, consists of an expander coupled to a motor through a gear ratio, and a compressor directly coupled to the opposite side of the motor. This configuration, instead of a non-geared direct drive design, is driven by the need to operate the compressor and expander at their individual optimized speeds, which are

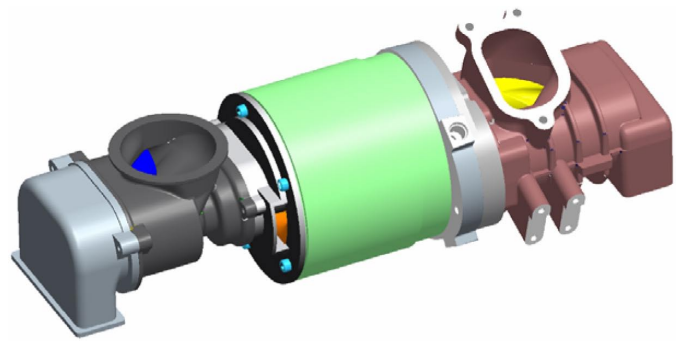

FIGURE 1. Fuel Cell Air System (Expander/Motor/Compressor)

not the same. Testing to date has shown that to optimize the complete system, a gear ratio between 1.7 and 3.0 is needed. The final ratio will be determined when the final compressor and expander testing is complete.

System performance utilizing exisiting hardware, a P400 compressor and V250 expander, is estimated to be 1.4 kW at 25% full flow and 10.9 kW at 100% full flow. After changing to an optimized compressor and expander combination, a P260 compressor and V250 optimzed expander, estimated system performance is 1.3 kW at 25% full flow and 9.9 kW at 100% full flow, Table 2.

Expander Plastic Rotor

The runner system for the rotor injector mold was optimized through mold flow simulation. Initial design was a pin gate located at the tip of each of the four lobes. Fibers were highly oriented at the gate location on the lobe tip and became increasingly more random towards the root. In an effort to increase fiber orientation at the root, and thereby increase the root strength, a second runner system was designed and evaluated. The final design has a runner system with eight pin gates that are located in the root at two points. The resulting fiber orientation increased the alignment in the root region with random fiber orientation at the tip. The 8-pin runner system was implemented into the final tool design and tool fabrication has been started.

TABLE 2. Predicted P260 Compressor, V250 Optimized System Performance

Predicted System Performance at DOE Conditions					
Unit		25% Target		100% Target	
		Power	System Pwr	Power	System Pwr
		kW	kW	kW	kW
Compressor	P260	1.67	**1.30**	13.8	**9.9**
Expander	V250 Opt	-0.38		-3.98	

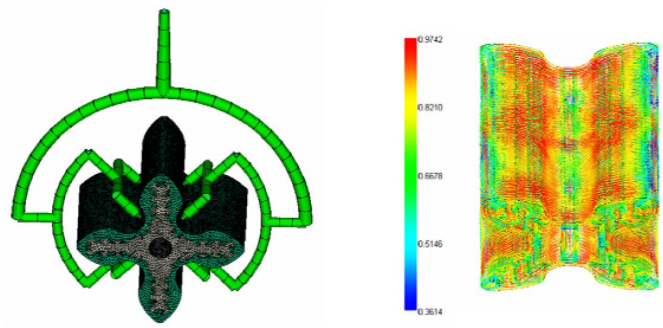

Red = highly oriented and Blue = random

FIGURE 2. 8-Pin Runner System and Fiber Orientation

CONCLUSIONS AND FUTURE DIRECTIONS

Period 1 Conclusions

Delivered concept design of the compressor/expander assembly with integrated motor that projected to meet the project performance targets of:

Full Flow Conditions

- Input power (with expander) projected to be 9.9 kW not 8 kW
- Input power (with expander and heat recovery) projected to be 9.4 kW not 8 kW
- Input power (without expander) projected to meet 13.8 kW vs 14 kW
- Motor plus motor controller efficiency projected to meet 90%

25% Flow Conditions

- Input power (with expander) projected to be 1.3 kW not 1 kW
- Input power (with expander and heat recovery) projected to be 1.2 kW not 1 kW
- Input power (without expander) projected to meet 1.7 kW vs. 2 kW
- Motor plus motor controller efficiency projected to be 70% not 80%

Idle Flow Conditions

- Input power (with expander) to be determined
- Input power (without expander) projected to be 270 W not 200 W
- Motor + motor controller efficiency to be determined

Future Directions

- Prototype Eaton compressor/expander with integrated motor:
  - Finalize detail drawing package and release for fabrication
  - Procure prototype components
  - Inspect, assemble, debug prototypes to verify functionality
  - Develop production cost estimates
  - Document volume production cost model and identify opportunities, design and process changes that will improve cost
- Design, build, procure and debug Eaton performance stand test rig
- Conduct performance and validation testing at Eaton:
  - Write test plan/determine test criteria
  - Measure and document using maps and excel data sheets
  - Conduct test at the specified target conditions
  - Document results with performance maps
  - Measure system weight and system volume including motor, controller, and system enclosure

FY 2013 PRESENTATIONS

1. Eybergen, Bill, Roots Air Management System with Integrated Expander, U.S. DRIVE Technical Meetings - Fuel Cell Tech Team (FCTT), December 19, 2012.

2. Stretch, Dale, Roots Air Management System with Integrated Expander, DOE Merit Review - Fuel Cell Tech Team (FCTT), May 14, 2013.

V.H.1 Fuel Cells Systems Analysis

Rajesh K. Ahluwalia (Primary Contact),
Xiaohua Wang
Argonne National Laboratory
9700 South Cass Avenue
Argonne, IL 60439
Phone: (630) 252-5979
Email: walia@anl.gov

DOE Manager
Nancy Garland
Phone: (202) 586-5673
Email: Nancy.Garland@ee.doe.gov

Project Start Date: October 1, 2003
Project End Date: Project continuation and direction determined annually by DOE

Overall Objectives

- Develop a validated model for automotive fuel cell systems, and use it to assess the status of the technology.
- Conduct studies to improve performance and packaging, to reduce cost, and to identify key R&D issues.
- Compare and assess alternative configurations and systems for transportation and stationary applications.
- Support DOE/U.S. DRIVE automotive fuel cell development efforts.

Fiscal Year (FY) 2013 Objectives

- Validate the stack model for fuel cells with 3M's nano-structured thin-film (NSTF) catalysts in membrane electrode assemblies (MEAs).
- Develop a model for air management system with Roots compressors and expanders.
- Validate the cross-flow humidifier model using data for a prototype unit with Gore's sandwich membranes.
- Update the performance of the reference automotive fuel cell system using recent data for system components.

Technical Barriers

This project addresses the following technical barriers from the Fuel Cells section of the Fuel Cell Technologies Office Multi-Year Research, Development, and Demonstration Plan:

(B) Cost

(C) Performance

Technical Targets

This project is conducting system level analyses to address the following DOE 2020 technical targets for automotive fuel cell power systems operating on direct hydrogen:

- Energy efficiency: 60% at 25% of rated power
- Q/ΔT: 1.45 kW/°C
- Power density: 850 W/L for system, 2,500 W/L for stack
- Specific power: 650 W/kg for system, 2,000 W/kg for stack
- Transient response: 1 s from 10% to 90% of maximum flow
- Start-up time: 30 s from –20°C and 5 s from +20°C ambient temperature
- Precious metal content: 0.125 g/kW (rated)

FY 2013 Accomplishments

- Collaborated with 3M in taking cell data to validate the model for NSTF catalyst-based MEAs and stacks.
- Developed a kinetic model for the oxygen reduction reaction on PtCoMn/NSTF catalyst.
- Developed a kinetic model for hydrogen oxidation and hydrogen evolution reactions on PtCoMn/NSTF catalyst.
- Developed a neural network model for mass transfer overpotentials in PtCoMn/NSTF cathode catalyst.
- Developed and validated a model for mass transfer overpotentials in PtCoMn/NSTF anode catalyst because of nitrogen buildup.
- Conducted a preliminary study to investigate the impact of the heat rejection constraint (Q/ΔT) on fuel cell system cost and performance.

✧ ✧ ✧ ✧ ✧

INTRODUCTION

While different developers are addressing improvements in individual components and subsystems in automotive fuel cell propulsion systems (i.e., cells, stacks, balance-of-plant components), we are using modeling and analysis to address issues of thermal and water management, design-point and part-load operation, and component-, system-, and vehicle-level efficiencies and fuel economies. Such analyses are essential for effective system integration.

APPROACH

Two sets of models are being developed. The GCtool software is a stand-alone code with capabilities for design, off-design, steady state, transient, and constrained optimization analyses of fuel cell systems (FCSs). A companion code, GCtool-ENG, has an alternative set of models with a built-in procedure for translation to the MATLAB®/Simulink® platform commonly used in vehicle simulation codes, such as Autonomie.

RESULTS

In FY 2013, we continued to collaborate with 3M to obtain reference performance data on 50-cm^2 active area single cells using MEAs that consisted of 3M 24-µm membrane (850 equivalent weight), ternary $Pt_{0.68}Co_{0.3}Mn_{0.02}$ NSTF catalyst, and 3M gas diffusion layers (GDLs) made by applying a hydrophobic treatment to a backing paper and a micro-porous layer [1]. The Pt loading was 0.050 $mg.cm^{-2}$ in the anode and 0.054, 0.103, 0.146, or 0.186 $mg.cm^{-2}$ in the cathode. All cells were first conditioned using a "thermal cycling" process, described in detail in Steinbach et al. [2], which consisted of repeated temperature and voltage cycles over a period of 2-3 days until stable performance was reached. The polarization curves were obtained for different temperatures (30-90°C), inlet pressures (1-2.5 atm), inlet relative humidities (25-100%), and stoichiometries for the cathode (1.5-10) and the anode (1.2-5) by running galvanodynamic scans at cell current densities varying from 0.02 to 2 $A{\cdot}cm^{-2}$. The cell was held for 120 s at each current step and the cell voltage and the high-frequency resistance (from alternating current impedance measurements) were recorded every 5 s. Prior to the start of the experiments, for each cell, the electrochemical surface area (ECSA) was determined by cyclic voltammetry, the hydrogen crossover current density and cell short resistance were determined by measuring the plateau currents, and the mass activity of Pt was measured in H_2/O_2 at 80°C, 1-atm reactant H_2 and O_2 pressures, and 100% relative humidity (RH).

Oxygen Reduction Reaction (ORR) Kinetics

We used the polarization data at low current densities (<0.5 $A{\cdot}cm^{-2}$) to determine the kinetic constants for the ORR on PtCoMn/NSTF catalyst. We found that the kinetic data could be correlated with a single Tafel equation and a transfer coefficient that is a function of the relative humidity [3]. The correlation indicates a 0.36 order for the O_2 partial pressure, 39.5 $kJ{\cdot}mol^{-1}$ activation energy for the temperature dependence, and an additional 0.9 order for RH dependence. The calculated mass activities and specific activities at 0.9 V ohmic resistance corrected cell voltage, 1 atm H_2 and O_2 partial pressures, 80°C and 100% RH agree well with the measured values of 0.13-0.25 $A{\cdot}mg_{Pt}^{-1}$ and 1.7-2.0 $mA{\cdot}cm_{Pt}^{-2}$ for the cells with different Pt loading.

Hydrogen Oxidation Reaction (HOR) Kinetics

We analyzed the kinetics of the HOR and hydrogen evolution reaction (HER) on PtCoMn/NSTF catalyst by operating the 50-cm^2 cells in H_2 pump mode with supersaturated feeds at 45-90°C and 0.7-2.5 atm H_2 partial pressures. The results showed that the HOR and HER are completely reversible, and that both of these reactions can be described by the same Butler-Volmer kinetics with first-order dependence on the H_2 partial pressure [4]. The specific exchange current density for the 2-electron HOR/HER on the NSTF ternary catalyst, derived from the measured polarization curves, is 489 $mA{\cdot}cm_{Pt}^{-2}$ at 80°C and 1-atm H_2 partial pressure. The temperature dependence of the exchange current density is consistent with an activation energy of 38.9 $kJ.mol^{-1}$. Compared to dispersed Pt/C catalyst with an ultralow 0.003 $mg.cm^{-2}$ Pt loading, the HOR kinetics on NSTF catalyst with 0.05-0.10 $mg.cm^{-2}$ Pt loading was 60-110% faster on an area-specific basis, but it was slower on a mass basis. The measured HOR/HER kinetics is a function of the state of the catalyst in that the specific exchange current density increased by 460% when the anode catalyst was conditioned with the same protocol normally used for the cathode catalyst.

Cathode Mass Transfer

We used the measured polarization curves, HFRs, mass activities, ECSAs, and H_2 crossover current density to develop, train, and validate an artificial neural network for cathode mass transfer and ohmic overpotentials. We determined the weights and biases for the multilayer perceptron feed-forward network with one hidden layer and 20 neurons using hyperbolic tangent as the activation function. Figure 1 compares the modeled artificial neural network mass transfer overpotentials with the data derived from four series of tests that varied cell temperature, cell pressure, inlet relative humidity and cathode Pt loading. In agreement with data, the model shows increasing mass transfer overpotentials (η_{mc}) as the cell temperature (Figure 1a) or pressure (Figure 1b) is lowered while maintaining exit RH at 100%. The dependence of η_{mc} on inlet RH is more complex in Figure 1c since the highest mass transfer overpotentials do not occur under wettest conditions. Similar to data for dispersed Pt/C, the NSTF catalyst system also shows higher mass transfer overpotentials as the Pt loading is decreased (Figure 1d).

Anode Mass Transfer

A special series of tests was designed to determine the anode mass transfer overpotentials (η_{ma}) due to N_2 buildup. These tests were run with 0-75% N_2 in feed H_2 and variable anode stoichiometry and cathode dew points. The temperature was varied between 70 to 85°C at 1.5-2.5 atm. Figure 2 shows the effect of N_2 buildup on anode overpotentials estimated as the differences in measured cell

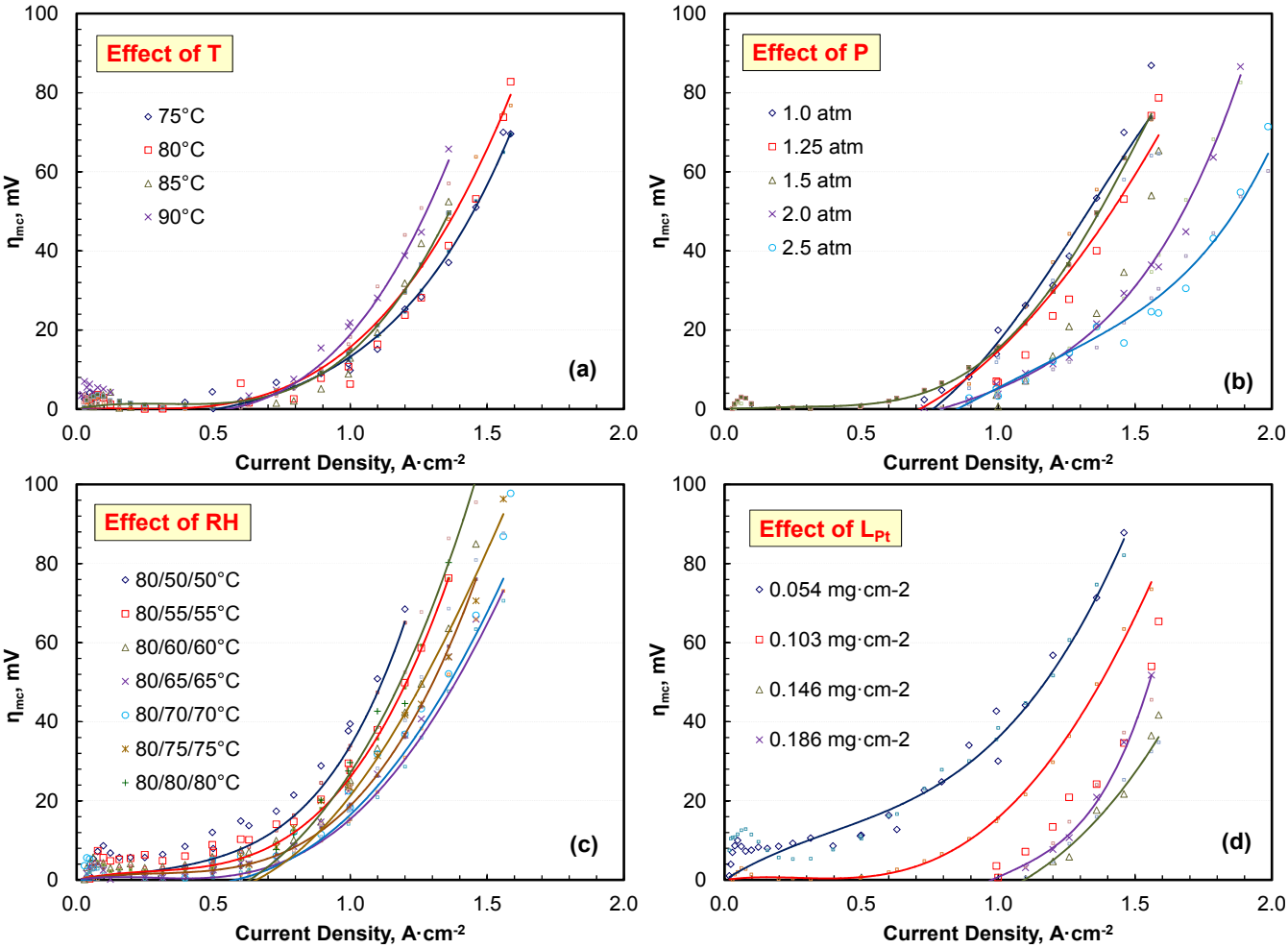

FIGURE 1. Validation of the artificial neural network model for cathode mass transfer overpotentials. The variables are: a) cell temperature and inlet RH (1.5 atm, 0.104 mg_{Pt}·cm^{-2} in cathode); b) inlet pressure and inlet RH (80°C, 0.104 mg_{Pt}.cm^{-2} in cathode); c) inlet relative humidity (1.5 atm, 80°C, 0.104 mg_{Pt}.cm^{-2} in cathode); and d) cathode Pt loading (1.5 atm, 80°C).

voltages with and without N_2 in feed H_2. The data in Figure 2 were used to derive and correlate anode mass transfer coefficient as a function of Reynolds number, pressure, temperature, and H_2 fraction. The correlation was used to develop a model to determine performance losses due to HOR kinetics, anode mass transfer and decrease in Nernst potential with N_2 buildup. The results from this model are shown as solid lines and compared with test data in Figure 2.

Model Validation

The above correlations for ORR kinetics, HOR kinetics, cathode mass transfer, and anode mass transfer have been incorporated in a multi-nodal model that determines the current density distribution along the cell, concentration (H_2, O_2, N_2, H_2O vapor) fields in the counter-flowing anode and cathode streams, liquid water movement across the catalyst layers and GDLs, water transport across the membrane, and temperature fields. The model was calibrated against the cell voltages measured in the 50-cm^2 performance tests. The calibration is shown as a parity plot in Figure 3 for the performance data at 1.5, 2.5, and 3 atm for different temperatures, RH, cathode/anode stoichiometries, and Pt loadings in cathode catalyst. In general, the model results compare well with the experimental data ($R^2 > 0.987$) and the agreement is even better at higher pressures.

System Performance

The cell model is being used to evaluate the performance of an NSTFC stack in an 80-kW_{net} fuel cell system (see [5,6] for system configuration). The initial focus of the study is on the effect of the heat rejection target ($Q/\Delta T = 1.45$) on system cost and performance. Here Q is the waste heat produced in the stack and ΔT is the difference between the coolant stack outlet temperature and the ambient (heat sink) temperature taken as 40°C. Figure 4 summarizes the results from an optimization study that minimized the system cost [7] subject to the constraint of specified $Q/\Delta T$. The variables to be optimized were coolant outlet temperature,

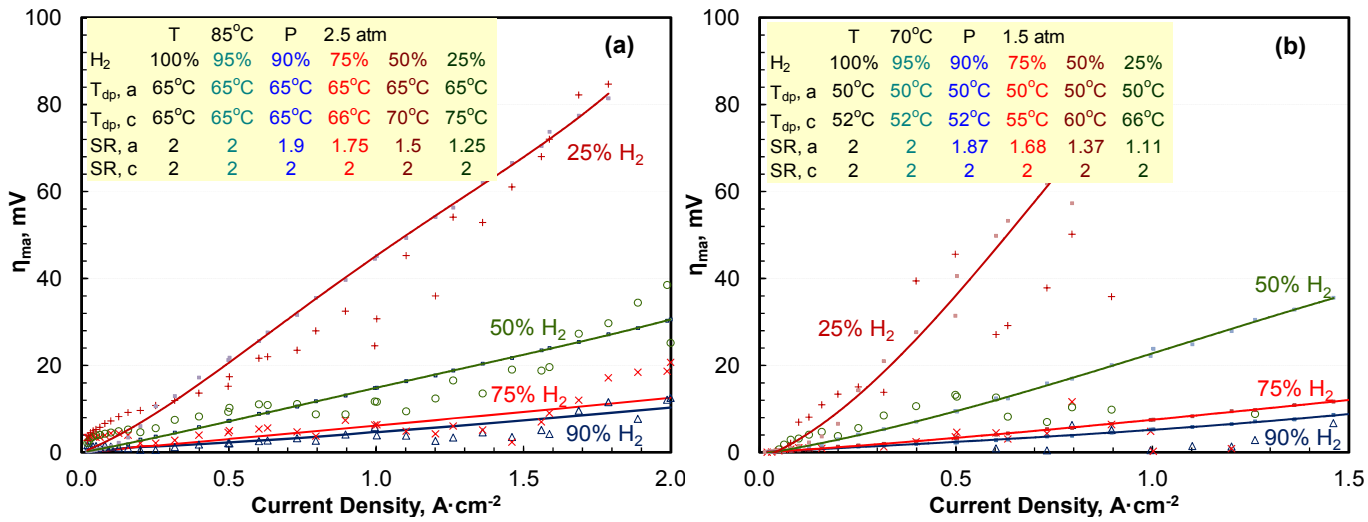

FIGURE 2. Anode mass transfer overpotentials in ternary NSTF catalyst: a) data at 85°C and 2.5 atm; b) data at 70°C and 1.5 atm anode stoichiometry (SR_a) and anode/cathode dew points (T_{dp}) are functions of the feed composition.

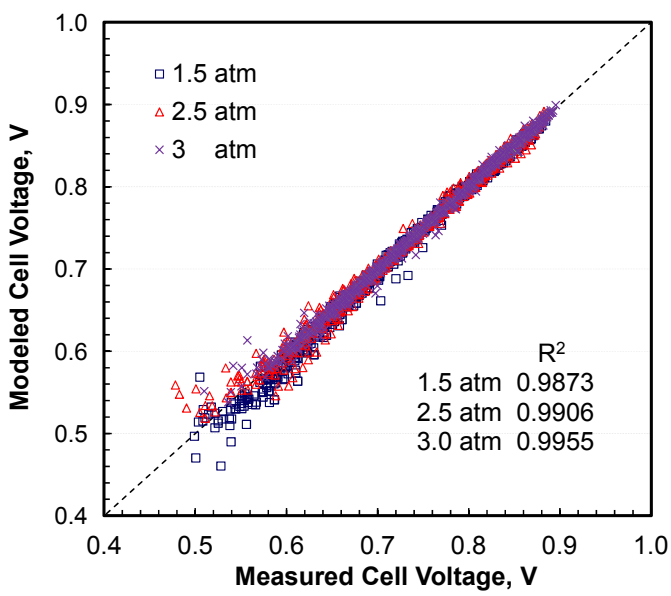

FIGURE 3. Validation of the cell model using all the data at 1.5, 2.5 and 3 atm inlet pressures.

dew-point temperature of cathode air at stack inlet, cathode stoichiometry and Pt loading in cathode. Stack inlet pressure was treated as a study parameter. As listed in the legend, Pt loading in anode (L_{Pt}), rise in coolant temperature across the stack (ΔT_c), and anode stoichiometries were held constant. Illustrative results in Table 1 for 2.5-atm stack inlet pressure indicate that constraining Q/ΔT to smaller values requires increasing system efficiency at rated power which in turn results in higher cell voltage, lower power density (not listed), and increased Pt content (g/kW) and system cost ($/kW). Meeting Q/ΔT=1.45 kW/°C target also required that the coolant temperature be raised to the 95°C allowable limit and this also contributed to decrease in stack power density. For comparison, Table 1 includes the Pt content and system cost for the same system efficiency but without the Q/ΔT constraint. For the same system efficiency, the differences in Pt content and system cost in Table 1 with and without the Q/ΔT constraint are measures of the decrease in power density because of the elevated stack temperature (ΔT effect). The differences in Pt content and system cost in Table 1 and Figure 4 for different Q/ΔT are measures of the decrease in power density because of higher cell voltages (Q effect).

CONCLUSIONS AND FUTURE DIRECTIONS

- The mass activities calculated from the ORR kinetic model are in agreement with the 0.13-0.25 $A \cdot mg^{-1}$ activities measured for the ternary NSTF catalyst with 0.054-0.186 $mg \cdot cm^{-2}$ Pt loadings.
- Specific exchange current densities for HOR/HER on ternary NSTF catalyst with 0.05 $mg \cdot cm^{-2}$ Pt loading are 60-110% higher than on Pt/C at much lower Pt loadings. The HOR/HER activities can be increased significantly if anode catalyst is conditioned more completely.
- As in dispersed Pt/C catalysts, the artificial neural network model indicates higher mass transfer overpotentials at lower Pt loadings in the ternary NSTF catalyst.
- A multi-variable optimization study showed that elevated stack temperatures and higher cell voltages are required as the stack operating conditions are changed to accommodate the target of 1.45 kW/°C Q/ΔT with resulting penalty in Pt content (g/kW) and system cost ($/kW).

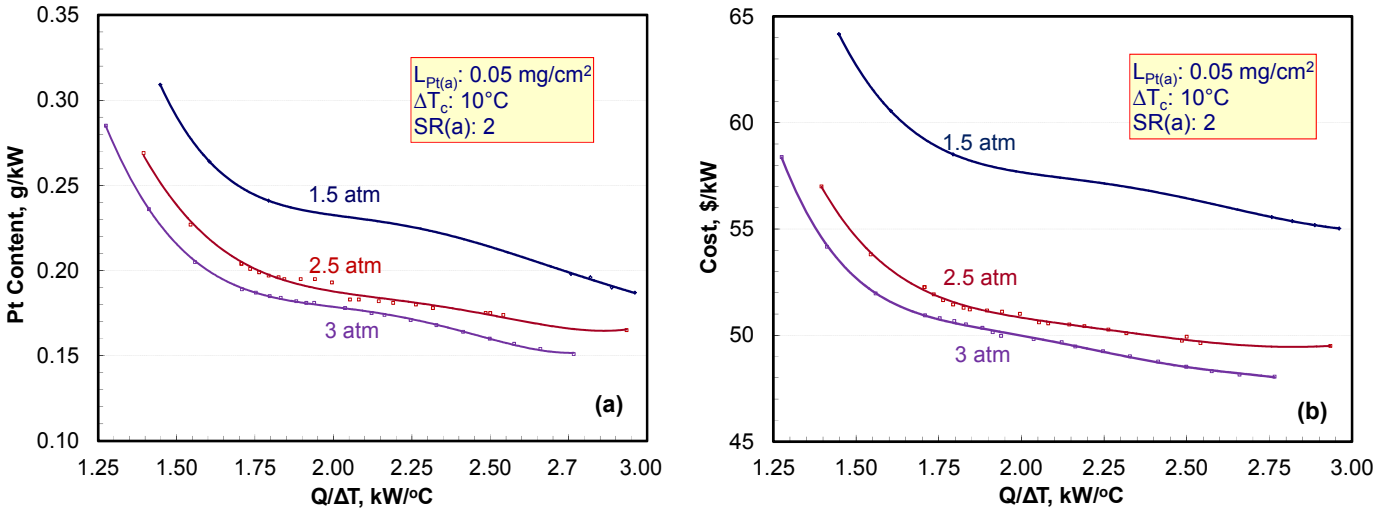

FIGURE 4. Effect of Q/ΔT constraint on system performance: a) Pt content; b) system cost.

TABLE 1. Effect of Q/ΔT target on system performance, 2.5 atm stack inlet pressure, 40°C ambient temperature

Minimum cost subject to Q/ΔT constraint, 95°C maximum stack temperature, 40°C ambient temperature					Minimum cost for given system efficiency (40°C)	
Q/ΔT	System	Cell V	Pt Content	Cost	Pt Content	Cost
kW/°C	Eff.,%	mV	g/kW	$/kW	g/kW	$/kW
3.0	40	574	0.17	49.5	0.17	49.5
1.7	45	640	0.20	52.3	0.19	50.2
1.5	47.5	670	0.23	53.8	0.20	51.6
1.4	50	700	0.27	57.0	0.24	54.6

- In FY 2014, we will investigate the effects of alternative NSTF catalysts and air management system on system performance and cost.

FY 2013 PUBLICATIONS/PRESENTATIONS

1. X. Wang, R.K. Ahluwalia, X. Wang, and A.J. Steinbach, "Kinetics of Hydrogen Oxidation and Hydrogen Evolution Reactions on Nanostructured Thin-Film Platinum Alloy Catalyst," J. Electrochemical Society, 160 (3) F251-F261, 2013.

2. R.K. Ahluwalia, S. Arisetty, X. Wang, X. Wang, R. Subbaraman, S.C. Ball, S. DeCrane, and D.J. Myers, "Thermodynamics and Kinetics of Platinum Dissolution from Carbon-Supported Electrocatalysts in Aqueous Media under Potentiostatic and Potentiodynamic Conditions," J. Electrochemical Society, 160 (4) F447-F455, 2013.

3. S. Ahmed, D.P. Papadias, and R.K. Ahluwalia, "Configuring a Fuel Cell based Residential Combined Heat and Power System," J. of Power Sources, 242, 884-894, 2013.

4. R.K. Ahluwalia, X. Wang, A. Lajunen, A.J. Steinbach, S.M. Hendricks, M.J. Kurkowski, and M.K. Debe, "Kinetics of Oxygen Reduction Reaction on Nanostructured Thin-Film Platinum Alloy Catalyst," J. of Power Sources, 215 (1) 77-88, 2012.

5. S. Arisetty, X. Wang, R.K. Ahluwalia, R. Mukundan, R. Borup, J. Davey, D. Langlois, F. Gambini, O. Polevaya, and S. Blanchet, "Catalyst Durability in PEM Fuel Cells with Low Platinum Loadings," J. Electrochemical Society, 159 (5) B455-B462, 2012.

6. R.K. Ahluwalia, X. Wang, A. Lajunen, A.J. Steinbach, S.M. Hendricks, M.J. Kurkowski, and M.K. Debe, "Performance of PEFC Stacks with Low-Pt Nanostructured Thin Film Catalysts at High Power Densities," 2012 Fuel Cell Seminar & Exposition, Mohegan Sun, Uncasville, CT, November 5–8, 2012.

7. R.K. Ahluwalia and X. Wang, "Reaction Kinetics and Transport Modeling for Nanostructured Thin Film Catalysts," 4th Transport Working Group Meeting, Lawrence Berkeley National Laboratory, Berkeley, CA, July 26–27, 2012.

8. R.K. Ahluwalia and N. Garland, "Report from the Annexes: Annex 26," IEA AFC ExCo 44th Meeting, Toronto, Canada, June 7–8, 2012.

9. R.K. Ahluwalia, "Fuel Cells for Transportation: Recent Progress in U.S.A.," IEA Annex 26 Meeting, Gothenburg, Sweden, May 22–23, 2012.

REFERENCES

1. M.K. Debe, "Advanced Cathode Catalysts and Supports for PEM Fuel Cells," Grant No. DE-FG36-07GO17007, FreedomCAR Technical Team Review, Detroit, MI, March 10, 2010.

2. A.J. Steinbach, C.V. Hamilton, and M.K. Debe, "Impact of Micromolar Concentrations of Externally-Provided Chloride and Sulfide Contaminants on PEMFC Reversible Stability," ECS Transactions 11(1), 889-897, 2007.

3. R.K. Ahluwalia, X. Wang, A. Lajunen, A.J. Steinbach, S.M. Hendricks, M.J. Kurkowski, and M.K. Debe, "Kinetics of Oxygen Reduction Reaction on Nanostructured Thin-Film Platinum Alloy Catalyst," J. Power Sources, 215, 77-88, 2012.

4. X. Wang, R. K. Ahluwalia, X. Wang, and A. J. Steinbach, "Kinetics of Hydrogen Oxidation and Hydrogen Evolution Reactions on Nanostructured Thin-Film Platinum Alloy Catalyst," J. Electrochemical Society, 160 (3) F251-F261, 2013.

5. R.K. Ahluwalia , X. Wang, J. Kwon, and A. Rousseau, "Drive-Cycle Performance and Life-Cycle Costs of Automotive Fuel Cell Systems," 2011 Fuel Cell Seminar & Exposition, Orlando, FL, October 31 – November 2, 2011.

6. R.K. Ahluwalia, X. Wang, J. Kwon, A. Rousseau, J. Kalinoski, B. James, and J. Marcinkoski, "Performance and Cost of Automotive Fuel Cell Systems with Ultra-Low Platinum Loadings," J. Power Sources, 196, 4619, 2011.

7. B.D. James, J.A. Kalinoski, and K.N. Baum, "Mass Production Cost Estimation for Direct H_2 PEM Fuel Cell Systems for Automotive Applications: 2009 Update," DTI Report GS-10F-0099J, January 2010.

V.H.2 Fuel Cell Transportation Cost Analysis

Brian D. James (Primary Contact), Jennie M. Moton, Whitney G. Colella
Strategic Analysis, Inc.
4075 Wilson Blvd. Suite 200
Arlington, VA 22203
Phone: (703) 778-7114
Email: bjames@sainc.com

DOE Managers
Jason Marcinkoski
Phone: (202) 586-7466
Email: Jason.Marcinkoski@ee.doe.gov
Gregory Kleen
Phone: (720) 356-1672
Email: Gregory.Kleen@go.doe.gov

Contract Number: DE-EE0005236

Project Start Date: September 30, 2011
Project End Date: September 30, 2016

Overall Objectives

- Define low-temperature proton exchange membrane (PEM) fuel cell system (FCS) operational and physical characteristics that reflect the current status of system performance and fabrication technologies.
- Estimate the production cost of the FCSs for automotive and bus applications at multiple rates of annual production.
- Identify key cost drivers of these systems and pathways to further cost reduction.

Fiscal Year (FY) 2013 Objectives

- Update 2012 automotive and bus FCS cost projections to reflect latest performance data and system design information.
- Define design and analyze cost of alternate catalyzed membrane fabrication methods.
- Define design and analyze cost of plate-frame air humidifier systems.

Technical Barriers

This project addresses the following technical barriers from the Fuel Cells section of the Fuel Cell Technologies Office Multi-Year Research, Development, and Demonstration Plan:

(B) Cost

Technical Targets

This project conducts cost modeling to attain realistic, process-based system cost estimates for integrated transportation FCSs operating on direct hydrogen. These values can help inform future technical targets:

- DOE fuel cell system cost target: $30/kWe

FY 2013 Accomplishments

- Updated automotive FCS cost analysis to include the most up-to-date fuel cell stack performance data provided by Argonne National Laboratory (ANL).
- Analyzed the W.L. Gore and Associates Inc. (Gore) low-cost catalyzed membrane fabrication process and compared its cost to nano-structured thin-film (NSTF) catalyst application using a more conventional Nafion® membrane.
- Analyzed a plate-frame membrane humidifier and compared its cost to the previously analyzed tubular membrane humidifier.
- Projected the FCS cost for an 80-kW light-duty vehicle application using a Design for Manufacturing and Assembly (DFMA®) methodology at an annual production rate of 500,000 FCSs per year.
- Projected the cost of a 160-kWe FCS for a bus.

✧ ✧ ✧ ✧ ✧

INTRODUCTION

This project represents an update to the ongoing PEM FCS cost model for 80-kWe automotive power systems. New technologies, materials data, and optimization modeling are incorporated to give an up-to-date value for system cost. In addition, costs of a PEM FCS for 160-kWe bus applications were analyzed.

FCSs for transportation applications are a longstanding area of fuel cell product development. Numerous prototype vehicles exist for a variety of transportation applications, and research continues into improving the competitiveness of fuel cells as compared to the internal combustion engine. To better assess the potential usefulness and market-worthiness of fuel cells for transportation applications, this work describes a DFMA®-style [1] analysis of the cost to manufacture two different transportation FCSs. The systems analyzed are low-temperature PEM FCSs with peak electrical capacities of 80 kWe for light-duty vehicle (automobile) applications and 160 kWe for bus applications. The FCSs consume a hydrogen gas fuel stream from an onboard

compressed hydrogen storage system. The impact of annual production rate on the cost of both systems is examined to assess the difference between a nascent and a mature product manufacturing base. The annual production rates analyzed are 1,000, 10,000, 30,000, 80,000, 100,000, and 500,000 FCSs per year for automotive systems and 400 and 1,000 systems per year for the bus systems.

This work focuses primarily on the efforts to update the existing DFMA® cost model of the automobile FCS as well as new efforts to design and cost-model the bus FCS. These systems' stack and balance-of-plant (BOP) designs and performance parameters are discussed and the methods of cost-modeling each explained. Cost trends are evaluated in terms of the capital costs per unit of installed electrical capacity ($/kWe) and system annual production rate.

APPROACH

A DFMA®-style analysis is conducted to attain cost estimates of PEM FCSs for automobiles and buses at various manufacturing production rates. Fuel cell stack polarization performance is supplied by ANL and included in the PEM FCS performance and cost model. In addition, industry partners provide feedback on the design, materials, and manufacturing and assembly of FCS components and overall system. Fuel cell stack polarization performance is based on output from a detailed, first principles stack model created by ANL and validated against 3M NSTF membrane electrode assembly (MEA) performance. Output from the detailed ANL model is used to create a simplified stack polarization model that returns predicted current density for a specified cell voltage, stack pressure, cathode Pt catalyst loading, air stoichiometry, and stack outlet coolant temperature. This simplified 5-variable model is incorporated into the overall FCS cost model to allow complete flexibility in specification of stack operating conditions. A sweep over the entire potential stack operating condition design space can then be used to determine conditions that lead to the lowest system cost. The FCS is sized based on rated power operating parameters. System performance is based on performance estimates of individual components, built up into an overall system energy budget. Overall system and component performance are cross checked against estimates made by the ANL detailed models [2]. DFMA® process-based cost estimation techniques are applied to the major system components (and other specialty components) such as the fuel cell stack, membrane humidifier, air compressor/expander/motor unit, and hydrogen recirculation ejectors. For each of these, a manufacturing process train details the specific manufacturing and assembly machinery, and processing conditions are identified and used to assess component cost. For lesser components such as valves, heat exchangers, sensors, and piping, less detailed methods of cost estimation are applied. These methods include simplified DFMA®-style techniques and price quotations from vendors. An approach of frequent communication with vendors to obtain price quotes, and to discuss component design characteristics and manufacturing methods, is used to ensure the validity of the assumptions used in the cost estimates.

RESULTS

The 2013 cost update of the automotive and bus fuel cell power system is currently underway but not yet complete. While complete system cost estimates are not yet available, substantial progress has been made on analyzing alternative component technologies, specifically catalyst-coated membranes (CCMs) and air humidifiers.

To explore potential cost reduction of the CCMs of the FCS, a novel low-cost catalyzed membrane fabrication method [2] developed by Gore was analyzed. The modeled system draws exclusively from non-proprietary input and is composed of three sequential roll-to-roll fabrication steps: 1) cathode formation, 2) supported electrolyte formation, and 3) anode formation. Cathode formation is modeled as deposition of cathode catalyst ink onto a reusable Mylar substrate via die-slot coating followed by a moderate-temperature drying furnace. Electrolyte formation is modeled as die-slot coating of a Nafion® ionomer onto the cathode layer followed by unrolling and lowering of an expanded polytetrafluoroethylene (ePTFE) layer onto the wet ionomer, followed by furnace drying. Anode formation is modeled as die-slot coating of anode catalyst ink onto the electrolyte layer followed by furnace drying. A full DFMA® analysis of each step was conducted based on capital cost of the equipment, processing speed, material usage, expected yields, labor usage, and utility consumption. The membrane is modeled as a "bought" item, meaning that it is purchased from a sub-tier vendor rather than being fabricated in-house by the fuel cell system integrator. As such, markup for profit, research and development, and other general and administrative expenses is included for the membrane only within the CCM cost projection.

For automotive systems, DFMA® results in Figure 1 compare the projected costs of the Gore CCM manufacturing method described previously with those of the CCM fabrication method used in the 2012 cost analysis. The 2012 CCM fabrication method is based on a 3M NSTF catalyst application onto an ePTFE-supported Nafion® ionomer membrane. Catalyst application is modeled as vacuum magnetron sputtering of Pt/Co/Mn catalyst onto a high-surface-area substrate of PR-149 whiskers grown by sublimation followed by annealing. Membrane fabrication is modeled as occlusion of ePTFE in Nafion® ionomer solution within a separate factory setting. A DFMA® analysis was conducted and yielded results detailing the final estimated capital cost of the CCMs at different manufacturing rates. As shown in Figure 1, the capital cost of both CCMs is seen to decrease with increasing automotive system annual

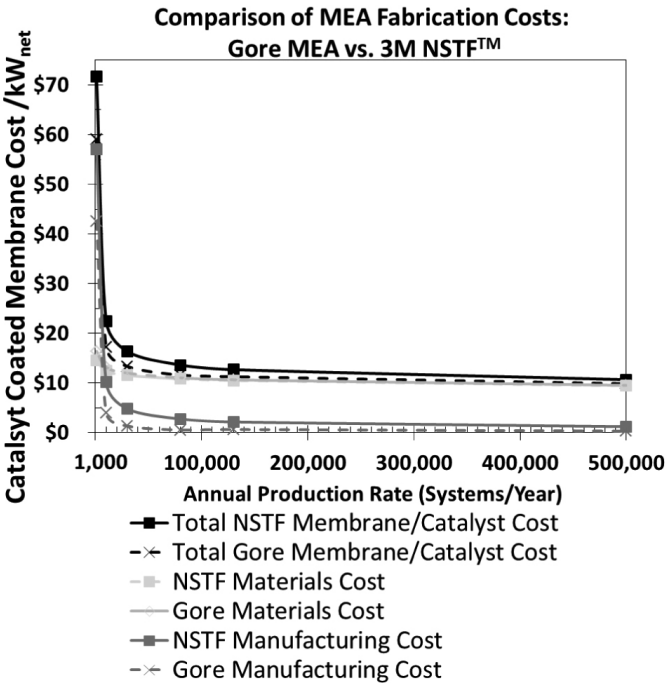

FIGURE 1. Cost Comparison of Gore and 3M MEAs

production rate. While the materials costs for both Gore and 3M CCMs are similar, the processing costs for the 3M CCM are greater than for the Gore CCM. Overall, the Gore CCM is estimated to be slightly less expensive than the 3M CCM. As production rate increases, the cost differential between the two different CCMs decreases in absolute terms. At the highest production rates considered (500,000 automotive systems per year), the Gore CCM processing costs are projected to approach just a few cents per kWe. Note that this analysis compares CCM costs on a per-square-meter-of-membrane basis, assuming the exact same engineering performance of the CCMs; the analysis does not capture potential differences in polarization performance and durability between the two CCMs.

A plate frame air humidifier is examined as a potentially lower cost and smaller volume alternative to the previously modeled tubular membrane humidifier. The plate frame humidifier design and projected manufacturing methods are based on publicly available information from Gore and dPoint Technologies Inc. [3]. For the automotive application, the modeled design is based on use of 80 "cell pouches" (loops of membrane with a metal spacer within the loop, total humidifier membrane area is 1.6 m^2) that allow dry primary inlet air to flow through the inside of the pouch and humid secondary outlet oxygen-depleted air from the cathode to flow cross-wise across the outside of the pouch. Stamped metal "ribs" are used to separate the pouches and thus enable gas flow between the pouches. The cells are arranged in a simple aluminum cast-metal housing to direct the gas flows. The postulated manufacturing process for the plate frame membrane humidifier is broken down into eight steps, as seen in Table 1, with costs further subdivided into materials, manufacturing, tooling, markup, and total costs. The greatest cost driver for the membrane humidifier is the material cost of the membrane at ~$29/humidifier. Consequently, costs are strongly impacted by the quantity of membrane material needed for the humidifier. The membrane is modeled as a four-layer integrated composite consisting of a 10-micron ePTFE layer, 5-micron Nafion® ionomer layer, 10-micron ePTFE layer, and 180-micron polyethylene terephthalate layer. The ePTFE layers bracket and mechanically support the very thin, and thus high water flux, ionomer layer and are arranged in a symmetrical orientation to minimize stresses during thermal cycling and thereby enhance lifetime. The much thicker polyethylene terephthalate layer provides

TABLE 1. Cost Analysis of a New Plate Frame Membrane Humidifier Design by Gore

All at 500k systems per year						
Component Costs per Humidifier System		**Materials**	**Manuf.**	**Tools**	**Markup**	**Total**
Station 1: Membrane Fabrication	$/stack	$28.99	$2.65	$0.16	$7.95	$39.75
Station 2: Humidifier Etching (Flow Field Plates)	$/stack	$15.09	$11.13	$0.00	$0.00	$26.21
Station 3: Pouch Forming	$/stack	$0.44	$1.30	$0.05	$0.00	$1.79
Station 4: Stamp SS ribs	$/stack	$0.64	$1.45	$3.60	$0.00	$5.69
Station 5: Stack Forming	$/stack	$4.33	$7.23	$0.00	$0.00	$11.57
Station 6: Stack Housing	$/stack	$5.05	$0.50	$1.21	$0.00	$6.76
Station 7: Assembly of Stack into Housing	$/stack	$0.00	$1.70	$0.00	$0.00	$1.70
Station 8: System Test	$/stack	$0.00	$0.32	$0.00	$0.00	$0.32
	Totals =	**$54.54**	**$26.28**	**$5.02**	**$7.95**	**$93.78**

additional mechanical support and abrasion resistance. Fabrication of the composite membrane uses roll-to-roll processing steps analogous to those postulated for the Gore low-cost CCM line discussed previously. The second largest cost driver is the etching process for the humidifier flow field plates based on a material cost (stainless steel 316L) of ~$15/humidifier and an electrochemical etching manufacturing cost of ~$11/humidifier. Electrochemical etching is selected for the metal spacers as it grants the design flexibility and dimensional tolerance critical to achieving low pressure drop and high membrane water transport performance. The total cost for the plate frame membrane humidifier at 500,000 systems per year is projected to be ~$94/humidifier.

FCS costs for bus applications were analyzed in late 2012 and are currently being updated for 2013 advances in technology. While cost results for 2013 are not yet available, DFMA® results for 2012 indicate that the projected capital costs for a fuel cell bus in mass production are consistent with industry projections and DOE R&D guidelines. Figure 2 shows the components contributing to the 2012 cost of the bus fuel cell stacks. The gas diffusion layers, membranes, and NSTF catalyst ink and application are the largest cost contributors, followed by stamped bipolar plates and MEA gaskets. The total stack cost at 1,000 systems per year is estimated to be $21,651 for two 80-kWe stacks. Figure 3 plots the BOP costs as function of component source, at the same annual production rate. The BOP cost is estimated to be $8,707, roughly 40% of the stack costs. The sensors and air loop are the most significant cost contributors to the BOP.

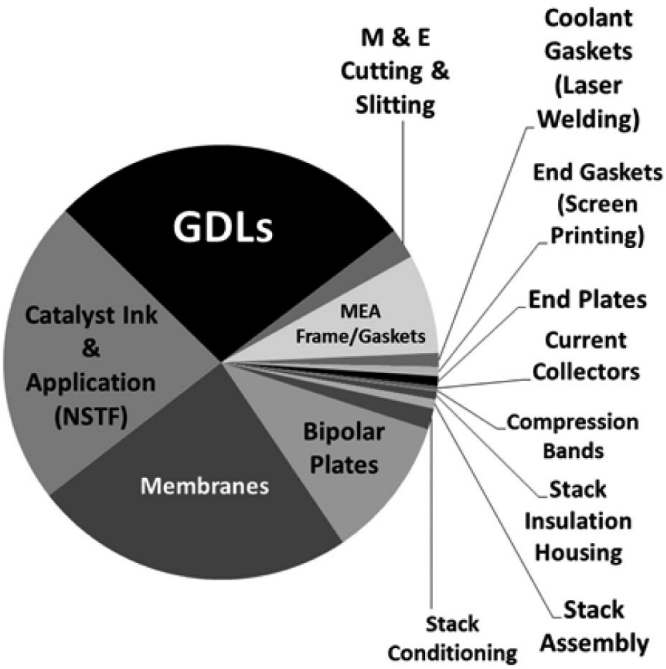

FIGURE 2. Cost Break-Down for PEM Fuel Cell Stacks for a Bus

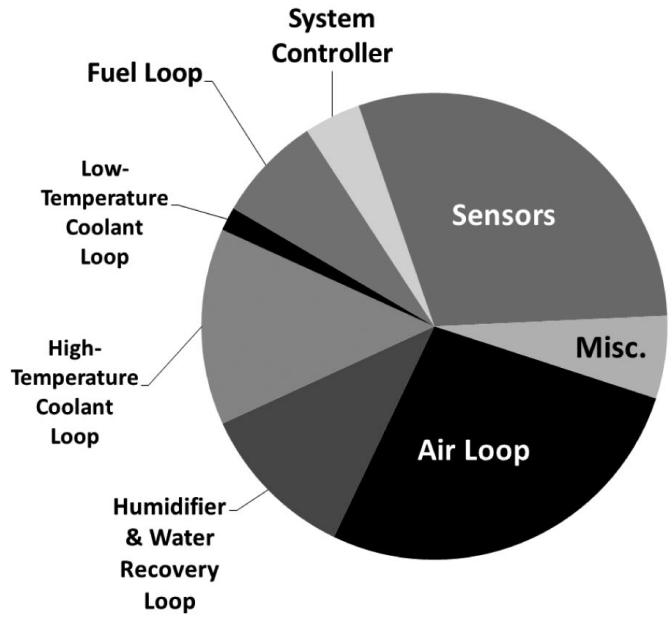

FIGURE 3. Cost Break-Down for PEM Fuel Cell Bus BOP

The projected DFMA® capital cost for both stacks and BOP is ~$170/kWe, consistent with both industry estimates and DOE goals.

CONCLUSIONS AND FUTURE DIRECTIONS

- Cost analysis of CCMs fabricated using the Gore roll-to-roll fabrication methods yields similar, but slightly lower costs than CCMs fabricated using previously analyzed fabrication methods (NSTF catalyst application on an ePTFE supported membrane), assuming that both CCMs have similar engineering and polarization performance.
- Costs of a plate frame air humidifier (based on designs from Gore and dPoint Technologies) are projected to be ~$100 per unit (sized for an 80-kWe automotive fuel cell system). The materials costs for the humidification membrane and the fabrication cost of the stainless steel spacers (fabricated by electrochemical etching) are the greatest cost drivers for the air humidifier.
- The 2012 projected cost of bus 160-kWe low-temperature PEM FCS is ~$170/kWe, consistent with both industry estimates and DOE goals. The three greatest cost drivers for the bus stack are the gas diffusion layers, membranes, and NSTF catalyst layer and application. The greatest cost drivers for the bus BOP are the sensors and air loop.
- An updated stack polarization model was obtained from ANL and integrated into the fuel cell cost models. A Monte Carlo analysis can then be used to identify FCS operating conditions that lead to the lowest FCS capital cost.

- Projections of the overall FCS cost for both automotive and bus applications will be made for a range of annual production rates.

FY 2013 PUBLICATIONS/PRESENTATIONS

1. James, B.D., Spisak, A.B., Colella, W.G., "Design for Manufacturing and Assembly (DFMA) Cost Estimates of Transportation Fuel Cell Systems," expected 2013 (accepted for publication).

2. Colella, W.G., "Advanced Electrochemical Systems," *California Renewable Energy and Storage Technology Conference*, California State University Northridge, Northridge, CA, May 4th, 2013.

3. James, B.D., Moton, J.M., Colella, W.G., "Energy Systems Design and Thermoeconomic Analysis of Advanced Vehicle Systems," *American Society of Mechanical Engineers (ASME) 2013 7th International Conference on Energy Sustainability*, Minneapolis, MN, July 14–19th, 2013.

4. James, B.D., Moton, J.M., Colella, W.G., "Fuel Cell Vehicle Design for Manufacturing and Assembly (DFMA) Analysis," *ASME 2013 11th Fuel Cell Science, Engineering and Technology Conference*, Minneapolis, MN, July 14–19th, 2013.

5. James, B.D., Spisak, A.B., Colella, W.G., "Hydrogen-fueled proton exchange membrane (PEM) fuel cell vehicles (FCVs) -- Conceptual and Physical Design and Capital Cost Estimates," *ASME 2012 International Mechanical Engineering Congress & Exposition*, Houston, Texas, Nov. 9th–15th, 2012, IMECE2012-88990.

6. James, B.D., Spisak, A.B., Colella, W.G., "Design for Manufacturing and Assembly (DFMA) Cost Estimates of Transportation Fuel Cell Systems," *Fuel Cell Seminar*, Uncasville, Connecticut, Nov. 5th–8th, 2012.

7. James, B.D., Moton, J.M., Colella, W.G., *Design for Manufacturing and Assembly of Fuel Cell Vehicles*, U.S. DOE EERE FCT Program Webinar Series, April 16th, 2013.

REFERENCES

1. Boothroyd, G., P. Dewhurst, and W. Knight. "Product Design for Manufacture and Assembly, Second Edition," 2002.

2. Busby, F. Colin. "Manufacturing of Low-Cost, Durable Membrane Electrode Assemblies Engineered for Rapid Conditioning," W.L. Gore & Associates, Inc., presentation at the 2012 DOE Hydrogen and Fuel Cell Program Annual Merit Review, Washington, DC, 16 May 2012.

3. Johnson, William B. "Materials and Modules for Low-Cost, High Performance Fuel Cell Humidifiers," W.L. Gore & Associates, Inc., presentation at the 2012 DOE Hydrogen and Fuel Cell Program Annual Merit Review, Washington, DC, 17 May 2012.

V.H.3 Characterization of Fuel Cell Materials

Karren More (Primary Contact), David Cullen, Miaofang Chi, Raymond Unocic
Oak Ridge National Laboratory (ORNL)
1 Bethel Valley Road
Building 4515 – Room 193
Oak Ridge, TN 37831-6064
Phone: (865) 574-7788
Email: morekl1@ornl.gov

DOE Manager
Donna Ho
Phone: (202) 586-8000
Email: Donna.Ho@ee.doe.gov

Project Start Date: October 1, 1999
Project End Date: Project continuation and direction determined annually by DOE

Overall Objectives

- Identify, develop, and optimize high-resolution imaging and microanalysis techniques, and unique specimen preparation methodologies, for the µm- to sub-Å-scale characterization of the material constituents comprising fuel cells (FCs) (e.g., electrocatalyst, catalyst support, ionomer, and membrane).
- Elucidate fundamental relationships between the material constituents within FC membrane electrode assemblies (MEAs) and correlate these data with MEA stability and performance using guidance from the FC community.
- Integrate microstructural characterization as a core resource within other DOE FC projects.
- Evaluate microstructural and microchemical changes contributing to FC performance loss, identify degradation mechanisms, and devise mitigation strategies related directly to material improvements.
- Make capabilities for advanced characterization and expertise available to the FC community outside of ORNL.

Fiscal Year (FY) 2013 Objectives

- Quantify extent of carbon corrosion in MEAs subjected to accelerated stress tests (ASTs) by building on previous observations related to carbon structural changes (e.g., formation of graphite oxide and its dependence on initial graphitic structure/content) using a combination of analytical microscopy techniques and X-ray photoelectron spectroscopy.
- Establish imaging and analysis parameters/conditions that should be used to best characterize and quantify the structure and composition of ionomer thin films (less than 10-nm thick) *within* the MEA electrodes without inducing artifacts/damage.
- Establish imaging and analysis parameters/conditions that should be used to image and quantify the structure and composition of individual electrocatalyst nanoparticles (as-synthesized, incorporated in MEAs, and post-aging) using large solid angle silicon drift detectors to minimize beam damage. These studies should be correlated with electron tomography experiments.
- Correlate µm-scale electrode architecture with processing to optimize microstructure for enhanced performance.
- Develop in situ liquid microscopy capabilities for electrochemistry of FC materials to study electrocatalyst coarsening and carbon corrosion.

Technical Barriers

This project addresses the following technical barriers from the Fuel Cells section of the Fuel Cell Technologies Office Multi-Year Research, Development, and Demonstration Plan:

(A) Durability

(C) Performance

Technical Targets

This project is focused on conducting fundamental characterization studies on the stability of individual material constituents comprising FC MEAs. Of primary importance is relating electrode microstructural/material changes occurring during aging with measured FC durability and performance. Insights gained through extensive microstructural studies will be applied toward the design and manufacture of catalysts and catalyst supports that meet the DOE 2017 and 2020 electrocatalyst targets listed in Table 1.

FY 2013 Accomplishments

- Based on input from the FC Tech Team, ORNL and Los Alamos National Laboratory (LANL) collaborated on a series of ASTs to quantitatively assess the extent of carbon oxidation as a function of carbon-support type used in the cathode. These MEAs were studied to correlate carbon-support oxidation (microstructural observations) with CO_2 evolution to further understand the critical parameters that govern both electrocatalyst and carbon support stability.

TABLE 1. Technical Targets: Electrocatalysts for Transportation Applications

Characteristic	Units	2011 Status	2017 Target	2020 Target
PGM total content (both electrodes	g/kW (rated)	0.19	0.125	0.125
PGM total loading	mg PGM/cm^2 electrode area	0.15	0.125	0.125
Loss in initial catalytic activity	% mass activity loss	48	<40	<40
Electrocatalyst support stability	% mass activity loss	<10	<10	<10
Mass Activity	A/mg Pt @ 900 mV	0.24	0.44	0.44
Non-Pt catalyst activity per volume of supported catalyst	A/cm^2 @ 800 mV	60 (at 0.8 V) 165 (extrapolated from > 0.85 V)	300	300

PGM – platinum-group metal

- Separate ionomer studies with General Motors (GM) and Ballard were continued during FY 2013, with particular attention paid to ionomer thin films on model substrates and identifying the proper microscopy conditions to reliably analyze thin ionomer films. This is ongoing work with the ultimate goal being the assessment of "real" ionomer films in catalysts layers.
- David Cullen spent one month at Commissariat à l'Energie Atomique (CEA) in Grenoble, France, collaborating on two primary FC studies: 3-dimensional tomography of nanostructured thin-film catalysts before and after aging, and mapping ionomer distributions within catalysts layers. CEA has unique capabilities that complement ORNL techniques, and this valuable visit will help us identify critical operating parameters necessary for our ongoing research.
- ORNL collaborated with Nuvera Fuel Cells on the Sustained Power Intensity with Reduced Electrocatalyst Program to quantify Pt electrocatalyst degradation in terms of Pt coarsening and migration. These data are currently being used as experimental input for models being developed by researchers at Argonne National Laboratory (ANL).

✧ ✧ ✧ ✧ ✧

INTRODUCTION

Polymer electrolyte membrane (PEM) FCs are being developed for future use as efficient, zero-emission power sources. However, the performance of PEMFCs degrades with time at elevated temperature and relative humidity during electrochemical aging in automotive and stationary applications. Performance degradation can be directly attributed to the durability of individual material constituents comprising the MEA, including the electrocatalyst, catalyst support, ionomer, polymer membrane, and the gas diffusion layer/microporous layer. The structural and chemical degradation mechanisms contributing to performance loss have not been fully elucidated and/or quantified. During the past several years, the Microstructural Characterization Project at ORNL has been focused on forming collaborative relationships with numerous MEA and FC developers/manufacturers, universities, and national laboratories, to apply ORNL's advanced electron microscopy capabilities and expertise to characterize as-synthesized (fresh) FC materials (individual constituents and/or materials incorporated in fresh MEAs), MEAs subjected to ASTs designed to degrade specific MEA components, and field-aged MEAs. These studies are used to establish critical processing-microstructure-performance relationships and to understand the individual materials changes contributing to measured MEA degradation, performance loss, and failure. Understanding the structural and compositional changes of the materials comprising the MEA during electrochemical aging will allow for the implementation of processing changes and critical materials development that are required for optimizing FC durability and performance.

APPROACH

The microstructural characterization task utilizes advanced electron microscopy analysis techniques to characterize the individual material components comprising FC MEAs, before and after incorporation into an MEA structure, and after electrochemical aging. ORNL's approach is focused on identifying and optimizing novel high-resolution imaging and compositional/chemical analysis techniques, and developing unique specimen preparation methodologies, for the µm- to Å-scale characterization of the material constituents (electrocatalyst, catalyst support, ionomer, membrane, etc.). ORNL applies these advanced analytical and imaging techniques for the evaluation of the microstructural and microchemical changes of each material constituent and correlates these observations with FC performance (aging studies—ASTs and field-aging—are conducted at a variety of collaborator's laboratories). These studies are designed to elucidate the microstructure-related degradation mechanisms contributing to FC performance loss. ORNL makes the techniques and extensive staff expertise and knowledge available to a broad community of

FC researchers outside of ORNL via several collaborative mechanisms: (1) work for others for proprietary research, (2) ORNL User Facilities (e.g., Shared Research Equipment User Facility), and (3) collaborative non-proprietary research projects supported via the Microstructural Characterization Project that are consistent with ORNL's research activities, which has been the primary mechanism for conducting collaborative research—partners have included: LANL, ANL, National Renewable Energy Laboratory, Brookhaven National Laboratory, Lawrence Berkeley National Laboratory, Sandia National Laboratory, GM, 3M, Automotive Fuel Cell Cooperation, Proton OnSite, W.L. Gore, Ballard, Nuvera Fuel Cells, Fuel Cell Energy, UTC-Power (now ClearEdge Power), and numerous universities.

RESULTS

During FY 2013, ORNL continued its efforts related to topics of interest to the FC community through collaborations with numerous partners, which have included research specific to understanding carbon corrosion mechanisms, the characterization of thin ionomer films, catalyst nanoparticle evaluation via electron microscopy, and progress made in the area of in situ liquid-cell electrochemical microscopy (the last two topics are not included in this report). These tasks build upon research conducted during the last several years to establish vital correlations between the structure-chemistry of individual MEA components and their durability and stability during electrochemical aging.

Carbon Corrosion (collaboration with LANL)

To better understand carbon corrosion in FC cathodes, LANL supplied ORNL with a series of MEAs having cathode layers that were prepared using three different carbon black (CB)-supported Pt inks:

- High surface area carbon (HSAC) + 20% Pt
- Vulcan carbon (VC) + 20% Pt
- Low surface area carbon (LSAC) + 20% Pt

These MEAS were subjected to the carbon corrosion AST, 1.2-V hold at 80°C and 100% relative humidity, for time increments ranging from 5 h to 400 h. After each test, MEAs were cut in cross-section by ultramicrotomy for examination by electron microscopy to microstructurally quantify the extent and mechanisms of carbon corrosion as a function of hold time at 1.2 V and type of CB used CO_2 evolution was measured during selected ASTs.

The cathode prepared using HSAC + 20% Pt exhibited the poorest durability and was characterized by extensive performance loss after only 20 h at 1.2 V, as shown in the polarization curves in Figure 1a, which could be directly correlated with severe cathode thinning (greater than 50% thickness loss after 20 h), Figure 1b, and loss of porosity (greater than 50% porosity loss after 20 h), Figure 1c. The MEA prepared with VC, on the other hand, exhibited somewhat enhanced durability compared to HSAC, as shown in Figure 2a, but some performance loss was observed after only 50 h at 1.2 V. Although extensive cathode thinning/compression was characteristic of both HSAC and VC, the extent of losses was significantly greater for the HSAC; after 100 h at 1.2 V, where less than 20% of the cathode thickness and only 2% porosity were retained, whereas after 400 h at 1.2 V, the VC retained 40% cathode thickness accompanied by less than 5% porosity. Examination of the structural components, specifically the structure of the carbon support and the Pt catalysts, showed evidence for carbon corrosion in terms of carbon structural changes, but these changes were non-homogeneous within the catalyst layer (extremely localized) and not as extensive as originally believed. Figure 3a shows that the most degraded regions within the cathode containing HSAC (exhibiting the highest carbon corrosion) were localized within compressed "bands" running parallel

(b) (c)

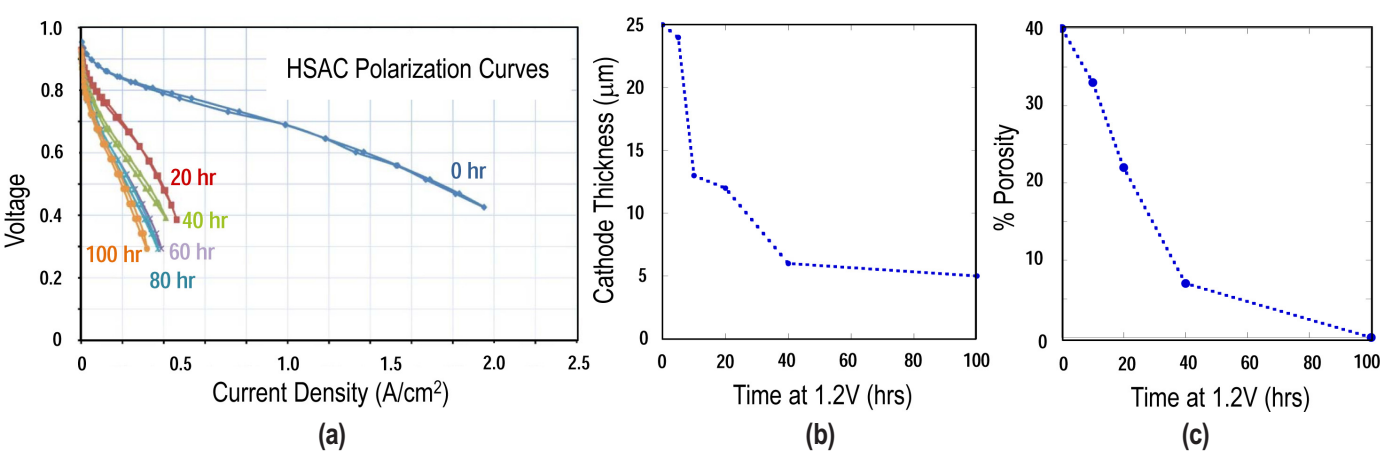

FIGURE 1. (a) Polarization curves for an MEA with HSAC + 20% Pt cathode tested at 1.2 V for 20, 40, 60, 80, and 100 h. (b) HSAC cathode thickness loss as a function of hold time at 1.2 V. (c) HSAC cathode porosity loss as a function of hold time at 1.2 V.

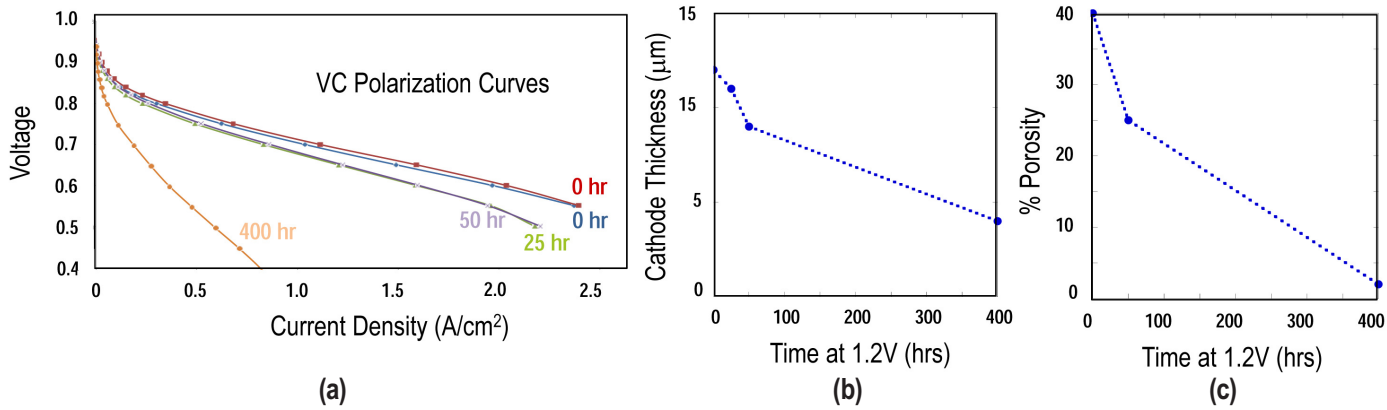

FIGURE 2. Polarization curves for an MEA with VC + 20% Pt cathode tested at 1.2 V for hold times of 25, 50, and 400 h. (b) VC cathode thickness loss as a function of hold time at 1.2 V. (c) VC cathode porosity loss as a function of hold time at 1.2 V.

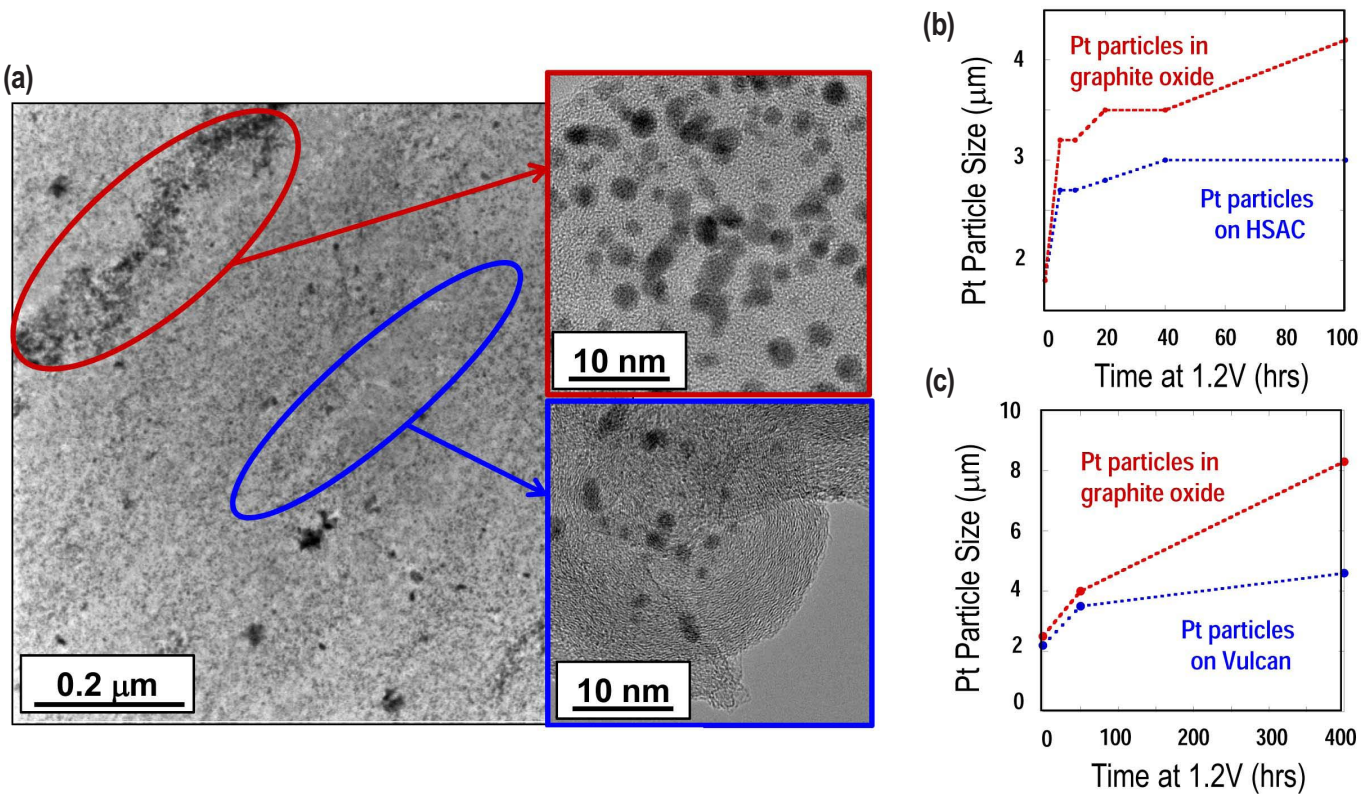

FIGURE 3. (a) HSAC cathode exhibiting formation of dense "bands" of graphite oxide formation embedded in regions showing limited oxidation of the HSAC meso-graphitic structure. (b) Pt particle sizes measured within dense graphite oxide "bands" and less-oxidized HSAC regions. (c) Pt particle sizes measured within dense graphite oxide "clusters" and less-oxidized VC regions.

to the cathode-membrane interface. These bands consisted of dense regions of amorphous, partially oxidized carbon (graphite/carbon oxide) with a significantly larger Pt particle size (Figure 3b). The highly oxidized bands comprised only ~10% of the entire cathode layer, whereas the remainder of the cathode layer exhibited much less carbon corrosion, and in fact, much of the HSAC structure was retained to some extent (much less incorporation of oxygen within the HSAC support). The cathode layer prepared with VC exhibited a similar trend of localized densification and graphite oxide formation, except that these regions appeared as much smaller "clusters" throughout the cathode rather than the densified "bands" observed for HSAC, as shown in Figure 3b, and the extent of corrosion of the VC appeared more

uniform than for the HSAC. Significantly greater Pt particle coalescence was associated with the highly oxidized regions of the VC cathode, similar to observations for the HSAC.

These microstructural observations are consistent with the CO_2 evolution measured during several ASTs; for both the HSAC and VC cathodes the evolved CO_2 was extremely low (less than 400 ppm after 100 h) supporting less carbon corrosion based strictly on correlating performance loss due only to loss of carbon through the

$$C + H_2O \rightarrow CO_2 + 4H^+ + 4e'$$

reaction. Current results clearly demonstrate a structural change to the carbon support particles, which is supported by the observation of a progressive and non-homogeneous formation of localized dense graphite oxide bands/regions within the catalyst layer, as the overriding carbon degradation mechanism. The regions of greatest graphite oxide formation are also associated with the most Pt coarsening; in fact, much of the loss of Pt electrochemically active surface area (ECSA) can be directly attributed to the localized areas exhibiting the most graphite oxide formation, as shown in Figures 3b (HSAC) and 3c (VC). When the localized changes in carbon structure are combined with the progressive loss of porosity and cathode thinning/compression observed after the carbon corrosion ASTs (1.2 V hold), the performance losses can be fully explained in terms of electrode and support structural changes.

The extent of carbon corrosion and Pt coarsening, and therefore overall FC performance, can be directly related to the starting structure of the CB+Pt used in the cathode. The structures of the various CB supports are illustrated for comparison in the schematics and associated high-resolution transmission electron microscopy (TEM) images shown in Figure 4. HSAC is characterized as having an extremely small particle size (typically 10-50 nm diameter) with a highly defective meso-graphitic outer shell and an amorphous core—the Pt particles are primarily within this core. The VC support particles, on the other hand, are denser with a much larger overall particle size (typically 30-100 nm) with a thicker, more graphitized outer shell and a smaller amorphous core—the Pt particles are on the surface of the VC particles. LSAC (results not discussed in this report, but this carbon support exhibits significantly enhanced resistance to carbon corrosion), which is graphitized HSAC, exhibits a graphitic outer shell with a hollow core—the Pt attaches to the surface of the LSAC non-homogeneously at edges/

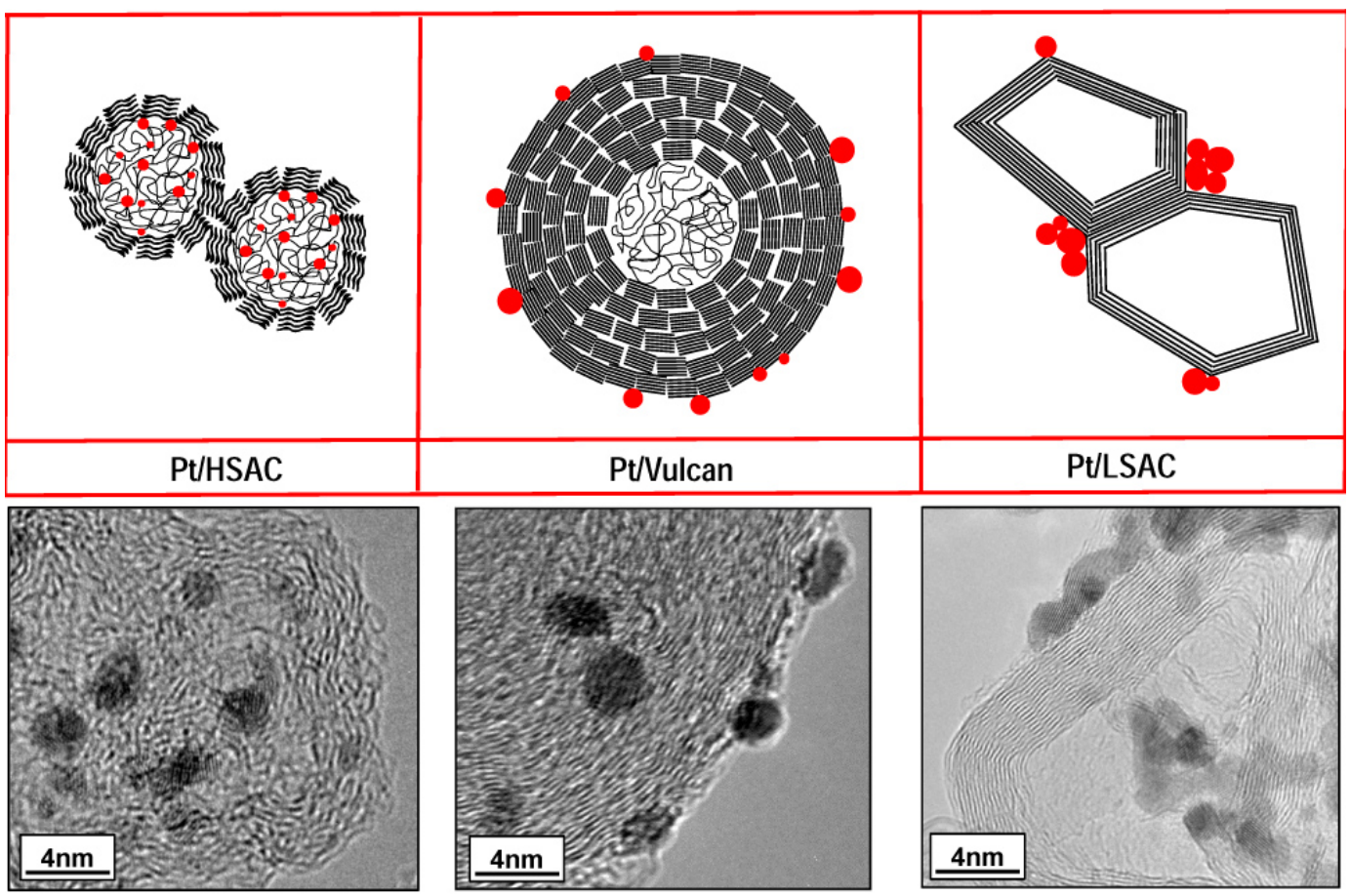

FIGURE 4. Schematics and associated high-resolution TEM images showing structure of HSAC + Pt, VC + Pt, and LSAC + Pt.

corners of the graphite shell. As a result of the number and type of surface defects associated with each of the different CBs, each carbon structure will exhibit a different corrosion behavior. The HSAC has the highest number of defects, which are primarily grain boundaries separating the meso-graphitic domains. These grain boundaries serve as rapid pathways for H_2O to enter the carbon structure and oxidize the amorphous core, and diffuse through the carbon edge planes, rapidly disrupting the meso-graphitic structure and forming graphite oxide. VC is a denser and more graphitic structure than HSAC, but is also characterized by a high number of defects (grain boundaries) between the meso-graphitic domains, making VC susceptible to oxidation, and this results in a slower, but still significant, rate of graphite oxide formation. LSAC is highly graphitized, with a large grain size, and few defects such as grain boundaries. LSAC particles are characterized by large, flat graphite basal plane surfaces, which are inherently oxidation resistant (no dangling edge bonds as associated with the less textured, misfit domain structure of VC) and have defects only associated with corners or edges where the large graphite surface facets adjoin/impinge. Clearly, a highly graphitized structure with a predominance of (002) surfaces and few defects will be more corrosion resistant.

Microscopy of Thin Ionomer Films

ORNL has established collaborations with GM and Ballard to use advanced microscopy techniques to study thin ionomer films, both on model substrates (silicon and Pt, for example) and within cathode layers. This research is focused on identifying the microscopy parameters that should be used to efficiently and non-destructively quantify the composition and structure of thin ionomer films before and after electrochemical aging. Ultimately, these studies are aimed at tracking ionomer stability and dispersions across the entire thickness of a catalyst layer and to determine how ionomer loading, thickness, and composition affect FC performance. Understanding ionomer distributions and changes to its structure and composition require that microscopy imaging and analysis methodologies be optimized to minimize beam damage. To date, many different microscope conditions have been evaluated for ionomer studies (voltage effects, current effects, temperature effects). This work will be continued in FY 2014, with the goal of quantifying the optimum microscope conditions needed to fully assess the nature of the ionomer within the cathode catalyst layer.

CONCLUSIONS AND FUTURE DIRECTIONS

ORNL's microstructural studies continue to provide insight regarding the structural and compositional characteristics of MEA material components that control stability and durability. We have focused primarily on carbon corrosion, electrocatalyst evaluation, and ionomer studies during FY 2013, and will continue to make progress on these issues in FY 2014:

- Carbon corrosion studies will continue in FY 2014, with greater emphasis placed on LSAC and mechanisms by which Pt dispersions may be improved on this corrosion-resistant support.
- Collaborations with GM and Ballard will continue and be expanded to determine the exact microscope conditions for reliably imaging and analyzing changes to ionomer thin films within catalyst layers. The primary goal of this work will be to "map" changes to the ionomer throughout the catalyst layer thickness and correlate these observations with carbon corrosion (graphite oxide formation) and Pt dispersions (especially lower Pt loadings).
- Perform/optimize in-house capabilities for in situ liquid-cell electrochemical microscopy. Several issues have delayed progress being made over the past two years, but ORNL is in a much better position now to perform experiments to study catalyst coarsening and carbon corrosion in real-time under potential hold and cycling conditions.
- Study field-aged PEMFCs to correlate materials degradation observations with results from ASTs.
- ORNL will continue to establish new collaborations with industrial and academic partners to provide characterization support and insight regarding FC materials durability and stability.

SPECIAL RECOGNITIONS & AWARDS/ PATENTS ISSUED

1. Karren L. More received the 2013 DOE Hydrogen and Fuel Cells Program R&D Award in Recognition of Outstanding Achievements in Microstructural Characterization of Fuel Cell Materials (May 2013).

2. K. Shawn Reeves received the 2013 Microscopy Society of America (MSA) Outstanding Technologist Award, Physical Sciences, in Recognition of (in part) her Development of Microtomy Techniques for Preparing Fuel Cell MEAs for Microscopy (August 2013).

FY 2013 PUBLICATIONS/PRESENTATIONS

1. A. Korvina, Y. Garsany, A. Epshteyn, A.P. Purdy, K.L. More, K.E. Swider-Lyons, and D.E. Ramaker, "Understanding Oxygen Reduction on Tantalum Oxyphosphate and Tantalum Oxide Supported Pt by X-Ray Absorbtion Spectroscopy," *Journal of Physical Chemistry C* **116**[34] 18175-18183 (2012).

2. K. Sykes Mason, K.C. Neyerlin, M.-C. Kuo, K.C. Horning, K.L. More, and A.M. Herring, "Investigation of a Silicotungstic Acid Functionalized Carbon on Pt Activity and Durability for the Oxygen Reduction Reaction," *Journal of the Electrochemical Society* **159**[12] F871-F879 (2012).

3. R.T. Atanasoski, L.L. Atanasoska, D.A. Cullen, G.M. Haugen, K.L. More, and G.D. Verstrom, "Fuel Cells Catalyst for Start-Up and Shutdown Conditions: Electrochemical, XPS, and STEM Evaluation of Sputter-Deposited Ru, Ir, and Ti on Pt-Coated NSTF Supports," *Electrocatalysis* **3**[3-4] 284-287 (2012).

4. L. Meng, D.A. Cullen, K. Sasaki, N.S. Marinkovic, K.L. More, and R.R. Adzic, "Ternary Electrocatalysts for Oxidizing Ethanol to Carbon Dioxide: Making Iridium Capable of Splitting C-C Bond," *Journal of the American Chemical Society* **135**[1] 132-141 (2013).

5. B.P. Pearman, N. Mohajeri, R.P. Brooker, M.P. Rodgers, D.K. Slattery, M.D. Hampton, D.A. Cullen, and S. Seal, "The Degradation Mitigation Effect of Cerium Oxide in Polymer Electrolyte Membranes in Extended Fuel Cell Durability Tests," *Journal of Power Sources* **225** 75-83 (2012).

6. G. Wu, K.L. More, P. Xu, H.-L. Wang, M. Ferrandon, A.J. Kropf, D.J. Myers, S. Ma, C.M. Johnston, and P. Zelenay, "A Carbon-Nanotube-Supported Graphene-Rich Non-Precious Metal Oxygen Reduction Catalyst with Enhanced Performance Durability," *Chemical Communications* **49**[32] 3265-3364 (2013).

7. C.-N. Sun, K.L. More, G.M. Veith, and T.A. Zawodzinski, "Composition Dependence of the Pore Structure and Water Transport of Composite Catalyst Layers for Polymer Electrolyte Fuel cells," *Journal of the Electrochemical Society* **160**[9] F1000-F1005 (2013).

8. M.P. Rodgers, B.P. Pearman, L.J. Bonville, D.A. Cullen, N. Mohajeri, and D.K. Slattery, "Evaluation of the Effect of Impregnated Platinum on PFSA Degradation for PEM Fuel Cells," *Journal of the Electrochemical Society* **160**[10] F1123-F1128 (2013).

9. Y. Garsany, A. Epshteyn, K.L. More, and K.E. Swider-Lyons, "Oxygen Electroreduction on Nanoscale Pt/[$TaOPO_4$]/VC] and Pt/[Ta_2O_5/VC] in Alkaline Electrolyte," *ECS Electrochemistry Letters* **2**[10] H46-H50 (2013).

10. S. Pylypenko, A. Borisevich, K.L. More, A.R. Corpuz, T. Holme, A.A. Dameron, T.S. olson, H.N. Dihn, T. Gennett, and R. O'Hayre, "Nitrogen: Unraveling the Secret to Stable Carbon-Supported Pt-Alloy Electrocatalysts," *Energy & Environmental Science* published on line DOI: 10.1039/c3ee40189h (2013).

11. ECS Short Course: K.L. More, "Advanced Microscopy Methods for Studying PEM Fuel Cell Materials" *223rd Meeting of the Electrochemical Society* Toronto, Canada – May 12, 2013.

12. Plenary Lecture: K.L. More, "Application of Advanced Microscopy Methods to Understand PEMFC-MEA Materials Degradation," Workshop on Advanced Characterization of Energy Conversion and Storage Materials, McMaster University, Hamilton, Ontario, Canada – May 17, 2013.

13. Invited Presentation: K.L. More and D.A. Cullen, "Application of Advanced Microscopy to Elucidate Materials Degradation Mechanisms in PEM Fuel Cells," Pacific Rim International Conference on Advanced Materials (PRICM-8), Waikoloa, HI – August 4–9, 2013.

14. Invited Presentation: D.A. Cullen, H.M. Meyer, K.S. Reeves, D.W. Coffey, and K.L. More, "Developing Fuel Cell Technologies Through Electron Microscopy," Microscopy & Microanalysis 2013, Indianapolis, IN – August 4–9, 2013.

15. Invited Presentation: K.L. More, "Characterization and Optimization of Cathode Materials for PEM Fuel Cells," 246th National Meeting of the American Chemical Society, Indianapolis, IN – September 8–12, 2013.

V.H.4 Neutron Imaging Study of the Water Transport in Operating Fuel Cells

Muhammad Arif (Primary Contact),
David L. Jacobson, Daniel S. Hussey
National Institute of Standards and Technology (NIST)
100 Bureau Drive
Gaithersburg, MD 20899
Phone: (301) 975-6303
Email: arif@nist.gov

DOE Manager
Nancy Garland
Phone: (202) 586-5673
Email: Nancy.Garland@ee.doe.gov

Contract Number: DE-AI-01-01EE50660

Project Start Date: Fiscal Year (FY) 2001
Project End Date: Project continuation and direction determined annually by DOE

Overall Objectives

- Provide state-of-the-art research and testing infrastructure to enable the fuel cell industry to design, test, and optimize prototype to commercial-grade fuel cells using in situ neutron imaging techniques.
- Provide a secure facility for proprietary research by industry. Provide beam time at no cost to non-proprietary research through a competitive proposal process. Make open research data available for beneficial use by the general fuel cell community.
- Continually improve and develop methods and technology to accommodate rapidly changing industry/academia needs.

FY 2013 Objectives

- Collaborate and support groups from the DOE Hydrogen and Fuel Cells Program performing water transport measurements with neutron imaging at NIST.
- Deploy new large-area detectors with high spatial resolution for fuel cell water transport measurements.
- Explore and develop high-resolution neutron imaging methods to enable water transport studies of catalyst and membrane electrode assemblies (MEAs).
- Employ a high resolution imaging method to achieve resolution approaching 1 micrometer to resolve water concentration in fuel cell electrodes.
- Determine and correct systematic effects due to spatial resolution effects.
- Build fuel cell infrastructure to enable testing of automotive-scale test sections.

Technical Barriers

This project addresses the following technical barriers from the Fuel Cells section of the Fuel Cell Technologies Office Multi-Year Research, Development, and Demonstration Plan:

(A) Durability

(B) Cost

(C) Performance

Technical Targets

This project is conducting fundamental studies of water transport in the fuel cell. Insights gained from these studies will be applied toward the design of components and operation strategies of proton exchange membrane fuel cells (PEMFCs) that meet the following DOE fuel cell targets:

- Durability with cycling at operating temperature of ≤80°C: 5,000 h
- System energy density: 650 W/L
- System specific power: 850 Watt/kg
- Energy efficiency: 60% at 25% rated power
- Cost: $30/kW$_e$
- Start-up time to 50% power: 30 seconds from -20°C, 5 seconds from 20°C
- Assisted start from low temperatures: -40°C
- Durability with cycling: 5,000 hrs

FY 2013 Accomplishments

- Published detailed analysis of making accurate measurements of the through-plane water content of proton exchange membranes using neutron radiography.
- Supported all target areas by imaging larger cell areas with high spatial resolution by acquiring and deploying large area high resolution neutron detectors for imaging MEA and gas diffusion layer (GDL) water content under a wide range of conditions for in situ testing of fuel cells.
- Designed, built and tested a high spatial resolution freeze chamber for testing unassisted starts from -40°C.
- Tested and developed new approaches to measure water related corrosion issues in catalyst membranes which can improve understanding of durability with cycling. To do this methods to achieve spatial resolution near 1 micrometer have been developed and tested.

INTRODUCTION

At NIST, we maintain the premier fuel cell neutron imaging facility in the world and continually seek to improve its capabilities to meet the changing needs of the fuel cell community. This facility provides researchers with a powerful and effective tool to visualize and quantify water transport inside operating fuel cells. Imaging the water dynamics of a PEMFC is carried out in real time with the required spatial resolution needed for fuel cells that are being developed today. From these images, with freely available NIST-developed image analysis routines, PEMFC industry personnel and researchers can obtain in situ, non-destructive, quantitative measurements of the water content of an operating PEMFC. Neutron imaging is the only in situ method for visualizing the water distribution in a "real-world" PEMFC. Unlike X-rays, whose interaction with materials increases with the number density of electrons, neutrons interact via the nuclear force, which varies somewhat randomly across the periodic table, and is isotopically sensitive. For instance, a neutron's interaction with hydrogen is approximately 100 times greater than that with aluminum, and 10 times greater than that with deuterium. It is this sensitivity to hydrogen (and insensitivity to many other materials) that is exploited in neutron imaging studies of water transport in operating fuel cells.

APPROACH

The typical length scales of interest in a PEMFC are channels approximately 1 mm wide and 1 mm deep, the diffusion media are 0.1 mm to 0.3 mm thick, the membrane is 0.01 mm to 0.02 mm thick, and the active area of test sections can range from 2 cm^2 to 500 cm^2. Though the study of water transport within these length scales are technically very challenging, the unique capabilities of neutron imaging have already successfully addressed many of the questions. However, as fuel cell research matures, the water transport questions become increasingly more demanding, requiring for instance resolving the water content in catalyst layers. To meet these demands, based on fuel cell community feedback and need, we continue to develop new facilities and improve existing capabilities for obtaining higher spatial and temporal resolution neutron images. These improvements will enable users to perform even more detailed, nondestructive, and in situ studies of the water and hydrogen transport in PEMFCs to meet DOE goals. In addition, employing mathematical models of neutron scattering, we will develop a software suite that enables users to obtain reliable, accurate, quantitative measurements of the water content in an operating PEMFC. Due to the complexity of PEMFCs and the large number of remaining open questions regarding water transport in PEMFCs, we will develop partnerships with industry, academia, and national laboratories to train them in the use of the facility, seek their feedback, and collaborate with them on research projects, to seek measurement breakthroughs that will facilitate the rapid, efficient, and robust development of fuel cells.

RESULTS

The NIST Neutron Imaging Facility provides year-to-year support for the DOE Hydrogen and Fuel Cells Program projects by providing beam time and by collaboration with users on a variety of related neutron imaging projects that support the DOE mission. For FY 2013, proposals from Los Alamos National Laboratory, Lawrence Berkeley National Laboratory, Rochester Institute of Technology, General Motors, Ford Motor Company, Ballard, University of Tennessee, Knoxville, University of Connecticut and University of Michigan have received project support for experiments at the facility accounting for more than 50 days of beam time. Published results from these and previous years experiments are reflected in the publication list attached to this report.

Meeting the requirements for imaging fuel cells has required constant innovation in neutron imaging technology and techniques. Usually one must trade high resolution for field of view of a fuel cell. For example, validation of down the channel models require a large field of view to visualize the channel's length. This means that longer flow channels (>4 cm) must be imaged with lower resolution because the number of pixels in the imaging detector is fixed. To improve the situation detectors with more pixels or larger fields of view are necessary. Until recently detectors that can image a 10 cm field of view with 10 micrometer pixels have not existed. However, recently both larger area microchannel plate detectors and charge-coupled device cameras have become available. Two new systems have been acquired for the user program. The first system is a large area 100 mega pixel charge-coupled device type detector with a pixel pitch of 9 µm by 9 µm shown in Figure 1. Using Gd_2O_2S:Tb scintillators, resolution near 20 micrometers is obtained. The second is a 256 megapixel microchannel plate detector with a 9 cm x 9 cm field of view. This detector is similar in design and capability of the existing NIST 40 mm microchannel plate detectors, with an expected spatial resolution of about 15 micrometers.

Understanding of flooding and degradation issues due to liquid water in catalysts is critical for improving durability and cycling of fuel cells. This requires even better spatial resolution than what has been achieved to date. Currently we can achieve near 13 µm, but to effectively study catalysts it will be necessary to achieve near 1 µm spatial resolution in one dimension of the image. This has pushed the need for innovation in neutron imaging that must go beyond the current limiting spatial resolution. This current resolution

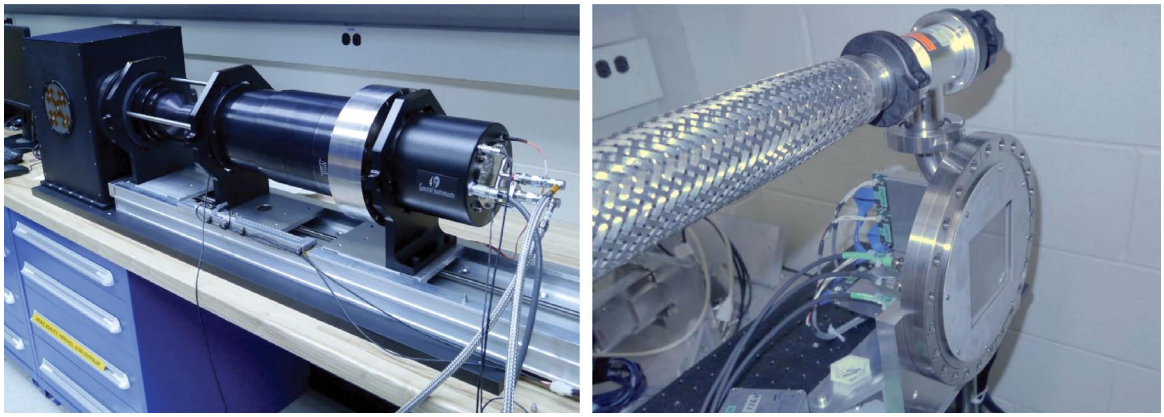

FIGURE 1. New large-area high-resolution detectors for validation of down the channel models of fuel cell operation.

limit is due to the range of charged particles that are used to detect neutrons (3.5 µm–150 µm) and fundamentally limits the spatial resolution. To overcome this limit we have been exploring two methods. The first called structured illumination uses neutron absorbing slits nanofabricated into gratings that are ~2 µm or less in width to define the neutron path illuminating the fuel cell with high spatial resolution in one dimension. The grating can then be translated across the object to obtain a high resolution image along the grating direction, overcoming the resolution limit of the detector. The resulting images can be combined to produce an image with spatial resolution defined by the slit width of the grating. Proof of principle measurements have shown this technique should work, but at a cost of increased integration time. This will require steady-state operation of the fuel cell for many hours.

A second avenue towards achieving 1 µm resolution has also been identified utilizing innovative X-ray lens technology developed by the National Aeronautics and Space Administration based on Wolter mirror optics. This innovation will eventually enable acquiring images with spatial resolution of ~1 µm, without reducing the signal rate to impractically low levels. As recently demonstrated by Liu et al. [1], these focusing neutron optics can be used to form images and show that high intensity will be possible.

Wolter focusing mirrors make the optical design of a neutron-imaging instrument similar to that of optical microscopes, where the resolution does not depend on the beam collimation, but rather on the optics itself. Consequently, the source size, and thus the number of neutrons illuminating the sample increase substantially, leading to higher signal rates. In addition, optical magnification would result in a better spatial resolution at the same pixel size of the detector. Therefore, the use of Wolter optics opens the possibility for significant progress in high resolution thermal neutron radiography, similar to the use of lenses in optical devices.

The use of large-magnification high-resolution optics would help neutron fuel cell imaging to reach 1 µm length scales with reasonable image acquisition times. An estimate of the increased signal rate for a 1:1 optic illustrates the potential gains. At the NIST neutron imaging facility, slit apertures of 2 mm x 20 mm are used to obtain images of fuel cells with about 10 µm spatial resolution. The short dimension of the slit provides high resolution along the through-plane of the fuel cell, while the long dimension provides a higher neutron fluence rate, which reaches about 2×10^6 cm^{-2} s^{-1}. This low fluence rate requires an image acquisition time of about 10 minutes for an accurate measurement of the water content in a fuel cell. Liu et al. [1] estimate the throughput of the Wolter optic would increase the effective neutron fluence rate to 2×10^8 cm^{-2} s^{-1} for a gain of 100 over the pinhole optics geometry. Further, the resolution of the image is the same in all directions, as opposed to being more blurred in one dimension, as is the case in the slit image. With such intensity gains it will possible to obtain high temporal (~5 s) and spatial resolution (~10 µm) images of transient processes in fuel cells. As well, tomography data sets with 10 µm voxel resolution could be obtained in a period of less than an hour as opposed to the current ~1 day. The possibility of 10x magnification, coupled with a detector spatial resolution of ~10 µm means that the system resolution could reach ~1 µm. Since the neutron density will be decreased by a factor of 100 from magnification, image acquisition times will be comparable to the current image acquisition time for ~10 µm resolution images (10 min). With this gain in resolution, one would be able to image the water content in standard Pt/C electrodes in fuel cells. Another advantage of an optic for imaging is that the sample no longer needs to be in direct contact with the detector, which allows for ample space both upstream and downstream of the sample, simplifying the experimental setup process. One could also perform simultaneous X-ray and neutron micro-tomography of porous media and in one unique instrument obtain the complementary information

from both probes; X-rays to measure the matrix and neutrons to measure the fluid.

The lens tested was not optimized for neutrons, but did demonstrate the potential for the lens to form neutron images with 4x magnification shown in Figure 2. Due to lower tolerances in the manufacture of the lens the resolution was limited to 70 µm; however the test showed that a practical neutron lens was feasible. The 4x magnified neutron image of a fuel cell is shown in Figure 3. Water content is plotted to demonstrate the feasibility of the lens to measure fuel cell water distributions.

High resolution imaging of the water transport during low temperature start-up impacts the DOE targets of unassisted startup from -40°C. Although the NIST freeze chamber has been able to achieve environmental conditions of -40°C to image flow fields, high spatial resolution at temperatures below -20°C has been challenging due to the design of the NIST freeze chamber. In order to extend high resolution freeze testing down to -40°C it was necessary to redesign the NIST freeze chamber to be compatible with high resolution detectors that could not run in a -40°C environment. A new environmental chamber was designed, built and tested to allow high resolution detectors to run at stable ambient room temperature while cooling a fuel cell in close proximity to -40°C with both air and liquid coolants. The fuel cell is located within 4 cm of the high resolution detector to avoid geometric blurring due to the neutron beam. Preliminary measurements were made with a fuel cell and a paper is in preparation describing the experimental setup and results.

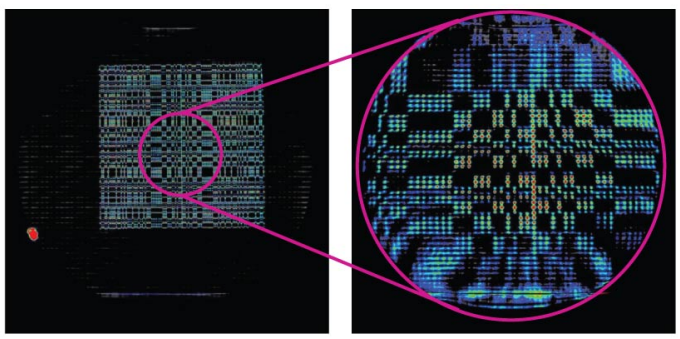

FIGURE 2. Contact radiograph of test pattern on left. Magnified 4x neutron image of test pattern on right.

Through the NIST partnership with General Motors a large-scale test stand was recently acquired and included into the testing infrastructure for the facility. The new large fuel cell test stand is capable operating fuel cells and small stacks at 800 W, 6-1,000 A @ 0.2 V, 0 V–50 V, hydrogen: 0.065 slpm–11.31 slpm, air: 0.239 slpm–26.92 slpm. The test stand is incorporated into the facility testing infrastructure and the facility technical staff are receiving training on calibration, operation and validation testing with the test stand in August 2013 with our testing partners from General Motors. Further reports of this capability and tests made with this stand will be presented at future Annual Merit Reviews.

CONCLUSIONS AND FUTURE DIRECTIONS

- Validation testing of down the channel models of fuel cell operation is now possible with large area, high resolution detectors for fuel cells:
  - Large field of view 10 cm x 10 cm

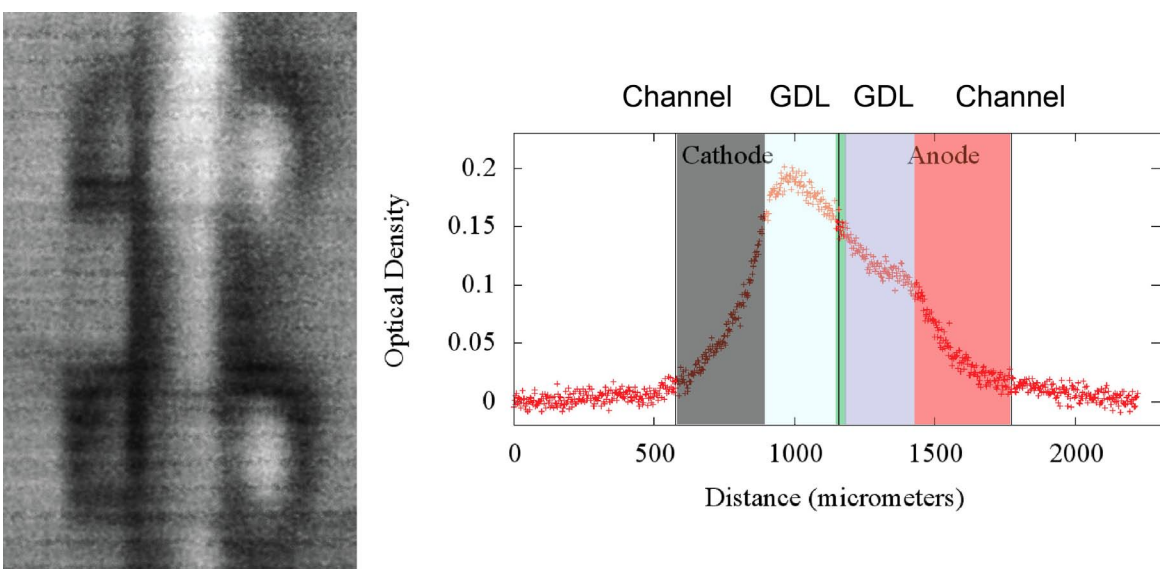

FIGURE 3. Left lens 4x magnified image of a dry fuel cell, right optical density is plotted, which is proportional to the water thickness. An additional calibration measurement is required to accurately convert to water thickness, but was not performed to limited beam time.

  - Spatial resolution 20 µm
  - Image flow fields and manifolds with high spatial resolution
  - Future—support imaging larger cells using large area detectors that maintain high spatial resolution.
- With the goal to study catalysts, we will continue to improve the image spatial resolution with a goal of 1 µm. We have identified new avenues toward high resolution MEA water content:
  - Steady progress made towards grating method
  - Demonstrated prototype neutron microscope to image catalyst/membrane layers
  - Future—deploy grating based structured illumination method to user program
  - Future—develop neutron lens to achieve higher spatial and time resolution
  - Future—develop measurement technique to image catalyst degradation mechanisms due to carbon corrosion and freeze thaw with neutrons
- We have published a detailed exploration of the accuracy and uncertainties associated with water distribution measurements using neutron imaging.
  - Future—incorporate systematic corrections to MEA water content measurements into the NIST analysis software in a user friendly way
- Through-plane freeze measurement
  - New environmental enclosure fabricated and ready for fuel cell testing
- Future general improvements
  - Provide a NIST set of high resolution testing hardware to ensure user testing compatibility with beam line setup
  - Provide support for automotive-sized fuel cell hardware testing
  - Future—incorporate systematic corrections to MEA water content measurements into the NIST analysis software in a user friendly way

FY 2013 PUBLICATIONS/PRESENTATIONS

1. Hussey, D.S., Spernjak, D., Fairweather, J., Spendelow, J., Mukundan, R., Weber, A.Z., Jacobson, D.L., and Borup, R., Accurate measurement of the through-plane water content of proton-exchange membranes using neutron radiography. Journal of Applied Physics, v. 112, 104906 (2012).

2. Selamet, O.F., Pasaogullari, U., Spernjak, D., Hussey, D.S., Jacobson, D.L., and Mat, M.D., Two-Phase Flow in a Proton Exchange Membrane Electrolyzer Visualized In Situ by Simultaneous Neutron Radiography and Optical Imaging, accepted International Journal of Hydrogen Energy (2013).

3. K.J. Coakley, D.F. Vecchia, D.S. Hussey, and D.L. Jacobson, Neutron Tomography of a Fuel Cell: Statistical Learning Implementation of a Penalized Likelihood Method, submitted, IEEE Transactions on Nuclear Science (2013).

4. D. Liu, D. Hussey, M.V. Gubarev, B.D. Ramsey, D. Jacobson, M. Arif, D.E. Moncton, and B. Khaykovich, Demonstration of Achromatic Cold-Neutron Microscope Utilizing Axisymmetric Focusing Mirrors, submitted, Applied Physics Letters (2013).

5. Hussey, D.S., E. Baltic, K.J. Coakley & D.L. Jacobson, Improving quantitative neutron radiography through image restoration. Submitted to NIMA (2013).

6. J.D. Fairweather, D. Spernjak, A.Z. Weber, D. Harvey, S. Wessel, D.S. Hussey, D.L. Jacobson, K. Artyushkov, R. Mukundan, and R.L. Borup, Effects of Cathode Corrosion on Through-Plane Water Transport in Proton Exchange Membrane Fuel Cells, Journal of the Electrochemical Society, 160 (9) F980-F993 (2013).

7. W.A. Rigdon, X. Huang, D.S. Hussey, D.L. Jacobson, Proton Conductivity of Polymer Electrolyte Membranes during Transient Hydration, Electrochemical Society Letters, In preparation (2013).

8. Spernjak, D., D.S. Hussey, A.Z. Weber, R. Mukundan, J. Fairweather, E.L. Brosha, J. Davey, J. Spendelow, D.L. Jacobson, and R. Borup, Environmental affects on PEM water content. Journal of the Electrochemical Society, In preparation (2013).

9. Spernjak, D., G. Wu, J. Fairweather, D. Hussey, R. Mukundan, R. Borup and P. Zelenay, In situ measurement of flooding in thick Pt and PANI-derived catalyst layers in PEM fuel cells. Journal of the Electrochemical Society, In preparation (2013).

10. Wood, B.M., Ham, K., Hussey, D.S., Jacobson, D.L., Faridani, A., Kaestner, A., Vajo, J.J., Liu, P., Dobbins, T.A. and Butler, L.G., Real-Time Observation of Hydrogen Absorption by $LaNi_5$ with Dynamic Neutron Tomography, Nucl. Instrum. Meth. B, In preparation (2013).

11. R. Mukundan, D. Spernjak, R. Lujan, J. Fairweather, D. Hussey, D. Jacobson, A. Steinbach, A. Weber, and R.L. Borup, Neutron imaging and performance of PEM fuel cells with nanostructured thin film electrodes at low temperatures, ECS Trans., submitted (2013).

12. R.S. Fu, N. Khajeh-Hosseini-Dalasm, and U. Pasaogullari, Numerical Validation of Water Transport in Polymer Electrolyte Membranes, ECS Trans. 2013 50(2): 967-978; doi:10.1149/05002.0967ecst.

13. D.S. Hussey, D. Spernjak, G. Wu, D.L. Jacobson, D. Liu, B. Khaykovich, M.V. Gubarev, J. Fairweather, R. Mukundan, R. Lujan, P. Zelenay, and R.L. Borup, Neutron Imaging Of Water Transport In Polymer-Electrolyte Membranes And Membrane-Electrode Assemblies, ECS Trans., submitted (2013).

14. Lu, Z., Waldecker, J., X. Xie, Lai, M., Hussey, D. S., and Jacobson, D.L., Investigation of Water Transport in Perforated Gas Diffusion Layer by Neutron Radiography, ECS Trans., submitted (2013).

15. D. Spernjak, R. Mukundan, P. Wilde, R. Schweiss, K.L. More, D. Langlois, J. Fairweather, D. Hussey and R.L. Borup, PEM Fuel Cell Performance and Durability with Different Treatments of Microporous Layer (MPL), 222nd Meeting of the ECS, October 2012.

16. D.S. Hussey, D.L. Jacobson, B. Khaykovich, M.V. Gubarev, D. Spernjak, J. Fairweather, R. Mukundan, R. Lujan, and R.L. Borup, Neutron imaging PEMFCs with ~1 µm spatial resolution, 222nd Meeting of the ECS, October 2012.

17. X. Liu, J. Lin, K. McConnaghy, T. Trabold, J. Gagliardo, J. Owejan, Investigation of Channel-to-Manifold Water Transport in PEM Fuel Cells, ASME, November 2012.

18. B. Carnes, K. Chen, D. Spernjak, G. Luo, L. Hao, and C-Y Wang, A Case Study of Validation of Multiphase PEMFC Computer Models Using Through-Plane Liquid Water Measurements, 222nd Meeting of the ECS, October 2012.

19. R.S. Fu, N. Khajeh-Hosseini-Dalasm, and U. Pasaogullari, Numerical Validation of Water Transport in Polymer Electrolyte Membranes, 222nd Meeting of the ECS, October 2012.

20. D. Jacobson, D. Hussey, E. Baltic, M. Arif, Next generation needs for neutron radiography detectors, International Workshop on Neutron Optics and Detectors, Munich (Ismaning), Germany, July 2012.

21. D.S. Hussey, D.L. Jacobson, E. Baltic, M. Arif, The NIST Neutron Imaging Facility: Capabilities and Opportunities, ASNT 22nd Research Symposium, Memphis, TN, 19 MAR 2013.

22. D.S. Hussey, D.L. Jacobson, E. Baltic, E. Binkley, M. Arif, D. Liu, B. Khaykovich, M. Gubarev, A neutron microscope at NIST, ICNS 2013, Edinburgh, UK, July 2013.

23. D.S. Hussey, Seeing the world with neutron vision, Michigan Technical University, 25 April, 2013.

REFERENCES

1. D. Liu, D. Hussey, M.V. Gubarev, B.D. Ramsey, D. Jacobson, M. Arif, D.E. Moncton, and B. Khaykovich, Demonstration of Achromatic Cold-Neutron Microscope Utilizing Axisymmetric Focusing Mirrors, submitted, Applied Physics Letters (2013).

V.H.5 Enlarging the Potential Market for Stationary Fuel Cells Through System Design Optimization

Chris Ainscough (Primary Contact),
Dustin McLarty (UCI), Jack Brouwer (UCI),
Sam Sprik (NREL)
National Renewable Energy Laboratory (NREL)
15013 Denver West Pkwy
Golden, CO 80401
Phone: (720) 431-7296
Email: chris.ainscough@nrel.gov

DOE Manager
Jason Marcinkoski
Phone: (202) 586-7466
Email: Jason.Marcinkoski@ee.doe.gov

Subcontractor:
University of California, Irvine (UCI), Irvine, CA

Project Start Date: January 1, 2011
Project End Date: Project continuation and direction determined annually by DOE

Overall Objectives

Build an open-source tool that helps combined heat and power (CHP) fuel cell developers, end users, and other stakeholders to do the following for their systems:

- Drive economies of scale and cost reduction
- Determine the appropriate sizing to reduce cost at single installations
- Integrate to commercial building control and heating, ventilation and cooling (HVAC) systems to maximize durability and minimize lifecycle cost
- Compare performance relative to incumbent technologies
- Determine optimum system configuration
- Evaluate potential market penetration for new or existing product lines.

Fiscal Year (FY) 2013 Objectives

- Implement updated dispatch for fuel cell system dispatch and control into the model.
- Model verification against actual building/CHP installations.
- Demonstrate the fuel cell model to the Fuel Cell Technologies Office. This demonstration will serve as the basis for a Go/No-Go decision on further work for the project.

Technical Barriers

This project addresses the following technical barriers from the Fuel Cell section of the Fuel Cell Technologies Office Multi-Year Research, Development, and Demonstration Plan:

(A) Durability

(B) Cost

(C) Performance

Technical Targets

This project is providing a tool to fuel cell manufacturers, end users and other stakeholders to help them reduce the cost of fuel cell CHP installations by optimizing their sizing, combining them with hybridizing technologies such as thermal energy storage and batteries, dispatching them in cost-optimal ways, and investigating the fuel cell sizes and features to best address the national market. Relevant DOE targets (2020) are:

- Installed cost, natural gas: $1,500/kW
- Operating lifetime: 40,000-80,000 hours
- CHP energy efficiency: 90%

FY 2013 Accomplishments

- This project successfully implemented four new dispatch strategies which can reduce the lifetime costs of installing and operating fuel cell CHP systems in commercial buildings.
- This project successfully formed a users' group which allows users to test, use and suggest modifications to the software. Compiled versions of the code are under evaluation with eight organizations including Advanced Research Projects Agency–Energy, other national labs, and industrial fuel cell developers.
- The project successfully passed a Go/No-Go stage gate in July 2013.

✧ ✧ ✧ ✧ ✧

INTRODUCTION

This project aims to create an open-source software tool which allows fuel cell developers, their potential customers and other stakeholders to evaluate the ability of fuel cell installations to save money relative to the grid/natural gas paradigm. The model includes 768 model building

profiles covering the major American Society of Heating, Refrigerating and Air-Conditioning Engineers climate zones in the United States.

The model can perform design optimizations on single fuel cells and building combinations, campuses of multiple buildings, chillers, energy storage technologies, and onsite renewables such as solar and wind.

APPROACH

The approach taken by the research team is to build a flexible, configurable model which allows users to create modules for the various components which make up a project scenario (fuel cells, energy storage, chillers, buildings and campuses). NREL has teamed with the University of California, Irvine as a sub-contractor to leverage their extensive expertise in this area. In addition, NREL is working cross-center within the lab drawing extensively on the expertise of the Commercial Building group within NREL, to provide model building profiles.

RESULTS

The modeling effort has greatly expanded the number and types of analyses which can be completed. Four new dispatch/control strategies were introduced which can help reduce overall lifecycle costs of stationary fuel cell installations. New modules include vapor compression and absorption chillers (Figure 1), thermal energy storage (Figure 2), on-site renewables, time-of-use pricing in 20+ cities, a sensitivity analysis capability (Figure 3), national impact assessment (Figure 4), and design based on real (as opposed to model) building data.

CONCLUSIONS AND FUTURE DIRECTIONS

Future work will include more outreach and expansion of the users' group to be more inclusive, and add a structured way to receive feedback. Ultimately the desire of the team is to make the software open source to the users' group.

Proposed new work for FY 2014 includes (note, not all of these may be adopted into the final plan):

- Cost optimization instead of area under demand curve (brute force for energy charges only)
- Scale installation to demand with fixed fuel cell sizes based on multiples of baseline system e.g., 4x300 kW
- Advanced controls (e.g., predictive control) with physical distributed generation system models and comparison to ideal dispatch:
  - Single installation level of analysis

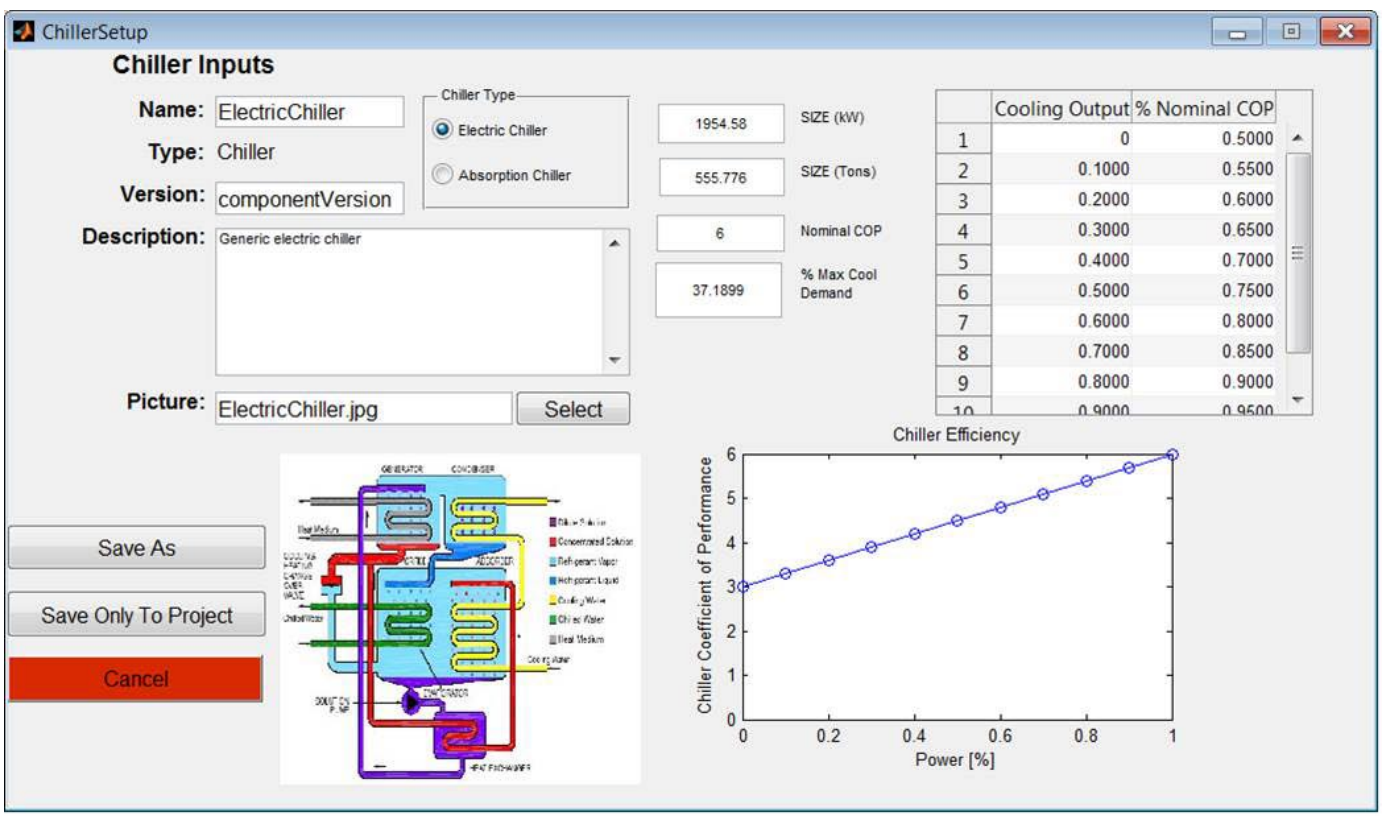

FIGURE 1. Module configuration screen for chillers, allowing users to easily configure both vapor compression and absorption chillers.

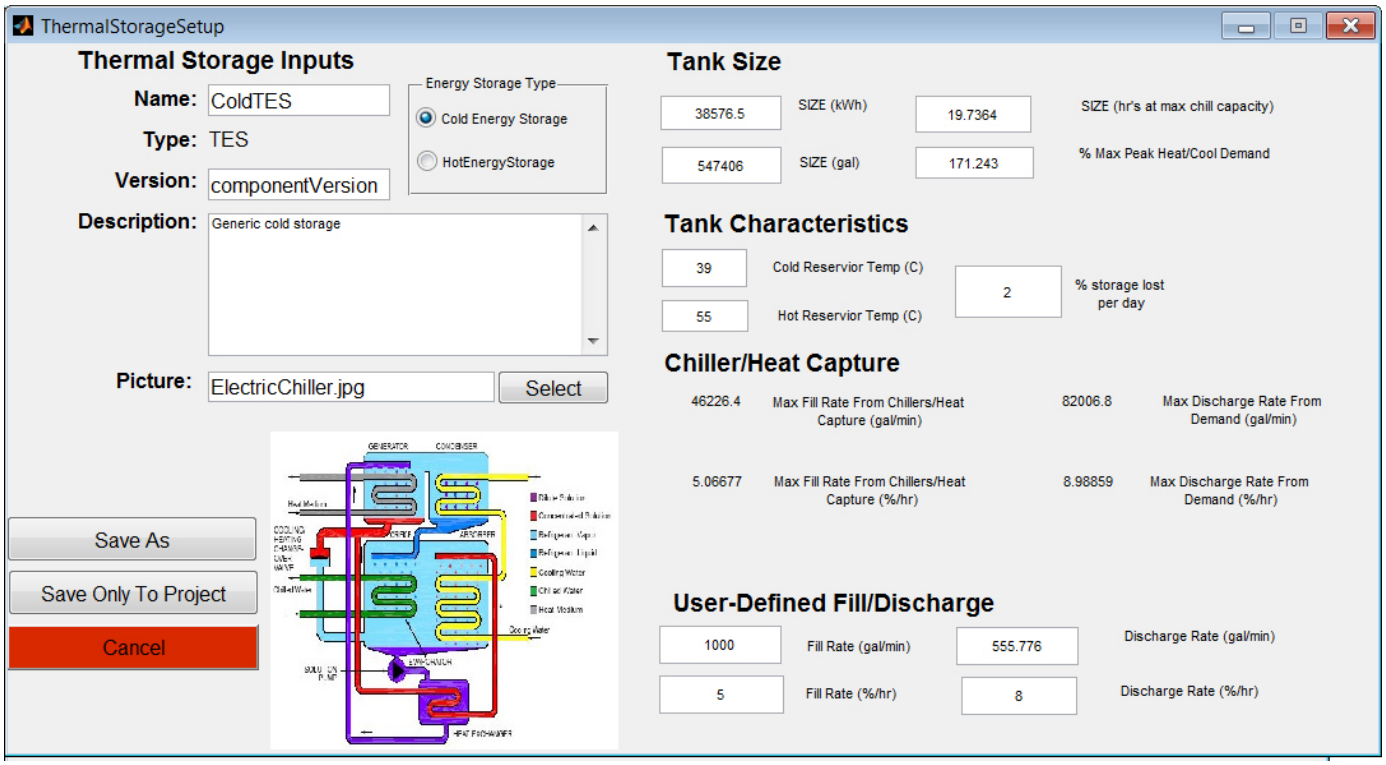

FIGURE 2. Module configuration screen for thermal energy storage, allowing users to easily configure both hot and cold water energy storage.

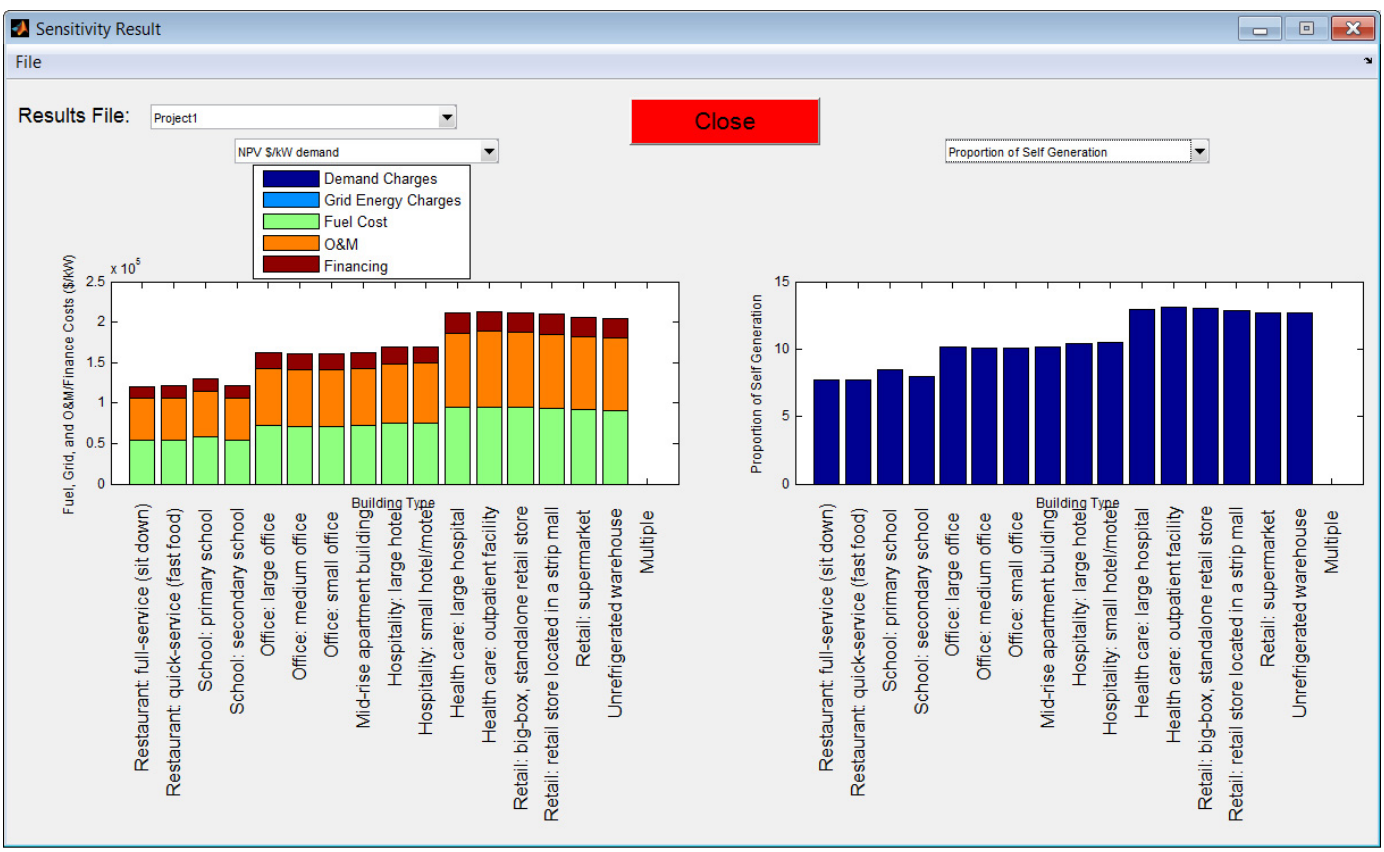

FIGURE 3. A sample sensitivity study showing net present value (NPV, $/kW) for the analysis scenario for various building types (left inset), and the proportion of self-generation (%) (right inset).

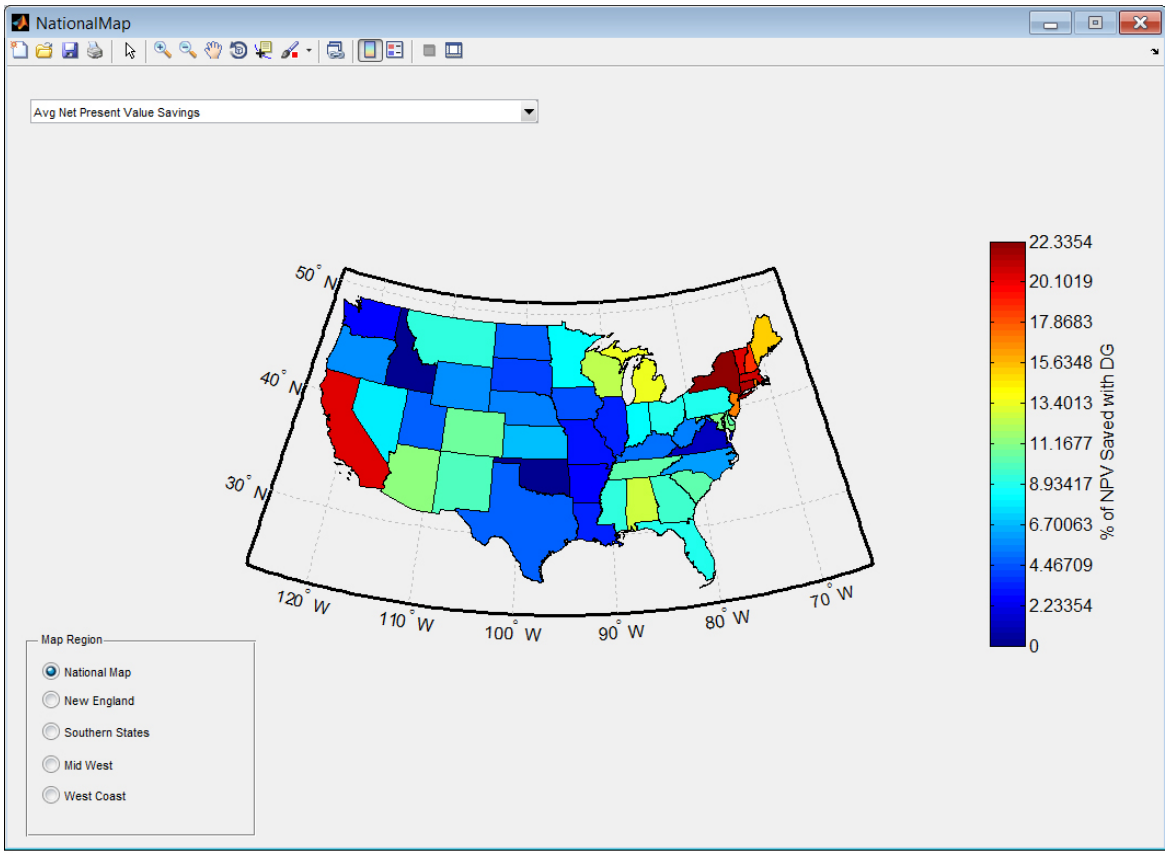

FIGURE 4. A sample map showing the average net present value savings in the continental United States for a sample analysis scenario.

- Building energy demand profiles:
  - Adoption of Pacific Northwest National Laboratory building profiles
  - Addition of American Society of Heating, Refrigerating and Air-Conditioning Engineers 90.1-2007 standard
  - Allow easy user upload of flat data files and conversion to Distributed Generation Building Energy Assessment Tool native format.
- Commercial Building Energy Consumption Survey (CBECS):
  - Update building inventories based on output from CBECS 2012.
- Refinement of economics for scenario analyses:
  - Database of State Incentives for Renewable Energy
  - Projections for changes in utility prices
  - Regional natural gas prices
  - Regional variation in energy vs. demand charges
  - Variation in utility costs and energy vs. demand costs with scale of installation
  - Variation in building sizes of same class (e.g., not all hospitals = 1,200 kW)

FY 2013 PUBLICATIONS/PRESENTATIONS

1. Enlarging Potential National Penetration for Stationary Fuel Cells through System Design Optimization, Fuel Cell Seminar, Uncasville, CT., November 2012.

2. Webinar with fuel cell OEMs, online, March 2013.

3. Enlarging Potential National Penetration for Stationary Fuel Cells through System Design Optimization, Annual Merit Review, Washington, D.C. May 2013.

4. Distributed Generation Build-out Economic Assessment Tool (DG-BEAT), University of California, Irvine, Irvine, CA. June 2013.

V.H.6 Stationery and Emerging Market Fuel Cell System Cost Analysis - Material Handling Equipment

Vince Contini (Primary Contact),
Kathya Mahadevan, Mike Jansen, and
Fritz Eubanks
Battelle
505 King Avenue
Columbus, OH 43201
Phone: (614) 424-7249
Email: continiv@battelle.org

DOE Managers
Donna Ho
Phone: (202) 586-8000
Email: Donna.Ho@ee.doe.gov
Reg Tyler
Phone: (720) 356-1805
Email: Reginald.Tyler@go.doe.gov

Contract Number: DE-EE0005250/001

Project Start Date: September 30, 2011
Project End Date: September 30, 2016

Overall Objectives

The objective of this project is to assist the U.S Department of Energy in developing fuel cell systems for stationary and emerging markets by developing independent cost models for manufacture and ownership.

- Identify the fundamental drivers of system cost and the sensitivity of the cost to system parameters.
- Help the DOE prioritize investments in research and development of components (e.g., metal bipolar plates versus composite graphite plates in polymer electrolyte membrane [PEM] fuel cells for low volume markets) to reduce the costs of fuel cell systems while considering systems optimization.
- Identify manufacturing processes that must be developed to commercialize fuel cells.
- Provide insights into the optimization needed for use of off-the-shelf components in fuel cell systems.

Fiscal Year (FY) 2013 Objectives

- Estimate cost of 1- and 5-kW solid oxide fuel cells (SOFCs) for auxiliary power unit applications at annual production volumes of 100 units, 1,000 units, and 10,000 units.
- Estimate cost of 1- and 5-kW PEM fuel cells for material handling equipment applications at annual production volumes of 100 units, 1,000 units, and 10,000 units.

Technical Barriers

This project addresses the following technical barriers from the Fuel Cell section of the Fuel Cell Technologies Office Multi-Year Research, Development, and Demonstration Plan:

(B) Cost

Technical Targets

To widely deploy fuel cells, significant strides must be made in lowering the cost of components and systems without compromising reliability and durability. This cost analysis will identify the fundamental drivers of component and system cost and the sensitivity of the cost to various component and system parameters. The cost analyses will provide the DOE information on the impact of production volumes on lowering costs of fuel cells and the types of high volume manufacturing processes that must be developed to enable the widespread commercialization. The study will also provide insights into the optimization needed for use of off-the-shelf components in fuel cell systems to drive down system costs. Finally, the study will analyze the lifecycle costs of owning and operating a fuel cell to estimate primary costs drivers to the end user in applicable markets.

FY 2013 Accomplishments

- Completed manufacturing cost analysis of 10-kW and 25-kW direct hydrogen PEM fuel cell systems for material handling applications.
- Completed the market assessment for the auxiliary power unit and material handling equipment markets.
  - Defined the application requirements
  - Selected appropriate fuel cell technologies and system sizes to meet requirements
- Detailed performance specifications and system requirements and completed preliminary system design of:
  - 1-kW and 5-kW SOFC for auxiliary power units
  - 1-kW and 5-kW PEM fuel cell for material handling equipment, specifically forklifts

Next Steps

In FY 2014 Battelle will:

- Complete full cost assessment of 1-kW and 5-kW SOFC systems for auxiliary power applications
- Complete full cost assessment of 1-kW and 5-kW PEM fuel cell systems for material handling applications

✧ ✧ ✧ ✧ ✧

APPROACH

Battelle will apply the established methodology used successfully on the previous fuel cell cost analysis study for the DOE [1-3]. The technical approach consists of four steps—market assessment, system design, cost modeling, and sensitivity analysis (Figure 1). The first step characterizes the potential market and defines the requirements for system design. The second step involves developing a viable system design and associated manufacturing process vetted by industry. The third step involves building the cost models and gathering inputs to estimate manufacturing costs. Manufacturing costs will be derived using the Boothroyd-Dewhurst Design for Manufacture Assembly Software. Custom manufacturing process models will be defined where necessary and parametrically modeled based on knowledge of the machine, energy, and labor requirements for individual steps that comprise the custom process. The fourth step will evaluate the sensitivity of stack and system costs to various design parameters. Both single-factor sensitivity analysis and Monte Carlo analysis will be performed. Single-factor sensitivity analysis helps determine the impact of individual parameters on system costs. The Monte Carlo analysis will help determine the impacts of cost variability. In addition to the sensitivity analysis, we will conduct a lifecycle cost analysis to estimate total cost of ownership for the target application and markets.

RESULTS

A high level summary of the final costs is shown below and emphasizes that the balance of plant (BOP) dominates the final cost—at most it is estimated to account for 83% of the final cost before markup at high production volumes. In all sizes and production rates analyzed, the BOP was responsible for approximately 80% of the pre-markup price. Overall the final cost is analyzed in four distinct categories: the capital cost of manufacturing equipment, the direct cost of material and assembly of the stack, the expense of BOP hardware, and the final cost of complete system assembly and testing it. Anticipated scrap is also captured in the stack manufacturing cost.

A standard sales markup of 50% was integrated at the end and is called out separately in Tables 1 and 2. At high production volumes, the final ticket price is estimated to be $2,918 per kW for a 10-kW MHE PEM system. This price decreases nearly 33% per kW for a 25-kW system.

CONCLUSIONS AND FUTURE DIRECTIONS

The primary driver of overall MHE system cost is the cost of BOP hardware, with battery, direct current to direct current (DC/DC) converter, hydrogen tank, and humidification system making up around 75% of the total BOP cost. The stack costs are most sensitive to change in current density and platinum loading.

Production volume considered in this report has negligible effect on stack cost, due to the fact that

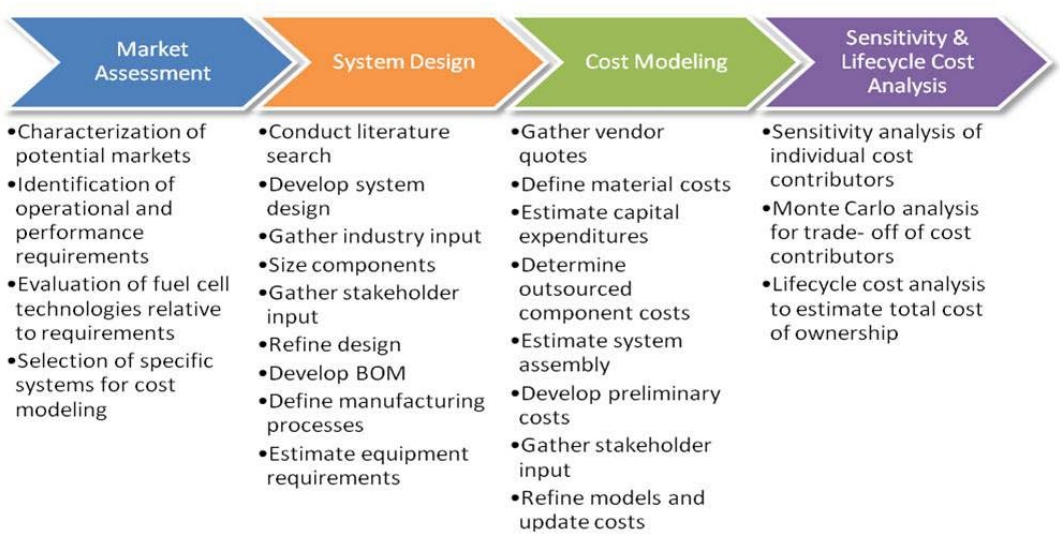

FIGURE 1. Battelle's Cost Analysis Methodology

TABLE 1. 10-kW MHE PEM Fuel Cell System per Unit Cost Summary

Description	100 Units	1,000 Units	10,000 Units
Total stack manufacturing cost, with scrap	$4,357	$3,974	$3,422
Stack manufacturing capital cost	$2,825	$283	$74
BOP	$27,272	$21,079	$17,856
System assembly, test, and conditioning	$279	$267	$266
Total system cost, pre-markup	**$34,733**	**$25,603**	**$21,618**
System cost per gross KW, pre-markup	**$3,158**	**$2,328**	**$1,965**
Sales markup	50.0%	50.0%	50.0%
Total system cost, with markup	**$52,100**	**$38,405**	**$32,427**
System cost per gross KW, with markup	$4,736	$3,491	$2,948

BOP – balance of plant

TABLE 2. 25-kW MHE PEM Fuel Cell System per Unit Cost Summary

Description	100 Units	1,000 Units	10,000 Units
Total stack manufacturing cost, with scrap	$8,815	$8,068	$6,851
Stack manufacturing capital cost	$2,825	$307	$121
BOP	$44,517	$34,571	$29,114
System assembly, test, and conditioning	$279	$267	$266
Total system cost, pre-markup	**$56,436**	**$43,213**	**$36,352**
System cost per gross KW, pre-markup	**$2,052**	**$1,571**	**$1,322**
Sales markup	50%	50%	50%
Total system cost, with markup	**$84,654**	**$64,820**	**$54,528**
System cost per gross KW, with markup	**$3,079**	**$2,357**	**$1,983**

platinum, graphite composite bipolar plate material, and commodity material costs are fairly constant across the range of purchased material quantities. Platinum is generally purchased at market spot price. Commodity material (e.g., aluminum, carbon black, methanol) markets are generally mature with price points fairly level over all but the smallest purchase quantities.

The manufacturing costs are also constrained to a lower cost bound by the material processing requirements, i.e., regardless of the volume being produced, the time required to produce each part is the same. For example, the bipolar plate material requires at least 120 seconds cure time in the mold, and another 15 minutes of post-bake time. This places an upper limit on throughput, and a corresponding lower limit on manufacturing cost, which is a function of the machine time required in producing each part. The same production time constraints are applicable to membrane electrode assembly hot pressing, and to a lesser extent, to catalyst application.

BOP component costs are driving total system cost and can potentially be reduced by:

- Eliminating DC/DC converter—requires invention/technical breakthrough
- Eliminating stack humidification
  - Required for operation at higher temperature and wider operating range

  - May require change of membrane material
- Using all steel hydrogen storage tank—also could help with ballast

FY 2013 PUBLICATIONS/PRESENTATIONS

1. F. Eubanks, V. Contini, Mahadevan, K,G. Stout, M. Jansen, J. Smith. November 2012. Manufacturing Cost Analysis of Fuel Cells for Forklift Applications. Fuel Cell Seminar, Uncasville, CT.

2. V. Contini, Mahadevan, K, F. Eubanks, M. Jansen, J. Smith. May 2013. Stationary and Emerging Market Fuel Cell System Cost Analysis – Material Handling Equipment. DOE Annual Peer Review, Washington, D.C.

REFERENCES

1. Battelle. 2011. The High Volume Manufacture Cost Analysis of 5 kW Direct Hydrogen Polymer Electrolyte Membrane (PEM) Fuel Cell for Backup Power Applications. Contract No. DE-FC36GO13110.

2. K. Mahadevan, K. Judd, H. Stone, J. Zewatsky, A. Thomas, H. Mahy, and D. Paul. 2007. Identification and characterization of near-term direct hydrogen proton exchange membrane fuel cell markets. Contract No. DE-FC36GO13110. Available at http://www1.eere.energy.gov/hydrogenandfuelcells/pdfs/pemfc_econ_2006_report_final_0407.pdf.

3. H. Stone, K. Mahadevan, K. Judd, H. Stein, V. Contini, J. Myers, J. Sanford, J. Amaya, and D. Paul. 2006. Economics of Stationary Proton Exchange Membrane Fuel Cells, Interim Report. Contract No. DE-FC36GO13110.

V.H.7 A Total Cost of Ownership Model for Design and Manufacturing Optimization of Fuel Cells in Stationary and Emerging Market Applications

Max Wei (Primary Contact), Thomas McKone, Timothy Lipman[1], Ahmad Mayyas[1], David Dornfeld[2], Joshua Chien[2], Shuk Han Chan[1], Michael Stadler, Paul Beattie[3], Patricia Chong[3], Anthony Kwong[1], Corinne Scown, Adam Weber, Whitney Collela[4], Brian James[4]
Lawrence Berkeley National Laboratory (LBNL)
1 Cyclotron Road
MS 90R-4000
Berkeley, CA 94706
Phone: (510) 486-5220
Email: mwei@lbl.gov

DOE Managers
Jason Marcinkoski
Phone: (202) 586-7466
Email: Jason.Marcinkoski@ee.doe.gov
Donna Ho
Phone: (202) 586-8000
Email: Donna.Ho@ee.doe.gov
Reg Tyler
Phone: (720) 356-1805
Email: Reginald.Tyler@go.doe.gov

Subcontractors:
1 University of California, Berkeley, Transportation Sustainability Research Center, Berkeley, CA
2 University of California, Berkeley, Laboratory for Manufacturing and Sustainability, Department of Mechanical Engineering, Berkeley, CA
3 Ballard Power Systems, Burnaby, B.C., Canada
4 Strategic Analysis, Inc., Arlington, VA

Project Start Date: October 1, 2011
Project End Date: September 30, 2016.

Overall Objectives

- Develop total cost of ownership (TCO) modeling tool for design and manufacturing of fuel cell systems in emerging non-automotive markets (e.g., stationary power, co-generation, and backup power systems) for low-temperature polymer electrolyte membrane (LT-PEM), high-temperature polymer electrolyte membrane (HT-PEM), and solid oxide fuel cell (SOFC) systems from 1-250 kW.
- Demonstrate expanded cost modeling framework by including life cycle analysis and possible ancillary financial benefits—including carbon credits, reductions of health and environmental externalities, end-of-life recycling, and reduced costs of building operation.
- Provide capability for sensitivity analysis to key cost assumptions, externality valuation, and policy incentive structures.

Fiscal Year (FY) 2013 Objectives

- Develop direct manufacturing cost model for LT-PEM combined heat and power (CHP) and backup power systems.
- Complete literature and patent search and functional specification definition for HT-PEM CHP systems.
- Develop TCO model for LT-PEM CHP and backup power systems.

Technical Barriers

This project addresses the following technical barriers from the Fuel Cells and Manufacturing R&D sections of the Fuel Cell Technologies Office Multi-Year Research, Development, and Demonstration Plan:

Fuel Cells

(B) Cost - Expansion of cost envelope to total cost of ownership including full life cycle costs and externalities

Manufacturing R&D

(A) Lack of High-Volume Membrane Electrode Assembly Processes

(B) Lack of High-Speed Bipolar Plate Manufacturing Processes

Technical Targets

This project is conducting TCO studies of LT-PEM, HT-PEM, and SOFC fuel cell systems in non-automotive applications. Insights gained from these studies can be applied toward the development of lower-cost, higher-volume manufacturing processes that can meet the following DOE CHP system equipment cost targets:

System	2015 Target	2020 Target
10 kW CHP System	$1,900/kW	$1,700/kW
100 kW CHP System	$2,300/kW	$1,000/kW

FY 2013 Accomplishments

- Developed system designs and functional specifications for LT PEM fuel cell systems for backup power (1-50 kW) and CHP applications (1-250 kW) and defined functional specifications for HT-PEM CHP systems (1-250 kW).
- Developed direct manufacturing cost model for LT-PEM fuel cell systems for CHP and backup power applications including key fuel cell stack component costing as a function of manufacturing volume and system size and automated roll-to-roll and assembly processing. The manufacturing and assembly process flow meets DOE cost targets for 2020 for 100-250 kW CHP systems.
- Literature search and patent review completed for HT-PEM fuel cell stack components.

✧ ✧ ✧ ✧ ✧

INTRODUCTION

The DOE has supported over the last decade several cost analysis studies for fuel cell systems for both automotive [1,2] and non-automotive systems [3,4]. These studies have primarily focused on the manufacturing costs associated with fuel cell system production. This project expands the scope and modeling capability from existing direct manufacturing cost modeling in order to quantify more fully the benefits of fuel cell systems by taking into account life cycle assessment, air pollutant impacts and policy incentives. The full value of fuel cell systems cannot be captured without considering the full range of TCO factors. TCO modeling becomes important in a carbon constrained economy and in a context where health and environmental impacts are increasingly valued. TCO is also critical as an input to industry and governments decisions on funding research, development and deployment as well as an input to organizations and individuals who make long term investment decisions.

Three components of the TCO model are (1) direct manufacturing costs, (2) life cycle or use-phase costs such as cost of operations and fuel, and (3) life cycle impact assessment costs such as health and environmental impacts. FY 2013 has been focused to date on the development of a direct manufacturing cost model for LT-PEM systems for application in CHP and backup power and demonstration of use-phase cost modeling.

APPROACH

Direct manufacturing costing utilizes bottom up, Design for Manufacturing and Assembly (DFMA®) techniques to optimize system design, materials and manufacturing flows for lowest manufacturing cost. Data for system designs and component costing is derived from (1) existing cost studies where applicable, (2) literature and patent sources, and (3) industry and national laboratory advisors. DFMA® manufacturing approaches for each stack component is summarized in Table 1a. Life cycle or use-phase costing will utilize existing LBNL tools [5], characterization of commercial building electricity and heating demand by geographical region, and earlier CHP modeling work by one of the authors [6].

Life cycle impact assessment is focused on use-phase impacts from energy use, carbon emissions and pollutant emissions [8], specifically on particulate matter emissions since they are the dominant contributor to life cycle impacts [9]. Health impact from particulate matter emissions will be characterized using existing LBNL health impact models [10]. A scenario analysis approach will be used where life cycle impact assessment will be characterized as a function of fuel cell system adoption by building type and geographic location. This approach allows the quantification of externalities (e.g. CO_2 and particulate matter) for varying degrees of fuel cell system market adoption in various regions of the U.S.

RESULTS

LT-PEM fuel cell systems and functional specifications have been developed for the range of systems sizes of 1-250 kW for CHP with direct H_2 and reformate fuel and 1-50 kW for backup power systems with direct H_2 fuel. System design for a 100-kW CHP system operating on reformate is shown in Figure 1. It includes an air slip input for greater CO tolerance, a liquid cooling sub-system, and larger stack sizing compared to the direct H_2 case due to slightly lower average stack electrical efficiency. Functional specifications for the 100-kW reformate case are shown in Table 1b. Backup power systems achieve cost reduction through simplification of balance-of-plant components with air cooled system design and once-through H_2 fuel supply.

Key fuel cell stack component costing and related balance-of-plant component costing has been completed as a function of manufacturing volume and system size. Both the catalyst coated membrane (CCM) and gaseous diffusion layer (GDL) are fully automated roll-to-roll processing; membrane electrode assembly (MEA) and stack assembly is fully automated at higher volume; and bipolar plates are semi-automated batch processing. The CCM and MEA frame/seal makes up 63% of overall stack costs at 1,000 systems/year with the plate and GDL at 18% each. The bipolar plate module is shown for illustration in Figure 2. To achieve lower cost at high volume, injection molding is utilized rather than the more common compression molding process. Material costs constitute over 80% of stack costs at high production volume.

TABLE 1. (a) DFMA® manufacturing approaches for LT-PEM CHP and backup power systems. Full DFMA® analysis has been completed on components marked with an asterisk (*). (b) Functional specifications for 100-kW CHP system operating with reformate fuel.

Component	Primary Approach	Reference
Membrane	Purchase Nafion®	Patent review, industry input
CCM*	Dual decal, slot die coating.	Literature, patents, industry input
GDL*	Spray coat MPL	[2,4]
Bipolar Plates*	Injection molded graphite –carbon composite	Literature, patents, industry input
Seal/Frame MEA*	Framed MEA	Patents, [7]
Stack Assembly*	Partial to fully automated	Patents, industry input
Endplate/Gaskets	Graphite composite/ Screen printed	Industry input, [4]
Test/Burn-in	Post assembly 3 hrs	Industry input

(a)

Parameter	Value	Unit
Gross system power	124	kW
Net system power	100	kW
Electrical output	480 V AC	Volts AC or DC
Waste heat grade	65	Temp. °C
Fuel utilization	80-95	%
Average system net electrical efficiency	32	% LHV
Thermal efficiency	51	% LHV
Total efficiency	83	Elect.+thermal (%)
Stack power	9.5	kW
Total plate area	360	cm^2
CCM coated area	232	cm^2
Single cell active area	198	cm^2
Gross cell inactive area	45	%
Cell amps	111	A
Current density	0.56	A/cm^2
Reference voltage	0.7	V
Power density	0.392	W/cm^2
Single cell power	78	W
Cells per stack	122	Cells
Stacks per system	13	Stacks

(b)

MPL – micro-porous layer; LHV – lower heating value; AC - alternating current; DC direct current

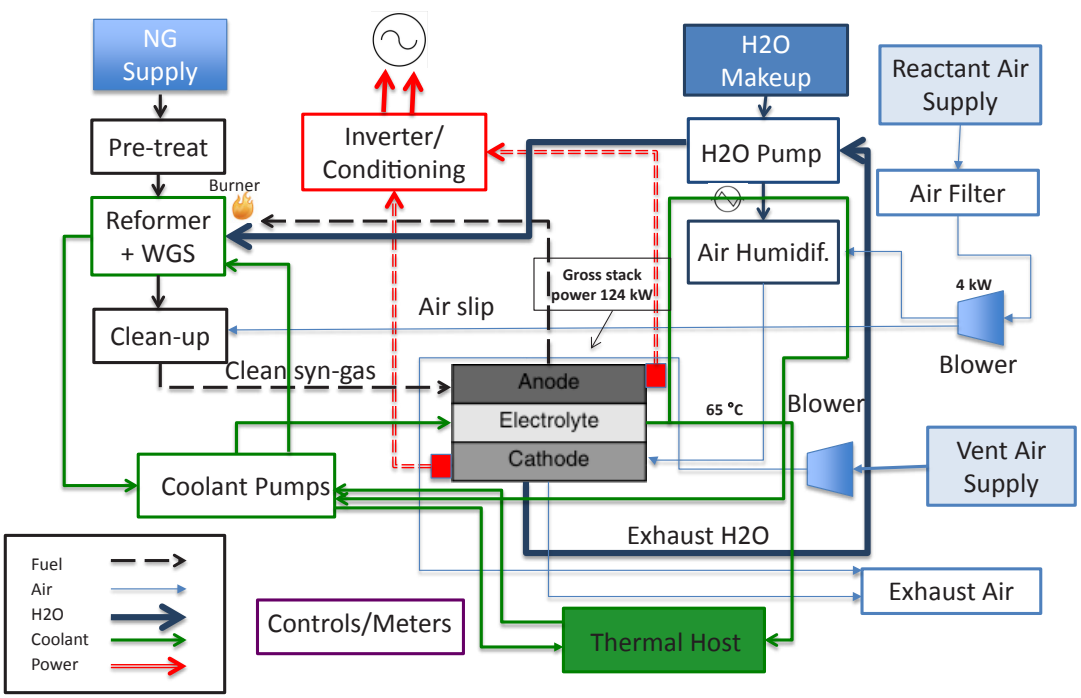

NG - natural gas; WGS - water-gas shift

FIGURE 1. System schematic design for 100-kW CHP system with reformate.

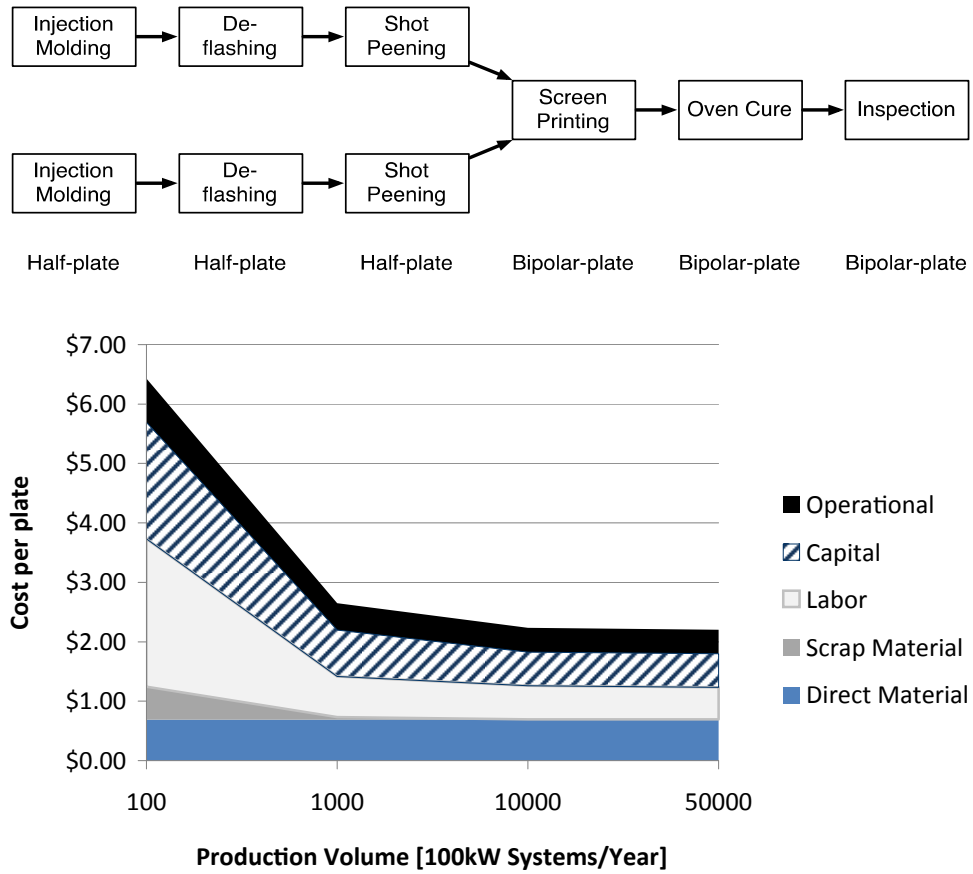

FIGURE 2. DFMA® example – bipolar plate injection molding process flow and cost per part as a function for annual production volume. Shown is the cost per plate for production volumes of 100-50,000 systems per year of 100-kW-size systems.

As manufacturing volume is increased, more cost reduction is achieved in the stack than balance of plant due to the automated production described in the proceeding for the stack. Equipment costs below $1,000/kW for 100-250 kW CHP systems are achieved, meeting the 2020 DOE target. Figure 3 shows cost estimates for the 100-kW CHP with reformate case, and Figure 4 shows cost results for 10-kW backup power systems. Stack cost for backup power systems is similarly reduced more rapidly than balance of plant with increasing production volume, and total cost per kW is estimated to be $1,262/kW at high volume production.

Use-phase modeling has been demonstrated with the LBNL DER-CAM tool [6] for commercial buildings in several different climate zones in California. This provides more realistic load-shapes for use phase modeling. We also developed a scenario analysis methodology for fuel cell system market penetration in commercial buildings using existing LBNL software tools (DER-CAM tool and APEEP models).

CONCLUSIONS AND FUTURE DIRECTIONS

Conclusions

- Stack cost is dominated by cost of materials at production volumes greater than a few thousands of systems per year.
- Stack cost is reduced more rapidly than balance-of-plant components as volume is increased due to the highly automated production process assumed for the stack.
- Mid-range power (100-250 kW) CHP system costs for volumes greater than 1,000 systems per year are consistent with 2020 DOE cost targets ($1,000/kW equipment cost).
- 10-kW backup power system costs are estimated to be less than $1,300/kW at high volume.

Future Directions

- Develop integrated model with scenario analysis and sensitivity analysis capability to assess the impacts

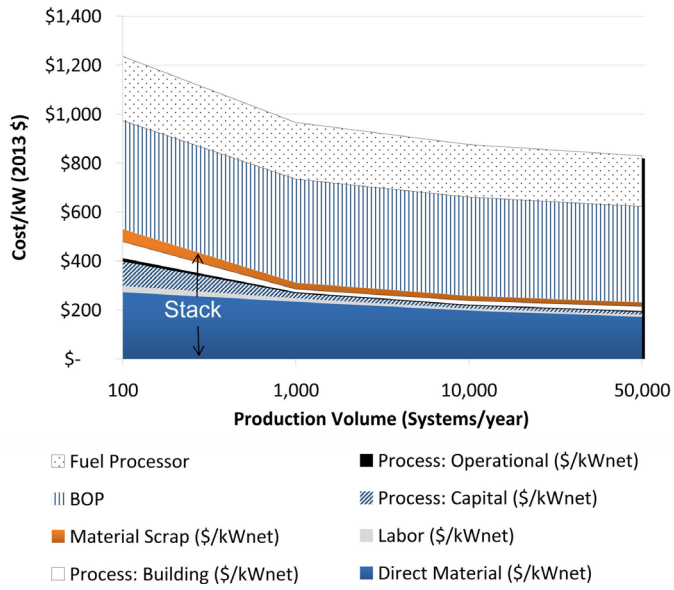

FIGURE 3. Cost results for 100-kW CHP system. Total Pt/Ru loading is assumed to be 0.5 mg/cm^2 Pt and 0.05 mg/cm^2 Ru.

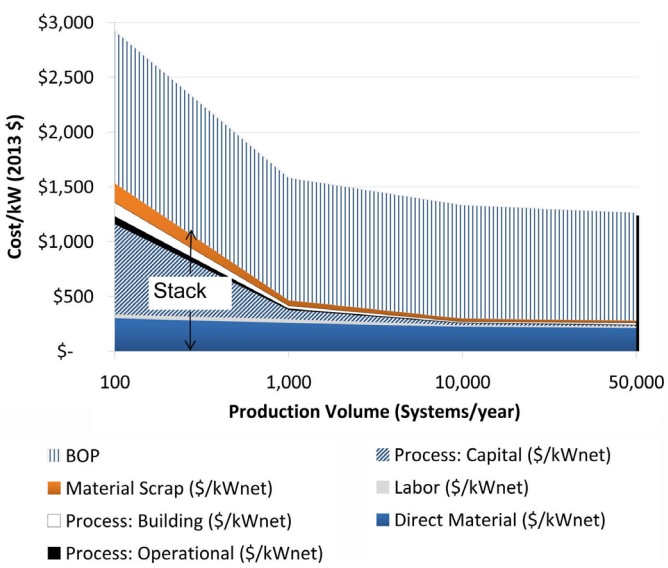

FIGURE 4. Cost results for 10-kW backup power system.

of varying levels of fuel cell system market adoption, externality valuation, and policy incentives.

- Extend the TCO model to include HT-PEM and SOFC in addition to LT-PEM.

FY 2013 PUBLICATIONS/PRESENTATIONS

1. M. Wei, T. McKone, T. Lipman, *A Total Cost of Ownership Model for Design and Manufacturing Optimization of Fuel Cells in Stationary and Emerging Market Applications*, 2013 Annual Merit Review, Arlington, Virginia, May 2013.

REFERENCES

1. James, Brian, Kalinoski, J., and K. Baum. Mass-Production Cost Estimation for Automotive Fuel Cell Systems. 2010 Annual Merit Review Proceedings, Department of Energy, Hydrogen and Fuel Cells Program. Washington, D.C. June 2010.

2. Sinha, Jayanti and Y. Yang. *Direct Hydrogen PEMFC Manufacturing Cost Estimation for Automotive Applications*. 2010 Annual Merit Review Proceedings, Department of Energy, Hydrogen and Fuel Cells Program. Washington, D.C. June 2010.

3. Mahadevan, Kathya, V. Contini, M. Goshe, J. Price, F. Eubanks, and F. Griesemer. Economic Analysis of Stationary PEM Fuel Cell Systems. 2010 Annual Merit Review Proceedings, Department of Energy, Hydrogen and Fuel Cells Program. Washington, D.C. June 2010.

4. James, B., Spisak, A., Colella, W. *Manufacturing Cost Analysis of Stationary Fuel Cell Systems*, Strategic Analysis Inc. Arlington, VA, September 2012.

5. Stadler, Michael, Marnay, C., Gonçalo Cardoso, G. et. al. The Carbon Dioxide Abatement Potential of California's Mid-Sized Commercial Buildings. California Energy Commission, PIER Program. CEC-500-2010-050 (2011).

6. Lipman, Timothy E., Jennifer L. Edwards, and Daniel M. Kammen, "Fuel Cell System Economics: Comparing the Costs of Generating Power with Stationary and Motor Vehicle PEM Fuel Cell Systems," Energy Policy 32(1): 101-125 (2004)

7. ACI Technologies, Inc. Manufacturing Fuel Cell Manhattan Project, U.S. Government Contract No. N00014-08-D-0758, November 2011.

8. Van Rooijen, Jaap. A Life Cycle Assessment of the PureCell™ Stationary Fuel Cell System: Providing a Guide for Environmental Improvement, Center for Sustainable Systems, Report No. CSS06-09 University of Michigan, Ann Arbor, Michigan, June 30, 2006.

9. National Research Council. Hidden Costs of Energy: Unpriced Consequences of Energy Production and Use. The National Academies Press: Washington, D.C., 2010.

10. Muller, N.Z., and R.O. Mendelsohn, The Air Pollution Emission and Policy Analysis Model (APEEP): Technical Appendix [online]. Yale University, New Haven, CT. December 2006. Available at: https://segueuserles.middlebury.edu/nmuller/APEEP_Tech_Appendix.pdf.

V.H.8 Technical Assistance to Developers

T. Rockward, R.L. Borup (Primary Contact), F. Garzon, R. Mukundan, K. Rau, Y.S. Kim, and D. Spernjak
Los Alamos National Laboratory (LANL)
P.O Box 1663
Los Alamos, NM 87545
Phone: (505) 667-2823
Email: borup@lanl.gov

DOE Manager
Nancy Garland
Phone: (202) 586-5673
Email: Nancy.Garland@ee.doe.gov

Project Start Date: October 2003
Project End Date: Project continuation and direction determined annually by DOE

Overall Objectives

- Support fuel cell component and system developers by providing access to LANL staff scientists and state-of-art characterization techniques
- Assess and characterize fuel cell materials and components and give feedback to developers
- Assist the DOE Durability Working Group with the development of various new material durability testing protocols
- Provide support to the U.S. Council for Automotive Research (USCAR) and the USCAR/DOE Fuel Cell Technical Team
- Report findings/results to the DOE

Fiscal Year (FY) 2013 Objectives

- Support the DOE Fuel Cell Technologies Office program and working groups:
  - Provide co-chairs for the Durability, Modeling Transport and Catalyst Working Groups
  - Provide a member to the Fuel Cell Technical Team
  - Provide support on developing protocols for membrane conductivity at low relative humidity (RH)
- Characterize degradation mechanisms of components:
  - Evaluate novel microporous layer (MPL) materials
    - Compare MPL materials performance and water content
  - Develop a correlation quantitating water content by in situ measurements of operating fuel cell components by small angle X-ray scattering (SAXS) and neutron imaging
  - Evaluate degradation mechanism of water transport membranes
  - Conduct hydrothermal ageing of membranes and characterize by Fourier transform infrared (FTIR) spectroscopy

Technical Barriers

This project addresses the following technical barriers from Section 3.4.5 of the Fuel Cell Technologies Office Multi-Year Research, Development, and Demonstration Plan:

(A) Durability

(B) Cost

(C) Performance

FY 2013 Accomplishments

- Evaluate novel compositions of MPL materials:
  - Compared/characterized traditional baseline MPL materials with those incorporating different composition of aluminosilicate or carbon nano-tube (CNT) fibers
  - Compared performance, mass transport resistance, water balance, and water content profiles
- Quantitate and compare in situ water content by neutron imaging and SAXS:
  - Performed in situ water content measurements with identical hardware utilizing neutron imaging and SAXS to quantitate the two techniques for water content
  - Defined water content at different current densities and spatially over the cell dimensions by both techniques.
- Conducted hydrothermal ageing of water transport membranes:
  - Aged different membranes at 25%, 50%, 75%, and 100% RH
  - Examining membrane processing conditions
  - Evaluated growth of membrane anhydride formation by FTIR
  - Designed new ageing sample holders for direct transfer from ageing chamber to FTIR

✧ ✧ ✧ ✧ ✧

INTRODUCTION

This task supports the allowance of technical assistance to fuel cell component and system developers as directed by the DOE. This task includes testing of novel materials and participation in the further development and validation of single cell test protocols. This task also covers technical assistance to DOE Working Groups, USCAR, and the USCAR/DOE Driving Research and Innovation for Vehicle efficiency and Energy sustainability (U.S. DRIVE) Fuel Cell Technical Team. Assistance includes technical validation of new fuel cell materials and methods, single-cell fuel cell testing to support the development of targets and test protocols, and regular advisory participation in other working groups and reviews. This assistance is made available to polymer electrolyte membrane (PEM) fuel cell developers by request and upon DOE approval.

APPROACH

The LANL fuel cell team has extensive knowledge and in-house analytical capabilities which can be made available to PEM fuel cell developers to support the U.S. DOE Fuel Cell Technologies Office. These capabilities, along with the personnel, uniquely allow us to conduct thorough diagnostics and confirm results of existing and novel materials. In FY 2013, several tasks were addressed. This included testing of novel MPL materials, examination of water transport membrane durability, and conducting experiments to relate in situ water measurements by neutron imaging and by SAXS. Detailed highlights of these projects will be further discussed below. Los Alamos has extensive experimental equipment available for testing and characterizing fuel cells that includes, but is not limited to:

- Approximately 40 single-cell fuel cell test stations
- Three-dimensional material imaging by X-ray tomography
- Scanning electron microscopy/energy dispersive X-ray analysis
- X-ray fluorescence spectroscopy
- Differential scanning calorimetry
- FTIR spectroscopy
- Tapered element oscillating microbalance
- Thermogravimetric analysis
- Simultaneous thermogravimetric analysis/differential scanning calorimetry
- Differential thermal analysis
- Solid-phase and liquid-phase nuclear magnetic resonance
- Gas chromatography
- Mass spectroscopy
- X-ray diffraction
- Solid-state diffuse reflectance infrared Fourier transform spectroscopy
- Raman spectrometer

RESULTS

In FY 2013, we completed testing and analysis and provided feedback to both the collaborator and the DOE technical development managers in several different major component areas. Some selected findings were as follows:

Novel MPL Material Characterization

Scanning electron microscopy characterization showed MPLs have 'loosely packed' carbon black + poly-tetrafluoroethylene (PTFE); upon incorporation of fibers, such as CNT and aluminosilicate fibers, the carbon black particles tend to surround CNT 'bundles,' and fibers such as CNTs are not homogeneously distributed within the MPL. The performance of these novel MPL materials was measured in terms of fuel cell performance and their effect on mass transport limitations. Figure 1 shows the performance for the materials in terms of (a) voltage-current-resistance (VIR) in H_2/Air, (b) VIR in H_2/HelOx, and (c) the impedance at 1.2 A/cm^2. 25BC is the traditional carbon black MPL mixed with PTFE binder, 25BL has hydrophilic aluminosilicate fibers in it, and 25BN has CNTs mixed into the MPL. Similar performance for three different MPL/gas diffusion layers (GDLs) is observed in H_2/HelOx up to about 2 A/cm^2 - (O_2 diffuses 3.7x faster in He vs. N_2 – see Figure 1b); this indicates that with the HelOx mixture, these MPLs show similar mass transport and water removal characteristics. In H_2/air, the VIR performance is best with the 25BN, followed by the 25BL, with the lowest performance for 25BC. The impedance (Figure 1c) verifies that the order of mass transport resistance is best with 25BN < 25BL < 25BC. Rationale for better performance of the BN is likely due to less flooding in the cathode catalyst layer due to better water removal characteristics of the MPL with CNT additives.

In situ high-resolution cross-sectional water imaging was performed to correlate the performance and impedance to water content; this is shown in Figure 2. The water content in the catalyst layer and GDL follow the same trend as the transport resistance measured in the impedance: 25BN < 25BL < 25BC.

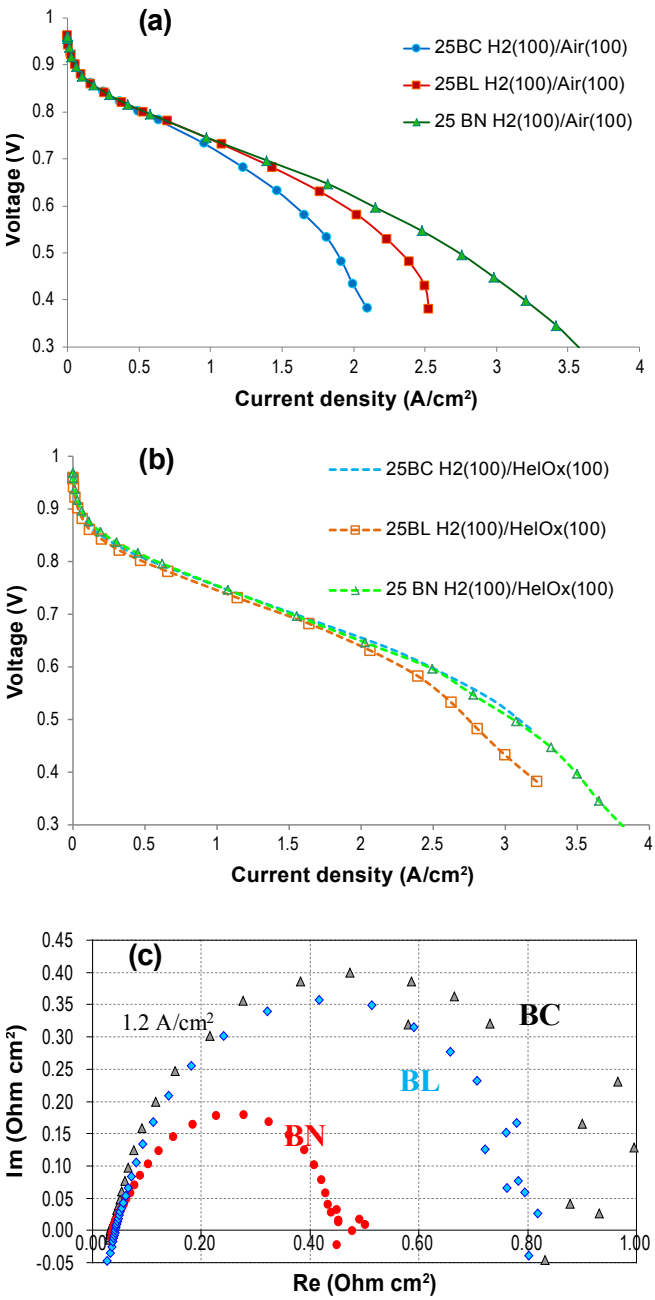

FIGURE 1. Polarization performance of 25BC, 25BL, and 25BN in (a) H_2/air, (b) H_2/HelOx, and (c) impedance at 1.2 A/cm^2 in H_2/air.

Correlating In Situ Water Content by SAXS and Neutron Imaging

In situ SAXS has been used by multiple groups to characterize fuel cell membranes and the effect of water content on structure; however, to date there has not been a method to correlate the in situ SAXS measurements directly to the water content of the membranes. To correlate the water content, an identical cell was operated while conducting SAXS and neutron imaging. The SAXS scattering profile is shown in Figure 3, showing (a) the top portion of the cell, (b) the middle portion of the cell, and (c) the lower portion of the cell when the cell was operated in a co-flow arrangement with the gas inlets at the top of the cell. The neutron imaging showing the water content for the same cell for six different current densities is illustrated in Figure 4, with the same operating geometry. The SAXS and neutron imaging both show maximum cell water content between 0.2–0.4 A/cm^2; above this current density the heat generated in the cell reduces the water content. The SAXS shows that the membrane water content below the ribs is greater than that below the channels. This is consistent with higher-resolution through-plane neutron imaging. The co-flow cells have maximum water content near the outlets, and the counter flow cells have maximum water content near the middle of the cells.

Water Transport Membrane Ageing

Preliminary measurements were made of the anhydride peak formation in a number of water transport membranes subjected to different pre-treatment conditions and ageing at different RHs and temperatures. These studies were to help define the degradation mechanism and correlate the chemical differences to changing water transport properties in membranes for humidification applications. To date, the pre-treatment of the membranes shows no significant differences in anhydride formation, nor does the type of membrane. Additional measurements will be made with thinner membranes to attempt to quantitate the degradation mechanism for water transport.

CONCLUSIONS AND FUTURE DIRECTIONS

In FY 2013 LANL

- Provided support for program interaction with DOE by supplying the co-chair of the DOE Fuel Cell Technologies Durability Working Group, the co-chair of the DOE Transport Modeling Working Group, and a permanent representative to the DOE Fuel Cell Technical Team. Work on defining protocols to properly measure proton conductivity at low RHs was accomplished and presented to the Fuel Cell Technical Team.
- Specific studies were carried out on:
  - Novel MPL material characterization
  - Correlating in situ water content by SAXS and neutron imaging
  - Water transport membrane ageing

For FY 2014, we will continue to support fuel cell developers as directed by DOE by providing capabilities that exist at LANL and are not readily available to many developers.

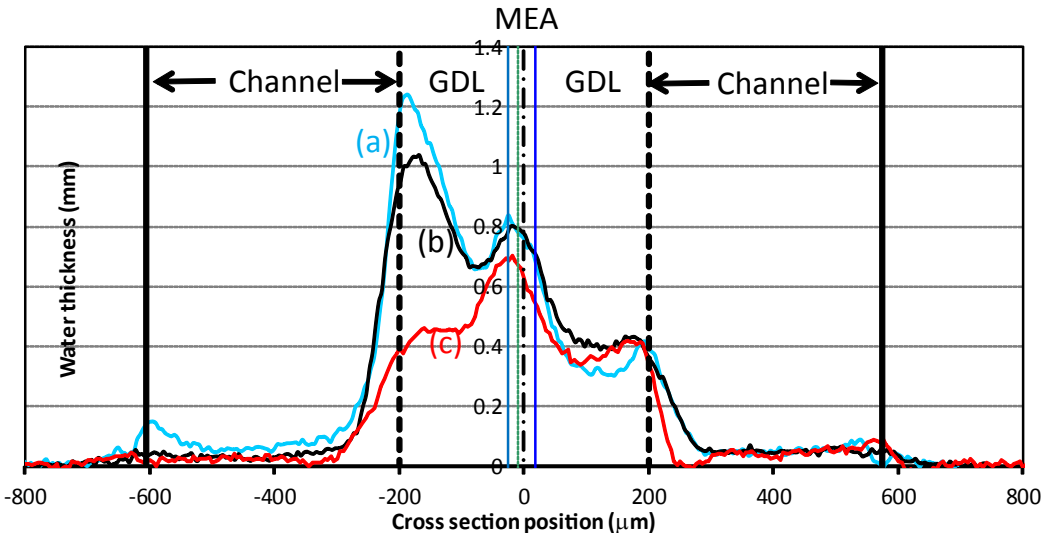

FIGURE 2. Neutron imaging water density profiles at 1.2 A/cm^2 of (a) 25BC, (b) 25BL, and (c) 25BN at 80°C and 100% RH.

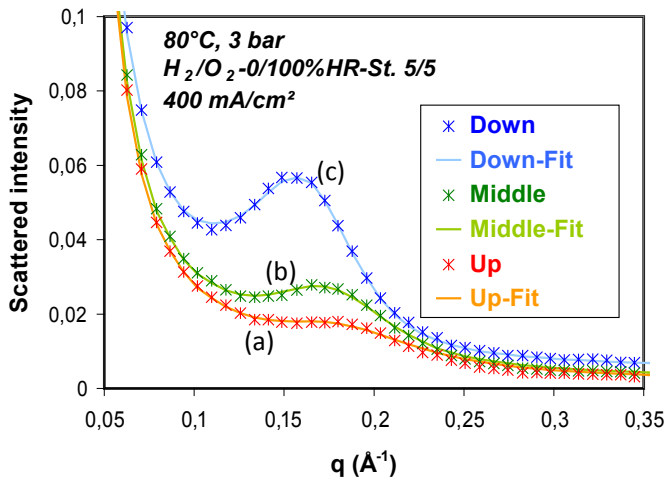

FIGURE 3. In situ small X-ray scattering of operating fuel cells showing average membrane water content (a) top portion, (b) middle portion, and (c) lower portion.

To request assistance, please contact Rod Borup (Borup@lanl.gov) or Tommy Rockward (Trock@lanl.gov), or the DOE Technology Development Managers: Nancy Garland (Nancy.Garland@ee.doe.gov) or Dimitrios Papageorgopoulos (Dimitrios.Papageorgopoulos@ee.doe.gov).

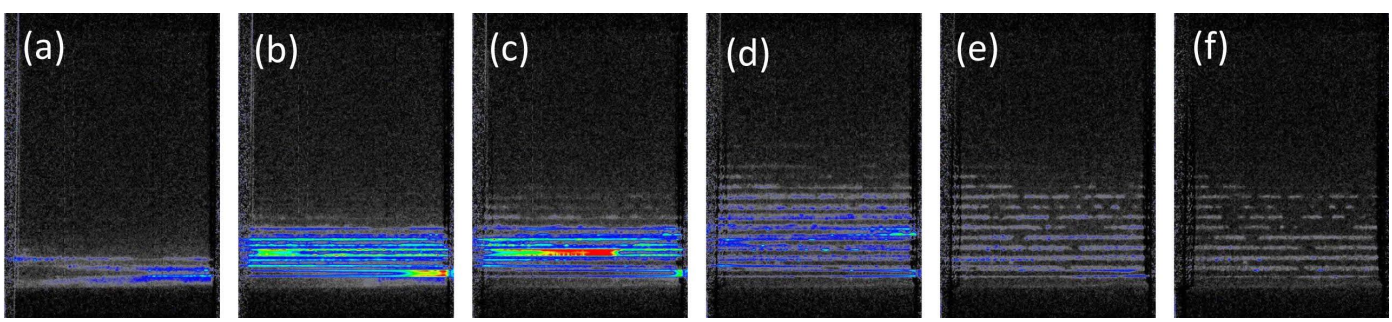

FIGURE 4. In situ water images by neutron scattering of identical cells used in Figure 3 at (a) 0.1 A/cm^2, (b) 0.2 A/cm^2, (c) 0.4 A/cm^2, (d) 0.6 A/cm^2, (e) 0.7 A/cm^2, (f) 0.8 A/cm^2.

V.I.1 Novel Materials for High Efficiency Direct Methanol Fuel Cells

Steve Carson (Primary Contact), David Mountz, Wensheng He, and Tao Zhang
Arkema Inc.
900 First Ave
King of Prussia, PA 19406
Phone: (610) 878-6707
Email: steve.carson@arkema.com

DOE Managers
Donna Ho
Phone: (202) 586-8000
Email: Donna.Ho@ee.doe.gov
Reg Tyler
Phone: (720) 356-1805
Email: Reginald.Tyler@go.doe.gov

Technical Advisor
John Kopasz
Phone: (630) 252-7531
Email: kopasz@anl.gov

Contract Number: DE-EE0000474

Subcontractors:
- IRD Fuel Cells, LLC, Albuquerque, NM
- Illinois Institute of Technology, Chicago, IL

Project Start Date: May 1, 2010
Project End Date: September 30, 2013

Overall Objectives

- Develop a membrane technology having low methanol crossover, high conductivity, and increased durability.
- Develop cathode catalysts that can operate with considerably reduced platinum loading and improved methanol tolerance.
- Combine the cathode catalyst and membrane into a membrane electrode assembly (MEA) having a performance of 150 mW/cm^2 at 0.4 V and a cost of less than $0.80/W for the two components.

Fiscal Year (FY) 2013 Objectives

- Develop a Generation 2 membrane with an areal resistance <0.0375 Ω∗cm^2 and a methanol permeation coefficient ≤1x10^{-7} cm^2/s.
- Demonstrate MEA performance with a developmental membrane of 150 mW/cm^2 @ 0.4 V (60°C, 1M methanol).
- Demonstrate an MEA with an Arkema membrane with ≥5,000 hours of durability testing.

Technical Barriers

This project addresses the following technical barriers from the Fuel Cells section (Portable Power) of the Fuel Cell Technologies Office Multi-Year Research, Development, and Demonstration Plan:

(A) Durability

(B) Cost

(C) Performance

Technical Targets

This project is conducting focused research on next-generation membrane and cathode catalyst materials for direct methanol fuel cells (DMFCs). Work on the cathode catalysts was stopped after a Go/No-Go decision in January 2012 and remaining work focused on membrane development and testing these materials in MEAs. Insights gained from these studies will be applied toward the design of an MEA for portable power devices that meet the DOE 2013 targets for a 10-50 W system:

- Performance: Specific Power (30 W/kg), Power Density (35 W/L), Specific Energy (430 Wh/kg), and Energy Density (500 Wh/L)
- Cost: $10/W
- Lifetime: 3,000 hours

In translating DOE targets, the following goals for the membrane and MEA performance were defined (Table 1). The progress towards meeting these goals is also summarized.

TABLE 1. Progress towards meeting the project technical targets for portable power applications. All targets were based on a methanol concentration of 1M.

Characteristic	Units	Industry Benchmark	Project Target	Status
Methanol Permeability	cm^2/s	3x10^{-6}	1x10^{-7}	5x10^{-7}
Areal Resistance, 70°C	Ω∗cm^2	0.120 (7 mil PFSA)	0.0375	0.03
MEA I-V Cell Performance (0.4 V)	mW/cm^2	90	150	140
MEA Lifetime	Hours	>3,000	5,000	1,500-3,000

I-V – current-voltage; PFSA – perfluorinated sulfonic acid

FY 2013 Accomplishments

- Achieved a 140 mW/cm^2 MEA power density using an optimized Generation 1 membrane and commercially available gas diffusion electrodes (GDEs).
- Optimized a Generation 1 membrane to have a 0.030 Ω*cm^2 areal resistance (AR) and a 5 x 10^{-7}cm^2/s methanol permeation coefficient.
- Continued work on the Generation 2 membranes to decrease their high water solubility.
- Obtained 1,500-3,000 hrs of MEA durability with Generation 1 membranes and commercial GDEs.
- IRD completed initial 600-hour durability evaluations of Arkema's reference MEAs.
- Based on findings from the reference MEA testing, and in conjunction with internal IRD knowledge regarding electrodes, catalyst loading, and gas diffusion layers (GDLs), IRD has fabricated a short stack and initiated testing.

✧ ✧ ✧ ✧ ✧

INTRODUCTION

There is a tremendous need for efficient portable power sources. The explosive growth of the lithium-ion battery market is fueled by the ever-growing demand for portable power used in consumer electronics. For the DMFC industry to emerge as an alternative to batteries, difficult technical hurdles have to be overcome. One hurdle is developing inexpensive membranes with reduced methanol cross-over and areal resistance that will contribute to more efficient DMFCs.

APPROACH

Arkema is developing new DMFC membranes with lower fuel cross-over and high conductivity. The membranes are formed from blends of poly(vinylidene fluoride) (PVDF) with a variety of highly sulfonated polyelectrolytes—technology that was initially developed in previous DOE-funded projects. A number of variables can be easily adjusted in the blending process to tailor properties such as conductivity and methanol permeation. The key to obtaining the desired properties resides in control of composition, architecture, and morphology of the membrane components. These are controlled on a practical level through polyelectrolyte chemistry processes, which are being systematically investigated.

In the past year, work has focused on refining the first and second membrane generations. These membranes were durability tested in MEAs with several different commercial GDEs. IRD was brought into the project at the end of 2012 to assist in evaluating the performance of Arkema membranes in MEAs and short stacks.

RESULTS

MEA Performance

MEA development work focused on screening commercial electrodes in 2012. Johnson Matthey ELE170/171 electrodes were used as the standard electrodes in this project. Two new sets of commercial electrodes were evaluated and the details of the electrodes are shown in Table 2.

TABLE 2. Details of commercial Johnson Matthey GDEs evaluated in this project.

Anode/ Cathode Series	Anode Catalyst Loading	Cathode Catalyst Loading	Remarks
ELE 170/171	3 mg Pt/cm² 1.5 mg Ru/cm²	1.5 mg Pt/cm²	Standard electrodes used in most of the testing to date.
ELE 156/157	2.5 mg Pt/cm² 1.25 mg Ru/cm²	1.0 mg Pt/cm²	Lower catalyst loadings. Same catalyst ink formulation as standard.
ELE 196/197	3 mg Pt/cm² 1.5 mg Ru/cm²	1.5 mg Pt/cm²	GDE designed for hydrocarbon membranes.

A performance of 140 mΩ/cm² was demonstrated with a 1.3-mil Arkema membrane and a combination of ELE156/197 electrodes, as shown in Figure 1. For comparison, a performance of 110 mΩ/cm² was typically obtained with

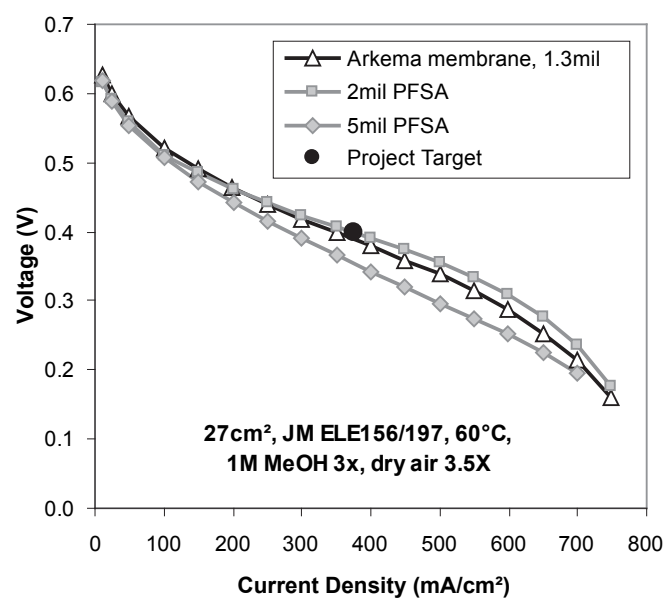

FIGURE 1. Beginning-of-life MEA performance of Arkema and PFSA membranes with the ELE156/197 electrodes.

ELE 170/171 electrodes in 1M methanol testing. The significant performance increase was attributed to improved mass transport in the new electrodes over the ELE170/171 electrodes. The performance using the ELE156/197 electrodes is close to the final project target of 150 mW/cm². We attempted to further increase the MEA performance by adjusting membrane composition and thickness, but no performance increase was observed. At this stage, the MEA performance is dominated by other variables such as the electrodes.

MEA Durability

A summary of the durability testing is shown in Table 3. There is some variation in the data due to several unexplained failures recently. The results suggest that MEAs with the Arkema membrane have less durability than ones with 2-mil PFSA. A comparison of MEA property changes between the two longest-lasting Arkema and PFSA MEAs is shown in Figure 2. The MEA with the Arkema membrane shows a steady increase in MEA resistance over time, while the PFSA membrane-based MEA show little to no increase. The result is consistent with that of Kim, et al., who compared the durability of MEAs based on PFSA and BPSH membranes [1]. They attributed the MEA resistance increase to the deterioration of the membrane/electrode interface.

TABLE 3. Summary of MEA durability test results and status. The failure criterion is a 20% in voltage loss at 0.2 A/cm^2 from the polarization curves. Arkema membranes have a thickness of 1-1.3 mils.

Membrane	# of Samples	Total Hours/comments
2-mil PFSA	1	4,500 hrs
Arkema (28-30 wt% PE)	5	1,000-2,000 hrs.
Arkema (35 wt% PE)	4	One ran 3,000 hrs and another <1,000 hrs. Two repeat tests started recently.
5-mil PFSA	3	1,400-2,600 hrs. Failed earlier than expected.

PE – polyelectrolyte

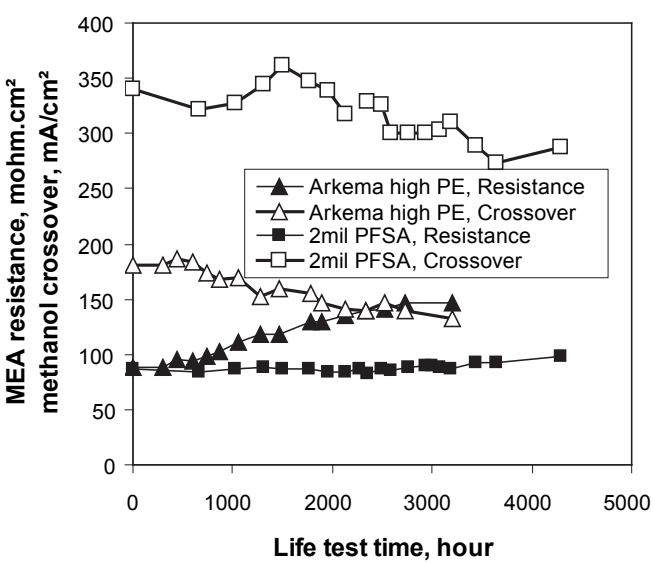

FIGURE 2. Change of MEA properties in durability testing for MEAs with Arkema high-PE and 2-mil PFSA membranes.

The Arkema membrane with a higher polyelectrolyte loading showed increased durability in one test, and more samples are running to validate the result. The higher loading may give more durability by providing a larger buffer for electrolyte degradation and lower MEA resistance.

IRD MEA Evaluation

IRD was contracted to complete a brief MEA development project and perform durability testing on the optimized MEA. Variations in MEA components and constructions were evaluated, inclusive of the Arkema membrane(s). Variations such as the air permeability of the GDLs, catalyst loadings, and modifications to the gasketing in the MEA were evaluated. Representative data for the Arkema membrane testing at IRD is provided in Figure 3, which shows how the changes in air permeability of the GDL can be used to improve the performance of the MEA. More specifically, increased air permeability provided better performance.

The results of the testing above led IRD to describe the Arkema membranes as being more similar to hydrocarbon membranes than to PFSA membranes. They felt this would allow them to select combinations of conditions, materials, and fabrication techniques to obtain improved performance of MEAs including Arkema membranes. From the results obtained, IRD created cells using the Arkema membranes (with IRD's knowledge of best MEA parameter choices) to fabricate short stacks and initiate performance and durability testing. Initial results are promising and the evaluations should be completed by the end of August 2013.

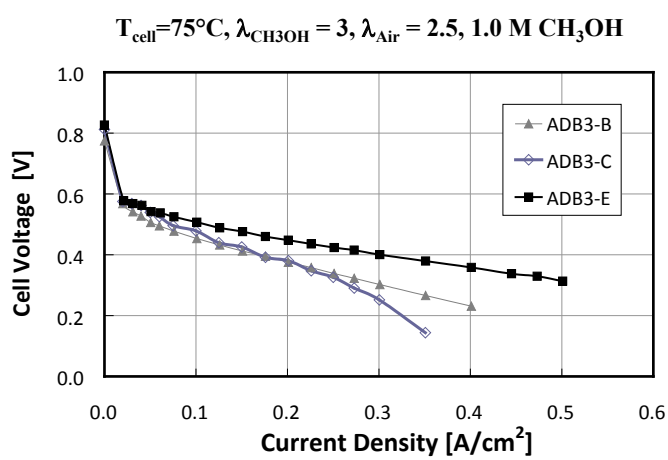

FIGURE 3. Performance of MEAs fabricated at IRD with different GDLs.

Membrane Development

The best performance was obtained with Generation 1 membranes that were modified from the work done last year. Specifically, the PVDF:PE ratio and thickness were optimized to produce lower AR at the expense of slightly raising the methanol permeability. The optimized membrane AR is 0.03 $\Omega*cm^2$ and the methanol permeability coefficient is 5 x 10^{-7} cm^2/s at 1.2 mils. This meets the AR project target, but not the methanol permeability coefficient target. Due to the inherent limitations with this membrane chemistry, both targets cannot be met with one composition. As discussed in an earlier report, the AR has a greater impact than methanol crossover on MEA performance which was factored into the membrane design.

Efforts also continued on the second generation of PE technology that can be used in membranes to form different microstructures than the ones used in the first generation. The microstructure may be a potent factor to increase membrane performance through changes in morphology. Various crosslinking technologies were employed in an attempt to reduce leaching of the water-soluble PE from the membrane after immersion in water. The approaches to crosslinking have not been effective at reducing leaching of the PE, which is leading to high AR values and poor performance.

CONCLUSIONS AND FUTURE DIRECTIONS

140 mW/cm² was demonstrated with an Arkema membrane and a combination of commercial electrodes, which is close to the project target. The best MEA durability results with an Arkema membrane is 3,000 hrs, which is lower than the 5,000 hr project target, but meets the DOE 2013 portable power target. Remaining project work includes completing on-going durability tests and performing post-mortem analysis.

FY 2013 PUBLICATIONS/PRESENTATIONS

1. Hou, J.; Mountz, D.; Hull, M.; Madsen, L. "Correlating Morphology, Proton Conductivity, and Water Transport in Polyelectrolyte-Fluoropolymer Blend Membranes," Accepted to the Journal of Membrane Science in August 2013.

2. "Novel Materials for High Efficiency Direct Methanol Fuel Cells," David Mountz, Wensheng He, Tao Zhang, and Steve Carson. Presentation at the 2012 DOE Hydrogen Program and Vehicle Technologies Program Annual Merit Review and Peer Evaluation Meeting, May 15.

3. He, W.; Mountz, D.; Zhang, T.; Roger, C. "Polyvinylidene Fluoride-Based Membranes for Direct Methanol Fuel Cell Applications," Presented at the Department of Energy Webinar on Fuel Cells for Portable Power, July 17th.

REFERENCES

1. Yu Seung Kim, Melinda Einsla, James E. McGrath, and Bryan S. Pivovar, "The Membrane–Electrode Interface in PEFCs II. Impact on Fuel Cell Durability", *J Electrochem. Soc.*, 2010, **157**, B1602-B1607.

V.I.2 Advanced Materials and Concepts for Portable Power Fuel Cells

P. Zelenay (Primary Contact), H. Chung, Y.S. Kim, Q. Li, G. Purdy, D. Spernjak, X. Wen, G. Wu
Materials Physics and Applications Division
Los Alamos National Laboratory
Los Alamos, NM 87545
Phone: (505) 667-0197
Email: zelenay@lanl.gov

DOE Manager
Nancy Garland
Phone: (202) 586-5673
Email: Nancy.Garland@ee.doe.gov

Subcontractors:
- R.R. Adzic, M. Li, M. Vukmirovic
  Brookhaven National Laboratory, Upton, NY
- Y. Yan, J. Zheng
  University of Delaware, Newark, DE
- J.E. McGrath, Y. Chen, J. Rowlett, A. Shaver
  Virginia Polytechnic and State University, Blacksburg, VA
- A.M. Bonastre, N.C. Moreno, G. Hards, E. Price, J. Sharman, G. Spikes
  Johnson Matthey Fuel Cells, Swindon, United Kingdom
- C. Böhm
  SFC Energy, Brunnthal, Germany
- K.L. More, D. Cullen
  Oak Ridge National Laboratory, Oak Ridge, TN (no-cost partner)

Project Start Date: September 2010
Project End Date: August 2014

Overall Objective

Develop advanced materials (catalysts, membranes, electrode structures, membrane electrode assemblies [MEAs]) and fuel cell operating concepts capable of fulfilling cost, performance, and durability requirements established by DOE for portable fuel cell systems; assure path to large-scale fabrication of successful materials.

Fiscal Year (FY) 2013 Objectives

- Demonstrate PtRu or PtRuSn methanol oxidation catalyst that exceeds final project anode mass activity target of 200 mA mg_{Pt}^{-1} cm^{-2} at ≤0.25 V at 80°C (internal resistance [iR]-corrected), with durability at least matching that of the state-of-the-art methanol oxidation catalyst (HiSPEC® 12100).
- Develop PtRu/CuNWs-based methanol oxidation catalysts with the onset potential <0.3 V vs. the reference hydrogen electrode (RHE) and mass activity at 0.40 V vs. RHE at least matching that of the benchmark PtRu catalyst (HiSPEC® 12100).
- Synthesize multi-block copolymer with methanol permeability reduced by at least 50% relative to Nafion® and maintained ionic conductivity and water uptake.
- Improve selectivity of the ternary $PtRhSnO_2$ electrocatalyst for 12-electron oxidation of ethanol to CO_2 up to 30% at E = 0.4 V, 60-80°C.
- Demonstrate 150 mA cm^{-2} at 0.50 V in a direct dimethyl ether fuel cell (DDMEFC) operating with a new-generation PtRuPd/C anode catalyst at a loading of <3.0 mg_{Pt} cm^{-2} (80°C).
- Characterize the most promising new direct methanol fuel cell (DMFC) anode catalyst and/or membrane developed in the project in a short stack under conditions simulating SFC Energy's commercial products.

Technical Barriers

This project addresses the following technical barriers in the Fuel Cells section (3.4.5, Technical Barriers) of the Fuel Cell Technologies Office Multi-Year Research, Development, and Demonstration Plan [1]:

(A) Durability (catalysts, membranes, electrode layers)

(B) Cost (catalysts, MEAs)

(C) Performance (catalysts, membranes, electrodes, MEAs)

Technical Targets

Portable fuel cell research in this project focuses on the DOE technical targets specified in Tables 3.4.7a, 3.4.7b, and 3.4.7c in Section 3.4.4 (Technical Challenges) of the Fuel Cell Technologies Office Multi-Year Research, Development, and Demonstration Plan [1]. Table 1 summarizes the latest DOE performance targets for portable power fuel cell systems in three power ranges.

Using DOE's Table 3.4.7 as guidance relevant to portable power systems, the following specific project targets have been devised:

- System cost target: $5/W
- Performance target: Overall fuel conversion efficiency (η_Σ) of 2.0-2.5 kWh/L
- In the specific case of a DMFC, the above assumption translates into a total fuel conversion efficiency (η_Σ) of 0.42-0.52, corresponding to a 1.6 to 2.0-fold improvement over the state of the art (ca. 1.250 kWh/L). Assuming fuel utilization (η_{fuel}) and balance-of-plant efficiency (η_{BOP}) of 0.96 and 0.90, respectively (efficiency

TABLE 1. DOE Performance Targets for Portable Power Fuel Cell Systems in Three Power Ranges

Technical Targets: Portable Power Fuel Cell Systems (< 2 W; 10-50 W; 100-250 W)				
Characteristics	**Units**	**2011 Status**	**2013 Targets**	**2015 Targets**
Specific power	**W/kg**	5; 15; 25	8; 30; 40	10; 45; 50
Power Density	**W/L**	7; 20; 30	10; 35; 50	13; 55; 70
Specific energy	**Wh/kg**	110; 150; 250	200; 430; 440	230; 650; 640
Energy density	**Wh/L**	150; 200; 300	250; 500; 550	300; 800; 900
Cost	**$/W**	150; 15; 15	130; 10; 10	70; 7; 5
Durability	**Hours**	1,500; 1,500; 2,000	3,000; 3,000; 3,000	5,000; 5,000; 5,000
Mean time between failures	**Hours**	500; 500; 500	1,500; 1,500; 1,500	5,000; 5,000; 5,000

numbers based on information obtained from DMFC systems developers), and using theoretical voltage (V_{th}) of 1.21 V at 25°C, the cell voltage (V_{cell}) targeted in this project can be calculated as:

$$V_{cell} = V_{th}\,[\eta_{\Sigma}\,(\eta_{fuel}\,\eta_{BOP})^{-1}] = 0.6\text{-}0.7\ \text{V}$$

- Thus, the ultimate target of the materials development effort in the DMFC part of this project is to assure an operating single fuel cell voltage of at least 0.60 V. Very similar voltage targets have been calculated for fuel cells operating on two other fuels, ethanol, and DME.

FY 2013 Accomplishments

- Ultra-thrifted catalysts (uTAAC and uT-PtRuSn) of methanol oxidation have been synthesized in 25 g batches; uT-PtRuSn meets the project anode activity target of 200 mA mg_{Pt}^{-1} at 0.25 V while ultra-thrifted Pt/Ru/C catalyst (uTAAC) is only 13 mV off that target.
- Thrifted PtRu/C catalyst (AAC) has come within 40 mV of the overall DMFC performance target of 0.15 A cm^{-2} at 0.60 V; AAC is ready for 50 cm^2 stack testing by SFC Energy.
- A very low onset potential target of methanol oxidation (0.288 V vs. RHE) has been achieved using PtRu/CuNW catalyst with optimized Pt-to-Ru ratio.
- Johnson Matthey Fuel Cells and Los Alamos National Laboratory data indicate that Ru crossover in MEAs with state-of-the-art carbon-supported PtRu catalysts, though detectable, is much reduced and does not impact oxygen reduction reaction (ORR) activity of the cathode.
- Cracking of metal-black or carbon-supported catalyst layers has little, if any, effect on performance; cracks may facilitate anode operation at high currents.
- Structural changes to the bisphenol unit are very effective in controlling the membrane water uptake and reducing methanol crossover (by as much as 54% with a tetramethyl bisphenol A-based multi-block copolymer).
- Pt_{ML}/Au/C catalysts of ethanol oxidation have been synthesized by displacing the Cu underpotential deposition (UPD) layer on Au/C and by the microemulsion approach; catalysts have been further altered with various modifiers to enhance activity via the bifunctional approach; Pt_{ML} supported on such nanocores as PdAuFe and PdAuCo shows interesting potential as lower-cost ethanol catalysts.
- $RhSnO_2/Pt_{ML}$/Au/C catalyst exhibits high ethanol oxidation selectivity; CO_2 is the only product in the potential range of 0.3-0.7 V; non-CO_2 byproducts are observed at very high, and not necessarily direct ethanol fuel cell-relevant electrode potentials (above 0.7 V).
- Current density of 0.15 A cm^{-2} at a DDMEFC voltage of 0.50 V has been reached with a high metal content ternary catalyst of DME oxidation ($Pt_{45}Ru_{45}Pd_{10}$/C); density functional theory (DFT) calculations confirm the effect of Pd addition on the kinetics of both the C-O and C-H bond scission.

✧ ✧ ✧ ✧ ✧

INTRODUCTION

This multitask, multi-partner project targets advancements to portable fuel cell technology through the development and implementation of novel materials and concepts for (i) enhancing performance, (ii) lowering cost, (iii) minimizing size, and (iv) improving durability of fuel cell power systems for consumer electronics and other mobile and off-grid applications. The primary focus of the materials research in this project is on electrocatalysts for the oxidation of methanol, ethanol, and dimethyl ether; on innovative nanostructures for fuel cell electrodes; and on advanced polyaromatic membranes for lower cost MEAs and enhanced

fuel cell performance (fuel crossover, proton conductivity). In parallel with new materials, this project targets development of various operational and materials-treatment concepts, concentrating among others on improvements to the long-term performance of individual components and the complete MEA.

APPROACH

The two primary research goals of this project are (i) the development of binary and ternary catalysts for the oxidation of methanol, ethanol, and DME; and (ii) synthesis of polyaromatic multiblock copolymers for lower cost and better fuel cell performance through reduced fuel crossover and increased protonic conductivity. Better understanding of the key factors impacting the performance of both catalysts and polymers is also pursued through a characterization effort including X-ray absorption spectroscopy, X-ray photoelectron spectroscopy, nuclear magnetic resonance, and transmission electron microscopy.

Development of new catalysts and polymers is closely tied to electrode nanostructures tailored to minimize precious metal content, maximize mass activity, and enhance durability. The electrode-structure component of the effort concentrates on two groups of materials: (i) solid-metal nanostructures (e.g., nanowires and nanotubes) and (ii) carbon-based nanostructures acting as supports for metal catalysts.

In addition to the short-term testing and initial performance assessment, the catalysts, membranes, supports, electrode structures, and MEAs developed in this project are subject to long-term performance (durability) testing. Performance-limiting factors and degradation mechanisms are being identified and, if possible, addressed. Fabrication and scale-up of viable catalysts, membranes, and supports is also being tackled through collaboration between partners in this project.

RESULTS

DMFC Catalysts—Development of new methanol oxidation catalysts continued in FY 2013 through "thrifting" of Pt in the advanced anode catalyst (AAC, thrifted binary PtRu/C catalyst developed in FY 2012). The newly developed ultra-thrifted PtRu/C catalyst (uTAAC) has been found to outperform the HiSPEC® 12100 benchmark and AAC in terms of methanol oxidation onset potential and mass activity. uTAAC nearly matches AAC in DMFC testing at a loading of only 0.3 mg_{pt} cm^{-2}, compared to the 1.0 mg_{pt} cm^{-2} catalyst loading of AAC (Figure 1). Furthermore, uTAAC maintains excellent mass activity (only 13 mV off the final project target) throughout the in situ accelerated anode stability test. The highest cycling durability (merely ca. 1% overall performance loss after 300 cycles) has been

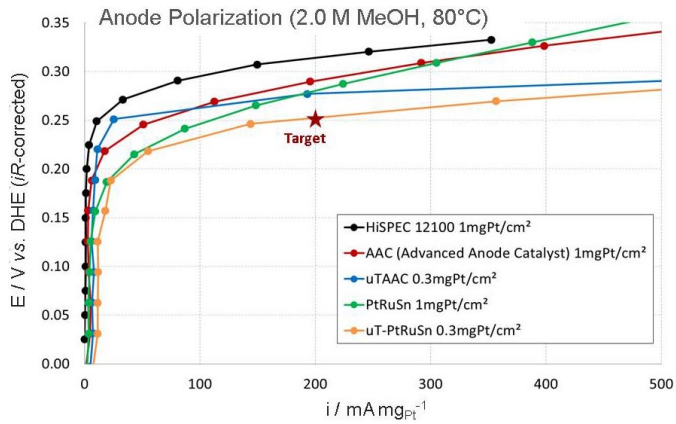

FIGURE 1. DMFC anode polarization plots recorded with new ultra-thrifted uTAAC and uT-PtRuSn catalysts with catalyst loading of 0.3 mg_{Pt} cm^{-2}. Polarization plots for AAC, PrRuSn/C and benchmark HiSPEC® 12100 PtRu catalysts with catalyst loading of 1.0 mg_{Pt} cm^{-2} shown for reference.

demonstrated with the AAC in accelerated MEA stability testing (Figure 2, bottom). Fuel cell performance has been found not to be affected by limited Ru migration to the cathode, as revealed by post-mortem X-ray tomography of MEAs (Figure 2, top). Anode catalysts are on track to reaching the activity required for meeting the overall DMFC performance target of 150 mA cm^{-2} at 0.60 V. This target is expected to be reached with AAC and/or uTAAC without a durability loss.

A highly active ternary PtRuSn/C catalyst was first introduced in FY 2012. Through Pt-thrifting and optimizing Sn content in this ternary catalyst, the new ultra-thrifted PtRuSn/C (uT-PtRuSn) catalyst has been developed in FY 2013. The new catalyst meets the mass-activity target of 200 mA mg_{Pt}^{-1} at ≤ 0.25 V (80°C) with the Pt loading as low as 0.3 mg_{Pt} cm^{-2} thanks to the effect of Sn at low methanol oxidation overpotentials (Figure 1). In order to become fully viable, the uT-PtRuSn catalyst needs stability improvements at higher operating potentials of the anode.

Future research will focus on further improvements in the DMFC performance and stability through optimization of AAC, uTAAC, and uT-PtRuSn-based anodes, and stabilizations of nano-particulate structures of the catalysts.

Innovative Electrode Structures—A very low onset potential of methanol oxidation of 0.288 V vs. RHE has been achieved by tuning the Pt-to-Ru ratio in the PtRu/CuNW catalyst. This result represents meeting (and exceeding) the onset potential target for the nanostructured PtRu catalysts of ≤0.3 V vs. RHE. The mass activity of the PtRu/CuNW catalyst based on the total precious metal content in the catalyst is higher than that of the PtRu/C benchmark catalyst (HiSPEC® 12100).

Multiblock Copolymers for Reduced Methanol Crossover—Poly(arylene ether benzonitrile) multiblock

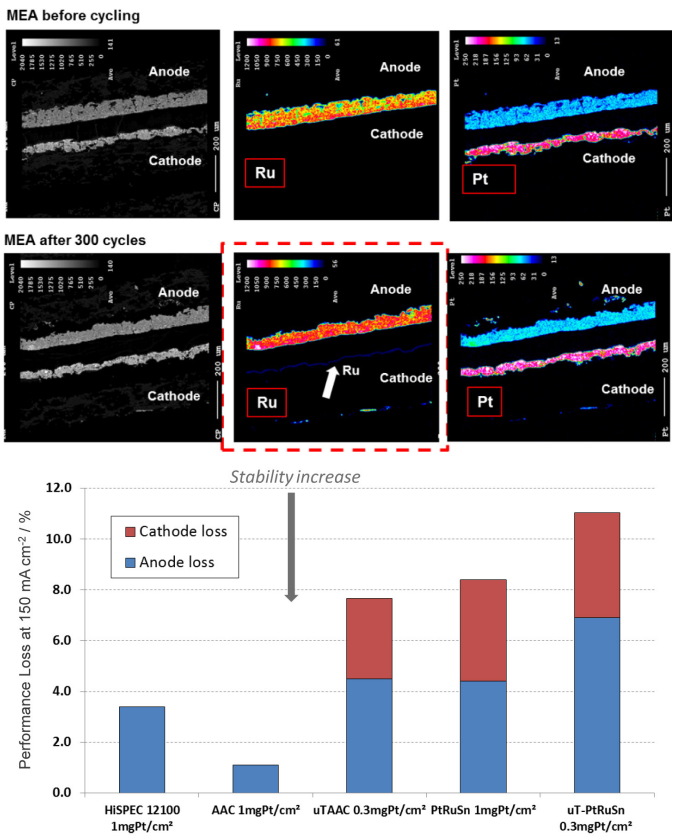

FIGURE 2. In situ accelerated MEA stability test. Post-mortem X-ray tomography of MEAs with an AAC anode revealing small amount of Ru at the cathode catalyst (top). Cathode/anode performance loss breakdown for MEAs after 300 cycles (0.05-0.85 V, 80°C) with different anode catalysts (bottom).

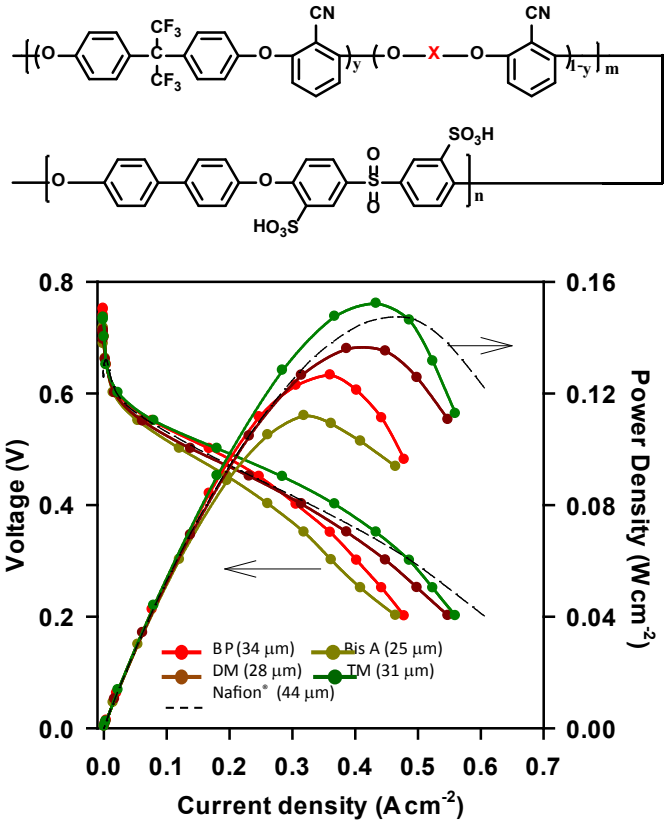

FIGURE 3. DMFC polarization plots recorded with four multiblock copolymer membranse and reference Nafion® 115 membrane; $c_{methanol}$ = 1.0 M; cell temperature 75°C. BP: biphenyl; Bis A: bisphenol A; DM: dimethyl bisphenol A; TM: tetramethyl bisphenol A.

copolymers with high proton conductivity and low methanol permeability were developed in FY 2011 and FY 2012. However, those copolymers had relatively high water uptake often causing delamination with Nafion®-bonded catalyst layers. Membrane research in FY 2013 has thus focused on synthesizing multiblock copolymers with reduced water uptake. Chemical modifications for this purpose include (i) control of the fluorination level and (ii) control of the bisphenol structure. In the first approach, the ratio of hexafluoro bisphenol A (6F) to biphenyl (BP) has been varied in the hydrophobic segment in multiblock copolymers. The water uptake of the copolymers has decreased from 54% to 45% as the 6F/BP ratio increased from 0.25 to 1. However, the methanol permeability has also increased, from 1.4 x 10^{-6} to 2.2 x 10^{-6} $cm^2 s^1$, due to the enhanced methanol solubility upon fluorination. In the second approach, modifications have been introduced to the biphenyl structure of the hydrophobic block segment. Multiblock copolymers having bisphenol A (Bis A), dimethyl bisphenol A (DM), tetramethyl bisphenol A (TM) have been synthesized. The bisphenol structural change turns out to be very effective in reducing both methanol permeability and water uptake. The TM-based multiblock copolymer shows very low methanol permeability (ca. 1.09 x 10^{-6}) and water uptake (ca. 20%), with good proton conductivity (ca. 0.1 S cm^{-1}). The TM-based multiblock copolymer exhibits excellent performance as shown in Figure 3. Further structural optimization and DMFC durability test using TM-based multi-block copolymer are ongoing.

DMFC Performance Degradation—The rate of DMFC performance degradation with electrodes based on metal-black and carbon-supported catalysts has been studied at three methanol concentrations: 0.5 M, 1.0 M, and 4.0 M. Cathode CO stripping after 100-hour life tests indicates that most of the Ru crossover takes place during a two-hour H_2-air MEA break-in. CO stripping potential is independent of methanol concentration in the following 100 hours of DMFC operation, regardless of the catalyst type (unsupported or supported). In turn, CO stripping from the anode points to no significant change to the surface composition of both catalyst types during the 100-hour test. MEAs with metal black catalysts suffer from more severe Ru crossover than carbon-supported catalysts, which correlates with the performance loss observed with the two catalysts. A very small Ru contamination of the cathode is observed with carbon-supported catalysts, which does not impact the cathode

operation. This agrees with the durability test data involving AAC above.

Post-mortem X-ray tomography of MEAs points to the presence of cracks in as-prepared and tested MEAs (16-19% anode, 8-12% cathode) in Johnson Matthey Fuel Cells carbon-supported catalysts used in gas diffusion electrodes. Los Alamos National Laboratory metal-black electrodes are initially crack-free, with cracks forming during life test (7-9%). The crack formation does not lead to any observable performance loss of metal-black electrodes.

Ethanol Oxidation Catalysts—The DFT prediction of the effect that lattice expansion has on the properties of a Pt monolayer (Pt_{ML}) supported on a single crystal of Au(111) vs. those of Pt(111) has been confirmed by single-crystal model catalyst studies. In agreement with the modeling, a considerable enhancement in the current density of ethanol oxidation is observed upon the Pt_{ML} lattice expansion. The Pt_{ML}/Au/C nanoparticle catalysts have been synthesized by displacing a Cu UPD layer pre-deposited on Au/C nanoparticles. The most active catalyst, with ca. 200 mV lower onset potential of ethanol oxidation and ca. 14 times higher current density at 0.5 V vs. RHE has been developed by further modifying the expanded Pt_{ML} on an Au/C core with SnO_2 to induce bifunctionality.

A one-pot and easily scalable microemulsion synthesis method of Au@Pt/C, which is less complex than the Cu UPD method, has been developed (Figure 4, top). The obtained Au@Pt nanoparticles are ca. 4 nm in average size. A SnO_2-modified bifunctional SnO_2/Au@Pt/C catalyst performs similarly to an analogous catalyst but obtained using the Cu UPD method (Figure 4, bottom). The microemulsion approach represents a new simple synthesis route for large-scale fabrication of Pt/Au core-shell catalysts.

In situ infrared reflection-absorption spectroscopy reveals that CO_2 is the only product of ethanol oxidation on $RhSnO_2/Pt_{ML}$/Au/C in the potential range of 0.30-0.70 V vs. RHE. CH_3COOH and CH_3CHO are observed at potentials higher than 0.70 V vs. RHE.

Dimethyl Ether Fuel Cell Research—PtRuPd/C catalysts with high metal content (~65 wt%) have been successfully synthesized by a modified polyol method using ethylene glycol as a reducing agent. Transmission electron microscopy data point to a uniform distribution of ca. 2.7 nm PtRuPd nanoparticles on the carbon support. The formation of a $Pt_{45}Ru_{45}Pd_{10}$/C alloy has been confirmed by the (111) peak shift relative to Pt in X-ray diffraction patterns. Electrochemical testing has shown that $Pt_{45}Ru_{45}Pd_{10}$/C is more active in DME oxidation than $Pt_{40}Ru_{40}Pd_{20}$/C, $Pt_{34}Ru_{33}Pd_{33}$/C, and HiSPEC®12100. 10 at% of Pd appears to effectively assist in the C-O bond scission without inhibiting the removal of surface CO by Ru hydroxide/oxides.

A DDMEFC operating with a $Pt_{45}Ru_{45}Pd_{10}$/C anode can generate 0.15 A cm^{-2} at 0.50 V, by ca. 70 mV outperforming

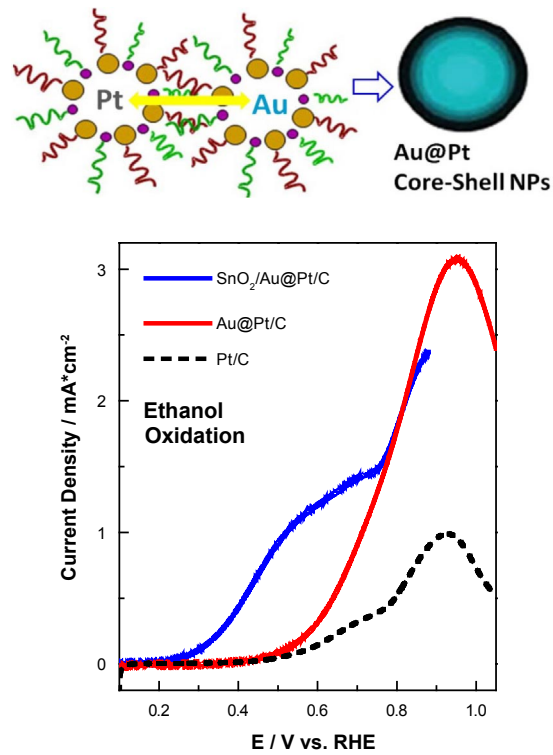

FIGURE 4. Schematic diagram of microemulsion synthesis of Au@Pt core-shell nanoparticles (top). Ethanol oxidation plots on Au@Pt/C and SnO_2/Au@Pt/C catalysts in aqueous 0.1 M $HClO_4$ at room temperature; $c_{ethanol}$ = 0.5 M (bottom).

PtRu/C reference catalyst (HiSPEC® 12100). No significant performance loss has been observed after 100 hours of the cell operation (Figure 5).

DFT calculation has confirmed that the addition of Pd to PtRu should result in a significant lowering of the activation energy for both C-H and C-O bond breaking during DME oxidation, by 0.19 eV and 0.25 eV, respectively.

CONCLUSIONS

- New ultra-thrifted catalysts (uTAAC and uT-PtRuSn) of methanol oxidation demonstrate high activity at a Pt loading of 0.3 mg cm^{-2}. uT-PtRuSn meets the project anode activity target of 200 mA mg_{Pt}^{-1} at 0.25 V while uTAAC is only 13 mV off that target.
- AAC shows excellent cycling durability, losing only ca. 1% of its performance after 300 cycles; small Ru migration to the cathode appears to have no effect on durability.
- While Sn enhances methanol oxidation activity at low overpotentials, Sn dissolution from the ternary catalyst needs to be addressed.
- CuNW support benefits the mass activity of PtRu/CuNW without a performance penalty in electrochemical

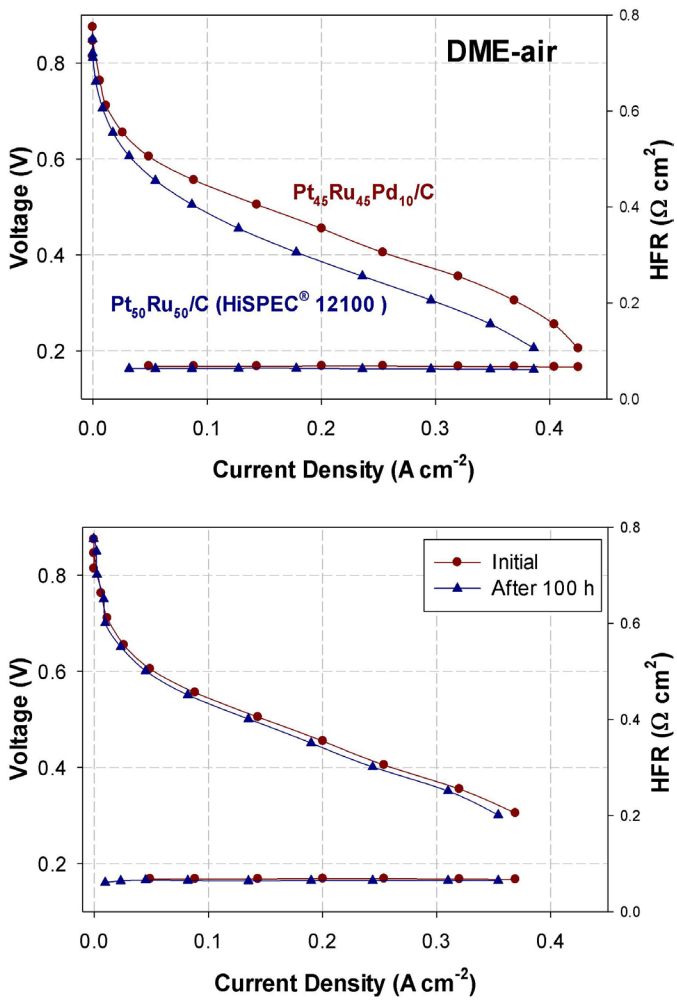

FIGURE 5. DDMEFC polarization plots measured with $Pt_{45}Ru_{45}Pd_{10}$/C and HiSPEC® 12100 catalysts (top); DDMEFC polarization plots measured with $Pt_{45}Ru_{45}Pd_{10}$/C before and after 100-hour life time at 0.4 V (bottom). Anode: 2.7 mg_{Pt} cm^{-2} $Pt_{45}Ru_{45}Pd_{10}$/C or HiSPEC® 12100, 40 sccm DME gas, 30 psig; cathode: 4.0 mg cm^{-2} Pt black, 500 sccm air, 20 psig; membrane: Nafion® 212; cell: 80ºC.

testing; that result warrants catalyst scale-up for fuel cell testing.

- Structural changes to the bisphenol unit provide an effective method of controlling the membrane water uptake and reducing methanol crossover; the most significant performance improvement has been achieved with a TM-modified membrane.
- One-pot, scalable, and simple microemulsion method yields an Au@Pt/C catalyst with the ethanol/methanol oxidation properties similar to those of an Au@Pt/C catalyst obtained using much more complex Cu UPD method.
- CO_2 is the only product of ethanol oxidation on the ternary $RhSnO_2/Pt_{ML}$/Au/C catalyst in the fuel cell-relevant potential range of 0.30-0.70 V vs. RHE.
- Ru crossover in DMFCs with carbon-supported PtRu anode catalysts is much reduced compared to fuel cells with metal-black anodes; the crossover in cells with carbon-supported PtRu catalysts has little effect on the ORR activity of the cathode over the operating times used in this research.
- A new, high metal-content ternary catalyst of DME oxidation ($Pt_{45}Ru_{45}Pd_{10}$/C) allows for 0.15 A cm^{-2} to be achieved in a DDMEFC at 0.50 V and shows no significant performance loss after 100 hours of operation.
- DFT calculation confirms the activation effect of Pd in both the C-O and C-H bond scission.

FUTURE DIRECTIONS

- Methanol oxidation catalysis and electrode structures: Improve mass activity of thrifted and ultra-thrifted AAC PtRu/C catalysts; stabilize the nano-particulate structures of PtRu/C and PtRuSn/C to minimize Ru and Sn dissolution; optimize AAC-based anodes; scale up and test in MEAs PtRu platelets and Pt monolayer catalysts; further improve mass activity of PtRu/CuNWs; scale up nanostructured catalyst synthesis; complete 50-cm^2 stack testing.
- Innovative membranes: Optimize membrane thickness and MEA processing with controlled hydrophobicity; improve durability of alternative membranes at higher methanol concentrations; identify the mechanism of DMFC performance degradation in prolonged life tests, up to 500 h; develop mitigation strategies.
- Ethanol oxidation catalysis: Develop catalysts based on expanded Pt monolayers decorated by SnO_2 and Rh islands and optimized such catalysts for ethanol oxidation; scale up ternary and Pt-monolayer catalysts for ethanol oxidation and test in MEAs.
- DME research: Optimize composition and morphology of ternary DME oxidation catalysts to improve mass activity.

SPECIAL RECOGNITIONS & AWARDS/ PATENTS ISSUED

1. Piotr Zelenay, The Electrochemical Society Energy Technology Division Research Award, The Electrochemical Society Meeting, Toronto, Canada, May 2013.

2. Piotr Zelenay, 2012 Los Alamos National Laboratory Patent & Licensing Award (August 2012; for year 2011).

FY 2013 PUBLICATIONS (UNTIL APRIL 2013)

1. M. Li, R.R. Adzic, "Low Platinum Content Electrocatalysts for Methanol and Ethanol Electrooxidation", Electrocatalysis in Fuel Cells: A Non and Low Platinum Approach, Edited by Minhua Shao, ISBN 978-1-4471-4911-8, Springer, 2013, Chapter 1, pp. 1-26.

2. M. Li, W.-P. Zhou, N.S. Marinkovic, K. Sasaki, R.R. Adzic, "The Role of Rhodium and Tin Oxide in the Platinum-based Electrocatalysts for Ethanol Oxidation to CO_2", *Electrochim. Acta*, in press.

3. K. Sasaki, M. Li, "Electrocatalysts for Anodic Reactions", Encyclopedia of Applied Electrochemistry, edited by Robert F. Savinell, Kenichiro Ota and Gerhard Kreysa. Springer, in press.

4. Q. Li, D. Spernjak, P. Zelenay, Y.S. Kim, "Electrode Degradation of Direct Methanol Fuel Cells Evidenced by X-ray Tomography;" *ECS Trans.*, 50 (2), 2199-2205 (2012).

5. Q. Li, G. Wu, Z. Bi, C.M. Johnston, P. Zelenay, "A Ternary Catalyst for Dimethyl Ether Electrooxidation" *ECS Trans.*, 50 (2), 1933-1941 (2012).

6. M. Li, P. Liu, Radoslav R. Adzic, "Platinum Monolayer Electrocatalysts for Anodic Oxidation of Alcohols", *J. Phys. Chem. Lett.* 3, 3480–3485 (2012).

7. M. Li, N.S. Marinkovic, K. Sasaki, "In Situ Characterization of Ternary Pt–Rh–SnO_2/C Catalysts for Ethanol Electrooxidation", *Electrocatalysis* 3, 376-385 (2012).

FY 2013 PRESENTATIONS (UNTIL APRIL 2013)

1. Q. Li, D. Spernjak, P. Zelenay, Y.S. Kim, "Electrode Degradation of Direct Methanol Fuel Cells Evidenced by X-ray Tomography", 222nd Meeting of the Electrochemical Society, Honolulu, Hawaii, October 7–12, 2012.

2. Q. Li, G. Wu, C.M. Johnston, P. Zelenay, "A Ternary Catalyst for Dimethyl Ether Electrooxidation", 222nd Meeting of the Electrochemical Society, Honolulu, Hawaii, October 7–12, 2012.

3. Y. Chen, J.R. Rowlett, C.H. Lee, Y.S. Kim, Q. Li, P. Zelenay, J.E. McGrath, "Controlled Fluorination Level Poly(arylene ether benzonitrile) Hydrophobic-Disulfonated Poly(arylene ether sulfone) Hydrophilic Multiblock Copolymer for Direct Methanol Fuel Cells (DMFCs)", 244th Meeting of the American Chemical Society, August 19–23, 2012, Philadelphia, Pennsylvania.

4. M. Li, R.R. Adzic, "Electrocatalysts for Electrochemical Oxidation of Small Organic Molecules", DARPA Workshop "Low-temperature Electrochemical Oxidation of Hydrocarbon Fuels". Broomfield, CO, July 2012.

5. M. Li, K. Sasaki, M.B. Vukmirovic, R.R. Adzic, "In situ XAS and IRRAS of Platinum Monolayer Fuel Cell Electrocatalysts", 221st Electrochemical Society Meeting. Seattle, WA, May 2012.

6. Q. Li, G. Wu, Y.S. Kim, C.M. Johnston, P. Zelenay, "Direct Dimethyl Ether Fuel Cell with Much Improved Performance", 221st Meeting of the Electrochemical Society, Seattle, Washington, May 6-10, 2012.

REFERENCE

1. *Multi-Year Research, Development and Demonstration Plan: Section 3.4 Fuel Cells*, Fuel Cell Technologies Program, 2011. http://www1.eere.energy.gov/hydrogenandfuelcells/mypp/pdfs/fuel_cells.pdf

V.J.1 Power Generation from an Integrated Biomass Reformer and Solid Oxide Fuel Cell (SBIR Phase III)

Quentin Ming (Primary Contact), Patricia Irving
InnovaTek, Inc.
3100 George Washington Way, Suite 108
Richland, WA 99354
Phone: (509) 375-1093
Email: ming@innovatek.com

DOE Managers
Kathi Epping Martin
Phone: (202) 586-7425
Email: Kathi.Epping@ee.doe.gov
Kelly R. Opatz
Phone: (865) 576-4173
Email: Opatzkr@oro.doe.gov

Contract Number: DE-EE0004535

Project Start Date: October 1, 2010
Project End Date: September 30, 2013

Overall Objectives

- Establish design to meet technical and operational needs for distributed energy production from renewable fuels
- Design, optimize, and integrate proprietary system components and balance of plant in a highly efficient system
- Demonstrate the technical and commercial potential of the technology for energy production, emissions reduction, and process economics

Fiscal Year (FY) 2013 Objectives

- Achieve 40% system operating efficiency with revised/optimized system design
- System performance proves superior energy efficiency and emissions reductions compared to conventional technology
- Analysis of process economics supports commercial feasibility

Technical Barriers

This project addresses the following technical barriers from the Fuel Cells section of the DOE Fuel Cell Technologies Office Multi-Year Research, Development, and Demonstration Plan:

(A) Durability

(B) Cost

(C) Performance

Because our system has an integrated reformer that will process both natural gas and renewable liquid feedstocks, it also addresses technical barriers in the Hydrogen Production section of the DOE Fuel Cell Technologies Office Multi-Year Research, Development, and Demonstration Plan:

(A) Reformer Capital Costs and Efficiency

(B) Operations and Maintenance (O&M)

(C) Biomass Feedstock Issues

(E) Control and Safety

(F) Capital Cost

(G) System Efficiency And Electricity Cost

Technical Targets

InnovaTek's research plan addresses several DOE technical targets for stationary applications for fuel cell power systems operating on natural gas and for hydrogen generation systems [1]. Progress in meeting DOE's technical targets is provided in Table 1.

TABLE 1. Progress toward Meeting Technical Targets for Integrated Stationary Fuel Cell Power Systems Operating on Reformate[a], and Distributed Forecourt Production of Hydrogen from Bio-Derived Renewable Liquids

Characteristic	Units	2015 Target[c]	2020 Target	InnovaTek 2013 Status[d]
Electrical Energy Efficiency[b] @ Rated Power	%	42.5	>45%	41
Equipment Cost, 5-kW System	$/kW$_e$	1,700	1,500	2,361
H_2 Production Energy Efficiency	%	70	75	70
H_2 Levelized Cost[e]	$/kg	5.90	2.30	6.31

[a] Includes fuel processor, stack, and all ancillaries.
[b] Regulated alternating current net/lower heating value of the fuel
[c] For a fuel cell system using natural gas as fuel
[d] For a solid oxide fuel cell and fuel reformer system using bio-kerosene as fuel
[e] Assumes ethanol cost of $2.41/gal for 2015, $0.85/gal for 2020, and $2.47/gal for 2013 (InnovaTek status) and volume production of capital equipment

FY 2013 Accomplishments

- Developed highly efficient thermally integrated system design for producing 43,800 kWh/yr of distributed power.
- Completed solid model, bill of materials (BOM), and piping and instrumentation diagram that was used to estimate manufacturing costs.

- Used Design for Manufacturing and Assembly (DFMA®) to reduce part count by approximately 74% and cost by 40%.
- Obtained 41% system efficiency.
- Completed analyses using the H2A and HOMER models to determine cost of hydrogen production and cost of power using InnovaTek's technology.
- Manufactured a proprietary prototype system, including hardware, software, and catalysts and used it to demonstrate 2.2 kW power from bio-kerosene, sending electricity to the grid.
- Supported three students and continued partnerships with Pacific Northwest National Laboratory, Washington State University, Boeing, City of Richland, Impact Washington, Breakthrough Technologies Institute, and the Mid-Columbia Energy Initiative.

✧ ✧ ✧ ✧ ✧

INTRODUCTION

Alternative energy sources must be sought to meet energy demand for our growing economy and to improve energy security while reducing environmental impacts. In addition to facilitating the use of a renewable fuel source, cost and durability are among the most significant challenges to achieving clean, reliable, cost-effective fuel cell systems. Therefore this project is focusing on lowering the cost and increasing the durability of a fuel cell distributed renewable energy system, while also assuring that its performance meets or exceeds that of competing technologies. Work was conducted to develop proprietary steam reforming technology that uses multiple fuel types, including renewable liquid bio-fuels, and integrates the fuel processor with a solid oxide fuel cell (SOFC). A highly efficient integrated system design with an SOFC was developed that reduces the loss of heat through an effective thermal design. Modeling and simulations were completed to compare designs for prototype components and to analyze process flow for alternative system configurations. A major effort to reduce system complexity and cost was completed using DFMA® software tools. An optimized integrated system design was selected, components were fabricated, and a prototype 2.2-kW system was assembled and tested during this period to determine costs and performance.

APPROACH

The technological approach utilizes a steam reforming reactor to convert bio-fuel derived from lignocellulosic biomass to hydrogen-rich reformate that fuels an integrated SOFC for power generation. The project has evolved through three developmental stages.

1. Optimization of SOFC and fuel processor integration – is completed using process simulation and analysis to optimize system design and produce a complete mass and energy balance for individual components of the system. Process flow and piping and instrumentation diagrams are prepared to analyze possible system configurations using MathCAD® and FEMLAB models to simulate the process flow paths in the system.
2. Design for manufacturing and field operation – requires continued modeling and analysis such as failure modes and effects analysis and DFMA® and several iterations of component manufacturing and tests to compare design options. The dimensions, geometries and flow patterns defined from optimization modeling work completed in Stage 1 are translated into three-dimensional computer-aided design (CAD) images and drawings.
3. System demonstration and validation for commercial applications – takes place after down-selection of the final design. Several complete systems are built for demonstration to gain performance data necessary to validate the design and operation of the system.

RESULTS

System Design and Fabrication

The system design produced in 2012 was further optimized in 2013 using manufacturability and integrated product development concepts to achieve cost and performance targets for a pre-commercial fuel cell energy system. Various design concept alternatives were evaluated against DFMA® objectives to help reduce both capital equipment costs and maintenance cost while increasing lifetime and robustness. CAD was used for cost effective development and analysis of design alternatives (Figure 1). All drawings, specifications, and price quotes were consolidated for subsystem components along with the specifications developed. This information formed the detailed design package for building a prototype system.

A BOM was prepared for all subsystems of the fuel cell power plant. This BOM was used to obtain cost estimates for prototype fabrication and for volume production from potential vendors and fabricators. Suppliers were down-selected based on pricing and quality of products. A solid model of the integrated system was prepared (Figure 2) and used as a guide for system assembly. Compared to the 2012 fuel processor prototype, part count was reduced by 74% and cost was reduced by 40% (Table 2). System efficiency was increased to 41% (from 37.5% in 2012) as a result of improved stack electrical efficiency, lower parasitic power due to lower stack pressure drop, less waste heat loss through improved thermal integration and heat transfer, and higher methane content in the reformate which reduced stack cooling needs.

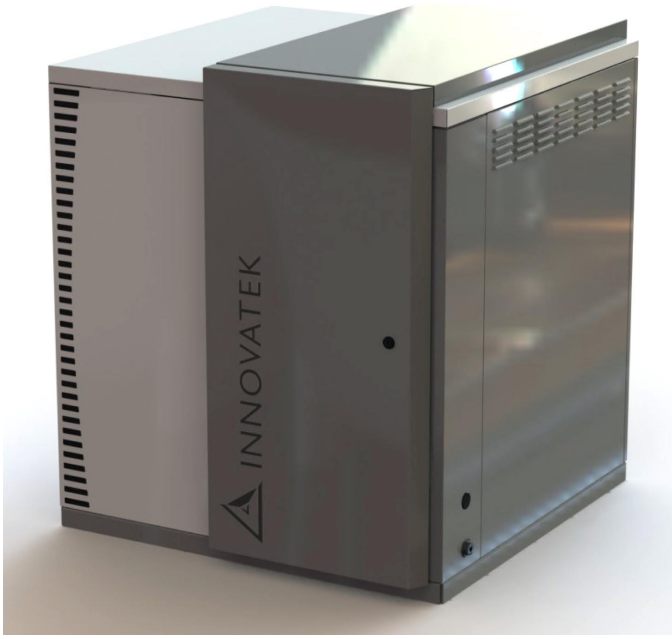

FIGURE 1. InnovaGen® Fuel Cell Power System

Performance Testing

Initial testing of the prototype fuel cell system was successful in achieving 2.2 kW net power production. Longer-term testing is continuing in order to determine durability and maintenance interval.

Cost Analysis

The H2A and HOMER models were used with data from our manufacturing cost analysis and system performance determinations to estimate cost of power and levelized cost of hydrogen using our technology. The results of these analyses are presented in Table 2.

TABLE 2. Fuel Processor Cost Reduction

Prototype System	Labor Cost	Material Cost	Total Cost	Number of Parts	Approximate Volume (L)
2012	$10,201	$4,951	$15,152	159	13.87
2013	$6,374	$3,997	$10,371	66	6.88

CONCLUSIONS AND FUTURE DIRECTIONS

- On the basis of careful systems modeling and component integration using CAD and thermal systems design an overall system electrical efficiency of 41% is possible.
- DFMA® analyses and demonstration results indicate that system cost, performance, and durability targets established by DOE are within feasibility for InnovaTek's technology.
- Results from prototype testing will be used to optimize the design for a field-ready system to utilize for long-term durability and performance testing.

FY 2013 PUBLICATIONS/PRESENTATIONS

1. Irving, P.M., Renewable Distributed Energy Generation, oral presentation, WA State Energy Symposium, Seattle WA, November 2012.

2. Irving, P.M., InnovaTek's Energy Systems Technology Development, oral presentation, Pasco Kennewick Rotary Club, July 10, 2013.

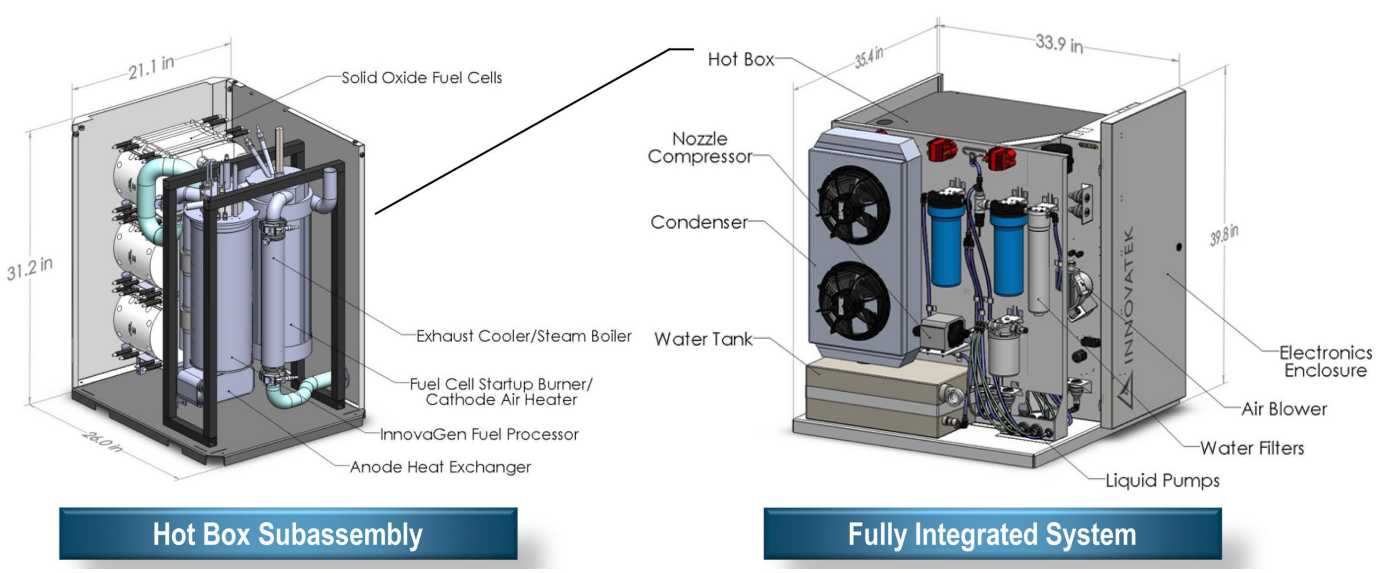

FIGURE 2. Solid Models used for Assembly of Fuel Cell Power System Components

3. Ming, Q., P.M. Irving, The role of the fuel cell system in sustainable power generation, oral presentation, IEEE Conference on Technologies for Sustainability, Portland OR, August 2013.

REFERENCES

1. Fuel Cell Technologies Office Multi-Year Research, Development, and Demonstration Plan, U.S. Department of Energy, 2013. http://www1.eere.energy.gov/hydrogenandfuelcells/mypp/

V.K.1 Low-Cost PEM Fuel Cell Metal Bipolar Plates

Conghua "CH" Wang
TreadStone Technologies, Inc.
201 Washington Rd.
Princeton, NJ 08543
Phone: (609) 734-3071
Email: cwang@TreadStone-Technolgoies.com

DOE Managers
Jason Marcinkoski
Phone: (202) 586-7466
Email: Jason.Marcinkoski@ee.doe.gov
David Peterson
Phone: (720) 356-1747
Email: David.Peterson@go.doe.gov

Technical Advisor
Thomas Benjamin
Phone: (630) 252-1632
Email: benjamin@anl.gov

Contract Number: 09EE0000463

Subcontractors:
- Ford Motor Company, Dearborn, MI
- Gas Technology Institute, Des Plaines, IL
- Stony Brook University, Stony Brook, NY
- IBIS Associates, Inc., Waltham, MA

Project Start Date: September 1, 2009
Project End Date: February 28, 2013

Overall Objectives

- Reduce or eliminate the small amount of gold used in TreadStone's current corrosion-resistant metal plate technology for proton exchange membrane (PEM) fuel cell applications.
- Develop low-cost metal bipolar plates using commercially available low-cost carbon steel or aluminum as the substrate materials.
- Optimize the fabrication process for large-scale manufacture.
- Demonstrate TreadStone's low-cost metal plate technology in the applications of portable, stationary and automobile fuel cell systems.

Fiscal Year (FY) 2013 Objectives

- Finish the 2,000-hour durability demonstration of 20-cell short stack at Ford.

Technical Barriers

This project addresses the following technical barriers from the Fuel Cells section of the Fuel Cell Technologies Office Multi-Year Research, Development, and Demonstration Plan:

(A) Durability

(B) Cost

(C) Performance

Technical Targets

The focus of this project is to further develop TreadStone's proprietary corrosion-resistant metal plate technology reducing the metal plate cost to <$3/kW, while still meet the performance requirements. There are a number of performance requirements for PEM fuel cell bipolar plates. The most challenging requirements for metal bipolar plates are summarized in Table 1. The status of TreadStone's low-cost metal plates is summarized in the table as well.

TABLE 1. TreadStone's Metal Plate Status and DOE's Targets

Parameter	Unit	TreadStone 2010 Status	DOE Targets	
			2010	2015
Plate Cost [a]	$/kW	3.82	5	3
Plate Weight [b]	kg/kW	<0.4	<0.4	<0.4
Corrosion Anode [c]	$\mu A/cm^2$	n/a	<1	<1
Corrosion Cathode [d]	$\mu A/cm^2$	<0.01	<1	<1
Resistance [e]	Ohm cm^2	<0.01	<0.02	<0.02

[a] Based on 50% utilization of active area on the whole plate surface, stainless steel foil cost at historical average of $2/lb, 1 W/cm^2 power density and projected 500,000 stacks per year production.
[b] Based on the 0.1-mm thick stainless steel foil.
[c] pH 3, 0.1 ppm hydrogen fluoride, 80°C, peak active current <1 X 10^{-6} A/cm^2 (potentiodynamic test at 0.1 mV/s, -0.4 V to +0.6 V (Ag/AgCl)) de-aerated with Ar purge.
[d] Includes contact resistance (on as-received and after potentiostatic experiment) measured.
n/a - not available

FY 2013 Accomplishments

Successfully demonstrated the application of TreadStone's metal plates in the 2,000-hour durability test using a 20-cell short automobile stack under dynamic operation conditions.

✧ ✧ ✧ ✧ ✧

INTRODUCTION

It has been reported that using metal bipolar separate plates can reduce the PEM fuel cell stack weight and volume by 40-50%, comparing with current graphite-based bipolar plates [1]. The major barrier to use metal bipolar plates in PEM fuel cells is the severe corrosion condition during stack operation. Most metals do not have the adequate corrosion resistance in PEM fuel cell environments, which results in rapid performance degradation due to the formation of the electrically resistive surface oxide scale, and potential contamination of the membrane electrode assembly (MEA) by the dissolved ions from the metal plates. Various corrosion protection techniques have been investigated to prevent metal plate corrosion in PEM fuel cell environments [2-7]. Some of these technologies have developed corrosion-resistant metal plates that can meet the performance requirements. However, it is still a challenge to have the metal bipolar plate that can meet both the performance and cost requirements. The focus of TreadStone's project is to develop corrosion-resistant metal bipolar plates at the low cost to meet DOE's 2015 targets.

APPROACH

Most researches on metal bipolar plates have been focused on covering the entire plate surface with an electronically conductive and corrosion-resistant material that protects the metal from corrosion and maintains the electrical conductance of the metal. The challenge of this approach is that there are only limited numbers of low-cost materials that can meet electrically conductive and corrosion-resistive requirements for PEM fuel cell applications. In addition, the processing required to apply these materials on the metal substrate are either difficult or high cost.

TreadStone takes a different approach to develop the metal bipolar plates for PEM fuel cell applications. It was found that it is unnecessary to have the entire surface electrically conductive to ensure the low interfacial contact resistance (<10 mΩ.cm^2) between the bipolar plate and the gas diffusion layer (GDL). TreadStone's approach is based on this principle, as shown in Figure 1.

The majority of the metal surface area is covered with the low-cost corrosion-resistant but non-(or poor) conductive material (purple layer in Figure 1). A corrosion-resistant and highly electrically conductive material (such as Au) forms a path for electron transport, in the form of small conductive dots (yellow bars in Figure 1) penetrating through the non-conductive layer. Electrons generated from the anode reaction will flow through the GDL to the conductive vias (illustrated as red arrows) passing through the metal plate to the other side for the cathode reaction on the cathode of the adjacent cell. The conductive vias, having a dimension as small as several micrometers, are distributed on the metal surface. The average distance between the conductive vias is 20-70 μm. The dense distribution of conductive vias ensures a uniform current distribution between the GDL and metal bipolar plate.

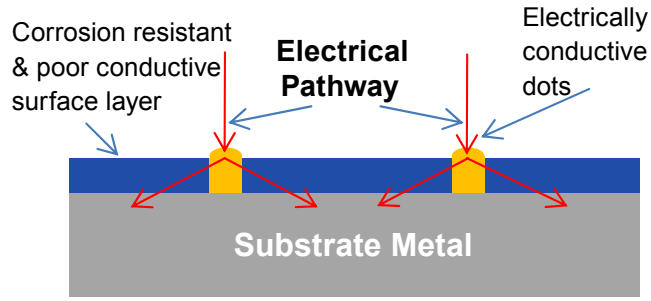

FIGURE 1. Schematic drawing of TreadStone's corrosion resistant metal plate design.

TreadStone's approach is unique because it uses only a small portion (<1-2%) of the plate surface for electrical contact. It was found that more than 500,000 via/in^2 cover the metal plate surface as the electrical contact point of metal plate with GDL, when small (<5 μm) conductive vias are used. It is because of the high amount of the contact points that enable the low contact resistance of metal plates.

RESULTS

The focus of this year's project is to finish the 2,000-hour durability test of TreatStone's metal plates in a full-size, 20-cell short stack under automobile dynamic operation conditions. The stack uses the metal plates from TreadStone and the MEA from W. L. Gore. During the test, the polarization curves were measured periodically. Figure 2 shows the polarization curves of the stack before and after 485, 750, 1,000, 1,500, 1,850, and 2,000 hours. It shows that stack voltage is slightly lower than the original stack voltage (0.624 V/cell at 1.3 A/cm^2 current density). The performance

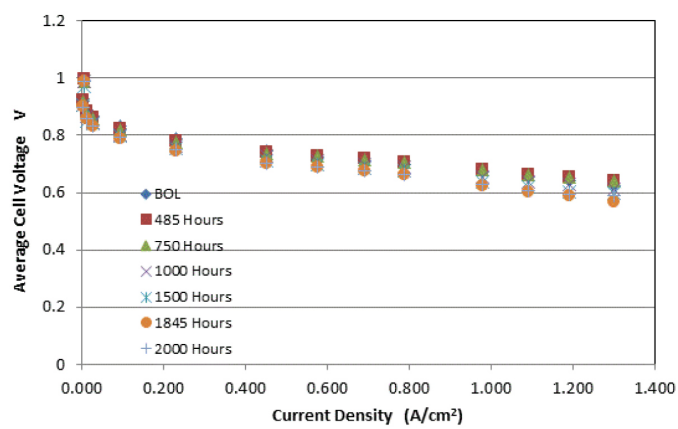

FIGURE 2. Performance comparison of the 20-cell stack using TreadStone's metal plates before (BOL) and during the 2,000-hour test.

degradation of this metal plate stack is due to the degradation of the MEAs under the testing condition using this prototype stack for components evaluation.

The direct parameter of the metal plate performance is the monitoring of the through-plate voltage (TPV) drop during the stack tests. In order to do it, one plate was taken out of the stack every 500 hours for the TPV measurement and visual inspection for any corrosion marks. By the end of the 2,000-hour test, the stack was dissembled for the TPV measurement and inspection of all plates. Table 2 summarizes the TPV of all plates (except the end plate on the first and last cell) under 1 A/cm^2 @ 90 psi compression force at the beginning of life (BOL) and the middle of life (MOL). It shows that there was not any increase of the plate TPV during the 2,000-hour test. Actually, the average plate TPV reduced from 8.83 mV (equal to through-plate resistance of 8.83 mΩ.cm^2) to 6.37 mV (equal to through plate resistance of 6.37 mΩ.cm^2) after the stack durability test. The reason for the TPV reduction is that gold splats were slowly compressed and turn flatter under the high compression force of the assembled stack, which would improve the electrical contact between the plates and GDL, resulting in the lower electrical contact resistance and TPV. Figure 3 shows the scanning electron microscope pictures of the gold splats in the valley (A) and land (B) areas of a tested plate. It shows that gold splats in the valley keep the original morphology because they were not pressed by the GDL. On the other hand, gold splats on the land area are flatter and bigger, after pressed by the GDL in the stack. The gold splat morphology change leads to the higher area coverage of gold on metal plates and results the lower plate resistance.

The reduction of the through-plate resistance after the 2,000-hour test indicates that TreadStone's metal plate is suitable for automobile fuel cell applications.

TABLE 2. Comparison of Plate TPV at BOL and MOL

Plate ID	Testing Time, hours	TPV mV	
		MOL	BOL
Average		6.37	8.83
# 01	2,000	7.53	9.68
# 02	2,000	6.52	10.32
# 03	2,000	6.28	8.52
# 04	2,000	5.73	9.15
# 05	2,000	5.88	8.32
# 06	2,000	7.80	8.79
# 07	2,000	7.38	9.55
# 08	2,000	6.10	9.52
# 09	2,000	5.58	8.59
# 10	2,000	7.42	9.25
# 11	2,000	6.50	7.69
# 12	2,000	6.15	10.72
# 13	2,000	5.82	8.25
# 14	2,000	5.92	8.39
# 15	2,000	5.68	7.99
# 16	2,000	5.67	8.12
#17	1,500	5.93	7.42
#18	500	5.90	9.09
#19	1,000	7.21	8.49

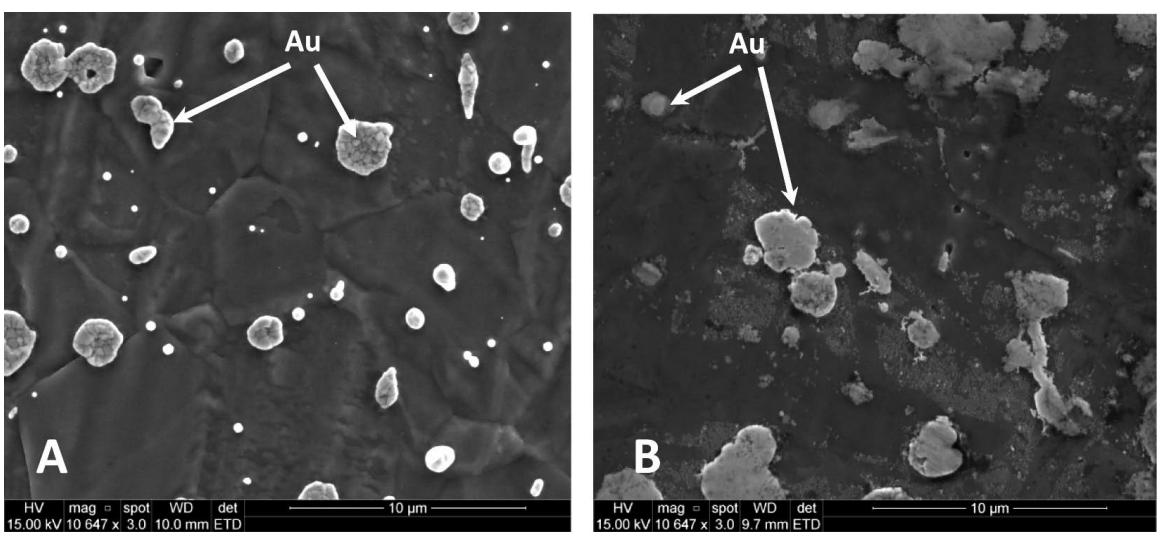

FIGURE 3. Scanning electron microscope picture of gold splats (A) in the valley, and (B) on the land area of a plate tested in the 20-cell short stack.

CONCLUSIONS AND FUTURE DIRECTIONS

TreadStone's unique corrosion-resistant metal bipolar plates have demonstrated stable operation for PEM fuel cell applications in portable, stationary and automobile applications. The process has been optimized for small-scale commercial production. In addition to the PEM fuel cell applications, we have demonstrated the application of this technology in other similar application, such as electrolyzer, anion exchange membrane fuel cells and flow batteries. Further development will be focused on:

- Identify a manufacturing partner for large-scale commercial fabrication of the metal plates.
- Further evaluation with more industrial partners.
- Extend the application into electrolyzer and flow battery markets.

REFERENCES

1. A.S. Woodman, E.B. Anderson, K.D. Jayne, and M.C. Kimble, AESF SUR/FIN '99 Proceedings, 6/21-24, 1999.

2. M.P. Brady, B. Yang, H. Wang, J.A. Tuner, K.L.More, M. Wilson, and F. Garzon, JOM, 2006, 58, 50.

3. H. Wang, M.P. Brady, K.L. More, H.M. Meyer and J.A. Turner, J. Power Sources, 2004, 138, 75.

4. Y. Wang, D.O. Northwood, Int. J. Hydrogen Energy 2007, 32, 895.

5. C.Y. Chung, S.K. Chen, P.J. Chiu, M.H. Chang, T.T. Hung, T.H. Ko, J. Power Sources 2008, 176, 276.

6. M.A.L. Garcia, M.A. Smith, J. Power Sources 2006, 158, 397.

7. D.G. Nam, H.C. Lee, J. Power Sources 2007, 170, 268.

8. R. Tian, J. Sun, L. Wang, Int. J. Hydrogen Energy 2006, 31, 1874.

V.L.1 Advanced Ionomers and MEAs for Alkaline Membrane Fuel Cells

Bryan Pivovar (Primary Contact), Dan Ruddy, Matt Sturgeon, Hai Long
National Renewable Energy Laboratory (NREL)
15013 Denver West Parkway
Golden, CO 80401
Phone: (303) 275-3809
Email: Bryan.Pivovar@nrel.gov

DOE Manager
Kathi Epping Martin
Phone: (202) 586-7425
Email: Kathi.Epping@ee.doe.gov

Subcontractors:
- Shimshon Gottesfeld, Dario Dekel, CellEra, Inc., Caesaria, Israel
- Krzysztof Lewinski, Mike Yandrasits, Steve Hamrock, 3M Company, St. Paul, MN
- Andy Herring, Mei-chen Kuo, Colorado School of Mines (CSM), Golden, CO

Project Start Date: April 22, 2013
Project End Date: April 22, 2015

Overall Objectives

- Synthesize novel perfluoro (PF) anion-exchange membranes (AEMs) with high-temperature stability and high water permeability
- Employ novel PF AEM materials in electrodes and as membranes in alkaline membrane fuel cells
- Demonstrate high performance, durability, and tolerance to ambient carbon dioxide

Fiscal Year (FY) 2013 Objectives

Synthesize three unique PF anion-exchange polymer chemistries from the sulfonyl fluoride form precursor

Technical Barriers

This project addresses the following technical barriers from the Fuel Cells section (3.4.4) of the Fuel Cell Technologies Office Multi-Year Research, Development, and Demonstration Plan:

(A) Durability (of membranes and membrane electrode assemblies, MEAs)

(B) Cost (of membranes and MEAs)

(C) Performance (of membranes and MEAs)

Technical Targets

This project will synthesize novel PF AEMs and ionomers and incorporate these MEAs for fuel cell testing. The project generally supports targets outlined in the Fuel Cell Technologies Office Multi-Year Research, Development, and Demonstration Plan in application to specific areas (portable, stationary, transportation). However, as alkaline membrane fuel cells are at an earlier stage of development, specific target tables have not yet been developed. There are two tasks in the Technical Plan of the Multi-Year Research, Development, and Demonstration Plan for alkaline membranes; this project seeks to address both.

	Task
1.4	Demonstrate an anion-exchange membrane that retains 99% of original ion exchange capacity for 1,000 hours in hydroxide form at T >80ºC. (2Q 2013)
3.8	Demonstrate anion-exchange membrane technologies in MEA/single cells with non-PGM catalysts that maintain performance higher than 350 mW/cm^2 for 2,000 hours at T >80°C. (4Q, 2016)

PGM – precious-grade metal

FY 2013 Accomplishments

None to date

✧ ✧ ✧ ✧ ✧

INTRODUCTION

Alkaline membrane fuel cells (AMFCs) are of interest primarily because they enable use of non-Pt catalysts, the primary cost/supply limitation of proton exchange membrane fuel cells PEMFCs. AMFCs, therefore, offer the potential of greatly decreased PEMFC cost. Operating AMFCs under ambient carbon dioxide conditions remains a challenge due to carbonate formation. An approach that has shown promise for carbon dioxide tolerance is increased operating temperature. Unfortunately, the stability of cations and water management both become more difficult as temperature rises.

The use of perflourinated ionomers, similar to those used in PEM systems, with tethered cations should help improve water transport properties and offer exceptional chemical durability of the backbone. The significant advances demonstrated in AMFC systems have been accomplished primarily through improving water management and the bonding between membrane and electrode. Both issues can be tackled much more effectively when employing PF AEMs and ionomers. This project consists of three sub-tasks: (1) synthesis of novel perfluorinated alkaline ionomers

(NREL, CSM, 3M); (2) membranes and dispersions (3M, NREL); and (3) MEA fabrication and fuel cell testing (CellEra, 3M, NREL).

APPROACH

The team will focus on achieving higher-temperature, higher-power-density AMFC operation through implementation of novel alkaline PF membranes and ionomeric dispersions. The PF materials proposed are expected to enhance water transport capabilities and electrode performance/durability significantly, thereby enabling higher temperature and power density operation. The combination of high current density and operating temperature will improve the ability of these devices to tolerate ambient CO_2, potentially enabling complete tolerance to ambient CO_2.

Most AEMs are based on hydrocarbon polymer chemistry. From significant work in the area of PEMs, water transport has been shown to be significantly higher in PF polymers, particularly at lower hydration levels [1].

Starting with the sulfonyl fluoride form of current PF ionomers (see Figure 1) we have identified and in several cases verified the ability to convert commercially available precursors into anion-exchange polymers and membranes. Synthesis work will focus on linkage chemistry with spacer groups to better mate the highly electron withdrawing backbone with the highly electropositive cation. This linkage and mating of dissimilar materials has been shown to be a major limitation for chemical stability in these systems. A handful of cations and linkage chemistries have already been identified for initial study. The synthesis of novel ionomers is the first critical task and will represent the majority of our initial efforts. This effort will focus on investigating different tethering chemistry/strategies, investigating different spacer groups, and different covalently tetherable cations.

The synthesized PF ionomers will be cast into membranes, made into polymeric dispersions, and characterized. The procedures will draw on existing membrane-making know-how and likely will be similar to that reported in the literature for Tosflex dispersion preparation. Most of the characterization performed on these materials is anticipated to be routine.

We will implement novel PF AEMs and dispersions into MEAs. Due to the experience of our team members with similar perfluorinated sulfonic acid materials, this implementation should be relatively straightforward when both ionomer and membrane are in PF form. While the use of non-precious catalysts are the primary driving force for AMFC study, in order to maximize efficiency most testing will involve Pt electrodes as a baseline material, as there is ample experimental justification that these results can be translated to non-precious catalyst systems once demonstrated with Pt.

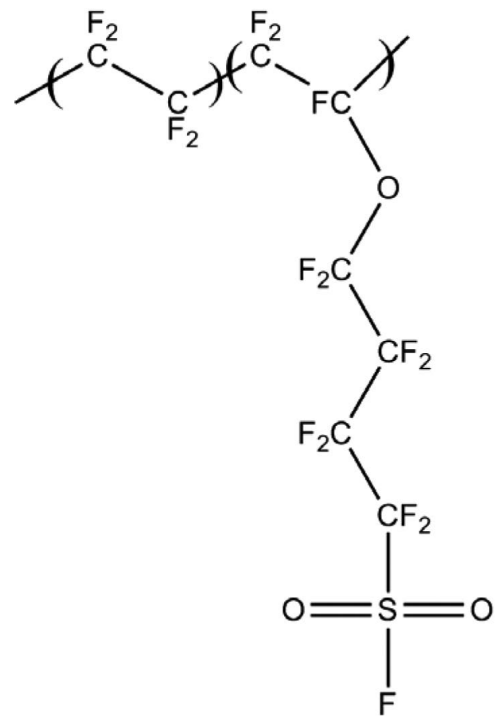

FIGURE 1. Sulfonyl Fluoride Precursor Form of PF Ionomers

RESULTS

The project started in April 2013. Subcontracting has been initiated with all of the subcontractors and the subcontract with CSM is in place and has active work occurring. Initial efforts on the project have focused on evaluating promising synthesis routes, obtaining materials, and characterizing reactions.

CONCLUSIONS AND FUTURE DIRECTIONS

As the project is just at its inception, we have little in terms of conclusions, and instead have a focus on future directions:

- PF Ionomer Synthesis (NREL/CSM, 3M)
  - Cation tethering to sulfonyl fluoride precursor form through sulfur-nitrogen linkage (NREL/CSM, 3M)
  - Development and application of alternative chemistries (NREL/CSM, 3M)
- PF AEMs and Ionomeric Dispersions (3M, NREL/CSM)
  - Membrane casting (3M, NREL/CSM)
  - Polymer dispersion preparation (3M, NREL/CSM)
  - Membrane characterization (NREL/CSM, 3M)
- MEA Fabrication/Fuel Cell Testing (CellEra, NREL, 3M)

  - Water management and CO_2 tolerance studies (CellEra)
  - PF AEM and ionomeric dispersions in MEA fabrication and fuel cell testing (CellEra, NREL, 3M)
- Detailed Assessment of Cost and Manufacturability (CellEra, 3M, NREL)

SPECIAL RECOGNITIONS & AWARDS/ PATENTS ISSUED

1. Principal Investigator, Bryan Pivovar, has been awarded the 2012 Charles Tobias Young Investigator Award (Electrochemical Society).

REFERENCES

1. Kreuer, K.D., et al., Chemical Reviews, 2004. **104**(10): p. 4637-4678.

V.M.1 Improving Fuel Cell Durability and Reliability

Prabhakar Singh
Center for Clean Energy Engineering
University of Connecticut (UConn)
44 Weaver Road, Unit 5233
Storrs, CT 06268-5233
Phone: (860) 486-8379
Email: singh@engr.uconn.edu

DOE Managers
Dimitrios Papageorgopoulos
Phone: (202) 586-5463
Email: Dimitrios.Papageorgopoulos@ee.doe.gov
Reg Tyler
Phone: (720) 356-1805
Email: Reginald.Tyler@go.doe.gov

Technical Advisor
Thomas Benjamin
Phone: (720) 356-1805
Email: benjamin@anl.gov

Contract Number: DE-EE00003226

Project Start Date: August 1, 2010
Project End Date: October 31, 2013

Overall Objectives

Overall objective of the research project is to develop an in-depth understanding of the degradation processes in advanced electrochemical energy conversion systems. It is also the objective of the research project to transfer the technology to participating industries for implementation in manufacturing of cost-effective and reliable integrated systems. The project aims to:

- Advance fuel cell-based power generation systems architecture, including renewable hybridized energy conversion and storage.
- Develop novel cell and stack structural and functional materials and validate their performance under the nominal and transient operational conditions for the evaluation of long-term bulk, interfacial, and surface stability.
- Gain a fundamental understanding of chemical, mechanical, electrochemical, and electrical processes related to:
  - The utilization of fuels ranging from bio-derived fuels to liquid petroleum to hydrogen.
  - The role of fuel impurities on degradation and processes for removal from feedstock.
  - Surface and interface phenomena related to surface adsorption, interfacial compound formation, and electron/ion generation and transport, electrodics, and electrochemistry.

Novel membranes, heterogeneous catalyst materials, and structures will be developed and validated through experimentation. Collaborative research projects with industry will be developed to improve the performance stability and long-term reliability of advanced fuel cells and other power generations systems.

Fiscal Year (FY) 2013 Objectives

- Quantify the role of fuel impurities on degradation processes in advanced electrochemical energy conversion systems.
- Optimize novel cell and stack structural and functional materials from a durability, cost, and performance perspective.
- Demonstrate and improve performance stability and reliability through advanced materials and fabrication processes.

Technical Barriers

This project addresses the following technical barriers from the Fuel Cells section of the Fuel Cell Technologies Office Multi-Year Research, Development, and Demonstration Plan:

(A) Durability

(B) Cost

(C) Performance

Technical Targets

The projects associated with this project address technical aspects of stationary fuel cells and stationary fuel processors. DOE 2011 targets are as follows:

Stationary Proton Exchange Membrane Fuel Cell Stack Systems (5-250 kW) Operating on Reformate:

- Cost: $530/kWe
- Durability: 40,000 hours

Stationary Fuel Processors (equivalent to 5-250 kW) to Generate Hydrogen-Containing Fuel Gas

- Cost: $220/kWe
- Durability: 40,000 hours
- H_2S content in product stream: <4 ppbv (dry)

FY 2013 Accomplishments

- The Center for Clean Energy Engineering has successfully developed, in total, 18 industrially sponsored research, development, and engineering projects in the field of clean and sustainable energy.
- These collaborative projects have leveraged DOE funds with industrial financial support to accelerate the development of advanced materials, cell and stack components, catalysts and fuel cleanup, and balance-of-plant sub-systems.
- The industrial projects support the mission of DOE through the development of reliable and cost-effective advanced clean and efficient fuel cell power generation systems.

✧ ✧ ✧ ✧ ✧

INTRODUCTION

The scope of this energy systems and technology research and development initiative will focus on the development and validation of the mechanistic understanding and subsequent creation of novel cost-effective materials to mitigate degradation processes. Through a unique collaborative project with industry we will solve technology gaps through joint industry/university projects. These relationships will accelerate the development and deployment of clean and efficient multi-fuel power generation systems.

The scope of the research projects will include identification and prioritization of the technology gaps and research needs along with the development of enabling technologies that meet the overall stack and balance-of-plant improvements from a durability, cost, and performance perspective. Specifically the performance stability and reliability of the power generation systems will be improved through the implementation of advanced materials and fabrication processes. Technical areas of interest, to be addressed by the industry/university collaborations, will include a) performance stability and reliability of fuel cell systems; b) fuels, fuel processing, and catalysis; c) advanced functional and structural materials, processes and systems; d) hydrogen storage and power management; and e) renewable energy and resources.

APPROACH

The approach used for this project was to develop collaborative industry/university research projects aimed specifically at accelerating the development and deployment of clean and efficient multi-fuel power generation systems. Through a competitive process, faculty developed relationships with industry that provided additional amounts of cash and in-kind support, thus leveraging funding available through this project. By requiring a financial commitment from industry this methodology ensured that technology problems of commercialization relevance would be addressed. Industry collaborative projects have been developed with UTC Power, FuelCell Energy, UTC Research Center, NanoCell Systems, APSI, Oasys Water, Nissan, Corning, Proton OnSite, BC Hydro, Sci-Tech, and WR Grace & Company. The project topics have addressed issues ranging from performance stability and reliability of fuel cell systems to fuels, fuel processing, and catalysis and finally including advanced functional and structural materials, processes, and systems.

RESULTS

Role of Multi-Scale Water Transport in Dynamic Performance of Polymer Electrolyte Fuel Cells (Project PI: Ugur Pasaogullari, Industry Partner: Nissan). The collaboration between Nissan and UConn focused on understanding the transport phenomena at very high current density operation of polymer electrolyte fuel cells (PEFCs). The work in the last year resulted in detailed understanding of the micro-structure of the gas diffusion layers (GDLs) in PEFCs. GDLs were responsible for ~50% of the oxygen transport losses in PEFCs and high current density operation which required very effective oxygen transport to active reaction sites. Numerical models that describe the multi-phase transport phenomena at very high current density conditions were developed, and the results have been compared with neutron radiography results obtained at the National Institute of Standards and Technology Center for Neutron Radiography.

High-Performance Phosphoric Acid Fuel Cell Electrodes for Soluble Polymers and Alternate Fabrication Methods (Project PI: Ned Cipollini, Industrial Partner: UTC Power). A new method of fabricating phosphoric acid fuel cell (PAFC) cathodes was developed which promises many advantages over the present state-of-the-art method: 1) less expensive, 2) more controllable in thickness and Pt loading, 3) fewer defects, and 4) produces free-standing electrodes. Mixtures of poly tetrafluoroethylene (PTFE) or PTFE/perfluoro alkoxy, catalyst, and hydrocarbon lubricant/vehicle were rolled, much like bread dough, into a layer of desired thickness, dried, and sintered at 349°C or 330°C, respectively. Sub-scale fuel cell tests show that even without composition optimization, the performances of these experimental electrodes exceed that of conventional electrodes. We expect the process to be scalable and also applicable to the anode and matrix (without sintering) layers and to lead to lower cost/kW PAFCs.

Mechanistic Understanding of Matrix Stability in MCFCs (Project PI: Prabhakar Singh, Industry Partner: FuelCell Energy). Technical discussions progressed during the reporting period to identify electrical performance

degradation mechanisms related to the electrolyte matrix stability under cell operation conditions. Role of the oxidant and fuel gas chemistry, fuel utilization, temperature, current density, and melt chemistry were examined using solid–gas–melt thermochemistry, microstructural, and chemical analysis of post tested samples. An experimental test matrix was designed in consultation with the industry partner and both short-term and long-term experiments were conducted using matrix constituents to examine the coarsening of the matrix. As received samples were examined at the matrix-anode and matrix-cathode interfaces. Samples were subsequently washed in glacial acetic acid-acetic anhydride mixture to dissolve and remove the electrolyte. Obtained samples were further analyzed for the morphology. Role of anode and cathode atmospheres, humidity level, and electrolyte basicity were experimentally evaluated. Nickel dissolution in the matrix was also analyzed.

Waste to Energy: Biogas Cleanup (Desulfurization) for Energy Generation (Project PI: Steven Suib, Industry Partner: FuelCell Energy). Over the past 12 months we have made significant progress in the area of sulfur getters for fuel cell systems. We have made adsorbents that work at various relative humidities and have excellent capacity. These unique cost-effective adsorbents are now being scaled.

Fuel Reforming Catalysts for Efficient Energy Usage (Project PI: Steven Suib, Industry Partner: APSI). Our work with APSI in the past 12 months has involved generation of novel catalysts for fuel reforming. We have also studied the mechanism of reaction of these catalysts. A final area of research has involved evaluation of such systems in combustion catalysis.

Structure-Activity Correlations in Soot Oxidation (Project PI: Steven Suib, Industrial Partner: Corning). In the last 12 months our work with Corning has involved the study of various carbonaceous materials that can ruin filer systems. Our work has fully characterized these different soot materials. We have also developed catalysts to destroy this soot.

Optimization of Fluid Catalytic Cracking (FCC) Selectivity Through Detailed Modeling of Catalyst Evaluation Experiments and the Contributions of Catalyst Components (Project PI: George Bollas, Industry Partner: W.R. Grace & Co.). Models of state-of-the-art catalyst evaluation procedures for the FCC process have been developed, incorporating key characteristics of different catalyst testing reactors. Model predictions (in good agreement with experimental data) have provided metrics for comparison and analysis of data from different reactors and for the study of the performance of catalyst decay functions on the same basis, and are providing theoretical insights to decoupling the effect of matrix type and zeolite diffusional properties on catalysts, as well as to the analysis of several different reaction kinetic networks. Predictive models have been developed capable of simulating FCC operation with catalyst blends, with using only pure catalyst experiments. Non-linearities of the blend catalyst performance were predicted successfully and understood. The effect of catalyst support (matrix) was decoupled from that of the active catalyst (USY zeolite) and the effect of each catalyst component was represented by sets of different lumped kinetics. It was shown that pre-cracking is a significant contribution from the matrix (yielding mostly light-cycle oil and naphtha) whereas the zeolite is responsible mainly for the selectivity to lighter products. Optimal catalyst formulations can be proposed through a user-friendly interface, developed for the analysis of FCC lab-scale data.

Nanostructured Catalyst Support Systems for Next Generation Electolyzers (Project PI: William Mustain, Industry Partner: Proton OnSite). During this project, the UConn/Proton team developed a new Pt/WC electro-catalyst that has very high activity and stability at a fraction of the Pt catalyst loading in the Proton commercial unit. The new catalyst reduces the total Pt loading by 80%, while retaining 96% of its activity during short-term operation. Both of these metrics are significantly better than existing commercial catalysts.

Reliability Evaluation and Enhancement of Synchronized Phasor Network (Project PI: Peng Zhang, Industrial Partner: BC Hydro). During 2012-2013, the project sponsored by DOE has resulted in a published U.S. patent and several innovations that improve the reliability of synchronized phasor networks and power grid. Approximate analytic variance for estimation method of phasor, frequency and rate of change of frequency were derived, which provided insight for reducing errors in phasor tracking algorithms. A generalized capacity outage tables approach was further studied to evaluate the reliability of active distribution systems considering different operation modes under single or multiple contingencies. The results have been published in the Institute of Electrical and Electronics Engineers journal and presented at the Institute of Electrical and Electronics Engineers PES General Meeting 2013 in Vancouver. Most recently, significant efforts were devoted to quantifying and enhancing the reliability of BC Hydro's synchronized phasor (synchrophasor) network which is planned to be connected as part of the Western Electric Coordinating Council wide area measurement system. Extensive sensitivity studies have been performed to identify the vulnerabilities in BC Hydro's synchrophasor network so as to provide the most cost-effective strategy to reinforce the network.

Plasmonic Nanostructures for Solar Energy Harvesting (Project PI: Brian Willis, Industry Partner: SciTech). A new nanofabrication procedure and reactor design has been completed to overcome a problem with shorting due to particulates. The new antenna design includes successively larger parallel arrays with minimal overlap area to enable multiple measurements per experiment. In situ analysis experiments were initiated to provide greater fundamental

understanding of the atomic layer deposition growth process to optimize antenna growth conditions.

Waste Heat Recover and Utilization Using the Osmotic Heat Engine (Project PI: Jeff McCutcheon, Industry Partner: Oasys Water). During the last year, we have successfully integrated our custom built pressure retarded osmosis testing unit into our lab for testing various membranes for their osmotic power potential. We have evaluated our chemically modified retarded osmosis membrane platforms as well as our newly developed nylon-supported thin-film composite membranes and achieved power densities of up to 2.5 watts/m^2. Our nano-fiber platforms have shown much better performance. Our recent nano-fiber-supported thin-film composite membranes have exhibited power densities of up to 7.5 watts/m^2, far exceeding industry target of 5 watts/m^2.

Gasification Technology and Clean-Up for Integration with Solid Oxide Fuel Cell (Project PI: Radenka Maric). During this past year, we have modified the pilot gasifier unit to decrease the feed rate to match the feedstock supply. In addition, we developed a method for pelletizing various feedstock such as; biosolids (wastewater residuals), food waste and animal waste. These larger pellets as well as modifications to air distribution resulted in better operational control and production of a combustible gas with values of between 130 and 160 Btus per pound. This project was described in a webcast presented by Dr. Maric as part of the Energy and Water Conference sponsored by the Water Environment Federation in March 2013.

CONCLUSIONS AND FUTURE DIRECTIONS

Of the 11 projects listed above four of them will continue into FY 2014. At this time the list of projects is stable and we do not anticipate additional projects. We do, however, continue to expect the following achievements to continue from the above list of activities:

- Advanced functional and structural materials R&D will continue to address long-term surface, interface and bulk instabilities at the engineered systems level. Research will continue in areas related to solid- and liquid-gas interactions as they relate to surface corrosion, electrochemical poisoning, agglomeration and coarsening of porous aggregates, and catalytic degradation.
- UConn and its partners will continue to develop advanced fuel cleanup and processing technologies to enable multi-fuel capabilities of advanced fuel cell systems. Cost-effective technologies for the removal of contaminants from gas phase will be developed and validated.
- Developed technologies will be transferred to industries to accelerate the development and deployment of advanced fuel cell systems.
- Research findings will be presented and published in technical meetings and peer reviewed journals. Intellectual property will be disclosed through invention disclosures and review by the university's center for science and technology commercialization.

SPECIAL RECOGNITIONS & AWARDS/ PATENTS ISSUED

Three invention disclosures have been filed with the University of Connecticut's Office of Economic Development and transferred to the client, UTC Power (now ClearEdge Power):

1. "Electrodes from Polymers Soluble at Elevated Temperatures." Case number 13-041.

2. "Phosphoric Acid Fuel-Cell (PAFC) Electrodes from Soluble or Meltable Polymers by Fibrillation of PTFE." Case number 13-042.

3. "Phosphoric Acid Fuel-Cell (PAFC) Electrodes by Fibrillation of PTFE." It has been assigned case number 13-043.

FY 2013 PUBLICATIONS/PRESENTATIONS

1. Lakshitha Pahalagedera, Hom N. Sharma, Chung-Hao Kuo, Saminda Dharmarathna, Ameya V. Joshi, Steven L. Suib, and Ashish B. Mhadeshwar, "Structure and Oxidation Activity Correlations for Carbon Blacks and Diesel Soot", in preparation for submission to Chemistry of Materials, 2012.

2. Y. Liu, and W.E. Mustain, "Evaluation of Tungsten Carbide as the Electrocatalyst Support for Platium Hydrogen Evolution/ Oxidation Catalysts", *Int. J. Hydrogen Energy*, 37 (2012) 8929

3. Fu, R.S., Khajeh-Hosseini-Dalasm, N., and Pasaogullari, U., "Numerical Validation of Water Transport in Polymer Electrolyte Membranes," ECS Transactions, 50 (2012).

4. McCutcheon, J.R., "Next Generation Membranes for Forward and Pressure Retarded Osmosis", 3rd Annual Water Industry Exhibition & Conference, May 2–4, 2012.

5. Arena, J., Manickam SS, Reimund, K.K., McCoskey, B.D., Freeman, B.D., McCutcheon, J.R., "Surface Modification of Thin Film Composite Membranes with Polydopamine for Engineered Osmosis", Oral Presentation at the North American Membrane Society Annual Meeting, New Orleans, LA, June 9–13, 2012.

6. A. Abdollahi, P. Zhang, and N. Zhou, "Generalized Subspace Least Mean Square Method for High-Resolution Accurate Power System Oscillation Mode Estimation," IEEE Trans. Power Systems, under review. Submission date: July, 2012.

7. H. Xue and P. Zhang, "Subspace-Least Mean Square Method for accurate harmonic and interharmonic measurement in power systems," *IEEE Trans. Power Delivery*, vol. 27, no. 3, Jul. 2012.

8. "Next Generation Membranes for Forward and Pressure Retarded Osmosis", International Union of Pure and Applied Chemistry. Blacksburg, VA, July 24–27, 2012.

9. Y. Wang, W. Li, P. Zhang and B. Wang, "Reliability analysis of Phasor Measurement Unit considering data uncertainty," IEEE Trans. Power Delivery, vol. 27, no. 3, pp. 1503-1510, Aug. 2012.

10. Huang, L., Bui, N.N., McCutcheon, J.R. "Nylon 6,6 Microfiltration Membranes as Supports for Thin Film Composite Membranes for Engineered Osmosis". American Institute of Chemical Engineers Annual Meeting, November 2012.

11. Bui, N.N., McCutcheon, J.R., "Hydrophilic Nanofibers as Supports for Thin Film Composite Membranes for Engineered Osmosis." American Institute of Chemical Engineers Annual Meeting, November 2012.

12. Bie, P.Zhang, G. Li, B. Hua, M. Meehan, and X. Wang, "Reliability evaluation of active distribution system including microgrids, " IEEE Trans. Power Systems, vol. 27, no. 4, pp. 2342-2350, Nov. 2012.

13. Y. Wang, P. Zhang, W. Li and W. Xiao, "Online overvoltage prevention control of photovoltaic generators in microgrids," IEEE Trans. Smart Grid, vol. 3, no. 4, pp. 2071-2078, Dec. 2012

14. McCutcheon, J.R., "Engineered Osmosis for Sustainable Water and Power", University of Kansas Department of Chemical and Petroleum Engineering Seminar Series, December 4, 2012.

15. McCutcheon, J.R.,"New Membrane Platforms for Pressure Retarded Osmosis", Statkraft, Oslo, Norway, December 12, 2012.

16. Y. Liu, T.G. Kelley, J.G. Chen and W.E. Mustain, "Metal Carbides as Alternative Electrocatalyst Supports", ACS Catalysis, 3 (2013) 1184

17. Lakshitha Pahalagedera, Hom N. Sharma, Chung-Hao Kuo, Saminda Dharmarathna, Ameya V. Joshi, Steven L. Suib, and Ashish B. Mhadeshwar, "Comparative Analysis of the Structure and Chemical Nature of Carbon", in preparation for submission to Analytical Chemistry, 2013.

18. A. Abdollahi, P. Zhang, and H. Xue, "Enhanced Subspace-Least Mean Square for fast and accurate power system measurement," IEEE Trans. Power Delivery, vol. 28, no. 1, pp. 383-393, Jan. 2013.

19. McCutcheon, J.R., "New Membrane Platforms for Engineered Osmosis", ACS Polymer Membrane Mediated Water Filtration Meeting, Pacific Grove, CA, February 28, 2013.

20. DOE visited Center for Clean Energy Engineering at University of Connecticut on March 28, 2013 to review projects associated with Fuel Cell Technology.

21. "Evaluation of Tungsten Carbide and Tungsten Oxide as Pt Supports for Oxygen Reduction Reaction", The Electrochemical Society, Toronto, May 2013. Presenting Author: Ying Liu.

V.N.1 Computer Simulation of Proton Transport in Fuel Cell Membranes

Principal Investigator: Gregory A. Voth
Department of Chemistry, James Franck Institute, and Computation Institute, University of Chicago
5735 S. Ellis Ave.,
Chicago, Illinois 60637, United States.
Phone: (773) 702-9092
Email: gavoth@uchicago.edu

DOE Program Manager: Larry A. Rahn
Phone: (301) 903-2508
Email: Larry.Rahn@science.doe.gov

Objectives

We seek to understand the multiscale coupling of proton transport and polymer morphology in proton exchange membrane (PEM) materials using a combination of detailed reactive molecular dynamics (MD) and mesoscale coarse-grained (CG) simulations, which will help guide future membrane development efforts.

Technical Barriers

The main technical barrier this year is to increase the scalability of the coarse-grained smoothed particle hydrodynamics (CG-SPH) method in order to simulate extremely large-scale systems. We foresee a positive outcome with input from specialists in Argonne National Lab through the INCITE program.

Abstract

Our major advancements this year using reactive MD have been in exploring the effects of morphology and side chain length on proton transport.

Using cylindrical, lamellar, and cluster model morphologies with our multistate empirical valence bond (MS-EVB) reactive MD method, we revealed two different proton translocation mechanisms. The prevalence of these mechanisms depended on the morphology used and the interfacial spacing for a given morphology.

Our investigation into the promising new short side chain 3M membrane using reactive MD also implicitly highlighted the effect of morphology, since there was essentially no difference in the local transport properties between 3M and Nafion®, even though 3M conducts much better in experiment.

We have also taken steps to examine these morphological effects at previously inaccessible length and time scales using our novel smoothed particle hydrodynamics (SPH) method. This method was validated using simple lamellar-like structures and also random morphologies derived from dissipative particle dynamics (DPD) simulations.

Progress Report

A. Proton Conductivity at the Mesoscale: Pushing the Limits of Simulation with Multiscale Modeling of Proton Exchange Membranes

We have completed the validation of our CG-SPH simulation method which has been parameterized using our reactive MD simulations and will provide closer connection to experimental results. [1,2] The method combines a CG model for the polyelectrolyte membrane [3] with a smoothed particle hydrodynamics (SPH) [4] description of the proton concentration diffusion in order to study proton conduction through heterogeneous materials. The SPH proton transport is parameterized using our previous Multistate Empirical Valence Bond (MS-EVB) reactive MD simulations [5,6] to capture the impact of local water environments on proton transport coefficients. The combined CG-SPH method gives a foundation for exploring the mesoscale regime for proton conduction that lies beyond atomistic approaches, while providing a higher resolution than traditional engineering calculations of transport properties. The goal is to achieve a higher degree of predictive capability at length scales that can capture the heterogeneity inherent to the phase-segregated morphology of hydrated Nafion®.

The CG-SPH method has recently been applied to the example of the Nafion® membrane at a variety of hydration levels. The CG model, in conjunction with dissipative particle dynamics, reveals phase-segregated structures with water channels that expand upon further hydration and are nanometers in width. Configurations from these simulations are used in the SPH algorithm to simulate proton transport under an applied concentration gradient. The SPH equations are integrated until a steady state is achieved and volume averaging can be used to extract an effective conductivity. Examination of the steady state concentration profiles shows the presence of significant variations in the proton distribution throughout the water channels of the membrane, in agreement with recent experiments, and demonstrates the important role of including local nanoscale effects to understand the mesoscale transport of protons. In comparing these results with experiments, nearly quantitative agreement was found at higher hydration levels where the CG model is expected to perform well.

B. Morphological Effect on Proton Solvation and Transport in Hydrated Nafion®

Simulations for three of the main morphological models of Nafion® currently proposed in the literature were

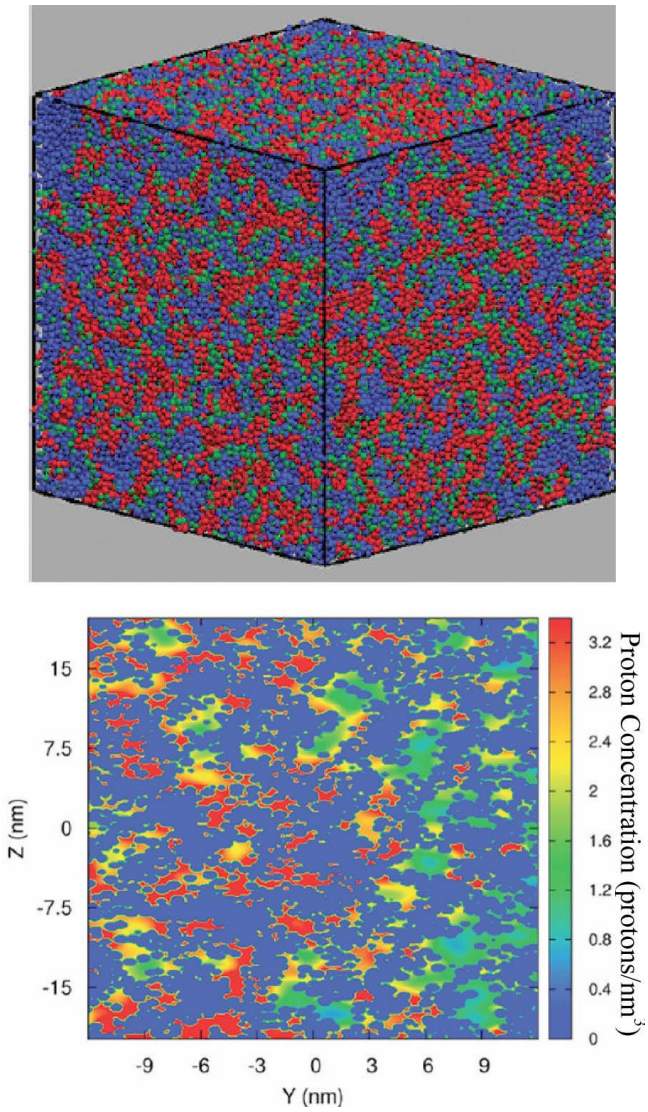

FIGURE 1. (Top) Equilibrated DPD morphology used for SPH simulations. Water beads are blue, polymer backbone red, and side chain green. (Bottom) Results from SPH simulation showing proton concentration in the above morphology.

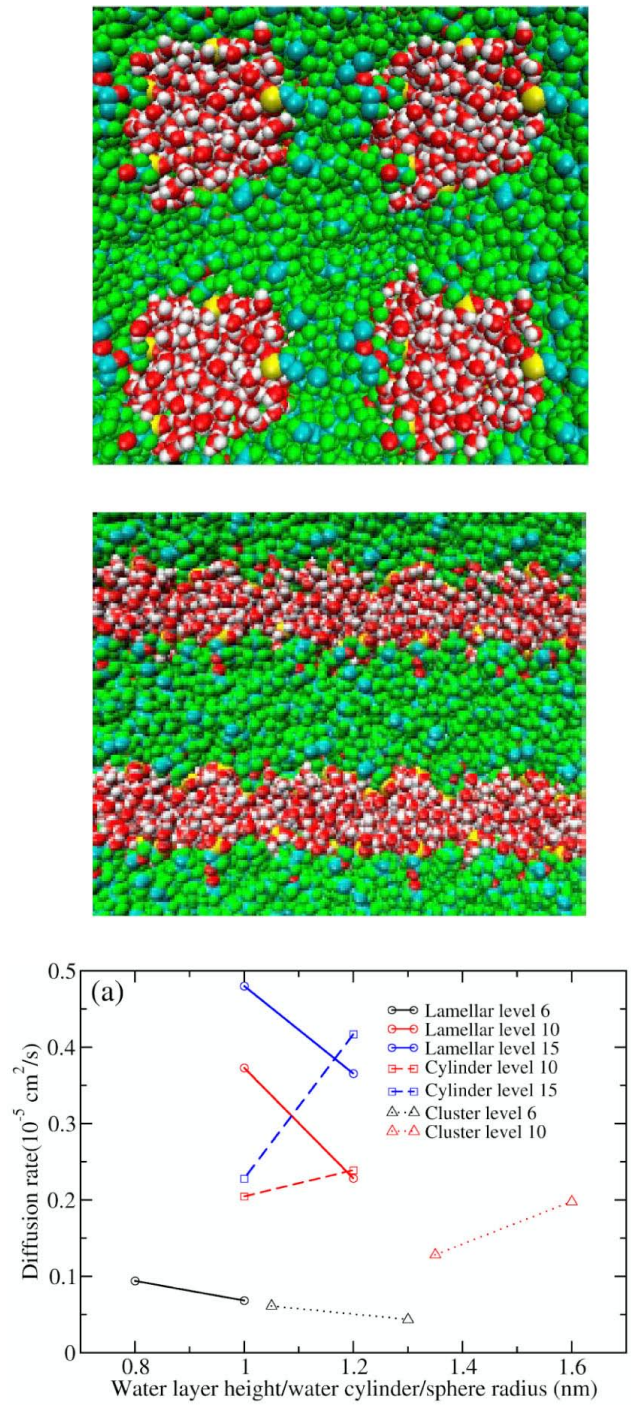

FIGURE 2. (Top) Snapshot of the cylinder-type model. (Middle) Snapshot of the lamellar-type model. (Bottom) Proton diffusion coefficients calculated for lamellar, cylinder, and cluster-channel models at hydration level 6, 10, and 15.

performed using the self consistent iterative MS-EVB (SCI-MS-EVB) method. [7] The three morphological models included the lamellar structure, the cylinder model, and the cluster-channel model. Each structure was studied at a series of hydration levels and the spacing between the interfaces of the hydrophilic and the hydrophobic regions was varied to extract the geometric factors affecting proton solvation and transport. It was found that for a given hydration level in the lamellar and cylindrical models, increasing the interfacial spacing resulted in greater concentrations of protons near the sulfonate groups. It was also found by examination of the amplitudes of the EVB states that the excess protons near the sulfonate groups tended to be in Zundel-like ($H_5O_2^+$) structures. Interestingly, in contrast to the lamellar and cylindrical models, the cluster-network model showed a decrease in interfacial protons as the interfacial spacing was increased. These results can be justified by the observation that while increasing the hydrophilic regions size results in a greater amount of non-interfacial water occupying the hydrophilic region, the sulfonate groups also become more

closely spaced. This results in an entropic force pushing the protons towards the bulk-like water, and an enthalpic force attracting the protons to the interface. In the lamellar and cylindrical models the attractive enthalpic force dominates. However, because of the larger relative increase in the bulk like water in the cluster network model the entropic force is comparatively larger.

Analysis of the proton transport showed a large dependence on geometry and hydration level, which varied depending on which morphological model was being employed. [8] These results suggested different transport mechanisms were occurring as the size of the water domains changed in the different models and so a detailed analysis of the diffusion pathways was carried out. In the lamellar and cylindrical models, the protons preferred to travel along the interface of the hydrophilic regions, especially at higher interfacial spacings, which agrees well with the structural results. The closer packing of sulfonate groups in the lamellar model resulted in higher diffusion rates, as the proton was more easily able to hop from sulfonate to sulfonate between the sheets. The cluster-network model showed markedly lower diffusion rates as the protons had some probability of being trapped in the connecting channel; however, diffusion within the water clusters showed similar mechanistic behavior to the other models.

C. Comparison of Local Proton Transport in 3M and Nafion® Membrane

The 3M membrane is a promising alternative proton exchange membrane to Nafion®. Even though their chemical structures are similar, the 3M membrane, whose side chain is shorter, conducts better than Nafion®. Previously, it was conjectured that a PEM membrane with a shorter side chain may promote the Grotthuss mechanism and that may be why the 3M conductivity is better than Nafion®. By including both vehicular and Grotthuss mechanisms in the SCI-MS-EVB simulations, [7] the conjecture can be directly tested.

In our study, [9] different equilibrium and dynamical properties of 3M and Nafion® were compared at three different hydration levels (5, 9, and 14) with two different temperatures (300 K and 353 K). The morphology of these membranes was chosen to be random. To isolate the differences coming from only the side chains, the backbones for both membranes were kept the same and the same equilibration process was performed. The most important result is that the biggest difference in the self-diffusion constant of the hydrated proton center of excess charge (CEC) was only 56% at hydration level 14 at 300 K, while the differences at other conditions were much smaller. We found no evidence that the local proton transport in the two membranes can cause a difference in their conductivity. Gaining insight from the work by Feng and Voth, [8] differences in the morphology globally can lead to very different diffusion constants of excess protons. The random morphology chosen for the systems is probably not an accurate description of the true structure(s). This reinforces the idea that a more complete picture of the actual morphology of these membranes is likely required to obtain a better understanding of proton transport in these membranes as well as to obtain better overall agreement between the calculated diffusion constants and the experimental measurements.

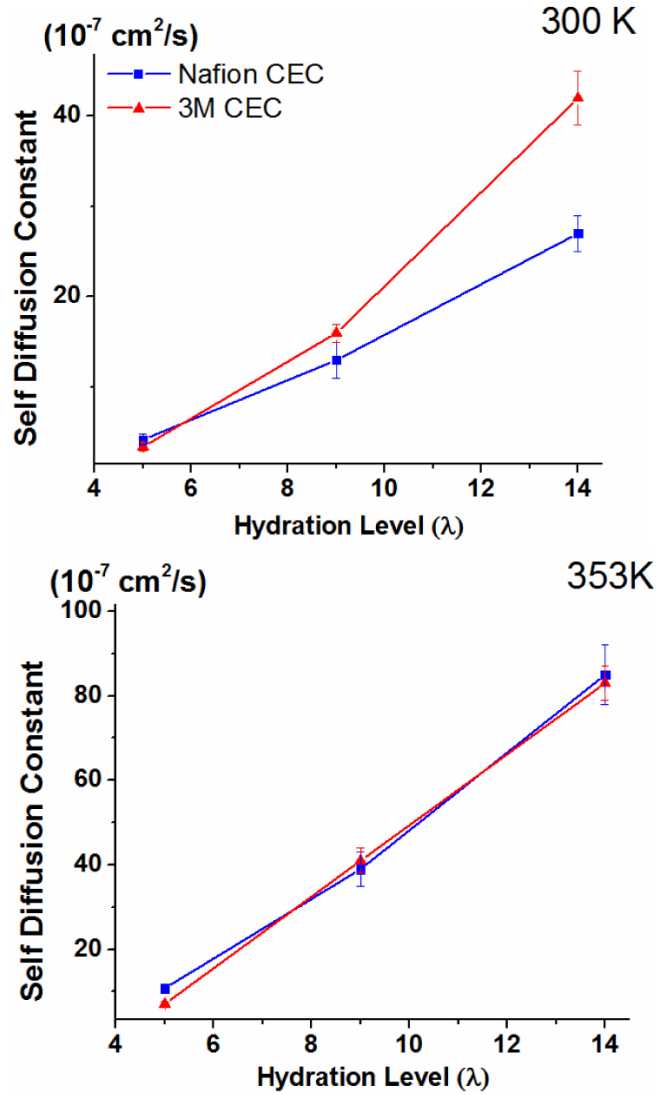

FIGURE 3. Calculated hydrated proton CEC in 3M and Nafion® as a function of hydration level at 300 K and 353 K.

Future Directions

The current development of the CG-SPH model is focused on introducing water and polymer movement to match physical systems more closely. This movement will be incorporated using methods similar to DPD to introduce thermal noise into the equations of motion. With this method validated, we can begin to explore the effect of morphology

on the large-scale proton transport through the membrane. Using a methodology similar to previous efforts in the group, we will choose several candidate morphologies and explore the differences in long-range transport across these morphologies, hopefully providing a clearer connection to conductivity experiments.

Recent algorithmic developments to our MS-EVB code have made longer length and time scales available. We plan to take this opportunity to investigate further the causes for the difference in conductivities between the various perfluorosulfonic acid membranes such as Nafion®, Hyflon®, and 3M, and to bridge those results into the CG-SPH model in a multiscale fashion.

References

1. Jorn, R.; Voth, G.A., Mesoscale Simulation of Proton Transport in Proton Exchange Membranes. *J. Phys. Chem. C.* **2012,** *116*, 10476-10489.

2. Jorn, R.; Savage, J.; Voth, G.A., Proton Conduction in Exchange Membranes across Multiple Length Scales. *Acc. Chem. Res.* **2012,** *45*, 2002-2010.

3. Wescott, J.T.; Qi, Y.; Subramanian, L.; Capehart, T.W. Mesoscale Simulaton of Morphology in Hydrated Perfluorosulfonic Acid Membranes. *J. Chem. Phys.* **2006,** *124,* 134702.

4. Monaghan, J.J. Smoothed Particle Hydrodynamics. *Rep. Prog. Phys.* **2005,** *68,* 1703-1759.

5. Petersen, M.K.; Voth, G.A. Characterization of the Solvation and Transport of the Hydrated Proton in the Perfluorosulfonic Acid Membrane Nafion. *J. Phys. Chem. B.* **2006,** *110,* 18594-18600.

6. Feng, S.; Voth, G.A. Proton Solvation and Transport in Hydrated Nafion. *J. Phys. Chem. B.* **2011,** *115,* 5903-5912.

7. Wang, F.; Voth, G.A. A Linear-Scaling Self-Consistent Generalization of the Multistate Empirical Valence Bond Method for Multiple Excess Protons in Aqueous Systems. *J. Chem. Phys.* **2005,** *122,* 144105-144109.

8. Feng, S.; Savage, J.; Voth, G.A., Effects of Polymer Morphology on Proton Solvation and Transport in Proton-Exchange Membranes. *J. Phys. Chem. C.* **2012,** *116*, 19104-19116.

9. Tse, Y.-L.S.; Herring, A.M.; Kim, K.; Voth, G.A., Molecular Dynamics Simulations of Proton Transport in 3M and Nafion Perfluorosulfonic Acid Membranes. *J. Phys. Chem. C.* **2013**. [Online early access] DOI: 10.1021/jp400693g

Publication list acknowledging the DOE grant in the past year

1. Jorn, R.; Voth, G.A., Mesoscale Simulation of Proton Transport in Proton Exchange Membranes. *J. Phys. Chem. C.* **2012,** *116*, 10476-10489.

2. Jorn, R.; Savage, J.; Voth, G.A., Proton Conduction in Exchange Membranes across Multiple Length Scales. *Acc. Chem. Res.* **2012,** *45*, 2002-2010.

3. Feng, S.; Savage, J.; Voth, G.A., Effects of Polymer Morphology on Proton Solvation and Transport in Proton-Exchange Membranes. *J. Phys. Chem. C.* **2012,** *116*, 19104-19116.

4. Tse, Y.-L.S.; Herring, A.M.; Kim, K.; Voth, G.A., Molecular Dynamics Simulations of Proton Transport in 3M and Nafion Perfluorosulfonic Acid Membranes. *J. Phys. Chem. C.* **2013**. [Online early access] DOI: 10.1021/jp400693g

V.N.2 Fluoropolymers, Electrolytes, Composites and Electrodes

Principal Investigator: Dr. Stephen Creager, PI
Department of Chemistry, Clemson University
Clemson SC 29634
Phone: (864) 656-2319
Email: screage@clemson.edu

Team Members

- Dr. Joseph Thrasher and Dr. Darryl DesMarteau, co-PIs
  Department of Chemistry, Clemson University
  Clemson SC 29634
  Phone: (864) 656-0627
  Email: thrash5@clemson.edu; fluorin@clemson.edu
- Dr. Iqbal Sharif, Postdoctoral Associate
  Department of Chemistry, Clemson University
  Clemson SC 29634
  Voice: (864) 656-1176
  Email: isharif@clemson.edu
- Mr. Hung-Pham Doc and Ms. Jamie Shetzline, Graduate Assistants
  Department of Chemistry, Clemson University
  Clemson SC 29634
  Voice: (864) 656-3065
  Email; hpham@clemson.edu; jshetzl@clemson.edu

DOE Program Manager: Dr. Larry Rahn
Separations and Analysis Program,
Chemical Sciences, Geosciences and Biosciences Division,
Office of Basic Energy Sciences
Phone: (301) 903-2508
Email: Larry.Rahn@science.doe.gov

Objectives

- The overall objective of this research is to create and understand the behavior of new fluoropolymer-based electrolytes and electrodes suitable for use in electrochemical energy storage and conversion devices such as batteries and fuel cells.
- This objective is pursued via work in three thrust areas as follows: (1) fluorinated monomers and ionomers for preparing new proton- and hydroxide-ion-conducting ionomers; (2) membrane separators made from these ionomers; and (3) nanocomposite electrodes prepared using these ionomers with carbon aerogels / xerogels to provide mixed electronic / ionic conduction functionality.
- Specific project objectives are as follows:
  - Synthesize and characterize high-ion-exchange-capacity (>1.25 meq/g) TFE-based copolymer and terpolymer ionomers with a broad range of functional groups including sulfonyl fluorides, sulfonic acids, sulfonimides, sulfonamides, and phosphonates to support proton conduction, and also quaternary ammonium and guanidinium cations to support hydroxide-ion conduction.
  - Fabricate and test membrane separators, carbon-based nanocomposite electrodes, and membrane-electrode assemblies by combining fluoroionomers with suitable crosslinking agents and/or mesoporous carbon supports. Work in this objective will include studies aimed at independently measuring ionic and electronic contributions to membrane and thin-film electrode conduction.
- Expected outcomes from the project are new fluoropolymer electrolyte and electrode materials having properties superior to existing materials, and also new knowledge regarding the behavior of such materials in energy storage and conversion applications.

Technical Barriers

- Proton exchange membranes (PEMs). Existing PEMs have low ionic conduction particularly under very hot and dry conditions (e.g. 120°C and 25% RH), as well as poor dimensional stability, high water swelling, and poor durability. Existing fluoroalkyl sulfonic acid ionomers have been in use for over 50 years and have been optimized about as much as they can be. New protogenic groups and new ionomer morphology approaches, e.g. involving crosslinking, are needed to improve properties.
- Crosslinked fluoroionomers. Ionomer crosslinking can mitigate problems from high water swelling / poor dimensional stability, particularly with high-IEC materials; however, few approaches provide crosslinks in a controllable way that could mitigate problems from swelling without introducing undesirable brittleness into membranes.
- Alkaline exchange membranes (AEMs). Alkaline ionomers are not widely used in fuel-cell devices due in part to low ionic conduction but particularly to poor ionomer stability when in contact with hydroxide-ion-containing electrolytes, especially under under hot and dry conditions. Fluoropolymer ionomers are widely used in PEM-based devices but are little used to prepare AEMs in part due to concerns about alkali stability.
- Electrodes. High-IEC ionomers are desired in electrodes to promote ionic conduction and thorough wetting of electrode surfaces, however most such materials are water-soluble and therefore unsuitable for PEM and AEM fuel cell use. Ionomer attachment to electrode surfaces could mitigate this problem however existing fluoroionomer materials offer no means for surface attachment.

Abstract

Project work is reported on the preparation and study of new fluorinated trifluorovinyl ether (TFVE) monomers for proposed proton-conducting ionomers, and new partially fluorinated model compounds relevant to proposed hydroxide-ion-conducting ionomers. TFVE monomers having sulfonyl fluoride, sulfonate, phosphonate, and sulfonimide functional groups have been prepared in multigram quantities and are available for project use. A new TFE handling facility is being constructed at Clemson and will be available for project use in summer 2013. Testing of model compounds for alkaline fluoroionomer hydroxide-ion conductors showed that the *N*-methyl sulfonamide, fluorocarbon-sulfonamide, hydrocarbon-sulfonamide, and hydrocarbon-amine linkages are all stable to strongly alkaline media at elevated temperatures, confirming that such linkages can be used to construct robust fluoropolymer-based hydroxide-ion conductors. Aliphatic quaternary ammonium groups decomposed in hot D_2O/KOD media via nucleophilic attack of hydroxide on methyl groups attached to quaternary nitrogen, as was expected from prior work on other aliphatic ammonium salts. Insights from this work are guiding efforts to understand the stability limits of cationic groups in potential fluoropolymer-based hydroxide-ion conductors. In related work, studies on first-generation carbon/zirconia/fluoroionomer nanocomposite materials were completed which provide guidance for studies on next-generation materials, and methods are being refined for studying mixed electronic / ionic conduction in thin-film electrodes prepared from these composite materials.

Progress Report

(1) Fluorinated monomers and ionomers. Fluorocarbon ionomers are being prepared by co-polymerization of one or more trifluorovinyl ether (TFVE) co-monomers with tetrafluoroethylene (TFE) gas. The TFVE monomers shown in Figure 1 have been prepared in multigram quantities and are available for use on the project.

The $–SO_2F$, $-SO_3(Na)$ and $–SO_2N(Na)SO_2CF_3$ monomers have long been known and used to prepare proton-conducting fluoroionomers. Ionomers based on the $–SO_2N(Na)SO_2CF_3$ monomer in particular have been extensively studied at Clemson. The phosphonate monomers are relatively new. They were recently prepared by DesMarteau and co-workers for use in making all-phosphonate ionomers as part of a separate project, but they have not until now been used to prepare terpolymers containing both protogenic groups (e.g. $-SO_3(H)$ and $–SO_2N(H)SO_2CF_3$) and phosphonate-based crosslinking / surface-anchoring agents co-polymerized with TFE. With multi-gram quantities of these monomers in hand we are positioned to start systematically preparing these terpolymer ionomers and studying their properties, particularly their propensity for crosslinking and surface grafting via the phosphonate groups.

TFE is a hazardous and highly explosive gas for which highly specialized handling techniques and facilities are needed. Clemson is in the late stages of completing a new facility under the direction of Joe Thrasher for generating and handling TFE. An opening ceremony is planned for spring/summer 2013. This facility will be used to perform TFE-based co-polymerizations with the monomers in Figure 1 to produce ionomers.

In other work, partially fluorinated model compounds were prepared having structures relevant to proposed alkaline fluoroionomers for accomplishing hydroxide ion transport. Figure 2 presents structures for three such compounds that have been prepared and their stability studied in strongly alkaline media.

The two neutral model compounds (X = -H and $–N(CH_3)_2$) were dissolved in a solution of 9:1 d_6-DMSO:D_2O into which approximately 1.5 M KOH had been dissolved, and the solutions were heated to 60C and 80C for 48 hrs each. No differences in the ^{19}F or ^{1}H NMR spectra were observed between the start and finish of heating. We conclude that all of the chemical linkages in these compounds, including the *N*-methyl sulfonamide, the fluorocarbon-sulfonamide, the hydrocarbon-sulfonamide, and the hydrocarbon-amine, are stable to strongly alkaline media at elevated temperatures. Ongoing studies involving

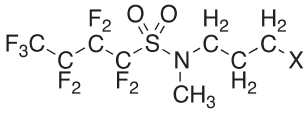

X = -H, $-N(CH_3)_2$, $-N(CH_3)_3^+ I^-$

FIGURE 2. Model compounds for studying alkaline stability of chemical linkages in proposed hydroxide-ion-conducting fluoroionomers.

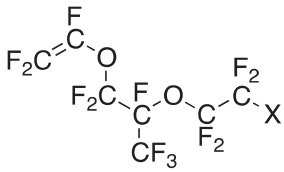

X = $-SO_2F$, $-SO_3(Na)$, $-SO_2N(Na)SO_2CF_3$, $PO_3(Na)_2$, $PO_3(CH_2CF_3)(Na)$

FIGURE 1. Structures of TFVE monomers suitable for co-polymerization with TFE to prepare fluorinated proton-conducting ionomers.

harsher conditions will explore the limits of stability for these linkages. We note that these results refute the commonly-held notion that fluorocarbon ionomers will not be well suited for preparing alkaline exchange membranes due to instability of the fluorocarbons on exposure to hot alkali. There may be stability limits for such materials but they will likely not involve the fluorocarbons or the sulfonamide groups linking anion-exchange groups to the ionomers.

In another stability study, the quaternary ammonium model compound ($X = -N(CH_3)_3^+ I^-$) was dissolved in a solution of KOD in D_2O (without d_6-DMSO) and heated to 60 and 80 C. In this case it was found that the ^{19}F NMR spectrum did not change but the ^1H NMR spectrum did change, in a manner consistent with decomposition by nucleophilic attack of hydroxide at one of the quaternary ammonium methyl groups to produce methanol (actually methoxide) and re-generate the tertiary amine. This decomposition pathway, illustrated in Figure 3, is consistent with known pathways for decomposition of other aliphatic quaternary ammonium ions in strongly alkaline media. Ongoing work is exploring the stability limits of this and other anion-exchange groups, e.g. guanidinium, to strongly alkaline media at elevated temperature, in an effort to understand materials decomposition pathways under such conditions and to down-select appropriate monomers for inclusion in hydroxide-ion-conducting fluoroionomers.

(2) Membrane separators. Most project work in this term was focused on monomers and ionomers so there was relatively little work on membranes. There will be more work in this area as ionomer synthesis work progresses to provide material for membrane and membrane-electrode-assembly fabrication.

3. Nanocomposite electrodes. In the past year work was completed on the use of telechelic perfluoro-cyclobutyl-based oligomer ionomers having aryl sulfonic acid groups on the main chain of the polymer and aryl phosphonates on the end groups. These polymers were grafted onto mesoporous carbons supports having large pore volumes (approximately 85% free volume), large internal surface areas (over 500 m^2/g), and integrated zirconia particles that allow for electrolyte attachment via terminal phosphonate groups. A publication describing this work appeared in *Chemical Communications* late in 2012 (see Figure 4).

In more recent work, a method is being developed for independently measuring the electronic and ionic contributions to conductivity in thin-film mixed-conductor electrodes. The method is illustrated in Figure 5. Formulations have been developed for all-electronic and all-ionic thin-film electrodes and the cell design is being optimized to ensure that measured cell resistances report principally on the properties of the thin-film electrodes and not on the contacts to the electrodes. Excellent progress is being made and a validated method is expected to be available by summer 2013.

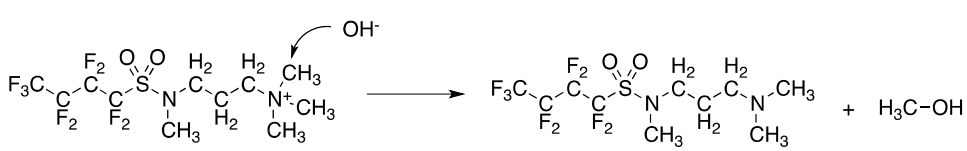

FIGURE 3. Proposed pathway for decomposition of a partially-fluorinated *N*-methyl sulfonamide quaternary ammonium salt in strongly alkaline KOD / D_2O media.

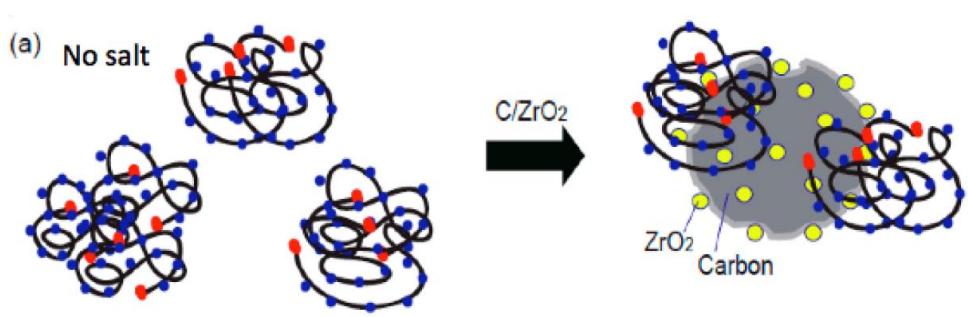

FIGURE 4. Grafting of telechelic oligomer ionomers onto the interior pore surfaces of mesoporous carbon/zirconia composite electrodes. Terminal phosphonate groups provide a means for anchoring polymer chains onto embedded zirconia particles in the carbon matrix.

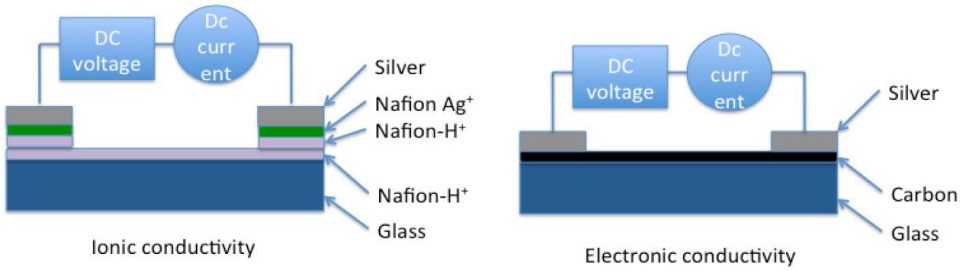

FIGURE 5. Proposed method for independently measuring ionic (left) and electronic (right) contributions to conductivity in thin-film electrodes.

Future Directions

Ongoing work is focused on improving synthesis of TFVE monomers, synthesizing fluorinated terpolymer ionomers having high ion-exchange capacity and desired compositions, continuing to explore alkali stability of model compounds for proposed alkaline exchange membrane ionomers, and continuing to refine and validate methods for studying mixed electronic and ionic conduction in nanocomposite thin-film electrodes. Some work is planned for summer 2013 aimed at preparing carbon / zirconia composites from other carbon sources besides carbon aerogels / xerogels, including carbon black and also graphene. This work will provide a wide range of carbon-based substrates to accommodate grafting of fluorinated ionomers with phosphonate groups incorporated into the polymer structure. As this work progresses, other future work will come into play including fabrication and study of membrane separators and membrane-electrode assemblies.

Publication list (including patents), acknowledging the DOE grant or contract

1. Park, Jiyoung; Jung-Min Oh; Stephen E. Creager; and Dennis W. Smith Jr. "Grafting of Chain-End-Functionalized Perfluorocyclobutyl (PFCB) Aryl Ether Ionomers onto Mesoporous Carbon Supports" *Chemical Communications*, **2012**, 48, 8225-8227

2. Oh, Jung-Min; Amar S. Kumbhar; Olt Geiculescu; and Stephen E. Creager, "Nanoscale ZrO_2 - embedded Mesoporous Carbon Composites: A Potential Route to Functionalized Mesoporous Carbon Composite Materials", *Langmuir*, **2012**, 28, 3259-3270

V.N.3 Gas Transport Across Hyperthin Membranes

Principal Investigator: Professor Steven L. Regen
Department of Chemistry
Lehigh University
Bethlehem, Pennsylvania
Phone: (610) 758-4842
Email: slr0@lehigh.edu

Mr. Minghui Wang
Department of Chemistry
Lehigh University
Bethlehem, Pennsylvania
Phone: (610) 758-3482
Email: miw308@lehigh.edu

Dr. Vaclav Janout
Department of Chemistry
Lehigh University
Bethlehem, Pennsylvania
Phone: (610) 758-3482
Email: vaj2@lehigh.edu

DOE Program Manager: Larry A. Rahn
Phone: (301) 903-2508
Email: Larry.Rahn@science.doe.gov

Objectives

The objectives of this research are to learn how to synthesize "hyperthin" (<<100 nm) Langmuir-Blodgett films and polyelectrolyte multilayers having minimal film defects, and to use such knowledge in the design of novel permeation-selective membranes that have potential for separating gaseous mixtures; e.g., H_2/CO_2 and CO_2/N_2.

Technical Barriers

One main technical barrier in this area is preventing the formation of defects in membranes that are much thinner than ca. 100 nm. A second technical barrier is finding ways to exploit differences in solubility and diffusivity among gaseous permeants for their effective separation.

Abstract

Single Langmuir-Blodgett (LB) bilayers derived from a calix[6]arene-based surfactant and poly(acrylic acid) exhibit exceptional H_2/CO_2 permeation selectivities (ca. 75) and significant CO_2/N_2 selectivities (ca. 30). In sharp contrast, hyperthin polyelectrolyte multilayers (PEMs), formed from poly(diallyldimethylammonium chloride) (PDADMAC) and poly(sodium 4-styrene sulfonate) (PSS) show very low H_2/CO_2 permeation selectivity (ca. 2) but exceptionally high CO_2/N_2 permeation selectivities (ca. 100). The H_2/CO_2 and CO_2/N_2 selectivity found with these LB bilayers is mainly due to differences in diffusivity, which reflect their kinetic diameters (H_2, 0.29 nm; CO_2, 0.33 nm; N_2, 0.36 nm), and also the tightness of the membrane. The very low H_2/CO_2 selectivity and high CO_2/N_2 selectivity associated with these PEMs is mainly the result of a high solubility of CO_2 relative to H_2 and N_2.

Progress Report

Two key requirements that must be met for a membrane to be considered as a candidate for gas separations are (i) that it exhibits high permeation selectivity and (ii) that it is capable of producing a high flux. In brief, the flux (J) of a gaseous permeant across a membrane is determined by a permeability coefficient (P), the pressure gradient (Δp) that is applied across the membrane, and the thickness (l) of that membrane, according to eq. 1. A normalized flux can also be expressed as a permeance, P/l, as shown in eq. 2. The ratio of the permeances for two gases, i and j, then represents the permeation selectivity, α, of the membrane (eq. 3). For nonporous membranes, the permeation selectivity is also related to diffusion and solubility coefficients, D and S, respectively according to eq. 4. Because of the inverse relationship that exists between J and l (eq. 1), creating membranes as thin as possible while maintaining permeation selectivity remains a primary goal.

$$J\ (\mathrm{cm^3/cm^2\text{-}sec}) = \frac{P \cdot \Delta p}{l} \qquad (1)$$

$$\frac{P}{l}\ (\mathrm{cm^3/cm^2 \cdot s \cdot cm\ Hg}) = \frac{J}{\Delta p} \qquad (2)$$

$$\alpha_{ij} = \frac{\left(\frac{P}{l}\right)_i}{\left(\frac{P}{l}\right)_j} \qquad (3)$$

$$\alpha_{ij} = \left(\frac{D_i}{D_j}\right) \times \left(\frac{S_i}{S_j}\right) \qquad (4)$$

1. Unexpected Barrier Properties of Polyelectrolyte Multilayers.

Background and Hypothesis

In previous work, we found that certain polyelectrolyte multilayers (PEMs) show CO_2/N_2 selectivities in excess of 100. [Wang, Y.; Stedronsky, E.; Regen, S. Defects in a Polyelectrolyte Multilayer: The Inside Story, *J. Am. Chem. Soc.*, **2008**, *130*, 16510-16511; (b) Wang, Y.; Janout, V.; Regen, S. L. Creating Poly(ethylene oxide)-based Polyelectrolytes for Thin Film Construction Using an Ionic Linker Strategy. *Chem. Mater.*, **2010**, *22*, 1285-12887]**.** Such CO_2/N_2 selectivity is exceptional and, therefore, warranted more detailed investigation. Since poly(allylamine hydrochloride) was common to the different PEMs showing this behavior, and since primary amine groups are capable of enhancing the permeation of CO_2 across polymeric membranes via a facilitated transport mechanism, we were led to hypothesize that these amine groups were playing a central role.

Results

To test this hypothesis, we fabricated a series of analogous PEMs that were devoid of primary amine groups. Specifically, 14 nm-thick PEMs were prepared using **1** and **2** as complementary polyelectrolytes and an anchor layer that consisted of a Langmuir-Blodgett monolayer of **3**, which was stabilized with **2** (Figure 1). Table 1 shows typical permeance values across composite membranes made from these PEMs on supports made from poly[1-(trimethylsilyl)-1-propyne] (PTMSP). Also shown are typical permeances across the supports themselves. The high CO_2/N_2 selectivity of these membranes is in sharp contrast to their very low H_2/CO_2 selectivity. This fact, together with the fact that size difference between CO_2 (0.33 nm) and N_2 (0.36 nm) is similar to the size difference between H_2 (0.29 nm) and CO_2, implies that it is the *solubility* of CO_2 that is largely responsible for such selectivities. More specifically, the permeation of the smaller and more soluble CO_2 molecule is strongly favored over N_2 due to favorable differences in diffusivity and solubility. In contrast, a favored diffusivity of the smaller H_2 molecule is offset by the favored solubility of a larger CO_2 molecule, resulting in low H_2/CO_2 selectivity. These results further show that primary amine groups are not required for high CO_2/N_2 permeation selectivity.

TABLE 1. Barrier Properties of Polyelectrolyte Multilayers (Δp=30 psi, $10^6 P/l$ (cm^3/cm^2-s-cm Hg)

PEM	H_2	CO_2	N_2	H_2/N_2	H_2/CO_2	CO_2/N_2
-----	620	1400	260	2.4	0.44	5.4
-----	620	1500	260	2.4	0.41	5.8
1 + **2**	48	28	0.25	190	1.7	110
1 + **2**	45	19	0.18	250	2.4	110

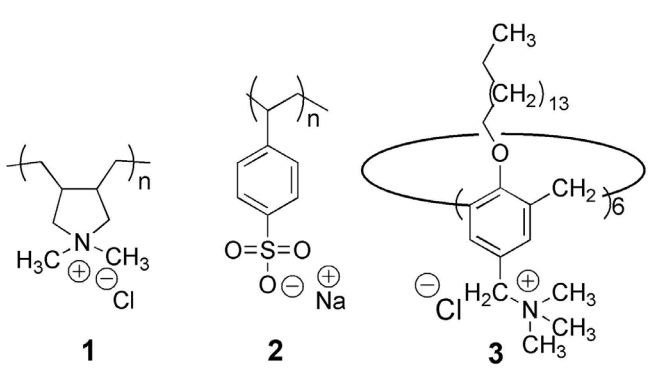

FIGURE 1. Structures of polymers and calix[6]arene-based surfactant used to fabricate PEMs and single LB bilayers.

2. Single Langmuir-Blodgett Bilayers Made from a Calix[6]arene-based Surfactant and Poly(acrylic acid).

Membrane design

In Figure 2 is shown our experimental design for hyperthin membranes that were expected to exhibit exceptional permeation selectivity based on molecular sieving. Here, a "porous surfactant" is used to form a monolayer on the surface of an aqueous subphase containing a polymeric counterion. The purpose of the polymer is to stabilize the assembly in its monolayer state and also in a corresponding Langmuir-Blodgett bilayer. If the polymeric network is sufficiently loose, the main barrier for gas transport is then expected to be the pores within the surfactants that make up each monolayer—a situation that

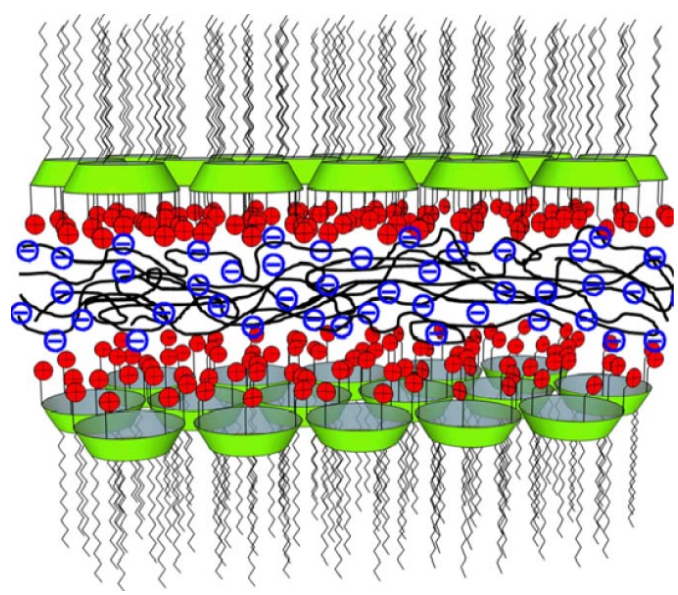

FIGURE 2. Stylized illustration of a perforated LB bilayer that has been stabilized with a polymeric counterion.

could result in molecular sieving action and exceptional size-selectivity.

Results

Single Langmuir-Blodgett bilayers containing poly(acrylic acid) (PAA) were fabricated using a pH of 3.1 and conditions similar to those previously reported (see publication #4). Table 2 summarizes the barrier properties of these membranes. In brief, significant H_2/CO_2 and CO_2/N_2 permeation selectivities were observed. The fact that these selectivities are similar implies that the permeation of all three gases is dominated by diffusion and permeant size. The slightly greater H_2/CO_2 selectivity is also consistent with a slightly greater difference in kinetic diameters between H_2 and CO_2 compared with CO_2 and N_2.

Table 2. LB Bilayer of 3/poly(acrylic acid) (Δp=30 psi, $10^6 P/l$ (cm^3/cm^2-s-cm Hg)

PEM	H_2	CO_2	N_2	H_2/N_2	H_2/CO_2	CO_2/N_2
-----	620	1400	260	2.4	0.44	5.4
-----	620	1500	260	2.4	0.41	5.8
3/PAA	5.7	0.081	0.0024	2400	70	34
3/PAA	4.0	0.054	0.0023	1700	74	23

Relationship to Existing Polymeric Membranes.

To judge the intrinsic permeability properties of these hyperthin membranes, we have employed the series resistance model. Thus, if one assumes that the resistance (i.e., the reciprocal of the permeance) of each composite membranes is equal to the sum of the resistances of the hyperthin membrane, itself, and that of the PTMSP support, then the permeance of the hyperthin membrane, $[P/l]_{ht}$, can be calculated from the equation, $1/[P/l]_{composite} = 1/[P/l]_{PTMSP} + 1/[P/l]_{ht}$. Based on the thicknesses of a given hyperthin membrane, one can then calculate its intrinsic permeability coefficient using the equation: $P_{ht} = [P/l]_{ht} \times l_{ht}$. To place these permeation properties into perspective, we have included them in "upper bound" plots for H_2/CO_2 and for CO_2/N_2 in which the permeation selectivity is plotted as a function of the permeability coefficient for the smaller gaseous permeant (not shown). Such plots have previously been constructed for a large series of polymeric membranes (Robeson, L.M. The Upper Bound Revisited. *J. Membr. Sci*., **2008**, *320*, 390-400). A straight line that can be drawn from such data then defines the highest performing polymeric membranes, and the negative slope reflects a "trade-off" between permeability and permeation selectivity; i.e., the higher selectivity the lower permeability and *vice versa*. The fact that the intrinsic barrier properties of these PEMs and LB bilayers lie *beneath this upper bound* implies that a solution-diffusion mechansim of permeation is dominant in both cases (see publications #2 and #4 for these plots).

Future Directions

The barrier properties of these hyperthin PEMs and LB bilayers that we have investigated are fundamentally different. Studies currently in progress are aimed at obtaining a deeper understanding of these differences, and at exploiting membrane solubility as a means of enhancing H_2/CO_2 and CO_2/N_2 permeation selectivities.

Publications

1. Wang, Minghui; Janout, Vaclav; Regen, Steven L. Gas Transport Across Hyperthin Membranes. *Accounts of Chemical Research,* **2013,** DOI: 10.1021/ar3002624.

2. Wang, Minghui; Janout, Vaclav; Regen, Steven L. Unexpected Barrier Properties of Structurally Matched and Unmatched Polyelectrolyte Multilayers. *Chem. Commun.,* **2013,** *49*, 3576-3578.

3. Wang, Minghui; Janout, Vaclav; Regen, Steven L. Minimizing Defects in Polymer-Based Langmuir-Blodgett Monolayers and Bilayers Via Gluing. *Langmuir*, **2012**, *28*, 4614-4617.

4. Wang, Minghui; Janout, Vaclav; Regen, Steven L. Hyperthin Organic Membranes with Exceptional H_2/CO_2 Permeation Selectivity: Importance of Ionic Crosslinking and Self-Healing. *Chem Commun*. **2011**, *47*, 2387-2389.

5. Wang, Minghui; Janout, Vaclav; Regen, Steven L. Glued Langmuir-Blodgett Bilayers From Calix[n]arenes: Influence of Calix[n]arene Size on Ionic Crosslinking, Film Thickness and Permeation Selectivity. *Langmuir*, **2010**, *26*, 12988-12993.

6. Wang, Yao; Janout, Vaclav; Regen, Steven L. Creating Poly(ethylene oxide)-based Polyelectrolytes for This Film Construction Using and Ionic Linker Strategy. *Chem. Mater*., **2010**, *22*, 1285-1287.

V.N.4 Theory-Guided Design of Nanoscale Multimetallic Nanocatalysts for Fuel Cells

Principal Investigator: Perla B. Balbuena
Texas A&M University
3122 TAMU
College Station, TX 77843,
Phone: (979) 845-3375
Email: balbuena@tamu.edu

Other team members:

- Jorge M. Seminario (Co-PI)
  Texas A&M University,
  3122 TAMU
  College Station, TX 77843
  Phone: (979) 845-3301
  Email: seminario@tamu.edu
- Graduate Students: Rafael Callejas-Tovar (graduated August 2012), Pussana Hirunsit (graduated August 2010), Gustavo Ramirez-Caballero (graduated December 2011), Julibeth M. Martinez de la Hoz
- Undergrad. students: Santosh Koirala, Birendra Adhikari, Diego F. Leon, Diego A. Guio, Wenta Liao, Hilda Mera, Ashish Mathkari, Carl Diaz
- Postdocs: Yuguang Ma and Juan Sotelo

DOE Program Manager: Raul Miranda
Phone: (301) 903-8014
Email: Raul.Miranda@science.doe.gov

Objectives

The aims of this project are: (a) characterizing the metal activity and dissolution process in alloy nanocatalysts used for the oxygen reduction reaction in acid medium and their effects on surface structure and composition during electrochemical surface oxidation and surface reduction, as a function of catalyst shape and size; (b) evaluating our hypothesis that electronic and geometric confinement are the reasons for the experimentally observed activity enhancement after the dissolution process takes place; (c) using the insights obtained from these studies to continue our efforts in the design of improved catalysts for this and other technologically relevant reactions.

Technical Barriers

The complexity of a catalytic surface constantly changing under harsh oxidative conditions poses a significant challenge for modeling and experiments.

Abstract

First-principles analyses of oxygen reduction catalysts are carried out to answer these questions: 1) How do the catalytic surface and its environment change as the reaction takes place, and how do these changes affect the activity and stability of the catalyst; 2) What are the effects of the dynamics of the catalyst and that of the surrounding medium on the catalytic activity and stability; and 3) What is the effect of important side reactions on the catalytic process?. We use a concerted multiscaled theoretical analysis of nanoscale multi-metallic catalysts including their environment. Our computational approach is directly applicable to other catalytic reactions taking place on nanoscale particles.

Progress Report

Surface segregation effects in alloy nanoparticles

A systematic study as a function of core composition starting with monometallic cores of the 3d, 4d, and 5d groups revealed that all the 4d and 5d pure cores may serve as stable cores, and their beneficial effect on the Pt monolayer may be further tuned by alloying the core to another element, here chosen from 3d or 5d groups. The Pd_3X cores enhance the stability of the surface Pt atoms both in vacuum and under adsorbed oxygen; however the high oxygen-philicity of some of the X elements induces their surface segregation causing surface poisoning with oxygenated species and dissolution of the X metals in acid medium.

Evolution of nanocatalyst surface under oxidation and reduction conditions

Buckling of surface Pt atoms is known to occur at high oxygen coverage on pure Pt and alloy surfaces. We developed a novel multi-scale modeling approach where we mimic the oxidation process of extended surfaces of pure Pt and Pt-alloys as a function of increasing oxygen coverage, yielding the time evolution of the surface at a given extent of oxidation. Such oxidation is given by various oxygenated species such as atomic oxygen and water dissociation products. The pH effect is also incorporated. We used the DFT results in force fields for classical MD simulations able to follow the evolution of the catalyst structure and dynamics in slabs and nanoparticles. In our most recent work, we developed a new approach integrating DFT and MD simulations to evaluate the degradation of alloy catalysts at harsh oxidation conditions. Our approach is able to reveal migration of O atoms into the subsurface and that of non-

noble atoms towards the surface, detachment and interactions with solvent and ionic species at the interface of the metal catalyst and the electrolyte. We characterized such catalytic degradation in extended surfaces and nanoparticles in acid medium.

Effects of geometric and electronic confinement on catalytic reactions

We investigated the origins of the enhanced catalytic activity found in nanoporous structures after dealloying. The proximity of two transition-metal surfaces separated by a subnanometer gap gives rise to new chemistry that could be potentially useful for enhanced reactivity in catalysis, separations, and sensing processes. Depending on the nature of the interacting surfaces, confined adsorbates may be strongly adsorbed, dissociated, or reacted with other species. Separation of mixed gases or liquids could be obtained by appropriately tuning the composition of the alloy surfaces and the gap geometry. Furthermore, the importance of local atomic disorder on reactivity has been pointed out based on X-Ray absorption spectroscopy experiments.

Recently we have studied the activity improvement on the dissociation of molecular oxygen confined between Pt surfaces separated by subnanometer distances. We found that at certain Pt surface-surface separation, the dissociation of molecular oxygen is spontaneous. We also studied interactions of X/Pt skin surfaces where X is a monolayer of a 3d, 4d, or 5d metal. In this case, the effect of the separation distance between X/Pt surfaces was analyzed in relation to the dissociation of molecular oxygen and water. It was found that the electronic structure of skin surfaces under confinement changes with respect to that of a single surface, becoming more active for catalysis. Changes in the electronic structure of the confined skin surfaces can be detected through other physical properties such as magnetic moments. The influence of the overlayer metal nature on these phenomena offers the possibility of designing specific materials for targeted catalytic applications by manipulation of control variables, such as the surface-surface separation between the skin surfaces but also the composition of the composite system. For example, the interaction between Ti/Pt surfaces separated by a small gap in the order of 0.4 to 0.8 nm facilitates the creation of an enhanced electron density in the gap between surfaces inducing the formation of an ethylene radical that readily reacts with another ethylene radical and starts polymerization without the need of an initiator. These examples illustrate the potential effect of confinement on the ORR. Many other intermediate steps such as coupled proton and electron transfers to the oxygenated species could be equally affected by geometric and electronic confinement. We investigate such effects in porous metallic structures. We found that the experimentally measured activity enhancement may result from the geometric and electronic confinement resulting from the nanoporous structure originated after the dealloying process. We carried out a systematic plan to verify our hypothesis and investigated additional details that can be applied to a more general class of catalytic processes. Results include density functional theory analysis of reactions occurring in metallic porous structures; Kinetic Monte Carlo simulations of the dealloying process; and formation of porous structures emulating synthesis processes and also emulating dealloying occurring during fuel cell operation, i.e., under oxygenated environments.

Future Directions

The results of these investigations indicate that the main lines of research that would be most promising for fuel cell electrocatalysis remain centered in the design of **active** and especially **durable** catalysts. Our experience with theoretical analyses of these systems points to the main topics that we suggest as future research directions: 1) design of the optimum alloy composition that could be used as a core under a Pt thin layer acting as a catalyst; 2) design of the best nanoarchitectures that could make such alloy compositions resistant to the acid (or alkaline) medium where the ORR takes place; 3) incorporate the effect of the substrate which, in nanosystems, can make a huge difference for supported catalysts.

Publication list (including patents) acknowledging the DOE grant or contract

1. Javier, A., Li, D., Balbuena, P.B., and Soriaga,M.P. "Simulation of scanning tunneling microscope image of benzene chemisorbed on a Pd(111) electrode surface by density functional theory," *Reports in Electrochemistry*, 2013, *3*, 1-5.

2. Martinez de la Hoz, J.M. and Balbuena, P.B. "Local surface structure effect on reactivity of molecules confined between metallic surfaces," *Phys. Chem. Chem. Phys.,* 2013, *15* (5), 1647-1654.

3. Callejas-Tovar, R., Diaz, C.A., Martinez de la Hoz, J.M., and Balbuena, P.B. "Dealloying of Platinum-Based Alloy Catalysts: Kinetic Monte Carlo Simulations," *Electrochim. Acta*, 2013, in press, http://dx.doi.org/10.1016/j.electacta.2013.01.053.

4. Callejas-Tovar, R. and Balbuena, P.B. "Effect of Metal Porosity on Oxygen Reduction Reaction Activity*," J. Phys. Chem. C*, 2012, *116*, 14414-14422.

5. Javier, A., Kim, J-G, Baricuatro, J.H., Balbuena, P.B., and Soriaga, M.P. "Adsorption structure of benzoquinone on Pd(111) surfaces: A study by density functional theory," *Electrocatalysis*, 2012, *3*, 353-359, DOI 10.1007/s12678-012-0110-5.

6. Ramirez-Caballero, G.E., Martinez de la Hoz, J.M., and Balbuena, P.B. "p-n Junction at the Interface between Metallic Systems," *J. Phys. Chem. Lett.*, 2012, *3*, 818-825.

7. Balbuena, P.B., Callejas-Tovar, R., Hirunsit, P., Martínez de la Hoz, J.M. Ma, Y. and Ramírez-Caballero, G.E., "Evolution of Pt and Pt-alloy catalytic surfaces under oxygen reduction reaction in acid medium," *Top. Catal.,* 2012, *55*, 322-335.

8. Callejas-Tovar, R., Liao, W., Mera, H., and Balbuena, P.B. "Molecular dynamics simulations of surface oxidation on Pt and Pt/PtCo/Pt3Co nanoparticles supported over carbon," *J. Phys. Chem. C*, 2011, *115*, 23768-23777.

9. Martinez de la Hoz, J.M., and Balbuena, P.B., "Geometric and electronic confinement effects on catalysis," *J. Phys. Chem. C*, 2011, *115*, 21324-21333.

10. Callejas-Tovar R., and Balbuena, P.B. "Molecular dynamics simulations of surface oxide-water interactions on Pt(111) and Pt/PtCo/Pt3Co(111)," *Phys. Chem. Chem. Phys*., 2011, *13*, 20461-20470.

11. Ramírez-Caballero G.E., and Balbuena, P.B. "Confinement-induced changes in magnetic behavior of a Ti monolayer on Pt," *Chem. Phys. Lett*.., 2011, *507*, 117-121.

12. Javier, A.C., Kim, Y.G. Soriaga, J.B., Balbuena, P.B., and Soriaga,M.P. "STM and DFT studies of anion adsorption at well-defined surfaces: Pd(111) in sulfuric acid solution" *Phil. Sci. Lett.* 2011, *4*, 18-23.

13. Callejas-Tovar, R., Liao, W., Martinez de la Hoz, J.M., and Balbuena, P.B. "Molecular dynamics simulations of surface oxidation on Pt(1 1 1) and Pt/PtCo/Pt3Co(1 1 1)" *J. Phys. Chem C*., 2011, *115*, 4104-4113.

14. Ramirez-Caballero, G., Mathkari, A., and Balbuena,P.B., "Confinement-induced polymerization of ethylene," *J. Phys. Chem C*., 2011, *115*, 2134-2139.

15. Callejas-Tovar R. and Balbuena, P. B. "Understanding Activity and Durability of Core/Shell Nanocatalysts for Fuel Cells", in M. Shao (Ed.) "Electrocatalysis in Fuel Cells", *Lecture Notes in Energy* 2013, *9*, DOI 10.1007-1-4471-4911-8_20, Springer Verlag, London.

16. Callejas-Tovar, R., Liao, W., Martinez de la Hoz, J.M., and Balbuena, P.B., "Modeling oxidation of Pt-based alloy surfaces for fuel cell cathode electrocatalysts," Royal Society of Chemistry, *Catalysis Books Series*, 2012, Vol. 24, J.J. Spivey and M. Gupta, Eds., 323-357.

V.N.5 Structure-Property Relationship in Metal Carbides and Bimetallic Alloys

Principal Investigator: Jingguang Chen
Department of Chemical Engineering
Columbia University
Phone: (212) 854-6166
Email: jgchen@columbia.edu

DOE Program Manager: Raul Miranda
Email: Raul.Miranda@science.doe.gov

Objectives

The main objective of the current DOE-sponsored research is to correlate the structure-property relationship in metal carbides and bimetallic alloys, with the aim of replacing or substantially reducing the loading of Pt-group metals in catalysis and electrocatalysis. It is well known that the electronic and catalytic properties of transition metals can be modified by alloying either with carbon to form carbides or with another metal to produce bimetallic alloys. The carbide and bimetallic materials are excellent model systems to demonstrate the feasibility of tuning the catalytic activity, selectivity, and stability as alternative electrocatalysts to replace Pt-group metal catalysts.

Technical Barriers

Fuel cells, electrolyzers, and photoelectrochemical cells are electrochemical devices that are commonly regarded as core technologies in a clean energy future. Central to the operation of all of these devices are electrocatalysts, which mediate charge transfer processes between the electrolyte and device electrodes with minimal losses in efficiency. Unfortunately, many state of-the-art catalysts used in these technologies are comprised of expensive Pt-group metals. The high prices and limited supplies of these precious metals create potentially prohibitive barriers to market penetration and scale-up production of devices requiring large catalyst loadings.

Abstract

In the current presentation we will discuss the utilization of metal-modified carbides as potentially low-cost electrocatalysts for several reactions, including hydrogen evolution reaction (HER) and alcohol oxidation. For example, by depositing one monolayer (ML) of Pt on a tungsten monocarbide (WC) substrate, the ML Pt/WC electrocatalysts show similar HER activity as bulk Pt, demonstrating the possibility of significantly reducing the Pt loading. The Pt/WC catalyst also shows enhanced CO-tolerance over Pt for alcohol oxidation. We will also present our recent results on alternative electrocatalysts using other monolayer metals (Pd, Cu) and on other metal carbide substrates (W_2C, Mo_2C, and TiC).

Progress Report

When powered by renewable energy sources, such as wind- or solar-based technologies, the generation of hydrogen from the electrolysis of water represents a means to produce a high energy density, mobile energy carrier without any associated carbon dioxide emissions. At low temperatures, this process can take place in a variety of electrochemical devices ranging from high-current density polymer electrolyte membrane (PEM) electrolyzers to low-current density, solar-driven photoelectrochemical cells (PECs). For all of these water-splitting applications, the choice of the HER catalyst employed at the cathode can have a profound influence on the cost, lifetime, and efficiency of the device. Pt is a very active and commonly used HER catalyst, but its high cost and limited world-wide supply make its use a barrier to mass production of H_2 by water electrolysis. One approach to overcoming the challenges associated with Pt HER catalysts is to increase the surface to bulk atomic ratio of Pt, allowing for a lower metal loading to be used without compromising electrolysis efficiency. At present Pt electrocatalysts are typically in the form of supported nanoparticles, in which most Pt atoms are located within the particle core where they are screened from being involved in the electrochemical reaction. During the past funding cycle we explored the lower limit of Pt loading by utilizing nearly all Pt atoms in the form of an atomic layer, or monolayer (ML), on low-cost tungsten monocarbide (WC) and other carbide substrates. Although Pt is still utilized, this ML Pt-WC electrocatalyst structure approaches the lower limit of Pt loading. By using a low cost support material such as WC, the ML Pt-WC structure offers great potential to drive down catalyst costs for various clean technology devices.

The main reason for choosing WC as the substrate is largely due to the fact that WC often shows “Pt-like” properties, as demonstrated by both our group and other researchers. There is a general agreement in the literature that WC has similar bulk electronic properties to Pt, but there is notable deviation in surface properties. These differences in surface electronic properties, which ultimately determine how a surface interacts with reactants, are small enough to translate into similar catalytic behavior for some reaction systems, but not for others, including most electrochemical applications. During the past funding cycle we have attempted to overcome the short-comings of pure WC

catalysts by modifying the WC surface with ML amounts of Pt. The hypothesis is that replacement of all but the top ML of bulk Pt catalysts with an electronically similar "Pt-like" WC core will result in a ML Pt-WC surface that should have electronic and catalytic properties more similar to Pt than WC. The significance of this concept is that it predicts that ML Pt-WC will exhibit catalytic activity that is comparable, though not identical, to bulk Pt catalysts while making full use of every Pt atom. A further expectation that follows from the similar electronic properties of Pt and WC is that they should intuitively result in good adhesion between the Pt ML and WC surface, suppressing the tendency for the Pt ML to agglomerate into bulk Pt particles that would lead to a reduction in catalytic activity.

In order to probe the electronic similarities of ML Pt-WC and bulk Pt catalysts, DFT calculations were used to determine the binding energies of reactant molecules that are relevant to key electrochemical applications. For example, we compared the binding energies for hydrogen (relevant to HER activity), oxygen (relevant to the oxygen reduction reaction (ORR) activity of polymer electrolyte membrane fuel cells), and methoxy (related to the direct methanol fuel cell (DMFC) activity) for Pt(111), WC(0001), and ML Pt-WC(0001) surfaces. These binding energies are chemical descriptors that are related to the HER, ORR, and DMFC activities, respectively. Previous work has shown that the hydrogen, oxygen, and methoxy binding energies all correlate strongly with the surface d-band density of states (DOS). It is well known that the distribution of the surface d-band DOS, approximated by the d-band center, plays a crucial role in determining how a surface interacts with adsorbed atoms and molecule. Our results show that the bare WC(0001) surface binds all three adsorbates much more strongly than Pt(111), but modification of the WC(0001) surface with 1 ML of Pt shifts all three binding energies to values that are similar to Pt. For the most simple adsorbates, hydrogen and oxygen, the calculated binding energies on ML Pt-WC(0001) are nearly identical to Pt(111), suggesting that ML Pt-WC should show similar HER and ORR activities to Pt. In comparison, it is seen that there is still a notable difference in the binding energy of the slightly more complex methoxy intermediate, suggesting different DMFC activity for ML Pt-WC and Pt. These predictions have been verified experimentally in our subsequent studies.

Based on DFT predictions of similar hydrogen binding energy on ML Pt-WC(0001) and Pt(111), we have evaluated the activity of ML Pt-WC for HER, which is the cathodic reaction that produces $H_{2(g)}$ during water electrolysis and is one of the most fundamental and commonly studied electrochemical reactions. To test these predictions, the HER activity of sub-ML to ML amounts of Pt on WC thin films was compared to a Pt foil sample by carrying out linear sweep voltammetry in 0.5 M H_2SO_4 at room temperature. Our results show that the HER activity of the bare WC surface is much lower than that of the Pt foil, but the addition of one ML of Pt to WC results in a surface with HER activity comparable to the bulk Pt foil. This finding is in excellent agreement with DFT predictions based on the expected correlation between hydrogen binding energy and HER activity, and demonstrates the potential of using ML Pt-WC to drastically decrease Pt loading for the HER application. Furthermore, the ML Pt-WC surfaces show excellent stability due to the strong binding between surface Pt atoms and the WC substrate.

In order to extend the promising results on thin films to real world applications, it is important to synthesize and evaluate core-shell Pt-WC catalysts in the powder form. The synthesis of ML Pt-WC powder catalysts is challenging, and until our recent study no established methods exist. Physical vapor deposition (PVD) has been shown to successfully produce monolayers on planar substrates, but PVD is a line-of-sight technique, and therefore, not applicable to particle substrates. To demonstrate the proof-of-principle, we explored the atomic layer deposition (ALD) of Pt over WC particles. The HER activity of the resulting core-shell Pt-WC particles was evaluated using similar methods for the thin film catalysts. Our results show that, as Pt coverage on WC increases to an equivalent of 1 ML, the value for HER activity of Pt-WC approaches that of 10 wt% Pt/C. Although an ideal single ML of Pt is not produced on the WC powder using ALD, the presence of a thin Pt layer on the WC substrate is sufficient to achieve HER activities that are comparable to the conventional Pt/C catalysts. The Pt wt% for each of the ALD Pt-WC catalysts was determined from atomic absorption spectroscopy (AAS) measurements. The Pt loading in the Pt-WC sample is determined to be about a factor of ten less than the 10 wt% Pt/C catalyst, confirming the possibility of substantially reducing the Pt loading while achieving HER activity similar to pure Pt catalysts.

In addition to the ML Pt/WC catalysts, several other metal-carbide modified systems, including ML Pt on W_2C, Mo_2C and TiC, have been evaluated for HER activity. These results demonstrate the possibility of extending knowledge learned from WC to other metal carbide substrates.

Future Directions

We plan to further unravel the structure-property relationship in carbide and metal-modified carbide catalysts, with a special focus on the fundamental understanding of using metal-modified carbides as electrocatalysts. We plan to search for metal-modified carbides as efficient electrocatalysts, using combined theoretical and experimental approaches to identify descriptors for predicting HER catalysts; the promising metal-modified carbides will also be evaluated for HER activity and stability in the presence of impurity ions that are typically present in tap water. We will also explore the utilization of metal-modified carbides as electrocatalysts for CO_2 reduction based on our hypothesis that the CO-tolerant nature of metal-modified carbides should

make them more active and stable than currently leading Pt- and Cu-based electrocatalysts.

Selected publications acknowledging the current DOE grant

1. Sheng, W., Myint, M., Chen, J.G. and Yan, Y., "Correlating Hydrogen Evolution Reaction Activity in Alkaline Electrolyte to Hydrogen Binding Energy on Monometallic Surfaces", *Energy & Environmental Science*, (2003) DOI:10.1039/C3EE00045A.

2. Lu, Q., Chen, J.G., and Xiao, J.Q., "Design Nanostructured Electrodes for High-performance Supercapacitors", *Angewandte Chemie International Edition*, 52 (2013) 1882-1889.

3. Esposito, D.V., Hunt, S.T., Kimmel, Y.C., and Chen, J.G. "A New Class of Electrocatalysts for Hydrogen Production from Water Electrolysis: Metal Monolayers Supported on Low-Cost Transition Metal Carbides", *Journal of the American Chemical Society*, 134 (2012) 3025-3033.

4. Kelly, T.G., and Chen, J.G., "Metal Overlayer on Metal Carbide Substrate: Unique Bimetallic Properties for Catalysis and Electrocatalysis", *Chemical Society Reviews*, 41 (2012) 8021-8034.

5. Stottlemyer, A.L., Kelly, T.G., Meng, Q., and Chen, J.G., "Reactions of Oxygen-Containing Molecules on Transition Metal Carbides: Surface Science Insight into Potential Applications in Catalysis and Electrocatalysis", *Surface Science Reports*, 67 (2012) 201-232.

6. Esposito, D.V., Forest, R.V., Chang, Y., Hou, S., McCandless, B.E., Gaillard, N., Lee, K.H., Birkmire, R.W. and Chen, J.G., "Photoelectrochemical Reforming of Glucose to Produce H_2 using a WO_3-based Tandem Cell Device", *Energy & Environmental Science*, 5 (2012) 9091-9099.

7. Hsu, I.J., Kimmel, Y.C., Willis, B.G., and Chen, J.G. "Atomic Layer Deposition Synthesis of Platinum-Tungsten Carbide Core-Shell Catalysts for Hydrogen Evolution", *Chemical Communications*, 48 (2012) 1063-1065.

8. Esposito, D.V., and Chen, J.G., "Monolayer Platinum Supported on Tungsten Carbides as Low-Cost Electrocatalysts: Opportunities and Limitations", *Energy & Environmental Science*, 4 (2011) 3900-3912.

9. Bosco, J.P., Sasaki, K., Sadakane, M., Ueda, W., and Chen, J.G., "Synthesis and Characterization of Three-Dimensionally Ordered Macroporous (3DOM) Tungsten Carbide: Application to Direct Methanol Fuel Cells", *Chemistry of Materials*, 22 (2010) 966-973.

10. Hansgen, D.A., Vlachos, D.G., and Chen, J.G, "First Principles-Based Bimetallic Catalyst Selection: An Application to the Ammonia Decomposition Reaction", *Nature Chemistry*, 2 (2010) 484-489.

11. Weidman, M.C., D.V. Esposito, D.V. and J.G. Chen, J.G., "The Electrochemical Properties of Tungsten and Tungsten Monocarbide (WC) Over Wide pH and Potential Ranges", *Journal of the Electrochemical Society*, 157 (2010) F179-F188.

12. Esposito, D.V., Hunt, S.T., Stottlemyer, A.L., Dobson, K.D., McCandless, B.E., Birkmire, R.W., and Chen, J.G., "Low-Cost Hydrogen Evolution Catalysts Based on Monolayer Platinum on Tungsten Monocarbide (WC) Substrates", *Angewandte Chemie International Edition*, 49 (2010) 9859-9862.

V.N.6 Nanostructured Catalysts for Hydrogen Generation from Renewable Feedstocks

Principal Investigator: Abhaya Datye
University of New Mexico (UNM)
Dept. of Chemical & Nuclear Engineering
MSC 01 1120
Albuquerque, NM 87131-0001
Email: datye@unm.edu

Co-Principal Investigator:
Yong Wang
Washington State University (WSU), Pullman, WA and
Pacific Northwest National Laboratory (PNNL)
902 Battelle Boulevard, P.O. Box 999
Richland, WA 99352
Email: yongwang@pnl.gov

Names of Team Members
Post-docs:
Zhang He (WSU), Junming Sun (WSU), Barr Halevi (UNM)
Graduate Students:
Jonathan Paiz (UNM), Angelica Benavidez (UNM),
Eric Petersen(UNM), Stephen Davison (WSU),
Yongchun Hong (WSU)
Undergrad Students:
Johnny Nogales, Aaron Jenkins, Monique Cordova
(all UNM).

Collaborators:
- Robert Schloegl, Fritz Haber Institute, Berlin, Germany.
- Timothy Boyle, Sandia National Laboratories
- Boris Kiefer, New Mexico State University
- Hua Guo, University of New Mexico, Dept. of Chemistry
- Corey Leclerc, New Mexico Tech
- Donghai Mei, Ayman Karim, Chuck Peden, and Ja Hun Kwak, PNNL
- Jean-Sabin McEwen, WSU
- Jeff Miller, Argonne National Laboratory
- Eric Stach and Dong Su, Center for Functional Nanomaterials, BNL

DOE Program Manager: Raul Miranda
Phone: (301) 903-8014
Email: Raul.Miranda@science.doe.gov

Objectives

The research program is directed towards the development of highly active and selective catalysts for the production of hydrogen from renewable alcohols. The objective is to gain fundamental understanding of complex, multi-component catalysts through an investigation of catalytic processes occurring on system sub-components (the metal phase and the support) and synergistic interactions among the catalyst system components. To facilitate the mechanistic and reaction studies, we synthesize catalysts that are well-defined: single phase, uniform composition metallic alloy powders. We also synthesize oxides of controlled morphology that expose well-defined single facets so that the role of the oxide phase can be studied. These catalysts are studied using novel analytical approaches including the use of in-situ microscopy and spectroscopy techniques.

Technical Barriers

Selective catalysts are increasingly multifunctional, and involve synergistic contributions from several components, including the catalyst support. The goal of achieving the ultimate performance in activity and selectivity demands control of particle size, composition, and achieving desired atomic connectivity, and structure in the catalytically active sites. Unraveling the contributions of each of these components in industrial catalysts is challenging because of the inherent heterogeneity of these catalysts. It is therefore necessary to find an approach that bridges the gap between the well-defined model catalysts used in surface science experiments and those that can be tested in a conventional flow reactor under industrially relevant conditions.

Abstract

Work carried out during this second year of the 3-year project renewal period continues to build on insight gained in the first year of this project, focusing on understanding the role played by ZnO as a promoter. Base metals (e.g., Co) and precious metals are active in C-C bond cleavage of ethanol, with metal oxide (e.g., ZrO_2, ZnO, CeO_2, etc) supported Co catalysts being less selective to CH_4 than precious metal catalysts. However, supported Co catalysts are prone to rapid deactivation, thus limiting their potential applications. On supported cobalt catalysts we have learnt that addition of the ZnO improves the selectivity towards CO_2 and suppresses methane formation. Although the mechanisms of CH_4 formation and catalyst deactivation are not fully understood yet, it is speculated that high oxygen mobility throughout the oxide support can facilitate the oxidation of CHx species formed from C-C bond cleavage of ethanol, leading to reduced CH_4 formation and improved catalyst life. Our work on aerosol synthesis has helped in generating single phase metal alloys in the PdZn system, allowing us to determine the role of phase and composition on reactivity for methanol steam reforming. In steam reforming of ethanol, we find that addition of Zn leads to improved H_2 yield in PdZn catalysts. Finally, we have learnt that isolated single atoms of Pd on

alumina show exceptionally high activity for CO oxidation. We highlight two of the projects we have carried out this past year.

Progress Report

Steam Reforming of Acetone

The formation of acetone in ethanol steam reforming (ESR) and its oligomerization on the acidic/basic sites of the oxide support and the subsequent carbon deposition (mainly as filaments) on the active sites responsible for H2O dissociation can result in insufficient oxygen-mobility, which causes catalyst deactivation under practical operating conditions. Therefore, acetone steam reforming (ASR) was studied to elucidate the detailed mechanisms on Co nanoparticles and to enable the rational design of highly active, selective, and stable catalysts for steam reforming of biomass-derived oxygenates. Co nanoparticles (~5 nm) were synthesized on an inert support (graphitized activated carbon) without addition of promoter to minimize the complications by either support and/or promoter. On the basis of experimental mechanistic investigations and theoretical understanding of the full reaction mechanism with density functional theory (DFT) calculations, we elucidated that Co nanoparticles (~5 nm) play dual roles of cleaving C-C bond of acetone while efficiently dissociating H2O to oxidize CHx* and C*. As a result, inert activated carbon-supported Co nanoparticle catalysts are very selective and stable for hydrogen production via ASR (Figure 1). The high selectivity is attributed to: 1) the facile C-H bond scission relative to the C-C bond cleavage of acetone suppresses the formation of CH3* species that lead to methane (Figure 2); 2) the hydrogenation of CHx* species has a higher barrier than dehydrogenation; and 3) the facile H2O dissociation resulting in a higher water-gas-shift activity. On the other hand, the factors responsible for the exceptional catalyst stability are: 1) enhanced oxygen mobility by facile water dissociation on the cobalt nanoparticles (~5 nm); and 2) the lack of acid/base sites on the inert support. This work suggests that acetone, either formed as a by-product or present as a reactant, can be selectively steam-reformed to produce hydrogen without the catalyst deactivation issue as previously reported in the literature. Our fundamental understanding of the nature of Co nanoparticles further provides the insight into the rational design of catalysts for steam reforming of biomass-derived oxygenates with minimized formation of coke and methane.

CO oxidation on Pd/La-alumina

In recent work on Pd/La-alumina automotive exhaust catalysts, there was evidence suggesting that lanthana, which is used to stabilize gamma alumina, may play a role in improved CO oxidation reactivity. Fig 3 shows the light off curve for CO oxidation on Pd/alumina and on Pd/La-alumina. We investigated the origins of this enhanced CO oxidation

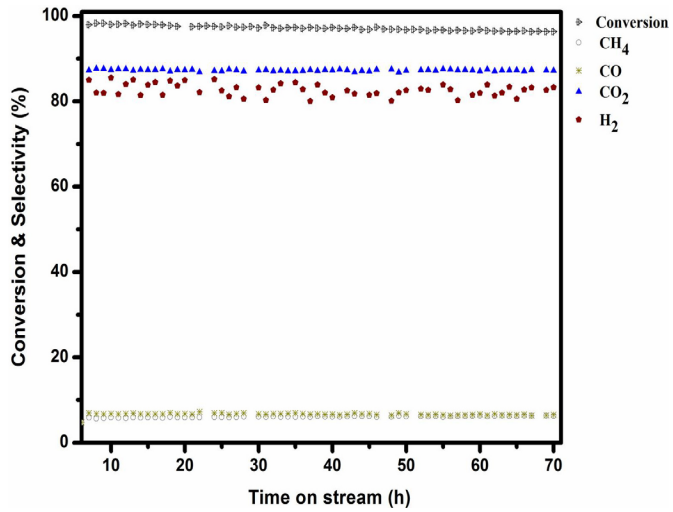

FIGURE 1. Co/C catalyst durability test during ASR (20 mg, 7.8 mol% C, steam/carbon=5, W/F= 0.094 g.s. STP mL-1, T= 450°C). With the high space velocity and acetone partial pressure, at a conversion below 100%, no observable deactivation was found after 70 hrs time on stream operation.

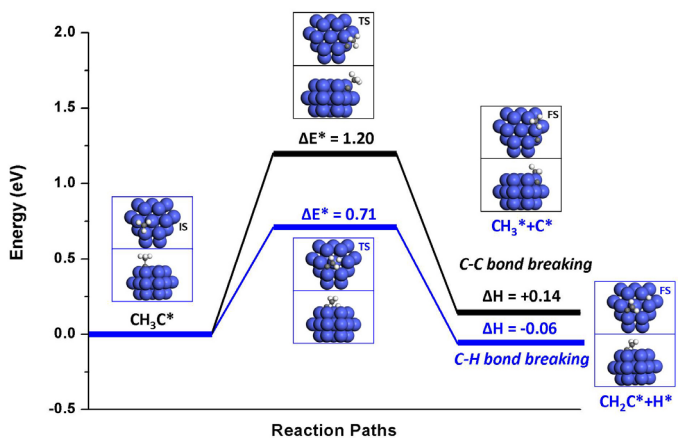

FIGURE 2. The C-H bond-breaking of CH_3C^* is more favorable than the C-C bond-breaking, indicating the CH_3 formation is least likely.

activity via EXAFS, XANES, FTIR and via HAADF STEM. It was found that the La-alumina support had smaller Pd particles than on Pd/alumina. More important, the Pd particles on La-alumina showed facile oxidation behavior, hence they allowed O_2 to compete with CO allowing for the onset of low temperature oxidation. Figure 4 shows a schematic of our observations.

To further investigate the reactivity of these Pd catalysts, we studied these catalysts via Aberration Corrected (AC) STEM. Fig. 5 shows how PdO was seen after heating the catalyst at 140°C, a temperature where we would only expect metallic Pd. These STEM images confirm the facile redox behavior of Pd that was also seen by FTIR of adsorbed CO. These images also provide evidence for existence of

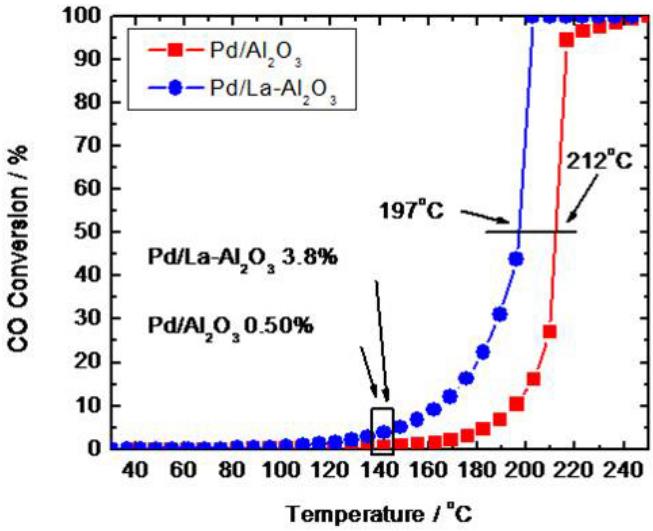

FIGURE 3. CO oxidation reactivity on Pd/alumina and Pd/La-alumina. The box shows % conversion at 140°C.

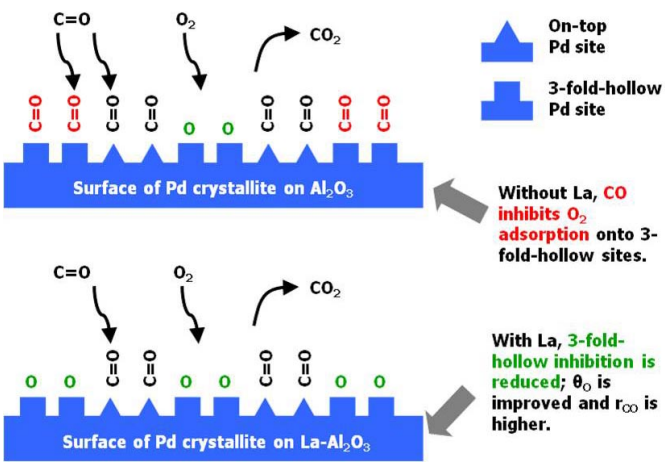

FIGURE 4. Schematic showing the observed behavior of Pd/La-alumina that leads to enhanced CO oxidation at 140°C.

atomically dispersed species, which we have confirmed to be La atoms as well as Pd atoms. To study the CO oxidation reactivity of the atomically dispersed species, we prepared a catalyst containing 0.5 wt% Pd. We saw a low onset temperature for reaction with significant CO oxidation reactivity at 60 °C. While the low onset temperature can also be seen on Pd/alumina, the Pd/La-alumina is much more stable. These results show that atomically dispersed Pd species can be stable and show high reactivity even on a non-reducible support like alumina. Understanding the conditions that lead to the stability of these isolated atoms of Pd should pave the way for future work on tapping the potential of atomically dispersed species in heterogeneous catalysis. It will also help us bridge the gap between homogeneous and hetergeneous catalysts.

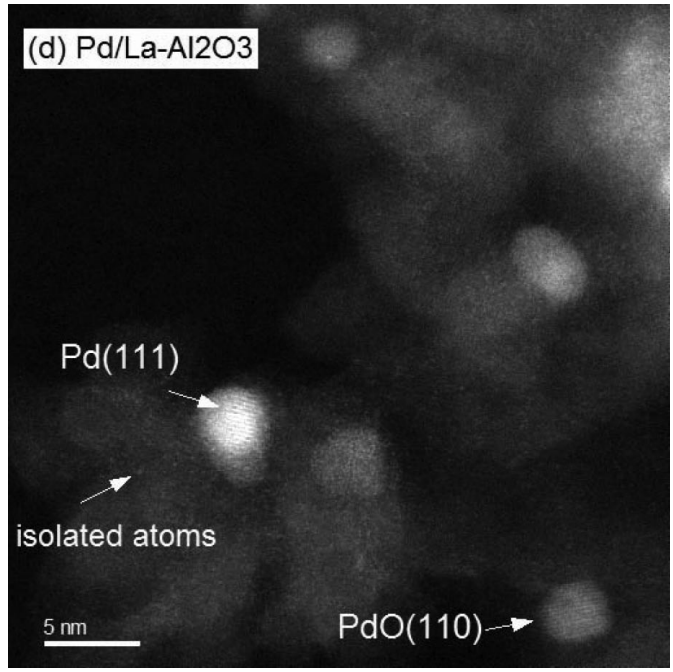

FIGURE 5. AC-STEM image of 2.5 wt% Pd/La-alumina. We see the presence of PdO in these catalysts at low temperatures. The facile oxidation of Pd helps explain the enhanced low temperature reactivity for CO oxidation.

Future Directions

We will continue our work on alcohol reforming for hydrogen production using aerosol derived model catalysts as well as supported catalysts. In-situ studies of phase evolution of bimetallic catalysts will be carried out using model supported catalysts. We plan to complete our studies of CO oxidation on atomically dispersed Pd and move on to other reactions where the dispersed Pd may provide enhanced reactivity.

Publication list acknowledging the DOE grant since the last annual report

1. Z. Wei, J. Sun, H. Zhang, Y. Li, A.K. Datye and Y. Wang, "Bimetallic nanocatalysts for hydrogen generation", *Chem.Soc. Review* 2012, Chemical Society Reviews, 41 (2012) 7994-8008

2. B. Halevi, E.J. Peterson, A. Roy, A. Delariva, E. Jeroro, F. Gao, Y. Wang, J.M. Vohs, B. Kiefer, E. Kunkes, M. Hävecker, M. Behrens, R. Schlögl, A.K. Datye, Catalytic reactivity of face centered cubic PdZn α for the steam reforming of methanol, Journal of Catalysis, 291 (2012) 44-54.

3. B. Halevi, S. Lin, A. Roy, H. Zhang, E. Jeroro, J. Vohs, Y. Wang, H. Guo, A.K. Datye, High CO_2 Selectivity of ZnO Powder Catalysts for Methanol Steam Reforming, The Journal of Physical Chemistry C, 117 (2013) 6493-6503.

4. J.R. Gaudet, A. de la Riva, E.J. Peterson, T. Bolin, A.K. Datye, Improved Low-Temperature CO Oxidation Performance of Pd Supported on La-Stabilized Alumina, ACS Catal., 3 (2013) 846-855.

5. J. Sun, D. Mei, A. Karim, A. Datye, Y. Wang, "Minimizing the formation of coke and methane on Co nanoparticles in steam reforming of biomass-derived oxygenates", *ChemCatChem*. DOI:10.1002/cctc.201300041.(cover page June 2013 issue).

6. R.S. Johnson, A. DeLaRiva, V. Ashbacher, B. Halevi, C.J. Villanueva, G.K. Smith, S. Lin, A.K. Datye, H. Guo, The CO oxidation mechanism and reactivity on PdZn alloys, Physical Chemistry Chemical Physics, (2013) in press.

7. S. Davidson, J. Sun, Y.Wang, "Ethanol steam reforming on Co/CeO_2: the effect of ZnO promoter", *Topics in Catalysis* (2013) (in press).

8. A.D. Benavidez, L. Kovarik, A. Genc, N. Agrawal, E.M. Larsson, T.W. Hansen, A.M. Karim, A.K. Datye, Environmental transmission electron microscopy study of the origins of anomalous particle size distributions in supported metal catalysts, ACS Catal., 2 (2012) 2349-2356.

9. B. Roy, U. Martinez, K. Loganathan, A.K. Datye, C.A. Leclerc, Effect of preparation methods on the performance of Ni/Al2O3 catalysts for aqueous-phase reforming of ethanol: Part I-catalytic activity, *International Journal of Hydrogen Energy*, 37 (2012) 8143-8153.

10. B. Roy, K. Artyushkova, H.N. Pham, L. Li, A.K. Datye, C.A. Leclerc, Effect of preparation method on the performance of the Ni/Al 2O3 catalysts for aqueous-phase reforming of ethanol: Part II-characterization, *International Journal of Hydrogen Energy*, 37 (2012) 18815-18826.

11. J. Sun, A.M. Karim, H. Zhang, L. Kovarik, Z. Wei, X.Li, Y. Wang, "Vapor phase hydrodeoxygenation of guaiacol on carbon supported metal catalysts", *Journal of Catalysis* (in press).

V.N.7 Fundamental Structure/Property Studies of Gas Separation Membrane Polymers

Principal Investigator: Benny D. Freeman
Department of Chemical Engineering
University of Texas at Austin
Center for Energy and Environmental Resources
10100 Burnet Road, Building 133
Austin, TX 78758
Phone: (512) 232-2803, Fax: (512) 232-2807
Email: freeman@che.utexas.edu

Names of Team Members:
Zachary P. Smith (zachary@che.utexas.edu),
David F. Sanders (sanders@che.utexas.edu),
Kevin A. Stevens (kstevens@che.utexas.edu),
Qiang Liu (qianglit@che.utexas.edu)
The University of Texas at Austin
10100 Burnet Road, Building 133
Austin, TX 78758
Phone: (512) 232-2802

DOE Program Manager: Larry A. Rahn
Phone: (301) 903-2508
Email: Larry.Rahn@science.doe.gov

Objectives

Refinery, petrochemical, and natural gas industries, in particular, offer large opportunities for membranes, but they could benefit from more robust, higher performance membrane materials. The overarching goal of this fundamental, experimental research program is to systematically synthesize, characterize, and, ultimately, rationally tailor a novel class of polymeric membrane materials with the chemical and thermal stability as well as separation properties required for gas separation applications. This program will exploit and further develop our discovery that polymers prepared by thermal rearrangement of soluble aromatic polyimides (PIs) containing *ortho*-positioned functional groups, such as OH, exhibit unusually high gas permeability and selectivity values. Furthermore, early studies of this class of materials suggest that they are very robust chemically (i.e., insoluble in all known solvents) and resistant to plasticization, which would be important in, for example, olefin/paraffin separation or natural gas purification, where high concentrations of hydrocarbons dissolved in the polymer can compromise separation properties due to plasticization.

Technical Barriers

Thermally rearranged polymers show promising separation characteristics for several gas pairs including CO_2/CH_4. The literature lacks substantive characterization studies of these materials for membrane applications, and therefore, a broad range of structure-functionality data must be compiled to develop a fundamental understanding of why these materials have property sets so far above those of other materials and to understand whether the fundamental, molecular-level characteristics that give these materials their high transport properties are general or specific to this class of polymers.

Abstract

Work in 2012-2013 focused on studying gas permeability, diffusivity and solubility of polyimides and thermally rearranged (TR) polymers based on 3,3'-dihydroxy-4,4'-diaminobiphenyl (HAB) and 2,2'-bis-(3,4-dicarboxyphenyl) hexafluoropropane dianhydride (6FDA). To determine the effect of temperature on gas sorption, we studied H_2 sorption in the HAB-6FDA polyimide and 3 partially converted HAB-6FDA TR polymers. Increasing conversion increased gas solubility by approximately a factor of 2.6, which is similar to that of other nonpolar gases. Furthermore, in comparing H_2 sorption in HAB-6FDA with that of other polymers commonly considered for membrane applications, the HAB-6FDA TR polymers had the highest H_2 sorption. Similar studies are under way with other gases relevant for gas separations applications. We also investigated the effect of the size of the reactive leaving group and synthesis route on transport properties in TR polymers. In general, bulkier reactive leaving groups contribute to increased gas permeability in TR polymers compared to TR polymers synthesized from hydroxyl-functional leaving groups. Furthermore, we investigated samples with identical leaving groups but synthesized from two different routes. These tests showed that the leaving group on the polyimide has more of an effect on gas transport than that of synthesis route. We are also measuring mixed gas performance of these polymers and have found, in many cases, situations where CO_2/CH_4 mixed gas selectivity is actually higher than the selectivity calculated based on pure gas permeability values. The fundamental basis for this observation is under investigation.

Progress Report

Hydrogen Sorption Polymers for Membrane Applications

Hydrogen separation is used in many industrially significant gas separation applications such as oxo-chemical synthesis, refinery off-gas purification, and syngas ratio adjustment. However, because H_2 has a small kinetic diameter (2.89Å) and one of the lowest critical temperatures, Tc (33K), the effect of polymer structure on hydrogen diffusion and solubility is difficult to determine because solubility is so low. Challenges in determining these fundamental gas transport parameters have hindered the polymer membrane field from advancing our understanding of polymer structure on hydrogen transport.

To investigate H_2 sorption, we used a high precision magnetic suspension balance to determine H_2 sorption as a function of temperature in a series of HAB-6FDA TR polymers with increasing conversion. As shown in Figure 1A, gas solubility increased by approximately a factor of 2.6 between the polyimide and most highly converted TR polymer (TR 450 30min), so the relative change in H_2 sorption as a function of thermal rearrangement is similar to that of other nonpolar gases such as O_2, N_2, and CH_4. Notably, the increase in H_2 sorption does not track with increases in gas sorption for quadrupolar gases, such as CO_2, whose solubility increases by a factor of 1.7 between the HAB-6FDA polyimide and TR 450 30min sample.

To broaden the framework of this study, we investigated H_2 sorption in other polymers commonly studied for membrane applications (c.f., Figure 1B). Matrimid®, which is of the same family of polymers as HAB-6FDA (i.e., polyimides), had nearly identical gas sorption to that of the HAB-6FDA polyimide. Amorphous Teflon® (AF 2400) had H_2 sorption between that of the TR 350 60min and TR 400 60min sample. Polysulfone had the lowest H_2 sorption, and poly(dimethylsiloxane) (PDMS), which was the only rubbery polymer considered, had a slightly endothermic enthalpy of sorption, as indicated by the negative correlation between gas solubility and 1000/T. From these results, accurate diffusion coefficients for H_2 sorption in these polymers can be determined. As we have shown for other gases in TR polymers, increases in gas permeability from thermal rearrangement for H_2 are largely a result of increases in gas diffusivity.

Effect of Reactive Leaving and Synthesis Route Group on Transport Properties

Thermal rearrangement occurs at elevated temperatures for precursor polyimides with reactive *ortho*-position functional groups. We have previously reported that there is an effect of precursor synthesis route and/or the reactive leaving group on TR polymer transport properties. To decouple these two variables, we pursued a unique organic synthesis approach to synthesize TR polymer precursors from identical synthesis routes but with different reactive

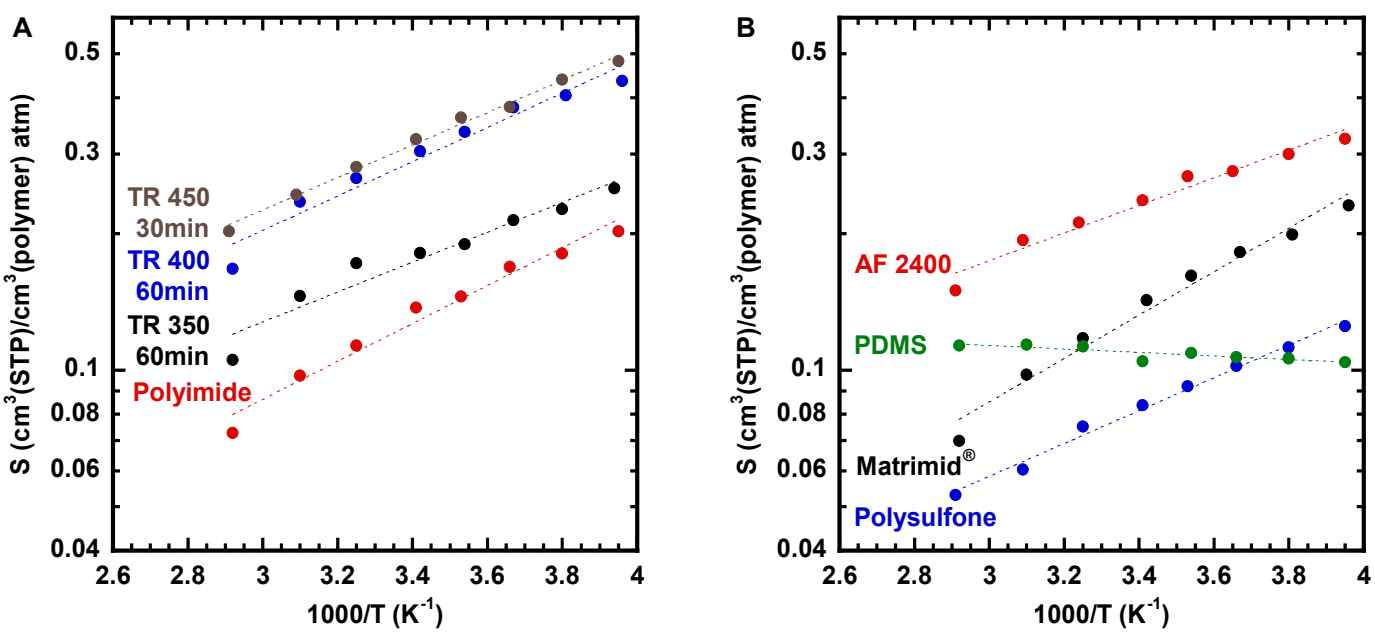

FIGURE 1. Hydrogen solubility in (A) HAB-6FDA as a function of thermal rearrangement, and (B) additional polymers frequently used for membrane applications. In Figure A, Polyimide stands for the HAB-6FDA polyimide, and partially converted TR polymers are represented by the temperature and time at which they have been rearranged. For example, TR 450 30min indicates a sample of HAB-6FDA that has been converted at 450°C for 30min. For Figure B, AF 2400 is amorphous Teflon® AF 2400 and PDMS is poly(dimethylsiloxane).

leaving groups. This synthesis approach was accomplished by first thermally imidizing HAB-6FDA to form a polyimide precursor with hydroxyl *ortho*-functionality. This precursor was chemically derivatized through a series of esterification reactions to synthesize an HAB-6FDA polyimide with variable reactive leaving groups.

As shown in Figure 2A, an HAB-6FDA polyimide can be converted to an HAB-6FDA TR polymer at elevated temperatures between 350°C and 450°C. Under these conditions, the reactive *ortho*-functional group, R, leaves the polymer. Regardless of which derivatized R group is used, upon thermal treatment, all forms of HAB-6FDA rearrange to form the polybenzoxazole (PBO) structure shown in Figure 2A. To compare the transport properties of TR polymers prepared from each of these derivatized precursors polyimides, we determined CO_2 permeability as a function of conversion for all of the derivatized products as shown in Figure 2B. Modifications to the leaving group of the polyimide change the CO_2 permeability for the unconverted samples. Upon conversion, samples with leaving groups that are bulkier than hydroxyl groups results in larger increases in CO_2 permeability. To compare transport properties of two polymers with identical leaving groups that were synthesized via diverse synthetic pathways, we compared the CO_2 permeability for two acetate-functional polymers, whereby the first was synthesized via the derivatization method described above (labeled Ac in Figure 2), and the second was synthesized via chemical imidization (labeled C in Figure 2). As shown in Figure 2B, there is almost no difference in CO_2 permeability between the samples of identical leaving groups but prepared from different synthesis routes. Therefore, the leaving group has a stronger influence on transport properties than the synthesis route.

Future Directions

We are furthering our basic structure property studies by investigating the effect of light gas permeability and CO_2 as well as olefin/paraffin plasticization effects for several TR polymers with different functionality in the chemical backbone. In addition to the HAB diamine, we are investigating a fluorinated diamine known as APAF, and in addition to the 6FDA dianhydride, we are investigating a dianhydride known as ODPA. Our plasticization studies for CO_2/CH_4 separation have extended to mixed gas plasticization experiments, whereby we have investigated the effect of thermal rearrangement on plasticization to pressures of approximately 50 atm in 50:50 mixed-gas feeds and temperatures between 15°C and 70°C.

In our continued efforts to characterize the chemical and morphological features of TR polymers, we have begun a series of fractional free volume measurements using positron annihilation lifetime spectroscopy (PALS).

Finally, to provide a broader framework for comparing our H_2 sorption and diffusion data, we are determining helium sorption in TR polymers and a number of other polymers commonly used for applications in gas separation membranes.

Publication list (including patents) acknowledging the DOE grant or contract

1. Smith, Z.P., Tiwari, R.R., Murphy, T.M., Sanders, D.F., Gleason, K.L., Gunawan, G., Paul, D.R., and Freeman, B.D., The Basis for Hydrogen and Helium Permselectivity in Hydrocarbon and Fluorocarbon Based Polymers. in preparation.

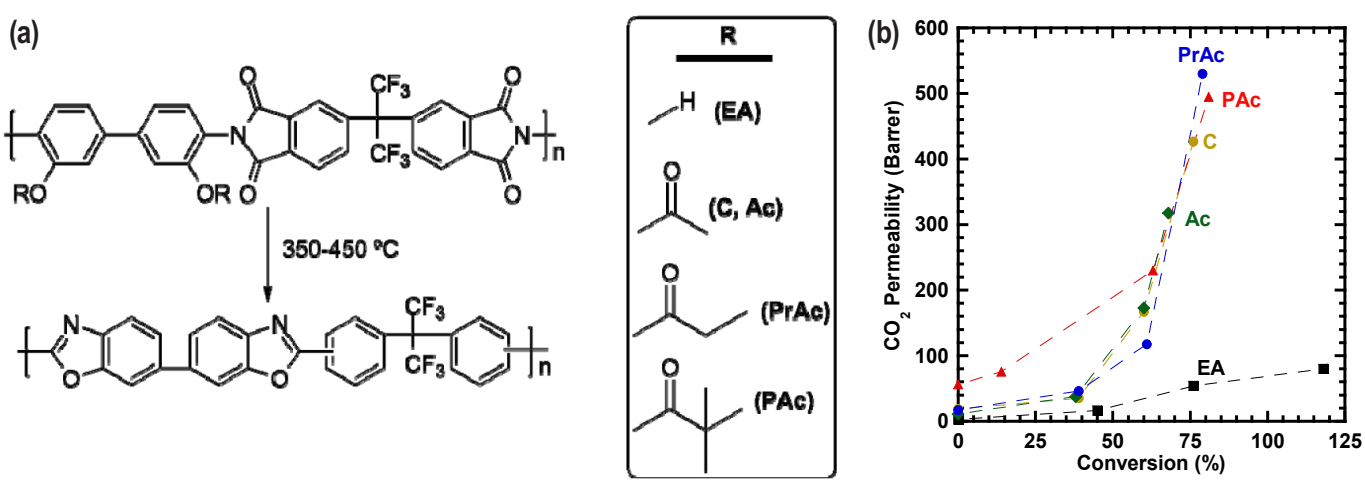

FIGURE 2. (A) Thermal rearrangement of an HAB-6FDA polyimide to form an HAB-6FDA TR polymer. Various R groups will all theoretically rearrange into identical TR polymers. (B) Comparison of CO_2 permeability as a function of conversion for HAB-6FDA prepared with various leaving groups and prepared by multiply synthetic routes (i.e., C versus Ac).

2. Sanders, D.F., Guo, R., Smith, Z.P., Stevens, K.A., Liu, Q., McGrath, J.E., Paul, D.R., and Freeman B.D., Influence of Polyimide Precursor Synthesis Route and ortho-Position Functional Group on Thermally Rearranged (TR) Polymer Properties: Pure Gas Permeability and Selectivity. in preparation.

3. Smith, Z.P., Tiwari, R.R., Murphy, T.M., Sanders, D.F., Gleason, K.L., Paul, D.R., and Freeman, B.D., Hydrogen sorption in polymers for membrane applications. *Polymer*, **2013,** in press, DOI: 10.1016/j.polymer.2013.04.006.

4. Sanders, D.F., Smith, Z.P., Ribeiro, C.P., Guo, R., McGrath, J.E., Paul, D.R., and Freeman, B.D., Permeability, diffusivity, and free volume of thermally rearranged polymers based on 3,3'-dihydroxy-4,4'-diamino-biphenyl (HAB) and 2,2'-bis-(3,4-dicarboxyphenyl) hexafluoropropane dianhydride (6FDA). *Journal of Membrane Science*, **2012,** 409-410.

5. Smith, Z.P., Sanders, D.F., Ribeiro Jr, C.P., Guo, R., Freeman, B.D., Paul, D.R., McGrath, J.E., and Swinnea, S., Gas sorption and characterization of thermally rearranged polyimides based on 3,3'-dihydroxy-4,4'-diamino-biphenyl (HAB) and 2,2'-bis-(3,4-dicarboxyphenyl) hexafluoropropane dianhydride (6FDA). *Journal of Membrane Science*, **2012,** 416.

V.N.8 Precisely Tunable High Performance Carbon Molecular Sieve Membranes for Energy Intensive Separations

Principal Investigator: W.J. Koros
Chemical Engineering
Georgia Institute of Technology
Atlanta, Georgia 30332-0100
Phone: (404) 385-2684
Email: wjk@che.gatech.edu

DOE Program Manager: Dr. Larry Rahn
Separations and Analysis Program
Chemical Sciences, Geosciences and Biosciences Division
Office of Basic Energy Sciences
Phone: (301) 903-2508
Email: Larry.Rahn@science.doe.gov

Abstract

In our previous project of "Synthesis and analysis of polymers with high permeabilities and permselectivities for gas separation applications", we focused on rational discovery and development of robust crosslinked polyimide membrane materials for energy-efficient purification of natural gas, and investigated the following areas: (1) synthesis of 6FDA-based polyimides with comparable chemical structures; (2) thermal properties and chemical structures of the polymers; (3) CO_2-induced plasticization response vs. chemical structure of the polymers; (4) gas separation properties vs. chemical structure of the polymers; (5) sub-Tg thermal cross-linking of the polymer membranes, and (6) physical aging and CO_2 exposure effects on gas permeation properties of thin films.

The current project's focus is to study advanced carbon molecular sieve (CMS) membranes. The overarching goal is to develop an improved fundamental framework to guide the systematic understanding and formation of carbon molecular sieve membrane materials appropriate for important energy intensive separations. Determination and analysis of the effects on penetrant sorption and transport properties caused by systematic variations in precursor polyimide structures and pyrolysis protocols will be key thrusts of the work. A diverse but systematic set of dianhydride and diamine monomers will be used to explore effects of matrix rigidity and packing of precursor polyimides on final carbon properties. We will analyze diffusion selectivities in terms of activation energies and activation entropies to improve the understanding of discrimination on the basis of shape of the penetrants. A special focus will be upon the interaction of pyrolysis temperatures and pyrolysis atmospheres. This aspect of the work will expand on an important recent discovery by our group that the presence of parts-per-million levels of oxygen enables exquisite control of permeability and selectivity in carbons. Finally, evaluation of the effects on separation performance for selected binary and ternary gas feeds is proposed to probe interactions between co-permeating components. These multicomponent gas studies, while difficult, provide valuable insights that are unavailable from single gas investigations alone.

To reach the goal, we need to design and synthesize precursor polymers with specific related structures; we need to tune pyrolysis protocols and atmospheres for optimization of CMS Properties; and finally, we need to compare the CMS membranes' gas separation performance to relate the performance with the structures and pyrolysis conditions.

Progress Report

The 6FDA dianhydride and DAM diamine monomers provide starting points that we know yield a highly open and conveniently processable polyimide precursor, which can be engineered to adjust matrix rigidity and packing. We designed 6FDA-based polyimide copolymers by using a symmetrical (indicated by the "s" prefix) or an asymmetric (indicated by the "a" prefix) dianhydride. These irregular asymmetric dianhydrides provide packing inhibiting components, and should give higher permeability CMS structures vs. the CMS from symmetric structures. The structures of the polymers are given in scheme 1.

We will also compare 3FDA-based copolymers with 6FDA-based copolymers, examples are shown in Scheme 2.

We have synthesized symmetrical copolymers by condensation of the dianhydrides with the diamine, DAM. This is a two-step reaction in which the first step produces a high molecular weight polyamic acid (PAA) at low temperature (~5°C), while the second step involves ring closure by releasing water to produce the chemical stable polyimide (PI). Chemical imidization was carried out for the PAA solution in the presence of beta picoline and acetic anhydride at ambient temperature for 24 h. The resulting polyimides were precipitated, washed with methanol, and dried at 210 °C under vacuum for 24 h. An example of the synthesis procedure is shown in Scheme 3.

Synthesis of the asymmetrical copolymers is currently underway. Asymmetric dianhydrides are not common chemicals; however, we have successfully obtained samples from a specialty commercial supplier and are starting to characterize these samples. With the analytic results, we will make a decision to buy asymmetric dianhydrides

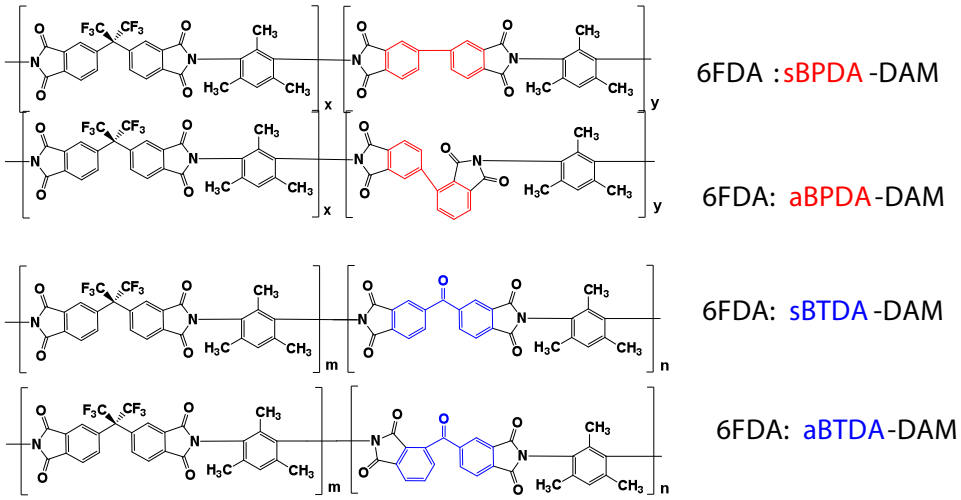

SCHEME 1. Chemical structures of symmetric and asymmetric copolymers

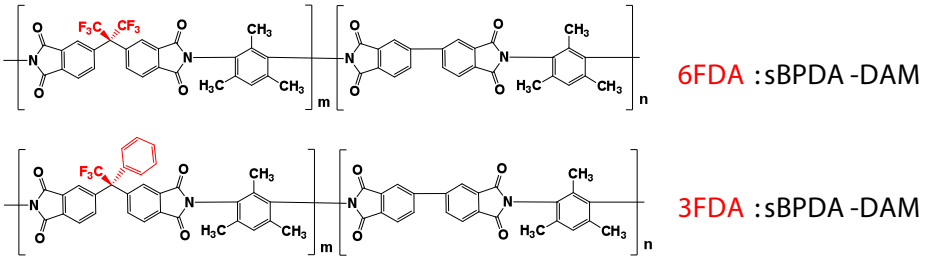

SCHEME 2. Chemical structures of 3FDA- and 6FDA-based copolymers

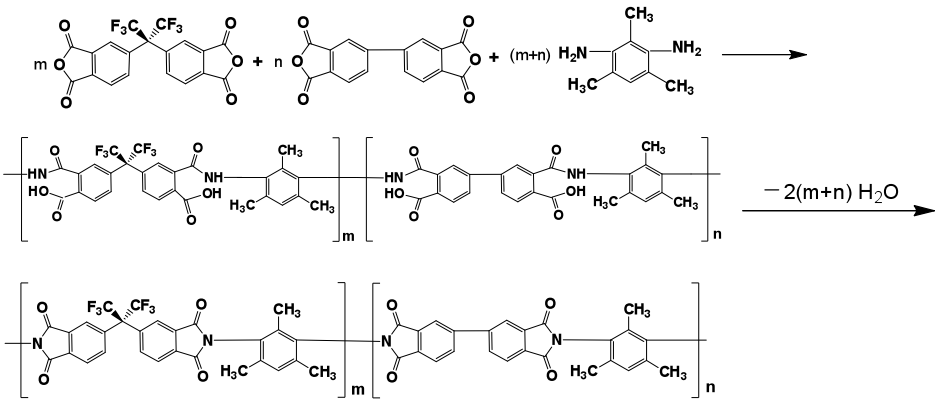

SCHEME 3. Synthesis of 6FDA:sBPDA-DAM copolymer

from a commercial source or to synthesize the asymmetric dianhydrides by ourselves.

Permeation performance of 6FDA:sBPDA-DAM membrane

6FDA:sBPDA-DAM(1:1) copolymer membrane was cast on a Teflon® covered glass plate from a THF solution (~20 wt%) inside a controlled environment glove bag to promote slow evaporation of the solvent. A casting knife with a 12 mil clearance was used to draw the solution into a film of uniform thickness. After completion of the evaporation of THF solvent, the membrane was removed from the plate, and dried at 180 °C for 24 h under vacuum. The resulting polymer precursor membrane will be used for making CMS membrane.

For comparison, the gas separation performance was also tested for the polymer precursor membrane. Both pure gases

and mixed gas were tested at 35°C with a feed pressure of 50 psia. The permeability is 282 barrers for He, 92.6 barrers for O_2, 24.3 barrers for N_2, 460 barrers for CO_2, 23 barrers for CH_4, 43.6 barrers for C_2H_4, 13.0 barrers for C_2H_6, 29 barrers for C_3H_6, and 2.2 barrers for C_3H_8. Selectivity is 12.3 for He/CH_4, 11.6 for He/N_2, 3.8 for O_2/N_2, 20.0 for CO_2/CH_4, 18.9 for CO_2/N_2, 4.0 for O_2/CH_4, 1.1 for N_2/CH_4, 3.3 for C_2H_4/C_2H_6, and 13.4 for C_3H_6/C_3H_8, respectively. For a mixed gas of CO_2/CH_4 (10/90), permeability was tested as 545 barrers and 23 barrers for CO_2 and CH_4, respectively, with a CO_2/CH_4 selectivity of 22.8; for CO_2/CH_4 (50/50) mixed gas, permeability was 493 barrers and 23.4 barrers for CO_2 and CH_4, respectively, with a CO_2/CH_4 selectivity of 21.

Preliminary results of CMS membrane from 6FDA:sBPDA-DAM precursor polymer

The CMS membrane was made through pyrolysis of the precursor membrane in a temperature and atmosphere controlled furnace. The final separation performance of a CMS membrane is influenced by the following parameters, including polymer precursor, pyrolysis temperature, thermal soak time, and pyrolysis atmosphere.

The thermal decomposition property was studied by TGA analysis. As shown in Figure 1, 6FDA:sBPDA-DAM(1:1) is stable until 450°C, then it starts to decompose. A weight loss of about 40wt% was found up to around 700°C in Argon. Beyond 700°C the weight loss is much smaller. Based on the decomposition behavior, the final pyrolysis temperatures were chosen as 500°C, 550°C, 675°C, and 800°C.

An example of a typical heating protocol for preparing CMS membranes at different pyrolysis temperature is shown in Figure 2. The polymer precursor membrane was heated from 50°C at 10 K/min to 250°C, followed by a rate of 3 K/min to a temperature of 15 degree below the final temperature, then heated at 0.25 K/min to the final temperature and soaked at that temperature for 2h in Argon with a flow rate of 200 mL/min. The furnace was then cooled down naturally to room temperature, and the resulting CMS membrane was used for gas permeation tests.

The gas separation performance was tested for CMS membranes, and the results were plotted against the experimental upper bound. As shown in Figure 3a, the 6FDA:sBPDA-DAM(1:1) precursor membrane showed a CO_2/CH_4 separation performance near the polymer upper bound, while the CMS membranes exhibited separation performance *greatly exceeding the upper bound.* CMS membranes from the lower pyrolysis temperatures, such as 550 °C, show quite high CO_2 permeability; however, the CO_2/CH_4 selectivity is not significantly increased. With the pyrolysis temperature increased to 675°C, the CMS membrane shows both improved CO_2 permeability and CO_2/CH_4 selectivity. With an increase in final pyrolysis temperature, the CO_2/CH_4 selectivity increased, while the CO_2 permeability decreased. The CMS membrane pyrolyzed at 800°C showed quite lower permeabilities (not shown in the Figure).

Compared with the precursor membrane, CMS membranes pyrolyzed at 500 °C had quite high C_2H_4 permeability with improvements in C_2H_4/C_2H_6 selectivity. CMS membranes pyrolyzed at 675 °C showedhigher C_2H_4/C_2H_6 selectivity, while the C_2H_4 permeability was almost the same as the precursor membrane, as can be seen in Figure 3b.

From Figure 3c, for the C_3H_6/C_3H_8 pair, the 6FDA:sBPDA-DAM(1:1) polymer precursor membrane showed a C_3H_6/C_3H_8 separation performance on the polymer

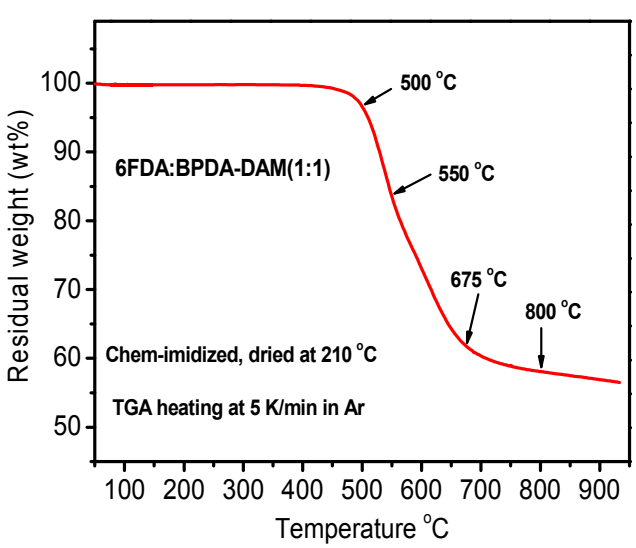

FIGURE 1. 6FDA:sBPDA-DAM copolymer TGA plot

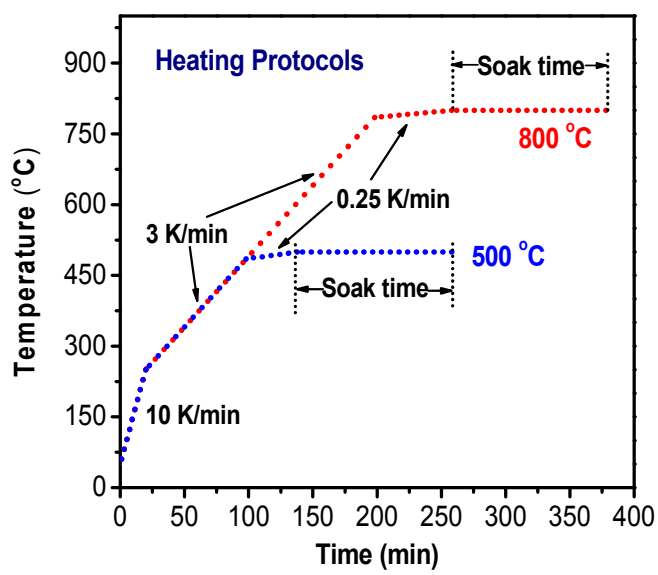

FIGURE 2. Example of pyrolysis protocols. Figure 1:6FDA:sBPDA-DAM copolymer TGA plot

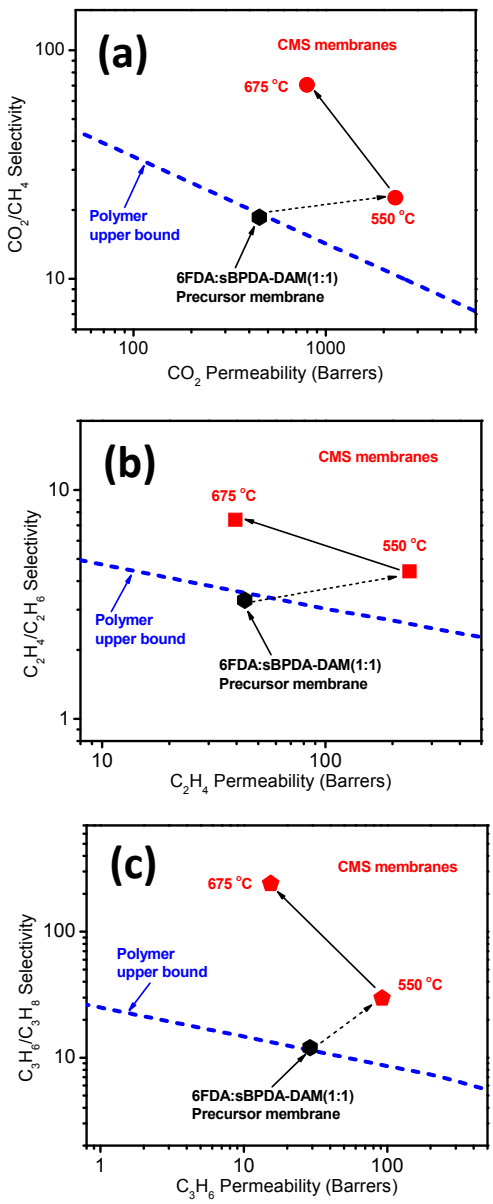

FIGURE 3. *Performance of CMS membrane from 6FDA:sBPDA-DAM copolymer for separation of (a)* CO_2/CH_4, (b) C_2H_4/C_2H_6, and (c) C_3H_6/C_3H_8.

upper bound. The CMS membranes showed extremely good separation performance based on pure gas permeation tests, but we must also study mixed gases, since competition between the two penetrants can be strong for this more condensable pair. With an increase of pyrolysis temperature, the C_3H_6/C_3H_8 selectivity increased markedly, although the C_3H_6 permeability decreased.

The above permeation results indicate that CMS membranes pyrolyzed at lower temperature have bigger ultramicropore size than the membranes pyrolyzed at higher temperature. There is a competition between the creation of pores and the reduction of pore size. The pyrolysis temperature can be grouped into two regions, the fast weight loss region and the slow weight loss region, as can be seen in Figure 4. With a pyrolysis temperature in the fast weight loss region, the creation of pores is dominant, while in the slow weight loss region, the reduction of pore size is dominant. It seems a pyrolysis temperature within the region where fast weight loss is ending while the slow weight loss is starting might yield the resulting CMS membrane with both good permeability as well as high selectivity.

The performance of CMS dense film membrane made from 6FDA:sBPDA-DAM(1:1) precursor membrane was influenced by aging time, as shown in Figure 5. The steady state was not reached in one month for a CMS membrane pyrolyzed at 500°C. This response appears to be somewhat related to aging phenomena seen in conventional glassy

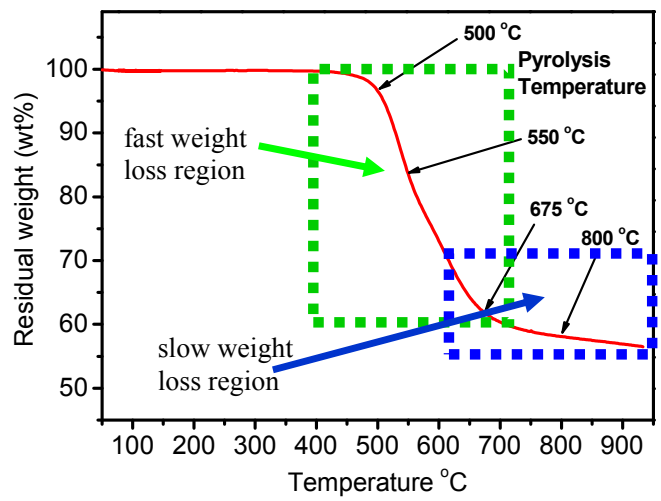

FIGURE 4. Wt. loss rate vs.CMS ultramicropore development

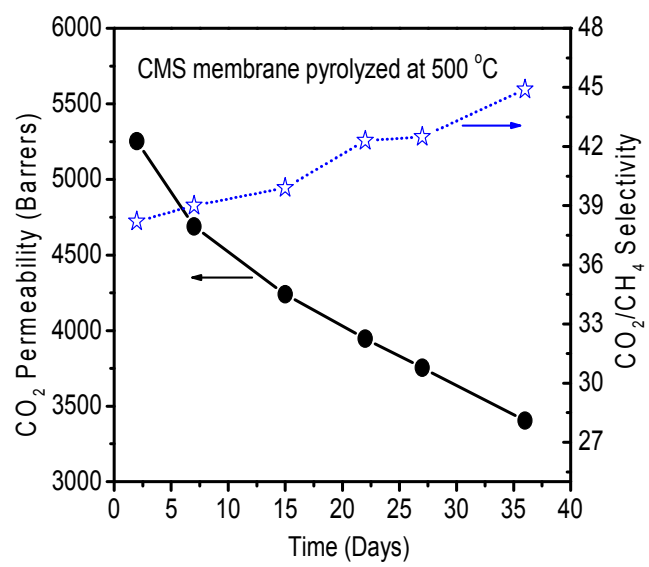

FIGURE 5. CO_2 permeability vs. aging time

polymers, and our goal is to accelerate the aging to enable focusing on the intrinsic stable properties of the high performance carbon glass. We will report more on this topic in our next update.

Publication list (including patents) acknowledging the DOE grant

Publications Under DE-FG02-04ER15510 (2011-2012)

1. W.J. Koros and R.P. Lively, "*Water and beyond: Expanding the spectrum of large-scale energy efficient separation processes*", *AIChE Journal*, 58(9) 2624-2633,2012.

2. Wulin Qiu, Liren Xu, William J Koros, *"Effects of Polymer Precursors and Pyrolysis Conditions on Carbon Molecular Sieve Membranes for Gas Separation"*, **40th Annual NATAS (North American Thermal Analysis Society) Conference**, Orlando, FL, United States, August 10–15, 2012.

3. Wulin Qiu, Chien-Chiang Chen, Liren Xu, William J Koros, *"6FDA-Based Polyimide Membranes with Different Chemical Structures for Gas Separation"*, **NAMS (The North American Membrane Society) 2012 meeting**, New Orleans, LA, United States, June 9–13, 2012.

V.N.9 Nanoporous Membranes for Hydrogen Production: Experimental Studies and Molecular Simulations

Principal Investigator: Muhammad Sahimi
University of Southern California, Los Angeles
Los Angeles, CA 90089-1211
Phone: (213)740-2064
Email: moe@usc.edu

Theodore Tsotsis, Co-Principal Investigator
University of Southern California, Los Angeles
Los Angeles, CA 90089-1211
Phone: (213) 740-2069
Email: tsotsis@usc.edu

DOE Program Manager: Dr. Larry Rahn
Separations and Analysis Program, Chemical Sciences, Geosciences and Biosciences Division, Office of Basic Energy Sciences
Phone: (301) 903-2508
Email: Larry.Rahn@science.doe.gov

Abstract

In this project, we study SiC nanoporous membranes, which exhibit the potential to overcome many of the difficulties other inorganic membranes face, particularly under conditions typically encountered in reactive separations for H_2 production, and in fuel-cell applications. In particular, we systematically investigate and further develop the technique of pre-ceramic polymer pyrolysis to produce nanoporous SiC membranes and films, which are both cost-efficient and industrially viable. Our efforts are motivated by the growing interest in the H_2 economy, which necessitates the development of robust nanoporous materials for use in high-temperature and pressure processes related to H_2 production. SiC is a promising material for such applications, due to its many unique properties, such as high thermal conductivity, thermal shock resistance, chemical inertness and high mechanical strength. The main focus of our project is on trying to understand the formation process of the membranes, namely, how the initial structure of the polymeric precursor and the pyrolysis conditions impact the final membrane characteristics. Our efforts involve extensive experimental investigation of the membrane formation process, as well as modeling of the pyrolysis process itself by molecular dynamics simulations, since the understanding must be at the molecular level. The new science that is being developed impacts not only the fabrication of SiC membranes, but also the general field of inorganic membranes, including carbon molecular-sieve (CMS) and mixed-matrix membranes. A key outcome of our effort will be the ability to prepare a membrane with certain "optimal" properties (e.g., permeance, separation factor, and surface characteristics) by being able to determine in a systematic way the type of polymeric precursor one needs to use, and the preparation method and procedure that one must utilize.

Progress Report

The results of the work accomplished in this project are summarized as follows:

Highly permeable macroporous SiC supports have been prepared. In our efforts we have investigated a variety of factors that impact the properties of these supports. They include, (i) the type and composition of the starting powders utilized; (ii) the type and quantity of sintering aids and the temperature and other conditions of sintering, and (iii) the impacts of various surface treatments. A novel dip-coating technique has been developed that involves modification of the slip-casting step using SiC nanofibers and nanotubes, which provides a more effective means for preventing infiltration in the underlying macroporous structure during both the slip-casting and the subsequent thin film deposition steps. Using this preparation technique, membranes have been prepared with very high (He/Ar) separation factors of more than 2000, while using substrates with significantly higher surface roughness. MD simulations were employed in order to examine the adsorption and diffusion of N_2, H_2, CO_2, CH_4, and n-C_4H_{10} in silicon carbide nanotubes (SiCNT's). The simulations indicated the strong effect of the nanotubes' chirality and curvature on the pressure-dependence of the adsorption isotherms and the self-diffusivities. Detailed comparison was made between the results and those for the CNT's, and the hydrogen adsorption capacity of the SiCNTs is higher than the CNTs' under the conditions that we have studied. A templating technique has also been developed for the preparation of high-surface area SiC materials with highly-interconnected pore structures. These materials, in addition to finding useful applications as membrane films, also show potential to find important applications as adsorbents, catalyst supports and energy storage media (e.g., supercapacitors).

In order to gain insight into the processes that prepare these nanoporous materials, we have developed a class of models, referred to as the *geometric models*, which aim to understand the effect of the material's morphology, such as its pore-size distribution (PSD) and pore interconnectivity, on its sorption and transport characteristics, and on its ability to separate molecular mixtures. These models make use of an annealing method to generate the solid matrix of the SiC material via the semi-empirical, extended Brenner force

field (FF), previously utilized to model various phenomena involving SiC bulk materials and surfaces by MD and MC simulations. The method consists of starting in the crystalline β-SiC state, raising the temperature until the crystal melts, and then decreasing the temperature gradually to the desired value. The material's pore structure is generated via a Voronoi space tessellation technique, which creates a 3-D pore network within the resulting material. Its characteristics (porosity, PSD, interconnectivity) are fine-tuned by fitting, via atomistic (GCMC) simulations, experimental single-gas (e.g., N_2 and CO_2) adsorption data. The resulting model membrane structures are then used to study the transport of single gases and binary gas mixtures. Due to the nano-scale size of the membrane pores, it is of paramount importance to understand the interactions between the molecules and the pore walls and their influence on the transport processes, as they determine the ability of the SiC materials to separate mixtures based on differences in molecular mobility. To accomplish that, we utilize non-equilibrium molecular dynamics (NEMD) simulations, and for certain gas pairs the results agree qualitatively with our experimental data.

Despite their modest success in matching experimental transport and separation data, the geometric models offer little in terms of predictive capabilities, as they do not use information about the chemical structure of the polymeric precursors and the membrane's preparation method. For modeling to be predictive, an accurate, detailed knowledge of the pore space, and a molecular-level understanding of the pore surfaces are of paramount importance. In addition, one must accurately mimic the processes that are involved in the fabrication of the membranes. This then requires the development of a reactive FF that correctly models the pyrolysis process that generates these materials. In our current efforts, we have begun to expand and to further improve the ReaxFF for PDMS, originally proposed by Professor William Goddard and his team at Caltech, who collaborate with us in our current efforts, and will adopt it for the investigation of the pyrolysis of allylhydridopolycarbosilane (AHPCS) at high temperatures. In our simulations so far we have focused attention on hydridopolycarbosilane (HPCS) as it prepares, in principle, a ceramic with a stoichiometric Si:C ratio. Experimentally, on the other hand, we have found during our present efforts that AHPCS provides better experimental flexibility in preparing SiC membranes. During the renewal period, therefore, we will extend our efforts to also simulate AHPCS pyrolysis. As a first step towards simulating the pyrolysis process of the pre-ceramic precursor that forms the SiC, we generate a realistic model of the polymer itself utilizing energy minimization and MD simulations and the polymer-consistent FF (PCFF). The figure below shows a HPCS amorphous polymer originally built by introducing four polymer chains, each having 482 atoms, in a periodic cell box of 28.9 Å in size using the modified self-avoid walk (SAW) method.

Our reactive (RMD) simulations using ReaxFF (below the SiC melting point) yield the initial pyrolysis products of the HPCS to be hydrogen and associated polymer fragments, indicating that decomposition and subsequent cross-linking of the polymer are initiated by Si-H and C-H bond cleavage. Secondary reactions (involving produced radicals) lead to cross-linking between Si and C atoms of adjacent chains, yielding eventually the formation of the amorphous SiC structure. We have studied the temperature-dependence of the HPCS pyrolysis by following the rate of production of the H radicals using reactive molecular dynamics (RMD) simulations with ReaxFF. We have also tracked the temperature dependence of the H radical production in order to extract the Arrhenius parameters for the failure modes of the HPCS. Further, we have validated the ability of ReaxFF to represent the equation of state of the SiC crystal by testing against its more than 250 crystalline structures, and its three major known polytypes.

The structure of SiC is generated by carrying out extensive RMD simulations in the NVT ensemble in the temperature range (2000 - 3000 K). During the simulations, the hydrogen radicals (key product of the pyrolysis process) are removed from the simulation box as a way of speeding up the simulations, and the structure is cooled down to 2000 K. Then, MD simulations in the NPT ensemble are utilized to compress the system at 2000 K. Eventually the system is relaxed at ambient temperature to arrive at the amorphous structure of SiC. To test the validity of the model, in addition to calculating the entropy and radial distribution function, we also computed the melting point, the X-ray diffraction (XRD) spectra, and other structural properties. In order to assess the ability of the ReaxFF simulations to be predictive, model validation via comparison with experiments is of critical importance, and will be a key focus of the proposed efforts in the future. Figure 2 presents a comparison between the computed radial distribution function and the experimental data.

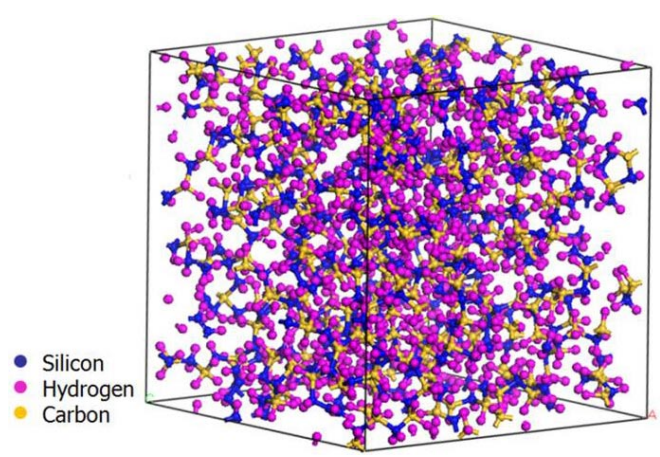

FIGURE 1. HPCS amorphous polymer structure

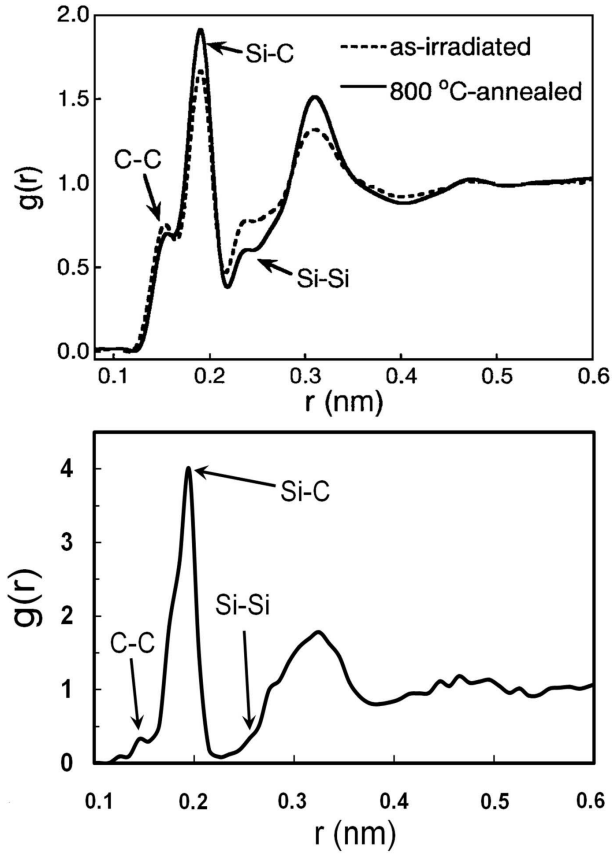

FIGURE 2. Comparison of the computed radial distribution function of the amorphous SiC (below) with the experimental data (top).

In an attempt to model the formation process of the membranes at a coarse scale, a pore network model has also been developed to study the evolution of the pore space of a nanoporous SiC membrane during its fabrication by (CVI/CVD) techniques. Good agreement was found between the simulation results and the experimental data. Thus, the model may be used, in conjunction with the molecular-scale model, for determining the optimal conditions under which a membrane may achieve a given value of permselectivity.

A network model was also developed to interpret the results of flow permporometry (FPP) that has been used widely for determining the pore size distribution of a broad class of porous materials, including our studies of the high-flux macroporous SiC supports. The model is the first of its kind, even though permporometry has been used for decades.

We have also begun to study other nanostructures, including SiC nanotubes, as a potential material for storage of hydrogen, as well as separation materials and sensors. So far, we have studied adsorption and diffusion of a variety of gases in SiC, both experimentally and by MD simulations. We have also measured adsorption of nitrogen in carbon nanotubes, in order to compare the data with those measured with SiC nanotubes. The preliminary results have been very encouraging.

Publication list (including patents) acknowledging the DOE grant

1. K. Malek and M. Sahimi, Molecular Dynamics Simulations of Adsorption and Diffusion of Gases in Silicon-Carbide Nanotubes, *Journal of Chemical Physics* **132**, 014310/1-014310/10 (**2010**).

2. R. Mourhatch, T.T. Tsotsis, and M. Sahimi, Network Model for the Evolution of the pore Structure of Silicon-Carbide Membranes During Their Fabrication, *Journal of Membrane Science* **356**, 138-146 (**2010**).

3. R. Mourhatch, T.T. Tsotsis, and M. Sahimi, Determination of the True Pore Size Distribution by Flow Permporometry Experiments: An Invasion Percolation Algorithm, *Journal of Membrane Science* **367**, 53-62 (**2010**).

4. M. Khademi and M. Sahimi, Molecular Dynamics Simulation of Pressure-Driven Water Flow in Silicon-Carbide Nanotubes, *Journal of Chemical Physics* **135**, 204509/1-204509/7 (**2011**).

5. S. Naserifar, L. Liu, W.A. Goddard, T.T. Tsotsis, and M. Sahimi, Toward a Process-Based Molecular Model of a SiC Membrane. I. Development of a Reactive Force Field, *Journal of Physical Chemistry C* **117**, 3308-3319 (**2013**).

6. S. Naserifar, W.A. Goddard, L. Liu, T.T. Tsotsis, and M. Sahimi, Toward a Process-Based Molecular Model of a SiC Membrane. II. Reactive Dynamics Simulation of the Pyrolysis of Polymer Precursor to form Amorphous SiC, *Journal of Physical Chemistry C* **117**, 3320-3329 (**2013**)

7. S. Soltani, M. Sahimi, and T.T. Tsotsis, Catalytic Membrane Reactors: A Brief Overview, in *Encyclopedia of Membrane Science and Technology* (Wiley-VCH, 2013).

V.N.10 Structure/Composition/Function Relationships in Supported Nanoscale Catalysts for Hydrogen

Investigators: Larry A. Curtiss, Jeffrey W. Elam, Jeffrey P. Greeley, Julius L. Jellinek, Christopher L. Marshall, Jeffrey T. Miller, Stefan Vajda, Peter C. Stair*
Argonne National Laboratory
9700 South Cass Avenue
Argonne, IL 60439
Phone: (630) 252-6499
Email: pstair@northwestern.edu

DOE Program Manager: Raul Miranda
Phone: (301) 903-8014
Email: Raul.Miranda@science.doe.gov

Objectives

The research is geared toward the development of new methods for the preparation of solid catalytic materials with atomic precision and the utilization of these materials for fundamental understanding of composition/structure/function relationships in supported, heterogeneous catalysts for reactions that produce hydrogen from hydrogen-rich molecules. The ability to control metal nanoparticle composition, size, and structure, as well as the supports and promoters, is investigated; along with roles in determining adsorptive and catalytic properties. One particular goal is to evaluate performance of novel catalyst material structures for hydrogen production from methanol. The catalysts are supported metal and alloy nanoparticles and clusters with an emphasis on sizes in the range <1 nm, i.e. ~2-50 atoms that have been stabilized by coating with ultrathin oxide layers.

Technical Barriers

Catalysts based on noble metal nanoparticles for reforming of hydrogen rich organic molecules, such as methanol, to produce molecular hydrogen exhibit poor activity at low temperature due to poisoning by CO and poor stability at higher temperature due to particle growth and carbon deposition. We hypothesize that catalyst activity and stability can be improved greatly by using subnanometer size metal and alloy particles on suitable supports combined with oxide overlayers that stabilize the particles against particle growth and selectively block surface sites that produce undesirable products. Advanced techniques for synthesis, stabilization, characterization, theory and testing are employed to prepare novel catalyst structures and understand their chemical and catalytic properties.

Abstract

The focus of this project is the synthesis, stabilization, characterization, catalytic evaluation and computation of supported metal particle catalysts in the size range ≤1 nm, i.e. ~2-50 atoms. New synthetic and stabilization methodologies, based on atomic layer deposition and computational understanding have been achieved for ultra-small, supported metal particles. These materials exhibit exceptional performance for catalytic transformations involving methanol and other small hydrocarbons. The novel structures that involve oxide coatings of the noble metal nanoparticles provide a wholly new and effective methodology for improving the performance of catalytic materials. The research integrates efforts in: 1) synthesis and stabilization of uniform, supported clusters and oxide promoters; 2) characterization of cluster size, atomic structure, stability, and electronic structure during synthesis, pretreatment, and catalytic reaction; 3) investigation of catalytic and chemical events on the clusters that are relevant to hydrogen production; 4) computational quantum chemical modeling to understand and predict experimental results.

Progress Report

New Catalyst Structures

The synthesis of new catalyst compositions and structures is a key to advancing the performance of practical catalytic processes. Atomic Layer Deposition (ALD) has been developed as an exceptionally powerful, flexible and precise method for synthesis of single-component and alloy metal nanoparticle catalyst materials with outstanding activity, selectivity and stability. The initial focus was synthesis of Pd nanoparticles supported on alumina because they exhibit high activity for conversion of methanol to hydrogen but suffer from lack of stability at reaction temperature. Using palladium (II) hexafluoroacetylacetonate [$Pd(hfac)_2$] as the Pd-precursor and formaldehyde (HCHO) as the reducing agent produced well-dispersed, uniform ~2 nm Pd nanoparticles. Starting with high-surface-area silica the support composition can be changed, as desired, by depositing a thin layer of oxide before the Pd deposition (e.g., Al_2O_3 to make alumina supported Pd) and/or the Pd particles can be stabilized by overcoating with oxide after the Pd deposition. The thickness of these oxide layers is controlled with atomic precision by the ALD chemistry. Our research has shown that, using deposition temperature and ALD support composition, Pd particles with uniform, selectable sizes from <1 to several nanometers can be formed. We have also shown that the scope of nanoparticle catalytic materials

that can be prepared by ALD includes single-component systems (Pt, Ir, Ru) and alloys (Pt-Ir, Pt-Ru, Ir-Ru, Pt-Pd).

Remarkable new catalyst structures with exceptional performance have been synthesized by overcoating the supported metal nanoparticles with alumina by ALD. Detailed studies of the alumina ALD overcoating chemistry show that the aluminum precursor reacts preferentially with edge and corner sites on the Pd nanoparticles. This blocks their participation in the reaction and results in a more structurally uniform catalytic metal surface consisting primarily of terrace site geometries. This picture has emerged based on combining *in-situ* experiments, *ex-situ* TEM, and DFT calculations of the initial stages of Al_2O_3 ALD on the Pd nanoparticle surfaces. We discovered that the Al_2O_3 ALD on Pd nanoparticles proceeds by a *self-poisoning, self-cleaning* process. The Pd surface becomes poisoned by adsorbed CH_3* species during the trimethyl aluminum exposures, which prevents the formation of a complete monolayer of adsorbed Al species. During the subsequent H_2O exposures, the Pd surface is cleaned of CH_3* species, and the net result is a porous Al_2O_3 film. This porous structure retains the catalytic activity of the Pd nanoparticles by providing reagent gases with access to the Pd surface sites. This is depicted schematically in Figure 1. Additional studies showed that even after complete encapsulation by thick alumina layers, new pores can also be opened in the overcoat by calcination/dehydration at 700 °C. This restores access to the Pd particle surface and provides a strategy for manipulating the pore structure of the catalyst.

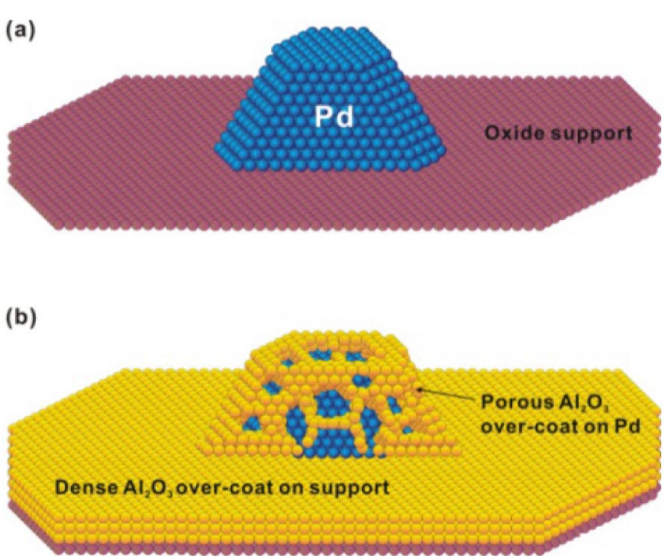

FIGURE 1. Schematic illustration of porous Al_2O_3 ALD over-coat on Pd nanoparticle: (a) supported Pd catalyst; (b) dense Al_2O_3 film on oxide support with porous Al_2O_3 overcoat on Pd nanoparticle formed by ALD.

Catalyst Performance

The performance of ALD-synthesized catalyst structures has been investigated for methanol decomposition and ethane dehydrogenation. The overcoated structure stabilizes nanoparticle size even under severe reaction conditions (e.g. 800 °C calcination, 270 °C methanol decomposition, or 675 °C ethane dehydrogenation). Figure 2 depicts the Pd particle size stability achieved for methanol reaction conditions. Without overcoating (0 ALD cycles) the particle size has doubled, resulting in lower catalytic activity. Particle size is stable for materials with 1-8 cycles of overcoating. Rather than causing an expected loss in catalytic activity Figure 3 shows that overcoating actually produces an increase in catalytic activity that is essentially constant up to the thickness produced by 16 ALD cycles. Beyond 16 cycles the Pd particles become increasingly encapsulated until by 32 cycles they are no longer accessible to the methanol reagent. Catalysts prepared by opening new pores in thick alumina overcoats (via calcination) were examined for ethane dehydrogenation activity, selectivity, and stability at 675 °C. Figure 4 shows that these materials exhibit high selectivity to ethylene, low selectivity to undesirable methane production and stable performance with no coking over time. This methodology may have far-reaching application to prolong catalyst lifetimes under severe reaction conditions.

Size and support effects in the oxidative decomposition of methanol by means of <1 nm palladium clusters on an amorphous alumina support were studied under realistic reaction pressures and temperatures. Smaller $Pd_{8\text{-}12}$ clusters were found to promote decomposition to CO and hydrogen; however, with mediocre activity due to CO poisoning. The larger $Pd_{15\text{-}18}$ clusters preferentially produce dimethyl ether

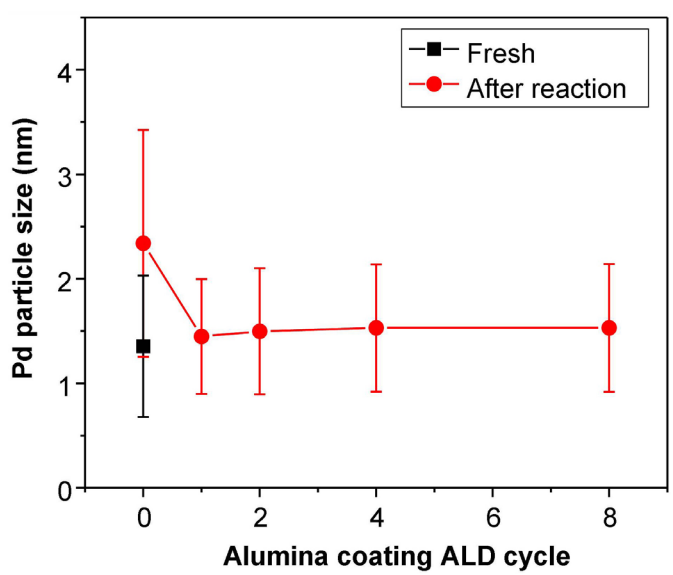

FIGURE 2. Pd particle size after methanol reaction (270°C, 6 hrs) with/without alumina overcoat

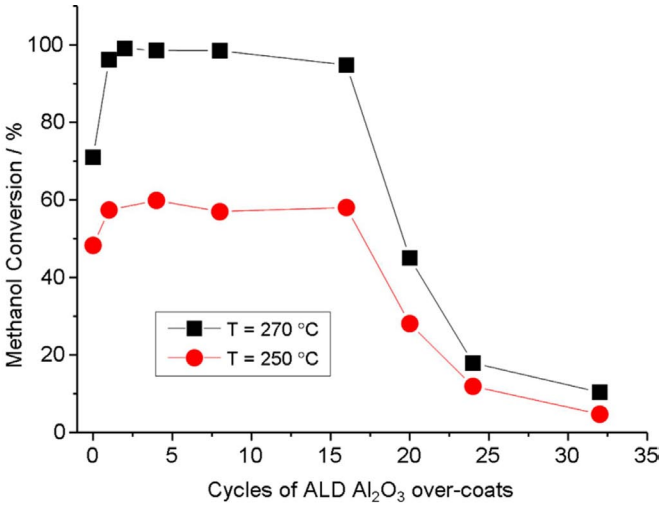

FIGURE 3. Methanol conversion vs. overcoating thickness

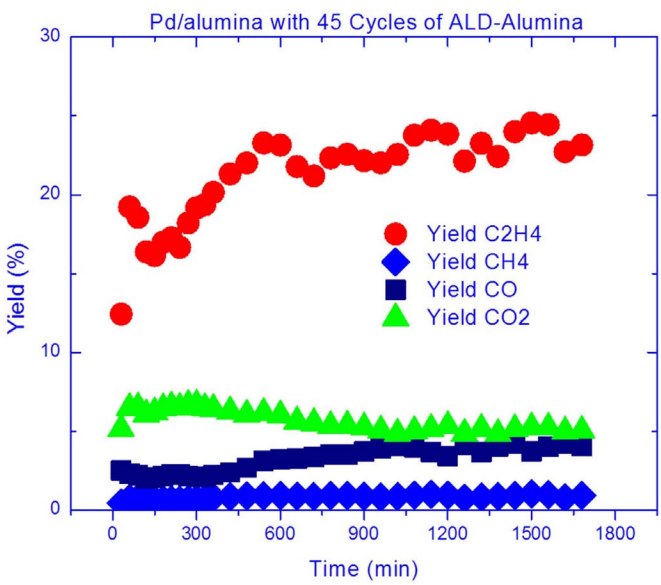

FIGURE 4. Product yields during ethane dehydrogenation catalyzed by overcoated Pd nanoparticles

and formaldehyde, without signs of poisoning. A thin ALD titania overcoat applied on the Pd_{15-18} improves the sintering resistance in a manner similar to the alumina overcoats on larger particles.

Understanding and Predicting Catalysts

The need to characterize these small particles led to the development of new X-ray based techniques at the Advanced Photon Source (APS) at Argonne. *In-situ* XAS has been used in combination with TEM to confirm the size, structure, and composition of metallic and alloy nanoparticles prepared by ALD. In addition to the standard structural characterization of nanoparticle metal and alloy hydrogen production catalysts, several new capabilities have been developed. An *in-operando* reactor, i.e., simultaneous measurement of reaction kinetics and XAS spectra has been developed. The plug-flow reactor can measure the reaction kinetics identically to that in the laboratory and has capabilities which allow for the XAS study of catalysts at temperatures up to about 400°C and 50 atm pressure. A recent improvement in the reactor materials from thick-walled quartz to vitreous carbon allows for *in-operando* XAS measurements of lower energy transition metals, e.g., 3d elements, at lower concentrations, or at faster acquisition times.

In-situ XAS spectroscopy has also been applied for understanding the details in the steps of ALD nanoparticle synthesis. We determined that the support hydroxyl groups react with the Pt-CH_3 bond of the trimethylcyclopentadienyl-methyl Pt (IV) ALD precursor forming CH_4 and the supported dimethylcyclopentadienyl-methyl Pt (IV) complex. Subsequent ALD cycles showed that the precursor preferentially reacts with the support, rather than with metallic or oxidized Pt previously deposited on the support. These insights into the formation of Pt nanoparticles led to ALD strategies for formation of sub-nanometer Pd nanoparticles and bimetallic Pt-Ru nanoparticles mentioned above.

Periodic plane wave calculations were employed to elementary reaction pathways and energetics for methanol decomposition by supported and unsupported M_4 and M_8 (M=Pd, Cu, and Co) clusters for methanol decomposition. For Pd (primarily Pd_4) clusters, the decomposition of methanol begins through CH bond breaking to form hydroxymethyl (CH_2OH), followed by steps involving the formation of hydroxymethylene (CHOH), formyl (CHO), and carbon monoxide (CO). An alternative dehydrogenation pathway with O-H bond breaking as the first step, followed by formation of methoxy (CH_3O) and formaldehyde (CH_2O), was slightly less favorable. In contrast, pathways involving C-O bond cleavage are much less energetically favorable, and no feasible pathways involving C-O bond formation to yield dimethyl ether (CH_3OCH_3) were found. By comparison to extended Pd surfaces, all reaction intermediates were found to bind slightly more strongly to the clusters than to the surfaces. Modeling the effects of an alumina support on methanol decomposition over Pd_4 and Pd_8 clusters indicated that larger Pd clusters and inclusion of the alumina support did not significantly affect the reaction pathways calculated for the Pd_4 cluster.

The reaction pathways on Cu_4 and Co_4 clusters provide a contrast to those of the Pd_4 clusters. The Co_4 cluster pathway is favorable both thermodynamically and kinetically for dehydrogenation, but since CO adsorption is also favorable, it is likely to poison methanol decomposition at low temperatures, similar to Pd clusters. In contrast, CO poisoning of the Cu_4 cluster is less of a problem, but the dehydrogenation steps are not favorable. This finding

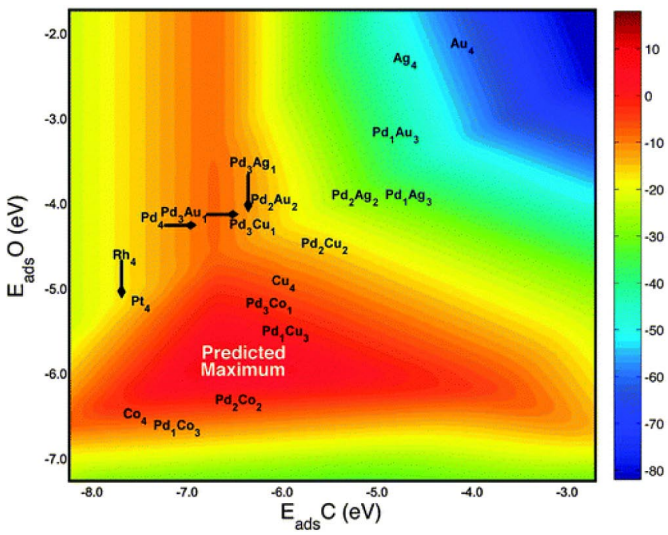

FIGURE 5. Volcano plot of methanol decomposition rate by two component clusters. Red is the highest rate. Blue is the lowest rate.

strongly indicates a need to find other clusters that combine the favorable aspects of the Co and Cu clusters for methanol decomposition while, at the same time, not suffering from the deficiencies of these elements. To this end Brønsted-Evans-Polanyi relationships have been calculated for two-component clusters using bond energies of atomic carbon and oxygen to the cluster as descriptors. The results shown in Figure 5 indicate that Pd-Cu and Pd-Co alloys should be active systems for methanol decomposition.

Future Directions

Formation of new catalyst structures and compositions by ALD appears to be a very promising direction for the future. The potential to create new pore structures with controlled length, diameter and wall composition could have a major impact on catalyst performance, regardless of the target reaction system. Given the extensive scope of materials possible with ALD, the exploration of its potential will benefit from high throughput experimentation. Associated characterization and theory will provide much needed guidance for identifying possible high performance combinations.

Publication list (including patents) acknowledging the DOE grant or contract

1. Vajda, S., Lee, S., Sell, K., Barke, I., Kleibert, A., von Oeynhausen, V., Meiwes-Broer K.-H., Rodríguez, A.F., Elam, J.W., Pellin, M.J., Lee, B., Seifert, S., Winans, R.E., Combined Temperature-Programmed Reaction and In Situ X-ray Scattering Studies of Size-Selected Silver Clusters Under Realistic Reaction Conditions in the Epoxidation of Propene, *Journal of Chemical Physics*, **2009,** *131,*121101.

2. Mehmood, F., J. Greeley, and L.A. Curtiss, Density Functional Studies of Methanol Decomposition on Sub-nanometer Pd Clusters, *Journal of Physical Chemistry C* **2009,** *113,* 21789.

3. Lee, S.; B. Lee, F. Mehmood, S. Seifert, J.A. Libera, J.W. Elam, J. Greeley, P. Zapol, L.A. Curtiss, M.J. Pellin, P.C. Stair, R.E. Winans, and S. Vajda, Oxidative Decomposition of Methanol on Sub-nanometer Palladium Clusters: The Effect of Catalyst Size and Support Composition. *Journal of Physical Chemistry C* **2010,** *114***,** 10342.

4. Mehmood, F., J.P. Greeley, P. Zapol, L.A. Curtiss, Comparative Density Functional Study of Methanol Decomposition on Cu_4 and Co_4 Clusters, *Journal of Physical Chemistry C* **2010,** *114,* 14458.

5. Setthapun, W., Williams, W.D., Kim, S.M., Feng, H., Elam, J.W., Rabuffetti, F.A., Poeppelmeier, K.R., Stair, P.C., Stach, E.A., Ribeiro, F.H., Miller, J.T., Marshall, C.L., Genesis and Evolution of Surface Species During Pt Atomic Layer Deposition on Oxide Supports Characterized by In-Situ XAFS Analysis and Water-Gas Shift Reaction, *Journal of Physical Chemistry C* **2010,** *114*, 9758.

6. Christensen, S.T., Feng, H., Libera, J.L., Guo, N., Miller, J.T., Stair, P.C., Elam, J.W., Supported Ru-Pt Bimetallic Nanoparticle Catalysts Prepared by Atomic Layer Deposition, *Nano Letters* **2010,** *10*, 3047.

7. Feng, H., Libera, J.A., Stair, P.C., Miller, J.T., Elam, J.W., Sub-nanometer Palladium Particles Synthesized by Atomic Layer Deposition, *ACS Catalysis* **2011,** *1*, 665.

8. Feng, H., Lu, J., Stair, P.C., Elam, J.W., Alumina Over-coating on Pd Nanoparticle Catalysts by Atomic Layer Deposition: Enhanced Stability and Reactivity. *Catalysis Letters* **2011,** *141*, 512.

9. Lei, Y., Jelic, J., Nitche, L., Meyer, R.J., Miller, J.T., The Effect of Particle Size and Adsorbates on L_3, L_2 and L_1 X-Ray Absorption Near-Edge Spectra of Supported Pt Nanoparticles, *Topics in Catalysis* **2011,** *54,* 334.

10. Lu, J., Fu, B., Kung, M.C., Xiao, G., Elam, J.W., Kung, H.H., Stair, P.C., Coking and Sintering Resistant Palladium Catalysts Achieved through Atomic Layer Deposition. *Science* 2012, *335,* 1205.

11. Lu, J., Liu, B., Greeley, J.P., Feng, Z., Libera, J.A., Lei, Y., Bedzyk, M.J., Stair, P.C., Elam, J.W., Porous Alumina Protective Coatings on Palladium Nanoparticles by Self-Poisoned Atomic Layer Deposition, *Chemistry of Materials* 2012, *24,* 2047.

12. Mehmood, F., Rankin, R.B., Greeley, J.P., and Curtiss, L.A.,Trends in Methanol Decomposition on Transition Metal Alloy Clusters from Scaling and Bronsted-Evans-Polyani Relationships, *Physical Chemistry Chemical Physics* 2012, *14,* 8644.

V.N.11 Metal and Metal Oxide-Supported Platinum Monolayer Electrocatalysts for Oxygen Reduction

Principal Investigator: Radoslav Adzic
Brookhaven National Laboratory
Upton, NY 11973-5000
Phone: (631) 344-4522
Email: adzic@bnl.gov

Team Members
Additional PIs: Jia Wang, Miomir Vukmirovic, Kotaro Sasaki, Ping Liu
Post-docs: Stoyan Bliznakov, Meng Li, Kurian Kuttiyiel
Graduate Students: Yu Zhang (Stony Brook U), Guangyu Chen (Beijing U. China)

DOE Program Manager: Paul Maupin
Phone: (301) 903-4355
Email: Paul.Maupin@science.doe.gov

Objectives

This program involves studies of basic problems of electrocatalysis of fuel cell reactions while focusing on platinum monolayer electrocatalysts for the O_2 reduction reaction (ORR) and the electrocatalysts for ethanol and methanol oxidation to CO_2. The goals include developing the fundametal understanding of these catalytic systems to allow syntheses of electrocatalysts with ultimately low Pt content. These catalysts have high activity and high stability facilitated by fine-tuning of the activity of Pt monolayer (Pt ML) in the interaction with cores. The nanoparticle, nanorod and nanowire cores will have tailored compositions and shapes, and modified surfaces and sub-surfaces. Kinetic modeling and theoretical calculations are carried out for a deeper insight into the kinetics of the ORR and ethanol oxidation. Studies using well-defined surfaces are carried out to gain understanding of the atomic-scale phenomena involved in the interactions of Pt monolayers with supports as well as developing new catalysts for ethanol and methanol oxidation.

Technical Barriers

The project is focused on developing several Pt ML catalysts that are likely to have the highest Pt mass activity and excellent potential to overcome the obstacles hindering the broad application of fuel cells. The results will enhance our understanding of the metal monolayer-support interactions for a viable approach for controlling chemical reactivity in the top atomic layer. They will also provide insights into catalytic behavior of core-shell nanoparticles and possibilities for designing their properties. In addition, we explore the catalyst capable of C – C bond splitting at low overpotentials in the oxidation of small organic molecules.

Progress Report

Strategies for improving Pt ML electrocatalysts for the ORR and designing catalysts for the oxidation of methanol and ethanol

Several methods for improving Pt ML catalysts have been developed based on earlier results and the current understanding of this topic. These include fine-tuning of the Pt ML-support interaction to enhance activity and stability using: i) noble metal-, and noble metal-non noble metal-alloy cores, ii) hollow metal or alloy cores, iii) ultra-thin nanowires, iv) electrodeposited nanowires on carbon nanoparticles, v) nitride-stabilization of Pt alloys, vi) tensile strain for increasing activity of Pt for methanol and ethanol oxidation. The methods ii)-vi) have been demonstrated in this project.

Pt ML on hollow Pd nanoparticles electrocatalysts for the ORR

We synthesized high-activity electrocatalysts for the ORR comprising a Pt monolayer shell on compact hollow Pd and Pd-Au nanoparticles. Pulse electrodeposited Ni nanoparticles were replaced galvanically by Pd and Pd–Au ions to obtain corresponding hollow nanoparticles. The hollow architecture of the Pd–Au particles was achieved by the delicate balance between galvanic displacement and Kirkendall effect in controlling reaction kinetics. Pt ML catalysts supported on such hollow cores exhibited total-metal mass activities ranging from 0.41 to 0.57 A mg^{-1}. We attribute this enhanced activity to the smooth surface morphology and hollow-induced lattice contraction, in addition to the mass-saving geometry of hollow particles.

Tuning the Pt ML activity by core alloy composition

Alloying Pd with Au increases the stability of such cores, which plays a role under condittion of potential excursions to high anodic values. EXAFS spectra show retardation of Pd oxidation with increasing potentials for $Pd_{90}Au_{10}/C$ and $Pd_{80}Au_{20}/C$ compared with Pd/C nanoparticles. The changes in coordination number of Pd-O demonstrate this tendency more clearly (left figure). This is not observed with $Pd_{70}Au_{30}/C$, presumably due to agglomeration of Au (as also suggested by XRD data). Importantly, Pd_9Au NPs, as well as NWs show significantly enhanced ORR after the deposition of a Pt monolayer. It has a volcano-type composition

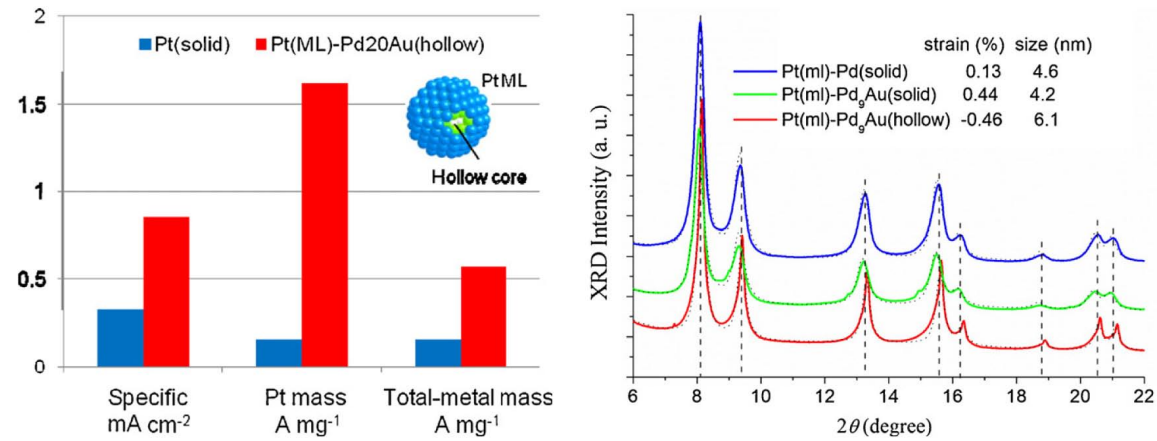

FIGURE 1. The ORR specific and mass activities derived from the kinetic currents at 0.9 V (vs. RHE) for hollow $Pt_{ML}/Pd_{20}Au(h)/C$ nanocatalysts (red) and solid Pt/C nanoparticles (blue) (left panel). Profiles of X-ray powder diffraction intensity for three Pt ML catalysts cores. The dotted lines are the fits, yielding the average particle diameters and lattice constants. The lattice strains listed are calculated with respect to the lattice constant of bulk Pt, 3.923A˚.

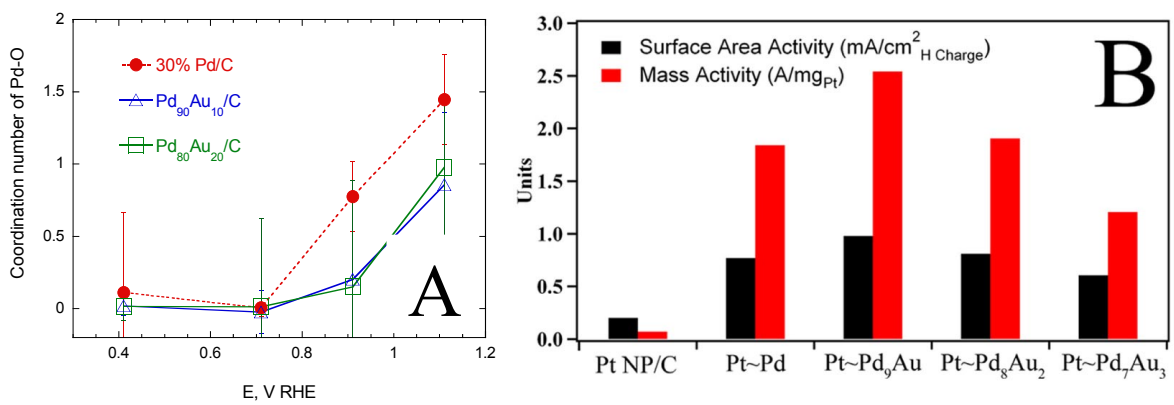

FIGURE 2. Coordination Pd-O number for Pd oxidation with increasing potentials of Pd/C and Pd_xAu_{1-x}/C (A); Kinetic currents at 0.9 V normalized to the measured ESA and the Pt mass for the Pt~Pd1−xAux NW/C and commercial Pt NP/C, respectively (B)

dependence, which likely results from the competition between the structural and electronic effects, as gold content increases.

Nitride stabilized PtNi core−shell nanocatalysts for high ORR activity

The PtNiN synthesis involves nitriding Ni nanoparticles and simultaneously encapsulating them by 2−4 monolayer-thick Pt shell. The experimental data and the DFT calculations indicate nitride has the bifunctional effect that facilitates formation of the core−shell structures and improves the performance of the Pt shell by inducing both geometric and electronic effects. Synchrotron XRD indicates the Ni_4N stoichiometry, while i*n situ* XAS shows the Ni_4N cores protected by Pt shell causing the delayed oxidation of Pt and high stability of the catalyst. Little change in ECSA and a small decrease in half-wave potential after 35,000 potential cycles indicate a high stability of Ni_4N@Pt core-shell NPs. The nitride core lowers the *d*-band center of Pt and promotes Pt diffusion to defect sites on the surface. High ORR activity for Ni, Fe, Co follows the sequence: PtNiN > PtFeN > PtCoN.

Electrocatalysts for ethanol and methanol oxidation

Further studies of the electrocatalysts capable of splitting the C-C bonds at room temperature found that Ir can be made activated in Pt-Ir-SnO_2/C catalyst.

Model catalyst study, supported by DFT calculation, showed that expansive strain caused by underlying Au substrate can dramatically improve the activity of Pt_{ML} for methanol and ethanol oxidation. Co-catalysts such as Ru, SnO_2, $RhSnO_2$ further improve Pt_{ML} due to the bi-functional mechanism, and shift the reaction onset to more negative values with practical interest. IR shows a high catalyst selectivity to CO_2 production. At the potential range of 0.3~0.7V, CO_2 is the only product observed; CH_3COOH

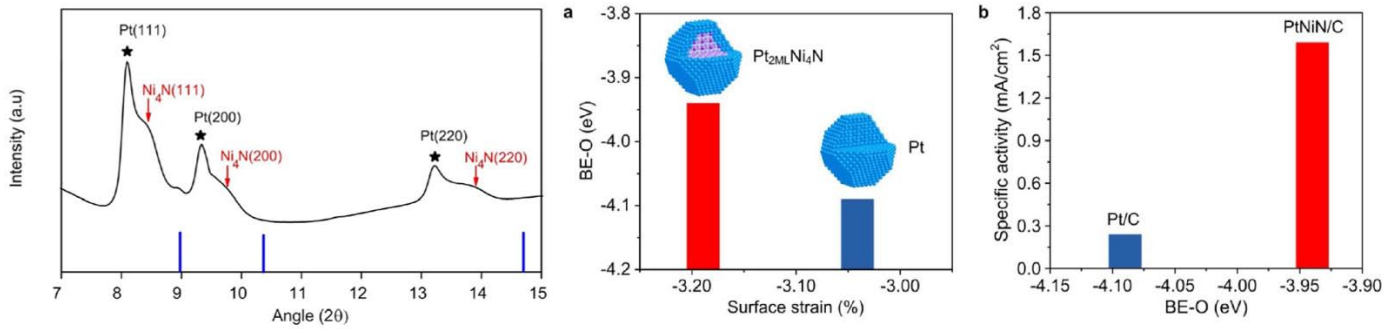

FIGURE 3. Synchrotron XRD pattern for PtNiN catalyst showing Pt and Ni4N phases. (blue line denotes Ni_3N phase). (a) Surface strain versus predicted BE-O on the Pt 2MLNi$_4$N and Pt nanoparticle models with ~1.7 nm. (b) Pt specific activity against BE-O on PtNiN/C and Pt/C.

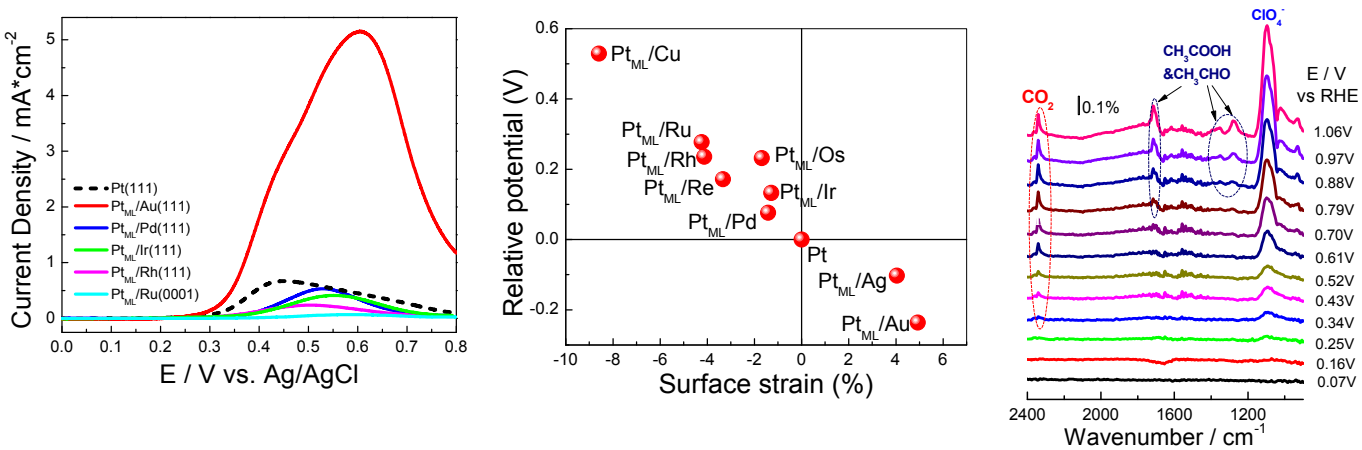

FIGURE 4. Model catalysts: Pt-monolayer supported on different single-crystal for MOR (left) DFT-calculated variation of the lowest potential for MOR to occur (middle), *In situ* FTIR of MOR on Pt/Au/C in 0.1M $HClO_4$, 0.5 M CH_3OH (right).

and CH_3CHO start to show when the potential is higher than 0.7V.

Future studies

The proposed future work is aimed to improve the most promising results obtained so far, to address the open basic questions of the interaction of Pt monolayer with supports and their effects on the kinetics of the ORR, to explore the possible solution to the barrier imposed by the low open circuit potential of the ORR, to increase our understanding of the mechanism of cores protecting the shells in core-shell catalysts, and to design and synthesize the second generation of core-shell catalysts with tuning the effect of core on a Pt monolayer shell by hetero-layered core structure. The supports will also involve refractory metals, and selected oxides, such as CeO_2, NbO_2 and Magneli phase oxides. Graphene oxide as support appears promising in our preliminary studies. We will start studies of supported pyrolized transition metal macrocycles. Preliminary results are very promising. How are the ORR activities of metal in the extended surface and in the form of supported-nanoparticles related?

Electrodeposition of selected alloys as stable, inexpensive cores and optimization of the cores shapes. Using non-aqueous solvents for electrodeposition of reactive metal cores, UPD of various MLs for Pt ML deposition on reactive metals and alloys.

Considerable effort will be focused on the electrocatalysts for ethanol oxidation. We will continue with theoretical studies to determine what are the geometries and energetics of reactants, possible intermediates and transition states? On which sites does the reaction take place? The critical size of ensemble of atoms for ethanol adsorption will be determined. To address these questions of ORR and EOR, theoretical calculations will be coordinated with our experiments on well-defined model catalysts. DFT calculations will be combined with micro-kinetic modeling, kinetic Monte Carlo (KMC) and molecular dynamic (MD) simulations.

Publications

1. Bliznakov, S., Vukmirovic, M., et al. Electrodeposition of Pd Nanowires and Nanorods on Carbon Nanoparticles. Maced. J. Chem. Chem. Eng. 2011 30 (1): 19-27.

2. Konopka, D.A., Li, M., et al. Platinum Supported on NbRuyOz as Electrocatalyst for Ethanol Oxidation in Acid and Alkaline Fuel Cells. J. Phys. Chem. C 2011 115 (7): 3043-3056.

3. Sasaki, K., Kuttiyiel, K., et al. Carbon-Supported IrNi Core-Shell Nanoparticles: Synthesis, Characterization, and Catalytic Activity. J. Phys. Chem. C 2011 115 (20): 9894-9902.

4. Sasaki, K., Kuttiyiel, K., et al. Platinum Monolayer on IrFe Core-Shell Nanoparticle Electrocatalysts for the Oxygen Reduction Reaction. Electrocatal. 2011 2 (2): 134-140.

5. Adzic, R. Platinum Monolayer Electrocatalysts: Tunable Activity, Stability, and Self-Healing Properties. Electrocataly. 2012 3 (3-4): 163-169.

6. Bliznakov, S.T., Vukmirovic, M.B., et al. Pt Monolayer on Electrodeposited Pd Nanostructures: Advanced Cathode Catalysts for PEM Fuel Cells. J. Electrochem. Soc. 2012 159 (9): F501-F506.

7. Chen, W.F., Sasaki, K., et al. Hydrogen-Evolution Catalysts Based on Non-Noble Metal Nickel-Molybdenum Nitride Nanosheets. Angew. Chem. Int. Ed. 2012 51 (25): 6131-6135.

8. Gong, K.P., Cho, Y., et al. Tetrahedral Palladium Nanocrystals: A New Support for Platinum Monolayer Electrocatalysts with High Activity and Stability in the Oxygen Reduction Reaction. Z. Phys. Chem. 2012 226 (9-10): 1025-1038.

9. Herron, J.A., Jiao, J., et al. Oxygen Reduction Reaction on Platinum-Terminated "Onion-structured" Alloy Catalysts. Electrocatal. 2012 3 (3-4): 192-202.

10. Huang, K., Sasaki, K., et al. Increasing Pt oxygen reduction reaction activity and durability with a carbon-doped TiO2 nanocoating catalyst support. J. Mater. Chem. 2012 22 (33): 16824-16832.

11. Kang, Y. J., Qi, L., et al. Highly Active Pt3Pb and Core-Shell Pt3Pb-Pt Electrocatalysts for Formic Acid Oxidation. ACS Nano 2012 6 (3): 2818-2825.

12. Karan, H. I., Sasaki, K., et al. Catalytic Activity of Platinum Mono layer on Iridium and Rhenium Alloy Nanoparticles for the Oxygen Reduction Reaction. ACS Catalysis 2012 2 (5): 817-824.

13. Koenigsmann, C., Sutter, E., et al. Size- and Composition-Dependent Enhancement of Electrocatalytic Oxygen Reduction Performance in Ultrathin Palladium-Gold (Pd1-xAux) Nanowires. J. Phys. Chem. C 2012 116 (29): 15297-15306.

14. Koenigsmann, C., Sutter, E., et al. Highly Enhanced Electrocatalytic Oxygen Reduction Performance Observed in Bimetallic Palladium-Based Nanowires Prepared under Ambient, Surfactantless Conditions. Nano Lett. 2012 12 (4): 2013-2020.

15. Kuttiyiel, K.A., Sasaki, K., et al. Bimetallic IrNi core platinum monolayer shell electrocatalysts for the oxygen reduction reaction. Energy Environ. Sci. 2012 5 (1): 5297-5304.

16. Kuttiyiel, K.A., Sasaki, K., et al. Nitride Stabilized PtNi Core-Shell Nanocatalyst for high Oxygen Reduction Activity. Nano Lett. 2012 12 (12): 6266-6271.

17. Zhou, W.P., An, W., et al. Electrooxidation of Methanol at SnOx-Pt Interface: A Tunable Activity of Tin Oxide Nanoparticles. J. Phys. Chem. Lett. 2012 3 (22): 3286-3290.

18. Li, M., Liu, P., et al. Platinum Monolayer Electrocatalysts for Anodic Oxidation of Alcohols. J. Phys. Chem. Lett. 2012 3 (23): 3480-3485.

19. Sasaki, K., Naohara, H., et al. Highly stable Pt monolayer on PdAu nanoparticle electrocatalysts for the oxygen reduction reaction. Nature Communications 2012 3 1115 1-9.

20. Yang, L.J., Vukmirovic, M.B., et al. Tuning the Catalytic Activity of Ru@Pt Core-Shell Nanoparticles for the Oxygen Reduction Reaction by Varying the Shell Thickness. J. Phys. Chem. C 2013 117 (4): 1748-1753.

21. Zhang, Y., Ma, C., et al. Hollow core supported Pt monolayer catalysts for oxygen reduction. Catal. Today 2013 202: 50-54.

22. Kang, Y.J., Ye, X.C., et al. Design of Pt-Pd Binary Superlattices Exploiting Shape Effects and Synergistic Effects for Oxygen Reduction Reactions. J. Am. Chem. Soc. 2013 135 (1): 42-45.

23. Chen, W.F., Wang, C.H., et al. Highly active and durable nanostructured molybdenum carbide electrocatalysts for hydrogen production. Energy Environ. Sci. 2013 6 (3): 943-951.

24. Li, M., Cullen, D.A., et al. Ternary Electrocatalysts for Oxidizing Ethanol to Carbon Dioxide: Making Ir Capable of Splitting C-C Bond. J. Am. Chem. Soc. 2013 135 (1): 132-141.

V.N.12 Active Sites and Mechanism for the Water-Gas Shift Reaction on Metal and Metal/Oxide Catalysts (BNL FWP CO-027)

Principal Investigator: José A. Rodriguez
Chemistry Department
Brookhaven National Laboratory
Upton, NY 11973
Phone: (631) 344-2246
Email: rodrigez@bnl.gov

Names of Team Members:

- Ping Liu
  Chemistry Department
  Brookhaven National Laboratory
  Upton, NY 11973
  Phone: (631) 344-5970
  Email: pingliu3@bnl.gov
- Jonathan C. Hanson
  Chemistry Department
  Brookhaven National Laboratory
  Upton, NY 11973
  Pone: (631) 344-4344
  Email: hanson1@bnl.gov
- Dario Stacchiola
  Chemistry Department
  Brookhaven National Laboratory
  Upton, NY 11973
  Phone: (631) 344-4378
  Email: djs@bnl.gov
- Sanjaya Senanayake
  Chemistry Department
  Brookhaven National Laboratory
  Upton, NY 11973
  Phone: (631) 344-4344
  Email: ssenanay@bnl.gov

DOE Program Manager: Raul Miranda
Phone: (301) 903-2508
Email: Raul.Miranda@science.doe.gov

Objectives

Most hydrogen is currently derived from steam reforming of hydrocarbons (reacting steam with natural gas): $C_nH_m + nH_2O \rightarrow nCO + (n\text{-}m/2)H_2$. The reformed fuel contains substantial CO, which degrades the performance of the platinum catalysts used in polymer electrolyte membrane (PEM) fuel cell systems. The water-gas shift reaction (WGS: $CO + H_2O \rightarrow H_2 + CO_2$) is a critical process in providing pure hydrogen for fuel cells and other applications. Our main objective is to obtain the knowledge necessary to predict the behavior, and ultimately design, improved cost-effective low temperature water-gas shift catalysts.

Technical Barriers

What is the active phase of WGS catalysts? A central challenge is the difficulty of characterizing the active state of the catalyst at the elevated pressure and temperatures used for WGS operation. *In-situ* studies are needed to characterize the composition of metal-oxide catalysts and establish the general role of reduced metal nanoparticles vs. cationic metal centers.

What is the reaction mechanism? A generally accepted mechanism for the WGS reaction does not yet exist. Alternatives include associative mechanisms (i.e. formation of HCOO, HOCO, CO_3 or HCO_3 intermediates) and the redox mechanism. Generally, the WGS involves the activation of water to release H_2 and the activation of CO to combine with the O left behind to release CO_2. However, the problem is complex since metal nanoparticles and the oxide support can work in a cooperative way, facilitating different reaction steps.

Abstract

Current industrial catalysts for the water-gas shift reaction are commonly mixtures of Fe-Cr and Zn-Al-Cu oxides, used at temperatures between 350-500°C and 180-250°C, respectively. These oxide catalysts are pyrophoric and normally require lengthy and complex activation steps before usage. Improved catalysts are being sought, particularly for lower temperature (e.g., at T<150°C, equilibrium lowers the product CO concentration into ranges suitable for direct

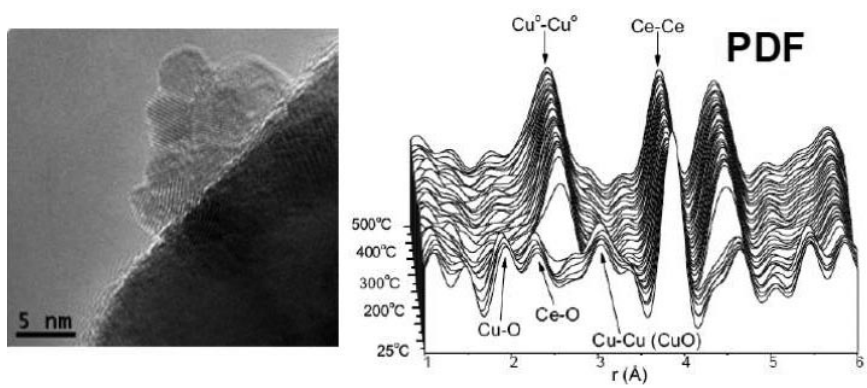

FIGURE 1. Left: TEM image of an inverse CeO_x/CuO catalysts. Right: *In-situ* time-resolved PDF data for a CeO_2/CuO catalyst during the WGS.

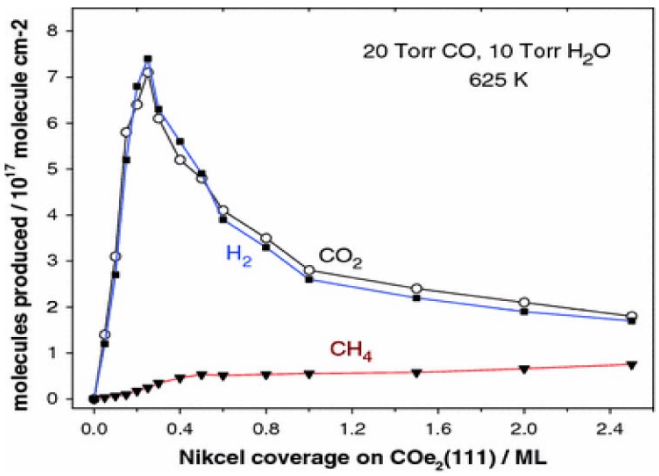

FIGURE 2. Water-gas shift activity of Ni/CeO_2(111) as a function of Ni coverage.

fuel cell use without further purification.). Ceria (Au, Cu or Pt on CeO_2), titania (Au, Pd or Pt on TiO_2) and molybdena (Ni, Cu and Au on MoO_2) based nanostructured catalysts are very promising new candidates for high activity, lower temperature operation in WGS systems. However, the design and optimization of these and other metal/oxide WGS nanocatalysts are hindered by controversy about basic questions regarding the nature of the active sites and the reaction mechanism. Here, we follow a coordinated experimental and theoretical effort to better understand these promising metal/oxide catalysts, and to develop concepts for their improvement. The project combines research in three thrusts: (i) *in-situ* studies to determine catalyst structure, oxidation state and chemistry under reaction conditions; (ii) studies of relevant model systems, primarily based on nanoparticles supported on single crystal substrates; and (iii) computational modeling. By closely linking these three research thrusts, our goal is to provide strongly validated mechanistic and structural conclusions for the future design and optimization of nanostructured WGS catalysts.

Progress Report

In-situ studies of WGS catalysts with XRD, PDF, XAFS and TEM: Evolution of metal/oxide catalysts

The active phase of a series of metal/oxide powder catalysts (Pt/CeO_2, Pt-Ru/CeO_2, Pt/CeOx/TiO_2, Au/CeO_x/TiO_2, $Ce_{1-x}Ni_xO_{2-y}$, CeO_x/CuO) was investigated using a combination of *in-situ* time-resolved X-ray diffraction (XRD), Pair-distribution function (PDF) analysis, X-ray absorption fine structure (XAFS) and environmental TEM. Under reaction conditions most of these WGS catalysts underwent chemical transformations that drastically modified their composition with respect to that obtained during the synthesis process. The active phase of catalysts which combine Cu, Ni, Au or Pt with oxides such as CeO_2, TiO_2 and CeO_x/TiO_2 essentially involved nanoparticles of the reduced metals. The oxide support underwent partial reduction and was not a simple spectator, facilitating the dissociation of water and in some cases modifying the chemical properties of the supported metal. Therefore, to optimize the performance of these catalysts one must take into consideration the properties of the metal and oxide phases. Figure 1 shows a TEM image and PDF data for an inverse CeOx/CuO powder catalysts. In the TEM image, taken for the as-prepared catalysts, one can see crystallites that in many cases exhibit a (111) surface termination. The PDF results for water-gas shift reaction conditions show a simultaneous disappearance of the Cu-O vector of CuO with the appearance of a Cu-Cu vector for metallic copper. These data, and in-situ results obtained for other catalysts in our group, indicate that a WGS metal/oxide catalyst is a dynamic entity that changes with reaction conditions.

Metal-oxide interactions and the activity of water-gas shift catalysts

A series of model catalysts {CeOx/Cu(111), CeOx/Au(111), Pt/CeO_2(111), Ni/CeO_2(111), Pt/TiO_2(110), Pt/CeOx/TiO_2(110)} was used to study fundamental aspects of the water-gas shift reaction. These studies revealed that the oxide component of the catalyst can affect the reaction process in two different ways. First, the presence of O vacancies in the oxide greatly facilitates the dissociation of water. Second, the electronic properties of the metal can be affected by interactions with the oxide producing special chemical properties. This is the case in the Ni/CeO_2(111), Pt/ CeO_2(111) and Pt/CeO_x/TiO_2(110) systems. In Figure 2, small coverages of Ni on CeO_2(111) are highly active for the water-gas shift reaction and do not produce methane, although bulk Ni is a very good catalyst for the methanation of CO. The electronic properties of Ni and Pt nanoparticles deposited on CeO_2(111) and CeO_x/TiO_2(110) have been examined using core and valence photoemission. The results of valence photoemission point to a new type of metal-support interaction which produces large electronic perturbations for small Ni and Pt particles in contact with ceria. The Ni/CeO_2(111), Pt/CeO_2(111) and Pt/CeO_x/TiO_2(110) systems exhibited a density of metal d states near the Fermi level that was much smaller than that expected for bulk metallic Ni or Pt. The electronic perturbations induced by ceria on Ni made this metal a very poor catalyst for CO methanation, but transformed Ni into an excellent catalyst for the production of hydrogen through the water-gas shift reaction(Figure 2) and the steam reforming of ethanol. Furthermore, the large electronic perturbations seen for small Pt particles in contact with ceria significantly enhanced the ability of the admetal to adsorb and dissociate water made it a highly active catalyst for the water-gas shift reaction(Figure 3). The behaviour seen for Ni/CeO_2(111), Pt/CeO_2(111) and Pt/CeO_x/TiO_2(110) systems illustrates the positive effects derived from electronic metal-support interactions and points to a promising approach for

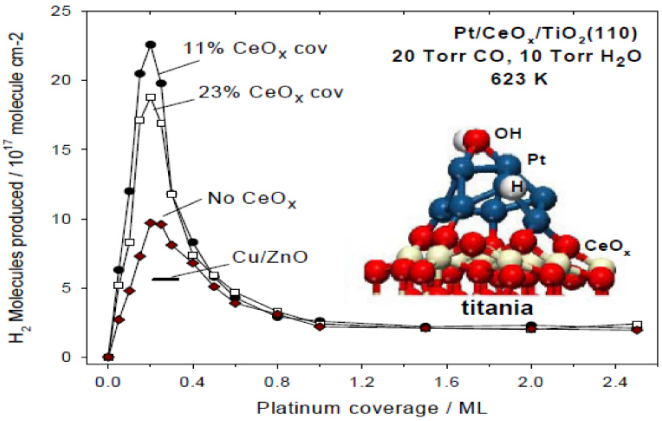

FIGURE 3. Water-gas shift activity of $Pt/TiO_2(110)$ and $Pt/CeO_x/TiO_2(111)$ as a function of Pt coverage.

improving or optimizing the performance of metal/oxide catalysts.

Future Directions

We will be using a combination of experiment and theory to continue our studies on the behavior of WGS nanocatalysts that contain three different types of oxides: Ceria- (Cu/CeO_2, Au/CeO_2, Pd/CeO_2, Pt/CeO_2), titania- (Au/TiO_2, Pd/TiO_2, Pt/TiO_2) and molybdena-based (Au/MoO_2, Cu/MoO_2, Ni/MoO_2) systems. The future research can be divided into three major thrusts:

i) In-situ Characterization of High-Surface Area Powder Catalysts. In the next years we will perform systematic experiments that will focus on examining the chemical state and structural/morphological properties of metal/oxide WGS catalysts using a unique suite of techniques (XAFS, XRD, TEM) for *in-situ* characterization. A new capability for environmental transmission electron microscopy (ETEM) is being established at the Center for Functional Nanomaterials (CFN) in BNL. The new ETEM is a custom-designed instrument for advanced *in-situ* electron microscopy, including experiments for chemical reaction and crystal growth in various gas environments. It is the first of its kind and will be applied for three dimensional (3D) tomography and near-edge x-ray absorption spectroscopy with powder catalysts. After the structural and morphological characterization of the catalysts, experiments that use IR spectroscopy to probe the WGS reaction mechanism will be carried out. We will be able to validate or discard controversial claims. The combination of *in-situ* XANES, XRD, TEM and IR spectroscopy will allow us to establish meaningful correlations between structure and reactivity that can be directly used to improve the performance of WGS industrial catalysts. The studies described in this part of the proposal will give basic information that will be used in the other two parts of the project for modeling the catalytic process at an atomic level and for testing fundamental concepts.

ii) Experimental Studies with Model Well-defined Catalysts. The powder nanocatalysts under study in the previous part are complex by nature. Investigators have a limited control over the structural and electronic properties that can affect the chemical reactivity of the system. This makes it difficult to study basic phenomena associated with the water-gas shift reaction: How does the reaction change with particle size, what is the nature of the electronic interaction between the admetal and oxide support,are electronic effects more important than structural or ensemble effects, is the oxide a simple spectator, how does the reaction rate depend on the oxide surface structure?

In this part of the project, we plan to do WGS studies on several well-defined model catalysts. These model systems will be used to examine fundamental issues that have been raised from *in-situ* studies of high-surface area powder catalysts and will provide results that are essential for the theoretical work described in the next section. Metal nanoparticles will be deposited by physical vapor deposition on single crystal oxide surfaces. Another type of model will involve "inverse" catalysts consisting of oxide nanoparticles supported on Au(111), Cu(111) and Pt(111) single crystals. We have been successful preparing nano-arrays of MoO_x, TiO_x and CeO_x on Au(111). We also know how to prepare $CeO_x/Cu(111)$ "inverse" model catalysts. The model systems are flexible and can be modified to test new concepts or hypothesis that will come from the future theoretical studies. Since we will be dealing with new materials or catalyst configurations, these studies also can give novel ideas on what should be considered when designing new industrial catalysts.

In-situ data collected with IR spectroscopy and moderate-pressure XPS on the well-defined metal/oxide and oxide/metal systems will point to key intermediates in the WGS reaction mechanism and will be extremely useful as a check-point in the theoretical studies described in the next section.

(iii) Theoretical Studies of WGS Reaction Mechanism and the Behavior of Active Sites. Despite extensive efforts, there are some issues involved in the WGS reaction that cannot be addressed directly by experiment. What is the detailed reaction pathway including the geometries and energetics of reactants, possible intermediates and transition states? On which sites does the reaction take place? How are the WGS activities of metal and metal oxide nanoparticles affected by differences in their electronic structure and geometry associated with particle size and shape, the metal oxidation state, the support, and particle↔support interactions?

We will be performing calculations on systems similar to those under study in the previous sections (i) and (ii). When going from extended surfaces to isolated nanoparticles and oxide supported nanoparticles, the effects of size, shape, and metal↔oxide interactions on the catalysis will

be determined. Our calculations on these materials will be coordinated with extensive experiments, especially for the model catalysts discussed in section (ii), so that meaningful comparisons can be made. Our DFT study of a system will start with the calculation of the reaction pathway, where the computationally identified possible intermediates can be compared with the results from our experimental *in-situ* studies. With the calculated information on the energetics of intermediates and transition states, a micro-kinetic model will be developed to estimate the catalytic activity. In addition, features of the reaction pathway obtained from static DFT studies will be explored by molecular dynamics (MD) simulations. With this close interaction between theory and experiment, we should be able to provide definitive information about the behavior of WGS catalysts. The DFT calculations will be carried out using the DMol^3, CASTEP and VASP codes. For a few of these systems, we will perform MD simulations using the algorithms available in CASTEP, VASP or CPMD. We will also augment the micro-kinetic model calculations with kinetic Monte Carlo (KMC) simulations.

Publication list: 20 papers published or in press

1. Gonzalez, Ines et al, A Comparative Study of the Water Gas Shift Reaction over Platinum Catalysts Supported on CeO_2, TiO_2 and Ce-modified TiO_2. *Catal. Today* **2010**, *149*, 372-379.

2. Rodriguez, Jose et al, Inverse Oxide/Metal Catalysts: A Versatile Approach for Activity Tests and Mechanistic Studies. *Surf. Sci.* **2010**, *604*, 241-244 **(invited)**.

3. Park, Joon et al, Gold, Copper and Platinum Nanoparticles dispersed on $CeO_x/TiO_2(110)$ Surfaces: High Water-Gas Shift Activity and the Nature of the Mixed-Metal Oxide at the Nanometer Level. *J. Am. Chem. Soc.* **2010**, *132*, 356-363.

4. Senanayake, Sanjaya et al, Probing the Reaction Intermediates for the Water-Gas Shift over Inverse CeO_x/Au(111) Catalysts. *J. Catal.* **2010**, *271*, 392 - 400.

5. Barrio, Laura et al, Unusual Physical and Chemical Properties of Ni in $Ce_{1-x}Ni_xO_{2-y}$ Oxides: Structural Characterization and Catalytic Activity for the Water Gas Shift Reaction. *J. Phys. Chem. C*, **2010**, *114*, 12689-12697.

6. Barrio, Laura et al, Unraveling the Active Site in Copper−Ceria Systems for the Water−Gas Shift Reaction: *In Situ* Characterization of an Inverse Powder CeO_{2-x}/CuO−Cu Catalyst. *J. Phys. Chem. C*, **2010**, *114*, 3580-3587.

7. Senanayake, Sanjaya et al, Water-Gas Shift and CO Methanation Reactions over Ni-CeO_2(111) Catalysts. *Topics in Catal.* **2011**, *54*, 34 - 41.

8. Barrio, Laura et al, *In situ* characterization of Pt catalysts supported on ceria modified TiO_2 for the WGS reaction: influence of ceria loading on catalytic behavior. *Phys. Chem. Chem. Phys.*, 2012, *14*, 2192-2202.

9. Rodriguez, Jose, Gold-based Catalysts for the Water–gas Shift Reaction: Active Sites and Reaction Mechanism. *Catal. Today*, **2011**, *160*, 3-10 **(invited)**. http://www.sciencedirect.com/science/article/pii/S092058611000444X - item1#item1

11. Rodriguez, Jose, Supported Gold in CO Oxidation, the Water-gas Shift, and DeSOx Reactions, book chapter for *Supported Metals in Catalysis*, 2nd Edition (Editors: James Anderson and Marcos Fernandez-Garcia), Imperial College Press, London, 2012 **(invited book chapter)**.

12. Senanayake, Sanjaya et al, Nanopatterning in CeO_x/Cu(111): A New Mechanism for Surface Reconstruction and Enhancement of Catalytic Activity. *J. Phys. Chem. Letters*, **2012**, *3*, 839-843.

13. Bruix, Albert et al., A New Type of Strong Metal-Support Interaction and the Production of H_2 through the Transformation of Water on Pt/CeO_2(111) and Pt/CeO_x/TiO_2(110) Catalysts. *J. Am. Chem. Soc.* **2012**, *134*, 8968-8974.

14. Xu, Weiqian et al. *In situ* Studies of CeO_2-supported Pt, Ru, and Pt–Ru Alloy Catalysts for the Water–gas Shift Reaction: Active Phases and Reaction Intermediates. *J. Catal.* **2012**, *291*, 117-126.

15. Kubacka, Anna et al, Tungsten as an Interface Agent Leading to Highly Active and Stable Copper-Ceria Water Gas Shift Catalyst. *Applied Catal. B : Environmental*, **2012**, *132/133*, 423-432.

16. Ramirez-Reina, Tomas et al, *Operando* Characterization of Iron-promoted Ceria-Alumina Gold Catalysts during the Water-gas Shift Reaction. *Catal. Today*, **2013**, *205*, 41-48.

17. Senanayake, Sanjaya et al, Unique Properties of Ceria Nanoparticles Supported on Metals: Novel Inverse Ceria/Copper catalysts for CO Oxidation and the Water-Gas Shift Reaction. *Accounts of Chemical Research*, 2013, in press **(invited)**.

18. Rodriguez, Jose et al, In-situ/Operando Studies for the Production of Hydrogen through the Water-Gas Shift on Metal Oxide/Catalysts. *Phys. Chem. Chem. Phys.* **2013**, in press (**invited**).

19. Si, Rui et al., Effect of Ceria on Gold-Titania Catalysts for the Water-Gas Shift Reaction: Fundamental Studies for Au/CeO_x/TiO_2(110) and Au/CeO_x/TiO_2 Powders. *J. Phys. Chem. C*, **2012**, *116*, 23547-23555.

20. Stacchiola, Dario et al. Importance of the Metal–Oxide Interface in Catalysis: *In Situ* Studies of the Water–Gas Shift Reaction by Ambient-Pressure X-ray Photoelectron Spectroscopy. *Angew. Chem. Int. Ed.* **2013**, in press.

V.N.13 Fundamentals of Catalysis and Chemical Transformations

Principal Investigator: Steven. H. Overbury
Oak Ridge National Laboratory
Chemical Sciences Division
1 Bethel Valley Rd
Oak Ridge, TN 37831
Phone: (865) 574 5040
Email: overburysh@ornl.gov

Co-investigators:
AC Buchanan, Sheng Dai, Edward W. Hagaman, De-en Jiang, Michelle Kidder, Danny Lutterman, David R. Mullins, Adyita Savara, Zili Wu

DOE Program Manager: Raul Miranda
Phone: (301) 903-8014
Email: Raul.miranda@science.doe.gov

Objectives

Our objective is to achieve a detailed understanding of how oxygenates adsorb, transform and react with one another and other functionalities on highly uniform model catalysts. The hypothesis is that this approach may lead to general methods for design of improved catalysts. A related objective is to elucidate the role of site geometry, oxygen availability, confinement, and metal support interactions in controlling selectivity in reactions catalyzed on oxides surfaces and supported metal particles.

Technical Barriers

The conversion of biomass is limited by a need for new, stable and more selective catalysts. Success in our project may lead to a general understanding of catalytic oxygenate transformations that may lead to improved catalysts.

Abstract

The overarching goal of this proposal is to learn how oxygenated molecules, relevant to the conversion of biomass, interact and react in fluid phases and at the surfaces of heterogeneous catalysts. We tailor new catalysts by original synthetic methods, probe their structures by a wide array of techniques before, during and after their use in catalytic reactors, examine their surface species during reaction using *operando* and flow pyrolysis techniques, determine their actual catalytic performance and computationally model the molecular and interfacial interactions that explain their behavior. We focus on oxide catalysis, especially CeO_2; catalysis by Au, especially with respect to structure and stabilization of supported Au and Au based catalysts; and reaction pathways of model lignin molecules tethered to SiO_2 surfaces. Our work combines computational methods to aid interpretation of experimental measurements and to create detailed models of reaction pathways.

Progress Report

Surface chemistry on monolithic CeO_2

Highly oriented films of $CeO_2(111)$ and $CeO_2(100)$ have been used as model surfaces to typify the surface chemistry of oxygenates on reducible oxides. Recently we have focused on the comparison of these two surface structures to explore the role of site geometry upon the surface chemical transformations. We have explored adsorption and evolution of methanol and water and find that the increased ease of vacancy formation on the (100) surface compared to the (111) surface plays a role in altering the selectivity for decomposition compared to desorption. Another focus area is the effect of structure on the transformations of the oxygenates, especially small alcohols and aldehydes.

We have examined the surface intermediates that form as a function of temperature, coverage and oxidation state of the surface on these two surfaces. Temperature-dependent adsorption and reaction of acetaldehyde (CH_3CHO) on a fully oxidized and a highly reduced thin-film $CeO_2(111)$ surfaces have been investigated using a combination of reflection-absorption IR spectroscopy (RAIRS) and periodic density functional theory (DFT+U) calculations. On the fully oxidized surface, acetaldehyde adsorbs weakly through its carbonyl O interacting with a lattice Ce^{4+} cation in the η1-O configuration. This state desorbs at 210 K without reaction. On the highly reduced surface, new vibrational signatures appear below 220 K due to a dimer state formed from the coupling of the carbonyl O and the acyl C of two acetaldehyde molecules. This dimer decomposed above 400 K to produce enolate (CH_2CHO^-). Calculated activation barriers for the coupling of acetaldehyde, the decomposition of the dimer state, and the recombinative desorption of enolate and H as acetaldehyde, agree with TPD for acetaldehyde adsorbed on reduced $CeO_2(111)$. The results demonstrate that surface oxygen vacancies play a crucial role in stabilizing and activating acetaldehyde for coupling reactions.

Acetaldehyde adsorption on $CeO_2(100)$ is stronger than on the (111) surface and desorption extends through a larger T range from 200 K to above 400 K. In addition to the parent molecule, above 400 K additional products are observed. Total decomposition to CO, CO_2 and H_2O are the principal pathways with a small amount of dehydration to produce acetylene at 700 K. In addition, a notable product is the small amount of crotonaldehyde that is evident at 430 K, a result of the aldol condensation coupling reaction between

two acetaldehyde molecules. The adsorption and reaction on CeO_2(100) is consistent with trends previously observed for the other oxygenates. Specifically, stronger adsorption results from a greater number of coordination vacancies around the Ce cation on CeO_2(100) compared to CeO_2(111). The CO and CO_2 products result from dehydrogenation of the adsorbed acetaldehyde by the basic O anions. The water desorption results from the relative ease with which the H reacts with the surface O.

Studies on shaped nanocrystals

Oriented single crystals have limited surface area and the UHV environment is challenging for probing catalytic pathways. To bridge this gap we have initiated studies of reactions chemisorption and reactions studies on shaped nanoparticles that have well defined surface structures including cubes that terminate on {100} surfaces, octahdedra that terminate on {111} and rods that terminate on a mixture of defective but low index terminations. Using these nanoshapes we have probed structure dependence in chemisorption and reaction rates.

Adsorption and desorption of a probe molecule, methanol, were followed by *in situ* IR and Raman spectroscopy to probe surface species and mass spectrometry to probe temperature dependent evolution of desorption products. Upon methanol adsorption, on-top, bridging and three-coordinate methoxy species are formed on rods and cubes while only on-top methoxy is present on the octahedra. The distribution of the methoxy species is believed to be determined by the coordination status of surface Ce cations and the amount of defect sites on the three nanoshapes. During the TPD the methoxy species are gradually dehydrogenated into H_2 and CO *via* formate intermediates. Formyl is also evident on the rods. Methoxy is more reactive on the rods, resulting in desorption of H_2 and CO at lower temperature (< 583 K) than on cubes and octahedra. Higher than stoichiometric H/CO ratio is observed in the methanol-TPD products, attributed to retention of some amount of formate and carbonate on the ceria nanoshapes as revealed by *in situ* IR. A small amount of methanol and formaldehyde desorbs below 423 K from the three surfaces due to the disproportionation of methoxy. UV Raman and IR results indicate that the ceria nanoshapes are slightly reduced at room temperature by methanol adsorption, and become more reduced during methanol desorption. The degree of reduction is dependent on the surface structure of the nanoshapes.

Shaped CeO_2 nanoparticles have also been used to explore the effect of surface structure upon the surface chemistry and catalytic selectivity for the ethanol selective oxidation reaction. CeO_2 octahedra, cubes and rods were synthesized using previously published methods. Adsorption and desorption behavior on these nanoshapes was determined by a combination of temperature programmed desorption (TPD) and in situ DRIFTS. Activity and selectivity were measured in steady state and in temperature programmed surface reaction (TPSR). Shape dependent differences are observed in surface adsorbates, their transformation temperatures and the selectivity for dehydration, dehydrogenation and decomposition. Ethoxide and acetate are the primary surface species present under both TPD and TPSR conditions for all shapes. Different rates of α- and β-CH bond scission on the different shapes are responsible for different product selectivity. Structure dependent, reductive vacancy formation and availability of reactant O_2 combine to control surface H which in turn plays a role in controlling product selectivity.

Au catalysts, clusters and bimetallic catalysts

We have explored various salts as supports, including phosphates and sulfates, that may stabilize Au catalysts for gas phase reactions such as CO oxidation. Au catalysts containing $BaSO_4$ nanocrystals (5–8 nm) were prepared by *in situ* growth method using amphiphilic sulfonate (SDBS) as the sulfate source, leading to new, highly stable, nonreducible but ‘‘active’’ Au catalyst supports that may be preferable to the typical reducible oxides for low-temperature CO oxidation. The results suggest a unique interaction between Au nanoparticles and nanosized $BaSO_4$ supports. We have also explored another strategy for stabilizing ultra-small gold clusters under thermal treatment. By this strategy, thiolated gold clusters (Au_{25}, Au_{144}), after removal of the protecting thiolate ligands by thermal treatment, can be stabilized onto heterostructured mesoporous supports. The essence of this strategy lies in use of the heterostructured binary oxide supports (M_xOy-$mSiO_2$) synthesized through a combination of a transition-metal oxide and an ordered mesoporous silica. Monodispersed Au clusters can be readily absorbed into the pores of this heterostructured oxide. The size of the clusters is maintained after removing the thiolate ligands by thermal treatment in air, making this method superior to *in vacuo* treatment. Small gold clusters supported on these heterostructured mesoporous supports were found to be active for CO oxidation.

We have developed a synthetic methodology to create supported, nanoscale AuCuPd ternary alloy nanoparticles through the diffusion of Cu^0 and Pd^0 atoms in an organic solvent using hexadecylamine as a reductant and ligand stabilizer. Subjecting the AuCuPd catalyst to reductive or oxidative pretreatment conditions greatly affected the catalytic activity for the oxidation of CO. In situ XRD and EXAFS indicated that oxidizing the catalyst to 300°C produced a AuPd alloy core that was separated from CuO and a small amount of PdO. Oxidation at 500°C resulted in the segregation of PdO and CuO to form a decorated Au rich particle. Forming a PdO and CuO rich surface on the AuPd or Au-rich core decreased O_{ads} spill over from Cu to Au or Pd sites and hindered access to the Au active sites resulting in decreased catalytic activity. Reducing the catalyst under H_2 formed a AuCuPd alloy with a Cu rich surface and

formed the most active catalyst. It is likely that Cu, a base metal, helped to lower the activation energy through the activation O_2 that could migrate to Au or Pd sites. However, $AuCu/SiO_2$ demonstrated an opposite structure-activity relationship. Reduced AuCu alloy was the least active catalyst and improved after it was oxidized to form a Au-CuO hybrid particle.

$Au_{15}(SR)_{13}$ is the smallest, stable thiolated gold nanocluster experimentally identified so far and its elusive structure may hold the key to the origin of the nucleus in the formation of thiolated gold nanoclusters. By an extensive exploration of possible isomers by DFT, we arrive at a novel structure for $Au_{15}(SR)_{13}$ with high stability and whose optical-absorption features match experiment. This structure features a cyclic [Au(I)-SR] pentamer interlocked with one staple trimer motif protecting the tetrahedral Au_4 nucleus, together with another trimer motif. This structure suggests that $Au_{15}(SR)_{13}$ is a transitional composition from the $[Au(I)\text{-}SR]_x$ polymer ($Au_{10}(SR)_{10}$) to larger $Au_n(SR)_m$ clusters that have only the staple motifs; and that the nucleation process starts from the Au_4 core. We have also explored the interaction between gold nanoclusters and a fully hydroxylated surface, $Mg(OH)_2$ basal plane, by using a DFT-enabled local basin-hopping technique for global-minimum search. We find strong interaction of Au clusters with the surface -OH *via* a short bond between edge Au atoms and O atoms of the OH groups. We expect that this strong interaction is ubiquitous on hydroxylated support surfaces and helps the gold clusters against sintering, thereby contributing to their CO-oxidation activity at low temperatures.

Future Directions

Additional DFT computations will be performed to understand better how surface site geometry affects the rates of α- and β-CH bond scission, and how this alters product selectivity. Probe molecules will be chosen to examine substituent group effects on the CH bond cleavage of the adsorbed reactants. Adsorption of various 'test' gases (pyridine, acetonitrile, CO, CO_2…) on the CeO_2 nanoshapes will be used to quantify how structure affects acid-base parameters and bonding interactions. We will examine increasingly more complicated oxygenates such as polyols to understanding how adjacent hydroxyls compete for sites. Experimental studies of reaction selectivity and surface intermediates on the CeO_2 shapes will be supplemented with computer simulations to build a detailed understanding of the reaction pathways. Following a similar approach, work will continue on characterizing ketonization of acids, especially acetic acid, on the ceria nanoshapes. We will initiate studies of Au clusters deposited on CeO_2 nanoshapes with the goal of creating highly uniform model catalysts that have known support structure and identically sized Au particles. The stability and temperature dependent evolution of these catalysts will be studied microscopically, and their reactivity/selectivity will be characterized and compared to the CeO_2 and Au reactivities to elucidate metal-support effects on the model surfaces.

Publication list

1. Tian, C.; Chai, S.-H.; Mullins, D.R.; Zhu, X.; Binder, A.; Guo, Y.; Dai, S., Heterostructured $BaSO_4$–SiO_2 mesoporous materials as new supports for gold nanoparticles in low-temperature CO oxidation. *Chem. Commun.* **2013,** *49* 3464-3466.

2. Poutsma, M.L., Evolution of Structure-Reactivity Correlations for the Hydrogen Abstraction Reaction by Chlorine Atom. *J. Phys. Chem. A* **2013,** *117*, 687-703.

3. Mullins, D.R.; Albrecht, P.M.; Calaza, F.C., Variations in Reactivity on Different Crystallographic Orientations of Cerium Oxide. *Topics in Catalysis* **2013,** *in press*.

4. Liu, Z.G.; Chai, S.H.; Binder, A.; Li, Y.Y.; Ji, L.T.; Dai, S., Influence of calcination temperature on the structure and catalytic performance of CuOx-CoOy-CeO_2 ternary mixed oxide for CO oxidation. *Appl. Catal. A - Gen.* **2013,** *451*, 282-288.

5. Beste, A.; Buchanan, A.C., III, Computational Investigation of the Pyrolysis Product Selectivity for alpha-Hydroxy Phenethyl Phenyl Ether and Phenethyl Phenyl Ether: Analysis of Substituent Effects and Reactant Conformer Selection. *J. Phys. Chem. A* **2013,** *117,* 3235–3242.

6. Albrecht, P.M.; Mullins, D.R., Adsorption and Reaction of Methanol over CeOx(100) Thin Films. *Langmuir* **2013,** *in press*.

7. Younker, J.M.B., A.; Buchanan, I., A.C., Computational Study of Bond Dissociation Enthalpies for Lignin Model Compounds: β-5 Arylcoumaran. *Chem. Phys. Lett* **2012,** *545*, 100-106.

8. Yang, X.; Wu, Z.; Moses-Debusk, M.; Mullins, D.R.; Mahurin, S.M.; Geiger, R.M.; Kidder, M.K.; Narula, C.K., Heterometal Incorporation in M-Exchanged Zeolites Enables Low Temperature Catalytic Activity of NOx Reduction. *J. Phys. Chem. C* **2012,** *116*, 23322-23331.

9. Wu, Z.; Schwartz, V.; Li, M.; Rondinone, A.; Overbury, S.H., Support Shape Effect in Metal Oxide Catalysis: Ceria Nanoshapes Supported Vanadia Catalysts for Oxidative Dehydrogenation of Isobutane. *J. Phys. Chem. Lett.* **2012,** *3* 1517–1522.

10. Wu, Z.; Li, M.; Overbury, S.H., Probing the surface sites of ceria nanoshapes via methanol adsorption and reaction. *ACS Catalysis* **2012,** *2*, 2224 - 2234.

11. Wu, Z.; Li, M.; Overbury, S.H., Raman Spectroscopic Study of the Speciation of Vanadia Supported on Ceria Nanocrystals with Defined Surface Planes. *ChemCatChem* **2012,** *4* (10), 1653-1661.

12. Wu, Z.; Li, M.; Overbury, S.H., On the Structure Dependence of CO Oxidation over CeO_2 Nanocrystals with Well-Defined Surface Planes. *J. Catal.* **2012,** *285*, 61-73.

13. Tian, C.C.; Chai, S.H.; Zhu, X.; Wu, Z.L.; Binder, A.; Bauer, J.C.; Brown, S.; Chi, M.F.; Veith, G.M.; Guo, Y.L.; Dai, S., In situ growth synthesis of heterostructured $LnPO_4$-SiO_2 (Ln = La, Ce, and Eu) mesoporous materials as supports for small gold particles used in catalytic CO oxidation. *J Mater Chem* **2012,** *22* (48)), 25227-25235.

14. Singh, J.A.; Overbury, S.H.; Dudney, N.J.; Li, M.; Veith, G.M., Gold Nanoparticles Supported on Carbon Nitride: Influence of Surface Hydroxyls on Low Temperature Carbon Monoxide Oxidation. *ACS Catalysis* **2012,** *2*, 1138−1146.

15. Qiao, Z.A.; Huo, Q.S.; Chi, M.F.; Veith, G.M.; Binder, A.J.; Dai, S., A "Ship-In-A-Bottle" Approach to Synthesis of Polymer Dots@Silica or Polymer Dots@Carbon Core-Shell Nanospheres. *Advanced Materials* **2012,** *24* (45), 6017.

16. Qian, H.F.; Jiang, D.E.; Li, G.; Gayathri, C.; Das, A.; Gil, R.R.; Jin, R.C., Monoplatinum Doping of Gold Nanoclusters and Catalytic Application. *J Amer. Chem. Soc.* **2012,** *134* (39), 16159-16162.

17. Poutsma, M.L., Review of Rate Constants and Exploration of Correlations of the Halogen Transfer Reaction of Tri-substituted Carbon-Centered Radicals with Molecular Halogens. *J. Org. Chem* **2012,** *77*, 2619-2636.

18. Mullins, D.R.; Albrecht, P.M.; Chen, T.-L.; Calaza, F.; Biegalski, M.D.; Christen, H.M.; Overbury, S.H., Water Dissociation on CeO_2(100) and CeO_2(111) Thin Films. *J. Phys. Chem. C* **2012,** *116*, 19419−19428.

19. Ma, G.C.; Binder, A.; Chi, M.F.; Liu, C.; Jin, R.C.; Jiang, D.E.; Fan, J.; Dai, S., Stabilizing gold clusters by heterostructured transition-metal oxide-mesoporous silica supports for enhanced catalytic activities for CO oxidation. *Chem. Commun.* **2012,** *48* (93), 11413-11415.

20. Kintzel, E.J.J.; Kidder, M.K.; Buchanan, A.C., III; Britt, P.F.; Mamantov, E.; Zamponi, M.; Herwig, K.W., The Dynamics of 1,3-Diphenylpropane Tethered to the Interior Pore Surfaces of MCM-41. *J. Phys. Chem. C* **2012,** *116*, 923.

21. Jiang, D.-e.; Overbury, S.H.; Dai, S., Structures and Energetics of Pt Clusters on TiO2: Interplay between Metal–Metal Bonds and Metal–Oxygen Bonds. *The Journal of Physical Chemistry C* **2012,** *116* (41), 21880-21885.

22. Fulvio, P.F.; Mayes, R.T.; Bauer, J.C.; Wang, X.Q.; Mahurin, S.M.; Veith, G.M.; Dai, S., "One-pot" synthesis of phosphorylated mesoporous carbon heterogeneous catalysts with tailored surface acidity. *Catalysis Today* **2012,** *186* (1), 12-19.

23. Calaza, F.C.; Xu, Y.; Mullins, D.R.; Overbury, S.H., Oxygen Vacancy-Assisted Coupling and Enolization of Acetaldehyde on CeO2(111). *J Amer. Chem. Soc.* **2012,** *134* (43), 18034-18045.

24. Beste, A.; Buchanan, A.C., III, Kinetic Simulation of the Thermal Degradation of Phenethyl Phenyl Ether, a Model Compound for the β-O-4 Linkage in Lignin. *Chem. Phys. Lett.* **2012,** *550*, 19-24.

25. Beste, A.; Buchanan, A.C., III, The Role of Carbon-Carbon Phenyl Migration in the Pyrolysis Mechanism of β-O-4 Lignin Model Compounds: Phenethyl Phenyl Ether and α-Hydroxy Phenethyl Phenyl Ether. *J. Phys. Chem. A* **2012,** *116*, 12242-12248.

26. Bauer, J.C.; Veith, G.M.; Allard, L.F.; Oyola, Y.; Overbury, S.H.; Dai, S., Silica-Supported Au-CuOx Hybrid Nanocrystals as Active and Selective Catalysts for the Formation of Acetaldehyde from the Oxidation of Ethanol. *ACS Catalysis* **2012,** *2* (12), 2537-2546.

27. Allard, L.F.; Overbury, S.H.; Bigelow, W.C.; Katz, M.B.; Nackashi, D.P.; Damiano, J., Novel MEMS-Based Gas-Cell/Heating Specimen Holder Provides Advanced Imaging Capabilities for In Situ Reaction Studies. *Microscopy and Microanalysis* **2012,** *18* (4), 656-666.

28. Yin, H.F.; Ma, Z.; Chi, M.F.; Dai, S., Heterostructured catalysts prepared by dispersing Au@Fe2O3 core-shell structures on supports and their performance in CO oxidation. *Catalysis Today* **2011,** *160* (1), 87-95.

29. Tenney, S.A.; He, W.; Ratliff, J.S.; Mullins, D.R.; Chen, D.A., Characterization of Pt-Au and Ni-Au Clusters on TiO_2(110). *Topics in Catalysis* **2011,** *54*, 42.

30. Pei, Y.; Shao, N.; Li, H.; Jiang, D.E.; Zeng, X.C., Hollow Polyhedral Structures in Small Gold–Sulfide Clusters. *ACS Nano* **2011,** *5*, 1441.

31. Ma, Z.; Dai, S., Development of Novel Supported Gold Catalysts: A Materials Perspective. *Nano Res* **2011,** *4*, 3-32.

32. Li, M.J.; Wu, Z.L.; Overbury, S.H., CO oxidation on phosphate-supported Au catalysts: Effect of support reducibility on surface reactions. *J. Catal.* **2011,** *278* (1), 133-142.

33. Jiang, D.E.; Overbury, S.H.; Dai, S., Interaction of Gold Clusters with a Hydroxylated Surface. *J. Phys. Chem. Lett.* **2011,** *2* (10), 1211-1215.

34. Jiang, D.E.; Dai, S., The Role of Low-coordinate Oxygen on Co_3O_4(110) in Catalytic CO Oxidation. *Phys. Chem. Chem. Phys.* **2011,** *13*, 978.

35. Chen, T.-L.; Mullins, D.R., Ethylene Glycol Adsorption and Reaction over CeO_x(111) Thin Films. *J. Phys. Chem. C* **2011,** *115* 13725-13733.

36. Chen, T.-L.; Mullins, D.R., Adsorption and Reaction of Acetaldehyde over CeO_X(111) Thin Films. *J. Phys. Chem. C* **2011,** *115*, 3385.

37. Calaza, F.C.; Chen, T.L.; Mullins, D.R.; Overbury, S.H., Structure and Reactivity of Alkyl Ethers Adsorbed on CeO(2)(111) Model Catalysts. *Topics in Catalysis* **2011,** *54* (1-4), 56-69.

38. Brooks, J.D.; Chen, T.-L.; Mullins, D.R.; Cox, D.F., Reactions of ethylidene on a model chromia surface: 1,1-dichloroethane on stoichiometric α-Cr_2O_3 (10-12). *Surface Science* **2011,** *605*, 1170.

39. Bauer, J.C.; Mullins, D.; Li, M.J.; Wu, Z.L.; Payzant, E.A.; Overbury, S.H.; Dai, S., Synthesis of silica supported AuCu nanoparticle catalysts and the effects of pretreatment conditions for the CO oxidation reaction. *Phys. Chem. Chem. Phys.* **2011,** *13* (7), 2571-2581.

V.N.14 Activation of Small Molecules with Bi-Functional Ambiphilic Catalyst Complexes

Principal Investigator: Tom Autrey
Pacific Northwest National Laboratory
Phone: (509) 375-3792
Email: tom.autrey@pnnl.gov
Donald Camaioni, Abhi Karkamkar,
Greg Schenter, Herman Cho, Shawn Kathmann,
Bojana Ginoska-Pangovska, Mark Bowden

DOE Program Manager: Raul Miranda
Catalysis Sciences Program
Office of Science, U.S. Dept. of Energy
E-mail: Raul.Miranda@science.doe.gov

Objectives

To determine and understand the factors controlling the energy landscapes describing the mechanism and the dynamics of catalyzed reaction pathways. Insight into quantitative structure-reactivity relationships will facilitate rational approaches to design and control the synthesis of new catalyst structures.

Technical Barriers

New research tools to measure kinetic and thermodynamic parameters in catalytic reactions. Development of computational methods to study solvent effects on reactions. Discovery of cheaper, *greener* catalyst materials.

Abstract

The objective of our research is to develop fundamental insight into catalysis and small molecule activation in molecular complexes that will provide the basis for developing rational approaches in new catalysis design. Our focus is bi-functional – ambiphilic centers – molecular complexes comprised of both electron-rich and electron-poor sites, that provide an environment for heterolytic activation of molecular hydrogen and other small molecules such as CO_2 for transformation to fuels for energy storage. Our research approach uses a combination of experimental spectroscopy and computational modeling to study trends in structure-function relationships that control the thermodynamics and kinetics of small molecule activation. The outcome of this research will be predictive models for controlling chemical transformations at the molecular level. This work has wide ranging implications in catalysis for energy storage and energy storage materials as well as alternative approaches to catalytic activation of small molecules *without using transition metals*.

Progress Report

Until recently, few chemists would have predicted that molecular hydrogen could be activated at ambient temperature and pressure using a combination of an amine or phosphine Lewis base with a borane Lewis acid. The accepted view had been that metals and d-electrons are required to activate hydrogen.[1] However, a paradigm shift in our appreciation of hydrogen activation and catalysis was initiated by the reports from the Stephan group[2] that a *frustrated Lewis pair* (FLP) – that is, an ambiphilic complex of a Lewis acid and Lewis base that cannot form a formal Donor – Acceptor dative bond provides a *vacancy* of latent reactivity, between the D and A to heterolytically activate molecular hydrogen –at room temperature. Recently the collaborative efforts by Stephan & Erker[3,4] and Soós & Papai[5] have demonstrated the use of FLPs in catalytic hydrogenation of polar functional groups. The novel reactivity afforded by a bi-functional catalyst, illustrated in Figure 1, demonstrates that there are new approaches to catalysis and small molecule activation that do not require metals.[6]

While H_2 activation and transfer to polar unsaturated substrates by non-metal catalysts is a provocative observation there is little insight into the mechanism or the properties that control the driving force for the catalytic reaction. In Stephens' pioneering work[7] it was noted that the reactivity

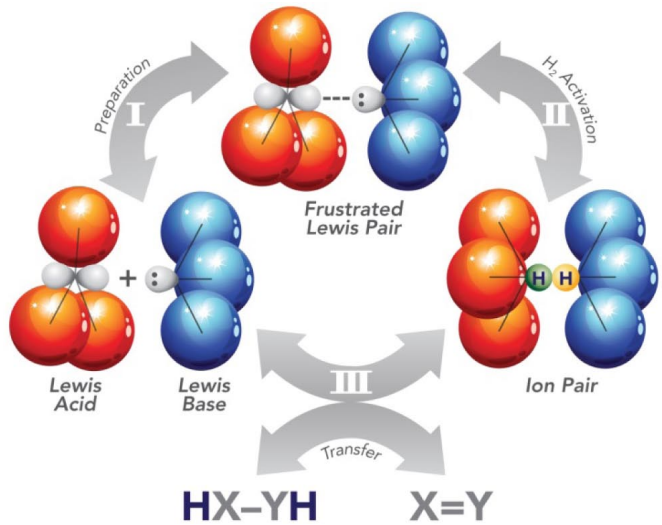

FIGURE 1. Illustration of the catalytic reduction cycle; step I, catalyst preparation; step II, H_2 activation; step III, H_2 transfer.

appeared to be correlated with the cumulative acidity and basicity of the Lewis pairs, however, it was not until recently that Rokob and co-workers provided evidence for this hypothesis.[8]

Recent computational studies suggested a few intriguing proposals to describe the unique reactivity of FLPs; Pápai and co-workers suggested that a loosely organized frustrated pair at an optimal acid-base distance provides *bifunctional cooperativity* for a synergistic interaction with molecular hydrogen.[9] Wang and co-workers suggest that *geometrical constraints* are important and optimal alignment of the Lewis acid and Lewis base can lower the activation barrier.[10] Pyykko describes an energy decomposition analysis (EDA) of H_2 activation by a FLP and suggests the attraction between the protonic and hydridic hydrogen in the products compensates for the energy required to split H_2 homolytic.[11] Finally, Grimme has put forth a provocative hypothesis - that the molecular or chemical nature of the FLP is not as important as the strong electrostatic attraction induced by the FLP.[12] He notes that the *electric field strength* in FLPs approaches the magnitude required to split H_2 in a vacuum without a barrier and that the rate limiting step for H_2 activation is diffusion into a *prepared Lewis pair* (PLP).

This computational work provides some thought provoking propositions to explain the latent reactivity afforded by bringing together in close proximity an electron rich Lewis base and an electron deficient Lewis acid species creating a new reactive *vacancy*; however, there is little experimental insight into either the thermodynamics or kinetics of FLP formation, H_2 activation by FLPs or H_2 transfer from FLPs to unsaturated substrates. **A central theme to our catalysis research program is to minimize the heights of the hills and the depths of the valleys along the reaction pathway**. To this end we use methods to determine reaction thermodynamics to understand the factors that control the depth of the valleys and measure activation barriers to understand the factors that control the height of the hills in the catalytic reaction cycle (*see PI publication list, references 1-3*). Further to this understanding there are a number of fundamental scientific questions that we will address in our research to maximize the potential of the catalytic cycle outlined in Figure 1:

- Is a sufficient electric field all that is necessary for H_2 activation or are bonding and other environmental factors just as important? Are there geometric constraints, e.g., specific angles and distances between the Lewis acid and Lewis base to enhance reactivity, both H_2 activation and catalytic H_2 transfer?
- How does the reactivity of a bidentate Lewis acid or base differ from the reactivity of an intramolecular Lewis acid-base complex?
- What parameters best describe the reactivity created in the vacancy, {}, between the Lewis base, D and Lewis acid, A, pair, i.e., D{}A? What is the rate limiting step in the catalytic reduction of polar molecules; hydride transfer, proton transfer, a concerted H^+/H^- transfer?

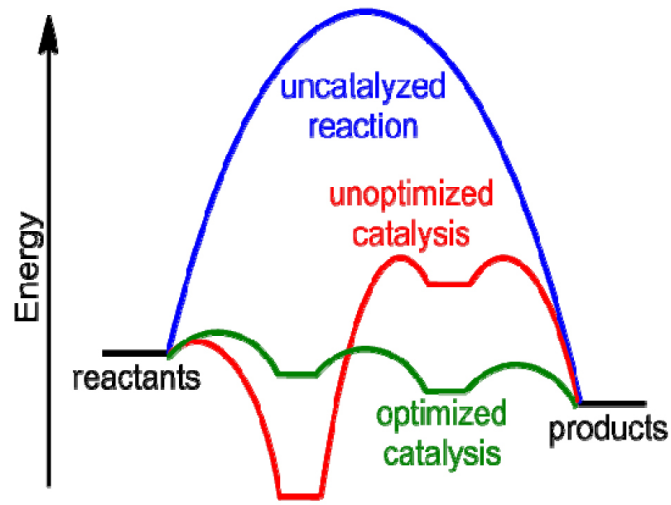

- How does this distinctive property, i.e., a quasi-open coordination site, {}, formed between an electron rich and electron poor site, correlate with vacancies and defects in heterogeneous catalysis structures and surfaces composed of Lewis acid and Lewis base sites? What properties in these molecular structures are essential to understand and enable the building of parallel properties in heterogeneous structures?
- What can we learn from fundamental studies of molecular complexes of FLPs combined with transition metals, i.e., 'tri-functional' sites to build new catalyst complexes, heterogeneous & homogeneous complexes for small molecule activation and catalysis?
- How general is this phenomena of small molecule activation without metals? How can these vacancies be optimized for the catalytic reduction of CO_2 or biomass functions, e.g., carbonyls?

These are critical questions relevant to the advancement of hydrogenation catalysis research. The need for novel approaches to catalytic hydrogenation are becoming more important as we consider alternate energy feed stocks – needs ranging from biomass upgrading to the conversion of wastes, e.g., CO_2, to usable liquid fuels, i.e., MeOH. The possibility of the catalytic reduction of carbon dioxide and CO to liquid fuels is not unreasonable given recent reports of reversible binding of CO_2 in FLPs[13] and the stoichiometric reduction of CO_2 to methanol using an FLP to activate carbon dioxide,[14] or hydrogen.[15] More recently Labinger and Bercaw have demonstrated the synergy of a combination of a metal and Lewis acid/base for the reduction of CO.[16]

Fundamental understanding of novel approaches to catalysis and small molecule activation are of direct relevance

to research missions supported by the U.S. Department of Energy to enable basic research science to predict and control matter and energy at the electronic, atomic and molecular levels in order to provide foundations for new energy technologies critical to energy, environment and national security.

Future Directions

Our research will build upon our previous accomplishments using experimental spectroscopy, thermodynamic and kinetic measurements combined with computational modeling to gain fundamental insight into the unique properties of bi-functional ambiphilic catalyst centers. We are interested in understanding structure-reactivity relationships for small molecule activation to elucidate the properties that control reactivity (**kinetics**) and driving force (**thermodynamics**) in catalytic reactions. The study of *homotopic*[17] catalytic reaction centers composed of well-defined Lewis acid/base pairs is readily controlled and tunable, both in complexity and function. We will investigate the mechanisms for all steps in the catalytic cycle, (i) catalyst preparation, i.e., the equilibrium between the Lewis acid, A, Lewis base, B, the Frustrated Lewis pair (FLP) and the activated or Prepared Lewis pair (PLP), (ii) H_2 activation by the PLP and (iii) H^+/H^- transfer from the Ionic pair (IP) to the unsaturated substrate, by intra- and inter-molecular and Lewis pairs.

Publication list

1. Abhi Karkamkar, Kshitij Parab, Doinita Neiner, Thomas K. Nielsen, Herman Cho, Donald M. Camaioni, Tom Autrey. Thermodynamic Study of Heterolytic Hydrogen Activation by Frustrated Borane-Amine Lewis Pairs. Invited *Dalton Trans*. **2013**, *42*, 615.

2. Liem X. Dang, Gregory K. Schenter, Tsun-Mei Chang, Shawn M. Kathmann and Thomas S. Autrey. The Role of Solvent on the Thermodynamics and Kinetics of Forming Frustrated Lewis Pairs. J. Phys. Chem. Letters. *J. Phys. Chem. Lett.* **2012**, *3*, 3312. DOI: 10.1021/jz301533a.

3. Donald M. Camaioni, Bojana Ginovska-Pangovska, Gregory K. Schenter, Shawn M. Kathmann, and Tom Autrey. Analysis of the Activation and Heterolytic Dissociation of H2 by "Frustrated" Lewis Pairs: NH3 and BX3 (X = H, F and Cl). *J. Phys Chem A*. **2012**, 116, 7228.

4. Arshad Aijaz, Abhi Karkamkar, Young Joon Choi, Nobuko Tsumori, Ewa Rönnebro, Tom Autrey, Hiroshi Shioyama, Qiang Xu. Immobilizing Highly Catalytically Active Pt Nanoparticles inside the Pores of Metal-Organic Framework. *J. Am. Chem. Soc*. **2012**, *134*, 13926.

5. Thomas K. Nielsen, Abhi Karkamkar, Mark Bowden, Flemming Besenbacher, Torben R. Jensen, Tom Autrey. Methods to stabilize and destabilize ammonium borohydride. Invited *Dalton Trans*, **2013**, *42*, 680.

6. Zhenguo Huang, Tom Autrey. Boron-nitrogen-hydrogen ("BNH") compounds: recent developments in hydrogen storage, applications in hydrogenation and catalysis, and new syntheses. *Energy Environ. Sci.*, **2012**, *5*, DOI:10.1039/C2EE23039A. Invited Review

References (Endnotes)

1. G Kubas. *Science* **2006**, *314*, 1096.

2. GC Welch, RRS Juan, JD Masuda, DW Stephan, *Science* **2006**, *314*, 1124.

3. DW Stephan, et al. Inorg. Chem. **2011**, *50*, 12338.

4. DW Stephan, Erker, G. *Angew. Chem. Int. Ed.* **2010,** *49*, 46.

5. G Erős, H Mehdi, I Pápai, TA Rokob, P Király, G Tárkányi, T Soós, *Angew. Chem. Int. Ed.* **2010,** *49.*

6. PP Power, Nature **2010**, 463.

7. GC Welch, DW Stephan, *J. Am. Chem. Soc.* **2007**, 129, 1880.

8. TA Rokob, Hamza, A.; Pápai, I. *J. Am. Chem. Soc*. **2009**, *131*, 10701.

9. TA Rokob, Bako, I.; Stirling, A.; Hamza, A.; Pápai, I. *J. Am. Chem. Soc.*, **2013**, *135*, 4425.

10. G Lu, Li, L.; Zhao, L.; Huang, F.; Wang, Z-X. *Inorg. Chem*. **2010**, *49*, 295.

11. P Pyykko, Wang. C. *Phys Chem. Chem. Phys.* **2010**, *12*, 149.

12. S Grimme, Kruse, H.; Goerigk, L.; Erker, G. *Angew. Chem. Int. Ed*. **2010,** *49*, 1402.

13. CM Mömming, E Otten, G Kehr, R Fröhlich, S Grimme, DW Stephan, G Erker. *Angew. Chem. Int. Ed*. **2009**, 48, 6643.

14. G Ménard, DW Stephan. *J. Am. Chem. Soc*. **2010**, 132, 1796.

15. A Ashley, L Thompson, D O'Hare. Angew. Chem. Int. Ed. **2009**, 48, 9839.

16. AJM Miller, JA Labinger, JE Bercaw. *J. Am. Chem. Soc.*, **2010**, *132*, 3301.

17. Robert Crabtree, *Chemical Reviews* **2011**, **DOI:** 10.1021/cr2002905

V.N.15 Bio-Inspired Molecular Catalysts for Oxidation of Hydrogen and Production of Hydrogen: Cheap Metals for Noble Tasks

Principal Investigator: R. Morris Bullock
Pacific Northwest National Laboratory
P.O. Box 999, K2-57
Richland, WA 99352
Phone (509) 372-6589
Email: morris.bullock@pnnl.gov

Names of Team Members
- PNNL Staff Colleagues: Daniel L. DuBois, Mary Rakowski DuBois
- Postdoctoral Research Associates (2010-present): Kevin Welch, Jenny Y. Yang, Eric Wiedner, Tianbiao "Leo" Liu, Elliott Hulley

DOE Program Manager: Dr. Raul Miranda
Office of Basic Energy Sciences
Chemical Sciences, Geosciences, & Biosciences (CSGB) Division
Email: Raul.Miranda@science.doe.gov

Objectives

Electrocatalysts based on inexpensive, earth-abundant metals are needed since most fuel cells are based on platinum, an expensive, precious metal. Our objective is to design and synthesize biologically inspired functional model complexes that catalyze the oxidation of hydrogen and the production of hydrogen. Our research focuses on molecular complexes containing ligands bearing pendant amines that function as proton relays.

Technical Barriers

It is now widely recognized that there is a need to develop catalysts that rely less on noble metals like platinum, particularly for use in large scale energy systems where the high cost and low abundance of precious metals will preclude their use. Our efforts focus on the rational development of new molecular catalysts based on inexpensive, abundant metals such as iron, manganese and cobalt. The technical barriers include synthesis and design of ligands and metal complexes, obtaining an understanding of mechanistic details of the reactions, and development of highly active electrocatalysts with low overpotentials. In addition, we seek to use thermodynamic data to guide the rational design of molecular catalysts. Such thermochemical data can come from equilibrium measurements by spectroscopic measurements (e.g., NMR spectroscopy) as well as electrochemical studies. Together, these measurements provide critical information required for the rational design of molecular catalysts, including acidity of protonated pendant amines of the ligands and hydride donor ability of metal hydrides. Understanding the thermodynamics allows the rational design of catalysts for oxidation of hydrogen or the reverse, production of H_2 by reduction of protons.

Abstract

Electrocatalysts for fast, efficient conversion between electrical and chemical energy is needed because of the temporal variations of renewable, carbon-free sources of energy such as solar and wind. Storing energy in the HH bond of hydrogen is attractive since oxidation of hydrogen in a fuel cell provides electricity efficiently and cleanly. Electrocatalysts based on inexpensive, earth-abundant metals are needed since most fuel cells are based on platinum, an expensive, precious metal. The cost of cobalt, manganese or iron is at least a thousand times less expensive than platinum, so dramatic cost savings would result from development of catalysts using these inexpensive, earth-abundant metals. Natural hydrogenase enzymes oxidize and produce H_2 using iron and nickel. Our objective is to design and synthesize biologically inspired functional models that catalyze the oxidation of hydrogen and production of hydrogen with high activity and low overpotentials. A comprehensive knowledge of the thermochemical properties of MH and NH bonds underpins our ability to produce highly active catalysts. Specifically, a key issue for catalysis is the ability to have the hydride (H^-) acceptor ability of the metal and the basicity (proton acceptor ability) of the amine appropriately matched so that the heterolytic cleavage of H_2 is close to thermoneutral. The facile reversibility of the heterolytic cleavage of H_2 in the active site of enzymes indicates that those systems have balanced thermodynamics.

Progress Report

The iron complexes $CpFe(P^{Ph}_2N^{Bn}_2)Cl$, $CpFe(P^{Ph}_2N^{Ph}_2)Cl$, $CpFe(P^{Ph}_2C_5)Cl$ (where $P^{Ph}_2N^{Bn}_2$ is 1,5-dibenzyl-1,5-diaza-3,7-diphenyl-3,7-diphosphacyclooctane, $P^{Ph}_2N^{Ph}_2$ is 1,3,5,7-tetraphenyl-1,5-diaza-3,7-diphosphacyclooctane, and $P^{Ph}_2C_5$ is 1,4-diphenyl-1,4-diphosphacycloheptane) have been synthesized and characterized by NMR spectroscopy, electrochemical studies, and X-ray diffraction. These chloride derivatives are readily converted to the corresponding hydride complexes $CpFe(P^{Ph}_2N^{Bn}_2)H$, $CpFe(P^{Ph}_2N^{Ph}_2)H$, $CpFe(P^{Ph}_2C_5)H$ and $Fe(H_2)^+$ complexes $[CpFe(P^{Ph}_2N^{Bn}_2)(H_2)]BAr^F_4$, (where BAr^F_4 is $B[(3,5-(CF_3)_2C_6H_3)_4]^-$), $[CpFe(P^{Ph}_2N^{Ph}_2)(H_2)]BAr^F_4$, and $[CpFe(P^{Ph}_2C_5)(H_2)]BAr^F_4$, and $[CpFe(P^{Ph}_2N^{Bn}_2)(CO)]BAr^F_4$. An attractive interaction was found by x-ray crystallography between the N

atom of the pendant amine and the C atom of the coordinated CO ligand for $[CpFe(P^{Ph}{}_2N^{Bn}{}_2)(CO)]BAr^F{}_4$. The N•••CO distance of 2.848 Å is shorter than the sum of van der Waals radii of N and C atoms (3.25 Å) by ca. 0.4 Å, indicating there is a significant bonding interaction between the N atom of the $P^{Ph}{}_2N^{Bn}{}_2$ ligand and the C atom of the carbonyl ligand.

Studies of H/D exchange by the complexes $[CpFe(P^{Ph}{}_2N^{Bn}{}_2)(H_2)]^+$, $[CpFe(P^{Ph}{}_2N^{Ph}{}_2)(H_2)]^+$, and $[CpFe(P^{Ph}{}_2C_5)(H_2)]^+$ carried out using H_2 and D_2 indicate that the relatively rapid H/D exchange observed for $[CpFe(P^{Ph}{}_2N^{Bn}{}_2)(H_2)]^+$ and $[CpFe(P^{Ph}{}_2N^{Ph}{}_2)(H_2)]^+$ compared to $[CpFe(P^{Ph}{}_2C_5)(H_2)]^+$ is consistent with *intramolecular heterolytic cleavage of H_2* mediated by the pendant amine. The hydrogenase enzymes have been shown to undergo exchange reactions to produce HD under an H_2/D_2 atmosphere. Computational studies for our synthetic complexes indicate a low barrier for heterolytic cleavage of H_2. These mononuclear Fe^{II} dihydrogen complexes containing pendant amines in the ligands mimic crucial features of the distal Fe site of the active site of the [FeFe]-hydrogenase required for H-H bond formation and cleavage. Requirements for heterolytic H_2 cleavage at the active site of [FeFe]-hydrogenases and synthetic catalysts based on Fe are a ferrous (Fe^{II}) center for binding of H_2, a properly positioned pendant amine in the ligand framework, and energy matching of the proton acceptor ability of the amine and the hydride acceptor ability of the metal, so that heterolytic cleavage of H_2 is thermodynamically favored. Our results indicate that suggesting *mononuclear* Fe complexes can be competent models of the active site of [FeFe]-hydrogenase enzymes.

The Fe complexes described above were shown to bind H_2 and heterolytically cleave H_2, but they were not electrocatalysts for oxidation of H_2. Rational modification of the ligand steric and electronic parameters was carried out by installing an alkyl group with larger steric bulk on phosphorus, with the intent of preventing binding of the external amine base, while still enabling binding of H_2 to the Fe^{II} center. An electron-withdrawing C_6F_5 substituent was added to the Cp ligand, with the intent of increasing the acidity of the $Fe(H_2)^+$ complex. The iron hydride complex $[Cp^{C_6F_5}Fe(P^{iBu}{}_2N^{Bn}{}_2)H]$ was synthesized and fully characterized by spectroscopic measurements as well as by single crystal x-ray crystallography. This complex is an electrocatalyst for oxidation of H_2 under 1 atmosphere H_2 in fluorobenzene solution at 22°C (Fig. 1).

The proposed mechanism for electrocatalytic oxidation of H_2 by $CpFe(P^{Ph}{}_2N^{Bn}{}_2)H$ is shown in Fig. 3.

Future Directions

Research on iron and manganese electrocatalysts for oxidation of hydrogen is continuing under the Center for Molecular Electrocatalysis, an Energy Frontier Research Center, and is focused on increasing the turnover frequency and decreasing the overpotential.

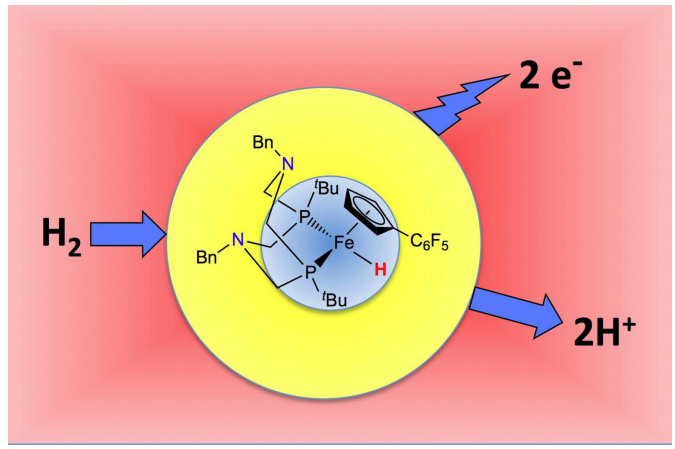

FIGURE 1. Schematic representation of the oxidation of H_2 by $[Cp^{C_6F_5}Fe(P^{iBu}{}_2N^{Bn}{}_2)H]$.

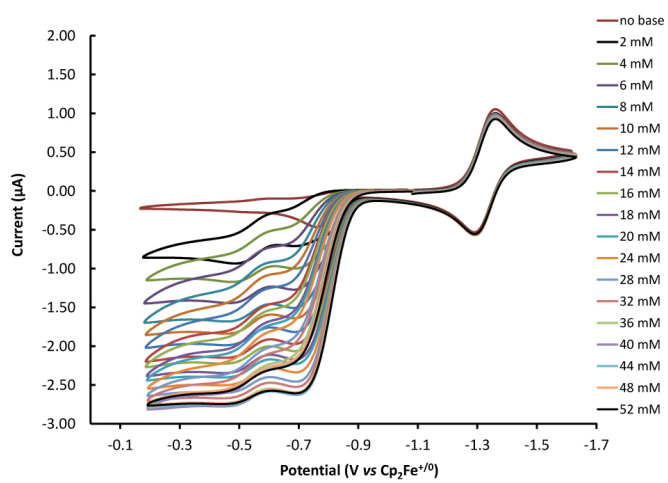

FIGURE 2. Cyclic voltammograms of a fluorobenzene solution of $[Cp^{C_6F_5}Fe(P^{iBu}{}_2N^{Bn}{}_2)H]$ (1.0 mM) under 1.0 atm H_2 at 22 °C with increasing concentrations of *N*-methylpyrrolidine, as indicated in the legend. The increase in current at higher concentrations of base indicates that the oxidation of H_2 is catalyzed by the iron complex. Conditions: scan rate, 20 mV/s, 0.1 M $^nBu_4NB(C_6F_5)_4$ supporting electrolyte, glassy carbon working electrode. Potentials are referenced to $Cp_2Fe^{+/0}$ at 0 V, and $Cp_2Co^+PF_6^-$ (-1.33 V) was used as a secondary internal reference.

Publications acknowledging DOE-BES Funding (2010-present)

1. Yang, J.Y.; Bullock, R.M.; Dougherty, W.G.; Kassel, W.S.; Twamley, B.; DuBois, D.L.; Rakowski DuBois, M., "Reduction of Oxygen Catalyzed by Nickel Diphosphine Complexes with Positioned Pendant Amines," *Dalton Trans.* **2010**, *39*, 3001-3010.

2. "*Catalysis Without Precious Metals*" R.M. Bullock, Ed.; Wiley-VCH, Weinheim, Germany, 2010; ISBN: 978-3-527-32354-8.

3. Welch, K.D.; Dougherty, W.D.; Kassel, W.S. DuBois, D.L.; Bullock, R.M. "Synthesis, Structures, and Reactions of Manganese

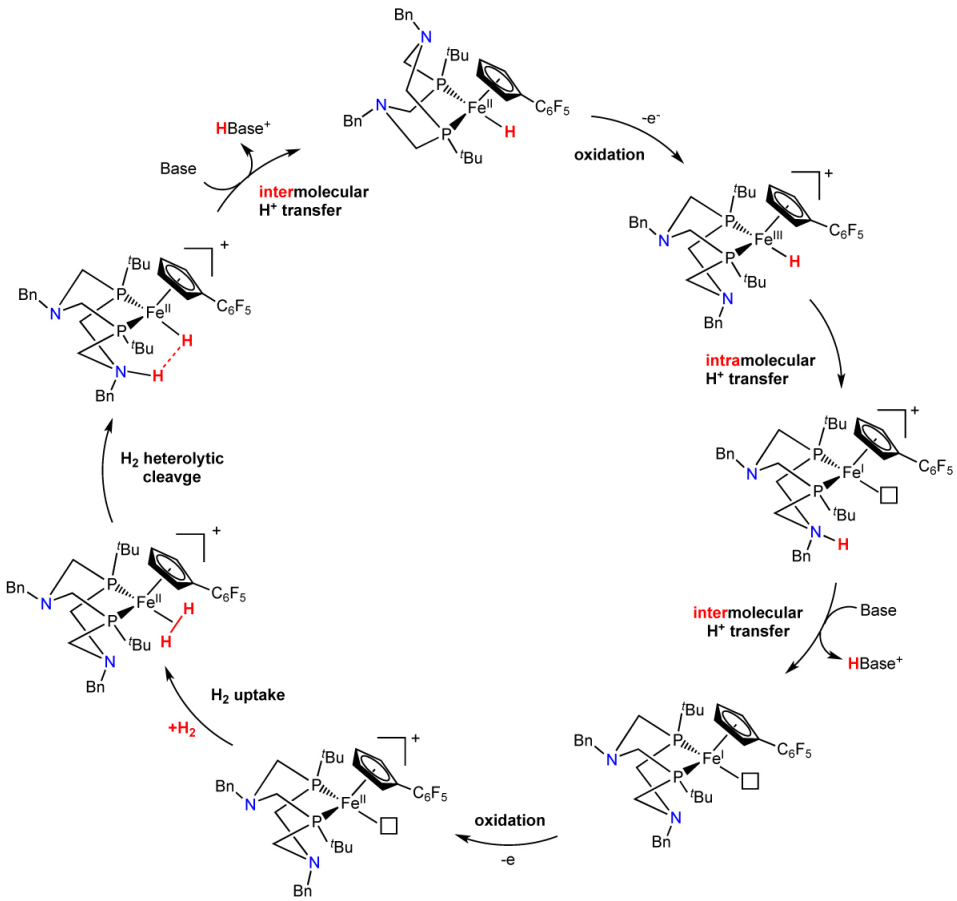

FIGURE 3. Proposed mechanism of electrocatalytic oxidation of H_2. Oxidation of Fe^{II}-H leads to an increased acidity of the Fe^{III}-H bond. Intramolecular proton transfer from iron to the pendent amine is followed by intermolecular deprotonation of the N-H by the external amine base. Electrochemical oxidation of the iron complex is followed by binding of H_2, which is heterolytically cleaved, with the hydride being transferred to iron and the proton to the pendent amine. Deprotonation by the external amine base completes the catalytic cycle and regenerates the iron hydride $CpFe(P^{Ph}_2N^{Bn}_2)H$.

Complexes Containing Diphosphine Ligands With Pendant Amines," *Organometallics*, **2010**, *29*, 4532-4540.

4. Wiedner, E.S.; Yang, J.Y.; Dougherty, W.G.; Kassel, W.S.; Bullock, R.M.; Rakowski DuBois, M.; DuBois; D.L., "Comparison of Cobalt and Nickel Complexes with Sterically Demanding Cyclic Diphosphine Ligands: Electrocatalytic H_2 Production by $[Co(P^{tBu}_2N^{Ph}_2)(CH_3CN)_3](BF_4)_2$," *Organometallics*, **2010**, *29*, 5390-5401.

5. Rakowski DuBois, M.; DuBois, D.L., "A Modular Approach to the Development of Molecular Electrocatalysts for H_2 Oxidation and Production Based on Inexpensive Metals," In "*Catalysis Without Precious Metals*:" R.M. Bullock, Ed.; Wiley-VCH, Weinheim, Germany, 2010.

6. Yang, J.Y.; Bullock, R.M. Rakowski DuBois, M.; DuBois, D. "Fast and Efficient Molecular Electrocatalysts for H_2 Production: Using Hydrogenase enzymes as Guides," *MRS Bulletin* **2011**, *36*, 39-47. (invited review article).

7. DuBois, D.L.; Bullock, R.M., "Molecular Electrocatalysts for the Oxidation of Hydrogen and the Production of Hydrogen –The Role of Pendant Amines as Proton Relays," *Eur. J. Inorg. Chem.* **2011**, 1017-1027. (invited review article for special issue on Hydrogenases).

8. Bullock, R.M. "A Mercurial Route to a Cobalt Dihydrogen Complex," *Angew. Chem. Intl. Ed.*, **2011**, *50*, 4050-4052.

9. Wiedner, E.S., Yang, J.Y., Chen, S., Raugei, S., Dougherty, W.G., Kassel, S., Helm, M.H., Bullock, R.M., Rakowski DuBois, M., DuBois, D.L., "Stabilization of Nickel Complexes with Ni^0•••H-N Bonding Interactions Using Sterically Demanding Cyclic Diphosphine Ligands," *Organometallics* **2012**, *31*, 144-156.

10. Liu, T.; Chen, S.; O'Hagan, M.J.; DuBois, M.R.; Bullock, R.M.; DuBois, D.L. "Synthesis, Characterization and Reactivity of Fe Complexes Containing Cyclic Diazadiphosphine Ligands: The Role of the Pendant Base in Heterolytic Cleavage of H_2" *J. Am. Chem. Soc.* **2012**, *134*, 6257-6272.

11. Liu, T.; DuBois, D.L.; Bullock, R.M. "An Iron Complex with Pendent Amines as a Molecular Electrocatalyst for Oxidation of Hydrogen," *Nature Chemistry*, **2013**, *5*, 228-233.

V.N.16 Platinum-Group Metal (PGM) Substituted Complex Oxide Catalysts

Principal Investigator: Ram Seshadri
Materials Department and Department of Chemistry and Biochemistry
Materials Research Laboratory, University of California
Santa Barbara, CA 93106
Phone: (805) 893-6129
Email: seshadri@mrl.ucsb.edu

Names of Team Members:

- Lauren Misch: Current graduate student.
  Email: lmisch@chem.ucsb.edu
- Dr. Alexander Birkel: Post-doctoral fellow.
  Email: abirkel@mrl.ucsb.edu
- Joshua Kurzman: Former graduate student, now post-doctoral fellow in France.
- Stephanie Moffitt: Former undergraduate student, now graduate student at Northwestern:

DOE Program Manager: Dr. Raul Miranda
Phone: (301) 903-8014
Email: Raul.Miranda@science.doe.gov

Objectives

The increasing costs of platinum group metals (PGMs), arising from their scarcity, and from their ever-growing use in catalytic converters provides the imperative for research into better use of PGMs in catalysis. PGMs are extensively implicated in hydrogen generation from (hydro)carbon feedstocks, in the conversion of hydrogen into electricity in fuel cells, and in counter electrodes for photocatalytic water splitting. Other drivers for PGM abatement are the potential environmental impact of dispersed PGM particles, wastefully ablated from catalytic converters, and the complex geopolitics of sourcing these metals. A significant body of work, including from Santa Barbara, has pointed to the effectiveness of complex transition metal oxides substituted with small amounts of noble metal ions (notably, Pd^{2+}) in oxidation catalysis. This area of research has yielded a number of important surprises, chief amongst which is the increasing body of evidence pointing to Pd^{2+} in the oxide lattice, rather than Pd nanoparticles on the surface of the oxide, that are the active sites for CO oxidation. This has led us to question the paradigm of oxide-supported PGM nanoparticle catalysis – at least for a large class of important oxidation and partial oxidation reactions – and to envisage the development of catalysts that obviate problems inherent to supported catalysts; inefficiencies due to only surface atoms being accessible, particle sintering with concurrent loss of active surface area, and ablation. The materials focus is on complex oxides; complex implying they possess at least two crystallographically distinct cation sites. It has been clear to us that a perovskite like $BaCeO_3$, which we have explored in some detail, behaves very differently from simple oxide supports like Al_2O_3. The objectives include exploring the catalytic role/activity of PGM ions such as Pd^{2+}, Pt^{2+}, and Au^{3+} substituted in complex oxide hosts. The target reactions are H_2, CO and hydrocarbon transformations, although the widespread use of PGM-based materials in many areas of catalysis means that the work will likely impact other areas of chemical conversion and energy as well. Our principal theme is the design of complex, multi-cation oxide hosts containing low quantities of substituted PGM ions, and their use as sinter- and poison-resistant replacements for conventional oxide-supported PGM catalysts.

Technical Barriers

The chief technical barrier to carrying out the work as described has been in learning how to prepare and stabilize the different oxides with either small PGM substitution, or that are stoichiometric in PGM-content. In general, PGM ions are oxophobic, which means that they do not easily form stable oxides, and the stability of the oxide decreases at increasing temperature. On the other hand, they are rather sluggish to react, which usually requires preparation at high temperatures, under conditions that push the limits of their stability. The second technical barrier is that many catalytic reactions take place under conditions wherein the PGM ion can be reduced to zerovalent (metal) nanoparticles. It is then important to distinguish reactions that are actually catalyzed by the PGM ion, rather than by the PGM nanoparticle.

Abstract

Substituted metal oxides containing ionic platinum group metal species have been attracting a great deal of attention because of their potential to reduce the amount of precious metals used in heterogeneous catalysis. To address questions surrounding catalytic activity of precious metal ions, we have continued to probe both well-defined model systems as well as lightly substituted simple and complex oxides. We continue to use CO oxidation as a test reaction, but in addition, we are employing a host of new, and industrially relevant reactions such as C–H bond activation, hydrocarbon combustion, and catalytic hydrogenation/dehydrogenation. We have used our understanding of experiments on known model compounds, in conjunction with detailed density functional electronic structure calculations, to determine potentially new catalytic systems based on markers of catalytic activity such as the d band position. In this past year, we have investigated Pd-substituted CeO_2. This substituted simple oxide has been well-studied for use in CO oxidation, NO_x reduction, and the water-gas shift reaction. We have investigated this compound, prepared by

ultrasonic spray pyrolysis, for partial oxidation and dry-reforming of CH_4. We have also, in this period, completed a comprehensive study of the electronic structure of gold compounds, in the search for new catalytic materials where the active element is gold. In this light, and as a precursor to further experiments, we have also examined the chemistry of Ir^{4+}. A survey of some of the progress is reported here.

Progress Report

4.1 $Ce_{1-x}Pd_xO_{2-\delta}$: Substituted ion *versus* supported metal

Pd-substituted CeO_2, $Ce_{1-x}Pd_xO_{2-\delta}$ was prepared as a high surface area powder using ultrasonic spray pyrolysis (USP). USP has been previously used for preparing mesoporous carbon materials; we have further developed this method to be applicable for substituted metal oxides. Metal nitrate precursors are mixed in a suitable molar ratio in water. The precursor solution is then nebulized into a fine mist and carried through a tube furnace at adjustable temperature, and the products are collected in water bubblers. The catalysts were extensively characterized using synchrotron X-ray diffraction and other techniques, confirming phase pure samples up to 10 mol% Pd substitution. $Ce_{0.95}Pd_{0.05}O_{2-\delta}$ was found to be active for the partial oxidation of CH_4 above 450°C. Partial oxidation of CH_4 over $Ce_{0.95}Pd_{0.05}O_{2-\delta}$ yields the expected combustion products along with non-stoichiometric synthesis gas in the form of excess hydrogen gas. The excess hydrogen is a result of several secondary reactions occurring after combustion, including dry reforming of CH_4, steam reforming of CH_4, and water gas shift. We found that this material becomes catalytically active for C–H bond activation only after the Pd^{2+} ions have been reduced to Pd metal supported on CeO_2. This observation was confirmed from post-reaction analyses including X-ray diffraction, X-ray photoelectron spectroscopy, and by verifying the activity of the reduced Pd^0/CeO_2 catalysts for ethylene hydrogenation, a reaction that is known to require Pd^0. We have identified USP as a facile method for the preparation of substituted metal oxides, and also for the preparation of well-dispersed metal nanoparticles on oxide supports via reduction of substituted materials. Ongoing efforts are focused on the preparation of complex oxides by USP, including Pd-substituted perovskites, and solid acids.

4.2 Studies of gold compounds – Why are nanoparticles special?

As a strategy for addressing questions surrounding the possible catalytic role of ionic gold and platinum group species, we have looked to well-defined model compounds, and reported a comparison of two highly stable oxides containing square planar and isoelectronic Au^{3+} and Pd^{2+}: La_4LiAuO_8 and La_2BaPdO_5. Given that Pd^{2+} and Pt^{2+} in the solid state are well known to catalyze a variety of reactions, a natural question is whether Au^{3+}can behave similarly. We determined that La_4LiAuO_8 is a very poor catalyst for the oxidation of CO to CO_2, in contrast to La_2BaPdO_5, which is quite a good catalyst for this reaction, despite being tested as a low surface area bulk powder. Electronic structure calculations revealed distinct differences in the average energy of the Pd 4d and Au 5d states – the Au d-states are held deep below the Fermi energy with the centroid positioned at approximately –5.0 eV. The Pd d-states of La_2BaPdO_5, on the other hand, are only about 2.5 eV below E_F. In the context of the Hammer–Nørskov d-band model, the distinct behaviors of these isoelectronic model compounds can be interpreted in terms of the differing abilities to interact with adsorbates: the d-states of La_4LiAuO_8 are not accessible, while the d-states of La_2BaPdO_5 are. Thus, we were led to the question: If the d-states of cationic $Au^{3+}$are too stabilized to be of interest for catalysis, where are the d-states located in compounds containing formally or partially anionic gold? Although a number of compounds of Au^- are known, none of them are sufficiently stable to warrant catalytic testing and many are air-sensitive; for example, dealloying of alkali-Au films exposed to O_2 has been found to occur near room temperature. $Au^{\delta-}$ species, however, which are encountered in polar intermetallics of Au with the early transition metals, are comparatively quite stable. As we began to study ordered gold alloys, however, similarities in the electronic structure of gold compounds containing Au in vastly different formal oxidation states quickly became apparent. It became clear that the formal oxidation state of Au was uninformative about the electronic structural features that dictate catalytic activity, namely, the energy of the Au d-states.

Using first principles bulk electronic structure calculations on a variety of Au compounds and species, encompassing a wide spectrum of formal oxidation states, coordination geometries, and chemical environments, we found that the center of the d band is linearly dependent on the degree of d-band filling. This is a general relationship for Au irrespective of its surroundings. Although changes in the d-band filling are small, the population of the d shell has a significant effect on the energy of the Au d-states. The ready formation of Au^- in compounds such as CsAu arises from Au possessing relatively stabilized s states, which also manifests as a relatively large Pauling electronegativity (for a metal) of 2.54. However, the destabilization of d-states results in Au readily forming compounds in the formal 3+ oxidation state (exemplified by La_4LiAuO_8). This schizophrenic behavior – summarized as s-electronegative but d-electropositive – is what results in the intermetallic compounds displaying such a wide variation in the Au d-band center position, and indeed, sharing the same range of d-band center positions as compounds of Au that are formally 3+.

4.3 Relativistic effects in the stability of Ir^{4+}

Relativistic effects lower the energy of (stabilize) the 6s orbital for an Ir atom, which is the result of the contraction of

the s wavefunction towards the nucleus. Unlike the 6s state, the energy of the 5d orbitals increases and the wavefunction is shifted outward by the repulsion of the contracted s orbital. Both the wavefunction and energy of the s orbital are almost identical at the full-relativistic (FR) and scalar-relativistic (SR) levels. For the d orbitals, there are two channels in the FR approach. The SR energies and wavefunctions are located at the middle of the two FR channels, indicating that the SR state represents the average of the FR states. A similar trend is also found for Rh, but to a significantly lesser extent. This is a general trend for the 4d and 5d transition metals and has been noted in discussions of relativistic effects for molecules and clusters containing 4d and 5d transition metal atoms. However, the manner in which this leads to higher oxidation states in extended crystalline oxides had not previously been examined within a completely *ab-initio* framework. The valence and conduction states around the Fermi levels consist of Ir 6d and O 2p orbitals. For non-relativistic (NR) and SR cases, the spin degrees of freedom do not mix with the orbital degrees of freedom and the d orbitals can split into two groupings of states with t_{2g} and e_g symmetries arising from the octahedral crystal field. There is a greater extent of mixing between the Ir-d and O-p orbitals in IrO_2, suggesting a greater degree of covalency. Ir_2O_3 is a semiconductor, with fully occupied t_{2g} states. The SR pDOS have similar features to the NR pDOS, but the widths are increased in the SR pDOS and the Fermi levels are shifted upward, which is caused by the destabilization of the Ir 5d levels and associated increase in the energy difference between the Ir 5d and O 2p energy levels. For this reason, there is a larger contribution of Ir 5d character near the Fermi level in the SR DOS than in the NR DOS. The significant destabilization of the Ir 5d energy is the origin of the categorical stability of the Ir^{4+} state.

Future Directions

Currently, we are exploring the ultrasonic spray pyrolysis and microwave preparative routes for the preparation of a number of substituted complex oxides with Pd^{2+} and Pt^{2+}/Pt^{4+}. One such example is $LaFeO_3$, the Pd- substituted variant of which seems to be catalytically active even at room temperature. We are also planning to make model compounds such as La_2BaPdO_5 with higher surface area using USP. Another strategy for new complex oxides being explored is the concurrent development of solid acidity and Pd^{2+} substitution for reactions relevant to C–H activation. A third direction that has proved very fruitful in the past six months, is the use of microwave-assisted preparative methods which are yielding significant reductions (from days to minutes) in the preparation time of the more sluggish PGM oxides.

Publication list (including patents) acknowledging the DOE grant or contract:

1. J.A. Kurzman, X. Ouyang, W.B. Im, J. Li, J. Hu, S.L. Scott, and R. Seshadri, La_4LiAuO_8 and La_2BaPdO_5: Comparing two highly stable d^8 square-planar oxides, *Inorg. Chem.* 49 (2010) 4670–4680.

2. J.A. Kurzman, S.L. Moffitt, A. Llobet, and R. Seshadri, Neutron diffraction study of La_4LiAuO_8: Understanding Au^{3+} in an oxide environment, *J. Solid State Chem.* 184 (2011) 1439–1444.

3. T.Z. Forbes, J.A. Kurzman, R. Seshadri, and A. Navrotsky, The energetics of La_4LiAuO_8, *J. Mater. Res.* 26 (2011) 1188–1192.

4. J.A. Kurzman, J. Li, T.D. Schladt, C.R. Parra, X. Ouyang, R. Davis, J.T. Miller, S.L. Scott, and R. Seshadri, Pd^{2+}/Pd^0 redox cycling in hexagonal $YMn_{0.5}Fe_{0.5}O_3$: Implications for catalysis by PGM-substituted complex oxides, *Inorg. Chem.* 50 (2011) 8073–8084.

5. J.A. Kurzman, M.-S. Miao, and R. Seshadri, Hybrid functional electronic structure of $PbPdO_2$, a small-gap semiconductor, *J. Phys. C: Condens. Matter* 23 (2011) 465501(1–7).

6. L.M. Misch, J.A. Kurzman, A.R. Derk, Y.-I. Kim, R. Seshadri, H. Metiu, E.W. McFarland, and G.D. Stucky, C–H bond activation by Pd substituted CeO_2: Substituted ions *versus* reduced species. *Chem. Mater.* 23 (2011) 5432–5439.

7. M.-S. Miao and R. Seshadri, Rh_2O_3 versus IrO_2: Relativistic effects and the stability of Ir^{4+}, *J. Phys. C: Condensed Matter.* 24 (2012) 215503(1–8).

8. M.-S. Miao, J.A. Kurzman, N. Mammen, S. Narasimhan, and R. Seshadri, Trends in the electronic structure of extended gold compounds: Implications for the use of gold in heterogeneous catalysis, *Inorg. Chem.* 51 (2012) 7569–7578.

V.N.17 Porous Transition Metal Oxides: Synthesis, Characterization, and Catalytic Activity

Principal Investigator: Steven L. Suib
The University of Connecticut
Unit 3060, Depts. of Chemistry and Chemical Engineering
55 N. Eagleville Rd., University of Connecticut,
Storrs, CT 06269-3060
Phone: (860) 486-2797
Email: Steven.Suib@uconn.edu

Names of Team Members:
Altug Poyraz, Chung Hao Kuo, Saminda Dharmarathna,
The University of Connecticut
Unit 3060, Depts. of Chemistry
55 N. Eagleville Rd., University of Connecticut
Storrs, CT 06269-3060
Phone: (860) 486-2797
Email: Altug.Poyraz@uconn.edu,
ChungHao.Kuo.Suib@uconn.edu,
Saminda Dharmarathna@uconn.edu

DOE Program Manager: Dr. Raul Miranda
Phone: (301) 903-8014
Email: Raul.Miranda@science.doe.gov

Objectives

The goals of this project are as follows:

a. To synthesize well ordered crystalline mesoporous transition metal oxide (MTMO) materials with monomodal uniform pore sizes.

b. To prepare and characterize ordered mesoporous thin films.

c. To optimize catalytic activity, selectivity, and stability in oxidation catalysis using amorphous porous oxides and crystalline microporous and mesoporous materials.

d. To investigate the role of mesoporous materials in battery systems.

e. To develop novel *in situ* characterization methods for syntheses, selective oxidations, and battery studies.

Technical Barriers

The technical barriers in this project include synthesis of catalysts and obtaining excellent catalytic yields and stabilities. The synthesis barriers are related to the generic preparation of metal and nonmetal oxide mesoporous systems. Some materials are more difficult to make than others. Right now some are not able to be made. The catalysis barriers involve optimizing the pore size of the catalysts, optimizing active sites, and understanding factors that give stability to the systems.

Abstract

This project concerns the synthesis of well-ordered crystalline mesoporous transition metal oxide (MTMO) materials with monomodal uniform pore sizes. Characterization of the physical and chemical properties of these materials is being done with a variety of methods. Several catalytic reactions are being studied such as photo-assisted catalytic water splitting, catalytic coupling of diamine and hydroxyketones, quinoxaline formation, selective catalytic oxidation of adamantane, and three component coupling Hantzsch reactions. In addition, such materials are being studied in battery applications.

Progress Report

Sub Topic 1: Synthesis of Mesoporous Materials.

Research in the area of synthesis of microporous and mesoporous materials is ongoing.[1-20] Unique University of Connecticut (UCT) type metal oxide materials have been prepared that have crystalline walls, monomodal mesopore size distributions, and high thermal stabilities. These materials are under development through a licensing agreement. In addition, several microporous materials have been prepared that are being studied in a variety of catalytic reactions like photo-assisted catalytic oxidation of water[7,14] and several selective and total oxidation reactions.[4-6,8,11,15,19] Activities of these systems are often controlled by the amount of defects, especially oxygen ion vacancies, as well as dopants. Another emphasis has been on the activation of CO_2 to produce useful chemicals and fuels by electrochemical methods.[10,16-17,20] Another active area has been studies of metal oxide and mixed metal oxides with the control of particle size and morphology and their influence on catalytic properties.[1,5,9,11,12]

Sub Topic 2: Photoassisted Water Splitting with Porous Metal Oxides.

Water oxidation is the bottleneck in artificial photosynthetic systems that aim to split water into hydrogen and oxygen. However, water oxidation occurs readily in plants, catalyzed by the Mn_4O_4Ca manganese cluster. Manganese minerals are ubiquitous in nature displaying layered and tunnel structures. In our studies,[7,14] mixed valent porous amorphous manganese oxides (AMO), along with cryptomelane type tunnel manganese oxides (OMS-2) and layered birnessite (OL-1) have been used as water oxidation

catalysts. Significantly higher turnovers were obtained with AMO (290 mmol O_2/mol Mn) compared to tunnel structure OMS-2 (110 mmol O_2/mol Mn) and layered structure OL-1 (27 mmol O_2/mol Mn) in water oxidation tests with Ce^{4+}. Oxygen evolution was also confirmed under photochemical conditions using $[Ru(bpy)_3]^{2+}$ as a photosensitizer and persulfate as a sacrificial agent. The differences in catalytic activity among these catalysts have been probed using X-ray diffraction, transmission electron microscopy, Raman and Fourier transform infrared (FTIR) spectroscopy, average oxidation state, and compositional analyses. Comparison of AMO against prominent manganese catalysts described in literature shows AMO provided the highest turnover numbers. AMO catalyst was also reusable after regeneration. O-18 labeling studies proved that water was the source of dioxygen and IR proved the structural stability of AMO after reaction. AMO is related to hexagonal birnessites such as layered biogenic manganese oxides or H^+-birnessite that have cation vacancies in the MnO_2 sheets rather than completely filled Mn^{3+}/Mn^{4+} sheets, and this is influential in catalytic activity. A reaction scheme, scanning electron micrograph of the best photocatalyst, and proposed structure is given in **Figure 1**.

Sub Topic Hydrocarbon Oxidations.

A representative study of catalytic oxidations involves the bi-modification *in situ* oxidation at interfaces (IOI) coupled with an ion-exchange synthesis method that has produced mesoporous silicon oxide (MPS) templates. Manganese oxide was formed at the internal surface of the MPS template by IOI. In this IOI method, high valent oxo-anions of Mn (MnO_4^-) were used for the selective oxidation of polyethyleneoxide (PEO) groups of Pluronic ($PEO_{20}PPO_{70}PEO_{20}$) surfactant and formed manganese oxide at the organic-inorganic (corona) interface. The oxide formation was restricted at the corona interface by a positively charged CTA^+ head group of the cationic surfactant CTABr. The second modification of the MPS template was done by introducing promoter ions (Cs^+, K^+) or H^+ by an ion-exchange reaction between CTA^+ and the ions. The bi-modified MPS-Mn-X (X = Cs, K, or H) samples preserved the mesoporosity and high surface area of the MPS template. The bi-modified MPS-Mn-X samples were found to be more active, selective, and stable than the singly modified MPS-Mn sample for gas phase oxidation of toluene.

This study illustrates the synthesis, characterization and catalytic performance of the bi-modified mesoporous silicon oxides (MPS-Mn-X where X= Cs, K, or H). First, manganese oxide clusters were formed and kept at the positively charged organic-inorganic interface of the as-synthesized mesoporous silicon oxide by the "*in-situ* oxidation at interface" method. Unlike traditional wet- impregnation methods, the newly developed method restricts manganese oxide formation in the mesopore structure and uses as-synthesized mesoporous templates rather than calcined ones. The second modification was then carried out using the singly modified MPS-Mn sample and introducing promoter cations (K^+ and Cs^+) or H^+ using ion-exchange reactions between the cations and CTA^+. The synthesized bi-modified MPS-Mn-X preserved the advantages of the MPS template such as having highly ordered mesopore structures, high surface areas, and regular-cylindrical mesopores. The synthesized bi-modified MPS-Mn-X samples were tested for catalytic total oxidation of toluene under oxygen deficient conditions. The bi-modified MPS-Mn-X catalysts exhibited higher performance, selectivity, and stability compared to the singly modified MPS-Mn catalysts. The higher performance of the bi-modified MPS-Mn-X catalysts in catalytic oxidation of toluene (**Figure 2**) is attributed to creation of more active Mn^{3+} sites on the catalyst surfaces by the promoter ions.

A different strategy to create selective oxidation catalyst has involved use of ultrasonic cavitation in the synthesis of

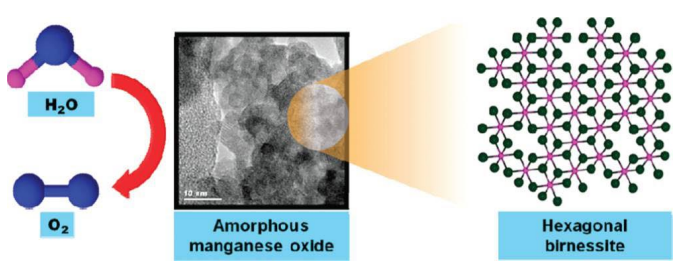

FIGURE 1. Photoassisted Catalytic Water Splitting, Scanning Electron Micrograph, and Proposed structure of the Active Catalyst.

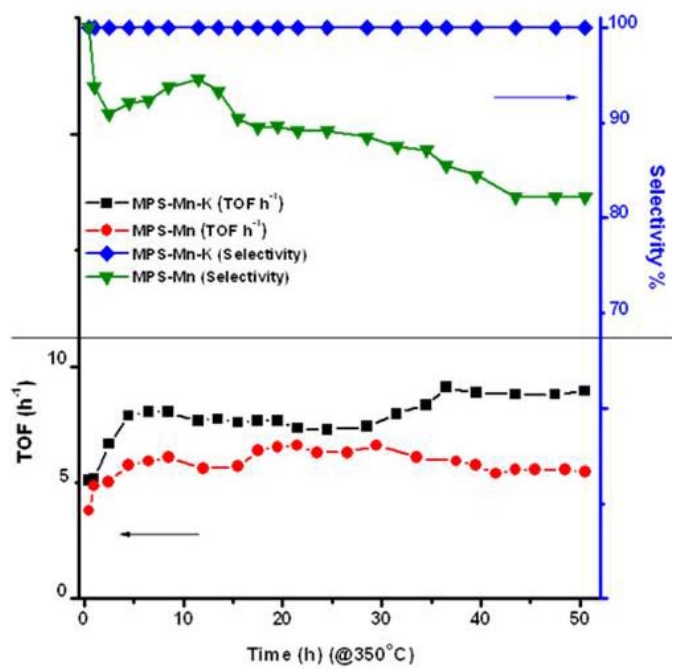

FIGURE 2. 50 h stability test TOF (h-1) and % CO2 selectivity results for MPS-Mn and MPS-Mn-K catalysts.

novel materials. A rapid, direct sonochemical method was successfully developed to synthesize cryptomelane-type manganese octahedral molecular sieve (OMS-2) materials. Very high surface area of 288 ± 1 m^2/g and small particle sizes in the range of 1–7 nm were produced under nonthermal conditions. No further processing such as calcination was needed to obtain the pure cryptomelane phase. A co-solvent system was utilized to reduce the reaction time and to obtain higher surface areas. Reaction time was reduced by 50% using water/acetone mixed phase solvent systems. The cryptomelane phase was obtained with 5% acetone after 2 h of sonication at ambient temperature. Reaction time, temperature, and acetone concentration were identified as the most important parameters in the formation of the pure cryptomelane phase. OMS materials synthesized using the above-mentioned method were characterized by X-ray diffraction, nitrogen sorption, scanning electron microscopy, transmission electron microscopy, and Fourier transformation infrared spectroscopy. OMS-2 materials synthesized using sonochemical methods possess greater amounts of defects and hence show excellent catalytic performances for oxidation of benzyl alcohol as compared to OMS-2 synthesized using reflux methods and commercial MnO_2. Surface areas and particle sizes are shown in Table 1. Table 2 shows some of the catalytic results for selective oxidation of toluene.

Future Directions

Future directions of this project include synthesis of new mesoporous materials that are difficult to make including some transition metal systems, nonmetal oxide systems, mixed metal systems, and doped Mesoporous materials. Characterization studies include determination of fundamental properties of these systems and using such information as feedback to the syntheses to make better materials as regards purity, controlled structures, and controlled compositions. Catalytic studies will involve optimization of selectivities and activities in the reactions described above.

TABLE 1. BET Surface Area of As Synthesized OMS-SC Samples[a]

OMS-sc Sample	BET s.a. ± 1 (m^2/g)	particle size (nm)	OMS-sc Sample	BET s.a. ± 1 (m^2/g)	particle size (nm)
4 h	245	2.8	10% ACE - 2 h	188	3.3
8 h	115	6.1	10% ACE - 3 h	199	2.7
12 h	118	5.4	10% THF - 3 h	200	1.0
3 h –55 °C	267	2.4	10% DMSO - 3 h	246	3.2
3 h –65 °C	177	6.6	10% DEE - 3 h	250	2.2
			10% SULF. - 3 h	286	4.2
K-OMS-2_{REF}	88	11.4	10% TOLU. - 3 h	288	5.4

[a]THF, tetrahydrofuran; DMSO, dimethylsulfoxide; DEE, diethyl ether; ACE, acetone; SULF., sulfolane; TOLU., toluene.

TABLE 2. Selective Oxidation of Benzyl Alcohol[a]

catalyst	BET s.a. ± 1 (m^2/g)	Conv. %[b]	Sel. %[c]	TON[d]
K-OMS-$2_{SC\text{-}10\%Toln.}$	288	52 (28[e])	100	8.32
1st recovery[f]		36 (39[h])	100	7.58
2nd recovery[g]		18 (20[h])	100	7.2
K-OMS-$2_{SC\text{-}12h}$	118	39	100	6.24
K-OMS-2_{REF}	88	21	100	3.36
commercial MnO_2	28	15	100	2.4

[a]Reaction conditions: 50.0 mg of catalyst; 1 mmol of benzyl alcohol t = 2 h and 15 mL of toluene as solvent; T = 110 °C. [b]Conversion (% based on benzyl alcohol. Conversion (%) based on substrate = [1 - ((concentration of substrate left after reaction) × (initial concentration of substrate))$^{-1}$] × 100. [c]Selectivity based on benzyl aldehyde no other products were detected. [d]TON – [$(mol_{substr})(mol_{catalyst})^{-1}$] where mol_{substr} is the moles of benzyl alcohol converted. [e]Conversion in inert (N_2) atmosphere. [f]First recovery, mass of the catalyst recovered was 38 mg. [g]Second recovery, mass of the catalyst recovered was 20 mg. [h]Calculated conversion for fresh catalyst.

Publication list (including patents) acknowledging the DOE grant or contract

1. Qiu, G.; Dharmarathna, S.; Zhang, Y.; Opembe, N.; Huang, H.; Suib, S., Facile Microwave-Assisted Hydrothermal Synthesis of CuO Nanomaterials and Their Catalytic and Electrochemical Properties, *J. Phys. Chem. C*, **2012**, *116*, 468-477.

2. Chen, C.H.; Suib, S.L., Control of Catalytic Activity Via Porosity, Chemical Composition, And Morphology of Nanostructured Porous Manganese Oxide Materials, *J. Ch. Chem. Soc*., 2012, *59*, 465-472.

3. Genuino, H.C.; Horvath, D.T.; King'ondu, C.K.; Hoag, G.E.; Collins, J.B.; Suib, S.L., Effects of visible and UV light on the characteristics and properties of crude oil-in-water emulsions, *Photochem. Photobiol. Sci*., **2012**, *11*, 692-702.

4. Dharmarathna, S.; King'ondu, C.K.; Pedrick, W.; Pahalagedara, L.; Suib, S.L., Direct Sonochemical Synthesis of Manganese Octahedral Molecular Sieve (OMS-2) Nanomaterials Using Cosolvent Systems, Their Characterization, and Catalytic Applications, *Chem. Mat*., **2012**, *24*, 705-712.

5. Njagi, E.C.; Genuino, H.C.; King'ondu, C.K.; Dharmarathna, S.; Suib, S.L., Catalytic Oxidation of Ethylene at Low Temperatures Using Porous Copper Manganese Oxides, *Appl. Catal. A*, **2012**, *421-422*, 154-160.

6. Opembe, N.N.; King'ondu, C.K.; Suib, S.L., Efficient Oxidation of 2,3,6-Trimethyl Phenol Non-Exchanged and H+ Exchanged Manganese Oxide Octahedral Molecular Sieves (K-OMS-2 and H–K-OMS-2) as Catalysts, *Catal. Lett*., **2012**, *142*, 427-432.

7. Iyer, A.; Del-Pilar, J.; King'ondu, C.; Kissel, E.; Garces, H.; Huang, H.; El-Sawy, A.; Dutta, P.; Suib, S., Water Oxidation Catalysis using Amorphous Manganese Oxides, Octahedral Molecular Sieves (OMS-2) and Octahedral Layered (OL-1) Manganese Oxide Structures, *J. Phys. Chem. C*, 2012, *116*, 6474-6483.

8. Suib, S.L., Novel catalysts for oxidations, biomass conversion, and alternative fuels, *Preprints – American Chemical Society, Division of Petroleum Chemistry*, **2012**, *57*, 173-174.

9. Garces, H.F.; Espinal, A.E.; Suib, S.L., Tunable Shape Microwave Synthesis of Zinc Oxide Nanospheres and Their Desulfurization Performance Compared with Nanorods and Platelet-Like Morphologies for the Removal of Hydrogen Sulfide, *J. Phys. Chem. C*, **2012**, *116*, 8465-8474.

10. Espinal, L.; Wong-Ng, W.; Kaduk, J.A.; Allen, A.J.; Snyder, C.R.; Chiu, C.; Siderius, D.W.; Li, L., Cockayne, E., Espinal, A.E.; Suib, S.L., Time dependent CO_2 sorption hysteresis by octahedral molecular sieves with manganese oxide framework, *J. Am. Chem. Soc*., **2012**, *134*, 7944-7951.

11. Genuino, H.; Dharmarathna, S.; Njagi, E.; Mei, M.; Suib, S., Gas-Phase Total Oxidation of Benzene, Toluene, Ethylbenzene, and Xylenes Using Shape-Selective Manganese Oxide and Copper Manganese Oxide Catalysts, *J. Phys. Chem*. C, **2012**, *116*, 12066-12078.

12. Genuino, H.; Hamal, D.; Fu, Y.J.; Suib, S., Synergetic Effects of Ultraviolet and Microwave Radiation for Enhanced Activity of TiO_2 Nanoparticles in Degrading Organic Dyes Using a Continuous-Flow Reactor, *J. Phys. Chem. C*, **2012**, *116*, 14040-14051.

13. Sharma, H.; Pahalagedara, L.; Joshi, A.; Suib, S.; Mhadeshwar, A., An Experimental Study of Carbon Black and Diesel Engine Soot Oxidation Kinetics using Thermogravimetric Analysis, *Energy Fuels*, 2012, in press.

14. Najafpour, M.M.; Sedigh, D.J.; King'ondu, C.K.; Suib, S.L., Nano-sized manganese oxide–bovine serum albumin as a promising and biomimetic catalyst for water oxidation, *RSC Adv*., **2012**, 1-5.

15. Poyraz, A.S.; Biswas, S.; Genuino, H.C.; Dharmarathna, S.; Kuo, C.H.; Suib, S.L., Bimodification of Mesoporous Silicon Oxide by Coupled "In Situ Oxidation at the Interface and Ion Exchange" and its Catalytic Activity in the Gas-Phase Toluene Oxidation, *ChemCatChem*, **2012**, in press.

16. Hu, B.; Frueh, S.; Garces, H.F.; Zhang, L.; Aindow, M.; Brooks, C.; Kreidler, E.; Suib, S.L., Selective Hydrogenation of CO_2 and CO to Useful Light Olefins over Octahedral Molecular Sieve Manganese Oxide Supported Iron Catalysts, Appl. Catal. B, **2012**, 54-61.

17. Hu, B.; Suib, S.L., Synthesis of Useful Compounds from CO_2, in Green CO_2: Advances in CO_2 Utilization, G. Centi, S. Perathoner, Eds., John Wiley and Sons, Inc., NY, Chapter 3, 2013, in press.

18. Najafpour , M.M.; Leonard , K.C.; Fan , F.F.; Tabrizi, M.A.; Bard, A.J.; King'ondu , C.; Suib, S.L.; Haghighi, B.; Allakhverdiev, S.I.; Nano-size layered manganese-calcium oxide as an efficient and biomimetic catalyst for water oxidation under acidic conditions: comparable to platinum *Dalton Trans*.**, 2013**, *42*, 5085-5091.

19. Genuino, H.; Meng, Y.; Horvath, D.T.; Kuo, C.H.; Seraji, M.S.; Morey, A.M.; ,Joesten, R.; Suib, S.L., Enhancement of Catalytic Activities of Octahedral Molecular Sieve Manganese Oxide for Total and Preferential CO Oxidation via Vanadium Ion Framework Substitution, *Chem Cat Chem*, **2013**, in press.

20. Hu, B.; Guild, C.; Suib, S.L., Thermal, Electrochemical, and Photochemical Conversion of CO_2 to Fuels and Value-added Products, *J. of CO_2 Util*., **2013**, in press.

V.N.18 Understanding the Effects of Surface Chemistry and Microstructure on the Activity and Stability of Pt Electrocatalysts on Non-Carbon Supports

Principal Investigator: William E. Mustain
Department of Chemical & Biomolecular Engineering
University of Connecticut
191 Auditorium Rd., Unit 3222
Storrs, CT 06269-3222

DOE Program Manager: Raul Miranda
Phone: (301) 903-8014
Email: raul.miranda@science.doe.gov

Objectives

The objective of this DOE/BES sponsored research is to use Pt nanoparticles supported on several carbon and non-carbon supports to elucidate the effects of the chemical composition and microstructure of the electrocatalyst support on the activity, stability and utilization of supported Pt clusters. The overall goal of this work is to develop the tools needed to design novel electrocatalysts that have ultra-low Pt content and excellent electrochemical stability. The work in this program is organized across 3 themes:

I. Elucidating the Role of Support Surface Chemistry on the Structure and Activity of Supported Pt

II. Understanding the Influence of Carbon Support Adatoms on Electrochemical Stability

III. Rational Design of the Catalyst-Support Microstructure

Technical Barriers

Use of intrinsically unstable materials: Due to the weak interaction between all known carbon-black catalyst support materials and Pt clusters and the thermodynamic instability of carbon at elevated surface potentials, it is currently in question whether the continued investigation of carbon black support materials will lead to high stability electrocatalysts. The weak interaction and support dissolution leads to catalyst agglomeration during operation and severe reduction in the number of electrochemically active sites, drastically lowering the reaction rate with time. Also, though Pt alloy electrocatalysts have shown enhanced activity for the ORR, they suffer from low chemical stability in acidic environments, such as the PEMFC cathode, due to leaching of the alloyed metal. Also, there is no evidence in the literature that alloying Pt has any appreciable effect on cluster agglomeration. Therefore, alloying does not address the fundamental issue with PEMFC catalysts: cluster stability.

Lack of guiding principles for catalyst and support design: Carbon offers many properties that make it nearly ideal for electrochemical applications including: i) tolerance to acidic and alkali media; ii) high electronic conductivity; iii) low cost; and iv) complex microporous structure, yielding high specific surface area and facile mass transport. Despite this, little is known about how the balance between porosity, microstructure, and surface chemistry of the support influences the dispersion of Pt, its utilization, and the mass transport of both reactants and products within the catalyst. This limited information regarding the catalyst support and its role in PEMFC performance has translated to non-carbon supports as well, which has stunted the advance and implementation of next-generation materials in PEMFCs. Therefore, a fundamental, systematic study carefully controlling the catalyst support porosity, microcrystallinity and surface chemistry is desperately needed.

Abstract

In the first 2 ½ years of this project, we have clearly shown that the electrocatalyst support has an impact on the activity and stability of Pt through at least two different mechanisms: 1) Electron transfer between the catalyst and support that shifted the binding energy of oxygen to more positive potentials, leaving a clean Pt surface for the ORR; and 2) Lattice matching, which led to preferential faceting of Pt (111), which has a very high ORR activity. In fact, preferential faceting and strong bonding between the catalyst and support led to a Pt/ITO catalyst with a specific activity of 750 $\mu A/cm^2_{Pt}$ and mass activity of 621 mA/mg_{Pt} (both exceed 2015 DOE targets) with no measurable reduction in activity over 1000 accelerated degradation cycles between 0.0V and 1.4 V. vs. NHE. Pt/WC also showed improved activity compared to Pt/C, though surface oxidation and dissolution led to low catalyst life. However, we were also able to report, for the first time, a detailed mechanism for the electrochemical dissolution and instability of WC and WO_3 in acid media. In addition, using templated carbon, we have found that pore sizes <5 nm are not useful for ORR electrocatalysts. We have also found that having an amorphous support nanostructure significantly improves the Pt utilization. In addition, we found that doping carbon-based supports with surface N functional groups improves the stability of the carbon relative to commercial carbon and allows for very small Pt particle sizes (<2 nm) even at very high Pt loading (50 wt%). This combination led to Pt/N-OMC (OMC = ordered mesoporous carbon) catalysts with better activity and stability than commercial Pt/C (BASF). We also found during degradation testing of the N-OMC that it has very high double layer capacitance for its surface area

(156 F/g; 25.1 μF/cm^2) and is competitive with commercial carbons for supercapacitor applications. Most importantly, our initial work has validated our overall approach, allowed us to develop reliable experimental protocols, has used fundamental discoveries to make contributions to real devices and has led to interesting new questions that will be the subject of our work moving forward.

Progress Report

To date, our team focused our efforts in two key areas: surface chemistry and microstructure. With regards to the surface chemistry work, we have started developing a fundamental understanding to learn if and how the support surface can influence the electrocatalytic activity of supported Pt nanoparticles. Also of great interest here was the ability of the support to dictate the dispersion and stability of supported Pt. Most of the work in this area was accomplished using non-carbon support materials (with Pt/Vulcan acting as our control material): WC/WO_3, Indium-Tin Oxides and TiAlN. Our microstructural work focused on using a silicate templating approach to control the pore size of an ordered mesoporous carbon (OMC). Carbon was selected due to its ease in preparation and similarity of its surface composition and bonding to the control material. We also developed a template modification technique to control the homogeneity and structural order of the OMC. In the following sections, it is impossible to provide all the work that was done; for this, we would like to invite readers to visit our publications and feel free to contact us with any questions.

High Activity, High Stability Pt/Sn-doped Indium Oxide Electrocatalysts for the ORR

We studied indium-tin oxides over a very broad range of composition, from 1% indium in tin oxide, which had rutile crystal structure with inserted In^{3+} to 1% Sn in indium oxide, which had a bixbyite cubic structure. We found that 5% Sn in indium oxide possessed the highest ORR activity and excellent stability. We will focus on the 5% Sn-In_2O_3 results here, which was reported in the Journal of the American Chemical Society [Publication 3], which will be denoted as ITO below.

The specific and mass activity of Pt supported on ITO was considerably higher than Pt/C. The Pt/ITO catalyst exhibited a specific activity of 0.750 ± 0.04 mA/cm2 at 0.9 V, which was 3 times greater than that of Pt/C (0.235 0.01 ± mA/ cm2). After normalization to the loading amount of Pt metal, the mass activity of Pt/ITO catalyst was found to be 621 ± 31 mA/mgPt, which was 4 times greater than that of Pt/C (156 ± 9 mA/mgPt) and far exceeded the 2015 DOE goal for Pt mass activity of 440 mA/mgPt. Characteristic voltammograms for Pt/ITO at various rotation rates are presented in Figure 1a. The higher specific activity of the Pt/ITO was found to be a result of synergistic effects between the surface Sn of ITO and the supported Pt NPs. Perhaps the most significant impact of the ITO was the preferential exposure of {111} facets on the Pt NPs on Pt/ITO compared to Pt NPs supported on carbon black, which typically contain mostly {100} facets. Interestingly, the Pt and ITO seemed to have similar cubic lattice spacing, which resulted in continuous lattice fringes from the ITO substrate to supported Pt particles, indicating that the Pt was grown epitaxially on the ITO surface The ORR activity on low-index crystallographic facets of Pt in a nonadsorbing electrolyte such as perchloric acid is known to increase on the order of Pt(100) ≪ Pt(111) < Pt(110), with a minor difference in catalytic activity between Pt(111) and Pt(110). This difference in ORR activity most likely arises from the structure-sensitive inhibiting effect of OH_{ad} species on Pt(hkl), which blocks the active site for O_2 adsorption and thus retards the ORR kinetics. The Pt/ITO catalyst also

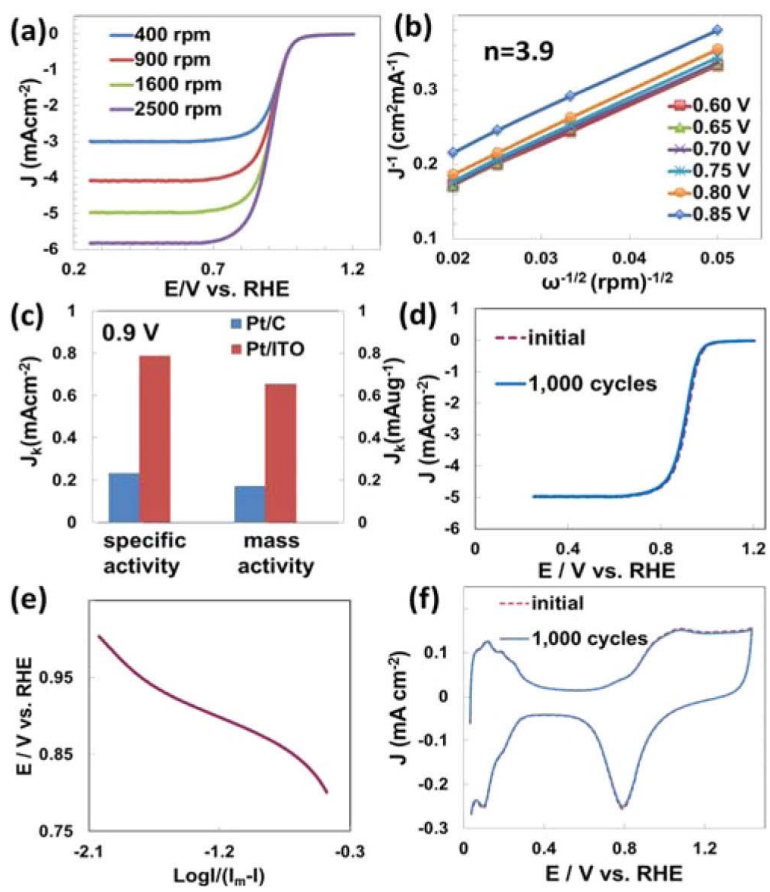

FIGURE 1. (a) Polarization curves for Pt/ITO. (b) Koutecky-Levich plots for the ORR on Pt/ITO. (c) measured specific and mass activity of Pt/ITO and its comparison to Pt/C. (d) ORR stability of Pt/ITO over 1000 Cycles. (e) ORR Tafel plot for Pt/ITO. (f) Voltammetry stability for Pt/ITO.

showed excellent ORR stability over 1000 cycles between 0 and 1.4 V vs. NHE (Figure 1d) and excellent retention in the electrochemically active area during cycling (Figure 1f).

Pt Nanoparticles Supported on WC and WO_3

Our interest in WC as an electrocatalyst support for Pt was born out of several papers in the recent literature that claimed that WC promoted the electrocatalytic activity of Pt for several reactions, including the ORR. However, none of the authors at that time were able to provide an adequate explanation, though it was noted that near the Fermi level, Pt and WC have similar electronic structures, which could allow for electron transfer between the catalyst and support, particularly when adsorbates approach the Pt surface. Another key limitation of the literature was that many authors failed to report the surface state of the WC and only reported one scan for the WC surface. This left significant doubt as to the real role of the WC surface state and its stability in highly acidic media at ORR relevant potentials.

One of the most significant findings of this study was that the ORR on Pt is enhanced by the presence of the WC support [Publication 7]. In fact, the onset potential for Pt/WC was higher than Pt/Vulcan (Pt/C) and that the ½ wave potential was shifted positive. The root cause for this was suggested by theTafel slope where a 120 mV/decade slope was observed over the entire potential window, up to 0.9V. This is an important finding since bulk Pt and Pt/C both typically show two Tafel slopes in this region: i) 120 mV/decade < ~0.7V vs. NHE where the Pt is nearly oxide free; and ii) 60 mV/decade > ~ 0.7 V vs. NHE where the surface coverage of oxygen on Pt is very high. The presence of only the 120 mV/decade Tafel slope for Pt supported on WC suggests that the WC support suppressed oxide formation on the Pt nanoparticles. Unfortunately, the enhancement was short-lived [Publication 5]. After the Pt/WC catalyst was cycled between 0.0 V and 0.8 V vs. NHE, we observed significant degradation in both the electrochemical response and the physical structure of the support and severe agglomeration of Pt. Extensive studies with both WC and WO_3 supports showed that Pt is very strongly bound to WC initially and Pt/WC shows excellent stability at potentials < 0.8 V vs. NHE. However, as the potential approaches 0.8 V vs. NHE, the WC is rapidly oxidized to WO_2, which we found by XPS. Finally, the WO_3 chemically reacts in the highly acidic environment to form tungsten bronze, H_xWO_3, which is water soluble. The solubility of the bronze physically isolates the Pt nanoparticles, which migrate and agglomerate into large superclusters.

Nitrogen-Doped Ordered Mesoporous Carbon

We also evaluated the influence of surface functional groups (primarily nitrogen and oxygen) on carbon and its microcrystallinity on the dispersion and activity of supported platinum particles [Publications 1-2, 9-13]. We prepared the carbon supports using an amorphized silicate template. The carbons were made by modifying SBA-15, filling the template with pyrrole, polymerization and carburization at various temperatures between 800°C and 1400°C to control the length of the graphitic domains and nitrogen content. The carbons are denoted as CPPy-X, where X is the heat treatment temperature in Celsius. The PSD profile of all of CPPy-X carbons were similar, signifying that the temperature treatment did not change their pore structure. The SBET and V_{tot} of all samples were within 5%. The SBET of CPPy-1000 was 593 m^2/g and its V_{tot} was 0.78 cm^3/g. We also performed extensive XRD and RAMAN analysis, which showed that, generally, the length of the graphitic domains of the carbon increased with temperature; however, this did not change the overall structure of the material. However, XPS showed significant changes in surface composition among CPPy-X samples. The atomic (at) % of C, N and O were determined from C 1s, N 1s and O 1s peaks of full survey spectra. The nitrogen content decreased from 10.5 at % (800 °C) to 0.5 at % (1400°C) while the oxygen content decreased from 8.4 at % (800 °C) to 0.3 at % (1400°C). In fact, at 1400°C, the nitrogen and oxygen contents were within the error limit of XPS (<1%).

50 wt% of Pt was deposited onto the CPPy-X supports without pre-activation (i.e. boiling in acid to increase the number of oxygen functionalities). Without such pre-activation, Pt NPs on CPPy-X were expected to be clustered, especially at high loadings such as 50 wt% which was the target loading in this work. High resolution TEM images of Pt/CPPy -800 and Pt/CPPy -1000 showed a uniform Pt NPs particle size distribution. However, particles in Pt/CPPy -1000 were larger than that of Pt/CPPy-800. Indeed, the average size of Pt NPs was 3.7 nm on Pt/CPPy -1000 while it was 1.5 nm on Pt/CPPy-800. Compared to Pt/CPPy-800 and Pt/CPPy-1000, agglomeration could be observed in Pt/CPPy-1200 and Pt/CPPy-1400 despite their high surface areas. However, the size of Pt NPs on Pt/CPPy-1200 and Pt/CPPy-1400 were 2.9 and 3.3 nm, respectively. We found that a very intricate mechanism of Pt NPs nucleation and growth existed on Pt/CPPy-X which warrants additional study.

The ORR activity of the Pt/CPPy-X electrocatalysts was determined by CV between 0.2 and 1.1 V vs. NHE. Overall, we found that the nitrogen content played a far more significant role in the ORR activity than the surface oxygen groups and some interesting trends were observed. The trends in the specific and mass activity of Pt are shown in Figures 2a and 2b, respectively. The specific ORR activity of supported Pt initially decreased with increasing N content, as the particle size decreased. However, after a minimum at 5% N, the specific activity again increases, which is very surprising since the Pt dispersion was enhanced with excess N, which gave the smallest Pt particle sizes. We would normally

have expected the specific activity to further drop. The enhancement in specific activity suggests some interaction

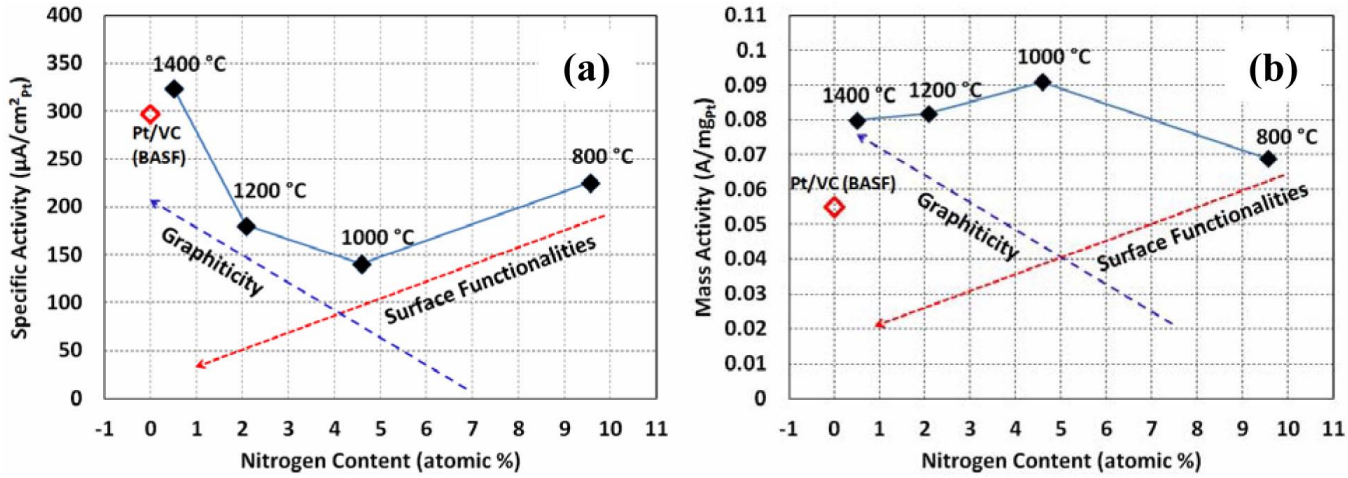

FIGURE 2. Trends in the specific (a) and mass (b) activity of Pt supported on N-functionalized carbon.

between Pt and the N groups, which needs to be understood. We have done some preliminary XAS work and have observed some variation of shape in the secondary peaks of the high energy (EXAFS) region, which suggests some electronic interaction between Pt and the functional groups. We expected the unusually high specific activity with small particle size to yield very high mass activity catalysts, however, we found that the Pt in the carbon pores were generally inaccessible, leading to very low electrochemically active area (only 31 m^2/g). Mechanisms to improve the accessibility of the nanosized Pt also require additional study.

Future Directions

Our future work with ITO and WC supports will focus on improving their long-term stability. We will also further study how the faceting of the non-carbon catalyst support influences how the Pt nanoparticles grow and some of our future work will be targeted in this area as well on model surfaces. We will also investigate new geometries to shield carbide-based supports from the electrolyte as well as the deposition of monolayer thickness Pt films. We will also investigate coupling a new physics-based model with a genetic algorithm to evaluate their performance with the goal of predicting novel catalyst layer microstructures.

Publication list (including patents) acknowledging the DOE grant or contract

1. Shrestha, Sujan; Asheghi, Sasha; Timbro, Jeffrey; Mustain, William E., "Effects of Pore Structure in Nitrogen Functionalized Mesoporous Carbon on Oxygen Reduction Reaction Activity of Platinum Nanoparticles.", *Carbon*, Accepted, In Press.

2. Shrestha, Sujan; Asheghi, Sasha; Timbro, Jeffrey; Morse, Nicholas; Mustain, William E., "Temperature Controlled Surface Chemistry of Nitrogen Doped Mesoporous Carbon and Its Influence on Pt ORR Activity", *Appl. Catal. A*, Accepted.

3. Liu, Ying; Mustain, William E., "High Stability, High Activity Pt/ITO Oxygen Reduction Electrocatalysts", *J. Am. Chem. Soc.*, 2013, **135** (2), 530.

4. Liu, Ying; Mustain, William E., "Evaluation of Tungsten Carbide as the Electrocatalyst Support for Platinum Hydrogen Evolution/Oxidation Catalysts", *Int. J. Hydrogen Energy*, 2012, **37**, 8929.

5. Liu, Ying; Shrestha, Sujan; Mustain, William E., "Synthesis of nano-size tungsten oxide and its evaluation as an electrocatalysts support for oxygen reduction in acid media", ACS Catalysis, 2012, **2**, 456.

6. Shrestha, Sujan; Liu, Ying; Mustain, William E., "Electrocatalytic Activity and Stability of Pt clusters on State-of-the-Art Supports: A Review, 2011, **53**, 256.

7. Liu, Ying; Mustain, William E., "Structural and Electrochemical Studies of Pt Clusters Supported on High Surface Area Tungsten Carbide for Oxygen Reduction", *ACS Catalysis*, 2011, **1**, 212.

8. Shrestha, Sujan; Mustain, William E., "Properties of Nitrogen-Functionalized Ordered Mesoporous Carbon Prepared Using Polypyrrole Precursor", *J. Electrochem. Soc.*, 2010, **157**, B1665.

9. Shrestha, Sujan; Morse, Nicholas; Mustain, William E., "Effect of Surface Chemistry on Double Layer Capacitance of Nitrogen Doped Ordered Mesoporous Carbon", Submitted for Review.

10. Shrestha, Sujan; Asheghi, Sasha; Timbro, Jeffrey; Mustain, William E., "Influence of Pore Structure of N-Doped Mesoporous Carbon in PEM Fuel Cells", *ECS Trans.*, 2013, 50 (2), 1287.

11. Shrestha, Sujan; Asheghi, Sasha; Timbro, Jeffrey; Lang, Christopher M.; Mustain, William E., "ORR and Fuel Cell Performance of Pt Supported on N-Functionalized Mesoporous Carbon", *ECS Trans.*, 2011, **41**(1), 1183.

12. Shrestha, Sujan; Mustain, William E., "Pt Nanoparticles Supported on Nitrogen Functionalized Ordered Mesoporous Carbon", *ECS Trans.*, 2010, **33**(1), 293.

13. Shrestha, Sujan; Mustain, William E., "Electrochemical Studies of N-functionalized Mesoporous Carbon", *ECS Trans.*, 2010, **28**(23), 27.

V.N.19 *In Situ* NMR/IR/Raman and *ab initio* DFT Investigations of Pt-Based Mono- and Bi-metallic Nanoscale Electrocatalysts: from Sulfur-Poisoning to Polymer Promoters to Surface Activity Indexes

Principal Investigator: YuYe J. Tong
Department of Chemistry
Georgetown University
37th & O Streets, NW
Washington, DC 20057
Phone: (202) 687-5872
Email: yyt@georgetown.edu

DOE Program Manage: Dr. Raul Miranda
Phone: (301) 903-8014
Email: Raul.Miranda@science.doe.gov

Objectives

The proposal targets two primary objectives:

1. Significantly advance our fundamental understanding of sulfur poisoning of Pt-based mono- and bi-metallic nanoscale electrocatalysts through careful interrogation of long and short range electronic effects caused by the poisonous sulfur-metal bonding.
2. Investigate and establish correlations among the surface *d* band center, the frontier orbitals of the metal surface as represented by the surface local density of states at the Fermi level (E_f –LDOS), and the associated electrochemical reactivity.

Achieving these objectives will lead one step closer to achieving the long-term goal of the PI. That is, by firmly establishing fundamentally-justified and experimentally-proved detailed electronic structure – surface reactivity relationships based on crosscutting *in situ* investigations of (real-world) nanoscale electrocatalysts, like these proposed in this project (*vide infra*), the PI strives to make substantial intellectual contributions to the development of unified predictive descriptions and concepts of heterogeneous catalysts (electronic) structure and activity by which new catalytic materials with desired functionalities (e.g., activity, selectivity, sustainability, and durability) can be rationally designed and developed

Technical Barriers

Although of great practical and fundamental importance in improving impurity tolerance of anode and cathode materials for both low temperature proton-exchanged membrane fuel cells and high temperature solid oxide fuel cells, systematic mechanistic investigations of sulfur-poisoning of Pt-based electrocatalysts in an electrochemical environment and its possible remedies have been surprisingly rare as compared to what has been done on heterogeneous catalysts in the gas phase in general. As asserted in the Feb. 2004 OBES report "Basic Research Needs for the Hydrogen Economy", *detailed mechanistic studies of the sulfur poisoning and tolerance of anode and cathode materials in general have yet to be undertaken*. Consequently, our current insufficient electronic-level understanding of the problem represents one of the most important contemporary challenges for the development of technologically viable fuel cells. Overcoming such a hurdle is urgently needed in the basic energy science research because it is a central issue underlying the practical durability and performance of fuel cells and also determining the fuel specifications.

Abstract

Over the current funding period (08/15/10 – present), we have achieved the following results: (1) identified the chemical state of adsorbed sulfur species on a Pt surface; (2) discovered that adsorbed sulfur species at low coverage can substantially enhance the oxygen reduction reaction (ORR), methanol oxidation reaction (MOR), and CO monolayer oxidation reaction (CMOR); (3) discovered that adsorption of PVP (polyvinylpyrrolidone) on commercial Pt black and carbon-supported Pt electrocatalysts can substantially enhance MOR and formic acid oxidation reaction (FAOR) activity. In addition, the adsorbed heavy PVP (360k) shows molecular switch-like behavior that can be used for freeing active sites for reactions at low potentials where the reactions take place and protecting and stabilizing the surface at high potentials where the bare Pt surface is most susceptible to corrosion; (4) demonstrated that the widely-used but unjustified current ratio criterion for CO tolerance in MOR is largely inadequate; (5) identified the most active surface water species in the MOR; (6) Studied the electronic properties of Pt shells in Au@Pt and Ru@Pt; and (7) Application of the condensed Fukui function to predict reactivity in core–shell transition metal nanoparticles (NPs).

Progress Report

1. The chemical state of adsorbed sulfur species on a Pt surface

The chemical state of adsorbed sulfur on a Pt surface was identified and investigated by a combination of detailed electrochemical (EC) measurements, in situ surface enhanced

Raman scattering (SERS) and ab initio density functional theory (DFT) calculations. The SERS data coupled with the DFT calculations provide the first convincing evidence showing that the adsorbed sulfur is in a sulfide (S^{2-}) state.

2. ORR, MOR, and CMOR enhanced by sulfur adsorption

We have reported a remarkable observation that robust activity enhancement in ORR (65 mV positive shift of the half-wave potential and 133% increase in kinetic current density at 0.6 V vs. Ag/AgCl) on commercial Pt electrocatalyst (Pt/C, 40 wt. %, d ~ 4.1 nm) could be achieved by adsorbing sulfide at low coverage ($\theta_{S,H}$ ~ 0.16), although the strong poisoning effect did prevail at high sulfide coverage as frequently observed. This unexpected activity enhancement was ascribed to a combination of an increase of the potential of surface oxidation and weakened surface bonding. Additionally, the effect of sulfide adsorption on the reactivity of core-shell (M@Pt, M=Au and Pd) NPs in the ORR was also investigated and compared with that of Pt/C so that possible remedies to the sulfur-poisoning of a pure Pt surface at high sulfide coverage may be identified. The results showed that the Pd@Pt NPs appeared to be the most tolerant electrocatalyst towards sulfur poisoning in ORR among the samples studied.

We have investigated the effect of adsorbed sulfide (S^{2-}_{ads}) on MOR taking place on Pt/C NPs using EC and attenuated total reflection-surface enhanced IR absorption spectroscopy (ATR-SEIRAS) techniques. The observed substantial enhancement in MOR activity per active site was rationalized by an enhanced parallel reaction pathway by the S^{2-} adsorption that did not lead to poisonous CO. Moreover, there was delayed/suppressed adsorption of electrolyte anions and oxygen-containing species and increased amounts of isolated free water monomers caused by the sulfide adsorption-induced more negatively charged Pt sites, which led to more available active sites, weakened bonding interaction between the Pt NPs and oxygen-containing species, and more active water species for MOR along the parallel reaction pathway.

We have also investigated the influence of adsorbed sulfide (S^{2-}_{ads}) on CMOR on carbon-supported Pt/C NPs using electrochemical and in situ ATR-SEIRAS techniques. An enhanced kinetics of CMOR on the S^{2-}_{ads}-Pt/C was observed by potentiodynamic CO stripping and potentiostatic CO oxidation analyses. EC impedance measurements revealed a weakened bonding of oxygen-containing species with the S^{2-}_{ads} -Pt/C surface as compared with the clean Pt/C surface, which we believe was the main reason for the observed enhanced CMOR by the S^{2-}_{ads}. The in situ SEIRAS data showed the existence of both linear- and bridge-bonded CO in all samples and that the sulfide adsorption substantially increased the fraction of the former on the available Pt sites and facilitated the conversion between them. Our results also indicate that the frequently observed pre-CMOR current most likely arises from oxidation of weakly-bonded CO rather than from reactions taking place at defect sites.

3. PVP Effects

We have discovered unexpected yet highly remarkable and intriguing observations of the PVP-enhanced electrocatalytic activity of the Pt nanoparticles for MOR and FAOR. In situ FTIR investigation suggests strongly that the observed activity enhancements are likely due to the PVP-induced additional reaction pathways. These observations may open up a new paradigm of research in which the protecting/stabilizing organic ligands can now be incorporated as an advantageous part of a nanocatalytic system.

We have also studied the effect of the commonly used 55k MW and a heavier chain of 360k MW PVP on commercial 40 wt% Pt/C using electrochemical methods and in situ SEIRAS experiments during the MOR and related gaseous CO oxidation. The PVP-modified samples exhibited an enhanced long- term CO tolerance with a small hindrance to the intrinsic activity of Pt/C. Increased water adsorption in the presence of polymer was observed to coincide with the oxidation of adsorbed CO and was related to the desorption of the surface-bound carbonyl of PVP via in situ SEIRAS. The notable differences between the adsorbate trends are indicative of adsorbed polymer interactions with the surface. Interestingly it is the strong dependence of the polymer molecular weight (Mw) that led to qualitatively different behavior. Understanding the effects of adsorbed PVP on electrocatalytic reactions is of fundamental and practical importance due to its widespread use in synthesized NPs targeted for fuel cell applications.

4. An unjustified current ratio criterion for CO tolerance in MOR

We have revisited a popular criterion that uses the ratio between the peak currents of the respective positive (anodic) and negative (cathodic) potential scans, If/Ib, in the cyclic voltammetry of methanol electro-oxidation to gauge CO-tolerance and catalytic activity of Pt-based electro-catalysts and its inadequacy was revealed by an in situ SERAIS study.

5. The most active surface water species in MOR

We have reported a detailed electrochemical in situ SEIRAS investigation of two different core-shell, Ru@Pt and Au@Pt/C, metal NPs. We were able to identify the most active sites and surface water species involved in the carbon monoxide oxidation reaction (COR) and MOR on these NPs. We discovered that exposing the as-synthesized Ru@Pt NPs to air could turn them into largely surface-ruthenated NPs whose structure was rather stable under multiple potential cycling between -0.2 and 0.7 V (vs. Ag/AgCl, 3 M) and

reduction at -0.3 V but could be annealed by the COR. The SEIRAS data enabled the identification of the Ru coordinated to Ru, Ru coordinated to Pt, and Pt-islands on Ru -core sites on the COR-annealed Ru@Pt NPs among which the most active sites were the Pt-islands on Ru-core sites for the COR and MOR, as evidenced by an onset potential as low as -0.1 V for the COR. For the Au@Pt/C NPs, the SEIRAS data showed a much higher onset potential (0.45 V) for the COR that accounted for their much lower activity observed as compared to that of the Ru@Pt in terms of COR and MOR. Among the three different surface water species, namely the water monomer, the weakly hydrogen-bonded water, and the strongly hydrogen-bonded water, the SEIRAS data pointed to the weakly hydrogen-bonded water as the dominant source that provided oxygen for the COR and MOR. Furthermore, the SEIRAS data showed that the surface water structure was very different in reaction media, i.e., with pre-adsorbed CO or methanol, from that in pure supporting electrolyte, an observation that strongly cautions the practice of using the latter to identify the active water species.

6. ^{195}Pt and ^{13}C NMR study of Au@Pt and Ru@Pt core-shell electrocatalysts

Pt-based core−shell (M@Pt where M stands for core element) NPs have recently been under increasing scrutiny in the fields of fuel cell and lithium air battery electrocatalysis due to their promising prospects in optimizing catalytic activity, reducing Pt loading and consequently lowering its cost. To achieve the latter, delineating spatially resolved local (surface) elemental distribution and associated variations in electronic properties under working condition (i.e., in situ) is arguably a prerequisite of fundamental importance in investigating electrocatalysis but unfortunately is still sorely missing. In this regard, in situ ^{195}Pt EC NMR of Pt-based NPs is unique in terms of accessing such information, particularly the spatially resolved partition between the s- and d-like Fermi level local density of states (E_f-LDOS) modified by the core elements. In this paper, we report a comparative in situ ^{195}Pt EC-NMR investigation of Ru@Pt vs. Au@Pt NPs which was complemented by in situ ^{13}C EC-NMR of the ^{13}CO adsorbed on the respective NPs generated via dissociation of methanol and by ab initio DFT calculations. The results showed opposing electronic effects between Ru vs. Au cores: the former substantially reduced the s-like but not the d-like E_f-LDOS of the Pt shell while the latter did the opposite. According to recent quantum calculations, a reduction in d-like partition would weaken the Pt−O bond while a reduction in s-like partition would weaken the Pt−H bond, which is largely in agreement with experimental observations.

7. The condensed Fukui function to predict reactivity in core–shell transition metal nanoparticles

Chemical reactivity descriptors are a powerful means for understanding reactivity in a wide variety of chemical compounds. These descriptors, rooted in density functional theory, have found broad application in organic chemical reactions, but have not been as widely applied for other classes of chemical species such as nanoparticles, which are the subject of this article. Specifically, we explore application of the Fukui function, the global hardness and softness, the local softness, and the dual descriptor to pure metallic and core–shell nanoparticles, with and without a CO molecule bound to the surface. We find that the Fukui function is useful in predicting and interpreting chemical reactivity, and that it correlates well with the results of the popular d-band center method. Differences in the Fukui function before and after bonding of a CO molecule to the surface of a nanoparticle reveal interesting information about the reactivity of the nanoparticle surface. The change in the Fukui function when an electric field is applied to the molecule is also considered. Though the results are generally good, some of the limitations of this approach become clear.

Future Directions

While continuing to focus on unraveling the surface chemistry of sulfur and other conventional poisonous species on Pt-based electrocatalysts, we will explore a novel perspective of it, which was inspired by some very interesting observations made over the current grant period. Specifically, it was observed that traditionally undesirable species, such as sulfur, can actually promote, rather than poison, catalytic activity of Pt-based electrocatalysts. For instance, at relatively low coverage (<20%), adsorbed sulfur species can promote considerably COR, MOR, and ORR activity; adsorbed PVP can substantially enhance MOR and formic acid oxidation reaction (FAOR) activity; and adsorbed iodine can significantly improve the stability of PtCu alloy electrocatalyst for ORR. These observations are along the line of a new emerging area of research in which many traditional poisoning species have been observed to promote catalytic reactions. However, much of the surface chemistry that governs such behavior remains to be uncovered and their potential practical applications are largely unexplored.

Publication list (including patents) acknowledging the DOE grant or contract[1-24]

1. Park, I.-S.; Tong, Y.Y.J., Sulfide–Adsorption-Enhanced Oxygen Reduction Reaction on Carbon-Supported Pt Electrocatalyst. *Electrocatal* **2013**, accepted.

2. Lica, G.C.; Tong, Y.J., Electrochemical impedance spectroscopic measurement of potential of zero charge of octanethiolate-protected Au and Pd nanoparticles. *J. Electroanal. Chem.* **2013,** *688*, 349.

3. Allison, T.C.; Tong, Y.Y.J., Application of the condensed Fukui function to predict reactivity in core–shell transition metal nanoparticles. *Electrochim. Acta* **2013**, 10.1016/j.electacta.2012.12.072.

4. Zaluzhna, O.; Li, Y.; Allison, T.C.; Tong, Y.Y.J., Inverse-micelle-encapsulated water-enabled bond breaking of dialkyl diselenide/

disulfide: a critical step for synthesizing high-quality gold nanoparticles. *J Am Chem Soc* **2012,** *134* , 17991.

5. Tong, Y.Y.J., Unconventional promoters of catalytic activity in electrocatalysis. *Chem. Soc. Rev.* **2012,** *41*, 8195.

6. Park, I.-S.; Chen, D.-J.; Atienza, D.O.; Tong, Y.Y.J., Enhanced CO monolayer electro-oxidation reaction on sulfide-adsorbed Pt nanoparticles: A combined electrochemical and in situ ATR-SEIRAS spectroscopic study. *Catalysis Today* **2012,** *202*, 175.

7. Park, I.; Atienza, D.O.; Hofstead-Duffy, A.M.; Chen, D.J.; Tong, Y.Y.J., Mechanistic Insights on Sulfide-Adsorption Enhanced Activity of Methanol Electro-Oxidation on Pt Nanoparticles. *ACS Catal*. **2012,** *2*, 168.

8. Hofstead-Duffy, A.M.; Chen, D.-J.; Tong, Y.Y.J., An in situ attenuated total reflection-surface enhanced infrared absorption spectroscopic study of enhanced methanol electro-oxidation activity on carbon-supported Pt nanoparticles by poly(vinylpyrrolidone) of different molecular weights. *Electrochim. Acta* **2012,** *82*, 543.

9. Hofstead-Duffy, A.M.; Chen, D.-J.; Sun, S.-G.; Tong, Y.Y.J., Origin of the current peak of negative scan in the cyclic voltammetry of methanol electro-oxidation on Pt-based electrocatalysts: a revisit to the current ratio criterion. *Journal of Materials Chemistry* **2012,** *22* (11), 5205.

10. Chen, D.-J.; Xu, B.; Sun, S.-G.; Tong, Y.Y.J., Electroless deposition of ultrathin Au film for surface enhanced in situ spectroelectrochemisrty and reaction-driven surface reconstruction for oxygen reduction reaction. *Catalysis Today* **2012,** *182*, 46.

11. Atienza, D.O.; Allison, T.C.; Tong, Y.Y.J., Spatially-Resolved Electronic Alterations as Seen by in situ195Pt and 13CO NMR in Ru@Pt and Au@Pt Core-Shell Nanoparticles. *J. Phys. Chem. C* **2012,** *116*, 26480.

12. Xu, B.; Park, I.-S.; Li, Y.; Chen, D.-J.; Tong, Y.Y.J., An in situ SERS investigation of the chemical states of sulfur species adsorbed onto Pt from different sulfur sources. *J. Electroanal. Chem.* **2011,** *662* (1), 52.

13. Susut, C.; Tong, Y.Y.J., Size-Dependent Methanol Electro-oxidation Activity of Pt Nanoparticles with Different Shapes. *Electrocatal* **2011,** *2*, 75.

14. Susut, C.; Chen, D.-J.; Sun, S.-G.; Tong, Y.Y.J., Capping polymer-enhanced electrocatalytic activity on Pt nanoparticles: a combined electrochemical and in situ IR spectroelectrochemical study. *Phys. Chem. Chem. Phys* **2011,** *13* (16), 7467.

15. Park, I.-S.; Xu, B.; Atienza, D.O.; Hofstead-Duffy, A.M.; Allison, T.C.; Tong, Y.Y.J., Chemical state of adsorbed sulfur on Pt nanoparticles. *ChemPhysChem* **2011,** *12* (4), 747.

16. Du, B.; Zaluzhna, O.; Tong, Y.Y.J., Electrocatalytic properties of Au@Pt nanoparticles: effects of Pt shell packing density and Au core size. *Phys. Chem. Chem. Phys* **2011,** *13*, 11568-11574.

17. Allison, T.C.; Tong, Y.Y.J., Evaluation of methods to predict reactivity of gold nanoparticles. *Phys. Chem. Chem. Phys* **2011,** *13* (28), 12858.

18. Xu, B.; Park, I.-S.; Li, Y.; Chen, D.-J.; Tong, Y.Y.J., In situ Surface Enhanced Raman Scattering Spectroscopic Study of Sulfur Adsorption on Polycrystaline Platinum Electrode Surface. *Electrochemistry* **2010,** *16*, 256.

19. Du, B.; Rabb, S.A.; Zangmeister, C.; Tong, Y.Y., A volcano curve: optimizing methanol electro-oxidation on Pt-decorated Ru nanoparticles. *Phys. Chem. Chem. Phys* **2009,** *11* (37), 8231.

20. Tan, F.; Du, B.; Danberry, A.L.; Park, I.-S.; Sung, Y.-E.; Tong, Y.Y., A comparative in situ195Pt electrochemical-NMR investigation of PtRu nanoparticles supported on diverse carbon nanomaterials. *Faraday Discuss.* **2008,** *140*, 139.

21. Susut, C.; Nguyen, T.; Chapman, G.; Tong, Y.Y., Shape and size stability of Pt nanoparticles for MeOH electro-oxidation. *Electrochim. Acta* **2008,** *53* (21), 6135.

22. Susut, C.; Chapman, G.B.; Samjeské, G.; Osawa, M.; Tong, Y.Y., An unexpected enhancement in methanol electro-oxidation on an ensemble of Pt(111) nanofacets: a case of nanoscale single crystal ensemble electrocatalysis. *Phys. Chem. Chem. Phys* **2008,** *10* (25), 3712.

23. Du, B.; Danberry, A.L.; Park, I.-S.; Sung, Y.-E.; Tong, Y.Y., Spatially resolved [sup 195]Pt NMR of carbon-supported PtRu electrocatalysts: Local electronic properties, elemental composition, and catalytic activity. *J. Chem. Phys.* **2008,** *128* (5), 052311.

24. Danberry, A.L.; Du, B.; Park, I.-S.; Sung, Y.-E.; Tong, Y.Y., Probing Spatially-Resolved Pt Distribution in PtRu Nanoparticles with 195Pt EC-NMR. *J Am Chem Soc* **2007,** *129* (45), 13806-13807.

V.N.20 Investigation of the Nature of Active Sites on Heteroatom-Containing Carbon Nano-Structures for Oxygen Reduction Reaction

Principal Investigator: Umit S. Ozkan
College of Engineering Distinguished Professor
Department of Chemical and Biomolecular Engineering
The Ohio State University
Phone: (614) 292-6623
Email: Ozkan.1@osu.edu

Post-doctoral Researchers:
- Xiaoguang Bao, Department of Chemistry, The Ohio State University
- Juan Tian, Burcu Mirkelamoglu and Bing Tan, Department of Chemical and Biomolecular Engineering, The Ohio State University

PhD Students:
Elizabeth J. Biddinger, Dieter von Deak, Deepika Singh, **Kuldeep Mamtani,** Department of Chemical and Biomolecular Engineering, The Ohio State University

Undergraduate Students:
Douglas S. Knapke, Katie Luthman, Jesaiah King, Dan Valco, Sai Uppati, Department of Chemical and Biomolecular Engineering, The Ohio State University

Collaborators:
- Aravind Asthagiri, Associate Professor, Department of Chemical and Biomolecular Engineering, The Ohio State University
- Christopher Hadad, Professor, Department of Chemistry, The Ohio State University
- Dr. Jeffrey Miller, Argonne National Laboratory
- Dr. Jean-Marc Millet, CNRS Catalysis Research Institute Lyon-France

DOE Program Manager: Raul Miranda
USDOE, Office of Basic Energy Sciences,
Catalysis Science Program
Phone: 301-903-8014
Email: raul.miranda@science.doe.gov

Objectives

To investigate the nature of the active sites in CN_x and Fe-N-C catalysts for the oxygen reduction reaction in proton exchange membrane (PEM) fuel cells

Technical Barriers

In PEM and direct methanol fuel cells, the oxygen reduction reaction at the cathode leads to the major overpotential and as a result major power loss. Pt catalysts, which are the state-of-the art cathode electro-catalysts, suffer from prohibitively high cost, making the wide-spread application of fuel cells difficult. Among the alternatives, nitrogen-containing carbon structures, with or without a metal center, show potential as possible replacements for Pt. What is lacking, however, is an understanding of the nature of the active sites in these materials.

Abstract

Nitrogen-containing carbon nanostructures (CN_x) have been synthesized and developed as cathode catalysts for proton exchange membrane (PEM) fuel cells in our research group at Ohio State as part of our previous work. In the last year, we have examined the growth process of CN_x catalysts on two different Co-doped substrates: Vulcan carbon and Magnesia, during the decomposition of acetonitrile using *in-situ* techniques such as X-ray absorption near edges spectroscopy (XANES), extended X-ray absorption fine structure spectroscopy (EXAFS), X-ray diffraction (XRD) and *ex-situ* techniques such as X-ray photon spectroscopy (XPS), and transmission electron microscopy (TEM). The structure of CN_x obtained as well as the nitrogen content was significantly different on the two substrates, which led to differences in activity, as shown by rotating ring disk electrode (RRDE). We have also recently begun synthesizing Fe-N-C catalysts, which are commonly known to be the most active non-precious metal catalysts for the oxygen reduction reaction (ORR). The active sites for Fe-N-C catalysts are thought to be $Fe\text{-}N_2$ and/or $Fe\text{-}N_4$ centers, which are possibly different from the active sites of CN_x catalysts which are most likely pyridinic nitrogen groups located on graphitic edge planes. We have compared CN_x and Fe-N-C catalysts in half cell and single cell tests along with the characterization techniques listed above, to elucidate the differences in the structure and active sites between the two types of catalysts.

Progress Report

1. In-situ characterization of the growth of CN_x carbon nano-structures as oxygen reduction reaction catalysts

In-situ XANES and EXAFS techniques were used to characterize the CN_x growth process over two substrates (Vulcan carbon and MgO) doped with Co. Changes taking place in the growth catalyst were examined during the heat treatment and decomposition of acetonitrile over the substrates. *In-situ* XANES provided information about the ease of reduction and coordination environment of Co over Co-VC and Co-MgO substrates. Linear combination (LC) fitting analysis was performed for the spectra obtained for the two substrates at room temperature, at 800°C, after 30 min and after 2 h of acetonitrile flow with cobalt acetate, CoO, Co foil as reference compounds.

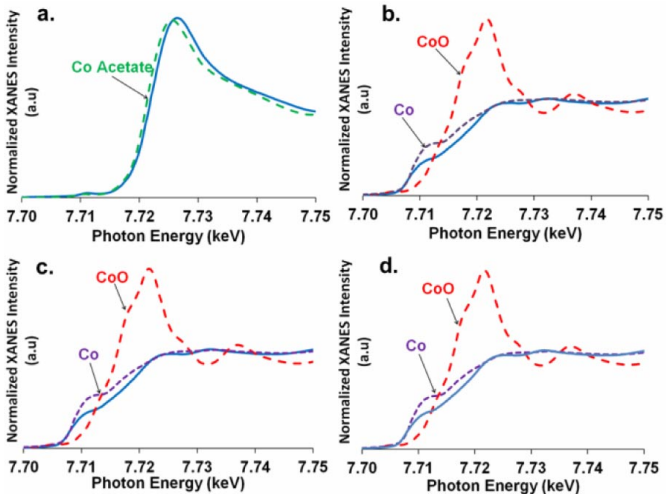

FIGURE 1. Normalized *in-situ* XANES spectra of Co K-edge taken during the growth of CN_x over Co-Vulcan Carbon growth substrate at different stages of pyrolysis a) room temperature, b) after treatment in N_2 at 800°C, c) after 30 min of CH_3CN pyrolysis, d) after 2 h of CH_3CN pyrolysis (Spectra for Co acetate, CoO and Co are shown as reference).

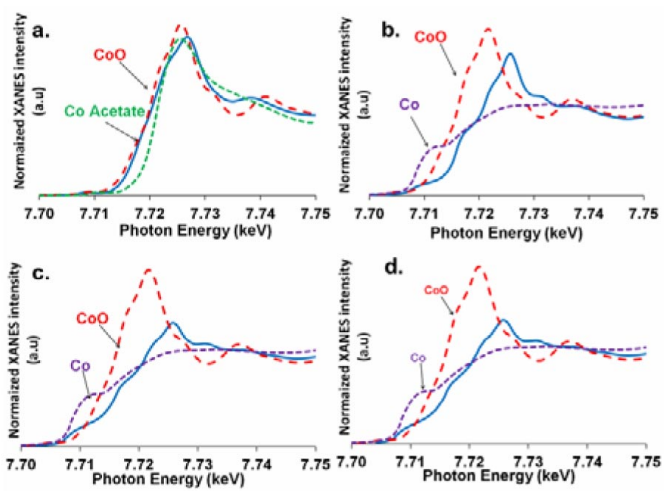

FIGURE 2. Normalized *in-situ* XANES spectra of Co K-edge taken during the growth of CN_x over Co-MgO substrate at different stages of pyrolysis a) room temperature, b) after treatment in N_2 at 800°C, c) after 30 min of CH_3CN pyrolysis, d) after 2 h of CH_3CN pyrolysis.

From LC-XANES analysis of the Co-VC spectra at room temperature, cobalt species were seen to exist as cobalt acetate prior to any heat treatment (Figure 1a). Under nitrogen at 800°C, the sample was reduced to a mostly metallic form and remained in this state even after introduction of acetonitrile for 30 min and 2 h (Figure 1b-d). The LC-XANES fits for the Co-MgO samples showed more oxidized states for cobalt (Figure 2a), which could be explained by the presence of the oxide support. At room temperature, Co in Co-MgO exists in Co^{2+} form. Up to 40% reduction was observed under nitrogen (Fig. 2b). Metallic cobalt became more evident upon introduction of acetonitrile for 30 min, and persisted with the same percentage contribution after 2h of acetonitrile treatment (Fig 2c and d). Co over MgO appeared to be less reduced at the end of acetonitrile treatment than over VC substrate. XANES spectra collected ex-situ for CN_x samples after acid washing was identical for both CN_x formed over MgO and Vulcan carbon (Figure 3), with over 90% metallic Co, demonstrating that although the type and abundance of cobalt phases that exist at the end of the acetonitrile pyrolysis may be different over the two growth substrates, once washed away in acid the cobalt phase left behind in CN_x is the same regardless of the substrate used.

The extended X-ray absorption fine structure (EXAFS) spectroscopy technique provides information about the coordination environment of the samples. The magnitudes of the k^2 weighted Fourier Transform of the Co K-edge EXAFS spectra for Co-VC samples are shown in Figure 4a. At room temperature, the peak at the uncorrected R-value of 1.59 Å can be attributed to the Co-O peak present in Co-acetate. After nitrogen treatment at 800°C, the Co-O peak disappeared with a concurrent appearance of the Co-Co peak at 2.1 Å in the uncorrected FT-magnitude. This Co-Co peak persisted in both of the spectra taken 30 min and 2h after acetonitrile introduction. EXAFS fits were carried out using the same experimental standards used in XANES fits. After heat treatment in N_2 only, and even after acetonitrile introduction for 30 mins, the cobalt particle size under *in-situ* conditions was very similar to that of bulk metallic cobalt, as indicated by the calculated coordination number (CN) values of 11.2 and 10.9 respectively.

Figure 4b shows the FT-magnitudes acquired over the Co-MgO substrate at four different stages during pyrolysis. At room temperature, there exists a peak at 1.59Å, which could correspond to the Co-O bond in CoO. At 800°C in nitrogen, a smaller peak appeared at 1.4 Å along with a peak at 2.6 Å, which could be due to the Co-O and Co-O-Co interactions, respectively. After reduction under acetonitrile atmosphere, the intensity of the peak at 1.59Å decreased, with the simultaneous occurrence of a broad peak at 2.27 Å (uncorrected), which could be due to conjunction of Co-Co with the Co-O-Co bond contributions. EXAFS fits carried out for the samples to provide further verification that the ratios of cobalt acetate, cobalt oxide, and metallic cobalt obtained for the different sample compositions were accurate.

Transmission electron microscopy imaging helped characterize the growth of acid-washed carbon nanostructures formed upon acetonitrile pyrolysis over Co-VC and Co-MgO substrates. As seen in Figure 5a-d, after acid washing, the carbon nanostructures grown over Co-VC are in the form of stacked cups, but with less order as compared to the CN_x grown on Co-MgO (Figure 5e-h). Carbon nanostructures are less abundant in the CN_x grown over the VC support due to the majority of growth medium

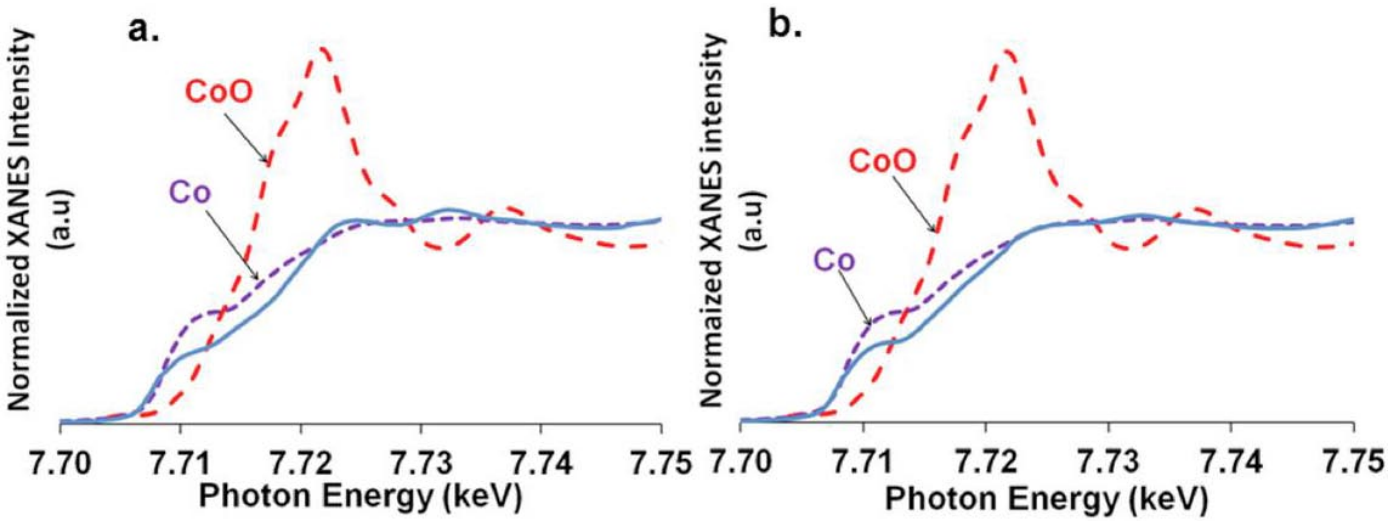

FIGURE 3. Normalized ex-situ XANES Co K-edge spectra of acid-washed CN_x grown on a) Co-VC and b) Co-MgO

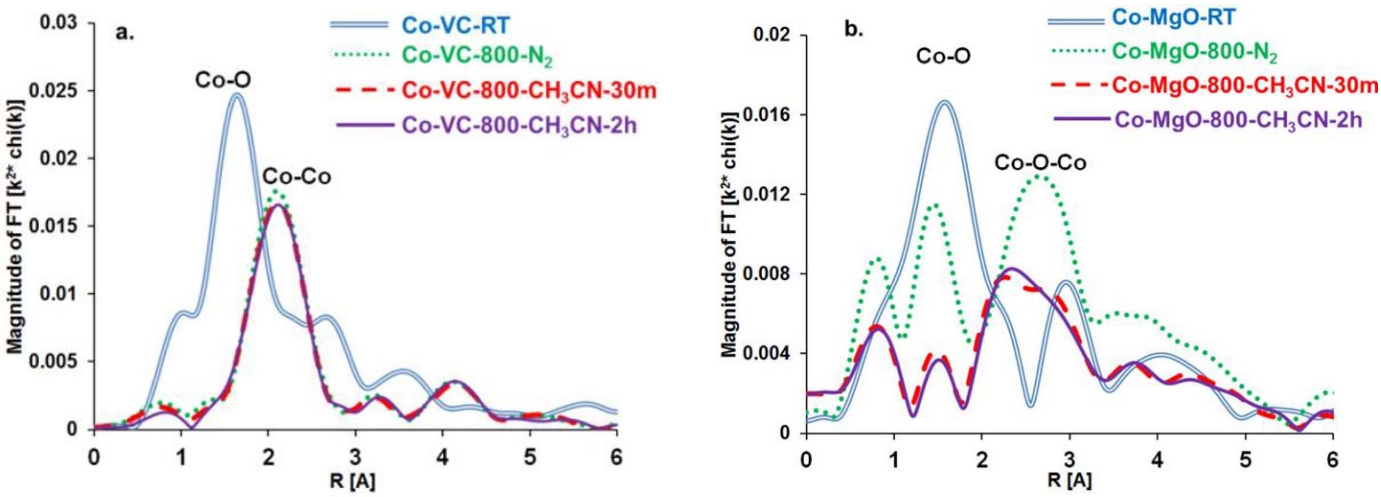

FIGURE 4. Magnitudes of k^2-weighted Fourier transforms of *in-situ* cobalt K-edge EXAFS spectra of (a) Co-VC and (b) Co-MgO growth substrates during different stages of pyrolysis

(i.e., Vulcan carbon) remaining after acid washing. The fibers are thick-walled (wall thickness~10nm), with relatively large cobalt particles encased within the carbon shell, with a diameter of approximately 25nm (Fig. 16c-d).

CN_x nano-structures grown over the Co-MgO, on the other hand, are more-ordered and better-defined stacked cups, as shown in Fig. 5e, f, and g. They are more abundant because the oxide support is washed away with acid leaching, leaving only the carbon nanostructures behind. Cobalt also appeared to be encased within the nanostructures, and the particle size and wall thickness were smaller than those seen in CN_x grown over Co-VC, as is the diameter of the stacked cups (Fig. 5d and h).

Electrochemical activity tests for washed and unwashed CN_x grown over Co-VC and Co-magnesia were performed using RRDE technique in acidic medium. Figure 6a shows the polarization curves for the washed and unwashed samples grown over the two different growth substrates. When washed samples were compared, the CN_x catalysts grown over Co-MgO were seen to be more active towards ORR than CN_x grown over Co-VC. There was a difference of 50 mV between the onset potentials (Figure 6. Inset) observed over these two washed catalysts.

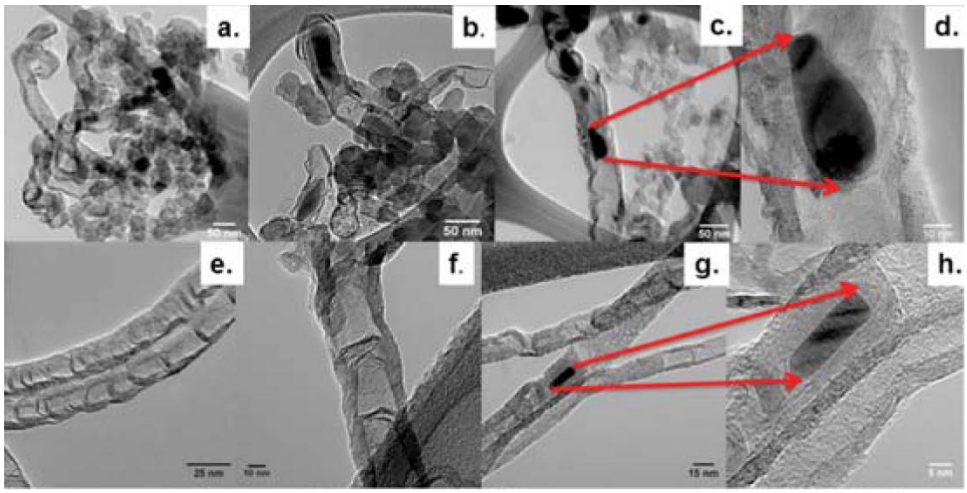

FIGURE 5. TEM images of acid-washed CN_x, grown on Co-Vulcan Carbon (a-d) and CO-MgO (e-h)

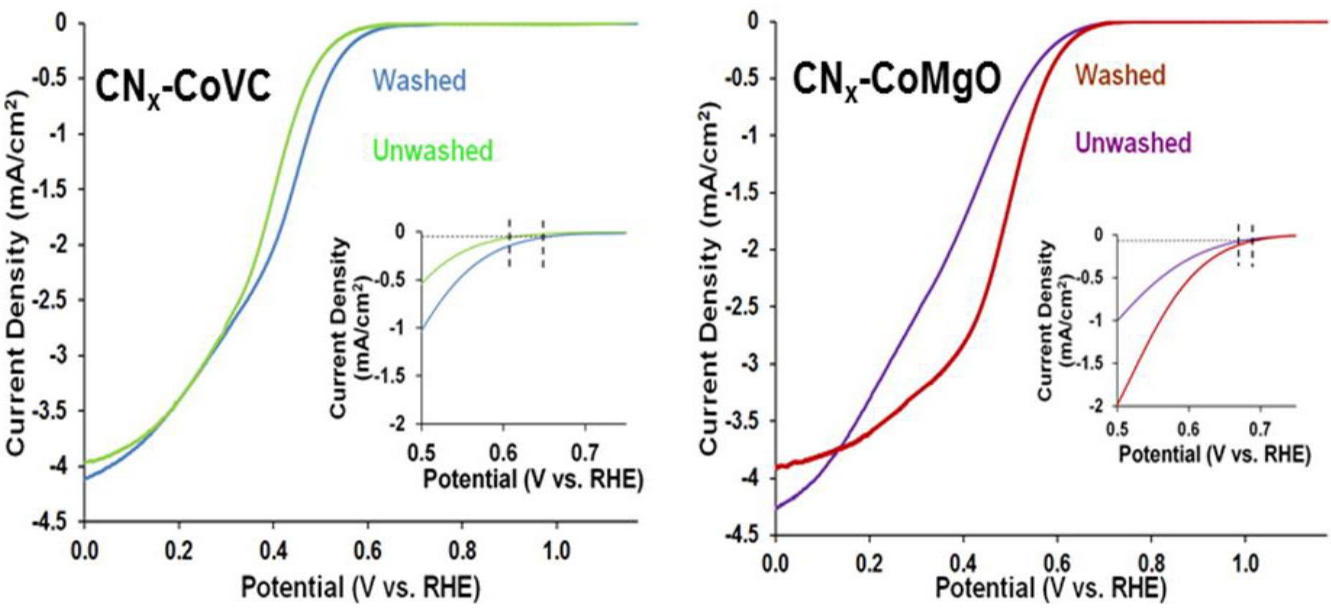

FIGURE 6. Rotating ring disk electrode (RRDE) tests of washed and unwashed CNx catalysts grown on Co-Vulcan Carbon and Co-MgO in O_2-saturated 0.5M H_2SO_4 at 25°C; rotation rate: 2500 rpm; scan rate 10 mV/s; scan direction: cathodic; catalyst loading 1.6 mg/cm^2 ; disk geometric area: 0.2472 cm^2

2. Investigation of differences between CNx and iron-nitrogen-carbon (Fe-N-C) catalysts for ORR

More recently reported non-precious metal ORR catalysts consist of a high surface area carbon support impregnated with 1% Fe and a nitrogen containing pore filler, heat treated in an inert atmosphere of Ar, followed by a second heat treatment in pure NH_3. The active sites in these catalysts are thought to be iron coordinated by two and/or four nitrogen atoms in a carbon matrix.

In our previous work, we have shown high ORR activity for nitrogen-doped carbon nanostructures (CN_x) synthesized by heat treatment of an oxide or carbon support impregnated with Fe or Co in acetonitrile. These carbon nano-structures were washed by an acid to leach out any exposed metal and non-conductive oxides. These catalysts had high pyridinic nitrogen content with significant graphitic edge plane exposure both of which correlated with ORR activity.

In an ongoing study, we are attempting to elucidate differences between Fe-N-C and CNx catalysts. Fuel cell activity tests performed on CN_x (grown on a Fe-doped supports by acetonitrile pyrolysis) and Fe-N-C (heat treated in Ar followed by NH_3) catalysts demonstrated that Fe-N-C catalysts were more active for ORR (Figure 7). However,

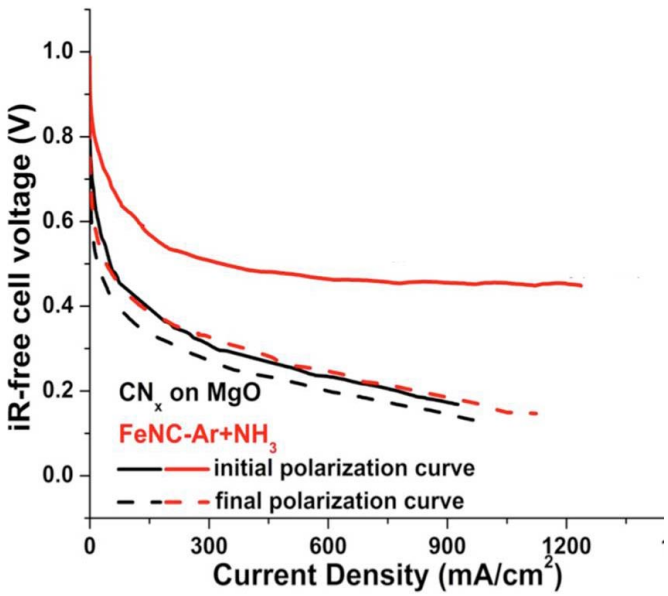

FIGURE 7. Fuel cell activity comparison for CNx and Fe-N-C before and after a 100-hour potential hold. Cell temperature: 80°C; Relative humidity: 100%; Backpressure: 15psig; Cathode catalyst loading 1mg/cm2 ; Anode catalyst: 0.5 mg Pt/cm^2

fuel cell stability tests performed for 100 h with a 0.5V potential hold revealed that while Fe-N-C catalysts have a high initial activity, they degrade rapidly within the first 24 h, beyond which their current density continued to decrease further. Whereas CN_x catalysts had a lower initial activity, but showed significantly less degradation in the first 24 h, following which the current density reached a plateau and remained constant thereafter. Figure 7 shows the polarization curves obtained before and after the 100-hour potential hold. We are currently investigating compositional and structural differences between the two classes of catalysts via XPS, TEM, EXAFS, XANES, TPO techniques.

Future Directions

In addition to investigating differences between CN_x and Fe-N-C catalysts, we are examining the effect of acid washing on Fe-N-C catalysts, as well as the effect of duration of acid washing on the activity and stability of these catalysts.

We have also obtained preliminary results to show that CN_x and Fe-N-C catalysts are active for ORR in alkaline medium, with activities comparable to platinum. This could have a direct implication on development of cathode catalysts for metal-air batteries or alkaline fuel cells. We will be developing button cells to test these materials as cathodes for zinc-air batteries.

Publication list in the last year acknowledging the DOE grant or contract

1. Von Deak, D., Singh, D., Biddinger, E.J., King, J.C., Bayram, B., Miller, J.T., Ozkan, U.S., "Investigation of sulfur poisoning of CNx oxygen reduction catalysts for PEM fuel cells," *Journal of Catalysis.* **2012**, 285, 145-151.

2. Von Deak, D. Singh, D., King, J.C., Ozkan, U.S., "Von Deak, D. Singh, D., King, J.C., Ozkan, U.S., "Use of carbon monoxide and cyanide to probe the active sites on nitrogen-doped carbon catalysts for oxygen reduction," *Applied Catalysis, B.,* **2012**, 113-114, 126-133.

3. Ozkan, U.S., "Bridging Heterogeneous Catalysis and Electro-catalysis: Catalytic Reactions Involving Oxygen," accepted for publication in *Topics in Catalysis*

4. Singh, D., Soykal, I.I., von Deak, D., Tian, J., King, J., Miller, J.T., Ozkan, U.S., "Operando and *in-situ* characterization of the growth of CN_x carbon nano-structures as oxygen reduction reaction catalysts," accepted to *Journal of Catalysis.*

5. Bao, X., Nie, X., von Deak, D., Biddinger, E.J., Luo, W., Asthagiri, A., Ozkan, U.S., Hadad, C.M., "A first-principles study of the role of quarternary-N doping on the oxygen reduction reaction activity and selectivity of graphene edge sites," accepted to *Topics in Catalysis*.

V.N.21 Oxide-Metal Interactions Studied on M@Oxide, Core-Shell Catalysts

Principal Investigator: Raymond J. Gorte
Chemical & Biomolecular Engineering
University of Pennsylvania
311 Towne Building, 220 South 33rd Street
Philadelphia, PA 19104
Phone: 215/898-4439
Email: gorte@seas.upenn.edu

Chen Chen
Chemical & Biomolecular Engineering
University of Pennsylvania
311 Towne Building, 220 South 33rd Street
Philadelphia, PA 19104
Phone: 215/898-4439
Email: chenc5@seas.upenn.edu

Lisandra Arroyo
Chemical & Biomolecular Engineering
University of Pennsylvania
311 Towne Building, 220 South 33rd Street
Philadelphia, PA 19104
Email: lisyarroyo@gmail.com

DOE Program Manager: Raul Miranda
Email: Raul.Miranda@science.doe.gov

Objectives

The primary objective of this work is to develop better catalysts through optimization of metal/metal-oxide interactions. The primary goals of the present work will be: 1) to investigate the catalytic properties of core-shell catalysts prepared by self-assembly methods to determine how the oxide shells affect the activity of metal catalysts, 2) to use these materials to characterize the energetics associated with oxide-metal interfaces in systems of catalytic interest, 3) to characterize the nature of the oxide-metal interface spectroscopically, and 4) to develop a better understanding of the role that oxide-metal interactions have on catalytic properties.

Abstract

Core-shell nanoparticles have been synthesized in organic solutions using self-assembly methods, with Pd or Pt at the core and ceria, zirconia, and titania as the shell. These are then adsorbed in monolayer form onto oxide supports that have been functionalized using silanes to make them hydrophobic. The primary goals of the present work are: 1) to investigate the catalytic properties of core-shell catalysts prepared by self-assembly methods to determine how the oxide shells affect the activity of metal catalysts, 2) to use these materials to characterize the energetics associated with oxide-metal interfaces in systems of catalytic interest, 3) to characterize the nature of the oxide-metal interface spectroscopically, and 4) to develop a better understanding of the role that oxide-metal interactions have on catalytic properties

Progress Report

Initial studies with Pd@ceria/alumina demonstrated that the activity of this catalyst is a strong function of calcination temperature, with catalysts showing greatly improved activity when heated to above 1073 K. To understand this, we have investigated the properties of a Pd@CeO_2/Si-Al_2O_3 catalyst after calcination at 773 K and after calcination at 1073 K.

Calcining to higher temperatures increased rates for the methane-oxidation reaction over Pd@CeO_2/Si-Al_2O_3 by a factor of more than three for measurements in 0.5% CH_4 and 5% O_2. The effect of increasing calcination temperature on this catalyst was even more dramatic for methane-steam reforming (MSR). The Pd@CeO_2/Si-Al_2O_3 catalyst calcined to 773 K was unstable for MSR, losing almost all of its activity over the period of an hour while the catalyst calcined at 1073 K showed reasonably stable rates. CO adsorption, monitored using volumetric uptakes, and FTIR indicated adsorption on the Pd was suppressed following reduction at 673 K in H_2 when the catalyst had been calcined at only 773 K, but not after 1073 K. Pulse-reactor measurements demonstrated that catalysts calcined at either 773 K or 1073 K were heavily reduced under MSR reaction conditions at 673 K but that the catalyst heated to 1073 K could be reoxidized by H_2O at this temperature, while the 773-K sample could not be. It is suggested that increasing calcination temperature modifies the structure of the ceria shell, which in turn changes the ceria redox properties.

Future Directions

We are continuing our investigations of the Pd@Ceria/alumina catalyst in order to understand why it shows exceptional activity for methane oxidation. We are also beginning similar studies of catalysts prepared with different metal cores and different oxide shells.

Publication list

1. Y. Kang, M. Li, Y. Cai, M. Cargnello, R.E. Diaz, T.R. Gordon, N.L. Wieder, R.R. Adzic, R.J. Gorte, E.A. Stach, C.B. Murray, "Heterogeneous catalysts need not to be so "heterogeneous": Monodisperse Pt nanocrystals by combining shape-controlled synthesis and purification by colloidal recrystallization", *Journal of the American Chemical Society*, **2013**, *135*, 2741-2747.

2. M. Cargnello, P. Fornasiero, R.J. Gorte, "Opportunities for Tailoring Catalytic Properties Through Metal-Support Interactions, *Catalysis Letters*, **2012**, *142*, 1048-1048.

3. K. Bakhmutsky, J. Imran Alsous, and R.J. Gorte, "A Thermodynamic Investigation of the Redox Properties of VPO Catalysts", *Catalysis Letters*, **2012**, *142*, 578-81.

4. Dianyuan Wang, Yijin Kang, Vicky Doan-Nguyen, Jun Chen, Rainer Kungas, Noah L. Wieder, Kevin Bakhmutsky, Raymond J. Gorte, and Christopher B. Murray, Synthesis and oxygen storage capacity of 2-D ceria nanocrystals", *Angewante Chemie, Int. Ed*., **2011**, *50*, 4378-4381.

5. K. Bakhmutsky, N.L. Wieder, T. Baldassare, M.A. Smith, and R.J. Gorte , "A Thermodynamic Study of the Redox Properties of Supported Co particles", *Applied Catalysis A*, **2011**, *397*, 266-71.

6. I. Baldychev, A. Javadekar, D.J. Buttrey, J.M. Vohs, and R.J. Gorte, "A Comparison of Redox Properties of Molybdenum-Based Mixed Oxides", *Applied Catalysis A*, 2011, *394*, 287-93.

7. I. Baldychev, J.M. Vohs, and R.J. Gorte, "The Effect of Support on Redox Properties and Methanol-Oxidation Activity of Vanadia Catalysts", *Applied Catalysis A*, **2011**, *391*, 86-91.

8. R.J. Gorte, "Ceria in Catalysis: From Automotive Applications to the Water-Gas Shift Reaction", *AIChE Journal*, **2010**, *56*, 1126-35.

9. I. Baldychev, R.J. Gorte, and J.M. Vohs, "The Impact of Redox Properties on the Reactivity of V_2O_5/Al_2O_3 Catalysts", *Journal of Catalysis*, **2010**, *269*, 397-403.

V.N.22 Fundamental Studies of the Steam Reforming of Alcohols on Pd/ZnO and Co/ZnO Catalysts

Principal Investigator: John M. Vohs
Department of Chemical and Biomolecular Engineering
University of Pennsylvania
220 S. 33rd Street
Philadelphia, PA 19104
Phone: (215) 898-6318
Email: vohs@seas.upenn.edu

Team Members:
Mr. Eddie Martono (graduate student)
Phone: (215) 898-7230
Email: martono@seas.upenn.edu

DOE Program Manager: Dr. Raul Miranda
Phone: (301) 903-8014
Email: Raul.Miranda@science.doe.gov

Objectives

The overall goal of this project was to provide fundamental insight into the factors that control the activity and selectivity of supported metal catalysts for the steam reforming of alcohols to produce hydrogen. Specific goals were to determine how metal- support interactions, including transfer of oxygen from reducible oxides to the metal, affect catalyst reactivity and stability, and to determine the mechanism by which alloying affects the selectivity of group VIII metal-based catalysts.

Abstract

In this project we are studying the relationships between the structure and reactivity of ZnO-supported Pd, Pt, and Co alcohol steam reforming catalysts and determining the origins of the their unique reactivity and high selectivity for producing H_2 and CO_2. In addition to identifying the relevant reaction pathways and intermediates, we are investigating how alloying Pd and Pt with Zn significantly alters the selectivity for methanol steam reforming and how interactions at the Co-ZnO interface influence the extent of oxidation of the Co and its reactivity. A surface science approach using model single crystal catalysts (e.g. Pd/ZnO(0001), Zn/Pd(111), Co(0001) and Co/ZnO(0001)) and an array of surface sensitive spectroscopic probes (HREELS, XPS, LEED, AES, TPD, AFM) is being used to characterize surface structures and adsorbed intermediates at the molecular level. In addition to determining the mechanisms of alcohol steam reforming reactions, this project is also providing fundamental insights that will be useful in designing a wide range of supported metals catalysts.

Progress Report

Structure-activity relationships for supported Co catalysts

XPS and TPD studies of the reaction of ethanol on Co films and CoO particles supported on non-reducible YSZ(100) (see Figure 1 for representative TPD data) show that the activation energy for the dehydrogenation of adsorbed ethoxide to produce acetaldehyde, which is a key intermediate in ethanol steam reforming (ESR), is a function of the oxidation state of the cobalt. The activation energy varies from 86 kJ/mol on O_2-dosed Co/YSZ(100) to 126 kJ/mol CoO/YSZ(100). These results along with those obtained from Co foils implicate Co^{2+} as the active site for dehydrogenation of ethoxide to produce acetaldehyde, and indicate that the most active surface for this reaction consists of either a two-dimensional oxide layer on metallic cobalt or an oxygen covered metallic cobalt surface. Studies of the reaction of ethanol on model Co/ZnO(0001) and Co/CeO_2(100) catalysts also show that partially oxidized cobalt films or particles that contain both Co^0 and Co^{2+} are the most active for the dehydrogenation of adsorbed ethoxide species to produce acetaldehyde. For these systems, however,

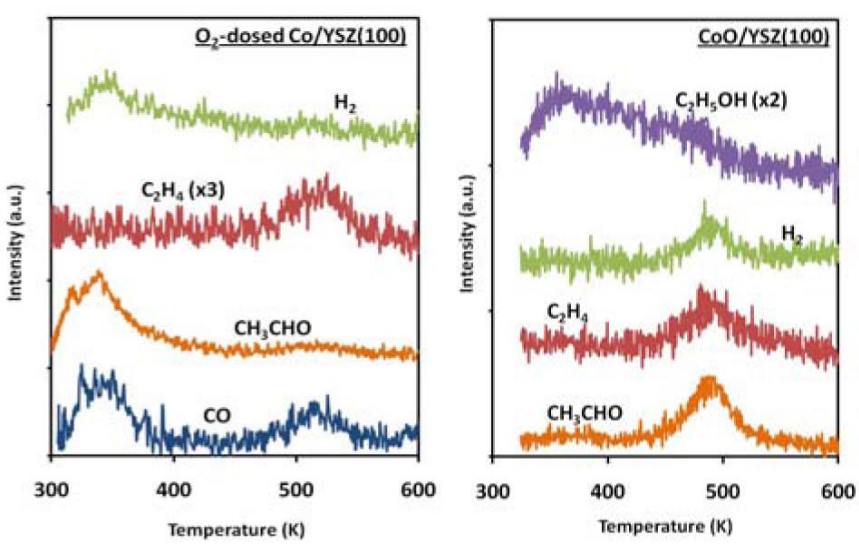

FIGURE 1. Ethanol TPD spectra obtained from O_2 pre-dosed Co/YSZ(100) and CoO/YSZ(100).

the Co can be maintained in a partially oxidized state via reaction with the reducible support.

The results obtained in our studies provide considerable insight into how the support influences the overall activity of Co-based SRE catalysts. In particular, they indicate that the high activity observed for Co on reducible supports is due to the fact that these supports facilitate the oxidative dehydrogenation of ethoxide to acetaldehyde by providing the oxygen required for this reaction. This pathway results in reduction of the support which is then reoxidized via reaction with water in a subsequent step. This pathway is shown schematically in Figure 2 for a $Co/CeO_2/YSZ(100)$ model catalyst. Our results also show that in addition to promoting this reaction, the facile transfer of oxygen from the support to the Co plays a role in removing carbon deposits and thereby helping to maintain activity.

PtZn alloy catalysts for alcohol steam reforming

In the previous 3-year grant cycle we investigated the mechanism by which alloying Pd with a small amount of Zn dramatically alters the selectivity of Pd-based methanol steam reforming catalysts. Our study showed that Zn formed two-dimensional ordered surface phases which had electronic properties significantly different than that of bulk Pd. These electronic effects were found to alter the activation energies for C-H bond cleavage thereby stabilizing adsorbed aldehyde intermediates, and to decrease the adsorption energy for CO. During the current grant cycle we have returned to the issue of alloying with Zn and have expanded our previous studies with Pd to include Pt. The goal here was to determine if the insights obtained for the Pd-Zn system are general and applicable to other group VIII metals. Pt/ZnO catalysts have high activity and selectively for methanol and ethanol steam reforming and PtZn alloys have been proposed as catalysts for both oxygen reduction and fuel oxidation in PEM fuel cells, and for the hydrogenation of aldehydes to produce α,β-unsaturated alcohols. Thus, this system is also technologically relevant.

Structural Characterization: We have collaborated with Bruce Koel's group at Princeton to determine the structure of near surface PtZn alloys formed by vapor deposition of Zn onto Pt(111) followed by annealing. Our group has collected detailed LEED, AES, and XPS data for Zn-modified Pt(111) surfaces, while Koel's group has performed an in-depth low energy ion scattering spectroscopy (LEIS) study. Our combined data show that Zn adlayers on Pt(111) substitute into the surface layer upon annealing above 600 K which is consistent with previous studies by Rodriguez. Ordered surface phases are not observed, however, and the Zn distributes itself into the first 2-3 atomic layers with the Zn concentration in the outermost layer being relatively low.

CO bonding on Zn-modified Pt(111): The heat of adsorption of CO was measured and used to assess how Zn addition affects the surface electronic properties. Consistent with our previous studies of PdZn, alloying Pt with Zn was found to decrease the heat of adsorption of CO. In a somewhat surprising result, however, just the opposite trend was observed for a Pt(111) surface decorated with Zn adatoms (Zn/Pt(111)) where the CO desorption temperature increased relative to that on clean Pt(111). HREELS data

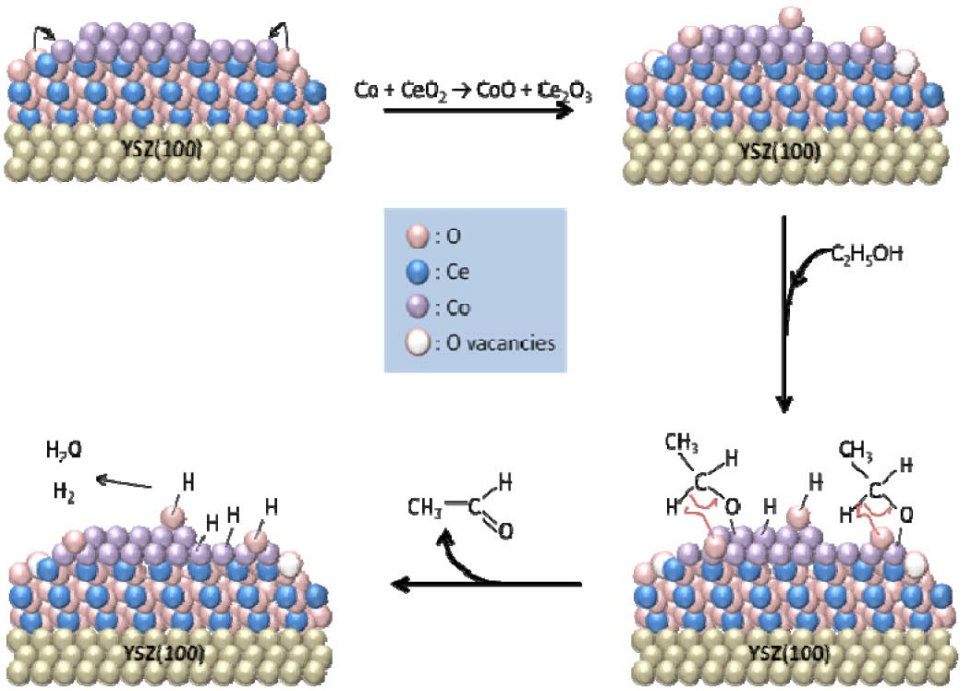

FIGURE 2. Pathway for the dehydrogenation of ethanol to produce acetaldehyde on $Co/CeO_2/YSZ(100)$.

indicate that at temperatures above 200 K, CO does not adsorb on the Zn adatoms on this surface. Thus, different perturbations of the surface electronic properties are observed for Zn adatoms and those incorporated into the surface layer.

Reactivity of PtZn/Pt(111) surfaces towards oxygenates: CH_3OH was found to adsorb only molecularly on Pt(111) (some reaction does occur at defect sites). In contrast on PtZn/Pt(111) it undergoes dissociative adsorption to form methoxide groups which decompose to CO and H at temperatures below 300 K. Since the Zn concentration in the outmost layer of the PtZn/Pt(111) surface is less than 5% of a monolayer, we attribute this enhanced reactivity for O-H bond scission to an electronic effect rather than reaction at the isolated Zn sites. These results further demonstrate the large effect that alloying with small amounts of Zn has on the reactivity of group VIII metals.

Much more interesting chemistry was observed for reaction of oxygenates on Pt(111) surfaces decorated with Zn adatoms. We have used TPD and HREELS to map out the reactivity of the surface towards methanol as a function of the Zn coverage. Several interesting trends were observed. First the Zn adatoms provide sites for O-H bond scission in adsorbed methanol to form methoxide groups which appear to reside on both Zn and Pt sites. Those adsorbed on the Zn adatoms undergo dehydrogenation near 300 K to produce adsorbed formaldehyde, while those on the Pt sites decompose completely to CO and H_2. These reaction pathways are summarized in Figure 3. We are currently using TPD and HREELS to study the adsorption and reaction of ethanol and acetaldehyde on the Zn-modified Pt(111) surfaces. Our preliminary results for these molecules suggest that at least under some conditions the Zn adatoms provide sites for C-O bond cleavage in adsorbed aldehydes. This result suggests that the Pt-alloy catalysts may also have some activity for the deoxygenating of both aldehydes and polyols which might be useful in the production of fuels and chemicals from cellulosic biomass.

While the Zn-adatom surfaces used here are not likely to be representative of those in real Pt/ZnO alcohol steam reforming catalysts it is noteworthy that high activity for PdZn and PtZn alloys for alcohol steam reforming is only observed for catalysts that contain Zn in excess of the stable 50:50 alloy composition. This is consistent with our hypothesis that that the presence of Zn adatoms on the alloy surface is required for high reforming activity.

Publication acknowledging the DOE grant or contract

1. Hyman, M., Martono, M., and Vohs, J.M., Studies of the Structure and Interfacial Chemistry of Co Layers on ZnO(0001) , *J. Phys. Chem. C*, **2010**, 114**,** 16892-16899.

2. Halevi, B., Peterson, E.J., Delariva, A., Jeroro, E., Lebarbier, V.M., Wang, Y., Vohs, J.M., Kunkes, E., Havecker, M., Behrens, M., Schlögl, R., and Datye, A.K., *J. Phys. Chem. C.*, **2010**, 114, 17181-17190.

3. Hyman, M.P. and Vohs, J.M., Reaction of Ethanol on Oxidized and Reduced Cobalt Surfaces, *Surface Science*, **2011**, 605, 383-389.

4. Martono, E. and Vohs, J.M., *Phys.* Reaction Pathways for Ethanol on Model Co/ZnO(0001) Catalysts, *Phys. Chem. Chem. Phys.*, **2011**, 13, 9880-9886.

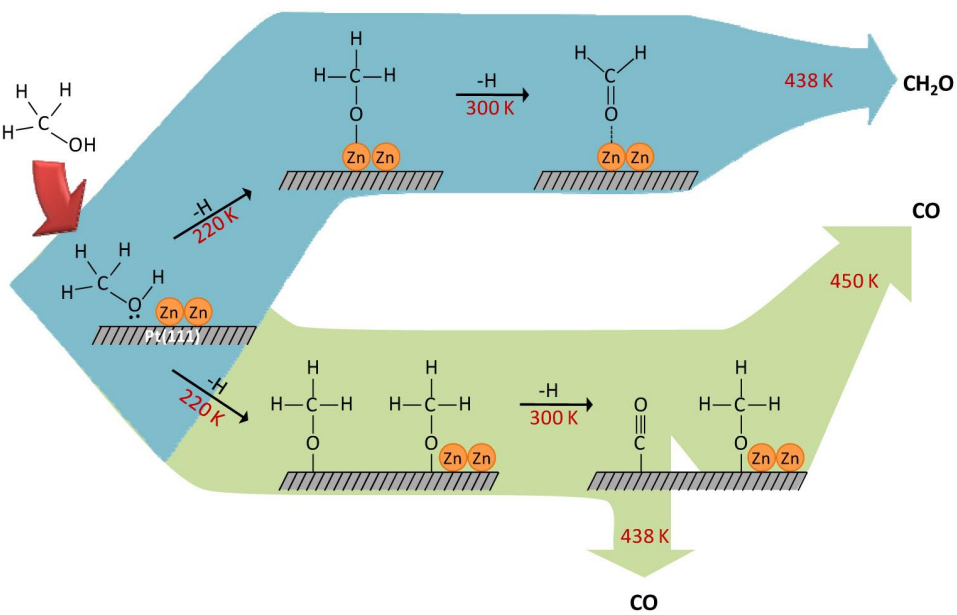

FIGURE 3. Pathways for the reaction of methanol on Zn-modified Pt(111) surfaces.

5. Martono, E. and Vohs, J.M., Active Sites for the Reaction of Ethanol to Acetaldehyde on Co/YSZ(100) Model Steam Reforming Catalysts, *ACS Catalysis*, **2011**, 1, 1414-1420.

6. Martono, E. and Vohs, J.M., Support Effects in Cobalt Based Ethanol Steam Reforming Catalysts: Reaction of Ethanol on Co/CeO_2/YSZ(100) Model Catalysts, *J. Catal.*, **2012**, 291, 79-86.

7. Halevi, B., Peterson, E.J., Roy1, A., DeLariva1, A., Jeroro, E., Gao, F., Wang, Y., Vohs, J.M., Kiefer, B., Kunkes, E., Havecker, M., Behrens, M., Schlögl, R., and Datye, A.K., Catalytic Reactivity of Face Centered Cubic PdZn for the Steam Reforming of Methanol, *J. Catal.*, **2012**, 291, 44-54.

8. Vohs, J.M., *Chemical Reviews*, Site Requirements for the Adsorption and Reaction of Oxygenates on Metal Oxide Surfaces, in press. (ASAP version available on-line DOI:10.1021/cr300328u).

9. Martono, E. and Vohs, J.M. , Reaction of CO, CH_2O, and CH_3OH on Zn-modified Pt(111), *J. Phys. Chem. C,* in press.

10. Ho, C.S., Martono, E., Banerjee, S., Roszell, J., Vohs, J.M., and Koel, B.E. Alloy Formation and Chemisorption at Zn/Pt(111) Bimetallic Surfaces using Alkali ISS, XPD, and TPD, *J. Phys. Chem. C,* in press.

11. Halevi, B., Lin, S., Roy, A., Zhang, H., Jeroro, E., Vohs, J.M., Wang, Y., Guo, H., and Datye, A.K., High CO_2 Selectivity of ZnO Powder Catalysts for Methanol Steam Reforming, *J. Phys. Chem C*, in press.

V.N.23 Theoretically Relating the Surface Composition of Pt Alloys to Their Perfromance as the Electrocatalysts of Low-Temperature Fuel Cells

Principal Investigator: Guofeng Wang
Assistant Professor
Department of Mechanical Engineering and Materials Science
University of Pittsburgh
Pittsburgh, PA 15261
Phone: (412) 624 3325
Email: guw8@pitt.edu

DOE Program Manager: Dr. Raul Miranda
Phone: (301) 903-4355
Email: raul.miranda@science.doe.gov

Objectives

The main goal of this project is to gain fundamental knowledge about the relation between surface composition and catalytic performance of Pt alloy catalysts for oxygen reduction reactions (ORR).

Specific objective 1: Develop and improve a first-principles based multiscale computation approach to simulating surface segregation phenomena in Pt alloy surfaces.

Specific objective 2: Evaluate the surface electronic structure and catalytic activity of Pt alloy catalysts.

Specific objective 3: Relate the surface composition to the catalytic performance of Pt alloy catalysts.

Technical Barriers

To accomplish the research objectives, the PI needs to develop the modified embedded atom method atomic interaction potentials for Pt alloys, improve the atomistic Monte Carlo simulation method for simulating surface segregation process in Pt alloys, perform the density functional theory transition state calculations to determine the reaction energetics of the ORR on Pt alloy surfaces, and develop kinetic Monte Carlo simulation codes to evaluate the rate of the ORR on the Pt alloy catalysts.

Abstract

The project was launched on September 15, 2009. Over the grant period, we have accomplished all the research objectives proposed in the proposal. Specifically, we have developed and performed Monte Carlo (MC) simulations predicting the surface composition of a series of Pt binary and ternary alloy catalysts, carried out first-principles transition state calculations of the ORR on Pt and Pt alloy surfaces, developed and performed kinetic Monte Carlo (KMC) simulations predicting the activity for the ORR on Pt surfaces, and derived the relation between surface composition and catalytic activity for the ORR on Pt alloys. As a result of our study, ten research articles supported by this grant have been published in peer-reviewed journals.

Progress Report

Monte Carlo simulations on surface segregation in Pt alloys

Supported by this grant, my research group has successfully developed the modified embedded atom method (MEAM) atomic interaction potentials for Pt-Ni, Pt-Re, Pt-Mo, Pt-Co, Pt-Ti, Pt-Fe, Pt-Pd, Pt-V, Pt-Au, and Pt-Mn binary alloys and Pt-Ni-Co, Pt-Ni-Fe, and Pt-Pd-Ni ternary alloys. Furthermore, we performed the Metropolis Monte Carlo (MC) simulations to accurately predict the surface segregation phenomena and surface composition profiles in these Pt alloys after annealing in vacuum. In Fig. 1, we show the predicted surface composition profiles of three representative alloys using the developed MEAM potentials and the MC simulation method. For ordered Pt3Ti alloys (Fig. 1(b)), the Pt concentration in the outermost (111) surface layer exhibits an abrupt change around the stoichiometric composition (75 at.% of Pt) and reaches 100 at.% even if the bulk Pt concentration is just slightly above 75 at.%. In the annealed Pt-Ni (111) surface (Fig. 1(c)), the surface Pt concentration varies in an oscillatory fashion from the outermost surface layer to the bulk material and Pt enriches the outermost layer. Fig. 1(d) shows that the surface Pt concentration varies gradually with increasing Pt in the annealed Pt-Pd (111) surface and Pd will enrich the outermost surface layer. Our theoretical predictions are in excellent agreement with available experimental data.

Density functional theory transition state calculations of ORRs on the surfaces of Pt catalysts

In this project, we examined the influence of both ligand effect and structure effect on the reaction energetics of the ORRs on Pt-based electrocatalysts. To this end, we calculated the reaction energetics (including surface adsorption energy, heat of reaction, and activation energy) of the ORRs on Pt(111), Pt/Ni(111), Pt(100), and Pt/Ni(100) surfaces using the DFT method. With the DFT structure optimization calculations, we first identified the most stable sites for the seven ORR intermediates adsorbed on the Pt and Pt/Ni surfaces. Then, we constructed the initial and final states of

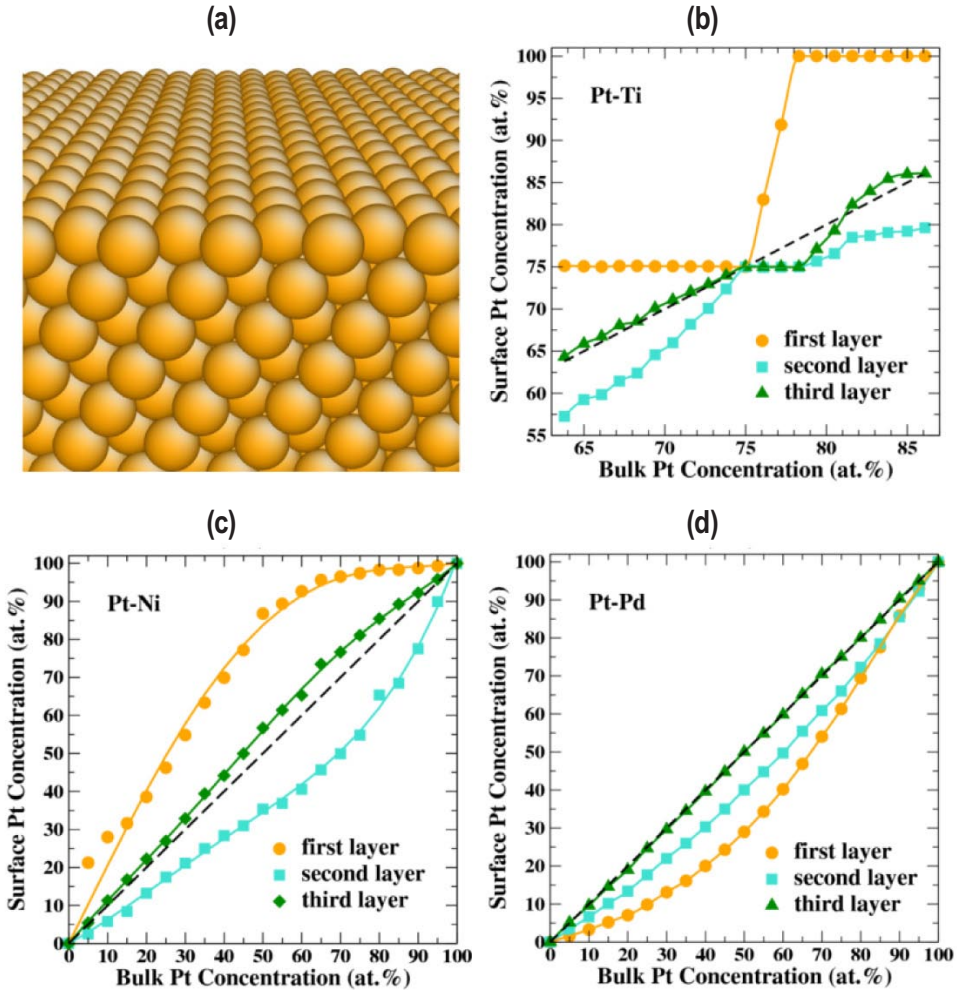

FIGURE 1. (a) Atomistic structure of the (111) surface of alloys with face-centered cubic lattice. Predicted chemical composition (expressed in atomic concentration of Pt) in the three outermost layers of the annealed fcc (111) surface of (b) Pt-Ti, (c) Pt-Ni, and (d) Pt-Pd alloys. In (b), (c), and (d), the black dashed lines indicate where surface compositions are equal to overall bulk compositions.

various ORR elementary steps on the Pt and Pt/Ni surfaces using these lowest-energy configurations and determined the corresponding transition states using the climbing image nudged elastic band method. In Fig. 2, we show the atomic structures for the ORR elementary steps on the Pt(100) surface attained in our DFT calculations. Furthermore, we calculated heat of reaction and activation energy for all the elementary steps of the ORRs on the Pt(111), Pt/Ni(111), Pt(100), and Pt/Ni(100) surfaces. In this study, we predicted that the rate-determining step for the ORR is the OH hydrogenation reaction with activation energy of 0.80 eV on the Pt (100) surface, the O hydrogenation reaction with activation energy of 0.79 eV on the Pt (111) surface, the OH hydrogenation reaction with activation energy of 0.79 eV on the Pt/Ni (100) surface, and the O2 hydrogenation reaction with activation energy of 0.15 eV on the Pt/Ni (111) surface. Since a low activation energy for the rate-determining step leads to high activity for the ORRs, our DFT results suggest that the catalytic activity for the ORR would be slightly higher on the Pt/Ni (100) than that on the Pt (100) surface, would be reasonably higher on the Pt (111) than that on the Pt (100) surface, and would be much higher on the Pt/Ni (111) than that on the Pt (111) surface. Our theoretical study provides a quantitative explanation to the experimentally measured trend of the ORR activity on the Pt and Pt-Ni (111) and (100) single crystals.

Correlation between surface composition of Pt alloys and catalytic activity for ORR

Supported by this grant, my research group has made great effort to establish the relationship between the surface chemical composition and the ORR activity of Pt alloy catalysts using both the first-principles DFT transition state calculation method and the kinetic Monte Carlo (KMC) method. In this research, we focused on studying the rate of

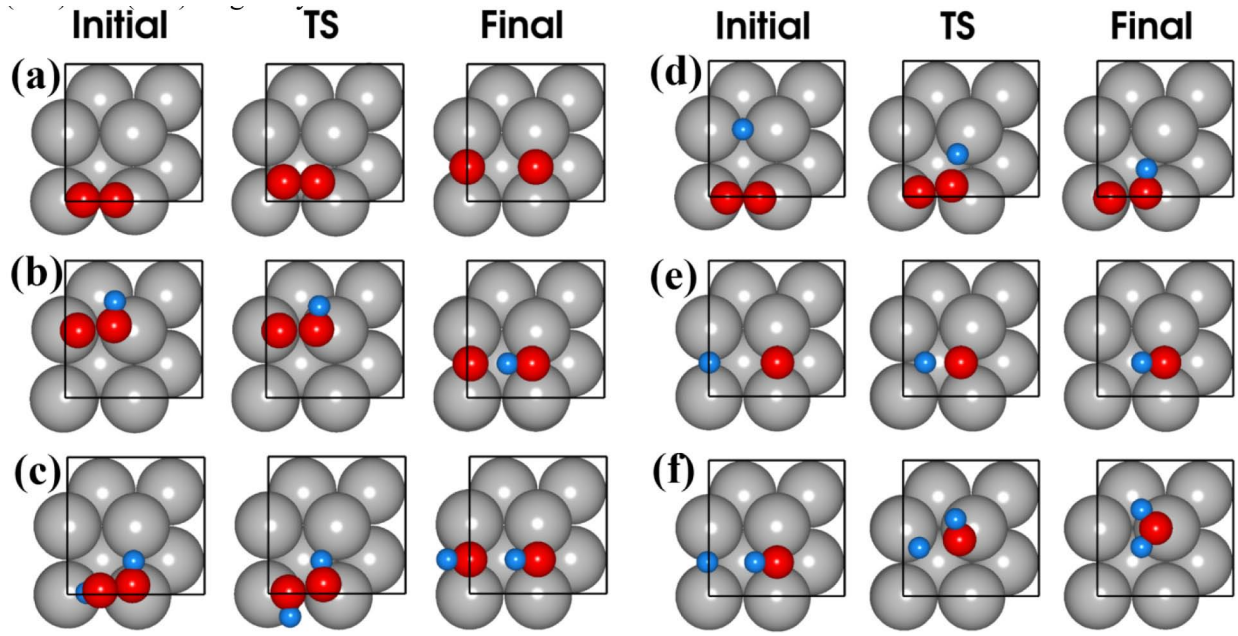

FIGURE 2. Atomic structures of the initial state, transition state, and final state for (a) O2 dissociation reaction, (b) OOH dissociation reaction, (c) H2O2 dissociation reaction, (d) O2 hydrogenation reaction, (e) O hydrogenation reaction, and (f) OH hydrogenation reaction on Pt (100) surface. In the figure, gray balls represent Pt atoms, red balls represent O atoms, and blue balls represent H atoms, respectively.

the ORRs on Pt-skin Pt-TM alloy (111) surfaces. Here, TM refers to transition metal element Ti, V, Fe, Co, and Ni. To this end, we determined all the surface adsorption energies, heats of reaction, and activation energies related to the ORRs on the Pt-TM alloy surfaces using the DFT calculation method. From our DFT data of activation energies, we have found that the ORR will favorably follow the peroxyl dissociation mechanism on the Pt and Pt3Fe (111) surfaces but adopt the peroxide dissociation mechanism on the Pt/Ti, Pt/V, Pt/Fe, Pt/V, Pt/Ni, Pt3Ti, and Pt3V (111) surfaces. For each modeled Pt catalyst surface, we found the activation energy for the rate determining step (denoted as "Ea"), which has the highest activation energy among all the elementary reaction steps within the preferred mechanism, of the ORR following the most preferable mechanism. Conceivably, the lower the value of Ea is, the higher the rate of the ORR would be. Consequently, we plotted in Fig. 3 the reciprocal value of Ea as a function of oxygen (O) binding energy on the Pt-based catalyst surfaces. In this way, we correlate the catalytic activity for the ORR with the surface electronic structure of the Pt-based catalysts.

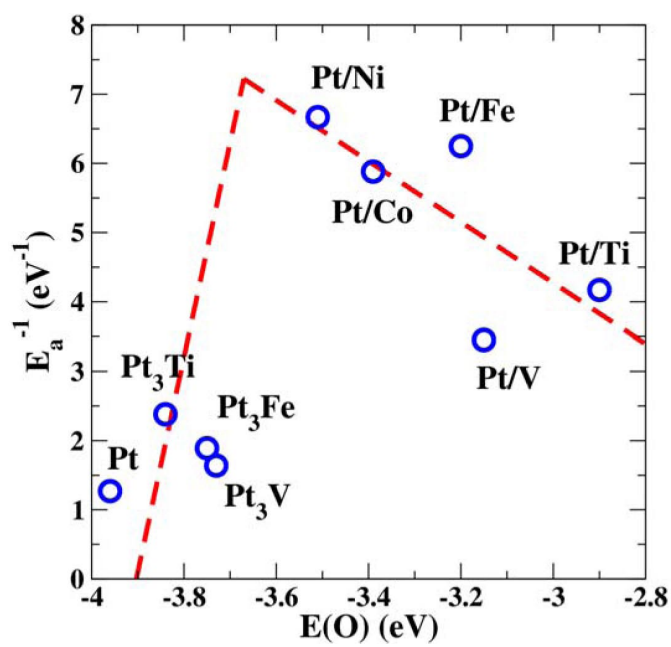

FIGURE 3. Plot of calculated activity (1/Ea) for ORR as a function of O binding energy on Pt-based electrocatalyst surfaces.

Future Directions

As a continuation of this grant, the PI will investigate the metal dissolution process, Ostwald ripening, and coalescence sintering processes, and the adsorbate-induced surface segregation process of Pt-based catalysts using atomistic simulation techniques. Moreover, the PI will theoretically correlate the change in metallic catalyst surface (such as, structure and composition) with the change in catalytic activity for electrochemical reactions related to renewable energy technology. In particular, we will simulate the structure evolution in Pt and Pt alloy nanoparticles with diameters ranging from 1.5 nm (about 200 atoms)

to 10 nm (about 30000 atoms) using the MEAM atomic interaction potentials, which are capable of accurately describing the surface and bulk structures of the catalysts. The structure evolution of metal catalysts is influenced by many interplaying effects (such as surface composition, crystal structure, morphology, particle shape, particle size, surface adsorbate, gas partial pressure, and temperature) and is closely related to the performance (such as activity and durability) of the catalysts. Consequently, this study is expected to fill the existing gap in our knowledge on how to better design and fabricate metallic catalysts in order to ensure their long-term catalytic activity.

Publication list (including patents) acknowledging the DOE grant or contract

1. Duan, Z.Y., Zhong, J. & Wang, G.F., Modeling surface segregation phenomena in the (111) surface of ordered Pt3Ti crystal. *The Journal of Chemical Physics* **2010**, *133*, 114701.

2. Wang, C., Wang, G.F., van der Vliet, D., Chang, K.C., Markovic, N.M., & Stamenkovic, V.R. Monodisperse Pt3Co nanoparticles as electrocatalyst: the effects of particle size and pretreatment on electrocatalytic reduction of oxygen. *Physical Chemistry Chemical Physics*, **2010**, *12*, 6933-6939.

3. Zhang, Y., Duan, Z.Y., Xiao, C., & Wang, G.F. Density functional theory calculation of platinum surface segregation energy in Pt3Ni (111) surface doped with a third transition metal. *Surface Science*, **2011**, *605*, 1574-1579.

4. Yang, Y., Wang, G.F., & Li, X.D. Water molecule-induced stiffening in ZnO nanobelts. *Nano Letters*, **2011**, *11*, 2845-2848.

5. Duan, Z.Y. & Wang, G.F. Monte Carlo simulation of surface segregation phenomena in extended and nanoparticle surface of Pt-Pd alloys. *Journal of Physics: Condensed Matter*, **2011**, *23*, 475301.

6. Duan, Z.Y. & Wang, G.F. A first principles study of oxygen reduction reaction on a Pt (111) surface modified by a subsurface transition metal M (M=Ni, Co, or Fe). *Physical Chemistry Chemical Physics*, **2011**, *13*, 20178-20187.

7. Datta, A., Duan, Z.Y., & Wang, G.F. Influence of surface segregation on the elastic properties of Pt-Ni alloy nanowires. *Computational Materials Science*, **2012**, *55*, 81-84.

8. He, H., Lei, Y., Xiao, C., Chu, D., Chen, R.R. & Wang, G.F. Molecular and electronic structure of transition-metal macrocyclic complexes as related to catalyzing oxygen reduction reactions: A density functional theory study. *Journal of Physical Chemistry C*, **2012**, *116*, 16038-16064.

9. Duan, Z.Y. & Wang, G.F. Comparison of reaction energetics for oxygen reduction reactions on Pt (100), Pt (111), Pt/Ni (100), and Pt/Ni (111) surfaces: A first-principles study. *Journal of Physical Chemistry C*, **2013**, appear on line, DOI: 10.1021/jp400388v.

10. Kattel, S., Duan, Z.Y. & Wang, G.F. Density functional theory study of oxygen reduction reaction on Pt3Ti alloy electrocatalyst. *Journal of Physical Chemistry C*, **2013**, appear on line, DOI: 10.1021/jp400158r.

V.N.24 Nanoscale Surface Chemistry and Electrochemistry of Clean and Metal-Covered Faceted Substrates: Structure, Reactivity and Electronic Properties

Principal Investigator: Robert A. Bartynski
Department of Physics & Astronomy
Laboratory for Surface Modification
136 Frelinghuysen Rd.
Piscataway, NJ 08854
Phone: 732-445-5500 x4839
Email: bart@physics.rutgers.edu

Postdocs:
- Wenhua Chen (Rutgers University)
- Quantong Shen (Rutgers University)

Undergraduate:
- Grant Junno (Rutgers University)

Collaborators:
- Timo Jacob (U. Ulm, Germany);
- Jingguang Chen (Columbia U.);
- Bruce Koel (Princeton University)

DOE Program Manager: Raul Miranda
Phone: (301) 903-8014
Email: Raul.Miranda@science.doe.gov

Objectives

The goal of this work is to explore new aspects of nanoscale phenomena in surface chemistry and electrochemistry with the aim of characterizing the relationships between nanoscale surface features (facets and clusters) and catalytic reactivity/selectivity. A long-term goal is to improve reactivity and selectivity by controlling the shape and size distribution of nanoscale surface features. Our emphasis is on atomically rough and morphologically unstable surfaces that undergo nanoscale faceting when covered by adsorbate (gas or metal) and annealed to elevated temperatures. There are three parts of the project: faceting of model catalytic surfaces, growth of metallic nanoparticles on the faceted surfaces, and reactivity/selectivity of the nanoscale facets in catalytic reactions

Technical Barriers

Recent work has demonstrated that reactivity and selectivity in catalysis can be tuned by controlling the nanoparticle size and shape. However, highly dispersed supported catalysts used in industry usually have a wide distribution of sizes and shapes of nanoparticles. Great progress has been recently made in controlling shape and size of nanoparticles. To elucidate the reaction mechanism, which is in turn beneficial to the design and development of new catalysts, macroscale model catalysts (planar single crystals) and nanoscale model catalysts are usually used to catalyze the reactions. These structures can exhibit new phenomena in heterogeneous catalysis, as well as in electrochemical reactions.

Abstract

We have performed experimental and theoretical studies of planar and faceted transition metal surfaces in an effort to explore structure-reactivity relationships, as well as nanoscale size effects, in catalytic reactions for hydrogen generation and NO reduction. Adsorbate-induced faceting of the Ir(210) and Re(11-21) surfaces was studied using scanning tunneling microscopy (STM) and low energy electron diffraction (LEED). Oxygen-induced faceting of Ir(210) is sustained after the oxygen overlayer if removed by exposure to hydrogen. Then, the recombination of H_{ads} and desorption of H_2 was monitored by temperature programmed desorption. In a similar fashion, the role of co-adsorbed hydrocarbons on the NO reduction reaction was studied by pre-adsorption of C_2H_2 on the planar and faceted Ir(210) surfaces. In the latter case, no size effects were found, which is in contrast to the influence of pre-adsorbed CO on this reaction where the reaction was very sensitive to facet size. In an effort to extend this approach to electrochemical reactions we studied the hydrogen evolution reaction (HER) on carbon-induced faceted Re(11-21) surfaces that were covered with a monolayer of Pt. These surfaces exhibited a higher reactivity than pure Re(11-21) [not surprising] but also a higher reactivity than Pt(111) [very encouraging].

Progress Report

Structure sensitivity in adsorption and desorption of hydrogen on Ir.

We have performed a combined theoretical and experimental study of hydrogen adsorption and desorption on planar Ir surfaces and nanoscale Ir facets. As indicated in Figure 1, at saturation coverage, two TPD peaks of H_2 appear at 360K and 440K from faceted Ir(210) while one peak is observed from planar Ir(210), indicating strong structure sensitivity in recombination and desorption of H_2. At fractional coverage, only one peak is seen at 440K on faceted Ir(210). No evidence has been found for size effects in desorption of H_2 from faceted Ir(210). Density functional theory (DFT) in combination with the *ab-initio* atomistic

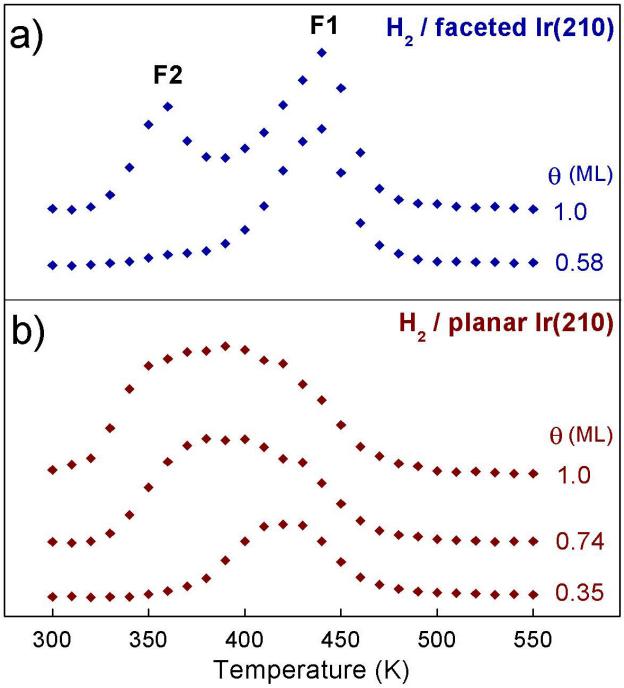

FIGURE 1. TPD spectra of H_2 from (a) planar and (b) faceted Ir(210), pre-dosed with H_2 at 300K.

thermodynamics approach is used to study hydrogen on planar Ir(210) and faceted Ir(210), consisting of {311} and (110) facets. We find that H prefers to bind at the two-fold short-bridge sites on Ir surfaces. The calculations also suggest that the higher temperature peak is related to H_2 desorption from (311) faces. For hydrogen on planar Ir(210), T_D is calculated to be 405 K, which lies between T_D values for hydrogen on Ir(110) and Ir(311). The DFT results of desorption temperatures for hydrogen from (210), (311), and (110) of Ir are in good agreement with those observed by TPD.

Reduction of nitric oxide by acetylene on Ir surfaces with different morphologies: Comparison with reduction of NO by CO.

Reduction of nitric oxide (NO) by acetylene (C_2H_2) has been investigated by temperature-programmed desorption (TPD) on planar Ir(210) and faceted Ir(210) with tunable sizes of three-sided nanopyramids exposing (311), (311□), and (110) faces. Upon adsorption, C_2H_2 dissociates to form acetylide (CCH) and H species on the Ir surfaces at low C_2H_2 precoverage. For adsorption of NO on C_2H_2-covered Ir, both planar and faceted Ir(210) exhibit high reactivity for reduction of NO with high selectivity to N_2 at low C_2H_2 precoverage, although the reaction is completely inhibited at high C_2H_2 precoverage. Coadsorbed C_2H_2 significantly influences dissociation of NO. The N-, H-, and C-containing TPD products are dominated by N_2, H_2, CO, and CO_2 together with small amounts of H_2O. For adsorption of NO

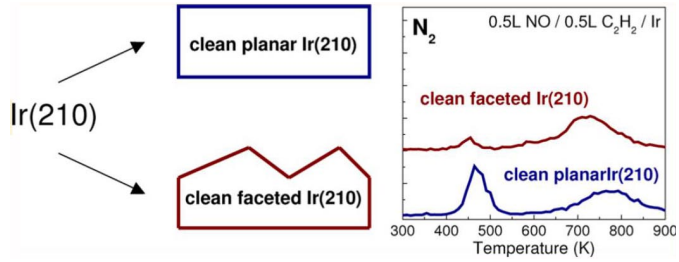

FIGURE 2. Schematic diagram of O-induced faceting of Ir(210) and a comparison of TPD spectra of N_2 from adsorption of 0.5L NO on planar and faceted Ir(210) pre-exposed to 0.5L C_2H_2 at 300K.

on C-covered Ir(210) at fractional C precoverage, formation of CO_2 is promoted while production of CO is reduced. Reduction of NO by C_2H_2 is structure sensitive on faceted Ir(210) versus planar Ir(210), but no evidence is found for size effects in the reduction of NO by C_2H_2 on faceted Ir(210) for average facet sizes of 5 nm and 14 nm. The results are compared with reduction of NO by CO on the same Ir surfaces. As for NO+C_2H_2, the Ir surfaces are very active for reduction of NO by CO with high selectivity to N_2 and the reaction is structure sensitive, but clear evidence is found for size effects in the reduction of NO by CO on the nanometer scale. Furthermore, coadsorbed CO does not affect dissociation of NO at low CO precoverage whereas coadsorbed CO considerably influences dissociation of NO at high CO precoverage. The adsorption sites of CCH+H on Ir are characterized by density functional theory.

Reduction of NO by C_2H_2 on planar and faceted Ir(210).

Motivated by the possibility that faceted C/Re(11-21) may be a promising substrate for synthesizing nanoscale model (electro)catalyst, we deposited Pt ML (monolayer) onto nano-faceted C/Re(11-21) surface, denoted as Pt-ML/C/Re(11-21), as shown in Figure 3 and then tested its reactivity in electrochemistry. We have found that Pt-ML/C/Re(11-21) exhibits higher reactivity for hydrogen evolution reaction (HER) than pure Re(11-21) and Pt(111). This finding illustrates the potential for future studies of nanostructured bimetallic system relevant to electrocatalytic reactions. A detailed characterization of the Pt monolayer on faceted C/Re(11-21) surface as a function of carbon coverage will be the subject of future studies to elucidate the role of carbon in stabilizing the Pt ML on faceted C/Re(11-21). Note that our previous studies show that Pt is not able to induce faceting of the Re surface due to the fact that Pt does not "float" on the Re surface.

Future Directions

In the coming year, we will build on our current results and continue our work on faceting of metal surfaces, growth of metallic nanoclusters on the faceted metal surfaces, synthesis of nanoscale model (electro)catalysts of metal

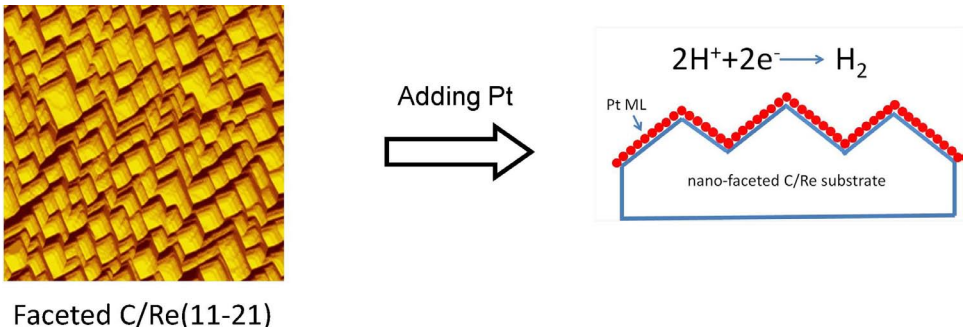

FIGURE 3. STM image of faceted C-covered Re(11-21) surface and a schematic diagram of synthesizing nanoscale model Pt electrocatalyst using nano-faceted C/Re metal substrate.

(Pt, Pd and Au) monolayer (ML) on clean and C- covered faceted metal surfaces, (electro)catalytic reactions on clean and metal-covered planar and faceted metal surfaces with focus on structure sensitivity and size effects in the reactions related to environmental applications and hydrogen production. It is important to note that the PI has long term collaboration with colleagues at the National Synchrotron Light Source (NSLS) to perform HRXPS studies, which allow us to identify the nature of surface oxygen on the oxygen-modified faceted metal surfaces.

Publication list

1. Chen, W., Shen, Q., Bartynski, R.A., Kaghazchi, P., and Jacob, T., Reduction of Nitric Oxide by Acetylene on Ir Surfaces with Different Morphologies: Comparison with Reduction of NO by CO *Langmuir* **2013** *29* (4) 1113-1121..

2. Yang, X., Koel, B.E., Wang, H., Chen, W., and Bartynski, R.A., Nano-faceted C/Re(11-21): Fabrication, structure and template for synthesizing nanostructured model Pt Electrocatalyst for hydrogen evolution reaction, *ACS Nano* **2012** *6* (2) 1404-1409.

3. Chen, W., Bartynski, R.A., Kaghazchi, P., and Jacob, T., Oxidation of CO by NO on planar and faceted Ir(210) *J. Chem. Phys. C* **2012** *136* (22) 224701.

4. Kaghazchi, P., Jacob, T., Ermanoski, I., Chen, W., and Madey, T.E., New surfaces stabilized by adsorbate-induced faceting *J. Phys.: Conden. Matter* **2012** *24* (26) 265003.

5. Shen, Q., Chen, W., Wang, H., and Bartynski, R.A., Morphological Stability of Oxygen- and Nitrogen-covered Ru(11-21) *J. Phys.: Conden. Matter* to be submitted

6. Kaghazchi, P., Jacob, T., Chen, W., and Bartynski, R.A., TPD and DFT studies of adsorption and desorption of hydrogen on planar and faceted Ir(210) *J. Am. Chem. Soc.* To be submitted.

7. Kaghazchi, P., Jacob, T., Junno, G., Chen, W., and Bartynski, R.A., Morphological Stability of C-covered Re(11-21) *Phys. Rev. B.* to be submitted

8. Wang, H., and Madey, T.E., O-induced metastable facet formation on Re(11-21) *Phys. Rev. B.* to be submitted

9. Yang, X., Feng, T., Hsueh, C.-L., Wang, H., Chen, W., Koel, B.E., and Bartynski, R.A., Au-induced Nano-faceting of Re(11$\bar{2}$1) in preparation.

10. Chen, W., and Bartynski, R.A., Applications of Nano-Faceted Metal Surfaces in preparation.

11. Shen, Q., Baier, R., Govind, Chen, W., Madey, T.E., Bartynski, R.A., Au-induced Faceting of Re(12-31), in preparation.

V.N.25 Correlation of Theory and Function in Well-Defined Bimetallic Electrocatalysts

Principal Investigator: Richard M. Crooks[1]
Phone: 512-475-8674
Email: crooks@cm.utexas.edu

Names of Team Members

- Graeme Henkelman,[1] Co-PI
  Phone: 512-471-4179
  Email: henkelman@cm.utexas.edu
- Rachel Anderson,[1] graduate student
  Email: rachel.anderson@utexas.edu
- Samuel T. Chill,[1] graduate student
  Email: samchill@utexas.edu
- Ravikumar Iyyamperumal,[1] postdoc
  Email: ravikumariyyamperumal@gmail.com
- Hyun-You Kim,[1] postdoc
  Email: hykim@cm.utexas.edu
- David Yancey,[1] graduate student
  Email: dfyancey@utexas.edu
- Liang Zhang,[1] graduate student
  Email: zhangbright1986@gmail.com

[1]The University of Texas at Austin
Department of Chemistry and Biochemistry
105 E. 24th St., Stop A5300
Austin, TX, USA 78712-1224

DOE Program Manager: Dr. Raul Miranda
Phone: 301-903-8014
Email: Raul.Miranda@science.doe.gov

Objectives

The objective of this research project is to correlate the structure of nanoparticles that are comprised of ~100-200 atoms to their catalytic function. The project is based on a growing body of evidence suggesting that catalytic properties can be tailored through controlled synthesis of nanoparticles. What is missing from many of these studies, and what we are contributing, is a model catalyst that is sufficiently small and well-characterized that its function can be directly predicted by theory. Specifically, our work seeks to develop a fundamental and detailed understanding of the relationship between the structure of nanoscopic electrocatalysts and their function. We have assembled a team with expertise in theory, synthesis, and advanced characterization methods to address the primary objective of this project. We anticipate the outcomes of the study to be: (1) a better theoretical understanding of how nanoparticle structure affects catalytic properties; (2) the development of advanced, *in-situ* and *ex-situ*, atomic-scale characterization methods that are appropriate for particles containing 100-200 atoms; and (3) improved synthetic methods that produce unique nanoparticle structures that can be used to test theoretical predictions.

Technical Barriers

Investigation of such small nanoparticles poses significant challenges both for experiment and theory. Dendrimers provide an excellent template for synthesis, but characterization of ~1-2 nm particles is much more difficult than for related materials having sizes >3 nm. For example, we have found that 1-2 nm particles can undergo structural deformations that may substantially change the rates of catalytic reactions and the stability of the catalytic surface itself. Because these structural changes may be driven by catalytic reactions, it is important that characterization be carried out *in operando* and that theory take into account catalytic substrates and intermediates bound to the nanoparticle surface. Coupling of theory and experiment simplifies the task of identifying subtle structural differences in these smallest of catalytic nanoparticles. Measurements of particle size and structure require high-resolution techniques such as aberration-corrected electron microscopy and x-ray absorption spectroscopy (e.g., EXAFS and XANES), as well as electrochemical techniques that can identify the presence of adsorbates on the nanoparticle surface. In some cases that we have investigated, assumptions of regular crystalline particles break down in ways that are not easy to detect experimentally. For example, in the case of Au@Pt nanoparticles, calculations show that the Pt shell favors a distortion of the (100) facets to (111). This structural change was predicted to be important for electrocatalytic formic acid oxidation, and subsequently this prediction was verified experimentally. In the following examples, we show how our combined experimental and theoretical approach is able to characterize and predict the structure and function of very small nanoparticle catalysts – particles that are in the exciting size regime where new chemistry is possible at the interface of homogeneous and heterogeneous catalysis.

Abstract

Our research directly addresses two of the DOE Grand Challenges for Basic Energy Sciences. Specifically, we endeavor to use synthesis and theory to develop first-principles rules for predicting the structure of new forms of matter that have predictable catalytic functions. The rules and principles discovered during this project will likely be useful for designing other (noncatalytic) materials as well. Within this broader context, our proposal specifically

addresses the Catalysis for Energy components of the DOE BES Use-Inspired Discovery Science research thrusts.

Progress Report

Design of Pt-shell Nanoparticles with Alloy Cores for the Oxygen Reduction Reaction

We reported that the oxygen binding energy of alloy-core@Pt nanoparticles can be linearly tuned by varying the elemental composition of the core. Using this tuning mechanism, we are able to predict optimal compositions for different alloy-core@Pt nanoparticles. **Figure 1** is a plot of the onset potential for the ORR for AuPd@Pt dendrimer-encapsulated nanoparticle (DEN) electrocatalysts having different ratios of Pd and Au in their cores. These findings are in near-exact agreement with theoretical predictions. Specifically, optimal activity is observed for an alloy core composition of 28% Au/72% Pd supporting a submonolayer Pt shell. Importantly, these findings represent an unusual case of first-principles theory presaging the experimental results. Continuous tuning of the shell metal by the underlying alloy-core provides a systematic means for designing nanoparticles that have desirable catalytic activity. Additional work, exploring different metal combinations and other reactions, is underway to determine the generality of these findings.

Efficient Electrocatalytic Oxidation of Formic Acid using Au@Pt Dendrimer-Encapsulated Nanoparticles

To determine the generality of the correlation between oxygen binding energy and ORR activity (discussed in the previous subsection), we have expanded the scope of our studies to include electrocatalytic formic acid oxidation

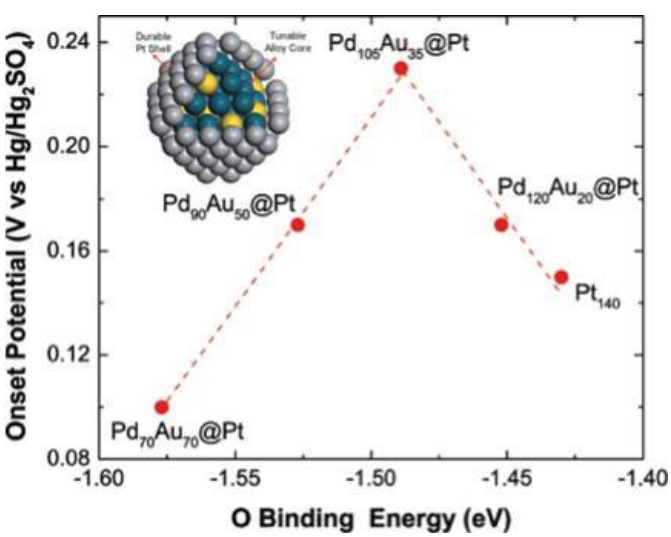

FIGURE 1. Measured onset potential for the ORR at Pd_xAu_{1-x}@Pt DENs plotted as a function of the corresponding oxygen binding energy calculated by DFT. Structure of alloy-core@Pt nanoparticles is illustrated at the upper left corner.

using monometallic and bimetallic DENs. As shown in Figure 2, the results indicate that Au147@Pt core@shell DENs exhibit better electrocatalytic activity and lower CO poisoning than Pt-only DENs of the same size. Theoretical calculations attribute the observed activity to the deformation of nanoparticle structure, slow dehydration of formic acid, and weak binding of CO on Au_{147}@Pt surface. Subsequent experiments confirmed the theoretical predictions. Perhaps the most significant outcome of this work, however, is that there appear to be major structural differences between particles in the 1-2 nm size range of DENs and the more commonly studied (and more experimentally tractable) nanoparticles having sizes >3 nm. This is likely due to the lower stability of the smaller particles, and thus their enhanced ability to deform in the presence of adsorbates during catalysis. Coupled theoretical/experimental studies of this sort will provide insight into the structural properties of active catalytic nanoparticles.

A Theoretical and Experimental Examination of Systematic Ligand-Induced Disorder in Au Dendrimer-Encapsulated Nanoparticles

An ongoing problem we have faced in this project is determination of the structure of 1-2 nm particles. This task has been exacerbated by deficiencies we have discovered in the theory used to interpret EXAFS spectra of structurally distorted DENs. Accordingly, we prepared DENs having controlled structural distortions and then compared experimentally and theoretically determined EXAFS spectra. Specifically, different numbers of thiols were introduced onto the surfaces of Au DENs, consisting of an average of 147 atoms, to systematically tune nanoparticle disorder. An analogous system was investigated using density functional theory molecular dynamics (DFT-MD). These MD trajectories were then used to produce theoretical EXAFS signals that could be directly compared to the experimental results by an iterative FEFF calculation over all atoms in the particle over the duration of the MD simulation. Validation of the theoretical results by comparing to experiment, as shown in **Figure 3**, allows us to infer previously unknown details of structure and dynamics of the nanoparticles. Additionally, the structural information arising from the theoretical studies can be compared with traditional EXAFS fitting results to identify and rationalize any errors in the experimental fit. There are two important outcomes of this study: (1) DFT-MD simulations accurately depict complex experimental systems in which we have control over nanoparticle disorder, and (2) representative theoretical EXAFS signals can be calculated from these DFT-MD trajectories. This study demonstrates the advantages of using a combined experimental/theoretical approach over standard EXAFS fitting methodologies for determining the structural parameters of metallic nanoparticles.

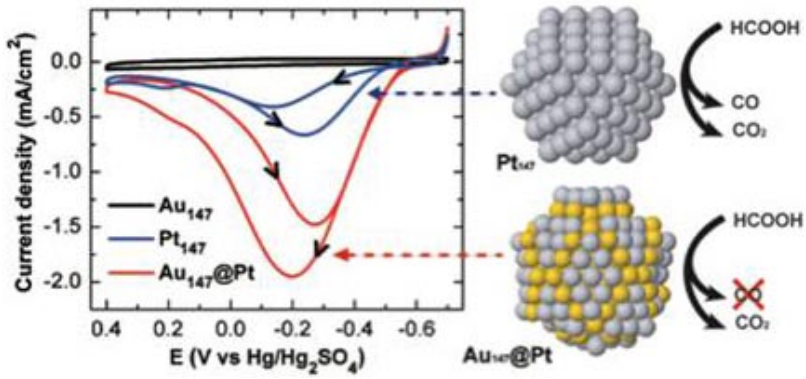

FIGURE 2. CVs for formic acid oxidation of Au_{147}, Pt_{147}, and Au_{147}@Pt DEN-modified glassy carbon electrodes.

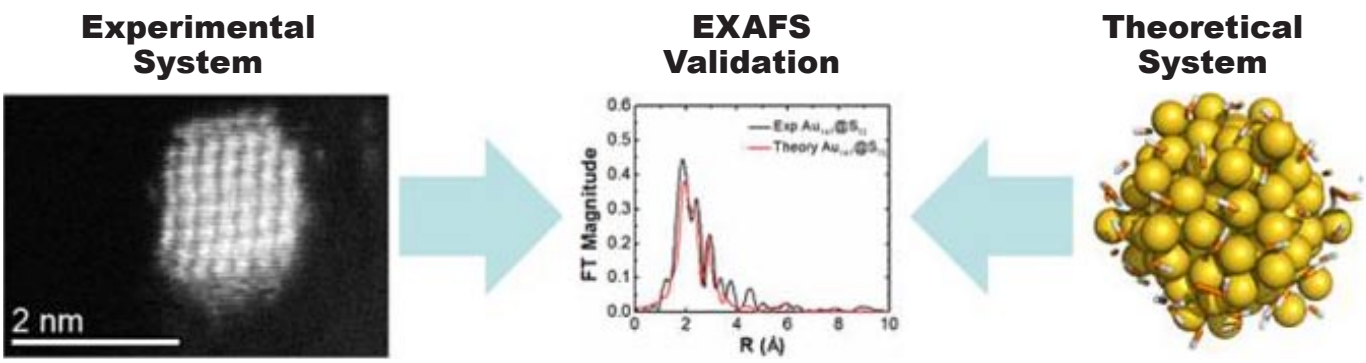

FIGURE 3. Graphical representation of the scheme for comparing theoretical and experimental systems via EXAFS.

An Experimental and Theoretical Investigation of the Inversion of Pd@Pt Core@Shell Dendrimer-Encapsulated Nanoparticles

For accurate correlation of theory and experiment, it is critically important that the structure of the catalytically active nanoparticle used for the experimental and theoretical activity determinations be the same. However, as alluded to earlier, 1-2 nm nanoparticles tend to be structurally unstable. Obviously, it is important to better understand the source of this instability, how it is affected by surface-bound ligands, and whether additional distortions occur in operando. Accordingly, we undertook a combined theoretical and experimental structural study of 1-2 nm core@shell Pd147@Pt162 DENs prepared by a homogeneous synthetic route. Note that larger (>3 nm) Pd@Pt nanoparticles are known to retain their core@shell structure. However, we have observed that the smaller DENs invert to form a Pt_{147}@$Pd_{147}Pt_{15}$ configuration as shown in **Figure 4**. The key finding of this study is that the final inverted structure, determined by *in-situ* EXAFS spectroscopy, correlates well with first-principles calculations. Specifically, DFT calculations predict that the inverted Pt_{147}@$Pd_{147}Pt_{15}$ structure is more thermodynamically stable than the original Pd_{147}@Pt_{162}

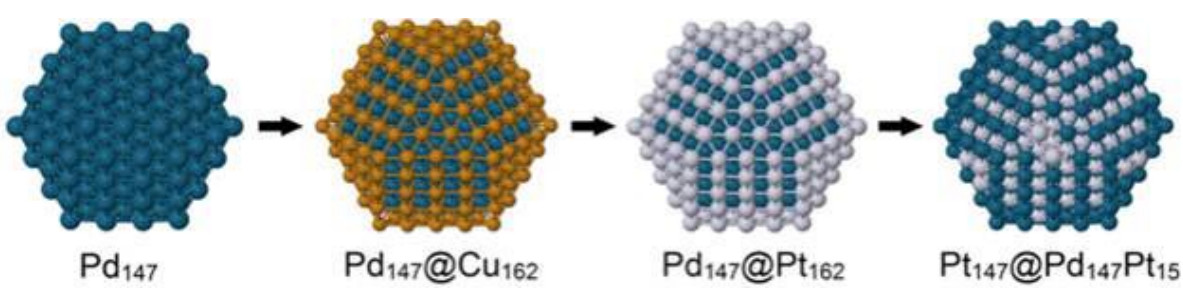

FIGURE 4. Synthesis procedure of Pd@Pt nanoparticle and its inversion

structure and that the increased disorder and high energy edge and corner sites that are present in the smaller DENs help to initiate the structural rearrangement.

Future Directions

The objective of this research project is to understand correlations between the atomic-level structure and the energetics of electrochemical reactions catalyzed by 1-2 nm nanoparticles. Our future plans involve direct correlation of theory with kinetic measurements obtained using accurate experimental models. This approach involves the following key steps: (1) ensuring that the structures of the experimental models are well-defined *in operando*; (2) understanding structural instabilities in nanoparticles that affect activity; and (3) developing more accurate experimental and theoretical methods for correlating structure and function. One specific thrust involves determining the generality of our finding that the catalytic activity of core@shell DENs can be tuned by changing the elemental composition of the core. Another important study involves our consistent finding that 1-2 nm nanoparticles can be structurally unstable, particularly in the presence of surface-adsorbed intermediates. We need to be able to better predict this behavior theoretically, and then develop better tools for *in-situ* analysis of the active structures of 1-2 nm catalysts.

Publication list (including patents) acknowledging the DOE grant or contract

1. Yancey, D.F.; Carino, E.V.; Crooks, R.M., Electrochemical Synthesis and Electrocatalytic Properties of Au@Pt Dendrimer-Encapsulated Nanoparticles. *J. Am. Chem. Soc.* **2010**, *132*, 10988-10989.

2. Weir, M.G.; Myers, V.S.; Frenkel, A.I.; Crooks, R.M., In-situ X-ray Absorption Analysis of ~1.8 nm Dendrimer-Encapsulated Pt Nanoparticles During Electrochemical CO Oxidation. *ChemPhysChem* **2010**, *11*, 2942-2950 (invited, special issue on electrochemistry).

3. Sheppard, D.; Henkelman, G.; Anatole von Lilienfeld, O., Alchemical Derivatives of Reaction Energetics. *J. Chem. Phys.* **2010,** *133*, 084104.

4. Tang, W.; Zhang, L.; Henkelman, G., Catalytic Activity Improvement in Pd/Cu Random Alloy Nanoparticles. *J. Phys. Chem. Lett.* **2011**, *2*, 1328-1331.

5. Lu, C.-Y.; Henkelman, G., The Role of Geometric Relaxation in Oxygen Binding to Metal Nanoparticles. *J. Phys. Chem. Lett.* **2011**, *2*, 1328-1331.

6. Myers, V.S.; Weir, M.G.; Carino, E.V.; Yancey, D.F.; Pande, S.; Crooks, R.M., Dendrimer-encapsulated Nanoparticles: New Synthetic and Characterization Methods and Catalytic Applications. *Chem. Sci.* **2011**, *2*, 1632-1646.

7. Welborn M.; Tang W.; Ryu J.; Petkov V.; Henkelman G., A Combined Density Functional and X-ray Diffraction Study of Pt Nanoparticle Structure. *J. Chem. Phys.* **2011**, *135*, 014503

8. Myers, V.S.; Frenkel, A.I.; Crooks, R.M., In-situ Structural Characterization of Platinum Dendrimer-Encapsulated Oxygen Reduction Electrocatalysts. *Langmuir* **2012**, *28*, 1596-1603.

9. Dumitrescu, I.; Yancey, D.F.; Crooks, R.M., Dual-Electrode Microfluidic Cell for Characterizing Electrocatalysts. *Lab Chip* **2012**, *12*, 986-993.

10. Carino, E.V.; Kim, H.Y.; Henkelman, G.; Crooks, R.M., Site-Selective Cu Deposition on Pt Dendrimer-Encapsulated Nanoparticles: Correlation of Theory and Experiment. *J. Am. Chem. Soc.* **2012**, *134*, 4153-4162.

11. Yancey, D.F.; Zhang, L.; Crooks, R.M.; Henkelman, G., Au@Pt Dendrimer Encapsulated Nanoparticles as Model Electrocatalysts for Comparison of Experiment and Theory. *Chem. Sci.* **2012**, *3*, 1033-1040.

12. Dumitrescu, I.; Crooks, R.M., Effect of Mass Transfer on the Oxygen Reduction Reaction Catalyzed by Platinum Dendrimer Encapsulated Nanoparticles. *Proc. Natl. Acad. Sci., USA* **2012**, *109*, 11493-11497.

13. Liu, H.; Crooks, R. M., Highly reproducible chronoamperometric analysis in microdroplets. *Lab Chip* **2013**, *13*, 1364-1370.

14. Zhang L.; and Henkelman G., Tuning the Oxygen Reduction Activity of Pd Shell Nanoparticles with Random Alloy Cores. *J. Phys. Chem. C* **2012**, *116*, 20860-20865

15. Kim H.-Y.; Henkelman G., CO oxidation at the interface between doped-CeO2 and supported Au nanoparticles. *J. Phys. Chem. Lett.* **2012**, *3*, 2194-2199

16. Kim H.-Y.; Lee H.-M.; Henkelman G.; CO oxidation mechanism on CeO2 supported Au nanoparticles. *J. Am. Chem. Soc.* **2012**, *134*, 1560-1570

17. Kim H.-Y.; Park J.-N.; Henkelman G.; Kim J.-M., Design of highly-nanodispersed Pd-MgO/SiO2 composite catalyst with multifunctional activity for CH4 reforming. *ChemSusChem*. **2012**, *5*, 1474-1481

18. Kim H.-Y.; Henkelman G., CO oxidation at the interface of Au nanoclusters and the stepped-CeO2(111) surface by the Mars-van Krevelen mechanism. *J. Phys. Chem. Lett.* **2013**, *4*, 216-221

19. Iyyamperumal R.; Zhang L.; Henkelman G.; Crooks R.M., Efficient Electrocatalytic Oxidation of Formic Acid using Au@Pt Dendrimer-Encapsulated Nanoparticles. *J. Am. Chem. Soc.* March, **2013** (published on the ACS website, DOI: 10.1021/ja4010305)

20. Garcia, S.; Anderson, R.M.; Celio, H.; Dahal, N.; Dolocan, A.; Zhou, J.; Humphrey, S.M., Microwave Synthesis of Au-Rh Core-Shell Nanoparticles and Implications of the Shell Thickness in Hydrogenation Catalysis. Chem. Commun. April, **2013** (published on the RSC website, DOI: 10.1039/C3CC40387D)

21. Zhang L.; Iyyamperumal R.; Crooks R.M.; Henkelman G., Design of Pt-shell Nanoparticles with Alloy Cores for the Oxygen Reduction Reaction. *J. Am. Chem. Soc.* April, **2013** (under revision)

22. Yancey D.F.; Chill S.T.; Zhang L.; Frenkel A.I.; Henkelman G.; Crooks R.M., Systematic Ligand-Induced Disorder in Au_{147} Dendrimer-Encapsulated Nanoparticles. *Chem. Sci.* March, **2013** (submitted)

V.N.26 Metal Ion Sites on Oxide Supports as Catalysts for the Water-Gas Shift and Methanol Steam Reforming Reactions

Principal Investigator:
Maria Flytzani-Stephanopoulos
Department of Chemical and Biological Engineering
Tufts University
4 Colby St., Medford, MA 02155
Phone: (617) 627-3048
Email: maria.flytzani-stephanopoulos@tufts.edu

Team Members:

- Charles E. Sykes
  Department of Chemistry
  Tufts University
  62 Talbot Ave., Medford, MA 02155
  Phone: (617) 627-3773
  Email: charles.sykes@tufts.edu
- Howard.Saltsburg
  Department of Chemical and Biological Engineering
  Tufts University
  4 Colby St., Medford, MA 02155
  Phone: (617) 627-5658
  Email: howard.saltsburg@tufts.edu
- Manos Mavrikakis
  Department of Chemical and Biological Engineering
  University of Wisconsin
  Madison, WI 53706
  Phone: (608) 262-9053
  Email: manos@engr.wisc.edu

Subcontractor:
George Flynn
Department of Chemistry
Columbia University
New York, NY 10027
Email: gwf1@columbia.edu

DOE Program Manager: Raul Miranda
Email: raul.miranda@science.doe.gov

Objectives

The overall goal of this project is to elucidate the atomic-level interaction of Au, Cu, and Pt, with oxide supports, such as CeO_2, ZrO_2, ZnO, FeO_x, and TiO_2 for reactions of interest in the production of hydrogen via the water-gas shift reaction and fuel processing reactions, especially methanol conversion reactions. One key objective is to understand the role of the support in these systems. Nanoshapes of the oxide supports are prepared to test structure sensitivity. Use of alkali promoters is investigated as a way to stabilize metal cations on any support, including earth-abundant oxides (silica, alumina) and even carbon surfaces. Another major objective is the synthesis and detailed study of single atom alloys of PdCu, PtCu, PdAu, containing trace amounts of platinum or palladium, as new highly selective catalysts for reactions of methanol and other biomass-derived oxygenates.

Abstract

The work conducted this year was multi-pronged. For both the water-gas shift (WGS) and the methanol steam reforming (SRM) reactions, understanding the role of water on the surface is crucial. This was examined by STM and DFT studies of the Au/Fe_3O_4(111) model catalyst for the WGS reaction. Strongly bound OH species on the Fe^{III} cations of the iron-terminated Fe_3O_4(111) surface do not allow CO adsorption. Only when Au adatoms are present (bound over the under-coordinated O atoms) on the iron oxide surface, is CO adsorption possible. This explains why the WGS reaction occurs at low temperatures on the Au/Fe_3O_4 surfaces, but not on the gold-free iron oxide surfaces. Methanol activation is also studied over the same surfaces. In the case of methanol activation on copper catalysts, water was found to play an important catalytic role. Using high-resolution STM and temperature programmed reaction analysis, we found that six or more water molecules in the form of hydrogen bonded clusters act cooperatively to deprotonate each methanol molecule on an *oxygen-free* Cu(111) surface, stabilizing methoxy species on the copper step edges. The addition of isolated Pd atoms to the Cu(111) surface promotes this reaction, with methoxy dehydrogenating selectively to formaldehyde at higher temperatures. These results are fundamentally important when considering the mechanism involved in methanol reforming to products including CO, CO_2 and H_2. In work with alkali promoted atomically dispersed Pt, we showed very high stability of core-shell Pt(Na)@SiO_2 materials under realistic WGS reaction conditions. More than half of the Pt existed as active Pt-O-(OH)-Na clusters in the silica shell and their activity was similar to that of Pt/CeO_2. Na-promoted Pt on TiO_2 was prepared also last year and tested for formaldehyde oxidation at ambient conditions. This work was in collaboration with the Hong He group, of the Research Center for Eco-Environmental Sciences, Chinese Academy of Sciences, Beijing. A new more efficient mechanistic pathway for the formaldehyde oxidation reaction was identified in that work. Alkali addition also effectively activates Pt on multi-wall carbon nanotubes, an otherwise inert material, to become an efficient catalyst for the WGS reaction at ~ 250-300°C. Work on alkali promotion of gold catalysts continued this year with new experimental as well as computational findings supporting the model of a single metal center stabilized by O and OH species supplied by the surrounding sodium

atoms. Au-O- species on ceria were also found to catalyze the dehydrogenation of formic acid at close to ambient conditions. These findings are general and can be extended to other supports.

Progress Report

1. Scanning Tunneling Microscopy and Theoretical Study of Water Adsorption on Fe_3O_4 and of the Water-Gas Shift Reaction on Au/Fe_3O_4

The adsorption of water on iron oxide single crystal surfaces was investigated via Scanning Tunneling Microscopy (STM) and first-principle theoretical simulations[1]. Water species are observed only on the Fe-terminated Fe_3O_4(111) surface at temperatures up to 235 K, Fig. 1. Between 235 and 245 K we observed a change in the surface species from intact water molecules and hydroxyl groups bound to the surface to only hydroxyl groups atop the surface terminating Fe^{III} cations. DFT calculations confirm the identity of the surface species proposed from the STM images, finding that the most stable water species are the dissociated one (OH + H), with OH atop surface terminating Fe^{III} sites and H atop under-coordinated oxygen sites. Attempts to simulate the adsorption of CO on the hydroxylated surface fail because the only binding sites for CO are the surface Fe^{III} sites, which are blocked by the much more strongly bound OH. In order to promote this reaction, we simulated a surface decorated with gold atoms, Fig. 2. The Au ad-atoms cap the under-coordinated oxygen sites and dosed CO is found to bind to the Au ad-atom. This newly created binding site for CO not only allows for coexistence of CO and OH on the surface of Fe_3O_4 but also provides co-location between the two species. These two factors explain the catalytic activity for the Water-Gas Shift Reaction on Au/Fe_3O_4(111) surfaces.

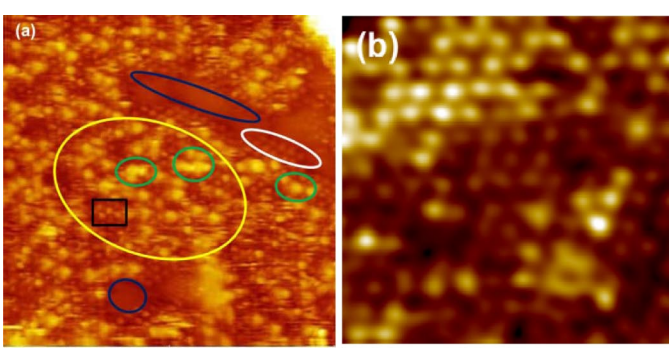

FIGURE 1. Topographic STM image of an iron oxide surface after dosing 0.15L of water at 235 K. (a) The image at 235K shows that the Fe-terminated Fe_3O_4(111) domain (yellow oval) has chemisorbed water species (marked by the black rectangle) and physisorbed water species (marked by green ovals) on it while the O-terminated FeO(111) (blue ovals) domains do not have any adsorbed water species; (b) The image at 245 K clearly shows only hydroxyl groups (bright features) on the Fe-terminated Fe_3O_4(111) surface.

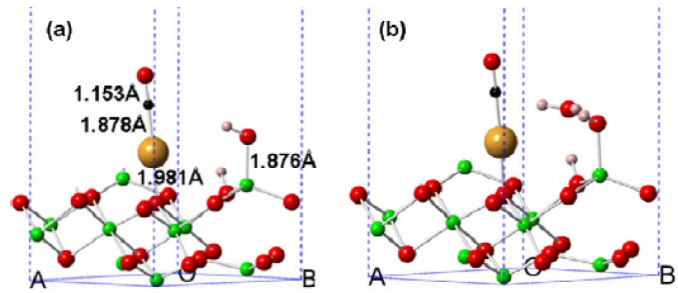

FIGURE 2. Optimized H_2O and CO adsorption on an Au-doped Fe_3O_4 (111) surface (a) Dissociative water adsorption (b) Two H_2O molecule adsorption (Red: O atoms; Green: Fe atoms; Black: C atom; Orange: Au atom; Pink: H atoms).

2. Water-Catalyzed Methanol Dehydrogenation to Formaldehyde

Copper catalysts have excellent activity and selectivity for methanol conversion to hydrogen and carbon dioxide by the SRM reaction. This product balance is dictated by the formation and weak binding of formaldehyde, the key reaction intermediate. It is widely accepted that oxygen adatoms or oxidized copper are required to activate methanol. By high-resolution STM and temperature programmed reaction testing, we found that six or more water molecules in the form of hydrogen bonded clusters act cooperatively to deprotonate each methanol molecule on an *oxygen-free* copper surface. Hydrogen-bonded networks of water comprise an active complex on which it is energetically favorable to bind a proton. On an atomically flat Cu(111) surface, where methoxy can only be formed as a transient species, the addition of hydrogen-bonded water complexes that stabilize H atoms drives O-H bond scission, leaving methoxy stabilized on Cu step edge atoms[2]. The addition of isolated Pd atoms to the Cu(111) surface promotes this reaction by allowing more methanol to remain on the surface at higher temperatures, where a greater degree of O-H bond activation can take place. Methoxy stabilized at Cu step edges and/or Pd atoms remains on the surface until it dehydrogenates selectively to formaldehyde at higher temperatures. The water-assisted dehydrogenation of methanol to formaldehyde comprises a new elementary step in the methanol steam reforming pathway. By studying well-defined surfaces, we have shown that both under-coordinated Cu step edge atoms and isolated Pd atoms at Cu(111) step edges can act as selective methanol dehydrogenation sites, as no decomposition of methanol to CO was observed[2].

3. Silica-encapsulated platinum catalysts for the low-temperature water-gas shift reaction

Encapsulated platinum in core-shell Pt@SiO_2 materials was prepared by a reverse microemulsion method. With alkali ion addition, the Pt-Na@SiO_2 or Na(IMP)-Pt@SiO_2 materials show very good activity for the low-temperature

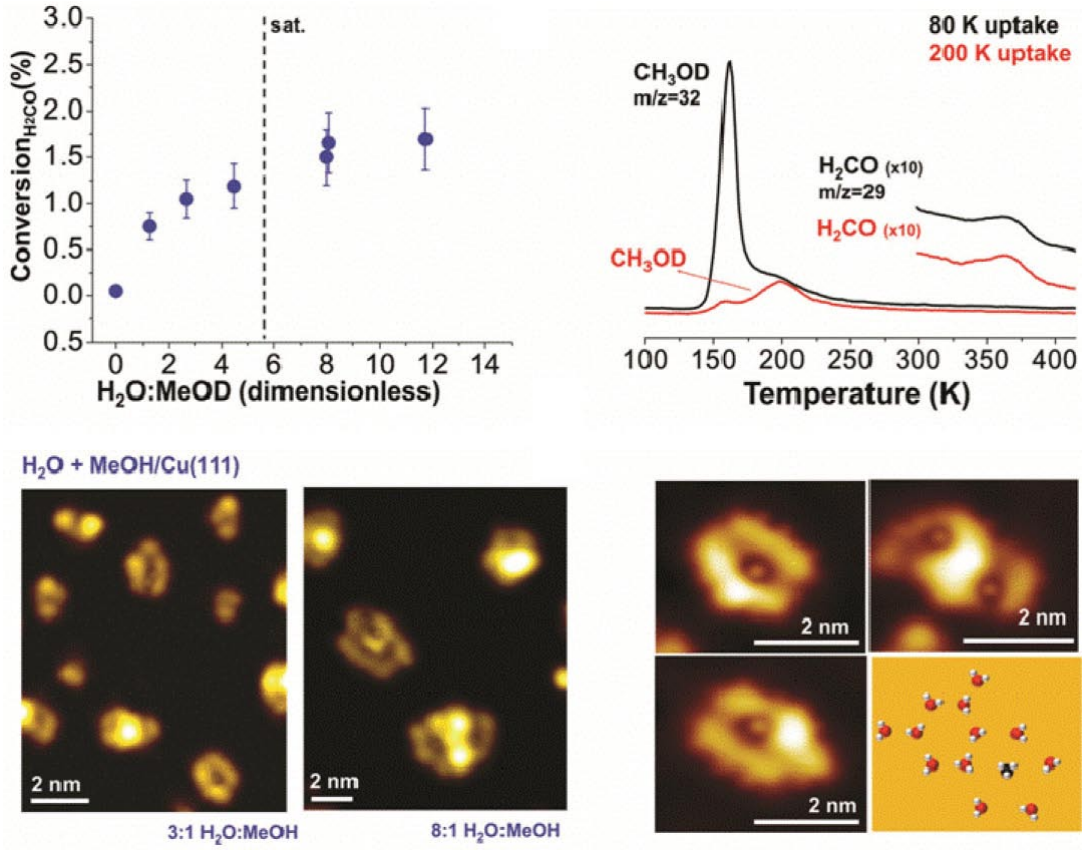

FIGURE 3. Upper left panel shows conversion of methanol to formaldehyde (370 K) as a function of water coverage adsorbed with 0.15 ML of partially deuterated methanol (CH_3OD) on Cu(111). The vertical line indicates saturation of the monolayer. The upper right panel shows TPR profiles of methanol adsorbed at 85 K and 200 K on Cu(111); in each case, water was co-adsorbed on the surface at 85 K. The lower STM panels show co-adsorption of methanol and water at 5 K after annealing to 60 K leads to the formation of new structures. High resolution STM images reveal a new structure consisting of a ring of hydrogen-bonded water molecules surrounding a deprotonated methanol molecule. In this configuration, the water molecules act in concert to deprotonate the methanol molecule to methoxy, which appears as a localized protrusion in the cluster[2].

WGS reaction, Fig. 4. Promotion by Na is independent of the point of addition[3].

The active Pt-O_x(OH)-Na species in the silica shell stabilize both the Pt and Na ions, dissociate water, and regenerate surface hydroxyl groups. The apparent activation energy for the WGS reaction over Pt-based catalysts is independent of the support structure and type.

4. Alkali-promoted Pt/TiO_2 opens a new pathway to formaldehyde oxidation at ambient temperatures

In work carried out with alkali-promoted Pt/TiO_2 catalysts, we found that the key steps for HCHO oxidation (including O_2, HCHO and H_2O activation) take place on the atomically dispersed Pt-O(OH)x-alkali species, which alters the ambient-temperature HCHO oxidation pathway by promoting the reaction between surface OH and formate species at room temperature, and thus greatly enhancing the HCHO oxidation activity[4]. Such OH activation by alkali ion addition may apply to other volatile organic compound oxidation reactions and to other metals.

5. Dehydrogenation of formic acid on atomically dispersed gold on ceria

In new work with supported gold on ceria, we have found that atomically dispersed gold species catalyze the decomposition of formic acid through the dehydrogenation pathway at near-ambient temperatures. Au-O-Ce sites on the {110} surfaces of ceria nanorods prepared by hydrothermal methods have high activity and excellent stability for formic acid dehydrogenation[5]. Mechanistic insights from this study point to the use of trace amounts of gold to achieve robust and cost-effective catalysts.

6. Other Work with atomically dispersed supported gold and platinum

Alkali addition was effective in activating Pt on any support, including platinum on multi-wall carbon nanotubes,

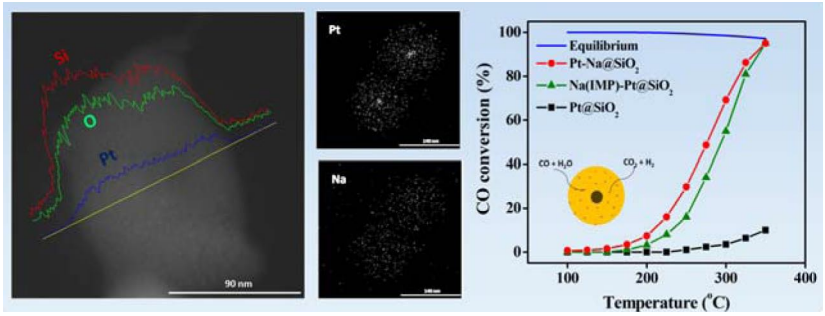

FIGURE 4. (left panel) Elemental linescans of as prepared Pt@SiO_2; after air calcination at 400°C; and STEM/EDS of Pt, Na in the same. (right panel) CO conversion profiles in steady-state tests of WGS reaction over Pt@SiO_2,Pt-Na@SiO_2 and Na(IMP)-Pt@SiO_2catalysts (2%CO–10%H_2O–He, 70 mL/min, contact time = 0.09 g s/mL).

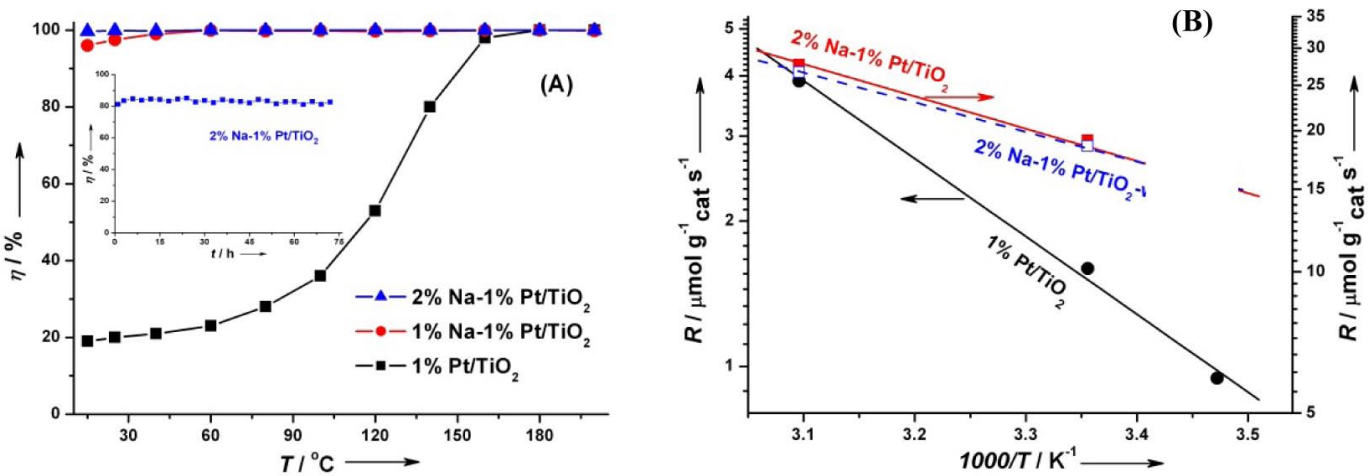

FIGURE 5. (A) HCHO conversion (η) over x wt.% Na-1 wt.% Pt/TiO_2 (x = 0, 1 and 2) catalysts as a function of temperature. HCHO 600 ppm, O_2 20 vol.%, RH: ~50%, He bal.; total flow rate: 50 cm^3 min^{-1}, and GHSV 120,000 h^{-1} (inset: stability test of 2% Na-1% Pt/TiO_2 at 25°C, GHSV = 300,000 h^{-1} with same other reaction conditions); (B) HCHO oxidation rate (*R*) over 1% Pt/TiO_2, 2% Na-1% Pt/TiO_2 and 2% Na-1% Pt /TiO_2-washed catalysts.

an otherwise inert material. Pt-O-(OH)-Na clusters on the carbon nanotube walls catalyze the WGS reaction at ~ 250-300°C[6]. Work on alkali promotion of gold catalysts continued this year with new experimental as well as computational findings supporting the model of a single gold atom stabilized by O and OH species supplied by the surrounding sodium atoms. Results from this work will be included in the annual report.

Future Directions

A comprehensive and complementary approach is followed to elucidate the metal-oxide interaction at the atomic scale. Since last year, we have also added an important new dimension to the project on the atomic metal-to-metal interaction with the preparation of single atom alloys. Work with methanol reactions on PdCu and PtCu SAAs will continue both with model catalysts and their nanoparticle analogs. In other STM work, methanol

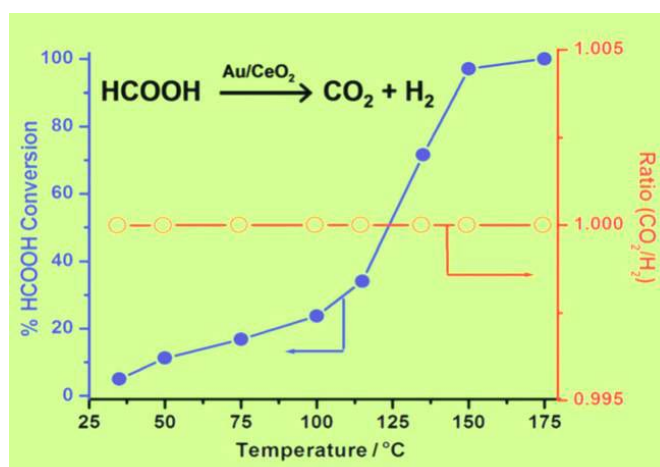

FIGURE 6. Decomposition of formic acid with dispersed gold on ceria

on the Au/Fe_3O_4(111) model catalyst is currently under investigation. This work will be concluded in the first part of the next reporting period; and the results will be transferred to nanoshapes for further study under ambient pressure. The synthesis, characterization and evaluation of Au and Cu and their surface alloys on nanoshapes of ZnO, TiO_2 and (Zn) ZrO_2 for WGS, SRM, and ethanol reactions will continue. The desired outcome is a good mechanistic understanding of the chemistries under investigation and the reaction-induced evolution of the key catalyst structures in order to propose general catalyst design guidelines for the reactions of interest to this project.

Publication list acknowledging the DOE grant DE-FG02-05ER15730— this reporting period

1. Rim, KT., Flytzani-Stephanopoulos, M, Flynn, GW, Batista, ER, et al., "Scanning Tunneling Microscopy and Theoretical Study of Water Adsorption on Fe_3O_4: Implications for Catalysis", *JACS,* **2012**, 134, 18979-18985.

2. Boucher, MB, Marcinkowski, MD, Liriano, ML, Murphy, CJ, Lewis, EA, Jewell, AD, Mattera, MFG, Kyriakou, G, Flytzani-Stephanopoulos, M., Sykes, ECH, "A Molecular-Scale Perspective of Water-Catalyzed Methanol Dehydrogenation to Formaldehyde" **2013**, submitted.

3. Wang, Y, Zhai Y, Pierre, D, Flytzani-Stephanopoulos, M., "Silica-encapsulated Platinum Catalysts for the low-temperature Water-gas Shift Reaction", *Appl. Cat. B* **2012**, 127, 342- 350.

4. Zhang, C, et al., "Alkali-Metal-Promoted Pt/TiO_2 Opens a More Efficient Pathway to Formaldehyde Oxidation at Ambient Temperatures", *Angewandte Chemie International Edition*, **2012**, 51, 9628-9632.

5. Yi, N, Saltsburg, H., Flytzani-Stephanopoulos, M, "Efficient and Stable Hydrogen Production through Dehydrogenation of Formic Acid on Atomically Dispersed Gold on Ceria", *ChemSusChem,* **2013**, DOI: 10.1002/cssc.201200957.

6. Zugic, B, Bell, DC, Flytzani-Stephanopoulos, M, Activation of Platinum Supported on Carbon for the Low-Temperature Water-Gas Shift Reaction, **2013**, submitted.

7. Flytzani-Stephanopoulos, M, Gates, BC, "Atomically Dispersed Supported Metal Catalysts", *Annu. Rev. Chem. Biomol. Eng.* **2012**, 3, 545–74.

8. Lawton, TJ, Carrasco, J, Baber, AE, Michaelides, A, Sykes, ECH, "Hydrogen-bonded Assembly of Methanol on Cu (111)" *Physical Chemistry Chemical Physics*, **2012**, *14*, 11846-11852

9. Lawton, TJ, Kyriakou, G, Baber, AE, Sykes, ECH, "An Atomic Scale View of Methanol Reactivity at the Cu(111)/CuO_x Interface" *ChemCatChem*, Accepted, **2013** DOI: 10.1002/cctc.201200810

10. Lessard, J, Valsamakis, I, Flytzani-Stephanopoulos, M, "Novel Au/La_2O_3 and Au/$La_2O_2SO_4$ Catalysts for the WGS Reaction Prepared via Anion Adsorption Method", *Chem Comm* **2012**, 48(40), 4857-4859.

11. Yang, M, Allard, LF, Flytzani-Stephanopoulos, M. "Atomically Dispersed Au-$(OH)_x$ Species Bound on Titania Catalyze the Low-temperature Water-Gas Shift Reaction", *J. Am. Chem. Soc.,* **2013**, DOI: 10.1021/ja312646d.

V.N.27 Hydrocarbon Oxidation, Dehydrogenation and Coupling over Model Metal Oxide Surfaces

Principal Investigator: David F. Cox
Department of Chemical Engineering
Virginia Tech
Blacksburg, VA 24060
Phone: 540-231-6829
Email: dfcox@vt.edu

Names of Team Members
Mr. Xu Feng
Chemical Enginering; Virginia Tech
Blacksburg, VA 24060
Email: Exufeng@vt.edu

Dr. Yujung Dong
Chemical Enginering; Virginia Tech
Blacksburg, VA 24060
Email: yjdong@vt.edu

DOE Program Manager: Dr. Raul Miranda
Office of Basic Energy Sciences
SC-22.1/Germantown Building
U.S. Department of Energy
1000 Independence Avenue, SW
Washington, D.C. 20585-1290
Phone: 301-903-8014
Email: Raul.Miranda@science.doe.gov

Objectives

The overall goal of the project is to develop an understanding of structure/function relationships in small alkane oxidation and dehydrogenation over transition metal oxide surfaces.

Technical Barriers

Selective heterogeneous catalysts for the dehydrogenation of ethane are limited by the equivalent C–H bonds which show no selectivity in ethane activation. A clear understanding of the elementary chemical steps in the reaction of the different possible intermediates may help us overcome these difficulties.

Abstract

The reaction of C_1 hydrocarbon fragments has been examined on α-$Cr_2O_3(10\bar{1}\bar{1}2)$, α-$Cr_2O_3(0001)$, α-$Fe_2O_3(10\bar{1}\bar{1}2)$ and manganese oxides. The material choices allow some separation of structural and electronic effects, and an examination of the surface chemistry of oxides with $3d^3$, $3d^4$ and $3d^5$ transition metal 3+ cations.

Progress Report

Work in past project periods has focused on understanding the reactivity of different C_1 and C_2 hydrocarbon surface intermediates that may play an important role in ethane dehydrogenation over transition metal oxide surfaces. Most recently we have focused on the C_1 species, methyl and methylene, because they show an important range of reactivity related to dehydrogenation, surface diffusion, and coupling reactions (carbon-carbon bond making). Our goal has been to understand both structural and electronic effects in the reactions of these species

Chromia Surfaces

Chromia was chosen as a target material because it exhibits an ability to selectively dehydrogenate butanes to butylenes, although the selectivity for ethane dehydrogenation or oxidative dehydrogenation is limited. For butane dehydrogenation, coordinately unsaturated Cr^{3+} centers are thought to be the primary reaction sites for the dehydrogenation chemistry.

Reactions were studied on the α-$Cr_2O_3(10\bar{1}\bar{1}2)$ and α-$Cr_2O_3(0001)$ surfaces to examine the structure sensitivity of the methyl, CH_3, dehydrogenation reaction and the diffusion and coupling of methylene, $:CH_2$, to ethylene, $CH_2{=}CH_2$. These chromia surfaces, because of the $3d^3$ electronic configuration of the Cr^{3+} cations, are highly nonreducible in UHV, even when exposed to hydrogen atoms. As a result, no oxygen-containing products are observed in TPD from these surfaces.

The $(10\bar{1}\bar{1}2)$ and (0001) surfaces expose Cr^{3+} cations with coordination numbers of five (one coordination vacancy relative to the bulk) and three (three coordination vacancies), respectively. We have shown experimentally that methyl dehydrogenation is structure insensitive, showing no significant variation in the activation barrier to dehydrogenation to methylene with changes in cation coordination or local site geometry. Methylene coupling to ethylene is associated with a rate-limiting surface diffusion step on both α-$Cr_2O_3(10\bar{1}\bar{1}2)$ and (0001) surfaces, and shows a significant structure sensitivity. The rate-limiting step shows an 85 K increase in the reaction temperature in TPD on the (0001) due to the lower accessibility of surface O atoms on the stoichiometric (0001) surface. The local site geometry also requires longer, less-stable bonds as the methylene diffuses across the surface.

For both surfaces, DFT gives an interesting picture of the methylene surface diffusion process. DFT suggests

methylene can π-bond to a surface cation, or bridge bond between a surface cation and anion on either surface. The diffusion process is simply a thermally-driven rehybridization in which methylene varies between π-bonded (sp^2) and bridge-bonded (sp^3) configurations, with the barrier to diffusion significantly lower than that for methylene dehydrogenation to surface carbon.

C_1 Reactions on α-Fe_2O_3

Because α-Cr_2O_3 and α-Fe_2O_3 both crystallize in the corundum bulk structure with only minor (less than 2%) differences in the lattice parameters, a comparison of surface chemistry over similar terminations of the two materials allows one to test the impact of a nearly-pure electronic effect associated with the $3d^3$ and $3d^5$ electronic structure of Cr^{3+} and Fe^{3+} cations, respectively. The iron oxide is known to be much more reducible than the chromia, so differences in selectivity due to the reactivity of surface lattice oxygen were anticipated.

Variations in the M^{3+} d-electron density cause dramatic but predictable changes in the surface chemistry of methylene, :CH_2, fragments on stoichiometric corundum-structure $(10\bar{1}\bar{1}2)$ surfaces when Cr^{3+} cations are replaced with Fe^{3+}. The reaction selectivity on stoichiometric α-Fe_2O_3 $(10\bar{1}\bar{1}2)$ is entirely towards the non selective oxidation products CO and CO_2 for small submonolayer doses of the reactant, consistent with the reducible nature of the surface. CO and CO_2 evolve simultaneously (often an indication of a carboxylate surface intermediate) at 630 K in TPD. The reaction of formate formed from the adsorption of formic acid occurs in a similar temperature range to give CO and CO_2, in support of this assignment. No other products are observed from the stoichiometric surface. However, for consecutive TPD runs, the production of CO and CO_2 drop off quickly with the first few doses of reactant, and formaldehyde ($H_2C{=}O$) and ethylene ($H_2C{=}CH_2$) appear as major products.

From the products formed, it is clear that methylene fragments reduce the surface via the extraction of lattice oxygen to make CO, CO_2 and $H_2C{=}O$. The shift in the product slate from nonselective oxidation products (CO, CO_2) to selective oxidation ($H_2C{=}O$) and $H_2C{=}CH_2$ occurs as the surface becomes reduced. For methylene coupling to ethylene, the generation of reduced Fe^{2+} surface sites is clearly important, although the specific site requirements (if any) for the coupling reaction are unclear because of a lack of information about the surface structure.

Reactions on Manganese Oxide Surfaces

The increase in *d* electron density for Fe_2O_3 ($3d^5$ for Fe^{3+} vs $3d^3$ for Cr^{3+}) leads to a highly reducible surface compared to the non-reducible Cr_2O_3. Given the dramatic differences in reaction selectivity observed between these two materials, we have wondered how a $3d^4$ configuration for a Mn^{3+} cation would compare in terms of selectivity. Unfortunately, Mn_2O_3 does not crystallize in the same corundum structure as α-Cr_2O_3 and α-Fe_2O_3, but given that we have found dramatic changes in selectivity associated with electronic changes and primarily kinetic effects from structural changes, we concluded an examination of Mn_2O_3 chemistry would be of interest, regardless of the structural differences. Macroscopic Mn_2O_3 single crystals are not available, but MnO can be purchased from commercial sources. Reports from Langell's group at UNL indicate that the surface of MnO(001) can be oxidized to Mn_2O_3. We have used this approach starting with a MnO(001) single crystal.

We have been able to produce the two higher oxides of manganese via high-temperature oxidation (to Mn_2O_3) and subsequent thermal reduction (to Mn_3O_4). Both higher oxides are disordered, and fail to give a clear diffraction pattern in LEED. Our initial work has focused on water and carbon dioxide adsorption as probe molecules to distinguish differences in the oxides. The higher oxides give very different CO_2 and water TPD signals than ordered MnO_2(001), but the differences for Mn_2O_3 and Mn_3O_4 are minimal.

Since Mn_3O_4 is a mixed valence oxide with both Mn^{2+} and Mn^{3+} cations, we have also tried to produce an ordered Mn^{3+} compound by oxidizing a Na pre-covered MnO surface to produce $NaMnO_2$. The synthesis is fairly straightforward in UHV, but also produces a disordered surface. While our work has failed to produce an ordered Mn^{3+} oxide film that we can characterize structurally, we are currently pursuing a set of TPD reaction studies with C_1 hydrocarbon fragments and oxygenates to test for any obvious differences in selectivity due to the $3d^4$ electronic structure of Mn^{3+} surface cations.

Future Directions

Following the examination of Mn_2O_3 chemistry, we will begin an investigation of mixed valence magnetite (Fe_3O_4) surface chemistry.

Publication list (since 2009) acknowledging the DOE grant or contract

1. Gibbs, G.V.; Ross, N.L.; Cox, D.F.; Rosso, K.M.; Iversen, B.B.; Spackman, M.A.; Bonded radii and the contraction of the electron density of the oxygen atom by bonded interactions. *The Journal of Physical Chemistry A* **2013**, *117*, 1632-1640.

2. Gibbs, G.V.; Wang, D.; Hin, C.; Ross, N.L.; Cox, D.F.; Crawford, T.D.; Spackman, M.A.; Angel, R.J.; Properties of atoms under pressure: Bonded interactions of the atoms in three perovskites. *The Journal of Chemical Physics* **2012**, *137*, 164313.

3. Gibbs, G.V.; Crawford, T.D.; Wallace, A.F.; Cox, D.F.; Parrish, R.M.; Hohenstein, E.G.; Sherrill, C.D.; Role of Long-Range Intermolecular Forces in the Formation of Inorganic Nanoparticle Clusters. *The Journal of Physical Chemistry A* **2011**, *115*, 12933-12940.

4. Brooks, J.D.; Chen, T.L.; Mullins, D.R.; Cox, D.F.; Reactions of ethylidene on a model chromia surface:1,1-dichloroethane on stoichiometric α-Cr_2O_3 $(10\bar{1}\bar{1}2)$. *Surface Science* **2011,** *605***,** 1170-1176.

5. Gibbs, G.V.; Wallace, A.F.; Downs, R.T.; Ross, N.L.; Cox, D.F.; Rosso, K.M.; Thioarsenides: van der Waals bonded Interactions and bond paths. *Physics and Chemistry of Minerals* **2011,** *38***,** 267-291.

6. Gibbs, G.V.; Wallace, A.F.; Zallen, R.; Downs, R.T.; Ross, N.L.; Cox, D.F.; Rosso, K.M.; Bond Paths and van der Waals Interactions in Orpiment, As_2S_3. *The Journal of Physical Chemistry A* **2010,** *114,* 6550-6557.

7. Gibbs, G.V.; Wallace, A.F.; Cox, D.F.; Downs, R.T.; Ross, N.L.; Rosso, K.M; Si-O Bonded Interactions, Silica Polymorphs and Siloxane Molecules. *American Mineralogist* **2009**, *94,* 1085-1102.

8. Brooks, J.D.; Ma, Q.; Cox, D.F.; Reactions of ethyl groups on a model chromia surface: ethyl chloride on stoichiometric α-Cr_2O_3 $(10\bar{1}\bar{1}2)$. *Surface Science* **2009**, *603,* 523-528.

9. McKee, M.A.; Ma, Q.; Mullins, D.R.; Neurock, M.; Cox, D.F.; Reactions of vinyl groups on a model chromia surface: vinyl chloride on stoichiometric α-Cr_2O_3 $(10\bar{1}\bar{1}2)$. *Surface Science* **2009,** *603,* 265-272.

10. Gibbs, G.V.; Wallace, A.F.; Cox, D.F.; Dove, P.M.; Downs, R.T; Ross, N.L.; Rosso, K.M; The role of directed van der Waals bonded interactions in the determination of the structures of molecular arsenate solids. *The Journal of Physical Chemistry A* **2009***, 113,* 736-749.

V.N.28 Atomic Level Studies of Advanced Catalysts for Hydrodeoxygenation

Principal Investigator: S. Ted Oyama
Virginia Tech, Dept. of Chemical Engineering
Blacksburg, VA 24061
Phone: 540-231-5309
Email: oyama@vt.edu

DOE Program Manager: Raul Miranda
Email: Raul.Miranda@science.doe.gov

Objectives

The utilization of biomass for the production of fuels and chemicals is currently an area of great activity because of the recognition that fossil fuels are a finite resource and because of the imminent threat of global warming from the release of carbon dioxide. Biomass pyrolysis has great potential for the production of drop-in replacements for petroleum products, but the pyrolysis oil product has low heating value and stability and high corrosivity, and improvements are needed. This project involves the development of advanced hydrodeoxygenation (HDO) catalysts to reduce the oxygen content of the oil.

Technical Barriers

A fundamental challenge is the design of catalysts that have high activity and selectivity in HDO. The biggest barriers in catalyst development is the formulation of compositions that do not deactivate with the bio-oil feedstock, which has high acidity and is highly functionalized.

Abstract

The catalysts that will be developed are a class of highly active and stable materials, the transition metal phosphides. Initial tests in our laboratory and elsewhere have demonstrated that the catalysts are highly effective in oxygen removal from model bio-oil compounds. We propose to build on these findings to develop advanced compositions using new preparation methods. The specific compounds will be bimetallic phosphide catalysts composed of the elements Ti, V, Cr, W, Fe, Co, Ni encompassing Groups 4-9 in the Periodic Table. The support will be fluid catalytic cracking materials with high Si-Al ratio, of interest because they have a bimodal mesoporous/microporous structure and are highly attrition resistant. The study of bimetallic compositions is motivated by our recent finding that NiFeP has outstanding catalytic properties. The catalysts will be highly dispersed and will be studied by x-ray absorption spectroscopy (XAS) and ^{31}P solid-state nuclear magnetic resonance spectroscopy.

The novel catalysts will be tested with model compounds and the best compositions will be tried in a pilot scale unit with real feeds at realistic pyrolysis conditions. The substrates to be used will be 2-methyltetrahydropyran (2-MTHP) and guaiacol (GCOL), which are, respectively, models for cellulose and lignin. The compounds are chosen because they can react by several pathways to give information about the reaction mechanism. The work will include detailed studies of kinetics and spectroscopy to understand the mechanism of the HDO reaction and to relate it to the structure of the catalysts in their working state. Knowledge of the partial pressure dependency of the rates of reaction on the reactants and various co-reactants (H_2, CO) and products (CO_2, H_2O, organics) will set the kinetic constraints to the mechanism. Then in situ studies by Fourier transform infrared and XAS will be used to identify key intermediates during reaction and will be used to distinguish between mechanisms. Importantly, these measurements will be carried out simultaneously at a synchrotron facility with specially designed equipment. Dynamic studies with methods we have developed will be used to establish the role of observed intermediates in the catalytic reactions. The overall objective is to obtain information that can be used to improve the catalyst action by understanding the key factors that govern reactivity.

Progress Report

Synthesis of Catalysts

A series of silica-supported metal phosphides was prepared by two methods involving the reduction of phosphite ("I") or phosphate ("A") precursors and was studied for the hydrodeoxygenation (HDO) of 2-methyltetrahydrofuran (2-MTHF). The "I" method required lower temperature than the "A" method and resulted in catalysts with higher surface area.

The activity was evaluated in a packed-bed reactor on the basis of equal CO chemisorption sites (30 μmol) loaded in the reactor with comparison made to a commercial Pd/Al_2O_3 catalyst. At 300 °C and 1 atm the order of activity was Ni_2P > WP > MoP > CoP > FeP > Pd/Al_2O_3. The principal HDO products for the iron group phosphides (Ni_2P and CoP) were pentane and butane, whereas for the group 6 metal phosphides (MoP and WP) the products were mostly pentenes and pentadienes. For the Pd/Al_2O_3 and the low-activity FeP/SiO_2 catalyst the products were mostly pentenes and C4 mixtures. There were no significant differences in the turnover frequency between materials prepared by the two methods, except possibly for the case of WP. There were likewise no great changes in selectivity towards HDO products at 5% total conversion, except for

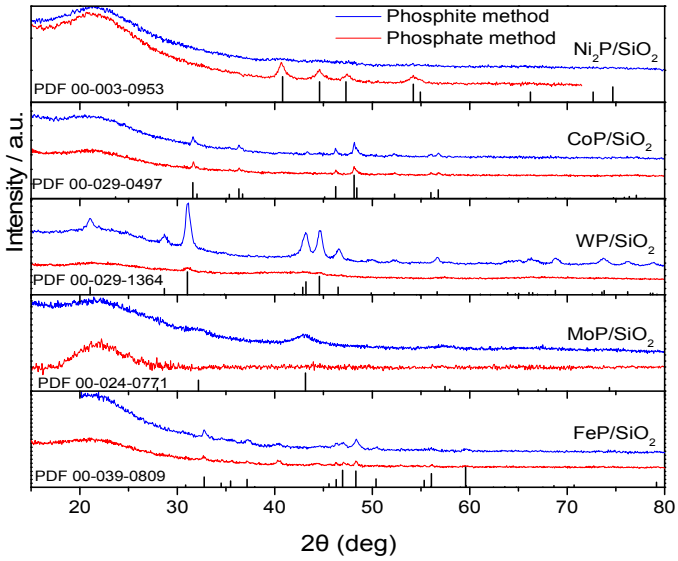

FIGURE 1. X-ray diffraction patterns of catalysts prepared by the phosphite and phosphate methods.

WP. The differences in the case of WP were attributed to the surface P/W ratio which x-ray photoelectron spectroscopy (XPS) showed to be twice as large for the I method than the A method. Contact time studies were used to develop reaction networks for the most active catalysts, Ni_2P/SiO_2 and WP/SiO_2. For Ni_2P/SiO_2 by both methods the selectivity profiles were similar, and could be explained by a rake mechanism with pentenes as primary products, 2-pentanone as a secondary product, and pentane as a final product. In contrast, for WP/SiO_2 the selectivity depended greatly on the preparation method, but produced a preponderance of unsaturated compounds. The results could be explained from the surface composition.

Reactions of 2-Methyltetrahydrofuran (cellulose model compound)

A series of supported nickel-iron phosphide catalysts were used to study the hydrodeoxygenation of 2-methyltetrahydrofuran (2-MTHF), a model compound for biomass-derived pyrolysis oil. The catalysts were prepared by incipient wetness impregnation of the active components onto potassium ion-exchanged USY zeolites followed by temperature-programmed reduction. The samples were denoted as Ni_2P/KUSY, NiFeP(3:1)/KUSY, NiFeP(1:1)/KUSY, NiFeP(1:3)/KUSY, and FeP/KUSY, where the numbers in parenthesis are the Ni:Fe molar ratios. The results of the studies can be understood from ensemble and ligand effects. X-ray diffraction analysis indicated the presence of alloys in the mixed composition samples, and this was supported by CO chemisorption and infrared measurements. Uptakes of CO decreased as the iron content increased, suggesting that iron present on the surface of the catalysts blocked chemisorption sites. Fourier transform infrared (FTIR) measurements showed a single peak for linearly adsorbed CO whose intensity decreased with Fe content, in agreement with the uptake results. Moreover, the FTIR peak shifted monotonically consistent with a ligand effect in an alloy formed in the Ni_2P and FeP particles. The reactivity in 2-MTHF HDO was studied at 250-325 °C and 0.5 MPa and it was found that the conversion was highest for the Ni_2P/KUSY sample and decreased steadily with Fe content. However, the turnover frequency did not change significantly, indicating that the rate-determing step was activation of 2-MTHF on single Ni sites.

The selectivity at low conversion (3%) changed from mostly n-pentane and n-butane for Ni_2P/KUSY to mostly 1-pentanol for the iron-containing samples, suggesting that in subsequent steps an ensemble effect was operational with the iron influencing the reaction chemistry. At high conversion (70%) all the samples produced mostly n-pentane and n-butane.

Reactions of Guaiacol (lignin model compound)

Several types of Ni phosphides with different phosphorus contents (Ni_2P, $Ni_{12}P_5$, and Ni_3P) were prepared by temperature-programmed reduction (TPR) and were tested for hydrodeoxygenation (HDO) of guaiacol at various temperatures, H_2 pressures, and contact times. Low phosphorus content in the precursors leads to the formation of Ni-rich phosphides such as Ni_3P and $Ni_{12}P_5$ with high concentration of metallic sites, while high phosphorus levels results in the formation of Ni_2P with low numbers of metallic sites. The reactivity of the catalysts for the HDO of guaiacol displays a strong dependence on the phosphorus content. At temperatures higher than 260 °C, high-phosphorus catalysts have higher turnover frequencies (TOFs) than low-phosphorus samples and carry out complete HDO to

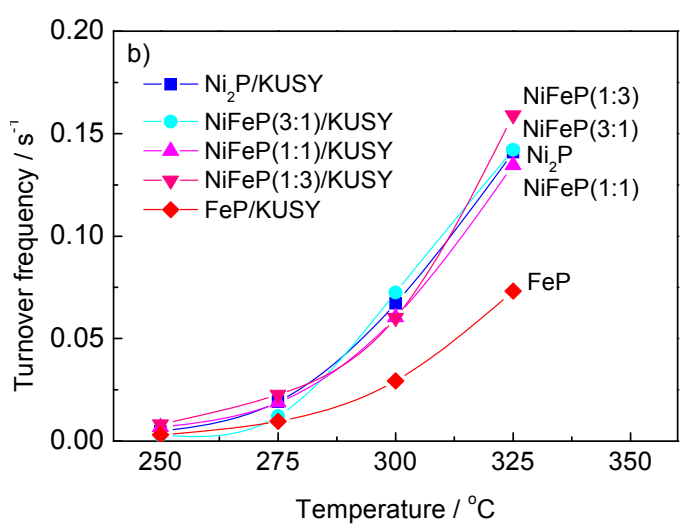

FIGURE 2. Activity of different Ni-Fe catalysts showing similar TOFs

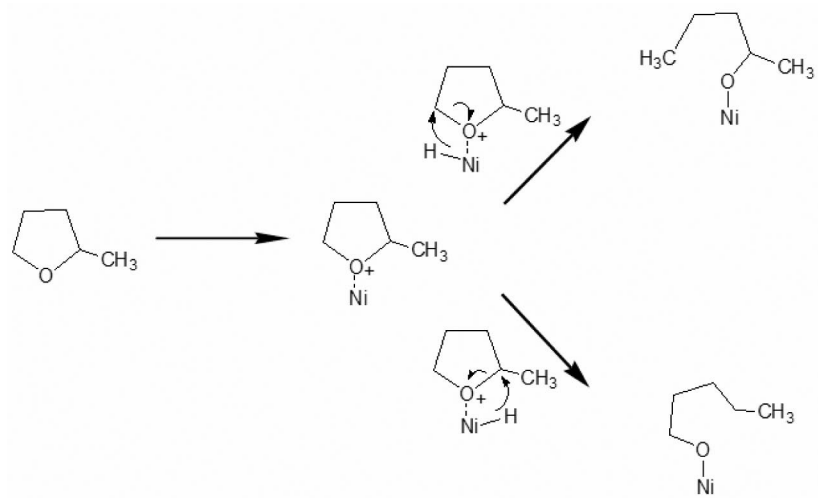

FIGURE 3. Reaction of 2-methyltetrahydrofuran involving a single Ni atom

the product benzene. In comparison, metallic Ni catalyst has little ability to produce benzene or hexane but produces only phenol, cyclohexanone, orcyclohexanol at different H_2 pressures. The reaction pathways for guaiacol HDO is proposed to involve catechol as primary product and phenol as secondary product, based on the effect of contact time on the product distribution (Fig. 4).

Future Directions

Understanding of the relationship between the physical properties of catalysts and their activity is important to develop new improved compositions. The objectives are given below.

1. Advanced preparation of bimetallic phosphide catalysts and atomic-level characterization.
   Materials will be prepared by combining the most active single-elements, Ni and W, with Ti, V, Cr, Mn, Fe, and Co. The catalysts will be highly dispersed, and x-ray absorption fine structure (XAFS) and ^{31}P NMR spectroscopy will be used to determine the structure of the active phase
2. Reactivity studies with model compounds and real feeds. Hydrodeoxygenation will use two compounds, guaiacol (GCOL and 2-methyltetrahydro-pyran (2-MTHP), which are models of lignin and cellulose-hemicellulose. Contact time measurements will provide the reaction network, and isotopic labeling the mode of ring-opening. The best catalysts will be evaluated in catalytic pyrolysis with actual biomass.
3. Studies of kinetics and mechanisms.
   For the best catalysts partial pressure dependency and contact time measurements will be used to derive a

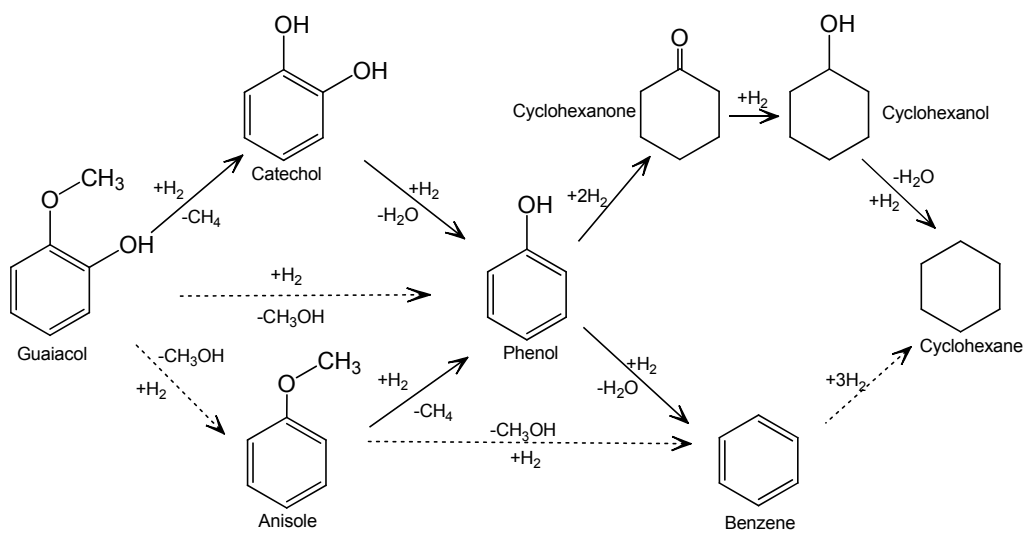

Figure 4. Reaction network for guaiacol hydrodeoxygenation

plausible reaction sequence which will be checked spectroscopically. Kinetic rate expressions will be tested statistically.

4. Studies with in situ Fourier transform infrared (FTIR) spectroscopy and XAFS.
   Adsorbed species will be probed by FTIR and XAFS spectroscopy using a dynamic method where changes in coverage ($d\theta/dt$) will be compared to the turnover frequency. In situ measurements will relate changes in catalyst structure with adsorption to identify active sites.

Publication list (including patents) acknowledging the DOE grant or contract

1. Phuong Bui, Juan Antonio Cecilia, Ted. S. Oyama, Atsushi Takagaki, Antonia Infantes-Molina, Haiyan Zhao, Dan Li, Enrique Rodríguez-Castellón, Antonio Jiménez López, Studies of the Synthesis of Transition Metal Phosphides and their Activity in the Hydrodeoxygenation of a Biofuel Model Compound J. Catal. **2012**, 294, 184-198.

2. Jieun Shin, Ara Cho, Atsushi Takagaki, Ryuji Kikuchi, S. Ted Oyama, Ligand and ensemble effects in bimetallic NiFe phosphide catalysts for the hydrodeoxygenation of 2-methyltetrahydrofuran *Topics Catal.* **2012**, 55, 969–980.

3. Oxygen-removal from dibenzofuran as a model compound in biomass derived bio-oil on nickel phosphide catalysts: Role of phosphorus
Juan Antonio Cecilia, Antonia Infantes-Molina, Enrique Rodríguez-Castellón, Antonio Jiménez-López, S. Ted Oyama, *Appl. Catal. B: Env.* **2013**, 136-137, 140-149.

V.N.29 Atomic-Scale Design of Metal and Alloy Catalysts: a Combined Theoretical and Experimental Approach

Principal Investigator: Manos Mavrikakis
Department of Chemical & Biological Engineering
University of Wisconsin-Madison
Madison, WI 53706
Phone/Fax: 608-262-9053
Email: manos@engr.wisc.edu

Co-PI:

- James A. Dumesic
  Department of Chemical & Biological Engineering
  University of Wisconsin-Madison
  Madison, WI 53706
  Phone: 608-262-1095
  Email: dumesic@engr.wisc.edu
- Younan Xia
  Department of Chemistry and Biochemistry
  Georgia Institute of Technology
  Atlanta, GA 30332
  Phone: 404-385-3209
  Email: younan.xia@bme.gatech.edu

Subcontractor
Younan Xia
Department of Chemistry and Biochemistry
Georgia Institute of Technology
Atlanta, GA 30332.
Phone: 404-385-3209
Email: younan.xia@bme.gatech.edu

DOE Program Manager: Raul Miranda
Phone: (301) 903-8014
Email: Raul.Miranda@science.doe.gov

Objectives

The main objective of this combined theoretical and experimental project is to: (i) *design* from first-principles, (ii) *synthesize* using advanced *nanosynthesis* techniques, and (iii) experimentally evaluate *new metal* and *alloy nanoparticles,* with unique *catalytic* properties for a number of important chemical reactions. We also want to address the fundamentals of reactivity at metal/metal oxide interfaces.

Technical Barriers

1. Low-temperature polymer electrolyte membrane (PEM) fuel cells present an attractive method of generating electricity for portable devices. However, the commercial feasibility of these systems is limited by the high cost of Pt-based catalysts. Experimental screening of catalytic materials is costly and time-consuming. From a fundamental understanding of reaction mechanisms, developed through first-principles calculations, we are able to identify promising materials using reactivity appropriate reactivity descriptors.
2. Water plays a significant role in surface reactions, even if only a spectator species, including at impurity levels. In addition, spillover of atoms from metal to metal oxide supports and the reverse has been shown to play a key role in heterogeneous catalysis. We address the role of water on hydrogen atom diffusion, and thereby spillover, at FeO/Pt interfaces.

Abstract

The catalysts designed in this project can impact a number of applications, including low temperature fuel cells, hydrogen production and purification, and liquid fuels production. The importance of the atomic-scale architecture of these new theoretically-designed catalysts to their unique properties is driving the development of *new inorganic materials synthesis* approaches, which are capable of synthesizing the theoretically determined optimal, and in some cases, metastable, nanoscale catalytic architectures.

Over the past year, we have made progress toward our objectives through a combination of theoretical and experimental studies. We have used DFT calculations to show that water is able to assist hydrogen diffusion on a FeO/Pt moire structure. This finding has substantial implications for reactions where water participates as a reactant, product, solvent, or impurity in the reaction mixture. We have also designed "onion"-structured alloy catalysts from first principles that demonstrate a high activity for the oxygen reduction reaction (ORR). These alloys, composed of a Pt monolayer deposited on a substrate metal (or alloy) with a number of 1-atom-thick Pd layers in between, have been synthesized experimentally and verified to have higher catalytic activity than pure Pt ORR catalysts.

Progress Report

Water-Mediated Proton Hopping on an Iron Oxide Surface[1] Science 2012, 336 (6083)

The diffusion of hydrogen is an important process in a number of applications, including catalytic hydrogen evolution and reforming, hydrogenation/dehydrogenation of hydrocarbons, and hydrogen storage. Hydrogen diffusion is practically important in cases where the "spillover" effect operates, where active sites for H_2 dissociation and association are spatially separated from the active sites for other reactions. Mechanisms involving hydrogen spillover

have been implicated in many industrially important catalytic reactions, including methanol synthesis and hydrogenation of benzene and toluene, for example. The presence of hydrogen spillover on oxides can also affect the catalytic activity of oxide catalysts, in some cases activating an otherwise inactive catalyst.

Enhanced rates of surface reactions involving hydrogen diffusion upon addition of water have been observed in a number of cases. However, the fundamental atomistic mechanisms underlying hydrogen diffusion on solid surfaces and the factors influencing them still remain unsettled. In a recent study, we revealed the underlying mechanism of an enormous hydrogen diffusion enhancement induced by trace amounts of water on a monolayer FeO thin film deposited on a Pt surface.

By using fast scanning tunneling microscopy (STM), rapid hydrogen diffusion on a FeO/Pt moiré structure (see Figure 1) at low temperature (105 K) was observed. To understand the underlying mechanism of the fast hydrogen diffusion on this surface, we used density functional theory corrected for on-site Coulomb interaction (DFT+U) on the natural $\left(\sqrt{91}\times\sqrt{91}\right)R5.2°$ (very large) unit cell. We studied intrinsic hydrogen diffusion on the FeO/Pt moire structure and found that hydrogen diffusion is highly activated, with an energy barrier of ~1 eV. By introducing a very small amount of water close to the surface, we found that a new channel for fast hydrogen diffusion opens up: this new channel goes via a proton transfer process mediated by H_2O, involving the transfer of the surface proton to the water molecule and the formation of short-lived hydronium ion (H_3O^+) species at the transition state. Subsequently, one of the original water protons is transferred to an O atom on the FeO surface. The H_2O-mediated hydrogen diffusion process needs an energy barrier of only ~0.2 eV, as shown in Figure 2. This finding, in contrast to the intrinsic H diffusion, clearly suggests that water can accelerate H diffusion by ~16 orders of magnitude at room temperature.

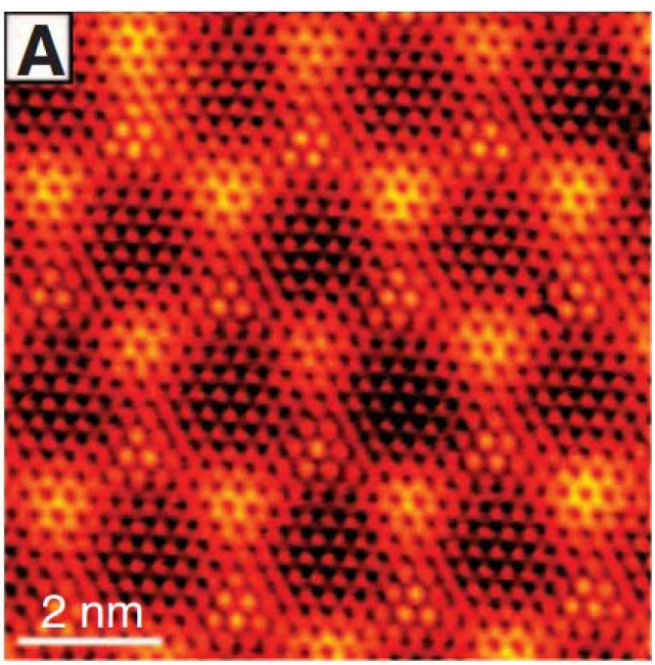

FIGURE 1. Atomically-resolved STM image of the bare FeO film on Pt(111) showing the moiré structure and protrusions due to individual Fe and O atoms. Figure from reference 1.

Oxygen Reduction on Pt-Terminated Alloy Catalysts[5] *Electrocatalysis* 2012, 3 (3-4)

Low-temperature polymer electrolyte membrane (PEM) fuel cells present an attractive method of generating electricity for portable devices. However, the commercial feasibility of these systems is limited by the high cost of Pt-based catalysts, which are necessary to catalyze the oxygen reduction reaction (ORR) at fuel cell cathodes with sufficiently low over-potentials. To overcome this materials challenge, we have been interested in developing Pt alloy catalysts that maintain or increase the high catalytic activity of Pt, while minimizing Pt-loading. Using first-principles calculations, we have identified a series of Pt-terminated alloy catalysts, which are predicted to have equal or better catalytic activity than pure Pt, while minimizing Pt-loading.

In previous work,[2] we studied a series of bimetallic catalysts featuring a Pt monolayer deposited on a substrate metal, denoted as Pt*/X (X = Au, Pd, Ru, Rh, or Ir). We found that Pt*/Pd had the highest activity, which was a 20-fold increase in Pt mass activity compared with pure Pt. In addition to their high activity, these catalysts utilized a fraction of the Pt necessary for the standard pure Pt catalyst. Our fundamental studies revealed that the activity of these catalysts was correlated with the strength of oxygen binding on the catalytic surfaces and that the optimal oxygen binding is slightly weaker than that of pure Pt. By depositing Pt on a substrate, its binding properties are modulated through electronic interactions with the substrate (referred to as the

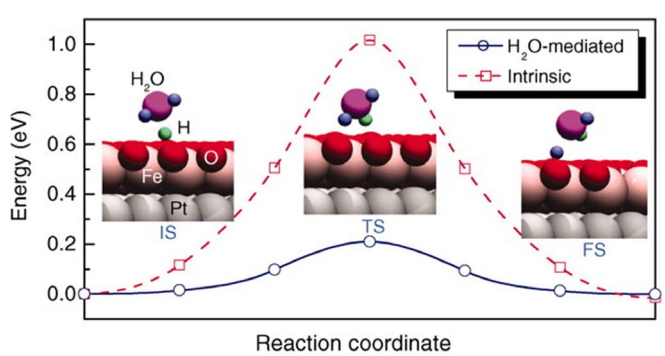

FIGURE 2. Energy profile for hydrogen atom diffusion on FeO/Pt(111): H_2O-mediated (blue solid line) and intrinsic (red dashed line); insets provide cross-sectional views of the initial (IS), transition (TS), and final state (FS) for the H_2O-mediated (fast) diffusion of H atoms. Figure from reference 1.

ligand effect[3]) and through lattice mismatch between Pt and the substrate (referred to as the strain effect[4]). In particular, for Pt*/Pd, these effects weaken oxygen binding slightly, so that Pt*/Pd gets closer to the optimal oxygen binding.

These initial studies revealed a strategy for improving the efficacy of these catalysts by taking advantage of ligand and strain effects. However, the cost of the Pd substrate was still high for commercial applications and the activity could be improved further. To address these challenges, we have now investigated a series of "onion-structured" alloys, which are composed of a Pt-monolayer deposited on a substrate with 0, 1 or 2 monolayers of Pd sandwiched between the Pt-monolayer and the substrate (denoted Pt*/M_2/M_3, see Figure 3).[5] The Pd sandwiched layers are important because they "shield" the Pt shell atoms from the ligand effect induced by the substrate material, while the substrate material was chosen to weaken the oxygen binding relative to Pt*/Pd by compressing the Pt*/Pd template slightly.

In Figure 4 we present the DFT-estimated catalytic activity (activity increases in the positive y-direction) of the onion-structured alloy catalysts, based on rigorous calculations of the reaction energetics on those surfaces, as a function of their oxygen binding affinity. This results in a "volcano curve". Additionally, we plot the theoretical activity of hypothetical catalysts over a continuum of binding properties with a purple line. This prediction is based on linear-scaling correlations[6] and Brønsted-Evans-Polanyi correlations[7], rather than through rigorous evaluations of all of the reaction energetics.

The optimal activity is found on surfaces that bind oxygen weaker (more positive in x-axis of Frig. 4) than both pure Pt and Pt*/Pd. We have found a number of candidate catalysts that are predicted to be significantly more active than Pt*/Pd (note that a change in activity of 0.06 eV corresponds to an order of magnitude change in the rate constant at room temperature). Of these active surfaces, Pt*/Pd/Pd_3Fe[8] and Pt*/PdIr[9] have now been synthesized and tested experimentally, verifying the predicted improvement in activity versus pure Pt.

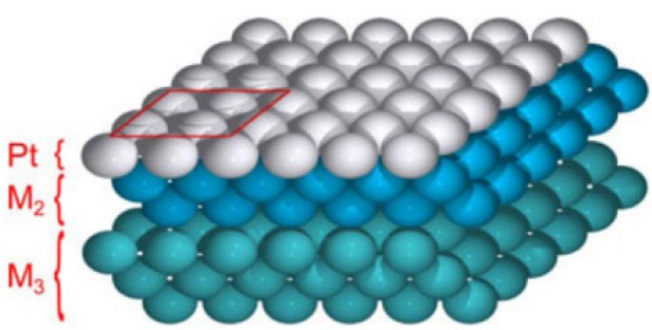

FIGURE 3. Cross-sectional view of "onion alloy" structures. M2 is typically Pd, while M_3 can be a monometallic or intermetallic alloy. Figure from reference 5.

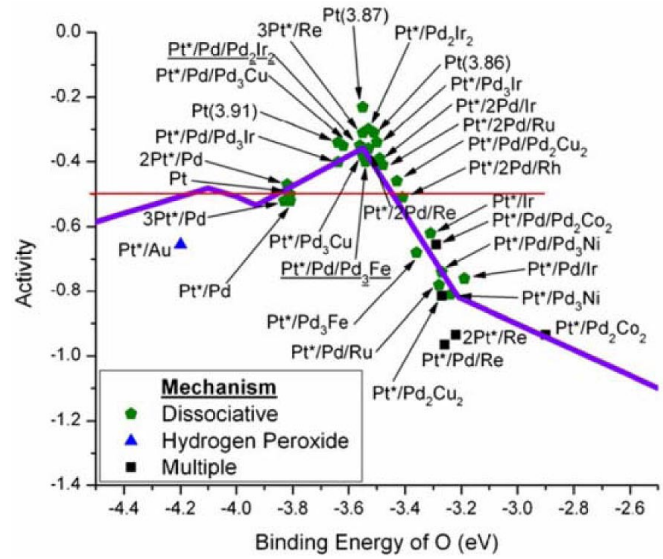

FIGURE 4. DFT-derived "volcano curve" for ORR activity (in eV) of close-packed surfaces versus oxygen binding energy. Activity of pure Pt is shown with the red horizontal line. Purple line represents the theoretical prediction of activity as a function of binding energy of oxygen. Figure from reference 5.

Future Directions

Our research plans for this coming year of the project have not changed from those described in detail in the most recent renewal proposal. In addition to furthering the work described here, we continue to pursue experimental and theoretical studies to test surface alloys for the vapor phase NO reduction by H_2. We also continue to investigate shape-selective nanoparticle synthesis, particularly through the variation of Br- ion concentration in the synthesis process, to yield nanocubes, truncated cubes, or cubotachedrons.

References

1. L.R. Merte, G.W. Peng, R. Bechstein, F. Rieboldt, C.A. Farberow, L.C. Grabow, W. Kudernatsch, S. Wendt, E. Laegsgaard, M. Mavrikakis, F. Besenbacher, "Water-Mediated Proton Hopping on an Iron Oxide Surface," *Science* **336**, 889-893 (2012).

2. J.L. Zhang, M.B. Vukmirovic, Y. Xu, M. Mavrikakis, R.R. Adzic, "Controlling the catalytic activity of platinum-monolayer electrocatalysts for oxygen reduction with different substrates," *Angewandte Chemie-International Edition* **44**, 2132-2135 (2005).

3. J.R. Kitchin, J.K. Norskov, M.A. Barteau, J.G. Chen, "Role of strain and ligand effects in the modification of the electronic and chemical properties of bimetallic surfaces," *Physical Review Letters* **93**, (2004).

4. M. Mavrikakis, B. Hammer, J.K. Norskov, "Effect of strain on the reactivity of metal surfaces," *Physical Review Letters* **81**, 2819-2822 (1998).

5. J.A. Herron, J. Jiao, K. Hahn, G. W. Peng, R.R. Adzic, M. Mavrikakis, "Oxygen Reduction Reaction on Platinum-Terminated "Onion-structured" Alloy Catalysts," *Electrocatalysis* **3**, 192-202 (2012).

6. F. Abild-Pedersen, J. Greeley, F. Studt, J. Rossmeisl, T.R. Munter, P.G. Moses, E. Skulason, T. Bligaard, J.K. Norskov, "Scaling properties of adsorption energies for hydrogen-containing molecules on transition-metal surfaces," *Physical Review Letters* **99**, (2007).

7. S.G. Wang, B. Temel, J.A. Shen, G. Jones, L.C. Grabow, F. Studt, T. Bligaard, F. Abild-Pedersen, C.H. Christensen, J.K. Norskov, "Universal Bronsted-Evans-Polanyi Relations for C-C, C-O, C-N, N-O, N-N, and O-O Dissociation Reactions," *Catalysis Letters* **141**, 370-373 (2011).

8. W.P. Zhou, X.F. Yang, M.B. Vukmirovic, B.E. Koel, J. Jiao, G.W. Peng, M. Mavrikakis, R.R. Adzic, "Improving Electrocatalysts for O-2 Reduction by Fine-Tuning the Pt-Support Interaction: Pt Monolayer on the Surfaces of a Pd3Fe(111) Single-Crystal Alloy," *Journal of the American Chemical Society* **131**, 12755-12762 (2009).

9. S.L. Knupp, M.B. Vukmirovic, P. Haldar, J.A. Herron, M. Mavrikakis, R.R. Adzic, "Platinum Monolayer Electrocatalysts for O-2 Reduction: Pt Monolayer on Carbon-Supported PdIr Nanoparticles," *Electrocatalysis* **1**, 213-223 (2010).

Publication list (including patents) acknowledging the DOE grant or contract:

1. Yang, L., Vukmirovic, M.B., Su, D., Sasaki, K., Herron, J.A., Mavrikakis, M., Liao, S., Adzic, R.R., Tuning the Catalytic Activity of Ru@Pt Core–Shell Nanoparticles for the Oxygen Reduction Reaction by Varying the Shell Thickness. *Journal of Physical Chemistry C* **2013**, *117* (4)

2. Merte, L.R., Peng, G., Bechstein, R., Rieboldt, F., Farberow, C.A., Grabow, L.C., Kudernatsch, W., Wendt, S., Lægsgaard, E., Mavrikakis, M., Besenbacher, F., Water-Mediated Proton Hopping on an Iron Oxide Surface. *Science* **2012,** *336* (6083)

3. Herron, J.A., Jiao, J., Hahn, K., Peng, G., Adzic, R.R., Mavrikakis, M., Oxygen Reduction Reaction on Platinum-Terminated "Onion-structured" Alloy Catalysts. *Electrocatalysis* **2012,** *3* (3-4)

4. Jewell, A.D., Peng, G., Mattera, M.F.G., Lewis, E.A., Murphy, C.J., Kyriakou, G., Mavrikakis, M., Sykes, E.C.H., Quantum Tunneling Enabled Self-Assembly of Hydrogen Atoms on Cu(111). *ACS Nano* **2012,** *6* (11)

5. Svenum, I.-H., Herron, J.A., Mavrikakis, M., Venvik, H.J., Adsorbate-Induced Segregation in a PdAg Membrane Model System: $Pd_3Ag(111)$. *Catalysis Today* **2012,** *193* (1)

6. Herron, J.A., Tonelli, S., Mavrikakis, M., Atomic and Molecular Adsorption on Pd(111). *Surface Science* **2012,** *606* (21-22)

7. Rossmeisl, J., Ferrin, P., Tritsaris, G.A., Nilekar, A.U., Koh, S., Bae, S.E., Brankovic, S.R., Strasser, P., Mavrikakis, M., Bifunctional Anode Catalysts for Direct Methanol Fuel Cells. *Energy & Environmental Science* **2012,** *5* (8)

8. Karan, H.I., Sasaki, K., Kuttiyiel, K., Farberow, C.A., Mavrikakis, M., Adzic, R.R., Catalytic Activity of Platinum Monolayer on Iridium and Rhenium Alloy Nanoparticles for the Oxygen Reduction Reaction. *ACS Catalysis* **2012,** *2* (5)

9. Peng, H.-C., Xie, S., Park, J., Xia, X., Xia, Y., Quantitative analysis of the coverage density of Br^- ions on Pd{100} facets and its role in controlling the shape of Pd nanocrystals. *Journal of the American Chemical Society* **2012,** *135* (10)

10. Xie, S., Choi, S.-I., Xia, X., Xia, Y., Catalysis on faceted noble-metal nanocrystals: both shape and size matter. *Current Opinion in Chemical Engineering* **2013,** *2*

11. Xia, Y., Xia, X., Wang, Y., Xie, S., Shape-controlled synthesis of metal nanocrystals. *MRS Bulletin* **2013**, in press

12. Patent Application: P120136US01 Mixed-metal platinum catalysts with improved carbon monoxide tolerance, Filed Date: Sept. 21, 2012; M. Mavrikakis, A.U. Nilekar, R.R. Adzic, K. Sasaki

VI. MANUFACTURING R&D

VI.0 Manufacturing R&D Program Overview

INTRODUCTION

The Manufacturing Research and Development (R&D) program supports activities needed to reduce the cost of manufacturing hydrogen and fuel cell systems and components. Manufacturing R&D will enable the mass production of components in parallel with technology development and will foster a strong domestic supplier base. The program's R&D activities address the challenges of moving today's technologies from the laboratory to high-volume, pre-commercial manufacturing to drive down the cost of hydrogen and fuel cell systems. The program focuses on the manufacturing of components and systems that will be needed in the early stages of commercialization. Research investments are focused on reducing the cost of components currently used or planned for use, as well as reducing overall processing times. Progress toward targets is measured in terms of reductions in the cost of producing fuel cells, increased manufacturing processing rates, and growth of manufacturing capacity.

In Fiscal Year (FY) 2013, manufacturing projects continued in the following areas: novel electrode deposition processes for membrane electrode assembly (MEA) fabrication, reduction in the number of assembly steps for MEAs, use of scatterfield microscopy and in-line diagnostics for cell and component quality control to measure catalyst loading and detect defects in catalyst-coated membranes and gas diffusion electrodes, and fabrication technologies for high-pressure composite storage tanks.

GOAL

Develop innovative technologies and processes that reduce the cost of manufacturing fuel cells and systems for hydrogen production, delivery, and storage.

OBJECTIVES[1]

Key objectives for Manufacturing R&D include:

- Develop manufacturing techniques to reduce the cost of automotive fuel cell stack assembly and testing at high volume (500,000 units/year) from the 2008 value of $38/kW to $21/kW by 2017.
- Develop processes that will reduce the fabrication and assembly costs for compressed-hydrogen storage systems by 12% from the current high-volume costs of $18/kWh by 2017.
- Support efforts to reduce the cost of manufacturing components and systems to produce hydrogen at $2–$4/gge (2007 dollars) (untaxed, delivered, and dispensed) by 2020.

FY 2013 TECHNOLOGY STATUS

Presently, fuel cell systems are fabricated in small quantities. The cost of 10 kW, low-temperature proton exchange membrane (PEM) fuel cell systems for backup power is projected to be ~$2,200/kW$_{net}$ at a volume of 100 systems per year.[2] For automotive applications using today's technology, the cost of an 80-kW PEM fuel cell system is projected to be $55/kW for high-volume manufacturing (500,000 systems/year).[3] Projected costs include labor, materials, and related expenditures, but do not account for manufacturing R&D investment.

FY 2013 KEY ACCOMPLISHMENTS

FY 2013 saw a number of advancements in the manufacture of fuel cells and hydrogen storage systems, including:

- **Electrode Deposition:** A cost analysis by Strategic Analysis predicts that W.L. Gore's MEAs would have similar costs to 3M's nanostructured thin film /membrane catalyst-coated membrane because the materials costs are about the same (dominated by Pt cost). Gore processing costs are expected to be lower due to non-vacuum processing and faster line speeds.

[1] Note: Targets and milestones were recently revised; therefore, individual project progress reports may reference prior targets.
[2] Wei, M., et al., http://www.hydrogen.energy.gov/pdfs/review13/fc098_wei_2013_o.pdf.
[3] James, B.D., et al., http://hydrogen.energy.gov/pdfs/13012_fuel_cell_system_cost_2013.pdf.

- **High-Pressure Storage:** Quantum improved the in-house computer program, mWind, which allows more composite shell layer options using advanced fiber placement methods, to generate finite element analysis models of composite shells; Quantum verified and confirmed the accuracy of the models with strain gage and optical strain measurements; measurements at the transition area between aft dome cap and cylinder section were within 10 to 25% of values obtained from strain gages at the same location. Quantum completed the latest hydrogen pressure vessel design with mWind to incorporate advanced fiber placement dome caps and baseline fiber.
- **MEA Manufacturing:** BASF demonstrated "one pass" microporous layer and catalyst coating on carbon paper, reduced labor and material costs by >30% for paper structures compared to best cloth gas diffusion electrodes, and demonstrated a 30% reduction in platinum loading compared to best cloth-based anodes without losing performance. All of its customers upgraded to new, more uniform, higher performing product (Celtec® P1100 W) based on this DOE project.
- **Component and Stack Measurement:** Using its optical reflectometry technique, the National Renewable Energy Laboratory detected surface defects and morphology in electrode layers, in both catalyst-coated membrane and gas diffusion electrode configurations, as well as surface defects in tubular solid oxide fuel cells. The National Renewable Energy Laboratory reached an agreement to demonstrate its optical reflectometry technique on Ion Power's catalyst coating line.
- **Ultrasound sealing of High Temperature MEAs:** Rensselaer Polytechnic Institute successfully demonstrated that the performance of a 10-cell stack consisting of MEAs bonded in less than 5 seconds using an ultrasonic bonding manufacturing approach is the same as MEAs bonded in 30 seconds using the traditional thermal bonding manufacturing approach. In addition, large area cells (140 cm^2) produced via ultrasonic bonding performed the same as those produced via the traditional thermal bonding approach.
- **Metrology for fuel cell manufacturing:** Based on the optical design work conducted in FY 2012, NIST constructed a new large aperture projection scatterometer specifically for fuel cell manufacturing metrology research. Using the new large aperture projection scatterometer instrument, NIST made dynamic (as a function of velocity or web-line speed) Pt loading measurements on Gore-provided catalyst-coated membrance samples; NIST collected data that showed good sensitivity and repeatability with no apparent dependence on velocity (1-4 ft/min). The tool will enable NIST to measure larger format samples at typical webline speeds (30 ft/min).

BUDGET

The President's FY 2014 budget request for the Fuel Cell Technologies Office includes $4 million for Manufacturing R&D. The FY 2013 appropriation for Manufacturing R&D was $2 million.

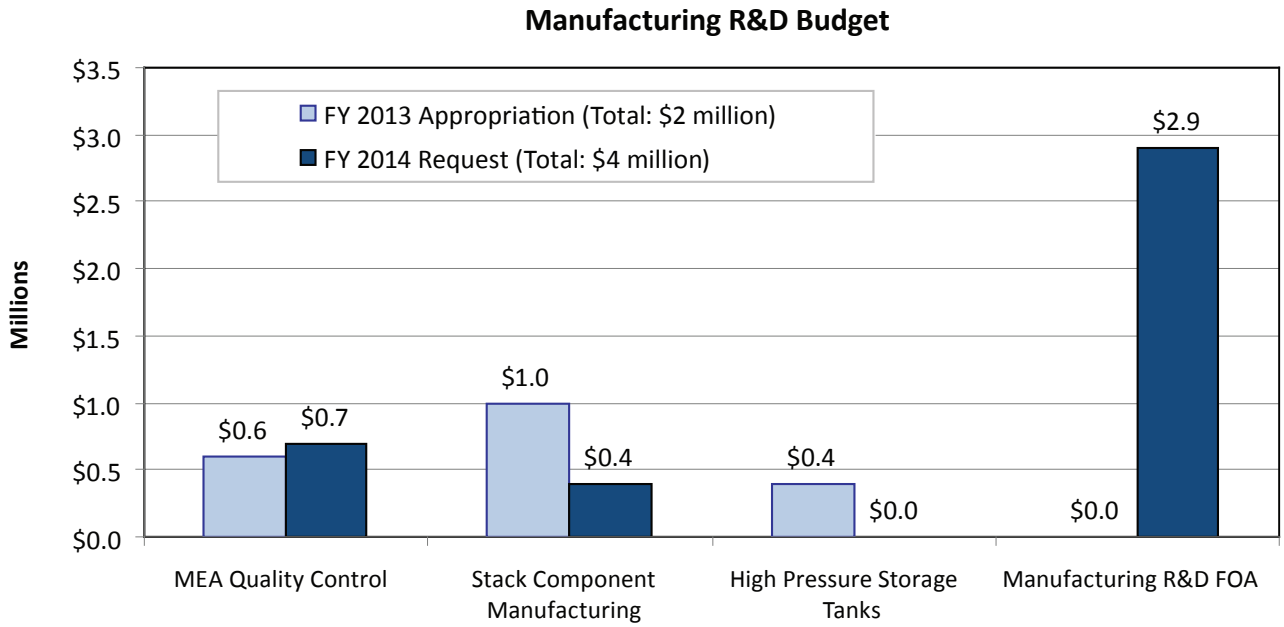

FOA - Funding Opportunity Announcement

FY 2014 PLANS

In FY 2014, activities in the Manufacturing R&D program will:

- Continue to use predictive modeling and single- and segmented-cell test methods to assist diagnostic development.
- Study the effect of as-manufactured defects on MEA lifetime using standard or modified accelerated stress tests.
- Work toward the implementation of techniques on industry production lines.

The Fuel Cell Technologies Office plans to work with other offices within Energy Efficiency and Renewable Energy to develop a cross-cutting workshop on quality control/metrology to leverage diagnostic capabilities and identify synergies and opportunities across other technology offices. The Office also plans to issue a request for information followed by a funding opportunity to be released in FY 2014, with awards subject to appropriation and announced later in the fiscal year. The Office will continue to coordinate with other agencies (including the National Institute of Standards and Technology and the U.S. Department of Defense) and with other technology offices within Energy Efficiency and Renewable Energy to identify synergies and leverage efforts.

Nancy Garland
Acting Manufacturing R&D Team Lead
Fuel Cell Technologies Office
U.S. Department of Energy
1000 Independence Ave., SW
Washington, D.C. 20585-0121
Phone: (202) 586-5673
Email: Nancy.Garland@ee.doe.gov

VI.1 Fuel Cell Membrane Electrode Assembly Manufacturing R&D

Michael Ulsh (Primary Contact), Guido Bender, Huyen Dinh
National Renewable Energy Laboratory (NREL)
15013 Denver West Parkway
Golden, CO 80401
Phone: (303) 275-3842
Email: michael.ulsh@nrel.gov

DOE Manager
Nancy Garland
Phone: (202) 586-5673
Email: Nancy.Garland@ee.doe.gov

Partners:
- Lawrence Berkeley National Laboratory (LBNL), Berkeley, CA
- Colorado School of Mines, Golden, CO
- Rensselaer Polytechnic Institute, Troy, NY
- 3M, St. Paul, MN
- Acumentrics, Westwood, MA
- BASF Fuel Cells, Somerset, NJ
- Delphi, Fenton, MI
- General Motors, Pontiac, MI
- Ion Power, New Castle, DE
- Proton OnSite, Wallingford, CT
- Ultra Electronics – Adaptive Materials Inc., Ann Arbor, MI
- W.L. Gore and Associates, Elkton, MD

Project Start Date: July 16, 2007
Project End Date: Project continuation and direction determined annually by DOE

Overall Objectives

- Evaluate and develop in-line diagnostics for cell and component quality control and validate diagnostics in-line.
- Investigate the effects of membrane electrode assembly (MEA) component manufacturing defects on MEA performance and durability to understand the required performance of diagnostic systems and contribute to the basis of knowledge available to functionally determine manufacturing tolerances for these materials.
- Use established models to predict the effects of local variations in MEA component properties, and integrate modeling of the operational and design characteristics of diagnostic techniques into the design and configuration of in-line measurement systems.
- These objectives have strong support from the industry. Specifically, the outcomes of the 2011 NREL/DOE Hydrogen and Fuel Cell Manufacturing R&D Workshop and the Office of Naval Research-funded Manufacturing Fuel Cell Manhattan Project confirmed the importance of continued development of in-line quality control techniques for cell manufacturing. Our specific development activities have been and will continue to be fully informed by direct input from industry. As new technologies emerge and as the needs of the industry change, the directions of this project will be adjusted.

Fiscal Year (FY) 2013 Objectives

- Prove the feasibility of the through-plane infrared/direct current (IR/DC) diagnostic using moving sheet material
- Prove the feasibility of optical reflectometry for detection of surface defects on solid oxide fuel cell (SOFC) tube cells
- Go/No-go decision for further work to implement the IR/reactive flow-through (RFT) technique on the web-line.

Technical Barriers

This project addresses the following technical barriers from the Manufacturing R&D section (3.5) of the Fuel Cell Technologies Office Multi-Year Research, Development, and Demonstration Plan:

(A) Lack of High-Volume Membrane Electrode Assembly Processes

(E) Lack of Improved Methods of Final Inspection of MEAs

(K) Low Levels of Quality Control

Contribution to Achievement of DOE Manufacturing R&D Milestones

This project contributes to the achievement of the following DOE milestones from the Manufacturing R&D section (3.5) of the Fuel Cell Technologies Office Multi-Year Research, Development, and Demonstration Plan:

- 6.2. Develop defect detection techniques in pilot scale applications for manufacturing MEAs and MEA components. (4Q, 2013)
- 6.3 Establish models to predict the effect of manufacturing variations on MEA performance. (4Q, 2014)
- 6.4. Demonstrate methods to inspect full MEAs and cells prior to assembly into stacks. (4Q, 2014)

FY 2013 Accomplishments

- Demonstrated detection of surface defects and morphology in electrode layers, in both catalyst-coated membrane (CCM) and gas diffusion electrode (GDE) configurations, using our optical reflectometry technique.
- Demonstrated the detection of surface defects in tubular SOFC cells on our bench-top motion stage using our optical reflectometry technique.
- Proved the feasibility of using our infrared/reactive flow-through (IR/RFT) technique to detect thermal responses from GDEs in open-environment, moving substrate operation with a prototype air knife.
- Demonstrated improved detectability and response time of our IR/RFT technique.
- Demonstrated the through-plane IR/DC technique to detect shorting through the membrane using two-side coated CCM sheets.
- Performed modeling of IR/DC and IR/RFT process variables and integrated modeling results into further improvement of the techniques.
- Performed feasibility studies of a new capacitance-based diagnostic aimed at measurement of ionomer-to-carbon ratio in electrodes.
- Used segmented and single cell testing to understand how defects in CCM catalyst layers affect local (spatially resolved) and total cell performance as well as failure development under accelerated aging.
- Developed a new cell hardware and methods for quasi-in situ spatial detection of failure development.
- Completed a detailed comparison of in situ performance between thermal and ultrasonically pressed proton exchange membrane MEAs.
- Continued collaboration with our industry partners, including three of DOE's competitively awarded manufacturing R&D projects, in accordance with our project charter.

✧ ✧ ✧ ✧ ✧

INTRODUCTION

In FY 2005–2007, NREL provided technical support to DOE in developing a new key program activity: manufacturing R&D for hydrogen and fuel cell technologies. This work included a workshop on manufacturing R&D, which gathered inputs on technical challenges and barriers from the fuel cell industry, and subsequent development of a roadmap for manufacturing R&D. In late FY 2007, NREL initiated a project to assist the fuel cell industry in addressing these barriers, initially focusing on in-line quality control of MEA components. The project is utilizing the unique and well-established capabilities of NREL's National Center for Photovoltaics for developing and transferring diagnostic and process technology to the manufacturing industry.

Defects in MEA components differ in type and extent depending on the fabrication process used. The effects of these defects also differ, depending on their size, location in the cell relative to the reactant flow-field, cell operating conditions, and which component contains the defect. Understanding the effects of these different kinds of defects is necessary in order to specify and/or develop diagnostic systems with the accuracy and data acquisition/processing rates required for the speed and size scales of high-volume continuous manufacturing methods. Furthermore, predictive capabilities for manufacturers are critical to assist in the development of tolerances and to enable assessment of the effects of material and process changes.

APPROACH

NREL and its partners are addressing the DOE manufacturing milestones listed above by evaluating, developing, and validating (in-line) diagnostics that will support the use of high-volume manufacturing processes for the production of MEAs and MEA component materials. Prioritization of this work is based on inputs from our industry partners on their critical manufacturing quality control needs. We are focusing on diagnostic capabilities not addressed by commercially available in-line systems; in particular we are evaluating methods to make areal rather than point measurements such that discrete defects can be identified. We are also developing test methodologies to study the effects of the size and/or extent of each important type of variability or defect. These results will assist our industry partners in validating manufacturing tolerances for these materials, ultimately reducing scrap rates and cost, and improving supply chain efficiency. Finally, predictive models are being used at LBNL to understand the operational and design characteristics of diagnostic techniques by simulating the behavior of MEA components in different excitation modes. These results are being fed back to our design effort in configuring the diagnostics for in-line implementation. MEA models are also being utilized to understand the in situ behavior of defect MEAs to guide and further elucidate experiments.

RESULTS

Over the past year we advanced the capabilities and applicability of previously developed techniques, explored new techniques, and continued to advance the understanding of the effects of defects in an operating cell. We proved that our optical reflectance diagnostic is very sensitive to both variability and morphology of electrode surfaces, despite

the black, low contrast nature of the surfaces. Figure 1 shows an example of a GDE with undispersed fiber bundles creating high spots and creases on the electrode surface. We also extended our previous work on planar SOFC cells and showed that optical reflectance can be used to detect surface defects in tubular cells.

In work to advance our infrared-based techniques, we successfully transitioned the IR/RFT technique from a totally enclosed measurement of a small sample to a measurement in an open environment, which would be required for an in-line measurement of a sheet or continuous web of GDE. We implemented these advancements on our bench-top roller system to demonstrate the operation of the technique on a moving (10 foot per minute) sheet of GDE. Figure 2 shows the roller system with a GDE sheet and the air knife used to impinge the reactive gas mixture onto the electrode surface. In addition, using a combination of both experimental and numerical methods, we and our partners at LBNL predicted and experimentally proved increased detection sensitivity and reduced response time by modifying the hydrogen concentration in our nonflammable excitation gas mixture. LBNL also continued modeling the excitation geometry of the IR/DC technique and showed that detection sensitivity to thin cracks, which were experimentally determined to be the most difficult type of defect to detect, could be greatly improved by application of a nonuniform electrical excitation.

In more developmental work, we proved the feasibility of using an ex situ capacitance technique to indicate relative changes in the ratio of ionomer to carbon in the electrode – an important parameter to cell performance. Continuing studies will address improving the sensitivity of the technique to small ionomer-to-carbon variations. We continued our studies of the effects of electrode bare spots, identifying a threshold of size below which total cell performance is not affected. Figure 3 shows a comparison of performance curves for electrodes with and without defects as well as

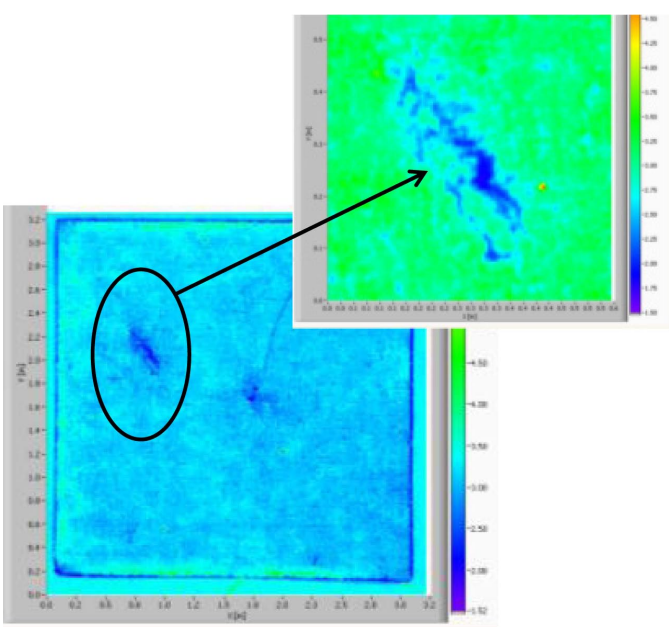

FIGURE 1. Optical reflectance images of surface irregularities in a GDE due to undispersed fiber bundles.

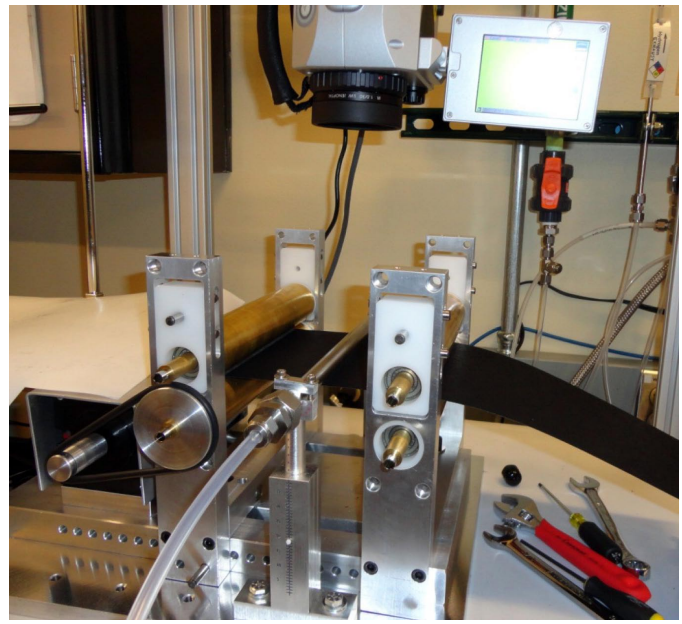

FIGURE 2. IR/RFT setup showing bench-top roller system, GDE sheet material, air knife to impinge reactive gas onto the GDE surface, and infrared charge-coupled device.

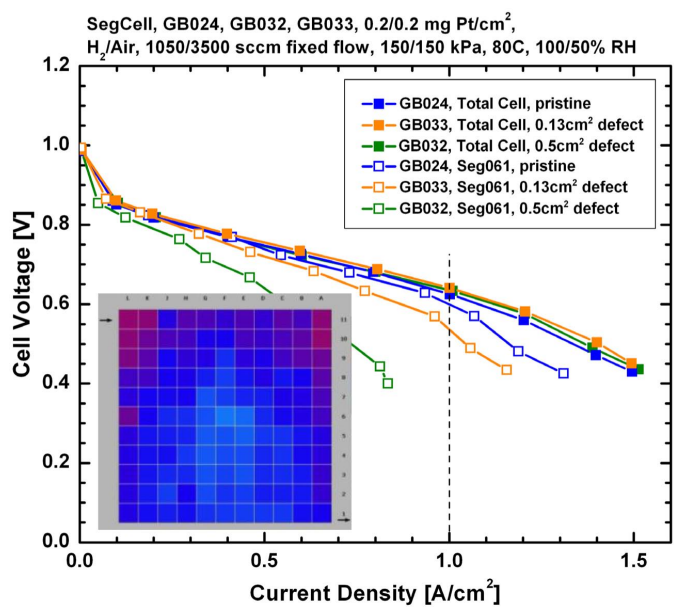

RH - relative humidity

FIGURE 3. Polarization data for a pristine and two defect MEAs showing that, while the performance at the location of the electrode bare spot (open symbols) varies greatly, the total cell performance (filled symbols) is the same; inset shows spatially resolved voltage data for the MEA with a 0.13 cm^2 defect.

spatially resolved performance data for an electrode with a small defect. In addition, we developed a novel cell hardware that enables typical cell operation and in situ electrical and electrochemical diagnostics, but also allows us, using an infrared charge-coupled device detector, to spatially observe the development of failures in the cell resulting from these defects under accelerated aging conditions. Using this hardware, we showed that a bare spot in the electrode acted as the initiation location for a mechanical failure of the cell.

FUTURE DIRECTIONS

- Demonstrate the IR/RFT technique on the research web-line
- Determine the feasibility of using the capacitance technique as a rapid, sufficiently sensitive quality measurement for electrode ionomer-to-carbon ratio
- Continue to use predictive modeling and single and segmented cell test methods to assist diagnostic development
- Study the effect of as-manufactured defects on MEA lifetime using standard or modified accelerated stress tests
- Work toward the implementation of our techniques on industry production lines

FY 2013 PUBLICATIONS AND PRESENTATIONS

1. "Fuel Cell MEA Manufacturing R&D," M. Ulsh; DOE Fuel Cell Technologies Program Annual Merit Review; Washington, D.C.; May, 2013.

2. "Challenges to High-volume Production of Fuel Cell Materials: Quality Control," M. Ulsh, B. Sopori, N. Aieta, G. Bender; ECS Fall Meeting, Honolulu, HI; October, 2012.

3. "The Spatial Performance Effect of Electrode Defects in PEMFC," G. Bender, W. Felt, M. Ulsh; ECS Fall Meeting, Honolulu, HI; October, 2012.

4. "Fuel Cell Manufacturing Diagnostic Techniques: IR Thermography with Reactive Flow Through Excitation," A. Manak, G. Bender, M. Ulsh; ACS National Meeting, Philadelphia, PA; August, 2012.

5. "Effects of local variations of the gas diffusion layer properties on PEMFC performance using a segmented cell system," T. Reshetenko, G. Bender, K. Bethune, R. Rocheleau; Electrochimica Acta, vol. 80, p. 368-376, 2012.

VI.2 Manufacturing of Low-Cost, Durable Membrane Electrode Assemblies Engineered for Rapid Conditioning

F. Colin Busby
W.L. Gore & Associates, Inc (Gore)
Gore Electrochemical Technologies Team
201 Airport Road
Elkton, MD 21921
Phone: (410) 392-3200
Email: CBusby@WLGore.com

DOE Managers
Nancy Garland
Phone: (202) 586-5673
Email: Nancy.Garland@ee.doe.gov
Jesse Adams
Phone: (720) 356-1421
Email: Jesse.Adams@go.doe.gov

Contract Number: DE-FC36-086018052

Subcontractors:
- UTC Power, South Windsor, CT
- University of Delaware (UD), Newark, DE
- University of Tennessee, Knoxville (UTK), Knoxville, TN

Project Start Date: October 1, 2008
Project End Date: June 30, 2014

Overall Objective

The overall objective of this project is to develop a unique, high-volume manufacturing process that will produce low-cost, durable, high-power density 5-layer membrane electrode assemblies (MEAs) that minimize stack conditioning:

- Manufacturing process scalable to fuel cell industry MEA volumes of at least 500k systems/year.
- Manufacturing process consistent with achieving $9/kWe DOE 2017 transportation MEA cost target.
- The product made in the manufacturing process should be at least as durable as the MEA made in the current process for relevant automotive-duty cycling test protocols.
- The product developed using the new process must demonstrate power density greater or equal to that of the MEA made by the current process for relevant automotive operating conditions.
- Product form is designed to be compatible with high-volume stack assembly processes: 3-layer MEA roll-good (anode electrode + membrane + cathode electrode) with separate rolls of gas diffusion media (GDM).
- The stack break-in time should be reduced to 4 hours or less.

Fiscal Year (FY) 2013 Objectives

- Low-cost MEA R&D
  - New 3-Layer (3-L) MEA Process Exploration
    - Investigate equipment configuration for low-cost MEA production
    - Investigate raw material formulations
    - Map out process windows for each layer of the MEA
  - Mechanical Modeling of Reinforced 3-L MEA
    - Use model to optimize membrane reinforcement for 5,000+ hour durability and maximum performance
    - Develop a deeper understanding of MEA failure mechanisms
  - 5-Layer (5-L) Heat and Water Management Modeling
    - Optimization of GDM thermal, thickness, and transport properties to enhance the performance of thin, reinforced membranes, and unique properties of direct-coated electrodes using a validated model
  - Optimization
    - Execute designed experiments which fully utilize UD and UTK modeling results to improve the new MEA process and achieve the highest possible performance and durability
  - MEA Conditioning
  - Evaluate potential for new process to achieve DOE cost targets prior to process scale up (Go/No-Go decision)
- Scale Up and Process Qualification
- Stack Validation

Technical Barriers

This project addresses the following technical barriers from the Manufacturing R&D section of the Fuel Cell Technologies Office Multi-Year Research, Development, and Demonstration Plan:

(A) Lack of High-Volume Membrane Electrode Assembly Processes

Contribution to Achievement of DOE Manufacturing R&D Milestones

This project will contribute to achievement of the following DOE milestones from the Manufacturing R&D section of the Fuel Cell Technologies Office Multi-Year Research, Development, and Demonstration Plan:

- 1.4: Develop processes for highly uniform continuous lamination of MEA components (4Q, 2014)
- 1.7: Demonstrate processes for highly uniform continuous lamination of MEA components (4Q, 2016)
- 1.8: Develop fabrication and assembly processes for PEM fuel cell MEA components leading to an automotive fuel cell system that cost $30/kW. (4Q, 2017)

FY 2013 Accomplishments

- Direct Coating Process Development
  - The primary path for the new 3-L MEA process has succeeded in incorporating the previously modeled process improvements which indicated potential for a 25% reduction in high-volume 3-L MEA cost.
  - Lab-scale development of the new 3-L MEA process is nearing completion:
    - Each layer in the primary path process has been sheet coated on control substrate materials
    - Gore scaled up a replacement for a discontinued backer which satisfies the following requirements:
      - Thickness uniformity
      - Mechanical stability up to max drying and piece-part conversion temperatures
      - Chemical stability
      - Cleanliness
      - Electrode release
      - Supply chain reliability
      - Cost
    - Cathode electrode coating on the new backer has been demonstrated on a roll-to-roll coating line and is equivalent to or better than the current commercial electrode in Gore's beginning-of-life test, start/stop accelerated stress test, and voltage cycling accelerated stress test.
- Gore has demonstrated mechanical durability of a 10-micron expanded polytetrafluoroethylene (ePTFE) reinforced membrane. In previous testing, GORE™ MEAs exceeded 2,000 hours of accelerated mechanical durability testing, which has been equated to achieving 9,000 hours of membrane durability in an 80°C automotive duty cycle. This exceeds the DOE 2015 membrane durability target of 5,000 hours. Gore's 10-micron ePTFE reinforced membrane technology has been successfully incorporated into the lab-scale new 3-L MEA process.
- A quasi-static elastic/plastic layered structure MEA mechanical model has been modified to include visco-elastic/plastic behavior. Mechanical property experiments which are required to calculate model input parameters are complete and modeling of different membrane reinforcement geometries is underway. The final model will be used to predict reinforced MEA mechanical lifetime for a variety of temperature and relative humidity cycling scenarios. The model will also be used to explore different reinforcement strategies and optimize mechanical durability of the MEA structure targeted by the new low-cost process.
- 5-Layer Heat & Water Management Model development at UTK is complete.

✧ ✧ ✧ ✧ ✧

INTRODUCTION

Over the past 20 years, great technical progress has been made in the area of improving power density and durability of fuel cell stacks, so much so that most of the requisite technical targets are now within reach. Yet, three major technical challenges remain. First and foremost is meeting the cost targets. The second challenge is producing components that are amenable for use in a high-speed, automotive assembly line. One impediment to this latter goal is that stack components must currently go through a long and tedious conditioning procedure before they produce optimal power. This so-called "break-in" can take many hours, and can involve quite complex voltage, temperature and/or pressure steps. These break-in procedures must be simplified and the time required reduced, if fuel cells are to become a viable power source. The third challenge is to achieve the durability targets in real-world operation. This project addresses all three challenges: cost, break-in time, and durability for the key component of fuel cell stacks: MEAs.

APPROACH

The overall objective of this project is to develop unique, high-volume manufacturing processes for low-cost, durable, high-power density 3-Layer MEAs that require little or no stack conditioning. In order to reduce MEA and stack costs, a new process will be engineered to reduce the cost of intermediate backer materials, reduce the number and cost of coating passes, improve safety and reduce process cost by minimizing solvent use, and reduce required conditioning time and costs. MEA mechanical durability will be studied and optimized using a combination of ex situ mechanical

property testing, non-linear mechanical model optimization, and in situ accelerated mechanical durability testing. Fuel cell heat and water management will be modeled to optimize electrode and GDM thermal, geometric, and transport properties and interactions. Unique enabling technologies that will be employed in new process development include:

- Direct coating which will be used to form at least one membrane–electrode interface.
- Gore's advanced ePTFE membrane reinforcement and advanced perfluorosulfonic acid ionomers which enable durable high-performance MEAs.
- Advanced fuel cell testing and diagnostics.

RESULTS

Low-Cost MEA Process Development

Primary path

Process step 1: Coat bottom electrode on low-cost, non-porous backer

Process step 2: Direct coat reinforced membrane on top of the bottom electrode

Process step 3: Direct coat top-side electrode on top of the reinforced membrane

The alternate path is to directly coat the anode electrode onto a backer-supported reinforced half-membrane to make an anode-side 1.5-layer intermediate rolled-good. The cathode electrode is then directly coated onto a backer-supported reinforced half-membrane in a similar process. In the final step, the backers are removed from the anode-side and cathode-side 1.5-layers intermediates and the webs are laminated together to form the 3-layer product.

Electrodes made using lab-scale versions of the current primary path process equipment have demonstrated performance equivalent to or better than the current commercial electrodes across a broad range of operating conditions.

Figures 1 and 2 show performance of direct-coated electrodes paired with opposing control electrodes in a range of operating conditions which can be used to assess the

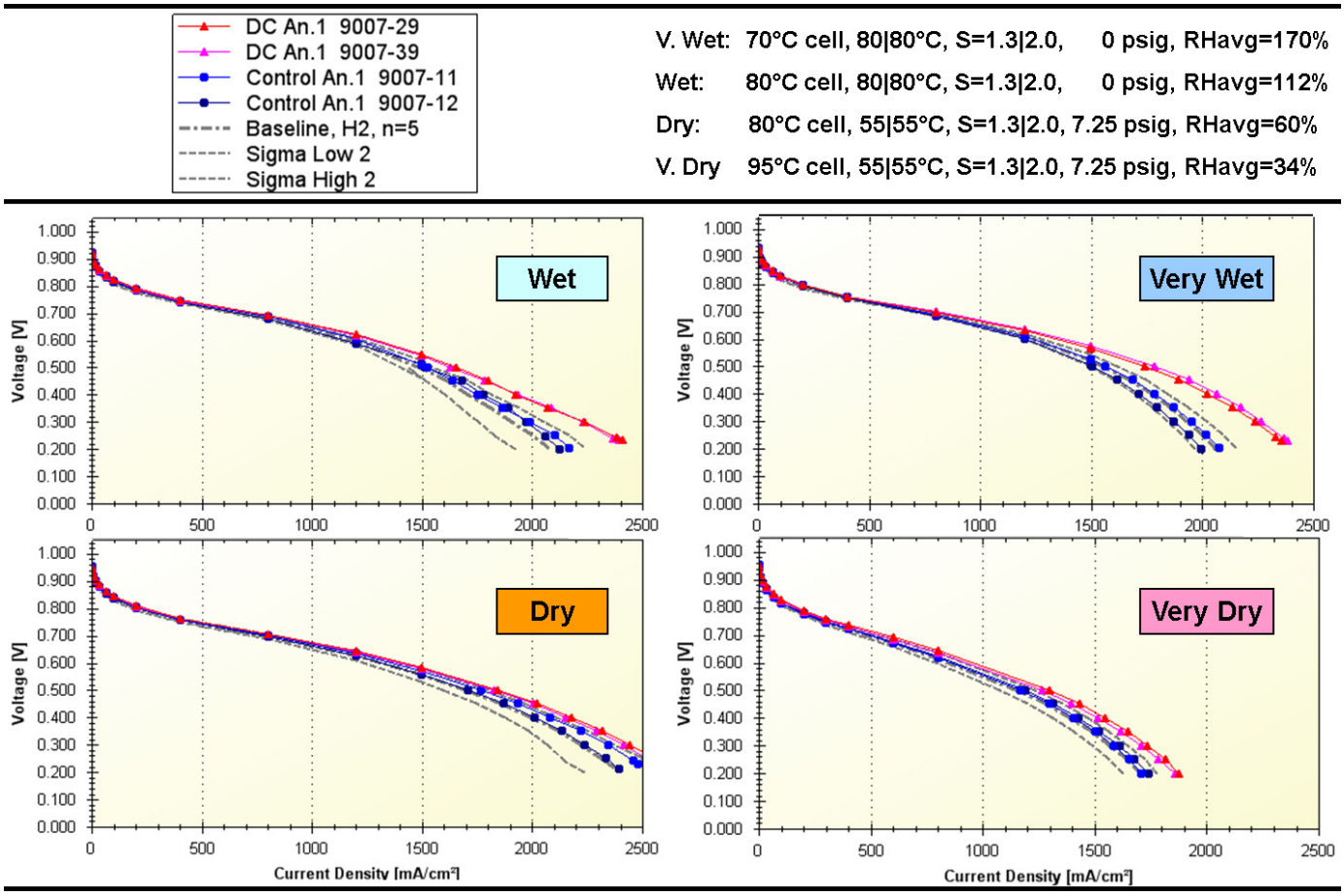

FIGURE 1. Direct-Coated Anode Performance (PL = Platinum loading in mg/cm^2)

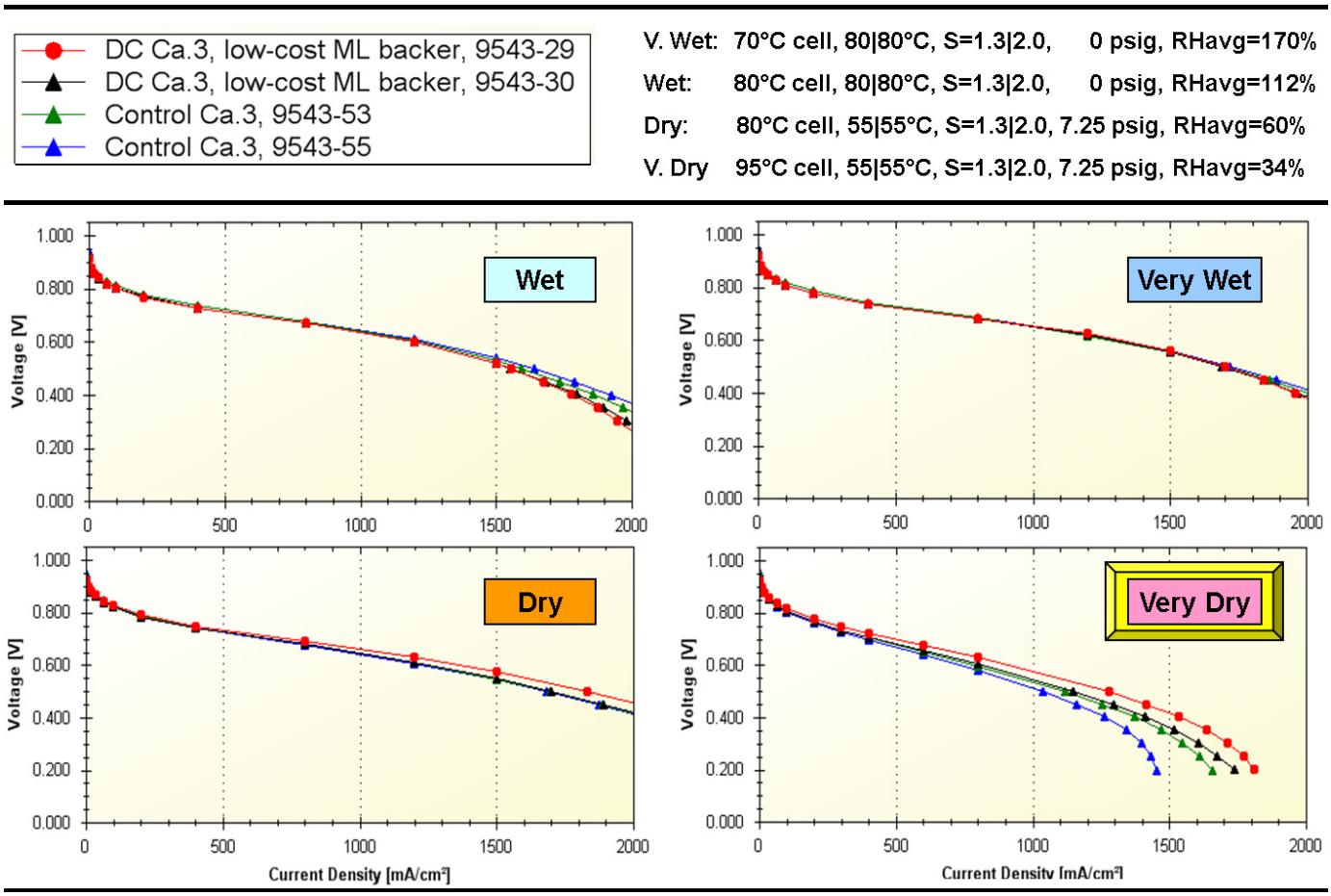

FIGURE 2. Direct-Coated Cathode Performance (PL = Platinum loading in mg/cm^2)

viability of an MEA for different applications (automotive, stationary, portable, etc.), or for dynamic operation within a single application.

Coating research during the past year focused on backer development and demonstration of cathode-on-backer coating on a roll-to-roll pilot line. Future experiments will combine direct-coated anodes and direct-coated cathodes and test the durability of direct-coated MEA.

Mechanically Durable 10-µm Reinforced Membrane

Gore has successfully incorporated a mechanically durable 10-µm reinforced membrane into the current primary path process. The 10-µm membrane construction has demonstrated high performance due to reduced resistance and increased water back-diffusion (see Figure 3). In previous testing, GORE™ MEAs exceeded 2,000 hours of accelerated mechanical durability testing, which has been equated to achieving 9,000 hours of membrane durability in an 80°C automotive duty cycle. This exceeds the DOE 2015 membrane durability target of 5,000 hours. The accelerated mechanical durability testing protocol is summarized in Table 1.

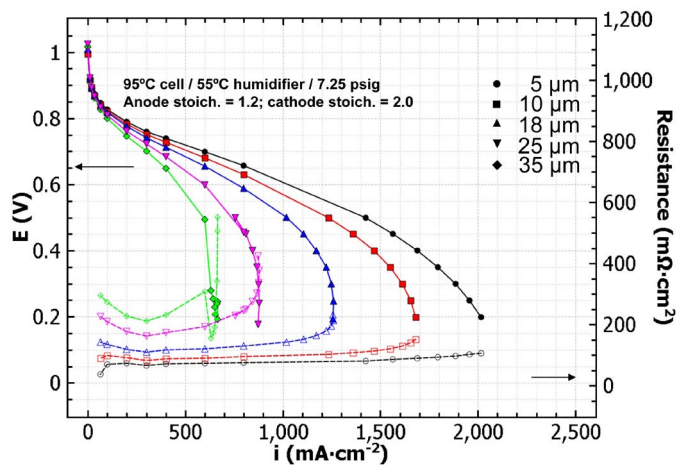

FIGURE 3. Performance of Thin, Mechanically Durable Reinforced Membranes

TABLE 1. Accelerated Mechanical Durability Testing Protocol

Tcell (°C)	Pressure (kPa)	Flow (Anode/Cathode, cc/min)
80	270	500 N2/1,000 N2

Cycle between dry feed gas and humidified feed gas (sparger bottle temp = 94˚C)
Dry feed gas hold time: 15 seconds
Humidified feed gas hold time: 5 seconds
For further protocol information, see: W. Liu, M. Crum, ECS Transactions **3**, 531-540 (2007).

Mechanical Modeling of Reinforced 3-L MEA (UD)

A quasi-static elastic/plastic layered structure MEA mechanical model has been modified to include visco-elastic/plastic behavior. Mechanical property experiments which are required to calculate model input parameters are complete and modeling of different membrane reinforcement geometries is underway.

Nafion® 211 membrane is used for the model membrane and the temperature, relative humidity (RH), and time dependent properties are calculated from the ongoing experimental results. The viscous properties are modeled using a 2-layer viscoplastic constitutive model. This material model consists of an elastoplastic "arm" that is in parallel with an elastoviscous "arm." The elastoplastic arm consists of an elastic spring (stiffness K_p) and a plastic component (yield stress, σ_y and hardening H'). Yielding according to the Mises criterion is used here. The elastoviscous arm has two elements, one spring (stiffness K_v) and one dashpot (using a time hardening law $\dot{\varepsilon}_v = A\sigma_v^n$). Thus, the instantaneous elastic stiffness of the material is the sum of the elastic elements, $K_p + K_v$. In summary, the parameters that are required for this model are K_p, σ_y, H', K_v, A and n. These properties are determined from the experimental results. Tensile testing was conducted for a range of displacement rates to investigate the influence of this parameter on the mechanical response. The rates were selected so that the full visco-elastic-plastic constitutive equations can be determined. The relationships obtained from the MEA testing are "composite properties," combining the properties of the membrane with the electrodes. The constitutive equations for the electrodes will be obtained via reverse analysis. The experimental results have shown that the mechanical response of Nafion® 211 membrane and the MEA is dependent on temperature and humidity as well as displacement rate. Figure 4 shows the dynamic response of modeled membrane stress as a function of RH in the flow channels. Peak stress after dehydration decreases by about 25% with a reduction of

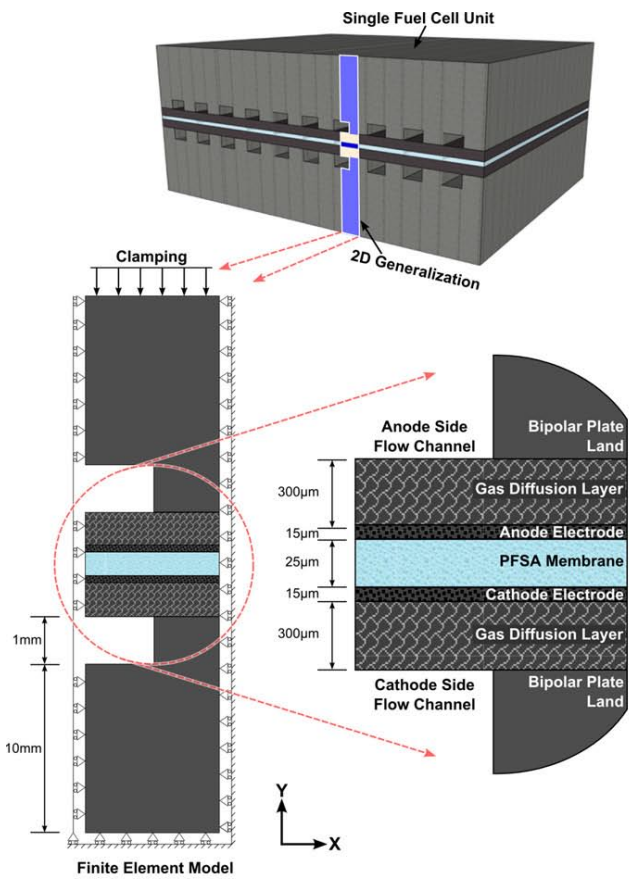

Water Volume Fraction	Swelling Strain	Thermal Strain
$\phi_w = \dfrac{18\lambda}{EW/\rho_P + 18\lambda}$	$\varepsilon^{sw} = \left(\dfrac{\theta+273}{\theta_0+273}\right)\ln(1-\phi_w)$	$\varepsilon^{th} = \alpha(\theta-\theta_0)$

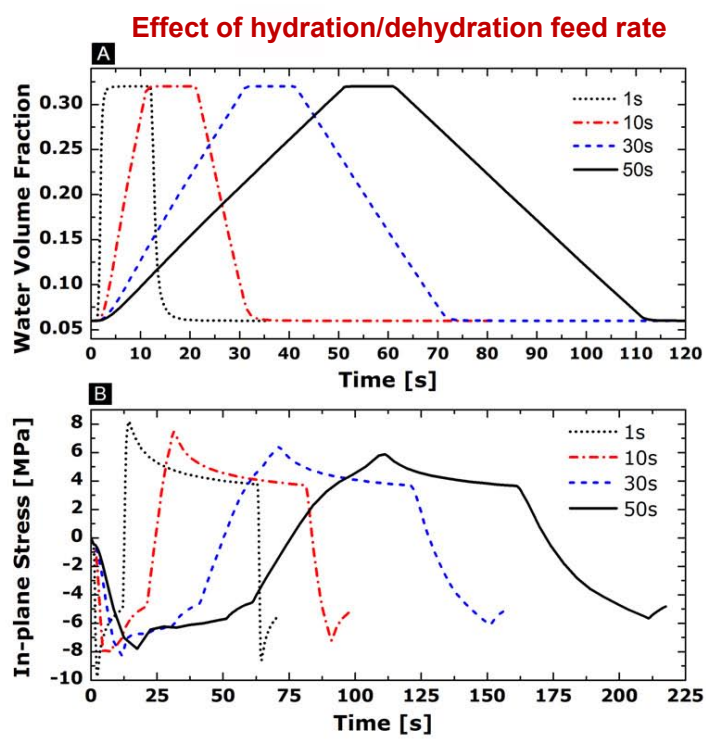

FIGURE 4. Two-Dimensional Plane Strain Finite Element Model for a Single Cell under RH Cycling

humidity transition time from 1 s to 50 s, indicating that an abrupt change in hydration is a more severe case than a gradual change in hydration. Results also indicate that lower temperature, lower humidity, or faster displacement rate result in a larger stress for a given strain.

5-L Heat & Water Management Modeling (UTK)

MEAs and diffusion media materials were selected and experimental testing was initiated. Computationally, an initial first round of two-dimensional single-phase computational model simulation was completed to simulate the impact of diffusion media and membrane thickness and thermal properties. This analysis has enabled some understanding of the consequences of the various micro/macro diffusion media designs. The thermal properties of the diffusion media and microporous layer were shown to be critical to facilitate proper water management and are critical engineering parameters.

CONCLUSIONS AND FUTURE DIRECTIONS

The combination of Gore's advanced materials, expertise in MEA manufacturing, and fuel cell testing with the mechanical modeling experience of University of Delaware and the heat and water management experience of University of Tennessee enables a robust approach to development of a new low-cost MEA manufacturing process.

- Electrodes made using lab-scale versions of the current primary path process equipment have demonstrated performance equivalent to or better than the current commercial electrodes across a broad range of operating conditions. Cathode coating on the new low-cost backer has been demonstrated on a roll-to-roll process. Future work will focus on combining direct-coated anodes and cathodes as well as accelerated stress testing to ensure that durability of the new, direct-coated MEAs are equivalent to or better than the current commercial control MEA.
- Fuel cell heat and water management modeling will be used to efficiently optimize electrode and GDM thermal, geometric, and transport properties and interactions. Direct-coated electrodes will be paired with the most appropriate GDM materials identified in this study. In this way, GDM will enable maximum performance and durability of the low-cost 3-layer MEA.
- A quasi-static elastic/plastic layered structure MEA mechanical model has been modified to include visco-elastic/plastic behavior. Mechanical property experiments which are required to calculate model input parameters are complete and modeling of different membrane reinforcement geometries is underway. Furthermore, UD is studying the growth of flaws under fatigue loading under a range of temperature-humidity operating conditions. The model will be validated with MEA accelerated durability testing. The final model will then be used to predict reinforced MEA lifetime for a variety of temperature and RH cycling scenarios. The model will also be used to optimize mechanical durability of the MEA structure targeted by the new low-cost process.

NAFION is a registered trademark of E. I. DuPont de Nemours & Company

GORE and designs are trademarks of W. L. Gore & Associates, Inc.

FY 2013 PUBLICATIONS/PRESENTATIONS

1. 2013 Hydrogen Program Annual Merit Review: mn004_busby_2013_o.pdf.

2. Khattra, N.S., Lu, Z., Karlsson, A.M., Santare, M.H., Busby, F.C., Schmiedel, T., "Time-Dependent Mechanical Response of a Composite PFSA Membrane," **Journal of Power Sources**, v. 228, p. 256-69, 2013.

3. Lu, Z., Lugo, M., Santare, M.H., Karlsson, A.M., Busby, F.C., Walsh, P., "An experimental Investigation of Strain Rate, Temperature and Humidity Effects on the Mechanical Behavior of a PFSA Membrane," **Journal of Power Sources**, v. 214, p. 130-36, 2012.

4. Khattra, N.S., Karlsson, A.M., Santare, M.H., Walsh, P., Busby, F.C., "Effect of Time-Dependent Material Properties on the Mechanical Behavior of PFSA Membranes Subjected to Humidity Cycling," **Journal of Power Sources**, v. 214, p. 365-76, 2012.

VI.3 Adaptive Process Controls and Ultrasonics for High Temperature PEM MEA Manufacture

Daniel F. Walczyk (Primary Contact),
Stephen J. Rock
Center for Automation Technologies and Systems
Rensselaer Polytechnic Institute
Suite CII 8015
110 8th Street
Troy, NY 12180-3590
Phone: (518) 276-2397
Email: walczd@rpi.edu

DOE Managers
Nancy Garland
Phone: (202) 586-5673
Email: Nancy.Garland@ee.doe.gov
Jesse Adams
Phone: (720) 356-1421
Email: Jesse.Adams@go.doe.gov

Contract Number: DE-FG36-08GO18053/A000

Subcontractor:
Arizona State University, Tempe, AZ

Project Start Date: September 1, 2008
Project End Date: September 30, 2013

Overall Objectives

- Significantly reduce pressing cycle time for high-temperature polymer electrolyte membrane (PEM) membrane electrode assembly (MEA) through the development of novel, robust ultrasonic bonding processes (also demonstrate for low-temperature [<100°C] PEM MEAs).
- Achieve greater manufacturing uniformity and performance through (a) an investigation into the causes of excessive variation in ultrasonically and thermally bonded MEAs using more diagnostics applied during the entire fabrication and cell build process, and (b) development of rapid, yet simple quality control measurement techniques for use by industry.

Fiscal Year (FY) 2013 Objectives

- Test ultrasonically and thermally bonded high-temperature MEAs, the latter with and without adaptive process control applied, in 5- and 10-cell short stacks.
- Test ultrasonically and thermally bonded MEAs with larger active area (140 cm^2) to obtain statistically significant performance data for comparison with the 'standard' 45-cm^2 MEA size.
- Investigate the causes of excessive variation in ultrasonically and thermally bonded high-temperature MEAs using more diagnostics applied during the entire fabrication and cell build process.
- Perform a cost analysis that compares roll-to-roll manufacturing and discrete manufacturing (current) approaches for high-temperature MEAs.
- Develop guidelines that allow manufacturing engineers to design/specify tooling (horn, anvil, registration fixture) and determine optimal process parameters for bonding high-temperature PEM MEAs using ultrasonics.

Technical Barriers

This project addresses the following Manufacturing R&D technical barriers in the Manufacturing R&D section (3.5.5) of the Fuel Cell Technologies Office Multi-Year Research, Development, and Demonstration Plan:

(A) Lack of High-Volume Membrane Electrode Assembly Processes

(K) Low Levels of Quality Control

Contribution to Achievement of DOE Manufacturing R&D Milestones

This project will contribute to achievement of the following DOE milestones from the Manufacturing R&D section (3.5.7) of the Fuel Cell Technologies Office Multi-Year Research, Development, and Demonstration Plan:

- 1.1: Develop continuous in-line measurement for MEA fabrication. (4Q, 2012)
- 6.3: Establish models to predict the effect of manufacturing variations on MEA performance. (4Q, 2014)

FY 2013 Accomplishments

The major accomplishments for FY 2013 are as follows:

- Successfully demonstrated operation of ultrasonically and thermally bonded MEAs in a 10-cell stack for efficient multi-cell testing and also correlated performance differences to stack conditions.
- Demonstrated that thermal bonding times for high-temperature MEAs can be drastically reduced from 30 to 5 seconds provided cells are annealed for at least

five minutes. MEA bonding strength was measured using peel testing and electrochemical capacitance measurement.

- Demonstrated that ultrasonically and thermally bonded MEAs with 140-cm^2 active area had equal performance.
- Ultrasonically bonded 605-cm^2 MEAs using the new large area 15 kHz welder, successfully demonstrated cell operation using BASF testing hardware, and demonstrated that performance exceeded that of equivalent thermally pressed cells.
- Demonstrated that cyclic voltammetry (CV) with ambient air and at room temperature can be used to measure shorts and the degree of electrode-to-membrane bonding in a MEA.
- Finished first draft of a design guide for manufacturing engineers to use when designing an ultrasonic or thermal bonding system for high- and low-temperature PEM MEAs.

✧ ✧ ✧ ✧ ✧

INTRODUCTION

To realize the tremendous potential of fuel cell technology, high-volume, high-quality manufacturing technologies must be developed in parallel with the materials and designs for MEAs, stacks, and the other stack components, which is currently not the case. There are currently three main barriers to the development of high-volume fuel cell manufacturing. First, the current practice involving extensive testing and burn-in of components and stacks will not allow the industry to achieve the necessary cost targets and throughput for stacks, components, and systems. Second, for the current process used to laminate low-temperature (e.g., Nafion®) MEAs for both PEM fuel cells and direct methanol fuel cells, it is common to thermally press for as long as 1½–5 minutes. Even the pressing process for high-temperature polybenzimidazole/phosphoric acid (PBI/PA) MEAs, although much shorter than for Nafion®-based MEAs at about one minute, is still too long for high-volume manufacture. Third is the variability of MEA performance. The component materials, including gas diffusion layer or gas diffusion electrode, membrane or catalyst-coated membrane, and gasketing materials all exhibit variations in key properties such as thickness, porosity, catalyst loading, and water or acid content and concentration. Yet, it is common practice to employ a fixed combination of pressing process parameter values (time, temperature, and pressure), regardless of these component variations, which leads to MEAs that exhibit different physical and performance-related properties.

APPROACH

The research being conducted for this project will help reduce the barriers to the development of high-volume fuel cell manufacturing by reducing the unit process cycle time for MEA pressing by the use of ultrasonic bonding, and by minimizing the variability in performance of MEAs produced using advanced diagnostics to gain insight into how process conditions and variables affect performance. This will in turn help lead to the reduction or elimination of the practice of burn-in testing of fuel cell stacks. All of these benefits will contribute to a reduction in manufacturing costs for MEAs.

High-Temperature MEA Stack Testing – A new stack architecture for testing up to ten 45-cm^2 high-temperature PEM fuel cell MEAs was designed, fabricated, debugged, and thoroughly tested. Each cell can be monitored for performance versus current, temperature, reactant composition, and time. The cell-to-cell variation is then analyzed and compared to variation observed when testing individual cells to determine if (1) the ultrasonic bonding process had an adverse effect on performance in stacks, and (2) defective cells detected using CV show up as poor performing cells during stack testing.

Testing of Scaled-Up MEAs – Not knowing if ultrasonic bonding would produce functional scaled-up MEAs (i.e., 140 cm^2), thermally pressed MEAs were produced for comparison. These MEAs were produced using larger tooling, but with parameters used for the 45-cm^2 MEAs scaled proportionally. Likewise, the ultrasonically bonded MEAs were produced with proportionally scaled energy flux and force. All scaled-up MEAs underwent voltage/current curve testing using similar test conditions as before.

Even larger high-temperature MEAs with 605 cm^2 active area were ultrasonically bonded using a new custom-designed 15-kHz press and associated tooling (horn and anvil) designed and fabricated at Rensselaer. The resulting MEAs were tested by BASF and compared to baseline performance.

Applying Advanced Diagnostics to PBI MEA Ultrasonic Bonding for Quality Control – Single defective fuel cells configured electronically in series in a fuel cell stack can require stack disassembly and cell replacement, resulting in wasted manufacturing resources and a risk of damaging additional cells. As a result, Rensselaer has developed a diagnostic technique capable of detecting defective fuel cells prior to stack assembly; specifically, the technique detects electronically shorted MEAs and poorly bonded MEAs prior to stack assembly. Such defects are detected using cyclic voltammetry, which can measure a current proportional to the degree of bonding and electronic shorting. The measurement time for this technique is on the order of 1-10 seconds—fast enough to be used in production-scale MEA manufacturing. The measurement is acquired at room temperature with ambient air exposed simultaneously

to both fuel cell electrodes on either side of the MEA, thereby simplifying the design of the test fixture. A range of simulated shorts and degrees of MEA bonding were tested using the CV technique. The voltage scanning rate was varied to characterize the effect of scan rate on the sensitivity of defect detection.

Advanced diagnostics were also used to validate the result that the manufacturing latitude is wide during MEA bonding as long as cells are annealed. MEA peel strength, capacitance, and cell performance were measured for MEAs fabricated with a range of bonding and annealing conditions.

Design Guide – Rensselaer is developing a comprehensive design guide that will allow manufacturing engineers to design/specify tooling (horn, anvil, registration fixture) and determine optimal process parameters for bonding high-temperature PEM MEAs using ultrasonics.

RESULTS

High-Temperature MEA Stack Testing – A stack consisting of five thermally bonded and five ultrasonically bonded MEAs was fabricated and tested. The stacks were constructed with the MEAs alternating, i.e., the odd cells were thermally pressed and the even were ultrasonically sealed. As shown in Figure 1, there was no significant difference in performance between cells when the stack was operated on H_2/O_2, but the H_2/air shows a very clear division between the odd and even numbered cells, which corresponds to a performance difference between the thermally bonded (slightly better) and ultrasonically bonded (slightly worse) MEAs. Same thickness gasketing was used for ultrasonically and thermally bonded MEAs.

Because of differences in starting thickness (ultrasonic were slightly thicker due to lower processing pressure), actual post lamination thickness compression for the mixed stack was 17% for the ultrasonic MEAs and 35% for the thermal MEAs. Hence, poorer ultrasonic MEA performance on air (21% O_2 concentration) is attributable to higher in-stack compression, which results in higher cathode gas diffusion media resistance and mass transport losses.

MEAs have been prepared for use in a simulation of the use of the air-air CV approach to manufacturing inspection of MEA active area and cross-shorting. Ten MEAs have been ultrasonically bonded, with one MEA having a partial short caused by membrane misalignment.

Testing of Scaled-Up MEAs – Fabrication of the larger 140-cm^2 cells required a redesigned ultrasonic press combined with a 15-kHz system. The original C-Frame-style press from Branson used for all previous research visually flexed when placed under loads required for 45-cm^2 cells. An H-Frame press, required for any larger MEAs, was brought on-line late in the fourth quarter of 2012, with debug continuing into the first quarter of 2013. The press was designed to maintain parallelism of the ultrasonic horn (top) and anvil (bottom) during loading. Tooling alignment is obtained through the use of matching spherical dome and

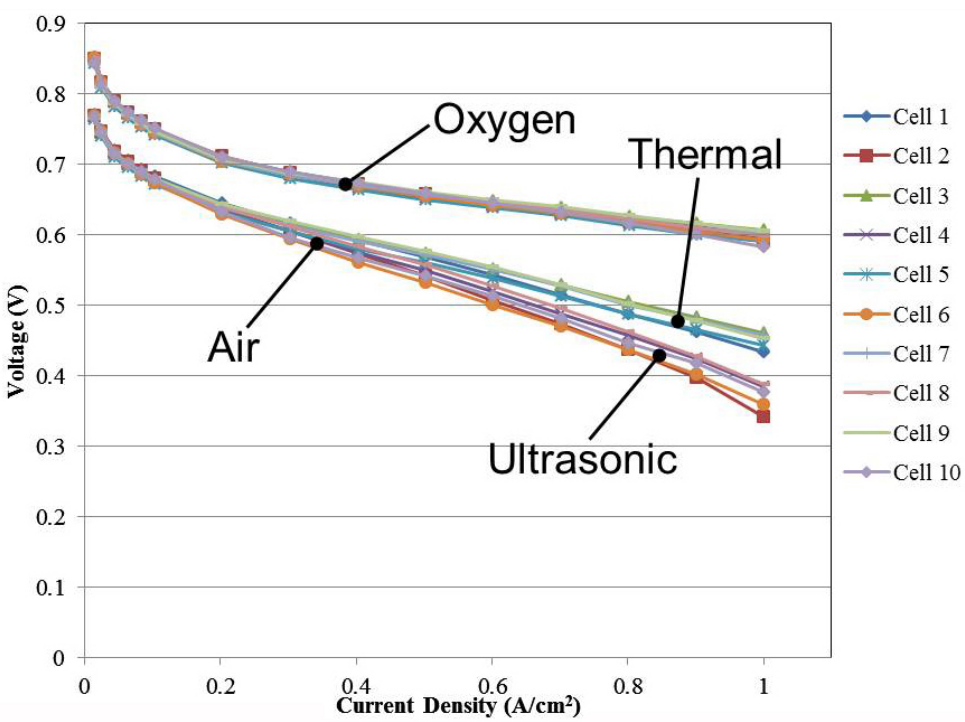

FIGURE 1. H_2/air polarization curve for stack with five each of thermal and ultrasonic MEAs.

seat supporting the bottom tooling. The large surface area of the geometry distributes high loads without damaging the structure.

Two small pneumatic guide cylinders (50-mm bore) are used to move the lower tooling into place, followed by a large load cylinder below (8-inch bore) to supply lamination force/pressure. The combined loads of the main and guide cylinders are capable of generating up to 5,600 lb_f at 100 psi, or 10,000 lb_f at 200 psi pressures. Lamination loads (at the MEA) range from 45-100 psi, thus requiring up to 9,400 lb_f to laminate a 605-cm^2 MEA, which is the maximum size envisioned for this press.

Thermally and ultrasonically bonded MEAs with 140-cm^2 active area had previously been shown to have negligible deviation. Due to improvements made to the custom-designed testing hardware, the polarization curve for the 140-cm^2 MEAs is approaching that of the baseline 45-cm^2 MEA, as shown in Figure 2 (thermally bonded 140-cm^2 MEA curve shown). Elevated ohmic losses are believed to be caused by insufficient current collector thickness and poor electrical interface between current collector and bipolar plate.

As further proof that the 140-cm^2 test hardware was responsible for the lower performance shown in Figure 2, MEAs with 605-cm^2 active area, the largest to date, were bonded ultrasonically using the 15-kHz machine, tested by project collaborator BASF Fuel Cell using their own test hardware, and performance was compared to thermally pressed MEAs made by BASF. The performance of the ultrasonically bonded MEAs was actually better than that of the thermally bonded ones, as shown in Figure 3.

Applying Advanced Diagnostics to PBI MEA Ultrasonic Bonding for Quality Control – Electronically shorted MEAs were successfully detected between 1-10 seconds (depending on scanning rate) prior to cell operation using the aforementioned CV technique as compared to 30-60 seconds using an ohmmeter (traditional method). Interestingly, the degree of MEA bonding could be detected but did not correlate to fuel cell performance for the PBI/phosphoric acid fuel cells tested.

Although the electrochemical capacitance provides an indication of interfacial contact area between the PA electrolyte and the electrocatalyst, which directly impacts cell performance, the electrochemical capacitance measured after thermal bonding did not correlate to cell performance. It is thought that additional acid permeation occurs during cell build and operation, increasing the surface area of catalyst in contact with electrolyte for cells which were bonded to a lesser extent during thermal bonding. Although electrochemical capacitance measurement following MEA thermal bonding does not indicate performance for PBI/PA fuel cells, the authors believe it may for PEM fuel cells and warrants future investigation.

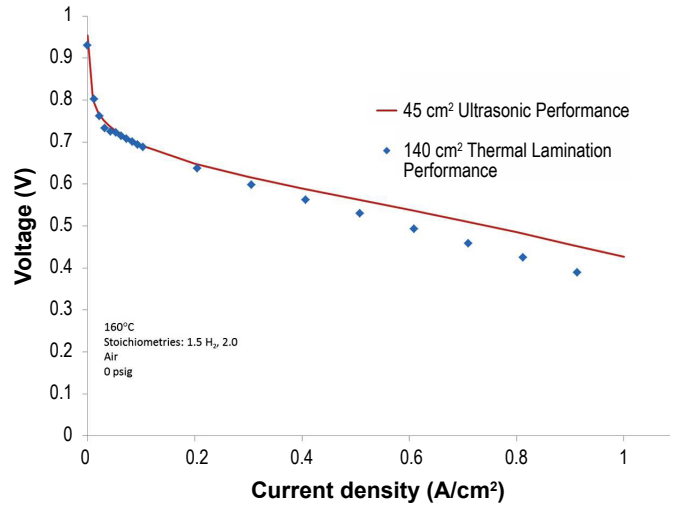

FIGURE 2. 140-cm^2 thermally laminated MEA performance compared to a baseline 45-cm^2 ultrasonic MEA.

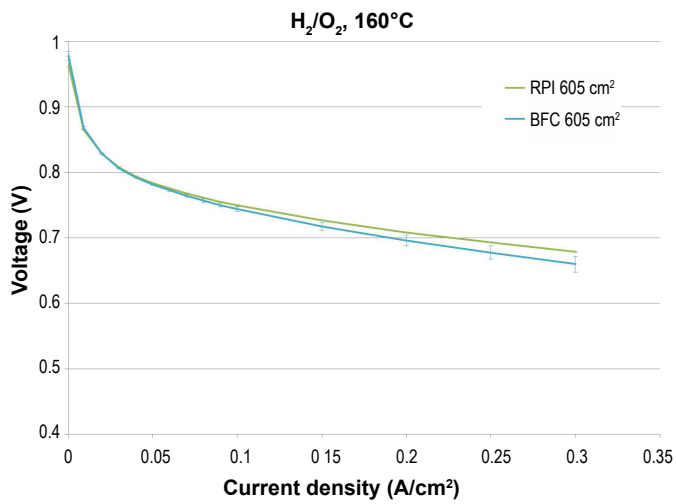

FIGURE 3. Comparison of 605-cm^2 ultrasonically bonded MEA to BASF Fuel Cell thermally bonded MEA.

This CV quality control technique may have value during manufacturing to ensure that electrodes, subgaskets (if used), and membrane comprising an MEA have been structurally unitized after the thermal bonding operation. Adequate MEA bonding, measured as minimum mechanical bond strength (e.g., shear lap or peel), is important from a manufacturing perspective, since MEAs are sold individually to customers and are handled extensively during fuel cell stack assembly. Although not the focus of this work, electrochemical capacitance measurement may provide a non-destructive measurement which could be correlated to mechanical bond strength.

The 15-kHz tooling was used to refine ultrasonic lamination of MEAs using a paper gas diffusion electrode

provided by BASF Fuel Cell. Process optimization resulted in very little performance deviation of ultrasonic lamination samples versus thermally laminated samples. A number of critical performance metrics of cells built with ultrasonically and thermally laminated MEAs are shown in Figure 4 for a relative comparison of the thermal and ultrasonic bonding processes. The chart shows the ratio of ultrasonic to thermal performance for each metric of interest. Gray bars indicate essentially equal performance. Green is substantially better. Red is somewhat worse. Performance is essentially the same for these samples, indicating that further process optimization is not necessary.

The effect of MEA thermal bonding and annealing time on electrochemically active anode catalyst area was studied to determine if reductions in the cycle time of these processes were likely to reduce the anode electrode performance when operating on reformate. MEAs were fabricated with standard thermal bonding and annealing times (30 seconds bonding and 30 minutes annealing) and with reduced cycle times (5 seconds bonding and no annealing). Reducing the thermal bonding time to 5 seconds and eliminating the annealing process step did not decrease the electrochemically active anode catalyst area relative to MEAs fabricated with standard processing conditions. It was also found that the electrochemically active cathode catalyst area and fuel cell performance were not affected by the reduction in bonding time and elimination of the annealing step. However, previous research reported in 2012 indicated other possible benefits to the annealing process such as normalization of MEA thickness and an increase in the mechanical bond strength between the electrodes. This research along with the results obtained through 2012 points toward the possibility of increasing the throughput of PBI/PA fuel cell manufacturing without negatively impacting performance by shortening the cycle times of existing processes.

CONCLUSIONS AND FUTURE DIRECTIONS

High-Temperature MEA Stack Testing – The stack can be used to quickly determine whether changes in processes or process parameters have any significant effect on performance. Using a single-cell testing fixture instead of the 10-cell stack, it would take ten times longer to gather enough data to be able to draw correlations between changes in MEA fabrication.

Parts will be run through the air-air CV test, in which CV will be applied at ambient conditions, with anode and cathode electrodes exposed to air. The test has been shown to have high sensitivity to electrical shorting and also reveals inadequate electrochemical interfaces or lack of electrochemically active surface area. After initial CV testing, the MEAs will be run through the standard thermal treatment (for PBI MEAs) and then a second round of air-air CV followed by functional testing as a 10-cell stack. Results from both CVs and stack testing will be compared to demonstrate relevance of the air-air CV as a manufacturing inspection method.

Testing of Scaled-Up MEAs – Equivalent performance was demonstrated for ultrasonically and thermally bonded MEAs with 140-cm^2 active area, although both were slightly below baseline performance of smaller MEAs due to non-optimized testing hardware. Conversely, performance of ultrasonically bonded 605-cm^2 MEAs was actually better than same-sized thermally bonded MEAs made by BASF Fuel Cell. The overall conclusion is that ultrasonic bonding provides at least equivalent performance to thermal bonding for a wide range of MEA sizes.

Applying Advanced Diagnostics to PBI MEA Ultrasonic Bonding for Quality Control

- The air-air, room temperature CV technique is a rapid diagnostic method (<10 sec) that can be used to identify

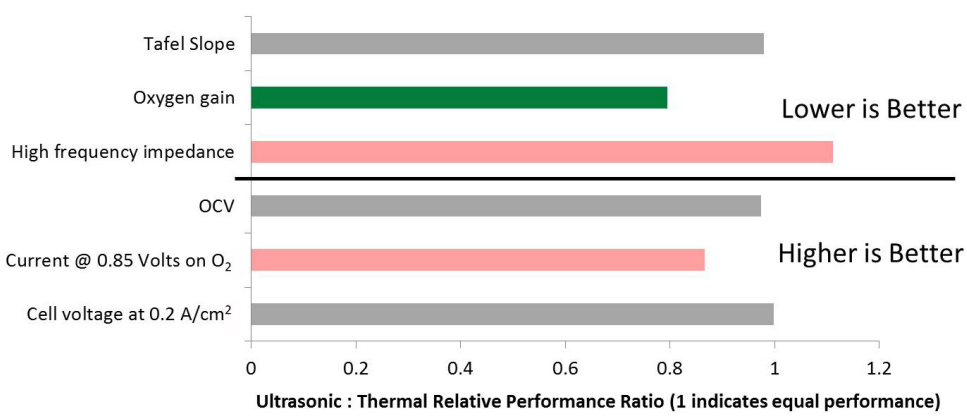

FIGURE 4. Relative performance of cells built with ultrasonically and thermally laminated MEAs. A value of one indicates equal performance. Lower scores are better for Tafel slope, oxygen gain, and high frequency impedance. Higher scores are better for the open circuit voltage (OCV), current at 0.85 V, and cell voltage at 0.2 A/cm^2.

MEA short circuits due to manufacturing defects and possibly the degree of electrode-to-membrane bonding.

- Advanced diagnostics have shown that performance of ultrasonically and thermally bonded MEAs using a new paper gas diffusion electrode is essentially the same.
- Annealing and bonding time were found to have little or no effect on anode or cathode surface area by taking CV measurements of the hydrogen oxidation peak area for MEAs fabricated with normal and reduced bonding and annealing cycle times. It is considered highly likely that the thermal bonding and annealing processes used by our commercial partners can be shortened significantly.

Expanded Cost Analysis – The cost analysis is on-going and will be completed in the third quarter of 2013.

Design Guide – A first draft of the design guide is currently under revision.

FY 2013 PUBLICATIONS/PRESENTATIONS

1. Buelte, S., Walczyk, D., and Sweeney, I., "Effect of MEA Bonding Technique on Fuel Cell Performance and Platinum Crystallite Size," *Journal of Fuel Cell Science and Technology* (Accepted for Publication).

2. Beck, J., Walczyk, D., Buelte, S., Hoffman, C., "Comparison of Performance Losses between Ultrasonic and Thermal Bonding of Membrane Electrode Assemblies in PEM Fuel Cells," *Journal of Fuel Cell Science and Technology,* Vol. 10, No. 4, June 2013, 041004 (10 pages).

3. Beck, J., Walczyk, D., Hoffman, C., Buelte, S., "Ultrasonic Bonding of Membrane Electrode Assemblies for Low Temperature PEM Fuel Cells," *Journal of Fuel Cell Science and Technology*, Vol. 9, No. 5, Oct. 2012, 051005 (8 pages).

4. Beck, J., Walczyk, D., Hoffman, C., and Buelte, S., "Ultrasonic Bonding of Membrane Electrode Assemblies for Low Temperature PEM Fuel Cells," *Proceedings of the ASME 2012 10th Fuel Cell Science, Engineering and Technology Conference* (FuelCell2012), Paper # FuelCell2012-91308, July 23-26, 2012, San Diego, CA, USA.

VI.4 Metrology for Fuel Cell Manufacturing

Michael Stocker
National Institute of Standards and Technology
100 Bureau Drive, Mail Stop 8212
Gaithersburg, MD 20899
Phone: (301) 975-5102
Email: stocker@nist.gov

DOE Managers
Nancy Garland
Phone: (202) 586-5673
Email: Nancy.Garland@ee.doe.gov
Jesse Adams
Phone: (720) 356-1421
Email: Jesse.Adams@ee.doe.gov

Contract Number: DE-EE0001047

Project Start Date: October 1, 2009
Project End Date: October 1, 2013

Overall Objectives

- Evaluate the scatterfield microscopy technique's sensitivity to performing catalyst loading and defect detection on industry supplied catalyst-coated membranes (CCMs) and gas diffusion electrodes (GDEs).
- Accurately measure the optical properties of the constituent materials in industry-supplied CCMs and GDEs.
- Build realistic theoretical models of CCMs and GDEs in order to generate accurate simulation data.
- Demonstrate quantitative theory-to-experiment agreement on CCM and GDE measurements.
- For dual-side catalyst coating operations, build and test a prototype optical device that will enable high-throughput simultaneous dual-side catalyst coating and defect detection measurements.

Fiscal Year (FY) 2013 Objectives

- Investigate other optics-based measurement approaches as in situ process control fuel cell manufacturing metrology solutions.
- Build and test a new scatterometry-based prototype optical measurement system for catalyst loading and defect measurements.
- Continue developing samples to allow accurate optical properties determination of CCM and GDE constituent materials.

Technical Barriers

This project addresses the following technical barriers from the Manufacturing R&D section of the Fuel Cell Technologies Office Multi-Year Research, Development, and Demonstration Plan:

(K) Low Levels of Quality Control

Contribution to Achievement of DOE Manufacturing R&D Milestones

This project will contribute to achieving the following DOE milestones from the Manufacturing R&D sections of the Fuel Cell Technologies Office Multi-Year Research, Development, and Demonstration Plan:

- 6.1 Develop continuous in-line measurements for PEM MEA fabrication. (4Q, 2012)
- 6.2 Develop defect detection techniques in pilot scale applications for manufacturing MEAs and MEA components. (4Q, 2013)
- 6.6 Demonstrate continuous in-line measurement for MEA and MEA component fabrication. (4Q, 2015)

FY 2013 Accomplishments

- Based on the optical design work conducted in FY 2012, constructed a new large aperture projection scatterometer (LAPS) specifically for fuel cell manufacturing metrology research.
- Using the new LAPS instrument, made dynamic (as a function of velocity or web-line speed) platinum (Pt) loading measurements on Gore-provided CCM samples.
- Using the new LAPS instrument, performed diffraction pattern scans of 3M-provided nanostructured thin film (NSTF) samples as a function of Pt loading.

✧ ✧ ✧ ✧ ✧

INTRODUCTION

Scatterfield microscopy is an optical technique developed at the National Institute of Standards and Technology (NIST) that extends the ability to extract useful dimensional and materials related information from optical microscopy data when measuring samples and targets with features and dimensions that are beyond the resolution limit of the microscope. Applying our scatterfield microscopy techniques, we have been successful in extracting relative catalyst loading values from angle-resolved reflectivity scans of CCM fuel cell products. We have successfully

demonstrated the ability of the technique to produce industrially relevant sensitivities to changes in Pt loading. In addition, building on our previous knowledge of and work in applying scatterfield microscopy in fuel cell manufacturing metrology, we designed and built a new scatterometry-based optical metrology tool for performing fuel cell catalyst loading and defect detection measurements.

APPROACH

The scatterfield microscopy approach has been successful in achieving industrially relevant sensitivities (0.01 mg Pt/cm^2) in performing Pt loading measurements on industry provided CCMs. Progress has also been made from the inception of the project in developing electromagnetic scattering models that would allow us to generate accurate simulation data of the CCM samples we are measuring. Work has continued this year in the modeling area, but the majority of our attention focused on developing a new scatterometry-based optical instrument. The reasons for developing this tool are rooted in the experience we gained in validating the scatterfield microscopy approach in fuel cell manufacturing metrology. This new instrument was designed to resolve some open issues with the scatterfield microscopy approach (including open issues with our spectroscopic ellipsometry measurements) while providing additional functionality. First, the vertical motion of the CCM samples may introduce measurement errors if not accounted for properly. Second, the sensitivity of the scatterfield microscope and spectroscopic ellipsometer measurements to local defects and sample variations has not been fully addressed. Third, we had not previously been able to make dynamic loading measurements (as function of velocity) of CCM samples. This new instrument, called the LAPS, addresses these three issues. This new instrument is shown in Figure 1.

RESULTS

The LAPS, a completely new optical instrument designed specifically for fuel cell manufacturing metrology, was built and tested. Preliminary data were acquired from this new instrument and reported at the DOE Annual Merit Review meeting May 15, 2013. The majority of the effort on this project this year involved the design, construction, and testing of the LAPS. The primary motivations for building this tool were the following: to engineer a bigger (adjustable) spot size for large area data averaging, to facilitate better signal to noise measurements (via a more powerful source and a more sensitive detector), to add the ability to make measurements at web-line speeds, and to be able to quantify the coupled vertical motions of the membranes during measurement. Accomplishments regarding the construction of the LAPS include: completing the mechanical design, procuring necessary instrumentation, fabricating required parts, developing optical and mechanical alignment procedures, and writing LabVIEW® motion control and data acquisition code.

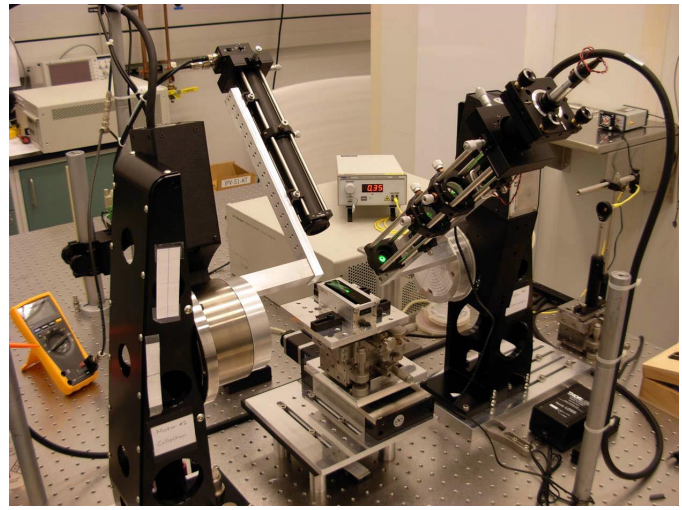

FIGURE 1. Newly Constructed LAPS Instrument

Preliminary dynamic CCM loading data were taken on a Gore sample set (A510/M710.18/C510) as a function of velocity, simulating web-line movement of the samples. Sample loadings in the set were 0.10, 0.20, 0.30 and 0.40 mg Pt/cm^2. The stage used in this round of data permitted sample velocities (web-line speeds) ranging from approximately 1.0 ft/min to 4.0 ft/min. These data are shown in Figure 2. The data show good sensitivity and repeatability with no apparent dependence on velocity. This tool will enable us to measure larger format samples at typical web-line speeds (30 ft/min) and we are currently in process of integrating a new stage capable of moving the samples at those speeds.

When illuminated, the 3M NSTF-type samples produce a diffraction pattern as seen in Figure 3. This diffraction presents a new measurement challenge that requires further study. The amplitude of the different peaks contains key information about the materials and surface properties of the sample. We successfully measured this diffraction pattern as a function of loading on a 3M sample set, including 0.10, 0.15, and 0.20 mg Pt/cm^2 loading values. In this particular measurement, the illumination arm is held at 80 degrees and the collection arm is scanned from 80 to 30 degrees. These diffraction pattern data, shown in Figure 4, demonstrate excellent sensitivity in certain peaks.

CONCLUSIONS AND FUTURE DIRECTIONS

In past reports, we have successfully demonstrated Pt loading measurement sensitivities at the level of competing technologies. There remains significant work to properly measure the optical properties of the CCM and GDE constituent materials to enable accurate simulations in order

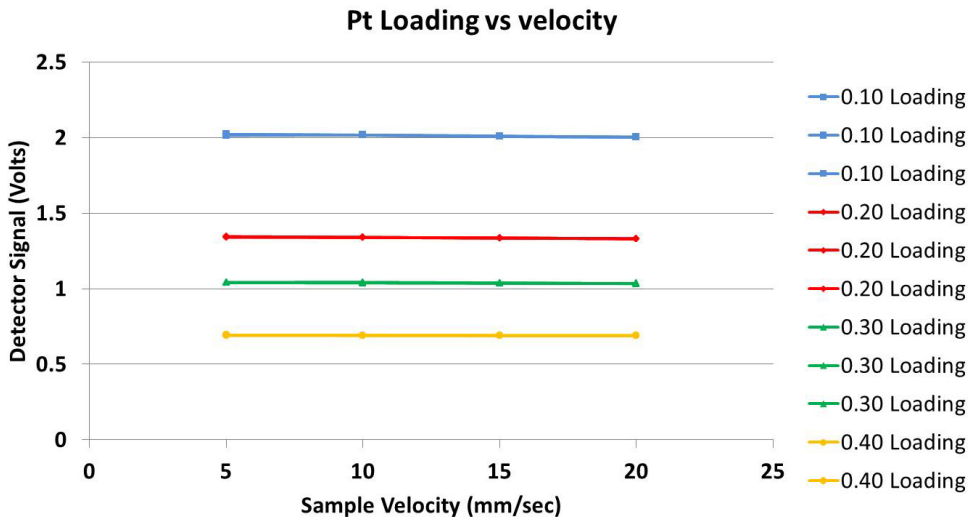

FIGURE 2. LAPS Dynamic Pt Loading Measurements

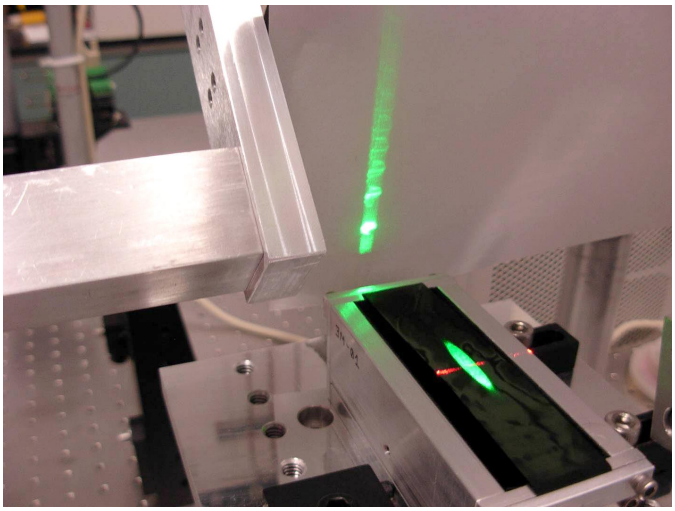

FIGURE 3. 3M NSTF Diffraction Pattern

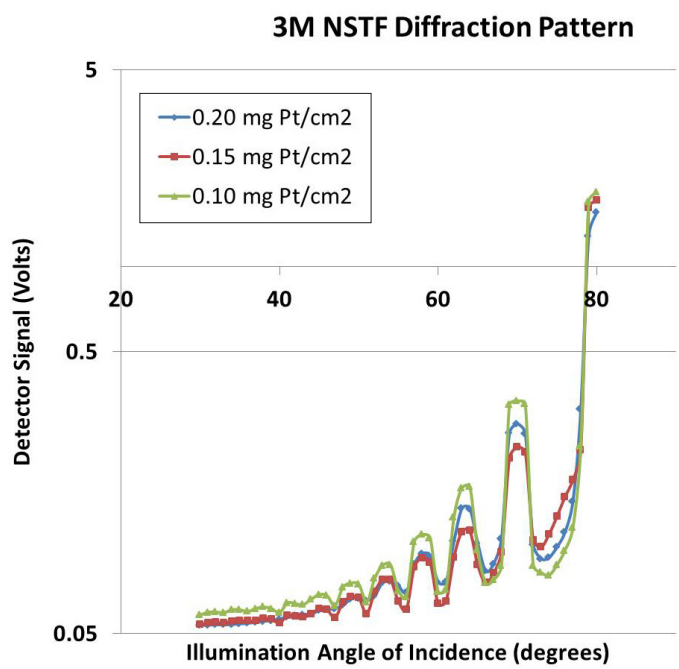

FIGURE 4. Measured 3M NSTF Diffraction Pattern as a Function of Pt Loading

to achieve quantitative theory-to-experiment agreement. For this methodology to become a robust effective metrology solution, we need to be able to accurately model the samples to generate quantitative simulation data. To further understand the underlying measurement science and develop the necessary rigor, we designed and built a custom optical metrology tool (LAPS). The tool is now operational. We still need to comprehensively characterize and calibrate the tool. We acquired preliminary LAPS data on Gore samples (as a function of velocity) and 3M samples (diffraction pattern).

The most pressing challenge to achieving quantitative fuel cell manufacturing metrology is to develop the simulation infrastructure to enable the underlying rigor with acceptable uncertainties and sensitivities. Although we have demonstrated initial theory to experiment data fits, different manufacturers using different methods and materials for their membranes require adaptability of the methodology. This necessitates a flexible model that allows different geometrical parameters and normalization procedures. Once a robust modeling and fitting algorithm has been established, the method is generally broadly applicable to different membrane types.

A multiple-beam and dual-side LAPS hardware architecture capable of dramatically increasing throughput will require significant further design work and research.

We will continue working with industrial collaborators to create samples that allow optical property measurements of CCM constituent materials. The next materials to characterize are the actual proton exchange membrane (Nafion® and 3M membrane) and amorphous carbon. We need to finish characterizing and calibrating the LAPS tool. We will measure larger format samples at web-line speeds. We already have another stage (Newport XMS160) to integrate that will increase travel to six inches and speeds in excess of 30 ft/min. It will be a priority to answer outstanding questions regarding the diffraction and scattering of the periodic 3M NSTF samples and optimize for Pt loading determination. We will continue to investigate the applicability of scatterfield microscopy and LAPS to fuel cell defect detection. Industry input is needed as to the types, sizes, and distributions of defects that cause real performance losses.

DISCLAIMER

Certain commercial equipment, instruments, or materials are identified in this paper in order to specify the experimental procedure adequately. Such identification is not intended to imply recommendation or endorsement by the National Institute of Standards and Technology, nor is it intended to imply that the materials or equipment identified are necessarily the best available for the purpose.

ACKNOWLEDGEMENTS

The work detailed in this report would not have been possible without the contributions of the following. All are NIST personnel and guest researchers unless otherwise noted: Mark Debe (3M), Judy Rudolf and Colin Busby (W.L. Gore), Mike Ulsh (National Renewable Energy Laboratory), Richard Silver, Francois Goasmat, Jing Qin, Bryan Barnes, John Kramar, Bin Ming, Brad Damazo, Hui Zhou, Prem Kavuri, Martin Sohn, and Eric Stanfield.

FY 2013 PUBLICATIONS/PRESENTATIONS

1. M. Stocker, "Metrology for Fuel Cell Manufacturing," DOE Annual Merit Review Proceedings, MN006, May 15, 2013, http://www.hydrogen.energy.gov/pdfs/review13/mn006_stocker_2013_o.pdf.

VI.5 High-Speed, Low-Cost Fabrication of Gas Diffusion Electrodes for Membrane Electrode Assemblies

Emory S. De Castro
BASF Fuel Cell, Inc.
39 Veronica Avenue
Somerset, NJ 08873
Phone: (848) 209-3509
Email: Emory.DeCastro@BASF.com

DOE Managers
Nancy Garland
Phone: (202) 586-5673
Email: Nancy.Garland@ee.doe.gov
Jesse Adams
Phone: (720) 356-1421
Email: Jesse.Adams@go.doe.gov

Contract Number: DE-EE0000384

Subcontractor:
Dr. Vladimir Gurau
Case Western Reserve University, Cleveland, OH

Project Start Date: July 1, 2009
Project End Date: June 30, 2013

Overall Objectives

- Reduce cost in fabricating gas diffusion electrodes through the introduction of high-speed coating technology, with a focus on materials used for the high-temperature membrane electrode assemblies (MEAs) that are used in combined heat and power generation.
- Relate manufacturing variations to actual fuel cell performance in order to establish a cost-effective product specification.
- Use advanced quality control methods previously developed to guide realization of these two objectives.

Fiscal Year (FY) 2013 Objectives

- Further decrease cost beyond that achieved with cloth substrates by developing paper substrates and single-pass applications.
- Exploit stable inks to promote platinum thrift with cloth-based substrates.

Technical Barriers

This project addresses the following technical barriers from the Manufacturing R&D section of the Fuel Cell Technologies Office Multi-Year Research, Development, and Demonstration Plan (Section 3.5):

(A) Lack of High-Volume Membrane Electrode Assembly Processes

(K) Low Levels of Quality Control

Contribution to Achievement of DOE Manufacturing R&D Milestones

This project will contribute to achievement of the following DOE milestones from the Manufacturing R&D section of the Fuel Cell Technologies Office Multi-Year Research, Development, and Demonstration Plan (Section 3.5.7):

(1.1) Develop continuous in-line measurement for MEA and MEA component fabrication. (4Q, 2012)

(1.3) Develop processes for direct coating of electrodes on membranes or gas diffusion media. (4Q, 2014)

(1.6) Demonstrate processes for direct coating of electrodes on membranes or gas diffusion media. (4Q, 2016)

This project addresses coating throughput and uniformity of gas diffusion electrodes (GDEs), a critical component for MEA fabrication. Achievement of this project's objectives would satisfy milestones 1.3 and 1.6, direct coating of electrodes on gas diffusion media. One sub-task is to develop a continuous X-ray fluorescence analyzer that directly measures catalyst deposition level and distribution on rolled goods, ultimately guiding improvements in through put and uniformity. This sub-task directly contributes to the fourth quarter 2012 goal for in-line measurement.

FY 2013 Accomplishments

- Demonstrated "one pass" micro-porous layer (MPL) and catalyst coating on carbon paper
- Reduced labor and material costs >30% for paper structures compared to best cloth GDEs
- Demonstrated 30% reduction in platinum loading compared to best cloth-based anodes without losing performance
- All customers changed over to new, more uniform, higher performing product based on this work (Celtec® P1100W)

✧ ✧ ✧ ✧ ✧

INTRODUCTION

The basis of this project is to create GDEs at a far lower cost than those currently available. GDEs are critical components of MEAs and represent the highest cost subcomponent of the MEA. Cost reduction will be accomplished through development of a higher throughput coating process, modeling the impact of defects due to the higher speed process, and overcoming these limitations while also providing a "six-sigma" based manufacturing specification. The main focus of the effort is creating next-generation inks through advanced additives and processing methodologies. As part of our approach, we will also develop on-line quality control methods such as determination of platinum concentration and distribution during the coating process. The on-line mapping of platinum will guide the ink development process and provide feedback on uniformity.

For this reporting period, we further reduced the cost of manufacturing GDEs as applied to paper substrates, and exploited the ink stability to reduce precious metal in the anode of a cloth-based GDE. The basis of this project is to produce stable inks of carbon black or catalyzed carbon black and hydrophobic binder. The use of a hydrophobic binder is critical to create GDEs for high-temperature MEAs. In this period we demonstrated that the new stability in these inks affords more concentrated suspensions and thus, for the paper system, reduces the number of applications needed per pass to a single application for the MPL and a single application for the catalyst layer. For the cloth-based materials, we used these new inks and developed an alternative anode structure that shows improved utilization and thus reduced precious metal loading without loss in performance. Both these efforts support additional cost reduction.

APPROACH

GDEs are comprised of a gas diffusion layer coated with catalyst. The gas diffusion layer is simply carbon cloth or a non-woven carbon that has been coated with carbon black and serves as a current collector for the catalyst as well as a gas distributer. For both the carbon black and catalyst, a hydrophobic binder is added to achieve critical porosity and hydrophobicity in the final structure. Of the carbon black, catalyst, or hydrophobic binder, none is soluble in aqueous solutions. Aqueous solutions as solvents are much preferred in order to reduce volatile organic emissions, and, more importantly, employing organic solvents with a highly active catalyst is too dangerous in a production environment. Also, the hydrophobic binder is shear-sensitive, meaning it becomes less stable when pumped or subjected to shear forces in the coating applicator. Thus, the challenge in this project is overcoming the inherent physical limitations in these materials through advanced formulations and processing.

Our approach to solving this challenge begins with identifying key quality GDE metrics that relate directly to ink performance, developing an understanding of the forces behind ink stability, and introducing solution measurement methods that relate ink performance to the quality metrics. With more stable ink formulations, we have shown ability to coat longer and wider webs at higher speeds with a lower incidence of defects. Since the ink can be made more concentrated and remain stable, we can use less application passes and save cost. The ink development process is supplemented by two other activities that ultimately lead to lower cost GDEs. We developed a model that will predict the impact of manufacturing variations on MEA performance and used this model to determine the level of coating quality needed to maintain consistent current and voltage. Also, we created an on-line analyzer to track the distribution of precious metal catalysts and guide more precise coating processes.

RESULTS

Conversion of Lower Cost Substrates

Last year we presented some early results on developing lower cost substrates into gas diffusion electrodes. Non-woven carbon fiber materials ("carbon paper") are believed to be ~30% lower in cost compared to the carbon cloth at higher volumes and are anticipated to be more uniform with lower material defects. The porosity, hydrophobicity, and absorption properties of the carbon papers are totally different than carbon cloth, and we had to develop an entirely new class of inks for the MPL, anode electrode layer, and cathode electrode layer. This year we demonstrated production scale coating of a single-pass MPL on paper and proof of principle for a single-pass catalyst coating at the pilot scale. Figure 1 illustrates this progress compared to the new carbon cloth-based materials developed in this project. Projecting cost savings from coating time and cost of the base materials, we exceed an additional cost reduction of 30% over the best carbon cloth systems developed in this project (for 3,000 5-kW systems).

Platinum Thrift on Cloth Substrates

Reducing the precious metal content in the MEA was not part of the original scope of this project. However, based on reviews of this project, it was suggested that the improved inks may lead to more uniform structures and thus greater utilization within the catalyst layer. We exploited properties of the new inks and developed a new anode structure that contains 30% less platinum, but performs the same or better than similar carbon-based anodes from this project. Figure 2 illustrates this point. At current above 0.3 A/cm^2, even with 2% CO in the reformate, there appears to be an improvement in mass transport due to these new structures.

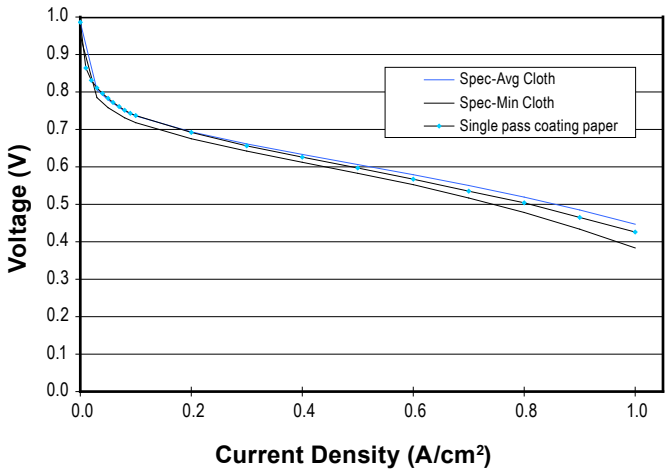

FIGURE 1. Comparison of single-pass applications (MPL and catalyst layer) on paper to multiple pass applications on woven materials from this project ("Spec Avg." & "Spec Min"), T = 160°C, pressure = 1 bar_a, stoich: 1.2/2 H_2/air.

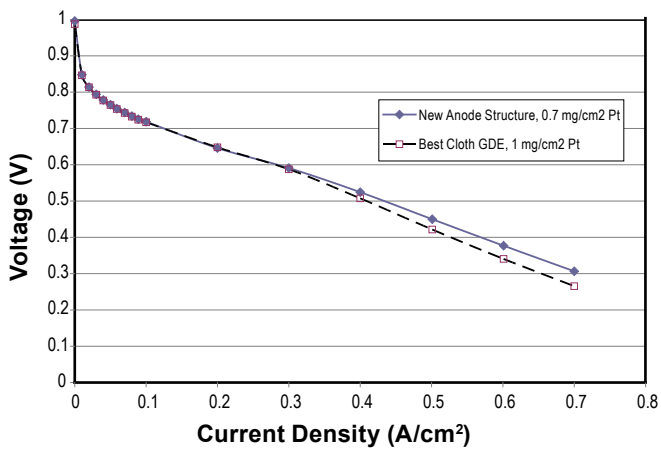

FIGURE 2. Comparison of new anode structure (lower precious metal) to best materials from this project, T = 160°C, pressure = 1 bar_a, stoich: 1.2/2 reformate/air, reformate = 70% H_2, 28% CO_2, 2% CO.

Create Specification Using "Six Sigma" Statistical Approach

One part of this project is to relate variations in performance to manufacturing variations, such as the distribution of precious metal. A basis for this approach is to test a statistically significant population of coating runs, and construct an average and process variation. Figure 3 shows the average +/-3σ of over 200 fuel cell tests on cloth-based cathodes developed in this project. For the first time, we are able to use statistical control processes to release the new product based on this project's advances, as opposed to selecting "high performers" at the cost of very low material yields. Figure 3 summarizes these results.

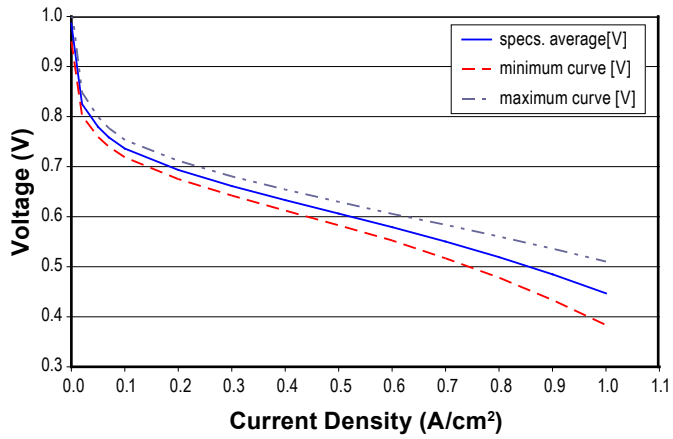

FIGURE 3. Cathode average +/-3σ, T = 160°C, pressure = 1 bar_a, stoich: 1.2/2 H_2/air.

CONCLUSIONS AND FUTURE DIRECTIONS

We have achieved DOE's milestone 1.6 for direct coating of catalyst on gas diffusion media and exceeded our project goal of three-fold improvement in material throughput for carbon cloth-based media. This improvement has led to a 75% reduction in labor cost to manufacture and produced very uniform, lower defect materials. A well-received new product (Celtec® P1100W) was launched based on this project. Through the gain in our understanding of formulating these materials in aqueous suspensions, we developed a new set of inks (MPL, anode catalyst, cathode catalyst) for use on carbon paper substrates and project an additional 30% savings over that achieved with cloth substrates. The development of an on-line X-ray fluorescence scanning instrument for measuring catalyst applications on gas diffusion media meets DOE milestone 1.1 – continuous in-line measurement for MEA component fabrication. Although our project concludes with this report, we will continue to work on cost reduction through developing a new product based on carbon paper substrates.

SPECIAL RECOGNITIONS & AWARDS/ PATENTS ISSUED

1. 2013 DOE Hydrogen and Fuel Cells Program R&D Award for reducing the cost of manufacturing gas diffusion electrodes (May Annual Merit Review).

FY 2013 PUBLICATIONS/PRESENTATIONS

1. Joerg Belak, "Improved Membrane Electrode Assemblies for High Temperature PEM Fuel Cells." ACS Meeting (Division of Polymer Chemistry): Advances in Materials for Proton Exchange Membrane Fuel Cell Systems, Feb. 17–20th, 2013, Asilomar Conference Grounds, Pacific Grove, California.

VI.6 Development of Advanced Manufacturing Technologies for Low-Cost Hydrogen Storage Vessels

Mark Leavitt
Quantum Fuel Systems Technologies Worldwide, Inc.
25242 Arctic Ocean Drive
Lake Forest, CA 92630
Phone: (949) 399-4584
Email: mleavitt@qtww.com

DOE Managers
Nancy Garland
Phone: (202) 586-5673
Email: Nancy.Garland@ee.doe.gov
Jesse Adams
Phone: (720) 356-1421
Email: Jesse.Adams@go.doe.gov

Contract Number: DE-FG36-08GO18055

Subcontractors:
- Boeing Research and Technology, Seattle, WA
- Pacific Northwest National Laboratory (PNNL), Richland, WA

Project Start Date: September 26, 2008
Project End Date: September 30, 2013

Overall Objectives

Develop new methods for manufacturing Type IV pressure vessels for hydrogen storage with the objective of lowering the overall product cost by:

- Optimizing composite usage through combining traditional filament winding (FW) and advanced fiber placement (AFP) techniques.
- Exploring the usage of lower-strength, higher-modulus fibers on the outer layers of FW.
- Building economic and analytical models capable of evaluating FW and AFP processes including manufacturing process variables and their impact on vessel mass savings, material cost savings, processing time, manufacturing energy consumption, labor and structural benefits.
- Studying polymer material degradation under high-pressure hydrogen environment to optimize storage volume.

Fiscal Year (FY) 2013 Objectives

- Refine the mWind software using data collected from vessels designed with mWind.
- Build and test hybrid vessels designed with mWind.
- Improve the quality of dome caps.
- Allow more control over the test process of liner material.

Technical Barriers

The project addresses the following technical barriers from the Manufacturing R&D section (3.5) of the Fuel Cell Technologies Office Multi-Year Research, Development, and Demonstration Plan:

(M) Lack of Low-cost Carbon Fiber

(N) Lack of Low-cost Fabrication Techniques for Storage Tanks

Contribution to Achievement of DOE Manufacturing R&D Milestones

This project will contribute to achievement of the following DOE milestone from the Manufacturing R&D section of the Fuel Cell Technologies Office Multi-Year Research, Development, and Demonstration Plan:

- Milestone 7.2: Develop fabrication and assembly processes for high pressure hydrogen storage technologies that can achieve a reduction of 10% off the baseline cost of $18/kWh for Type IV, 700 bar tanks. (4Q, 2015)

FY 2013 Accomplishments

- Improved the in-house computer program, mWind, which allows more composite shell layer options using AFP methods to generate finite element analysis (FEA) models of composite shells.
- Verified and confirmed the accuracy of mWind with strain gage and optical strain measurements.
- Completed the latest vessel design with mWind to incorporate AFP dome caps and baseline fiber.
- Conceptualized a three-piece layup tool to allow an easy extraction of the composite dome cap from the mandrel tool.
- Installed a new smart-motor control system and a newly designed dancer system to allow for better control, high torque output and consistent tension on each tow.
- Upgraded in situ tester for testing liner material by adding a programmable logic controller to apply a constant strain rate.

INTRODUCTION

The goal of this project is to develop an innovative manufacturing process for Type IV high-pressure hydrogen storage vessels, with the intent to significantly lower manufacturing costs. The development is to integrate the features of high-precision AFP and commercial FW while satisfying design requirements.

APPROACH

The hybrid vessel designs were based on FEA results to optimize strain distribution and achieve uniform displacement in the domes of the vessel. The modified in-house software for generating FEA models of the composite shells with the option of using AFP methods was further refined and improved based on computed tomography (CT) scans, strain gage, and optical strain measurements last year. AFP dome caps were manufactured by Boeing according to Quantum designs based on FEA results. A series of testing to national standards will be conducted to validate the hybrid designs.

RESULTS

Vessel Design Iterations

Vessel 12: At the time of writing the 2012 annual report, the Vessel 12 design was just completed with the latest version of mWind at that time. This design incorporated AFP with baseline and lower-cost fibers. The major difference on this design was that the AFP dome cap terminations were further into the cylinder section to improve load transfer between AFP and FW, eliminating the fiber strain spikes in the forward and aft transition areas between AFP and FW. The burst pressure reached 144.5 MPa (20,958 psi), short of meeting the minimum requirement of 157.5 MPa (22,843 psi). The burst location was in the transition area between AFP and FW. It was discovered that the vessel was not built per design—more baseline fiber layers were replaced by lower-cost fiber. Since the tensile strength of the lower-cost fiber is not significantly different from that of the baseline fiber, the proper number of lower-cost fiber layers would not have made up the 13 MPa deficit during the burst test. In addition, the calculated hoop thickness between dome caps did not match the height of the dome caps at tangent points, resulting an uneven surface for bridging to occur when applying the first helical pattern. In the last annual report, it was mentioned that the baseline fiber was the most cost-effective option in terms of performance per dollar. The remaining designs would focus on passing the burst test and other national standard tests without using lower-cost fiber.

Before the start of Vessel 13 design, the features not working correctly previously in mWind were debugged and fixed. Bugs encountered included the composite thickness in the dome and start and end points of non-continuous fiber layers.

Vessel 13: The Vessel 13 design increased the number of initial hoop layers to eliminate the bridging issue seen in Vessel 12. The additional hoop layers caused extra bending into the dome near the tangent line. The dome caps needed additional layers (from 12 to 20) to counter the additional stress. Increasing the number of dome caps layer maximizes the benefits of AFP, eliminating the unnecessary fibers that would have been in place if those were filament wound.

The dome caps were built at Boeing with a process using a solid, sealed foam tool and a freezing approach for extracting the dome caps from the tool. The layup was successfully completed with no visible wrinkles or defects. Figure 1 shows the in-process layup of the aft dome cap on the sealed, foam tool. This picture shows a ply placement that will be later covered with additional fiber-placed plies.

Upon installing the dome caps onto the liner, it was discovered that the length of the dome caps on the cylinder section was one inch longer than the design value. The difference was due to how the tangent point was defined. Boeing defined the tangent point of each dome by measurement of the liner with a coordinate measuring machine, while Quantum based their tangent point on geometry of the tooling used to manufacture the liner.

The number of hoop layers per design that was applied between the dome caps did not provide the required thickness to match the dome cap thickness at the tangent points. The winding layup was adjusted to relocate some hoop layers from the outer layers to the inner layers to avoid fiber bridging in the dome-cylinder transition areas. In addition, bridging between layers was observed in the aft end during winding. This type of buildup was a concern for Vessel 13 to have low burst strength.

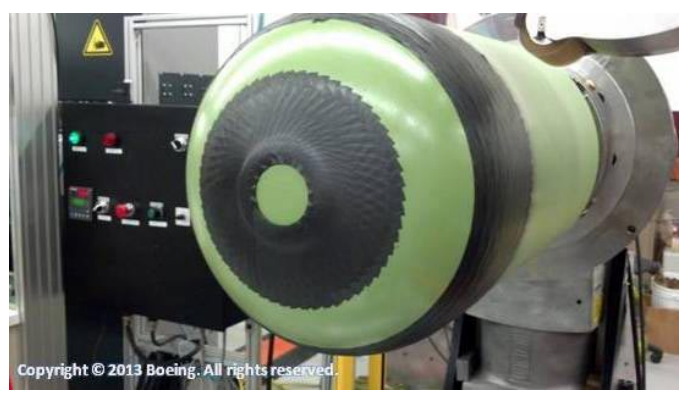

FIGURE 1. Layup of Aft Dome Cap on Foam Mandrel—the Mandrel has a Released Coating (Green) to Facilitate the Removal of the Layup

Before performing the burst test, CT scanning was completed on the domes. The CT scans of the aft end revealed bridging. When compared to the build up near the aft polar boss between CT scan images and FEA design layup, it was very similar. However, small adjustments were made to the material buildup in mWind to better correlate the predicted and measured profiles in the future.

Optical and physical strain measurements were performed on the vessel prior to burst test. Optical measurements were performed with ARAMIS, supported by the Boeing Company. The surface strains were calculated from the measured displacements at specific pressure loads. The strain gages were mounted in the transition areas between domes and cylinder section, as well as in mid cylinder. Strain gage measurements showed the value was approximately 5,000 micro strain for hoop strain at the aft dome and cylinder transition, while ARAMIS measured 4,000-5,000 micro strain at the same location. The results showed that ARAMIS was sufficiently accurate that its measurements could be used to analyze the design and help verify the strain calculations from mWind.

Figure 2 shows the hoop and axial strains measured and predicted by the FEA model of Vessel 13 with correct material buildup. There was good correlation in the upper portion of the dome section. The predicted and measured strains tend to diverge near the polar opening part of the dome due to voids in this area and effects of dome curvature. These results showed that FEA models provided a good prediction of the actual stress/strain conditions in a composite pressure vessel. The dome caps are generally farther away for the polar region and do not have the bridging and voids seen in this area. Thus, mWind and ANSYS are adequate to design the composite knuckle region which contains both FW and AFP layers.

The burst pressure reached 142.6 MPa (20,679 psi), which was below the requirement. Rupture occurred in the aft dome polar boss, as shown in Figure 3. The location was consistent with where bridging occurred.

Vessel 14: The focus of the Vessel 14 design was to reduce the voids in the aft end polar opening area. The stresses and strains in other areas of the dome increased as layers were reduced in the polar opening. A significant

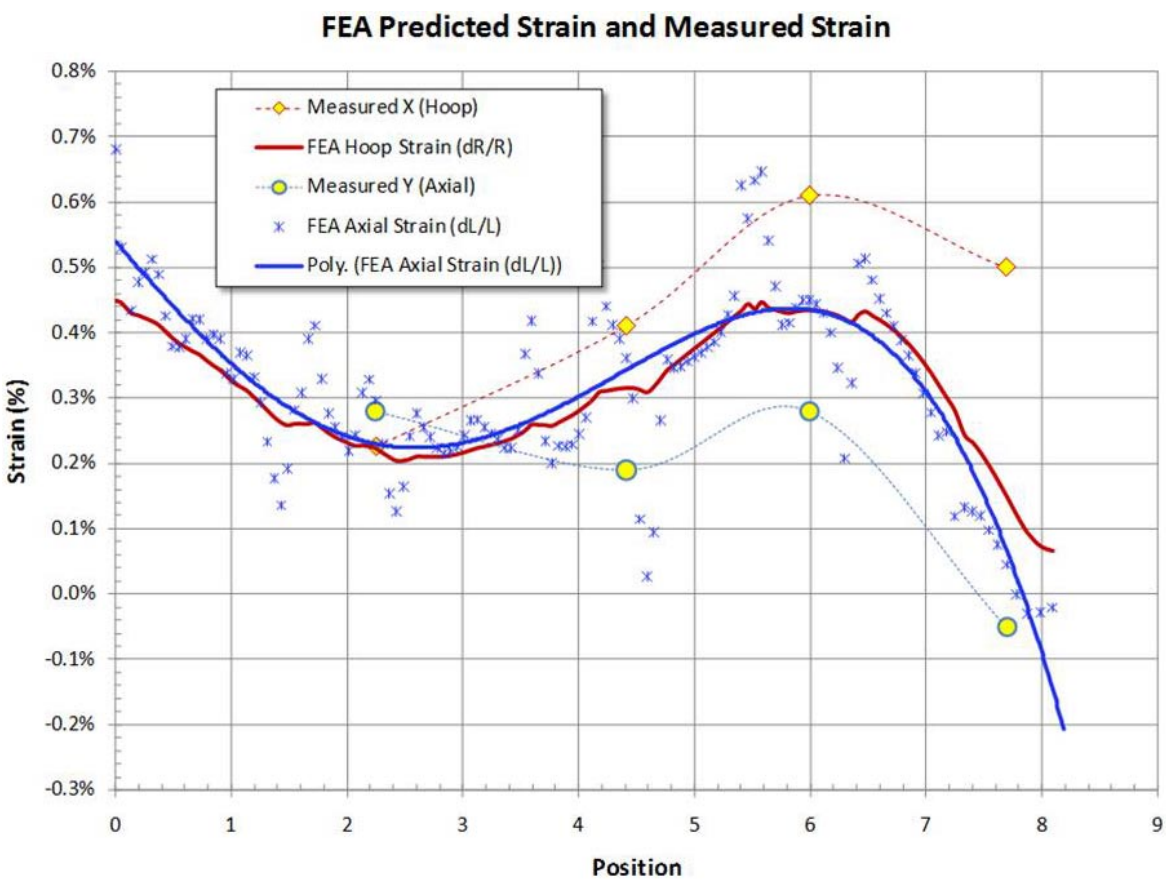

FIGURE 2. Measured and Predicted Hoop and Axial Strains of Vessel 13

FIGURE 3. Vessel 13 Burst Test High-Speed Video Frame

reduction of layers was accomplished with the latest design, which reduced 3.6 kg (7.9 lbs) of weight when compared to Vessel 13. FEA showed the maximum fiber strain was in the hoop section without any spikes in the helical layers in the dome section.

Boeing built the latest dome caps, which reduced from 20 to 14 plies with different layup sequence per design. The tangent point was also clarified to resolve an earlier issue associated with differing definitions between FW and AFP. Fabrication of these dome caps was successful and demonstrated a continual improvement over previous versions.

During the build, when a partial helical layer was applied on the liner to pull the dome caps tight onto the liner ends, fiber bridging was observed across two different layers of the aft dome cap. Upon removing the partial helical, chopped fiber mixed with resin was used to fill the air gap. As the partial helical was re-applied onto the liner, small wrinkles were observed on the aft dome cap. Instead of winding a partial helical, a complete helical layer was applied onto the vessel, with the expectation the helical pattern would be able to flatten out the wrinkles. The fiber tension eventually "collected" all the small wrinkles to form two larger wrinkles. This most likely was caused by a small difference in size of the AFP tooling and the liner geometry thus resulting in a gap between the liner and the dome cap. This full helical was removed before winding the vessel per design. After the first helical pattern per design was applied, the vessel was allowed to cure at room temperature overnight while rotating on the winding machine. The wrinkles on the aft dome were then solid which allowed the dome to be smoothed by filing of the high spots. The wrinkle size was kept to a minimal this way without affecting the next filament wound layers. For potential design improvements, strain gage and optical strain measurements and usage of high speed camera during burst test have been planned. The burst test is tentatively scheduled for early August 2013.

Continuous Process Improvement–Collapsible Tool Concept

Boeing's AFP process "lays" prepreg material onto a hard tool surface, forming the exact shape of the dome while eliminating wrinkling–a significant problem identified earlier in our project. Because the layup tool is a single, solid piece, it requires a difficult freezing step in order to release the layup from the tool. To solve this problem, a three-piece layup tool has been conceptualized. The tooling concept uses three pieces. The first piece is a wedge that slides out from the back of the tool, after which the remaining two sections will hinge together to allow for an easy extraction of the composite dome cap from the mandrel tool. By incorporating this collapsible tool into the robotic cell, the fixture will easily be removed with little downtime, increasing the overall efficiency of the cell and processes. Building the collapsible tool is pending coordination of the effort.

Fiber Creel System Upgrade

Boeing installed a new smart-motor control system from Animatics onto their existing creel system, along with a newly designed dancer system. The Animatics motors allow for better control and higher torque output as compared to previous systems. This system also allows for a dynamically controlled, closed-loop-active tow tensioning, allowing for consistent tension on each tow regardless of tow direction or speed.

Cost Model

PNNL updated the cost model during FY 2013 to use material cost assumptions that are consistent with DOE's other hydrogen storage programs. Strategic Analysis was contracted by DOE to compile consensus values of material costs for comparison of vessel costs across DOE projects. PNNL incorporated Strategic Analysis's carbon fiber cost information into the cost model used by the project. Increasing the carbon fiber cost from $11/lb to $13/lb further accentuates the cost savings of the project's optimized vessel designs that reduce the total mass of carbon fiber used.

Characterization of Polymer Liner Materials

PNNL has developed a miniature in situ test frame for characterizing the strength and modulus of vessel liner materials—high-density poly-ethylene. The tensile load

frame fits into PNNL's high-pressure hydrogen autoclave for testing materials in the real-world environment of a pressurized vessel. Previous ex situ tests show a strong time dependence on material properties indicating that in situ properties could be different. PNNL built the prototype in situ tensile rig in FY 2012 and performed proof of concept testing in hydrogen. The system has been upgraded significantly in FY 2013 by adding a programmable logic controller to control the solenoid power, giving the ability to apply a constant strain rate. The tensile tester was also repackaged in a more rigid frame to reduce the system compliance that was observed on closer review of the tensile test data. Figure 4 shows the excellent repeatability of the system in performing nine in-air tests of commercial high-density poly-ethylene liner material.

CONCLUSIONS AND FUTURE DIRECTIONS

- mWind is sufficiently accurate for hybrid vessel designs.
- FEA on the latest vessel design provides high confidence on passing the burst pressure requirement, but bridging and wrinkles on the aft dome are factors that could affect the outcome.
- Boeing's manufacturing process for dome caps has improved to show insignificant amount of wrinkles on the parts before installation.
- The carbon fiber cost used in the cost model now matches with the consensus value used in other DOE hydrogen storage projects.
- PNNL's improved in situ tester shows excellent repeatability of test results.
- Perform burst test, ambient temperature cycle test, drop test, extreme temperature cycle test, and accelerated stress rupture test to validate process/material changes critical to hybrid vessel design.
- Boeing will continue to support dome cap manufacturing.
- Update cost model with the cost and amount of fiber used in the final hybrid design.
- Perform high-density poly-ethylene tensile tests in high-pressure hydrogen.

FY 2013 PUBLICATIONS/PRESENTATIONS

1. Development of Advanced Manufacturing Technologies for Low Cost Hydrogen Storage Vessels, Annual Merit Review and Peer Evaluation Meeting, Department of Energy, May 13–17, 2013, Arlington, Virginia.

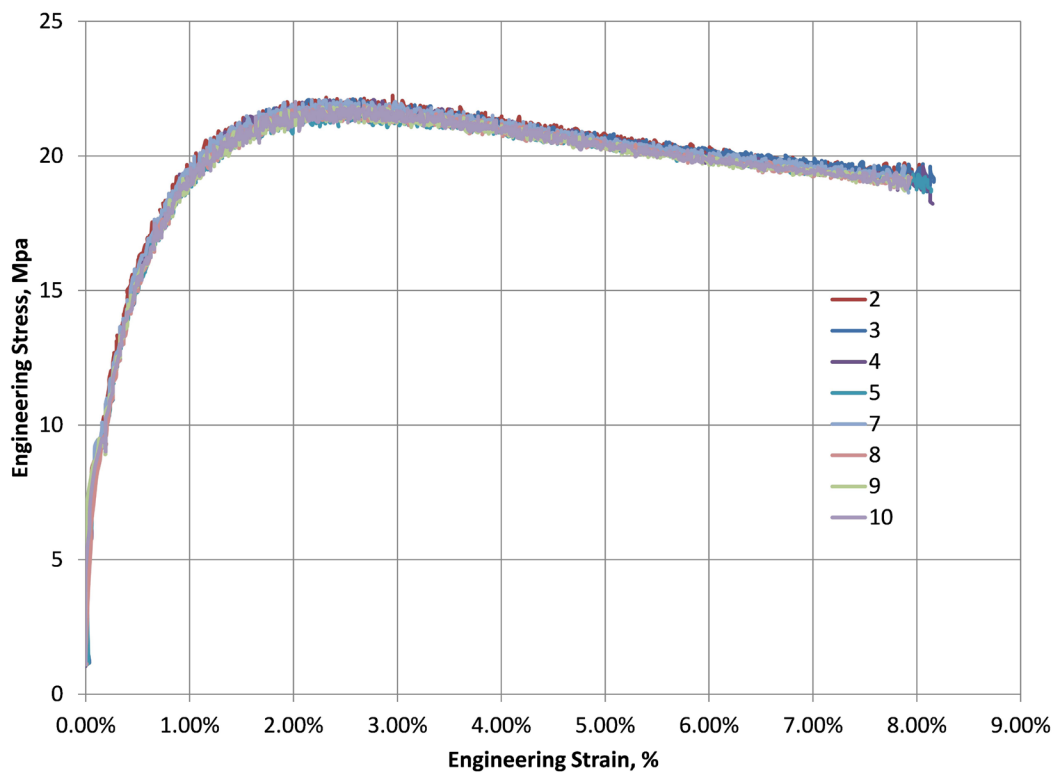

FIGURE 4. Repeatability of High-Density Poly-Ethylene Tensile Tests Performed in Air using the In Situ Test Frame

VII. TECHNOLOGY VALIDATION

VII.0 Technology Validation Program Overview

INTRODUCTION

The Technology Validation program demonstrates, tests, and validates hydrogen and fuel cell technologies and uses the results to provide feedback to the Fuel Cell Technologies Office's research and development (R&D) activities.

Continuing efforts include the real-world evaluation and monitoring of fuel cells in stationary power, backup power, buses, and material handling equipment applications. In Fiscal Year (FY) 2013, the program awarded new projects in which data are collected to track technological progress in the performance, durability, and reliability of refueling stations, advanced refueling components, and fuel cell electric vehicles (FCEVs). The program also solicited proposals on the topics of fuel cell hybrid electric medium-duty trucks, rooftop backup power, and advanced hydrogen refueling components.

GOAL

Validate the state of the art of fuel cell systems in transportation and stationary applications as well as hydrogen production, delivery, and storage systems. Assess technology status and progress to determine when technologies should be moved to the market transformation phase.

OBJECTIVES[1]

- By 2017, validate commercial stationary fuel cells (100 kW to 3 MW) against 2015 system targets (50,000 h, 45% electrical efficiency).
- By 2017, validate durability of auxiliary power units against 2015 fuel cell system target (15,000 h, 35% electrical efficiency).
- By 2019, validate hydrogen FCEVs with greater than 300-mile range and 5,000 hours fuel cell durability.
- By 2019, validate a hydrogen fueling station capable of producing and dispensing 200 kg H_2/day (at 5 kg/3 min; 700 bar) to cars and/or buses.
- By 2020, validate large-scale systems for grid energy storage that integrate renewable hydrogen generation and storage with fuel cell power generation—operating for more than 10,000 hours, with a round-trip efficiency of 40%.

FY 2013 TECHNOLOGY STATUS

FCEV Evaluation

The National Renewable Energy Laboratory (NREL) is validating light-duty FCEV performance and durability through analysis of dynamometer and real-world vehicle performance data. Multiple real-world sites and customers are included in this demonstration project. Data (operation, maintenance, and safety) are collected onsite by project partners for the fuel cell system(s) and infrastructure. NREL receives the data quarterly and stores, processes, and analyzes the data. An internal analysis of all available data is completed quarterly and a set of technical composite data products (representing aggregated data) is published every six months. The prior light-duty FCEV validation effort—the National Learning Demo—concluded in FY 2012. Much of the activity in FY 2013 focused on getting projects started—preparing data templates and security procedures, interacting with project partners, and prioritization of data to be collected.

Fuel Cell Bus Evaluation

NREL has been collecting and analyzing data from fuel cell buses from three transit agencies; AC Transit (Oakland, CA), CTTRANSIT (Hartford, CT), and SunLine (Thousand Palms, CA). The objective of this effort is to determine the status of fuel cell systems for buses and to aid other fleets with the implementation of next-generation

[1] Note: Targets and milestones were recently revised; therefore, individual project progress reports may reference prior targets.

fuel cell buses. New fuel cell bus designs demonstrated improved fuel economy over diesel and compressed natural gas buses. NREL reported on fuel cell power plants that had accumulated fuel cell stack operating hours in excess of 10,000. A measure of reliability—the miles between road call—has room for improvement, but the highest percentage of road calls realized was not associated with the fuel cell system itself. The majority of road calls were due to bus-related issues such as problems with doors, air conditioning, and windshield wipers, while fuel cell-related issues made-up approximately 22% of the road calls.

Hydrogen Component Validation

The main objectives of this project include the independent validation and systems integration of commercial and advanced prototype hydrogen production, compression, dispensing, and fuel cell technologies. In FY 2013, the project focused on performing accelerated life testing of both diaphragm and piston hydrogen compressors. NREL has formed agreements with different manufacturers and will track and evaluate performance of multiple piston-type gas boosters from these manufacturers under an accelerated duty cycle. The project work scope also includes quantifying, under near-real-world operating conditions, operation and maintenance, durability, and reliability of renewable electrolysis systems as they are applied to energy storage and vehicle refueling. NREL will monitor system faults and maintenance, and also analyze the performance of renewable electrolysis.

Hydrogen Station Analysis

The objective of this project is to collect data from state-of-the-art hydrogen fueling facilities, such as those operated by the California Air Resources Board (CARB), Proton OnSite, and GTI, providing valuable feedback on sensitive data related to hydrogen infrastructure for industry and the Office.

- CARB's Newport Beach, California station features onsite generation of hydrogen through a small-scale natural gas steam methane reformer, demonstrating the footprint and equipment arrangement of such a retail facility. Evaluation results will be used to make recommendations on how to optimize discrete station components.
- Proton OnSite's fully containerized station deployments (located in Wallingford, Connecticut and Braintree, Massachusetts) demonstrate advanced technologies, including 1) higher-pressure hydrogen generation with electrochemical compression, 2) higher-efficiency generation with lower resistance electrolyte and advanced catalyst, 3) higher addressable capacity composite storage, and 4) advanced packaging concepts for reduced footprint. This project goes beyond data collection; it aims to validate the first full-scale demonstration of a higher-pressure water electrolyzer.
- GTI has partnered with Linde to demonstrate deployments in five California locations, where new 900 bar ionic compression technology is utilized.

Sustainable Hydrogen Fueling Station

The California State University, Los Angeles (CSULA) is operating a hydrogen station based on electrolysis from renewable electricity on their campus to test, collect data, and validate hydrogen refueling architecture and individual components in a real-world operating environment. Performance evaluations data are being provided to NREL. The project also serves educational purposes, as it provides a living lab environment for engineering and technology students.

Stationary Fuel Cell Evaluation

This project informs the Office, the public, fuel cell manufacturers, and other stakeholders about the performance of stationary fuel cell systems operating under real-world conditions, while reporting on the baseline, progress, and technical challenges. Operation, maintenance, and safety data are collected and analyzed quarterly by NREL for stationary fuel cell systems. In FY 2013, installation data from California's Self Generation Incentive Program were collected from five companies, for 249 units (totaling 97 MW). Natural gas was seen as the most popular fuel choice, but renewable fuels (digester gas, landfill gas, etc.) accounted for 43% of capacity. Average installed cost was found to be $10,223/kW.

Early Markets Analysis

Early market application of fuel cell technologies includes validating material handling equipment (MHE) and backup power fuel cell performance through analysis and reporting of real-world operation and value proposition metrics. MHE were found to be operating with average availability of about 98% at eight end-user facilities, with most systems operating at least six hours a day. The American Recovery and Reinvestment Act had an objective to deploy approximately 1,000 fuel cell systems in key early markets, and this was met within two years from the first deployment. Early market end users are operating 1,326 fuel cell units at 407 sites in 22 states. By the first quarter of FY 2013, 504 MHE fuel cell units were deployed at eight facilities, and 820 backup power fuel cell units were operating at 398 sites. Among components related to the infrastructure, hydrogen compressors contributed the highest number of maintenance events and maintenance labor hours.

Hydrogen Recycling System Evaluation

This project involves the validation of a system of reclamation and recycling of hydrogen that is wasted (flared or vented) in various industrial operations. The main project objective is to demonstrate product readiness and to quantify the benefits and customer value proposition of H2Pump's Hydrogen Recycling System (HRS-100™) by installing and analyzing the operation of multiple prototype 100 kg hydrogen per day systems in real-world customer locations. Modified fuel cell technology is utilized, providing up to 90% recovery of hydrogen. All of the data acquired by the systems will be made available for NREL for analysis, including factors such as stack voltage and current, system power, and hydrogen flow rate, as well as maintenance and repair logs.

FY 2013 KEY ACCOMPLISHMENTS

Fuel Cell Vehicles and Hydrogen Infrastructure: Awarded $5.3M for five years to demonstrate advanced light-duty FCEVs, where data will be collected from approximately 70 vehicles. To develop hydrogen fueling infrastructure for FCEVs, $2.4M was awarded for evaluating hydrogen stations (in CA, MA, and CT) and advanced refueling components.

Fuel Cell Buses: New fuel cell bus designs were demonstrated to have approximately 1.9 times the fuel economy of diesel buses, and about 2.3 times the fuel economy of compressed natural gas buses. As of May 2013, the highest-hour fuel cell power plant had surpassed 13,000 hours, while several others accumulated significant hours, such as 10,686, 8,770, and 5,300 hours.

Early Markets: The number of fuel cell backup power systems deployed increased more than 18-fold from the beginning to the end of The American Recovery and Reinvestment Act, with start reliability reaching as high as 99.6%. One unit successfully demonstrated a continuous run time of 65 hours during the data collection period, while the average run time was 39 minutes. MHE fuel cell systems accumulated nearly 1.5 million hours by the end of 2012. High operation hours were observed on the 490 systems. The ultimate durability of fuel cell MHE is still being determined and will continue to be tracked by NREL. On an annualized cost per MHE per year, the fuel cell has approximately 10% savings for a Class I/II MHE.

BUDGET

The funding portfolio for Technology Validation enables the program to continue to collect and analyze data from fuel cells operating in transportation and stationary applications, as well as hydrogen production and delivery technologies. In FY 2013, $8.5 million in funding was appropriated for the Technology Validation program, and $7 million was requested for FY 2014 (subject to congressional appropriations).[2]

[2] The majority of the FY 2014 funding is likely to be focused on projects resulting from proposals submitted in response to a funding opportunity announcement that was issued for a variety of application areas.

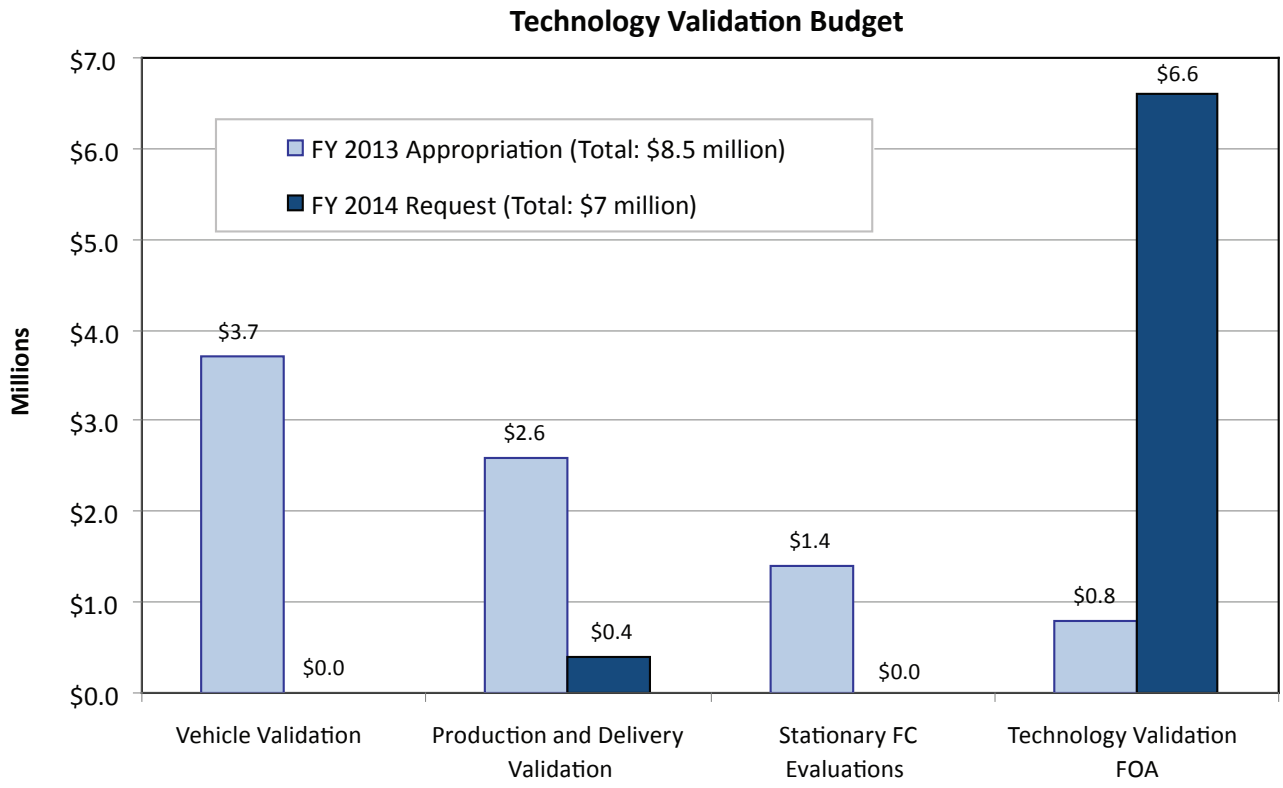

FC - fuel cell; FOA - Funding Opportunity Announcement
* Subject to appropriations, project Go/No-Go decisions and competitive selections. Exact amounts will be determined based on R&D progress in each area and the relative merit and applicability of projects competitively selected through planned funding opportunity announcements.

FY 2014 PLANS

In FY 2014, the Technology Validation program will continue its detailed evaluations of hydrogen and fuel cell technologies in transit buses, next generation hydrogen fueling stations, stationary power deployments, and early market applications. The program will also award several new projects resulting from its funding opportunities issued in June 2013. Further funding opportunities may also be developed in FY 2014, subject to appropriations.

Jason Marcinkoski
Acting Technology Validation Team Lead
Fuel Cell Technologies Office
U.S. Department of Energy
1000 Independence Ave., SW
Washington, D.C. 20585-0121
Phone: (202) 586-7466
Email: Jason.Marcinkoski@ee.doe.gov

VII.1 Technology Validation: Fuel Cell Bus Evaluations

Leslie Eudy
National Renewable Energy Laboratory (NREL)
15013 Denver West Parkway
Golden, CO 80401
Phone: (303) 275-4412
Email: leslie.eudy@nrel.gov

DOE Manager
Jason Marcinkoski
Phone: (202) 586-7466
Email: Jason.Marcinkoski@ee.doe.gov

Subcontractors:
Kevin Chandler, Battelle, Columbus, OH

Project Start Date: March 2001
Project End Date: Project continuation and direction determined annually by DOE

Overall Objectives

- Validate fuel cell electric bus (FCEB) performance and cost compared to DOE and Department of Transportation (DOT) targets and conventional technologies.
- Coordinate with the DOT's Federal Transit Administration (FTA) on the data collection for the National Fuel Cell Bus Program (NFCBP) and with international work groups to harmonize data-collection methods and enable the comparison of a wider set of vehicles.

Fiscal Year (FY) 2013 Objectives

- Document performance results from each current FCEB demonstration site.
- Complete annual status report comparing results from the different demonstrations.

Technical Barriers

This project addresses the following technical barriers from the Technology Validation section of the Fuel Cell Technologies Office Multi-Year Research, Development, and Demonstration Plan:

(A) Lack of Fuel Cell Electric Vehicle and Fuel Cell Bus Performance and Durability Data

(D) Lack of Hydrogen Fueling Infrastructure Performance and Availability Data

Contribution to Achievement of DOE Technology Validation Milestones

This project has contributed to achievement of the following DOE milestone from the Technology Validation section of the Fuel Cell Technologies Office Multi-Year Research, Development, and Demonstration Plan:

- *Milestone 2.3: Validate fuel cell electric vehicles achieving 5,000-hour durability (service life of vehicle) and a driving range of 300 miles between fuelings. (4Q, 2019)* By the end of May 2013, NREL had documented four FCEB fuel cell systems with operation in excess of 5,000 hours. One of these systems has logged more than 13,000 hours in service, and a second system has surpassed 10,600 hours. Bus fuel economy is dependent on duty-cycle. Based on in-service fuel economy values between 5 and 7 miles per kilogram, the hybrid FCEBs currently in service can achieve a range between 200 and 320 miles per fill.

FY 2013 Accomplishments

- Published reports on performance and operational data covering 18 full-size FCEBs in revenue service in the United States.
- Documented more than 13,000 hours on a single fuel cell power plant.

✧ ✧ ✧ ✧ ✧

INTRODUCTION

Transit agencies continue to aid the FCEB industry in developing and optimizing advanced transportation technologies. These in-service demonstration programs are a vital part of the process to validate the performance of fuel cell systems in buses and to determine issues that require resolution. Using fuel cells in a transit application can help accelerate the learning curve for the technology because of the high mileage accumulated in short periods of time. During the last year, the project teams have made progress in improving fuel cell durability, availability, and reliability. More work is still needed to meet the performance needs of transit agencies, lower capital and operating costs, and transition the maintenance to transit staff.

APPROACH

NREL uses a standard evaluation protocol to provide:

- Comprehensive, unbiased evaluation results of advanced technology vehicle development and operations.

- Evaluations of hydrogen infrastructure development and operation.
- Descriptions of facility modifications required for the safe operation of FCEBs.
- Detailed performance and durability results of FCEBs to validate status against technical targets, educate key stakeholders, and further DOE goals.

The evaluation protocol includes two levels of data: operation and maintenance data on the bus and infrastructure, and more detailed data on the fuel cell, system, and components. The first set of data is considered non-sensitive and is obtained mainly from the transit fleet. The analysis, which consists of economic, technical, and safety factors, focuses on performance and use, including progress over time and experience with vehicle systems and supporting infrastructure.

The detailed data are collected with cooperation from the bus and fuel cell system manufacturers and are considered highly sensitive. Results include aggregate data products that protect each manufacturer's specific data. To date, NREL has collected this type of data from two fuel cell manufacturers. Aggregate results will be published if and when enough data are available to protect each company's identity and source data.

RESULTS

During FY 2013, NREL collected and analyzed data on the following four FCEB demonstrations at three transit agencies in the United States:

- Zero Emission Bay Area (ZEBA) Demonstration – five Bay Area transit agencies led by Alameda-Contra Costa Transit (AC Transit in Oakland, California) are demonstrating twelve 40-foot Van Hool buses with ClearEdge Power fuel cells in a Siemens hybrid system. The hybrid system was integrated by Van Hool and uses lithium-ion batteries from EnerDel.
- Advanced Technology FCEB Project (AT FCEB) – SunLine (Coachella Valley area, California) is operating one New Flyer 40-foot bus with a Bluways hybrid system and Ballard fuel cell. This bus was the pilot bus from a fleet of 20 buses operating in Whistler, British Columbia, Canada.
- American Fuel Cell Bus Project (AFCB) – in December 2012 SunLine began operating an ElDorado 40-foot bus with a BAE Systems hybrid propulsion system using Ballard fuel cells and lithium batteries. This project is part of FTA's NFCBP.
- 'Nutmeg' Fuel Cell Electric Bus Demonstration – named for Connecticut's state nickname, the Nutmeg project is also part of the NFCBP. The four buses, which are identical to the 12 ZEBA buses, were operated by Connecticut Transit (CTTRANSIT) in Hartford, Connecticut. One bus was moved to Flint, Michigan, for at least one year of demonstration.

All of these buses are fuel cell dominant hybrid buses. The first two of these evaluations were funded by DOE, and the other evaluations were covered by funding from FTA. NREL published results from each of these demonstrations. A summary of selected results is included in this report.

NREL completed reports on operational and performance data from these FCEBs and conventional baseline buses at each agency. The results are also compared to technical targets for FCEB performance established by DOE/DOT and published in a Fuel Cell Technologies Record in September 2012. Tables 1 through 3 provide a summary of the reported results from the operation at each agency, including data from the baseline buses.

TABLE 1. 2013 Summary Data Results for ZEBA FCEBs

Vehicle data	FCEB	Diesel
Number of buses	12	3
Data period (month, year)	Sep 11 – Apr 12	Sep 11 – Apr 12
Number of months	8	8
Total fleet miles	147,069	82,098
Average miles per month	1,690	3,635
Total fuel cell hours	17,619	
Fuel economy (mi/kg)	6.68	
Fuel economy (mi/diesel gallon equivalent)	7.55	4.00
Average speed (mph)	8.3	N/A
Availability (%)	56	77

TABLE 2. 2013 Summary Data Results for Nutmeg FCEBs

Vehicle data	FCEB	Diesel
Number of buses	4	3
Data period (month, year)	Aug 11 – Jan 13	Aug 11 – Jul 12
Number of months	18	12
Total fleet miles	83,996	112,308
Average miles per month	1,235	3,120
Total fuel cell hours	7,305	
Fuel economy (mi/kg)	6.42	
Fuel economy (mi/diesel gallon equivalent)	7.24	3.79
Average speed (mph)	13.2	N/A
Availability (%)	53	85

TABLE 3. 2013 Summary Data Results for SunLine FCEBs

Vehicle data	AFCB	AT FCEB	CNG
Number of buses	1	1	5
Data period (month, year)	Mar 12 – Jan 13	Aug 11 – Jan 13	Aug 11 – Jan 13
Number of months	11	18	18
Total fleet miles	37,896	27,970	377,318
Average miles per month	3,445	1,554	4,192
Total fuel cell hours	2,422	2,399	
Fuel economy (mi/kg)	6.45	5.34	
Fuel economy (mi/diesel gallon equivalent)	7.29	6.03	3.23
Average speed (mph)	15.6	11.7	15.7
Availability (%)	84	60	80

CNG – compressed natural gas

One of the performance targets for FCEBs is to demonstrate fuel economy that is two times that of conventional bus technology. The FCEBs included in this report showed fuel economy improvements ranging from 87% to 126% compared to conventional buses, depending on duty-cycle. Figure 1 shows the fuel economy of the buses at each of the three transit agencies in miles per diesel gallon equivalent. (Note that the baseline buses at SunLine are compressed natural gas [CNG] buses.) These data show that the FCEBs are demonstrating fuel economy values about two times those of the baseline buses. The chart also includes data on hybrid buses at CTTRANSIT.

One key challenge for the fuel cell bus industry is increasing the durability and reliability of the fuel cell system to meet FTA life cycle requirements for a full-size bus—12 years or 500,000 miles. DOE and FTA have set an early fuel cell power plant (FCPP) performance target of 4–6 years (or 25,000 hours) durability for the fuel cell propulsion system, which would be approximately half the life of the bus. The FCPP would be rebuilt or replaced at that time—similar to what transit agencies typically do for diesel engines. Last year, NREL reported on FCPPs that had accumulated hours in excess of 10,000. These FCPPs have continued to accumulate hours in service. Figure 2 shows the hours accumulated on the FCPPs by fleet over the last few years. As of May 2013, the highest-hour FCPP had surpassed 13,000 hours. Several other FCPPs have accumulated significant hours, the highest of which have achieved 10,686; 8,770; and 5,300 hours. This shows significant improvement in durability toward meeting the 25,000 hour target.

Another measure of reliability for the transit industry is miles between roadcall (MBRC). Figure 3 provides a summary of MBRC for the four FCEB demonstrations and includes the MBRC for the bus as a whole, MBRC for the propulsion system, and MBRC for the fuel cell system. The targets for each category are included on the chart. While the current status for MBRC has risen over the last year, there are still improvements to be made to meet the targets. The highest percentage of roadcalls was due to bus-related

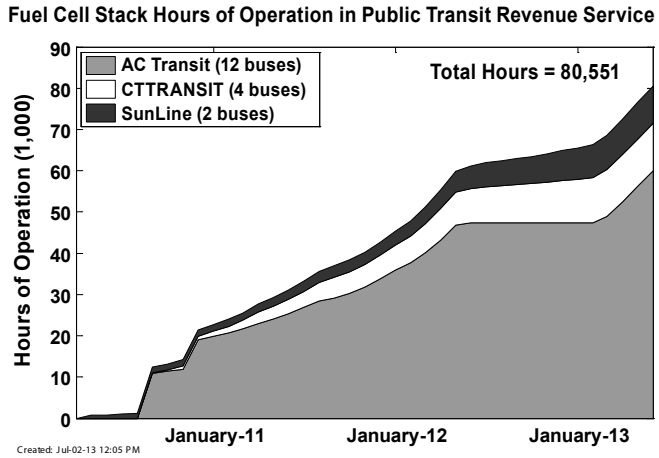

FIGURE 2. Total FCPP Hours Accumulated by Fleet

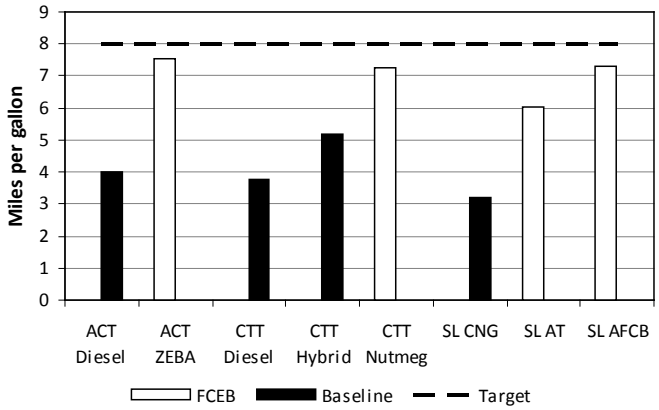

FIGURE 1. Fuel Economy Comparison by Fleet (Diesel Equivalent)

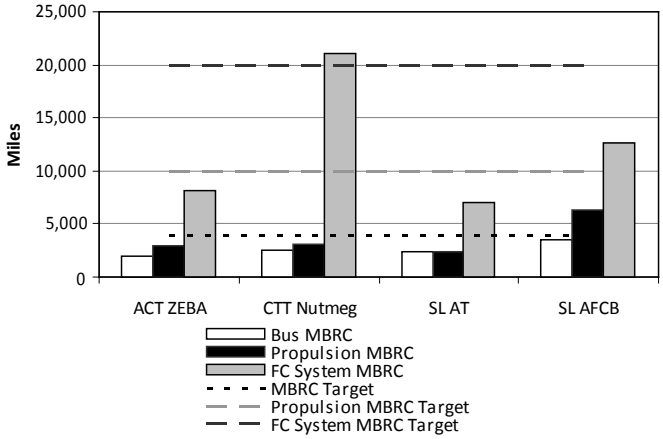

FIGURE 3. Miles between Roadcall Comparisons by Fleet

issues such as problems with doors, air conditioning, and windshield wipers. Fuel cell-related issues made up approximately 22% of the roadcalls during the period.

CONCLUSIONS AND FUTURE DIRECTION

Fuel cell propulsion systems in buses have continued to show progress in increasing the durability and reliability of FCEBs and the primary components. The current technology already meets fuel economy targets and is showing promise to exceed the fuel cell durability target. Table 4 summarizes the current status compared to the DOE/DOT performance targets. There are still challenges to overcome before fuel cell buses can match the current performance standard of diesel buses. These include:

- Continuing operation to validate durability and reliability of the fuel cell systems and other components to match transit needs.
- Optimizing the propulsion system to maximize operation and resolve integration issues.
- Transferring all maintenance work to transit personnel.
- Lowering the costs of purchasing, operating, and maintaining buses and infrastructure.
- Integrating hydrogen fueling procedures into the existing fueling process.
- Transferring the lead role for fuel cell system integration to transit bus builders.

Future work by NREL includes:

- Continuing data collection, analysis, and reporting on performance data for FCEBs in service at the following sites:
  - ZEBA FCEB Demonstration led by AC Transit
  - SunLine
  - City of Burbank
  - Additional sites as funding allows
- Investigating reliability, durability, and life cycle of FCEBs as a part of ongoing evaluations.
- Coordinating with FTA to collect data on the demonstrations funded under the NFCBP.
- Coordinating with national and international FCEB demonstration sites.

FY 2013 PUBLICATIONS/PRESENTATIONS

1. L. Eudy, K. Chandler, 2013, *SunLine Transit Agency Advanced Technology Fuel Cell Bus Evaluation: Fourth Results Report*, National Renewable Energy Laboratory, Golden, CO, NREL/TP-5600-57560, January.

2. L. Eudy, K. Chandler, C. Gikakis, 2012, *Fuel Cell Buses in U.S. Transit Fleets: Current Status 2012*, National Renewable Energy Laboratory, Golden, CO, NREL/TP-5600-52927, November.

3. K. Chandler, L. Eudy, 2012*, Zero Emission Bay Area (ZEBA) Fuel Cell Bus Demonstration: Second Results Report*, National Renewable Energy Laboratory, Golden, CO, NREL/TP-5600-55367, July.

4. L. Eudy, K. Chandler, 2012, *Connecticut Nutmeg Fuel Cell Bus Project: First Analysis Report*, Federal Transit Administration, Washington, DC, FTA Report No. 0020, July.

5. L. Eudy, 2012, *Fuel Cell Electric Bus Evaluations: Recent Results*, Presentation at the California Fuel Cell Partnership Bus Team Meeting, June.

6. L. Eudy, 2012, *Technology Validation: Fuel Cell Bus Evaluations*, Presentation at the DOE Hydrogen and Fuel Cells Program Annual Merit Review, Arlington, VA, May.

REFERENCES

1. Fuel Cell Technologies Program Record # 12012, Sep. 2012, www.hydrogen.energy.gov/pdfs/12012_fuel_cell_bus_targets.pdf.

TABLE 4. 2013 Summary of Progress Toward Meeting DOE/DOT Targets [1]

	Units	2013 Status	2016 Target	Ultimate Target
Bus lifetime	Years/miles	5/100,000	12/500,000	12/500,000
Power plant lifetime	Hours	1,000–13,000	18,000	25,000
Bus availability	%	53–84	85	90
Bus Roadcall Frequency	Miles between road call	2,000–3,500	3,500	4,000
Fuel Cell System Roadcall Frequency	Miles between road call	7,000–20,000	15,000	20,000
Operation time	Hours per day/days per week	19/7	20/7	20/7
Maintenance cost	$/mile	0.39–1.30	0.75	0.40
Fuel economy	Miles per diesel gallon equivalent	6–7.5	8	8
Range	Miles	220–325	300	300

VII.2 Stationary Fuel Cell Evaluation

Chris Ainscough (Primary Contact), Genevieve Saur
National Renewable Energy Laboratory (NREL)
15013 Denver West Pkwy
Golden, CO 80401
Phone: (720) 431-7296
Email: chris.ainscough@nrel.gov

DOE Manager
Jason Marcinkoski
Phone: (202) 586-7466
Email: Jason.Marcinkoski@ee.doe.gov

Project Start Date: October 1, 2011
Project End Date: Project continuation and direction determined annually by DOE

Overall Objectives

Independently assess, validate, and report operation targets and stationary fuel cell system performance under real operating conditions

Fiscal Year (FY) 2013 Objectives

- Quarterly analysis of available data in the NREL Hydrogen Secure Data Center (HSDC)
- Publication of eleven composite data products (CDPs)
- Update of a public website for disseminating the CDPs

Technical Barriers

This project addresses the following technical barrier from the Technology Validation section of the Fuel Cell Technologies Office Multi-Year Research, Development, and Demonstration Plan:

(B) Lack of Data on Stationary Fuel Cells in Real-World Operation

Contribution to Achievement of DOE Technology Validation Milestones

This project will contribute to achievement of the following DOE milestones from the Technology Validation section of the Fuel Cell Technologies Office Multi-Year Research, Development, and Demonstration Plan:

- Milestone 1.1: Complete validation of residential fuel cell micro combined heat and power (CHP) systems that demonstrate 40% efficiency and 25,000 hour durability. (4Q, 2015)
- Milestone 1.2: Complete validation of commercial fuel cell CHP systems that demonstrate 45% efficiency and 50,000 hour durability. (4Q, 2017)

FY 2013 Accomplishments

- This project published an initial set of CDPs in October 2012
- This project published an updated, expanded set of CDPs in March 2013
- This project completed the publication of a website to help disseminate the above results in November 2012, http://www.nrel.gov/hydrogen/proj_fc_systems_analysis.html (Figure 1)
- Published a report, "Stationary Fuel Cell Deployments in California: Interim Technology Status, Deployments and Eligible Incentive Costs

✧ ✧ ✧ ✧ ✧

INTRODUCTION

This project aims to provide status on stationary fuel cell systems to inform DOE, the public, fuel cell manufacturers and other stakeholders. This is the only project directly working on technical barrier (B): Lack of Data on Stationary Fuel Cells in Real-World Operation.

FIGURE 1. A screenshot of the website where all CDPs for stationary fuel cells can be seen and disseminated to stakeholders.

APPROACH

The project's data collection plan builds on other technology validation activities. Data (operation, maintenance, and safety) are collected onsite by the project partners for the fuel cell system(s) and infrastructure. NREL receives the data quarterly and stores, processes, and analyzes the data in NREL's HSDC.

The HSDC is an off-network room with access for a small set of approved users. An internal analysis of all available data is completed quarterly and a set of technical CDPs is published every six months. The CDPs present aggregated data across multiple systems, sites, and teams in order to protect proprietary data and summarize the performance of hundreds of fuel cell systems.

A review cycle is completed before the publication of CDPs. The review cycle includes providing detailed data products of individual system and site performance results to the individual data provider. Detailed data products also identify the individual contribution to CDPs. The NREL Fleet Analysis Toolkit is an internally developed tool for data processing and analysis structured for flexibility, growth, and simple addition of new applications. Analyses are created for general performance studies as well as application- or technology-specific studies.

RESULTS

California's Self-Generation Incentive Program (SGIP) has helped deploy 249 fuel cell systems, for a total of 97 MW, since 2001. These fuel cell deployments have shown that they may be applied to a wide variety of fuels, including renewable biogases from landfill, biomass and digester sources. Deployment numbers have increased even in a climate of declining incentive spending. However, current fuel cell installation costs are significantly higher than the 2020 DOE target; ~$10,000/kW compared to a DOE target of $1,500 (running on natural gas), Figure 2.

Throughout the 12 year history of California's SGIP, nearly 250 fuel cell units have been deployed, accounting for almost 100 MW of installed electrical capacity. The progression of the deployments (count and capacity) can be seen in detail in Figure 3. Deployment activities were relatively slow until the 2010 program year when a sharp increase took place. The number of deployments in 2010 (145) was greater than the number that had been deployed in all the prior years combined (55). This spike was partially fueled by the arrival of a new supplier.

Looking at the deployment trends of fuels over the span of the program's history (Figure 4), we see the greatest diversity of fuels in the 2009 and 2010 program years.

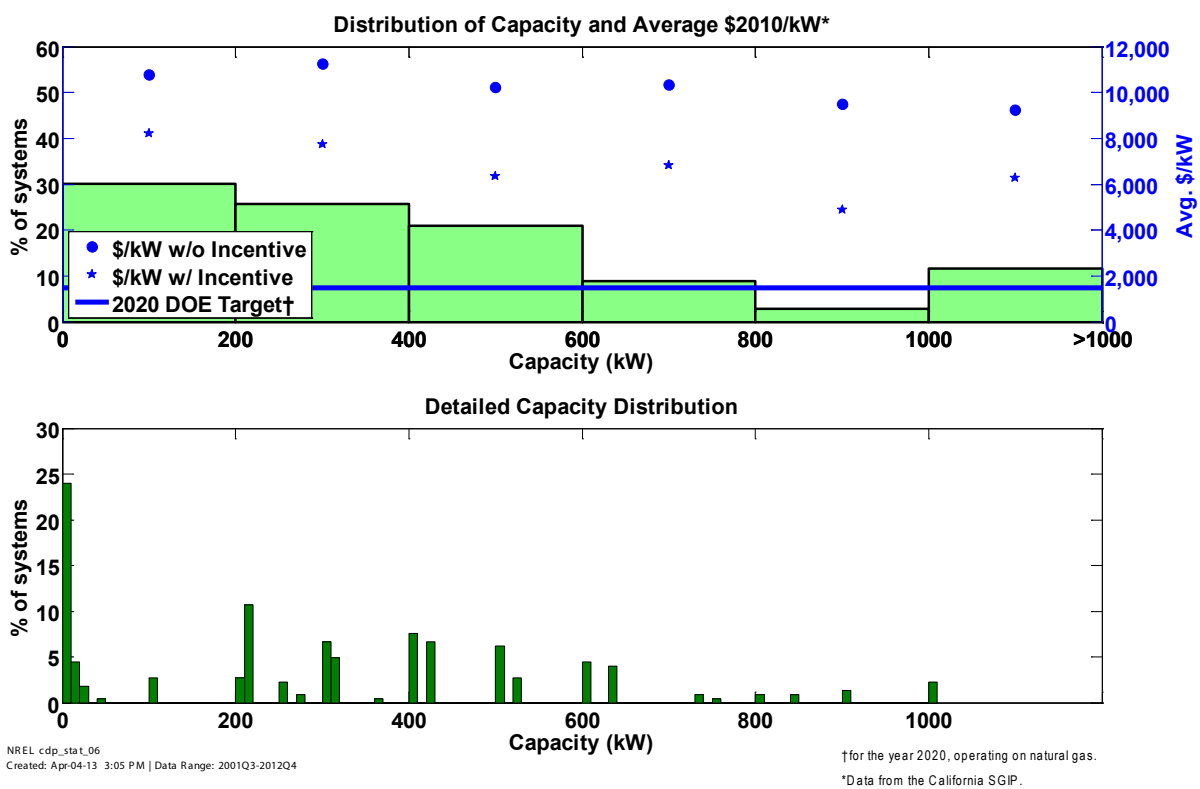

FIGURE 2. Distribution of capacity and average $/kW, relative to DOE 2020 targets running on natural gas.

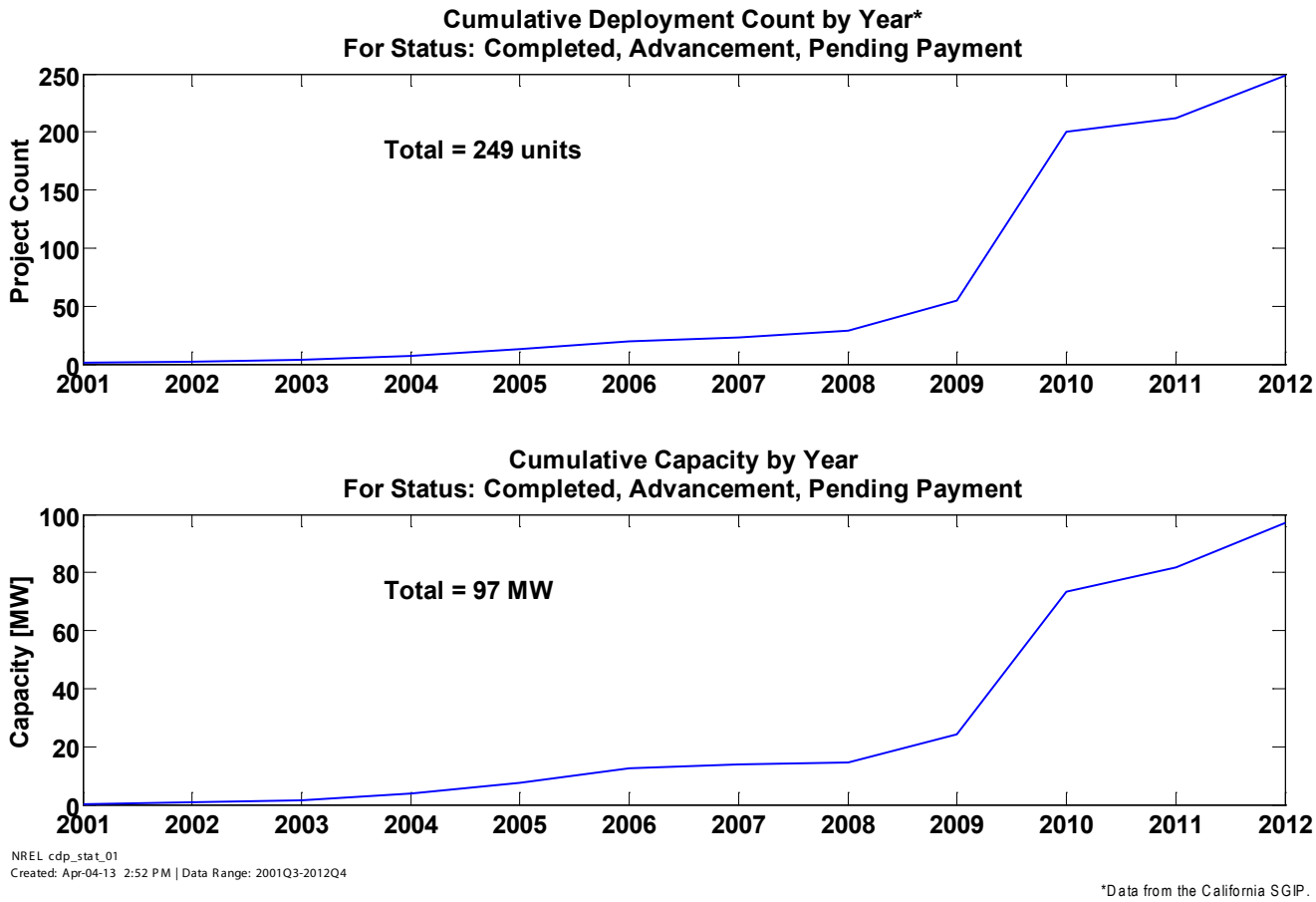

FIGURE 3. Total SGIP deployment count and kWh of installed capacity 2001-2012.

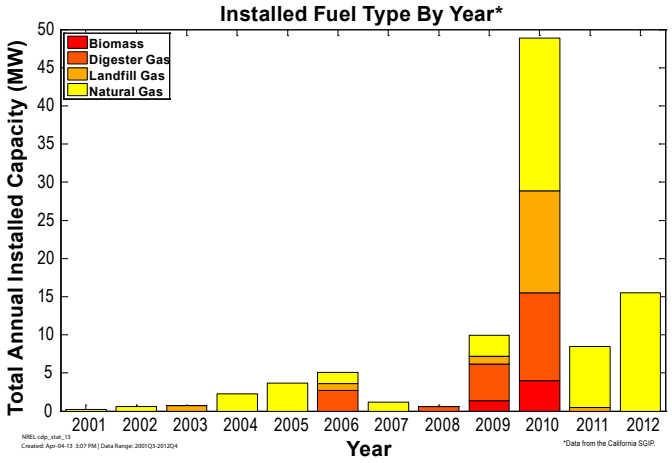

FIGURE 4. Installed fuel type by year which shows the recent domination of the market by natural gas installations.

During the 2009 program year, the incentive level for fuel cells operating on renewable fuels (biogas) was $4.5/W1, or 17% higher than the 2013 program year. Additionally, the fuel source was only required to be available for five years in 2009, as opposed to ten in 2013, and out-of-state directed biogas was not expressly forbidden. These reductions in the attractiveness of incentives, technical challenges related to reforming biogas, as well as the low cost of natural gas may contribute to the fact that from 2011 on, most systems are powered by natural gas, with all systems in 2012 falling into that category.

CONCLUSIONS AND FUTURE DIRECTIONS

Stationary fuel cells have seen wide deployments in the state of California sponsored in part by the SGIP. This program has deployed systems from 5 kW up to 2,800 kW in a variety of applications, using at least one system from each of the common commercially available fuel cell chemistries such as polymer electrolyte membrane, solid oxide, molten carbonate, phosphoric acid, and phosphoric acid doped polybenzimidazole (aka high-temperature polymer electrolyte membrane).

Despite the numbers deployed, total installed costs eligible for incentive dollars continue to rise in recent years, moving away from 2020 DOE targets, which they are already far from meeting. The causes of this trend are as yet unknown, and require further investigation.

Incentive spending by SGIP will continue to decline for fuel cells in the coming years. The effect that will have on deployments is uncertain, as the largest gains in total deployments have happened in the last five years, in a regime of declining incentives. It will be important to continue to analyze trends in California's SGIP as an indicator of larger national trends in the coming years and performance status as data are available.

For future work, this project aims to develop additional data sets to that available from SGIP, and continuing the regular cadence of results publication.

FY 2013 PUBLICATIONS/PRESENTATIONS.

1. Stationary Fuel Cell Evaluation, Annual Merit Review, Washington, D.C. May 2013.

VII.3 Hydrogen Recycling System Evaluation and Data Collection

Rhonda Staudt
H2Pump LLC
11 Northway Lane North
Latham, NY 12110
Phone: (518) 783-2241
Email: Rhonda.staudt@h2pumpllc.com

DOE Managers
Jason Marcinkoski
Phone: (202) 586-7466
Email: Jason.Marcinkoski@ee.doe.gov
Jim Alkire
Phone: (720) 356-1426
Email: James.Alkire@go.doe.gov

Contract Number: DE-EE0006091

Project Start Date: January 2013
Project End Date: June 2014

Overall Objectives

The objective of this project is to demonstrate the product readiness and to quantify the benefits and customer value proposition of H2Pump's Hydrogen Recycling System (HRS-100™) by installing and analyzing the operation of multiple prototype 100-kg per day systems in real world customer locations. The data gathered will be used to measure reliability, demonstrate the value proposition to customers, and validate our business model. H2Pump will install, track and report multiple field demonstration systems in industrial heat treating and semi-conductor applications. The customer demonstrations will be used to develop case studies and showcase the benefits of the technology to drive market adoption. The objectives of the project are to:

- Validate commercial assumptions around the Hydrogen Recycling Agreement including customer assumptions and system performance.
- Build case studies of the HRS-100™ in customer operations that can be used as credible demonstrations quantifying the operating cost savings, emissions reduction and production efficiency improvement.
- Expand the Beta test fleet into additional customer environments to accelerate learning, problem identification, resolution and reduce the risk of product launch
- Provide data to the National Renewable Energy Laboratory (NREL) for in-depth analysis of system performance characteristics and identify areas for improved data gathering and performance causal analysis. All of the data acquired by the systems will be made available for NREL. The minimum data includes stack voltage and current, system power, and hydrogen flow rate. Data frequency can be no less than a one minute interval. Maintenance and repair logs should also be provided to NREL, specifying time, maintenance item, or reason for repair. NREL will also be provided with all gas analysis to help determine whether certain gases result in higher degradation.
- Prepare and test commercial infrastructure elements such as installation, commissioning, reporting, operation, and maintenance.

Fiscal Year (FY) 2013 Objectives

- Create and deploy a database tool for retrieval of data logs to monitor and analyze system performance.
- Install and commission four of the eight systems in the first quarter of 2013 and provide data to NREL to perform degradation calculations.
- Execute Go/No-Go review.
- Install and commission the four remaining systems in the second half of 2013 and provide data to NREL to perform degradation calculations.

Technical Barriers

This project addresses the following technical barriers from the Technology Validation section of the Fuel Cell Technologies Office Multi-Year Research, Development, and Demonstration Plan:

(D) Lack of Hydrogen Refueling Infrastructure Performance and Availability Data

(G) Hydrogen from Renewable Resources

FY 2013 Accomplishments

- Installed and commissioned an HRS-100™ system at Ulbrich Stainless Steel in Wallingford, CT.
- Installed and commissioned an HRS-100™ system at Pall Corporation in Cortland, NY.
- Installed and debugged two HRS-100™ systems at Rome Strip Steel in Rome, NY in conjunction with a gas treatment system for oil removal and CO reduction.
- Implemented method for data retrieval, sharing and analysis with NREL while database development is underway.

✧ ✧ ✧ ✧ ✧

INTRODUCTION

Hydrogen is used in numerous industrial applications including metallurgical and semiconductor processing. Hydrogen intensive metal heat treating applications include stainless steel annealing, brazing, and metal production from ore. Each industrial application uses hydrogen for different purposes; however, in general, hydrogen is used to create an oxygen-free reducing atmosphere and is not consumed by the industrial process. H2Pump has developed a unique hydrogen recycling solution capable of reclaiming nearly 100 kg per day from such industrial processes.

Figure 1 shows how the HRS integrates with a typical industrial furnace or semi-conductor manufacturing tool. The HRS receives the furnace or tool exhaust which is normally flared or exhausted to atmosphere. The HRS requires certain utilities including electricity, water, and nitrogen. The heart of the HRS system is the electrochemical pump stack. The electrochemical process involves the extraction of hydrogen from a gas stream containing hydrogen followed by the formation of "new" hydrogen. This transformational approach is accomplished without mechanical compression. The new hydrogen is returned to the original process.

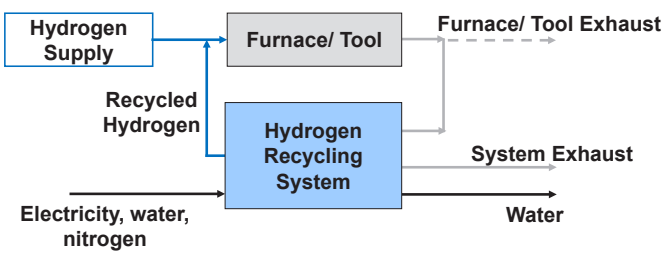

FIGURE 1. Integration of a Hydrogen Recycling System with an Industrial Process

The HRS-100™ system design is represented in Figure 2. The main subsystems and components include incoming gas clean-up, humidification, the pump stack, power supply, heat rejection and the dryer. Most heat treating processes require very low dew point in the hydrogen supply. To ensure adequate quality of the recycled product, H2Pump measures the dew point of the product before returning the hydrogen to the customer's process.

APPROACH

H2Pump is fortunate to have the support of the New York State Energy Research and Development Authority (NYSERDA) as a cost-sharing partner in this project. The NYSERDA award funds 50% of the system material cost, the installation cost, and the ongoing operation and maintenance costs of the demonstration. The DOE award shares the costs of the systems, the database development, and analysis performed by NREL.

A total of eight systems are planned to be installed and monitored during the project. For each site H2Pump follows the steps shown in Figure 3. The first step is establishing the site requirements and installation plan. Activities to uncover site specific issues, including potential gas contaminates are undertaken early in the planning process. Mitigation plans are put in place for known contaminates and the systems are installed and commissioned. Following commissioning, the system will be monitored and the data logs will be given to NREL for analysis.

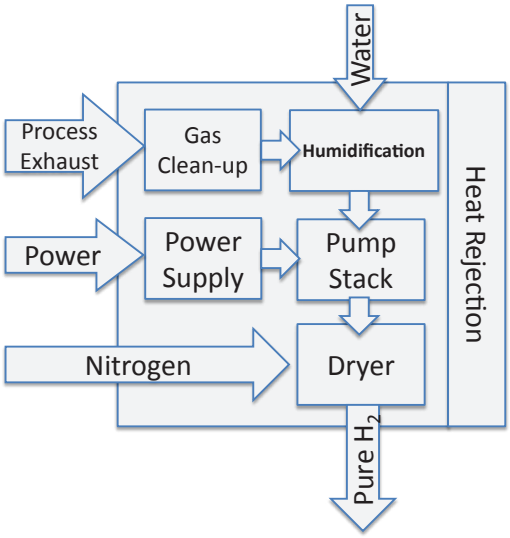

FIGURE 2. HRS-100™ Subsystems and Components

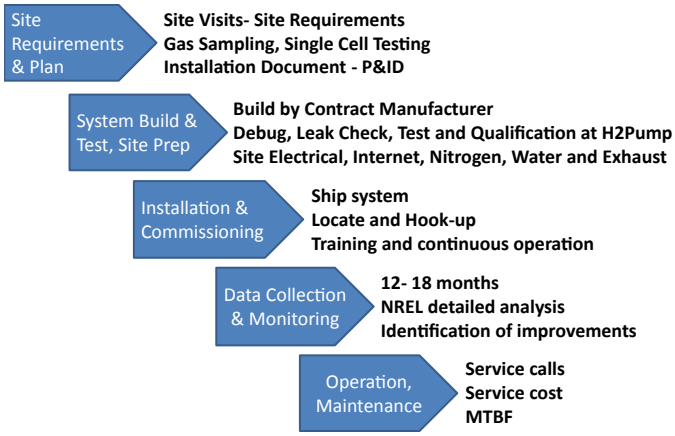

FIGURE 3. Program Approach

RESULTS

As of this report, the first four systems are installed, with only two fully commissioned and reporting only two months of operational data. The installed systems are shown in Figure 4. The final two systems should achieve continuous operation in the third quarter of 2013. Once more systems are reporting data H2Pump will be able to summarize the results and NREL will be able to report their analysis. This has delayed the Go/No-Go decision for a quarter.

CONCLUSIONS AND FUTURE DIRECTIONS

The site planning and commissioning steps are proving to be the most critical and time intensive part of the project. For the remaining four installations in the second part of the project, greater emphasis will be placed on understanding the site actual operational characteristics.

FY 2013 PUBLICATIONS/PRESENTATIONS

1. 2013 U.S. DOE Hydrogen and Fuel Cells Program and Vehicle Technologies Program Annual Merit Review and Peer Evaluation Meeting, May 13–17, 2013, Crystal City, Virginia.

FIGURE 4. Completed HRS-100™ Installs

VII.4 Hydrogen Component Validation

Kevin Harrison (Primary Contact), Michael Peters, Chris Ainscough
National Renewable Energy Laboratory (NREL)
15013 Denver West Parkway
Golden, CO 80401
Phone: (303) 384-7091
Email: Kevin.Harrison@nrel.gov

DOE Manager
Jason Marcinkoski
Phone: (202) 586-7466
Email: Jason.Marcinkoski@ee.doe.gov

Subcontractor:
Marc Mann, Spectrum Automation Controls, Arvada, CO

Project Start Date: October 1, 2011
Project End Date: Project continuation and direction determined annually by DOE

Overall Objectives

- Collaborate with industry to test and validate the commercial readiness of hydrogen systems components and systems.
- Develop and work with industry to provide advanced functionality and innovative solutions of near-commercial hydrogen systems.
- Working with DOE and other key stakeholders, by 2020, validate large-scale systems for grid energy storage that integrate renewable hydrogen generation and storage with fuel cell power generation by operating for more than 10,000 hours with a round-trip efficiency of 40%.

Fiscal Year (FY) 2013 Objectives

- Install, perform accelerated testing on, and analyze performance of hydrogen compressors.
- Establish cooperative research agreements with industry partners to enable equipment loans and testing of advanced systems at NREL.
- Monitor system faults and downtime of the Hydrogen Component Validation Project system and report composite data products alongside comparable sites.

Technical Barriers

This project addresses the following technical barriers from the Technology Validation section of the Fuel Cell Technologies Office 2012 Multi-Year Research, Development, and Demonstration Plan:

(D) Lack of Hydrogen Refueling Infrastructure Performance and Availability Data

(G) Hydrogen from Renewable Resources

Technical Targets

This project is focused on testing and validation efforts to better integrate hydrogen systems and measure their ability to deliver low-cost hydrogen from production through dispensing. However, the project is flexible and has been retargeted in FY 2013 to focus on performing accelerated life testing of both diaphragm and piston hydrogen compressors. Projects in the Technology Validation sub-program are both "learning demonstrations" to help guide and manage the hydrogen and fuel cell component and materials research and development activities, and a validation of the technology under real-world operating conditions against durability and performance targets. While compressor performance metrics are being developed and integrated with this Technology Validation work plan, hydrogen compression can be found included in Task 3 of the Technology Validation section of the Fuel Cell Technologies Office Multi-Year Research, Development, and Demonstration Plan.

Task 3 – Hydrogen Delivery, Production, and Refueling

- Milestone 3.3: Validate large scale (>100 kg/day) integrated wind-to-hydrogen production system. (2Q, 2015)
- Milestone 3.9: Validate large-scale system for grid energy storage that integrates renewable hydrogen generation and storage with fuel cell power generation by operating for more than 10,000 hours with a round-trip efficiency of 40%. (4Q, 2020)

FY 2013 Accomplishments

- Installed and began accelerated life testing of pneumatically-driven piston hydrogen gas booster.
- Established a Cooperative Research and Development Agreement (CRADA) with PDC Machines. Started process for a second CRADA with Proton Onsite.
- Reported detailed reliability metrics for the Xcel Energy/NREL demonstration project relative to other hydrogen stations operating at 350 bar.

✧ ✧ ✧ ✧ ✧

INTRODUCTION

The Hydrogen Component Validation project is advancing the integration of renewable electricity sources with state-of-the-art hydrogen production, compression, storage, and dispensing systems. The project work scope includes quantifying the operation and maintenance, durability, and reliability under near-real-world operating conditions to support DOE validation of these metrics. Insights gained from this work benefit the hydrogen-based industry and relevant stakeholders as the market for this equipment and products expands. Progress in on-site production, compression, and storage at fueling stations will continue to be validated as the technology improves and is scaled up.

Today, one of the project's primary goals is to validate the performance and reliability of hydrogen production (via renewable electrolysis) and compression systems as they are applied to hydrogen as an energy storage medium and for vehicle refueling. The project includes optimization of the electrical pathway (i.e., power conversion) between renewable sources and the electrolyzer and compression systems of hydrogen at various pressures.

APPROACH

This project provides a flexible, independent testing platform and verification of the technical readiness of advanced integrated systems by operating them from the grid and renewable electricity sources. Real-world data from daily system operation are revealing opportunities for improved system design, optimization, and unique hardware configurations to advance the commercialization of these technologies. Lessons learned and data-driven results provide feedback to DOE, industry, and the analytical and modeling components of other sub-programs.

RESULTS

In FY 2013, NREL, using various funding mechanisms (e.g., work for others, internal, and CRADA), expanded the capabilities of the Hydrogen Component Validation project. The system was designed as a flexible platform enabling quick installation, testing, and reporting of critical equipment performance for DOE and industry.

In FY 2013, NREL established a CRADA with PDC Machines, a leading manufacturer of diaphragm compressors. This CRADA is focused on a fully instrumented 700-bar compressor and performing highly accelerated life testing at NREL. The system is expected to be fully integrated with NREL's system, including data acquisition to improve reporting of test results and to feed back lessons learned to PDC. NREL also started the process towards a second CRADA with Proton Onsite, a leading manufacturer of polymer electrolyte membrane electrolyzer systems. The focus of this CRADA will revolve around advanced grid integration techniques, increasing system efficiency, and improved coupling with renewable sources of electricity.

Figure 1 shows the results of reliability tracking at the Hydrogen Component Validation project, as compared to other 350-bar stations for which NREL collects data. Values of the shape parameter above 1 indicate an increasing failure rate, while those below 1 indicate a decreasing failure rate. The rate of failures at the Hydrogen Component Validation project is increasing as a result of its mission to provide highly accelerated life testing of hydrogen components, yet its shape parameter is within the range of other stations its age, indicating that the results, while accelerated, are relevant.

A pneumatically-driven hydrogen gas booster was operated with an accelerated duty cycle and required a rebuild after 200 hours of operation. It was at this point that the high-pressure seals were no longer building pressure above about 3,500 psig, but the seals didn't fail completely. The manufacturer was contacted after the seals were determined to be ineffective and indicated that this situation was very rare after this short duration. They also recommended replacement of both sets of seals and checking the valves.

Worn high-pressure seals leak into a 'dead zone' where the hydrogen gas is ported out a vent. The premature wearing of the seals is attributed to the extremely cold operational conditions the gas booster faced during the first 200 hours of operation—namely, the winter months of December 2012 and January 2013. The gas booster is mounted outdoors in an enclosure but has no heating or cooling to keep it within any temperature range.

The manufacturer (MaxPro Technologies) has indicated that the operational temperature isn't specified, but requires the dew point of the drive air remain below ambient to avoid freezing of the input drive mechanism and vent leak-off port. To assure dry drive air, NREL added an active cooler at the output of the 20-horsepower air compressor to reduce the dew point of the air that drives the gas booster. In addition, a 120-gallon buffer tank was added to reduce the cycling of the compressor.

One significant lesson learned from this initial high-pressure seal rebuild event is that, with the right system controls (e.g., hand valves) and proper analysis equipment (e.g., graduated cylinder), the high-pressure seal degradation can be monitored at the leak-off port. NREL installed the proper system controls and created a process to monitor seal integrity. Full details to these findings will be provided in the DOE CPS 58055 Milestone Report which will be available at the end of August 2013. Figure 2 shows the compressor flow rate versus outlet pressure. The data reveal that the high-pressure seals required replacement because they were not capable of compressing hydrogen above 3,500 psig.

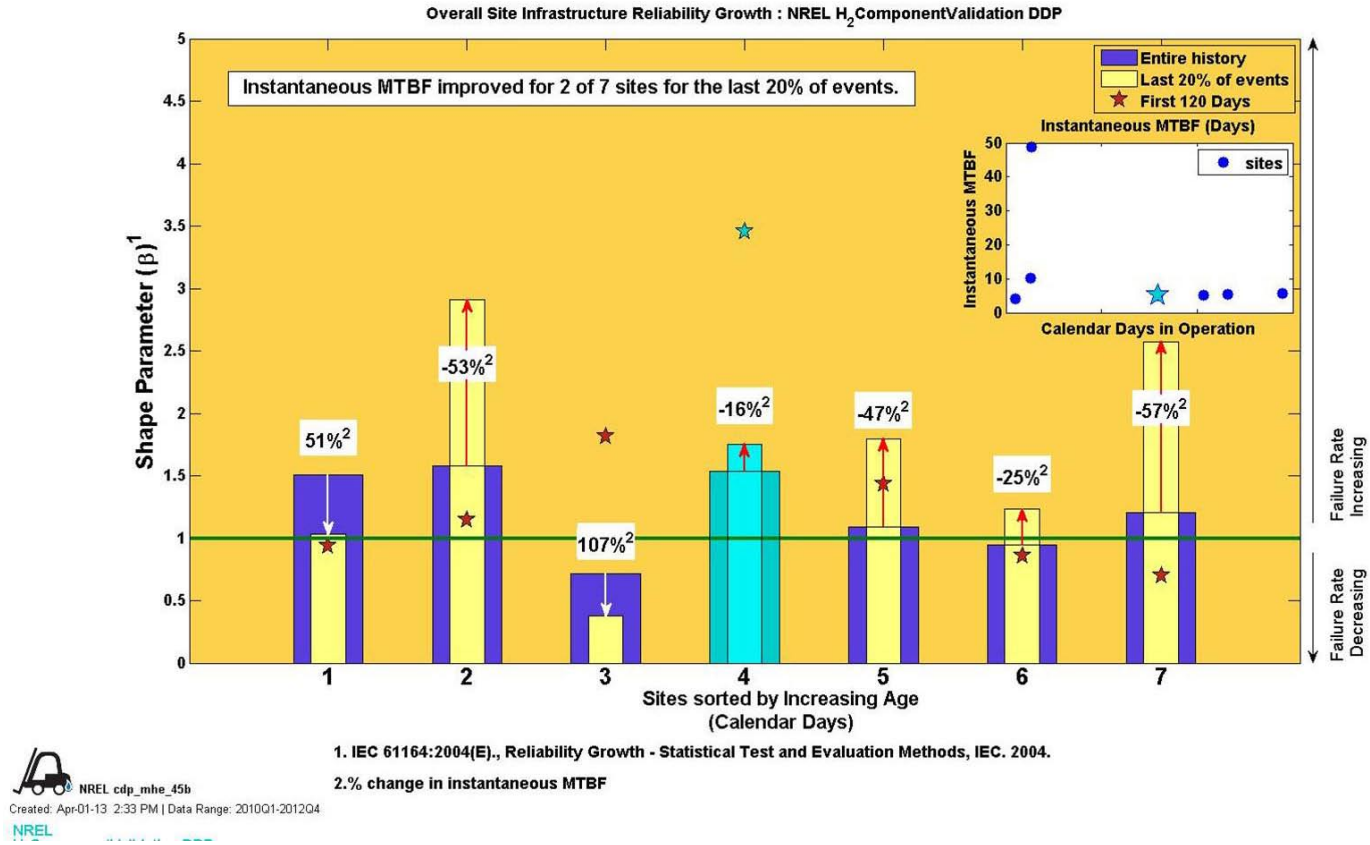

MTBF - mean time between failure

FIGURE 1. NREL's Detailed Data Product Comparing the Hydrogen Component Validation Project

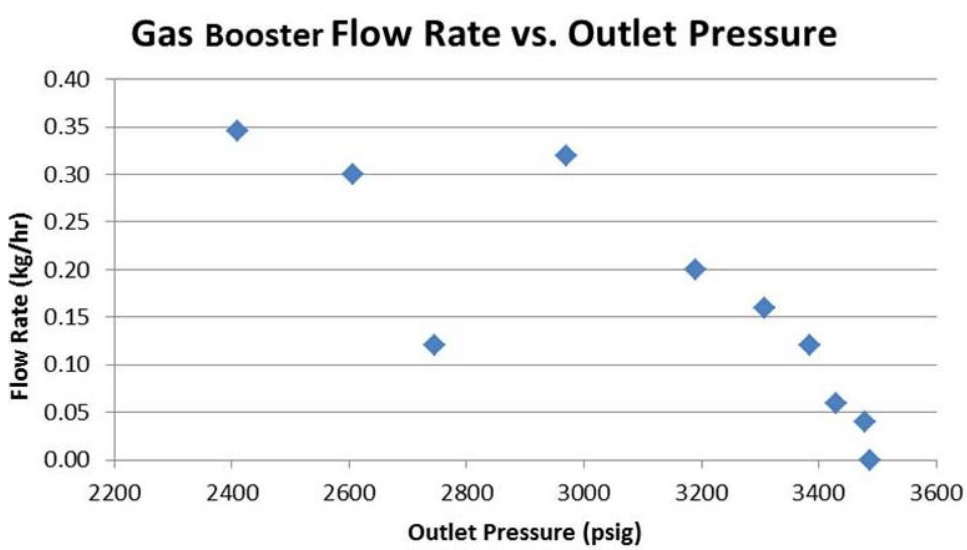

FIGURE 2. Hydrogen Flow Rate versus Gas Booster Outlet Pressure just before Seal Replacement

A work for others project with California's Department of Food and Agriculture, Division of Measurement Standards, allowed the addition of high-pressure storage (13,500 psig) from FIBA Technologies. In addition, two new high-pressure piston gas boosters, from Hydraulics International, were procured using NREL overhead budget

from the Transportation and Hydrogen Systems Center. Performance and maintenance of these new systems will be tracked alongside the existing system components.

CONCLUSIONS AND FUTURE DIRECTION

NREL, using various funding mechanisms, expanded the capabilities of the Hydrogen Component Validation project. NREL established a CRADA with PDC Machines and is finalizing another with Proton Onsite. Both agreements will focus on improving their equipment reliability and validate system performance. Tracking of reliability data shows that while the project is successful in accelerating failures of the components under test, the failure rates are within reason for other stations of its type and age and are therefore relevant. A pneumatically-driven hydrogen gas booster was operated with an accelerated duty cycle for 200 hours before rebuilding of the high-pressure seals was required. It was at this point that these seals were no longer building pressure above about 3,500 psig. A process was established to periodically monitor the integrity of the high-pressure seals to better predict the next maintenance event.

In the coming year the team will complete the following:

- Track and evaluate performance of multiple piston-type gas boosters from different manufacturers under an accelerated duty cycle.
- Monitor system faults and maintenance and analyze performance of Xcel Energy/NREL renewable electrolysis, compression, storage, and refueling demonstration project.
- Follow through with CRADAs established in FY 2013 and expand industry involvement in the validation testing being conducted at NREL.

VII.5 Validation of an Advanced High-Pressure PEM Electrolyzer and Composite Hydrogen Storage, With Station Operating Data Reporting, at the SunHydro Stations

Larry Moulthrop (Primary Contact), Luke Dalton
Proton Energy Systems dba Proton OnSite
10 Technology Drive
Wallingford, CT 06492
Phone: (203) 678-2188
Email: lmoulthrop@protononsite.com

DOE Managers
Jason Marcinkoski
Phone: (202) 586-7466
Email: Jason.Marcinkoski@ee.doe.gov
Jim Alkire
Phone: (720) 356-1426
Email: James.Alkire@go.doe.gov

Contract Number: DE-EE0005887

Subcontractor:
SunHydro LLC, CT

Project Start Date: December 1, 2012
Project End Date: November 30, 2013
(Go/No-Go decision for next phase)

Overall Objectives

- Validate energy savings of up to 11 kWh/kg H_2 through system and stack advancements
- Double usable hydrogen storage per unit volume by increasing pressure cycling range
- Provide advanced packaging design to reduce station footprint
- Collect and report station performance for up to 24 months

Fiscal Year (FY) 2013 Objectives

- Build full-scale advanced cell stack for stack portion of energy savings
- Install system upgrades for reduced dryer losses for system portion of energy savings
- Complete analysis of codes and standards for advanced packaging arrangement
- Complete instrumentation of station and initiate reporting of station performance

Technical Barriers

This project addresses the following technical barriers from the Technology Validation section of the Fuel Cell Technologies Office Multi-Year Research, Development, and Demonstration Plan:

(C) Hydrogen Storage

(D) Lack of Hydrogen Refueling Infrastructure Performance and Availability Data

(E) Codes and Standards

Technical Targets

Advanced Electrolysis-Based Fueling Systems: There is not a specific target table in the Technology Validation section of the Multi-Year Research, Development, and Demonstration Plan specific to hydrogen refueling infrastructure. This project is conducting technology validation of improved cell stack, system, and storage components for an electrolysis-based hydrogen refueling station. These improvements will support the following targets:

- Reduce station energy use by up to 11 kWh/kg
- Reduce the storage volume by 50% per kg of hydrogen dispensed
- Package a station based on proton exchange membrane (PEM) electrolysis within a 12-meter International Organization for Standardization (ISO) container

FY 2013 Accomplishments

- Procured new tooling for the high-efficiency electrolyzer cell stack and ordered long-lead system and stack parts
- Finalized system design approach for 55-bar upgrade
- Built test system for high-efficiency cell stack, to be modified for 55-bar operation
- Reviewed safety codes and zoning standards for compact component arrangements
- Completed design review with Air Products for storage upgrades
- Ordered Type II extended pressure cycle range storage tubes and ancillaries
- Ordered major fueling system components for compact station arrangement

INTRODUCTION

This project primarily leverages Proton's SunHydro#1 station in Wallingford CT, with access to over 100 kg/day in generation capacity, and a new containerized SunHydro#2 station deploying to Braintree, MA, for technology validation of improved components for hydrogen fueling stations (Figure 1). Since its grand opening in 2010, SunHydro#1 has generated and dispensed in excess of 5,800 kg of hydrogen over thousands of fueling events. Our compact, containerized SunHydro™ station design embodied by SunHydro#2 can address initial demand for small, manufactured H_2 fueling infrastructure in a manner that affords rapid, scalable deployment. The SunHydro station product 'skid', integrating H_2 generation, compression, storage, and dispensing in an intermodal transport ISO container, mitigates significant site permitting issues by virtue of its small 40' x 8' footprint and an innovative application of hydrogen code that drastically reduces required clearances.

Proton and SunHydro LLC are ready to continue down this pathway to demonstrate advanced generation/compression/storage component technologies, including 1) higher pressure hydrogen generation with electrochemical compression, 2) higher efficiency generation with lower resistance electrolyte and advanced catalyst, 3) higher addressable capacity composite storage, and 4) advanced packaging concepts for reduced footprint. Testing will be performed on the compression and drying efficiency as part of the higher generation pressure improvement. The station will also be monitored quarterly for hydrogen produced, stored, and dispensed as well as for the resulting energy consumption by major station subcomponents.

APPROACH

These hydrogen fueling improvements will be accomplished based on the following approaches. For higher pressure/higher efficiency PEM cell stacks, Proton has recently qualified a 30% reduction in PEM membrane thickness for 15- and 30-bar hydrogen generator product lines. The thinner material has been fully qualified with over 5,000 hours of continuous operation in a commercial-scale cell stack and is now ready for introduction to the fueling scale product line, to be operated at 55 bar. Furthermore, Proton has been developing advanced catalyst materials and processes that simultaneously reduce the cost of the product and improve the electrochemical performance. Ongoing work on Proton's Phase II Small Business Innovative Research project through the Department of Energy has been successful in developing an alternate catalyst application technique resulting in 50% less catalyst usage as well as efficiency gains due to the lower ohmic resistance. This change is going through production release at the smaller scale commercial stack level. Through this technology validation effort, the tooling is also being procured for the larger size for phase-in after the initial production qualification. A 55-bar militarized cell stack design will be built using the thinner material and advanced catalyst

FIGURE 1. SunHydro#1 and SunHydro#2 Stations

deposition to show the performance improvement at full scale compared to previous technology stacks. A 55-bar capable balance-of-plant system that can accept multiple 55-bar cell stacks is required to validate these improvements at fueling station scale. We will upgrade a commercial 30-bar C series electrolyzer's hydrogen-water management system to operate at 55 bar by strengthening the gas drying components. An increase in hydrogen generation pressure from 30 bar to 55 bar can improve hydrogen fueling system efficiency in two areas – H2 gas drying and dried H2 compression into station storage. With increased H2 generation pressure the relative fraction of water present in the gas decreases, positively impacting the performance of the hydrogen gas dryer since it has less water vapor to remove. As a result of the lower water concentration, the dryer purge losses can be expected to decrease substantially since the water vapor concentration at 55 bar will be about 55% of the concentration at 30 bar. Higher dry H2 pressure into the station mechanical compressor will result in better combined compression energy and higher throughput capability.

For higher addressable capacity storage and reduced station footprint, Proton will install and validate new compact Type II composite storage tubes and apply fresh interpretations of hydrogen safety code to design a complete fueling station within the compact footprint of an ISO container. Proton will apply these new rules to the design of SunHydro#2 station.

The impact of all performance improvements will be reported through instrumentation of the station before and after the design changes. The impact of new compact station arrangements will be reported in site approval time and in station operability data.

RESULTS

As this project is technology validation, most results of cell stack and system technology performance will be reported after technology deployment and test scheduled for late FY 2013 and FY 2014.

The build of the Proton C Series 30 hydrogen generator that will act as the test bed for the advanced cell stack was completed in late 2012. This system completed its verification testing and is currently supplying the hydrogen used by the Sun Hydro#1 station at Proton. The hydrogen gas management portion of the commercial C series 30 bar pressure hydrogen generator is comprised primarily of proprietary design hydrogen/water phase separator and a pressure swing absorber. Proton engineering completed a mechanical design analysis of these components to learn that only minor changes to valve seats, retaining bolts, and pressure sensors are needed to operate at 55 bar. This allows Proton to proceed with the modifications.

Modifications to model code that can affect containerized hydrogen solutions were discussed during a first draft revision working meeting of the National Fire Protection Association (NFPA) 2 Hydrogen Technology Code committee in June 2013 on which Proton is a member. Hydrogen infrastructure stakeholders in attendance – industry, enforcement authorities, code developers, national labs, vehicle manufacturers – recognized a code gap concerning larger containerized hydrogen solutions for storage, energy production, and fueling systems. Containerization is being implemented as a means to reduce site requirements and approval time for hydrogen infrastructure. Existing model code treats shipping containers as a building, which can impose additional equipment, site, and clearance requirements not typically required of industrial equipment that can limit enforcer latitude in approving containerized systems, especially when in close proximity to existing buildings and occupancies. Clear and specific code language addressing containerized equipment as equipment can serve to help the code enforcer accelerate approvals. At the meeting an outline of new code language was put forth by membership and a working subcommittee formed with Proton as chair to develop the language favorable to providing code enforcers appropriate guidance when considering containerized systems. This work will aid approval and deployment of SunHydro#2 station in a 12-meter ISO container. Initial meetings with authorities in Braintree, MA, the site of SunHydro#2, have been very favorable already due to local zoning laws that regard a shipping container footprint as needing very little consideration in terms of setbacks and other building site constraints.

Work on a compact fueling station arrangement for the SunHydro#2 station has advanced to where major components are on order. Typical fueling station arrangements use explosion-proof equipment and housings to contain electrical power and controls. This approach limits accessibility for service and maintenance. Typical model code application forces significant separation distances from high pressure storage to personnel, adjacent buildings, and equipment, on the order of 25 to 35 feet. These tend to drive up station material and build costs and increase station footprint beyond acceptable limits. Proton has developed fueling-class water electrolyzers that, due to their minimal hydrogen content, do not require or introduce hazardous location classification on their own. Our analysis of compact hydrogen station component arrangements under this work shows an advantage to using the non-classified area immediately around our PEM hydrogen generator to house almost all electrical power and control equipment. Further, the NFPA 2 hydrogen code permits reduction of separation distances from hydrogen storage to electrical exposures and unclassified areas to be reduced to near zero when a 2-hour rated firewall is interposed. Proton has identified relatively inexpensive materials and construction that can be used to compactly create a 2-hour firewall in between two containers or to demise one container. Our arrangement analysis to date

shows significant space saving advantages in placing this firewall in between the non-classified electrolyzer generator container space and the classified container space housing compression, storage, and a built-in dispenser. Ancillary cooling equipment may be placed on the roof of the non-classified H2 generation container section, with a firewall interposed line-of-site to the classified compression, storage, and a built-in dispenser (Figure 2). This approach will be validated to meet the 8' x 40' goal in the SunHydro#2 station under construction as of this report.

CONCLUSIONS AND FUTURE DIRECTIONS

- Conclusions to date:
  - Modeling of component arrangements aided by application of up-to-date model code show that a full-size hydrogen fueling station can be implemented within a 8'x 40' container space and incorporate PEM H2 generation, H2 compression, storage, and dispensing with cooling ancillary components mounted on the roof.
- Future directions:
  - An advanced full-size 55-bar PEM cell stack will be built and tested along previous designs to validate higher pressure and efficiencies improve station efficiency by up to 11 kwh/kg H2
  - Higher addressable storage tanks will be installed and validated in two stations
  - A compact containerized fueling station will be deployed and permitted
  - Both stations will be instrumented to facilitate reporting of station performance.

FY 2013 PUBLICATIONS/PRESENTATIONS

1. AMR 2013 moulthrop, TV012

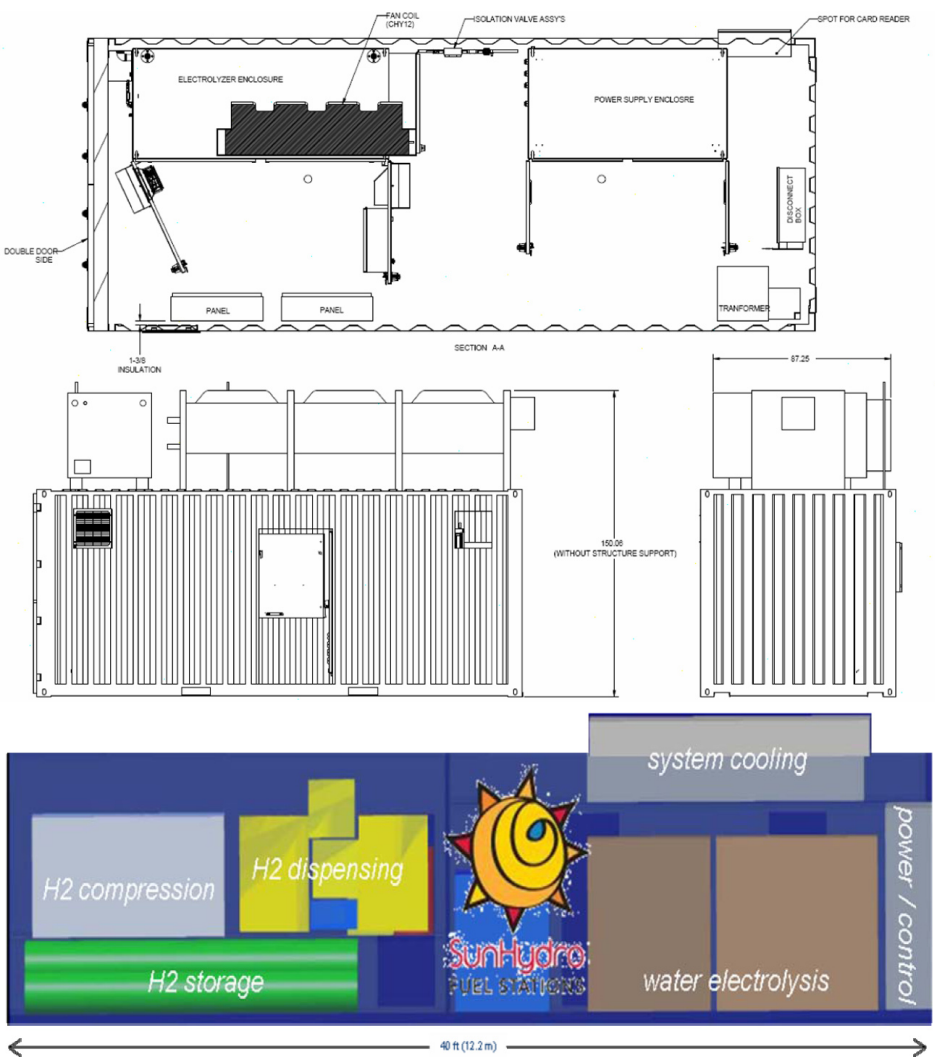

FIGURE 2. Arrangement, H2 Generator Container Section and SunHydro Concept

VII.6 Forklift and Backup Power Data Collection and Analysis

Jennifer Kurtz (Primary Contact), Sam Sprik, Todd Ramsden, Genevieve Saur, Chris Ainscough, Matt Post, and Mike Peters
National Renewable Energy Laboratory (NREL)
15013 Denver West Parkway
Golden, CO 80401-3305
Phone: (303) 275-4061
Email: jennifer.kurtz@nrel.gov

DOE Manager
Jason Marcinkoski
Phone: (202) 586-7466
Email: Jason.Marcinkoski@ee.doe.gov

Project Start Date: October 2012
Project End Date: September 2014

Overall Objectives

- Perform an independent assessment of technology in "real-world" operation conditions, focusing on fuel cell systems and hydrogen infrastructure
- Leverage data processing and analysis capabilities developed under the Fuel Cell Vehicle Learning Demonstration
- Support market growth through reporting on technology status to key stakeholders and performing analyses relevant to the markets' value proposition
- Study fuel cell systems operating in material handling equipment (MHE), backup power, portable power, and stationary power applications; the project includes approximately 1,000 deployed fuel cell systems

Fiscal Year (FY) 2013 Objectives

- Conduct quarterly analysis of operation and maintenance data for fuel cell systems and hydrogen infrastructure (x4)
- Prepare bi-annual technical composite data products (x2)
- Publish interim draft report of status and performance of fuel cell MHE and backup power systems
- Complete performance analyses on durability, reliability, and infrastructure utilization

Technical Barriers

This project addresses the following technical barriers from the Technology Validation section of the Fuel Cell Technologies Office Multi-Year Research, Development, and Demonstration Plan:

(D) Lack of Hydrogen Refueling Infrastructure Performance and Availability Data

(E) Codes and Standards

Contribution to Achievement of DOE Technology Validation Analysis Milestones

This project will contribute to achievement of the following DOE milestones from the Technology Validation section of the Fuel Cell Technologies Program Multi-Year Research, Development and Demonstration Plan:

- Milestone 4.3: Report safety event data and information from ARRA projects (3Q, 2013)

FY 2013 Accomplishments

- By December 2012, 1,302 fuel cell systems were in operation throughout the United States, more than double the number of systems that were in operation at the end of 2010. Seven of the eight MHE sites are fully operational (one site completed its project) and the number of fuel cell backup power systems deployed increased more than 18-fold—from 44 to 806—from 2010 to 2012.
- The technical results published in April 2013 [1] include 21 backup power composite data products (CDPs) and 72 MHE CDPs. The results are categorized as deployment, fuel cell operation, infrastructure operation, fuel cell safety, infrastructure safety, fuel cell durability, fuel cell maintenance, infrastructure maintenance, fuel cell reliability, infrastructure reliability, and cost of ownership.
- The basic deployment and use statistics analyzed for MHE are 490 units in operation; 1,445,558 operation hours; average 4.6 hours between fills; 246,997 fills; and 187,426 kilograms of hydrogen dispensed in 2.3 minutes, on average.
- The basic deployment and use statistics analyzed for backup power are 1.86 MW installed capacity; 806 systems in operation; average site capacity between 4 and 6 kW; and a successful start percentage of 99.6% from the 134 systems that reported detailed operation data.
- A continuous run time of 65 hours was demonstrated for at least one backup power system.
- An interim report summarizing the performance status for fuel cell backup power was completed.

- An interim report summarizing the performance status for fuel cell MHE was completed.

✧ ✧ ✧ ✧ ✧

INTRODUCTION

The U.S. Department of Energy (DOE) designated more than $40 million in American Recovery and Reinvestment Act (ARRA) funds for the deployment of up to 1,000 fuel cell systems. This investment is enabling fuel cell market transformation through development of fuel cell technology, manufacturing, and operation in strategic markets where fuel cells can compete with conventional technologies. The strategic markets include MHE, backup power, stationary power, and portable power, and the majority of the deployed systems are in the MHE and backup power markets. NREL is analyzing operational data from these key deployments to better understand and highlight the business case for fuel cell technologies and report on the technology status.

APPROACH

The project's data collection plan builds on other technology validation activities. Data (operation, maintenance, and safety) are collected on-site by the project partners for the fuel cell system(s) and infrastructure. NREL receives the data quarterly and stores, processes, and analyzes the data in NREL's Hydrogen Secure Data Center (HSDC). The HSDC is an off-network room with access for a small set of approved users. An internal analysis of all available data is completed quarterly and a set of technical CDPs is published every six months. The CDPs present aggregated data across multiple systems, sites, and teams in order to protect proprietary data and summarize the performance of hundreds of fuel cell systems and thousands of data records. A review cycle is completed before the publication of CDPs. The review cycle includes providing detailed data products (DDPs) of individual system and site performance results to the individual data provider. DDPs also identify the individual contribution to CDPs. The NREL Fleet Analysis Toolkit is an internally developed tool for data processing and analysis structured for flexibility, growth, and simple addition of new applications. Analyses are created for general performance studies as well as application- or technology-specific studies.

RESULTS

An objective of the ARRA fuel cell project—to deploy approximately 1,000 fuel cell systems in key early markets—was met within two years from the first deployments. Early market end users are operating 1,302 fuel cell units (Figure 1) at 301 sites in 20 states. At the end of 2012, 490 MHE fuel cell units were operating at seven facilities, and 806 backup power fuel cell units were operating at 385 sites.

The data provided a great deal of information regarding deployment numbers, installed capacity, reliability, and operation trends and characteristics. The number of fuel cell backup power systems deployed increased more than

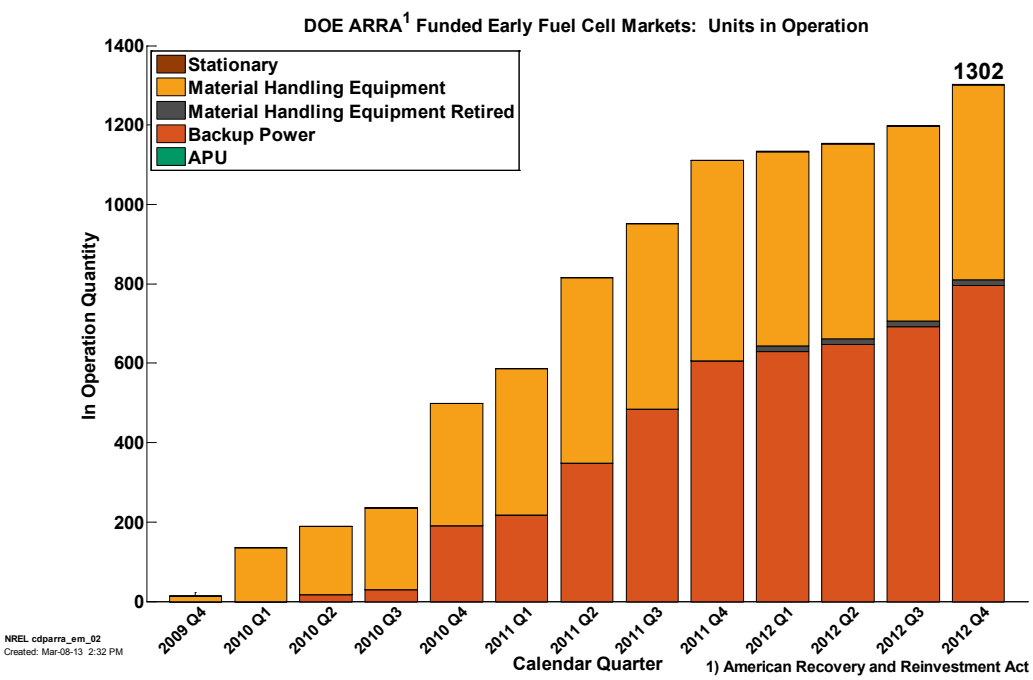

FIGURE 1. DOE ARRA-Funded Early Fuel Cell Markets: Units in Operation

18-fold—from 44 to 806—from the beginning to the end of the project. The start reliability of those systems was 99.6%. While system size ranged to greater than 10-kilowatt (kW) systems, 78% of the systems were in the 4–6 kW size range. Modules of smaller fuel cell units could be combined to adjust the system size to the individual site's needs. The fuel cells accumulated more than 1,153 hours of operation time with one unit successfully demonstrating a continuous run time of 65 hours during the data collection period. The average run time was 39 minutes, and the backup fuel cells were typically started less than once a month. The operational data were also used to characterize the interactions with grid outages and how best to use the systems for critical backup power applications.

There were only eight unsuccessful operations during the 2-year monitoring period. The major cause of five unsuccessful starts was system failure. These systems failures vary in cause, some related to the system and integration with the site. Three of the five system failures were related to a software error in certain situations, which was subsequently fixed. This real-world situational feedback is a critical product development step for fuel cell system manufacturers. The other three causes for unsuccessful starts were once for an emergency stop and twice for no fuel. Additional lessons learned here are based on how sites receive low-fuel alarms and training of site personnel. The emergency stop was likely the result of an operator testing the system and not a safety incident.

Many of the operation characteristics are driven by grid outages and stability. In order to better understand this dynamic, we analyzed grid data from a DOE database, the Electric Disturbance Event Annual Summaries [2] from 2002 to 2012. The data were analyzed to show numbers of incidents and average outage time. While the local grid will affect specific backup power unit operation, these national data can help illustrate what systems face. The number of incidents has seen an increasing trend, while the duration has decreased some. Over the 10-year period, the average number of incidents was 118, while the average duration by year was about 42 hours, or 38 hours when averaging per incident.

An animated movie was also developed that shows a visual representation of the grid incidents and the fuel cell operation [3,4]. The major grid outages are overlaid with installation locations and dates as well as operation data for select fuel cell backup power units and synthesized into a time-lapse geographical visualization map. The interactive map allows the user to click or play through the highlighted events to analyze usage patterns in conjunction with major grid outages (Figure 2).

The MHE fuel cell systems accumulated nearly 1.5 million hours by the end of 2012. High operation hours on the 490 systems indicate these systems are successfully performing and making an impact at the high-productivity facilities. These end-user facilities have had experience with

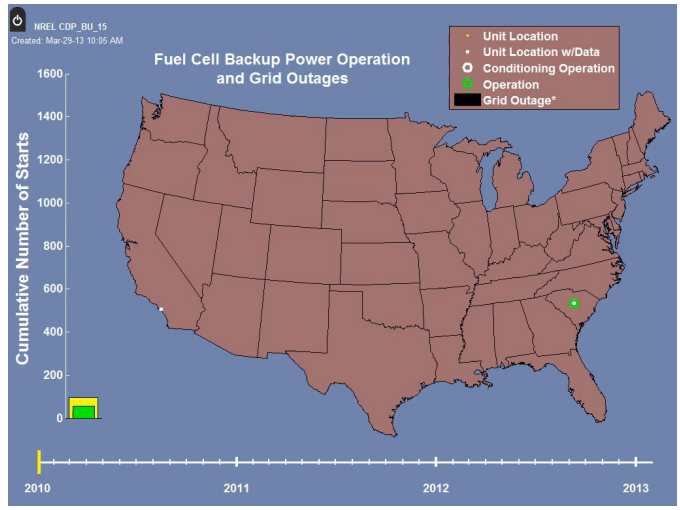

FIGURE 2. Snapshot of the Fuel Cell Backup Power Operation and Grid Outages Movie

battery and propane lifts and expected the fuel cell systems to meet and exceed performance expectations in a few key areas for both the retrofit and greenfield sites. These key performance areas include fill amount, operation per fill, operation per day (and year), mean time between failure, and voltage degradation (or fuel cell operation durability). These areas were studied in detail for each system, fleet, and lift classification.

The ultimate durability of fuel cell MHE is still being determined and will continue to be tracked by NREL. This is a key metric to the value proposition—if MHE are unable to meet the expectations of 2–3 times the life of a battery system, the value proposition may be in jeopardy. At least six systems had already demonstrated durability past the interim target of 10,000 hours. However, the majority (60%) of systems are currently projected to experience 10% voltage decay prior to reaching 10,000 hours of operation (Figure 3). It is important to note that the 10% level is a benchmark only and does not necessarily represent end-of-life for the fuel cell stack, and certainly not for the entire power plant, of which the stack is only one part.

The cost of ownership analysis studied the costs for maintenance, equipment, and refueling labor. This analysis compared these costs between fuel cell MHE and battery MHE. On an annualized cost per MHE per year, the fuel cell has approximately 10% savings for a Class I/II MHE. Factors that have a significant impact on the cost of ownership analysis results include deployment size, operation hours, and facility requirements.

Among components related to the infrastructure, hydrogen compressors contributed the highest number of maintenance events and maintenance labor hours, as well as the greatest number of hydrogen leaks. Half of all unscheduled maintenance events and nearly 60% of the repair

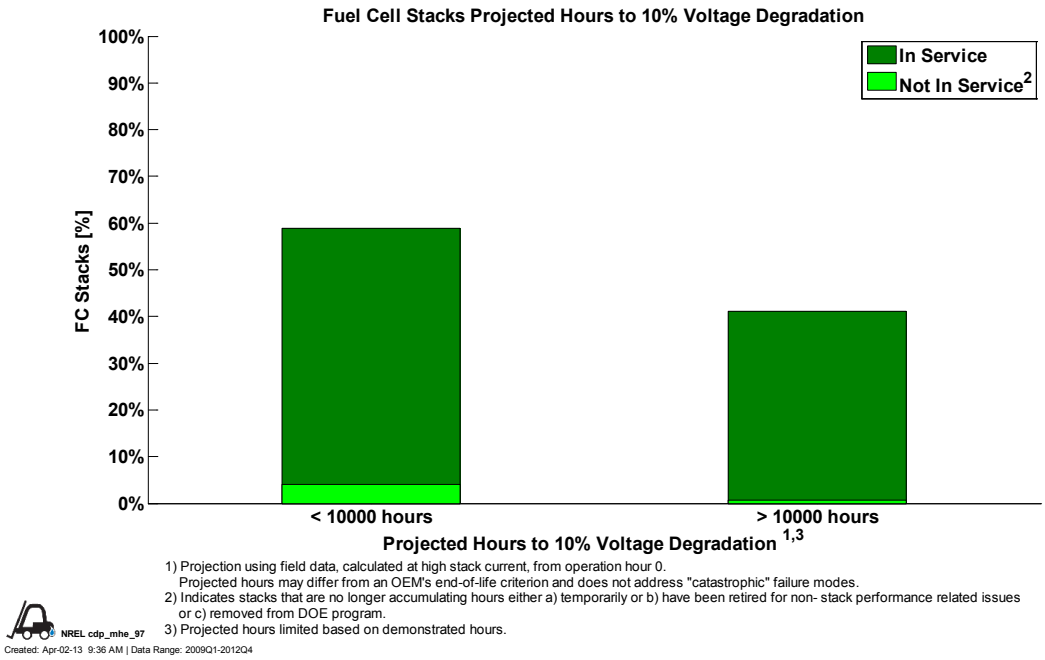

FIGURE 3. Study of Fuel Cell MHE Voltage Degradation Against an Interim Metric Of 10,000 Hours

labor hours were attributed to the hydrogen compressor (Figure 4). Some sites, in fact, have redundant compressors because the reliability of the machines is the limiting factor in station reliability, and they are crucial to the station's mission.

Reliability improved for many of the sites over time and allowed fuel cell power module original equipment manufacturers (OEMs) to learn valuable lessons that cannot be learned in a lab setting. These deployments allowed OEMs to improve their products, while giving them a real-world stage on which to prove their value. This ultimately enabled repeat orders from customers in the absence of ARRA funding.

Despite drive-offs, collisions, and even a few (non-hydrogen) fires, the hydrogen systems of the MHE and the infrastructure were never compromised, safety systems worked as intended, and no serious injuries related to the technologies were reported.

CONCLUSIONS AND FUTURE DIRECTIONS

The results have shown that MHE and backup power are two markets where fuel cells are capable of meeting the operating demands, and these deployments can be leveraged to accelerate fuel cell commercialization. Analysis by NREL of the hydrogen fuel cell MHE and associated infrastructure deployed under ARRA shows that these systems are safe, productive, cost effective, available, durable, and add value to their respective facilities.

The deployment of 1,302 fuel cell units has established a significant data set of successful and safe operation in the hands of end users, has increased fuel cell manufacturing and support capabilities, and has translated lessons learned from the field into improved fuel cell systems for future operation. The aggregated data showcase the significant use and status at end-user sites over the last two years in MHE and backup power applications. The CDPs address a need for published results on the technology status that can be utilized by industry, developers, and end users. The analyses have evolved as the accumulated time and hydrogen dispensed both have increased, providing an insight into market behaviors and expectations. Continued analyses will be covered under Technology Validation and include the following:

- Quarterly analysis of operation data for MHE and backup power systems
- Publication of bi-annual technical CDPs
- Demonstration of a 72-hour continuous run time for a backup power fuel cell system
- Analysis of backup power value proposition

FY 2013 PUBLICATIONS/PRESENTATIONS

1. Ramsden, T., "Fuel Cell-Powered Material Handling Equipment Cost of Ownership Analysis," Golden, CO: National Renewable Energy Laboratory, published April 2013. (report)

2. Kurtz, J., Sprik, S., Ainscough, C., Saur, G., Post, M., Peters, M., "ARRA Material Handling Equipment Composite Data Products:

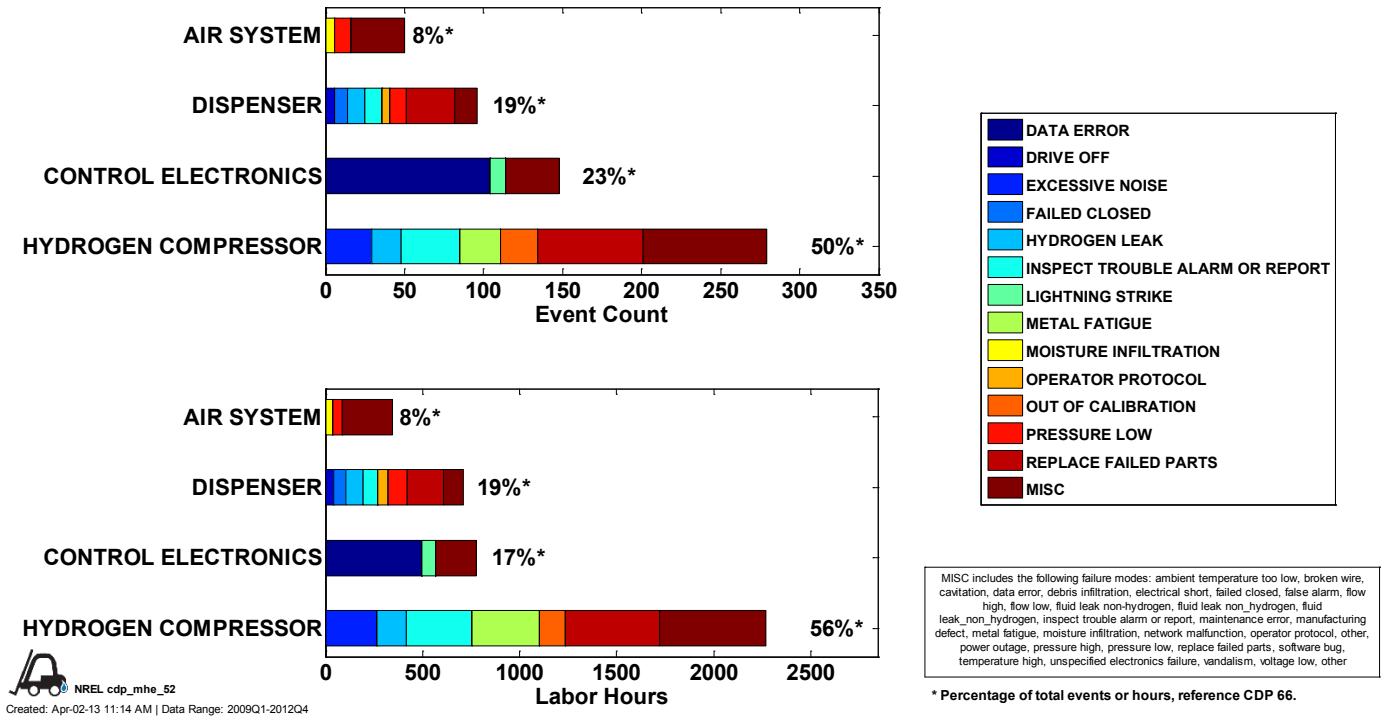

FIGURE 4. Breakdown of Failure Modes for the Top Four MHE Infrastructure Maintenance Categories

Data Through Quarter 4 of 2012," Golden, CO: National Renewable Energy Laboratory, published April 2013. Composite data products produced by NREL's early fuel cell market demonstrations team. (report)

3. Kurtz, J., Sprik, S., Ainscough, C., Saur, G., Post, M., Peters, M., "Spring 2013 Composite Data Products: Backup Power," Golden, CO: National Renewable Energy Laboratory, published April 2013. Composite data products produced by NREL's early fuel cell market demonstrations team. (report)

4. Harrison, K., Rivkin, C., Ainscough, C., Burgess, R., Peters, M., "CSD Safety and Reliability Data," Forecourt CSD Workshop, March 20, 2013. (presentation)

5. Kurtz, J., Sprik, S., Ainscough, C., Saur, G., Post, M., Peters, M., "Early Fuel Cell Market Deployments: ARRA and Combined (IAA, DLA, ARRA) – Quarter 4 2012 Composite Data Products," Golden, CO: National Renewable Energy Laboratory, published March 2013. Composite data products produced by NREL's early fuel cell market demonstrations team. (report)

6. Kurtz, J., Wipke, K., Sprik, S., Ramsden, T., Ainscough, C., Saur, G., Post, M., "Early Fuel Cell Market Deployments: ARRA and Combined (IAA, DLA, ARRA) - Quarter 3 2012 Composite Data Products," Golden, CO: National Renewable Energy Laboratory, published January 2013. Composite data products produced by NREL's early fuel cell market demonstrations team. (report)

7. Kurtz, J., Sprik, S., Ramsden, T., Saur, G., Ainscough, C., "What We've Learned from 2.5 Years of Early Market Fuel Cell Operation," 2012 Fuel Cell Seminar, November 6, 2012. (presentation)

8. Kurtz, J., Ainscough, C., Simpson, L., Caton, M., "Hydrogen Storage Needs for Early Motive Fuel Cell Markets," Golden, CO: National Renewable Energy Laboratory, published November 2012. Report on NREL's analyses of hydrogen storage performance needs and technology gaps. (report)

9. Kurtz, J., Sprik, S., Ramsden, T., Ainscough, C., Saur, G., "ARRA Material Handling Equipment Composite Data Products: Data Through Quarter 2 of 2012," Golden, CO: National Renewable Energy Laboratory, published October 2012. Composite data products produced by NREL's early fuel cell market demonstrations team. (report)

10. Kurtz, J., Sprik, S., Ramsden, T., Saur, G. "Fuel Cell Backup Power Technology Validation," 2012 International Telecommunications Energy Conference, October 1, 2012. (presentation)

11. Kurtz, J., Wipke, K., Sprik, S., Ramsden, T., Ainscough, C., Saur, G., "Fall 2012 Composite Data Products: Backup Power," Golden, CO: National Renewable Energy Laboratory, published October 2012. Composite data products produced by NREL's early fuel cell market demonstrations team. (report)

12. Kurtz, J., "Secure Data Center," Golden, CO: National Renewable Energy Laboratory, published August 2012. Introductory fact sheet about the Secure Data Center at NREL's Energy Systems Integration Facility. (fact sheet)

13. Kurtz, J., Wipke, K., Sprik, S., T., Ramsden, T., Ainscough, C., Saur, G., "Analysis Results for ARRA Projects: Enabling Fuel Cell Market Transformation," 2012 U.S. DOE Hydrogen Program and Vehicle Technologies Program Annual Merit Review and Peer Evaluation Meeting, Washington, D.C, May 2012. (presentation)

REFERENCES

1. "Early Fuel Cell Market Demonstrations," website, Golden, CO: National Renewable Energy Laboratory, http://www.nrel.gov/hydrogen/proj_fc_market_demo.html.

2. Electric Disturbance Events (OE-417) are recorded by DOE's Office of Electricity Delivery & Energy Reliability. Annual summaries are available at http://www.oe.netl.doe.gov/oe417.aspx.

3. "Fuel Cell Backup Power Geographical Visualization Map," fact sheet, Golden, CO: National Renewable Energy Laboratory, December 2012, available at http://www.nrel.gov/docs/fy13osti/56740.pdf.

4. "Grid Outages and Fuel Cell Usage for Back-up Power," animated movie, Golden, CO: National Renewable Energy Laboratory, available at http://youtu.be/GZBLzP5Ka0Q.

VII.7 Fuel Cell Electric Vehicle Evaluation

Jennifer Kurtz (Primary Contact), Keith Wipke, Sam Sprik, Genevieve Saur, and Chris Ainscough
National Renewable Energy Laboratory (NREL)
15013 Denver West Parkway
Golden, CO 80401-3305
Phone: (303) 275-4061
Email: Jennifer.Kurtz@nrel.gov

DOE Manager
Jason Marcinkoski
Phone: (202) 586-7466
Email: Jason.Marcinkoski@ee.doe.gov

Project Start Date: October 2012
Project End Date: Project continuation and direction determined annually by DOE

Overall Objectives

- Validate hydrogen fuel cell electric vehicles (FCEVs) in real-world setting
- Identify current status and evolution of the technology

Fiscal Year (FY) 2013 Objectives

- Complete the update of data templates
- Complete a priority rating for existing FCEV analyses and Composite Data Products (CDPs)
- Complete the first round of processing and analyses of data from multiple FCEV original equipment manufacturers (OEMs)

Technical Barriers

This project addresses the following technical barriers from the Technology Validation section of the Fuel Cell Technologies Office Multi-Year Research, Development, and Demonstration Plan:

(A) Lack of Fuel Cell Electric Vehicle and Fuel Cell Bus Performance and Durability Data

Contribution to Achievement of DOE Technology Validation Analysis Milestones

This project contributes to the achievement of the following DOE milestones from the Technology Validation section of the Fuel Cell Technologies Office Multi-Year Research, Development, and Demonstration Plan:

- Milestone 2.3: Validate fuel cell electric vehicles achieving 5,000-hour durability (service life of vehicle) and a driving range of 300 miles between fuelings. (4Q, 2019)

FY 2013 Accomplishments

- Completed a prioritized list of FCEV data analyses and CDPs for current project
- Completed the update of data templates (vehicle operation, maintenance, safety, and specification templates were updated based on previous templates, discussions with stakeholders, and validation-topic priorities)
- Received and processed vehicle data from multiple FCEV OEMs
- Supported kick-off meetings with individual project partners and detailed conversations on the provided data
- Completed the update of security procedures for the Hydrogen Secure Data Center (HSDC)

✧ ✧ ✧ ✧ ✧

INTRODUCTION

The DOE has funded projects for the collection and delivery of FCEV data submitted to the National Renewable Energy Laboratory (NREL) for analysis, aggregation, and reporting. Multiple real-world sites and customers are included in this FCEV demonstration project. This activity addresses the lack of on-road FCEV data and seeks to validate improved performance and longer durability from comprehensive sets of early FCEVs, including first-production vehicles. NREL's objective in this project is to support DOE in the technical validation of hydrogen FCEVs under real-world conditions. This is accomplished through evaluating and analyzing data from the FCEVs to identify the current status of the technology, compare it to DOE program targets, and assist in evaluating progress between multiple generations of technology, some of which will include commercial FCEVs for the first time.

APPROACH

The project's data collection plan builds on other technology validation activities. Data (operation, maintenance, and safety) are collected onsite by project partners for the fuel cell system(s) and infrastructure. NREL receives the data quarterly and stores, processes, and analyzes the data in NREL's HSDC. The HSDC is an off-network room with access provided to a small set of approved users. An internal analysis of all available data is completed quarterly and a set of technical CDPs is published every six

months. The CDPs present aggregated data across multiple systems, sites, and teams in order to protect proprietary data and summarize the performance of hundreds of fuel cell systems and thousands of data records. A review cycle is completed before the CDPs are published. This review cycle includes providing Detailed Data Products (DDPs) of individual system- and site-performance results to the specific data provider. DDPs also identify the individual contribution to the CDPs. The NREL Fleet Analysis Toolkit is an internally developed tool for data processing and analysis structured for flexibility, growth, and simple addition of new applications. Analyses are created for general performance studies as well as application- or technology-specific studies.

RESULTS

Much of the activity in FY 2013 focused on the steps necessary to get the projects started. NREL supported these steps through data templates (see Figure 1), the HSDC security procedures, project partner interactions, and analyses prioritization. The following priorities were the result of targets, feedback, and discussions between NREL, DOE, and project partners.

The priorities identified as critical were:

- Fuel cell durability
- Vehicle operation (hours and miles)
- Specifications (power density and specific power)
- Range, fuel economy, and efficiency
- Fill performance
- Reliability

The priorities identified as important were:

- Drive behaviors
- Fill behaviors
- Power management
- Energy
- Transients
- Comparisons to conventional vehicles

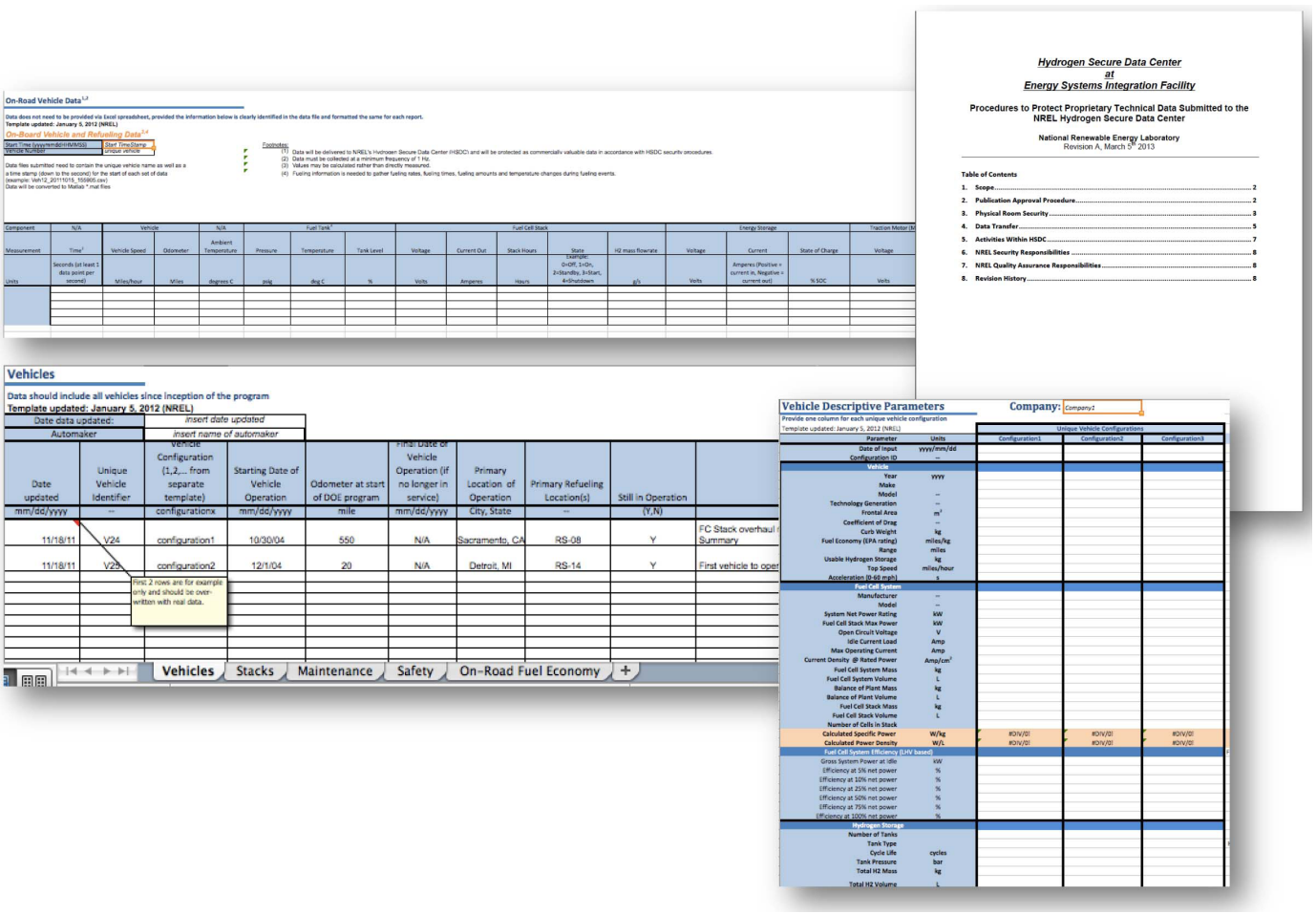

FIGURE 1. Updated FCEV Data Templates and HSDC Security Procedures Document

NREL supported project kick-offs and one-on-one meetings to gain consensus on the methods for data transfer and the steps for building and maintaining trust, such as sending fake CDPs to demonstrate the review process.

Data has been received and processed from multiple OEMs, and data from the remaining project partners is expected by the end of FY 2013.

CONCLUSIONS AND FUTURE DIRECTIONS

This project is still in the early stage. By the end of FY 2013, we expect to complete the first quarterly processing of data from enough OEMs to produce and publish the first, limited set of CDPs in early FY 2014. This first analysis round will rely heavily on the analysis work completed in the FCEV Learning Demonstration project (see Figure 2). Analysis results will focus on the critical and important topics and will validate the performance of current FCEVs against DOE targets and Learning Demonstration benchmarked performance (see Figure 3).

FY 2013 PUBLICATIONS/PRESENTATIONS

1. Kurtz, J.; Wipke, K.; Sprik, S.; Ainscough, C.; Saur, G. (May 2013). "Fuel Cell Electric Vehicle Evaluation." NREL poster prepared for the 2013 DOE Hydrogen and Fuel Cells Program and Vehicle Technologies Office Annual Merit Review and Peer Evaluation.

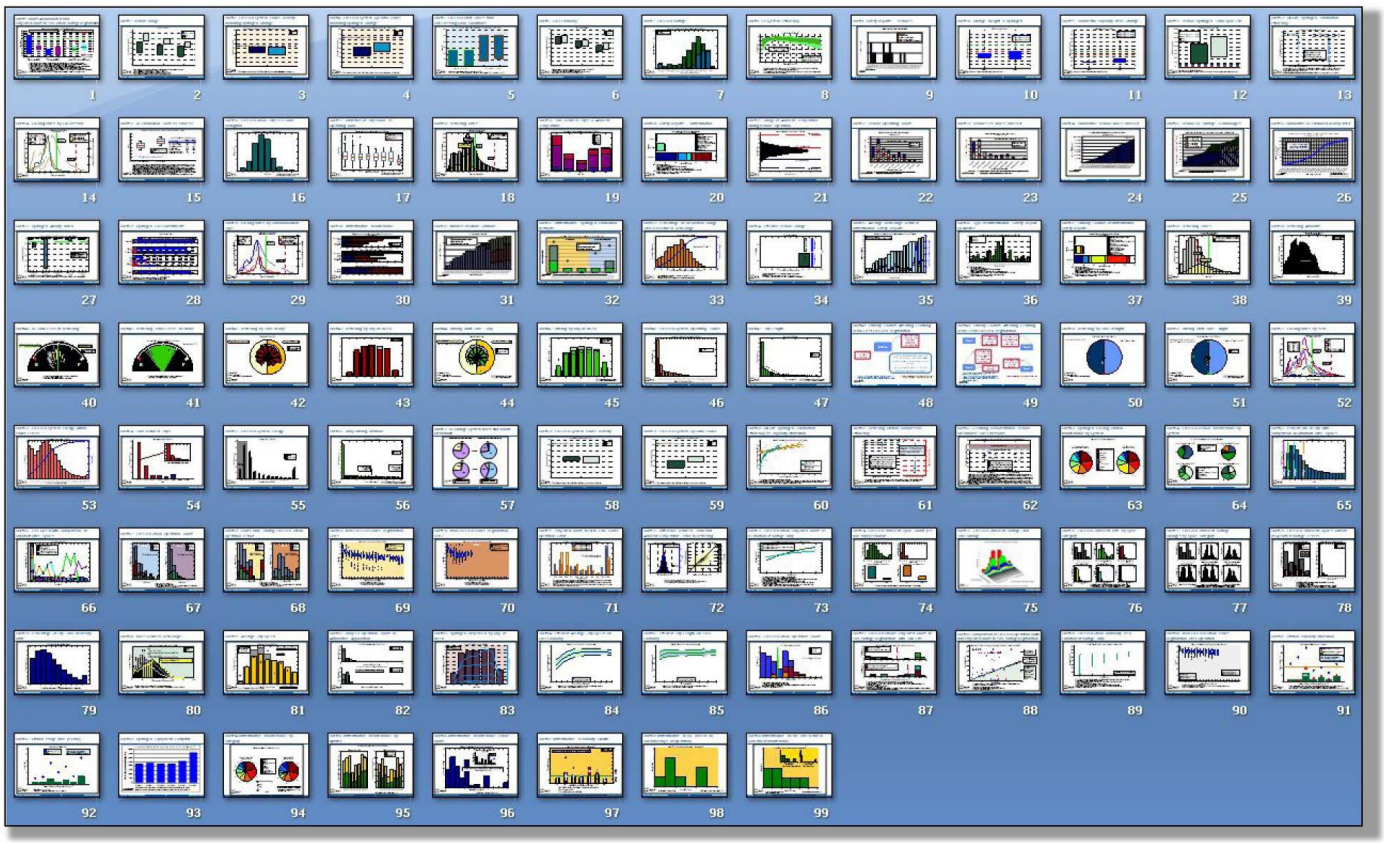

FIGURE 2. Snapshot of 99 FCEV CDPs from Learning Demonstration Project

Vehicle Performance Metrics	Gen 1 Vehicle	Gen 2 Vehicle	2009 Target	After 2009Q4
Fuel Cell Stack Durability			**2,000 hours**	
Max Team Projected Hours to 10% Voltage Degradation	**1,807 hours**	**2,521 hours**		--
Average Fuel Cell Durability Projection	821 hours	1,062 hours		1,748 hours
Max Hours of Operation by a Single Fuel Cell Stack to Date	2,375 hours	1,261 hours		1,582 hours
Driving Range			**250 miles**	
Adjusted Dyno (Window Sticker) Range	**103 - 190 miles**	**196 - 254 miles**		--
Median On-Road Distance Between Fuelings	56 miles	81 miles		98 miles
Fuel Economy (Window Sticker)	42 – 57 mi/kg	43 – 58 mi/kg	no target	--
Fuel Cell Efficiency at ¼ Power	51% – 58%	53% – 59%	60%	--
Fuel Cell Efficiency at Full Power	30% – 54%	42% – 53%	50%	--

Infrastructure Performance Metrics			2009 Target	After 2009Q4
H_2 Cost at Station (early market)	On-Site Natural Gas Reformation **$7.70 – $10.30/kg**	On-Site Electrolysis **$10.00 – $12.90/kg**	**$3/gge**	--
Average H_2 Fueling Rate	0.77 kg/min		1.0 kg/min	0.65 kg/min

Outside of this project, DOE independent panels concluded at 500 replicate stations/year:
Distributed natural gas reformation at 1,500 kg/day: **$2.75-$3.50/kg** (2006)
Distributed electrolysis at 1,500kg/day: **$4.90-$5.70** (2009)

Outside review panel

FIGURE 3. Learning Demonstration Key Performance Metrics and Targets

VII.8 Next Generation Hydrogen Infrastructure Evaluation

Sam Sprik (Primary Contact), Jennifer Kurtz, Chris Ainscough, Genevieve Saur, Matt Post, and Mike Peters
National Renewable Energy Laboratory (NREL)
15013 Denver West Parkway
Golden, CO 80401-3305
Phone: (303) 275-4431
Email: sam.sprik@nrel.gov

DOE Manager
Jason Marcinkoski
Phone: (202) 586-7466
Email: Jason.Marcinkoski@ee.doe.gov

Project Start Date: October 1, 2011
Project End Date: Project continuation and direction determined annually by DOE

Overall Objectives

- Study current, state-of-the-art hydrogen fueling stations. Analyze efficiency, performance, cost and reliability of station components and systems from existing stations.
- Perform an independent assessment of technology in real-world operating conditions, focusing on hydrogen infrastructure for on-road vehicles.
- Leverage data processing and analysis capabilities developed under the Fuel Cell Vehicle Learning Demonstration as well as from forklift, backup power and bus projects.

Fiscal Year (FY) 2013 Objectives

- Collect data from state-of-the-art hydrogen (H2) fueling facilities, such as those funded by the California Air Resources Board (CARB), to enrich the analyses and composite data products (CDPs) on H2 fueling originally established by the Learning Demonstration project.
- Work with codes and standards activities and fueling facility owners/operators to benchmark performance of the fueling events relative to current SAE International (SAE) procedures.
- Perform analysis and provide feedback on sensitive data from hydrogen infrastructure for industry and DOE. Aggregate these results for publication.
- Participate in technical review meetings and site visits with industry partners to discuss results from NREL's analysis in an interactive manner.
- Maintain an accurate database (location and status) of all online hydrogen stations in the United States, and provide periodic updates to other online resources, specifically NREL's Alternative Fuels Data Center (AFDC) station locator, the Fuel Cell and Hydrogen Energy Association, the California Fuel Cell Partnership (CaFCP), and FuelCells.org.

Technical Barriers

This project addresses the following technical barrier from the Technology Validation section of the Fuel Cell Technologies Office Multi-Year Research, Development, and Demonstration Plan:

(D) Lack of Hydrogen Refueling Infrastructure Performance and Availability Data

Contribution to Achievement of DOE Technology Validation Milestones

This project will contribute to achievement of the following DOE milestones from the Technology Validation section of the Fuel Cell Technologies Office Multi-Year Research, Development, and Demonstration Plan:

- Milestone 4.4: Complete evaluation of 700-bar fast fill fueling stations and compare to SAE J2601 specifications and DOE fueling targets. (3Q, 2016)

FY 2013 Accomplishments

- Created new fall 2012 CDPs based on previously supplied data.
- Updated NREL's internal database of stations and their locations and submitted updates to AFDC.
- Participated in the CaFCP working group meetings.
- Internally processed and analyzed quarterly infrastructure data in the HSDC for later inclusion in CDPs once aggregation is possible.
- Provided assistance in filling out and modifying templates for those providing infrastructure data.
- Gathered and provided updates on stations under the DOE Funding Opportunity Announcement 626 projects that are not providing data yet.
- Updated NREL Fleet Analysis Toolkit code to accept data in multiple formats from stations outside the DOE Funding Opportunity Announcement 626 stations.
- Analyzed data from station provider outside DOE Funding Opportunity Announcement 626 projects.

- Gathered additional data outside the standard template to provide SAE J2601 with data on idle times during fueling events.
- Presented this project at Fuel Cell Seminar 2012 and at the 2013 Annual Merit Review.

✧ ✧ ✧ ✧ ✧

INTRODUCTION

In the past decade, approximately 60 hydrogen fueling stations supported a few hundred fuel cell electric vehicles (FCEVs) in the United States. Of these stations, 25 supported the 183 DOE Learning Demonstration vehicles. As original equipment manufacturers are ramping up FCEV bus, forklift, and car production, there is an effort to build additional stations, increase individual station fueling output, and cluster stations to cover the area where vehicles are located.

California has been a leader in supporting additional hydrogen infrastructure through multiple state agencies, including CARB and the California Energy Commission. Two separate actions by CARB funded seven stations of which several are online with the remainder soon to be open in 2012. California Energy Commission is also working on funding stations, moving the state toward the CaFCP goal of 68 stations by 2015 when FCEVs will be introduced in larger numbers. These stations are expected to be included in subsequent evaluations.

Keys to success for improving hydrogen fueling availability are selecting the fueling location, ensuring public access, and providing adequate output to support the vehicles. Developing multi-use facilities that can serve cars, buses, and/or forklifts may help the economics and capacity utilization. Hydrogen output from existing and upcoming facilities varies from 12 to 140 kg/day, with most new fueling facilities being in the 100 kg/day range. There is an effort to focus on clusters of stations near population centers in the Los Angeles area. Using available hydrogen energy from landfills and wastewater treatment plants is one way to make use of a renewable feedstock and to lower greenhouse gas emissions. As more vehicles come online, all fueling facilities will need to be accessible to anyone with a hydrogen vehicle. Long construction lead times need to be accounted for when planning for the upcoming vehicles. As these optimized fueling facilities are developed, there is a need to continue data collection and analysis to track the progress and determine future technology development needs.

APPROACH

The emphasis of this project is documenting the innovations in hydrogen fueling and how it will meet vehicle customer needs. This includes analysis that captures the technology capability (such as back-to-back filling capability, impact of pre-cooling temperature, and radio-frequency identification of vehicles to allow unique fueling profiles) as well as the customer perspective (such as fueling times and rates, safety, and availability). Individual components such as compressors will be evaluated with the available data to establish current status and research needs. Station locations will be evaluated within the context of both available vehicles and future vehicles and their fueling patterns. NREL will also use the analysis results to support DOE in identifying trends from the data that will help guide DOE's research and development activities.

Data analysis will be performed on sensitive industry hydrogen fueling data in NREL's HSDC and recommendations will be provided to DOE on opportunities to refocus or supplement research and development activities. Aggregation of the analyzed data allows for creation of composite results for public dissemination and presentation. Some existing CDPs from the previous learning demonstration will be updated with new data, as appropriate. All this involves working with industry partners to create and publish CDPs that show the current technology status without revealing proprietary data. Feedback to industry takes form in detailed data products (protected results) and provides direct benefit to them from the NREL analysis performed on their data. We will continue exercising the fueling analysis functionality of the NREL Fleet Analysis Toolkit to preserve and archive a snapshot of the analysis results from each quarter. This allows a deeper level of results to be stored in an easy-to-access form within the HSDC.

Using unique analysis capabilities and tools developed at NREL, researchers are providing valuable technical recommendations to DOE based on real-world experiences with the technology. NREL will continue to provide multiple outputs in the form of CDPs and presentations and papers at technical conferences.

RESULTS

The hydrogen station locations in the U.S. can be seen in Figure 1. As stations are built or retired, updates are made to the internal database and shared with others including the AFDC. There are currently 53 stations in the U.S. and 10 are considered open to the public at this point with most of those in California. Recently, for this project, a few more stations have started providing data to NREL so there is now data from four stations which means that aggregation is possible and CDPs can be created for public dissemination in the fall.

Although the primary goal of the early stations is for coverage, we still want to show how the stations are being used in regards to capacity utilization and usage per hour. The capacity utilization CDPs have been presented in the past with updates expected this fall and can be found

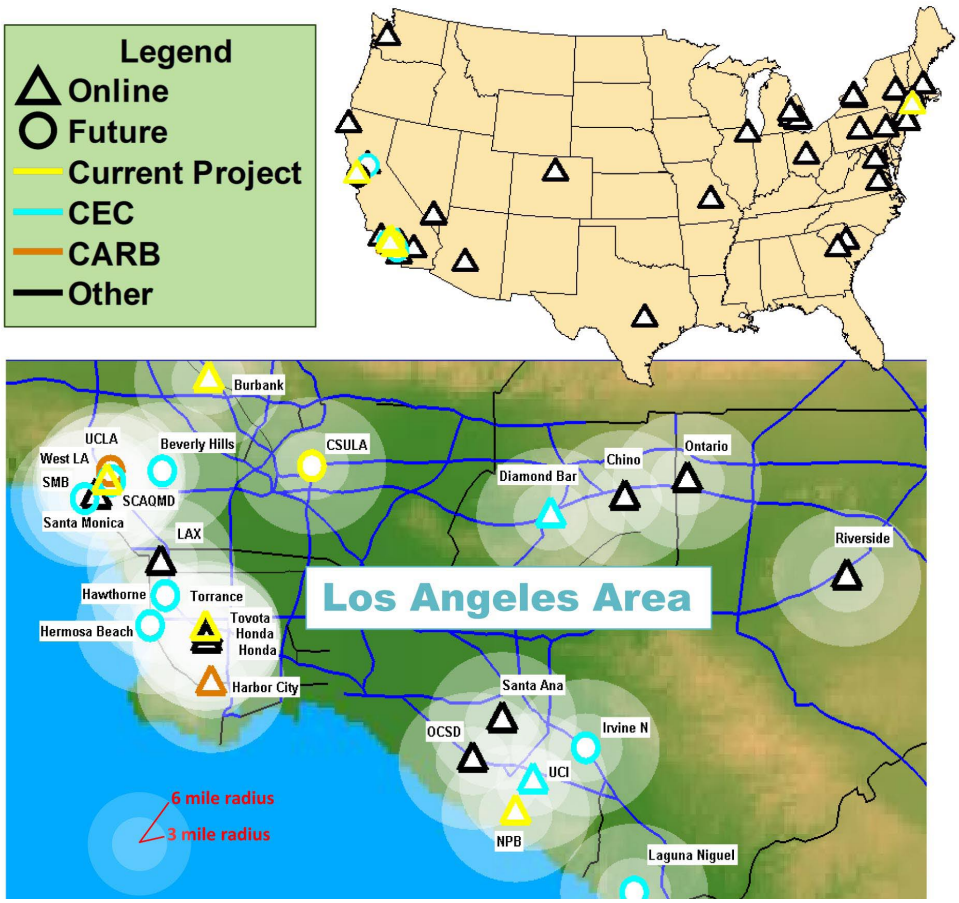

FIGURE 1. Hydrogen Station Locations

on the website. A new analysis (based on older data) was created this year to show the station usage per hour. The number of fills in an hour (only for hours for which there was dispensing) are presented in Figure 2. There were 1 to 7 fills per hour with an average of 1.5 per hour and a median of 1 per hour. This shows low usage compared with the material handling projects where there are many forklifts filling per hour. A second analysis was created to show how much hydrogen has been dispensed per hour and can be seen in Figure 3. On average there are 4.1 kilograms of hydrogen dispensed per hour with a median of 3.5 kilograms and a maximum of 14.9 kilograms. Figure 4 shows the graphical comparison with material handling equipment and reveals about the same amount being dispensed per hour for cars and forklifts even though there are many more fills per hour for the forklifts. This is a result of the cars having larger tanks than the forklifts allowing them to have more hydrogen per fill. As more data comes in there will be more analysis focusing on the usage of the stations.

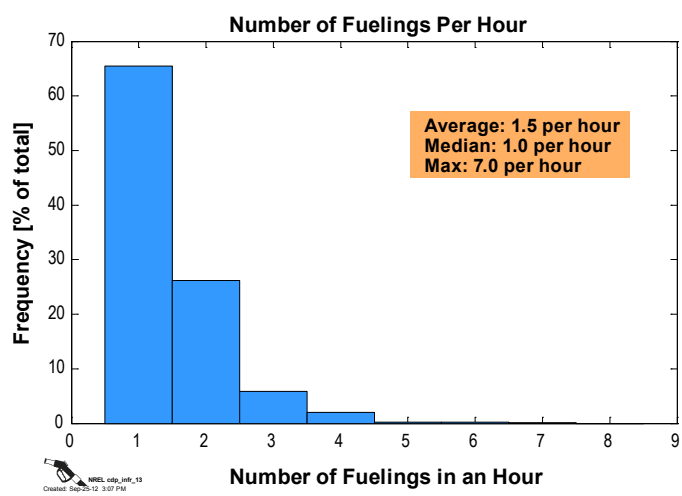

FIGURE 2. Number of Fueling Events per Hour

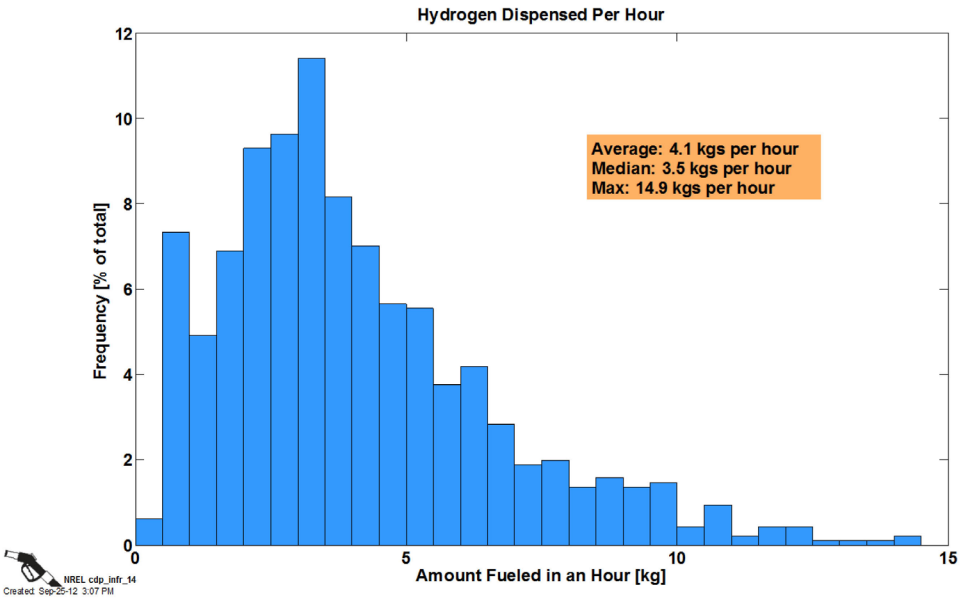

FIGURE 3. Amount of Hydrogen Dispensed per Hour

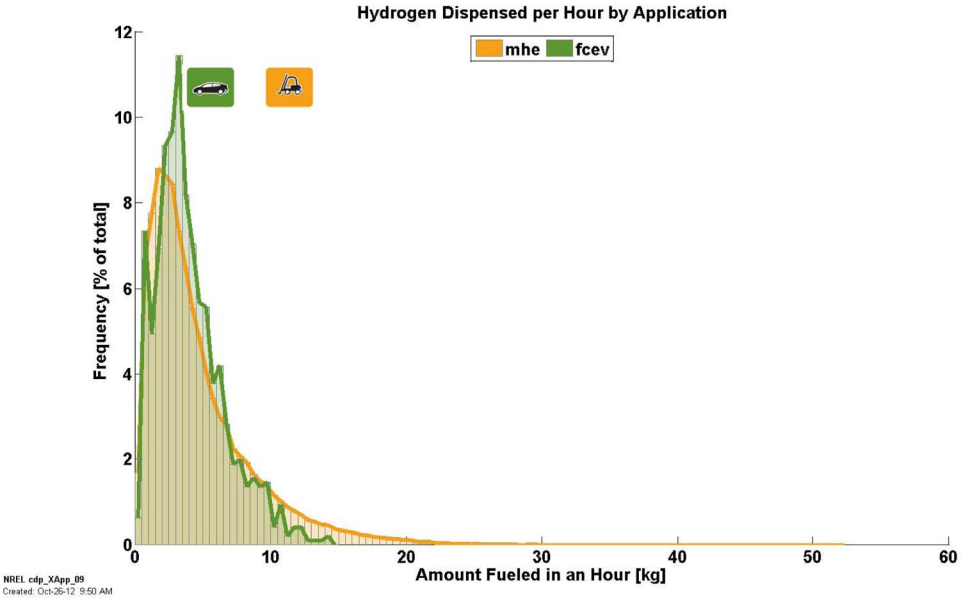

FIGURE 4. Amount of Hydrogen per Hour across Applications

CONCLUSIONS AND FUTURE DIRECTIONS

As new stations come online or are updated, their performance and availability will affect how successfully they support the current and upcoming fleet of fuel cell vehicles. Continual data collection, analysis, and feedback will provide DOE and the hydrogen and fuel cell community with awareness of the technology readiness and identify research areas for improvement. Few stations have been providing data during this project startup but that is starting to change and NREL is receiving more and more data making it possible to start aggregating the data in CDPs without revealing individual station identity, and to identify general trends in the industry. As more data become available from more stations, there will be an increase in data analysis possibilities to validate the technology for hydrogen infrastructure.

FY 2013 PUBLICATIONS/PRESENTATIONS

1. "Next Generation Hydrogen Infrastructure Evaluation," poster presented at the 2013 DOE Annual Merit Review and Peer Evaluation Meeting, May 16, 2013, Washington, D.C.

2. "Analyzing the Next Generation of Hydrogen Stations," presentation at 2012 Fuel Cell Seminar, November 6, 2012, Uncasville, CT.

3. CDPs and other publications available on the Hydrogen Infrastructure section of NREL's Technology Validation website, http://www.nrel.gov/hydrogen/proj_tech_validation.html.

VII.9 Data Collection and Validation of Newport Beach Hydrogen Station Performance

Michael J. Kashuba
California Air Resources Board
1001 I Street, P.O. Box 2815
Sacramento, CA 95812
Phone: (916) 323-5123
Email: mkashuba@arb.ca.gov

DOE Managers
Jason Marcinkoski
Phone: (202) 586-7466
Email: Jason.Marcinkoski@ee.doe.gov
Jim Alkire
Phone: (720) 356-1426
Email: James.Alkire@go.doe.gov

Contract Number: DE-EE0005889

Subcontractor:
Hydrogenics, Mississauga, ON, Canada

Project Start Date: October 2012
Project End Date: March 2015

Overall Objectives

- Specify and install correct instrumentation to increase the amount of data collected
- Validate new data and conduct initial analysis
- Increase overall station/equipment up time
- Reduce non-scheduled maintenance visits
- Make component optimization recommendations
- Check/validate station optimization

Fiscal Year (FY) 2013 Objectives

- Specify and install correct instrumentation to increase the amount of data collected
- Validate new data and conduct initial analysis

Technical Barriers

This project addresses the following technical barriers from the Technology Validation section of the Fuel Cell Technologies Office Multi-Year Research, Development, and Demonstration Plan:

(D) Lack of Hydrogen Refueling Infrastructure Performance and Availability Data

(F) Centralized Hydrogen Production from Fossil Resources

Contribution to Achievement of DOE Technology Validation Milestones

This project will contribute to achievement of the following DOE milestones from the Technology Validation section of the Fuel Cell Technologies Office Multi-Year Research, Development, and Demonstration Plan:

- Milestone 3.2: Validate novel hydrogen compression technologies or systems capable of >200 kg/day that could lead to more cost-effective and scalable (up to 500 kg/day fueling station solutions for motive applications. (4Q, 2014)

FY 2013 Accomplishments

Specified 16 pieces of instrumentation to effectively increase data collection.

✧ ✧ ✧ ✧ ✧

INTRODUCTION

The hydrogen fueling station located at 1600 Jamboree Boulevard in Newport Beach, CA, was designed and built to refuel light-duty fuel cell electric vehicles (FCEVs). The station features the on-site generation of hydrogen through a small-scale natural gas steam methane reformer. All the hydrogen-related equipment was added to an existing retail gasoline/diesel station. The station is an early demonstration of what the footprint and equipment arrangement of a retail on-site steam methane reformer facility might look like.

Only a few hundred FCEVs are on the road in California. As a result, hydrogen throughput is relatively low at the few early pre-commercial hydrogen stations that are currently open. As a result, the stations are underutilized. This project aims to collect additional data to allow the operator to potentially adjust various station component and operational parameters in order to improve the overall efficiency of the station and lower operation and maintenance costs and to help improve air quality and reduce greenhouse gas emissions.

APPROACH

The first phase of the project involves specifying and installing the correct instrumentation to increase the amount of data collected. This involves installing (3) mass flow

meters, (2) hour meters, (9) power meters, and (2) water flow meters. The new data collected will be validated and the initial analysis will be conducted.

The second phase of the project aims to improve the efficiency of the station. The intent is to increase the overall station and equipment up time and reduce non-scheduled maintenance visits. The data collected will be used to make recommendations on how to optimize discrete station components. The recommendations will be acted upon, and continually monitored to validate the optimization of the station.

RESULTS

The results of this project have yet to be derived. Final contract/grant agreement negotiation between subcontractor, station owner, real estate owner, and hydrogen station operator has taken much longer than anticipated.

CONCLUSIONS AND FUTURE DIRECTIONS

Data collection at the station is in progress. Research is expected to continue as planned until 2015.

VII.10 California State University Los Angeles Hydrogen Refueling Facility Performance Evaluation and Optimization

David Blekhman
California State University Los Angeles (CSULA)
Los Angeles, CA 90032
Phone: (323) 343-4569
Email: blekhman@calstatela.edu

DOE Managers
Jason Marcinkoski
Phone: (202) 586-7466
Email: Jason.Marcinkoski@ee.doe.gov
James Alkire
Phone: (720) 356-1426
Email: James.Alkire@go.doe.gov

Contract Number: DE-EE0005890

Subcontractor:
Hydrogenics, Mississauga, ON, Canada

Project Start Date: October 1, 2012
Project End Date: September 30, 2016

Overall Objectives

Technical Objectives

- Test, collect data, and validate hydrogen refueling architecture deployed at CSULA and its individual components in a real-world operating environment
- Provide the performance evaluations data to the Hydrogen Secure Data Center (HSDC) at the National Renewable Energy Laboratory (NREL)
- Contribute to the development of new industry standards
- Develop and implement fueling station system performance optimization

Educational objectives:

- Conduct outreach and training activities promoting the project and hydrogen and fuel cell technologies
- Provide a living-lab environment for engineering and technology students pursuing interests in hydrogen and fuel cell technologies

Fiscal Year (FY) 2013 Objectives

Design and install data collection system for the station and its major components (Figure 1).

Technical Barriers

This project addresses the following technical barriers from the Fuel Cell Technologies Office Multi-Year Research, Development, and Demonstration Plan:

Hydrogen Production

(B) Operations and Maintenance (O&M)

(E) Control and Safety

Technology Validation

(D) Lack of Hydrogen Refueling Infrastructure Performance and Availability Data

Contribution to Achievement of DOE Hydrogen Production and Technology Validation Milestones

This project will contribute to achievement of the following DOE milestones from the Fuel Cell Technologies Office Multi-Year Research, Development, and Demonstration Plan:

Hydrogen Production

- Milestone 2.6: Verify the total capital investment for a distributed electrolysis system against the 2015 targets using H2A. (Q2, 2016)
- Milestone 2.7: Verify 2015 distributed hydrogen production levelized cost target through pilot scale testing coupled with H2A analysis to project economies of scale cost reduction. (Q3, 2017)

Technology Validation

- Milestone 3.4: Validate station compression technology provided by delivery team. (4Q, 2018)

FY 2013 Accomplishments

This is the first year of the project with its accomplishments listed as follows:

- Reviewed existing instrumentation and equipment for data acquisition available at the station
- Designed enhancements for data acquisition that will enable station performance evaluation
- Procured equipment according to the design

✧ ✧ ✧ ✧ ✧

FIGURE 1. CSULA Hydrogen Fueling Facility, from left to right: storage tanks, PDC 350-bar compressor, two Hydro Pac 700-bar compressors, and Quantum chiller.

INTRODUCTION

The CSULA hydrogen station deploys the latest technologies with the capacity to produce and dispense 60 kg/day, sufficient to fuel 15-20 vehicles. The station utilizes a Hydrogenics electrolyzer, first- and second-stage compressors enabling 350- and 700-bar fueling and 60 kg of hydrogen storage. The station is grid-tied and to be supplied by 100% renewable power.

Coupling the station and the academic background of the research team presents a strong partner for DOE and NREL in conducting a hydrogen refueling facility performance evaluation and optimization project. This also includes multiple activities and subprojects listed in the objectives section.

APPROACH

To enable effective data collection on the station performance, the team utilizes some of the sensors already available at the station and introduces a number of additional meters for completed system. A software package is being developed to achieve maximum automation in data collection and processing per NREL requirements.

As data are collected and analyzed for a period of time, the station performance will be evaluated for potential optimization and other technical enhancements. The goals would be to reduce maintenance cost, reduce hydrogen costs and improve user experience.

RESULTS

As stated in achievements, this is a new project that in a short time evaluated current station design, specified data acquisition enhancements and procured additional equipment. The equipment will be installed and software developed for data acquisition.

CONCLUSIONS AND FUTURE DIRECTIONS

This is a new project that is well underway. The research team looks forward to collaborating with DOE and NREL in evaluating the station performance and contributing to the development of a robust and economically viable hydrogen infrastructure.

VII.11 Performance Evaluation of Delivered Hydrogen Fueling Stations

Mike Tieu
Gas Technology Institute
1700 S. Mt. Prospect Rd.
Des Plaines, IL 60018
Phone: (847) 768-0940
Email: michael.tieu@gastechnology.org

DOE Managers
Jason Marcinkoski
Phone: (202) 586-7466
Email: Jason.Marcinkoski@ee.doe.gov
Jim Alkire
Phone: (720) 356-1426
Email: James.Alkire@go.doe.gov

Contract Number: DE-EE0005886

Subcontractor:
Linde LLC, Hayward, CA

Project Start Date: March 1, 2013
Project End Date: August 31, 2016

Overall Objectives

- Confirm performance of systems in real world applications through data collection
- Provide the public with aggregated data presented in composite data products, and secure confidential data in the National Renewable Energy Laboratory Hydrogen Secure Data Center
- Benchmark station capacity utilization, maintenance, and safety

Fiscal Year (FY) 2013 Objectives

- Perform station assessments—an evaluation of stations' adequacy to ensure deliverables are achievable and development of associated data acquisition plan
- Data acquisition engineering design and packaging—station design packages to be reviewed for data acquisition integration
- System fabrication and installation (initial three sites)—specification of project materials, execution of hazards and operability analysis, and fabrication and installation of equipment

Technical Barriers

This project addresses the following technical barriers from the Technology Validation section of the Fuel Cell Technologies Office Multi-Year Research, Development and Demonstration Plan:

(D) Lack of Hydrogen Refueling Infrastructure Performance and Availability Data

Contribution to Achievement of DOE Technology Validation Milestones

This project will contribute to achievement of the following DOE milestones from the Technology Validation section of the Fuel Cell Technologies Office Multi-Year Research, Development and Demonstration Plan:

- Milestone 2.3: Validate fuel cell electric vehicles achieving 5,000 hr. durability (service life of vehicle) and a driving range of 300 miles between fuelings. (4Q, 2019)
- Milestone 3.2: Validate novel hydrogen compression technologies or systems capable of 200> kg/day that could lead to more cost-effective and scalable (up to 500 kg/day fueling station for motive applications. (4Q, 2014)
- Milestone 3.4: Validate station compression technology provided by delivery team. (4Q, 2018)
- Milestone 4.4: Complete evaluation of 700 bar fast fill fueling stations and compare to SAE J2601specifications and DOE fueling targets. (3Q, 2016)

FY 2013 Accomplishments

- Secured funding for all five project locations in California
- Agreed to terms with project partner and subcontractor
- Obtained station technical specifications and commenced review
- General project approach and software was selected providing the project the data format requirements
- Completed a preliminary design and approach for integration of data collection systems in station design in order to meet project objectives and deliverables set forth by the National Renewable Energy Laboratory (Figure 1)

✧ ✧ ✧ ✧ ✧

FUTURE DIRECTIONS

- Complete station site reviews and finalize data acquisition plan
- Obtain station engineering drawings for specific stations and complete detailed integration approach

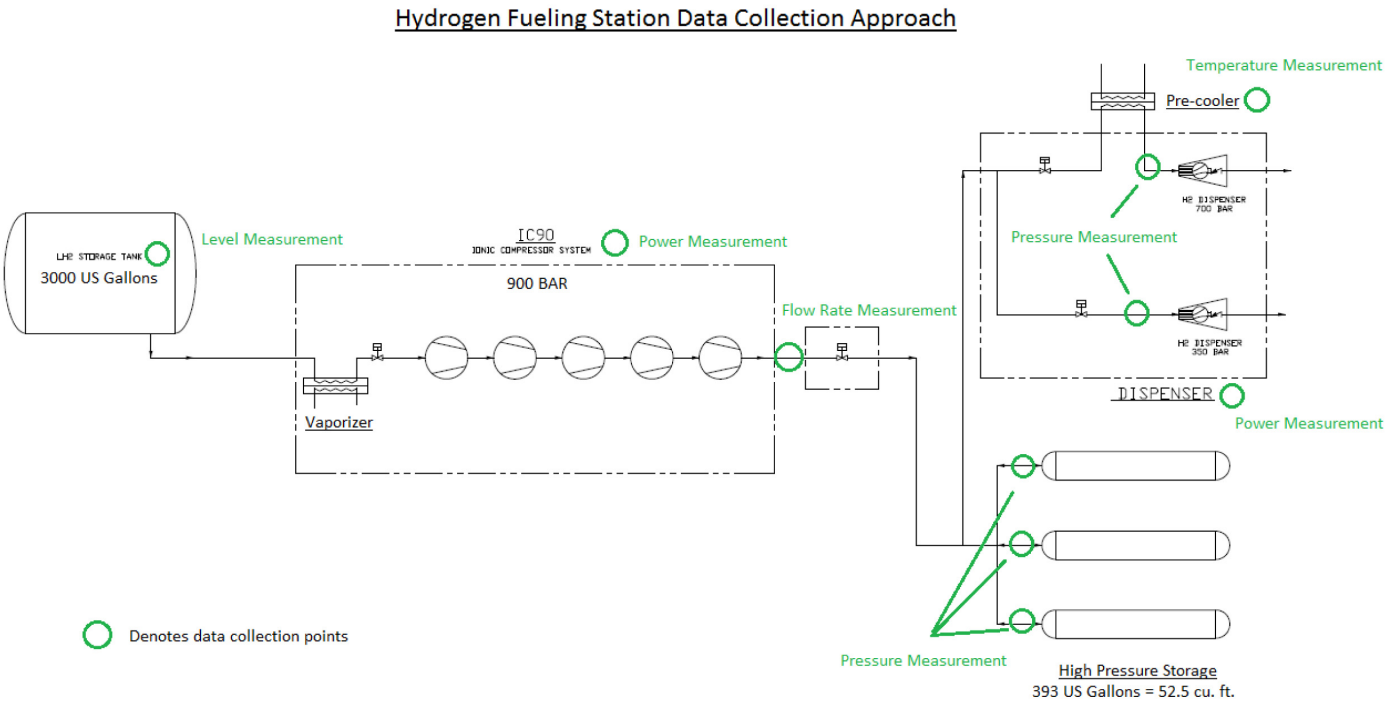

FIGURE 1. Hydrogen Fueling Station Data Collection Approach

- Develop LabVIEW® data acquisition software and data storage/handling process
- Create site-specific engineering drawings for hardware installation and data collection system integration to station equipment
- Identify, specify, and procure materials required for data acquisition system fabrication
- Complete hazards and operability analysis of each of the preliminary locations identified in the statement of project objectives
- Fabrication of electrical panels and onsite installation/start-up/commissioning of units

FY 2013 PUBLICATIONS/PRESENTATIONS

1. tv025_tieu_2013_p.pptx – Poster Presentation 2013 AMR.

VIII. SAFETY, CODES & STANDARDS

VIII.0 Safety, Codes & Standards Program Overview

INTRODUCTION

The Safety, Codes and Standards program identifies and performs high priority research and development (R&D) to provide an experimentally validated and fundamental understanding of the relevant physics, critical data, and safety information needed to define the requirements for technically sound and defensible codes and standards. In Fiscal Year (FY) 2013, the program continued to identify and evaluate safety and risk management measures that can be used to define the requirements and close the gaps in codes and standards in a timely manner.

Communication and collaboration among codes and standards stakeholders (e.g., government, industry, codes and standards development organizations, universities, and national laboratories) is emphasized in order to maximize the impact of the program's efforts and activities in harmonizing domestic and international regulations, codes, and standards (RCS).

Internationally, efforts continue through the testing activities of the Regulations, Codes and Standards Working Group (RCSWG) of the International Partnership for Hydrogen and Fuel Cells in the Economy (IPHE). Domestically, the program utilizes the expertise of the Hydrogen Safety Panel (HSP) to disseminate relevant information and implement safe practices pertaining to the operation, handling, and use of hydrogen and fuel cell technologies. The HSP, with over 400 years of combined member experience in the hydrogen industry, provides recommendations on the safe conduct of project work as well as lessons learned and best practices that can be of broad benefit to the industry. The program continues to share current safety information and knowledge with the community.

In addition, extensive external stakeholder input—from the fire-protection community, academia, automobile manufacturers, and energy, insurance, and aerospace sectors—is used to create and enhance safety knowledge tools for emergency responders and authorities having jurisdiction. The program works to enable the continual availability of safety knowledge tools, distributed online or in-person in order to reach the largest number of personnel possible.

GOALS

The program's key goals are to provide the validated scientific and technical basis required for the development of codes and standards, to promulgate safety practices and procedures to allow for the safe deployment of hydrogen and fuel cell technologies, and to ensure that best safety practices are followed by Fuel Cell Technologies Office-funded projects.

OBJECTIVES[1]

The program's key objectives are to:

- Develop and validate test measurement protocols and methods to support and facilitate international harmonization of codes and standards for high-pressure tanks.
- Conduct materials R&D to provide the technical underpinning to enable fault-tolerant system designs for use with hydrogen infrastructure rollout by 2015.
- Conduct a quantitative risk assessment (QRA) study to address indoor refueling requirements to be adopted by code developing organizations (e.g., National Fire Protection Association [NFPA] and International Code Council [ICC]) by 2015.
- Support and facilitate development and promulgation of essential codes and standards by 2015 to enable widespread deployment and market entry of hydrogen and fuel cell technologies and completion of all essential domestic and international RCS by 2020.
- Ensure that best safety practices underlie research, technology development, and market deployment activities supported through Office-funded projects.
- Develop and enable widespread sharing of safety-related information resources and lessons-learned with first responders, authorities having jurisdiction, and other key stakeholders.

[1] Note: Targets and milestones were recently revised; therefore, individual project progress reports may reference prior targets.

FY 2013 STATUS

The program continues to support R&D to provide the technical basis for codes and standards development, with projects in a wide range of areas including fuel specification, separation distances, materials and components compatibility, and hydrogen sensor technologies. Utilizing the results from these R&D activities, the program continues to actively participate in discussions with standards development organizations such as the NFPA, ICC, SAE International, the CSA Group, and the International Organization for Standardization (ISO) to promote domestic and international collaboration and harmonization of RCS.

The following websites provide additional, up-to-date information relevant to the status of the program's activities:

- Technical Reference for Hydrogen Compatibility of Materials (www.ca.sandia.gov/matlsTechRef/)
- Hydrogen Incident Reporting and Lessons Learned Database (www.h2incidents.org/)
- Hydrogen Bibliographic Database (www.hydrogen.energy.gov/biblio_database.html)
- Hydrogen Safety Best Practices Manual (www.h2bestpractices.org/)
- Hydrogen Safety Training for Researchers (www-training.llnl.gov/training/hc/HS5094DOEW/index.html)
- Introduction to Hydrogen for Code Officials (www.hydrogen.energy.gov/training/code_official_training/)
- Hydrogen Safety for First Responders (www.hydrogen.energy.gov/firstresponders.html)

FY 2013 KEY ACCOMPLISHMENTS

The program continued to make progress in several areas, including the following:

- International and Domestic Regulations, Codes, and Standards Harmonization
  - Submitted the Global Technical Regulation on hydrogen-fuelled vehicles to the United Nations Economic Commission for Europe Working Party 29 (UN ECE WP.29). Accepted in June 2013, this regulation was led by the U.S. Department of Transportation National Highway Transportation Safety Administration and will serve as the technical underpinning for the United States Federal Motor Vehicle Safety Standard.
  - Performed hydraulic cycle tests (up to 35 MPa) with the IPHE working group using a harmonized test measurement protocol which was established for consistent results independent of the test facility. Testing was conducted by the United States and China under the RCSWG and lessons learned were implemented in a revised test method protocol for a second tank, which will be completed in FY 2014.
  - Provided a science-based approach for the development of an ISO (14687-2) standard for hydrogen fuel quality, which was published by ISO in December 2012. This standard is now harmonized with the SAE International domestic standard on fuel quality (SAE J2719).
  - Supported the standardization of SAE J2579, *Standard for Fuel Systems in Fuel Cell and Other Hydrogen Vehicles*, which was published by SAE in March of 2013.
- Hydrogen Behavior, Risk Assessment, and Materials Compatibility (Sandia National Laboratories [SNL])
  - Developed integrated algorithms for conducting QRA for gaseous hydrogen facilities and vehicles that are applied to identified risk drivers and associated consequences, including further reducing separation distances.
  - Identified ignition and jet light-up boundaries of jet flames for circular unintended releases with increased confidence and initiated a study on non-circular releases.
  - Updated *Technical Reference for Hydrogen Compatibility of Materials* (SAND2012-7321) and developed datasets for fatigue crack growth of materials in gaseous hydrogen.
- Hydrogen Quality (Los Alamos National Laboratory, LANL)
  - Determined that low-loaded anodes (0.03 mg-Pt/cm^2) have a ≈100 mV loss at 1 A/cm^2 when exposed to 100 ppm CO for 50 hours and ≈200 mV loss when exposed to 4 ppb of H_2S for 50 hours at steady state.
- Codes and Standards Development and Outreach (National Renewable Energy Laboratory, NREL)

  - Published a technical report *Regulations, Codes, and Standards (RCS) Template for California Hydrogen Dispensing Stations* to help the deployment and commercialization of hydrogen infrastructure.
  - Supported the referencing of the NFPA 2 Hydrogen Technologies Code chapter in the International Fire Code and Uniform Fire code in order to create a national hydrogen code.
- Component Testing (NREL)
  - Completed the validation testing of Hydrogen Pressure Relief Device 1 Phase, which includes modified test protocols that include worst case conditions during cycling tests.
- Hydrogen Safety Panel, Databases, Props, and First Responders (Pacific Northwest National Laboratory, PNNL)
  - Developed the first mobile app for the Fuel Cell Technologies Office with the following features:
    - Integrates H_2incidents.org and H_2bestpractices.org into a single, searchable, iPad and iPhone application.
    - Includes safety planning guidance and checklist features.
    - Access to all tools (except H_2incidents.org) available without a data connection.
  - Added six new safety event records from national laboratories, universities, and private-sector firms in the United States and other countries since the 2012 Annual Merit Review and Peer Evaluation Meeting, for a total of 207 records currently in the database.
  - Updated H_2bestpractices.org to include the safety checklist for outdoor storage with an indoor use, which was developed by the HSP.
  - Developed training material for first responders and code officials, bringing the total educated to over 25,000 first responders to date (online and in-person)
- Sensors
  - Developed, optimized, and characterized working electrode and electrolyte layers grown using electron beam (e-beam) evaporation methods, demonstrating a significant reduction in sensor manufacturing time that suggest decreases in projected manufacturing costs. (LANL and Lawrence Livermore National Laboratory)
  - Completed a review on the use of oxygen sensors to correlate changes in oxygen concentration to hydrogen levels, which are recommended in the current text of the Global Technical Regulation. (NREL)

BUDGET

The program received an appropriation of $6.6 million in FY 2013. This allowed for sustained progress in key R&D and codes and standards development work. The President's FY 2014 budget request includes $7.0 million for Safety, Codes and Standards, which will ensure continuity in key R&D and focus areas as shown below.

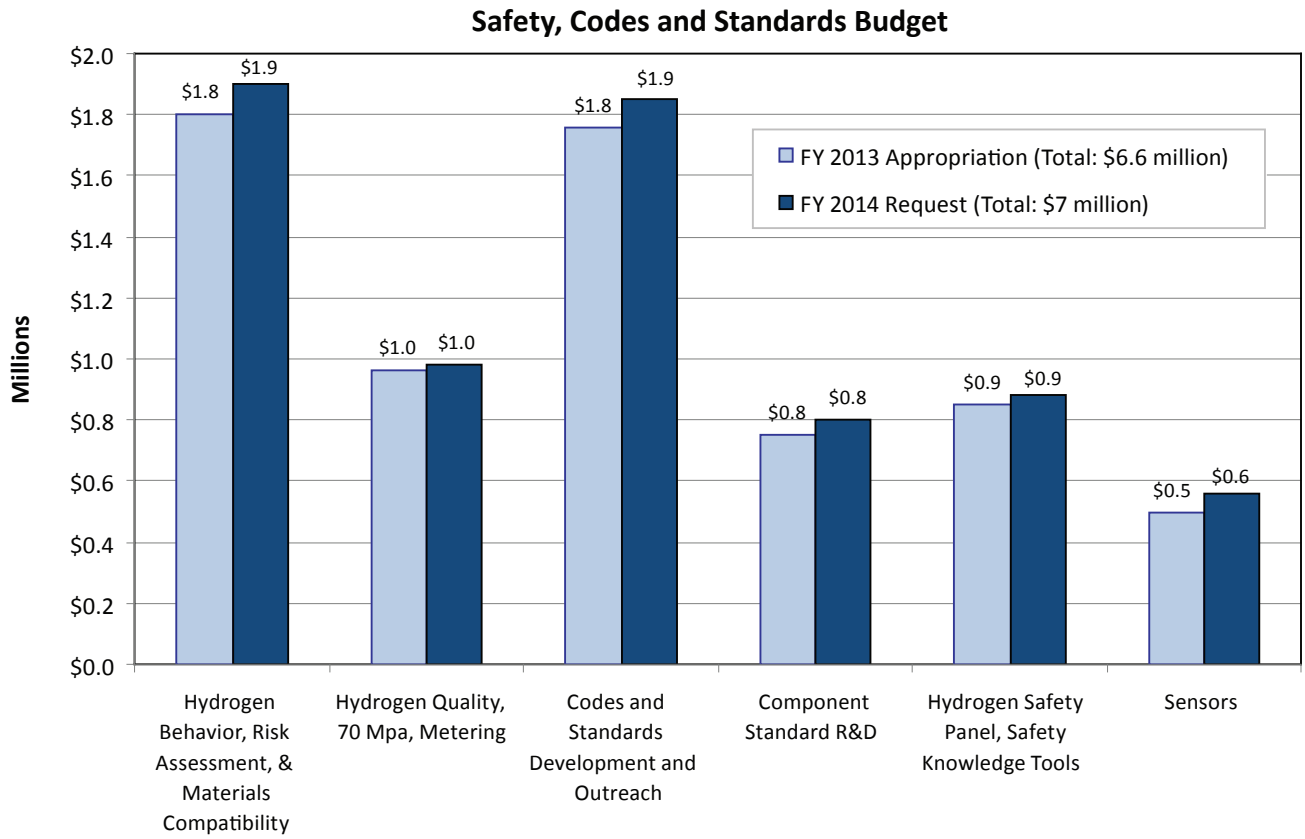

FY 2014 PLANS

The Safety, Codes and Standards program will continue to work with codes and standards organizations to develop technical information and performance data to enhance hydrogen-specific codes and standards. To address these needs, the program will continue to support a rigorous technical R&D program—including assessment of materials compatibility for component designs and high-pressure tank cycle testing—and continue to promote a QRA approach to identify risks and establish protocols to mitigate those risks. Future work will also focus on the permitting of hydrogen fueling stations and early market applications and testing, measurement, and verification of hydrogen fuel specifications.

The program will also continue to promote the domestic and international harmonization of test protocols for qualification and certification as well as the harmonization of RCS for hydrogen fuel quality and other key international standards. This will be enabled by working with the appropriate domestic and international organizations such as the NFPA, ICC, SAE International, CSA Standards, and the ISO. The program will also continue to participate in IPHE's Regulations, Codes and Standards Working Group and the International Energy Agency's Hydrogen Implementing Agreement, both of which are engaged in hydrogen safety work.

Charles James Jr.
Safety, Codes & Standards Team Lead
Fuel Cell Technologies Office
U.S. Department of Energy
1000 Independence Ave., SW
Washington, D.C. 20585-0121
Phone: (202) 287-6223
Email: Charles.James@ee.doe.gov

VIII.1 Fuel Cell Technologies National Codes and Standards Development and Outreach

Carl Rivkin (Primary Contact), Chad Blake, Robert Burgess, William Buttner
National Renewable Energy Laboratory (NREL)
15301 Denver Parkway West
Golden, CO 80401
Phone: (303) 275-3839
Email: carl.rivkin@nrel.gov

DOE Manager
Rick Farmer
Phone: (202) 586-1623
Email: Richard.Farmer@ee.doe.gov

Subcontractors:
- Compressed Gas Association, Chantilly, VA
- Davidson Code Concepts, Easley, SC
- Fuel Cell and Hydrogen Energy Association, Washington, D.C.
- Kelvin Hecht, Avon, CT
- National Fire Protection Association, Quincy, MA
- SAE International (SAE), Troy, MI

Project Start Date: October 1, 2002
Project End Date: Project continuation and direction determined annually by DOE

Overall Objectives

- Support the deployment of hydrogen technologies for hydrogen fuel cell vehicles and stationary applications
- Make critical safety information readily available through webinars, workshops, safety reports, and technical presentations
- Inform key stakeholders of the safety, codes and standards requirements for the safe use of hydrogen technologies
- Develop sensor technologies to support the safe use of hydrogen technologies
- Identify and resolve safety issues associated with hydrogen technologies infrastructure

Fiscal Year (FY) 2013 Objectives

- Publish NREL Guide to Hydrogen Safety
- Support the development of the next edition of the National Fire Protection Association (NFPA) 2 Hydrogen Technologies Code and SAE J2601 Fueling Protocol
- Present webinars on codes and standards progress and hydrogen fueling protocols
- Update codes and standards citations for the DOE Hydrogen and Fuel Cells website
- Present codes and standards information at California hydrogen technologies deployment meetings and workshops
- Implement 2020 plan for the deployment of hydrogen technologies infrastructure

Technical Barriers

This project addresses the following technical barriers from the Hydrogen Safety, Codes and Standards section of the Fuel Cell Technologies Office Multi-Year Research, Development, and Demonstration Plan:

(A) Safety Data and Information: Limited Access and Availability

(D) Lack of Hydrogen Knowledge by Authorities Having Jurisdiction

(F) Enabling National and International Markets Requires Consistent Regulations, Codes, and Standards

(G) Insufficient Technical Data to Revise Standards

(H) Insufficient Synchronization of National Codes and Standards

(I) Lack of Consistency in Training of Officials

(K) No Consistent Codification Plan and Process for Synchronization of R&D and Code Development

(L) Usage and Access Restrictions

Contribution to Achievement of DOE Safety, Codes and Standards Milestones

This project will contribute to achievement of the following DOE milestones from the Hydrogn Safety, Codes and Standards section of the Fuel Cell Technologies Office Multi-Year Research, Development and Demonstration Plan:

- Milestone 4.4: Complete National Codes and Standards Chronological Development Plan. (4Q, 2014)
- Milestone 4.5: Complete fueling station codes and template. (4Q, 2014)
- Milestone 4.6: Completion of standards for critical infrastructure components and systems. (4Q, 2014)

- Milestone 4.7: Complete risk mitigation analysis for advanced transportation infrastructure systems. (1Q, 2015)
- Milestone 4.8: Revision of NFPA 2 to incorporate advanced fueling and storage systems and specific requirements for infrastructure elements such as garages and vehicle maintenance facilities. (3Q, 2016)
- Milestone 4.9: Completion of Global Technical Regulation (GTR) Phase 2. (1Q, 2017)

FY 2013 Accomplishments

- NREL provided broad coordination of codes and standards development by:
  - Supported Codes and Standards Tech Team–develop and maintain the "2020" plan for defining and tracking codes and standards work required for deployment of hydrogen fuel cell vehicles.
  - Managed the National Hydrogen and Fuel Cells Codes and Standards Coordinating Committee. This group has monthly meetings that serve as a forum for the codes and standards development community to share information.
  - Led Hydrogen Sensor Task Group monthly meetings.
  - Acted as liaison between codes and standards development committees to assist in coordination between fire codes and standards development projects.
- NREL worked to have references to NFPA 2 Hydrogen Technologies Code placed in the Fire Codes (The International Fire Code and the Uniform Fire Code) to create a national hydrogen code.
- NREL developed a Hydrogen Safety Handbook that will be published by the end of FY 2013.
- Updated the codes and standards reference material for both stationary fuel cells and infrastructure for fuel cell vehicles that resides on the DOE Hydrogen and Fuel Cells website.
- Published NREL technical report "Regulations, Codes, and Standards (RCS) Template for California Hydrogen Dispensing Stations."
- Published NREL Technical Report Steering Committee Progress Report on Hydrogen Sensor Performance Testing and Evaluation under the memorandum of understanding between NREL, DOE, Joint Research Centre-Institute for Energy and Transport, and the European Commission.

✧ ✧ ✧ ✧ ✧

INTRODUCTION

The fundamental purpose of this work is to support the safe deployment of hydrogen technologies. To achieve this objective codes and standards must be in place to protect public safety and any significant safety issues must be resolved.

The work under this project has helped develop a national set of codes and standards to safely deploy hydrogen technologies. Additionally, key safety issues have been identified and are in the process of being resolved. Safety, codes, and standards information has been distributed to interested parties using a variety of techniques including webinars, NREL technical reports, workshops, in-person presentations, and Web-based products.

APPROACH

The project approach has been to involve as many key stakeholders as possible in codes and standards development and coordination and outreach activities to achieve maximum effectiveness. These stakeholders include industry partners, standards development organizations, research organizations including other national laboratories, authorities having jurisdiction, local government in locations where projects will be deployed, and trade organizations involved in technology development and deployment.

RESULTS

Figure 1 illustrates the progress that has been made towards developing the key codes and standards required to deploy hydrogen technologies. The reference of NFPA 2 in the International Fire Code effectively creates a national hydrogen code. This simplification and coordination of code requirements will make it easier to develop permit application, review and approve applications, and ensure a high level of public safety. This accomplishment helps meet several DOE milestones including 4.4 and 4.8.

NREL published the technical report "Regulations, Codes, and Standards (RCS) Template for California Hydrogen Dispensing Stations" that will help in moving infrastructure deployment forward in California. California appears to be on the leading edge of hydrogen fueling station deployment because of state regulations that mandate the use of zero emission vehicles (hydrogen fuel cell vehicles are classified as zero emission vehicles). This report will help both project developers and code officials write and approve permit applications for hydrogen fueling stations. This work helps meet DOE milestone 4.5.

NREL's ongoing support of standards development has resulted in all of the key codes and standards being promulgated for the deployment of hydrogen technologies. This point is illustrated in the far right column of Figure 1.

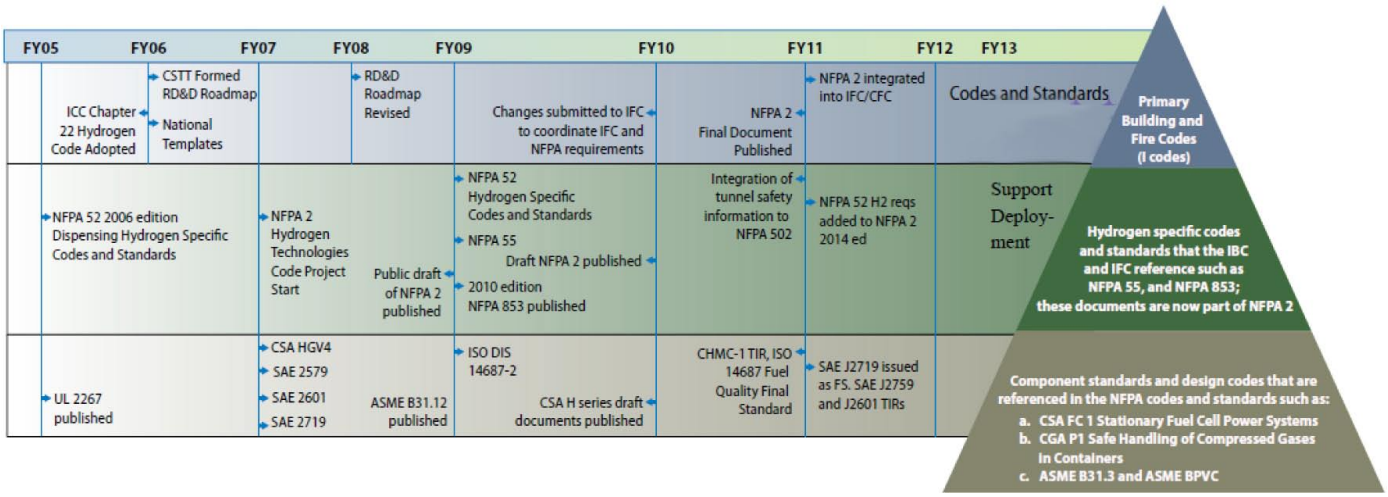

FIGURE 1. Hydrogen Codes and Standards Progress

This effort addresses DOE milestones 4.4, 4.5, 4.6, 4.7, 4.8, and 4.9. The reason this work addresses the GTR is that the SAE J2579 standard that was supported through this coordination work is used as the basis for the GTR.

NREL performed a Process Hazard Analysis on a hydrogen fueling station to help prioritize the risks presented by the construction and operation of a high pressure fueling station. The results of this analysis directly address Milestone 4.7.

NREL prioritized codes and standards development projects through the use of the "2020 Hydrogen Infrastructure Deployment Plan." The plan was developed with the input of the DOE Codes and Standards Technical Team.

CONCLUSIONS AND FUTURE DIRECTIONS

Conclusions

Codes and Standards

- Codes and standards development support will continue at a reduced level through direct support of standards development organizations and participation on or operation of coordination committees.
- Ongoing coordination of the fire codes and key hydrogen codes and standards is a priority.

Outreach

- Deployment support will be focused on infrastructure at locations with project activity and concrete deployment plans, for example jurisdictions in California.
- These goals can only be accomplished through collaborations with key stakeholders at all levels.
- NREL will continue to support deployment of hydrogen and fuel cell technologies through programs such as the technical reports, webinars, safety reviews, and the Web-based information compendium.

Future Directions

Codes and Standards Coordination/Development

- Continue work to coordinate codes and standards on a smaller scale with special focus on taking information from deployment projects back to code development committees.
- Resolve infrastructure codes and standards issues.

Outreach

- Continue to publish NREL technical reports, deliver webinars, and provide Web-based information on key safety issues required to support hydrogen technologies deployment.
- Assist code officials, project developers, and other interested parties in use of new codes and standards and safety information through outreach activities, with special focus on key jurisdictions such as California.
- Work with interested parties to provide information to assist in infrastructure deployment.

FY 2013 PUBLICATIONS/PRESENTATIONS

1. Buttner, W.J.; Burgess, R.; Rivkin, C.; Post, M.B.; Boon-Brett, L.; Black, G.; Harskamp, F.; Moretto, P.(2012). Inter-Laboratory Assessment of Hydrogen Safety Sensors Performance under Anaerobic Conditions.International Journal of Hydrogen Energy. Vol. 37(22), November 2012; pp. 17540-17548; NREL Report No. JA-5600-55065. http://dx.doi.org/10.1016/j.ijhydene.2012.03.165.

2. Buttner, W.; Post, M.; Burgess, R.; Rivkin, C.; Boon-Brett, L.; Palmisano, V.; Bonato, C.; Harskamp, F.(2012). Steering Committee Progress Report on Hydrogen Sensor Performance Testing and Evaluation under the Memorandum of Agreement between NREL, U.S. DOE and JRC-IET, EC. 24 pp.; NREL Report No. MP-5600-57207.

3. Rivkin, C.; Blake, C.; Burgess, R.; Buttner, W.; Post, M. (2012). Regulations, Codes, and Standards (RCS) Template for California Hydrogen Dispensing Stations. 30 pp.; NREL Report No. TP-5600-56223.

4. Rivkin, C; California Unified Program (CUPA) conference Regulations, Codes, and Standards (RCS) for Hydrogen Fueling Stations, February 7, 2013 Anaheim, CA.

5. Rivkin, C; National Hydrogen and Fuel Cell Coordinating Committee (NHFCCC) Meeting webinar, Codes and Standards: Progress to Date and the Path Forward, February 6, 2013.

VIII.2 Component Standard Research and Development

Robert Burgess (Primary Contact), William Buttner, Carl Rivkin
National Renewable Energy Laboratory (NREL)
15013 Denver West Parkway
Golden, CO 80401
Phone: (303) 275-3823
Email: robert.burgess@nrel.gov

DOE Manager
Rick Farmer
Phone: (202) 586-1623
Email: Richard.Farmer@ee.doe.gov

Project Start Date: Fiscal Year (FY) 2012
Project End Date: Project continuation and direction determined annually by DOE

Overall Objectives

- Support development of new codes and standards required for commercialization of hydrogen technologies.
- Support code development that is based on the latest scientific knowledge by providing analytical, technical, and contractual support.
- Participate directly on codes and standards committees to identify technology gaps, then work to define research and development needs required to close those gaps.
- Conduct laboratory testing to provide a basis for improved code language.
- Collaborate with industry, university and government researchers to develop improved analytical and experimental capabilities.

FY 2013 Objectives

- Collect safety/reliability data through direct communication with stakeholders and by utilizing NREL Technology Validation data to identify failure modes with highest statistical probability.
- Compile information into a report summarizing findings of failure mode investigation.
- Provide support for webinar on fueling protocols in conjunction with SAE International (SAE) interface committee, referencing SAE J2601 path forward.
- Build industry partnerships to conduct high-pressure hydrogen component and system level testing designed to understand root cause failure modes and to provide guidance for engineering best practices.
- Facilitate utilization of the new DOE Energy Systems Integration Facility (ESIF) laboratory space by identifying best use of laboratory and testing capabilities and by supporting ESIF user facility designation through interface with DOE/NREL user facility personnel.

Technical Barriers

This project addresses the following technical barriers identified in the DOE Fuel Cell Technologies Office, Safety Codes and Standards, Multi-Year Research, Development, and Demonstration (MYRD&D) Plan:

(A) Safety Data and Information: Limited Access and Availability

(C) Safety is Not Always Treated as a Continuous Process

(F) Enabling National and International Markets Requires Consistent Regulations, Codes and Standards

(G) Insufficient Technical Data to Revise Standards

(H) Insufficient Synchronization of National Codes and Standards

(J) Limited Participation of Business in the Code Development Process

(K) No Consistent Codification Plan and Process for Synchronization of R&D and Code Development

Contribution to Achievement of DOE Safety, Codes & Standards Milestones

This project contributes to achievement of the following DOE milestones from the Hydrogen Safety, Codes and Standards section of the Fuel Cell Technologies Office's Multi-Year Research, Development, and Demonstration Plan:

- Milestone 2.3: Publish protocols for identifying potential failure modes. (2Q, 2013)
- Milestone 2.11: Publish draft protocol for identifying potential failure modes and risk mitigation. (4Q, 2014)
- Milestone 2.15: Develop holistic design strategies. (4Q, 2017)
- Milestone 2.19: Validate inherently safe design for hydrogen fueling infrastructure. (4Q, 2019)
- Milestone 3.1: Develop, validate, and harmonize test measurement protocols. (4Q, 2014)
- Milestone 4.1: Complete determination of safe refueling protocols for high pressure systems. (1Q, 2012)
- Milestone 4.3: Identify and evaluate failure modes. (3Q, 2013)

FY 2013 Accomplishments

- Collected safety/reliability data through direct communication with stakeholders and by utilizing NREL Technology Validation data to identify failure modes with highest statistical probability.
- Published NREL peer reviewed report "Component Testing Report" to provide information summarizing findings of failure mode investigation.
- Participated as moderator at DOE webinar on hydrogen fueling protocols. Webinar was held in conjunction with SAE interface committee providing the technical experts who presented talks on the webinar.
- Built industry partnerships to conduct high-pressure hydrogen component and system level testing designed to understand root cause failure modes and to provide guidance for engineering best practices.
- Developed utilization plans for DOE ESIF laboratory space by identifying best use of new capabilities and by supporting ESIF user facility designation through interface with DOE/NREL user facility personnel.
- Conducted industry workshops to match industry needs with DOE/ESIF laboratory capability.

✧ ✧ ✧ ✧ ✧

INTRODUCTION

Hydrogen safety, codes and standards has been identified in the DOE MYRD&D plan as an area where significant barriers need to be addressed. Codes and standards help ensure that hydrogen systems are safe and reliable, thereby enabling the acceptance of commercialization and growth of hydrogen technologies. NREL is providing research and development support to these codes and standards through validation testing, analytical modeling, and product commercialization efforts. NREL has been tasked with these responsibilities as defined in the DOE MYRD&D plan.

APPROACH

Hydrogen safety is being addressed by first identifying safety concerns, then developing appropriate test and analysis tasks that provide a technical basis for improved engineering methods and practices. Safety concerns are being compiled by direct discussion with key stakeholders, by leveraging existing data available through NREL's Technology Validation Sub-Program and by utilizing public outreach activities such as workshops and webinars. Identified safety concerns are prioritized, and then research and development tasks are aligned with the highest risk safety concerns. In general, the risk is defined by the combination of the severity and the likelihood of occurrence. Research and development results are then published for general use by stakeholders. Information is further disseminated through NREL outreach activities. Published results are then used as a basis for improved hydrogen codes and standards.

NREL is also participating on relevant codes and standards committees to help identify gaps and define research and development needs to close those gaps. Working at the committee level allows us to quickly identify areas that need R&D support and to work directly with the technical experts in planning a path forward. This process is instrumental in avoiding delays and setbacks in the development of new codes and standards and in the revision of existing codes and standards. By providing support from a national lab we are able to help establish codes and standards language with solid technical basis.

RESULTS

NREL has been working toward identifying safety gaps and supporting research and development efforts for developing new and improved hydrogen codes and standards. Results reported here are for efforts specifically directed at component level standards and identified hydrogen safety concerns.

Codes and Standards Technical Committee Support – NREL has supported the development of SAE J2601 (Fueling Protocols for Light Duty Gaseous Hydrogen Surface Vehicles) fueling protocols by providing technical basis for several key sections of the document. This includes the hot soak conditions from NREL's Technology Validation Composite Data Product #72 that was used as worst-case assumptions for onboard system temperatures when formulating the non-communication fill tables. SAE J2601 is planned for balloting by the end of FY 2013. NREL has also supported the release of SAE J2579 (Standard for Fuel Systems in Fuel Cell and Other Hydrogen Vehicles), which successfully balloted as a full standard in December of 2012. NREL also supported National Fire Prevention Association (NFPA) 2 Hydrogen Technologies Code while undergoing the first major revision through participation on the technical committee and several working groups. Material for reserved applications chapters is being added. The first draft meeting was held during the first week of June 2013 at NFPA headquarters in Quincy, MA.

DOE Hydrogen Refueling Webinar (22 February, 2013) – NREL acted as moderator for this event and supported planning and logistics activities. Speakers were selected from the SAE interface committee, and included Jesse Schneider of BMW and Steve Mathison of Honda. The event was well attended and generated valuable stakeholder comments and questions. This information has been valuable input for use in developing J2601 into a full standard.

Component Testing Report (NREL report no. PR-560-48070, 31 August, 2012) – This report compiles information from stakeholders, regulations codes and standards technical committees and outreach activities to itemize needs and gaps for safety and reliability of hydrogen systems. Leveraging of NREL Technology Validation data was also used to identify safety and reliability issues that have shown through field evaluation to be statistically higher occurrence and therefore of greater safety concern.

ESIF Laboratory Planning – NREL took occupancy of a new DOE laboratory building, ESIF, in December of 2012. This laboratory building provides the Hydrogen Safety, Codes and Standards Sub-Program with a valuable resource for conducting research and development activities. As part of this effort, a process hazard analysis was conducted and a five-year plan was produced.

Research and Development Outreach Activities – Numerous outreach activities were conducted in conjunction with the DOE/NREL Hydrogen Safety, Codes and Standards Sub-Program. These activities are used as a resource in soliciting feedback from industry and identifying priorities for research and development tasks. Significant outreach activities include: 1) conducting SAE J2601/NFPA 2 joint call to coordinate references and interrelated content in these documents; 2) participation on DOE-organized relief valve field failure task torce, which led to NREL removing similar relief valves from hydrogen service and reserving them for future root cause validation testing; 3) work for Others activity through the California Department of Food and Agriculture weights and measures project which has been instrumental in identifying gaps and needs for hydrogen metering; 4) participation on NREL Pressure Safety Panel to identify DOE laboratory protocols for the safe use of high-pressure hydrogen at a DOE laboratory; and 5) participation on Non-Metallic Materials workshop led by Sandia, addressing issues with elastomers used in high-pressure hydrogen service and the need to produce safe, leak tight systems.

CONCLUSIONS AND FUTURE DIRECTION

NREL has identified numerous opportunities to further improve the inherent safety of high-pressure hydrogen systems that are designed to serve fuel cell electric vehicle markets. These opportunities must be pursued through a variety of means, including failure mode testing investigations, root cause analysis and codes and standards development. Proposed future direction will utilize existing data generated by the Technology Validation Sub-Program and include research and development tasks that are aimed at improving the safety and reliability of high-pressure hydrogen systems. The new ESIF laboratory includes capability for component and system level testing that can be leveraged in support of fuel cell electric vehicle deployment activities.

FY 2013 PUBLICATIONS

1. "Component Standard Research and Development", DOE Annual Merit Review, May 14th, 2013.

2. "NREL Hydrogen Safety Plan, Annex II Hydrogen Component Testing", March 2013.

3. "DOE Workshop Series" sponsored by Secretary Chu, Poster Presentation "NREL Sensor Testing", Chicago IL, September 24–25, 2012.

4. "Component Testing Report, Hydrogen Safety Codes and Standards, FY12 AOP Deliverable 7.5", August 31st, 2012.

VIII.3 Hydrogen Safety, Codes and Standards: Sensors

Eric L. Brosha[1] (Primary Contact), Fernando H. Garzon[1], Robert S. Glass[2] (Primary Contact), Cortney Kreller[1], Rangachary Mukundan[1], and Leta Woo[2]

[1]Los Alamos National Laboratory (LANL)
MS D429, P.O Box 1663
Los Alamos, NM 87545
Phone: (505) 665 4008
Email: Brosha@lanl.gov

[2]Lawrence Livermore National Laboratory (LLNL)

DOE Manager
Rick Farmer
Phone: (202) 586-1623
Email: Richard.Farmer@ee.doe.gov

Project Start Date: Fiscal Year (FY) 2008
Project End Date: FY 2014

Overall Objectives

- Develop a low-cost and low-power electrochemical hydrogen safety sensor for a wide range of vehicle and infrastructure applications with focus on high durability and reliability
- Continually advance test prototypes guided by materials selection, sensor design, electrochemical research and development (R&D) investigation, fabrication, and rigorous life testing
- Disseminate packaged sensor prototypes and control systems to DOE laboratories and commercial parties interested in testing and fielding advanced prototypes for cross-validation
- Evaluate manufacturing approaches for commercialization
- Engage an industrial partner and execute technology transfer

FY 2013 Objectives

- Perform third round of validation and verification at the National Renewable Energy Laboratory (NREL)
- Acquire new lot of sensor platforms from ESL ElectroScience and fabricate sensors for NREL testing
- Test heater control boards at LANL and validate performance and sensor temperature response at NREL
- Initiate industrial partner search for sensor field trials

Technical Barriers

This project addresses the following technical barriers from the Hydrogen Safety section (3.8) of the Fuel Cell Technologies Office Multi-Year Research, Development, and Demonstration Plan:

(A) Safety Data and Information: Limited Access and Availability

(C) Safety is Not Always Treated as a Continuous Process

(K) No Consistent Codification Plan and Process for Synchronization of R&D and Code Development

(L) Usage and Access Restrictions

Technical Targets

Technical targets vary depending on the application [1,2], but in general include:

- Sensitivity: 1-4 vol% range in air
- Accuracy: ± 1% full scale in the range of 0.04-4 vol%
- Response Time: <1 min at 1% and <1 sec at 4%; recovery <1 min
- Temperature Operating Range: -40ºC to 60ºC
- Durability: Minimal calibration or no calibration required over sensor lifetime (as defined by particular application)
- Cross-Sensitivity: Minimal interference to humidity, H_2S, CH_4, CO, and volatile organic carbons

FY 2013 Accomplishments

- Tested sensor power supplies together with cheaper, more simplified sensor platforms incorporating integrated, unitary heater/temperature sensor platforms.
- Developed, optimized, and characterized working electrode and electrolyte layers grown using electron beam evaporation methods. A significant reduction in sensor manufacturing time was demonstrated that would eventually mean a reduction in projected manufacturing costs.
- New sensors were prepared using e-beam methods and packaged for Round 3 testing at NREL.
- Identified and tested La-Sr-Cr-O electrode as a candidate for applications that may involve anaerobic operations: solves a weakness identified in Round 2 NREL testing last year.
- Conducted last round of verification and validation at NREL: data show that the sensor signal changes

due to changes in ambient temperature are effectively eliminated.

- Interference testing performed on sensors indicated negligible interference in the presence of H_2 for the standard interferences tested.
- Demonstrated that the electrochemical mixed potential sensor technology exhibits a high degree of sensor device-to-device response reproducibility.

✧ ✧ ✧ ✧ ✧

INTRODUCTION AND APPROACH

Recent developments in the search for sustainable and renewable energy coupled with the advancements in fuel cell vehicles have augmented the demand for hydrogen safety sensors [2]. There are several sensor technologies that have been developed to detect hydrogen, including deployed systems to detect leaks in manned space systems and hydrogen safety sensors for laboratory and industrial usage. Among the several sensing methods, electrochemical devices [3-9] that utilize high temperature-based ceramic electrolytes are largely unaffected by changes in humidity and are more resilient to electrode or electrolyte poisoning. The desired sensing technique should meet a detection threshold of 1% (10,000 ppm) H_2 and response time of ≤1 min [10], which is a target for infrastructure and vehicular uses. Further, a review of electrochemical hydrogen sensors by Korotcenkov et al. [11] and the report by Glass et al. [10, 12] suggest the need for inexpensive, low-power, and compact sensors with long-term stability, minimal cross-sensitivity, and fast response. This view has been largely validated and supported by the fuel cell and hydrogen infrastructure industries at the NREL/DOE Hydrogen Sensor Workshop held on June 8, 2011 [13]. Many of the issues preventing widespread adoption of best-available hydrogen sensing technologies available today besides cost derive from excessive false positives and false negatives arising from signal drift and unstable sensor baseline; both of these problems necessitate unacceptably frequent calibration [13].

As part of the Hydrogen Codes and Standards sub-program, LANL and LLNL are working together to develop and test inexpensive, zirconia-based, electrochemical (mixed potential) sensors for H_2 detection in air. Previous work conducted at LLNL [9] showed that indium tin oxide (ITO) electrodes produced a stable mixed potential response in the presence of up to 5% H_2 in air with very low response to CO_2 and water vapor. The sensor also showed desirable characteristics with respect to response time, resistance to aging, and degradation due to thermal cycling.

In this investigation, the development and testing of an electrochemical H_2 sensor prototype based on '(ITO)/yttria-stabilized zirconia (YSZ)/platinum (Pt) configuration is detailed.

The device was fabricated using commercial ceramic sensor manufacturing methods on an alumina substrate with an integrated Pt resistance heater to achieve precise control of operating temperature while minimizing heterogeneous catalysis and loss of hydrogen sensitivity. Targeting fuel cell-powered automotive applications, the safety sensor was subjected to interference studies, temperature cycling, operating temperature variations, and long-term testing now exceeding over 6,000 hrs for some sensor configurations. In FY 2011, FY 2012, and FY 2013, the mixed potential electrochemical technology was independently validated at the hydrogen safety sensor-testing lab at NREL in three separate rounds of testing. In each round, two packaged pre-commercial prototypes were tested against a standard testing protocol, including the effects of changes in ambient temperature, pressure, humidity, and oxygen partial pressure (non-anaerobic) and sensor resistance to cross-interferences such as CO, CO_2, CH_4, and NH_3. In general, NREL testing showed a fast response to H_2 with exceptional low-level sensitivity and high signal-to-noise, very little deviation in sensor response to changes in ambient conditions such as humidity and barometric pressure, and minimal response to some common interference gases. However, potential weaknesses were found in the first two rounds of testing such as changes in sensor calibration with ambient temperature changes and complete sensor failure under the most harsh operating environment tested (anaerobic conditions).

FY 2011 testing at NREL uncovered an unanticipated interaction of the sensor element with the data acquisition system used in the hydrogen sensor testing system. The first sensor testing and validation experiments showed data with an anomalously high baseline (when no H_2 was present) and poor sensitivity to H_2 (when H_2 was present). These behaviors were never seen in LANL or LLNL laboratory sensor development work and could only be explained if there was insufficient input impedance on the data acquisition system. As a result, a high-impedance buffer (HIB) circuit board was designed and built to isolate the naked electrochemical sensor from stray electric currents that would generate a high baseline voltage which, depending on the direction of the current flow, would induce an offset voltage that would reduce the sensor voltage generated in response to H_2 exposure. The HIB is designed around a Burr Brown INA116 electrometer amplifier integrated circuit and is designed to minimize leakage between the electrodes and from the sensor itself to the electrometer circuit. The major success of FY 2012 were the successful verification and validation of the sensor/HIB package at NREL.

For FY 2013, a newly designed and constructed heater board was tested that changed sensor heater power according to ambient temperature. Scanning electron microscopy (SEM) and energy dispersive X-ray spectroscopy (EDS) analysis of the sensor that was exposed to anaerobic conditions were performed, and the post-testing evaluation was conducted to understand and interpret NREL findings.

The salient features of the H_2 sensor prototype developed by LANL and LLNL are (a) low power consumption, (b) compactness to fit into critical areas for some applications, (c) simple operation, (d) fast response, (e) a direct voltage read-out circumventing the need for complicated signal processing, (f) a low-cost sensor platform, and (g) excellent stability and reproducibility, all of which are conducive to commercialization using common ceramic manufacturing methods.

RESULTS REPORTED IN FY 2013

(a) Temperature feedback and heater control circuit development: In FY 2013, the principal goal for the third round of NREL testing was to test performance of the LANL/LLNL H_2 safety sensor prototype with active temperature feedback and control. NREL test results in FY 2011, Round 1 testing returned the anticipated results for ambient temperature testing. Because the sensor was tested using a fixed applied heater voltage throughout all of the Round 1 NREL testing, changes in the temperature of the NREL test chamber caused the sensor's temperature also to rise and fall commensurately. The variation in sensor voltage with temperature is well known since the response of mixed potential sensors is governed by electrode kinetics and the electrochemical reactions are a strong function of temperature. The small changes in the sensor Pt heater resistance were used to provide feedback to a heater control circuit designed and constructed for this project by Custom Sensor Solutions (Tucson, AZ). Figure 1 shows the experimental setup used for Round 3 testing at LANL. This circuit used a voltage output from a simple analog bridge to add/subtract to the heater voltage using the resistance from the sensor's Pt resistive heater as the control point. It is a very simple circuit and mode of operation that effectively maintained sensor temperature despite large changes in ambient T (over 90°C range in NREL test protocol) or local changes in sensor element temperature due to heat generated by H_2 combustion. While a 30°C change in test chamber temperature led to a 136% change in sensor voltage at 1% H_2 levels, this large temperature-induced shift in sensor voltage was not seen this year, indicating that the circuit worked very well.

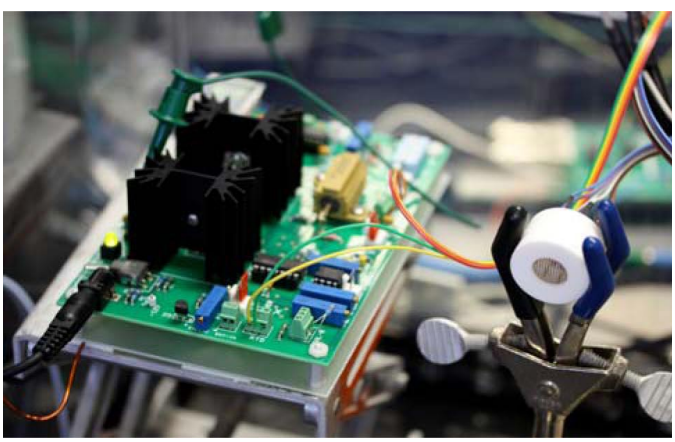

FIGURE 1. A packaged mixed potential, electrochemical sensor (shown in clamp on right) together with heater control electronics (left) used in FY 2013, Round 3 NREL testing to maintain precise sensor operating temperature commensurate with changes in ambient sensor temperature and temperature changes resulting from liberation of heat of combustion of the H_2 test gas.

(b) NREL testing: Figure 2 shows the results of NREL testing during the linear hydrogen range test performed as part of normal protocol. Given the exceptionally high signal-to-noise and high low-level sensitivity, NREL added several lower H_2 concentration levels to the test protocol. The sensors exhibited a normal baseline and response when measured at LANL or LLNL sensor laboratories in all cases. The HIB electronics developed in FY 2012 by Custom Sensor Solutions to counter undesirable sensor-data acquisition system interactions worked well, and a side benefit is the ability to control sensor baseline off-set and to adjust a desired amount of voltage amplification or gain. This latter feature is illustrated in Figure 2. The two sensors show different voltage levels for the same set of test gas concentrations because the gain was deliberately set at two different levels. The working voltage out is more than adequate for future final development and field trials, even for inexpensive recording of signal using either analog or digital circuits.

(c) Faster and less expensive methods of sensor fabrication demonstrated: In FY 2013, the methodology used to fabricate the safety sensor electrodes and electrolyte layers was changed from a combination of radio frequency magnetron sputtering (for the ITO working electrode) and electron beam evaporation (e-beam, for the YSZ electrolyte) to all e-beam. E-beam methods are used in commercial fabrication of sensors and devices. It is less expensive and a much faster method for film growth, although maintaining the stoichiometry of complex oxide materials may be more difficult. Figure 3a shows the EDS results of a test film grown in less than 10 minutes from a commercially sourced ITO target. The EDS confirmed the presence of the ITO film in a composition suitable for this application and similar in composition to those films prepared by sputtering. Also this FY, a new faceplate holder and machined shadow masks were procured to accommodate the ESL-prepared platforms and to apply the working electrode and electrolyte layers with more precision, leading to less change of substrate slippage resulting in unusable devices. Figure 3b is an SEM image using backscatter detector showing the ESL-prepared platform and wire bonding pads and counter electrode extension, together with the LANL-prepared ITO and YSZ layers.

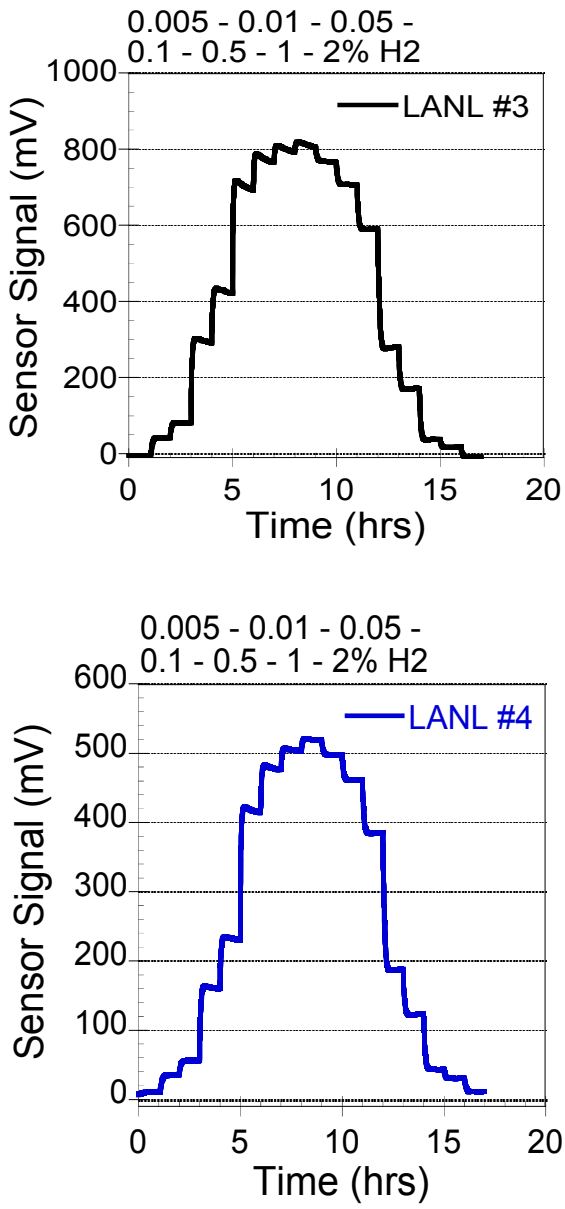

FIGURE 2. NREL "linear hydrogen test" performed on two packaged LANL/LLNL electrochemical hydrogen sensors. The use of HIB circuit boards isolated the two sensors from leakage currents in the data acquisition system at NREL discovered in Round 1 of testing. The HIB circuits isolate the sensors from stray leakage currents and permit normal sensor function. The different signal voltage levels for equivalent H_2 concentrations are a demonstration of the variable gain (signal amplification) built into the HIB circuitry.

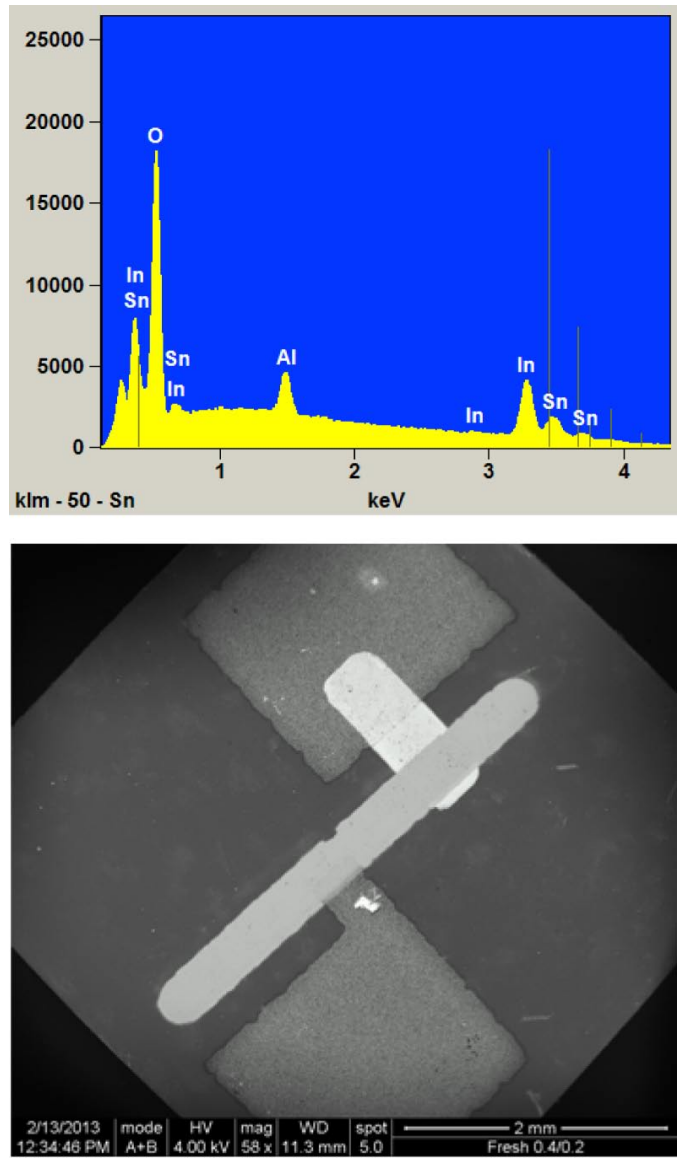

FIGURE 3A (TOP) AND 3B (BOTTOM). EDS spectra showing the elemental analysis of an ITO working electrode prepared from a single target, electron beam evaporation source (3a) and an electron backscatter detector image of the an actual H_2 sensor prepared at LANL on a commercially prepared, ESL sensor platform (3b). The final sensor layer (YSZ) can be seen in this image to cover the ITO working electrode (bright contrast) and the Pt counter electrode extension from the Pt pad used for electrical connection to the sensor.

(d) Comparison of FY 2012 and FY 2013 devices and demonstrated device-to-device reproducibility: One of the LANL/LLNL sensors prepared for NREL testing in FY 2012 was retrieved and placed into an improved sensor test stand constructed in FY 2013 at LANL. A newly prepared and packaged sensor was also tested under identical conditions. Not only were the working electrode and electrolyte prepared using different methods and equipment, the sensors tested at NREL in FY 2013 were also fabricated using a new ESL platform production lot. Despite the opportunity for substantial variations in sensor construct, the fundamental underpinnings of the sensor design and flexibility imparted though use of the HIBs permits exceptional high-level device-to-device reproducibility. This is shown in Figure 4a. Moreover, Figure 4b illustrates that precise temperature control during operation reveals a true logarithmic response not seen up to now. In past reports, a plot of sensor voltage vs. H_2 concentration would show deviations from logarithmic behavior with increasing H_2 levels. This was because

the sensor heater voltage was not automatically reduced commensurate with heating due to heat of combustion of the hydrogen. The data in Figure 4b are another indication as to how well the combined sensor/heater control has improved the performance of the safety sensor.

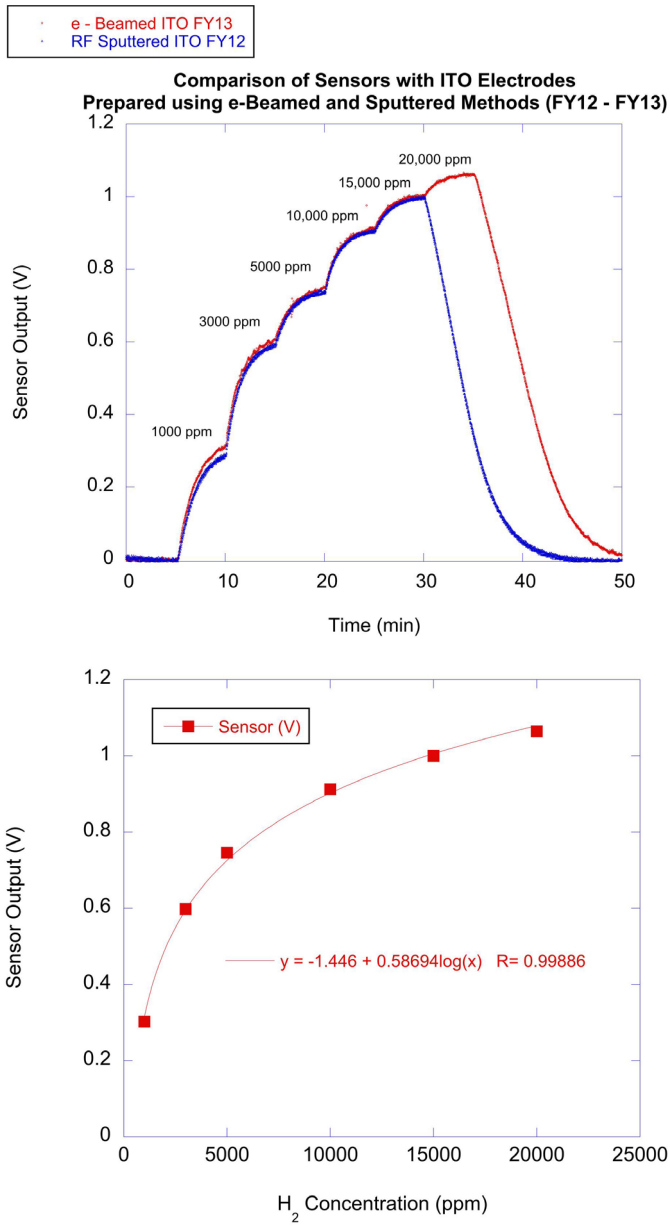

FIGURE 4A (TOP) AND 4B (BOTTOM). H_2 response comparison of a packaged H_2 safety sensor prepared and tested in Round 2 NREL testing in FY 2012 to a sensor prepared in FY 2013 using all electron beam evaporation methods (4a). The FY 2012 ITO sensor-working electrode was prepared using radio frequency magnetron sputtering and more than an order of magnitude slower deposition rate. Bottom, 4b: a plot of H_2 voltage level vs. H_2 concentration of a packaged LANL/LLNL H_2 safety sensor prepared in FY 2013; this year the high quality of fit to a logarithmic curve is the result of using temperature feedback from the sensor to control heater voltage applied to the sensor.

(e) Interference testing protocol at NREL: The packaged H_2 safety sensor prototype was tested at NREL using its interference protocol. The standard NREL test focuses on four interference gases: CH_4, CO_2, CO, and NH_3. Figure 5 shows the NREL testing results for 1%, 0.5%, 50 ppm, and 50 ppm, respectively. In these tests, the sensor baseline is first established, and 1% of H_2 is cycled. The interference gas is then turned on for 1 hr, after which 1% H_2 is reestablished together with the interference gas. After an additional hour, the H_2 is switched off and, after one more additional hour, the flow of interference gas is terminated. Finally, the sensor is cycled with one more exposure of 1% H_2. With this protocol, the sensor performance before and after interference exposure is measured together with the potential to measure the effects of simultaneous target/interference gas exposure. Figure 5 shows minimal interference effects for CO_2, CO, and ammonia. Methane produces an interesting response curve. The sensor shows a response to 1% CH_4; however, when hydrogen is introduced, Figure 5 shows that the voltage level for neat 1% H_2 is recovered and the apparent response to CH_4 is rejected. All interference gases tested impart no deleterious effects or poisoning to the sensor.

(f) Oxygen partial pressure testing; NREL anaerobic testing component of protocol: The effect of changing oxygen partial pressure on sensor H_2 sensitivity was investigated as part of the NREL standard test protocol. What was not conveyed to us was the fact that part of this protocol looked at testing in the absence of oxygen. Mixed potential electrochemical sensors using zirconia electrolytes rely on oxygen in the environment to establish competing electrode reactions and mediate the transfer of electrons that enable communication of electric potentials using a potentiostat or sourcemeter. However, the sensor will function in oxygen partial pressures ranging from roughly a fraction of a percent to 100% PO_2. This was confirmed by NREL. Figure 6 shows the sensor response to 1% H_2 cycling while the fraction of air was reduced in the experiment leading to PO_2 levels of 20%, 10%, 5%, and finally 0%. The sensor response to 1% H_2 remained unchanged as the PO_2 was reduced. However, as expected, the sensor voltage became unstable in the absence of oxygen. Moreover, the sensor response did not recover, and post mortem investigations quickly showed that the indium tin oxide sensor working electrode was not stable in anaerobic conditions, and the reducing environment produced by lack of oxygen, 1% H_2, and roughly 450-500°C sensor temperature led to reduction of the oxide to metal. The anaerobic testing duration was on the order of 5 hours, so it is quite possible that short periods of operation (e.g., <10 or 20 minutes) may not produce these irreversible effects. Once this occurred, SEM/EDS analysis showed that the metal cations diffused into the platform or alloyed with the Pt sensor pad. While the sensor cannot tolerate extended periods in such reducing conditions, the sensor nevertheless

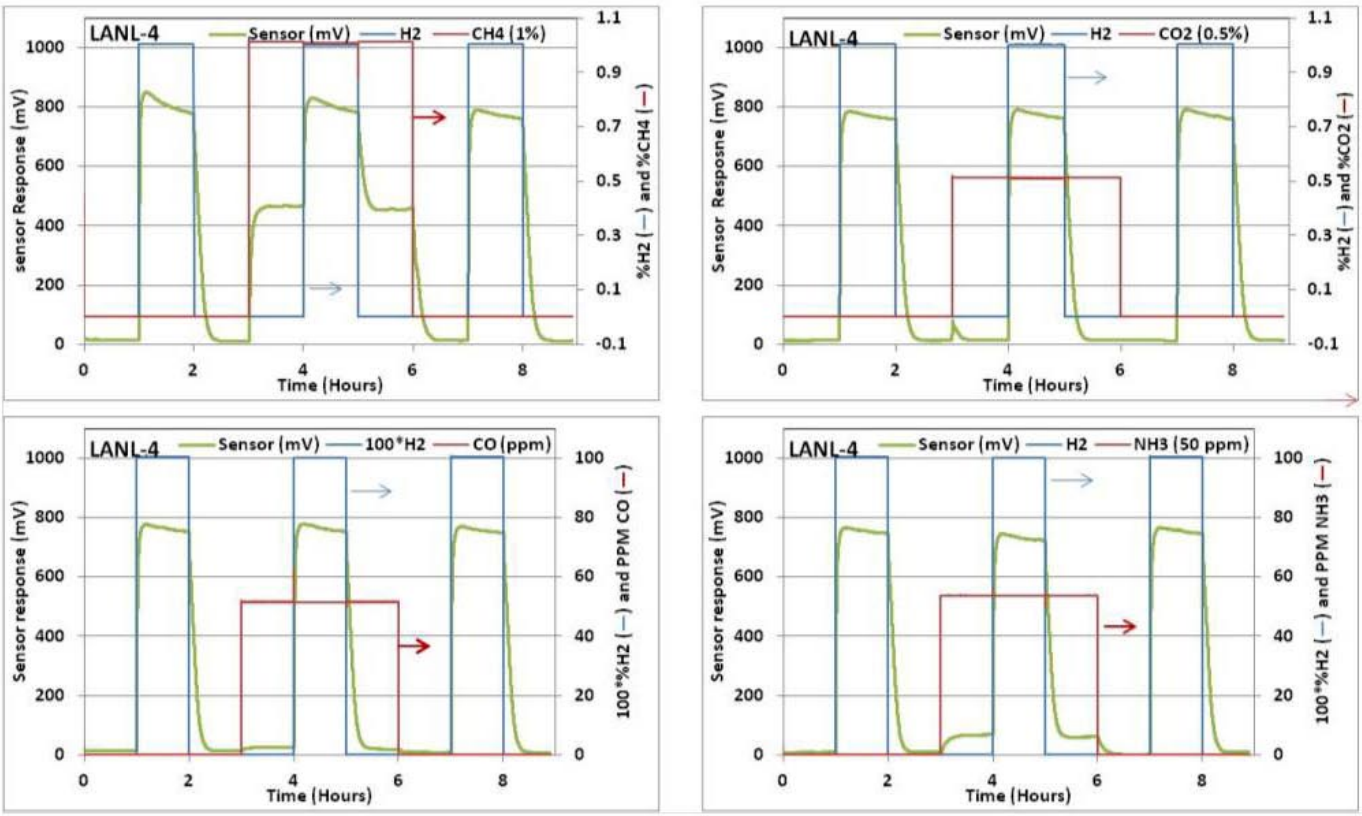

FIGURE 5. The results of standard NREL interference tests for methane (upper left), CO_2 (upper right), CO (lower left), and ammonia (lower right) at 1%, 0.5%, 50 ppm, and 50 ppm, respectively. The sensor showed minimal interference to CO_2, CO, and ammonia in these tests. The unusual response to methane (the complete rejection of CH_4 interference in the presence of H_2) is under investigation.

performed very well, and response was essentially invariant to PO_2 changes short of 0% O_2.

In FY 2013, a new working electrode material candidate was identified as a possible substitute for ITO. Lanthanum strontium chromite is a very stable electronically conducting oxide material that has been used for other applications (e.g., solid oxide fuel cells and automotive electrochemical sensor research and development) where exceptionally harsh conditions are anticipated. LANL investigations strongly indicate that this material may be substituted for the ITO for sensors that require extended anaerobic exposure periods. Though not required for the present safety application, it is available as an option for future development.

In summary, the third round of NREL testing was completed in April 2013, and all concerns identified in Rounds 1 and 2 were successfully ameliorated. Data produced in FY 2013 indicates that the technology has been validated to advance to field trials in collaboration with commercial hydrogen partners. Optimization of support electronics and improvements to the sensor technology continue to progress with the available funding.

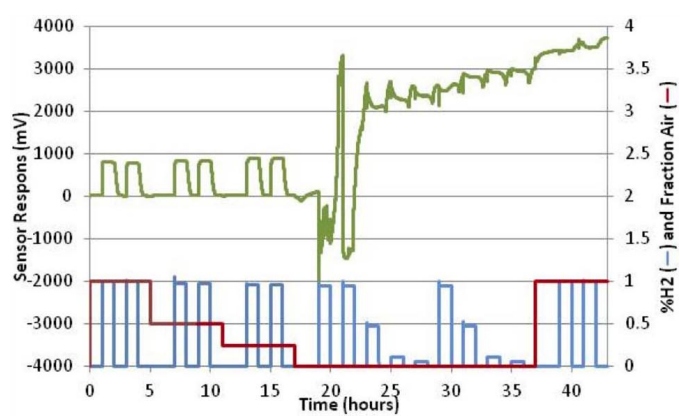

FIGURE 6. NREL anaerobic testing experiment that tests ability of H_2 sensors to withstand operation without air or oxygen. The LANL/LLNL electrochemical sensor H_2 response is invariant to PO_2 changes, but some O_2 is required based on sensor design incorporating use of oxygen ion-conducting solid electrolyte (YSZ).

CONCLUSIONS

- All FY 2013 milestones were completed this year.
- A viable H_2 safety sensor technology has been developed on an advanced sensor platform that continues to improve. An advanced H_2 sensor prototype was fabricated on an alumina substrate with ITO and Pt electrodes and YSZ electrolyte with an integrated Pt heater to achieve precise operating temperature and minimize heterogeneous catalysis.
- Multiple sensors were prepared using new electron beam vapor deposition methods and packaged. Devices may be fabricated in a fraction of the time as devices prepared by a combination of radio frequency magnetron sputtering (working electrode) and e-beam evaporation (electrolyte). Sensors prepared in FY 2013 showed identical response to sensors prepared in FY 2012, e.g., excellent response, signal-to-noise, and device-to-device reproducibility.
- Two sensors, heater control boards, and impedance buffers were tested in a third round of validation/verification conducted at NREL.
- The new heater control feedback effectively eliminated the temperature response reported by NREL in Round 1 testing.
- A combination of NREL Round 2 and 3 testing shows excellent sensitivity to H_2, reproducible device response with high signal-to-noise, minimal interferences to changes in relative humidity and barometric pressure, minimal response to changes in ambient temperature, and good to excellent rejection of potential interference gases CO_2, CO, NH_3, and CH_4.
- NREL testing showed minimal changes in sensor response over a wide range of oxygen partial pressures. H_2 response was constant until all oxygen was removed from the test chamber, showing oxygen displacement will not affect sensor response. Post mortem analysis of the device subjected to NREL anaerobic testing revealed that the highly reducing environment at operating temperature affected the ITO electrode. A new working electrode material was identified and tested and is available for applications where periods of anaerobic operation may be envisioned.

FUTURE DIRECTIONS

- Identify potential partners to plan and conduct field trials and testing at a commercial H_2 production or filling station in collaboration with NREL.
- Identify commercialization partners and plan for a path forward.
- Develop new version of sensor electronics optimized for field-testing.
- Reduce size and power consumption of the sensor element.
- Work with NREL partners to develop testing protocols for mixed potential type, electrochemical gas sensors.
- Prepare and test new sensors for field trials, test with new electronics and field packaging.
- Place sensors and data acquisition computers/data loggers at field-test location(s).

COLLABORATION AND COORDINATION WITH OTHER INSTITUTIONS

- National Renewable Energy Laboratory
- ESL ElectroScience, Inc.
- Custom Sensor Solutions, Inc.
- BJR Sensors, LLC

FY 2013 PUBLICATIONS AND PRESENTATIONS

1. P.K. Sekhar, C. Kreller, R. Mukundan, W. Buttner, M. Post, and E.L. Brosha, "Independent Testing of Hydrogen Prototype Sensors," Int. J. of Hydrogen Energy, in preparation July 2013.

2. L.Y. Woo, R.S. Glass, E.L. Brosha, R. Mukundan, F.H. Garzon, W.J. Buttner, M.B. Post, C. Rivkin, and R. Burgess, "Humidity Tolerance of Electrochemical Hydrogen Safety Sensors Based on Yttria- Stabilized Zirconia (YSZ) and Tin-doped Indium Oxide (ITO)," *Transactions of the ECS* **45** (16) (2013) 19-31.

3. P.K. Sekhar, E.L. Brosha, R. Mukundan, H. Mekonen, B. Farber, C. Kreller, and F.H. Garzon, "Packaging and Testing of a Hydrogen Safety Sensor Prototype," *Int. J. of Hydrogen Eng.* **37** No. 19 (2012) 14707-14713.

4. E.L. Brosha, "Leak Detection and Hydrogen Sensor Development," Pathways to Commercial Success: Technologies and Products Supported by the Fuel Cell Technologies Program, DOE EERE, September 2012, p. 238 (E-54).

REFERENCES

1. W.J. Buttner, M.B. Post, R. Burgess, C. Rivkin, *Int. J. Hydrogen Energy*, **36**, 2462 (2011).

2. L. Boon-Brett, J. Bousek, G. Black, P. Moretto, P. Castello, T. Hübert, and U. Banach, Identifying performance gaps in hydrogen safety sensor technology for automotive and stationary applications, International Journal of Hydrogen Energy, 35 (2010), 373-384.

3. H. Iwahara, H. Uchida, K. Ogaki, and H. Nagato, Nernstian Hydrogen Sensor Using $BaCeO_3$-Based, Proton-Conducting Ceramics Operative at 200-900°C, Journal of The Electrochemical Society, 138 (1991), 295-299.

4. Y. Tan and T.C. Tan, Characteristics and Modeling of a Solid State Hydrogen Sensor, The Journal of Electrochemical Society, 141 (1994), 461-466.

5. Z. Samec, F. Opekar, and G.J.E.F. Crijns, Solid-state Hydrogen Sensor Based on a Solid-Polymer Electrolyte, Electroanalysis, 7 (1995), 1054-1058.

6. Y-C.Liu, B-J. Hwang, and I.J. Tzeng, Solid-State Amperometric Hydrogen Sensor Using Pt/C/Nafion Composite Electrodes Prepared by a Hot-Pressed Method, Journal of The Electrochemical Society, 149 (2002), H173-H178.

7. L.B. Kriksunov and D.D. Macdonald, Amperometric hydrogen sensor for high-temperature water, Sensors and Actuators B, 32 (1996), 57-60.

8. G. Lu, N. Miura, and N. Yamazoe, High-temperature hydrogen sensor based on stabilized zirconia and a metal oxide electrode, Sensors and Actuators B, 35-36 (1996), 130-135.

9. L.P. Martin and R.S. Glass, Hydrogen Sensor Based on Yttria-Stabilized Zirconia Electrolyte and Tin-Doped Indium Oxide Electrode, Journal of The Electrochemical Society, 152 (2005), H43-H47.

10. R.S. Glass, J. Milliken, K. Howden, R. Sullivan (Eds.), Sensor Needs and Requirements for Proton-Exchange Membrane Fuel Cell Systems and Direct-Injection Engines, 2000, pp. 7 – 15. DOE, UCRL-ID-137767.

11. G. Korotcenkov, S.D. Han and J.R. Stetter, Review of Electrochemical Hydrogen Sensors, Chemical Review, 109 (2009), 1402-1433.

12. L.P. Martin and R.S. Glass, Electrochemical Sensors for PEMFC Vehicles, presented at The 2004 DOE Hydrogen, Fuel Cells, and Infrastructure Technologies Program Review, Philadelphia, PA (May 27, 2004).

13. NREL/DOE Hydrogen Sensor Workshop, June 8, 2011, Chicago IL. http://www.hydrogen.energy.gov/pdfs/progress11/viii_3_burgess_2011.pdf

14. F.H. Garzon, R. Mukundan, and E.L. Brosha, Solid state mixed potential gas sensors: theory, experiments and challenges, Solid State Ionics, 136-137 (2000), 633-638.

15. P.K. Sekhar, E.L. Brosha, R. Mukundan, M.A. Nelson, and F.H. Garzon, Application of Commercial Automotive Sensor Manufacturing Methods for NO_x/NH_3 Mixed Potential Sensors for Emission Control, ECS Transactions. 19 (2009), 45-49.

VII.4 R&D for Safety, Codes and Standards: Materials and Components Compatibility

Aaron Harris (Primary Contact), Brian Somerday
Sandia National Laboratories
P.O. Box 969
Livermore, CA 94551-0969
Phone: (925) 294-4530
Email: apharri@sandia.gov

Sandia National Laboratories is a multi-program laboratory managed and operated by Sandia Corporation, a wholly owned subsidiary of Lockheed Martin Corporation, for the U.S. Department of Energy's National Nuclear Security Administration under contract DE-AC04-94AL85000.

DOE Manager
Rick Farmer
Phone: (202) 586-1623
Email: Richard.Farmer@ee.doe.gov

Project Start Date: October 1, 2003
Project End Date: Project continuation and direction determined annually by DOE

Overall Objectives

- Understand the effects of hydrogen on structural materials
- Support the development and improvement of design and safety qualification standards for material use and materials evaluation

Fiscal Year (FY) 2013 Objectives

- Support the development of design and safety qualification standards for components (SAE International [SAE] J2579, American Society of Mechanical Engineers [ASME] Article KD-10) and materials testing standards (Canadian Standards Association [CSA] CHMC1)
- Develop more efficient and reliable materials test methods in standards
- Execute materials testing to address targeted data gaps in standards and critical technology development
- Develop and maintain material property database and identify material property data gaps

Technical Barriers

This project addresses the following technical barriers from the Hydrogen Safety, Codes ,and Standards section 3.8 of the Fuel Cell Technologies Office Multi-Year Research, Development, and Demonstration Plan:

(A) Safety Data and Information: Limited Access and Availability

(F) Enabling National and International Markets Requires Consistent Regulations, Codes, and Standards

(G) Insufficient Technical Data to Revise Standards

Contribution to Achievement of DOE Safety, Codes and Standards Milestones

This project will contribute to achievement of the following DOE milestones from the Hydrogen Safety, Codes and Standards section of the 2012 Fuel Cell Technologies Office Multi-Year Research, Development, and Demonstration Plan:

- Milestone 2.9: Publish technical basis for optimized design methodologies of hydrogen containment vessels to account appropriately for hydrogen attack. (4Q, 2014)
- Milestone 2.16: Demonstrate the use of new high-performance materials for hydrogen applications that are cost-competitive with aluminum alloys. (4Q, 2017)
- Milestone 2.18: Implement validated mechanism-based models for hydrogen attack in materials (4Q 2018)
- Milestone 3.3: Reduce the time required to qualify materials, components, and systems by 50% relative to 2011 with optimized test method development. (1Q 2017)
- Milestone 3.4: Develop hydrogen material qualification guidelines including composite materials (Q4, 2017)
- Milestone 4.9: Completion of the GTR Phase 2. (1Q, 2017)
- Milestone 5.2: Update materials compatibility technical reference (4Q, 2011-2020)
- Milestone 5.4: Develop and publish database for properties of structural materials in hydrogen gas. (2Q, 2013)

FY 2013 Accomplishments

- Completed test matrix to evaluate fatigue crack growth rate (da/dN) relationship corrections—two steels (SA372 Grade J and 34CrMo4) at three pressures (10, 45, 100 MPa):
  - For higher-strength steel, da/dN correction depends on hydrogen pressure and delta K level

  - For lower-strength steel, da/dN correction is less sensitive to hydrogen pressure
- Investigated effects of welding practice on hydrogen-exposed orbital welds in Type 316L tube:
  - Effect of low temperature evaluated for orbital tube welds
  - Tensile ductility of tubing and welds similar to data for bar materials
- Updated full public report on Technical Reference for Hydrogen Compatibility of Materials (SAND2012-7321), available on the Sandia National Laboratories' website (www.sandia.gov/matlsTechRef):
  - Data contributed to the White House OpenEI website (en.openei.org/wiki/Gateway:Hydrogen) initiative

✧ ✧ ✧ ✧ ✧

INTRODUCTION

A principal challenge to the widespread adoption of hydrogen infrastructure is the lack of quantifiable data on its safety envelope and worries about additional risk from hydrogen. To convince regulatory officials, local fire marshals, fuel suppliers, and the public at large that hydrogen refueling is safe for consumer use, the risk to personnel and bystanders must be quantified and minimized to an acceptable level. Such a task requires strong confidence in the safety performance of high pressure hydrogen systems. Developing meaningful materials characterization and qualification methodologies in addition to enhancing understanding of performance of materials is critical to eliminating barriers to the development of safe, low-cost, high-performance high-pressure hydrogen systems for the consumer environment.

APPROACH

The Materials and Components Compatibility project leverages decades of experience in high-pressure hydrogen systems, well-developed industry partnerships, world class technical expertise, and unique experimental equipment to focus on three critical activities: 1) optimize materials characterization methodologies, 2) generate critical hydrogen compatibility data for materials to enable technology deployment, and 3) provide international leadership by assembling and maintaining a technical reference that is populated with vetted data and includes a technical assessment of the data and its application.

RESULTS

Completed test matrix to evaluate correction method applied to fatigue crack growth relationships for two steels at three pressures

Hydrogen embrittlement has a great impact on the durability of metal components exposed to high-pressure hydrogen gas. Fatigue testing in high-pressure hydrogen helps ascertain material performance properties which inform the design of many parts and components used in high-pressure hydrogen service (i.e., ASME Article KD-10). The current fatigue crack growth test procedures in Article KD-10 are impractical, since test durations can be excessive at the prescribed load-cycle frequency (0.1 Hz). The test method can be improved to balance efficiency and data reliability. In FY 2011 and FY 2012 a modified test method was proposed and a validation test matrix was defined. The FY 2013 results represent completion of the validation test matrix consisting of two common pressure vessel steels in a range of hydrogen gas pressures. Table 1 provides a summary of the testing completed in FY 2013.

Figure 1 shows results from testing on the high-strength steel (34CrMo4) carried out following the matrix in Table 1. The results suggest that a possible test method modification could be implemented which would increase the efficiency of the test by applying a load-cycle frequency of 10 Hz (higher frequency = shorter test time). In concert, a correction factor to this high-rate data is determined by measuring the crack growth rate (da/dN) as a function of frequency at selected stress-intensity factor levels. There is a limiting frequency for the upper-bound da/dN, for example in the top graph of Figure 1 the 10-MPa pressure test reaches its upper-bound da/dN at approximately 1 Hz for both stress-intensity factors. The correction applied to the higher frequency test could be based upon the upper-bound da/dN measured at the limiting frequency. For the higher-strength 34CrMo4 steel, the correction factor applied to the high-frequency test data is dependent upon the pressure and the stress-intensity factor (delta K).

Similar to the high strength steels, the crack growth rate for the lower-strength SA372 Gr. J steel reaches an upper bound da/dN which is also defined by a limiting load cycle frequency (Figure 2). However, unlike the high-strength steel, the upper bound da/dN for the low-strength steel is similar for both 45 MPa and 100 MPa at both stress-intensity factors, which suggests that there is less sensitivity to hydrogen pressure. A modification to the test method may be the definition of a limiting test pressure in addition to the limiting frequency. These boundary conditions could enhance the efficiency of the test while ensuring that testing appropriately characterizes the material performance.

TABLE 1. Results of FY 2013 Testing

Steel	S_u (MPa)	H_2 Pressure (MPa)	Test Frequency (Hz)	Load Ratio	Status
SA372 Gr. J	890	10	10	0.1	Complete FY 2012-2013
		10	Variable	0.1	Complete FY 2012-2013
		45	10	0.1	Complete FY 2011-2012
		45	Variable	0.1	Complete FY 2011-2012
		100	10	0.1	In progress
		100	Variable	0.1	Complete FY 2012-2013
34CrMo4	1045	10	10	0.1	Complete FY 2012-2013
		10	Variable	0.1	Complete FY 2012-2013
		45	10	0.1	Complete FY 2012-2013
		45	Variable	0.1	Complete FY 2012-2013
		100	10	0.1	Complete FY 2012-2013
		100	Variable	0.1	Withdrawn

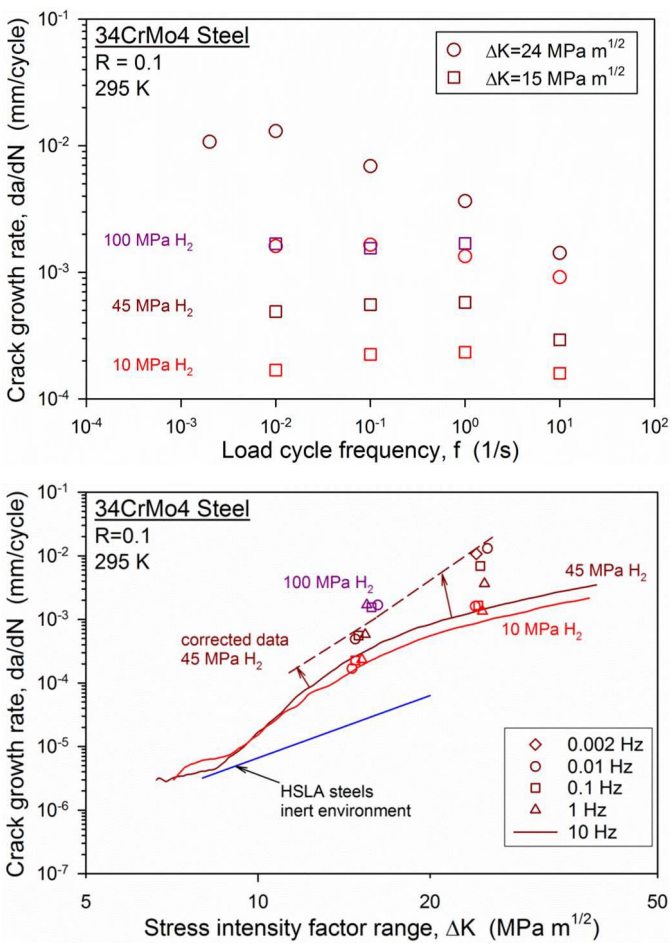

FIGURE 1. Top: summary of results for high strength steels shown as crack growth rate as a function of cycle frequency at different pressures for selected stress intensity factors. Bottom: test results for high strength steel demonstrating the validation of the correction factor applied to high-frequency data (improved efficiency).

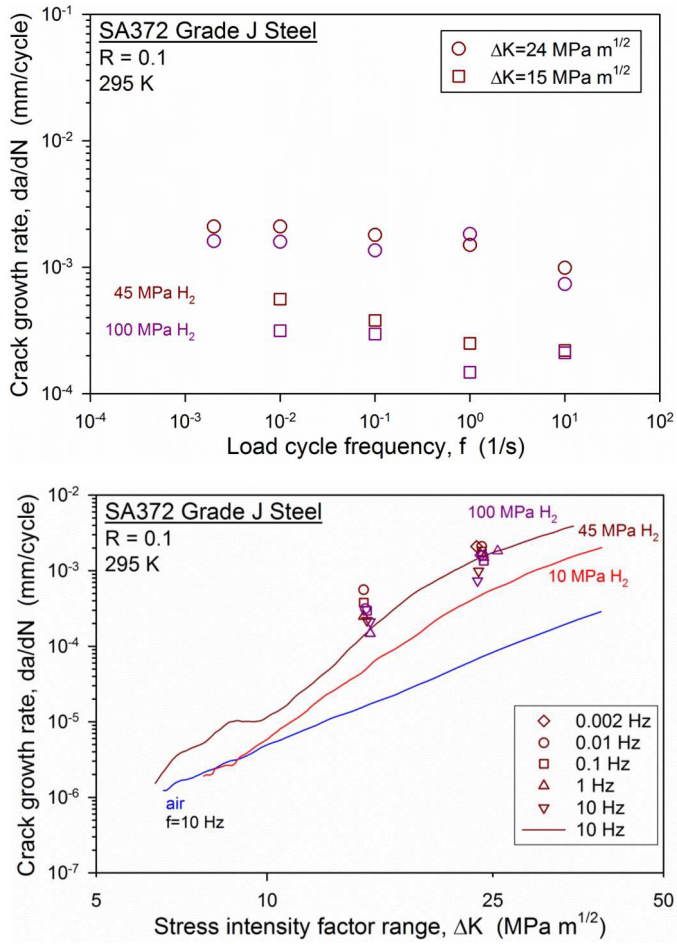

FIGURE 2. Top: summary of results for low strength steels shown as crack growth rate as a function of cycle frequency at different pressures at selected stress intensity factors. Bottom: test results for low strength steel demonstrating the validation of the correction factor applied to higher frequency testing (improved efficiency).

Investigation of welding practice for hydrogen-exposed orbital tube welds in Type 316L

While material characterization establishes safety margins for the performance of materials there are other factors which must be considered with regard to the practical use of those materials in the application. Orbital welding is a popular and well trusted method for joining tubing. This process is often automated and highly repeatable. All welding practices, regardless of automation, introduce microstructure alterations and residual stress to the material in and around the weld location. This activity investigated the performance of orbital tube welds with respect to non-welded tubes and traditional coupon samples from bar stock. Figure 3 shows the results of the testing. Weld A was produced by the industry partner and Weld B was created at Sandia using commercial welding equipment. Although the data set from these experiments is limited, the results suggest that welding practice can affect resistance to hydrogen embrittlement. Weld A retained ductility similar to the non-welded sample while Weld B shows a greater effect of hydrogen. Despite the manifestation of hydrogen embrittlement (reduced tensile ductility) in both welds, the absolute ductility values remain quite high (a key factor in safety of the tubing). The correlation of nickel content with greater resistance to hydrogen embrittlement has been substantiated with the results of tensile tests on the tubing and the orbital welded specimens compared to bar material as shown in Figure 4. The unexpected performance of Weld B is under investigation.

Investigation of temperature on hydrogen-exposed orbital tube welds

Another consideration with regard to the performance of welds in high-pressure hydrogen environments is the effect of low service temperatures. It is well known that hydrogen embrittlement of stainless steels is maximum at sub-ambient temperature, thus this environmental variable must be explored for stainless steel weld performance as well. Figure 5 shows that hydrogen-affected ductility at sub-ambient temperature is similar for the orbital tube welds compared to the non-welded tube and bar stock.

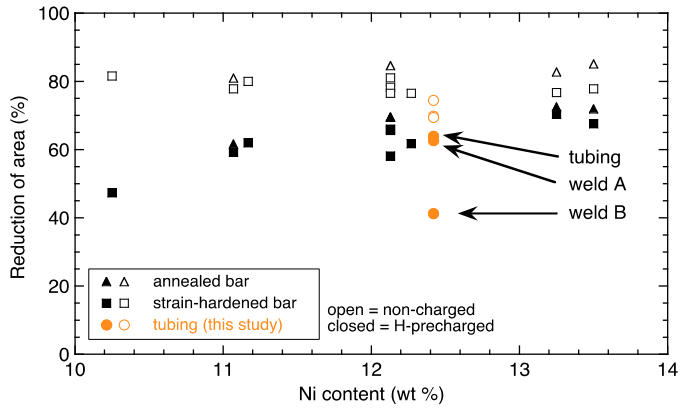

FIGURE 4. The results of the tubing and orbital tube welds is consistent with the correlation of nickel content with greater resistance to hydrogen embrittlement.

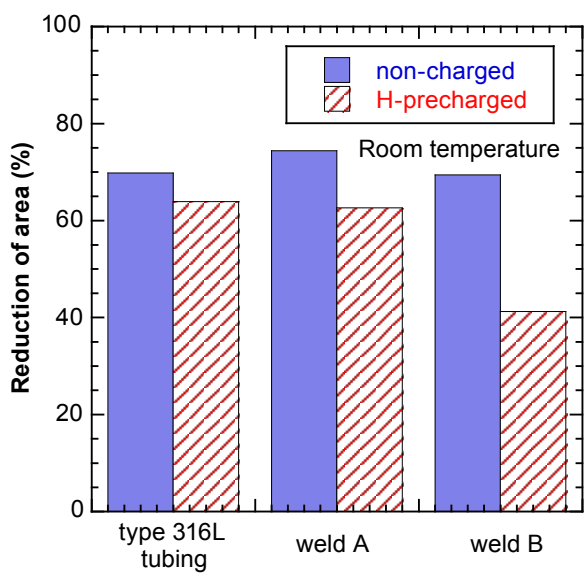

FIGURE 3. Results of weld practices upon the performance of welds in Type 316L tubing. The Type 316L tubing is non-welded, Weld A was produced by the industrial partner and Weld B was produced at Sandia using commercial welding equipment.

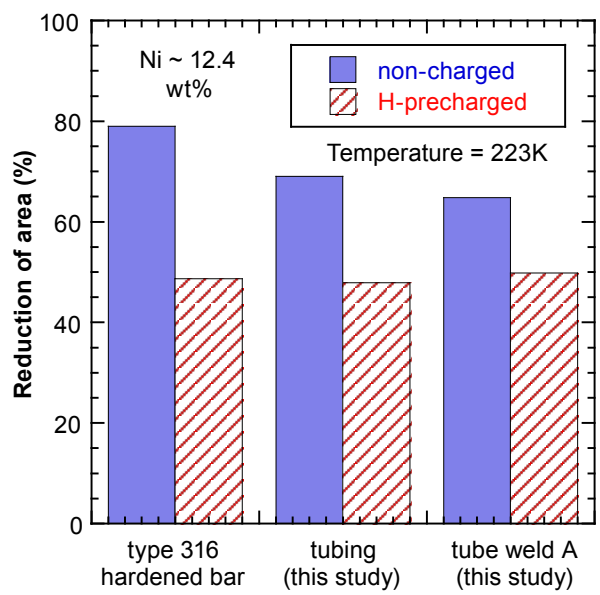

FIGURE 5. Tensile ductility results for 316 stainless steel bar stock, tubing and welded tubing at low temperatures.

Updates to the Technical Reference for Hydrogen Compatibility of Materials

The White House, in collaboration with the Department of Energy, initiated a project to publish energy data, called OpenEI. The OpenEI initiative hopes to leverage the success of publication of U.S. Geological Survey data that spawned the mobile GPS industry. In support of this initiative, Sandia posted two sets of information to the OpenEI website (en.openei.org/wiki/Gateway:Hydrogen). The Technical Reference for Hydrogen Compatibility of Materials was updated as a full public report and made available through the website (www.sandia.gov/matlsTechRef) and the OpenEI (en.openei.org/wiki/Gateway:Hydrogen). In addition, new datasets for fatigue crack growth in gaseous hydrogen not yet featured in the Technical Reference were included in the OpenEI database.

International Institute for Carbon-Neutral Energy Research (I2CNER)

Sandia provides leadership for the Hydrogen Structural Materials Division within the I2CNER. This research division in I2CNER is focused on understanding fundamental mechanisms of hydrogen embrittlement and developing new materials for hydrogen service—two areas that are critical to the Safety, Codes and Standards sub-program. Support of this task will enable Brian Somerday (division lead principal investigator) to interface the research performed in I2CNER with the DOE Fuel Cell Technologies Office, providing a conduit for research information between this international institute and the Fuel Cell Technologies Office.

Brian Somerday attended the I2CNER Annual Symposium at Kyushu University, Japan, in January 2013, presenting an overview of research progress in the Hydrogen Structural Materials Division. In addition, he served as a session chair at the HYDROGENIUS & I2CNER Research Symposium on Structural Materials, which featured presenters from eight different countries. Brian Somerday also met with collaborators in I2CNER, exchanging views and providing guidance on basic research that complements the applied research in the Materials Compatibility activity.

In June 2013, Brian Somerday traveled to Kyushu University for the Ministry of Education, Culture, Sports, Science, and Technology Site Visit, essentially an annual review of the Institute. As lead principal investigator, he represented the Hydrogen Structural Materials Division in the review.

National Institute of Advanced Industrial Science and Technology (AIST)

The DOE and the Ministry of Economy, Trade and Industry have coordinated R&D efforts in the area of hydrogen safety, codes, and standards. One of these coordinated activities is collaboration between AIST-Tsukuba and Sandia to develop standardized test methods for fracture threshold and fatigue crack growth measurements of steels in high-pressure hydrogen gas and to define the mechanisms of hydrogen-assisted fracture in stainless steels. An evolving project plan initiated in FY 2012 outlines the details of coordinated research between AIST-Tsukuba and Sandia in these two topic areas. The collaboration is expected to involve reciprocal visits to the U.S. and Japan.

This activity was reduced due to budget constraints. The reduction eliminated experiments on pressure vessel steels at Sandia that complement companion experiments at AIST. Brian Somerday met twice with his project-lead counterpart at AIST, once at AIST and another time at Sandia, to discuss progress on testing pressure vessel steels in hydrogen gas at AIST. Chris San Marchi visited AIST/Tsukuba for two weeks in March (expenses paid by AIST), presenting seminars at AIST and at Kyushu University (Hydrogenius). Chris San Marchi also visited Nippon Steel and Sumitomo Metals to share experience with testing in gaseous hydrogen and explore opportunity for collaboration with a steel manufacturer.

AIST-Tsukuba continued to conduct experiments on pressure vessel steels in hydrogen gas which formed the basis for discussions in project meetings hosted at Sandia throughout FY 2013. Sandia is provided test specimens from a U.S. pressure vessel steel specification for inclusion in the AIST test matrix. Dr. Bai An from AIST visited Sandia in May 2013 to continue the collaboration.

Codes and Standards Support

This project affects many codes and standards, both directly and indirectly. The following list summarizes that direct participation:

- CSA CHMC1
  - Materials testing and data application standard
  - Sandia provides leadership in technical committee and document preparation
  - Publication of Part 3 expected in 2013
- SAE J2579
  - Hydrogen vehicle fuel system standard
  - Sandia serves as U.S. technical lead on addressing hydrogen embrittlement
  - Publication expected in 2013
- ASME Article KD-10
  - Standard on high-pressure hydrogen tanks for transport and storage
  - Sandia provides data on exercising and improving materials test methods

- Reporting progress on optimizing fatigue crack growth testing to former chair of ASME Project Team on Hydrogen Tanks

CONCLUSIONS AND FUTURE DIRECTIONS

- Fatigue crack growth results for high strength steel (34CrMo4) and low-strength steel (SA372 Gr.J) in three hydrogen gas pressures suggest that test method efficiency could be improved without compromise of data reliability.
  - Future work – communicate the results of testing to ASME and support further action by the technical committee.
  - Future work – Develop validated methodology to account for fatigue crack initiation life in steel H_2 pressure vessels for consideration in ASME Article KD-10.
  - Future work – Leverage results on fatigue crack growth of pressure vessel steels in H_2 to enhance understanding of basic physics in collaboration with I2CNER.
  - Future work – Develop R&D project with industry partner(s) to evaluate and improve resistance of high-strength structural metals to H_2-assisted fracture.
  - Future work - Critically evaluate test method ("safety factor method") in CHMC1 Part 3 for qualifying materials for hydrogen service.
- Orbital tube welding practices for stainless steels may have an influence on the performance in hydrogen gas, however all welds retained significant tensile ductility. The performance of hydrogen-exposed orbital tube welds at strong sub-ambient temperature is similar to non-welded tubes and stainless steel bar stock.
  - Future work – Measure fatigue crack initiation resistance of H_2-exposed stainless steel tube welds.
  - Future work – Develop R&D program with industry partner(s) to evaluate and improve resistance of high-strength structural metals to H_2-assisted fracture.

FY 2013 PUBLICATIONS/PRESENTATIONS

1. K. Nibur, B. Somerday, C. San Marchi, J. Foulk, M. Dadfarnia, and P. Sofronis, "The Relationship Between Crack-Tip Strain and Subcritical Cracking Thresholds for Steels in High-Pressure Hydrogen Gas", *Metallurgical and Materials Transactions A*, vol. 44A, 2013, pp. 248-269.

2. T. Michler, C. San Marchi, J. Naumann, S. Weber, M. Martin: "Hydrogen environment embrittlement of stable austenitic steels". *Int J Hydrogen Energy*, vol. 37, 2012, pp.16231-16246.

3. C. San Marchi, B. Somerday. "Technical Reference for Hydrogen Compatibility of Materials", Sandia National Laboratories Report SAND2012-7321, 2012.

4. (invited presentation) C. San Marchi, "Overview of Gaseous Hydrogen Embrittlement Testing at Sandia", Korean Society of Mechanical Engineering, Annual Fall Meeting, Special International Session on Hydrogen Effects in Materials, Chagwon, Korea, Nov. 2012.

5. (invited presentation) C. San Marchi, A. Harris, D. Dedrick, "Investigation of the Hydrogen Release Incident at the AC Transit Emeryville Facility", Korea Research Institute of Standards and Science (KRISS), Daejeon, Korea, Nov. 2012.

6. (invited presentation) C. San Marchi, "Standards for Qualifying Materials for Hydrogen Service", Korea Research Institute of Standards and Science (KRISS), Daejeon, Korea, Nov. 2012.

7. B. Somerday, K. Nibur, and C. San Marchi, "Measurement of Fatigue Crack Growth Rates for SA-372 Gr. J Steel in 100 MPa Hydrogen Gas Following Article KD-10", ASME PVP2013, Paper No. 97455, 2013, submitted.

8. B. An, H. Itouga, T. Iijima, C. San Marchi, and B. Somerday, "Hydrogen-assisted twin boundary fracture of type 304 austenitic stainless steel at low temperature investigated by scanning probe microscopy", ASME PVP2013, Paper No. 97355, 2013, submitted.

9. C. San Marchi, L. Hughes, B. Somerday, and X. Tang, "Hydrogen-Assisted Fracture of Type 316L Tubing and Orbital Welds, ASME PVP2013, Paper No. 97538, submitted.

VIII.5 Hydrogen Fuel Quality

T. Rockward (Primary Contact), C. Quesada, K. Rau, E. Brosha, F. Garzon, and R. Mukundan
P.O Box 1663
Los Alamos National Laboratory (LANL)
Los Alamos, NM 87545
Phone: (505) 667-9587
Email: trock@lanl.gov

DOE Manager
Rick Farmer
Phone: (202) 586-1623
Email: Richard.Farmer@ee.doe.gov

Project Start Date: October 2006
Project End Date: Project continuation and direction determined annually by DOE

Overall Objectives

- To support the Hydrogen Safety Codes and Standards sub-program through:
  - Participation in working groups e.g., Working Group 12
  - Providing leadership to hydrogen fuel quality efforts
  - Performing the research and development (R&D) needed to develop science-based codes and standards
  - Develop tools that can remove safety and hydrogen fuel quality barriers to the commercialization of fuel cells

Fiscal Year (FY) 2013 Objectives

- To carry out the duties of ASTM International (ASTM) sub-committee chair for D03.14 gaseous hydrogen fuel efforts.
- To help determine levels of impurity constituents for the development of an international standard for hydrogen fuel quality—International Organization for Standardization Technical Committee (ISO TC) 197 WG12.
- Investigate the impact of fuel impurities on polymer electrolyte fuel cell performance using state-of-the-art membrane electrode assemblies (MEAs).
- To demonstrate proof-of-concept of an electrochemical analyzer to detect low levels of impurities in hydrogen fuel.
- Report findings/results to the DOE.

Technical Barriers

This project addresses the following technical barriers from the Hydrogen Safety, Codes and Standards section (3.7.5) of the Fuel Cell Technologies Office Multi-Year Research, Development, and Demonstration Plan:

(F) Enabling National and International Markets Requires Consistent Regulations, Codes, and Standards

(G) Insufficient technical Data to Revise Standards

(H) Insufficient Synchronization of National Codes and Standards

(K) No Consistent Codification Plan and Process for Synchronization of R&D and Code Development

Technical Targets

Most Hydrogen Safety, Codes and Standards activities do not have quantifiable technical targets.

FY 2013 Accomplishments

- Contributions to ASTM
  - Sub-committee Chair D03.14
  - Multiple standards developed and/or under development
  - Chaired two separate ASTM national meetings
- Inline Fuel Quality Analyzer
  - Proof of concept demonstrated for CO analyzer using sputtered platinum electrode
    - Improved sensitivity
    - Improved durability
    - CO dosage monitoring possible—analyzer under construction
- Impurity testing expanded to state-of-the-art MEAs
  - Hydrogen fuel standard developed based on common MEA
  - Lower loading results in significantly higher performance loss
  - State-of-the-art nano-structured thin-film (NSTF) MEAs also exhibit significantly higher losses than the common MEA
- U.S. DOE/Japanese Automotive Research Institute Meeting on Fuel Quality and Durability
  - Potential collaborations identified: drive cycle testing, exchange of MEAs and protocols

✧ ✧ ✧ ✧ ✧

INTRODUCTION

The work performed is divided into three tasks: a) contributions to ASTM standards development, b) inline fuel quality analyzer development, and c) R&D for fuel quality standards development.

Recently, an international team (ISO TC197 WG-12) developed hydrogen fuel product specifications for use in proton exchange membrane fuel cell (PEMFC) applications for road vehicles (ISO 14687-2:2012). Fuel cells tested with the fuel specification indicated that ammonia, carbon monoxide and hydrogen sulfide were the critical contaminants; i.e. the impurities that were the most harmful to PEMFC performance and/or its durability. While the fuel specification was based on actual PEMFC data from MEAs using conventional dispersed Pt/C catalysts; the DOE target loading for platinum has been continuously lowered and is currently based on novel materials that were unavailable during the development of the ISO standard. The current status of PEMFC technology as monitored by the DOE Fuel Cell Program is based on NSTF materials. MEAs based on these novel materials show great promise for reduced cost (better performance at lower precious metal loadings) and greater durability over conventional Pt/C electrodes [1]. However, their thin electrode structure may face water management challenges, especially during low temperature operations [2]. In addition, LANL scientists showed that an increase in local water can enhance performance with certain impurities [3]. Therefore, there is still uncertainty in whether or not the fuel standards may need revising to accommodate these novel catalyst layers and low loadings. In FY 2013 we evaluated PEMFC performance utilizing these novel materials in the presence of surface adsorbing contaminants.

Once science-based defendable standards are established, there is still a need to provide the tools necessary to implement this standard. LANL is helping this effort by providing leadership to ASTM to develop methods to determine the impurity content in the fuel. Finally LANL is also developing an inline fuel quality analyzer capable of quick and cheap detection of the key impurities in the H_2 fuel at various points in the supply chain. For example, carbon monoxide and hydrogen sulfide are impurities in hydrogen reformed from fossil fuels, or bio gas. While steam reforming natural gas will make hydrogen affordable and available, it will produce trace amounts of CO and H_2S. The ISO has set a fuel standard of 99.97% H_2 as applicable to PEMFC vehicles with a maximum allowance of 0.2 ppm for CO and 4 ppb for H_2S [4]. In addition to the hydrogen grade being certified, it would be prudent to have inline analyzers to protect expensive fuel cell components from these contaminants. Previous publications have demonstrated that Nafion®-based sensors using platinum electrodes respond to CO [5]. This response can be used to quantitatively analyze the amount of CO present in the hydrogen fuel stream. In FY 2013 LANL demonstrated a proof of concept CO dose monitor that has that the potential to be incorporated into an inline analyzer.

APPROACH

R&D for Fuel Quality Standards

Tests were conducted on 50-cm^2 MEAs using a total platinum loading of 0.15 mg/cm^2. The NSTF anode was 0.03 mg Pt/cm^2, the NSTF cathode was 0.125 mg Pt/cm^2 (Pt_3Ni_7, de-alloyed and annealed), and the electrode was a 24-µm 3M 850 equivalent weight electrolyte-PEM. The gas diffusion layers (GDLs) used were also provided by 3M—2979 GDL at both the cathode and anode. The MEAs were subjected to 50 hours of exposure to either 4 ppb H_2S or 100 ppm CO in the anode feed stream of a fuel cell operating at 50A constant current held at 80°C.

Inline Fuel Quality Analyzer

Carbon monoxide chemisorbs on platinum surfaces preventing hydrogen dissociation from occurring, and inherently reducing the current output that can be measured as increasing resistance of the system. The fuel quality analyzer is a 5-cm^2 MEA with platinum electrodes. One electrode is low surface area Pt sputtered on carbon cloth with 0.1 mg Pt/cm^2 loading. The opposing electrode is a BASF Pt-Vulcan higher surface area 0.2 mg Pt/cm^2. Both were hot-pressed onto a Nafion® 117 membrane. The higher surface area electrode is positioned as the counter/reference electrode and exposed to ultra-high purity hydrogen only, while CO/H_2 is introduced at the sputtered electrode. Stripping voltammetry is used to verify the presence of CO, its amount, and to oxidize CO off the electrode's surface, which inherently regenerates the analyzer for subsequent uses.

RESULTS

Contributions to ASTM Standards Development

Sub-Committee Chair: Officer Duties: The sub-committee chair is responsible for preparing items for Sub- and Main-Committee ballots, resolving negative votes on the website, hosting meetings and recording minutes. Furthermore, the duties include registration of a work items, organizing collaboration areas, submitting items for ballot, scheduling virtual meetings, and handling negatives and comments and organizing inter-laboratory studies (ILS).

On-Going Standards Development: The D03 Subcommittee D03.14 on Hydrogen and Fuel Cells is responsible for developing standards, specifications, practices, and guidelines relating to hydrogen used in

energy generation or as feed gas to low-, medium- and high-temperature fuel cells**.** Table 1 lists the on-going standards being developed under ASTM D03.14.

Inter-Laboratory Studies [6]: The ultimate goal of ILS is to enhance the quality of ASTM standard test methods by assisting technical committees as they develop precision statements backed by high quality laboratory data for their test method, so as to incorporate at least a repeatability statement.

Inline Analyzer Development

The analyzer is designed to be operated as a hydrogen pump, with H_2 flowing on both sides. A potentiostat is used to probe the electrode with a voltage and to measure the current response from hydrogen oxidizing on one side and protons reducing on the other. The inverse of the slope of the resulting line gives the resistance of the cell that is strongly affected by any poisoning of the Pt electrode. Figure 1 demonstrates resistance increases over time of a standard Pt electrode (0.2 mg-Pt/cm^2) in the presence of 0.5 ppm CO for two hours. While the standard Pt electrode does get poisoned over time, decreasing the Pt loading and/or the Pt surface area can dramatically improve sensitivity. This is demonstrated in Figure 2a illustrating the performance of a sputtered Pt electrode operated under the same conditions as the conventional Pt/C electrode. The decrease in loading and surface area of the sputtered electrode resulted in a >100% improvement in the CO sensitivity. Figure 2b illustrates the performance of this same device exposed to 0.1 ppm CO for

TABLE 1. On-Going Standards being Developed under ASTM D03.14

Work Item	Title	Constituents (Detection Limit)	Update
Published	Standard Test Method for Determination of Trace Carbon Dioxide, Argon, Nitrogen, Oxygen and Water in Hydrogen Fuel by Jet Pulse Injection and Gas Chromatography/Mass Spectrometer Analysis	CO_2 (0.5 ppm), nitrogen (5 ppm), argon (1 ppm), oxygen (2 ppm), and water (1 ppm)	Published official item: D7649-10 Awaiting test samples
Published	Standard Practice for Sampling of High Pressure Hydrogen and Related Fuel Cell Feed Gases	Gaseous sampling	Published official item: D7606-11
Published	Standard Test Method for Determination of Ammonium, Alkali and Alkaline Earth Metals in Hydrogen and Other Cell Feed Gases by Ion Chromatography	Formic Acid (low ppb to ppm)	Published official item: D7550-09
Published	Standard Test Method for Sampling of Particulate Matter in High Pressure Hydrogen used as a Gaseous Fuel with an In Stream Filter	Particulate sampling	Published official item: D7650-10 Addressed
Published	Standard Test Method for Determination of Trace Gaseous Contaminants in Hydrogen Fuel by Fourier Transform Infrared (FTIR) Spectroscopy	Ammonia, CO_2, CO, formaldehyde, formic acid, and water (defined by EPA 40 CFR part 136 Appendix A "meet detection limits of SAE TIR J2719")	Published official item: D7653-10 ILS complete, collecting data on going
21162	Standard Test Method for the Characterization of Particles from Hydrogen Fuel Streams by Scanning Electron Microscope	Particulates	N/A
Published	Standard Test Method for Visualizing Particulate Sizes and Morphology of Particles Contained in Hydrogen Fuel by Microscopy	Particulates	Published official item: D7634-10
Published	Standard Test Method for Gravimetric Measurement of Particulate Concentration of Hydrogen Fuel	Particulates	Published official item: D7651-10
Published	Standard Test Method for Test Method for the Determination of Total Hydrocarbons in Hydrogen by FID Based Total Hydrocarbon (THC) Analyzer	Total hydrocarbons (0.1 ppm)	Published official item: D7675-11 Editorial changes
23815	Determination of Total Halocarbons contained in Hydrogen and other gaseous fuels	Total halogenated compounds ("halocarbon determination requirements contained in SAE J2719" 0.1 ppb)	Editorial changes address, negatives need resolution (D.Bartel)
Published	Standard Test Method for Determination of Trace Hydrogen Sulfide, Carbonyl Sulfide, Methyl Mercaptan, Carbon Disulfide and Total Sulfur in Hydrogen Fuel by Gas Chromatography and Sulfur Chemiluminescence Detection	Total sulfur (0.02 ppb)	Published official item: D7652-11
34574	Standard Test Method for Determination of Trace Hydrogen Bromide, Hydrogen Chloride, Chlorine and organic halides in Hydrogen Fuel by Gas Chromatography with Electrolytic Conductivity Detector and Mass Spectrometer	Trace hydrogen bromide, hydrogen chloride, chlorine and organic halides	Ballot closed Dec 12, New Standard

EPA – Environmental Protection Agency

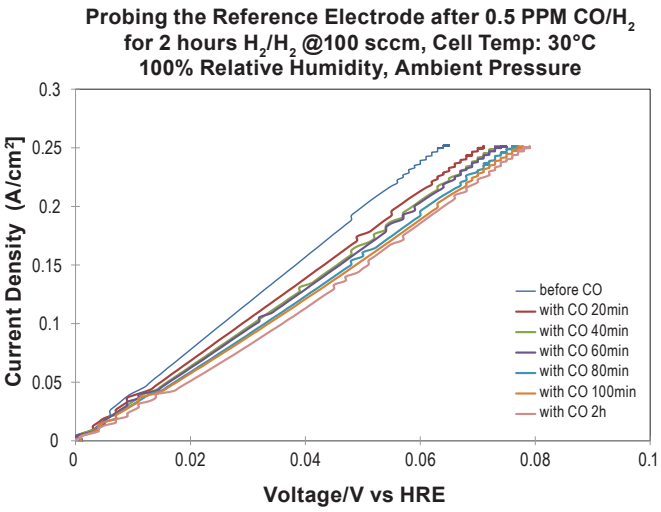

FIGURE 1. Resistance increase of the reference electrode (0.2 mg-Pt/cm^2) in the presence of 0.5 ppm CO over 2 hours

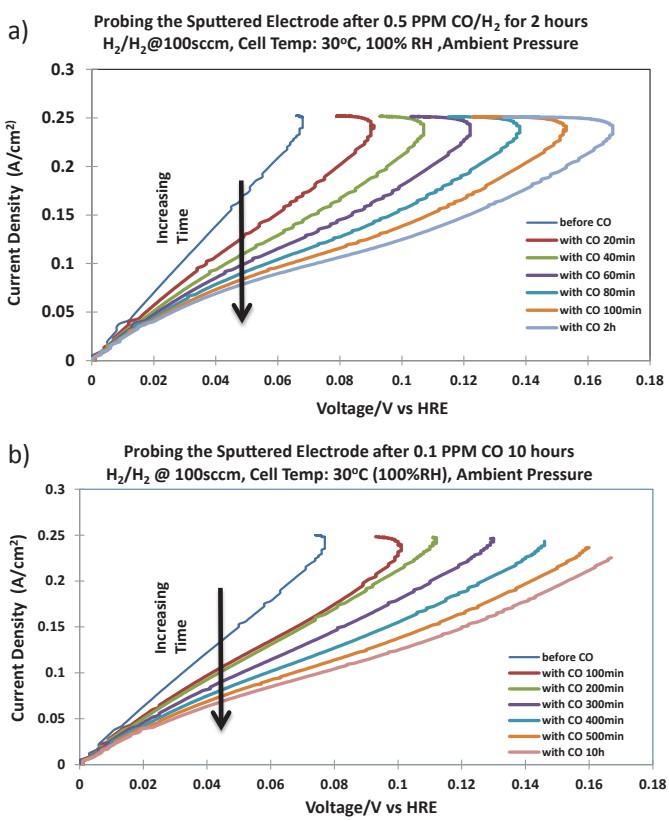

FIGURE 2. Resistance increase of the sputtered platinum sensing electrode in the presence of a) 0.5 ppm CO over 2 hours and b) 0.1 ppm over 10 hours

10 hours. Extensive studies on this device suggest that this sputtered electrode could serve as the sensing electrode of a CO dosage monitor. Operating conditions were varied in an effort to find optimal conditions for increased sensitivity of

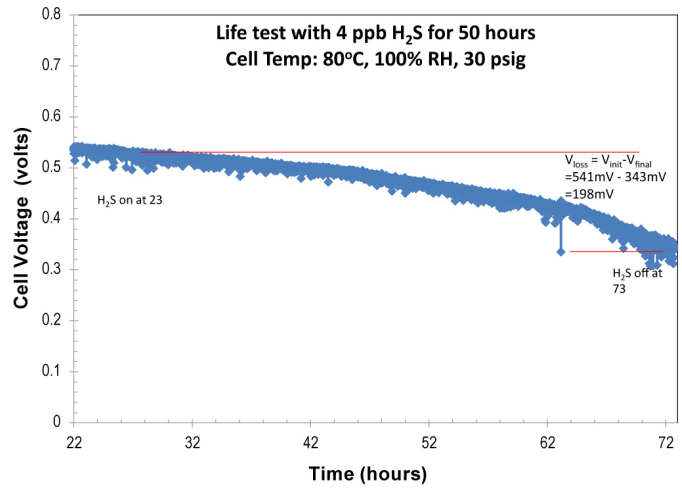

FIGURE 3. Voltage loss during 50 hours of exposure to 4 ppb H_2S at an operating current of 1 A/cm^2 (total losses observed ≈198 mV)

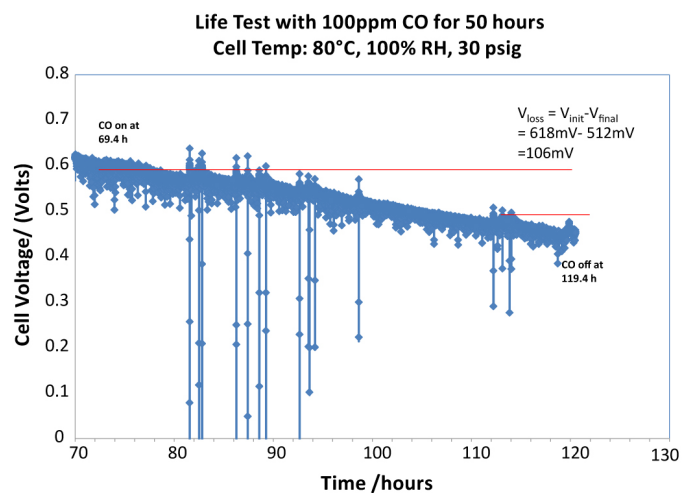

FIGURE 4. Voltage loss during 50 hours of exposure to 100 ppm CO at an operating current of 1 A/cm^2 (total losses observed ≈106 mV)

CO. The operating conditions tested were 30°C and 60°C and an applied voltage bias of 0.0 V and 0.2 V. The sensitivity of the device was lower at 0.2 V than at 0.0 V and the use of a voltage >0.6 V resulted in complete CO clean up. Therefore the device could be used as a dosage monitor for CO that can be reset by the use of high potentials.

R&D for Fuel Quality Standards

Figures 3 and 4 highlight the voltage response over time of fuel cells operated at 100% relative humidity (RH) and 30 psig back pressure with CO and H_2S concentrations at or below the current fuel quality standards limit. The hydrogen sulfide caused approximately 198 mV drop (at 1 A/cm^2) in the fuel cell performance, while an approximate 106 mV drop (at 1 A/cm^2) was observed when the fuel cell

was exposed to carbon monoxide. The fuel quality standards were determined using a common MEA with a 0.1 mg-Pt/cm^2 loading. The lower-loaded anodes (0.03 mg-Pt/cm^2) used in this study resulted in significantly more degradation under the same conditions. Further studies are underway using state-of-the-art MEAs subjected to fuel cell testing in the presence of fuel impurities. These results will be further augmented with testing under non steady state conditions (drive cycle transients) to determine the real impact of CO and H_2S on fuel cell performance.

CONCLUSIONS AND FUTURE DIRECTIONS

In FY 2013, a proof of concept for a CO dosage monitor capable of detecting <0.1 ppm·hour of CO was demonstrated. Fuel quality testing with low-loaded anodes (0.03 mg-Pt/cm^2) indicate ≈100 mV loss at 1 A/cm^2 when exposed to 100 ppm CO for 50 hours and ≈200 mV loss when exposed to 4 ppb of H_2S for 50 hours. In FY 2013 LANL also provided leadership to the ASTM Subcommittee D03.14 on Hydrogen and Fuel Cells. LANL will work on the following tasks in FY 2014.

- Continue providing leadership to ASTM efforts
- Construct an electrochemical analyzer-based on the proof of concept demonstrated for the CO dosage monitor
- Expand inline analyzer proof of concept to H_2S and NH_3
- Perform tests with ultra-low platinum loading and state-of-the-art materials using the ISO concentration levels
- Understand recovery mechanisms in state-of-the-art MEAs
- Explore DOE/Japanese Automotive Research Institute/ LANL collaboration that incorporates durability and drive cycle tests in the presence of impurities

COLLABORATORS/PARTNERS

- WG -12 Members
- Japanese Automotive Research Institute
- ASTM International
- Air Liquide
- California Fuel Cell Partnership
- CONSCI

REFERENCES

1. M.K. Debe, "Electrocatalyst approaches and challenges for automotive fuel cells", *Nature*, V486, 43 (2012).

2. M.K. Debe, "Nanostructures thin film electrocatalysts for PEM fuel cells – A tutorial on the fundamental characteristics and practical properties of NSTF catalysts", *ECS Trans*., 45(2), 47 (2012).

3. Tommy Rockward, John Davey, Eric L. Brosha, and Fernando H. Garzon, "*Investigating the Impact of Low Levels of Sulfur Compounds on the Fuel Cell Performance"*, 218th ECS Meeting, Las Vegas, NV (2010).

4. Organization, I.S., *Hydrogen fuel — Product specification — Part 2: Proton exchange membrane (PEM) fuel cell applications for road vehicles*, in *ISO TC 197*2012, ISO copyright office: Case postale 56 • CH-1211 Geneva 20.

5. Mukundan, R., Brosha, E.L. and Garzon, F.H., *A low temperature sensor for the detection of carbon monoxide in hydrogen*. Solid State Ionics, 2004. **175**(1-4): p. 497-501.

6. http://www.astm.org/ILS/index.html.

VIII.6 R&D for Safety Codes and Standards: Hydrogen Release Behavior

Aaron Harris (Primary Contact), Isaac Ekoto
Sandia National Laboratories
P.O. Box 969
Livermore, CA 94551-0969
Phone: (925) 294-4530
Email: apharri@sandia.gov

Sandia National Laboratories is a multi-program laboratory managed and operated by Sandia Corporation, a wholly owned subsidiary of Lockheed Martin Corporation, for the U.S. Department of Energy's National Nuclear Security Administration under contract DE-AC04-94AL85000.

DOE Manager
Rick Farmer
Phone: (202) 586-1623
Email: Richard.Farmer@ee.doe.gov

Project Start Date: October 1, 2003
Project End Date: Project continuation and direction determined annually by DOE

Overall Objectives

- Quantify fluid mechanics and combustion behavior of unintended hydrogen releases in support of consequence analysis for safety assessments.
- Perform relevant experiments to validate fluid mechanics and combustion behavior in both controlled laboratory and full-scale, worst-case, representative experiments.
- Support the development of regulations, codes, and standards (RCS) related to the use of hydrogen as a vehicle fuel with presentation of experimental and modeled release and combustion behavior, specific scenario analysis, and expert opinion.

Fiscal Year (FY) 2013 Objectives

- Complete validation of initial set of reduced order models to enable development of quantitative and hazard evaluation tools for high pressure hydrogen unintended releases.
- Conduct experiments to understand dominant release, ignition and combustion phenomena for unintended hydrogen releases for development and revision of RCS and best practices:
  - Support consequence analysis in the "risk informed" approach
  - Model release dynamics from relevant leak scenarios
  - Determine ignition and flame-up probabilities
  - Quantify thermal radiation and overpressure hazards

Technical Barriers

This project addresses the following technical barriers from the Hydrogen Safety, Codes and Standards section 3.8 of the Fuel Technologies Office Multi-Year Research, Development, and Demonstration Plan:

(F) Enabling National and International Markets Requires Consistent RCS

(G) Insufficient Technical Data to Revise Standards

(L) Usage and Access Restrictions – parking structures, tunnels, and other usage areas

Contribution to Achievement of DOE Safety, Codes and Standards Milestones

This project will contribute to achievement of the following DOE milestones from the Hydrogen Safety, Codes and Standards section of the 2011 Fuel Cell Technologies Office Multi-Year Research, Development, and Demonstration Plan:

- Milestone 2.7: Provide critical understanding of hydrogen behavior relevant to unintended releases in enclosures. (4Q, 2013)
- Milestone 2.10: Understand flame acceleration leading to transition to detonation. (4Q, 2014)
- Milestone 2.13: Develop and validate simplified predictive engineering models of hydrogen dispersion and ignition. (4Q 2015)

FY 2013 Accomplishments

- Improved confidence identifying the hazard development boundaries for circular aperture unintended releases.
- Performed experiments to examine the dispersion characteristics from non-circular releases.
- Developed layer model for concentration build-up within an enclosure, which uses the previously developed jet integral model as an input and will be the input boundary condition for a steady-state overpressure module within the quantitative risk assessment (QRA) toolkit.
- Improved radiative heat flux boundaries and associated harm prediction from hydrogen jet fires, leading to potential recommendations for reduced separation distances.

✧ ✧ ✧ ✧ ✧

INTRODUCTION

A principal challenge to the widespread adoption of hydrogen infrastructure is the lack of quantifiable data on its safety envelope and perception of any additional risk from hydrogen. To convince regulatory officials, local fire marshals, fuel suppliers, and the public at large that hydrogen refueling is safe for consumer use, the risk to personnel and bystanders must be quantified and minimized to an acceptable level. Such a task requires validated methods to assess the harm potential from credible failure modes and a good understanding of effective mitigation measures to control any associated hazards.

Understanding release and ignition behavior for hydrogen provides the scientific foundation necessary to perform QRAs—the use of past failures to predict the likelihood of future failures—and thereby estimate the risk of harm from an accident. The hydrogen specific QRA approach is incorporated in the development of model codes and standards to appropriately regulate the retail/commercial use of hydrogen.

Simulations and models, validated with experimental data, are the cornerstone of the hydrogen specific QRA. These simulations and models provide critical input to the overall risk evaluation. While risk is classically defined as the product of frequency and consequences, a more detailed definition, specific to hydrogen hazards, is shown in Equation 1 below. For hydrogen systems, the major hazards involve the release of hydrogen gas with subsequent ignition. Equation 1 characterizes the various factors of risk for ignition of a hydrogen release as a function of probability of a release, probability of ignition given the release type, probability of a hazard given a specific release and ignition type, and finally the probability of harm given the associated hazard. Release behavior models and experiments provide insight to factors (shown in red in Equation 1) for predicting risk.

APPROACH

Using advanced laser-based diagnostics and imaging capabilities in the Turbulent Combustion Lab, Sandia and its partners provide quantifiable data to help accelerate the development of hydrogen fuel infrastructure.

Working with stakeholders Sandia identifies research topics to address research gaps which the science of unintended hydrogen release, ignition, and combustion might close. Research gaps are identified by multiple stakeholders, for example the U.S. DRIVE Codes and Standards Technical Team Roadmap updated in June 2013, highlighted the need for critical data on unintended releases of liquid hydrogen and cryogenic hydrogen gas. Research topics, such as liquid hydrogen releases, are incorporated into strategic research planning activities.

Sandia developed a 5-year roadmap in 2010 with the explicit goal of addressing short-, medium-, and long-term hydrogen behavior safety research needs. The plan was based on an analysis of the current knowledge base, key SNL contributions to this knowledge base, and critical gaps that serve as barriers to the creation of future standards which can be informed by leveraging unique SNL capabilities. Research topics were divided into five main areas:

1. General release behavior (relevant release geometries, storage states, jet dynamics)
2. Ignition mechanisms (diffusion ignition, electrostatic discharge, conduction)
3. Necessary ignition conditions (minimum ignition energy, mixture ignitability)
4. Necessary flame light-up conditions (ignition characteristics, flow strain rates)
5. Light-up consequences (flame radiation, pressure, flame impingement)

To execute this plan, Sandia recreates representative hydrogen leaks using custom burners and a laser spark apparatus to pinpoint ignition at different locations within the release plume. These capabilities enable statistical characterization of the release plume and insight into phenomenological processes during ignition and transition to sustained flame light-up. Critical data generated in these experiments and the models validated with this data are not explicitly useful to the codes and standards development committees.

To ensure clear comprehension of the scientific results, Sandia works with code development organizations (National Fire Protection Association [NFPA], Canadian Standards Association, etc.) and industry partners or industry groups (such as the Compressed Gas Association). This critical communication effort uses reports, scientific journal articles or conference presentations, and may also directly participate in code development committees or provide presentations to industry partners or industry groups.

The overarching goal of behavior science is the determination of consequences from unintended hydrogen releases. Accurately predicting the consequences of

$$Risk \propto \sum_{i,j,k} P(\text{Release}_i) P(\text{Ignition}_j | \text{Release}_i) P(\text{Hazard}_k | \text{Ignition}_j \cap \text{Release}_i) P(\text{Harm} | \text{Hazard}_k)$$

EQUATION 1. Risk as a function of probability of a release, probability of ignition given a release, probability of a hazard given a release and ignition, and finally the probability of harm given the hazard.

unintended hydrogen release is critical to the development of a comprehensive QRA toolkit that aggregates arbitrary system failure mode analysis with quantifiable consequence modeling. Ultimately this toolkit would be used to improve existing codes and standards as well as provide flexibility in the application of the codes, thus accelerating development of hydrogen fuel infrastructure.

RESULTS

Improved Accuracy of Ignition Conditions

Current analysis techniques used to develop regulations, codes and standards traditionally use the 1% mean concentration boundary, which corresponds to ¼ of the hydrogen lower flammability limit, to determine separation distances for electrical equipment, sensor placement, and other ignition sources. The ignition probability boundary, or the boundary where ignition is possible, has been reliably determined based on our recent work and highlighted in Figure 1. This metric is a more suitable approach to be used to by the codes and standards community to define separation distances based on concerns about proximity to ignition sources. This work has highlighted boundaries based on mean concentration envelopes are overly conservative since the potential for ignition is prohibitively low in a large portion of this boundary. Further measurements of the jet light-up boundary, defined as the region where incipient ignition kernels can transition into sustained flames with true hazard, have revealed additional potential to reduce separation distances further. Analytic determination of this separation boundary remains an ongoing area of research. Understanding the physical behavior in this context provides critical data to the RCS developers and allows them to understand to what degree the regulations are conservative.

Evaluation of Unintended Releases from Non-circular Openings

Most experimental investigations of underexpanded hydrogen jets have been limited to circular nozzles in an attempt to better understand the fundamental jet-exit flow physics and model this behavior with pseudo source models. However, many realistic compressed storage leak exit geometries, such as those from component housing cracks

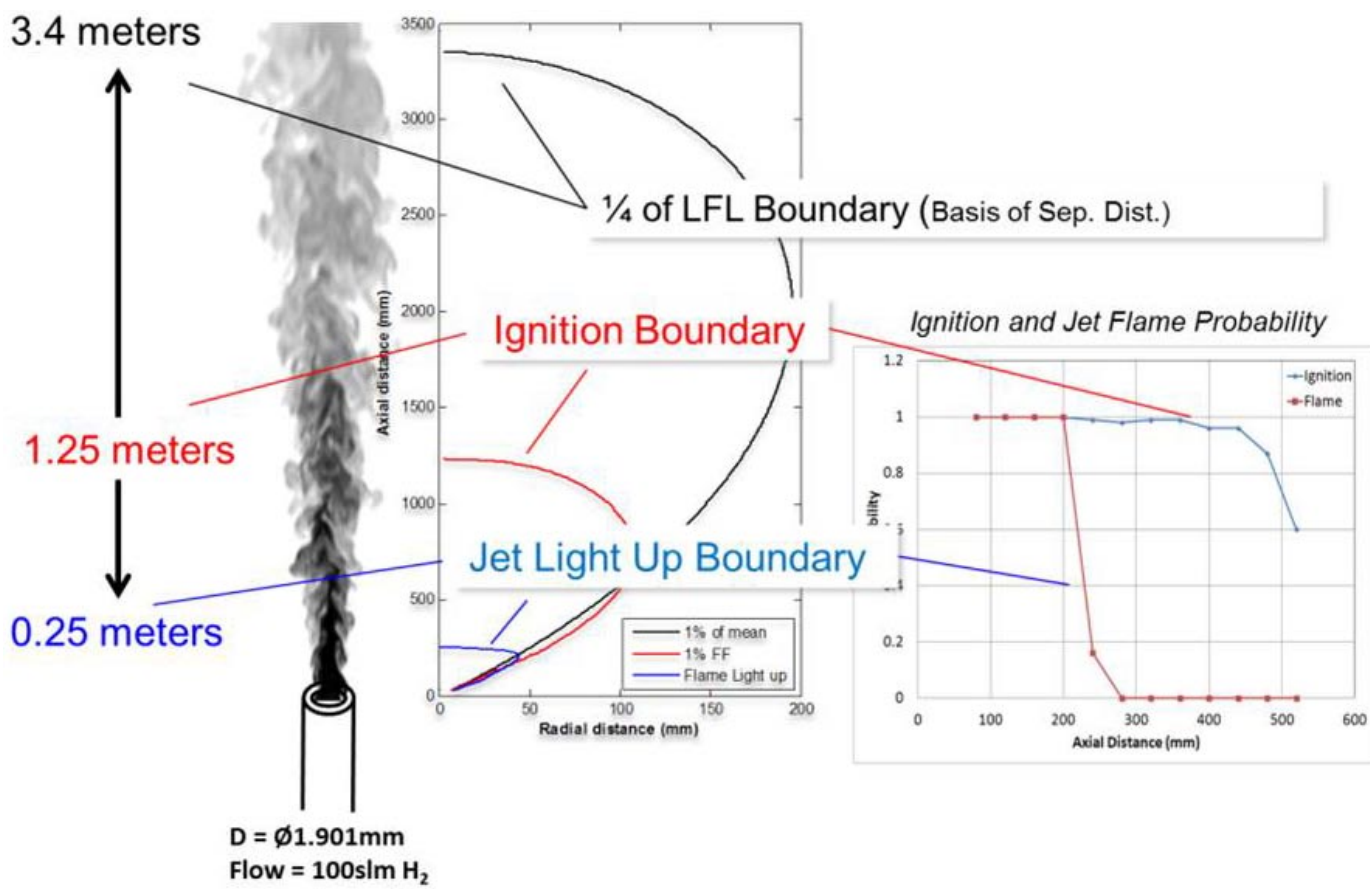

FIGURE 1. Schematic of the measured safety boundaries for to a given low pressure release (1.9 mm release diameter, 100 slm flow rate) (1) Traditional Exclusion Zone Boundary: ¼ of the lower flammability limit, (2) Ignition Boundary: the envelope where ignition is possible (3) Jet Light-Up Boundary: the envelope where flame sustainment is possible.

or leaky fittings, are not expected to be circular. This past year, jet dispersion characteristics from choked rectangular slot nozzles with aspect ratios from 2 to 8 were investigated and compared with an equivalent circular nozzle. Schlieren imaging was used to observe the jet-exit shock structure while quantitative planar laser Rayleigh scattering was used to measure downstream dispersion characteristics. The top image of Figure 2 is a Schlieren image of the shock structure from a circular nozzle along with corresponding images from major and minor axes views of a slot nozzle. The

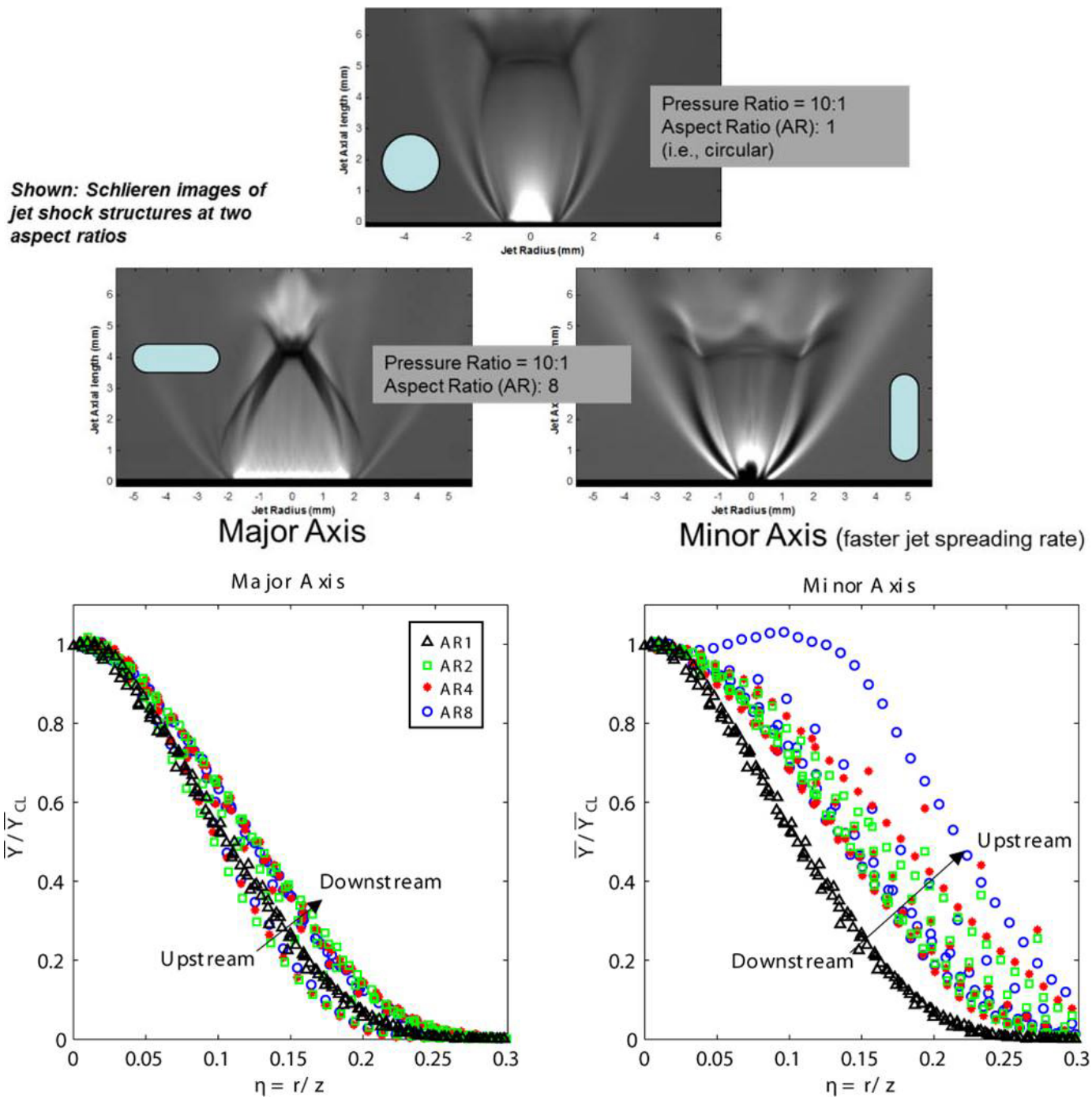

FIGURE 2. Top: Schlieren images of releases with different aspect ratios, with the planar nozzle view indicated by the light blue shape. The top image is of a symmetric circular release, while the bottom two images are of the major and minor axes of a slot nozzle with an aspect ratio of 1:8. These images highlight the asymmetric nature of the shock structure at the release exit for slot nozzles. Bottom: Radial mean mass fraction profiles in the major (left) and minor (right) axes planes for the circular nozzle and three slot jets with respective aspect ratios of 2, 4, and 8 that were extracted at discrete downstream radial locations and were plotted against the non-dimensional radial coordinate, η.

bottom image shows the influence of downstream dispersion characteristics relative to the characteristic circular nozzle. The current QRA method does not account for these differences, which can result in unrealistic predictions for modeled failure modes. These results provide physical insight and much needed model validation data for model development.

Developed Layer Model for Accumulation of Hydrogen from an Unintended Releases

Overpressure hazards can result from two different mechanisms. The first involves the rapid blowdown from a high pressure reservoir within a sufficiently confined volume—ignition is not necessary since a substantial pressure rise is possible from the rapidly expanding gas into the ambient. The second mechanism results from delayed ignition and subsequent development of a deflagration/detonation wave from accumulated flammable gas layers, typically due to slower leaks into larger confined volumes. Prediction of the hazard require accurate modeling of all phenomena related to the hazard, which includes the initial release blowdown and dispersion, the development of an accumulation layer at the ceiling, and (if required) the combustion of this flammable layer. Both hazards take advantage of Sandia developed network flow models, source models, and integral dispersion models. This past year an additional model that predicts the accumulation of gas and buildup of pressure within a confined space that accounts for passive ventilation (such as a warehouse or repair facility) was developed. At the moment, the developed layer model is only accurate for steady state prediction, but will be improved to accommodate unsteady releases in FY 2014. Furthermore, the layer model output is being used as an input boundary condition for a lean flame deflagration model for hazards that involve ignition of flammable mixture, necessary requirements for developed QRA toolkits.

Improved Flame Radiation Evaluation

Radiative heat fluxes from small to medium-scale hydrogen jet flames (<10 m) compare favorably to theoretical predictions provided the product species thermal emittance and optical flame thickness are corrected for. However, recent heat flux measurements from two large-scale horizontally orientated hydrogen flames (17.4 and 45.9 m) revealed that current methods underpredicted the flame radiant fraction, defined as the radiative energy escaping relative to chemical energy released, by 40% or more. Newly developed weighted source flame radiation models have demonstrated substantial improvement in the heat flux predictions, particularly in the near-field, and allow for a sensible way to correct potential ground surface reflective irradiance. Results depicted in Figure 3 show that inaccuracies in the experimental measurement were partially explained when the model type is changed from a single-point source model (simplified

d_j [mm]	[kg/s]	L_{vis} [m]	p_0 [barg]	T_0 [K]	T_{amb} [K]	p_{amb} [bar]
50.8	7.4	48.5	62.1	288	280	1.01

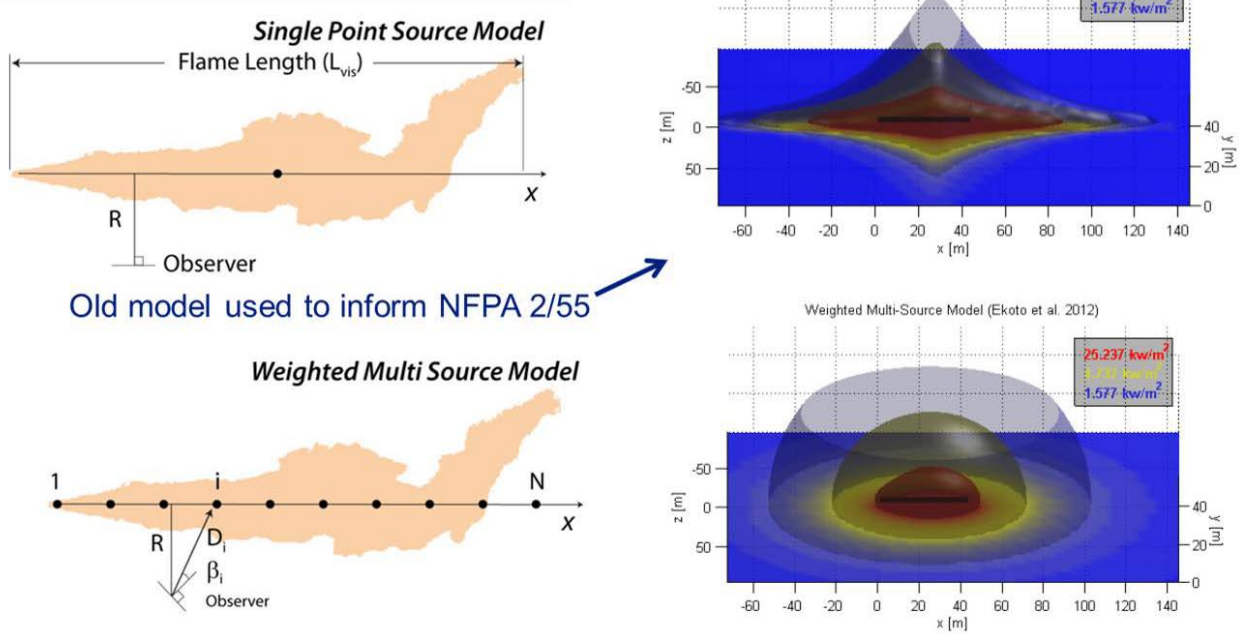

FIGURE 3. Summary of the results for prediction of radiation surface using two model techniques: single-point source model and weighted multi-source model.

radiation model) to a weighted multi-source model. In particular, near-field radiative heat flux predictions (within ½ of the visible flame length) where hazards are greatest had substantially better agreement with the measurements. Additional radiative addition corrections from partially reflective surfaces were developed and found to be potentially large contributors to the overall heat flux budget. Further model improvements are possible if the impact of flame trajectory from wind/buoyancy considerations are incorporated and are under development in FY 2014. Since the single-point source model was previously used to generate scientific justification for fire codes (i.e., NFPA 2) the improved accuracy of the weighted multi-source model can further address commercial barriers within safety, codes, and standards such as separation distances. The next step for this work is interaction with fire code development committees to ensure that they are provided the current scientific understanding of the hazards of hydrogen releases.

CONCLUSIONS AND FUTURE DIRECTIONS

- Conclusion: The jet light-up boundary is finite, predictable and provides a much more accurate prediction of light-up probability than either the lower flammability limit or the ignition boundary.
  - Future work: Fully define the jet light-up boundary and incorporate into prediction tools for QRA.
- Conclusion: Circular nozzles are not sufficient to cover the range of possible realistic release scenarios and it is important to be able to model the downstream characteristics of slot nozzles.
  - Future Work: Fully characterize the effect of higher aspect ratios and determine an appropriate distribution for release shapes to more accurately predict dispersion, ignition and subsequent hazards within QRA.
- Conclusion: Overpressures from hazards within enclosure can be accurately modeled using Sandia developed release, dispersion, accumulation, and deflagration models.
  - Future Work: Continue development on the deflagration combustion model and update the modeling framework to accept non-steady releases. A substantial validation campaign is needed to test the model accuracy and improve where needed.
- Conclusion: The single-point source model is insufficient in prediction of radiation from large flames. A weighted multi-source model shows better prediction capabilities in the near-field where hazards are greatest.
  - Future Work: Provide a brief report on the results of the experiment to NFPA 2 working groups for consideration in the current code revision cycle.

FY 2013 PUBLICATIONS/PRESENTATIONS

1. Ekoto IW, Ruggles AJ, Creitz LW, Li JX, Updated Jet Flame Radiation Modeling with Corrections for Buoyancy, ICHS, (accepted).

2. Ruggles AJ, Ekoto IW, Experimental investigation of nozzle aspect ratio effects on underexpanded hydrogen jet release characteristics, ICHS, (accepted).

3. Ruggles AJ, Ekoto IW, Radial probability density function characterization for self-similar turbulent hydrogen jets, J Fluid Mech, (submitted).

4. Houf WG, Evans GH, Ekoto IW, Merilo EG, Groethe MA, Hydrogen fuel-cell forklift vehicle releases in enclosed spaces. Int J Hydrogen Energy, 2013;39:8179-89.

5. Ekoto IW, Houf WG, Evans GH, Merilo EG, Groethe MA, Experimental investigation of hydrogen release and ignition from fuel cell powered forklifts in enclosed spaces. Int J Hydrogen Energy, 2012;37:17446-56.

6. Ruggles AJ, Ekoto IW, Ignitability and mixing of underexpanded hydrogen jets. Int J Hydrogen Energy, 2012;37:17549-60.

7. Ekoto, IW, R&D Needs for Reduced Order H2 Release/Ignition Behavior Models - The Sandia Perspective, HySafe Research Priorities Workshop , BAM, Berlin, Oct 16, 17, 2012.

8. Ekoto, IW, Large Scale Flame Radiation Modeling, IEA Experts Meeting, BAM, Berlin, Oct 4, 5, 2012.

9. Ekoto IW, Houf WG, Ruggles AJ, Creitz LW, Li JX, Large-Scale Hydrogen Jet Flame Radiant Fraction Measurements and Modeling. Proc International Pipeline Conference, Calgary, Canada, Sept 24-28, 2012.

VIII.7 R&D for Safety Codes and Standards: Risk Assessment

Aaron Harris (Primary Contact), Katrina Groth
Sandia National Laboratories
P.O. Box 969
Livermore, CA 94551-0969
Phone: (925) 294-4530
Email: apharri@sandia.gov

Sandia National Laboratories is a multi-program laboratory managed and operated by Sandia Corporation, a wholly owned subsidiary of Lockheed Martin Corporation, for the U.S. Department of Energy's National Nuclear Security Administration under contract DE-AC04-94AL85000.

DOE Manager
Rick Farmer
Phone: (202) 586-1623
Email: Richard.Farmer@ee.doe.gov

Contract Number: DE-AC04-94AL85000

Project Start Date: October 1, 2003
Project End Date: Project continuation and direction determined annually by DOE

Overall Objectives

- Establish quantitative risk assessment (QRA) as an acceptable method to assess hazards associated with widespread use of hydrogen as a fuel.
- Use hydrogen-specific QRA in a risk informed decision making process to support the development of regulations, codes, and standards for hydrogen fuel.
- Develop and support the creation of a hydrogen-specific risk assessment toolkit.

Fiscal Year (FY) 2013 Objectives

- Scope and initiate work on a quantitative risk assessment (QRA) toolkit to enable sustained use of QRA by code developers, in site-specific hazard reviews and in development of broad deployment strategies in line with project objectives.
- Participate as experts for National Fire Protection Association (NFPA) 2, International Energy Agency (IEA) Task 31 and other international programs.
- Provide QRA results for specific scenarios (e.g., indoor fueling, bulk storage, effect of passive or active mitigation features, etc.) needed for revision of regulations, codes, and standards (RCS).

Technical Barriers

This project addresses the following technical barriers from the Hydrogen Safety, Codes and Standards section of the Fuel Cell Technologies Office Multi-Year Research, Development, and Demonstration Plan:

(A) Safety Data and Information: Limited Access and Availability

(F) Enabling National and International Markets Requires Consistent RCS

(G) Insufficient Technical Data to Revise Standards

(L) Usage and Access Restrictions – parking structures, tunnels and other usage areas

Contribution to Achievement of DOE Safety, Codes and Standards Milestones

This project will contribute to achievement of the following DOE milestones from the Safety, Codes and Standards section of the 2011 Fuel Cell Technologies Office Multi-Year Research, Development, and Demonstration Plan:

- Milestone 2.4: Publish a method for estimating accident likelihood. (2Q, 2013)
- Milestone 2.8: Publish risk mitigation strategies. (2Q, 2014)
- Milestone 2.11: Publish a draft protocol for identifying potential failure modes and risk mitigation. (4Q 2014)
- Milestone 2.19: Validate inherently safe design for hydrogen fueling infrastructure. (4Q, 2019)
- Milestone 4.7: Complete risk mitigation analysis for advanced transportation infrastructure systems. (1Q, 2015)
- Milestone 4.8: Revision of NFPA 2 to incorporate advanced fueling storage systems and specific requirements for infrastructure elements such as garages and vehicle maintenance facilities. (3Q, 2016)

FY 2013 Accomplishments

- Conducted QRA for indoor fueling of hydrogen-powered industrial trucks which determined that the risk introduced by fueling hydrogen-powered industrial trucks inside of the large warehouse space does not increase the risk of the occupation and the warehouse environment.
- Documented new QRA methods and QRA needs for use in development of codes and standards requirements through the publication of a Sandia National

Laboratories report focused on indoor fueling. The new methods were used for the indoor fueling assessment.

- Created initial version of hydrogen specific QRA toolkit by integrating previously disparate activities, including manual data manipulation, under a single algorithm. Included ability to perform sensitivity analysis using the single algorithm increasing the efficiency and improving the value of the assessment to the end user.
- Hosted hydrogen QRA workshop for stakeholders. Gathered participants from industry, government, and research to determine the requirements of the next version of the QRA toolkit and to determine the applicability of such a toolkit to other flammable gas fuels such as compressed natural gas (CNG).

✧ ✧ ✧ ✧ ✧

INTRODUCTION

A principal challenge to the widespread adoption of hydrogen infrastructure is the lack of quantitative data regarding safety and property risks from hydrogen. To convince regulatory officials, local fire marshals, fuel suppliers, and the public at large that hydrogen refueling is safe for consumer use, the risk to personnel and bystanders must be quantified and minimized to an acceptable level. Such a task requires validated methods to assess the harm potential from credible failure modes and a good understanding of effective mitigation measures to control associated hazards.

APPROACH

Using unique skills quantitative risk assessment, Sandia and its partners are working to develop a scientific-based, hydrogen-specific, adaptable process for risk informed decision making. This process will help eliminate deployment barriers within regulations, codes, and standards to hydrogen fuel infrastructure by facilitating site-specific risk considerations for stakeholders to determine appropriate risk mitigation measures versus the traditional approach of prescriptive code requirements.

QRA can be used to identify risk drivers and the associated consequences in step-out hydrogen technologies. Sandia is developing data and tools for risk assessment of hydrogen fuel cell systems and infrastructure. This entails the development of safety scenarios, benchmark experiments, technical data, and subsequently, tools and techniques for integrating these pieces into technical data for codes and standards decision.

Development of a comprehensive QRA tool that aggregates arbitrary system failure mode analysis with quantifiable consequence modeling obtained from improved hydrogen behavior understanding of this project remains the overarching goal. Ultimately this tool would be used to improve existing codes and standards as well as provide flexibility in the application of the codes.

RESULTS

Conduct QRA for Indoor Fueling of Hydrogen-Powered Industrial Trucks

Hydrogen powered industrial trucks have gained a market foothold as a niche application of hydrogen fueled electric vehicles. The increased usage and commercial viability of these vehicles has inspired increased scrutiny of the risk of fueling these vehicles indoors. A QRA was conducted to evaluate the risk introduced by fueling the vehicles in the warehouse environment.

In order to conduct the QRA, Sandia in close cooperation with industry stakeholders, first developed a generic system model for indoor fueling equipment and the vehicle fuel system. Industry partners also participated in a generic failure modes and effects analysis for both the indoor fueling system (dispenser) and the vehicle fuel system. This project team then constructed an integrated algorithm to perform the QRA including the ability to perform sensitivity analysis.

The QRA concluded that the predicted fatal accident rate, a common measurement of risk for a specific occupation, was around 0.17. Table 1 shows the fatal accident rate values for several occupations from the Bureau of Labor Statistics, 2010. For the scenarios considered and with a large margin of error, fueling hydrogen-powered industrial trucks inside of the warehouse does not increase the risk experienced by those operators.

TABLE 1. Bureau of Labor Statistics, 2010 Fatal Accident Rate Data for Several Occupations

Occupation	FAR
U.S. workforce total	1.8
Construction and extraction occupations	5.9
Industrial machinery, installation, repair, and maintenance workers	10.4
Industrial truck and tractor operators	3.0
Laborers and freight, stock, and material movers, hand	3.1
Farming, fishing, and forestry occupations	13.5

FAR – fatal accident rate

Create Initial Version of Hydrogen-Specific QRA Toolkit

Many of the initial elements of the QRA toolkit were developed concurrently with the indoor fueling assessment effort. Using commercially available software tools (MATLAB®) an algorithm was developed that integrated multiple process steps into a single program. In addition

to the evaluation of the indoor fueling scenarios, previous scenarios were evaluated to ensure the accuracy of the integrated tool.

Several elements, particularly a prediction of overpressure have not yet been incorporated into the tool. Analysis for such elements must be conducted using a separate model or program. The future work for this task will be a full integration of the elements into a single program with some functionality for sensitivity analysis.

Figure 1 is a block diagram that shows the various sub-programs used within the toolkit. The entire program is referred to as a toolkit as many of the subprogram models may function for stand-alone analysis of particular consequences, therefore the toolkit is both a single QRA program and multiple independent subprograms.

Host Hydrogen-Specific QRA Workshop for Stakeholders

The QRA Toolkit Introduction Workshop was held at Energetics on June 11-12. The workshop was co-hosted by Sandia National Laboratories and HySafe, the International Association for Hydrogen Safety. The objective of the workshop was twofold: (1) present a methodology and toolkit (currently under development) for conducting QRA to support the development of codes and standards and safety assessments of hydrogen-fueled vehicles and fueling stations, and (2) improve understanding of the needs of early-stage alternative fuel users (hydrogen, CNG, and liquefied natural gas [LNG]) and set priorities for "Version 1" of the toolkit in the context of the commercial evolution of hydrogen fuel cell electric vehicles. The workshop consisted of an introduction and three technical sessions: Risk Informed Development and Approach, CNG/LNG Applications and Introduction of a Hydrogen-Specific QRA toolkit.

Document New QRA Methods and Needs for use in Development of Codes and Standards Requirements

A report documenting the workshop and outcomes of the workshop is planned for publication in September 2013.

CONCLUSIONS AND FUTURE DIRECTIONS

Conclusion: Application of the integrated toolkit in a preliminary form was successful in performing a quantitative risk assessment of indoor hydrogen fueling activities and the results of the analysis suggest there is no additional risk for the exposed population.

- Future work: Further development of the algorithm including the incorporation of an overpressure module. FY 2014 goal of producing Version 1 of the algorithm.

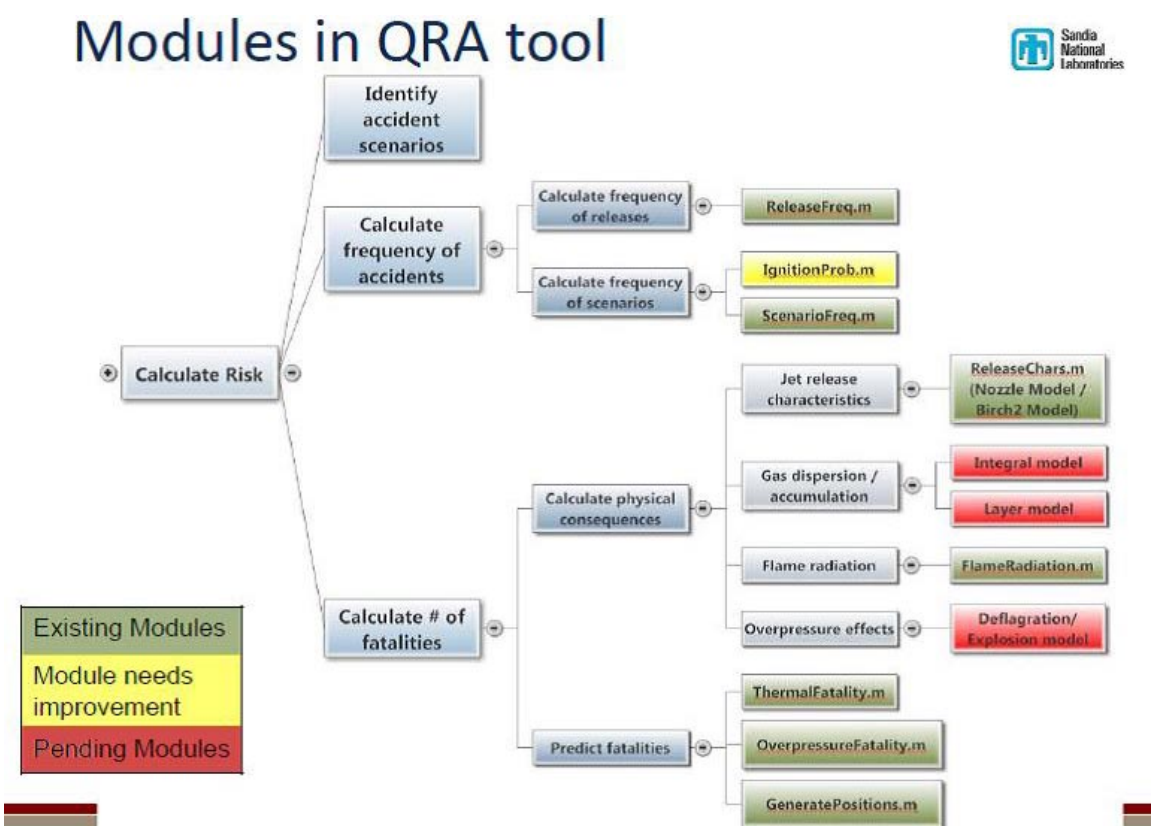

FIGURE 1. Sandia Hydrogen-Specific QRA Toolkit Block Diagram, Version 0

- Future Work: Collaborate with industry stakeholders using both the toolkit and previous risk informed decision making process concepts to validate the performance-based requirements of NFPA 2, Chapter 5 for the purpose of siting hydrogen fueling infrastructure. The requirements of this code chapter rely heavily on risk assessment. Despite publication in 2010 Chapter 5 has not yet been used for siting a fueling station.

FY 2013 PUBLICATIONS/PRESENTATIONS

1. Groth, K., Lachance, J., Harris, A. "Early-Stage Quantitative Risk Assessment to Support Development of Codes and Standard Requirements for Indoor Fueling of Hydrogen Vehicles" Sandia National Laboratories Report, SAND2012-10150.

2. LaChance, J.L.; Middleton, B. & Groth, K.M. Comparison of NFPA and ISO approaches for evaluating separation distances International Journal of Hydrogen Energy, 2012, 37, 17488-17496.

3. LaChance, J. "Risk Informed Development of Hydrogen Codes and Standards" IEA Task 31 Experts meeting, Bethesda, MD, Oct, 4-5, 2012).

4. Groth, K.M.; LaChance, J.L. & Harris, A.P. Design-stage QRA for indoor vehicular hydrogen fueling systems. Proceedings of the European Society for Reliability Annual Meeting (ESREL 2013), 2013.

VIII.8 Hydrogen Emergency Response Training for First Responders

Monte R. Elmore
Pacific Northwest National Laboratory (PNNL)
902 Battelle Blvd.
Richland, WA 99352
Phone: (509) 372-6158
Email: monte.elmore@pnnl.gov

DOE Manager
Rick Farmer
Phone: (202) 586-1623
Email: Richard.Farmer@ee.doe.gov

Subcontractors:
- Jennifer Hamilton, California Fuel Cell Partnership (CaFCP), Sacramento, CA
- Hanford Fire Department, Richland, WA
- Hazardous Materials Management and Emergency Response (HAMMER) Training Facility, Richland, WA

Project Start Date: October 2004
Project End Date: Project continuation and direction determined annually in consultations with DOE

Overall Objective

Support the successful implementation of hydrogen and fuel cell technologies by providing technically accurate hydrogen safety and emergency response information to first responders.

Fiscal Year (FY) 2013 Objectives

- Provide a one-day first responder training course, "Hydrogen Emergency Response Training for First Responders," that integrates the use of DOE's mobile hydrogen fuel cell vehicle (FCV) prop.
- Continue to support the Web-based awareness-level course, "Introduction to Hydrogen Safety for First Responders." www.hydrogen.energy.gov/firstresponders.
- Disseminate first responder hydrogen safety educational materials at appropriate fire fighter conferences to raise awareness.

Technical Barriers

This project addresses the following technical barriers from the Safety Codes and Standards section of the Fuel Cell Technologies Office Multi-Year Research, Development, and Demonstration Plan:

(A) Safety Data and Information: Limited Access and Availability

(D) Lack of Hydrogen Knowledge by Authorities Having Jurisdiction

(E) Lack of Hydrogen Training Materials and Facilities for Emergency Responders

Contribution to Achievement of DOE Hydrogen Safety Milestones

This project will contribute to achievement of the following DOE milestone from the Safety Codes and Standards section of the Fuel Cell Technologies Office Multi-Year Research, Development, and Demonstration Plan:

- 5.3 Enhance hydrogen safety training props and deliver classroom curriculum for emergency response training. (4Q, 2012)

FY 2013 Accomplishments

- **Prop-Based Course**: This operations-level course was presented at two fire training centers in Honolulu and Hilo, Hawaii in the past year. Three consecutive one-day training classes were held at each location. Approximately 300 first responders from the above sites received this training. Extremely positive feedback from each of the sites continues to reinforce the value of this course to first responder organizations.
- **Awareness-Level Course**: After almost seven years, our website continues to receive ~200-300 unique visits per month from almost every state and some foreign countries. The course is registered on the Training finder Realtime Affiliate Network website for broader dissemination to first responders.
- **Outreach**: Compact disks (CDs) of the awareness-level course were distributed through the DOE Energy Efficiency and Renewable Energy Information Center, and upon receipt of individual requests.

✧ ✧ ✧ ✧ ✧

INTRODUCTION

Safety in all aspects of a future hydrogen infrastructure is a top priority, and safety concerns influence all DOE hydrogen and fuel cell projects. Despite the most concerted effort, however, no energy system can be made 100% risk-free. Therefore, for any fuel and energy system, a suitably trained emergency response force is an essential component of a viable infrastructure. The Fuel Cell Technologies Office has identified training of emergency response personnel as a high priority, not only because these personnel need to understand how to respond to a hydrogen incident, but also

because firefighters and other emergency responders are influential in their communities and can be a positive force in the introduction of hydrogen and fuel cells into local markets.

This project employs the Occupational Safety and Health Administration and National Fire Protection Association frameworks for hazardous materials emergency response training to provide a tiered hydrogen safety education program for emergency responders. The effort started with development and distribution of the awareness-level Web-based course in FY 2006-2007. A more advanced course and materials to facilitate education were developed in FY 2008-2009, complementing the design, construction, and operation of an FCV prop (developed under PNNL's Hydrogen Safety project). The overall first-responder education program will continue to be updated. In addition, PNNL has implemented outreach efforts to key stakeholder groups to facilitate delivery of the training to a broad audience.

APPROACH

PNNL works with subject matter experts in hydrogen safety and first responder training to develop hydrogen safety course materials. Draft materials undergo considerable review and revision before being released. The PNNL team works with DOE to make stakeholder groups aware of training opportunities and to provide "live" training when appropriate. The Web-based awareness-level course is available "online" or on CDs and provides the student with a basic understanding of hydrogen properties, uses, and appropriate emergency response actions. The prop-based course, a more advanced operations-level course, was initially presented at the HAMMER training facility in Richland, WA. Subsequently, the mobile prop has enabled the course to be delivered at several offsite fire training centers (in California during 2010-12, and Hawaii in 2013) in order to reach larger audiences in areas where hydrogen and fuel cell technologies are being deployed.

RESULTS

Prop-Based Course: The focus of the curriculum is on teaching first responders what is the same and what is different about hydrogen and FCVs as compared to conventional fuels and vehicles. Feedback is requested at each class to help us improve the course content and delivery. Based on feedback from all the training sessions held this past year, we conclude that following the training, first responders are more familiar with the properties and behavior of hydrogen, and are prepared to operate in a safe and effective manner if a hydrogen incident should occur in their jurisdiction.

The FCV prop has been integrated into the "Hydrogen Emergency Response Training for First Responders" course. The prop demonstrates potential conditions that could be encountered during the control and suppression of a FCV fire.

CONCLUSIONS AND FUTURE DIRECTIONS

The introductory Web-based course has been highly successful, based on the usage recorded and feedback received. The course is fulfilling a need expressed by the first responder community to receive more information about hydrogen and fuel cells so they will be prepared in the rare event of a hydrogen incident. The in-depth prop-based course builds on that success and is very useful in giving first responders a hands-on experience with simulated FCV incidents that integrates well with classroom training. PNNL will continue to update both courses as needed to reflect current applications and markets for hydrogen and fuel cells.

H2USA launched at the U.S. Department of Energy's Annual Merit Review in May 2013. Through H2USA, the partners will focus on identifying actions to encourage early adopters of fuel cell electric vehicles, conduct coordinated technical and market analysis, and evaluate alternative fueling infrastructure that can enable cost reductions and economies of scale. Although the structure and activities of H2USA are still being defined, the new partnership will consider infrastructure, hydrogen production and vehicle deployment at a national level. It will also look at how other fuel cells deployments, such as back-up power and material handling, can help pave the way for mainstream hydrogen vehicle infrastructure.

A properly trained first responder community is critical to the success of this transformation to hydrogen fuel cell applications. First responders represent two demographics: a potential rescuer in a hydrogen incident and a potential consumer of fuel cell technology. It is critical that the information they receive is up to date, accurate, factual and technically correct. The national template for emergency responder education on hydrogen and fuel cells will aid in eliminating misinformation, and potentially assist with information about other vehicle technologies, as well.

Hydrogen and fuel cell emergency response information has been included in multiple training programs, such as the U.S. Department of Energy's Hydrogen Emergency Response Training for First Responders, developed and managed by PNNL, and a program developed for the California Office of the State Fire Marshal by the CaFCP. Additionally, emergency responder education for alternative fueled and electric vehicles, including hydrogen, has been developed and delivered by a number of other organizations around the country. However, consistency in the content and messaging about hydrogen and fuel cells varies across these programs, and may not be contemporary with the activities in early markets. Reasons for such discrepancies are many; however, in general may be attributed to the amount of hydrogen and

fuel cell activities in a given region, and access to industry-vetted information.

A single repository of information related to hydrogen and fuel cells (a National Hydrogen Emergency Response Template) is necessary to provide current and accurate information and to avoid duplication of efforts among various training programs. The primary goal for developing a national 'template' for hydrogen and fuel cell vehicle emergency response is to provide current, factual, relevant information with consistent messaging and for ease of review/updates on an annual or semi-annual basis. Once developed, the template must reside in a single location and be disseminated from that location as needed in various forms, depending on the level of information needed (i.e. awareness vs. operations level).

PNNL currently manages the DOE program on Hydrogen Emergency Response Training for First Responders, and has done so for several years, providing both internet-based awareness-level and classroom-based operations-level training (with hands-on demonstrations). PNNL would develop and maintain the National Emergency Responder Template for hydrogen and fuel cell applications. Maintaining the template would include keeping a single source of information updated on fuel cell applications and on the proper response to hydrogen emergencies.

The training materials would be made available to other agencies wishing to include hydrogen safety training for first responders in their curricula. Example agencies may include the National Fire Protection Agency, Federal Emergency Management Agency's National Fire Academy, and the National Alternative Fuels Training Consortium (West Virginia University). These organizations all have excellent training deployment capabilities.

FY 2013 PUBLICATIONS/PRESENTATIONS

1. Elmore, M.R. "Hydrogen Emergency Response Training for First Responders" PNNL-SA-86615. Presented at the 2013 DOE Annual Merit Review, May 14, 2013. Washington, D.C.

VIII.9 Hydrogen Safety Panel and Hydrogen Safety Knowledge Tools

Nick Barilo
Pacific Northwest National Laboratory (PNNL)
P.O. Box 999
Richland, WA 99354
Phone: (509) 371-7894
Email: nick.barilo@pnnl.gov

DOE Manager
Rick Farmer
Phone: (202) 586-1623
Email: Richard.Farmer@ee.doe.gov

Subcontractors:
- Addison Bain, NASA (ret), Melbourne, FL
- David J. Farese, Air Products and Chemicals, Inc., Allentown, PA
- William C. Fort, Shell Global Solutions (ret), Houston, TX
- Larry Fluer, Fluer, Inc., Paso Robles, CA
- Don Frikken, Becht Engineering, St. Louis, MO
- Richard A. Kallman, City of Santa Fe Springs, CA
- Glenn W. Scheffler, GWS Solutions of Tolland, LLC, Tolland, CT
- Andrew J. Sherman, Powdermet Inc., Euclid, OH
- Ian Sutherland, General Motors, Warren, MI
- Robert G. Zalosh, Firexplo, Wellesley, MA

Project Start Date: 2004
Project End Date: Project continuation and direction determined annually by DOE

Overall Objectives

- Provide expertise and recommendations to DOE and assist with identifying safety-related technical data gaps, best practices, and lessons learned.
- Help DOE integrate safety planning into funded projects to ensure that all projects address and incorporate hydrogen and related safety practices.
- Collect information and share lessons learned from hydrogen incidents and near-misses, with a goal of preventing similar safety events from occurring in the future.
- Capture the vast and growing knowledge base of hydrogen experience and make it publicly available to the "hydrogen community" and stakeholders.

Fiscal Year (FY) 2013 Objectives

- Conduct ongoing safety assessments of DOE projects through safety plan reviews and site visits.
- Engage other hydrogen and fuel cell technology stakeholders through Hydrogen Safety Panel (HSP) meetings and targeted outreach.
- Increase number of records in database by encouraging "incident owners" to share lessons learned with the hydrogen community.
- Enhance utility of the safety knowledge tools.

Technical Barriers

This project addresses the following technical barriers from the Hydrogen Safety section of the Fuel Cell Technologies Office Multi-Year Research, Development, and Demonstration Plan:

(A) Safety Data and Information: Limited Access and Availability

(C) Safety is Not Always Treated as a Continuous Process

(D) Lack of Hydrogen Knowledge by Authorities Having Jurisdiction

(G) Insufficient Technical Data to Revise Standards

Contribution to Achievement of DOE Safety, Codes and Standards Milestones

This project contributes to achievement of the following DOE tasks and milestones from the Hydrogen Safety, Codes and Standards section (3.7) of the Fuel Cell Technologies Office Multi-Year Research, Development, and Demonstration Plan:

- Task 1: Address Safety of DOE R&D Projects (ongoing)
- Task 5: Dissemination of Data, Safety Knowledge, and Information (ongoing)
- Milestone 5.1: Update safety bibliography and incidents databases. (4Q, 2011-2020)

FY 2013 Accomplishments

- Conducted the 18th HSP meeting in Honolulu, HI, February 4–7, 2013, in conjunction with "Hydrogen Emergency Response Training for First Responders."
- Issued a final report, "Hydrogen Safety Panel Review of DOE Fuel Cell Projects," for the HSP's American Recovery and Reinvestment Act (ARRA) project.
- Contributed to early safety review activities for the University of Hawaii's Hawaii Natural Energy Institute (HNEI) two projects (Power Park Project; Geothermal Hydrogen Grid Management Project) on Oahu and the Big Island.

- Collaborated with DOE to present the educational session, "Deployment of Hydrogen Fuel Cells – Safety Considerations and Resources," at the 2013 National Fire Protection Association (NFPA) Conference & Expo, in Chicago, IL, on June 11, 2013.
- Reviewed seven safety plans since July 1, 2013, for projects in fuel cell and hydrogen storage research and development (R&D).
- Completed a safety checklist for an outdoor supply system providing hydrogen for an indoor application to be utilized as a resource for hazard analysis.
- Added four new safety event records to H2Incidents.org since the 2012 Annual Merit Review and Peer Evaluation Meeting, for a total of 210 records currently in the database.
- Developed a first-of-its-kind iPad/iPhone app to enhance the utility and integration of the safety knowledge tools (H2Incidents.org and H2bestpractices.org) with other safety planning resources.

✧ ✧ ✧ ✧ ✧

INTRODUCTION

Safety is an essential element for realizing the "hydrogen economy" – safe operation in all of its aspects from hydrogen production through storage, distribution and use; from research, development, and demonstration to deployment and commercialization. As such, safety is given paramount importance in all facets of the research, development, demonstration, and deployment work of the DOE Fuel Cell Technologies (FCT) Office. This annual report summarizes activities associated with two projects, the Hydrogen Safety Panel and Hydrogen Safety Knowledge Tools.

Recognizing the nature of the DOE FCT Program and the importance of safety planning, the HSP was formed in December 2003 to bring a broad cross-section of expertise from the industrial, government and academic sectors to help ensure the success of the program as a whole. The experience of the HSP resides in industrial hydrogen production and supply, hydrogen R&D and applications, process safety and engineering, materials technology, risk analysis, accident investigation and fire protection. The HSP provides expertise and recommendations on safety-related issues and technical data gaps, reviews individual DOE-supported projects and their safety plans and explores ways to bring best practices and lessons learned to broadly benefit the FCT Program.

PNNL continues to improve the safety knowledge software tools as well as develop new techniques for dissemination of this information. This report covers the Hydrogen Incident Reporting and Lessons Learned database (H2Incidents.org) and the Hydrogen Safety Best Practices online manual (H2bestpractices.org). These web-based resources play a key role in reaching, educating, and informing stakeholders whose contributions will help enable the deployment of new hydrogen and fuel cell technologies.

APPROACH

The HSP strives to raise safety consciousness most directly at the project level. Safety should be driven at the project level by organizational policies and procedures, safety culture and priority. Project safety plans are reviewed in order to encourage thorough and continuous attention to safety aspects of the specific work being conducted. Panel-conducted safety reviews focus on engagement, learning, knowledge-sharing, and active discussion of safety practices and lessons learned, rather than as audits or regulatory exercises. Through this approach, DOE and the HSP are trying to achieve safe operation, handling, and use of hydrogen and hydrogen systems for all DOE projects.

The Hydrogen Incident Reporting and Lessons Learned (H2Incidents.org) facilitates open sharing of lessons learned from hydrogen safety events to help avoid similar events from occurring in the future. DOE-funded project teams and others are encouraged to voluntarily submit records of incidents and near-misses, along with specific lessons learned. The addition of new records is also pursued by actively seeking news reports on hydrogen events, searching existing databases, and encouraging self-submittals by "incident owners."

Hydrogen Safety Best Practices (H2bestpractices.org) is an easy-to-use web-based manual focusing on the safe use of hydrogen. It has been compiled from learnings and observations from HSP site visits, safety plan reviews and other work, and available reference materials tailored specifically to working with hydrogen. Links are provided to other web-based resources and supporting information to enhance the usefulness of this resource. Experts from the HSP, national laboratories, and other subject matter experts contribute and review new material added to the site. PNNL staff members, with assistance from the HSP, respond to user questions and comments.

RESULTS

The HSP was formed in FY 2004 and the first meeting was held in Washington, D.C., December 11–12, 2003. The HSP is comprised of 14 members having over 400 years of industry and related experience (see Table 1 for FY 2013 Panel membership).

The 18th HSP meeting was held in Honolulu, HI, during the week of February 4, 2013. The meeting provided a unique opportunity to hold a first-of-its-kind meeting with local stakeholders and authorities having jurisdiction to discuss

the barriers to the safe commercial deployment of hydrogen technologies in Hawaii. One outcome of this meeting was an initiative to create a local hydrogen stakeholder network. Two HSP task groups were formed to address technical safety gaps related to certifications and outdoor enclosures. Also, the concurrent timing of the meeting and first responder training was beneficial for bringing focused attention to hydrogen and fuel cell technologies to Hawaii. Many of the guests expressed thanks and shared that the meetings, interactions, and related activities were a great benefit.

TABLE 1. HSP Members

Nick Barilo, Project Manager*	PNNL
Bill Fort, Chair*	Shell Global Solutions (ret)
Addison Bain	NASA (ret)
David Farese	Air Products and Chemicals
Larry Fluer*	Fluer, Inc.
Don Frikken	Becht Engineering
Aaron Harris	Sandia National Laboratories
Richard Kallman*	City of Santa Fe Springs, CA
Miguel Maes	NASA White Sands Test Facility
Glenn Scheffler	GWS Solutions of Tolland, LLC
Andrew Sherman	Powdermet Inc.
Ian Sutherland	General Motors
Steven Weiner*	PNNL
Robert Zalosh	Firexplo

* Changes in HSP membership/responsibility

A final report, "Hydrogen Safety Panel Review of DOE Fuel Cell Projects," was issued for the HSP's ARRA project [1]. The report includes recommendations in the areas of project integration/safety planning, hazard analysis, codes and standards requirements, and third-party certification. Dissemination of this report will help bring the safety learnings to a broader set of stakeholders who also play an essential role in helping accelerate fuel cell commercialization.

During the past year the HSP has provided various safety review and support to projects as noted in Table 2. Since 2004, the HSP has reviewed 325 safety plans, conducted 48 safety reviews, and performed 16 follow-up interviews.

The HSP's most recent safety review work has focused on project investments intended to accelerate the commercialization and deployment of fuel cells and fuel cell manufacturing, installation, maintenance, and support services. The timing of the HSP's safety plan reviews and subsequent site visits has often occurred after equipment was deployed or operational. This resulted in safety recommendations on safety planning, equipment design, and configuration that were often difficult to implement. A new approach for earlier project involvement was utilized in support of safety review activities for the HNEI hydrogen production and fuel station projects. The activities included piping and instrumentation diagram reviews, design reviews, and a certification study review. The concept proved successful and the project teams were able to realize the benefits of:

- Understanding and evaluating the safety issues and code requirements.
- Implementing significant design changes based on input from the HSP.
- Enhancing the confidence of project managers and stakeholders in approving the final design configuration.

This new model for HSP interaction with project teams is shown in Figure 1. Implementation of this approach will help ensure that HSP recommendations and safety considerations are integrated into the project to influence the final equipment configuration. To promote this model, PNNL worked with the DOE Golden Office to expand contract language to encourage projects to integrate the HSP into additional project activities. Additionally, the HSP is now participating in project kickoff meetings in order to help the projects understand the safety planning requirements and how the HSP may be a resource for ensuring that safety is integrated into all aspects of their project scope (Table 2 identifies where those activities have occurred).

Engagement in the project planning phase enables the HSP to identify technical safety gaps. As a result of the HSP's ARRA and HNEI project work, an HSP task group was established to consider the "Safety of Hydrogen Systems Installed in Outdoor Enclosures." The HSP's learnings regarding incomplete code requirements for equipment enclosures has already been impactful on the NFPA 2, "Hydrogen Technologies Code," committee which has formed its own task group to evaluate possible changes for the 2015 edition of that document.

Sharing and disseminating safety information and knowledge continues to be an important aspect of HSP work. For example, HSP members collaborated with DOE to present the educational session, "Deployment of Hydrogen Fuel Cells – Safety Considerations and Resources," at the 2013 NFPA Conference & Expo, in Chicago, IL, on June 11, 2013 [10]. This session addressed the current status of hydrogen fuel cells and the applicable codes and standards that enable their deployment. The resources which play a key role in reaching, educating and informing stakeholders whose contributions will help enable a broad set of fuel cell applications were also presented.

International collaboration is also an important theme. Leadership was provided to the International Energy Agency Hydrogen Implementing Agreement Task 31 (Hydrogen Safety) for the work under Subtask D, Knowledge Analysis,

TABLE 2. HSP Project Safety Work since July 1, 2012

Work	Project Title	Contractor
Process diagram, on-location site layout and conceptual design reviews (July 2012)	Renewable Hydrogen Production Research Projects	Hawaii Natural Energy Institute
HNEI Certification Study Review [2]	Renewable Hydrogen Production Research Projects	Hawaii Natural Energy Institute
Safety plan reviews [3,4]	Hydrogen Storage in Metal-Organic Frameworks	NIST, GM, LBNL, UC Berkeley
Safety plan review [5]	Room Temperature Hydrogen Storage in Nano-Confined Liquids	HRL Laboratories
Safety plan reviews [6,7,8]	Roots Air Management System with Integrated Expander	Eaton Corp., Ballard
Safety evaluation follow-up report [9]	Fuel-Cell Powered Lift Truck Fleet Deployment	Coca-Cola, Bottling Co., Plug Power
Safety evaluations final report [1]	HSP Review of DOE Fuel Cell Projects	Various contractors
Safety guidance at project kickoff (March 2013)	Hydrogen Recycling System Demonstration	H2Pump
Safety guidance at project kickoff (March 2013)	Fuel Cell Ground Support Equipment Development and Demonstration	Plug Power
Safety guidance at project kickoff (May 2013)	Fuel Cell Auxiliary Power Unit for Refrigerated Trucks	Nuvera

NIST – National Institute of Standards and Technology; GM – General Motors; LBNL – Lawrence Berkeley National Laboratory; UC Berkeley – University of California, Berkeley

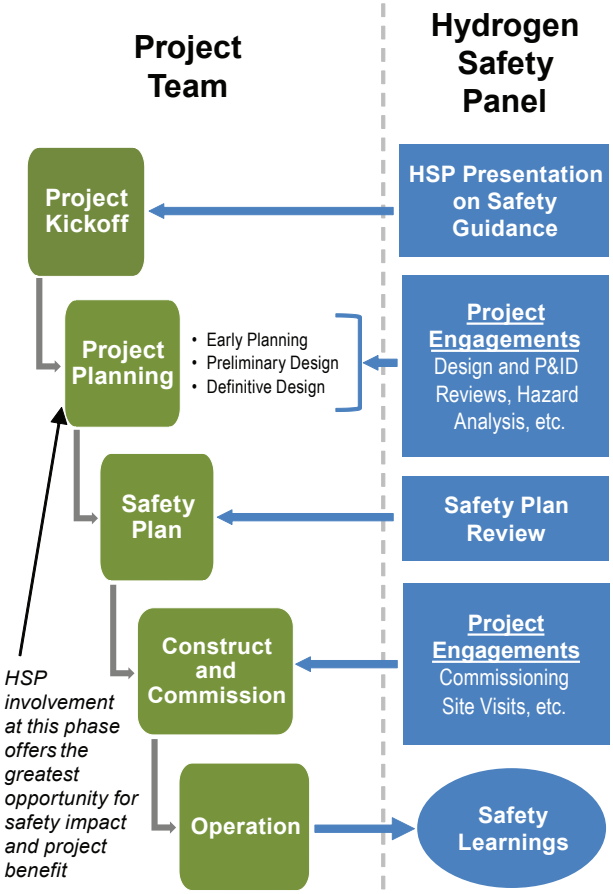

FIGURE 1. Hydrogen Safety Panel Reviews for Deployment Projects

Dissemination and Use. Under this task, a white paper was authored to illustrate how technology information and knowledge dissemination are an integral part of this international collaboration [11]. Two talks were contributed to the Hydrogen Safety Stakeholder Workshop, *Sharing Knowledge, Identifying Needs, Celebrating Progress,* in Bethesda, MD, on October 2-3, 2012 [12,13]. PNNL also contributed two manuscripts for presentation at the International Conference on Hydrogen Safety in Brussels, Belgium, on September 9-11, 2013 [14,15].

The safety knowledge tools H2incidents.org and H2bestpractices.org websites continue to see a steady number of visitors. To increase visibility and get this information in the hands of a greater audience, the project has integrated information from the websites into a mobile application (see Figure 2). The "Hydrogen Tools" application brings added value by combining information from the websites (H2incidents.org and H2bestpractices.org) as well as other project resources (safety planning guidance and a safety checklist), calculators and related tools. The mobile app also allows for search capabilities across the incidents and database resources and the best practices can be viewed offline.

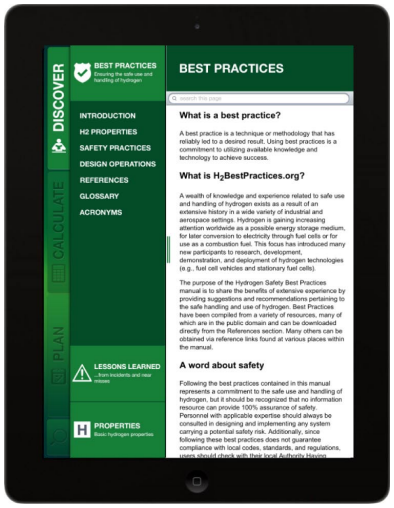

FIGURE 2. Hydrogen Tools iPad App

CONCLUSIONS AND FUTURE DIRECTIONS

The work and approaches taken by the HSP will continue to focus on how safety knowledge, best practices and lessons learned can be brought to bear on the safe conduct of project work and the deployment of hydrogen technologies and systems in applications of interest and priority in the DOE FCT Office. The HSP can also be used more broadly as an asset for safe commercialization by reaching out to new stakeholders and users involved in early deployment activities.

The HSP will undertake a number of initiatives over the next year including:

- Support project activities with the focus on early engagement including kickoff meetings, safety plan reviews, site visits and other relevant interactions with project teams.
- Submit a white paper to DOE on "Safety of Hydrogen Systems Installed in Outdoor Enclosures."
- Achieving an appropriate mix of safety expertise and perspective is important for the Panel to perform safety reviews and address relevant issues. PNNL will continue to evaluate the HSP membership to maintain its leadership role in hydrogen safety.
- Seek opportunities to share safety knowledge with new audiences to facilitate the safe deployment of hydrogen and fuel cell technologies. Some examples include the 2014 NFPA Conference and Expo and potential collaboration with the U.S. Fire Administration.

Our hydrogen safety knowledge tools help remove barriers to the deployment and commercialization of hydrogen and fuel cell technologies. Feedback on both of our websites has been extremely positive. In order to remain vital and useful, databases and websites require a concerted effort beyond just general maintenance. The content must be current, relevant to the community being served, and valuable to the users.

- Continue to encourage DOE projects and private-sector incident owners to submit records of incidents and near-misses to share their lessons learned with the hydrogen community.
- Issue the "Hydrogen Tools" app for the iPhone.
- Evaluate additional resources that could be added to the mobile application to enhance its usefulness for projects and permitting officials.

FY 2013 PUBLICATIONS

1. Weiner, S.C. and Fassbender L.L., "Lessons Learned from Safety Events," PNNL-SA-86551, International Journal of Hydrogen Energy, Volume 37, Issue 22, November 2012, pp. 17358-17363.

2. Kallman, R.A., Barilo, N.F. and Murphy, W.F., "Permitting of a Project Involving Hydrogen – A Code Official's Perspective," PNNL-SA-87780, Energy Procedia, Volume 29, November 2012, pp. 265-275.

3. Weiner, S.C., Fassbender, L.L., Blake, C., Aceves, S., Somerday, B.P. and Ruiz, A., "Web-Based Resources Enhance Hydrogen Safety Knowledge," PNNL-SA-82812, International Journal of Hydrogen Energy, Volume 38 (2013), pp 7583-7593.

REFERENCES

1. Weiner, S.C. and N.F. Barilo, "Hydrogen Safety Panel Review of DOE Fuel Cell Projects," PNNL-22075, December 18, 2012.

2. Barilo, N. F. to Ewan, M., "Re: Boyd Report on Hydrogen Safety Design Review held at Powertech," December 5, 2012.

3. Weiner, S.C. to Adams, J., "Safety Plan Review for Hydrogen Storage in Metal-Organic Frameworks," September 5, 2012.

4. Weiner, S.C. to Adams, J., "Revised Safety Plan for UC/LBNL Hydrogen Storage in Metal-Organic Frameworks," December 4, 2012.

5. Weiner, S.C. to Randolph, K., "HRL Safety Plan Reviewed by Hydrogen Safety Panel," September 25, 2012.

6. Weiner, S.C. to Tyler, R., "Eaton Corp. Safety Plan Reviewed by Hydrogen Safety Panel," November 28, 2012.

7. Weiner, S.C. to Tyler, R., "Ballard Safety Plan Reviewed by Hydrogen Safety Panel," December 5, 2012.

8. Barilo, N.F. to Tyler, R., "Revised Eaton Corp. Safety Plan," February 20, 2013.

9. Weiner, S.C., Follow-up Report for "Safety Evaluation Report: Fuel-Cell Powered Lift Truck Fleet Deployment, Coca-Cola Bottling Company Consolidated, Charlotte, NC," October 19, 2012.

10. Barilo, N.F., Weiner, S.C., and James, C., "Deployment of Hydrogen Fuel Cells – Safety Considerations and Resources," PNNL-SA-92552, 2013 NFPA Conference & Expo, June 11, 2013.

11. Weiner, S.C., "Advancing the Hydrogen Safety Knowledge Base," A White Paper of the International Energy Agency Hydrogen Implementing Agreement Task 31 – Hydrogen Safety, PNNL-22159, January 15, 2013.

12. Barilo, N.F., "Hydrogen Safety Program," IEA Hydrogen Implementing Agreement Hydrogen Safety Stakeholders Workshop, Bethesda, MD, October 2–3, 2012.

13. Weiner, S.C., "Safety Knowledge Tools Overview and Examples," PNNL-SA-90919, IEA Hydrogen Implementing Agreement Hydrogen Safety Stakeholders Workshop, Bethesda, MD, October 2–3, 2012.

14. Barilo, N.F. and Weiner, S.C., "Deploying Fuel Cell Systems: What Have We Learned?" PNNL-SA-92591, International Conference on Hydrogen Safety, Brussels, Belgium, September 9–11, 2013.

15. Weiner, S.C., "Advancing the Hydrogen Safety Knowledge Base," PNNL-SA-91531, International Conference on Hydrogen Safety, Brussels, Belgium, September 9–11, 2013.

VIII.10 International Partnership for Hydrogen and Fuel Cells in the Economy—Regulations, Codes and Standards Working Group

Jay Keller
Zero Carbon Energy Solutions
Email: Jay.O.Keller@gmail.com

DOE Manager
Sunita Satyapal
Phone: (202) 586-2336
Email: Sunita.Satyapal@ee.doe.gov

Fiscal Year (FY) 2013 Objectives

- Complete Phase I of the Type IV tank hydraulic test measurement multi-national round robin (RR)
- Advance the Type IV tank pneumatic test measurement multi-national RR
- Initiate new RR activities on fuel quality effects on fuel cell stacks
- Initiate a focus on safety for our meetings and the International Partnership for Hydrogen and Fuel Cells in the Economy Steering Committee (IPHE SC) website

Technical Barriers

This project addresses the following technical barriers from the Codes and Standards section of the Fuel Cell Technologies Office Multi-Year Research, Development, and Demonstration Plan section 3.7.5:

(A) Safety Data and Information: Limited Access and Availability

(F) Enabling National and International Markets Requires Consistent Regulations, Codes, and Standards

(G) Insufficient Technical Data to Revise Standards

(H) Insufficient Synchronization of National Codes Standards (by extension International Standards)

(K) No Consistent Codification Plan and Process for Synchronization of R&D and Code Development

Contribution to Achievement of DOE Codes and Standards Milestones

This project will contribute to achieving the following DOE milestones from the Safety Codes and Standards sections of the Fuel Cell Technologies Office Multi-Year Research, Development, and Demonstration Plan (Section 3.7.7)

- 2.1 Publish a system for classifying accident types. (2Q, 2012)
  - Safety data base portal, incident highlights during Regulations Codes and Standards Working Group (RCSWG) meetings
- 2.2 Publish a draft international hydrogen fuel specification standard. (4Q, 2012)
  - Initiated a task force to investigate a fuel quality on stack behavior RR
- 2.9 Publish technical basis for optimized design methodologies of hydrogen containment vessels to account appropriately for hydrogen attack. (Q4, 2014)
  - Hydraulic and pneumatic Type IV tank testing measurement RR
- 3.1 Develop, validate, and harmonize test measurement protocols. (4Q, 2014)
  - Hydraulic and pneumatic Type IV tank testing measurement RR
- 3.2 Publish hydrogen quality testing protocols. (4Q, 2015)
  - Initiated a task force to investigate fuel quality effects on stack performance
- 4.2 Develop supporting research programs (round robins) to provide data and technologies. (2Q, 2012)
  - Tank measurement and fuel quality RR
- 5.1 Update safety bibliography and incidents databases. (4Q, 2011 – 2020)
  - IPHE safety Web portal to international data bases

FY 2013 Accomplishments

- Hydraulic testing successfully completed on the first of two 35-MPa tanks by the U.S.
  - Successfully performed analysis of the combined results, drafted improvements to the measurement protocol. Execution of the improved measurement protocol on the second 35-MPa tank is in progress by both participants as of the writing of this document.
- Hydraulic testing successfully completed on both 35-MPa tanks by China.
- Held two RCSWG face-to-face meetings which accomplished the following:

- Advanced the tank measurement RR
- Launched a RR on fuel quality for stack behavior
- Made a safety discussion a standing agenda item
- Launched a IPHE RCSWG presence on the IPHE SC website
- Launched a RCSWG activity to produce an incidents/safety portal to international databases

• Provided two reports to the IPHE SC at the Fall and Spring SC Face-to-Face

✧ ✧ ✧ ✧ ✧

INTRODUCTION

The IPHE was established in 2003 as an international intergovernmental organization to accelerate the use of hydrogen and fuel cells in the economy. It provides a mechanism for partners to organize, coordinate and implement effective, efficient, and focused international research, development, demonstration, and commercial utilization activities. The following countries are members of IPHE:

- Australia
- Germany
- New Zealand
- Brazil
- Iceland
- Norway
- Canada
- India
- Norway
- China
- Italy
- Republic of South Africa
- European Commission
- Japan
- United Kingdom
- France
- Republic of Korea
- United States

At the May 2010 IPHE SC meeting in Essen Germany the IPHE SC endorsed the importance of the RCSWG in taking a leading role in harmonizing RCS, from an IPHE top-down perspective. The IPHE/RCSWG is now one of two standing working groups for the IPHE; the other is the Education working group. The RCSWG's role is to create and conduct a forum where potentially contentious and controversial issues of RCS are identified and handled. The RCSWG can recommend a consensus solution and promote resolution of these contentious issues. The RCSWG also conducts pre-normative work to globally harmonize the execution of testing relevant to RCS.

BACKGROUND

The RCSWG has currently one RR in progress on measurement protocol for testing Type IV tanks. Additional activities are planned for the future. The RCSWG chose to pursue the tank testing issue first. There have been issues raised about the lack of uniformity in test measurement protocol related to Type IV composite overwrap pressure vessels. The RCSWG response was to launch a RR to define a harmonized test measurement protocol. Successful completion of this RR will result in the creation of a harmonized test measurement protocol suitable for use by testing facilities around the world. This protocol will ensure uniformity of testing procedures and subsequently uniformity in the results of these tests, regardless of where they are being performed. Also, the protocol will be suitable for smaller testing facilities as opposed to multi-million dollar research facilities.

APPROACH

A representative cycle stress test protocol was developed drawing from the three draft standards and regulations (SAE International J2579, the Global Technical Regulation, and the European Integrated Hydrogen Project Rev 12B). Our representative cycle stress tests will be or were applied both hydraulically and pneumatically. The testing will occur at several different RCSWG members' facilities around the world. The currently identified RCSWG participating countries in this RR are Brazil, China, the European Union (EU), France, and the U.S. Brazil has been active in helping to draft the protocol. China, France, and the U.S. are active in the hydraulic testing, the EU, France, and the U.S. are active in the pneumatic testing phase. Hexagon Lincoln has supplied four 35-MPa tanks for the hydraulic testing; Commissariat à l'Energie Atomique, France, is supplying six 70-MPa tanks for both the hydraulic and pneumatic phases of this project.

RESULTS

RCSWG has successfully completed the first test campaign on 35-MPa Type IV tanks, in China and the U.S. (see Figures 1 and 2). A total of four different test configurations were executed. Results from this first test campaign were analyzed and used to improve the test measurement protocol.

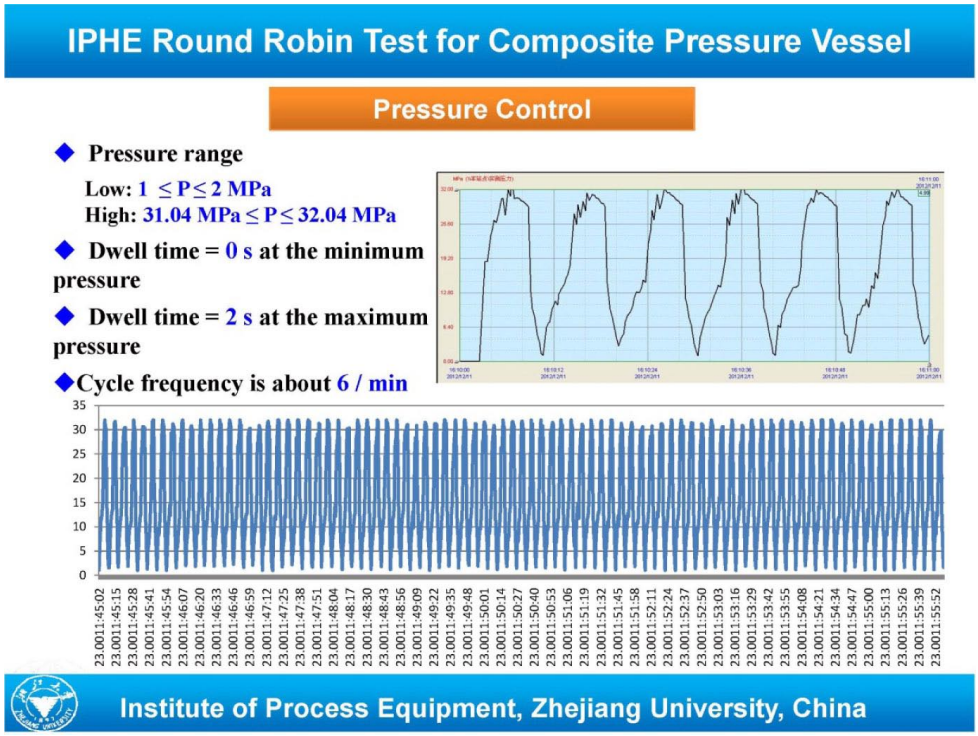

FIGURE 1. Test results from the Institute of Process Equipment, Zhejiang University, China. The figure shows tank pressure (ordinate) for a 100 cycles (abscissa) (bottom plot) and an expanded pressure vs. cycle for six cycles (top plot).

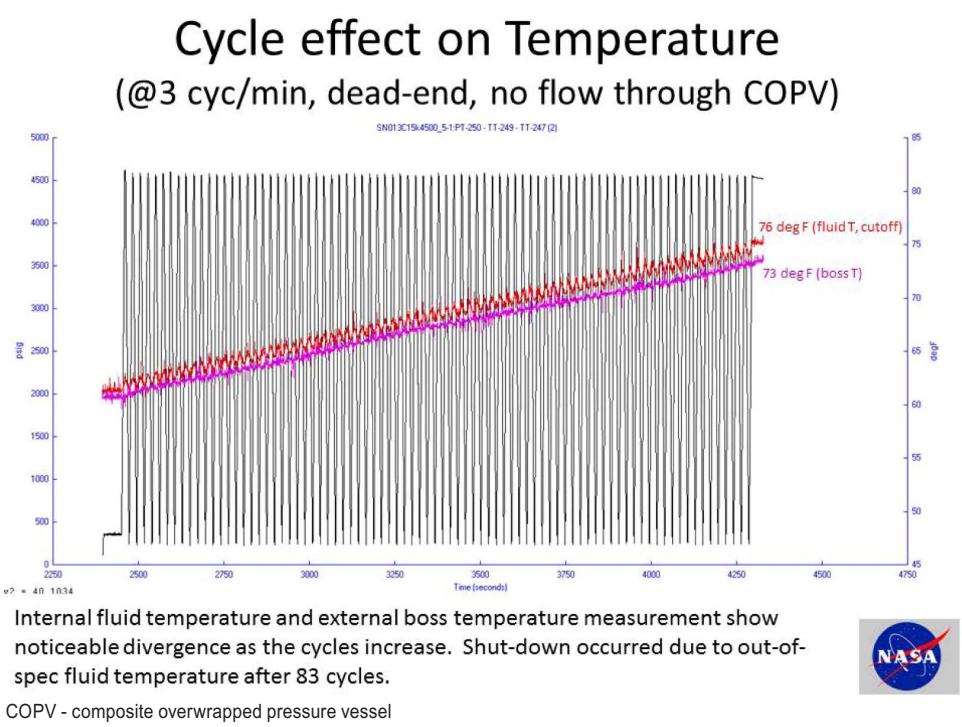

FIGURE 2. This figure shows the rise in temperature (ordinate) of the working fluid inside the tank at for the end-boss for a dead-ended configuration as a function of cycle number (abscissa). Note: the temperature deviation between the boss temperature (lower plot) and the in-tank fluid temperature (upper plot), and note that deviation grows with the number of cycles.

CONCLUSIONS AND FUTURE DIRECTIONS

This current phase of the RR on tank measurement protocol has been a success in that we have developed a test measurement protocol that, when applied, will ensure uniformity in results independent of the facility. We have also successfully demonstrated that when the modified test measurement protocol is used, the test campaign can be executed and maintained with in the cycle test specifications.

We have recently initiated the pneumatic phase of this RR and anticipate similar results from this effort. We have also initiated a RR focused on fuel quality effects on stack performance. Five member countries have been identified to comprise a task force to define this new RR. This RR has received official endorsement from the IPHE SC. We will officially launch at our Fall 2013 face-to-face meeting.

An additional benefit of the tank measurement RR will be the creation of two research laboratories which will have the capability to address the measurement of hydrogen dispensing suitable for metrology needs, as specified in International Organization of Legal Metrology R139 in the EU and National Institute of Standards and Technology Handbook 44 in the U.S. We will consider an activity addressing the pre-normative issues related to metering at the conclusion of the pneumatic phase of the Type IV tank RR.

VIII.11 NREL Hydrogen Sensor Testing Laboratory

William Buttner (Primary Contact), Carl Rivkin, Robert Burgess
National Renewable Energy Laboratory
15013 Denver West Parkway
Golden, CO 80401
Phone: (321) 275-3903
Email: William.Buttner@nrel.gov

DOE Manager
Rick Farmer
Phone: (202) 586-1623
Email: Richard.Farmer@ee.doe.gov

Project Start Date: October 1, 2012
Project End Date: Project continuation and direction determined annually by DOE

Overall Objectives

- Quantify performance of commercial hydrogen safety sensors relative to DOE metrics.
- Collaborate with industry, universities, and government researchers to develop improved hydrogen sensor technologies.
- Educate the hydrogen community on the proper use of hydrogen sensors.
- Support development and updating of hydrogen sensors codes and standards.
- Support infrastructure deployment by providing expert guidance on the use of hydrogen sensors.

Fiscal Year (FY) 2013 Objectives

- Quantify performance metrics of developmental sensor technologies supported by DOE.
- Support infrastructure deployment by providing sensor testing capability and guidance to stakeholders.
- Support fuel cell electric vehicle deployment by assessing safety sensor requirements specified in the Global Technical Regulation (GTR) for hydrogen-powered vehicles.
- Facilitate the commissioning of the NREL Energy System Integration Facility (ESIF) by working with NREL Environmental, Health and Safety to review and validate the chemical detection system.
- Transfer and establish the NREL Sensor Laboratory to ESIF.

Technical Barriers

This project addresses the following technical barriers identified in the Hydrogen Safety, Codes and Standards section of the Fuel Cell Technologies Office Multi-Year Research, Development, and Demonstration Plan:

(A) Safety Data and Information: Limited Access and Availability

(C) Safety is Not Always Treated as a Continuous Process

(F) Enabling National and International Markets Requires Consistent Regulations, Codes and Standards

(G) Insufficient Technical Data to Revise Standards

(H) Insufficient Synchronization of National Codes and Standards

(K) No Consistent Codification Plan and Process for Synchronization of R&D and Code Development

Contribution to Achievement of DOE Safety, Codes and Standards Milestones

This project contributes to achievement of the following DOE milestones from the Hydrogen Safety, Codes and Standards section of the Fuel Cell Technologies Office's Multi-Year Research, Development, and Demonstration Plan:

- Milestone 2.6: Develop sensors meeting technical targets (4Q, 2013)
- Milestone 2.12: Develop leak detection devices for pipelines (4Q, 2015)
- Milestone 2.15: Develop holistic design strategies (4Q, 2017)
- Milestone 3.1: Develop, validate, and harmonize test measurement protocols (4Q, 2014)
- Milestone 4.9: Completion of GTR Phase 2 (1Q, 2017)
- Milestone 5.1: Update safety bibliography and incidents databases (4Q, 2011-2020)

FY 2013 Accomplishments

- NREL and the European Union Joint Research Centre's Institute for Energy and Transport (IET) completed a 2-year Memorandum of Agreement (MOA) to collaborate on hydrogen safety sensor research; the MOA is being renewed.
- Completed numerous topical studies on the proper use of hydrogen sensors under the auspices of the NREL-IET MOA.

  - Completed a critique on the use of oxygen sensors to correlate changes in oxygen concentration to hydrogen levels with strong arguments as to why this approach should not be used.
  - Completed a survey of the impact of depressed oxygen on sensor performance for the major sensor platform types. Some sensors will not function in the absence of oxygen, which can lead to a potentially dangerous situation. Many stakeholders are not aware of this requirement.
  - Completed a study of the impact of miniaturization via micro-machining on sensor performance.
  - Initiated a fourth topical study surveying the impact of interferences and poisons on performance of the major sensor platform types.
  - Completed the round robin testing with IET of commercial hydrogen sensors.
- Contributed to the white paper "Advancing the Hydrogen Safety Knowledge Base" summarizing the accomplishments of the International Energy Agreement, Hydrogen Implementation Agreement--Task 31 Hydrogen Safety.
- The NREL sensor laboratory proposed to the U.S. representative on the GTR (Nha Nguyen, Department of Transportation) that endorsement on the use of oxygen measurements to track hydrogen/helium leaks be removed from the GTR text.
- Supported the commissioning of the NREL ESIF by reviewing the chemical sensor detection system and assisting in validating its performance.
- Established the NREL sensor laboratory in the ESIF.

✧ ✧ ✧ ✧ ✧

INTRODUCTION

Safety is a major concern for the emerging hydrogen infrastructure. A reliable safety system is comprised of various elements that can include intrinsic design features (e.g., pressure control systems), engineering controls (e.g., sample size minimization), and the use of hydrogen sensors to monitor for releases. Both the IFC 2009 and National Fire Protection Association (NFPA) 2 require hydrogen sensors for numerous applications, thus sensors will be mandatory in all jurisdictions that adopt either IFC or NFPA. To assure the availability of reliable safety sensors, NREL established the Sensor Test Facility. The NREL Sensor Test Facility provides stakeholders (e.g., sensor developers and manufacturers, end users and code officials) an independent, unbiased evaluation of hydrogen sensor technologies. Test protocols are guided by the requirements in national and international sensor standards, as well as sensor performance targets established by DOE. In addition to laboratory assessment of sensor performance, a critical mission of the NREL sensor testing laboratory is to educate end users on the proper use of hydrogen sensors. This is achieved, in part, through topical studies designed to illustrate fundamental properties and limitations of various hydrogen sensor technologies. The NREL sensor laboratory also facilitates deployment by partnering with end-users to assist in the design of their sensor system.

APPROACH

Evaluation of hydrogen safety sensors is an on-going activity at NREL. The NREL sensor test apparatus was designed with advanced capabilities, including parallel testing of multiple hydrogen sensors, sub-ambient to elevated temperature, sub-ambient to elevated pressure, active humidity control and accurate control of gas parameters with multiple precision digital mass flow meters operating in parallel. The test apparatus is fully automated for control and monitoring of test parameters and for data acquisition with around-the-clock operation capability. Selected sensors are subjected to an array of tests to quantify the impact of variation of environmental parameters and chemical matrix on performance. Results are reported back to the developer or manufacturer to support their future development work. NREL sensor testing also supports end-users by qualifying technology for their application and by educating the hydrogen community on the proper use of hydrogen sensors. The importance of hydrogen safety sensors has been internationally recognized. The IET has also established a sensor test facility. To facilitate sensor analysis and dissemination of the results, the NREL and the IET sensor testing laboratories have formalized collaboration under an inter-laboratory MOA. The MOA synergizes the laboratories' independently programmed activities to maximize the benefit of their respective institutional interests through cooperative activities. Under the auspices of the MOA, numerous topical studies have been initiated and jointly presented at meetings and published.

RESULTS

In order to support hydrogen deployment, the NREL Sensor Test Facility strives to assure the availability of hydrogen sensors to meet stakeholder needs. This is achieved in part by providing an unbiased assessment of performance to sensor developers and manufacturers as well as end-users. NREL has also performed numerous topical studies aimed at educating the hydrogen community on the proper use of hydrogen sensors. Results reported here summarize major studies completed in FY 2013 on the characterization and use of hydrogen sensors.

A round-robin test (RRT) of hydrogen sensors between NREL and IET produced quantitatively equivalent results,

thereby cross-validating the respective test systems and protocols. IET and NREL thus agreed to coordinate all future sensor evaluations so as to explicitly eliminate duplicate activity. The RRT also indicated a disparity between actual sensor performance and manufacture specifications; nearly one-third of the models considered for RRT did not meet the manufacturer accuracy specification. The protocol developed for the RRT stipulated that commercial, factory-calibrated sensors would be used without adjustment; on-site calibration would have lowered the number of sensors that were out of specification. Nevertheless, this observation emphasizes the need to verify sensor metrics prior to deployment.

One emerging approach to measure hydrogen releases has been to use oxygen sensors to monitor changes in ambient oxygen levels and then to equate this change to hydrogen. This approach has been explicitly cited in the draft GTR proposed for hydrogen-fueled vehicles {Section B.6.1.2: "Sensors are selected to measure either the build-up of the hydrogen or helium gas or the reduction in oxygen (due to displacement of air by leaking hydrogen/helium)"}. The use of oxygen sensors to measure hydrogen levels was evaluated. In spite of the endorsement in the GTR, this approach was found to be inappropriate for closed systems, such as automobile passenger compartments. This is shown in Figure 1 which plots the O_2 sensor reading in air (21 vol% O_2) at 0.8 bar (region A). At 0.4 hours, the system was pressurized with helium to 1.0 bar; no response was observed on the oxygen sensor in spite of the presence of 20 vol% helium (region B). At 0.75 hours, the chamber was maintained at 1.0 bar while purged with air (region C). As a result, NREL has recommended to the U.S. representative on the GTR panel to remove the endorsement of this approach from the GTR. In addition, it was found that the natural drift in the oxygen sensor response precludes using this approach for safety monitoring applications (e.g., indoor monitors). Complete details of this study, including recommendations for alternative technologies will be presented at the 2013 International Conference for Hydrogen Safety and published in the International Journal of Hydrogen Energy.

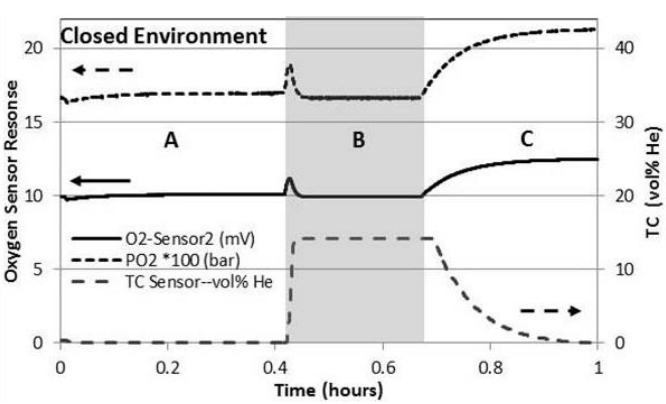

FIGURE 1. Insensitivity of the Oxygen Sensor to a Hydrogen Surrogate in a Closed Environment

Several critical sensor performance metrics remain elusive, such as the DOE target response time of 1 s. To achieve fast kinetics, sensor developers have invoked advanced manufacturing techniques such as micro-machining to produce miniaturized devices. Such an approach can yield low-cost sensors through economy of scale manufacturing. It can also improve response times by minimizing the impact of bulk properties on the sensor response. NREL, in collaboration with IET and the Université du Québec à Trois-Rivières, evaluated the impact of miniaturization on sensor performance. Miniaturized sensors did indeed exhibit improved response times, however some developers tended to overemphasize the response time specification at the expense of other parameter since it was also observed that at least for some platform types, micro-machining resulted in significant degradation in overall sensor performance. Preliminary results were presented at the World Hydrogen Energy Conference 2012 and a complete study was submitted to the International Journal of Hydrogen Energy in August 2013.

Hydrogen operations are often performed under an anaerobic atmosphere in order to minimize risks associated with the use of hydrogen. As an integral element in a safety system, sensor performance should not be compromised by operational parameters, but unfortunately many sensor platforms are deactivated when operated in an anaerobic atmosphere. On several occasions the NREL sensor laboratory had to inform an end-user that the sensor they proposed to use to measure hydrogen in a nitrogen purge would not work. This could lead to a false negative and potentially dangerous situation once the nitrogen purge is mixed with air. To educate the hydrogen community on the choice of hydrogen sensor platforms compatible for use in inert atmospheres, NREL and the IET completed an assessment of the oxygen requirements for the major sensor platform types. Preliminary results were presented at the 2011 International Conference for Hydrogen Safety and recently published in the International Journal of Hydrogen Energy.

In addition to topical studies, the NREL Sensor Test Facility supports sensor development by providing sensor developers and manufacturers with advanced sensor test capability. NREL provides reports and verbal briefings to sensor developers on the performance of their technology. The summary also includes an assessment of possible failure modes. The NREL Sensor Test Facility personnel have extensive experience in the design and use of chemical sensors, and can often identify faults that are missed by developers. Inasmuch as it is the policy of NREL not to identify a specific manufacturer, these reports are confidential and cannot be openly presented in an open forum such as the Annual Merit Review, but the data can be used, without reference to the sensor model, in topical studies and presentations. The NREL Sensor Test Facility has also worked with end-users on the design and verification of their

hydrogen safety sensor system. Recently, the NREL Sensor Test Facility worked with the NREL Environmental Health and Safety Group to check out and validate the gas detection system implemented in ESIF.

CONCLUSIONS AND FUTURE DIRECTIONS

In the next year, the NREL sensor laboratory will build off its current accomplishment and capabilities via two main avenues—continued evaluation of commercial and developing sensor technologies and support of deployment by expanded collaborations with end-users of sensors.

- Manufacture/Developer Support
  - Commercial and developmental sensor technology performance validation
  - Wide area monitoring/distributed sensors
  - Process control sensors/fuel quality sensors (sensors for 0 to 100 vol% hydrogen)
- End-User Support to Support Deployment
  - Guidance on the use of hydrogen sensors in infrastructure deployments
  - Department of Transportation and the GTR on hydrogen vehicles
  - Barriers to sensor certification and the impact

FY 2013 PUBLICATIONS/PRESENTATIONS

1. Assessment of Commercial Micro-machined Hydrogen sensors to guide the Next Generation, H. El Matbouly, F. Domingue, V. Palmisano, L. Boon-Brett, M.B. Post, C. Rivkin, R. Burgess, and W.J. Buttner; presented at World Hydrogen Energy Conference 2012 and submitted to the International Journal of Hydrogen Energy (2013).

2. An Assessment on the Quantification of Hydrogen Releases Through Oxygen Displacement Using Oxygen Sensors, W. Buttner, M. Post, R. Burgess, C. Rivkin, L. Boon-Brett, V. Palmisano; to be presented at the International Conference on Hydrogen Safety (September 9–11, 2013) and published in the proceedings.

3. Evaluation of Selectivity and Resistance to Poisons of Commercial Hydrogen Sensors, V. Palmisano, L. Boon-Brett, W. Buttner, M. Post, R. Burgess, C. Rivkin, to be presented at the International Conference on Hydrogen Safety (September 9–11, 2013) and published in the proceedings.

4. Inter-laboratory assessment of hydrogen safety sensors performance under anaerobic conditions, W.J. Buttner, R. Burgess, C. Rivkin, M.B. Post, L. Boon-Brett, G. Black, F. Harskamp, P. Moretto, International Journal of Hydrogen Energy 37 (2012) 17540-17548.

5. Steering Committee Progress Report on Hydrogen Sensor Performance Testing and Evaluation under the Memorandum of Agreement between NREL, U.S. DOE and JRC-IET, EC W. Buttner, M. Post, R. Burgess, C. Rivkin, L. Boon-Brett, V. Palmisano, C. Bonato and F. Harskamp Technical Report NREL/TP-5600-57207 (December 2012).

6. NREL/JRC MoA Steering Committee Meeting--Hydrogen Sensor Testing and Evaluation, W. Buttner, R. Burgess, C. Rivkin, M. Post L. Boon-Brett, P. Moretto, G. Black, V. Palmisano, F. Harskamp, C. Bonato, NREL/JRC Steering Committee-Annual Review Meeting (December 3, 2012).

7. U.S. Hydrogen Sensor Standards and Their Impact on Infrastructure Implementation, Kathleen O'Malley, William J. Buttner, H. Lopez, Julie Cairns, Robert Burgess, Carl Rivkin, and Robert Wichert, to be published as an NREL Technical Report (2013).

IX. MARKET TRANSFORMATION

IX.0 Market Transformation Program Overview

INTRODUCTION

The Market Transformation program is conducting activities to help promote and implement commercial and pre-commercial hydrogen and fuel cell systems in real-world operating environments to provide feedback to research programs, U.S. industry manufacturers, and potential technology users. One of the program's goals is to achieve sufficient manufacturing volumes in emerging commercial applications to enable cost reductions through economies of scale, which will help address the current high cost of fuel cells. These early fuel cell deployments will also address other market acceptance factors, which will result in further expansion of market opportunities.

Current key objectives of the Market Transformation program are to build on past successes in material handling equipment (MHE) (e.g., lift trucks) and emergency backup power applications that were part of the American Reinvestment and Recovery Act of 2009 (Recovery Act), by exploring other emerging applications for market viability. Fiscal Year (FY) 2013 activities were primarily focused on completing projects using FY 2010 appropriations, launching a new project to demonstrate commercial viability of fuel cell-powered airport ground support baggage tractors, and preparing and issuing a new solicitation using FY 2013 appropriations to demonstrate fuel cell-powered electric medium-duty hybrid trucks for parcel delivery applications. These projects are highly leveraged, with an average of more than half of the projects' funds being provided by DOE's partners. Partners providing resources to these projects have shown a high level of interest in exploring these applications and markets, and this level of industry interest is very promising for the potential growth of the domestic fuel cell industry.

GOALS

Market Transformation activities provide financial and technical assistance for the use of hydrogen and fuel cell systems in early market applications, with the key goals of achieving sales volumes that will enable cost reductions through economies of scale, supporting the development of a domestic industry, and providing feedback to testing programs, manufacturers, and potential technology users.

OBJECTIVES[1]

The program's key objectives include:

- Conduct market transformation deployment projects to enable life cycle cost and performance of fuel cell-powered lift trucks and emergency backup power systems to be on par with conventional technologies by 2020.
- Establish baseline energy efficiency and reliability performance metrics for commercially available emergency backup power systems, MHE, and light commercial/residential power systems and provide feedback to component suppliers regarding cost reduction opportunities by 2013.
- Test emerging approaches to grid management using renewable hydrogen storage and fuel cell systems in coordination with the DOE's Office of Electricity Delivery and Energy Reliability by 2014.
- Advance the knowledge and expertise of waste-to-energy stationary fuel cells, shipboard auxiliary power unit (APU) applications, and aviation applications through targeted testing and evaluation efforts in coordination with technology validation activities and in partnership with the U.S. Department of Defense, the U.S. Navy, the U.S. Army, and civilian agencies such as the U.S. Department of Agriculture and the Federal Aviation Administration by conducting design requirements planning for aircraft APUs by 2012, shipboard APUs by 2013, and waste-to-energy fuel cells by 2014.
- Identify lessons learned from promulgated policies and regulations and promote the development of the most effective and applicable incentives for hydrogen and fuel cell technologies by 2016.

[1] Note: Targets and milestones were recently revised; therefore, individual project progress reports may reference prior targets.

FY 2013 STATUS

Fuel cells have been enjoying growing success in key early markets, particularly MHE and backup power applications. The Fuel Cell Technologies Office's early market deployment efforts—including Market Transformation funding and Recovery Act funding—have successfully catalyzed a significant level of market activity in these areas, which has been accompanied by substantial reductions in the price of fuel cells. The Office is actively pursuing additional opportunities for effective stimulation of market activity. Ongoing activities and additional areas of interest include the following:

- **MHE Project:** As a complement to the hydrogen fuel cell lift truck deployments currently underway, the program continues to investigate the market viability of using direct methanol fuel cell (DMFC) technologies. The DMFC MHE project is now being completed and operational benefits and reduced infrastructure costs are being verified.
- **Micro-CHP (combined heat and power) Project:** To document the market viability of fuel cells for small facilities, the program is working with fuel cell developers and system users to monitor the long-term performance and evaluate the engineering, economic, and environmental impacts of micro-CHP systems at five commercial facilities. Clear Edge Power has provided 15 fuel cells.
- **Hydrogen Energy Storage Project:** In partnership with the Naval Research Laboratory and the State of Hawaii, the program is supporting the demonstration of a hydrogen energy storage system as a grid management tool. While hydrogen produced from the system could be used in a variety of value-added applications, during the initial phase of the project, the hydrogen will be used in fuel cell buses operated by the County of Hawaii Mass Transportation Agency and the National Park Service.
- **South Carolina Landfill Gas Purification Project:** The program is demonstrating the business case and technical viability of using landfill gas (LFG) as a source of renewable hydrogen production, with BMW's assembly plant in South Carolina as the host site. This project represents a first-of-its-kind LFG-to-hydrogen production plant in the nation and is expected to serve as a model for future adoption of renewable biogas as a feedstock for hydrogen production.
- **Ground Support Equipment (GSE) Demonstration Project:** This project is demonstrating the value proposition of using fuel cell-powered tow tractors as a cost-competitive and more energy-efficient solution when compared to incumbent internal combustion engine-powered vehicles. This effort will address concerns regarding the weatherproofing of fuel cell-powered GSE and enable end-users at FedEx's busiest airport to accomplish their daily tasks while reducing consumption of gasoline and diesel fuels. This project was kicked off in Latham, New York in March 2013.
- **Cost-Benefit Analysis of Fuel Cells in Hybrid Electric Vehicles Project:** The program is demonstrating the cost-benefit tradeoffs of adding a fuel cell APU to double the range of existing battery electric vehicles and aims to quantify the cost-benefit of using a fuel cell APU for different vehicle classes based on the levelized cost of driving.

FY 2013 KEY ACCOMPLISHMENTS

In FY 2013, the program developed deployment tools and business cases for various fuel cell applications, conducted public outreach activities, and analyzed and tested potential new early markets in mobile lighting, DMFC-powered lift trucks, and auxiliary power. The following are some of the key milestones the program achieved in FY 2013:

- In FY 2013, this project analyzed 251,000 hours of operational data from 131 DMFC lift trucks operating at five food distribution sites. Durability analysis and operation analysis of the DMFC units has been completed. The estimated median time of DMFC unit operation was 1,391 hours.
- Performance data for 15 micro-CHP fuel cells were collected and analyzed indicating an average of over 11,000 hours per system. The project team also made recommendations and adjustments to the fuel cell operation that improved fuel cell power output stability.
- In 2013, as part of a demonstration of a hydrogen energy storage system as a grid management tool, a fuel cost analysis based on project equipment in fuel cell bus applications resulted in fuel cost estimates that are competitive (~$8/kg) with conventional fuels on a cents per mile basis.

- Awarded two projects and began design development of fuel cell APUs for refrigerated trucks.
- By the end of FY 2013, the LFG-to-hydrogen project team completed development of an LFG clean-up system, conducted startup and troubleshooting activities, and demonstrated, using project equipment, that the fuel cost estimate is competitive (~5.50/kg) with off-site commercial vendors. This project—the world's first demonstration of LFG-to-hydrogen fuel for fuel cell powered lift trucks—is continuing at the BMW plant in Greer, South Carolina, home to the world's largest fuel cell-powered lift truck fleet (over 300 MHE units).
- In FY 2013, the GSE demonstration project was kicked off in Latham, New York and the project team completed system modeling, tracked and shared data with the baggage tow tractor manufacturer, coordinated with FedEx Express sites for hydrogen permits, and signed a hydrogen supply agreement.
- At the end of FY 2013, the project team developed a vehicle-level energy management system to properly evaluate benefits of using fuel cell system power and onboard hydrogen storage, quantified the trade-off between energy consumption and cost on the Urban Dynamometer Driving Schedule, and demonstrated benefits of using fuel cell systems to double the range of current battery electric vehicles for medium-duty vehicle applications.

BUDGET

FY 2013 appropriation was $3 million and $3 million was requested in FY 2014.

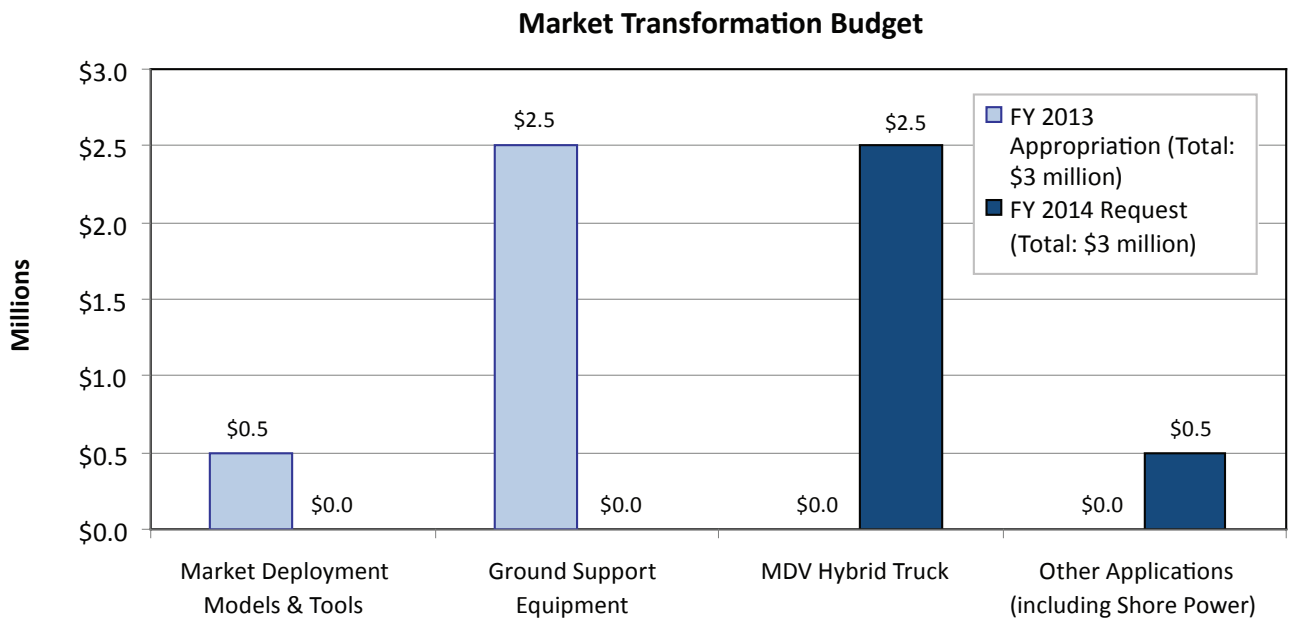

FY 2014 PLANS

In FY 2014, the program will continue to document lessons learned associated with previously funded projects, including the strategies developed for market entry and for risk management with respect to safety, environmental, and siting requirements. Business analysis and case studies will be initiated. Collection and evaluation of data from these projects will provide the basis for verifying the business cases for various early market fuel cell systems, as well as providing an assessment of the performance of these integrated systems. Data will be made publicly available so that more potential customers will become aware of the benefits of integrated hydrogen and fuel cell systems. In addition, a near-term priority will be to continue collaborating with other federal agencies—in accordance with existing interagency cooperative agreements such as the DOE-Department of Defense memorandum of understanding—to increase the use of fuel cells in market-ready applications and to increase awareness of the benefits of these deployments. Competitive award(s) will be made and design and deployment of fuel cell-powered medium-duty trucks for parcel delivery will begin.

Pete Devlin
Market Transformation and Interagency Coordination Manager
Fuel Cell Technologies Office
U.S. Department of Energy
1000 Independence Ave., SW
Washington, D.C. 20585-0121
Phone: (202) 586-4905
Email: Peter.Devlin@ee.doe.gov

IX.1 Direct Methanol Fuel Cell Material Handling Equipment Demonstration

Todd Ramsden (Primary Contact), Mike Ulsh, Jen Kurtz, Sam Sprik, Huyen Dinh, Chris Ainscough
National Renewable Energy Laboratory
15013 Denver West Parkway
Golden, CO 80401
Phone: (303) 275-3704
Email: todd.ramsden@nrel.gov

DOE Manager
Peter Devlin
Phone: (202) 586-4905
Email: Peter.Devlin@ee.doe.gov

Subcontractors:
Oorja Protonics, Inc., Fremont, CA

Project Start Date: June 1, 2010
Project End Date: March 31, 2013

Overall Objectives

- Operate and maintain fuel-cell-powered material handling equipment (MHE) using direct methanol fuel cell (DMFC) technology.
- Compile operational data of DMFCs and validate their performance under real-world operating conditions.
- Provide an independent technology assessment that focuses on DMFC system performance, operation, and safety.
- Evaluate the market viability of using DMFCs in material handling applications.

Fiscal Year (FY) 2013 Objectives

- Complete regular analysis of operation data through December 2012.
- Complete validation of operation against the operational project target for calendar days and hours of operation per unit.
- Complete durability and reliability analyses of units.
- Complete value proposition analysis of DMFCs MHE technology.

Barriers

This project addresses non-technical issues that prevent full commercialization of fuel cells.

Technical Targets

No specific technical targets have been set.

FY 2013 Accomplishments

- Analyzed 251,000 hours of operation from 131 units operating at five sites.
- Completed operation analysis against calendar time and hours (median hours of DMFC unit operation was 1,391).
- Completed durability analysis of DMFC units.

✧ ✧ ✧ ✧ ✧

INTRODUCTION

The National Renewable Energy Laboratory (NREL) and the U.S. Department of Energy (DOE) are interested in supporting the development of early market applications for fuel cell technologies. A study by Battelle Memorial Institute, "Identification and Characterization of Near-term Direct Hydrogen Proton Exchange Membrane Fuel Cell Markets," showed that fuel cells have the potential to power material handling equipment (also known generically as forklifts) at a lower overall cost than lead-acid batteries for certain types of operations [1]. Battery-powered forklifts typically use lead-acid batteries that can only provide enough power for one 8-hour shift. Multi-shift operations therefore generally require additional battery packs and battery change-outs, which reduces productivity and increases costs of operation.

NREL and DOE are currently evaluating the benefits of hydrogen-fueled polymer electrolyte membrane (PEM) fuel cells for MHE and have found that PEM fuel-cell-powered MHE can have a lower total cost of ownership compared to battery-powered forklifts [2,3]. As a supplement to the hydrogen-fueled PEM fuel-cell-powered forklift deployment testing, NREL is investigating the use of DMFC technologies in material handling applications. DMFCs, which use a liquid methanol fuel, hold promise to deliver many of the same operational benefits of hydrogen-powered fuel cell MHE, including long run times, short fueling times, and increased productivity. Liquid alcohol fuels such as methanol offer reduced infrastructure costs, high energy density, and low overall fueling costs.

APPROACH

NREL has partnered with Oorja Protonics on a project to demonstrate and evaluate DMFCs to provide power for MHE in four commercial wholesale distribution centers. In total, 75 DMFC-powered Class III pallet jacks have been deployed

in warehouses operated by Unified Grocers, Testa Produce, and Earp Distribution. DMFC lifts are being operated two shifts per day for a 15-month deployment, with 3,500 to 5,000 total operational hours expected on each unit.

As part of the project, Oorja built, tested, and deployed its OorjaPac Model 3 DMFC power pack into Class III pallet jacks. The DMFC system delivers an output power of approximately 1.5 kW and includes a 3-gallon methanol storage tank expected to provide approximately 12 hours of autonomy between fuelings. Methanol fuel is being dispensed to the DMFC MHE using the OorjaRig methanol dispenser, which is designed to meet all relevant fire and safety codes for indoor methanol dispensing. Oorja is collecting data on both the DMFC systems and the supporting methanol fueling infrastructure. NREL has compiled and analyzed these data and is providing a third-party assessment on the performance of DMFCs used in material handling applications. As part of the 15-month deployment, DMFCs lifts were operated for two shifts per day, with a total operational target of 3,500 hours of use for each unit.

RESULTS

In total, the DMFC MHE fleet had more than 251,000 hours of operation as of December 2012. DMFC systems had significant usage, with over half of the units logging more than 1,500 hours of operation, and nearly 25% of the systems reaching more than 2,370 hours (see Figure 1). A few systems have surpassed the minimum operational target of 3,500 hours.

The OorjaPac Model 3 DMFC power packs used in this deployment project act in concert with traditional MHE battery systems. Unlike traditional battery systems that have limited run time and require frequent battery changes and charging from the electricity grid, the OorjaPac DMFC system acts as an onboard battery charger, maintaining the battery pack state-of-charge and eliminating electric-grid-based battery charging. Under this configuration, actual DMFC operation time depends on the battery state-of-charge. With a high charge level, the DMFC system may turn off while the pallet jack continues to be used. Hence, the operation hours noted above reflect actual run-time of the DMFC systems but may underestimate actual MHE hours of operation.

The DMFC Class III pallet jacks are deployed in warehouses operating two shifts per day. Data provided indicate that DMFC systems are typically operated 7 to 12 hours per day (with actual MHE operation hours potentially higher). NREL found that DMFC systems operate for an average of 8.7 hours between methanol fuelings (see Figure 2). Thus, the DMFC systems can easily operate for a full shift on a single methanol fill, and given their typical

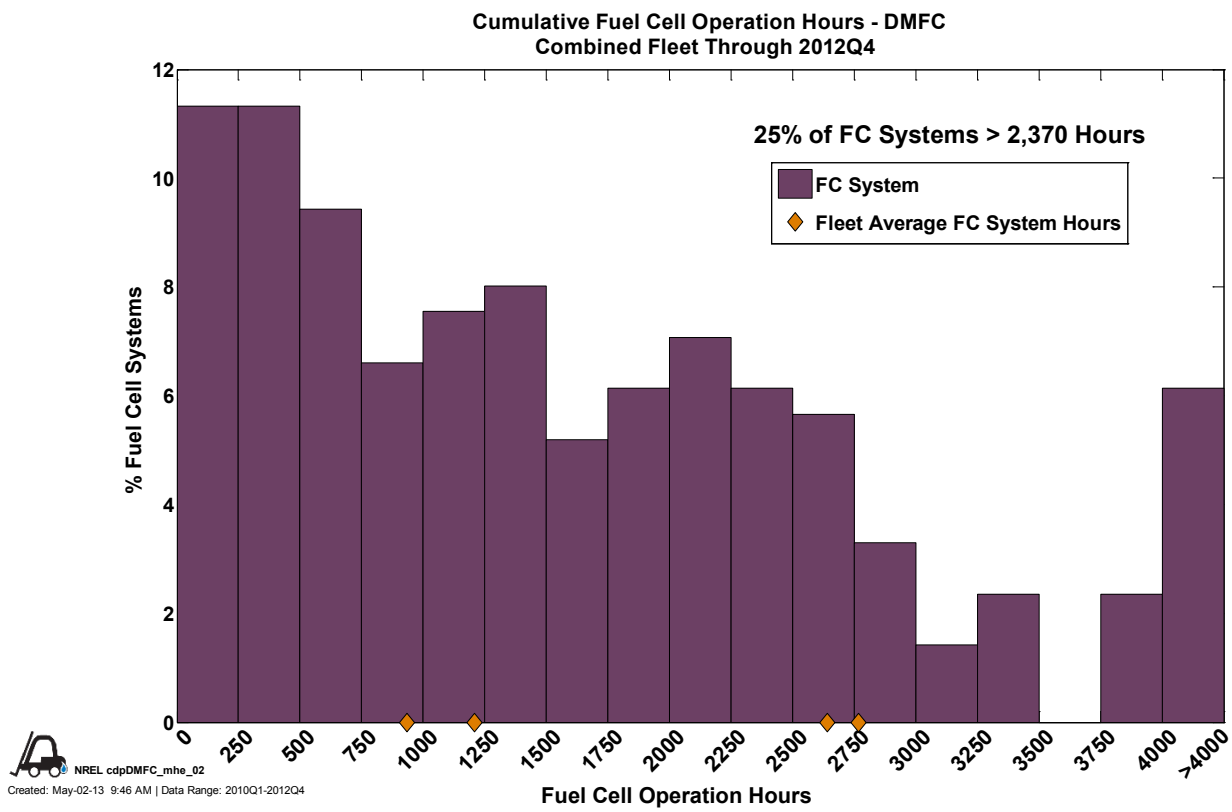

FIGURE 1. Fuel Cell Unit Operational Hours

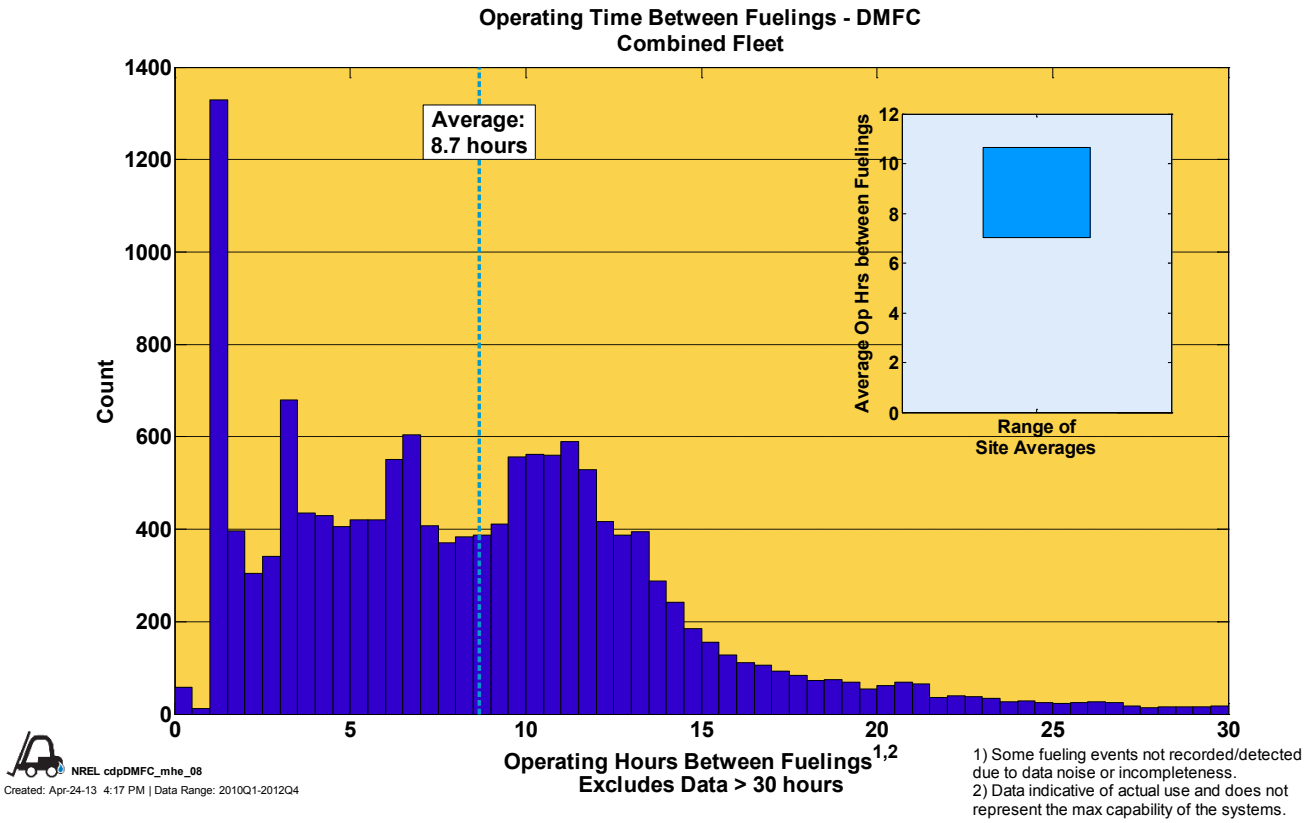

FIGURE 2. DMFC Operation Hours between Fuelings

use pattern, they can often operate for a complete two-shift day on a single fill. Reflecting this, analysis of the methanol fueling data shows that the DMFC systems are filled one time per day on average.

NREL analyzed individual DMFC systems to characterize system voltage, current, and power; maximum voltage and power over time; and stack voltage decay. A voltage and power degradation analysis is completed for each unit and fleet. The degradation analyses are projected times to 10% voltage degradation and a lower power limit. Actual results not published because the results are proprietary.

TABLE 1. Performance Summary of the Oorja DMFC Systems

Sites	5
Number of fuel cell forklift power units analyzed	131
Total hours of operation	251,000
Total methanol fueling events	>14,000
Average hours of operation between fueling	~9
Average daily hours of operation per system	8-10
Average daily methanol fills per system	~1
Median DMFC system hours of operation	1,391

NREL has completed the technology durability analysis. The technology reliability and MHE value proposition analyses are not completed due to insufficient data.

CONCLUSIONS AND FUTURE DIRECTION

Overall, although NREL received a great deal of stack-level DMFC system data, NREL received very limited data from Oorja on maintenance and costs. Due to this, NREL cannot provide a thorough verification of maintenance and infrastructure costs. Based on the limited summary data provided, it appears that DMFC units that had been upgraded with system improvements had 40% fewer unscheduled maintenance events compared to the initial generation of DMFC systems that were deployed as part of this demonstration. Methanol infrastructure costs appear to be on the order of $75,000 per site. In comparison, hydrogen infrastructure costs to support PEM fuel cell MHE are expected to be in the range of $500,000 to $1M per site.

Suggested DMFC research and development pathways to address improving DMFC durability:

- Improve anode catalyst durability by minimizing Ru loss. PtRu alloy is the state-of-the art DMFC anode catalyst but performance degrades over time because

of the loss of Ru. Furthermore, some Ru crosses over from anode to cathode via the membrane and lowers the cathode performance.

- Higher methanol tolerant membrane, that is also durable, conductive and low cost, is needed to minimize mixed potential issue when methanol solution crosses over from anode to cathode. This lowers the fuel cell voltage, fuel utilization and overall fuel cell performance over time. Higher methanol tolerant membrane will also enable higher methanol concentration fuel to be used and result in smaller methanol fuel storage. This could save space in fueling station and cost.
- Methanol tolerant cathode catalyst. Cathode catalyst that does not oxidize the methanol that crosses over from the anode would improve fuel cell performance and durability.
- Engineer DMFC systems to operate over a range of environmental temperatures, including below freezing to 100°C.
- Optimize the DMFC system to have good water and methanol concentration management. This will increase fuel cell voltage, fuel utilization & performance, along with lower maintenance cost.

FY 2013 PUBLICATIONS/PRESENTATIONS

1. Ramsden, T., Ulsh, M., Kurtz, J., Sprik, S., Ainscough, C., "Direct Methanol Fuel Cell Material Handling Equipment Deployment," DOE Hydrogen and Fuel Cells Program Annual Merit Review, May 16, 2012, Washington, D.C.

REFERENCES

1. K. Mahadevan et al., "Identification and Characterization of Near-Term Direct Hydrogen Proton Exchange Membrane Fuel Cell Markets," Battelle. April 2007.

2. National Renewable Energy Laboratory, "Hydrogen and Fuel Cells Research: Early Fuel Cell Market Demonstrations." http://www.nrel.gov/hydrogen/proj_fc_market_demo.html.

3. National Renewable Energy Laboratory, Hydrogen Technologies and Systems Center's Technology Validation Program, "Total Cost of Ownership for Class I, II, & III Forklifts," March 2012. http://www.nrel.gov/hydrogen/cfm/images/cdp_mhe_58_totalcostofownership.jpg.

IX.2 Fuel Cell Combined Heat and Power Commercial Demonstration

Kriston Brooks (Primary Contact), Siva Pilli
Pacific Northwest National Laboratory
P.O. Box 999
Richland, WA 99352
Phone: (509) 372-4343
Email: kriston.brooks@pnnl.gov

DOE Manager
Peter Devlin
Phone: (202) 586-4905
Email: Peter.Devlin@ee.doe.gov

Subcontractor:
ClearEdge Power, Hillsboro, OR

Project Start Date: August 2010
Project End Date: Project continuation and direction determined annually by DOE

Overall Objectives

- Deploy and monitor combined heat and power fuel cell systems (CHP FCSs) in the range of 5-50 kWe in commercial applications.
- Evaluate the engineering, economics, and environmental impact to provide end-users with an independent assessment of the technology.
- Monitor the long-term performance of the systems. As funding allows, we have a contract in place to monitor the systems for five years.
- Demonstrate the viability of the technology to potential customers by developing a business case.

Fiscal Year (FY) 2013 Objectives

- Monitor fuel cell performance and share the results at conferences and in other forums.
- Demonstrate the impact of updated balance of plant (BOP) on the micro-CHP FCS availability.
- Prepare business case for micro-CHP FCSs and incorporate comments from an industrial review.

Technical Barriers

This project addresses the following technical barriers from the Market Transformation section of the Fuel Cell Technologies Office Multi-Year Research, Development, and Demonstration Plan:

(F) Inadequate user experience for many hydrogen and fuel cell applications

(H) Utility and other key industry stakeholders lack awareness of potential renewable hydrogen storage application

(I) Lack of cross cutting information on how to use hydrogen and fuel cell systems in combination with energy efficiency and renewable energy technologies with existing projects

Technical Targets

Applicable DOE 2015 Technical Targets for 1-10 kWe CHP FCSs operating on natural gas:

- Electrical efficiency at rated power = 38.4% (higher heating value)
- System equipment cost, 5 kW = $1,700/kW
- Degradation with cycling = 0.5%/1,000 hrs
- Operating Lifetime = 40,000 hrs
- System Availability = 98%

FY 2013 Accomplishments

- Analyzed 11,255 hours (average hours per system as of July 1, 2013), for 15 micro-CHP FCSs in terms of net electrical and thermal power and system efficiency and availability.
- Recommended changes in the fuel cell operation that resulted in improved fuel cell stability.
- Developed an approach to compare the economics of the micro-CHP FCS to conventional technologies.
- Prepared a draft micro-CHP FCS business case describing the anticipated growth of the FCS market, applications where CHP FCSs would be beneficial and economic conditions that favor their use.

✧ ✧ ✧ ✧ ✧

INTRODUCTION

PNNL provides support to the Market Transformation sub-program with the objective to aid in the development of the fuel cell and associated hydrogen markets. The strategy is to identify near term niche markets where fuel cells have potential, work with the DOE and stakeholders to develop activities in those areas, analyze the business case, and present the results to the community.

APPROACH

The objective of this project is to demonstrate micro-CHP FCSs and assess their performance to help determine and document market viability. PNNL has worked with a vendor to provide micro-CHP FCS at several small industrial buildings. The purpose of these installations is to gather performance data over the course of 1-5 years. The gathered information is being analyzed, to provide "real-world" data from units "in the customer's hands" to validate performance, durability, and reliability; installation, operations, and maintenance costs; and identify advantages to their commercialization.

This project also is developing a business case that could be provided to industry to estimate the size of the market and its growth potential, identify possible niche markets, and compare the micro-CHP FCS with its alternatives in terms of economics, engineering and environmental impact. It has also utilized techno-economic-environmental optimization models to analyze the business case for micro-CHP FCSs. Model results can elucidate competitive strengths of this technology by building type, load curve, and climate. Analyses under this effort incorporate market characteristics that will strengthen the business case such as spark spread and environmental regulations. It also addresses the FCS characteristics such as capital cost, payback period, and reliability. The micro-CHP fuel cell systems being monitored under this project are being used as a case study within the business case.

FIGURE 1. Two Micro-CHP FCS Units Tested for this Study in Portland, Oregon

RESULTS

The micro-CHP FCS subcontractor provided 15 micro-CHP FCSs that were installed at four different deployment sites: two sites in Northern California, one site in Southern California, one site in Oregon (for a sample deployment see Figure 1). Independent evaluation of manufacturer-stated economic, engineering, and environmental performance of the CHP FCSs was performed.

Economic Performance

Cost analyses of micro-CHP FCS installations were performed to quantify their current and expected future profitability. Cost data gathered from the manufacturer include the FCS capital cost, additional equipment cost, installation, sales tax, and decommissioning costs, and the total cost of fuel over the lifetime of the project. All costs are recorded in present day dollars. The total project cost along with the DOE cost share for each site is shown in Table 1. The DOE cost share varied from 36 to 44 percent depending on the location. The differences in cost per unit/DOE cost share arise from the differences in additional equipment costs (vary depending on the infrastructure at a given site), variable sales tax, and fuel costs. On average, the cost of one unit is approximately $83,500. Figure 2 shows the average cost distribution among the micro-CHP FCSs in the deployed

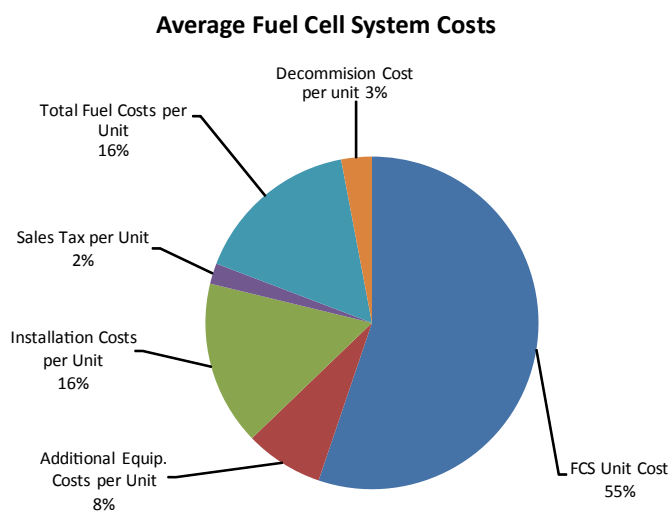

FIGURE 2. Cost Distribution for an Average Micro-CHP FCS in the Deployed Fleet

TABLE 1. Total Project Costs and Cost Share Information for Individual Sites

Partner/Site	Location	Number of FCSs	Total Project Cost [$]	DOE Cost Share		Payback (Years)	
				$	%	Without Incentives	With Incentives
College	Portland, OR	2	$188K	$82K	44%	8.66	N/A
Nursery	Corona Del Mar, CA	3	$228K	$83K	36%	4.95	3.75
Recreation	Oakland, CA	5	$409K	$150K	37%	5.32	4.06
Grocery	San Francisco, CA	5	$427K	$158K	37%	5.43	3.99
Total		**15**	**$1252K**	**$473K**	**38%**	**6.09**	**5.12**

fleet. Capital costs include an estimate for operation and maintenance costs for replacement of the stack and BOP components.

Two different payback analyses (one including incentives in the life cycle cost [LCC] analysis and the other excluding incentives from the LCC analysis) were performed to calculate the payback time (see Table 1). The payback period varied from 4.95 years to 8.66 years when incentives were excluded from the LCC analysis. The payback period varied from 3.75 years to 4.06 years when incentives were included from the LCC analysis. Note that "college" is not eligible for incentives because of the financial nature and location of this organization.

Figure 3 shows the average payback period based on current and projected (next five years) sales of micro-CHP FCS units. The projected costs are based on an estimated production of 4,000 systems/year and represent a 25% cost decrease. Assuming no incentives, the average payback periods for the current and projected costs are 6.09 and 4.71 years, respectively. The cost reduction with increased production is consistent with a previous study that predicted that the cost of 5-kW stationary proton exchange membrane fuel cells would decrease by 32% by increasing the production of systems from 100/year to 10,000/year [1].

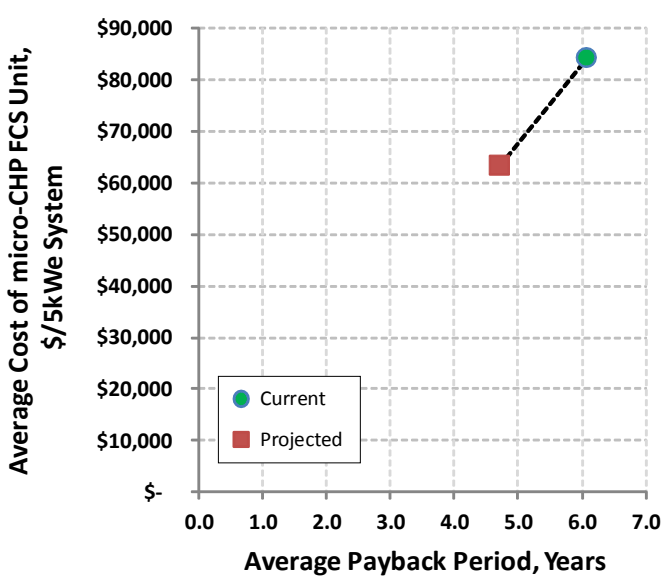

FIGURE 3. Average Payback Period versus Average Cost of the Micro-CHP FCS Unit

Engineering Performance

Engineering performance parameters identified and used in the economic analysis, were independently monitored and analyzed by PNNL. This analysis led to several recommendations which resulted in system improvements and system upgrades. The analysis is presented in Table 2 to document all the improvements and upgrades to date.

- Data analysis of as-installed FCS units: A total of 10 systems were installed between September and December 2011. Initial data indicated that the FCSs have a long-term average production of about 4.5 kWe of power. This was slightly below the manufacturer's stated rated electric power output of 5 kWe. Furthermore, the power output declined for all units over this time period. The rate of decline averaged over the fuel cells evaluated is near 3.2% per 1,000 hours. This decline was primarily the result of high-temperature polybenzimidazole fuel cell stack degradation.
- Data analysis after set-point changes: Based on PNNLs recommendation, the micro-CHP FCS set points were changed from 5 kWe to 4 kWe for the short term. Between March 2012 and June 2012, data analysis indicated that the FCSs have relatively stable performance and a long-term average production of about 4 kWe of power, consistent with the new set-point. However, there were some reliability issues, which are reflected in a decreased availability (88.9%). This availability reduction was attributed to the BOP system failures. Based on this analysis, the project team started to make BOP upgrades in late-June/early-July 2012.
- Data analysis after BOP upgrades: BOP upgrades for eight systems were done during June 2012 and July 2012. The project team is currently working on system upgrades for the rest of the systems/units. Data analysis of the systems with BOP upgrades indicated that the FCSs continue to have relatively stable power performance but now

TABLE 2. Micro-CHP FCS Performance Summary

	Unit	Stated Value	Initial Data	After Set-Point Changes	After BOP Upgrades
Period of Operation	--	--	**Oct. 2011 to Feb. 2012**	**Mar. 2012 to June 2012**	**July 2012 to July 2013**
Number of Operating Units Measured	--	--	10	15	8
Average Net Electric Power Output	kWe	5.0[c]	4.5±0.3	4.0 ± 0.2	4.0 ± 0.2
Average Net Heat Recovery[b]	kWth	5.5[c]	5.1 ± 0.4	4.6 ± 0.3	4.5 ± 0.2
Temperature to Site	°C	Up to 65	56.3 ± 3.8	49.6 ± 3.9	48.3 ± 5.1
Average Net System Electric Efficiency[a]	%	36	33.0 ± 2.1	33.5 ± 2.5	33.3 ± 2.4
Average Net Heat Recovery Efficiency[a]	%	40	37.4 ± 2.3	38.0 ± 2.8	37.8 ± 2.8
Overall Net System Efficiency[a]	%	76	70.4 ± 4.4	71.6 ± 5.4	71.1 ± 5.2
Availability, A_o	%	--	95.7 ± 2.8	88.9 ± 7.4	96.5 ± 1.3

(a) Efficiencies are based on higher heating value.
(b) The average heat recovery values are calculated by the manufacturer, and do not represent a measured value.
(c) The 5.0 kWe and 5.5 kWth set-points were changed to 4.0 kWe and 4.5 kWth during March/April of 2012.

also have increased system reliability as reflected in an increased availability (96.5%).

Environmental Performance

The environmental impacts of CHP FCSs are quantified by applying a life cycle assessment methodology [2-5]. In brief, this methodology quantifies the environmental impact of both GHG emissions and air pollution emissions.

- Greenhouse Gas (GHG) Emissions: The CHP FCS was compared to a conventional coal-fired power plant, an average gas-fired plant, and an advanced cogeneration plant. A CHP FCS can produce as little as one-third the emissions of a conventional energy system composed of a coal power plant and a coal-fired boiler, producing the same quantity of electricity and heat. A CHP FCS can emit just one-half the GHG emissions of an average gas-fired system. Table 3 shows the GHG mitigation cost comparison for all cases using the 2010 annual total electricity consumption in the United States [6]. Values of \$20/metric tonne of CO_2 equivalent emissions and \$100/metric tonne of CO_2 equivalent emissions, based on United Nations Intergovernmental Panel on Climate Change estimates [7-9], are considered here to provide both low and high estimates for GHG mitigation cost. These are proportional to the changes in the GHG gas emissions for the systems shown.
- Human Health Effects: The exhaust gas composition from a CHP FCS was analyzed to quantify the change in air pollution emissions. Based on the methodology presented by Colella [5], the human health costs associated with air pollution emissions from a CHP FCS were compared with the same conventional, average, and advanced systems described above assuming all the electricity in the U.S. is being generated from that single source. This comparison is also shown in Table 3. The human health costs decrease significantly when switching from a conventional coal-powered system to a CHP FCS. For example, the total human health costs stemming from air pollution from electricity production in the United States based on the use of a conventional coal-powered system is estimated to be approximately \$505 billion per year. By contrast, the same human health costs using CHP FCSs instead for electricity generation are estimated to be only \$0.57 billion per year. The costs between Case 1 and Case 4 differ by a factor of approximately 1,000.

Micro-CHP FCS Business Case

A business case was also developed for a micro-CHP FCS. In this business case, parameters that determine their competitive advantage were identified. Places with high electricity prices and low natural gas prices are ideal

TABLE 3. GHG Mitigation Cost and Human Health Cost Comparison of CHP FCS and Other Energy Generators

	CO_2 Equivalent (g/kWhr)	CO_2 Equivalent for Total Energy (Billion tonnes/kWhr)	GHG Mitigation Cost (in Billion \$)		Total Human Health Costs due to Air Pollution (in Billion \$/year)
			Low Estimate (\$20/ metric tonne)	High Estimate (\$100/ metric tonne)	
Case 1: Conventional System	1,696	6.49	\$132	\$659	\$505
Case 2: Average System	1,188	4.54	\$92	\$462	\$485
Case 3: Advanced System	602	2.52	\$47	\$234	\$146
Case 4: Micro-CHP FCS	528	2.05	\$41	\$205	\$0.57

locations for using these systems. These conditions make a high "spark spread" and are generally in the northeastern area of the United States and California where government incentives are already in place to offset the current high cost of these FCSs. Fuel cell systems differentiate themselves from other CHP generating technologies by being more efficient and having fewer environmental impacts. Although micro-turbines and reciprocating engines are less expensive, they are not as efficient as fuel cells, thus their fuel costs are higher. Forecasts suggest that the micro-CHP fuel cell market will grow at a compound annual growth rate of over 30% over the next five years.

CONCLUSIONS AND FUTURE DIRECTIONS

The real-time monitoring of FCSs installations over a 20-month period (September 2011 – June 2013) has provided a variety of insights about the system performance.

- Assuming no incentives, the average payback periods of micro-CHP FCSs for the current and projected costs are 6.1 and 4.7 years respectively.
- Analyzed 11,255 hours (average hours per system as of July 1, 2013) for 15 micro-CHP FCSs in terms of net electrical and thermal power and system efficiency and availability which led to several recommendations resulting in system improvements and system upgrades.
  - Recommended changes in the fuel cell operation that resulted in improved fuel cell stability.
- Prepared a draft micro-CHP FCS business case describing the anticipated growth of the FCS market, applications where CHP FCS would be beneficial and economic conditions that favor their use.

Future Directions

- Continue monitoring and analyzing engineering and economic performance data from all the demonstration systems. Heat and electricity usage is also monitored at two installations.
- Share the results at conferences and in other forums.
- Demonstrate the impact of updated BOP on the micro-CHP FCS availability.
- Incorporate comments from the industrial review and finalize business case for micro-CHP FCSs.

SPECIAL RECOGNITIONS & AWARDS/ PATENTS ISSUED

1. Received Best Poster Award at the Fuel Cell Seminar & Exposition, November 2012.

FY 2013 PUBLICATIONS/PRESENTATIONS

1. Kriston Brooks, et.al; "Business Case for a 5 kW Combined Heat and Power Fuel Cell System" - For Industry Review, June 2013.

2. Holladay, Jamie, "Independent Analysis of Real-Time Performance Data from Co-Generative Fuel Cell Systems Installed in Commercial Buildings," Invited speaker to the U.S. DOE CHP R&D Meeting, February 13, 2013.

3. Pilli, Siva, "Thermo-Economic & Real-Time Measured Performance Analysis of Micro Combined Heat & Power Fuel Cell Systems," Fuel Cell Seminar & Exposition, November 7, 2012.

REFERENCES

1. James BD. 2012. "Fuel Cell Transportation Cost Analysis, Preliminary Results." 2012 DOE Annual Merit Review Meeting, May 17, 2012, Washington, D.C. Retrieved from: http://www.hydrogen.energy.gov/pdfs/review12/fc018_james_2012_o.pdf.

2. O'Hayre R, SW Cha, W Colella, and FB Prinz. 2009. "Fuel Cell Fundamentals." Second Edition, ISBN 978-0-470-25843-9, John Wiley & Sons, Inc., Hoboken, New Jersey, pp. 451–482.

3. Jacobson MZ, WG Colella, and DM Golden. 2005. "Air pollution and health effects of switching to hydrogen fuel cell and hybrid vehicles." Science 308:1901.

4. Colella WG, MZ Jacobson, and DM Golden. 2005. "Switching to a U.S. Hydrogen Fuel Cell Vehicle Fleet: The Resultant Change in Energy Use, Emissions, and Global Warming Gases." Journal of Power Sources 150:150–181.

5. Colella WG. 2010. "Designing Energy Supply Chains Based on Hydrogen." Chapter 45 in Climate Change Science and Policy, 2nd edition, SH Schneider, A Rosencranz, and MD Mastrandrea (eds.), Island Press, Washington, D.C., pp. 456–466.

6. U.S. Energy Information Administration, Table 7.2. Retail Sales and Direct Use of Electricity to Ultimate Customers by Sector. Available at: http://www.eia.gov/electricity/annual/pdf/table7.2.pdf.

7. Working Group III Intergovernmental Panel on Climate Change (IPCC). 2007. Working Group III Contribution to the Intergovernmental Panel on Climate Change (IPCC) Fourth Assessment Report, Climate Change 2007: Mitigation of Climate Change, Summary for Policy Makers, Bangkok, Thailand, 20 April – 4 May, 2007, Table SPM1, Table SPM2, p. 12; Figure SPM 5B, p. 13. Available at: http://www.mnp.nl/ipcc/docs/FAR/ApprovedSPM0405rev4b.pdf.

8. Intergovernmental Panel on Climate Change (IPCC). 2001. "Climate Change 2001: The Scientific Basis." Cambridge University Press, Cambridge, United Kingdom.

9. Levine, M, D Ürge-Vorsatz, K Blok, L Geng, D Harvey, S Lang, G Levermore, A Mongameli Mehlwana, S Mirasgedis, A Novikova, J Rilling, and H Yoshino. 2007. "Residential and Commercial Buildings." In Climate Change 2007: Mitigation. Contribution of Working Group III to the Fourth Assessment Report of the Intergovernmental Panel on Climate Change, B Metz, OR Davidson, PR Bosch, R Dave, and LA Meyer (eds.), Cambridge University Press, Cambridge, United Kingdom and New York.

IX.3 Landfill Gas-to-Hydrogen

Russ Keller
SCRA Applied R&D dba Advanced Technology International
5300 International Blvd.
Charleston, SC 29418
Phone: (843) 760-4358
Email: russ.keller@scra.org

DOE Managers
Pete Devlin
Phone: (202) 586-4905
Email: Peter.Devlin@ee.doe.gov
Greg Kleen
Phone: (720) 356-1672
Email: Gregory.Kleen@go.doe.gov

Contract Number: DE-FG36-08GO18113

Subcontractors:
- Gas Technology Institute (GTI), Des Plains, IL
- Ameresco, Inc., Framingham, MA

Project Start Date: March 1, 2011
Project End Date: December 31, 2013 (no-cost extension from July 31, 2013 to December 31, 2013 is in progress)

Overall Objectives

- Validate that a financially viable business case exists for a full-scale deployment of commercially available equipment capable of converting landfill gas (LFG) to hydrogen under the specific BMW operating environment.
- Validate that commercially available clean-up and reformation equipment can convert BMW's LFG to hydrogen at purity levels consistent with fuel cell industry standards.
- Conduct a side-by-side operational verification of fuel cell material handling equipment (MHE) performance and durability between a test group operating on LFG-supplied hydrogen and a control group operating on delivered hydrogen supplied by an industrial gas provider.

Fiscal Year (FY) 2013 Objectives

- Deliver Mobile Hydrogen Unit and gas clean-up skid to site.
- Complete all necessary electrical and mechanical connections for all equipment.
- Conduct startup activities, commission and shake-down the equipment.
- Produce and validate H2 output meets required specifications.
- Initiate side-by-side trial.

Technical Barriers

This project addresses the following technical barriers from the Market Transformation and Technology Validation sections of the Fuel Cell Technologies Office Multi-Year Research, Development, and Demonstration Plan:

Market Transformation

(E) A lack of flexible, simple, and proven financing mechanisms
  - Lack of life cycle cost and performance data to demonstrate low investor risks

(I) Lack of cross-cutting information on how to use hydrogen and fuel cell systems in combination with energy efficiency and renewable energy technologies with existing projects

(K) Inadequate installation expertise

Technology Validation

(F) Centralized Hydrogen Production from Fossil Resources

(G) Hydrogen from Renewable Resources

Technical Targets

There are no specific technical targets associated with this particular project. Rather, the landfill gas-to-hydrogen project will focus on validating that integrated systems comprised of commercially available equipment can deliver cost-competitive hydrogen from an initial LFG source under real-world operating conditions.

FY 2013 Accomplishments

- Delivered all project equipment to the host site.
- Completed all necessary electrical and mechanical connections for all equipment.
- Conducted startup activities and initial equipment shakedown.
- Conducted troubleshooting activities to bring product gas constituents into specification.

✧ ✧ ✧ ✧ ✧

INTRODUCTION

BMW Manufacturing Company incorporated more than 100 pieces of fuel cell-powered MHE into a new assembly line that become operational 2010. While BMW currently is purchasing hydrogen services from an established industrial gas supplier, they strongly desire a future option where they could produce their own hydrogen, preferably from a renewable source—and ideally as a follow-on effort from their nationally acclaimed 2002 landfill methane project. BMW's original LFG project was implemented in December 2002, and the infrastructure currently allows for collecting and cleaning methane gas from the Palmetto Landfill near Spartanburg, SC, transporting it through a 9.5-mile pipeline to the BMW plant, removing siloxane contaminants on-site, compressing and then using it as fuel for gas turbine electrical generators.

Assessments by BMW of the available quantity of LFG beyond that currently devoted to electrical power generation confirm that, should the LFG-to-hydrogen production initiative prove viable, there would be sufficient LFG available to fuel the entire BMW MHE fleet in both their existing and new facilities. (Note: subsequent management decisions by BMW leadership after commencing this project have raised the on-site fuel cell MHE inventory to 270 units, representing a 100% site-wide conversion from battery power to fuel cell power.)

APPROACH

The over-arching objective of this effort is to validate there is a viable business case for BMW to move forward with a full-scale LFG-to-hydrogen conversion operation should the proposed LFG-to-hydrogen conversion technology prove financially and technically viable. The project would execute in three distinct phases: (1) conduct a feasibility study to examine the potential cost-competitiveness of hydrogen generated from LFG through a capital investment in commercially available equipment compared with hydrogen delivered at current market prices; (2) deploy and test a pilot-scale system (LFG clean-up and hydrogen production) to demonstrate the technical feasibility of converting BMW's unique LFG composition to hydrogen at purity levels consistent with fuel cell industry standards; and (3) provide "real-world" evidence via a "side-by-side" trial that fuel cell-powered MHE performance and durability are consistent between LFG-sourced hydrogen and hydrogen supplied by an industrial gas provider.

Successfully meeting the project objectives will give BWM leadership the confidence to move forward with scale up should they so choose. Additionally, this effort will lay the groundwork for proving the business case for future adopters. As of this writing, two different private sector organizations have approached the project team, expressing interest in potentially adapting the project's results to LFG-to-hydrogen business opportunities in their respective locations.

RESULTS

The project commenced officially on June 17, 2011, with the first phase of an anticipated three phase program of work. This initial phase was an economic feasibility study and business case analysis designed to assess whether a capital equipment investment in on-site LFG clean-up and methane conversion to hydrogen would enable production of hydrogen at or below the cost of having hydrogen delivered to the host site by an industrial gas company. This study completed on October 26, 2011, and was delivered to BMW management. BMW approved the study's conclusions on November 21, 2011, and authorized the project team to proceed to the second phase of the project. A copy of the feasibility study has been provided to DOE.

The "bottom line" conclusion from the feasibility study was that, at BMW's anticipated "full-scale" hydrogen production requirement, the existing LFG supply and front-end gas clean-up equipment at the BMW facility and on-site production of hydrogen using LFG as the hydrocarbon feedstock appears to be cost competitive, if not advantageous, versus hydrogen sourced from vendors, produced offsite and transported to the facility.

Implication for DOE Fuel Cell Technologies Office: Although the analysis presented within the feasibility study is specific to the LFG equipment and constituents at the BMW facility, the basic principles of hydrocarbon feedstock clean-up and reformation to hydrogen should apply to other LFG sources, as well as to agricultural waste streams, wastewater systems, digester gases, and other process off-gases.

(Note: Current incentive policies established by the Environmental Protection Agency regarding "qualified" renewable transportation fuels are under review. Should these reviews extend the existing renewable fuels incentives to hydrogen derived from LFG, the economic advantages that flow from the conclusions drawn above concerning cost competitiveness will become more pronounced at the higher daily production levels, and also might serve to lower the economic competitiveness threshold to smaller daily hydrogen production volumes.)

Throughout the current fiscal year the team has been experiencing difficulty with the performance of the gas clean-up system, initially during post-fabrication testing and currently during post-installation commissioning and acceptance testing. While this technology is well-proven in large-scale applications, the need to scale *down* to pilot size components and systems has proven challenging. Figure 1 depicts the hydrogen generation equipment and LFG clean-up equipment after their arrival at the BMW site.

Hydrogen Generation Equipment
November 12, 2012

Landfill Gas Clean-Up Equipment
November 26, 2012

FIGURE 1. Gas Cleanup Skid And Mobile Hydrogen Unit

Since landing the equipment at the BMW site the team has executed a series of field trials focused on equipment adjustments and adsorbent change-outs in an attempt to achieve the necessary product gas composition. To date, these actions have proven unsuccessful in lowering concentrations of oxygen and nitrogen to acceptable levels. Table 1 summarizes the constituent components of the LFG clean-up system effluent versus the required specifications obtained during troubleshooting trials.

TABLE 1. LFG Clean-Up Skid Product Gas Specifications and Composition

Component	CO_2	CH_4	O_2	N_2
Target Specs	<10%	>90%	<0.2%	<3.5%
Dec 2012	*	*	*	*
Jan 2013	25.0%	63.0%	2.5%	9.5%
Feb 2013	3.6%	77.8%	3.2%	15.4%
Mar 2013	0.7%	68.0%	4.6%	26.7%

In May 2013 the project team initiated a dedicated diagnostic and troubleshooting effort in concert with a third party vendor having specific expertise in removing nitrogen from pipeline methane streams.

CONCLUSIONS AND FUTURE DIRECTIONS

- Complete the troubleshooting protocol currently underway.
- Once the equipment performance meets required specifications, initiate a monitoring period of approximately six to eight weeks to validate the purity of the LFG-sourced hydrogen.
- Secure follow-on funding and execute a "side-by-side" trial comparing the performance of a control group of MHE fuel cells operating on delivered hydrogen with a test group running on LFG-sourced hydrogen.

FY 2013 PUBLICATIONS/PRESENTATIONS

1. DOE Annual Merit Review – 15 May 2013

IX.4 Hydrogen Energy Systems as a Grid Management Tool

Richard (Rick) E. Rocheleau (Primary Contact), Mitch Ewan
Hawaii Natural Energy Institute (HNEI)
School of Ocean and Earth Science and Technology
University of Hawaii at Manoa
1680 East-West Road, POST 109
Honolulu, HI 96822
Phone: (808) 956-8346
Email: rochelea@hawaii.edu

DOE Manager
Pete Devlin
Phone: (202) 586-4905
Email: Peter.Devlin@ee.doe.gov

Technical Advisor
Karen Swider-Lyons
Naval Research Laboratory
Phone: (202) 404-3314
Email: karen.lyons@nrl.navy.mil

Project Start Date: September 30, 2010
Project End Date: September 29, 2013

Overall Objectives

- Demonstrate the use of electrolyzers to mitigate the impacts of intermittent renewable energy by regulating grid frequency
- Characterize performance/durability of commercially available electrolyzers under dynamic load conditions
- Supply hydrogen to fuel cell shuttle buses operated by County of Hawaii Mass Transit Agency (MTA), and Hawaii Volcanoes National Park
- Conduct performance/cost analysis to identify benefits of integrated system including grid ancillary services and off-grid revenue streams
- Evaluate effect on reducing overall hydrogen costs offset by value-added revenue streams

Fiscal Year (FY) 2013 Objectives

- Contract the Hawaii Center for Advanced Transportation Technologies to convert the El Dorado bus to a fuel cell electric vehicle (FCEV) utilizing a Hydrogenics fuel cell power system
- Finalize Puna Geothermal Ventures (PGV) agreement
- Develop a project hydrogen safety plan
- Engage the DOE Hydrogen Safety Panel to support hydrogen safety including equipment installation, project hydrogen safety plans, outreach to the authorities having jurisdiction, and first responder training
- Respond to questions posed by the public on the draft Environmental Assessment (EA) for the installation of a hydrogen system at the PGV power plant on the Island of Hawaii prepared in FY 2012 and complete the final draft of the EA
- Install site improvements and utilities at the PGV geothermal plant to support the operation of the hydrogen system
- Hire a contractor to operate and maintain the hydrogen system
- Install, commission, and operate the hydrogen system at PGV
- Procure two Powertech 450-bar tube trailers to transport hydrogen from PGV to the County of Hawaii MTA bus yard in the town of Hilo, and Hawaii Volcanoes National Park
- Purchase a Ford F-450 diesel truck to tow the tube trailer
- Install a 350-bar hydrogen fuel dispenser at the MTA base yard in Hilo
- Purchase an El Dorado 2012 ENC AeroElite 290, 19-seat shuttle bus
- Supply hydrogen for a FCEV shuttle bus for local community bus service operated by the County of Hawaii MTA
- Characterize performance/durability of the Proton polymer electrolyte membrane electrolyzer under dynamic load conditions
- Conduct performance/cost analysis to identify benefits of integrated systems including grid services and off-grid revenue streams

Technical Barriers

This project addresses non-technical issues that prevent full commercialization of fuel cells and hydrogen infrastructure as indicated in the following sections of the July 2013 amendments to the Fuel Cell Technologies Office Multi-Year Research, Development and Demonstration Plan:

Section 3.1.5 - Hydrogen Production Technical Barriers

(J) Renewable Electricity Generation Integration (for central)

(K) Manufacturing

(M) Control & Safety

Section 3.2.5 - Hydrogen Delivery Technical Barriers

(E) Gaseous Hydrogen Storage and Tube Trailer Delivery Costs

(K) Safety, Codes, and Standards

Section 3.3.5 - Hydrogen Storage Technical Barriers

(B) System Cost

(C) Efficiency

(F) Codes & Standards

(H) Balance-of-Plant (BOP) Components

(I) Dispensing Technology

Section 3.7.5 - Hydrogen Safety, Codes, & Standards

(B) Availability and Affordability of Insurance

(D) Lack of Hydrogen Knowledge by Authorities Having Jurisdiction

Section 3.8.5 – Education and Outreach Technical Barriers

(D) Lack of Educated Trainers and Training Opportunities

Section 3.9.5 – Market Transformation Barriers

(A) Inadequate Standards and Complex & Expensive Permitting Procedures

(B) High Hydrogen Infrastructure Capital Costs for Polymer Electrolyte Membrane (PEM) Fuel Cell Applications

(C) Inadequate Private Sector Resources Available for Infrastructure Development

(G) Lack of Knowledge Regarding the Use of Hydrogen Inhibits Siting

(H) Utility and Other Stakeholders Lack Awareness of Potential Hydrogen Production and Storage Applications

(J) Insufficient Numbers of Trained and Experienced Servicing Personnel

(K) Inadequate Installation Expertise

(L) Lack of Qualified Technicians for Maintenance

(M Lack of Certified Service Providing Organizations for Installation and Maintenance

FY 2013 Accomplishments

- Completed site designs for installation of equipment at PGV and MTA sites
- Prepared a draft EA and made an initial "Finding of No Significant Impact"
- Published "Finding of No Significant Impact" on the internet and presented project to the local community
- Prepared draft responses to public comments
- Prepared a draft operations and maintenance contract to support daily operation of the hydrogen systems
- Developed a draft Memorandum of Agreement with MTA
- Engaged DOE Hydrogen Safety Team to support hydrogen safety
- Conducted First Responder Training to over 150 County of Hawaii firefighters utilizing the Pacific Northwest National Laboratory training program
- Completed a "Factory Acceptance Trial" of the Powertech hydrogen system equipment and control systems comprised of:
  - Autonomous data acquisition, monitoring and control system
  - Hydrogen production and compression module
  - Hydrogen transport trailer
  - Hydrogen dispensing system
- Continued to work with PGV to progress Memorandum of Agreement

✧ ✧ ✧ ✧ ✧

INTRODUCTION

While solar and wind resources offer a major opportunity for supplying energy for electrical grid electricity production and delivery systems, their variability and intermittency can raise challenges for the cost-effective and high-reliability integration of these renewable sources on electrical grids. In Hawaii, the curtailment and grid management-related challenges experienced by these renewable sources are a challenge at today's level of generation capacity, and these costs will hinder the substantive additional penetration of electricity generation supplied by these renewable resources. Hydrogen production through electrolysis may provide an opportunity to mitigate curtailment and grid management costs by serving as a controllable load allowing real-time control in response to changes in electricity production. The renewable hydrogen product can also create new and incremental revenue streams to the power producers through the sale of hydrogen products to customers outside of the electricity delivery system. Accordingly, hydrogen energy production at a utility scale offers the potential for increasing the levels of variable renewable energy that can be harnessed by the power producers or systems operators.

APPROACH

A four-step process is required to evolve island energy systems:

- Develop and validate rigorous analytic models for electricity and transportation.
- Develop and model scenarios for the deployment of new energy systems including additional renewables.
- Identify and analyze mitigating technologies (demand side management, storage, smart grid, advanced controls, forecasting, future gen) to address systems integration (grid stability) and institutional issues.
- Conduct testing and evaluation to validate potential solutions to facilitate utility acceptance.

Under separate and ongoing DOE and industry-funded efforts, HNEI has been conducting energy roadmapping and technology validation to identify economically viable technologies to transform island energy infrastructures. A full network model incorporating generator governors and automatic generator control was developed that provided the following capabilities:

- Transient stability simulation looks at challenging times with fluctuating renewables to check transient stabilities.
- Long-term dynamic simulation.

A production cost model was developed that provided the following capabilities:

- Representation of dispatch and unit commitment rules
- Hour-by-hour simulation of grid operations for a full year taking into account ramp rates and dispatch rules—for example minimum percentage load for baseload units.
- Yields cumulative fuel usage, emissions, and variable costs.

Frequency variability due to wind fluctuation of the Big Island grid was used as the initial test of the models. The Big Island grid has the following characteristics:

- 100 to 200 MW with early evening peak
- 30 MW wind
- 38 MW regulated geothermal
- Significant and growing photovoltaics

To explore the potential of the hydrogen production opportunity, this project will evaluate the value proposition of using utility-scale electrolyzers to both regulate the grid and use excess electricity from renewables to make hydrogen for various products. In this initial phase of the project, an electrolyzer will be installed at the PGV geothermal plant on the Big Island. In this first phase, it will not be connected to the grid. The electrolyzer will be operated in a dynamic mode designed to simulate future operation as a grid-connected variable load that can be quickly ramped up and down to provide frequency regulation. Data will be collected to analyze the ability of the electrolyzer to ramp up and down, and to determine its durability and performance under dynamic operating conditions. The hydrogen produced by the system will be used to fuel one bus operated by the County of Hawaii MTA. Schematics of the project concept are shown in Figures 1 and 2.

RESULTS

- Developed a model that shows the dynamic operation of the electrolyzer for managing grid frequency compared to a one-megawatt battery energy storage system that is installed on the Hawaii Electric Light Company grid (Figure 3).
- Completed site designs for the PGV and MTA dispensing sites.

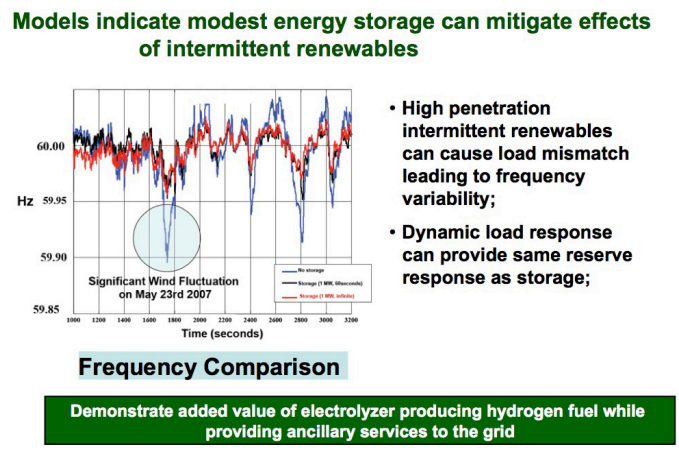

FIGURE 1. Effect of Dynamic Load Response on Grid Frequency

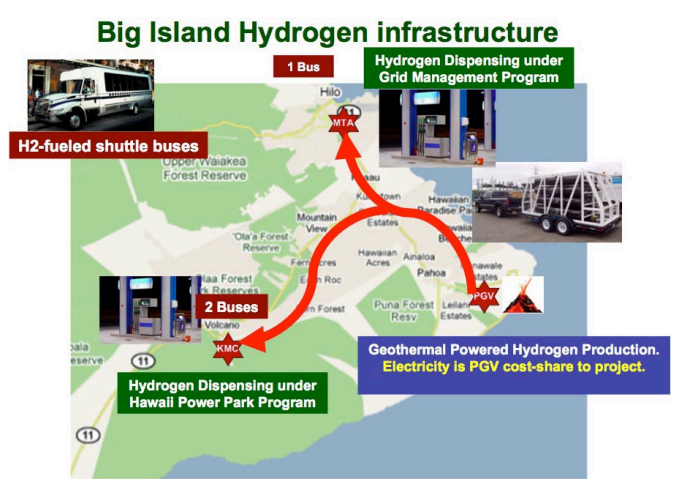

FIGURE 2. Hydrogen Production and Delivery System

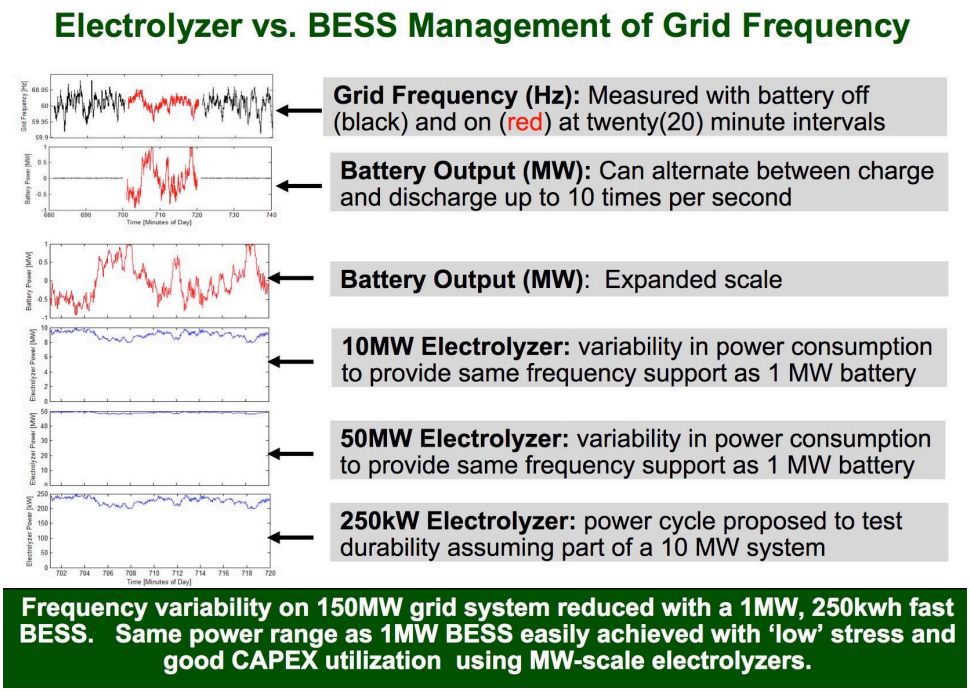

FIGURE 3. Comparison of a Battery Energy Storage System (BESS) with a Dynamically Operated Electrolyzer on Managing Grid Frequency

- Progressed legal agreements among project participants (PGV, MTA) including resolution of liability, indemnification, and insurance issues and requirements.
- Completed the construction of the hydrogen systems equipment and autonomous monitoring and control system and conducted a factory acceptance trial (Figure 4).
- Completed site designs for the PGV and MTA sites.
- Developed a scope of supply for the site improvements contractor.
- Completed a draft State of Hawaii Environmental Assessment, published a draft Finding of No Significant Impact, conducted a briefing to the local community where the project will be situated, and developed responses to community questions/comments.
- Completed First Responder training for over 300 first responders on the Island of Hawaii and Oahu utilizing the Pacific Northwest National Laboratory training program team and live fire "burn prop" that were deployed to Hawaii.

CONCLUSIONS AND FUTURE DIRECTIONS

- The project is underway but equipment and infrastructure need to be installed and operated before any results can be evaluated.

FIGURE 4. Hydrogen System Equipment

- Future work involves the procurement, installation, and operation of the following:
  - Installing hydrogen production systems and infrastructure at the PGV geothermal site
  - Installing hydrogen dispensing systems and infrastructure at the MTA bus depot site in Hilo
  - Procuring and operating a 19-passenger fuel cell electric bus
  - Operating the electrolyzer and hydrogen systems at the PGV and MTA sites

- Collecting and analyzing hydrogen system and fuel cell electric bus performance data
- Preparing performance reports and sharing it with project sponsors and industry

A major project challenge to the timely deployment of hydrogen infrastructure and equipment necessary to conduct operations has been the amount of time required to develop legal agreements to address liability issues. This is approaching two years in this project. This in turn has required our requesting no-cost extensions to extend the project to meet operational test duration requirements. This represents a large investment in outreach and education of all parties concerned including the legal profession, risk managers, first responders, and authorities having jurisdiction.

FY 2013 PUBLICATIONS/PRESENTATIONS

1. R. Rocheleau and M. Ewan, "*Hawaii Energy Systems as a Grid Management Tool*", *US DOE Annual Merit Review*, Washington, D.C., May 2012.

2. R. Rocheleau and M. Ewan, "*Hawaii Energy Systems as a Grid Management Tool*", *World Hydrogen Energy Conference*, Toronto, Canada. June 2012.

IX.5 Ground Support Equipment Demonstration

James Petrecky
Plug Power
968 Albany-Shaker Road
Latham, NY 12110
Phone: (518) 817-9124
Email: James_Petrecky@plugpower.com

DOE Managers
Pete Devlin
Phone: (202) 586-4905
Email: Peter.Devlin@ee.doe.gov
Jim Alkire
Phone: (720) 356-1426
Email: James.Alkire@go.doe.gov

Contract Number: DE-EE0006093

Subcontractor:
Nuvera Fuel Cells, Billerica, MA

Project Start Date: January 2013
Project End Date: December 2015

Overall Objectives

- To create a hydrogen fuel cell-based solution as a cost-competitive and more energy-efficient baggage tow tractors (airport vehicle) compared to the incumbent internal combustion engine-powered vehicles.
- To enable airport end users to accomplish their daily tasks with a hydrogen fuel cell solution while reducing consumption of gasoline and diesel fuels, reducing U.S. demand for petroleum.
- To demonstrate lower carbon emissions with the fuel cell solution.
- To demonstrate a value proposition that shows decreased energy expenditures when compared to diesel-powered airport vehicles.

See Table 1.

Fiscal Year (FY) 2013 Objectives

- Plug Power develops the 80-V fuel cell product for baggage tow tractor
- Testing with Charlatte CT5E baggage tow tractor
- Factory acceptance test to demo equivalent operation as battery/internal combustion engine
- Nuvera conducts site planning to install hydrogen at two locations

Technical Barriers

- Upsizing GenDrive architecture from current 48-V product to 80 V
- Outdoor application – need for weatherproofing

Technical Targets

See Table 1.

FY 2013 Accomplishments

- Fuel cell testing
- Systems engineering - collection of requirements
- Data logging of CT5E in FedEx Express application (Ontario, CA)
- Sharing of information with baggage tow tractor manufacturer
- System modeling
- Coordination with FedEx Express sites for hydrogen prep/permits
- Kickoff meeting with DOE and Partners in Latham on March 27, 2013
- Receipt of Charlatte CT5E at Plug Power for weatherproofing and interconnect design
- Hydrogen supply agreement

TABLE 1. Specific Project Objectives and Expectations

DOE Project Objectives	Plug Power-FedEx Project Expectations
Reduce petroleum consumption	Each BTT uses ~2 gal/hr. Total BTT run time of 15 BTT's over 2 years will be upwards of **175,200 gallons of diesel fuel reduced.**
Reduce emissions at airports	AT 9.8 kg CO2 per gal of diesel, there will be upwards of **1717 metric tonnes of CO2 eliminated at airports.**
Operate 10 hrs/day & 5,000+ hours	BTT operation occurs during two shifts: day (11 AM-3 PM) and night (10 PM-2 AM). The total clock day is 11AM-2PM (15 hours). **Actual BTT activity is 8 hours per day. Total run time of 15 BTT's over 2 years will be upwards of 87,600 fleet hours.**
Towing capability of 3,000 to 6,000 lbs.	The BTT will be able to tow 4 FedEx containers each weighing 40,000 lbs. The corresponding **drawbar capacity of the fuel cell-powered BTT is 5,000 lbs.**
Accelerated development of FC-powered GSE	**Fleet of 15 80V fuel cell systems in real world application in 2013 gaining significant field experience while allowing a premier BTT end user to evaluate for larger deployments.**

FC - fuel cell; GSE - ground support equipment; BTT - baggage tow tractor

- Site planning at Memphis

✧ ✧ ✧ ✧ ✧

INTRODUCTION

This project will deploy 15 fuel cell-powered units for two years at FedEx's busiest airport. The project is planned for two phases. The first is a one-year development phase where Plug Power develops, builds and tests the 80-V (~20 kW) fuel cell system for the baggage tow tractor application. The second is a two-year demonstration where a fleet of baggage tow tractors are integrated into Charlatte CT5E electric tow tractors and deployed at the FedEx locations under real-world conditions. The two fuel cell fleets will be fueled by a Nuvera PowerTap steam methane reformer and compression, storage, and dispensing solution at each site.

APPROACH

Plug Power will design an 80-V battery as a drop in place replacement of an electric Charlatte tug (see Figure 1).

Hydrogen will be supplied to the tugs via Nuvera PowerTap hydrogen generators, which will provide onsite hydrogen at 350 bar to be dispensed directly to the fuel cell in the tug (see Figure 2).

- Definition of requirements – already in process
- Alpha prototype – second quarter testing/third quarter design improvements
- Baggage tow tractor beta builds – fourth quarter demo builds
- Baggage tow tractor testing and certification – by end of year
- Site preparation
- Commissioning
- Demonstration
- Assessment after Year 1
- Demonstration
- Assessment after Year 2

RESULTS

The kickoff of the project occurred on March 27, 2013. Results will be communicated in quarterly reports later this year.

CONCLUSIONS AND FUTURE DIRECTIONS

The demonstration of 15 baggage tow tractor units at Memphis will begin early in 2014.

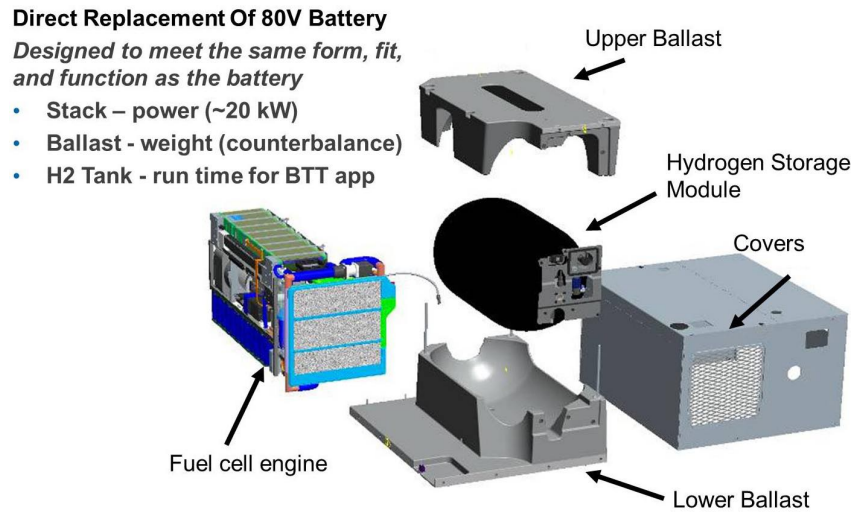

FIGURE 1. Direct Replacement of 80-V Battery

FIGURE 2. Hydrogen Solution

IX.6 Fuel Cells as Range Extenders for Battery Electric Vehicles

Aymeric Rousseau (Primary Contact), Phil Sharer
Argonne National Laboratory
9700 South Cass Avenue
Argonne, IL 60439-4815
Phone: (630) 252-7261
Email: arousseau@anl.gov

DOE Manager
Pete Devlin
Phone: (202) 586-4905
Email: Peter.Devlin@ee.doe.gov

Project Start Date: June 1, 2011
Project End Date: February 1, 2013

Overall Objectives

- Demonstrate the cost–benefit tradeoffs of adding a fuel cell auxiliary power unit (APU) to double the range of existing battery electric vehicles (BEVs)
- Quantify the cost benefit of using a fuel cell APU for different vehicle classes based on levelized cost of driving

Fiscal Year (FY) 2013 Objectives

- Optimize the component sizing and vehicle level energy management of each individual vehicle considered
- Quantify the cost benefit of using a fuel cell APU for one compact car and one medium-duty vehicle
- Write a report summarizing the benefits of using a fuel cell APU to double the range of current BEVs

Technical Barriers

This project addresses the following technical barriers from the Market Transformation section of the Fuel Cell Technologies Office Multi-Year Research, Development, and Demonstration Plan:

(F) Inadequate user experience for many hydrogen and fuel cell applications

FY 2013 Accomplishments

- Developed vehicle-level energy management to properly evaluate the benefits of using fuel cell system power and onboard hydrogen storage.
- Quantified the trade-off between energy consumption and cost on the Urban Dynamometer Driving Schedule.
- Demonstrated the benefits of using fuel cell systems to double the range of current BEVs for medium-duty applications.

✧ ✧ ✧ ✧ ✧

INTRODUCTION

The goal of this project is to analyze the cost–benefit tradeoffs of adding a fuel cell APU to a BEV to double its range. Doubling battery size is an option, but it comes with a considerable increase in vehicle cost. A novel approach that addresses this cost increase is to supplement the stored electrical energy of the BEV with a hydrogen fuel cell APU. The addition of a low-power APU, providing tractive power to double the range of the BEV, could be a cost-effective alternative for doubling the battery energy. This paper explores such an architecture for a Class 4 medium-duty pickup and delivery (P&D) truck using two different vehicle-level control strategies and using the levelized cost of driving (LCOD) as the basis for a cost comparison.

APPROACH

The APU power and APU fuel mass were allowed to change independently of each other. Figure 1 is a flow chart illustrating this approach.

A BEV was the starting point. This vehicle was created using future 2015 DOE assumptions for each powertrain component. The BEV was then sized to have a range twice that of the baseline BEV. This new BEV is referred to in this paper as a 2X BEV. A fuel cell APU with storage was added to this vehicle, thereby allowing the battery to then be downsized in power and in energy. Since the fuel mass was decoupled from the power, a two-dimensional parametric sweep of

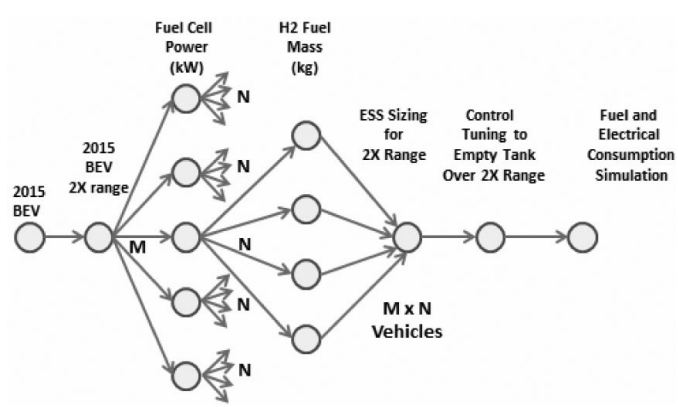

FIGURE 1. Number of Vehicles Considered – Control Strategy Based on Fuel Cell Rated Power

power versus fuel mass could be performed on the APU. The assumptions of the Class 4 P&D are similar to the Navistar EStar [1]. The cost assumptions for the fuel cell system and the hydrogen storage were provided by Strategic Analysis.

RESULTS

Two separate vehicle level control strategies were developed as part of the study. The following paragraph focuses on the control where the fuel cell system is used at its rated power. That approach has the advantage of minimizing fuel cell system cost and consequently maximize the benefits of using a fuel cell APU.

Figure 2 shows the electrical and fuel consumption of the vehicles. In Figure 2a, one notices that as the amount of onboard hydrogen to consume increased, the electrical consumption decreased proportionally until the onboard fuel mass reached 6 kg, at which point the electrical energy consumption was close to zero. Any additional fuel beyond 6 kg forced the range out of bounds, since the fuel energy exceeded the energy that the vehicle needed to complete the 2X range. Thus, at the 6 kg point, the vehicle transitioned from net charge-depleting to net charge-sustaining operation. Beyond 6 kg, the trip was not long enough to consume the entire mass of fuel, so the range constraint was exceeded to meet the constraint that the APU fuel tank had to be empty at the end of the trip. Figure 2b shows that, as expected, increasing the fuel mass increased the fuel consumption, because an increasingly larger mass of fuel had to be consumed over the trip distance in order to end the trip with an empty tank. Basically, fuel energy from the APU displaced electrical energy from the battery.

The top dashed line in Figure 3a shows the battery cost for a BEV, without the APU, using the baseline assumption

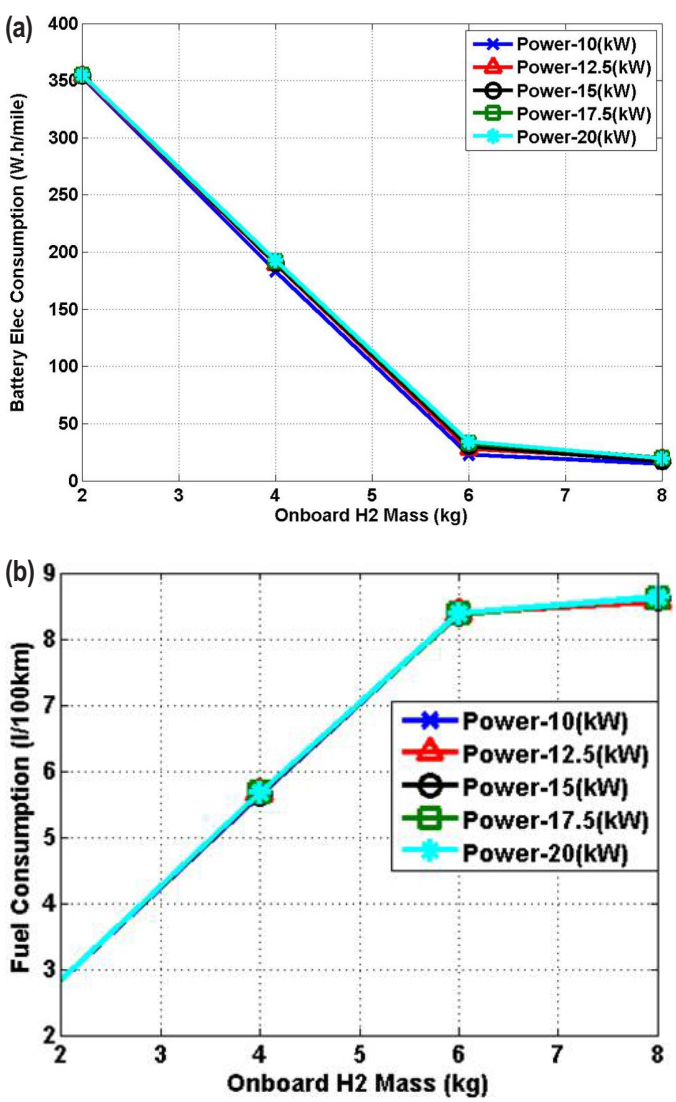

FIGURE 2. Battery Electrical Consumption (a) and Fuel Cell Fuel Consumption (b)

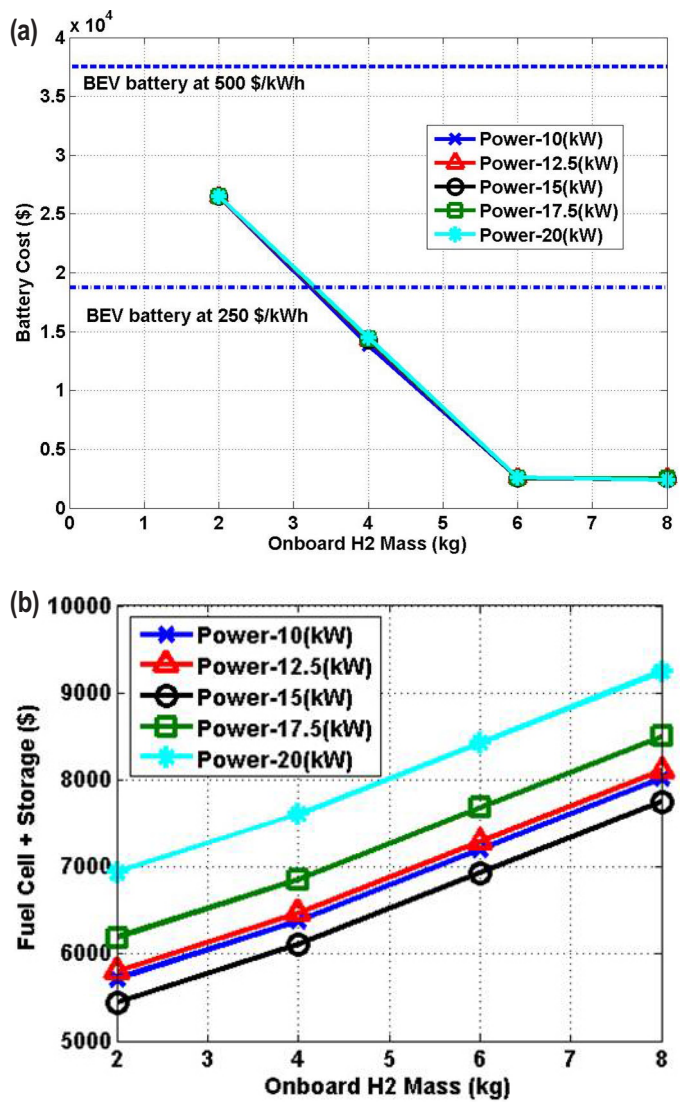

FIGURE 3. Battery Cost (a) and Fuel Cell System with Hydrogen Storage Cost (b)

of $500/kWh. For comparison, the bottom dashed line shows the battery cost for a 2X BEV if an assumption of $250/kWh is used for the battery's specific cost. Halving the specific cost for a BEV halves the battery cost. The fuel cell APU cost equation had two terms: one dependent on APU power, and the second dependent on hydrogen storage fuel mass. The APU cost linearly increased by $2,500 when the hydrogen mass increased from 2 to 8 kg. The cost overall increased by $1,500 when the power increased from 10 to 20 kW, but the relationship was nonlinear, and a local minimum was reached at 15 kW, as shown in Figure 3b.

The total manufacturing cost savings over the BEV for the Class 4 P&D truck is close to $30,000 for a 15-kW APU with 6 kg of onboard storage. Figure 4 shows this result. Four other interesting vehicle cost cases are also shown in Figure 4 for comparison to the APU option. Case A is the manufacturing cost for a 2X BEV assuming the base specific battery is $500/kWh. Case B is the manufacturing cost of a 2X BEV, assuming the specific battery cost is $250/kWh instead of $500/kWh. Case C is the manufacturing cost of a fuel cell hybrid electric vehicle (HEV) using the same production numbers as the APU of 10,000 units/year. Case D is the manufacturing cost of a fuel cell HEV using a production number of 500,000 units/year. This figure indicates that adding a fuel cell APU is always a viable option when the battery cost is $500/kWh. Even if the battery cost matches the DOE cost targets, the APU still adds some benefit to reducing the cost of the BEV when supplying 6 kg of onboard storage. However, if the production numbers were to increase significantly by a factor of 50, the fuel cell HEV would become the most cost-effective option.

The LCOD is shown in Figure 5; it decreased by 38% compared to that of a 2X BEV, when using 6 kg of hydrogen. This figure uses the following assumptions: 5-year vehicle

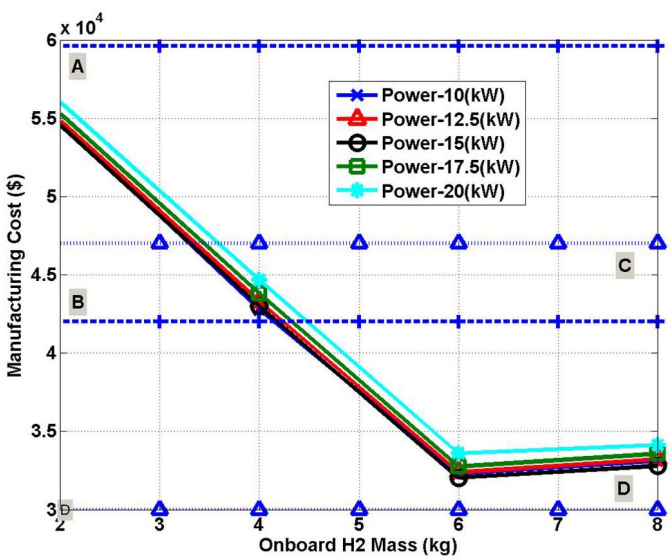

FIGURE 4. Manufacturing Cost for APU Vehicles

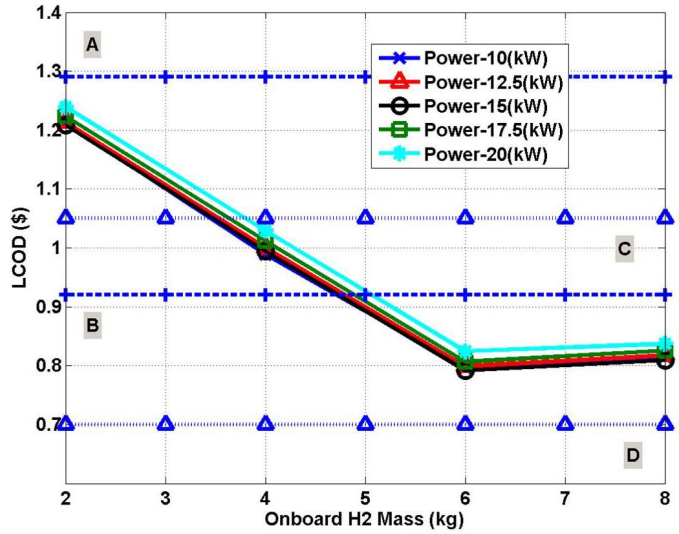

FIGURE 5. LCOD for APU Vehicles

life with 15,000 miles traveled per year. For comparison, line A shows the 2X BEV LCOD. Line B shows the 2X BEV assuming $250/kWh. Line C shows the fuel cell HEV case assuming 10,000 units/year. Line D shows the fuel cell HEV case assuming 500,000 units/year.

CONCLUSIONS AND FUTURE DIRECTIONS

On the basis of the cost assumptions and drive cycles considered in this project, the following statements can be made regarding this specific combination of assumptions for a Class 4 P&D truck:

- Using a fuel cell system and storage is cheaper than using a battery to store energy.
- However, a Li-ion battery is cheaper than a fuel cell system for delivering power.
- Using a fuel cell that is close to its rated power (i.e., maximum power control) provides the lowest LCOD.
- For the Heavy-duty Hybrid Utility Trucks drive cycle considered and when the default LCOD assumptions in this paper are used, a 10-kW fuel cell system with 6 kg of onboard hydrogen would provide an optimum solution.
- Increasing vehicle lifetime, annual miles traveled, and fuel cost did not significantly change the relative benefit comparison between the maximum power strategy and the maximum efficiency strategy.
- The optimum onboard mass dropped to 2 kg for both the maximum power strategy and the maximum efficiency strategy when the fuel cost was $8/gasoline gallon equivalent (in 2010 $).
- The results are affected by the cost of hydrogen, vehicle lifetime, driving distance, and cost of the battery.

However, the fuel cell APU option consistently reached a lower LCOD when compared with a BEV with twice the original electric range when the cost of the fuel cell was considered at a production level of 10,000 units.

- When the production level was increased to greater numbers (e.g., 500,000), the fuel cell as a system was cheaper overall than the battery. At 500,000 units, it appears that it would be more cost effective to produce the fuel cell vehicle than a BEV and APU combination that has a 2X range

FY 2013 PUBLICATIONS/PRESENTATIONS

1. P. Sharer, A. Rousseau, "Benefits of Fuel Cell Range Extender for Medium-Duty Vehicle Applications", EVS27, Barcelona, Nov 17–20 2013.

REFERENCES

1. Navistar, *eSTAR*™, http://www.estar-ev.com accessed April 2012.

IX.7 Hawaii Hydrogen Initiative (H2I) Financial Scenario Analysis

Michael Penev (Primary Contact), Marc Melaina, Aaron Brooker
National Renewable Energy Laboratory (NREL)
15013 Denver West Parkway
Golden, CO 80401
Phone: (303) 275-3880
Email: mike.penev@nrel.gov

DOE Manager
Pete Devlin
Phone: (202) 586-4905
Email: Peter.Devlin@ee.doe.gov

Project Start Date: October 1, 2011
Project End Date: December 31, 2012

Overall Objectives

- Support Hawaii Hydrogen Initiative (H2I) [1] team with technology guidance for hydrogen fueling infrastructure
- Evaluate fuel cell vehicle deployment potential in Oahu
- Evaluate hydrogen resource supply options and delivery pathways
- Produce scenario analysis of fueling infrastructure deployment
- Produce financial analysis and incentive requirements for infrastructure deployment

Fiscal Year (FY) 2013 Objectives

- Produce financial projection scenarios:
  - Consider vehicle adoption rates
  - Determine infrastructure support requirements
  - Evaluate full range of expenses
  - Apply competitive revenue ceiling
  - Perform accounting cycle analysis
  - Perform multi-year financing projections
- Provide H2I team with scenario analysis:
  - Communicate risk and sensitivities
  - Facilitate strategic planning
  - Evaluate incentive requirements

Technical Barriers

This project addressed the following technical barriers from the Market Transformation and Systems Analysis sections of the Fuel Cell Technologies Office Multi-Year Research, Development, and Demonstration Plan:

Market Transformation:

(C) Inadequate private sector resources available for infrastructure development

(D) Market uncertainty around the need for hydrogen infrastructure versus timeframe and volume of commercial fuel cell applications

(E) A lack of flexible, simple, and proven financing mechanisms

(N) Policies and incentives (e.g., Investment Tax Credit) are not available to government or other non-profit entities - impeding early market adoption in the public sector

Systems Analysis:

(A) Future Market Behavior

(B) Stove-piped/Siloed Analytical Capability

(D) Insufficient Suite of Models and Tools

(E) Unplanned Studies and Analysis

Contribution to Achievement of DOE Market Transformation and Systems Analysis Milestones

This project will contribute to achievement of the following DOE milestones from the Market Transformation and Systems Analysis sections of the Fuel Cell Technologies Office Multi-Year Research, Development, and Demonstration Plan:

Market Transformation:

- Milestone 2.5: Develop third party financing model for Federal users to aggregate and multiply power needs. (2Q, 2012)

Systems Analysis:

- Milestone 1.4: Complete evaluation of fueling station costs for early vehicle penetration to determine the cost of fueling pathways for low and moderate fueling demand rates. (4Q, 2012)

FY 2013 Accomplishments

- Developed an Excel-based infrastructure deployment model that was integrated with Automotive Deployment Options Projection Tool (ADOPT), a vehicle sales model based on economic conditions and calibrated to past market vehicle purchasing behavior
- Produced multiple infrastructure deployment scenarios for internal H2I team support

- Produced two scenarios for external reporting (covered under this report):
  - Baseline scenario (low vehicle sales)
  - Optimistic scenario (high vehicle sales)
- Deployment scenarios were evaluated with new modeling algorithms accounting for annual dispensing infrastructure capital deployment, feedstock usage, financing requirements, and incentives

✧ ✧ ✧ ✧ ✧

INTRODUCTION

Early market hydrogen infrastructure deployment requires synchronization of the proverbial chicken and egg. When fuel cell electric vehicles (FCEVs) are not available, fueling infrastructure providers have no business case to provide hydrogen. In our analysis, we model an annual approach to infrastructure deployment in which infrastructure leads vehicle sales.

APPROACH

Analysis for hydrogen infrastructure roll-out assumes that vehicle sales will not occur if fueling infrastructure is not available to the Oahu population. The overall strategy of roll-out thus preempts vehicle sales with infrastructure deployment. Vehicle sales were projected via the ADOPT model, which was calibrated to past vehicle purchasing behavior on Oahu. Such behavior is driven by vehicle characteristics such as size, cost, and fuel efficiency. Additional considerations were included in the model for infrastructure availability and vehicle range. A vehicle stock model was used to track the number of vehicles on the road. Fuel efficiency projections along with vehicle-miles-traveled profiles were used to derive annual aggregate hydrogen demand. The demand was allocated to individual fueling stations through 2050, and each station's financial performance was projected for the same period based on the cost of delivered hydrogen to the station over time and a maximum price the market can bear for hydrogen (based on competitive pricing with gasoline). Initial revenue shortfalls were used as an indicator for required incentives.

RESULTS

Modeling infrastructure roll-out incorporates a minimal station coverage required to initiate vehicle sales. In the presented scenarios, 15 stations were deployed preemptively to demand growth. Demand for hydrogen was distributed among stations in a statistical manner, which then drove station upgrades and new station builds throughout the length of the analysis (see Figure 1).

Each station's performance was tracked on an annual basis. Generally accepted accounting principles framework analysis was used to evaluate each station's financial performance each year. Three projections using generally accepted accounting principles were used for financial analysis:

- Projected income statement: accounts for revenues and expenses to arrive at annual net income
- Projected statement of cash flows: accounts for annual cash flows, including financing activities such as acquisition of additional debt or equity investment
- Projected balance sheet: accounts for business structure according to the following equation:

$$\text{Assets} = \text{Liabilities} + \text{Owners Equity}$$

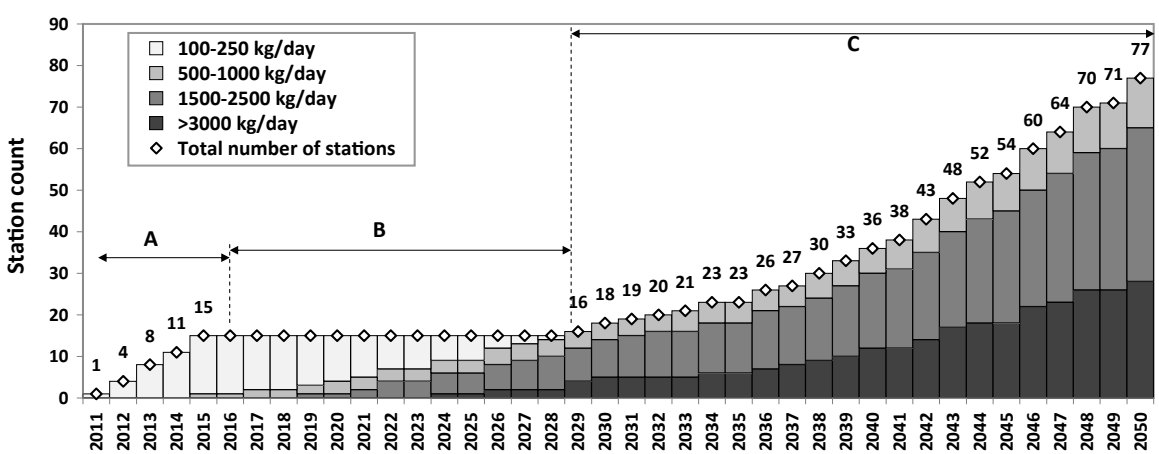

FIGURE 1. Station stock size distribution for the optimistic hydrogen roll-out scenario: (A) coverage stations build-out, (B) coverage stations saturation, (C) upgrading and infrastructure expansion.

The balance sheet arrives at capital structure and maintains financing sourcing to comply with covenant debt-to-equity limit (see Figure 2)

Financial analysis finds that revenue shortfalls will be experienced for an extended period after the initial infrastructure deployment. Such shortfall is expected to impede investment into hydrogen infrastructure. In order to encourage private sector participation in infrastructure roll-out, an after-tax internal rate of return of 10% was solved for by our financial solver by introducing a "production incentive" (see Figure 3). Such an incentive acts as a revenue supplement for station owners and makes return on investment into hydrogen similar to other owner investments.

The financial performance in the scenarios was benchmarked by the relative amount of required incentives. Scenarios requiring more incentives were not as attractive. Figure 4 shows the incentive requirements for the optimistic scenario presented in this report.

CONCLUSIONS AND FUTURE DIRECTIONS

NREL analysts have worked closely with the H2I analysis team to produce a streamlined model for analyzing hydrogen infrastructure deployment and financial scenarios. The modeling effort has outlined timelines for infrastructure deployment requirements, as well as financial incentive projections to support such activities. Our analysis projects potential sales of FCEVs in Oahu and a schedule of station deployments necessary to support the fleet. Detailed financial analysis was performed on a station-by-station basis and was aggregated for an island-wide infrastructure outlook. Infrastructure incentives for this scenario totaled $18.5 million through 2050. NREL's findings quantify

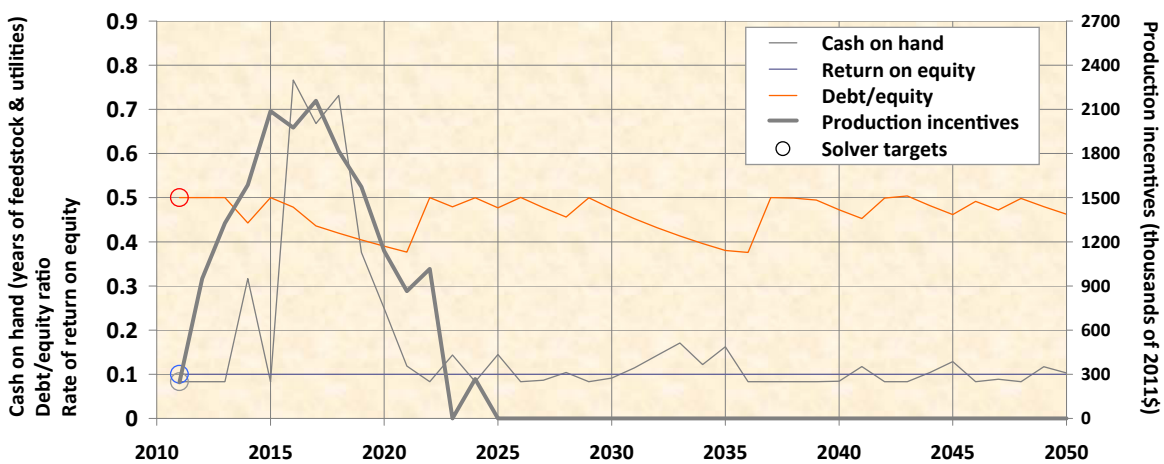

FIGURE 2. Financial performance evaluation performed annually to drive financing activities and to conform to capital structure requirements.

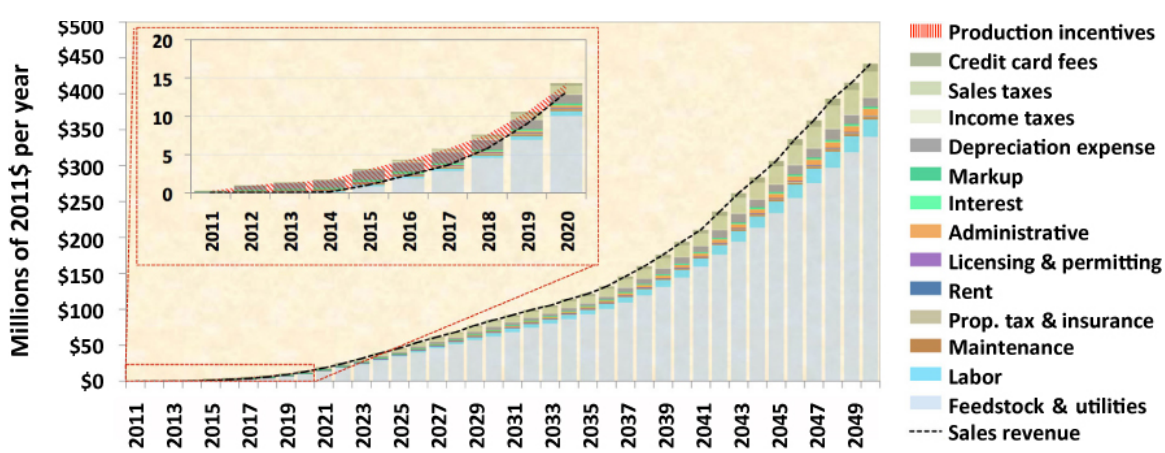

FIGURE 3. Hydrogen fueling station network revenues and expenses through 2050. Early revenue shortfalls constitute the need for incentives (labeled as "production incentives"). Production incentives close the gap between total revenues and total expenses.

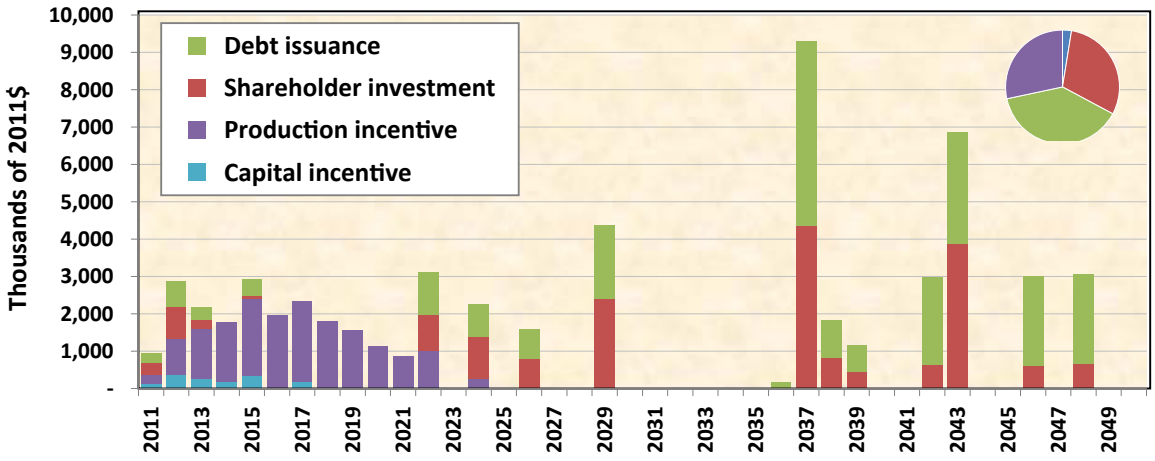

FIGURE 4. Annual incentives and new financing need projections. Pie-chart shows relative amounts of total investment by type.

funding opportunity projections by four sources: equity investment, debt investment, capital incentives, and production incentives. Work on this project concluded in the first quarter of FY 2013. Analytical results were used in decision making by the H2I team, and positive feedback on the usefulness of the methodology has spawned additional activities. The NREL team used this modeling framework to evaluate financial performance of the California Fuel Cell Partnership roadmap [2]. In addition, the model was used to evaluate the potential for hydrogen infrastructure in the northeastern United States, and screening results were presented at a working meeting of stakeholders [3].

Feedback from H2I members has been very positive about the modeling framework. The model algorithms will be further enriched and will be embedded in NREL's Scenario Evaluation, Regionalization and Analysis model [4]. This will allow complete supply chain analysis for hydrogen production using a geospatially and temporally resolved framework. Work with this model will be used on regional and national scales to inform DOE and other stakeholders.

FY 2013 PUBLICATIONS/PRESENTATIONS

1. Penev, M., Melaina, M., Brooker, A., "Hawaii Hydrogen Initiative Financial Scenario Analysis," Fuel Cell Seminar, November 6, 2012.

REFERENCES

1. "H2I, Hawaii Hydrogen Initiative." Accessed [7/10/13]: http://www.hydrogen2hawaii.com/.

2. "A California Road Map." (2012). California Fuel Cell Partnership. Accessed [7/10/13]: http://cafcp.org/carsandbuses/caroadmap.

3. "Ticket to Ride: A Regional Roadmap for Hydrogen Infrastructure and Fuel Cell Vehicles." (2012). Working meeting, open to the public. September 11, 2012, Albany, NY.

4. Brian Bush et. al. "Optimal Regional Layout of Least-Cost Hydrogen Infrastructure," Proceedings of the 2010 NHA Hydrogen Conference & Expo, 2010, volume 28.

X. AMERICAN RECOVERY AND REINVESTMENT ACT ACTIVITIES

X.0 American Recovery and Reinvestment Act Activities

INTRODUCTION

In April 2009, the U.S. Department of Energy (DOE) announced the investment of $41.6 million in American Recovery and Reinvestment Act (Recovery Act) funding for fuel cell technologies. These investments were made to accelerate the commercialization and deployment of fuel cells and to spur the growth of a robust fuel cell manufacturing industry in the United States, with accompanying jobs in fuel cell manufacturing, installation, maintenance, and support services. Twelve grants were awarded to develop and deploy a variety of fuel cell technologies, including polymer electrolyte membrane (PEM), solid oxide, and direct-methanol fuel cells in auxiliary power, backup power, combined heat and power, material handling equipment, and portable-power applications. The cost share provided by the project teams is over $54 million, more than 56% of the total cost of the projects.

All Recovery Act project teams submit quarterly reports, which are available to the public through the Recovery.gov website. These reports include technology and deployment status as well as data on jobs created and funds spent. Collection and analysis of operational data from the fuel cell deployments are being performed by the National Renewable Energy Laboratory's (NREL's) National Fuel Cell Technology Evaluation Center (NFCTEC), formerly the Hydrogen Secure Data Center, to assess the performance and commercial readiness of the fuel cell technologies. Data are aggregated across multiple systems, sites, and teams, and are made available on a quarterly basis through Composite Data Products (CDPs), published on NREL's website. Seventeen presentations containing all CDPs have been published thus far, with the latest CDPs including performance, reliability, maintenance, and safety data for material handling equipment and backup power.

GOALS & OBJECTIVES

The Recovery Act fuel cell projects are addressing the objectives stated above as well as the overall Recovery Act goals of creating new jobs and saving existing ones, spurring economic activity, and investing in long-term economic growth. These deployments have also required project teams to address key challenges, including siting and permitting, fueling infrastructure, and fuel cell lifetime and reliability. These deployments have also attracted significant attention, with media events taking place at three of the Recovery Act deployment sites.

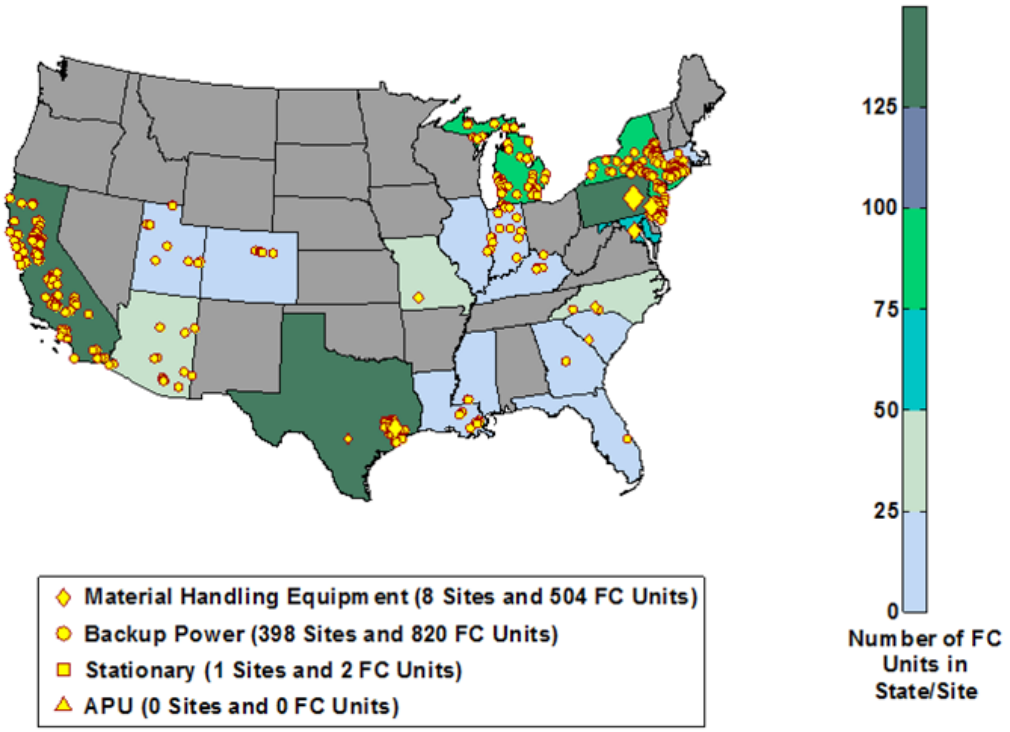

DOE Recovery Act-Funded Fuel Cell Deployment Locations

FISCAL YEAR (FY) 2013 STATUS AND PROGRESS

As of October 2013, more than 500 fuel cell lift trucks and a total of 820 fuel cell backup power systems for cellular communications towers and stationary backup power systems had been deployed—surpassing the original deployment goal of up to 1,000 fuel cells—and over 95% of the Recovery Act project funds had been spent by the projects. NREL's NFCTEC has established data reporting protocols with each of the project teams. CDPs and Detailed Data Products showing progress to date have been prepared. The CDPs are available on the NREL NFCTEC website, http://www.nrel.gov/hydrogen/proj_fc_market_demo.html. Of the original twelve projects, nine have been successfully completed.

Auxiliary Power

Delphi Automotive (Troy, MI and Rochester, NY): Delphi has been developing a 3- to 5-kW solid oxide fuel cell (SOFC) auxiliary power unit (APU) for heavy-duty commercial Class-8 trucks at their laboratory in Rochester, New York, demonstrating the potential of the SOFC APU as an anti-idle solution for truck manufacturers and their fleet owners. During SOFC APU testing, Delphi discovered a significant issue with the desulfurizer during repeated thermal cycles. As trials of alternative desulfurizer materials failed to meet requirements, Delphi opted to remove the desulfurizer from the system, providing a lower net power unit as designed with the volume for the desulfurizer bed not utilized. Delphi demonstrated 3.5 kW net power with zero sulfur fuel and 2.0 kW net power with ultra-low sulfur diesel fuel which is regulated to contain <15 ppm sulfur. Delphi completed vehicle demonstration testing with the APU operating in a typical driver usage scenario by providing power for rest stops and overnight cabin comfort and power demands. This project has been completed.

Backup Power

Sprint Nextel, Inc. (Reston, VA): Sprint is demonstrating the technical and economic viability of deploying 1- to 10-kW PEM hydrogen fuel cells with 72 hours of onsite fuel storage (using a new Medium Pressure Hydrogen Storage Solution with onsite refueling) to provide backup power for multiple access cell sites on the Sprint Wireless network. Deployments were planned for 260 new hydrogen fuel cell systems at sites in eight different states. Sprint has completed over 736 site surveys at potential deployment sites for their fuel cell backup-power systems. As of June 2013, Sprint had installed and commissioned 501 new PEM backup-power fuel cells at 260 sites.

Plug Power Inc. (Latham, NY): Plug Power has been demonstrating the market viability of low-temperature, 6-kW PEM GenCore® fuel cells fueled by liquid petroleum gas (LPG) to provide clean and reliable primary power and emergency backup power (72 hours or more). The objective of this project was to install and operate 20 fuel cell systems at Fort Irwin in Barstow, CA, and Warner Robins Air Force Base in Warner Robins, GA. These units run continuously on LPG, providing power to the grid and switching to emergency backup power during grid failure. A small battery pack is used to accommodate spikes in power demand. As of April 2013, the 10 GenCore® fuel cells installed at the Warner Robins Air Logistics Center at Warner Robins Air Force Base generated about 39 MWh of power at an average efficiency of approximately 25.4%. The units were providing backup power for lighting within the building. Plug Power has installed 10 additional fuel cells at an engineering building at Fort Irwin. These 10 additional systems should be operational in late 2013.

Combined Heat and Power

Plug Power Inc. (Latham, NY): Plug Power has been evaluating the performance of high-temperature, natural gas-fueled, 5-kW micro-combined heat and power fuel cell units (GenSys Blue®). The objective of the project is to validate the durability of the fuel cell system and verify its commercial readiness. Six units have undergone internal Plug Power testing to estimate failure rates, and three units were installed and tested in a real-world environment at the National Fuel Cell Research Center at the University of California, Irvine. These systems have logged over 31,000 hours in two years and have met their 30% electrical efficiency and 99% heat availability targets. Due to membrane electrode assembly supply and quality issues, Plug Power did not meet the durability target of >8,700 hours per unit. Plug Power has since transferred the role of deploying units at customer sites in California to ClearEdge Power, Inc. Two ClearEdge units were installed in California in 2012 and have completed the year of operation. Both units operated successfully with one achieving greater than 92% availability and one achieving greater than 95% availability. Combined, the two units produced 65.5 MWh of electricity and 74.7 MWh of heat. This project has been completed.

Portable Power

Acumentrics (Westwood, MA): Acumentrics is developing portable, propane-fueled SOFC generators as potential replacement for traditional gas/diesel generators. The project was originally led by Jadoo Power but was novated to Acumentrics in June of 2013. Two 1,000-W cart-mounted and two 250-W man-portable SOFC units fueled by propane will be demonstrated for three weeks at NASCAR events in Daytona, Florida in February of 2014. The demonstrations will include sufficient operating hours and start-up/shut-down cycles with data collection such that overall power, fuel efficiency, and noise of operation can be evaluated and compared with conventional technologies.

Data Collection & Analysis

National Renewable Energy Laboratory (Golden, CO): NREL is analyzing operational data (operation, maintenance, and safety) from the Recovery Act fuel cell deployments to better understand and highlight the business case for fuel cell technologies. Data collected by the project partners is being stored, processed, and analyzed in NREL's NFCTEC. Reports on the technology status are generated on a quarterly basis, while technical composite data products are published every six months. NREL has published ten deployment-focused CDPs and seven cycles of technical CDPs—currently composed of 72 CDPs for material handling equipment and 21 CDPs for backup power. In addition, they have provided hundreds of detailed data results to the individual projects. NREL has created a website to host these published results and presentations. Analysis and publication of Recovery Act deployment data will continue in FY 2014.

BUDGET

FROM the LABORATORY to DEPLOYMENT:

DOE funding has supported R&D by all of the fuel cell suppliers involved in these projects.

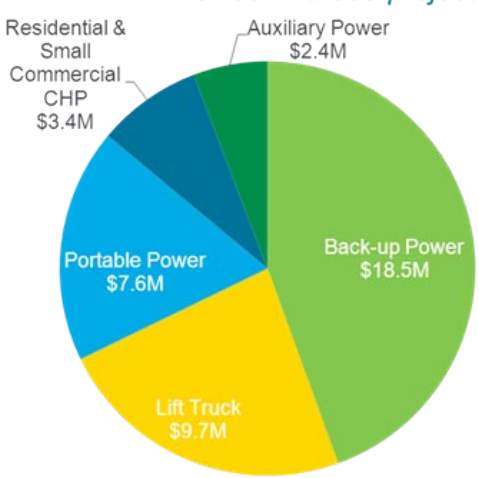

Approximately $54 million in cost-share funding from industry participants—for a total of about $96 million.

COMPANY	AWARD	APPLICATION
Delphi Automotive	$2.4 M	Auxiliary Power
FedEx Freight East	$1.3 M	Lift Truck
GENCO	$6.1 M	Lift Truck
Acumentrics	$2.2 M	Portable
MTI MicroFuel Cells	$3.0 M	Portable
Nuvera Fuel Cells	$1.1 M	Lift Truck
Plug Power, Inc.	$3.4 M	CHP
Plug Power, Inc.	$2.7 M	Back-up Power
Univ. of N. Florida	$2.4 M	Portable
ReliOn, Inc.	$8.5 M	Back-up Power
Sprint Nextel	$7.3 M	Back-up Power
Sysco of Houston	$1.2 M	Lift Truck

FY 2014 PLANS

All on-going projects will complete deployment activities in 2013 or 2014.

Finally, in FY 2014, the Fuel Cell Technologies Office will continue to document the lessons learned associated with the Recovery Act projects, including strategies developed for market entry and management of risks relating to safety, environmental, and siting requirements. The Office will finalize its evaluation of early-stage "market change" impacts (for the period of 2010 through the end of 2012) of the Recovery Act fuel cell deployments.

Jim Alkire
Project Officer and Lead for Recovery Act Activities
Fuel Cell Technologies Office
U.S. Department of Energy
1000 Independence Ave., SW
Washington, D.C. 20585-0121
Phone: (720) 356-1426
Email: James.Alkire@go.doe.gov

Sara Dillich
Fuel Cell Technologies Office
U.S. Department of Energy
1000 Independence Ave., SW
Washington, D.C. 20585-0121
Phone: (202) 586-7925
Email: Sara.Dillich@ee.doe.gov

X.1 Solid Oxide Fuel Cell Diesel Auxiliary Power Unit Demonstration

Gail Geiger (Primary Contact), Rick Kerr
Delphi Automotive Systems, LLC
5725 Delphi Drive
Troy, MI 48098
Phone: (585) 359-6187
Email: gail.e.geiger@delphi.com

DOE Managers
Dimitrios Papageorgopoulos
Phone: (202) 586-5463
Email: dimitrios.papageorgopoulos@ee.doe.gov
David Peterson
Phone: (720) 356-1747
Email: David.Peterson@go.doe.gov

Contract Number: DE-EE0000478

Subcontractors:
- Electricore Inc., Valencia CA
- PACCAR, Inc., Bellevue, WA
- TDA Research, Inc., Wheat Ridge, CO

Project Start Date: August 1, 2009
Project End Date: September 30, 2013

Objectives

- Design, develop, and demonstrate a 3-5 kW Solid Oxide Fuel Cell (SOFC) Auxiliary Power Unit (APU) for heavy-duty commercial Class 8 trucks (Figure 1).
- Utilize Delphi's next generation SOFC system as the core power plant and prove the viability of the market opportunity for a 3-5 kW diesel SOFC APU system.

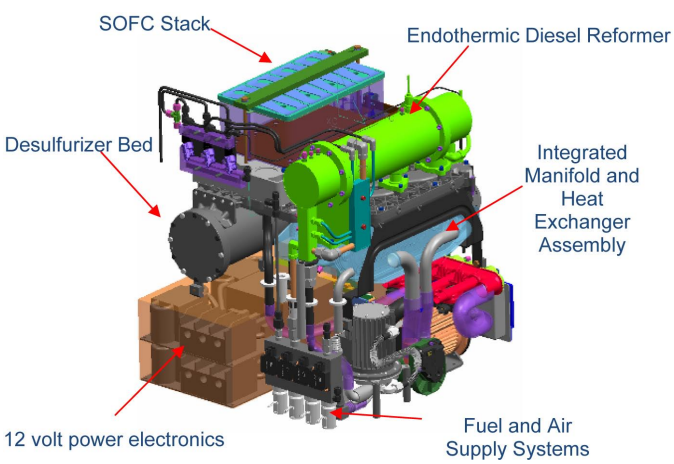

FIGURE 1. Delphi SOFC APU Schematic

- Test and demonstrate the diesel SOFC APU system in a high visibility fleet customer vehicle application that will support hotel loads and other real world operating conditions.

Relevance to the American Recovery and Reinvestment Act (ARRA) of 2009 Goals

During this phase of the project, a total of four jobs were created/maintained;

- Delphi: three full-time employees
- PACCAR: one full-time employee

As a result of this project, Delphi's SOFC APU was installed on a highly visible fleet truck. The demonstration provided Delphi, and their partner and fleet customer, with real world experience of the technology in the application. This demonstration should increase the overall awareness of SOFC APUs and help to facilitate commercialization of the product. Additionally, this project supported further development of Delphi's SOFC stack with additional exposure and testing in a different environmental application.

Technical Barriers

As a result of the successful execution of this project, Delphi addressed:

- System vibration robustness
- Overall system packaging
- System weight
- System cost
- System manufacturability
- System durability/reliability

During SOFC APU system testing, Delphi discovered a significant issue with the desulfurizer during repeated thermal cycles. Trials of alternative desulfurizing materials failed to meet requirements. Delphi opted to remove the desulfurizer from the system, providing a lower net power unit as designed with the volume for the desulfurizer bed not utilized. Future development in the area of high temperature desulfurization materials is still needed.

Technical Targets and Milestones

- Install the SOFC APU on a vehicle in service and complete real-world application demonstration.
- Provide 3-5 kW of power during truck idle periods allowing for reduced fuel consumption and harmful emissions.

- Specific power ≥15 w/kg
- Power density ≥10 w/l
- Net system efficiency ≥35%
- ≥2,000 hours of operation

Accomplishments

- Operator Instructions, Safety and Training Manual prepared
- Driver training completed
- APU Field Service Plan developed and included:
  - Frequency of checks by Delphi Engineers
  - Training of technicians on site
- Field data collection plan developed
- Desulfurizer removed due to difficulty with sorbent
- System modified and recalibrated to operate without sorbent
- SOFC APU operation confirmed in the lab
- SOFC APU mounted on Peterbilt Class 8 Truck and driven on demonstration loop (Figure 2)
- SOFC APU demonstration was completed with 1,098 truck miles and 1,125 hours of operation
  - Demonstration unit performance: 22% net efficiency, 8 W/l power density, 7 W/kg specific power

✧ ✧ ✧ ✧ ✧

INTRODUCTION

Delphi's SOFC system, installed on heavy-duty commercial trucks providing auxiliary power, addresses the growing concerns about emissions, fuel consumption, and noise. In the United States today, there are more than one million long-haul, heavy-duty commercial trucks with sleeper cabs on the road. When drivers stop for their mandatory rest periods or loading/unloading, they often leave their engines idling in order to heat/cool the sleeping areas and operate other vehicle systems. This idling practice is costly to the driver, the fleet owner, and harmful to the environment. The Environmental Protection Agency's Smart Way Transport Partnership estimates that each year, long duration idling of truck engines consumes approximately 960 million gallons of diesel fuel and emits 11 million tons of carbon dioxide, 180 thousand tons of nitrogen oxides, and 5 thousand tons of particulate matter into the air. In addition to the consumed fuel and emissions, idling trucks create elevated noise levels. The SOFC APU has the potential to decrease idling fuel consumption by up to 85%, reduce exhaust emissions below federal regulation emission standards, and decrease radiated noise levels to less than 60 decibels when compared to the truck's main engine.

FIGURE 2. Delphi SOFC Demonstration Truck

As a result of the on-road demonstration under this project, Delphi will be able to present user profile data to its fleet customer. This data will reinforce the lab-generated data showing that use of an SOFC APU as an anti-idling solution will provide drivers and fleets with reduced fuel consumption as well as reduced emissions and noise. This demonstration should increase the overall awareness of SOFC APUs and provide positive momentum in preparing to commercialize this product.

APPROACH

Under this project, Delphi pursued a three-phase approach to conduct its development. During Phase 1, Delphi worked with its partner, PACCAR, to establish the application's specifications and commercial requirements for the SOFC APU. Phase 2 work focused on design verification and system testing (lab and on-vehicle). Phase 3 included the demonstration of the SOFC APU on a heavy-duty Class 8 vehicle. The data collected during the demonstration phase was analyzed and reported.

All Delphi facilities involved in the project were required to meet Delphi's stringent safety requirements and are in alignment with the Safety Planning Guidance documentation specified by DOE. Additionally, there are no changes to the information contained within the National Environmental Policy Act forms submitted.

RESULTS

During this report period, Delphi:

- Evaluated and gained a better understanding of the effects of sulfur and the impact it has on SOFC APU performance.

- Demonstrated 3.5 kW net power with zero sulfur fuel and 2.0 kW net power with ultra-low sulfur diesel fuel which is regulated to contain <15 ppm sulfur.
- Completed several of the tasks necessary to provide a road-ready SOFC APU and completed a demonstration test.
- Completed SOFC APU system integration into the truck including mounting APU controls in the sleeper and adding data logging systems to the vehicle (Figure 3).
- Completed vehicle demonstration testing with the APU operating in a typical driver usage scenario by providing power for rest stops and overnight cabin comfort/power demands. Figure 4 shows the power output of the APU during a 24-hour period from the demonstration test, which included APU start-up while driving and 17 hours of providing auxiliary power during a typical overnight resting period.

FIGURE 3. "In-Cab" APU Control Interface

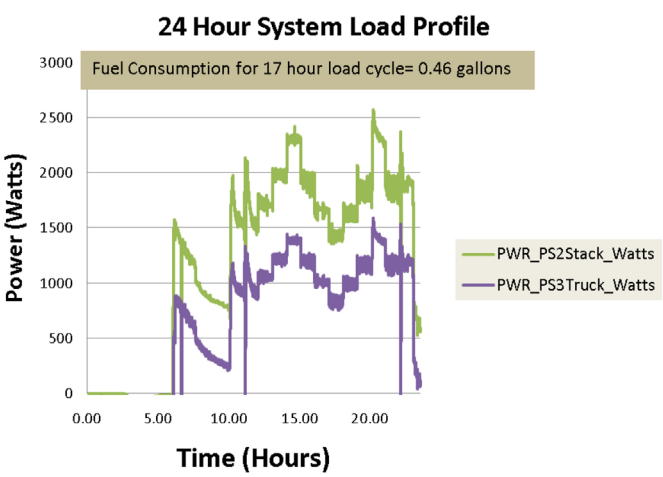

FIGURE 4. Demonstration Data

CONCLUSIONS AND FUTURE DIRECTIONS

Delphi demonstrated the potential of the SOFC APU as an anti-idle solution for truck manufacturers and their fleet owners and completed this project. While feedback for the technology was positive, significant commercial pull driven by anti-idling regulations, is still lacking. Delphi is currently putting the developed APU technology on the shelf, and will continue to develop its SOFC stack for other applications.

SPECIAL RECOGNITIONS & AWARDS/ PATENTS ISSUED

1. 2012/964806 Published: Combustor for a Fuel Cell System

2. 2013/152533 Pending: Fuel Reformer reactor without intersecting flow paths

3. 2013/363760 Pending: Heat Exchanger Reformer with Thermal Expansion Management

4. 2013/713039 Pending: Fuel Reformer with Thermal Management

5. 2013/527631 Pending: Multi-Fuel Combustor with Swirl Flame Stabilization

6. 2013/711834 Pending: Fuel Reformer Catalyst Arrangement

FY 2013 PUBLICATIONS/PRESENTATIONS

1. May 2013 DOE Hydrogen Program Peer Review Presentation: "Solid Oxide Fuel Cell Diesel Auxiliary Power Unit", Dan Hennessy.

X.2 Highly Efficient, 5-kW CHP Fuel Cells Demonstrating Durability and Economic Value in Residential and Light Commercial Applications

Jim Petrecky
Plug Power
968 Albany-Shaker Road
Latham, NY 12110
Phone: (518) 817-9124
Email: James_Petrecky@plugpower.com

DOE Manager
Reginald Tyler
Phone: (720) 356-1805
Email: Reginald.Tyler@go.doe.gov

Subcontractor:
ClearEdge Power, Sunnyvale, CA

Project Start Date: June 2009
Project End Date: September 2013

Objectives

- Create new jobs as well as save existing ones; spur economic activity
- Invest in long-term economic growth
- Accelerate the commercialization and deployment of fuel cells, fuel cell manufacturing, installation, maintenance, and support services

Relevance to the American Recovery and Reinvestment Act (ARRA) of 2009 Goals

- Jobs created at Plug Power including engineering, testing, sales, marketing, program management
- Improved reliability and efficiency of hydrogen fuel cell systems
- Decreased fossil fuel dependencies for power generation
- Used demonstrations to overcome the fuel cell development hurdles of durability, cost, system complexity, and temperature
- Substantiated the durability of Plug Power's 5 kW stationary proton exchange membrane fuel cell system and verify its commercial readiness for the marketplace:
  - Task 1 - internal fleet testing
  - Task 2 - external customer demos in real-world locations in California

Technical Barriers

- Stack Quality Issues
  - GenSys Blue membrane electrode assembly production was moved to another manufacturing process
  - Hydrogen tests looked strong
  - Reformate test: cell-to-cell variability
  - Stacks would have multiple weak cells

Technical Targets and Milestones

See Table 1.

Accomplishments

- Design Improvements
  - Efficiency: 89% total peak to 94%

TABLE 1. Performance Targets and Results

6A Target Performance and Go/No-Go Decision Chart					
Characteristic	**Units**	**Goal**	**1st GO - 2Q10**	**1st GO Actual**	**2nd GO - 2Q11**
Electrical efficiency at rated power	%	40	>30	32%	>30
CHP efficiency at rated power	%	90	>80	90%	>80
Cost (qnty < 15)	$/kWe	10,000	20,000	10,400	20,000
Durability at < 10% rated power degradation	hr	10,000	2,000	3,000	8,700
Noise	dB(A)	<55 at 10m	<55 at 10m	55 at 1m	<55 at 10m
Emissions (combined NOx, CO, SOx, hydrocarbon, particulates)	g/MWhr	< 1.5	< 1.5	< 1.5	< 1.5
				GO	NO GO

CHP - combined heat and power.

  - Manufacturing: Build reduced from >120 to <50 hr
  - Direct Material Cost Reduction: ~$90k to $53k in volumes <20
- Fleet of six GenSys combined heat and power (CHP) units at: 31k+ run hours; 53 MW-hrs electric, 633 MW-hrs heat

✧ ✧ ✧ ✧ ✧

INTRODUCTION

This demonstration project is intended to test multiple units of high-temperature, proton exchange membrane fuel cell systems in residential and light commercial micro-combined heat and power (μ-CHP) applications in California. The specific objective of the demonstration project is to substantiate the durability of GenSys Blue, and, thereby, verify its technology and commercial readiness for the marketplace. Plug Power is working with the University of California, Irvine (UCI), Sempra, and ClearEdge during this project.

APPROACH

From 2009 to 2012, Plug Power led the development through internal customer acceptance testing. However, in May of 2010, Plug Power announced that the Company would "focus commercial activity on material handling market." In 2012, Plug Power subcontracted ClearEdge to demo ClearEdge CHP units in California.

RESULTS

See Figure 1 and Table 2.

ClearEdge CHP Units

UCI Irvine (Comm. 7/25/12)
Irvine, CA
- **Availability: 98.2%**
- **Run Time: 5,134 hrs.**
- **Elec: 20,532 kW-hr (36% Eff.)**
- **Heat: 23,269 kW-hr (78% Eff.)**

- **Taco Bell (Comm. 9/28/12)**

San Juan Capistrano, CA
- **Availability: 95.6%**
- **Run Time: 3,482 hrs.**
- **Elec: 13,962 kW-hr (35% Eff.)**
- **Heat: 15,825 kW-hr (76% Eff.)**

FIGURE 1. ClearEdge Unit Performance

TABLE 2. Plug Power CHP System Performance Metrics

Plug Power CHP System Performance Metrics (Through December 2011)								
System S/N	E8	E9	E10	F2	F3	F4	Totals	Average
Commissioned Date	Jan-10	Jan-10	Apr-10	Jan-10	Mar-10	Jun-10		
System Runtime (Hours)	7,823	4,381	1,777	8,977	5,011	3,249	31,219	5,203
Current Stack Runtime	6,058	3,802	1,777	1,651	3,098	3,249	19,635	3,273
Burner Runtime	11,443	9,910	8,344	7,958	11,191	8,264	57,109	9,518
Electrical kWh	15,247	7,349	2,520	15,109	6,679	6,002	52,905	8,818
Thermal kWh	117,862	101,859	95,252	112,070	122,348	83,607	632,998	105,500
Startup Reliability	60.0%	70.0%	71.4%	64.0%	56.3%	54.5%		62.7%
Heat Operational	100.0%	100.0%	100.0%	100.0%	100.0%	100.0%		100.0%
CHP Operational	71.9%	39.2%	55.7%	70.4%	53.8%	46.9%		56.3%

CONCLUSIONS AND FUTURE DIRECTIONS

The continuity of supply for the high-temperature stacks needs to remain a focus of this market to meet and continue to improve the stack life requirements for this technology to be competitive with incumbent technology.

FY 2013 PUBLICATIONS/PRESENTATIONS

1. H2RA003_PETRECKY_2013_o (Annual Merit Review)

X.3 Accelerating Acceptance of Fuel Cell Backup Power Systems

Jim Petrecky
Plug Power
968 Albany-Shaker Road
Latham, NY 12110
Phone: (518) 817-9124
Email: James_Petrecky@plugpower.com

DOE Manager
Reginald Tyler
Phone: (720) 356-1805
Email: Reginald.Tyler@go.doe.gov

Subcontractor:
IdaTech, Bend, OR

Project Start Date: June 2009
Project End Date: September 2013

Objectives

- Create new jobs as well as save existing ones; spur economic activity
- Accelerate the commercialization and deployment of fuel cells, fuel cell manufacturing, installation, maintenance, and support services
- Demonstrate market viability and increase market pull of fuel cell systems within our government customers/partners

Relevance to the American Recovery and Reinvestment Act (ARRA) of 2009 Goals

- Jobs created at Plug Power including engineering, testing, sales, marketing, program management
- Commercialization and enablement of the fuel cell supply chain, including DANA, BASF, 3M, etc. as well as collaborations with other partners such as IdaTech and site installation support subcontractors
- Increased distributed power generation through the deployment of 20 GenSys systems
- Improved reliability and efficiency of mission critical backup power (>72 hours)
- Decrease fossil fuel dependencies for power generation

Technical Barriers

- Obtaining permitting from utility companies to operate fuel cells in a grid parallel (grid tied) configuration.

The following body of work was provided to the utility however the utility decided it was not sufficient.

  - Generating Facility Interconnection Application
  - Scope of Work for Fuel Cell Installation
  - Project Scope
  - Description of Work
  - Proposed Location and Build Layout
  - Concrete Pad Detail
  - Equipment Grounding Detail
  - Location of Fuel Cell Systems, Gas Piping, and Electrical Components
  - Site Electrical Wiring Diagram
  - Inverter Electrical Wiring Diagram
  - Equipment List and Specification
  - Contractor Requirements
  - Building Plans for Original Construction of Building (Host Site)
  - Map of Existing Renewable Energy Currently Installed at Host Base
  - Safety Plan and Emergency Procedure for GenSys Fuel Cell Fleet at Host Base

- The following was requested before permitting would be available:
  - Entire map of site host's interconnected generation - A complete and comprehensive single-line diagram of the entire generating facility's electrical configuration will be required. This application requires substantially more detailed information to ensure compliance of all tariffs and standards.
  - Single-Line Diagram - comprehensive diagram of the complete electrical configuration of the entire facility.
  - Three-Line Diagram - detailed protection study; phase and polarity identification.
  - Elementary Diagram - comprehensive representation of the entire facility containing information of all components electrically connected.
  - Plot Plan Drawing - needs update to include physical location and distances of all components
  - Relay Diagram - Diagrams and written descriptions regarding protective relays that will be used to detect faults or abnormal operating conditions for distribution system.

- Proposed Relay Settings - Demonstrate how the unscheduled and uncompensated export of real power from a generating facility for a duration exceeding two seconds but less than 60 seconds will be accomplished; for the proposed transfer switch, details to ensure that the automatic transfer switch and scheme comply with Rule 21 requirements.
- Relay test report will be required once the proposed relay settings have been reviewed and approved by protection engineering.

Technical Targets and Milestones

- Install 20 proton exchange membrane fuel cells for backup power at two site hosts by September 2012
- Backup power >72 hours

Accomplishments

- Successful installation, commissioning, and decommissioning of the first fleet of 10 GenSys units at Site Host 1, resulting in the following metrics for backup power:
  - 13,506 operating hours
  - 39.07 MW-hr electricity produced
  - Electrical efficiency = 25.4%
- A network outage simulation occurred on Saturday, January 19, 2013, 5:00 PM. The fuel cells powered the lighting in the building without issue. The commercial utility power was turned off - main disconnect switch SW1. Within ~20 s, the relays transferred and lighting was restored by fuel cell system power. Network outage simulation was roughly 30 minutes.
- Successfully installed the second fleet of 10 GenSys unit at Site Host 2.

✧ ✧ ✧ ✧ ✧

INTRODUCTION

Extending the amount of backup power that is available to U.S. agencies provides flexibility to their emergency planning. If an outage occurs due to a natural disaster, for example, these agencies have more time to react to the issue at hand instead of applying resources to regaining power. The intent of this project is to demonstrate two fleets of backup-power fuel cells as a validate solution for backup power requirements of greater than 72 hours.

APPROACH

The approach for extended backup is the merging of two Plug Power products – the GenCore and GenSys systems. By combining the field experience of the GenCore in backup applications with the long run time of the GenSys system, extended backup is achieved (see Figure 1).

RESULTS

As outlined in the Accomplishment sections, the fleet of 10 GenSys units at Site Host 1 was successful in providing

FIGURE 1. Approach

backup power and continuing to maintain power to the facilities through a network outage simulation.

A list of future work has been compiled based on the field experience in operating this micro fleet. This list includes the definition of failure modes, failure signatures/symptoms for future work to create early detection and recovery methods (see Figure 2):

- RPM: Autothermal oxidizer timeout waiting for catalyst activation
- CM: Electronic board failures, some possible connection to software
- RPM: Loss of fuel flow (related to flow meter/valve issues)
- TMM: Coolant leak, loss of coolant
- RPM: Anode air pump failed to start, known issue
- RPM: Gas leak during commissioning
- CM: Unknown, attributed to electronic boards
- RPM: Fuel flow issue with occasional dropout or flow spikes
- PGM: Max low cell trips, stack protection due to either CO or cell performance
- RPM: Desulfurization needed excessive time for conditioning/equilibration
- CM: Firmware update and boot failure

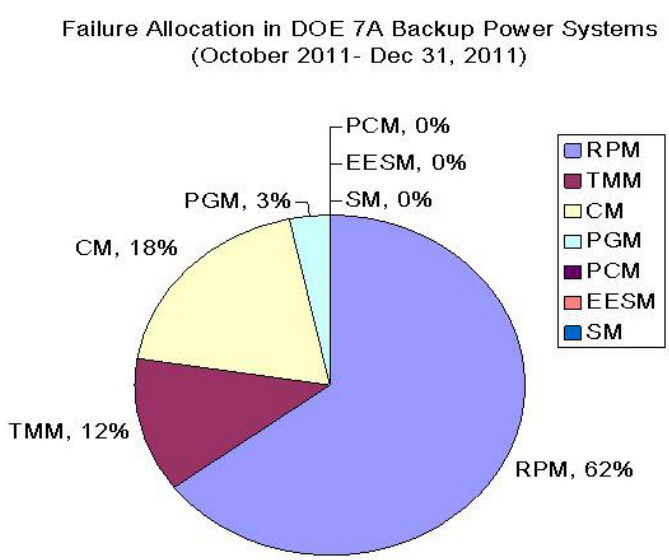

RPM - reactive processing; TMM - thermal management;
CM - controls & electronics; PGM - power generation; PCM - power controls;
EESM - electrical energy storage; SM - structure

FIGURE 2. Failure Allocation

CONCLUSIONS AND FUTURE DIRECTIONS

- Permitting is a case-by-case situation. Working with the utility for one site host was a straightforward process provided that the application requirements were met. Working with the utility for the second site host has been extremely problematic and has caused very significant delays.
- It is difficult to project the timing requirements for permitting, therefore future direction is to start the permitting process as soon as possible in any project.

FY 2013 PUBLICATIONS/PRESENTATIONS

1. H2RA007_PETRECKY_2013_o (Annual Merit Review)

X.4 Use of 72-Hour Hydrogen PEM Fuel Cell Systems to Support Emergency Communications

Kevin Kenny
Sprint Nextel
12000 Sunrise Valley Drive
MS: VARESQ0401-E4064
Reston, VA 20191
Phone: (703) 592-8272
Email: kevin.p.kenny@sprint.com

Jerry Haley – Deployment Project Manager
Ericsson Services, Inc.
Phone: (678) 523-0788
Email: jerry.haley@ericsson.com

DOE Managers
Sara Dillich
Phone: (202) 586-7925
Email: Sara.Dillich@ee.doe.gov
Jim Alkire
Phone: (720) 356-1426
Email: James.Alkire@go.doe.gov

Contract Number: EE-0000486

Subcontractors:
- Air Products & Chemicals, Inc., Allentown, PA (Fuel Project Partner)
- Altergy Systems, Folsum, CA (Fuel Cell Project Partner)
- Black & Veatch Corporation, Overland Park, KS (A&E Project Partner)
- Burns & McDonnell Engineering Co., Inc., Kansas City, MO (A&E Project Partner)
- Ericsson Services, Inc., Overland Park, KS (Deployment Management Project Partner)
- ReliOn, Inc., Spokane, WA (Fuel Cell/A&E Project Partner)

Project Start Date: March 18, 2010
Project End Date: December 31, 2013

Objectives

- Eliminate barriers to siting and permitting 72 hours of hydrogen fuel storage
- Eliminate barriers to refueling sites at the required level of performance
- Collect and analyze data sample to evaluate economic and operational metrics

Relevance to the American Recovery and Reinvestment Act (ARRA) of 2009 Goals

Sprint, through this deployment effort, seeks to:

- Support the creation of new jobs
- Maintain existing jobs
- Bring proton exchange membrane (PEM) fuel cell technology into the market, which will foster job training opportunities:
  - Installation
  - Service
  - Repair

Relevance to the DOE Fuel Cell Technologies Office's ARRA Project Goals

Through the successful deployment of this technology, it is expected that the following goals shall be achieved:

- Demonstrate the operational acceptance and financial viability of using PEM fuel cell technology to support critical emergency power requirements:
  - Telecommunications
  - Health care/life-support systems
  - Critical government operations
- Expanded user community offers many positive market opportunities:
  - Increased demand prompts greater production volume and lowers unit cost.
  - Cross-industry adoption spurs "services" growth (construction, maintenance, ancillary support) as more units are deployed – costs are lowered due to competition.
  - Fueling infrastructure is "pulled" into the market by true demand rather than being "pushed" into the market to support speculative potential.

Technical Barriers

Major barriers being addressed under this project are summarized as follows:

- Higher costs: initial capital cost, as well as operational expenditures (increased site lease costs to support code-mandated hydrogen setbacks), is higher than incumbent technology (diesel generator).

- Siting and permitting: due to variations in the applicable code requirements and versions recognized by the authorities having jurisdiction, each market launch requires time with the local officials (e.g., building, fire) to help them understand the referenced codes and how Sprint interprets/complies with code requirements.
- Fueling infrastructure: this project deploys a new model for stationary hydrogen fuel cells, relying upon an onsite refillable medium-pressure storage solution rather than the low-pressure hydrogen cylinder exchange model. Our project partner, Air Products, has invested in a small fleet of transport vehicles to deliver bulk compressed hydrogen to small, geographically diverse, remote cell sites.

Technical Targets and Milestones

The following performance targets and associated milestones have been set for this project.

- Install 260 additional PEM fuel cells for backup power by end of December 2012.
  - California – 100 units
  - Connecticut – 30 units
  - New Jersey – 65 units
  - New York – 65 units
- Retrofit a total of 70 existing low-pressure hydrogen storage systems with the new medium-pressure onsite refillable hydrogen storage solution in the following states:
  - California
  - Louisiana
  - Texas

Accomplishments

To date, our team has:

- Completed the required documentation for National Environmental Policy Act clearance and received the requested comprehensive categorical exclusion on May 12, 2011.
- Thus far, our team has conducted site surveys at 736 candidate sites to support new PEM fuel cell deployments at 260 locations.
- A total of 392 of the 583 candidates were removed from consideration for a variety of reasons during Phase 1 (site survey, entitlement review).
  - Space constraints within the cell site compound (real estate and setbacks).
  - Access restrictions for hydrogen fueling vehicle.
- An additional 79 candidates "fell out" during Phase 2 (site acquisition) due to:
  - Cost
  - Zoning issues
- Commissioned the first new unit on May 11, 2011, in Alloway, NJ. As of June 3, 2013, a total of 259 new PEM fuel cells have been commissioned into service.
- Expect to have 260 new PEM fuel cells commissioned by the end of the third quarter of 2013.

✧ ✧ ✧ ✧ ✧

INTRODUCTION

The relevance of this project to the goals of the ARRA of 2009 is threefold. First, Sprint seeks to support the creation of new jobs, as well as maintain existing jobs, to successfully complete this deployment effort. Second, Sprint intends to spur economic activity through the positive impact to various industries and service providers at all levels of the supply chain. And finally, Sprint is confident that this investment in PEM hydrogen fuel cells, to provide emergency power to our critical wireless network facilities, will truly benefit our nation's long-term economic growth.

APPROACH

After reviewing the Code Division Multiple Access Network Site Inventory, a master candidate site list was created based upon the restoration priority of the facility and whether or not the site was equipped with a fixed generator. Sprint focused on specific markets to exploit the sites' proximity to the hydrogen distribution facility (within 200 miles), as well as to concentrate on market clusters to minimize site acquisition, siting/permitting, installation, commissioning, and training expenditures. In addition, this cluster approach helps to minimize costs associated with the maintenance of a PEM fuel cell spare parts inventory. Finally, this concentration permits a consistent presentation to the local building officials, which in turn helps to clarify applicable code (Uniform Building Code, National Fire Protection Association, etc.) interpretations. In theory, all of these efforts should help to facilitate a rapid, safe, and successful deployment in the market.

Our Hydrogen Safety Plan was submitted to DOE on July 13, 2010. On January 18, 2011, feedback from the safety panel team at DOE was received. A National Environmental Policy Act comprehensive categorical exclusion was secured on May 12, 2011.

RESULTS

On May 11, 2011, Sprint successfully commissioned the first PEM fuel cell funded by this project. This unit was the first fuel cell system to be deployed in the network which was equipped with the Medium Pressure, Refillable On-Site, Hydrogen Storage Solution. Since that initial installation, a grand total of 259 such devices have been commissioned. When this project completes, we will have more than doubled the number of sites in our network with emergency power provided by PEM fuel cells! Figure 1 provides the deployment schedule for this project.

To date, a total of 736 sites have been evaluated to determine if the locations are suitable for new PEM fuel cell deployment or, if equipped with a PEM fuel cell today, if it can support the use of the new hydrogen fuel storage solution. Figure 2 provides a summary of the various reasons so many sites are dropped from consideration following the completion of Phase 1 (site survey) activities.

Once the candidate site makes it through Phase 1, it can be dropped from consideration during Phase 2 (site acquisition and zoning). Figure 3 provides a summary of the various reasons a site can be dropped at this stage of deployment. Interestingly, it appears that the education of

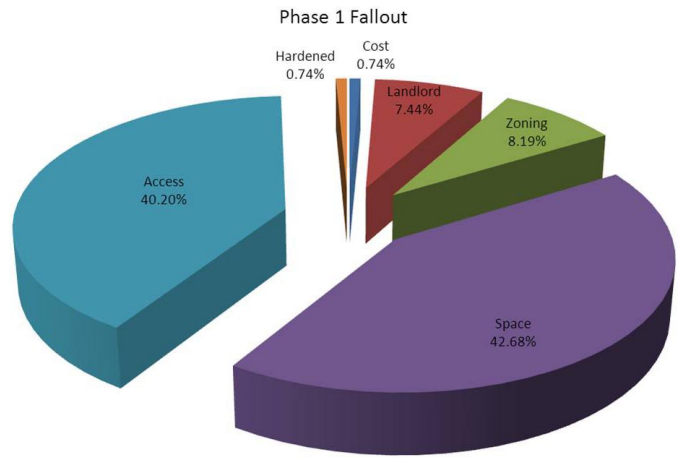

FIGURE 2. Phase 1 (Site Survey/Entitlement Review) Fallout Summary

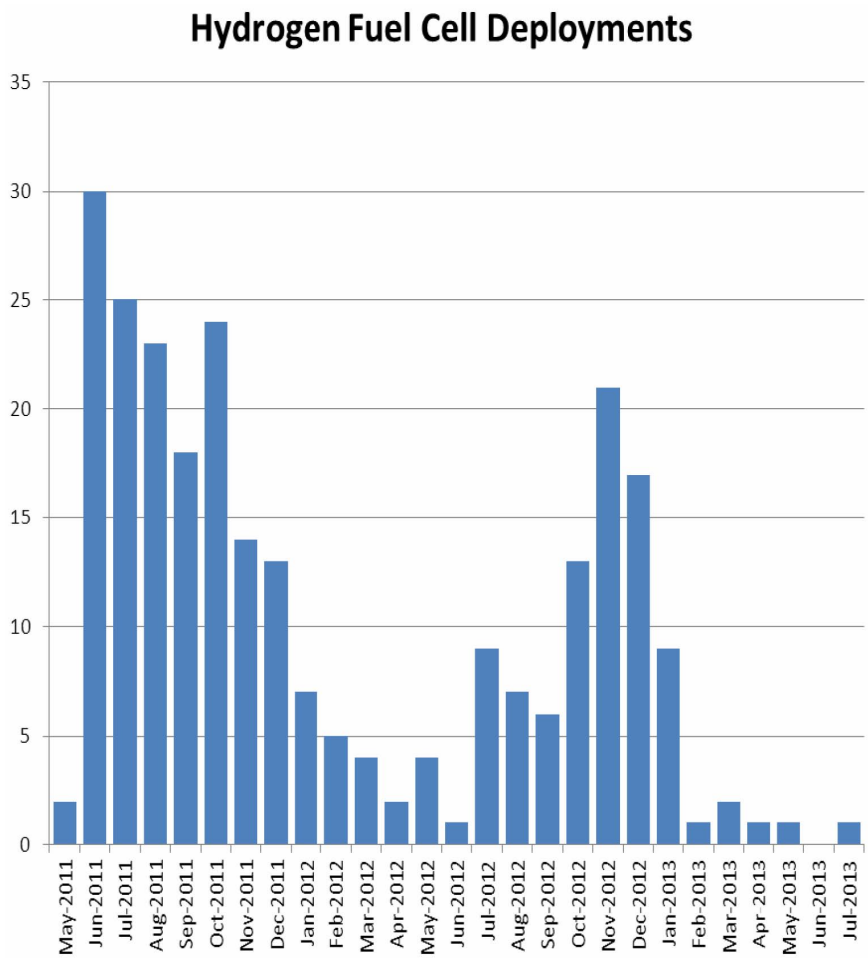

Month	Quantity
May-2011	2
Jun-2011	30
Jul-2011	25
Aug-2011	23
Sep-2011	18
Oct-2011	24
Nov-2011	14
Dec-2011	13
Jan-2012	7
Feb-2012	5
Mar-2012	4
Apr-2012	2
May-2012	4
Jun-2012	1
Jul-2012	9
Aug-2012	7
Sep-2012	6
Oct-2012	13
Nov-2012	21
Dec-2012	17
Jan-2013	9
Feb-2013	1
Mar-2013	2
Apr-2013	1
May-2013	1
Jun-2013	0

FIGURE 1. Deployment Schedule

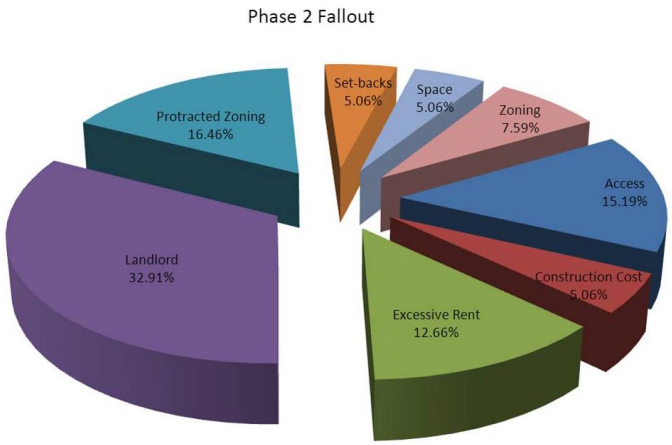

FIGURE 3. Phase 2 (Site Acquisition/Zoning) Fallout Summary

property owners (landlords, tower aggregators), municipal officials, and/or the zoning board might permit more sites to remain in consideration.

CONCLUSIONS AND FUTURE DIRECTIONS

We recognized going into this project that the fallout rate for candidate sites would be in the 40% range due to the limited amount of space available in the typical cell site compound. Limited real estate, in the case of PEM fuel cell deployment, can be a double-edged sword. There may be physical space to permit the placement of the equipment onsite; however, code-mandated setback distances may or may not be able to be supported at the facility. Without uniform, recognized hydrogen/fire codes, it appears that PEM fuel cells will continue to require more time/effort/money to deploy versus the incumbent diesel generator solution.

XI. SYSTEMS ANALYSIS

XI.0 Systems Analysis Program Overview

INTRODUCTION

The Systems Analysis program supports decision-making by providing a greater understanding of technology gaps, options and risks, and the contribution of individual technology components to the overall system (i.e., from fuel production to utilization, as well as the interaction of the components and their effects on the system). Analysis is also conducted to assess cross-cutting issues, such as integration with the electrical sector and use of renewable fuels. Particular emphasis is given to assessing onboard storage options and infrastructure implications.

The Systems Analysis program made several significant contributions to the program during Fiscal Year (FY) 2013. The cost of infrastructure was compared to infrastructure for other advanced fuel vehicles and opportunities of reducing the infrastructure costs were examined by using stakeholder input and exploring synergies with other fuels such as natural gas. The JOBS and economic impacts of Fuel Cells (JOBS FC) model continues to be enhanced by Argonne National Laboratory (ANL) and RCF Economic and Financial Consulting as they add the capability to assess employment impacts of infrastructure development. Infrastructure and early market analyses were conducted to better understand hurdles such as cash flow and station utilization, and supply and demand issues. The Greenhouse Gases, Regulated Emissions, and Energy Use in Transportation (GREET) model is being enhanced to evaluate greenhouse gas emissions and petroleum on a well-to-wheels basis for hydrogen pathways with various onboard storage options, and to incorporate water consumption analysis capability to conduct life-cycle analysis of various hydrogen production pathways.

GOAL

The program's goal is to provide system-level analysis to support hydrogen and fuel cell development and technology readiness by evaluating systems and pathways including resources and infrastructure issues to help guide the selection and estimate potential value of research, development, and deployment projects and efforts.

OBJECTIVES

- By 2014, complete environmental studies that are necessary for technology readiness.
- By 2017, complete analysis of program performance, cost status, and potential for use of fuel cells for a portfolio of commercial applications.
- By 2019, complete analysis of the potential for hydrogen, stationary fuel cells, fuel cell electric vehicles (FCEVs) and other fuel cell applications such as material handling equipment. The analysis will address necessary resources, hydrogen production, transportation infrastructure, performance of stationary fuel cells and FCEVs, and the system effects resulting from the growth of fuel cell market share in the various sectors of the economy.
- Provide milestone-based analysis, including risk analysis, independent reviews, financial evaluations, and environmental analysis to support the program's needs prior to technology readiness.
- Periodically update the life-cycle energy, petroleum use, greenhouse gas, and criteria emissions analysis for technologies and pathways for the program to include technological advances or changes.

FY 2013 STATUS

The Systems Analysis program focuses on examining the economics, benefits, opportunities, and impacts of fuel cells and renewable fuels with a consistent, comprehensive analytical framework. Analysis conducted in FY 2013 included socio-economic impacts such as increased employment from fuel cell deployment, life-cycle cost of various vehicle platforms including FCEVs with the Vehicle Technologies Office, renewable biogas resources for hydrogen production, potential benefits of emerging onboard storage options, life-cycle impacts of water use in hydrogen production pathways, identification of early markets for fuel cells and opportunities to reduce cost through various mechanisms, and options to reduce infrastructure cost. The Systems Analysis program has transitioned from developing key models to completing critical program analyses. As evidenced by the completed and ongoing analysis

activities, the initial strategy of the Systems Analysis program was effective in enabling the completion of a portfolio of analytical projects.

FY 2013 ACCOMPLISHMENTS

Develop and Maintain Models and Systems Integration

- ANL, with assistance from RCF, continues to estimate job creation as a result of program projects and enhance the JOBS FC model to estimate employment and revenue impacts of infrastructure development. JOBS FC uses an input-output methodology to estimate changes in industry expenditures as a result of fuel cell deployment and calculates the effects of those changes throughout the economy. Version 1.0 of the model was released for public use in May 2012 and includes forklift and backup power applications of polymer electrolyte membrane fuel cells and prime power applications of phosphoric acid and molten carbonate fuel cells for user-specified analyses at the state, regional, or national level. It is available for download at www.jobsfc.es.anl.gov.
- The model is being used to continue to assess the employment impacts of the American Reinvestment and Recovery Act of 2009 (Recovery Act) funding for fuel cell deployments for backup power. The figure below illustrates that Recovery Act created or retained approximately 950 job-years of employment during the 2009 to 2012 timeframe. Note that a job-year is one year of work by one person (e.g., 5 job-years can be 5 years of work by 1 person, 1 year of work by 5 persons).

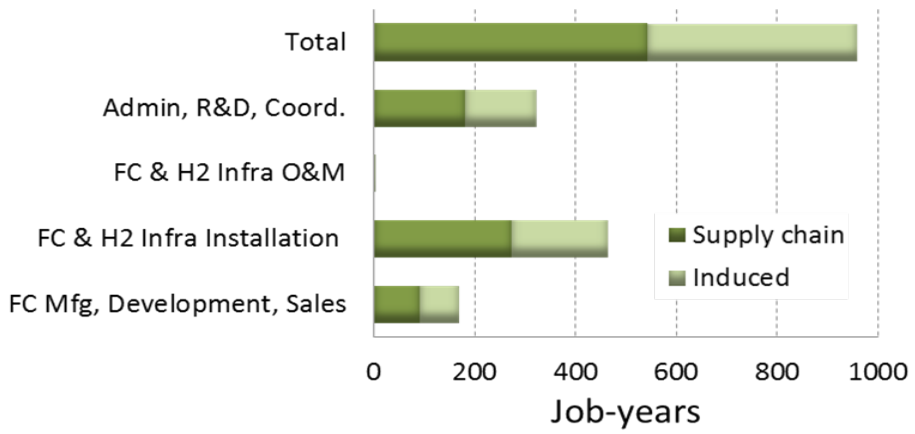

FC – fuel cell; H2 – hydrogen; O&M – operations and maintenance; Infra – infrastructure; Mfg - manufacturing
Source: Argonne National Laboratory

Market Analysis

- Navigant Research continues to assess global and domestic market analysis of the fuel cell markets for portable, stationary power, and transportation applications. The analysis identified increased growth in the fuel cell market in the domestic and international markets as shown in the following figure. As exhibited, the fuel cell market remains strong with over ~30,000 systems shipped in 2012, an increase of greater than 35% over 2011.

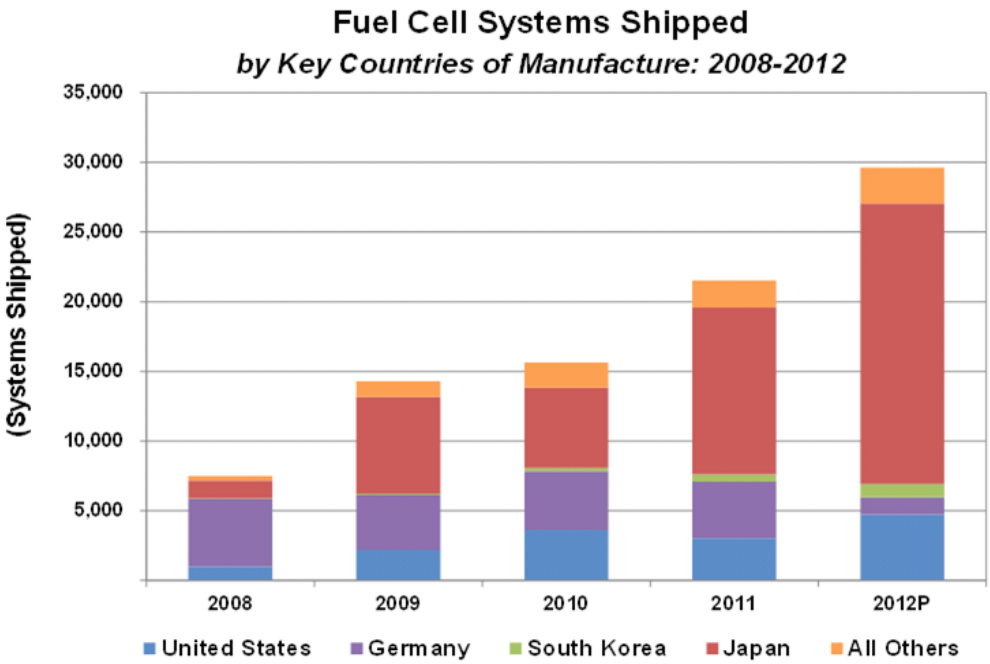

2012P – 2012 projected
Sources: Navigant Research and DOE 2012 Fuel Cell Technologies Market Report

Infrastructure Analysis

- The University of California at Davis assessed alternative strategies for introducing FCEVs and hydrogen infrastructure in Southern California over the next decade to satisfy the zero emission vehicle regulation while taking into consideration station placement, quantity, size, and type. The analysis studies infrastructure economics from multiple perspectives including network, station owner, and consumer. The project analyzed rollout strategies for FCEVs and hydrogen infrastructure including station cash flow in Southern California over

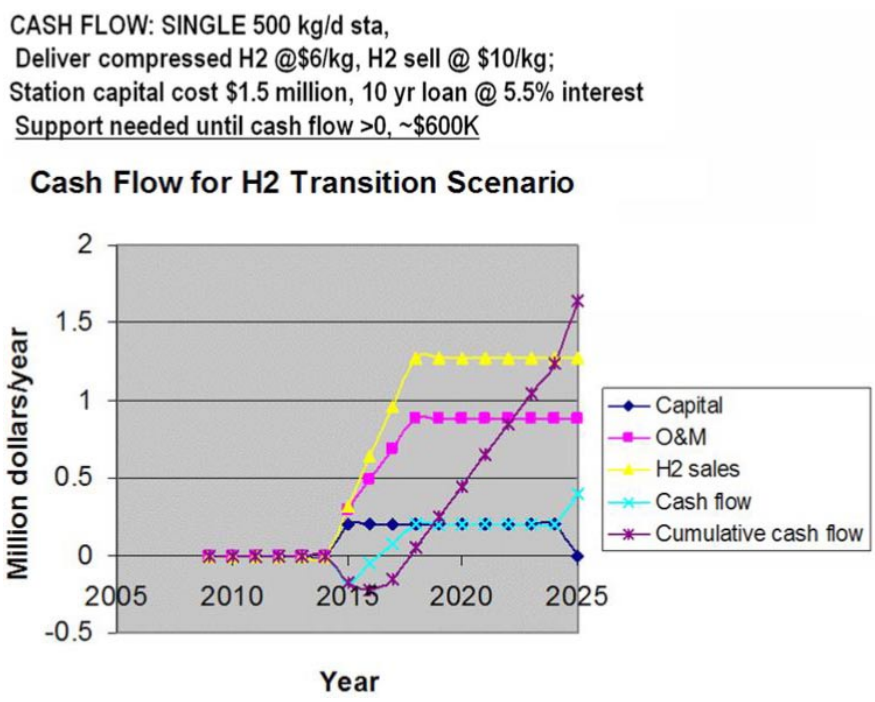

Source: University of California, Davis

the next decade through input and discussion with stakeholders in the auto industry, energy industry, industrial gas industry, state agencies, and national labs. The analysis showed that a single 500 kg/d station costing $1.5 million has a positive cash flow within a few years, once the hydrogen demand for the station increases to the station capacity. The station could experience a negative cash flow totaling ~$400K-700K in the early stages.

Fueling Pressure Analysis

- Oak Ridge National Laboratory (ORNL) began examining the optimal delivered hydrogen pressure for refueling FCEVs by including the values of consumer choice. The project assessed the balance between storage and delivery pressure and station quantity to determine the best deployment of infrastructure to support consumer refueling needs. The analytical framework assesses the complicated relationships between onboard hydrogen storage pressure and range, costs, consumer acceptance, and industry risks. ORNL found that the optimal pressure is most sensitive to the value that consumers place on their time, incremental cost of hydrogen, and number of FCEVs. For example, with 100 stations and 50,000 FCEVs in Southern California, 700-bar fueling offers lower combined costs than either 350 bar or 500 bar. This conclusion provides insight to the uncertainty of high-pressure incremental costs (0.2-0.6 $/kg for high-pressure upgrade) or the value of refueling travel time (25-75 $/hour).

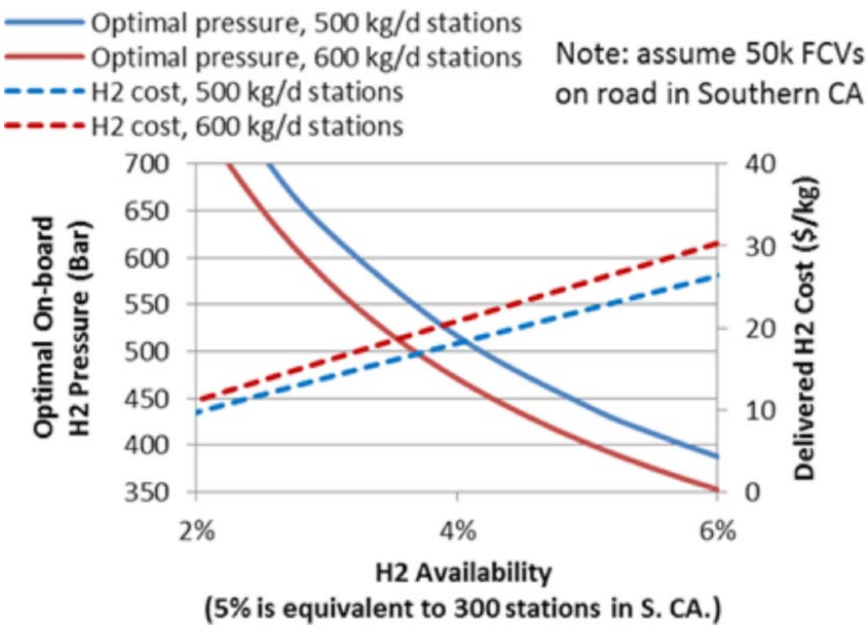

FCV – fuel cell vehicle
Source: Oak Ridge National Laboratory

Environmental Analysis

- **Vehicle Portfolio Well-to-Wheel Analysis**
  Analysis was conducted in collaboration with the Bioenergy Technologies and Vehicle Technologies Offices to estimate the lifecycle greenhouse gas (GHG) emissions resulting from several fuel/vehicle pathways, for a portfolio of future mid-size cars. Major inputs to the calculation of GHG emissions included the fuel economy of each vehicle and fuel production pathway efficiency. The data and major assumptions and results are documented in a DOE record[1]. The results of the analysis show that GHG emissions could be reduced to a range of 30-190 g of CO_2e per mile compared to the current gasoline internal combustion engine of 430 g of CO_2e per mile. This reinforces the point that a portfolio of advanced vehicles and renewable fuels will be needed to reduce the GHG emissions from the current vehicle fleet to meet future reduction targets.

[1] http://hydrogen.energy.gov/pdfs/13005_well_to_wheels_ghg_oil_ldvs.pdf.

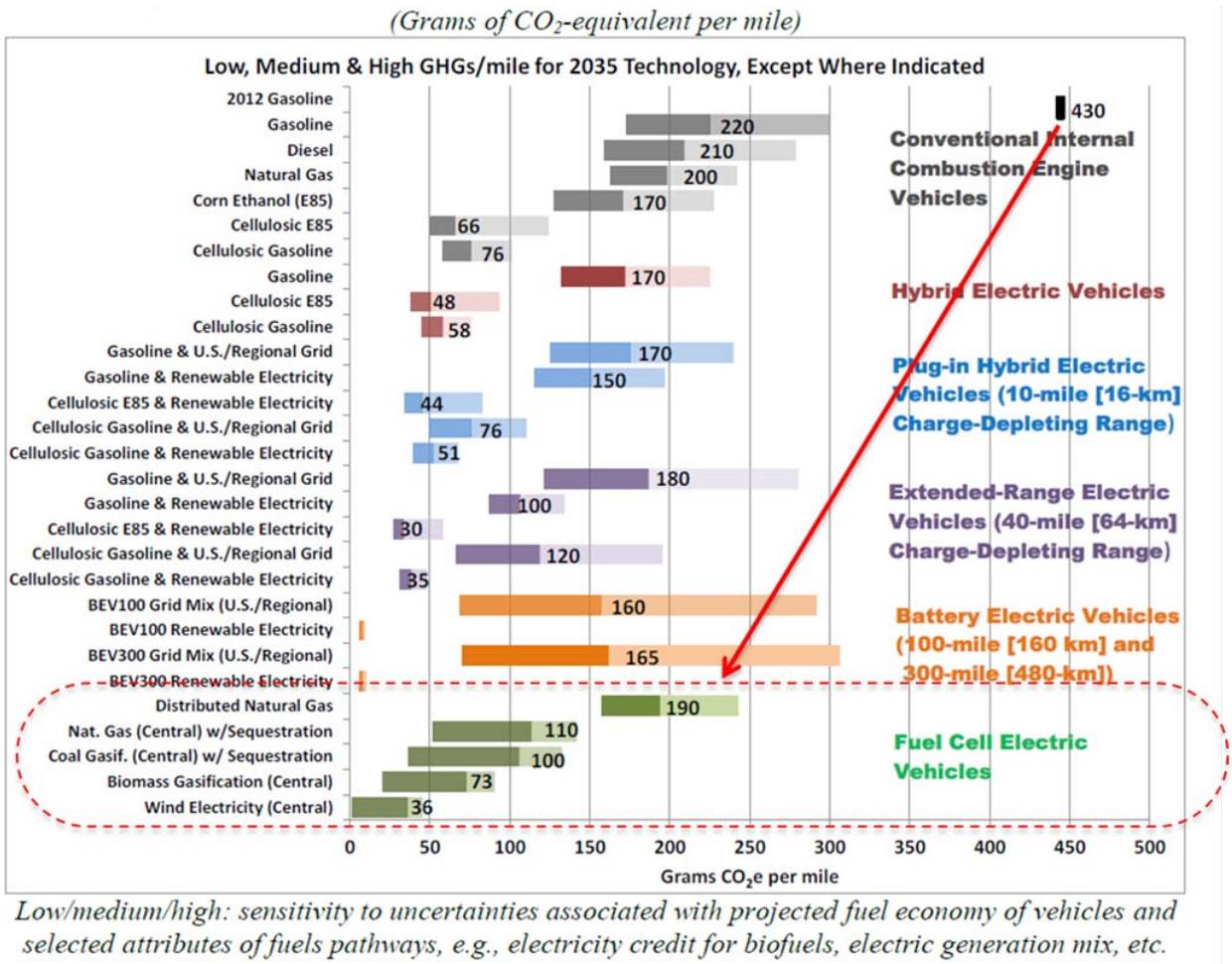

E85 – 85% ethanol 15% gasoline; BEV – battery electric vehicle
Source: http://hydrogen.energy.gov/pdfs/13005_well_to_wheels_ghg_oil_ldvs.pdf

- **Onboard Storage Well-to-Wheel Analysis**
  ANL revised the GREET model to include new onboard storage options with a central natural gas reforming production pathway. The onboard storage options added to the model included the following:
  - Cryo-compressed storage system
  - Metal organic framework (MOF-5) sorption storage system

  As shown in the figure to the right, the life-cycle GHG emissions associated with 350 and 700 bar gaseous storage and the new onboard hydrogen storage systems were estimated to be between 315 and 373 g_{CO2e}/mi. Systems that require significant precooling (e.g., cryo-compressed and MOF-5) at their current technology state exhibited GHG emissions of 370 to 400 gCO_2e/mi compared with GHG emissions of 315 to 330 gCO_2e/mi from systems that require less precooling (i.e., 700-bar system) or no precooling (i.e., 350-bar system). The same methodology will be applied to evaluate the environmental impacts of other new and emerging hydrogen onboard storage systems.

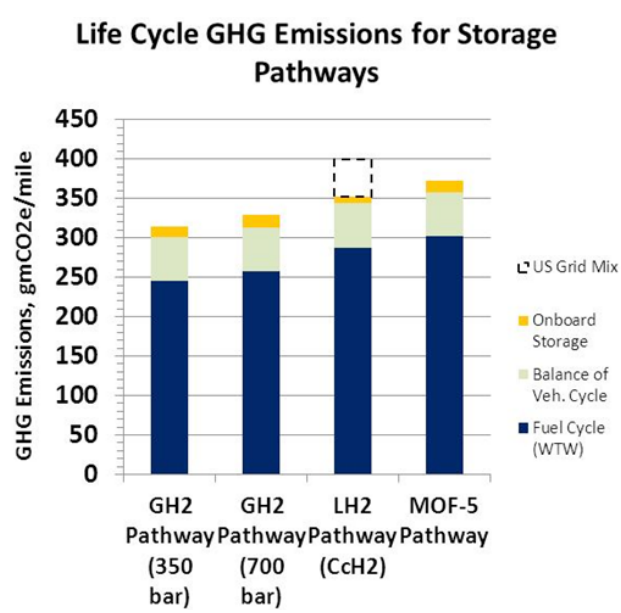

GH2 – gaseous hydrogen; LH2 – liquefied hydrogen; CcH2 – cryo-compressed hydrogen; WTW – well to wheels
Source: ANL

Resource Analysis

- **Water Life Cycle Analysis**
  ANL enhanced the GREET model's life cycle analysis capabilities to examine water consumption for hydrogen production and delivery pathways from natural gas. The production of energy feedstocks and fuels requires water use. Feedstocks like natural gas, crude oil, and oil sands require significant volumes of water for drilling, extraction, and conversion into energy products. Also, biofeedstocks such as corn and cellulosic sources need water for growth. Converting these conventional and new feedstocks to fuel requires additional water consumption. Similarly, water is needed for heat rejection in thermo-electric power generation cycles. Producing hydrogen from electricity (via electrolysis), natural gas (via steam methane reformation), or biomass (via gasification) requires additional use of water for the conversion process as well as for cooling. Analysis will continue to examine water consumption for other hydrogen production and delivery pathways such as coal, biogas, and nuclear feedstock sources. The analysis will include liquefaction and compression processes along these pathways, as compared to other fuel pathways on a life-cycle basis, including baseline petroleum gasoline, bioethanol, and battery electric vehicles pathways.

- **Biogas Resource Analysis**
  National Renewable Energy Laboratory examined resource availability for renewable hydrogen produced from net biogas from landfills and wastewater treatment plants, which provides alternatives to traditional sources of hydrogen, hedges against fluctuation in costs and demand for fossil fuels, and aids compliance with state policies for renewable fuels. The total methane potential from industrial, institutional and commercial organic waste is estimated to be 6.2 million tonnes per year, which, if converted to hydrogen, would yield approximately 1.6 million tonnes of hydrogen per year. The project updates prior studies on hydrogen production from methane from wastewater treatment, landfills, and manure management, and expands analysis to include methane from industrial processes and organic food waste.

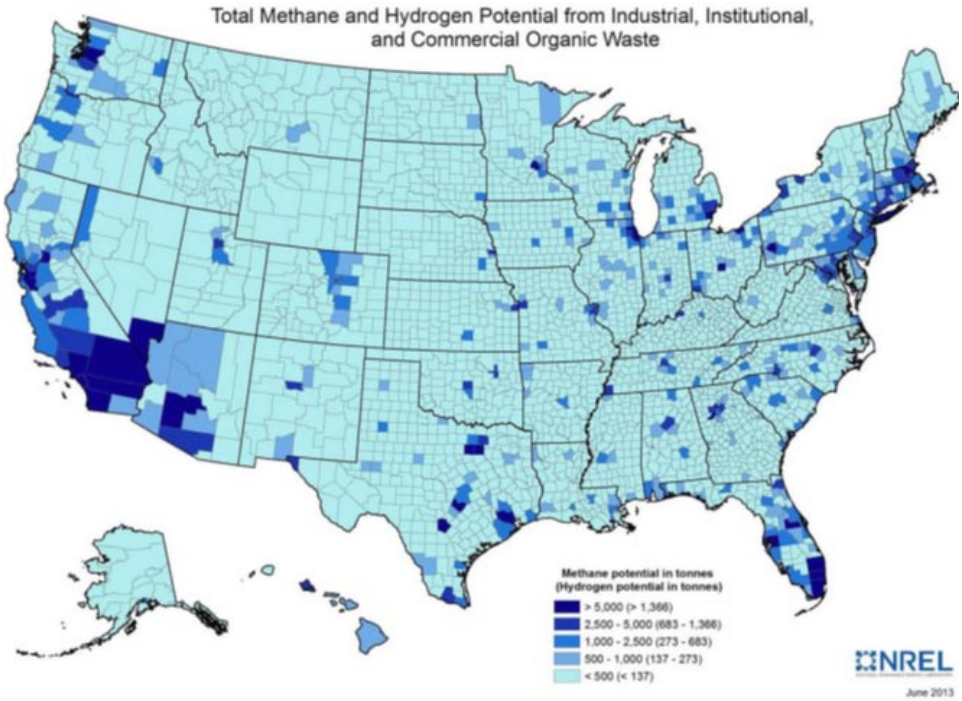

Source: National Renewable Energy Laboratory

Programmatic Analysis

- **Cost per Mile Analysis**
  Analyses were conducted in conjunction with the Vehicle Technologies Office to estimate the life-cycle costs resulting from several fuel/vehicle pathways, for a portfolio of future mid-size cars. Major inputs to the calculation of costs of ownership included the price of each vehicle and the annual fuel costs. The data and major assumptions and results are documented in a DOE record[2]. As shown below, projected R&D advances will drive future cost competitiveness between advanced vehicles and fuels.

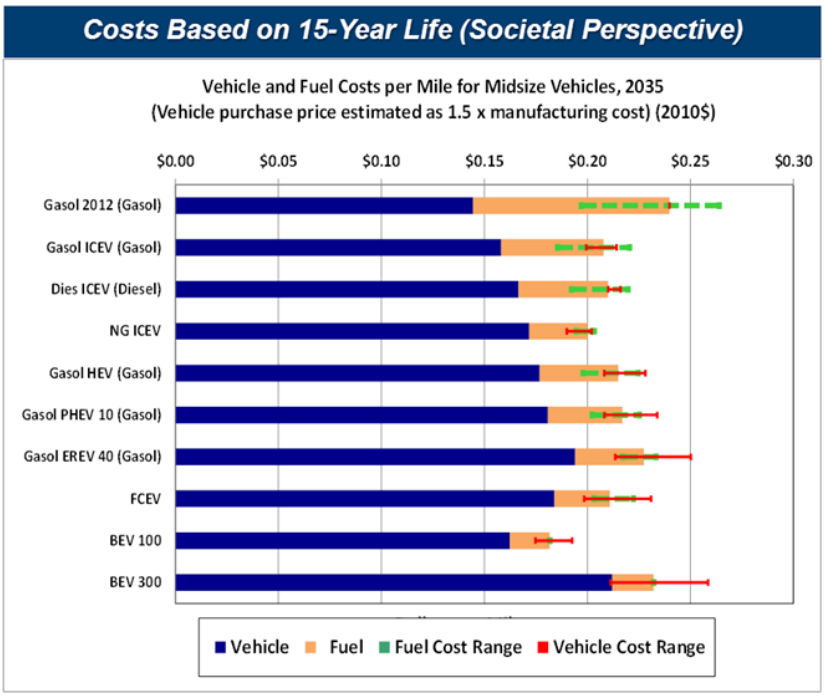

- **Worldwide Status of Hydrogen FCEV Technology and Prospects for Commercialization**
  ORNL examined the status of FCEV technology and commercialization plans in Japan, Korea, the European Union, and the United States. Benchmark progress has been seen by original equipment manufacturers (OEMs) in the performance of FCEV technology, manufacturing costs, and the timing of commercialization. Government and industry plans for deployment of FCEVs were documented, and the data collected were used to recalibrate the market transition models. FCEV performance will be ready for commercial introduction by OEMs in 2013, 2015, 2017, and 2020, depending on the availability of refueling stations. There is general agreement that the performance of FCEVs with respect to durability, cold start, packaging, acceleration, refueling time, and range has progressed to the point where vehicles that could be brought to market in 2015 will satisfy customer expectations.

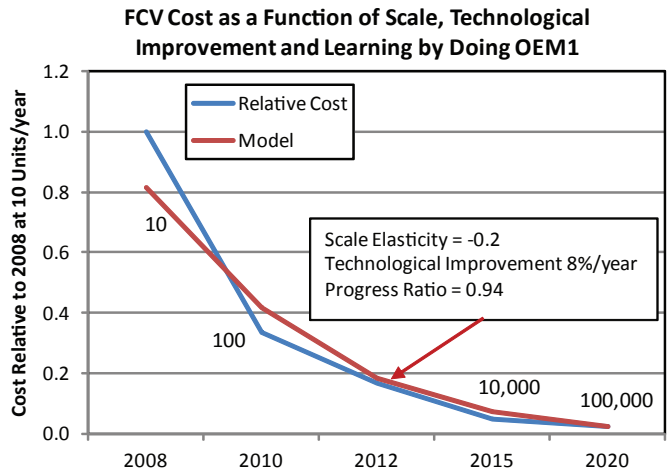

Source: Oak Ridge National Laboratory

[2] http://hydrogen.energy.gov/pdfs/13006_ldv_life_cycle_costs.pdf.

- **Commercial Products and Patents Resulting from DOE Sponsored R&D**
  Pacific Northwest National Laboratory continues to analyze the commercial benefits of the program by tracking the commercial products and technologies, and patents developed from the Energy Efficiency and Renewable Energy Office (EERE) funding. The benefits of EERE-funded projects continue to grow as illustrated in the figures below. Over 450 patents were awarded and 41 products were commercialized by 2013 as a result of research funded by EERE in the areas of storage, production, delivery, and fuel cells which will be highlighted in the FY 2013 Pathways to Commercial Success Report[3].

Cumulative Number of Patents Awarded

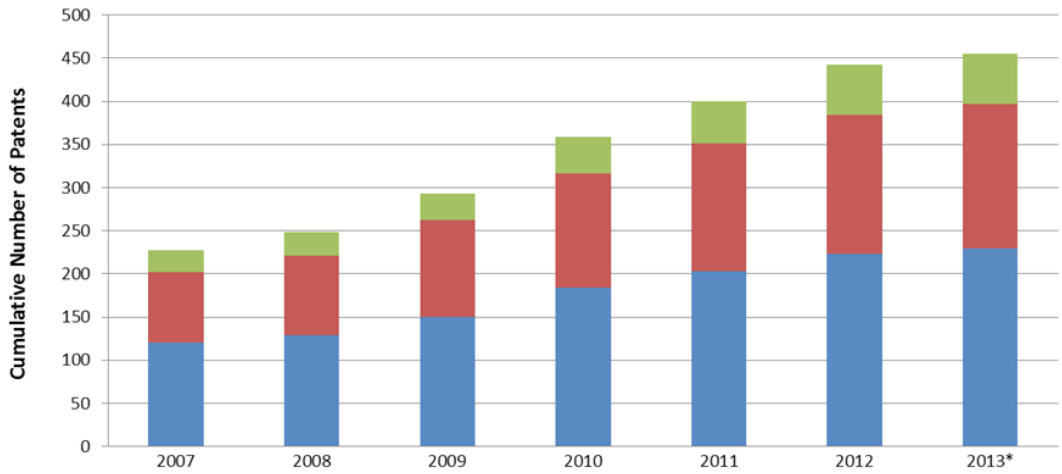

	2007	2008	2009	2010	2011	2012	2013*
Storage	24	26	30	41	47	57	58
Production/Delivery	82	93	112	132	148	161	167
Fuel Cell	121	129	151	185	204	224	230
Total	227	248	293	358	399	442	455

*Partial data for 2013

Source: Pacific Northwest National Laboratory

Cumulative Number of Commercial Products Entering the Market

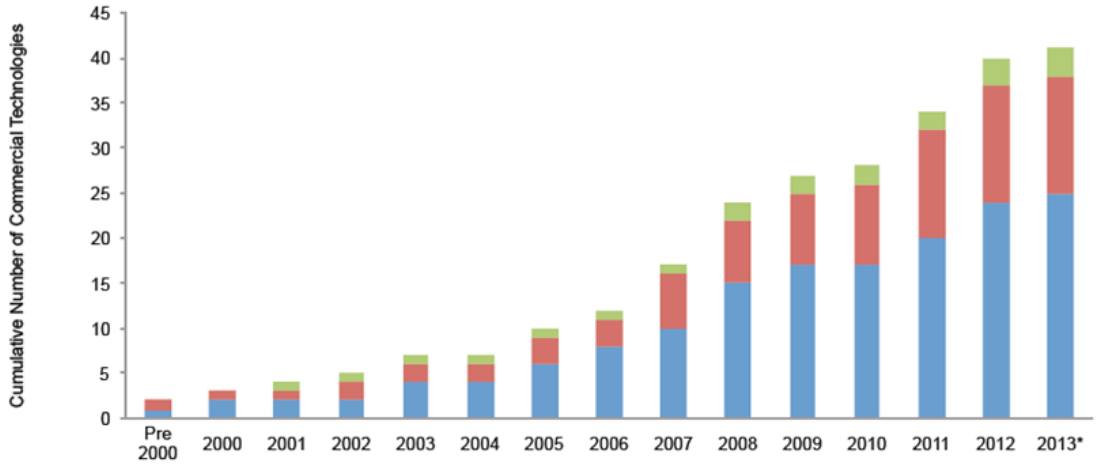

	Pre 2000	2000	2001	2002	2003	2004	2005	2006	2007	2008	2009	2010	2011	2012	2013*
Storage	0	0	1	1	1	1	1	1	1	2	2	2	2	3	3
Production/Delivery	1	1	1	2	2	2	3	3	6	7	8	9	12	13	13
Fuel Cell	1	2	2	2	4	4	6	8	10	15	17	17	20	24	25
Total	2	3	4	5	7	7	10	12	17	24	27	28	34	40	41

*Partial data for 2013.

Source: Pacific Northwest National Laboratory

[3] http://www1.eere.energy.gov/hydrogenandfuelcells/pdfs/pathways_2013.pdf.

BUDGET

The budget for the Systems Analysis program is consistent with the goals and objectives of the program and is responsive to assessing fuel cell applications for energy storage, stationary power generation, specialty applications, and light duty transportation. The FY 2014 budget request includes funding for early fuel cell and hydrogen market and infrastructure analysis, as well as renewable resource evaluation, environmental and resource life cycle analysis, overall program analysis, socio-economic analysis of fuel cell and hydrogen market growth, modeling, and systems integration. New fuel cell opportunities for energy storage and integration with existing energy supply networks such as natural gas transmission will continue to be evaluated.

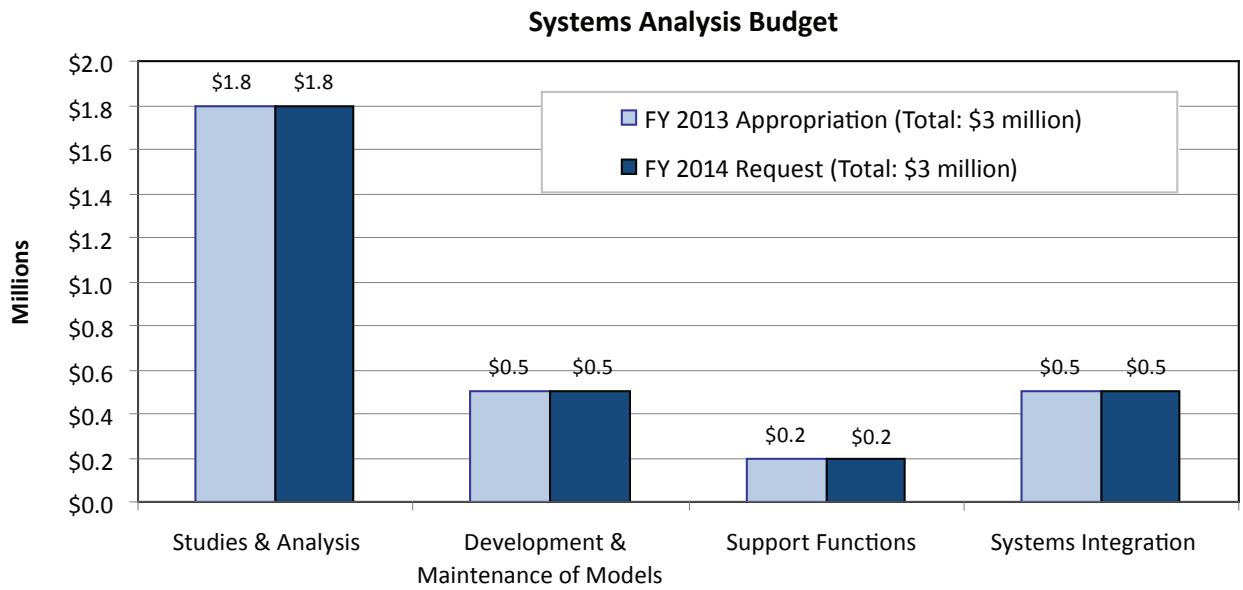

FY 2014 PLANS

The Systems Analysis activity for FY 2014 will focus on conducting analyses to determine technology gaps for fuel cell systems and infrastructure for different applications, benefits, and opportunities for new onboard storage options and utilizing fuel cells for energy storage and transport. Analyses will be focused on understanding the tradeoffs and regional impacts of fuel cells with other alternative fuels, light-duty vehicle life cycle costs for multiple platforms, socio-economic impacts of job creation based on hydrogen supply infrastructure development and other fuel cell technologies, and the synergies of linking stationary fuel cell power generation and hydrogen generation from combined heat, hydrogen and power applications with early market power and light-duty vehicle electricity and hydrogen demands. The FY 2013 appropriation included $3 million for Systems Analysis; the FY 2014 request is also $3 million. The budget request for FY 2014 reflects the focus on early market analysis, fuel cell technology evaluations, and renewable fuel benefits, as well as biogas and water resource and infrastructure analysis.

Fred Joseck
Systems Analyst
Fuel Cell Technologies Office
U.S. Department of Energy
1000 Independence Ave., SW
Washington, D.C. 20585-0121
Phone: (202) 586-7932
Email: Fred.Joseck@ee.doe.gov

XI.1 Worldwide Status of Hydrogen Fuel Cell Vehicle Technology and Prospects for Commercialization

David L. Greene
Oak Ridge National Laboratory (ORNL)
2360 Cherahala Boulevard
Knoxville, TN 37932
Phone: (865) 946-1310
Email: dlgreene@ornl.gov

DOE Manager
Fred Joseck
Phone: (202) 586-7932
Email: Fred.Joseck@ee.doe.gov

Subcontractor:
Gopal Duleep, HD Systems, Washington, DC

Project Start Date: August 2012
Project End Date: September 2013

Overall Objectives

- Describe the worldwide status of automotive fuel cell technology.
- Estimate the likely costs of automotive fuel cell systems and components.
- Assess current worldwide plans for deployment of hydrogen refueling infrastructure.

Fiscal Year (FY) 2013 Objectives

- Document the status of automotive fuel cell technology based on discussions with experts at automobile manufacturers, public presentations, and the published literature.
- Estimate the likely costs of automotive fuel cell systems and components in 2015 and 2020 at low (20,000/year) and high (200,000/year) production volumes.
- Describe current plans for deployment of hydrogen refueling infrastructure and expectations for early sales of hydrogen fuel cell vehicles (FCVs).
- Obtain thorough review by original equipment manufacturers (OEMs) of the information they provided. Publish a final report as an ORNL Technical Memorandum summarizing confidential information in such a way that manufacturer-specific data is not identified.

Technical Barriers

This project addresses the following technical barriers from the Systems Analysis section of the Fuel Cell Technologies Office Multi-Year Research, Development, and Demonstration Plan:

(A) Future Market Behavior

(C) Inconsistent Data, Assumptions and Guidelines

Contribution to Achievement of DOE Systems Analysis Milestones

This project contributes to achievement of the following DOE milestones from the Systems Analysis section of the Fuel Cell Technologies Office Multi-Year Research, Development, and Demonstration Plan:

- Milestone 1.12: Complete an analysis of the hydrogen infrastructure and technical target progress for technology readiness. (4Q, 2015)
- Milestone 1.16: Complete analysis of program performance, cost status, and potential use of fuel cells for a portfolio of commercial applications. (4Q, 2018)
- Milestone 1.17: Complete analysis of program technology performance and cost status, and potential to enable use of fuel cells for a portfolio of commercial applications. (4Q, 2018)
- Milestone1.18: Complete life cycle analysis of vehicle costs for fuel cell electric vehicles compared to other vehicle platforms. (4Q, 2019)
- Milestone 1.19: Complete analysis of the potential for hydrogen, stationary fuel cells, fuel cell vehicles (FCVs), and other fuel cell applications such as material handling equipment including resources, infrastructure and system effects resulting from the growth in hydrogen market shares in various economic sectors. (4Q, 2020)

By documenting the current status of automotive fuel cell technology in terms of performance and cost, this study provides an updated benchmark of progress toward program research and development (R&D) targets that explains progress to date and informs analyses of future market potential.

FY 2013 Accomplishments

- Completed a written review of the current status of automotive fuel cell technology performance and cost based on published and publicly available sources.

- Obtained input from U.S., Japanese, Korean and German OEMs about status of fuel cell technology.
- Published final report on status and prospects for worldwide automotive fuel cells and deployment of hydrogen refueling infrastructure, after thorough review.

✧ ✧ ✧ ✧ ✧

INTRODUCTION

At least eight of the world's largest automobile manufacturers have plans to bring FCVs to market sometime between 2013 and 2020. Governments in the Members of the European Union (EU), United States, Japan and Korea have developed plans to deploy hydrogen refueling infrastructure to support the early market introduction of hydrogen FCVs. This study assesses the current status of automotive fuel cell technology and the plans for deploying of refueling infrastructure.

APPROACH

Interviews with the leading OEMs and with governmental agencies and non-governmental organizations in the United States, Japan, South Korea and Germany were conducted in late summer and fall of 2012. The information obtained was combined with data from the open literature and public meetings, and analyzed with the objective of providing a comprehensive view of the current status of the industry and its future prospects.

RESULTS

The performance of FCVs with respect to durability, cold start, packaging, acceleration, refueling time and range has progressed to the point where vehicles that could be brought to market in 2015 will satisfy customer expectations. However, cost and the lack of refueling infrastructure remain significant barriers. Costs have been dramatically reduced over the past decade, yet are still about twice what appears to be needed for sustainable market success. While all four countries have plans for the early deployment of hydrogen refueling infrastructure, the roles of government, industry and the public in creating a viable hydrogen refueling infrastructure remain unresolved. The existence of an adequate refueling infrastructure and supporting government policies are likely to be the critical factors that determine when and where hydrogen FCVs are brought to market.

Estimates of the costs of 85-kW automotive fuel cell systems, produced in volumes of 20,000 units per year and 200,000 units per year in model year 2016 are shown in Table 1. The estimates are based on the published literature [1-3] and information provided in discussions with OEMs. By far the largest component of total cost in low volume, near future production will be the fuel cell stack. Hydrogen storage tanks will be the third largest component after the cost of the vehicle glider.

TABLE 1. Central Tendency Estimates of FCV Cost at 20K/yr Production Volume Extrapolated to 200K/yr Volume

Cost in $	2016 (20K/yr)	2016 (200K/yr)
Fuel cell stack (85 kW)	24,000	15,150
Hydrogen storage (5 kg)	6,700	5,300
Battery (35 kW,2 kWh)	1,500	1,300
Electric Motor/Inverter/Drive (110 kW peak, 60 kW continuous)	3,600	3,150
Gearbox	400	350
Total Powertrain	**36,200**	**25,250**
Electric HVAC/Regenerative Brakes (incremental)	800	750
Glider	11,000	11,000
Total FCV cost	**48,000**	**37,000**

HVAC – heating, ventilation and air conditioning

High volume (200,000 units/year) cost estimates for 2016 and beyond 2020 are compared in Table 2. If high volumes could be achieved after 2020, fuel cell stack costs would still be in the neighborhood of $13,000 to $14,000, given today's technology. With significant advances in areas such as platinum loadings and membranes, fuel cell stack and balance of plant costs could be halved relative to high volume, 2016 costs (Table 1).

TABLE 2. Estimates of FCV Cost at 200K/yr Production Volume for 2016 and 2020+

Cost in $	2016 (200K/yr)	2020+ (200K/yr) without breakthrough	2020+ (200K/yr) with technology breakthrough
Fuel cell stack (85 kW)	15,150	13,650	7,575
Hydrogen storage (5 kg)	5,300	4,750	3,500
Battery (35 kW,2 kWh)	1,300	975	975
Electric Motor/Inverter/Drive (110 kW peak, 60kW continuous)	3,150	2,825	2,400
Gearbox	350	350	350
Total Powertrain	**25,250**	**22,550**	**14,800**
Electric HVAC/Regenerative Brakes (incremental)	750	650	650
Glider (constant weight)	11,000	11,000	11,000
Total FCV cost	**37,000**	**33,200**	**26,300**

The advances that are needed to achieve competitive costs for FCVs by 2020 are consistent with reasonably

conservative estimates of scale economies, learning by doing and technological progress driven by R&D. Based on data provided by OEMs, it is estimated that a scale elasticity (percent change in cost with a 1% increase in production volume) of approximately -0.2 together with a progress ratio of approximately 0.95 (5% cost reduction for each doubling of production volume) and R&D driven technological progress of 5% to 8% per year would be sufficient to achieve the post 2020 high volume cost estimates (Table 2, "with breakthrough"). Estimates of the three parameters based on information provided by three different OEMs are shown in Figures 1-3.

California, Germany, Japan, South Korea and other countries intending to create markets for FCVs have developed plans for deploying hydrogen refueling infrastructure. At present, the hydrogen stations in operation are few and intended for demonstration purposes but their numbers are increasing. As the study was being completed in early 2013, the internet site H2Stations.org reported 18 stations operating in California, 30 in Germany, 29 in Japan and 12 in South Korea (as of August 2013, 24 stations were in operation in California: http://hydrogen.pnl.gov/cocoon/morf/hydrogen/article/707). In general, both planning and funding is being carried out cooperatively by automotive and energy industries, non-governmental organizations and governments. Coordinating station deployments and vehicle sales will be a major challenge. Every region is facing major uncertainties about how consumers will respond to hydrogen FCVs and limited fuel availability, the costs and availability of vehicles and hydrogen fuel, how the construction and operation of stations will be funded and what other supporting policies may be needed.

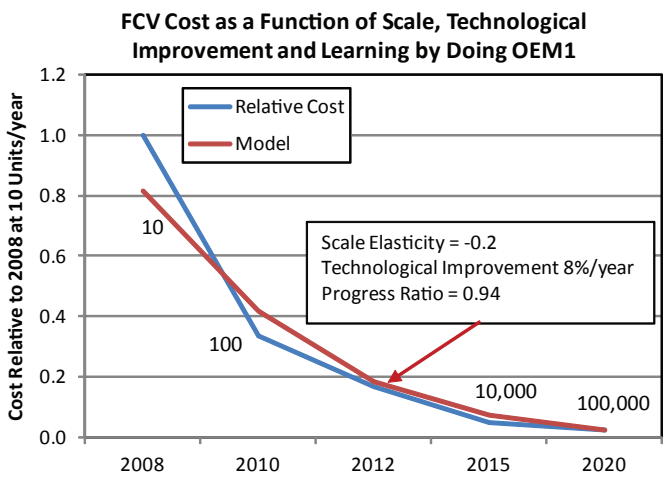

FIGURE 1. FCV Cost as a Function of Scale, Technological Improvement and Learning by Doing: OEM1.

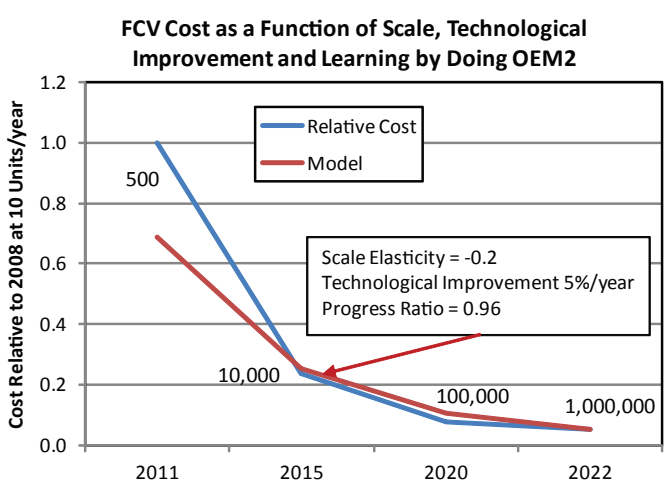

FIGURE 2. FCV Cost as a Function of Scale, Technological Improvement and Learning by Doing: OEM2.

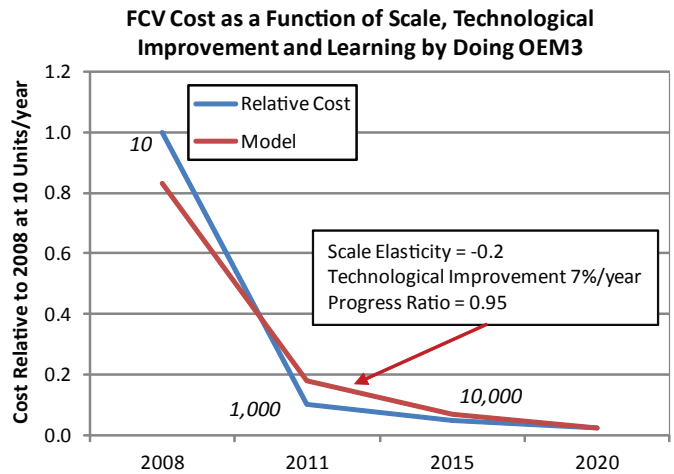

FIGURE 3. FCV Cost as a Function of Scale, Technological Improvement and Learning by Doing: OEM3.

Together with the cost of FCVs, availability of hydrogen refueling stations is the OEMs' greatest concern at the present time and will strongly affect their plans for producing FCVs. Public and private statements by OEMs and independent evaluations of FCV technology all indicate that FCVs have met the performance benchmarks necessary for sales to the public to begin in 2015, if not sooner. Durability, energy efficiency, cold start, acceleration, refueling, packaging, and range goals have all been met.

OEMs are now focused on cost reduction and the deployment of an adequate refueling infrastructure. Midsize fuel cell passenger cars introduced in 2015-2017 could sell for $50,000 to $60,000, assuming manufacturers do not attempt to recoup full overhead costs. However, further technological progress will be necessary to reduce fuel cell system costs by another 50%, as is generally believed to be required for a sustainable FCV market. These goals could be achieved by

2020-2025, assuming plausible scale economies, and rates of learning and technological progress.

CONCLUSIONS AND FUTURE DIRECTIONS

- There is general agreement that the performance of FCVs with respect to durability, cold start, packaging, acceleration, refueling time and range has progressed to the point where vehicles that could be brought to market in 2015 will satisfy customer expectations.
- Fuel cell system cost and the lack of refueling infrastructure remain significant barriers to market success for FCVs. Costs have been dramatically reduced over the past decade, yet are still about twice what appears to be needed for sustainable market success.
- The U.S. (especially California), Germany, Japan and South Korea all have plans for the early deployment of hydrogen refueling infrastructure, yet the roles of government, industry and the public in creating a viable hydrogen refueling infrastructure remain unresolved.
- The existence of an adequate refueling infrastructure and supporting government policies are likely to be the critical factors that determine when and where hydrogen FCVs are brought to market.

It is recommended that this assessment be carried out bi-annually to provide updated information on progress towards commercialization and market success.

FY 2013 PUBLICATIONS/PRESENTATIONS

1. Greene, D.L. and G. Duleep, 2013. "Status and Prospects of the Global Automotive Fuel Cell Industry and Plans for Deployment of Fuel Cell Vehicles and Hydrogen Refueling Infrastructure", ORNL/TM-2013/222, Oak Ridge National Laboratory, Oak Ridge, Tennessee, June.

2. Greene, D.L., C. Liu and S. Park, 2013. "Transition from Petro-Mobility to Electro-Mobility", in D. Stolten and V. Scherer, eds., *Transition to Renewable Energy Systems,* Wiley-VCH, Weinheim, Germany.

3. Greene, D.L., "The Transition from Petro-mobility to Electro-mobility", presented at the 3rd International Conference on Energy Process Engineering, Frankfurt, Germany, June 6, 2013.

4. Greene, D.L. and G. Duleep, "Worldwide Status of Hydrogen Fuel Cell Vehicle Technology and Prospects for Commercialization", presentation at the DOE Fuel Cell Technologies Annual Merit Review and Peer Evaluation Meeting, Arlington, VA, May 14, 2013.

5. Greene, D.L., "Transitions to Alternative Vehicles and Fuels", presentation to the Hydrogen Technical Advisory Committee, Washington, D.C., April 23, 2013.

REFERENCES

1. McKinsey & Co. 2011. A Portfolio of Powertrains for Europe: A Fact-Based Analysis, sponsored in part by National Organisation Wasserstoff, Berlin, available on the internet at http://ec.europa.eu/research/fch/pdf/a_portfolio_of_power_trains_for_europe_a_fact_based__analysis.pdf.

2. (NRC) National Research Council. 2013. Transitions to Alternative Vehicles and Fuels, Appendix F, "Vehicles," National Academies Press, Washington, DC.

3. James, B.D., J.M. Moton and W.G. Colella. 2013. "Fuel Cell Transportation Cost Analysis," U.S. Department of Energy 2013 Annual Merit Review and Peer Evaluation Meeting for the Hydrogen and Fuel Cell Technologies Program, Arlington, Virginia, May 14.

XI.2 Siting Strategies for Early H_2 Refueling Infrastructure in California: Learning from the Gasoline Experience

Michael Nicholas
Institute of Transportation Studies
University of California
1605 Tilia Street
Davis, CA 95616
Phone: (530) 754-4408
Email: mianicholas@ucdavis.edu

DOE Manager
Fred Joseck
Phone: (202) 586-7932
Email: Fred.Joseck@ee.doe.gov

Contract Number: 1F-30841

Project Start Date: January 1, 2011
Project End Date: December 31, 2014

Overall Objective

Provide analysis to support hydrogen and fuel network development.

Fiscal Year (FY) 2013 Objectives

- Determine the minimum number of stations necessary for the maximum number of customers to reduce investment necessary.
- Analyze strategies for early hydrogen fueling station placement, numbers, and network development to enable fuel accessibility for initial rollout of hydrogen fuel cell passenger cars.
- Conduct case studies for H_2 fuel cell vehicle rollout in California utilizing geographic information system (GIS)-based analysis for station siting and consumer convenience from the perspective of the network.

Technical Barriers

This project addresses the following technical barriers from the Systems Analysis section of the Fuel Cell Technologies Office Multi-Year Research, Development, and Demonstration Plan:

(A) Future Market Behavior

(C) Inconsistent Data, Assumptions and Guidelines

(D) Insufficient Suite of Models and Tools

Contribution to Achievement of DOE Systems Analysis Milestones

This project will contribute to achievement of the following DOE milestones from the Systems Analysis section of the Fuel Cell Technologies Office Multi-Year Research, Development, and Demonstration Plan:

- Milestone 1.20: Complete review of fuel cell and hydrogen markets. (4Q, 2011 through 4Q, 2020)
- Milestone 1.4: Complete evaluation of fueling station costs for early vehicle penetration to determine the cost of fueling pathways for low and moderate fueling demand rates. (4Q, 2012)

FY 2013 Accomplishments

- Assessed alternative strategies for introducing fuel cell vehicles and H_2 infrastructure in Southern California over the next decade to satisfy the California Zero Emission Vehicle regulation. Considered station placement, number, size, and type of stations.
- Assessed tradeoffs in terms of convenience from the home and while travelling around the Los Angeles region.
- Presented results in reports and talks at meetings.
- Collaborated with California Fuel Cell Partnership (CAFCP) and other stakeholders and analysts.

✧ ✧ ✧ ✧ ✧

INTRODUCTION

What constitutes a sufficient hydrogen network to initiate a market launch of vehicles has evolved over time. Most approaches have centered around a percentage of stations—for example, "a network should have 10% of existing gasoline stations offering an alternative fuel" or similar. However, such a transformation has an inherent boundary problem. Would this mean 10% of stations in a state? In the entire world? A city? This paper attempts to decouple the percentage of stations from the area which is being studied into the important metrics that the percentage is supposed to embody. In this way, smaller areas can be considered for market launch, and the capital outlay can be reduced.

APPROACH

In order to explore how many stations are needed for a market launch, we considered a likely early market area, Los Angeles, and examined the necessary number of stations from two perspectives important to owners and drivers: distance of the station from home (Figure 1) and distance while travelling around (Figure 2). For this study, we looked only at likely market deployment areas in Los Angeles by the California Fuel Cell Partnership which we called "market clusters" (Figure 3) and examined the population and traffic patterns for which these clusters were responsible. If this strategy can provide convenience for those vehicle owners based on these metrics, then a more far-reaching percentage of stations is not needed.

RESULTS

Clustering demand reduces the number of stations that are required to satisfy a given number of customers. Restricting stations solely to clusters has no detrimental effects on home-based refueling, but it reduces regional mobility. Although the majority of refueling is local, smaller stations that enable travel throughout the region, and perhaps in nearby regions, provide flexibility in planning how to refuel and ease the fear of running out of fuel.

Redundancy and reliability can be addressed in several ways. First, the number of stations can be increased. Second, backup capacity in the form of mobile refuelers can supplement the network when stations go down. Third, the redundancy and reliability concerns can be ameliorated with an integrated navigation and refueling information system.

The minimum number of stations per cluster in the scenarios is two to provide redundancy in the case of a station failure. However, the number of stations necessary for convenience in each cluster needs to be evaluated for every cluster separately. Generally, customers are currently about one minute away from their nearest gasoline station. Siting two hydrogen stations in downtown Los Angeles results in a 2.1 minute average travel time, whereas siting two stations in the Torrance cluster results in a 3.7 minute average travel time to a station. Creating parity in the number of minutes to the nearest station among regions may be more important than creating parity in the number of stations among clusters. As mentioned before, the size of the area in which vehicles are marketed could be reduced to bring parity in terms of travel time from home to station.

Varying the number of clusters from four to 12 presents some interesting tradeoffs given a fixed number of stations. Given 16 stations, and the choice of four, six, or eight clusters, the anomalous drop in home to station time because

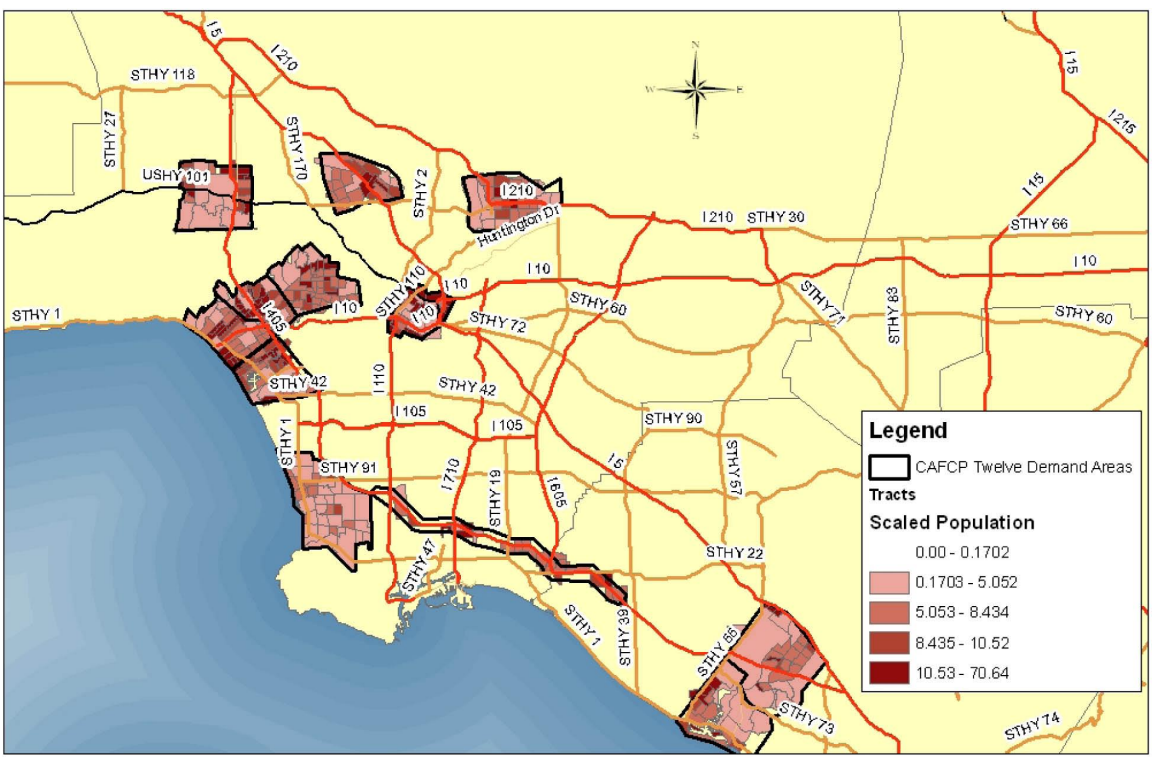

FIGURE 1. Population distribution scaled within the clusters so that each cluster represents the same number of people. Population is a proxy for attractiveness of vehicle placement. Having each cluster represent the same number of vehicles implies that each cluster is equally attractive.

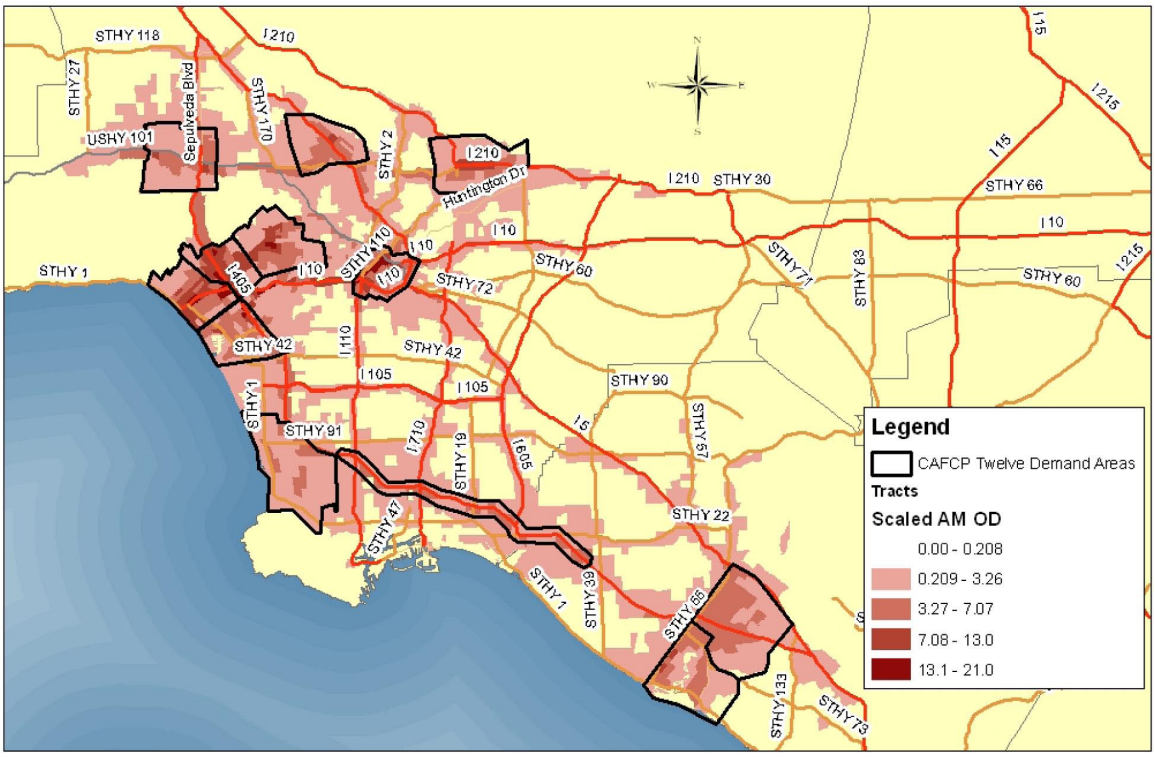

FIGURE 2. Scaled vehicle miles traveled using only trips originating within the 12 clusters during the AM period. Data were aggregated to census tracts and display was normalized by tract land area.

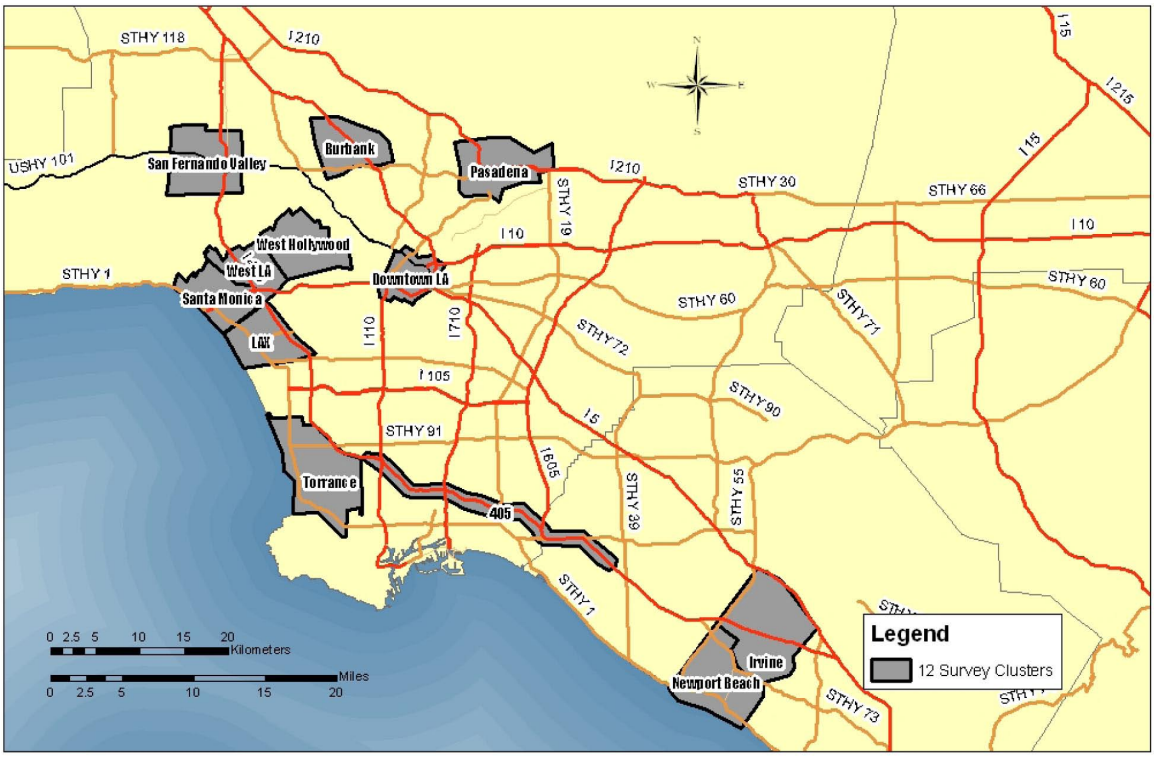

FIGURE 3. The shaded regions define the possible clusters where vehicles will be placed.

of Irvine notwithstanding, adding connector stations reduced diversion time more than adding new clusters. However, it is recognized that adding stations where there are not future market clusters presents a problem with finding partners to help site and construct the station. Stations sited outside of future market clusters may also not find a sufficient load to make them cost-effective. Therefore, a strategy of siting connector stations in future market clusters may be the most effective strategy. Interestingly, using the traffic from the four-cluster scenario, some connector stations fell into future market areas such as downtown Los Angeles, west Los Angeles, and the I-405 corridor, pointing to a possible bridging strategy to progress from rollouts in one cluster to the next.

CONCLUSIONS AND FUTURE DIRECTIONS

Overall, we find that a cluster strategy provides good refueling convenience and reliability with a relatively small number of strategically placed stations, reducing infrastructure costs. There are some limitations to this work in that it relies solely on modeling of people's needs rather that surveying respondents. We expect to find that customers would like a few stations placed far away from home for infrequent but very important trips. However, for most driving, the cluster strategy is a promising path towards reducing initial infrastructure needs in terms of total number of stations needed.

Future work

- Extend the California rollout analysis to analyze H_2 infrastructure build-out in other U.S. regions.
- Determine the market for hydrogen vehicles as a function of distance from station.
- Examine clusters that grow organically rather than decide them a priori.

FY 2013 PUBLICATIONS/PRESENTATIONS

1. Michael Nicholas and Joan Ogden, "Analysis of Rollout Strategies for Fuel Cell Vehicles and Hydrogen Infrastructure in California," presented at the UC-DOE Hydrogen Technical Advisory Committee Meeting, November 15, 2012, Alexandria, VA.

2. Joan Ogden and Michael Nicholas, "Tools for Modeling Rollout Strategies for Fuel Cell Vehicles and H2 Infrastructure," presented at NREL Hydrogen System Analysis meeting, March 12, 2013.

3. Joan Ogden, "Design and Economics of an Early Hydrogen Refueling Network for California," USDOE, project an032, Hydrogen and Fuel Cells Annual Merit Review, Arlington, VA, May 14, 2013.

4. Michael Nicholas, "Siting Strategies for Early H2 Refueling Infrastructure in California: Learning from the Gasoline Experience," project an031. USDOE, Hydrogen and Fuel Cells Annual Merit Review, Arlington, VA, May 14, 2013.

XI.3 Design and Economics of an Early Hydrogen Refueling Network for California

Joan Ogden
Institute of Transportation Studies
University of California
1715 Tilia Street
Davis, CA 95616
Phone: (530) 752-2768
Email: jmogden@ucdavis.edu

DOE Manager
Fred Joseck
Phone: (202) 586-7932
Email: Fred.Joseck@ee.doe.gov

Contract Number: 1F-30841

Project Start Date: January 1, 2011
Project End Date: December 31, 2014

Overall Objectives

Provide system-level technical and economic analysis to support initial rollout of hydrogen and fuel cell technologies.

Fiscal Year (FY) 2013 Objectives

- Analyze strategies for early hydrogen fueling station placement, numbers and network development, to enable fuel accessibility for initial rollout of hydrogen fuel cell passenger cars.
- Develop robust data on costs and performance for early stations and scenarios and strategies for deployment.
- Conduct case studies for H2 fuel cell vehicle (FCV) rollout California, utilizing GIS-based analysis for station siting and consumer convenience and economics from perspective of the network, individual station owners and consumers (fuel cost).

Technical Barriers

This project addresses the following technical barriers from the Systems Analysis section of the Fuel Cell Technologies Office Multi-Year Research, Development, and Demonstration Plan:

(A) Future Market Behavior

(C) Inconsistent Data Assumptions and Guidelines

(D) Insufficient Suite of Models and Tools

Contribution to Achievement of DOE Systems Analysis Milestones

This project will contribute to achievement of the following DOE milestones from the Systems Analysis section of the Fuel Cell Technologies Office Multi-Year Research, Development, and Demonstration Plan:

- Milestone 1.20: Complete review of fuel cell and hydrogen markets. (4Q, 2011 through 4Q, 2020)
- Milestone 1.4: Complete evaluation of fueling station costs for early vehicle penetration to determine the cost of fueling pathways for low and moderate fueling demand rates. (4Q, 2012)

FY 2013 Accomplishments

- Assessed alternative strategies for introducing FCVs and H2 infrastructure in Southern California over the next decade to satisfy the California Zero Emission Vehicle regulation. Considered station placement, number, size, and type of stations.
- Analyzed infrastructure economics from multiple perspectives: network, station owner, consumer. A spreadsheet model was developed to analyze different rollout scenarios.
- Presented results in reports and talks at meetings.
- Collaborated with California Fuel Cell Partnership and other stakeholder and analysts.

✧ ✧ ✧ ✧ ✧

INTRODUCTION

The cost and logistics of building early hydrogen refueling infrastructure are key barriers to the commercialization of hydrogen FCVs. Finding attractive infrastructure strategies is important to enable the initial introduction of hydrogen vehicles, when demand is small, and infrastructure must be closely coordinated with vehicle deployment. In this research, we explore the economics of a ‘‘cluster strategy’’ for introducing hydrogen vehicles and refueling infrastructure. Clustering refers to coordinated introduction of hydrogen vehicles and refueling infrastructure in a few focused geographic areas such as smaller cities (e.g. Santa Monica, Irvine) within a larger region (e.g. Los Angeles Basin) [1]. We analyze the design and economics of early hydrogen infrastructure networks over the next 10 years focusing on California, a likely site

for introduction of hydrogen FCVs in support of the state's Zero Emission Vehicle regulation. Several DOE Systems Analysis goals are addressed in this work. It contributes to understanding future markets by illuminating how hydrogen might be supplied to early adopters of FCVs. Further, it helps fill gaps in station cost data and modeling.

APPROACH

To analyze alternative scenarios for building up hydrogen infrastructure over time, we developed an EXCEL-based hydrogen infrastructure rollout spreadsheet model (called HIR). Current and future hydrogen station capital and operation and maintenance (O&M) costs were estimated based on input from industry, the California Fuel Cell Partnership, the California Energy Commission and DOE analysts at the National Renewable Energy Laboratory, Oak Ridge National Laboratory and Argonne National Laboratory. We consider a range of station sizes (100 kg/d to 1000 kg/d), station types (compressed gas truck delivery, liquefied H2 truck delivery, onsite reformer, onsite electrolyzer), and technical maturity (current, 2014-5, 2015+). Our model is flexible and allows the user to run cases rapidly, to analyze a variety of hydrogen supply options, station sizes and types, and conduct sensitivity studies.

We analyzed infrastructure economics from several perspectives: the whole network, the individual station owner and the consumer (delivered hydrogen cost at the pump). Our modeling estimates how many stations would be needed and how much it will cost to develop cost competitive hydrogen supply. Outputs from the model include numbers and types of stations built, capital costs and O&M costs, hydrogen sales and cash flow over at each year. From the cash flow analysis we estimate a break-even year (the year when the station produces H2 competitively with gasoline on a cents per mile basis) and the subsidies required for various stakeholders.

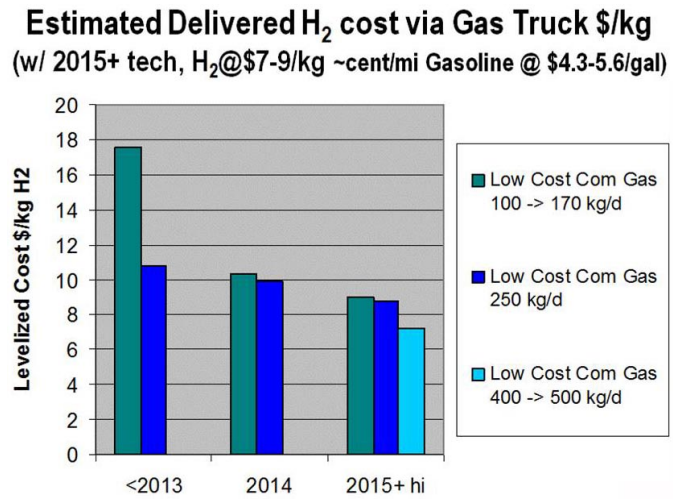

FIGURE 1. Estimated Delivered H2 Cost via Gas Truck $/kg

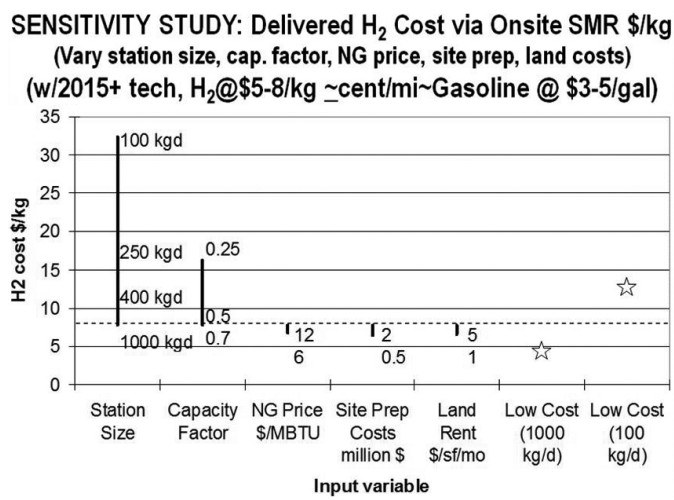

FIGURE 2. Sensitivity Study: Delivered H2 Cost via Onsite SMR $/kg

RESULTS

First we used our model to compare the cost of hydrogen from different types and sizes of hydrogen stations under steady-state conditions when stations are fully utilized.

- Results are shown in Figure 1 for stations based on compressed gas truck delivery. The levelized hydrogen cost ($/kg) is plotted for three time periods corresponding to present, 2014, and 2015+ technology and three different station sizes, from 100-500 kg/d. The cost of hydrogen decreases over time with technology improvement and with increased station size. For large stations beyond 2015, we find hydrogen costs of $7-9/kg equivalent on a cents per mile basis to gasoline at $4.3-5.6/gallon.
- Figure 2 illustrates a hydrogen cost sensitivity study for onsite reformer stations for changes in station size, utilization, natural gas cost, and other factors. For 1,000 kg/d onsite steam methane reformer (SMR) stations, we estimate costs of $5-8/kg depending on the input assumptions.

Alternative rollout scenarios were analyzed for introducing tens of thousands of FCVs and 60 to 80 stations in Southern California over the next 5-10 years, varying numbers and types of stations over time (an example station build-out schedule is shown in Figure 3: we analyzed many variations on this). The rollout analysis yielded the following key results:

- We estimate that 60-80 hydrogen stations would be needed to support 34,000 FCVs in Southern California c. 2018. (This fuel cell vehicle population was estimated by the California Fuel Cell Partnership based on a 2010 survey of automakers.) In the first few years relatively

small stations are built, in later years larger stations are added (Figure 3).

- Capital investments of $113-160 million would be needed to build a station network depending on the sizes and types of stations assumed (based on 700 bar stations ranging in size from 100 to 1,000 kg/d). This is about $3,000-5,000 per car served for the first 60-80 stations. As more vehicles are deployed, the network expands, larger stations are built and the cost of hydrogen becomes competitive on a cents per mile basis with gasoline.
- Cash flow calculations were carried out for the whole network (Figure 4) and for an individual 500 kg/d station (Figure 5). Annual costs for station capital and operating costs and the annual revenue from hydrogen sales are shown (assuming that the station demand ramps up to 100% over four years as more FCVs arrive).
  - For the first few years, the network cash flow is negative, but it becomes positive after about 2017 as stations are better utilized (more hydrogen sales) and larger stations are added. The network breaks even in 5-7 years (Figure 4).
  - An early strategy using gas truck delivery yields H2 costs of <$10/kg. If (H2 selling price) – (truck delivered H2 cost) ≥$4/kg, the network breaks even in less than eight years.
  - The individual 500 kg/d station costing $1.5 million has cash flow >0 within a few years (assuming rapid market growth). Support to compensate for early negative cash flow ~$400-700K per station.
- We estimated a subsidy of $50-70 million would be sufficient to support early network development to launch a competitive supply network. This accounts for capital + O&M for 18 small stations (100-250 kg/d) and support for sixty 500 kg/d stations until the cash flow becomes positive. Beyond this point, new 500 kg/d stations would make money selling H2 at competitive prices, assuming continued rapid market growth.

This research helps illustrate viable scenarios for H2 infrastructure rollout and highlight sensitivities. It contributes to understanding future markets by illuminating how hydrogen might be supplied to early adopters of FCVs. Further, it helps fill gaps in station cost data and modeling tools.

FIGURE 3. Scenario for Introducing 78 Stations in Southern California by Station Size and Type

#New Sta	2011	2012	2013	2014	2015	2016	2017
Mobile Refueler	4	0	0	0	0	0	0
Compressed Gas Truck Delivery							
170 kg/d	0	0	4	0	0	0	0
250 kg/d	0	0	0	10	0	0	0
400 kg/d	0	0	0	0	20	20	20
Total sta. capacity (kg/y)	400	400	1080	3580	11580	21580	31580
# FCVs in fleet	197	240	347	1161	12106	23213	34320
H2 demand (kg/y)	137	168	250	800	8500	16000	24000

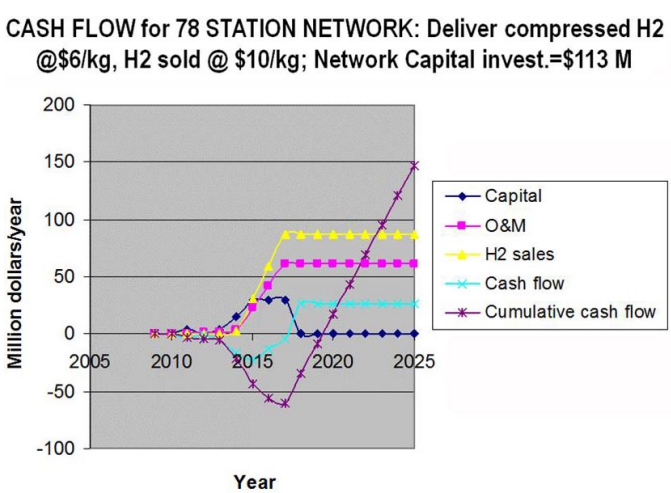

FIGURE 4. Cash Flow for 78 Station Network

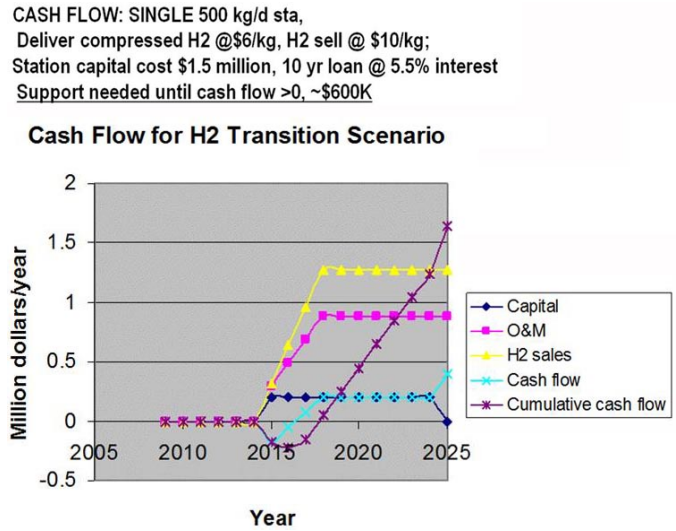

FIGURE 5. Cash Flow for Single 500 kg/d station

CONCLUSIONS AND FUTURE DIRECTIONS

Overall, we find that a cluster strategy provides good refueling convenience and reliability with a relatively small number of strategically placed stations, reducing infrastructure costs. There appear to be viable paths toward a cost competitive hydrogen supply network beyond 2017, assuming that markets for FCVs grow rapidly.

Future work

- Extend California rollout analysis to analyze H2 Infrastructure build out in other U.S. regions.
- Look at the potential role of tri-generation systems that co-produce electricity and heat for buildings and hydrogen for vehicles in early H2 infrastructure development (residential and commercial buildings).
- Examine longer term transition from early hydrogen supply based on natural gas derived hydrogen to "green" H2 from low net carbon pathways such as renewables and fossil with carbon capture and storage. Conduct case studies for California, U.S.

FY 2013 PUBLICATIONS/PRESENTATIONS

1. Tyson Eckerle, Remy Garderet, Ken Gunn ,Catherine Dunwoody, Jackie Birdsall, Bill Elrick, Joan Ogden, Tim Brown, "Incentivizing Hydrogen Infrastructure Investment, Phase 1: An Analysis of Cash Flow Support To Incentivize Early Stage Hydrogen Station Investment," Report to the California Fuel Cell Partnership, June 18, 2012.

2. Michael Nicholas and Joan Ogden, "Analysis of Rollout Strategies for Fuel Cell Vehicles and Hydrogen Infrastructure in California," presented at the UCDOE Hydrogen Technical Advisory Committee Meeting, November 15, 2012, Alexandria, VA.

3. Joan Ogden and Michael Nicholas, "Tools for Modeling Rollout Strategies for Fuel Cell Vehicles and H2 Infrastructure," presented at NREL Hydrogen System Analysis meeting, March 12, 2013.

4. Joan Ogden, "Design and Economics of an Early Hydrogen Refueling Network for California, "USDOE, project an032, Hydrogen and Fuel Cells Annual Merit Review, Arlington, VA, May 14, 2013.

5. Michael Nicholas, "Siting Strategies for Early H2 Refueling Infrastructure in California: Learning from the Gasoline Experience", project an031. USDOE, Hydrogen and Fuel Cells Annual Merit Review, Arlington, VA, May 14, 2013.

REFERENCES

1. Joan Ogden and Michael Nicholas, "Analysis of a 'Cluster' Strategy for Introducing Hydrogen Vehicles in Southern California", *Energy Policy*, 39 (2011) 1923–1938.

XI.4 Analysis of Optimal Onboard Storage Pressure for Hydrogen Fuel Cell Vehicles

Zhenhong Lin (Primary Contact), David Greene
Oak Ridge National Laboratory
2360 Cherahala Boulevard
Knoxville, TN 37932
Phone: (865) 946-1308
Email: linz@ornl.gov, dlgreene@ornl.gov

DOE Manager
Fred Joseck
Phone: (202) 586-7932
Email: Fred.Joseck@ee.doe.gov

Project Start Date: October 1, 2012
Project End Date: September 30, 2013

Overall/Fiscal Year (FY) 2013 Objectives

- Optimize delivered H_2 pressure
- Analyze sensitivity of optimal pressure
- Compare different pressure options for California

Technical Barriers

This project addresses the following technical barriers from the Hydrogen Storage section of the Fuel Cell Technologies Office Multi-Year Research, Development, and Demonstration Plan:

(B) System Cost

(F) Codes and Standards

(K) System Life-Cycle Assessments

This project also addresses the following technical barriers from the Market Transformation section:

(B) High hydrogen fuel infrastructure capital costs for Polymer Electrolyte Membrane (PEM) fuel cell applications

Contribution to Achievement of DOE Hydrogen Storage/Market Transformation Milestones

This project will contribute to achievement of the following DOE milestones from the Hydrogen Storage and Market Transformation sections of the Fuel Cell Technologies Office Multi-Year Research, Development, and Demonstration Plan:

- Storage 3.3: Transportation: Complete economic evaluation of cold hydrogen storage against targets. (4Q, 2015)
- Storage 3.6: Update early market storage targets. (4Q, 2017)
- Storage 3.7: Transportation: Complete analysis of onboard storage options compared to ultimate targets. (4Q, 2020)
- Market Transformation 1.13: Deploy, test, and develop business cases for renewable hydrogen energy systems for power, building, and transportation sectors. (1Q, 2015)

FY 2013 Accomplishments

- Developed a spreadsheet tool to determine the optimal onboard hydrogen pressure in a regional context.
- Explained interactions between pressure, station size, and station number.
- Recommended 700 bar for Southern California after comparing the combined costs of infrastructure and refueling inconvenience resulting from 350, 500, and 700 bar, assuming 100 stations and 50,000 fuel cell electric vehicles (FCEVs) on the road as the California Fuel Cell Partnership 2017 deployment plan envisions.
- Analyzed sensitivity of optimal pressure against high-pressure incremental cost, value of time, FCEV market share, vehicle efficiency, and driving intensity.

✧ ✧ ✧ ✧ ✧

INTRODUCTION

The pressure of hydrogen delivered to hydrogen vehicles can be an important parameter that has great impact on the delivered cost of hydrogen and the range limitation obstacle of hydrogen vehicles. On one hand, higher hydrogen pressure allows more hydrogen to be stored onboard, enabling a longer driving range between hydrogen refills, but the cost of hydrogen supply infrastructure, and therefore the delivered cost of hydrogen, will be higher. However, while lower hydrogen pressure shortens the driving range and results in higher refueling frequency, the delivered hydrogen cost can be lower. Also importantly, the lower capital cost of low-pressure stations will encourage investment activities in developing more stations, resulting in better refueling convenience for consumers.

The objectives of this project are:

- Develop an optimization model to identify the delivered pressure of hydrogen that reflects tradeoff among hydrogen cost, infrastructure capital cost requirement, driving range, refueling frequency, and refueling convenience. The objective of optimization is maximization of consumer acceptance of hydrogen vehicles.
- Analyze and recommend the delivered hydrogen pressure as a function of technology cost, regional geography, hydrogen demand, and driving patterns.

APPROACH

The optimization method is formulated to reflect tradeoff between consumer refueling convenience and infrastructure costs. Higher pressure increases hydrogen storage and driving range between hydrogen refills, but increases the cost of delivery infrastructure and the cost of hydrogen. To simplify the problem, FCEVs are assumed to be equipped with high-pressure-capable tanks. A region-wide optimal infrastructure roll-out scheme, as opposed to cluster strategies, is implicitly assumed. That is, hydrogen stations are implicitly assumed to be optimally located to minimize the expected refueling travel time of a random motorist.

Specifically, the optimal pressure is solved for by equating the marginal value of increased range due to increased pressure to the marginal H_2 delivered cost due to increased pressure. This is equivalent to minimization of combined costs of refueling inconvenience and stations. The marginal value of increased range due to higher pressure is measured by reduction of net present value of total refueling time over 5 years. Refueling time includes access time to station (depends on availability) and refueling time at station. The marginal cost of increased pressure includes the resulting increased cost of pumps, tanks, and energy use. Based on discussions with the Fuel Pathway Integration Technical Team of U.S. DRIVE, these metrics are assumed for the baseline: a mid-size FCEV car with 60 miles per gasoline gallon equivalent fuel economy; a representative driver who drives 12,800 miles per year and values refueling travel time at $50/hour; a dispenser linger time of 2.4 minutes; hydrogen filling time of 1.6 kg/min; $4.50/kg delivered hydrogen cost at 700 bar and $4.00/kg at 350 bar, both with full utilization (based on H2A models); and Southern California as the regional context.

RESULTS

The optimal pressure is found to decrease with availability of more hydrogen stations or larger stations. As shown in Figure 1, the optimal pressure decreases from over 700 bar to 350 bar when the hydrogen availability increases from 2.5% to 6%. With more stations, consumers spend less time on the road to refueling each time they need a refill. A shorter driving range becomes more tolerable, allowing lower hydrogen pressure. But because the number of FCEVs, 50,000 in this example, is held constant, higher hydrogen availability results in lower infrastructure utilization and thus higher hydrogen cost. But with the same number of stations and FCEVs on the road, smaller stations (from 600 kg/d to 500 kg/d in Figure 1) allow higher utilization and lower the delivered hydrogen cost, making room for higher pressure to raise the driving range.

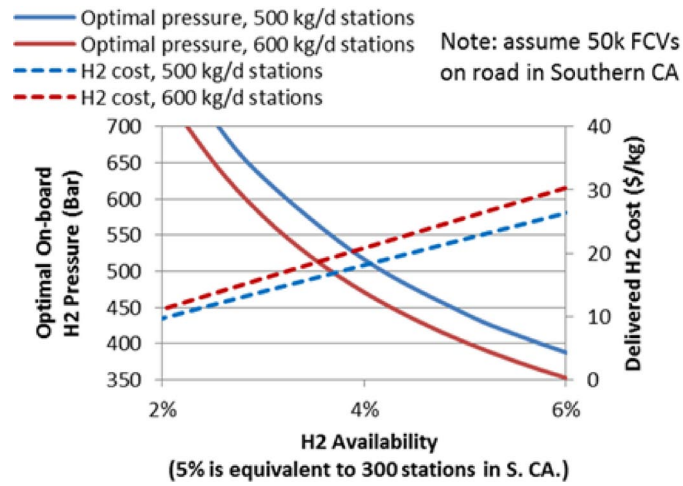

FIGURE 1. Response of Optimal Pressure and Hydrogen Cost

The optimal pressure is found to be sensitive to the high-pressure incremental cost, value of refueling travel time and the number of FCEVs on the road. The reference case for the sensitivity analysis is based on the assumptions of 4% hydrogen availability; 50,000 FCEVs on the road; an average station size of 500 kg/day; an average vehicle fuel economy of 60 miles per gasoline gallon equivalent; an average 12,800 miles of annual driving distance; a time value at $50/hour; and $0.4/kg incremental cost of hydrogen from 350 bar to 700 bar. The resulting optimal pressure is about 500 bar. As shown in Figure 2, a 50% decrease in the incremental cost of hydrogen would drive the optimal pressure up to about 700 bar. Reducing the time value to $25/hour or the number of FCEVs to 25,000 would reduce the optimal pressure to about 350 bar.

Three pressure levels are compared to find the best for Southern California based on the near-term FCEV and infrastructure deployment scenario envisioned by California Fuel Cell Partnership. The pressure of 700 bar is found to be the best among the three. The comparison is based on the assumptions of 100 stations, each 350 kg/day, and 50,000 FCEVs on the road. The three levels of pressure being compared are 350, 500, and 700 bar. In all cases involving variation of time value from $25 to $75 per hour and the incremental cost from $0.2 to $0.6 per kg H_2, as shown on Figure 3, the pressure level 700 bar results in lowest

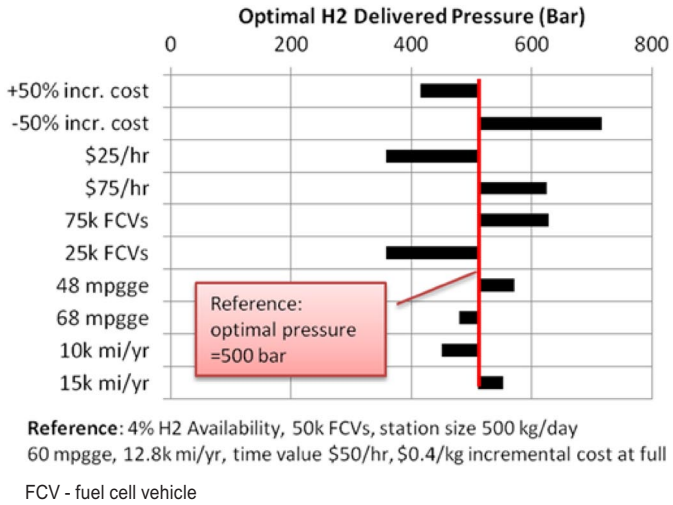

FIGURE 2. Sensitivity of Optimal Pressure

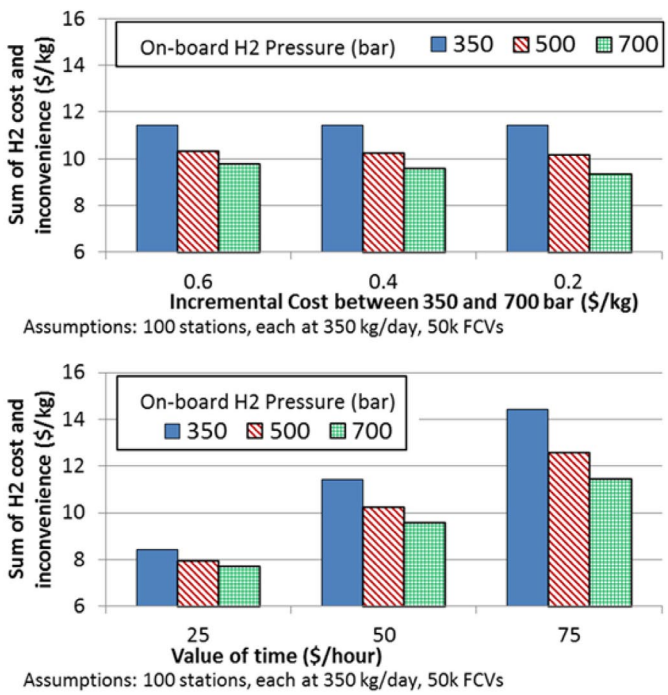

FIGURE 3. Compare Three Hydrogen Pressures for Southern California

combined cost of station and consumer inconvenience, regardless of the incremental cost of hydrogen and the value of time.

CONCLUSIONS AND FUTURE DIRECTIONS

This project determined and analyzed the optimal onboard hydrogen pressure as a function of vehicle and driver attributes, infrastructure availability and cost, and FCEV penetration in a regional context. Key quantitative findings are:

- A sub-optimal pressure leads to a higher combined cost, including infrastructure cost and refueling inconvenience cost, and therefore bigger barriers for market acceptance.
- With everything else held constant, including the number of FCEVs on the road, more hydrogen stations lead to lower onboard pressure and higher delivered hydrogen costs, due to lower infrastructure utilization.
- With everything else held constant, smaller hydrogen stations lead to higher onboard pressure and lower delivered hydrogen costs, due to higher infrastructure utilization.
- The optimal pressure is most sensitive to value of time, incremental cost of hydrogen, and number of FCEVs.
- With 100 stations and 50,000 FCEVs in Southern California, consistent with the California Fuel Cell Partnership 2017 deployment plan, 700 bar offers lower combined costs than either 350 bar or 500 bar. This conclusion is robust against uncertainty of high-pressure incremental costs (0.2-0.6 $/kg for high-pressure upgrade) or value of refueling travel time (25-75 $/hour).

The caveats of this study include:

- No representation of demand response to H_2 cost and pressure
- Limited analysis on uncertainty
- No consideration of cluster roll-out strategy

Thus, we propose an extended study to estimate the optimal delivered pressure that maximizes station profitability and FCEV acceptance and minimizes investment risks, via the following next tasks:

- Define and measure station profitability and investment risk
- Model cluster roll-out strategies
- Integrate with consumer choice models (e.g., MA3T)
- Estimate required subsidy and analyze station business models
- Conduct comprehensive uncertainty analysis
- Expand the study to beyond 100 stations to understand the point when the fueling pressure decreases
- Update the analysis with new station and fueling pressure costs from H2A Delivery Scenario Analysis Model

FY 2013 PUBLICATIONS/PRESENTATIONS

1. Zhenhong Lin, David Greene. Optimal Delivered H_2 Pressure: preliminary results. Presented to the FPITT team, Houston, Texas, Jan. 26, 2013.

2. Zhenhong Lin, David Greene. Impacts of Range and Refueling Pressure. Presented to the FPITT team, Fairfax, Virginia, Mar. 18, 2013.

3. Zhenhong Lin, David Greene. Analysis of Optimal On-Board Storage Pressure for Hydrogen Fuel Cell Vehicles. Presented at the DOE Hydrogen and Fuel Cells Program 2013 Annual Merit Review meeting, Crystal City, Virginia, May 14, 2013.

REFERENCES

1. Karl J. Gross, et al. (2012). Recommended Best Practices for the Characterization of Storage Properties of Hydrogen Storage Materials. H2 Technology Consulting, LLC.

2. The Department of Energy Hydrogen Analysis (H2A) Cost models are available online: http://www.hydrogen.energy.gov/h2a_analysis.html

3. Department of Energy. The Fuel Cell Technologies Office Multi-Year Research, Development, and Demonstration Plan.

4. Zhenhong Lin, Joan Ogden, Yueyue Fan, Chien-Wei Chen (2008). The fuel-travel-back approach to hydrogen station siting. International Journal of Hydrogen Energy, 33(2008), 3096 – 3101.

XI.5 Life-Cycle Analysis of Hydrogen Onboard Storage Options

Amgad Elgowainy (Primary Contact),
Krishna Reddi, Michael Wang
Argonne National Laboratory
9700 South Cass Avenue
Argonne, IL 60439
Phone: (630) 252-3074
Email: aelgowainy@anl.gov

DOE Manager
Fred Joseck
Phone: (202) 586-7932
Email: Fred.Joseck@ee.doe.gov

Project Start Date: October 2012
Project End Date: October 2013

Overall Objectives

Quantify environmental impacts of various physical and material-based hydrogen (H2) onboard storage technologies.

Fiscal Year (FY) 2013 Objectives

Quantify life-cycle greenhouse gas (GHG) emissions of the following physical and material-based H2 onboard storage technologies:

- 350-bar compressed gaseous storage system
- 700-bar compressed gaseous storage system
- Cryo-compressed hydrogen (CcH2) storage system
- Metal organic framework (MOF)-5 sorption storage system

Technical Barriers

This project addresses the following technical barriers from the Systems Analysis section of the Fuel Cell Technologies Office Multi-Year Research, Development, and Demonstration Plan:

(C) Inconsistent Data, Assumptions and Guidelines

(D) Insufficient Suite of Models and Tools

(E) Unplanned Studies and Analysis

Contribution to Achievement of DOE Systems Analysis Milestones

This project contributes to achievement of the following DOE milestone from the Systems Analysis section of the Fuel Cell Technologies Office Multi-Year Research, Development, and Demonstration Plan:

- Task 1.13: Complete environmental analysis of the technology environmental impacts for hydrogen and fuel cell scenarios and technology readiness. (4Q, 2015)

FY 2013 Accomplishments

- Quantified the energy use associated with the manufacturing and charging of four hydrogen onboard storage system technologies including the 350- and 700-bar compressed gaseous storage systems, CcH2 storage system, and gaseous storage in the MOF-5 sorption system.
- Quantified the GHG emissions associated with the manufacturing of fuel cell electric vehicles (FCEVs), including the manufacturing of the various onboard storage systems.
- Quantified the fuel cycle GHG emissions associated with hydrogen production, delivery, distribution, dispensing to the onboard storage system.

✧ ✧ ✧ ✧ ✧

INTRODUCTION

The stages included in the life-cycle of any product include its raw material acquisition, transportation and processing, as well as its manufacturing, distribution, use and disposal or recycling. Life-cycle analysis (LCA) of a fuel is known as fuel-cycle analysis or well-to-wheels (WTW) analysis, while LCA of vehicle manufacturing is known as vehicle-cycle analysis, Figure 1. Combining the environmental impacts of the fuel cycle with the vehicle cycle facilitates the comparison of alternative H2 fuel production, delivery, dispensing and onboard storage pathway options, including the manufacturing of FCEV components, on a common (i.e., life cycle) basis. The LCA of hydrogen FCEV systems depends on the vehicle's onboard storage technology. For example the CcH2 storage option requires the liquefaction of H2 and the manufacturing of super-insulated cryogenic vehicle's storage tank, while the 350- and 700-bar compressed gaseous storage options require compression, precooling and the manufacturing of high-pressure storage tanks. The MOF-5 storage option requires both precooling and compression to dispense an equivalent amount of hydrogen (5.8 kg) at a specified fill rate (1.67 kg/min). The manufacturing of the onboard storage system is part of the vehicle cycle which includes other FCEV components such as the fuel cell, transmission, chassis, traction motor, generator, electronic controller, fuel cell auxiliaries, body, tires, batteries, and fluids. The vehicle cycle also includes the vehicle's assembly process, and disposal or recycling at the end of the vehicle's life. The fuel cycle includes the production, compression/

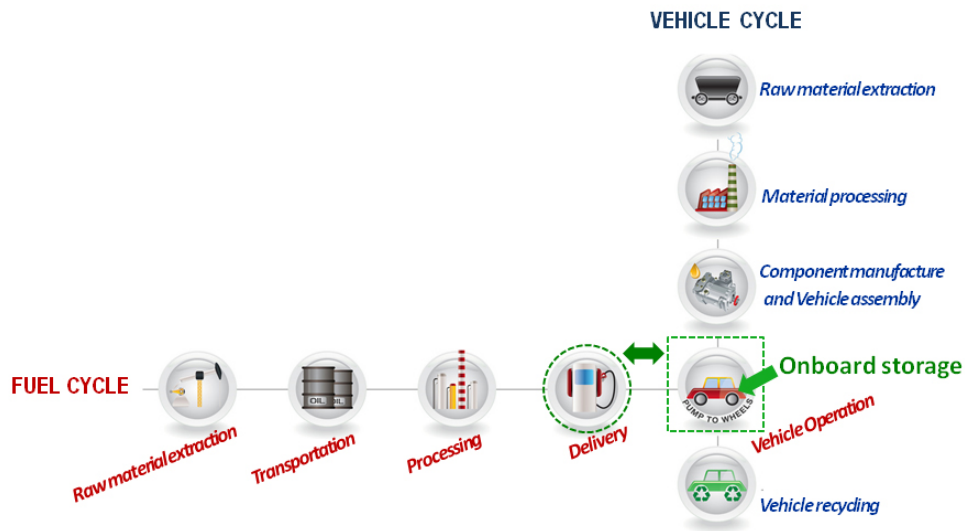

FIGURE 1. Fuel Cycle and Vehicle Cycle Stages in the GREET Model

precooling/liquefaction, delivery and consumption of hydrogen. The LCA of FCEVs combines the fuel cycle with the vehicle cycle to assess the environmental impacts associated with various hydrogen onboard storage options.

APPROACH

The material balance for the physical 350- and 700-bar compressed gas storage systems was obtained from the technical assessment of these systems conducted by Argonne National Laboratory and TIAX [1-2]. The material balance for the MOF-5 sorption storage system (200 liter, Type I tank) was obtained from the technical assessment done by the Hydrogen Storage Engineering Center of Excellence as shown in Table 1. The advanced materials in these storage systems, such as carbon fiber and MOF, were examined to determine the composition as well as the energy and carbon intensities of the basic materials used in the manufacturing process of these advanced materials. The carbon intensities of all vehicle components, including storage tank materials, e.g., aluminum and stainless steel, were obtained from the Greenhouse gases, Regulated Emissions, and Energy in Transportation (GREET) model for vehicle cycle evaluation. The GHG emissions associated with hydrogen production, liquefaction, compression, precooling, and delivery were obtained from the GREET fuel cycle model.

TABLE 1. Material Balance of MOF-5 Storage System

MOF-5 System Components	Weight (kg)	Material
Pressure vessel	62.2	Al
Vacuum shell	14.8	Al
Heat exchanger	4.3	Al
Insulation	7.7	PET
Adsorbent	24.4	MOF-5
Balance of plant	17.4	SS
Total	130.8	

Al – aluminum; PET – polyethylene terephthalate; SS – stainless steel

RESULTS

Table 2 lists the life cycle GHG emissions associated with the manufacturing of each H2 onboard storage system. Figure 2 shows vehicle cycle GHG emissions for various onboard storage options. As shown in the figure, it is assumed that the only difference in the vehicles' components is the onboard storage system. The total GHG emissions over the vehicle cycle range from 11.5 ton of carbon dioxide equivalent (CO_{2e}) for the cryo-compressed option to 12.8 ton of CO_{2e} for the 700 bar storage option. It should be noted that different onboard storage systems have different implications on the fuel cycle GHG emissions because of the different H2 packaging requirement for each system. For example, the 350-bar compressed gas system requires compression while the cryo-compressed system requires liquefaction. The 700-bar compressed gas requires additional precooling at 233 K to overcome the heat of compression while the MOF-5 system requires precooling at 80 K to overcome the heat of adsorption and reach the required energy density at 100 bar.

TABLE 2. Life-Cycle GHG Emissions of Various Hydrogen Onboard Storage Options

Onboard Storage Option	GHG Emissions
350-bar compressed gas storage	2,210 kg_{CO2e}
700-bar compressed gas storage	2,670 kg_{CO2e}
Cryo-compressed storage	1,490 kg_{CO2e}
MOF-5 storage	2,440 kg_{CO2e}

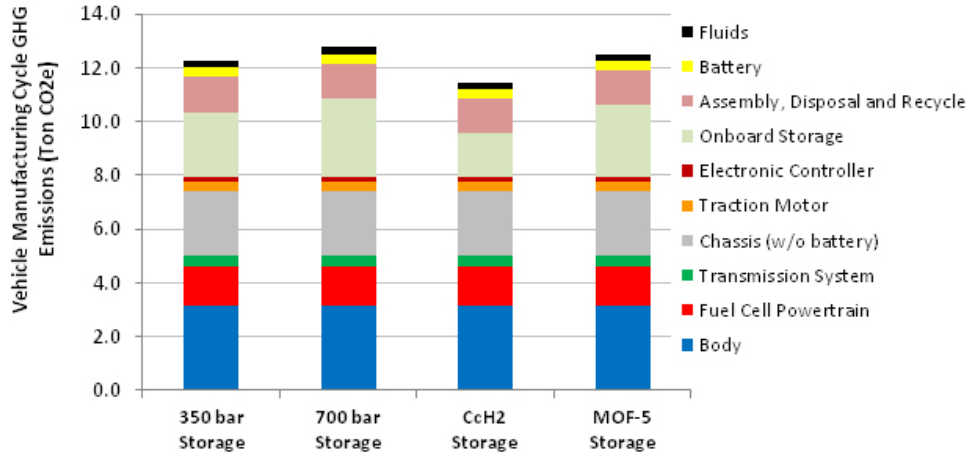

FIGURE 2. Vehicle Cycle GHG Emissions of Various Onboard Storage Systems

For the cryo-compressed storage option, the liquefaction GHG emissions from current plants in North America are estimated at 5 kg_{CO2e} per kg of H2 (instead of 8 kg_{CO2e} per kg of H2 when the U.S. average electricity generation mix is assumed as the source for liquefaction energy). The precooling to 80 K for the MOF-5 system requires approximately 10 kg of liquid nitrogen per kg of H2 and results in GHG emissions of 5.4 kg_{CO2e} per kg of precooled hydrogen. Table 3 shows the GHG emissions associated with the fuel cycle of hydrogen for various onboard storage systems, including the hydrogen production from steam methane reforming (SMR). In order to combine the vehicle cycle results in Table 2 with the fuel cycle results in Table 3, a common functional unit (e.g., vehicle's travelled mile) is required. A FCEV's fuel economy of 60 miles per kg of H2 is assumed to estimate the fuel cycle GHG emissions on a per mile basis. The vehicle's travelled distance over its lifetime is assumed to be 160,000 miles in order to estimate the vehicle cycle GHG emissions on a per mile basis. Table 4 shows per-mile combined fuel cycle and vehicle cycle GHG emissions associated with each onboard storage system. The hydrogen production via SMR is responsible for 200 g_{CO2e}/mi of the total life-cycle GHG emissions.

TABLE 3. Fuel Cycle GHG Emissions of H2 Associated with Various Onboard Storage Options (kg_{CO2e}/kg_{H2})

H2 Pathway (storage option)	Production (via SMR)	Transport (via trucks)	Compression/ liquefaction	Total
GH2 Pathway (350 bar)	12	0.7	2.0	14.7
GH2 Pathway (700 bar)	12	0.7	2.9	15.6
LH2 Pathway (CcH2)	12	0.1	5.2	17.3
GH2 Pathway (MOF-5)	12	0.7	5.4	18.1

GH2 – gaseous hydrogen; LH2 – liquefied hydrogen

TABLE 4. Combined Fuel Cycle and Vehicle Cycle GHG Emissions Associated with Various H2 Onboard Storage Systems (g_{CO2e}/mi)

H2 Pathway (storage option)	Onboard Storage	Balance of Vehicle Cycle	Fuel Cycle (WTW)	Total
GH2 Pathway (350 bar)	14	56	245	315
GH2 Pathway (700 bar)	17	56	257	330
LH2 Pathway (CcH2)	9	56	288	353
GH2 Pathway (MOF-5)	15	56	302	373

CONCLUSIONS AND FUTURE DIRECTIONS

Life-cycle GHG emissions associated with various hydrogen onboard storage systems were estimated between 315 and 373 g_{CO2e}/mi. Systems that require significant precooling (e.g., cryo-compressed and MOF-5) exhibited more GHG emissions compared with systems that require less precooling (i.e., 700-bar system) or no precooling (i.e., 350-bar system). The same methodology can be applied to evaluate the environmental impacts of new and emerging hydrogen onboard storage systems.

SPECIAL RECOGNITIONS & AWARDS/ PATENTS ISSUED

1. Amgad Elgowainy and Michael Wang received the DOE Joint Vehicle Technologies and Fuel Cell Technologies R&D Award in recognition for their outstanding contributions to life-cycle assessment of alternative fuel vehicles pathways, including fuel cell and battery electric vehicles (2013).

REFERENCES

1. Hua, T. and R. Ahluwalia et al., 2010, Technical Assessment of Compressed Hydrogen Storage Tank Systems for Automotive Applications, Argonne National Laboratory, Nuclear Engineering Division, Report No. ANL/10-24.

2. Ahluwalia, R. and T. Hua et al., 2009, Technical Assessment of Cryo-Compressed Hydrogen Storage Tank Systems for Automotive Applications, Argonne National Laboratory, Nuclear Engineering Division, Report No. ANL/09-33.

XI.6 Employment Impacts of Infrastructure Development for Hydrogen and Fuel Cell Technologies

Marianne Mintz
Argonne National Laboratory
9700 S. Cass Ave.
Argonne, IL 60439
Phone: (630) 252-5627
Email: mmintz@anl.gov

DOE Manager
Fred Joseck
Phone: (202) 586-7932;
Email: Fred.Joseck@ee.doe.gov

Subcontractor:
RCF Economic and Financial Consulting, Inc., Chicago, IL

Project Start Date: October 2010
Project End Date: Project continuation and direction determined annually by DOE

Overall Objectives

- Facilitate early market deployment of fuel cells by developing a downloadable, user-friendly tool to estimate economic impacts.
- Identify opportunities for enhancing the economic impact of fuel cell production and deployment by better understanding where and how impacts occur and how infrastructure deployment produces economic benefits in addition to facilitating fuel cell market success.
- Meet stakeholder needs for estimating impacts of fuel cell and infrastructure deployment on state, regional, and national employment, earnings, and economic output.

Fiscal Year (FY) 2013 Objectives

- Quantify employment impacts of fuel cell deployment under the American Recovery and Reinvestment Act (ARRA).
- Update and validate the JOBS and economic impacts of Fuel Cells (JOBS FC) model.
- Initiate work to understand the effect of infrastructure development on job creation.

Technical Barriers

This project addresses the following technical barriers from the Systems Analysis section of the Fuel Cell Technologies Office Multi-Year Research, Development and Demonstration Plan:

(B) Stove-piped/Siloed Analytical Capability

(C) Inconsistent Data, Assumptions and Guidelines

(D) Insufficient Suite of Models and Tools

Contribution to Achievement of DOE Systems Analysis Milestones

- 1.7: Complete analysis of job impact for fuel cell growth in material handling equipment sector through 2020. (4Q, 2013)
- 1.10: Complete analysis of job impact for fuel cell growth in distributed power generation sector through 2020. (4Q, 2014)
- 1.14: Complete analysis of the job impact from fuel cell growth in stationary power generation sector through 2020. (4Q, 2015)
- 2.2 Annual model update and validation. (4Q, 2011 through 4Q, 2020)
- 2.3: Complete development of job estimation model. (2Q, 2012)
- 2.4: Complete validation of job estimation model for material handling equipment sector. (4Q, 2013)
- 2.5: Complete validation of job estimation model for distributed fuel cell power generation. (4Q, 2014)
- 2.6: Complete validation of job estimation model for stationary fuel cell power generation. (4Q, 2015)

FY 2013 Accomplishments

- Continued close collaboration with stakeholders, fuel cell producers, and other researchers via a series of meetings, teleconferences, and webinars. Demonstrated beta versions of the JOBS FC model to this group to validate data and obtain feedback on desired functionality, granularity, and outputs. Added hydrogen producers to stakeholder group to gain further insight into infrastructure development cost, deployment, and other issues.
- Completed revisions to phosphoric acid fuel cells (PAFCs) and molten carbonate fuel cells (MCFCs), and launched version 1.1 of the JOBS FC model. That activity involved development of the following deliverables:
  - A user's guide.

- A dedicated website for users to register and download the model and User's Guide.
- A webinar introducing JOBS FC 1.1.

- Began initial design and development of JOBS and economic impacts of Hydrogen (JOBS H2) model.
- Analyzed the employment impacts of deploying proton exchange membrane (PEM) fuel cells in forklifts and for backup power applications with support from the ARRA. Issued a report documenting methodology and results.

✧ ✧ ✧ ✧ ✧

INTRODUCTION

The project is developing and applying a computer model to estimate economic impacts of deploying fuel cells and associated infrastructure in early markets. Insights from the model will assist the Fuel Cell Technologies Office and its stakeholders in estimating employment and other economic impacts from DOE technology development and in identifying fuel cell markets and regions that are most likely to generate jobs and economic activity.

RESULTS

In FY 2011–2012, Argonne National Laboratory and RCF Economic and Financial Consulting designed and implemented a spreadsheet tool to calculate state, regional, and national economic impacts of fuel cell production, installation, and utilization in early markets (i.e., 2015–2020). Known as JOBS FC, that tool is a user-friendly, spreadsheet-based model. In FY 2013, an updated and expanded version of that tool, JOBS FC 1.1, was launched, and employment impacts associated with ARRA-funded fuel cell projects were examined using the same input-output methodology.

JOBS Model Development and Stakeholder Collaboration

A considerable portion of FY 2013 was devoted to enhancement and quality assurance of JOBS FC—including data validation, development of the user interface, and outreach. Supply chains were characterized using information from the literature, fuel cell suppliers, and stakeholders. Default values for fuel cell costs and operating parameters were obtained from these sources as well as through fundamental engineering design calculations.

Work also began on JOBS H2, a separate tool focusing specifically on hydrogen infrastructure. In its initial version, JOBS H2 estimates employment impacts associated with the deployment of hydrogen fueling stations for early markets. FY 2013 accomplishments include the formation of a stakeholder advisory group to guide model development, design of the conceptual model, and initial data collection.

For both JOBS models, the effect of fuel cell and hydrogen infrastructure deployment can be examined on any of 60 geographies—50 states, nine census regions, and the nation as a whole. The models estimate changes in employment, earnings, and economic output by adjusting the dollar flows among economic sectors within the relevant geography. As fuel cell systems (or H_2 infrastructure) are deployed, the purchases send dollars up the supply chain for PEM fuel cell, PAFC, or MCFC technologies or H_2 fuel as well as to the relevant supply chains for system integrators, installers, fuel suppliers, and businesses providing operation and maintenance services. These incremental purchases flow to other sectors which represent purchases from their supply chains. In the aggregate, the resulting web of transactions represents a nascent fuel cell industrial sector. Purchases include not only the fuel cell (or hydrogen) itself, but all transactions required to install, fuel, and operate the fuel cell system, as well as to build a facility to manufacture the fuel cell. To illustrate, a set of base or "reference scenarios" have been postulated and used to generate an initial set of JOBS FC results. Results for the MCFC prime power reference scenario are shown in Figure 1.

Employment Impacts of ARRA-Funded Fuel Cell Projects

In FY 2013, a detailed analysis of the employment impact of the ARRA-funded fuel cell program was completed. Data on DOE and industry cost-share expenditures under the program for 2009–2012 (Table 1) were obtained and allocated to industrial sectors. Results are shown in Figures 2 and 3.

For forklift applications, the ARRA program created or retained approximately 350 job-years of employment, approximately 56% of which occurred in the fuel cell and

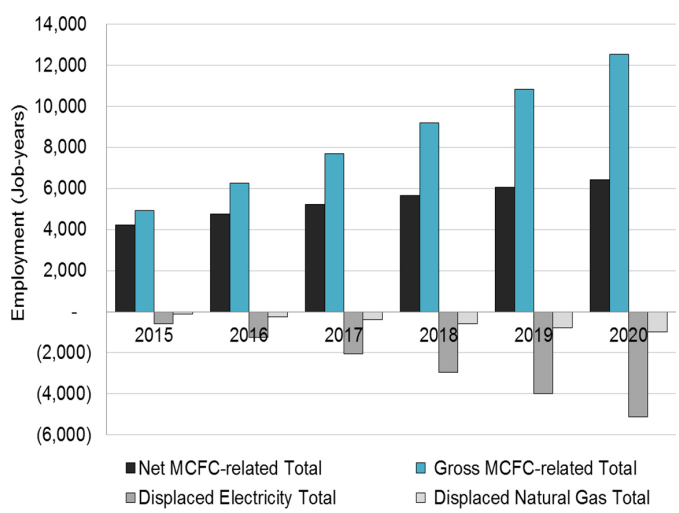

FIGURE 1. Gross and Net Employment Impacts of MCFC Fuel Cell Deployment under the Reference Case

TABLE 1. Expenditures under the ARRA-Supported Fuel Cells Program, 2009–2012

Expenditures (million $)	Forklift Projects	BUP Projects	Total
DOE	$9.7	$18.5	$28.2
Industry	$11.8	$30.8	$42.6
TOTAL	$21.5	$49.3	$70.8

BUP – Backup Power

infrastructure supply chain. The remainder, induced job-years, occurred from the ripple effect of re-spending in the economy by supply chain workers. Similarly, the ARRA program created or retained approximately 950 job-years of employment for backup power applications. Note that a job-year is one year of work by one person (e.g., 5 job-years can be 5 years of work by 1 person, 1 year of work by 5 persons or any person x year product equal to 5).

Note also that the estimates in Figures 2 and 3 do not include impacts from post-2012 fuel cell operation or from any (i.e., 2009–2012 plus post-2012) expenditures for hydrogen fuel. These expenditures are outside the scope of the ARRA program. In a separate analysis, impacts were estimated for these "out-of-scope" expenditures. The results suggest an additional 35 job-years per year are required to sustain fuel cell operation. Over five years, these activities result in over 150 additional job-years of impact associated with the ARRA-supported fuel cell program.

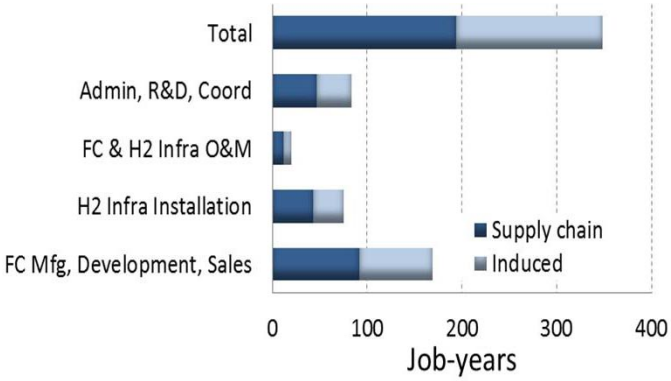

FIGURE 2. Domestic Employment from ARRA-Supported Deployment of Fuel Cells in Forklifts

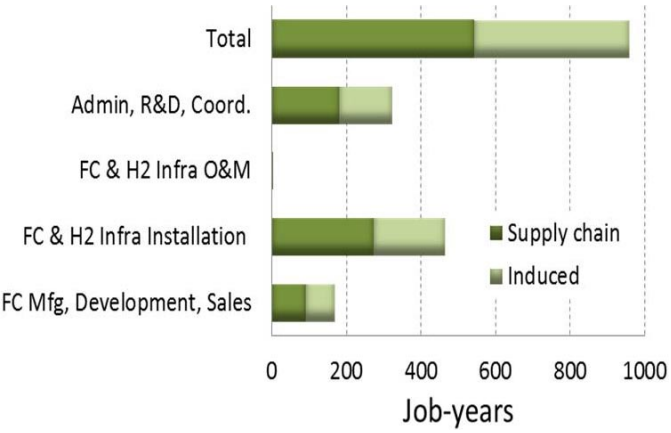

FIGURE 3. Domestic Employment from ARRA-Supported Deployment of Fuel Cells in Backup Power

CONCLUSIONS AND FUTURE DIRECTIONS

FY 2013 work focused on completion of the JOBS FC model, initial design and development of the JOBS H2 model, and analysis of the employment impact of the ARRA fuel cell program. Work on JOBS FC included outreach to industry and stakeholders to develop and validate input data and refine the user interface; model testing and quality assurance via a series of webinars, beta tests and sensitivity analyses; and model launch. Analysis of fuel cell deployments under the ARRA program produced a set of "top down" estimates based on total expenditures. FY 2014 work will build on these efforts, incorporating stakeholder recommendations for enhancements to the functionality and scope of both models, as well as developing estimates of employment impacts to support ongoing fuel cell deployment programs.

Potential future model enhancements include adding solid oxide fuel cell and high-temperature PEM technologies for prime power applications; distributed hydrogen production and biologically-derived hydrogen as options for fueling fuel cells in forklift, prime power, or vehicle applications; various options for delivering and dispensing hydrogen fuel to serve emerging vehicle markets; and analyzing the impacts of alternative hydrogen station rollout scenarios.

PUBLICATIONS

1. Mintz, M., C. Mertes, and E. Stewart, *Employment Impacts of Fuel Cell Deployment in Early Markets*, 92nd Annual Meeting of the Transportation Research Board, Washington, DC, January 16, 2013.

2. Mintz, M., J. Molburg, J. Gillette, C. Mertes, and E. Stewart, *JOBS FC 1.1 (JOBS and economic impacts of Fuel Cells)*, EERE webinar, December 12, 2012.

3. *JOBS and Economic Impacts of Fuel Cells (JOBS FC 1.1): User's Guide,* Argonne National Laboratory Report, ANL-12/24 Rev. 01, December 2012.

4. Mintz, M., J. Molburg, C. Mertes, and E. Stewart, *Employment Impacts of Early Markets for Fuel Cells: Initial Results of JOBS FC*, Fuel Cell Seminar and Exposition, Uncasville, CT, November 8, 2012.

XI.7 Pathway Analysis: Projected Cost, Well-to-Wheels Energy Use and Emissions of Current Hydrogen Technologies

Todd Ramsden (Primary Contact), Mark Ruth
National Renewable Energy Laboratory
15013 Denver West Pkwy.
Golden, CO 80401
Phone: (303) 275-3704
Email: todd.ramsden@nrel.gov

DOE Manager
Fred Joseck
Phone: (202) 586-7932
Email: Fred.Joseck@ee.doe.gov

Project Start Date: January 1, 2012
Project End Date: August 30, 2013

Overall Objectives

- Conduct cost and life-cycle energy and emissions analyses of full current-technology hydrogen pathways to evaluate hydrogen cost, energy requirements and greenhouse gas (GHG) emissions.
- Provide detailed reporting of assumptions and data used to analyze hydrogen production, delivery, and dispensing technologies, enabling consistent and transparent understanding of results.
- Evaluate potential of current technologies to meet $2-$4/kg hydrogen cost target.
- Validate DOE's Fuel Cell Technologies Office (FCTO) Macro-System Model (MSM) and its underlying component models (in particular, the H2A Production model, the Hydrogen Delivery Scenario Analysis Model [HDSAM], and the Greenhouse gas, Regulated Emissions, and Energy use in Transportation [GREET] model) through industry review.

Fiscal Year (FY) 2013 Objectives

- Finalize and publish the current-technologies pathway analysis which began in FY 2012.
- Conduct detailed sensitivity analyses, including cost, energy use, and emissions analyses based on a fuel cell electric vehicle (FCEV) on-road fuel economy of 48 miles per gasoline gallon equivalent (gge) and 68 miles/gge.
- Complete technical report on the analysis, providing a detailed reporting of hydrogen cost and capital costs of the full hydrogen pathways to support FCEV's, upstream energy and feedstock usage and GHG emissions.
- Conduct a companion pathway analysis to consider future hydrogen technologies that are expected to be available in the 2020 to 2030 timeframe, assessing the impact technology improvements will have on hydrogen cost and well-to-wheels (WTW) energy use and emissions.

Technical Barriers

This project addresses the following technical barriers from the Systems Analysis section of the Fuel Cell Technologies Office Multi-Year Research, Development, and Demonstration Plan:

(B) Stove-piped/Siloed Analytical Capability

(C) Inconsistent Data, Assumptions and Guidelines

(D) Insufficient Suite of Models and Tools

Contribution to Achievement of DOE Systems Analysis Milestones

This project will contribute to achievement of the following DOE milestones from the Systems Analysis section of the Fuel Cell Technologies Office Multi-Year Research, Development, and Demonstration Plan:

- Milestone 1.12: Complete an analysis of the hydrogen infrastructure and technical target progress for technology readiness. (4Q, 2015)
- Milestone 1.13: Complete environmental analysis of the technology environmental impacts for hydrogen and fuel cell scenarios and technology readiness. (4Q, 2015)
- Milestone 1.15: Complete analysis of program milestones and technology readiness goals - including risk analysis, independent reviews, financial evaluations, and environmental analysis - to identify technology and risk mitigation strategies. (4Q, 2015)
- Milestone 1.18: Complete life cycle analysis of vehicle costs for fuel cell electric vehicles compared to other vehicle platforms. (4Q, 2019)
- Milestone 2.2: Annual model update and validation. (4Q, 2011 through 4Q, 2020)
- Milestone 3.4: Review Hydrogen Threshold Cost status. (4Q, 2014; 4Q, 2017; 4Q, 2020)

FY 2013 Accomplishments

- Estimated the total cost of fuel cell vehicle ownership for two hydrogen production, delivery and dispensing pathways, including the cost of hydrogen fuel and FCEV

purchase and operating costs. Distributed hydrogen production from natural gas reformation pathway resulted in lowest costs, with costs of $0.10 per mile driven for hydrogen fuel and total vehicle ownership and operational cost of $0.66 per mile (in a mature market).

- Ten current-technology hydrogen production, delivery and dispensing pathways analyzed, providing evaluations of WTW costs, energy use and GHG emissions:
  - Estimated the cost of hydrogen in a mature market, with costs ranging from $4.60/kg-H2 for the distributed natural gas reformation pathway to $8.80/kg for the distributed ethanol reforming pathway.
  - Estimated the total lifecycle GHG emissions of all pathways, including upstream fuel- and feedstock-related emissions and vehicle production-related emissions. The distributed ethanol-reforming pathway had the lowest emissions, with 50 g CO_2-equivalent per mile at an assumed 68 miles/gge fuel economy (70 g CO_2-eq/mi at 48 miles/gge). The lowest cost distributed natural gas reforming pathway yielded 250 g CO_2/mi at 68 miles/gge fuel economy (350 g CO_2/mi at 48 miles/gge).
- Extensive industry review of overall results, modeling results, and input parameters provided external validation of the MSM and the related component models (H2A Production, HDSAM, and GREET).
- Conducted an initial assessment of future-technology hydrogen pathways expected to be available in the 2020 to 2030 timeframe.

✧ ✧ ✧ ✧ ✧

INTRODUCTION

DOE's FCTO had identified a need to understand the cost, energy use, and emissions tradeoffs of various hydrogen production, delivery, distribution, and use options under consideration for FCEVs. This study assesses 10 complete hydrogen production, delivery, and dispensing pathways to evaluate total dispensed hydrogen cost, total cost of ownership for a FCEV, and lifecycle assessments of total energy use and GHG emissions. The study considers the potential of current hydrogen technologies if they were brought to commercial scale in a mature fuel cell vehicle market; it is not an assessment of transition scenarios where equipment may not be fully utilized.

This study will help FCTO evaluate the potential of current technologies to meet the $2-$4/kg cost target for dispensed hydrogen. By providing a common framework for modeling using consistent data and assumptions, this study provides a detailed and transparent understanding of hydrogen technologies and will assist FCTO with goal setting and research and development decisions. Finally, this analysis will aid in understanding and assessing technology needs and progress, potential environmental impacts, and the energy-related economic benefits of various hydrogen pathways.

APPROACH

This study evaluated 10 hydrogen production, delivery, and dispensing pathways for hydrogen cost, energy requirements and GHG emissions (see Table 1). Considering plausible hydrogen production and delivery scenarios for mature hydrogen transportation-fuel markets combined with market penetration of hydrogen fuel cell vehicles, the study uses a common set of assumptions to provide a consistent assessment of all pathways. Major assumptions include:

- 2015 start-up year with 2015 FCEV purchase
- Currently available hydrogen technologies, projected to a commercial scale
- Costs reported in $2007
- 40-year analysis period for central production; 20-year analysis for distributed cases
- Feedstock and utility costs from the Annual Energy Outlook 2009, based on national averages
- On-road FCEV fuel economy of 48 miles/gge (with sensitivity analyses at 68 miles/gge)
- Urban demand area with a population of 1.25 million (nominally Indianapolis)
- 15% FCEV penetration
- Conventional, mid-sized FCEV (not light-weighted)
- 15,000 miles/year vehicle miles traveled per FCEV

TABLE 1. Hydrogen Pathways Evaluated

Path	Production Feedstock / Technology	Delivery Mode	Dispensing Mode
1	Natural Gas Reforming	Distributed Production	700 Bar, gaseous
2	Ethanol Reforming	Distributed Production	700 Bar, gaseous
3	Grid Electrolysis	Distributed Production	700 Bar, gaseous
4	Biomass Gasification	Gaseous H_2 in Pipelines	700 Bar, gaseous
5	Biomass Gasification	Gaseous H_2 Truck	700 Bar, gaseous
6	Biomass Gasification	Liquid H_2 Truck	700 Bar, gaseous
7	Biomass Gasification	Liquid H_2 Truck	Cryo-compressed
8	Natural Gas Reforming	Gaseous H_2 in Pipelines	700 Bar, gaseous
9	Wind Electrolysis	Gaseous H_2 in Pipelines	700 Bar, gaseous
10	Coal Gasification (with carbon capture)	Gaseous H_2 in Pipelines	700 Bar, gaseous

- Hydrogen dispensed for 700-bar, high-pressure storage (except cryo-compressed case)

The analysis was conducted using the MSM, which acts as a central transfer station, linking together the H2A Production model, HDSAM, GREET, and the Cost-Per-Mile tool. Making use of the discounted cash flow, rate of return features of H2A Production and HDSAM, the MSM provides cost results in terms of a levelized cost of hydrogen (incorporating a 10% real rate of return on investments) in a $/kg basis. The MSM also outputs well-to-pump, pump-to-wheels, and WTW efficiencies, GHG emissions, and energy use for each pathway. Emissions and energy use results include upstream energy use required for feedstock production, processing, and delivery. For all pathways evaluated, the key assumptions, modeling parameters, and analysis inputs were reviewed by industry partners through the U.S. DRIVE Fuel Pathways Integration Technical Team.

RESULTS

The MSM evaluation of the 10 current-technology hydrogen pathways presents the cost of hydrogen and the performance of the pathways in terms of total energy use, fossil energy use, and GHG emissions. Figure 1 shows the levelized cost of hydrogen from the 10 different pathways. DOE's FCTO has set a hydrogen cost target of $2-$4/gge dispensed at the pump. The distributed natural gas reformation pathway comes closest to this target, with a projected hydrogen cost of $4.60/gge. To achieve the $4/gge target, DOE has a hydrogen production target of $2/gge. The hydrogen pathways evaluation shows that four production pathways (distributed natural gas reformation, central biomass gasification, central natural gas reformation, and central coal gasification) achieve or approach this target, with production costs of $2.20/gge or less. Hydrogen station compression, storage, and dispensing costs for 700-bar dispensing (not including delivery) range from approximately $1.00/gge to $2.50/gge, showing that compression, storage, and dispensing is a critical area for research in order to meet overall hydrogen cost targets.

The study also evaluated the total cost of FCEV ownership including the costs of the hydrogen fuel and the costs of vehicle purchase and operation. The lowest cost of FCEV ownership resulted from hydrogen fuel produced and dispensed from the distributed natural gas reformation pathway. Assuming a 5-year ownership period and fuel economy of 48 miles/gge, the distributed natural gas pathway resulted in total ownership costs of $0.66 per mile. With fuel costs of $0.10/mi, the hydrogen fuel accounts for about 15% of ownership costs. The purchase of the FCEV (represented as finance and depreciation costs) account for about 50% of ownership costs.

Figure 2 illustrates that for a 48 miles/gge FCEV, all the pathways (except the distributed electrolysis pathway) result in GHG emissions (on a gram CO_2-equivalent per mile basis) lower than 350 g/mile, demonstrating a significant improvement over a conventional gasoline vehicle. Figure 2 also shows that when a higher fuel economy of 68 miles/gge is considered, all of the pathways except distributed

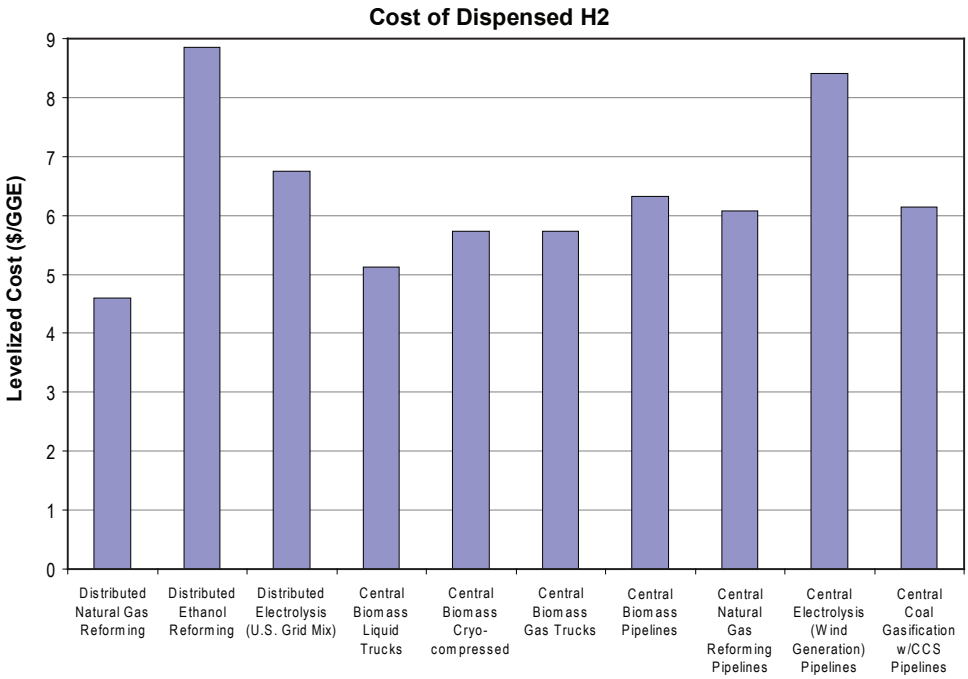

FIGURE 1. Cost of Dispensed Hydrogen from All Pathways

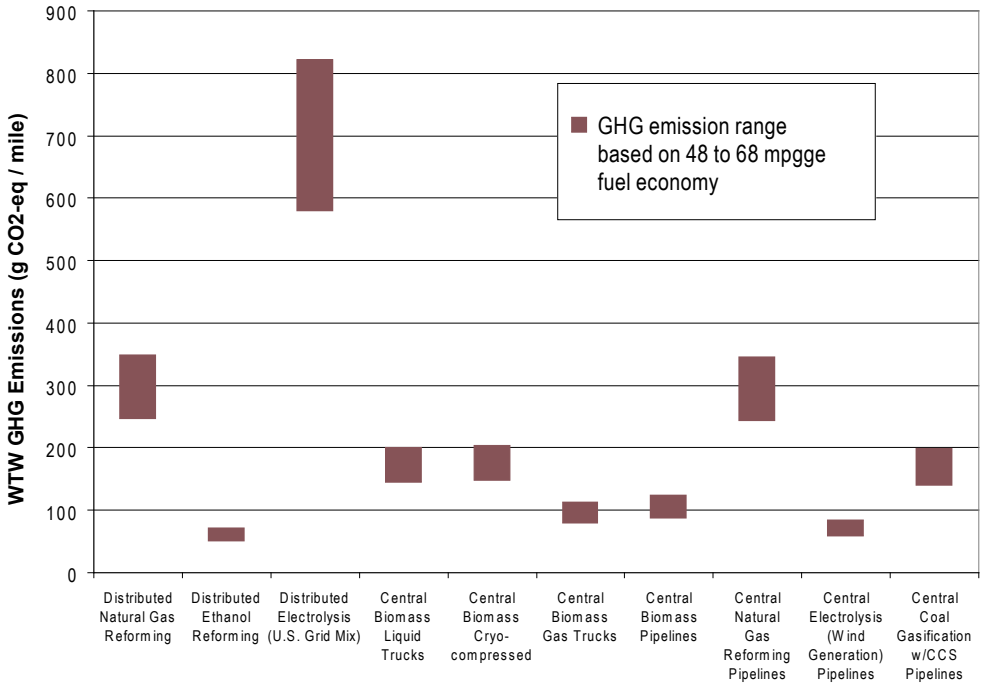

FIGURE 2. WTW GHG Emissions from All Pathways

electrolysis result in GHG emissions lower than 250 g/mile and four pathways have GHG emissions lower than 100 g/mile. Distributed electrolysis has high GHG emissions when compared to the other hydrogen pathways because of the assumed electricity grid mix (the U.S. average grid mix is assumed). The pathways that use natural gas as a feedstock use little petroleum but have high GHG emissions compared to most of the other pathways due to the GHGs released in producing hydrogen from natural gas. The coal pathway has slightly lower GHG emissions than the natural gas pathways because of the efficient sequestration system that is assumed. Of the four options for delivering hydrogen from a centralized production plant, pipeline delivery has the lowest GHG emissions and lowest petroleum use. The two liquid truck delivery options have higher GHG emissions because of the high electricity consumption of the liquefaction process (the U.S. average grid mix is assumed).

CONCLUSIONS AND FUTURE DIRECTIONS

The WTW analysis shows that based on current hydrogen production, delivery, and dispensing technologies, none of the pathways can achieve the $4/gge DOE target, even extrapolated out to full commercialization in a mature hydrogen market. However, almost all pathways demonstrate significant improvements in WTW GHG emissions compared to conventional gasoline vehicles.

In the latter part of FY 2013 and early FY 2014, the WTW pathways analysis will be extended to consider process and cost improvements that might be expected to be available in the 2020-2030 timeframe. This evaluation of future hydrogen technologies will project where hydrogen costs and associated energy and GHG emissions might be expected to fall based on continued research and development activities. This companion analysis should therefore provide a better picture of the potential of achieving DOE's $4/gge hydrogen cost target.

FY 2013 PUBLICATIONS/PRESENTATIONS

1. Todd Ramsden, "Pathway Analysis: Projected Cost, Well-to-Wheels Energy Use and Emissions of Current Hydrogen Technologies". Presentation at the 2013 DOE Hydrogen and Fuel Cell Technologies Program Annual Merit Review, Arlington, VA.

XI.8 Hydrogen from Biogas: Resource Assessment

Genevieve Saur (Primary Contact), Anelia Milbrandt
National Renewable Energy Laboratory
15013 Denver West Parkway
Golden, CO 80401-3305
Phone: (303) 275-3783
Email: genevieve.saur@nrel.gov

DOE Manager
Fred Joseck
Phone: (202) 586-7932
Email: Fred.Joseck@ee.doe.gov

Project Start Date: October 2012
Project End Date: September 2013

Overall Objectives

Address resources availability for renewable hydrogen which provides alternatives to traditional sources of hydrogen, hedges again fluctuating costs and demand for fossil fuels, and aids compliance with state policies for renewable fuels.

Fiscal Year (FY) 2013 Objectives

- Update prior study on methane from wastewater treatment, landfills, and manure management.
- Expand analysis to include methane from industrial processes and organic food waste.

Technical Barriers

This project addresses the following technical barriers from the Systems Analysis section of the Fuel Cell Technologies Office Multi-Year Research, Development, and Demonstration Plan:

(A) Future Market Behavior - Expand analysis to include current net availability by assessing sources currently in use.

(C) Inconsistent Data, Assumptions, and Guidelines - The resource assessment collects data from several sources into one place and uses consistent conversion methods to obtain the hydrogen potential.

Contribution to Achievement of DOE Systems Analysis Milestones

This project will contribute to achievement of the following DOE milestones from the Systems Analysis section of the Fuel Cell Technologies Office Multi-Year Research, Development, and Demonstration Plan:

- Milestone 1.6: Complete analysis of biogas availability for stationary power generation and hydrogen production. (4Q, 2013)

FY 2013 Accomplishments[1]

- Collected data from several sources: Environmental Protection Agency Clean Watersheds Needs Survey, 2007; Environmental Protection Agency Landfill Methane Outreach Program; Department of Agriculture Census, 2007; U.S. Census Bureau County Business Patterns 2011; and the Homeland Security Infrastructure Program Gold Dataset 2012 to estimate biogas from wastewater treatment plants, landfills, animal manure, and industrial, institutional, and commercial (IIC) sites [1-5]. Preliminary estimates of net methane availability are 1.9, 2.5, 1.8, and 1.2 (total) million tonnes annually for wastewater treatment plants, landfills, animal manure, and IIC, respectively.
- Developed hydrogen estimates for the four biogas sources using biogas purification efficiency of 87% and methane-to-hydrogen conversion of 3.3 kg CH_4/kg H_2 from DOE's H2A Production Hydrogen from Steam Methane Reforming Central case study [6]. Preliminary estimates of hydrogen for biogas from wastewater treatment plants, landfills, animal manure, and IIC are 508, 648, 486, and 305 thousand tonnes of hydrogen, respectively.
- Produced estimates for fuel cell electric vehicles (FCEVs) supported using efficiency of 57 miles/gasoline gallon equivalent and annual usage of 10,000 miles driven/yr [5]. Preliminary estimates of FCEVs supported by wastewater treatment plants, landfills, animal manure, and IIC are 2.9, 3.7, 2.7, and 1.7 million vehicles annually.
- Developed U.S. national maps and two regional maps (Sacramento, CA, and Boston, MA) for understanding the geographic distribution of the resources.

✧ ✧ ✧ ✧ ✧

INTRODUCTION

This analysis includes a resource assessment of four sources of biogas in the U.S. that updates and expands a previous study on the subject; wastewater treatment plants (WWTPs), landfills, animal manure, and industrial, institutional and commercial source of organic waste (IIC) [1-5]. Biogas is produced by anaerobic digestion of organic matter in an oxygen-free environment. This addresses both the total resource as well as a net availability against some

[1] Results are updated from the AMR 2013 presentation.

of the competing demands for the biogas. From this resource assessment the potential for renewable hydrogen from biogas is calculated as well as the FCEVs that it might support. The geographic distribution is also provided to help consider regional policies that might support increased utilization of the resource.

APPROACH

The analysis uses databases of biogas resources from the Environmental Protection Agency, Department of Agriculture, and U.S. Census Bureau to calculate the methane potential of each resource in a consistent manner. The total potential of each source is calculated on either a point source or county basis dependent on the data; WWTP and landfills by point source, animal manure and IIC by county. A net availability is also estimated by either cross-referencing existing applications or by candidate sites recommended for development. WWTP and animal manure net availability is estimated using a database of combined heat and power plants and the animal manure by existing anaerobic digestion plants. Candidate landfills assessed by the Environmental Protection Agency are used to calculate the net availability of the resource. National and regional maps are used to show the geographic distribution of resources.

From the methane availability the amount of hydrogen and FCEVs supported can be estimated. The hydrogen potential is calculated from the methane potentials in the resource assessment by assuming an 87% methane purification efficiency in the process to make biomethane and a usage of 3.3 kg CH_4/kg H_2 in steam methane reforming of the biomethane to produce hydrogen. Annual FCEVs supported were calculated using an estimate of 56.5 miles/kg H_2 and 10,000 miles driven annually [7].

RESULTS[2]

The U.S. potential for methane and hydrogen is shown in Table 1. The total annual potential from all sources was about 16 million tonnes of methane or 4.2 million tonnes of hydrogen if purified and converted. However, the net availability was estimated at only about 6.2 million tonnes of methane or 1.6 million tonnes of hydrogen annually. Landfills had the highest potential, but when estimating net availability all resources showed between 300-650 thousand tonnes of hydrogen potential annually. The methane and hydrogen potentials could enhance the renewable portfolio of either stationary power expansion or vehicle infrastructure.

From the methane and hydrogen estimate, maps were developed by point sources for WWTP and landfills (Figure 1) or at the county level for animal manure and IIC (Figure 2). The geographic distribution of resources is important for considering policies, incentives, and techno-economic system design of diverse biogas sources. To understand some of the local geographic elements of biogas sources maps regional maps were also made of the Sacramento, CA, and Boston, MA, (Figure 3) areas. These maps help highlight the distribution of resources and how targeted policy might foster development as well as the system design intricacies for making economically feasible projects.

TABLE 1. U.S. Methane and Hydrogen Potentials by Source

Source	Methane Potential (thousand tonnes/yr)		Hydrogen Potential (thousand tonnes/yr)	
	Total	Available	Total	Available
WWTP*	2,339	1,927	618	509
Landfills**	10,586	2,455	2,795	648
Animal Manure***	1,905	1,842	503	486
IIC Organic Waste	1,158	Not Available	306	N/A
Total	15,989	6,224	4,222	1,643

* Total potential for WWTP is higher, given that the analysis was done for only half of the WWTPs in the country (water flow data for the rest is missing).
** Total potential for landfills could be higher given that the estimate accounts for only the waste in place recorded for a given year and doesn't take into account additional waste that may have come in since the record was taken (as it was done for available potential estimate). It is an approximate value. Available potential for landfills is estimated using candidate landfills only. Available potential could be higher if we include "other" and "potential" landfills.
*** Existing digesters (dairy, poultry, and swine) capture about 62,942 tonnes/yr [2,3].

In order to facilitate future studies some distribution plots of plant sizes were created for WWTP and landfills (Figure 4). These help to understand the size considerations for developing economically feasible projects. They can help target certain size plants or analyze the impact of co-digestion and economies of scale for biogas purification. Knowledge of both the spatial and size elements of biogas sources can help inform strategies for their development.

The impact on early market FCEV rollout was also considered in relation to how many vehicles the renewable hydrogen from biogas might support. Table 2 shows the estimated FCEV supported by hydrogen from the biogas sources. This is also taken in comparison to the U.S. fleet estimates for 2010 for cars and light-duty trucks of about 230 million vehicles [8]. Overall, the net availability of biogas could support about 11 million FCEVs which would be about 5% of the U.S. fleet in 2010 if that portion were replaced by FCEVs.

CONCLUSIONS AND FUTURE DIRECTIONS

The updated resource assessment for methane and hydrogen production from biogas was completed, which included three sources previously studied and one new source of organic matter. The conclusions of the analysis are that biogas can be a significant source of renewable fuel, but it

[2] Results are updated from the AMR 2013 presentation.

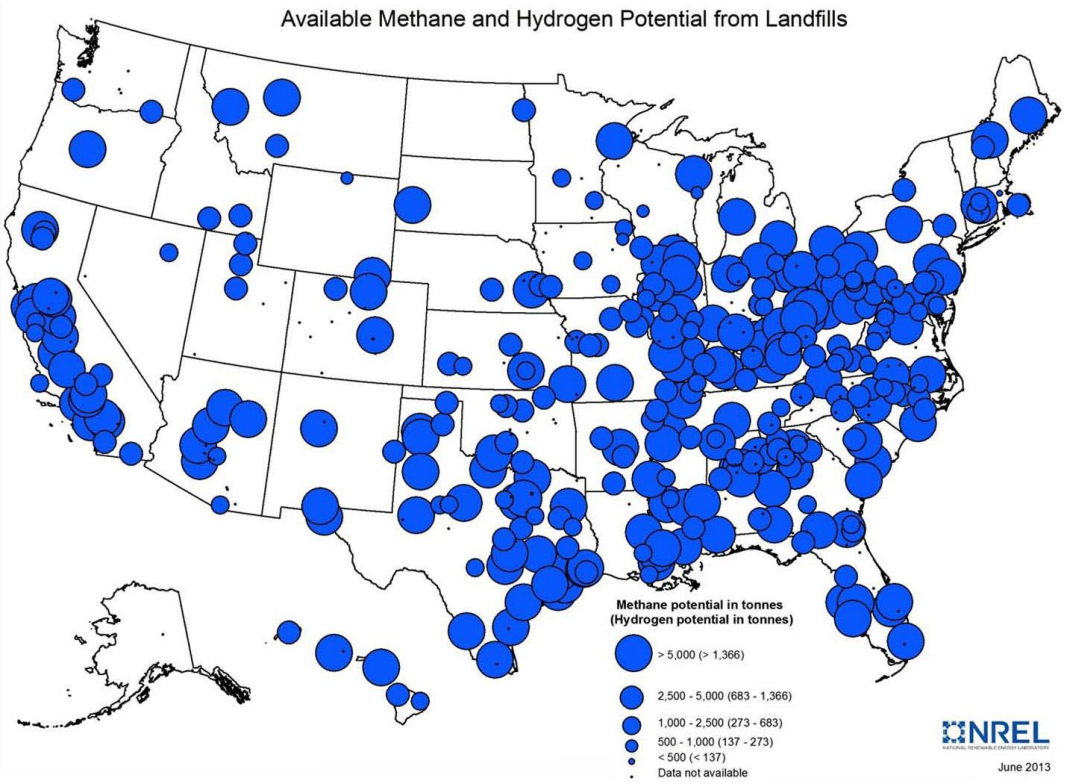

FIGURE 1. Net Availability of Methane and Hydrogen Potential from Landfills

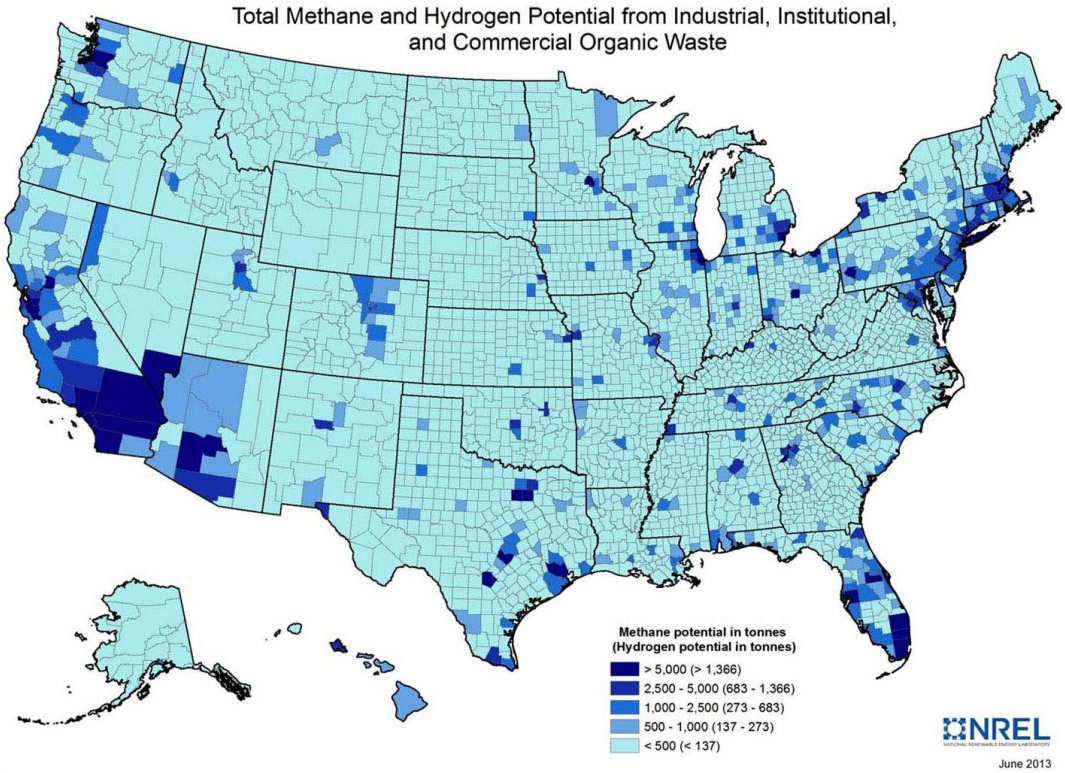

FIGURE 2. Total Methane and Hydrogen Potential from Industrial, Institutional, and Commercial sources of Organic Waste

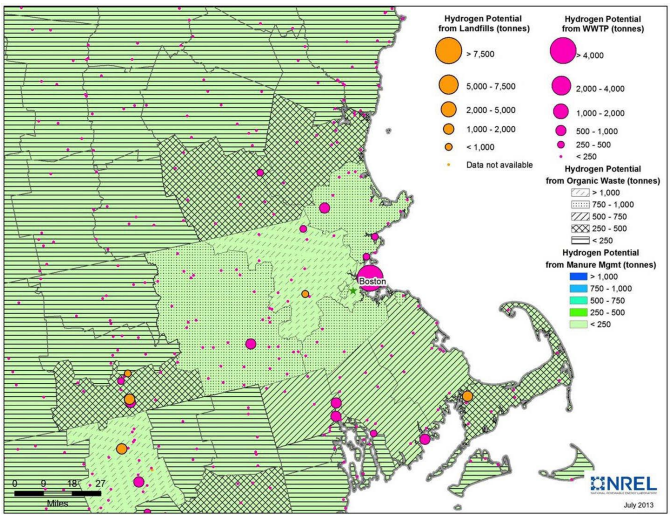

FIGURE 3. Hydrogen Potential from Biogas in Boston, MA

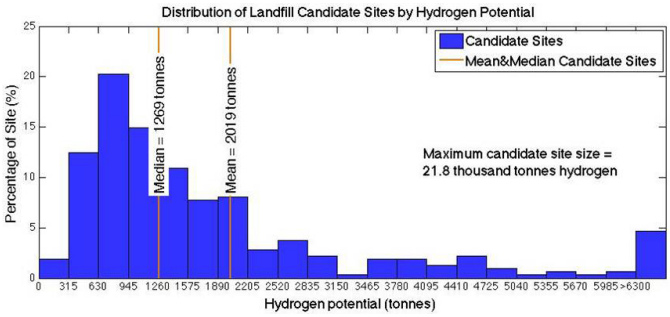

FIGURE 4. Size Distribution of Landfill Candidate Sites by Hydrogen Potential

TABLE 2. FCEVs Supported by Biogas Source Net Availability

Biogas Source	FCEVs Supported (millions annually)	Percentage of 2010 U.S. Light-Duty Fleet (%)
WWTP	2.9	1%
Landfills	3.7	2%
Animal Manure	2.7	1%
IIC*	1.7	1%
Total	11.0	5%

* IIC is total potential.

is not going to meet all of our energy needs. As a fuel it has challenges both in the techno-economic system feasibility as well as for policy and incentives. The diverse nature of the resources may make designing systems that span sources more viable. For that purpose, information about the spatial and size distribution of sources is an important step.

Future work could include:

- Resource assessment of lipids (fats, oils, grease)
- Inclusion into (http://en.openei.org/wiki/Main_Page), an energy data repository, for better collaboration
- Techno-economic analysis of biogas production and purification
- Cost and quality implications in biogas and biomethane
- Regional differences in cost, policy & incentives
- Pathways assessment of spatial distribution for combining multiple sources

FUTURE DIRECTIONS

The following will be completed in FY 2013:

- Finalize methodology and estimates for methane and hydrogen potential from wastewater treatment plants, landfills, and animal manure.
- Estimate net potential of the different biogas sources.
- Estimate methane and hydrogen potential from industrial and commercial processes and facilities that have organic waste using U.S. Census Bureau data on business patterns.
- Generate U.S. maps using the geographic data to show distribution and intensity of the different biogas sources.
- Estimate the FCEVs supported in the U.S. by biogas.
- Complete final report on the biogas assessment from wastewater treatment plants, landfills, animal manure, and industrial/commercial processes.

FY 2013 PUBLICATIONS/PRESENTATIONS

1. Hydrogen from Biogas: Resource Assessment, presented at DOE Annual Merit Review, May 13–17, 2013, Washington, D.C.

REFERENCES

1. U.S. EPA's Clean Watersheds Needs Survey (CWNS) 2008.

2. U.S. EPA's Landfill Methane Outreach Program (LMOP) (2012).

3. U.S. Department of Agriculture 2007 Census.

4. U.S. Census Bureau County Business Patterns 2011.

5. Homeland Security Infrastructure Program (HSIP) Gold Dataset 2012.

6. U.S. DOE (2012) H2A: Current Central Hydrogen Production from Natural Gas without CO2 Sequestration v. 3.0. U.S. Department of Energy. http://www.hydrogen.energy.gov/h2a_prod_studies.html

7. U.S. DOE (2012). Total Costs of Ownership of Future Light-Duty Vehicles, U.S. Department of Energy. Report Number DE-FOA-0000592: https://www.fedconnect.net/fedconnect/?doc=DE-FOA-0000592&agency=DOE

8. Davis, S.C., S.W. Diegel, and R.G. Boundy, *Transportation Energy Data Book: Edition 31*, 2012, Oak Ridge National Laboratory: Oak Ridge, TN.

XI.9 Global Hydrogen Resource Analysis

Thomas Drennen
Earth Systems Analysis, Department 6926
Sandia National Laboratories
Albuquerque, NM 87185
Phone: (315) 781-3419
Email: Drennen@hws.edu

Todd West
Systems Research and Analysis II
Sandia National Laboratories
P.O. Box 969 M/S 9406
Livermore, CA 94551-0969
Phone: (925) 294-3145
Email: thwest@sandia.gov

DOE Manager
Fred Joseck
Phone: (202) 586-7932
Email: Fred.Joseck@ee.doe.gov

Project Start Date: June 2010
Project End Date: December 31, 2013

Overall Objectives

This project is a subtask of the International Energy Agency (IEA) Hydrogen Implementing Agreement (HIA) Task 30 (Global Hydrogen Systems Analysis). The overall objectives of Subtask 30A (Global Hydrogen Resource Analysis) are to:

- Analyze potential hydrogen production and distribution pathways for participating countries.
- Develop a user-friendly pathways analysis tool that allows users the ability to:
  - Understand the resource options and constraints to meeting future hydrogen demand for various fuel cell vehicle market shares.
  - Estimate potential petroleum savings and greenhouse gas emission reductions associated with various scenarios.
- Collaborate with IEA analysts as appropriate to support global hydrogen resource analysis.

The objective for U.S. participation in this international effort is to inform ongoing analysis in regards to international efforts to identify pathways and assumptions for the widespread implementation of hydrogen in the transportation sector.

Fiscal Year (FY) 2013 Objectives

- Completion of pathways analysis tool and final report.
- Demonstrate value of pathways tool for understanding country and regional-level resource availability to support large-scale rollout of hydrogen vehicles and the associated greenhouse gas (GHG) emission reductions over a business-as-usual scenario.
- Gather feedback on analysis results from relevant stakeholders through final report and webinar.

Technical Barriers

This project addresses the following technical barriers from the Systems Analysis section of the Fuel Cell Technologies Office Multi-Year Research, Development, and Demonstration Plan:

(A) Future Market Behavior

(C) Inconsistent Data, Assumptions, and Guidelines

(D) Insufficient Suite of Models and Tools

Contribution to Achievement of DOE Systems Analysis Milestones

This project will contribute to achievement of the following DOE milestones from the Systems Analysis section of the Fuel Cell Technologies Office Multi-Year Research, Development, and Demonstration Plan:

- Milestone 1.9: Complete analysis and studies of resource/feedstock, production/delivery, and existing infrastructure for technology readiness. (4Q, 2014)
- Milestone 1.13: Complete environmental analysis of the technology environmental impacts for hydrogen and fuel cell scenarios and technology readiness. (4Q, 2015)

FY 2013 Accomplishments

- Completed development of version 1.0 of the Global Pathways Resource Analysis Tool (GPAT). GPAT is a user-friendly tool to help participants in HIA Task 30 and other interested stakeholders understand resource options and constraints to meeting future hydrogen demand for various market share scenarios for hydrogen fuel cell vehicles.
- Presented initial results from GPAT to the HIA Task 30 experts, the HIA Executive Committee, and to IEA analysts.
- Results demonstrate a large range of potential pathways for providing hydrogen to fuel a significant hydrogen fuel

cell fleet and that resource availability is not the limiting factor in a hydrogen economy. For example, for a scenario where the fuel cell vehicle market share reaches 40% by 2050, if natural gas was the sole feedstock used for hydrogen production in the U.S. and Germany, the additional natural gas demand would be limited to about 25% of current demand for natural gas in those countries. In the more likely case where hydrogen would be produced from a variety of feedstocks, the added demand for natural gas would be considerable less. See results for additional scenarios.

✧ ✧ ✧ ✧ ✧

INTRODUCTION

The IEA established the HIA to pursue collaborative hydrogen research and development and information exchange among its member countries. The goal of Task 30 (Global Hydrogen Systems Analysis) is to "perform comprehensive technical and market analysis of hydrogen technologies and resources and supply and demand related to the projected use of hydrogen." Task 30 includes four main subtasks. Subtask A, the focus of this effort, focuses on the potential hydrogen production and distribution pathways for participating countries. Subtask B is developing a harmonized hydrogen technology database. Subtask C is focused on collaboration with IEA analysts regarding the potential future role for hydrogen in a clean energy future.

APPROACH

The GPAT calculates least-cost pathways for H2 supply for eight participating countries: France, Germany, Italy, Norway, Spain, Sweden, the United Kingdom, and the United States. The pathways include consideration of feedstock, conversion, distribution (regional and long-distance), and carbon costs. For each country, hydrogen demand is calculated based on assumptions about future hydrogen vehicle market shares. Hydrogen production costs are calculated based on country-supplied data on feedstock availability for hydrogen production by type, cost, and quantity from 2010 to 2050, and assumptions about hydrogen production technology assumptions (efficiencies, costs, etc.). Where country-level data was not available, U.S.-based analysis estimates derived from H2A [1], the Hydrogen Delivery Scenario Analysis Model [2], and the Macro-System Model [3] were used. Integration of results from Subtask 30B (Technology Database) and HIA Task 28 (Distribution) is expected by in first quarter 2014.

GPAT also estimates petroleum savings and GHG reductions and compares the feedstock use for H2 production through 2050 with 2010 primary energy consumption. The tool includes consideration of inter-regional transfers of hydrogen based on total cost of producing and delivering hydrogen.

A key feature of GPAT is the ability for users to vary key assumptions, including resource availability and price, vehicle shares and efficiencies, carbon taxes, and renewable portfolio standards, and view real-time results, making the tool ideal for policy-level discussions.

RESULTS

Our analysis shows that there are a large number of potential pathways for providing hydrogen to fuel a significant vehicle fleet and that resource availability is not the limiting factor in a hydrogen economy. Using GPAT, each participating country has identified multiple options for producing hydrogen domestically.

GPAT results are presented at both the regional (i.e., Europe) and then country-level (France, Denmark, Sweden, Spain, Norway, and Germany). Illustrative, preliminary results for Europe are shown in Figures 1-3. Comparable graphs exist at the country level, or, in the U.S., at the regional level. Figure 1 shows the least-cost pathways for supplying the required hydrogen for a 40% hydrogen fuel vehicle (HFV) 2050 market share scenario in the absence of either carbon taxes or country-level renewable portfolio standards. In the absence of the carbon taxes, natural gas, coal, and wind are the dominant feedstocks used for the production of hydrogen, with small contributions from biomass and hydro. Distributed steam methane reforming is the lowest cost option in the early years; in later years, electrolysis using onshore wind resources and centralized coal gasification play a more dominant role. Because of the increasing reliance on coal in this scenario, annual CO_2 emissions from the light-duty vehicle sector are just 12.5% lower than for the non-H2 case in 2050.

Figure 2 shows the least-cost pathways with $100 per ton CO_2 price phased in over time, beginning in 2015. For this case, natural gas is the dominant feedstock initially, but as the CO_2 tax increases, H2 production begins to shift to onshore wind and centralized coal gasification with Carbon capture and storage. For this case, CO_2 emissions in 2050 from light-duty vehicles are reduced 24% over the base case.

Figure 3 shows the projected delivered hydrogen costs ($/kg) in 2050 for one European country (country not identified here due to preliminary nature of results) for the $100/ton CO_2 tax case. Costs are broken down by feedstock, conversion, distribution, and carbon tax component. The lowest cost option in this year is biomass gasification. In the absence of the CO_2 tax, centralized coal would be the low-cost option.

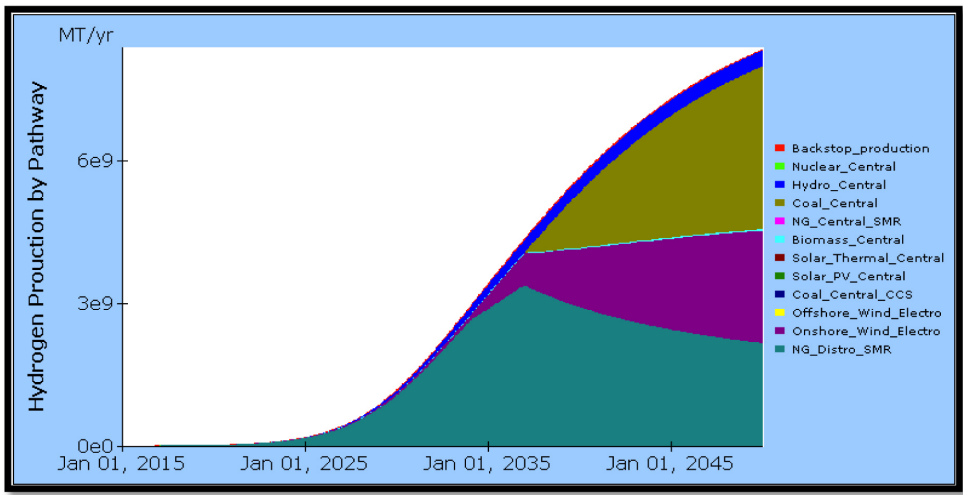

FIGURE 1. Least-cost H2 pathways in Europe for HFV market share of 40% by 2050.

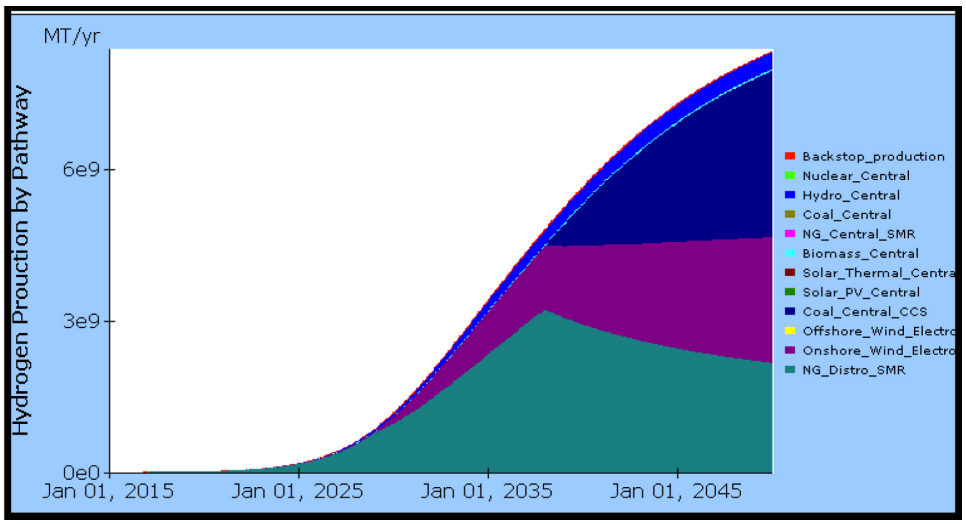

FIGURE 2. Least-cost H2 pathways in Europe for HFV market share of 40% by 2050 with $100 per ton CO_2 tax.

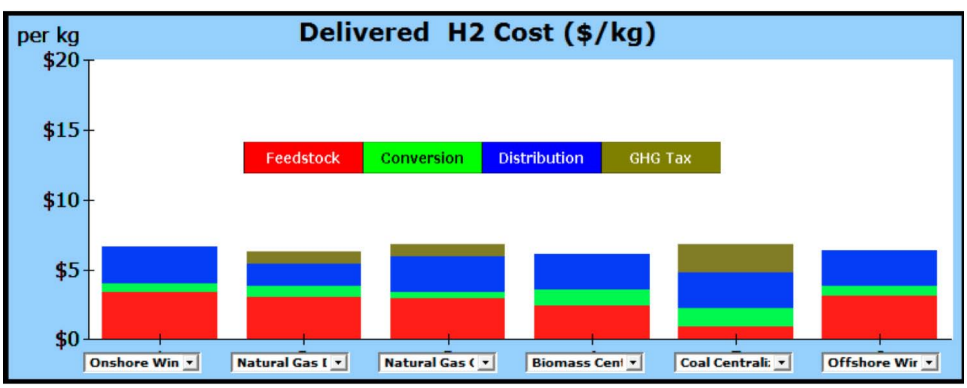

FIGURE 3. Illustrative H2 production costs in 2050 ($/kg).

CONCLUSIONS AND FUTURE DIRECTIONS

This global resource analysis work is a subtask of the IEA HIA Task 30 (Global Hydrogen Systems Analysis). The main objective is to analyze potential hydrogen production and distribution pathways for participating countries. To accomplish this objective, we developed a user-friendly pathways tool to help participants understand the resource options and constraints to meeting future hydrogen demand for various scenarios. The results show there are a large number of potential pathways for providing hydrogen to fuel significant fuel cell fleets and that resource availability is not the limiting factor for a hydrogen economy. While one of the stated goals for pursuing fuel cell vehicles are reduced GHG emissions, access to cheap supplies of fossil fuels could limit the GHG emission reductions. For this reason, many countries expect their countries to require some percentage of their hydrogen production to come from low-carbon intensity fuels such as wind or biomass. The final results will be presented to the HIA participating countries in October 2013 for approval and will be presented in a final report.

FY 2013 PUBLICATIONS/PRESENTATIONS

1. T. Drennen, "Global Hydrogen Resource Analysis", DOE/EERE Annual Merit Review, Project ID: AN038, Washington, D.C., May 14, 2013.

2. T. Drennen and S. Schoenung, "Hydrogen Resource Analysis Update", HIA Task 30, Spring meeting, Paris, March 10, 2013.

3. T. Drennen and S. Schoenung, "Task 30, Subtask A Update for HIA ExCo", Paris, March 11, 2013.

4. T. Drennen, D. Reichmuth, T. West, "Hydrogen Analysis Update", HIA Task 30, Fall meeting, Oslo, September 27, 2013.

REFERENCES

1. The Department of Energy Hydrogen Analysis (H2A) Cost models are available online at: www.hydrogen.energy.gov/h2a_analysis.html.

2. The Department of Energy Hydrogen Analysis Delivery Scenario Analysis Model (HDSAM) is available at: http://www.hydrogen.energy.gov/analysis_repository/project.cfm/PID=218.

3. The Department of Energy Macro System Model (MSM) is available at: http://www.hydrogen.energy.gov/macro_system_model.html.

XI.10 Life-Cycle Analysis of Water Use for Hydrogen Production Pathways

Amgad Elgowainy (Primary Contact),
Michael Wang, and May Wu
Argonne National Laboratory
9700 South Cass Avenue
Argonne, IL 60439
Phone: (630) 252-3074
Email: aelgowainy@anl.gov

DOE Manager
Fred Joseck
Phone: (202) 586-7932
Email: Fred.Joseck@ee.doe.gov

Project Start Date: April 2013
Project End Date: Project continuation and direction determined annually by DOE

Overall Objective

Quantify water consumption associated with various hydrogen production pathways

Fiscal Year (FY) 2013 Objectives

- Evaluate water consumption for various hydrogen production processes
- Identify approaches to efficient water use
- Assess impacts of feedstock source on life-cycle water consumption for hydrogen production
- Identify major contributors to water consumption in the upstream supply chain of hydrogen

Technical Barriers

This project addresses the following technical barriers from the Systems Analysis section of the Fuel Cell Technologies Office Multi-Year Research, Development, and Demonstration Plan:

(C) Inconsistent Data, Assumptions and Guidelines

(D) Suite of Models and Tools

(E) Unplanned Studies and Analysis

Contribution to Achievement of DOE Systems Analysis Milestones

This project contributes to achievement of the following DOE milestone from the Systems Analysis section of the Fuel Cell Technologies Office Multi-Year Research, Development, and Demonstration Plan:

- Task 1.13: Complete environmental analysis of the technology environmental impacts for hydrogen and fuel cell scenarios and technology readiness. (4Q, 2015)

FY 2013 Accomplishments

- Quantified the water consumption associated with central and distributed production of hydrogen via steam methane reformation (SMR).
- Quantified the water consumption associated with central and distributed production of hydrogen via electrolysis of water.

✧ ✧ ✧ ✧ ✧

INTRODUCTION

One emerging category of interest to the life-cycle analysis (LCA) of alternative fuels is water consumption. The production of most energy feedstocks and fuels require significant water use. Competing fuel production pathways strain available water resources and raise the potential of water supply and demand imbalance at a regional level. Addressing the potential regional imbalance requires the examination of the growing needs for water use in different energy production systems. Fossil feedstock sources such as natural gas and crude oil require significant volumes of water for extraction. Similarly, biofeedstocks such as corn and cellulosic biomass need water for growth, Figure 1. Converting conventional and biofeedstocks to fuels require additional water consumption. Producing hydrogen from electricity (via electrolysis), natural gas (via SMR), or biomass (via gasification) requires the use of water for the conversion process as well as for cooling.

The stages included in the life cycle of any product include its raw material acquisition, transportation and processing, as well as its manufacturing, distribution, use and disposal or recycling. LCA of a fuel is known as fuel-cycle analysis or well-to-wheels (WTW) analysis. With support from DOE Energy Efficiency and Renewable Energy offices, including the Fuel Cell Technologies Office Argonne National Laboratory developed the Greenhouse gases, Regulated Emissions, and Energy in Transportation (GREET) model to evaluate the environmental impacts of various fuel-vehicle systems on a life-cycle basis. The life cycle stages in the GREET model are shown in Figure 2. This phase of the project will focus only on the fuel cycle water consumption. LCA metrics in GREET include energy use by type (e.g., fossil, petroleum, natural gas, coal, nuclear, renewable), greenhouse gases emissions (e.g., CO_2, N_2O, CH_4), and criteria air pollutants emissions (e.g., CO, VOC,

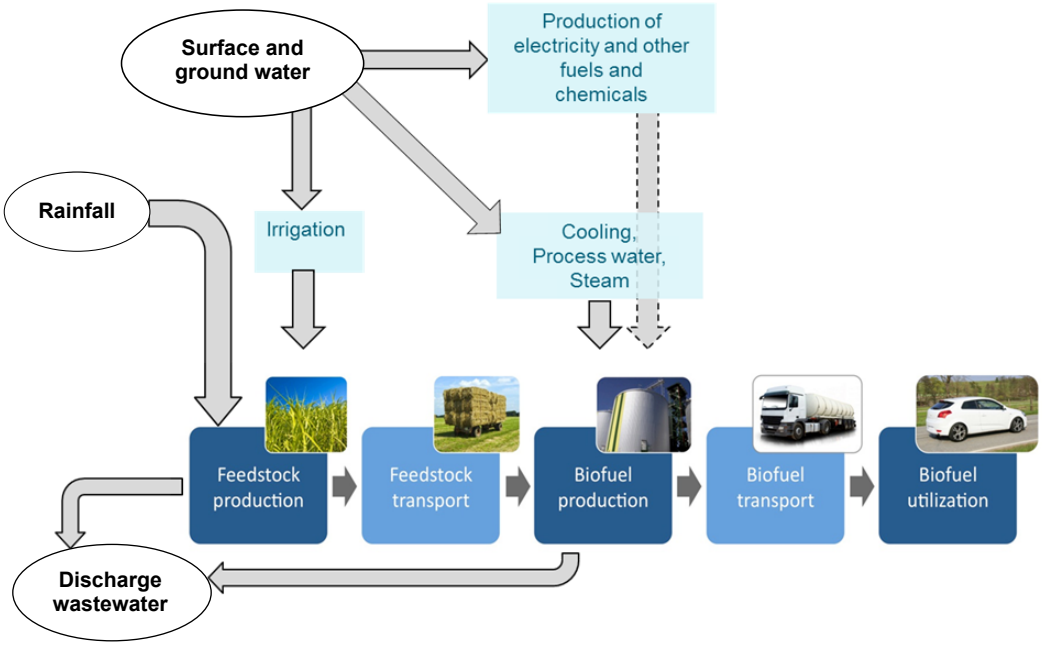

FIGURE 1. Example of Water Accounting in the Biofuel Production Pathway

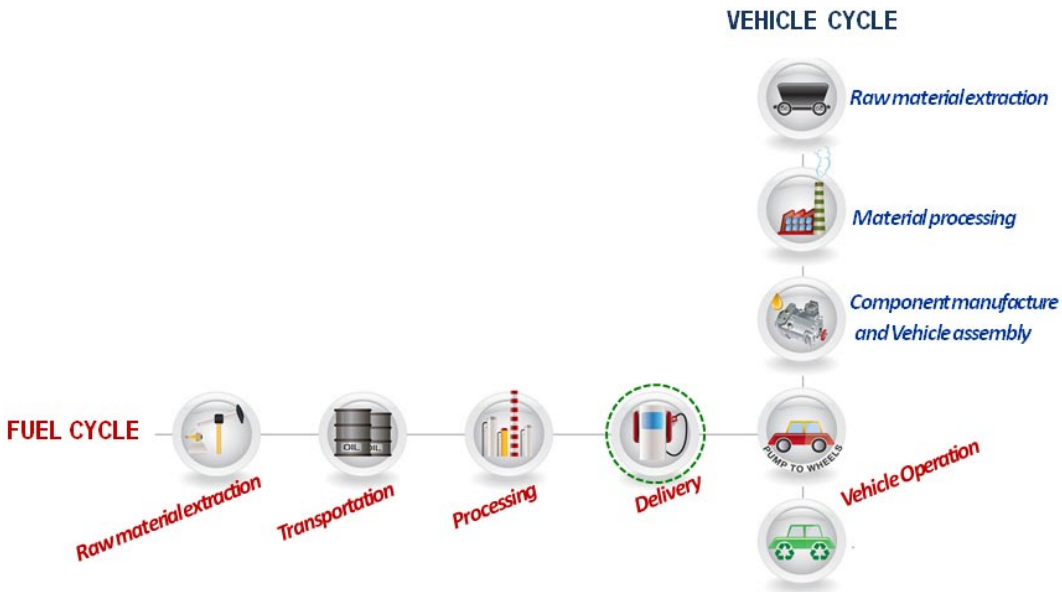

FIGURE 2. Life-Cycle Stages in the GREET Model

NOx, SOx, particulate matter. With the help of this effort, water consumption will be added as a new metric to the GREET model. Water consumption will account only for fresh surface and ground water (also known as "blue" water). Water consumption is defined as fresh water withdrawal from a given surface or ground source minus the fresh water returned to the same withdrawal source.

APPROACH

The water consumption during hydrogen production processes can be attributed to three main factors: (1) water rejection at water treatment plant, (2) water consumption needed for the energy conversion process, and (3) water consumption during cooling process. Data sources for this

project include open literature, Fuel Cell Technologies Office H2A models, industrial sources, and engineering process calculations. Once water consumption is estimated for the hydrogen production processes, the indirect water use in the upstream supply chain will be evaluated and incorporated in the life-cycle water consumption assessment.

RESULTS

The rejection rate at the water treatment plant depends on the quality of supply water and on the employed purification technology. While municipal water's total dissolved solids are typically below 500 ppm, total dissolved solids in surface and ground waters typically exceed 1,000 ppm. Deionization systems use ion selective membranes that allow the positive ions to separate from the water toward the negative electrode and the negative ions toward the positive electrode, and achieve nearly 100% water recovery rate. Reverse osmosis systems remove nonionic organic contaminants by forcing water under pressure through a semi-permeable membrane while excluding most contaminants. The water recovery rate in such systems depends on the quality of supplied water and can achieve water recovery rate up to 75-80%. The water required for the conversion process to H_2 fuel depends on the feedstock source and the employed technology, and is typically higher than the water consumption calculated from stoichiometric chemistry (1.2 and 2.4 gallon of water per kg of H_2 for SMR and electrolysis, respectively) due to the frequent blow down operations to remove the accumulated impurities which negatively impacts the system performance. Cooling towers require water circulation rate of approximately 10 gal/min for each 100 kg/day hydrogen production [1]. The water consumption rate in cooling towers is typically less than 2% of the water circulation rate. However, dry cooling technologies do not consume any water but are more expensive. The water consumption for hydrogen production via SMR and electrolysis is typically in the range of 9-12 gallon of water per kg of H_2. Rejection at water treatment plants and water loss in cooling towers represent more than 50% of the total water consumption. Future water conservation technologies can practically reduce the water consumption rate to 5-7 gallon of water per kg of H_2 with the lower end for production via SMR and the higher end for production via electrolysis.

CONCLUSIONS AND FUTURE DIRECTIONS

Water consumption during industrial hydrogen production via SMR is in the range of 9-12 gallon of water per kg of H_2. Further analysis is required to evaluate water consumption in other hydrogen production pathways (e.g., biomass and coal gasification). In the next project step, indirect water consumption in the upstream supply chain (e.g., natural gas recovery, electricity generation, biomass growth, transportation and distribution, etc.) will be evaluated. Finally, the water consumption by process will be incorporated in the GREET model to estimate life-cycle water consumption for each production pathway.

SPECIAL RECOGNITIONS & AWARDS/ PATENTS ISSUED

1. Amgad Elgowainy and Michael Wang received the DOE Joint Vehicle Technologies and Fuel Cell Technologies R&D Award in recognition for their outstanding contributions to life-cycle assessment of alternative fuel vehicles pathways, including fuel cell and battery electric vehicles (2013).

REFERENCES

1. Simon, A., Daily, W., White, R. 2010, Hydrogen and Water: An Engineering, Economic, and Environmental Analysis, Lawrence Livermore National Laboratory, Report# LLNL-TR-422193.

XI.11 Analysis of Fuel Cell Integration with Biofuels Production

Mark F. Ruth (Primary Contact), Mark Antkowiak
National Renewable Energy Laboratory
15013 Denver West Pkwy.
Golden, CO 80401
Phone: (303) 384-6874
Email: mark.ruth@nrel.gov

DOE Manager
Fred Joseck
Phone: (202) 586-7932
Email: Fred.Joseck@ee.doe.gov

Project Start Date: May 1, 2012
Project End Date: July 1, 2013

Overall Objectives

- Identify opportunities for using fuel cells in biorefineries
- Analyze potential benefits of fuel cells in biorefineries
- Report the effects of integration on levelized costs, capital costs, and operating costs

Fiscal Year (FY) 2013 Objectives

- Finalize analysis which was performed in FY 2012
- Report on analysis

Technical Barriers

This project addresses the following technical barriers from the Systems Analysis section of the Fuel Cell Technologies Office Multi-Year Research, Development, and Demonstration Plan:

(B) Stove-piped/Siloed Analytical Capability

(D) Insufficient Suite of Models and Tools

(E) Unplanned Studies and Analysis

Contribution to Achievement of DOE Systems Analysis Milestones

This project will contribute to achievement of the following DOE milestones from the Systems Analysis section of the Fuel Cell Technologies Office Multi-Year Research, Development, and Demonstration Plan:

- Milestone 1.13: Complete environmental analysis of the technology environmental impacts for hydrogen and fuel cell scenarios and technology readiness. (4Q, 2015)
- Milestone 1.14: Complete analysis of the job impact from fuel cell growth in stationary power generation sector through 2020. (4Q, 2015)
- Milestone 1.16: Complete analysis of program performance, cost status, and potential use of fuel cells for a portfolio of commercial applications. (4Q, 2018)
- Milestone 1.17: Complete analysis of program technology performance and cost status, and potential to enable use of fuel cells for a portfolio of commercial applications. (4Q, 2018)
- Milestone 1.19: Complete analysis of the potential for hydrogen, stationary fuel cells, fuel cell vehicles, and other fuel cell applications such as material handling equipment including resources, infrastructure and system effects resulting from the growth in hydrogen market shares in various economic sectors. (4Q, 2020)
- Milestone 1.20: Complete review of fuel cell and hydrogen markets. (4Q, 2011 through 4Q, 2020)
- Milestone 3.3: Complete review of status and outlook of non-automotive fuel cell industry. (biennially from 4Q, 2011 through 4Q, 2019)

FY 2013 Accomplishments

- Analyzed potential of fuel cells for combined heat and power (CHP) and combined heat, hydrogen, and power (CHHP) application in emerging biorefineries by focusing on the cost competitiveness of molten carbonate fuel cells (MCFC) and phosphoric acid fuel cells (PAFC) systems in fast-pyrolysis biorefineries.
- Estimated effects on levelized costs of the product pyrolysis oil. None of the four basic fuel cell scenarios studied resulted in a levelized cost of the pyrolysis oil lower than the non-fuel cell case's $2.11/gal ($2005). With a pyrolysis oil levelized cost of $2.17/gal, the MCFC fuel cell in CHHP mode scenario had the lowest levelized cost of the four fuel cell scenarios. It was followed by the MCFC fuel cell in CHP mode scenario at $2.19/gal. The PAFC scenarios in CHHP and CHP modes resulted in levelized costs of $2.22 and $2.29/gal, respectively.
- Estimated effects on fixed capital investment (FCI) on the fast pyrolysis biorefinery. The FCI of the base case without a fuel cell is $172M ($2005). Adding a MCFC increases the FCI to $199M and $202M in CHP and CHHP configurations, respectively. Adding a PAFC system increases the FCI to $223M and $255M in CHP and CHHP configurations, respectively.

✧ ✧ ✧ ✧ ✧

INTRODUCTION

This study provides a preliminary examination of the possibility of inserting one or more fuel cells into a fast pyrolysis-based biofuels production facility. Biomass pyrolysis systems have the potential to produce liquid transportation fuels in an economically competitive manner. Wright et al. (2010) estimated that, for an nth generation fast-pyrolysis plant that purchased all of its hydrogen necessary for hydrocracking and hydrotreating from offsite, the fixed capital investment is $172M and the levelized cost (assuming a 10% discount rate) is $2.11/gal pyrolysis oil. Wright et al. considered two separate production scenarios.

As shown in Figure 1, fuel cell systems were added to the Wright case to estimate the potential of fuel cells within such processes. In each case, the fuel cell systems converted natural gas and fuel gas produced in the pyrolysis process to power and heat for use in the system thus offsetting all the power required during normal operation and much of the heat. Those scenarios are referred to as CHP scenarios. In some cases, the fuel cell systems also produced hydrogen offsetting merchant hydrogen purchased to upgrade the pyrolysis oil. Those scenarios are referred to as CHHP scenarios. Two types of fuel cell systems were analyzed: MCFC systems with reforming of hydrocarbons to hydrogen within the fuel cell and PAFC systems with an external reformer.

APPROACH

The techno-economic models developed for the merchant hydrogen scenario of Wright's study was the basis for this effort. The Fuel Cell Power (FCPower) Model—a techno-economic model for the analysis of high-temperature fuel cell systems in distributed applications—was added to Wright's model to incorporate fuel cell costs. Scenarios with both MCFCs and PAFCs were developed. Scenarios were also developed for each fuel cell type in two modes: CHP and CHHP. In each scenario, the fuel cell is integrated into the pyrolysis process. The fuel cell system uses merchant natural gas and fuel gas produced by the pyrolysis process to produce heat and electricity and, in some scenarios, hydrogen. Heat from the fuel cell is used directly in the pyrolysis reactor. Heat generated from the fuel cell offsets char combusted for heat thus increasing income from selling the char byproduct and reducing the capital and operating expenses of the char combustor. The fuel cell system is sized to meet all electricity requirements of the plant thus eliminating the need to purchase electricity.

In the CHHP scenarios with MCFCs, hydrogen produced by the fuel cell systems offset the hydrogen purchase but the amount of heat produced is reduced. In PAFC CHHP scenarios, hydrogen production is decoupled from heat and electricity production because reforming is external from the fuel cell; thus, the full hydrogen requirement is

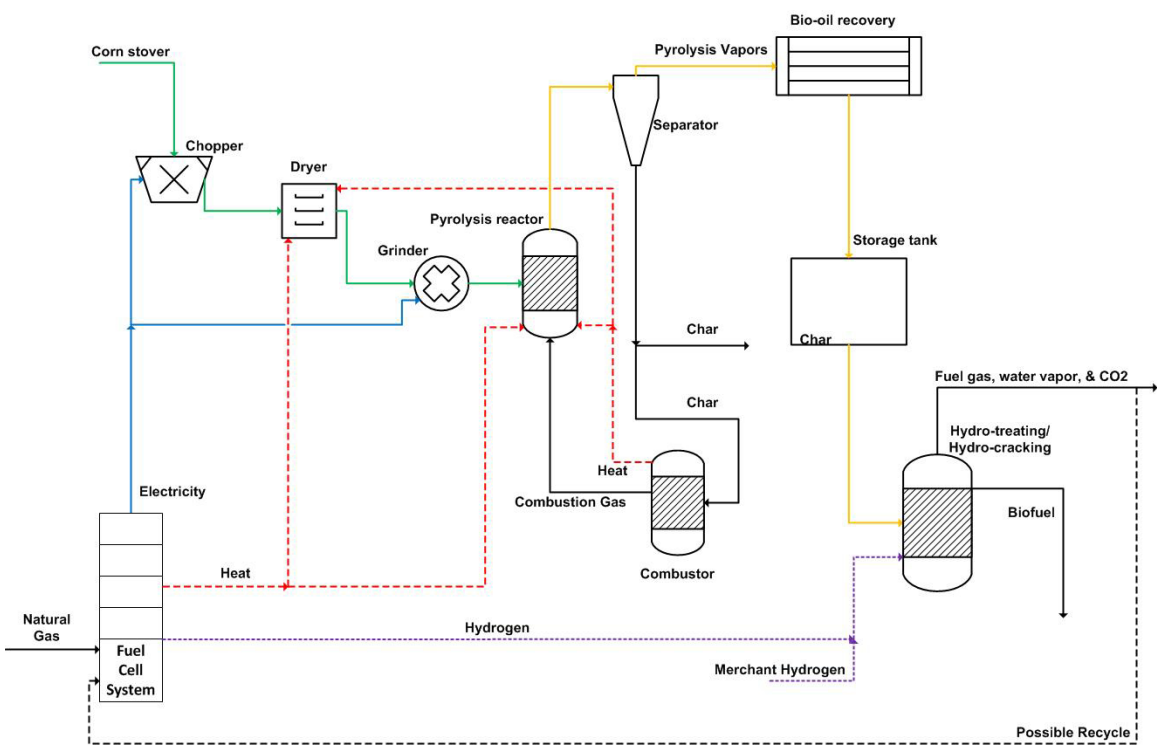

FIGURE 1. Process flow diagram for pyrolysis biorefinery integrated with fuel cell system. Red lines indicate heat flow, blue lines indicate electric power flow. All other lines are material streams.

met by the fuel cell system and no hydrogen is purchased. Sensitivity analyses were conducted on multiple parameters in each scenario.

RESULTS

Each configuration's resulting fuel cell cost, fuel cell system cost (including reforming), combustion system cost, total installed equipment cost, FCI, and levelized cost of the product pyrolysis oil are summarized in Table 1. The MCFC CHP configuration that is sized to meet the pyrolysis plant's electricity requirement of 11.49 MW requires 86 MMBtu/hr natural gas or fuel gas. The system produces 7.8 MW of usable heat and reduces char utilization by 1,027 kg/hr and ash production by 196 kg/hr. The MCFC CHHP configuration requires the same size MCFC system and thus the fuel cell cost and natural gas requirement are the same as the CHP configuration. Because 65% of the available heat is used for hydrogen production, 152 kg/hr of hydrogen are produced but the production of usable heat is only 2.7 MW. The hydrogen production offsets a portion of the 2,041 kg/hr hydrogen required for hydrotreating. The reduced heat production results in a reduction in char utilization of only 359 kg/hr.

The PAFC CHP system that is sized to meet the pyrolysis plant's electricity demand of 11.49 MW requires 105 MMBtu/hr natural gas or fuel gas. The system produces 8.8 MW of usable heat and reduces char utilization by 1,146 kg/hr and ash production by 219 kg/hr. The PAFC CHHP configuration requires the same size fuel cell but the reformer is sized to meet the full hydrogen demand. As a result, the reformer has four times the capacity of the one for the CHP system and four times as much natural gas is required. The resulting fuel cell system's natural gas requirement is 407 MMBtu/hr. Note that the reformer in the PAFC CHHP case needs to be four times larger than that in the CHP case because of the high demand for hydrogen for treating the pyrolysis oil. Also, note that the increased proceeds from additional sales of char and reduced ash disposal costs (not shown) are small when compared to other costs.

The levelized cost for all fuel cell configurations is higher than the base case because the effects of a higher capital cost more than offset the lower operating costs in those cases. A key reason the capital cost is higher in each fuel cell configuration is that the combustion system's size and cost are reduced but not fully eliminated in the fuel cell system configurations. Note that the levelized costs in the CHHP configurations are lower than those in the corresponding CHP configurations because reducing the amount of hydrogen, which is purchased at $5.00/gasoline gallon equivalent (gge) in the base case, is financially beneficial.

Figure 2 displays levelized fuel cost results from single-point sensitivities in the base case (above the solid, horizontal line) and the MCFC CHHP configuration (below the solid, horizontal line). A high electricity price of $0.10/kWh results in a higher cost for the base case system than for the MCFC CHHP because the MCFC case produces all of its own electricity in the fuel cell. In addition, if the natural gas price is low ($2.00/MMBtu is shown in the figure) or the 30% federal tax credit is allowed, the levelized cost difference between the base case and the MCFC CHHP case becomes small as well (about $0.03/gal pyrolysis biofuel). Because fuel gas is a byproduct from the pyrolysis process, a high value such as $8.00/MMBtu results in a lower levelized cost of pyrolysis oil than a low value such as $3.00/MMBtu.

Figure 3 displays a similar sensitivity analysis for the PAFC CHHP configuration. Even though the difference between the baseline costs for the base case and the PAFC CHHP configuration are greater than the MCFC CHHP configuration, there are scenarios where the PAFC CHHP configuration are the lowest cost. One of those scenarios is high-cost merchant hydrogen. If the merchant hydrogen cost is $2.50/gge instead of $1.50/gge (as in the base case) the no

TABLE 1. Financial Comparison of MCFC- and PAFC-Based Systems with the Base Case

PARAMETER ($2005)	MCFC CHP	MCFC CHHP	PAFC CHP	PAFC CHHP	Base Case (no fuel cell)
Fuel Cell Uninstalled Cost	$16,600,000	$16,600,000	$24,900,000	$24,900,000	N/A
Fuel Cell Installed Cost	$19,900,000	$19,900,000	$28,600,000	$28,600,000	N/A
Fuel Cell System Uninstalled Cost	$16,800,000	$16,800,000	$31,100,000	$49,100,000	N/A
Fuel Cell System Installed Cost	$20,200,000	$20,200,000	$35,800,000	$56,500,000	N/A
Combustion System Uninstalled Cost*	$14,400,000	$14,900,000	$14,300,000	$14,300,000	$15,200,000
Combustion System Installed Cost*	$43,500,000	$45,100,000	$43,200,000	$43,200,000	$45,900,000
Total Installed Cost, Complete Pyrolysis Plant	$128,300,000	$129,900,000	$143,700,000	$164,400,000	$110,600,000
Total Fixed Capital Investment	$199,300,000	$201,800,000	$223,300,000	$255,400,000	$171,800,000
Levelized Cost of Pyrolysis Oil ($2005/Gallon)	$2.19	$2.17	$2.29	$2.22	$2.11

* Does not include fuel cell cost

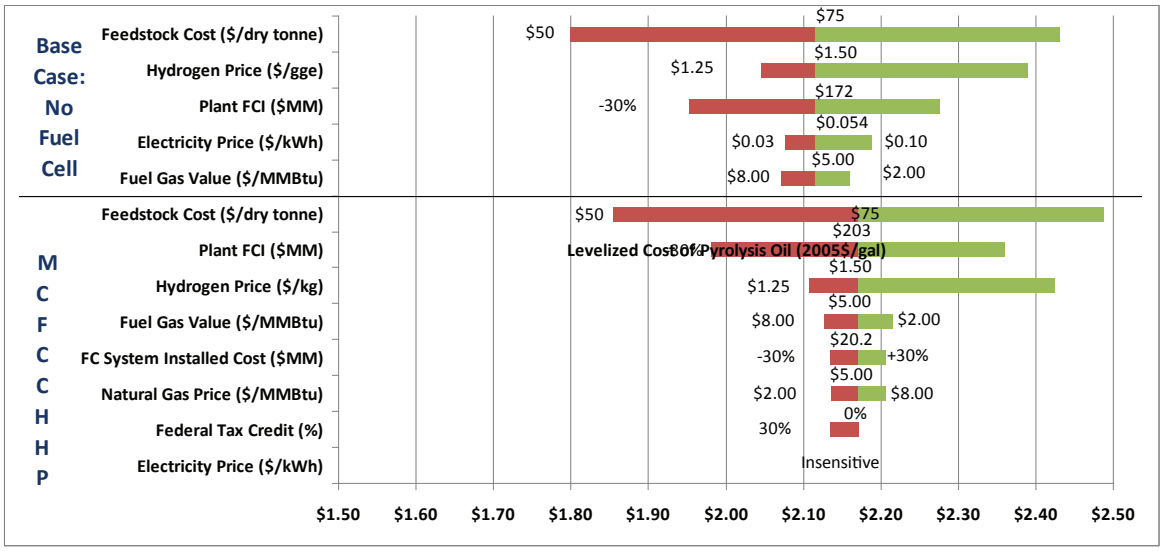

FIGURE 2. Sensitivity analysis of single points in the base case and the MCFC CHHP case.

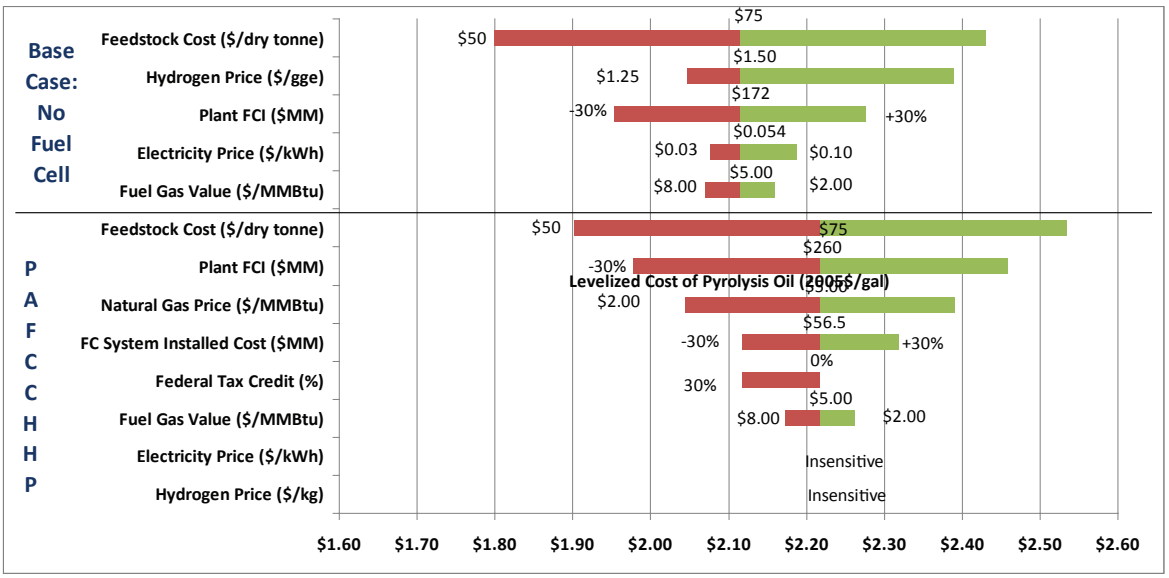

FIGURE 3. Sensitivity analysis of single points in the base case and the PAFC CHHP case.

fuel cell configuration levelized cost increases to $2.39/gal where the PAFC CHHP case stays at $2.22/gal because its hydrogen demand is met internally as is the electricity demand. As with the MCFC CHHP system, if the 30% federal tax credit is allowed, the difference between levelized costs for the fuel cell and non-fuel cell systems converge.

CONCLUSIONS AND FUTURE DIRECTIONS

None of the four basic fuel cell scenarios studied resulted in a levelized cost of the pyrolysis oil lower than the non-fuel cell case's $2.11/gal. With a pyrolysis oil levelized cost of $2.17/gal, the MCFC fuel cell in CHHP mode scenario had the lowest levelized cost of the four fuel cell scenarios. It was followed by the MCFC fuel cell in CHP mode scenario at $2.19/gal. The PAFC scenarios in CHHP and CHP modes resulted in levelized costs of $2.22 and $2.29/gal, respectively. MCFC's scenarios resulted in lower levelized costs than PAFCs because they are more efficient and CHHP scenarios resulted in lower levelized costs than CHP scenarios because of the value of produced hydrogen.

A key reason the fuel cell systems resulted in higher levelized costs is that they require a larger capital investment. The fuel cell costs were partially offset by reducing the char combustion system size; however, since the combustion system could not be completely eliminated without producing

much more electricity than the system needs, both systems were still required. A second reason the fuel cell systems resulted in a higher levelized cost is that they produced electricity and hydrogen (in the CHHP cases) that are competing against projected costs of $0.054/kWh electricity and $1.50/gge for hydrogen.

Sensitivity results show that fuel cell system configurations may be more cost competitive if the electricity cost is closer to $0.10/kWh than the initial estimate of $0.054/kWh; the hydrogen cost is closer to $2.50/gge than the initial estimate of $1.50/gge; or a 30% federal tax credit for fuel cells is in place (not assumed because the projected startup year in this analysis is 2017 which is after the current tax incentive expires). When determining if a fuel cell system should be included in the design or not, the plant designer needs to consider confidence levels in each of those estimates as well as the desire to hedge costs to prevent losses if electricity or hydrogen prices were to change unexpectedly.

No additional work is planned; however, if funding were available activities should be considered including:

- Quantification of other benefits of fuel cell systems within biorefineries. Benefits such as potential greenhouse gas emission reductions; the ability to hedge against potential electricity and H_2 market volatility; and improvements to system reliability and resilience should be considered.
- CHP opportunities for near-term biomass processes should be investigated. Those processes include both first generation (e.g., corn dry mills) and second generation (e.g., lignocellulosic ethanol production) facilities. Ideally, the focus of such analyses should be on processes that produce biogas that can be used as feed to the fuel cell system.
- Identification of additional options where fuel cells can be used in conjunction with other renewable energy technologies.

FY 2013 PUBLICATIONS/PRESENTATIONS

1. Annual Merit Review Presentation on May 14, 2013.

XI.12 Analysis of Community Energy

Darlene Steward
National Renewable Energy Laboratory
15013 Denver West Parkway
Golden, CO 80401
Phone: (303) 275-3837
Email: Darlene.Steward@nrel.gov

DOE Manager
Fred Joseck
Phone: (202) 586-7932
Email: Fred.Joseck@ee.doe.gov

Project Start Date: September 2011
Project End Date: Project continuation and direction determined annually by DOE

Overall Objective

Evaluate the potential benefits of integrating renewable (photovoltaic [PV]) electricity generation with hydrogen-based transportation fueling

Fiscal Year (FY) 2013 Objectives

- Model performance and economics of hydrogen production and storage for capturing peak PV generation and fueling hydrogen-powered vehicles
- Compare system based on PV-generated hydrogen fueling fuel cell electric vehicles (FCEVs) versus system based on PV-generated electricity fueling battery-electric vehicles (EVs)
- Produce draft report of analyses

Technical Barriers

This project addresses the following technical barriers from the Systems Analysis section of the Fuel Cell Technologies Office Multi-Year Research, Development, and Demonstration Plan:

(B) Stove-piped/Siloed Analytical Capability

(D) Insufficient Suite of Models and Tools

(E) Unplanned Studies and Analyses.

Contribution to Achievement of DOE Systems Analysis Milestones

This project has contributed to achievement of the following DOE milestones from the Systems Analysis section of the Fuel Cell Technologies Office Multi-Year Research, Development, and Demonstration Plan:

- Milestone 1.5: Complete evaluation of hydrogen for energy storage and as an energy carrier to supplement energy and electrical infrastructure. (4Q, 2012)
- Milestone 1.17: Complete analysis of program technology performance and cost status and potential to enable use of fuel cells for a portfolio of commercial applications. (4Q, 2018)

FY 2013 Accomplishments

- Created two distributed PV/vehicle-fueling system models: one using PV to supply electricity to buildings and produce hydrogen for FCEV fuel, and one using PV to supply electricity to buildings and produce electricity for EV fuel.
- Performed hourly modeling of all system energy flows using modeled building load and measured solar resource data, highlighting the time-dependent impacts of distributed PV generation.
- Analyzed realistic grid impacts for three levels of PV electricity generation (1,200-, 4,000-, and 7,000-m^2 PV systems) "behind the meter," showing that the largest PV system provides the best vehicle-fueling economics, especially for the hydrogen/FCEV system.
- Showed that capturing PV-generated energy for vehicle fueling could eliminate reverse flow of electricity to the grid.
- Compared performance and economics of hydrogen/FCEV system versus electricity/EV system, finding, in the best-case scenario, a vehicle-fueling cost of $0.19/mile for FCEVs versus $0.13/mile for EVs; the EV economics are better largely because EVs use less energy per mile than FCEVs, but the hydrogen/FCEV system provides potential for greater flexibility than the electricity/EV system[1].

✧ ✧ ✧ ✧ ✧

INTRODUCTION

Because PV generation is intermittent, strategies must be implemented to integrate high levels of PV into the electricity system. In particular, high penetration of distributed, residential rooftop PV systems could affect loading and capacity margins for community-level electricity-distribution systems. PV output typically peaks slightly before the

[1]Hydrogen vehicle: midsize 2012 Honda FCX Clarity, 60 miles/GGE (approx. 55.6 kWh/100 miles), 240 mile range. Electric only vehicle: midsize 2013 Nisson Leaf, 29 kWh/100 miles, 75 miles/charge. Source: Fueleconomy.gov accessed 6/20/2013.

peak daily electricity demand, and this offset could cause overloading of local distribution equipment at high PV penetration.

Hydrogen and fuel cell technologies offer possible PV-integration strategies that could enhance the economic viability—and thus deployment—of both distributed PV and hydrogen/fuel cell technologies. This study modeled and analyzed the costs and benefits of using PV-generated electricity to power homes and produce hydrogen fuel for FCEVs. The study also compared this system to a system that powers homes and stores PV-generated electricity in batteries to fuel EVs.

APPROACH

First, simulated systems integrating PV with hydrogen/FCEV and electricity/EV fueling were created using a modified version of DOE's Fuel Cell Power Model. The PV provides electricity to the buildings and all the electricity for vehicle fuel; when PV output is less than building load, the grid supplies the difference. In addition to PV systems of three different sizes (1,200, 4,000, and 7,000 m^2), the hydrogen/FCEV system includes an electrolyzer, compressor, storage, and dispenser, and the electricity/EV system includes battery storage and a charger (Figure 1).

An hourly building load profile for about 100 single-family homes was established based on modeled load data for a hotel (which has a load profile similar to housing) in Boulder, Colorado. Empirical solar resource data for this location were used to determine PV output for each modeled PV system. Vehicle-fueling profiles and hydrogen and battery system performance and costs were developed from a variety of sources [1-11]. Two fueling cases were analyzed. In Case 1, all PV output in excess of building load is directed to vehicle fueling. In Case 2, all PV output before noon plus all output in excess of building load is directed to vehicle fueling. Finally, hourly energy flows—PV output, electricity to buildings (from PV and the grid), electricity to storage (from PV), and stored electricity to vehicles—were modeled for the simulated systems, and system electricity and fuel costs were calculated.

RESULTS

Figure 2 shows an example of system energy flows for a day in July for Case 1 with the 4,000-m^2 PV system. Both building and vehicle peak demands are offset from the peak PV output. During the PV peak, the system draws no electricity from the grid and produces hydrogen or electricity for storage, which is then used to supply the later-peaking vehicle demand. In this example, PV produces the equivalent of 167% of building electricity demand while directly supplying 47% of building demand; the grid supplies the

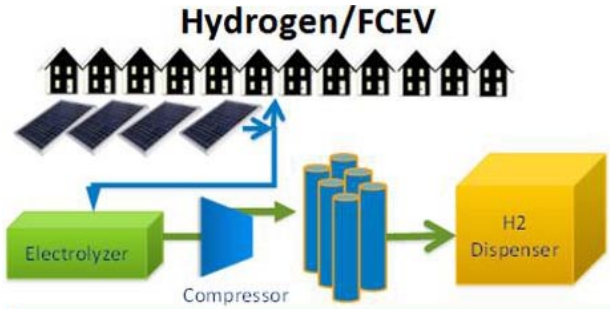

Electrolyzer	Sized to maximum difference between PV output and building load
Compressor	Sized to peak hourly hydrogen rate
Hydrogen storage	Assumed daily full cycling of storage system (no multi-day storage)
Hydrogen dispenser	One assumed in all cases (350-bar dispensing)

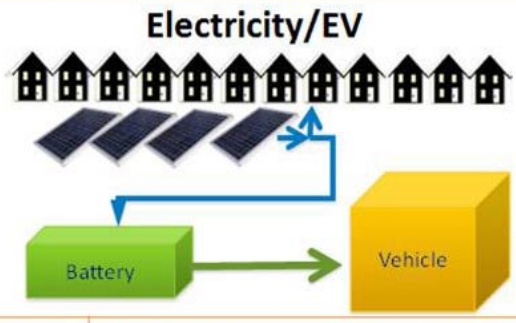

Zinc-air battery	Sized to maximum kWh in storage + 50% assuming full discharge of the battery daily (no multi-day storage)
Level I charging	Assume home vehicle charging (comparable to 350-bar hydrogen system)

FIGURE 1. Schematics of Hydrogen/FCEV and Electricity/EV Systems

remaining 53% of building demand. Table 1 summarizes the energy flows for the 4,000-m^2 PV Case 1 systems.

Figure 3 and Figure 4 show the total system capital costs for Case 1 and Case 2, respectively. The PV system dominates the capital costs followed, for the larger systems, by the electrolyzer. When the PV system costs are excluded, the electrolyzer accounts for 16% (1,200-m^2 PV system), 40% (4,000-m^2 system), and 45% (7,000-m^2 system) of the hydrogen system costs. For the smallest PV system, hydrogen storage accounts for the largest capital cost (22%). Hydrogen system capital costs are higher for Case 2 than for Case 1. However, this difference decreases as the PV system size increases because the difference in annual hydrogen production between the two cases (and thus the difference

TABLE 1. Energy Flows for Hydrogen/FCEV and Electricity/EV Systems, Case 1, 4,000-m^2 PV

Equipment/ System	System Size	Yearly Output	Capacity Factor (% of max output during operation [hrs/year])	Percent of Building Load
PV System	4,000 m^2 (~611 kW peak rated output)	955,681 kWh	18	167 (total) 47 (direct supply)
Electrolyzer (H_2 system)	560 kW input	14,564 kg	40 [3,265]	—
Hydrogen Storage (H_2 system)	85 kg	~ 1 cycle per day	—	—
Vehicle Electricity (battery system)	—	500,755 kWh	—	—
Battery Storage (battery system)	2,954 kWh	~ 1 cycle per day	—	—
Grid	—	303,744 kWh	—	53

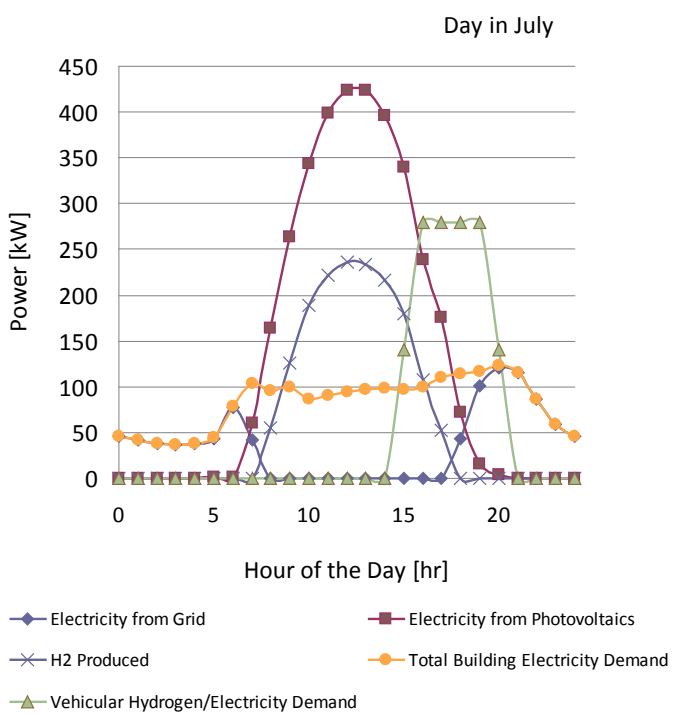

FIGURE 2. Building Electricity Demand, Vehicular Hydrogen/Electricity Demand, PV and Grid Electricity Supply, and Hydrogen Produced (or Electricity to Storage) During a Typical Day in July (4,000-m^2 PV system), Case 1

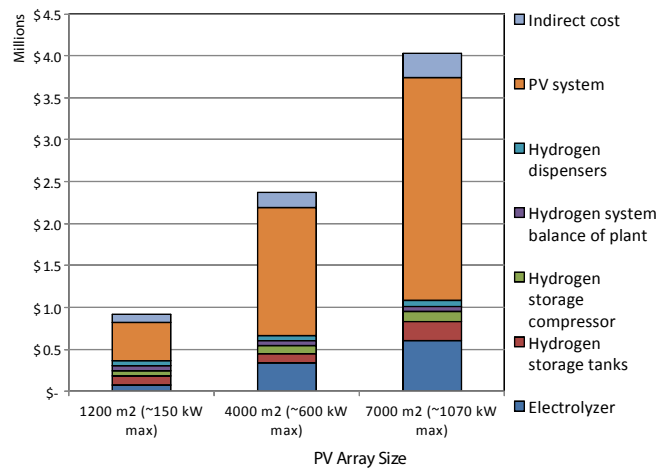

PV system is largest cost item @ $2.50/watt

Other System Cost Assumptions (installed):

- Dispensers: $64,000
- Compressor: $2,600 - $11,000/kW (depending on size)
- H2 storage: ~$1,400/kg
- Electrolyzer: ~$600/kWin ($750/kW incl indirect costs)

FIGURE 3. Total Hydrogen/FCEV System Capital Costs, Including PV Panels, Case 1

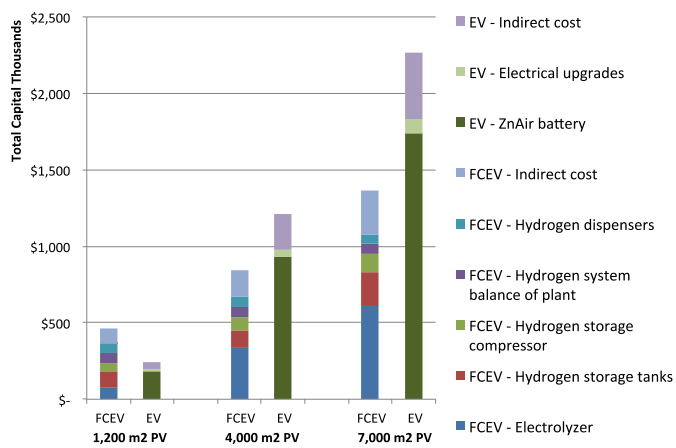

Battery system produces ~3% more energy than hydrogen system because of its higher efficiency.

Other System Cost Assumptions (installed):

- Dispensers: $64,000
- Compressor: $2,600 - $11,000/kW (depending on size)
- H2 storage: ~$1,400/kg
- Electrolyzer: ~$600/kWin ($750/kW incl indirect costs)
- Battery: $315/kWh

FIGURE 4. CapitalCosts of Hydrogen/FCEV and Electricity/EV Systems, Case 2

in the size of the required hydrogen production and storage components) decreases as the PV system size increases. For the 7,000-m^2 system, the Case 1 and Case 2 capital costs are almost identical.

The vehicle-refueling analysis shows the potential for community-level hydrogen refueling using only renewably generated electricity. Table 2 summarizes the Case 1 and Case 2 cost results for both the hydrogen/FCEV and electricity/EV systems. With the 4,000-m^2 PV system, the number of FCEVs served (70–80) roughly matches the modeled community size (100 households). The levelized hydrogen cost ranges from $34/kg ($1.01/kWh) for the 1,200-m^2 Case 1 system to $11/kg ($0.34/kWh) for the 7,000-m^2 Case 2 system. The cost of battery storage of electricity for electric vehicles ranges from $0.57/kWh–$0.39/kWh, also decreasing with increasing system size. The hydrogen system cost reduction for the larger systems is due to better utilization of the equipment. The hydrogen system configuration is also more flexible than the battery system because there are more independent pieces of equipment. For small systems, this is a disadvantage, but for larger systems the increased flexibility reduces costs because an incremental increase in hydrogen storage capacity per kWh (hydrogen tank) is less expensive than an incremental (per kWh) increase in electrochemical storage. Even though the hydrogen system is lower cost than the battery system for the largest storage case, the electric vehicle is less expensive on a fuel ¢/mile basis because of its higher efficiency in this scenario in comparison to the FCEV.

In both cases for both the hydrogen and battery systems, diverting more electricity from the PV system for vehicle fueling improves the economics; this effect is more pronounced for the hydrogen/FCEV system than for the battery/EV system. The best hydrogen cost is from the Case 2, 7,000-m^2 PV system. In this scenario, about 90% of the PV output goes to hydrogen production or battery storage, and the PV system supplies 28% of the building load. The hydrogen system produces about 32,000 kg of hydrogen per year (about 90 kg/day), enough to supply 159 vehicles at a cost of $11/kg or $0.19/mile.

CONCLUSIONS AND FUTURE DIRECTIONS

This analysis shows that community-level hydrogen fueling using only PV-generated electricity could be accomplished. For the 4,000-m^2 PV system case, the number of FCEVs that could be fueled roughly matches the total number of vehicles expected for the community size modeled (100 households). By capturing excess peak PV electricity generation as vehicle fuel (instead of feeding excess electricity back onto the grid), the system also provides the smoothing of PV/grid interactions that could be vital for integrating high levels of distributed PV. Although the analysis did not explicitly address seasonal variations in production or demand, it is likely that the additional storage modeled would be sufficient to accommodate them.

With the 4,000-m^2 PV system, the number of FCEVs served (70–80) roughly matches the modeled community size (100 households). The levelized hydrogen cost ranges from $34/kg ($1.01/kWh) for the 1,200-m^2 Case 1 system to $11/kg ($0.34/kWh) for the 7,000-m^2 Case 2 system. The cost of battery storage of electricity for electric vehicles ranges from $0.57/kWh–$0.39/kWh, also decreasing with increasing system size. Even though the hydrogen system is lower cost than the battery system for the largest storage case, the electric vehicle is less expensive on a fuel ¢/mile basis ($0.11/mile and $0.19/mile, respectively) because of its higher efficiency in this scenario in comparison to the FCEV.

TABLE 2. Summary of Vehicle Fueling Cost Results

Hydrogen for FCEVs								
	Case 1 (Excess Electricity)				Case 2 (Excess Electricity + Morning Output)			
PV Size (m^2) [% of bldg load]	Production (kg H_2/yr)	Vehicles Served	H_2 Cost ($/kg)	H_2 Cost (¢/mi)	Production (kg H_2/yr)	Vehicles Served	H_2 Cost ($/kg)	H_2 Cost (¢/mi)
1,200 [~50%]	1,804	9	34	56	3,541	17	22	38
4,000 [~170%]	14,564	72	13	22	16,985	84	12	21
7,000 [~300%]	29,274	146	12	20	31,898	159	11	19
Electricity for EVs								
	Case 1 (Excess Electricity)				Case 2 (Excess Electricity + Morning Output)			
PV Size (m^2)	Production (kWh/yr)	Vehicles Served	Elec. Cost ($/kWh)	Elec. Cost (¢/mi)	Production (kWh/yr)	Vehicles Served	Elec. Cost ($/kWh)	Elec. Cost (¢/mi)
1,200	61,726	17	0.57	17	121,936	35	0.45	13
4,000	500,755	143	0.41	12	585,475	168	0.40	12
7,000	1,008,212	289	0.39	11	1,100,877	316	0.39	11

Note: ¢/mile values are for fuel only and do not include vehicle cost or maintenance.

Thus this analysis does not present a compelling economic case for community-scale hydrogen fueling for very small systems in comparison to battery storage and EV charging. However, several characteristics of hydrogen/FCEV systems could be attractive despite the higher cost. The hydrogen/FCEV system provides more flexibility in its configuration than the electricity/EV system because the power (per kW) component (the electrolyzer) is decoupled from the capacity (per kWh) component of the system (the hydrogen storage tanks). In the battery storage system, the power-to-capacity ratio is fixed, so the system configuration is less flexible, and additional storage is more expensive on a per-kWh basis than additional hydrogen storage capacity. Overall system costs are highly dependent on the relationships between component sizes/capacities, so a more flexible system may prove to be more cost effective when carefully optimized for the particular situation and goals.

Future work in this area could include the following:

- Explore more realistic scenarios for addressing seasonal variation in PV output
- Explore methodologies for optimizing hydrogen system configuration
- Explore the impact of incentives and net metering for system economics

FY 2013 PUBLICATIONS/PRESENTATIONS

1. Steward, Analysis of Community Energy; Project ID AN043, Poster presentation at the U.S. Department on Energy Office of Energy Efficiency and Renewable Energy Fuel Cell and Vehicle Technologies Annual Merit Review. Washington DC May 13–17, 2013.

2. Hydrogen Community Energy; Hydrogen Energy Storage and Community-Level Refueling for Grid Integration of Distributed PV (Expected publication September 2013).

REFERENCES

1. Barbose, G.; Darghouth, N.; Wiser, R. (November 2012). *Tracking the Sun V: An Historical Summary of the Installed Cost of Photovoltaics in the United States from 1998 to 2011.* Berkeley, CA: Lawrence Berkeley National Laboratory.

2. DOE Independent Review. (September 2009). *Current (2009) State-of-the-Art Hydrogen Production Cost Estimate Using Water Electrolysis*. NREL/BK-6A1-46676. Golden, CO: National Renewable Energy Laboratory. http://www.nrel.gov/docs/fy10osti/46676.pdf.

3. FCPower Model. (2012). Molten Carbonate Fuel Cell, version 1.2 (Excel file). http://www.hydrogen.energy.gov/fc_power_analysis.html.

4. Field, K.; Deru, M.; Studer, D. (2010). *Using DOE Commercial Reference Buildings for Simulation Studies*. Preprint. SimBuild 2010. Golden, CO: National Renewable Energy Laboratory.

5. H2A Production Model. (2012). Current Forecourt Grid Electrolysis 1500 kg per day version 3.0 (Excel file). http://www.hydrogen.energy.gov/h2a_prod_studies.html.

6. HTAC. (September 2011). HTAC Energy Storage Working Group discussions.

7. James, B. D.; Perez, J.; Baum, K.N.; Spisak, A.; Sanders, M. (May 2011). *Low Temperature PEM Stationary Fuel Cell System Cost Analysis: Preliminary Results*. DTI Subcontract Report; page 35.

8. "Fuel Cell Power Model Case Study Data." (2009). National Renewable Energy Laboratory. http://www.hydrogen.energy.gov/cf/fc_power_analysis_model_data.cfm.

10. Rastler, D. (December 2010). *Electricity Energy Storage Technology Options: A White Paper Primer on Applications, Costs, and Benefits*. EPRI Technical Update.

11. Steward, D.; Saur, G.; Penev, M.; Ramsden, T. (November 2009). *Lifecycle Cost Analysis of Hydrogen versus Other Technologies for Electrical Energy Storage*. NREL/TP-560-46719. Golden, CO: National Renewable Energy Laboratory. http://www.nrel.gov/docs/fy10osti/46719.pdf.

XII. SMALL BUSINESS INNOVATION RESEARCH (SBIR) FUEL CELL TECHNOLOGIES OFFICE NEW PROJECTS AWARDED IN FY 2013

XII.0 Small Business Innovation Research (SBIR) Fuel Cell Technologies Office New Projects Awarded in FY 2013

The Small Business Innovation Research (SBIR) program provides small businesses with opportunities to participate in DOE research activities by exploring new and innovative approaches to achieve research and development (R&D) objectives. The funds set aside for SBIR projects are used to support an annual competition for Phase I awards of up to $225,000 each for about nine months to explore the feasibility of innovative concepts. Phase II R&D efforts further demonstrate the technologies to move them into the marketplace, and these awards are up to $1,500,000 over a two-year period. Small Business Technology Transfer (STTR) projects include substantial (at least 30%) cooperative research collaboration between the small business and a non-profit research institution.

Table 1 lists the SBIR Phase I and Table 2 lists the STTR Phase II projects awarded in FY 2013 related to the Fuel Cell Technologies Office. Brief descriptions of each project follow.

TABLE1. FY 2013 SBIR Phase I Projects Related to the Hydrogen and Fuel Cells Program

Title	Company	City, State
XII.1 Cryogenically Flexible, Low Permeability Thoraeus Rubber H2 Dispenser Hose	Nanosonic, Inc.	Pembroke, VA
XII.2 Hydrogen Leak Detector for Hydrogen Dispenser	Applied Nanotech, Inc.	Austin, TX
XII.3 Nanostructured Catalysts for Alkaline PEM Fuel Cells	Giner, Inc.	Newton, MA

TABLE 2. FY 2013 STTR Phase II Projects Related to the Hydrogen and Fuel Cells Program

Title	Company	City, State
XII.4 Low-Noble-Metal-Content Catalysts/Electrodes for Hydrogen Production by Water Electrolysis	Proton Energy Systems	Wallingford, CT

PHASE I PROJECTS

XII.1 Cryogenically Flexible, Low Permeability Thoraeus Rubber H2 Dispenser Hose

Nanosonic, Inc.
158 Wheatland Drive
Pembroke, VA 24136-3645

This project will offer Thoraeus Rubber™ as a flexible, tough, low-permeability H2 dispenser hose. Thoraeus Rubber™ has been demonstrated to maintain low air permeability (<1.58 cc/100 in^2/day/atm) upon the triple-fold cold flex test conducted at -50ºC. Herein, an innovative reinforced version would be developed to optimize ultra-low hydrogen permeability and embrittlement.

XII.2 Hydrogen Leak Detector for Hydrogen Dispenser

Applied Nanotech, Inc.
3006 Longhorn Blvd, Ste 107
Austin, TX 78758-7631

There is a need for hydrogen leak detection on hydrogen fuel stations. Hydrogen detectors can be integrated in hydrogen dispensers for reliability and safety during operation. In this project, we will develop a low-cost, long-lifetime, miniature hydrogen detector capable of detecting hydrogen in low concentrations.

XII.3 Nanostructured Catalysts for Alkaline PEM Fuel Cells

Giner, Inc.
89 Rumford Avenue
Newton, MA 02466-1311

The objective is to develop a high-porosity, fibrous composite air cathode with a low-cost catalyst and a designed mechanism to manage electrolyte flooding.

PHASE II PROJECTS

XII.4 Low-Noble-Metal-Content Catalysts/Electrodes for Hydrogen Production by Water Electrolysis

Proton Energy Systems
10 Technology Drive
Wallingford, CT 06492-1955

Proton OnSite manufactures hydrogen generation systems which can be integrated with renewable energy sources to generate hydrogen fuel while producing minimal carbon footprint. This project aims to reduce the cost and energy required to manufacture these units through development of improved electrode application methods and reduction in platinum group metal usage.

XIII. Acronyms, Abbreviations, and Definitions

α-AlH_3	Alpha polymorph of aluminum hydride
~	Approximately
@	At
°C	Degrees Celsius
°F	Degrees Fahrenheit
Δ	Change, delta
ΔG	Gibbs free energy of reaction
ΔH	Enthalpy of reaction, Enthalpy of hydrogenation
$\Delta H°_f$	Standard heat of formation
ΔK	Stress intensity factor
ΔP	Pressure drop, pressure change
≈	Equals approximately
>	Greater than
≥	Greater than or equal to
<	Less than
≤	Less than or equal to
μ	Micro (one-millionth; 0.000001)
μA	Microampere(s)
$\mu A/cm^2$	Microampere(s) per square centimeter
μc-Si	Microcrystalline silicon
μg	Microgram(s)
μCHP	Micro-combined heat and power
μCHX	Microscale combustor/heat exchanger
μCHP	Micro-combined heat and power
μm	Micrometer(s); micron(s)
μM	Micromolar
μmol	Micromole(s)
$\mu\Omega\text{-}cm^2$	Micro-ohm(s)-square centimeter
μV	Microvolt(s)
η	Viscosity
#	Number
Ω	Ohm(s)
Ω/cm^2	Ohm(s) per square centimeter
$\Omega\text{-}cm^2$	Ohm-square centimeter(s)
%	Percent
®	Registered trademark
$	United States dollars
^{11}B-NMR	Boron 11 nuclear magnetic resonance
1-D, 1D	One-dimensional
1Q	First quarter of the fiscal year
2-D, 2D	Two-dimensional
2Q	Second quarter of the fiscal year
3-D, 3D	Three-dimensional
3DSM	Dimensionally stable membrane with 3-dimensional porous support
3-L	Three-layer
3-MPAB	3-methoxypropylamineborane
3-PPAB	3-phenylpropylamine-borane
3Q	Third quarter of the fiscal year
4Q	Fourth quarter of the fiscal year
5-L	Five-layer
6FBPS0	Hexafluoro biphenol sulfone
6FCN-x	Hexafluoro bisphenol A based disulfonated polybenzonitrile (H+ form) (x denotes degree of sulfonation)
6FK	Hexafluoro ketone; Partially fluorinated poly(arylene ether ketone)
6FPAEB	Hexafluoro bisphenol a benzonitrile
8YSZ	8 mol% yttria-stabilized zirconia
A	Ampere(s), amp(s)
Å	Angstrom(s)
AAE	Adsorbent acceptability envelope
AB	Ammonia-borane, NH_3BH_3
ABH_2	Ammonium borohydride, NH_4BH_4
AC	Alternating current; Activated carbon
ACF	Activated carbon fibers
A/cm^2	Amps per square centimeter
ACN	Acetonitrile
ACNT	Aligned carbon nanotube
ADG	Anaerobic digester gas
AEM	Anion exchange membrane; Analytical electron microscopy
AEO	Annual Energy Outlook
AFDC	Alternative Fuels Data Center
AFM	Atomic force microscopy; Anti-ferromagnetic
AFP	Automated fiber placement
AFV	Alternative fuel vehicle
Ag	Silver
AGC	Activated graphitic carbon
AgCl	Silver chloride
A-h	Amp-hour(s)
AHJ	Authorities having jurisdiction
AISI	American Iron & Steel Institute
AIST	Japanese National Institute of Advanced Industrial Science and Technology
AK	Alkali

a.k.a.	Also known as
Al	Aluminum
Al_2O_3	Aluminum oxide
Al-AB	Aluminum-ammonia-borane
$AlCl_3$	Aluminum chloride
ALD	Atomic layer deposition
AlH_3	Aluminum hydride; Alane
ALL-CRAFT	Alliance for Collaborative Research in Alternative Fuel Technology
ALS	Advanced Light Source at Lawrence Berkeley National Laboratory
ALT	Accelerated life test
AM	Air mass
AM 1.5	Air Mass 1.5 solar illumination
AM1.5G	Air Mass 1.5 Global (solar spectrum)
AMBH	Amine metal borohydride
AMC	Aminomethyl-cyclohexane
AMFC	Anion exchange membrane fuel cell; Alkaline membrane fuel cell
AMR	Annual Merit Review
AN	Acrylonitrile
ANL	Argonne National Laboratory
ANOVA	Analysis of variance
ANSI	American National Standards Institute
A_o	Arrhenius constant, ml/[cm^2-min-atm½]; Availability
APCI, APCi	Air Products and Chemicals, Inc.
APD	3-aminopropane-1,2-diol
APR	Aqueous-phase reforming
APU	Auxiliary power unit
AQMD	Air Quality Management District
Ar	Argon
AR	Areal resistance
ARPA-E	Advanced Research Projects Agency–Energy
ARRA	American Recovery and Reinvestment Act
As	Arsenic
ASAXS	Anomalous small-angle X-ray scattering
a-Si	Amorphous silicon
a-SiC	Amorphous silicon carbide
a-SiGe	Amorphous silicon germanium
a-SiN	Amorphous silicon nitride
ASME	American Society of Mechanical Engineers
ASPEN	Modeling software, computer code for process analysis
ASR	Area-specific resistance
AST	Accelerated stress test
ASTM	ASTM International, originally known as the American Society for Testing and Materials
AT	Ammonia triborane
at%	Atomic percent
atm	Atmosphere(s)
ATP	Adenosine triphosphate; Advanced Technology Program
ATPase	Adenosine triphosphatase
ATR	Autothermal reformer; Autothermal reforming; Attenuated total reflection
ATR-FTIR	Attenuated total reflectance Fourier transform infrared
a.u.	Arbitrary units
Au	Gold
AuS	Gold sulfide
$AuSnO_x$	Gold supported on hydrous tin oxide
$AuTiO_x$	Gold supported on titanium oxide
Autonomie	Plug-and-Play Powertrain and Vehicle Model Architecture and Development Environment software model by Argonne National Laboratory to support the rapid evaluation of new powertrain/propulsion technologies for improving fuel economy through virtual design and analysis in a math-based simulation environment
Avg	Average
AZO	Aluminum zinc oxide
^{11}B-NMR	Boron 11 nuclear magnetic resonance
B	Boron
B_2O_3	Boron oxide; Diboron trioxide
Ba	Barium
Bara	Bar absolute
barg	Bar gauge
BBC	4,4',4''-(benzene-1,3,5-triyl-tris(benzene-4,1-diyl))tribenzoate
BCC	Body-centered cubic
BCN	Boron carbon nitride
Be	Beryllium
BES	Basic Energy Sciences office within the DOE Office of Science
BET	Brunauer-Emmett-Teller surface area analysis method
BEV	Battery electric vehicle
BFZ0	$BaFe_{0.975}Zr_{0.025}O_3$
BFZ1	$BaFe_{0.90}Zr_{0.10}O_3$
BG-DW	65% bio-glycol-35% distilled water
B-G	Boron doped graphitic material
B-H	Boron/hydrogen bond

B-H, BH, BH_4	Borohydride
BHP	Butyl perhydropyrolidine
Bi	Bismuth
$bmimBF_4$	1-butyl-3-methyl-imidazolium tetrafluoroborate
bmimCl	1-butyl-3-methyl-imidazolium chloride
bmimOTf	1-butyl-3-methyl-imidazolium triflate
$bmimPF_6$	1-butyl-3-methyl-imidazolium hexafluorophosphate
BMPFFP	1-butyl-1-methyl-pyrrolidinium tris(pentafluoroethyl)trifluorophosphate
BN	Boron-nitrogen
BNH	Boron-nitrogen-hydrogen
BNHx	Dehydrogenated ammonia-borane
BNL	Brookhaven National Laboratory
BNNT	Boron nitride nanotubes
B-O	Any oxidized boron species, borate
Boc	Tert-butoxycarbonyl
BOC	Best of class
$B(OH)_3$	Boric acid
BOL	Beginning of life
BOP, BoP	Balance of plant
BOT	Beginning of test
BP	Bisphenol; Biphenyl
bpe	Bis(4-pyridyl)ethane
BPEE	1,2-bipyridylethene
BPDC	Biphenyl-4,4'-dicarboxylate
BPP	Bipolar plate
BPPPO	Biphenol-based phenyl phosphine oxide
BPPPO-35	Biphenol-based phenyl phosphine oxide copolymer, 35% molar fraction of disulfonic acid unit (35% level of sulfonation)
BPS	Ballard Power Systems
BPS	Bi Phenyl Sulfone
BPS100	Fully disulfonated poly(arylene ether sulfone)
BPSH	Block polysulfone ether polymer
BPSH	Bi Phenyl Sulfone: H Form
BPSH-30	Biphenyl sulfone H form, 30% molar fraction of disulfonic acid unit (30% level of sulfonation)
BPSH-x	BiPhenyl based disulfonated polySulfone (H+ form) (x denotes degree of sulfonation)
BPVC	Boiler and Pressure Vessel Code
BPVE	Perfluorocyclobutane-biphenyl vinyl ether
BPVE-6F	Perfluorocyclobutane-biphenyl vinyl ether hexafluoroisopropylidene
BPy	2,2'-bipyridine
BPY	4,4'-bypyridine
Br	Bromine
Br_2	Diatomic bromine
BTB	1,3,5-benzenetribenzoate
BTC	1,3,5-benzenetricarboxylate
BTE	4,4',4''-(benzene-1,3,5-triyltris(ethyne-2,1-diyl))tribenzoate
BTT	Benzene tris-tetrazole
BTTCD	Octa-carboxylate ligand
BTU, Btu	British thermal unit(s)
Bu_3SnCl	Tributyltin chloride
$Bu_3SnSnBu_3$	Hexabutyldistannane
BV	Benzyl viologen
BxHy	Polyhedral boranes
BZYC	$BaZr_{0.1}Ce_{0.7}Y_{0.1}Yb_{0.1}O_{3-\delta}$
C	Carbon
C	Couloumb
C_2H_4	Ethylene
C_2H_6	Ethane
C_3H_8	Propane
Ca	Calcium
CA	Carbon aerogel; Chronoamperometry
$CaBr_2$	Calcium bromide
$CaCO_3$	Calcium carbonate
CAD	Computer-aided design
CAE	Computer-assisted engineering
CAER	Center for Applied Energy Research
CaFCP	California Fuel Cell Partnership
CaI	*Clostridium acetobutylicum* hydrogenase
CaO	Calcium oxide
CARB	California Air Resources Board
CaS	Calcium sulfide
CaSFCC	California Stationary Fuel Cell Collaborative
CB	Conduction band; Carbon black
CBECS	Commercial Building Energy Consumption Survey
CbHS	Carbon-based hydrogen storage
CBM	Conduction band minimum
CBN	Carbon-boron-nitrogen
CBS	Casa Bonita strain; Complete basis set
cc	Cubic centimeter(s)
CCC	Carbon composite catalyst
CCD	Charge-coupled device
CCF	Complex coolant fluid

cc/g cat/hr	Cubic centimeter(s) per gram catalyst per hour
CcH2	Cryo-compressed hydrogen
CCHSS	Complex Compound Hydrogen Storage System
CCL	Cathode catalyst layer
CCM	Catalyst-coated membrane
cc/min, ccm	Cubic centimeters per minute
ccp	Cubic close-packing
CCS	Carbon capture and storage
CC&S	Carbon capture and sequestration
CCVJ	9-([E]-2-carboxy-2-cyanovinyl)julolidine
Cd	Cadmium
CD	Compact disk; Charge depleting; Cathode dewpoint
Cdl	Double layer capacitance
cDNA	Complementary DNA
CDO	Code development organization
CDP	Composite data product
CdS	Cadmium sulfide
C-DSM™	Chemically etched dimensionally stable membrane
Ce	Cerium
CEA	Commissariat à l'Energie Atomique
CEC	California Energy Commission
CEM	Compressor/expander motor (module)
CeO_2	Ceric oxide
CF	Carbon fiber; Carbon foam
CFC	Chlorofluorocarbon
CFD	Computational fluid dynamics
CFF	Complex coolant fluid
cfm	Cubic feet per minute
CGA	Compressed Gas Association
CGH2	Compressed gaseous hydrogen
CGM	Charge-generating material
CGO	Cerium gadolinium oxide, Gd-doped CeO_2
CGS	Copper gallium diselenide, $CuGaSe_2$
$CGSe_2$	Copper gallium diselenide
CH	Chemical hydride
cH_2	Compressed hydrogen gas
CH_4	Methane
CHEX	Continuous catalytic heat exchanger
CHHP	Combined heat, hydrogen, and power
Chl	Chlorophyll
CHMC1	Test Method for Evaluating Material Compatibility for Compressed Hydrogen Applications–Phase I-Metals
CHP	Combined heat and power
CHPFC	Combined heat and power fuel cell
CHS	Chemical hydrogen storage
CHSCoE	Chemical Hydrogen Storage Center of Excellence
CI	Compression ignition
$CIGSe_2$	Copper indium gallium diselenide
CIGS	Copper indium gallium diselenide
Cl	Chlorine
CL	Catalyst layer; ε-caprolactone
cm	Centimeter
CM	Controls module
cm^2	Square centimeter
CMO	Conductive metal oxides
CMWNT	Carbon multi-walled nanotube
CN	Carbon-nitrogen
CNC	Carbon nanocage
CNF	Carbon nano-fiber
CNG	Compressed natural gas
CNT	Carbon nanotube
Co	Cobalt
CO	Carbon monoxide
CO_2	Carbon dioxide
CO_{2e}	Carbon dioxide equivalent
COD	Chemical oxygen demand
COE	Cost of electricity
COF	Covalent-organic framework
COF_2	Carbonyl fluoride
COGS	Cost of goods sold
COMSOL	Multiphysics modeling and engineering simulation software
COPV	Composite overwrapped pressure vessel
COS	Carbon oxysulfide; Carbonyl sulfide
COx	Oxides of carbon
c_p	Specific heat
cp	Commercial purity
cP	Centipoise
CpI	*Clostridium pasteurianum* [FeFe]- hydrogenase
CPMAS	Cross polarization magic angle spinning
CPO, CPOX	Catalytic partial oxidation
c.p.s.	Counts per second

CPU	Computer processing unit
CPV	Composite pressure vessel
Cr	Chromium
CRADA	Cooperative Research and Development Agreement
CRCC	Corrosion-resistant conducting catalytic
CRTP	Corrosion-resistant transparent protective
Cs	Cesium
C&S	Codes and standards
CSA	Canadian Standards Association; Cell stack assembly
CSMP	Cabot Superior MicroPowders
CSTT	Codes and Standards Tech Team
CSU	California State University
CSULA	California State University Los Angeles
CT	Computed tomography
CTA	Charge transfer agent
CTAB	Cetyl trimethyl ammonium bromide
CTB	Cyclotriborazane
CTE	Coefficient of thermal expansion
CTTRANSIT	Connecticut Transit
Cu	Copper
CU	University of Colorado
Cu_2O	Cuprous oxide
$CuBiW_2O_8$	Copper bismuth tungstate
cu in.	Cubic inch
$CuInGaS_2$	Copper indium gallium sulfide
CuNW	Copper nanowire
CuO	Cupric oxide; Copper(II) oxide
$CuWO_4$	Copper tungstate
cu.yd.	Cubic yard(s)
CV	Cyclic voltammetry; Cyclic voltammogram
CVD	Chemical vapor deposition
CVS	Chemical vapor synthesis
CWRU	Case Western Reserve University
CY	Calendar year
CZO	Ceria-zirconia
d	Day(s)
D_2	Deuterium
D-A	Dubinin-Astakhov
DAC	Diamond anvil cell
DADB	Diammoniate of diborane, $[(NH_3)_2BH_2][BH_4]$
DAKOTA	Design Analysis Kit for Optimization and Terascale Applications
DB	Diborane (B_2H_6)
dB(A)	Decibel(s) A scale
DBBPDSA	4, 4'-dibromobiphenyl 3, 3'-dislufonic acid, monomer
DBPDSA	1, 4-dibromo phenylene 2, 5-disulfonic acid
DC	Direct current
DCTDD	1,8-diazacyclotetradecane-2,7-dione
DDMEFC	Direct dimethyl ether fuel cell
DDP	Detailed Data Product
d_{DR}	Dubini-Radushkevich average micropore diameter
DDR	A zeolite structure code
DEF	Diethylformamide
Deg	Degree
DEGDBE	Diethylene glycol dibutyl ether
ΔB_a	The difference in magnetic induction at high and low applied magnetic fields
ΔG	Gibbs free energy of reaction
ΔH	Enthalpy of reaction; Enthalpy of hydrogenation
$\Delta H°_f$	Standard heat of formation
ΔK	Stress intensity factor
ΔP	Pressure drop; Pressure change
DEMS	Differential electrochemical mass spectroscopy
DFM	Design for manufacturing
DFMA®	Design for Manufacturing and Assembly
DFT	Density functional theory
DGDE	Di-ethylene glycol di-butyl ether
DHBC	2,5-dihydroxybenzene dicarboxylate
DI	Deionized; De-ionized water
DLC	Diamondlike carbon
dL/g	Deciliters per gram
DM	Diffusion media
DMA	Dimethylacetamide
DMAc	Dimethyl acetamide
DMC	Diffusion Monte Carlo; Direct manufactured cost
DMDF	2,5-dimethoxy 2,5-dihydrofuran
DMDS	Dimethyldisulfide
DME	Dimethyl ether; Dimethoxyethane
DMEA	Dimethlethylamine
DMEAA	Dimethlethylamine alane
DMF	n, n-di-methyl formamide
DMFC	Direct methanol fuel cell
$dmimMeSO_4$	1,3-dimethyl-imidazolium methylsulfate

dmpe	Dimethylphosphinoethane
DMPO	5,5-Dimethylpyrroline-N-oxide
DMSO	Dimethyl sulfoxide
DMT	Dimethyltrityl
DMTHF	Dimethyltetrahydrofuran
DNA	Deoxyribonucleic acid
DNG	Desulfurized natural gas
DNI	Direct normal insolation
DOD	Depth of discharge; Department of Defense
DOE	Department of Energy
DOT	Department of Transportation
DP	Dew point
DRIFTs	Diffuse reflectance infrared Fourier transform spectroscopy
DSC	Differential scanning calorimetry; Dynamic scanning calorimetry
DSM™	Dimensionally stable membrane
DSM-MC	Distance scaling method Monte Carlo
DVBPC	Divinyl aryl ether monomer
DVD	Digital video disk
DVMT	Daily vehicle miles traveled
e^-	Electron
E	Activation energy, kJ/mol
E_0xE_1	Utilization efficiency of incident solar light energy
$E_{1/2}$	Half-wave potential
E85	85%-15% blend of ethanol with gasoline
Ea	Activation energy
EA	Environmental assessment
E_{ad}	Hydrogen adsorption heat
EAN	Ethylammonium nitrate
EASA	Electrochemically active surface area
E-BOP	Electrical balance of plant
EBSD	Electron backscatter diffraction
EC	European Commission; Electro-chemical; Evaportive-cooled; Efficiency of conversion; Electrochemical capacitance
ECA	Electrochemical area
ECB	Ethylcyclobutane
ECC	Electrochemical compressor; Engineered cementitious composite
ECE	Economic Commission for Europe
ECS	Equilibrium crystal shape
ECSA	Electrochemically active surface area; Electrochemical surface area; Effective catalyst surface area
ECV	Electrochemical capacitance voltage
ED	Ethylenediamine
EDA	Ethylene diamine; Energy decomposition analysis
EDAX	Manufacturer of energy dispersive X-ray hardware and software
EDBB	Ethylenediamine bisborane
EDC	Energy distribution curve
edmimCl	2-ethyl-1,3-dimethyl-imidazolium ethylsulfate
EDP	Electrophoretic deposition
EDS	Energy dispersive X-ray spectroscopy; Energy dispersive spectrum
EDTA	Ethylenediamine tetraacetic acid
EDX	Energy dispersive X-ray
EELS	Electron energy loss spectroscopy
EERE	U.S. DOE Office of Energy Efficiency and Renewable Energy
EFR-AHJ	Emergency first responder-authorities having jurisdiction
EFTE	Ethylene-tetrafluoroethylene
e.g.	*Exempli gratia*: for example
EGR	Exhaust gas recirculation
EHC	Electrochemical hydrogen compressor
EHS	Environmental Health and Safety
EIA	Energy Information Administration of the U.S. Department of Energy
EIGA IGC	European Industrial Gases Association/ Industrial Gases Council
EIHP	European Integrated Hydrogen Project
EIS	Electrochemical impedance spectroscopy
EISF	Elastic incoherent structure factor
ELAT®	Registered Trademark of De Nora North America, Inc., covers GDLs and GDEs
EMA	Effective medium approximation
EMF	Electromagnetic field
EMI	Electro magnetic interference
EMPA	Electron microprobe analysis
ENABLE	Energetic neutral atom beam lithography/ epitaxy
ENG	Expanded natural graphite
eNMR	Electrochemical nuclear magnetic resonance
EODC	Electro-osmotic drag coefficient
EOL	End of life
EOT	End of test
EPA	Environmental Protection Agency
EPD	Electrophoretic deposition

EPDM	Ethylene propylene diene monomer
EPHC	Ethylperhydrocarbazole
ePTFE	Expanded polytetrafluoroethylene
ER	Emergency responder
ERW	Electric resistance weld
ES	Energy storage
ESA	Electrochemical surface area
ESEM	Environmental scanning electron microscope
ESIF	Energy Systems Integration Facility
et al.	*Et Alii:* and others
ETA	Event tree analysis
etc.	*Et cetera*: and so on
E-TEK	Division of De Nora North America, Inc.
ETFE	Ethylene-tetrafluoroethylene
ETFECS	Extended thin film electrocatalyst structures
EtOH	Ethanol
EU	European Union
eV	Electron volt
EVD	Extreme value distributions
EVOH	Ethylene vinyl alcohol
EVSE	Electric vehicle supply equipment
EW	Equivalent weight
EXAFS	Extended X-ray absorption fine structure analysis
F	Fluorine
F	Faraday constant, the amount of electric charge in one mole of electrons (96,485.3383 coulomb/mole)
F^-	Fluorine ion
FA	Furfyl alcohol
FANS	Filter analyzer neutron spectroscopy
FAT	Fleet Analysis Toolkit; Factory acceptance test
FBMR	Fluidized bed membrane reactor
FC	Fuel cell
FCB	Fuel cell bus
FCC	Face-centered cubic; Fuel Cell Catalyst; Fluid catalytic cracking
FCEB	Fuel cell electric bus
FCEV	Fuel cell electric vehicle
FCI	Fixed capital investment
FC POWER	Fuel Cell Power Model
FCPP	Fuel cell power plant
FCS	Fuel cell system
FCSMR	Forecourt steam methane reformer (ing)
FCT	Fuel Cell Technologies
$FCTES^{QA}$	Fuel Cell Testing, Safety and Quality Assurance (an international effort to harmonize fuel cell testing procedures)
FCTO	Fuel Cell Technologies Office
FCTT	Fuel Cell Technical Team
FCV	Fuel cell vehicle
Fd	Ferredoxin
Fe	Iron
FE	U.S. DOE Office of Fossil Energy
Fe_2O_3	Ferric oxide
FEA	Finite element analysis
FEM	Finite element model
FEP	Fluorinated ethylene propylene; Teflon®
FESEM	Field emission scanning electron microscope
fg-ELAT	Fine gradient ELAT
FIB	Focused ion beam
FISIPE	Fibras Acrilicas Portugese
FLiNaK	LiF-NaF-KF eutectic salt
FLP	Frustrated Lewis pair
Fluent	Computer code for computational fluid dynamics
FMEA	Failure modes and effects analysis
^{19}FNMR	^{19}Fluorine nuclear magnetic resonance
FNR	Ferredoxin NADP+ oxidoreductase
FOM	Federated object model
FOM	Figure of merit
FPA	Fluoroalkyl phosphonic and phosphinic acids
fpi	Fins per inch
fpm	Feet per minute
FPS	Bis(4-fluorophenyl)sulfone; Fuel processing system
FRP	Fiber-reinforced composite piping; Fiber-reinforced polymer; Full rate production
FRR	Fluoride release rate
F-SPEEK	Fluorosulfonic acid of polyetheretherketone
FSW	Friction stir welding
ft	Feet
FT	Fault tree
ft^2	Square feet
ft^3	Cubic feet
FTA	Federal Transit Administration
FT-IR, FTIR	Fourier transform infrared
FTIR-ATR	Fourier transform infrared attenuated total reflection
FTO	Fluorine-doped tin oxide
FTP, FTP-75	Federal Test Procedure

FWS	Fixed-window scan
FW	Formula weight; Filament winding
FWHM	Full width at half maximum
FY	Fiscal year
g	Gram; acceleration of gravity
G	Graphite
Ga	Gallium
GaAs	Gallium arsenic
GADDS	General area diffraction system
gal	Gallon
GaP	Gallium phosphide
GB	Gigabyte
GC	Gas chromatograph; General computational
GC	Glassy, or vitreous carbon: a pure carbon that is amorphous (non-crystalline)
g/cc	Grams per cubic centimeter
GCLP	Grand-canonical linear programming
GCMC	Grand Canonical Monte Carlo
GCMS	Gas chromatograph-mass spectroscopy
GCNF	Graphitized carbon nano-fiber
GCNT	Graphitized carbon nanotubes
GCtool	Software package developed at ANL for analysis of fuel cells and other power systems
Gd	Gadolinium
GDC	Gadolinium-doped ceria
GDE	Gas diffusion electrode
GDL	Gas diffusion layer
GDM	Gas diffusion media
GDS	Galvanodynamic scan
Ge	Germanium
GES	Giner Electrochemical Systems, LLC
GF	Glass fiber
GFC	Gas flow channel
GFP	Green fluorescent protein
GGA	Generalized gradient approximation
GGE, gge	Gasoline gallon equivalent
GH_2	Gaseous hydrogen
GHG	Greenhouse gas
GHSV	Gas hourly space velocity
GIS	Geographic information system
GJ	Gigajoule(s)
g/kW	Gram(s) per kilowatt
GLACD	Glancing angle co-deposition
GLAD	Glancing angle deposition
GLS	Gas-liquid separator
GLY	Glycerol
Glyme	Dimethoxyethane
gm	Gram(s)
GM	General Motors
gm/day	Gram(s) per day
g/min	Gram(s) per minute
GNF	Graphite nanofiber
GO	Graphene oxide
GODC	Graphene oxide derived carbon
GOF	Graphene-oxide framework
GPa	Gigapascal(s)
GPAT	Global Pathways Resource Analysis Tool
GPC	Gel permeation chromatography
GPS	Global positioning system
GPU	Gas permeation units
GRC	Glass-reinforced concrete
GREC	Graphite reinforced epoxy composite (IM6 continuously wound)
GREET2	Greenhouse gases, Regulated Emissions and Energy use in Transportation model
GRPE	Working Party on Pollution and Energy
g/s	Grams per second
GTI	Gas Technology Institute
GTR	Global Technical Regulations
GUI	Graphical user interface
GV	Gasoline vehicle
GVW	Gross vehicle weight
GW	An approximation permitting practical calculation of excitation energies in metals, semi-conductors and insulators
GWe, GW_e	Gigawatt(s) electric
h	Hour(s)
H	Hydrogen
H+	Proton
H^-	Hydride
H_2	Diatomic hydrogen
H2A	Hydrogen Analysis project sponsored by DOE
H_2BPyDC	2,2'-bipyridine-5,5'-dicarboxylic acid
H_2cat	Catechol, 1,2 dihydroxybenzene
H_2-FCS	Stationary fuel cell system designs that co-produce hydrogen
H_2(hfipbb)	4,4'-(hexafluoroisopropylidene)bis(benzoic acid)
H2I	Hawaii Hydrogen Initiative
H2-ICE, H_2 ICE	Hydrogen internal combustion engine

H_2Lib	Library of H_2 component models in Simulink®
H_2O	Water
H_2O_2	Hydrogen peroxide
H_2oba	4,4'-oxybis-benzoic acid
H2QWG	DOE Hydrogen Quality Working Group
H_2S	Hydrogen sulfide
H_2SO_4	Sulfuric acid
H2V	Hydrogen vehicle
H_3BBC	1,3,5-tris(4'-carboxy[1,1'-biphenyl]-4-yl-) benzene
H_3BTB	4,4',4''-benzene-1,3,5-triyl-tribenzoic acid
H_3PO_4	Phosphoric acid
HAADF	High-angle annular dark-field
HAADF-STEM	High angle annular dark field scanning transmission electron microscopy
HAMMER	Hazardous Materials Management and Emergency Response
HATCI	Hyundai America Technical Center, Inc.
HAVO	Hawaii Volcanoes National Park
HAZ	Heat-affected zone
HAZID	Hazard Identification Analysis
HAZOP	Hazards and Operational Safety Analysis; Hazards and operability analysis
HB	Hydrazine borane
HBr	Hydrogen bromide
HBTU	o-Benzotriazol-1-yl-N,N,N',N'-tetramethyluronium hexafluorophosphate
HCC	Hybrid cathode catalyst
HCl, HCL	Hydrochloric acid; Hydrogen chloride
$HClO_4$	Perchloric acid
HCN	Hydrogen coordination number
HCNG	Hydrogen-compressed natural gas
HCO_3^-	Bicarbonate
hcp	Hexagonal close-packing
HC&S	Hawaiian Commercial and Sugar Company
HD	Deuterium hydride
HDF	Hydrogen dispensing facility
HDPE	High-density polyethylene
HDS	Hydrogen desulfurization
HDSAM	Hydrogen Delivery Scenario Analysis Model
He	Helium
HE	Hydrogen embrittlement
HEMA	2-hydroxylethyl methacrylate
HEN	Heat exchange network
HEPA	High efficiency particulate air filter
HER	Hydrogen evolution reaction
HES	Hydrogen energy station
HEV	Hybrid electric vehicle
HEX	Heat exchanger
Hf	Hafnium
HF	Hydrogen Fueler
HF	Hydrofluorhydric acid; Hydrogen fluoride; Hartree-Fock
HFB	Hexafluorobenzene
HFC	Hydrogen fuel cell
HFCTF	Hawaii Fuel Cell Test Facility
HFCV	Hydrogen fuel cell vehicle
HFI	Hydrogen Fuel Initiative
HFP	Hexafluoropropylene
HFP	1,1,1,3,3,3 hexafluoro-2-propanol
HFR	High-frequency resistance
HFS	Hydrogen fueling station
HFSS	High-flux solar simulator
HFV	Hydrogen-fueled vehicle
HGEF	Hawaii Gateway Energy Center
HGM	Hydrogen Generation Module
HGMs	Hollow glass microspheres
HGV	Hydrogen gaseous vehicle
HHV	Higher heating value
HI	Hydrogen iodide, hydriodic acid
HIA	Hydrogen-induced amorphization; Hydrogen Implementing Agreement
HIAD	Hydrogen Incidents and Accidents Database
HIB	High-impedance buffer
HIC	Hydrogen-induced cracking
HICE	Hydrogen internal combustion engine
HiPCO, HiPCo	High-pressure carbon monoxide
HIPOC	Hydrogen Industry Panel on Codes
HIx	Blend of hydrogen iodide, iodine, and water
HIZ	Perhydro-indolizidine
HKUST	1 Cu_3(1,3,5-benzenetricarboxylate)$_2$
HLA	High level architecture
HMC	Hyundai Motor Company
HNEI	Hawaii Natural Energy Institute
HNO_3	Nitric acid
HOMO	Highest occupied molecular orbital
HOPG	Highly-ordered pyrolytic graphite
HOR	Hydrogen oxidation reaction
hp	Horsepower
HP	High pressure

HPA	Heteropoly acid
HPA-C	Heteropoly acid
HPC	Highly porous carbon
HPEP	Hydrogen Production Expert Panel
HPIT	Hydrogen-powered industrial truck
HPLC	High performance liquid chromatography
HPPH	1,6-di(4-hydroxyl)phenylperfluorohexane
HPPS	*N,N*-diisopropylethylammonium 2,2-bis(*p*-hydroxyphenyl) pentafluoropropanesulfonate
HPRD	Hydrogen pressure relief device
HQS100	Hydroquinone sulfone
hr	Hour(s)
HRA	Home refueling appliance
HRS	Hydrogen refueling stations
HRT	Hydraulic retention time
HRTEM	High-resolution transmission electron microscopy
HR-STEM	High resolution scanning transmission electron microscopy
HRXRT	High-resolution X-ray tomography
HS	Hydrogen sorption
HSAC	High surface area carbon
HSC	Database name derived from the letters for enthalpy, entropy, and heat capacity
HSCC	Hydrogen Station Cost Calculator
HSCoE	Hydrogen Sorption Center of Excellence
HSDC	Hydrogen Secure Data Center
HSE	High surface area electrode
HSECoE	Hydrogen Storage Engineering Center of Excellence
HSMCoE	Hydrogen Storage Material Center of Excellence
HSO_4	Bisulfate anion
HSP	Hydrogen safety plan
HSRP	Hydrogen Safety Review Panel
HSSIM	Hydrogen Storage SIMulator
HSU	Hydrogen separation unit
HT	High temperature
H-T-NT	Hierarchical TiO_2 nanotubes
HTAC	Hydrogen and Fuel Cell Technical Advisory Committee
HTFC	High-temperature fuel cell
HTFSA	Trifluomethylsulfonic acid
HTGR	High-temperature gas-cooled reactor
HTHX	High-temperature heat exchanger
HTM	High-temperature membrane; Hydrogen transport membrane
HTMWG	High Temperature Membrane Working Group
HTPEM	High-temperature polymer electrolyte membrane
HTWGS	High-temperature water-gas shift
HTXRD	High-temperature X-ray diffraction
HVAC	Heating, ventilation, and cooling
HWCVD	Hot-wire chemical vapor deposition
HWD	Hot wire deposition
HWFET	Highway Fuel Economy Test
HX	Heat exchanger
HyARC	Hydrogen Analysis Resource Center
HYDA	*Chlamydomonas reinhardtii* [FeFe] hydrogenase
Hydrofill™	GTI hydrogen dispenser filling control algorithm
HyDRA	Hydrogen Demand and Resource Analysis
HyPro, HYPRO	Analysis tool
HyQRA	Hydrogen quantitative risk assessment
HyS	Hybrid sulfur
HYSYS®	Process simulation software by Aspentech, computer code for flowsheet analysis
HyTEx	Hydrogen Technical Experimental (database)
HyTRANS	DOE's market simulation model for the transition to hydrogen vehicles
Hz	Hertz
HZM	Hot zone module
i	Current density (mA/cm^2)
I	Current
I_2	Diatomic iodine
I2CNER	International Institute for Carbon-Neutral Energy Research
IBAD	Ion beam assisted deposition
IBS	Ion beam sputtering
I/C	Ionomer to catalyst
IC	Internal combustion
ICC	International Code Council
ICE	Internal combustion engine
ICEV	Internal combustion engine vehicle
ICMS	Integrated ceramic membrane system
ICP	Inductively coupled plasma
ICPAE	Inductively coupled plasma atomic emission
ICP-AES	Inductively coupled plasma atomic emission spectroscopy

ICP-MS	Inductively coupled plasma mass spectrometry
ICP-OES	Inductively coupled plasma optical emission spectroscopy
ICR	Interfacial contact resistance
ID	Inside diameter
i.e.	*id est*: that is
IE	Intelligent Energy
IEA	International Energy Agency
IEA-HIA	International Energy Agency Hydrogen Implementing Agreement
IEC	International Electrotechnical Commission
IEC	Ion exchange capacity, milliequivalents of acid groups per gram of material
IECV	Integrated end cap vessel
IEEE	Institute of Electrical and Electronics Engineers, Inc.
IET	Institute for Energy and Transport
IFC	International Fire Code
IGBT	Insolated-gate bipolar transistor
IGCC	Integrated gasification combined cycle
IGCC-CMR	Integrated gasification combined cycle-catalytic membrane reactor
IGCC-MR	Integrated gasification combined cycle-membrane reactor
IGCC-PBR	Integrated gasification combined cycle-paladium-based reactor
IGT	Institute of Gas Technology
IIC	Industrial, institutional, and commercial
IINS	Inelastic incoherent neutron scattering
IIT	Illinois Institute of Technology
IL	Ionic liquid
ILS	Inter-laboratory studies
ILTA	Ionic liquids tethered to amineboranes
In	Indium
In., in	Inch
in^2	Square inch
INER	Institute of Nuclear Energy Research
INERI	International Nuclear Energy Research Initiative
InP	Indium phosphorus
INS	Inelastic neutron scattering
I-O	Input-output
IOS	Intelligent Optical Systems, Inc.
IP	Induction period; Intellectual property
IPA	Isopthalate; Isopropyl alcohol
IPCC	Intergovernmental Panel on Climate Change
IPCE	Incident photon conversion to electrons; Incident photon conversion efficiency
IPE	Integrated photovoltaic electrolysis
IPES	Inverse photoemission spectroscopy
IPHE	International Partnership for the Hydrogen Economy
IPNS	Intense Pulse Neutron Scattering Facility at Argonne National Laboratory
IQE	Internal quantum efficiency
IR	Infrared
iR	Internal resistance
Ir	Iridium
IRMOF	Isoreticular metal organic framework
IrO_x	Iridium oxide
IRR	Internal rate of return
IRRAS	Infrared reflection-absorption spectroscopy
ISIS	World's leading pulsed neutron and muon source located at the UK Rutherford Appleton Laboratory near Oxford
ISO	International Organization for Standardization
ISO TC197	International Standards Organization Technical Committee
ISS	Ion scattering spectroscopy
ITM	Ion transport membrane
ITO	Indium tin oxide
ITP	Indium tin phosphate
ITWS	Isothermal water splitting
IV	Current-voltage
J	Current; Joule(s)
JHQTF	Joint Hydrogen Quality Task Force (U.S. Fuel Cell Council)
JM	Johnson Matthey
JMFC	Johnson-Matthey Fuel Cells, Inc.
JNAIST	Japanese National Institute of Advanced Industrial Science and Technology
JOBS FC	JOBS and economic impacts of Fuel Cells
JOBS H2	JOBS and economic impacts of Hydrogen
JPL	Jet Propulsion Laboratory
JRC	Joint Research Centre
J-V, JV	Current density-voltage
K	Sievert's constant, ml/[cm^2-min-atm½]
K	Kelvin, absolute temperature
K	Potassium
kÅ	1,000 angstroms
KAERI	Korea Atomic Energy Research Institute

KAIST	Korea Advanced Institute of Science and Technology
kA/m^2	Kilo-ampere(s) per square meter
kb	Kilo-base pair, a unit of measurement used in genetics equal to 1,000 nucleotides
KBr	Potassium bromide
kcal	Kilocalorie(s)
kcal/mol	Kilocalorie(s) per mole
KeV	Kilo electron volt(s)
kg	Kilogram(s)
kg/d	Kilogram(s) per day
kg/hr	Kilogram(s) per hour
kg/m^3	Kilogram(s) per cubic meter
KH	Potassium hydride
KHTC	Hydrotalcites; Potassium-promoted hydrotalcite
kHz	Kilohertz
K_{IH}	Fracture toughness measured in hydrogen gas
kJ	Kilojoule(s)
K_{JIC}	Fracture toughness
kJ/mol	Kilojoule(s) per mole
km	Kilometer(s)
KMC	Kinetic Monte Carlo
KOH	Potassium hydroxide
kPa	Kilopascal(s)
kph	Kilometer(s) per hour
ksi	1,000 pound-force per square inch
kT/y	Kiloton(s) per year
Kth, K_{th}	Fracture toughness threshold
K_{TH}	Hydrogen-assisted crack growth threshold
kVA	Kilovolt-amp(s) (units of apparent power)
kW	Kilowatt(s)
kWe, kW_e	Kilowatt(s) electric
kWh	Kilowatt-hour(s)
kWh/kg	Kilowatt-hour(s) per kilogram
kWh/L	Kilowatt-hour(s) per liter
kW/kg	Kilowatt(s) per kilogram
kWt	Kilowatt(s) thermal
L, l	Liter(s)
La	Lanthanum
LAGP	Lithium aluminum germanium phosphate
LAH	Lithium aluminum hydride ($LiAlH_4$)
λ	Lambda, hydration number
LAMH	Lithium amide and magnesium hydride
LAMOX	Lanthanum molybdenum oxide (*e.g.*, $La_2Mo_2O_9$)
LANL	Los Alamos National Laboratory
LAO	Lanthanum-modified alumina
LAPS	Large aperture projection scatterometer
LAS	Large aperture scatterometry
lb	Pound(s)
LBM	Lattice Boltzmann method
lbmol	Pound(s)-mole
LBNL	Lawrence Berkeley National Laboratory
LC	Liquid carrier; Low concentration
LCA	Life cycle assessment; Life-cycle analysis
LCC	Life cycle cost
LCC	$La_{0.7}Ca_{0.3}CrO_{3-\delta}$
LCH_2	Hydrogenated liquid carrier; Compressed hydrogen produced from liquid hydrogen
LCHPP	Low Cost Hydrogen Production Platform (DOE Program Title)
LCMS	Liquid chromatography-mass spectroscopy
LCOD	Levelized cost of driving
LCOE	Levelized cost of electricity
L/D	Length to diameter ratio
LDV	Light-duty vehicle
LED	Light emitting diode
LEED	Low-energy electron diffraction
LEL	Lower explosion limit
LFG	Landfill gas
LFL	Lower flammability limit
L/h, l/h	Liter(s) per hour
LH2, LH_2	Liquid hydrogen
LHC	Light-harvesting chlorophyll
LHSV	Liquid hourly space velocity, h^{-1}
LHV	Lower heating value
Li	Lithium
Li_3N	Lithium nitride
Li-AB	Lithium amidoborane, $Li\text{-}NH_2\text{-}BH_3$
$LiBH_4$	Lithium borohydride
LIBS	Laser-induced breakdown spectroscopy
LiH	Lithium hydride
LLC	Limited Liability Company; Lessons Learned Corner
LLNL	Lawrence Livermore National Laboratory
L/min, l/min	Liter(s) per minute
LMWO	Lanthanum molybdenum tungsten oxide (*e.g.*, $La_2Mo_{1.8}W_{0.2}O_{9-x}$)
LN_2	Liquid nitrogen
LNG	Liquefied natural gas
LOC	Liquid organic carrier

LOHC	Liquid organic hydrogen carrier
LP	Lattice parameter
LPG	Liquefied petroleum gas
LPM	Liter(s) per minute
LPR	Liquid-phase reforming
LQ*	Dehydrogenated liquid carrier
LQ*H2	Hydrogenated liquid carrier
LRIP	Low rate initial production
LRS	Laser raman spectroscopy
LSAC	Low surface area carbon
LSC	Lanthanum strontium cobalt oxide, (La, Sr) CoO_3, strontium-doped lanthanum cobaltite, $La_{0.8}Sr_{0.2}CoO_{3+\delta}$
LSCF	Lanthanum strontium cobalt iron oxide, (La, Sr)(Co, Fe)O_3
LSCF7328	La-Sr-Cu-Fe-O
LSCM	Lanthanum strontium chromium manganese oxide, (La, Sr)(Cr, Mn)O_3
LSCr	Lanthanum strontium chromium oxide, (La, Sr)CrO_3
LSM	Lanthanum strontium manganese
LSMO	Lanthanum strontium manganese oxide, (La, Sr)MnO_3, strontium-doped lanthanum manganite, $La_{0.8}Sr_{0.2}MnO_{3+\delta}$
LST	Lanthanum strontium titanium oxide, (La, Sr) TiO_3
LSV	Lanthanum strontium vanadate; Linear sweep voltammetry
LT	Low-temperature
LTDMS	Laser induced thermal desorption mass spectrometry
LUMO	Lowest unoccupied molecular orbital
m	Meter(s)
M	Mole, Molar; Million
m^2	Square meter(s)
m^2/g	Square meter(s) per gram
m^2/s	Square meter(s) per second
m^3	Cubic meter(s)
M31	Arkema's first-generation membrane candidate
M41	Arkema's second-generation membrane candidate
M43	Arkema's third-generation membrane candidate
M51, M52, M53	Arkema's membanes incorporating phosphonic acid
M70	Arkema's fourth-generation membrane candidate
MA	Mass activity; methyl acrylate
MA3T	Market Acceptance of Advanced Automotive Technologies
μA	Microampere(s)
mA	Milliamp(s)
MA	Mass activity
M-AB	Metal ammonia-borane
MAB, M-AB	Metal amidoboranes
$\mu A/cm^2$	Microampere(s) per square centimeter
mA/cm^2	Milliamp(s) per square centimeter
MARKAL	Market Allocation Model—A generic, multi-sector energy model developed by the Energy Technology Systems Analysis Program of the International Energy Agency
MAS	Magic angle spinning
MAS ^{11}B-NMR	Magic angle spinning boron-11 nuclear magnetic resonance spectroscopy
MAS-NMR	Magic angle spinning nuclear magnetic resonance
MATI	Modular Adsorption Tank Insert
MAWP	Maximum allowable working pressure
MB	Megabyte
MBE	Molecular beam epitaxy
MBMS	Molecular beam mass spectrometry
M-BOP	Mechanical balance of plant
MBRC	Miles between roadcall
MBWR	Modified Benedict Webb Rubin
MC	Monte Carlo; Methyl cellulose
mC^2	Multi-component composite (membrane)
MCB	Marine Corps Base
$mC\text{-}cm^{-2}$	Millicoulomb(s) per square centimeter
MCEL	Millenium Cell, Inc.
MCFC	Molten carbonate fuel cell
mCHP	Micro-combined heat and power
μCHP	Micro-combined heat and power
μCHX	Microscale combustor/heat exchanger
MCM	Mobile crystalline material
μc-Si	Microcrystalline silicon
MDES	Methyl-diethoxy silane
mdip	5,5′-methylene-di-isophthalate
MEA	Membrane electrode assembly
MeAB	Methylamine borane
MEAM	Modified embedded atom method

MEC	Microbial electrolysis cell; Minimum explosive concentration
MeCN	Acetonitrile
MEIC	Mixed electronic and ionic conducting (membranes)
MEMS	Micro-electro-mechanical systems
MeOH	Methanol
meq	Milliequivalents
meq/g	Milliequivalents/gram
MES	Microstructered electrode scaffold
MeV	Mega electron volt
mf	Mass fraction
Mg	Megagram(s)
μg	Microgram(s)
mg	Milligram(s)
$MgCl_2$	Magnesium chloride
mg/cm^2	Milligram(s) per square centimeter
MgH_2	Magnesium hydride
MgH_2@C	MgH_2 incorporated in carbon scaffold
MgO	Magnesium oxide
$Mg(OH)_2$	Magnesium hydroxide
$mgPt/cm^2$	Milligram(s) of platinum per square centimeter
MH, M-H	Metal hydride
MHC	Metal hydride-based compressor
MHCoE	Metal Hydride Center of Excellence
MHE	Material handling equipment
MHI	Methylperhydroindole
MHz	Megahertz
mi	Mile(s)
MIE	Minimum ignition energy
MIEC	Mixed ionic and electronic conduction
mi/kg	Mile(s) per kilogram
mil	Millimeter(s)
min	Minute(s)
MIT	Massachusetts Institute of Technology
MiTi®	Mohawk Innovative Technologies Inc.
MJ	Megajoule(s)
mL, ml	Milliliter(s)
ML	Monolayer
μCHP	Micro-combined heat and power
μm	Micrometer(s); micron(s)
μM	Micromolar
mM	Millimolar
mm	Millimeter(s)
MMBtu	Million British thermal units
MM-FSW	Multi-pass, multi-layer friction stir welding
MMOF	Microporous metal-organic framework
mmol	Millimole(s)
μmol	Micromole(s)
MMSCFD	Million standard cubic feet/day
MMT	Million metric tonnes
Mn	Manganese
Mn_2O_3	Manganese oxide
M-N-H	Amide/imide
MnO	Manganese oxide
$\mu\Omega\text{-}cm^2$	Micro-ohm(s)-square centimeter
Mo	Molybdenum
MO	Molecular orbital; metal oxide
MOA	Memorandum of Agreement
MOF	Metal-organic framework
mol	Mole(s)
MOL	Middle of life
mol%	Mole percent
mol/min	Mole(s) per minute
mΩ	Milli-ohm(s)
MΩ	Mega-ohm(s)
$m\Omega/cm^2$	Milli-ohm(s) per square centimeter
MoPc	Molybdenum phthalocyanine
MOR	Methanol oxidation reaction
MPa	Megapascal(s)
MPG, mpg	Mile(s) per gallon
MPGGE	Miles per gasoline gallon equivalent
mph	Mile(s) per hour
MPHI	Methylperhydroindole
MPL	Microporous layer
MPMC	Massively Parallel Monte Carlo
mpy	Miles per year
MQMAS	Multiple quantum magic angle spinning
MR	Membrane reactor
MRCAT	Materials Research Collaborative Access Team
MREC	Microbial reverse-electrodialysis electrolysis cell
MRI	Magnetic resonance imaging
MRL	Manufacturing readiness level
ms	Millisecond(s)
MS	Mass spectroscopy; Mass spectrometry; More Stations
MSAC	Mid-range carbon support; Medium surface area carbon

mS/cm	Milli-Siemen(s) per centimeter
MS-H_2	Hydrogen mass spectrometry
MSM	Macro-System Model
MSR	Membrane steam reformer
MSRI	Materials and Systems Research, Inc.
MSTF	Mesostructured thin films
MTA	Metric tonne per annum; Mass Transportation Agency
MTBF	Mean time between failure
MTBR	Mean time between repairs
M/TC	Metal-doped templated carbon
M-TCPP	M = Fe, Mn, Co, Ni, Cu, Zn, H2, tetrakis(4-carboxyphenyl)porphyrin
mtorr	Millitorr
µV	Microvolt(s)
mV	Millivolt(s)
MV	Methyl viologen
mW	Milliwatt(s)
MW	Megawatt(s)
MW	Molecular weight
mW/cm^2	Milliwatt(s) per square centimeter
MWCNT	Multiple-wall carbon nanotube
MWe	Megawatt(s) electric
MWh	Megawatt-hour(s)
MWNT	Multi-wall carbon nanotube
MWOE	Midwest Optoelectronics, LLC
MWth	Megawatt(s) thermal
MYPP	Multi-Year Program Plan (the Fuel Cell Technologies Office's Multi-Year Research, Development, and Demonstration Plan)
MYRDD, MYRD&DP	Multi-Year Research, Development and Demonstration Plan
N	Normal (e.g., 1N H_3PO_4 is 1 normal solution of phosphoric acid)
N	Nitrogen atom
N	Newton (unit of force)
N112	Nafion® 1100 equivalent weight, 2 millimeter thick membrane
N_2	Diatomic nitrogen
N_2O	Nitrous oxide
Na	Sodium
NA	North American
Na_2S	Sodium sulfide
Na_3AlH_6	Trisodium hexahydroaluminate
$NaAlH_4$	Sodium aluminum hydride; Sodium tetrahydroaluminate; Sodium alanate
$NaBH_4$	Sodium borohydride
$NaBO_2$	Sodium metaborate
NACE	National Association of Corrosion Engineers
NaCl	Sodium chloride
NACS	North American Catalysis Society
NADH	(reduced) Nicotinamide adenine dinucleotide
NADP	Nicotinamide adenine dinucleotide phosphate
NADPH	Nicotinamide adeninine dinucleotide phosphate
Nafion®	Registered Trademark of E.I. DuPont de Nemours
NaH	Sodium hydride
NA NG	North American natural gas
NaOH	Sodium hydroxide
NAS	National Academy of Sciences
NASA	National Aeronautics and Space Administration
Nb	Niobium
Ncc	Normal cubic centimeters
N/cm^2	Newton(s) per square centimeter
NCNR	NIST Center for Neutron Research
ND	Not determined at this time
NDC	New delivery concept, Naphthalene-2,6-dicarboxylate
nDDB	N-dodecyl benzene
NDE	Non-destructive examination
NE	U.S. DOE Office of Nuclear Energy, Science, and Technology
NEB	Nudged elastic band
NEC	National Electrical Code
NEF	N-ethylformamide
NEMS	National Energy Modeling System
NEPA	National Environmental Policy Act
NETL	National Energy Technology Laboratory
NEU	Northeastern University
NEXAFS	Near edge X-ray absorption fine structure
NFCBP	National Fuel Cell Bus Program
NFCRC	National Fuel Cell Research Center
NFM	Nanoporous framework material
Nfn-Pt/C	Nafion®-loaded Pt/C
NFPA	National Fire Protection Association
ng	Nanogram
NG	Natural gas
NGCC	Natural gas combined cycle
NGNP	Next Generation Nuclear Plant
NGV	Natural gas vehicle

NH_3	Ammonia
NHA	National Hydrogen Association
NHE	Normal hydrogen electrode
NHFC4	National Hydrogen and Fuel Cells Codes and Standards Coordinating Committee
NHI	Nuclear Hydrogen Initiative
NHTSA	National Highway Traffic Safety Administration of the U.S. Department of Transportation
Ni	Nickel
NICC	Natural gas Infrastructure Component Cost model
NILS	Normal interstitial lattice sites
NiMH	Nickel metal hydride
NIR	Near infra-red
NIST	National Institute of Standards and Technology
NL	Normal liter(s)
NLDFT	Non-local density functional theory
nm	Nanometer(s)
NM	Noble metal
Nm^3	Normal cubic meter(s)
NMHC	Non-methane hydrocarbons
NMOC	Non-methane organic carbons
nmol	Nanomole(s)
NMP	N-methylpyrrolidone
NMR	Nuclear magnetic resonance
NMSU	New Mexico State University
NMT	New Mexico Tech
NNA	Non-North American
NNA NG	Non-North American natural gas
NNIF	NIST neutron imaging facility
NNSA	National Nuclear Security Administration
NO_2	Nitric oxide
NOA	Norland Optical Adhesive
nOB	N-octyl benzene
NOx, NO_x	Oxides of nitrogen
NP	Nanoparticle
NPB	Neopentyl benzene
NPC	Nanoporous carbon; Normalized photocurrent
NPGM	Non-precious metal group
NPMC	Non-precious metal catalyst
NPD	Neutron powder diffraction
NPDF	Neutron powder diffraction
NPM	Nanostructured polymeric materials; Non-precious metal
NPPD	n-phenyl-phenylenediamine
NPS	National Park Service
NPT	Normal pressure and temperature
NPV	Net present value
NR	Nanorod
NR_3	Tertiary amine
NRC	National Research Council
NREL	National Renewable Energy Laboratory
NRELFAT	NREL Fleet Analysis Toolkit
NRVS	Nuclear resonance vibrational spectroscopy
NSF	National Science Foundation
NSTF	Nano-structured thin-film
NSTFC	Nano-structured thin film catalyst
NT	Nanotube
NTCNA	Nissan Technical Center, North America
NTE	Negative thermal-expansion
N-T-NT	Nano-grass type titania nanotube
NV	Neutron vibrational
NVS	Neutron vibrational spectroscopy
NW	Nanowire
NWM	Natural Water Management, UTC Power's system and cell stack design which utilizes evaprotative cooling in the cell stack assembly
NYSERDA	New York State Energy Research and Development Authority
NZVI	Nano zerovalent iron
Ω	Ohm(s)
Ωcm^2	Ohm(s)-square centimeter
O	Oxygen
O_2	Diatomic oxygen
O/C	Oxygen-to-carbon ratio
OCP	Open circuit potential
OCSD	Orange County Sanitation District
OCV	Open-circuit voltage
o.d.,OD	Outer diameter
ODA	Oxygenated form of diamine
ODE	Ordinary differential equation
OEC	Oxygen evolving complex
OEM	Original equipment manufacturer
OER	Oxygen evolution reaction
OGMC	Ordered graphitic mesoporous carbon
OH^-	Hydroxyl radical
O&M	Operation and maintenance
OMC	Ordered mesoporous carbon
Ω	Ohm(s)

Ωcm^2	Ohm(s)-square centimeter
ONR	Office of Naval Research
ORF	Opening Reading Frame indicating the occurence of a protein coding region in the DNA sequence
ORNL	Oak Ridge National Laboratory
ORNL-HTML	Oak Ridge National Laboratory High Temperature Materials Laboratory
ORR	Oxygen reduction reaction
OSC	Oxygen storage capability
OSHA	Occupational Safety and Health Administration
OSM	Optical scatterfield microscopy
o-SWNH	Oxidized single-walled nanohorn
OSU	Ohio State University
OSU	Oregon State University (Microproducts Breakthrough Institute)
OTM	Oxygen transport membrane
P	Phosphorus
P	Pressure
Pa	Pascal(s)
PA	Phosphoric acid, Phenylacetylene; Polyamide
PAA	Poly(acrylic acid)
P&D	Pickup and delivery
PAD	Polymer-assisted deposition
PADD	Petroleum Administration for Defense District
PAES	Poly(arylene-ether-sulfone)
PAFC	Phosphoric acid fuel cell
P&ID	Piping and instrumentation diagram
PAN	Peroxyacetyl nitrate; Polyacrylonitrile
PANI	Polyaniline
PAN-MA	Polyacrylonitrile with methyl acrylate
PAN-VA	Polyacrylonitrile with vinyl acetate
PA/PBI	Phosphoric-acid-doped polybenzimidazole
PAR	Photosynthetically-active radiation
PAS	Photoactive semiconductor; Photo acoustic
Pb	Lead
PB	Polyborazylene
PBI	Polybenzimidazole
PBPDSA	poly(biphenylene disulfonic acid)
P-C	Pressure-composition
PC	Polycarbonate
PCA	Pyrenecarboxylic acid
PCE	Perchloroethylene
PCF	Polycarbonate film
PCHD	Poly(cyclohexadiene)
PCI	Pressure-composition isotherm
PCL	Polycaprolactone
PCM	Power control module
PCN	Porous coordination network
P-C-P	Phosphorus-carbon-phosphorus
PCR	Polymerase chain reaction
PCS	Power conditioning system
PCT, P-C-T	Pressure-concentration-temperature
PCTFE	Polychlorotrifluoroethylene
Pd	Palladium
PDA	Phenyldiacetylene
PdAg	Palladium-silver alloy
Pd-ACF	Pd-modified activated carbon fibers
Pd-CR	Palladium-based chemical resistor
PdCu, Pd-Cu	Palladium-copper alloy
PdCuTM	Palladium copper transition metal
PDF	Probability density function; Pair distribution function
PdHg/CF	Carbon foam doped with palladium-mercury compound
PDI	Polydispersity index
Pd-MIS	Palladium-based metal-insulator-semiconductor
PDMS	Polydimethylsiloxane
PDS	Potentiodynamic scan
PDU	Process development unit
PE	Polyelectrolyte; Polyethylene
PEC	Photoelectrochemical; Photoelectrocatalyst; Photoelectrochemical cell
PECH	Polyepichlorohydrin
PECVD	Plasma-enhanced chemical vapor deposition
PED	Pulsed electrodeposition
PEDOT:ClO_4	Poly(3,4-ethylenedioxythiophene):perchlorate
PEEK	Polyether ether ether ketone
PEFC	Polymer electrolyte fuel cell; Proton exchange fuel cell
PEG	Polyethylene glycol
PEGMEMA	Monomethoxypoly(ethyleneglycol) methacrylate
PEGS	Prototype electrostatic ground state
PEI	Polyetherimide; Polyethylene imine
PEKK	Poly (ether ketone ketone)
PEM	Proton exchange membrane; Polymer electrolyte membrane

PEMFC	Polymer electrolyte membrane fuel cell; Proton exchange membrane fuel cell
PEN	Polyethylene naphthalate
PEO	Poly(ethylene oxide)
PES	Polyether sulfone
PES	Proton Energy Systems, Inc.
PES	Polyethersulfone
PET	Polyethylene teraphthalate
PetF1	*Synechocystis* host ferredoxin
PEV	Plug-in electric vehicle
PF	Perfluoro
PFA	Perfluoroalkoxy (a type of fluoropolymer)
PFA	Polyfurfuryl alcohol
PFAC	PFA-derived carbon
PFAE	Perfluoroalkylether
PFC	Polymer electrolyte membrane fuel cell
PFCS	Poly-generative fuel cell systems
PFD	Process flow diagram
PFGB	Perfluorinated guanidine base
PFG-NMR	Pulse field gradient nuclear magnetic resonance
PFGSE	Pulse field gradient spin echo
PFGSE NMR	Pulsed field gradient spin echo nuclear magnetic resonance
PFIA	Perfluoro imide acid
PFPO	Perfluorinated propylene oxide
PFPO-PSS	Poly(perfluoropropylene oxide)-b-poly(styrene sulfonate)
PFSA	Perfluorinated sulfonic acid, perfluorosulfonic acid, poly(fluorosulfonic acid)
PFSI	Perfluorosulfonate ionomer
PFSHQ	2-(5-fluorosulfonyl-3-oxaoctafluoropentyl)-1,4-dihydroxy-benzene
PG	Propylene glycol
PGAA	Prompt-gamma activation analysis
PGE	Platinum group element
PGM	Precious group metal; Platinum-group metal
PGSE	Pulsed-field gradient spin-echo
PGV	Puna Geothermal Ventures
pH	Power of the hydronium ion
p-H_2	Para-hydrogen
Ph_3SnCl	Triphenyltin chloride
$Ph_3SnSnPh_3$	Hexaphenyldistannane
PHA	Process hazard analysis; Preliminary hazard analysis
PHEC	Perhydro-ethylcarbazole
PHEV	Plug-in hybrid electric vehicle
PHI	Perhydro-indolizidine
PHIP	Para-hydrogen induced polarization
PHMI	Perhydro-methylindole
PhOH	Phenol
PI	Principal investigator
PI	Polyimide
P&ID	Piping and instrumentation diagram; Process and instrumentation diagram
PIL, pIL	Protic ionic liquid
PIM, pIM	Protic ionic membrane
pK_a	Acid dissociation constant
PLC	Programmable logic controller
PLLA	Poly-L-lactic acid
PLP	Prepared Lewis pair
PLRS	Planar laser Raleigh scatter
PLS	Polymer-layered silicate
PM	Precious metal such as platinum
PM	Particulate matter
PMG	Glycidyl methacrylate-type copolymer
PMMA	Poly(methyl methacrylate)
PND	Polymerized nitrogen donor
PNNL	Pacific Northwest National Laboratory
pO_2	Oxygen partial pressure
POC	Proof of concept
POCOP	*P*,*P*-*bis*(1,1-dimethylethyl)-,3-[[*bis*(1,1-dimethylethyl)phosphino]oxy]phenyl ester
POF	Polymeric-organic framework; Porous organic framework
POM	Polyoxometallate
POP	Porous organic polymers
POSS	Polyhedral oligomeric silsesquioxane
POX	Partial oxidation
PP	Polyphosphazene; Polypropylene; Poly(phenylene)
PPA	Polyphosphoric acid; Polyphthalamide
ppb	Part(s) per billion
ppbv	Part(s) per billion by volume
PPDSA	Poly (p-phenylene disulfonic acid)
PPE	Porous polyethylene
PPI	Plug Power, Inc.; Pore(s) per inch
ppm, PPM	Part(s) per million
ppmv	Part(s) per million by volume
ppmw	Part(s) per million by weight
PPN	Porous polymer network
PPO	Phenyl phosphine oxide

PPOR	Metalloporphyrin porous organic polymer
P-POSS	Phosphonic acid polyhedral oligomeric silsesquioxane
PPS	Polyphenylene sulfide
PPSA	Poly (p-phenylene sulfonic acid)
PPSA	Partial pressure swing adsorption
PPSU	Polyphenylsulfone
PPy	Polypyrrole
Pr	Praseodymium
PR	Pressure ratio
PRA	Probabilistic risk assessment
PRD	Pressure relief device
PrOx	Preferential oxidation
PRSV	Peng-Robinson Stryjek-Vera
PS	Proton sponge (bis- (dimethyamino) naphthalene)
PS	Polysiloxane
PSA	Pressure swing adsorption, adsorber
PSAT	Powertrain Systems Analysis Toolkit, a vehicle simulation software package developed at Argonne National Laboratory
PSD	Particle size distribution, pore size distribution
PSEPVE	Perfluoro (4-methyl-3,6-dioxaoct-7-ene) sulfonyl fluoride
PSf	Poly(arylene ether sulfone)
psi, PSI	Pound(s) per square inch
PSI	Photosystem I
psia	Pound(s) per square inch absolute
psid	Pound(s) per square inch differential
psig, PSIG	Pound(s) per square inch gauge
PSOFC	Planar solid oxide fuel cell
PSS	Porous stainless steel; Potentiostatic scan
PSU	Polysulfone
PSU	Pennsylvania State University
Pt	Platinum
PT	Phosphazene trimer
P-T	Pressure-temperature
Pt_3Co	Platinum-cobalt alloy
Pt_3Fe	Platinum-iron alloy
Pt_3Ni	Platinum-nickel alloy
PTA	Phosphotungstic acid
Pt/AC/BC/IRMOF-8	Isoreticular metal organic framework (MOF) doped with platinum supported on activated carbon, and further coupled to MOF with a bridging compound
Pt/AX-21	Pt-doped microporous carbon AX-21
Pt/C	Platinum/carbon
PTC	Production tax credit
PTFE	Teflon® – poly-tetrafluoroethylene
Pt-FePO	Platinum iron phosphate
PTM	Proton transport membrane
PtML	Platinum monolayer
Pt-MM	Platinum group mixed metal
Pt-NH	Platinum decorated carbon nano-horns
PtO	Platinum oxide
PtO_2	Platinum dioxide
PtRu	Platinum ruthenium
Pt-SWNH	Platinum decorated single-walled nanohorns
Pt-TaPO	Platinum tantalum phosphate
PTTPP	Poly-tetrakis(3,5-dithiophen-2-ylphenyl)-porphyrin
PTW	Pump to wheels
PV	Photovoltaic; Present value
PVA	Polyvinyl alcohol
PVC	Polyvinyl chloride
PVD	Physical vapor deposition
PVDC	Polyvinylidene chloride
PVDF	Polyvinylidene fluoride
PVP	Polyvinylpyrrolidone
PVPP	Polyvinyl pyridinium phosphate
PVT, P-V-T	Pressure-Volume-Temperature
PXRD	Powder X-ray diffraction
PyC	4-pyrazole carboxylate
PzDC	2,8-pyrazabole dicarboxylate
Q	Neutron momentum transfer
Q1, Q2, Q3, Q4	Quarters of the year
QC	Quality control
QCM	Quartz crystal microbalance
QE	Quantum efficiency
QENS	Quasielastic neutron scattering
QLRA	Qualitative risk analysis
QMC	Quantum Monte Carlo
QNS	Quasielastic neutron scattering
QRA	Quantitative risk assessment
qRT-PCR	Quantitative reverse transcriptase-polymerase chain reaction
*Q*st	Isosteric heat of adsorption
R	Universal or ideal gas constant, 8.314472 $J \cdot K^{-1} \cdot mol^{-1}$
RAMAN	A spectroscopic technique

RAS	Russian Academy of Sciences
RBS	Rutherford back scattering
RC	Resistance-capacitance; Research cluster
RCD	Rated current density
RCS	Regulations codes and standards
RCSWG	Regulations, Codes, and Standards Working Group
Rct	Charge transfer resistance
RCWA	Rigorous couples waveguide analysis
R&D	Research and development
RD&D, R,D&D	Research, development & demonstration
RDE	Rotating disk electrode
Re	Rhenium
ReaxFF	Reactive force field large-scale molecular dynamic calculations
REC	Renewable energy credit
RED	Reverse electrodialysis
REWP	Renewable Energy Working Party
Rf	Generic fluoroalkyl group
RF, rf	Radio frequency
RFC	Regenerative fuel cell
RFP	Request for proposals
RFT	Reactive flow-through
RGA	Residual gas analyzer (analysis)
Rh	Rhodium
RH	Relative humidity
RHE	Reference hydrogen electrode; Reversible hydrogen electrode
RHLC	Relative humidity/load cycle test
ρ_a	Apparent density of activated carbon
$\rho_{ad.H_2}$	Adsorbate hydrogen density in micropores
RIXS	Resonant inelastic X-ray scattering spectra
RMS	Root mean square
RNA	Ribo nucleic acid
RNG	Renewable natural gas
ROI	Return on investment
ROM	Rough order of magnitude
ROMP	Ring-opening metathesis polymerization
ROW	Right of way
RPC	Ruthenium-polypridyl complex
RPI	Rensselaer Polytechnic Institute
rpm	Revolution(s) per minute
RPN	Risk priority number
RPS	Renewable portfolio standard
RPSA	Rapic pressure swing adsorption
RR	Round robin
RRDE	Rotating ring disc electrode
RSOFC	Reversible solid oxide fuel cell
RT	Room temperature
RTD	Resistive temperature device
RTIL	Room temperature ionic liquid
RTO	Ruthenium-titanium oxide
Ru	Ruthenium
s	Second(s)
S	Siemen(s)
S	Sulfur
-S	Sulfur-deprived
SA	Specific amperage
SA	Surface area
SA	Sulfur-ammonia thermochemical water-splitting cycle; System Architect
SAC	Super-activated carbon
SAE	SAE International, originally known as the Society of Automotive Engineers
SAFC	Solid acid fuel cell
SAH	Sodium aluminum hydride
SAM	Scanning Auger microscopy
SAMPE	Society for the Advancement of Material and Process Engineering
SANS	Small angle neutron scattering
SAS	Styrene-acrylonitrile-vinylsulfate
SASSP	Solvent assisted solid state processing
SAXS	Small angle X-ray scattering
SBAB	Sec-butylamineborane
S_{BET}	BET specific surface area
SBH	Sodium borohydride
SBIR	Small Business Innovation Research
Sc	Scandium
S/C	Steam to carbon ratio
SCC	Stress corrosion cracking
sccm, SCCM	Standard cubic centimeter(s) per minute
SCCV	Steel/concrete composite vessel
SCE	Saturated calomel electrode
SCF, scf	Standard cubic feet; Supercritical fluid
scfd	Standard cubic feet per day
SCFH, scfh	Standard cubic feet per hour
SCFM	Standard cubic feet per minute
S/cm	Siemen(s) per centimeter
SCOF	Single cell with open flowfield
SCR	Selective catalytic reduction; Semi-conductor rectifier

ScSZ	Scandia-stabilized zirconia
SD	Standard deviation; System dynamics
SDAPP	Sulfonated Diels-Alder polyphenylene
SDAPPe	Sulfonated Diels-Alder polyphenylene ether
SDC	Samarium-doped ceria
sDCDPS	3,3′-disulfonate-4,4′-dichlorodiphenylsulfone
SDE	SO_2-depolarized electrolyzer
SDO	Standards development organization
Se	Selenium
SE	Secondary electron; spectroscopic ellipsometry
sec	Second(s)
SECA	Solid State Energy Conversion Alliance
SECM	Scanning electrochemical microscope
SEM	Scanning electron microscopy; Scanning electron microscope
SEOS	Simple equation of state
SERA	Scenario Evaluation, Regionalization, and Analysis
SERC	Schatz Energy Research Center
SET	Surface energy treatment
SF	Safety factor; Polystyrene-b-PFPO
SF_6	Sulfur hexafluoride
SFA	Sulfonic acid
SFC2	$SrFeCo_{0.5}O_x$
SFM	$Sr_2Fe_{1.5}Mo_{0.5}O_{6-\delta}$
SFT	Sr-Fe-Ti oxide
SFTI	$Sr_{0.1}Fe_{0.9}Ti_{0.10}O_x$
SG	Shale gas
SGD	Spontaneous galvanic displacement; System gravimetric density
SGIP	Self-Generation Incentive Program
Sh	Sherwood
SHE	Standard hydrogen electrode
Si	Silicon
S-I	Sulfur-iodine
SI	Sulfur-iodine cycle; Spectrum image
Si^3N^4	Silicon nitride
SiC	Silicon carbide
SiCN	Silicon carbonitride
SIMS	Secondary ion emission spectroscopy
Si-NS	Silica nanosprings
SiO_2	Silicon dioxide
SIU	Southern Illinois University
sL	Standard liter (0°C, 1 atm)
SLAC	Stanford Linear Accelerator Center
SLMA	Sr- and Mn-doped $LaAlO_3$
SLPH	Standard liter(s) per hour
SLPM	Standars liter(s) per minute
slpm, slm, sL/min	Standard liter(s) per minute
SLT	Strontium-doped lanthanum titanate
SMART	Specific, measurable, attainable, relevant, timely
SMR	Steam methane reformer; Steam methane reforming
SMR-ECM	Steam methane reformer with electrochemical purifier
SMR-PSA	Steam methane reformer with pressure swing adsorption
SMT	Single-molecule trap
Sn	Tin
SNG	Substitute natural gas
SNL	Sandia National Laboratories
SNLL	Sandia National Laboratory Livermore
SnO	Tin oxide
SnO_2	Tin oxide
SNR	Signal-to-noise ratio
SNS	Spallation neutron source
SNTT	Spiral notch torsion test
SO_2	Sulfur dioxide
SO_3	Sulfur trioxide
SOC	State-of-charge
SOEC	Solid oxide electrolysis cell; Solid oxide electrolyzer cell
SOFC	Solid oxide fuel cell
SOFEC	Solid oxide fuel-assisted electrolysis cell
SOM	Solid-oxide oxygen-ion-conducting membrane
SORFC	Solid oxide regenerative fuel cell
SOTA	State of the art
SOW	Statement of work
SOx	Oxides of sulfur
sPAES	Sulfonated poly(arylene ether sulfone)
SPE	Solid phase epitaxial
SPEEK	Sulfonated poly(ether ether ketone)
SPEK	Sulfonated poly-etherketone-ketone
SPEKK	Sulfonated polyether(ether ketone ketone)
SPEX	Type of milling machine
SPM	Scanning probe microscope
sPOSS	Sulfonated octaphenyl polyhedral oligomeric silsesquioxanes

S-PPSU	Sulfonated polyphenylsulfone
SPS	Spark plasma sintering
sq. in.	Square inch(es)
Sr	Strontium
SR	Steam reformer; Steam reforming; Salinity ratio; Stoichometric ratio
SRNL	Savannah River National Laboratory
SrO	Strontium oxide
SRR	Solar receiver-reactor
$SrTiO_3$	Strontium titanate
SS	Stainless steel
SSA	Specific surface area
SSAWG	Storage System Analysis Working Group
SSC	Short side-chain; Structure, system, and component
SSM	Sacrificial support method
SSNMR	Solid-state nuclear magnetic resonance
SSRL	Stanford Synchrotron Radiation Laboratory
SSWAG	Storage System Working Analysis Group
STCH	Solar thermochemical hydrogen
STEM	Scanning transmission electron microscopy
STH	Solar-to-hydrogen
STM	Scanning tunneling microscopy
STMBMS	Simultaneous thermogravimetric modulated beam mass spectrometer
STP	Standard temperature and pressure
STS	Scanning tunneling spectroscopy
STTP	Shared Technology Transfer Project
STTR	Small Business Technology Transfer
S_u	Ultimate tensile strength
SU/SD	Start-up and shut-down
SUNY-ESF	State University New York Environmental Science Forestry
SV	Space velocity
SVD	System volumetric density
SW	Square wave
SWCNH	Single-wall carbon nanohorn
SWCNT	Single-walled carbon nanotube
SWNH	Single-walled nanohorn
SWNT	Single-wall nanotube
SwRI®	Southwest Research Institute®
S_y	Yield strength
SYT	Yttrium-doped strontium titanate
T	Temperature
T, t	Ton, tonne
T	Tesla (unit of magnetic induction)
t	Time
T_{1bar}	Temperature at which equilibrium pressure of hydrogen is 1 bar for a hydrogen exchange reaction
Ta	Tantalum
TA	Terephthalic acid
TAG	Technical Advisory Group
TAMU	Texas A&M University
TaON	Tantalum oxynitride
TaPO	Tantalum phosphate
TBAB	Tetra-n-butylammonium bromide
$TBA_2B_{12}H_{12}$	Tetra-*n*-butylammonium dodecahydrododecaborate
TBABh	Tetra-n-butylammonium borohydride
$TBA\text{-}PF_6$	Tetra-*n*-butylammonium hexafluorophosphate
TBD	To be determined
TBMD	Tight-binding molecular dynamic
TC	Templated carbon
TC	Thermocouple
TCCR	Transparent, conducting and corrosion resistant
TCD	Thermal conductivity detector
TCNE	Tetracyanoethylene
TCO	Transparent conductive oxide
TDDFT	Time-dependent density functional theory
TDLAS	Tunable diode laser absorption spectroscopy
TDS	Transitional demand scenario
Te	Tellurium
te	Metric ton or tonne (1,000 kg)
TEA	Triethylamine
$TEA_2B_{12}H_{12}$	Triethylammonium dodecahydrododecaborate
TEAA	Triethylamine alane adduct
TEAB	Tetraethyl ammonium borohydride
TEAH	Tetraethylammonium hydroxide
TEAMS	tetraethylammonium methane sulfonic
TED	Triethylene-diamine
TEDA	Triethylenediamine
TEM	Transmission electron microscopy
TEOA	Triethanolamine
TEOM	Tapered element oscillating microbalance
TEOS	Tetra-ethoxy silane
tf	Thin film
Tf	Trifluormethane sufonate, or triflate anion (CF_3SO_3-)
TFA	Trifluoromethanesulfonic acid
TFAc	Trifluoroacetate

TFE	Tetrafluoroethylene
TFMPA	Trifluoromethylphosphonic acid
TFMSA	Trifluoromethane sulfonic acid
TF-RDE	Thin film rotating disk electrode
tf-Si	Thin-film silicon
TFSI	bis(Trifluoromethylsulfonyl)imide
TFVE	Trifluorovinyl ether
Tg, T_g	Glass transition temperature
TG	Thermogravimetric; Theory Group
TGA	Thermal gravimetric analysis; Thermogravimetric analysis; Thermogravimetric analyzer
TGA-DSC	Thermo-gravimetric analysis-differential scanning calorimetry
TGA-MS	Thermogravimetric analysis-mass spectrometer
TG-DTA	Thermo-gravimetric/differential thermal analyzer
THF	Tetrahydrofuran
Ti	Titanium
$TiCl_3$	Titanium trichloride
TiF_3	Titanium trifluoride
TiH_2	Titanium hydride
Ti-IRMOF-16	Titanium (Ti) intercalated IRMOF-16
TiO_2	Titanium dioxide (anatase)
TIVM	Toroidal intersecting vane machine
TKK	Tanaka Kikinzoku Kogyo K. K.
TLA, *Tla*	Truncated light-harvesting chlorophyll antenna
tla1	Mutant of the Tla1 gene (GenBank Assession No. AF534570)
tlaR	Mutant of unknown gene with a truncated light-harvesting chlorophyll antenna
tlaX	Mutant of unknown gene with a truncated light-harvesting chlorophyll antenna
TLCP	Thermotropic liquid crystal polymer
TM	Tetramethyl bisphenol A
TM	Transition metal
TMA	Trimethylamine; Trimethylaluminum
TMA	Thermal mechanical analyzer
TMAA	Trimethylamine alane adduct
TMAB	Tetramethylammonium borohydride
TMAH	Tetramethylammonium hydroxide
TMB	Trimethylborate
TMEDA	Tetramethylethane-1,2-diamine; N^1,N^1,N^2,N^2-tetramethylethane-1,2-diamine
TMG	Tetramethyl guanidine
TMOS	Tetramethoxy silane
TMPP	Tetramethoxyphenyl porphyrins
TMPS	Trimethoxyl phenyl silane
TMPyP	Tetramethylpyridylporphine
TNA	Titania nanotube array
TNT	Trinitrotoluene
TN-T	TiO_2 nanotubes
TOC	Total organic content
TOF	Turnover frequency
ToF-SIMS	Time-of-flight secondary ion spectroscopy
TPA	Tripropylamine; Temperature-programmed adsorption
TPAH	Tetra-n-propylammonium hydroxide
TPB	Triple phase boundary
TPD	Tonne(s) per day
TPD	Thermally programmed desorption; Temperature-programmed desorption
TPDMS	Temperature-programmed desorption mass spectrometry
TPO	Temperature-programmed oxidation
TPP	Tetraphenyl porphyrin
TPPS	5,10,15,20-tetrakis(4-sulfonatophenyl) porphyrin
TPR	Temperature-programmed reduction
TPRD	Thermally-activated pressure relief device
TPS	3-(trihydroxysilyl)-1-propane-sulfonic acid
TPV	Through-plate voltage
TRA	Technology Readiness Assessment
TRAIN	TrainingFinder Realtime Affiliate Network
TRL	Technology readiness level
TRO	RuO_2-TiO_2
Trityl	Chemical blocking group used to protect amines
tr. oz.	Troy ounce
TSWS	Temperature-swing water splitting
TVS	Twin Vortices Series
TW	Triangel wave
UC	University of California
UCB	University of California, Berkeley
UCF	University of Central Florida
UCI	University of California, Irvine
UCLA	University of California, Los Angeles
UCONN	University of Connecticut
UCSB	University of California, Santa Barbara
UDDS	Urban Dynamometer Driving Schedule
UEL	Upper explosive limit

UFL	Upper flammability limit
UGA	University of Georgia, Athens
UH	University of Hawaii
UHP	Ultra-high purity
UHV	Ultra-high vacuum
UIUC	University of Illinois, Urbana-Champaign
UL	Underwriters Laboratory
ULAM	Ultra-low-angle microtomy
ULSD	Ultra-low sulfur diesel
UM	University of Michigan
UMC	Unsaturated metal centers
UMC	Ultramicroporous carbon
UMCP	University of Maryland College Park
UMSL	University of Missouri, St. Louis
UN	United Nations
UNB	University of New Brunswick
UNCC	University of North Carolina at Charlotte
UNECE	United Nations Economic Commission for Europe
UNLV	University of Nevada, Las Vegas
UNLVRF	UNLV Research Foundation
UNM	University of New Mexico
UNR	University of Nevada, Reno
UPD	Underpotential deposition
UP-DW	Ultra-pure distilled water
UPE	Ultra-high molecular weight polyethylene
UPL	Upper potential limit
UPS	Ultraviolet photoelectron spectroscopy
U.S.	United States
US06	Environmental Protection Agency vehicle driving cycle
USA	United States of America
USANS	Ultra-small angle neutron scattering
USAXS	Ultra-small angle X-ray scattering
USB	Universal serial bus
USC	University of South Carolina; University of Southern California
USCAR	United States Council for Automotive Research, U.S. Cooperative Automotive Research
U.S. DRIVE	United States Driving Research and Innovation for Vehicle efficiency and Energy sustainability
USFCC	United States Fuel Cell Council
USM	University of Southern Mississippi
USTAG	U.S. Technical Advisory Group
UT	University of Toledo; University of Tennessee
UTC, UTC FC	United Technologies Corporation Fuel Cells
UTC	University of Tennessee, Chattanooga
UTCP	UTC Power
UTRC	United Technologies Research Center
UV	Ultraviolet
UV-vis	Ultraviolet-visual
UW	University of Washington
V	Vanadium
V	Volt
VA	Vinyl acetate
VAC	Volts alternating current
VACNTs	Vertically aligned carbon nanotubes
VANTA	Vertically aligned nanotube arrays
VASP	Vienna ab initio simulation package
VaTech	Virginia Polytechnic Institute and State University
VB	Valence band
VBM	Valence band minimum, Valence band maximum
VC	Vanadium carbide
VC	Vulcan carbon
VDC	Volts direct current
VDF	Vinylidene fluoride
VDOS	Vibrational density of states
vdW	van der Waals
vdW-DF	van der Waals density function
VFA	Volatile fatty acid
VFS	Vehicle fueling station
$V(H_2)$	Volumetric hydrogen adsorption capacity; Volumetric hydrogen storage capacity
VHSV	Volumetric hourly space velocity
VHTR	Very high temperature gas-cooled nuclear reactor
VHTS	Virtual high-throughput screening
VI	Venter Institute
V-I, V/I	Voltage–current
VIM/VAR	Vacuum induction melting/vacuum arc remelting
VIR	Voltage-current-resistance
VIS	Visible light at 400-700 nm
V_{mp}	Micropore volume
VMT	Vehicle miles traveled
VOC	Volatile organic compound, Voltage open circuit
Vol., vol.	Volume

vol%	Volume percent
V_{pore}	Total pore volume
VT	Virginia Tech
W	Tungsten
W	Watt(s)
WAXD	Wide-angle X-ray diffraction
WAXS	Wide angle X-ray scattering
WBS	Work breakdown schedule
WC	Tungsten carbon; Tungsten carbide
W/cm^2	Watt(s) per square centimeter
WDD	Water displacement desorption
We, W_e	Watt(s) electric
WG	Working group
WG-12	Working Group 12
WGS	Water-gas shift
WGSMR	Water-gas shift membrane reactor
WGSR	Water-gas shift reactor
Wh	Watt-hour(s)
$W(H_2)$	Gravimetric hydrogen storage capacity
W-h/kg	Watt-hour(s) per kilogram
W-h/L, Wh/liter, Wh/L	Watt-hour(s) per liter
WHSV	Weight hourly space velocity
Wind2H2	Wind to hydrogen demonstration project
W/kg	Watt(s) per kilogram
W/L, W/l	Watt(s) per liter
W/m-K, W/m.K, W/mK	Watt(s) per meter-Kelvin (unit of thermal conductivity)
WMO	World Meteorological Organization
WO_3	Tungsten trioxide
WO_x	Tungsten oxide
WP.29	Working Party 29 - World Forum for Harmonization of Vehicle Regulations
Wppm	Weight part(s) per million
WSTF	White Sands Test Facility
wt	Weight
Wt	Watt(s) thermal
wt%, wt.%	Weight percent (percent by weight)
WTP	Well to pump
WTP	Water transport plate
WTPP	Well-to-power plant
WTT	Well-to-tank
WTW	Well-to-wheels
w/v	Weight by volume
WWTP	Waste water treatment plant
X-	an anionic ligand such as chloride
XAFS	X-ray absorption fine structure
XANES	X-ray absorption near-edge spectroscopy
XAS	X-ray absorption spectroscopy
XC72	High-surface-area carbon support made by Cabot
XES	X-ray emission spectroscopy
XPS	X-ray photoelectron spectroscopy, X-ray photon spectroscopy, X-ray photoemission spectroscopy, X-ray photoluminescence spectroscopy
XPS-UPS	X-ray photoelectron-ultraviolet photoelectron spectroscopy
XRD	X-ray diffraction
XRF	X-ray fluorescence
Y	Yttrium
yr, YR	Year
YSZ	Yttria-stablized zirconia
Z	Atomic number
ZEBA	Zero Emission Bay Area
ZEV	Zero emission vehicle
ZHS	Zinc hydroxystannate
ZIF	Zeolitic imidazolate framework
ZIO	Zirconium-doped indium oxide
ZMOF	Zeolite(-type) metal-organic framework
Zn	Zinc
ZnO	Zinc oxide
ZPE	Zero point energy
zpp	Zirconium phenyl phosphonate
Zr	Zirconium
ZrO_2	Zirconium dioxide
ZrSPP	Zirconium phosphate sulfophenylphosphonate
ZVI	Zerovalent iron

XIV. Primary Contacts Index

A

Aceves, Salvador . . . III-42
Adzic, Radoslav . . . V-26, V-280
Ahluwalia, Rajesh . . . IV-11, V-175
Ainscough, Chris . . . V-199, VII-11
Anton, Don . . . IV-29
Ardo, Shane . . . II-97
Arif, Muhammad . . . V-193
Atanasoski, Radoslav . . . V-9
Autrey, Thomas . . . V-292
Ayers, Katherine . . . II-18, II-22, II-26, II-39

B

Balbuena, Perla . . . V-254
Baldwin, Don . . . III-21
Barilo, Nick . . . VIII-46
Bartynski, Robert . . . V-328
Blanchet, Scott . . . V-104
Blekhman, David . . . VII-43
Borup, Rod . . . V-98
Brooks, Kriston . . . IX-11
Brosha, Eric . . . V-37, VIII-14
Bullock, Morris . . . V-295
Burgess, Robert . . . VIII-11
Busby, Colin . . . VI-11
Buttner, William . . . VIII-55

C

Cai, Mei . . . IV-63
Carson, Steve . . . V-216
Chen, Jingguang . . . V-257
Chidambaram, Dev . . . II-89
Conti, Amedeo . . . V-159
Contini, Vince . . . V-203
Cox, David . . . V-340
Creager, Stephen . . . V-247
Crooks, Richard . . . V-331
Czernik, Stefan . . . II-119

D

Dalton, Luke . . . II-35
Datye, Abhaya . . . V-260
Davis, Benjamin . . . IV-131
De Castro, Emory . . . VI-27
Deutsch, Todd . . . II-70
Di Bella, Frank . . . III-48
Dinh, Huyen . . . V-129
Drennen, Tom . . . XI-44
Drost, Kevin . . . IV-71

E

Elgowainy, Amgad . . . III-11, XI-29, XI-48
Elmore, Monte . . . VIII-43
Eudy, Leslie . . . VII-7

F

Feng, Zhili . . . III-37
Flytzani-Stephanopoulos, Maria . . . V-335
Freeman, Benny . . . V-264

G

Garzon, Fernando . . . V-31
Geiger, Gail . . . X-7
Gennett, Thomas . . . IV-103
Ghirardi, Maria . . . II-105
Gorte, Raymond . . . V-318
Goudy, Andrew . . . IV-121
Greene, David . . . XI-13
Gross, Karl . . . IV-24
Grot, Stephen . . . V-86
Gu, Wenbin . . . V-153

H

Hamdan, Monjid . . . II-11
Harris, Aaron . . . VIII-22, VIII-33, VIII-39
Harrison, Kevin . . . II-15, VII-18
Heshmat, Hooshang . . . III-16
Holladay, Jamie . . . IV-38
Hu, Jian . . . II-75

J

James, Brian . . . IV-18, V-181
Jensen, Craig . . . IV-135

K

Kashuba, Michael . . . VII-41
Keller, Jay . . . VIII-51
Keller, Russ . . . IX-16
Kenny, Kevin . . . X-16
King, David . . . II-124

Kongkanand, Anusorn V-61
Koros, William V-268
Kurtz, Jennifer V-116, VII-26, VII-32

L

Leavitt, Mark VI-30
Lewis, Michele II-43
Lin, Zhenhong XI-25
Lipp, Ludwig. III-33, V-83
Liu, Shih-Yuan IV-140
Long, Jeffrey. IV-89
Lueking, Angela IV-107

M

Maness, Pin-Ching II-108, II-116
Markovic, Nenad V-19
Mavrikakis, Marios V-347
McDaniel, Anthony II-62
Melis, Tasios II-101
Ming, Quentin. V-227
Mintz, Marianne XI-33
Mittelsteadt, Cortney V-79
Mittelsteadt, Cortney V-147
Moen, Chris III-46
Mohapatra, Satish V-162
Mondloch , Joseph IV-99
More, Karren V-186
Moulthrop, Larry VII-22
Mukerjee, Sanjeev V-54
Mukundan, Rangachary V-109
Mustain, William V-305
Myers, Deborah V-95

N

Newhouse, Norman IV-76
Nicholas, Michael XI-17
Norman, Timothy II-31
Norris, Bob IV-160

O

Ogden, Joan XI-21
Ogitsu, Tadashi II-84
Olsen, Raina IV-93
Overbury, Steve V-288
Oyama, S. Ted V-343
Ozkan, Umit V-313

P

Parilla, Phil IV-80
Penev, Michael IX-30
Petrecky, James. IX-24, X-10, X-13
Pivovar, Bryan V-14, V-235
Popov, Branko. V-68

R

Ramani, Vijay V-50
Ramsden, Todd IX-7, XI-36
Rawls, George. III-25
Regen, Steven V-251
Rivkin, Carl VIII-7
Rocheleau, Richard. IX-19
Rockward, Tommy V-212, VIII-28
Rodriguez, Jose. V-284
Rohatgi, Aashish. III-53
Rousseau, Aymeric IX-26
Ruth, Mark XI-51

S

Sahimi, Muhammad V-273
Saur, Genevieve XI-40
Semelsberger, Troy IV-53
Seshadri, Ram. V-298
Simmons, Kevin IV-171
Singh, Prabhakar V-238
Smith, Barton IV-154
Somerday, Brian III-29
Sprik, Sam VII-36
Stair, Peter. V-276
Staudt, Rhonda VII-15
Steinbach, Andrew V-90
Steward, Darlene. XI-56
Stocker, Mike VI-23
St-Pierre, Jean V-135
Stretch, Dale V-170
Suib, Steven V-301
Summers, William II-68

T

Taylor, Robin. II-48
Thornton, Matthew. IV-57
Tieu, Michael VII-45
Tong, YuYe V-309
Turner, John V-44

U

Udovic, Terry IV-126
Ulsh, Michael VI-7

V

Vajo, John IV-84
van Hassel, Bart IV-46
Veenstra, Michael IV-67
Vohs, John V-320
Voth, Gregory V-243

W

Wagener, Earl V-166
Walczyk, Dan VI-17
Wang, Conghua V-231
Wang, Guofeng V-324
Warren, Dave IV-165
Weber, Adam V-141
Wegrzyn, Jim IV-146
Wei, Max V-207
Weimer, Al II-57
Wessel, Silvia V-121
Weyman, Phil II-113
Williamson, Todd II-93
Wolverton, Christopher IV-112

X

Xu, Liwei II-79

Z

Zelenay, Piotr V-74, V-220
Zidan, Ragaiy IV-150

XV. Hydrogen and Fuel Cells Program Contacts

Sunita Satyapal, Director
Fuel Cell Technologies Office
Office of Energy Efficiency and Renewable Energy
U.S. Department of Energy
Phone: (202) 586-2336
Email: Sunita.Satyapal@ee.doe.gov

Rick Farmer, Operations Supervisor
Fuel Cell Technologies Office
Office of Energy Efficiency and Renewable Energy
U.S. Department of Energy
Phone: (202) 586-1623
Email: Richard.Farmer@ee.doe.gov

John Vetrano
Materials Sciences and Engineering Division
Basic Energy Sciences Program
Office of Science
U.S. Department of Energy
Phone: (301) 903-5976
Email: John.Vetrano@science.doe.gov

Guido B. Dehoratiis, Jr.
Division of Advanced Energy Systems
DOE Office of Fossil Energy
Phone: (202) 586-2795
Email: Guido.B.Dehoratiis@hq.doe.gov

Carl Sink
Office of Gas Cooled Reactor Technologies
DOE Office of Nuclear Energy
Phone: (301) 903-5131
Email: Carl.Sink@nuclear.energy.gov

Hydrogen Production and Delivery

Sara Dillich, Acting Hydrogen Production and Delivery Team Leader
Fuel Cell Technologies Office
Office of Energy Efficiency and Renewable Energy
U.S. Department of Energy
Phone: (202) 586-7925
Email: Sara.Dillich@ee.doe.gov

Hydrogen Storage

Ned Stetson, Hydrogen Storage Team Leader
Fuel Cell Technologies Office
Office of Energy Efficiency and Renewable Energy
U.S. Department of Energy
Phone: (202) 586-9995
Email: Ned.Stetson@ee.doe.gov

Fuel Cells

Dimitrios Papageorgopoulos, Fuel Cells Team Leader
Fuel Cell Technologies Office
Office of Energy Efficiency and Renewable Energy
U.S. Department of Energy
Phone: (202) 586-5463
Email: Dimitrios.Papageorgopoulos@ee.doe.gov

Manufacturing R&D

Nancy Garland, Acting Manufacturing R&D Team Leader
Fuel Cell Technologies Office
Office of Energy Efficiency and Renewable Energy
U.S. Department of Energy
Phone: (202) 586-5673
Email: Nancy.Garland@ee.doe.gov

Technology Validation

Jason Marcinkoski, Acting Technology Validation Team Leader
Fuel Cell Technologies Office
Office of Energy Efficiency and Renewable Energy
U.S. Department of Energy
Phone: (202) 586-7466
Email: Jason.Marcinkoski@ee.doe.gov

Safety, Codes & Standards

Charles James Jr., Team Lead
Fuel Cell Technologies Office
Office of Energy Efficiency and Renewable Energy
U.S. Department of Energy
Phone: (202) 287-6223
Email: Charles.James@ee.doe.gov

Education

Gregory J. Kleen, Acting Education Team Leader
Fuel Cell Technologies Office
Golden Field Office
U.S. Department of Energ
Phone: (720) 356-1672
Email: Gregory.Kleen@go.doe.gov

Market Transformation

Pete Devlin, Market Transformation and Interagency Coordination Manager
Fuel Cell Technologies Office
Office of Energy Efficiency and Renewable Energy
U.S. Department of Energy
Phone: (202) 586-4905
Email: Peter.Devlin@ee.doe.gov

Systems Analysis

Fred Joseck, Systems Analysis Team Leader
Fuel Cell Technologies Office
Office of Energy Efficiency and Renewable Energy
U.S. Department of Energy
Phone: (202) 586-7932
Email: Fred.Joseck@ee.doe.gov

American Recovery and Reinvestment Act (ARRA) Activities

Jim Alkire, Project Officer and Leader of Recovery Act Activities
Fuel Cell Technologies Office
Office of Energy Efficiency and Renewable Energy
U.S. Department of Energy
Phone: (720) 356-1426
Email: James.Alkire@go.doe.gov

XVI. Project Listings by State

Alabama

IV.E.3 University of Alabama: Novel Carbon(C)-Boron(B)-Nitrogen(N)-Containing H2 Storage Materials IV-140

IV.F.4 Toray Composites America: Synergistically Enhanced Materials and Design Parameters for Reducing the Cost of Hydrogen Storage Tanks IV-171

Arizona

VI.3 Arizona State University: Adaptive Process Controls and Ultrasonics for High-Temperature PEM MEA Manufacture VI-17

Arkansas

II.C.5 University of Arkansas at Little Rock: Metal Oxide Semiconductor Nanotubular Arrays for Photoelectrochemical Hydrogen Generation II-89

California

II.B.2 Science Applications International Corporation: Solar High-Temperature Water-Splitting Cycle with Quantum Boost II-48

II.B.2 Thermochemical Engineering Solutions: Solar High-Temperature Water-Splitting Cycle with Quantum Boost II-48

II.B.2 University of California, San Diego: Solar High-Temperature Water-Splitting Cycle with Quantum Boost. II-48

II.B.4 Sandia National Laboratories: Solar Hydrogen Production with a Metal Oxide-Based Thermochemical Cycle. II-62

II.C.4 Lawrence Livermore National Laboratory: Characterization and Optimization of Photoelectrode Surfaces for Solar-to-Chemical Fuel Conversion II-84

II.C.5 University of Nevada, Reno: Metal Oxide Semiconductor Nanotubular Arrays for Photoelectrochemical Hydrogen Generation II-89

II.C.7 California Institute of Technology: Next-Generation Si Microwire Array Devices for Unassisted Photoelectrosynthesis. II-97

II.D.1 University of California, Berkeley: Maximizing Light Utilization Efficiency and Hydrogen Production in Microalgal Cultures II-101

II.D.4 J. Craig Venter Institute: Hydrogen from Water in a Novel Recombinant Oxygen-Tolerant Cyanobacterial System. II-113

III.5 Sandia National Laboratories: Hydrogen Embrittlement of Structural Steels III-29

III.7 Ben C. Gerwick Inc.: Vessel Design and Fabrication Technology for Stationary High-Pressure Hydrogen Storage. III-37

III.8 Lawrence Livermore National Laboratory: Rapid High-Pressure Liquid Hydrogen Refueling for Maximum Range and Dormancy. III-42

III.8 Linde LLC: Rapid High-Pressure Liquid Hydrogen Refueling for Maximum Range and Dormancy. III-42

III.9 Sandia National Laboratories: Polymer and Composite Material Performance in Hydrogen III-46

III.10 HyGen Industries: Development of a Centrifugal Hydrogen Pipeline Gas Compressor III-48

IV.A.3 H2 Technology Consulting LLC: Best Practices for Characterizing Engineering Properties of Hydrogen Storage Materials IV-24

IV.B.1 Jet Propulsion Laboratory: Hydrogen Storage Engineering Center of Excellence IV-29

IV.B.1 California Institute of Technology: Hydrogen Storage Engineering Center of Excellence IV-29

IV.C.1 H2 Technology Consulting LLC: Hydrogen Sorbent Measurement Qualification and Characterization IV-80

IV.C.2 HRL Laboratories, LLC: Room Temperature Hydrogen Storage in Nano-Confined Liquids IV-84

California (Continued)

IV.C.3 Lawrence Berkeley National Laboratory: Hydrogen Storage in Metal-Organic Frameworks IV-89

IV.D.1 California Institute of Technology: Design of Novel Multi-Component Metal Hydride-Based Mixtures for Hydrogen Storage IV-112

V.A.2 Stanford University: Extended, Continuous Pt Nanostructures in Thick, Dispersed Electrodes. V-14

V.A.3 Jet Propulsion Laboratory: Nanosegregated Cathode Catalysts with Ultra-Low Platinum Loading V-19

V.A.5 University of California, Riverside: The Science and Engineering of Durable Ultra-Low PGM Catalysts . . . V-31

V.C.1 Lawrence Berkeley National Laboratory: High-Performance, Durable, Low-Cost Membrane Electrode Assemblies for Transportation Applications V-90

V.D.1 Lawrence Berkeley National Laboratory: Durability Improvements through Degradation Mechanism Studies V-98

V.D.3 Lawrence Berkeley National Laboratory: Accelerated Testing Validation. V-109

V.F.1 Lawrence Berkeley National Laboratory: Fuel Cell Fundamentals at Low and Subzero Temperatures V-141

V.F.4 Lawrence Berkeley National Laboratory: Transport Studies Enabling Efficiency Optimization of Cost-Competitive Fuel Cell Stacks V-159

V.G.3 Electricore, Inc.: Roots Air Management System with Integrated Expander. V-170

V.H.5 University of California, Irvine: Enlarging the Potential Market for Stationary Fuel Cells Through System Design Optimization V-199

V.H.7 Lawrence Berkeley National Laboratory: A Total Cost of Ownership Model for Design and Manufacturing Optimization of Fuel Cells in Stationary and Emerging Market Applications V-207

V.H.7 University of California, Berkeley: A Total Cost of Ownership Model for Design and Manufacturing Optimization of Fuel Cells in Stationary and Emerging Market Applications. V-207

V.N.9 University of Southern California, Los Angeles: Nanoporous Membranes for Hydrogen Production: Experimental Studies and Molecular Simulations V-273

V.N.16 University of California, Santa Barbara: Platinum-Group Metal (PGM) Substituted Complex Oxide Catalysts V-298

VI.6 Quantum Fuel Systems Technologies Worldwide, Inc.: Development of Advanced Manufacturing Technologies for Low-Cost Hydrogen Storage Vessels. VI-30

VII.11 Linde LLC: Performance Evaluation of Delivered Hydrogen Fueling Stations VII-45

VIII.4 Sandia National Laboratories: R&D for Safety, Codes and Standards: Materials and Components Compatibility VIII-22

VIII.6 Sandia National Laboratories: R&D for Safety Codes and Standards: Hydrogen Release Behavior. VIII-33

VIII.7 Sandia National Laboratories: R&D for Safety Codes and Standards: Risk Assessment VIII-39

VIII.8 California Fuel Cell Partnership: Hydrogen Emergency Response Training for First Responders VIII-43

VIII.9 Fluer, Inc. : Hydrogen Safety Panel and Hydrogen Safety Knowledge Tools. VIII-46

VIII.9 City of Santa Fe Springs: Hydrogen Safety Panel and Hydrogen Safety Knowledge Tools. VIII-46

VIII.10 Zero Carbon Energy Solutions: International Partnership for Hydrogen & Fuel Cells in the Economy - Regulations Codes and Standards Working Group VIII-51

IX.1 Oorja Protonics, Inc.: Direct Methanol Fuel Cell Material Handling Equipment Deployment IX-7

X.1 Electricore, Inc.: Solid Oxide Fuel Cell Diesel Auxiliary Power Unit Demonstration. X-7

X.2 ClearEdge Power: Highly Efficient, 5-kW CHP Fuel Cells Demonstrating Durability and Economic Value in Residential and Light Commercial Applications X-10

X.4 Altergy Systems: Use of 72-Hour Hydrogen PEM Fuel Cell Systems to Support Emergency Communications X-16

XI.2 University of California: Siting Strategies for Early H2 Refueling Infrastructure in California: Learning from the Gasoline Experience XI-17

XI.3 University of California: Design and Economics of an Early Hydrogen Refueling Network for California XI-21

California (Continued)

XI.9 Sandia National Laboratories: Global Hydrogen Resource Analysis XI-44

Colorado

II.A.2 National Renewable Energy Laboratory: Renewable Electrolysis Integrated Systems Development and Testing II-15
II.A.2 Spectrum Automation Controls: Renewable Electrolysis Integrated Systems Development and Testing II-15
II.B.3 University of Colorado: Solar-Thermal Redox-Based Water Splitting Cycles II-57
II.B.4 University of Colorado: Solar Hydrogen Production with a Metal Oxide-Based Thermochemical Cycle II-62
II.B.4 Colorado School of Mines: Solar Hydrogen Production with a Metal Oxide-Based Thermochemical Cycle II-62
II.C.1 National Renewable Energy Laboratory: Semiconductor Materials for Photoelectrolysis. II-70
II.C.2 MVSystems, Incorporated: Photoelectrochemical Hydrogen Production II-75
II.C.3 National Renewable Energy Laboratory: Critical Research for Cost-Effective Photoelectrochemical Production of Hydrogen II-79
II.C.5 National Renewable Energy Laboratory: Metal Oxide Semiconductor Nanotubular Arrays for Photoelectrochemical Hydrogen Generation II-89
II.D.2 National Renewable Energy Laboratory: Biological Systems for Hydrogen Photoproduction II-105
II.D.3 National Renewable Energy Laboratory: Fermentation and Electrohydrogenic Approaches to Hydrogen Production II-108
II.D.5 National Renewable Energy Laboratory: Probing O2-Tolerant CBS Hydrogenase for Hydrogen Production II-116
II.E.1 National Renewable Energy Laboratory: Distributed Bio-Oil Reforming II-119
III.8 Engineering, Procurement & Construction : Rapid High-Pressure Liquid Hydrogen Refueling for Maximum Range and Dormancy. III-42
IV.B.1 National Renewable Energy Laboratory: Hydrogen Storage Engineering Center of Excellence. IV-29
IV.B.5 National Renewable Energy Laboratory: System Design, Analysis, Modeling, and Media Engineering Properties for Hydrogen Energy Storage IV-57
IV.C.1 National Renewable Energy Laboratory: Hydrogen Sorbent Measurement Qualification and Characterization IV-80
IV.C.6 National Renewable Energy Laboratory: Weak Chemisorption Validation IV-103
V.A.2 National Renewable Energy Laboratory: Extended, Continuous Pt Nanostructures in Thick, Dispersed Electrodes V-14
V.A.2 Colorado School of Mines: Extended, Continuous Pt Nanostructures in Thick, Dispersed Electrodes V-14
V.A.7 National Renewable Energy Laboratory: Tungsten Oxide and Heteropoly Acid-Based Systems for Ultra-High Activity and Stability of Pt Catalysts in PEM Fuel Cell Cathodes. V-44
V.A.7 Colorado School of Mines: Tungsten Oxide and Heteropoly Acid-Based Systems for Ultra-High Activity and Stability of Pt Catalysts in PEM Fuel Cell Cathodes V-44
V.A.7 University of Colorado, Boulder: Tungsten Oxide and Heteropoly Acid-Based Systems for Ultra-High Activity and Stability of Pt Catalysts in PEM Fuel Cell Cathodes V-44
V.D.4 National Renewable Energy Laboratory: Analysis of Laboratory Fuel Cell Technology Status – Voltage Degradation V-116
V.E.1 National Renewable Energy Laboratory: Effect of System Contaminants on PEMFC Performance and Durability V-129
V.E.1 Colorado School of Mines: Effect of System Contaminants on PEMFC Performance and Durability V-129
V.H.5 National Renewable Energy Laboratory: Enlarging the Potential Market for Stationary Fuel Cells Through System Design Optimization V-199
V.L.1 National Renewable Energy Laboratory: Advanced Ionomers and MEAs for Alkaline Membrane Fuel Cells V-235

Colorado (Continued)

V.L.1 Colorado School of Mines: Advanced Ionomers and MEAs for Alkaline Membrane Fuel Cells V-235

VI.1 National Renewable Energy Laboratory: Fuel Cell Membrane Electrode Assembly Manufacturing R&D VI-7

VII.1 National Renewable Energy Laboratory: Technology Validation: Fuel Cell Bus Evaluations VII-7

VII.2 National Renewable Energy Laboratory: Stationary Fuel Cell Evaluation. VII-11

VII.4 National Renewable Energy Laboratory: Hydrogen Component Validation VII-18

VII.4 Spectrum Automation Controls: Hydrogen Component Validation VII-18

VII.5 Proton OnSite: Validation of an Advanced High-Pressure PEM Electrolyzer and Composite Hydrogen Storage, with Data Reporting, for SunHydro Stations VII-22

VII.6 National Renewable Energy Laboratory: Forklift and Backup Power Data Collection and Analysis VII-26

VII.7 National Renewable Energy Laboratory: Fuel Cell Electric Vehicle Evaluation VII-32

VII.8 National Renewable Energy Laboratory: Next Generation Hydrogen Infrastructure Evaluation VII-36

VII.9 California Air Resources Board: Data Collection and Validation of Newport Beach Hydrogen Station Performance VII-41

VII.10 California State University, Los Angeles: California State University Los Angeles Hydrogen Refueling Facility Performance Evaluation and Optimization VII-43

VII.11 Gas Technology Institute: Performance Evaluation of Delivered Hydrogen Fueling Stations. VII-45

VIII.1 National Renewable Energy Laboratory: Fuel Cell Technologies National Codes and Standards Development and Outreach VIII-7

VIII.2 National Renewable Energy Laboratory: Component Standard Research and Development VIII-11

VIII.11 National Renewable Energy Laboratory: NREL Hydrogen Sensor Testing Laboratory VIII-55

IX.1 National Renewable Energy Laboratory: Direct Methanol Fuel Cell Material Handling Equipment Deployment IX-7

IX.7 National Renewable Energy Laboratory: Hawaii Hydrogen Initiative (H2I) Financial Scenario Analysis IX-30

X.1 TDA Research, Inc.: Solid Oxide Fuel Cell Diesel Auxiliary Power Unit Demonstration. X-7

XI.7 National Renewable Energy Laboratory: Pathway Analysis: Projected Cost, Well-to-Wheels Energy Use and Emissions of Current Hydrogen Technologies XI-36

XI.8 National Renewable Energy Laboratory: Hydrogen from Biogas: Resource Assessment XI-40

XI.11 National Renewable Energy Laboratory: Analysis of Fuel Cell Integration with Biofuels Production XI-51

XI.12 National Renewable Energy Laboratory: Analysis of Community Energy XI-56

Connecticut

II.A.3 Proton OnSite: High-Performance, Low-Cost Hydrogen Generation from Renewable Energy. II-18

II.A.4 Proton OnSite: Low-Cost Large-Scale PEM Electrolysis for Renewable Energy Storage II-22

II.A.5 Proton OnSite: Economical Production of Hydrogen through Development of Novel, High Efficiency Electrocatalysts for Alkaline Membrane Electrolysis II-26

II.A.7 Proton OnSite: Hydrogen by Wire - Home Fueling System II-35

II.A.8 Proton OnSite: Low-Noble-Metal-Content Catalysts/Electrodes for Hydrogen Production by Water Electrolysis II-39

III.6 FuelCell Energy, Inc.: Electrochemical Hydrogen Compressor III-33

III.6 Sustainable Innovations, LLC: Electrochemical Hydrogen Compressor III-33

IV.B.1 United Technologies Research Center: Hydrogen Storage Engineering Center of Excellence IV-29

IV.B.3 United Technologies Research Center: Advancement of Systems Designs and Key Engineering Technologies for Materials-Based Hydrogen Storage IV-46

V.B.2 FuelCell Energy, Inc.: High-Temperature Membrane with Humidification-Independent Cluster Structure . . . V-83

Connecticut (Continued)

V.C.2 United Technologies Research Center: Rationally Designed Catalyst Layers for PEMFC Performance Optimization. V-95

V.E.2 University of Connecticut: The Effect of Airborne Contaminants on Fuel Cell Performance and Durability V-135

V.E.2 UTC Power: The Effect of Airborne Contaminants on Fuel Cell Performance and Durability. V-135

V.F.1 United Technologies Research Center: Fuel Cell Fundamentals at Low and Subzero Temperatures V-141

V.M.1 University of Connecticut: Improving Fuel Cell Durability and Reliability. V-238

V.N.17 University of Connecticut: Porous Transition Metal Oxides: Synthesis, Characterization, and Catalytic Activity. V-301

V.N.18 University of Connecticut: Understanding the Effects of Surface Chemistry and Microstructure on the Activity and Stability of Pt Electrocatalysts on Non-Carbon Supports V-305

VI.2 UTC Power: Manufacturing of Low-Cost, Durable Membrane Electrode Assemblies Engineered for Rapid Conditioning. VI-11

VII.5 SunHydro LLC: Validation of an Advanced High-Pressure PEM Electrolyzer and Composite Hydrogen Storage, with Data Reporting, for SunHydro Stations VII-22

VIII.1 Kelvin Hecht: Fuel Cell Technologies National Codes and Standards Development and Outreach VIII-7

VIII.9 GWS Solutions of Tolland, LLC: Hydrogen Safety Panel and Hydrogen Safety Knowledge Tools. VIII-46

Delaware

IV.D.2 Delaware State University: Hydrogen Storage Materials for Fuel Cell-Powered Vehicles. IV-121

IV.D.2 University of Delaware: Hydrogen Storage Materials for Fuel Cell-Powered Vehicles IV-121

V.A.2 University of Delaware: Extended, Continuous Pt Nanostructures in Thick, Dispersed Electrodes. V-14

V.B.3 Ion Power Inc.: Corrugated Membrane Fuel Cell Structures V-86

V.D.1 Ion Power Inc.: Durability Improvements through Degradation Mechanism Studies V-98

V.D.3 Ion Power Inc.: Accelerated Testing Validation. V-109

V.I.2 University of Delaware: Advanced Materials and Concepts for Portable Power Fuel Cells V-220

VI.2 University of Delaware: Manufacturing of Low-Cost, Durable Membrane Electrode Assemblies Engineered for Rapid Conditioning. VI-11

Florida

VIII.9 Addison Bain: Hydrogen Safety Panel and Hydrogen Safety Knowledge Tools VIII-46

Georgia

IV.E.5 Savannah River National Laboratory: Electrochemical Reversible Formation of Alane IV-150

V.D.5 Georgia Institute of Technology: Development of Micro-Structural Mitigation Strategies for PEM Fuel Cells: Morphological Simulations and Experimental Approaches V-121

V.N.8 Georgia Institute of Technology: Precisely Tunable High Performance Carbon Molecular Sieve Membranes for Energy Intensive Separations. V-268

Hawaii

II.C.2 University of Hawaii at Manoa: Photoelectrochemical Hydrogen Production II-75

IV.C.6 University of Hawaii: Weak Chemisorption Validation IV-103

IV.E.2 Hawaii Hydrogen Carriers, LLC: Development of a Practical Hydrogen Storage System Based on Liquid Organic Hydrogen Carriers and a Homogeneous Catalyst IV-135

V.E.1 University of Hawaii: Effect of System Contaminants on PEMFC Performance and Durability V-129

V.E.2 Hawaii Natural Energy Institute: The Effect of Airborne Contaminants on Fuel Cell Performance and Durability V-135

Hawaii (Continued)

IX.4 Hawaii Natural Energy Institute: Hydrogen Energy Systems as a Grid Management Tool IX-19

Illinois

II.A.5 Illinois Institute of Technology: Economical Production of Hydrogen through Development of Novel, High Efficiency Electrocatalysts for Alkaline Membrane Electrolysis II-26
II.B.1 Argonne National Laboratory: Electrolyzer Development in the Cu-Cl Thermochemical Cycle II-43
II.B.1 Gas Technology Institute: Electrolyzer Development in the Cu-Cl Thermochemical Cycle II-43
II.B.1 Orion Enterprises, Inc.: Electrolyzer Development in the Cu-Cl Thermochemical Cycle II-43
III.1 Argonne National Laboratory: Hydrogen Delivery Infrastructure Analysis III-11
IV.A.1 Argonne National Laboratory: System Analysis of Physical and Materials-Based Hydrogen Storage Options IV-11
IV.C.5 Northwestern University: Metallation of Metal–Organic Frameworks: En Route to Ambient Temperature Storage of Molecular Hydrogen IV-99
IV.D.1 Northwestern University: Design of Novel Multi-Component Metal Hydride-Based Mixtures for Hydrogen Storage IV-112
V.A.3 Argonne National Laboratory: Nanosegregated Cathode Catalysts with Ultra-Low Platinum Loading V-19
V.A.8 Illinois Institute of Technology: Synthesis and Characterization of Mixed-Conducting Corrosion Resistant Oxide Supports V-50
V.C.1 Argonne National Laboratory: High-Performance, Durable, Low-Cost Membrane Electrode Assemblies for Transportation Applications V-90
V.C.2 Argonne National Laboratory: Rationally Designed Catalyst Layers for PEMFC Performance Optimization V-95
V.D.1 Argonne National Laboratory: Durability Improvements through Degradation Mechanism Studies V-98
V.D.2 Argonne National Laboratory: Durability of Low-Platinum Fuel Cells Operating at High Power Density V-104
V.H.1 Argonne National Laboratory: Fuel Cells Systems Analysis V-175
V.I.1 Illinois Institute of Technology: Novel Materials for High Efficiency Direct Methanol Fuel Cells V-216
V.K.1 Gas Technology Institute: Low-Cost PEM Fuel Cell Metal Bipolar Plates V-231
V.N.1 University of Chicago: Computer Simulation of Proton Transport in Fuel Cell Membranes V-243
V.N.10 Argonne National Laboratory: Structure/Composition/Function Relationships in Supported Nanoscale Catalysts for Hydrogen V-276
IX.3 Gas Technology Institute: Landfill Gas-to-Hydrogen IX-16
IX.6 Argonne National Laboratory: Fuel Cells as Range Extenders for Battery Electric Vehicles IX-26
XI.5 Argonne National Laboratory: Life-Cycle Analysis of Hydrogen Onboard Storage Options XI-29
XI.6 Argonne National Laboratory: Employment Impacts of Infrastructure Development for Hydrogen and Fuel Cell Technologies XI-33
XI.6 RCF Economic and Financial Consulting, Inc.: Employment Impacts of Infrastructure Development for Hydrogen and Fuel Cell Technologies XI-33
XI.10 Argonne National Laboratory: Life-Cycle Analysis of Water Use for Hydrogen Production Pathways XI-48
V.C.2 Indiana University Purdue University: Rationally Designed Catalyst Layers for PEMFC Performance Optimization V-95

Kansas

X.4 Black & Veatch Corporation: Use of 72-Hour Hydrogen PEM Fuel Cell Systems to Support Emergency Communications X-16
X.4 Ericsson Services, Inc.: Use of 72-Hour Hydrogen PEM Fuel Cell Systems to Support Emergency Communications X-16

Maryland

IV.B.5 Mark Paster: System Design, Analysis, Modeling, and Media Engineering Properties for Hydrogen Energy Storage . . . IV-57

IV.C.3 National Institute of Standards and Technology: Hydrogen Storage in Metal-Organic Frameworks . . . IV-89

IV.D.3 National Institute of Standards and Technology: Neutron Characterization in Support of the DOE Hydrogen Storage Sub-Program . . . IV-126

V.C.1 Johns Hopkins University: High-Performance, Durable, Low-Cost Membrane Electrode Assemblies for Transportation Applications . . . V-90

V.D.1 National Institute of Standards and Technology: Durability Improvements through Degradation Mechanism Studies . . . V-98

V.H.4 National Institute of Standards and Technology: Neutron Imaging Study of the Water Transport in Operating Fuel Cells . . . V-193

VI.2 W. L. Gore & Associates, Inc.: Manufacturing of Low-Cost, Durable Membrane Electrode Assemblies Engineered for Rapid Conditioning . . . VI-11

VI.4 National Institute of Standards and Technology: Metrology for Fuel Cell Manufacturing . . . VI-23

Massachusetts

II.A.1 Giner, Inc.: PEM Electrolyzer Incorporating an Advanced Low-Cost Membrane . . . II-11

II.A.6 Giner, Inc.: Unitized Design for Home Refueling Appliance for Hydrogen Generation to 5,000 psi . . . II-31

III.10 Concepts NREC: Development of a Centrifugal Hydrogen Pipeline Gas Compressor . . . III-48

IV.E.3 Protonex Technology Corporation: Novel Carbon(C)-Boron(B)-Nitrogen(N)-Containing H2 Storage Materials . . . IV-140

V.A.4 Massachusetts Institute of Technology: Contiguous Platinum Monolayer Oxygen Reduction Electrocatalysts on High-Stability Low-Cost Supports . . . V-26

V.A.9 Northeastern University: Development of Novel Non-PGM Electrocatalysts for Proton Exchange Membrane Fuel Cell Applications . . . V-54

V.A.10 Massachusetts Institute of Technology: High-Activity Dealloyed Catalysts . . . V-61

V.A.10 Northeastern University: High-Activity Dealloyed Catalysts . . . V-61

V.B.1 Giner, Inc.: Dimensionally Stable High Performance Membrane . . . V-79

V.B.2 Giner, Inc.: High-Temperature Membrane with Humidification-Independent Cluster Structure . . . V-83

V.D.2 Nuvera Fuel Cells, Inc.: Durability of Low-Platinum Fuel Cells Operating at High Power Density . . . V-104

V.F.2 Giner, Inc.: Transport in PEMFCs . . . V-147

V.F.2 Tech-Etch: Transport in PEMFCs . . . V-147

V.F.2 Ballard Material Products, Inc.: Transport in PEMFCs . . . V-147

V.F.4 Nuvera Fuel Cells, Inc.: Transport Studies Enabling Efficiency Optimization of Cost-Competitive Fuel Cell Stacks . . . V-159

V.G.1 Protonex Inc.: Large-Scale Testing, Demonstration and Commercialization of the Nanoparticle-Based Fuel Cell Coolant (SBIR Phase III) . . . V-162

V.K.1 IBIS Associates, Inc.: Low-Cost PEM Fuel Cell Metal Bipolar Plates . . . V-231

V.N.26 Tufts University: Metal Ion Sites on Oxide Supports as Catalysts for the Water-Gas Shift and Methanol Steam Reforming Reactions . . . V-335

VIII.1 National Fire Protection Association: Fuel Cell Technologies National Codes and Standards Development and Outreach . . . VIII-7

VIII.9 Firexplo: Hydrogen Safety Panel and Hydrogen Safety Knowledge Tools . . . VIII-46

IX.3 Ameresco, Inc.: Landfill Gas-to-Hydrogen . . . IX-16

IX.5 Nuvera Fuel Cells, Inc.: Ground Support Equipment Demonstration . . . IX-24

Michigan

III.7 University of Michigan: Vessel Design and Fabrication Technology for Stationary High-Pressure Hydrogen Storage . . . III-37

IV.B.1 General Motors Company: Hydrogen Storage Engineering Center of Excellence . . . IV-29

IV.B.1 Ford Motor Company: Hydrogen Storage Engineering Center of Excellence . . . IV-29

IV.B.1 University of Michigan: Hydrogen Storage Engineering Center of Excellence . . . IV-29

IV.B.6 General Motors Company: Thermal Management of Onboard Cryogenic Hydrogen Storage Systems . . . IV-63

IV.B.7 Ford Motor Company: Ford/BASF-SE/UM Activities in Support of the Hydrogen Storage Engineering Center of Excellence . . . IV-67

IV.B.7 University of Michigan: Ford/BASF-SE/UM Activities in Support of the Hydrogen Storage Engineering Center of Excellence . . . IV-67

IV.C.3 General Motors Company: Hydrogen Storage in Metal-Organic Frameworks . . . IV-89

IV.D.1 Ford Motor Company: Design of Novel Multi-Component Metal Hydride-Based Mixtures for Hydrogen Storage . . . IV-112

IV.E.2 General Motors Company: Development of a Practical Hydrogen Storage System Based on Liquid Organic Hydrogen Carriers and a Homogeneous Catalyst . . . IV-135

IV.F.4 Ford Motor Company: Synergistically Enhanced Materials and Design Parameters for Reducing the Cost of Hydrogen Storage Tanks . . . IV-171

V.A.8 Nissan Technical Center: Synthesis and Characterization of Mixed-Conducting Corrosion Resistant Oxide Supports . . . V-50

V.A.9 Michigan State University: Development of Novel Non-PGM Electrocatalysts for Proton Exchange Membrane Fuel Cell Applications . . . V-54

V.A.9 Nissan Technical Center: Development of Novel Non-PGM Electrocatalysts for Proton Exchange Membrane Fuel Cell Applications . . . V-54

V.A.10 General Motors Company: High-Activity Dealloyed Catalysts . . . V-61

V.B.3 General Motors Company: Corrugated Membrane Fuel Cell Structures . . . V-86

V.C.1 Michigan Technological University: High-Performance, Durable, Low-Cost Membrane Electrode Assemblies for Transportation Applications . . . V-90

V.C.1 General Motors Company: High-Performance, Durable, Low-Cost Membrane Electrode Assemblies for Transportation Applications . . . V-90

V.D.5 Michigan Technological University: Development of Micro-Structural Mitigation Strategies for PEM Fuel Cells: Morphological Simulations and Experimental Approaches . . . V-121

V.F.3 General Motors Company: Investigation of Micro- and Macro-Scale Transport Processes for Improved Fuel Cell Performance . . . V-153

V.G.3 Kettering University: Roots Air Management System with Integrated Expander . . . V-170

V.K.1 Ford Motor Company: Low-Cost PEM Fuel Cell Metal Bipolar Plates . . . V-231

VIII.1 SAE International: Fuel Cell Technologies National Codes and Standards Development and Outreach . . . VIII-7

VIII.9 General Motors Company: Hydrogen Safety Panel and Hydrogen Safety Knowledge Tools . . . VIII-46

X.1 Delphi Automotive Systems, LLC: Solid Oxide Fuel Cell Diesel Auxiliary Power Unit Demonstration . . . X-7

Minnesota

II.A.3 Entegris, Inc.: High-Performance, Low-Cost Hydrogen Generation from Renewable Energy . . . II-18

II.A.4 3M Company: Low-Cost Large-Scale PEM Electrolysis for Renewable Energy Storage . . . II-22

V.A.1 3M Company: Durable Catalysts for Fuel Cell Protection during Transient Conditions . . . V-9

V.A.3 3M Company: Nanosegregated Cathode Catalysts with Ultra-Low Platinum Loading . . . V-19

V.C.1 3M Company: High-Performance, Durable, Low-Cost Membrane Electrode Assemblies for Transportation Applications . . . V-90

V.F.1 3M Company: Fuel Cell Fundamentals at Low and Subzero Temperatures . . . V-141

Minnesota (Continued)

V.L.1 3M Company: Advanced Ionomers and MEAs for Alkaline Membrane Fuel Cells V-235

Missouri

VIII.9 Becht Engineering: Hydrogen Safety Panel and Hydrogen Safety Knowledge Tools VIII-46

X.4 Burns & McDonnell Engineering Co., Inc.: Use of 72-Hour Hydrogen PEM Fuel Cell Systems to Support Emergency Communications X-16

Nebraska

III.3 Hexagon Lincoln: Development of High-Pressure Hydrogen Storage Tank for Storage and Gaseous Truck Delivery III-21

IV.B.1 Hexagon Lincoln: Hydrogen Storage Engineering Center of Excellence IV-29

IV.B.9 Hexagon Lincoln: Development of Improved Composite Pressure Vessels for Hydrogen Storage IV-76

IV.F.4 Hexagon Lincoln: Synergistically Enhanced Materials and Design Parameters for Reducing the Cost of Hydrogen Storage Tanks IV-171

Nevada

II.C.1 University of Nevada, Las Vegas: Semiconductor Materials for Photoelectrolysis II-70

II.C.5 University of Nevada, Las Vegas: Metal Oxide Semiconductor Nanotubular Arrays for Photoelectrochemical Hydrogen Generation II-89

New Jersey

IV.C.7 Rutgers University: Hydrogen Trapping through Designer Hydrogen Spillover Molecules with Reversible Temperature and Pressure-Induced Switching IV-107

V.K.1 TreadStone Technologies, Inc.: Low-Cost PEM Fuel Cell Metal Bipolar Plates V-231

V.N.24 Rutgers University: Nanoscale Surface Chemistry and Electrochemistry of Clean and Metal-Covered Faceted Substrates: Structure, Reactivity and Electronic Properties V-328

VI.5 BASF Fuel Cell, Inc.: High-Speed, Low-Cost Fabrication of Gas Diffusion Electrodes for Membrane Electrode Assemblies VI-27

New Mexico

II.C.6 Los Alamos National Laboratory: Photoelectrochemical Material Synthesis at LANL II-93

IV.B.1 Los Alamos National Laboratory: Hydrogen Storage Engineering Center of Excellence IV-29

IV.B.4 Los Alamos National Laboratory: Chemical Hydride Rate Modeling, Validation, and System Demonstration IV-53

IV.E.1 Los Alamos National Laboratory: Fluid Phase Chemical Hydrogen Storage Materials IV-131

V.A.2 Los Alamos National Laboratory: Extended, Continuous Pt Nanostructures in Thick, Dispersed Electrodes V-14

V.A.5 Los Alamos National Laboratory: The Science and Engineering of Durable Ultra-Low PGM Catalysts. V-31

V.A.5 University of New Mexico: The Science and Engineering of Durable Ultra-Low PGM Catalysts V-31

V.A.6 Los Alamos National Laboratory: Engineered Nano-Scale Ceramic Supports for PEM Fuel Cells V-37

V.A.6 University of New Mexico: Engineered Nano-Scale Ceramic Supports for PEM Fuel Cells V-37

V.A.9 University of New Mexico: Development of Novel Non-PGM Electrocatalysts for Proton Exchange Membrane Fuel Cell Applications V-54

V.A.9 Pajarito Powder: Development of Novel Non-PGM Electrocatalysts for Proton Exchange Membrane Fuel Cell Applications V-54

V.A.9 Los Alamos National Laboratory: Development of Novel Non-PGM Electrocatalysts for Proton Exchange Membrane Fuel Cell Applications. V-54

New Mexico (Continued)

V.A.12 Los Alamos National Laboratory: Non-Precious Metal Fuel Cell Cathodes: Catalyst Development and Electrode Structure Design . . . V-74

V.A.12 IRD Fuel Cells, LLC: Non-Precious Metal Fuel Cell Cathodes: Catalyst Development and Electrode Structure Design . . . V-74

V.D.1 Los Alamos National Laboratory: Durability Improvements through Degradation Mechanism Studies . . . V-98

V.D.1 University of New Mexico: Durability Improvements through Degradation Mechanism Studies . . . V-98

V.D.2 Los Alamos National Laboratory: Durability of Low-Platinum Fuel Cells Operating at High Power Density . . . V-104

V.D.3 Los Alamos National Laboratory: Accelerated Testing Validation. . . . V-109

V.D.3 University of New Mexico: Accelerated Testing Validation . . . V-109

V.D.5 Los Alamos National Laboratory: Development of Micro-Structural Mitigation Strategies for PEM Fuel Cells: Morphological Simulations and Experimental Approaches . . . V-121

V.D.5 University of New Mexico: Development of Micro-Structural Mitigation Strategies for PEM Fuel Cells: Morphological Simulations and Experimental Approaches . . . V-121

V.E.1 Los Alamos National Laboratory: Effect of System Contaminants on PEMFC Performance and Durability . . . V-129

V.F.1 Los Alamos National Laboratory: Fuel Cell Fundamentals at Low and Subzero Temperatures . . . V-141

V.H.8 Los Alamos National Laboratory: Technical Assistance to Developers. . . . V-212

V.I.1 IRD Fuel Cells, LLC: Novel Materials for High Efficiency Direct Methanol Fuel Cells. . . . V-216

V.I.2 Los Alamos National Laboratory: Advanced Materials and Concepts for Portable Power Fuel Cells . . . V-220

V.N.6 University of New Mexico: Nanostructured Catalysts for Hydrogen Production from Renewable Feedstocks . . . V-260

VIII.3 Los Alamos National Laboratory: Hydrogen Safety, Codes and Standards: Sensors. . . . VIII-14

VIII.5 Los Alamos National Laboratory: Hydrogen Fuel Quality . . . VIII-28

New York

II.A.8 Brookhaven National Laboratory: Low-Noble-Metal-Content Catalysts/Electrodes for Hydrogen Production by Water Electrolysis. . . . II-39

II.B.2 Electrosynthesis Co. Inc.: Solar High-Temperature Water-Splitting Cycle with Quantum Boost . . . II-48

III.2 Mohawk Innovative Technologies, Inc.: Oil-Free Centrifugal Hydrogen Compression Technology Demonstration . . . III-16

IV.E.4 Brookhaven National Laboratory: Aluminum Hydride: the Organometallic Approach . . . IV-146

V.A.2 State University of New York, Albany: Extended, Continuous Pt Nanostructures in Thick, Dispersed Electrodes. . . . V-14

V.A.4 Brookhaven National Laboratory: Contiguous Platinum Monolayer Oxygen Reduction Electrocatalysts on High-Stability Low-Cost Supports . . . V-26

V.A.12 General Motors Company: Non-Precious Metal Fuel Cell Cathodes: Catalyst Development and Electrode Structure Design . . . V-74

V.A.12 University of Rochester: Non-Precious Metal Fuel Cell Cathodes: Catalyst Development and Electrode Structure Design . . . V-74

V.E.1 General Motors Company: Effect of System Contaminants on PEMFC Performance and Durability . . . V-129

V.F.3 Rochester Institute of Technology: Investigation of Micro- and Macro-Scale Transport Processes for Improved Fuel Cell Performance. . . . V-153

V.F.3 University of Rochester: Investigation of Micro- and Macro-Scale Transport Processes for Improved Fuel Cell Performance . . . V-153

V.I.2 Brookhaven National Laboratory: Advanced Materials and Concepts for Portable Power Fuel Cells . . . V-220

V.K.1 Stony Brook University: Low-Cost PEM Fuel Cell Metal Bipolar Plates. . . . V-231

New York (Continued)

V.N.5 Columbia University: Structure-Property Relationship in Metal Carbides and Bimetallic Alloys V-257

V.N.11 Brookhaven National Laboratory: Metal and Metal Oxide-Supported Platinum Monolayer Electrocatalysts for Oxygen Reduction V-280

V.N.12 Brookhaven National Laboratory: Active Sites and Mechanism for the Water-Gas Shift Reaction on Metal and Metal/Oxide Catalysts. V-284

VI.3 Rensselaer Polytechnic Institute: Adaptive Process Controls and Ultrasonics for High-Temperature PEM MEA Manufacture VI-17

VII.3 H2Pump LLC: Hydrogen Recycling System Evaluation and Data Collection VII-15

IX.5 Plug Power Inc.: Ground Support Equipment Demonstration IX-24

X.2 Plug Power Inc.: Highly Efficient, 5-kW CHP Fuel Cells Demonstrating Durability and Economic Value in Residential and Light Commercial Applications X-10

X.3 Plug Power Inc.: Accelerating Acceptance of Fuel Cell Backup Power Systems X-13

Ohio

II.C.3 Midwest Optoelectronics, LLC: Critical Research for Cost-Effective Photoelectrochemical Production of Hydrogen II-79

II.C.3 Xunlight Corporation: Critical Research for Cost-Effective Photoelectrochemical Production of Hydrogen II-79

II.C.3 University of Toledo: Critical Research for Cost-Effective Photoelectrochemical Production of Hydrogen II-79

IV.D.1 Ohio State University: Design of Novel Multi-Component Metal Hydride-Based Mixtures for Hydrogen Storage. IV-112

V.B.3 Graftech International Holdings Inc.: Corrugated Membrane Fuel Cell Structures V-86

V.H.6 Battelle: Stationery and Emerging Market Fuel Cell System Cost Analysis - Material Handling Equipment V-203

V.N.20 Ohio State University: Investigation of the Nature of Active Sites on Heteroatom-Containing Carbon Nano-Structures for Oxygen Reduction Reaction. V-313

VI.5 Case Western Reserve University: High-Speed, Low-Cost Fabrication of Gas Diffusion Electrodes for Membrane Electrode Assemblies. VI-27

VII.1 Battelle: Technology Validation: Fuel Cell Bus Evaluations VII-7

VIII.9 Powdermet Inc.: Hydrogen Safety Panel and Hydrogen Safety Knowledge Tools VIII-46

Oregon

IV.B.1 Oregon State University: Hydrogen Storage Engineering Center of Excellence IV-29

IV.B.8 Oregon State University: Microscale Enhancement of Heat and Mass Transfer for Hydrogen Energy Storage IV-71

IV.E.3 University of Oregon: Novel Carbon(C)-Boron(B)-Nitrogen(N)-Containing H2 Storage Materials IV-140

IX.2 ClearEdge Power: Fuel Cell Combined Heat and Power Commercial Demonstration. IX-11

X.3 IdaTech, LLC: Accelerating Acceptance of Fuel Cell Backup Power Systems X-13

Pennsylvania

II.A.3 Pennsylvania State University: High-Performance, Low-Cost Hydrogen Generation from Renewable Energy II-18

II.B.1 Pennsylvania State University: Electrolyzer Development in the Cu-Cl Thermochemical Cycle II-43

II.B.4 Bucknell University: Solar Hydrogen Production with a Metal Oxide-Based Thermochemical Cycle. II-62

II.D.3 Pennsylvania State University: Fermentation and Electrohydrogenic Approaches to Hydrogen Production II-108

Pennsylvania (Continued)

IV.C.7 Pennsylvania State University: Hydrogen Trapping through Designer Hydrogen Spillover Molecules with Reversible Temperature and Pressure-Induced Switching IV-107
V.A.3 University of Pittsburgh: Nanosegregated Cathode Catalysts with Ultra-Low Platinum Loading V-19
V.A.12 Carnegie Mellon University: Non-Precious Metal Fuel Cell Cathodes: Catalyst Development and Electrode Structure Design V-74
V.F.1 Pennsylvania State University: Fuel Cell Fundamentals at Low and Subzero Temperatures V-141
V.F.3 Pennsylvania State University: Investigation of Micro- and Macro-Scale Transport Processes for Improved Fuel Cell Performance V-153
V.F.4 Pennsylvania State University: Transport Studies Enabling Efficiency Optimization of Cost-Competitive Fuel Cell Stacks V-159
V.G.1 Dynalene Inc.: Large-Scale Testing, Demonstration and Commercialization of the Nanoparticle-Based Fuel Cell Coolant (SBIR Phase III) V-162
V.I.1 Arkema Inc.: Novel Materials for High Efficiency Direct Methanol Fuel Cells V-216
V.N.3 Lehigh University: Gas Transport Across Hyperthin Membranes V-251
V.N.21 University of Pennsylvania: Oxide-Metal Interactions Studied on M@Oxide, Core-Shell Catalysts V-318
V.N.22 University of Pennsylvania: Fundamental Studies of the Steam Reforming of Alcohols on PdZnO and Co/ZnO Catalysts V-320
V.N.23 University of Pittsburgh: Theoretically Relating the Surface Composition of the Pt Alloys to Their Performance as the Electrocatalysts of Low-Temperature Fuel Cells V-324
VIII.9 Air Products and Chemicals, Inc.: Hydrogen Safety Panel and Hydrogen Safety Knowledge Tools VIII-46
X.4 Air Products and Chemicals, Inc.: Use of 72-Hour Hydrogen PEM Fuel Cell Systems to Support Emergency Communications X-16

Rhode Island

V.A.3 Brown University: Nanosegregated Cathode Catalysts with Ultra-Low Platinum Loading V-19

South Carolina

II.B.5 Savannah River National Laboratory: Electrolyzer Development for the HyS Thermochemical Cycle II-68
III.4 Savannah River National Laboratory: Fiber Reinforced Composite Pipeline III-25
IV.B.1 Savannah River National Laboratory: Hydrogen Storage Engineering Center of Excellence IV-29
IV.E.5 Greenway Energy, LLC: Electrochemical Reversible Formation of Alane IV-150
V.A.11 University of South Carolina: Development of Ultra-Low Platinum Alloy Cathode Catalyst for Polymer Electrolyte Membrane Fuel Cells V-68
V.E.1 University of South Carolina: Effect of System Contaminants on PEMFC Performance and Durability V-129
V.F.2 University of South Carolina: Transport in PEMFCs V-147
V.G.2 Tetramer Technologies, LLC: New High-Performance Water Vapor Membranes To Improve Fuel Cell Balance-of-Plant Efficiency and Lower Costs V-166
V.N.2 Clemson University: Fluoropolymers, Electrolytes, Composites and Electrodes V-247
VIII.1 Davidson Code Concepts: Fuel Cell Technologies National Codes and Standards Development and Outreach VIII-7
IX.3 Advanced Technology International: Landfill Gas-to-Hydrogen IX-16

Tennessee

II.A.3 Oak Ridge National Laboratory: High-Performance, Low-Cost Hydrogen Generation from Renewable Energy II-18
III.7 Oak Ridge National Laboratory: Vessel Design and Fabrication Technology for Stationary High-Pressure Hydrogen Storage III-37
IV.C.4 Oak Ridge National Laboratory: The Quantum Effects of Pore Structure on Hydrogen Adsorption IV-93

Tennessee (Continued)

IV.F.1 Oak Ridge National Laboratory: Lifecycle Verification of Polymeric Storage Tank Liners IV-154

IV.F.2 Oak Ridge National Laboratory: Melt Processable PAN Precursor for High-Strength, Low-Cost Carbon Fibers IV-160

IV.F.3 Oak Ridge National Laboratory: Development of Low-Cost, High-Strength Commercial Textile Precursor (PAN-MA) IV-165

IV.F.4 AOC, LLC: Synergistically Enhanced Materials and Design Parameters for Reducing the Cost of Hydrogen Storage Tanks IV-171

V.A.1 Oak Ridge National Laboratory: Durable Catalysts for Fuel Cell Protection during Transient Conditions V-9

V.A.2 Oak Ridge National Laboratory: Extended, Continuous Pt Nanostructures in Thick, Dispersed Electrodes V-14

V.A.2 University of Tennessee: Extended, Continuous Pt Nanostructures in Thick, Dispersed Electrodes V-14

V.A.3 Oak Ridge National Laboratory: Nanosegregated Cathode Catalysts with Ultra-Low Platinum Loading V-19

V.A.6 Oak Ridge National Laboratory: Engineered Nano-Scale Ceramic Supports for PEM Fuel Cells V-37

V.A.9 University of Tennessee: Development of Novel Non-PGM Electrocatalysts for Proton Exchange Membrane Fuel Cell Applications V-54

V.A.12 Oak Ridge National Laboratory: Non-Precious Metal Fuel Cell Cathodes: Catalyst Development and Electrode Structure Design V-74

V.D.1 Oak Ridge National Laboratory: Durability Improvements through Degradation Mechanism Studies V-98

V.D.3 Oak Ridge National Laboratory: Accelerated Testing Validation V-109

V.F.3 University of Tennessee: Investigation of Micro- and Macro-Scale Transport Processes for Improved Fuel Cell Performance V-153

V.G.1 University of Tennessee: Large-Scale Testing, Demonstration and Commercialization of the Nanoparticle-Based Fuel Cell Coolant (SBIR Phase III) V-162

V.H.3 Oak Ridge National Laboratory: Characterization of Fuel Cell Materials V-186

V.I.2 Oak Ridge National Laboratory: Advanced Materials and Concepts for Portable Power Fuel Cells. V-220

V.N.13 Oak Ridge National Laboratory: Fundamentals of Catalysis and Chemical Transformations. V-288

VI.2 University of Tennessee: Manufacturing of Low-Cost, Durable Membrane Electrode Assemblies Engineered for Rapid Conditioning VI-11

XI.1 Oak Ridge National Laboratory: Worldwide Status of Hydrogen Fuel Cell Vehicle Technology and Prospects for Commercialization. XI-13

XI.4 Oak Ridge National Laboratory: Analysis of Optimal Onboard Storage Pressure for Hydrogen Fuel Cell Vehicles. XI-25

Texas

III.10 Texas A&M University: Development of a Centrifugal Hydrogen Pipeline Gas Compressor. III-48

V.C.2 University of Texas at Austin: Rationally Designed Catalyst Layers for PEMFC Performance Optimization. V-95

V.N.4 University of Texas: Theory-Guided Design of Nanoscale Multi-Metallic Catalysts For Fuel Cells. V-254

V.N.7 University of Texas at Austin: Fundamental Structure/Property Studies of Gas Separation Membrane Polymers V-264

V.N.25 University of Texas: Correlation of Theory and Function in Well-Defined Bimetallic Electrocatalysts V-331

VIII.9 William C. Fort: Hydrogen Safety Panel and Hydrogen Safety Knowledge Tools. VIII-46

Utah

III.7 MegaStir Technologies: Vessel Design and Fabrication Technology for Stationary High-Pressure Hydrogen Storage. III-37

Virginia

II.A.1 Virginia Polytechnic Institute and State University: PEM Electrolyzer Incorporating an Advanced Low-Cost Membrane II-11

IV.A.2 Strategic Analysis, Inc.: Hydrogen Storage Cost Analysis IV-18

IV.B.5 Strategic Analysis, Inc.: System Design, Analysis, Modeling, and Media Engineering Properties for Hydrogen Energy Storage. IV-57

IV.F.2 Virginia Polytechnic Institute and State University: Melt Processable PAN Precursor for High-Strength, Low-Cost Carbon Fibers IV-160

V.F.2 Virginia Polytechnic Institute and State University: Transport in PEMFCs V-147

V.H.2 Strategic Analysis, Inc.: Fuel Cell Transportation Cost Analysis V-181

V.H.7 Strategic Analysis, Inc.: A Total Cost of Ownership Model for Design and Manufacturing Optimization of Fuel Cells in Stationary and Emerging Market Applications V-207

V.I.2 Virginia Polytechnic Institute and State University: Advanced Materials and Concepts for Portable Power Fuel Cells. V-220

V.N.27 Virginia Tech: Hydrocarbon Oxidation, Dehydrogenation and Coupling over Model Metal Oxide Surfaces V-340

V.N.28 Virginia Tech: Atomic Level Studies of Advanced Catalysts for Hydrodeoxygenation. V-343

VIII.1 Compressed Gas Association: Fuel Cell Technologies National Codes and Standards Development and Outreach VIII-7

X.4 Sprint Nextel: Use of 72-Hour Hydrogen PEM Fuel Cell Systems to Support Emergency Communications X-16

Washington

II.E.2 Pacific Northwest National Laboratory: Biomass-Derived Liquids Distributed Reforming II-124

III.7 Global Engineering and Technology: Vessel Design and Fabrication Technology for Stationary High-Pressure Hydrogen Storage. III-37

III.11 Pacific Northwest National Laboratory: Investigation of H2 Diaphragm Compressors to Enable Low-Cost Long-Life Operation III-53

IV.B.1 Pacific Northwest National Laboratory: Hydrogen Storage Engineering Center of Excellence IV-29

IV.B.2 Pacific Northwest National Laboratory: Systems Engineering of Chemical Hydrogen Storage, Pressure Vessel, and Balance of Plant for Onboard Hydrogen Storage IV-38

IV.E.3 Pacific Northwest National Laboratory: Novel Carbon(C)-Boron(B)-Nitrogen(N)-Containing H2 Storage Materials IV-140

IV.F.4 Pacific Northwest National Laboratory: Synergistically Enhanced Materials and Design Parameters for Reducing the Cost of Hydrogen Storage Tanks IV-171

V.J.1 InnovaTek: Power Generation from an Integrated Biomass Reformer and Solid Oxide Fuel Cell (SBIR Phase III Xlerator Program) V-227

V.N.14 Pacific Northwest National Laboratory: Activation of Small Molecules with Bi-Functional Ambiphilic Catalyst Complexes V-292

V.N.15 Pacific Northwest National Laboratory: Bio-Inspired Molecular Catalysts for Oxidation of Hydrogen and Production of Hydrogen: Cheap Metals for Noble Tasks V-295

VI.6 Boeing Research and Technology: Development of Advanced Manufacturing Technologies for Low-Cost Hydrogen Storage Vessels. VI-30

VI.6 Pacific Northwest National Laboratory: Development of Advanced Manufacturing Technologies for Low-Cost Hydrogen Storage Vessels VI-30

VIII.8 Pacific Northwest National Laboratory: Hydrogen Emergency Response Training for First Responders. . . VIII-43

VIII.8 Hanford Fire Department: Hydrogen Emergency Response Training for First Responders VIII-43

VIII.8 Hazardous Materials Management and Emergency Response Training and Eduction Center: Hydrogen Emergency Response Training for First Responders VIII-43

Washington (Continued)

VIII.9 Pacific Northwest National Laboratory: Hydrogen Safety Panel and Hydrogen Safety Knowledge Tools . . . VIII-46

IX.2 Pacific Northwest National Laboratory: Fuel Cell Combined Heat and Power Commercial Demonstration . . . IX-11

X.1 PACCAR, Inc.: Solid Oxide Fuel Cell Diesel Auxiliary Power Unit Demonstration . . . X-7

X.4 ReliOn, Inc.: Use of 72-Hour Hydrogen PEM Fuel Cell Systems to Support Emergency Communications . . . X-16

Washington, D.C.

V.A.10 George Washington University: High-Activity Dealloyed Catalysts . . . V-61

V.N.19 Georgetown University: In Situ NMR/IR/Raman and ab initio DFT Investigations of Pt-Based Mono- and Bi-metallic Nanoscale Electrocatalysts: from Sulfur-Poisoning to Polymer Promoters to Surface Activity Indexes . . . V-309

VIII.1 Fuel Cell and Hydrogen Energy Association: Fuel Cell Technologies National Codes and Standards Development and Outreach . . . VIII-7

XI.1 HD Systems: Worldwide Status of Hydrogen Fuel Cell Vehicle Technology and Prospects for Commercialization . . . XI-13

Wisconsin

V.G.3 Eaton Corporation: Roots Air Management System with Integrated Expander . . . V-170

V.N.29 University of Wisconsin: Atomic-Scale Design of Metal and Alloy Catalysts: A Combined Theoretical and Experimental Approach . . . V-347

II.A.4 University of Wyoming: Low-Cost Large-Scale PEM Electrolysis for Renewable Energy Storage . . . II-22

Foreign Countries

Canada

IV.B.1 Université du Québec à Trois-Rivières: Hydrogen Storage Engineering Center of Excellence . . . IV-29

V.A.1 Dalhousie University: Durable Catalysts for Fuel Cell Protection during Transient Conditions . . . V-9

V.A.1 Automotive Fuel Cell Cooperation: Durable Catalysts for Fuel Cell Protection during Transient Conditions . . . V-9

V.A.5 Ballard Fuel Cells: The Science and Engineering of Durable Ultra-Low PGM Catalysts . . . V-31

V.A.12 University of Waterloo: Non-Precious Metal Fuel Cell Cathodes: Catalyst Development and Electrode Structure Design . . . V-74

V.D.1 Ballard Power Systems: Durability Improvements through Degradation Mechanism Studies . . . V-98

V.D.3 Ballard Power Systems: Accelerated Testing Validation . . . V-109

V.D.5 Ballard Power Systems: Development of Micro-Structural Mitigation Strategies for PEM Fuel Cells: Morphological Simulations and Experimental Approaches . . . V-121

V.D.5 Queen's University: Development of Micro-Structural Mitigation Strategies for PEM Fuel Cells: Morphological Simulations and Experimental Approaches . . . V-121

V.E.2 Ballard Power Systems: The Effect of Airborne Contaminants on Fuel Cell Performance and Durability . . . V-135

V.G.3 Ballard Power Systems: Roots Air Management System with Integrated Expander . . . V-170

V.H.7 Ballard Power Systems: A Total Cost of Ownership Model for Design and Manufacturing Optimization of Fuel Cells in Stationary and Emerging Market Applications . . . V-207

VII.9 Hydrogenics Corporation: Data Collection and Validation of Newport Beach Hydrogen Station Performance . . . VII-41

Canada (Continued)

VII.10 Hydrogenics Corporation: California State University Los Angeles Hydrogen Refueling Facility Performance Evaluation and Optimization VII-43

France

V.D.3 Université de Lorraine: Accelerated Testing Validation V-109

Germany

V.A.10 Technical University Berlin: High-Activity Dealloyed Catalysts V-61

V.I.2 SFC Energy: Advanced Materials and Concepts for Portable Power Fuel Cells V-220

Israel

V.L.1 CellEra, Inc.: Advanced Ionomers and MEAs for Alkaline Membrane Fuel Cells V-235

Japan

III.2 Mitsubishi Heavy Industries, Ltd: Oil-Free Centrifugal Hydrogen Compression Technology Demonstration III-16

South Korea

V.A.11 Yonsei University: Development of Ultra-Low Platinum Alloy Cathode Catalyst for Polymer Electrolyte Membrane Fuel Cells. V-68

United Kingdom

II.A.1 Parker Hannifin Ltd domnick hunter Division: PEM Electrolyzer Incorporating an Advanced Low-Cost Membrane II-11

V.A.4 Johnson Matthey Fuel Cells: Contiguous Platinum Monolayer Oxygen Reduction Electrocatalysts on High-Stability Low-Cost Supports V-26

V.A.10 Johnson Matthey Fuel Cells: High-Activity Dealloyed Catalysts V-61

V.C.2 Johnson Matthey Fuel Cells: Rationally Designed Catalyst Layers for PEMFC Performance Optimization. V-95

V.F.4 Johnson Matthey Fuel Cells: Transport Studies Enabling Efficiency Optimization of Cost-Competitive Fuel Cell Stacks V-159

V.I.2 Johnson Matthey Fuel Cells: Advanced Materials and Concepts for Portable Power Fuel Cells V-220

XVII. Project Listings by Organization

3M Company

II.A.4 Low-Cost Large-Scale PEM Electrolysis for Renewable Energy Storage II-22
V.A.1 Durable Catalysts for Fuel Cell Protection during Transient Conditions V-9
V.A.3 Nanosegregated Cathode Catalysts with Ultra-Low Platinum Loading V-19
V.C.1 High-Performance, Durable, Low-Cost Membrane Electrode Assemblies for Transportation Applications V-90
V.F.1 Fuel Cell Fundamentals at Low and Subzero Temperatures V-141
V.L.1 Advanced Ionomers and MEAs for Alkaline Membrane Fuel Cells. V-235

Addison Bain

VIII.9 Hydrogen Safety Panel and Hydrogen Safety Knowledge Tools. VIII-46

Advanced Technology International

IX.3 Landfill Gas-to-Hydrogen IX-16

Air Products and Chemicals, Inc.

VIII.9 Hydrogen Safety Panel and Hydrogen Safety Knowledge Tools. VIII-46
X.4 Use of 72-Hour Hydrogen PEM Fuel Cell Systems to Support Emergency Communications. X-16

Altergy Systems

X.4 Use of 72-Hour Hydrogen PEM Fuel Cell Systems to Support Emergency Communications. X-16

Ameresco, Inc.

IX.3 Landfill Gas-to-Hydrogen IX-16

AOC, LLC

IV.F.4 Synergistically Enhanced Materials and Design Parameters for Reducing the Cost of Hydrogen Storage Tanks IV-171

Argonne National Laboratory

II.B.1 Electrolyzer Development in the Cu-Cl Thermochemical Cycle II-43
III.1 Hydrogen Delivery Infrastructure Analysis III-11
IV.A.1 System Analysis of Physical and Materials-Based Hydrogen Storage Options IV-11
V.A.3 Nanosegregated Cathode Catalysts with Ultra-Low Platinum Loading V-19
V.C.1 High-Performance, Durable, Low-Cost Membrane Electrode Assemblies for Transportation Applications V-90
V.C.2 Rationally Designed Catalyst Layers for PEMFC Performance Optimization. V-95
V.D.1 Durability Improvements through Degradation Mechanism Studies V-98
V.D.2 Durability of Low-Platinum Fuel Cells Operating at High Power Density V-104
V.H.1 Fuel Cells Systems Analysis V-175
V.N.10 Structure/Composition/Function Relationships in Supported Nanoscale Catalysts for Hydrogen V-276
IX.6 Fuel Cells as Range Extenders for Battery Electric Vehicles IX-26
XI.5 Life-Cycle Analysis of Hydrogen Onboard Storage Options XI-29
XI.6 Employment Impacts of Infrastructure Development for Hydrogen and Fuel Cell Technologies XI-33
XI.10 Life-Cycle Analysis of Water Use for Hydrogen Production Pathways XI-48

Arizona State University
VI.3 Adaptive Process Controls and Ultrasonics for High-Temperature PEM MEA Manufacture VI-17

Arkema Inc.
V.I.1 Novel Materials for High Efficiency Direct Methanol Fuel Cells V-216

Automotive Fuel Cell Cooperation
V.A.1 Durable Catalysts for Fuel Cell Protection during Transient Conditions V-9

Ballard Fuel Cells
V.A.5 The Science and Engineering of Durable Ultra-Low PGM Catalysts. V-31

Ballard Material Products, Inc.
V.F.2 Transport in PEMFCs V-147

Ballard Power Systems
V.D.1 Durability Improvements through Degradation Mechanism Studies V-98
V.D.3 Accelerated Testing Validation V-109
V.D.5 Development of Micro-Structural Mitigation Strategies for PEM Fuel Cells: Morphological Simulations and Experimental Approaches. V-121
V.E.2 The Effect of Airborne Contaminants on Fuel Cell Performance and Durability V-135
V.G.3 Roots Air Management System with Integrated Expander V-170
V.H.7 A Total Cost of Ownership Model for Design and Manufacturing Optimization of Fuel Cells in Stationary and Emerging Market Applications V-207

BASF Fuel Cell, Inc.
VI.5 High-Speed, Low-Cost Fabrication of Gas Diffusion Electrodes for Membrane Electrode Assemblies. VI-27

Battelle
V.H.6 Stationery and Emerging Market Fuel Cell System Cost Analysis - Material Handling Equipment. V-203
VII.1 Technology Validation: Fuel Cell Bus Evaluations VII-7

Becht Engineering
VIII.9 Hydrogen Safety Panel and Hydrogen Safety Knowledge Tools. VIII-46

Ben C. Gerwick Inc.
III.7 Vessel Design and Fabrication Technology for Stationary High-Pressure Hydrogen Storage III-37

Black & Veatch Corporation
X.4 Use of 72-Hour Hydrogen PEM Fuel Cell Systems to Support Emergency Communications. X-16

Boeing Research and Technology
VI.6 Development of Advanced Manufacturing Technologies for Low-Cost Hydrogen Storage Vessels VI-30

Brookhaven National Laboratory
II.A.8 Low-Noble-Metal-Content Catalysts/Electrodes for Hydrogen Production by Water Electrolysis II-39
IV.E.4 Aluminum Hydride: the Organometallic Approach IV-146
V.A.4 Contiguous Platinum Monolayer Oxygen Reduction Electrocatalysts on High-Stability Low-Cost Supports. V-26
V.I.2 Advanced Materials and Concepts for Portable Power Fuel Cells V-220

Brookhaven National Laboratory (Continued)
V.N.11 Metal and Metal Oxide-Supported Platinum Monolayer Electrocatalysts for Oxygen Reduction. V-280
V.N.12 Active Sites and Mechanism for the Water-Gas Shift Reaction on Metal and Metal/Oxide Catalysts V-284

Brown University
V.A.3 Nanosegregated Cathode Catalysts with Ultra-Low Platinum Loading V-19

Bucknell University
II.B.4 Solar Hydrogen Production with a Metal Oxide-Based Thermochemical Cycle II-62

Burns & McDonnell Engineering Co., Inc.
X.4 Use of 72-Hour Hydrogen PEM Fuel Cell Systems to Support Emergency Communications. X-16

California Air Resources Board
VII.9 Data Collection and Validation of Newport Beach Hydrogen Station Performance VII-41

California Fuel Cell Partnership
VIII.8 Hydrogen Emergency Response Training for First Responders VIII-43

California Institute of Technology
II.C.7 Next-Generation Si Microwire Array Devices for Unassisted Photoelectrosynthesis II-97
IV.B.1 Hydrogen Storage Engineering Center of Excellence IV-29
IV.D.1 Design of Novel Multi-Component Metal Hydride-Based Mixtures for Hydrogen Storage IV-112

California State University, Los Angeles
VII.10 California State University Los Angeles Hydrogen Refueling Facility Performance Evaluation and Optimization. VII-43

Carnegie Mellon University
V.A.12 Non-Precious Metal Fuel Cell Cathodes: Catalyst Development and Electrode Structure Design V-74

Case Western Reserve University
VI.5 High-Speed, Low-Cost Fabrication of Gas Diffusion Electrodes for Membrane Electrode Assemblies. VI-27

CellEra, Inc.
V.L.1 Advanced Ionomers and MEAs for Alkaline Membrane Fuel Cells. V-235

City of Santa Fe Springs
VIII.9 Hydrogen Safety Panel and Hydrogen Safety Knowledge Tools. VIII-46

ClearEdge Power
IX.2 Fuel Cell Combined Heat and Power Commercial Demonstration. IX-11
X.2 Highly Efficient, 5-kW CHP Fuel Cells Demonstrating Durability and Economic Value in Residential and Light Commercial Applications X-10

Clemson University
V.N.2 Fluoropolymers, Electrolytes, Composites and Electrodes. V-247

Colorado School of Mines
II.B.4 Solar Hydrogen Production with a Metal Oxide-Based Thermochemical Cycle II-62
V.A.2 Extended, Continuous Pt Nanostructures in Thick, Dispersed Electrodes. V-14

Colorado School of Mines (Continued)

V.A.7 Tungsten Oxide and Heteropoly Acid-Based Systems for Ultra-High Activity and Stability of Pt Catalysts in PEM Fuel Cell Cathodes . . . V-44

V.E.1 Effect of System Contaminants on PEMFC Performance and Durability . . . V-129

V.L.1 Advanced Ionomers and MEAs for Alkaline Membrane Fuel Cells. . . . V-235

Columbia University

V.N.5 Structure-Property Relationship in Metal Carbides and Bimetallic Alloys . . . V-257

Compressed Gas Association

VIII.1 Fuel Cell Technologies National Codes and Standards Development and Outreach . . . VIII-7

Concepts NREC

III.10 Development of a Centrifugal Hydrogen Pipeline Gas Compressor. . . . III-48

Dalhousie University

V.A.1 Durable Catalysts for Fuel Cell Protection during Transient Conditions . . . V-9

Davidson Code Concepts

VIII.1 Fuel Cell Technologies National Codes and Standards Development and Outreach . . . VIII-7

Delaware State University

IV.D.2 Hydrogen Storage Materials for Fuel Cell-Powered Vehicles . . . IV-121

Delphi Automotive Systems, LLC

X.1 Solid Oxide Fuel Cell Diesel Auxiliary Power Unit Demonstration. . . . X-7

Dynalene Inc.

V.G.1 Large-Scale Testing, Demonstration and Commercialization of the Nanoparticle-Based Fuel Cell Coolant (SBIR Phase III) . . . V-162

Eaton Corporation

V.G.3 Roots Air Management System with Integrated Expander. . . . V-170

Electricore, Inc.

V.G.3 Roots Air Management System with Integrated Expander. . . . V-170

X.1 Solid Oxide Fuel Cell Diesel Auxiliary Power Unit Demonstration. . . . X-7

Electrosynthesis Co. Inc.

II.B.2 Solar High-Temperature Water-Splitting Cycle with Quantum Boost . . . II-48

Engineering, Procurement & Construction

III.8 Rapid High-Pressure Liquid Hydrogen Refueling for Maximum Range and Dormancy. . . . III-42

Entegris, Inc.

II.A.3 High-Performance, Low-Cost Hydrogen Generation from Renewable Energy . . . II-18

Ericsson Services, Inc.

X.4 Use of 72-Hour Hydrogen PEM Fuel Cell Systems to Support Emergency Communications. . . . X-16

Firexplo

VIII.9 Hydrogen Safety Panel and Hydrogen Safety Knowledge Tools. VIII-46

Fluer, Inc.

VIII.9 Hydrogen Safety Panel and Hydrogen Safety Knowledge Tools. VIII-46

Ford Motor Company

IV.B.1 Hydrogen Storage Engineering Center of Excellence IV-29

IV.B.7 Ford/BASF-SE/UM Activities in Support of the Hydrogen Storage Engineering Center of Excellence. IV-67

IV.D.1 Design of Novel Multi-Component Metal Hydride-Based Mixtures for Hydrogen Storage IV-112

IV.F.4 Synergistically Enhanced Materials and Design Parameters for Reducing the Cost of Hydrogen Storage Tanks IV-171

V.K.1 Low-Cost PEM Fuel Cell Metal Bipolar Plates V-231

Fuel Cell and Hydrogen Energy Association

VIII.1 Fuel Cell Technologies National Codes and Standards Development and Outreach VIII-7

FuelCell Energy, Inc.

III.6 Electrochemical Hydrogen Compressor III-33

V.B.2 High-Temperature Membrane with Humidification-Independent Cluster Structure V-83

Gas Technology Institute

II.B.1 Electrolyzer Development in the Cu-Cl Thermochemical Cycle II-43

V.K.1 Low-Cost PEM Fuel Cell Metal Bipolar Plates V-231

VII.11 Performance Evaluation of Delivered Hydrogen Fueling Stations VII-45

IX.3 Landfill Gas-to-Hydrogen IX-16

General Motors Company

IV.B.1 Hydrogen Storage Engineering Center of Excellence IV-29

IV.B.6 Thermal Management of Onboard Cryogenic Hydrogen Storage Systems IV-63

IV.C.3 Hydrogen Storage in Metal-Organic Frameworks. IV-89

IV.E.2 Development of a Practical Hydrogen Storage System Based on Liquid Organic Hydrogen Carriers and a Homogeneous Catalyst IV-135

V.A.10 High-Activity Dealloyed Catalysts V-61

V.A.12 Non-Precious Metal Fuel Cell Cathodes: Catalyst Development and Electrode Structure Design V-74

V.B.3 Corrugated Membrane Fuel Cell Structures V-86

V.C.1 High-Performance, Durable, Low-Cost Membrane Electrode Assemblies for Transportation Applications V-90

V.E.1 Effect of System Contaminants on PEMFC Performance and Durability V-129

V.F.3 Investigation of Micro- and Macro-Scale Transport Processes for Improved Fuel Cell Performance. V-153

VIII.9 Hydrogen Safety Panel and Hydrogen Safety Knowledge Tools. VIII-46

George Washington University

V.A.10 High-Activity Dealloyed Catalysts V-61

Georgetown University

V.N.19 In Situ NMR/IR/Raman and ab initio DFT Investigations of Pt-Based Mono- and Bi-metallic Nanoscale Electrocatalysts: from Sulfur-Poisoning to Polymer Promoters to Surface Activity Indexes V-309

Georgia Institute of Technology

V.D.5 Development of Micro-Structural Mitigation Strategies for PEM Fuel Cells: Morphological Simulations and Experimental Approaches V-121

V.N.8 Precisely Tunable High Performance Carbon Molecular Sieve Membranes for Energy Intensive Separations V-268

Giner, Inc.

II.A.1 PEM Electrolyzer Incorporating an Advanced Low-Cost Membrane II-11

II.A.6 Unitized Design for Home Refueling Appliance for Hydrogen Generation to 5,000 psi II-31

V.B.1 Dimensionally Stable High Performance Membrane V-79

V.B.2 High-Temperature Membrane with Humidification-Independent Cluster Structure V-83

V.F.2 Transport in PEMFCs V-147

Global Engineering and Technology

III.7 Vessel Design and Fabrication Technology for Stationary High-Pressure Hydrogen Storage III-37

Graftech International Holdings Inc.

V.B.3 Corrugated Membrane Fuel Cell Structures V-86

Greenway Energy, LLC

IV.E.5 Electrochemical Reversible Formation of Alane IV-150

GWS Solutions of Tolland, LLC

VIII.9 Hydrogen Safety Panel and Hydrogen Safety Knowledge Tools. VIII-46

H2 Technology Consulting LLC

IV.A.3 Best Practices for Characterizing Engineering Properties of Hydrogen Storage Materials. IV-24

IV.C.1 Hydrogen Sorbent Measurement Qualification and Characterization IV-80

H2Pump LLC

VII.3 Hydrogen Recycling System Evaluation and Data Collection VII-15

Hanford Fire Department

VIII.8 Hydrogen Emergency Response Training for First Responders VIII-43

Hawaii Hydrogen Carriers, LLC

IV.E.2 Development of a Practical Hydrogen Storage System Based on Liquid Organic Hydrogen Carriers and a Homogeneous Catalyst. IV-135

Hawaii Natural Energy Institute

V.E.2 The Effect of Airborne Contaminants on Fuel Cell Performance and Durability V-135

IX.4 Hydrogen Energy Systems as a Grid Management Tool IX-19

Hazardous Materials Management and Emergency Response Training and Eduction Center

VIII.8 Hydrogen Emergency Response Training for First Responders VIII-43

HD Systems

XI.1 Worldwide Status of Hydrogen Fuel Cell Vehicle Technology and Prospects for Commercialization XI-13

Hexagon Lincoln

III.3 Development of High-Pressure Hydrogen Storage Tank for Storage and Gaseous Truck Delivery III-21

Hexagon Lincoln (Continued)

IV.B.1 Hydrogen Storage Engineering Center of Excellence IV-29

IV.B.9 Development of Improved Composite Pressure Vessels for Hydrogen Storage IV-76

IV.F.4 Synergistically Enhanced Materials and Design Parameters for Reducing the Cost of Hydrogen Storage Tanks IV-171

HRL Laboratories, LLC

IV.C.2 Room Temperature Hydrogen Storage in Nano-Confined Liquids IV-84

Hydrogenics Corporation

VII.9 Data Collection and Validation of Newport Beach Hydrogen Station Performance VII-41

VII.10 California State University Los Angeles Hydrogen Refueling Facility Performance Evaluation and Optimization. VII-43

HyGen Industries

III.10 Development of a Centrifugal Hydrogen Pipeline Gas Compressor III-48

IBIS Associates, Inc.

V.K.1 Low-Cost PEM Fuel Cell Metal Bipolar Plates V-231

IdaTech, LLC

X.3 Accelerating Acceptance of Fuel Cell Backup Power Systems. X-13

Illinois Institute of Technology

II.A.5 Economical Production of Hydrogen through Development of Novel, High Efficiency Electrocatalysts for Alkaline Membrane Electrolysis II-26

V.A.8 Synthesis and Characterization of Mixed-Conducting Corrosion Resistant Oxide Supports V-50

V.I.1 Novel Materials for High Efficiency Direct Methanol Fuel Cells V-216

Indiana University Purdue University

V.C.2 Rationally Designed Catalyst Layers for PEMFC Performance Optimization. V-95

InnovaTek

V.J.1 Power Generation from an Integrated Biomass Reformer and Solid Oxide Fuel Cell (SBIR Phase III Xlerator Program) V-227

Ion Power Inc.

V.B.3 Corrugated Membrane Fuel Cell Structures V-86

V.D.1 Durability Improvements through Degradation Mechanism Studies V-98

V.D.3 Accelerated Testing Validation V-109

IRD Fuel Cells, LLC

V.A.12 Non-Precious Metal Fuel Cell Cathodes: Catalyst Development and Electrode Structure Design V-74

V.I.1 Novel Materials for High Efficiency Direct Methanol Fuel Cells V-216

J. Craig Venter Institute

II.D.4 Hydrogen from Water in a Novel Recombinant Oxygen-Tolerant Cyanobacterial System II-113

Jet Propulsion Laboratory

IV.B.1 Hydrogen Storage Engineering Center of Excellence IV-29

Jet Propulsion Laboratory (Continued)

V.A.3 Nanosegregated Cathode Catalysts with Ultra-Low Platinum Loading V-19

Johns Hopkins University

V.C.1 High-Performance, Durable, Low-Cost Membrane Electrode Assemblies for Transportation Applications V-90

Johnson Matthey Fuel Cells

V.A.4 Contiguous Platinum Monolayer Oxygen Reduction Electrocatalysts on High-Stability Low-Cost Supports V-26

V.A.10 High-Activity Dealloyed Catalysts V-61

V.C.2 Rationally Designed Catalyst Layers for PEMFC Performance Optimization. V-95

V.F.4 Transport Studies Enabling Efficiency Optimization of Cost-Competitive Fuel Cell Stacks V-159

V.I.2 Advanced Materials and Concepts for Portable Power Fuel Cells V-220

Kelvin Hecht

VIII.1 Fuel Cell Technologies National Codes and Standards Development and Outreach VIII-7

Kettering University

V.G.3 Roots Air Management System with Integrated Expander. V-170

Lawrence Berkeley National Laboratory

IV.C.3 Hydrogen Storage in Metal-Organic Frameworks. IV-89

V.C.1 High-Performance, Durable, Low-Cost Membrane Electrode Assemblies for Transportation Applications V-90

V.D.1 Durability Improvements through Degradation Mechanism Studies V-98

V.D.3 Accelerated Testing Validation V-109

V.F.1 Fuel Cell Fundamentals at Low and Subzero Temperatures. V-141

V.F.4 Transport Studies Enabling Efficiency Optimization of Cost-Competitive Fuel Cell Stacks V-159

V.H.7 A Total Cost of Ownership Model for Design and Manufacturing Optimization of Fuel Cells in Stationary and Emerging Market Applications V-207

Lawrence Livermore National Laboratory

II.C.4 Characterization and Optimization of Photoelectrode Surfaces for Solar-to-Chemical Fuel Conversion II-84

III.8 Rapid High-Pressure Liquid Hydrogen Refueling for Maximum Range and Dormancy. III-42

Lehigh University

V.N.3 Gas Transport Across Hyperthin Membranes. V-251

Linde LLC

III.8 Rapid High-Pressure Liquid Hydrogen Refueling for Maximum Range and Dormancy. III-42

VII.11 Performance Evaluation of Delivered Hydrogen Fueling Stations VII-45

Los Alamos National Laboratory

II.C.6 Photoelectrochemical Material Synthesis at LANL II-93

IV.B.1 Hydrogen Storage Engineering Center of Excellence IV-29

IV.B.4 Chemical Hydride Rate Modeling, Validation, and System Demonstration. IV-53

IV.E.1 Fluid Phase Chemical Hydrogen Storage Materials IV-131

V.A.2 Extended, Continuous Pt Nanostructures in Thick, Dispersed Electrodes. V-14

Los Alamos National Laboratory (Continued)

V.A.5 The Science and Engineering of Durable Ultra-Low PGM Catalysts. V-31
V.A.6 Engineered Nano-Scale Ceramic Supports for PEM Fuel Cells V-37
V.A.9 Development of Novel Non-PGM Electrocatalysts for Proton Exchange Membrane Fuel Cell Applications V-54
V.A.12 Non-Precious Metal Fuel Cell Cathodes: Catalyst Development and Electrode Structure Design V-74
V.D.1 Durability Improvements through Degradation Mechanism Studies V-98
V.D.2 Durability of Low-Platinum Fuel Cells Operating at High Power Density V-104
V.D.3 Accelerated Testing Validation V-109
V.D.5 Development of Micro-Structural Mitigation Strategies for PEM Fuel Cells: Morphological Simulations and Experimental Approaches. V-121
V.E.1 Effect of System Contaminants on PEMFC Performance and Durability V-129
V.F.1 Fuel Cell Fundamentals at Low and Subzero Temperatures V-141
V.H.8 Technical Assistance to Developers. V-212
V.I.2 Advanced Materials and Concepts for Portable Power Fuel Cells V-220
VIII.3 Hydrogen Safety, Codes and Standards: Sensors VIII-14
VIII.5 Hydrogen Fuel Quality. VIII-28

Mark Paster

IV.B.5 System Design, Analysis, Modeling, and Media Engineering Properties for Hydrogen Energy Storage IV-57

Massachusetts Institute of Technology

V.A.4 Contiguous Platinum Monolayer Oxygen Reduction Electrocatalysts on High-Stability Low-Cost Supports V-26
V.A.10 High-Activity Dealloyed Catalysts V-61

MegaStir Technologies

III.7 Vessel Design and Fabrication Technology for Stationary High-Pressure Hydrogen Storage III-37

Michigan State University

V.A.9 Development of Novel Non-PGM Electrocatalysts for Proton Exchange Membrane Fuel Cell Applications V-54

Michigan Technological University

V.C.1 High-Performance, Durable, Low-Cost Membrane Electrode Assemblies for Transportation Applications V-90
V.D.5 Development of Micro-Structural Mitigation Strategies for PEM Fuel Cells: Morphological Simulations and Experimental Approaches. V-121

Midwest Optoelectronics, LLC

II.C.3 Critical Research for Cost-Effective Photoelectrochemical Production of Hydrogen II-79

Mitsubishi Heavy Industries, Ltd

III.2 Oil-Free Centrifugal Hydrogen Compression Technology Demonstration. III-16

Mohawk Innovative Technologies, Inc.

III.2 Oil-Free Centrifugal Hydrogen Compression Technology Demonstration. III-16

MVSystems, Incorporated

II.C.2 Photoelectrochemical Hydrogen Production II-75

National Fire Protection Association

VIII.1 Fuel Cell Technologies National Codes and Standards Development and Outreach VIII-7

National Institute of Standards and Technology

IV.C.3 Hydrogen Storage in Metal-Organic Frameworks. IV-89
IV.D.3 Neutron Characterization in Support of the DOE Hydrogen Storage Sub-Program IV-126
V.D.1 Durability Improvements through Degradation Mechanism Studies V-98
V.H.4 Neutron Imaging Study of the Water Transport in Operating Fuel Cells V-193
VI.4 Metrology for Fuel Cell Manufacturing VI-23

National Renewable Energy Laboratory

II.A.2 Renewable Electrolysis Integrated Systems Development and Testing II-15
II.C.1 Semiconductor Materials for Photoelectrolysis II-70
II.C.3 Critical Research for Cost-Effective Photoelectrochemical Production of Hydrogen II-79
II.C.5 Metal Oxide Semiconductor Nanotubular Arrays for Photoelectrochemical Hydrogen Generation II-89
II.D.2 Biological Systems for Hydrogen Photoproduction. II-105
II.D.3 Fermentation and Electrohydrogenic Approaches to Hydrogen Production. II-108
II.D.5 Probing O2-Tolerant CBS Hydrogenase for Hydrogen Production. II-116
II.E.1 Distributed Bio-Oil Reforming II-119
IV.B.1 Hydrogen Storage Engineering Center of Excellence IV-29
IV.B.5 System Design, Analysis, Modeling, and Media Engineering Properties for Hydrogen Energy Storage IV-57
IV.C.1 Hydrogen Sorbent Measurement Qualification and Characterization IV-80
IV.C.6 Weak Chemisorption Validation IV-103
V.A.2 Extended, Continuous Pt Nanostructures in Thick, Dispersed Electrodes. V-14
V.A.7 Tungsten Oxide and Heteropoly Acid-Based Systems for Ultra-High Activity and Stability of Pt Catalysts in PEM Fuel Cell Cathodes V-44
V.D.4 Analysis of Laboratory Fuel Cell Technology Status – Voltage Degradation V-116
V.E.1 Effect of System Contaminants on PEMFC Performance and Durability V-129
V.H.5 Enlarging the Potential Market for Stationary Fuel Cells Through System Design Optimization V-199
V.L.1 Advanced Ionomers and MEAs for Alkaline Membrane Fuel Cells. V-235
VI.1 Fuel Cell Membrane Electrode Assembly Manufacturing R&D VI-7
VII.1 Technology Validation: Fuel Cell Bus Evaluations VII-7
VII.2 Stationary Fuel Cell Evaluation VII-11
VII.4 Hydrogen Component Validation. VII-18
VII.6 Forklift and Backup Power Data Collection and Analysis VII-26
VII.7 Fuel Cell Electric Vehicle Evaluation VII-32
VII.8 Next Generation Hydrogen Infrastructure Evaluation VII-36
VIII.1 Fuel Cell Technologies National Codes and Standards Development and Outreach VIII-7
VIII.2 Component Standard Research and Development. VIII-11
VIII.11 NREL Hydrogen Sensor Testing Laboratory VIII-55
IX.1 Direct Methanol Fuel Cell Material Handling Equipment Deployment IX-7
IX.7 Hawaii Hydrogen Initiative (H2I) Financial Scenario Analysis IX-30
XI.7 Pathway Analysis: Projected Cost, Well-to-Wheels Energy Use and Emissions of Current Hydrogen Technologies. XI-36
XI.8 Hydrogen from Biogas: Resource Assessment XI-40
XI.11 Analysis of Fuel Cell Integration with Biofuels Production XI-51

National Renewable Energy Laboratory (Continued)

XI.12 Analysis of Community Energy XI-56

Nissan Technical Center

V.A.8 Synthesis and Characterization of Mixed-Conducting Corrosion Resistant Oxide Supports V-50

V.A.9 Development of Novel Non-PGM Electrocatalysts for Proton Exchange Membrane Fuel Cell Applications V-54

Northeastern University

V.A.9 Development of Novel Non-PGM Electrocatalysts for Proton Exchange Membrane Fuel Cell Applications V-54

V.A.10 High-Activity Dealloyed Catalysts V-61

IV.C.5 Metallation of Metal–Organic Frameworks: En Route to Ambient Temperature Storage of Molecular Hydrogen. IV-99

IV.D.1 Design of Novel Multi-Component Metal Hydride-Based Mixtures for Hydrogen Storage IV-112

Nuvera Fuel Cells, Inc.

V.D.2 Durability of Low-Platinum Fuel Cells Operating at High Power Density V-104

V.F.4 Transport Studies Enabling Efficiency Optimization of Cost-Competitive Fuel Cell Stacks V-159

Nuvera Fuel Cells, Inc.

IX.5 Ground Support Equipment Demonstration IX-24

Oak Ridge National Laboratory

II.A.3 High-Performance, Low-Cost Hydrogen Generation from Renewable Energy II-18

III.7 Vessel Design and Fabrication Technology for Stationary High-Pressure Hydrogen Storage III-37

IV.C.4 The Quantum Effects of Pore Structure on Hydrogen Adsorption. IV-93

IV.F.1 Lifecycle Verification of Polymeric Storage Tank Liners IV-154

IV.F.2 Melt Processable PAN Precursor for High-Strength, Low-Cost Carbon Fibers. IV-160

IV.F.3 Development of Low-Cost, High-Strength Commercial Textile Precursor (PAN-MA). IV-165

V.A.1 Durable Catalysts for Fuel Cell Protection during Transient Conditions V-9

V.A.2 Extended, Continuous Pt Nanostructures in Thick, Dispersed Electrodes. V-14

V.A.3 Nanosegregated Cathode Catalysts with Ultra-Low Platinum Loading V-19

V.A.6 Engineered Nano-Scale Ceramic Supports for PEM Fuel Cells V-37

V.A.12 Non-Precious Metal Fuel Cell Cathodes: Catalyst Development and Electrode Structure Design V-74

V.D.1 Durability Improvements through Degradation Mechanism Studies V-98

V.D.3 Accelerated Testing Validation V-109

V.H.3 Characterization of Fuel Cell Materials. V-186

V.I.2 Advanced Materials and Concepts for Portable Power Fuel Cells V-220

V.N.13 Fundamentals of Catalysis and Chemical Transformations V-288

XI.1 Worldwide Status of Hydrogen Fuel Cell Vehicle Technology and Prospects for Commercialization XI-13

XI.4 Analysis of Optimal Onboard Storage Pressure for Hydrogen Fuel Cell Vehicles. XI-25

Ohio State University

IV.D.1 Design of Novel Multi-Component Metal Hydride-Based Mixtures for Hydrogen Storage IV-112

V.N.20 Investigation of the Nature of Active Sites on Heteroatom-Containing Carbon Nano-Structures for Oxygen Reduction Reaction V-313

Oorja Protonics, Inc.

IX.1 Direct Methanol Fuel Cell Material Handling Equipment Deployment IX-7

Oregon State University

IV.B.1 Hydrogen Storage Engineering Center of Excellence IV-29

IV.B.8 Microscale Enhancement of Heat and Mass Transfer for Hydrogen Energy Storage IV-71

Orion Enterprises, Inc.

II.B.1 Electrolyzer Development in the Cu-Cl Thermochemical Cycle II-43

PACCAR, Inc.

X.1 Solid Oxide Fuel Cell Diesel Auxiliary Power Unit Demonstration X-7

Pacific Northwest National Laboratory

II.E.2 Biomass-Derived Liquids Distributed Reforming II-124

III.11 Investigation of H2 Diaphragm Compressors to Enable Low-Cost Long-Life Operation III-53

IV.B.1 Hydrogen Storage Engineering Center of Excellence IV-29

IV.B.2 Systems Engineering of Chemical Hydrogen Storage, Pressure Vessel, and Balance of Plant for Onboard Hydrogen Storage IV-38

IV.E.3 Novel Carbon(C)-Boron(B)-Nitrogen(N)-Containing H2 Storage Materials IV-140

IV.F.4 Synergistically Enhanced Materials and Design Parameters for Reducing the Cost of Hydrogen Storage Tanks IV-171

V.N.14 Activation of Small Molecules with Bi-Functional Ambiphilic Catalyst Complexes V-292

V.N.15 Bio-Inspired Molecular Catalysts for Oxidation of Hydrogen and Production of Hydrogen: Cheap Metals for Noble Tasks V-295

VI.6 Development of Advanced Manufacturing Technologies for Low-Cost Hydrogen Storage Vessels VI-30

VIII.8 Hydrogen Emergency Response Training for First Responders VIII-43

VIII.9 Hydrogen Safety Panel and Hydrogen Safety Knowledge Tools VIII-46

IX.2 Fuel Cell Combined Heat and Power Commercial Demonstration IX-11

Pajarito Powder

V.A.9 Development of Novel Non-PGM Electrocatalysts for Proton Exchange Membrane Fuel Cell Applications V-54

Parker Hannifin Ltd domnick hunter Division

II.A.1 PEM Electrolyzer Incorporating an Advanced Low-Cost Membrane II-11

Pennsylvania State University

II.A.3 High-Performance, Low-Cost Hydrogen Generation from Renewable Energy II-18

II.B.1 Electrolyzer Development in the Cu-Cl Thermochemical Cycle II-43

II.D.3 Fermentation and Electrohydrogenic Approaches to Hydrogen Production II-108

IV.C.7 Hydrogen Trapping through Designer Hydrogen Spillover Molecules with Reversible Temperature and Pressure-Induced Switching IV-107

V.F.1 Fuel Cell Fundamentals at Low and Subzero Temperatures V-141

V.F.3 Investigation of Micro- and Macro-Scale Transport Processes for Improved Fuel Cell Performance V-153

V.F.4 Transport Studies Enabling Efficiency Optimization of Cost-Competitive Fuel Cell Stacks V-159

Plug Power Inc.

IX.5 Ground Support Equipment Demonstration IX-24

X.2 Highly Efficient, 5-kW CHP Fuel Cells Demonstrating Durability and Economic Value in Residential and Light Commercial Applications X-10

X.3 Accelerating Acceptance of Fuel Cell Backup Power Systems. X-13

Powdermet Inc.

VIII.9 Hydrogen Safety Panel and Hydrogen Safety Knowledge Tools. VIII-46

Proton OnSite

II.A.3 High-Performance, Low-Cost Hydrogen Generation from Renewable Energy II-18

II.A.4 Low-Cost Large-Scale PEM Electrolysis for Renewable Energy Storage II-22

II.A.5 Economical Production of Hydrogen through Development of Novel, High Efficiency Electrocatalysts for Alkaline Membrane Electrolysis II-26

II.A.7 Hydrogen by Wire - Home Fueling System. II-35

II.A.8 Low-Noble-Metal-Content Catalysts/Electrodes for Hydrogen Production by Water Electrolysis II-39

VII.5 Validation of an Advanced High-Pressure PEM Electrolyzer and Composite Hydrogen Storage, with Data Reporting, for SunHydro Stations. VII-22

Protonex Inc.

V.G.1 Large-Scale Testing, Demonstration and Commercialization of the Nanoparticle-Based Fuel Cell Coolant (SBIR Phase III) V-162

Protonex Technology Corporation

IV.E.3 Novel Carbon(C)-Boron(B)-Nitrogen(N)-Containing H2 Storage Materials. IV-140

Quantum Fuel Systems Technologies Worldwide, Inc.

VI.6 Development of Advanced Manufacturing Technologies for Low-Cost Hydrogen Storage Vessels VI-30

Queen's University

V.D.5 Development of Micro-Structural Mitigation Strategies for PEM Fuel Cells: Morphological Simulations and Experimental Approaches. V-121

RCF Economic and Financial Consulting, Inc.

XI.6 Employment Impacts of Infrastructure Development for Hydrogen and Fuel Cell Technologies XI-33

ReliOn, Inc.

X.4 Use of 72-Hour Hydrogen PEM Fuel Cell Systems to Support Emergency Communications. X-16

Rensselaer Polytechnic Institute

VI.3 Adaptive Process Controls and Ultrasonics for High-Temperature PEM MEA Manufacture VI-17

Rochester Institute of Technology

V.F.3 Investigation of Micro- and Macro-Scale Transport Processes for Improved Fuel Cell Performance. V-153

Rutgers University

IV.C.7 Hydrogen Trapping through Designer Hydrogen Spillover Molecules with Reversible Temperature and Pressure-Induced Switching IV-107

V.N.24 Nanoscale Surface Chemistry and Electrochemistry of Clean and Metal-Covered Faceted Substrates: Structure, Reactivity and Electronic Properties V-328

SAE International

VIII.1 Fuel Cell Technologies National Codes and Standards Development and Outreach VIII-7

Sandia National Laboratories

II.B.4 Solar Hydrogen Production with a Metal Oxide-Based Thermochemical Cycle II-62
III.5 Hydrogen Embrittlement of Structural Steels III-29
III.9 Polymer and Composite Material Performance in Hydrogen III-46
VIII.4 R&D for Safety, Codes and Standards: Materials and Components Compatibility VIII-22
VIII.6 R&D for Safety Codes and Standards: Hydrogen Release Behavior VIII-33
VIII.7 R&D for Safety Codes and Standards: Risk Assessment VIII-39
XI.9 Global Hydrogen Resource Analysis XI-44

Savannah River National Laboratory

II.B.5 Electrolyzer Development for the HyS Thermochemical Cycle II-68
III.4 Fiber Reinforced Composite Pipeline III-25
IV.B.1 Hydrogen Storage Engineering Center of Excellence IV-29
IV.E.5 Electrochemical Reversible Formation of Alane IV-150

Science Applications International Corporation

II.B.2 Solar High-Temperature Water-Splitting Cycle with Quantum Boost II-48

SFC Energy

V.I.2 Advanced Materials and Concepts for Portable Power Fuel Cells V-220

Spectrum Automation Controls

II.A.2 Renewable Electrolysis Integrated Systems Development and Testing II-15
VII.4 Hydrogen Component Validation. VII-18

Sprint Nextel

X.4 Use of 72-Hour Hydrogen PEM Fuel Cell Systems to Support Emergency Communications. X-16

Stanford University

V.A.2 Extended, Continuous Pt Nanostructures in Thick, Dispersed Electrodes. V-14

State University of New York, Albany

V.A.2 Extended, Continuous Pt Nanostructures in Thick, Dispersed Electrodes. V-14

Stony Brook University

V.K.1 Low-Cost PEM Fuel Cell Metal Bipolar Plates V-231

Strategic Analysis, Inc.

IV.A.2 Hydrogen Storage Cost Analysis IV-18
IV.B.5 System Design, Analysis, Modeling, and Media Engineering Properties for Hydrogen Energy Storage IV-57
V.H.2 Fuel Cell Transportation Cost Analysis. V-181
V.H.7 A Total Cost of Ownership Model for Design and Manufacturing Optimization of Fuel Cells in Stationary and Emerging Market Applications V-207

SunHydro LLC

VII.5 Validation of an Advanced High-Pressure PEM Electrolyzer and Composite Hydrogen Storage, with Data Reporting, for SunHydro Stations. VII-22

Sustainable Innovations, LLC
III.6 Electrochemical Hydrogen Compressor III-33

TDA Research, Inc.
X.1 Solid Oxide Fuel Cell Diesel Auxiliary Power Unit Demonstration X-7

Tech-Etch
V.F.2 Transport in PEMFCs V-147

Technical University Berlin
V.A.10 High-Activity Dealloyed Catalysts V-61

Tetramer Technologies, LLC
V.G.2 New High-Performance Water Vapor Membranes To Improve Fuel Cell Balance-of-Plant Efficiency and Lower Costs V-166

Texas A&M University
III.10 Development of a Centrifugal Hydrogen Pipeline Gas Compressor III-48
V.N.4 Theory-Guided Design of Nanoscale Multi-Metallic Catalysts For Fuel Cells V-254

Thermochemical Engineering Solutions
II.B.2 Solar High-Temperature Water-Splitting Cycle with Quantum Boost II-48

Toray Composites America
IV.F.4 Synergistically Enhanced Materials and Design Parameters for Reducing the Cost of Hydrogen Storage Tanks IV-171

TreadStone Technologies, Inc.
V.K.1 Low-Cost PEM Fuel Cell Metal Bipolar Plates V-231

Tufts University
V.N.26 Metal Ion Sites on Oxide Supports as Catalysts for the Water-Gas Shift and Methanol Steam Reforming Reactions V-335

United Technologies Research Center
IV.B.1 Hydrogen Storage Engineering Center of Excellence IV-29
IV.B.3 Advancement of Systems Designs and Key Engineering Technologies for Materials-Based Hydrogen Storage IV-46
V.C.2 Rationally Designed Catalyst Layers for PEMFC Performance Optimization V-95
V.F.1 Fuel Cell Fundamentals at Low and Subzero Temperatures V-141

Université de Lorraine
V.D.3 Accelerated Testing Validation V-109

Université du Québec à Trois-Rivières
IV.B.1 Hydrogen Storage Engineering Center of Excellence IV-29

University of Alabama
IV.E.3 Novel Carbon(C)-Boron(B)-Nitrogen(N)-Containing H2 Storage Materials IV-140

University of Arkansas at Little Rock

II.C.5 Metal Oxide Semiconductor Nanotubular Arrays for Photoelectrochemical Hydrogen Generation II-89

University of California

II.B.2 Solar High-Temperature Water-Splitting Cycle with Quantum Boost II-48

II.D.1 Maximizing Light Utilization Efficiency and Hydrogen Production in Microalgal Cultures II-101

V.A.5 The Science and Engineering of Durable Ultra-Low PGM Catalysts. V-31

V.H.5 Enlarging the Potential Market for Stationary Fuel Cells Through System Design Optimization V-199

V.H.7 A Total Cost of Ownership Model for Design and Manufacturing Optimization of Fuel Cells in Stationary and Emerging Market Applications V-207

V.N.16 Platinum-Group Metal (PGM) Substituted Complex Oxide Catalysts V-298

XI.2 Siting Strategies for Early H2 Refueling Infrastructure in California: Learning from the Gasoline Experience XI-17

XI.3 Design and Economics of an Early Hydrogen Refueling Network for California XI-21

University of Chicago

V.N.1 Computer Simulation of Proton Transport in Fuel Cell Membranes V-243

University of Colorado

II.B.3 Solar-Thermal Redox-Based Water Splitting Cycles II-57

II.B.4 Solar Hydrogen Production with a Metal Oxide-Based Thermochemical Cycle II-62

V.A.7 Tungsten Oxide and Heteropoly Acid-Based Systems for Ultra-High Activity and Stability of Pt Catalysts in PEM Fuel Cell Cathodes V-44

University of Connecticut

V.E.2 The Effect of Airborne Contaminants on Fuel Cell Performance and Durability V-135

V.M.1 Improving Fuel Cell Durability and Reliability. V-238

V.N.17 Porous Transition Metal Oxides: Synthesis, Characterization, and Catalytic Activity V-301

V.N.18 Understanding the Effects of Surface Chemistry and Microstructure on the Activity and Stability of Pt Electrocatalysts on Non-Carbon Supports V-305

University of Delaware

IV.D.2 Hydrogen Storage Materials for Fuel Cell-Powered Vehicles IV-121

V.A.2 Extended, Continuous Pt Nanostructures in Thick, Dispersed Electrodes. V-14

V.I.2 Advanced Materials and Concepts for Portable Power Fuel Cells V-220

VI.2 Manufacturing of Low-Cost, Durable Membrane Electrode Assemblies Engineered for Rapid Conditioning. VI-11

University of Hawaii

II.C.2 Photoelectrochemical Hydrogen Production II-75

IV.C.6 Weak Chemisorption Validation IV-103

V.E.1 Effect of System Contaminants on PEMFC Performance and Durability V-129

University of Michigan

III.7 Vessel Design and Fabrication Technology for Stationary High-Pressure Hydrogen Storage III-37

IV.B.1 Hydrogen Storage Engineering Center of Excellence IV-29

IV.B.7 Ford/BASF-SE/UM Activities in Support of the Hydrogen Storage Engineering Center of Excellence. IV-67

University of Nevada

II.C.1 Semiconductor Materials for Photoelectrolysis II-70

II.C.5 Metal Oxide Semiconductor Nanotubular Arrays for Photoelectrochemical Hydrogen Generation II-89

University of New Mexico

V.A.5 The Science and Engineering of Durable Ultra-Low PGM Catalysts. V-31

V.A.6 Engineered Nano-Scale Ceramic Supports for PEM Fuel Cells V-37

V.A.9 Development of Novel Non-PGM Electrocatalysts for Proton Exchange Membrane Fuel Cell Applications V-54

V.D.1 Durability Improvements through Degradation Mechanism Studies V-98

V.D.3 Accelerated Testing Validation V-109

V.D.5 Development of Micro-Structural Mitigation Strategies for PEM Fuel Cells: Morphological Simulations and Experimental Approaches. V-121

V.N.6 Nanostructured Catalysts for Hydrogen Production from Renewable Feedstocks. V-260

University of Oregon

IV.E.3 Novel Carbon(C)-Boron(B)-Nitrogen(N)-Containing H2 Storage Materials. IV-140

University of Pennsylvania

V.N.21 Oxide-Metal Interactions Studied on M@Oxide, Core-Shell Catalysts V-318

V.N.22 Fundamental Studies of the Steam Reforming of Alcohols on PdZnO and Co/ZnO Catalysts V-320

University of Pittsburgh

V.A.3 Nanosegregated Cathode Catalysts with Ultra-Low Platinum Loading V-19

V.N.23 Theoretically Relating the Surface Composition of the Pt Alloys to Their Performance as the Electrocatalysts of Low-Temperature Fuel Cells. V-324

University of Rochester

V.A.12 Non-Precious Metal Fuel Cell Cathodes: Catalyst Development and Electrode Structure Design V-74

V.F.3 Investigation of Micro- and Macro-Scale Transport Processes for Improved Fuel Cell Performance. V-153

University of South Carolina

V.A.11 Development of Ultra-Low Platinum Alloy Cathode Catalyst for Polymer Electrolyte Membrane Fuel Cells V-68

V.E.1 Effect of System Contaminants on PEMFC Performance and Durability V-129

V.F.2 Transport in PEMFCs V-147

University of Southern California, Los Angeles

V.N.9 Nanoporous Membranes for Hydrogen Production: Experimental Studies and Molecular Simulations V-273

University of Tennessee

V.A.2 Extended, Continuous Pt Nanostructures in Thick, Dispersed Electrodes. V-14

V.A.9 Development of Novel Non-PGM Electrocatalysts for Proton Exchange Membrane Fuel Cell Applications V-54

V.F.3 Investigation of Micro- and Macro-Scale Transport Processes for Improved Fuel Cell Performance. V-153

V.G.1 Large-Scale Testing, Demonstration and Commercialization of the Nanoparticle-Based Fuel Cell Coolant (SBIR Phase III) V-162

VI.2 Manufacturing of Low-Cost, Durable Membrane Electrode Assemblies Engineered for Rapid Conditioning. VI-11

University of Texas

V.C.2 Rationally Designed Catalyst Layers for PEMFC Performance Optimization V-95
V.N.7 Fundamental Structure/Property Studies of Gas Separation Membrane Polymers V-264
V.N.25 Correlation of Theory and Function in Well-Defined Bimetallic Electrocatalysts V-331

University of Toledo

II.C.3 Critical Research for Cost-Effective Photoelectrochemical Production of Hydrogen II-79

University of Waterloo

V.A.12 Non-Precious Metal Fuel Cell Cathodes: Catalyst Development and Electrode Structure Design V-74

University of Wisconsin

V.N.29 Atomic-Scale Design of Metal and Alloy Catalysts: A Combined Theoretical and Experimental Approach V-347

University of Wyoming

II.A.4 Low-Cost Large-Scale PEM Electrolysis for Renewable Energy Storage II-22

UTC Power

V.E.2 The Effect of Airborne Contaminants on Fuel Cell Performance and Durability V-135
VI.2 Manufacturing of Low-Cost, Durable Membrane Electrode Assemblies Engineered for Rapid Conditioning VI-11

Virginia Polytechnic Institute and State University

II.A.1 PEM Electrolyzer Incorporating an Advanced Low-Cost Membrane II-11
IV.F.2 Melt Processable PAN Precursor for High-Strength, Low-Cost Carbon Fibers IV-160
V.F.2 Transport in PEMFCs V-147
V.I.2 Advanced Materials and Concepts for Portable Power Fuel Cells V-220

Virginia Tech

V.N.27 Hydrocarbon Oxidation, Dehydrogenation and Coupling over Model Metal Oxide Surfaces V-340
V.N.28 Atomic Level Studies of Advanced Catalysts for Hydrodeoxygenation V-343

W.L. Gore & Associates, Inc.

VI.2 Manufacturing of Low-Cost, Durable Membrane Electrode Assemblies Engineered for Rapid Conditioning VI-11

William C. Fort

VIII.9 Hydrogen Safety Panel and Hydrogen Safety Knowledge Tools VIII-46

Xunlight Corporation

II.C.3 Critical Research for Cost-Effective Photoelectrochemical Production of Hydrogen II-79

Yonsei University

V.A.11 Development of Ultra-Low Platinum Alloy Cathode Catalyst for Polymer Electrolyte Membrane Fuel Cells V-68

Zero Carbon Energy Solutions

VIII.10 International Partnership for Hydrogen & Fuel Cells in the Economy - Regulations Codes and Standards Working Group VIII-51

U.S. DEPARTMENT OF
ENERGY

www.hydrogen.energy.gov